Comprehensive Coordination Chemistry II

FROM BIOLOGY TO NANOTECHNOLOGY

EDITORS-IN-CHIEF

Jon A McCleverty
Thomas J Meyer

Edited by
L. Que, Jr., W.B. Tolman

Volume 8
Bio-coordination Chemistry

Introduction to Volume 8

Since the publication of CCC (1987), bioinorganic chemistry has blossomed and matured as an interdisciplinary field, which is surveyed in this volume from the perspective of coordination chemistry. Fully comprehensive coverage of biological inorganic chemistry is not possible, so a subset of topics is presented that captures the excitement of the field and reflects the scope and diversity of the systems and research approaches used. As an introduction, a summary of structural motifs that pervade bioinorganic systems is presented (Chapter 1). Subsequent chapters focus on the nature of the metal sites in proteins that participate in electron transfer (Chapters 2–4) and on the transport and storage of metal ions within the biological milieu (Chapters 5–9). The diverse and biologically important array of metalloproteins that bind and activate dioxygen and perform oxidation reactions are then discussed (Chapters 10–18). To complete the presentation of metal–dioxygen chemistry, superoxide processing systems and photosynthetic oxygen evolution are portrayed (Chapters 19–20). The following sections focus on the activation of other small molecules (H_2, Chapter 21; N_2, Chapter 22), mono- and dinuclear metal sites that perform hydrolysis reactions (Chapters 23–24), and the burgeoning bio-organometallic area (Chapter 25). Proteins with synergistic metal–radical sites are discussed in Chapter 26. Iron–sulfur clusters are revisited in Chapter 27, which presents those that are involved in enzyme catalysis rather than simple electron transfer. The role of metal ions in the environmentally significant process of denitrification is the focus of Chapter 28. Finally, the binding of metal ions to DNA and RNA are emphasized in Chapter 29. Together, the array of topics presented in this volume illustrates the importance of coordination chemistry in the biological realm and the breadth of current bioinorganic chemistry research.

L Que, Jr.
Minnesota, USA
March 2003

W B Tolman
Minnesota, USA
March 2003

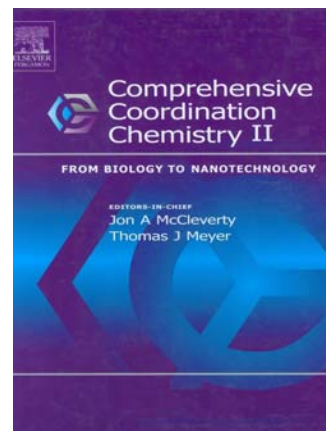# COMPREHENSIVE COORDINATION CHEMISTRY II

From Biology to Nanotechnology

Second Edition

Edited by

J.A. McCleverty, University of Bristol, UK
T.J. Meyer, Los Alamos National Laboratory, Los Alamos, USA

Description

This is the sequel of what has become a classic in the field, Comprehensive Coordination Chemistry. The first edition, CCC-I, appeared in 1987 under the editorship of Sir Geoffrey Wilkinson (Editor-in-Chief), Robert D. Gillard and Jon A. McCleverty (Executive Editors). It was intended to give a contemporary overview of the field, providing both a convenient first source of information and a vehicle to stimulate further advances in the field. The second edition, CCC-II, builds on the first and will survey developments since 1980 authoritatively and critically with a greater emphasis on current trends in biology, materials science and other areas of contemporary scientific interest. Since the 1980s, an astonishing growth and specialisation of knowledge within coordination chemistry, including the rapid development of interdisciplinary fields has made it impossible to provide a totally comprehensive review. CCC-II provides its readers with reliable and informative background information in particular areas based on key primary and secondary references. It gives a clear overview of the state-of-the-art research findings in those areas that the International Advisory Board, the Volume Editors, and the Editors-in-Chief believed to be especially important to the field. CCC-II will provide researchers at all levels of sophistication, from academia, industry and national labs, with an unparalleled depth of coverage.

Bibliographic Information

10-Volume Set - Comprehensive Coordination Chemistry II
Hardbound, ISBN: 0-08-043748-6, 9500 pages
Imprint: ELSEVIER
Price:
USD 5,975
EUR 6,274 Books and electronic products are priced in US dollars (USD) and euro (EUR). USD prices apply world-wide except in Europe and Japan.EUR prices apply in Europe and Japan. See also information about conditions of sale & ordering procedures -http://www.elsevier.com/wps/find/bookconditionsofsale.
cws_home/622954/conditionsofsale, and links to our regional sales officeshttp://www.elsevier.com/wps/find/contact.cws_home/regional
GBP 4,182.50
030/301
Last update: 10 Sep 2005

Volumes

Volume 1: Fundamentals: Ligands, Complexes, Synthesis, Purification, and Structure
Volume 2: Fundamentals: Physical Methods, Theoretical Analysis, and Case Studies
Volume 3: Coordination Chemistry of the s, p, and f Metals
Volume 4: Transition Metal Groups 3 - 6
Volume 5: Transition Metal Groups 7 and 8
Volume 6: Transition Metal Groups 9 - 12
Volume 7: From the Molecular to the Nanoscale: Synthesis, Structure, and Properties
Volume 8: Bio-coordination Chemistry
Volume 9: Applications of Coordination Chemistry
Volume 10: Cumulative Subject Index
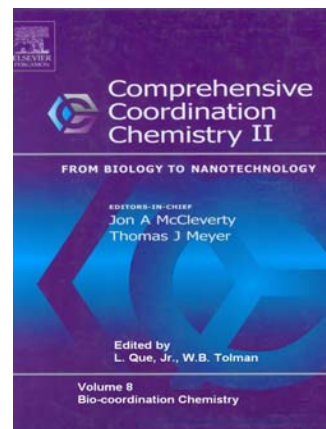
10-Volume Set: Comprehensive Coordination Chemistry II

COMPREHENSIVE COORDINATION CHEMISTRY II

Volume 8:
Bio-coordination Chemistry

Edited by
L. Que, Jr., W.B. Tolman

Contents

8.1
Recurring Structural Motifs in Bioinorganic Chemistry

L. QUE, JR. and W. B. TOLMAN
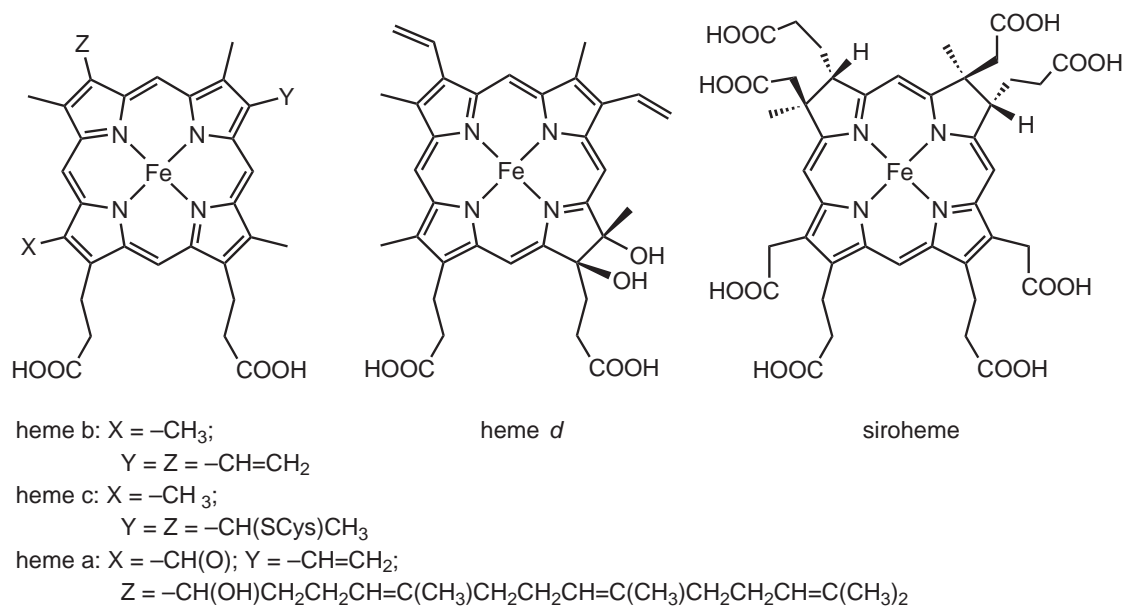### University of Minnesota, Minneapolis, Minnesota, USA
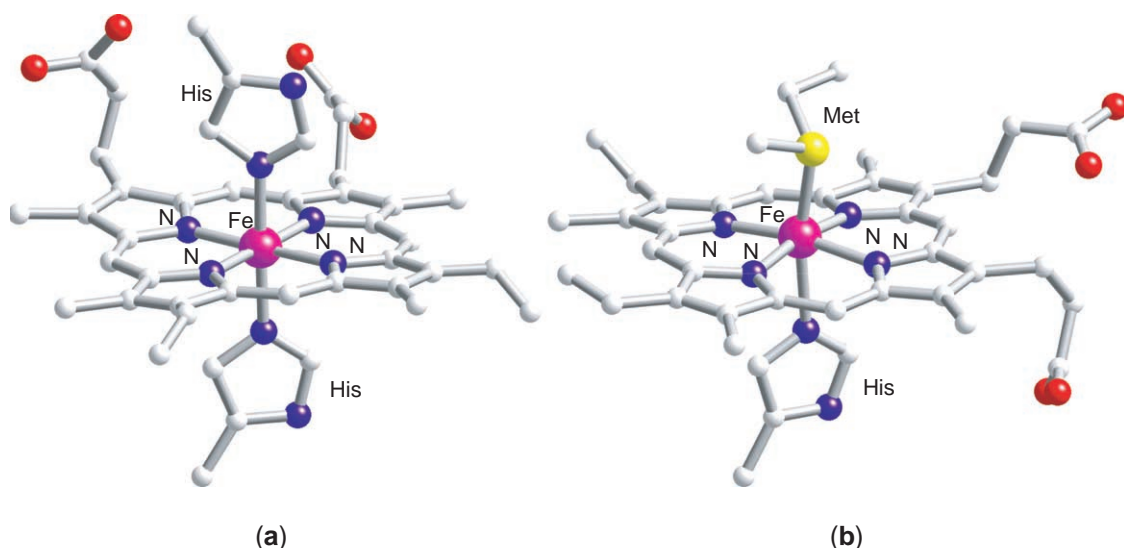
8.1.1   INTRODUCTION

In the sixteen years since the publication of *Comprehensive Coordination Chemistry* (*CCC*, 1987) bioinorganic chemistry has undergone significant development and matured into a multidisciplinary field with coordination chemistry at its locus.[1–6] The field has greatly benefited from advances in macromolecular crystallography, which have led to the structural characterization of many metalloenzyme active sites. From this ever-expanding database can be discerned a number of recurring structural motifs, whose physical and reactivity properties can be further modulated by secondary protein interactions.[7] We present the following overview and accompanying gallery of active-site structures to serve as a framework for the more detailed discussions in the component chapters of this volume. The coverage of topics is not comprehensive; rather, the choice of examples is meant solely to be illustrative of motifs common to multiple metalloprotein systems with often diverse functions.

8.1.2   COMMON MOTIFS WITH NON-AMINO-ACID LIGANDS

Perhaps the most recognizable active-site motif in metalloproteins is the tetradentate porphyrin macrocycle, the organic cofactor associated with heme proteins. The most commonly encountered is protoporphyrin IX or heme b (Figure 1), found in the active sites of dioxygen-binding globins, dioxygen-activating cytochrome P450, H_2O_2-activating peroxidases, and b-type cytochromes involved in electron transfer (see Chapters 8.2, 8.10–8.12, and 8.17). Addition of cysteinyl residues to the two vinyl groups on the porphyrin periphery converts heme b to heme c (Figure 1), which are found in c-type cytochromes that are also involved in electron transfer. With four equatorial sites of a potentially octahedral metal center occupied by this tetrapyrrole macrocycle, the chemistry of the iron can be modulated principally by changing the nature of the fifth and sixth ligands. In electron-transfer proteins, both sites are occupied, usually by His/His or His/Met residues, as in cytochromes b_5[8] and c_{553},[9] respectively (Figure 2). For oxygen-binding globins and heme enzymes, only the fifth (or proximal) site is occupied by a protein residue, leaving the sixth site available for binding small molecules such as O_2, CO, NO, or H_2O_2. The proximal ligand is

heme b: X = –CH$_3$;
        Y = Z = –CH=CH$_2$
heme c: X = –CH$_3$;
        Y = Z = –CH(SCys)CH$_3$
heme a: X = –CH(O); Y = –CH=CH$_2$;
        Z = –CH(OH)CH$_2$CH$_2$CH=C(CH$_3$)CH$_2$CH$_2$CH=C(CH$_3$)CH$_2$CH$_2$CH=C(CH$_3$)$_2$

Figure 1   Drawings of various heme derivatives.

Figure 2   Structures of the active sites of (a) cytochrome b$_5$ (PDB 1CYO); (b) cytochrome c$_{553}$ (PDB 1B7 V).

typically His (myoglobin,[10] hemoglobin, horseradish peroxidase), Tyr (catalase[11]), or Cys (cyto-chrome P450[12] and chloroperoxidase) (Figure 3). The chemistry of the active site can be further affected by second-sphere residues such as Glu or Gln that can hydrogen-bond to the proximal His to modulate its basicity, or those on the distal side that can serve as acids and/or bases to aid in the binding of dioxygen or the cleavage of the O—O bond. The presence or absence of the latter can in fact determine whether a dioxygen moiety in the active site becomes an electrophilic oxidant, as in the case of hydrocarbon-oxidizing cytochrome P450,[13] or acts as a nucleophile, as in the case of the estradiol-producing enzyme aromatase.[14] The rich chemistry of heme proteins and enzymes is discussed in Chapters 8.11, 8.12, and 8.17.

There are other tetrapyrrole macrocycles found in nature besides protoporphyrin IX (Figure 1). Differences with the latter can be as simple as changes in the substituents on the porphyrin periphery, such as in heme a and heme a$_3$, which are key components of the mammalian respiratory enzyme cytochrome oxidase (see Chapter 8.17). Other disparities can entail changes in the oxidation level of the macrocycle, such as the two-electron reduced heme d of cytochrome
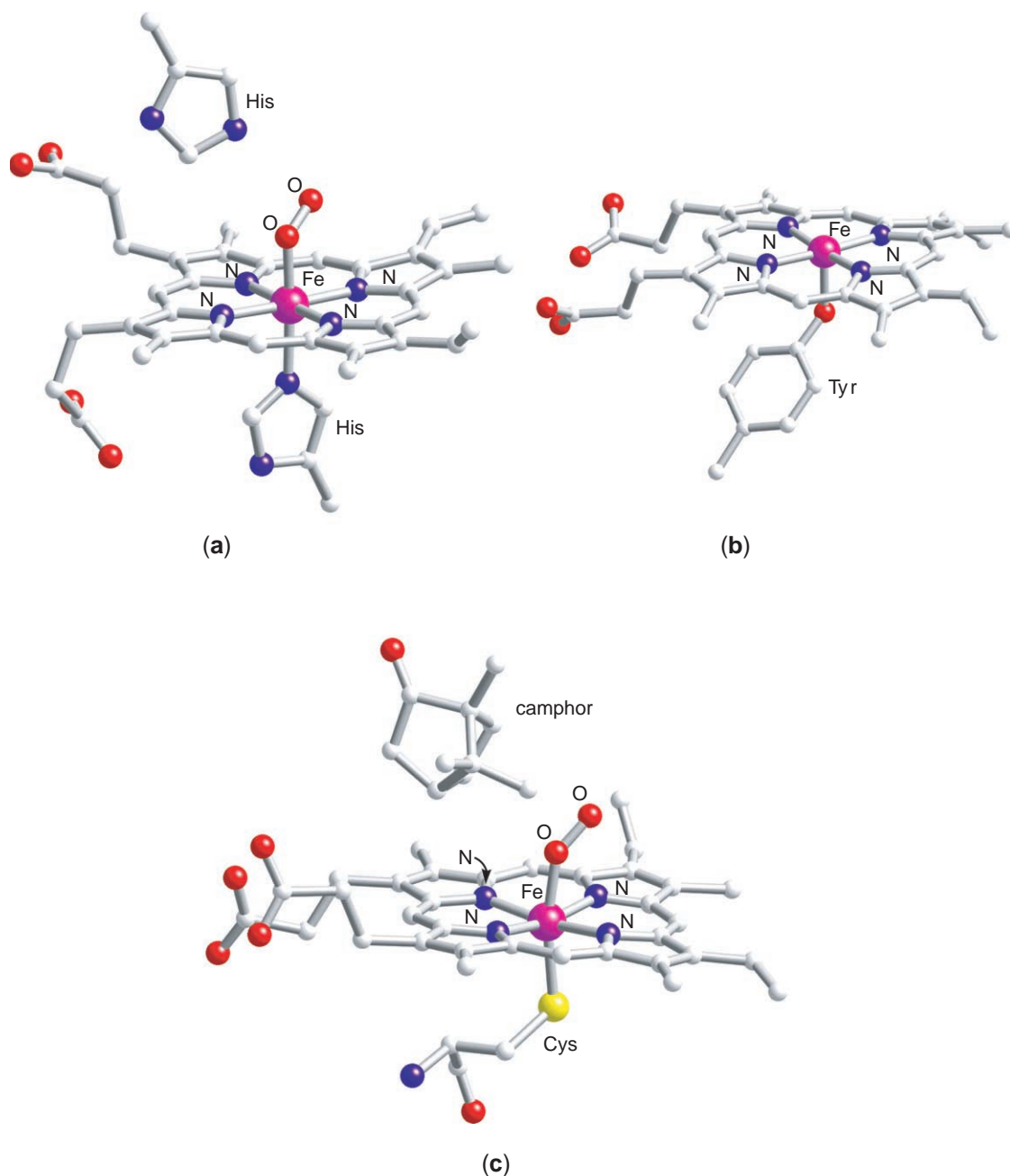
Figure 3 Structures of the metal-containing portion of (a) oxymyoglobin (PDB 1A6M); (b) catalase (PDB 1DGF); (c) the oxygen adduct of reduced cytochrome P450 with camphor substrate bound (PDB 1DZ4).

bd of *E. coli*, and the four-electron reduced sirohemes of sulfite oxidase and nitrite reductase (see Chapter 8.28). Factor F430 is a highly reduced tetrapyrrole ligand that binds nickel and is involved in methanogenesis, while cobalt-containing coenzyme B_{12} has a corrin ring with one fewer carbon than in the macrocyle (see Chapter 8.25).

Another easily recognizable bioinorganic motif is the iron–sulfur cluster exemplified by the Fe_2S_2 rhomb and the Fe_4S_4 cubane (Figure 4), most often found in ferredoxins involved in low-potential electron transfer (see Chapter 8.3).[15] The iron ions in these clusters typically have a distorted tetrahedral geometry, with cysteine residues serving as terminal ligands. The Fe_2S_2 cluster (Figure 4a) cycles between the +2 and +1 oxidation states, with redox potentials in the −200 mV range.[16] A variation is the Rieske cluster found in the respiratory electron-transfer chain and some dioxygenases that operates in the +200 mV range (Figure 4b).[17] In this cluster, the two terminal cysteinates on one iron are replaced by neutral histidine ligands, resulting in the upshift

(a)

(c)
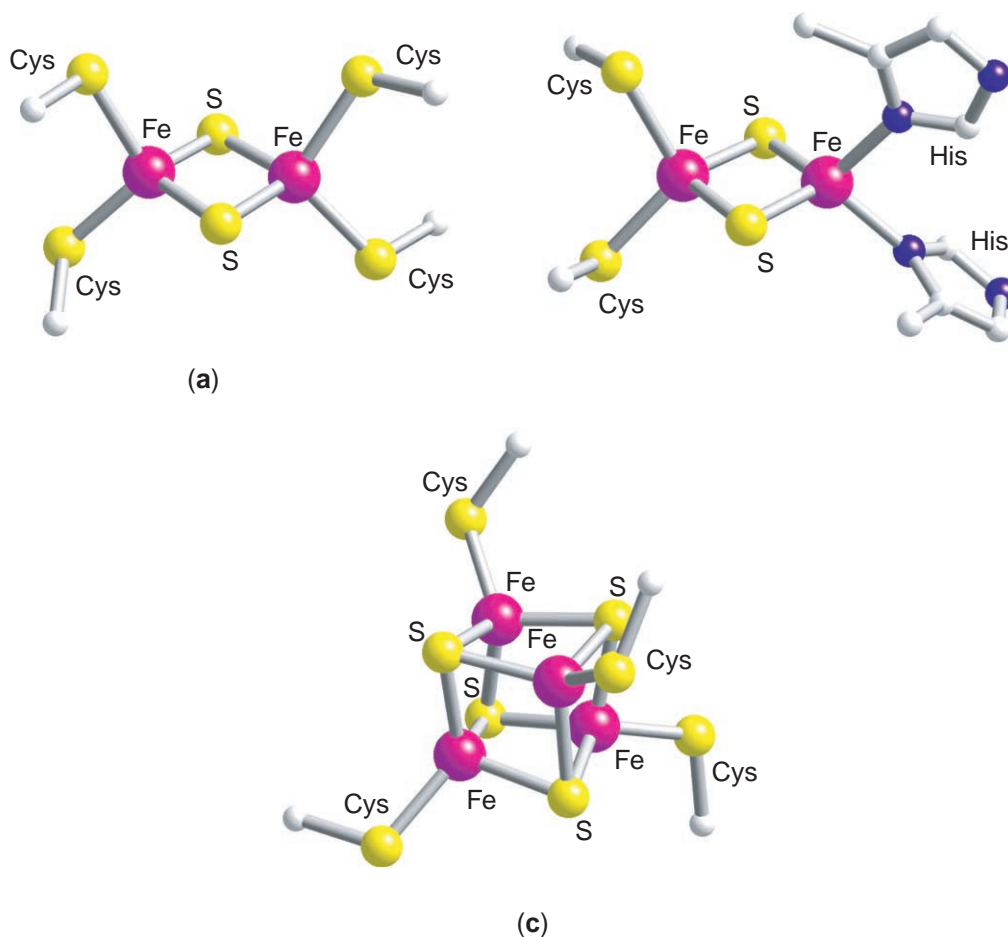
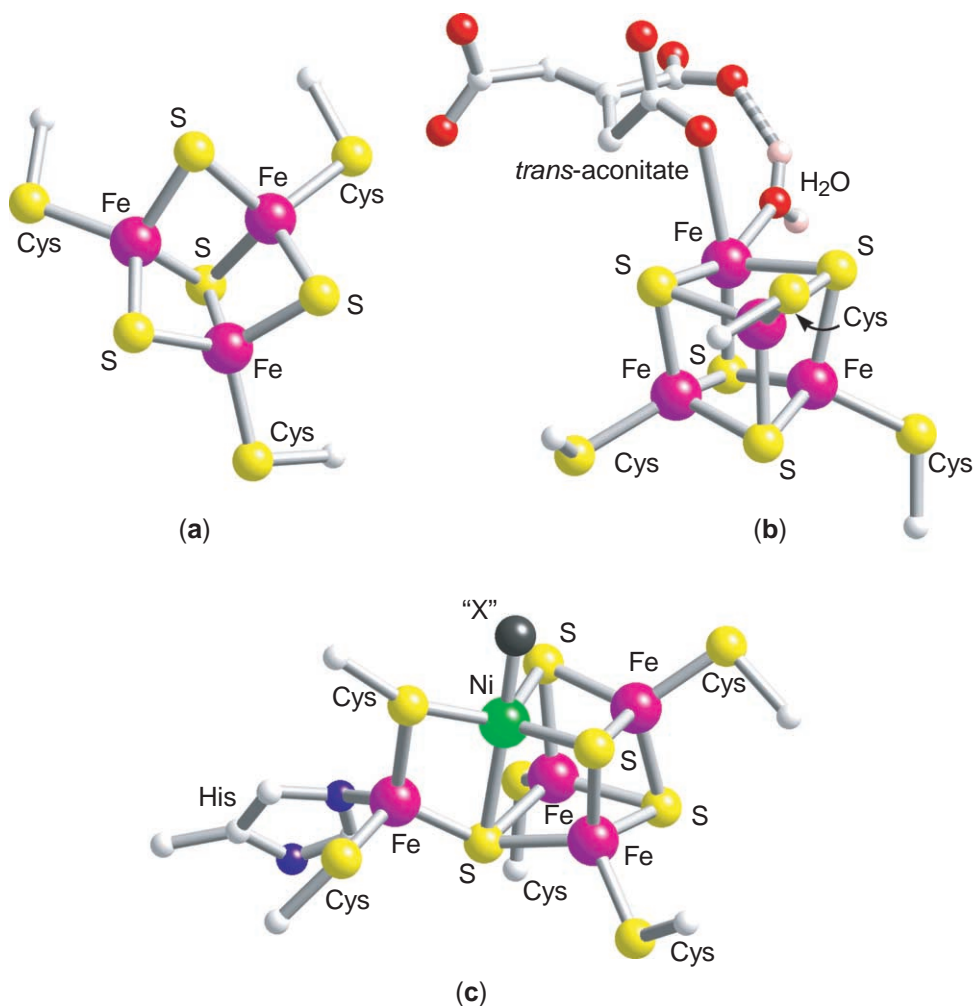**Figure 4** Structures of the (a) $Fe_2S_2(Cys)_4$ ferrodexin site (PDB 1AWD); (b) $Fe_2S_2(Cys)_2(His)_2$ "Rieske" site (PDB 1JM1); (c) $Fe_4S_4(Cys)_4$ ferrodoxin site (PDB 2FDN).

in potential. The Fe_4S_4 cluster (Figure 4c)[18] also typically cycles between the +2 and +1 oxidation states, but can access the +3 oxidation state in some cases and the 0 oxidation state in the Fe protein of nitrogenase.[19] Iron–sulfur clusters thus provide Nature with considerable flexibility in the potentials of electrons they can transfer.

There are also cuboidal FeS clusters in which one of the iron sites is significantly different from the other three. The extreme example is the Fe_3S_4 cluster, where one of the Fe corners is missing. Although originally considered to be an artifact of oxidative damage to iron–sulfur proteins, as in the ferredoxin from *Azotobacter vinelandii* (Figure 5a),[20] such clusters have been found in active enzymes, e.g., the NiFe hydrogenase,[21] and are presumably involved in the electron-transfer chain needed to deliver electrons to the heterodinuclear NiFe enzyme active site. Aconitase is another enzyme with a site-differentiated Fe_4S_4 cluster. This key enzyme of the Krebs cycle catalyzes the isomerization of citrate to isocitrate (see Chapter 8.27). The isomerization occurs on one specific Fe of the Fe_4S_4 cluster. Instead of having a terminal Cys ligand, the unique Fe has a terminal aqua ligand in the resting state and binds the substrate, thereby increasing its coordination number during the catalytic cycle (Figure 5b).[22] Thus, the aconitase Fe_4S_4 cluster does not work as an electron-transfer site in this enzyme, but instead provides a metal center that functions as a Lewis acid. There is also recent evidence that an Fe_4S_4 cluster can act both as an electron-transfer site and a Lewis acid center. In S-adenosylmethionine-dependent iron–sulfur enzymes, one Fe of the cluster acts to bind the carboxylate of the S-adenosylmethionine cofactor prior to the redox reaction (see Chapter 8.27).

One Fe is replaced by another metal ion in other site-differentiated Fe_4S_4 clusters. Many of these examples derive from the chemical reconstitution of an Fe_3S_4 cluster with another metal ion, e.g., $ZnFe_3S_4$, $CoFe_3S_4$, $CdFe_3S_4$, etc.[15] In addition, CO dehydrogenase has been found to have an $NiFe_4S_5$ cluster that is presumably involved in CO binding and activation (Figure 5c)

Figure 5 Structures of the (a) $Fe_3S_4(Cys)_4$ ferredoxin site (PDB 7FD1); (b) aconitase active site with bound trans-aconitate (PDB 1ACO); (c) $NiFe_4S_5$ cluster in carbon monoxide dehydrogenase (PDB 1JQK).

(see Chapter 8.25).[23] The novel cluster has a structure that significantly deviates from the postulated model in which the Ni ion is appended to an intact Fe_4S_4 cluster; instead, the Ni ion is integrated into the cluster structure, which could be construed as arising from the coordination of a (Cys)Ni-μ-S(R)-Fe(Cys)(His) unit to three of four μ-S atoms of an Fe_3S_4 cluster.

The iron–sulfur clusters of the MoFe protein of nitrogenase illustrate another variation on the cuboidal M_4S_4 theme. The P and M clusters of this protein can be formulated as vertex-shared bicubane units, perhaps required because the fixation of dinitrogen is thought to occur in two-electron reduction steps (see Chapter 8.22). For the P cluster, which serves as an electron-storage and -transfer site, two Fe_4S_4 clusters combine to share a common μ_6-S vertex (Figure 6a).[24] On the other hand, the M cluster, which is believed to be the locus of nitrogen-fixing activity, is a combination of an Fe_4S_3 and an $MoFe_3S_3$ cuboidal unit sharing a common, newly discovered μ_6-vertex, which cannot be a sulfur atom (Figure 6b).[24] The electron density associated with this atom identifies it as a low Z atom, and a μ_6-N is mechanistically the most attractive possibility.

The third recurring structural motif with non-amino-acid components found in metalloproteins is the metal–dithiolene unit found in molybdenum- and tungsten-containing oxidases or dehydrogenases (see Chapter 8.18). The dithiolene is typically a pterin derivative (often with phosphate and/or nucleotide appendages) and coordinated to Mo or W in a 1:1 or 2:1 stoichiometry (Figure 7).[25,26] These units usually function in two-electron redox reactions (cf. "oxo transfer"), shuttling between M^{IV} and M^{VI} oxidation states.

The most recent addition to this group of motifs is the $Fe(CO)_x(CN)_y$ fragment found in the active sites of both NiFe and Fe-only hydrogenases (Figure 8).[21,27] This organometallic fragment is connected to a $Ni(Cys)_4$ unit in the NiFe enzyme via two thiolate bridges (Figure 8a) and to

(**a**)

(**b**)
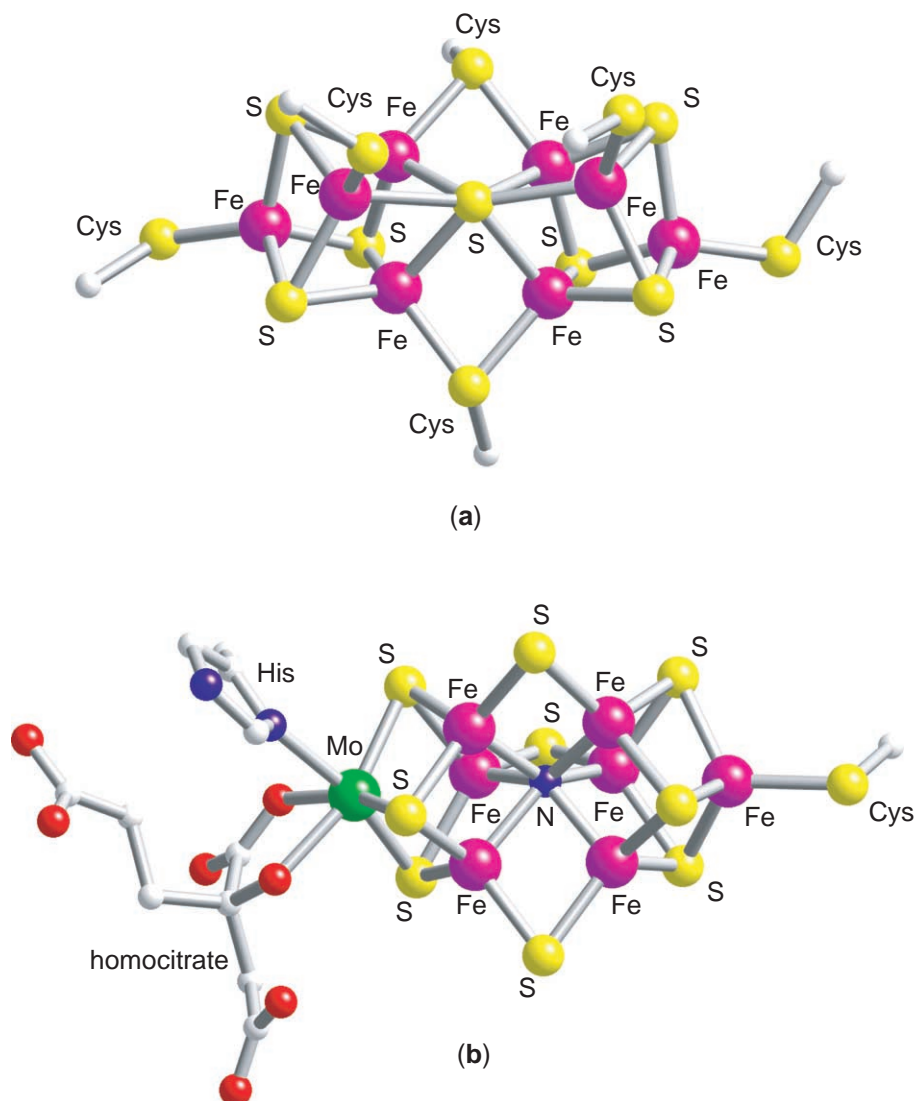
Figure 6   Structures of the nitrogenase (a) P cluster; (b) molybdenum-iron cofactor (PDB 1M1 N).

another organometallic Fe fragment via a dithiolate bridge in the Fe-only enzyme (Figure 8b). The unusual organometallic nature of this fragment suggests an important role for H_2 activation, but more work is required to establish the mechanisms of action for these fascinating enzymes (see Chapter 8.21).

8.1.3   COMMON MOTIFS WITH AMINO-ACID LIGANDS

The tetrahedral $M(Cys)_4$ unit is a commonly found structure in metalloproteins. Besides the Ni center in NiFe hydrogenases (Figure 8a),[21] this motif is also found for M = Fe, Zn, and Cd. An $Fe(Cys)_4$ site is present in rubredoxin (Figure 9a),[28] one of the earliest characterized iron–sulfur proteins. It also is found in dinuclear superoxide reductases,[29] where it is proposed to serve as an electron-storage site for the superoxide-reducing active site (see Chapter 8.19). The $M(Cys)_4$ unit is a structural component in Zn-containing alcohol dehydrogenase[30] and a fragment of the Zn/Cd clusters of metallothioneins (Figure 9b; see Chapter 8.9).[31] Variations of this tetrahedral motif occur in Zn-finger proteins where a $Zn(His)_2(Cys)_2$ unit is commonly found (Figure 9c).[32]

   The trigonal $Cu(Cys)(His)_2$ unit is a recurring motif in cupredoxins, more commonly known as "blue" copper proteins, which are principally involved in electron transfer in the high potential
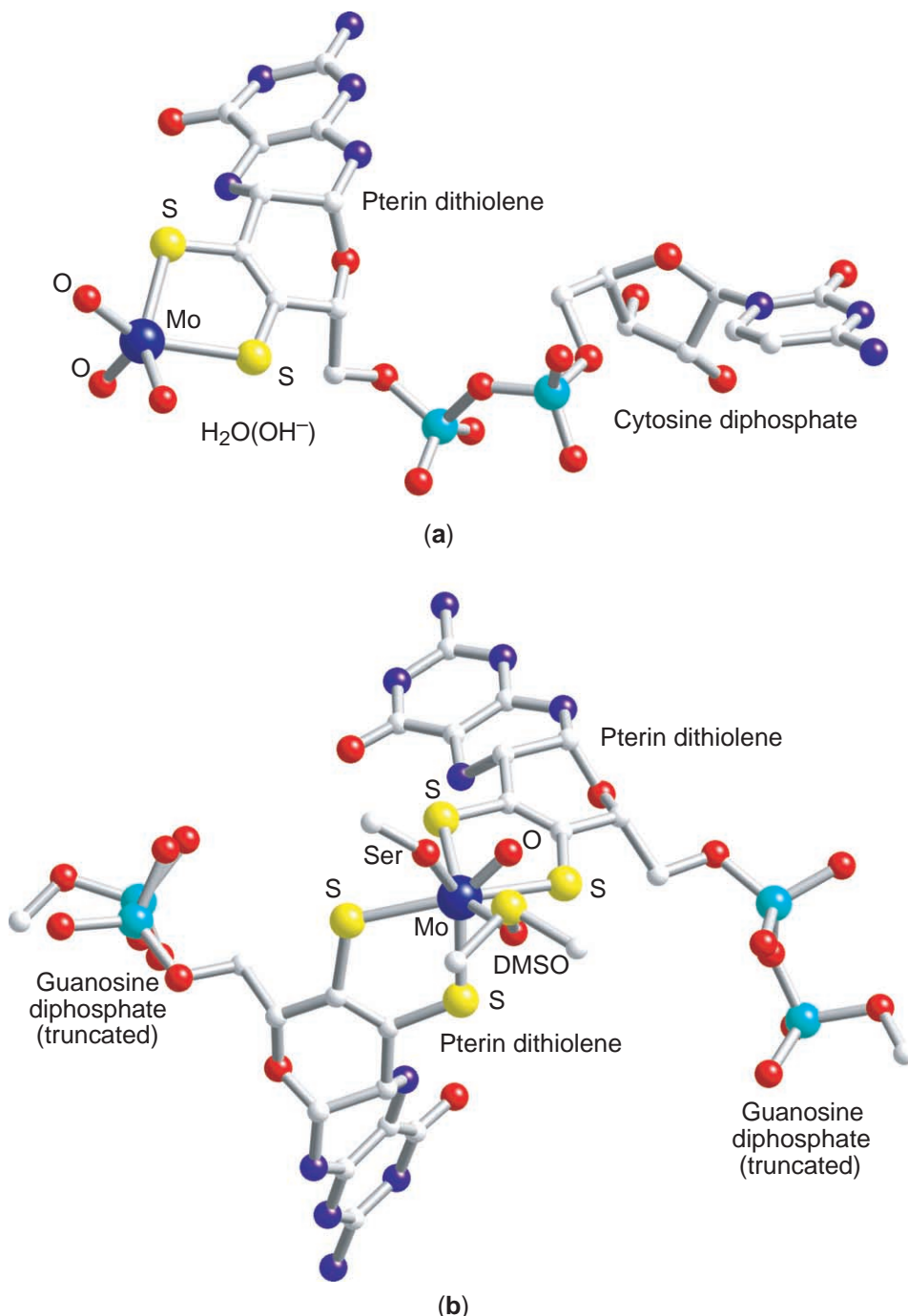
Figure 7 Structures of the (a) Mo^{VI} site of aldehyde oxidoreductase (PDB 1HLR); (b) DMSO adduct to the Mo^{IV} site of dimethylsulfoxide reductase (PDB 4DMR). The guanine portions of the pterin cofactors in (b) are omitted for clarity.

range (see Chapter 8.4). The presence of axial ligation and the strength of such interactions with the copper center modulate the redox potential to provide the range observed for these proteins.[33] As illustrated in Figure 10, the cupredoxin site can be trigonal (Figure 10a),[34] trigonal pyramidal (Figure 10b),[35] or trigonal bipyramidal (Figure 10c).[36] A closely related motif is found in the delocalized, mixed-valence dicopper(I,II) centers of cytochrome oxidase (Figure 10d)[37] and nitrous oxide reductase,[38] which may be construed as a dimeric derivative in which one His on each Cu is replaced by another ligand (see Chapter 8.17).

The facial M(Xaa)$_3$ unit is another versatile building block, which is suitable for a variety of metal ions and accommodates tetrahedral, trigonal-bipyramidal, square-pyramidal, and octahedral
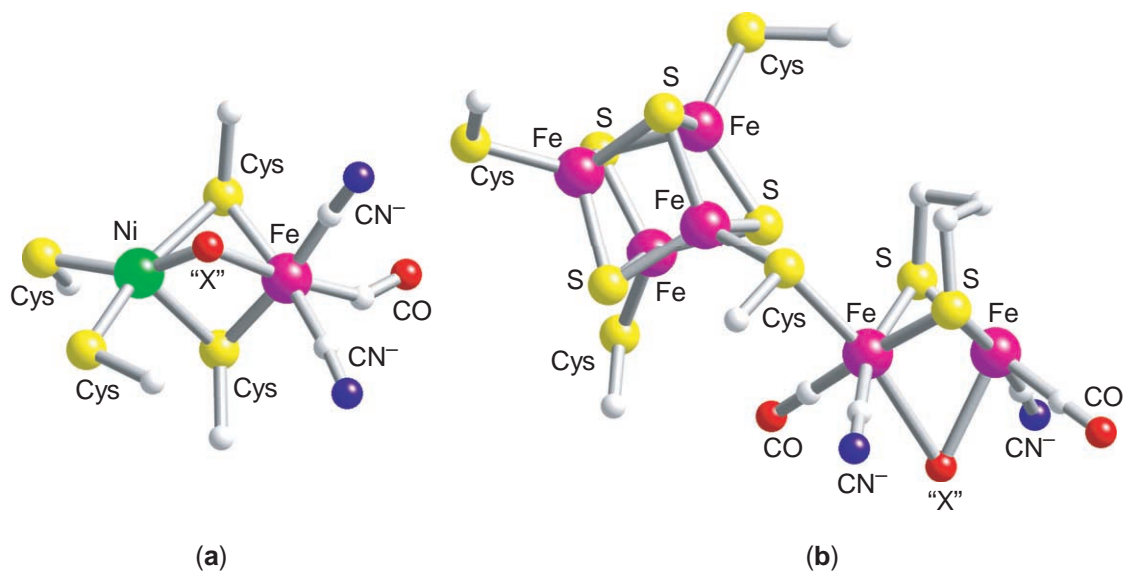
Figure 8   Structures of the active sites of (a) Ni–Fe hydrogenase (PDB 2FRV); (b) Fe-only hydrogenase (PDB 1HFE).
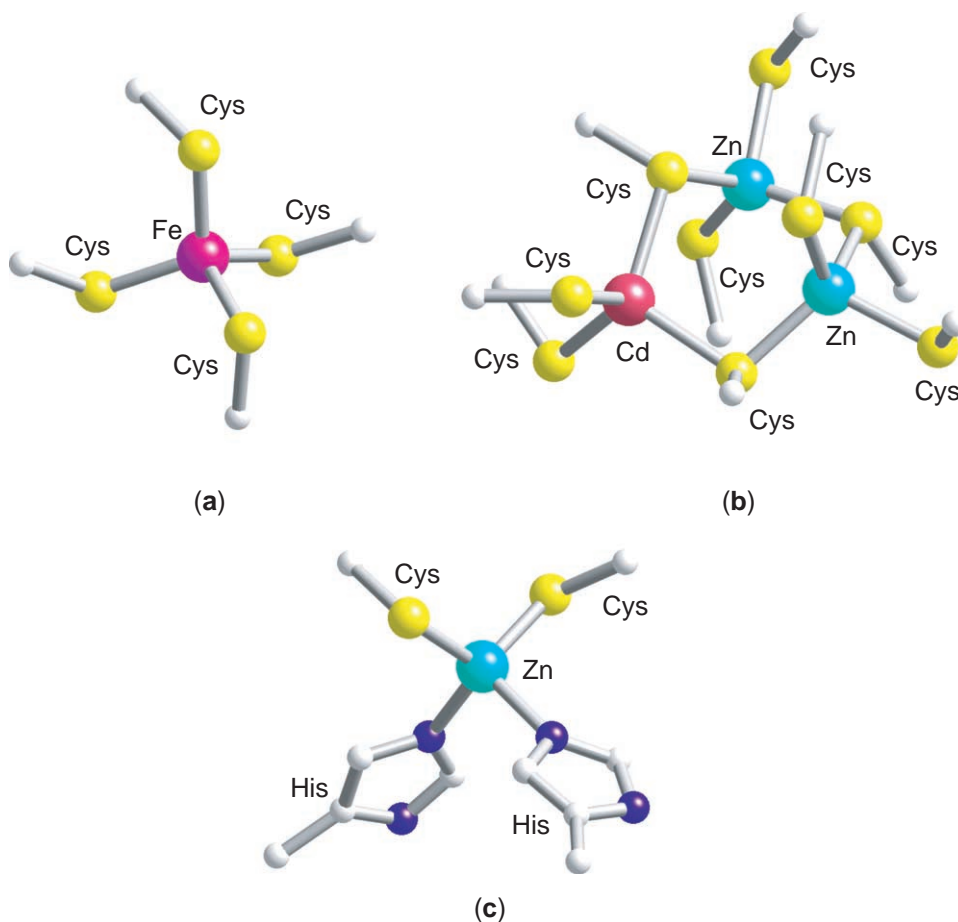
Figure 9   Structures of the (a) rubredoxin Fe(Cys)$_4$ site (PDB 1BRF); (b) Zn$_2$Cd(Cys)$_9$ metallothionein site (PDB 4MT2); (c) Zn(His)$_2$(Cys)$_2$ "zinc finger" site (PDB 1A1H).
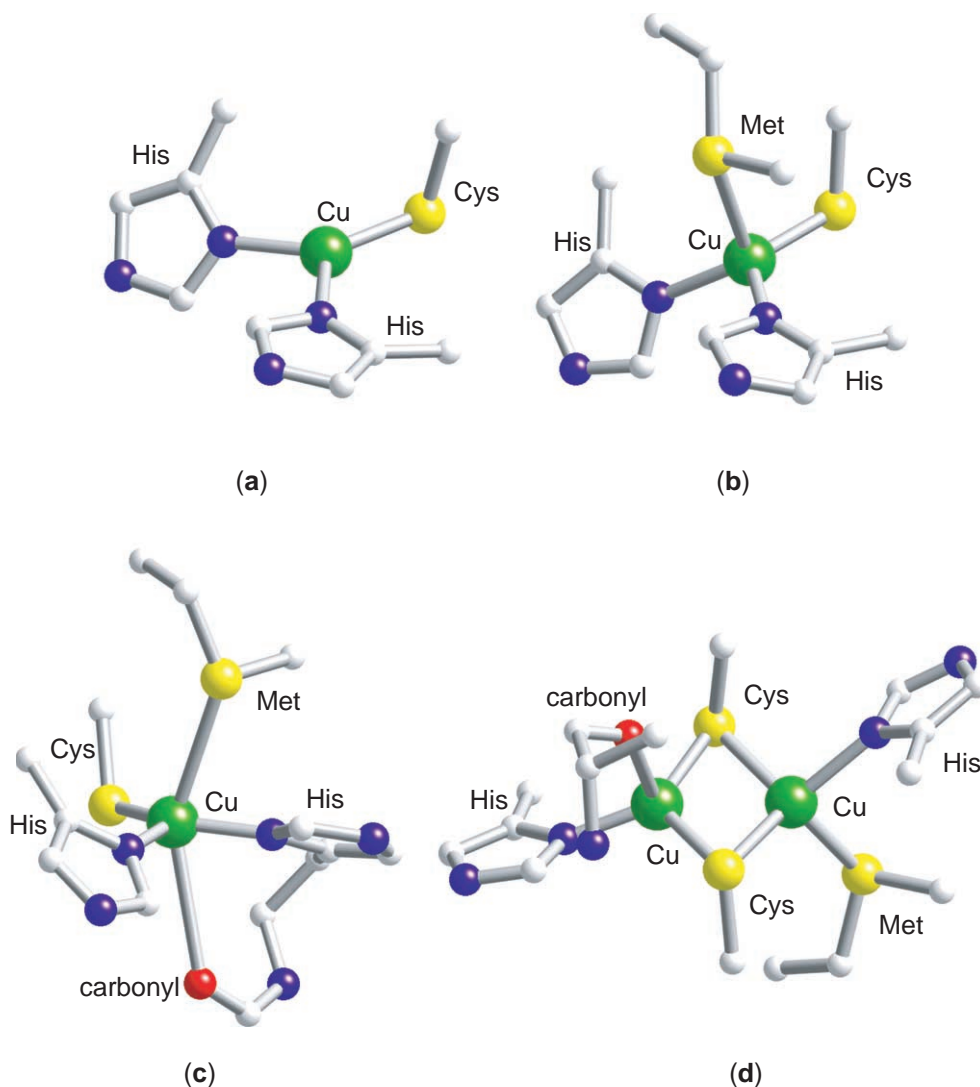
Figure 10 Structures of the copper–thiolate electron-transfer sites in (a) laccase (PDB 1HFU); (b) plasto-cyanin (PDB 1KDJ); (c) azurin (PDB 1NWP). Also shown: (d) the delocalized, mixed-valent dicopper(I,II) "Cu$_A$" electron-transfer site from cytochrome ba3 (PDB 2CUA).

geometries. The M(His)$_3$ motif is found in the tetrahedral metal sites of several metalloenzymes, such as carbonic anhydrase (Zn^{II}, Figure 11a),[39] nitrite reductase (Cu^{II}, Figure 11b),[40] and cytochrome *c* oxidase (Cu, Figure 11c).[41] The fourth position is used to activate the water nucleophile in carbonic anhydrase, to bind nitrite in nitrite reductase, and to serve as the initial binding site for O$_2$ (or CO) in cytochrome *c* oxidase. This motif also provides the remaining ligands of the square-pyramidal ions of the Cu$_2(\mu$-η^2:η^2-O$_2$) core in oxyhemocyanin (Figure 12a)[42] and one six-coordinate iron ion of the diiron site in oxyhemerythrin (Figure 12b).[43]

An additional recurring facial motif is the 2-His-1-carboxylate triad found in a number of mononuclear nonheme iron enzymes that activate O$_2$.[44,45] This triad serves to hold the iron(II) center in the active site and provides three solvent-accessible sites to bind exogenous ligands. This superfamily of enzymes can catalyze a range of oxidative transformations, including the *cis*-dihydroxylation of arene double bonds and the oxidative cleavage of catechols in the biodegrad-ation of aromatics, the formation of the β-lactam and thiazolidine rings of penicillin, the hydroxylation of Phe, Tyr, and Trp with the help of a tetrahydrobiopterin cofactor, and the oxidative decarboxylation of an α-ketoglutarate co-substrate to generate an oxidant capable of functionalizing C—H bonds (see Chapter 8.14). The coordinative versatility of this active-site motif is illustrated in Figure 13. Figures 13a and 13b show the active-site structures of binary enzyme–bidentate substrate complexes, an extradiol cleaving catechol dioxygenase with its

(**a**)   (**b**)

(**c**)
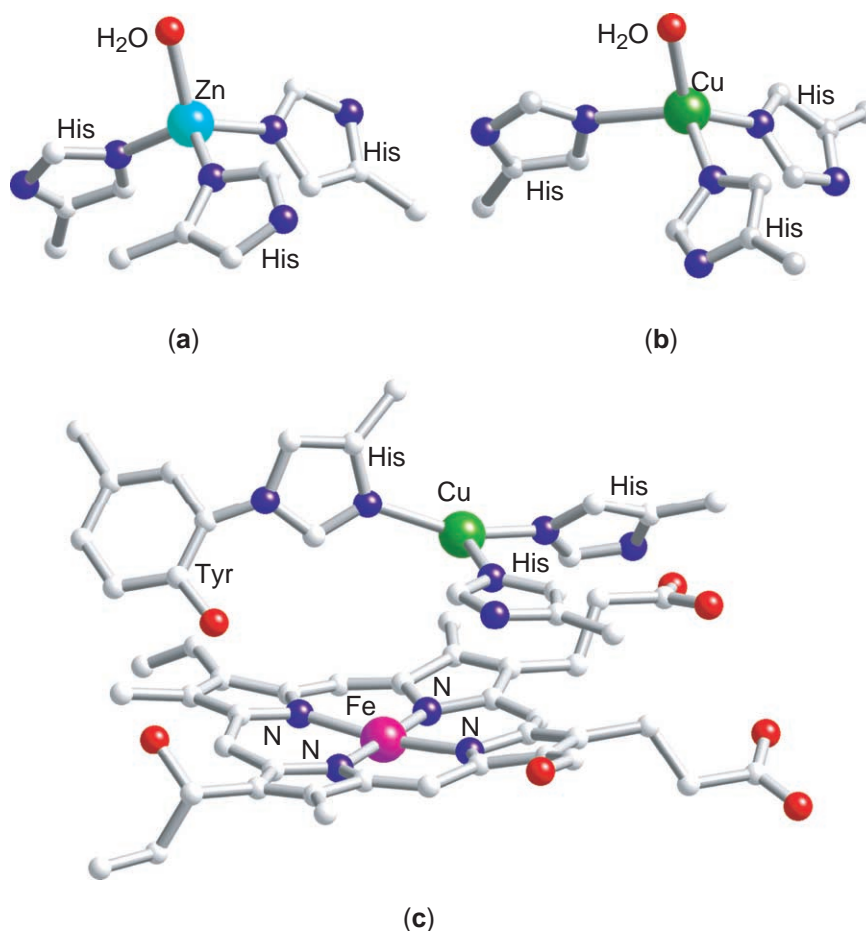
Figure 11   Structures of the active sites of (a) carbonic anhydrase (PDB 1CA2); (b) nitrite reductase (PDB 2NRD); (c) cytochrome c oxidase (heme a_3-Cu_B pair; PDB 1OCR).

(**a**)   (**b**)
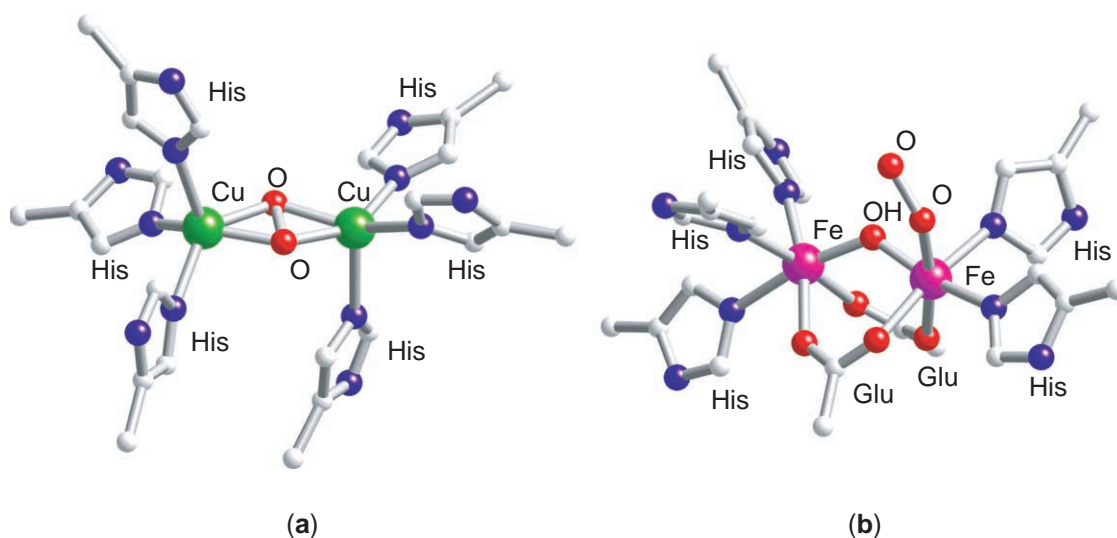
Figure 12   Structures of the active sites of (a) oxyhemocyanin (PDB 1OXY); (b) oxyhemerythrin (PDB 1HMO).

catecholate substrate (Figure 13a)[46] and deacetoxycephalosporin synthase (DAOCS) with its α-ketoglutarate cofactor (Figure 13b),[47] both with a sixth site available for O_2 binding. Figures 13c and 13d show the active sites of ternary complexes: isopenicillin N synthase (IPNS) with the coordinated thiolate of its tripeptide substrate and NO bound as a surrogate for O_2[48] and
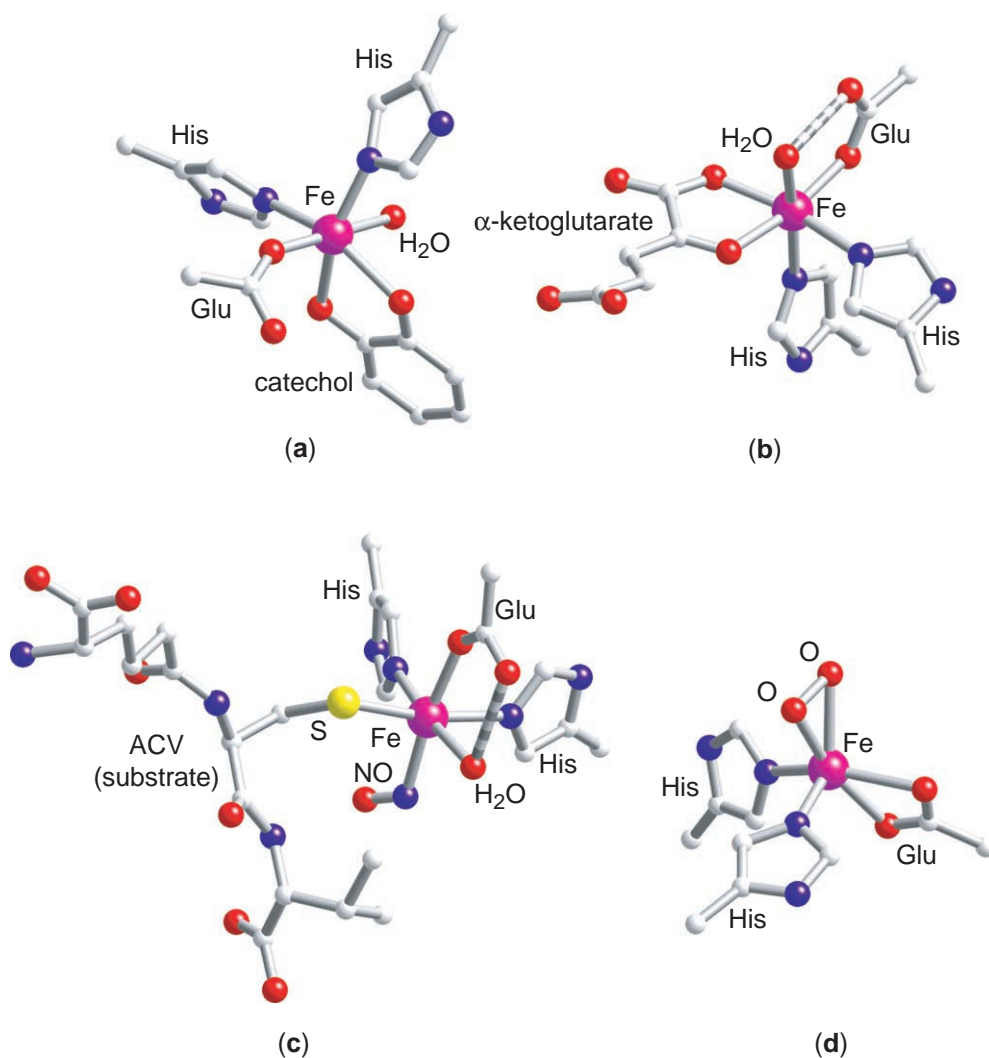
Figure 13 Structures of the active sites of (a) 2,3-dihydroxybiphenyl 1,2-dioxygenase complexed with catechol (PDB 1KND); (b) deacetoxycephalosporin synthase with bound α-ketoglutarate (PDB 1RXG); (c) isopenicillin N synthase with coordinated substrate and NO (PDB 1BLZ); (d) naphthalene dioxygenase with bound dioxygen in the presence of substrate (not shown) (PDB 1O7M).

naphthalene dioxygenase with a side-on bound dioxygen,[49] presumably poised to effect the *cis*-dihydroxylation of a double bond on the nearby arene substrate (not shown). These examples illustrate how a diversity of reactions can be obtained from the flexibility of the 2-His-1-carboxylate motif, which enables the iron(II) center to bind and activate substrates, cofactors and/or O_2.

   Other combinations of histidine and carboxylate ligands also can be found in a number of metalloenzymes. Quercetinase is a copper enzyme that uses a 3-His-1-carboxylate combination arranged in a square-pyramidal geometry, with one basal site available for the coordination of substrate (Figure 14a).[50] Fe and Mn superoxide dismutases utilize a 3-His-1-carboxylate combination in a sawhorse arrangement to provide coordination sites for two exogenous ligands (Figure 14b).[51] These coordination environments can in fact be construed as combinations of $M(His)_3$ and $M(His)_2$(carboxylate) triads. Alternatively, some dimetal hydrolases like the β-lactamase from *S. maltophilia* (see Chapter 8.24) combine the two triad types via a hydroxo bridge to generate a $(His)_3Zn$-μ-OH-$Zn(His)_2(Asp)$ active site (Figure 14c).[52] Note how, in most examples, the monodentate carboxylate ligand hydrogen bonds to a bound water or hydroxide.

   A number of other metalloenzymes have $M^{II}_2(His)_2(O_2CR)_4$ active sites (see Chapter 8.13). Most prominent of these are the di-iron enzymes, including the hydroxylase component of methane monooxygenase (MMOH, Figure 15a)[53] and class 1 ribonucleotide reductase R2 proteins (Figure 15b).[54] These enzymes have two conserved Asp/Glu(Xaa)$_n$GluXaaXaaHis sequence motifs in a four-helix bundle that provide the six amino-acid ligands for the di-iron
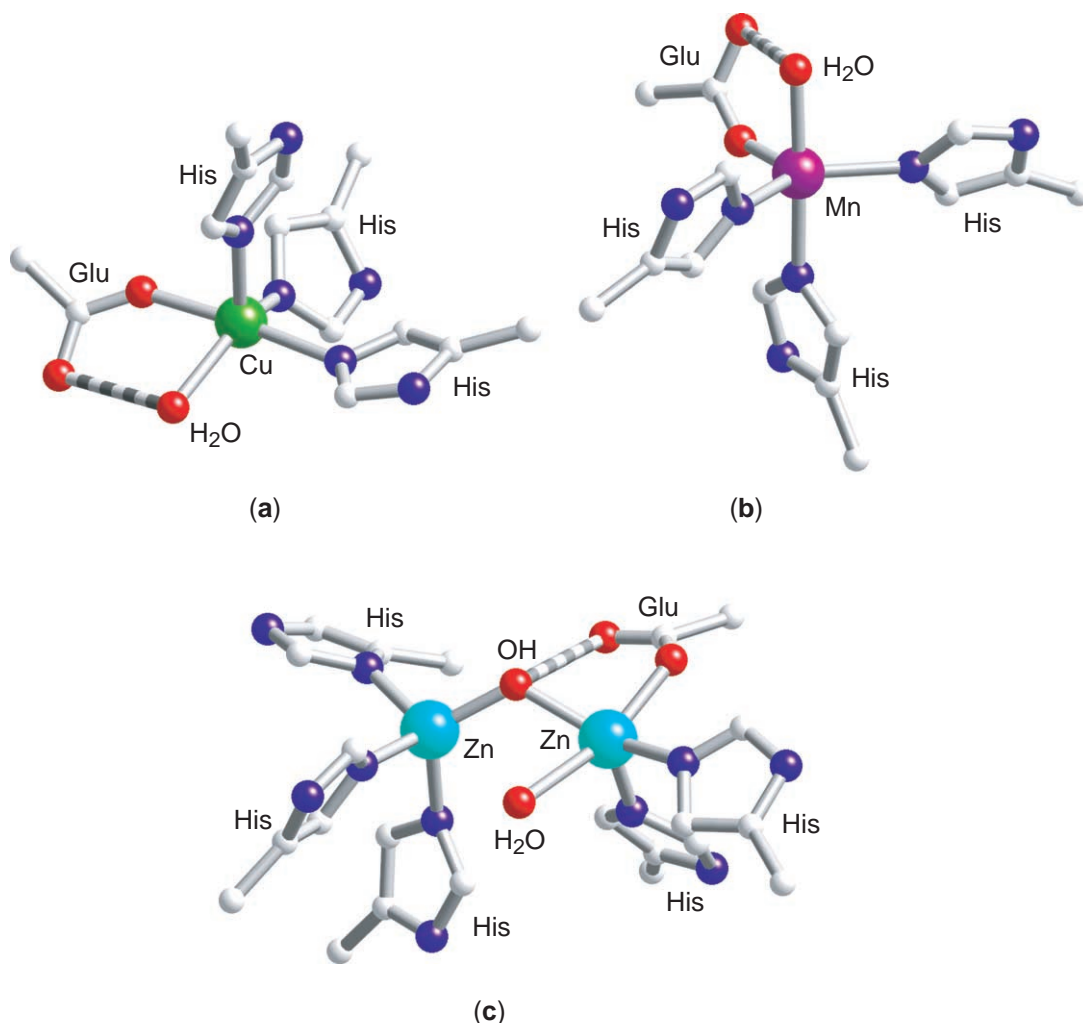
Figure 14 Structures of the active sites of (a) quercetinase (PDB 1JUH); (b) Mn superoxide dismutase (PDB 3MDS); (c) a dizinc β-lactamase (PDB 1SML).

active site. The di-iron center activates O_2 and carries out the hydroxylation of alkanes and the formation of a catalytically essential tyrosyl radical for the conversion of ribonucleotides to deoxyribonucleotides, respectively. The carboxylates more distant in sequence from the other two residues act as terminal ligands, while the two near in sequence to the His ligands act to bridge the iron atoms, with both monodentate and bidentate modes observed. Upon oxidation of these di-iron(II) enzymes to the di-iron(III) state, there is a change in core structure, resulting in the shift of one carboxylate bridge to a terminal position (the so-called carboxylate shift[55]) and the introduction of an oxo bridge or two hydroxo bridges to neutralize the Lewis acidity of the iron(III) ions (Figures 15c and 15d).[53,56] (An oxo bridge is also observed in the oxidized form of an unrelated diiron protein hemerythrin (Figure 12b).) Related dinuclear active sites are found for fatty acid desaturases,[57] rubrerythrin,[58] the ferroxidase site in ferritins,[59] and the dimanganese catalase.[60]

The crystal structures of nitrile hydratase and acetyl CoA synthase both show a metal center coordinated to a planar N_2S_2 unit derived from a CysXaaCys tripeptide, with the nitrogen ligands arising from the peptide amidates of the Xaa residue and the latter Cys residue. These results emphasize a point originally made in the explorations of the coordination chemistry of peptide ligands: that the peptide nitrogen can bind to metal centers, particularly in its anionic form. In the recently reported structures of acetyl CoA synthase, there is a planar $Ni(N_2S_2)$ unit derived from a $Cys_{595}Gly_{596}Cys_{597}$ tripeptide segment (Figure 16a).[61,62] This unit is in turn connected to an Fe_4S_4 cluster via an intervening metal ion, which can be Ni, Cu, or Zn in the three structures reported. In nitrile hydratase, the low-spin iron(III) ion is coordinated to the planar N_2S_2 unit from $Cys_{112}Ser_{113}Cys_{114}$ and additionally ligated by an axial thiolate from nearby Cys_{109} (Figure 16b).[63] The sixth site can be occupied by a solvent molecule, which presumably is involved in
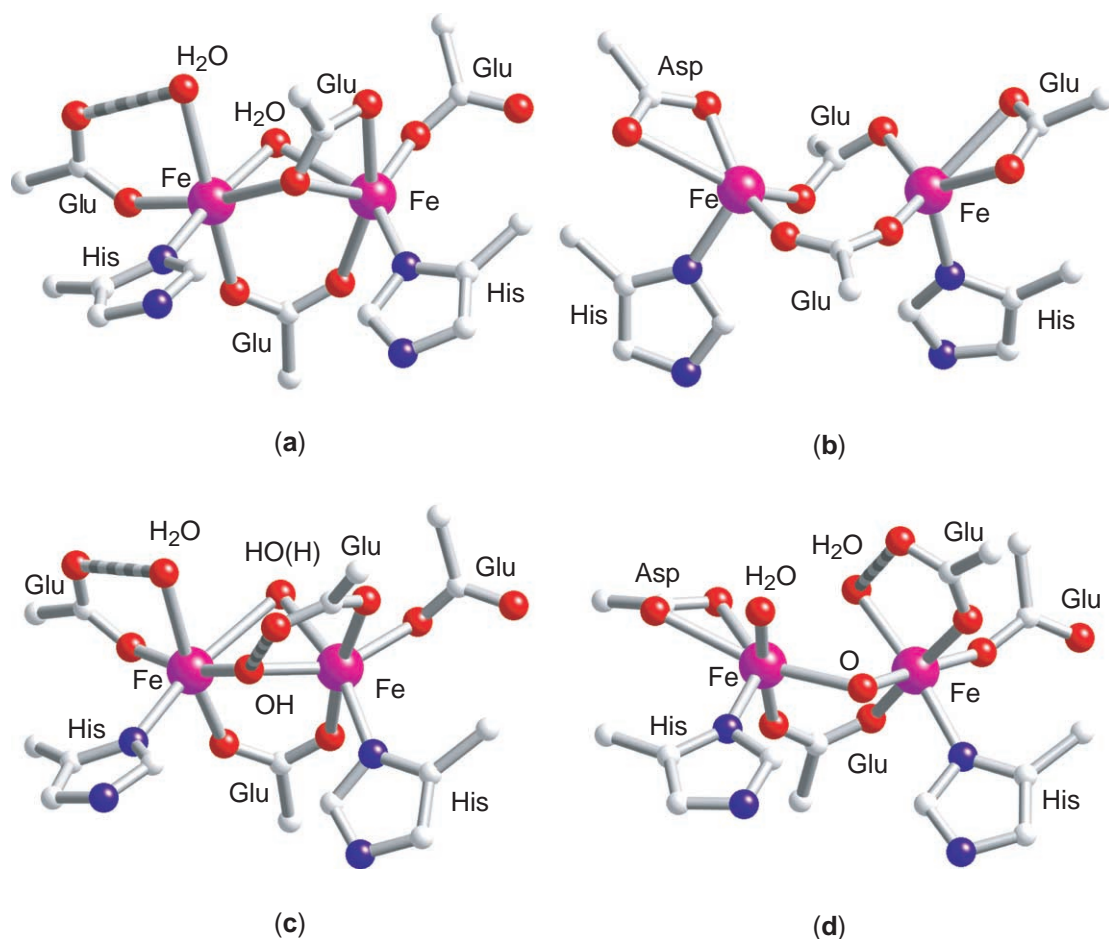
Figure 15 Structures of the di-iron active sites of (a) reduced MMOH (PDB 1FYZ); (b) reduced ribonucleotide reductase (PDB 1XIK); (c) oxidized MMOH (PDB 1FZ1); (d) oxidized ribonucleotide reductase (PDB 1AV8).
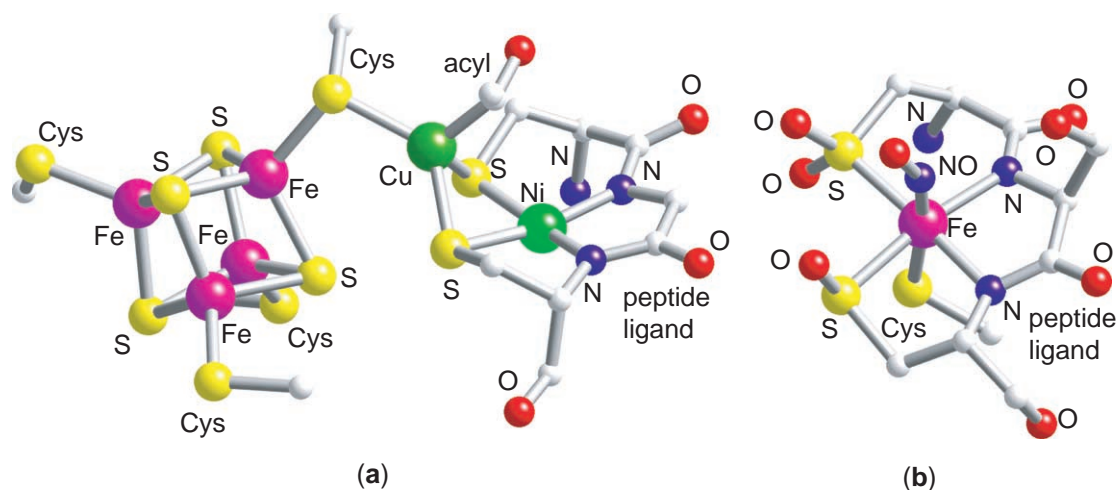
Figure 16 Structures of (a) the multimetallic site of acetyl CoA synthase (PDB 1MJG); (b) the active site of the NO adduct of nitrile hydratase (PDB 2AHJ).

nitrile hydrolysis, or NO, which is an inhibitor. Further making this active-site structure unique is the observed post-translational oxidation of the thiolates of Cys$_{112}$ and Cys$_{114}$ to a sulfinate (RSO$_2^-$) and a sulfenate (RSO$^-$), respectively, required for enzyme activity.
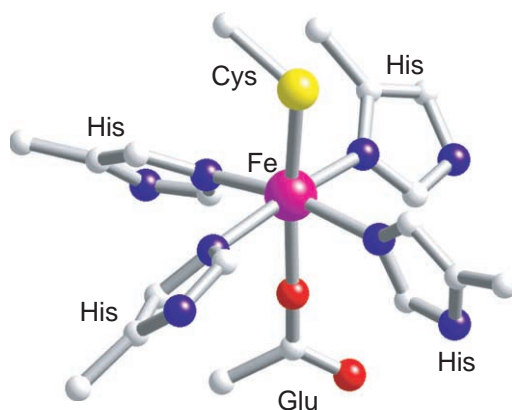
Figure 17 Structure of the catalytic active site of superoxide reductase (PDB 1DQI).

As a final example, we note the similarity of the square-pyramidal $FeN_4(Cys_{axial})$ site found in superoxide reductase[29] (Figure 17) to those of cytochrome P450 (Figure 3c) and chloroperoxidase. While the N4 units in cytochrome P450 and chloroperoxidase derive from a porphyrin, the four nitrogens of superoxide reductase are from four His residues. Interestingly, this motif is used in the two heme enzymes to bind and activate dioxygen moieties to generate a high-valent oxoiron species capable of substrate oxidations, while the corresponding site in superoxide reductase is used to protect anaerobes from the toxic effects of superoxide by reducing it to H_2O_2.

8.1.4 CONCLUDING REMARKS

In this introductory overview, we have attempted to point out structural similarities among metalloprotein active sites to emphasize how Nature has utilized coordination chemistry to her advantage, particularly in generating related active sites with different functions. In highlighting common features, we have necessarily de-emphasized unique sites such as the unusual $Cu_4(\mu_4\text{-}S)$ cluster of nitrous oxide reductase (see Chapter 8.28) and the critical Mn_4 cluster in the oxygen-evolving complex of photosynthesis (see Chapter 8.20), whose precise structure is still developing as higher resolution crystallographic data become available. Also excluded are possible motifs that may emerge in the areas of metal-ion transport and homeostasis (see Chapters 8.5, 8.6, and 8.8) and metal ion/nucleic acid interactions (see Chapter 8.28). It is our hope that this overview provides a sufficient basis for underscoring the importance of coordination chemistry in bioinorganic chemistry.

ACKNOWLEDGMENT

8.1.5 REFERENCES

1. Lippard, S. J.; Berg, J. M. *Principles of Bioinorganic Chemistry*; University Science: Mill Valley, CA, 1994.
2. Kaim, W.; Schwederski, B. *Bioinorganic Chemistry: Inorganic Elements in the Chemistry of Life*; Wiley: New York, 1991.
3. Bertini, I.; Gray, H. B.; Lippard, S. J.; Valentine, J. S., Eds. *Bioinorganic Chemistry*; University Science Books: Mill Valley, CA, 1994.
4. Fraústo da Silva, J. J. R.; Williams, R. J. P. *The Biological Chemistry of the Elements: The Inorganic Chemistry of Life*; Clarendon Press: Oxford, UK, 1991.
5. Cowan, J. A. *Inorganic Biochemistry: An Introduction*; 2nd ed.; Wiley-VCH: New York, 1997.
6. Holm, R. H.; Solomon, E. I. *Chem. Rev.* **1996**, *96*, 2239–3042, entire issue, edited by Holm Solomon.
7. Holm, R. H.; Kennepohl, P.; Solomon, E. I. *Chem. Rev.* **1996**, *96*, 2239–2314.
8. Durley, R. C. E.; Mathews, F. S. *Acta Crystallogr. D Biol. Crystallogr.* **1996**, *52*, 65–66.
9. Benini, S.; Gonzalez, A.; Rypniewski, W. R.; Wilson, K. S.; Van-Beeumen, J. J.; Ciurli, S. *Biochemistry* **2000**, *39*, 13115–13126.
10. Vojtechovsky, J.; Chu, K.; Berendzen, J.; Sweet, R. M.; Schlichting, I. *Biophys. J.* **1999**, *77*, 2153–2174.
11. Putnam, C. D.; Arvai, A. S.; Bourne, Y.; Tainer, J. A. *J. Mol. Biol.* **2000**, *296*, 295–309.
12. Schlichting, I.; Berendzen, J.; Chu, K.; Stock, A. M.; Maves, S. A.; Benson, D. E.; Sweet, R. M.; Ringe, D.; Petsko, G. A.; Sligar, S. G. *Science* **2000**, *287*, 1615–1622.

13. Ortiz de Montellano, P. R., Ed. *Cytochrome P450: Structure, Mechanism, and Biochemistry*; 2nd ed.; Plenum: New York, 1995.
14. Wertz, D. L.; Valentine, J. S. *Struct. Bonding* **2000**, *97*, 38–60.
15. Beinert, H.; Holm, R. H.; Münck, E. *Science* **1997**, *277*, 653–659.
16. Bes, M. T.; Parisini, E.; Inda, L. A.; Saraiva, L.; Peleato, M. L.; Sheldrick, G. M. to be published (PDB 2FDN).
17. Boenisch, H.; Schmidt, C. L.; Schaefer, G.; Ladenstein, R. *J. Mol. Biol.* **2002**, *319*, 791–805.
18. Dauter, Z.; Wilson, K. S.; Sieker, L. C.; Meyer, J.; Moulis, J. M. *Biochemistry* **1997**, *36*, 16065–16073.
19. Yoo, S. J.; Angove, H. C.; Burgess, B. K.; Hendrich, M. P.; Münck, E. *J. Am. Chem. Soc.* **1999**, *121*, 2534–2545.
20. Schipke, C. G.; Goodin, D. B.; McRee, D. E.; Stout, C. D. *Biochemistry* **1999**, *38*, 8228–8239.
21. Volbeda, A.; Garcia, E.; Piras, C.; deLacey, A. L.; Fernandez, V. M.; Hatchikian, E. C.; Frey, M.; Fontecilla Camps, J. C. *J. Am. Chem. Soc.* **1996**, *118*, 12989–12996.
22. Lauble, H.; Kennedy, M. C.; Beinert, H.; Stout, C. D. *J. Mol. Biol.* **1994**, *237*, 437–451.
23. Drennan, C. L.; Heo, J.; Sintchak, M. D.; Schreiter, E.; Ludden, P. W. *Prod. Nat. Acad. Sci. USA* **2001**, *98*, 11973–11978.
24. Einsle, O.; Tezcan, F. A.; Andrade, S. L. A.; Schmid, B.; Yoshida, M.; Howard, J. B.; Rees, D. C. *Science* **2002**, *297*, 1696–1700.
25. Rebelo, J. M.; Dias, J. M.; Huber, R.; Moura, J. J.; Ramao, M. J. *J. Biol. Inorg. Chem.* **2001**, *6*, 791–800.
26. McAlpine, A. S.; McEwan, A. G.; Bailey, S. *J. Mol. Biol.* **1998**, *275*, 613–623.
27. Nicolet, Y.; Piras, C.; Legrand, P.; Hatchikian, C. E.; Fontecilla-Camps, J. C. *Structure Fold. Des.* **1999**, *7*, 13–23.
28. Bau, R.; Rees, D. C.; Kurtz, D. M.; Scott, R. A.; Huang, H. S.; Adams, M. W. W.; Eidsness, M. K. *J. Biol. Inorg. Chem.* **1998**, *3*, 484–493.
29. Yeh, A. P.; Hu, Y.; Jenney, F. E., Jr.; Adams, M. W. W.; Rees, D. C. *Biochemistry* **2000**, *39*, 2499–2508.
30. Eklund, H.; Samma, J. P.; Wallen, L.; Branden, C. I.; Akeson, A.; Jones, T. A. *J. Mol. Biol.* **1981**, *146*, 561–587.
31. Braun, W.; Vasak, M.; Robbins, A. H.; Stout, C. D.; Wagner, G.; Kagi, J. H.; Wuthrich, K. *Proc. Natl. Acad. Sci. USA* **1992**, *89*, 10124–10128.
32. Elrod-Erickson, M.; Benson, T. E.; Pabo, C. O. *Structure* **1998**, *6*, 451–464.
33. Gray, H. B.; Malmstrom, B. G.; Williams, R. J. P. *J. Biol. Inorg. Chem.* **2000**, *5*, 551–559.
34. Ducros, V.; Brzozowski, A. M.; Wilson, K. S.; Ostergaard, P.; Schneider, P.; Svendson, A.; Davies, G. J. *Acta Crystallogr. D* **2001**, *57*, 333–336.
35. Kohzuma, T.; Inoue, T.; Yoshizaki, F.; Sasakawa, Y.; Onodera, K.; Nagatomo, S.; Kitagawa, T.; Uzawa, S.; Isobe, Y.; Sugimura, Y.; Gotowda, M.; Kai, Y. *J. Biol. Chem.* **1999**, *274*, 11817–11823.
36. Chen, Z. W.; Barber, M. J.; McIntire, W. S.; Mathews, F. S. *Acta Crystallogr. D* **1998**, *D54*, 253–268.
37. Williams, P. A.; Blackburn, N. J.; Sanders, D.; Bellamy, H.; Stura, E. A.; Fee, J. A.; McRee, D. E. *Nat. Struct. Biol.* **1999**, *6*, 509–516.
38. Brown, K.; Tegon, M.; Prudencio, M.; Pereira, A. S.; Besson, S.; Moura, J. J.; Moura, I.; Cambillau, C. *Nat. Struct. Biol.* **2000**, *7*, 191–195.
39. Eriksson, A. E.; Jones, T. A.; Liljas, A. *Proteins* **1988**, *4*, 274–282.
40. Adman, E. T.; Godden, J. W.; Turley, S. *J. Biol. Chem.* **1995**, *270*, 27458–27474.
41. Yoshikawa, S.; Shinzawa-Itoh, K.; Nakashima, R.; Yaono, R.; Yamashita, E.; Inoue, N.; Yao, M.; Fei, M. J.; Libeu, C. P.; Mizushima, T.; Yamaguchi, H.; Tomizake, T.; Tsukihara, T. *Science* **1998**, *280*, 1723–1729.
42. Magnus, K. A.; Hazes, B.; Ton-That, H.; Bonaventura, C.; Bonaventura, J.; Hol, W. G. J. *Proteins* **1994**, *19*, 302–309.
43. Holmes, M. A.; Le Trong, I.; Turley, S.; Sieker, L. C.; Stenkamp, R. E. *J. Mol. Biol.* **1991**, *218*, 583–593.
44. Hegg, E. L.; Que, L., Jr. *Eur. J. Biochem.* **1997**, *250*, 625–629.
45. Que, L., Jr. *Nat. Struct. Biol.* **2000**, *7*, 182–184.
46. Vaillancourt, F. H.; Han, S.; Fortin, P. D.; Bolin, J. T.; Eltis, L. D. *J. Biol. Chem.* **1998**, *273*, 34887–34895.
47. Valegard, K.; van Scheltinga, A. C.; Lloyd, M. D.; Hara, T.; Ramaswamy, S.; Perrakis, A.; Thompson, A.; Lee, H. J.; Baldwin, J. E.; Schofield, C. J.; Hajdu, J.; Andersson, I. *Nature* **1998**, *394*, 805–809.
48. Roach, P. L.; Clifton, I. J.; Hensgens, C. M.; Shibata, N.; Schofield, C. J.; Hajdu, J.; Baldwin, J. E. *Nature* **1997**, *387*, 827–830.
49. Karlsson, A.; Parales, J. V.; Parales, R. E.; Gibson, D. T.; Eklund, H.; Ramaswamy, S. *Science* **2003**, *299*, 1039–1042.
50. Fusetti, F.; Schroeter, K. H.; Steiner, R. A.; Van Noort, P. I.; Pijning, T.; Rozeboom, H. J.; Kalk, K. H.; Egmond, M. R.; Dijkstra, B. W. *Structure* **2002**, *10*, 259–268.
51. Ludwig, M. L.; Metzger, A. L.; Pattridge, K. A.; Stallings, W. C. *J Mol. Biol.* **1991**, *219*, 335–358.
52. Ullah, J. H.; Walsh, T. R.; Taylor, I. A.; Emery, D. C.; Verma, C. S.; Gamblin, S. J.; Spencer, J. *J. Mol. Biol.* **1998**, *284*, 125–136.
53. Whittington, D. A.; Lippard, S. J. *J. Am. Chem. Soc.* **2001**, *123*, 827–836.
54. Logan, D. T.; Su, X. D.; Aberg, A.; Regnstrom, K.; Hajdu, J.; Eklund, H.; Nordlund, P. *Structure* **1996**, *4*, 1053–1064.
55. Rardin, R. L.; Tolman, W. B.; Lippard, S. J. *New J. Chem.* **1991**, *15*, 417–430.
56. Tong, W.; Burdi, D.; Riggs-Gelasco, P.; Chen, S.; Edmondson, D.; Huynh, B. H.; Stubbe, J.; Han, S.; Arvai, A.; Tainer, J. *Biochemistry* **1998**, *37*, 5840–5848.
57. Lindqvist, Y.; Huang, W.; Schneider, G.; Shanklin, J. *EMBO J.* **1996**, *15*, 4081–4092.
58. Jin, S.; Kurtz, D. M., Jr.; Liu, Z.-J.; Rose, J.; Wang, B.-C. *J. Am. Chem. Soc.* **2002**, *124*, 9845–9855.
59. Stillman, T. J.; Hempstead, P. D.; Artymiuk, P. J.; Andrews, S. C.; Hudson, A. J.; Treffry, A.; Guest, J. R.; Harrison, P. M. *J. Mol. Biol.* **2001**, *307*, 587–603.
60. Whittaker, M. M.; Barynin, V. V.; Antonyuk, S. V.; Whittaker, J. W. *Biochemistry* **1999**, *38*, 9126–9136.
61. Doukov, T. I.; Iverson, T. M.; Seravalli, J.; Ragsdale, S. W.; Drennan, C. L. *Science* **2002**, *298*, 567–572.
62. Darnault, C.; Volbeda, A.; Kim, E. J.; Legrand, P.; Vernède, X.; Lindahl, P. A.; Fontecilla-Camps, J. C. *Nat. Struct. Biol.* **2003**, 271–279.
63. Nagashima, S.; Nakasako, M.; Dohmae, N.; Tsujimura, M.; Takio, K.; Odaka, M.; Yohda, M.; Kamiya, N.; Endo, I. *Nat. Struct. Biol.* **1998**, *5*, 347–351.

8.2
Electron Transfer: Cytochromes

K. R. RODGERS and G. S. LUKAT-RODGERS
North Dakota State University, Fargo, USA

8.2.1 INTRODUCTION

The cytochromes are ubiquitous heme proteins ($>75,000$ known)[1] that play essential roles in biological electron transfer. They were originally classified on the basis of optical absorbance maxima characteristic of their prosthetic heme groups.[2,3] The chemical structures of the most common biological hemes are shown in Figure 1. Several classes of biological metal-chelating ligands, macrocyclic tetrapyrroles, include the porphyrins ($22\pi e^-$ ligands in hemes *a*, *b*, and *c*), chlorins ($20\pi e^-$ ligands in heme *d*), isobacteriochlorins ($18\pi e^-$ ligands as in heme d_1), and corrins ($20\pi e^-$ ligands). Heme *b* in *b*-type cytochromes is an iron protoporphyrin IX complex in which the iron atom is ligated to the four pyrrole nitrogen atoms. Hemes *a* and *c* are derivatives of heme *b*.
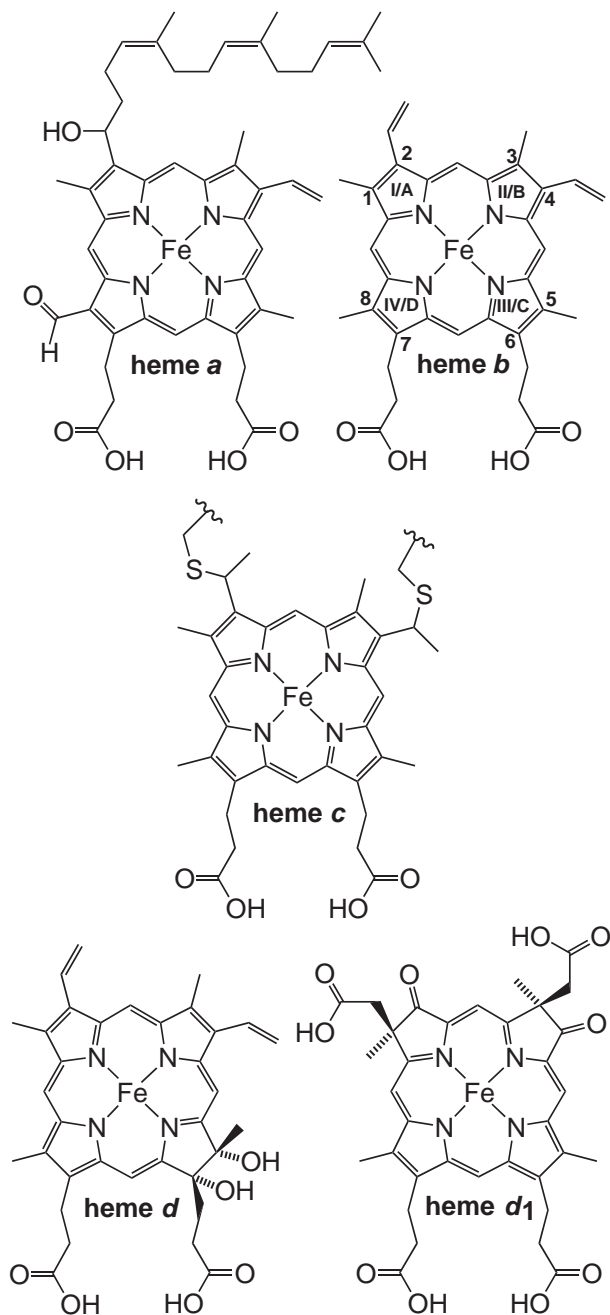
Figure 1 Common biological heme structures. The labeling conventions indicated on the heme *b* structure are those commonly found in the literature on solution studies. The Roman numeral designations are used here. The crystallographic literature uses an Arabic letter labeling scheme that is rotated by $-90°$ (90° counterclockwise) from that shown here.

Cross-linking of the heme *b* vinyl groups at β-pyrrole positions 2 and 4, with Cys side chains, covalently links the heme to the proteins in *c*-type cytochromes. Cross-linking occurs at highly conserved –Cys–Xxx–Yyy–Cys–His– sequences. In heme *a*, hydroxyl and farnesyl groups are added to the vinyl side chain at position 2, with a formyl group at position 8. Heme *a* is found in proteins like cytochrome *c* oxidase. Heme d_1 contains ketone groups in place of the position 2 and 4 vinyl groups. In cytochrome cd_1 nitrite reductase, the *d*-type cytochrome has been identified as 3,8-dioxo-17-acrylate-porphyrindione.[4] As this chapter will focus on electron-transfer cytochromes, a subset of the proteins containing porphyrin-based heme complexes, the discussion of the interplay between coordination chemistry and electronic structure will focus on their porphyrinate ligands and their iron complexes.
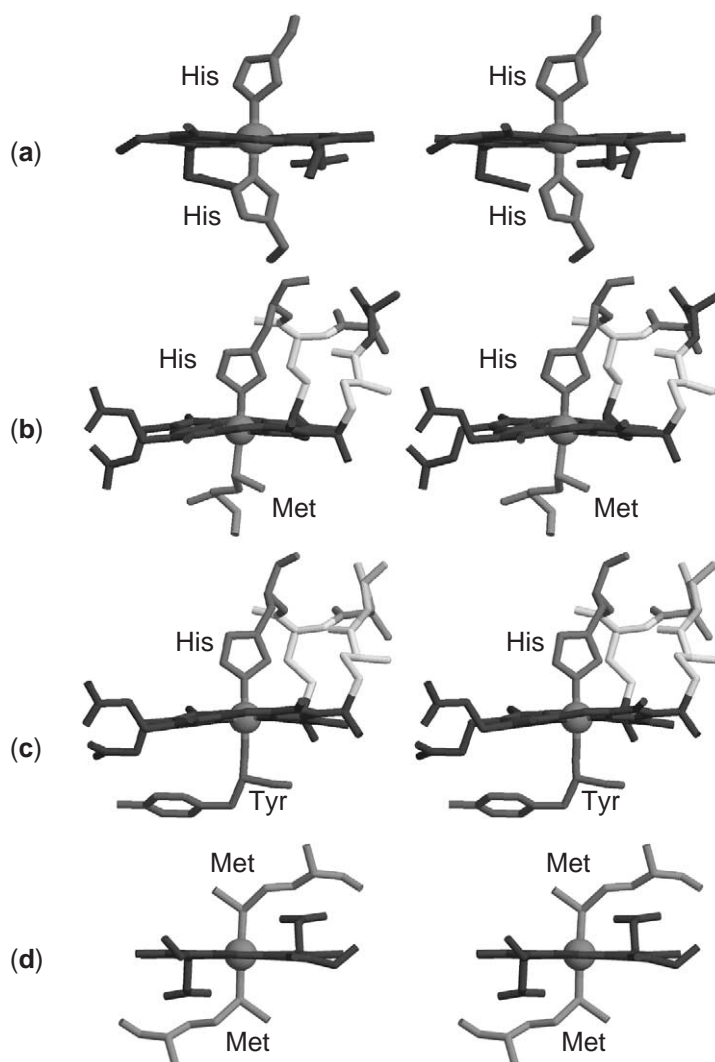
Figure 2 Cross-eyed stereo views of the hemes and their axial ligands found in electron-transfer cyto-chromes. (a) Bis–His ligation is generally found in cyts *b* and multiheme cyts *c* (PDB code1WDB). (b) His/Met ligation is common in class I cyts *c* (PDB code 1YCC). (c) His/amine ligation has been observed only in cyt *f* (PDB code 1CTM). For *c*-type cytochromes, the conserved Cys–Xxx–Yyy–Cys–His sequence and its covalent linkages to the heme are shown. (d) Bis–Met ligation is found in bacterioferritin (PDB code 1BCF) and has been engineered into some cyt b_{562} mutants. Note the variation in amplitudes and compositions of out-of-plane distortion.

Electron-transfer cytochromes are, with one exception (cytchromes *c'*), six-coordinate, low-spin (6cLS) with axial ligands being supplied by Lewis-basic amino-acid side chains or, less commonly, N-terminal amine groups. The known axial ligand pairs are illustrated in Figure 2. In *b*-type cytochromes, the heme is bound to the protein via two axial ligands of the heme iron, usually histidines (His). A His residue is also one of the axial ligands in *c*-type cytochromes. It is found in the conserved –Cys–Xxx–Yyy–Cys–His– sequence, which also anchors the porphyrin macrocycle to the protein. In *c*-type cytochromes, the most common second axial ligand for the heme iron is the thioether side chain of a methionine (Met). However, bis-His heme coordination is known and occurs most frequently in multiheme *c*-type cytochromes.[5] The His ligands are coordinated to the iron through the Nε, although there is at least one example of Nδ coordination.[6] In the unique case of cyt *f*, a *c*-type cytochrome in the photosynthetic cyt b_6f complex, the heme iron is coordinated by a His residue and the amine of the N-terminal tyrosine (Tyr).[7] Finally, the iron-storage protein, bacterioferritin, contains a *b*-type cytochrome thought to be involved in redox-coupled release of iron from the bacterioferritin iron core.[8] This cytochrome exhibits bis-Met axial ligation, with the thioether ligands being supplied by symmetry-related pairs of bacterio ferritin subunits.[9,10]

## 8.2.2 HEME ELECTRONIC STRUCTURE AND AXIAL-LIGAND GEOMETRIES

8.2.2.1 Structural Aspects of 6cLS Iron Porphyrinates

In early studies of cytochromes, spectroscopic methods were relied upon for determination of spin state, coordination number, and axial-heme ligation. Model hemes in which metal-ion size, charge, and d-orbital occupancy, as well as ligand structure and composition, could be systematically varied, were spectrally characterized for comparison to cytochromes. Synthetic 6cLS Fe^{II} and Fe^{III} porphyrinates have been studied for many years with the goal of clarifying structure–function relationships observed in cytochromes.

The structures of many 6cLS Fe^{II} and Fe^{III} porphyrinates are available.[11] The Fe^{III} complexes exhibit several characteristic structural properties. There is little or no displacement (~ 0.09 Å) of the Fe^{III} center from the mean heme plane, even in complexes with different axial ligands. The Fe–N_{prrole} (Fe—N_p) bond lengths depend upon the charge of the complex, with Fe—N_p being ~ 1.990 Å for neutral or positively charged complexes, and ~ 2.000 Å for complexes with a single negative charge.[11] The Fe—N_p distances within a given complex can be inequivalent if axial ligands are coplanar and nearly aligned with the Fe—N_p bonds ($\phi \sim 0$, Figure 3), those perpendicular to the ligand plane being shorter by ~ 0.02 Å. Axial Fe^{III}—L bond lengths depend upon orientation if the ligand is planar. Steric interactions of axial ligands like pyridines and hindered imidazoles with the porphyrin ring tend to lengthen the Fe^{III}—L bond. Finally, π-acceptor ligands can induce ruffling of the porphyrin core by electronic stabilization.

Equatorial Fe—N_p bond lengths in the 6cLS Fe^{II} porphyrinates are only slightly longer (~ 0.0102 Å) than their Fe^{III} counterparts, and in the complexes with identical axial ligands, the Fe^{II} atom is in the plane of the porphyrin core.[11] In the LS d^6 configuration of the ferrous cytochromes and model hemes, filling of the d_π orbitals is expected to favor increased π-bonding in these complexes. This is borne out by shortening of bonds with π-acceptor ligands by hundredths of angstrom relative to the corresponding Fe^{III} complexes.[11] In model hemes, the Fe—S bond lengths for neutral sulfur ligands appear to be insensitive to whether the iron is in the $+2$ or $+3$ oxidation state. Bonds to neutral nitrogen donor ligands such as imidazoles, pyrazoles, and pyridines exhibit longer bonds in the Fe^{II} complexes.[11]

8.2.2.2 Out-of-plane Porphyrin Deformation

One of the more extensively studied and discussed structural variables has been equilibrium out-of-plane distortion of the porphyrin. Out-of-plane porphyrin deformation typically results in a bathochromic (red) shift of the optical absorption spectrum and a shift to more negative reduction potentials (easier to oxidize).[12–15] These tantalizing correlations, based upon studies of model complexes comprising porphyrin ligands such as octaethyltetraphenylporphyrinate ($OETPP^{2-}$), having sterically crowded peripheries that force large out-of-plane deformations, have driven
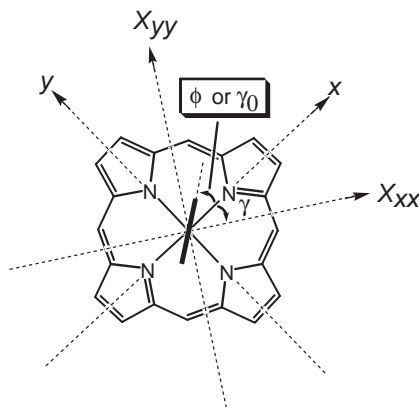
Figure 3 Heme core showing rotation angle of planar axial ligand(s) with respect to the Fe–N_p (positive x) axis, ϕ or γ_0. Also shown is the equivalent counterrotation, γ, of the magnetic susceptibility tensor axes. Adapted from ref. 27.
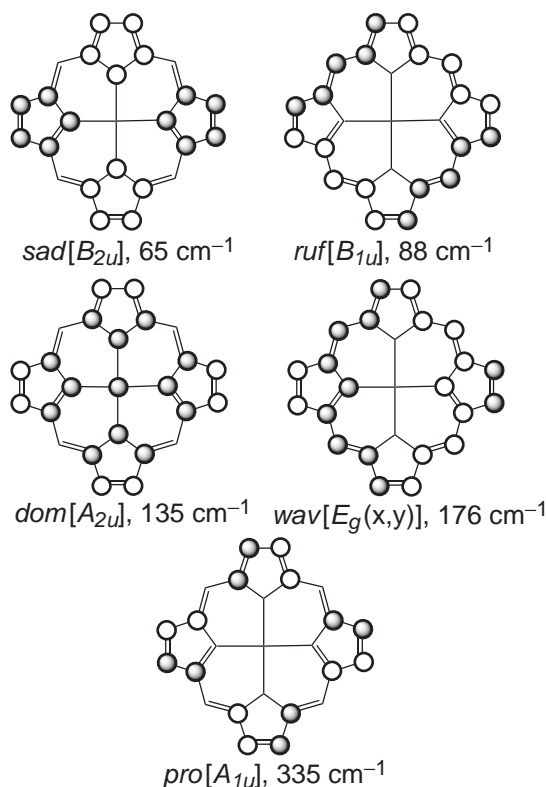
Figure 4 Six out-of-plane vibrational coordinates of a D_{4h} metalloporphyrin used in normal structural decompositions to reveal compositions of equilibrium out-of-plane heme deformations. Mulliken symbols are of the D_{4h} point group and the abbreviations *sad*, *ruf*, *dom*, *wav*, and *pro* indicate saddled, ruffled, domed, wave, and propeller distortions, respectively. (Note that wav_x and wav_y derive from a doubly degenerate pair of E_g vibrational modes of the D_{4h} porphyrin.) The dark and light circles indicate atoms on opposite sides of the mean heme plane. Adapted from ref. 11.

widespread investigation of the relationships between out-of-plane deformation, redox potential, and optical spectra of porphyrins and metalloporphyrins.[12–14]

Several reports have called into question the correlation between sterically enforced, out-of-plane deformation and the electronic properties, redox potential and spectroscopic signatures.[16–18] Based on UV–visible spectra, structural analysis, and TD-DFT calculations, it has been suggested that the shifts in UV–visible transitions result from electronic effects of the peripheral substituents on the aromatic porphyrin core. These effects drive a bond-alternating rearrangement of the porphyrin core atoms called "in-plane nuclear reorganization."[16]

Regardless of the driving force(s), out-of-plane porphyrin deformations invariably occur along low-frequency, normal coordinates. A recent computational method, normal-coordinate structural decomposition (NSD), yields linear combinations of equilibrium distortions along the lowest-frequency out-of-plane normal vibrational coordinates of the heme.[15,19,22] The six out-of-plane vibrational coordinates of a D_{4h} metalloporphyrin used in the linear combinations are illustrated in Figure 4. NSD results show that hemes in many cytochromes exhibit equilibrium out-of-plane distortions of nearly 1 Å along the *ruf* and/or *sad* coordinates, and it has been estimated that these distortions require heme protein interaction energies substantially greater than 2 kcal mol^{-1} [1] and up to 8 kcal mol^{-1} [1,23,24] Interestingly, out-of-plane deformations are largely conserved within classes of cytochromes.[21,22,25,26] It has been suggested that expenditure of energy by a protein to enforce a particular out-of-plane distortion is unlikely to be accidental, and could play an important role in biological function.[15,23]

8.2.2.3 The Frontier Orbitals and Fe–Ligand Bonding

Figure 5 shows the nodal patterns of the four highest occupied and the two lowest unoccupied porphyrin molecular orbitals (MOs)[27] and the energy ordering and symmetry designations of
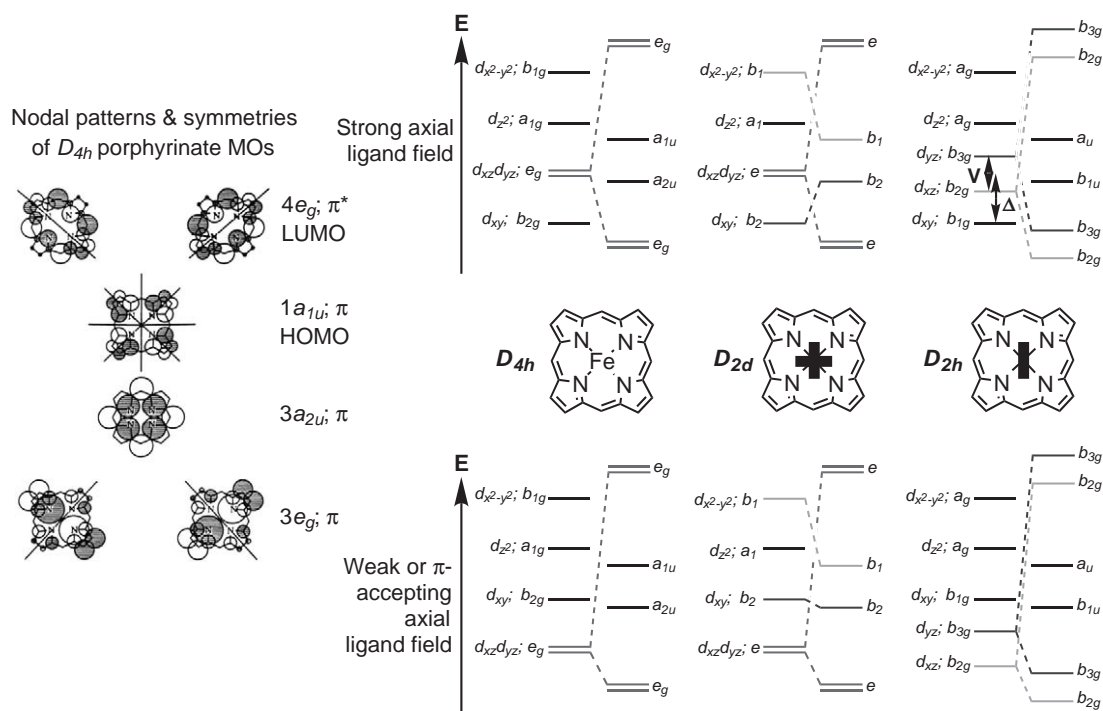
Figure 5 Nodal patterns of the four highest occupied and the two lowest unoccupied porphyrinate π MOs are shown at the left (adapted from reference 27). At the right are shown the iron *d*-orbitals and porphyrin MOs, along with their symmetries in the D_{4h}, D_{2d}, and D_{2h} point groups. Symmetry-allowed bonding/ antibonding orbital interactions are shown by dashed lines connecting porphyrinate and *d*-orbitals of the same symmetries. Heme structures are shown for each point group to illustrate the effect of axial ligand orientation on the symmetry of the molecule, whether or not the porphyrin experiences out-of-plane distortion. If the axial ligands are not identical, the heme has either C_{2v} or lower symmetry. In these cases all of the *d*- and porphyirn π-orbitals shown are allowed by symmetry to participate in bonding/antibonding interactions. The relative energies shown are arbitrary and are not intended to accurately reflect energy match or mismatch of metal *d*- and porphyrin π-orbitals.

metal-centered *d*-orbitals in octahedral and tetragonal ligand fields, along with the frontier MOs of the porphyrin. Sigma bonding between iron and the porphyrin is based on interactions between the d_{z^2} (a_{1g} in D_{4h}) and $d_{x^2-y^2}$ (b_{1g} in D_{4h}) orbitals of iron and porphyrin MOs with respective symmetries. The degenerate d_{xz}, d_{yz} pair (e_g in D_{4h}) can combine with the porphyrin π MOs of e_g symmetry.[27] The d_{xy} orbital is nonbonding in D_{4h} metalloporphyrins. Of particular interest is the bonding interaction between the d_{xy} orbital (b_2 symmetry) and the porphyrinate b_2 MO (correl- ates with the a_{2u} MO in D_{4h} complexes) in hemes of D_{2d} symmetry.[24,27–32] Symmetry lowering to D_{2d} is usually associated with the ruffling distortion shown in Figure 4. This deformation involves counterrotation of adjacent pyrrole rings about their Fe—N_p bonds, which results in a nonzero projection of pyrrole N p_z-derived MOs onto the mean porphyrin plane. The resulting π–d_{xy} bonding represents an electronic contribution to the stability of some ruffled 6cLS Fe[III] porphy- rinates with $(d_{xz},d_{yz})^4(d_{xy})^1$ Fe[III] ground states. This stabilization is not possible for Fe[II] com- plexes, because the d_{xy} orbital is filled.

Sigma bonding between Fe and axial ligands generally involves $3d_{z^2}$, $4s$, and $4p_z$ orbitals of the metal and occupied orbitals of the axial ligands. Axial ligands can also participate in π bonding with Fe[III] and Fe[II] centers by interaction of their π orbitals with the partially or completely filled d_{xz} and d_{yz} orbitals.[27]

In most 6cLS Fe[III] hemes, the ordering is that of the $(d_{xy})^2(d_{xz},d_{yz})^3$ ground state.[27] This state is subject to stabilization by Jahn–Teller splitting of the e_g set, which results in symmetry lowering from fourfold to twofold rotational symmetry. The stabilization due to Jahn–Teller splitting in 6cLS Fe[III] porphyrinates can manifest itself as experimentally discernible symmetry lowering, including the thermodynamic preference for parallel orientations of planar axial ligands and asymmetry in Fe—N_p bond lengths when the ligands align with two opposing Fe—N_p bonds.[11,25,33,34] Such complexes give rise to rhombic (type II) EPR spectra,[27,28,35] as shown in Figure 6. Although according to the Jahn–Teller theorem, d_{xz} and d_{yz} cannot be degenerate in
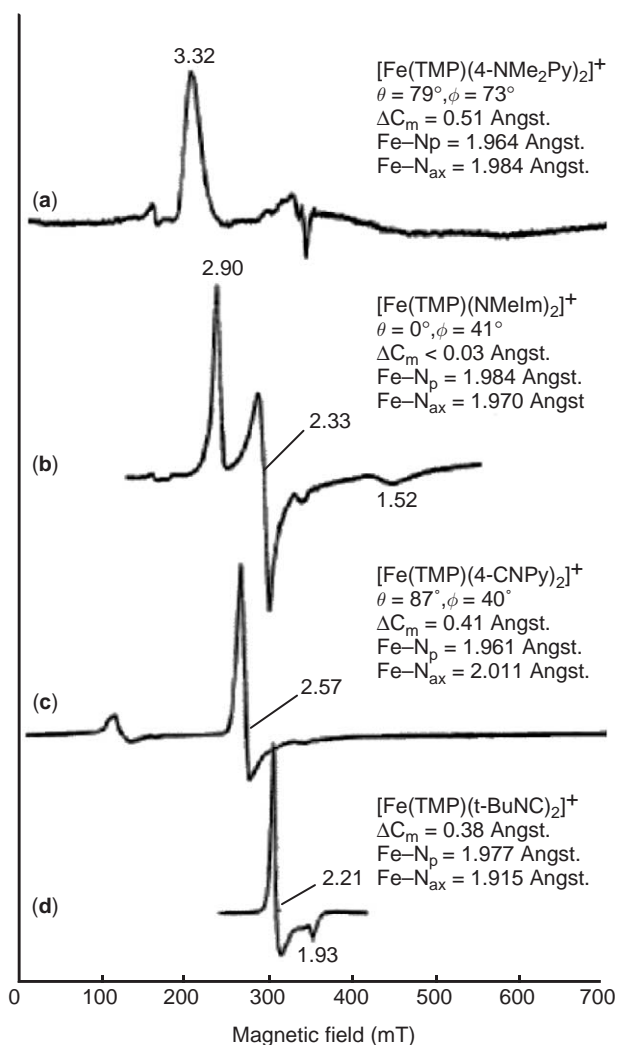
Figure 6 X-band EPR spectra of 6cLS ferric hemes. (a) Type I or "large g_{max}" spectrum typical of complexes with mutually perpendicular axial ligands. (b) Type II or normal rhombic spectrum typical of complexes with mutually parallel axial ligands. (c) Type III axial spectrum with large, and (d) small difference between g_I and g_{II}. Type III spectra are typical of 6cLS complexes having axial π-acceptor ligands such as isocyanides. Figure adapted from reference 27.

6cLS Fe^{III} hemes, the effects of Jahn–Teller splitting can be masked by strong steric interactions between the porphyrin and axial ligands, due either to out-of-plane deformation of the porphyrin or to sterically demanding axial ligands[11] such as 2-methylimidazole, which force the axial ligands to be mutually perpendicular. These complexes also have $(d_{xy})^2(d_{xz},d_{yz})^3$ ground states and give rise to highly anisotropic (type I or "g_{max}") EPR spectra.[27,28,35] In complexes with strong axial-ligand fields imposed by weak σ-donor and/or π-acceptor ligands, such as 4-cyanopyridine and the organic isocyanides, the MOs having contributions from the d_{xz} and d_{yz} AOs are stabilized. These complexes have axial $(d_{xz},d_{yz})^4(d_{xy})^1$ ground states,[11,27] which are not susceptible to Jahn–Teller distortion and exhibit type III EPR spectra.[27] This ground state is further evidenced by substantial weakening of the porphyrin πd ($^2B_2 \rightarrow {}^2A_1$) NIR-CT MCD transition, which is symmetry forbidden for $(d_{xz},d_{yz})^4(d_{xy})^1$ ground states.[28]

8.2.2.4 Cause and Effect Roles of Axial Ligation

Planar axial ligands can adopt mutually parallel or mutally perpendicular orientations in 6cLS Fe^{III} complexes, with their orientations relative to the Fe—N_p bonds ranging from $0°$ to $45°$.[27]

Relevant angles are shown in Figure 3. There are two principal aspects of axial ligation to consider, steric and electronic. Planar axial ligands prefer mutually orthogonal orientations if Fe—L bonding causes steric interactions between the axial ligands and the porphyrin. These interactions are stronger for the six-membered pyridine and sterically hindered 2-methylimidazole ligands than for imidazole.[11,27] They can involve atoms in the porphyrin core and/or bulky peripheral substituents, and usually result in ruffling of the porphyrin core (see Figure 4).

A distinct situation arises in persubstituted porphyrins, wherein strong steric interactions occur between adjacent substituents at the porphyrin periphery. These porphryins exhibit an inherent saddling deformation, even as metal-free macrocycles, and exhibit such narrow clefts that steric constraints dictate orthogonal, or nearly orthogonal, orientations of axial ligands.[27,36] Most orthogonal axial-ligand orientations in 6cLS Fe^{III} porphyrinates are attributable to the relief of costly intramolecular steric interactions.[11,34,37–39] This is an important point with regard to the heme structures and deformations in cytochromes, as their hemes exhibit little intrinsic intramolecular steric strain.[23] Furthermore, since all type b, c, and f cytochromes characterized to date have $(d_{xy})^2(d_{xz},d_{yz})^3$ ground states,[27,40,41] there is no electronic stabilization of the ruffling distortion as described above in these cytochromes. Hence, equilibrium deviations from planarity must be attributable to exogenous forces brought to bear on the heme by the protein.

In the absence of steric encumbrance at the porphyrin periphery, the parallel axial-ligand conformation is favored for ligands such as unhindered imidazoles. This is attributed to stabilization of the Jahn–Teller distorted ground state.[11,27,34] In these complexes, the porphyrin is invariably flat and ϕ, the ligand angle, can range from $0°$ to $45°$ (Figure 3). The complexes having ϕ near $0°$ exhibit rhombic EPR spectra and a B_{1g}-distorted porphyrin core (nonequivalent adjacent Fe^{III}—N_p bond lengths). Those with ϕ near $45°$ exhibit equivalent Fe^{III}—N_p bond lengths, but still yield rhombic EPR spectra wherein the rhombicity, V (see Figure 5), has been shown to track inversely with ϕ.[42] Six-coordinate, low-spin Fe^{II} complexes strongly prefer parallel axial ligands and a planar porphyrin ligand.[11,27,29] This is thought to be because of the inability of low-spin Fe^{II} to stabilize a ruffled porphyrin conformation. Several examples of ruffled 6cLS Fe^{II} complexes have been reported.[43] Ruffling has been ascribed to steric interactions between bulky porphyrin substituents and axial ligands. Some work has suggested that Fe—N_{ax} bonding is independent of π-accepting ability of the axial ligands; these results were interpreted to mean that d_{xz}- and d_{yz}-orbitals are not strongly involved in π-bonding.[29] Consistent with this reasoning, a series of 4-substituted pyridines with varying pK_as and π-acceptor abilities show the same thermodynamic stabilities, suggesting that axial bond strengths do not vary significantly in this series. This is in contrast to the analogous Fe^{III} complexes, wherein the Fe—N_{ax} bond strength varies predictably.[44] Since the redox potential depends upon the ratio of Fe^{III} and Fe^{II} stability constants, $\log(\beta_2^{III}/\beta_2^{II})$,[44] tunability of the contribution of bond strengths to redox potential seems to be confined to tunability of β_2^{III} in model complexes. It is worth noting that this may not be the case in cytochromes, because the proteins have control over porphyrin conformation and axial-ligand orientation, which can differ from the lowest-energy conformations of the model complexes where there are no exogenous forces.

8.2.3   CYTOCHROMES c

8.2.3.1   Function

Cyt c has an important role in the production of ATP; in the mitochondrial respiratory electron-transfer chain, cyt c transfers electrons from the transmembrane cyt bc_1 complex to cytochrome c oxidase.[45,46] Cyt c also delivers electrons to cytochrome c peroxidase, which facilitates the reduction of hydrogen peroxide to water. In addition to its life-sustaining electron-transfer functions, cyt c is required for activation of the cell-death protease, caspase-3, in apoptosis.[47–49] Defects in cyt c biogensis have been implicated in pathogenic responses related to copper[50] and iron metabolism,[51] and prokaryotic heme biosynthesis.[52]

Similar c-type cytochromes are involved in many kinds of energy metabolism in bacteria, such as phototrophes, methylotrophes, sulfate reducers, nitrogen-fixers, and denitrifiers. For example, in the anaerobic electron chain of the denitrification system in Gram-negative bacteria, c-type cytochromes transfer electrons from the cyt bc_1 complex to cytochrome cd_1 nitrite reductase, N_2O

reductase, and NO reductase.[53] In plants and cyanobacteria, *c*-type cytochromes shuttle electrons from the cyt $b_6 f$ complex to photosystem I.[54]

Due to its central role in the vital processes of living organisms, and the large database of physical and biochemical information available on cyt *c*, it has become one of the paradigms in the study of biological electron-transfer processes.[55,56] Functional studies on cyt *c* and numerous cyt *c* point mutants have been used to identify residues and regions of the protein that influence electron-transfer properties.[55–57] In order to study intraprotein electron transfer and the pathways involved in cyt *c*, numerous donor–acceptor complexes have been generated by covalently linking various redox-active inorganic complexes to surface amino-acid residues of cyt *c*.[58–60] Interprotein electron transfer has also been examined using cyt *c* complexes with cytochrome *c* oxidase,[61–65] plastocyanin,[66–69] cyt b_5,[70–72] and cytochrome *c* peroxidase.[73–76] Since cyt *c* is ubiquitous, easy to isolate, stable, and soluble, it has also become a system for the study of protein folding[77–86] and protein dynamics.[87–90]

8.2.3.2 General Classifications

Cyts *c* fall into at least four general classes.[5,91,92] The largest class, class I, consists of small (8–20 kDa), monoheme cyts *c* that are homologous to mitochondrial cyt *c*. Sequence and structural data have been used to divide class I into sixteen subclasses.[92] Mitochondrial cyts *c* and purple bacterial cyts c_2 make up the largest subclass. Additional subclasses include *Pseudomonas* cyts c_{551}, cyts c_4, cyts c_5, cyts c_6 (algal cyts c_{553}), *Chlorobium* cyt c_{555}, *Desulfovibrio* cyts c_{553}, cyanobacterial and algal cyts c_{550}, *Ectothiorhodospira* cyts c_{551}, flavocytochromes *c*, methanol dehydrogenase-associated cyt c_{550} or c_L, cytochrome cd_1 nitrite reductase, alcohol dehydrogenase and its associated cytochrome subunit, *Pseudomonas* nitrite reductase-associated cyt *c*, *Bacillus* cyt *c*, and *Bacillus* cytochrome oxidase subunit II. With the large number of cyts *c* presently being characterized structurally, proteins that fall into new additional subclasses continue to be found.[93,94] Most class I cyts *c* are water soluble and contain a 6cLS heme. Their heme-attachment site (–Cys–Xxx–Yyy–Cys–His–) is towards the N-terminus. The axial heme iron ligation is provided by the His residue of the heme-attachment site and a Met residue found near the C-terminus. Figure 7(a) illustrates the general fold for class I cyts *c*.

Class II cyts *c* have a single *c*-type heme covalently linked to the highly conserved –Cys–Xxx–Yyy–Cys–His– sequence near their C-termini.[5] While the number of conserved amino-acid residues among class II cyts *c* is relatively small,[5,95] the structural motif of a left-twisted, four-α-helix bundle is characteristic of these proteins (Figure 7(b)).[96,97] A His residue occupies one axial coordination site of the heme iron, while the second axial coordination site is variable. This class has two subclasses that are distinguished by the spin state of the heme. Subclass IIa consists of cyts *c′*, which have high-spin (HS) configurations in the reduced form [Fe^{II}, $S = 2$] and either HS ($S = 5/2$)[98–101] or a quantum-admixed spin (admixture of $S = 5/2$ and $S = 3/2$) states[98,100,102–104] in the ferric form. For example, the observed *g*-values for ferric *Chromatium vinosum* cyt *c′* ($g_1 = 5.32$, $g_2 = 4.67$, $g_3 = 1.97$) are not typical for a purely high-spin ferric heme, and simulation of this EPR spectrum reveals that the electronic ground state of this cyt *c′* consists of 51% $S = 3/2$ and 49% $S = 5/2$.[100] These cyts *c′* are found in photosynthetic and denitrifying bacteria. Subclass IIb includes proteins like cyt c_{556} from *Rhodopseudomonas (Rps.) palustris*,[105] *Rhodobacter (Rb.) sulfidophilus*[106] and *Agrobacterium tumefaciens*,[5] and cyt c_{554} from *Rb. sphaeroides*[107] that contain low-spin hemes. In these cases, the sixth heme ligand, a Met, is found near the N-terminus.

Triheme, tetraheme, octaheme, nonaheme, and 16-heme cyts *c* from sulfate and sulfur-reducing bacteria are included in class III.[5,92,108–112] Gene duplication of tri- and tetraheme units is clearly apparent. In *Desulfovibrio* species, the tetraheme proteins (~15 kDa) are part of the electron-transfer chain that couples the oxidation of molecular hydrogen by hydrogenase to sulfate reduction.[113] These multiheme proteins, also known as cyts c_3, generally have bis-His heme ligation. Although the conserved amino acids in this class appear to be limited to the heme-binding cysteines and the heme iron axial histidines, the three-dimensional structures of *Desulfovibrio* tetraheme cyts c_3[40,114–121] reveal that the overall protein fold with two short β-strands and 3 to 5 α-helices is conserved.[92] Interestingly, the heme–heme distances and heme–heme angles are evolutionarily highly conserved. The hemes are in close proximity to one another, with adjacent pairs of heme planes nearly perpendicular to one another (Figure 7(c)). There is, however, considerable variability in the dihedral angle between the axial His planes in *Desulfovibrio (D.)* cyts c_3.[119,120,122]

Class IV consists of large (40 kDa) tetraheme photosynthetic reaction center (THRC) cyts *c*. *Rsp. viridis* THRC cyt *c* is the electron donor to the bacteriochlorophyll special pair. The structure of this membrane-associated *Rsp. viridis* cyt *c* exemplifies the tertiary structure of this class (Figure 7d).[5] Its four hemes are in a linear arrangement, with alternating high- and low-potential sites . While *Rsp. viridis* THRC cyt *c* has three hemes with bis-His ligation and one with His/Met ligation, the homologous THRC cyts *c* from *Chloroflexus aurantiacus*[92] and *Rubrivivax (Rv.) gelatinosus*[123] appear to contain only His/Met heme ligation.

Nitrosomonas (N.) europaea cyt c_{554} is a tetraheme that is not homologous to either class III or class IV multiheme cytochromes, and is considered to be in a class of its own (Figure 7e). Involved in the biological nitrification pathway, this cyt c_{554} accepts two electrons from hydroxylamine oxidoreductase (HAO) upon generation of nitrite. Its one high-spin heme and three 6cLS hemes (+47, +47, −147, and −276 mV vs. SHE) are arranged in two types of pairs where the hemes are in van der Waals contact. Hemes III/IV have their porphyrin planes nearly perpendicular to one another in an arrangement similar to that in cyts c_3.[6] Heme pairs I/III and II/IV have nearly parallel porphyrin rings that overlap at one edge, similar to the heme arrangement in HAO and cytochrome *c* nitrite reductase.[6] Sequence similarities between these seemingly unrelated proteins are found in the polypeptide near the hemes when the heme-stacking arrangement is used to align the protein chains.[124] Based on this and the conserved nature of the heme organization, it has been suggested that *N. europaea* cyt c_{554}, HAO, and cytochrome *c* nitrite reductase have a common evolutionary origin, but have diverged to fulfill different functions.

A sixth class of *c*-type cytochromes consists of the cyts *f* from the cyt b_6f complex of oxygenic photosynthesis. The crystal structure cyt *f* on the lumin-side reveals two elongated domains made up primarily of β-sheet secondary structure, with the heme attached to the larger domain close to

(a)   (a)

(b)   (b)

(c) (c)

(d) (d)

(e) **(e)**

(f) **(f)**
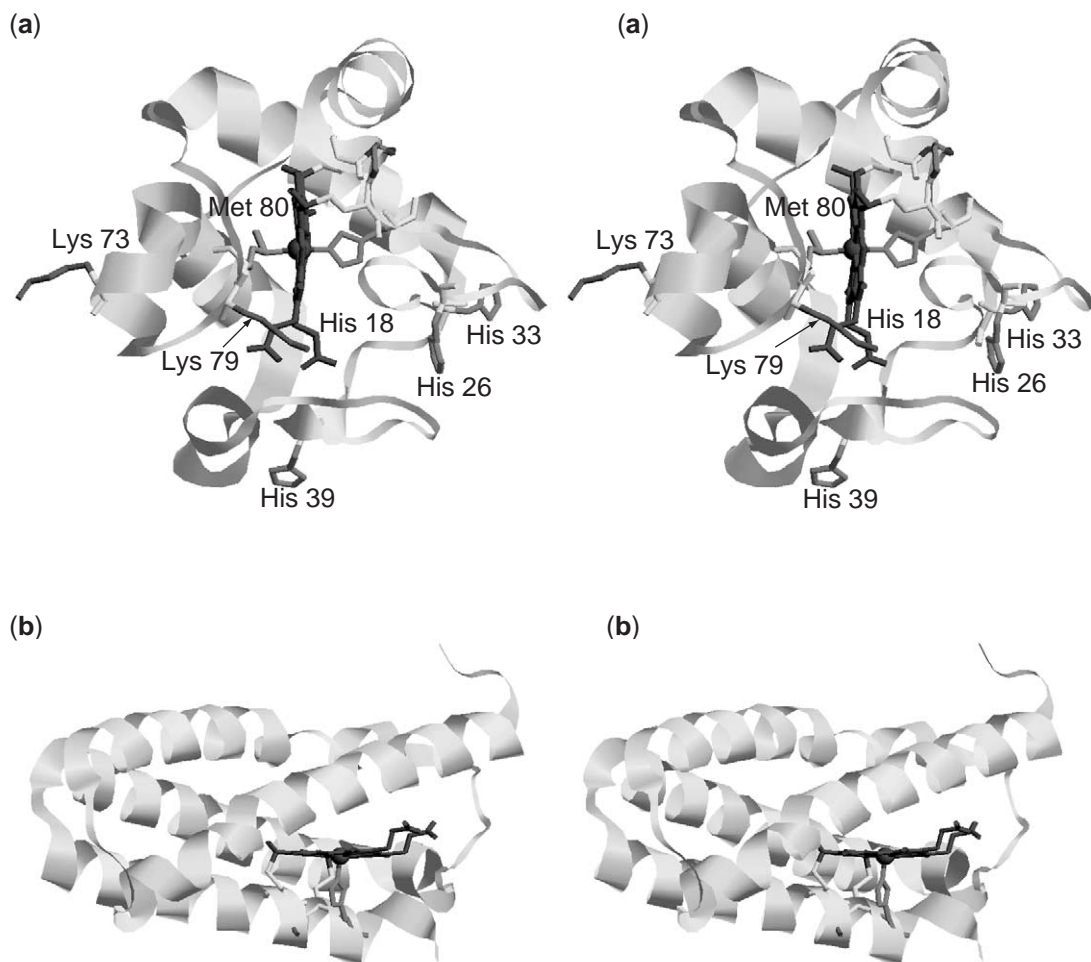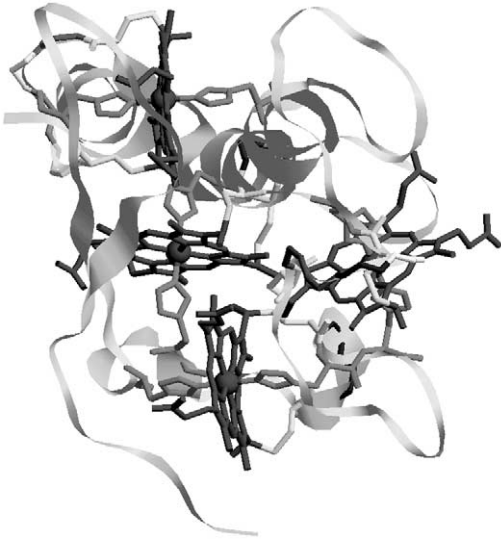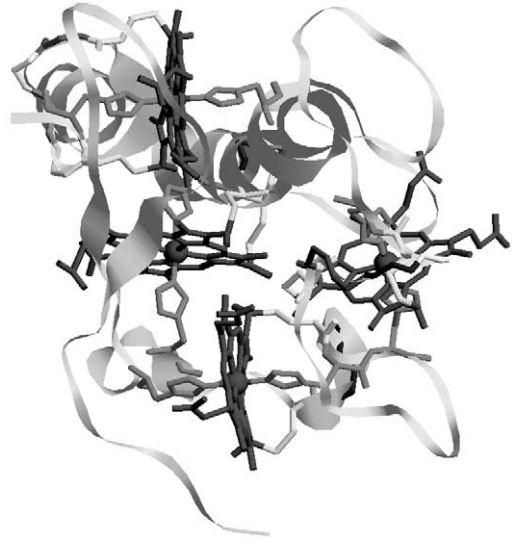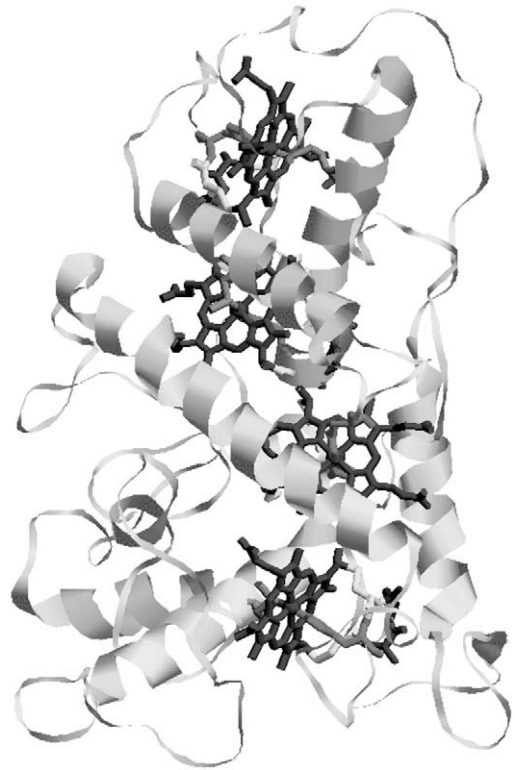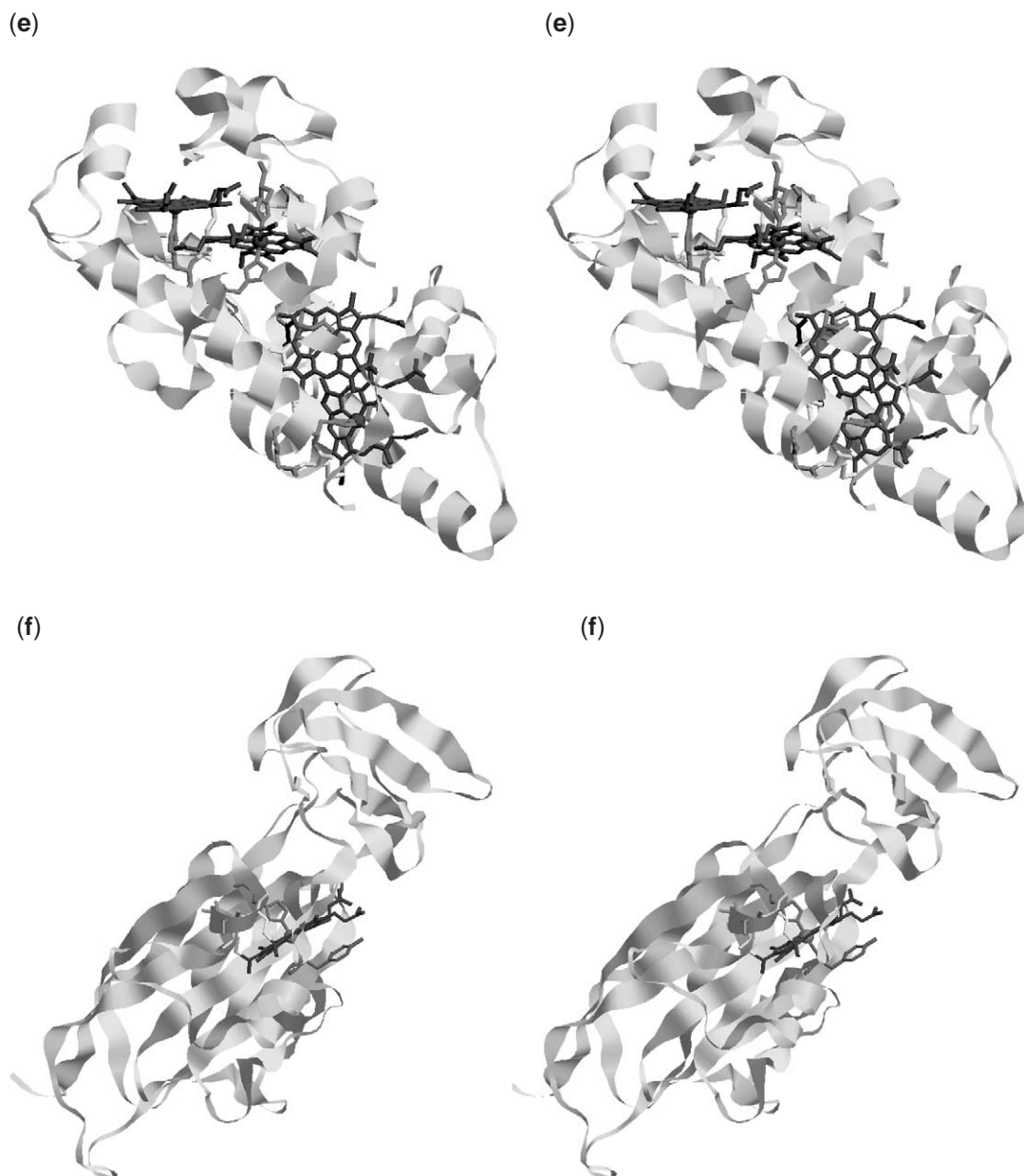
Figure 7 Cross-eyed stereo views of protein folds for *c*-type cytochromes. (a) Class I, *iso*-1-cyt *c* (PDB code 2YCC); (b) class II, cyt *c'* (PDB code 1E84); (c) class III, cyt c_3 (PDB code 1WAD); (d) class IV, THRC cyt *c* (PDB code 3PRC); (e) Cyt c_{554} (PDB code 1FT6); (f) cyt *f* (PDB code 1CI3).

the interface of the two domains (Figure 7f).[7] Its β-sheet content and axial-heme ligation (His and the α-amino group of the N-terminal Tyr) make this structure unlike that of any other class of *c*-type cytochrome already discussed.[7,125]

8.2.3.3 Structural Studies of Mitochondrial Cytochromes *c*

As a protein subgroup of class I, mitochondrial cyts *c* have sequence homologies that are evolutionarily conserved.[5,126] This sequence homology translates into a high degree of structural similarity. Crystal structures are available for tuna,[127–129] horse,[130] rice,[131] and yeast (*iso*-1 and *iso*-2 of *Saccharomyces (S.) cerevisiae*)[132–134] mitochondrial cyts *c*. The typical cyt *c* fold consists of a series of α-helices and fairly extended loop structures. The heme is almost completely enclosed in

a hydrophobic pocket. Only five atoms at the edge of the heme pyrrole rings II and III are exposed to the surface, while the heme propionates are shielded from bulk solvent by interactions with polar side chains. In some bacterial class I cyts the propionates are exposed to solvent, due to variations in surface loops on the common class-I core structure.[5] The features common to all five mitochondrial cyt *c* structures include the heme attachment site at Cys14 and Cys17, His18 and Met80 as fifth and sixth heme iron ligands, hydrogen bonding from Pro30 to His18, hydrogen bonding from Tyr67 to Met80, heme propionate-7 hydrogen bonded by Gly41, Tyr48, and Trp59, and heme propionate-6 hydrogen bonded by Thr/Ser49, Thr78, Lys79. Cyt *c* from tuna, horse, and yeast (both isozymes) also has hydrogen bonds between Asn52 and propionate-7.[135]

The axial ligand bonds to Met80 and His18 are almost perpendicular to the pyrrole nitrogen plane of the heme. The axial His orientation, as defined by an angle ϕ (with respect to the Fe–N_{pII} bond vector in Figure 1), is 46.5° in reduced *iso*-1-cyt *c* and 55.8° in oxidized *iso*-1-cyt *c*.[133] The stereochemistry of the Met80 sulfur atom in eukaryotic cyts *c*, as demonstrated by X-ray crystallography and NMR NOE experiments, is generally in the R configuration.[136]

The heme is slightly saddled with pyrrole rings involved in the thioether bonds to the polypeptide chain showing the greatest deviation from the mean porphyrin plane.[133] This distortion is observed in mitochrondial cyts *c* from various sources[137] and when significant heme structural differences are observed, they correlate with amino-acid variations in the –Cys–Xxx–Yyy–Cys–His– sequence.[21] NSD results for wild-type *iso*-1-cyt *c* from yeast indicate that ruffling is the major out-of-plane deformation. Negative saddling and small positive amounts of waving deformations also contribute.[20] Examination of 16 *iso*-1-cyt *c* mutants indicates that the relative contribution of each out-of-plane deformation to the total distortion is fairly constant. Thus, the nature of heme conformational distortion appears relatively insensitive to alterations in the heme pocket or conserved amino-acid residues. Shelnutt and co-workers have hypothesized that the heme distortion in cyts *c* is due to strain introduced through the covalent thioether linkages[137] by the five residues, –Cys–Xxx–Yyy–Cys–His–,[20,21,138] of the heme attachment sequence. Recently, the *iso*-1-cyt *c* (Cys14Ser) variant with a single thioether bond between the heme and the protein has been shown to retain its Met80/His18 axial ligation.[139] An NSD analysis of *iso*-1-cyt *c* (Cys14Ser) should be useful in evaluating the above hypotheses.

8.2.3.4 Redox-linked Conformational Changes in Class I Cytochromes *c*

The first structural determinations of redox-dependent conformational changes were reported for tuna cyt *c* in 1980.[127] Comparison of high-resolution structures currently available for reduced cyts *c*[129,132,134] and oxidized cyts *c*[128,130,131,133] yields similar conclusions: namely, that the overall protein fold of mitochrondial cyts *c* is not significantly altered upon oxidation. However, there are conformational changes localized in the heme pocket that have been extensively discussed within the context of redox potential. The largest consistently observed, redox-dependent changes occur in the vicinity of a conserved water molecule (Wat166) and involve the side chains of Tyr67, Thr78, and Asn52. These side chains are highly conserved among eukaryotic cyts *c*[126] and participate in hydrogen-bonding networks involving the conserved water molecule, the Met80 heme ligand, and propionate-7.

The redox-coupled movement of Wat166[135] is shown for *S. cerevisiae iso*-1-cyt *c* in Figure 8. In reduced *iso*-1-cyt *c*, Wat166 is hydrogen-bonded to the side chain of Asn52, which is also linked via hydrogen bonding to propionate-7. In oxidized *iso*-1-cyt *c*, Wat166 moves 1.6 Å closer to the heme, and the hydrogen bond to Asn52 is lost. Possible reorientation of the Wat166 dipole and its movement toward the heme iron in oxidized *iso*-1-cyt *c* suggest that it helps stabilize the positive charge on the heme iron. Oxidation of *iso*-1-cyt *c* also results in weakening of the Trp59/propionate-7 hydrogen bonding, movement of the Asp60 side chain, and strengthening of propionate-7 interactions with Gly41 and an internal water molecule, Wat121.[133]

The immediate environment of Met80 also exhibits redox-dependent changes. The Met80 sulfur-to-heme-iron bond length increases upon oxidation (2.35 Å, reduced; 2.43 Å, oxidized), while the His18 nitrogen-to-heme-iron bond changes by only 0.02 Å (1.99 Å, reduced; 2.01 Å, oxidized).[133] In the reduced form, the OH of Tyr67 hydrogen bonds to the sulfur of Met80. Loss of this hydrogen bond upon oxidation stabilizes the positively charged heme by making Met80 less electron-withdrawing and allowing Tyr67 to hydrogen bond with Wat166. Phe82 is within van der Waals contact of the Met80 side chain. The Phe82 side chain is parallel to the plane of the
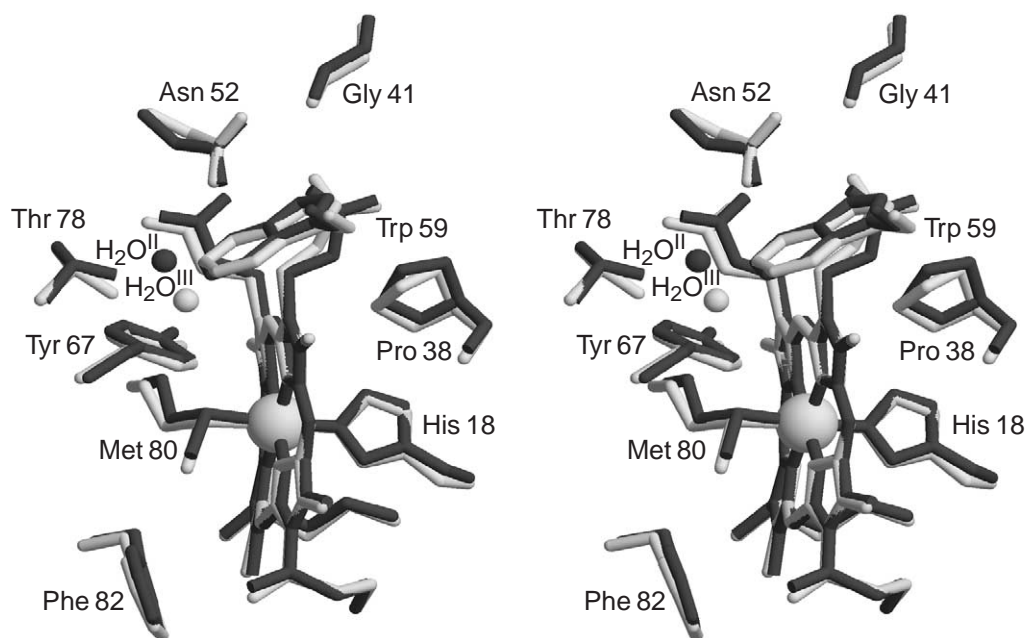
Figure 8 Overlay of residues and the conserved water molecule in the heme pockets of reduced (dark or red, PDB code 1YCC) and oxidized (light or green, PDB code 2YCC) *iso*-1-cyt *c*. Cross-eyed stereo view.

heme close to its solvent-exposed edge; its position with respect to the heme plane changes slightly upon oxidation.[133]

The increased out-of-plane distortion of the ferric heme in the *iso*-1-cyt *c*[132,133] suggests that heme distortion could be correlated to change of oxidation state. However, this is not observed for tuna cyt *c*.[127] Evaluation of the out-of-plane heme distortions in ten crystal structures of mitochondrial ferro- and ferricyts *c* reveals no conserved redox-dependent differences in the ruffling or *x*- and *y*-waving deformations.[21]

Examination of redox-dependent structural changes in solution by NMR spectroscopy is facilitated by the availability of proton assignments for horse cyt *c*,[140–142] tuna cyt *c*,[143] and yeast *iso*-1-cyt *c* (Cys102Thr),[144] a variant that does not dimerize. Analysis of NMR pseudo-contact shifts suggests only subtle differences between oxidized and reduced cyt *c*.[145–148] Solution structures determined for both oxidation states of horse cyt *c*[149–152] and *iso*-1-cyt *c*[153,154] have the general secondary structural features and overall protein fold found in the crystal structures. The NMR structures for horse cyt *c* show a difference in backbone atom positions (2.4 Å r.m.s. variation[150]; 1.4 Å r.m.s. variation[151,152]) upon oxidation. High-angle solution X-ray scattering experiments[155] detect comparable oxidation-dependent protein conformational changes. The solution structures of horse cyt *c* indicate that the percentage of the solvent-exposed heme surface area increases from 7.53% to 14.6% upon oxidation.[150] The dynamical features of horse and yeast cyt *c*, as probed by proton exchange and ^{15}N heteronuclear relaxation NMR experiments, are responsive to the redox state of the heme.[88,89,152–154] These data have been interpreted as increased flexibility of the protein fold in the oxidized form.

Pseudo-two-dimensional NOESY-TOCSY spectra[149,156] and ePHOGSY-NOESY experiments[157] have been used to detect water molecules with long residence times in the structure. Although the general location of the conserved water (Wat166, *iso*-1; Wat1, horse) is similar to its position in the crystal structure, its movement upon oxidation appears to be 3.7 Å away from the heme iron,[150,156] rather than 1.6 Å toward the heme as in the crystal structure. This translates into differences in the Wat166/Wat1-protein hydrogen-bonding network when comparing solution and crystal structures of oxidized cyt *c*.

In a fashion similar to mitochondrial cyts *c*, heme propionate conformations are redox-linked in some prokaryotic class I cyts *c* like *Rb. capsulatus* cyt *c*₂[158–162] and *Monoraphidium brunii* cyt *c*₆.[163–165] However, the role of a conserved water analogous to Wat166 in *iso*-1-cyt *c* is not clear. For example, the position of the conserved water molecule in *Rsp. palustris* cyt *c*₂ is relatively insensitive to oxidation state.[166] In cyts *c*₆ from *Chlamydomonas (C.)reinhardtii*[167] and *Scenedesmus obliquus*,[168] an internal water molecule is positioned between the two heme propionates. Its

position is not equivalent to that of *iso*-1-cyt *c* Wat166, and it is insensitive to the heme oxidation state. *Methylobacterium extorquens* cyt c_H, an electron donor to methanol oxidase in methylotropic bacteria, and *Thermus thermophilus* cyt c_{552}, an electron donor to a ba_3-type cytochrome *c* oxidase, are two examples of prokaryotic class I cyts *c* where the conserved water molecule, or hydrogen-bonding equivalent, is missing from their heme pockets.[169–171] These observations suggest that the usual hydrogen-bonding network involving the heme pocket water molecule is not essential to electron transfer.[171]

8.2.3.5 Conformational Changes as a Function of pH in Class I Cytochromes *c*

Five states identified as a result of reversible, pH-induced, conformational transitions in oxidized horse cyt *c*[172] are summarized in Scheme 1. Since these states were first reported in 1941, considerable work has gone into their characterization. At near-physiological pH, the 6cLS state III is the predominant form and is considered to be the native protein conformation. Formation of state II can be monitored by the appearance of new absorbance bands at 530 nm and 625 nm, and the concomitant appearance of NMR features typical of an HS ferric heme.[5,173] Resonance Raman data also indicate the presence of a 6cHS ferric heme and an additional 6cLS ferric heme for state II.[174] The 6cHS ferric heme is consistent with displacement of Met80 by a water molecule. The 6cLS ferric heme is proposed to have less out-of-plane distortion and His18/His33 axial ligation. At pH 0.3, a 5cHS species predominates (state I). Particular attention has been paid to the conformational change between states III and IV, known as the alkaline transition, which has a pKa of 8.5–9.5 depending on the species and solution conditions.[5] Resonance Raman evidence suggests that a similar conformational change occurs in cyt *c* when it interacts with cytochrome *c* oxidase.[64,65] The sulfur-to-iron charge-transfer band at 695 nm characteristic of Met–Fe^{III} ligation is lost at alkaline pH, indicating that Met80 is no longer ligated to the heme iron. EPR and MCD data for alkaline horse ferricyt *c* indicate that the heme iron is still 6cLS.[175] Chemical shifts reported for alkaline horse ferricyt *c* are consistent with lysine (Lys) coordination to the heme.[176] Both EPR[175] and 2D NMR studies[176] indicate the presence of at least two alkaline species in horse ferricyt *c* above pH 9.5. Studies involving chemical modification of Lys residues did not yield unambiguous identification of the sixth axial ligand in alkaline horse ferricyt *c*.[177]

Since the late 1980s, the ability to generate site-directed mutants of *S. cerevisiae iso*-1-cyt *c* has facilitated characterization of transitions of state III → IV and state IV → V. Studies of *iso*-1-cyt *c* and variants, (Lys73Ala), (Lys79Ala), (Lys86Ala), (Lys87Ala), and double mutant (Lys73Ala/Lys79Ala), involving ^{1}H-NMR, EPR, resonance Raman, and UV-visible spectroscopies, have demonstrated that Lys73 and Lys79 replace Met80 as the sixth heme iron ligand in two conformers of state IV.[178–180] The coordinated lysines in these two alkaline conformers are replaced, most likely, by a hydroxide ion provided by Wat166 to form two conformers with pK_as above 10 (state V).[180] Scheme 2 illustrates the conformational equilibria of wild-type *iso*-1-cyt *c* between pH 7 and 12, as characterized by component analysis of their resonance Raman spectra.[180]

In wild-type *iso*-1-cyt *c* isolated from yeast, Lys72 is trimethylated; when this *S. cerevisiae* protein is expressed in *Escherichia (E.) coli*, Lys72 is not trimethylated. Although the *iso*-1-cyts *c* expressed in *E. coli* and in *S. cerevisiae* have the same spectroscopic properties at neutral pH, the pK_a for the state III → IV transition is ~0.6 pK_a units lower for the protein expressed in *E. coli*. ^{1}H NMR data for *iso*-1-cyt *c* and its (Lys72Ala) variant expressed in *E. coli* have identified a third alkaline conformer, which has Lys72 coordinated to the heme.[181] Since cyts *c* from higher eukaryotes are not trimethylated at Lys72, this suggests that Lys72 could be an axial ligand in alkaline horse and other higher eukaryotic ferricyts *c*.[179,181]

Kinetics of the alkaline transition have been characterized with pH-jump experiments.[175,182–184] The two-step mechanism in Scheme 3 accounts for the pH dependence of the monoexponential rate constants observed from neutral pH to pH 10.[184] The first step in the alkaline isomerization, deprotonation of a titratable group in the native protein, "triggers" the second step, which is heme iron ligand exchange. This minimal kinetic mechanism does not consider five-coordinate intermediates or multiple alkaline conformers. Biphasic behavior observed in pH-jump experiments above pH 10 suggests the formation of a transient HS heme intermediate in ferricyt *c* from yeast[183] and higher eukaryotes[175] within the first 100 ms. A species with similar spectroscopic features is observed in the *iso*-1-cyt *c* (Phe82Trp) variant as a thermodynamically stable, HS form maximized at pH 8.5. Resonance Raman data for the (Phe82Trp) protein suggest that, in addition to

state I

state II

state III

state IV

state V

His 18

OH$_2$

Fe^{3+}

His 18

His 33

Fe^{3+}

His 18

Met 80

S

Fe^{3+}

His 18

Lys 72, 73, or 79

NH$_2$

Fe^{3+}

His 18

OH

Fe^{3+}

His 18

Fe^{3+}

His 18

pK_a 0.42

pK_a 2.5

pK_a 9.35

pK_a 12.76

Scheme 1

state IVa   **state Va**
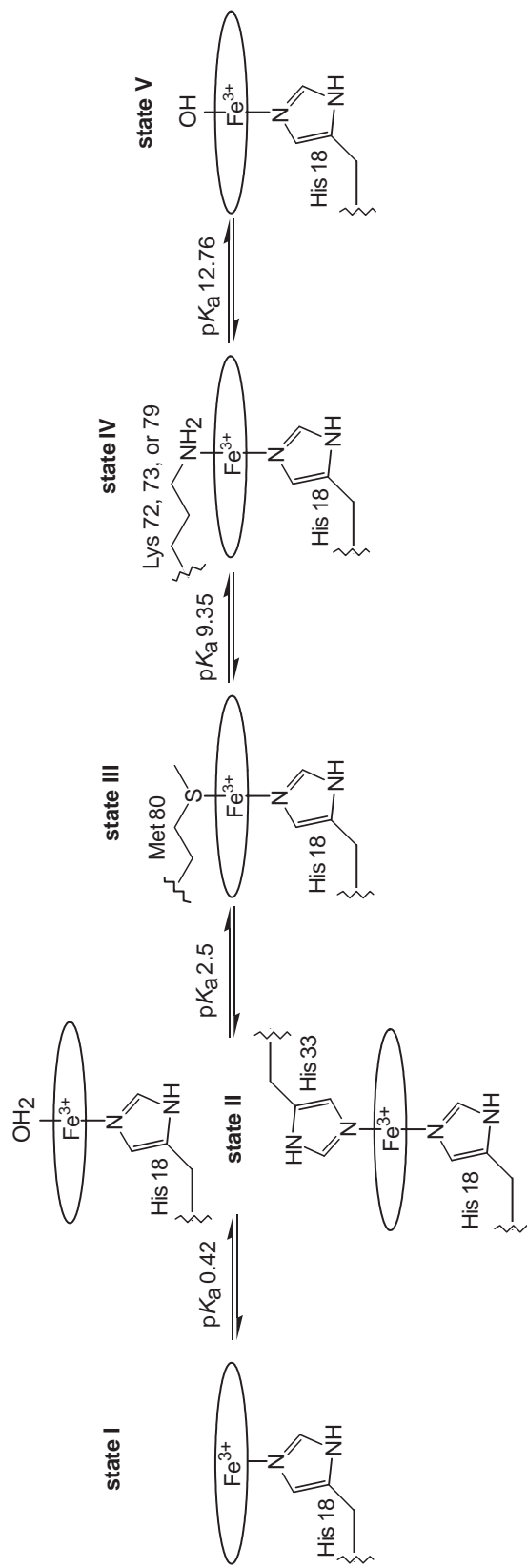
Scheme 2
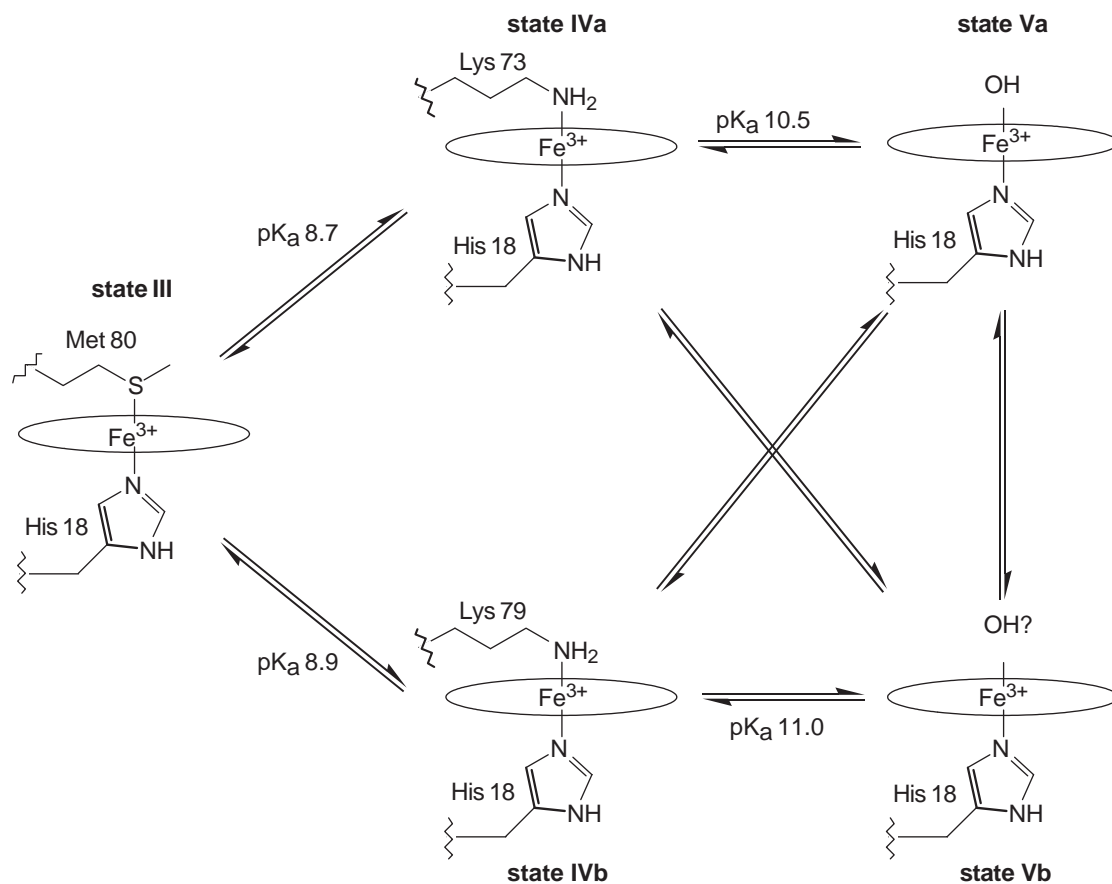
an obligatory 5cHS intermediate, there is a six-coordinate intermediate in which either Wat166 or Tyr67 is coordinated to the heme before displacement by Met80 to form state III, or by Lys73 or Lys79 to generate state IV.[183]

The reduction potential for alkaline cyt *c* is substantially lower than that for the native protein (*iso*-1-cyt *c*, pH 10.4: $E_{native} = +230$ mV, $E_{alkaline} = -230$ mV; horse cyt c, pH 10.0: $E_{native} = +255$, $E_{alkaline} = -205$ mV vs. SHE).[185] Although cyts c_2 exhibit a more positive reduction potential than their mitochondrial counterparts (Table 1), the ΔE ($E_{alkaline} - E_{native}$), -407 mV to -440 mV, is similar.[186] This large reduction potential difference is attributed to the Met80 heme ligation in state III, and a proposed lower percentage of solvent-exposed heme in state III relative to state IV (see Section 8.2.7). This difference in redox potential is coupled to a difference in conformational energy between native and alkaline states of ~ 10 kcal mol^{-1} for *iso*-1-cyt *c*.[185] It has been proposed that this constitutes a binary molecular switch.[179,185]

The identification of two state IV conformers suggests the existence of two such switching mechanisms in *iso*-1-cyt *c*.[179] The identity of the "trigger" group(s) whose protonation state dictates the conformation of the protein is presently unknown. The titratable groups Lys73/Lys79,[179] Tyr67,[184,187] His18,[188] heme propionate-7,[189,190] and the conserved water in the heme pocket[128] have been suggested as possibilities. The character of the pH-linked conformations is also affected by the phylogenetically conserved Phe82. Phe82 replacement by Ser, Tyr, Gly, Ile, or Leu results in destabilization of ferricyt *c* by lowering the pK_a for the alkaline transition.[182] The basis of this effect will probably be revealed with identification of the trigger group.

Thermal titration of cyts *c* from horse, cow, and tuna monitored by FTIR shows conformational transitions akin to the alkaline transition at 54 °C, 57 °C, and 50 °C, respectively.[191] The reversible disappearance of the 695 nm band of state III in *iso*-1-cyt *c* upon moderate heating correlates with the loss of the heme iron Met80 sulfur bond. The rate constant for site exchange between iron-bound and free Met is 1.8 s^{-1}. These data, along with NMR data, suggest that the

Scheme 3

high-temperature conformation at neutral pH and the alkaline conformation at room temperature are the same with a Lys as with the sixth heme ligand.[192] However, comparison of resonance Raman spectra of Lys 73 and Lys 79 ligated alkaline states (IVa and IVb) with those of the high-temperature species do not support this conclusion.[180,193,194]

8.2.3.6 Intramolecular Heme Ligand Rearrangements

8.2.3.6.1 *Mitochrondrial cytochrome c folding intermediates*

Heme ligand switching as a mechanism for converting redox energy into "conformational" energy has been observed in the alkaline transition (described in Section 8.2.3.5), in folding intermediates with non-native heme ligands converting back to native Met/His coordination upon folding, and in *iso*-1-cyt *c* (Phe82His). Although a detailed discussion of cyt *c* folding is beyond the scope of this chapter, the coordination chemistry of the heme plays an important role. Apo-cyt *c* is substantially unfolded in neutral solution. Cyt *c* containing H_2PPIX but no iron takes on a folded structure known as the "molten globule state,"[195] which has a significant amount of native-like secondary structure, but its tertiary structure fluctuates. Hence, maintenance of the rigid native cyt *c* fold requires heme iron axial ligation. Although the Fe—Met80 bond is not absolutely required for native structure and function,[196,197] the difficulty in obtaining cyt *c* His18 mutants[198] suggests that the Fe—His18 bond is essential.

Unfolded cyt *c* generated in urea or guanidine hydrochloride (GuHCl) contains a low-spin, bis-His heme adduct. In unfolded *iso*-1-cyt *c*, native axial ligand His18 and one of His26, 33, or 39 ligate the heme iron.[199–201] Upon folding, Met80 replaces the non-native His heme ligand. Kinetic folding studies have suggested that slow-folding phases are due to non-native His heme ligation.[201–204] This is substantiated by studies of cyts *c* that lack the proposed non-native ligands. Folding kinetics for class I cyts *c* that contain only one His residue, like *D. vulgaris* cyt c_{553} and *Rb. capsulatus* cyt c_2, are not complicated by ligand-dependent kinetic phases.[205,206] At neutral pH cyt c_{553} folds within 220 μs,[206] approximately a thousandfold faster than other cyts *c* under similar conditions.[207–210] A dramatic increase in folding rate is also observed for the *iso*-2-cyt *c* (His33Asn/His39Lys) double mutant relative to wild-type protein.[211] Equilibrium and stopped-flow kinetics with horse cyt *c* (His26Gln) and (His33Asn) mutants indicate that His33 is the predominant heme iron ligand in GuHCl-unfolded horse cyt *c* (pH 5.0).[201,212]

The heme ligation states observed under varying conditions for ferricyt *c* are summarized in Scheme 4a. For horse ferricyt *c*, ^{1}H NMR was used to identify the heme ligands in partially and fully denatured protein in neutral solution. The species observed were dependent on the identity of the denaturant and its concentration.[213,214] In low concentrations of GuHCl, two intermediates with Lys/His heme ligation were observed.[214] Protein-folding kinetics and pH titration data for tuna cyt *c*, which lacks His33, suggest that Lys/His coordination also occurs in the misligated

Table 1 Selected reduction potentials for various cytochromes and their heme pocket mutants.

Cytochrome	$E^{0'}$(mV)	Cytochrome variant	$E^{0'}$ (mV)	Class	References
Rhodocyclus tenuis THRC cyt *c*				Class IV	274
HP$_1$	420				
HP$_2$	420				
LP$_1$	110				
LP$_2$	60				
Rsp. Viridis THRC cyt *c*				Class IV	275,276
H1 (c_{559})	380				
H3 (c_{556})	330				
H2 (c_{552})	20				
H4 (c_{554})	−60				
Rb. Capsulatus cyt c_2	373	Gly29Ser[a]	330	Class I	277,278,279
		Pro30Ala[a]	258		
		Tyr67Cys[a]	348		
		Tyr67Phe[a]	308		
C. reinhardtii cyt *f*[i]	370	Tyr1Phe	369	cyt *f*	280
		Tyr1Ser	313		
		Val3Phe	373		
		Phe4Leu	348		
		Phe4Trp	336		
		Tyr1Phe/Phe4Tyr	370		
		Tyr1Ser/Phe4Leu	289		
		Val3Phe/Phe4Trp	342		
R. rubrum cyt c_2	324			Class I	275
Arthrospira maxima cyt c_6	314			Class I	281
P. laminosum cyt *f*[i]	297	Trp4Phe	323	cyt *f*	280
		Trp4Leu	300		
		Phe3Val/Trp4Phe	316		
S. cerevisiae iso-2 cyt *c*	288[d]	Asn52Ile	243	Class I	282

Table 1 continued

Cytochrome	$E^{0'}$(mV)	Cytochrome variant	$E^{0'}$ (mV)	Class	References
S. cerevisiae iso-1 cyt c[b]	272[e], 285[c], 290[d]			Class I	179,180, 182,183,259,283,284, 285,286,287
		Arg38Lys	249[e]		
		Arg38His	245[e]		
		Arg38Gln	242[e]		
		Arg38Asn	238[e]		
		Arg38Leu	231[e]		
		Arg38Ala	225[e]		
			239[c]		
		Asn52Ala	257[d]		
		Asn52Ile	231[c]		
		Tyr67Phe	234[d]		
		Phe82Leu	286[d]		
		Phe82Tyr	280[d]		
		Phe82Ile	273[d]		
		Phe82Trp	266[d]		
		Phe82Ala	260[d]		
		Phe82Ser	255[d]		
		Phe82Gly	247[d]		
P. aeruginosa cyt c551	276			Class I	275
horse cyt c	262			Class I	268,277
		Met80Ala	82[c]		
		Met80His	41[c]		
		Met80Leu	−45[c]		
		Met80Cys	−390[c]		
rat cyt c	260	Pro30Ala[a]	258	Class I	277,288,289,290
		Pro30Val[a]	261		
		Tyr67Phe[a]	224		
Rps. palustris cyt c556	230			Class II	5
E. coli cyt b562	168	Phe61Gly	90	cyt b (Class II)	291,292
		Phe65Val	173		
		Phe61Ile/Phe65Tyr	68		
		His102Met	240		
		Arg98Cys/His102Met	440[k]		
Alc. denitrificans cyt c' (ADCP)	132			Class II	5
Rps. palustris cyt c' (RPCP)	102			Class II	5
D. vulgaris cyt c553	37			Class I	275,293
	20S5	Met23Cys	29		
		Gly51Cys	28		
		Met23Cys/Met23Cys	88		
		Gly51Cys/Gly51Cys	105		

Table 1 Selected reduction potentials for various cytochromes and their heme pocket mutants.

Cytochrome	$E^{0'}$(mV)	Cytochrome variant	$E^{0'}$ (mV)	Class	References
Rhodocyclus tenuis THRC cyt *c*				Class IV	274
HP$_1$	420				
HP$_2$	420				
LP$_1$	110				
LP$_2$	60				
Rsp. Viridis THRC cyt *c*				Class IV	275,276
H1 (c_{559})	380				
H3 (c_{556})	330				
H2 (c_{552})	20				
H4 (c_{554})	−60				
Rb. Capsulatus cyt c_2	373	Gly29Ser[a]	330	Class I	277,278,279
		Pro30Ala[a]	258		
		Tyr67Cys[a]	348		
		Tyr67Phe[a]	308		
C. reinhardtii cyt f^i	370	Tyr1Phe	369	cyt *f*	280
		Tyr1Ser	313		
		Val3Phe	373		
		Phe4Leu	348		
		Phe4Trp	336		
		Tyr1Phe/Phe4Tyr	370		
		Tyr1Ser/Phe4Leu	289		
		Val3Phe/Phe4Trp	342		
R. rubrum cyt c_2	324			Class I	275
Arthrospira maxima cyt c_6	314			Class I	281
P. laminosum cyt f^i	297	Trp4Phe	323	cyt *f*	280
		Trp4Leu	300		
		Phe3Val/Trp4Phe	316		
S. cerevisiae iso-2 cyt *c*	288[d]	Asn52Ile	243	Class I	282

Table 1 continued

Cytochrome	$E^{0\prime}$(mV)	Cytochrome variant	$E^{0\prime}$ (mV)	Class	References
S. cerevisiae iso-1 cyt c[b]	272[e] 285[c] 290[d]	Arg38Lys	249[e]	Class I	179,180, 182,183,259,283,284, 285,286,287
		Arg38His	245[e]		
		Arg38Gln	242[e]		
		Arg38Asn	238[e]		
		Arg38Leu	231[e]		
		Arg38Ala	225[e]		
			239[c]		
		Asn52Ala	257[d]		
		Asn52Ile	231[c]		
		Tyr67Phe	234[d]		
		Phe82Leu	286[d]		
		Phe82Tyr	280[d]		
		Phe82Ile	273[d]		
		Phe82Trp	266[d]		
		Phe82Ala	260[d]		
		Phe82Ser	255[d]		
		Phe82Gly	247[d]		
P. aeruginosa cyt c_{551}	276			Class I	275
horse cyt c	262	Met80Ala	82[c]	Class I	268,277
		Met80His	41[c]		
		Met80Leu	−45[c]		
		Met80Cys	−390[c]		
rat cyt c	260	Pro30Ala[a]	258	Class I	277,288,289,290
		Pro30Val[a]	261		
		Tyr67Phe[a]	224		
Rps. palustris cyt c_{556}	230			Class II	5
E. coli cyt b_{562}	168	Phe61Gly	90	cyt b (Class II)	291,292
		Phe65Val	173		
		Phe61Ile/Phe65Tyr	68		
		His102Met	240		
		Arg98Cys/His102Met	440[k]		
Alc. denitrificans cyt c′ (ADCP)	132			Class II	5
Rps. palustris cyt c′(RPCP)	102			Class II	5
D. vulgaris cyt c_{553}	37 20S5	Met23Cys	29	Class I	275,293
		Gly51Cys	28		
		Met23Cys/Met23Cys	88		
		Gly51Cys/Gly51Cys	105		

Table 1 Selected reduction potentials for various cytochromes and their heme pocket mutants.

Cytochrome	$E^{0'}$(mV)	Cytochrome variant	$E^{0'}$ (mV)	Class	References
Rhodocyclus tenuis THRC cyt *c*				Class IV	274
HP$_1$	420				
HP$_2$	420				
LP$_1$	110				
LP$_2$	60				
Rsp. Viridis THRC cyt *c*				Class IV	275,276
H1 (c_{559})	380				
H3 (c_{556})	330				
H2 (c_{552})	20				
H4 (c_{554})	−60				
Rb. Capsulatus cyt c_2	373	Gly29Ser[a]	330	Class I	277,278,279
		Pro30Ala[a]	258		
		Tyr67Cys[a]	348		
		Tyr67Phe[a]	308		
C. reinhardtii cyt f[i]	370	Tyr1Phe	369	cyt f	280
		Tyr1Ser	313		
		Val3Phe	373		
		Phe4Leu	348		
		Phe4Trp	336		
		Tyr1Phe/Phe4Tyr	370		
		Tyr1Ser/Phe4Leu	289		
		Val3Phe/Phe4Trp	342		
R. rubrum cyt c_2	324			Class I	275
Arthrospira maxima cyt c_6	314			Class I	281
P. laminosum cyt f[i]	297	Trp4Phe	323	cyt f	280
		Trp4Leu	300		
		Phe3Val/Trp4Phe	316		
S. cerevisiae iso-2 cyt *c*	288[d]	Asn52Ile	243	Class I	282

Table 1 Selected reduction potentials for various cytochromes and their heme pocket mutants.

Cytochrome	$E^{0\prime}$ (mV)	Cytochrome variant	$E^{0\prime}$ (mV)	Class	References
Rhodocyclus tenuis THRC cyt *c*				Class IV	274
HP$_1$	420				
HP$_2$	420				
LP$_1$	110				
LP$_2$	60				
Rsp. Viridis THRC cyt *c*				Class IV	275,276
H1 (c_{559})	380				
H3 (c_{556})	330				
H2 (c_{552})	20				
H4 (c_{554})	−60				
Rb. Capsulatus cyt c_2	373	Gly29Ser[a]	330	Class I	277,278,279
		Pro30Ala[a]	258		
		Tyr67Cys[a]	348		
		Tyr67Phe[a]	308		
C. reinhardtii cyt *f*[i]	370	Tyr1Phe	369	cyt *f*	280
		Tyr1Ser	313		
		Val3Phe	373		
		Phe4Leu	348		
		Phe4Trp	336		
		Tyr1Phe/Phe4Tyr	370		
		Tyr1Ser/Phe4Leu	289		
		Val3Phe/Phe4Trp	342		
R. rubrum cyt c_2	324			Class I	275
Arthrospira maxima cyt c_6	314			Class I	281
P. laminosum cyt *f*[i]	297	Trp4Phe	323	cyt *f*	280
		Trp4Leu	300		
		Phe3Val/Trp4Phe	316		
S. cerevisiae iso-2 cyt *c*	288[d]	Asn52Ile	243	Class I	282

Table 1 Selected reduction potentials for various cytochromes and their heme pocket mutants.

Cytochrome	$E^{0'}$(mV)	Cytochrome variant	$E^{0'}$ (mV)	Class	References
Rhodocyclus tenuis THRC cyt *c*				Class IV	274
HP$_1$	420				
HP$_2$	420				
LP$_1$	110				
LP$_2$	60				
Rsp. Viridis THRC cyt *c*				Class IV	275,276
H1 (c_{559})	380				
H3 (c_{556})	330				
H2 (c_{552})	20				
H4 (c_{554})	−60				
Rb. Capsulatus cyt c_2	373	Gly29Ser[a]	330	Class I	277,278,279
		Pro30Ala[a]	258		
		Tyr67Cys[a]	348		
		Tyr67Phe[a]	308		
C. reinhardtii cyt *f*[i]	370	Tyr1Phe	369	cyt *f*	280
		Tyr1Ser	313		
		Val3Phe	373		
		Phe4Leu	348		
		Phe4Trp	336		
		Tyr1Phe/Phe4Tyr	370		
		Tyr1Ser/Phe4Leu	289		
		Val3Phe/Phe4Trp	342		
R. rubrum cyt c_2	324			Class I	275
Arthrospira maxima cyt c_6	314			Class I	281
P. laminosum cyt *f*[i]	297	Trp4Phe	323	cyt *f*	280
		Trp4Leu	300		
		Phe3Val/Trp4Phe	316		
S. cerevisiae iso-2 cyt *c*	288[d]	Asn52Ile	243	Class I	282

Table 1 continued

Cytochrome	$E^{0\prime}$(mV)	Cytochrome variant	$E^{0\prime}$ (mV)	Class	References
S. cerevisiae iso-1 cyt c[b]	272[e] 285[c] 290[d]	Arg38Lys	249[e]	Class I	179,180, 182,183,259,283,284, 285,286,287
		Arg38His	245[e]		
		Arg38Gln	242[e]		
		Arg38Asn	238[e]		
		Arg38Leu	231[e]		
		Arg38Ala	225[e]		
			239[c]		
		Asn52Ala	257[d]		
		Asn52Ile	231[c]		
		Tyr67Phe	234[d]		
		Phe82Leu	286[d]		
		Phe82Tyr	280[d]		
		Phe82Ile	273[d]		
		Phe82Trp	266[d]		
		Phe82Ala	260[d]		
		Phe82Ser	255[d]		
		Phe82Gly	247[d]		
P. aeruginosa cyt c_{551}	276			Class I	275
horse cyt c	262	Met80Ala	82[c]	Class I	268,277
		Met80His	41[c]		
		Met80Leu	−45[c]		
		Met80Cys	−390[c]		
rat cyt c	260	Pro30Ala[a]	258	Class I	277,288,289,290
		Pro30Val[a]	261		
		Tyr67Phe[a]	224		
Rps. palustris cyt c_{556}	230			Class II	5
E. coli cyt b_{562}	168	Phe61Gly	90	cyt b (Class II)	291,292
		Phe65Val	173		
		Phe61Ile/Phe65Tyr	68		
		His102Met	240		
		Arg98Cys/His102Met	440[k]		
Alc. denitrificans cyt c' (ADCP)	132			Class II	5
Rps. palustris cyt c'(RPCP)	102			Class II	5
D. vulgaris cyt c_{553}	37 205	Met23Cys	29	Class I	275,293
		Gly51Cys	28		
		Met23Cys/Met23Cys	88		
		Gly51Cys/Gly51Cys	105		

Table 1 Selected reduction potentials for various cytochromes and their heme pocket mutants.

Cytochrome	$E^{0'}$(mV)	Cytochrome variant	$E^{0'}$ (mV)	Class	References
Rhodocyclus tenuis THRC cyt *c*				Class IV	274
HP$_1$	420				
HP$_2$	420				
LP$_1$	110				
LP$_2$	60				
Rsp. Viridis THRC cyt *c*				Class IV	275,276
H1 (c_{559})	380				
H3 (c_{556})	330				
H2 (c_{552})	20				
H4 (c_{554})	−60				
Rb. Capsulatus cyt c_2	373	Gly29Ser[a]	330	Class I	277,278,279
		Pro30Ala[a]	258		
		Tyr67Cys[a]	348		
		Tyr67Phe[a]	308		
C. reinhardtii cyt *f*[i]	370	Tyr1Phe	369	cyt *f*	280
		Tyr1Ser	313		
		Val3Phe	373		
		Phe4Leu	348		
		Phe4Trp	336		
		Tyr1Phe/Phe4Tyr	370		
		Tyr1Ser/Phe4Leu	289		
		Val3Phe/Phe4Trp	342		
R. rubrum cyt c_2	324			Class I	275
Arthrospira maxima cyt c_6	314			Class I	281
P. laminosum cyt *f*[i]	297	Trp4Phe	323	cyt *f*	280
		Trp4Leu	300		
		Phe3Val/Trp4Phe	316		
S. cerevisiae iso-2 cyt *c*	288[d]	Asn52Ile	243	Class I	282

Table 1 Selected reduction potentials for various cytochromes and their heme pocket mutants.

Cytochrome	$E^{0'}$(mV)	Cytochrome variant	$E^{0'}$ (mV)	Class	References
Rhodocyclus tenuis THRC cyt *c*				Class IV	274
HP$_1$	420				
HP$_2$	420				
LP$_1$	110				
LP$_2$	60				
Rsp. Viridis THRC cyt *c*				Class IV	275,276
H1 (c_{559})	380				
H3 (c_{556})	330				
H2 (c_{552})	20				
H4 (c_{554})	−60				
Rb. Capsulatus cyt c_2	373	Gly29Ser[a]	330	Class I	277,278,279
		Pro30Ala[a]	258		
		Tyr67Cys[a]	348		
		Tyr67Phe[a]	308		
C. reinhardtii cyt *f*[i]	370	Tyr1Phe	369	cyt *f*	280
		Tyr1Ser	313		
		Val3Phe	373		
		Phe4Leu	348		
		Phe4Trp	336		
		Tyr1Phe/Phe4Tyr	370		
		Tyr1Ser/Phe4Leu	289		
		Val3Phe/Phe4Trp	342		
R. rubrum cyt c_2	324			Class I	275
Arthrospira maxima cyt c_6	314			Class I	281
P. laminosum cyt *f*[i]	297	Trp4Phe	323	cyt *f*	280
		Trp4Leu	300		
		Phe3Val/Trp4Phe	316		
S. cerevisiae iso-2 cyt *c*	288[d]	Asn52Ile	243	Class I	282

Table 1 continued

Cytochrome	$E^{0'}$ (mV)	Cytochrome variant	$E^{0'}$ (mV)	Class	References
S. cerevisiae iso-1 cyt c[b]	272[e]	Arg38Lys	249[e]	Class I	179,180, 182,183,259,283,284, 285,286,287
	285[c]	Arg38His	245[e]		
	290[d]	Arg38Gln	242[e]		
		Arg38Asn	238[e]		
		Arg38Leu	231[e]		
		Arg38Ala	225[e]		
			239[c]		
		Asn52Ala	257[d]		
		Asn52Ile	231[c]		
		Tyr67Phe	234[d]		
		Phe82Leu	286[d]		
		Phe82Tyr	280[d]		
		Phe82Ile	273[d]		
		Phe82Trp	266[d]		
		Phe82Ala	260[d]		
		Phe82Ser	255[d]		
		Phe82Gly	247[d]		
P. aeruginosa cyt c_{551}	276			Class I	275
horse cyt c	262	Met80Ala	82[c]	Class I	268,277
		Met80His	41[c]		
		Met80Leu	−45[c]		
		Met80Cys	−390[c]		
rat cyt c	260	Pro30Ala[a]	258	Class I	277,288,289,290
		Pro30Val[a]	261		
		Tyr67Phe[a]	224		
Rps. palustris cyt c_{556}	230			Class II	5
E. coli cyt b_{562}	168	Phe61Gly	90	cyt b (Class II)	291,292
		Phe65Val	173		
		Phe61Ile/Phe65Tyr	68		
		His102Met	240		
		Arg98Cys/His102Met	440[k]		
Alc. denitrificans cyt c' (ADCP)	132			Class II	5
Rps. palustris cyt c' (RPCP)	102			Class II	5
D. vulgaris cyt c_{553}	37	Met23Cys	29	Class I	275,293
	205	Gly51Cys	28		
		Met23Cys/Gly51Cys	88		
		Gly51Cys/Gly51Cys	105		

Table 1 Selected reduction potentials for various cytochromes and their heme pocket mutants.

Cytochrome	$E^{0'}$(mV)	Cytochrome variant	$E^{0'}$ (mV)	Class	References
Rhodocyclus tenuis THRC cyt *c*				Class IV	274
HP$_1$	420				
HP$_2$	420				
LP$_1$	110				
LP$_2$	60				
Rsp. Viridis THRC cyt *c*				Class IV	275,276
H1 (c_{559})	380				
H3 (c_{556})	330				
H2 (c_{552})	20				
H4 (c_{554})	−60				
Rb. Capsulatus cyt c_2	373	Gly29Ser[a]	330	Class I	277,278,279
		Pro30Ala[a]	258		
		Tyr67Cys[a]	348		
		Tyr67Phe[a]	308		
C. reinhardtii cyt f[i]	370	Tyr1Phe	369	cyt f	280
		Tyr1Ser	313		
		Val3Phe	373		
		Phe4Leu	348		
		Phe4Trp	336		
		Tyr1Phe/Phe4Tyr	370		
		Tyr1Ser/Phe4Leu	289		
		Val3Phe/Phe4Trp	342		
R. rubrum cyt c_2	324			Class I	275
Arthrospira maxima cyt c_6	314			Class I	281
P. laminosum cyt f[i]	297	Trp4Phe	323	cyt f	280
		Trp4Leu	300		
		Phe3Val/Trp4Phe	316		
S. cerevisiae iso-2 cyt *c*	288[d]	Asn52Ile	243	Class I	282

Table 1 continued

Cytochrome	$E^{0'}$(mV)	Cytochrome variant	$E^{0'}$ (mV)	Class	References
S. cerevisiae iso-1 cyt c[b]	272[e]	Arg38Lys	249[e]	Class I	179,180, 182,183,259,283,284, 285,286,287
	285[c]	Arg38His	245[e]		
	290[d]	Arg38Gln	242[e]		
		Arg38Asn	238[e]		
		Arg38Leu	231[e]		
		Arg38Ala	225[e]		
			239[c]		
		Asn52Ala	257[d]		
		Asn52Ile	231[c]		
		Tyr67Phe	234[d]		
		Phe82Leu	286[d]		
		Phe82Tyr	280[d]		
		Phe82Ile	273[d]		
		Phe82Trp	266[d]		
		Phe82Ala	260[d]		
		Phe82Ser	255[d]		
		Phe82Gly	247[d]		
P. aeruginosa cyt c_{551}	276			Class I	275
horse cyt c	262	Met80Ala	82[c]	Class I	268,277
		Met80His	41[c]		
		Met80Leu	−45[c]		
		Met80Cys	−390[c]		
rat cyt c	260	Pro30Ala[a]	258	Class I	277,288,289,290
		Pro30Val[a]	261		
		Tyr67Phe[a]	224		
Rps. palustris cyt c_{556}	230			Class II	5
E. coli cyt b_{562}	168	Phe61Gly	90	cyt b (Class II)	291,292
		Phe65Val	173		
		Phe61Ile/Phe65Tyr	68		
		His102Met	240		
		Arg98Cys/His102Met	440[k]		
Alc. denitrificans cyt c′ (ADCP)	132			Class II	5
Rps. palustris cyt c′ (RPCP)	102			Class II	5
D. vulgaris cyt c_{553}	37	Met23Cys	29	Class I	275,293
	20S5	Gly51Cys	28		
		Met23Cys/Met23Cys	88		
		Gly51Cys/Gly51Cys	105		

Table 1 Selected reduction potentials for various cytochromes and their heme pocket mutants.

Cytochrome	$E^{0'}$(mV)	Cytochrome variant	$E^{0'}$ (mV)	Class	References
Rhodocyclus tenuis THRC cyt *c*				Class IV	274
HP$_1$	420				
HP$_2$	420				
LP$_1$	110				
LP$_2$	60				
Rsp. Viridis THRC cyt *c*				Class IV	275,276
H1 (c_{559})	380				
H3 (c_{556})	330				
H2 (c_{552})	20				
H4 (c_{554})	−60				
Rb. Capsulatus cyt c_2	373	Gly29Ser[a]	330	Class I	277,278,279
		Pro30Ala[a]	258		
		Tyr67Cys[a]	348		
		Tyr67Phe[a]	308		
C. reinhardtii cyt f^i	370	Tyr1Phe	369	cyt *f*	280
		Tyr1Ser	313		
		Val3Phe	373		
		Phe4Leu	348		
		Phe4Trp	336		
		Tyr1Phe/Phe4Tyr	370		
		Tyr1Ser/Phe4Leu	289		
		Val3Phe/Phe4Trp	342		
R. rubrum cyt c_2	324			Class I	275
Arthrospira maxima cyt c_6	314			Class I	281
P. laminosum cyt f^i	297	Trp4Phe	323	cyt *f*	280
		Trp4Leu	300		
		Phe3Val/Trp4Phe	316		
S. cerevisiae iso-2 cyt *c*	288[d]	Asn52Ile	243	Class I	282

Table 1 Selected reduction potentials for various cytochromes and their heme pocket mutants.

Cytochrome	$E^{0'}$(mV)	Cytochrome variant	$E^{0'}$ (mV)	Class	References
Rhodocyclus tenuis THRC cyt *c*				Class IV	274
HP$_1$	420				
HP$_2$	420				
LP$_1$	110				
LP$_2$	60				
Rsp. Viridis THRC cyt *c*				Class IV	275,276
H1 (c_{559})	380				
H3 (c_{556})	330				
H2 (c_{552})	20				
H4 (c_{554})	−60				
Rb. Capsulatus cyt c_2	373	Gly29Ser[a]	330	Class I	277,278,279
		Pro30Ala[a]	258		
		Tyr67Cys[a]	348		
		Tyr67Phe[a]	308		
C. reinhardtii cyt *f*[i]	370	Tyr1Phe	369	cyt *f*	280
		Tyr1Ser	313		
		Val3Phe	373		
		Phe4Leu	348		
		Phe4Trp	336		
		Tyr1Phe/Phe4Tyr	370		
		Tyr1Ser/Phe4Leu	289		
		Val3Phe/Phe4Trp	342		
R. rubrum cyt c_2	324			Class I	275
Arthrospira maxima cyt c_6	314			Class I	281
P. laminosum cyt *f*[i]	297	Trp4Phe	323	cyt *f*	280
		Trp4Leu	300		
		Phe3Val/Trp4Phe	316		
S. cerevisiae iso-2 cyt *c*	288[d]	Asn52Ile	243	Class I	282

Table 1 Selected reduction potentials for various cytochromes and their heme pocket mutants.

Cytochrome	$E^{0\prime}$(mV)	Cytochrome variant	$E^{0\prime}$ (mV)	Class	References
Rhodocyclus tenuis THRC cyt *c*				Class IV	274
HP$_1$	420				
HP$_2$	420				
LP$_1$	110				
LP$_2$	60				
Rsp. Viridis THRC cyt *c*				Class IV	275,276
H1 (c_{559})	380				
H3 (c_{556})	330				
H2 (c_{552})	20				
H4 (c_{554})	−60				
Rb. Capsulatus cyt c_2	373	Gly29Ser[a]	330	Class I	277,278,279
		Pro30Ala[a]	258		
		Tyr67Cys[a]	348		
		Tyr67Phe[a]	308		
C. reinhardtii cyt f^i	370	Tyr1Phe	369	cyt *f*	280
		Tyr1Ser	313		
		Val3Phe	373		
		Phe4Leu	348		
		Phe4Trp	336		
		Tyr1Phe/Phe4Tyr	370		
		Tyr1Ser/Phe4Leu	289		
		Val3Phe/Phe4Trp	342		
R. rubrum cyt c_2	324			Class I	275
Arthrospira maxima cyt c_6	314			Class I	281
P. laminosum cyt f^i	297	Trp4Phe	323	cyt *f*	280
		Trp4Leu	300		
		Phe3Val/Trp4Phe	316		
S. cerevisiae iso-2 cyt *c*	288[d]	Asn52Ile	243	Class I	282

Table 1 continued

Cytochrome	$E^{0'}$ (mV)	Cytochrome variant	$E^{0'}$ (mV)	Class	References
S. cerevisiae iso-1 cyt *c*[b]	272[e], 285[c], 290[d]	Arg38Lys	249[e]	Class I	179,180, 182,183,259,283,284, 285,286,287
		Arg38His	245[e]		
		Arg38Gln	242[e]		
		Arg38Asn	238[e]		
		Arg38Leu	231[e]		
		Arg38Ala	225[e]		
			239[c]		
		Asn52Ala	257[d]		
		Asn52Ile	231[c]		
		Tyr67Phe	234[d]		
		Phe82Leu	286[d]		
		Phe82Tyr	280[d]		
		Phe82Ile	273[d]		
		Phe82Trp	266[d]		
		Phe82Ala	260[d]		
		Phe82Ser	255[d]		
		Phe82Gly	247[d]		
P. aeruginosa cyt *c*551	276			Class I	275
horse cyt *c*	262	Met80Ala	82[c]	Class I	268,277
		Met80His	41[c]		
		Met80Leu	−45[c]		
		Met80Cys	−390[c]		
rat cyt *c*	260	Pro30Ala[a]	258	Class I	277,288,289,290
		Pro30Val[a]	261		
		Tyr67Phe[a]	224		
Rps. palustris cyt *c*556	230			Class II	5
E. coli cyt *b*562	168	Phe61Gly	90	cyt *b* (Class II)	291,292
		Phe65Val	173		
		Phe61Ile/Phe65Tyr	68		
		His102Met	240		
		Arg98Cys/His102Met	440[k]		
Alc. denitrificans cyt *c'* (ADCP)	132			Class II	5
Rps. palustris cyt *c'* (RPCP)	102			Class II	5
D. vulgaris cyt *c*553	37, 205	Met23Cys	29	Class I	275,293
		Gly51Cys	28		
		Met23Cys/Gly51Cys	88		
		Gly51Cys/Gly51Cys	105		

Table 1 Selected reduction potentials for various cytochromes and their heme pocket mutants.

Cytochrome	$E^{0'}$(mV)	Cytochrome variant	$E^{0'}$ (mV)	Class	References
Rhodocyclus tenuis THRC cyt c				Class IV	274
HP$_1$	420				
HP$_2$	420				
LP$_1$	110				
LP$_2$	60				
Rsp. Viridis THRC cyt c				Class IV	275,276
H1 (c_{559})	380				
H3 (c_{556})	330				
H2 (c_{552})	20				
H4 (c_{554})	−60				
Rb. Capsulatus cyt c_2	373	Gly29Ser[a]	330	Class I	277,278,279
		Pro30Ala[a]	258		
		Tyr67Cys[a]	348		
		Tyr67Phe[a]	308		
C. reinhardtii cyt f[i]	370	Tyr1Phe	369	cyt f	280
		Tyr1Ser	313		
		Val3Phe	373		
		Phe4Leu	348		
		Phe4Trp	336		
		Tyr1Phe/Phe4Tyr	370		
		Tyr1Ser/Phe4Leu	289		
		Val3Phe/Phe4Trp	342		
R. rubrum cyt c_2	324			Class I	275
Arthrospira maxima cyt c_6	314			Class I	281
P. laminosum cyt f[i]	297	Trp4Phe	323	cyt f	280
		Trp4Leu	300		
		Phe3Val/Trp4Phe	316		
S. cerevisiae iso-2 cyt c	288[d]	Asn52Ile	243	Class I	282

Table 1 continued

Cytochrome	$E^{0\prime}$(mV)	Cytochrome variant	$E^{0\prime}$ (mV)	Class	References
S. cerevisiae iso-1 cyt *c*[b]	272[e]	Arg38Lys	249[e]	Class I	179,180,
	285[c]	Arg38His	245[e]		182,183,259,283,284,
	290[d]	Arg38Gln	242[e]		285,286,287
		Arg38Asn	238[e]		
		Arg38Leu	231[e]		
		Arg38Ala	225[e]		
			239[c]		
		Asn52Ala	257[d]		
		Asn52Ile	231[c]		
		Tyr67Phe	234[d]		
		Phe82Leu	286[d]		
		Phe82Tyr	280[d]		
		Phe82Ile	273[d]		
		Phe82Trp	266[d]		
		Phe82Ala	260[d]		
		Phe82Ser	255[d]		
		Phe82Gly	247[d]		
P. aeruginosa cyt c_{551}	276	Met80Ala	82[c]	Class I	275
horse cyt *c*	262	Met80His	41[c]	Class I	268,277
		Met80Leu	−45[c]		
		Met80Cys	−390[c]		
rat cyt *c*	260	Pro30Ala[a]	258	Class I	277,288,289,290
		Pro30Val[a]	261		
		Tyr67Phe[a]	224		
Rps. palustris cyt c_{556}	230			Class II	5
E. coli cyt b_{562}	168	Phe61Gly	90	cyt *b*	291,292
		Phe65Val	173	(Class II)	
		Phe61Ile/Phe65Tyr	68		
		His102Met	240		
		Arg98Cys/His102Met	440[k]		
Alc. denitrificans cyt *c′* (ADCP)	132			Class II	5
Rps. palustris cyt *c′*(RPCP)	102			Class II	5
D. vulgaris cyt c_{553}	37	Met23Cys	29	Class I	275,293
	20⁵	Gly51Cys	28		
		Met23Cys/Met23Cys	88		
		Gly51Cys/Gly51Cys	105		

Table 1 continued

Cytochrome	$E^{0'}$(mV)	Cytochrome variant	$E^{0'}$ (mV)	Class	References
S. cerevisiae iso-1 cyt c[b]	272[e]	Arg38Lys	249[e]	Class I	179,180, 182,183,259,283,284, 285,286,287
	285[c]	Arg38His	245[e]		
	290[d]	Arg38Gln	242[e]		
		Arg38Asn	238[e]		
		Arg38Leu	231[e]		
		Arg38Ala	225[e]		
			239[c]		
		Asn52Ala	257[d]		
		Asn52Ile	231[c]		
		Tyr67Phe	234[d]		
		Phe82Leu	286[d]		
		Phe82Tyr	280[d]		
		Phe82Ile	273[d]		
		Phe82Trp	266[d]		
		Phe82Ala	260[d]		
		Phe82Ser	255[d]		
		Phe82Gly	247[d]		
P. aeruginosa cyt c_{551}	276			Class I	275
horse cyt c	262	Met80Ala	82[c]	Class I	268,277
		Met80His	41[c]		
		Met80Leu	−45[c]		
		Met80Cys	−390[c]		
rat cyt c	260	Pro30Ala[a]	258	Class I	277,288,289,290
		Pro30Val[a]	261		
		Tyr67Phe[a]	224		
Rps. palustris cyt c_{556}	230			Class II	5
E. coli cyt b_{562}	168	Phe61Gly	90	cyt b (Class II)	291,292
		Phe65Val	173		
		Phe61Ile/Phe65Tyr	68		
		His102Met	240		
		Arg98Cys/His102Met	440[k]		
Alc. denitrificans cyt c' (ADCP)	132			Class II	5
Rps. palustris cyt c'(RPCP)	102			Class II	5
D. vulgaris cyt c_{553}	37			Class I	275,293
	20S5	Met23Cys	29		
		Gly51Cys	28		
		Met23Cys/Met23Cys	88		
		Gly51Cys/Gly51Cys	105		

Table 1 Selected reduction potentials for various cytochromes and their heme pocket mutants.

Cytochrome	$E^{0'}$(mV)	Cytochrome variant	$E^{0'}$ (mV)	Class	References
Rhodocyclus tenuis THRC cyt *c*				Class IV	274
HP₁ → HP$_1$	420				
HP₂ → HP$_2$	420				
LP₁ → LP$_1$	110				
LP₂ → LP$_2$	60				
Rsp. Viridis THRC cyt *c*				Class IV	275,276
H1 (c_{559})	380				
H3 (c_{556})	330				
H2 (c_{552})	20				
H4 (c_{554})	−60				
Rb. Capsulatus cyt c_2	373	Gly29Ser[a]	330	Class I	277,278,279
		Pro30Ala[a]	258		
		Tyr67Cys[a]	348		
		Tyr67Phe[a]	308		
C. reinhardtii cyt f[i]	370	Tyr1Phe	369	cyt f	280
		Tyr1Ser	313		
		Val3Phe	373		
		Phe4Leu	348		
		Phe4Trp	336		
		Tyr1Phe/Phe4Tyr	370		
		Tyr1Ser/Phe4Leu	289		
		Val3Phe/Phe4Trp	342		
R. rubrum cyt c_2	324			Class I	275
Arthrospira maxima cyt c_6	314			Class I	281
P. laminosum cyt f[i]	297	Trp4Phe	323	cyt f	280
		Trp4Leu	300		
		Phe3Val/Trp4Phe	316		
S. cerevisiae iso-2 cyt *c*	288[d]	Asn52Ile	243	Class I	282

Table 1 Selected reduction potentials for various cytochromes and their heme pocket mutants.

Cytochrome	$E^{0'}$(mV)	Cytochrome variant	$E^{0'}$ (mV)	Class	References
Rhodocyclus tenuis THRC cyt *c*				Class IV	274
HP$_1$	420				
HP$_2$	420				
LP$_1$	110				
LP$_2$	60				
Rsp. Viridis THRC cyt *c*				Class IV	275,276
H1 (c_{559})	380				
H3 (c_{556})	330				
H2 (c_{552})	20				
H4 (c_{554})	−60				
Rb. Capsulatus cyt c_2	373	Gly29Ser[a]	330	Class I	277,278,279
		Pro30Ala[a]	258		
		Tyr67Cys[a]	348		
		Tyr67Phe[a]	308		
C. reinhardtii cyt *f*[i]	370	Tyr1Phe	369	cyt *f*	280
		Tyr1Ser	313		
		Val3Phe	373		
		Phe4Leu	348		
		Phe4Trp	336		
		Tyr1Phe/Phe4Tyr	370		
		Tyr1Ser/Phe4Leu	289		
		Val3Phe/Phe4Trp	342		
R. rubrum cyt c_2	324			Class I	275
Arthrospira maxima cyt c_6	314			Class I	281
P. laminosum cyt *f*[i]	297	Trp4Phe	323	cyt *f*	280
		Trp4Leu	300		
		Phe3Val/Trp4Phe	316		
S. cerevisiae iso-2 cyt *c*	288[d]	Asn52Ile	243	Class I	282

Table 1 continued

Cytochrome	$E^{0'}$ (mV)	Cytochrome variant	$E^{0'}$ (mV)	Class	References
S. cerevisiae iso-1 cyt c[b]	272[e]	Arg38Lys	249[e]	Class I	179,180, 182,183,259,283,284, 285,286,287
	285[c]	Arg38His	245[e]		
	290[d]	Arg38Gln	242[e]		
		Arg38Asn	238[e]		
		Arg38Leu	231[e]		
		Arg38Ala	225[e]		
			239[c]		
		Asn52Ala	257[d]		
		Asn52Ile	231[c]		
		Tyr67Phe	234[d]		
		Phe82Leu	286[d]		
		Phe82Tyr	280[d]		
		Phe82Ile	273[d]		
		Phe82Trp	266[d]		
		Phe82Ala	260[d]		
		Phe82Ser	255[d]		
		Phe82Gly	247[d]		
P. aeruginosa cyt c_{551}	276			Class I	275
horse cyt c	262	Met80Ala	82[c]	Class I	268,277
		Met80His	41[c]		
		Met80Leu	−45[c]		
		Met80Cys	−390[c]		
rat cyt c	260	Pro30Ala[a]	258	Class I	277,288,289,290
		Pro30Val[a]	261		
		Tyr67Phe[a]	224		
Rps. palustris cyt c_{556}	230			Class II	5
E. coli cyt b_{562}	168	Phe61Gly	90	cyt b (Class II)	291,292
		Phe65Val	173		
		Phe61Ile/Phe65Tyr	68		
		His102Met	240		
		Arg98Cys/His102Met	440[k]		
Alc. denitrificans cyt c' (ADCP)	132			Class II	5
Rps. palustris cyt c' (RPCP)	102			Class II	5
D. vulgaris cyt c_{553}	37	Met23Cys	29	Class I	275,293
	20S5	Gly51Cys	28		
		Met23Cys/Met23Cys	88		
		Gly51Cys/Gly51Cys	105		

Table 1 continued

Cytochrome	$E^{0\prime}$ (mV)	Cytochrome variant	$E^{0\prime}$ (mV)	Class	References
S. cerevisiae iso-1 cyt *c*[b]	272[e], 285[c], 290[d]	Arg38Lys	249[e]	Class I	179,180, 182,183,259,283,284, 285,286,287
		Arg38His	245[e]		
		Arg38Gln	242[e]		
		Arg38Asn	238[e]		
		Arg38Leu	231[e]		
		Arg38Ala	225[e]		
			239[c]		
		Asn52Ala	257[d]		
		Asn52Ile	231[c]		
		Tyr67Phe	234[d]		
		Phe82Leu	286[d]		
		Phe82Tyr	280[d]		
		Phe82Ile	273[d]		
		Phe82Trp	266[d]		
		Phe82Ala	260[d]		
		Phe82Ser	255[d]		
		Phe82Gly	247[d]		
P. aeruginosa cyt *c*551	276			Class I	275
horse cyt *c*	262	Met80Ala	82[c]	Class I	268,277
		Met80His	41[c]		
		Met80Leu	−45[c]		
		Met80Cys	−390[c]		
rat cyt *c*	260	Pro30Ala[a]	258	Class I	277,288,289,290
		Pro30Val[a]	261		
		Tyr67Phe[a]	224		
Rps. palustris cyt *c*556	230			Class II	5
E. coli cyt *b*562	168	Phe61Gly	90	cyt *b* (Class II)	291,292
		Phe65Val	173		
		Phe61Ile/Phe65Tyr	68		
		His102Met	240		
		Arg98Cys/His102Met	440[k]		
Alc. denitrificans cyt *c'* (ADCP)	132			Class II	5
Rps. palustris cyt *c'* (RPCP)	102			Class II	5
D. vulgaris cyt *c*553	37 20S5	Met23Cys	29	Class I	275,293
		Gly51Cys	28		
		Met23Cys/Met23Cys	88		
		Gly51Cys/Gly51Cys	105		

Protein			Notes	Class	Ref.
bovine liver Mc cyt b_5[l]	3	70	Protoheme IX dimethyl ester	cyt b	294
S. cerevisiae cyt b_2	−2			cyt b	275
C. vinosum cyt c′ (CVCP)	−5			Class II	5
rat liver Mc cyt b_5	−7 ± 1			cyt b	295,296
R. rubrum cyt c′ (RRCP)	−8			Class II	5
tryptic bovine hepatic cyt b_5	−10 ± 3	17 11 −25 −33	Val61Lys Val61His Val61Glu Val61Tyr	cyt b	297
rat liver OM cyt b_5[f]	−102	110 −148	His63Met Val45Leu/Val61Leu protoheme IX dimethyl ester	cyt b	298,299
D. desulfuricans Norway cyt c_3	−132 −255 −320 −360	−36		Class III	275
Ectothiorhodospira shaposhnikovii cyt b_{558}	−210			cyt b	300
Azotobacter vinelandii bacterioferritin	−225	−475	In presence of nonheme iron core	cyt b	301

D. vulgaris Hildenborough cyt c_3[j]

	His22Met	His25Met	His35Met	His70Met	Class	Ref.
−250	−210	−90	−205	−65		
−310	−250	−285	−265	−240		
−310	−250	−305	−280	−295	Class III	302,303
−330	−290	−310	−350	−320		

Protein			Notes	Class	Ref.
Arthrospira maxima cyt c_{549}	−260			Class I	281

Protein	Description / Variant	E (mV)		Class / type	Ref
bovine liver Mc cyt b_5[l]	Protoheme IX dimethyl ester	3	70	cyt b	294
S. cerevisiae cyt b_2		-2		cyt b	275
C. vinosum cyt c' (CVCP)		-5		Class II	5
rat liver Mc cyt b_5		-7 ± 1		cyt b	295,296
R. rubrum cyt c' (RRCP)		-8		Class II	5
tryptic bovine hepatic cyt b_5		-10 ± 3		cyt b	297
	Val61Lys		17		
	Val61His		11		
	Val61Glu		-25		
	Val61Tyr		-33		
rat liver OM cyt b_5[f]	His63Met		110	cyt b	298,299
	Val45Leu/Val61Leu protoheme IX dimethyl ester	-102	-148		
D. desulfuricans Norway cyt c_3		-132; -255; -320; -360	-36	Class III	275
Ectothiorhodospira shaposhnikovii cyt b_{558}		-210		cyt b	300
Azotobacter vinelandii bacterioferritin	In presence of nonheme iron core	-225	-475	cyt b	301
D. vulgaris Hildenborough cyt c_3[j]	(see matrix below)	-250; -310; -310; -330		Class III	302,303
Arthrospira maxima cyt c_{549}		-260		Class I	281

D. vulgaris Hildenborough cyt c_3[j]:

His22Met	His25Met	His35Met	His70Met
-210	-90	-205	-65
-250	-285	-265	-240
-250	-305	-280	-295
-290	-310	-350	-320

[a] Numbering of the residues corresponds to that of horse cyt c. [b] Iso-1-cyt c reported here all contain a mutation at Cys102Thr(Ser/Ala) to prevent dimerization. [c] Reduction potentials measured at pH 7.0, 0.1 M ionic strength, 25 EC versus SHE. [d] Reduction potentials measured at pH 6.0, 0.1 M ionic strength, 25 EC versus SHE. [e] Reduction potentials measured at 0.1 M sodium phosphate pH 7.0, 0.1 M NaCl, 25 EC versus SHE. [f] Recombinant rat OM cyt b_5. [g] Reduction potential for the State III of this variant. Reduction potentials measured at pH 6.0, 0.1 M ionic strength, 25 EC versus SHE. [h] Reduction potential measured in the b_6f complex. [i] Reduction potential measured at pH 7.0 in 50mM K_2HPO_4/KH_2PO_4 buffer. [j] Reduction potentials determined by CV and DPV methods in 0.1 M phosphate buffer, pH 7.6. [k] Reduction potential at pH 4.8. [l] Recombinant bovine liver cyt b_5.
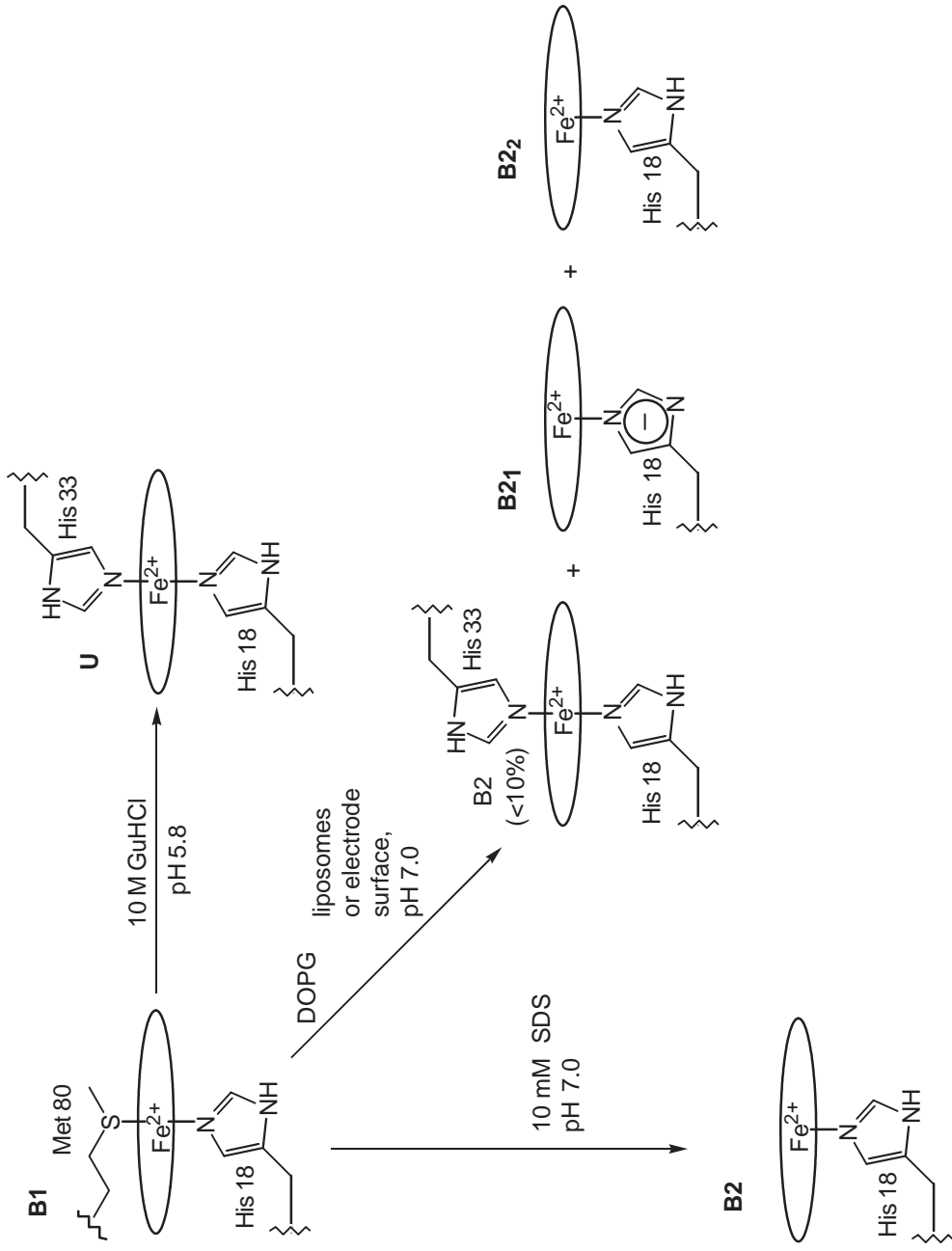
Scheme 4a

Scheme 4b

tuna protein.[215] At concentrations of GuHCl which fully denature horse cyt *c*, the Lys/His coordination is replaced by the His/His heme ligation discussed earlier.[213,214] In unfolded *iso*-1-cyt *c*, the N-terminal amino group can also ligate the heme.[207] This is not observed for horse cyt *c*, because its N-terminus is acetylated.[212] As the pH of unfolded cyt *c* is lowered, the non-native His is replaced by water yielding a 6cHS heme.[212,216] A further drop in pH results in a 5cHS species in which water is the axial ligand.[79,193,217–219] Acidic denaturing conditions are required for His18 displacement from the heme, suggesting that significant loss of secondary structure is required for structural rearrangement on the His18 side of the heme. There is no evidence of His18 replacement in unfolded ferrocyt *c* at pH > 3 (Scheme 4b).[193] This is consistent with ferrocyt *c* being $\sim 10\,\mathrm{kcal\,mol^{-1}}$ more stable towards unfolding than its ferric form, and a ΔE ($E_{\mathrm{native}} \sim 260\,\mathrm{mV}$; $E_{\mathrm{unfolded}} \sim -150\,\mathrm{mV}$ vs. SHE) of $410\,\mathrm{mV}$.[220–224]

In addition to the native (B1) and unfolded (U) cyt *c* conformations, a conformational state designated B2, in which the native secondary structure is preserved but the Met80 side of the heme pocket has a more open structure, has been detected upon binding of cyt *c* to electrodes,[193,225–227] micelles,[193,226] polyanions,[226] anionic surfaces of phospholipid vesicles,[226,228] and cytochrome *c* oxidase.[64,65] In the B2 conformation, 5cHS and 6cLS heme configurations in both oxidation states were identified by global analysis of resonance Raman spectra[193] (Scheme 4a and 4b). Redox potentials for the B2(5cHS) and B2(6cLS) configurations (−0.31 and −0.41 V vs. a saturated calomel electrode, respectively) are significantly lower than the redox potential of the native protein (B1(6sLS), +0.02 V vs. SCE).[225]

Since heme ligand substitution processes affect cyt *c* folding, substitution of the Fe[III] with a substitution-inert Co[III] in the cyt *c* heme significantly slows down the folding process (from hundreds of ms to hours) and facilitates separation of ligand substitution coupled folding from the protein backbone dynamics.[215,229] The crystal structure of tuna Co[III]-cyt *c* demonstrates that the metal substitution does not alter the native fold and the heme axial ligation (Met80/His18) is maintained.[229] Two misligated folding intermediates have been proposed for horse (His33/His18, Lys$_a$/His18) and tuna (Lys$_a$/His18, Lys$_b$ or His26/His18) Co[III]-cyts *c*.[215,229]

The folding of ferrous cyt *c* has been studied by several optically triggered techniques. The secondary structure of ferrous cyt *c* in 4.6 M GuHCl pH 6.5 is similar to that of the native protein, while the ferrous CO adduct generated under the same conditions is predominantly unfolded. Thus, photodissociation of the CO adduct triggers the folding reaction and has been used to initiate protein-folding and ligand-rebinding reactions for kinetics studies with time-resolved optical absorption, time-resolved circular dichroism, and fluorescence spectroscopy.[230–233] A kinetic model for time-resolved optical absorption data suggests that intermolecular binding of Met80 or Met65 ($k = 2.5 \times 10^4\,\mathrm{s^{-1}}$, $\tau = 40\,\mathrm{\mu s}$) is faster than binding of His33 or His26 ($k = 2.5 \times 10^3\,\mathrm{s^{-1}}$, $\tau = 400\,\mathrm{\mu s}$).[230] Folding intermediates with lifetimes of 2 μs, 50 μs, 225 μs, and 880 μs were identified with time-resolved circular dichroism. The 2 μs and 50 μs processes have been proposed to involve Fe[II]—Met80 and Fe[II]–His33 or His26 coordination, respectively. The two slowest phases are due to CO rebinding.[233] This method of studying folding intermediates is complicated by loss of the Fe[II]—His18 bond upon CO photolysis. Rebinding of CO to the resulting four-coordinate heme yields kinetic intermediates that are unrelated to folding.[234]

The difference in the stabilities of oxidized and reduced cyt *c* facilitates initiation of folding experiments by photo-induced electron transfer. Photoexcitation of Ru(2,2′-bipyridine)$_3^{2+}$ or NADH yields a long-lived excited state capable of reducing unfolded ferricyt *c*. Upon reduction of the heme, the ferrocyt *c* folding process begins.[82,208,209,223,224] In neutral solution and 3.2 M GuHCl, the kinetics of ferrocyt *c* folding can be fitted to a single exponential phase that corresponds to the displacement of the non-native His in unfolded ferrocyt *c* by Met80 in the folded protein. In acidic solution, the heme is five-coordinate until Met80 binds to generate the native fold.[208] The Met binding rate ($k = 16 \pm 5\,\mathrm{s^{-1}}$ at pH 5.0, 3.2 M GuHCl)[208] is significantly different from the fast Met binding rate obtained from CO-photolysis-triggered folding kinetics.[230] This difference has been ascribed to differences in the unfolded protein prior to electron-transfer-triggered folding (unfolded ferricyt *c*) and CO-photolysis-triggered folding (unfolded carbonmonoxy ferrocyt *c*).[208,231]

8.2.3.6.2   *Redox-driven heme ligand switching in iso-1-cytochrome* c *(Phe82His)*

Although the native heme ligand Met80 is present in the *iso*-1-cyt *c* (Phe82His/Cys102Ser(or Thr)) variant, EPR and NIR-MCD data indicate bis-His coordination with His82 as the sixth heme ligand in the oxidized mutant.[235] ^{1}H-NMR characterization of the reduced mutant

demonstrates that Met80 is the sixth heme iron ligand in the ferrous state.[236] Ferric *iso*-1-cyt *c* (Phe82His/Cys102Ser(or Thr)) has a conformation analogous to the B2 conformation in wild-type cyt *c*; this results in a less distorted heme in the ferric form relative to the ferrous protein.[237] The redox-driven, reversible, heme-ligand switching between Met80–Fe^{II}–His18 and His82–Fe^{III}–His18 has been demonstrated by cyclic and square-wave voltammetry.[238] Similar heme coordination rearrangements are observed in the cytochromes in cd_1 nitrite reductase. The ferric enzyme has His/Tyr side chains ligating the d_1-heme, and the *c*-type heme has bis-histidine coordination. Reduction of cd_1 nitrite reductase causes the loss of d_1-heme Tyr coordination and the *c*-type heme iron coordination rearranges from His17/His69 to Met106/His69.[239]

8.2.3.7 Exogenous Ligand Complexes of Class I Cytochromes *c*

8.2.3.7.1 *Exogenous ligand complexes of ferricytochromes c*

Ferricyt *c* forms complexes with small ligands such as cyanide, ammonia, azide, imidazole, and pyridine. These ligands bind to the heme iron by displacement of Met80.[240–243] Association constants are given in Table 2. In general, exogenous ligand binding results in localized conformational changes in the heme pocket, increasing its size.[191,248–252]

In the ferricyt *c* cyanide adduct, the cyanide is hydrogen bonded to a protein residue.[253] Tyr67 is a likely candidate, because of the short T_1 and slow exchange with bulk water of its hydroxyl proton,[254] and its hydroxyl proton is within hydrogen-bond distance of the cyanide nitrogen.[252] Movement of Met80 upon cyanide binding leaves its bulky side chain pointing away from the center of the heme cavity toward the protein surface, and the backbone of residues 77–85 moves away from the heme, thereby increasing the size of the heme pocket. In contrast, *iso*-1-cyt *c* (His29Gln/Met80Ala/Cys102Ser) cyanide adduct has the conformation of the backbone residues 79–81 comparable to that of the native protein.[254–257]

^{1}H-NMR spectra of the ferricyt *c* ammonia complex are similar to those observed for alkaline cyt *c*. The crystal structure of the ammonia adduct of *Rps. palustris* cyt c_2 shows only three residues (Lys92–Met93–Thr94; *Rps. palustris* numbering, Met93 is the heme axial ligand in the native form) involved in the conformational change caused by NH_3 complexation.[166] It has been proposed that the weak hydrogen bond between the sulfur of Met93 and the Tyr66 OH (3.34 Å) stabilizes the native form of the protein. This hydrogen bond and the more flexible Met loop in *Rps. palustris* cyt c_2 due to a six-residue insertion (Gly82–Ala87) facilitate formation of the ammonia complex.[166] In *Rps. viridis* cyt c_2 which has a strong hydrogen bond between Met93 and Tyr66 (3.12 Å), ammonia does not displace Met93.[258]

Azide-binding studies of *iso*-1-cyt *c* and its Phe82 variants (Phe82Tyr, ($K_f = 31$ M^{-1}); Phe82Ser, (52 M^{-1}); Phe82Ile, (64 M^{-1}); Phe82Leu, (96 M^{-1}); Phe82Gly, (105 M^{-1})) demonstrate that features favoring the alkaline transition also enhance azide binding.[245] Kinetic data for azide binding is consistent with a two-step mechanism (Scheme 5), in which fluctuation of the polypeptide chain controls access to the heme and is rate limiting. This model was proposed because no correlation between Phe82 substitution and Fe—Met80 bond strength is obvious,[245] and increased azide affinity is observed for variants with greater solvent accessibility of the heme.[132,182,259]

Table 2 Association constants for exogenous ligand complexes of *c*-type cytochromes.

Ligand	Protein	K_a(M^{-1})	References
Cyanide	Horse cyt *c*	~10^6	244
Azide	Horse cyt *c*	4.5	240,245
	iso-1-cyt *c*	16.7	245
	Rb. sphaeroides cyt c_2	48	246
Ammonia	cyt *c*	1.5–4	243
Imidazole	Horse cyt *c*	30	242,247
	Rb. capsulatus cyt c_2	1,440	246,247
	Rb. sphaeroides cyt c_2	1,420	246,247
Pyridine	Horse cyt *c*	2.5	240
	Rb. sphaeroides cyt c_2	7.8	246
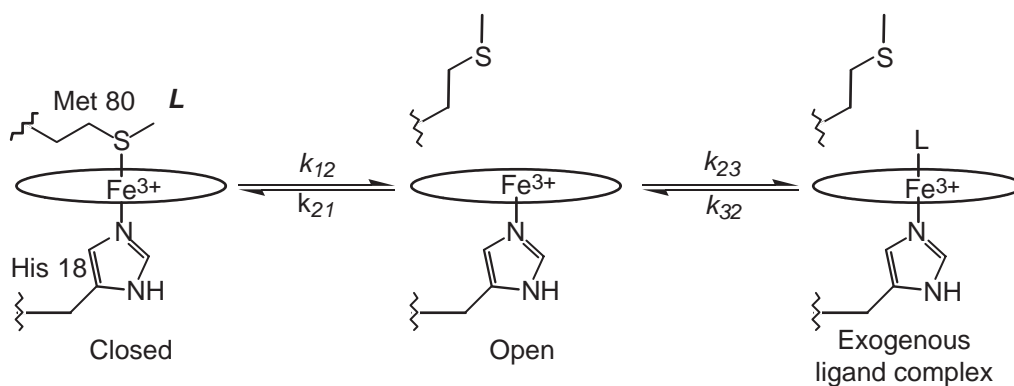
Scheme 5

The same mechanism with a rate-limiting conformational change that results in loss of the Fe—Met bond[242,246,247] has been proposed for imidazole binding to ferricyts c and c_2. Imidazole binds to cyts c_2 from *Rb. capsulatus* and *Rb. sphaeroides* fifty times more strongly than to horse cyt c.[242,246,247] It has been proposed that the cyt c_2 imidazole adduct is stabilized by a hydrogen-bonding network in which an internal water molecule is hydrogen bonded to both the bound imidazole hydrogen and the backbone carbonyl oxygen of Phe102 (*Rb. sphaeroides* numbering).[246] The crystal structure of the *Rb. sphaeroides* cyt c_2 imidazole adduct is consistent with this description of hydrogen bonding.[260] Differences in the dissociation rate constant between cyts c_2 (0.06–0.09 s^{-1}) and horse cyt c (1.6–1.7 s^{-1}) suggest that exogenous imidazole binding in horse cyt c is not stabilized by hydrogen bonding.[246]

NMR and EPR data for the ferricyt c imidazole adduct indicate that the axial-ligand (imidazole and His18) planes are oriented in a nearly parallel arrangement similar to cyt b_5 and the model compound (TPP)Fe(Im)$_2$.[25,248,251,261,262] Large negative shifts of the midpoint potential are seen for imidazole, 1-methylimidazole, and 1-ethylimidazole complexes relative to native ferricyt c ($E_{\text{Im}} - E_{\text{native}} = -426$ mV, -359 mV, -327 mV, respectively).[263]

Horse ferricyt c and *Rb. sphaeroides* ferricyt c_2 have similar binding affinities for pyridine suggesting that, unlike the cyt c_2 imidazole adduct, bound pyridine is not stabilized by hydrogen bonding.[246] Equilibrium constants for binding of pyridine, 3-methylpyridine, and 4-methylpyridine and an increasing $\Delta S°$ term (py, 148 J K^{-1} mol^{-1}; 3MePy, 273 J K^{-1} mol^{-1}; 4MePy, 548 J K^{-1} mol^{-1}) suggest that 4-methylpyridine causes the most extensive conformational change.[264] Thermodynamic parameters for pyridine binding obtained from NMR data ($\Delta H = 44.0$ kJ mol^{-1}; $\Delta S° = 148$ J K^{-1} mol^{-1} at pH 7.0) suggest that a favorable entropy change is the driving force for adduct formation.[265] Evidence from 2D EXSY ^{1}H-NMR experiments suggest that pyridine stabilizes the alkaline form of cyt c. In the presence of pyridine at neutral pH, a lysine-bound form is observed in addition to the native cyt c and the pyridine adduct.[266]

8.2.3.7.2 *Exogenous ligand complexes of ferrocytochrome* c

In neutral solution, the ferrocyt c iron—Met80 bond is not readily broken. Cyanide and CO adducts of the ferrocyt c can be generated only under extreme conditions of temperature or pH.[267] Binding of π-acid ligands to ferrous heme is observed for cyt c variants with substitutions at Met80. Horse ferrocyt c (Met80Leu) and (Met80Cys) variants bind CO. These CO derivatives are similar to wild-type cyt c CO adducts at pH 13.7, for which spectroscopic data are consistent with residue 80, not His18, being displaced by the CO.[268,269] Ferrocyt c (Met80Ala)[196,197,270] binds O$_2$ with a higher affinity than myoglobin. The resulting O$_2$ adduct also has a lower autoxidation rate than myoglobin.[197,270] A stabilizing Phe82 interaction with the bound dioxygen has been proposed, based on the observation of such an interaction in the myoglobin (Leu29Phe) variant, which exhibits an unusually large oxygen binding constant and low autoxidation rate.[270] Solution structure data for the ferricyt c (Met80Ala) cyanide adduct indicate that such an interaction may occur.[255] However, hydrogen bonding between the Tyr67 OH and bound O$_2$ is thought to be the major stabilizing cavity interaction.[254,255]

8.2.3.8 Class II Cytochromes c'

The physiological role of cytochromes c' is unknown. Since they are found in a wide variety of bacteria with different metabolic pathways, roles in photosynthetic electron transfer,[5] nitrogen assimilation,[271] and NO detoxification[272] have been proposed. These class II cyts c have redox potentials varying from -10 mV to $+150$ mV (Table 1).[5,271,273]

8.2.3.8.1 Structure of cytochromes c'

Crystal structures for ferricyts c' from *Rhodospirillum molischianum* (RMCP),[304] *Rhodospirillum rubrum* (RRCP),[305] *Chromatium vinosum* (CVCP),[306] *Alcaligenes xyloseoxidans* (AXCP),[307] *Alcaligenes denitrificans* (ADCP),[307] *Rhodocyclus gelatinosus* (RGCP),[95] *Rhodobacter capsulatus* (RCCP),[96,308,309] and *Rhodopseudomonas palustris* (RPCP)[97] indicate that they all have a characteristic antiparallel four-α-helix (A, B, C, and D helices) bundle structure ($\sim$14 kDa) (Figure 7b). The heme is covalently attached to helix D; it makes nonbonded contacts with residues on helices A, C, and D. Based on the hydrophobic character of the surfaces of helices A and B, cyts c' have been organized into two types.[97] The hydrophobic A–B surfaces of type I cyts c' result in globular dimers; type II cyts c' have hydrophilic A–B surfaces and form flattened dimers or remain monomeric. RMCP, CVCP, AXCP, and ADCP are type I. Type II RCCP is dimeric in the solid state,[96] but is monomeric in solution.[310] RPCP is monomeric in solution.[97]

Ferricyts c' are divided into two groups based on solvent accessibility of the sixth (distal) coordination site of the heme. The first group includes CVCP, RCCP, and RGCP.[95,96] In these proteins, a deep channel between helices B and C leads to the vacant heme coordination site, which is protected from solvent exposure by an aromatic amino-acid side chain. This channel is missing in the second group of ferricyts c' (RMCP, RRCP, AXCP, ADCP, RPCP),[97,304,305,307] and their distal pocket is buried, with Leu16 blocking access to the sixth coordination site of the heme. The affinity of this second group for alkylisocyanides is about a 1,000-fold lower than observed for group I.[311] Presumably the channel facilitates the binding of large heme ligands like n-butylisocyanide to ferrocyts c' of group I.[308,311]

The five-coordinate heme iron is displaced by $\sim$0.3 Å out of the porphyrin plane towards the axial His ligand (Figure 9a). Out-of-plane distortions of the heme in ferricyts c' are described by linear combination of saddling (-0.3 Å to -0.4 Å) and ruffling (0.1 Å to 0.3 Å) deformations. The distortion is conserved among the ferricyts c' that have been examined.[21] The orientation of the axial His (ϕ is $\sim$33°)[312] is suggested as a contributing influence to the observed heme distortions.[21] A linear, negative correlation between ϕ and ν(Fe-His) frequency for ferrous high-spin hemoproteins indicates that ν(Fe-His) is downshifted $\sim$0.5 cm^{-1} deg^{-1}.[313] Thus, the ν(Fe-His) mode of ferrocyts c' at 228–231 cm^{-1} [313–315] and ϕ of $\sim$33° place these proteins on the correlation line that is consistent with a proximal His having significant imidazolate character.[313,314] In most of the ferricyts c' crystal structures, the solvent-exposed axial His has a hydrogen-bonding contact between its Nδ1 and a well-ordered water molecule.[95–97,307,312] Although this hydrogen-bonding interaction is also observed in the crystal structure of ferrous AXCP,[312] it alone is unlikely to generate imidazolate character at the axial His. Stabilization of a proximal imidazolate ionically by a positively charged residue has been proposed. A likely candidate is either an Arg or a Lys residue in close proximity to the axial His in all the cyts c' examined to date.[96,97,304–309,312]

No significant difference in the secondary structure composition between oxidized and reduced cyts c' is detected by NMR,[101,316,317] and crystallographic data for oxidized and reduced AXCP indicate that there is very little difference between their overall structures.[312] However, a redox-dependent change in AXCP is observed on the proximal side of the heme. In ferricyt c' the quanidinium group of Arg124 (AXCP numbering) is perpendicular to the imidazole ring of His120 (axial heme ligand) and practically parallel to a heme pyrrole ring. This allows overlap of the positive charge of the Arg with the heme π-system. Upon reduction, the Arg124 side chain moves into a position parallel to His120.[312]

8.2.3.8.2 Ligand adducts of reduced cytochromes c'

Ferrocyts c' form stable adducts with NO and CO, but not with O_2. The affinities and rates of CO binding to ferrocyts c' at pH 7.0 range from 1.3×10^3 M^{-1} to 1.7×10^6 M^{-1} and 8.4 to 2.6×10^3 M^{-1} s^{-1}, respectively, and are 10^2- to 10^5-fold smaller than those of globins and
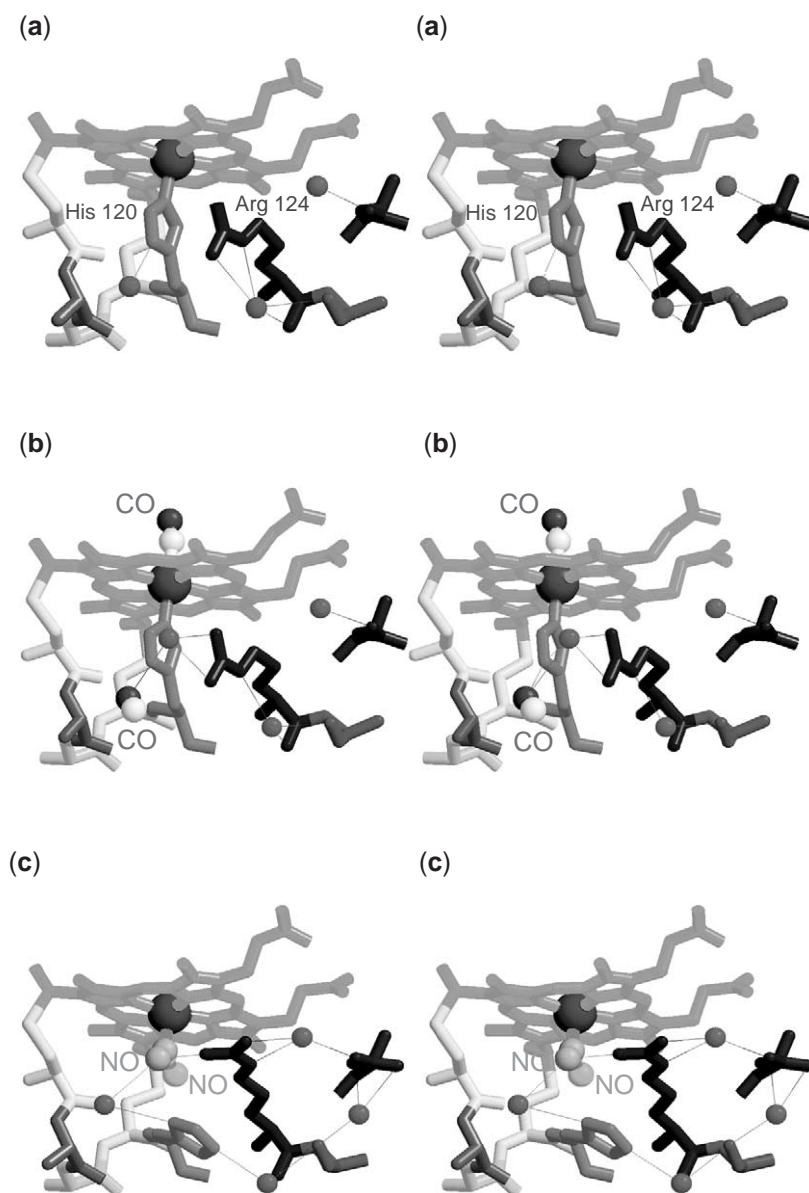
Figure 9 Cross-eyed stereo views showing axial coordination environments in ferrocyt c'. (a) 5cHS ferrous cyt c' (PDB code 1E84); (b) ferrous cyt c'-CO (PDB code 1E86) showing a molecule of CO bound to the protein in the distal heme pocket; and (c) ferrous cyt c'-NO (PDB code 1E85) showing the disordered proximal NO ligand and the imidazole ligand of the proximal His being stabilized in its unbound arrangement by a network of hydrogen bonds involving water molecules shown as (violet) spheres.[312] Dashed lines show hydrogen-bonding interactions.

peroxidases.[311] These ligand binding characteristics reflect the fact that the bulky amino-acid side chain limiting access to the sixth coordination site of the heme must move prior to ligand binding.[306,308] Reduced RMCP dimer binds CO in a noncooperative manner,[318] but CO binding to ferrous CVCP is cooperative and induces dissociation of the CVCP dimers.[319] This dissociation is postulated to be driven by a ligand-binding-induced conformational change.[306]

The ferrocyt c' CO adduct is 6cLS, with the CO bound on the distal side of the heme (Figure 9b).[312,314,315] The ν(Fe–CO) and ν(C–O) frequencies for CO adducts of AXCP (491 cm^{-1}, 1,966 cm^{-1})[314] and CVCP (492 cm^{-1}, 1,978 cm^{-1})[315] are indicative of CO adducts with a neutral His as the proximal ligand and a nonpolar environment around the distal CO ligand. The Fe–CO unit is almost linear, with an Fe–C–O angle of 167°. A second CO binds in the proximal heme pocket and is stabilized by hydrogen bonding to His120.[312]
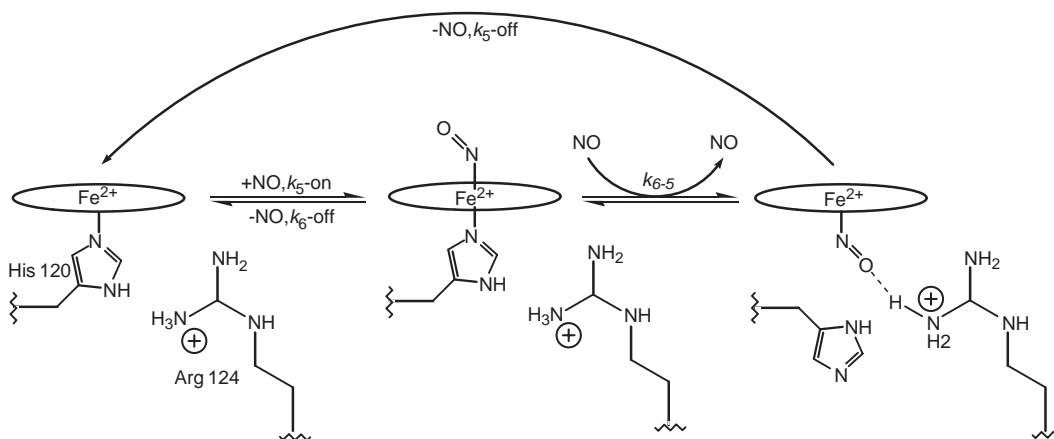
Scheme 6

Both five- and six-coordinate nitrosyl adducts of ferrocyt c' have been observed. The fraction of six-coordinate nitrosyl adduct is an indication of the Fe—His bond stability, and both decrease in the following order: RCCP $\sim$ RPCP $>$ CVCP $>$ RRCP $>$ AXCP (AXCP–NO is predominantly five-coordinate).[320,321] A crystallographic study of the ferrous AXCP–NO reveals that the NO generates a five-coordinate complex by displacing His120 and binding to the proximal side of the heme (Figure 9c). Two NO conformers are reported. One has an Fe–N–O angle of 124° and no specific interactions of the NO with the protein; the second conformer has an Fe–N–O angle of 132° and forms a hydrogen bond with $N^{\eta 1}$ of Arg124.[312] The ν(Fe–NO) and ν(N–O) frequencies (526 cm^{-1} and 1,661 cm^{-1}, respectively) are consistent with a five-coordinate nitrosyl heme having relatively strong π-backbonding. These frequencies suggest that the NO ligand is in a positively polarized environment.[314] Kinetic studies of NO binding to ferrous AXCP, monitored by stopped-flow infrared[322] and UV-visible[323] spectroscopies, indicate that initially a six-coordinate nitrosyl intermediate is formed, followed by conversion to the five-coordinate NO adduct. The relatively slow formation rate for this six-coordinate nitrosyl intermediate ($4.4 \pm 0.5 \times 10^4$ M^{-1} s^{-1}) and the high ν(Fe–NO) frequency (579 cm^{-1}) observed for the freeze-trapped, six-coordinate intermediate are indicative of NO binding in a sterically crowded distal heme pocket. Conversion of the 6cLS NO adduct to the thermodynamically favored proximal 5cLS complex is slow, having a half time on the order of hours. The conversion rate is NO dependent, suggesting that NO catalyzes formation of the proximal five-coordinate nitrosyl complex. The proposed mechanism is illustrated in Scheme 6.[322,323] The kinetics of formation of the five-coordinate proximal nitrosyl heme in AXCP are similar to those of five-coordinate sGC–NO formation.[323,324] Based on this similarity, it has been hypothesized that activated sGC could contain proximal NO adduct.[312,323]

8.2.3.8.3   *Folding intermediates of cytochromes* c'

Visible spectral features of GuHCl-unfolded ferric RPCP are consistent with a 6cHS heme having His and water as axial ligands.[325] Unlike mitochondrial cyts c, heme misligation of ferricyt c' does not affect the kinetics of its folding. A single kinetic phase is observed for stopped-flow, triggered ferricyt c' folding in neutral solution ($\tau = 0.4$ ms).[325] In alkaline solution (pH $>$ 10), thermal or chemical unfolding of ferricyt c' yields a 6cLS heme.[325,326] Since cyt c' contains only one His residue, it has been proposed that the alkaline 6cLS heme is due to His/Lys axial ligation.[325]

Folding of ferrocyt c' has been studied by taking advantage of the greater stability of the reduced form toward unfolding([GuHCl]$_{1/2}$ = 2.9 M) relative to the oxidized protein ([GuHCl]$_{1/2}$ = 1.9 M). Ferrocyt c' folding was initiated by photoreduction of unfolded ferricyt c' in 2.02–2.54 M GuHCl. The observed folding was kinetically heterogeneous with fast-folding ($k = 7.0 \times 10^3$ s^{-1}, 5.7×10^3 s^{-1}), intermediate-folding ($k = 9.0 \times 10^2 - 1.5 \times 10^1$ s^{-1}), and slow-folding ($k = 5.9 \times 10^{-1}$ s^{-1}, 4.8×10^{-1} s^{-1}) components. Visible spectra of unfolded ferrocyt c' between pH 4 and 10 indicate a 6cLS heme with coordination of a methionine sulfur. Misligated states involving two methionines (Met15 and Met25) are probably responsible for the intermediate and slow phases of the ferrocyt c' folding.[325]

8.2.3.8.4 Cytochrome b_{562}

E. coli cyt b_{562}, a protein of unknown function, is a four-helix-bundle protein (12 kDa) containing a single heme coordinated by Met7 on helix 1 and His102 on helix 4.[327,328] While it is structurally homologous to cyt c', it is the only protein in this structural class that does not have a covalently bound heme.[5,327] The low-spin d^5 and d^6-hemes of the oxidized and reduced forms of cyt b_{562} are converted to 5cHS hemes in the GuHCl-unfolded protein, with the His102 being the likely axial ligand.[329] Folding studies analogous to those discussed for cyt c' (Section 8.2.3.8.3) indicate that ferrocyt b_{562} folding is dominated by a single kinetic phase ($k = 800 \pm 200\,\mathrm{s}^{-1}$).[329] Non-native ligation states are not observed. Rapid heme dissociation in unfolded ferrocyt b_{562} ($k_{\mathrm{diss}} = 3\text{--}7 \times 10^3\,\mathrm{s}^{-1}$) competes with protein folding and limits the time scale for the observation of folding kinetics.[330]

Cyt b_{562} (Met7Ala) has a 5cHS heme, and its folding characteristics are comparable to those of apocyt b_{562}, indicating that bis-ligation contributes significantly to the free energy of unfolding.[331] A more stable axial-ligand mutant is generated by changing the polar interactions between the heme propionates and Glu residues in the heme pocket. Mutation of cyt b_{562} has produced a cytochrome P450-like protein with Met7Glu creating a cavity, His102Cys providing the axial ligation, and Glu4Ser and Glu8Ser stabilizing the heme.[332]

Conversion of cyt b_{562} into a *c*-type cytochrome has been accomplished by introducing (Arg98Cys) and (Tyr101Cys) mutations, which generate the conserved –Cys–Xxx–Yxx–Cys–His– sequence. Covalent attachment of the heme does not significantly alter the protein fold or the axial heme ligation, but it does impart an increased stability toward thermal and chemical denaturation relative to that of wild type.[333,334] The double mutant cyt b_{562} (Arg98Cys/His102-Met) ($pK_a = 7.1$) is a high-spin, *c*-type cytochrome at high pH and is converted to a 6cLS bis-Met species at low pH.[291] NMR analysis of cyt b_{562} (Arg98Cys/His102Met) suggests that the conformation of Met7, with its R stereochemistry at the chiral sulfur ligand, is analogous to that in wild-type protein, while the sulfur of Met102 has S stereochemistry. This arrangement results in a torsional angle of 110° between the Met7 and Met102 sulfur lone pairs.[335] The resulting ligand field symmetry in cyt b_{562} (Arg98Cys/His102Met) is close to purely axial,[291] consistent with a $(d_{xz}, d_{yz})^4(d_{xy})^1$ ground state. This is in contrast to bacterioferritin, the only other known bis-Met ligated cytochrome, for which the ferric form is a highly rhombic $(d_{xy})^2(d_{xz}, d_{yz})^3$ ground state.[9,336] However, these factors alone are unlikely to account for the $\sim$600 mV redox potential difference between these two bis-Met ligated systems (cyt b_{562} (Arg98Cys/His102Met), 440 mV at pH 4.8; *Azotobacter vinelandii* bacterioferritin, -225 mV).[291]

Formation of *c*-type cytochromes requires formation of stereospecific thioether cross-links between the heme and protein. The processes and proteins involved in this post-translational cyt *c* maturation are being elucidated.[337–339] The proteins encoded by the cyt *c* maturation operons have been identified. They are involved in heme transport, chaperoning, and attachment to apocyt *c*. Although the mechanistic details of cyt *c* maturation are unknown, the steps will undoubtedly involve a series of axial-ligand exchange reactions as the heme is chaperoned and crosslinked to apocyt *c*.

8.2.3.9 Multiheme Cytochromes *c*

In tetraheme cyts c_3, hemes are numbered relative to their attachment to the polypeptide, i.e., the sequence order of their binding cysteinyl residues. Hemes I and III are generally attached to the protein via a –Cys–(Xxx)$_2$–Cys–His– peptide segment, while the covalently linked peptide segment for hemes II and IV is –Cys–(Xxx)$_4$–Cys–His–.[340,341] The macroscopic redox potentials for these low-redox-potential proteins have been determined by electrochemical and spectrochemical methods.[302,303,340,342] NMR and EPR methods have been employed to measure the microscopic redox potentials of each heme and the heme interaction potentials in tetraheme cyt c_3.[117,342–348] Resonance Raman spectroscopy and NSD have also been used to assign hemes to measured redox potentials, based on heme ruffling and total heme distortion.[341] Although the overall relative orientation of the hemes is conserved, the order of heme oxidation varies among cyts c_3 from different sources.[117,342,348] Cyts c_3 exhibit homotropic redox cooperativity, in which the redox potential of a given heme is dependent on the redox states of the other hemes. The redox potentials of the cyts c_3 hemes are also pH dependent (redox-Bohr effect).[343,348,349] The molecular basis for this redox-Bohr effect in cyts c_3 appears to involve heme propionates and their interactions with hydrogen-bonding networks and/or charged residues in their vicinity.[121,349–357] The interactions between the four hemes and one ionizable center in cyts c_3 from *D. gigas*[356] and

D. vulgaris[358] and two ionizable centers in *D. desulfuricans ATCC27774* [348] that result in concerted two-electron/two-proton transfer steps has been called "proton-thrusting," because it is akin to the redox-linked proton-transfer mechanisms seen in membrane-bound protein complexes involved in proton pumping.[113,358]

A group of multiheme *c*-type cytochromes, members of the NapC/NirT family, are membrane bound via a hydrophobic N-terminal region and contain 4–5 heme-binding sequences.[359] The tetraheme proteins, *Paracoccus denitrificans* NapC, *Pseudomonas stutzeri* NirT, *Wolinella succinogenes* NrfH, *Shewanella putrefaciens* CymA, and *N. europaea* CycB, have 45–49% sequence homology.[359,360] Analysis of the primary sequences suggests duplication of two di-heme domains.[361] Spectroscopic characterization of NapC[361] and CymA[362] indicates that they each have four 6cLS hemes with mutually parallel bis-His axial ligation. Consistent with bis-His ligation, the reduction potentials of the hemes in NapC and CymA range from $+10\,mV$ to $-235\,mV$.[361,362] The lack of structural information for any NapC/NirT homologue precludes classification of the proteins.

8.2.4 CYTOCHROME b_5

In erythrocytes, a soluble 11 kDa cyt b_5 reduces methemoglobin to a functional-oxygen-binding ferrous form.[363,364] A similar function for cyt b_5 in muscle, reduction of metmyoglobin to deoxymyoglobin, has been suggested.[365,366] The amino-acid sequence of the soluble erythrocyte cyt b_5 is identical to that of the heme-binding domain of microsomal cyt b_5. Microsomal cyt b_5 (Mc cyt b_5) is associated with the membrane of the endoplasmic reticulum and has been found in mammals, insects, plants, and other eukaryotes.[367,368] It provides reducing equivalents for desaturation of fatty acids, cholesterol biosynthesis, and hydroxylation reactions involving cytochrome P450.[369–371] Two distinct forms of cyt b_5 exist in rat hepatocytes, and the genes encoding them have been identified.[372–374] One is a Mc cyt b_5, and the second is bound to the outer membrane of the liver mitochondria (OM cyt b_5).[375] Rat OM cyt b_5 participates in the reduction of cytosolic semidehydroascorbate.[376] A prokaryotic homologue of cyt b_5, *Ectothiorhodospira vacuolata* cyt b_{558}, has also been reported.[300]

The mammalian Mc cyts b_5 contain 134 amino-acid residues and show 93–98% sequence similarity.[376] OM cyt b_5 (146 residues) is larger than Mc cyts b_5 and shares only 68% sequence similarity with bovine Mc cyt b_5.[376] Both Mc cyts b_5 and OM cyt b_5 have three domains: an N-terminal hydrophilic domain, a medial hydrophobic domain, and a C-terminal hydrophilic domain. In the cytosol, the 100-amino-acid N-terminal domain, which binds the *b*-type heme,[377] participates in electron-transfer reactions.[378–380] The heme-binding domains of Mc cyt b_5 and OM cyt b_5 exhibit very similar protein folds.[381,382] They have six α-helices and four β-strands, two of which form a short β-sheet. The heme is located in a pocket formed by four α-helices and a β-sheet, with its propionates pointing towards the solvent and the opposite heme edge buried in a hydrophobic pocket. The planes of the heme axial His ligands are in a near-parallel orientation (Figure 10).

8.2.4.1 Heme Orientation Isomers

Since the porphyrin of the *b*-type heme is not covalently attached to the protein, the heme in cyt b_5 can bind to the protein in two orientations, related to one another by a 180° rotation about the porphyrin α, γ-meso axis. Upon reconstitution of apo-cyt b_5 with hemin, isomers A and B are present in approximately a 1:1 ratio, and with time an equilibrium mixture is obtained. The equilibrium A:B ratio varies, depending on the protein source. For example, the A:B ratios for rat OM cyt b_5, rat Mc cyt b_5, bovine Mc cyt b_5, and chicken Mc cyt b_5 are 1:1, 1.6:1, 9:1, and 20:1, respectively.[383–385] The free-energy difference between the isomers in Mc cyts b_5 is $\sim620\,cal\,mol^{-1}$ ($\Delta E^{0'} = 27\,mV$).[386] Solution structures of the A and B isomers indicate that structural differences between the isomers are localized around the heme.[90,385] In isomer A, the two hydrogen bonds from the Ser64 backbone NH and its side chain –OH to propionate-7 are important in stabilizing the heme protein interaction. The major difference between forms A and B and the dominant effector of the reduction potential difference between them is a hydrogen bond, between propionate-7 and the Ser64 amide in form A, that is absent in form B.[387] In protoheme IX dimethylester cyt b_5[388] and cyt b_5 (Ser64Ala) variant, these hydrogen bonds are absent and the rate of heme dissociation increases six- to tenfold over that of wild type.[389]
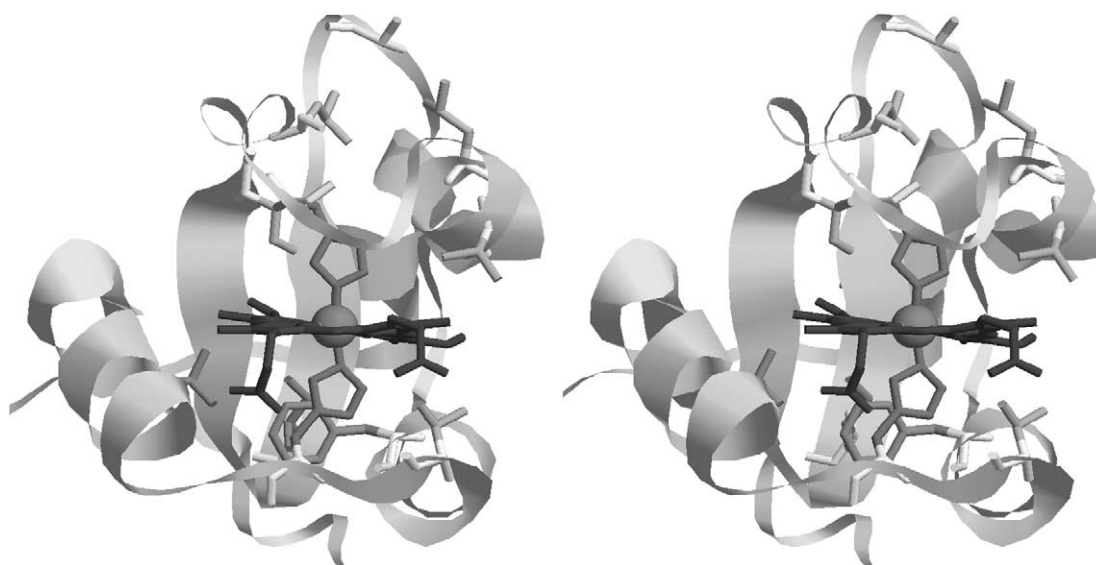
Figure 10 Cross-eyed stereo view of rat OM cyt b_5 fold (PDB code 1B5M). Val61 and Val45 are shown (in violet) to the right of the heme. Two hydrophobic networks responsible for OM cyt b_5 stability are also shown. The first consists of the side chains of Ala18, Ile32, Leu36, and Leu47, (shown in gold) above and behind the heme.[376] The second includes Ile25, Phe58, Leu71, (shown in green) below and behind the heme.[393] The corresponding residues in Mc cyt b_5 are Ser18, Leu32, Leu36, Arg47, Leu25, and Ser71, respectively.

8.2.4.2 Comparison of Mc and OM Cytochromes b_5

In contrast to Mc cyts b_5, the thermodynamic equilibrium ratio of A:B isomers of 1:1.3 in OM cyt b_5 favors isomer B, and is obtained only after hours at 65 °C. At physiological temperature, the OM cyt b_5 heme is kinetically trapped.[390] Several other properties of rat OM cyt b_5 differ from those of rat Mc cyt b_5.: (i) OM cyt b_5 has a significantly lower redox potential[298,299] than Mc cyt b_5 (Table 2); (ii) OM cyt b_5 (T_m, 83.6 °C) is more stable toward thermal denaturation than Mc cyt b_5 (T_m, 65.2 °C).[297,390,391]; (iii) OM cyt b_5 is about $10 \, \text{kJ mol}^{-1}$ ($\sim 2.5 \, \text{kcal mol}^{-1}$) more stable than Mc cyt b_5 towards chemical denaturation;[390,392] (iv) while bovine Mc cyt b_5 will release heme to apo-myoglobin at pH 7.0,[389] heme is not transferred from rat OM cyt b_5 to apo-myoglobin even at pH values as low as 5.2.[390,392] Two hydrophobic networks responsible for the stability and slow heme dissociation and reorientation in OM cyt b_5 have been identified.[392,393] Mutation of the five residues involved in these hydrophobic networks in OM cyt b_5 yields a protein with the structural elements of Mc cyt b_5.[393] Molecular dynamics simulations predict two conformers of Mc cyt b_5 in solution, a cleft-open and a cleft-closed form; and only one, the cleft-closed form, for OM cyt b_5.[392,394] It is proposed that OM cyt b_5 is held in the cleft-closed conformation by one of its hydrophobic networks.

8.2.4.3 Axial Heme Ligand Mutants of Cytochrome b_5

The axial His residues in cyt b_5 are His39 at the end of helix $\alpha 2$ and His63 in a loop region connecting helices $\alpha 4$ and $\alpha 5$. The cyt b_5 (His63Ala) variant binds heme with a drastically diminished affinity relative to wild-type protein. However, the mutant protein achieves the holoprotein structure, suggesting that the Fe—His63 bond is not essential for complete protein folding.[395] Mutants cyt b_5 (His63Leu) and (His39Leu) were used to study heme incorporation into apocyt b_5. The formation constants of the heme with cyt b_5 (His63Leu) and (His39Leu) were $2.5 \times 10^3 \, \text{mM}^{-1}$ and $7.3 \times 10^4 \, \text{mM}^{-1}$, respectively, indicating that the His63/heme interaction generates the most stable structure. Further kinetic studies indicate that the dominant pathway for heme incorporation into apo-cyt b_5 involves initial coordination of His63.[396]

Some axial-ligand mutants of OM cyt b_5 activate oxygen and are capable of coupled oxidation of the heme in the presence of a reducing agent and O_2,[299,397] similar to heme oxygenase chemistry. This reaction yields intermediates like hydroxyheme and verdoheme, and finally

biliverdin. Coupled oxidation of heme by OM cyt b_5 (His63Met) and (His63Val) variants stop at verdoheme. In these mutants, the ferric hemes are six-coordinate complexes with His39 and water as axial ligands. Upon reduction, a 6cLS species having His39 and Met63 ligands is formed for cyt b_5 (His63Met),[299] while ferrocyt b_5 (His63Val) contains a 5cHS.[397] In contrast, the OM cyt b_5 (His39Val) mutant catalyzes the coupled oxidation of heme to biliverdin. During this coupled oxidation, a metastable ferrocyt b_5 (His39Val) oxy complex is observed.[397] Mechanistic aspects of the coupled oxidation of heme catalyzed by these OM cyt b_5 mutants may be relevant to heme oxygenation performed by heme oxygenase.

8.2.5 CYTOCHROME bc_1 COMPLEX

Many cytochromes in energy-transducing organelles are membrane-bound proteins. Present in mitochondria and in purple photosynthetic bacteria, the cyt bc_1 complex (also called ubiquinol-cytochrome c oxidoreductase, or complex III) catalyzes the electron transfer from ubiquinol to ferricyt c and pumps protons from the matrix to the cytosol.[46,398,399] The catalytic core of the cyt bc_1 complex comprises three redox-active subunits: they are a cyt b with two b-type hemes (b_H and b_L), a cyt c_1, and a Reiske iron sulfur protein. While this catalytic core has enzymatic activity in some α proteobacteria like *Paracoccus*, *Rhodospirillum rubrum*, and *Rb. capsulatus*, mitochondrial cyt bc_1 complexes have an additional seven or eight subunits.[45]

The structures of the cyt bc_1 complexes from chicken,[400] cow,[400–402] rabbit,[400] and yeast[403] have been reported. Its cyt b has eight transmembrane helices (A–H) connected by loops. Hemes b_H and b_L are bound in a four-helix bundle formed by helices A–D; they come within 8.2 Å of one another. Their axial His ligands are on helices B and D, His83-heme b_L-His182, and His97-heme b_H-His196. Cyt c_1 has a C-terminal transmembrane helix that anchors the large cytoplasmic domain to the membrane. Examination of the protein fold of the cytoplasmic domain of cyt c_1 reveals that it is indeed a class I cyt c.[400] The pyrrole II corner of the heme in cyt c_1 is exposed like that in the mitochondrial cyts c. It is at this protein surface that electron transfer to cyt c is thought to occur. Crystal-structure data suggest that there is a conformation in which the Fe_2S_2 cluster of the Reiske protein is close enough to cyt c_1 heme propionate-6 (4.0 Å) and the heme edge (8.2 Å) to efficiently transfer electrons. Based on this distance, an electron-transfer rate of between 4.8 and $80 \times 10^6 \, s^{-1}$ has been calculated. A model for electron transfer from the Reiske protein into cyt c_1 via propionate-6 and out of cyt c_1 through the pyrrole II of its heme to cyt c has been proposed.[400]

The crystal structure for the complex between the *S. cerevisae* cyt bc_1 complex and cyt c indicates that cyt c binds to the cyt c_1 subunit at a compact contact site through nonpolar forces.[404] The edge-to-edge distance between the two hemes is 9.4 Å. This short distance facilitates direct heme-to-heme electron transfer. An electron-transfer rate constant between $8.3 \times 10^6 \, s^{-1}$ and $9.7 \times 10^5 \, s^{-1}$ was calculated using an electron-tunneling model for redox proteins.[404,405] Although a structural pathway involving 16 covalent bonds and one van der Waals interaction can be drawn from the heme pyrrole II of cyt c_1 through the Met80 of cyt c to its heme, the direct heme-to-heme electron transfer rate is significantly faster than protein-mediated electron-transfer rates known for cyt c.

8.2.6 CYTOCHROME b_6f COMPLEX

During oxygenic photosynthesis, the cyt b_6f complex couples electron transfer with proton translocation across the thylakoid membrane of the chloroplast to generate the electrochemical potential which drives ATP synthesis.[54] It couples electron transfer from photosystem II (via plastoquinol) to photosystem I (via plastocyanin or cyt c_6).[406] The cyt b_6f complex or plastoquinol–plastocyanin oxidoreductase consists of seven subunits: a cyt b_6, a cyt f, a Reiske iron sulfur protein, subunit IV, and three low-molecular-weight ($\leq 4\,kDa$) transmembrane subunits.[54] Cyt b_6 contains a high potential heme ($-45\,mV$) on the lumenal side of the thylakoid membrane and a low potential heme ($-150\,mV$) on the stromal side. Both hemes are bis-His coordinated. EPR and Mössbauer spectra reveal that the axial histidine planes are perpendicular, a characteristic of type I 6cLS ferriheme complexes.[41] While cyt b_6 and subunit IV share a common ancestor with the larger cyt b of the cyt bc_1 complex,[407] cyt f and cyt c_1 are not related.[7,400]
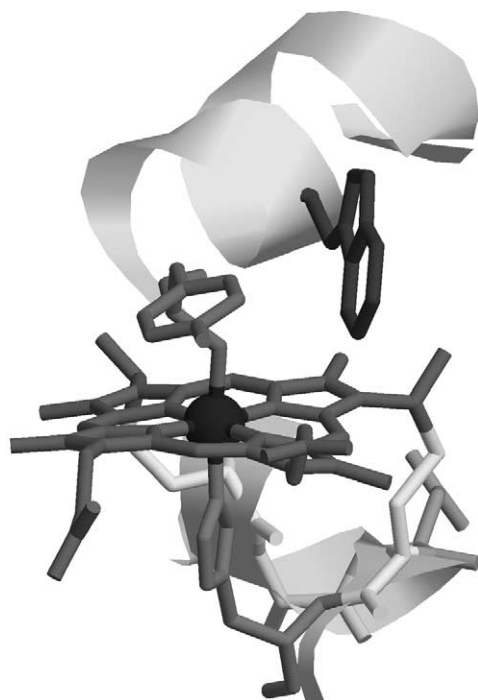
Figure 11   Heme of cyt *f* (PDB code 1CI3) showing coordination of the N terminus to the ferric heme iron. The edge-to-face interaction between Trp4 and the porphyrin macrocycle are also shown. This interaction is thought to modulate redox potential by interaction with porphyrin π MOs.[7,280]

On the His-ligated side of the heme in cyt *f*, there is a highly conserved, L-shaped chain of five water molecules.[54,125,408] These five water molecules form hydrogen bonds with ten amino-acid residues, seven of which are also highly conserved. One of the internal waters forms a hydrogen bond with the heme. Mutation of these conserved residues alters the *in vivo* function of cyt *f*.[409] Coupling of electron- and proton transfer via this "proton wire" has been proposed as the function of the water chain.[408,409]

The hydrophobic heme environment of cyt *f* in plants (and algae) is generated by Tyr1, Pro2, Ile3, and Phe4(Tyr4) shielding the heme from solvent. In cyanobacteria, residue 4 is typically a tryptophan.[280] The planes of the heme and the aromatic side chain of residue 4 are almost orthogonal (81–86°), and the side chain of residue 4 is in contact with the heme (Figure 11).[7] This type of edge-to-face interaction has also been observed in cyt b_5 (Phe58, Phe35),[381,382] cyt b_{562} (Phe61),[327] and peptide-sandwich mesohemes (hemoprotein models, Trp or Phe).[410,411] In the peptide-sandwich mesohemes, the Trp heme interaction stabilizes α-helical structure and the oxidized state.[412] Comparison of the reduction potentials for cyanobacterium *Phlormidium (P.) laminosum* cyt *f* (Trp4), its (Trp4Phe) mutant, green alga *C. reinhardtii* cyt *f* (Phe4) and its (Phe4Trp) variant, reveals that the Trp heme interaction in cyt *f* also stabilizes the oxidized form (Table 2).[280]

8.2.7   FACTORS REGULATING REDOX POTENTIAL IN CYTOCHROMES

Iron protoporphyrin IX (FePPIX) in neutral aqueous solution has a midpoint potential of −115 mV vs. SHE.[5] The corresponding bis-imidazole complex at pH 8.5 has a midpoint potential of −235 mV.[413] Once FePPIX is placed into a protein environment, the reduction potentials range from −475 mV (bacterioferritin) to +420 mV (THRC cyt *c*) vs. SHE (Table 1). The factors responsible for controlling hemoprotein redox potentials have been investigated extensively.[295,414–418] The level of understanding of the interplay between these factors is still such that it is not possible to predict the redox potential of a given cytochrome structure, or how evolutionary pressures (mutagenesis) tap the range of potentials available to a structural motif.

The most important factors contributing to the Gibbs free energy change for the reduction of ferrihemoproteins, ΔG_{redox} are shown in Equation (1):[5,295]

$$\Delta G_{redox} = \Delta G_{cen} + \Delta G_{el} + \Delta G_{lig} + \Delta G_{conf} \qquad (1)$$

Equation (1) includes bonding interactions at the redox center (ΔG_{cen}), electrostatic interactions between the redox center and polar groups within the protein and the solvent (ΔG_{el}), differences in ligand affinity (ΔG_{lig}), and redox-dependent conformational energy differences (ΔG_{conf}). In the following discussion, selected examples illustrating how factors involving the heme and its immediate environment contribute to ΔG_{redox} are given.

Chelation of iron by the porphyrin, substituents at the periphery of the porphyrin ring, axial heme ligands, and geometry of the coordination sphere contribute to ΔG_{cen}.[5] Reconstitution of cyt b_5 with a variety of modified hemins has been used to evaluate the effect of the vinyl and propionate groups on its reduction potential.[294,419] Destabilization of the oxidized form by the electron-withdrawing ability of the vinyl groups increases the reduction potential.[420] The positive charge on the ferric heme in cyt b_5 is stabilized by the heme propionates. This stabilization is lost in protoheme IX dimethylester cyt b_5, and its reduction potential increases by 66–67 mV relative to that of cyt b_5.[294,298] A 300 mV range in reduction potential can be accessed in synthetic cytochromes known as heme protein maquettes by changing the electron-donating or -withdrawing character of the peripheral substituents on the prophyrin ring.[1,413]

Change in the axial ligation of horse cyt c in its (Met80His), (Met80Leu), and (Met80Cys) mutants results in a significant drop in reduction potential ($5.1 < \Delta\Delta G_{redox} < 15.0\,kcal\,mol^{-1}$).[268] Interestingly, change in the axial ligation at the His18 position in *iso*-2-cyt c (His18Arg) does not affect its reduction potential.[421] Natural variations in the sixth heme ligand also cause positive shifts in ΔG_{redox}. For five-coordinate class II cyts c with redox potentials in the range of -10 mV to 150 mV, ΔG_{redox} is shifted positively by 2.5 to 6.2 kcal mol^{-1} relative to class I cyts c.[277] Larger shifts in ΔG_{redox} ($8.3 < \Delta\Delta G_{redox} < 15.2\,kcal\,mol^{-1}$) are observed in class III cyts c with bis-His ligation. In cyt c_3 (class III)[302,303] and cyt b_5[298,299] mutants where axial His/Met and bis-Met coordination has been engineered, respectively, large increases in the reduction potential are observed (Table 1). Based on axial ligation only, reduction potentials are expected to increase in the following order: bis-His < His/Met < bis-Met.

Contributions to ΔG_{el} include the effects of ions in solution,[5,422–424] the dipolar interactions within the protein and with the solvent, interaction of buried charges with the redox center, and interaction of solvent-exposed charges with the redox center.[5] In the early 1970s, Kassner proposed that increases in heme-environment polarity result in increased stability of the more highly charged oxidized state and, therefore, a decrease in reduction potential.[425] The effect of mixed solvents on the redox potential of cyt c supports this hypothesis.[426] Analysis of two series of *iso*-1-cyt c heme-pocket mutants, in which either Arg38 or Phe82 has been replaced with residues of varying side-chain hydrophobicities, indicates that the characteristics of the Phe82 mutants are consistent with this hypothesis, while those of the Arg38 mutants are not.[295]

Correlation of reduction potential with area of solvent-exposed heme for a number of structurally characterized cytochromes indicates that reduction potential increases as heme exposure decreases.[427] A recent analysis including various cytochromes suggests that potentials can be modulated over a 500 mV range by variation in heme solvent exposure.[428] To test this within a given cytochrome system, the heme solvent accessibility of the highly exposed heme in *D. vulgaris* cyt c_{553} was attenuated by homodimer formation in cyt c_{553} mutants (Met23Cys) and (Glu51Cys). The mutant redox potentials increased by 68–85 mV (Table 1).[293]

The dielectric constant of the OM cyt b_5-exposed heme-edge microenvironment modulates its reduction potential. Exclusion of water from the solvent-exposed heme and neutralization of charge on heme propionates by complexation of OM cyt b_5 with a modified electrode surface result in a positive shift in its reduction potential.[298] Electrochemical studies of cyt b_5 (Val45Ile/Val61Ile), wherein Ile side chains block solvent access to the heme pocket and to a significant portion of the heme edge, indicate that dehydration of the heme edge has at least as much influence on the reduction potential as the neutralizing charges of the propionates.[429] Conversely, increased dielectric constant (increased solvent exposure) of the heme microenvironment results in a negative shift in heme reduction potential, as illustrated by the cyt b_5 (Val45Leu/Val61Leu) variant. The isopropyl groups of Val45 and Val61 restrict access of solvent molecules to the heme pocket. Replacement of these valines by leucines results in channels that increase the accessibility of water to the heme pocket, and a shift of -46 mV in the reduction potential relative to wild-type cyt b_5 results (Table 1).[298]

In tryptic bovine hepatic cyt b_5, the effect of mutation at Val61, located at the rim of the heme pocket, has been explained in terms of charge density at the exposed heme edge. Introduction of negatively charged (Tyr or Glu) at this position increases the electrostatic potential at the exposed heme edge, decreasing the reduction potential at the heme iron (Table 1).[297] Replacement of Val61 with positively charged residues reduces the electrostatic potential at the heme edge, and the reduction potential increases by 21–27 mV.[297] The crystal structure of cyt b_5 (Val61His) shows the His61 side chain pointing away from the heme pocket out into the solvent, but its configuration is such that it may also function as a gate to block access to the heme pocket.[297,430]

Redox-dependent conformational energy differences (ΔG_{conf}) contribute to the ΔG_{redox} in tetraheme cyt c_3. Comparison of the structures of oxidized and reduced forms indicates that there are small, localized, redox-coupled conformational changes[120,350,351] that result in the network of cooperativities. For *D. desulfuricans* ATCC27774 cyt c_3, the coupling energies of several pairs of hemes and deprotonation sites have noncoulombic contributions. This has been interpreted as "mechanochemical coupling" which arises from the local redox-coupled conformational changes, and is postulated to be important in controlling the thermodynamic properties of the proteins involved in energy-transducing processes.[348]

Protein–protein complex formation between cytochromes and other proteins can affect their redox potential by contributing to ΔG_{lig}.[5] As discussed in Section 8.2.3.6.1, the B2 conformation of cyt c that is observed upon binding to cytochrome c oxidase shows a significant drop in reduction potential.[225] Another example is the THRC cyt c–reaction-center complex. Reaction-center-bound *Rv. gelatinosus* THRC cyt c heme reduction potentials of +320 mV, +300 mV, +130 mV, and +70 mV vs SHE drop significantly when the THRC cyt c is not bound to the reaction center (+118 mV, +118 mV, +28 mV, +8 mV).[123]

8.2.8 CONCLUDING REMARKS

The hemes constitute a versatile set of redox centers. The broad spectrum of variability in combinations of environmental factors such as solvent exposure, electrostatic fields, axial-ligand identity and conformation, deformations of the heme, and proximity to other redox centers, gives rise to a large dynamic range in redox potential. The difficulty in predicting redox potential of the cytochromes and elucidating the mechanistic details of their functions stems largely from this extensive dynamic range. Future progress in our ability to predict cytochrome potentials and to design redox centers will depend upon the continued growth in our understanding of the interdependencies among the aforementioned factors.

8.2.9 REFERENCES

1. Gibney, B. R.; Dutton, P. L. In *Advances in Inorganic Chemistry*; Sykes, A. G., Mauk, G., Eds.; Academic Press: New York, 2000; Vol. 51; pp 409–455.
2. Keilin, D.; Keilin, J. *The History of Cell Respiration and Cytochromes* **1966**, Cambridge University Press: London.
3. Cramer, W. A.; Knaff, D. B. *Energy Transduction in Biological Membranes* **1990**, Springer-Verlag: New York.
4. Cutruzzola, F. *Biochim. Biophys. Acta* **1999**, *1411*, 231–249.
5. Moore, G. R.; Pettigrew, G. W. *Cytochromes c: Evolutionary, Structural and Physicochemical Aspects* **1990**, Springer-Verlag: Berlin.
6. Iverson, T. M.; Arciero, D. M.; Hsu, B. T.; Logan, M. S. P.; Hooper, A. B.; Rees, D. C. *Nature Struct. Biol.* **1998**, *5*, 1005–1012.
7. Martinez, S. E.; Huang, D.; Szczepaniak, A.; Cramer, W. A.; Smith, J. L. *Structure* **1994**, *2*, 95–105.
8. Le Brun, N. E.; Thomson, A. J.; Moore, G. R. *Structure and Bonding* **1997**, *88*, 103–138.
9. Frolow, F.; Kalb, A. J.; Yariv, J. *Nature, Struct. Biol.* **1994**, *1*, 453–460.
10. Geroge, G. N.; Richards, T.; Bare, R. E.; Gea, Y.; Prince, R. C.; Stiefel, E. I.; Watt, G. D. *J. Am. Chem. Soc.* **1993**, *115*, 7716–7718.
11. Scheidt, W. R. In *The Porphyrin Handbook*; Kadish, K. M., Smith, K. M., Guilard, R., Eds.; Academic Press: New York, 2000; Vol. 3, pp 49–112.
12. Barkigia, K. M.; Chantranupong, L.; Smith, K. M.; Fajer, J. *J. Am. Chem. Soc.* **1988**, *110*, 7566–7567.
13. Gudowska-Nowak, E.; Newton, M. D.; Fajer, J. *J. Phys. Chem.* **1990**, *94*, 5795–5801.
14. Fajer, J. J. *Porphyrins and Phthalocyanines* **2000**, *4*, 382–385.
15. Shelnutt, J. A. In *The Porphyrin Handbook*; Kadish, K. M., Smith, K. M., Guilard, R., Eds.; Academic Press: New York, 2000; Vol. 7, pp 167–223.
16. Wertsching, A. K.; Koch, A. S.; DiMagno, S. G. *J. Am. Chem. Soc.* **2001**, *123*, 3932–3939.
17. Parusel, A. B. J.; Wondimagegn, T.; Ghosh, A. *J. Am. Chem. Soc.* **2000**, *122*, 6371–6374.
18. DiMagno, S. G.; Wertsching, A. K.; Ross, C. R. II *J. Am. Chem. Soc.* **1995**, *117*, 8279–8280.

19. Jentzen, W.; Simpson, M. C.; Hobbs, J. D.; Song, X.-Z.; Ema, T.; Nelson, N. Y.; Medforth, C. J.; Smith, K. M.; Veyrat, M.; Mazzanti, M.; Ramasseul, R.; Marchon, J.-C.; Takeuchi, T.; Goddard, W. A. III.; Shelnutt, J. A. *J. Am. Chem. Soc.* **1995**, *117*, 11085–11097.
20. Jentzen, W.; Song, X.-Z.; Shelnutt, J. A. *J. Phys. Chem. B* **1997**, *101*, 1684–1699.
21. Jentzen, W.; Ma, J. G.; Shelnutt, J. A. *Biophys. J.* **1998**, *74*, 753–763.
22. Shelnut, J. A.; Song, X. Z.; Ma, J. G.; Jia, S. L.; Jentzen, W.; Medforth, C. J. *Chem. Soc. Rev.* **1998**, *27*, 31–41.
23. Anderson, K. K.; Hobbs, J. D.; Luo, L.; Stanley, K. D.; Quirke, J. M. E.; Shelnutt, J. A. *J. Am. Chem. Soc.* **1993**, *115*, 12346–12352.
24. Safo, M. K.; Walker, F. A.; Raitsimring, A. M.; Walters, W. P.; Dolata, D. P.; Debrunner, P. G.; Scheidt, W. R. *J. Am. Chem. Soc.* **1994**, *116*, 7760–7770.
25. Walker, F. A.; Huynh, B. H.; Scheidt, W. R.; Osvath, S. R. *J. Am. Chem. Soc.* **1986**, *108*, 5288–5297.
26. Howes, B. D.; Scheidt, C. B.; Welinder, K. G.; Marjocchi, M. P.; Ma, J. G.; Zhang, J.; Shelnutt, J. A.; Smulivich, G. *Biophys. J.* **1999**, *77*, 478–492.
27. Walker, F. A. *Coord. Chem. Rev.* **1999**, *185–186*, 471–534.
28. Cheesman, M. R.; Walker, F. A. *J. Am. Chem. Soc.* **1996**, *118*, 7373–7380.
29. Safo, M. K.; Nesset, M. J. M.; Walker, F. A.; Debrunner, P. G.; Scheidt, W. R. *J. Am. Chem. Soc.* **1997**, *119*, 9438–9448.
30. Ghosh, A.; Gonzalez, E.; Vangberg, T. *J. Phys. Chem. B* **1999**, *103*, 1363–1367.
31. Simonneaux, G.; Schünemann, V.; Morice, C.; Carel, L.; Toupet, L.; Winkler, H.; Trautwein, A. X.; Walker, F. A. *J. Am. Chem. Soc.* **2000**, *122*, 4366–4377.
32. Astashkin, A. V.; Raitsimring, A. M.; Kennedy, A. R.; Shokhireva, T. K.; Walker, F. A. *J. Phys. Chem. A* **2002**, *106*, 74–82.
33. Collins, D. M.; Countryman, R.; Hoard, J. L. *J. Am. Chem. Soc.* **1972**, *94*, 2066–2072.
34. Munro, O. Q.; Serth-Guzzo, J. A.; Turowska-Tyrk, I.; Mohanrao, K.; Shokhireva, T. K.; Walker, F. A.; Debrunner, P. G.; Scheidt, W. R. *J. Am. Chem. Soc.* **1999**, *121*, 11144–11155.
35. Walker, F. A.; Nasri, H.; Turowska-Tyrk, I.; Mohanrao, K.; Watson, C. T.; Shokhirev, N. V.; Debrunner, P. G.; Scheidt, W. R. *J. Am. Chem. Soc.* **1996**, *118*, 12109–12118.
36. Ogura, H.; Yatsunyk, L.; Medforth, C. J.; Smith, K. M.; Barkigia, K. M.; Renner, M. W.; Melamed, D.; Walker, F. A. *J. Am. Chem. Soc.* **2001**, *123*, 6564–6578.
37. Safo, M. K.; Gupta, G. P.; Walker, F. A.; Scheidt, W. R. *J. Am. Chem. Soc.* **1991**, *113*, 5497–5510.
38. Safo, M. K.; Gupta, G. P.; Watson, C. T.; Simonis, U.; Walker, F. A.; Scheidt, W. R. *J. Am. Chem. Soc.* **1992**, *114*, 7066–7075.
39. Munro, O. Q.; Marques, H. M.; Debrunner, P. G.; Mohonrao, K.; Scheidt, W. R. *J. Am. Chem. Soc.* **1995**, *117*, 935–954.
40. Einsle, O.; Foerster, S.; Mann, K.; Fritz, G.; Messerschmidt, A.; Kroneck, P. M. H. *Eur. J. Biochem.* **2001**, *268*, 3028–3035.
41. Schünemann, V.; Trautwein, A. X.; Illerhaus, J.; Haehnel, W. *Biochemistry* **1999**, *38*, 8981–8991.
42. Soltis, S. M.; Strouse, C. E. *J. Am. Chem. Soc.* **1988**, *110*, 2824–2829.
43. Grodzicki, M.; Flint, H.; Winkler, H.; Walker, F. A.; Trautwein, A. X. *J. Phys. Chem. A* **1997**, *101*, 4202–4207.
44. Nesset, M. J. M.; Shokhirev, N. V.; Enemark, P. D.; Jacobson, S. E.; Walker, F. A. *Inorg. Chem.* **1996**, *35*, 5188–5200.
45. Berry, E. A.; Guergova-Kuras, M.; Huang, L.; Crofts, A. R. *Ann. Rev. Biochem.* **2000**, *69*, 1005–1075.
46. Schultz, B. E.; Chan, S. I. *Ann. Rev. Biophys. Biomol. Struct.* **2001**, *30*, 23–65.
47. Lui, X.; Kim, C. N.; Yang, J.; Jemmerson, R.; Wang, X. *Cell* **1996**, *86*, 147–157.
48. Yang, J.; Liu, X.; Bhalla, K.; Kim, C. N.; Ibrado, A. M.; Cai, J.; Peng, I.-I.; Jones, D. P.; Wang, X. *Science* **1997**, *275*, 1129–1132.
49. Kluck, R. M.; Bossy-Wetzel, E.; Green, D. R.; Newmeyer, D. D. *Science* **1997**, *275*, 1132–1136.
50. Yang, C.-H.; Azad, H. R.; Cooksey, D. A. *Proc. Natl. Acad. Sci. USA* **1996**, *93*, 7315–7320.
51. Yeoman, K. H.; Delgado, M. J.; Wexler, M.; Downie, J. A.; Johnston, A. W. B. *Microbiology* **1997**, *143*, 127–134.
52. Biel, S. W.; Biel, A. J. *J. Bacteriol.* **1990**, *172*, 1321–1326.
53. Zumft, W. G. *Microbiol. Mol. Biol. Rev.* **1997**, *61*, 533–616.
54. Cramer, W. A.; Soriano, G. M.; Pononmarev, M.; Huang, D.; Zhang, H.; Martinez, S. E.; Smith, J. L. *Ann. Rev. Plant Physiol.* **1996**, *47*, 477–508.
55. Mauk, A. G. *Structure and Bonding* **1991**, *75*, 132–157.
56. Scott, R. A.; Mauk, A. G. *Cytochrome c: A Multidisciplinary Approach* **1996**, University Science Books: Sausalito, CA.
57. Mauk, A. G.; Moore, G. R. *J. Biol. Inorg. Chem.* **1997**, *2*, 119–125.
58. Therien, M. J.; Chang, J.; Raphael, A. L.; Bowler, B. E.; Gray, H. B. *Structure and Bonding* **1991**, *75*, 109–129.
59. Winkler, J. R.; Gray, H. B. *Chem. Rev.* **1992**, *92*, 369–379.
60. Bjerrum, M. J.; Casimiro, D. R.; Chang, I.; Di Bilio, A. J.; Gray, H. B.; Hill, M. G.; Langen, R.; Mines, G. A.; Skov, L. K.; Winkler, J. R.; Wuttke, D. S. *J. Bioenerg. Biomemb.* **1995**, *27*, 295–302.
61. Brzezinski, P.; Wilson, M. T. *Proc. Natl. Acad. Sci. USA* **1997**, *94*, 6176–6179.
62. Döpner, S.; Hildebrandt, P.; Rosell, F. I.; Mauk, A. G.; von Walter, M.; Buse, G.; Soulimane, T. *Eur. J. Biochem.* **1999**, *261*, 379–391.
63. Weber, C.; Michel, B.; Bosshard, H. R. *Proc. Natl. Acad. Sci. USA* **1987**, *84*, 6687–6691.
64. Hildebrandt, P.; Heimburg, T.; Marsh, D.; Powell, G. L. *Biochemistry* **1990**, *29*, 1661–1668.
65. Hildebrandt, P.; Vanhecke, F.; Buse, G.; Soulimane, T.; Mauk, A. G. *Biochemistry* **1993**, *32*, 10912–10922.
66. Crnogorac, M. M.; Ullmann, G. M.; Kosti, N. M. *J. Am. Chem. Soc.* **2001**, *123*, 10789–10798.
67. Pletneva, E. V.; Fulton, D. B.; Kohzuma, T.; Kosti, N. M. *J. Am. Chem. Soc.* **2000**, *122*, 1034–1046.
68. Ullmann, G. M.; Kosti, N. M. *J. Am. Chem. Soc.* **1995**, *117*, 4766–4774.
69. Zhou, J. S.; Kosti, N. M. *J. Am. Chem. Soc.* **1992**, *114*, 3562–3563.
70. Durham, B.; Fairris, J. L.; McLean, M.; Millett, F.; Scott, J. R.; Sligar, S. G.; Willie, A. *J. Bioenerg. Biomemb.* **1995**, *27*, 331–340.
71. Mauk, A. G.; Mauk, M. R.; Moore, G. R.; Northrup, S. H. *J. Bioenerg. Biomemb.* **1995**, *27*, 311–330.

72. Rodriguez-Maranon, M. J.; Qui, F.; Stark, R. E.; White, S. P.; Zhang, X.; Foundling, S. I.; Rodriguez, V.; Schilling, C. L. III.; Bunce, R. A.; Rivera, M. *Biochemistry* **1996**, *35*, 16378–16390.
73. Liang, N.; Mauk, A. G.; Pielak, G. J.; Johnson, J. A.; Smith, M.; Hoffman, B. M. *Science* **1988**, *240*, 311–313.
74. Hoffman, B. M.; Natan, M. J.; Nocek, J. M.; Wallin, S. A. *Structure and Bonding* **1991**, *75*, 85–108.
75. McLendon, G. *Structure and Bonding* **1991**, *75*, 159–174.
76. Nocek, J. M.; Zhou, J. S.; De Forest, S.; Priyadarshy, S.; Beratan, D. N.; Onuchic, J. N.; Hoffman, B. M. *Chem. Rev.* **1996**, *96*, 2459–2489.
77. Bai, Y.; Sosnick, T. R.; Mayne, L.; Englander, S. W. *Science* **1995**, *269*, 192–197.
78. Nall, B. T. In *Cytochrome c: A Multidisciplinary Approach*; Scott, R. A., Mauk, A. G., Eds.; University Science Books: Sausalito, CA, 1996; pp 167–200.
79. Yeh, S. R.; Han, S.; Rousseau, D. L. *Acc. Chem. Res.* **1998**, *31*, 727–736.
80. Englander, S. W.; Sosnick, T. R.; Mayne, L. C.; Shtilerman, M.; Qi, P. X.; Bai, Y. *Acc. Chem. Res.* **1998**, *31*, 737–744.
81. Shastry, M. C. R.; Sauder, J. M.; Roder, H. *Acc. Chem. Res.* **1998**, *31*, 717–725.
82. Telford, J. R.; Wittung-Stafshede, P.; Gray, H. B.; Winkler, J. R. *Acc. Chem. Res.* **1998**, *31*, 755–763.
83. Eaton, W. A.; Muoz, V.; Thompson, P. A.; Henry, E. R.; Hofrichter, J. *Acc. Chem. Res.* **1998**, *31*, 745–753.
84. Akiyama, S.; Takahashi, S.; Ishimori, K.; Morishima, I. *Nature Struct. Biol.* **2000**, *7*, 514–520.
85. Akiyama, S.; Takahashi, S.; Kimura, T.; Ishimori, K.; Morishima, I.; Nishikawa, Y.; Fujisawa, T. *Proc. Natl. Acad. Sci. USA* **2002**, *99*, 1329–1334.
86. Lyubovitsky, J. G.; Gray, H. B.; Winkler, J. R. *J. Am. Chem. Soc.* **2002**, *124*, 5481–5485.
87. Hagen, S. J.; Hofrichter, J.; Szabo, A.; Eaton, W. A. *Proc. Natl. Acad. Sci. USA* **1996**, *93*, 11615–11617.
88. Fetrow, J. S.; Baxter, S. M. *Biochemistry* **1999**, *38*, 4480–4492.
89. Baxter, S. M.; Fetrow, J. S. *Biochemistry* **1999**, *38*, 4493–4503.
90. Banci, L.; Presenti, C. *J. Biol. Inorg. Chem.* **2000**, *5*, 422–431.
91. Ambler, R. P. *Biochim. Biophys. Acta* **1991**, *1058*, 42–47.
92. Meyer, T. E. In *Cytochrome c: A Multidisciplinary Approach*; Scott, R. A., Mauk, A. G., Eds.; University Science Books: Sausalito, CA, 1996; pp 33–99.
93. Klarskov, K.; Van Driessche, G.; Backers, K.; Dumortier, C.; Meyer, T. E.; Tollin, G.; Cusanovich, M. A.; Van Beeumen, J. J. *Biochemistry* **1998**, *37*, 5995–6002.
94. Frazao, C.; Enguita, F. J.; Coelho, R.; Sheldrick, G. M.; Navarro, J. A.; Hervas, M.; De la Rosa, M. A.; Carrondo, M. A. *J. Biol. Inorg. Chem.* **2001**, *6*, 324–332.
95. Archer, M.; Banci, L.; Dikaya, E.; Romao, M. J. *J. Biol. Inorg. Chem.* **1997**, *2*, 611–622.
96. Tahirov, T. H.; Misaki, S.; Meyer, T. E.; Cusanovich, M. A.; Higuchi, Y.; Yasuoka, N. *J. Mol. Biol.* **1996**, *259*, 467–479.
97. Shibata, N.; Iba, S.; Misaki, S.; Meyer, T. E.; Bartsch, R. G.; Cusanovich, M. A.; Morimoto, Y.; Higuchi, Y.; Yasuoka, N. *J. Mol. Biol.* **1998**, *284*, 751–760.
98. La Mar, G. N.; Jackson, J. T.; Dugad, L. B.; Cusanovich, M. A.; Bartsch, R. G. *J. Biol. Chem.* **1990**, *265*, 16173–16180.
99. Fujii, S.; Yoshimura, T.; Kamada, H.; Yamaguchi, K.; Suzuki, S.; Shidara, S.; Takakuwa, S. *Biochim. Biophys. Acta* **1995**, *1251*, 161–169.
100. Zahn, J. A.; Arciero, D. M.; Hooper, A. B.; Dispirito, A. A. *Eur. J. Biochem.* **1996**, *240*, 684–691.
101. Tsan, P.; Caffrey, M.; Daku, M. L.; Cusanovich, M.; Marion, D.; Gans, P. *J. Am. Chem. Soc.* **2001**, *123*, 2231–2242.
102. Yoshimura, T.; Suzuki, S.; Nakahara, A.; Iwasaki, H.; Masuko, M.; Matsubara, T. *Biochim. Biophys. Acta* **1985**, *831*, 267–274.
103. Korszun, Z. R.; Bunker, G.; Khalid, S.; Scheidt, W. R.; Cusanovich, M. A.; Meyer, T. E. *Biochemistry* **1989**, *28*, 1513–1517.
104. Monkara, F.; Bingham, S. J.; Kadir, F. H. A.; McEwam, A. G.; Thomson, A. J.; Thurgood, A. G. P.; Moore, G. R. *Biochim. Biophys, Acta* **1992**, *1100*, 184–188.
105. Ambler, R. P.; Bartsch, R. G.; Daniel, M.; Kamen, M. D.; McLellan, L.; Meyer, T. E.; Van Beeumen, J. J. *Proc. Natl. Acad. Sci. USA* **1981**, *78*, 6854–6857.
106. Ambler, R. P.; Meyer, T. E.; Bartsch, R. G.; Cusanovich, M. A. *Arch. Biochem. Biophys.* **2001**, *388*, 25–33.
107. Bartsch, R. G.; Ambler, R. P.; Meyer, T. E.; Cusanovich, M. A. *Arch. Biochem. Biophys.* **1989**, *271*, 433–440.
108. Banci, L.; Bertini, I.; Bruschi, M.; Sompornpisut, P.; Turano, P. *Proc. Natl. Acad. Sci. USA* **1996**, *93*, 14396–14400.
109. Pereira, I. A. C.; Pacheco, I.; Liu, M.-Y.; LeGall, J.; Xavier, A. V.; Tereira, M. *Eur. J. Biochem.* **1997**, *248*, 323–328.
110. Assfalg, M.; Banci, L.; Bertini, I.; Bruschi, M.; Giudici-Orticoni, M. T.; Turano, P. *Eur. J. Biochem.* **1999**, *266*, 634–643.
111. Matias, P. M.; Coelho, R.; Pereira, I. A. C.; Coelho, A. V.; Thompson, A. W.; Sieker, L. C.; Le Gall, J.; Carrondo, M. A. *Structure* **1999**, *7*, 119–130.
112. Umhau, S.; Fritz, G.; Diederichs, K.; Breed, J.; Welte, W. Kroneck P. M. H. *Biochemistry* **2001**, *40*, 1308–1316.
113. Louro, R. O.; Catarino, T.; LeGall, J.; Xavier, A. V. *J. Biol. Inorg. Chem.* **1997**, *2*, 488–491.
114. Higuchi, Y.; Kusunoki, M.; Matsuura, Y.; Yasuoka, N.; Kakudo, M. *J. Mol. Biol.* **1984**, *172*, 109–139.
115. Matias, P. M.; Frazão, C.; Morais, J.; Coll, M.; Carrondo, M. A. *J. Mol. Biol.* **1993**, *234*, 680–699.
116. Czjzek, M.; Payan, F.; Guerlesquin, F.; Bruschi, M.; Haser, R. *J. Mol. Biol.* **1994**, *243*, 653–667.
117. Morais, J.; Palma, P. N.; Frazão, C.; Caldeira, J.; LeGall, J.; Moura, I.; Moura, J. J. G.; Carrondo, M. A. *Biochemistry* **1995**, *34*, 12830–12841.
118. Matias, P. M.; Morais, J.; Coelho, R.; Carrondo, M. A.; Wilson, K.; Dauter, Z.; Sieker, L. *Protein Sci.* **1996**, *5*, 1342–1354.
119. Simões, P.; Matias, P. M.; Morais, J.; Wilson, K.; Dauter, Z.; Carrondo, M. A. *Inorg. Chim. Acta* **1998**, *273*, 213–224.
120. Nørager, S.; Legrand, P.; Pieulle, L.; Hatchikan, C.; Roth, M. *J. Mol. Biol.* **1999**, *290*, 881–902.
121. Louro, R. O.; Bento, I.; Matias, P. M.; Catarino, T.; Baptista, A. M.; Soares, C. M.; Carrondo, M. A.; Turner, D. L.; Xavier, A. V. *J. Biol. Chem.* **2001**, *276*, 44044–44051.

122. Louro, R. O.; Correia, I. J.; Brennan, L.; Coutinho, I. B.; Xavier, A. V.; Turner, D. L. *J. Am. Chem. Soc.* **1998**, *120*, 13240–13247.
123. Agalidis, I.; Othman, S.; Boussac, A.; Reiss-Husson, F.; Desbois, A. *Eur. J. Biochem.* **1999**, *261*, 325–336.
124. Iverson, T. M.; Arciero, D. M.; Hooper, A. B.; Rees, D. C. *J. Biol. Inorg. Chem.* **2001**, *6*, 390–397.
125. Carrell, C. J.; Schlarb, B. G.; Bendall, D. S.; Howe, C. J.; Cramer, W. A.; Smith, J. L. *Biochemistry* **1999**, *38*, 9590–9599.
126. Banci, L.; Bertini, I.; Rosato, A.; Varani, G. *J. Biol. Inorg. Chem.* **1999**, *4*, 824–837.
127. Takano, T.; Dickerson, R. E. *Proc. Natl. Acad. Sci USA* **1980**, *77*, 6371–6375.
128. Takano, T.; Dickerson, R. E. *J. Mol. Biol.* **1981**, *153*, 95–155.
129. Takano, T.; Dickerson, R. E. *J. Mol. Biol.* **1981**, *153*, 79–94.
130. Bushnell, G. W.; Louie, G. V.; Brayer, G. D. *J. Mol. Biol.* **1990**, *214*, 585–595.
131. Ochi, H.; Hata, Y.; Tanaka, N.; Kakudo, M.; Sakuri, T.; Achara, S.; Morita, Y. *J. Mol. Biol.* **1983**, *166*, 407–418.
132. Louie, G. V.; Brayer, G. D. *J. Mol. Biol.* **1990**, *214*, 527–555.
133. Berghuis, A. M.; Brayer, G. D. *J. Mol. Biol.* **1992**, *223*, 959–976.
134. Murphy, M. E. P.; Nall, B. T.; Brayer, G. D. *J. Mol. Biol.* **1992**, *227*, 160–176.
135. Brayer, G. D.; Murphy, M. E. P. In *Cytochrome c: A Multidisciplinary Approach*; Scott, R. A., Mauk, A. G., Eds.; University Science Books: Sausalito, CA, 1996; pp 103–166.
136. Pielak, G. J.; Auld, D. S.; Betz, S. F.; Hilgen-Willis, S. E.; Garcia, L. L. In *Cytochrome c: A Multidisciplinary Approach*; Scott, R. A., Mauk, A. G., Eds.; University Science Books: Sausalito, CA, 1996; pp 203–284.
137. Hobbs, J. D.; Shelnutt, J. A. *J. Protein Chem.* **1995**, *14*, 19–25.
138. Ma, J. G.; Laberge, M.; Song, X. Z.; Jentzen, W.; Jia, S. L.; Zhang, J.; Vanderkooi, J. M.; Shelnutt, J. A. *Biochemistry* **1998**, *37*, 5118–5128.
139. Rosell, F. I.; Mauk, A. G. *Biochemistry* **2002**, *41*, 7811–7818.
140. Wand, A. J.; Di Stefano, D. L.; Feng, Y.; Roder, H.; Englander, S. W. *Biochemistry* **1989**, *28*, 186–194.
141. Feng, Y.; Roder, H.; Englander, S. W.; Wand, A. J.; Di Stefano, D. L. *Biochemistry* **1989**, *28*, 195–203.
142. Feng, Y.; Wand, A. J.; Roder, H.; Englander, S. W. *Biophys. J.* **1991**, *59*, 323–328.
143. Gao, Y.; Lee, A. D. J.; Williams, R. J. P.; Williams, G. *Eur. J Biochem.* **1989**, *182*, 57–65.
144. Gao, Y.; Boyd, J.; Williams, R. J. P.; Pielak, G. J. *Biochemistry* **1990**, *29*, 6994–7003.
145. Feng, Y.; Roder, H.; Englander, S. W. *Biochemistry* **1990**, *29*, 3505–3509.
146. Gao, Y.; Boyd, J.; Pielak, G. J.; Williams, R. P. J. *Biochemistry* **1991**, *30*, 1928–1934.
147. Santos, H.; Turner, D. L. *Eur. J. Biochem.* **1992**, *206*, 721–728.
148. Turner, D. L.; Williams, R. P. J. *Eur. J. Biochem.* **1993**, *211*, 555–562.
149. Qi, P. X.; Di Stefano, D. L.; Wand, A. J. *Biochemistry* **1994**, *33*, 6408–6417.
150. Qi, P. X.; Beckman, R. A.; Wand, A. J. *Biochemistry* **1996**, *35*, 12275–12286.
151. Banci, L.; Bertini, I.; Gray, H. B.; Luchinat, C.; Reddig, T.; Rosato, A.; Turano, P. *Biochemistry* **1997**, 36, 9867–9877.
152. Banci, L.; Bertini, I.; Huber, J. G.; Spyroulias, G. A.; Turano, P. *J. Biol. Inorg. Chem.* **1999**, *4*, 21–31.
153. Baistrocchi, P.; Banci, L.; Bertini, I.; Turano, P.; Bren, K. L.; Gray, H. B. *Biochemistry* **1996**, *35*, 13788–13796.
154. Banci, L.; Bertini, I.; Bren, K. L.; Gray, H. B.; Sompornpisut, P.; Turano, P. *Biochemistry* **1997**, *36*, 8992–9001.
155. Tiede, D. M.; Zhang, R.; Seifert, S. *Biochemistry* **2002**, *41*, 6605–6614.
156. Qi, X. P.; Urbauer, J. L.; Fuentes, E. J.; Leopold, M. F.; Wand, A. J. *Nature Struct. Biol.* **1994**, *1*, 378–382.
157. Bertini, I.; Dalvit, C.; Huber, J. G.; Luchinat, C.; Piccioli, M. *FEBS Lett.* **1997**, *415*, 45–48.
158. Benning, M. M.; Wesenberg, G.; Caffrey, M. S.; Bartsch, R. G.; Meyer, T. E.; Cusanovich, M. A.; Rayment, I.; Holden, H. M. *J. Mol. Biol.* **1991**, *220*, 673–685.
159. Gooley, P. R.; Zhao, D.; MacKenzie, N. E. *J. Biomol. NMR* **1991**, *1*, 145–154.
160. Zhao, D.; Huton, H. M.; Cusanovich, M. A.; MacKenzie, N. E. *Protein Sci.* **1996**, *5*, 1816–1825.
161. Cordier, F.; Caffrey, M.; Brutscher, B.; Cusanovich, M. A.; Marion, D.; Blackledge, M. *J. Mol. Biol.* **1998**, *281*, 341–361.
162. Zhao, D.; Hutton, H. M.; Gooley, P. R.; MacKenzie, N. E.; Cusanovich, M. A. *Protein Sci.* **2000**, *9*, 1828–1837.
163. Frazao, C.; Soares, C. M.; Carrondo, M. A.; Pohl, E.; Dauter, Z.; Wilson, K. S.; Hervás, M.; Navarro, J. A.; De la Rosa, M. A.; Sheldrick, G. *Structure* **1995**, *3*, 1159–1170.
164. Banci, L.; Bertini, I.; Quacquarini, G.; Walter, O.; Diaz, A.; Hervás, M.; De la Rosa, M. A. *J. Biol. Inorg. Chem.* **1996**, *1*, 330–340.
165. Banci, L.; Bertini, I.; De la Rosa, M. A.; Koulougliotis, D.; Navarro, J. A.; Walter, O. *Biochemistry* **1998**, *37*, 4831–4843.
166. Geremia, S.; Garau, G.; Vaccari, L.; Sgarra, R.; Viezzoli, M. S.; Calligaris, M.; Randaccio, L. *Protein Sci.* **2002**, *11*, 6–17.
167. Kerfeld, C. A.; Anwar, H. R.; Interrante, R.; Merchant, S.; Yeates, T. O. *J. Mol. Biol.* **1995**, *250*, 627–647.
168. Schnackenberg, J.; Than, M. E.; Mann, K.; Wiegand, G.; Huber, R.; Reuter, W. *J. Mol. Biol.* **1999**, *290*, 1019–1030.
169. Anthony, C. *Biochim. Biophys. Acta* **1992**, *1099*, 1–15.
170. Than, M. E.; Hof, P.; Huber, R.; Bourenkov, G. P.; Bartunik, H. D.; Buse, G.; Soulimane, T. *J. Mol. Biol.* **1997**, *271*, 629–644.
171. Read, J.; Gill, R.; Dales, S. L.; Cooper, J. B.; Wood, S. P.; Anthony, C. *Protein Sci.* **1999**, *8*, 1232–1240.
172. Theorell, H.; Åkesson, A. . *J. Am. Chem. Soc.* **1941**, *63*, 1804–1811.
173. Battistuzzi, G.; Borsari, M.; Cowan, J. A.; Eicken, C.; Loschi, L.; Sola, M. *Biochemistry* **1999**, *38*, 5553–5562.
174. Indiana, C.; de Sanctis, G.; Neri, F.; Santos, H.; Smulevich, G.; Coletta, M. *Biochemistry* **2000**, *39*, 8234–8242.
175. Wilson, M. T.; Greenwood, C. In *Cytochrome c: A Multidisciplinary Approach*; Scott, R. A., Mauk, A. G., Eds.; University Science Books: Sausalito, CA, 1996; pp 611–634.
176. Hong, X. L.; Dixon, D. W. *FEBS Lett.* **1989**, *246*, 105–108.
177. Theodorakis, J. L.; Garber, E. A. E.; McCracken, J.; Peisach, J.; Schejter, A.; Margoliash, E. *Biochim. Biophys. Acta* **1995**, *1252*, 103–113.
178. Ferrer, J. C.; Guillemette, J. G.; Bogumil, R.; Inglis, S. C.; Smith, M.; Mauk, G. A. *J. Am. Chem. Soc.* **1993**, *115*, 7505–7508.

179. Rosell, F. I.; Ferrer, J. C.; Mauk, A. G. *J. Am. Chem. Soc.* **1998**, *120*, 11234–11245.
180. Döpner, S.; Hildebrandt, P.; Rosell, F. I.; Mauk, A. G. *J. Am. Chem. Soc.* **1998**, *120*, 11246–11255.
181. Pollock, W. B. R.; Rosell, F. I.; Twitchett, M. B.; Dumont, M. E.; Mauk, A. G. *Biochemistry* **1998**, *37*, 6124–6131.
182. Pearce, L. L.; Gartner, A. L.; Smith, M.; Mauk, A. G. *Biochemistry* **1989**, *28*, 3152–3156.
183. Rosell, F. I.; Harris, T. R.; Hildebrand, D. P.; Döpner, S.; Hildebrandt, P.; Mauk, A. G. *Biochemistry* **2000**, *39*, 9047–9054.
184. Davis, L. A.; Schejter, A.; Hess, G. P. *J. Biol. Chem.* **1974**, *249*, 2624–2632.
185. Barker, P. D.; Mauk, G. A. *J. Am. Chem. Soc.* **1992**, *114*, 3619–3624.
186. Battistuzzi, G.; Borsari, M.; Francia, F. *Biochemistry* **1997**, *36*, 16247–16258.
187. Luntz, T. L.; Schejter, A.; Garber, E. A. E.; Margoliash, E. *Proc. Natl. Acad. Sci. USA* **1989**, *86*, 3524–3528.
188. Gadsby, P. M.; Peterson, J.; Foote, N.; Greenwood, C.; Thomson, A. J. *Biochem. J.* **1987**, *246*, 43–54.
189. Hartshorn, R. T.; Moore, G. R. *Biochem. J.* **1989**, *258*, 595–598.
190. Tonge, P.; Moore, G. R.; Wharton, C. W. *Biochem. J.* **1989**, *258*, 599–605.
191. Filosa, A.; Ismail, A. A.; English, A. M. *J. Biol. Inorg. Chem.* **1999**, *4*, 717–727.
192. Taler, G.; Schejter, A.; Navon, G.; Vig, I.; Margoliash, E. *Biochemistry* **1995**, *34*, 14209–14212.
193. Oellerich, S.; Wackerbarth, H.; Hildebrandt, P. *J. Phys. Chem. B* **2002**, *106*, 6566–6580.
194. Hildebrandt, P.; Pielak, G. J.; Williams, R. J. P. *Eur. J. Biochem.* **1991**, *201*, 211–216.
195. Hamada, D.; Kuroda, Y.; Kataoka, M.; Aimoto, S.; Yoshimura, T.; Goto, Y. *J. Mol. Biol.* **1996**, *256*, 172–186.
196. Wallace, C. J. A.; Clark-Lewis, I. *J. Biol. Chem.* **1992**, *267*, 3852–3861.
197. Lu, Y.; Casimiro, D. R.; Bren, K. L.; Richards, J. H.; Gray, H. B. *Proc. Natl. Acad. Sci. USA* **1993**, *90*, 11456–11459.
198. Fumo, G.; Spitzer, J. S.; Fetrow, J. S. *Gene* **1995**, *164*, 33–39.
199. Babul, J.; Stellwagen, E. *Biopolymers* **1971**, *10*, 2359–2361.
200. Muthukrishnan, K.; Nall, T. *Biochemistry* **1991**, *30*, 4706–4710.
201. Elöve, G. A.; Bhuyan, A. K.; Roder, H. *Biochemistry* **1994**, *33*, 6925–6935.
202. Roder, H.; Elöve, G. A.; Englander, S. W. *Nature* **1988**, *335*, 700–704.
203. Sosnick, T. R.; Mayne, L.; Hiller, R.; Englander, S. W. *Nat. Struct. Biol.* **1994**, *1*, 149–156.
204. Takahashi, S.; Yeh, S. R.; Das, T. K.; Chan, C. K.; Gottfried, D. S.; Rousseau, D. L. *Nature Struct. Biol.* **1997**, *4*, 44–50.
205. Sauder, J. M.; MacKenzie, N. E.; Roder, H. *Biochemistry* **1996**, *35*, 16852–16862.
206. Guidry, J.; Wittung-Stafshede P. *J. Mol. Biol.* **2000**, *301*, 769–773.
207. Hammack, B.; Godbole, S.; Bowler, B. E. *J. Mol. Biol.* **1998**, *275*, 719–724.
208. Telford, J. R.; Tezcan, F. A.; Gray, H. B.; Winkler, J. R. *Biochemistry* **1999**, *38*, 1944–1949.
209. Chen, E.; Wittung-Stafshede, P.; Kliger, D. S. *J. Am. Chem. Soc.* **1999**, *121*, 3811–3817.
210. Bai, Y. *Proc. Natl. Acad. Sci. USA* **1999**, *96*, 477–480.
211. Pierce, M. M.; Nall, B. T. *Protein Sci.* **1997**, *6*, 618–627.
212. Colón, W.; Wakem, L. P.; Sherman, F.; Roder, H. *Biochemistry* **1997**, *36*, 12535–12541.
213. Russell, B. S.; Melenkivitz, R.; Bren, K. L. *Proc. Natl. Acad. Sci. USA* **2000**, *97*, 8312–8317.
214. Russell, B. S.; Bren, K. L. *J. Biol. Inorg. Chem.* **2002**, *7*, 909–916.
215. Tezcan, F. A.; Winkler, J. R.; Gray, H. B. *J. Am. Chem. Soc.* **1999**, *121*, 11918–11919.
216. Yeh, S. R.; Takahashi, S.; Fan, B.; Rousseau, D. L. *Nature Struct. Biol.* **1997**, *4*, 51–56.
217. Yeh, S. R.; Rousseau, D. L. *Nature Struct. Biol.* **1998**, *5*, 222–228.
218. Yeh, S. R.; Rousseau, D. L. *J. Biol. Chem.* **1999**, *274*, 17853–17859.
219. Boffi, A.; Das, T. K.; Della Longa, S.; Spagnuolo, C.; Rousseau, D. L. *Biophys. J.* **1999**, *77*, 1143–1149.
220. Bixler, J.; Bakker, G.; McLendon, G. *J. Am. Chem. Soc.* **1992**, *114*, 6938–6939.
221. Hilgen-Willis, S.; Bowden, E. F.; Pielak, G. J. *J. Inorg. Biochem.* **1993**, *51*, 649–653.
222. Cohen, D. S.; Pielak, G. J. *J. Am. Chem. Soc.* **1995**, *117*, 1675–1677.
223. Pascher, T.; Chesick, J. P.; Winkler, J. R.; Gray, H. B. *Science* **1996**, *271*, 1558–1560.
224. Mines, G. A.; Pascher, T.; Lee, S. C.; Winkler, J. R.; Gray, H. B. *Chem. Biol.* **1996**, *3*, 491–497.
225. Hildebrandt, P.; Stockburger, M. *Biochemistry* **1989**, *28*, 6710–6721.
226. Hildebrandt, P.; Stockburger, M. *Biochemistry* **1989**, *28*, 6722–6728.
227. Murgida, D. H.; Hildebrandt, P. *J. Phys. Chem. B* **2001**, *105*, 1578–1586.
228. Hildebrandt, P.; Heimburg, T.; Marsh, D. *Eur. J. Biophys.* **1990**, *18*, 193–201.
229. Tezcan, F. A.; Findley, W. A.; Crane, B. R.; Ross, S. A.; Lyubovitsky, J. G.; Gray, H. B.; Winkler, J. R. *Proc. Natl. Acad. Sci. USA* **2002**, *99*, 8626–8630.
230. Jones, C. M.; Henry, E. R.; Hu, Y.; Chan, C. K.; Luck, S. D.; Bhuyan, A.; Roder, H.; Hofrichter, J.; Eaton, W. A. *Proc. Natl. Acad. Sci. USA* **1993**, *90*, 11860–11864.
231. Chen, C. K.; Hofrichter, J.; Eaton, W. A. *Science* **1996**, *274*, 628–629.
232. Hagen, S. J.; Hofrichter, J.; Eaton, W. A. *J. Phys. Chem. B* **1997**, *101*, 2352–2365.
233. Chen, E.; Wood, M. J.; Fink, A. L.; Kliger, D. S. *Biochemistry* **1998**, *37*, 5589–5598.
234. Arcovito, A.; Gianni, S.; Brunori, M.; Travaglini-Allocatelli, C.; Bellelli, A. *J. Biol. Chem.* **2001**, *276*, 41073–41078.
235. Hawkins, B. K.; Hilgen-Willis, S.; Pielak, G. J.; Dawson, J. H. *J. Am. Chem. Soc.* **1994**, *116*, 3111–3112.
236. Schejter, A.; Taler, G.; Navon, G.; Liu, X.-J.; Margoliash, E. *J. Am. Chem. Soc.* **1996**, *118*, 477–478.
237. Zheng, J.; Ye, S.; Lu, T.; Cotton, T. M.; Chumanov, G. *Biopolymers* **2000**, *57*, 77–84.
238. Feinberg, B. A.; Liu, X.; Ryan, M. D.; Schejter, A.; Zhang, C.; Margoliash, E. *Biochemistry* **1998**, *37*, 13091–13101.
239. Williams, P. A.; Fulop, V.; Garman, E. F.; Saunders, N. F. W.; Ferguson, S. J.; Hajdu, J. *Nature* **1997**, *389*, 406–412.
240. Sutin, N.; Yandell, J. K. *J. Biol. Chem.* **1972**, *247*, 6932–6936.
241. Aviram, I.; Schejter, S. *J. Biol. Chem.* **1980**, *255*, 3020–3024.
242. Das, G.; Hickey, D. R.; McLendon, D.; McLendon, G.; Sherman, F. *Proc. Natl. Acad. Sci. USA* **1989**, *86*, 496–499.
243. Banci, L.; Bertini, I.; Spyroulias, G. A.; Turano, P. *Eur. J. Inorg. Chem.* **1998**, *5*, 583–591.
244. George, P.; Tsou, C. L. *Biochem. J.* **1952**, *50*, 440–448.
245. Rafferty, S. P.; Smith, M.; Mauk, A. G. *Inorg. Chim. Acta* **1996**, *242*, 171–177.
246. Dumortier, C.; Meyer, T. E.; Cusanovich, M. A. *Arch. Biochem. Biophys.* **1999**, *371*, 142–148.
247. Dumortier, C.; Holt, J. M.; Meyer, T. E.; Cusanovich, M. A. *J. Biol. Chem.* **1998**, *273*, 25647–25653.

248. Shao, W.; Sun, H.; Yao, Y.; Tang, W. *Inorg. Chem.* **1995**, *34*, 680–687.
249. Liu, G.; Shao, W.; Huang, X.; Wu, H.; Tang, W. *Biochim. Biophys. Acta* **1996**, *1277*, 61–82.
250. Ma, D.; Lu, J.; Tang, W. *Biochim. Biophys. Acta* **1998**, *1384*, 32–42.
251. Banci, L.; Bertini, I.; Liu, G.; Lu, J.; Reddig, T.; Tang, W.; Wu, Y.; Yao, Y.; Zhu, D. *J. Biol. Inorg. Chem.* **2001**, *6*, 628–637.
252. Yao, Y.; Qian, C.; Ye, K.; Wang, J.; Bai, Z.; Tang, W. *J. Biol. Inorg. Chem.* **2002**, *7*, 539–547.
253. Behere, D. V.; Ales, D. C.; Goff, H. M. *Biochim. Biophys. Acta* **1986**, *871*, 285–292.
254. Bren, K. L.; Gray, H. B.; Banci, L.; Bertini, I.; Turano, P. *J. Am. Chem. Soc.* **1995**, *117*, 8067–8073.
255. Banci, L.; Bertini, I.; Bren, K. L.; Gray, H. B.; Sompornpisut, P.; Turano, P. *Biochemistry* **1995**, *34*, 11385–11398.
256. Banci, L.; Bertini, I.; Bren, K. L.; Cremonini, M. A.; Gray, H. B.; Luchinat, C.; Turano, P. *J. Biol. Inorg. Chem.* **1996**, *1*, 117–126.
257. Banci, L.; Bertini, I.; Savellini, G. G.; Romagnoli, A.; Turano, P.; Cremonini, M. A.; Luchinat, C.; Gray, H. B. *Protein Struct. Funct. Genet.* **1997**, *29*, 68–76.
258. Sogabe, S.; Miki, K. *J. Mol. Biol.* **1995**, *252*, 235–247.
259. Rafferty, S. P.; Pearce, L. L.; Barker, P. D.; Guillemette, J. G.; Kay, C. M.; Smith, M.; Mauk, A. G. *Biochemistry* **1990**, *29*, 9365–9369.
260. Axelrod, H. L.; Feher, G.; Allen, J. P.; Chirino, A. J.; Day, M. W.; Hsu, B. T.; Rees, D. C. *Acta Crystallogr.* **1994**, *D50*, 596–602.
261. Shokhirev, N. V.; Walker, F. A. *J. Biol. Inorg. Chem.* **1998**, *3*, 581–594.
262. Walker, F. A.; Reis, D.; Balke, V. L. *J. Am. Chem. Soc.* **1984**, *106*, 6888–6898.
263. Liu, G. H.; Shao, W. P.; Zhu, S. M.; Tang, W. X. *J. Inorg. Biochem.* **1995**, *60*, 123–131.
264. Lu, J.; Ma, D.; Hu, J.; Tang, W.; Zhu, D. *J. Chem. Soc., Dalton Trans.* **1998**, 2267–2274.
265. Shao, W.; Yao, Y.; Liu, G.; Tang, W. *Inorg. Chem.* **1993**, *32*, 6112–6114.
266. Liu, G.; Chen, Y.; Tang, W. *J. Chem. Soc., Dalton Trans.* **1997**, 795–802.
267. Schejter, A. In *Cytochrome c: A Multidisciplinary Approach*; Scott, R. A., Mauk, A. G., Eds,; University Science Books: Sausalito, CA, 1996; pp 335–345.
268. Raphael, A. L.; Gray, H. B. *J. Am. Chem. Soc.* **1991**, *113*, 1038–1040.
269. Smulevich, G.; Bjerrum, M. J.; Gray, H. B.; Spiro, T. G. *Inorg. Chem.* **1994**, *33*, 4629–4634.
270. Bren, K. L.; Gray, H. B. *J. Am. Chem. Soc.* **1993**, *115*, 10382–10383.
271. Yamanaka, T. *The Biochemistry of Bacterial Cytochromes* **1992**, 89–168. Japan Scientific Societies Press: Tokyo.
272. Cross, R.; Aish, J.; Paston, S. J.; Poole, R. K.; Moir, J. W. B. *J. Bacteriol.* **2000**, *182*, 1442–1447.
273. Meyer, T.; Kamen, M. *Adv. Protein Chem.* **1982**, *35*, 105–212.
274. Menin, L.; Schoepp, B.; Garcia, D.; Parot, P.; Verméglio, A. *Biochemistry* **1997**, *36*, 12175–12182.
275. Bertrand, P.; Mbarki, O.; Asso, M.; Blanchard, L.; Guerlesquin, F.; Tegoni, M. *Biochemistry* **1995**, *34*, 11071–11079.
276. Gunner, M. R.; Honig, B. *Proc. Natl. Acad. Sci. USA* **1991**, *88*, 9151–9155.
277. Caffrey, M. C.; Cusanovich, M. A. *Biochim. Biophys. Acta* **1994**, *1187*, 277–288.
278. Zhao, D.; Hutton, H. M.; Meyer, T. E.; Walker, F. A.; MacKenzie, N. E.; Cusanovich, M. A. *Biochemistry* **2000**, *39*, 4053–4061.
279. Caffrey, M. S.; Daldal, F.; Holden, H.; Cusanovich, M. A. *Biochemistry* **1991**, *30*, 4119–4125.
280. Ponamerev, M. V.; Schlarb, B. G.; Howe, C. J.; Carrell, C. J.; Smith, J. L.; Bendall, D. S.; Cramer, W. A. *Biochemistry* **2000**, *39*, 5971–5976.
281. Sawaya, M. R.; Krogmann, D. W.; Serag, A.; Ho, K. K.; Yeates, T. O.; Kerfeld, C. A. *Biochemistry* **2000**, *40*, 9215–9225.
282. McGee, W. A.; Rosell, F. I.; Liggins, J. R.; Rodriguez-Ghidarpour, S.; Luo, Y.; Chen, J.; Brayer, G. D.; Mauk, A. G.; Nall, B. T. *Biochemistry* **1996**, *35*, 1995–2007.
283. Komar-Panicucci, S.; Bixler, J.; Bakker, G.; Sherman, F.; McLendon, G. *J. Am. Chem. Soc.* **1992**, *114*, 5443–5445.
284. Rafferty, S. P.; Guillemette, J. G.; Berghuis, A. M.; Smith, M.; Brayer, G. D.; Mauk, A. G. *Biochemistry* **1996**, *35*, 10784–10792.
285. Lett, C. M.; Berghuis, A. M.; Frey, H. E.; Lepock, J. R.; Guillemette, J. G. *J. Biol. Chem.* **1996**, *271*, 29088–29093.
286. Hickey, D. R.; Berghuis, A. M.; Lafond, G.; Jaeger, J. A.; Cardillo, T. S.; McLendon, D.; Das, G.; Sherman, F.; Brayer, G. D.; McLendon, G. *J. Biol. Chem.* **1991**, *266*, 11686–11694.
287. Cutler, R. L.; Davis, A. M.; Creighton, S.; Warshel, A.; Moore, G. R.; Smith, M.; Mauk, A. G. *Biochemistry* **1989**, *28*, 3188–3197.
288. Schejter, A.; Luntz, T. L.; Koshy, T. I.; Margoliash, E. *Biochemistry* **1992**, *31*, 8336–8343.
289. Koshy, T. I.; Luntz, T. L.; Schejter, A.; Margoliash, E. *Proc. Natl. Acad. Sci. USA* **1990**, *87*, 8697–8701.
290. Luntz, T. L.; Schejter, A.; Garber, E. A. E.; Margoliash, E. *Proc. Natl. Acad. Sci. USA* **1989**, *86*, 3524–3528.
291. Barker, P. D.; Nerou, E. P.; Cheesman, M. R.; Thomson, A. J.; de Oliveira, P.; Hill, H. A. O. *Biochemistry* **1996**, *35*, 13618–13626.
292. Springs, S. L.; Bass, S. E.; McLendon, G. L. *Biochemistry* **2000**, *39*, 6075–6082.
293. Fantuzzi, A.; Sadeghi, S.; Valetti, F.; Rossi, G. L.; Gilardi, G. *Biochemistry* **2002**, *41*, 8718–8724.
294. Funk, W. D.; Lo, T. P.; Mauk, M. R.; Brayer, G. D.; MacGillivray, R. T. A.; Mauk, A. G. *Biochemistry* **1990**, *29*, 5500–5508.
295. Mauk, A. G.; Moore, G. M. *J. Bio. Inorg. Chem.* **1997**, *2*, 119–125.
296. Rodgers, K. K.; Sligar, S. G. *J. Am. Chem. Soc.* **1991**, *113*, 9419–9421.
297. Xue, L.-L.; Wang, Y.-H.; Xie, Y.; Wang, W.-H.; Qian, W.; Huang, Z.-X.; Wu, J.; Xia, Z.-X. *Biochemistry* **1999**, *38*, 11961–11972.
298. Rivera, M.; Seetharaman, R.; Girdhar, D.; Wirtz, M.; Zhang, X.; Wang, X.; White, S. *Biochemistry* **1998**, *37*, 1485–1494.
299. Rodriguez, J. C.; Rivera, M. *Biochemistry* **1998**, *37*, 13082–13090.
300. Kostanjeveki, V.; Leys, D.; Van Driessche, G.; Meyer, T. E.; Cusanovich, M. A.; Fischer, U.; Guisez, Y.; Van Beeumen, J. *J. Biol. Chem.* **1999**, *274*, 35614–35620.
301. Watt, G. D.; Frankel, R. B.; Papaefthymious, G. C.; Spartalian, L.; Stiefel, E. I. *Biochemistry* **1986**, *25*, 4330–4336.

302. Mus-Veteau, I.; Dolla, A.; Guerlesquin, F.; Payan, F.; Czjzek, M.; Haser, R.; Bianco, P.; Haladjian, J.; Rapp-Giles, B. J.; Wall, J. D.; Voordouw, G.; Bruschi, M. *J. Biol. Chem.* **1992**, *267*, 16851–16858.
303. Dolla, A.; Florens, L.; Bianco, P.; Haladjian, J.; Voordouw, G.; Forest, E.; Wall, J.; Guerlesquin, F.; Bruschi, M. *J. Biol. Chem.* **1994**, *269*, 6340–6346.
304. Finzel, B. C.; Weber, P. C.; Hardman, K. D.; Salemme, F. R. *J. Mol. Biol.* **1985**, *186*, 627–643.
305. Yasui, M.; Harada, S.; Kai, Y.; Kasai, N.; Kusunoki, M.; Mastuura, Y. *J. Biochem. (Tokyo)* **1992**, *111*, 317–324.
306. Ren, Z.; Meyer, T.; McRee, D. E. *J. Mol. Biol.* **1993**, *234*, 433–445.
307. Dobbs, A. J.; Anderson, B. F.; Faber, H. R.; Baker, E. N. *Acta Crystallog. sect. D* **1996**, *52*, 356–368.
308. Tahirov, T. H.; Misaki, S.; Meyer, T. E.; Cusanovich, M. A.; Higuchi, Y.; Yasuoka, N. *Nature Struct. Biol.* **1996**, *3*, 459–464.
309. Tahirov, T. H.; Misaki, S.; Meyer, T. E.; Cusanovich, M. A.; Higuchi, Y.; Yasuoka, N. *Acta Crystallog. sect. D* **1997**, *53*, 658–664.
310. Déméné, H.; Tsan, P.; Gans, P.; Marion, D. *J. Phys. Chem. B* **2000**, *104*, 2559–2569.
311. Kassner, R. J. *Biochim. Biophys. Acta* **1991**, *1058*, 8–12.
312. Lawson, D. M.; Stevenson, C. E. M.; Andrew, C. R.; Eady, R. R. *EMBO J.* **2000**, *19*, 5611–5671.
313. Othman, S.; Richaud, P.; Verméglio, A.; Desbois, A. *Biochemistry* **1996**, *35*, 9224–9234.
314. Andrew, C. R.; Green, E. L.; Lawson, D. M.; Eady, R. R. *Biochemistry* **2001**, *40*, 4115–4122.
315. Hobbs, J. D.; Larsen, R. W.; Meyer, T. E.; Hazzard, J. H.; Cusanovich, M. A.; Ondrias, M. R. *Biochemistry* **1990**, *29*, 4166–4174.
316. Tsan, P.; Caffrey, M.; Daku, M. L.; Cusanovich, M.; Marion, D.; Gans, P. *J. Am. Chem. Soc.* **1999**, *121*, 1795–1805.
317. Caffrey, C.; Simorre, J. P.; Brutscher, B.; Cusanovich, M.; Marion, D. *Biochemistry* **1995**, 34, 5904–5912.
318. Doyle, M. L.; Weber, P. C.; Gill, S. J. *Biochemistry* **1985**, *24*, 1987–1991.
319. Doyle, M. L.; Gill, S. J.; Cusanovich, M. A. *Biochemistry* **1986**, *25*, 2509–2516.
320. Yoshimura, T.; Suzuki, S.; Nakahara, A.; Iwasaki, H.; Masuko, M.; Matsubara, T. *Biochemistry* **1986**, *25*, 2436–2442.
321. Yoshimura, T.; Fujii, S.; Kamada, H.; Yamaguchi, K.; Suzuki, S.; Shidara, S.; Takakuwa, S. *Biochim. Biophys. Acta* **1996**, *1292*, 39–46.
322. George, S. J.; Andrew, C. R.; Lawson, D. M.; Thorneley, R. N. F.; Eady, R. R. *J. Am. Chem. Soc.* **2001**, *123*, 9683–9684.
323. Andrew, C. R.; George, S. J.; Lawson, D. M.; Eady, R. R. *Biochemistry* **2002**, *41*, 2353–2360.
324. Zhoa, Y.; Brandish, P. E.; Ballou, D. P.; Marletta, M. A. *Proc. Natl. Acad. Sci. USA* **1999**, *96*, 14753–14758.
325. Lee, J. C.; Gray, H. B.; Winkler, J. R. *Proc. Natl. Acad. Sci. USA* **2001**, *98*, 7760–7764.
326. Clark, K.; Dugad, L. B.; Bartsch, R. G.; Cusanovich, M. A.; La Mar, G. N. *J. Am. Chem. Soc.* **1996**, *118*, 4654–4664.
327. Hamada, K.; Bethge, P. H.; Mathews, F. S. *J. Mol. Biol.* **1995**, *247*, 947–962.
328. Arnesano, F.; Banci, L.; Bertini, I.; Faranone-Mennella, J.; Rosato, A.; Barker, P. D.; Fersht, A. R. *Biochemistry* **1999**, *38*, 8657–8670.
329. Wittung-Stafshede, P.; Gray, H. B.; Winkler, J. R. *J. Am. Chem. Soc* **1997**, *119*, 9562–9563.
330. Wittung-Stafshede, P.; Lee, J. C.; Winkler, J. R.; Gray, H. B. *Proc. Natl. Acad. Sci. USA* **1999**, *96*, 6587–6590.
331. Kamiya, N.; Okimoto, Y.; Ding, Z.; Ohtomo, H.; Shimizu, M.; Kitayama, A.; Morii, H.; Nagamune, T. *Protein Engineering* **2001**, *14*, 415–419.
332. Uno, T.; Yukinari, A.; Tomisugi, Y.; Ishikawa, Y.; Makino, R.; Brannigan, J. A.; Wilkinson, A. J. *J. Am. Chem. Soc.* **2001**, *123*, 2458–2459.
333. Barker, P. D.; Nerou, E. P.; Freund, S. M. V.; Fearnley, I. M. *Biochemistry* **1995**, *34*, 15191–15203.
334. Arnesano, F.; Banci, L.; Bertini, I.; Ciofi-Baffoni, S.; Woodyear, T. L.; Johnson, C. M.; Barker, P. D. *Biochemistry* **2000**, *39*, 1499–1514.
335. Barker, P. D.; Freund, S. M. V. *Biochemistry* **1996**, *35*, 13627–13635.
336. Cheesman, M. R.; Kadir, F. H. A.; Al-Basseet, J.; Al-Massad, F.; Farrar, J.; Greenwood, C.; Thomson, A. J.; Moore, G. R. *Biochem. J.* **1992**, *286*, 361–367.
337. Thöny-Meyer, L. *Biochim. Biophys. Acta* **2000**, *1459*, 316–324.
338. O'Brian, M. R.; Thöny-Meyer, L. *Adv. Microb. Phys.* **2002**, *46*, 257–318.
339. Thöny-Meyer, L. *Biochem. Soc. Trans.* **2002**, *30*, 633–638.
340. Pieulle, L.; Haladjian, J.; Bonicel, J.; Hatchikian, E. C. *Biochim. Biophys. Acta* **1996**, *1273*, 51–61.
341. Ma, J.-G.; Zhang, J.; Franco, R.; Jia, S.-L.; Moura, I.; Moura, J. J. G.; Kroneck, P. M. H.; Shelnutt, J. A. *Biochemistry* **1998**, *37*, 12431–12442.
342. Coutinho, I. B.; Xavier, A. V. *Meth. Enzymol.* **1994**, *243*, 119–140.
343. Park, J.-S.; Ohmura, T.; Kano, K.; Sagara, T.; Niki, K.; Kyogoku, Y.; Akutsu, H. *Biochim. Biophys. Acta* **1996**, *1293*, 45–54.
344. Fan, K.; Akutsu, H.; Kyogoku, Y.; Niki, K. *Biochemistry* **1990**, *29*, 2257–2263.
345. Salgueiro, C. A.; Turner, D. L.; LeGall, J.; Xavier, A. V. *J. Biol. Inorg. Chem.* **1997**, *2*, 343–349.
346. Turner, D. L.; Salgueiro, C. A.; Catarino, T. LeGall J.; Xavier, A. V. *Biochim. Biophys. Acta* **1994**, *1187*, 232–235.
347. Turner, D. L.; Salgueiro, C. A.; Catarino, T.; LeGall, J.; Xavier, A. V. *Eur. J. Biochem.* **1996**, *241*, 723–731.
348. Louro, R. O.; Catarino, T.; LeGall, J.; Turner, D. L.; Xavier, A. V. *ChemBioChem* **2001**, *2*, 831–837.
349. Martel, P. J.; Soares, C. M.; Baptista, A. M.; Fuxreiter, M.; Náray-Szabó, G.; Louro, R. O.; Carrondo, M. A. *J. Biol. Inorg. Chem.* **1999**, *4*, 73–86.
350. Messias, A. C.; Kastrau, D. H. W.; Costa, H. S.; LeGall, J.; Turner, D. L.; Santos, H.; Xavier, A. V. *J. Mol. Biol.* **1998**, *281*, 719–739.
351. Brennan, L.; Turner, D. L.; Messias, A. C.; Teodoro, M. L.; LeGall, J.; Santos, H.; Xavier, A. V. *J. Mol. Biol.* **2000**, *298*, 61–82.
352. Harada, E.; Fukuoka, Y.; Ohmura, T.; Fukunishi, A.; Kawai, G.; Fujiwara, T.; Akutsu, H. *J. Mol. Biol.* **2002**, *319*, 767–778.
353. Salgueiro, C. A.; da Costa, P. N.; Turner, D. L.; Messias, A. C.; van Dongen, W. M. A. M.; Saraiva, L. M.; Xavier, A. V. *Biochemistry* **2001**, *40*, 9709–9716.

354. Savaiva, L. M.; Salgueiro, C. A.; da Costa, P. N.; Messias, A. C.; LeGall, J.; van Dongen, W. M. A. M.; Xavier, A. V. *Biochemistry* **1998**, *37*, 12160–12165.
355. Kazanskaya, I.; Lexa, D.; Bruschi, M.; Chottard, G. *Biochemistry* **1996**, *35*, 13411–13418.
356. Louro, R. O.; Catarino, T.; Turner, D. L.; Picarra-Pereira, M. A.; Pacheco, I.; LeGall, J.; Xavier, A. V. *Biochemistry* **1998**, *37*, 15808–15815.
357. Salgueiro, C. A.; da Costa, P. N.; Turner, D. L.; Messias, A. C.; van Dongen, W. M. A. M.; Saraiva, L. M.; Xavier, A. V. *Biochemistry* **2001**, *40*, 9709–9716.
358. Louro, R. O.; Catarino, T.; Salgueiro, C. A.; LeGall, J.; Xavier, A. V. *J. Biol. Inorg. Chem.* **1996**, *1*, 34–38.
359. Simon, J.; Pisa, R.; Stein, T.; Eichler, R.; Klimmek, O.; Gross, R. *Eur. J. Biochem.* **2001**, *268*, 5776–5782.
360. Meyers, C. R.; Myers, J. M. *J. Bact.* **1997**, *179*, 1143–1152.
361. Roldán, M. D.; Sears, H. J.; Cheesman, M. R.; Ferguson, S. J.; Thomson, A. J.; Berks, B. C.; Richardson, D. J. *J. Biol. Chem.* **1998**, *273*, 28785–28790.
362. Field, S. J.; Dobbin, P. S.; Cheesman, M. R.; Watmough, N. J.; Thomson, A. J.; Richardson, D. J. *J. Biol. Chem.* **2000**, *275*, 8515–8522.
363. Mauk, M. R.; Mauk, A. G. *Biochemistry* **1982**, *21*, 4730–4734.
364. Bunn, H. F.; Forget, B. G. *Hemoglobin: Molecular, Genetic, and Clinical Aspects*; W. B. Saunders: Philadelphia, PA, 1986.
365. Livingston, D. J.; McLachlan, S. J.; La Mar, G. N.; Brown, W. D. *J. Biol. Chem.* **1985**, *260*, 15699–15707.
366. Arihara, K.; Cassens, R. G.; Greaser, M. L.; Luchansky, J. B.; Mozdziak, P. E. *Meat Sci.* **1995**, *39*, 205–213.
367. Guzov, V. M.; Houston, H. L.; Murataliev, M. B.; Walker, F. A.; Feyereisen, R. *J. Biol. Chem.* **1996**, *271*, 26637–26645.
368. Yu, Y.; Yamasaki, H.; Kita, K.; Takamiya, S. *Arch. Biochem. Biophys.* **1996**, *328*, 165–172.
369. Strittmatter, P.; Spatz, L.; Corcoran, D.; Rogers, M. J.; Setlow, B.; Redline, R. *Proc. Natl. Acad. Sci. USA* **1974**, *71*, 4565–4569.
370. Bonfils, C.; Balny, C.; Maurel, P. *J. Biol. Chem.* **1981**, *256*, 9457–9465.
371. Canova-Davis, E.; Waskell, L. *J. Biol. Chem.* **1984**, *259*, 2541–2546.
372. Mitoma, J.; Ito, A. *EMBO J.* **1992**, *11*, 4197–4203.
373. Borgese, N.; D'Arrigo, A.; De Silvestris, M.; Pietrini, G. *FEBS Lett.* **1993**, *325*, 70–75.
374. Kuroda, R.; Ikenoue, T.; Honsho, M.; Tsujomoto, S.; Mitoma, J.; Ito, A. *J. Biol. Chem.* **1998**, *273*, 31097–31102.
375. Fukushima, K.; Sato, R. *J. Biochem.* **1973**, *74*, 161–173.
376. Altuve, A.; Silchenko, S.; Lee, K.-H.; Kuczera, K.; Terzyan, S.; Zhang, X.; Benson, D. R.; Rivera, M. *Biochemistry* **2001**, *40*, 9469–9483.
377. De Silvestris, M.; D'Arrigo, A.; Borgese, N. *FEBS Lett.* **1995**, *370*, 69–74.
378. Ozols, J. *Biochim. Biophys. Acta* **1989**, *997*, 121–130.
379. Smith, M. A.; Jonsson, L.; Stymne, S.; Stobart, K. *Biochem. J.* **1992**, *287*, 141–144.
380. Deodutta, R.; Strobel, H. W.; Liehr, J. G. *Arch. Biochem. Biophys.* **1991**, *285*, 331–338.
381. Rodriguez-Maranon, M. J.; Qiu, F.; Stark, R. E.; White, S. P.; Zhang, X.; Foundling, S. I.; Rodriguez, V.; Schilling, C. L. III; Bunce, R. A.; Rivera, M. *Biochemistry* **1996**, *35*, 16378–16390.
382. Durley, R. C. E.; Mathews, F. S. *Acta Crystallogr.* **1996**, *D52*, 65–76.
383. Rivera, M.; Barillas-Mury, C.; Christensen, K. A.; Little, J. W.; Wells, M. A.; Walker, F. A. *Biochemistry* **1992**, *31*, 12233–12240.
384. La Mar, G. N.; Burns, P. D.; Jackson, J. T.; Smith, K. M.; Langry, K. C.; Strittmatter, P. *J. Biol. Chem.* **1981**, *256*, 6075–6079.
385. Lee, K.-B.; La Mar, G. N.; Kehres, L. A.; Fujinari, E. M.; Smith, K. M.; Pochapsky, T. C.; Sligar, S. G. *Biochemistry* **1990**, *29*, 9623–9631.
386. Walker, F. A.; Emrick, D.; Rivera, J. E.; Hanquet, B. J.; Buttlaire, D. H. *J. Am. Chem. Soc.* **1988**, *110*, 6234–6240.
387. Dangi, B.; Sarma, S.; Yan, C.; Banville, D. L.; Guiles, R. D. *Biochemistry* **1998**, *37*, 8289–8302.
388. Banci, L.; Bertini, I.; Branchini, B. R.; Hajieva, P.; Spyrouliasm, G. A.; Turano, P. *J. Biol. Inorg. Chem.* **2001**, *6*, 490–503.
389. Hunter, C. L.; Lloyd, E.; Eltis, L. D.; Rafferty, S. P.; Lee, H.; Smith, M.; Mauk, A. G. *Biochemistry* **1997**, *36*, 1010–1017.
390. Silchenko, S.; Sippel, M. L.; Kuchment, O.; Benson, D. R.; Mauk, A. G.; Altuve, A.; Rivera, M. *Biochem. Biophys. Res. Comm.* **2000**, *273*, 467–472.
391. Hewson, R.; Newbold, R. J.; Whitford, D. *Protein Eng.* **1993**, *6*, 953–964.
392. Manyusa, S.; Mortuza, G.; Whitford, D. *Biochemistry* **1999**, *38*, 14352–14362.
393. Cowley, A. B.; Altuve, A.; Kuchment, O.; Terzyan, S.; Zhang, X.; Rivera, M.; Benson, D. R. *Biochemistry* **2002**, *44*, 11566–11581.
394. Storch, E. M.; Daggett, V. *Biochemistry* **1995**, *34*, 9682–9693.
395. Falzone, C. J.; Wang, Y.; Vu, B. C.; Scott, N. L.; Bhattacharya, S.; Lecomte, J. T. J. *Biochemistry* **2001**, *40*, 4879–4891.
396. Ihara, M.; Takahashi, S.; Ishimori, K.; Morishima, I. *Biochemistry* **2000**, *39*, 5961–5970.
397. Avila, L.; Huang, H.; Rodriguez, J. C.; Moënne-Loccoz, P.; Rivera, M. *J. Am. Chem. Soc.* **2000**, *122*, 7618–7619.
398. Trumpower, B. L. *Microbiol. Rev.* **1990**, *54*, 101–129.
399. Trumpower, B. L.; Gennis, R. B. *Ann. Rev. Biochem.* **1994**, *63*, 675–716.
400. Zhang, Z.; Huang, L.; Schulmeister, V. M.; Chi, Y.-I.; Kim, K. Y.; Hung, L.-W.; Crofts, A. R.; Berry, E. A.; Kim, S.-H. *Nature* **1998**, *392*, 677–684.
401. Iwata, S.; Lee, J. W.; Okada, K.; Lee, J. K.; Iwata, M.; Rasmussen, B.; Link, T. A.; Ramaswamy, S.; Jap, B. K. *Science* **1998**, *281*, 64–71.
402. Xia, D.; Yu, C.-A.; Kim, H.; Xia, J.-Z.; Kachurin, A. M.; Zhang, L.; Yu, L.; Deisenhofer, J. *Science* **1997**, *277*, 60–66.
403. Hunte, C.; Koepke, J.; Lange, C.; Roβmanith, T.; Michel, H. *Structure* **2000**, *8*, 669–684.
404. Lange, C.; Hunte, C. *Proc. Natl. Acad. Sci. USA* **2002**, *99*, 2800–2805.
405. Page, C. C.; Moser, C. C.; Chen, X.; Dutton, P. L. *Nature* **1999**, *402*, 47–52.

406. Kerfeld, C. A.; Krogmann, D. W. *Ann. Rev. Plant Physiol. Plant Mol. Biol.* **1998**, *49*, 397–425.
407. Widger, W. R.; Cramer, W. A.; Herrmann, R. G.; Trebst, A. *Proc. Natl. Acad. Sci. USA* **1984**, *81*, 674–678.
408. Martinez, S. E.; Huang, D.; Ponomarev, M.; Cramer, W. A.; Smith, J. L. *Protein Sci.* **1996**, *5*, 1081–1092.
409. Ponamarev, M. V.; Cramer, W. A. *Biochemistry* **1998**, *37*, 17199–17208.
410. Williamson, D. A.; Benson, D. R. *Chem. Commun.* **1998**, 961–962.
411. Liu, D.; Williamson, D. A.; Kennedy, M. L.; Williams, T. D.; Morton, M. M.; Benson, D. R. *J. Am. Chem. Soc.* **1999**, *121*, 11798–11812.
412. Kennedy, M. L.; Silchenko, S.; Houndonoughbo, N.; Gibney, B. R.; Dutton, P. L.; Rodgers, K. R.; Benson, D. R. *J. Am. Chem. Soc.* **2001**, *123*, 4635–4636.
413. Shifman, J. M.; Gibney, B. R.; Sharp, R. E.; Dutton, P. L. *Biochemistry* **2000**, *39*, 14813–14821.
414. Armstrong, F. A. *J. Biol. Inorg. Chem.* **1997**, *2*, 139–142.
415. Gunner, M. R.; Alexov, E.; Torres, E.; Lipovaca, S. *J. Biol. Inorg. Chem.* **1997**, *2*, 126–134.
416. Warshel, A.; Papazyan, A.; Muegge, I. *J. Biol. Inorg. Chem.* **1997**, *2*, 143–152.
417. Zhou, H.-X. *J. Biol. Inorg. Chem.* **1997**, *2*, 109–113.
418. Fedurco, M. *Coord. Chem. Rev.* **2000**, *209*, 263–331.
419. Lee, K.-B.; Jun, E.; La Mar, G. N.; Rezzano, I. N.; Pandey, R. K.; Smith, K. M.; Walker, F. A.; Buttlaire, D. H. *J. Am. Chem. Soc.* **1991**, *113*, 3576–3583.
420. Reid, L. S.; Lim, A. R.; Mauk, A. G. *J. Am. Chem. Soc.* **1986**, *108*, 8197–8201.
421. Sorrell, T. N.; Martin, P. K.; Bowden, E. F. *J. Am. Chem. Soc.* **1989**, *111*, 766–767.
422. Ohmura, T.; Nakamura, H.; Niki, K.; Cusanovich, M. A.; Akutsu, H. *Biophys. J.* **1998**, *75*, 1483–1490.
423. Caffrey, M. S.; Cusanovich, M. A. *Arch. Biochem. Biophys.* **1991**, *285*, 227–230.
424. Reid, L. S.; Mauk, M. R.; Mauk, A. G. *J. Am. Chem. Soc.* **1984**, *106*, 2182–2185.
425. Kassner, R. J. *J. Am. Chem. Soc.* **1973**, *95*, 2674–2677.
426. Sivakolundu, S. G.; Mabrouk, P. A. *J. Am. Chem. Soc.* **2000**, *122*, 1513–1521.
427. Stellwagen, E. *Nature* **1978**, *275*, 73–74.
428. Tezcan, F. A.; Winkler, J. R.; Gray, H. B. *J. Am. Chem. Soc.* **1998**, *120*, 13383–13388.
429. Wirtz, M.; Oganesyan, V.; Zhang, X.; Studer, J.; Rivera, M. *Faraday Discussions* **2000**, *116*, 221–234.
430. Wu, J.; Gan, J.-H.; Xia, Z.-X.; Wang, Y.-H.; Wang, W.-H.; Xue, L.-L.; Xie, Y.; Huang, Z.-X. *Proteins: Struct., Funct. and Gene.* **2000**, *40*, 249–257.

8.3
Electron Transfer: Iron–Sulfur Clusters

R. H. HOLM

Harvard University, Cambridge, MA, USA

8.3.1 SCOPE AND FUNDAMENTAL LIGAND TYPES

The impetus for the development of iron–sulfur cluster chemistry over the last three decades derives largely from the occurrence of iron–sulfur clusters in an extensive variety of proteins and enzymes.[1–5] Five cluster types (**1**)–(**5**) have been demonstrated by protein crystallography and are shown in Figure 1. Clusters (**1**)–(**3**) represent the fundamental set found in proteins (ferredoxins) from a variety of prokaryotic and eucaryotic sources. Rhomb-like cluster (**1**) is especially prevalent in green plants. Cuboidal cluster (**2**) and cubane-type cluster (**3**) are found in bacterial sources
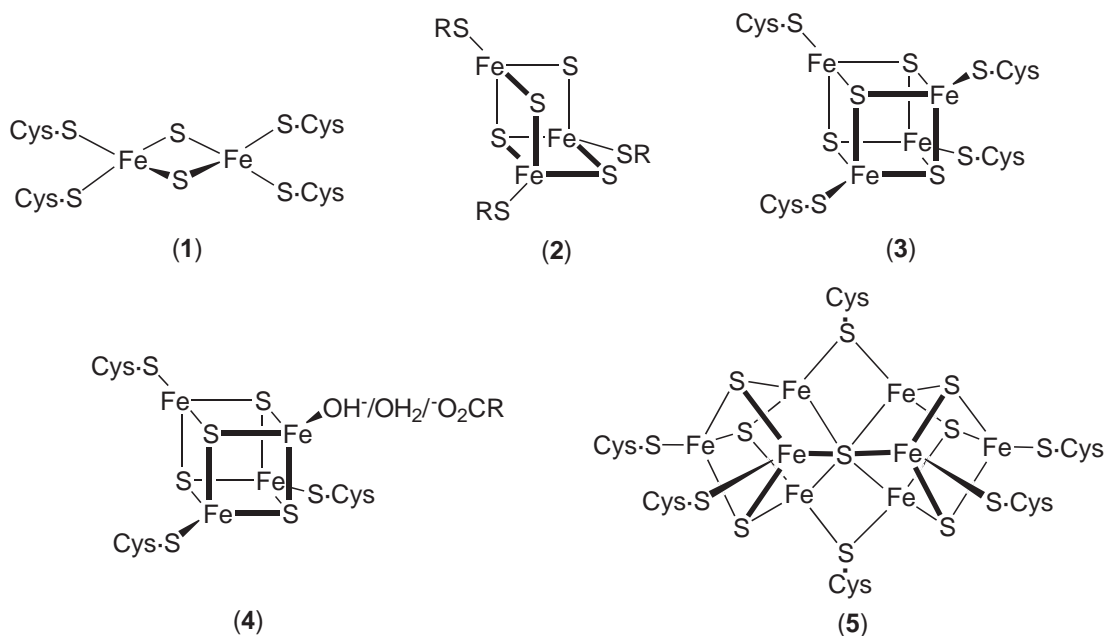
Figure 1 Structurally defined native clusters.

and differ by a single iron atom and its terminal ligand. Cluster (**4**) is a variation of (**3**) in which a terminal cysteinate is replaced by an exogenous ligand or a carboxylate sidechain, and (**5**), the most complex protein-bound cluster, is the **P** cluster of nitrogenase in the as-isolated form of the iron–molybdenum protein.[6,7] In addition, there are variations on these themes in which terminal cysteinate is replaced by alkoxide from serinate, the imidazole ring of histidine, and carboxylate from glutamate or aspartate. However, the great majority of protein-bound clusters feature tetrahedral four-coordinate iron sites with terminal cysteinate ligation. Except for oxidized (**1**), the clusters are mixed-valence $Fe^{III,II}$, often with delocalized electronic structures and coupled magnetic interactions.[8,9]

Provided here is an account of synthetic iron–sulfur cluster chemistry intended to summarize leading results since the subject was briefly treated in *Comprehensive Coordination Chemistry* (*CCC*, 1987), Volume 4, but also contains certain earlier findings. Structural types and synthetic reactions affording them are emphasized. Synthetic methods are selective, not exhaustive. Reactions are presented in minimal form; indicated stoichiometries are not necessarily those used in practice. Methods for and structures of sulfide clusters generally extend to selenide clusters, which are not included. Space does not allow detailed consideration of electronic properties. Not included are iron thiolates, organometallic, carbonyl, nitrosyl, or certain other types of abiological clusters which have been treated recently,[10] and iron–sulfur proteins themselves. As will become evident, the scope of synthetic clusters far exceeds the biological set (**1**)–(**5**). Presented in Scheme 1 are synthetic reactions for four clusters of varying nuclearity by reaction of elemental sulfur with a common mononuclear precursor, $[Fe(SEt)_4]^{2-}$.[11] These reactions have the common theme of sulfur as a source of sulfide by reduction with thiolate and/or Fe^{II}, a frequent reaction in synthesis. Clusters are generally isolated as dark red or black salts of quaternary ammonium or phosphonium cations, soluble in polar solvents such as acetonitrile, Me_2SO, and DMF, and unstable to air, particularly in solution. Throughout, *cluster* refers to the entire molecule $[Fe_mS_pL_l]^z$ with generalized terminal ligands L and *core* to the Fe_mS_p portion thereof. Redox potentials are referenced to the standard calomel electrode. As will become evident, the Fe_2S_2 rhomb is the fundamental building block in iron–sulfur cluster chemistry.

8.3.2 [Fe₂S₂] CLUSTERS

As prepared, these clusters are in the oxidized form, contain the planar rhombic $[Fe_2(\mu_2\text{-S})_2]^{2+}$ core, and are of three general types. Thiolate-ligated cluster (**6a**) is an analogue of protein site (**1**) and may be prepared by reactions (1)[11] and (2)[12] from mononuclear precursors and by ligand

$$[FeCl_4]^{2-}$$

4NaSEt, MeCN

$$[Fe(SEt)_4]^{2-}$$

1S, MeCN   1.5S, 85 °C, MeCN

1.4S, Me$_2$CO

$$[Fe_2S_2(SEt)_4]^{2-} \qquad [Fe_3S_4(SEt)_4]^{3-} \xrightarrow{60\,°C,\ MeCN} [Fe_6S_9(SEt)_2]^{4-}$$

80 °C
MeCN   1FeCl$_2$, 1NaSEt

4RSH
MeCN   2RSH
MeCN

MeCN

$$[Fe_4S_4(SEt)_4]^{2-} \qquad [Fe_3S_4(SR)_4]^{3-} \qquad [Fe_6S_9(SR)_2]^{4-}$$
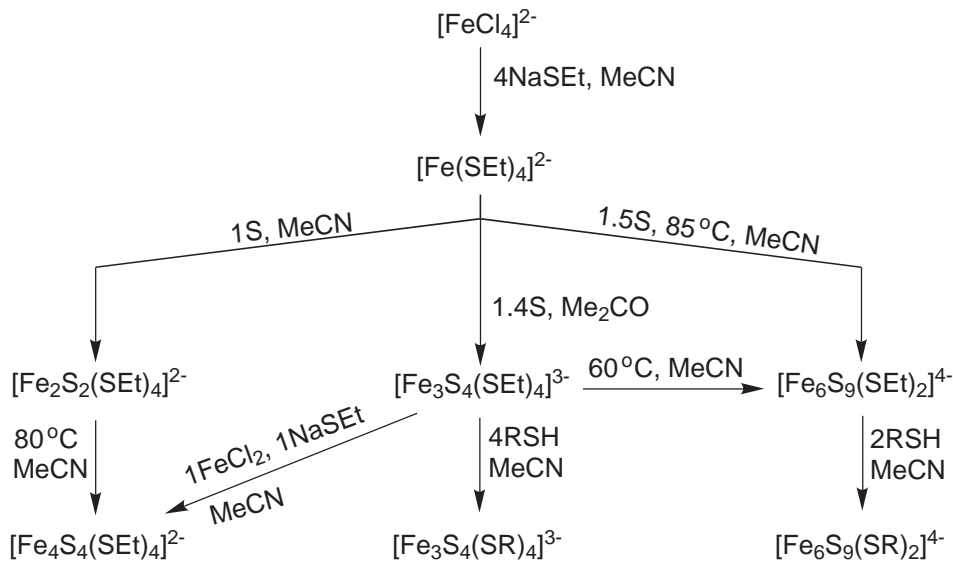
Scheme 1

substitution reaction (3)[13] (R = alkyl, R′ = aryl), which may be shifted toward product by removal of RSH. Related methods starting from FeCl$_3$, sulfur, and NaSR are also available.[14]

$$2[Fe(SR)_4]^{2-} + 2S \rightarrow [Fe_2S_2(SR)_4]^{2-} + RSSR + 2RS^- \tag{1}$$

$$2[Fe(SR)_4]^{1-} + 2S \rightarrow [Fe_2S_2(SR)_4]^{2-} + 2RSSR \tag{2}$$

$$[Fe_2S_2(SR)_4]^{2-} + 4R′SH \rightleftharpoons [Fe_2S_2(SR′)_4]^{2-} + 4RSH \tag{3}$$
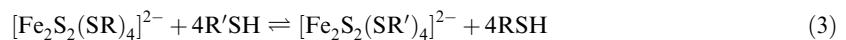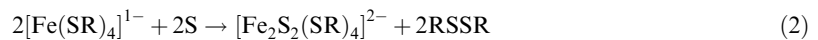
Clusters (**6b**) with L = halide have been obtained from (**6a**) by reaction (4)[19], and are useful starting materials for the preparation of clusters (**6b**) with L = ArO$^-$ and C$_4$H$_4$N$^-$, as in ligand substitution reaction (5)[20–22]. This reaction has also been used with NaSR to prepare thiolate clusters (**6a**), including those containing short cysteinyl peptides as closer models of protein site (**1**).[15–17] Peptide clusters are also accessible by reaction (3). Bis(pentasulfide) cluster (**6c**) is obtained by the reaction of [Fe(SPh)$_4$]$^{2-}$ with five equivalents of (PhCH$_2$S)$_2$S.[18]

$$[Fe_2S_2(SR)_4]^{2-} + 4R′COX \rightarrow [Fe_2S_2X_4]^{2-} + 4R′COSR \tag{4}$$

$$[Fe_2S_2X_4]^{2-} + 4NaL \rightarrow [Fe_2S_2L_4]^{2-} + 4NaX \tag{5}$$
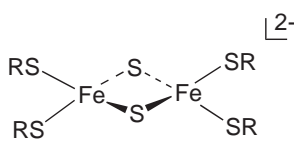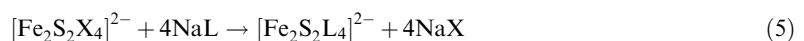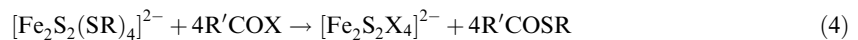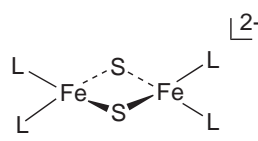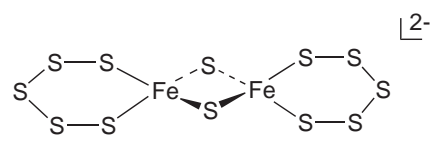
(6a)   (6b)   (6c)

As a class, [Fe$_2$S$_2$]$^{2+}$ clusters are air sensitive, exhibit a diamagnetic ground state with thermally accessible excited states arising from antiferromagnetic coupling of two $S = 5/2$ spins, and characteristic absorption and isotropically shifted ^{1}H NMR spectra that allow their

identification.[11,14] Cores are essentially isometric with the usual bond distances Fe–S ≈ 2.30 Å and Fe–Fe ≈ 2.70 Å; iron sites exhibit distorted tetrahedral stereochemistry. Clusters (**6a**) can be reduced chemically or electrochemically to $[Fe_2S_2(SR)_4]^{3-}$.[13,23–25] These species can be examined *in situ* but none has ever been isolated because of their extreme reactivity, one aspect of which is spontaneous reaction (6)[26] where both reactant and product have the same mean oxidation state ($Fe^{2.5+}$). As for reduced protein site (**1**), $[Fe_2S_2(SR)_4]^{3-}$ species are characterized by an antiferromagnetically coupled $S = 1/2$ ground state, an axial or rhombic EPR spectrum observable at or below ca. 100 K[23–25] and a trapped-valence $Fe^{III}Fe^{II}$ ground state. Consequently, this state is an intrinsic property and not a consequence of protein structure and environment:

$$2[Fe_2S_2(SR)_4]^{3-} \rightarrow [Fe_4S_4(SR)_4]^{2-} + 4RS^- \tag{6}$$
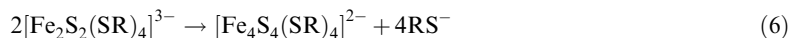
8.3.3   [Fe₃S₄] CLUSTERS

Two types of trinuclear clusters, linear $[Fe_3S_4(SR)_4]^{3-}$ (**7**) and cuboidal $[Fe_3S_4(SR)_3]^{3-}$ (**8**), have been prepared and differ in core structure, oxidation state, and stability. Both clusters have been observed in proteins; cluster (**8**) is an analogue of protein site (**2**):

        (**7**)   (**8**)
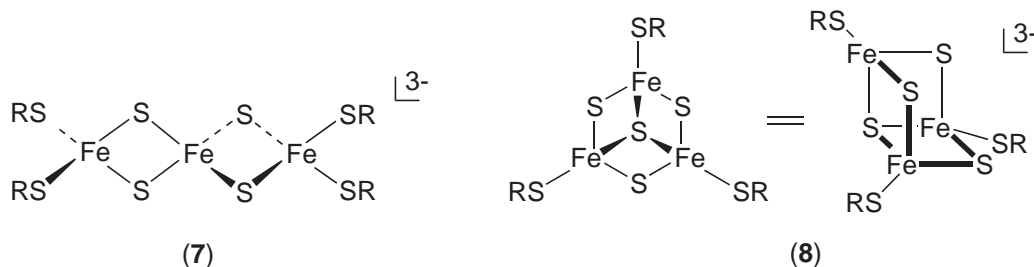
8.3.3.1   Linear Clusters

The first trinuclear cluster (**7**) prepared was $[Fe_3S_4(SEt)_4]^{3-}$ in 1983,[11] obtained by careful control of stoichiometry and scale in reaction (7)[11,27]. The initial complex may be used as such or generated *in situ*.[27] Isolated clusters with R = Ph[11] and mes[28] have been prepared by ligand substitution analogous to reaction (3). The structure of $[Fe_3S_4(SPh)_4]^{3-}$ contains the all-ferric core $[Fe_3S_4]^{1+}$ built of two nearly planar Fe_2S_2 rhombs sharing a common iron atom and disposed at a dihedral angle of 89.4°. The rhombs are nearly isometric with those in (**6a**), and the three Fe^{III} sites have distorted tetrahedral geometry.[11] These sites ($S = 5/2$) are antiferromagnetically coupled to generate an $S = 1/2$ ground state; $[Fe_3S_4(SEt)_4]^{3-}$ behaves as a Curie paramagnet at 5–300 K.[29] Linear cluster (**7**) has been found in a partially unfolded form of the enzyme aconitase where it was identified by comparison of spectroscopic properties with those of $[Fe_3S_4(SEt)_4]^{3-}$.[30] Subsequent comparative MCD spectra further support the presence of (**7**).[31] Recently, reconstitution of recombinant human cytosolic iron regulatory protein 1 (cytosolic aconitase) with Fe^{II} and Na_2S afforded a product containing (**7**), as shown by EPR and EXAFS analysis.[32] It is probable that the cluster is fully ligated by cysteinate in both proteins. An Fe_4S_4 cluster is present in the functional protein; no examples of the linear cluster *in vivo* have been found. A minor amount of the linear cluster has also been detected in pyruvate formate-lyase activating enzyme:[33]

$$3[Fe(SEt)_4]^{2-} + 4S \rightarrow [Fe_3S_4(SEt)_4]^{3-} + 5/2\ EtSSEt + 3EtS^- \tag{7}$$
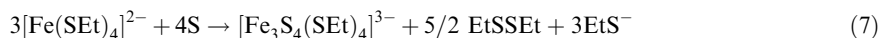
    The fully oxidized nature of cluster (**7**) generates significant reactivity properties. The cluster cannot be reversibly reduced, but it does react with $FeCl_2$ to form an Fe_4S_4 cluster and with reduced metal complexes to afford heterometal cubane-type clusters.[1,34] Reaction (8)[11] proceeds in high yield. Reaction (9)[27] produces a cluster containing a loosely bound diamagnetic $Mo(CO)_3$ unit and a paramagnetic ($S = 2$) $[Fe_3S_4]^0$ core fragment which serves as an electronic analogue of protein site (**2**) in the same oxidation state. Reaction (10)[28,35,36]

(R = Et, mes) conveys one of the two routes to NiFe$_3$S$_4$ clusters. Reactions (8)–(10) and those in Scheme 2 are ones of fragment condensation in which rearranged Fe$_3$S$_4$ is a fragment of the product cluster. EPR and Mössbauer spectra support the core formulations [CoFe$_3$S$_4$]$^{2+}$ ($S = 1/2$) ≡ {Co^{II} ($S = 3/2$) + [Fe$_3$S$_4$]^0 ($S = 2$)} and [NiFe$_3$S$_4$]$^{1+}$ ($S = 3/2$) ≡ {Ni^{II} ($S = 1$) + [Fe$_3$S$_4$]$^{1-}$ ($S = 5/2$)},[28,35] indicating that (9) is formed by a one-electron reduction and (10)/(11) by two-electron reduction of [Fe$_3$S$_4$]$^{1+}$. Cluster (10) is isolated with four thiolate ligands because of the lability of ligated AsPh$_3$. While PPh$_3$ is bound in (11), it is readily displaced in the absence of free phospine by a variety of ligands.[35] These reductive rearrangement reactions are characterized by core reduction, structural alteration from a linear to a cuboidal geometry, and binding of the incoming metal. The reactions in Scheme 2 can be likened to inner sphere electron transfer in which there is a persistent intermediate that resembles the final product:

$$[Fe_3S_4(SEt)_4]^{3-} + FeCl_2 + EtS^- \rightarrow [Fe_4S_4(SEt)_4]^{2-} + 1/2\ EtSSEt + 2Cl^- \tag{8}$$

$$[Fe_3S_4(SEt)_4]^{3-} + [Mo(CO)_3(MeCN)_3] \rightarrow [(CO)_3MoFe_3S_4(SEt)_3]^{3-} + 1/2\ EtSSEt + 3MeCN \tag{9}$$

$$[Fe_3S_4(SR)_4]^{3-} + [Ni(PPh_3)_4] \rightarrow [(Ph_3P)NiFe_3S_4(SR)_3]^{2-} + EtS^- + 3PPh_3 \tag{10}$$
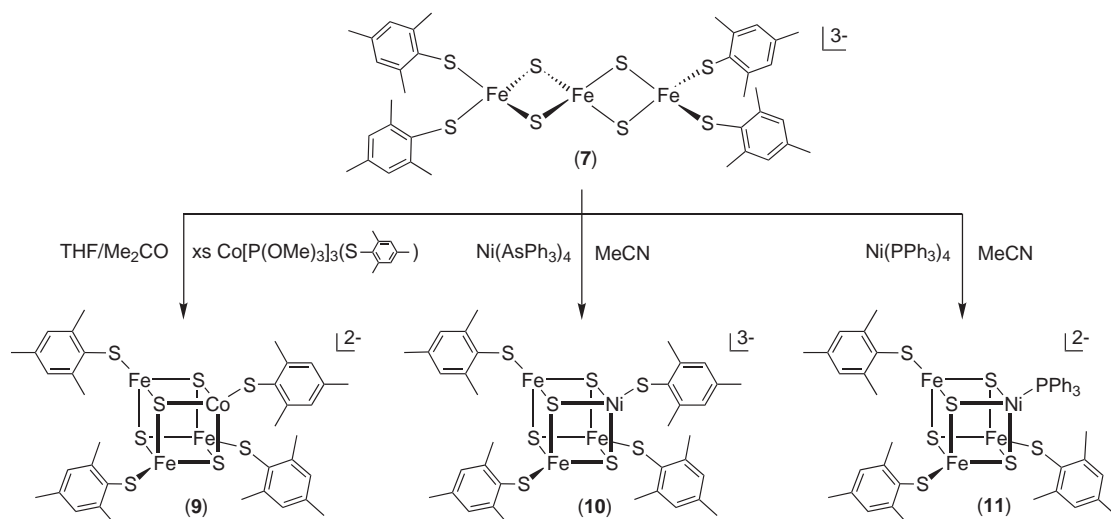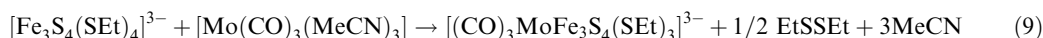
Scheme 2

8.3.3.2 Cuboidal Clusters

Protein site (2) was discovered after sites (1) and (3) were well established. An analogue of (2) proved more difficult to synthesize than those of the other two sites. Despite numerous earlier attempts, an analogue cluster (8) was not prepared until 1995.[37,38] The key to obtaining this cluster in substance is the use of the trifunctional semirigid cavitand ligand LS$_3$ to form the 3:1 site-differentiated cluster (12) (Section 8.3.4.7) in Scheme 3. This cluster undergoes the regiospecific substitution reactions (12) → (13) → (14). Further reaction with N-methylmidodiacetate removes the unique iron atom, yielding [Fe$_3$S$_4$ (LS$_3$)]$^{3-}$ (15), the only isolated example of cuboidal (8). The structure of (15) resembles closely the cubane cluster [Fe$_4$S$_4$(LS$_3$)Cl]$^{2-}$, showing that removal of an iron atom does not cause any major changes in the remainder of the core structure. Cluster (15) exhibits the three-member electron transfer series (11);[38] only the central member has been isolated. All attempts to prepare examples of (8) with monofunctional thiolate ligands have thus far been unsuccessful.

$$[Fe_3S_4(LS_3)]^{4-} \leftrightarrow [Fe_3S_4(LS_3)]^{3-} \leftrightarrow [Fe_3S_4(LS_3)]^{2-} \tag{11}$$
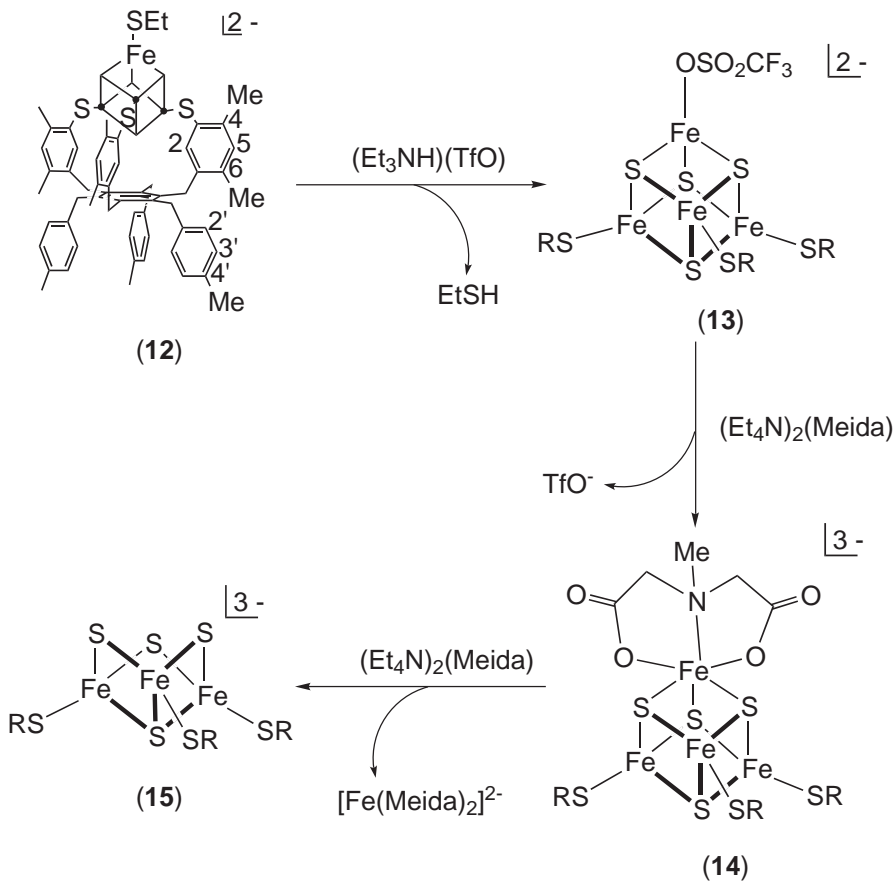
Scheme 3

Cluster (**2**) is usually found in proteins that lack a fourth cysteinyl residue in a normal position for binding to an Fe_4S_4 cluster. Cluster (**15**) is a structural and electronic analogue of site (**2**) in the mixed-valence $[Fe_3S_4]^0$ oxidation state.[38] Double exchange between the two sites of a delocalized $Fe^{III}Fe^{II}$ pair produces a spin $S = 9/2$ which is antiferromagnetically coupled to the $S = S/2$ spin at the Fe^{III} site to generate an $S = 2$ ground state. The existence of this state in (**15**), established by Mössbauer spectroscopy and comparison with proteins, is thus an intrinsic property of the cluster and is independent of protein structure. Protein clusters are generally isolated in the fully oxidized $[Fe_3S_4]^{1+}$ state, which is characterized by an EPR signal near $g \approx 2.01$ corresponding to an $S = 1/2$ ground state. When this cluster is treated with Fe^{II} under reducing conditions in reaction (12), an $[Fe_4S_4]^{2+}$ cluster is formed in which one iron atom is coordinated by an exogenous ligand (water, hydroxide) or a noncysteinate residue. Reaction (13)[38] is closely related to this process. The reverse of reaction (12), probably passing through $[Fe_4S_4]^{3+}$ which releases the iron atom not bound by cysteinate, is the means of formation of protein cluster (**2**) in the oxidized state. Chemical oxidation of $[Fe_4S_4(Stibt)_4]^{2-}$ generates an EPR signal attributed to an $[Fe_3S_4]^{1+}$ cluster[39]. The initial cluster has been oxidized and isolated in the $[Fe_4S_4]^{3+}$ state.[40] In proteins, the reduced nucleophilicity of the $[Fe_3S_4]^{1+}$ portion of $[Fe_4S_4]^{3+}$ and the lack of a terminal cysteinate ligand contribute to the ease of removal of Fe^{II}:

$$[Fe_3S_4]^{1+} + Fe^{2+} + e^- \rightarrow [Fe_4S_4]^{2+} \tag{12}$$

$$[Fe_3S_4(LS_3)]^{3-} + [FeCl_4]^{2-} \rightarrow [Fe_4S_4(LS_3)Cl]^{2-} + 3Cl^- \tag{13}$$
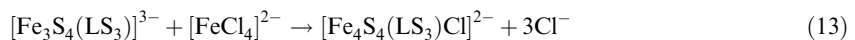
The structures of (**8**) and (**15**) suggest that the clusters might bind a metal at the voided site, thereby forming cubane-type cores. This expectation has been realized for both the native and synthetic clusters. Incubation of proteins having Fe_3S_4 sites with excess metal ion under reducing

conditions leads to the formation of MFe_3S_4 clusters with divalent ions of the first transition series and Cu^I, Cd^{II}, Pb^{II}, and Tl^I.[34,41–43] Reaction (14)[44] occurs with certain reduced metal compounds and thiophilic metals to afford a series of heterometal cubanes with $L-M = Ph_3P-Co^{II}/Ni^{II}/Cu^I/Ag^I$, $(OC)_3Mo^0/W^0$, and $NC-Cu^I/Ag^I$, and $M = Tl^I$. This reaction affords the $[CoFe_3S_4]^{1+}$ oxidation level, one electron more reduced than (**9**). Both reaction (14) and those of Scheme 2 produce isoelectronic $[NiFe_3S_4]^{1+}$ clusters. Reaction (14) includes nonredox binding of thiophilic metals and inner-sphere redox reactions with Co^I and Ni^I. Products of the first reaction type are formulated as $\{M^{1+}+[Fe_3S_4]^0\}$ and retain the $S = 2$ ground state of (**15**). Those of the second are $\{M^{2+}+[Fe_3S_4]^{1-}\}$ with $S = 1$ (Co) and $3/2$ (Ni). A significant feature of these clusters is that the heterometal is incorporated into cores with the reduced fragments $[Fe_3S_4]^{0,1-}$, which function as cluster ligands. The fully oxidized core $[Fe_3S_4]^{1+}$ is evidently insufficiently nucleophilic to act as a general ligand. Only the soft thiophiles Tl^I [45] (weakly) and Cu^I [41,46] have been shown to coordinate to this oxidation state of protein-bound clusters. Electrochemical potentials for metal ion release are consistent with a low binding affinity of $[Fe_3S_4]^{1+}$.[43] Lastly, ground spin states of heterometal protein clusters are interpretable in terms of antiparallel spin coupling between tetrahedral M^{II} and $[Fe_3S_4]^{0,1-}$ fragments.[34] The large majority of synthetic $[MFe_3S_4]^z$ clusters also follow this regularity:[28,35]

$$[Fe_3S_4(LS_3)]^{3-} + [ML'_n]^z \rightarrow [LMFe_3S_4(LS_3)]^{2-,3-} + (n-1)L' \tag{14}$$
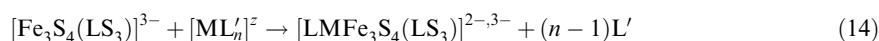
8.3.4 [Fe_4S_4] CLUSTERS

Cubane-type clusters (**16**) constitute the largest family of iron–sulfur clusters. The first examples were synthesized in 1972–73.[47,48] Hundreds of clusters with variant ligands and different oxidation states have been prepared subsequently, those with the $[Fe_4S_4]^{2+}$ core being by far the most common. These clusters are considered in three basic groups followed by other types containing specialized ligation.

(**16**)
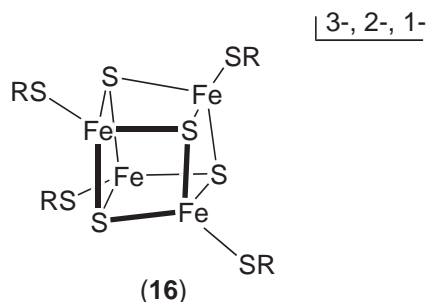
8.3.4.1 Thiolate, Halide, and Related Clusters

As shown in Figure 2, homoleptic thiolate-ligated clusters constitute a four-member electron transfer series whose core oxidation state ranges from all-ferrous $[Fe_4S_4]^0$ to $[Fe_4S_4]^{3+}$ with mean oxidation state $Fe^{2.75+}$. The all-ferric state $[Fe_4S_4]^{4+}$ remains hypothetical. Isoelectronic protein sites and synthetic clusters, illustrated by thiolate-ligated species, are arranged vertically. Thus the clusters $[Fe_4S_4(SR)_4]^{2-}$ (**16**) are analogues of protein site (**3**) in the same oxidation state in ferredoxin and high-potential proteins. The $[Fe_4S_4(SR)_4]^{3-,2-,1-}$ oxidation states have been isolated. Several examples of $[Fe_4S_4(SR)_4]^{4-}$, containing the all-ferrous core $[Fe_4S_4]^0$, have been detected electrochemically, but at potentials indicative of extreme sensitivity to oxidation (e.g., $[Fe_4S_4(SAr)_4]^{3-/4-}$ at -1.5 V to -1.7 V.[26,49]). Because other oxidation states are usually obtained by oxidation or reduction of $[Fe_4S_4(SR)_4]^{2-}$, these clusters are first considered.

Clusters in the $[Fe_4S_4]^{2+}$ state were originally prepared by the self-assembly reaction (15)[47,48]. Subsequently, convenient reactions (16)[52,53] and (17)[52,53] were introduced in which sulfur is the source of sulfide. These reactions are among the very few in which cluster assembly has been resolved into detectable steps.[50] Thus, under the stoichiometry of reaction (17), reaction (18a)

core oxidation state:	$[Fe_4S_4]^0$	$[Fe_4S_4]^{1+}$	$[Fe_4S_4]^{2+}$	$[Fe_4S_4]^{3+}$
	4Fe(II)	3Fe(II) + Fe(III)	2Fe(II) +2Fe(III)	Fe(II) + 3Fe(III)
proteins:	Fe protein† $\longleftarrow$	Fd$_{red}$ $\rightleftharpoons$	Fd$_{ox}$/HP$_{red}$ $\rightleftharpoons$	HP$_{ox}$
analogues:	$[Fe_4S_4(SR)_4]^{4-}$ $\rightleftharpoons$	$^*[Fe_4S_4(SR)_4]^{3-}$ $\rightleftharpoons$	$^*[Fe_4S_4(SR)_4]^{2-}$ $\rightleftharpoons$	$^*[Fe_4S_4(SR)_4]^{1-}$

Fd = ferredoxin. HP = "high-potential" protein. *Isolated. †Nitrogenase.

Figure 2 Electron transfer series of native and synthetic $[Fe_4S_4]$ clusters, showing core oxidation states and formal metal oxidation states. The $[Fe_4S_4]^0$ state in a protein is known only in the Fe protein of nitrogenase.

forms the adamantaine-like complex $[Fe_4(SR)_{10}]^{2-}$,[51] which reacts quantitatively with sulfur to give the product cluster in reaction (18b).[50] The sum (18a) + (18b) = (17). If the reactant mole ratio is increased to RS$^-$:Fe^{III}: S $\geq$ 5:1:1, a different pathway described by sequential reacations (19a), (1), and (19b)[26,50] is followed. The product is generated in the last step by spontaneous dimerization in methanol solution. The sum 4(19a) + 2(1) + (19b) = (17). Reactions (16) and (17) have been conducted in methanol and water. Many of the reactions leading to the formation of $[Fe_4S_4(SR)_4]^{2-}$ have been summarized.[50] Reaction (20)[54,55] is particularly useful for, but not restricted to, the formation of arythiolate clusters. The reaction may be shifted completely to the right by a suitable amount of R$'$SH or removal of product thiol. In this and related systems, mixed clusters of monofunctional ligands are detectable by NMR but are not separable owing to the facile ligand redistribution reaction (21)[54] ($n = 1$–3).

$$4FeCl_3 + 6RS^- + 4HS^- + 4OMe^- \rightarrow [Fe_4S_4(SR)_4]^{2-} + RSSR + 12Cl^- + 4MeOH \qquad (15)$$

$$4FeCl_2 + 10RS^- + 4S \rightarrow [Fe_4S_4(SR)_4]^{2-} + 3RSSR + 8Cl^- \qquad (16)$$

$$4FeCl_3 + 14RS^- + 4S \rightarrow [Fe_4S_4(SR)_4]^{2-} + 5RSSR + 12Cl^- \qquad (17)$$

$$4FeCl_3 + 14RS^- \rightarrow [Fe_4(SR)_{10}]^{2-} + 2RSSR + 12Cl^- \qquad (18a)$$

$$[Fe_4(SR)_{10}]^{2-} + 4S \rightarrow [Fe_4S_4(SR)_4]^{2-} + 3RSSR \qquad (18b)$$

$$FeCl_3 + 5RS^- \rightarrow [Fe(SR)_4]^{2-} + 1/2 \ RSSR + 3Cl^- \qquad (19a)$$

$$2[Fe_2S_2(SR)_4]^{2-} \rightarrow [Fe_4S_4(SR)_4]^{2-} + RSSR + 2RS^- \qquad (19b)$$

$$[Fe_4S_4(SR)_4]^{2-} + nR'SH \rightleftharpoons [Fe_4S_4(SR)_{4-n}(SR')_n]^{2-} + nRSH \qquad (20)$$

$$(4-n)[Fe_4S_4(SR)_4]^{2-} + n[Fe_4S_4(SR')_4]^{2-} \rightleftharpoons 4[Fe_4S_4(SR)_{4-n}(SR')_n]^{2-} \qquad (21)$$
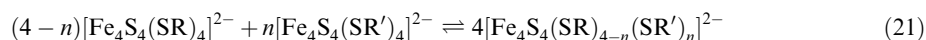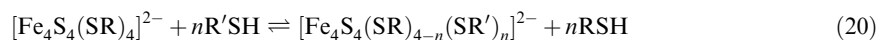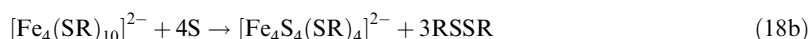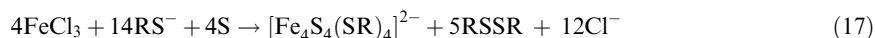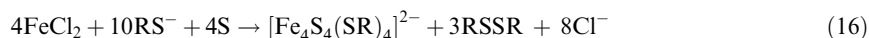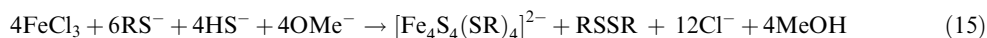
The nucleophilic nature of coordinated thiolate sustains reaction with electrophiles such as weak protonic acids,[56] acyl halides,[19] and sulfonium cations.[57] Reaction (22)[19] is illustrative; intermediate species with $n = 1$–3 are detectable by NMR. The reaction is irreversible; the clusters $[Fe_4S_4X_4]^{2-}$ (X = Cl$^-$, Br$^-$) are available in high yield by this method. These clusters can be directly assembled in the reaction systems FeX$_3$/H$_2$S/Ph$_4$PX[58] and FeCl$_3$/Na$_2$S/R$_4$NBr.[59] The iodo cluster was first made by the reaction of $[Fe_4S_4Cl_4]^{2-}$ with NaI in acetonitrile,[19] and

subsequently by the assembly reaction (23)[60,61] Halide clusters have been isolated only in the $[Fe_4S_4]^{2+}$ state. Their principal feature is ligand lability, leading to extensive use in generalized reaction (24) as precursors to differently substituted clusters. By substitution reactions (20), (24) and others, clusters with a diverse array of ligands have been prepared or generated in solution:

$$[Fe_4S_4(SR)_4]^{2-} + nR'COCl \rightarrow [Fe_4S_4(SR)_{4-n}Cl_n]^{2-} + nR'COSR \qquad (22)$$

$$4Fe(CO)_5 + 4S + I_2 + 2I^- \rightarrow [Fe_4S_4I_4]^{2-} + 20CO \qquad (23)$$

$$[Fe_4S_4X_4]^{2-} + 4L^z \rightarrow [Fe_4S_4L_4]^{z'} + 4X^- \qquad (24)$$
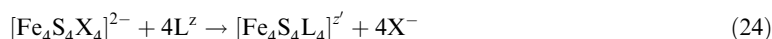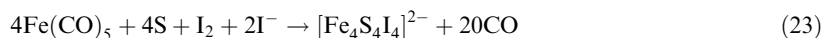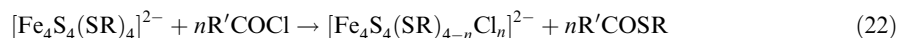
The family of thiolate cluster $[Fe_4S_4(SR)_4]^{2-}$ is exceptionally large, including among others those with the simplest ligand (R = H),[62–64] exceptionally bulky ligands (R = 2,4,6-triisopropyl-benzenethiolate,[39,40] 2,4,6-triisopropylbenzylthiolate,[65] adamantane-1-thiolate[66]), water-solubilizing ligands (R = CH_2CH_2OH,[67,68] $(CH_2)_2CO_2^-$[69]), crown ether ligands,[70,71] macrocyclic tetrathiolates,[72–74] and dendrimeric thiolates (R = dendron).[75,76] Clusters with other ligand types such as phenolate[77] and dithiocarbamate[78] have been prepared. Based on kinetics investigations, mechanisms have been proposed for the substitution of bound thiolate with another thiolate in the presence of weak acid,[79,80] and for reaction (24) with X = Cl^- or Br^- and L = RS^-.[81–83]

8.3.4.2 The $[Fe_4S_4]^{3+}$ Oxidation State

This state is an analogue of the oxidized form of cluster (3) of high-potential iron–sulfur proteins, a subset of ferredoxins demarcated by access to this state. It was first detected by electrochemical oxidation of $[Fe_4S_4(SBu^t)_4]^{2-}$ and related clusters with bulky ligands.[84–86] Thereafter, the redox couple $[Fe_4S_4(Stibt)_4]^{2-/1-}$ was found to be chemically reversible, and $[Fe_4S_4-(Stibt)_4]^{1-}$ was isolated from the oxidation of the cluster dianion in dichloromethane with $[Cp_2Fe](BF_4)$.[40] Other oxidants of moderate strength also effect this oxidation.[39] In some instances, $[Fe_4S_4(SR)_4]^{1-}$ clusters have been generated by γ-irradiation in host single crystals of $[Fe_4S_4(SR)_4]^{2-}$ salts for spectroscopic study.[87,88] While certain $[Fe_4S_4-(SR)_4]^{1-}$ clusters can be generated by chemical or electrochemical oxidation of $[Fe_4S_4(SR)_4]^{2-}$ at moderate potentials (near 0 V), they are clearly much less stable than the precursor dianions. The great majority of oxidation reactions observed electrochemically are irreversible. Conditions have been found with aqueous polymer dispersions that permit observation of the redox couples $[Fe_4S_4-(SAd)_4]^{3-/2-/1-}$ and demonstration of proton-coupled electron transfer reactions.[66,89] Overall, $[Fe_4S_4(SR)_4]^{1-}$ clusters are best stabilized in dry weakly basic solvents such as dichloromethane and with large hydrophobic ligands that protect the electrophilic $[Fe_4S_4]^{3+}$ core from nucleophilic attack.[90,91] Only $(Bu_4N)[Fe_4S_4(Stibt)_4]$ has been isolated in substance. Its EPR and Mössbauer spectroscopic properties establish an $S = 1/2$ ground state and sustain the description of the cluster as an analogue of the HP_{ox} site.

8.3.4.3 The $[Fe_4S_4]^{1+}$ Oxidation State

This state is an analogue of the reduced form of protein cluster (3), and in isolable form is found mainly as the thiolate clusters $[Fe_4S_4(SR)_4]^{3-}$. These species are strongly reducing, and in aprotic solvents show reversible $[Fe_4S_4(SR)_4]^{3-/2-}$ couples at ca. −1.0 V to −1.5 V. The clusters are usually prepared by reduction of $[Fe_4S_4]^{2+}$ clusters, as in reaction (25)[26,95,96] which utilizes the reductant sodium acenaphthylenide in solvents such as acetonitrile/THF. The clusters can also be conveniently obtained in a single-step synthesis using the reaction system $FeCl_2/2NaSR/4NaSH$ in DMF.[92] Excess thiolate is added to neutralize the protons released from hydrosulfide. The oxidant, which removes one electron per four equivalents of Fe^{II}, has not been identified. Reduction of $[Fe_4S_4-(SCH_2CH_2OH)_4]^{2-}$ with dithionite[68] and $[Fe_4S_4(SCH_2CH_2CO_2)_4]^{6-}$ with $[Cr(EDTA)]^{4-}$[93] in aqueous solution to the $[Fe_4S_4]^{1+}$ state have been reported. Redox potentials of $[Fe_4S_4]^{2+/1+}$ couples of thiolate clusters are markedly increased upon passing from a non-aqueous solvent to water. For example, the $[Fe_4S_4(SCH_2CH_2CO_2)_4]^{6-/7-}$ potential in methanol[94] and the $[Fe_4S_4(SCH_2CH_2OH)_4]^{2-/3-}$ potential

in Me_2SO^{67} are raised by ca. 200 mV and 400 mV, respectively, in aqueous solution. Evidently, solvation and attendant hydrogen bonding are effective in attenuating increased negative charge, thereby stabilizing the reduced clusters:

$$[Fe_4S_4(SR)_4]^{2-} + C_{12}H_8{}^{1-} \rightarrow [Fe_4S_4(SR)_4]^{3-} + C_{12}H_8 \tag{25}$$
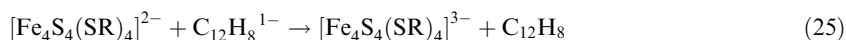
As a class, $[Fe_4S_4(SR)_4]^{3-}$ clusters are unstable to air and are slowly oxidized[97,98] or decomposed by protic molecules. They are usually found with $S = 1/2$ ground states but examples of pure $S = 3/2$ ground states[96] and physical mixtures of the two states[99] are well documented. Both spin states have been found in proteins with EPR spectra that are similar to those of analogue clusters. Electron self-exchange in the systems $[Fe_4S_4(SR)_4]^{2-/3-}$ is very fast ($k \approx 10^6$ M^{-1} s^{-1} at 300 K in acetonitrile).[100] Core chalcogenide exchange reaction (26)[101] occurs spontaneously in acetonitrile at 300 K. All $(4-n, n)$ species have been identified by their isotropically shifted NMR spectra in approximately statistical amounts after several hours of reaction in 10 mM acetonitrile solutions. The reaction is the core analogue of ligand redistribution reaction (21), and signifies core lability. The mechanism of the reaction remains unknown. The same reaction occurs for $[Fe_4Q_4(SR)_4]^{2-}$ clusters $Q = S$, Se but is much slower and requires elevated temperatures:

$$(4-n)[Fe_4S_4(SR)_4]^{3-} + n[Fe_4Se_4(SR)_4]^{3-} \rightleftharpoons 4[Fe_4S_{4-n}Se_n(SR)_4]^{3-} \tag{26}$$
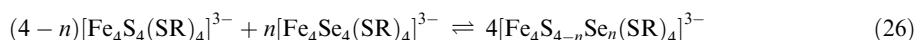
8.3.4.4 Structural Trends of Fe$_4$S$_4$ Clusters

The cubane-type cluster structure (**16**) holds over the preceding three oxidation states. Over 80 crystal structures have been reported, the large majority for $[Fe_4S_4]^{2+}$ clusters. In general, core dimensions are not strongly affected by different types of terminal ligands. Cluster cores are built of concenric interlocking Fe_4 and S_4 tetrahdra or, alternatively, by six edge-shared Fe_2S_2 rhombs; the highest possible symmetry is cubic (T_d). This symmetry is rarely achieved, tetragonal (D_{2d}) or rhombic distortions being frequently encountered. Shape parameters have been described that afford a concise description of structures with D_{2d} symmetry.[102] The term "cubane type" is inclusive of all types of relatively small distortions from cubic symmetry. Cores contain non planar Fe_2S_2 rhomboidal faces and S_4 units whose volume is ca. 2.3 times larger than the volume of the Fe_4 units, with the result that the sulfur atoms are on the outside of the core structure. Each iron site has distorted tetrahedral stereochemistry. Typical core dimensions for early structures in the field have been tabulated.[102] In no case is there any indication of localized Fe^{II} or Fe^{III} valence states, consistent with all spectroscopic data. Structural data for three oxidation states are accessible only with homoleptic thiolate clusters, and reveal several trends and certain irregularities. Clusters (**17a**), (**17b**), and (**17c**) convey typical mean bond lengths (Å) over the three states. Across the series, mean Fe–Fe and Fe–S bond lengths and core volumes tend to increase slightly, consistent with occupation of antibonding orbitals with substantial Fe/S character. Terminal Fe–SR bond lengths increase, in accord with increased Fe^{II} character of the core.

The only $[Fe_4S_4]^{3+}$ structure available is $(Bu_4N)[Fe_4S_4(Stibt)_4]^{40}$ (**17a**). There is no crystallographically imposed symmetry; the core tends toward a tetragonally compressed structure with four Fe–S bonds about 0.06 Å shorter than the other eight. This distortion is particularly clear in $(Et_4N)_2[Fe_4S_4(SCH_2Ph)_4]$ (**17b**), the first $[Fe_4S_4]^{2+}$ structure determined.[48] Under D_{2d} symmetry, core bond lengths and angles divide as Fe–S and S···S $(4+8)$, Fe–Fe $(2+4)$, and Fe–Fe–Fe, S–Fe–S, Fe–S–Fe $(4+8)$. Here four short and eight long Fe–S distances are approximately parallel and perpendicular, respectively, to the idealized $\bar{4}$-axis. A compressed tetragonal distortion is entirely common for $[Fe_4S_4]^{2+}$ clusters, as in, for example, $(Me_4N)_2[Fe_4S_4$-$(SPh)_4]$,[54] $(Me_3NCH_2Ph)_2[Fe_4S_4(SBu^t)_4]$,[85] and $(Ph_4As)_2[Fe_4S_4(SAd)_4]^{66}$ where it is idealized, and in $(Bu_4N)_2[Fe_4S_4(SBu^t)_4]^{103}$ and $(Et_4N)_2[Fe_4S_4(SBu^t)_4]^{85}$ where it is imposed. In $[Fe_4S_4]^{1+}$ clusters, numerous core distortions are observed, many of which are compared elsewhere.[99,104] Among them is that observed in $(Et_4N)_3[Fe_4S_4(SCH_2Ph)_4]^{105}$ (**17c**), where mean Fe–S distances divide into six long and six short, affording an idealized C_2-axis. Exact core shapes and dimensions and also RS–Fe–S angles external to the core for $[Fe_4S_4]^{2+,1+}$ clusters are clearly dependent on forces in the crystalline state. Among the many indications are distortions in monoclinic and orthorhombic forms of $(Bu_4N)_2[Fe_4S_4(SPh)_4]^{106-108}$ that depart from the D_{2d} distortion of the Me_4N^+ salt, small core dimensional differences (Fe–Fe, Fe–S distances) in three salts of $[Fe_4S_4(SBu^t)_4]^{2-}$ with

(17a)   **(17b)**   **(17c)**
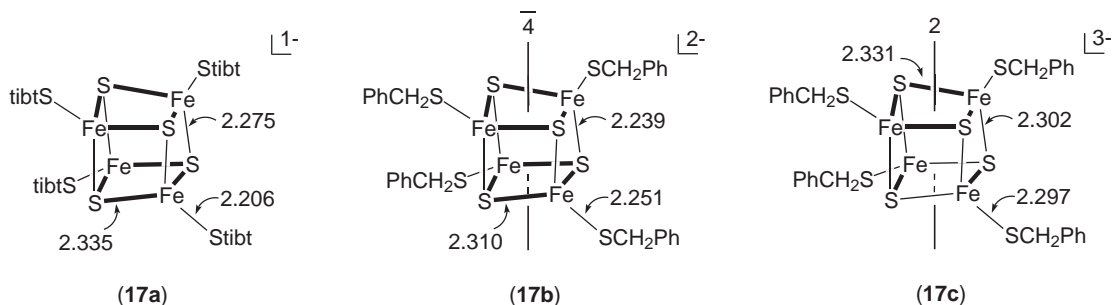
imposed or idealized D_{2d} symmetry, and an $S = 1/2$ ground state in crystalline $(Et_4N)_3$-$[Fe_4S_4(SCH_2Ph)_4]\cdot DMF$ compared to an $S = 3/2$ ground state in the unsolvated compound. It is clearly evident from structural and spectroscopic information that the fine details of $[Fe_4S_4]^{1+}$ cluster structures and the accompanying stabilization of a ground state spin are enormously sensitive to environment. As yet, no correlation has been established between the type(s) of distortion and spin state. Manifold distortions are among the most remarkable features of reduced clusters. They convey a core structure plasticity that may promote the spontaneous core chalcogenide exchange reaction (26).

8.3.4.5 Reactions with π-acceptor Ligands

Generalized ligand substitution reaction (24) proceeds with a variety of anionic ligands such as halides, thiolates, and arene oxides. Certain neutral ligands also substitute on the $[Fe_4S_4]^{2+}$ core, notably isonitriles and tertiary phosphines. Although nitrosyl clusters are not within the purview of this section, we note the existence of cubane-type $[Fe_4S_4(NO)_4]^{0,1-}$[109]. Iron–sulfur–nitrosyl clusters are treated elsewhere.[10,110]

8.3.4.5.1 Isonitrile clusters

In reaction (27),[111,113] a terminal chloride is substituted by three isonitriles (R = Me, Et, Bu^t, Cy, 2,6-Me$_2$C$_6$H$_3$NC) in a regiospecific reaction of a 3:1 site-differeniated cluster. Equilibrium constants in acetonitrile range from 3.8 (R = Me) to 4,900 (R = 2,6-Me$_2$C$_6$H$_3$NC).[111] In reaction (28)[114] with a large excess of isonitrile, two sites are substituted to afford cluster (**18**) (X = Cl$^-$, Br$^-$; R = Me, Et, Bu^t). When the exceptionally labile cluster $[Fe_4S_4I_4]^{2-}$ was reacted with 9 equiv of 2,6-Me$_2$C$_6$H$_3$NC in the presence of cobaltocene, the product is the $[Fe_4S_4]^{1+}$ cluster $[Fe_4S_4(2,6-Me_2C_6H_3NC)_9I]$.[112] Halide ligands in isonitrile clusters undergo normal displacement reactions with thiolate or phenolate ligands. The structure of the latter complex was established as its benzenethiolate substitution product:[112]

$$[Fe_4S_4(LS_3)Cl]^{2-} + 3RNC \rightarrow [Fe_4S_4(LS_3)(RNC)_3]^{1-} + Cl^- \tag{27}$$

$$[Fe_4S_4X_4]^{2-} + 6RNC \rightarrow [Fe_4S_4X_2(RNC)_6] + 2X^- \tag{28}$$
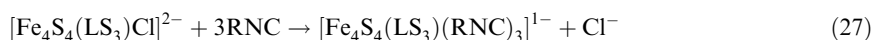
Isonitrile binding produces the six-coordinate diamagnetic sites Fe^{II}S$_3$(RNC)$_3$ in the $[Fe_4S_4]^{2+}$ core, a feature made clear by Mössbauer and structural data.[111,113] These sites are separated from the remaining paramagnetic iron atoms by Fe $\cdots$ Fe distances of 3.0–3.1 Å, compared to normal values of 2.7–2.8 Å between paramagnetic sites. In addition, the two diamagnetic Fe^{II} atoms are separated by 3.45 Å and their mutual Fe–S bond lengths are 2.35–2.38 Å compared to Fe–S distances of 2.23–2.27 Å at the paramagnetic sites. The diamagnetic sites resemble the Fe^{II}S$_3$(CO)$_3$ units in $[Fe_4S_4(CO)_{12}]$, which has crystallographically imposed T_d symmetry, Fe–S bond lengths of 2.33 Å, and nonbonding Fe $\cdots$ Fe distances of 3.47 Å.[115] The formation of low-spin Fe^{II} sites by isonitrile ligation has significant consequences. The clusters $[Fe_4S_4(LS_3)(RNC)_3]^{1-}$ contain the cuboidal $[Fe_3S_4]^0$ core fragment electronically analogous to protein site (**2**) in the same oxidation state.[111,113] Stabilization

(**18**)
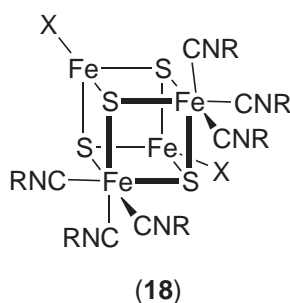
of this fragment by reaction (27) preceded the syntheseis of site analogue $[Fe_3S_4(LS_3)]^{3-}$ (**15**) by six years. Cluster (**18**) has as one face the fragment $[Fe^{III}_2S_2]^{2+}$, which is the core of oxidized protein site (**1**) and contains the bridged $Fe^{III}Fe^{III}$ pair in the $[Fe_4S_4]^{3+}$ core of oxidized HP proteins. Unlike the situation in the latter proteins, the $Fe^{III}Fe^{III}$ pair in (**18**) is isolated from further intracluster magnetic interaction and affords an opportunity to determine the exchange constant J for $[Fe^{III}_2S_2]^{2+}$ within the cubane-type geometry of the protein site. For two clusters, $J = 240$ and $280\,cm^{-1}$ ($H = JS_1 \cdot S_2$), values that should be useful in fitting magnetic data of $[Fe_4S_4]^{3+}$ clusters.[116]

8.3.4.5.2 *Phosphine clusters*

Treatment of $[Fe_4S_4X_4]^{2-}$ in acetonitrile with 4 equiv of PBu^t_3 in THF affords the 3:1 site-differentiated clusters $[Fe_4S_4(PBu^t_3)_3X]$ (**19**, $X = Cl^-$, Br^-, I^-).[117] Reaction of $[Fe_4S_4Cl_4]^{2-}$ with 4.4 equiv of PR_3 ($R = Pr^i$, Cy, Bu^t) in acetonitrile/THF yields the fully substituted clusters $[Fe_4S_4(PR_3)_4]^{1+}$ (**20**).[118] The cause of different extents of subsition is not clear. The product clusters have three notable features: (i) they are in the reduced ($[Fe_4S_4]^{1+}$) state, as indicated by their axial or rhombic EPR spectra arising from an $S = 1/2$ ground state with $g_{av} = 1.99$–2.01 and substantial g-value anisotropy ($g = 1.9$–2.1); (ii) they are formed by tertiary phosphines with cone angles $\gtrsim 160°$. Because R_3PS was detected as a product of the foregoing reactions, the phosphine is the probable reductant, with electrons generated in the formal half-reaction $R_3P + S^{2-} \rightleftharpoons R_3PS + 2e^-$. A ^{31}P NMR study of one reaction system found that phosphine sulfide was formed in an amount consistent with reaction (29),[119] in which the product in quotes is hypothetical. Large phosphine cone angles can be accommodated in cubane-type structures with tetrahedral metal sites. However, phosphines with smaller cone angles, particularly PEt_3 (132°), form clusters of a different structural type (Section 8.3.5.2) Lastly, (iii), $[Fe_4S_4(PR_3)_4]^{1+}$ clusters sustain the reversible three-member electron transfer series (30).[118] For $R = Bu^t$ in dichloromethane, $E_{1/2} = -0.98\,V$ (1+/0) and $0.16\,V$ (2+/1+), placing both the reduced and oxidized members within the range of isolation. However, neither has been isolated. The neutral cluster is susceptible to ligand loss and formation of higher nuclearity species. (Section 8.3.7). The isolation of this cluster is a matter of some interest for its all-ferrous ($[Fe_4S_4]^0$) core is isoelectronic with the cluster in the fully reduced iron protein of nitrogenase.[120]

(**19**)   (**20**)

$$2[Fe_4S_4Cl_4]^{2-} + 5Ppr^i_3 \rightarrow [Fe_4S_4(Ppr^i_3)_4]^{1+} + Pr^i_3PS + 4Cl^- + \text{``}[Fe_4S_3Cl_4]^{1-\text{''}} \tag{29}$$

$$[Fe_4S_4(PR_3)_4]^{2+} \leftrightarrow [Fe_4S_4(PR_3)_4]^{1+} \leftrightarrow [Fe_4S_4(PR_3)_4]^0 \tag{30}$$
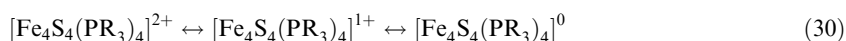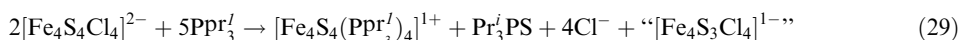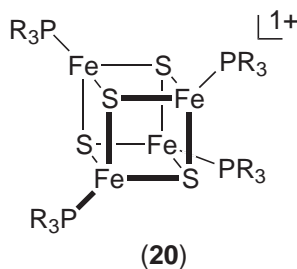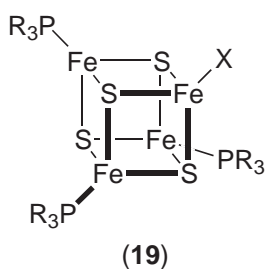
8.3.4.6 Fe$_4$S$_4$ Peptide Clusters

The logical extension of $[Fe_4S_4(SR)_4]^{2-}$ clusters to more realistic analogues of protein site (**3**) by the binding of cysteine derivations or cysteinyl peptides was made early in the development of the field. Ligand substitution reaction (31)[121] proceeds in Me$_2$SO. It is an extension of reaction (20) in which R′SH = Ac-Cys-NHMe or a glycyl–cysteinyl oligopeptide such as 12-(Cys)$_4$peptide = *t*Boc–Gly–Cys–(Gly)$_2$–Cys–(Gly)$_2$–Cys–(Gly)$_2$–Cys–Gly–NH$_2$. The peptide carries the Cys–X–X–Cys spacing found in many Fd sequences. This protocol was extended to other Gly-Cys peptides[122] and to short mono- and dicysteinyl peptides,[123–125] often to demonstrate that N–H···S hydrogen bonding to core sulfur atoms effects small positive shifts in $[Fe_4S_4]^{2+,1+}$ redox potentials. Thereafter, clusters with longer and more physiologically realistic peptides were prepared. The cluster derived from the totally synthetic apoprotein of *Clostridium pasteurianum* Fd, which contains two Fe$_4$S$_4$ clusters, was shown to be essentially identical in properties to the native protein.[126] Mutant peptides were prepared in order to examine the effects of residue variations on stability and redox potentials.[127,128] Further, a 31-residue version of the 58-residue apoprotein of *Desulfovibrio gigas* Fd II was successfully designed to bind an Fe$_4$S$_4$ cluster.[129] In these cases, the clusters were reconstituted from FeCl$_3$, Na$_2$S, and a thiol (often HOCH$_2$CH$_2$SH) in the presence of a peptide using the classic procedure of Rabinowitz:[130]

$$[Fe_4S_4(SBu^t)_4]^{2-} + 12\text{-}(Cys)_4\text{peptide} \rightarrow [Fe_4S_4\{12\text{-}(Cys)_4\text{peptide}\}]^{2-} + 4Bu^tSH \qquad (31)$$
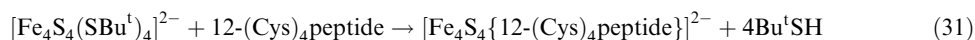
The 16-residue peptide H$_2$N–Lys–Leu–Cys–Glu–Gly–Gly–Cys–Ile–Ala–Cys–Gly–Ala–Cys–Gly–Gly–Trp, containing part of the foregoing sequence and Cys residue spacing common to Fds, has been found to be effective in supporting an $[Fe_4S_4]^{2+}$ cluster generated by the reconstitution procedure, and stabilizing the reduced state $[Fe_4S_4]^{1+}$ formed by reaction with dithionite.[131] Replacement of one or more Cys residues with noncoordinating or potentially coordinating residue (Asp, His) greatly reduced or eliminated cluster incorporation. Further, the effects of residue variation within the consensus sequence and truncation of peptide length were examined.[132] Among the findings are stabilization of the cluster by the consensus motif Cys–Ile–Ala–Cys–Gly–Ala–Cys in a 2:1 complex, requirement of the spacing pattern Cys–X–X–Cys–X–X–Cys and a favorable effect of bulky hydrophobic residues in the consensus motif for cluster formation, and the importance of non-ligating residues on cluster formation with 16-residue peptides. These and other results lead to the identification of factors stabilizing an Fe$_4$S$_4$ cluster in short peptides where cluster binding and stability is not influenced by protein folding.

Tetranuclear clusters have been reconstituted or inserted into proteins of some complexity. A cluster was reconstituted in a four-α helix protein related to the domain of the F$_x$ cluster in the photosystem I reaction center.[133] Using water-soluble $[Fe_4S_4(SCH_2CH_2OH)_4]^{2-}$, a cluster was inserted into an engineered form of thioredoxin rationally designed to bind an Fe$_4$S$_4$ cluster with four Cys residues appropriately juxtaposed in the folded protein structure.[134] Here the protein acts as a scaffold for binding of the cluster. Protein maquettes have been designed to bind an Fe$_4$S$_4$ cluster and two heme groups.[135] The 67-residue peptide consists of two helices with ca. 27 residues connected by a loop containing the sequences Cys–Glu–Gly–Gly–Cys–Ile–Ala–Cys–Gly–Ala–Cys, whose last seven residues constitute part of the primary structure of *Peptococcus aerogenes* Fd. The cluster was introduced in the apoprotein by the reconstituition procedure. Two His residues were included in appropriate positions in the helices such that heme groups bind to one residue from each helix. The molecular assembly with one cluster and two hemes is intended to approach the juxtaposition of redox centers in certain oxidoreductases. In a related approach, a 63-residue helix-loop-helix peptide was synthesized as a scaffold for the stabilization of metal ions bridged by a Cys residue to an Fe$_4$S$_4$ cluster.[136] The loop contains the part of the foregoing consensus sequence and Cys–Glu, affording ^{26}Cys–Glu–^{28}Cys–Ile–Ala–^{31}Cys–Gly–Ala–^{34}Cys. The helices contain additionally His or His and Cys binding residues near the consensus loop. One target molecular assembly is (**21**), in which the cluster is coordinated to three Cys residues of the consensus sequence. The fourth Cys residue bridges the cluster to Ni^{II}, which is additionally bound to three imidazole ligands from His residues forming a planar NiN$_3$S coordination unit. The cluster was introduced by ligand substitution of $[Fe_4S_4(SCH_2CH_2OH)_4]^{2-}$ with the 63mer; Ni^{II} was bound in a subsequent step. The structure, which is intended to simulate the spectroscopically deduced A-Cluster structure of nickel-containing carbon monoxide dehydrogenase, is supported by analytical and spectroscopic evidence, including Ni EXAFS results.[137]
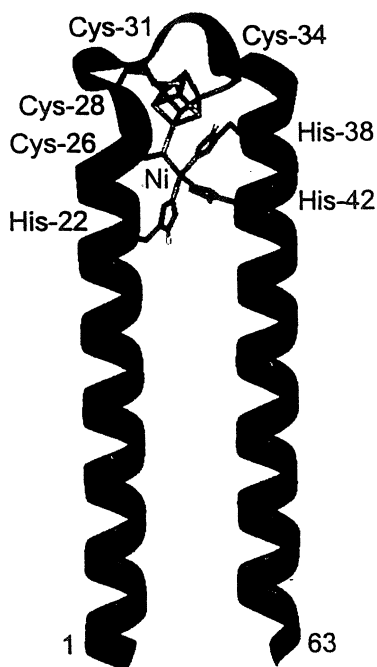
(21)

8.3.4.7 Site-differentiated Fe$_4$S$_4$ Clusters

Clusters of this type depart from homoleptic terminal ligation. Clusters (**18**) and (**19**) are examples of 2:2 and 3:1 site-differentiated clusters. Others, such as [Fe$_4$S$_4$(SPh)$_2$Cl$_2$]$^{2-}$ and [Fe$_4$S$_4$(SPh)$_2$-(O-p-tol)$_2$]$^{2-}$,[138,139] have been obtained as crystalline salts. Additionally, the neutral clusters [Fe$_4$S$_4$-I$_2$L$_2$](L = Ph$_3$PS, thioureides, and related ligands) have been isolated.[140–143] However, in general mixed-ligand clusters tend to disproportionate in processes analogous to the reverse of reaction (21) of homoleptic thiolate clusters. This type of ligand substitution is to be expected with charged clusters in solvents of moderate (or higher) dielectric constant, such as acetonitrile, DMF, and Me$_2$SO. It may be repressed with neutral clusters in low dielectric media in which the disproportionation products are ions. The motivation to prepare site-differentiated clusters free of disproportionation first arose with demonstration of the 3:1 cluster (**4**) (Figure 1) in aconitase, which is the catalytic site.[144] Citrate is bound, activated, and transformed to isocitrate at the unique iron site.

The first ligand to form controlled 3:1 clusters is (**22**) (LS$_3$), in which alternate groups around the central benzene ring are sterically forced above and below the ring.[145] Thus the three thiol-containing "arms" and forced to the same side by the three p-tolylthio "legs." What results is a semirigid trigonally symmetric cavitand-type ligand whose thiol groups are preorganized to capture an Fe$_4$S$_4$ cluster.[146] The tris(indolylthiol) ligand (**23**) appears to utilize the same steric principle,[147] whereas the ligands (**24**) are based on the bowl-shaped cyclotriveratrylene stereochemistry.[148] The structure of [Fe$_4$S$_4$(LS$_3$)(SEt)]$^{2-}$ is shown schematically as (**12**) (Scheme 3). X-ray structure proofs of (**22**)[38,145,146,149,150] and (**23**)[147] functioning as tridentate ligands to a single cluster are available. In addition, a macrocyclic polyether trithiol[151] and a ligand based on tacn with three N-substituents -C(O)-p-C$_6$H$_4$SH,[152] which impose mirror and trigonal symmetry, respectively, on their cluster complexes have been synthesized. X-ray structures have not been reported for complexes of these ligands or of (**24**). Cluster complexes were prepared by ligand substitution reaction (20) (3R'SH = trithiol) or (24) (L^{3-} = trithiolate). All isolated clusters supported by these ligands are in the [Fe$_4$S$_4$]$^{2+}$ oxidation state. Many [Fe$_4$S$_4$(LS$_3$)L']^z clusters undergo reversible electrochemical reduction to the [Fe$_4$S$_4$]$^{1+}$ state and several to the [Fe$_4$S$_4$]^0 state.[49,150,153]

The primary purpose of site differentiation is regiospecific ligand substitution, a property that has been extensively demonstrated for [Fe$_4$S$_4$(LS$_3$)L']$^{2-}$ (L' = Cl$^-$, RS$^-$). Much of the initial work

(22)   **(23)**   **(24)**

$R = CH_2CH_2SH$,
$m\text{-}CH_2C_6H_4CH_2SH$
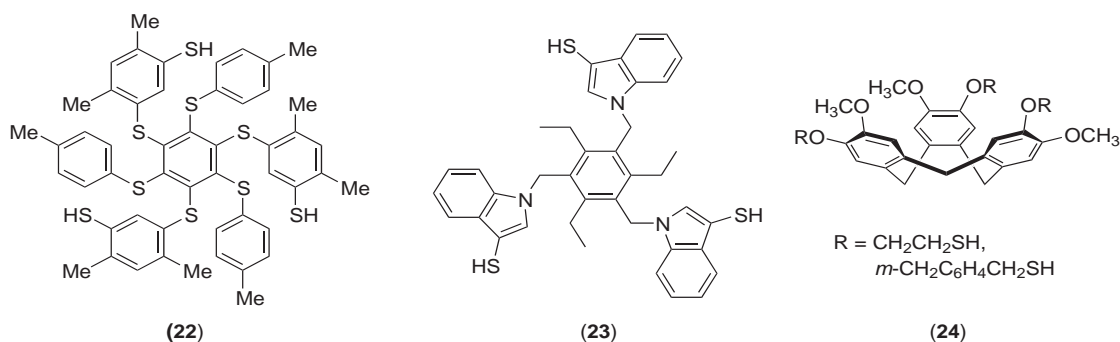
in the area has been summarized.[154] The chloride cluster is obtained from $[Fe_4S_4(LS_3)(SEt)]^{2-}$ by reaction (22) ($n = 1$).[145] Substitution reactions can be monitored by chemical shift changes of 5-H and the methyl groups of the coordinating arms (**12**, Scheme 3), which are exquisitely sensitive to ligand changes at the unique iron site, and/or by shifts in redox potential. A partial summary of such reactions is contained in Scheme 4. Reaction (27) and Scheme 3 also present site-specific reactions. Examples include substitution of chloride by uninegative anions,[153] creation of five- and six-coordinate sites with bi- and tridentate ligands,[155] respectively, formation of double cubanes linked by dithiolate[156], oxo[153] and sulfido[156] bridges, and attachment of coordination units through thiolate[157] and sulfide[158,159] bridges. Reaction (32)[159] illustrates formation of bridged assembly (**25**), related to the catalytic site of a subclass of sulfite reductases, by an unsymmetrical coupling reaction that takes advantage of ca. 35 kcal mol^{-1} energy difference between Si—Cl and Si—S bond strengths, and should be capable of extension. Site-specific substitution reactions have also been described for clusters supported by ligand (**24**)[160] and for the reaction of amino acids with the cluster based on the tacn-derived ligand.[161] $[Fe_4S_4(LSe_3)Cl]^{2-}$ undergoes extensive substitution reactions analogous to those of its sulfur congener.[150] Substitution reactions of 3:1 site-differentiated clusters has led to a large family of mixed-ligand clusters, thereby permitting elucidation of the effects of ligand type, charge, and coordination number on properties such as NMR isotropic shifts, redox potentials, and charge distribution as assessed from ^{57}Fe isomer shifts.

$$[Fe_4S_4(LS_3)(SSiMe_3)]^{2-} + Fe(OEiBC)Cl] \rightarrow \{[Fe_4S_4(LS_3)]S[Fe(OEiBC)]\}^{2-} + Me_3SiCl \qquad (32)$$

(25)
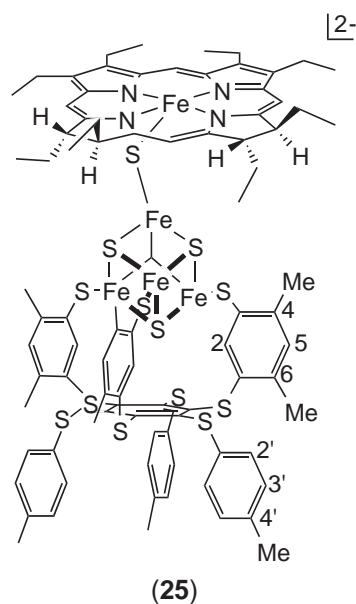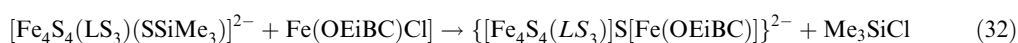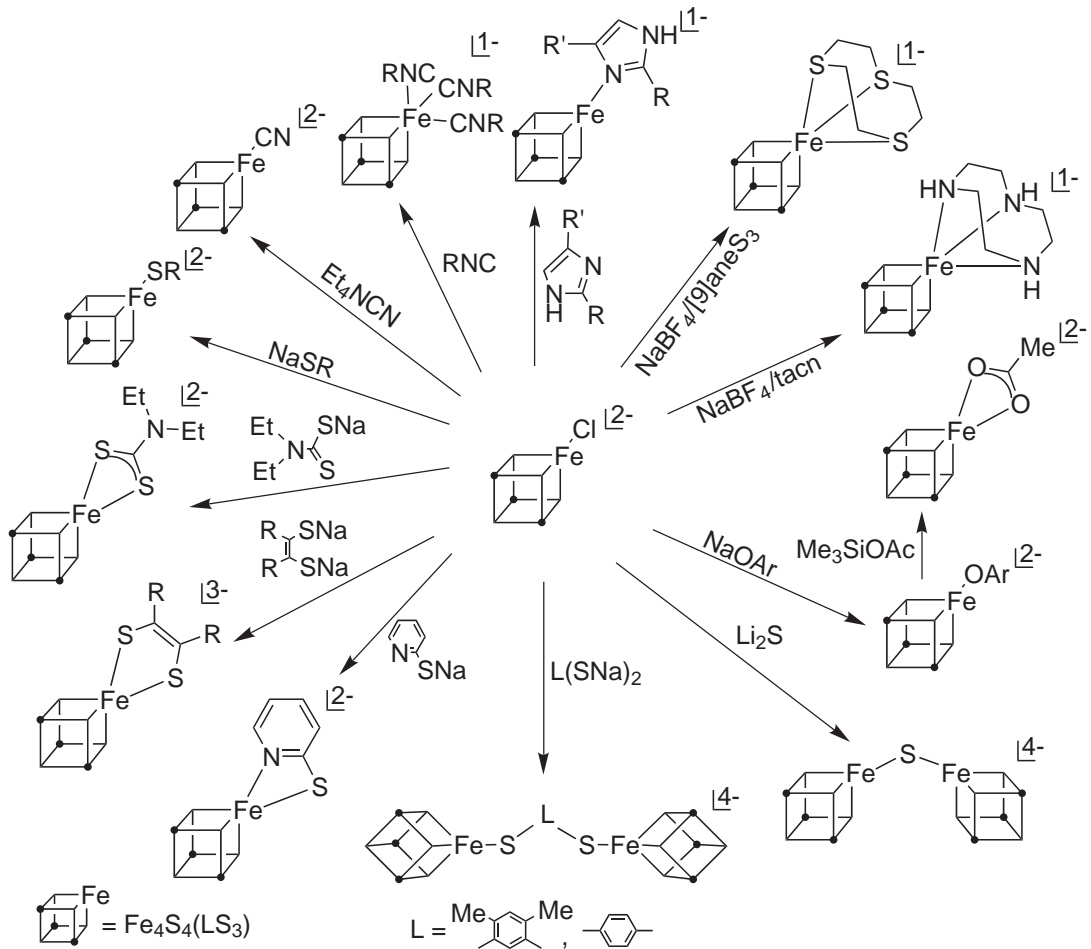
Scheme 4

8.3.4.8 Fe$_4$S$_6$ Clusters

Two clusters containing the all-ferric [Fe$_4$S$_6$]^0 core have been prepared by reaction (33)[162] in acetonitrile (R = Et, 2R = 4,5-Me$_2$C$_6$H$_2$-1,2-(CH$_2$)$_2$). [Fe$_4$S$_6$(SEt)$_4$]$^{2-}$ has also been isolated as a by-product of reaction (7).[162] It has the linear structure (**26**) and is homologous with (**7**):

$$4[Fe(SR)_4]^{2-} + 6S \rightarrow [Fe_4S_6(SR)_4]^{4-} + 4RS^- + 4RSSR \qquad (33)$$
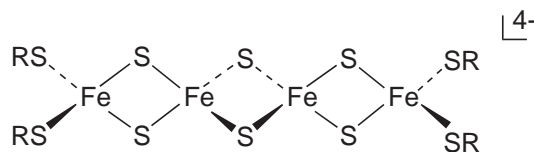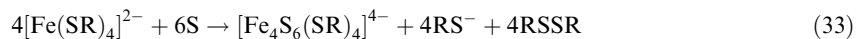
(**26**)

Both of these clusters are solubilized fragments of the solid state compound M^{I}FeS$_2$, which contain chains of edge-shared FeS$_4$ tetrahedra with Fe–S, Fe–Fe, and S$\cdots$S distances very similar to those of the molecular clusters. Only limited reactivity information is available.[162] In aceto-nitrile solution, [Fe$_4$S$_6$(SEt)$_4$]$^{4-}$ slowly converts to mixture of [Fe$_2$S$_2$(SEt)$_4$]$^{2-}$, [Fe$_4$S$_4$(SEt)$_4$]$^{2-}$, and [Fe$_6$S$_9$(SEt)$_2$]$^{4-}$. The durene-α,α'-dithiolate cluster is described as stable. Reaction of [Fe$_4$S$_6$-(SEt)$_4$]$^{4-}$ with FeCl$_2$ in acetonitrile forms [Fe$_4$S$_4$(SEt)$_4$]$^{2-}$. If antiferromagnetic coupling extends to these clusters, a diamagnetic ground state is expected. In that event, the isotropically shifted ^{1}H NMR spectrum of [Fe$_4$S$_6$(SEt)$_4$]$^{4-}$ requires occupation of excited spin state(s).

8.3.5 HEXANUCLEAR (Fe$_6$S$_6$, Fe$_6$S$_8$, Fe$_6$S$_9$) CLUSTERS

Clusters of nuclearity six exhibit the three core compositions indicated and four structural types, two being associated with Fe$_6$S$_6$. In addition, two mixed-valence clusters with lesser sulfur content have been characterized.[163] Treatment of thiolate-bridged [Fe$_2$(EtN$_2$S$_2$)$_2$] with [Fe$_4$S$_4$I$_4$)]$^{2-}$ in dichloromethane affords {[Fe$_2$(EtN$_2$S$_2$)$_2$]$_2$Fe$_4$S$_4$I$_2$}, which contains a stair-like valence-delocalized Fe$_6$(μ_3-S)$_4$ core with mean oxidation state Fe$^{2.5+}$ and two high-spin Fe^{II}N$_2$S$_3$ sites in which the iron atom is coordinated by the tetradentate ligand and one μ_3-S atom. A solution of this cluster in DMF deposits crystalline {[Fe$_2$(EtN$_2$S$_2$)$_2$]$_2$Fe$_4$S$_5$} whose nonplanar delocalized Fe$_4$(μ_4-S)(μ_3-S)$_2$(μ_2-S)$_2$ core also contains Fe$^{2.5+}$. Oxidation states were deduced from isomer shifts.

8.3.5.1 Prismane (Fe$_6$S$_6$) Clusters

The first two examples of prismane clusters [Fe$_6$S$_6$L$_6$]$^{2-,3-}$ (27) were prepared by reactions (34)[164,166] and (35).[165,167] In reaction (34) in acetonitrile, the presence of Et$_4$N$^+$ as the cluster counterion is essential; with other cations, salts of [Fe$_4$S$_4$Cl$_4$]$^{2-}$ are isolated. This reaction extends to the preparation of bromo and iodo clusters when conducted in dichloromethane.[164] Reaction (35), appealing because of the elementary reactants, has been scrutinized after its initial report and found to require carefully controlled workup conditions to obtain pure product.[165] Under ambient conditions, reaction (36)[164,166] is slow, allowing ligand substitution reaction (37)[168] to proceed (L$^-$ = Br$^-$, ArS$^-$, ArO$^-$), analogous to reaction (24). Phenolate-type clusters, typified by [Fe$_6$S$_6$(O-p-tol)$_6$]$^{3-}$, are relatively stable; reaction (36) proceeds to only ca. 40% completion in refluxing acetonitrile in 30 min.[168] Prismane clusters show one quasireversible oxidation at −0.2 V to 0.2 V and reduction at −0.7 V to −1.0 V.[168] No reduced ([Fe$_6$S$_6$]$^{2+}$) cluster has been isolated; oxidized ([Fe$_6$S$_6$]$^{4+}$) clusters can be obtained in high yield by reaction (38)[169,170] (L = Cl$^-$, Br$^-$) and the oxidized iodo prismane directly by reaction (35).

(27)

$$6FeCl_2 + 9PhS^- + 3(Et_4N)Cl + 6S \rightarrow (Et_4N)_3[Fe_6S_6Cl_6] + 9/2\ PhSSPh + 9Cl^- \qquad (34)$$

$$6Fe + 6S + 2I_2 + 2I^- \rightarrow [Fe_6S_6I_6]^{2-} \qquad (35)$$

$$2[Fe_6S_6L_6]^{3-} \rightarrow 3[Fe_4S_4L_4]^{2-} \qquad (36)$$

$$[Fe_6S_6Cl_6]^{3-} + 6L^- \rightarrow [Fe_6S_6L_6]^{3-} + 6Cl^- \qquad (37)$$

$$3[Fe_4S_4L_4]^{2-} + 2[Cp_2Fe]^{1+} \rightarrow 2[Fe_6S_6L_6]^{2-} + 2[Cp_2Fe] \qquad (38)$$
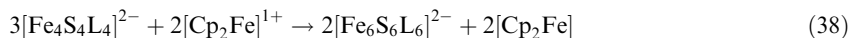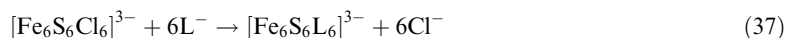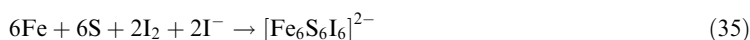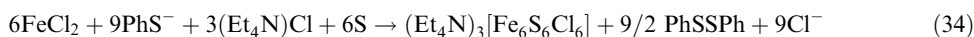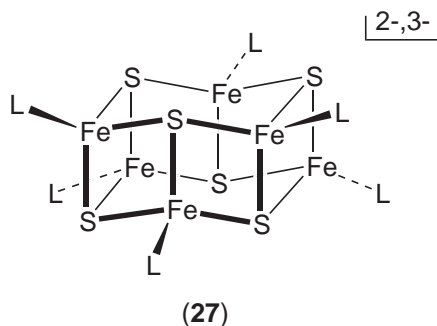
Prismane clusters (27) are distorted hexagonal prisms made up of two Fe$_3$S$_3$ rings in the chair configuration, and eclipsed such that a sulfur atom in one ring binds an iron atom in the other ring. Alternatively, the cluster consists of a cycle of six edge-bridged planar Fe$_2$S$_2$ rhombs. The FeS$_3$L units

have distorted tetrahedral coordination. The highest idealized core symmetry is D_{3d}. Dimensions within the rhombs are quite similar to those in Fe_2S_2 and Fe_4S_4 clusters; Fe–Fe separations are ca. 2.75 Å within a rhomb and ca. 3.8 Å to an iron atom in an adjacent rhomb. Structural and spectroscopic[164,171] evidence are consistent with an electronically delocalized structure for $[Fe_6S_6]^{3+}$ clusters, which have an $S = 1/2$ ground state. Some evidence exists for a temperature-dependent charge localization and structural differentiation of iron sites in two $[Fe_6S_6]^{2+}$ clusters at $\lesssim 20$ K;[170] these clusters have a diamagnetic ground state. The proposal that a protein apparently incorporating six iron atoms contains a prismane cluster has been invalidated by a crystal structure that reveals one cluster (**3**) and a noncubance Fe_4 unit with mixed ligation.[172] Other than in the clusters (**27**), the isolated hexagonal prismane core exists only in $[Fe_6S_6(NO)_6]^{2-}$.[173,174]

The remarkable reaction (39)[176,177] results in the capping of a prismane to afford the reduced $[Fe_6S_6]^{2+}$ clusters (**28**) (L = Cl^-, Br^-, ArO^-; M = Mo, W) in which the Fe_6S_6 core remains intact. The tricarbonyl, used in excess, acts as a ligand and as a reductant when the 3-/4- potential of the product cluster is above ca. −0.25 V. The putative carbonyl cation product has not been identified. Oxidized clusters $[Fe_6S_6L_6(M(CO)_3)_2]^{3-}$ can be obtained by reaction of the reduced clusters with $[Cp_2Fe]^{1+}$ or by using a more nearly stoichiometric quantity of tricarbonyl. The reaction of $[Fe_6S_6I_6]^{2-}$ with $[NiI_4]^{2-}$ forms $[Fe_3Ni_5S_6I_8]^{4-}$, in which the prismane core has been disrupted and a doubly capped structure is formed.[175] These noteworthy reactions indicate the potential of prismanes in the formation of high-nuclearity clusters:

$$[Fe_6S_6L_6]^{3-} + 3[M(CO)_3(MeCN)_3] \rightarrow [Fe_6S_6L_6\{(M(CO)_3)_2\}]^{4-} + 6MeCN + [M(CO)_3(MeCN)_3]^{1+} \quad (39)$$
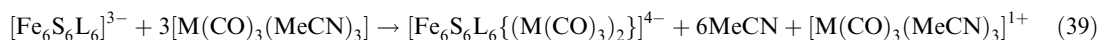
8.3.5.2   Basket (Fe_6S_6) Clusters

The clusters $[Fe_6S_6(PR_3)_4L_2]$ (**29**) as depicted resemble an inverted basket with an Fe-(μ_2-S)-Fe handle. They are readily formed in the assembly systems $[Fe(PEt_3)_2X_2]/(Me_3Si)_2S$ or Li_2S and $2[Fe(PEt_3)_2X_2]/[Fe_4S_4X_4]^{2-}$ or $[Fe_6S_6Cl_6]^{3-}$ (X = Cl^-, Br^-, I^-).[178] The system containing the cubane cluster is the method of choice. In a related approach, the reaction of $[Fe_4S_4I_4]^{2-}$ with a large excess of PMe_2Ph or $PMePh_2$ yields the corresponding iodo basket clusters in high yield.[143] Analogous reaction systems containing $[Fe(PEt_3)_2(SPh)_2]$ (generated *in situ*) and $(Me_3Si)_2S$ or $[Fe_4S_4(SPh)_4]^{2-}$ afford $[Fe_6S_6(PEt_3)_4(SPh)_2]$.[179] Alternatively, the chloride ligands in $[Fe_6S_6(PR_3)_4Cl_2]$ are displayed by PhS^- to give the thiolate cluster; benzoyl chloride converts this species to the chloride cluster. While the clusters $[Fe_4S_4(SR)_4]^{2-}$ do not react with tertiary phosphines at room temperature, the neutral mixed-ligand clusters $[Fe_4S_4(SR)_2(tmtu)_2]$ lead to $[Fe_6S_6(PR_3)_4(SR)_2]$.[143] Halide clusters containing the $[Fe_6S_6]^{2+}$ core with mean oxidation state $Fe^{2.33+}$ have an $S = 1$ ground state.[180] With cubane reactants, the apparent stoichiometry of basket core formation is given by reaction (40),[143] marking another case where a tertiary

(**28**)

(**29**)
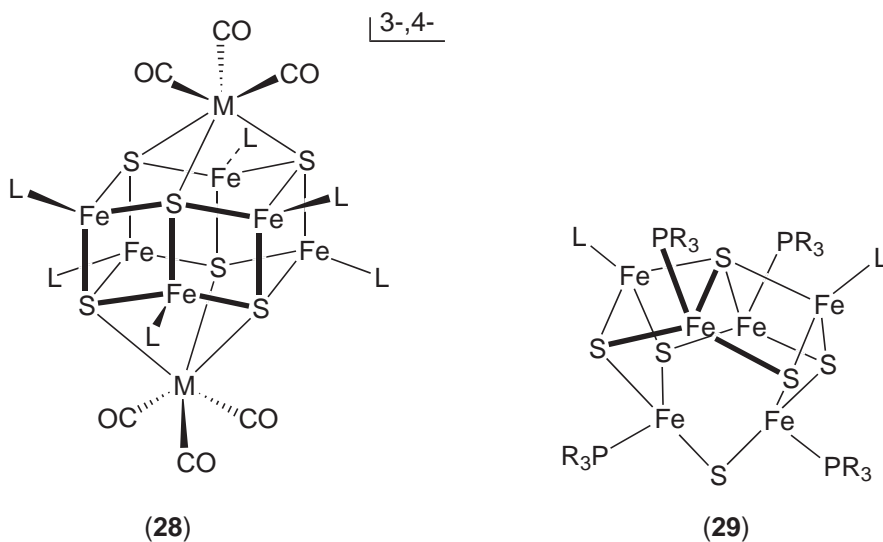
phosphine functions both as ligand and a reductant. The reaction system $[Fe(OH_2)_6](BF_4)_2/Li_2S/$ $4PEt_3$ in THF yields the homoleptic phosphine cluster $[Fe_6S_6(PEt_3)_6]^{1+}$ as the BF_4^- salt.[181] The $[Fe_6S_6]^{1+}$ core of this cluster has mean oxidation state $Fe^{2.17+}$; the source of oxidation of the Fe^{II} starting material has not been identified. The ground state is $S = 1/2$.[180] $[Fe_6S_6(PEt_3)_4Cl_2]$ undergoes acid-catalyzed substitution of chloride by PhS^- in acetonitrile solution; a mechanism has been proposed in which the initial site of protonation is a μ_3-S atom:[182]

$$5[Fe_4S_4]^{2+} + 2PR_3 \rightarrow 3[Fe_6S_6]^{2+} + 2R_3PS + 2Fe^{2+} \tag{40}$$

The structures of a representative set of basket clusters have been determined.[143,178,179,181] Bond distances for three clusters have been tabulated.[10] The $[Fe_6(\mu_2\text{-}S)(\mu_3\text{-}S)_4(\mu_4\text{-}S)]^{2+,1+}$ cores have idealized C_{2v} symmetry and are built by fusion of six nonplanar Fe_2S_2 rhombs to form an open basket with an Fe–S–Fe handle whose bond angle is 74–76°. The FeS_3Cl sites are normal, showing trigonally distorted tetrahedral coordination with the iron atoms ca. 1.0 Å above the S_3 plane. The FeS_3P sites are quite different, with trigonal pyramidal coordination, iron atoms ca. 0.10 Å above the S_3 plane, and two markedly obtuse S–Fe–S angles (127–141°). These flattened trigonal sites appear to be essential to core stability. Although the matter has not been systematically investigated, basket clusters thus far are formed by phosphines with cone angles of $\lesssim 140°$[183] whereas the cubane-type clusters $[Fe_4S_4(PR_3)_4]^{1+}$ are stabilized by phosphines with cone angles in excess of this value (160–182°). Bulky phosphines would tend to destabilize flattened pyramidal sites and therewith the basket core sterochemistry. Basket and prismane cores are isomeric, but clusters with isoelectronic cores have not been isolated. In dichloromethane, $[Fe_6S_6(PEt_3)_4Cl_2]$ exhibits a chemically reversible reduction at -0.78 V and oxidation at $+0.18$ V.[178] Oxidation produces the $[Fe_6S_6]^{3+}$ state, isoelectronic with that in prismanes such as $[Fe_6S_6Cl_6]^{3-}$. Coulometrically generated solutions of $[Fe_6S_6(PEt_3)_4Cl_2]^{1+}$ do not show electrochemical features attributable to other clusters, indicating that the oxidized cluster has not converted to another species. It remains to be demonstrated whether there can exist a basket version of $[Fe_6S_6L_6]^z$ or a prismane version of $[Fe_6S_6(PR_3)_4L_2]^z$ in any oxidation states(s) z.

The reaction system $4.5[Fe(PBu_3)_2(SPh_2)]/[Fe_4S_4(SPh)_4]^{2-}$ in acetonitrile/THF produces $[Fe_6S_6(\mu_2\text{-}SPh)(PBu_3)_4(SPh)_2]$.[184] This cluster has the basket topology with the handle containing a thiolate instead of sulfide bridge and a bond angle of 75°. Evidently, arylation, and possibly alkylation or protonation, at the handle sulfur site preserves the basket topology.

8.3.5.3   Fe$_6$S$_8$ Clusters

Clusters with this core composition have the generic core M_6Q_8 structure of idealized O_h symmetry found in the halide clusters of molybdenum and tungsten and the chalcogenide clusters of rhenium. All isolated clusters are of the type $[Fe_6(\mu_3\text{-}S)_8(PEt_3)_6]^z$ (**30**, $z = 0$ to 3+) in which an Fe_6 octahedron is surrounded by an S_8 cube. Each iron atom has square pyramidal FeS_4P coordination and is displaced by 0.25–0.31 Å toward the phosphorus atom. The first clusters prepared were $[Fe_6S_8(PEt_3)_6]^{2+,1+}$, obtained in low (15–20%) yield from the assembly system $[Fe(OH_2)_6]^{2+}/$ $3PEt_3/H_2S$ and isolated as BF_4^- or BPh_4^- salts.[185–187] The five-member electron transfer series (**41**)[187] was established by cyclic voltammetry; in dichloromethane it extends over the potential

(30)
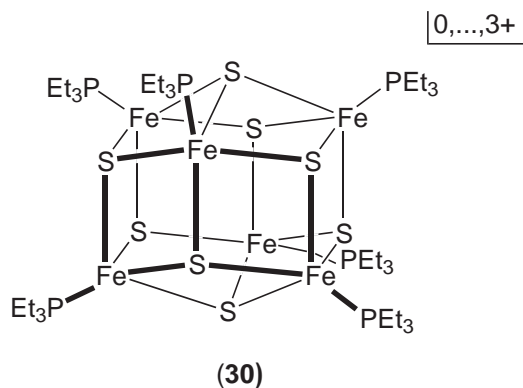
range 1.36 V (4+/3+) to −1.03 V (1+/0), indicating that all members except $[Fe_6S_8(PEt_3)_6]^{4+}$ are sufficiently stable for isolation. Thereafter, the protocol in Scheme 5 was developed,[188] leading to the isolation of $[Fe_6S_8(PEt_3)_6]^{3+,0}$ as well as the clusters $[Fe_6S_8(PEt_3)_6]^{2+,1+}$ prepared earlier. The principal difficulty in synthesis is the low yield of $[Fe_6S_8(PEt_3)_6]^{2+}$, from which other clusters are derived by oxidation or reduction reactions:

$$[Fe_6S_8(PEt_3)_6]^{4+} \leftrightarrow [Fe_6S_8(PEt_3)_6]^{3+} \leftrightarrow [Fe_6S_8(PEt_3)_6]^{2+} \leftrightarrow [Fe_6S_8(PEt_3)_6]^{1+} \leftrightarrow [Fe_6S_8(PEt_3)_6]^{0} \quad (41)$$
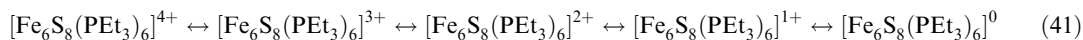
Cluster structure is presented in the orientation (**30**) to emphasize its relation to prismanes by the formal capping of (**27**) with two μ_3-S atoms. Structures have been determined for the four isolated members of series (41).[186–189] All members are mixed valence except the all-ferric 2+ cluster. Proceeding from the 3+ to the neutral cluster, Fe–Fe bond lengths steadily increase from 2.58 Å to 2.67 Å, Fe–P distances shorten by 0.06 Å, and Fe–S and nonbonding S⋯S distances do not show clear-cut trends. The Fe–Fe distances are indicative of direct, albeit weak, bonding interactions. Isomer shifts at 4.2 K increase from 0.22 mm s^{-1} to 0.36 mm s^{-1}, reflecting increasing reduction (Fe$^{3.17+}$ to Fe$^{2.67+}$).[188] The clusters are delocalized and paramagnetic in all oxidation states with the ground-state spins $S = 3/2$ (3+), 3 (2+), 7/2 (1+), and 3 (0). Few clusters exceed in redox capacity $[Fe_6S_8(PEt_3)_6]^{z}$, which possess the structural and electronic features requisite to extensive electron tranfer. Series (41) presents the first example of a cluster type isolated and structurally characterized over four sequential oxidation states.

8.3.5.4   Fe$_6$S$_9$ Clusters

The initial example of cluster (**31**) is $[Fe_6S_9(SBu^t)_2]^{4-}$, which was prepared in the assembly system $6FeCl_3/9Li_2S/4-8LiSBu^t/12LiOMe$ in methanol and was isolated as the $(Me_3NCH_2Ph)^+$ salt.[190,191] Cluster formation is circumscribed by a narrow range of reaction conditions; otherwise, $[Fe_4S_4 (SBu^t)_4]^{2-}$ is formed. Thereafter, a second assembly system in methanol was devised in which Na_2S_2 is the source of sulfide. The apparent stoichiometry in this system, which affords $[Fe_6S_9 (SR)_2]^{4-}$ (R = Me, Et, CH$_2$Ph) as Et$_4$N$^+$ salts and avoids cubane cluster formation, is given by reaction (42).[193] Clusters have also been obtained by another assembly system, $6[Fe(SEt)_4]^{2-}/9S$ in acetonitrile at 85 °C, which proceeds by reaction (43).[11] The same cluster is also formed by heating a solution of $[Fe_3S_4(SEt)_4]^{3-}$ in acetonitrile (Scheme 1). The cluster $[Fe_6S_9(SBu^t)_2]^{4-}$ undergoes ligand substitution with benzenethiol;[191] it and $[Fe_6S_9(SEt)_2]^{4-}$ show a one-electron oxidation and reduction at ca. −0.6 V and −1.8 V, respectively, in acetonitrile.[191,192]

6 [Fe(OH$_2$)$_6$](BF$_4$)$_2$/5 Li$_2$S/ $\frac{1}{2}$Na$_2$S$_2$/xs PEt$_3$

| THF

[Fe$_6$S$_6$(PEt$_3$)$_6$]$^{1+}$

2 S | THF

[Fe$_6$S$_8$(PEt$_3$)$_6$]$^{1+}$

O$_2$ | THF

[Fe$_6$S$_8$(PEt$_3$)$_6$]$^{2+}$ (15%)

Na$^+$Ph$_2$CO$^-$ | MeCN   Na$^+$Ph$_2$CO$^-$ or Zn | CH$_2$Cl$_2$ MeCN   I$_2$ | CH$_2$Cl$_2$

[Fe$_6$S$_8$(PEt$_3$)$_6$]   [Fe$_6$S$_8$(PEt$_3$)$_6$]$^{1+}$ [Fe$_6$S$_8$(PEt$_3$)$_6$]$^{3+}$

Scheme 5

(31)

$$6FeCl_3 + 6Na_2S_2 + 18RS^- \rightarrow Na_4[Fe_6S_9(SR)_2] + 7RSSR + 3Na_2S + 2NaSR + 18Cl^- \qquad (42)$$

$$6[Fe(SEt)_4]^{2-} + 9S \rightarrow [Fe_6S_9(SEt)_2]^{4-} + 7EtSSEt + 8EtS^- \qquad (43)$$
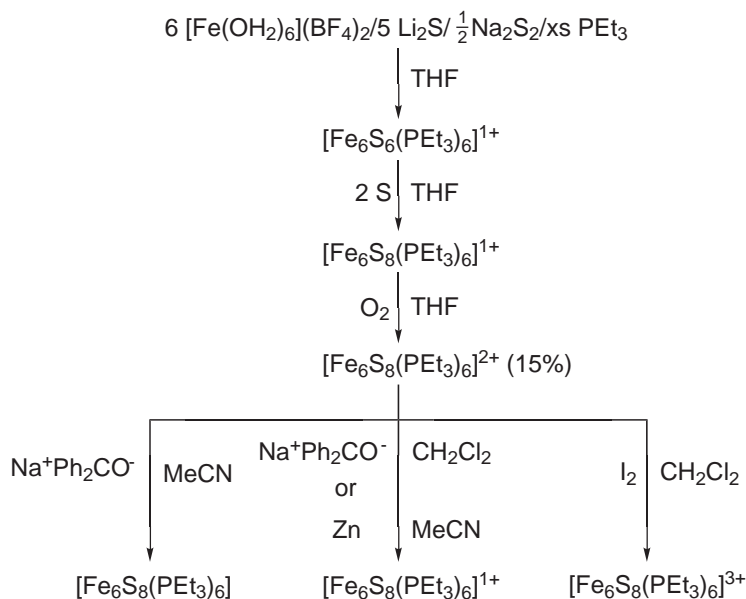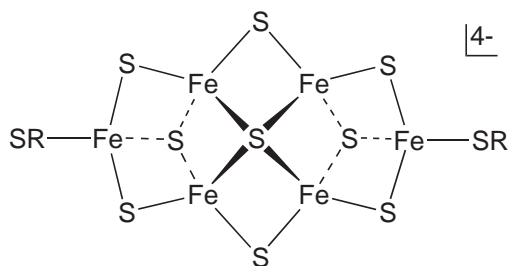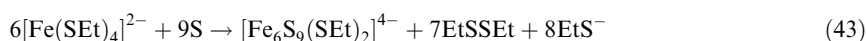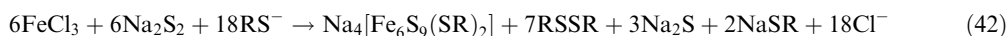
Structure (**31**) has been established for five clusters.[11,191,193,194] The $[Fe_6S_9]^{2-}$ core has idealized C_{2v} symmetry and the unusual bridging pattern $[Fe_6(\mu_4\text{-}S)(\mu_3\text{-}S)_2 (\mu_2\text{-}S)_6]$. It is formed of eight Fe_2S_2 rhombs that are fused such that two rhombs share all their edges and the other six present two unshared edges at the exterior of the cluster. The central Fe_4 rectangle is planar and the Fe_6 portion is coplanar within ca. 0.2 Å. The μ_4-S atom is displaced by ca. 1.3 Å directly above Fe_4 plane. The clusters are mixed-valence ($Fe^{2.67+}$). The assignment $(Fe^{3+})_2(Fe^{2.5+})_4$ is consistent with Mössbauer data.[192] Core symmetry implies delocalization of the central Fe_4 rectangle. The core topology subsumes cores of other clusters, including Fe_2S_2 (**6**), linear Fe_3S_4 (**7**), cuboidal Fe_3S_4 (**8**), and Fe_4S_6 (**26**). It does not occur in any other molecular iron–sulfur cluster or in solid state compounds. The same topology is found in the heterometal clusters $[(edt)_2 Mo_2Fe_4S_9]^{3-,4-}$, in which molybdenum atoms occupy the positions of the terminal iron atoms in (**31**).[192,195]

8.3.6 HEPTANUCLEAR (Fe_7S_6) AND OCTANUCLEAR (Fe_8S_6, Fe_8S_8, Fe_8S_9, Fe_8S_{12}) CLUSTERS

Clusters with nuclearities 7 and 8 comprise some five types, of which few examples of each have been synthesized. Reactivity properties of these clusters are largely unexplored.

8.3.6.1 Fe₇S₆ Cluster

The only example of this cluster type is $[Fe_7S_6(PEt_3)_4Cl_3]$ (**32**).[196] The cluster is assembled in 60% yield by the system $FeCl_2/(Me_3Si)_2S/2PEt_3$ in THF, which is very closely related to that which affords the basket cluster $[Fe_6S_6(PEt_3)_4Cl_2]$. Consequently, this cluster is also formed and has been separated from the desired product by fractional crystallization. Cluster (**32**) contains the core $[Fe_7(\mu_4\text{-}S)_3(\mu_3\text{-}S)_3]^{3+}$ of idealized C_{3v} symmetry, which is also the molecular symmetry (excluding ethyl groups). Iron sites are tetrahedrally coordinated. The cluster is paramagnetic with an $S = 1/2$ ground state.[180]

8.3.6.2 Fe₈S₆ Clusters

The first cluster synthesized was $[Fe_8S_6I_8]^{3-}$ (**33**) from the assembly system $[Fe_6S_6I_6]^{2-}/2Fe/I^-/1/2$ I_2 in dichloromethane in a sealed flask at 60 °C.[197] The reaction mixture was allowed to stand for several weeks; the cluster as its Et_4N^+ salt was separated mechanically in 40% yield. Subsequently, reaction (44)[198] in acetonitrile/THF was found to produce the reduced cluster in 40% yield after six days and a tedious workup. The structures of $[Fe_8S_6I_8]^{4-,3-}$ have been determined.[197,198] The cores $[Fe_8S_6]^{5+,4+}$ have idealized O_h symmetry and consist of a concentric Fe_8 cube and an S_6 octahedron. The sulfur atoms cap the faces of the cube and generate 12 Fe_2S_2

quadrilateral faces. Dimensions are normal and vary only slightly with oxidation level; Fe–Fe distances average 2.70 Å. This cluster type has been obtained in two other ways. Reaction of double cubane $[Fe_8S_8(PCy_3)_6]$ (Section 8.3.6.3) with chloroform affords $[Fe_8S_6(PCy_3)_4Cl_4]$ in low yield.[118] One isomer was isolated; crystalline D_{2d} symmetry requires adjacent iron atoms to have different terminal ligands. Treatment of the basket cluster $[Fe_6S_6(PMePh_2)_4Cl_2]$ in dichloromethane with two equivalents of $[RuI_2(MeCN)_4]$ results in the high-yield formation of $\{[(MeCN)_4(Ph_2MePS)Ru]_2Fe_8S_6I_8\}$ in which trans μ_5-S atoms bind Ru^{II} and four iron atoms of opposite faces of the Fe$_8$ cube.[199] Mixed-metal clusters having $[Fe_6Ni_2S_6]^{4+}$ and $[Fe_4Ni_4S_6]^0$ cores with the M$_8$S$_6$ structure of (33) and terminal iodide and phosphine ligands have been prepared.[199]

$$[Fe_4S_4I_4]^{2-} + 3FeI_2 + 3I^- + 4PMePh_2 \rightarrow {}^1/_2[Fe_8S_6I_8]^{4-} + Ph_2MePS + 3[FeI_3(PMePh_2)_3]^{1-} \quad (44)$$
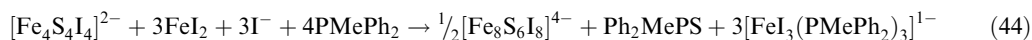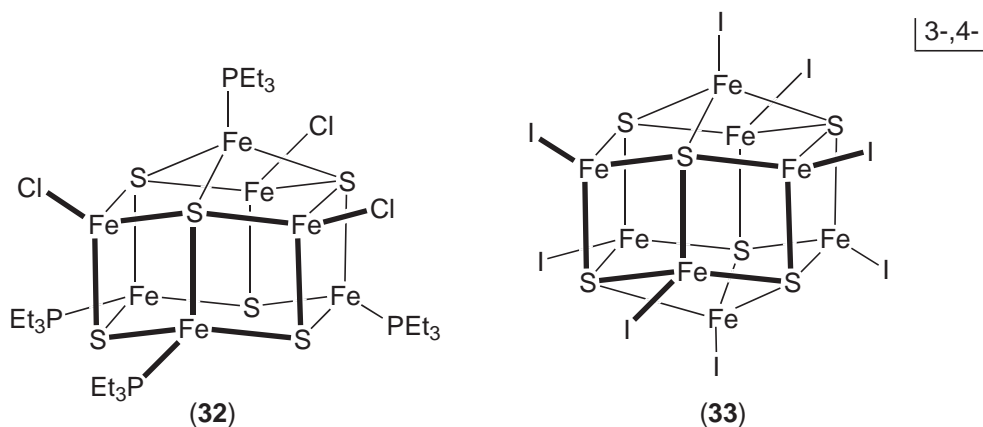
8.3.6.3 Fe$_8$S$_8$ Clusters

With reference to Scheme 6, cubane cluster (20) can be reduced to the neutral cluster, which has resisted isolation as such. Instead, upon standing in the indicated solvent mixture, benzene, or toluene the double cubane $[Fe_8S_8(PR_3)_6]$ (34, R = Pr^i, Cy) or tetracubane $[Fe_{16}S_{16}(PR_3)_8]$ (35) crystallizes.[118,200,201] The former contains the all-ferrous core $[Fe_8(\mu_4\text{-}S)_2(\mu_3\text{-}S)_6]$ of idealized C_{2h} symmetry. Structure (34) is that of an edge- or rhomb-bridged double cubane, a motif that extends to certain other metal–sulfur clusters such as $[(Cl_4cat)_2(Et_3P)_2Mo_2Fe_6S_8(PEt_3)_4]^{0,1-}$.[202,203] The bridging Fe$_2$S$_2$ rhomb has normal metric features (Fe–Fe, 2.68 Å; Fe–S, 2.31 (intercubane), 2.41 (intracubane) Å; S–Fe–S, 111°) as does the remainder of the molecule. Iron sites are tetrahedrally coordinated. $[Fe_8S_8(PCy_3)_6]$ is sparingly soluble; the only reported reactivity property is formation of $[Fe_8S_6(PCy_3)_4Cl_4]$ by reaction with chloroform. Reaction of 3:1 site-differentiated $[Fe_4S_4(2,4,6\text{-}Me_3C_6H_2NC)_9I]$ with $K[B(4\text{-}ClC_6H_4)_4]$ in THF precipitates KI and yields the only other known edge-bridged iron–sulfur double cubane, $[Fe_8S_8(2,4,6\text{-}Me_3C_6H_2NC)_{18}]^{2+}$, in which each nonbridging iron atom has the six-coordinate binding mode found in (18).[112]

8.3.6.4 Fe$_8$S$_9$ Clusters

Clusters of this type are sulfido-bridged double cubanes formed by the coupling reactions (45) (L = Cl$^-$, L$_3$ = LS$_3$)[149,156,204] and the reversible reaction (46).[158] The bridged structure (36) has been proven for $[(Fe_4S_4Cl_3)_2S]^{4-}$, for which the bridge Fe–S distance is 2.21 Å and the Fe–S–Fe angle is 102°.[204] Within the cubanes, the Fe–S bond lengths average to 2.23 Å, indicating an unstrained bridge bond. The related cluster $\{[Fe_4Se_4(LS_3)]_2Se\}^{4-}$ has an equivalent structure, with larger bridge angles of 113° and 115° in crystallographically inequivalent molecules. A conspicuous feature of the double cubanes is coupled reduction reactions. In acetonitrile, reductions occur at −1.10 V and −1.41 V for $[(Fe_4S_4Cl_3)_2S]^{4-}$, and at −1.26 V and −1.50 V for $\{[Fe_4S_4\text{-}(LS_3)]_2S\}^{4-}$.[149] Heterometal MoFe$_3S_4$ clusters can be coupled to double cubanes by chloride substitution analogous to reaction (45); the reaction

$[Fe_4S_4(PR_3)_4]^{1+}$ (**20**)

$K^+Ph_2CO^-$

THF

$[Fe_4S_4(PR_3)_4]^0$

standing in THF/MeCN ~7days

(**34**)

(**35**)
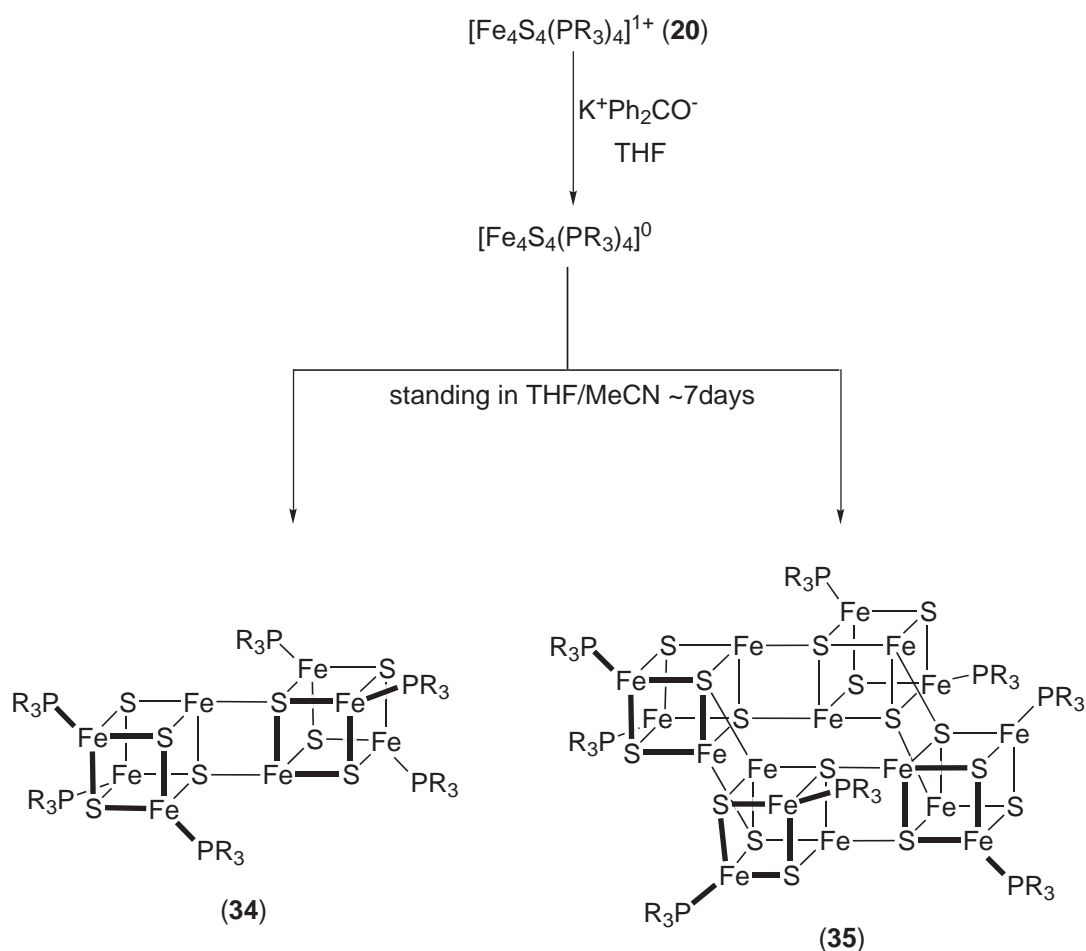
Scheme 6

products also display coupled reductions.[149,205,206] Potential separations of ca. 240–320 mV are one diagnostic property of sulfide-bridged double cubanes. The same is true for the oxo-bridged double cubane. $\{[Fe_4S_4(LS_3)]_2O\}^{4-}$, which reduces at -1.24 V and -1.47 V in Me_2SO.[153] Sulfide bridges are cleaved by water and by protic acids and other electrophiles.

$$2[Fe_4S_4L_3Cl]^{2-} + Li_2S \rightarrow [(Fe_4S_4L_3)_2S]^{4-} + 2LiCl \tag{45}$$

$$2[Fe_4S_4(LS_3)(SH)]^{2-} \rightarrow [Fe_4S_4(LS_3)]_2S^{4-} + H_2S \tag{46}$$

(**36**)
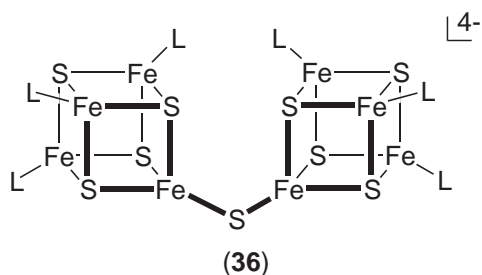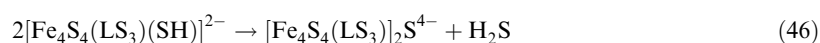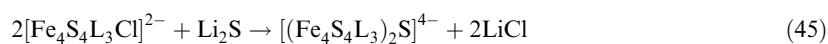
Self-condensation of the fundamental cubane cluster, $[Fe_4S_4(SH)_4]^{2-}$, in acetonitrile forms sulfide-bridged cubanes.[63] The simplest process is the reversible reaction (47). However, unlike reaction (46) further condensations are possible. On the basis of NMR and mass spectroscopic-results, it was concluded that the prevalent species under the experimental conditions employed is $\{[Fe_4S_4(SH)_3]_2[Fe_4S_4(SH)_2](\mu_2\text{-}S)_2\}^{6-}$, a cluster of nuclearity 12 with proposed structure (**37**). This species was not isolated in substance:

$$2[Fe_4S_4(SH)_4]^{2-} \rightarrow [Fe_4S_4(SH)_3]_2S^{4-} + H_2S \qquad (47)$$

(**37**)
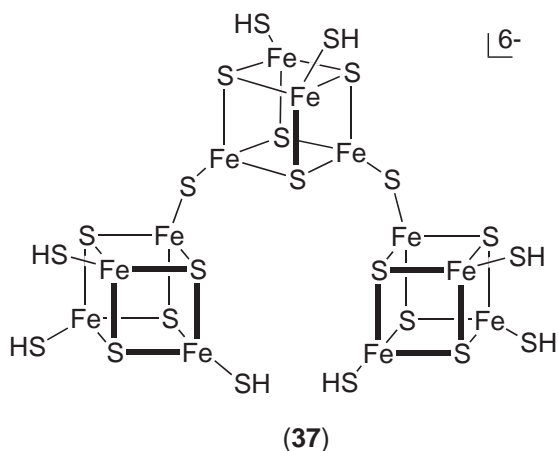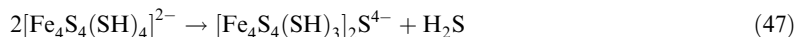
8.3.6.5 Fe$_8$S$_{12}$ Cluster

The only cluster of this type is an unexpected product of the reaction system $[Fe_4S_4(SEt)_2\text{-}(Bu^tNC)_6]/6.3$ $(PhCH_2S)_2S$ in benzene.[207] $[Fe_8S_{12}(CNBu^t)_6]$ (**38**) contains two "cubanoid" units $Fe_4S_5 = Fe_4(\mu_3\text{-}S)_3(\mu_3:\eta^2\eta^1\text{-}S_2)$ bridged by two μ_2-S atoms and related by an inversion center. Certain features of the precursor cluster are retained in the product. Each cubanoid unit contains two low-spin distorted octahedral $Fe^{II}S_3(Bu^tNC)_3$ and two distoted tetrahedral Fe^{III} $(\mu_3\text{-}S)_3(\mu_2\text{-}S)$ sites, which are clearly detectable in the Mössbauer spectrum. The persulfide coordination mode has been found in other iron–sulfur clusters such as $Cp_4Fe_4S_3(S_2)$ and $Cp_4Fe_2(S_2)_2$.[10] The bridged cubanoid motif has not been encountered previously. The cluster is antiferromagnetically coupled with an $S = 0$ ground state. It shows two well-defined reductions at -1.40 V and -1.80 V and oxidations at -0.30 V and 0.04 V, likely attributable to the tetrahedral Fe^{III} and octahedral Fe^{II} sites, respectively. No other reactivity properties are known.

L = CNBu^t

(**38**)
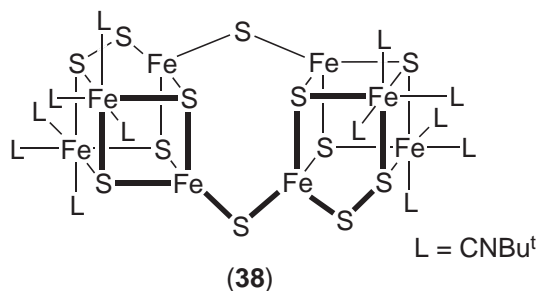
8.3.7 HIGHER NUCLEARITY CYCLIC CLUSTERS

Other than solution species (**37**), all clusters with nuclearity exceeding 8 possess ring structures.

8.3.7.1 Fe$_{16}$S$_{16}$ Clusters

Formation of [Fe$_{16}$S$_{16}$(PR$_3$)$_8$] (**35**, R = Pr^i, Cy, Bu^t) occurs by the association of individual cubanes upon dissociation of labile phosphine ligands as shown in Scheme 6.[118,201] Isolation of both (**34**) and (**35**) is assisted by their low solubility under the conditions employed. The synthesis of [Fe$_{16}$S$_{16}$(PPr$^i_3$)$_8$] has been optimized to 60% yield.[201] Cluster (**35**) is a cyclic tetracubane built by the edge-sharing of eight Fe$_2$S$_2$ rhombs, such that the cluster has D_4 symmetry. It is a unique structure. The central portion consists of two Fe$_4$(μ_4-S)$_4$ rings. The core is all-ferrous with the bridging modality [Fe$_{16}$(μ_4-S)$_8$(μ_3-S)$_8$]^0. Clusters (**34**) and (**35**) are members of a potentially extensive family of polycubanes [Fe$_{4n}$S$_{4n}$(PR$_3$)$_p$] for which structural principles have been described.[118] Enumeration of these clusters proceeds by fusing a single cubane with each of the distinct (n−1) cubanes in all possible edge-bridging arrangements and eliminating duplicates. The acyclic tricubane [Fe$_{12}$S$_{12}$(PR$_3$)$_8$] is one such cluster, and may be an intermediate in the formation of a tetracubane. This cluster, which can exist as three isomers, has not been detected.

8.3.7.2 Fe$_{18}$S$_{30}$ Clusters

In the course of seeking self-assembly systems that might not yield one or more of the clusters considered in preceding sections because of the exclusion of strongly binding terminal ligands, the system FeCl$_3$/3.1Na[PhC(O)Me]/1.8Li$_2$S in ethanol:methanol (2:1 v/v) was examined.[208,209] Addition of R$_4$NBr (R = Pr, Bu) after three hours reaction time followed by standing of the reaction mixture for five days afforded the corresponding salt of α-[Na$_2$Fe$_{18}$S$_{30}$]$^{8-}$ (**39**) in 60–75% yield. Small alteration of reaction conditions and workup procedure gave a second cluster, β-[Na$_2$Fe$_{18}$S$_{30}$]$^{8-}$ (**40**), in 70–75% yield.[210] Unlike all preceding species, these clusters contain no terminal ligands and are isomers in the same oxidation state (14Fe^{III} + 4Fe^{II}, Fe$^{2.78+}$). All iron sites have distorted tetrahedral coordination. The clusters assume that shape of a disc or toroid with the approximate dimensions $l \times w \times h = 13 \times 16 \times 3.3$ Å. Two Na$^+$ are encapsulated within. The pathway of formation of these clusters is obscure, but appears to pass through the sodium salt of the dark green-brown colloidal [FeS$_2$]$_n^{n-}$ whose formation is promoted by sodium acetanilate. Sodium ions may exert a template effect on ring closure and reduce negative charge; intractable products are obtained upon substituting Li$^+$ or K$^+$ for Na$^+$.

(**39**)　　　　　　　　　　(**40**)
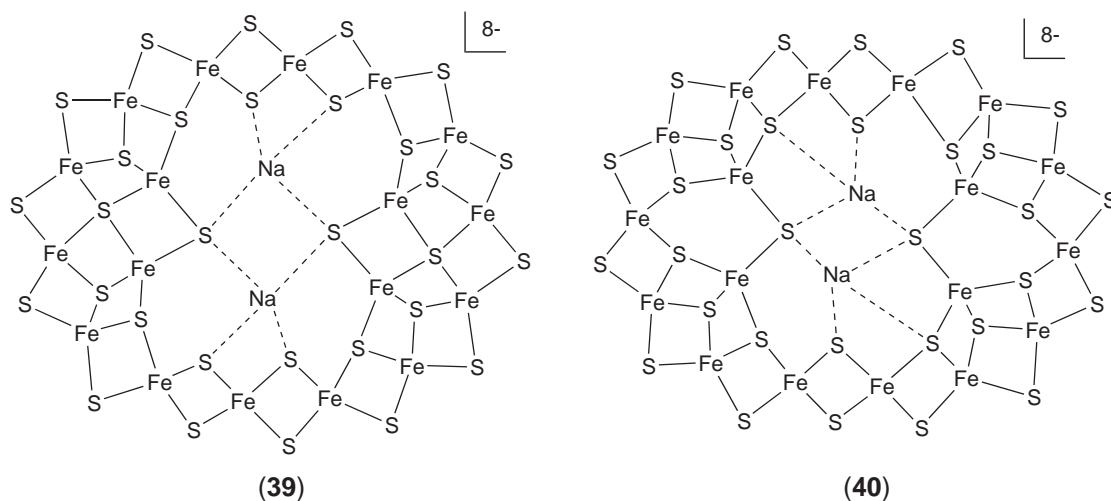
The two clusters have different Fe–S connectivity patterns, leading to isomers. The α-isomer is built up entirely of 24 vertex- and edge-shared Fe$_2$S$_2$ rhombs. Alternatively, it is conceptually constructed by the sequential connection of two linear Fe$_3$S$_4$ and two Fe$_6$S$_9$ units. The core structure is [Fe$_{18}$(μ_4-S)$_2$(μ_3-S)$_8$(μ_2-S)$_{20}$]$^{10-}$. The β-isomer contains two sulfur atoms that do not belong to rhombs, but instead are in two Fe$_3$S$_3$ rings. It is the second example, together with the basket (**29**), of a cluster not wholly constructed by the sharing of Fe$_2$S$_2$ rhombs. The prismanes (**27**) also contain such rings, but all atoms are included in rhombs. The core structure is [Fe$_{18}$(μ_3-S)$_{12}$(μ_2-S)$_{18}$]$^{10-}$. In addition to Fe$_2$S$_2$, both clusters contain as fragments the linear

and cuboidal Fe_3S_4 and Fe_4S_6 cores; as noted, Fe_6S_9 is included in the α-isomer. The clusters exhibit intense absorption extending through the visible region, a diamagnetic ground state and antiferromagnetically coupled excited states, two quasireversible or chemically reversible oxidations at ca. $-0.4\,V$ and $-0.6\,V$ in DMF, and a band-like extended Hückel molecular orbital structure.[209,210] The ring structures of clusters (**39**) and (**40**) are unique. An even larger cluster with no terminal ligands, $[Na_9Fe_{20}Se_{38}]^{9-}$, built up from 21 Fe_2Se_2 rhombs and possessing a bicyclic ring structure with the shape of a prolate ellipsoid, has been prepared and structurally characterized.[210]

8.3.8 SUMMARY

No other two elements in combination generate the diversity of cluster types as do iron and sulfur. The situation derives from two stable oxidation states of iron, bridging multiplicities of two to six for sulfide, and formation of significantly covalent Fe–S bonds.[211] Further, the large majority of cluster types stabilize more than one oxidation state linked by chemically reversible reactions, and two (or more) states are sometimes isolable. Beinert,[5] in remarking on the evolution, pervasive occurrence, and unusual properties of biological iron-sulfur clusters, has emphasized the chemical versatility of sulfur. The fundamental building block is the $Fe_2(\mu_2\text{-}S)_2$ rhomb; edge and/or vertex sharing with other rhombs occurs in all clusters and, except for two cases, provides the connectivities responsible for the entire core structure. Alternatively, many structures are describable as edge-shared tetrahedral (including terminal ligands). The prevalent stereochemistry at iron sites is tetrahedral or variously distorted versions thereof, the intrinsically preferred geometry for $Fe^{II,III}$ with weak-field ligands such as sulfide, thiolate, and halide. The structural flexibility of iron and sulfur is responsible for conversions between different core structures of the same and different compositions; examples are summarized elsewhere.[3]

Certain systematics are evident in cluster structures in addition to rhomb sharing, which is maximized in cyclic (**39**) and (**40**). Consider the formal core conversions and topologies in Figure 3.[212] Isomeric prismane and basket cores differ by placement of one iron atom. Capping the Fe_3S_3 face of a prismane generates the monocapped prismane Fe_7S_6 core. A second capping step produces the Fe_8S_6 core, variously described as a cuboctahedron or stellated octahedron, or as a rhombic dodecahedron in a distortion from cubic symmetry. This structure type occurs not only in (**33**) and $[Fe_8S_6(PCy_3)_4Cl_4]$ but also in the heterometal clusters (**28**) and in $Fe_{8-n}Ni_nS_6$ species ($n = 2, 4, 5$).

As extensive as the current set of iron–sulfur clusters is, there remain many other structural possibilities. A theory of enumeration and structure classification for metal chalcogenide clusters based on edge-sharing of tetrahedra has been developed.[213,214] Structures are predicted and computer-generated for a given stoichiometry $M_m(\mu_n\text{-}Q)_pL_l$ ($m \leq 8$, $l > 0$). These constitute a database of real or potential cluster topologies. The number of structures becomes unmanageably large above $m = 4$. Given that all structurally proven clusters with $m > 4$ exhibit uniterminal ligation at each iron atom, and in the entire set of synthetic clusters the bridging multiplicity rarely exceeds 4, the restrictive criteria $l = 1$ and $n \leq 4$ for any m may be imposed. Among the findings, there are unique solutions for $M_3Q_4L_3$ (**8**), $M_4Q_4L_4$ (**16**), and $M_6Q_9L_2$ (**31**), and three solutions for $M_6Q_6L_6$. Two of these are the prismane (**27**) and basket (**29**) topologies, together with an unknown cluster having the core $[Fe_6(\mu_4\text{-}S)(\mu_3\text{-}S)_3(\mu_2\text{-}S)_2]$. In the case of isomers, recourse may be taken to electronic structure calculations to determine the structure of lowest energy. For example, the structure of $[Fe_6S_6Cl_6]^{2-,3-}$ is correctly predicted as the prismane by extended Hückel results.[213] If the $l = 1$ restriction is dropped, a single solution appears for $M_3Q_4L_4$ (**7**) and $M_4Q_6L_4$ (**26**), and three more structures for $M_6Q_9L_2$. Further, for certain members of the sets $M_4Q_{3-6}L_{4-7}$, $M_5Q_{4-8}L_{4-8}$, and $M_6Q_{4-10}L_{2-10}$, a total of 13 (2), 57 (6) and 342 (16) structures, respectively, are enumerated. The numbers in parentheses satisfy the restrictions $l = 1$ and $n \leq 4$.

An abundance of synthetic targets in iron–sulfur cluster remains, especially in unexplored areas such as pentanuclear clusters. Whether known clusters represent all energetically feasible topologies under ordinary conditions for nuclearities $m = 4$, 6, and 8, remains an open issue. Given that the nitrogenase P-cluster structure (**5**) (Figure 1) was not correctly predicted and is unprecedented, it is reasonable to assume that not all iron–sulfur cluster products of biosynthesis have been discovered.
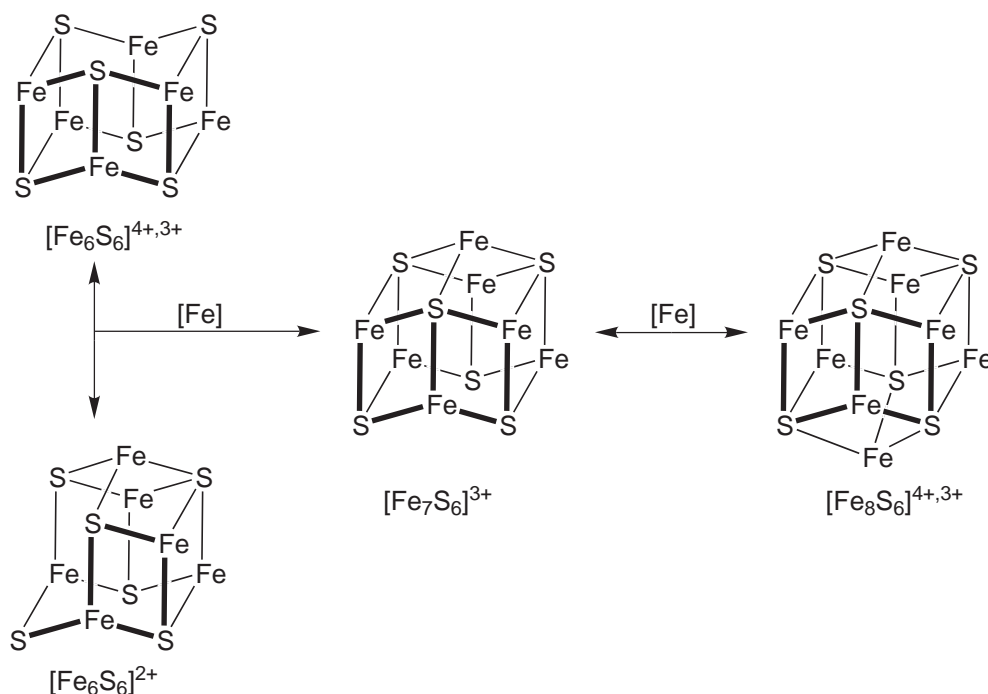
Figure 3 Formal relationship among Fe_6S_6, Fe_7S_6, and Fe_8S_6 cores by rearrangement and capping events.

8.3.9 REFERENCES

1. Holm, R. H. *Adv. Inorg. Chem.* **1992**, *38*, 1–71.
2. Cammack, R. *Adv. Inorg. Chem.* **1992**, *38*, 281–322.
3. Beinert, H.; Holm, R. H.; Münck, E. *Science* **1997**, *277*, 653–659.
4. Beinert, H.; Kiley, P. J. *Curr. Opin. Chem. Biol.* **1999**, *3*, 152–157.
5. Beinert, H. *J. Biol. Inorg. Chem.* **2000**, *5*, 2–15.
6. Peters, J. W.; Stowell, M. H. B.; Soltis, S. M.; Finnegan, M. G.; Johnson, M. K.; Rees, D. C. *Biochemistry* **1997**, *36*, 1181–1187.
7. Mayer, S. M.; Lawson, D. M.; Gormal, C. A.; Roe, S. M.; Smith, B. E. *J. Mol. Biol.* **1999**, *292*, 871–891.
8. Bertini, I.; Ciurli, S.; Luchinat, C. *Struct. Bonding* **1995**, *83*, 1–53.
9. Mouesca, J.-M.; Lamotte, B. *Coord. Chem. Rev.* **1998**, *178–180*, 1573–1614.
10. Ogino, H.; Inomata, S.; Tobita, H. *Chem. Rev.* **1998**, *98*, 2093–2121.
11. Hagen, K. S.; Watson, A. D.; Holm, R. H. *J. Am. Chem. Soc.* **1983**, *105*, 3905–3913.
12. Han, S.; Czernuszewicz, R. S.; Spiro, T. G. *Inorg. Chem.* **1986**, *25*, 2276–2277.
13. Mayerle, J. J.; Denmark, S. E.; DePamphilis, B. V.; Ibers, J. A.; Holm, R. H. *J. Am. Chem. Soc.* **1975**, *97*, 1032–1045.
14. Reynolds, J. G.; Holm, R. H. *Inorg. Chem.* **1980**, *19*, 3257–3260.
15. Balasubramanian, A.; Coucouvanis, D. *Inorg. Chim. Acta* **1983**, *78*, L35–L36.
16. Ueyama, N.; Ueno, S.; Nakata, M.; Nakamura, A. *Bull. Chem. Soc. Jpn.* **1984**, *57*, 984–988.
17. Ueno, S.; Ueyama, N.; Nakamura, A.; Tukihara, T. *Inorg. Chem.* **1986**, *25*, 1000–1005.
18. Coucouvanis, D.; Swenson, D.; Stremple, P.; Baenziger, N. C. *J. Am. Chem. Soc.* **1979**, *101*, 3392–3394.
19. Wong, G. B.; Bobrik, M. A.; Holm, R. H. *Inorg. Chem.* **1978**, *17*, 578–584.
20. Cleland, W. E.; Averill, B. A. *Inorg. Chem.* **1984**, *23*, 4192–4197.
21. Beardwood, P.; Gibson, J. F. *J. Chem. Soc., Chem. Commun.* **1985**, 102–104.
22. Salifoglou, A.; Simopoulos, A.; Kostikas, A.; Dunham, R. W.; Kanatzidis, M. G.; Coucouvanis, D. *Inorg. Chem.* **1988**, *27*, 3394–3406.
23. Beardwood, P.; Gibson, J. F.; Johnson, C. E.; Rush, J. D. *J. Chem. Soc., Dalton Trans.* **1982**, 2015–2020.
24. Mascharak, P. K.; Papaefthymiou, G. C.; Frankel, R. B.; Holm, R. H. *J. Am. Chem. Soc.* **1981**, *103*, 6110–6116.
25. Beardwood, P.; Gibson, J. F. *J. Chem. Soc., Dalton Trans.* **1983**, 737–747.
26. Cambray, J.; Lane, R. W.; Wedd, A. G.; Johnson, R. W.; Holm, R. H. *Inorg. Chem.* **1977**, *16*, 2565–2571.
27. Coucouvanis, D.; Al-Ahmad, S. A.; Salifoglou, A.; Papaefthymiou, V.; Kostikas, A.; Simopoulos, A. *J. Am. Chem. Soc.* **1992**, *114*, 2472–2482.
28. Zhou, J.; Scott, M. J.; Hu, Z.; Peng, G.; Münck, E.; Holm, R. H. *J. Am. Chem. Soc.* **1992**, *114*, 10843–10854.
29. Girerd, J.-J.; Papaefthymiou, G. C.; Watson, A. D.; Gamp, E.; Hagen, K. S.; Edelstein, N.; Frankel, R. B.; Holm, R. H. *J. Am. Chem. Soc.* **1984**, *106*, 5941–5947.
30. Kennedy, M. C.; Kent, T. A.; Emptage, M.; Merkle, H.; Beinert, H.; Münck, E. *J. Biol. Chem.* **1984**, *259*, 14463–14471.
31. Richards, A. J. M.; Thomson, A. J.; Holm, R. H.; Hagen, K. S. *Spectrochim. Acta* **1990**, *46A*, 987–993.
32. Gailer, J.; George, G. N.; Pickering, I. J.; Prince, R. C.; Kohlhepp, P.; Zhang, D.; Walker, F. A.; Winzerling, J. J. *J. Am. Chem. Soc.* **2001**, *123*, 10121–10122.

33. Krebs, C.; Henshaw, T. F.; Cheek, J.; Huynh, B. H.; Broderick, J. B. *J. Am. Chem. Soc.* **2000**, *122*, 12497–12506.
34. Johnson, M. K.; Duderstadt, R. E.; Duin, E. C. *Adv. Inorg. Chem.* **1999**, *47*, 1–82.
35. Ciurli, S.; Ross, P. K.; Scott, M. J.; Yu, S.-B.; Holm, R. H. *J. Am. Chem. Soc.* **1992**, *114*, 5415–5423.
36. Ciurli, S.; Yu, S.-B.; Holm, R. H.; Srivastava, K. K. P.; Münck, E. *J. Am. Chem. Soc.* **1990**, *112*, 8169–8171.
37. Zhou, J.; Holm, R. H. *J. Am. Chem. Soc.* **1995**, *117*, 11353–11354.
38. Zhou, J.; Hu, Z.; Münck, E.; Holm, R. H. *J. Am. Chem. Soc.* **1996**, *118*, 1966–1980.
39. Roth, E. K. H.; Jordanov, J. *Inorg. Chem.* **1992**, *31*, 240–243.
40. O'Sullivan, T.; Millar, M. M. *J. Am. Chem. Soc.* **1985**, *107*, 4096–4097.
41. Staples, C. R.; Dhawan, I. K.; Finnegan, M. G.; Dwinell, D. A.; Zhou, Z. H.; Huang, H.; Verhagen, M. F. J. M.; Adams, M. W. W.; Johnson, M. K. *Inorg. Chem.* **1997**, *36*, 5740–5749.
42. Butt, J. N.; Fawcett, S. E. J.; Breton, J.; Thomson, A. J.; Armstrong, F. A. *J. Am. Chem. Soc.* **1997**, *119*, 9729–9737.
43. Fawcett, S. E. J.; Davis, D.; Breton, J. L.; Thomson, A. J.; Armstrong, F. A. *Biochem. J.* **1998**, *335*, 357–368.
44. Zhou, J.; Raebiger, J. W.; Crawford, C. A.; Holm, R. H. *J. Am. Chem. Soc.* **1997**, *119*, 6242–6250.
45. Butt, J. N.; Sucheta, A.; Armstrong, F. A.; Breton, J.; Thomson, A. J.; Hatchikian, E. C. *J. Am. Chem. Soc.* **1991**, *113*, 8948–8950.
46. Butt, J. N.; Niles, J.; Armstrong, F. A.; Breton, J.; Thomson, A. J. *Nature Struct. Biol.* **1994**, *1*, 427–433.
47. Herskovitz, T.; Averill, B. A.; Holm, R. H.; Ibers, J. A.; Phillips, W. D.; Weiher, J. F. *Proc. Natl. Acad. Sci. USA* **1972**, *69*, 2437–2441.
48. Averill, B. A.; Herskovitz, T.; Holm, R. H.; Ibers, J. A. *J. Am. Chem. Soc.* **1973**, *95*, 3523–3534.
49. Zhou, C.; Raebiger, J. W.; Segal, B. M.; Holm, R. H. *Inorg. Chim. Acta* **2000**, *300–302*, 892–902.
50. Hagen, K. S.; Reynolds, J. G.; Holm, R. H. *J. Am. Chem. Soc.* **1981**, *103*, 4054–4063.
51. Hagen, K. S.; Stephan, D. W.; Holm, R. H. *Inorg. Chem.* **1982**, *21*, 3928–3936.
52. Christou, G.; Garner, C. D. *J. Chem. Soc., Dalton Trans.* **1979**, 1093–1094.
53. Bonomi, F.; Werth, M. T.; Kurtz, D. M. Jr. *Inorg. Chem.* **1985**, *24*, 4331–4335.
54. Que, L., Jr.; Bobrik, M. A.; Ibers, J. A.; Holm, R. H. *J. Am. Chem. Soc.* **1974**, *96*, 4168–4178.
55. Wong, G. B.; Kurtz, D. M. Jr.; Holm, R. H.; Mortenson, L. E.; Upchurch, R. G. *J. Am. Chem. Soc.* **1979**, *101*, 3078–3090.
56. Johnson, R. W.; Holm, R. H. *J. Am. Chem. Soc.* **1978**, *100*, 5338–5344.
57. Daley, C. J. A.; Holm, R. H. *Inorg. Chem.* **2001**, *40*, 2785–2793.
58. Müller, A.; Schladerbeck, N.; Krickemeyer, E.; Bögge, H.; Bill, E.; Trautwein, A. X. *Z. Anorg. Allgem. Chem.* **1989**, *570*, 7–36.
59. Rutchik, S.; Kim, S.; Walters, M. A. *Inorg. Chem.* **1988**, *27*, 1513–1515.
60. Saak, W.; Pohl, S. *Z. Naturforsch.* **1985**, *40b*, 1105–1112.
61. Saak, W.; Pohl, S. *Z. Naturforsch.* **1988**, *43b*, 457–462.
62. Müller, A.; Schladerbeck, N.; Bögge, H. *J. Chem. Soc., Chem. Commun.* **1987**, 35–36.
63. Hoveyda, H. R.; Holm, R. H. *Inorg. Chem.* **1997**, *36*, 4571–4578.
64. Segal, B. M.; Hoveyda, H. R.; Holm, R. H. *Inorg. Chem.* **1998**, *37*, 3440–3443.
65. Lenormand, A.; Iveson, P.; Jordanov, J. *J. Inorg. Chim. Acta* **1996**, *251*, 119–123.
66. Kambayashi, H.; Nagao, H.; Tanaka, K.; Nakamoto, M.; Peng, S.-M. *Inorg. Chim. Acta* **1993**, *209*, 143–149.
67. Hill, C. L.; Renaud, J.; Holm, R. H.; Mortenson, L. E. *J. Am. Chem. Soc.* **1977**, *99*, 2549–2557.
68. Christou, G.; Garner, C. D.; Drew, M. G. B.; Cammack, R. *J. Chem. Soc., Dalton Trans.* **1981**, 1550–1555.
69. Carrell, H. L.; Glusker, J. P.; Job, R.; Bruice, T. C. *J. Am. Chem. Soc.* **1977**, *99*, 3683–3690.
70. Gebbink, R. J. M. K.; Klink, S. I.; Feiters, M.; Nolte, R. J. M. *Eur. J. Inorg. Chem.* **2000**, 253–264.
71. Gebbink, R. J. M. K.; Klink, S. I.; Feiters, M.; Nolte, R. J. M. *Eur. J. Inorg. Chem.* **2000**, 2087–2099.
72. Tomohiro, T.; Okuno, H. *Inorg. Chim. Acta* **1993**, *204*, 147–152.
73. Tomohiro, T.; Uoto, K.; Okuno, H. *J. Chem. Soc., Dalton Trans.* **1990**, 2459–2463.
74. Okuno, H.; Uoto, K.; Tomohiro, T.; Youinou, M.-T. *J. Chem. Soc., Dalton Trans.* **1990**, 3375–3381.
75. Gorman, C. B.; Hager, M. W.; Parkhurst, B. L.; Smith, J. C. *Macromolecules* **1998**, *31*, 815–822.
76. Gorman, C. B.; Smith, J. C.; Hager, M. W.; Parkhurst, B. L.; Sierzputowska-Gracz, H.; Haney, C. A. *J. Am. Chem. Soc.* **1999**, *121*, 9958–9966.
77. Cleland, W. E.; Holtman, D. A.; Sabat, M.; Ibers, J. A.; DeFotis, G. C.; Averill, B. A. *J. Am. Chem. Soc.* **1983**, *105*, 6021–6031.
78. Kanatzidis, M. G.; Coucouvanis, D.; Simopoulos, A.; Kostikas, A.; Papaefthymiou, V. *J. Am. Chem. Soc.* **1985**, *107*, 4925–4935.
79. Henderson, R. A.; Oglieve, K. E. *J. Chem. Soc., Dalton Trans.* **1993**, 1467–1472.
80. Davies, S. C.; Evans, D. J.; Henderson, R. A.; Hughes, D. L.; Longhurst, S. *J. Chem. Soc., Dalton Trans.* **2002**, 3470–3477.
81. Henderson, R. A.; Oglieve, K. E. *J. Chem. Soc., Chem. Commun.* **1994**, 377–378.
82. Henderson, R. A.; Oglieve, K. E. *J. Chem. Soc., Chem. Commun.* **1998**, 1731–1733.
83. Henderson, R. A.; Oglieve, K. E. *J. Chem. Soc., Dalton Trans.* **1999**, 3927–3934.
84. DePamphilis, B. V.; Averill, B. A.; Herskovitz, T.; Que, L., Jr.; Holm, R. H. *J. Am. Chem. Soc.* **1974**, *96*, 4159–4167.
85. Mascharak, P. K.; Hagen, K. S.; Spence, J. T.; Holm, R. H. *Inorg. Chim. Acta* **1983**, *80*, 157–170.
86. Ueyama, N.; Sugawara, T.; Fuji, M.; Nakamura, A. *Chem. Lett.* **1984**, 1290.
87. Gloux, J.; Gloux, P.; Lamotte, B.; Mouesca, J.-M.; Rius, G. *J. Am. Chem. Soc.* **1994**, *116*, 1953–1961.
88. Mouesca, J.-M.; Rius, G.; Lamotte, B. *J. Am. Chem. Soc.* **1993**, *115*, 4714–4731.
89. Nakamoto, M.; Fukaishi, K.; Tagata, T.; Kambayashi, H. *Bull. Chem. Soc. Jpn.* **1999**, *72*, 407–414.
90. Ohno, R.; Ueyama, N.; Nakamura, A. *Chem. Lett.* **1989**, 399–402.
91. Blonk, H. L.; Kievit, O.; Roth, E. K. H.; Jordanov, J.; van der Linden, J. G. M.; Steggerda, J. J. *Inorg. Chem.* **1991**, *30*, 3231–3234.
92. Hagen, K. S.; Watson, A. D.; Holm, R. H. *Inorg. Chem.* **1984**, *23*, 2984–2990.
93. Henderson, R. A.; Sykes, A. G. *Inorg. Chem.* **1980**, *19*, 3103–3105.
94. Maskiewicz, R.; Bruice, T. C. *J. Chem. Soc., Chem. Commun.* **1979**, 703–704.
95. Laskowski, E. J.; Frankel, R. B.; Gillum, W. O.; Papaefthymiou, G. C.; Renaud, J.; Ibers, J. A.; Holm, R. H. *J. Am. Chem. Soc.* **1978**, *100*, 5322–5337.

96. Carney, M. J.; Papaefthymiou, G. C.; Whitener, M. A.; Spartalian, K.; Frankel, R. B.; Holm, R. H. *Inorg. Chem.* **1988**, *27*, 346–352.
97. Yamamura, T.; Christou, G.; Holm, R. H. *Inorg. Chem.* **1983**, *22*, 939–949.
98. Grönberg, K. L. C.; Henderson, R. A.; Oglieve, K. E. *J. Chem. Soc., Dalton Trans.* **1998**, 3093–3104.
99. Carney, M. J.; Papaefthymiou, G. C.; Spartalian, K.; Frankel, R. B.; Holm, R. H. *J. Am. Chem. Soc.* **1988**, *110*, 6084–6095.
100. Reynolds, J. G.; Coyle, C. L.; Holm, R. H. *J. Am. Chem. Soc.* **1980**, *102*, 4350–4355.
101. Reynolds, J. G.; Holm, R. H. *Inorg. Chem.* **1981**, *20*, 1873–1878.
102. Berg, J. M.; Holm, R. H. In *Iron-Sulfur Proteins*; Spiro, T. G., Ed.; Wiley-Interscience: New York, 1982, Chapter 1.
103. Hu, N.-H.; Liu, Y.-S.; Xu, J.-Q.; Yan, Y.-Z.; Wei, Q. *Chinese J. Struct. Chem.* **1991**, *10*, 117–120.
104. Carney, M. J.; Papaefthymiou, G. C.; Frankel, R. B.; Holm, R. H. *Inorg. Chem.* **1989**, *28*, 1497–1503.
105. Berg, J. M.; Hodgson, K. O.; Holm, R. H. *J. Am. Chem. Soc.* **1979**, *101*, 4586–4593.
106. Gloux, J.; Gloux, P.; Hendriks, H.; Rius, G. *J. Am. Chem. Soc.* **1987**, *109*, 3220–3224.
107. Lin, G.; Zhang, H.; Hu, S.-Z.; Mak, T. C. W. *Acta Crystallogr.* **1987**, *C43*, 352–353.
108. Excoffon, P.; Laugier, J.; Lamotte, B. *Inorg. Chem.* **1991**, *30*, 3075–3081.
109. Chu, C. T. W.; Lo, F. Y. K.; Dahl, L. F. *J. Am. Chem. Soc.* **1982**, *104*, 3409–3422.
110. Butler, A. R.; Glidewell, C.; Li, M. *Adv. Inorg. Chem.* **1988**, *32*, 335–393.
111. Weigel, J. A.; Srivastava, K. K. P.; Day, E. P.; Münck, E.; Holm, R. H. *J. Am. Chem. Soc.* **1990**, *112*, 8015–8023.
112. Harmjanz, M.; Saak, W.; Pohl, S. *J. Chem. Soc., Chem. Commun.* **1997**, 951–952.
113. Weigel, J. A.; Holm, R. H.; Surerus, K. K.; Münck, E. *J. Am. Chem. Soc.* **1989**, *111*, 9246–9247.
114. Goh, C.; Weigel, J. A.; Holm, R. H. *Inorg. Chem.* **1994**, *33*, 4869–4877.
115. Nelson, L. L.; Lo, F. Y. K.; Rae, A. D.; Dahl, L. F. *J. Organometal. Chem.* **1982**, *225*, 309–329.
116. Yoo, S. J.; Hu, Z.; Goh, C.; Bominaar, E. L.; Holm, R. H.; Münck, E. *J. Am. Chem. Soc.* **1997**, *119*, 8732–8733.
117. Tyson, M. A.; Demadis, K. D.; Coucouvanis, D. *Inorg. Chem.* **1995**, *34*, 4519–4520.
118. Goh, C.; Segal, B. M.; Huang, J.; Long, J. R.; Holm, R. H. *J. Am. Chem. Soc.* **1996**, *118*, 11844–11853.
119. Osterloh, F.; Segal, B. M.; Achim, C.; Holm, R. H. *Inorg. Chem.* **2000**, *39*, 980–989.
120. Strop, P.; Takahara, P. M.; Chiu, H.-J.; Angove, H. C.; Burgess, B. K.; Rees, D. C. *Biochemistry* **2001**, *40*, 651–656.
121. Que, L., Jr.; Anglin, J. R.; Bobrik, M. A.; Davison, A.; Holm, R. H. *J. Am. Chem. Soc.* **1974**, *96*, 6042–6048.
122. Burt, R. J.; Ridge, B.; Rydon, H. N. *J. Chem. Soc., Dalton Trans.* **1980**, 1228–1235.
123. Ueyama, N.; Terakawa, T.; Nakata, M.; Nakamura, A. *J. Am. Chem. Soc.* **1983**, *105*, 7098–7102.
124. Ueyama, N.; Kajiwara, A.; Terakawa, T.; Ueno, S.; Nakamura, A. *Inorg. Chem.* **1985**, *24*, 4700–4704.
125. Ohno, R.; Ueyama, N.; Nakamura, A. *Inorg. Chem.* **1991**, *30*, 4887–4891.
126. Smith, E. T.; Feinberg, B. A.; Richards, J. H.; Tomich, J. M. *J. Am. Chem. Soc.* **2001**, *113*, 688–689.
127. Smith, E. T.; Tomich, J. M.; Iwamoto, T.; Richards, J. H.; Mao, Y.; Feinberg, B. A. *Biochemistry* **1991**, *30*, 11669–11676.
128. Feinberg, B. A.; Lo, X.; Iwamoto, T.; Tomich, J. M. *Protein Engineering* **1997**, *10*, 69–75.
129. Sow, T.-C.; Pedersen, M. V.; Christensen, H. E. M.; Ooi, B.-L. *Biochem. Biophys. Res. Commun.* **1996**, *223*, 360–364.
130. Rabinowitz, J. *Methods Enzymol.* **1972**, *24*, 431–446.
131. Mulholland, S. E.; Gibney, B. R.; Rabanal, F.; Dutton, P. L. *J. Am. Chem. Soc.* **1998**, *120*, 10296–10302.
132. Mulholland, S. E.; Gibney, B. R.; Rabanal, F.; Dutton, P. L. *Biochemistry* **1999**, *38*, 10442–10448.
133. Scott, M. P.; Biggins, J. *Protein Sci.* **1997**, *6*, 340–346.
134. Coldren, C. D.; Hellinga, H. W.; Caradonna, J. P. *Proc. Natl. Acad. Sci. USA* **1997**, *94*, 6635–6640.
135. Gibney, B. R.; Mulholland, S. E.; Rabanal, F.; Dutton, P. L. *Proc. Natl. Acad. Sci. USA* **1996**, *93*, 15041–15046.
136. Laplaza, C. E.; Holm, R. H. *J. Am. Chem. Soc.* **2001**, *123*, 10255–10264.
137. Musgrave, K. B.; Laplaza, C. E.; Holm, R. H.; Hedman, B.; Hodgson, K. O. *J. Am. Chem. Soc.* **2002**, *124*, 3083–3092.
138. Coucouvanis, D.; Kanatzidis, M. G.; Simhom, E. D.; Baenziger, N. C. *J. Am. Chem. Soc.* **1982**, *104*, 1874–1882.
139. Kanatzidis, M. G.; Baenziger, N. C.; Coucouvanis, D.; Simopoulos, A.; Kostikas, A. *J. Am. Chem. Soc.* **1984**, *106*, 4500–4511.
140. Saak, W.; Pohl, S. *Z. Naturforsch.* **1988**, *43b*, 813–817.
141. Pohl, S.; Bierbach, U. *Z. Naturforsch.* **2002**, *46b*, 68–74.
142. Pohl, S.; Bierbach, U. *Z. Naturforsch* **1992**, *47b*, 1266–1270.
143. Harmjanz, M.; Junghans, C.; Optiz, U.-A.; Bahlmann, B.; Pohl, S. *Z. Naturforsch.* **1996**, *51b*, 1040–1048.
144. Beinert, H.; Kennedy, M. C.; Stout, C. D. *Chem. Rev.* **1996**, *96*, 2335–2373.
145. Stack, T. D. P.; Holm, R. H. *J. Am. Chem. Soc.* **1988**, *110*, 2484–2494.
146. Stack, T. D. P.; Weigel, J. A.; Holm, R. H. *Inorg. Chem.* **1990**, *29*, 3745–3760.
147. Walsdorff, C.; Saak, W.; Pohl, S. *J. Chem. Soc., Dalton Trans.* **1997**, 1857–1861.
148. van Strijdonck, G. P. F.; van Haare, J. A. E. H.; Hönen, P. J. M.; van den Schoor, R. C. G. M.; Feiters, M. C.; van der Linden, J. G. M.; Steggerda, J. J.; Nolte, R. J. M. *J. Chem. Soc., Dalton Trans.* **1997**, 449–461.
149. Huang, J.; Mukerjee, S.; Segal, B. M.; Akashi, H.; Zhou, J.; Holm, R. H. *J. Am. Chem. Soc.* **1997**, *119*, 8662–8674.
150. Zhou, C.; Holm, R. H. *Inorg. Chem.* **1997**, *36*, 4066–4077.
151. Whitener, M. A.; Peng, G.; Holm, R. H. *Inorg. Chem.* **1991**, *30*, 2411–2417.
152. Evans, D. J.; Garcia, G.; Leigh, G. J.; Newton, M. S.; Santana, M. D. *J. Chem. Soc., Dalton Trans.* **1992**, 3229–3234.
153. Weigel, J. A.; Holm, R. H. *J. Am. Chem. Soc.* **1991**, *113*, 4184–4191.
154. Holm, R. H.; Ciurli, S.; Weigel, J. A. *Progr. Inorg. Chem.* **1990**, *38*, 1–74.
155. Ciurli, S.; Carrié, M.; Weigel, J. A.; Carney, M. J.; Stack, T. D. P.; Papaefthymiou, G. C.; Holm, R. H. *J. Am. Chem. Soc.* **1990**, *112*, 2654–2664.
156. Stack, T. D. P.; Carney, M. J.; Holm, R. H. *J. Am. Chem. Soc.* **1989**, *111*, 1670–1676.
157. Liu, H. Y.; Scharbert, B.; Holm, R. H. *J. Am. Chem. Soc.* **1991**, *113*, 9529–9539.
158. Cai, L.; Holm, R. H. *J. Am. Chem. Soc.* **1994**, *116*, 7177–7188.
159. Zhou, C.; Cai, L.; Holm, R. H. *Inorg. Chem.* **1996**, *36*, 2767–2772.
160. van Strijdonck, G. P. E.; ten Have, P. T. J. H.; Feiters, M. C.; van der Linden, J. G. M.; Steggerda, J. J.; Nolte, R. J. M. *Chem. Ber.* **1997**, *130*, 1151–1157.

161. Barclay, J. E.; Diaz, M. I.; Evans, D. J.; Garcia, G.; Santana, M. D.; Torralba, M. C. *Inorg. Chim. Acta* **1997**, *258*, 211–219.
162. Al-Ahmad, S. A; Kampf, J. W.; Dunham, W. R.; Coucouvanis, D. *Inorg, Chem.* **1991**, *30*, 1163–1164.
163. Osterloh, F.; Saak, W.; Pohl, S.; Kroeckel, M.; Meier, C.; Trautwein, A. X. *Inorg. Chem.* **1998**, *37*, 3581–3587.
164. Kanatzidis, M. G.; Hagen, W. R.; Dunham, W. R.; Lester, R. K.; Coucouvanis, D. *J. Am. Chem. Soc.* **1985**, *107*, 953–961.
165. Evans, D. J.; Garcia, G.; Santana, M. D.; Torralba, M. C. *Inorg. Chim. Acta* **1999**, *284*, 296–299.
166. Kanatzidis, M. G.; Dunham, W. R.; Hagen, W. R.; Coucouvanis, D. *J. Chem. Soc., Chem. Commun.* **1984**, 356–358.
167. Saak, W.; Henkel, G.; Pohl, S. *Angew. Chem. Int. Ed. Engl.* **1984**, *23*, 150–151.
168. Kanatzidis, M. G.; Salifoglou, A.; Coucouvanis, D. *Inorg. Chem.* **1986**, *25*, 2460–2468.
169. Coucouvanis, D.; Kanatzidis, M. G.; Dunham, W. R.; Hagen, W. R. *J. Am. Chem. Soc.* **1984**, *106*, 7998–7999.
170. Coucouvanis, D.; Kanatzidis, M. G.; Salifoglou, A.; Dunham, W. R.; Simopoulos, A.; Sams, J. R.; Papaeftymiou, V.; Kostikas, A. *J. Am. Chem. Soc.* **1987**, *109*, 6863–6865.
171. Kröckel, M.; Trautwein, A. X.; Winkler, H.; Coucouvanis, D.; Kostikas, A.; Papaefthymiou, V. *Inorg. Chim. Acta* **1998**, *283*, 111–117.
172. Arendsen, A. F.; Hadden, J.; Card, G.; McAlpine, A. S.; Bailey, S.; Zaitsev, V.; Duke, E. H. M.; Lindley, P. F.; Kröckel, M.; Trautwein, A. X.; Feiters, M. C.; Charnock, J. M.; Garner, C. D.; Marritt, S. J.; Thomson, A. J.; Kooter, I. M.; Johnson, M. K.; van den Berg, W. A. M.; van Dongen, W. M. A. M.; Hagen, W. R. J. *Inorg. Biochem.* **1998**, *3*, 81–95.
173. Scott, M. J.; Holm, R. H. *Angew. Chem. Int. Ed. Engl.* **1993**, *32*, 564–566.
174. Geiser, U.; Williams, J. H. *Acta Crystallogr.* **1998**, C54, 292–293.
175. Saak, W.; Pohl, S. *Angew. Chem. Int. Ed. Engl.* **1991**, *30*, 881–883.
176. Coucouvanis, D.; Salifoglou, A.; Kanatzidis, M. G.; Dunham, W. R.; Simopoulos, A.; Kostikas, A. *Inorg. Chem.* **1988**, *27*, 4066–4077.
177. Al-Ahmad, S.; Salifoglou, A.; Kanatzidis, M. G.; Dunham, W. R.; Coucouvanis, D. *Inorg Chem.* **1990**, *29*, 927–938.
178. Snyder, B. S.; Holm, R. H. *Inorg. Chem.* **1988**, *27*, 2339–2347.
179. Reynolds, M. S.; Holm, R. H. *Inorg. Chem.* **1998**, *27*, 4494–4499.
180. Snyder, B. S.; Reynolds, M. S.; Holm, R. H.; Papaefthymiou, G. C.; Frankel, R. B. *Polyhedron* **1991**, *10*, 203–213.
181. Snyder, B. S.; Holm, R. H. *Inorg Chem.* **1990**, *29*, 274–279.
182. Almeida, V. R.; Gormal, C. A.; Henderson, R. A.; Oglieve, K. E.; Smith, B. E. *Inorg. Chim. Acta* **1999**, *291*, 212–225.
183. Woska, D.; Prock, A.; Giering, W. P. *Organometallics* **2000**, *19*, 4629–4638.
184. Cai, J.-H.; Chen, C.-N.; Liu, Q.-T.; Zhuang, B.-T.; Kang, B.-S.; Lu, J.-X. *J. Struct. Chem.* **1989**, *8*, 220–224.
185. Cecconi, F.; Ghilardi, C. A.; Midollini, S. *J. Chem. Soc., Chem. Commun.* **1981**, 640–641.
186. Agresti, A.; Bacci, M.; Cecconi, F.; Ghilardi, C. A.; Midollini, S. *Inorg. Chem.* **1985**, *24*, 689–695.
187. Cecconi, F.; Ghilardi, C. A.; Midollini, S.; Orlandini, A.; Zanello, P. *J. Chem. Soc., Dalton Trans.* **1987**, 831–835.
188. Goddard, C. A.; Long, J. R.; Holm, R. H. *Inorg. Chem.* **1996**, *35*, 4347–4354.
189. Bencini, A.; Ghilardi, C. A.; Midollini, S.; Orlandini, A.; Russo, U.; Uytterhoeven, M. G.; Zanchini, C. *J. Chem. Soc., Dalton Trans* **1995**, 963–974.
190. Christou, G.; Holm, R. H.; Sabat, M.; Ibers, J. A. *J. Am. Chem. Soc.* **1981**, *103*, 6269–6271.
191. Christou, G.; Sabat, M.; Ibers, J. A.; Holm, R. H. *Inorg. Chem.* **1982**, *21*, 3518–3526.
192. Zhou, H.-C.; Su, W.; Achim, C.; Rao, P. V.; Holm, R. H. *Inorg. Chem.* **2002**, *41*, 3191–3201.
193. Strasdeit, H.; Krebs, B.; Henkel, G. *Inorg. Chem.* **1984**, *23*, 1816–1825.
194. Fan, Y; Guo, C.; Zhang, Z.; Liu, X. *Sci. Sin., Ser. B:* **1988**, *31*, 161–170.
195. Zhang, Z.; Fan, Y.; Li, Y.; Niu, S.; Li, S. *Kexue Tongbao* **1987**, *32*, 1405–1409.
196. Noda, I.; Snyder, B. S.; Holm, R. H. *Inorg. Chem.* **1986**, *25*, 3851–3853.
197. Pohl, S.; Saak, W *Angew. Chem. Int. Ed. Engl.* **1984**, *23*, 907–908.
198. Pohl, S.; Opitz, U. *Angew. Chem. Int. Ed. Engl.* **1993**, *32*, 863–864.
199. Junghans, C.; Saak, W.; Pohl, S. *J. Chem. Soc., Chem. Commun.* **1994**, 2327–2328.
200. Cai, L.; Segal, B. M.; Long, J. R.; Scott, M. J. *J. Am. Chem. Soc.* **1995**, *117*, 8863–8864.
201. Zhou, H.-C.; Holm, R. H. *Inorg. Chem.* **2003**, *42*, 11–21.
202. Demadis, K. D.; Campana, C. F.; Coucouvanis, D. *J. Am. Chem. Soc.* **1995**, *117*, 8863–8864.
203. Osterloh, F.; Achim, C.; Holm, R. H. *Inorg. Chem.* **2001**, *40*, 224–232.
204. Challen, P. R.; Koo, S. M.; Dunham, W. R.; Coucouvanis, D. *J. Am. Chem. Soc.* **1990**, *112*, 2455–2456.
205. Huang, J.; Holm, R. H. *Inorg. Chem.* **1998**, *37*, 2247–2254.
206. Fomitchev, D. V.; McLauchlan, C. C.; Holm, R. H. *Inorg. Chem.* **2002**, *41*, 958–966.
207. Goh, C.; Novorozhkin, A.; Yoo, S. J.; Bominaar, E. L.; Münck, E.; Holm, R. H. *Inorg. Chem.* **1998**, *37*, 2926–2932.
208. You, J.-F.; Snyder, B. S.; Holm, R. H. *J. Am. Chem. Soc.* **1988**, *110*, 6589–6591.
209. You, J.-F.; Snyder, B. S.; Papaefthymiou, G. C.; Holm, R. H. *J. Am, Chem. Soc.* **1990**, *122*, 1067–1076.
210. You, J.-F.; Papaefthymiou, G. C.; Holm, R. H. *J. Am. Chem. Soc.* **1992**, *114*, 2697–2710.
211. Rose, K.; Shadle, S. E.; Glaser, T.; de Vries, S.; Cherepanov, A.; Canters, G. W.; Hedman, B.; Hodgson, K. O.; Solomon, E. I. *J. Am. Chem. Soc.* **1999**, *121*, 2353–2363.
212. Snyder, B. S.; Reynolds, M. S.; Noda, I.; Holm, R. H. *Inorg. Chem.* **1988**, *27*, 595–597.
213. Long, J. R.; Holm, R. H. *J. Am. Chem. Soc.* **1994**, *116*, 9987–10002.
214. Long, J. R.; Holm, R. H. *Inorg. Chim. Acta* **1995**, *229*, 229–239.

8.4
Electron Transfer: Cupredoxins

Y. LU
University of Illinois at Urbana-Champaign, IL, USA

8.4.1 OVERVIEW

Cupredoxins refer to a group of copper proteins that share the same overall structural fold and perform biological electron transfer (ET) through their redox reactivity.[1,2] The term cupredoxin comes from "ferredoxin," the Fe-containing redox proteins. Cupredoxins comprise one of the three classes of metalloproteins known to carry out biological electron transfer, after cytochromes (see Chapter 8.2) and ferredoxins (see Chapter 8.3).

8.4.1.1 Scope of the Chapter

Copper centers in proteins were initially classified into three types (types 1–3, see Table 1).[3,4] The classification was based mainly on their spectroscopic features, particularly those in electronic absorption and electron paramagnetic resonance spectra. Since the initial classification, two new copper centers, Cu_A[5,6] and Cu_Z,[7] have been discovered and characterized. Their unique structures do not belong to any of the three known types of copper centers and now those centers form their own classes.

Type 1 copper proteins are the class of proteins for which cupredoxins were originally named.[1,2] Type 1 copper proteins include both proteins with known electron transfer function (e.g., plastocyanin and rusticyanin), and proteins whose biological functions have not been determined conclusively (e.g., stellacyanin and plantacyanin). Although these proteins with unknown function cannot be called cup*redox*ins by the strict functional definition, they have been classified as cupredoxins because they share the same overall structural fold and metal-binding sites as cupredoxins. In addition, many multidomain proteins, such as laccase, ascorbate oxidase, and ceruloplasmin, contain multiple metal centers, one of which is a type 1 copper. Those cupredoxin *centers* are also included here. Finally, both the Cu_A center in cytochrome *c* oxidase (C*c*O) and nitrous oxide reductase (N_2OR), and the red copper center in nitrocyanin will be discussed in this chapter because their metal centers are structurally related to the type 1 copper center and the protein domain that contains both centers share the same overall structural motif as those of cupredoxins. The Cu_A center also functions as an electron transfer agent. Like ferredoxins, which contain either dinuclear or tetranuclear iron–sulfur centers, cupredoxins may include either the mononuclear or the dinuclear copper center in their metal-binding sites.

Comprehensive reviews on cupredoxins[1–4,8–20] and cupredoxin centers in multicopper oxidases[21–23] have appeared, as well as reviews on the Cu_A centers.[16,17,20,24–28]

8.4.1.2 The Cupredoxin Fold

All cupredoxins discussed in this chapter share a similar overall structural fold, commonly called the cupredoxin fold.[1,2,29] This is in spite of the fact that sequence homology among those cupredoxins vary greatly, some of which are less than 10% homologous to each other. The cupredoxin fold is an example of a protein structural motif called a Greek key β barrel,[30] which is one of the most common protein structural motifs shared in metalloproteins (such as superoxide dismutase and hemocyanin) as well as nonmetalloproteins (such as immunoglobulins and pyruvate kinase). A typical Greek key β barrel consists of six or eight antiparallel β strands with one or more connections that cross the top or bottom of a barrel, most often skipping two intervening strands (see Figure 1a).[30] The topology resembles the pattern of a Greek key (see Figure 1b). The loops connecting different strands vary in length and sequence identity. They also may be replaced by helices. The cupredoxin fold differs from the typical Greek key β barrel motif in that it contains two parallel strands, between its first and the third strands and between the eighth strand and half of its second strand (see Figures 1c and 1d).[1,2,29] The second parallel strand can form because, in cupredoxins, the second β strand is always broken into two small separate β strands so that the first half is antiparallel to the first strand while the second half is parallel to the eighth strand. The cupredoxin centers always reside in a pocket between three loops connecting the strands, with two of the three loops providing ligands to the copper center. Despite its proximity to the protein surface, the cupredoxin center is completely shielded from the solvent, a structural feature that is important for its electron transfer function because it contributes to lowering of the reorganization energy in ET.

8.4.1.3 The Colorful World of Cupredoxins and Structurally Related Proteins

One interesting feature of cupredoxins is that members of its family display a variety of intense and beautiful colors, from blue (e.g., plastocyanin and azurin), to green (e.g., plantacyanin and some nitrite reductases), to red (e.g., nitrosocyanin), to yellow (e.g., some model cupredoxin proteins and compounds), and to purple (e.g., Cu_A center from cytochrome *c* oxidase and nitrous oxide reductase). This rainbow of colors makes cupredoxins both fun to work with and challenging to study. The structure and function of each of the cupredoxin and structurally related centers will be described below and the origin of the color will be explained.

Table 1 Classification of copper centers in copper proteins.

Type	Mononuclear		Dinuclear		Tetranuclear
	Type 1	*Type 2*	*Type 3*	*Cu_A*	*Cu_Z*
UV-vis Spectrum	Strong absorption ~600 nm (in some proteins, 450 nm)	Weak absorption ~700 nm	Weak absorption ~700 nm	Strong absorption ~480 and 530 nm	Strong absorption ~640 nm
EPR spectrum	4-line ($A_\| < 80 \times 10^{-4}$ cm^{-1})	4-line ($A_\| \sim (130-180) \times 10^{-4}$ cm^{-1})	non-detectable	7-line ($A_\| \sim 30-70 \times 10^{-4}$ cm^{-1})	2 × 4-line ($A_\| \sim 61 \times 10^{-4}$ cm^{-1} & $A_\| \sim 24 \times 10^{-4}$ cm^{-1})
Common ligands	His, Cys, (Met)	His, Asp, (Tyr)	His, (Tyr)	His, Cys, (Met)	His, S^{2-}
Active site geometry	Distorted tetrahedral	Distorted tetragonal	Tetragonal	Trigonal planar	μ_4-S^{2-} tetracopper cluster
Examples	Azurin Plastocyanin Stellacyanin Nitrite reductase Laccase	Superoxide dismutase Galactose oxidase Amine oxidase Nitrite reductase Laccase	Hemocyanin Tyrosinase Catechol oxidase Laccase	Cyt *c* oxidase N$_2$O reductase Menaquinol NO- reductase	N$_2$O reductase

Figure 1 Schematic illustration of overall fold (a) and topology (b) of a typical Greek key β barrel motif, and overall structure (c) and topology (d) of a typical cupredoxin motif, using azurin as an example.

8.4.2 BLUE COPPER CENTERS

Blue copper centers exhibit an intense blue color, due to a strong absorption around 600 nm ($\varepsilon_{max} \sim 3,000$–$6,000\,M^{-1}\,cm^{-1}$) (see Table 2), which is 100–1,000 times more intense than that of normal copper ligand field transitions.[9,13] They also display a weak absorption around 450 nm. Their EPR spectra are almost invariably axial (i.e., $g_x \sim g_y$) with a narrow copper parallel hyperfine coupling constant ($A_\| < 80 \times 10^{-4}\,cm^{-1}$) instead of $(130$–$180) \times 10^{-4}\,cm^{-1}$ for a normal Cu^{II} center. The reduction potentials vary from 180 mV to 800 mV (vs. NHE-normal hydrogen electrode). They are the most well-characterized copper proteins upon which the type 1 copper center classification and cupredoxin names are based.

8.4.2.1 Plastocyanin

Plastocyanin has been isolated from cyanobacteria, algae, and all higher plants.[31] It transfers electrons from cytochrome f to P700$^+$, the double chlorophyll pigment of photosystem I. The plastocyanin of poplar tree (*populus nigra*) was the first cupredoxin to have its three-dimensional structure elucidated by X-ray crystallography.[32–34] In oxidized plastocyanin, the Cu^{II} is coordinated to three strong ligands, one cysteine and two histidines, and one weak ligand, methionine, in a distorted tetrahedral geometry (see Structure A in Figure 2). The three strong ligands form a trigonal plane, with Cu^{II} positioned slightly (0.36 Å) above the plane (Table 4). While the Cu^{II}—$N_{\delta(His)}$ bond distances (1.91 Å and 2.06 Å) are in the normal range for cupric-imidazole bonds, the Cu^{II}—$S_{\gamma(Cys)}$ distance (2.07 Å) is shorter than a normal cupric-thiolate bond, which usually has a bond distance of 2.3–2.9 Å.[35] This structural feature has been shown to be responsible for its unusually narrow $A_\|$ in EPR (see Section 8.4.8.2.2) and its high ET efficiency (see Section 8.4.8.3). In contrast, the fourth ligand, methionine, coordinates Cu^{II} at an unusually long distance, anywhere from 2.69 to 2.94 Å, depending on the source of plastocyanin. Interestingly, the reduced plastocyanin maintains almost the same geometry as the oxidized plastocyanin, with expected elongation of all bond distances (see Table 4).[36] In contrast to the situation for other electron transfer proteins, no significant difference in the dynamic properties is found between the two redox forms.[282,283] Another remarkable feature of plastocyanin is that the geometry of the cupredoxin center is preserved when the center is free of metal ion,[37] or when other metal ions (such as Hg^{II})[38] occupy the center.

8.4.2.2 Azurin

Azurin is found in gram-negative bacteria such as *Alcaligenes denitrificans* and *Pseudomonas aeruginosa*.[39] While its exact biological function remains unclear, it has been implicated in ET processes in several biological systems. It is the focus of many biochemical and biophysical studies because its gene and mutant proteins are readily obtainable, thanks in part to advances in biological techniques such as molecular cloning, polymerase chain reaction, and site-directed mutagenesis.[14,39] In the oxidized form,[40–43] the Cu^{II} is in a pseudotrigonal bipyramidal coordination environment, with one cysteine and two histidines in the trigonal plane, and a distant

Table 1 Classification of copper centers in copper proteins.

Type	Mononuclear		Dinuclear		Tetranuclear
	Type 1	Type 2	Type 3	Cu_A	Cu_Z
UV-vis Spectrum	Strong absorption ~ 600 nm (in some proteins, 450 nm)	Weak absorption ~ 700 nm	Weak absorption ~ 700 nm	Strong absorption ~ 480 and 530 nm	Strong absorption ~ 640 nm
EPR spectrum	4-line ($A_\| < 80 \times 10^{-4}$ cm^{-1})	4-line ($A_\| \sim (130{-}180) \times 10^{-4}$ cm^{-1})	non-detectable	7-line ($A_\| \sim 30{-}70 \times 10^{-4}$ cm^{-1})	2 × 4-line ($A_\| \sim 61 \times 10^{-4}$ cm^{-1} & $A_\| \sim 24 \times 10^{-4}$ cm^{-1})
Common ligands	His, Cys, (Met)	His, Asp, (Tyr)	His, (Tyr)	His, Cys, (Met)	His, S^{2-}
Active site geometry	Distorted tetrahedral	Distorted tetragonal	Tetragonal	Trigonal planar	μ_4-S^{2-} tetracopper cluster
Examples	Azurin Plastocyanin Stellacyanin Nitrite reductase Laccase	Superoxide dismutase Galactose oxidase Amine oxidase Nitrite reductase Laccase	Hemocyanin Tyrosinase Catechol oxidase Laccase	Cyt c oxidase N$_2$O reductase Menaquinol NO- reductase	N$_2$O reductase

Table 2 Spectroscopic properties of blue/green copper proteins and their biomimetic model proteins and compounds.

Protein	Source	Electronic absorption $(M^{-1}\,cm^{-1})$	R_ε^{a}	EPR $(A_\parallel)$ $(10^{-4}\,cm^{-1})$	Cu–Met (Å)	References
Plastocyanin	*Populus nigra*	$\varepsilon_{460\,nm}=300;\ \varepsilon_{597\,nm}=5{,}200$	0.06	axial (63)	2.90	221
Umecyanin	*Armoracia lapathifolia*	$\varepsilon_{460\,nm}=300;\ \varepsilon_{595\,nm}=3{,}400$	0.09	axial (35)	N/A	263
Azurin	*Alcaligenes denitrificans*	$\varepsilon_{460\,nm}=580;\ \varepsilon_{619\,nm}=5{,}100$	0.11	axial (60)	3.13	264
Amicyanin	*Paracoccus denitrificans*	$\varepsilon_{464\,nm}=520;\ \varepsilon_{595\,nm}=4{,}610$	0.11	axial	2.90	265
Amicyanin	*Thiobacillus versutus*	$\varepsilon_{460\,nm}=524;\ \varepsilon_{596\,nm}=3{,}900$	0.13	axial (59)	2.88	266,267
Nitrite Reductase	*Alcaligenes Sp.* NC1B 11015	$\varepsilon_{470\,nm}=640;\ \varepsilon_{594\,nm}=3{,}700$	0.17	axial (67)	N/A	268
Stellacyanin	*Rhus vernicifera*	$\varepsilon_{448\,nm}=1150;\ \varepsilon_{604\,nm}=4{,}000$	0.29	rhombic (37)	(amide)	269,270
Auracyanin	*Chloroflexus aurantiacus*	$\varepsilon_{455\,nm}=900;\ \varepsilon_{596\,nm}=2{,}900$	0.31	rhombic (47)	2.84	87,92
Mung Bean Blue Protein	*Phaseolus aureus*	$A_{450\,nm}=0.03;^{\text{b}}$ $A_{598\,nm}=0.09^{\text{b}}$	0.33	rhombic	N/A	271
Mavicyanin	*Cucurbita pepo medullosa*	$\varepsilon_{445\,nm}=1900;\ \varepsilon_{600\,nm}=5{,}000$	0.38	rhombic (37)	N/A	272

Table 2 Spectroscopic properties of blue/green copper proteins and their biomimetic model proteins and compounds.

Protein	Source	Electronic absorption $(M^{-1}\,cm^{-1})$	$R_\varepsilon{}^a$	EPR $(A_\parallel)$ $(10^{-4}\,cm^{-1})$	Cu–Met (Å)	References
Plastocyanin	*Populus nigra*	$\varepsilon_{460\,nm} = 300;\ \varepsilon_{597\,nm} = 5{,}200$	0.06	axial (63)	2.90	221
Umecyanin	*Armoracia lapathifolia*	$\varepsilon_{460\,nm} = 300;\ \varepsilon_{595\,nm} = 3{,}400$	0.09	axial (35)	N/A	263
Azurin	*Alcaligenes denitrificans*	$\varepsilon_{460\,nm} = 580;\ \varepsilon_{619\,nm} = 5{,}100$	0.11	axial (60)	3.13	264
Amicyanin	*Paracoccus denitrificans*	$\varepsilon_{464\,nm} = 520;\ \varepsilon_{595\,nm} = 4{,}610$	0.11	axial	2.90	265
Amicyanin	*Thiobacillus versutus*	$\varepsilon_{460\,nm} = 524;\ \varepsilon_{596\,nm} = 3{,}900$	0.13	axial (59)	2.88	266,267
Nitrite Reductase	*Alcaligenes Sp.* NC1B 11015	$\varepsilon_{470\,nm} = 640;\ \varepsilon_{594\,nm} = 3{,}700$	0.17	axial (67)	N/A	268
Stellacyanin	*Rhus vernicifera*	$\varepsilon_{448\,nm} = 1150;\ \varepsilon_{604\,nm} = 4{,}000$	0.29	rhombic (37)	(amide)	269,270
Auracyanin	*Chloroflexus aurantiacus*	$\varepsilon_{455\,nm} = 900;\ \varepsilon_{596\,nm} = 2{,}900$	0.31	rhombic (47)	2.84	87,92
Mung Bean Blue Protein	*Phaseolus aureus*	$A_{450\,nm} = 0.03;^b$ $A_{598\,nm} = 0.09^b$	0.33	rhombic	N/A	271
Mavicyanin	*Cucurbita pepo medullosa*	$\varepsilon_{445\,nm} = 1900;\ \varepsilon_{600\,nm} = 5{,}000$	0.38	rhombic (37)	N/A	272

Table 2 continued

Protein	Source	Electronic absorption ($M^{-1}\,cm^{-1}$)	R_ε[a]	EPR $(A_\parallel)$ ($10^{-4}\,cm^{-1}$)	Cu–Met (Å)	References
Pseudoazurin	Alcaligenes faecalis S-6	$\varepsilon_{450\,nm} = 1180;\ \varepsilon_{595\,nm} = 2{,}900$	0.41	rhombic	2.69	273
Rusticyanin	Thiobacillus ferro-oxidans	$\varepsilon_{450\,nm} = 1060;\ \varepsilon_{597\,nm} = 1{,}950$	0.54	rhombic (47)	2.88	274,275
Plantacyanin	Spinacea oleracea	$\varepsilon_{443\,nm} = 2030;\ \varepsilon_{597\,nm} = 3{,}400$	0.60	rhombic	2.62	276
Nitrite Reductase	Rhodopseudomonas sphaeroides forma sp. denitrificans	$\varepsilon_{464\,nm} = 3660;\ \varepsilon_{584\,nm} = 4{,}860$	0.75	rhombic (79)	N/A	277
Nitrite Reductase	Achromobacter cycloclastes	$\varepsilon_{458\,nm} = 2200;\ \varepsilon_{585\,nm} = 1{,}800$	1.22	rhombic (73)	2.56	278,279
CuZnSOD H80C	Saccharomyces cerevisiae	$\varepsilon_{459\,nm} = 1460;\ \varepsilon_{595\,nm} = 1{,}420$	1.03	rhombic (139)	(Asp)	70
Compound (1)	Synthetic model	$\varepsilon_{536\,nm} = 40;\ \varepsilon_{625\,nm} = 6{,}340$	N/A	axial (66)	2.119(N)	151,153
Compound (2)	Synthetic model	$\varepsilon_{749\,nm} = 5{,}800$	N/A	axial (111)	N/A	154
Compound (3)	Synthetic model	$\varepsilon_{430\,nm} = 1900;\ \varepsilon_{691\,nm} = 2{,}300$	0.826	rhombic (98)	2.403	156

Source: adapted from Lu et al. [70,71]

a R_ε is the ratio between the absorption around 460 nm and the absorption around 600 nm. b The extinction coefficient was not available from the reference [271].
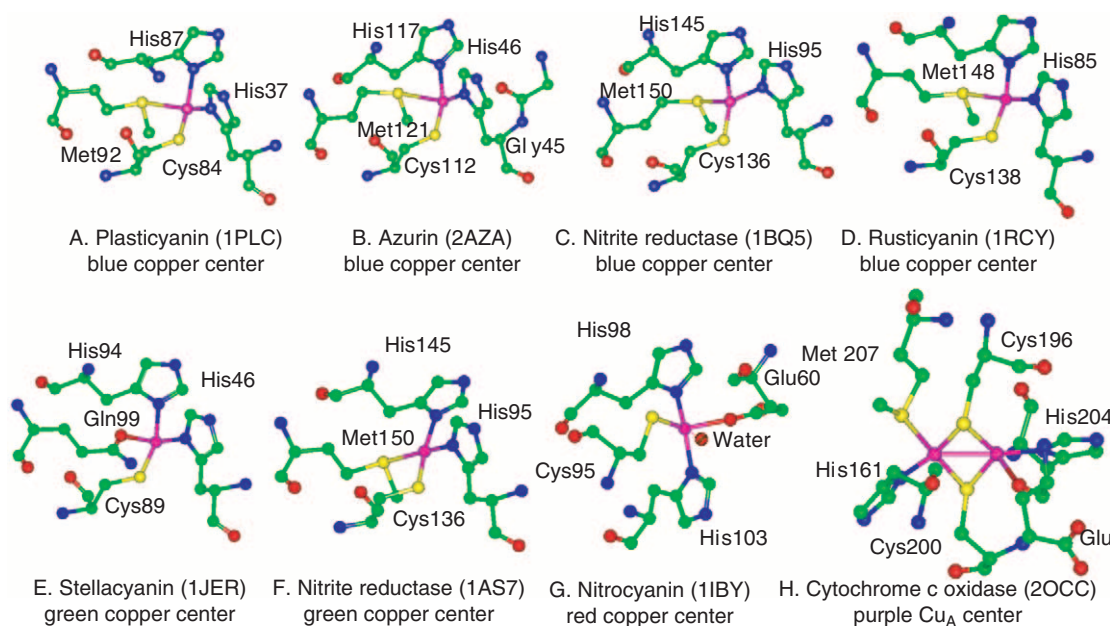
Figure 2 Copper centers in cupredoxins and related proteins (see Table 4 for details).

carbonyl oxygen from Gly45 and a thioether sulfur from Met121 in the axial positions (see Structure B in Figure 2). The Cu^{II} is displaced only 0.13 Å away from the trigonal plane, toward the axial methionine. The bond distances between Cu^{II} and the cysteine and two histidines are similar to those of plastocyanin while the Cu^{II}-methionine distance is longer (at 3.11 Å, see Table 4). Azurin is unique among cupredoxins in that it has an additional interaction with the backbone oxygen from Gly45 at 3.13 Å; this has been defined as weakly ionic.[17,44]

8.4.2.3 Other Small Blue Copper Proteins

Other small blue copper proteins include structurally well-characterized amicyanins,[45] as well as structurally unknown halocyanins[46] and uclacyanins.[47] Amicyanins have been isolated from methylotrophic and denitrifying bacteria. The primary function of the amicyanins is to transfer electrons from methylamine dehydrogenase to cytochrome c_{551}. The blue copper center in amicyanins[48,49] is quite similar to that of plastocyanin. Only fine differences are observed in terms of the Cu^{II}–S_{Met} axial ligand interactions and extent to which the Cu^{II} is displaced out of the trigonal plane defined by the $(N_{His})_2S_{Cys}$ ligands (see Table 4). Data from Table 4 also indicate only small structural changes when Cu^{II} is reduced to Cu^{I}.[50]

Halocyanins have been isolated from a haloalkaliphillic archaebacterium.[46] They may be involved in electron transfer in respiration chains that include cytochrome *bc* and a terminal oxidase cytochrome ba_3.[51] Uclacyanins have been isolated from *Arabidopsis* plant.[47] They have been shown to be members of the phytocyanin family (see Section 8.4.3.2).[47] While no three-dimensional structure is available, sequence alignments suggest that they share a similar primary coordination sphere as plantacyanins (see Section 8.4.3.2), with a methionine as the conserved axial ligand. This finding is interesting because uclacyanins have been shown to be more closely related to stellacyanins than to plantacyanins with respect to their gene domain organization, overall sequence homology, and protein glycosylation.[47]

8.4.2.4 Blue Copper Centers in Multidomain, Multicopper Enzymes

The blue copper center in cupredoxins is also found in multidomain, multicopper enzymes[21–23] such as ascorbate oxidase (AO),[52] laccase (Lc),[53] human ceruloplasmin (Cp),[54] and a subfamily of copper-containing nitrite reductase.[55,56] Nitrite reductase (NiR) catalyzes reduction of nitrite (NO_2^-) to nitric oxide (NO), a step in the biological dinitrification cycle.[57] Two distinct types of NiR are known: multiheme NiR (see Chapter 8.29) and multicopper NiR. The multicopper

NiR can be further classified as NiRs containing a green copper center (see Section 8.4.3.4) and NiRs containing a blue copper center (this section) such as NiR from *Alcaligenes xylosoxidans* NCIB 11015 and from *Alcaligenes xylosoxidans* GIFU 1051. The enzymes AO, Lc, and Cp are oxidases that catalyze the four-electron reduction of dioxygen to water *in vitro* (see Chapter 8.17). The precise functional roles of each of the proteins have not been determined conclusively.

The multicopper NiR is a homotrimer, in which each monomer contains two domains.[55,56] On the other hand, AO and Lc contain three domains while human Cp contains six domains.[21–23] Each domain of these enzymes has a typical cupredoxin fold. The blue copper center resides in the first domain of NiR, the third domain of AO and Lc, and the second, fourth, and sixth domains of human Cp. The blue copper centers in domain 1 of NiR (see Structure C in Figure 2),[58,59] domain 3 of AO[60–62] and in domains 4 and 6 of human Cp[63,64] are quite similar to that in plastocyanin, consisting of $Cu^{II}(N_{His})_2S_{Cys}S_{Met}$ in a flattened tetrahedral geometry. While the distance of $Cu^{II}–S_{\delta(Met)}$ is shorter for the blue copper center in NiR (2.62–2.64 Å) than in plastocyanin, the distances in AO and Cp (2.8–3.0 Å) are unusually longer (see Table 4). Furthermore, the axial methionine ligand in domain 3 of Lc[65–68] and domain 2 of human Cp[63,64] is replaced with a leucine. This replacement of methionine with a more hydrophobic leucine residue may be partially responsible for the unusually high reduction potentials of Lc from *polyporus versicolor* (785 mV vs. NHE) as well as the blue copper in domain 2 of human Cp (~1,000 mV vs. NHE).[69] The reduction potential in domain 2 of human Cp is so high that it is always in the reduced form under physiological conditions and it is not expected to play a role in the function of the enzyme.[69] With the exception of this redox inactive center, other blue copper centers in multicopper oxidases function by electron transfer from the physiological partners of the oxidases to the trinuclear copper center where oxidase reactions take place.

8.4.3 GREEN COPPER CENTERS

Green copper centers display not only an intense absorption around 600 nm, but also an increased absorption around 450 nm.[14,70–73] They are also called type 1.5 centers to indicate that their spectral and structural properties are somewhere between type 1 and type 2 copper centers.[14,73] The ratio of the two absorption bands ($R_\varepsilon = \varepsilon_{450}/\varepsilon_{600}$) varies greatly among cupredoxins (see Table 2);[70,71] it can be as low as 0.15 for plastocyanin, or as high as 1.2 for NiR from *Achromobacter cycloclastes*. The R_ε is so large for some proteins (such as NiR from *Achromobacter cycloclastes* and plantacyanins) that they exhibit an intense green color. The name "green copper center" is generally defined as those cupredoxin centers with $R_\varepsilon > 0.15$. More importantly, all green copper centers display a rhombic EPR signal ($\Delta g_\perp = g_x - g_y > 0.01$). The high ratio R_ε was found to correlate with the rhombicity of the EPR signal.[70,71]

8.4.3.1   Rusticyanin

Rusticyanin[74] is found in acidophilic sulfur bacterium *Thiobacillus ferrooxidans*. It is a key component of the iron-dependent energy-harvesting system; it is responsible for the transfer of electrons from Fe^{II} to cytochrome c_4, which then transfers electrons to a terminal oxidase. Rusticyanin has an unusually high stability at low pH ($pH_{optimum} \sim 2$) and it has the highest reduction potential (680 mV) among single-domain, single copper cupredoxins, lower only than those of the cupredoxin center in fungal Lc and in domain 2 of human Cp (see Section 8.4.2.4).

Despite the above unique properties, the primary coordination sphere of the cupredoxin center in rusticyanin is quite similar to that in plastocyanin, including the three strong ligands (($N_{His})_2S_{Cys}$) and one weak ligand (S_{Met}) in a distorted tetrahedral geometry (see Structure D in Figure 2 and Table 4).[75–77] NMR[75] and X-ray crystallographic[76,77] studies have revealed several factors that may contribute to the acid stability and high reduction potential of rusticyanin. These include a more extensive internal hydrogen-bonding network, more hydrophobic interactions, and a decrease in the number of charged residues surrounding the copper binding site, compared with other cupredoxins. Perhaps the major difference between rusticyanin and other cupredoxins is the position of the backbone carbonyl oxygen opposite to the axial methionine. In most cupredoxins, such as plastocyanin and azurin (see Figure 3), the backbone carbonyl oxygen points to the copper ion, and in azurin it binds via a weak ionic interaction. However, the protein fold in rusticyanin forces the backbone carbonyl oxygen to point away from the copper ion such that the
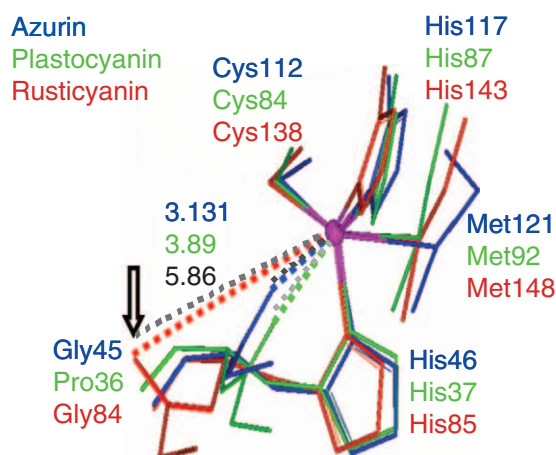
Figure 3 Overlay of copper centers in azurin, plastocyanin, and rusticyanin.

influence of this oxygen is completely eliminated (see Figure 3). Upon copper reduction, only small structural changes were observed.[77,78]

8.4.3.2 Plantacyanin and Stellacyanin: Two Members of the Phytocyanin Family

Phytocyanins are a family of blue copper proteins found exclusively in plants.[11,47] They are further classified into three subfamilies: plantacyanins (PNC), stellacyanins (STC), and uclacyanins (UCC).[47] Spectroscopic properties of uclacyanins are closer to those of blue copper centers and thus they were covered in Section 8.4.2.3. The function of phytocyanins has not been determined conclusively.

Plantacyanins are highly basic cupredoxins (pI ~ 11) found in various plant species, including spinach and cucumber seedlings and peelings. The plantacyanins found in the latter species are also called cucumber basic proteins or cusacyanins.[79] Its primary coordination sphere is similar to those of plastocyanin and rusticyanin, possessing a flattened tetrahedral geometry with $(N_{His})_2$ $S_{Cys}S_{Met}$ as ligands.[80–82] The Cu–$S_{\delta(Met)}$ distance (2.61 Å) in plantacyanins is the shortest Cu–$S_{\delta(Met)}$ distance so far observed in cupredoxins.

Stellacyanins[83] are different from other phytocyanins and cupredoxins by the nature of the axial ligand coordinated to the copper; the axial ligand is a conserved glutamine instead of methionine. They also exhibit lower reduction potentials (180–280 mV vs. NHE) than other cupredoxins, and undergo redox reactions with small inorganic complexes or at electrodes at unusually fast rates.[10,84] The stellacyanin subfamily includes stellacyanins from lacquer tree *Rhus Vernicifera* and cucumber *Cucumis sativus*, mavicyanin from green zucchini, and umecyanin from horseradish root.

The crystal structure of a recombinant, nonglycosylated stellacyanin from cucumber *Cucumis sativus* is now available.[85] The primary coordination sphere consists of two N_δ from histidines, one S_γ from cysteine, and one ε-amide oxygen from glutamine (see Structure E in Figure 2). The distance between Cu^{II} and the ε-amide oxygen (2.21 Å) is much shorter than the Cu–$S_{\delta(Met)}$ distances (2.6–3.1 Å) in other cupredoxins (see Table 4). As a result of this strong interaction, the Cu^{II} atom is displaced from the trigonal plane defined by the two histidines and one cysteine. Together, these interactions make the coordination geometry of stellacyanins nearly ideal tetrahedral. The structure also reveals that the cupredoxin site in stellacyanins is more exposed to solvent than other cupredoxins. This finding may explain its unusually fast redox reactions with small inorganic complexes or at electrodes.[10,84]

8.4.3.3 Other Small Green Copper Proteins

Other small green copper proteins include pseudoazurin[86] and auracyanin.[87,88] Pseudoazurins have been isolated from methylotrophic and denitrifying bacteria. In methylotrophs, while amicyanins are synthesized when methylamine is the sole source of carbon and energy,

pseudoazurins are synthesized instead when cells are grown in methanol. In denitrifying bacteria, pseudoazurins function as an electron donor to green copper-containing nitrite reductase (see Section 8.4.3.4). Auracyanins have been isolated from a phototrophic green bacterium. They have been implicated as an electron donor to the photosynthetic center.

The metal-binding site structures of pseudoazurin[89–91] and auracyanin[92] are similar to that of other cupredoxins, with one cysteine and two histidines forming a trigonal plane and a weak axial methionine to complete the distorted tetrahedral geometry. The $Cu-S_{\delta(Met)}$ distance (2.76 Å) in pseudoazurin is shorter than those of blue copper centers in plastocyanin and azurin, and is still longer than those in plantacyanin and NiR (see Table 4).

8.4.3.4 Green Copper Centers in Multidomain, Multicopper Enzymes

Nitrite reductases are unique among cupredoxin center-containing enzymes in that either blue copper or green copper centers are found in different members of the family. The blue copper-containing NiRs have been discussed in Section 8.4.2.4. Nitrite reductases from *Achromobacter cycloclastes*[93] and from *Alcaligenes faecalis* S-6[94,95] display a strong green color and are representative of green copper centers. Surprisingly the overall structure and metal-binding site of the green copper NiRs[93–95] and the blue copper NiRs[58,59] are quite similar, including the three strong $(N_{His})_2S_{Cys}$ ligands and a weak S_{Met} axial ligand in a distorted tetrahedral geometry (see Structure F in Figure 2 and Table 4). The only notable differences are slight differences in the orientation of the Met ligand and in the secondary coordination sphere.[55,56,58] The structural origins of the blue and green copper centers will be discussed in detail in Section 8.4.8.2.1.

8.4.4 RED COPPER CENTERS

Nitrosocyanin (NC) is a mononuclear copper protein with a brilliant red color due to a strong absorption at 390 nm ($\varepsilon_{max} \sim 7{,}000 \, M^{-1} \, cm^{-1}$).[96] It was isolated from the ammonia-oxidizing autotrophic bacterium *Nitrosomonas europaea*, and shares high sequence homology with other cupredoxins. For example, the C-terminal 69 amino acid sequence of NC is 65% homologous to those in the corresponding region of plastocyanin from cyanobacterium *Phormidium laminosum*. This high sequence homology resulted in NC exhibiting the same cupredoxin fold as found in other cupredoxins. A superposition of the crystal structures of NC[97] and plastocyanin gives a root mean square (r.m.s.) difference of 2.0 Å for 78 Cα coordinates, with the two copper centers occupying similar positions within the overall fold. Similar superposition with cupredoxin domains in multicopper enzymes such as AO, Lc, Cp, NiR, and N_2OR resulted in a r.m.s. of $\sim$1.5 Å.

There are some major differences between NC and other cupredoxins.[97] First, NC exhibits an unprecedented trimer of single domain cupredoxin folds and the copper center within the fold is less solvent accessible than other cupredoxin centers. Second, in contrast to the distorted tetrahedral geometry in other cupredoxins, the copper center in NC is in a square pyramid, with a single carboxylate oxygen of glutamate sitting at the pyramid apex and the one $S_{\gamma(Cys)}$, two $N_{\delta(His)}$, and a solvent (water) molecule forming the pyramid base (see Structure G in Figure 2). Significantly, NC lacks the long $Cu-S_{\delta(Met)}$ and short $Cu-S_{\gamma(Cys)}$ bond distances characteristic of most cupredoxins. Third, while the EPR copper parallel hyperfine coupling constant ($A_\parallel = 144 \times 10^{-4} \, cm^{-1}$) is much higher than those of other cupredoxins, the reduction potential of NC (85 mV vs. NHE) is much lower. These parameters are more typical of a "normal" type 2 copper center. Although the physiological function of NC is still unknown as of 2003, the above data, together with observation of an open coordination site in the crystal structure, suggest a possible catalytic, rather than electron transfer, function for NC.

8.4.5 PURPLE CU_A CENTERS

Purple Cu_A centers display an intense purple color with strong electronic absorption bands around 480 ($\varepsilon_{max} \sim 5{,}000 \, M^{-1} \, cm^{-1}$) and 530 nm ($\varepsilon_{max} \sim 4{,}000 \, M^{-1} \, cm^{-1}$) (Table 3).[25–28,98–101] Another moderately strong absorption around 800 nm ($\varepsilon_{max} \sim 1{,}600 \, M^{-1} \, cm^{-1}$) has also been observed. They are found in cytochrome *c* oxidase (C*c*O),[102–104] a terminal oxidase in the

Table 3 Electronic absorption data for selected purple Cu_A centers.

Protein	Source	Absorption (nm)	EPR $A_{\parallel}$ (10^{-4} cm^{-1})	References
Cu_A in N_2OR[a]	*Pseudomonas stutzeri*	350, 480, 540, 780	39	124
Cu_A in N_2OR[a]	*Achromobacter cycloclastes*	350, 481, 534, 780	N/A	280
Cu_A from caa_3[b]	*Bacillus subtilis*	365, 480, 530, 790	39	107
Cu_A from ba_3[b]	*Thermus thermophilus*	363, 480, 530, 790	31	108,202
Cu_A from aa_3[b]	*Paracoccus denitrificans*	354, 485, 530, 808	32	100,106
Cu_A in azurin[c]	*Pseudomonas aeruginosa*	360, 485, 530, 770	56	143,144
Cu_A in amicyanin[c]	*Thiobacillus versutus*	360, 483, 532, 790	33	142
Cu_A in CyoA[c]	*Escherichia coli*	358, 475, 536, 765	70,54[d]	140,100
Cu_A synthetic complex	Synthetic model	358, 602, 786, 1466	51	166

[a] native Cu_A protein.   [b] soluble Cu_A domain.   [c] engineered Cu_A protein.   [d] The parameters are from two slightly inequivalent copper nuclei.

Table 4　Metal–ligand bond distances of blue and green copper centers (Å).

Protein (source)	N-His	S-Cys	N-His	Axial ligand	Cu_{NNS}	PDB Code	References
Plastocyanin							
(poplar)	**His37**	**Cys87**	**His87**	**Met92**			
Cu^{II}, pH 6.0	1.91	2.07	2.82	2.81	0.36	1PLC	34
Cu^{I}, pH 7.0	2.12	2.17	2.39	2.87	0.47	5PCY	34
Azurin							
(A. denitrificans)	**His46**	**Cys112**	**His117**	**Met121-Gly45**			
Cu^{II}, pH 5.0	2.08	2.14	2.00	3.11(M) 3.13(G)	0.13	2AZA	41
Cu^{I}, pH 6.0	2.13	2.26	2.05	3.23(M) 3.23(G)	0.14	N/A	42
Azurin							
(P. aeruginosa)	**His46**	**Cys112**	**His117**	**Met121-Gly45**			
Cu^{II}, pH 5.5	2.08	2.24	2.01	3.15(M) 2.97(G)	0.10	4AZU	43
Cu^{I}, pH 5.55	2.14	2.25	2.04	2.97(M) 3.15(G)	N/A	N/A	22
Amicyanin							
(A. denitrificans)	**His53**	**Cys92**	**His95**	**Met98**			
Cu^{II}, pH 7.0	1.95	2.11	2.03	2.90	0.30	1AAC	49
Cu^{I}, pH 4.4	1.91	2.09	5.45	2.90	N/A	1BXA	50
Pseudoazurin							
(A. faecalis)	**His40**	**Cys78**	**His81**	**Met86**			
Cu^{II}, pH 6.8	2.16	2.16	2.12	2.76	0.43	1PAZ	89
Cu^{I}, pH 7.8	2.16	2.17	2.29	2.91	0.37	1PZA	90
Pseudoazurin							
(A. cycloclases)	**His40**	**Cys78**	**His81**	**Met86**			
Cu^{II}, pH 6.0	1.95	2.13	1.92	2.71	N/A	1BOK	91
Cu^{I}, pH 6.0	2.04	2.19	2.11	2.85	N/A	1BQR	91
Rusticyanin							
(T. ferroxidans)	**His85**	**Cys138**	**His143**	**Met148**			
Cu^{II}, pH 4.6	2.04	2.26	1.89	2.88	0.33	1RCY	76
Cu^{I}, pH 4.6	2.22	2.25	1.95	2.74	N/A	1A3Z	77
Plantacyanin							
(cucumber)	**His39**	**Cys79**	**His84**	**Met89**			
Cu^{II}	1.93	2.16	1.95	2.61	0.39	2CBP	81
Stellacyanin							
(cucumber)	**His46**	**Cys89**	**His94**	**Gln99**			
Cu^{II}, pH 7.0	1.96	2.18	2.04	2.21	0.33	1JER	85
Laccase							
(C. cinereus)	**His396**	**His452**	**His457**				
Cu^{II}	1.19	2.27	1.87	N/A	N/A	1A65	66
Ascorbate oxidase							
(zucchini)	**His445**	**Cys507**	**His512**	**Met517**			
Cu^{II}, pH 6.0	2.11	2.08	2.08	2.87	N/A	1AOZ	61
Cu^{I}, pH 6.0	2.12	2.14	2.08	2.95	N/A	1ASO	62
Nitrite Reductase							
(A. faecalis)	**His95**	**Cys136**	**His145**	**Met150**			
Cu^{II}, pH 4.0	2.06	2.08	1.98	2.64	0.48	1AS7	95
Cu^{I}, pH 4.0	2.07	2.19	2.08	2.58	0.64	1AQ8	95
Compound (**1**)	**N1**	**S**	**N2**	**N apical**			
Cu^{II}	1.930	2.176	2.037	2.119	0.34	N/A	152
Compound (**2**)	**N1**	**S**	**N2**				
Cu^{II}	1.923	2.1243	1.921	N/A	0.220	N/A	154
Compound (**3**)	**N1**	**S1**	**N2**	**S2**			
Cu^{II}	1.987	2.242	1.952	2.403	N/A	N/A	156

respiratory chain of eukaryotic mitochondria and some aerobic bacteria, nitrous oxide reductase (N_2OR),[24,28] an enzyme responsible for the reduction of N_2O in denitrifying bacteria, and menaquinol NO reductase.[105] In addition, soluble domains of C*c*O containing the Cu_A center have been obtained through expression of a truncated gene.[106–111] The purple Cu_A center is

involved in biological electron transfer,[24,28,103,104,112] and is believed to be responsible for ET from cytochrome *c* to heme *a* in C*c*O, and from cytochrome *c* to the catalytic Cu_Z center in N_2OR. The exact redox partner of the Cu_A center in menaquinol NO reductase remains to be defined. In addition to the purple color, the Cu_A centers also exhibit a seven-line EPR signal that is typical of a Class III[113] mixed-valence dinuclear copper center.[114,115]

Despite a poor amino acid sequence homology, the mononuclear cupredoxin copper and purple Cu_A centers share strong structural homology of the cupredoxin fold as indicated by amino acid sequence alignment.[102,116] This similarity has been confirmed by the availability of the crystal structures of proteins containing the purple Cu_A sites in native C*c*O,[5,6,117] N_2OR,[7] soluble domain of native C*c*O,[118] and engineered model Cu_A proteins.[119,120] The major difference resides in the ligand loop, which results in a dinuclear rather than mononuclear copper center. The Cu_A center contains two copper ions at a copper distance of ∼2.4 Å bridged by two μ_2 S_{Cys} thiolates, with short $Cu–S_{\gamma(Cys)}$ distances (2.27–2.42 Å) (see Structure H in Figure 2). The short Cu–Cu distance (2.4 Å) is indicative of a weak Cu—Cu bond, which is now supported by several spectroscopic studies and calculations.[16,17,101,121–123] Each copper is also coordinated by a $N_{\delta(His)}$ at a normal $Cu–N_{\delta(His)}$ distance (1.88–2.11 Å). Like in the mononuclear cupredoxins, weak axial ligand interactions are observed approximately perpendicular to the plane defined by the $Cu_2(S_{Cys})_2$ core. Those interactions originate from a $S_{\delta(Met)}$ for one copper at a distance of 2.46–3.16 Å on one side of the plane and a backbone carbonyl oxygen for the other copper at a distance of 2.15–2.62 Å on the other side of the plane. Under physiological conditions, only the redox couple of $[Cu(1.5)\cdots Cu(1.5)]$ and $[Cu^I\cdots Cu^I]$ is accessible. The reduction potential of this couple (∼240 mV vs. NHE)[106,124–127] is generally lower than most mononuclear cupredoxin centers.

8.4.6 CUPREDOXIN MODEL PROTEINS

The unusual and interesting structural and spectroscopic properties of cupredoxin centers stimulated the synthesis of a number of biomimetic proteins (this section) and compounds (see Section 8.4.7). This research endeavor has contributed to the fundamental understanding of the role of each essential structural element in the formation of the cupredoxin center, in the display of its spectroscopic signatures, and in performance of its functions. It also helped to advance the field of metalloprotein design and engineering.[128] Because of space limitation, only those model proteins and compounds that closely mimic the spectroscopic and/or structural properties of cupredoxin centers in their oxidized states (i.e., Cu^{II} for mononuclear and $[Cu(1.5)\cdots Cu(1.5)]$ for dinuclear centers) will be discussed in this chapter.

8.4.6.1 Mononuclear Cupredoxin Model Proteins

The first model protein to be discovered to mimic the spectroscopic properties of mononuclear cupredoxins is a Cu^{II}-substituted horse liver alcohol dehydrogenase.[129–132] Horse liver alcohol dehydrogenase is a dimer with each monomer containing a catalytic and a noncatalytic zinc site. The catalytic zinc ion is coordinated in a distorted tetrahedral geometry by two S_{Cys}, one N_{His}, and one O_{H_2O}. Replacing the catalytic zinc with Cu^{II} resulted in a protein with an intense blue color due to a strong absorption at 623 nm ($\varepsilon_{max} \sim 2,450 \, M^{-1} cm^{-1}$), and a rhombic EPR spectrum that resembles those of green copper centers in proteins such as stellacyanin. Even though there are two cysteines in the putative Cu^{II}-binding site of the model protein, rather than the one cysteine in cupredoxin centers, the study suggested that the unique spectroscopic properties of the cupredoxin center can be replicated by cysteines and histidines in a distorted tetrahedral environment.

Another close mimic of cupredoxin centers are Cu^{II}-substituted R-state insulins incorporating an exogenous thiolate ligand.[133–135] X-ray crystallographic studies of the Zn^{II}-insulin R_6 hexamer revealed that it contains two identical zinc sites, each coordinated to three N_{His} and one chloride or phenolate ion in a distorted tetrahedral geometry. Upon addition of thiolate ligands (such as pentafluorobenzenethiolate or tetrafluorobenzenethiolate), the Cu^{II}-substituted insulin R_6 hexamer exhibits strong absorption around 630 nm and an axial EPR spectrum that is similar to those of blue copper proteins, such as plastocyanin and azurin. Interestingly, addition of benzenethiolate or 4-methylbenzenethiolate to the protein resulted in derivatives with rhombic EPR spectra that resemble those of green copper centers.

The red and green copper centers have been engineered into the type 2 copper protein copper–zinc superoxide dismutase (CuZnSOD).[70,71,136,137] CuZnSOD is a dimeric enzyme with two identical subunits, each of which contains a normal type 2 copper and a zinc ion (see Chapter 8.19). The overall structure of each subunit is a Greek key β barrel, similar to those of cupredoxin folds. The metal-binding site contains a Cu^{II} coordinated to four N_{His} and a water molecule in a distorted square pyramidal geometry, and a Zn^{II} ligated by three N_{His} and one O_{Asp} in a distorted tetrahedral geometry. The Cu^{II} and Zn^{II} ions share a bridging histidine ligand. To elucidate the relationship between the type 1 and type 2 copper proteins and to take advantage of predefined scaffolds and metal-binding sites in the design of the unusual type 1 copper center, cysteines were incorporated into the metal-binding sites of yeast CuZnSOD. When a cysteine was substituted at either His46 or His120 of the copper site, a site having a distorted square pyramidal geometry and strong new absorption bands around 400 nm were observed (H46C CuZnSOD, $\varepsilon_{379nm} = 1,940\,M^{-1}\,cm^{-1}$ and H120C CuZnSOD, $\varepsilon_{406nm} = 1,250\,M^{-1}\,cm^{-1}$).[71,136,137] In addition, the proteins displayed a typical type 2 or "normal" EPR, with $A_{\parallel} = 150–170 \times 10^{-4}\,cm^{-1}$.[71,136,137]

While introducing cysteine into the copper site of CuZnSOD resulted in a red copper model protein, substitution of a cysteine for a histidine in the zinc site, a site possessing a distorted tetrahedral geometry, resulted in a protein with UV-vis and EPR spectral features of the green copper centers.[70,71,136] The magnetic circular dichroism[70] and resonance Raman (RR) spectra[138] of the copper derivative, as well as the electronic absorption spectrum of the cobalt derivative[70] of this protein also resembled those of other cupredoxin centers. Interestingly, all three His-to-Cys mutant proteins of yeast CuZnSOD reacted with ascorbate much faster than the wild-type protein, indicating that the presence of a thiolate greatly increased the redox reactivity of the metal binding sites, consistent with the thiolate providing an efficient super exchange pathway for electron transfer.[139]

8.4.6.2 Dinuclear Cupredoxin Model Proteins

The dinuclear purple Cu_A center has been designed and engineered into three different structurally related proteins using a technique called loop-directed mutagenesis.[15,128] First, it was introduced into the *CyoA* subunit of cytochrome *o* quinol oxidase.[140,141] This work was based on close structural and functional homology between subunit II of cytochrome *c* oxidase (C*c*OII) and the *CyoA* subunit of cytochrome *o* quinol oxidase. A careful sequence alignment revealed that the amino acids capable of forming the Cu_A center were replaced by those that could not coordinate copper and those amino acids were clustered in a loop between two β strands F and G (called the FG loop). Because the loop sequences between the two proteins were different and, without structural information, it was difficult to pinpoint which amino acids were responsible for the Cu_A site formation, the whole loop sequence of the *CyoA* subunit was replaced with the corresponding loop sequence of C*c*OII in order to restore the Cu_A center.[140,141] Spectroscopic[140,141] and X-ray crystallographic[119] studies confirmed that the Cu_A center, similar to that in C*c*O, was restored in CyoA.

Similar sequence alignments also revealed that C*c*OII shared similar structural homology with the mononuclear cupredoxins[102,116] and the main difference between the two families of proteins resided in the FG loop sequence. The difference in loop sequence is even bigger between Cu_A and mononuclear cupredoxins, such as amicyanin and azurin, than the difference between those of Cu_A and *CyoA*. In addition to differences in amino acid identities, the lengths of the loop are also different. For example, the total number of amino acids in the loop from cysteine to methionine is 7, 10, and 12, respectively, for *P. versutus* amicyanin, *P. aeruginosa* azurin and Cu_A in *P. Denitrificans* C*c*O.[142–144] Therefore, it is interesting that replacing the loop in either amicyanin[142] or azurin[143,144] with the loop in C*c*O resulted in proteins containing the Cu_A center. Comprehensive spectroscopic studies[101,142–145] and X-ray crystallography[120] indicated that the Cu_A centers in the amicyanin and azurin model proteins were almost identical to the native Cu_A centers, including the $Cu_2(S_{Cys})_2$ diamond core, the terminal N_{His} to each copper ion, the short Cu—Cu bond distance, and the weak axial ligand interactions from either a methionine or a backbone carbonyl. In addition to providing a simple alternative system for studying the Cu_A center, the study provided experimental support for the close structural and evolutionary relationship between the mononuclear and dinuclear cupredoxins. This relationship was further strengthened by a study in which a Cu_A center in C*c*O was converted to a mononuclear cupredoxin center through loop directed mutagenesis.[146]

8.4.7 CUPREDOXIN MODEL COMPOUNDS

Intrigued by the intense colors and unusual structural features of cupredoxins, inorganic chemists have tried for many years to make synthetic model compounds of these proteins.[147–150] While compounds with spectroscopic and structural properties similar to the normal red copper protein nitrosocyanin are known, making close mimics of the oxidized blue, green, and purple copper proteins proved to be challenging. The trigonally distorted tetrahedral geometry in the cupredoxins is quite different from the tetragonal geometry preferred by most Cu^{II} complexes. However, through clever ligand design and skillful synthetic execution, synthetic compounds that closely mimic the blue, green, and purple Cu_A compounds have been successfully obtained and characterized.

8.4.7.1 Mononuclear Cupredoxin Model Compounds

The first group of synthetic compounds to be found to closely mimic the spectroscopic and structural properties of the blue copper center were made through the use of a tridentate tris(pyrazolyl)hydroborate $\{HB(pz')_3^-\}$ ligand system.[148,151,152] Addition of a thiolate ligand completed the coordination and resulted in trigonally distorted tetrahedral complexes, such as complex (**1**) (see Figure 4). This intensely blue-colored model complex mimicked the blue copper center in many respects, including a strong absorption around 600 nm, a narrow EPR $A_\parallel$ (Table 2), and a short Cu^{II}-thiolate distance (2.1 Å, see Table 4). Interestingly, S K-edge X-ray absorption spectroscopy (XAS) measurement showed an even stronger covalent thiolate interaction in the HOMO of complex (**1**) (52%) than in plastocyanin (38%).[153]

Since studies have shown that the core structure of mononuclear cupredoxins is the three-coordinate trigonal-planar $Cu^{II}(N_{His})_2(S_{Cys})$, it is desirable to mimic this structural feature, such as in fungal laccase. The first such structure was synthesized using a bidentate β-diketiminate ligand and a triphenylmethylthiolate (**2**) (see Figure 4).[154] The short Cu—N (1.922(3) Å) and Cu—S (2.124(1) Å) bond lengths in (**2**) are very similar to those in blue copper centers in fungal laccase (1.9 Å and 2.2 Å, respectively), ceruloplasmin, and other blue copper and green copper proteins (Table 4). A detailed spectroscopic and electronic structural study indicated that elimination of the axial ligand can affect the covalency of the Cu^{II}-thiolate bond and its spectroscopic properties.[155] Finally, a compound (**3**) (see Figure 4) that reproduces the complete $N_2S_{thiolate}S_{thioether}$ ligation and geometry of mononuclear cupredoxins was made by replacing the triphenylmethylthiolate ligand in Structure (**2**) with $NaSC(Ph)_2CH_2SCH_3$.[156] As a result of the new thioether binding, the metal–ligand distances in Structure (**3**) are lengthened and the metal-binding site adopts a flattened tetrahedral geometry, similar to that in green copper centers. The reduced S-to-Cu^{II} CT intensity and rhombic EPR of Structure (**3**) are also consistent with Structure (**3**) being a close mimic of green copper centers.
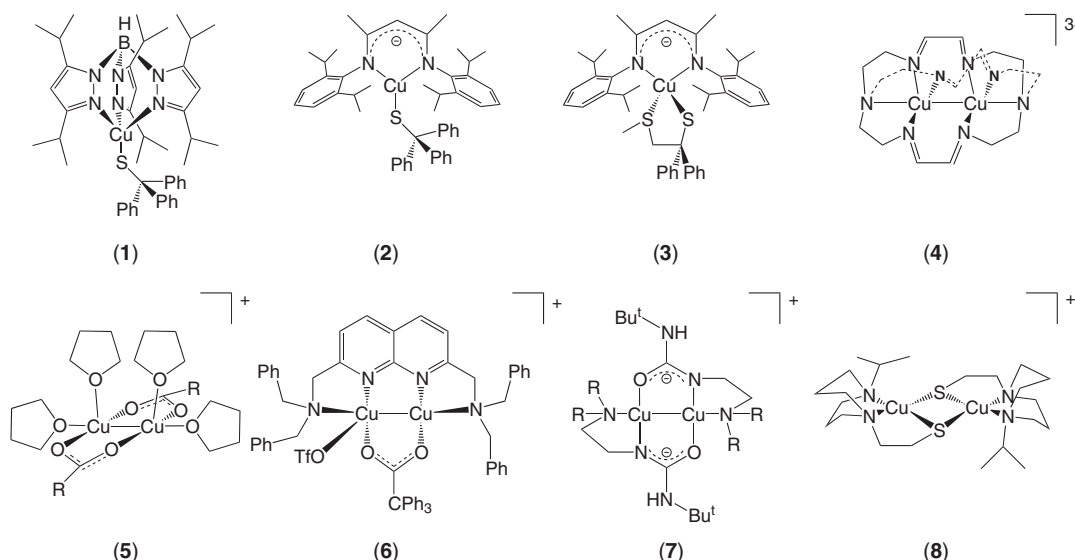
Figure 4 Mononuclear and dinuclear cupredoxin model complexes.

Table 5 Metal–ligand bond distances of purple Cu_A centers (Å).

Cu_A Source	Cu_1–Cu_2	Cu_1–S_1	Cu_1–S_2	Cu_1–N_1	Cu_2–S_1	Cu_2–S_2	Cu_2–N_2	Cu_2–S_3	Cu_1–O_1[b]	Cu_2–O_2[b]	Cu_2–O_3[b]	PDB	References
Native CcO (*P. denitrificans*)	2.55	**C216** 2.24	**C220** 2.23	**H181** 2.10	**C216** 2.25	**C220** 2.16	**H224** 2.11	**M227** 2.56	**(E218)** 2.77	**(H224)** 3.36	**(1180)** 4.82	**1AR1**	5
Native CcO (**Bovine**)	2.45	**C196** 2.17	**C200** 2.27	**H161** 1.93	**C196** 2.28	**C200** 2.21	**H204** 1.92	**M207** 2.66	**(E198)** 2.39	**(H204)** 3.67	**(L160)** 4.56	**2OCC**	6,117
Soluble domain (*T. thermophilus*)	2.51	**C149** 2.35	**C153** 2.42	**H114** 2.11	**C149** 2.29	**C153** 2.27	**H157** 1.88	**M160** 2.47	**(Q151)** 2.64	**(H157)** 4.31	**(I113)** 4.73	**2CUA**	118
Engineered Cu_A (*in CyoA*)	2.48	**C207** 2.12	**C211** 2.27	**H172** 1.83	**C207** 2.19	**C211** 2.20	**H215** 1.73	**M218** 3.00	**(E209)** 2.28	**(H215)** 4.47	**(M171)** 4.75	**1CYW**	119
Engineered Cu_A (*in Azurin*)	2.42 / 2.35	**C112** 2.42 / 2.30	**C116** 2.29 / 2.44	**H46** 2.01 / 2.08	**C112** 2.17 / 2.15	**C116** 2.30 / 2.33	**H120** 2.06 / 2.26	**M123** 2.98 / 3.16	**(E114)** 2.17 / 2.15	**(H120)** 4.07 / 4.42	**(G45)** 3.13 / 3.04	**1CC3**	120
Compound (4) Nitrate Acetate	**Cu_1–Cu_2** 2.364 / 2.415	**Cu_1–N_eq** 2.065–2.080 / 2.085		**Cu_1–N_1** 2.068 / 2.060		**Cu_2–N_eq** 2.065–2.045 / 2.075	**Cu_2–N_2** 2.065 / 2.068						158–160
Compound (5)	**Cu_1–Cu_2** 2.4246	**Cu_1–O_102** 1.885	**Cu_1–O_202** 1.883	**Cu_1–O_402** 2.087	**Cu_2–O_101** 1.883	**Cu_2–O_201** 1.881	**Cu_2–O_502** 2.042	**Cu_1–O_401** 2.285	**Cu_2–O_402** 2.270				161,162
Compound (6)	**Cu_1a–Cu_1b** 2.4493	**Cu_1a–O_1b** 1.872	**Cu_1b–N_1b** 1.911	**Cu_1b–N_3b** 2.090	**Cu_2b–O_2b** 1.883	**Cu_2b–N_2b** 1.907	**Cu_2b–N_4b** 2.113	**Cu_1b–O_3b** 2.257					163
Compound (7) R=Me	**Cu_1a–Cu_1b** 2.3876	**Cu_1a–O_7b** 1.867	**Cu_1a–N_8a** 1.869	**Cu_1a–N_11a** 2.087	**Cu_1b–O_7a** 1.852	**Cu_1b–N_8b** 1.858	**Cu_1b–N_11b** 2.080						165
Compound (8)	**Cu_1–Cu_1'** 2.9306	**Cu_1–S_1** 2.292	**Cu_1–S_1'** 2.250	**Cu_1–N_1'** 2.115	**Cu_1–S_1** 2.250	**Cu_1–S_1'** 2.292	**Cu_1–N_1** 2.115	**Cu_1–N_2** 2.125	**Cu_1–N_2** 2.125				166

[a] The structure and definition of each metal-ligand distance is shown in the figure below.
[b] The O is from the peptide carbonyl oxygen.
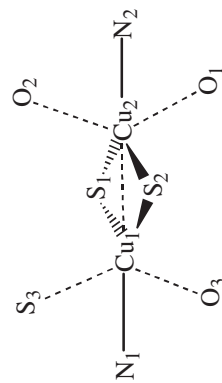
8.4.7.2 Dinuclear Cupredoxin Model Compounds

The dinuclear cupredoxin purple Cu_A contains a fully delocalized "class III"[113] mixed-valence dinuclear [Cu(1.5)···Cu(1.5)] center. While dinuclear or multinuclear mixed-valence copper complexes with the unpaired electron completely localized (class I) or partially delocalized (class II) were known for many years,[35,157] copper complexes with fully delocalized class III mixed valence, such as in Cu_A, are rare. Important progress has been made in synthesizing those model compounds. For example, mixed-valence dinuclear copper complexes (such as structure (**4**) in Figure 4) were synthesized by using the octa-azacryptand macrobicyclic ligand.[158–160] Visible absorption, EPR, XAS, and crystallographic studies all indicated that an unpaired electron is delocalized over a short Cu—Cu bond (e.g., 2.364(2) Å for nitrate and 2.415(2) Å for acetate complexes).[158–160] Direct σ-bonding interaction between the two coppers was revealed through a Fenske–Hall MO analysis.[159] Several other class III mixed-valence dinuclear copper complexes have also been synthesized by using either μ-1,3-carboxylate ligands (such as in compound (**5**) in Figure 4), 1,8-naphthyridine-based dinucleating ligands (such as in compound (**6**) in Figure 4), or μ-1,3-($\kappa N{:}\kappa O$) ureate ligand (such as in compound (**7**) in Figure 4).[161–165] In those model compounds, the electron spin coupling is through the direct Cu—Cu bond.

The model compound that is closest to modeling the purple Cu_A center to date is the bis-thiolate bridged, fully delocalized mixed-valence dinuclear copper complex (**8**) (see Figure 4)[161] through the use of a (*N*-thioethyl)daco ligand.[166] It contains the Cu_2S_2 planar diamond core as in the Cu_A center. The geometry of each metal ion is best described as distorted trigonal pyramidal, with each copper in an N_2S_2 coordination mode. The Cu–Cu distance of 2.92 Å is longer than those ($\sim$2.5 Å) in native Cu_A centers, which may explain the lack of Cu—Cu bonding in this model compound.[101] Therefore, unlike the model compounds (**3**)–(**7**) in Figure 4 mentioned above, the model compound (**8**) in Figure 4 achieved the electron spin coupling through the bridging sulfur ligand superexchange.[101] Study of this and other model compounds played a critical role in the elucidation of the electronic structure of purple Cu_A centers.[16,101]

8.4.8 SUMMARY

8.4.8.1 Structures

8.4.8.1.1 General features

A recent survey of small copper complexes having CuN_2S, $CuN_2S(X)$, $CuN_2S(XY)$, or $CuN_2S(XYZ)$ ligand donor sets in the Cambridge Structural Database System revealed that Cu^{II} favors tetragonal coordination, whereas Cu^I strongly prefers tetrahedral and trigonal planar geometries.[18] The resting Cu^{II} state of the red copper protein nitrosocyanin, with a square pyramidal geometry consisting of one $S_{\gamma(Cys)}$, two $N_{\delta(His)}$, and a solvent molecule at the pyramid base, and a single carboxylate oxygen of glutamate sitting at the pyramid apex, belongs to this normal type 2 copper category. Interestingly, upon reduction, the solvent molecule disappears in the crystal structure, together with a shift of one His away from the copper ion.[97] This structural change may be attributable to the preference of Cu^I for a lower coordination number. It is also consistent with a putative catalytic rather than electron transfer role for the type 2 copper center in red copper proteins, because significant structural changes upon redox activity increases reorganization energy and decreases electron transfer efficiency.

All blue and green copper centers have three strong ligands consisting of one $S_{\gamma(Cys)}$ and two $N_{\delta(His)}$. Although the three strong ligands form a trigonal coordination plane to the copper in many cases, this structural feature is not essential for the copper centers as the copper ion is often displaced from the trigonal plane, and the distance between the copper ion and the center of the trigonal planes varies among the copper centers. In the majority of blue and green copper centers, there is a fourth weak axial ligand, most often a $S_{\delta(Met)}$ and, in rare cases, such as in stellacyanin, a ε-amide oxygen from a glutamine side chain. The fourth ligand forms, together with the three strong ligands, a distorted tetrahedral geometry. In the case of azurin, a fifth interacting moiety from a backbone carbonyl oxygen is present opposite to the position of the fouth ligand. While weak covalent interactions have been confirmed between the copper ion of the fourth ligand, only weak ionic but no covalent interaction can be detected between the Cu^{II} and the fifth backbone oxygen.[17,44]

Although it appears that azurin is unique in having the fifth weak backbone oxygen ligand, a close inspection of other blue and green copper centers indicates that most of the copper centers contain a backbone carbonyl oxygen at a similar position as in azurin (see Figure 3). However, the backbone oxygen in those proteins is even further from the copper ion than that in azurin, so that the weak ionic interaction observed in azurin becomes much less significant in those proteins. In rusticyanin, the protein fold forces the backbone carbonyl oxygen to point away from the copper center (see Figure 3). Apparently the weak fourth and fifth ligands are not obligatory for the blue and green copper centers because certain centers in laccase and human ceruloplasmin contain no axial ligands, with leucine in place of methionine. They do, however, modulate the structural and functional properties of the centers (see below).

The dinuclear purple Cu_A center is structurally related to the mononuclear copper centers in that it resembles a dimer of blue or green copper centers, in which each copper ion replaces the missing imidazole on the other copper center.[167] This merging of two blue or green copper centers results in a $Cu_2(S_{Cys})_2$ diamond core with each copper ion coordinated to one histidine. Weak axial ligand interactions from $S_{\delta(Met)}$ and a backbone carbonyl oxygen are also observed above or below the plane defined by the $Cu_2(S_{Cys})_2$ core. As in the case of blue and green copper centers, these axial ligand interactions are not essential for the purple Cu_A center, but can modulate their structural and functional properties.

In all cupredoxins, the primary coordination sphere is surrounded by a network of hydrogen bonds.[2,20] This network includes NH–S_γ hydrogen bonds between backbone amide nitrogens and the cysteine ligand. For example, a hydrogen bond between the cysteine ligand and an asparagine (or serine in rusticyanin) residue next to the *N*-terminal histidine ligand at the $(n+1)$ position (called extra-loop H-bond)[20] is found in most blue and green copper proteins with the exception of laccase, ascorbate oxidase, and ceruloplasmin. In those latter proteins, this hydrogen bond is not possible due to the presence of a proline reside at the $(n+1)$ position. Instead, another hydrogen bond is found between the $S_{\gamma(Cys)}$ ligand and the backbone amide nitrogen located in the $(n+2)$ position with respect to the cysteine ligand within the ligand loop (called within-loop H-bond)[20] in laccase and ascorbate oxidase. Many blue and green copper proteins do not contain this within-loop H-bond because of the presence of a proline residue at the $(n+2)$ position. However, both hydrogen bonds are present in several blue or green copper proteins such as azurin, plantacyanin, and rusticyanin.

A remarkable feature of blue, green, and purple cupredoxins is that very little structural change is observed upon reduction. In the case of the blue and green copper centers, the same observation holds true for proteins when the copper ion is removed, or is substituted by a variety of other metal ions (such as Hg^{II}, Co^{II}, and Zn^{II}) with totally different preferences for coordination geometry and ligand donor sets.

8.4.8.1.2   *The role of each structural feature in determining the spectroscopic and functional properties of cupredoxins*

(i) Geometry

Perhaps the most important structure feature that defines cupredoxins and related proteins is their geometries. Red copper centers are in a tetragonal geometry while blue and green copper centers are in a distorted tetrahedral geometry. The difference between the blue and green copper centers lies in the degree of either tetragonal or tetrahedral distortion. These differences are reflected in their color and other spectroscopic properties (see Section 8.4.8.2 for a detailed discussion). Furthermore, the geometry also affects the reorganization energy in electron transfer reactions of cupredoxins, which will be discussed in Section 8.4.8.3.2.

(ii) Cysteine

The next most important structural feature is the cysteine coordination. The large Cu^{II}-S_{Cys} bonding covalency is responsible for the intense color, narrow $A_\parallel$, and strong donor–acceptor coupling factor (H_{AB}) for efficient ET.[13,16,17] Most mutations of the cysteine to other residues result in either a loss of copper-binding capability or greatly perturbed structural, functional, and spectroscopic characteristics. For example, the C112D mutation in azurin lacks the spectral features of type 1 copper centers and thus results in a type 2 copper center.[168] Furthermore,

this mutation results in a dramatically decreased covalency at the active site and reduced ET rates.[169] Interestingly an azurin variant containing selenocysteine in place of cysteine at the blue copper center has been obtained[170] through expressed protein ligation.[171] The variant displays a significantly increased $A_\parallel$ and red-shifted CT band, while maintaining the general type 1 copper characteristics, including similarity in reduction potentials.[170] In the case of the Cu_A center, the bridging cysteines are also responsible for maintaining the class III mixed-valence character of the site, despite unsymmetrical axial ligand interactions.[16,17,100,101] Mutations on one of the two cysteine residues in Cu_A, to serine or methionine, generally results in a mononuclear coppercenter resembling type I copper proteins.[141,146,172,173] However, some mutations result in a loss of all copper binding capability[141,174] or in a dinuclear species with valence trapped character.[146,172]

(iii) Axial ligands

Methionine is the highly conserved axial ligand in cupredoxins while other amino acids such as asparagine and leucine are found in a few proteins such as stellacyanin and laccase. The role of the axial ligand in mononuclear cupredoxins has been investigated through spectroscopic studies [13,16,17,44] and site-directed mutagenesis.[14] For example, mutations of the axial ligand have been performed.[175–182] In addition, certain axial ligand mutants have allowed the incorporation of free exogenous ligands into the axial position.[180,183,184] Together, these mutagenesis and comparison studies have yielded a wealth of information regarding the proposed role of the axial ligand. For example, structurally, the methionine is believed to protect the copper ion from interaction with water and exogenous ligands,[180,181,184–186] and prevent a large dependence on pH and temperature.[187] Electronically, the axial S_{Met}–Cu^{II} interaction is proposed to influence the stability of the oxidation states of the copper ion,[175,188] fine-tune the "in-plane" S_{Cys}—Cu^{II} interaction,[155,189–191] and change the geometry of the blue copper center.[70,138,191–194] A shorter S_{Met}—Cu^{II} bond distance is thought to result in more destabilization of the Cu^{II} state, a weaker S_{Cys}—Cu^{II} bond, and a more tetragonal (or flattened tetrahedral) distortion of the trigonal blue copper center.[13,16,17,44] The influences are manifested by different absorption intensity ratios of A_{460nm} to A_{600nm}, different rhombicity of the EPR signals, different Cu^{II}–S(Cys) covalency, and thus different functional properties.[16,17,70,138,194] On the other hand, paramagnetic ^{1}H-NMR studies on perturbed cupredoxin sites have indicated that, if generally a stronger axial interaction weakens the S(Cys)-Cu^{II} bond, in certain blue copper proteins the metal-lignad distances may be governed by beta-barrel structure.[195,196] Perhaps the most prominent role of the axial ligand is its ability to tune the reduction potential of the cupredoxins, over a range as large as 300 mV.[179,185,197–199] Recent work of replacing the methionine in azurin with isostructural selenomethionine and unnatural amino acids norleucine allowed a more systematic deconvolution of factors affecting the reduction potential, and pointed to hydrophobicity as the dominant factor in tuning the reduction potentials of cupredoxins by an axial ligands.[281]

Similar investigations on the role of the axial ligand in the dinuclear Cu_A center have also been carried out.[101,198,200–202] Spectroscopic characterization and theoretical calculation studies have shown that a strong axial ligand interaction from methionine favors longer Cu—Cu bond distances in Cu_A centers, which shifts more electron spin from the ligands to the copper ions and affects the reduction potential, reorganization energy, spin density distribution, and thus electron transfer rate.[100,101] On the other hand, results from calculations using density functional theory suggest that variations in the strength of axial ligand interactions will unlikely change the structure and reduction potentials of the Cu_A center.[203] Mutations of methionine in CyoA quinol oxidase,[141] and CcO from *S. cerevisiae*[174] and *P. denitrificans*[172] resulted in colorless and inactive proteins. Mutation of methionine in the *P. denitrificans* CcO[200] resulted in a valence trapped species for the Cu_A site and decreased the reduction potential by 100 mV. Mutation of methionine to glutamate and glutamine in the *Thermus thermophilus* subunit II of CcO[202] resulted in mutants with an increased $A_\parallel$ (31–42 G), but the Cu_A center maintained its class III, mixed-valence[113] character. In contrast to the situation found in the evolutionarily related blue copper proteins, the Cu-Cys bonds are not substantially altered by the Met-to-Gln mutation.[284] Interestingly, substitution of methionine to selenomethionine, also in the soluble subunit II of *T. thermophilus* CcO,[204] resulted in little change in the UV-vis, EPR, and reduction potential properties, even though a Cu–Se interaction was detected by EXAFS. On the other hand, the same mutation in mononuclear cupredoxin azurin resulted in a ~25 mV increase in reduction potential.[175] Therefore it appears that the axial ligand exerts less influence on the reduction potential of dinuclear Cu_A center than that of the mononuclear blue copper center.

(iv) Equatorial histidines

There are two histidines in either mononuclear cupredoxins or the dinuclear Cu_A center. Based on their location on the peptide, one is named an *N*-terminal histidine and another is called the C-terminal histidine. It is interesting to note that almost all histidines in cupredoxins use $N_{\delta(His)}$ for copper coordination while $N_{\varepsilon(His)}$ is more common in other types of copper centers. The role of histidine ligands in the electron transfer function of blue copper proteins was studied primarily by utilizing site-directed mutations. The results suggest that the histidine ligands play structural roles, such as protecting the redox active site,[205,206] and providing rigidity for the copper ion,[207,208] as well as functional roles, such as modulating the electronic structure[206,207,209] and participating in the electron transfer reaction.[205,207,210] Interestingly, titration of exogenous ligands into the His117Gly mutant yielded a series of perturbed copper sites ranging from blue, to green, to normal "red" copper as observed by EPR and UV-vis spectroscopy.[205,207,211]

A comparison of different Cu_A X-ray structures shows that the angular position of the histidine rings with respect to the $Cu_2(S_{Cys})_2$ core can influence the axial ligand interactions.[120] Since both the axial ligands and the angular position of the histidine ring are important for modulating the Cu–Cu distance, the three structural elements critical in modulating the Cu_A center can be traced to the angular position of the histidine rings. Therefore, mutations were made on native Cu_A systems to probe the role of these equatorial histidine ligands in this electron transfer site. The *N*-terminal histidine was mutated to asparagine, which resulted in a complete loss of copper bonding and protein misfolding in the engineered *CyoA* quinol oxidase,[141] *S. cerevisiae* mitochondrial C*c*O,[174] and the soluble subunit II of *Paracoccus denitrificans* C*c*O.[172] However, the same mutation in the entire *P. denitrificans* C*c*O enzyme resulted in a protein resembling the wild type with a blue-shifted 800 nm band and 60% of the wild-type activity.[146] On the other hand, mutation of the C-terminal histidine resulted in a loss of the structure and activity in *S. cerevisiae* mitochondrial[174] and *P. denitrificans* C*c*O.[146] However, dinuclear, valence trapped species were observed for soluble subunit II of *P. denitrificans* C*c*O[172] and the engineered CyoA quinol oxidase mutants,[141] and were characterized by a brown color with absorption peaks near 370 nm, 440 nm, and 800 nm. Finally, mutation of the C-terminal histidine in Cu_A azurin to Asn, Asp, Ala, and Gly resulted in dinuclear derivatives whose UV-vis, MCD, and ENDOR spectra were still very similar to the those of parent Cu_A azurin.[212,213] The only detectable difference was that the mutant proteins displayed a four-line EPR hyperfine, suggesting the presence of a trapped valence center rather than mixed-valence dinuclear center in the mutant proteins. These results indicate that histidines are important in stabilizing the dinuclear Cu_A structure, or minimally, maintaining the fully delocalized character of the center.

(v) Backbone carbonyl oxygen

Backbone carbonyl oxygens are present in the copper-binding sites of all cupredoxins (see Figure 3). However, most of them are far away from the copper center except those in azurin (at 3.1 Å) and in the Cu_A center (2.15 Å). While no covalent interaction with the copper center is detectable, calculations show that weak ionic interactions are present in azurin.[17,44] At ~2.15 Å, the effect of the backbone carbonyl oxygen of Glu114 in Cu_A azurin could be even larger. These backbone carbonyl oxygens have been implicated as playing a role in tuning the reduction potentials of the cupredoxins (see Section 8.4.8.3.1).[18,198] However, their roles have not been addressed experimentally because it is difficult to replace or perturb the oxygen using site-directed mutagenesis.

(vi) Hydrogen bonding network around the primary coordination sphere

The conserved hydrogen bond network in cupredoxins is believed to play a role in maintaining the geometry of the copper center and in determining the relative constraints of the Cu^{II} and Cu^I sites, which in turn influences the relative stability of the two states of the protein and, ultimately, the reduction potential.[20,214] Indeed, mutations of the Asn in the extra-loop H-bond (i.e., the Asn next to the N-terminal His ligand) in both azurin[215] and plastocyanin[216] resulted in reduced stability and, in the case of azurin, an increase of the reduction potential from 286 mV for wild-type azurin to 396 mV for the variant protein. In rusticyanin, the Asn residue in the extra-loop H-bond is replaced with a Ser residue.[217] Mutation of this Ser in rusticyanin resulted in reduced stability and a decrease of reduction potential by ~110 mV. Based on these results, the authors

attributed this Ser residue to be at least partially responsible for the high acid stability and reduction potential of rusticyanin. Finally, since the presence of a Pro in the ligand loop prevented the second within-loop H-bond formation, mutation of this Pro was carried out in pseudoazurin[218,219] and in amicyanin.[214] The mutations resulted in a marked increase in reduction potentials to close to the value for the unconstrained Cu $(N_{His})_2S_{Cys}S_{Met}$ site found in denatured blue copper proteins (see Section 8.4.8.3.1). These results may support the proposition[214] that in the low potential (less than 400 mV vs. NHE) blue and green copper centers, the hydrogen bond network may provide more constraint on Cu^I than Cu^{II}. Mutation of this network to relax the constraint is responsible for the increase of the reduction potentials.

8.4.8.2 Spectroscopic Properties

8.4.8.2.1 *Origin of the red, blue, green, and purple colors*
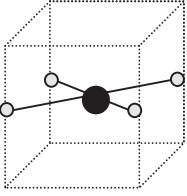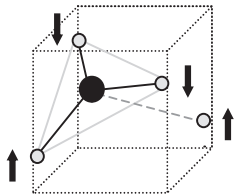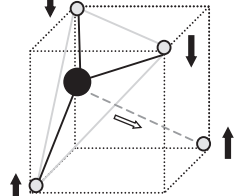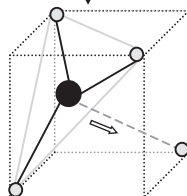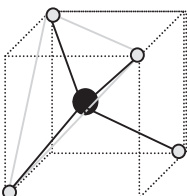
As mentioned in the above section, Cu^{II} ions normally prefer tetragonal geometries with four strong ligands in the equatorial plane (defined as the xy plane) and weak axial ligands above and below the plane (along the z-axis) (see Figure 5).[18] Interactions with the ligands result in splitting of the five d-orbitals of copper such that the $d_{x^2-y^2}$ level has the highest energy. With a d^9-configuration, the Cu^{II} ion has one unpaired electron in the highest occupied $d_{x^2-y^2}$ orbital. Although electric dipole selection rules forbid ligand field transitions in centrosymmetric tetragonal molecules, vibronic coupling makes it possible to observe weak absorptions in the 600–700 nm region. These weak absorptions cannot explain the intense color of cupredoxins.

The most likely origin of the intense color is ligand to metal charge transfer (LMCT) bands, as they are electric dipole allowed.[9,13,16,17] Most LMCT transitions occur in the ultraviolet region, with the thiolate ligand to Cu^{II} CT being an exception. The presence of a $S_{\gamma(Cys)}$ in a tetragonal geometry results in a normal case for ligand–copper bonding interaction, i.e., one lobe of the $d_{x^2-y^2}$ orbital orients along the ligand–metal bond, producing an intense, high-energy S_{Cys} pseudo-σ to Cu^{II} CT transition, and a weak, low-energy S_{Cys} π to Cu^{II} CT transition (see Figure 6).[13,17] The high energy, intense S_{Cys} pseudo-σ to Cu^{II} CT transition is the origin of the red color in the red copper protein nitrosocyanin, and is also responsible for the red or yellow colors in all model protein and compounds that possess tetragonal geometries.

The distorted tetrahedral geometry, particularly the three strong ligands in the trigonal plane and weak axial ligand interactions of the blue copper site (see Figure 5), results in a 45° rotation of the $d_{x^2-y^2}$ orbital in the xy-plane such that its lobes are bisected by the Cu—S_{Cys} bond, rather than along the bond (see Figure 6).[13,16,17,220,221] This orientation produces CT transitions that are opposite to those in the normal type 2 copper-cysteinate proteins, i.e., a weak, high-energy S_{Cys} pseudo-σ to Cu^{II} CT transition, and a strong, low-energy S_{Cys} π to Cu^{II} CT transition. Thus, the strong, low-energy S_{Cys} π to Cu^{II} CT transition is responsible for the intense blue color of blue copper proteins.

In most green copper centers (such as those in pseudoazurin, plantacyanin, and nitrite reductase), it is now believed that a coupled angular movement of the Cys and Met residues from an ideal blue copper center toward a more flattened tetragonal structure (see Figure 5) results in a rotation of the $d_{x^2-y^2}$ orbital in the xy-plane to somewhere between the positions in red copper center and blue copper centers (see Figure 6).[192,194] This rotation causes an increase in S_{Cys} pseudo-σ and a corresponding decrease of S_{Cys} π-interactions with the Cu^{II} $d_{x^2-y^2}$ orbital, and thus an intense green color is observed. In addition, the mixing of some Met sulfur character into the HOMO may also contribute to the green color. The cause of the coupled angular movement of the Cys and Met residues and the increased mixing of Met sulfur character into the HOMO could be the shorter $Cu–S_{\delta(Met)}$ and longer $Cu–S_{\gamma(Cys)}$ distances, which produces a Jahn–Teller distorting force that favors a more tetragonal geometry (see Section 8.4.8.3.2 for a more detailed discussion of the relationship between metal–ligand interactions and Jahn–Teller distorting force).[16,17,192,194] Different strengths of $Cu–S_{\delta(Met)}$ and $Cu–S_{\gamma(Cys)}$ interactions dictate different degrees of Jahn–Teller distortions, which in turn cause different coupled angular movement of the Cys and Met residues and thus different overlaps between Cu^{II} $d_{x^2-y^2}$-S_{Cys} pseudo-σ and Cu^{II} $d_{x^2-y^2}$-Cu^{II}-S_{Cys} π-orbitals. Therefore, different R_ξ can be observed.

Stellacyanin is an exception to the above rule.[194] The strong axial interaction from the ε-amide oxygen of glutamine side chain results in displacement of the Cu^{II} ion further away from the trigonal plane defined by the three strong $S_{Cys}(N_{His})_2$ ligands, to a more tetrahedral geometry (see Figure 5). As a result, only a minor decrease in S_{Cys} π overlap and a slight increase in S_{Cys}

Figure 5 Summary of Cu^{II}-thiolate centers (after Lu *et al.*).[70]

pseudo-σ overlap with the Cu^{II} $d_{x^2 - y^2}$ orbital occurs. This difference observed in stellacyanin has been attributed to a more constrained active site structure posed by the protein than those found in the green copper proteins.[16,194] This tetrahedral distortion has only a small effect on CT transitions (the colors of stellacyanins are still blue). However, the distortion results in large rhombic EPR spectra, just like other green copper proteins (see the next section below).

The purple color of the Cu_A center originates from two S-to-Cu^{II} CT transitions of approximately equal intensity.[16,17,100,101] In a dinuclear center like Cu_A, the valence d orbitals split into pairs with phases that are bonding (ψ) and antibonding (ψ^*) with respect to metal–metal interactions (see Figure 7). The energy separation of the two orbitals, related to the electronic coupling matrix element between the two copper ions ($2H_{AB}$, see Section 8.4.8.3.3),[222,223] is determined by
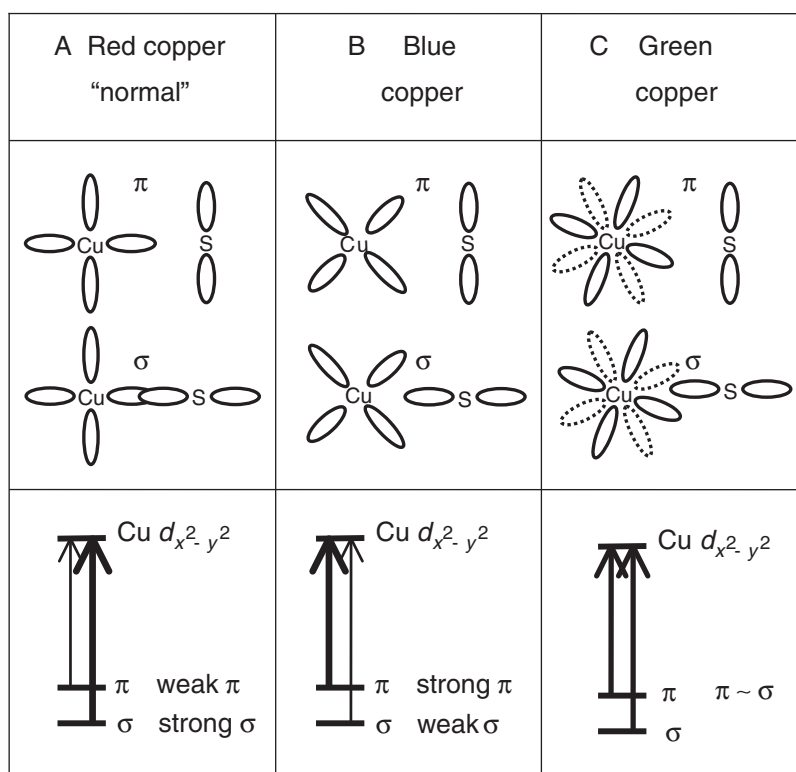
Figure 6 Possible Cu^{II}—S_γ(Cys) bonding interactions in red, blue, and green copper proteins (after Lu *et al.*).[70]

the bridging S_{Cys} ligands via an indirect superexchange pathway and by the direct metal orbital overlap via a metal–metal bond.[16,17,100,101] The 450 nm and 530 nm absorption bands have been attributed to $S(p_x)_g$ $Cu \rightarrow \psi^*$ (HOMO), and $S(p_y)_g$ $Cu \rightarrow \psi^*$ (HOMO) CT transitions, while the 800 nm absorption band has been assigned to be the $\psi \rightarrow \psi^*$ transition.

8.4.8.2.2 Origin of the narrow copper hyperfine coupling constants

In addition to the intense colors, the blue copper, green copper, and purple Cu_A centers also exhibit unusually narrow copper hyperfine constants ($A_\parallel < 80 \times 10^{-4} \, cm^{-1}$). It was proposed that
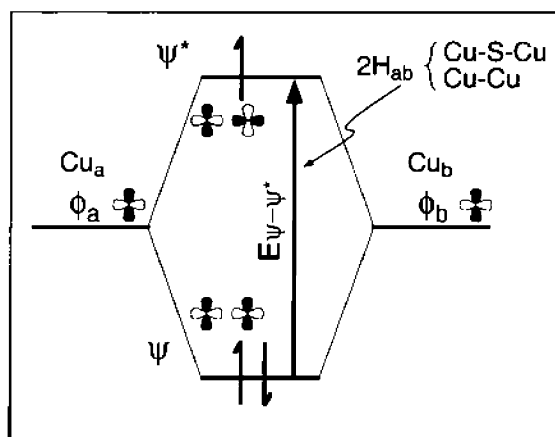
Figure 7 Splitting of metal *d*-orbitals in a dinuclear metal complex due to a combination of superexchange through bridging ligands and direct orbital overlap and the associated $\psi \rightarrow \psi^*$ transition (reproduced by permission of Elsevier from Solomon *et al.*[17]).

Cu $4p_z$ mixing into the Cu $d_{x^2-y^2}$ orbital may explain the narrow $A_\parallel$, as an electron in a p_z orbital has a spin dipolar interaction with the copper nuclear spin that is opposite to that of an electron in a $d_{x^2-y^2}$ orbital.[224–226] However, a polarized single-crystal XAS study showed that all Cu $4p$ mixing involves only the $4p_{x,y}$ orbitals.[227] Instead, the reduction in $A_\parallel$ was attributed mainly to the highly covalent Cu—S_{Cys} bond, which results in delocalization of the unpaired electron onto the ligands and thus reduces its coupling to the nuclear spin of Cu^{II}.[13] The high covalency has been confirmed by both Cu L-edge[228] and S K-edge[227] X-ray absorption studies. For example, a Cu L-edge study indicated that the total copper d-character in the HOMO is 41% and 44% for the blue copper in plastocyanin and Cu_A in engineered azurin, respectively.[229] These copper d characters are much less than the 61% copper d-character in a reference compound, $CuCl_4{}^{2-}$. In addition, a S K-edge study showed that the total S_{Cys} character in the HOMO is 38% and 46% for the blue copper in plastocyanin and Cu_A in engineered azurin, respectively.[229] Self-consistent field $X\alpha$-scattered wave calculations also are in excellent agreement with the experimental observations. The high Cu–S_{Cys} covalency also explains the unusually high intensity of the S_{Cys}-to-Cu^{II} CT bands of mono- and dinuclear cupredoxins.

8.4.8.3   Electron Transfer Properties

The blue, green, and purple copper centers discussed in this chapter are redox proteins that play important roles in biological electron transfer. According to the semiclassical Marcus equation,[230] the rate of biological electron transfer depends on three factors: driving force (or reduction potential differences between the donor and acceptor, ΔE°), reorganization energy (λ), and the donor–acceptor electronic coupling (H_{AB}). In this section, we will examine how the above cupredoxins are fine-tuned with respect to the three factors.

8.4.8.3.1   *Reduction potentials*

The reduction potential of a normal aqueous Cu^{II}/Cu^I couple is $\sim$150 mV (vs. NHE). The potential of the red copper protein nitrosocyanin (85 mV)[96] is consistent with it being a type 2 copper center with a negatively charged residue (Glu) coordinating the copper center. The negative charge further stabilizes the Cu^{II} state and thus lowers the reduction potential. In contrast, the reduction potentials of blue, green, and purple Cu_A centers are usually higher than that of the normal aqueous Cu^{II}/Cu^I couple. While the potentials of the purple Cu_A centers appear to be in a limited range (240–280 mV), the potentials of blue and green copper centers vary greatly, from 184 mV for stellacyanin to 785 mV for one of the blue copper centers in laccase (one of the blue copper centers in human ceruloplasmin has a potential of over 1,000 mV and it is believed that the center is always in the reduced state and does not play a functional role under physiological conditions). This wide range of potentials is required to efficiently match the physiological redox partners. Even a small (less than 100 mV) potential shift could adversely affect the normal function of biological electron transfer chains.

Many factors may contribute to the variation of the reduction potentials. It was proposed that the high reduction potentials of cupredoxins may be due to a strain[231–235] posed by the rigid protein fold onto the Cu^{II} center, which destabilizes Cu^{II} more than Cu^I. However, calculation of optimal geometries of the blue copper center in vacuum suggests that the trigonal core formed by the $S_{Cys}(N_{His})_2$ ligand set is a stable arrangement for Cu^{II},[19,236,237] and no distortion force was detected in the oxidized blue copper center.[188,238] Furthermore, folding studies showed that oxidized azurin was more stable than the reduced azurin.[201,239] Finally, the reduction potentials of an unfolded blue copper azurin and a purple Cu_A domain from *Thermus thermophilus* have been determined.[240] The potentials are higher than those of folded proteins (azurin: $E^\circ{}_{folded} = 320$ mV, $E^\circ{}_{unfolded} = 456$ mV; Cu_A center: $E^\circ{}_{folded} = 240$ mV, $E^\circ{}_{unfolded} = 453$ mV, vs. NHE).

Based on the above observations, two main factors have been identified as playing important roles in tuning the reduction potentials of cupredoxins. These are hydrophobic encapsulation and axial ligand coordination.[16,18,198] An X-ray absorption study indicated that the cysteine and at least one of the two histidines remained coordinated to the copper in the unfolded azurin,[241] which defined the intermediate potential of 456 mV vs. NHE. For cupredoxins with potentials higher than 456 mV, the hydrophobic encapsulation must be important; it increases reduction potentials by exclusion of water and encloses the positively charged metal center in a low

dielectric protein medium. However, axial ligand coordination may counter the effect of hydrophobic encapsulation by lowering the potentials through stabilization of the Cu^{II} state. For example, stellacyanin, with the ε-amide oxygen of glutamine side chain within a short distance of copper, has the strongest axial ligand coordination among all cupredoxins and has the lowest reduction potential (184 mV). With the presence of a long S_{Met} (3.1 Å) and a backbone carbonyl oxygen (3.1 Å), the axial ligand interactions are weaker in azurin than in stellacyanin; these weaker interactions destabilize Cu^{II} more than Cu^{I}, resulting in a higher reduction potential (320 mV) in azurin. The backbone carbonyl oxygen is even further from copper in plastocyanins and is forced to point away from copper by the protein fold in rusticyanins (see Figure 3). These differences may explain higher reduction potentials for plastocyanins (370 mV) and even higher potentials for rusticyanins (680 mV). Finally, in fungal laccase, leucine is present at the axial position. This complete lack of axial ligand coordination coupled with the hydrophobicity of the residue makes the blue copper center in fungal laccase possess one of the highest reduction potentials. In addition to the above two factors, other factors, such as solvent exposure[242] and hydrogen bonding networks[20,214] around the center may also play important roles.

The reduction potentials of Cu_A centers are influenced by the same factors that contribute to those of mononuclear cupredoxins discussed above, including hydrophobic encapsulation and axial ligand interactions from a weak methionine and a backbone carbonyl oxygen. However, the presence of two covalent S_{Cys} ligands would significantly stabilize the oxidized center and further lower the reduction potentials. This effect is believed to be countered by the presence of a Cu—Cu bond in the oxidized Cu_A; the presence of a second copper ion in close proximity would tend to increase the effective nuclear charge felt by the redox active electron and thus would increase the reduction potentials of the Cu_A centers.[16,17,101]

8.4.8.3.2 Reorganization energy

Many cupredoxins transfer electrons over a long (>10 Å) distance with a driving force as low as 0.1 eV. To transfer electrons efficiently, the reorganization energy must be minimized. Unlike heme systems, copper redox reactions in aqueous solution can exhibit reorganization energies as high as 2.4 eV,[243] due to significant geometric changes from the tetrahedral preferred for Cu^{I} to tetragonal preferred by Cu^{II} associated with unconstrained copper complexes. These geometric changes originate from a Jahn–Teller distorting force typical of a d^9 Cu^{II} ion in a ligand field where its partially unoccupied valence d-orbitals are degenerate.[16,17] For example, when placing a Cu^{II} ion in a tetrahedral field preferred by Cu^{I} ions, the three-fold degenerate HOMO will be subject to a large Jahn–Teller distorting force that will cause significant geometrical changes and thus high reorganization energies.

The reorganization energies of mononuclear cupredoxins, however, are much lower than those of unconstrained copper complexes. For example, the reorganization energy of azurin was estimated to be ~0.7 eV.[244] This low λ has been attributed to the unique geometry of mononuclear cupredoxins that influence the valence d-orbital splitting, which removes orbital degeneracy and minimizes or eliminates the Jahn–Teller distortion.[16,17] First, the weak axial ligand bond results in a trigonal geometry with $\sim C_{3v}$ symmetry (see Figure 8). This factor alone does not
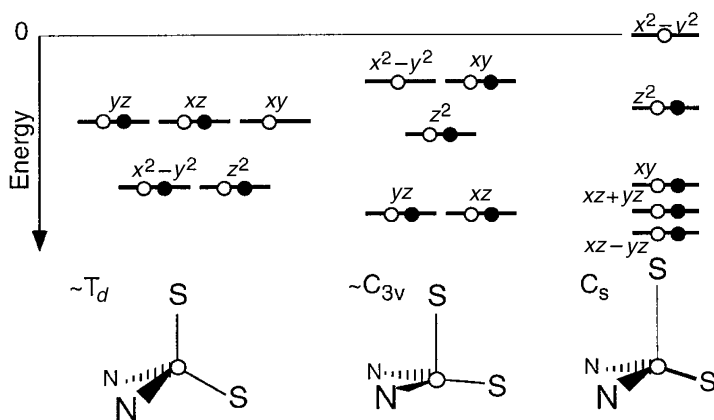
Figure 8 Depiction of how the ligand field of a classic blue copper center minimizes reorganization energy (after Randall *et al.*).[16]

eliminate the Jahn–Teller distorting force because this ligand field still results in a doubly degenerate HOMO. However, the shorter Cu^{II}—S_{Cys} bond, which charge compensates for the weak Cu^{II}-axial ligand bond, produces a site with C_s symmetry. The HOMO degeneracy is finally lifted and Jahn–Teller distortion is eliminated.

The reorganization energies for ET between the dinuclear Cu_A center and cytochrome a in cytochrome c oxidase have been estimated to be between 0.15–0.5 eV from ET experiments.[112] This estimate means that the λ for the Cu_A center is even lower than that for the mononuclear cupredoxin center. An electron transfer study of an engineered Cu_A azurin showed that the calculated λ for Cu_A in the engineered azurin is $\sim$0.4 eV, which is about half that of the blue copper center in native azurin.[245] Furthermore, an excited-state distortion analysis of a resonance Raman enhancement profile for Cu_A also confirmed that the inner-sphere λ for Cu_A is about 50% that of a blue copper center.[16,17,101] The lower λ for Cu_A can be attributed to the valence delocalization of the dinuclear center; the bond length distortions associated with the redox reaction can be spread over two metal ions and thus reduced to $\sim$1/2 that of the mononuclear copper or valence-trapped dinuclear centers.[101,203]

The above results and analysis on the low λ in mononuclear and dinuclear cupredoxins have also been supported by numerous structural analyses of both oxidized and reduced cupredoxins. Both X-ray crystallography[2,8] and XAS[246] of the metal-binding sites in the cupredoxins clearly show minimal difference between the oxidized and reduced proteins. Finally, in addition to the unique geometry and valence delocalization discussed above, which affect inner-sphere reorganization energy, other factors that may influence outer-sphere reorganization energy may also play an important role in cupredoxins. The factors include exclusion of water or solvent from the copper center in the folded proteins. This factor rules out electron transfer as a putative function for the red copper protein nitrosocyanin because its copper center is solvent accessible.

8.4.8.3.3 *Donor–acceptor electronic coupling factor*

In addition to the driving force and reorganization energy, the donor–acceptor electronic coupling factor, H_{AB}, is also important for efficient electron transfer. To elucidate H_{AB} in cupredoxins, both intra- and intermolecular electron transfer studies have been carried out. For intramolecular ET studies, the cupredoxin redox partners are generated either internally through a disulfide anion radical (through pulse radiolysis),[10,247] or externally through attachment of a metal complex (such as $[Ru(bpy)_2Im]^{2+}$ and $[Re^I(CO)_3(phen)]^+$) to a surface histidine,[248–250] or an organic molecule (such as thiouredopyrenetrisulfonate) through a surface lysine.[251] The intermolecular ET studies have been carried out using metal complexes, another redox enzyme, or through electron self-exchange reactions between oxidized and reduced cupredoxins.[252–255] Organic molecules or disulfide bonds have also been introduced to covalently link cupredoxins with either another redox partner or with another cupredoxin at a different oxidation state.[256] Due to space limitations and the focus on the coordination chemistry of cupredoxins, the results will not be presented here. Instead, only the contribution of the cupredoxin center to the H_{AB} is covered below.

Many cupredoxins such as azurin use the surface exposed C-terminal histidine ligand located in a hydrophobic patch as the ET conduit of the copper center to or from its redox partners.[15,257–260] In several other cupredoxins, such as plastocyanin, nitrite reductase, and ascorbate reductase, a remote site that is $\sim$13 Å away from the copper center may also be operative.[16,17] This remote site requires ET through S_{Cys} of the copper center. Interestingly, ET rates to both the adjacent site involving the C-terminal histidine and the remote site involving the cysteine are similar in plastocyanin,[261] despite the large difference in the ET path length. This result has been attributed to the anisotropic covalency of the redox active orbitals in the cupredoxin site.[16,17] Because the S_{Cys} covalency ($\sim$38%) is $\sim$10-fold greater than that of N_{His} ($\sim$4%), S_{Cys} contributes to H_{AB} much more than N_{His}. This finding, combined with the fact that H_{AB} affects the ET rate quadratically based on the Marcus equation, may explain why the longer pathway is competitive with the shorter pathway. Similar observations have also been made in the Cu_A-containing proteins.[16,17,101]

Finally, since both mononuclear cupredoxin and dinuclear Cu_A centers use similar cupredoxin scaffolds to perform similar ET functions, one may wonder why Nature would want to use the dinuclear Cu_A center to carry out the same function that the mononuclear blue or green copper centers perform remarkably well. This question is interesting especially considering that the assembly of the dinuclear Cu_A center is more difficult than that of the mononuclear one and

thus the process must be tightly controlled.[262] Although many studies have pointed to Cu_A being a more efficient redox center than mononuclear cupredoxin centers,[112] a direct comparison of the two classes of copper centers is desirable. The engineered Cu_A azurin made it possible by placing either the Cu_A center or the blue copper center in the same protein network.[143] X-ray crystal structural analysis showed that one of the coppers in Cu_A azurin is superimposable on the mononuclear blue copper in azurin, and the same ET pathways are operative in both proteins.[120] In this way, the difference in the H_{AB} factor between the two proteins, which is often difficult to define, is greatly minimized. ET studies by pulse radiolysis indicated that the Cu_A center in azurin transfers electrons about three times faster than the blue copper center in azurin, despite a lower driving force (0.69 eV for Cu_A vs. 0.76 eV for blue copper).[245] Therefore, the more efficient Cu_A center may be needed in some cases to perform faster ET reactions than the blue or green copper centers under lower driving force.

ACKNOWLEDGEMENTS

8.4.9   REFERENCES

1. Adman, E. T. Structure and function of small blue copper proteins. In *Topics in Molecular and Structural Biology: Metalloproteins*; Harrison, P., Ed.; MacMillan: New York, 1985; Vol. 1, pp 1–42.
2. Adman, E. T. *Adv. Protein Chem.* **1991**, *42*, 145–197.
3. Malkin, R.; Malmström, B. G. *Advan. Enzymol. Relat. Areas Mol. Biol.* **1970**, *33*, 177–244.
4. Fee, J. A. *Struct. Bond.* **1975**, *23*, 1–60.
5. Iwata, S.; Ostermeier, C.; Ludwig, B.; Michel, H. *Nature* **1995**, *376*, 660–669.
6. Tsukihara, T.; Aoyama, H.; Yamashita, E.; Tomizaki, T.; Yamaguchi, H.; Shinzawa-Itoh, K.; Nakashima, R.; Yaono, R.; Yoshikawa, S. *Science* **1995**, *269*, 1069–1074.
7. Brown, K.; Tegoni, M.; Prudencio, M.; Pereira, A. S.; Besson, S.; Moura, J. J.; Moura, I.; Cambillau, C. *Nat. Struct. Biol.* **2000**, *7*, 191–195.
8. Freeman, H. C. *Coord. Chem.* **1981**, *21*, 29–51.
9. Gray, H. B.; Solomon, E. I. Electronic structures of blue copper centers in proteins. In *Copper Proteins;* Spiro, T. G., Ed.; Wiley: New York, 1981; pp 1–39.
10. Farver, O.; Pecht, I. Electron transfer process of blue copper proteins. In *Copper Proteins;* Spiro, T. G., Ed.; Wiley: New York, 1981; pp 151–192.
11. Rydén, L. Structure and evolution of the small blue proteins. In *Copper Proteins and Copper Enzymes;* Lontie, R., Ed.; CRC Press: Boca Raton, FL, 1984; Vol. 1, pp 157–182.
12. Sykes, A. G. *Adv. Inorg. Chem.* **1991**, *36*, 377–408.
13. Solomon, E. I.; Baldwin, M. J.; Lowery, M. D. *Chem. Rev.* **1992**, *92*, 521–542.
14. Canters, G. W.; Gilardi, G. *FEBS Lett.* **1993**, *325*, 39–48.
15. Canters, G. W.; Kolczak, U.; Armstrong, F.; Jeuken, L. J. C.; Camba, R.; Sola, M. *Faraday Discuss.* **2000**, *116*, 205–220.
16. Randall, D. W.; Gamelin, D. R.; LaCroix, L. B.; Solomon, E. I. *J. Biol. Inorg. Chem.* **2000**, *5*, 16–29.
17. Solomon, E. I.; Randall, D. W.; Glaser, T. *Coord. Chem. Rev.* **2000**, *200–202*, 595–632.
18. Gray, H. B.; Malmström, B. G.; Williams, R. J. P. *J. Biol. Inorg. Chem.* **2000**, *5*, 551–559.
19. Ryde, U.; Olsson, M. H. M.; Pierloot, K. *Theor. Comp. Chem.* **2001**, *9*, 1–55.
20. Vila, A. J.; Fernández, C. O. Copper in electron trasfer protein. In *Handbook on Metalloproteins;* Bertini, I.; Sigel, A.; Sigel, H. Eds.; Marcel Dekker: New York, 2001; pp 813–856.
21. Messerschmidt, A. *Adv. Inorg. Chem.* **1994**, *40*, 121–185.
22. Messerschmidt, A. *Struct. Bonding (Berlin)* **1998**, *90*, 37–68.
23. Lindley, P. Multi-copper oxidases. In *Handbook on Metalloproteins;* Bertini, I.; Sigel, A.; Sigel, H., Eds.; Marcel Dekker: New York, NY, 2001; pp 763–811.
24. Kroneck, P. M. H.; Riester, J.; Zumft, W. G.; Antholine, W. E. *Biol. Metals* **1990**, *3*, 103–109.
25. Lappalainen, P.; Saraste, M. *Biochim. Biophys. Acta Bioenerg.* **1994**, *1187*, 222–225.
26. Dennison, C.; Canters, G. W. *J. Royl. Netherl. Chem. Soc.* **1996**, *115*, 345–351.
27. Beinert, H. *Eur. J. Biochem.* **1997**, *245*, 521–532.
28. Kroneck, P. M. H. Binuclear copper A. In *Handbook on Metalloproteins;* Messerschmid, A.; Huber, R.; Poulos, T.; Wieghardt, K., Eds.; Wiley: Chichester, UK, 2001; Vol. 2, pp 1333–1341.
29. Murphy, M. E. P.; Lindley, P. F.; Adman, E. T. *Protein Sci.* **1997**, *6*, 761–770.
30. Richardson, J. S. *Methods Enzymol.* **1985**, *115*, 341–358.
31. Freeman, H. C.; Guss, J. M. Plastocyanin. In *Handbook of Metalloproteins;* Messerschmid, A.; Huber, R.; Poulos, T.; Wieghardt, K., Eds.; Wiley: Chichester, UK, 2001; pp 1153–1169.
32. Colman, P. M.; Freeman, H. C.; Guss, J. M.; Murata, M.; Norris, V. A.; Ramshaw, J. A. M.; Venkatappa, M. P. *Nature* **1978**, *272*, 319–324.

33. Guss, J. M.; Freeman, H. C. *J. Mol. Biol.* **1983**, *169*, 521–563.
34. Guss, J. M.; Bartunik, H. D.; Freeman, H. C. *Acta Crystallogr., Sect. B: Struct. Sci.* **1992**, *B48*, 790–811.
35. Hathaway, B. J. Copper. In *Comprehensive Coordination Chemistry, the Synthesis, Reactions, Properties & Application of Coordination Compounds*; 1st ed.; Wilkinson, G.; Gillard, R. D.; McCleverty, J. A., Eds.; Pergamon: Oxford, UK, 1987; Vol. 5, pp 533–774.
36. Guss, J. M.; Harrowell, P. R.; Murata, M.; Norris, V. A.; Freeman, H. C. *J. Mol. Biol.* **1986**, *192*, 361–387.
37. Garrett, T. P. J.; Clingeleffer, D. J.; Guss, J. M.; Rogers, S. J.; Freeman, H. C. *J. Biol. Chem.* **1984**, *259*, 2822–2825.
38. Church, W. B.; Guss, J. M.; Potter, J. J.; Freeman, H. C. *J. Biol. Chem.* **1986**, *261*, 234–237.
39. Kolczak, U.; Dennison, C.; Messerschmid, A.; Canters, G. W. Azurin and azurin mutants. In *Handbook of Metalloproteins*; Messerschmid, A.; Huber, R.; Poulos, T.; Wieghardt, K. Eds.; Wiley: Chichester, UK, 2001; Vol. 2, pp 1170–1194.
40. Adman, E. T.; Stenkamp, R. E.; Sieker, L. C.; Jensen, L. H. *J. Mol. Biol.* **1978**, *123*, 35–47.
41. Baker, E. N. *J. Mol. Biol.* **1988**, *203*, 1071–1095.
42. Shepard, W. E. B.; Anderson, B. F.; Lewandoski, D. A.; Norris, G. E.; Baker, E. N. *J. Am. Chem. Soc.* **1990**, *112*, 7817–7819.
43. Nar, H.; Messerschmidt, A.; Huber, R.; van der Kamp, M.; Canters, G. W. *J. Mol. Biol.* **1991**, *221*, 765–772.
44. Lowery, M. D.; Solomon, E. I. *Inorg. Chim. Acta* **1992**, *198–200*, 233–243.
45. Mathews, F. S. Amicyanin and complexes of amicyanin with methylamine dehydrogenase and cytochrome c_{55}. In *Handbook of Metalloproteins*; Messerschmid, A.; Huber, R.; Poulos, T.; Wieghardt, K. Eds.; Wiley: Chichester, UK, 2001; Vol. 2; pp 1203–1214.
46. Scharf, B.; Engelhard, M. *Biochemistry* **1993**, *32*, 12894–12900.
47. Nersissian, A. M.; Immoos, C.; Hill, M. G.; Hart, P. J.; Williams, G.; Herrmann, R. G.; Valentine, J. S. *Protein Sci.* **1998**, *7*, 1915–1929.
48. Durley, R.; Chen, L.; Lim, L. W.; Mathews, F. S.; Davidson, V. L. *Protein Sci.* **1993**, *2*, 739–752.
49. Cunane, L. M.; Chen, Z.-W.; Durley, R. C. E.; Mathews, F. S. *Acta Crystallogr., Sect. D: Biol. Crystallogr.* **1996**, *D52*, 676–686.
50. Zhu, Z.; Cunane, L. M.; Chen, Z.-W.; Durley, R. C. E.; Mathews, F. S.; Davidson, V. L. *Biochemistry* **1998**, *37*, 17128–17136.
51. Scharf, B.; Wittenberg, R.; Engelhard, M. *Biochemistry* **1997**, *36*, 4471–4479.
52. Messerschmid, A. Ascorbate oxidase. In *Handbook of Metalloproteins*; Messerschmid, A.; Huber, R.; Poulos, T.; Wieghardt, K., Eds.; Wiley: Chichester, UK, 2001; Vol. 2, pp 1345–1358.
53. Davies, G. J.; Ducros, V. Laccase. In *Handbook of Metalloproteins*; Messerschmid, A.; Huber, R.; Poulos, T.; Wieghardt, K. Eds.; Wiley: Chichester, UK, 2001; Vol. 2, pp 1359–1368.
54. Lindley, P. F. Multi-copper oxidases. In *Handbook of Metalloproteins*; Messerschmid, A.; Huber, R.; Poulos, T.; Wieghardt, K. Eds.; Wiley: Chichester, UK, 2001; Vol. 2, 1369–1380.
55. Suzuki, S.; Kataoka, K.; Yamaguchi, K. *Acc. Chem. Res.* **2000**, *33*, 728–735.
56. Adman, E. T.; Murphy, M. E. P. Copper nitrite reductase. In *Handbook of Metalloproteins*; Messerschmid, A.; Huber, R.; Poulos, T.; Wieghardt, K., Eds.; Wiley: Chichester, UK, 2001; Vol. 2, pp 1381–1390.
57. Averill, B. A. *Chem. Rev.* **1996**, *96*, 2951–2964.
58. Inoue, T.; Gotowda, M.; Deligeer; Kataoka, K.; Yamaguchi, K.; Suzuki, S.; Watanabe, H.; Gohow, M.; Kai, Y. *J. Biochem.* **1998**, *124*, 876–879.
59. Dodd, F. E.; Van Beeumen, J.; Eady, R. R.; Hasnain, S. S. *J. Mol. Biol.* **1998**, *282*, 369–382.
60. Messerschmidt, A.; Rossi, A.; Ladenstein, R.; Huber, R.; Bolognesi, M.; Gatti, G.; Marchesini, A.; Petruzzelli, R.; Finazzi-Agro, A. *J. Mol. Biol.* **1989**, *206*, 513–529.
61. Messerschmidt, A.; Ladenstein, R.; Huber, R.; Bolognesi, M.; Avigliano, L.; Petruzzelli, R.; Rossi, A.; Finazzi-Agro, A. *J. Mol. Biol.* **1992**, *224*, 179–205.
62. Messerschmidt, A.; Luecke, H.; Huber, R. *J. Mol. Biol.* **1993**, *230*, 997–1014.
63. Zaitseva, I.; Zaitsev, V.; Card, G.; Moshkov, K.; Box, B.; Ralph, A.; Lindley, P. *J. Biol. Inorg. Chem.* **1996**, *1*, 15–23.
64. Lindley, P. F.; Card, G.; Zaitseva, I.; Zaitsev, V.; Reinhammar, B.; Selin-Lindgren, E.; Yoshida, K. *J. Biol. Inorg. Chem.* **1997**, *2*, 454–463.
65. Ducros, V.; Davies, G. J.; Lawson, D. M.; Wilson, K. S.; Brown, S. H.; Ostergaard, P.; Pedersen, A. H.; Schneider, P.; Yaver, D. S.; Brzozowski, A. M. *Acta Crystallogr., Sect. D: Biol. Crystallogr.* **1997**, *D53*, 605–607.
66. Ducros, V.; Brzozowski, A. M.; Wilson, K. S.; Brown, S. H.; Østergaard, P.; Schneider, P.; Yaver, D. S.; Pedersen, A. H.; Davies, G. J. *Nat. Struct. Biol.* **1998**, *5*, 310–316.
67. Ducros, V.; Brzozowski, A. M.; Wilson, K. S.; Ostergaard, P.; Schneider, P.; Svendson, A.; Davies, G. J. *Acta Crystallogr., Sect. D: Biol. Crystallogr.* **2001**, *D57*, 333–336.
68. Bertrand, T.; Jolivalt, C.; Briozzo, P.; Caminade, E.; Joly, N.; Madzak, C.; Mougin, C. *Biochemistry* **2002**, *41*, 7325–7333.
69. Machonkin, T. E.; Zhang, H. H.; Hedman, B.; Hodgson, K. O.; Solomon, E. I. *Biochemistry* **1998**, *37*, 9570–9578.
70. Lu, Y.; LaCroix, L. B.; Lowery, M. D.; Solomon, E. I.; Bender, C. J.; Peisach, J.; Roe, J. A.; Gralla, E. B.; Valentine, J. S. *J. Am. Chem. Soc.* **1993**, *115*, 5907–5918.
71. Lu, Y.; Roe, J. A.; Gralla, E. B.; Valentine, J. S. Metalloprotein ligand redesign: characterization of copper-cysteinate proteins derived from yeast copper-zinc superoxide dismutase. In *Bioinorganic Chemistry of Copper*; Karlin, K. D.; Tyeklar, Z., Eds.; Chapman and Hall: New York, 1993; pp 64–77.
72. Sanders-Loehr, J. Investigation of Type I copper site geometry by spectroscopy and molecular redesign. In *Bioinorganic Chemistry of Copper*; Karlin, K. D.; Tyeklar, Z., Eds.; Chapman and Hall: New York, 1993; pp 51–63.
73. Andrew, C. R.; Sanders-Loehr, J. *Acc. Chem. Res.* **1996**, *29*, 365–372.
74. Scholham, M. Rusticyanin. In *Handbook of Metalloproteins*; Messerschmid, A.; Huber, R.; Poulos, T.; Wieghardt, K., Eds.; Wiley: Chichester, UK, 2001; pp 1235–1241.
75. Botuyaan, M. V.; Toy-Palmer, A.; Chung, J.; Blake, R. C. II.; Beroza, P.; Case, D. A.; Dyson, H. J. *J. Mol. Biol.* **1996**, *263*, 752–767.
76. Walter, R. L.; Ealick, S. E.; Friedman, A. M.; Blake, R. C. II; Proctor, P.; Shoham, M. *J. Mol. Biol.* **1996**, *263*, 730–751.

77. Harvey, I.; Hao, Q.; Duke, E. M. H.; Ingledew, W. J.; Hasnain, S. S. *Acta Crystallogr., Sect. D: Biol. Crystallogr.* **1998**, *D54*, 629–635.

78. Grossmann, J. G.; Ingledew, W. J.; Harvey, I.; Strange, R. W.; Hasnain, S. S. *Biochemistry* **1995**, *34*, 8406–8414.

79. Guss, J. M.; Freeman, H. C. Cucumber basic protein. In *Handbook of Metalloproteins*; Messerschmid, A.; Huber, R.; Poulos, T.; Wieghardt, K., Eds.; Wiley: Chichester, UK, 2001; Vol. 2; pp 1215–1218.

80. Guss, J. M.; Merritt, E. A.; Phizackerley, R. P.; Hedman, B.; Murata, M.; Hodgson, K. O.; Freeman, H. C. *Science* **1988**, *241*, 806–811.

81. Guss, J. M.; Merritt, E. A.; Phizackerley, R. P.; Freeman, H. C. *J. Mol. Biol.* **1996**, *262*, 686–705.

82. Einsle, O.; Mehrabian, Z.; Nalbandyan, R.; Messerschmidt, A. *J. Biol. Inorg. Chem.* **2000**, *5*, 666–672.

83. Nersissian, A. M.; Hart, P. J.; Valentine, J. S. Stellacyanin, a member of the phytocyanin family of plant proteins. In *Handbook of Metalloproteins*; Messerschmid, A.; Huber, R.; Poulos, T.; Wieghardt, K., Eds.; Wiley: Chichester, UK, 2001; Vol. 2, pp 1219–1234.

84. Wherland, S.; Gray, H. B. Biological aspects of inorganic chemistry. In *Biological Aspects of Inorganic Chemistry*; Addison, A. W.; Cullen, W. R.; Dolphin, D., Eds.; Wiley: New York, 1977; pp 289–368.

85. Hart, P. J.; Nersissian, A. M.; Herrmann, R. G.; Nalbandyan, R. M.; Valentine, J. S.; Eisenberg, D. *Protein Sci.* **1996**, *5*, 2175–2183.

86. Adman, E. T. Pseudoazurin. In *Handbook of Metalloproteins*; Messerschmid, A.; Huber, R.; Poulos, T.; Wieghardt, K., Eds.; Wiley: Chichester, UK, **2001;** Vol. 2,1195–1202.

87. Trost, J. T.; McManus, J. D.; Freeman, J. C.; Ramakrishna, B. L.; Blankenship, R. E. *Biochemistry* **1988**, *27*, 7858–7863.

88. Van Driessche, G.; Hu, W.; Van De Werken, G.; Selvaraj, F.; McManus, J. D.; Blankenship, R. E.; Van Beeumen, J. J. *Protein Sci.* **1999**, *8*, 947–957.

89. Petratos, K.; Banner, D. W.; Beppu, T.; Wilson, K. S.; Tsernoglou, D. *FEBS Lett.* **1987**, *218*, 209–214.

90. Vakoufari, E.; Wilson, K. S.; Petratos, K. *FEBS Lett.* **1994**, *347*, 203–206.

91. Inoue, T.; Nishio, N.; Suzuki, S.; Kataoka, K.; Kohzuma, T.; Kai, Y. *J. Biol. Chem.* **1999**, *274*, 17845–17852.

92. Bond, C. S.; Blankenship, R. E.; Freeman, H. C.; Guss, J. M.; Maher, M. J.; Selvaraj, F. M.; Wilce, M. C. J.; Willingham, K. M. *J. Mol. Biol.* **2001**, *306*, 47–67.

93. Godden, J. W.; Turley, S.; Teller, D. C.; Adman, E. T.; Liu, M. Y.; Payne, W. J.; LeGall, J. *Science* **1991**, *253*, 438–442.

94. Kukimoto, M.; Nishiyama, M.; Murphy, M. E. P.; Turley, S.; Adman, E. T.; Horinouchi, S.; Beppu, T. *Biochemistry* **1994**, *33*, 5246–5252.

95. Murphy, M. E. P.; Turley, S.; Kukimoto, M.; Nishiyama, M.; Horinouchi, S.; Sasaki, H.; Tanokura, M.; Adman, E. T. *Biochemistry* **1995**, *34*, 12107–12117.

96. Arciero, D. M.; Pierce, B. S.; Hendrich, M. P.; Hooper, A. B. *Biochemistry* **2002**, *41*, 1703–1709.

97. Lieberman, R. L.; Arciero, D. M.; Hooper, A. B.; Rosenzweig, A. C. *Biochemistry* **2001**, *40*, 5674–5681.

98. Greenwood, C.; Hill, B. C.; Barber, D.; Eglinton, D. G.; Thomson, A. J. *Biochem. J.* **1983**, *215*, 303–316.

99. Farrar, J. A.; Thomson, A. J.; Cheesman, M. R.; Dooley, D. M.; Zumft, W. G. *FEBS Lett.* **1991**, *294*, 11–15.

100. Farrar, J. A.; Neese, F.; Lappalainen, P.; Kroneck, P. M. H.; Saraste, M.; Zumft, W. G.; Thomson, A. J. *J. Am. Chem. Soc.* **1996**, *118*, 11501–11514.

101. Gamelin, D. R.; Randall, D. W.; Hay, M. T.; Houser, R. P.; Mulder, T. C.; Canters, G. W.; de Vries, S.; Tolman, W. B.; Lu, Y.; Solomon, E. I. *J. Am. Chem. Soc.* **1998**, *120*, 5246–5263.

102. Saraste, M. *Q. Rev. Biophys.* **1990**, *23*, 331–366.

103. Babcock, G. T.; Wikstrom, M. *Nature* **1992**, *356*, 301–309.

104. Garcia-Horsman, J. A.; Barquera, B.; Rumbley, J.; Ma, J.; Gennis, R. B. *J. Bacteriol.* **1994**, *176*, 5587–5600.

105. Suharti; Strampraad, M. J. F.; Schroeder, I.; de Vries, S. *Biochemistry* **2001**, *40*, 2632–2639.

106. Lappalainen, P.; Aasa, R.; Malmström, B. G.; Saraste, M. *J. Biol. Chem.* **1993**, *268*, 26416–26421.

107. von Wachenfeldt, C.; de Vries, S.; van der Oost, J. *FEBS Lett.* **1994**, *340*, 109–113.

108. Slutter, C. E.; Sanders, D.; Wittung, P.; Malmström, B. G.; Aasa, R.; Richards, J. H.; Gray, H. B.; Fee, J. A. *Biochemistry* **1996**, *35*, 3387–3395.

109. Bertini, I.; Bren, K. L.; Clemente, A.; Fee, J. A.; Gray, H. B.; Luchinat, C.; Malmström, B. G.; Richards, J. H.; Sanders, D.; Slutter, C. E. *J. Am. Chem. Soc.* **1996**, *118*, 11658–11659.

110. Luchinat, C.; Soriano, A.; Djinovic-Carugo, K.; Saraste, M.; Malmström, B. G.; Bertini, I. *J. Am. Chem. Soc.* **1997**, *119*, 11023–11027.

111. Salgado, J.; Warmerdam, G.; Bubacco, L.; Canters, G. W. *Biochemistry* **1998**, *37*, 7378–7389.

112. Ramirez, B. E.; Malmström, B. G.; Winkler, J. R.; Gray, H. B. *Proc. Natl. Acad. Sci. USA.* **1995**, *92*, 11949–11951.

113. Robin, M. B.; Day, P. *Adv. Inorg. Chem. Radiochem.* **1967**, *10*, 247–422.

114. Kroneck, P. M. H.; Antholine, W. A.; Riester, J.; Zumft, W. G. *FEBS Lett.* **1989**, *248*, 212–213.

115. Kroneck, P. M. H.; Antholine, W. E.; Kastrau, D. H. W.; Buse, G.; Steffens, G. C. M.; Zumft, W. G. *FEBS Lett.* **1990**, *268*, 274–276.

116. Steffens, G. J.; Buse, G. *Hoppe-Seyler's Z. Physiol. Chem.* **1979**, *360*, 613–619.

117. Tsukihara, T.; Aoyama, H.; Yamashita, E.; Tomizaki, T.; Yamaguchi, H.; Shinzawa-Itoh, K.; Nakashima, R.; Yaono, R.; Yoshikawa, S. *Science* **1996**, *272*, 1136–1144.

118. Williams, P. A.; Blackburn, N. J.; Sanders, D.; Bellamy, H.; Stura, E. A.; Fee, J. A.; McRee, D. E. *Nat. Struct. Biol.* **1999**, *6*, 509–516.

119. Wilmanns, M.; Lappalainen, P.; Kelly, M.; Sauer-Eriksson, E.; Saraste, M. *Proc. Natl. Acad. Sci. USA* **1995**, *92*, 11955–11959.

120. Robinson, H.; Ang, M. C.; Gao, Y.-G.; Hay, M. T.; Lu, Y.; Wang, A. H. J. *Biochemistry* **1999**, *38*, 5677–5683.

121. Blackburn, N. J.; Barr, M. E.; Woodruff, W. H.; van der Oost, J.; de Vries, S. *Biochemistry* **1994**, *33*, 10401–10407.

122. Wallace-Williams, S. E.; James, C. A.; de Vries, S.; Saraste, M.; Lappalainen, P.; van der Oost, J.; Fabian, M.; Palmer, G.; Woodruff, W. H. *J. Am. Chem. Soc.* **1996**, *118*, 3986–3987.

123. Williams, K. R.; Gamelin, D. R.; LaCroix, L. B.; Houser, R. P.; Tolman, W. B.; Mulder, T. C.; de Vries, S.; Hedman, B.; Hodgson, K. O.; Solomon, E. I. *J. Am. Chem. Soc.* **1997**, *119*, 613–614.

124. Riester, J.; Zumft, W. G.; Kroneck, P. M. H. *Eur. J. Biochem.* **1989**, *178*, 751–762.

125. Chan, S. I.; Li, P. M. *Biochemistry* **1990**, *29*, 1–12.
126. Morgan, J. E.; Wikstrom, M. *Biochemistry* **1991**, *30*, 948–958.
127. Immoos, C.; Hill, M. G.; Sanders, D.; Fee, J. A.; Slutter, S. E.; Richards, J. H.; Gray, H. B. *J. Biol. Inorg. Chem.* **1996**, *1*, 529–531.
128. Lu, Y.; Berry, S. M.; Pfister, T. D. *Chem. Rev.* **2001**, *101*, 3047–3080.
129. Maret, W.; Dietrich, H.; Ruf, H. H.; Zeppezauer, M. *J. Inorg. Biochem.* **1980**, *12*, 241–252.
130. Maret, W.; Zeppezauer, M.; Desideri, A.; Morpurgo, L.; Rotilio, G. *FEBS Lett.* **1981**, *136*, 72–74.
131. Maret, W.; Shiemke, A. K.; Wheeler, W. D.; Loehr, T. M.; Sanders-Loehr, J. *J. Am. Chem. Soc.* **1986**, *108*, 6351–6359.
132. Maret, W.; Kozlowski, H. *Biochim. Biophys. Acta* **1987**, *912*, 329–337.
133. Brader, M. L.; Dunn, M. F. *J. Am. Chem. Soc.* **1990**, *112*, 4585–4587.
134. Brader, M. L.; Borchardt, D.; Dunn, M. F. *J. Am. Chem. Soc.* **1992**, *114*, 4480–4486.
135. Brader, M. L.; Borchardt, D.; Dunn, M. F. *Biochemistry* **1992**, *31*, 4691–4696.
136. Lu, Y.; Gralla, E. B.; Roe, J. A.; Valentine, J. S. *J. Am. Chem. Soc.* **1992**, *114*, 3560–3562.
137. Lu, Y.; Roe, J. A.; Bender, C. J.; Peisach, J.; Banci, L.; Bertini, I.; Gralla, E. B.; Valentine, J. S. *Inorg. Chem.* **1996**, *35*, 1692–1700.
138. Han, J.; Loehr, T. M.; Lu, Y.; Valentine, J. S.; Averill, B. A.; Sanders-Loehr, J. *J. Am. Chem. Soc.* **1993**, *115*, 4256–4263.
139. Lu, Y., Ph.D. Thesis, University of California, Los Angeles, CA, USA, 1992.
140. van der Oost, J.; Lappalainen, P.; Musacchio, A.; Warne, A.; Lemieux, L.; Rumbley, J.; Gennis, R. B.; Aasa, R.; Pascher, T.; Malmström, B. G.; Saraste, M. *EMBO J.* **1992**, *11*, 3209–3217.
141. Kelly, M.; Lappalainen, P.; Talbo, G.; Haltia, T.; van der Oost, J.; Saraste, M. *J. Biol. Chem.* **1993**, *268*, 16781–16787.
142. Dennison, C.; Vijgenboom, E.; de Vries, S.; van der Oost, J.; Canters, G. W. *FEBS Lett.* **1995**, *365*, 92–94.
143. Hay, M.; Richards, J. H.; Lu, Y. *Proc. Natl. Acad. Sci. USA* **1996**, *93*, 461–464.
144. Hay, M. T.; Ang, M. C.; Gamelin, D. R.; Solomon, E. I.; Antholine, W. E.; Ralle, M.; Blackburn, N. J.; Massey, P. D.; Wang, X.; Kwon, A. H.; Lu, Y. *Inorg. Chem.* **1998**, *37*, 191–198.
145. Dennison, C.; Berg, A.; Canters, G. W. *Biochemistry* **1997**, *36*, 3262–3269.
146. Zickermann, V.; Wittershagen, A.; Kolbesen, B. O.; Ludwig, B. *Biochemistry* **1997**, *36*, 3232–3236.
147. Bouwman, E.; Driessen, W. L.; Reedijk, J. *Coord. Chem. Rev.* **1990**, *104*, 143–172.
148. Kitajima, N. *Adv. Inorg. Chem.* **1992**, *39*, 1–77.
149. Karlin, K. D. *Science* **1993**, *261*, 701–708.
150. Mandal, S.; Das, G.; Singh, R.; Shukla, R.; Bharadwaj, P. K. *Coord. Chem. Rev.* **1997**, *160*, 191–235.
151. Kitajima, N.; Fujisawa, K.; Morooka, Y. *J. Am. Chem. Soc.* **1990**, *112*, 3210–3212.
152. Kitajima, N.; Fujisawa, K.; Tanaka, M.; Morooka, Y. *J. Am. Chem. Soc.* **1992**, *114*, 9232–9233.
153. Randall, D. W.; DeBeer George, S.; Hedman, B.; Hodgson, K. O.; Fujisawa, K.; Solomon, E. I. *J. Am. Chem. Soc.* **2000**, *122*, 11620–11631.
154. Holland, P. L.; Tolman, W. B. *J. Am. Chem. Soc.* **1999**, *121*, 7270–7271.
155. Randall, D. W.; George, S. D.; Holland, P. L.; Hedman, B.; Hodgson, K. O.; Tolman, W. B.; Solomon, E. I. *J. Am. Chem. Soc.* **2000**, *122*, 11632–11648.
156. Holland, P. L.; Tolman, W. B. *J. Am. Chem. Soc.* **2000**, *122*, 6331–6332.
157. Dunaj-Jurco, M.; Ondrejovic, G.; Melnik, M.; Garaj, J. *Coord. Chem. Rev.* **1988**, *83*, 1–28.
158. Harding, C.; McKee, V.; Nelson, J. *J. Am. Chem. Soc.* **1991**, *113*, 9684–9685.
159. Barr, M. E.; Smith, P. H.; Antholine, W. E.; Spencer, B. *J. Chem. Soc., Chem. Commun.* **1993**, 1649–1652.
160. Harding, C.; Nelson, J.; Symons, M. C. R.; Wyatt, J. *J. Chem. Soc., Chem. Commun.* **1994**, 2499–2500.
161. LeCloux, D. D.; Davydov, R.; Lippard, S. J. *J. Am. Chem. Soc.* **1998**, *120*, 6810–6811.
162. LeCloux, D. D.; Davydov, R.; Lippard, S. J. *Inorg. Chem.* **1998**, *37*, 6814–6826.
163. He, C.; Lippard, S. J. *Inorg. Chem.* **2000**, *39*, 5225–5231.
164. Zhang, X.-M.; Tong, M.-L.; Chen, X.-M. *Angew. Chem., Int. Ed.* **2002**, *41*, 1029–1031.
165. Gupta, R.; Zhang, Z. H.; Powell, D.; Hendrich, M. P.; Borovik, A. S. *Inorg. Chem.* **2002**, *41*, 5100–5106.
166. Houser, R. P.; Young, V. G., Jr.; Tolman, W. B. *J. Am. Chem. Soc.* **1996**, *118*, 2101–2102.
167. Larsson, S.; Källebring, B.; Wittung, P.; Malmström, B. G. *Proc. Natl. Acad. Sci. USA* **1995**, *92*, 7167–7171.
168. Mizoguchi, T. J.; Di Bilio, A. J.; Gray, H. B.; Richards, J. H. *J. Am. Chem. Soc.* **1992**, *114*, 10076–10078.
169. DeBeer, S.; Kiser, C. N.; Mines, G. A.; Richards, J. H.; Gray, H. B.; Solomon, E. I.; Hedman, B.; Hodgson, K. O. *Inorg. Chem.* **1999**, *38*, 433–438.
170. Berry, S. M.; Gieselman, M. D.; Nilges, M. J.; Van der Donk, W. A.; Lu, Y. *J. Am. Chem. Soc.* **2002**, *124*, 2084–2085.
171. Muir, T. W.; Sondhi, D.; Cole, P. A. *Proc. Natl. Acad. Sci. USA* **1998**, *95*, 6705–6710.
172. Farrar, J. A.; Lappalainen, P.; Zumft, W. G.; Saraste, M.; Thomson, A. J. *Eur. J. Biochem.* **1995**, *232*, 294–303.
173. Malatesta, F.; Nicoletti, F.; Zickermann, V.; Ludwig, B.; Brunori, M. *FEBS Lett.* **1998**, *434*, 322–324.
174. Speno, H.; Taheri, M. R.; Sieburth, D.; Martin, C. T. *J. Biol. Chem.* **1995**, *270*, 25363–25369.
175. Frank, P.; Licht, A.; Tullius, T. D.; Hodgson, K. O.; Pecht, I. *J. Biol. Chem.* **1985**, *260*, 5518–5525.
176. Karlsson, B. G.; Aasa, R.; Malmström, B. G.; Lundberg, L. G. *FEBS Lett.* **1989**, *253*, 99–102.
177. Chang, T. K.; Iverson, S. A.; Rodrigues, C. G.; Kiser, C. N.; Lew, A. Y. C.; Germanas, J. P.; Richards, J. H. *Proc. Natl. Acad. Sci. USA* **1991**, *88*, 1325–1329.
178. Murphy, L. M.; Strange, R. W.; Karlsson, B. G.; Lundberg, L. G.; Pascher, T.; Reinhammar, B.; Hasnain, S. S. *Biochemistry* **1993**, *32*, 1965–1975.
179. Romero, A.; Hoitink, C. W. G.; Nar, H.; Huber, R.; Messerschmidt, A.; Canters, G. W. *J. Mol. Biol.* **1993**, *229*, 1007–1021.
180. Bonander, N.; Karlsson, B. G.; Vänngård, T. *Biochemistry* **1996**, *35*, 2429–2436.
181. Kroes, S. J.; Hoitink, C. W. G.; Andrew, C. R.; Ai, J.; Sanders-Loehr, J.; Messerschmidt, A.; Hagen, W. R.; Canters, G. W. *Eur. J. Biochem.* **1996**, *240*, 342–351.
182. Veselov, A.; Olesen, K.; Sienkiewicz, A.; Shapleigh, J. P.; Scholes, C. P. *Biochemistry* **1998**, *37*, 6095–6105.

183. Vidakovic, M.; Germanas, J. P. *Angew. Chem., Int. Ed.* **1995**, *34*, 1622–1624.
184. Tsai, L.-C.; Bonander, N.; Harata, K.; Karlsson, G.; Vänngård, T.; Langer, V.; Sjölin, L. *Acta Crystallogr., Sect. D: Biol. Crystallogr.* **1996**, *D52*, 950–958.
185. Farver, O.; Skov, L. K.; Pascher, T.; Karlsson, B. G.; Nordling, M.; Lundberg, L. G.; Vänngård, T.; Pecht, I. *Biochemistry* **1993**, *32*, 7317–7322.
186. Bauer, R.; Danielsen, E.; Hemmingsen, L.; Bjerrum, M. J.; Hansson, O.; Singh, K. *J. Am. Chem. Soc.* **1997**, *119*, 157–162.
187. Salgado, J.; Kroes, S. J.; Berg, A.; Moratal, J. M.; Canters, G. W. *J. Biol. Chem.* **1998**, *273*, 177–185.
188. Solomon, E. I.; Penfield, K. W.; Gewirth, A. A.; Lowery, M. D.; Shadle, S. E.; Guckert, J. A.; LaCroix, L. B. *Inorg. Chim. Acta* **1996**, *243*, 67–78.
189. Karlsson, B. G.; Nordling, M.; Pascher, T.; Tsai, L.-C.; Sjolin, L.; Lundberg, L. G. *Protein Eng.* **1991**, *4*, 343–349.
190. Palmer, A. E.; Randall, D. W.; Xu, F.; Solomon, E. I. *J. Am. Chem. Soc.* **1999**, *121*, 7138–7149.
191. DeBeer, S.; Randall, D. W.; Nersissian, A. M.; Valentine, J. S.; Hedman, B.; Hodgson, K. O.; Solomon, E. I. *J. Phys. Chem. B* **2000**, *104*, 10814–10819.
192. LaCroix, L. B.; Shadle, S. E.; Wang, Y.; Averill, B. A.; Hedman, B.; Hodgson, K. O.; Solomon, E. I. *J. Am. Chem. Soc.* **1996**, *118*, 7755–7768.
193. Messerschmidt, A.; Prade, L.; Kroes, S. J.; Sanders-Loehr, J.; Huber, R.; Canters, G. W. *Proc. Natl. Acad. Sci. USA* **1998**, *95*, 3443–3448.
194. LaCroix, L. B.; Randall, D. W.; Nersissian, A. M.; Hoitink, C. W. G.; Canters, G. W.; Valentine, J. S.; Solomon, E. I. *J. Am. Chem. Soc.* **1998**, *120*, 9621–9631.
195. Donaire, A.; Jimenez, B.; Fernandez, C. O.; Pierattelli, R.; Niizeki, T.; Moratal, J.-M.; Hall, J. F.; Kohzuma, T.; Hasnain, S. S.; Vila, A. J. *J. Am. Chem. Soc.* **2002**, *124*, 13698–13708.
196. Fernandez, C. O.; Niizeki, T.; Kohzuma, T.; Vila, A. J. *J. Biol. Inorg. Chem.* **2003**, *8*, 75–82.
197. Diederix, R. E. M.; Canters, G. W.; Dennison, C. *Biochemistry* **2000**, *39*, 9551–9560.
198. Malmström, B. G.; Wittung-Stafshede, P. *Coord. Chem. Rev.* **1999**, *185–186*, 127–140.
199. Olsson, M. H. M.; Ryde, U. *J. Biol. Inorg. Chem.* **1999**, *4*, 654–663.
200. Zickermann, V.; Verkhovsky, M.; Morgan, J.; Wikstrom, M.; Anemuller, S.; Bill, E.; Steffens, G. C. M.; Ludwig, B. *Eur. J. Biochem.* **1995**, *234*, 686–693.
201. Wittung-Stafshede, P.; Malmström, B. G.; Sanders, D.; Fee, J. A.; Winkler, J. R.; Gray, H. B. *Biochemistry* **1998**, *37*, 3172–3177.
202. Slutter, C. E.; Gromov, I.; Richards, J. H.; Pecht, I.; Goldfarb, D. *J. Am. Chem. Soc.* **1999**, *121*, 5077–5078.
203. Olsson, M. H. M.; Ryde, U. *J. Am. Chem. Soc.* **2001**, *123*, 7866–7876.
204. Blackburn, N. J.; Ralle, M.; Gomez, E.; Hill, M. G.; Pastuszyn, A.; Sanders, D.; Fee, J. A. *Biochemistry* **1999**, *38*, 7075–7084.
205. Gorren, A. C. F.; den Blaauwen, T.; Canters, G. W.; Hopper, D. J.; Duine, J. A. *FEBS Lett.* **1996**, *381*, 140–142.
206. Germanas, J. P.; Di Bilio, A. J.; Gray, H. B.; Richards, J. H. *Biochemistry* **1993**, *32*, 7698–7702.
207. den Blaauwen, T.; Canters, G. W. *J. Am. Chem. Soc.* **1993**, *115*, 1121–1129.
208. den Blaauwen, T.; Hoitink, C. W. G.; Canters, G. W.; Han, J.; Loehr, T. M.; Sanders-Loehr, J. *Biochemistry* **1993**, *32*, 12455–12464.
209. Van Gastel, M.; Coremans, J. W. A.; Mol, J.; Jeuken, L. J. C.; Canters, G. W.; Groenen, E. J. J. *J. Biol. Inorg. Chem.* **1999**, *4*, 257–265.
210. den Blaauwen, T.; Van de Kamp, M.; Canters, G. W. *J. Am. Chem. Soc.* **1991**, *113*, 5050–5052.
211. Danielsen, E.; Bauer, R.; Hemmingsen, L.; Bjerrum, M. J.; Butz, T.; Troger, W.; Canters, G. W.; Den Blaauwen, T.; Van Pouderoyen, G. *Eur. J. Biochem.* **1995**, *233*, 554–560.
212. Wang, X.; Berry, S. M.; Xia, Y.; Lu, Y. *J. Am. Chem. Soc.* **1999**, *121*, 7449–7450.
213. Berry, S. M.; Wang, X.; Lu, Y. *J. Inorg. Biochem.* **2000**, *78*, 89–95.
214. Machczynski, M. C.; Gray, H. B.; Richards, J. H. *J. Inorg. Biochem.* **2002**, *88*, 375–380.
215. Hoitink, C. W. G.; Canters, G. W. *J. Biol. Chem.* **1992**, *267*, 13836–13842.
216. Dong, S.; Ybe, J. A.; Hecht, M. H.; Spiro, T. G. *Biochemistry* **1999**, *38*, 3379–3385.
217. Hall, J. F.; Kanbi, L. D.; Harvey, I.; Murphy, L. M.; Hasnain, S. S. *Biochemistry* **1998**, *37*, 11451–11458.
218. Nishiyama, M.; Suzuki, J.; Ohnuki, T.; Chang, H. C.; Horinouchi, S.; Turley, S.; Adman, E. T.; Beppu, T. *Protein Eng.* **1992**, *5*, 177–184.
219. Libeu, C. A. P.; Kukimoto, M.; Nishiyama, M.; Horinouchi, S.; Adman, E. T. *Biochemistry* **1997**, *36*, 13160–13179.
220. Penfield, K. W.; Gewirth, A. A.; Solomon, E. I. *J. Am. Chem. Soc.* **1985**, *107*, 4519–4529.
221. Gewirth, A. A.; Solomon, E. I. *J. Am. Chem. Soc.* **1988**, *110*, 3811–3819.
222. Gamelin, D. R.; Bominaar, E. L.; Kirk, M. L.; Wieghardt, K.; Solomon, E. I. *J. Am. Chem. Soc.* **1996**, *118*, 8085–8097.
223. Gamelin, D. R.; Bominaar, E. L.; Mathoniere, C.; Kirk, M. L.; Wieghardt, K.; Girerd, J.-J.; Solomon, E. I. *Inorg. Chem.* **1996**, *35*, 4323–4335.
224. Bates, C. A.; Moore, W. S.; Standley, K. J.; Stevens, K. W. H. *Proc. Phys. Soc. (London)* **1962**, *79*, 73–83.
225. Brill, A. S.; Bryce, G. F. *J. Chem. Phys.* **1968**, *48*, 4398–4404.
226. Roberts, J. E.; Brown, T. G.; Hoffman, B. M.; Peisach, J. *J. Am. Chem. Soc.* **1980**, *102*, 825–829.
227. Shadle, S. E.; Penner-Hahn, J. E.; Schugar, H. J.; Hedman, B.; Hodgson, K. O.; Solomon, E. I. *J. Am. Chem. Soc.* **1993**, *115*, 767–776.
228. George, S. J.; Lowery, M. D.; Solomon, E. I.; Cramer, S. P. *J. Am. Chem. Soc.* **1993**, *115*, 2968–2969.
229. George, S. D.; Metz, M.; Szilagyi, R. K.; Wang, H.; Cramer, S. P.; Lu, Y.; Tolman, W. B.; Hedman, B.; Hodgson, K. O.; Solomon, E. I. *J. Am. Chem. Soc.* **2001**, *123*, 5757–5767.
230. Marcus, R. A.; Sutin, N. *Biochim. Biophys. Acta* **1985**, *811*, 265–322.
231. Malmström, B. G. Two forms of copper in copper-containing oxidases. In *Oxidases and Related Systems*; King, T. E.; Mason, H. S.; Morrison, M., Eds.; Wiley: New York, 1965; pp 207–216.
232. Vallee, B. L.; Williams, R. J. *Proc. Natl. Acad. Sci. USA* **1968**, *59*, 498–505.
233. Gray, H. B.; Malmström, B. G. *Comments Inorg. Chem.* **1983**, *2*, 203–209.
234. Malmström, B. G. *Eur. J. Biochem.* **1994**, *223*, 711–718.

235. Williams, R. J. P. *Eur. J. Biochem.* **1995**, *234*, 363–381.
236. Ryde, U.; Olsson, M. H. M.; Pierloot, K.; Roos, B. O. *J. Mol. Biol.* **1996**, *261*, 586–596.
237. Pierloot, K.; De Kerpel, J. O. A.; Ryde, U.; Roos, B. O. *J. Am. Chem. Soc.* **1997**, *119*, 218–226.
238. Guckert, J. A.; Lowery, M. D.; Solomon, E. I. *J. Am. Chem. Soc.* **1995**, *117*, 2817–2844.
239. Leckner, J.; Wittung, P.; Bonander, N.; Karlsson, B. G.; Malmström, B. G. *J. Biol. Inorg. Chem.* **1997**, *2*, 368–371.
240. Wittung-Stafshede, P.; Hill, M. G.; Gomez, E.; Di Bilio, A. J.; Karlsson, B. G.; Leckner, J.; Winkler, J. R.; Gray, H. B.; Malmström, B. G. *J. Biol. Inorg. Chem.* **1998**, *3*, 367–370.
241. DeBeer, S.; Wittung-Stafshede, P.; Leckner, J.; Karlsson, G.; Winkler, J. R.; Gray, H. B.; Malmström, B. G.; Solomon, E. I.; Hedman, B.; Hodgson, K. O. *Inorg. Chim. Acta* **2000**, *297*, 278–282.
242. Battistuzzi, G.; Borsari, M.; Loschi, L.; Righi, F.; Sola, M. *J. Am. Chem. Soc.* **1999**, *121*, 501–506.
243. Winkler, J. R.; Wittung-Stafshede, P.; Leckner, J.; Malmström, B. G.; Gray, H. B. *Proc. Natl. Acad. Sci. USA* **1997**, *94*, 4246–4249.
244. Di Bilio, A. J.; Hill, M. G.; Bonander, N.; Karlsson, B. G.; Villahermosa, R. M.; Malmström, B. G.; Winkler, J. R.; Gray, H. B. *J. Am. Chem. Soc.* **1997**, *119*, 9921–9922.
245. Farver, O.; Lu, Y.; Ang, M. C.; Pecht, I. *Proc. Natl. Acad. Sci. USA.* **1999**, *96*, 899–902.
246. Blackburn, N. J.; de Vries, S.; Barr, M. E.; Houser, R. P.; Tolman, W. B.; Sanders, D.; Fee, J. A. *J. Am. Chem. Soc.* **1997**, *119*, 6135–6143.
247. Farver, O.; Pecht, I. *Adv. Chem. Phys.* **1999**, *107*, 555–589.
248. Winkler, J. R.; Gray, H. B. *Chem. Rev.* **1992**, *92*, 369–379.
249. Winkler, J. R.; Di Bilio, A. J.; Farrow, N. A.; Richards, J. H.; Gray, H. B. *Pure Appl. Chem.* **1999**, *71*, 1753–1764.
250. Gray, H. B.; Winkler, J. R. Electron trasfer in metalloproteins. In *Electron Transfer in Chemistry*; Balzani, V., Ed.; Wiley-VCH: Weinheim, Germany, 2001; Vol. 3, pp 3–23.
251. Borovok, N.; Kotlyar, A. B.; Pecht, I.; Skov, L. K.; Farver, O. *FEBS Lett.* **1999**, *457*, 277–282.
252. Gray, H. B. *Chem. Soc. Rev.* **1986**, *15*, 17–30.
253. Sykes, A. G. *Chem. Soc. Rev.* **1985**, *14*, 283–315.
254. Groeneveld, C. M.; Canters, G. W. *J. Biol. Chem.* **1988**, *263*, 167–173.
255. Groeneveld, C. M.; Ouwerling, M. C.; Erkelens, C.; Canters, G. W. *J. Mol. Biol.* **1988**, *200*, 189–199.
256. van Pouderoyen, G.; den Blaauwen, T.; Reedijk, J.; Canters, G. W. *Biochemistry* **1996**, *35*, 13205–13211.
257. Van de Kamp, M.; Silvestrini, M. C.; Brunori, M.; Van Beeumen, J.; Hali, F. C.; Canters, G. W. *Eur. J. Biochem.* **1990**, *194*, 109–118.
258. Van de Kamp, M.; Floris, R.; Hali, F. C.; Canters, G. W. *J. Am. Chem. Soc.* **1990**, *112*, 907–908.
259. Van Pouderoyen, G.; Mazumdar, S.; Hunt, N. I.; Hill, H. A. O.; Canters, G. W. *Eur. J. Biochem.* **1994**, *222*, 583–588.
260. Qin, L.; Kostic, N. M. *Biochemistry* **1996**, *35*, 3379–3386.
261. Kyritsis, P.; Lundberg, L. G.; Nordling, M.; Vänngård, T.; Young, S.; Tomkinson, N. P.; Sykes, A. G. *J. Chem. Soc., Chem. Commun.* **1991**, 1441–1442.
262. Wang, X.; Ang, M. C.; Lu, Y. *J. Am. Chem. Soc.* **1999**, *121*, 2947–2948.
263. Paul, K. G.; Stigbrand, T. *Biochim. Biophys. Acta* **1970**, *221*, 255–263.
264. Ainscough, E. W.; Bingham, A. G.; Brodie, A. M.; Ellis, W. R.; Gray, H. B.; Loehr, T. M.; Plowman, J. E.; Norris, G. E.; Baker, E. N. *Biochemistry* **1987**, *26*, 71–82.
265. Husain, M.; Davidson, V. L. *J. Biol. Chem.* **1985**, *260*, 14626–14629.
266. Van Houwelingen, T.; Canters, G. W.; Stobbelaar, G.; Duine, J. A.; Frank, J., Jr.; Tsugita, A. *Eur. J. Biochem.* **1985**, *153*, 75–80.
267. Romero, A.; Nar, H.; Huber, R.; Messerschmidt, A.; Kalverda, A. P.; Canters, G. W.; Durley, R.; Mathews, F. S. *J. Mol. Biol.* **1994**, *236*, 1196–1211.
268. Masuko, M.; Iwasaki, H.; Sakurai, T.; Suzuki, S.; Nakahara, A. *J. Biochem. (Tokyo)* **1984**, *96*, 447–454.
269. Peisach, J.; Levine, W. G.; Blumberg, W. E. *J. Biol. Chem.* **1967**, *242*, 2847–2858.
270. Malmström, B. G.; Reinhammar, B.; Vänngård, T. *Biochim. Biophys. Acta* **1970**, *205*, 48–57.
271. Shichi, H.; Hackett, D. P. *Arch. Biochem. Biophys.* **1963**, *100*, 185–191.
272. Marchesini, A.; Minelli, M.; Merkle, H.; Kroneck, P. M. H. *Eur. J. Biochem.* **1979**, *101*, 77–84.
273. Kakutani, T.; Watanabe, H.; Arima, K.; Beppu, T. *J. Biochem. (Tokyo)* **1981**, *89*, 463–472.
274. Cox, J. C.; Boxer, D. H. *Biochem. J.* **1978**, *174*, 497–502.
275. Cox, J. C.; Aasa, R.; Malmström, B. G. *FEBS Lett.* **1978**, *93*, 157–160.
276. Aikazyan, V. T.; Nalbandyan, R. M. *FEBS Lett.* **1975**, *55*, 272–274.
277. Michalski, W. P.; Nicholas, D. J. D. *Biochim. Biophys. Acta* **1985**, *828*, 130–137.
278. Liu, M. Y.; Liu, M. C.; Payne, W. J.; Legall, J. *J. Bacteriol.* **1986**, *166*, 604–608.
279. Iwasaki, H.; Noji, S.; Shidara, S. *J. Biochem. (Tokyo)* **1975**, *78*, 355–361.
280. Hulse, C. L.; ; Averill, B. A. *Biochem. Biophys. Res. Commun.* **1990**, *166*, 729–735.
281. Berry, S. M.; Ralle, M.; Low, D. W.; Blackburn, N. J.; Lu, Y. *J. Am. Chem. Soc.* **2003**, *125*, 8760–8768.
282. Bertini, I.; Ciurli, S.; Dikiy, A.; Fernandez, C. O.; Luchinat, C.; Safarov, N.; Shumilin, S.; Vila, A. J. *J. Am. Chem. Soc.* **2001**, *123*, 2405–2413.
283. Bertini, I.; Bryant, D. A; Ciurli, S.; Dikiy, A.; Fernandez, C. O.; Luchinat, C.; Safarov, N.; Vila, A. J.; Zhao, J. *J. Biol. Chem.* **2001**, *276*, 47217–47226.
284. Fernandez, C. O.; Cricco, J. A.; Slutter, C. E.; Richards, J. H.; Gray, H. B.; Vila, A. J. *J. Am. Chem. Soc.* **2001**, *123*, 11678–11685.

8.5
Alkali and Alkaline Earth Ion Recognition and Transport

J. A. COWAN
Ohio State University, Columbus, OH, USA

8.5.1 INTRODUCTION

This chapter takes up the topic of "alkali metals and group IIA metals" that was so ably covered by Fenton in the *Comprehensive Coordination Chemistry* (*CCC*, 1987) series.[1] In this earlier volume the biological aspects of alkali and alkaline earth metal ions were barely addressed. In great measure this reflected the level of understanding of the biological chemistry of these metals. While much was known concerning the functional roles of the alkali and alkaline earth metals in cellular chemistry, this was often unsupported by structural insight. While there has been much effort and success made in the design of ligands that coordinate these metals, particularly the alkali metal ions, these are typically macrocycles and have been well covered in other review series and will not be discussed in detail in this section. The companion series *Comprehensive Supramolecular Chemistry* is an excellent source of information in this area.[2]

The chemistry of the alkali and alkaline earth metal ions has often been viewed with disinterest relative to the chemistry of the transition metals. However, these ions are among the most abundant in cellular organisms. A useful text describing the biological chemistry of magnesium has been published.[3] The need to maintain homeostatic balance of the concentrations of these ions is vital for cellular survival through the important roles these play in bioenergetics, catalysis, and the requirement for magnesium, calcium, and occasionally potassium ions, as regulators or promoters of enzyme or protein function. This in turn dictates a need for selective transport and binding recognition. In this chapter the focus rests on topics where insight on biologically relevant coordination chemistry of the alkali and alkaline earth ions has emerged; primarily from structural studies. The aim is to summarize those key findings that have resulted in significant advances in understanding the coordination chemistry of these metal ions with biological ligands.

8.5.2 PHYSICOCHEMICAL PROPERTIES THAT UNDERLIE FUNCTION

The distinct biological roles for the alkali and alkaline earth ions (Table 1) reflect fundamental differences in their coordination chemistries and include variations in their structural, thermodynamic, and kinetic properties (Table 2). The functional role of each ion also underpins to a great extent the intra- and extracellular distribution of the alkali and alkaline earth ions (Table 3) since it is the distribution that dictates both availability and the necessary concentration gradients that underlie many important cellular functions of these ions. Extending from this, the binding affinity of biological ligands (large and small) typically correlates with the available concentration of free metal ions at a given locus. For example, binding affinities for intracellular magnesium ligands show K_D's ~ 0.5 mM, and K_D's ~ 2–4 mM for extracellular calcium ligands, while the K_D's for intracellular calcium ligands are on the order of nanomoles. In turn, such variations in cellular distribution also underlie mechanisms of selectivity. Abundant cations are selectively bound relative to other ions of much lesser abundance even if their binding affinities are greater.[4]

With the exception of magnesium, which may coordinate nitrogen donor ligands under special circumstances, the alkali and alkaline earth metal ions bind to oxygen ligands and adopt octahedral coordination. Both potassium and calcium commonly expand their coordination numbers and adopt irregular geometries.[4]

The ionic radius of Mg^{2+} is among the smallest of all cations; however, its hydrated radius is the largest and is approximately 400-fold larger than the free ion (Table 2).[5] In contrast, there is only a 25-fold change for Na^+ and Ca^{2+} and only a fourfold change for K^+. Solvent exchange rates also vary by almost five orders of magnitude (Table 2). These properties underpin the distinct functional roles of the cations and their binding sites on proteins and other biological molecules (Table 3). The coordination number and solvent exchange rate also play important

Table 1   Summary of cellular roles for the alkali and alkaline earth cations.

Ion	Intracellular	Transmembrane	Extracellular
Na^{++}	Electrolyte (protein/RNA/DNA)	Ion gradient	Electrolyte
K^+	Electrolyte (protein/RNA/DNA)	Ion gradient	
	Structural (RNA/DNA)		
Ca^{2+}	Structural (protein)	Ion gradient	Structural (protein)
	Catalytic (enzyme)		Catalytic (enzyme)
	Secondary messenger		
Mg^{2+}	Structural (RNA)		Structural (protein)
	Structural (protein)		Catalytic (enzyme)
	Catalytic (enzyme)		

Table 2   Physicochemical properties of the alkali and alkaline earth cations.[5]

Ion	Ionic radius (Å)[a]	Hydrated radius(Å)	Ionic volume (Å^3)	Hydrated volume (Å^3)	Coordination number	Water exchange rate(s^{-1})[b]
Na^+	0.95	2.75	3.6	88.3	6	8×10^8
K^+	1.38	2.32	11.0	52.5	6–8	10^9
Ca^{2+}	0.99	2.95	4.1	108	6–8	3×10^8
Mg^{2+}	0.65	4.76	1.2	453	6	10^5

[a] Ionic and hydrated radii are taken from refs. 83 and 84.   [b] Solvent exchange rates are taken from 83.

Table 3   Intra- and extracellular concentrations of the alkali and alkaline earth cations.

Ion	[total]$_{INTRA}$(mM)	[free]$_{INTRA}$(mM)	[total]$_{EXTRA}$(mM)
Na^{++}	12	8	145
K^+	140	120	5
Ca^{2+}	3	0.0001	4
Mg^{2+}	30$^+$	0.3	1

roles in determining biochemical recognition and function. For example, calcium ion finds use as a secondary messenger as a result of its rapid exchange kinetics and flexibility of coordination mode. Divalent magnesium is invariably hexacoordinate, as is sodium ion. By contrast, calcium and potassium ions can adopt six-, seven-, or eight-coordinate bonding arrangements.[4] Even nine-coordinate arrangements are known for Ca^{2+}.[6] Moreover, the coordination sphere is highly flexible with the larger ions Ca^{2+}, but much more constrained with Mg^{2+} and Na^+. The high charge density of Mg^{2+} gives rise to its strong Lewis acid character and makes it suitable to serve as such in enzyme catalysis,[7,8] typically in hydrolysis of phosphate esters and phosphoryl transfers.[9,10]

Structural definition of binding sites on biological ligands is less common for weak binding monovalents, but is better defined for the divalent ions. With Ca^{2+}, the distances between the cation and the oxygen atom of proteins and small molecules, as determined by crystal structure studies, vary widely between 2.2 and 2.7 Å. For Mg^{2+} this variation is only 2.05 to 2.25 Å.[11] The much greater flexibility in structures formed in part with Ca^{2+} allows a much greater angular deviation from the 90° angle expected of an octahedral geometry. Deviations from the expected 90° bond angle are as much as 40° with Ca^{2+} and less than half that with Mg^{2+}.[11] Structural flexibility underlies the use of Ca^{2+} as a signaling species, since it must bind to a variety of proteins and modulate a conformational change. This is consistent with the flexible coordination geometry of the Ca^{2+} ion that can accommodate different ligand arrangements for at least two states of the protein in question.[12,13]

8.5.3 COORDINATION COMPLEXES WITH PROTEINS

8.5.3.1 Calcium

Several calcium-binding motifs have been characterized for proteins; especially those with regulatory roles. The structural chemistry of EF hands and the coordination chemistry of calcium and other spherical metal ions, and related models, have been reviewed by Falke.[14]

Frequently, Ca^{2+} binding to such motifs resulted in perturbation of bonding interactions between the two principal elements of secondary structure. Such perturbations underlie the cooperativity often observed in proteins carrying such motifs. The best known is the so-called EF hand motif, first identified in carp parvalbumin,[15] and named after the E and F alpha helices of the structure that adopt a structural form resembling the thumb and index finger of a hand. The EF hand captures Ca^{2+} in a loop region between two α helices, with the side chains of residues 1, 3, 5, and 9 within the loop, residue 12 in the following helix, and the carbonyl of residue 7 making contacts (Figure 1).[16,17] Residue 9 is often in the outer sphere and stabilizes a Ca^{2+}-bound H_2O. Based on the structural understanding of calcium ion binding to EF hands, the binding affinity and metal ion selectivity have been tuned through rational amino acid substitutions.[18–21]

A β-hairpin motif shows residues 1–7 in well-conserved structural positions relative to the EF hand (Figure 1). Residue 9 typically moves and delivers two oxygens from a carboxylate to take up the site previously taken by residue 12. Divalent calcium can also be bound by a structurally similar loop bound by an α helix and β strand. Overall, the residues 1, 3, 5, and 9 are conserved in all of these structures and appear sufficient to define the Ca^{2+} binding motif. Putative Ca^{2+} binding sequences in integrins resemble those found in EF hands[16] and have been termed "EF hand-like" (Figure 1). The α helix/β strand defined motif common to integrins also lacks the need for residue 12.

No distinct structural motif is used by calcium-dependent nucleases such as staphylococcal nuclease.[22] Since these enzymes are extracellular, where Ca^{2+} concentrations are high, the binding affinities are normally low and in the millimolar range (Table 1).

8.5.3.2 Magnesium

For alkali and alkaline earth ions the most common protein ligands are the carboxylate groups in glutamate and aspartate residues. Figure 2 summarizes possible binding modes.[23,24] Larger cations favor the syn configuration with anti only identified for smaller ions with M—O distances <1.98 Å, and for very large ions such as Cs^+.[25] Alkali and alkaline earths, unlike transition metals, also bind the carboxylate out of plane. Some metal ions with M—O distances in the range 2.3–2.8 Å may bind in the bidentate mode, including Ca^{2+}.[25]
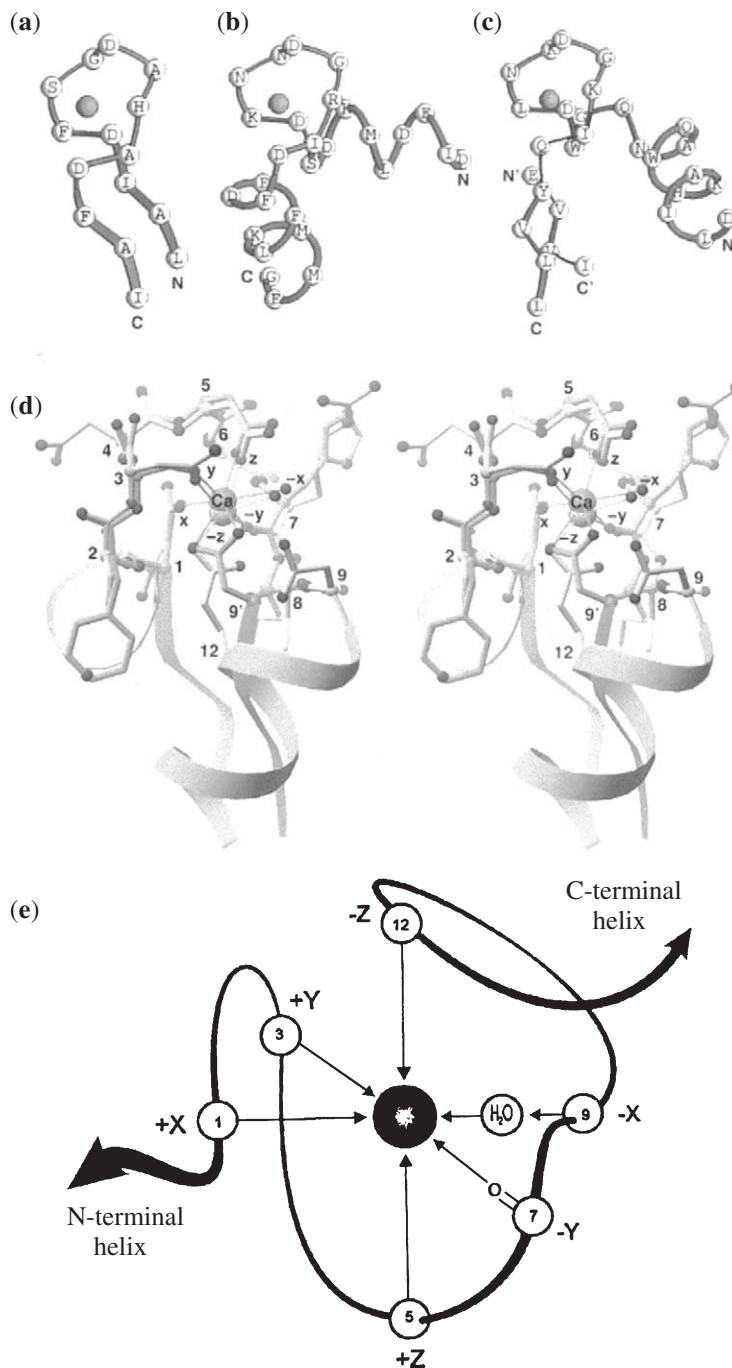
Figure 1 Structural binding motifs for Ca^{2+}. (a)–(c) show the β-strand motif, EF-hand motif, and helix turn motif, respectively. (d) shows a stereodiagram of the calcium binding domains in (a) and (b). (e) illustrates the ligand sites noted in the text. Backbone atoms are shown in yellow for (a) and green for (b) (reproduced with permission from Springer *et al.*[16] and Reid *et al.*[17]).

Computational methods have been brought to bear on the question of what controls coordination mode and geometry. Results from computational studies of crystallographically defined coordination complexes are compared with experimental structural data and further compared with similar structural configurations in protein structures. The assumption that gas-phase calculations might mimic protein environments has been tested on model complexes and generally found to be valid.[23,24,26]

(a)

(b)
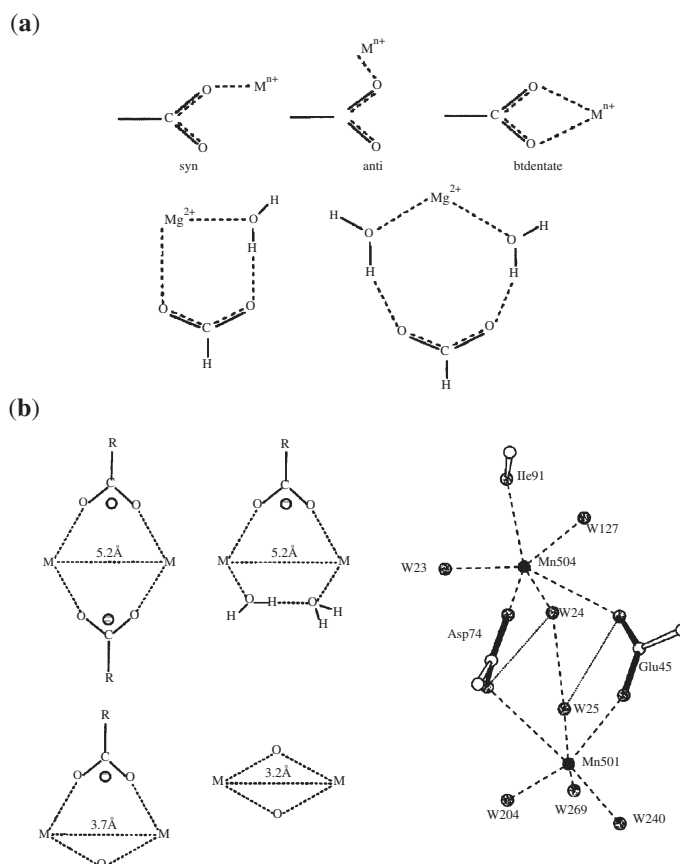
Figure 2 Magnesium binding motifs on proteins illustrated for one metal (a) and two metal (b) binding sites. The proposed binuclear site from *E. coli* EcoRV is illustrated in (b) (reproduced with permission from Katz *et al.*[23] and Glusker *et al.*[24]).

Binuclear metal centers are commonly found for transition metal-containing systems.[27] Several have been cited for magnesium[7] and even calcium ion.[28] The relevance of these crystallographically defined ions to the functional state in solution has been debated;[7,29,30] however, in this chapter we shall focus simply on the details of coordination chemistry (Figure 2). The close proximity of two divalent metal ions in a low dielectric medium, such as a protein, requires the close proximity of negatively charged groups to alleviate the electrostatic repulsion. The occurrence of a bridging carboxylate or carboxylates(s) yields an inter-metal distance of ~5.2 Å; however, an additional bridging hydroxide or phosphate oxygen can reduce the inter-site distance to ~3.3–3.6 Å.[24] Typically when a single carboxylate bridges magnesium the metal lies in an anti orientation relative to the carboxylate. When two carboxylates bridge, the geometry is syn.[24]

Certain proteins may use two metal ions in close proximity to maintain a preferred shape, or assist in enzyme catalysis.[7,27] As noted previously, metal–ligand interactions are structurally more precise than H bonds, and so their use better assures a specific structural orientation that may be required for protein function. Such an idea may be extended to all of the examples described in this chapter. There has been some effort to synthetically model such binuclear magnesium centers. For example, three novel carboxylate-bridged dimagnesium(II) complexes have been reported that use a ligand design based on *m*-xylenediamine bis(Kemp's triacid imide) as the binucleating ligand.[31] The crystallographically determined structure of the carboxylate complex shows a Mg⋯Mg distance of 4.783(2) Å. Reaction with sodium diphenyl phosphate yielded two new compounds. One contained the binuclear core with a bridging bidentate phosphate ligand and a metal–metal distance of 4.240(5) Å, while the other showed one bridging and one terminal phosphate ligand with a metal–metal distance of 4.108(3) Å.[31] The ligand exchange rates for the binuclear magnesium complexes were found to be two orders of magnitude slower relative to exchange results for the equivalent dinuclear zinc complex, consistent with the relative exchange rates for the individual Mg^{2+} and Zn^{2+} ions.

The role of Mg^{2+} and Ca^{2+} in biological catalysis commonly involves mediating hydrolysis of phosphate esters.[4,7,27] To this end the divalent ion often contains a bound H_2O that is then located proximally to the bound ester function (the so-called template effect). A second proposed role for the divalent metal ion is to promote ionization of the bound H_2O.[23] It is well recognized that in completely hydrated ions, charged metal ions lower the acidity constant (pK_a) of bound H_2O. For $Mg(H_2O)_6^{2+}$ the energy to remove a proton is 40% of that required to deprotonate bulk H_2O (the pK_a is lowered).[23] Commonly, however, alkali and alkaline earths are bound to proteins by carboxylates. It has been shown that replacement of a bound H_2O by carboxylate increases the energy to deprotonate an Mg^{2+}-bound H_2O by ~ 80 kcal/mole^{-1}, making it intermediate between the bulk water and fully hydrated Mg^{2+}(aq).[23] This change appears to originate entirely from electrostatics rather than the direct perturbation of the electronic structure of the metal ion. Further substitution by additional carboxylates further increases the pK_a with clear implications for enzymes that carry such motifs (Figure 3) where ionization of bound water to form hydroxide is often invoked.

Computational studies of magnesium binding to proteins have established that the dielectric properties of the solvent medium play a critical role in defining whether magnesium binds in an inner or outer sphere fashion.[26] When $\varepsilon \leq 4$, carboxylate may replace water, although additional stabilizing interactions are required for the carboxylate if deprotonation of the acid is required before coordination. This also rationalizes the observed outer sphere coordination preferred by divalent magnesium to nucleic acids[32,33] since the binding sites tend to be extensively solvent accessible with a higher dielectric constant. Coordination of charged carboxylate is strongly preferred relative to neutral acids, amides, or alcohol ligands. Stabilization of bound carboxylate stems from electrostatic factors and hydrogen bonding from the Mg-bound carboxylate to either water or H-bond acceptor groups bound to Mg^{2+}. Electrostatic demands dictate a maximum of four carboxylate ligands to magnesium. Additional carboxylate may bind only if there is an additional metal cofactor to bridge to, or if the ligand binds in the neutral protonated form. The latter is quite feasible since the grouping of several charged carboxylates tends to increase the effective pK_a of one of them. Water is the favored co-ligand for carboxyl ligated magnesium as a result of its small size and hydrogen bonding capacity. It was concluded also that magnesium binding to proteins most likely occurs stepwise with an initially hydrated metal entering the pocket with subsequent stepwise replacement of inner sphere waters.

Proteins typically bind metal ions with binding affinities (K_D) that match physiological availability.[3,7,33] In the case of intracellular free Ca^{2+} this is sub-micromolar, and so such Ca^{2+}
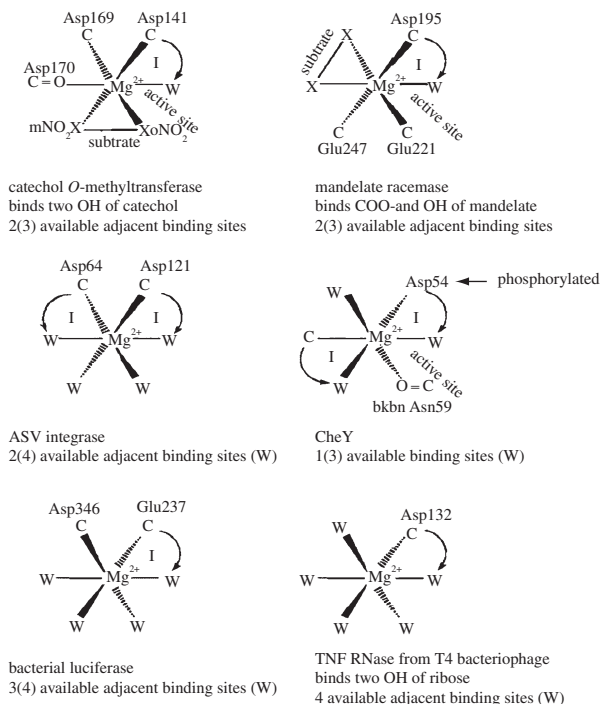
Figure 3   Coordination modes for magnesium ion binding to a variety of *E. coli* proteins (reproduced with permission from Katz *et al.*[23]).

binding proteins show $K_D \leq 1\,\mu M$, while extracellular Ca^{2+} proteins show $K_D > 1\,mM$, again reflecting the higher extracellular concentrations of this cation. The intracellular concentration of free Mg^{2+} is ~0.5 mM, and so K_D's typically lie in this range. Despite this similarity in K_D, many metal binding proteins, and magnesium-dependent enzymes in particular, show a rich variety of coordination motifs. These variations tailor the K_D as described, but also accommodate the diverse functional roles of the metal cofactor. In this regard, the availability of high-resolution structural data on several metal-dependent nuclease enzymes allows a critical analysis of the coordination chemistry of the bound cofactor and implications for the functional mechanism.[7] There is an apparent and interesting relationship between the requirements for metal-bound solvent interactions with the substrate and the coordination number with protein ligands, which ultimately controls the hydration state of the bound metal.[34]

Metal binding pockets of surface magnesium sites typically show poor selectivity and can accommodate a large variation in metal size.[35,36] Such relationships have been investigated intensively by Falke and co-workers, who have shown that such sites show strong charge selectivity, but weak size selectivity.[37] A comparison of calcium binding EF hands versus magnesium-dependent enzymes that Mg^{2+} and Ca^{2+} sites exhibit similar charge selectivity, but the Ca^{II} site is highly size-selective, preferring divalent and trivalent ions with radii similar to that of Ca^{II}. A structural comparison of the Mg^{2+} and Ca^{2+} sites suggested that these distinct size specificities stem from fundamentally different coordination schemes. The Ca^{2+} site surrounds the bound ion with a pentagonal bipyramidal array of seven protein oxygens, thereby fixing the coordination number and controlling the radius of the substrate cavity, while the flexible nature of the Mg^{2+} site was proposed to stem from its use of solvent oxygens to coordinate one hemisphere of the bound ion with variable coordination numbers and radius resulting to accommodate substrate ions of different size.

The metal binding pockets for the magnesium-dependent enzymes (several are summarized in Figure 3) differ markedly. The coordination environment and charge density in the metal binding pockets are distinct. The number of carboxylate ligands varies from none to three (additional carboxylates may derive from bound substrate, such as the case for mandelate racemase). Nevertheless, the binding affinity for Mg^{2+} is similar (0.5 mM) for each of these magnesium binding proteins. How does this arise, and why should it be so?

It appears that the solvation state of the metal cofactor is of critical importance for the proper functioning of these enzymes. The solvation state in turn is defined by the coordination state. Note that in the case of RNase H, not only the number of bound H_2O, but also the facial geometry, was found to be required for catalytic activity.[38] Since the metal binding affinities of metal-dependent nucleases are tuned to the normal physiological concentration, Nature has evolved a structural mechanism that permits permutation of the ligand environment of the essential metal cofactor, while optimizing the binding affinity to physiological requirements. In particular, the metal binding pockets of metal-dependent nucleases have evolved to allow a large variation in the number of protein ligands (and thereby solvent water), while optimizing the binding affinity to physiological requirements.

For many metallonucleases the metal cofactor appears to activate substrate by outer-sphere stabilization of the transition state. This is consistent with crystallographic precedent[33,39] based on the ground-state binding geometry of Mg^{2+}–oligonucleotide complexes. Experimental data clearly show that transition state stabilization is effected by hydrogen bonding with essentially no contribution from electrostatic stabilization through the charge on the cofactor.[38]

8.5.4 COORDINATION COMPLEXES WITH NUCLEIC ACIDS

8.5.4.1 DNA

Cation binding to nucleic acids can be viewed at two extremes. First, there exists a "cloud of cations", usually monovalents, that condense with and are displaced along the length of the polynucleic acid.[40,41] They are fully solvated and are exchangeable, serving mainly to electrostatically stabilize the polyanion. At the other extreme are tightly bound, partially dehydrated cations that bind at specific locations—usually to nucleic acids (especially RNA motifs) with well-defined tertiary structures.[33,40,42] More recently, evidence has emerged for an intermediate state (especially for DNA) where fully hydrated ions exhibit preferential binding to certain sequences (Figure 4). These often lie in the minor groove of AT-rich sequences and the major groove of GC-rich sequences.[41,43] This mode is especially observed for divalent ions.
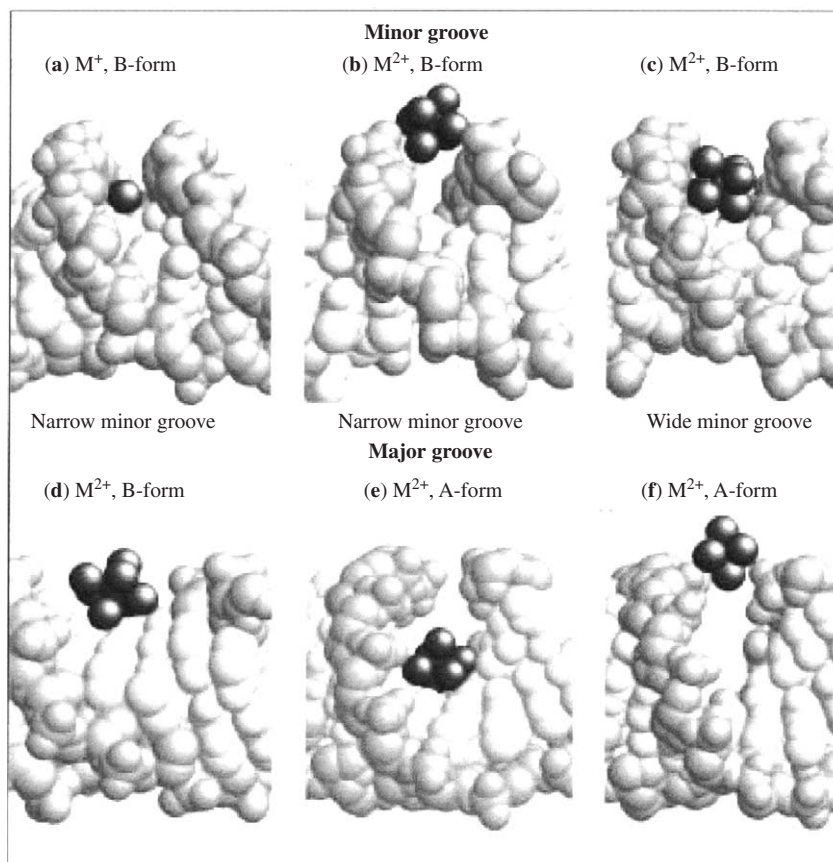
Figure 4 The correlation between DNA groove width and cation coordination sites is illustrated. The metal species shown are (a) Rb^+, (b) $Mg(H_2O)_6^{2+}$, (c) $Mg(H_2O)_6^{2+}$, (d) $Ca(H_2O)_8^{2+}$, (e) $Mg(H_2O)_6^{2+}$, and (f) $Co(NH_3)_6^{3+}$. (reproduced with permission from Hud *et al.*[41]; © 2001, Society of Biological Inorganic Chemistry).

Crystallographic characterization of the *B*-DNA sequence, CGCGAATTCGCG, has been reported at $\sim$1.5 Å resolution, with one Mg^{2+} per duplex.[44] Improved structures of this *B*-form DNA in the presence of Mg^{2+} and Ca^{2+} have been recently solved with atomic resolutions of 1.1 Å and 1.3 Å, respectively[45] (Figure 5). Duplexes in the crystal lattice are surrounded by 13 Mg^{2+} and 11 Ca^{2+}, respectively. Each cation generates a different DNA crystal lattice and stabilizes different end-to-end overlaps and lateral contacts between duplexes. Mg^{2+} ion allows the two outermost base pairs at either end to interact laterally via minor-groove H bonds, turning the 12-mer into an effective 10-mer. A Mg^{2+} ion coordinates in the major groove contributing to the kinking of the duplex at one end, while the Ca^{2+} ions reside in the minor groove, coordinating to the bases through their hydration shells. Mg^{2+} ions were also found at the periphery of the minor groove, bridging phosphate groups from opposite strands and contacting the groove at one border of the A tract. Several other Mg^{2+} ions bridge oxygen atoms of bases via coordinated water molecules, forming an extensive network of H bonds. Only two direct Mg–phosphate oxygen bonds have been identified with an Mg—O distance of $\sim$2.1 Å. A comparison of Mg^{2+} and Ca^{2+} coordination modes reveals some important distinctions, with the cations residing in the major and minor grooves, respectively, while calcium ions are more likely to form inner-sphere complexes. This is consistent with the lower hydration enthalpy of Ca^{2+} relative to Mg^{2+}.[3,9] In both cases, the divalent ions mediate contacts between multiple strands. Thus, it is possible that Mg^{2+} ions mediate specific contacts between DNA and small molecules (groove binding drugs) or proteins.

Sequence-specific binding and groove-specific bending of *B*-DNA by Mg^{2+} and Ca^{2+} has been observed crystallographically.[45–47] The 1 Å resolution structures of the decamers CCAACGTTGG and CCAGCGCTGG reveal binding of Mg^{2+} and Ca^{2+} to the major and minor grooves of DNA, respectively, as well as nonspecific binding to backbone phosphate oxygen atoms. Minor-groove binding involves H-bonds interactions between cross-strand DNA
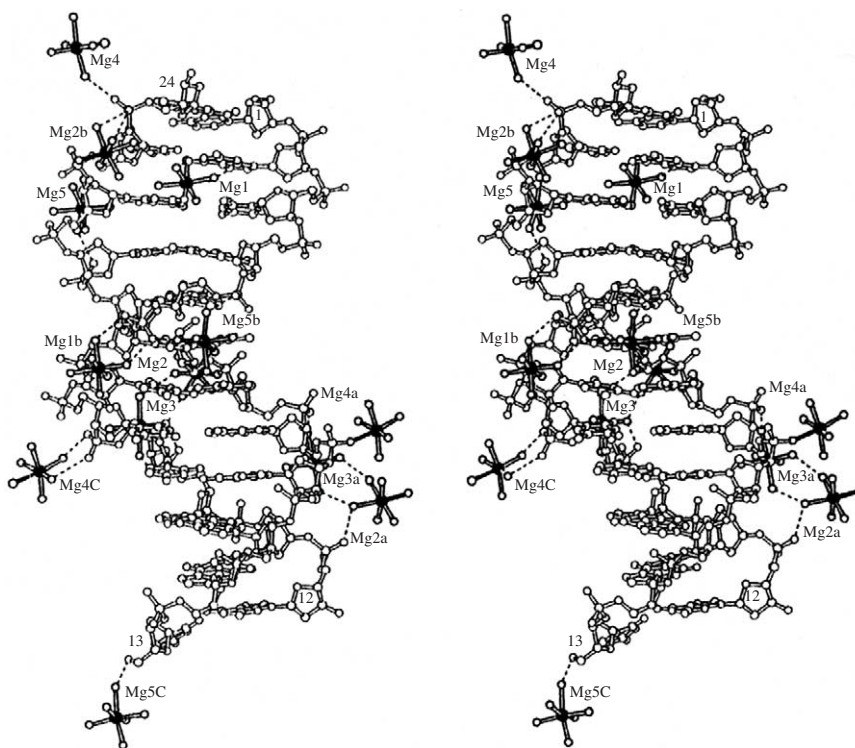
Figure 5 Stereoview of the B-DNA, CGCGAATTCGCG, in the presence of Mg^{2+}. Filled bonds indicate direct ion–DNA contacts, broken lines indicate hydrogen bonds (reproduced with permission from Minasov *et al.*[45]).

base atoms of adjacent base pairs and the metal-bound water ligands. In the major groove, the hydrated metal ion H bonds with O and N atoms from adjacent bases.

Divalent Mg interacts with DNA in a more specific manner, since waters of solvation can both donate and accept H bonds to base atoms. Mg^{2+} is drawn electrostatically to both major and minor grooves of DNA, as well as to the sugar–phosphate backbone. At GGCC/GGCC sequences, binding of magnesium to the major groove GG residues, and to the minor groove at the GC step, results in a bending of the helix toward the major groove. Ca^{2+} ion has been found to form polar covalent bonds bridging adjacent N7 and O6 atoms of GG bases. In addition to having higher affinity to DNA, Ca^{2+} binding to DNA results in greater DNA bending and thermal stabilization than Mg^{2+}.[45–47]

Of considerable importance are the structural motifs termed telomeres that have been identified at the ends of chromosomal DNA. Such motifs provide chromosomal stability and have been implicated in cell replications and a putative role in the mechanism of aging. Such structures (illustrated in Figure 6) are formed when four guanine bases form stable four-stranded helices. Such tetrads are stabilized principally by potassium ion, although sodium ion stabilization has also been characterized.[48,49] A cubic coordination motif is generated by the eight O6 atoms from the guanine bases.

8.5.4.2 RNA

Highly structured RNA domains are often stabilized by either K^+,[50] or especially Mg^{2+}.[42] Divalent magnesium may bind in either an outer-sphere or by an inner-sphere mode (Figure 7).[51] The former requires hexahydrated magnesium $[Mg(H_2O)_6]^{2+}$ to interact with RNA and base centers by hydrogen bonding to the waters of solvation. These waters are consequently stabilized to exchange with bulk water. Often, binding is to the O6 and N7 atoms of guanosine.[51,52] In a few cases the hydrated metal ion is stabilized by a negative electrostatic potential surface, with no direct bonding contacts. For inner-sphere ligation, common ligands to Mg^{2+} include the phosphate oxygens, N7 on purine bases, base keto groups such as O6 of guanosine and O4 of uracil, and the ribose 2′-OH.[51] Typically from 1 to 3 waters are displaced and octahedral coordination in maintained.
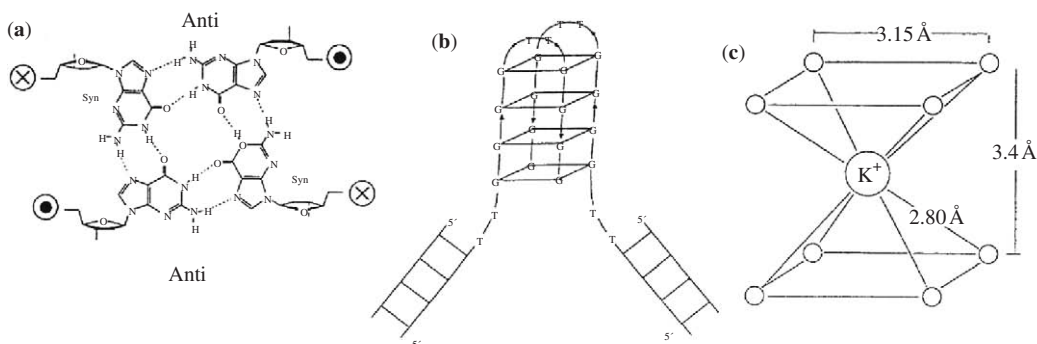
Figure 6 Stabilization of telomeric DNA by K^+. (a) A guanine tetrad within an antiparallel quadruplex. Strand orientations (5′ to 3′) are represented by (X) or (·), respectively. Structural requirements at the ribose rings are indicated. (b) A proposed structure for the overlapping ends of telomeric DNA. (c) An octacoordinate potassium chelation cage created by the O6 oxygen atoms of the stacked guanine bases. Interatomic distances are derived from fiber diffraction studies and model building (reproduced with permission from Sundquist and Klug[48]; © 1989, Society of Biological Inorganic Chemistry).

Several binding motifs on RNA have been characterized. These include the major groove of tandem G–U pairs (Figure 7) which provides a surface with strong negative potential and a series of potential ligands to the metal ion, and H-bound acceptors for metal-bound H_2O. Such sites readily bind hydrated magnesium ion.[53] The deep major groove of A-form RNA, and internal loops such as the loop E motif (Figure 8) are regions of high negative charge density and are attractive binding sites for hydrated Mg^{2+}. The loop E motif shows a number of magnesium ions that crosslink neighboring backbones, forcing them into close proximity, and include an unusual binuclear cluster.[54]

The adenine–adenine platform RNA motif has been shown to define a monovalent ion-binding site that is important for ribozyme folding (Figure 8).[40,42] Such binding motifs complement the general association of counter ions that are required to minimize electropositive repulsion between phosphates, and are likely to be more common than current evidence suggests. Selectivity mechanisms for ion binding include Coulomb attraction and van der Waals interactions arising from size variations and changes in RNA conformation. However, differences in solvation energies for bound and free solution ions play a major role. The calculated selectivity $(K^+ > Na^+ > Rb^+ > Cs^+ > Li^+)$[40] reflects experimental hydration energies.[55] Experimentally, the preferred ion is K^+. The binding site for K^+ is illustrated in Figure 8 and can be contrasted with the G tetrad identified in telomeric DNA (Figure 6).

8.5.4.3 Drug–Mg^{2+}–DNA Ternary Complexes

Many DNA-binding drugs use a divalent cofactor to mediate binding of the two partners. The metal cofactor typically bridges the phosphate of the DNA backbone with a metal chelate motif on the ligand. The metal cofactor may also perturb the conformation of the ligand and/or the DNA to optimize the drug–DNA interaction. For example, mithramycin (Figure 9) is a member of the aureolic acid group of antitumor antibiotics. They contain an aureolic acid core that chelates Mg^{2+}. Divalent magnesium appears to promote the selective binding to a cognate DNA sequence (5′-XXGCXX-3′) by a coupled mechanism requiring local conformation changes in the DNA backbone and a structural rearrangement of the mithramycin dimer.[56] Molecular modeling suggested that sequence selectivity arises from preferential coordination of Mg^{2+} to d(GpC) domains in the minor groove of Z-type DNA. Magnesium stabilizes a local Z-type conformation, which opens up binding pockets on the DNA for the sugar chains. Additionally, Mg^{2+} was also found to realign and stabilize the MTC dimer in a manner that optimizes the position of both the aureolic acid core and the sugar chains for DNA binding.

Similar examples of synergy between drug and DNA binding through a metal cofactor have been identified. In each case the drug contains a chelate motif (Figure 9) for a metal cofactor (typically Mg^{2+}), such as quinobenzoxazine and derivatives, quinolones (norfloxacin), and UK-1.[57–60]

(a)

(b)

5´-NN GU NN-3´
3´-NN GU NN-5´

major groove
edge

(c)

5´ GCGAGAGUAGGG
GUGAUGGUAGCC
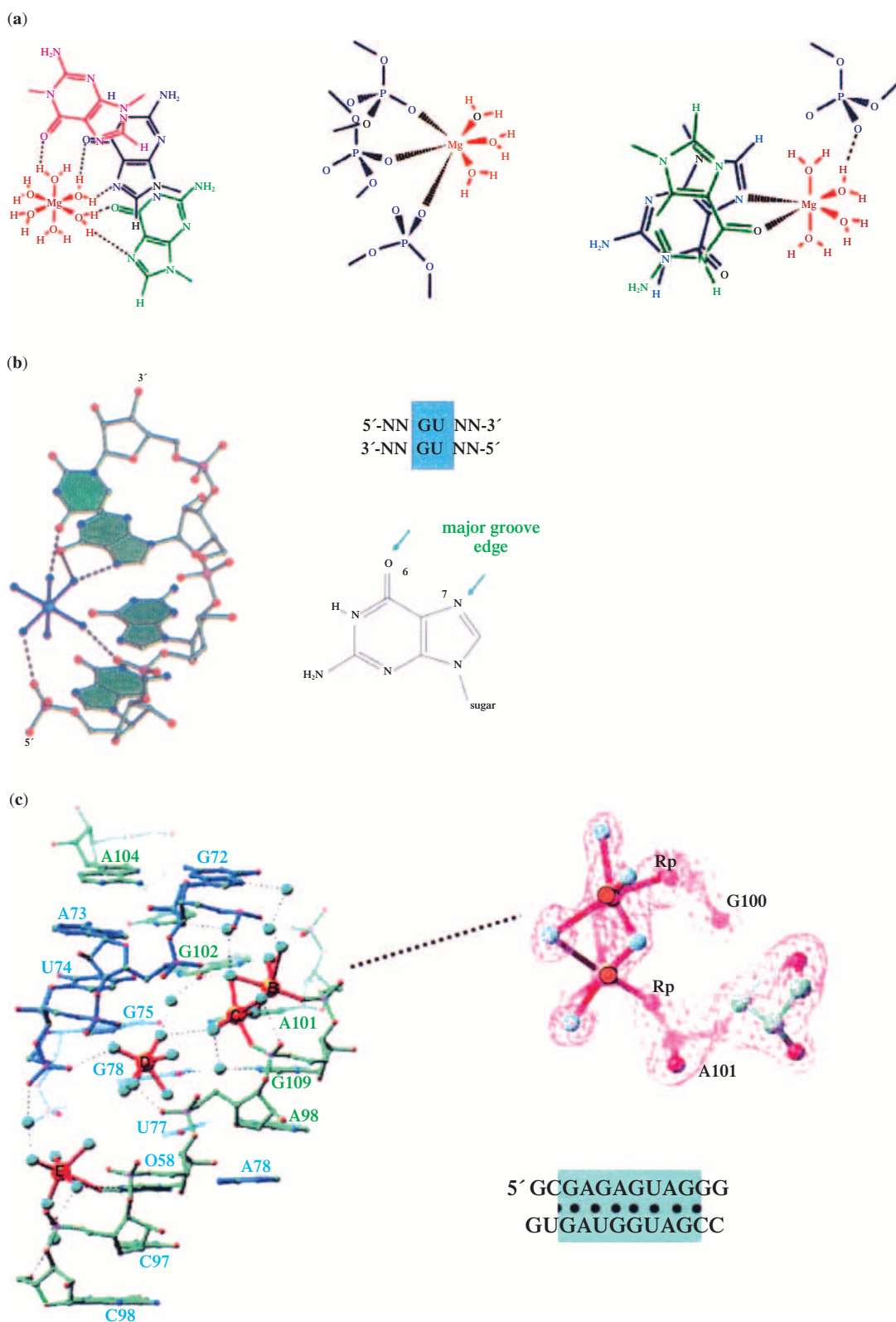
Figure 7 (a) A variety of magnesium binding sites on RNA structures, showing outer-sphere binding through solvent waters, and direct inner-sphere binding to phosphates. (b) A tandem GU motif that is favorable for major groove binding of metal cofactors through the O6 and N7 of guanosine. Outer-sphere binding by $Os(NH_3)_6^{3+}$, a mimic of $Mg(H_2O)_6^{2+}$, is shown. (c) The loop E motif possesses a narrow minor groove that appears able to stabilize binuclear magnesium centers (reproduced with permission from Pyle [42]; © 2002, Society of Biological Inorganic Chemistry).
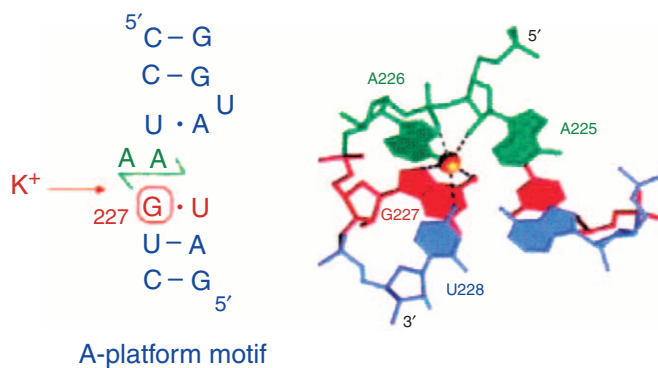
A-platform motif

Figure 8 Adenine platform for potassium ion binding. A pair of nucleotides are offset such that contiguous bases in a strand lie side by side (green). Together with adjacent bases, these form a binding motif for a partially dehydrated potassium ion, with ligand contacts to phosphate and base oxygen atoms (reproduced with permission from Pyle[42]; © 2002, Society of Biological Inorganic Chemistry).
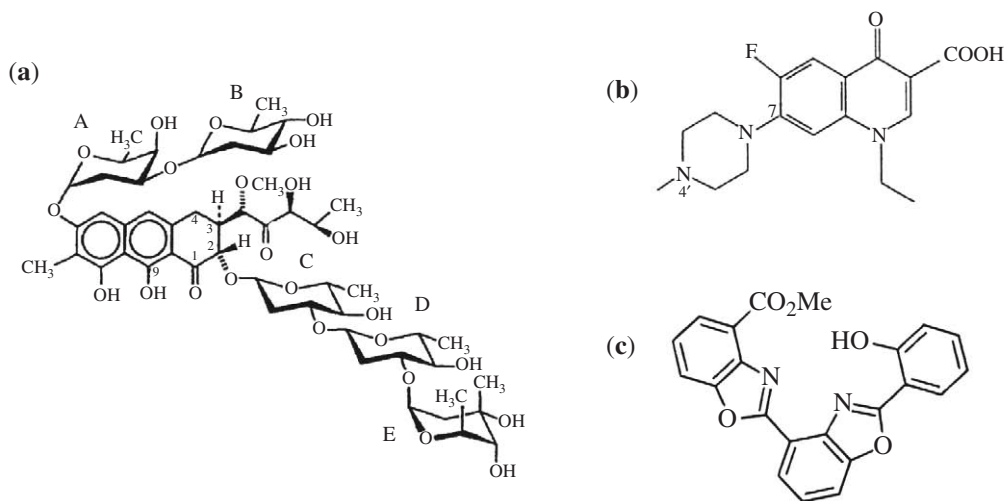
Figure 9 Chemical structures of (a) mithramycin; (b) perfloxacin; and (c) UK-1.

8.5.5 COORDINATION COMPLEXES WITH ION CARRIERS (IONOPHORES)

The coordination chemistry of ionophores has been extensively described, both in the first edition of this series, and the series *Comprehensive Supramolecular Chemistry*.[1] Such ligands are natural transmembrane ion carriers for the alkali and alkaline earth metal ions. Much of the earlier work in this area has focused on characterization of relative binding affinities and X-ray structure determination and evaluation. Since the mid-1980s, there has been increasing effort to characterize the kinetic properties of these metal complexes; especially by use of dynamic NMR methods,[61] and the functional aspects of membrane migration by direct conductivity measurements.[62] Such studies have provided significant insight on mechanisms underlying binding stability, kinetic lability, membrane transport, and selectivity.[61,63–65] For example, in the case of monensin it has been shown that dissociation of the complex is the rate-determining step, with relatively fast rates of diffusion of the complex through a membrane.[64,65] While K^+ is transported more rapidly in the absence of Na^+, the latter is preferentially transported in a mixture as a result of its enhanced stability in a membrane environment.[66] This is a clear demonstration of how a more rigorous understanding of the dynamics of ionophore complexes and their stability in the context of membrane environments is necessary for a more complete understanding of biological function.

Much of the progress in this area has been made possible by use of NOESY distance constraints and molecular modeling. Molecular dynamics calculations of the derived structures

at increasing relative permittivity provide insight on how ions bind to ionophores in a membrane versus solution environment.[58] It has become increasingly clear that a knowledge of the solution conformations is vital for an adequate understanding of membrane association and metal ion selectivity.[61] Moreover, it is of some significance that recent work contrasting solution NMR structures with those defined by X-ray crystallography[58,61,66–68] show functionally important differences. The solution structure of monensin A shows five oxygens closely attracted to the central metal ion (Na$^+$ or K$^+$) with a sixth oxygen more weakly attached (Figure 10).[66] For the larger Rb$^+$ ion, the terminal oxygen is replaced by one further along the chain to accommodate the larger ion. By contrast, the X-ray structure of monensin shows the central metal ion to be ligated by ether or hydroxy oxygens in a distorted octahedral arrangement, but no carboxylate binding. Rather, the latter is involved in H bonding to hydroxy groups and closes the macrocyclic structure.

For norasin, six oxygen atoms ligate, including carboxylate, and these ligand atoms are retained irrespective of the size of the metal ion. Rather, the conformations of the rings change to accommodate the metal ions and the metal–oxygen distances are similar.[67]
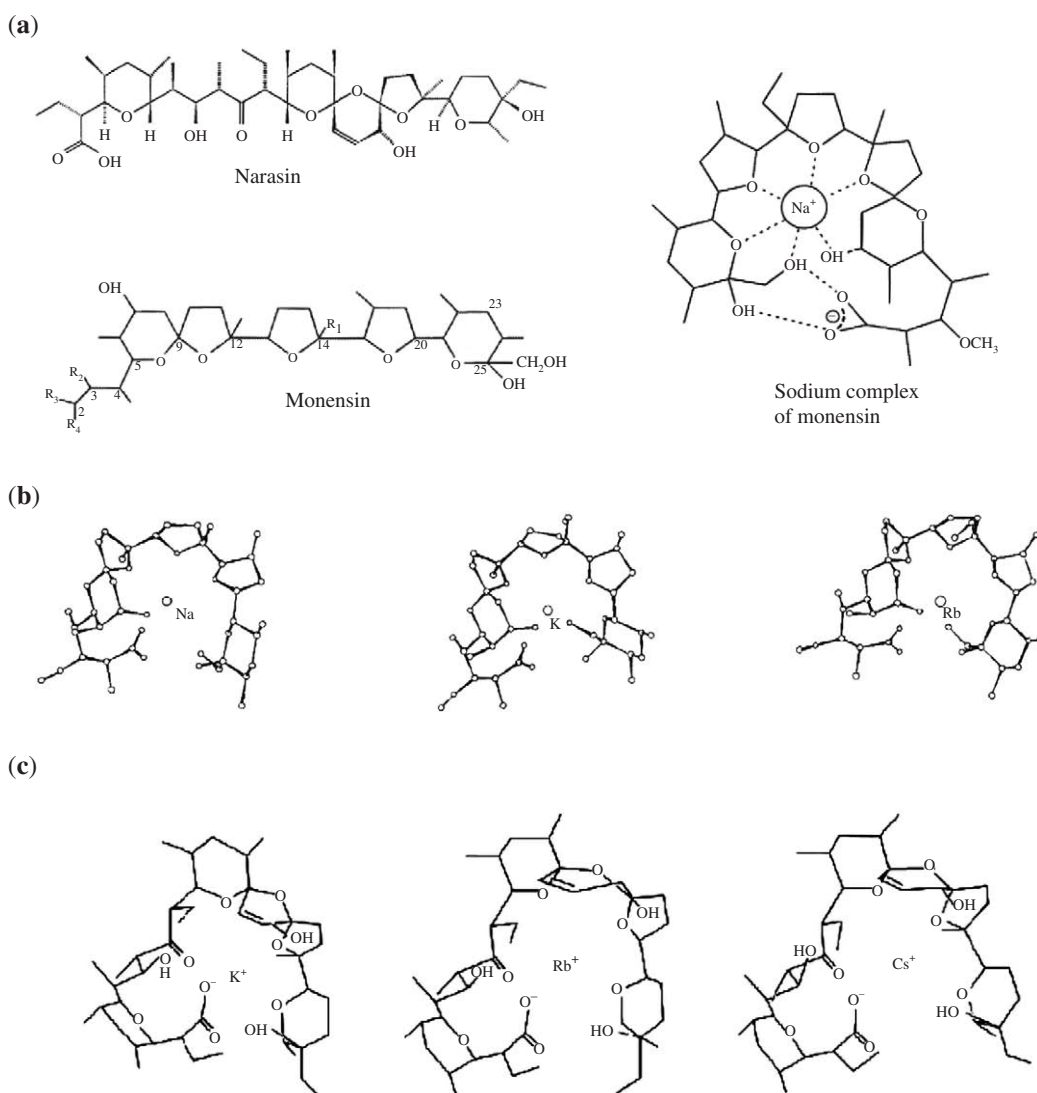
Figure 10 Monovalent ion coordination to monensin and narasin. (a) Structures of the ionophore ligands and an X-ray image of the sodium complex of monensin. (b) Solution conformations for the Na$^+$, K$^+$, and Rb$^+$ bound form of monensin. The terminal ligand changes to accommodate larger ligands. (c) Solution conformations for the Na$^+$, K$^+$, and Rb$^+$ bound form of narasin. The ligands stay the same, but the core expands to accommodate the larger ions. Carboxylate binding is not observed for either monensin or narasin (reproduced with permission from Martinek *et al.*[66,67]).

8.5.6 COORDINATION CHEMISTRY OF ION CHANNELS

Transmembrane metal ion transport is a poorly understood phenomenon. Several key questions to be answered include: how does a channel dehydrate and stabilize the presumably solvent-free metal cation (not an insignificant achievement for divalent magnesium, as section 8.5.2 revealed); how is transport gated (switched on and off) and made directional; and how is selectivity achieved? Channels presumably first recognize the hydrated cation, remove the hydration shell, and deliver the bare ion into the transport pathway through the membrane. Our understanding of ion channels has improved immeasurably with the recent crystallographic structural determinations of several potassium channels.[69–75] These studies support, in molecular detail, many of the hypotheses, predictions, and models that have been developed over decades of research.[76] A critical realization from this work is that the selectivity for potassium ion does not arise entirely from coordination effects. That is, a series of direct ligand contacts that define a space or passage with a specific diameter that selects for the metal ions that might pass through. Rather, selection also involves a subtle balancing of ligation/dehydration energies and electrostatic interaction of the charged monovalent with its environment.

   The high-resolution structure of these channels shows an aqueous pore, or cavity, on the intracellular side of the channel that contains ~50 water molecules and is surrounded by four α helices (Figure 11).[69,72] Detailed calculations of electrostatic stabilization and solvation energies suggest that the free energy of the potassium ion is balanced between stabilizing electrostatic interactions with solvent and especially the α helices, and destabilizing electrostatic contacts with the hydrophobic membrane.[69] Of the ~50 water molecules in the solvated cavity, eight are crystallographically defined as waters of hydration for K^+. The octahedrally coordinated $K(H_2O)_5^+$ in the cavity is the first example of structural definition of an aquated cation.[77]
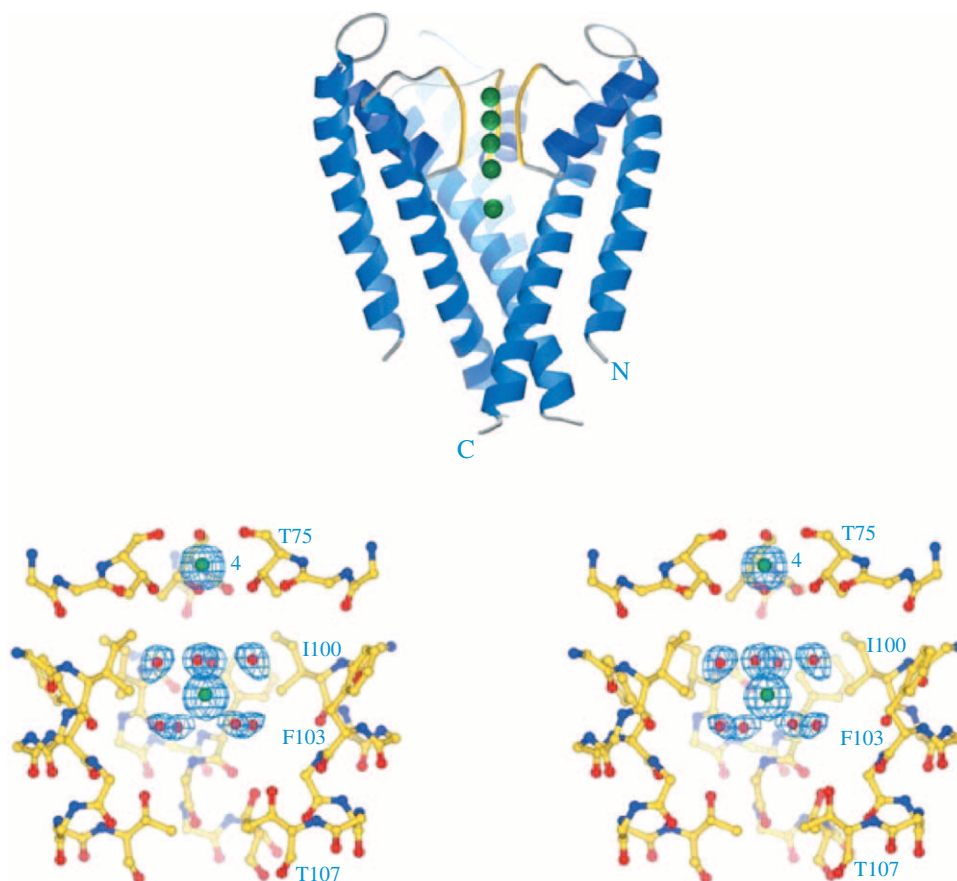
Figure 11 Structural biology of potassium channels. An illustration of the Kcsa K^+ channel showing protein backbone and the pore-forming helices (top). In the central cavity a fully solvated potassium ion is observed (bottom) (reproduced with permission from Roux and MacKinnon[69]).

Between the solvent-filled cavity and the extracellular environment lies the selectivity filter (Figure 12). Several coordination sites have been structurally characterized in this filter. These represent the motion of K^+ through the filter.[72,77–79] In each case the cation is held in a cubic eight-coordinate fashion by oxygen atoms from protein ligands. Structural studies have localized seven major binding sites for cations along the pore axis of the filter. These include one in the pore cavity, four in the selectivity filter, and two lying outside of the pore exit. The mechanism of K^+ transport involves an interesting rail car pathway. As illustrated in Figure 12 the cavity site is typically populated; however, only half of the remaining sites are populated at any instance with the ions being pushed through in a concerted manner.[72,77–79] The pairs of ions are separated by approximately one water molecule. The ions are ligated in a cubic fashion through coordination to backbone carbonyls. As the potassium ions move between sites the intervening waters maintain at least transient six-coordination before the cubic arrangement returns (Figure 13). The similarity in free energy for these sites minimizes the energy barriers to ion motion between them. The retention of fourfold symmetry throughout suggests optimization for K^+.

Movement occurs within the filter as a third ion enters and electrostatically interacts with the other two ions in the selectivity filter and facilitate displacements from the opposite side.[78,79] Other ions (such as Rb^+) do not display this thermodynamic balance and are conducted more slowly.
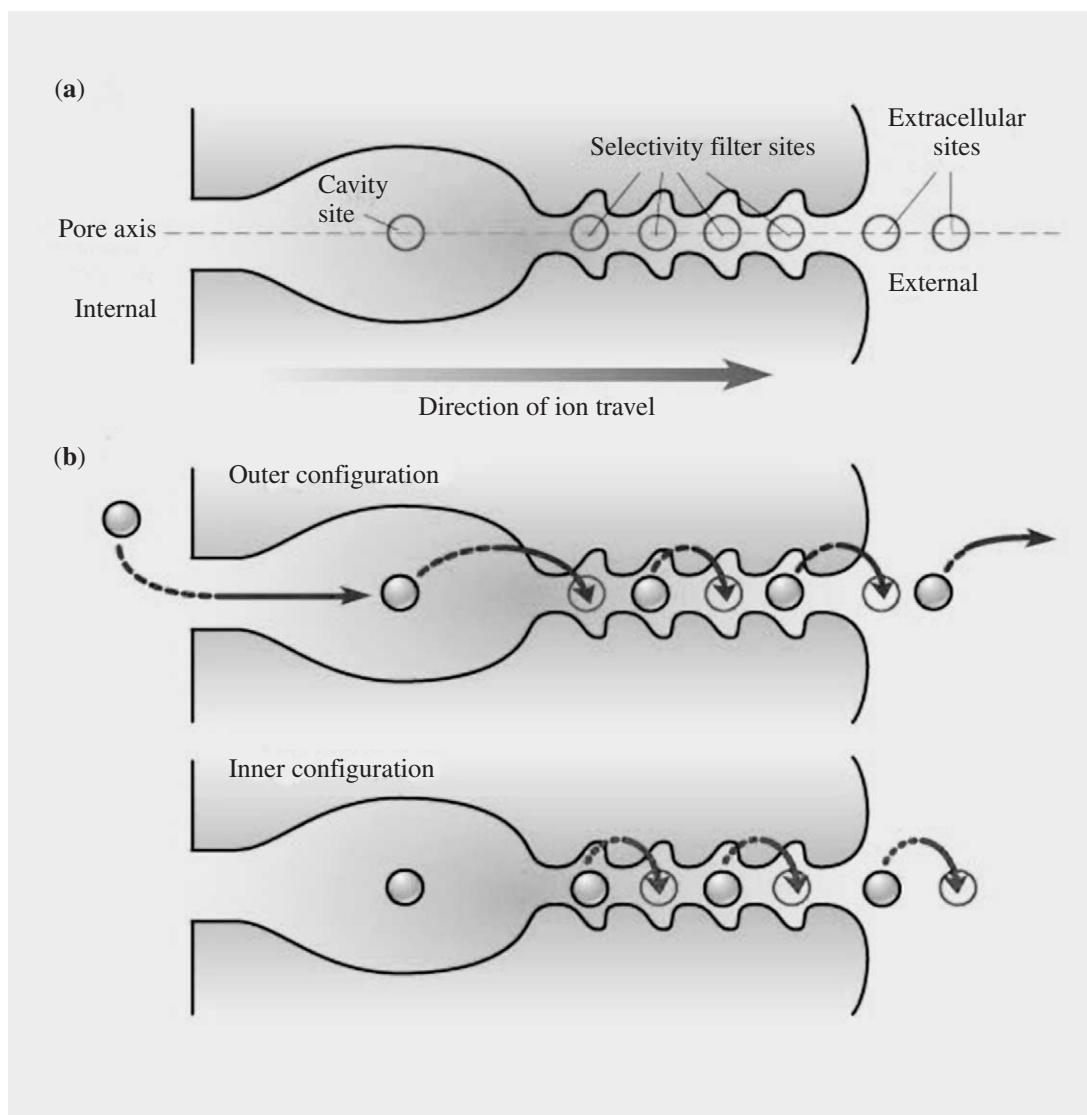
Figure 12 Illustration of the mode of action of the selectivity filter in potassium channel structures. (a) Illustration of the seven crystallographically located potassium ions. (b) Movement of the ions by a hopping mechanism (reproduced with permission from Miller[79]).

(a)
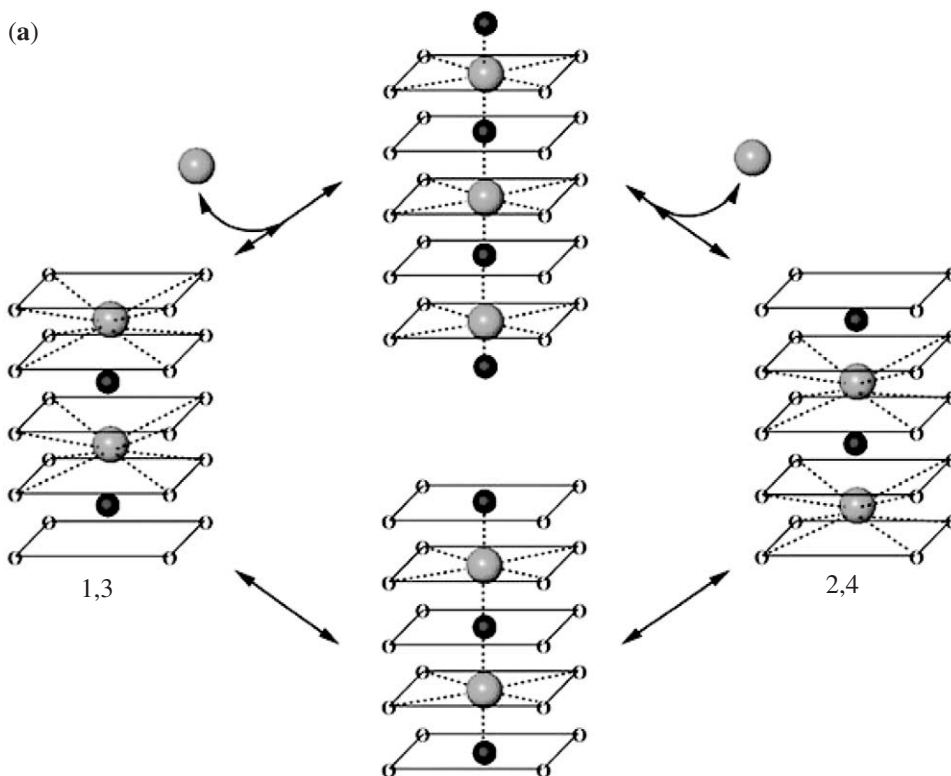
Figure 13 Potassium ion migration showing the retention of six- and eight-coordination through backbone carbonyls or inter-cation waters (reproduced with permission from Roux[69] and Morais-Cabral[72]).

Divalent barium is similar in size to K^+ and can fit in the selectivity filter, but is bound too tightly, thereby inhibiting the flow of K^+.[71] The appearance of two additional ion sites lying outside of the filter on the extracellular side (the latter of which is entirely solvated) (Figures 12 and 14) speaks to the strong electrostatic influence of the pore.

At either end of the selectivity pore, a partially solvated K^+ is seen to be coordinated by four carbonyl groups, while the other half of the ion is bound by four waters.[80] This represents either the dehydration step as the ion enters the filter, or the solvation step as it emerges into the extracellular or cavity environments, depending on the direction of flow. This directionality suggests that gating must occur and the structural mechanisms for this, which ultimately depend on local potassium concentrations and binding affinities, have begun to be addressed.[73,74] Ultimately, the structure, and therefore coordination motif, is dependent on potassium ion concentration.[80]

8.5.7   FUTURE PERSPECTIVES

Much has been achieved in the arena of structural characterization of alkali and alkaline earth chemistry with biological ligands. While much more needs to be defined, especially in the area of ion channels, increasingly the focus will tend toward studies of real-time function and dynamics, and exploring the influence of ligand conformational flexibility on function. Of particular significance are understanding the roles of ion cofactors in stabilizing specific protein conformations and regulating dynamic stability; the synergy between metals and their protein environment in promoting catalysis by enzymes; the roles of metal cofactors in promoting structure (local and global), catalysis, stability and bending, and protein and drug interactions of nucleic acids; ion uptake and release and transmembrane migration by ionophores; and the chemistry of ion channels, including gating, selectivity, and signaling. To address these questions a variety of physicochemical and spectroscopic tools must be brought to bear, with NMR, conductivity, and fluorescence methods likely to play central roles.[12,62,81,82] Elaboration of these important problems is well underway and rapid progress is to be expected. The foundations have been solidly planted.

(a)

(b)
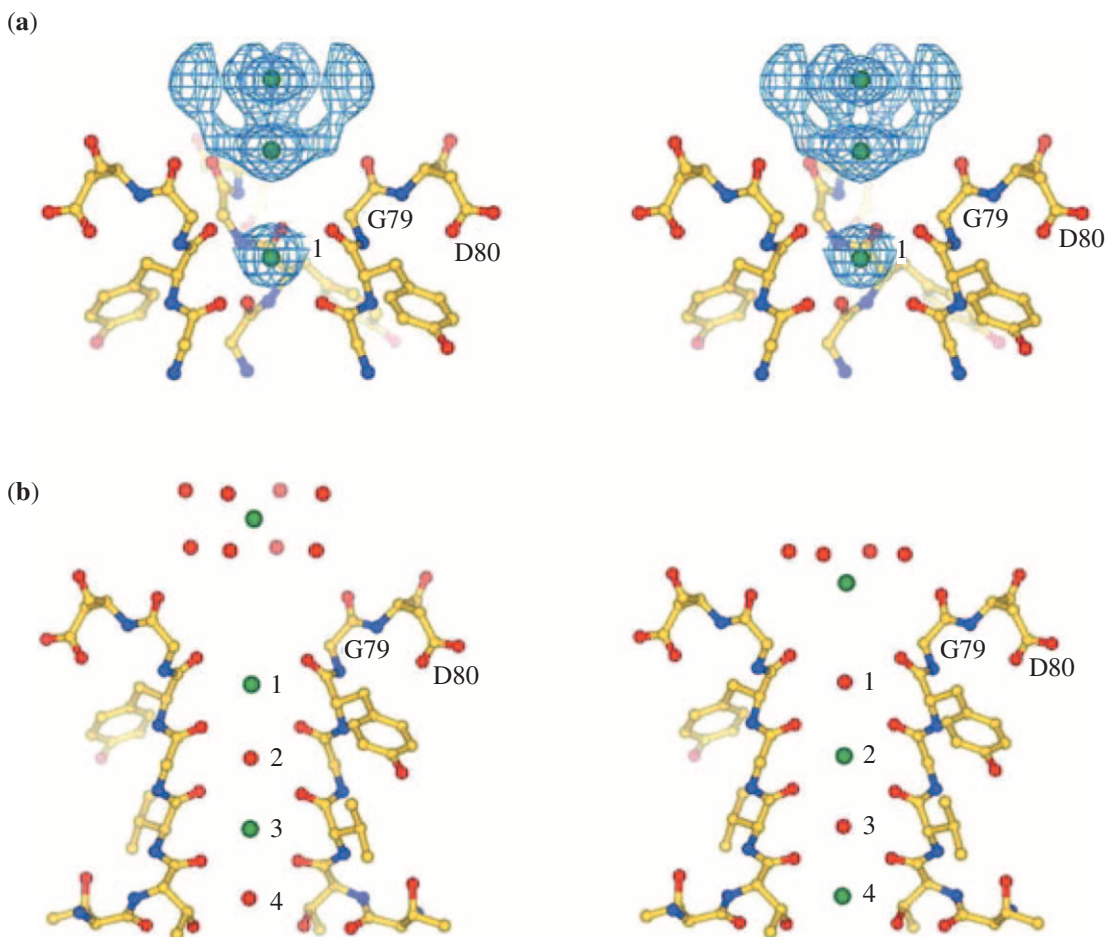
Figure 14 External potassium coordination sites (upper) showing the four principal ligand contacts (Gly backbone carbonyls) to a surface-bound K^+ ion and the fully solvated external ion that are held in the vicinity of the pore by electrostatics. Stereoviews (lower) showing the positions of potassium ions (green) and potassium-bound waters (red) in the central cavity, selectivity filter, and two extracellular ions (reproduced with permission from Zhou *et al.*[77]).

8.5.8 REFERENCES

1. Fenton, D. E. In *Comprehensive Coordination Chemistry*; Wilkinson, G., Gillard, R. D., McCleverty, J. A., Ed.; Pergamon: Oxford, U.K., 1987, Vol. 3, Chap. 23.
2. Atwood, J. L.; Lehn, J.-M., Eds. *Comprehensive Supramolecular Chemistry*. Pergamon: Oxford, U.K., 1996.
3. Cowan, J. A. *The Biological Chemistry of Magnesium*. Wiley-VCH: NY, 1995.
4. Cowan, J. A. *Inorganic Biochemistry*, 2nd ed. Wiley-VCH: NY, 1996.
5. Maguire, M. E.; Cowan, J. A. *Biometals* **2002**, *15*, 203–210.
6. Demadis, K. D.; Sallis, J. D.; Raptis, R. G.; Baran, P. *J. Am. Chem. Soc.* **2001**, *123*, 10129–10130.
7. Cowan, J. A. *Chem. Rev.* **1998**, *98*, 1067–1087.
8. Cowan, J. A. *Biometals* **2002**, *15*, 225–235.
9. Cowan, J. A. *Inorg. Chem.* **1991**, *30*, 2740–2747.
10. Cowan, J. A. *J. Inorg. Biochem.* **1993**, *49*, 171–175.
11. Einspahr, H.; Bugg, C. E. *Met. Ions. Biol. Syst.* **1984**, *17*, 51–97.
12. Malmendal, A. J. E.; Thulin, E.; Gippert, G. P.; Drakenberg, T.; Forsén, S. *J. Biol. Chem.* **1998**, *273*, 28994–29001.
13. Brown, E. M.; MacLeod, R. *J. Physiol. Rev.* **2001**, *81*, 239–297.
14. Falke, J. J.; Drake, S. K.; Hazard, A. L.; Peersen, O. B. *Q. Rev. Biophys.* **1994**, *27*, 219–290.
15. Kretsinger, R. H. *Annu. Rev. Biochem.* **1976**, *45*, 239–266.
16. Springer, T. A.; Jing, H.; Takagi, J. *Cell* **2000**, *102*, 115–119.
17. Reid, R. E.; Procyshyn, R. M. *Arch. Biochem. Biophys.* **1995**, *323*, 275–277.
18. Drake, S. K.; Zimmer, M. A.; Miller, C. L.; Falke, J. J. *Biochemistry* **1997**, *36*, 9917–9926.
19. Drake, S. K.; Lee, K. L.; Falke, J. J. *Biochemistry* **1996**, *35*, 6697–6705.
20. Drake, S. K.; Falke, J. J. *Biochemistry* **1996**, *35*, 1753–1760.
21. Drake, S. K.; Zimmer, M. A.; Kundrot, C.; Falke, J. J. *J. Gen. Phys.* **1997**, *110*, 173–184.

22. Libson, A. M.; Gittis, A. G.; Lattman, E. E. *Biochemistry* **1994**, *33*, 8007–8016.
23. Katz, A. K.; Glusker, J. P.; Markham, G. D.; Bock, C. W. *J. Phys. Chem.* **1998**, *102*, 6342–6350.
24. Glusker, J. P.; Katz, A. K.; Bock, C. W. *Struct. Chem.* **2001**, 12.
25. Carrell, C. J.; Carrell, H. L.; Erlebacher, J.; Glusker, J. P. *J. Am. Chem. Soc.* **1988**, *110*, 8651–8656.
26. Dudev, T.; Cowan, J. A.; Lim, C. *J. Am. Chem. Soc.* **1999**, *121*, 7665–7673.
27. Wilcox, D. E. *Chem. Rev.* **1996**, *96*, 2435–2458.
28. Horton, J. R.; Cheng, X. *J. Mol. Biol.* **2000**, *300*, 1049–1056.
29. Cowan, J. A.; Ohyama, T.; Howard, K.; Rausch, J. W.; Cowan, S. M. L.; Le Grice, S. F. J. *J. Biol. Inorg. Chem.* **2000**, *5*, 67–74.
30. Black, C. B.; Cowan, J. A. *J. Biol. Inorg. Chem.* **1998**, *3*, 292–299.
31. Yun, J. W.; Tanase, T.; Pence, L. E.; Lippard, S. J. *J. Am. Chem. Soc.* **1995**, *117*, 4407–4408.
32. Black, C. B.; Cowan, J. A. *J. Am. Chem. Soc.* **1994**, *116*, 1174–1178.
33. Black, B.; Huang, H.-W.; Cowan, J. A. *Coord. Chem. Rev.* **1994**, *135/136*, 165–202.
34. Cowan, J. A. *Inorg. Chim. Acta* **1998**, *275-276*, 24–27.
35. Huang, H. W.; Cowan, J. A. *Eur. J. Biochem.* **1994**, *219*, 253–260.
36. Casareno, R. L. B.; Cowan, J. A. *Chem. Commun.* **1996**, 1813–1814.
37. Needham, J. V.; Chen, T. Y.; Falke, J. J. *Biochemistry* **1993**, *32*, 3363–3367.
38. Black, C. B.; Foster, M.; Cowan, J. A. *J. Am. Chem. Soc.* **1996**, *1*, 500–506.
39. Sreedhara, A.; Cowan, J. A. *Biometals* **2002**, *15*, 211–223.
40. Burkhardt, C.; Zacharias, M. *Nucl. Acids Res.* **2001**, 29.
41. Hud, N. V.; Polak, M. *Curr. Opin. Struct. Biol.* **2001**, *11*, 293–301.
42. Pyle, A. M. *J. Biol. Inorg. Chem.* **2002**, *7*, 679–690.
43. Cowan, J. A.; Huang, H. W.; Hsu, L. Y. *J. Inorg. Biochem.* **1993**, *52*, 121–129.
44. Berger, I.; Tereshki, V. e.a. *Nucl. Acids. Res.* **1998**, *26*, 2473–2480.
45. Minasov, G.; Tereshko, V.; Egli, M. *J. Mol. Biol.* **1999**, *291*, 83–99.
46. Chiu, T. K.; Dickerson, R. E. *J. Mol. Biol.* **2000**, *301*, 915–945.
47. Tereshko, V.; Wilds, C. J.; Minasov, G.; Prakash, T. P.; Maier, M. A.; Howard, A.; Wawrzak, Z.; Manoharan, M.; Egli, M. *Nucl. Acids Res.* **2001**, *29*, 1208–1215.
48. Sundquist, W. I.; Klug, A. *Nature* **1989**, *342*, 825–829.
49. Phillips, K.; Dauter, Z.; Murchie, A. I. H.; Lilley, D. M. J.; Luisi, B. *J. Mol. Biol.* **1997**, *273*, 171–182.
50. Shiman, R.; Draper, D. *J. Mol. Biol.* **2000**, *302*, 79–91.
51. Tinoco, I.; Kieft, J. *Nat. Struct. Biol.* **1997**, *4*, 509.
52. Rudisser, S.; Tinoco, I. *J. Mol. Biol.* **2000**, *295*, 1211–1223.
53. Cate, J. H.; Doudna, J. A. *Structure* **1996**, *4*, 1221–1229.
54. Correll, C. C.; Freeborn, B.; Moore, P. B.; Steitz, T. A. *Cell* **1997**, *91*, 705–712.
55. Burgess, J. *Ions in Solution: Basic Principles of Chemical Interactions*. Halsted Press: New York, 1988.
56. Huang, H. W.; Li, D.; Cowan, J. A. *Biochimie* **1995**, *77*, 729–738.
57. Reynolds, M. B.; DeLuca, M. R.; Kerwin, S. M. *Bioorg. Chem.* **1999**, *27*, 326–337.
58. Paulus, E. F.; Kurz, M.; Matter, H.; Vertesy, L. *J. Am. Chem. Soc.* **1998**, *120*, 8209–8221.
59. Lecomte, S.; Moreau, N. J.; Chenon, M.-T. *Int. J. Pharm.* **1998**, *164*, 57–65.
60. Fan, J. Y.; Sun, D.; Yu, H.; Kerwin, S. M.; Hurley, L. H. *J. Med. Chem.* **1995**, *38*, 408–424.
61. Riddell, F. G. *Chirality* **2002**, *14*, 121–125.
62. Jin, T. *J. Chem. Soc. Perkin Trans. 2* **2002**, 151–154.
63. Riddell, F. G.; Arumagam, S.; Brophy, P. J.; Cox, B. G.; Payne, M. C. *J. Am. Chem. Soc.* **1988**, *110*, 734–738.
64. Riddell, F. G.; Arumagam, S.; Cox, B. G. *Biochim. Biophys. Acta* **1988**, *944*, 279.
65. Riddell, F. G.; Arumagam, S. *Biochim. Biophys. Acta* **1988**, *945*, 65.
66. Martinek, T.; Riddell, F. G.; Wilson, C. F.; Weller, C. T. *J. Chem. Soc. Perkin Trans. 2* **2000**, 35–41.
67. Martinek, T.; Riddell, F. G.; Wilson, C. F. *J. Chem. Soc. Perkin Trans. 2* **2000**, 2192–2198.
68. Mronga, S.; Muller, G.; Fischer, J.; Riddell, F. G. *J. Am. Chem. Soc.* **1993**, *115*, 8414–8420.
69. Roux, B.; MacKinnon, R. *Science* **1999**, *285*, 100–102.
70. Gulbis, J. M.; Zhou, M.; Mann, S.; MacKinnon, R. *Science* **2000**, *289*, 123–127.
71. Jiang, Y.; MacKinnon, R. *J. Gen. Physiol.* **2000**, *115*, 269–272.
72. Morais-Cabral, J. H.; Zhou, Y.; MacKinnon, R. *Nature* **2001**, *414*, 37–42.
73. Jiang, Y.; Lee, A.; Chen, J.; Cadene, M.; Chalt, B. T.; MacKinnon, R. *Nature* **2002**, *417*, 515–522.
74. Jiang, Y.; Lee, A.; Chen, J.; Cadene, M.; Chalt, B. T.; MacKinnon, R. *Nature* **2002**, *417*, 523–526.
75. Valiyaveetil, F. I.; MacKinnon, R.; Muir, T. W. *J. Am. Chem. Soc.* **2002**, *124*, 9113–9120.
76. Moczydlowski, E. *Chem. & Biol.* **1998**, *5*, R291–R301.
77. Zhou, Y.; Morais-Cabral, J. H.; Kaufman, A.; MacKinnon, R. *Nature* **2001**, *414*, 43–48.
78. Sansom, M. S. P.; Shrivastava, I. H. *Curr. Biol.* **2002**, *12*, R65–R67.
79. Miller, C. *Nature* **2001**, *414*, 23–24.
80. Zhou, Y.; Morais-Cabral, J. H. *Nature* **2001**, *414*, 43–48.
81. Drakenberg, T. *Biol. Chem. Magnesium* **1995**, 25–51.
82. Malmendal, A.; Linse, S.; Evenäs, J.; Forsén, S.; Torbjörn, D. *Biochemistry* **1999**, *38*, 11844–11850.
83. Diebler, H.; Eigen, M.; Ilgenfritz, G.; Maass, G.; Winkler, R. *Pure Appl. Chem.* **1969**, *20*, 93–115.
84. Eigen, M. *Pure Appl. Chem.* **1963**, *6*, 97–115.

8.6
Siderophores and Transferrins

E. A. DERTZ and K. N. RAYMOND

University of California, Berkeley, CA, USA

8.6.1 INTRODUCTION

The acquisition and transport of iron is a challenge common to essentially all organisms. Many organisms select iron over other transition metals to perform functions such as dioxygen transport and electron-transfer reactions, due to its abundance in the earth's crust and its tunable redox potential. However, the use of iron presents hazards. Its low solubility in an aqueous aerobic environment renders it difficult to obtain, and the biologically accessible reduction potential of the Fe^{3+}/Fe^{2+} couple promotes the generation of free radicals via Fenton chemistry.[1] The iron balance is delicate; several human diseases result from too much (β-thalassaemia,[2] hemochromatosis,[3] sickle cell[4]) or too little (anaemia[5]). To resist hydrolysis and prevent radical formation, iron needs to be appropriately bound and stored until needed. Accessible iron can also allow invading microbial pathogens to thrive. Many deadly pathogens (e.g., *M. tuberculosis*[6] and *V. cholera*[7]), responsible for the deaths of millions worldwide, require iron for full virulence. Even outside the host environment, iron is often the limiting nutrient. Open-ocean experiments have shown enormous phytoplankton blooms when the area was supplemented with iron.[8–11] Understanding the mechanisms by which organisms acquire and transport iron is of paramount importance to combating disease and understanding environmental cycles.

In order to stave off infectious microbial growth within the host organism, preventative measures must also be used to stop pathogenic organisms from scavenging iron from the host organism. Vertebrates, and some invertebrates, utilize ferric-ion-binding proteins called transferrins, in part to meet this challenge. While at any one time the amount of iron bound to human transferrin is less than 0.1% ($\sim$3 mg) of the total iron present, the high turnover of the transferrin-bound iron results in 30 mg being transported daily.[12] Present in bodily secretions such as saliva, milk, and tears, lactoferrin provides a potent bacteriostatic agent by binding any excess iron, thus preventing uptake by invading pathogens. Ovotransferrin offers a similar protection within the egg whites of birds. In addition, proteolitic peptides of these proteins appear to provide an even more proactive antimicrobial action, by disrupting the bacterial cell membrane.[13–17]

The solubility of ferric hydroxide limits the concentration of the ferric ion to 10^{-18} M in an aerobic environment at physiological pH. A bacterial cell of 10^{-9} cm^3 requires 10^5 to 10^6 ferric ions per generation to maintain the required 10^{-6} M internal concentration.[18] This is approximately ten orders of magnitude greater than the concentration available, forcing bacteria to engineer more aggressive iron-acquisition processes, including the production and secretion of powerful iron chelators, called siderophores. Microorganisms later reincorporate the ferric siderophore complexes via specific membrane-receptor proteins, through an energy-dependent process.[19] Typically, membrane receptors specific for the iron coordination center of a given siderophore type facilitate this energy-dependent process by binding the complex with an extraordinarily high affinity.[20,21] The recent availability of crystal structures of proteins involved in the recognition and transport events has greatly enhanced knowledge of siderophore-mediated iron transport. In addition to producing siderophores, bacteria express transferrin receptors on their cell surface, allowing theft of host iron bound by transferrins. Another *in vivo* iron source is heme,[22] but this is beyond the scope of this review. While siderophore- and transferrin-mediated iron transport have been studied in many Gram-negative bacteria, the mechanisms are largely unstudied in Gram-positive bacteria.

In this chapter we will describe the fundamental coordination chemistry, solution thermodynamic properties, and transport properties of these primary iron-transport agents: the siderophores and transferrins.

8.6.2 SIDEROPHORE TYPES

As noted, microorganisms produce low-molecular-weight iron chelators called siderophores, in order to overcome the immense difference between environmentally available and nutritionally required iron.[19,21,23–25] Even organisms unable to produce siderophores themselves can still utilize them, suggesting that the recognition process is common throughout the microbial world. Although many different siderophore structures have been characterized, the iron-binding moieties generally contain catecholate, hydroxamate, or α-hydroxycarboxylate groups. Structure variation helps prevent loss of the siderophore complex to competing organisms, since features not required for iron binding are often relevant for receptor recognition. Regardless of the chelating motif employed, the high iron-formation constants of siderophores enable them to solubilize iron from mineral or complexed sources, or to steal it from host proteins such as transferrin or lactoferrin.
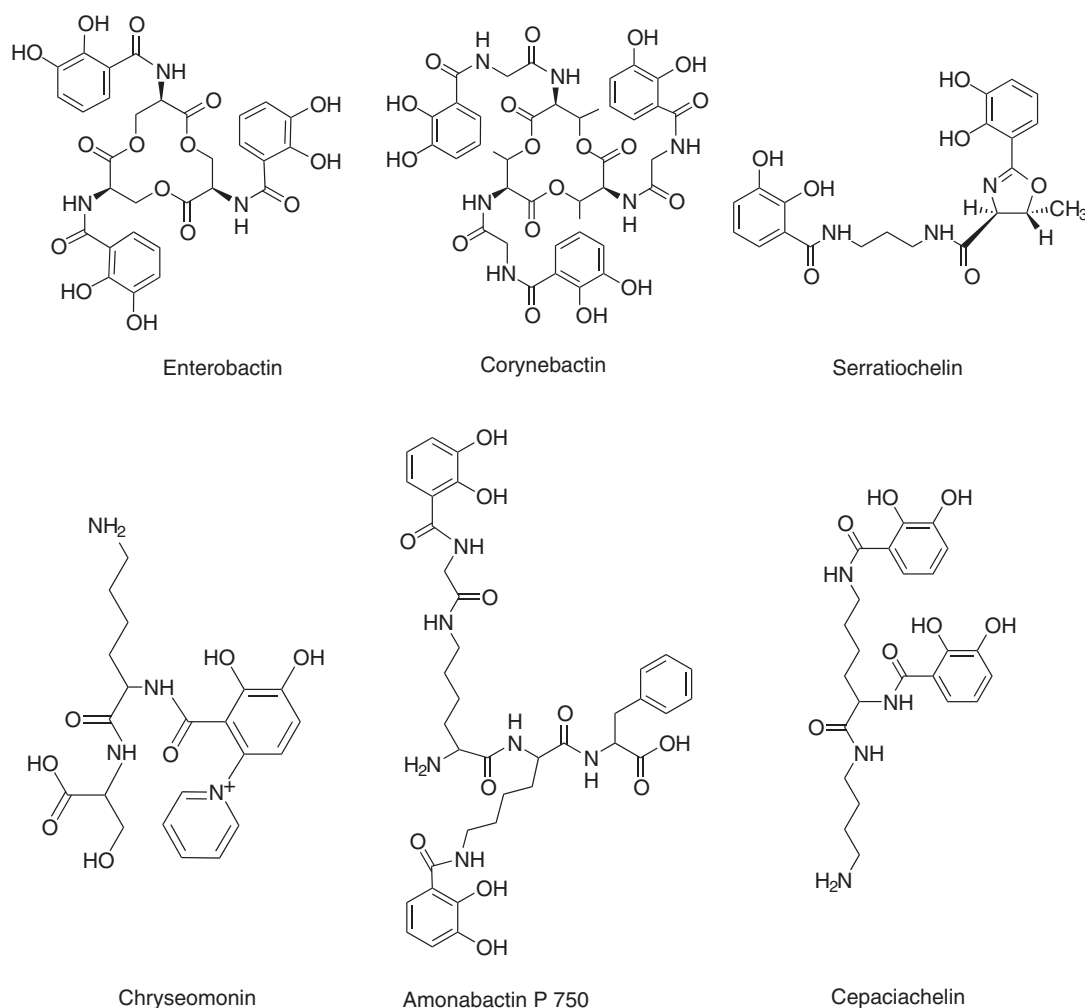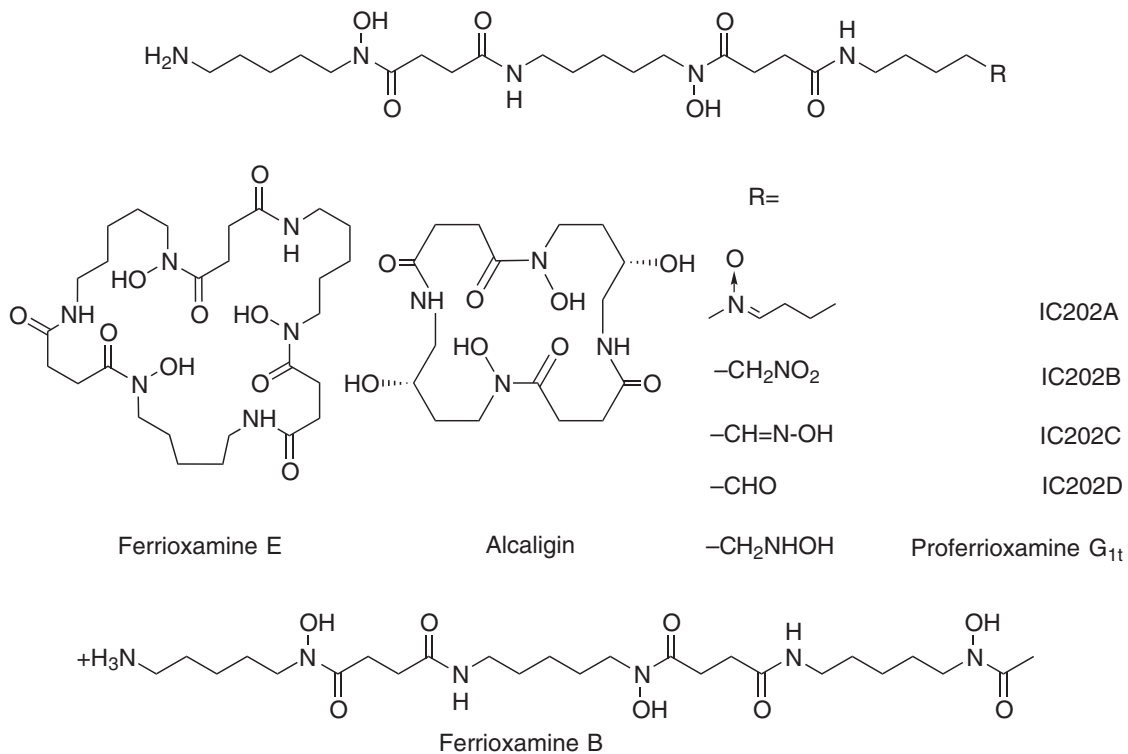
8.6.2.1 Catecholates

Catecholate siderophores (Figure 1) often provide the organism with a highly stable, negatively charged ferric complex. Complexation of the ferric ion requires deprotonation of the two phenolic hydrogens. However, the catecholate-binding domain is usually attached to the backbone via an amide linkage, yielding pK_a values (from 6 to 8.5 for the first dissociation, and approximately 11.5 for the second) slightly lower than expected for a free catechol (9 and 13, respectively). First isolated in 1971,[26,27] hexadentate enterobactin is primarily produced by Gram-negative bacteria. However, isolation of enterobactin from two Gram-positive *Streptomyces* species[28] suggests production of this powerful siderophore may be more universal than previously thought. The serine–trilactone backbone was thought unique to enterobactin. However, corynebactin, isolated from *Corynebacterium glutamicum*[29] and *Bacillus subtilis*,[30] also incorporates a trilactone back-bone; this backbone is based upon threonine rather than serine, and glycine spacers elongate the three chelating arms as compared to enterobactin. Other recently characterized catecholate sidero-phores include amonabactin[31,32] from the freshwater bacterium *Aeromonas hydrophila*, chryseo-monin[33] from *Chryseomonas luteola*, serratiochelin[34] from *Serratia marcescens*, and cepaciachelin[35] from *Burkholderia (Pseudomonas) cepacia*.

8.6.2.2 Hydroxamates

A wide variety of bacteria and fungi utilize hydroxamates (Figure 2) to sequester iron from their environment.[19,24,36] Formation of the ferric complex from these chelating groups requires the

Enterobactin Corynebactin Serratiochelin

Chryseomonin Amonabactin P 750 Cepaciachelin

Figure 1 Representative catecholate siderophores.

Figure 2 Representative hydroxamate siderophores.

deprotonation of the hydroxyl moiety, which has pK_a values from 8 to 9. Unlike tris-catecholates, tris-hydroxamates often form neutral ferric complexes. Recently, investigations of new siderophores (IC202 A-D and proferrioxamine G_{1t}) isolated from *Streptoalloteichus* sp. 1454-19 revealed that several of these siderophores possess immunosuppressive activity.[37–39] Also medically relevant, ferrioxamine B from *Streptomyces pilosus* is employed as a therapeutic iron chelator for β-thalassemia.[2] Although ferrioxamine B is the most studied member of the ferrioxamine family, the crystal structure of the ferric complex was solved only recently and it was suggested that the pendant amine arm may play a role in receptor recognition.[40] The crystal structure of another member of the ferrioxamine family, ferrioxamine E, has also been determined, but chelating plutonium (IV)[41] rather than iron.[42] The crystal structure of the dihydroxamate siderophore alcaligin, isolated from *Rhodotorula pilimanae*, revealed an interesting and unique monobridged (rather than triple helicate) structure.[43]

8.6.2.3 Carboxylates

Carboxylic acids represent another common iron-chelating motif (Figure 3). While the lower pK_a values (from 3.5 to 5) render these siderophores less efficient chelators at physiological pH, carboxylate siderophores remain effective iron chelators at much lower pH ranges than either catecholates or hydroxamates. Organisms thriving in mildly acidic environments tend to employ carboxylate-containing siderophores for this reason. S,S-rhizoferrin, the enantiomer of a common fungal siderophore, R,R-rhizoferrin, has been characterized from the bacterium *Ralstonia (Pseudomonas) picketti* DSM 6297.[44] Although recognition and uptake of the bacterial rhizoferrin was limited in fungi, the bacterial producer did not discriminate between the two enantiomers, incorporating each at similar rates. Enhanced uptake of the R,R-rhizoferrin in fungi suggests specific enantiomeric recognition by the iron-transport system. However, it is not clear whether bacteria, which do not differentiate between the enantiomers, possess two receptors capable of recognizing each enantiomer, or a completely different nonstereospecific uptake system. Several other α-hydroxycarboxylate siderophores that have been characterized include achromobactin[45] from *Erwinia chrysanthemi*, corrugatin[46] from *Pseudomonas corrugata*, and staphyloferrin B[47] from *Ralstonia eutropha*.
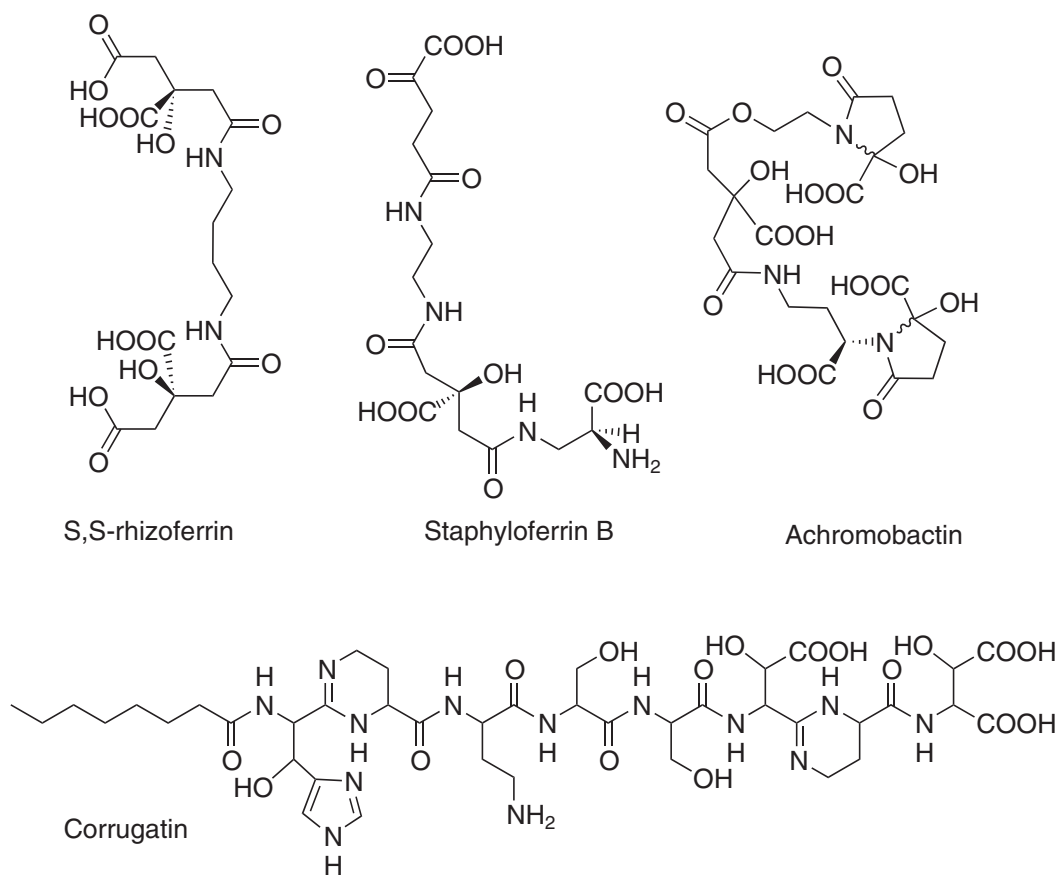
Figure 3 Representative α-hydroxycarboxylate siderophores.

8.6.2.4 Marine

Although siderophores secreted by terrestrial microorganisms comprise the vast majority of studies, recent experiments indicating that low ocean iron concentrations limit the growth of marine microorganisms have increased interest in marine siderophores (Figure 4).[8,9,11] With the bulk of marine iron present as suspended particles of varying sizes, the "dissolved" iron represents a small fraction of uncertain concentration (0.2 nM to 1 nM).[48,49] Marine organisms must overcome both low iron concentration and high dilution of the secreted siderophore in marine environments.[50] More than 99% of the dissolved iron is strongly complexed by uncharacterized organic ligands.[51] While these organic ligands help solubilize the ferric ion, they may also impede microorganisms from utilizing the iron, exacerbating the problem. Isolation and characterization of these iron-binding ligands, present in extremely low concentrations in the aquatic environment, presents a formidable task. The conditional stability constants for these ligands indicate that two major ligand types (L1 and L2) exist. While the concentration of the weaker-chelating L2 class increases with depth, the stronger-chelating L1 class is found only in the marine surface layer.[52] Improved extraction techniques led to the discovery of more than 50 different siderophore-like compounds from the coastal waters of Northern California. Preliminary screening indicates that these ligands possess hydroxamate and/or catecholate functionalities, and are within the expected molecular weight range (300–1,000 Da) of characterized siderophores.[51] Although these iron chelators have stability constants within the range of known siderophores, the use of specific membrane receptors by marine organisms has yet to be established. Further characterization and isolation of these ligands from discrete organisms will help to elucidate their role in the marine iron cycle.

Siderophores isolated from marine microorganisms contain iron-binding moieties similar to their terrestrial counterparts: catecholates, hydroxamates, and α-hydroxycarboxylates. Isolated hydroxamates include Ferrioxamine G[53] from *Vibrio* strain BLI-4, the aquachelins[54] from *Halomonas aquamaria*, and the marinobactins[54] from *Marinobacter* species DS40M6 and DS40M8. Petrobactin[55] from *Marinobacter hydrocarbonoclasticus* includes both catecholate and citrate
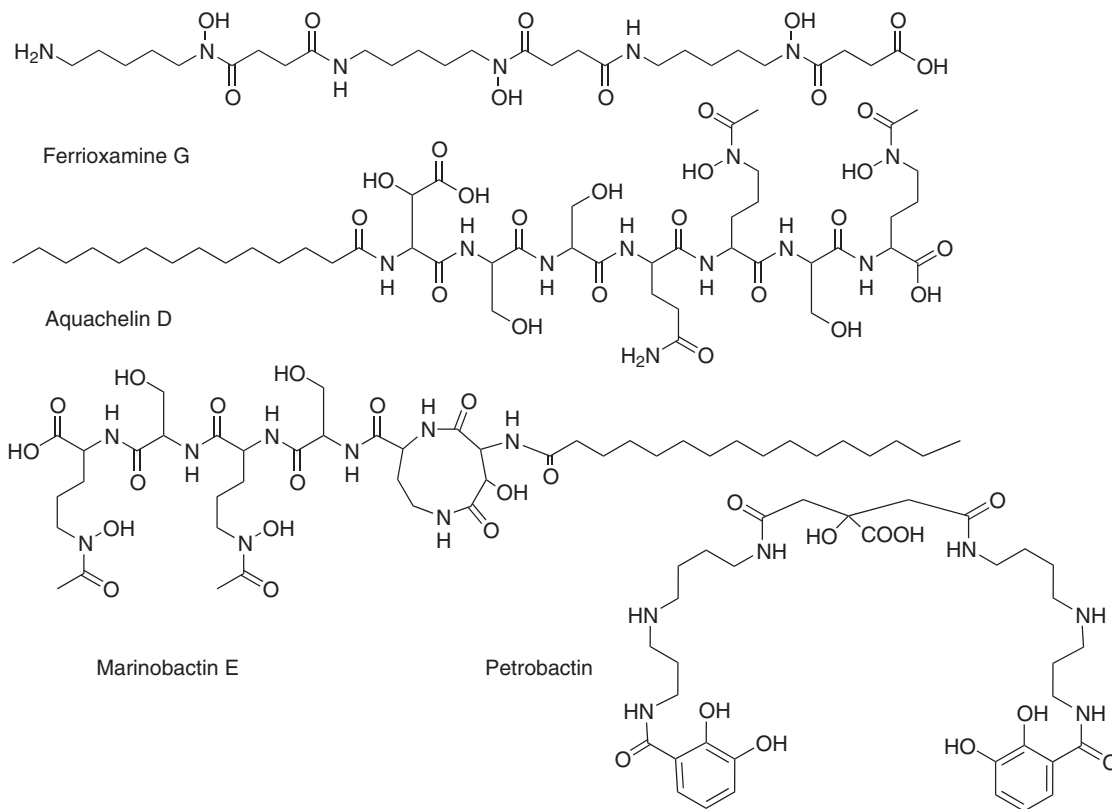
Figure 4 Representative marine siderophores.

iron-binding moieties. Current research suggests that phytoplankton, heterotrophic bacteria, and cyanobacteria play vital roles in the biogeochemical cycling of iron in the ocean, and future research will be needed to characterize their iron chelators.

8.6.2.5 Mixed Ligands

Many organisms produce siderophores that utilize more than one type of iron-binding moiety (Figure 5). Several species of *Pseudomonas* produce siderophores called pyoverdines (or pseudo-bactins) with subtle structural modifications that inhibit recognition by other bacteria. The structure of pyoverdine siderophores can be divided into three sections: the dihydroxyquinoline chromophore, the peptide chain, and the dicarboxylic acid or its monoamide. While the chromophore is fairly well conserved between species, the peptide linker varies and is important for the ferric complex recognition by the cell, in addition to providing four of the six hydrox-amate iron-binding sites. Half of the amino acids are in the D-configuration to prevent degradation by proteolytic enzymes; polar amino acids are also incorporated to enhance water solubility. About 50 pyoverdine structures have been reported, several since 1997.[56–62] Similar in structure to the pyoverdines, but with a different chromophore, azotobactin 87 was isolated from *Azotobacter vinelandii*.[63] *Rhodococcus erythropolis*, a Gram-positive bacterium considered for biodesulfurization of fuel oils on an industrial scale, produces a class of sider-ophores termed heterobactins, which incorporate both hydroxamate and catecholate-binding groups.[64] Gram-positive *Mycobacterium tuberculosis* produces two classes of siderophores: mycobactins, high-affinity iron-binding molecules within the cell wall, and exochelins, hydrox-amate-based molecules secreted into the environment to chelate iron and transfer it to the membrane-bound mycobactins.[65–67] Anachelin, the siderophore of freshwater cyanobacterium *Anabaena cylindrica*, has both a catecholate and a 2-*o*-hydroxyphenyloxazoline moiety to chelate iron.[68,69]
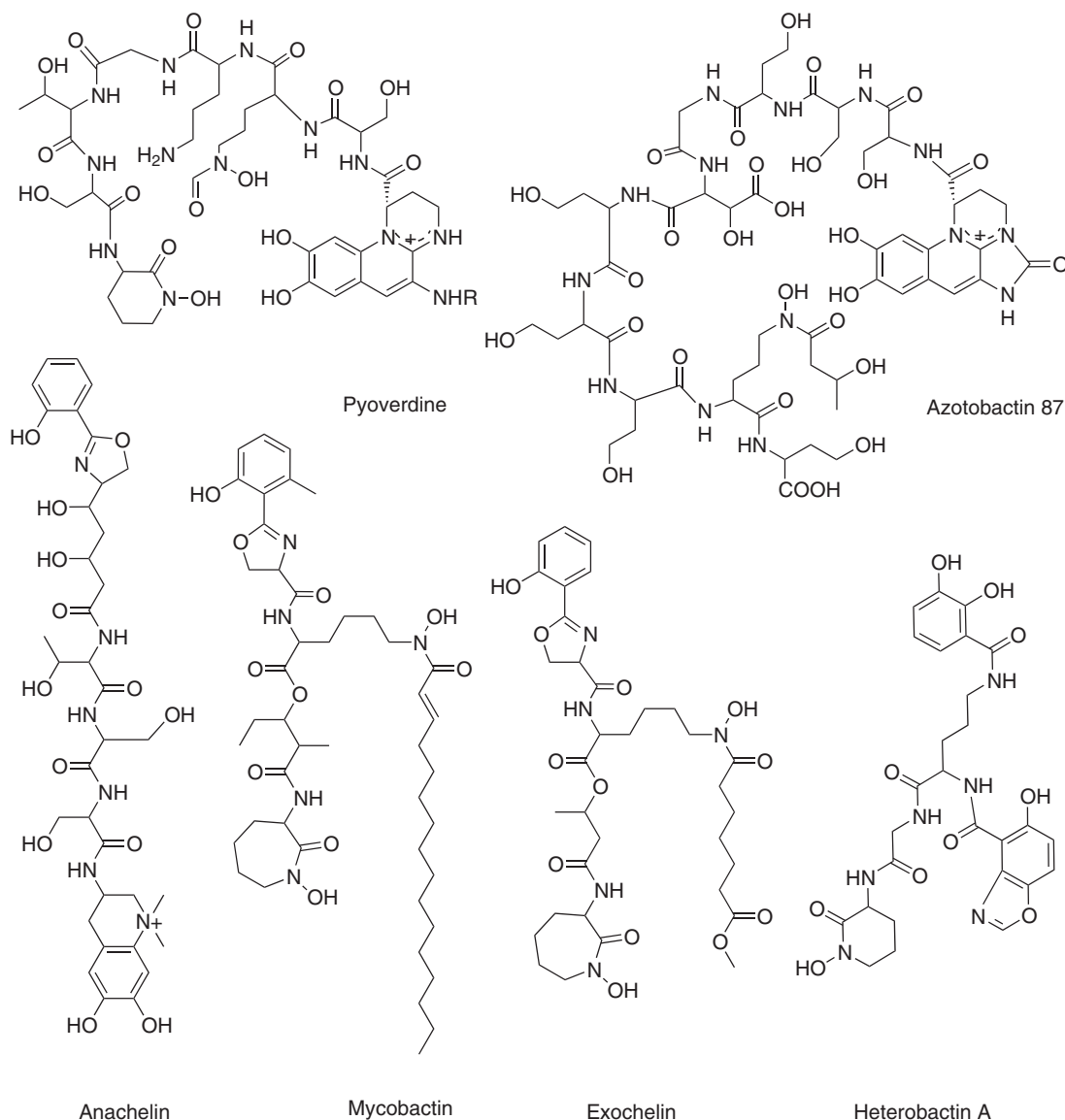
Figure 5 Representative mixed ligand siderophores.

8.6.2.6 Siderophore Analogs

The relevance of individual components of the siderophore structure is difficult to accurately determine by studying only the natural siderophore products.[19] Synthetic analogs of naturally occurring siderophores provide a way to isolate key structural features, in order to highlight the contribution of different components to the overall stability of the ferric complex. In addition, synthetic analogs can probe siderophore-receptor recognition via alteration of specific structural features or chirality. Over the last few decades, synthetic siderophore analogs have provided information regarding stability, recognition and uptake.[70–73] Space limitations allow us to highlight only a few current examples here. All analogs discussed are shown in Figure 6.

The mechanisms of iron release within an organism have been studied using various synthetic analogs. The very low reduction potential of ferric enterobactin ($-750\,\text{mV NHE}^{-1}$)[74] precludes reduction of the ferric ion as a viable mode of intracellular iron release, prompting the question of how the organism achieves this seemingly impossible feat. Several mechanisms seem plausible, including ligand hydrolysis and protonation of the ferric complex to yield a less thermodynamically stable product. Support for the ligand-hydrolysis mechanism includes the isolation of the enzyme esterase, which is able to hydrolyze the ester backbone.[75,76] However, enterobactin
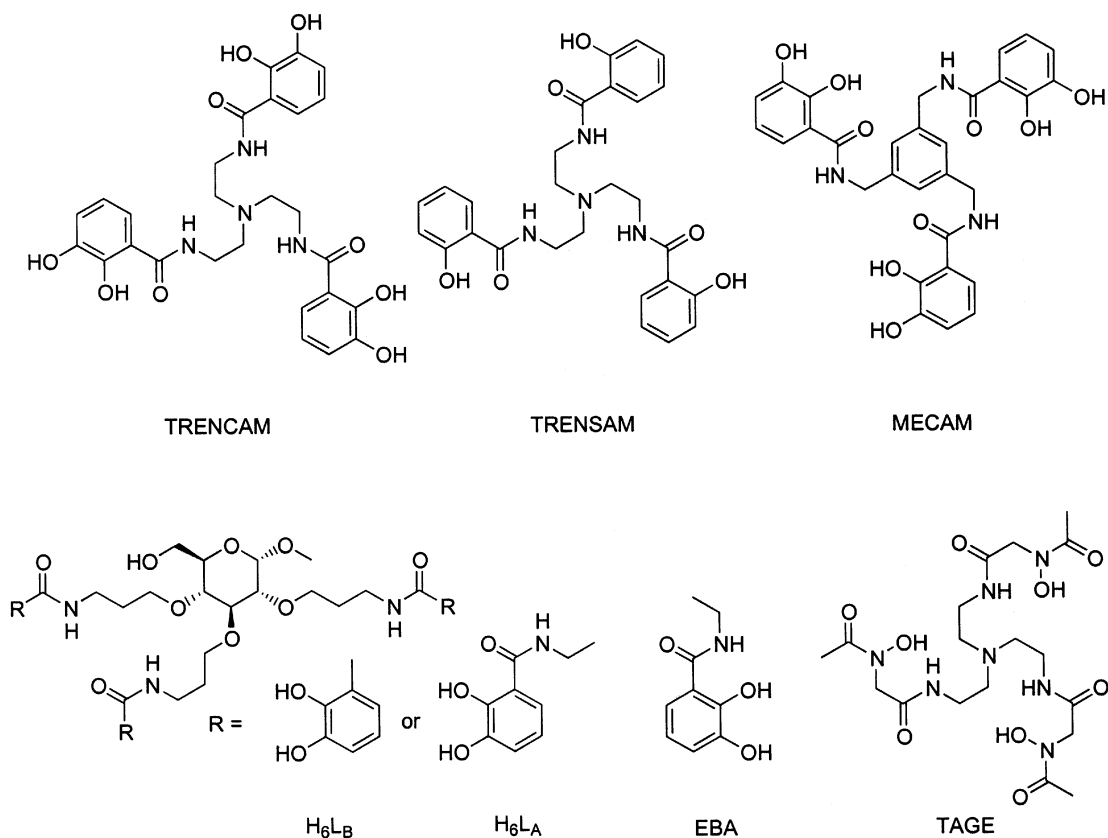
Figure 6 Representative siderophore analogs.

analogs with low reduction potentials but without a hydrolytically unstable backbone, such as MECAM, also provide iron to the organism, suggesting that another method for iron release must be available.[77]

Although protonation of the *meta* phenolic oxygen atoms would yield less stable ferric complexes ($FeLH_3$) than the triscatecholate metal (FeL^{3-}) complex, controversy regarding the biological relevance of this triprotonated metal complex persisted for years.[78] Although incorrectly reported as the coordination mode for enterobactin and the mechanism for iron release at biological pH,[79] the $FeLH_3$ species is neither the major species present at physiological pH nor the major pathway for iron release from enterobactin. However, an explanation for the ability of nonhydrolyzable analogs to deliver iron to the cell is still missing. Studies suggest that stepwise protonation of the FeL^{3-} species shifts the coordination of the iron from the *meta* phenolic oxygen of the catecholate to the carbonyl moiety of the amide, forming the $FeLH_3$ complex. A variety of experimental evidence supports this "salicylate-binding mode" as a secondary mechanism for iron release for nonhydrolyzable analogs.[77,80–82] The stability constants of two enterobactin analogs, the salicylamide, TRENSAM complex, and the catecholamide, TRENCAM, can be compared to determine the importance of the salicylate-binding mode at physiological pH. The stability constant of the TRENSAM ($\log \beta_{110} = 25.4$) is much lower than that of the TRENCAM complex ($\log \beta_{110} = 43$), and in the same range as the stability constant for the triprotonated enterobactin analog MECAM ($\log \beta_{113} = 25.3$).[82] Ferric triscatecholate complexes posses a strong LMCT band between 450 nm and 500 nm. While many catecholate siderophores remain intact (as indicated by the presence of the LMCT band) up to pH values of 9 or higher, the LMCT band for TRENSAM disappears above pH 7, due to the formation of iron hydroxide.[82] A variety of structural[83,84] and spectroscopic data[78,80,81] for ferric enterobactin and analogs show that at physiological pH, iron is coordinated via the three catecholate moieties in both enterobactin and nonhydrolyzable analogs outside the cell. The major pathway for iron release from enterobactin is hydrolysis of the backbone via the enzyme esterase, not ligand protonation. The salicylate-binding mode is relevant only for a select group of nonhydrolyzable enterobactin analogs at low pH during the *in vivo* Fe-extraction process.

The high affinity and selectivity of siderophores for ferric ion has prompted their use as prototypes for therapeutic iron chelators. For example, the current therapeutic regimen for the treatment of β-thalassemia[2] includes continuous infusion of the siderophore desferrioxamine B (Figure 2) to remove the excess iron accumulated from regular blood transfusions. Unfortunately, siderophores are far from ideal drugs, warranting the design of new agents. Enterobactin analogs designed for use as iron chelators include a series based upon a saccharide scaffold, rather than the triserine backbone (H_6L_A and H_6L_B).[71] Carbohydrates provide both increased hydrophilicity and high hydrolytic stability over the enterobactin trilactone. These analogs retain siderophore activity, as evident from bacterial growth-promotion studies,[71] and form highly stable ferric complexes ($\log \beta_{110} = 46.1$, pM = 28.3).[85]

Analogs also can highlight structural features important for the overall stability of the iron complex. Inter- and intrastrand hydrogen-bonding networks found in a tripodal hydroxamic acid analog (TAGE) of ferrichrome appear to contribute to tight iron binding and shielding of the iron from outer-sphere ligands. The amide N—H bond vectors point toward the coordinating aminohydroxyl oxygens, forming intrastrand hydrogen-bond networks with an average N···O (H···O) distance of 2.88 Å (2.14 Å). Interstrand N···O (H···O) distances average 3.2 Å (2.13 Å). The structural features provide insight into the key parameters that yield these highly stable ferric siderophore complexes.

8.6.3 SOLUTION THERMODYNAMICS

Formation of a ferric siderophore complex requires deprotonation of the phenolic hydrogen (catecholates) or hydroxyl proton (hydroxamates and carboxylates). Therefore, determination of ligand pK_a values is crucial to meaningfully interpret the stability of ferric complexes. Proton acidity varies considerably among the three major iron-chelating moieties. The high pK_a values of the catechol (9.2 and 13) make it the most basic ligand; addition of the amide moiety lowers these values substantially (7.3 and 12.1 for bidentate analog EBA, Figure 6).[86] Hydroxamate siderophores deprotonate near pH 8 to 9, while the cyclic version, hydroxypyridinonate, deprotonates near pH 5.8. Amino carboxylates are the most acidic ligands, with pK_a values from pH 3.5 to 5. Stepwise deprotonation of a hexadentate catecholate siderophore is described using Equation (1), and hydroxamate and carboxylates siderophores are described by Equation (2):

$$H_nL^{n-6} \rightleftharpoons H^+ + H_{n-1}L^{n-7} \qquad K_n = [H_{n-1}L^{n-7}][H^+]/[H_nL^{n-6}] \qquad \text{for } n = 1\text{--}6 \qquad (1)$$

$$H_nL^{n-3} \rightleftharpoons H^+ + H_{n-1}L^{n-4} \qquad K_n = [H_{n-1}L^{n-4}][H^+]/[H_nL^{n-3}] \qquad \text{for } n = 1\text{--}3 \qquad (2)$$
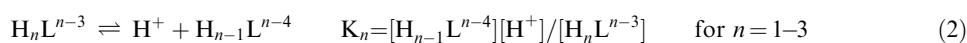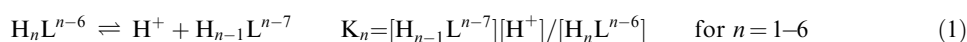
Most ligand pK_a values can be determined via a potentiometric titration, where the pH is monitored after sequential additions of either acid or base. The requirement of millimolar ligand concentration is a major drawback of this method, especially for ligands with poor water solubility. Another common method for determination of protonation constants when a potentiometric titration is not possible is a spectrophotometric titration, where both pH and spectral changes are monitored upon the addition of acid or base.

Siderophores form extremely stable ferric complexes, greatly enhancing the organism's ability to meet its iron requirement. Six coordinating atoms are required to fully complex iron in its preferred octahedral geometry. The denticity of the siderophores can vary, depending upon the number of chelating sites. Amonabactin has four sites for iron chelation, and forms neutral Fe_2L_3 complexes, while enterobactin, a hexadentate catecholate siderophore, forms an FeL^{3-} complex. At lower ligand concentrations, hexadentate siderophores form more stable complexes than analogous siderophores of lower denticity.

With its high charge-to-radius ratio, the ferric ion is quite acidic. Formation of insoluble iron hydroxides is favored in pH ranges over 2, leaving free Fe^{3+} concentrations as low as 10^{-18} M at pH 7.4. However, iron is often solubilized through chelation by organic ligands or proteins. Siderophores must be thermodynamically able to remove the complexed iron from environmental sources such as transferrin, citrate, hydroxide, and minerals. Knowledge of the iron-formation constant of a ligand indicates the strength of a siderophore to act as a ferric chelator. The stability constant for a ferric tris-catecholate siderophore complex is defined as:
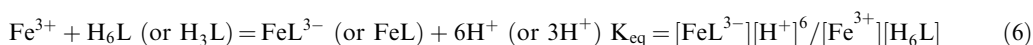
$$Fe^{3+} + L^{6-} \rightleftharpoons FeL^{3-} \quad K_f = [FeL^{3-}]/[Fe^{3+}][L^{6-}] \qquad (3)$$
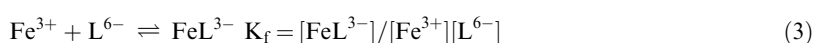
Or for the tris-hydroxamate or tris-α hydroxycarboxylate ferric siderophore as:

$$Fe^{3+} + L^{3-} \rightleftharpoons FeL \quad K_f = [FeL]/[Fe^{3+}][L^{3-}] \tag{4}$$
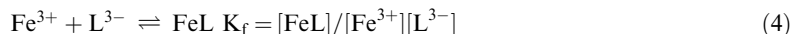
Since these ligands chelate ferric ion efficiently, direct measurement of the free Fe^{3+} after chelation is usually impossible. However, the stability of the complexes can be determined indirectly via a competition experiment with a chelator able to form strong iron complexes at lower pH ranges, such as ethylenediamine tetraacetic acid (EDTA).[87] The ferric EDTA complex is typically used for competition titrations because of its well-known stability constants and lack of absorbance in the visible region. By monitoring the LMCT at 480–500 nm of a FeL^{3-} triscatecholate complex (or 425 nm for a FeL trihydroxamate complex), where

$$FeEDTA^- + H_6L \text{ (or } H_3L) = FeL^{3-} \text{ (or FeL)} + H_2EDTA + 4H^+ \text{ (or } H^+) \tag{5}$$
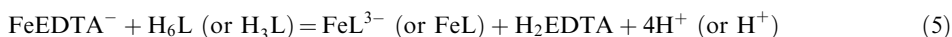
one can determine the amount of ferric siderophore complex formed. The resulting proton-dependent formation constant is:

$$Fe^{3+} + H_6L \text{ (or } H_3L) = FeL^{3-} \text{ (or FeL)} + 6H^+ \text{ (or } 3H^+) \quad K_{eq} = [FeL^{3-}][H^+]^6/[Fe^{3+}][H_6L] \tag{6}$$

Enterobactin has the highest formation constant measured (10^{49});[72] by comparison, ferrioxamine B has a formation constant of only $10^{30.6}$.[88] However, formation constants alone are not an accurate method for ranking the iron-binding ability of siderophores, because of the differences in ease of deprotonation. Because ligands having different functional groups and denticities will have different pK_a values, a better way to compare the iron-binding strength of various siderophores is to use pM values.[19] The pM value ($pM = -\log [Fe^{3+}]$), similar to pH, is employed to compare amounts of free iron remaining in solution in the presence of an iron chelator at a stated standard condition. Using the standard [L] of 10^{-5} M and [Fe^{3+}] of 10^{-6} M and pH of 7.4, pM allows for direct comparison of iron chelators, regardless of ligand denticity or chelating groups present.[89] (A different pH standard is needed in order to best compare marine siderophores, which exist in slightly more basic (8.3) seawater.) Enterobactin has a pM of 35.5, as compared to 26.6 for ferrioxamine B, showing an 8.9 order-of-magnitude enhancement in ferric complex stability. The high denticity and the predisposition of enterobactin toward metal binding[90] explain this staggering difference in stability of the ferric complex.

In addition to being an indirect measurement of the formation constant (K_f) of the iron complex, the reduction potential of the ferric siderophore complex is an important factor in developing the iron-release mechanism for siderophore-mediated iron transport. Under standard conditions, the reduction potentials for most known siderophores (ferric enterobactin -750 mV NHE^{-1},[74] ferriferrioxamine B -450 mV NHE^{-1} [88]) seem to preclude the use of biological reductants (NAD(P)H/NAD(P)$^+$ -324 mV NHE^{-1}) to reduce the ferric ion to the ferrous ion and therefore prompt release of the ion from the siderophore. However, this potential is highly sensitive to the ratio of [Fe^{3+}]/[Fe^{2+}], as predicted by the Nernst equation,

$$E = E^0 + 0.059 \log[Fe^{3+}]/[Fe^{2+}] \tag{7}$$

Addition of a ferrous sequestering agent (e.g., porphyrins) can drastically shift the reduction potential toward more positive values and into the range of biological reductants, favoring reduction of the ferric ion.[1] Addition of a ferrous chelator with formation constant greater than 10^3 theoretically allows transferrin ($E = -526$ mV NHE^{-1})[91] to be reduced by NADH.[92]

8.6.4 SIDEROPHORE-MEDIATED IRON TRANSPORT

Discussion of siderophore-mediated iron transport will be divided between the two structural classes of bacteria (Figure 7). Novel uptake systems will also be briefly covered. This review will not be able to cover the details of such a large and well-studied field, which has been covered in many good reviews.[19–21,23,36,66,93]
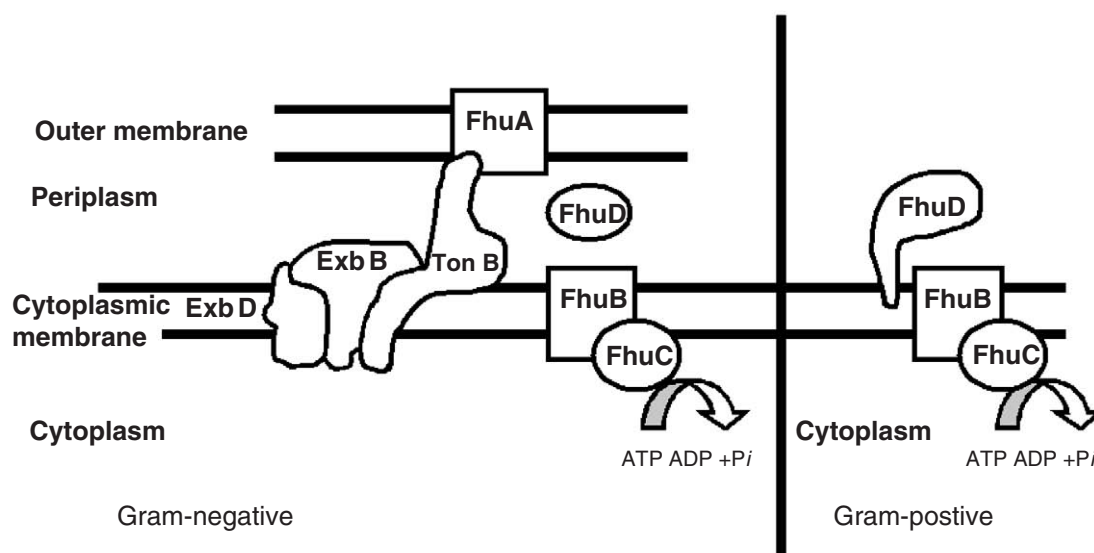
Figure 7 Gram-negative (left) and Gram-positive (right) siderophore-mediated iron uptake. In Gram-negative bacteria: the proteins are specific for hydroxamate siderophore transport. The OM receptor protein (FhuA) binds the ferric siderophore and transports it through the OM via energy transduced by the TonB-ExbBD system. The BP FhuD shuttles the ferric siderophore complex from the OM to the CM protein FhuB. ATPase FhuC hydrolyzes ATP, transporting the ferric siderophore complex into the cytoplasm. In Gram-positive bacteria: the lipoprotein FhuD binds the ferric siderophore and directs it to the CM protein FhuB. Hydrolysis of ATP by FhuC permits passage into the cytoplasm through the transmembrane protein FhuB.

8.6.4.1 Gram-negative Iron Transport

8.6.4.1.1 Outer membrane

Although passive diffusion, via nonspecific porins, mediates passage across the outer membrane (OM) in Gram-negative bacteria, the low concentration and large size of ferric siderophore complexes require an energized active transport process in order to fulfill the iron requirements of the cell. Recognition and incorporation of the ferric siderophore complex begins at an OM receptor, and this is the rate-limiting step for the entire siderophore-mediated iron-transport process.[21,94] Under periods of iron deprivation, organisms express highly specific receptors capable of binding a very narrow subset of ferric siderophores.[23,95] However, several bacteriophages (T1, T5, φ80, UC-1) and bacteriocins (colicin M and microcin 25) opportunistically utilize these OM receptors for entry into the cell.[24] Once the ferric siderophore complex is recognized, transport across the membrane is accomplished through transduction of the cytoplasmic proton motive force by the cytoplasmic membrane (CM) TonB-ExbB-ExbD complex.[20,93] Thus, ferric siderophore receptors are referred to as the TonB-dependent class of OM receptor proteins.[96] The crystal structure of the C-terminal domain of TonB has been reported.[97] Binding of the ferric siderophore to the OM receptor induces a conformational change in the receptor protein. Most notably, the unwinding of the switch helix in the receptor protein yields a flexible extended conformation. This unwinding of the switch helix allows facile distinction between receptors with and without bound siderophore complex, facilitating contact between TonB and the activated receptor. TonB transduces the electrochemical potential of the cytoplasmic membrane, resulting in a second conformational change in the receptor protein, and lowering the affinity of TonB for the receptor. The ferric siderophore is then released into the periplasmic space and TonB is retrieved and recycled by the cytoplasmic proteins ExbB and ExbD.[20,93]

The crystal structures of three OM proteins of *Escherichia coli*, each responsible for the recognition of a different type of ferric siderophore, have been described. FhuA[98,99] binds ferrichrome; FepA[100] recognizes ferric enterobactin, and similar tris-catecholate analogs. In 2002, the structure of the ferric citrate receptor, FecA (Figure 8),[101] appeared. Each of these receptors consists of approximately 700 residues organized into a C-terminal, 22-stranded β-barrel and an N-terminal plug domain located within the barrel channel. This N-terminal plug serves to block passage through the barrel. The unfolded plug domain of FepA binds ferric enterobactin, though
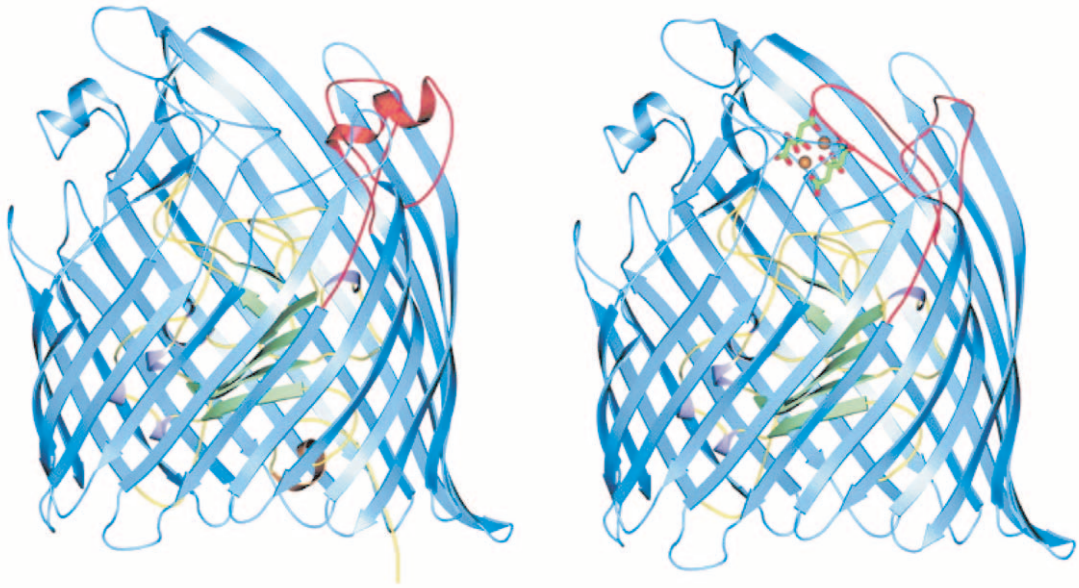
Figure 8 The bacterial ferric citrate uptake protein, FecA, without ferric citrate bound (left) and with ferric citrate (right). The 22-stranded β barrel (in blue) forms the transmembrane channel; the plug domain (in green) blocks passage of non-ferric citrate substrates; the switch helix (in orange, not seen in the ligated structure) unwinds to signal binding of ferric citrate.[101]

at a hundredfold lower affinity than the intact protein, suggesting that the plug domain rearranges to allow the ferric enterobactin to pass through the channel, rather than moving out as the intact plug.[94] Interestingly, FecA contains a third domain residing completely within the periplasm, termed the N-terminal extension. This periplasmic domain is responsible for signaling the presence of substrate bound to FecA. Binding of ferric citrate to FecA results in the interaction of the N-terminal extension with the transmembrane protein FecR, which in turn controls the activity of FecI and directs the transcription of genes required for the uptake of ferric citrate.[101]

8.6.4.1.2 *ATP-binding cassette (ABC) transport system*

Following passage through the gated channel formed by the OM protein, the ferric siderophore complex binds to a substrate-binding protein (BP), a part of the ATP-binding cassette (ABC) transport system responsible for the translocation of the complex across the periplasm CM.[102] While the interaction of the BP with the OM receptor protein has been postulated, experimental evidence for such an interaction has not yet been documented. The specificity and affinity of the BP for the ferric siderophore complex is far lower than their OM counterparts. While three separate OM receptors are required to transport ferric complexes of ferrichrome (FhuA), aerobactin (Iut), and coprogen (FhuE), the same FhuBCD ABC transporter can transport all of these complexes. The generalized mechanism for transport of ferric siderophores via the widely conserved ABC transport system includes: (i) binding of the substrate by the periplasmic-binding protein (BP); (ii) interaction of the BP with the CM spanning protein; and (iii) hydrolysis of ATP via a membrane-bound protein to transport ferric siderophore across the CM.

8.6.4.1.3 *Periplasm*

The crystal structure of the BP FhuD receptor protein with gallichrome (the gallium complex of ferrichrome),[103] albomycin,[104] coprogen,[104] and Desferal (ferrioxamine B, Figure 2)[104] reveals the greater flexibility of this protein as compared to the OM counterparts. A long α-helix connects the two dissimilar lobes of FhuD, forming a shallow-binding pocket lined with hydrophobic residues. The "classic" BP fold (causing a "Venus flytrap" closing upon substrate binding) is absent,[102]

resulting in a smaller structural difference between the FhuD holo and apo forms. Most of the substrate–protein interactions center on the iron core, leaving the majority of the complex exposed.[104] Increased hydrogen-bond contacts seem to correlate with increased substrate affinity (e.g., FhuD has more contacts and a higher affinity for coprogen ($0.3\,\mu M$) than for ferrichrome ($1.0\,\mu M$)).[104] Accommodation of a large variety of structural types is accomplished through recognition of only the central iron hydroxamate core of the ferric siderophore complex, and then adjusting BP around the rest of the substrate. This follows a prediction made almost 20 years ago regarding this hydroxamate uptake system and the establishment of its stereospecific recognition of the metal center: "...we conclude that only the hydroxamate iron center and its direct surroundings are important for recognition and uptake."[219]

Transport of catecholate siderophores also employs the same type of transport system. Although the structure of BP FepB has not yet been determined, binding studies suggest that this protein is far more specific for enterobactin ($K_d = 30\,nM$)[105] than the similar catecholate siderophores vibriobactin[106] and agrobactin.[105] Perhaps the tertiary structure of FepB contains a deeper and more shielded-binding pocket for the ferric complex, allowing more hydrogen-bonding contacts to the complex. Less solvent exposure would protect the ferric siderophore from dissociation from the BP, resulting in a higher-binding affinity for ferric siderophore complexes with the BP.

8.6.4.1.4 *Cytoplasmic membrane*

The periplasmic-binding protein (FhuD, FecB, or FepB) delivers the substrate (Fe-hydroxamate, Fe-citrate, or Fe-enterobactin), to the cytoplasmic transmembrane protein (FhuB, FecCD, or FepDG). Transport across the CM is driven by hydrolysis of ATP, achieved via ATP-binding proteins (FhuC, FecE, or FepC), attached to the CM. Interaction between FhuD and FhuB is evident from several studies.[107,108] Based upon these experimental results, a mechanism emerges whereby FhuD interacts with both the periplasmic loops and transmembrane segments of FhuB, perhaps forming a channel for FhuD to deposit the substrate into the cytoplasm. Direct contact between FhuD and FhuC within this channel, or a conformational change of the FhuB upon FhuD binding, could trigger the ATPase activity of FhuC, which allows transport of the ferric siderophore complex across the CM.[18]

8.6.4.2 Gram-positive Transport

8.6.4.2.1 *Comparison to Gram-negative iron transport*

Gram-positive bacteria lack the lipopolysaccharide layer encasing the cell, and therefore do not require the OM receptors such as FepA or FhuA to transport their siderophores into the cell (Figure 4).[21,95,109] Passage via diffusion is possible through the thick but porous peptidoglycan cell wall, eliminating the need for the energy-transducing TonB-ExbBD proteins. Transport across the CM likely occurs via the ABC transport system, as described for Gram-negative bacteria. One modification to the transport system between Gram-negative and Gram-positive bacteria is the probable use of a membrane-bound lipoprotein for transporting the ferric siderophore complex to the transmembrane component of the ABC system, rather than utilizing a soluble periplasmic-binding protein as in Gram-negative bacteria. The lipoprotein would provide the same high affinity for the ferric siderophore complex, but tethering it to the CM would prevent loss to the surrounding medium.

8.6.4.2.2 *Cytoplasmic membrane receptors*

Gram-positive siderophore receptor proteins are not as well documented as the Gram-negative receptor proteins. In 1993, Hantke reported a binding protein anchored via a glyceryl–cysteine–lipid residue to the CM of a Gram-positive bacterium.[110] This lipoprotein had sequence homology with both FepB (22.9%) and FhuD (16.2%) and was proposed to transport a wide variety of hydroxamate siderophores. More recently, at least three ABC transport systems have been reported for the Gram-positive *Staphylococcus aureus*. *S. aureus* produces two carboxylate

siderophores, staphyloferrin A[111] and B,[112] and the incompletely characterized aureochelin,[113] but is also able to utilize exogenous siderophores such as the hydroxamates ferrichrome and aerobactin, as well as catecholates such as enterobactin and 2,3-dihydroxybenzoic acid. Although each of the three transport systems appears to transport a different type of siderophore, all three posses a lipid-anchored binding protein, a transmembrane protein, and an ATPase protein. The ferric hydroxamate transporter, FhuCBG[114,115] (or FhuCBD[116]), indicated that *S. aureus* FhuC (29.5 kDa) was an ATPase similar to FhuC from *B. subtilis*. The *S. aureus* transmembrane permease proteins FhuB (36 kDa) and FhuG (36.1 kDa) are also very similar to their *B. subtilis* protein counterparts.[115] The more recently identified FhuD2 is a lipoprotein responsible for shuttling ferric hydroxamate complexes to the transmembrane protein.[114] Two other putative ABC transport systems, SirABC[117] and SstABCD[118], have been reported, although their siderphore substrates, in early 2003, have yet to be identified.

8.6.4.3 Iron Regulation

Both Gram-negative and Gram-positive bacteria produce siderophores, and their corresponding receptor proteins, only in response to iron-poor environments. Hantke recently reviewed this area,[95] and only a brief description will be included here. Fur (ferric uptake regulator), and Fur-like proteins, regulate iron uptake in many bacterial species. Some Gram-positive bacteria, such as streptomyces, corynebacteria, and mycobacteria, use the DtxR (diphtheria toxin regulator) protein. The two-domain Fur protein regulates iron metabolism in *E. coli*; similar proteins have been found in other bacteria. The protein contains two metal-binding sites: Zn^{2+} and Fe^{2+} (however, other divalent metals such as Mn^{2+} and Co^{2+} can also bind in the Fe^{2+} sites). Binding of Fe^{2+} to Fur suppresses the transcription of genes regulating siderophore production. The sequences for DtxR and Fur are different, but some structural similarity exists, including the presence of two metal-binding sites. However, in the DtxR protein, both sites are occupied by iron.

8.6.4.4 Novel Transport Mechanisms

8.6.4.4.1 Siderophore shuttle

In 2000, Stintzi *et al.* published a novel iron-transport mechanism (the "siderophore shuttle") that employs ligand exchange to provide the organism *Aeromonas hydrophila* with a flexible mechanism to satisfy its iron requirement (Figure 9).[119] An iron-free siderophore first binds the OM receptors. When a ferric siderophore complex subsequently binds, the iron-free siderophore is pushed into the receptor channel. The iron-bound siderophore transfers its iron to the iron-free ligand, prompting the release of this new ferric siderophore complex into the periplasmic space. The second siderophore, now without iron, remains bound to the receptor, waiting to accept iron from the next ferric siderophore complex in the same manner. This siderophore recognition and transport mechanism provides *Aeromonas hydrophila* with great flexibility, since a wide variety of siderophore types can be bound to the receptor protein instead of selectively recognizing only one. This ability to utilize iron from a wide variety of ferric complexes makes it a fierce competitor for iron. A similar mechanism involving the initial binding of an iron-free siderophore to the OM receptor has been reported for *Pseudomonas aeruginosa*.[120] In this system, however, the iron-bound siderophore displaces the iron-free siderophore, rather than transferring its iron as found in the siderophore shuttle.

8.6.4.4.2 Photodecarboxylation

Transition-metal complexes of α-hydroxy acids can be photolabile. The oil-degrading marine bacterium *Marinobacter hydrocarbonoclasticus* produces a siderophore, which appears to exploit photodecarboxylation to facilitate iron release. Petrobactin (Figure 4) forms a stable ferric complex through iron chelation by two catecholate moieties and a citryl group. Decarboxylation of the citryl moiety via photolysis of ferric petrobactin yields a less stable ferric complex than the
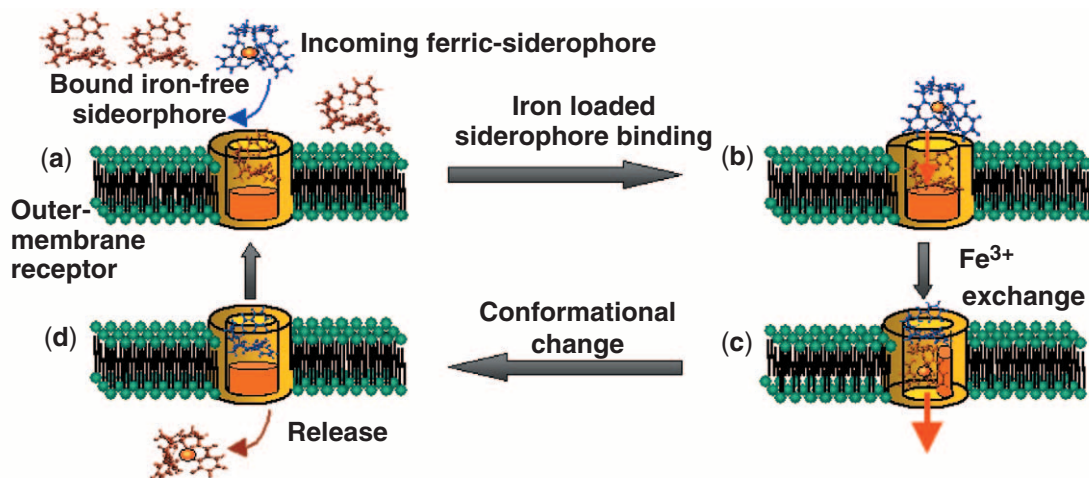
Figure 9 The "Siderphore Shuttle": (a) Binding of a siderophore to OM receptor protein; (b) Ferric siderophore finds to second site on OM receptor protein; (c) Iron exchange between siderophores, initiating a conformational change; (d) Release of the ferric siderophore complex into the periplasmic space. The second siderophore remains bound to the receptor protein, ready to begin the cycle again.

parent complex.[55] Photodecomposition of siderophores incorporating α-hydroxy acids may provide marine microorganisms with an effective iron-release pathway.

8.6.5 TRANSFERRINS

8.6.5.1 Types of Transferrins

The transferrin (Tf) family of proteins contains five members: serum transferrin, lactoferrin, ovotransferrin, melanotransferrin (also called p97), and the ferric-binding protein found in Gram-negative bacteria (Table 1).[121–126]

8.6.5.2 Transferrins with Two Iron-binding Sites

The vertebrate serum transferrin (sTfo), lactoferrin (Lf), and ovotransferrin (oTf) are glycoproteins containing 670–690 amino acids, with molecular weights around 80 kDa. A proposed gene-duplication event[127] resulted in these proteins containing a two-fold internal repeat, yielding an N-terminal domain with ~40% sequence homology with the C-terminal domain. The ability to bind ferric ion securely but reversibly, as well as the presence of a synergistic carbonate anion, characterizes these proteins. These three classes of transferrins (sTf, Lf, oTf) exhibit the most common structural type, consisting of two similar lobes tethered together. Each lobe is folded into two dissimilar domains (I and II), yielding two iron-binding sites within each interdomain cleft

Table 1 The five classes of transferrins.

Protein	Source	Ligands; Iron Sites	References
Transferrin	Vertebrate blood serum	Asp, 2 Tyr, His, carbonate; 2	121
	Insects	Asp, 2 Tyr, Gln or Thr, carbonate; 1	137
Lactoferrin	Secretions (milk, tears, saliva)	Asp, 2 Tyr, His, carbonate; 2	123
Ovotransferrin	Egg whites	Asp, 2 Tyr, His, carbonate; 2	121
Melanotransferrin	Vertebrates	Asp, 2 Tyr, His, carbonate; 1	128
Ferric Binding Protein	Gram-negative bacteria	Glu, 2 Tyr, His, phosphate, water; 1	148
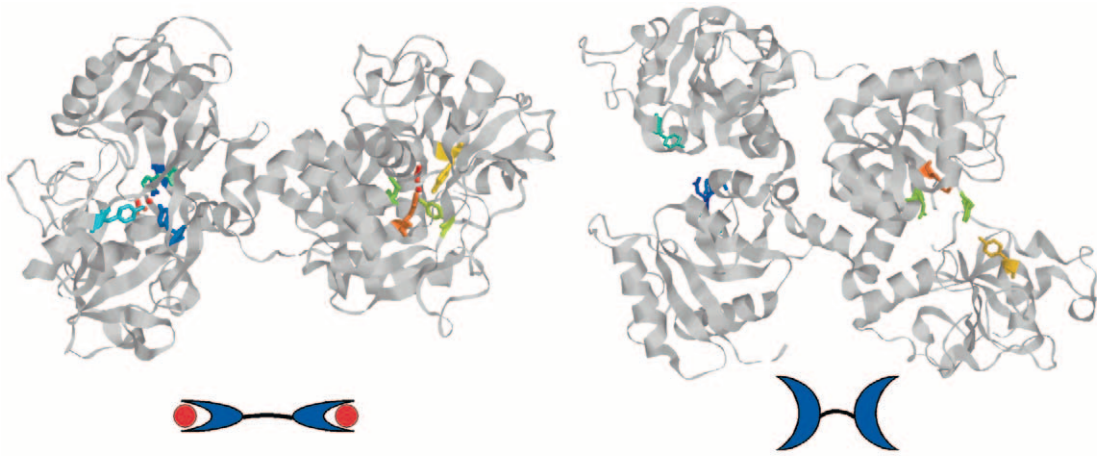
Figure 10 The crystal structure (top) and cartoon (bottom) of diferric ovotransferrin (left) and apo ovotransferrin (right). The coordinates were obtained from the Protein Data Bank under the identifiers 1DOT and 1AOV, respectively.

(Figure 10).[126] Both the sequence and tertiary structures of these three glycoproteins are very similar, and all three vertebrate proteins utilize the same four residues and synergistic carbonate anion to provide a distorted octahedral Fe^{3+}-binding site.

8.6.5.3 Transferrins with One Iron-binding Site

Studies have revealed a second common structural type of transferrin found in vertebrates, insects, and Gram-negative bacteria, where the iron-binding capability of the C-terminal has been lost. Although the ~40% sequence homology between melanotransferrin (mTf) and other transferrins suggest the functions of these proteins are similar, the loss of key iron-coordinating residues in the C-terminus renders mTf unable to bind more than one Fe per molecule.[128] Most insect transferrins also have major changes in the C-lobe, preventing iron binding. Octahedral coordination of iron is achieved through similar residues.[126] Finally, the monolobed, ferric-binding proteins found in several strains of pathogenic bacteria shuttle iron scavenged from host sTf, Lf, or oTf across the periplasmic space and share similar polypeptide topology with vertebrate Tfs. However, the low sequence homology (10%) of the monolobal and bilobal Tfs suggests a distant, anion binding, common ancestor and convergent evolution of iron binding.

8.6.5.4 Serum Transferrin

Recent crystal structures (2002) include hen,[129] rabbit,[130] and porcine[130] serum transferrins. The primary function of human serum transferrin is to safely transport iron to cells.[121,126,131–134] To accomplish this task, the bilobal Tf protein binds ferric ion very tightly ($K = 10^{22}$).[133] The potential loss of the smaller, monolobal Tf molecule through the kidney in vertebrates[135,136] was thought to prompt the gene-duplication event which created a bilobal form of serum transferrin.[127] Isolation of similarly sized bilobal proteins in invertebrates, however, indicates that the gene-duplication event, which created a bilobal protein, may be more ancient than previously thought.[124] Although sequence identity between the vertebrate and insect serum transferrins is only 25–30%, the iron-binding sites in the N-terminal lobes of each are remarkably similar. Only one amino-acid-binding site is altered: histidine in human Tf, and glutamine or threonine in insect Tfs.[137] However, deletions and alterations in the C-terminal lobes prevent most insect transferrins (except that of *Blaberus discoidalis*[138]) from binding the second ferric ion. Although the role of transferrins in invertebrates is unclear, these proteins likely function in iron transport or homeostasis.

8.6.5.5 Lactoferrin

The structure and function of lactoferrin (Lf) have been extensively reviewed,[123,139] and will not be covered here in detail. These proteins retain iron to a much lower pH than serum transferrins; absence of the pH-sensitive dilysine trigger (see below) enhances the acid stability of ferric Lf.[140] Retention of iron provides a bacteriostatic environment, highly effective in limiting microbial growth. A highly cationic molecule, Lf also binds anions such as DNA and heparin.[123] Despite high sequence identity (60%) between sTf and Lf, the major function of Lf does not appear to be iron transport. While a variety of mammalian cells express receptors for Lf, the function of Lf for those cells is still not well defined.[15,139,141] A recent (2001) crystal structure indicates that Lf may be involved with the polymerization of melanin monomers, proteins responsible for the coloration of animal skin and hair.[142]

8.6.5.6 Ovotransferrin

The major protein in egg white, ovotransferrin (oTf or conalbumin), is the iron-binding protein found in birds, which differs from serum transferrins only in the glycosylation pattern.[121,126] While sequestering iron from invading pathogens within eggs is a well-known function of oTf,[143] the 92-residue N-terminal domain called OTAP-92 also shows antibacterial activity.[17] OTf showed greater antiviral activity than Lf in the inhibition of Marel's disease virus (MDV), an avian herpes virus.[16] The kinetics of iron release from ovotransferrin have also been examined, suggesting a dual function of iron transport and iron sequestration for oTf.[144–147]

8.6.5.7 Ferric-binding Protein

The ferric-binding protein (Fbp) found in pathogenic Gram-negative bacteria shuttles the iron scavenged from the host transferrin or lactoferrin across the periplasmic space to the CM of the bacterium.[122,148] Fbp binds ferric ion (affinity constant of 10^{19} M^{-1}) almost as strongly as transferrin (10^{22} M^{-1}).[149] Fbps are more similar to non-iron-binding proteins (e.g., maltose- or phosphate-binding proteins) than other periplasmic iron transporters (e.g., FhuD, FepB, FecB).[148] Fbps show less than 20% homology with other Fbps. Despite sharing less than 10% sequence identity with transferrins, the iron-binding site is remarkably similar to that of vertebrate transferrins. The crystal structures of hFbp (or HitA) from *Haemophilus influenzae* and nFbp (or FbpA) from *Neisseria meningitidis* show nearly identical iron-binding sites. The protein iron coordination is through two tyrosyl oxygens, one histidyl nitrogen, and one glutamyl carboxylate; one oxygen from phosphate and water complete the nearly ideal octahedral coordination.[150] From the crystal structure of apo-hFbp,[151] an iron-binding mechanism has been developed; iron first binds to the well-ordered C-terminal half-site, causing the protein to rotate 21° around the central hinge and complete the coordination sphere of the initially disordered N-terminal half-site. Just as carbonate binds to the apo vertebrate transferrin proteins to prepare the site for iron binding,[152–155] phosphate binds to the open apo bacterial ferric-binding protein,[151] indicating that the protein requires iron, not the synergistic anion, to accomplish domain closing.

Although surprisingly similar to the bilobal transferrin protein family, several differences distinguish Fbp from other Tfs. Fbp is a monolobal protein, resulting in a much smaller molecular weight (~35 kDa) than Tfs, and it is capable of binding only one ferric ion per protein. Transferrins employ bidentate carbonate rather than monodentate phosphate and water as synergistic anions. The iron-chelating residues come from different areas of the protein, resulting in an iron-binding site that is far more solvent exposed in Fbp.[150] Despite the similar iron-binding capabilities of Fbp and Tf, their last common ancestor is thought to be an anion-binding protein.[150] Observations substantiating this hypothesis include different iron-binding locations for these proteins, inability of proteins more closely related to Fbp than Tf to bind iron, and the conservation of the anion-binding site between the two proteins. However, the independent development of similar iron-binding sites suggests that these four residues are nearly optimal to achieve tight, but reversible, iron binding.[150]

8.6.5.8 Melanotransferrin

Although initial studies reported melanotransferrin (or p97 from its apparent molecular mass) expression on only the surface of neoplastic cells,[156,157] later reports describe the identification of

mTf in normal tissues, including sweat gland ducts,[158,159] liver endothelial cells,[158,160] and the capillary endothelium and microglia of the brain.[161–163] The high sequence homology between human mTf and sTf suggests a role in iron transport; however, the iron-transport functions of mTf have yet to be fully established. While sTf circulates in the blood, mTf is bound to the cell membrane (although a second, soluble form has also been isolated[164]). The N-terminal of human, rabbit, and mouse mTf and human sTf and Lf have conserved iron-binding residues; the sequence of the C-terminals of mTf is dissimilar.[128] As a direct consequence of this modification, the C-terminal lobe is unable to bind iron. Iron- and anion-binding amino acids in the N-terminal half (Fe: aspartate, two tyrosines, and histidine; anion: arginine) are conserved in mammalian mTf. Replacement of arginine for histidine may prevent chicken mTf from binding iron, suggesting that during the evolution of this protein, the high-affinity iron-binding site was no longer required for proper functioning. Although increased iron transport was reported for Chinese hamster ovary cells transfected with mTf,[165] other evidence suggests mTf is not involved in iron transport. First, mTf binds iron but does not donate it to the cell.[166] Second, mTf expression is not regulated by intracellular Fe concentrations as are the sTf receptor proteins.[125] Third, removal of the cell-bound mTf only slightly reduced the ^{59}Fe uptake of the melanoma cells.[125] While the role of mTf in iron transport seems unlikely, other functions have been suggested, such as protection of membrane-lipid peroxidation by sequestering free iron to prevent Fenton chemistry,[128] metallo-protease activity,[167] or as an intercellular adhesion molecule, interacting with the transferrin receptor (TfR) to target metalloprotease activity.[128] Finally, mTf appears to be a biochemical marker of Alzheimer's disease. Several studies report elevated serum p97 levels in patients with Alzheimer's disease, compared to normal patients or those suffering from other forms of dementia.[162,168,169]

8.6.5.9 Vertebrate Transferrin Iron-binding Sites

The crystal structures of several transferrins have been solved and have been reviewed.[123,126] The iron-binding site is highly conserved for both lobes of the vertebrate sTf, oTf, and Lf (Figure 11). The protein provides four residues for iron binding: two tyrosyl phenolic oxygens (Tyr 95 and 188 in N-lobe hTf), one aspartic carboxylate oxygen (Asp 63), and one histidyl nitrogen (His 249). The distorted octahedral coordination sphere is completed by the synergistic bidentate carbonate anion, which provides two oxygen atoms.

8.6.5.10 Transferrin Cycle

The transfer of iron from transferrin to the cell is a well-characterized process (Figure 12).[12,126,131,170–173] Diferric transferrin binds to a transferrin receptor situated on the surface of the cell within a clathrin-coated pit, initiating endocytosis. The pit buds from the cell membrane and becomes an endosome after fusing with internal vesicles. An ATP-driven proton pump infuses protons into the endosome, acidifying the interior to a pH of 5.5. Under these conditions, iron dissociates from transferrin and is transported out of the endosome, likely by association with the divalent metal transporter DMT1 (also called Nramp2 and DCT1) and is stored in ferritin or incorporated into proteins. At low pH, the apo-transferrin/transferrin receptor complex is stable, and remains intact throughout this process. Exocytosis of the apo-Tf/TfR complex returns the apo-Tf back to the cell surface. The low affinity of the receptor for the empty Tf at physiological pH prompts release of apo-Tf back into the serum. With a half-life of approximately 8–10 days, a single transferrin protein may undergo 100–200 cycles, with each cycle lasting only 2–3 minutes.[126]

8.6.5.11 Vertebrate Transferrin Receptor Proteins

The transmembrane transferrin-receptor protein (TfR) provides access to the interior of the cell, allowing diferric serum transferrin to deliver iron quickly and safely.[174] Although cells requiring large amounts of iron (e.g., placental tissue, immature erythroid and rapidly dividing cells) express the highest levels of TfR,[173] the transferrin receptor is ubiquitous in nucleated cells in the body.[134] The transferrin/transferrin-receptor binding constant correlates with the degree of iron saturation of the transferrin: diferric > monoferric > apo.[175] Although identification of the
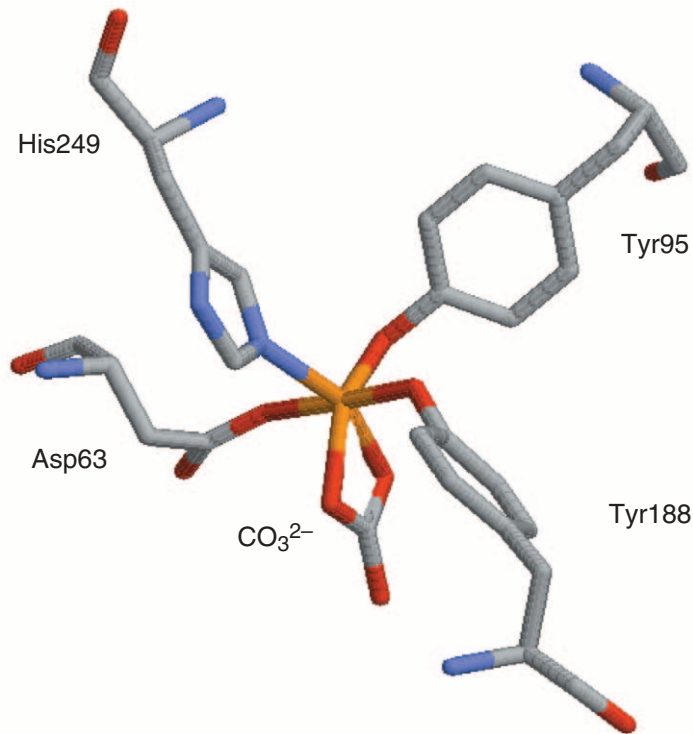
Figure 11 The iron-binding site of recombinant N-lobe human transferrin expressed in *Pichia pastoris*. Five oxygen (red) atoms and one nitrogen (blue) coordinate the iron (yellow). The oxygen donors are Tyr 95, Tyr 188, Asp 63, and carbonate. The nitrogen donor is His249. The coordinates were obtained from the Protein Data Bank under the identifier 1B3E.
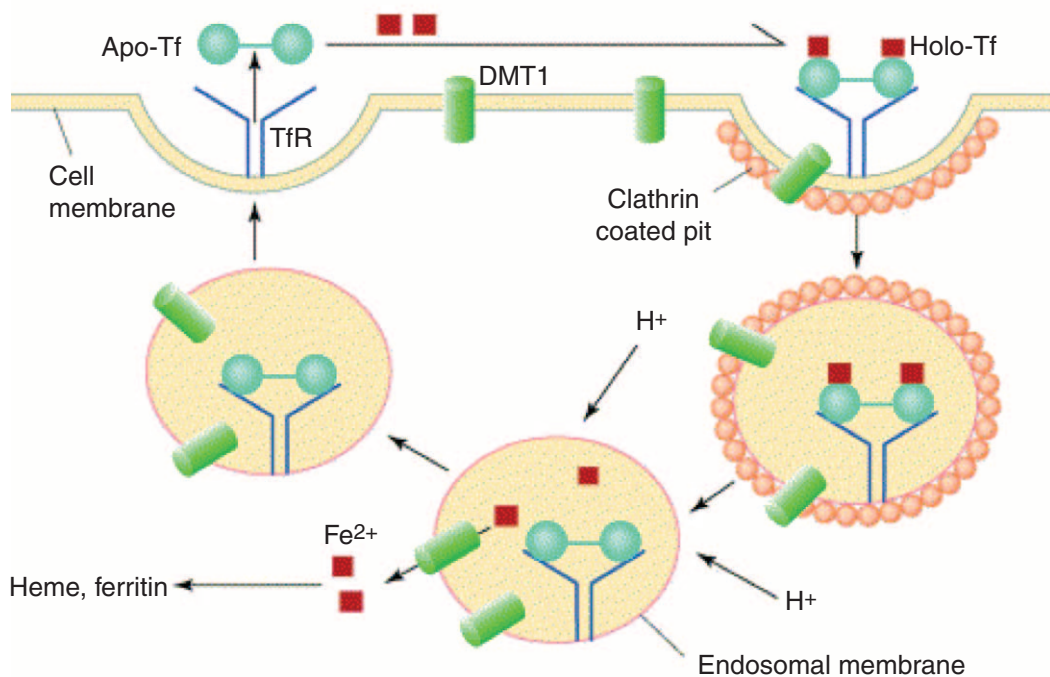
TRENDS in pharmacological sciences

Figure 12 The Transferrin Cycle. Diferric transferrin binds to the transferrin receptor expressed on the cellular surface. Clathrin facilitates endocytosis of the pit, forming an endosome. Transferrin, while remaining bound to the receptor, releases the iron upon acidification of the endosome. Ferrous ion leaves the endosome via a metal transporter (DMT1). The endosome is exocytosed, and the apo-transferrin is released.[134]
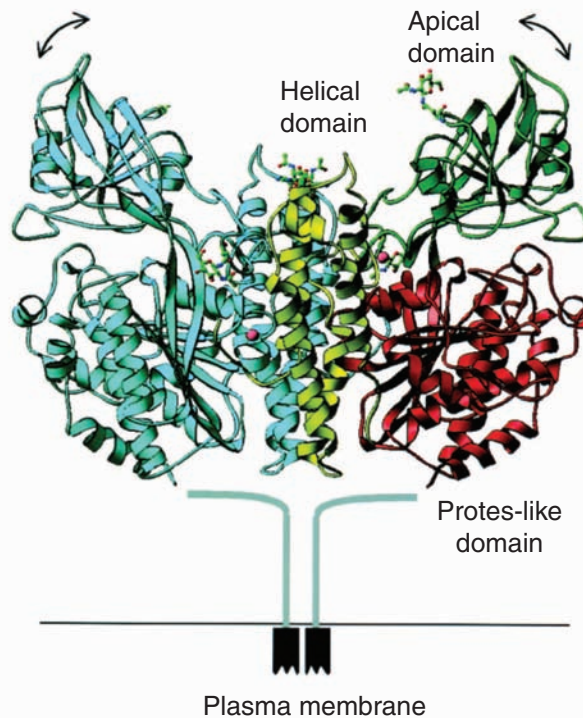
Figure 13 The transferrin receptor protein dimer. One monomer is in blue, while the other is colored according to domain. Sm^{3+} ions (pink spheres) facilitate the solution of the crystal structure. Arrows show direction of (small) displacements of the apical domain in noncrystallographically related molecules.[176]

region of direct interaction between iron-loaded sTf and the transferrin receptor is still ongoing (2003), the crystal structure of the ectodomain of the human TfR provides valuable clues. Two disulfide bonds join two protein monomers, forming an extracellullar TfR capable of binding two transferrins (Figure 13).[176] The monomer contains three domains: the protease-like, the apical, and the helical domains, that when dimerized resemble a butterfly. Combining structural, theoretical, and experimental evidence, plausible binding sites for transferrin to the TfR protein can be suggested. Recognition of transferrin by the receptor requires functional N- and C-lobes, indicating both lobes interact with the receptor.[177] While the C-terminal fragment of Tf provided iron to cells via the TfR, the N-terminal fragment did not; a greater number of contacts between the receptor and the C-lobe should be seen.[178] Release of iron into the endosome does not displace the transferrin molecule from the receptor, so rotation of the hinge in each domain needs to be unimpeded in the TfR-bound transferrin. Binding of only the NI or CI domain from each lobe allows the complementary half of each lobe to open easily. Conformational changes of the TfR during acidification of the endosome could possibly lead to corresponding movements of Tf, facilitating domain opening and iron release.

A second transferrin receptor (TfR2), sequenced in 1999,[179] appears to have similar functions to TfR.[180] In contrast to TfR, however, expression levels and binding constants with transferrin are lower.[181] In addition, transcription of TfR2 is not dependent on iron levels as is TfR, but rather on the cell cycle or cellular proliferation status.[180] Initial,[182] but controversial,[183] studies indicate that mutation of TfR2 may be a factor in the onset of the genetic disorder hemochromatosis.

8.6.5.12 Mechanism of Iron Chelation and Release

Biochemical experiments and crystal structures of apo, mono, and diferric serum transferrin greatly enhance our understanding of the mechanism by which Tfs strongly chelate ferric ion and then release it within the endosome. These processes are inherently related; the iron-binding steps occur in the opposite order to the steps leading to iron release from transferrin. Binding of iron to the tyrosine residues and to the synergistic anion while the Tf lobe is in the open conformation appears to be the first step.[184–186] Once the ferric-loaded domain samples the closed
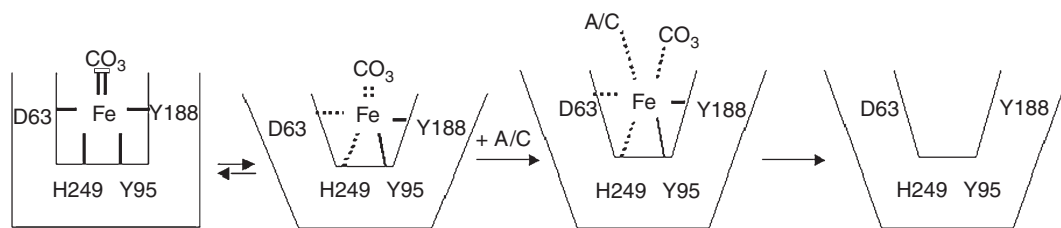
Figure 14 Iron release from transferrin. Iron is coordinated through four protein residues (D63, H249, Y95, and Y188) and the synergistic bidentate carbonate anion. The lobe continually samples the open and closed conformations. Partial loss of the carbonate, aspartate, and histidine are the first steps in the process. Coordination of the anion or chelator (A/C) forms a quaternary complex between the protein, iron, carbonate and the chelator/anion. Decay of the quaternary complex yields apo transferrin.

conformation, interaction with the remaining two residues, aspartate and histidine, locks the domain in the closed conformation.[187] The cycle continues as chelators and anions facilitate iron release within the endosome. Formation of a quaternary complex among the chelator, iron, carbonate, and remaining tyrosine residues follows the protonation and loss of the synergistic anion and histidine residue. Decay of the quaternary complex results in apo transferrin and the ferric chelator complex. Although the two lobes of human Tf are highly homologous, iron remains bound to the C-terminal at a much lower pH than the N-terminal site. Recombinant N-lobe mutants help elucidate the mechanism for iron release, resulting in a better understanding of the process for the N-terminal than for the C-terminal (Figure 14).

8.6.5.12.1 *Iron-binding residues*

Inspection of sTf, Lf, and oTf crystal structures, in conjunction with biochemical studies, provides a model for iron binding. Two conformations of apo-transferrin exist in equilibrium in solution, interconverted via rotation about a hinge to yield "open" and "closed" conformations. Rather than a dramatic snapping shut of the two halves of the domain only upon iron binding, the apo-Tf domain continually opens and closes. Crystal structures of apo-Tfs reveal this equilibrium.[126] Domain closing and tight iron binding is facilitated by the location of the residues within the protein. For N-lobe hTf, Asp 63 is on the NI domain, Tyr 188 on the NII domain, and Tyr 95 and His 249 are located within the hinge region. Studies of the N-lobe of human sTf indicate that the two tyrosyl ligands (Tyr 95 and Tyr 188) are not equivalent. Mutation of Tyr 95 to noncoordinating phenylalanine weakens, but does not destroy, the iron-binding capability. The Tyr 95 mutant also utilizes tridentate NTA (nitrilotriacetate) preferentially to the bidentate bicarbonate as the synergistic anion, completing the octahedral coordination of iron. Complete loss of iron-binding ability, accompanied by enhancement of copper affinity, characterizes the Tyr 188 phenylalanine mutant.[188] Loss of the Tyr 188 ligand may prevent the lobe from closing, destroying the ability of the protein to bind iron. Mutation of Asp 63[189] or His 249[190] weakens iron binding, with mutants again showing a higher affinity for tridentate NTA over bidentate carbonate as the synergistic anion.

8.6.5.12.2 *Synergistic anion*

The synergistic anion (usually carbonate), which provides two coordinating ligands, is absolutely necessary for the formation of a stable iron complex. N-lobe residues Arg124 and Thr120, and C-lobe Arg456 and Thr452, hold the anion in place via electrostatic and hydrogen bonds. Mutation of the threonine, and to a greater extent arginine, weakens anion binding and overall iron binding. Individual lobes of diferric transferrin arginine and threonine double mutants do not bind iron at all. However, mutagenesis of one lobe does not affect the iron-binding ability of the other lobe. These monoferric double mutants can still supply cells with iron, indicating recognition by the TfR.[191] High-resolution crystal structures of the human Fe-N-lobe at pH 5.8 show two conformations, depending upon the pH. At low pH, Arg124 moves away from the carbonate ligand, which has rotated by 30° as compared to the high-pH conformation. Partial protonation of carbonate to yield bicarbonate provides a plausible explanation for these results, suggesting the first step in the iron release mechanism involves protonation and partial loss of the synergistic anion.[192]

8.6.5.12.3   Dilysine trigger

The N-lobe of transferrin releases iron at a higher pH ($\sim$5.7) as compared to the C-terminal ($\sim$4.8). The close proximity of Lys 209 and 301 in the crystal structure of Fe-N-terminal ovotransferrin led to the proposal of the "dilysine trigger" as a pH-sensitive mechanism for iron release.[193] Protonation of the lysine residues at low pH pushes the two residues and their corresponding domains apart, opening the lobe and promoting release of the iron. An analogous lysine pair (Lys 206 and 296) was found in the N-lobe of human serum Tf, but not in the C-lobe or in lactoferrin, which may explain why iron removal is more difficult in those protein environments. Mutations of one or both of the lysines to neutral alanine[194,195] and glutamine[196] or anionic glutamate[196] disrupt the dilysine trigger and slow iron release. Since alanine cannot be protonated and does not push the domains apart, alanine mutants retain iron until pH 4.5, as compared to pH 5.5 for the native N-lobe.[195] Especially stable is the Glu 206–Lys 296 interaction, where formation of a salt bridge holds the two domains tightly together.[196]

8.6.5.12.4   Chelator- and anion-mediated Fe release from transferrin

Release of iron from transferrin requires a secondary anion or chelator.[197] A 2002 review covers the many studies investigating the effect of the anion (referred to as a nonsynergistic anion) on the rate of release.[198] The effect of the anion is complicated, but appears to include binding to an allosteric site termed the kinetically significant anion-binding site (KISAB site). Although the locations and the numbers of KISAB sites are not known, several residues have been implicated in nonsynergistic anion binding.[196,199–201] Anion binding affects iron release from both lobes, but release rates differ depending on the lobe, concentration, and type of anion.[197,202,203]

The kinetics of chelator-mediated iron release are often complicated, since the chelating ligands can act as both anions and iron chelators. Recently, a series of ligands were monitored for their ability to remove iron from diferric transferrin. At high ligand concentrations, hydroxypyridonate-based ligands effect the fastest iron-removal rates, followed by catecholates. At concentrations closer to therapeutic doses, iron removal correlates with the stability of the iron complex (pM). Comparable rates of iron and Ga^{3+} removal indicate that reduction of ferric to ferrous ion is not involved in the release mechanism, since gallium cannot be reduced to the 2+ state.[204] Chelators can selectively remove iron from either the N-lobe (e.g., enterobactin)[205] or the C-lobe (e.g., aerobactin)[205] from diferric transferrin. Several studies have indicated a significant amount of cooperation between the two lobes. Iron removal is possible (with the appropriate chelator) from the C-lobe of monoferric transferrin, but not possible from the N-lobe of monoferric transferrin. Amonabactin initially removes iron from either lobe of diferric transferrin, yielding either N-lobe or C-lobe monoferric transferrin. While amonabactin continues to remove iron from the C-lobe of the monoferric transferrin, iron remains bound by the N-lobe monoferric transferrin. The conformation of the empty C-lobe may prevent amonabactin from successfully accessing the iron in the N-lobe.[206] The presence of kinetically inert Co^{+3} in the C-lobe slows removal of iron by EDTP (ethylenediaminetetra(methylenephosphonic acid) from the N-lobe. In this case, the conformation of the filled C-lobe may prevent access to the iron in the N-lobe.[207]

8.6.5.13   Fe Release from Insect Transferrin

The N-terminal substitution of glutamine (or threonine) for histidine in insect Tf results in a more weakly coordinated iron, as evidenced by a longer Fe–glutamine bond in the crystal structure of an N-terminal hTf mutant with histidine exchanged for glutamine.[137] Weaker iron bonds should facilitate iron release from transferrin at higher pH ranges, but insect transferrins release iron in a pH range ($\sim$5.5) similar to vertebrate transferrins.[138] However, the weaker iron binding may be compensated by the loss of the dilysine trigger present in human Tf.[137]

8.6.5.14   Bacterial Transferrin Receptor Proteins

Pathogenic bacteria express transferrin, ovotransferrin, and lactoferrin receptors as a means to scavenge iron from the host organisms.[143,208] Pirating the iron from sTf, oTf, or Lf frees the organism from the energetically expensive process of synthesizing siderophores and ensures a
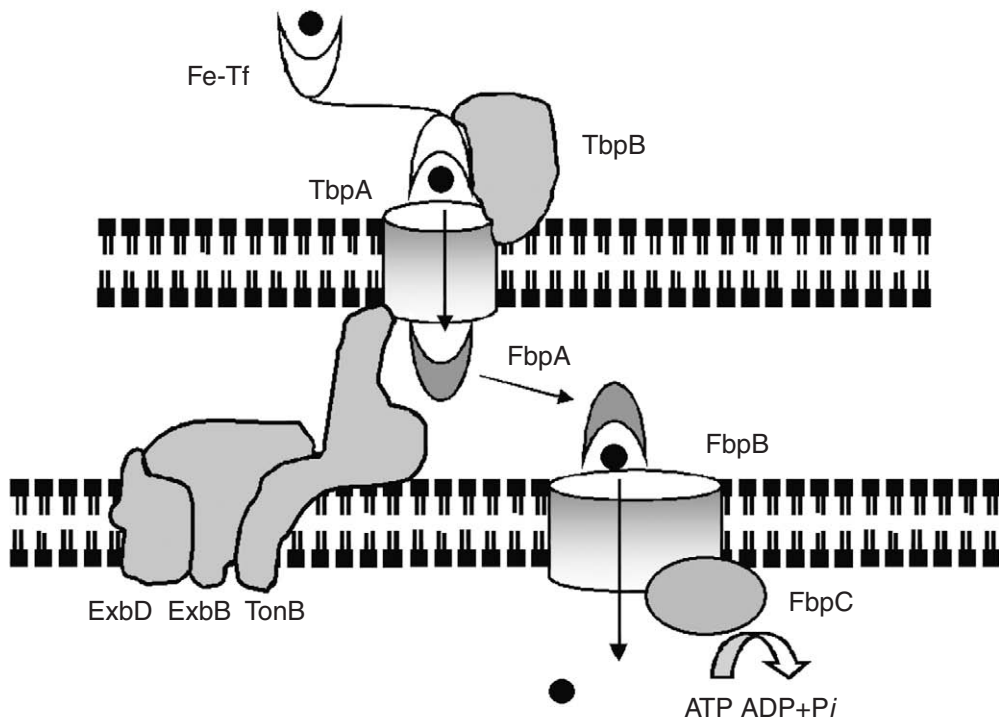
Figure 15 Transferrin-mediated iron uptake by bacteria. One lobe of ferric transferrin binds to the OM transmembrane receptor protein TbpA; TbpB facilitates binding. The unchelated ferric ion passes through the membrane and is then bound by the ferric-binding protein (FbpA), located in the periplasm. A TonB-ExbBD-like protein system provides the energy required for this process. FbpA shuttles the iron to the CM transmembrane protein FbpB. The iron moves into the cytoplasm following hydrolysis of ATP by FbpC.

consistent source of iron. Despite these advantages, limiting acquisition to only iron acquired from host proteins greatly reduces the number of environments hospitable to the organism, since the receptor expression is specific only to a few host Tf or Lf proteins. Unlike mammalian Tf transport, iron is released at the bacterial cell surface rather than endocytosis of the ferric-Tf. In contrast to siderophore-mediated transport, unchelated iron is transported across the periplasmic space via a ferric-binding protein (Fbp), a member of the transferrin superfamily.

Acquisition of iron by Gram-negative bacteria from transferrin (or lactoferrin[209] or ovotransferrin[143]) is accomplished by two OM receptors, which work in concert (Figure 15).[210,211] Transmembrane protein TbpA (or LbpA) is similar to the TonB-dependent OM receptors responsible for ferric siderophore recognition.[208,212,213] Lipoprotein TbpB (or LbpB) is tethered to the OM and is likely responsible for the early transferrin recognition events. TonB (or a TonB-like protein) provides the required energy to translocate free iron across the OM, likely in a manner similar to ferric siderophore transport. FbpA then chaperones the free ferric ion across the periplasmic space; the inner-membrane complex FbpB/FbpC acts as typical ABC transporter and moves the ferric ion across the CM.[148] The thick peptidoglycan wall of Gram-positive bacteria should prevent the passage of a large, 80 kDa Tf protein.[214,215] Transferrin-mediated uptake would require a cell wall-associated receptor able to facilitate iron release from transferrin. There are reports identifying cell wall proteins, StbA[216] and Tpn,[217] in *Staphylococcus aureus* and *S. epidermidis* that are able to bind human transferrin and may promote iron acquisition from transferrin.

8.6.5.15 Fe Release from Ferric-binding Protein in Gram-negative Bacteria

The dilysine trigger is unlikely to facilitate iron release from Fbp because the two lysine residues analogous to those in human Tf are located in different domains, outside the protein core. Repulsion between the two lysine residues is unlikely to be enough to force the opening to initiate iron release from Fbp.[151] Instead, a periplasmic ferric reductase may be responsible for facilitating

iron release. The use of phosphate and water in Fbp, instead of carbonate as in Tf, increases solvent exposure of the iron-binding site, resulting in a dramatic positive shift ($\sim$200 mV) in reduction potential as compared to human Tf (-526 mV/NHE).[91] The less negative potential (-290 mV NHE^{-1})[218] of ferric-Fbp compared to diferric sTf is within the range for NADH- or NADPH-driven reduction. Although reduction is not the mechanism of iron release from serum transferrin, it could be the mechanism of iron release from Fbp.

8.6.6 CONCLUSION

Iron is important for both microorganisms and animals, and complex systems have evolved to handle the demand. Fields as varied as ocean ecology and human health have the availability of iron as a critical issue. Without a constant source of iron, the growth of both marine microorganisms and human pathogens is limited. Understanding the iron metabolism of bacteria can help in combating disease by providing new targets that can limit the growth of invading pathogens. Chaperones such as transferrins allow for this potentially dangerous metal to be used safely *in vivo*. Improving our understanding of chelator-mediated iron removal from transferrin has many applications, such as drug development for the treatment of diseases like β-thalassemia. Detailing the mechanism by which iron is gained, bound, and lost in animals and microbes can help guide medical approaches.

ACKNOWLEDGMENTS

8.6.7 REFERENCES

1. Pierre, J. L.; Fontecave, M. *Biometals* **1999**, *12*, 195–199.
2. Olivieri, N. F.; Brittenham, G. M. *Blood* **1997**, *89*, 739–761.
3. Fleming, R. E.; Sly, W. S. *Annu. Rev. Physiol.* **2002**, *64*, 663–680.
4. Davies, S. C.; Roberts-Harewood, M. *Blood Rev.* **1997**, *11*, 57–71.
5. Andrews, N. C. *N. Engl. J. Med.* **1999**, *341*, 1986–1995.
6. De Voss, J. J.; Rutter, K.; Schroeder, B. G.; Su, H.; Zhu, Y. Q.; Barry, C. E. *Proc. Natl. Acad. Sci. USA.* **2000**, *97*, 1252–1257.
7. Henderson, D. P.; Payne, S. M. *Infect. Immun.* **1994**, *62*, 5120–5125.
8. Behrenfeld, M. J.; Kolber, Z. S. *Science* **1999**, *283*, 840–843.
9. Coale, K. H.; Johnson, K. S.; Fitzwater, S. E.; Gordon, R. M.; Tanner, S.; Chavez, F. P.; Ferioli, L.; Sakamoto, C.; Rogers, P.; Millero, F.; Steinberg, P.; Nightingale, P.; Cooper, D.; Cochlan, W. P.; Landry, M. R.; Constantinou, J.; Rollwagen, G.; Trasvina, A.; Kudela, R. *Nature* **1996**, *383*, 495–501.
10. Nakabayashi, S.; Kuma, K.; Sasaoka, K.; Saitoh, S.; Mochizuki, M.; Shiga, N.; Kusakabe, M. *Limnol. Oceanogr.* **2002**, *47*, 885–892.
11. Tortell, P. D.; Maldonado, M. T.; Granger, J.; Price, N. M. *FEMS Microbiol. Ecol.* **1999**, *29*, 1–11.
12. Ponka, P. *J. Trace Elem. Exp. Med.* **2000**, *13*, 73–83.
13. Nibbering, P. H.; Ravensbergen, E.; Welling, M. M.; van Berkel, L. A.; van Berkel, P. H. C.; Pauwels, E. K. J.; Nuijens, J. H. *Infect. Immun.* **2001**, *69*, 1469–1476.
14. Qiu, J. Z.; Hendrixson, D. R.; Baker, E. N.; Murphy, T. F.; St. Geme, J. W.; Plaut, A. G. *Proc. Natl. Acad. Sci. USA.* **1998**, *95*, 12641–12646.
15. Ward, P. P.; Uribe-Luna, S.; Conneely, O. M. *Biochem. Cell Biol.* **2002**, *80*, 95–102.
16. Giansanti, F.; Rossi, P.; Massucci, M.; Botti, D.; Antonini, G.; Valenti, P.; Seganti, L. *Biochem. Cell Biol.* **2002**, *80*, 125–130.
17. Ibrahim, H. R.; Sugimoto, Y.; Aoki, T. *Biochim. Biophys. Acta* **2000**, *1523*, 196–205.
18. Braun, V.; Killmann, H. *Trends Biochem. Sci.* **1999**, *24*, 104–109.
19. Stintzi, A.; Raymond, K. N. In *Molecular and Cellular Iron Transport*; Templeton, D. M., Ed.; Marcel Dekker: New York, 2002; pp 273–320.
20. Moeck, G. S.; Coulton, J. W. *Mol. Microbiol.* **1998**, *28*, 675–681.
21. Braun, V.; Hantke, K. In *Molecular and Cellular Iron Transport*; Templeton, D. M., Ed.; Marcel Dekker: New York, 2002; pp 395–426.
22. Wandersman, C.; Stojiljkovic, I. *Curr. Opin. Microbiol.* **2000**, *3*, 215–220.
23. Braun, V. *Int. J. Med. Microbiol.* **2001**, *291*, 67–79.
24. Braun, V.; Hantke, K.; Koster, W. In *Metal Ions in Biological Systems: Iron Transport and Storage in Microorganisms, Plants, and Animals*; Sigel, A., Sigel, D., Eds.; Marcel Dekker: New York, 1998; Vol. 35, pp 67–145.
25. Drechsel, H.; Jung, G. *J. Pept. Sci.* **1998**, *4*, 147–181.
26. Pollack, J. R.; Neilands, J. B. *Biochem. Biophys. Res. Commun.* **1970**, *38*, 989–992.

27. O'Brien, I. G.; Gibson, F. *Biochem. Biophys. Acta* **1970**, *215*, 393–402.
28. Fiedler, H. P.; Krastel, P.; Muller, J.; Gebhardt, K.; Zeeck, A. *FEMS Microbiol. Lett.* **2001**, *196*, 147–151.
29. Budzikiewicz, H.; Boessenkamp, A.; Taraz, K.; Pandey, A.; Meyer, J. M. *Z. Naturforsch.* **1997**, *52*, 551–554.
30. May, J. J.; Wendrich, T. M.; Marahiel, M. A. *J. Biol. Chem.* **2001**, *276*, 7209–7217.
31. Telford, J. R.; Raymond, K. N. *J. Biol. Inorg. Chem.* **1997**, *2*, 750–761.
32. Telford, J. R.; Leary, J. A.; Tunstad, L. M. G.; Byers, B. R.; Raymond, K. N. *J. Am. Chem. Soc.* **1994**, *116*, 4499–4500.
33. Adolphs, M.; Taraz, K.; Budzikiewicz, H. *Z. Naturforsch.* **1996**, *51*, 281–285.
34. Ehlert, G.; Taraz, K.; Budzikiewicz, H. *Z. Naturforsch.* **1994**, *49*, 11–17.
35. Barelmann, I.; Meyer, J. M.; Taraz, K.; Budzikiewicz, H. *Z. Naturforsch.* **1996**, *51*, 627–630.
36. Howard, D. H. *Clin. Microbiol. Rev.* **1999**, *12*, 394–404.
37. Iijima, M.; Someno, T.; Amemiya, M.; Sawa, R.; Naganawa, H.; Ishizuka, M.; Takeuchi, T. *J. Antibiot.* **1999**, *52*, 25–28.
38. Iijima, M.; Someno, T.; Imada, C.; Okami, Y.; Ishizuka, M.; Takeuchi, T. *J. Antibiot.* **1999**, *52*, 20–24.
39. Iijima, M.; Someno, T.; Amemiya, M.; Ishizuka, M.; Naganawa, H.; Takeuchi, T. *J. Antibiot.* **2000**, *53*, 1411–1415.
40. Dhungana, S.; White, P. S.; Crumbliss, A. L. *J. Biol. Inorg. Chem.* **2001**, *6*, 810–818.
41. Neu, M. P.; Matonic, J. H.; Ruggiero, C. E.; Scott, B. L. *Angew. Chem., Int. Ed. Engl.* **2000**, *39*, 1341, 1442–1444.
42. van der Helm, D.; Poling, M. *J. Am. Chem. Soc.* **1976**, *98*, 82–86.
43. Hou, Z. G.; Sunderland, C. J.; Nishio, T.; Raymond, K. N. *J. Am. Chem. Soc.* **1996**, *118*, 5148–5149.
44. Muenzinger, M.; Taraz, K.; Budzikiewicz, H.; Drechsel, H.; Heymann, P.; Winkelmann, G.; Meyer, J.-M. *Biometals* **1999**, *12*, 189–193.
45. Muenzinger, M.; Budzikiewicz, H.; Expert, D.; Enard, C.; Meyer, J.-M. *Z. Naturforsch.* **2000**, *55*, 328–332.
46. Risse, D.; Beiderbeck, H.; Taraz, K.; Budzikiewicz, H.; Gustine, D. *Z. Naturforsch.* **1998**, *53*, 295–304.
47. Muenzinger, M.; Taraz, K.; Budzikiewicz, H. *Z. Naturforsch.* **1999**, *54*, 867–875.
48. Wells, M. L.; Price, N. M.; Bruland, K. W. *Mar. Chem.* **1995**, *48*, 157–182.
49. Wu, J.; Boyle, E.; Sunda, W.; Wen, L.-S. *Science* **2001**, *293*, 847–849.
50. Butler, A. *Science* **1998**, *281*, 207–210.
51. Macrellis, H. M.; Trick, C. G.; Rue, E. L.; Smith, G.; Bruland, K. W. *Mar. Chem.* **2001**, *76*, 175–187.
52. Rue, E. L.; Bruland, K. W. *Mar. Chem.* **1995**, *50*, 117–138.
53. Martinez, J. S.; Haygood, M. G.; Butler, A. *Limnol. Oceanogr.* **2001**, *46*, 420–424.
54. Martinez, J. S.; Zhang, G. P.; Holt, P. D.; Jung, H. T.; Carrano, C. J.; Haygood, M. G.; Butler, A. *Science* **2000**, *287*, 1245–1247.
55. Barbeau, K.; Zhang, G.; Live, D. H.; Butler, A. *J. Am. Chem. Soc.* **2002**, *124*, 378–379.
56. Ongena, M.; Jacques, P.; Thonart, P.; Gwose, I.; Fernandez, D. U.; Schaefer, M.; Budzikiewicz, H. *Tetrahedron Lett.* **2001**, *42*, 5849–5851.
57. Amann, C.; Taraz, K.; Budzikiewicz, H.; Meyer, J.-M. *Z. Naturforsch.* **2000**, *55*, 671–680.
58. Weber, M.; Taraz, K.; Budzikiewicz, H.; Geoffroy, V.; Meyer, J.-M. *Biometals* **2000**, *13*, 301–309.
59. Mossialos, D.; Meyer, J.-M.; Budzikiewicz, H.; Wolff, U.; Koedam, N.; Baysse, C.; Anjaiah, V.; Cornelis, P. *Appl. Environ. Microbiol.* **2000**, *66*, 487–492.
60. Khalil–Rizvi, S.; Toth, S. I.; Van Der Helm, D.; Vidavsky, I.; Gross, M. L. *Biochemistry* **1997**, *36*, 4163–4171.
61. Ruangviryachai, C.; Barelmann, I.; Fuchs, R.; Budzikiewicz, H. *Z. Naturforsch.* **2000**, *55*, 323–327.
62. Fernandez, D. U.; Fuchs, R.; Taraz, K.; Budzikiewicz, H.; Munsch, P.; Meyer, J.-M. *Biometals* **2001**, *14*, 81–84.
63. Schaffner, E. M.; Hartmann, R.; Taraz, K.; Budzikiewicz, H. *Z. Naturforsch.* **1996**, *51*, 139–150.
64. Carrano, C. J.; Jordan, M.; Drechsel, H.; Schmid, D. G.; Winkelmann, G. *Biometals* **2001**, *14*, 119–125.
65. Vergne, A. F.; Walz, A. J.; Miller, M. J. *Nat. Prod. Rep.* **2000**, *17*, 99–116.
66. De Voss, J. J.; Rutter, K.; Schroeder, B. G.; Barry, C. E. *J. Bacteriol.* **1999**, *181*, 4443–4451.
67. Gobin, J.; Moore, C. H.; Reeve, J. R.; Wong, D. K.; Gibson, B. W.; Horwitz, M. A. *Proc. Natl. Acad. Sci. USA* **1995**, *92*, 5189–5193.
68. Beiderbeck, H.; Taraz, K.; Budzikiewicz, H.; Walsby, A. E. *Z. Naturforsch.* **2000**, *55*, 681–687.
69. Itou, Y.; Okada, S.; Murakami, M. *Tetrahedron* **2001**, *57*, 9093–9099.
70. Braun, V. *Drug Resist. Update* **1999**, *2*, 363–369.
71. Heggemann, S.; Schnabelrauch, M.; Klemm, D.; Moellmann, U.; Reissbrodt, R.; Heinisch, L. *Biometals* **2001**, *14*, 1–11.
72. Loomis, L. D.; Raymond, K. N. *Inorg. Chem.* **1991**, *30*, 906–911.
73. Matsumoto, K.; Ozawa, T.; Jitsukawa, K.; Einaga, H.; Masuda, H. *Chem. Commun.* **2001**, 978–979.
74. Cooper, S. R.; McArdle, J. V.; Raymond, K. N. *Proc. Natl. Acad. Sci. USA* **1978**, *75*, 3551–3554.
75. O'Brien, I. G.; Cox, G. B.; Gibson, F. *Biochim. Biophys. Acta* **1971**, *237*, 537–549.
76. Brickman, T. J.; McIntosh, M. A. *J. Biol. Chem.* **1992**, *267*, 12350–12355.
77. Matzanke, B. F.; Ecker, D. J.; Yang, T. S.; Huynh, B. H.; Mueller, G.; Raymond, K. N. *J. Bacteriol.* **1986**, *167*, 674–680.
78. Cass, M. E.; Garrett, T. M.; Raymond, K. N. *J. Am. Chem. Soc.* **1989**, *111*, 1977–1682.
79. Ratledge, C.; Dover, L. G. *Ann. Rev. Microbiol.* **2000**, *54*, 881–941.
80. Pecoraro, V. L.; Harris, W. R.; Wong, G. B.; Carrano, C. J.; Raymond, K. N. *J. Am. Chem. Soc.* **1983**, *105*, 4623–4633.
81. Pecoraro, V. L.; Wong, G. B.; Kent, T. A.; Raymond, K. N. *J. Am. Chem. Soc.* **1983**, 4617–4623.
82. Cohen, S. M.; Meyer, M.; Raymond, K. N. *J. Am. Chem. Soc.* **1998**, *120*, 6277–6286.
83. Karpishin, T. B.; Dewey, T. M.; Raymond, K. N. *J. Am. Chem. Soc.* **1993**, *115*, 1842–1851.
84. Stack, T. D. P.; Karpishin, T. B.; Raymond, K. N. *J. Am. Chem. Soc.* **1992**, *114*, 1512–1514.
85. Dhungana, S.; Heggemann, S.; Heinisch, L.; Mollmann, U.; Boukhalfa, H.; Crumbliss, A. L. *Inorg. Chem.* **2001**, *40*, 7079–7086.
86. Hou, Z. G. In *Chemistry*; University of California Press: Berkeley, CA, 1995; p 152.
87. Schwarzenbach, G.; Flaschka, H. *Complexometric Titrations*, 2nd ed.; Methuen: London, 1969.
88. Anderegg, G.; L'Eplattenier, F.; Schwarzenbach, G. *Helv. Chim. Acta* **1963**, *46*, 1409–1422.

89. pM $= -\log [Fe^{3+}]$; $[L] = 10^{-5}M$, $[M] = 10^{-6}M$.
90. Hou, Z. G.; Stack, T. D. P.; Sunderland, C. J.; Raymond, K. N. *Inorg. Chim. Acta* **1997**, *263*, 341–355.
91. Kretchmar, S. A.; Reyes, Z. E.; Raymond, K. N. *Biochim. Biophys. Acta* **1988**, *956*, 85–94.
92. Kraiter, D. C.; Zak, O.; Aisen, P.; Crumbliss, A. L. *Inorg. Chem.* **1998**, *37*, 964–968.
93. Braun, V. *FEMS Microbiol. Rev.* **1995**, *16*, 295–307.
94. Usher, K. C.; Ozkan, E.; Gardner, K. H.; Deisenhofer, J. *Proc. Natl. Acad. Sci. USA.* **2001**, *98*, 10676–10681.
95. Hantke, K. *Curr. Opin. Microbiol.* **2001**, *4*, 172–177.
96. Koebnik, R.; Locher, K. P.; Van Gelder, P. *Mol. Microbiol.* **2000**, *37*, 239–253.
97. Chang, C. S.; Mooser, A.; Pluckthun, A.; Wlodawer, A. *J. Biol. Chem.* **2001**, *276*, 27535–27540.
98. Ferguson, A. D.; Hofmann, E.; Coulton, J. W.; Diederichs, K.; Welte, W. *Science* **1998**, *282*, 2215–2220.
99. Locher, K.; Rees, B.; Koebnik, R.; Mitschler, A.; Moulinier, L.; Rosenbusch, J. P.; Moras, D. *Cell* **1998**, *95*, 771–778.
100. Buchanan, S. K.; Smith, B. S.; Venkatramani, L.; Xia, D.; Esser, L.; Palnitakar, M.; Chakraborty, R.; Van Der Helm, D.; Deisenhofer, J. *Nat. Struct. Biol.* **1999**, *6*, 56–63.
101. Ferguson, A. D.; Chakraborty, R.; Smith, B. S.; Esser, L.; Van Der Helm, D.; Deisenhofer, J. *Science* **2002**, *295*, 1715–1719.
102. Koster, W. *Res. Microbiol.* **2001**, *152*, 291–301.
103. Clarke, T. E.; Ku, S.-Y.; Dougan, D. R.; Vogel, H. J.; Tari, L. W. *Nat. Struct. Biol.* **2000**, *7*, 287–291.
104. Clarke, T. E.; Rohrbach, M. R.; Tari, L. W.; Vogel, H. J.; Koester, W. *Biometals* **2002**, *15*, 121–131.
105. Sprencel, C.; Cao, Z.; Qi, Z.; Scott, D. C.; Montague, M. A.; Ivanoff, N.; Xu, J.; Raymond, K. M.; Newton, S.M. C.; Klebba, P. E. *J. Bacteriol.* **2000**, *182*, 5359–5364.
106. Wyckoff, E. E.; Valle, A.-M.; Smith, S. L.; Payne, S. M. *J. Bacteriol.* **1999**, *181*, 7588–7596.
107. Rohrbach, M. R.; Braun, V.; Koester, W. *J. Bacteriol.* **1995**, *177*, 7186–7193.
108. Mademidis, A.; Killmann, H.; Kraas, W.; Flechsler, I.; Jung, G.; Braun, V. *Mol. Microbiol.* **1997**, *26*, 1109–1123.
109. Lim, Y.; Shin, S. H.; Lee, S. I.; Kim, I. S.; Rhee, J. H. *FEMS Microbiol. Lett.* **1998**, *163*, 19–24.
110. Schneider, R.; Hantke, K. *Mol. Microbiol.* **1993**, *8*, 111–121.
111. Meiwes, J.; Fiedler, H. P.; Haag, H.; Zahner, H.; Konetschnyrapp, S.; Jung, G. *FEMS Microbiol. Lett.* **1990**, *67*, 201–205.
112. Drechsel, H.; Freund, S.; Nicholson, G.; Haag, H.; Jung, O.; Zahner, H.; Jung, G. *Biometals* **1993**, *6*, 185–192.
113. Courcol, R. J.; Trivier, D.; Bissinger, M. C.; Martin, G. R.; Brown, M. R. W. *Infect. Immun.* **1997**, *65*, 1944–1948.
114. Sebulsky, M. T.; Heinrichs, D. E. *J. Bacteriol.* **2001**, *183*, 4994–5000.
115. Sebulsky, M. T.; Hohnstein, D.; Hunter, M. D.; Heinrichs, D. E. *J. Bacteriol.* **2000**, *182*, 4394–4400.
116. Cabrera, G.; Xiong, A.; Uebel, M.; Singh, V. K.; Jayaswal, R. K. *Appl. Environ. Microbiol.* **2001**, *67*, 1001–1003.
117. Heinrichs, J. H.; Gatlin, L. E.; Kunsch, C.; Choi, G. H.; Hanson, M. S. *J. Bacteriol.* **1999**, *181*, 1436–1443.
118. Morrissey, J. A.; Cockayne, A.; Hill, P. J.; Williams, P. *Infect. Immun.* **2000**, *68*, 6281–6288.
119. Stintzi, A.; Barnes, C.; Xu, L.; Raymond, K. N. *Proc. Natl. Acad. Sci. USA.* **2000**, *97*, 10691–10696.
120. Schalk, I. J.; Abdallah, M. A.; Pattus, F. *Biochem. Soc. Trans.* **2002**, *30*, 702–705.
121. MacGillivray, R. T. A.; Mason, A. B. In *Molecular and Cellular Iron Transport*; Templeton, D. M., Ed.; Marcel Dekker: New York, 2002; pp 41–70.
122. Ferreiros, C.; Criado, M. T.; Gomez, J. A. *Comp. Biochem. Physiol. B* **1999**, *123*, 1–7.
123. Baker, E. N.; Baker, H. M.; Kidd, R. D. *Biochem. Cell Biol.* **2002**, *80*, 27–34.
124. Nichol, H.; Law, J. H.; Winzerling, J. J. *Ann. Rev. Entomol.* **2002**, *47*, 535–559.
125. Richardson, D. R. *Eur. J. Biochem.* **2000**, *267*, 1290–1298.
126. Sun, H. Z.; Li, H. Y.; Sadler, P. J. *Chem. Rev.* **1999**, *99*, 2817–2842.
127. Park, I.; Schaeffer, E.; Sidoli, A.; Baralle, F. E.; Cohen, G. N.; Zakin, M. M. *Proc. Natl. Acad. Sci. USA.* **1985**, *82*, 3149–3153.
128. Sekyere, E.; Richardson, D. R. *FEBS Lett.* **2000**, *483*, 11–16.
129. Choudhury, D.; Thakurta, P. G.; Dasgupta, R.; Sen, U.; Biswas, S.; Chakrabarti, C.; Dattagupta, J. K. *Biochem. Biophys. Res. Commun.* **2002**, *295*, 125–128.
130. Hall, D. R.; Hadden, J. M.; Leonard, G. A.; Bailey, S.; Neu, M.; Winn, M.; Lindley, P. F. *Acta Crystallogr. D: Biol. Cryst.* **2002**, *58*, 70–80.
131. Aisen, P. *Metal Ions Biol. Syst.* **1998**, *35*, 585–631.
132. Conrad, M. E. *J. Trace Elem. Exp. Med.* **2001**, *14*, 115–117.
133. Harris, D. C.; Aisen, P. In *Iron Carriers and Iron Proteins*; Loehr, T., Ed.; VCH: New York, 1989; Vol. 5, pp 241–351.
134. Li, H. Y.; Qian, Z. M. *Med. Res. Rev.* **2002**, *22*, 225–250.
135. Williams, J. *TIBS* **1982**, *7*, 394–397.
136. Williams, J.; Grace, S. A.; Williams, J. M. *Biochem. J.* **1982**, *201*, 417.
137. Baker, H. M.; Mason, A. B.; He, Q. Y.; MacGillivray, R. T. A.; Baker, E. N. *Biochemistry* **2001**, *40*, 11670–11675.
138. Gasdaska, J. R.; Law, J. H.; Bender, C. J.; Aisen, P. *J. Inorg. Biochem.* **1996**, *64*, 247–258.
139. Brock, J. H. *Biochem. Cell Biol.* **2002**, *80*, 1–6.
140. Peterson, N. A.; Anderson, B. F.; Jameson, G. B.; Tweedie, J. W.; Baker, E. N. *Biochemistry* **2000**, *39*, 6625–6633.
141. Suzuki, Y.; Lonnerdal, B. *Biochem. Cell Biol.* **2002**, *80*, 75–80.
142. Sharma, A. K.; Kumar, S.; Sharma, V.; Nagpal, A.; Singh, N.; Tamboli, I.; Mani, I.; Raman, G.; Singh, T. P. *Proteins* **2001**, *45*, 229–236.
143. Alcantara, J.; Schryvers, A. B. *Microb. Pathog.* **1996**, *20*, 73–85.
144. Abdallah, F. B.; Chahine, J. M. E. *Eur. J. Biochem.* **1998**, *258*, 1022–1031.
145. Abdallah, F. B.; Chahine, J. M. E. *Eur. J. Biochem.* **1999**, *263*, 912–920.
146. Mizutani, K.; Muralidhara, B. K.; Yamashita, H.; Tabata, S.; Mikami, B.; Hirose, M. *J. Biol. Chem.* **2001**, *276*, 35940–35946.
147. Muralidhara, B. K.; Hirose, M. *J. Biol. Chem.* **2000**, *275*, 12463–12469.
148. Mietzner, T. A.; Tencza, S. B.; Adhikari, P.; Vaughan, K. G.; Nowalk, A. J. In *Bacterial Infection: Close Encounters at the Host Pathogen Interface*; Vogt, P. K., Mahan, M. J., Eds.; Springer: Berlin, 1998; Vol. 225, pp 113–135.
149. Nowalk, A. J.; Tencza, S. B.; Mietzner, T. A. *Biochemistry* **1994**, *33*, 12769–12775.

150. Bruns, C. M.; Nowalk, A. J.; Arvai, A. S.; McTigue, M. A.; Vaughan, K. G.; Mietzner, T. A.; McRee, D. E. *Nat. Struct. Biol.* **1997**, *4*, 919–924.
151. Bruns, C. M.; Anderson, D. S.; Vaughan, K. G.; Williams, P. A.; Nowalk, A. J.; McRee, D. E.; Mietzner, T. A. *Biochemistry* **2001**, *40*, 15631–15637.
152. Baker, E. N.; Rumball, S. V.; Anderson, B. F. *Trends Biochem. Sci.* **1987**, *12*, 350–353.
153. Anderson, B. F.; Baker, H. M.; Norris, G. E.; Rice, D. W.; Baker, E. N. *J. Mol. Biol.* **1989**, *209*, 711–734.
154. Cowart, R. E.; Kojima, N.; Bates, G. W. *J. Biol. Chem.* **1982**, *257*, 7560–7565.
155. Kojima, N.; Bates, G. W. *J. Biol. Chem.* **1981**, *256*, 12034–12039.
156. Brown, J. P.; Hewick, R. H.; Hellstrom, I.; Hellstrom, K. E.; Doolittle, R. F.; Dreyer, W. J. *Nature* **1982**, *296*, 171–173.
157. Rose, T. M.; Plowman, G. D.; Teplow, D. B.; Dreyer, W. J.; Hellstrom, K. E.; Brown, J. P. *Proc. Natl. Acad. Sci. USA.* **1986**, *83*, 1261–1265.
158. Alemany, R.; Vila, M. R.; Franci, C.; Egea, G.; Real, F. X.; Thomson, T. M. *J. Cell Sci.* **1993**, *104*, 1155–1162.
159. Natali, P. G.; Roberts, J. T.; Difilippo, F.; Bigotti, A.; Dent, P. B.; Ferrone, S.; Liao, S. K. *Cancer* **1987**, *59*, 55–63.
160. Sciot, R.; De Vos, R.; Van Eyken, P.; Van der Steen, K.; Moerman, P.; Desmet, V. J. *Liver* **1989**, *9*, 110–119.
161. Rothenberger, S.; Food, M. R.; Gabathuler, R.; Kennard, M. L.; Yamada, T.; Yasuhara, O.; McGeer, P. L.; Jefferies, W. A. *Brain Res.* **1996**, *712*, 117–121.
162. Jefferies, W. A.; Food, M. R.; Gabathuler, R.; Rothenberger, S.; Tamada, T.; Yasuhara, O.; McGeer, P. L. *Brain Res.* **1996**, *712*, 122–126.
163. Kwok, J. C.; Richardson, D. R. *Crit. Rev. Oncol. Hematol.* **2002**, *42*, 65–78.
164. Sekyere, E.; Food, M. R.; Richardson, D. R. *FEBS Lett.* **2002**, *512*, 350–352.
165. Kennard, M. L.; Richardson, D. R.; Gabathuler, R.; Ponka, P.; Jefferies, W. A. *EMBO J.* **1995**, *14*, 4178–4186.
166. Richardson, D. R.; Baker, E. *Biochim. Biophys. Acta* **1991**, *1091*, 294–304.
167. Garratt, R. C.; Jhoti, H. *FEBS Lett.* **1992**, *305*, 55–61.
168. Kennard, M. L.; Richardson, D. R.; Gabathuler, R.; Ponka, P.; Jefferies, W. A. *Nature Med.* **1996**, *2*, 1230–1235.
169. Kim, D. K.; Seo, M. Y.; Lim, S.-W.; Kim, S.; Kim, J.-W.; Carroll, B. J.; Kwon, D. Y.; Kwon, T.; Kang, S. S. *Neuropsychopharm.* **2001**, *25*, 84–90.
170. Trinder, D.; Morgan, E. In *Molecular and Cellular Iron Transport*; Templeton, D. M., Ed.; Marcel Dekker: New York, 2002; pp 427–449.
171. Aisen, P.; Enns, C.; Wessling-Resnick, M. *Inter. J. Biochem. Cell Biol.* **2001**, *33*, 940–959.
172. Andrews, N. C. *Curr. Opin. Chem. Biol.* **2002**, *6*, 181–186.
173. Ponka, P.; Lok, C. N. *Inter. J. Biochem. Cell Biol.* **1999**, *31*, 1111–1137.
174. Enns, C. A. In *Molecular and Cellular Iron Transport*; Templeton, D. M., Ed.; Marcel Dekker: New York, 2002; pp 71–94.
175. Young, S. P.; Bomford, A.; Williams, R. *Biochem. J.* **1984**, *219*, 505–510.
176. Lawrence, C. M.; Ray, S.; Babyonyshev, M.; Galluser, R.; Borhani, D. W.; Harrison, S. C. *Science* **1999**, *286*, 779–782.
177. Mason, A. B.; Tam, B.; Woodworth, R. C.; Oliver, R. W. A.; Green, B. N.; Lin, L. N.; Brandts, J. F.; Savage, K. J.; Linbeack, J. A.; MacGillivray, R. T. A. *Biochem. J.* **1997**, *326*, 77–85.
178. Zak, O.; Trinder, D.; Aisen, P. *J. Biol. Chem.* **1994**, *269*, 7100–7114.
179. Kawabata, H.; Yang, S.; Hirama, T.; Vuong, P. T.; Kawano, S.; Gombart, A. F.; Koeffler, H. P. *J. Biol. Chem.* **1999**, *274*, 20826–20832.
180. Kawabata, H.; Germain, R. S.; Vuong, P. T.; Nakamaki, T.; Said, J. W.; Koeffler, H. P. *J. Biol. Chem.* **2000**, *275*, 16618–16625.
181. West, A. P.; Bennett, M. J.; Sellers, V. M.; Andrews, N. C.; Enns, C. A.; Bjorkman, P. J. *J. Biol. Chem.* **2000**, *275*, 38135–38138.
182. Camaschella, C.; Roetto, A.; Cali, A.; De Gobbi, M.; Garozzo, G.; Carella, M.; Majorano, N.; Totaro, A.; Gasparini, P. *Nat. Genet.* **2000**, *25*, 14–15.
183. Beutler, E. *Blood* **2001**, *27*, 294–295.
184. Mizutani, K.; Yamashita, H.; Kurokawa, H.; Mikami, B.; Hirose, M. *J. Biol. Chem.* **1999**, *274*, 10190–10194.
185. Kuser, P.; Hall, D. R.; Haw, M. L.; Neu, M.; Evans, R. W.; Lindley, P. F. *Acta Crystallogr. D–Biol. Cryst.* **2002**, *58*, 777–783.
186. Khan, J. A.; Kumar, P.; Srinivasan, A.; Singh, T. P. *J. Biol. Chem.* **2001**, *276*, 36817–36823.
187. Mizutani, K.; Mikami, B.; Hirose, M. *J. Mol. Biol.* **2001**, *309*, 937–947.
188. He, Q. Y.; Mason, A. B.; Woodworth, R. C.; Tam, B. M.; MacGillivray, R. T. A.; Grady, J. K.; Chasteen, N. D. *Biochemistry* **1997**, *36*, 14853–14860.
189. He, Q. Y.; Mason, A. B.; Woodworth, R. C.; Tam, B. M.; Wadsworth, T.; MacGillivray, R. T. A. *Biochemistry* **1997**, *36*, 5522–5528.
190. He, Q. Y.; Mason, A. B.; Pakdaman, R.; Chasteen, N. D.; Dixon, B. K.; Tam, B. M.; Nguyen, V.; MacGillivray, R. T. A.; Woodworth, R. C. *Biochemistry* **2000**, *39*, 1205–1210.
191. Zak, O.; Ikuta, K.; Aisen, P. *Biochemistry* **2002**, *41*, 7416–7423.
192. MacGillivray, R. T. A.; Moore, S. A.; Chen, J.; Anderson, B. F.; Baker, H.; Luo, Y. G.; Bewley, M.; Smith, C. A.; Murphy, M. E. P.; Wang, Y.; Mason, A. B.; Woodworth, R. C.; Brayer, G. D.; Baker, E. N. *Biochemistry* **1998**, *37*, 7919–7928.
193. Dewan, J. C.; Mikami, B.; Hirose, M.; Sacchettini, J. C. *Biochemistry* **1993**, *32*, 11963–11968.
194. Steinlein, L. M.; Ligman, C. M.; Kessler, S.; Ikeda, R. A. *Biochemistry* **1998**, *37*, 13696–13703.
195. Nurizzo, D.; Baker, H. M.; He, Q. Y.; MacGillivray, R. T. A.; Mason, A. B.; Woodworth, R. C.; Baker, E. N. *Biochemistry* **2001**, *40*, 1616–1623.
196. He, Q. Y.; Mason, A. B.; Tam, B. M.; MacGillivray, R. T. A.; Woodworth, R. C. *Biochemistry* **1999**, *38*, 9704–9711.
197. Kretchmar, S. A.; Raymond, K. N. *Inorg. Chem.* **1988**, *27*, 1436–1441.
198. He, Q. Y.; Mason, A. B. In *Molecular and Cellular Iron Transport*; Templeton, D. M., Ed.; Marcel Dekker: New York, 2002; pp 95–124.
199. Zak, O.; Tam, B.; MacGillivray, R. T. A.; Aisen, P. *Biochemistry* **1997**, *36*, 11036–11043.

200. Li, Y.; Harris, W. R.; Maxwell, A.; Macgillivray, R. T. A.; Brown, T. *Biochemistry* **1998**, *37*, 14157–14166.
201. Harris, W. R.; Cafferty, A. M.; Trankler, K.; Maxwell, A.; MacGillivray, R. T. A. *Biochim. Biophys. Acta* **1999**, *1430*, 269–280.
202. He, Q. Y.; Mason, A. B.; Nguyen, V.; MacGillivray, R. T. A.; Woodworth, R. C. *Biochem. J.* **2000**, *350*, 909–915.
203. Marques, H. M.; Walton, T.; Egan, T. J. *J. Inorg. Biochem.* **1995**, *57*, 11–21.
204. Turcot, I.; Stintzi, A.; Xu, J. D.; Raymond, K. N. *J. Biol. Inorg. Chem.* **2000**, *5*, 634–641.
205. Ford, S.; Cooper, R. A.; Evans, R. W.; Hider, R. C.; Williams, P. H. *Eur. J. Biochem.* **1988**, *178*, 477–481.
206. Stintzi, A.; Raymond, K. N. *J. Biol. Inorg. Chem.* **2000**, *5*, 57–66.
207. Harris, W. R.; Bao, G. *Polyhedron* **1997**, *16*, 1069–1079.
208. Gray-Owen, S. D.; Schryvers, A. B. *Trends Microbiol.* **1996**, *4*, 185–191.
209. Yu, R. H.; Schryvers, A. B. *Biochem. Cell Biol.* **2002**, *80*, 81–90.
210. Gomez, J. A.; Criado, M. T.; Ferreiros, C. M. *Res. Microbiol.* **1998**, *149*, 381–387.
211. Fuller, C. A.; Yu, R.; Irwin, S. W.; Schryvers, A. B. *Microb. Pathog.* **1998**, *24*, 75–87.
212. Prinz, T.; Meyer, M.; Pettersson, A.; Tommassen, J. *J. Bacteriol.* **1999**, *181*, 4417–4419.
213. Schryvers, A. B.; Stojiljkovic, I. *Mol. Microbiol.* **1999**, *32*, 1117–1123.
214. Demchick, P.; Koch, A. L. *J. Bacteriol.* **1996**, *178*, 768–773.
215. Dijkstra, A. J.; Keck, W. *J. Bacteriol.* **1996**, *178*, 5555–5562.
216. Taylor, J. M.; Heinrichs, D. E. *Mol. Microbiol.* **2002**, *43*, 1603–1614.
217. Modun, B.; Williams, P. *Infect. Immun.* **1999**, *67*, 1086–1092.
218. Taboy, C. H.; Vaughan, K. G.; Mietzner, T. A.; Aisen, P.; Crumbliss, A. L. *J. Biol. Chem.* **2001**, *276*, 2719–2724.
219. Müller, G.; Matzanke, B. F.; Raymond, K. N. *J. Bacteriol.* **1984**, *160*, 313–318.

8.7
Ferritins

A. K. POWELL
Universität Karlsruhe, Germany

8.7.1   INTRODUCTION

Iron is an essential element for life with diverse roles such as in oxygen transport and storage, electron cycling and storage, and a variety of catalytic functions; these aspects are reviewed elsewhere in this volume. Because of the insolubility of iron(III) under hydrolyzing conditions where it forms oxyhydroxides and oxides it was necessary for living organisms to develop efficient mechanisms for the acquisition of iron from the environment and for its storage and protection from unwanted iron-mediated toxicity where free radical production leads to cell damage. Since iron is difficult to acquire in most organisms it is recycled with the iron excess to immediate requirements stored within the protein ferritin. Since the early 1980s much has been learnt about the protein with many methods applied to investigating the various aspects associated with iron storage, and in this chapter the progress made is reviewed with particular emphasis on the aspects relevant to coordination chemistry.

Ferritins are metalloproteins that can contain unusually large amounts of metal, since their principal function is the storage of iron in an inert but accessible form. Ferritins are found in all phyla, but those deriving from animals have been the most extensively studied. The motivation of studying iron homeostasis in humans has also resulted in a thorough investigation of the distribution of ferritin proteins and this reveals that while ferritins occur throughout the body, those found in the liver and spleen have much greater storage roles than those found in, for example, the brain and heart.[1]

While research has shown that the iron oxyhydroxide cores in animal ferritins have the sole purpose of acting as iron storage sites, phosphate can also be associated with these cores and the levels depend on local conditions. In the case of bacterioferritins the native cores always seem to incorporate phosphate and there is some debate as to whether the molecules also perform the further function of phosphate storage.[1] Interestingly, the cavity of bacterioferritins such as those from *Eschirichia coli* can also be used as a reaction vessel to lay down a variety of other mineral cores. Studies indicate that while details of the protein sequence and structure can vary, overall ferritin proteins can be regarded as possessing a constant set of structural motifs and it is these which are of particular relevance to coordination chemistry.

8.7.2   GENERAL STRUCTURAL AND CHEMICAL ASPECTS

8.7.2.1   Details of the Tertiary and Quaternary Protein Structure

In Table 1 some details and references for the 26 structures for which coordinates have been deposited in the Protein Data Bank are summarized. All of the systems listed have the ability to deposit mineralized iron oxyhydroxide cores and many of them have been engineered to probe certain structural or mechanistic features of the native systems. Three of the entries concern the ferritin-like proteins from *Listeria innocua* and *Helicobacter pylori* as well as the dps DNA-binding protein from *Eschirichia coli*, which are smaller than the "true" ferritins having only 12 rather than 24 protein subunits enclosing the central cavity. These proteins are used by the relevant bacteria to sequester iron especially under iron starvation conditions and have been recognized to have important health implications in a variety of infections. Since the iron uptake, storage, and release from these have not been studied in any great detail these will not be discussed further here and are included in Table 1 for completeness and also with the expectation that future studies will shed light on the nature of iron storage and the mineral core which is expected to contain around 500 iron centers.

The other structures that have been deposited derive from both animal and bacterial forms. One important aspect in which these forms differ is that the native bacterial forms from *E. coli* and *Rhodobacter capsulatus* are found to have heme groups associated with them whereas horse, mouse, and frog ferritins are heme free. Binding studies show that heme groups can be bound to the animal proteins and for this reason the study to assess protoporphyrin IX binding (as a tin complex) to apoferritin from horse spleen (PDB code 1hrs) was performed. In addition, bacterio-ferritins from *E. coli* can be engineered to crystallize without heme (PDB code 1eum), thus acting like an animal ferritin, and providing a useful system for investigating iron reaction chemistry in a ferritin system which can be readily produced in the laboratory rather than having to be obtained commercially as is generally the case for animal ferritins. In addition, other engineered ferritins have been produced in order to test mechanistic and binding hypotheses as will be discussed later in this chapter.

Looking back at the unfolding of the ferritin story up to our current level of knowledge it can be seen how the development of analytical techniques has helped to improve our understanding of the structural and functional aspects of iron homeostasis. The progress made in protein crystal-lography over the years provides a particularly striking example. Thus, although ferritin was first isolated from mammalian spleen and liver by Laufberger[2] in 1937, the crystallization of the protein from horse spleen was first reported in 1963 by Harrison.[3] These crystals were of loaded ferritin and only very low-resolution data at 6 Å could be obtained[4,5] on this orthorhombic form. Subsequently it was found that better data could be obtained on the apoferritin (i.e., free of the metal core) which crystallizes in the cubic space group $F432$.[6,7] Several structures for horse, mouse, human, and frog ferritins have now been determined and the coordinates deposited in the Protein Data Bank (see Table 1[8-29]) in some cases on recombinant forms. So far for animal ferritins, only HoSF crystallizing in space groups other than $F432$ has been investigated and the

Table 1 Summary of ferritin and related structures with coordinates deposited at the PDB.

PDB code	Source	Resolution (Å)	Comments	References
1aew	Horse apoferritin	1.95	Cubic form. Engineered and expressed in *E. coli*	8
1bcf	*E. coli*	2.9	Identification of heme binding	9
1bfr	*E. coli*	2.94	Monoclinic form of bfr	10
1bg7	Frog	1.85	Engineered and expressed in *E. coli* with mutation lys82gln and leu134pro	11
1dat	Horse apoferritin	2.05	Cubic form. Engineered and expressed in *E. coli*	12[a]
1dps	*E. coli*	1.6	Ferritin 12-mer homologue that binds and protects DNA. Mutation of ser164cys. 23 symmetry	13
1eum	*E. coli*	2.05	Engineered to remove heme groups. Known as ecFTN	14
1f61	*Mycobacterium tuberculosis*	2.0	Isocitrate lyase. Engineered and expressed in *E. coli*	15
1fha	Human	2.4	Recombinant H-chain expressed in *E. coli* with mutation lys86gln	16
1gwg	Horse	2.01	HoSF light chain expressed in *E. coli*. Used as part of a test for triiodide heavy atom phasing	17
1h96	Mouse	1.6	Mouse light chain expressed in *E. coli* with thr121ala	18
1hrs	Horse	2.6	HoLF cocrystallized with Sn-protoporphyrin IX to investigate heme binding	19
1ier	Horse	2.26	Cubic form of HoSF	20[a]
1ies	Horse	2.5	Tetragonal form of HoSF	20[a,b]
1jgc	*Rhodobacter capsulatus*	2.6	M-free ferroxidase center and observation of heme groups	21
1ji4	*Helicobacter pylori*	2.52	12-mer compare with 1dps and 1qgh	22
1krq	*Campylobacter jejuni*	2.70	Nonheme bacfer	23
1lbr	Mouse	1.21	L-chain expressed in *E. coli*	24
1mfr	Frog	2.8	Studies on diiron site in frog "M" ferritin	25
1qgh	*Listeria innocua*	2.35	12-mer compare with 1dps and 1ji4	26, 27
1rcc	Frog	2.4	L-chain at pH 5.5 with glu57ala, glu58ala, glu59ala, glu61ala, and betaine	28
1rcd	Frog	2.0	L-chain at pH 5.5 plus betaine	28
1rce	Frog	2.4	L-chain at pH 6.3 with glu57ala, glu58ala, glu59ala, glu61ala, and betaine	28
1rcg	Frog	2.2	L-chain at pH 5.5 plus betaine	28
1rci	Frog	2.0	L-chain at pH 5.5 with his25tyr and betaine	28
2fha	Human	1.9	Expressed in *E. coli* with lys86gln	8

[a] Compare the structures 1dat, 1ier, and 1ies. [b] A higher-resolution study on the tetragonal from is reported in Granier *et al.*[29]

symmetry relations to the cubic form discussed. The ferritins from bacterial sources have been structurally investigated by X-ray crystallography and so far no high-resolution single-crystal studies on plants have been reported.

By way of introduction it is helpful to summarize the current level of understanding in regard to iron storage in ferritins. Many review articles concentrating on various aspects of the story have appeared.[30–51] As will be seen in the following discussion, there remain many unanswered questions, perhaps requiring the development of new experiments and equipment before the picture can be completed.

The first protein structure determination on horse spleen ferritin (HoSF) performed by Harrison and co-workers[6,7,37] revealed that 24 subunits, each comprising four helices, which can also be regarded as 12 dimeric subunits, connect together to form a spherical protein shell encapsulating a
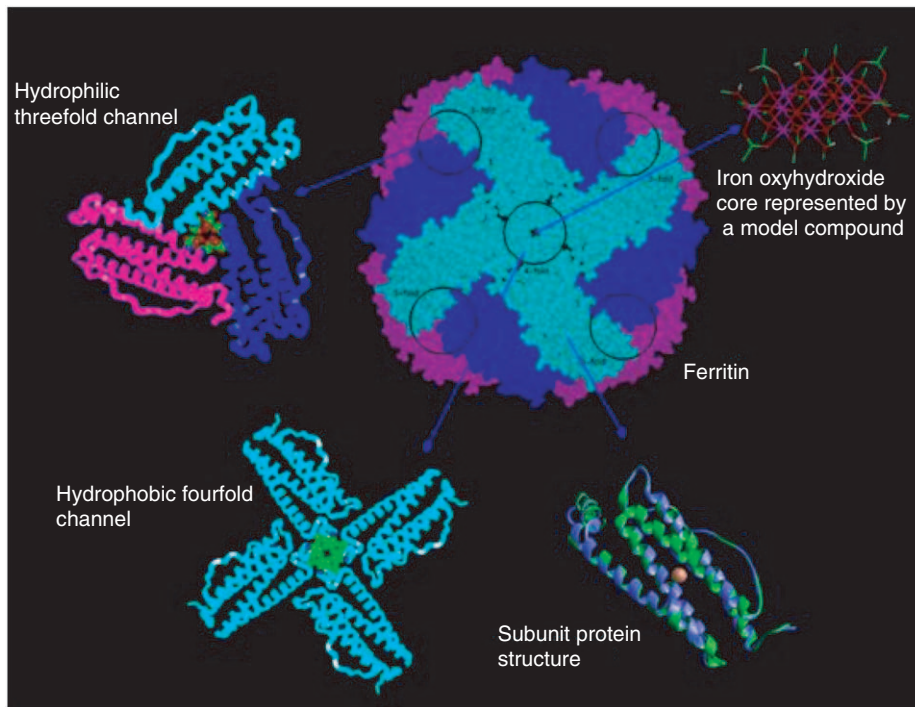
Figure 1 The structural features of ferritin with a ribbon diagram illustrating the tertiary and quaternary structure of the protein shell viewed down the fourfold axis.

spherical cavity 7.8 nm in diameter (Figure 1). In this case the protein crystallized with 432 symmetry and the arrangement of the subunits is such that threefold and fourfold channels (also a consequence of the site symmetry) lead into (or out of) the cavity. It was initially assumed that these would be the pathways for iron and water movement with the cavity acting as the iron storage site. Subsequent studies revealed that it is the threefold, hydrophilic channels in animal ferritins that are likely to allow for iron movement both into and out of the central cavity.

8.7.2.2 A Structural Model for Loaded Ferritins

Since the protein structure could not reveal the details of the contents of the cavity, a number of complementary techniques were used to establish the form of the iron storage. It is generally accepted that the iron is stored in the form of an iron(III) oxyhydroxide mineral which is structurally similar to ferrihydrite and that the cavity can hold up to 4,500 iron centers. The actual number of iron centers stored *in vivo* depends to some extent on the location of the protein in the organism, with more storage taking place in the liver and spleen than the brain, for example. These aspects will be discussed further in the following sections and for the present we can visualize the iron-loaded ferritin molecule as consisting of the following motifs (Figure 2):

(i)   an organic shell which is made up of the 24 protein subunits,
(ii) nucleation sites on the interior of the shell to which iron(III) centers will coordinate, and
(iii) an inorganic mineral core of iron(III) oxyhydroxide.

From this structural model we can see that a loaded ferritin molecule is an organic/inorganic hybrid nanoparticle. Furthermore, the inorganic core represents a nano-sized portion of a solid-state structure and is thus of interest to researchers in the area of nanoscience where the properties of systems cannot be described using conventional ideas from molecular or from solid-state science. Also noteworthy is the control over the properties of the core which is exerted by the protein shell and which effectively provides a nanoreactor for the production of the iron(III) oxyhydroxide nanoparticle. Thus, the ferritin system provides insights into many aspects of nanoscience which are at the forefront of research in this field. Also, if we look back on how
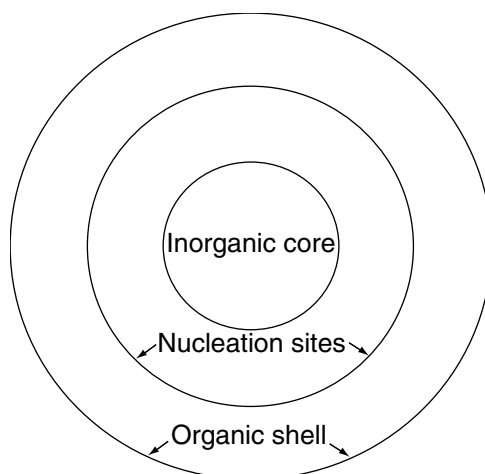
Figure 2 A schematic representation of the structural elements of loaded ferritins.

the secrets of ferritins were uncovered we find that progress here has been directly linked to progress and developments in the instrumentation available for investigating such materials. For example, as techniques such as electron microscopy have improved so has our knowledge of the details of the core structure and this will be discussed further below.

8.7.2.3 Current Knowledge on Structural and Physical Properties of Loaded Ferritins

The following description summarizes the knowledge on ferritins which has been reviewed since the early 1970s[30–51] and is designed to provide an introduction to the more detailed discussion on the coordination chemistry aspects which appears in Section 8.7.4.

Although the overall structural features of ferritins are fairly clear, some of the details are harder to resolve. This concerns principally the metallo components. Firstly and as stated above, it has not proved possible to elucidate the structure of the core using single-crystal protein crystallography, which is largely a result of the scale of the problem.

Indeed, it is a typical nanoscale problem, since locating up to 4,500 iron centers and their associated oxide and hydroxide oxygen atoms is not really feasible, while a powder pattern for such a small portion of an iron(III) oxyhydroxide mineral (which is probably also disordered) is not going to give much information on the detailed structure either, i.e., it lies between the molecular and solid-state descriptions.

In addition to the iron core, higher-resolution structural studies revealed that there can be further metallosites in the threefold channels (see Sections 8.7.4.1 and 8.7.4.4.2). These dinuclear ferroxidase centers are thought to be responsible for oxidizing the Fe^{II} (which is delivered and released from transferrin) for storage in the mineral core. The exact nature of these dinuclear sites at all stages of this process in the native system is not entirely clear from the available crystallography. Nevertheless, the fact that these sites exist is not in dispute. However, the questions concerning the mechanisms by which iron is taken up and released prove rather harder to address. These points will be discussed further below, but for the present we can note that studies point to the iron being transported to the ferritin by transferrin. In order for the iron to be released from the transferrin it must be reduced from iron(III) to iron(II). The iron(II) then moves down the threefold channels where it encounters the ferroxidase center and is oxidized to iron(III). It then enters the cavity where hydrolysis reactions lead to the formation of the iron(III) oxyhydroxide mineral. At this point, the question has been posed as to whether all of the iron(III) within the core has been oxidized by the ferroxidase centers or whether it is only those which attach to the nucleation sites and then the rest are oxidized by the driving force of the mineral formation. The idea that it is only the relatively small number needed for nucleation that are oxidized at the ferroxidase centers arises from the observation that oxidizing each and every iron center at the ferroxidase site could not only represent a bottleneck in the system (catalytic oxidation at the formation of an iron(III) oxyhydroxide mineral is well known in mineralogy), but also that the quantities of hydrogen peroxide produced in the animal systems, which is believed to be a

product of the oxidation process, should be kept to a minimum. Additionally, the possibilities for creating free radicals via Fenton-type chemistry should be minimized. The difficulty here lies in following the system in experiments that represent what is occurring *in vivo*. This is, of course, true of most mechanistic studies on metalloenzymes.

Much less is known about iron release from the ferritin mineral core *in vivo*. Experiments performed *in vitro* show that the iron(III) core can be removed by dialyzing with a reducing or chelating agent. Subsequently in these *in vitro* experiments it is then possible to lay down new cores of mineralized species, showing the utility of the apoprotein to act as a nanoreactor as mentioned above. These results are discussed further in Section 8.7.4. For the present we note that the favored mechanism for iron release involves reducing the iron(III) to iron(II).

Thus, overall, the details of core formation are not entirely clear, the exact nature of the core is still open to speculation, and the details of core dissolution need much more study.

First the techniques used to probe the structures and chemistry of the various aspects of ferritins will be described in Section 8.7.3. Then the coordination chemistry aspects in regard to the questions posed above will be discussed in Section 8.7.4.

8.7.3   TECHNIQUES OF STUDY APPLIED TO FERRITINS

Ferritin proteins are in theory accessible to a wide range of spectroscopic, structural, and kinetic methods, but in spite of the fact that there are numerous seemingly ideal features to be subjected to investigation, with the presence of paramagnetic metal centers there are significant difficulties associated with the presence of polydisperse, nanoscopic iron oxyhydroxide cores. These can be avoided if the apoprotein is studied, but this in turn means any information about the core is lost. Naturally, if the aim of the research is to look at iron uptake and release great care must be taken in having a well-defined system in the first place. If the aim is to measure the protein crystal structure, then the issue of any core loading turns out to be less problematic as the disordered cores can be treated as diffuse electron density and effectively ignored. So, although the structural information regarding the core is lost it does not affect the validity of the structural model for the rest of the protein.

8.7.3.1   X-ray Protein Structures

In order to appreciate the coordination chemistry aspects of ferritins, it is important to discuss the nature of the "ferritin reaction vessel." In effect, the protein shell of ferritins provides a complete and self-contained system that controls the chemistry of iron in exquisite detail. The construction of the shell is such that specialized environments are provided to ensure that each of the functions associated with the storage of iron in an inert but accessible form can be realized. Put another way, different groups of ligands for the iron centers can modulate redox potential, solubility, and local pH to stabilize the required form for the iron. It is thus necessary to discuss the features of the protein shell first.

Several important points have emerged from the structural analyses performed on single crystals of ferritins. The identification of the ferroxidase centers is one, the similarities and differences between ferritins from different parts of the same organism another, and the differences between, for example, mammalian and bacterioferritins a third. Another relevant consideration is the fact that very little is really known about the iron sites *in vivo*, especially the construction of the core. Most of what has been suggested about the coordination environments of the iron centers has been inferred from a combination of mutagenesis studies, comparison with better-characterized systems, e.g., diiron protein sites to compare with the ferroxidase center or iron oxyhydroxide minerals for the core, and some model compound studies.

8.7.3.1.1   *Features of the protein shell*

The best-studied ferritins are those from animal sources and these will be discussed first here. The subunits have relative masses of around 20,000 Da and turn out to come in two different forms distinguished as heavy (H) and light (L) with about 54% homology in amino acid sequence between the two.[1,52] The H:L ratio depends on the tissue of origin with more H subunits (about 2/3)

for ferritins from the brain and heart than those from the liver or spleen where the L subunit dominates with up to 90% composition.[53,54] The production of recombinant H or L subunit homopolymers has made the determination of the individual subunit structures possible. Thus, the structures for human H (HuHF) and horse L (HoLF) as well as bullfrog H (FrHF) and L ferritins (FrLF)[8,11,28] prove to be very similar in terms of their α-carbon backbones with superposition to within 0.5 Å r.m.s.[39] In all cases the subunits are folded into four-helix bundles which are over 5 nm in length with a long nonhelical loop connecting opposite ends of the bundle (Figure 1). A fifth, shorter helix is disposed at about 60° to the bundle. These subunits assemble into shells with the shorter helices from four different subunits arranged about a crystallographic fourfold axis giving rise to the fourfold channels. A further feature of the subunits is that they assemble into antiparallel pairs. Comparison of the primary structures of HuHF and HuLF shows that the amino acids that participate in interunit interactions in HuHF are largely conserved in HuLF with 79% identity between them.[8] This probably explains the ability of the two types of subunit to coassemble. A further important feature is the conservation of the glutamates and aspartates which are directed towards the threefold axis common to both subunit types and "funnel" into the threefold, hydrophilic channels.[55] This is also a feature of other animal ferritins, but not bacterial ferritins.[1,9,10,21,56] These threefold channels turn out to have different internal structures between the two subunit types with the H subunits having a dinuclear metal binding site, now known as the ferroxidase center, whereas in the L subunits this feature is replaced by electrostatic interactions between oppositely charged side chains.[16] The inner surface residues also differ between the two types with L subunits presenting a cluster of four glutamates to the inner surface while there are only two in the H subunits. The conjecture is that these differences are utilized to enhance the function of the different sorts of heteropolymers. For ferritins found in the brain or heart higher ferroxidase activity is expected, whereas for those in the liver or spleen, with high levels of L subunits, the primary function is nucleation and storage.

The ferroxidase center, important for rapid oxidation of Fe^{II} to Fe^{III}, was discovered relatively recently in the history of research into the metal sites in ferritins.[57–60] Ferroxidase activity within H subunits appears to occur at a dinuclear site situated within a four-helix bundle and resembling the dinuclear centers found in ribonucleotide reductase, methane monooxygenase, fatty acid desaturases, and ruberythrin (Chapter 8.11).[61,62] In bacterioferritins, for which protein crystal structures have been reported for ferritin from *Escherichia coli*[9,10] and *Rhodobacter capsulatus*,[21] the overall motif of a shell of 24 subunits with relative masses of about 18,500 Da is preserved but there are also 12 protoporphyrin IX heme groups present with unknown function which might have a role in connecting the dimer units and are buried within the shell between identical subunits related by twofold symmetry. In these bacterioferritins the subunits are all identical and contain both ferroxidase and nucleation sites.

8.7.3.2 Spectroscopic Techniques

Electronic spectroscopy is a useful means for identifying certain important chromophores which can occur in ferritins such as heme groups found in bacterioferritins,[41,63] the "signature" of the mineral core which results from charge transfer transitions from oxides and hydroxides to the metal centers at around 420 nm,[1,64] and the blue or purple colors associated with the peroxo intermediates of ferroxidase activity.[65] Spectrophotometric methods have also been important in kinetic and mechanistic studies. Other spectroscopic methods which have been applied to the study of ferritins include magnetic circular dichroism (MCD) spectroscopy,[66] electron paramagnetic resonance (EPR) spectroscopy,[67–69] NMR spectroscopy, e.g., using the ^{113}Cd nucleus for the investigation of the ferroxidase centers,[70] Mössbauer spectroscopy to probe both the ferroxidase center[71,72] and the crystallinity of the core,[46,47] and EXAFS spectroscopy to probe the local structure of the core.[73–77]

8.7.3.3 Magnetic Measurements

In addition to MCD and EPR spectroscopies, which in the past only furnished rather limited information being local rather than bulk probes, and complementary to the Mössbauer studies, bulk susceptibility studies have been performed on ferritins which have led to the observation of some phenomena with their origin in the nanoscopic properties of the core.[78,79] With the

availability of very high fields for EPR measurements it is now possible to use EPR to examine the spin structure of the whole core rather than trying to probe the local iron(III) environments. Using MCD in a similar way is a possibility for the future.

8.7.3.4 Kinetic and Mechanistic Studies

In addition to stopped-flow techniques to follow iron uptake and oxidation a range of other evidence for the mechanisms discussed in the following sections has been applied to ferritins. These include important pHstat/oximetry studies which have been used to investigate the stoichiometry of reactions involving dioxygen.[56,80–82] Also important have been competition experiments with various other metal ions to study the characteristics of the ferroxidase centers[83] as well as site-directed mutagenesis to quantify the roles of various amino acid side chains.[84,85]

8.7.3.5 Electron Microscopy

Scanning electron microscopy and tunneling electron microscopy both proved important techniques to apply to the study of ferritins from an early stage. As these techniques have become more powerful, it is possible to approach shorter length scales and obtain more detailed information on ferritin cores. Many of these advances have been driven by the needs of nanotechnology. It has proved possible to obtain images of loaded ferritins and judge core sizes as well as to get electron diffraction patterns to help with the rather thorny problem of identifying the nature of the mineral core.[46] Doubtless the newer nanoscience-driven techniques of STM and AFM will find application if it proves possible to produce well-defined ferritin nanoparticles with, for example, high-temperature magnetic properties.

8.7.3.6 General Chemical Aspects

In order to explore the progress that has been made in terms of understanding the coordination chemistry within the ferritin system it is useful to look at the underlying general chemistry that appears to be in operation. From what has been discussed above it can be concluded that the redox chemistry and aqueous chemistry of iron play key roles in the formation of ferritin cores. Of course, it has long been appreciated that the presence of coordinating ligands affects both redox potentials and hydrolytic chemistry and a major tenet of bioinorganic chemistry is that protein side chains provide particularly well-suited ligands for tuning metal ion function. While these aspects are relevant both to the ferroxidase centers and to the core formation and dissolution it is particularly instructive to apply these considerations to the situation of the buildup of the core and this is discussed in detail in Section 8.7.4.3.

8.7.4 COORDINATION CHEMISTRY ASPECTS

8.7.4.1 Iron(II) Uptake

In mammals, iron is delivered to ferritin by the well-studied transport protein transferrin (Chapter 8.6).[86] Transferrin binds the iron as an Fe^{III} center with a coordinating bicarbonate anion thought to be a necessary adjunct. It is possible that this bicarbonate has a buffer function on release of the iron in the form of iron(II). The considerations presented in Section 8.7.4.3 on iron redox chemistry and core formation examine such aspects in greater depth. The uptake is probably via receptor-mediated endocytosis and the majority view is now that ferroxidase activity is the next step in the uptake process with the overall process being an oxidative one starting from Fe^{II}.

Initially, iron(II) must travel into the protein shell and reach the ferroxidase centers. The X-ray crystallographic observation of metals such as Tb^{3+}, Cd^{2+}, Ca^{2+}, and Zn^{2+} binding to the six conserved carboxylate residues supports the idea that the threefold channels are the likely entry route for iron into the protein shell in animal ferritins.[16,87] Other experimental evidence to support this comes from ^{113}Cd NMR studies[70] indicating that Fe^{2+} ions compete with Cd^{2+} binding to HoSF in the channels. Other studies have shown that substitution of the threefold

channel carboxylates with other amino acids such as alanine, histidine, or leucine inhibits iron incorporation into ferritin.[84,85] Further support for the threefold route comes from calculations of electrostatic potentials in HuHF showing that the negative outer entrance is surrounded by patches of positive potential leading to an arrangement where electrostatic fields direct cations towards the channel entrance. This region of negative potential extends down the threefold channels to the interior.[55] The high degree of conservation of the three glutamate and three aspartate residues mentioned above in both the H and L subunits means that these channels will be similar in the heteropolymer ferritins.

8.7.4.2 Iron(II) Oxidation

8.7.4.2.1 *Coordination chemistry of the ferroxidase centers*

The ferroxidase centers of mammalian H subunits and bacterioferritin subunits appear to have rather different structures from the results of the X-ray studies. Although the two metals at the ferroxidase site are iron ions in the native system, in all published structures the sites have been occupied by metal ions different from iron as a result of the way in which samples are prepared for diffraction experiments. Thus, for example, for the structure on *E. coli* bacterioferritins (ecBFR) the sites are occupied by Mn centers,[9] whereas for HuHF Tb^{3+} is present.[1,16] The structure of *Rh. capsulatus* bacterioferritins has only partially occupied ferroxidase sites as the result of using EDTA in the sample purification and preparation.[21]

Kinetic experiments with recombinant HuHF as well as with HuLF and HoLF have further substantiated the proposal that the dinuclear center is the ferroxidase center[52,59,84,88,89] (see Figure 3). In addition, substituting amino acids at the center in HuHF greatly reduces oxidation, e.g., the mutations glu27ala, glu26lys and his65gly, glu107ala.[52,59,82,90–93] Binding of Fe^{II} at both sites seems to be necessary for fast oxidation. For HuHF oxidation is complete within 10s for 48 Fe^{II} per protein at pH 6.5.[59,90]

The picture that has emerged shows the motif of two iron centers linked by a carboxylate bridge from a glutamate residue for both ecBFR and HuHF (Figure 3). In the bacterial ferritin from *E. coli*, ecBFR, both iron centers have histidine coordination whereas in HuHF only one does, the other having a glutamate at the equivalent position. Furthermore, the iron sites are bridged by a second carboxylate residue in bacterioferritins, but there is a complicated network of hydrogen bonded water, carboxylate, amino, and tyrosinate moieties linking the iron centers in HuHF. The overall result is that one of the two sites is almost identical in both ecBFR and HuHF whereas the other is very different. These differences might have an important bearing on the iron oxidation and hydrolysis chemistry which, as discussed below, produces hydrogen peroxide for animal ferritin and water for bacterial.

8.7.4.2.2 *Mechanism of Fe^{II} oxidation at the ferroxidase center*

Studies on the H-type animal ferritins to elucidate the mechanism of Fe^{II} oxidation show that the ferroxidase center catalytically converts two Fe^{II} and one dioxygen to a diferric oxo/hydroxo mineral precursor and hydrogen peroxide via a diferric peroxo intermediate.[1,32,56,65,80–82,94] Overall these reactions can be summarized in Equations (1) and (2), where P^z represents the apoprotein of net charge z, $[Fe_2-P]^{z+4}$ a diferrous ferroxidase complex, and $[Fe_2O(OH)_2-P]^{z+2}$ a hydrolyzed μ-oxo-bridged iron(III) complex at the same site.[1,32,56] Thus in the ferroxidation reaction hydrogen peroxide is produced from the two-electron reduction of dioxygen at the diiron site (Equation (3)).[80] E° for this reaction is 0.682 V under standard conditions. The hydrogen peroxide thus produced is removed by reaction with catalase. This suggestion has been substantiated by following the effect of the presence of catalase on the reaction stoichiometry:[80–82,95]

$$2Fe^{2+} + P^z \longrightarrow [Fe^{II}_2\text{-}P]^{z+4} + 4H^+ \qquad (1)$$
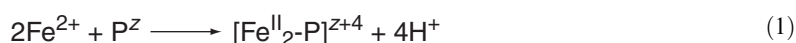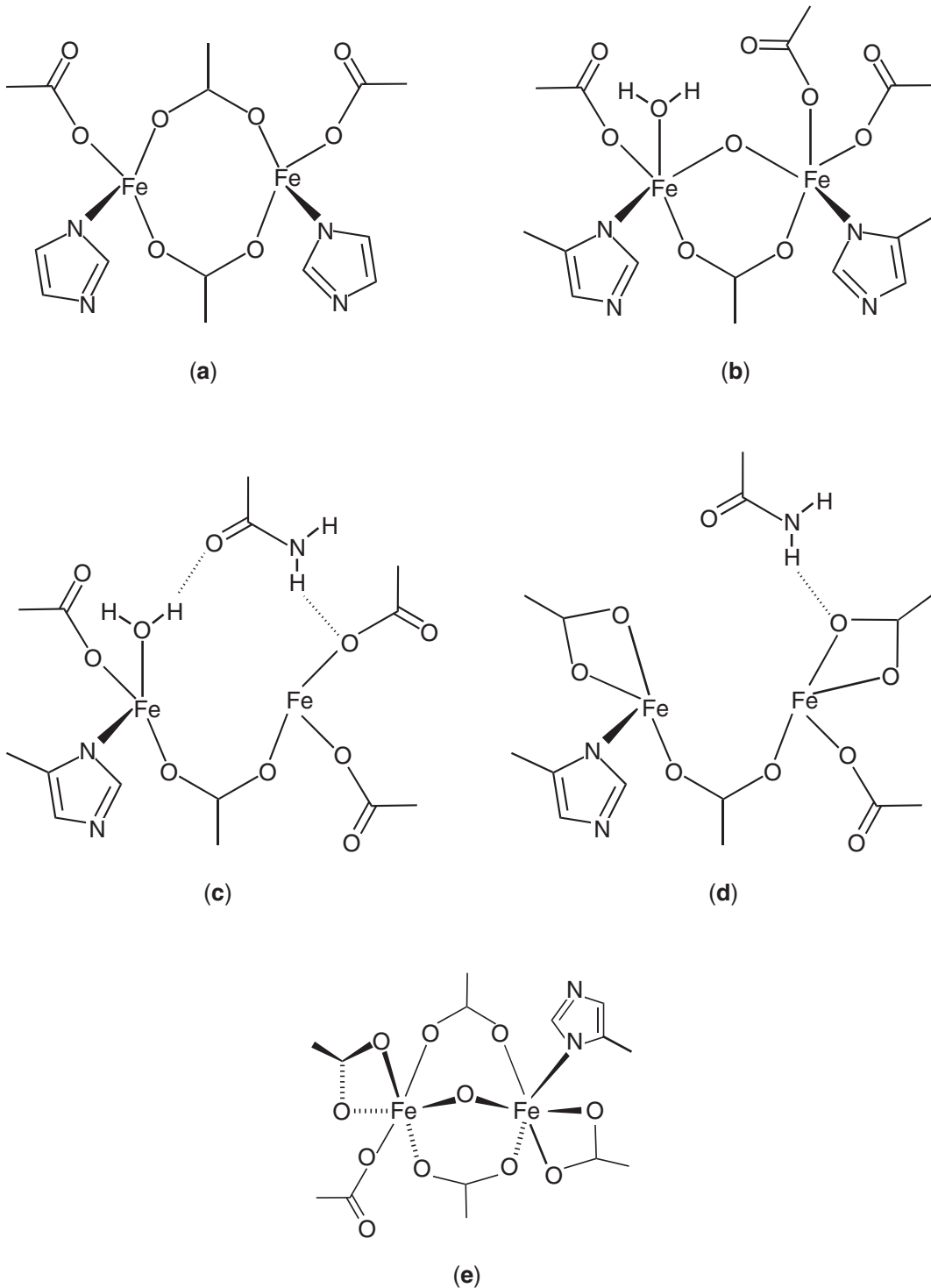
Figure 3 The suggested coordination environments of the iron centres in ferritin ferroxidase sites for: (a) bacterioferritin reduced form, 2 x Fe(II); (b) bacterioferritin oxidized form, 2 x Fe(III); (c) human ferritin (H-chain) both oxidized and reduced forms; (d) *E. coli* ferritin (ecFTN) oxidized and reduced forms; and (e) ruberythrin.

$$[Fe^{II}_2\text{-}P]^{z+4} + O_2 + 3H_2O \longrightarrow [Fe^{III}_2O(OH)_2\text{-}P]^{z+2} + H_2O_2 + 2H^+ \tag{2}$$

$$O_2 + 2H^+ + 2e^- \longrightarrow H_2O_2 \tag{3}$$
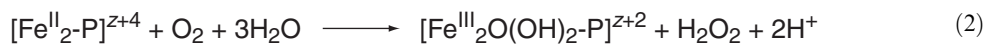
Transfer of iron thus oxidized to the core of mammalian ferritins occurs on a timescale of 5–10 min regenerating the ferroxidase center for further oxidation of Fe^{II}[80] until sufficient core has formed for the oxidation and mineralization to proceed via an autocatalytic route involving the mineral surface and obviating the need to remove peroxide from the system. This also makes it possible to avoid free radical production via Fenton-type chemistry.

The suggested intermediates in these reactions have been further investigated in mechanistic studies. As noted above, the requirement for two iron centers at the ferroxidase site for efficient catalytic activity and the stoichiometry of two Fe^{II} per O_2 led to the suggestion of a two-electron transfer to the dioxygen.[80] Further support for this comes from stopped flow studies on HuHF[59,60] showing that maximal oxidation rates are achieved with two Fe^{II} per H subunit. A blue intermediate species with an absorption maximum at about 650 nm was observed for which the color decays within a few seconds after the addition of 48 Fe^{II} per apoferritin, i.e., after all the ferroxidase centers have been occupied once.[65] Previous to this a blue-purple intermediate had been described for FrHF with the color ascribed to an Fe–tyrosinate complex on the basis of Raman studies.[96] In studies on ecBFR[97] and the ferritin from *E. coli* with the heme groups removed, ecFTN,[59] this blue color proved hard to detect with no evidence presented for it until 1997.[65] It was found in this study that using site-specific mutagenesis the color could either be enhanced fivefold or diminished depending on the substitutions. Thus it was found that removal of negatively charged side chains in the vicinity of the dinuclear center enhanced the absorbance observed at 600 nm, whereas introduction of a negative charge diminished the absorbance. These experiments led to the conclusion that at least in the ecFTN system the blue color did not derive from an Fe–tyrosinate charge transfer or from a tryptophan radical but was rather the signature of protein-catalyzed iron(II) oxidation in which the ligand to metal charge transfer of a diiron(III)–peroxo intermediate was the species responsible. Support for this view comes from the similar observations in a number of other di-iron proteins and their model compounds[61,62] and these are discussed in detail in Chapter 8.13. It is possible that the species that had previously been observed in the Raman studies on FrHF was indeed correctly identified as an Fe–tyrosinate, the discrepancy between that result and the results on the ecFTN being explicable by the rather different experimental conditions used in the different studies (the Raman experiment requiring significantly greater concentrations of sample in order to detect the signals satisfactorily). This is perhaps another case where care needs to be exercised in the interpretation of results on biological systems under conditions far removed from those *in vivo*.

The situation in heme-containing bacterioferritins turns out to be somewhat different. Extensive studies on ecBFR have been performed in attempts to unravel the details of the oxidation reactions and also to gauge the effect of possible inhibition by M^{II} species.[41,56,58,83,98,99] From the results of kinetic, spectroscopic, potentiometric, and pH-stat/oximetry studies obtained on wild-type as well as site-directed variants it has been found that the intrasubunit dinuclear metal sites are essential for core formation to proceed at normal rates. The process can be regarded as going through three kinetically distinct phases. The first and fastest phase is where two Fe^{II} centers bind at each of the dinuclear sites of the protein with the release of two protons per metal ion (Equation (4); cf. Equation (1)). In the presence of dioxygen this is followed by the rapid oxidation of the iron to Fe^{III} (Equation (5); cf. Equation (2)) but now the product is water rather the hydrogen peroxide observed for HuHF.[56] This reaction is only a summary of what has been observed. In fact the iron(II):O_2 stoichiometry established so far requires four iron(II) ions per dioxygen, i.e., at least two ferroxidase centers. Two mechanistic models have been proposed.[83] The "transient peroxide" model suggests that the reaction of oxygen at one ferroxidase center results in the formation of a μ-oxo-bridged iron(III) dimer and hydrogen peroxide. In other words, it is a similar situation as seen in Equation (2) for mammalian ferritins, but without a peroxo intermediate and now with the difference that the hydrogen peroxide reacts rapidly at a second ferroxidase center to give another μ-oxo-bridged iron(III) dimer and an oxide ion which forms water with the spare protons in the system (Equation (6)):

$$2Fe^{2+} + P^z \longrightarrow [Fe^{II}_2\text{-}P]^{z+4} + 4H^+ \tag{4}$$

$$[Fe^{II}_2\text{-}P]^{z+4} + O_2 + 2H^+ \longrightarrow [Fe^{III}_2O\text{-}P]^z + H_2O \tag{5}$$

$$H_2O_2 + [Fe^{II}_2] \longrightarrow [Fe^{III}_2O] + H_2O \qquad (6)$$
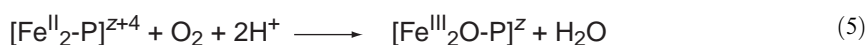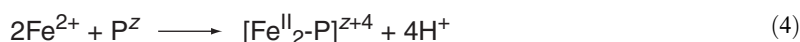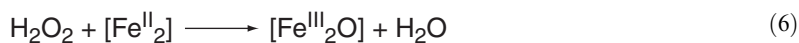
The alternative "high valent intermediate" model initially requires the sort of peroxo intermediate that has been observed in mammalian ferritins. The reaction of oxygen at one ferroxidase center results in a peroxo-bridged iron(III) dimer which then decays to form a μ-oxo-bridged iron(IV) dimer (Equation (7)). This high valent intermediate then undergoes a redox reaction with a second ferroxidase center containing iron(II) resulting in the formation of two μ-oxo-bridged iron(III) dimers (Equation (8)). In both cases water rather than hydrogen peroxide is produced. Further evidence that no hydrogen peroxide forms was provided by studies in the presence of catalase[56] where it was found that this had no effect on any of the reaction stages in contrast to the findings for mammalian ferritins (see above). These findings were also supported by evidence from spectroscopic measurements, in particular the production of Fe^{III} using EPR and the fact that the heme groups play no direct role in ferroxidase activity. This was shown by studying the heme-free variant, which had the same activity as the wild-type protein from pH stat/oximetry measurements, also in agreement with earlier studies using spectrophotometry to follow iron oxidation:[100]

$$[Fe^{III}_2(O_2)] \longrightarrow [Fe^{IV}_2O] + H_2O \qquad (7)$$

$$[Fe^{IV}_2O] + [Fe^{II}_2] + H_2O \longrightarrow 2[Fe^{III}_2O] + 2H^+ \qquad (8)$$
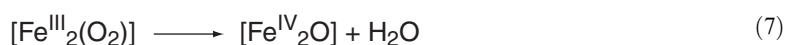
8.7.4.2.3 *Other studies*

It should be clear from the results discussed above that several features important to coordination chemistry have distinctive effects on the way in which the metal ions at the ferroxidase centers behave. For example, the studies where the "ligands" (here amino acid side chains) are altered using mutagenesis can show profound effects in terms of reactivity. Also relevant here is the fact that the ferroxidase sites in mammalian and bacterial ferritins have different coordination environments which might explain why the product of the oxidation for one is hydrogen peroxide and for the other water. The biological reasons behind this are probably what has dictated the choice just as the presence of heme groups in bacterioferritins must have a good biological reason even if this is not yet clear to us. There are two other avenues of enquiry that are helpful in understanding the coordination chemistry aspects of the system. The first is the substitution of Fe^{II} by other M^{II} ions in order to investigate the effect of Lewis acidity, redox activity, stability, inertness, and stereochemical flexibility on the reactions. Several studies have been performed on both HoSF and ecBFR. Competition binding studies using difference absorption spectroscopy showed that while Co^{II} and Cu^{II} have high affinity for binding at the ferroxidase sites, contrary to expectation from the Irving–Williams series Co^{II} is more tightly bound.[83] In other studies Co^{II} had been shown to bind less tightly than Zn^{II}.[98] The effect of then adding Fe^{II} and following core formation was studied. The presence of Co^{II} was found to lead to the loss of the second phase of the ferroxidase activity (Equation (5)) and it was concluded that Fe^{II} displaces the Co^{II} as oxidation activity was observed and it was possible to build up the iron oxyhydroxide core. Not surprisingly, addition of redox inactive Zn^{II} with its tight binding affinity effectively blocks core formation. The situation with Cu^{II} was somewhat more ambiguous as it can apparently be displaced from the centers, but in the competition studies was found to enable "ferroxidase-type" activity. The assumption was that the copper must be bound elsewhere since it was known not to be able to displace Zn^{II} in an experiment where the Zn^{II} was added, followed by Cu^{II} and then Fe^{II} and core formation was observed.[83]

A second relevant aspect here is the consideration of "models" for the various dimetal species that could be important in the reactions at the ferroxidase centers. The area of di-iron metallosites has received a great deal of attention from the early 1980s since the identification of such sites in hemerythrin and the production of the first coordination chemistry model compounds for these (Chapters 8.12 and 8.13). Subsequently several other systems with this motif have been studied and the ones of most relevance to the ferroxidase centers would appear to be those involved in oxygen activation rather than transport.[61,62]

A report has highlighted the delicate interplay between Fe⋯Fe distances in such systems and the chemistry that results with the point made that this distance has been found to be particularly short at 2.53 Å in the peroxo intermediate of ferroxidase activity as deduced from X-ray absorption studies.[101] Although other techniques have been applied and compared to support this result, caution in placing too much reliance on metrical data from EXAFS should be exercised. Nonetheless, the hypothesis that this short distance and the strain that is introduced into the system might account for the fact that in ferroxidase activity the peroxo intermediate is a substrate intermediate rather than a catalytic cofactor as is the case in the related diferric enzymes such as methane monooxygenase.

8.7.4.3 Formation of the Mineral Core: Redox Reactions and Core Formation

Core formation requires that Fe^{II} is oxidized to Fe^{III}. As stated above, for animal ferritins the initial oxidation takes place at ferroxidase centers in H subunits with the production of a peroxo intermediate. Subsequently it is believed that once a certain number of iron centers have been oxidized and stored in the core, the mineral provides the catalytic surface for further oxidation thus avoiding excess production of hydrogen peroxide. In general it is believed that in animal ferritins the H and L subunits have complementary roles, the former allowing for rapid oxidation of a critical number of iron centers and the latter encouraging mineral formation.[102] In the case of L-only ferritins, where no ferroxidase centers are present, it was found that HuLF takes up Fe^{II} at pH 7 converting it slowly to the Fe^{III} mineral within its cavity. However, this was not found to be possible at pH 5.5.[52] In the heteropolymer proteins only between 18% and 30% H subunit is required for maximum iron incorporation and mineralization.[53] In addition, L-rich ferritins such as found in the liver and spleen yield iron core particles of greater average size, crystallinity, and magnetic ordering than the H-rich ones.[82,92] If the ferroxidase and cavity mineralization residues are altered ferritins that neither oxidize nor incorporate iron can be produced.[82,103]

Mechanistic studies on animal and bacterial ferritins show that formation of the core is the slowest phase in the buildup of loaded ferritin. Cores only form when more than two Fe^{II} ions are added per subunit (i.e., more than 48). The first part of core formation involves nucleation and this takes place at carboxylate residues. In the previous section we followed the path of iron assimilation as far as oxidation at ferroxidase centers. Exactly what happens next is still open to interpretation, but there is a general consensus that some sort of hydrolyzed iron(III) species form which give the basis for the core. This is summarized in Equation (9), where $[Fe^{III}_2O(OH)_2-P]^{z+2}$ is the μ-oxo-bridged iron(III) dimer formed in Equation (2) and the hydrolysis initially has the function of vacating the ferroxidase site. Subsequently once sufficient core has been laid down Fe^{II} oxidation proceeds at the mineral surface along with hydrolysis to give the overall reaction shown in Equation (10) for both animal and bacterial ferritins.[56,102] Furthermore, studies on ecBFR showed that while the initial rate for the phase two oxidation step is essentially pH independent, for core formation this is very sensitive to pH with practically zero rate at pH 6.0 and increasing rates as pH is increased. The initial pH independence for phase two is in disagreement with an earlier report,[100] but this is probably a result of more limited data in the earlier paper:

$$[Fe^{III}_2O(OH)_2-P]^{z+2} + H_2O \longrightarrow P^z + 2FeO(OH)_{(core)} + 2H^+ \qquad (9)$$

$$4Fe^{2+} + O_2 + 6H_2O \longrightarrow 4FeO(OH)_{(core)} + 8H^+ \qquad (10)$$
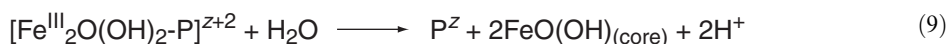
Finally, a possible third iron-binding site in the vicinity of the ferroxidase center of ecFTN appears to increase the rate of oxidation of Fe^{II} after 48 irons have been oxidized, but further studies are probably required on this system.[104]

In order to understand the chemistry behind the oxidation and storage of the iron better it is helpful to look at the redox and hydrolytic chemistry of iron.

The relative stabilities of the +2 and +3 oxidation states of iron are such that only small deviations from "normal" conditions can favor oxidation of Fe^{II} to Fe^{III} or reduction of Fe^{III} to Fe^{II} with accompanying large changes in solubility. The parameters that influence this are the

relative values of the electrode (reduction) potential, E, and the pH value: one a measure of the potential of electron activity, the other of the potential of proton activity in the system. The value of E is found using the Nernst equation and thus the activities (often approximated by concentrations) need to be taken into consideration. For metal ions these are often affected by the presence of coordinating species which can alter the electrode potential for oxidation or reduction though molecular orbital interactions (e.g., by changing the splitting of d orbitals in transition metal ions) or else overall pH through the release of protons into the medium as, for example, in hydrolysis reactions. For iron in a biological (or, indeed, terrestrial) environment the available range of E and pH is governed by the stability range for water, so redox potentials which would either reduce or oxidize water need not be considered. A useful way to illustrate the stable forms of chemical species at various values of E and pH is in a Pourbaix diagram. Relevant to the situation for the formation of the iron oxyhydroxide core is the Pourbaix diagram which combines the data for water and iron shown in Figure 4. In this diagram it is assumed that the water is pure and has a constant activity value of 1.

The standard reduction potential for dioxygen to give water at $25\,^{\circ}$C, 1 atm, and pH $=0$ is $E^{\circ}=1.23$ V. Substitution into the Nernst equation gives

$$E = 1.23 + \frac{RT}{nF}\ln[O_2][H^+]^4 \text{ V} \tag{11}$$

Now substituting for the various constants, the temperature, and the number of moles of electrons transferred and converting from natural logarithms so that the concentration of H^+ can be replaced by the negative value of pH gives

$$E = 1.23 + 0.0148\log[O_2] + (4 \times 0.0148 \times \log[H^+]) \text{ V} \tag{12}$$
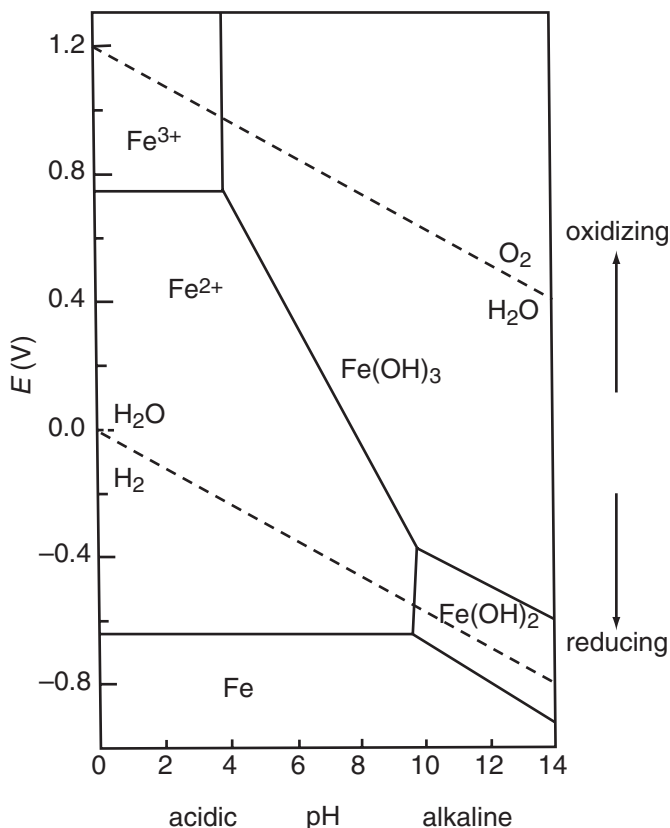
Figure 4   The Pourbaix diagram for the iron–water system. The solid line is drawn for $[Fe^{2+}] = 10^{-7}$M. The dashed line shows the limits of stability of water with respect to oxidation and reduction.

The concentration of oxygen is given by the partial pressure, which at the earth's surface is 0.21 atm, which gives

$$E = 1.23 + 0.0148\log(0.21) - 0.059.\text{pH V} \tag{13}$$

$$E = 1.22 - 0.059.\text{pH V} \tag{14}$$

The Pourbaix diagram shown in Figure 4 has been drawn for the situation where the solid lines represent an Fe^{II} concentration of 10^{-7} M. It is necessary to construct diagrams for the iron concentration of interest and also for other values of temperature and pressure. The diagram given is useful in the context of iron(III) biochemistry because it gives a good indication of the iron species that are relevant under the conditions found in natural waters and thus of the bioavailabilty of iron. We can see that at low potentials and pH values Fe^{II} is quite stable giving iron in a highly soluble form whereas at pH values around physiological and normal environmental Fe^{III} predominates in the form of insoluble oxyhydroxide species unless conditions are highly reducing. It can also be seen that in the region between pH 5 and pH 9 the interplay between the two oxidation states depends critically on the balance between pH and E and this is where biology has developed systems capable of tuning electrode potentials and local pH to favor the required oxidation state. This is obviously of direct relevance to the situation in ferritin in regard to iron storage and mobilization.

The next important process to consider in terms of trying to unravel the way in which iron is stored and mobilized is the hydrolytic chemistry of iron species. If we compare the oxidation states of +2 and +3 we can identify four species that could be important if we assume that the metal ions are in octahedral coordination geometries: Fe^{II} high and low spin and Fe^{III} high and low spin. However, the ligands that have been identified as relevant are expected to favor the high-spin forms. In this case the Fe^{III} ion becomes dominant because of the highly insoluble nature of the hydroxide which has the effect of removing the concentration of the oxidized species, $Fe(OH)_3$, from the Nernst equation for the system (Equations (15) and (16)):

$$Fe^{2+} + 3H_2O \rightleftharpoons Fe(OH)_3 + 3H^+ + e^- \tag{15}$$
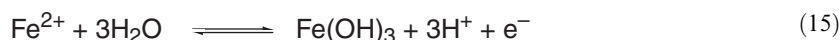
$$E = E^o + 0.059\log\frac{[Fe(OH)_3][H^+]^3}{[Fe^{2+}][H_2O]^3} \text{ V} \tag{16}$$

and taking the activity of water as unity and also the activity of the solid $Fe(OH)_3$ as unity for which the log values become zero gives

$$E = E^o - 0.059\log[Fe^{2+}] - (3 \times 0.0059\text{pH}) \text{ V} \tag{17}$$

Thus we see that the potential is dependent only on the concentration of Fe^{II} and the pH value. In this way, the formation of a solid-state phase for Fe^{III} within the ferritin core offers a means of controlling available iron levels in the organism. This is an important point since free iron ions are unwanted species in biological contexts where they can catalyze free radical reactions which in turn lead to cell damage. However, it is also important to maintain sufficient levels of iron within organisms which generally find it hard to sequester iron from their surroundings or foodstuffs and thus require a means of storing the metal to maintain their biochemistry. Thus the specialized mineral core provides an accessible store of iron which is mobilized as and when required by means which we do not yet understand.

It is perhaps helpful at this stage to look at the reactions which free iron ions catalyze. This is chemistry which was originally developed by Fenton in 1894 in order to improve the oxidizing power of hydrogen peroxide by the production of hydroxyl radicals, $OH^{\cdot}$, which have a standard electrode potential of 2.8 V which is more positive than those of ozone, hydrogen peroxide itself (1.8 V) potassium permanganate and chlorine and only marginally less than the standard reduc-

tion potential for fluorine (3.0 V). The two reactions which summarize the catalysis producing these radicals are (Equations (18) and (19)):

$$Fe^{2+} + H_2O_2 \rightarrow Fe^{3+} + OH^{\cdot} + OH^- \qquad (18)$$

$$Fe^{3+} + H_2O_2 \rightarrow Fe^{2+} + OOH^{\cdot} + OH^+ \qquad (19)$$

Furthermore, as well as causing oxidative damage to organic species these radicals can also transfer electrons to Fe(II) to give Fe(III) species and this is probably one reason why the ferroxidase activity is kept to the minimum necessary to allow for core formation. On the other hand, "Fe(OH)$_3$" itself (i.e, some mineralized oxyhydroxide species) is able to destroy hydrogen peroxide, decomposing it to dioxygen (effectively the reverse of Equation (2) in the presence of far larger quantities of hydrolyzed iron(III) species) and thus storage of iron in this form is an effective means of avoiding oxidative damage.

8.7.4.4 Iron(III) Storage and the Nature of the Mineral Core

The way in which the iron core in ferritin might build up and the structure of the mineral and its properties have been considered by many researchers over the years and yet there are still many questions that remain to be answered satisfactorily. From one viewpoint the subject belongs in the area of biomineralization, from a different standpoint the nanoscale properties have been of interest, and a third important area of research concerns the health aspects of iron storage and homeostasis. For this latter field the problems of "too much or too little" are to the fore, with iron overload disease a serious problem in much of Africa and the Middle East while in the Western world iron deficiency is more likely to be a problem. A key aspect to such health problems concerns the response of the organism to local iron levels and is regulated in healthy subjects by an "iron response element" (IRE) which also seems to involve metalloproteins within the so-called "iron response protein."[1,105] However, this has but little bearing on coordination chemistry aspects of ferritins that we are considering here whereas the chemical questions behind the mineralization processes and the measurement and interpretation of the physical properties of such nanoscale particles are of intense interest. It turns out to be helpful to consider these two aspects in tandem, as one tends to inform the other.

8.7.4.4.1 *Nature of the core and iron(III) hydrolysis*

In the following discussion the mineral core of ferritin will be regarded as an iron(III) oxyhydroxide mineral. Experiments performed on native animal systems suggest that varying degrees of phosphate can be associated with the mineral cores, but the ratio of P to Fe seems to depend more on local conditions than on any particular requirement for phosphate for core formation.[1] Conversely, for bacterioferritins phosphate seems to be an essential component of the wild-type mineral core and the resulting material is amorphous.[102] It is possible to contain exclusively metal oxide and oxyhydroxide cores within any apoferritin "reaction vessel" and these can be relatively crystalline. Given that the cores are difficult to investigate in the first place and that the cores in wild-type bacterioferritins are very poorly characterized, the following discussion is limited to the situation relevant to coordination and nanoscale chemistry where the species is a relatively well-defined nanoscopic portion of an extended mineral.

Opinion favors the formulation of the mineral species in the cores of loaded mammalian ferritins as a ferrihydrite species. It should be noted that "ferrihydrite" is a name that covers a variety of formulations depending on degrees of hydration and particle size being investigated and that the structure in terms of the coordination environments of the iron centers is by no means certain. This has been discussed at some length over the years in the literature, both in terms of a satisfactory structural model for ferrihydrite and in terms of what might be contained within ferritin cores,[37,40,42,43,46,47,73–77] but the following may at least underline the difficulties in resolving this with our current levels of physical techniques. For the present we can give this species the formula $5Fe_2O_3 \cdot 9H_2O$,[106,107] which is the formula most often seen in the literature on ferritins, but this has also been written as $Fe_2O_3 \cdot 2FeO(OH) \cdot 2.6H_2O$ on the basis of a number of studies suggesting the presence of both hematite and oxyhydroxide environments for the iron centers,[108] which emphasizes the "oxyhydroxy" nature of the material and also the fact that there are probably several different chemical environments for the iron centers. It is expected that some of these will have water ligands, in particular those at the mineral surface.

The spherical cavity in ferritins imposes a maximum size for an iron oxyhydroxide mineral particle forming within this shell of about 7.8 nm in diameter. This in turn imposes certain limits on the techniques that can be used to probe the structure and properties of such particles. There is the additional problem that it is possible to have more than one particle in any one core and also that loading studies show that while up to an average of 4,500 iron centers per ferritin can be loaded experimentally this does not give any information regarding the dispersion of the loading. This can be better appreciated if estimates of the maximum number of iron centers possible within a 7.8 nm diameter sphere containing various minerals are compared. This is most easily seen by calculating the density that would be observed for a mineral core of 7.8 nm in diameter akin to the suggested ferrihydrite form of the iron oxyhydroxide. This turns out to be about 2.9 g cm^{-3}, which, although somewhat lower than the range of densities reported for ferrihydrite phases,[109] is much better than if we do the same calculation based on 4,500 FeO(OH) units, which would have a density of only 2.7 g cm^{-3} in this volume and is significantly short of the observed and calculated densities of 4.27 g cm^{-3} for goethite (α-FeO(OH)) or 3.97 g cm^{-3} for lepidocrocite (γ-FeO(OH)). To illustrate this in another way, if the mineral were in the form of hematite (α-Fe$_2$O$_3$) we would expect about 9,800 iron centers to be present in this space to give the required density of 5.26 g cm^{-3}.[110] This suggests that minerals with increased amounts of hydroxides and hydration fit the observed loading better than the dehydrated forms, which, given the fact that the iron core is known to be accessible and soluble (whereas minerals such as hematite are the thermodynamically most stable and insoluble oxide forms), is not surprising. Such well-defined mineral species are, however, relevant in the history of investigating core mineral models since they provide important comparisons with the observed experimental data.

At this point it is instructive to look at iron(III) hydrolysis in more detail. As was discussed earlier, at electrode potentials and pH values likely to be found in the ferritin cavity iron(III) dominates and will be expected to undergo hydrolysis reactions. Starting from a hexaaquo [Fe(H$_2$O)$_6$]$^{3+}$ species successive proton loss from coordinated water molecules in conjunction with condensation reactions quickly leads to the precipitation of the "hydroxide" Fe(OH)$_3$. This formula is used to describe the gelatinous precipitate which forms virtually instantaneously in hydrolyzed iron(III) aqueous solutions and as we saw above is rather insoluble. Experimentally, however, it is known that "freshly precipitated ferric hydroxide" can be useful under the right conditions in synthesis and catalytic reactions until it "goes off." This loss of reactivity is the result of the material aging to form better-defined mineral phases, the first of which corresponds to something like our formula for ferrihydrite. Taking either of the formulas given above for ferrihydrite and normalizing to the 10 iron centers implicit in the first formula gives a relative formula of Fe$_{10}$O$_{24}$H$_{18}$ for both. If we compare this with 10 units of "Fe(OH)$_3$" then it corresponds to the freshly precipitated material with the loss of six water molecules for every 10 iron centers. Subsequently the mineral can age further and produce an iron oxyhydroxide, FeO(OH), usually goethite under standard conditions and ultimately, but perhaps after many years with no further intervention, hematite, Fe$_2$O$_3$, which for five hematite units corresponds to the loss of a total of 15 water molecules from the original 10 units of "Fe(OH)$_3$." Thus it seems that the ferritin core consists of a mineralized intermediate corresponding to a relatively reactive iron(III) hydrated oxyhydroxide nanoparticle which is only mobilized in response to a specific biological call, but otherwise is held safely within the ferritin molecule.

One important factor here will be the nature of the inside of the protein shell. As was discussed earlier, it is believed that clusters of carboxylate residues are important for nucleation of the core. These provide binding sites for, perhaps partially hydrolyzed, iron(III) species and then further iron(III) species join via the sorts of condensation reactions seen in normal hydrolysis to give hydroxide and maybe also oxide linkages and so on until the cavity is at capacity. What is not known is whether several crystallites form in this way or if one crystallite dominates. However, the usual models of nucleation and crystal growth used to describe the formation of a solid phase from another phase are modified here by the presence of the spherical protein cavity. Thus, the model usually applied to nucleation stresses the importance of overcoming the unfavorable energy term arising from the boundary between the phases and is usually called the surficial energy term. This is offset by the favorable lattice energy term resulting from the formation of the solid phase. Normally a nucleus of species must reach a certain size before it is stable here in the solid state with respect to existing in the other phase (here, in solution) and once it has done this it is expected that smaller nuclei will tend to redissolve and join to the larger particle resulting in crystal growth.[111–113] Obviously, the fewer surfaces the better with regard to minimizing surficial energy terms. However, the situation here has the added factor that bound iron(III) centers at the nucleation sites add stability to the growing mineral phase and since these are found regularly

over the inner surface of the protein it is possible that the mineralized cores are made up of several smaller crystallites growing out from these sites. These nucleation sites effectively remove some of the unfavorable surficial energy since coordination of the metal ions is expected to be a favorable process, but attempts to probe the core structure are literally complicated by the "scale" of the problem. Too many iron sites with too much symmetry and too many possibilities for disorder are embedded within the structure of loaded ferritin molecules in a single crystal to make protein X-ray crystallography very helpful, i.e., the problem is too large. One or several crystal-lites of an ill-defined mineral phase of nanometer proportions contain too few centers to define an extended (infinite) structure, i.e., the structure contains too small a portion of the extended phase to be resolved using solid-state techniques such as X-ray powder diffraction. In other words, we have the problem of gaining atomic resolution for a nanoscale structure.

8.7.4.4.2 *Methods used to probe iron core structures and their limitations*

(i) *Diffraction experiments and electron microscopy*

The difficulties associated with gaining structural details of the iron oxyhydroxide cores using the chemist's "method of choice" of X-ray crystallography have been discussed above. Nonetheless, powder diffraction data have helped to some extent in characterizing the cores in loaded horse spleen ferritin (HoSF) for which two- and six-line traces like those observed for ferrihydrite minerals were measured.[37] Unfortunately considerable debate regarding the experiments on the ferrihydrite phases themselves has arisen[109,114,115] and it is perhaps safer simply to draw compari-sons rather than try to name the mineral definitively. The root of this problem is that ferrihydrite phases also suffer from being polydisperse and nanoparticulate which results in boundary effects being present in materials where the interpretation of diffraction data relies on being able to regard the lattice as infinite. Indeed, diffraction line broadening is a means of gauging particle size using X-ray diffraction but this relies on the mineral phase being well defined in the solid state, so is of less help here.

Of particular help in the study of the cores have been techniques associated with electron microscopy. Most notably, TEM and electron diffraction from the cores have established ranges of particle size and given further evidence regarding the crystallinity of cores.[46] Caution should also be exercised here, however, as the technique has the potential to provide a great deal of information, most of which tends to remain unobserved and unanalyzed as it depends on the operator searching the micrograph for clues rather than any systematic survey. In addition, it is possible to observe diffraction from very small portions of crystal lattices, as little as an $\{M_7(OH)_{12}\}$ portion of a brucite structure,[116] because of the nature of electron diffraction which does not require significant long-range order.

(ii) *Magnetic measurements*

One of the many unusual aspects of nanoscopic systems containing unpaired spins is manifested in their magnetic behavior. In common with other physical properties this cannot be described "classically" from either the molecular or the solid-state point of view. These aspects are also discussed in detail in Chapter 7.13, but for our purposes it is sufficient to note that the problem is again one of "scale," the description of the coupling of many paramagnetic centers from the molecular point of view is too large a problem and trying to describe the situation from the standpoint of an extended structure cannot allow for the boundary effect of a nanoparticle. The fact that the cores of ferritins are also not monodisperse adds a further complication, but some interesting results have emerged and also the possibility for laying down mineral cores with different compositions holds some intriguing possibilities[103,117–120] which might be easier to realize if more control over core size could be exercised.

Two main probes of the magnetic behavior of ferritin cores have been used. Mössbauer studies provided a useful means of gauging the crystallinity of iron cores with the onset of superparamagnetic behavior used as a guide. These aspects have been extensively reviewed and were important contribu-tions to early investigations on ferritin cores.[46,47,121] Subsequently the observation of "single-molecule magnetism" in rather small aggregates of coupled paramagnetic centers,[122–124] which is really a manifestation of slow relaxation of the magnetization, but can also be found associated with quantum

tunneling effects,[125,126] has fuelled interest in the ferritin system and observations of similar effects have been reported.[78,79] The loaded ferritin system can be described as an antiferromagnetically coupled system with an overall nonzero ground state spin. Synthesis of much smaller examples of such systems is an area of much activity and the goal is to produce molecules where a combination of anisotropy and large ground state spin (well separated from excited states) lead to the observation of "single-molecule magnetism" at relatively high temperature.[122–124]

(iii) Model systems

Another approach to understanding the nature of the iron mineral core is through the use of model compounds. These should provide better-defined systems which can be used for comparative purposes. This approach was reviewed in an article published in 1997 where the following conclusions were drawn:[42]

- The models required should reproduce as many of the features associated with loaded ferritins without compromising the definition of the structure at a molecular level.
- Models based on nanoparticles such as "naked" iron oxyhydroxides,[109,127] iron oxyhydroxides contained within micelles, sugar coats and used for iron delivery drugs or citrate/nitrate coats[45,73,128–130] are unsuitable because they reproduce the situation in loaded ferritins rather than simplifying it so that all the problems associated with the characterization of ferritin cores are still present.

This led to the suggestion that a change in scale is required and that the model compounds should be accessible to single-crystal X-ray structure determinations, which at our current level of ability means that they should be molecular cluster aggregates (i.e., angstrom scale) which reproduce features of the nanoscopic systems.

For the model to reproduce successfully the features of loaded ferritins the following criteria should be fulfilled:

- the system should contain a mineralized but bounded nanoscale (or at least identifiable as a mineral portion) core;
- the core should be enclosed in an organic shell;
- the approximate relative proportions of Fe and C, H, N, and O should be reproduced;
- the different sorts of iron environment should be reproduced (see Figure 2) with iron centers at nucleation sites, on the mineral surface, and within the core; and
- the model should display unusual properties associated with nanoscale particles such as anomalous magnetic behavior.

Clearly, for the model to be both structural and fully functional it should be able to take up and release iron, but since certain aspects of this are still unclear in the native system and also rely on the presence of other protein machinery this is perhaps rather more than can be expected.

An examination of the reported iron oxyhydroxide aggregates that might fulfill these criteria was conducted. Of these, some had been suggested as models for loaded ferritins in the original literature while others had not, but all consist of aggregated iron centers enclosed in organic ligand "shells." It was found that there were some examples of cluster aggregates that reproduced some of the structural elements of loaded ferritins[131–139] (see Figure 2). Reproducing the relative ratios of C:N:O:H:Fe for a ferritin loaded with 4,500 iron(III) ions proved to be more difficult. Of the clusters considered only two incorporated nitrogen in the ligand shell[131–133] and of these $[Na_2Fe_{10}O_6(OH)_4(O_2CPh)_{10}(chp)_6(OCMe_2)_2(H_2O)_{12}]^{2+}$ (Figure 5),[133] where chp = 2-chloropyridonate, did not provide a particularly close agreement with the ratios found for the organic shell in ferritin or for the overall proportion of iron. However, the system produced hydrolytically which crystallizes as interpenetrating lattices of Fe_{17} and Fe_{19} aggregates[132] of formula $[Fe_{17}(heidi)_8O_4(OH)_{16}(H_2O)_{12}]^{3+}$ and $[Fe_{19}(heidi)_{10}O_6(OH)_{14}(H_2O)_{12}]^+$ (Figure 6), where heidi = hydroxyethyliminodiacetate, reproduces all the relative ratios excellently, and also has an identifiable close-packed AX_2 core which corresponds to a portion of the brucite $(Mg(OH)_2)$ structure. Another molecule, $[Fe_{10}O_4(OCH_3)_{16}(dbm)_6]$ (dbm = dibenzolylmethane, Figure 7) which unfortunately has no nitrogen present in the ligand shell but does have a core related to brucite with the OH groups replaced by OR groups, could also be useful for comparisons.[134] As yet the relevance of this system to elucidating the situation in loaded ferritin has not been explored further.
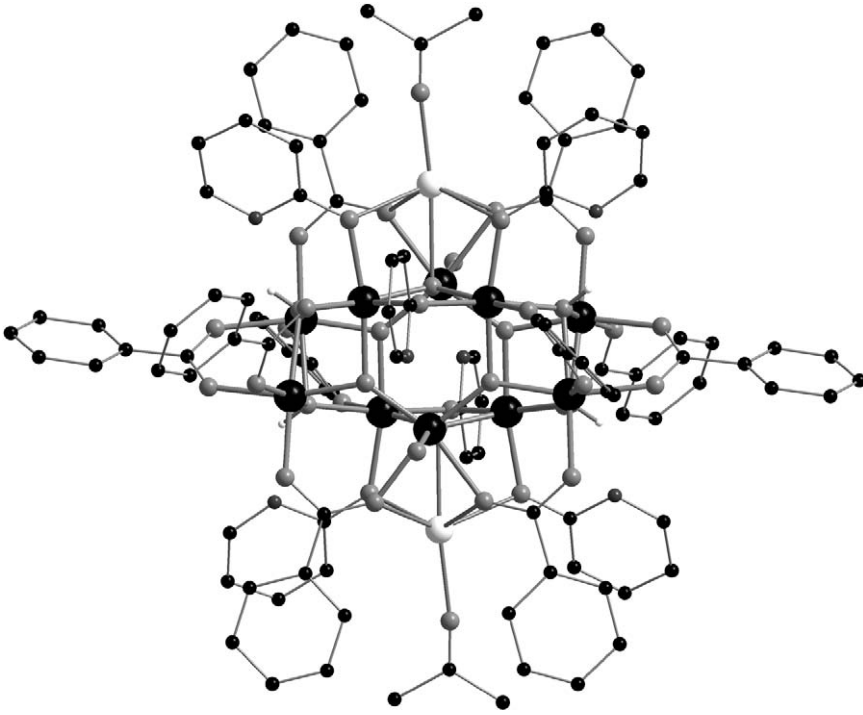
Figure 5 The molecular structure of the $[Na_2Fe_{10}O_6(OH)_4(O_2CPh)_{10}(chp)_6(OCMe_2)_2(H_2O)_2]$ model for loaded ferritin.
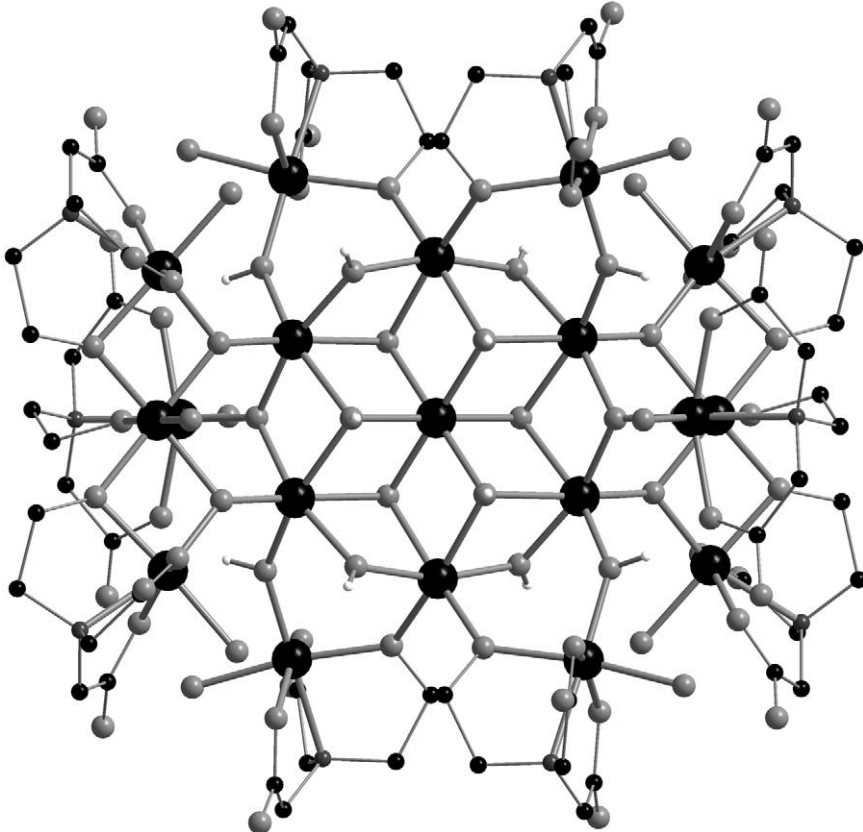
Figure 6 The molecular structure of the $[Fe_{19}(heidi)_{10}O_6(OH)_{14}(H_2O)_{12}]^+$ model for loaded ferritin.
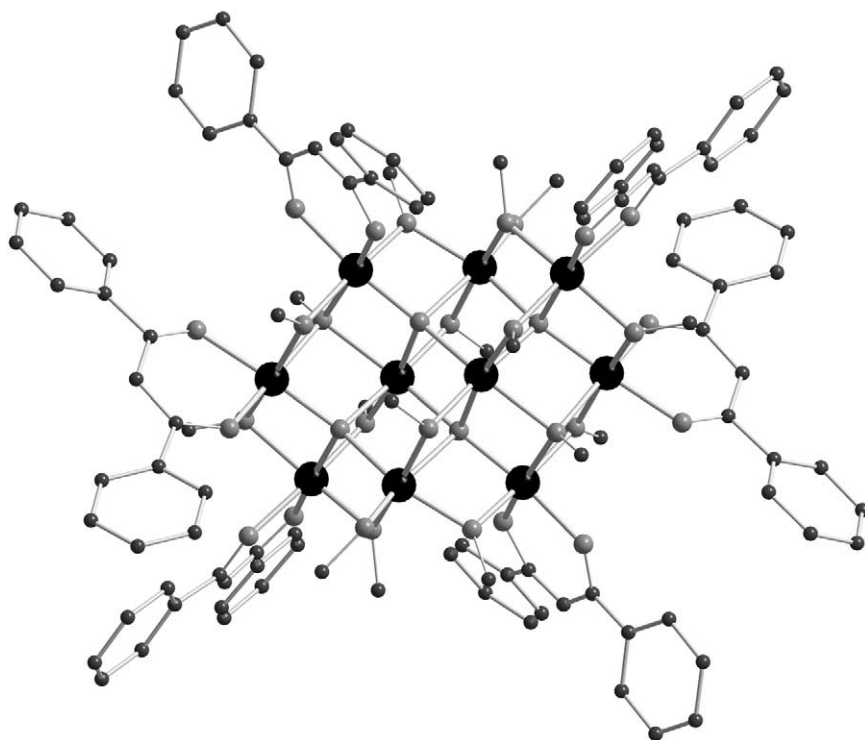
Figure 7 The molecular structure of the $[Fe_{10}O_4(OCH_3)_{16}(dbm)_6]$ model for loaded ferritin.

A mixed-valent cluster $[Fe^{III}_4Fe^{II}_8O_2(OCH_3)_{18}(O_2CCH_3)_6(CH_3OH)_{4.67}]$[135,136] (Figure 8) has an AX-type close-packed core again with hydroxides modeled with methoxides. The fact that this system is mixed valent might make it more relevant to the questions associated with the nature of the "iron pool" which describes the small molecular weight iron aggregates which appear to be present in healthy individuals and might be representative of iron species newly released from ferritin. The proportion of iron present in this aggregate is much greater than would be observed in a loaded ferritin. Other aggregates with ligand shells made up of carboxylates include the Fe_{11} compound $[Fe_{11}O_6-(OH)_6(O_2CPh)_{15}]$[137,138] (Figure 9) and the Fe_{17} aggregates which are related to this with the inclusion of M^{II} ions between two Fe_8 fragments of the Fe_{11} structure (Figure 10),[139] but in all cases the amount of iron trapped within the ligand coat is too high to reproduce satisfactorily the situation in ferritin.

Nonetheless, the Fe_{11} compound was examined using EXAFS spectroscopy[140] and was found to model certain features of the Fe···O environments. Subsequently[77] the EXAFS data for HoSF, the minerals goethite and lepidocrocite, the Fe_{11} aggregate, and the Fe_{17}/Fe_{19} systems were examined in detail. In this study, the Fe_{17}/Fe_{19} system was used to calibrate the parameters used in the interpretation of the EXAFS data with the rationale that the metrical details of the molecular structure were known to a high level of resolution for the model system. Previous work[74] had demonstrated that the Fe···Fe interactions are much more reliable in the interpretation of EXAFS data on ferritins and model compounds and this approach was applied here and tested on the very well-defined mineral models goethite and lepidocrocite. Overall the analysis for the various models and the comparison with the EXAFS on HoSF revealed that the bounded cluster models provided much better fits to the data than the mineral models. This is not surprising in view of the few iron environments in the minerals (one or two) compared with the many in the bounded systems. Finally, the Fourier transformed data of HoSF and the Fe_{17}/Fe_{19} system showed a remarkable degree of congruence with shells of oxygen and iron atoms with similar occupancies and almost identical distances with the only real difference being the better resolution of the data for the model system. The structural similarities of this model are clear when Figure 2 is compared with the molecular structure of the Fe_{19} aggregate shown in Figure 6. Subsequently it has been shown that adding alkyl side chains to the ligand in this system allows for the isolation of Fe_{19} aggregates without the cocrystallization of the Fe_{17} clusters.[141]

A further property to model was the presence of anomalous magnetic behavior with several of the models exhibiting nonzero ground state spins and the Fe_{17}/Fe_{19} system having the highest at $33/2$.[132] Subsequently a more detailed study on the Fe_{17}/Fe_{19} system[142] has revealed an
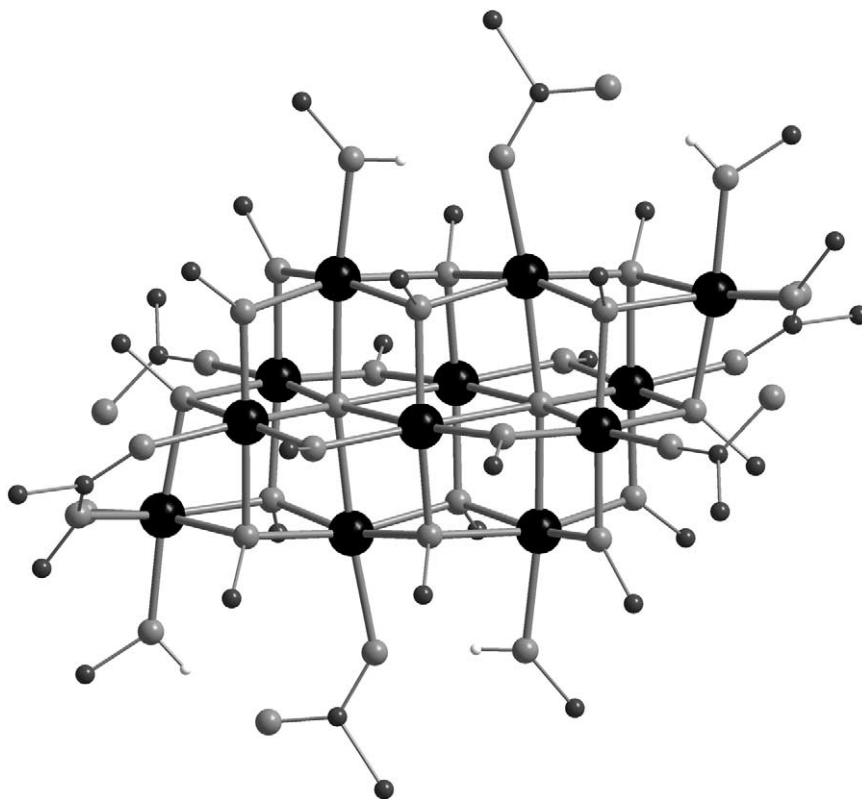
Figure 8   The molecular structure of the [Fe$^{III}_4$Fe$^{II}_8$O$_2$(OCH$_3$)$_{18}$(O$_2$CCH$_3$)$_6$(CH$_3$OH)$_{4.67}$] model for loaded ferritin.
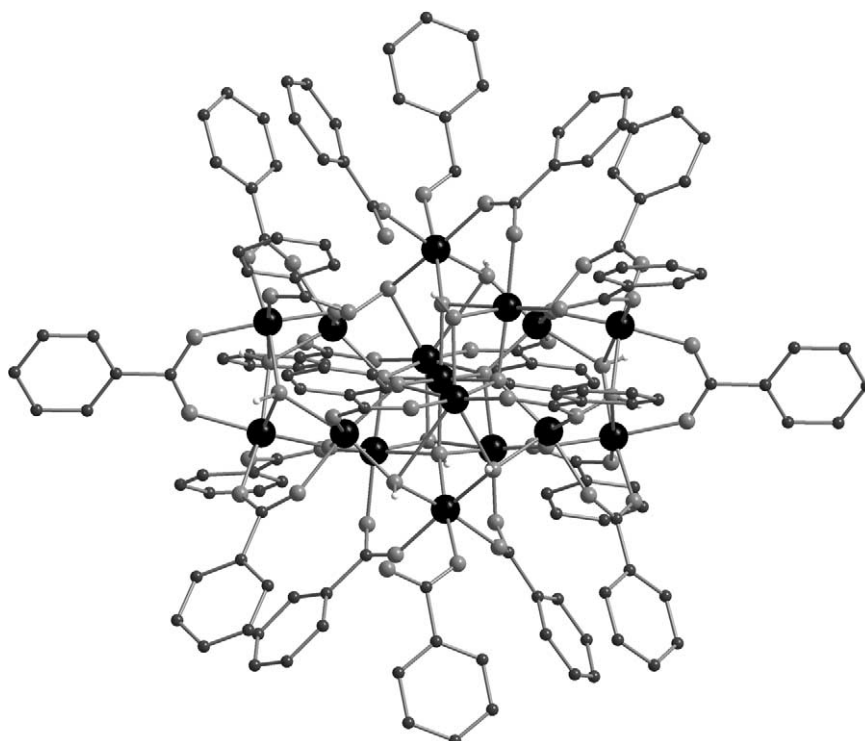
Figure 9   The molecular structure of the [Fe$_{11}$O$_6$(OH)$_6$(O$_2$CPh)$_{15}$] model for loaded ferritin.
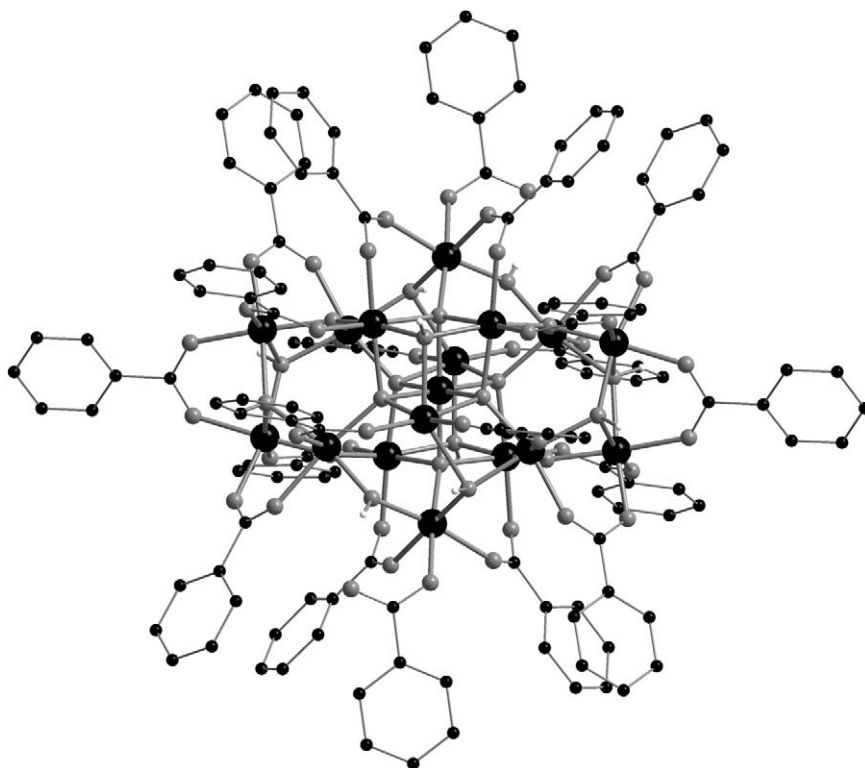
Figure 10   The molecular structure of the $[M^{II}Fe^{III}_{16}O_{10}(OH)_{10}(O_2CPh)_{15}]$ model for loaded ferritin.

anomalous hysteresis with similarities to that observed for loaded HoSF, although, as in the case of the studies on loaded ferritin,[78,79] the origin of this is still open to question.

8.7.4.5   Iron(III) Release

The release of iron from ferritin cores is an area demanding much more study.[1] Clearly an effective means for releasing iron from the mineral core is required for rapid response to iron-deficient situations. Although it is known that *in vitro* in the presence of reducing agents chelating agents such as 2,2′-bipyridine,[143,144] phenanthroline,[145] or ferrozine[93,146] can remove the iron from loaded ferritins, nothing is really known about the mechanism *in vivo*. For example, the identity of any *in vivo* reducing agent is uncertain and whether there is a need for a chelating species is not known. Considering the parameters summarized in the Pourbaix diagram (Figure 4) it can be seen that around physiological pH a shift from the situation of the solid-phase iron(III) oxyhydroxide mineral to a soluble iron species is most easily achieved either through a small change in pH or in the reduction potential if the system lies sufficiently close to the line separating "Fe(OH)$_3$" from Fe^{2+}. It is difficult to design experiments that can address these issues for the *in vivo* situation satisfactorily although comparisons with *in vitro* studies should help. The general "ferritin iron entry and exit problem" has been reviewed[147] where it was noted that although our level of knowledge concerning uptake it quite well advanced, the investigation into the mechanism for release is still at a speculative stage. However, a study has suggested that it is the threefold channels that allow for the passage of iron out of ferritin as well as for its entry. A "shutter" mechanism has been proposed on the basis of an X-ray crystallographic study where proline was substituted for a leucine and led to partial unfolding and increased exit rates of iron from ferritin.[148]

8.7.5   CONCLUSION AND OUTLOOK

A great deal of research effort has been expended since the early 1980s in trying to unravel the details of the structures and the iron uptake, storage, and release of ferritins. Much progress has

been made on investigating the uptake of iron into the core. Coordination chemistry has a defining role here in balancing local redox and pH requirements to optimize the efficiency of the process at every stage. The form of the mineralized cores used to store the iron is still not clear, but the fascinating properties of these nanoparticles and the expanding capabilities in instrumentation used in nanoscience should lead to rapid progress in this area. The chemistry associated with iron release is an area ripe for thorough research and could yield useful insights into the chemical aspects of mineral dissolution with implications in medicinal and materials applications. Again, coordination chemistry has a major role to play in this regard.

Overall this chapter has attempted to illustrate the diverse roles that coordination chemistry plays in the vital process of iron storage in organisms. This process is remarkable and we can again marvel at and learn from the way in which biology can control inorganic chemistry so exquisitely.

8.7.6 REFERENCES

1. Harrison, P. M.; Arosio, P. *Biochim. Biophys. Acta* **1996**, *1275*, 161–203.
2. Laufberger, E. V. *Bul. Soc. Chim. Biol.* **1937**, *19*, 1576–1582.
3. Harrison, P. M. *J. Mol. Biol.* **1963**, *6*, 404–422.
4. Hoare, R. J.; Harrison, P. M.; Hoy, T. G. *Nature* **1975**, *255*, 653–654.
5. Hoy, T. G.; Harrison, P. M.; Hoare, R. J. *J. Mol. Biol.* **1974**, *86*, 301–308.
6. Clegg, G. A.; Stansfield, R. F. D.; Bourne, P. E.; Harrison, P. M. *Nature* **1980**, *288*, 298–300.
7. Rice, D. W.; Ford, G. C.; White, J. L.; Smith, J. M. A.; Harrison, P. M. *Adv. Inorg. Biochem.* **1983**, *5*, 39–49.
8. Hempstead, P. D.; Yewdall, S. J.; Fernie, A. R.; Lawson, D. M.; Artymiuk, P. J.; Rice, D. W.; Ford, G. C.; Harrison, P. M. *J. Mol. Biol.* **1997**, *268*, 424–448.
9. Frolow, F.; Kalb, A. J.; Yariv, J. *Nature Struct. Biol.* **1994**, *1*, 453–460.
10. Dautant, A.; Meyer, J-B.; Yariv, J.; Précigoux, G.; Sweet, R. M.; Kalb, J. A.; Frolow, F. *Acta Crystallogr. D* **1999**, *54*, 16–24.
11. Takagi, H.; Shi, D.; Ha, Y.; Allwell, N. M.; Theil, E. C. *J. Biol. Chem.* **1998**, *273*, 18685–18688.
12. Gallois, B.; Langlois d'Estaintot, B.; Michaux, M. A.; Dautant, A.; Granier, T.; Précigoux, G.; Soruco, J.-A.; Roland, F; Chavas-Alba, O.; Herbas, A.; Crichton, R. R. *J. Biol. Inorg. Chem.* **1997**, *2*, 360–367.
13. Grant, R. A.; Filman, D. J.; Finkel, S. E.; Kolter, R.; Hogle, J. M. *Nature Struct. Biol.* **1998**, *5*, 294–303.
14. Stillman, T. J.; Hempstead, P. D.; Artymiuk, P. J.; Andrews, S. C.; Hudson, A. J.; Treffry, A.; Guest, J. R.; Harrison, P. M. *J. Mol. Biol.* **2001**, *307*, 587–603.
15. Sharma, V.; Sharma, S.; Zu Bentrup, K. H.; McKinney, J. D.; Russell, D. G.; Jacobs, W. R. Jr.; Sacchettini, J. C. *Nature Struct. Biol.* **2000**, *7*, 663.
16. Lawson, D. M.; Artymiuk, P. J.; Yewdall, S. J.; Smith, J. M. A.; Livingstone, J. C.; Treffry, A.; Luzzago, A.; Levi, S.; Arosio, P.; Cesareni, G.; Thomas, C. D.; Shaw, W. V.; Harrison, P. M. *Nature* **1991**, *349*, 541–544.
17. Evans, G.; Bricogne, G. *Acta Crystallogr. D* **2002**, *58*, 976–991.
18. Granier, T.; Gallois, B.; Langlois d'Estaintot, B.; Dautant, A.; Chevalier, J.-M.; Mellado, J.-M.; Beaumont, C.; Santambrogio, P.; Arosio, P.; Précigoux, G. *Acta Crystallogr. D* **2001**, *57*, 1491–1497.
19. Précigoux, G.; Yariv, J.; Gallois, B.; Dautant, A.; Courseille, C; Langlois d'Estaintot, B. *Acta Crystallogr. D* **1994**, *50*, 739–743.
20. Granier, T.; Gallois, B.; Dautant, A.; Langlois d'Estaintot, B.; Précigoux, G. *Acta Crystallogr. D* **1997**, *53*, 580–587.
21. Cobessi, D.; Huang, L.-S.; Ban, M.; Pon, N. G.; Daldal, F.; Berry, E. A. *Acta Crystallogr. D* **2002**, *58*, 29–38.
22. Zanotti, G.; Papinutto, E.; Dundon, W. G.; Batistutta, R.; Seveso, M.; Del Giudice, G.; Rappuoli, R.; Montecucco, C. *J. Mol. Biol.* **2002**, *323*, 125–130.
23. Clerté, S.; Dautant, A.; Langlois d'Estaintot, B.; Gallois, B.; Mizunoe, Y.; Wai, S. N.; Précigoux, G. *Acta Crystallogr. D* **1999**, *55*, 299–301.
24. Granier, T.; Gallois, B.; Langlois d'Estaintot, B.; Gallois, B.; Chevalier, J.-M.; Précigoux, G.; Santambrogio, P.; Arosio, P. *J. Biol. Inorg. Chem.* **2003**, *8*, 105–111.
25. Ha, Y.; Shi, D. S.; Small, G. W.; Theil, E. C.; Allewell, N. M. *J. Biol. Inorg. Chem.* **1999**, *4*, 243–256.
26. Ilari, A.; Savino, C; Stefanini, S.; Chiancone, E.; Tsernoglou, D. *Acta Crystallogr. D* **1999**, *55*, 552–553.
27. Ilari, A.; Stefanini, S.; Chiancone, E.; Tsernoglou, D. *Nature Struct. Biol.* **2000**, *7*, 38–43.
28. Trikha, J.; Thiel, E. C.; Allewell, N. M. *J. Mol. Biol.* **1995**, *248*, 949–967.
29. Granier, T.; Comberton, G.; Gallois, B.; Langlois d'Estaintot, B.; Dautant, A.; Crichton, R. R.; Précigoux, G. *Proteins* **1998**, *31*, 477–485.
30. Aisen, P.; Listowsky, I. *Annu. Rev. Biochem.* **1980**, *49*, 357–393.
31. Andrews, S. C.; Arosio, P.; Bottke, W.; Briat, J. F.; von Darl, M.; Harrison, P. M.; Laulhere, J. P.; Levi, S.; Lobreaux, S.; Yewdall, S. J. *J. Inorg. Biochem.* **1992**, *47*, 161–174.
32. Chasteen, N. D.; Sigel, A.; Sigel, H., Ed., *Metal Ions in Biological Systems* **1998**, *35*, 479–514, Chapter 12, Marcel Dekker, New York.
33. Clegg, G. A.; Fitton, J. E.; Harrison, P. M.; Treffry, A. *Prog. Biophys. Mol. Biol.* **1980**, *36*, 56–86.
34. Crichton, R. R. *New Engl. J. Med.* **1971**, *284*, 1413–1422.
35. Crichton, R. R. *Struct. Bonding (Berlin)* **1973**, *17*, 67–134.
36. Crichton, R. R. *Angew. Chem., Int. Ed. Engl.* **1973**, *12*, 57–65.
37. Ford, G. C.; Harrison, P. M.; Rice, D. W.; Smith, J. M. A.; Treffry, A.; White, J. L.; Yariv, J. *Phil. Trans. Roy. Soc. B* **1984**, *304*, 551–564.
38. Harrison, P. M.; Ford, G. C.; Rice, D. W.; Smith, J. M. A.; Treffry, A.; White, J. L. *Biochem. Soc. Trans.* **1987**, *15*, 744–748.

39. Harrison, P. M.; Hempstead, P. D.; Artymiuk, P. J.; Andrews, S. C.; Sigel, A.; Sigel, H., Ed., *Metal Ions in Biological Systems* **1998**, *35*, 435–477, Chapter 13, Marcel Dekker, New York.
40. Harrison, P. M.; Artymiuk, P. J.; Ford, G. C.; Lawson, D. M.; Smith, J. M. A.; Treffry, A.; White, J. L.; Ferritin, *Function and Structural Design of an Iron-storage Protein* Mann, S.; Webb, J.; Williams, R. J. P., Ed., *Biomineralization. Chemical and Biochemical Perspectives* **1989**, VCH, Weinheim, 257–294.
41. Le Brun, N. L.; Moore, G. R.; Thomson, A. J. *Struct. Bonding (Berlin)* **1987**, *88*, 103–138.
42. Powell, A. K.; *Struct. Bonding (Berlin)* **1997**, *88*, 1–38.
43. Powell, A. K.; Sigel, A.; Sigel, H., Ed., *Metal Ions in Biological Systems* **1998**, *35*, 515–561, Chapter 13, Marcel Dekker, New York.
44. Proulx-Curry, P. M.; Chasteen, N. D. *Coord. Chem. Rev.* **1995**, *144*, 347–368.
45. Spiro, G.; Saltman, P. *Struct. Bonding* **1969**, *6*, 116–156.
46. Pierre, T. G.; Webb, J.; Mann, S. Mann, S.; Webb, J.; Williams, R. J. P., Ed., *Biomineralization. Chemical and Biochemical Perspectives* **1989**, VCH, Weinheim, 294.
47. Pierre, T. G.; Chan, P.; Bauchspiess, K. R.; Webb, J.; Betteridge, S.; Walton, S.; Dickson, D. P. E. *Coord. Chem. Rev.* **1996**, *151*, 125–143.
48. Theil, E. C. *Adv. Inorg. Biochem.* **1983**, *5*, 1–38.
49. Theil, E. C. *ACS Symp. Ser.* **1988**, *372*, 179–195.
50. Theil, E. C. *Annu. Rev. Biochem.* **1987**, *56*, 289–315.
51. Theil, E. C.; Ferritin, Messerschmidt, A.Huber, R.Poulos, T.Wieghardt, K., Ed., *Handbook of Metalloproteins* **2001**, 771–790.
52. Levi, S.; Yewdall, S. J.; Harrison, P. M.; Santambrogio, P.; Cozzi, A.; Rovida, E.; Albertini, A.; Arosio, P. *Biochem. J.* **1992**, *288*, 591–596, Wiley, New York.
53. Levi, S.; Santambrogio, P.; Cozzi, A.; Rovida, E.; Corsi, B.; Tamborini, E.; Spada, S.; Albertini, A.; Arosio, P. *J. Mol. Biol.* **1994**, *238*, 649–654.
54. Arosio, P.; Adelman, T. G.; Drysdale, J. W. *J. Biol. Chem.* **1978**, *253*, 4451–4458.
55. Douglas, T.; Ripoli, D. R. *Protein Sci.* **1998**, *7*, 1083–1091.
56. Yang, X.; Le Brun, N. E.; Thomson, A. J.; Moore, G. R.; Chasteen, N. D. *Biochemistry* **2000**, *39*, 4915–4932.
57. Hempstead, P. D.; Hudson, A. J.; Artymiuk, P. J.; Andrews, S. C.; Banfield, M. J.; Guest, J. R.; Harrison, P. M. *FEBS Lett.* **1994**, *350*, 258–262.
58. Le Brun, N. E.; Andrews, S. C.; Guest, J. R.; Harrison, P. M.; Moore, G. R.; Thomson, A. J. *Biochem. J.* **1995**, *312*, 385–392.
59. Treffry, A.; Zhao, Z.; Quail, M. A.; Guest, J. R.; Harrison, P. M. *Biochemistry* **1995**, *34*, 15204–15213.
60. Treffry, A.; Zhao, Z.; Quail, M. A.; Guest, J. R.; Harrison, P. M. *Biochemistry* **1997**, *36*, 432–441.
61. Kurtz, D. M. Jr. *J. Biol. Inorg. Chem.* **1997**, *2*, 159–167.
62. Nordlund, P.; Eklund, H. *Curr. Opin. Struct. Biol.* **1995**, *5*, 758–766.
63. Yariv, J. *Biochem. J.* **1983**, *211*, 527.
64. Webb, J.; Gray, H. B. *Biochim. Biophys. Acta* **1974**, *351*, 224–229.
65. Zhao, Z.; Treffry, A.; Quail, M. A.; Guest, J. R.; Harrison, P. M. *J. Chem. Soc., Dalton Trans.* **1997**, 3977–3978.
66. Le Brun, N. L.; Moore, G. R.; Thomson, A. J. *Mol. Phys.* **1995**, *85*, 1061–1068.
67. Boas, J. F.; Troup, G. J. *Biochim. Biophys. Acta* **1971**, *229*, 68–74.
68. Weir, M. P.; Peters, T. J.; Gibson, J. F. *Biochim. Biophys. Acta* **1985**, *828*, 298–305.
69. Deighton, N.; Abu-Raqabah, A.; Rowland, I. J.; Symons, M. J.; Peters, T. J.; Ward, R. J. *J. Chem. Soc., Faraday Trans.* **1991**, *87*, 3193–3197.
70. Stefanini, S.; Desideri, A.; Vecchini, P.; Drakenberg, T.; Chiancone, E. *Biochemistry* **1989**, *28*, 378–382.
71. Ostrakh, M. I.; Milder, O. B.; Semionkin, V. A.; Prokopenko, P. G.; Livshits, A. B.; Kozlov, A. A.; Pikulev, A. I. *Z. Naturforsch.* **2002**, *57a*, 566–574.
72. Bauminger, E. R.; Treffry, A.; Quail, M. A.; Zhao, Z.; Nowik, I.; Harrison, P. M. *Inorg. Chim. Acta* **2000**, *297*, 171–180.
73. Thiel, E. C.; Sayers, D. E.; Brown, M. A. *J. Biol. Chem.* **1979**, *254*, 8132–8134.
74. Mackle, P. Garner C. D.; Ward, R. J.; Peters, T. J. *Biochim. Biophys. Acta* **1991**, *1115*, 145–150.
75. Heald, S. M.; Stern, E. A.; Bunker, B.; Holt, E. M.; Holt, S. J. *J. Am. Chem. Soc.* **1979**, *101*, 76.
76. Rohrer, J. S.; Quazi, T. I.; Watt, G. D.; Sayers, D. E.; Theil, E. C. *Biochemistry* **1990**, *29*, 259–264.
77. Heath, S. L.; Charnock, J. M.; Garner, C. D.; Powell, A. K. *Chem. Eur. J.* **1996**, *2*, 634–639.
78. Tejada, J.; Ziolo, R. F.; Zhang, X. X. *Chem. Mater.* **1996**, *8*, 1784.
79. Friedman, J. R.; Voskoboynik, U.; Sarachik, M. P. *Phys. Rev. B* **1997**, *56*, 10793–10796.
80. Yang, X.; Chen-Barrett, Y.; Arosio, P.; Chasteen, N. D. *Biochemistry* **1998**, *37*, 9743–9750.
81. Sun, S.; Chasteen, N. D. *J. Biol. Chem.* **1992**, *267*, 25160–25166.
82. Sun, S.; Arosio, P.; Levi, S.; Chasteen, N. D. *Biochemistry* **1993**, *32*, 9362–9369.
83. Baaghil, S.; Thomson, A. J.; Moore, G. R.; Le Brun, N. E. *J. Chem. Soc., Dalton Trans.* **2002**, 811–818.
84. Treffry, A.; Bauminger, E. R.; Hechel, D.; Hodson, N. W.; Nowik, I.; Yewdall, S. J.; Harrison, P. M. *Biochem. J.* **1993**, *296*, 721–728.
85. Levi, S.; Santambrogio, P.; Corsi, B.; Cozzi, A.; Arosio, P. *Biochem. J.* **1996**, *317*, 467–473.
86. Aisen, P.; Sigel, A.; Sigel, H.; Ed., *Metal Ions in Biological Systems* **1998**, *35*, 585–631, Chapter 15, Marcel Dekker, New York.
87. Hempstead, P. D.; Yewdall, S. J.; Fernie, A. R.; Lawson, D. M.; Artymiuk, P. J.; Rice, D. W.; Ford, G. C.; Harrison, P. M. *J. Mol. Biol.* **1997**, *268*, 424–448.
88. Levi, S.; Luzzago, A.; Cesareni, G.; Cozzi, A.; Franceschinelli, F.; Albertini, A.; Arosio, P. *J. Biol. Chem.* **1988**, *268*, 18086–18092.
89. Levi, S.; Salfeld, J.; Franceschinelli, F.; Cozzi, A.; Dorner, M. H.; Arosio, P. *Biochemistry* **1998**, *28*, 5179–5185.
90. Treffry, A.; Zhao, Z.; Quail, M. A.; Guest, J. R.; Harrison, P. M. *Biochemistry* **1997**, *36*, 432–441.
91. Lawson, D. M.; Treffry, A.; Artymiuk, P. J.; Harrison, P. M.; Yewdall, S. J.; Luzzago, A.; Cesareni, G.; Levi, S.; Arosio, P. *FEBS Lett.* **1989**, *254*, 207–210.
92. Bauminger, E. R.; Harrison, P. M.; Hechel, D.; Nowik, I.; Treffry, A. *Biochim. Biophys. Acta* **1991**, *1118*, 48–58.
93. Bauminger, E. R.; Harrison, P. M.; Hechel, D.; Hodson, N. W.; Nowik, I.; Treffry, A.; Yewdall, S. J. *Biochem. J.* **1993**, *296*, 709–719.
94. Pereira, A. S.; Small, W.; Krebs, C.; Tavares, P.; Edmondson, D. E.; Theil, E. C.; Huynh, B. H. *Biochemistry* **1998**, *37*, 9871–9876.

95. Xu, B.; Chasteen, N. D. *J. Biol. Chem.* **1991**, *266*, 19965–19970.
96. Waldo, G. S.; Ling, J.; Sanders-Loehr, J.; Theil, E. C. *Science* **1993**, *259*, 796–798.
97. Le Brun, N. E.; Wilson, M. T.; Andrews, S. C.; Guest, J. R.; Harrison, P. M.; Thomson, A. J.; Moore, G. R. *FEBS Lett.* **1993**, *333*, 197–202.
98. Keech, A. M.; Le Brun, N. L.; Wilson, M. T.; Andrews, S. C.; Moore, G. R.; Thomson, A. J. *J. Biol. Chem.* **1997**, *272*, 422–429.
99. Le Brun, N. L.; Keech, A. M.; Mauk, M. R.; Mauk, A. G.; Andrews, S. C.; Thomson, A. J.; Moore, G. R. *FEBS Lett.* **1996**, *397*, 159–163.
100. Andrews, S. C.; Le Brun, N. L.; Barynin, V.; Thomson, A. J.; Moore, G. R.; Guest, J. R.; Harrison, P. M. *J. Biol. Chem.* **1995**, *270*, 23268–23274.
101. Hwang, J.; Krebs, C.; Huynh, B. H.; Edmondson, D. E.; Theil, E. C.; Penner-Hahn, J. E. *Science* **2000**, *287*, 122–125.
102. Chasteen, N. D.; Harrison, P. M. *J. Struct. Biol.* **1999**, *126*, 182–194.
103. Wade, V. J.; Levi, S.; Arosio, P.; Harrison, P. M.; Mann, S. *J. Mol. Biol.* **1991**, *221*, 1443–1452.
104. Treffry, A.; Zhao, Z.; Quail, M. A.; Guest, J. R.; Harrison, P. M. *FEBS Lett.* **1998**, *432*, 213–218.
105. Cozzi, A.; Corsi, B.; Levi, S.; Santamborgio, P.; Albertini, A.; Arosio, P. *J. Biol. Chem.* **2000**, *275*, 25122–25129.
106. Towe, K. M.; Bradley, W. F. *J. Colloid. Inter. Sci.* **1967**, *24*, 384–392.
107. Chukrov, F. V.; Zvygagin, B. B.; Gorshkov, A. I.; Ermilova, L. P.; Balashova, V. V. *Int. Geol. Rev.* **1973**, *16*, 1131–1143.
108. Russell, J. D. *Clay. Miner.* **1979**, *14*, 109–114.
109. Eggleton, R. A.; Fitzpatrick, R. W. *Clays Clay Miner.* **1988**, *36*, 111–124.
110. Robie, R. A.; Bethke, P. M.; Beardsley, K. M Weast, R. C., Ed., 61st ed.*CRC Handbook of Chemistry and Physics* **1980**, B-208. CRC Press.
111. Zettlemoyer, A. C., Ed., *Nucleation* **1969**, Marcel Dekker: New York.
112. Nancollas, G. H.; Purdie, N. *Chem. Soc. Lond. Q. Rev.* **1964**, *18*, 1–20.
113. Garside, J. Nancollas, G. H., Ed., *Biological Mineralization and Demineralization* **1982**, Springer, Berlin, 37–77.
114. Manceau, A.; Combes, J.-M.; Calas, G. *Clays Clay Miner.* **1990**, *38*, 331–334.
115. Eggleton, R. A.; Fitzpatrick, R. W. *Clays Clay Miner.* **1990**, *38*, 335–336.
116. Womack, T.G.; Evans-Smith, R.; Powell, A.K. Unpublished work..
117. Ringeling, P. L.; Davy, S. L.; Monkara, F. A.; Hunt, C.; Dickson, D. P. E.; McEwan, A. G.; Moore, G. R. *Eur. J. Biochem.* **1994**, *233*, 847–855.
118. Meldrum, F. C.; Heywood, B. R.; Mann, S. *Science* **1992**, *257*, 522–523.
119. Mann, S.; Williams, J. M.; Treffry, A.; Harrison, P. M. *J. Mol. Biol.* **1987**, *198*, 405–416.
120. Meldrum, F. C.; Wade, V. J.; Nimmo, D. L.; Heywood, B. R.; Mann, S. *Nature* **1991**, *349*, 684–687.
121. Pierre, T. G.; Bell, S. H.; Dickson, D. P. E.; Mann, S.; Webb, J.; Moore, G. R.; Williams, R. J. P. *Biochim. Biophys. Acta* **1986**, *870*, 127–134.
122. Gatteschi, D.; Sessoli, R.; Cornia, A. *Chem. Commun.* **2000**, 725–732.
123. Caneschi, A.; Gatteschi, D.; Sessoli, R.; Barra, A. L.; Brunel, L. C.; Guillot, M. *J. Am. Chem. Soc.* **1991**, *113*, 5873–5874.
124. Sessoli, R.; Gatteschi, D.; Caneschi, A.; Novak, M. A. *Nature* **1993**, *365*, 141–413.
125. Thomas, L.; Lionti, F.; Ballou, R.; Gatteschi, D.; Sessoli, R.; Barbara, B. *Nature* **1996**, *383*, 145–147.
126. Friedman, J. R.; Sarachik, M. P.; Tejada, J.; Ziolo, R. *Phys. Rev. Lett.* **1996**, *76*, 3830–3833.
127. Flynn, C. M. *Chem. Rev.* **1984**, *48*, 31–41.
128. Yang, C.; Bryan, A. M.; Theil, E. C.; Sayers, D. E.; Bowen, L. H. *J. Inorg. Biochem.* **1986**, *28*, 393–405.
129. Spiro, T. G.; Allerton, S. E.; Renner, J.; Terzis, A.; Bils, R.; Saltman, P. *J. Am. Chem. Soc.* **1966**, *88*, 2721–2726.
130. Spiro, T. G.; Pape, L.; Saltman, P. *J. Am. Chem. Soc.* **1967**, *89*, 5555–5559.
131. Heath, S. L.; Powell, A. K. *Angew. Chem., Int. Ed. Engl.* **1992**, *31*, 191–192.
132. Powell, A. K.; Heath, S. L.; Gatteschi, D.; Pardi, L.; Sessoli, R.; Spina, G.; Del Giallo, F.; Pieralli, F. *J. Am. Chem. Soc.* **1995**, *117*, 2491–2502.
133. Benelli, C.; Parsons, S.; Solan, G. A.; Winpenny, R. E. P. *Angew. Chem., Int. Ed. Engl.* **1996**, *35*, 1825–1828.
134. Caneschi, A.; Cornia, A.; Fabretti, A. C.; Gatteschi, D. *Angew. Chem., Int. Ed. Engl.* **1995**, *34*, 2716–2718.
135. Taft, K. L.; Papaefthymiou, G. C.; Lippard, S. J. *Science* **1993**, *259*, 1302–1305.
136. Taft, K. L.; Papaefthymiou, G. C.; Lippard, S. J. *Inorg. Chem.* **1994**, *33*, 1510–1520.
137. Gorun, S. M.; Lippard, S. J. *Nature* **1986**, *319*, 666.
138. Gorun, S. M.; Papaefthymiou, G. C.; Frankel, R. B.; Lippard, S. J. *J. Am. Chem. Soc.* **1987**, *109*, 3337–3348.
139. Micklitz, W.; McKee, V.; Rardin, R. L.; Pence, L. E.; Papaefthymiou, G. C.; Bott, S. G.; Lippard, S. J. *J. Am. Chem. Soc.* **1994**, *116*, 8061–8069.
140. Islam, Q. T.; Sayers, D. E.; Gorun, S. M.; Theil, E. C. *J. Inorg. Biochem.* **1989**, *36*, 51–62.
141. Goodwin, J. C.; Sessoli, R.; Gatteschi, D.; Wernsdorfer, W.; Barra, A. L.; Powell, A. K.; Heath, S. L. *J. Chem. Soc., Dalton Trans.* **2000**, 1835–1840.
142. Price, D. J.; Lionti, F.; Ballou, R.; Wood, P. T.; Powell, A. K. *Phil. Trans. Roy. Soc. A* **1999**, *357*, 3099–3118.
143. Watt, G. D.; Frankel, R. B.; Papaefthymiou, G. C. *Proc. Natl. Acad. Sci.* **1985**, *82*, 3640–3643.
144. Granick, S.; Michaelis, L. *J. Biol. Chem.* **1943**, *147*, 91–97.
145. Bolann, B. J.; Ulvik, R. J. *Biochem. J.* **1987**, *243*, 55–59.
146. Boyer, R. F.; Grabile, T. W.; Petrovich, R. M. *Anal. Biochem.* **1988**, *174*, 17–22.
147. Theil, E. C.; Takagi, H.; Small, G. W.; He, L.; Tipton, A. R.; Danger, D. *Inorg. Chim. Acta* **2000**, *297*, 242–251.
148. Takagi, H.; Shi, D.; Ha, Y.; Allwell, N. M.; Theil, E. C. *J. Biol. Chem.* **1998**, *273*, 18685–18688.

8.8
Metal Ion Homeostasis

R. L. LIEBERMAN and A. C. ROSENZWEIG
Northwestern University, Evanston, IL, USA

8.8.1 INTRODUCTION

Transition metal ions are essential cofactors for proteins with diverse functions, including electron transfer, dioxygen binding and activation, nitrogen fixation, and antioxidant defense.[1] However, metal ions can also be deleterious. The dual nature of metal ions derives from two properties. First, redox active metal ions such as copper and iron can generate highly reactive hydroxyl radicals and cause oxidative damage to proteins, nucleic acids, and lipids. Second, metal ions can bind nonspecifically to amino acid residues, replacing existing metal ions in enzyme active sites or key structural sites, leading to aberrant activity or protein misfolding. Therefore, intracellular transition metal ion concentrations must be controlled carefully to ensure that metal ions are provided to essential metalloproteins and metalloenzymes, but do not accumulate to toxic levels. Since the early 1980s, a number of metal homeostatic systems in both eukaryotes and prokaryotes have been discovered by genetic techniques. Understanding these systems on the molecular level is a fundamental problem in biological coordination chemistry. Moreover, an increasing number of human diseases are linked to deficiencies in metal handling.[2]

Proteins involved in metal ion homeostasis can be divided into two broad families, metal trafficking proteins and metalloregulatory proteins. The metal trafficking proteins include membrane transporters that translocate metal ions across cell membranes[2] and soluble metallochaperone proteins that deliver metal ions to specific target proteins.[3] The metalloregulatory proteins utilize metal ions to regulate gene expression.[4,5] Proteins in both families maintain concentrations of both essential and nonessential metal ions. The coordination chemistry of metal homeostatic

proteins is not well understood due to a lack of biochemical and biophysical data. In the past decade, however, some details of metal binding have begun to emerge from spectroscopic and crystallographic studies. This chapter focuses on those systems for which information about metal ion coordination is available. More comprehensive reviews of copper,[4,6] zinc,[4,7] iron,[4,8] and heavy metal[9,10] metabolism can be found elsewhere.

8.8.2 METAL TRAFFICKING PROTEINS

8.8.2.1 Membrane Transporters

Membrane-bound metal ion transporters are responsible for maintaining proper concentrations of metal ions in different cellular compartments. These proteins can be involved in metal uptake or metal efflux. Transport is driven either by an electrochemical gradient or by ATP hydrolysis. In addition, both high affinity and low affinity transporters exist for many metal ions. The high affinity transporters are more specific and function when metal ion concentrations are limited, whereas the low affinity transporters are less specific and function under metal replete conditions.[4] Although transporters for a variety of metal ions have been identified in bacteria, yeast, plants, and humans, the details of metal binding have not been elucidated. In many transporters, conserved sequence motifs are postulated to bind metal ions. Examples of these motifs include methionine-rich sequences in the copper transporter Ctr1[11,12] and conserved histidines in the ZIP family of zinc transporters.[7] A major impediment to studying the coordination chemistry of the transporters is the presence of multiple transmembrane domains which render protein purification and *in vitro* characterization difficult.

Some transporters contain soluble metal binding domains that are more amenable to biophysical analysis. In particular, copper translocating *P*-type ATPases have an extended soluble amino terminus containing multiple copies of an MXCXXC sequence motif (single letter amino acid code where C is cysteine, M is methionine, and X is any amino acid).[13] Metal binding by this motif has been demonstrated for the human Wilson and Menkes disease proteins and for their yeast homologue Ccc2. The human proteins, mutations in which lead to disorders of copper metabolism,[14] contain six MXCXXC motifs and have been studied by various spectroscopic methods. The NMR structure of the fourth repeat of the Menkes protein in the presence of Ag^I reveals a 4.8 Å separation between the two cysteine sulfur atoms, consistent with linear coordination of Ag^I.[15] According to X-ray absorption spectroscopic (XAS) data for all six domains of the Menkes protein, copper binds as Cu^I and is coordinated in a distorted linear fashion by two sulfur atoms at a distance of 2.16 Å.[16] XAS data for the Wilson protein are consistent with two-coordinate Cu^I, and yield a Cu$\cdots$S distance of 2.18 Å.[17] The NMR structure of the *N*-terminal domain of yeast Ccc2, which contains only two MXCXXC repeats, suggests that Ccc2 binds Cu^I in a similar manner (Figure 1).[18]

Other copper ATPases with soluble *N*-terminal MXCXXC-containing domains are expected to contain analogous Cu^I-binding sites. These include two bacterial copper transporters designated CopA,[19,20] and other homologues discovered genetically or by sequence analysis.[13] In addition, CXXC-containing ATPases such as ZntA[21,22] and CadA[22,23] are specific for Zn^{II}, Cd^{II}, and Pb^{II}. The coordination chemistry of the *N*-terminal domains of the Zn^{II}/Cd^{II}/Pb^{II} transporters has not been established.

Furthermore, the specific function of the multiple MXCXXC-containing domains is not clear for any of the transporters. Several MXCXXC repeats can be deleted in the Wilson[24] and Menkes ATPases[25] without affecting transport activity. The ZntA *N*-terminus is not required for function, although ATPase activity is decreased in its absence.[26] It is also not known how these ATPases or any of the other metal ion transporters confer metal ion specificity. Understanding how the transmembrane domains of these transporters coordinate metal ions is crucial and constitutes a major goal for future research.
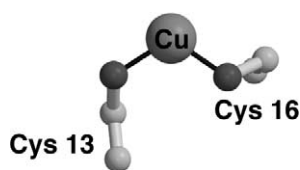
Figure 1 Metal-binding site in the soluble *N*-terminal domain of the yeast copper transporter Ccc2 (PDB accession code 1FVS). The Cu^I ion is coordinated by Cys 13 and Cys 16.

8.8.2.2 Atx1-like Copper Chaperones

Metallochaperone proteins are soluble metal-binding proteins that deliver metal ions to target proteins or enzymes via direct protein–protein interactions.[27] The yeast copper chaperone Atx1[28] delivers Cu^I to the Ccc2 transport ATPase for translocation across intracellular membranes and insertion into the multicopper oxidase Fet3.[29] Like its target protein, Atx1 contains a conserved MXCXXC sequence motif that binds metal ions. According to extended X-ray absorption fine structure (EXAFS) spectroscopic studies on Atx1 loaded with Cu^I, the Cu^I ion is three-coordinate with two sulfur ligands at a distance of 2.25 Å and a third sulfur, suggested to be from methionine or an exogenous thiol, at 2.40 Å.[30] The solution structure of a bacterial Atx1 homologue called CopZ is consistent with three-coordinate Cu^I.[31]

The high-resolution crystal structure of the Hg^{II} form of Atx1 has been determined.[32] Since Atx1 can transfer Hg^{II} as well as Cu^I to Ccc2,[32] this structure is a functionally useful model. The Hg^{II} ion is coordinated linearly by the two cysteines in the MXCXXC motif at distances of 2.33 Å and 2.34 Å (Figure 2). This coordination geometry is similar to that of Ag^I in the fourth repeat of the Menkes protein[15] and of Hg^{II} in MerP, a related bacterial mercury detoxification protein.[33] The Atx1 structure does not resolve the identity of the third Cu^I sulfur ligand observed in the EXAFS data. The sulfur atom of the methionine residue in the MXCXXC motif is located 8 Å from the Hg^{II} ion, indicating that this methionine is probably not a ligand. Crystal structures of the human homologue of Atx1, Hah1, provide another possibility for the third ligand. In three structures of Hah1, determined in the presence of Cu^I, Hg^{II}, and Cd^{II}, the metal ion is coordinated by cysteine residues from two Hah1 molecules (Figure 3).[34] Thus, the third ligand is likely a cysteine from an adjacent Atx1 molecule.

The Hah1 structures provide insight into the molecular mechanism of metal transfer between the Atx1-like chaperones and their partner ATPases. The target proteins of Hah1 are the Menkes and Wilson disease proteins (Section 8.8.2.1). In the Cu^I Hah1 structure, the coordination geometry is distorted tetrahedral with three Cu···S distances of 2.3 Å and the fourth sulfur at 2.4 Å (Figure 3a). These distances are within experimental error for a 1.8 Å resolution structure, suggesting that the Cu^I is four-coordinate. Nevertheless, the 2.3 Å distances are in the range for three-coordinate Cu^I observed in model compounds and metallothioneins[35,36] whereas four-coordinate Cu^I thiolate centers have not been reported in biology. Therefore, this Cu^I site might also be described as three-coordinate with a weakly bound fourth ligand. By contrast, the Hg^{II} center is clearly three-coordinate with three Hg···S distances of 2.3–2.5 Å and the fourth sulfur at 2.8 Å (Figure 3b).

These coordination geometries are consistent with a proposed mechanism in which the metal ion is transferred from chaperone to target protein by the formation of two- and three-coordinate
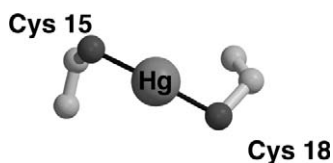
Figure 2 Metal-binding site in the Hg^{II} form of the yeast copper chaperone Atx1 (PDB accession code 1CC8). The Hg^{II} ion is coordinated linearly by Cys 15 and Cys 18.
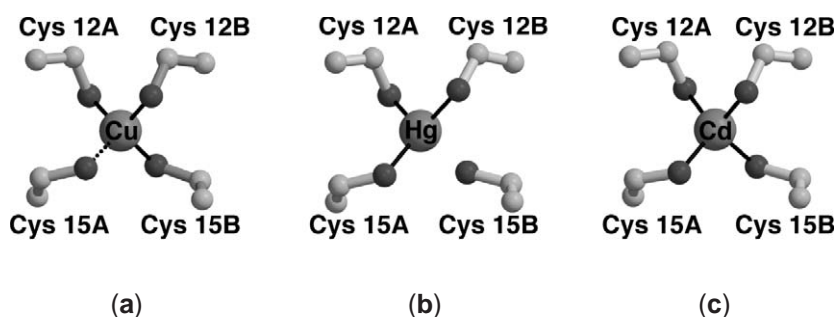
Figure 3 Metal-binding site in the human copper chaperone Hah1. Each metal ion is coordinated by Cys 12 and Cys 15 from two Hah1 molecules. (a) Cu^I coordination (PDB accession code 1FEE), (b) Hg^{II} coordination (PDB accession code 1FE4), and (c) Cd^{II} coordination (PDB accession code 1FE0).
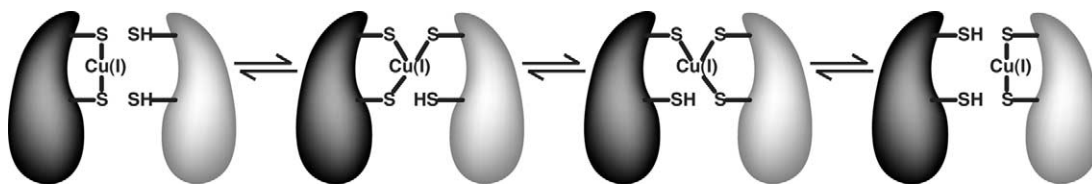
Figure 4 Proposed mechanism of Cu^I transfer between Hah1 and a domain of the Menkes or Wilson protein. Hah1 is shown in dark gray and the target domain is shown in light gray. Ligand exchange reactions lead to the formation of three-coordinate intermediates. The coordination in the first intermediate resembles that in the Hg^{II} Hah1 structure (Figure 3b), and the coordination in the second resembles that in the Cu^I Hah1 structure (Figure 3a).

intermediates involving cysteines from both MXCXXC motifs.[30] The Hah1 structures demonstrate that two MXCXXC-containing domains can dock with the cysteines in close proximity. Furthermore, these structures are good models for the metal exchange complex since the chaperones and their target domains have the same overall protein fold.[32] Metal transfer is envisioned to proceed through two three-coordinate intermediates modeled by the Hg^{II} and Cu^I structures (Figure 4)[34] Interestingly, Hah1 incubated with Cd^{II} does not interact with the Wilson protein.[37] The Cd^{II} complex of two Hah1 molecules is four-coordinate with Cd$\cdots$S distances of 2.4–2.5 Å (Figure 3c) and may be so stable that docking with the Wilson protein and subsequent metal exchange is precluded.

8.8.2.3 Copper Chaperones for Superoxide Dismutase

The copper chaperone for superoxide dismutase (CCS)[38] delivers copper to copper, zinc superoxide dismutase (SOD1) which catalyzes the disproportionation of superoxide to hydrogen peroxide and dioxygen.[39] CCS comprises three domains and binds Cu^I. Although the X-ray structure of copper-loaded CCS is not available, structures of the apo chaperone combined with spectroscopic data indicate that the copper ion is ligated by cysteine residues (Figure 5). The *N*-terminal domain (domain I) is structurally homologous to the Atx1-like chaperones and contains an MXCXXC sequence motif. In the yeast CCS crystal structure, the two cysteines form a disulfide bond, but the loop closely resembles the equivalent loop in Atx1, suggesting that this domain binds metal ions.[40] The middle domain (domain II) resembles the target enzyme SOD1. In yeast CCS, this domain lacks the residues that form the SOD1 copper and zinc-binding sites.[40] However, domain II of human CCS binds one zinc ion.[41] The *C*-terminal 30 residues of yeast CCS (domain III) form an extended loop[42] which includes a CXC sequence motif. The two cysteines in this motif are essential for metal transfer activity.[43] Addition of Co^{II} to tomato CCS, which contains only the four cysteines in the domain I MXCXXC and the domain III CXC motifs, results in an optical spectrum typical of tetrahedral four-coordinate Co^{II}.[44] EXAFS data for human CCS are best fit by a dinuclear copper cluster with a Cu$\cdots$Cu distance of 2.7 Å. Each Cu^I ion is ligated by three sulfur ligands at 2.26 Å.[45] These spectroscopic data suggest that the metal-binding site is located between domains I and III.

There are two potential problems with the hypothesis that Cu^I binds to both domains I and III. First, the two cysteines from domain III are positioned ~ 30 Å from the domain I MXCXXC motif in the structure of a heterodimeric complex between yeast CCS and yeast SOD1 (Figure 5).[42] Domain III forms an extended loop structure, however, and might adopt another conformation in which the four cysteines are proximal. Second, domain I is not required *in vivo*,[43] and its cysteines are not conserved in all CCS homologues,[42] implying that an essential role is unlikely. It is conceivable that Cu^I is usually coordinated by the two domain III cysteines, and that domain I participates in copper binding only under certain conditions. How copper bound by domain III or by domains I and III is transferred to the SOD1 active site remains an intriguing problem in coordination chemistry. In the structure of the heterodimeric complex, domain III is located adjacent to the SOD1 active site, poised to deliver the copper ion (Figure 5). Conformational changes in domain III could bring the cysteines within 5 Å of the closest histidine in the SOD1 active site, resulting in an intermediate coordination complex involving both cysteine and histidine ligands. The oxidation state of copper during transfer is also an open question. Although CCS only binds Cu^I, the transfer process is oxygen dependent[46] and might involve oxidation to Cu^{II}.
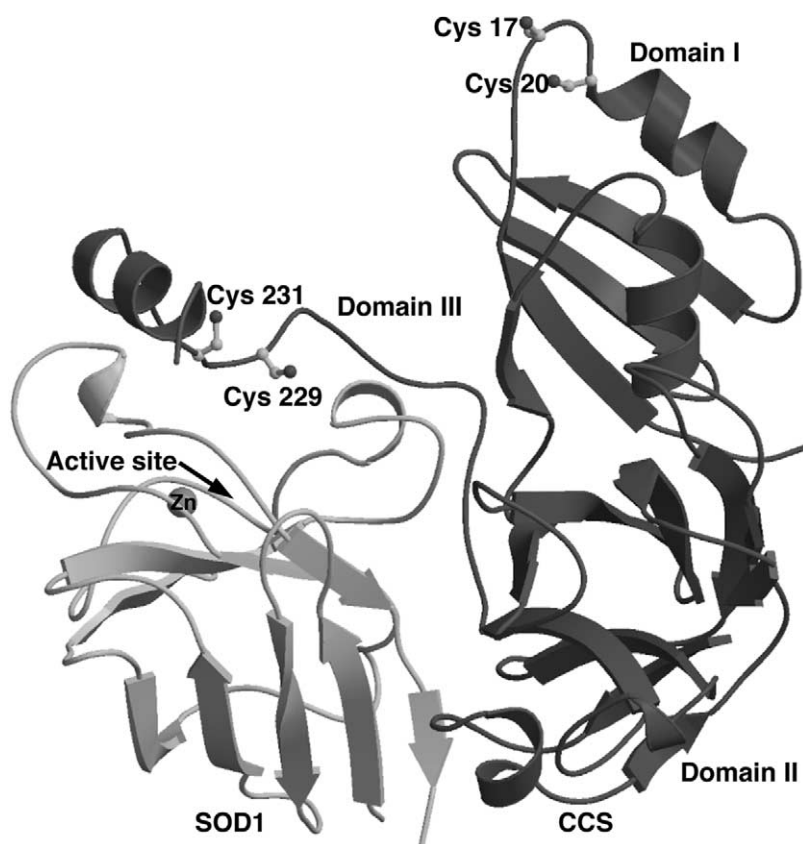
Figure 5 Heterodimeric complex between yeast CCS and yeast SOD1 (PDB accession code 1JK9). Potential CCS Cu^I ligands include Cys 17, Cys 20, Cys 229, and Cys 231. Only zinc is bound to SOD1 because one of the copper ligands has been mutated to trap the complex.

8.8.2.4 Copper Chaperones for Cytochrome *c* Oxidase

The four electron reduction of O_2 to H_2O is catalyzed by cytochrome *c* oxidase, the terminal enzyme in the mitochondrial respiratory chain. The electrons donated by cytochrome *c* enter this multisubunit complex at its dinuclear Cu$_A$ site and are transferred successively to heme *a*, to the heme a_3-Cu$_B$ center, and to O_2. Three proteins involved in the assembly of the two copper centers have been identified, Cox11, Cox17, and Sco1. Cox11 is implicated in assembly of the Cu$_B$ site[47] whereas Sco1 is involved in assembly of the Cu$_A$ site.[48] Cox17 is proposed to function as a copper chaperone, shuttling copper between the cytosol and the mitochondrial intermembrane space.[49] Binding of Cu^I by Sco1 and Cox17 has been studied by biochemical and spectroscopic methods. Sco1 contains a conserved CXXXC motif. Mutation of these two cysteines and a conserved histidine result in a nonfunctional yeast Sco1, implicating these three residues as ligands to the copper ion. EXAFS data indicate that the protein binds Cu^I with two sulfurs and one nitrogen.[50] These results are consistent with mutagenesis studies on a *Bacillus subtilis* Sco1 homologue called YpmQ.[48]

Cox17 binds three Cu^I ions.[51] The presence of S → Cu ligand-to-metal charge transfer (LMCT) bands in the optical spectrum and luminescence upon excitation at 300 nm indicate that the copper ions are arranged in a solvent shielded polycopper cluster like those in copper metalloregulatory proteins (Section 8.8.3.1) and metallothionein (Chapter 8.9). XAS data are suggestive of trigonal coordination and are best fit by three sulfur ligands at 2.25 Å and a 2.7 Å Cu⋯Cu vector.[52] Mutation of any two of three cysteines in a conserved CCXC sequence motif abolishes Cu^I binding.[51] Finally, Cox17 can form both dimers and tetramers, but the nature of the polycopper cluster in these oligomers has not been resolved.[52] The Cox17 dimer could contain either a hexanuclear cluster at the subunit interface or two separate trinuclear clusters.

8.8.2.5 Nickel Chaperones

The nickel-containing enzyme urease catalyzes the hydrolysis of urea to ammonia and carbamate.[53] The reaction occurs at a dinuclear nickel center bridged by a carbamylated lysine residue and a solvent molecule.[54] Assembly of this active site requires at least four accessory proteins, designated UreD, UreF, UreG, and UreE. The system from the bacterium *Klebsiella aerogenes* has been well characterized. Apo urease forms a complex with the UreD, UreF, and UreG proteins and can then be activated by the addition of UreE, nickel, bicarbonate, and GTP. UreE is proposed to function as a metallochaperone by directly transferring nickel ions to the urease active site.[55] Similar proteins are believed to participate in nickel insertion into the active sites of hydrogenase[56] and CO dehydrogenase.[57] The intact UreE binds six Ni^{II} ions, but removal of a 15 residue histidine-rich *C*-terminus yields a fully functional protein that only binds two Ni^{II} ions.[58] These two sites are proposed to be involved in assembly of the dinuclear nickel center. Truncated UreE also binds Cd^{II}, Co^{II}, Zn^{II}, and Cu^{II} *in vitro*.[58]

According to optical, NMR, and X-ray absorption spectroscopic data, the two Ni^{II} sites in truncated UreE are distinct. Both sites are five- or six-coordinate, but they differ in the number of histidine donors.[59] A model in which both metal sites are housed at the dimer interface has been proposed based on site directed mutagenesis studies.[60] In this model, one Ni^{II} ion is coordinated by four histidines and the other by two histidines. The site with four histidines is postulated to be crucial in the urease activation mechanism. The Cu^{II} substituted UreE also has two distinct metal-binding sites, but optical and resonance Raman data indicate the presence of a cysteine ligand not detected for the Ni^{II} loaded protein.[59]

The truncated forms of UreE from *K. aerogenes* and another microorganism, *Bacillus pasteurii*, have been crystallographically characterized. The *K. aerogenes* structure was determined in the presence of Cu^{II} because attempts to co-crystallize the protein with Ni^{II} or to soak preexisting apo crystals in Ni^{II}-containing solutions were unsuccessful.[61] The structure reveals a dimer with three metal-binding sites, all ligated by the histidine residues identified previously by mutagenesis experiments.[60] One Cu^{II} ion is located at the dimer interface and coordinated by two histidine ε nitrogens and one or two water molecules (Figure 6a). The average $Cu \cdots N$ distances are 2.03 Å and 2.08 Å for the two histidines. The other two Cu^{II} ions are found in surface exposed sites coordinated by two histidine ε nitrogens and one or two water molecules. The putative cysteine ligand identified by spectroscopy and mutagenesis[60] does not bind Cu^{II} in the structure and is quite distant from the metal-binding sites. It may be that this interaction occurs in solution between a cysteine residue from one dimer and a Cu^{II} ion from a second dimer, and is precluded in the structure by crystal packing. The dimer interface site is proposed to deliver Ni^{II} ions one at a time to the urease active site, and the other two sites are proposed to play a more secondary role, serving as reservoirs for Ni^{II}.[61]

The *B. pasteurii* UreE structure reveals the same dimer interface metal-binding site, but two dimers have crystallized as a tetramer.[62] Two different coordination geometries are observed in structures determined from two crystal forms. In the first structure, the Zn^{II} ion is pseudoocta-hedrally coordinated by four histidine ε nitrogens in the equatorial plane and two water molecules

(a)   **(b)**   **(c)**
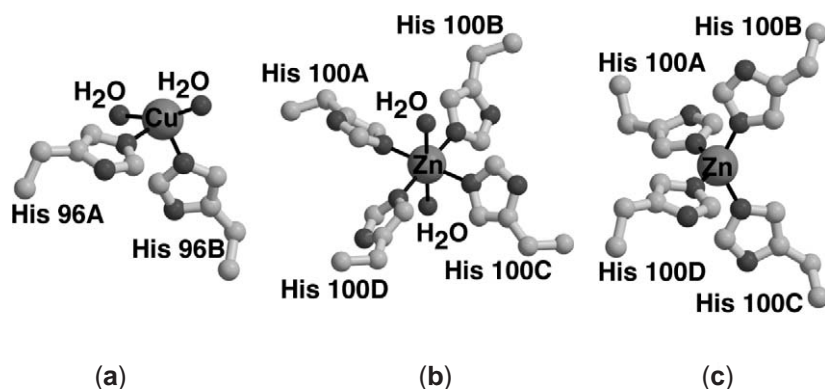
Figure 6 Metal-binding sites in the Ni^{II} chaperone UreE. (a) Cu^{II} site in *K. aerogenes* UreE (PDB accession code 1GMW). The Cu^{II} ion is coordinated by one His 96 residue from each monomer in the dimer and two solvent molecules. (b) Zn^{II} site in *B. pasteurii* UreE. The Zn^{II} is coordinated by four His 100 residues from two UreE dimers and by two solvent molecules (PDB accession code 1EB0). (c) Zn^{II} site in a second crystal form of *B. pasteurii* UreE. The Zn^{II} is coordinated by four His 100 residues from two UreE dimers (PDB accession code 1EAR).

in the axial coordination sites (Figure 6b). In the second structure, the geometry is tetrahedral with four coordinated histidines (Figure 6c). The Zn^{II} site is postulated to represent the Ni^{II}-binding site because soaking crystals used to obtain the first structure (Figure 6b) in high concentrations of $NiCl_2$ yielded a strong peak at the Zn^{II} site in anomalous difference Fourier maps, indicating that Ni^{II} can displace Zn^{II}. The additional surface-binding sites observed in the *K. aerogenes* structure are not present. Although the UreE structures provide valuable information about metal binding, the molecular mechanism of Ni^{II} delivery has not been elucidated. It is not clear which of the observed metal-binding sites is physiologically relevant. In addition, it is not known how UreE recognizes the apo urease UreDFG complex, although an extended hydrophobic region on the UreE surface of UreE may be important.[61,62]

8.8.2.6 Other Metal Co-factor Assembly Proteins

In addition to the copper and nickel metallochaperones described above, numerous other metal-binding proteins assist in metal co-factor formation. For copper, several auxiliary proteins are required to assemble the nitrous oxide reductase catalytic Cu_Z cluster.[63] One of these proteins, NosL, binds a Cu^I ion. EXAFS data are consistent with one histidine nitrogen and two sulfur ligands, one of which is probably a conserved cysteine.[64] NosL could be a metallochaperone, but evidence of metal transfer activity or interaction with nitrous oxide reductase has not been reported. For iron, bacterial iron–sulfur clusters are assembled on scaffold proteins such as NifU, which is involved in activating nitrogenase.[65] Similarly, IscU[66] and IscA[67] are believed to function in general Fe–S cluster biosynthesis. Transient formation of [2Fe–2S] and [4Fe–4S] clusters in these proteins has been observed by optical, resonance Raman, and Mössbauer spectroscopies. The homologous eukaryotic proteins, Isu[68] and Isa,[69] are likely to perform a similar function. The nitrogenase iron–molybdenum co-factor (FeMoco) is also preassembled by accessory proteins.[70] However, it is not clear how the clusters assembled on these scaffold proteins are ultimately transferred to target proteins.

8.8.3 METALLOREGULATORY PROTEINS

8.8.3.1 Copper

Metalloregulatory transcription factors sense metal ions and translate this information into signals that regulate gene expression. Although copper sensing is not well understood in most organisms, two transcription factors central to yeast copper homeostasis, Mac1 and Ace1 from *Saccharomyces cerevisiae*, have been characterized.[71] At high copper concentrations, copper-loaded Ace1 binds to DNA and activates expression of copper metallothioneins[72,73] and superoxide dismutase,[74] proteins that protect the cell from copper toxicity. A homolog from *Candida glabrata*, Amt1, functions in a similar fashion.[75] At low copper concentrations, Mac1 activates transcription of genes for the copper importers Ctr1 and Ctr3 and the metalloreductase Fre1.[76,77] Unlike Ace1 and Amt1, copper binding to Mac1 inhibits its function and leads to degradation of both Mac1[78] and the copper transporters.[79]

The N-terminal domains of Ace1 and Amt1 comprise a zinc binding module (residues 1–40) and a copper binding module (residues 41–100 in Ace1 and 41–110 in Amt1). Both modules interact with DNA.[80] Eleven of 12 cysteines found in the N-terminal domain are essential for activity. Ten of these cysteines are arranged in CXXC or CXC sequence motifs.[71] Both Ace1 and Amt1 bind four Cu^I ions and one Zn^{II} ion,[81,82] although early analysis of Ace1 indicated the presence of approximately eight Cu^I ions and no zinc.[83,84] Eight cysteines found in the copper module are proposed to ligate four Cu^I ions in a polynuclear Cu^I cluster, similar to that found in Cu^I metallothioneins. Formation of this cluster is essential for DNA binding. Another important feature of the cluster is that it binds copper ions cooperatively,[81,84] thereby allowing even a very small increase in copper concentration to activate Ace1/Amt1 and initiate metallothionein expression. Zinc is not required for DNA binding, but might affect function by altering protein-DNA contacts.[81]

Details of copper and zinc coordination by Ace1 and Amt1 have been elucidated by spectroscopic techniques. The N-terminal domains of both proteins exhibit a cysteine $S \rightarrow Cu$ LMCT band at ~260 nm and room temperature luminescence with an emission maximum of 580 nm and an excitation maximum of 310 nm.[81,83–85] This luminescence, also observed for Cu^I metallothionein,
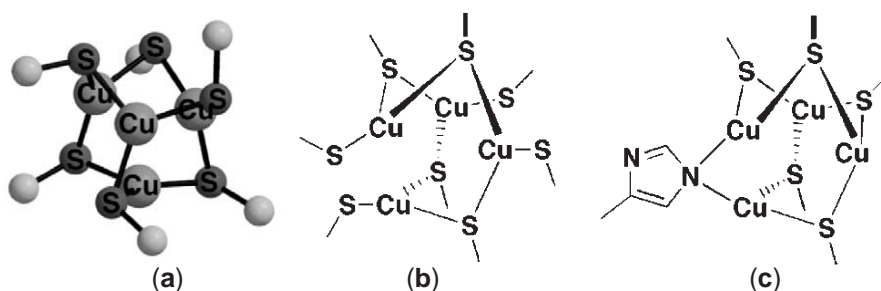
Figure 7 Proposed cluster structures in yeast copper metalloregulatory proteins. (a) $[Cu_4(SPh)_6]^{2-}$ model compound. The phenyl rings have been omitted for clarity. Six thiolates bridge the four Cu^I ions. The sites in Ace1 and Amt1 might resemble this complex. (b) Alternative structure for Ace1 and Amt1 cluster involving eight rather than six cysteines. In this arrangement, only four thiolates are bridging. (c) Proposed structure of the Mac1 Cu^I cluster.
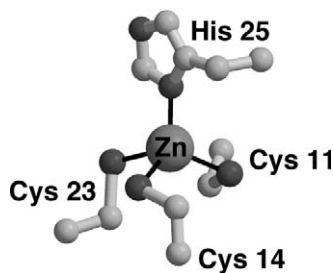
Figure 8 Zinc-binding site in the copper metalloregulatory protein Amt1. The Zn^{II} ion is coordinated tetrahedrally by His 25, Cys 11, Cys 14, and Cys 23 (PDB accession code 1CO4).

is indicative of a polynuclear, solvent shielded Cu^I thiolate cluster. EXAFS data for both Ace1[36,83,86] and Amt1[81,85] indicate that the Cu^I ions are trigonally coordinated with Cu—S distances of ~ 2.26 Å. The presence of a 2.7 Å Cu—Cu distance suggests that the cluster is polynuclear, and the EXAFS data closely resemble those for $[Cu_4(SPh)_6]^{2-}$, a synthetic tetracopper(I) thiolate cluster (Figure 7a).[36] The clusters in Ace1 and Amt1 are expected to be less symmetric than the $[Cu_4(SPh)_6]^{2-}$ complex.[85] This type of cluster only utilizes six of the eight cysteines in the copper module. An alternative structure involving eight cysteines, four of which are nonbridging, is also possible (Figure 7b).[86] Although the nuclearity of the cluster cannot be determined by EXAFS, the all-or-nothing formation of a four Cu^I loaded Amt1 detected by mass spectrometry is consistent with a tetranuclear cluster.[81]

Zinc binding by Amt1 and Ace1 has been probed by NMR, optical, and X-ray absorption spectroscopies. The solution structure of the Amt1 zinc module reveals a three-stranded anti-parallel β sheet with two short α-helical segments. A basic surface for docking with DNA is also evident.[87] The Zn^{II} ion is ligated by three cysteines and a histidine arranged in a CX_2CX_8XCXH motif (Figure 8).[87] These residues are conserved in Ace1 and four other yeast proteins, including Mac1.[80] The coordination determined from the Amt1 solution structure is consistent with mutagenesis data and ^{13}Cd NMR studies suggesting the presence of one histidine and three sulfur ligands.[82] EXAFS data and optical spectroscopy on the Co^{II} substituted Amt1 are compatible with either one nitrogen and three sulfur or four sulfur ligands.[81]

A homologous 40-residue zinc module is found at the N-terminus of Mac1 and likely binds a Zn^{II} ion with the analogous ligands. Mac1 also binds a second Zn^{II} ion, the coordination environment of which has not yet been determined.[88] The Mac1 copper-binding motifs comprise two C-terminal $CXCX_4CXCX_2CX_2H$ sequences, which together bind eight Cu^I ions. Mutagenesis studies indicate that the first such sequence is important for copper activation.[89] Two lines of spectroscopic data suggest that Mac1 contains a polynuclear Cu^I thiolate cluster similar to those postulated for Ace1 and Amt1. First, the copper form of Mac1 luminesces with an emission maximum near 570 nm.[90] Second, EXAFS data for a polypeptide including only the first metal binding sequence are best fit with three sulfur ligands at 2.25 Å and a 2.7 Å Cu···Cu distance. Since this copper-binding motif contains five cysteines and one histidine, a bridging histidyl nitrogen is proposed to replace one thiolate in a $[Cu_4(SR)_6]^{2-}$-like cluster (Figure 7c).[86] Further understanding of the copper coordination chemistry of Mac1, Ace1, and Amt1 will require X-ray

structure determinations. A number of additional questions regarding the copper metalloregulatory proteins remain unresolved. For example, the physiological relevance and function of the zinc module has not been well established. In addition, it is not known how copper ions are delivered to the nucleus for binding to Ace1, Amt1, and Mac1.

8.8.3.2 Iron

8.8.3.2.1 *Fur proteins*

The ferric uptake regulator (Fur) protein controls expression of proteins involved in siderophore biosynthesis and iron uptake. At high iron concentrations, iron-loaded Fur binds to DNA and inhibits transcription. When iron is limiting, Fur does not bind Fe^{II} or DNA, and gene expression is activated.[91] The *Escherichia coli* Fur is the best studied to date, but homologous proteins are found in a wide variety of other gram-negative bacteria.[92] The *E. coli* Fur protein comprises an *N*-terminal DNA binding domain and a *C*-terminal metal-binding domain which also mediates dimer formation.[93] Although Fur loaded with Fe^{II}, Mn^{II}, Co^{II}, Zn^{II}, and Cd^{II} binds DNA *in vitro*, only Fe^{II}, Mn^{II}, and Co^{II} regulate expression *in vivo*.[91,94] In addition to the functionally important Fe^{II}-binding site, Fur contains a Zn^{II} site, which may be structural.[95,96] Potential ligands for both sites include 12 conserved histidines and four conserved cysteines, a subset of which are implicated in metal binding by site-directed mutagenesis studies.[97]

The Zn^{II} form of Fur, which is sometimes called apo Fur, contains 0.5–2.0 zinc ions per protein monomer.[95,96] One Zn^{II} ion is easily removed and may occupy the Fe^{II}-binding site whereas removal of the second Zn^{II} ion requires low pH or denaturing conditions.[96] According to Zn XAS data, the tightly bound Zn^{II} ion is coordinated tetrahedrally by two sulfur donors at 2.3 Å and two N/O ligands at 2.0 Å (Figure 9a). Analysis of the EXAFS data suggests further that imidazole ligands are present, although carboxylate or water oxygen donors cannot be excluded. Notably, the Zn^{II} site is mononuclear, with no evidence of a second metal ion within 3–4 Å.[98]

The Fur Fe^{II} site has been characterized by EPR, Mössbauer, and X-ray absorption spectroscopies as well as by magnetic susceptibility measurements.[99] These data indicate that the iron is present as an isolated high-spin Fe^{II} center. EXAFS data are best fit with five nitrogen or oxygen donors at 2.13 Å, although a sixth ligand may also be present at a longer distance (Figure 9b).[99] These results are consistent with spectroscopic studies of the Co^{II} form of Fur.[100] The Co^{II} protein exhibits an optical spectrum indicative of a pentacoordinate or hexacoordinate site. The absence of S → Co LMCT bands suggests that cysteine residues are not coordinated to the metal ion, an observation corroborated by ^{1}H NMR studies implicating histidine and carboxylate ligands. The Co^{II} protein is similar to the Fe^{II} protein by EXAFS analysis, with five nitrogen or oxygen donors at 2.11 Å. Taken together, the spectroscopic data suggest a five- or six-coordinate Fe^{II} site with at least two histidines and one carboxylate ligand,[99] similar to the sites in mononuclear nonheme iron enzymes such as lipoxygenase and isopenicillin *N* synthase (Figure 9c).[101] Although the metal binding properties of Fur have been well characterized,
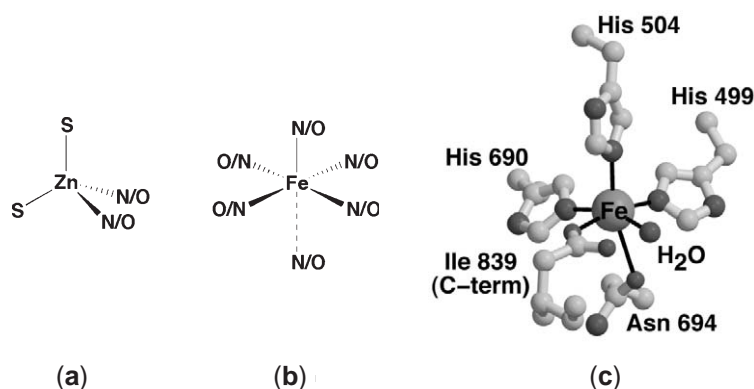
Figure 9 Proposed coordination geometries for the metal-binding sites in the *E. coli* iron metalloregulatory protein Fur. (a) Zn^{II} site, (b) Fe^{II} site, and (c) Fe^{II} site in soybean lipoxygenase-1 (PDB accession code 1F8N). The last residue in the polypeptide, Ile 839, coordinates via a C^- terminal oxygen.

many questions still need to be addressed. It is unclear how Fur distinguishes between Fe^{II} and other divalent metal ions that may be present *in vivo*. Although it is likely to be structural,[98] the function of the Zn^{II} ion has not been established.

8.8.3.2.2 *IdeR proteins*

Gram-positive bacteria control iron levels by iron-dependent regulator (IdeR) proteins that are functionally analogous to the Fur protein (Section 8.8.3.2.1). Like Fur, these proteins use Fe^{II} as a co-repressor, binding to DNA in the presence of metal ions and repressing transcription of genes encoding iron uptake systems, heme oxygenase, and virulence determinants. One of the best-characterized IdeR proteins is DtxR, the *Corynebacterium diphtheriae* diphtheria toxin repressor. DtxR controls expression of siderophore biosynthetic genes and of the *tox* gene which encodes diphtheria toxin. The structures of DtxR[102–107] and of the related IdeR from *Mycobacterium tuberculosis*[108,109] reveal an *N*-terminal DNA-binding domain and a flexible *C*-terminal regulatory domain. The *N*-terminal domain comprises two subdomains and houses two metal-binding sites. The first subdomain exhibits a helix-turn-helix motif common to DNA binding proteins, and the second subdomain forms a dimerization interface between two protein monomers. *In vitro* DNA binding is also promoted by Mn^{II}, Co^{II}, Ni^{II}, and Zn^{II},[110,111] and structures have been determined in the presence of all these metal ions.

The two metal-binding sites, which are separated by 10 Å, are designated "ancillary" and "primary".[112] The "ancillary" site, also called metal site 1, is not essential for repressor activity whereas the "primary" site, or metal site 2, must be filled for DNA binding. Metal site 1 is occupied in all the available structures. In the DtxR structures, Fe^{II}, Mn^{II}, Co^{II}, Zn^{II}, and Ni^{II} are coordinated tetrahedrally by two histidines, one with its δ nitrogen and the other with its ε nitrogen, a glutamic acid, and a sulfate or phosphate ion (Figure 10a).[103,105,113] Similar coordination is observed for Zn^{II} IdeR.[108] The sulfate or phosphate anions are hydrogen bonded to conserved residues, leading to the proposal that phosphate functions as a corepressor.[105] By contrast, the structures of Co^{II} DtxR[114] and Co^{II} IdeR[109] reveal trigonal bipyramidal coordination geometry at this site, with side chain oxygens from a glutamic acid and a glutamine from the *C*-terminal domain replacing the exogenous anion (Figure 10b). The physiological role of this metal site is unclear, but a hydrogen-bonding network between the two sites suggests that site 1 may modulate the activity of site 2.[102]

Site 2 is essential for activity.[112] This site is unoccupied in most of the DtxR structures, probably because a putative cysteine ligand[115] has been chemically modified.[103,105,113] The structures of Cd^{II}[103] and Mn^{II}[105] DtxR reveal a partially occupied site with distorted tetrahedral coordination by the carbonyl oxygen of the cysteine, a glutamic acid side chain oxygen, a histidine ε nitrogen, and a solvent molecule. This environment is probably not biologically relevant because the cysteine has been modified. The site is fully occupied in the Ni^{II} structure of a mutant protein in which the cysteine has been replaced with aspartic acid.[112] The Ni^{II} ion is coordinated octahedrally by a histidine ε nitrogen, side chain oxygens from glutamic acid and aspartic acid,
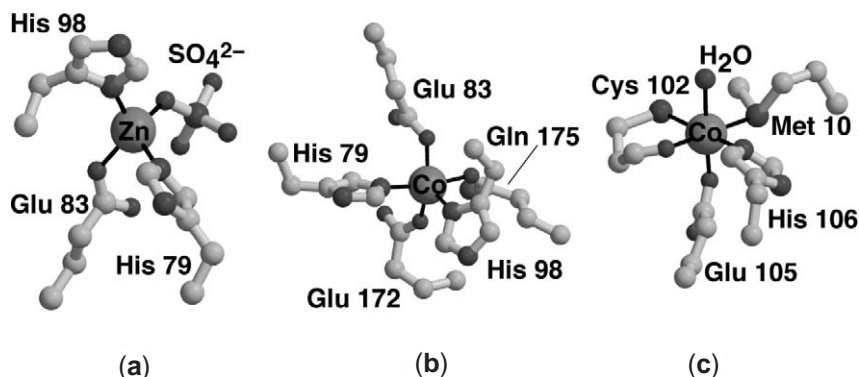
Figure 10 Metal-binding sites in bacterial IdeR proteins. (a) Ancillary site in Zn^{II} DtxR (PDB accession code 1BI0). The Zn^{II} ion is coordinated tetrahedrally by His 79, Glu 83, His 98, and a sulfate ion. (b) Ancillary site in Co^{II} IdeR (PDB accession code 1FX7). The Co^{II} ion is coordinated in trigonal bipyramidal geometry by His 79, Glu 83, His 98, Glu 172, and Gln 175. (c) Primary site in Co^{II} IdeR (PDB accession code 1FX7). The Co^{II} ion is coordinated octahedrally by Met 10, Cys 102, Glu 105, His 106, and a solvent molecule.

a solvent molecule, and a methionine sulfur. In the IdeR structures, metal site 2 is fully occupied. Both Co^{II} [109] and Zn^{II} [108] are coordinated by sulfurs from cysteine and methionine, the cysteine carbonyl oxygen, a glutamic acid side chain oxygen, and a histidine ε nitrogen (Figure 10c). The Zn^{II} coordination geometry is distorted square pyramidal whereas a solvent molecule completes the octahedral coordination for Co^{II}.

The structural data provide insight into how metal binding may activate these repressors. A comparison of apo and metal-bound DtxR reveals that metal binding induces a rotation of the two monomers with respect to one another.[104] This change aligns the *N*-terminal recognition helices with the major grooves of the target DNA, as evident in the structures of Ni^{II} [107] and Co^{II} [114] DtxR complexed with DNA. A second effect of metal binding is an unwinding of the *N*-terminal helix, alleviating what would otherwise be an unfavorable steric interaction with the DNA.[107]

8.8.3.2.3 Iron–sulfur proteins

Iron–sulfur proteins also regulate gene expression in response to iron levels. The *E. coli* IscR protein, which represses expression of genes encoding Fe–S cluster assembly proteins (Section 8.8.2.6), exhibits optical and EPR spectroscopic features typical of a [2Fe–2S] cluster.[116] This [2Fe–2S] cluster is proposed to play a key role in IscR function. Proteins that need Fe–S clusters are postulated to compete with IscR for available clusters. When enough clusters become available, IscR is loaded with its [2Fe–2S] cluster and represses further expression of the assembly proteins. Thus, cluster formation is synchronized with the demand for Fe–S-containing proteins.[117] Several other Fe–S transcription factors, including FNR and SoxR,[118] respond not to iron levels, but instead use the clusters to sense small molecules (Chapter 8.27). Under anaerobic conditions, FNR exists as a dimer containing a [4Fe–4S] cluster and binds to DNA, inducing expression of proteins required for anaerobic respiration. Exposure to oxygen results in a monomeric [2Fe–2S] or apo protein that does not interact with DNA.[119] In the case of SoxR, the redox state of its [2Fe–2S] cluster controls gene expression.[120] The reduced form is inactive, but oxidation by superoxide or nitric oxide activates transcription of the SoxS protein which in turn activates transcription of oxidative stress response genes.

Iron regulatory protein 1 (IRP1), a eukaryotic regulator protein that operates at the translational level, represents another type of Fe–S metalloregulatory protein.[121] When iron levels are low, the apo form of IRP1 binds to specific stem loop structures in mRNA called iron-responsive elements (IREs). Binding of IRP1 both inhibits ferritin translation and prevents degradation of transferrin receptor mRNA, permitting increased iron uptake.[122] In iron replete cells, IRP1 contains a cubane [4Fe–4S] cluster and functions as a cytosolic aconitase.[123] Assembly of the Fe–S cluster, therefore, not only regulates iron uptake and storage, but also switches the activity of IRP1 from RNA-binding to enzymatic.[124] It is not known exactly how the [4Fe–4S] cluster is assembled and disassembled, but oxidants are proposed to cause release of a single Fe^{II} ion and the formation of an intermediate [3Fe–4S] cluster.[125] Recent EXAFS and EPR data on an IRP1 [3Fe–4S] cluster reconstituted *in vitro* indicate that the three iron ions are arranged in a linear fashion.[126] It is not known whether a linear cluster forms *in vivo*.

8.8.3.3 Zinc, Cadmium, and Mercury

8.8.3.3.1 Zur

A Fur (Section 8.8.3.2.1) homologue that regulates expression of zinc uptake proteins has been identified in *E. coli*.[127] This protein, called Zur (zinc uptake regulator), binds to DNA in the presence of Zn^{II} and represses expression of the ZnuABC zinc import system.[128,129] Zur binds two Zn^{II} ions per monomer. According to EXAFS data, the first Zn^{II} ion, which is tightly bound, is coordinated by three sulfurs and one N/O ligand (Figure 11a). The second Zn^{II}, which is more easily removed, is ligated tetrahedrally by one sulfur and three N/O donors (Figure 11b). This second site can also be filled with Co^{II}, and both optical spectroscopy and Co EXAFS are consistent with one sulfur and three N/O ligands.[130] Although the metal binding affinities of the two sites are similar to what is observed for Fur,[96] the coordination is different. In Fur, the tight binding site is occupied by Zn^{II} in an $S_2(N/O)_2$ environment (Figure 9a).[98] The Fur site that
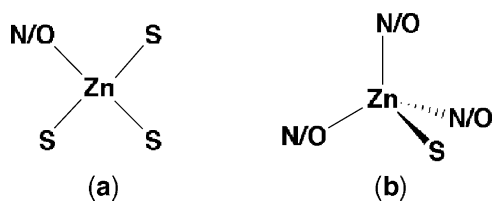
Figure 11 Proposed coordination for the Zn^{II}-binding sites in the *E. coli* zinc metalloregulatory protein Zur. (a) Tight binding site. This site can be compared to the Zn^{II} site in Fur (Figure 9a). (b) Site comparable to the Fe^{II} site in Fur (Figure 9b).

corresponds to second site in Zur binds Fe^{II} with five or six N/O ligands (Figure 9b).[99] The abilities of Zur and Fur to distinguish between metal ions might derive from these differences.[130]

8.8.3.3.2 ZntR and MerR

Whereas Zur controls expression of the zinc import system, another *E. coli* zinc metalloregulatory protein, ZntR,[131] activates expression of the zinc export system. In the presence of metal ions, ZntR activates transcription of the gene encoding ZntA, a *P*-type ATPase that exports Zn^{II}, Cd^{II}, and Pb^{II}.[21] All three metal ions induce expression of ZntA *in vivo*.[132] Unlike Zur, both the apo- and metal-loaded forms of ZntR bind to DNA. Conformational changes upon Zn^{II} binding are believed to distort the bound DNA in such a way as to promote RNA polymerase open complex formation. ZntR binds up to two Zn^{II} ions per monomer, but it is unclear whether both are required for activity.[133]

Although the Zn^{II} coordination environment in ZntR has not been elucidated, the metal binding site in a homologous protein, MerR, has been characterized in detail. MerR regulates expression of genes involved in bacterial Hg^{II} resistance. In the absence of Hg^{II}, MerR binds to DNA and represses transcription. Upon Hg^{II} binding, the DNA bound to MerR undergoes untwisting and unbending which facilitates open complex formation.[134,135] MerR binds one Hg^{II} ion per dimer. The binding site involves one cysteine from the first monomer and two cysteines from the second monomer, forming an asymmetric, subunit bridging coordination complex.[136] These three cysteines are conserved in all MerR proteins[136] as well as in ZntR.[131] Spectroscopic data are consistent with three-coordinate Hg^{II}. LMCT bands in the UV region are similar to those observed for a trigonal Hg^{II} thiolate model compound (Figure 12),[137] and EXAFS data are best fit with three sulfur ligands at 2.43 Å.[138] In addition, a comparison of ^{199}Hg NMR chemical shifts for MerR with those for model complexes and other Hg^{II}-loaded metalloproteins is consistent with trigonal planar thiolate coordination.[139] Finally, UV resonance Raman spectra indicate that the Hg^{II} coordination geometry is trigonal.[140]

8.8.3.3.3 SmtB and CadC

The metalloregulatory proteins SmtB and CadC belong to the ArsR family of repressors.[141] The original member of this family, *E. coli* ArsR, negatively regulates expression of proteins involved
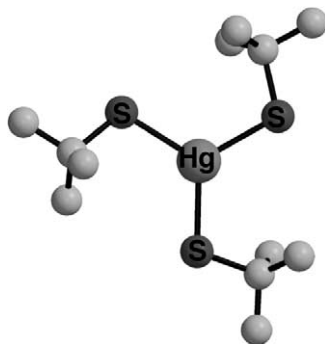
Figure 12 Synthetic model for the Hg^{II}-binding site in the bacterial metalloregulatory protein MerR. The Hg^{II} ion in $[Hg(SBu^t)_3]^{1-}$ is coordinated in a trigonal planar fashion by three aliphatic thiolates.

in arsenic resistance and binds As[III] via three cysteine residues.[142] The dimeric SmtB protein regulates expression of SmtA, a metallothionein that sequesters zinc in *Synechococcus* PCC7942. In the absence of metal ions, SmtB binds to DNA and represses transcription of the gene encoding SmtA. DNA binding is inhibited by Zn[II].[143,144] Titrations with zinc indicators demonstrate the presence of a single high affinity Zn[II] site.[145] EXAFS data for both Zn[II]- and Co[II]-substituted SmtB are best fit with one or two sulfurs, two histidines, and one carboxylate ligand arranged in tetrahedral geometry. The presence of a thiolate ligand in this site is apparent from the S → Co LMCT band in the optical spectrum of Co[II] SmtB.[145] The biological significance of this site is unclear, however, because mutagenesis indicates that none of the SmtB cysteines is essential for metal responsive regulation.[146]

According to the results of metal-binding titrations using mutant proteins, Co[II] and Zn[II] partition between two sites in each SmtB monomer.[144] Even though the homodimeric SmtB protein[147] contains four possible metal-binding sites, the observed stoichiometry is always one metal ion per monomer, implying that only two sites in the dimer can be occupied at once.[144] The first site, designated $\alpha 3N$, corresponds to the spectroscopically characterized site described above. The Zn[II] ion is ligated by two cysteines, a histidine, and an aspartic acid. Ligands for the second site, located at the dimer interface and designated the $\alpha 5$ site, include two histidines, an aspartic acid, and a glutamic acid (Figure 13). The glutamic acid might be replaced with a nearby cysteine for Co[II] binding. The $\alpha 5$ site was first identified from the locations of Hg[II] ions in a heavy atom derivative used to solve the apo SmtB structure.[147] Most importantly, mutation of a histidine residue in the $\alpha 5$ site completely abrogates Zn[II] promoted dissociation from DNA whereas mutation or derivatization of the cysteines in the $\alpha 3N$ site has no effect. Therefore, the $\alpha 5$ site is proposed to function as the primary Zn[II] sensing site in SmtB.[148]

The CadC protein from *Staphylococcus aureus* pI258 functions similarly to SmtB. In the absence of metal ions, CadC represses transcription of the gene encoding CadA, a *P*-type ATPase that exports Cd[II], Pb[II], and Zn[II].[149] Upon binding Cd[II], Pb[II], or Bi[III], the affinity of CadC for DNA is decreased significantly,[150,151] leading to expression of CadA. CadC, which is a dimer, binds one Cd[II] or Pb[II] per monomer. The optical spectrum of Cd[II] CadC exhibits a S → Cd LMCT band with an extinction coefficient consistent with four cysteine ligands. Similarly, the optical spectra of the Pb[II] [150] and Bi[III] [151] forms of CadC suggest three or four-coordinated cysteines. Cadmium EXAFS data are consistent with four sulfur scatterers at 2.53 Å,[150] whereas Pb EXAFS data are indicative of three sulfur ligands. The results of [113]Cd NMR experiments are less definitive, with possible interpretations including a S_3N, a S_3O, or an unusual S_4 coordination geometry.[150] Four cysteines have been identified as ligands by mutagenesis.[151,152] Based on structural homology modeling, these cysteines are located in positions comparable to those of the ligands to the SmtB $\alpha 3N$ site (Figure 13).[152]
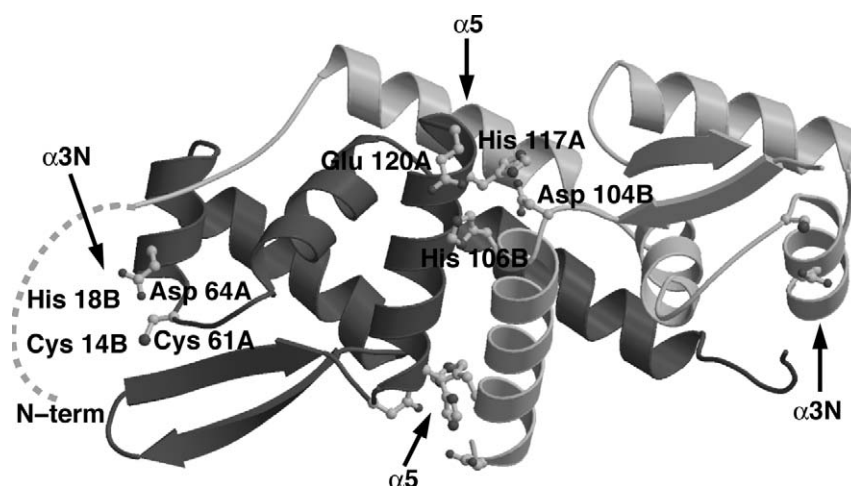
Figure 13 Structure of the apo form of the bacterial zinc metalloregulatory protein SmtB (PDB accession code 1SMT) showing the locations of the metal-binding sites. According to spectroscopic and biochemical data, ligands to the $\alpha 3N$ site include Cys 14 and His 18 from one monomer and Cys 61 and Asp 64 from the second monomer. Cys 14 and His 18 were not visible in the crystal structure. The ligands to the $\alpha 5$ site include Asp 104 and His 106 from one monomer and His 117 and Glu 120 from the second monomer.

Like SmtB, CadC also contains a second metal-binding site, which was detected by spectroscopic characterization of Co[II] substituted CadC.[152] Whereas CadC binds a single Cd[II] or Pb[II] ion, two Co[II] ions bind in distinct coordination environments. The first environment is cysteine rich and corresponds to the site described above. The second site, which is probably equivalent to the SmtB α5 site (Figure 13), exhibits an optical spectrum indicative of a distorted tetrahedral center comprising oxygen and nitrogen ligands. Whereas Cd[II], Pb[II], and Bi[III] can only bind at the thiolate-rich α3N site, Zn[II] and Co[II] can bind at both sites. In contrast to SmtB, mutagenesis data indicate that only the α3N site is required for negative regulation of DNA binding by metal ions. Thus, CadC and SmtB have the same two sites, but a different site is important for regulation in each protein. It is not clear why the proteins retain both sites, but one possibility is that CadC may have evolved from an SmtB-like protein whose function was to sense Zn[II] and Co[II].[152] Nevertheless, the different coordination environments suggest one way in which members of the ArsR metalloregulatory family confer metal ion specificity.

8.8.3.4   Zinc finger proteins

Another family of zinc metalloregulatory proteins includes the eukaryotic zinc finger proteins Zap1[153] and MTF-1 (metal response element-binding transcription factor-1).[154] Zap1, which regulates expression of zinc transporters,[155] contains five zinc finger domains, and is postulated to contain additional zinc sensing sites.[153] Mouse MTF-1 binds to DNA in the presence of zinc, inducing expression of metallothioneins, zinc transporters, and the heavy chain of the enzyme γ-glutamyl-cysteine synthetase. MTF-1 is also found in humans, chickens, and *Drosophila melanogaster*.[156] The protein comprises six zinc finger domains, each with a conserved $CX_4CX_{12}HX_2H$ sequence motif. These zinc fingers are predicted to form $\beta\beta\alpha$ finger structures with the Zn[II]-coordinated tetrahedrally by two cysteines and two histidines.[154] Some of the zinc fingers are proposed to be structural whereas others may be metalloregulatory. In support of this model, three or four domains bind zinc with high affinity, consistent with a folding role, and the others bind Zn[II] with a considerably lower affinity, consistent with a sensor role.[157] The mechanism by which Zn[II] regulates MTF-1 activity has not yet been elucidated.

8.8.4   CONCLUSIONS

The coordination chemistry of both metal trafficking proteins and metalloregulatory proteins is central to understanding metal ion homeostasis on the molecular level. Recent X-ray crystallographic and spectroscopic studies have revealed details of metal binding by soluble domains of copper transporters, by copper and nickel chaperones, and by copper, iron, zinc, mercury, and cadmium metalloregulatory proteins. In some cases, these data have also provided insight into homeostatic mechanisms. For the metal trafficking proteins, structures of the Atx1 and CCS chaperones suggest detailed mechanisms for copper transfer from chaperone to target protein. The details of metal ion transfer by other putative metallochaperones, including Cox17, Sco1, and UreE, remain unknown. For the metalloregulatory proteins, structures of DtxR show how metal binding facilitates interaction with DNA. The relationship between metal binding and gene regulation is less clear for the other systems. Another outstanding issue regarding the metalloregulatory proteins is that of metal ion specificity. Proteins such as Fur, the IdeRs, SmtB, and CadC bind multiple metal ions. Specificity may be tuned by the coordination environment as suggested for SmtB and CadC. Addressing these questions as well as pursuing biochemical characterization of additional genetically identified systems are important goals for future research.

8.8.5   ABBREVIATIONS

Ccc2 = yeast P-type ATPase cation transporter
Atx1 = yeast copper chaperone for Ccc2
Hah1 = human copper chaperone for the Menkes and Wilson disease proteins
SOD1 = copper, zinc superoxide dismutase
CCS = copper chaperone for superoxide dismutase
Cox17 = copper chaperone for cytochrome *c* oxidase

Sco1 = protein implicated in assembly of cytochrome *c* oxidase copper site
UreE = proposed nickel chaperone for urease
Ace1 = yeast copper metalloregulatory protein
Mac1 = yeast copper metalloregulatory protein
Amt1 = yeast copper metalloregulatory protein
Fur = ferric uptake regulator protein
IdeR = iron dependent regulator protein
DtxR = diphtheria toxin repressor
IscR = bacterial iron–sulfur metalloregulatory protein
IRP1 = iron regulatory protein 1
Zur = bacterial zinc uptake regulator protein
ZntR = bacterial zinc metalloregulatory protein
MerR = bacterial mercury metalloregulatory protein
SmtB = bacterial zinc metalloregulatory protein
CadC = bacterial cadmium metalloregulatory protein
MTF-1 = metal response element-binding transcription factor-1

8.8.6 REFERENCES

1. Holm, R. H.; Kennepohl, P.; Solomon, E. I. *Chem. Rev.* **1996**, *96*, 2239–2314.
2. Nelson, N. *EMBO J.* **1999**, *18*, 4361–4371.
3. Rosenzweig, A. C. *Accounts Chem. Res.* **2001**, *34*, 119–128.
4. Radisky, D.; Kaplan, J. *J. Biol. Chem.* **1999**, *274*, 4481–4484.
5. O'Halloran, T. V. *Science* **1993**, *261*, 715–725.
6. Labbé, S.; Thiele, D. J. *Trends Microbiol.* **1999**, *7*, 500–505.
7. Gaither, L. A.; Eide, D. J. *Biometals* **2001**, *14*, 251–270.
8. Andrews, N. C.; Fleming, M. D.; Levy, J. E. *Curr. Opin. Hematol.* **1999**, *6*, 61–64.
9. Gatti, D.; Mitra, B.; Rosen, B. P. *J. Biol. Chem.* **2000**, *275*, 34009–34012.
10. Silver, S.; Phung, L. T. *Annu. Rev. Microbiol.* **1996**, *50*, 753–789.
11. Dancis, A.; Yuan, D. S.; Haile, D.; Askwith, C.; Eide, D.; Moehle, C.; Kaplan, J.; Klausner, R. D. *Cell* **1994**, *76*, 393–402.
12. Lee, J.; Peña, M. M. O.; Nose, Y.; Thiele, D. J. *J. Biol. Chem.* **2002**, *277*, 4380–4387.
13. Solioz, M.; Vulpe, C. *Trends Biochem. Sci.* **1996**, *21*, 237–241.
14. Sarkar, B. *Chem. Rev.* **1999**, *99*, 2535–2544.
15. Gitschier, J.; Moffat, B.; Reilly, D.; Wood, W. I.; Fairbrother, W. J. *Nature Struct. Biol.* **1998**, *5*, 47–54.
16. Ralle, M.; Cooper, M. J.; Lutsenko, S.; Blackburn, N. J. *J. Am. Chem. Soc.* **1998**, *120*, 13525–13526.
17. DiDonato, M.; Hsu, H.-F.; Narindrasorasak, S.; Que, L., Jr.; Sarkar, B. *Biochemistry* **2000**, *39*, 1890–1896.
18. Banci, L.; Bertini, I.; Ciofi-Baffoni, S.; Huffman, D. L.; O'Halloran, T. V. *J. Biol. Chem.* **2001**, *276*, 8415–8426.
19. Rensing, C.; Fan, B.; Sharma, R.; Mitra, B.; Rosen, B. P. *Proc. Natl. Acad. Sci. USA* **2000**, *97*, 652–656.
20. Wunderli-Ye, H.; Solioz, M. *Biochem. Biophys. Res. Commun.* **2001**, *280*, 713–719.
21. Sharma, R.; Rensing, C.; Rosen, B. P.; Mitra, B. *J. Biol. Chem.* **2000**, *275*, 3873–3878.
22. Rensing, C.; Sun, Y.; Mitra, B.; Rosen, B. P. *J. Biol. Chem.* **1998**, *273*, 32614–32617.
23. Nucifora, G.; Chu, L.; Misra, T. K.; Silver, S. *Proc. Natl. Acad. Sci. USA* **1989**, *86*, 3544–3548.
24. Forbes, J. R.; Hsi, G.; Cox, D. W. *J. Biol. Chem.* **1999**, *274*, 12408–12413.
25. Payne, A. S.; Gitlin, J. D. *J. Biol. Chem.* **1999**, *273*, 3765–3770.
26. Mitra, B.; Sharma, R. *Biochemistry* **2001**, *40*, 7694–7699.
27. Rosenzweig, A. C.; O'Halloran, T. V. *Curr. Opin. Chem. Biol.* **2000**, *4*, 140–147.
28. Lin, S.; Pufahl, R.; Dancis, A.; O'Halloran, T. V.; Culotta, V. C. *J. Biol. Chem.* **1997**, *272*, 9215–9220.
29. Yuan, D. S.; Stearman, R.; Dancis, A.; Dunn, T.; Beeler, T.; Klausner, R. D. *Proc. Natl. Acad. Sci. USA* **1995**, *92*, 2632–2636.
30. Pufahl, R. A.; Singer, C. P.; Peariso, K. L.; Lin, S.-J.; Schmidt, P.; Culotta, V. C.; Penner-Hahn, J. E.; O'Halloran, T. V. *Science* **1997**, 853–856.
31. Banci, L.; Bertini, I.; Conte, R. D.; Markey, J.; Ruiz-Dueñas, F. J. *Biochemistry* **2001**, *40*, 15660–15668.
32. Rosenzweig, A. C.; Huffman, D. L.; Hou, M. Y.; Wernimont, A. K.; Pufahl, R. A.; O'Halloran, T. V. *Structure* **1999**, *7*, 605–617.
33. Steele, R. A.; Opella, S. J. *Biochemistry* **1997**, *36*, 6885–6895.
34. Wernimont, A. K.; Huffman, D. L.; Lamb, A. L.; O'Halloran, T. V.; Rosenzweig, A. C. *Nature Struct. Biol.* **2000**, *7*, 766–771.
35. Coucouvanis, D.; Murphy, C. N.; Kanodia, S. K. *Inorg. Chem.* **1980**, *19*, 2993–2998.
36. Pickering, I. J.; George, G. N.; Dameron, C. T.; Kurz, B.; Winge, D. R.; Dance, I. G. *J. Am. Chem. Soc.* **1993**, *115*, 9498–9505.
37. Larin, D.; Mekios, C.; Das, K.; Ross, B.; Yang, A.-S.; Gilliam, T. C. *J. Biol. Chem.* **1999**, *274*, 28497–28504.
38. Culotta, V. C.; Klomp, L. W. J.; Strain, J.; Casareno, R. L. B.; Krems, B.; Gitlin, J. D. *J. Biol. Chem.* **1997**, *272*, 23469–23472.
39. McCord, J. M.; Fridovich, I. *J. Biol. Chem.* **1969**, *244*, 6049–6055.
40. Lamb, A. L.; Wernimont, A. K.; Pufahl, R. A.; O'Halloran, T. V.; Rosenzweig, A. C. *Nature Struct. Biol.* **1999**, *6*, 724–729.
41. Lamb, A. L.; Wernimont, A. K.; Pufahl, R. A.; O'Halloran, T. V.; Rosenzweig, A. C. *Biochemistry* **2000**, *39*, 1589–1595.
42. Lamb, A. L.; Torres, A. S.; O'Halloran, T. V.; Rosenzweig, A. C. *Nature Struct. Biol.* **2001**, *8*, 751–755.

43. Schmidt, P. J.; Rae, T. D.; Pufahl, R. A.; Hamma, T.; Strain, J.; O'Halloran, T. V.; Culotta, V. C. *J. Biol. Chem.* **1999**, *274*, 23719–23725.
44. Zhu, H.; Shipp, E.; Sanchez, R. J.; Liba, A.; Stine, J. E.; Hart, P. J.; Gralla, E. B.; Nersissian, A. M.; Valentine, J. S. *Biochemistry* **2000**, *39*, 5413–5421.
45. Eisses, J. F.; Stasser, J. P.; Ralle, M.; Kaplan, J. H.; Blackburn, N. J. *Biochemistry* **2000**, *39*, 7337–7342.
46. Torres, A. S.; Petri, V.; Rae, T. D.; O'Halloran, T. V. *J. Biol. Chem.* **2001**, *276*, 38410–38416.
47. Hiser, L.; Di Valentin, M.; Hamer, A. G.; Hosler, J. P. *J. Biol. Chem.* **2000**, *275*, 619–623.
48. Mattatall, N. R.; Jazairi, J.; Hill, B. C. *J. Biol. Chem.* **2000**, *275*, 28802–28809.
49. Beers, J.; Glerum, D. M.; Tzagoloff, A. *J. Biol. Chem.* **1997**, *272*, 33191–33196.
50. Nittis, T.; George, G. N.; Winge, D. R. *J. Biol. Chem.* **2001**, *276*, 42520–42526.
51. Heaton, D.; Nittis, T.; Srinivasan, C.; Winge, D. R. *J. Biol. Chem.* **2000**, *275*, 37582–37587.
52. Heaton, D. N.; George, G. N.; Garrison, G.; Winge, D. R. *Biochemistry* **2001**, *40*, 743–751.
53. Hausinger, R. P.; Karplus, P. A. In *Urease Handbook of Metalloproteins*; Weighardt, K., Huber, R., Poulos, T. L. Messerschmidt A., Eds., Wiley: Chichester, UK, 2001; pp 867–879.
54. Jabri, E.; Carr, M. B.; Hausinger, R. P.; Karplus, P. A. *Science* **1995**, *268*, 998–1004.
55. Hausinger, R. P.; Colpas, G. J.; Soriano, A. *ASM News* **2001**, *67*, 78–84.
56. Olson, J. W.; Maier, R. J. *J. Bacteriol.* **2000**, *182*, 1702–1705.
57. Watt, R. K.; Ludden, P. W. *J. Biol. Chem.* **1998**, *273*, 10019–10025.
58. Brayman, T. G.; Hausinger, R. P. *J. Bacteriol.* **1996**, *178*, 5410–5416.
59. Colpas, G. J.; Brayman, T. G.; McCracken, J.; Pressler, M. A.; Babcock, G. T.; Ming, L.-J.; Colangelo, C. M.; Scott, R. A.; Hausinger, R. P. *J. Biol. Inorg. Chem.* **1998**, *3*, 150–160.
60. Colpas, G. J.; Brayman, T. G.; Ming, L.-J.; Hausinger, R. P. *Biochemistry* **1999**, *38*, 4078–4088.
61. Song, H. K.; Mulrooney, S. B.; Huber, R.; Hausinger, R. P. *J. Biol. Chem.* **2001**, *276*, 49359–49364.
62. Remaut, H.; Safarov, N.; Ciurli, S.; Van Beeumen, J. *J. Biol. Chem.* **2001**, *276*, 49365–49370.
63. Zumft, W. G.; Viebrock-Sambale, A.; Braun, C. *Eur. J. Biochem.* **1990**, *192*, 591–599.
64. McGuirl, M. A.; Bollinger, J. A.; Cosper, N.; Scott, R. A.; Dooley, D. M. *J. Biol. Inorg. Chem.* **2001**, *6*, 189–195.
65. Yuvaniyama, P.; Agar, J. N.; Cash, V. L.; Johnson, M. K.; Dean, D. R. *Proc. Natl. Acad. Sci. USA* **2000**, *97*, 599–604.
66. Agar, J. N.; Krebs, C.; Frazzon, J.; Huynh, B. H.; Dean, D. R.; Johnson, M. K. *Biochemistry* **2000**, *39*, 7856–7862.
67. Krebs, C.; Agar, J. N.; Smith, A. D.; Frazzon, J.; Dean, D. R.; Huynh, B. H.; Johnson, M. K. *Biochemistry* **2001**, *40*, 14069–14080.
68. Garland, S. A.; Hoff, K.; Vickery, L. E.; Culotta, V. C. *J. Mol. Biol.* **1999**, *294*, 897–907.
69. Kaut, A.; Lange, H.; Diekert, K.; Kispal, G.; Lill, R. *J. Biol. Chem.* **2000**, *275*, 15955–15961.
70. Shah, V. K.; Rangaraj, P.; Chatterjee, R.; Allen, R. M.; Roll, J. T.; Roberts, G. P.; Ludden, P. W. *J. Bacteriol.* **1999**, *181*, 2797–2801.
71. Winge, D. R. *Adv. Exp. Med. Biol.* **1999**, *448*, 237–246.
72. Furst, P.; Hu, S.; Hackett, R.; Hamer, D. *Cell* **1988**, *55*, 705–717.
73. Thiele, D. J. *Mol. Cell. Biol.* **1998**, *8*, 2745–2752.
74. Gralla, E. B.; Thiele, D. J.; Silar, P.; Valentine, J. S. *Proc. Natl. Acad. Sci. USA* **1991**, *88*, 8558–8562.
75. Zhou, P. B.; Thiele, D. J. *Proc. Natl. Acad. Sci. USA* **1991**, *88*, 6112–6116.
76. Labbé, S.; Zhu, Z.; Thiele, D. J. *J. Biol. Chem.* **1997**, *272*, 15951–15958.
77. Yamaguchi-Iwai, Y.; Serpe, M.; Haile, D.; Yang, W.; Kosman, D. J.; Klausner, R. D.; Dancis, A. *J. Biol. Chem.* **1997**, *272*, 17711–17718.
78. Zhu, Z.; Labbé, S.; Pena, M. M. O.; Thiele, D. J. *J. Biol. Chem.* **1998**, *273*, 1277–1280.
79. Yonkovich, J.; McKenndry, R.; Shi, X.; Zhu, Z. *J. Biol. Chem.* **2002**, *277*, 23981–23984.
80. Winge, D. R.; Graden, J. A.; Posewitz, M. C.; Martins, L. J.; Jensen, L. T.; Simon, J. R. *J. Biol. Inorg. Chem.* **1997**, *2*, 2–10.
81. Thorvaldsen, J. L.; Sewell, A. K.; Tanner, A. M.; Peltier, J. M.; Pickering, I. J.; George, G. N.; Winge, D. R. *Biochemistry* **1994**, *33*, 9566–9577.
82. Farrell, R. A.; Thorvaldsen, J. L.; Winge, D. R. *Biochemistry* **1996**, *35*, 1571–1580.
83. Dameron, C. T.; Winge, D. R.; George, G. N.; Sansone, M.; Hu, S.; Hamer, D. *Proc. Natl. Acad. Sci. USA* **1991**, *88*, 6127–6131.
84. Casas-Finet, J. R.; Hu, S.; Hamer, D.; Karpel, R. L. *Biochemistry* **1992**, *31*, 6617–6626.
85. Graden, J. A.; Posewitz, M. C.; Simon, J. R.; George, G. N.; Pickering, I. J.; Winge, D. R. *Biochemistry* **1996**, *35*, 14583–14589.
86. Brown, K. R.; Keller, G. L.; Pickering, I. J.; Harris, H. H.; George, G. N.; Winge, D. R. *Biochemistry* **2002**, 6469–6476.
87. Turner, R. B.; Smith, D. L.; Zawrotny, M. E.; Summers, M. F.; Posewitz, M. C.; Winge, D. R. *Nature Struct. Biol.* **1998**, *5*, 551–555.
88. Jensen, L. T.; Posewitz, M. C.; Srinivasan, C.; Winge, D. R. *J. Biol. Chem.* **1998**, *273*, 23805–23811.
89. Keller, G.; Gross, C.; Kelleher, M.; Winge, D. R. *J. Biol. Chem.* **2000**, *275*, 29193–29199.
90. Jensen, L. T.; Winge, D. R. *EMBO J* **1998**, *17*, 5400–5408.
91. Bagg, A.; Neilands, J. B. *Biochemistry* **1987**, *26*, 5471–5477.
92. Ratledge, C.; Dover, L. G. *Annu. Rev. Microbiol.* **2000**, *54*, 881–941.
93. Stojiljkovic, I.; Hantke, K. *Mol. Gen. Genet.* **1995**, *247*, 199–205.
94. Ochsner, U. A.; Vasil, A. I.; Vasil, M. L. *J. Bacteriol.* **1995**, *177*, 7194–7201.
95. Michaud-Soret, I.; Adrait, A.; Jaquinod, M.; Forest, E.; Touati, D.; Latour, J. M. *FEBS Lett.* **1997**, *413*, 473–476.
96. Althaus, E. W.; Outten, C. E.; Olson, K. E.; Cao, H.; O'Halloran, T. V. *Biochemistry* **1999**, *38*, 6559–6569.
97. Coy, M.; Doyle, C.; Besser, J.; Neilands, J. B. *Biometals* **1994**, *7*, 292–298.
98. Jacquamet, L.; Aberdam, D.; Adrait, A.; Hazemann, J. L.; Latour, J. M.; Michaud-Soret, I. *Biochemistry* **1998**, *37*, 2564–2571.
99. Jacquamet, L.; Dole, F.; Jeandey, C.; Oddou, J. L.; Perret, E.; Le Pape, L.; Aberdam, D.; Hazemann, J. L.; Michaud-Soret, I.; Latour, J. M. *J. Am. Chem. Soc.* **2000**, *122*, 394–395.
100. Adrait, A.; Jacquamet, L.; Le Pape, L.; Gonzalez de Peredo, A.; Aberdam, D.; Hazemann, J. L.; Latour, J. M.; Michaud-Soret, I. *Biochemistry* **1999**, *38*, 6248–6260.

101. Hegg, E. L.; Que, L., Jr. *Eur. J. Biochem.* **1997**, *250*, 625–629.
102. Ringe, D.; White, A.; Chen, S.; Murphy, J. R. Diphtheria toxin repressor: metal ion mediated control of transcription. In *Handbook of Metalloproteins*; Messerschmidt, A., Ed.; Wiley: Chichester, UK, 2001, pp 929–938.
103. Qiu, X.; Verlinde, C. L. M. J.; Zhang, S. P.; Schmitt, M. P.; Holmes, R. K.; Hol, W. G. J. *Structure* **1995**, *3*, 87–100.
104. Schiering, N.; Tao, X.; Zeng, H.; Murphy, J. R.; Petsko, G. A.; Ringe, D. *Proc. Natl. Acad. Sci. USA* **1995**, *92*, 9843–9850.
105. Qiu, X.; Pohl, E.; Holmes, R. K.; Hol, W. G. J. *Biochemistry* **1996**, *35*, 12292–12302.
106. Pohl, E.; Holmes, R. K.; Hol, W. G. J. *J. Biol. Chem.* **1998**, *273*, 22420–22427.
107. White, A.; Ding, X.; vanderSpek, J. C.; Murphy, J. R.; Ringe, D. *Nature* **1998**, *394*, 502–506.
108. Pohl, E.; Holmes, R. K.; Hol, W. G. J. *J. Mol. Biol.* **1999**, *285*, 1145–1156.
109. Feese, M. D.; Ingason, B. P.; Goranson-Siekierke, J.; Holmes, R. K.; Hol, W. G. J. *J. Biol. Chem.* **2001**, *276*, 5959–5966.
110. Tao, X.; Murphy, J. R. *J. Biol. Chem.* **1992**, *267*, 21761–21764.
111. Schmitt, M. P.; Holmes, R. K. *Mol. Microbiol.* **1993**, *9*, 173–181.
112. Ding, X.; Zeng, H.; Schiering, N.; Ringe, D.; Murphy, J. R. *Nat. Struct. Biol.* **1996**, *3*, 382–387.
113. Pohl, E.; Qui, X.; Must, L. M.; Holmes, R. K.; Hol, W. G. J. *Protein Sci.* **1997**, *6*, 1114–1118.
114. Pohl, E.; Holmes, R. K.; Hol, W. G. J. *J. Mol. Biol.* **1999**, *292*, 653–667.
115. Tao, X.; Murphy, J. R. *Proc. Natl. Acad. Sci. USA* **1993**, *90*, 8524–8528.
116. Schwartz, C. J.; Giel, J. L.; Patschkowski, T.; Luther, C.; Ruzicka, F. J.; Beinert, H.; Kiley, P. J. *Proc. Natl. Acad. Sci. USA* **2001**, *98*, 14895–14900.
117. Frazzon, J.; Dean, D. R. *Proc. Natl. Acad. Sci. USA* **2001**, *98*, 14751–14753.
118. Aono, S.; Nakajima, H. *Prog. React. Kinet. Mech.* **2000**, *25*, 65–107.
119. Khoroshilova, N.; Popescu, C.; Münck, E.; Beinert, H.; Kiley, P. J. *Proc. Natl. Acad. Sci. USA* **1997**, *94*, 6087–6092.
120. Ding, H.; Hidalgo, E.; Demple, B. *J. Biol. Chem.* **1996**, *271*, 33173–33175.
121. Eisenstein, R. S. *Annu. Rev. Nutr.* **2000**, *20*, 627–662.
122. Beinert, H.; Kennedy, M. C.; Stout, C. D. *Chem. Rev.* **1996**, *96*, 2335–2373.
123. Kennedy, M. C.; Mende-Mueller, L.; Blondin, G. A.; Beinert, H. *Proc. Natl. Acad. Sci. USA* **1992**, *89*, 11730–11734.
124. Haile, D.; Rouault, T. A.; Harford, J. B.; Kennedy, M. C.; Blondin, G. A.; Beinert, H.; Klausner, R. D. *Proc. Natl. Acad. Sci. USA* **1992**, *89*, 11735–11739.
125. Brown, N. M.; Kennedy, M. C.; Antholine, W. E.; Eisenstein, R. S.; Walden, W. E. *J. Biol. Chem.* **2002**, *277*, 7246–7254.
126. Gailer, J.; George, G. N.; Pickering, I. J.; Prince, R. C.; Kohlhepp, P.; Zhang, D.; Walker, F. A.; Winzerling, J. J. *J. Am. Chem. Soc.* **2001**, *123*, 10121–10122.
127. Patzer, S. I.; Hantke, K. *Mol. Microbiol.* **1998**, *28*, 1199–1210.
128. Patzer, S. I.; Hantke, K. *J. Biol. Chem.* **2000**, *275*, 24321–24332.
129. Outten, C. E.; O'Halloran, T. V. *Science* **2001**, *292*, 2488–2492.
130. Outten, C. E.; Tobin, D. A.; Penner-Hahn, J. E.; O'Halloran, T. V. *Biochemistry* **2001**, *40*, 10417–10423.
131. Brocklehurst, K. R.; Hobman, J. L.; Lawley, B.; Blank, L.; Marshall, S. J.; Brown, N. L.; Morby, A. P. *Mol. Microbiol.* **1999**, *31*, 893–902.
132. Binet, M. R. B.; Poole, R. K. *FEBS Lett.* **2000**, *473*, 67–70.
133. Outten, C. E.; Outten, F. W.; O'Halloran, T. V. *J. Biol. Chem.* **1999**, *274*, 37517–37524.
134. Ansari, A. Z.; Chael, M. L.; O'Halloran, T. V. *Nature* **1992**, *355*, 87–89.
135. Ansari, A. Z.; Bradner, J. E.; O'Halloran, T. V. *Nature* **1995**, *374*, 371–375.
136. Helmann, J. D.; Ballard, B. T.; Walsh, C. T. *Science* **1990**, *247*, 946–948.
137. Watton, S. P.; Wright, J. G.; MacDonnell, F. M.; Bryson, J. W.; Sabat, M.; O'Halloran, T. V. *J. Am. Chem. Soc.* **1990**, *112*, 2824–2826.
138. Wright, J. W.; Natan, M. J.; MacDonnell, F. M.; Ralston, D. M.; O'Halloran, T. V. *Prog. Inorg. Chem.* **1990**, *38*, 323–412.
139. Utschig, L. M.; Bryson, J. W.; O'Halloran, T. V. *Science* **1995**, *268*, 380–385.
140. Fleissner, G.; Reigle, M. D.; O'Halloran, T. V.; Spiro, T. G. *J. Am. Chem. Soc.* **1998**, *120*, 12690–12691.
141. Shi, W.; Wu, J.; Rosen, B. P. *J. Biol. Chem.* **1994**, *269*, 19826–19829.
142. Shi, W.; Dong, J.; Scott, R. A.; Ksenzenko, M.; Rosen, B. P. *J. Biol. Chem.* **1996**, *271*, 9291–9297.
143. Morby, A. P.; Turner, J. S.; Huckle, J. W.; Robinson, N. J. *Nucleic Acids Res.* **1993**, *21*, 921–925.
144. VanZile, M. L.; Chen, X.; Giedroc, D. P. *Biochemistry* **2002**, *41*, 9765–9775.
145. VanZile, M. L.; Cosper, N. J.; Scott, R. A.; Giedroc, D. P. *Biochemistry* **2000**, *39*, 11818–11829.
146. Turner, J. S.; Glands, P. D.; Samson, A. C. R.; Robinson, N. J. *Nucleic Acids Res.* **1996**, *24*, 3714–3721.
147. Cook, W. J.; Kar, S. R.; Taylor, K. B.; Hall, L. M. *J. Mol. Biol.* **1998**, *275*, 337–346.
148. VanZile, M. L.; Chen, X.; Giedroc, D. P. *Biochemistry* **2002**, *41*, 9776–9786.
149. Endo, G.; Silver, S. *J. Bacteriol.* **1995**, *177*, 4437–4441.
150. Busenlehner, L. S.; Cosper, N. J.; Scott, R. A.; Rosen, B. P.; Wong, M. D.; Giedroc, D. P. *Biochemistry* **2001**, *40*, 4426–4436.
151. Busenlehner, L. S.; Apuy, J. L.; Giedroc, D. P. *J. Biol. Inorg. Chem.* **2002**, *7*, 551–559.
152. Busenlehner, L. S.; Weng, T.-C.; Penner-Hahn, J. E.; Giedroc, D. P. *J. Mol. Biol.* **2002**, *319*, 685–701.
153. Bird, A. J.; Zhao, H.; Luo, H.; Jensen, L. T.; Srinivasan, C.; Evans-Galea, M.; Winge, D. R.; Eide, D. J. *EMBO J* **2000**, *19*, 3704–3713.
154. Giedroc, D. P.; Chen, X.; Apuy, J. L. *Antioxid. Redox Sign.* **2001**, *3*, 577–596.
155. Zhao, H.; Eide, D. J. *Mol. Cell. Biol.* **1997**, *17*, 5044–5052.
156. Andrews, G. K. *Biometals* **2001**, *14*, 223–237.
157. Chen, X.; Agarwal, A.; Giedroc, D. P. *Biochemistry* **1998**, *37*, 11152–11161.

8.9
Metallothioneins

P. GONZÁLEZ-DUARTE
Universitat Autònoma de Barcelona, Spain

8.9.1 INTRODUCTION

Metallothioneins (MTs) constitute a very wide family of ubiquitous proteins with features that are exceptional from the perspectives both of biology and coordination chemistry. If compared with all other metalloproteins, MTs are wholly unconventional because of their small size (2–7 kDa), their extremely high thiolate sulfur and metal content, both in the order of 10% (w/w), and the lack of tertiary structure in their apo form (apo-MT or thionein). The structural properties that distinguish all MTs are based on the metal-thiolate aggregates that give rise either to a single metal-binding domain, as in yeast, or to two such domains, as in mammals. These can be regarded as polynuclear homo- or heterometallic complexes of a multidentate ligand, involving terminal and/or bridging cysteinyl thiolate groups, and thus their study could be related to the field of metal thiolate complexes. However, from the perspective of coordination chemistry, MTs are unique as well as intriguing, given the different number and nature of the metal centers in MTs, the possible coexistence of several coordination geometries even for the same metal, and the influence of the peptide chain on the ligation modes of the thiolate sulfur.

Even though MTs exist naturally with zinc and/or copper bound to them, the discovery of the first MT in 1957 from horse kidney was the result of a search for a cadmium protein.[1] Since then, MTs have continuously challenged the interest of chemists and life scientists. A search in the SciFinder database with *metallothionein* as the entry yields about 15,000 publications and reveals more than 700 articles per year over the 1991–2001 decade. It also shows that developments in MT research have been covered by about 300 reviews. The widespread occurrence of MTs in nature suggests that they serve an important biological function not yet completely established. It would appear that MTs have no enzymatic activity, nor do they perform any catalytic role in known metabolic processes. Precise identification of the function of MTs accounts for the outstanding number of works available (as indicated by the search results) and prompts most of the research currently being undertaken.

This section is intended as a broad overview of the present knowledge of MTs from the perspective of coordination chemistry; the main developments with respect to their metal content, structure, spectroscopic features and chemical properties will therefore be summarized. Moreover, the structural patterns of the metal–sulfur aggregates in MTs will be compared with those found

in synthetic metal thiolates. A recent review of the structure and chemistry of MTs includes the most relevant literature prior to 2001.[2] Progress in the study of MTs by scientists from different fields has been covered in the proceedings of the four international conferences devoted exclusively to MTs.[3–6] Standard operating procedures for the isolation, quantification, and the chemical, physical, and spectroscopic characterization of MTs have been compiled in a methodological contribution.[7] General reviews covering all aspects of MT research are also available.[8–12]

8.9.1.1   Sources, Classification, and Function

MTs have been isolated from a wide range of living systems, from eukaryotic—and some prokaryotic—microorganisms through plants and invertebrates to mammals. A remarkable biological feature of MTs is that their genes are induced by a variety of agents. Their biosynthesis is therefore greatly enhanced both *in vivo* and in cultured cells by metal ions, certain hormones, and many cytotoxic agents. In animals, MTs are most abundant in parenchymatous tissues, i.e., liver, kidney, pancreas, and intestines.[8] Procedures for the isolation and characterization of MTs from biological sources, and special precautions that avoid oxidation of the cysteinyl residues forming disulfide bridges, as well as the randomization of metals, have all been reported.[7]

Less frequently, conventional chemical peptide synthesis has been used to produce the entire apo-MT protein (when the amino acid sequence is relatively short) or in the production of the separate MT domains. Thus, the metal-binding features of synthetic MTs from fungi[13,14] or the individual domains of crustacean[15] and mammalian[13,16–19] MTs have been characterized. Additionally, as peptide synthesis provides the methodology for a facile sequence modification, studies on designed MT-related peptides have also been carried out.[20,21]

The expression of MTs in recombinant systems has recently been proven as an effective alternative to their isolation from natural sources, thereby giving further stimulus to the study of MTs. After some early attempts,[22–24] current heterologous expression systems (essentially in *E. coli*) provide significant quantities of the desired MT, avoiding whatever constraint may be imposed by the availability of the corresponding native organisms.[19,25–31] In addition, by adapting the metal content in the culture media, MTs containing different metal ions can be recovered.[32,33] Furthermore, the expression and purification of separate MT domains afford an adequate alternative to proteolytic digestion procedures in the entire protein, which may compromise the integrity of the isolated peptides.[21,34–36] Finally, the DNA recombinant techniques allow the expression and purification both of wild-type and mutant forms, thus facilitating the analysis of the relative contribution that individual residues make to the *in vivo* and *in vitro* functions of MTs.[19,37–41]

Historically, three different classes were proposed in order to classify the extremely heterogeneous amino acid sequences of MTs: class I, comprising all MTs with clear sequence similarity to mammalian MT; class II, including polypeptides that are only distantly related to mammalian MT; and class III, for the enzymatically synthesized peptides of general formula (γ-Glu-Cys)$_n$Gly (the values of *n* ranging from 2 to 8), variously known as phytochelatins and cadystins and denoted as (γ-Glu-Cys)$_n$Gly(γ-EC) peptides.[42] More recently, a new classification consisting of a singular set for each individual taxon has been proposed (www.unizh.ch/~mtpage/classif.html). Both schemes are based on primary structure data, but do not include any functional or evolutionary information.[26] With respect to the primary structure of all MTs, the most remarkable feature is the recurrence of Cys–X–Cys tripeptide sequences, where X stands for an amino acid residue other than cysteine. To date, all vertebrates examined contain two or more distinct MT isoforms, denoted MT-1 through MT-4, which differ in amino acid residues other than the conserved cysteines. In mammals, MT-1 and MT-2 are found in all organs, MT-3 is expressed mainly in the brain, and MT-4 is most abundant in certain stratified tissues.[8]

Due to both the origin of their discovery and to their high metal-inducibility, it has long been suggested that one of the primary roles of MTs is to serve as a heavy-metal detoxification system.[43] However, it seems likely that this is not the primary function of MTs, but rather is simply a consequence of their high cysteine content.[44] A more physiological view generally considers that MTs could be involved in the homeostasis of copper and (especially) zinc ions.[45,46] There has been mounting evidence in recent years to suggest that MTs could be significant antioxidant and antiapoptotic proteins,[47,48] being especially important within the central nervous system.[49] Furthermore, other studies suggest that these proteins are also involved in the control of the redox status of cells and in energy metabolism.[50–53]

8.9.1.2 Spectroscopic Characterization and Stoichiometry of the Metal–Sulfur Aggregates in Metallothioneins

Unlike other metalloproteins, there is no specific metal-to-MT stoichiometry that defines MTs. Consequently, determination of the metal content is a primary step in the characterization of a new member of this large family of proteins, consisting of 197 sequences from 103 organisms (Swiss-Prot: www.expasy.ch/sprot/sprot-top.html). Within the MT family, differences in the length of the primary sequence and in the number of cysteines they encompass account for the highly variable metal-to-MT stoichiometries reported to date. Furthermore, not only is there no unique metal preference shown by mammalian and nonmammalian MTs[15,26,54] but—additionally—they can bind a mixture of different metal ions.[10] This complexity is added to by the fact that proteins with different metal contents are obtained depending both on the source and on the induction, isolation, and purification procedures.[7]

The analysis of the metal content in MTs includes determination of the number and nature of the bound metal ions[55] and elucidation of the coordination geometry around the different metal centers enfolded by the polypeptide chain. To this end, optical spectroscopies (UV-Vis, c.d. MCD and luminescence) have played a significant role,[10,56–58] despite providing information on the predominant species present in solution. Conversely, electrospray mass spectrometry (ES MS) allows determination of the molecular distribution of the various complex species coexisting within the sample.[59–61] However, in ES MS, the formation of artifacts due to operational features should not be disregarded.[62–64] A summary of the techniques more commonly used in the study of the metal-binding features of MTs can be found elsewhere.[65] Additionally, relevant information on the application and possible limitations of the X-ray absorption spectroscopy within the study of MTs has been reported.[10,66–69]

As regards the metal preferences of MTs, vertebrates and higher invertebrates naturally give rise either to Zn- or mixed Zn,Cu-loaded species, while yeast and fungi give rise to Cu-containing proteins. Concomitantly, it is widely accepted that in higher organisms the binding of the essential metals, Zn and Cu, occurs in two separate domains as opposed to lower organisms, where Cu is accommodated in only one domain.[2,70] Both features, the nature of the bound metal (Zn or Cu) and the one- or two-domain cluster structure, are probably essential for the MTs' different potential roles.[26] Within this context and in the absence of 3D structures of mixed Zn,Cu–MT species, recent studies suggest that Zn^{II} is essential for the *in vivo* and *in vitro* folding of mouse copper MT-1 in two domains.[33]

Whereas extensive information on the metal-binding abilities of mammalian MTs has been compiled,[10] current knowledge of those of non-mammalian species is more limited and rather dispersed. In order to fill this gap, existing data have been summarized in Table 1. A feature commonly found in several MTs is that they contain heterometallic mixtures of two (Zn,Cd; Cu,Cd; Zn,Cu) or three (Zn,Cd,Cu) metal ions. Still more striking is the great diversity of stoichiometries reported for certain homometallic metal-MT species, as shown in *S. cerevisiae*, where the copper-to-MT mole ratios range from 4 to 10, and in *N. crassa*, with a cadmium-to-MT mole ratio of 2 or 3. With this information on the metal-binding properties of MTs, it seems reasonable to conclude that the systematization of these data is hard indeed to achieve.

8.9.1.3 Three-dimensional Structures

Despite the discovery of MTs in 1957,[1] and also many of the subsequent studies being directed towards its metal content,[113] the first detailed knowledge of the 3D structure for the metal-thiolate clusters was not reported until almost 30 years later. Currently, this knowledge is only available for a small number of MTs, if compared with the already reported primary structure sequences (Swiss-Prot), and includes mammalian, invertebrate, and bacterial forms exclusively containing Zn and/or Cd ions (Table 2). To date, only limited structural data are available on copper-containing MTs,[85] attributable to the failure to obtain single crystals of the protein and to the unsuitability of the ^{63}Cu and ^{65}Cu isotopes for NMR studies.[18]

The key to understanding the 3D structure of MTs was the detailed analysis of the ^{113}Cd NMR spectra of rabbit liver Cd,Zn-MT-2,[114] which was reconfirmed by studies of rabbit liver Cd$_7$-MT-2.[115] Subsequent multidimensional/multinuclear NMR studies on ^{113}Cd-reconstituted Cd$_7$-MT-2 from rabbit,[116] rat,[117] and human,[118] and X-ray crystallographic studies of native rat Cd$_5$,Zn$_2$-MT-2[119] (Figure 1) allowed determination of the first 3D MT structures. These showed identical metal-thiolate cluster architectures and closely comparable polypeptide folds in crystals and in solution.

Table 1 Metal-to-MT stoichiometries reported for all known MTs except for mammalian forms.

Taxon/organism	M-MT stoichiometry	Taxon/organism	M-MT stoichiometry
Bacteria:		**Nematoda:**	
Synechococcus PCC 7942	Zn_4; Cd_4,Zn-SmtA[71]	*Caenorhabditis elegans*	M^{II}_6-CeMT-II (M = Cd, Zn)[29,62]
Fungi:		**Gastropoda:**	
Neurospora crassa	Cu_6-MT;[13,72,73] Cd_2-MT[13] M^{II}_3-MT (M = Zn, Cd, Hg, Co, Ni)[72,74]	*Helix pomatia* (Roman snail or Edible snail)	Cd_5,Zn-MT[75] Cu_{12}-MT;[62] Cu_6-MT[54]
Agaricus bisporus	Cu_6-MT[76], $Cu_{4,4}$-MT[14]	**Bivalvia:**	
Yeast:		*Mytilus edulis*	Cd_7-MT-10-IV[62]
Saccharomyces cerevisiae	Cu_{10}-CUP1[78,79] M_8-CUP1 (M = Cu, Ag)[80–83] M_7-CUP1 (M = Cu, Ag)[83–86] Cu_4-CUP1[87]M^{II}_4-CUP1 (M = Zn, Cd, Fe)[81,88] $Cu_{11–12}$-CRS5; Cd_6-CRS5[89]	*Mytilus galloprovincialis*	Cd_5-MT[77]
		Crassostrea virginica	Cd_5,$Zn_{1.7}$,$Cu_{0.1}$-CdBP1[90] $Cd_{4.7}$,$Zn_{1.6}$,$Cu_{0.1}$-CdBP2[90]
Candida glabrata	$Cu_{11–12}$-MT I; Cu_{10}-MT II[91]	**Insecta:**	
Plants:		*Orchesella cincta*	Cd_{7-8}-MT[92]
Pisum sativum (Pea)	$Cd_{5.6–6.1}$-PsMTA[93] Cd_4; $Zn_{6–11.5}$; $Cu_{3.5}$-PsMTA[94]	*Drosophila melanogaster*	M^{II}_3- + M^{II}_4-MTN (M = Zn, Cd)[25] Cu_8-MTN[25]
Lycopersicon esculentum (Tomato)	$Cd_{5.8}$-MT[95]	**Echinodermata:**	
		Strongylocentrotus purpuratus (Sea urchin)	Cd_7-MTA [$(Cd_4)^\alpha(Cd_3)^\beta$-MTA][62,97]

Organism	Metallothioneins
Fucus vesiculosus (Algae)	Cd_7-MT; Cu_{13}-MT[96]
Tritricum aestium (Wheat)	Zn_5-MT[98]
Vicia fava (Broad bean)	$Cd_{1.7}$,Cu,$Zn_{0.1}$-MT 1a[99]; Cd_2,$Cu_{0.4}$,$Zn_{0.02}$-MT 1b[99]; Cd_2,$Cu_{0.4}$,$Zn_{0.1}$-MT 2[99]
Zea mays (Maize)	Cd_8-MT[100]
Arabidopsis thaliana	$Cu_{8.4}$-MT 1, $Cu_{7.3}$-MT 2, $Cu_{5.5}$-MT 3[104]
Protozoa:	
Tetrahymena pigmentosa	Cd_{12}-MT 1; Cd_{12}-MT 2[106]; Cu_7-MT[107]
Tetrahymena pyriformis	Cd_{12}-MT 1; Cd_{12}-MT 2[106]
Annelida:	
Lumbricus rubellus	Cd_6-wMT-1; Cd_6-wMT-2[31]
Eisenia foetida	Cd_4-MT[62,111]
Crustacea:[a]	
Homarus americanus (American lobster)	Cd_3-$\beta\beta$MTH; Cd_3-$\beta\alpha$MTH[101,102]; M^{II}_6- + M^{II}_7-MTH (M = Zn, Cd)[26]; M^{II}_3- + M^{II}_4-$\beta\beta$; M^{II}_3- + M^{II}_4-$\beta\alpha$[26]; Cu_9,Cd_6-MT 1;[103]; Cd_9,Cu_{2-x},Zn_x-MT 2[103]; Cd_5,Cu-; Cd_6-MT 2[101]
Cancer pagurus	M^{II}_6- + M^{II}_7-MT (M = Cd, Co)[105]
Callinectes sapidus (Blue crab)	Cd_6-MT I[62]
Scilla serrata (Mud crab)	Cd_6-MT I; Cd_6-MT II[108]; $Cd_{3.1-3.7}$,$Zn_{1.6-1.8}$-MT[109]
Fishes:	
Notothenia coriiceps (Antarctic fish)	M^{II}_7-MTA (M = Zn, Cd)[110]
Aves:	
Gallus gallus (Chicken)	$Cd_{9-x}Zn_x$-MT; Cu_{15}-MT[112]

a In these organisms the $M^{II}_3(SCys)_9$ cluster in the N-terminal β domain is variously denoted as β_N or $\beta\beta$. Analogously, the $M^{II}_3(SCys)_9$ cluster in the C-terminal α domain is denoted as β_C or $\beta\alpha$.

Table 2   Structurally characterized MTs and corresponding amino acid sequences.[a,b]

Mouse Cd_7-MT-1[121]	(1DFT, 1DFS)	MDPN**C**S**C**STG GS**C**T**C**TSS**CA** **C**KN**C**K**C**TS**C**K KS**CC**S**CC**PVG **C**SK**C**AQG**C**V**C** KGAADK**C**T**CC** A
Human Cd_7-MT-2[118]	(1MHU, 2MHU)	MDPN**C**S**C**AAG DS**C**T**C**AGS**C**K **C**KE**C**K**C**TS**C**K KS**CC**S**CC**PVG **C**AK**C**AQG**C**I**C** KGASDK**C**S**CC** A
Rabbit Cd_7-MT-2[116]	(1MRB, 2MRB)	MDPN**C**S**C**AAA GDS**C**T**C**ANS**C** T**C**KA**C**K**C**TS**C** KKS**CC**S**CC**PP G**C**AK**C**AQG**C**I **C**KGASDK**C**S**CC C** A
Rat Cd_5Zn_2-MT-2 and Cd_7-MT-2[117,119]	(4MT2 and 1MRT, 2MRT)	MDPN**C**S**C**ATD GS**C**S**C**AGS**C**K **C**KQ**C**K**C**TS**C**K KS**CC**S**CC**PVG **C**AK**C**SQG**C**I**C** KEASDK**C**S**CC** A
Mouse Cd_7-MT-3[c,123]	(1JI9)	MDPET**C**P**C**PT GGS**C**T**C**SDK**C** K**C**KG**C**K**C**TN**C** KKS**CC**S**CC**PA G**C**EK**C**AKD**C**V **C**KGEEGAKAE AEK**C**S**CC**Q
Blue crab Cd_6-MT-1[125]	(1DMC, 1DME)	MPGP**CC**NDK**C** V**C**QEGG**C**KAG **C**Q**C**TS**C**R**C**SP **C**QK**C**TSG**C**K**C** ATKEE**C**SKT**C** TKP**C**S**CC**PK
American lobster Cd_6–MT–1[102,126]	(1HZQ, 1HZR)	PGP**CC**KDK**C**E **C**AEGG**C**KTG**C** K**C**TS**C**R**C**AP**C** EK**C**TSG**C**K**C**P SKDE**C**AKT**C**S KP**C**S**CC**XX
Sea urchin Cd_7-MTA[124]	(1QJK, 1QJL)	MPDVK**C**V**CC**K EGKE**C**A**C**FGQ D**CC**KTGE**CC**K DGT**CC**GI**C**TN AA**C**K**C**ANG**C**K **C**GSG**C**S**C**TEG N**C**A**C**
Synechococcus Zn_4-SmtA[71]	(1JJD)	MTSTTLVK**C**A **C**EP**C**L**C**NVDP SKAIDRNGLY Y**C**SEA**C**ADGH TGGSKG**C**GHT G**C**N**C**HG
S. cerevisiae Ag_7-MT and Cu_7-MT[84,85]	(1AOO and 1AQR,[d] 1FMY[d])	QNEGHE**C**Q**C**Q **C**GS**C**KNNEQ**C** QKS**C**S**C**PTG**C** NSDDK**C**P**C**GN KSEETKKS**CC** SGK

---

[a]   See text for details.   [b]   Protein Data Bank ID codes are given in parenthesis (www.rcsb.org).   [c]   Only the 3D structure of the α domain.   [d]   Only the polypeptide fold.

They also evidenced an astonishing property of MTs, namely, the flexibility of the polypeptide chain and the dynamic fluctuation of the metal ions within the clusters.[120]

The 3D NMR solution structure of Cd_7-MT-1 from recombinant mouse has recently been reported.[121] It shows the same metal-to-Cys connectivities and the same structural organization of clusters as those found in Cd_7-MT-2. Therefore, all currently structurally characterized mammalian MT-1 and MT-2 containing either Zn^{II} or Cd^{II} ions[122] share common structural features. They are monomeric, dumb-bell-like shaped proteins with uniformly sized and almost spherical C-terminal α- and N-terminal β-domains. The α-domain is composed of amino acid residues 31–61 and enfolds the $M_4(SCys)_{11}$ aggregate, while the β-domain includes residues 1–30 and harbors the $M_3(SCys)_9$ cluster, both being connected by the conserved Lys30–Lys31 segment. The absence of inter-domain constraints in all the reported NMR structures of mammalian MTs has been attributed to an increased flexibility in the linker region between the two domains of MT in solution, as compared with the crystal structure of rat liver MT-2.[44] In each domain, all the metal centers are tetrahedrally coordinated to both terminal and μ_2-bridging thiolate sulfur ligands (Figure 1), the central core of the metal–sulfur aggregates being formed by two fused $M_3(\mu\text{-}S)_3$ rings (α-domain) or by one $M_3(\mu\text{-}S)_3$ ring (β-domain), whose conformation is commented on below.

Relevant information is also available on the structure of the mammalian isoform MT-3,[123] having unique functional features when compared to MT-1 and 2.[8] Solution NMR of the α-domain of Cd_7-MT-3, which consists of the amino acid residues Lys32–Gln68, has revealed a tertiary fold that is very similar to MT-1 and 2, except for the Lys52–Glu60 loop that accommodates an acidic insertion relative to these isoforms. The Cd-to-Cys connectivities proposed for this domain compare well to those in the $Cd_4(SCys)_{11}$ aggregates of the other two isoforms. With respect to the β-domain of MT-3, NMR-detectable dynamic processes have
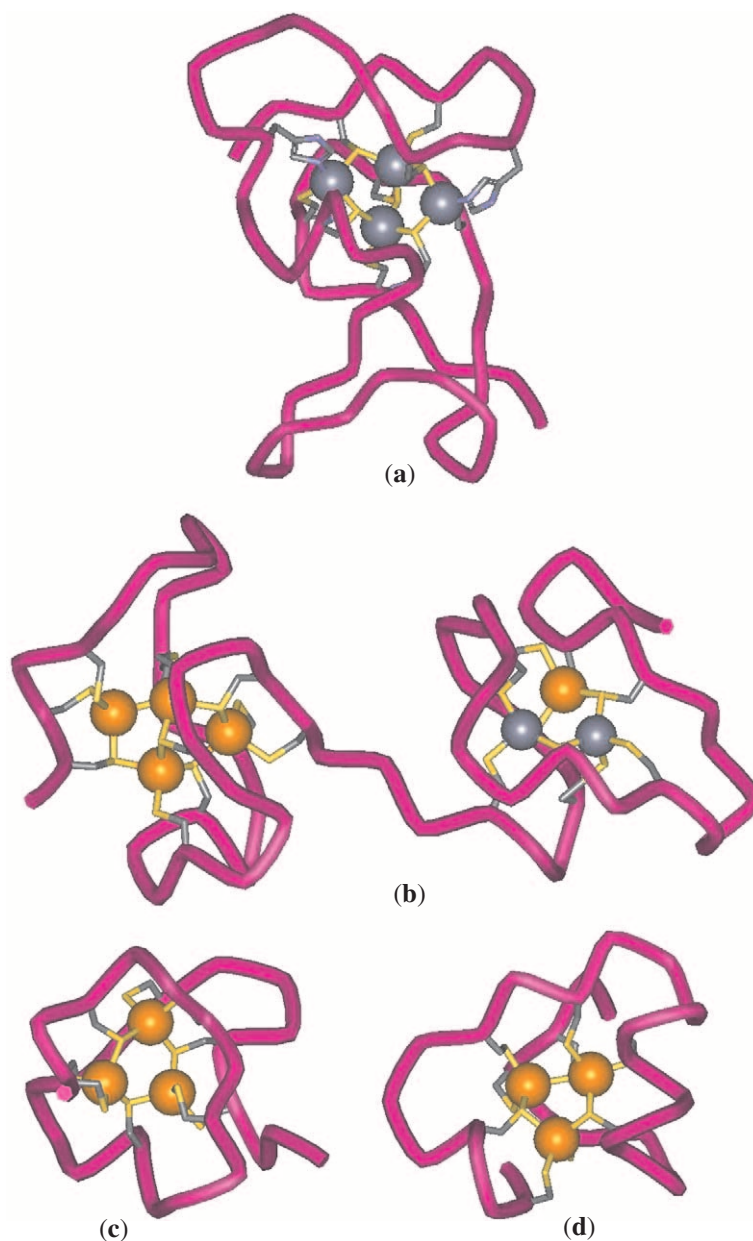
Figure 1 The three-dimensional structure of various MTs: (a) *Synechococcus* Zn_4-SmtA; (b) rat liver Cd_5,Zn_2-MT-2; (c) and (d), the isolated $Cd_3 \beta_N$ and $Cd_3 \beta_C$ domains of American lobster MTH, respectively. Zinc and cadmium ions are shown as blue and orange spheres, respectively. (Adapted from entries made to the Protein Data Bank, ID codes given in Table 2.)

hindered its structure determination. However, models calculated by homology modeling are consistent with this domain having the same backbone fold as MT-1 and 2.

Complete 3D solution structures have been determined by NMR experiments for three invertebrate Cd^{II}-MT forms, one from echinoidean and two from crustacean species. The structure of the sea urchin (*S. purpuratus*) $^{113}Cd_7$-MTA consists of two globular domains, an N-terminal $Cd_4(SCys)_{11}$ and a C-terminal $Cd_3(SCys)_9$, whose metal cluster topology compares well with the corresponding analogues in mammalian MT. Combined with this similarity, there is an inverted arrangement of the three and four metal clusters, and thus of the α and β domains, as well as a significantly different connectivity pattern for the Cys–metal coordination bonds in the two proteins.[124]

Crustacean MTs differ from the above-mentioned structures in that they only have 18 Cys residues within their sequences (Table 2). The blue crab (*C. sapidus*) $^{113}Cd_6$-MT-1, whose solution

structure determination is the first reported for MTs from a non mammalian source, has two separate domains, each containing a $Cd_3(SCys)_9$ cluster with three bridging and six terminal thiolate ligands. The metal-to-Cys stoichiometry and the $M^{II}_3(\mu\text{-}S)_3$ ring framework in both clusters compare well with those in the mammalian N-terminal β domain. In particular, the tertiary structure of crab MT-1 N-terminal β domain bears a close resemblance to the same domain in mammalian MT-2.[125] Previous studies on $^{111}Cd_6$-MT-1 from lobster (*H. americanus*), which allowed only the metal-cluster topology to be characterized, had already confirmed that the protein consists of two $Cd_3(SCys)_9$ clusters and established the corresponding Cd–SCys connectivities.[126] This information has recently been extended to the full structure determination of the two isolated chemically synthesized $^{113}Cd_3$ β domains from the same protein[102] (Figure 1).

The recent NMR structure of the bacterial MT SmtA, synthesized by the cyanobacterium *Synechococcus* PCC 7942, has provided evidence for the first metal core in MT where the Cys residues are not uniquely responsible for metal coordination.[71] In addition, the inorganic core of the $Zn_4(SCys)_9(NHis)_2$ cluster in SmtA (Figure 1) strongly resembles the $Zn_4(SCys)_{11}$ cluster of mammalian MT, despite the lack of sequence similarity and the presence of His ligands. Another interesting finding in SmtA is the topology surrounding one of the Zn sites, whose unprecedented elements of secondary structure in MTs resemble the zinc finger portions of GATA and LIM proteins.

The only reported structure for a copper metallothionein, also unique for an Ag-substituted derivative, is for yeast (*S. cerevisae*), which includes 12 Cys and 1 His out of the 53 amino acid residues. The NMR solution structure of both forms allowed determination of the backbone fold for the first 40 residues of the protein. In addition, based on the fact that only seven major Ag^I resonances were observed for the reconstituted protein, the Ag-to-Cys connectivities were derived and assumed identical for Cu-MT. Overall, it was concluded that yeast binds seven Cu^I or Ag^I ions in a single cluster, using 10 out of the 12 available Cys residues.[84,86] A recent NMR reinvestigation of Cu_7-MT from the same species has shown that a number of different arrangements of the seven copper ions is consistent with the highly refined structure of the polypeptide fold. This, together with the different coordination preferences of Cu^I and Ag^I with thiolate sulfur ligands (see below), casts doubt on the isostructurality of both metalloforms in yeast MT.[85]

Existing data on phytochelatins and related polypeptides show that they differ from MT not only in biosynthesis but also in structure. Whereas no 3D structure has yet been reported, electronic spectroscopy (c.d. and UV-Vis) and EXAFS data on Cd-γ-EC peptides led to different proposals as to the nature of the cadmium binding in such peptides, polynuclear cadmium thiolate aggregates versus isolated $Cd(SCys)_4$ units, respectively.[9] However, contrary to the conclusion of the previous work, a recent X-ray absorption spectroscopy study on Cd-γ-EC peptides and model systems provides evidence for the formation of a polynuclear cadmium cluster.[67]

8.9.1.4   Metal Thiolates as Models of the Metal–Sulfur Aggregates in Metallothioneins

Present structural and spectroscopic data on the metal coordination in MTs indicate that metal binding is almost exclusively due to the cysteinyl thiolate sulfur atoms of the peptide chain: the corresponding metal aggregates should therefore find a parallel in metal-thiolate chemistry. The only exception to this is the bacterial SmtA, in which it might be considered that two histidine residues play the role of two terminal cysteine ligands.[71] In fact, interest in the extensive family of metal thiolates has mainly been fuelled in recent decades by structural or bioinorganic objectives,[127,128] the high cysteine content in MTs serving as an important impetus.

Although binary transition metal thiolates $[M(SR)_n]$, most frequently of polymeric nature, have been long known, it is since the 1970s that significant advances have been made in the synthesis and structural chemistry of discrete thiolate complexes of general formula $[M_x(SR)_y]^z$.[127] Different synthetic approaches, such as the use of thiol ligands (RSH) including a low-coordinating solubilizing group (i.e., amine function) or sterically demanding substituents—or alternatively, of chelating dithiol ligands—have been most successful for the structural characterization of metal thiolate complexes of intermediate nuclearity ($2 \leq x \leq 14$). The investigation of mononuclear and polymeric complexes is more difficult because of the high solubility of the former and the well-known insolubility of the latter in common solvents. However, while the structural patterns found in $[M_x(SR)_y]^z$ complexes have been systematized,[127] it is still difficult to predict the stoichiometry and the stereochemistry around the metal centers in the complexes obtained at a given metal-to-thiol

molar ratio. The diverse coordination preferences of metal ions and their coexistence in the same complex species, the various ligation modes of the thiolate ligands (i.e., terminal, μ_2- or μ_3-bridging) and the possibility of secondary metal–sulfur interactions account for the main difficulties encountered in the synthesis of a particular complex. Overall, the search for synthetic models of metal–sulfur aggregates in MTs, which should facilitate knowledge of their chemical and spectroscopic features, is hampered by the inherent difficulties of metal-thiolate chemistry.

With respect to the metal–sulfur aggregates in MTs, it is remarkable that, despite the significant differences in amino acid composition and in the number and location of cysteine residues among the structurally characterized MTs (Table 2), only two basic types of Zn^{II} and/or Cd^{II} metal–sulfur aggregates have been found: $M_3(SCys)_9$ and $M_4(SCys)_{11}$. As previously indicated, the latter could also represent the $M_4(SCys)_9(NHis)_2$ cluster found in SmtA. Surprisingly, among the extensive family of homoleptic thiolate complexes, those of formula $[M_3(SR)_9]^{3-}$ and $[M_4(SR)_{11}]^{3-}$ (M = Zn or Cd) are unreported not only in the solid phase, according to the Cambridge Structural Database (CSD),[129] but also in solution.[130] On the other hand, structural information on Cu^I MTs is limited to the solution NMR studies of Cu_7-MT from yeast. As previously commented upon, these studies assumed that this metalloform was isostructural with the ^{107}Ag-substituted protein.[84,131] Overall, both issues—the lack of synthetic models for the metal(II)–sulfur aggregates in MT and the recently questioned[2,85] suitability of the ^{107}Ag isotope as a probe for the study of Cu-MTs—deserve further examination.

The steric arrangement of the Zn^{II} and/or Cd^{II} ions and bridging thiolate sulfur ligands in the $M_3(SCys)_9$ and $M_4(SCys)_{11}$ clusters of MT can be described according to the six torsion angles that define the conformation of a six-membered ring (Figure 2).[132] These values in structurally characterized MTs, obtained from Protein Data Bank (PDB) data (Table 2), show that most of the cyclohexane-like M_3S_3 rings in the $M_3(SCys)_9$ clusters have a distorted boat conformation, except for the β_N and β_C domains in lobster MTH, which show a sofa and a twist-boat conformation, respectively.[102] Moreover, the bicyclo[3.3.1]nonane-like cluster in $M_4(SCys)_{11}$ may be considered as being formed by two-fused six-membered M_3S_3 rings in twist-boat/sofa conformations (Figure 3), except for two cases where it is boat/twist-boat[71] or boat/chair.[124] This predominance of boat-type conformations in MTs contrasts with the chair-type usually found in metal thiolate complexes with simple thiolate ligands and tetrahedrally coordinated Zn or Cd.[128] Thus, a search of the CSD[129] on synthetic models of the $M_3(SCys)_9$ cluster reveals that the $M_3^{II}(\mu\text{-}S)_3$ ring is mainly found as a fragment of polynuclear metal thiolates with adamantanoid structure (19 out of 28 examples), and therefore in chair conformation. In a few complexes, the chelating nature of the thiolate ligand or the high nuclearity of the complex species accounts for the sofa or boat conformation of the fragment mentioned; overall, however, no structurally related synthetic model of the $M_3(SCys)_9$ cluster has been reported. Analogously, for the $M_4(SCys)_{11}$ cluster, most of the metal thiolate complexes (17 out of 24) contain the $M_4^{II}(\mu\text{–}S)_5$ unit as a fragment of adamantanoid structures, where the two-fused M_3S_3 rings are in chair conformations.[133,134] By extending the search to species containing the same unit but replacing the thiolate sulfur that belongs to both of the two-fused M_3S_3 rings by either a sulfide or a halide ion, complexes with the core $[M_8(\mu_4\text{-}X)(SR)_{16}]$[135–139] and $[S_4M_{10}(SPh)_{16}]^{4-}$,[140] M = Zn, Cd; X = S, halide, can be included. In all these examples, the two-fused rings show the same conformation, i.e., twist-boat/twist-boat, as opposed to the twist-boat/sofa conformations in the $M_4(SCys)_{11}$ clusters of MTs (Figure 3). Overall, the different conformational preferences shown by the $M_3^{II}S_3$ rings in the $M_3(SCys)_9$ and $M_4(SCys)_{11}$ clusters of MTs and in the inorganic metal thiolates emphasize the special role of the peptide chain enfolding the metal-thiolate cluster. Notwithstanding this, the presence of only two basic types of metal–sulfur aggregates in evolutionarily distant MTs emphasizes the functional relevance of the $M_3(SCys)_9$ and $M_4(SCys)_{11}$ structural motifs.

An analysis of the data deposited on the CSD[129] for the structurally characterized homoleptic thiolate complexes of general formula $M_x^I(SR)_y$, M = Ag or Cu, allows the following conclusions

Boat (C_{2v})	Sofa(C_s)	Chair(D_{3d})	Half-chair(C_2)	Twist boat(D_2)
(52,0,-52,52,0,-52)	(7,28,-62,62,-28,-7)	(54,-54,54,-54,54,-54)	(12,8,-47,67,-47,8)	(30,-63,30,30,-63,30)
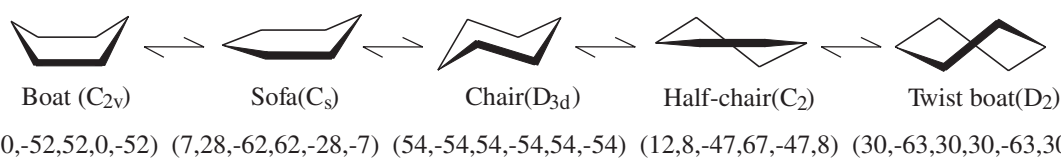
Figure 2 Interconversion between the conformational isomers of a six-membered ring with indication of the corresponding symmetry and set of torsion angles.
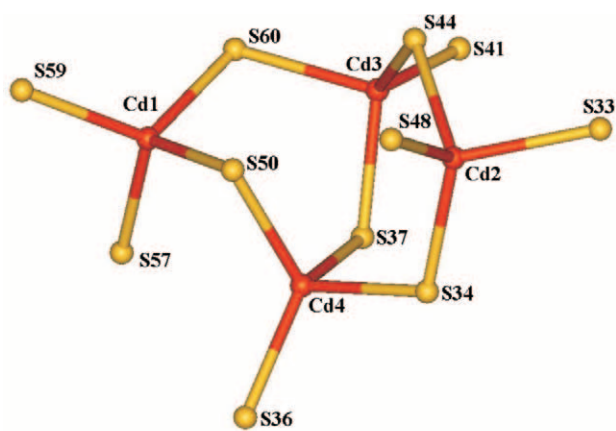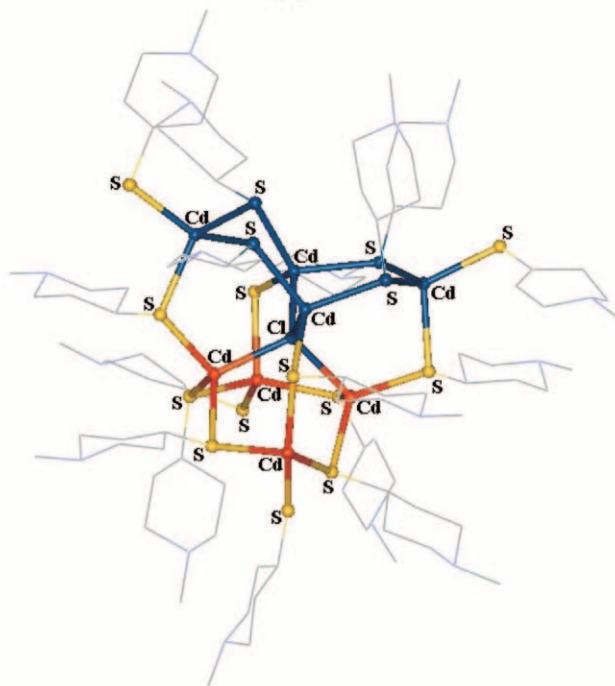
Figure 3 Comparison of: (a) the $Cd_4(SCys)_{11}$ cluster of the α domain of rat liver Cd_5,Zn_2-MT (Figure 1) with (b) a fragment (darkest shading) of the cage skeleton of the $[ClCd_8\{SCH(CH_2CH_2)_2N(H)Me\}_{16}]^{15+}$ cation.[135] The two fused Cd_3S_3 rings (see text) show twist-boat (left)/sofa (right) conformations in the $M_4(SCys)_{11}$ cluster of MT and twist-boat/twist-boat conformations in the cation.

to be drawn: (i) the number of thiolates with known structure is significantly higher for Cu than for Ag, this difference being mainly due to the high number of $Cu_4^I(SR)_6$ species; (ii) the coordination geometry around copper is exclusively trigonal in more than 50% of the complexes; in the rest it is either linear or there is coexistence of both trigonal and linear (however, there is no example of tetrahedral coordination); (iii) the coordination geometry around silver is exclusively linear in 50% of the complexes, followed by the coexistence of different combinations of linear, trigonal, and tetrahedral geometries; (iv) unlike for copper, silver thiolates show a tendency to form polymeric species[141] and secondary metal–sulfur interactions;[142] and (v) copper and silver complexes with the same thiolate ligand may have different formulae[143,144] and, even with the same formula, may show a different structure[142,145,146] as is shown in Figure 4. All these data strongly support the uncertainty surrounding the notion of Cu/Ag isomorphous replacement in MTs.
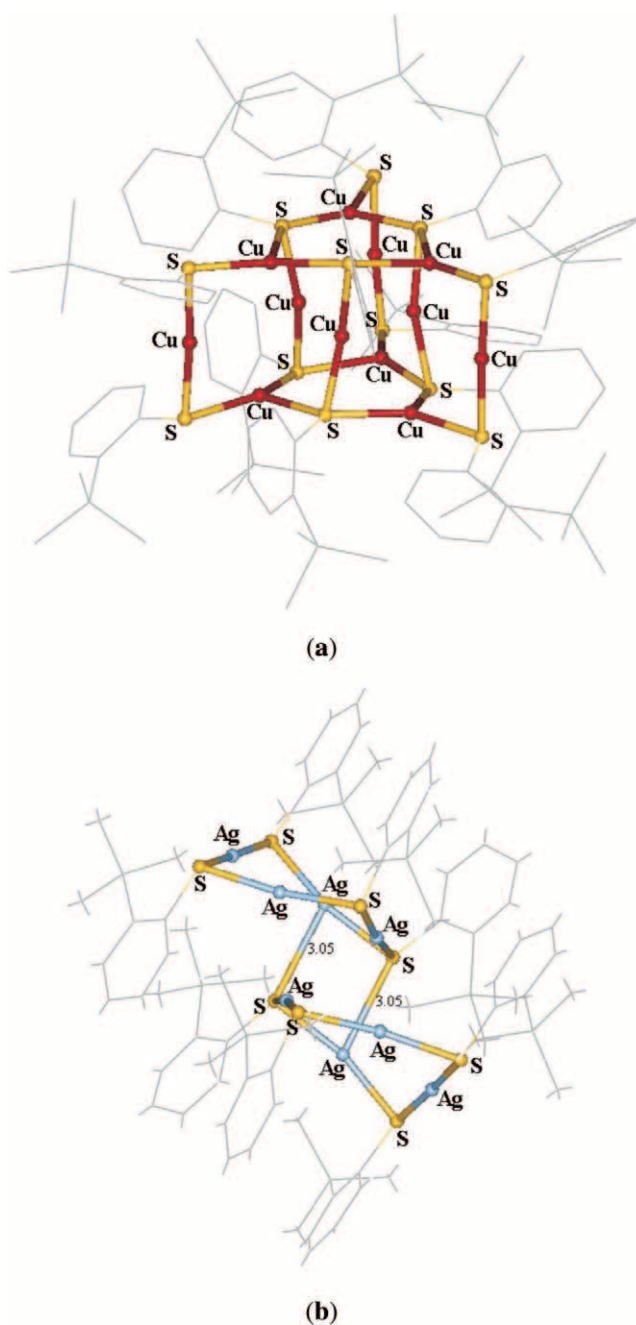
Figure 4 Comparison of copper and silver thiolate complexes of the same thiolate ligand and with the same formula unit. Perspective view of: (a) $[Cu(SC_6H_4-o-SiMe_3)]_{12}$ and (b) $[\{Ag(SC_6H_4-o-SiMe_3)\}_4]_2$, highlighting the $Cu_{12}S_{12}$ core and the fusing of two Ag_4S_4 units via $Ag\cdots S$ secondary interactions (3.05 Å).[142]

8.9.1.5 Dynamic Aspects and Reactivity

As research continues to seek out the physiological functions of MTs, their unusual dynamic properties acquire greater significance.[2,44,123] These were evidenced from 2D NMR[117] and crystallographic[119] studies on mammalian M^{II}_7-MT-2, where the calculated root-mean-square deviation (rmsd) values and the B-factors, respectively, showed a significant degree of dynamic structural disorder. Present data on MTs from different sources indicate that they are flexible molecules undergoing structural fluctuations within the metal clusters, as well as involving the polypeptide loops between the cysteine residues of the protein chain. Detailed analysis of the structural

flexibility and reactivity of MTs[2] and the study of the dynamics of interdomain and intermolecular interactions in mammalian MT have recently been reported.[44]

Structural non rigidity is often manifested in the M_xS_y cores of $[M_x(SR)_y]^z$ aggregates.[127] The degree of mechanical flexibility in these $[M_x(SR)_y]^z$ species is inversely related to the connectivity, i.e., the number of framework M—S bonds, and increases with the size of the $M_n(SR)_n$ rings that constitute the aggregate. As a result, inherently floppy $[M_x(SR)_y]^z$ complexes give rise to configurational isomers (those which can be distinguished in terms of the relative orientation of bonds)[147] as has been crystallographically observed for the $[M_5^I(SR)_6]^z$ complexes with M = Cu ($z = -1$),[148] and Ag ($z = 2$)[149] (Figure 5). Furthermore, in the case of metal thiolate complexes with an adamantane-like cluster structure, a mechanism for the intramolecular interconversion of terminal and bridging thiolate ligands has been proposed.[150] In addition to these dynamic features, the group 12 metal thiolates in solution show kinetic lability and (consequently) continuous breaking and re-forming of the metal–sulfur bonds.[65] By extending these features of metal thiolate complexes to MTs, it could be concluded that both the high structural flexibility and the kinetic lability of the M_xS_y cores in the $[M_x(SCys)_y]$ aggregates should substantially contribute to the dynamic properties of the entire protein. In other words, it seems likely that the metal-thiolate nature of the metal clusters in MTs is not only responsible for the unusual dynamic features of their metal cores when compared to other metalloproteins, but also for the mobility of the peptide chain, whose folding is essentially determined by the binding of the cysteine residues to the metal centers.

In all the mammalian MT structures characterized to date, the amino-terminal β-domains have been found to be more flexible than the carboxy-terminal α-domains.[123] Similarly, the structure of the backbone in the β-domain of the sea urchin MTA is less rigid than its α counterpart.[124] This enhanced flexibility of the β-domain in mammalian MT and in MTA is consistent with the predictions operating in $[M_x(SR)_y]^z$ species,[127] where a greater degree of mechanical flexibility should be expected for an M_3S_3 fragment consisting of six core atoms, six bonds, and one $M_3(SR)_3$ cycle than that for M_4S_5 with nine core atoms, ten bonds, and two-fused $M_3(SR)_3$ cycles. However, the strikingly different flexibility encountered in the β-domain of mammalian MTs (MT-3 $\gg$ MT-2 > MT-1),[123] the different kinetic stability of the two β-domains in lobster MTH[15] and the enhanced flexibility of cold-adapted MT as compared to mouse MT[151] reveal—among other examples—the special role of the peptide chain in tuning the chemical and structural features of the metal–sulfur aggregates.

MTs are unusually reactive metalloproteins, in which the high thermodynamic stability of the metal–sulfur bonds is coupled to a high kinetic lability. The latter accounts for the easy exchange of metal ions within the metal clusters, with metal ions in solution and also with
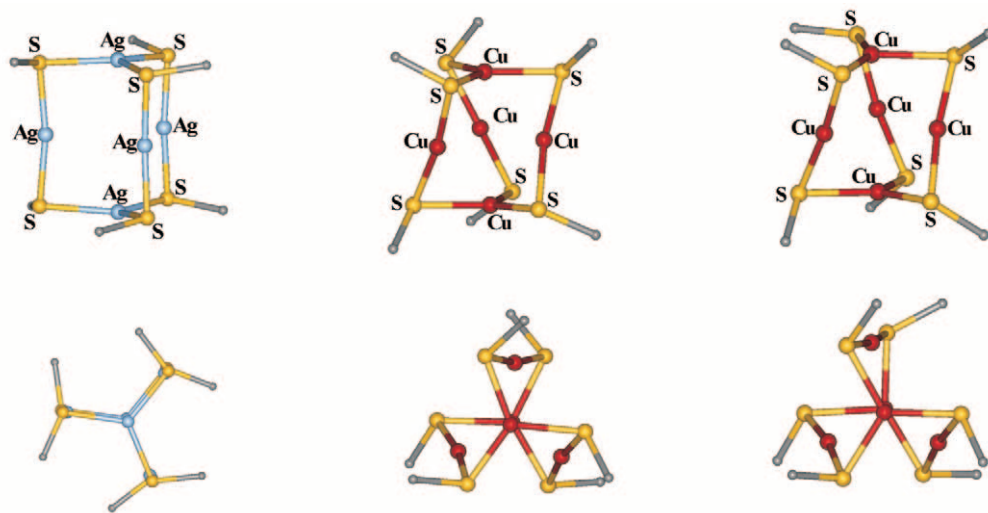
Figure 5 Perspective view of the metal–sulfur core in $[M_5(SR)_6]^z$ complexes: (a) $[Ag_5\{\mu\text{-}S(CH_2)_3\text{-}NHMe_2\}_3\{\mu\text{-}S(CH_2)_3NMe_2\}_3](ClO_4)_2$,[149] (b) $(Et_4N)[Cu_5(\mu\text{-}SBu^t)_6]$ and (c) $(Et_3NH)[Cu_5(\mu\text{-}SBu^t)_6]$,[148] and corresponding views along the M_{trig}–M_{trig} axis, showing the nonrigidity of the M_5S_6 cages. Carbon atoms are shown as gray spheres.

metal ions in clusters of other MT molecules.[2,44,65] The thermodynamic stability dictates the affinity of the metal ions for the binding sites as well as the order of their replacement in MTs, which is consistent with that found for inorganic thiolates: $Hg^{II} > Ag^{I} \sim Cu^{I} > Cd^{II} > Zn^{II}$.[2] In addition to the metal binding and exchange processes, the removal of the metal ions in MTs by competing ligands has also been analyzed with the aim of elucidating the interactions of MTs with cellular components and the role of Zn-MT as an intracellular metal donor.[152,153] In this context, i.e., the putative cellular chemistry of MTs, the metal transfer between MTs and enzymes,[154,155] and the nucleophilic reactivity of the coordinated cysteines toward electrophiles, including alkylating and oxidizing agents[153] and radical species,[156–162] are the object of intense study. In summary, current experimental data show that both the inherent kinetic lability of the metal thiolates and the nucleophilicity of the thiolate sulfur account for the chemical reactivity of the MTs. The influence of the peptide chain on the control and modulation of such properties is probably essential for the still undisclosed functional roles of these unique metalloproteins.

8.9.2 REFERENCES

1. Margoshes, M.; Vallee, B. L. *J. Am. Chem. Soc.* **1957**, *79*, 4813–4814.
2. Romero-Isart, N.; Vašák, M. *J. Inorg. Biochem.* **2002**, *88*, 388–396.
3. Kägi, J. H. R.; Nordberg, M., Eds. *Metallothionein I*; Experientia Suppl.; Birkhäuser Verlag: Basel, 1979; Vol. 34.
4. Kägi, J. H. R.; Kojima, Y., Eds. *Metallothionein II*; Experientia Suppl.; Birkhäuser Verlag: Basel, 1987; Vol. 52.
5. Suzuki, K. T.; Imura, N.; Kimura, M., Eds. *Metallothionein III. Biological roles and medical implications*; Birkhäuser Verlag: Basel, 1993.
6. Klaasen, C. D, Ed. *Metallothionein IV*; Birkhäuser Verlag: Basel, 1999.
7. Riordan, J. F.; Vallee, B. L., Eds. *Methods in Enzymology*; Academic Press: San Diego, 1991; Vol. 205.
8. Vašák, M.; Hasler, D. W. *Curr. Opin. Chem. Biol.* **2000**, *4*, 177–183.
9. Vašák, M.; Kägi, J. H. R. Metallothioneins. In *Encyclopedia of Inorganic Chemistry*; Bruce King, R., Ed., Wiley: Chichester, UK, 1994; Vol. 4, pp 2229–2241.
10. Stillman, M. J. *Coord. Chem. Rev.* **1995**, *144*, 461–511.
11. Stillman, M. J.; Shaw III, C. F.; Suzuki, K. T., Eds. *Metallothioneins*; VCH: New York, 1992.
12. Coyle, P.; Philcox, J. C.; Carey, L. C.; Rofe, A. M. *Cell. Mol. Life Sci.* **2002**, *59*, 627–647.
13. Kull, F. J.; Reed, M. F.; Elgren, T. E.; Ciardelli, T. L.; Wilcox, D. E. *J. Am. Chem. Soc.* **1990**, *112*, 2291–2298.
14. Nishiyama, Y.; Nakayama, S.; Okada, Y.; Min, K.-S.; Onosaka, S.; Tanaka, K. *Chem. Pharm. Bull.* **1990**, *38*, 2112–2117.
15. Muñoz, A.; Petering, D. H.; Shaw III, C. F. *Inorg. Chem.* **2000**, *39*, 6114–6123.
16. Okada, Y.; Ohta, N.; Iguchi, S.; Tsuda, Y.; Sasaki, H.; Kitagawa, T.; Yagyu, M.; Min, K.-S.; Onosaka, S.; Tanaka, K. *Chem. Pharm. Bull.* **1986**, *34*, 986–998.
17. Hartmann, H.-J.; Li, Y.-J.; Weser, U. *Biometals* **1992**, *5*, 187–191.
18. Li, Y.-J.; Weser, U. *Inorg. Chem.* **1992**, *31*, 5526–5533.
19. Sewell, A. K.; Jensen, L. T.; Erickson, J. C.; Palmiter, R. D.; Winge, D. R. *Biochemistry* **1995**, *34*, 4740–4747.
20. Okada, Y.; Tanaka, K.; Sawada, J.; Kikuchi, Y. Synthetic Metallothioneins. In *Metallothioneins*; Stillman, M. J.; Shaw III, C. F.; Suzuki, K. T., Eds.; VCH: New York, 1992, Chapter 9, pp 195–225.
21. Pan, P. K.; Zheng, Z. F.; Lyu, P. C.; Huang, P. C. *Eur. J. Biochem.* **1999**, *266*, 33–39.
22. Morooka, Y.; Nagaoka, T. *Appl. Environ. Microb.* **1987**, *53*, 204–207.
23. Hou, T. M.; Kim, R.; Kim, S. H. *Biochim. Biophys. Acta* **1988**, *951*, 230–234.
24. Berka, T.; Shatzman, A.; Zimmerman, J.; Strickler, J.; Rosenberg, M. *J. Bacteriol.* **1988**, *170*, 21–26.
25. Valls, M.; Bofill, R.; Romero-Isart, N.; González-Duarte, R.; Abián, J.; Carrascal, M.; González-Duarte, P.; Capdevila, M.; Atrian, S. *FEBS Lett.* **2000**, *467*, 189–194.
26. Valls, M.; Bofill, R.; González-Duarte, R.; González-Duarte, P.; Capdevila, M.; Atrian, S. *J. Biol. Chem.* **2001**, *276*, 32835–32843.
27. Shi, J.; Lindsay, W. P.; Huckle, J. W.; Morby, A. P.; Robinson, N. J. *FEBS Lett.* **1992**, *303*, 159–163.
28. Wang, Y.; Mackay, E. A.; Kurasaki, M.; Kägi, J. H. R. *Eur. J. Biochem.* **1994**, *225*, 449–457.
29. Erickson, J. C.; Sewell, A. K.; Jensen, L. T.; Winge, D. R.; Palmiter, R. D. *Brain Res.* **1994**, *649*, 297–304.
30. You, C.; Mackay, E. A.; Gehrig, P. M.; Hunziker, P. E.; Kägi, J. H. R. *Arch. Biochem. Biophys.* **1999**, *372*, 44–52.
31. Stürzenbaum, S. R.; Winters, C.; Galay, M.; Morgan, A. J.; Kille, P. *J. Biol. Chem.* **2001**, *276*, 34013–34018.
32. Cols, N.; Romero-Isart, N.; Bofill, R.; Capdevila, M.; González-Duarte, P.; González-Duarte, R.; Atrian, S. *Prot. Eng.* **1999**, *12*, 265–269.
33. Bofill, R.; Capdevila, M.; Cols, N.; Atrian, S.; González-Duarte, P. *J. Biol. Inorg. Chem.* **2001**, *6*, 408–417.
34. Capdevila, M.; Cols, N.; Romero-Isart, N.; Gonzàlez-Duarte, R.; Atrian, S.; Gonzàlez-Duarte, P. *Cell. Mol. Life Sci.* **1997**, *53*, 681–688.
35. Kurasaki, M.; Emoto, T.; Linde Arias, A. R.; Okabe, M.; Yamasaki, F.; Oikawa, S.; Kojima, Y. *Prot. Eng.* **1996**, *9*, 1173–1180.
36. Kurasaki, M.; Yamaguchi, R.; Linde Arias, A. R.; Okabe, M.; Kojima, Y. *Prot. Eng.* **1997**, *10*, 413–416.
37. Thrower, A. R.; Byrd, J.; Tarbet, E. B.; Mehra, R. K.; Hamer, D. H.; Winge, D. R. *J. Biol. Chem.* **1988**, *263*, 7037–7042.
38. Chernaik, M. L.; Huang, P. C. *Proc. Natl. Acad. Sci. USA* **1991**, *88*, 3024–3028.
39. Emoto, T.; Kurasaki, M.; Oikawa, S.; Suzuki-Kurasaki, M.; Okabe, M.; Yamasaki, F.; Kojima, Y. *Biochem. Genet.* **1996**, *34*, 239–251.
40. Pan, P. K.; Hou, F.; Cody, C. W.; Huang, P. C. *Biochem. Biophys. Res. Commun.* **1994**, *202*, 621–628.

41. Romero-Isart, N.; Cols, N.; Termansen, M. K.; Gelpi, J. L.; González-Duarte, R.; Atrian, S.; Capdevila M.; González-Duarte, P. *Eur. J. Biochem.* **1999**, *259*, 519–527.
42. Fowler, B. A.; Hildebrand, C. E.; Kojima, Y.; Webb, M. Nomenclature of Metallothionein. In *Metallothionein II*; Kägi, J. H. R.; Kojima, Y., Eds.; Experientia Suppl.; Birkhäuser Verlag: Basel, 1987; Vol. 52, pp 19–22.
43. Klaassen, C. D.; Liu, J.; Choudhuri, S. *Annu. Rev. Pharmacol. Toxicol.* **1999**, *39*, 267–294.
44. Zangger, K.; Armitage, I. M. *J. Inorg. Biochem.* **2002**, *88*, 135–143.
45. Cousins, R. J. *Physiol. Rev.* **1985**, *65*, 238–309.
46. Bremner, I. Nutritional and Physiological Significance of Metallothionein. In *Metallothionein II*; Kägi, J. H. R.; Kojima, Y, Eds.; Experientia Suppl., Birkhäuser Verlag: Basel, 1987; Vol. 52, pp 81–107.
47. Sato, M.; Bremner, I. *Free Radic. Biol. Med.* **1993**, *14*, 325–337.
48. Kang, Y. J. *Proc. Soc. Exp. Biol. Med.* **1999**, *222*, 263–273.
49. Hidalgo, J.; Aschner, M.; Zatta, P.; Vašák, M. *Brain Res. Bull.* **2001**, *55*, 133–145.
50. Maret, W.; Vallee, B. L. *Proc. Natl. Acad. Sci. USA* **1998**, *95*, 3478–3482.
51. Beattie, J. H.; Wood, A. M.; Newman, A. M.; Bremner, I.; Choo, K. H.; Michalska, A. E.; Duncan, J. S.; Trayhurn, P. *Proc. Natl. Acad. Sci. USA* **1998**, 358–363.
52. Maret, W.; Heffron, G.; Hill, H. A.; Djuricic, D.; Jiang, L. J.; Vallee, B. L. *Biochemistry* **2002**, *41*, 1689–1694.
53. Zangger, K.; Öz, G.; Armitage, I. M. *J. Biol. Chem.* **2000**, *275*, 7534–7538.
54. Dallinger, R.; Berger, B.; Hunziker, P.; Kägi, J. H. R. *Nature* **1997**, *338*, 237–238.
55. Bongers, J.; Walton, C. D.; Richardson, D. E.; Bell, J. U. *Anal. Chem.* **1988**, *60*, 2683–2686.
56. Vašák, M.; Kägi, J. H. R.; Hill, H. A. O. *Biochemistry* **1981**, *20*, 2852–2856.
57. Willner, H.; Vašák, M.; Kägi, J. H. R. *J. Chem. Soc., Chem. Commun.* **1987**, *26*, 6287–6292.
58. Schäffer, A. Absorption, Circular Dichroism, and Magnetic Circular Dichroism Spectroscopy of Metallothionein. In *Methods in Enzymology*, Riordan, J. F.; Vallee, B. L., Eds.; Academic Press: San Diego, 1991; Vol. 205, pp 529–540.
59. Jensen, L. T.; Peltier, J. M.; Winge, D. R. *J. Biol. Inorg. Chem.* **1998**, 3, 627–631.
60. Polec, K.; Palacios, O.; Capdevila, M.; González-Duarte, P.; Lobinski, R. Talanta **2002**, *57*, 1011–1017.
61. Hathout, Y.; Reynolds, K. J.; Szilagyi, Z.; Fenselau, C. *J. Inorg. Biochem.* **2002**, *88*, 119–122.
62. Gehrig, P. M.; You, C.; Dallinger, R.; Gruber, C.; Brouwer, M.; Kägi, J. H. R.; Hunziker, P. E. *Protein Science* **2000**, *9*, 395–402.
63. Yu, X.; Wojciechowski, M.; Fenselau, C. *Anal. Chem.* **1993**, *65*, 1355–1359.
64. Zaia, J.; Fabris, D.; Wei, D.; Karpel, R. L.; Fenselau, C. *Protein Science* **1998**, *7*, 2398–2404.
65. Kägi, J. H. R. Overview of Metallothionein. In *Methods in Enzymology*; Riordan, J. F.; Vallee, B. L., Eds.; Academic Press: San Diego, 1991, Vol. 205, pp 613–626.
66. Clark-Baldwin, K.; Tierney, D. L.; Govindaswamy, N.; Gruff, E. S.; Kim, C.; Berg, J.; Koch, S. A.; Penner-Hahn, J. E. *J. Am. Chem. Soc.* **1998**, *120*, 8401–8409.
67. Pickering, I. J.; Prince, R. C.; George, G. N.; Rauser, W. E.; Wickramasinghe, W. A.; Watson, A. A.; Dameron, C. T.; Dance, I. G.; Fairlie, D. P.; Salt, D. E. *Biochim. Biophys. Acta* **1999**, *1429*, 351–364.
68. Winge, D. R. Copper Coordination in Metallothionein. In *Methods in Enzymology*; Riordan, J. F.; Vallee, B. L., Eds.; Academic Press: San Diego, 1991; Vol. 205, pp 458–469.
69. Bogumil, R.; Faller, P.; Binz, P.-A.; Vašák, M.; Charnock, J. M.; Garner, D. *Eur. J. Biochem.* **1998**, *255*, 172–177.
70. Nielson, K. B.; Atkin, C. L.; Winge, D. R. *J. Biol. Chem.* **1985**, *260*, 5342–5350.
71. Blindauer, C. A.; Harrison, M. D.; Parkinson, J. A.; Robinson, A. K.; Cavet, J. S.; Robinson, N. J.; Sadler, P. J. *Proc. Natl. Acad. Sci. USA* **2001**, *98*, 9593–9598.
72. Beltramini, M.; Lerch, K. *Environ. Health Perspect.* **1986**, *65*, 21–27.
73. Lerch, K. *Nature* **1980**, *284*, 368–370.
74. Beltramini, M.; Lerch, K.; Vašák, M. *Biochemistry* **1984**, *23*, 3422–3427.
75. Dallinger, R.; Wang, Y.; Berger, B.; Mackay, E. A.; Kägi, J. H. R. *Eur. J. Biochem.* **2001**, *268*, 4126–4133.
76. Münger, K.; Lerch, K. *Biochemistry* **1985**, *24*, 6751–6756.
77. Raspor, B.; Pavicic, J. *Fresenius J. Anal. Chem.* **1996**, *354*, 529–534.
78. Prinz, R.; Weser, U. *Hoppe-Seyler's Z. Physiol. Chem.* **1975**, *356*, 767–776.
79. Sayers, Z.; Brouillon, P.; Svergun, D. I.; Zielenkiewicz, P.; Koch, M. H. J. *Eur. J. Biochem.* **1999**, *262*, 858–865.
80. Weser, U.; Hartman, H.-J.; Fretzdorff, A.; Strobel, G.-J. *Biochim. Biophys. Acta* **1977**, *493*, 465–477.
81. Winge, D. R.; Nielson, K. B.; Gray, W. R.; Hamer, D. H. *J. Biol. Chem.* **1985**, *260*, 14464–14469.
82. Sayers, Z.; Brouillon, P.; Vorgias, C. E.; Nolting, H. F.; Hermes, C.; Koch, M. H. J. *Eur. J. Biochem.* **1993**, *212*, 521–528.
83. Byrd, J.; Berger, R. M.; McMillin, D. R.; Wright, C. F.; Hammer, D.; Winge, D. R. *J. Biol. Chem.* **1988**, *263*, 6688–6694.
84. Peterson, C. W.; Narula, S. S.; Armitage, I. M. *FEBS Lett.* **1996**, *379*, 85–93.
85. Bertini, I.; Hartman, H.-J.; Klein, T.; Liu, G.; Luchinat, C.; Weser, U. *Eur. J. Biochem.* **2000**, *267*, 1008–1018.
86. Narula, S. S.; Winge, D. R.; Armitage, I. M. *Biochemistry* **1993**, *32*, 6773–6787.
87. Bordas, J.; Koch, M. H. J.; Hartmann, H.-J.; Weser, U. *FEBS Lett.* **1982**, *140*, 19–21.
88. Ding, X.-Q.; Bill, E.; Trautwein, A. X.; Hartmann, H. J.; Weser, U. *Eur. J. Biochem.* **1994**, *223*, 841–845.
89. Jensen, L. T.; Howard, W. R.; Strain, J. J.; Winge, D. R.; Culotta, V.C. *J. Biol. Chem.* **1996**, *271*, 18514–18519.
90. Roesijadi, G.; Kielland, S.; Klerks, P. *Arch. Biochem. Biophys.* **1989**, *273*, 403–413.
91. Mehra, R. K.; Garey, J. R.; Butt, T. R.; Gray, W. R.; Winge, D. R. *J. Biol. Chem.* **1989**, *264*, 19747–19753.
92. Hensbergen, P. J.; van Velzen, M. J. M.; Nugroho, R. A.; Donker, M. H.; van Straalen, N. M. *Comp. Biochem. Physiol. C* **2000**, *125*, 17–24.
93. Kille, P.; Winge, D. R.; Harwood, J. L.; Kay, J. *FEBS Lett* **1991**, *295*, 171–175.
94. Tommey, A. M.; Shi, J.; Lindsay, W. P.; Urwin, P. E.; Robinson, N. J. *FEBS Lett.* **1991**, *292*, 48–52.
95. Rauser, W. E. The Cd-Binding Protein from Tomato Compared to Those of Other Vascular Plants. In *Metallothionein II*; Kägi, J. H. R., Kojima, Y., Eds.; Experientia Suppl.; Birkhäuser Verlag: Basel, 1987; Vol. 52, pp 301–308.
96. Morris, C. A.; Nicolaus, B.; Sampson, V.; Harwood, J. L.; Kille, P. *Biochem. J.* **1999**, *338*, 553–560.
97. Wang, Y.; Hess, D.; Hunzinker, P. E.; Kägi, J. H. R. *Eur. J. Biochem.* **1996**, *241*, 835–839.

98. Robinson, N. J.; Tommey, A. M.; Kuske, C.; Jackson, P. J. *Biochem. J.* **1993**, *295*, 1–10.
99. Foley, R. C.; Liang, Z. M.; Singh, K. B. *Plant Mol. Biol.* **1997**, *33*, 583–591.
100. Bernhard, W. R.; Kägi, J. H. R. Purification and Characterization of Atypical Cadmium-Binding Polypeptides from ZeaMays. In *Metallothionein II*; Kägi, J. H. R., Kojima, Y., Eds.; Experientia Suppl.; Birkhäuser Verlag: Basel, 1987; Vol. 52, pp 309–315.
101. Zhu, Z.; Goodrich, M.; Isab, A. A.; Shaw III, C. F. *Inorg. Chem.* **1992**, *31*, 1662–1667.
102. Muñoz, A.; Försterling, F. H.; Shaw III, C. F.; Petering, D. H. *J. Biol. Inorg. Chem.* **2002**, *7*, 713–724.
103. Chou, C. L.; Guy, R. D.; Uthe, J. F. *Sci. Total Environ.* **1991**, *105*, 41–59.
104. Murphy, A.; Zhou, J.; Golsbrough, P. B.; Taiz, L. *Plant Physiol.* **1997**, *113*, 1293–1301.
105. Overnell, J.; Good, M.; Vašák, M. *Eur. J. Biochem.* **1988**, *172*, 171–177.
106. Piccinni, E.; Staudenmann, W.; Albergoni, V.; de Gabrieli, R.; James, P. *Eur. J. Biochem.* **1994**, *226*, 853–859.
107. Santovito, G.; Irato, P.; Palermo, S.; Boldrin, F.; Sack, R.; Hunziker, P.; Piccinni, E. *Protist* **2001**, *152*, 219–229.
108. Otvos, J. D.; Olafson, R. W.; Armitage, I. M. *J. Biol. Chem.* **1982**, *257*, 2427–2431.
109. Law, A. C. Y.; Cherian, M. G.; Stillman, M. J. *Biochim. Biophys. Acta* **1984**, *784*, 53–61.
110. D'Auria, S.; Carginale, V.; Scudiero, R.; Crescenzi, O.; di Maro, D.; Temussi, P. A.; Parisi, E.; Capasso, C. *Biochem. J.* **2001**, *354*, 291–299.
111. Gruber, C.; Stürzenbaum, S.; Gehrig, P.; Sack, R.; Hunziker, P.; Berger, B.; Dallinger, R. *Eur. J. Biochem.* **2000**, *267*, 573–582.
112. Rupp, H.; Voelter, W.; Weser, U. *Hoppe-Seyler's Z. Physiol. Chem.* **1975**, *356*, 755–765.
113. Vallee, B. L.; Maret, W. The Functional Potential and Potential Functions of Metallothioneins: A Personal Perspective. In *Metallothionein III. Biological roles and medical implications*; Suzuki, K. T.; Imura, N.; Kimura, M., Eds.; Birkhäuser Verlag: Basel, 1993, pp 1–9.
114. Otvos, J. D.; Armitage, I. M. *Proc. Natl. Acad. Sci. USA* **1980**, *77*, 7094–7098.
115. Otvos, J. D.; Engeseth, H. R.; Wehrli, S. *Biochemistry* **1985**, *24*, 6735–6739.
116. Arseniev, A.; Schultze, P.; Wörgötter, E.; Braun, W.; Wagner, G.; Vašák, M.; Kägi, J. H. R.; Wüthrich, K. *J. Mol. Biol.* **1988**, *201*, 637–657.
117. Schultze, P.; Wörgötter, E.; Braun, W.; Wagner, G.; Vašák, M.; Kägi, J. H. R.; Wüthrich, K. *J. Mol. Biol.* **1988**, *203*, 251–268.
118. Messerle, B. A.; Schäffer, A.; Vašák, M.; Kägi, J. H. R.; Wüthrich, K. *J. Mol. Biol.* **1990**, *214*, 765–779.
119. Robbins, A. H.; McRee, D. E.; Williamson, M.; Collett, S. A.; Xuong, N. H.; Furey, W. F.; Wang, B. C.; Stout, C. D. *J. Mol. Biol.* **1991**, *221*, 1269–1293.
120. Braun, W.; Vašák, M.; Robbins, A. H.; Stout, C. D.; Wagner, G.; Kägi, J. H. R.; Wüthrich, K. *Proc. Natl. Acad. Sci. USA* **1992**, *89*, 10124–10128.
121. Zangger, K.; Öz, G.; Otvos, J. D.; Armitage, I. M. *Protein Sci.* **1999**, *8*, 2630–2638.
122. Messerle, B. A.; Schäffer, A.; Vašák, M.; Kägi, J. H. R.; Wüthrich, K. *J. Mol. Biol.* **1992**, *225*, 433–443.
123. Öz, G.; Zangger, K; Armitage, I. M. *Biochemistry* **2001**, *40*, 11433–11441.
124. Riek, R.; Prêcheur, B.; Wang, Y.; Mackay, E. A.; Wider, G.; Güntert, P.; Liu, A.; Kägi, J. H. R.; Wüthrich, K. *J. Mol. Biol.* **1999**, *291*, 417–428.
125. Narula, S. S.; Brouwer, M.; Hua, Y.; Armitage, I. M. *Biochemistry* **1995**, *34*, 620–631.
126. Zhu, Z.; DeRose, E. F.; Mullen, G. P.; Petering, D. H.; Shaw III, C. F. *Biochemistry* **1994**, *33*, 8858–8865.
127. Dance, I. G. *Polyhedron* **1986**, *5*, 1037–1104.
128. Dance, I. G.; Fisher, K.; Lee, G. Metal–Thiolate Compounds. In *Metallothioneins*; Stillman, M. J.; Shaw III, C. F.; Suzuki, K. T. Eds.; VCH: New York, 1992, Chapter 13, pp 284–345.
129. Allen, F. H.; Kennard, O. *Chem. Des. Autom. News* **1993**, *8*, 31–37.
130. González-Duarte, P.; Vives, J. *Inorg. Chem.* **1989**, *28*, 25–30.
131. Narula, S. S.; Mehra, R. K.; Winge, D. R.; Armitage, I. M. *J. Am. Chem. Soc.* **1991**, *113*, 9354–9358.
132. Dale, J. *Stereochemistry and Conformational Analysis*; Verlag Chemie: New York, 1978, Chapter 5, pp 147–153.
133. Dean, P. A. W.; Vittal, J. J. Adamantane-like Cages. In *Metallothioneins*; Stillman, M. J.; Shaw III, C. F.; Suzuki, K. T., Eds.; VCH: New York, 1992, Chapter 14, , pp 346–386.
134. Vittal, J. J. *Polyhedron* **1996**, *15*, 1585–1642.
135. González-Duarte, P.; Clegg, W.; Casals, I.; Sola, J.; Rius, J. *J. Am. Chem. Soc.* **1998**, *120*, 1260–1266.
136. Dance, I. G. *Aust. J. Chem.* **1985**, *38*, 1391–1411.
137. Guo, S.; Ding, E.; Chen, H.; Yin, Y.; Li, X. *Polyhedron* **1999**, *18*, 735–740.
138. Burth, R.; Gelinsky, M.; Vahrenkamp, H. *Inorg. Chem.* **1998**, *37*, 2833–2836.
139. Ka-Luo, T.; Xiang-Lin, J.; Shao-Juan, J.; You-Qi, T. *Chin. J. Struct. Chem.* **1995**, *14*, 399–404.
140. Lee, G. S. H.; Fisher, K. J.; Craig, D. C.; Scudder, M. L.; Dance, I. G. *J. Am. Chem. Soc.* **1990**, *112*, 6435–6437.
141. Casals, I.; González-Duarte, P.; Sola, J.; Vives, J.; Font-Bardia, M.; Solans, X. *Polyhedron* **1990**, *9*, 769–771.
142. Block, E.; Gernon, M.; Kang, H.; Ofori-Okai, G.; Zubieta, J. *Inorg. Chem.* **1989**, *28*, 1263–1271.
143. Tang, K.; Aslam, M.; Block, E.; Nicholson, T.; Zubieta, J. *Inorg. Chem.* **1987**, *26*, 1488–1497.
144. Ka-Luo, T.; Qingchuan, Y.; Jianping, Y.; You-Qi, T. *Acta Sci. Nat. Univ. Pek.* **1988**, *24*, 398–403.
145. Tang, K.; Yang, J.; Yang, Q.; Tang, J. *J. Chem. Soc., Dalton Trans.* **1989**, 2297–2302.
146. Schroter-Schmid, I.; Strähle, J. *Z. Naturforsch., Teil B* **1990**, *45*, 1537–1542.
147. Harrowfield, J. M.; Wild, S. B. Isomerism in Coordination Chemistry. In *Comprehensive Coordination Chemistry*, 1st ed.; Wilkinson, G., Gillard, R. D., McCleverty, J. A., Eds.; Pergamon Press: New York, 1987; Vol. 1, pp 179–208.
148. Bowmaker, G. A.; Clark, G. R.; Seadon, J. K.; Dance, I. G. *Polyhedron* **1984**, *3*, 535–544.
149. González-Duarte, P.; Sola, J.; Vives, J.; Solans, X. *J. Chem. Soc., Chem. Commun.* **1987**, 1641–1642.
150. Hagen, K. S.; Stephan, D. W.; Holm, R. H. *Inorg. Chem.* **1982**, *21*, 3928–3936.
151. Capasso, C.; Abugo, O.; Tanfani, F.; Scire, A.; Carginale, V.; Scudiero, R.; Parisi, E.; D'Auria, S. *Proteins* **2002**, *46*, 259–267.
152. Petering, D. H.; Krezoski, S.; Chen, P.; Pattanaik, A.; Shaw III, C. F. Kinetic Reactivity of Metallothionein. In *Metallothioneins*; Stillman, M. J.; Shaw III, C. F.; Suzuki, K. T., Eds.; VCH: New York, 1992, Chapter 7, pp 164–185.
153. Shaw III, C. F.; Savas, M. M.; Petering, D. H. Ligand Substitution and Sulfhydryl Reactivity of Metallothionein. In *Methods in Enzymology*; Riordan, J. F., Vallee, B. L., Eds.; Academic Press: San Diego, 1991; Vol. 205, pp 401–419.

154. Jacob, C.; Maret, W.; Vallee, B. L. *Proc. Natl. Acad. Sci. USA* **1998**, *95*, 3489–3494.
155. Maret, W.; Jacob, C.; Vallee, B. L.; Fisher, E. H. *Proc. Natl. Acad. Sci. USA* **1999**, *96*, 1936–1940.
156. Thornalley, P. J.; Vašák, M. *Biochim. Biophys. Acta* **1985**, *827*, 36–44.
157. Felix, K; Lengfelder, E.; Hartmann, H.-J.; Weser, U. *Biochim. Biophys. Acta* **1993**, *1203*, 104–108.
158. Kröncke, K.-D.; Fehsel, K.; Schmidt, T.; Zenke, F. T.; Dasting, I.; Wesener, J. R.; Bettermann, H.; Breuing, K. D.; Kolb-Bachofen, V. *Biochem. Biophys. Res. Commun.* **1994**, *200*, 1105–1110.
159. Aravindakumar, C. T.; Ceulemans, J.; de Ley, M. *Biochem. J.* **1999**, *344*, 253–258.
160. Hartmann, H.-J.; Weser, U. *Biometals* **2000**, *13*, 153–156.
161. Montoliu, C.; Monfort, P.; Carrasco, J.; Palacios, O.; Capdevila, M.; Hidalgo, J.; Felipo, V. *J. Neurochem.* **2000**, *75*, 266–273.
162. Warthen, C. R.; Hammes, B. S.; Carrano, C. J.; Crans, D. C. *J. Biol. Inorg. Chem.* **2001**, *6*, 82–90.

8.10
Dioxygen-binding Proteins

D. M. KURTZ, JR.
University of Georgia, Athens, GA, USA

8.10.1   INTRODUCTION

8.10.1.1   The Functions of Dioxygen-binding Proteins

Dioxygen-binding proteins can be defined as those capable of undergoing the reversible reaction (1), and for which the equilibrium lies far to the right at ambient temperatures and partial pressures of O_2:

$$\text{Protein} + O_2 \rightleftharpoons [\text{Protein} - O_2] \tag{1}$$

These proteins are classically described as either O_2 carriers or O_2 storage reservoirs. The physiological function implied by these descriptors stems from the fact that both vertebrates and invertebrates derive most of their energy by "combustion" of organic compounds, and thus require large amounts of O_2. Given the surface-to-volume ratio of most higher organisms, simple diffusion of O_2 across body surfaces at ambient partial pressures would result in internal O_2 concentrations that are insufficient to sustain life. Furthermore, in response to various stresses, certain tissues or organs require a rapid infusion of O_2, for which passive diffusion would be insufficient. The existence of O_2-carrying proteins and their presence in large concentrations (approaching 20 mM for hemoglobin in red blood cells[1]) in higher organisms is thus rationalized. All known O_2-carrying proteins contain either iron or copper at their active sites; therefore, some relevant chemical properties of O_2 and transition metal ions are first summarized.

8.10.1.2   Some Properties of Dioxygen and its Reaction with Transition Metal Ions

8.10.1.2.1   Redox properties of dioxygen species

The standard reduction potentials for interconversions between various dioxygen species in aqueous solution at pH 7 are shown in Figure 1. Although molecular oxygen has the capacity to be quite reactive thermodynamically, it is quite sluggish in its reactions with most organic molecules. The sluggish reactivity is due to the triplet ground state of O_2, which is spin-forbidden from reacting with spin singlet molecules. The stability of the spin triplet state of O_2 is rooted in the degeneracy of the highest occupied molecular orbitals (HOMOs), which are π^*_{2p} in character, as shown in Figure 2. The spin singlet state of O_2, while very reactive with organic molecules, can be obtained only with a large input of energy.[2]

8.10.1.2.2   Types of $M-O_2$ complexes and frontier orbital interactions

Many, if not most, transition metal ions form dioxygen complexes, although examples of reversibility are rarer.[3–9] The three most common coordination geometries of dioxygen in synthetic transition metal complexes are shown in Figure 3A, and the orbital overlaps involved are shown in Figure 3B. The interactions with the π^* HOMOs on O_2 provide a low-energy pathway for overcoming the spin restrictions to reactivity and, thus, the kinetic inertness of O_2. While O_2 has a thermodynamic propensity to accept two or more electrons, it is not readily oxidized under ambient conditions in aqueous solution. These redox propensities of O_2, coupled with the
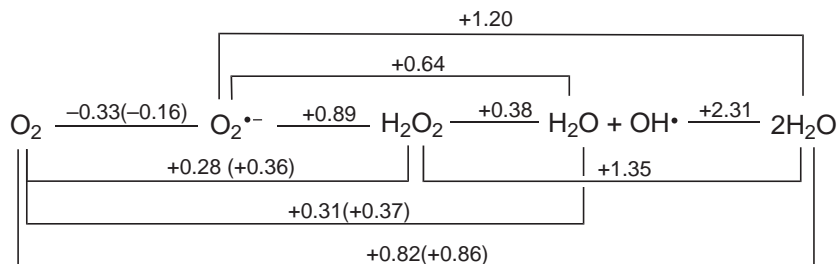
Figure 1   Standard reduction potentials (in volts) of dioxygen species in water at pH 7. Formal potentials are listed at 1 atm or (in parenthesis) at unit activity (redrawn from ref. 2).

	(a)	**(b)**	**(c)**
O_2 oxidation state:	O_2	O_2^-	O_2^{2-}
O—O bond order:	2	1.5	1
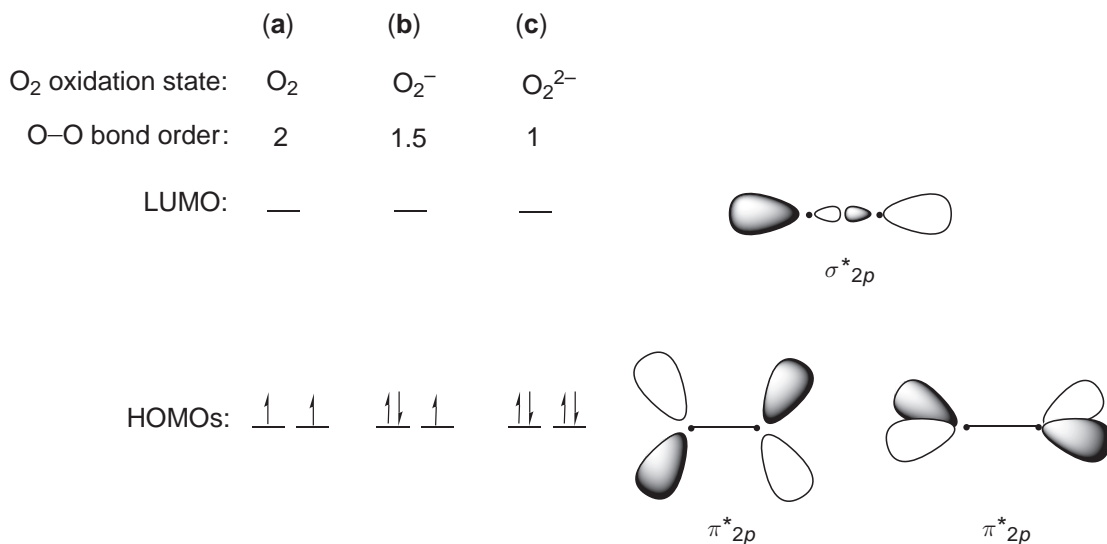
Figure 2 HOMOs and LUMO of the dioxygen molecule and its one- and two-electron reduced forms: (a) dioxygen; (b) superoxide; (c) peroxide. Shapes of the HOMOs and LUMO are shown to the right of the π^* and σ^* energy levels, respectively, with the O—O bond axis (defined as the z-axis) oriented horizontally.

multiple, readily accessible oxidation states of many transition metal ions, usually result in net transfer of electron density from metal ion to dioxygen upon complex formation. As shown in Figures 2 and 3B, this electron transfer occurs into effectively antibonding orbitals on O_2, which lowers the O—O bond order. The weaker bond is manifested in lower O—O stretching frequencies and longer O—O distances in metal–dioxygen adducts compared to molecular oxygen (cf. Table 1). The comparisons to stretching frequencies of superoxide and hydrogen peroxide show that most metal–dioxygen complexes can be classified as either superoxo or peroxo. The reduction potentials in Figure 1 show that two-electron reduction of dioxygen is thermodynamically more favorable than one-electron reduction, and, in fact, metal–peroxo complexes are more common than metal–superoxo. In order for O_2-binding to be reversible, however, the extent of electron transfer from metal ion to dioxygen must be delicately balanced, i.e., enough to form a stable complex, but not so much that the O—O bond is irreversibly cleaved.

Iron and copper are the only metals known to occur at the active sites of O_2-carrying proteins. This natural selection could not necessarily have been predicted from studies of synthetic complexes. Although synthetic iron and copper complexes that reversibly bind O_2 are known, synthetic cobalt complexes that reversibly bind O_2 have also been known for many years,[5] but have no known biological counterpart. One rationale for nature's selection of iron and copper over other transition metals for reversible O_2-binding is that the large concentrations of O_2-binding proteins necessary for life in higher organisms can be attained only by using metals with relatively high bioavailabilities, such as copper and particularly iron.

8.10.2 THE O_2-CARRYING PROTEINS

Three general types of O_2-carrying or -storage proteins are known: hemoglobin (Hb)/myoglobin (Mb), which contains a non-covalently attached heme, hemerythrin (Hr)/myohemerythrin (myoHr), which contains a non-heme di-iron site held to the protein via ligands furnished by

Table 1 O—O stretching frequencies and bond lengths of dioxygen and its metal complexes.

	νO—O (cm^{-1})	O—O bond length (Å)
Dioxygen	1,555	1.21
Metal-superoxo	1,100–1,150	1.24–1.31
Metal-peroxo	800–900	1.35–1.5
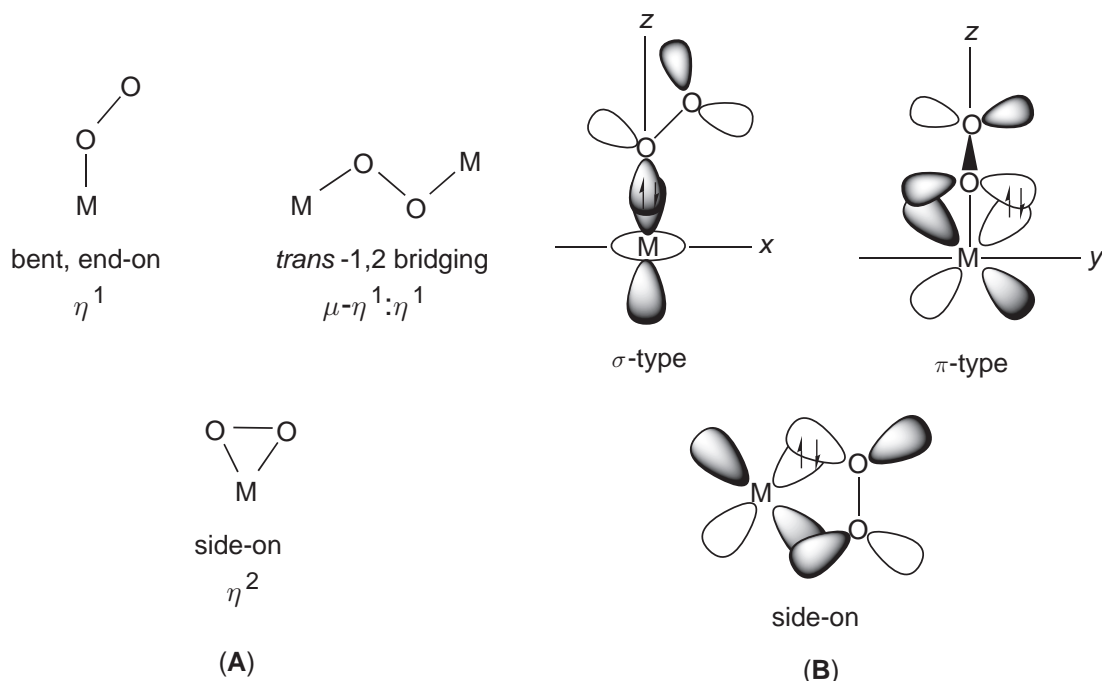
Figure 3 (A) The most commonly encountered dioxygen coordination modes. (B) Frontier molecular orbitals involved in metal–dioxygen bonding. The overlaps labeled σ-type and π-type correspond to both the η^1 and μ-η^1:η^1 coordination modes, and that labeled side-on to the η^2 coordination mode, respectively, in (A).

amino acid side chains, and hemocyanin (Hc) which contains a dicopper site, once again attached to the protein via amino acid side chain ligands. Fairly high resolution X-ray crystal structures are now available for all three types of O_2-carrying proteins in both their oxy and deoxy forms. The three types of O_2-carrying proteins bear no readily detectable structural similarities to each other at either subunit-fold or active-site levels.[10] Furthermore, there is no detectable amino acid sequence homology among the three types. Nature has, thus, apparently found three distinct solutions to the problem of binding O_2 reversibly.

8.10.2.1 Heme Type: Myoglobins and Hemoglobins

8.10.2.1.1 Early history and scope

Hb and Mb are among the most revered icons in bioinorganic chemistry. They were the first two proteins for which X-ray crystal structures were obtained.[11,12] Their well-established and thoroughly studied function of reversible O_2 binding and transport are familiar to most inorganic chemists. The literature on Hb and Mb is truly voluminous. The reader is, therefore, referred to leading references[1,13–15] for historical background and fundamental properties of Hb and Mb. An attempt is made here to present aspects that have been of interest to bio-inorganic chemists.

8.10.2.1.2 Properties of heme and iron-porphyrins

Since the active sites of all known Mbs and Hbs contain a non-covalently bound heme at their active sites, some relevant chemistry of this prosthetic group is first summarized. Several monographs and reviews are available on various aspects of heme and iron-porphyrin chemistry and spectroscopy.[16–18] Heme is an iron chelate of the tetrapyrrole macrocycle, protoporphyrin IX. The structure of heme is shown in Figure 4. In some invertebrate Hbs one of the vinyl substituents is replaced by a formyl group.[19] The heme ring is approximately planar and highly conjugated. Electronic transitions between π and π^* levels give heme a characteristic and intense absorption spectrum (and blood its intense color), which are sensitive to the iron oxidation and
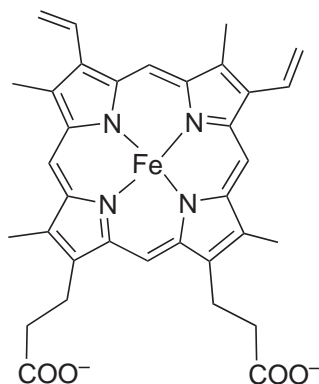
Figure 4 Schematic structure of the heme group (iron protoporphyrin IX) found at the active site of Mbs and Hbs.

spin state, and to exogenous axial ligands. Except in the most non-coordinating solvents or extreme steric hindrance, either one or two exogenous axial ligands occupy coordination positions approximately perpendicular to the heme plane. The planar geometry and the size of the iron binding cavity results in a fairly strong ligand field exerted by the four pyrrole nitrogen ligands to the iron. Both Fe^{II} or Fe^{III} oxidation states of heme are readily accessible under a variety of conditions.

Isolated Fe^{II}-heme readily reacts with O_2. However, under ambient conditions the reaction of Fe^{II}-heme or synthetic Fe^{II}-porphyrins is not the reversible one analogous to reaction (1), but rather the irreversible reaction (2), resulting in formation of the so-called μ-oxo dimer:

$$4[Fe^{II}-heme] + O_2 \longrightarrow 2[heme-Fe^{III}-O^{2-}-Fe^{III}-heme] \tag{2}$$
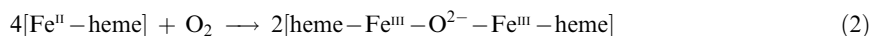
An obvious way to prevent reaction (2) is to keep two heme/porphyrin irons from closely approaching each other. Outside of a protein, this separation and reversible O_2-binding to heme was first accomplished more than 50 years ago using a polystyrene matrix derivatized with an imidazole to provide an axial heme ligand.[20] It was subsequently shown that an unhindered Fe^{II}-porphyrin could undergo reversible binding of O_2 in solution, but only at temperatures much below ambient, in order to slow reaction (2), and only in the presence of an "axial base," i.e., ligands such as imidazole or pyridine.[21] Reversible O_2-binding to Fe^{II}-porphyrins at room temperature was achieved by attaching bulky groups to the periphery of the macrocycle, thereby sterically hindering reaction (2). Numerous such derivatives have been described,[17,18] perhaps the most famous of which is the "picket-fence" porphyrin,[22] in which steric hindrance was achieved by attaching pivalamide groups to the phenyl rings of tetraphenyl-porphyrin. This fame is due not only to the remarkable synthetic achievement but also because a structure of the O_2 adduct, shown in Figure 5, was obtained. This structure anticipated the now well-established bent, end-on Fe−O−O geometry of dioxygen bound to Hb and Mb several years before sufficiently high-resolution crystal structures of oxyMb or oxyHb were obtained.

8.10.2.1.3 Distribution and general features of myoglobins and hemoglobins

In all vertebrates and many invertebrates, Hb circulates through the body within red blood cells, whereas Mb occurs within muscle tissues. Many invertebrates also contain tissue and/or extra-cellular Hbs which appear to serve mainly as either O_2 storage reservoirs or O_2 scavengers.[15] Plants also contain Hbs, typically referred to as leghemoglobins, because they occur most often in the roots of legumes, where they apparently regulate O_2 levels during N_2 fixation.[23] Bacterial Hbs have also been described, but their function is currently obscure.[24] All known Hbs and Mbs contain a common tertiary structure, which is illustrated in Figure 6 for sperm whale Mb, the paradigm for heme O_2-carrying proteins.[25] The 17-kilodalton (kDa) polypeptide of sperm whale Mb surrounds the heme in a characteristic "globin fold". This fold contains eight helical regions of secondary structure, typically identified as helices A through H from N- to C-terminus. Mammalian Hb is tetrameric ($\alpha_2\beta_2$), and each subunit is structurally and functionally very similar
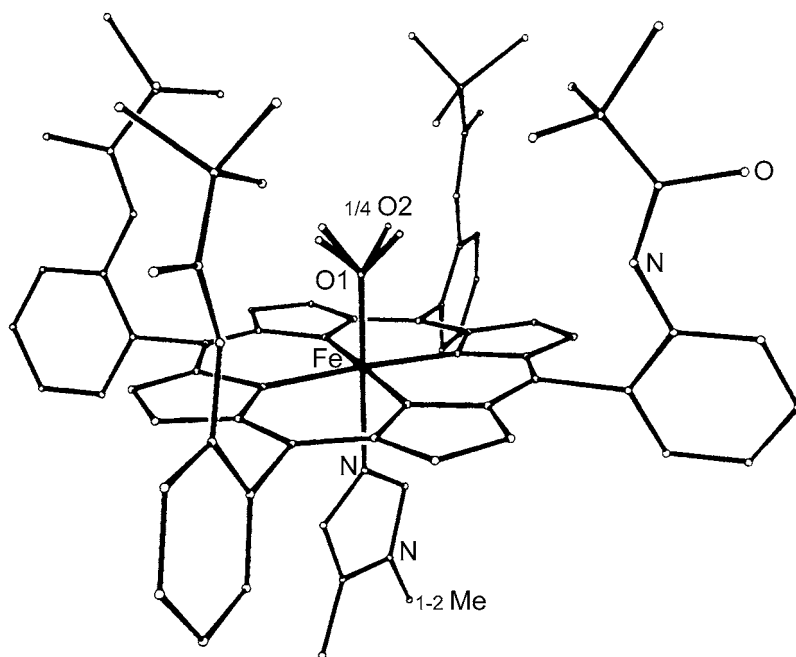
Figure 5 Structure of the O_2 adduct of the Fe^{II} picket fence porphryin/1−methylimidazole complex.[22]
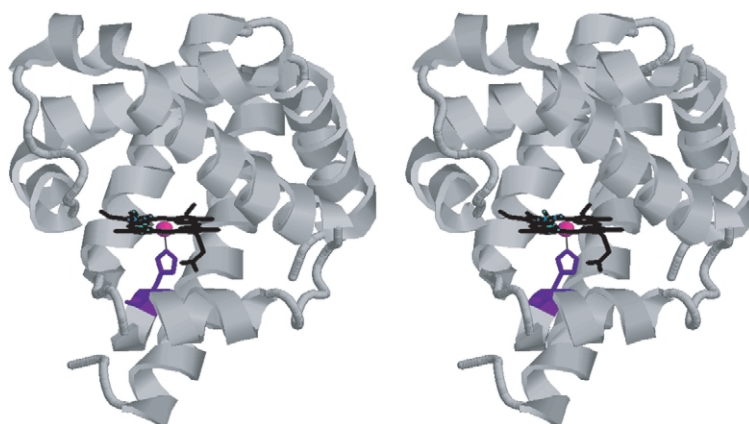
Figure 6 Stereo view of the tertiary structure of sperm whale deoxyMb. The polypeptide chain is traced as a ribbon structure and the heme group is shown in wireframe representation with iron represented as a purple sphere. The proximal histidine ligand is shown in blue wireframe. Structure was drawn using RASMOL[27] and coordinates from 1BZP[28] deposited in the Protein Data Bank.

to the monomeric Mb. Some invertebrate Hbs consist of large oligomers of the basic subunit structure with molecular masses exceeding 3×10^6 kDa.[15,26] Although the heme is non-covalently attached, it does not readily dissociate from the globin under ambient, non-denaturing conditions. This tight binding is due, in part, to the iron-axial ligand bond. All known Hbs and Mbs provide a fifth, axial nitrogen ligand from a histidine residue, referred to as the "proximal" histidine, in both deoxy and oxy forms (shown below the hemes in Figures 6 and 7). The sixth coordination position *trans* to the proximal histidine is unoccupied in the deoxygenated (deoxy) form, i.e., the Fe^{II} heme iron is five-coordinate, as illustrated in Figure 6.

The X-ray crystal structures of the active sites of sperm whale oxyMb and an invertebrate oxyHb are shown in Figure 7. As anticipated from the "picket-fence" model, O_2 binds to the active sites in a bent, end-on fashion *trans* to the proximal histidine. A comparison of the structures in Figures 5 and 7 shows that the torsional disorder of the Fe−O−O unit around the Fe—O bond axis in the picket-fence porphyrin O_2 adduct is quenched in Mb/Hb, apparently by hydrogen bonding interactions with residues lining the O_2-binding pocket—the so-called "distal"
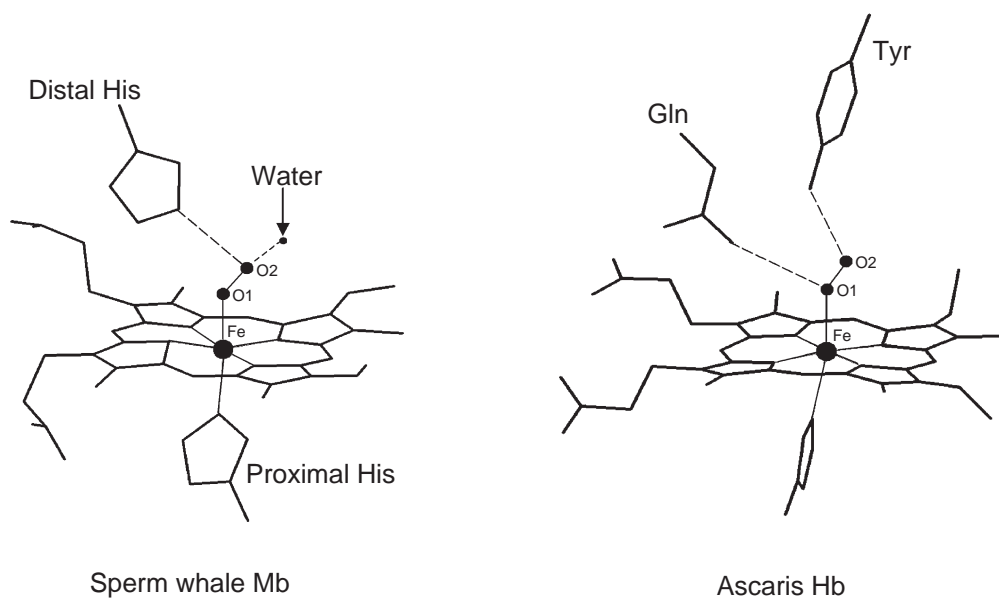
Figure 7 Wireframe representations of the X-ray crystal structures of the active sites of the oxy forms of sperm whale Mb[25] and Hb from the nematode, *Ascaris suum*.[29] Proximal His ligands are at bottom (with epsilon nitrogen coordinated to iron) and distal pockets are at top. Fe, O1, O2, and water label the heme iron, bound O_2 atoms, and pocket water, respectively, represented as spheres. Dashed lines represent hydrogen bonding interactions. Drawings were generated using RASMOL[27] and coordinates from 1MBO and 1ASH deposited in the Protein Data Bank.

pocket, above the heme. In mammalian Mbs and Hbs, the Nε of a conserved "distal" histidine serves as a hydrogen bond donor to the O2 (and perhaps also the O1) atom of the bound O_2. In some invertebrate Hbs, side chains of other residues in the distal pocket, such as a tyrosine and glutamine (shown in Figure 7, right), can replace histidine as hydrogen bond donors to the bound O_2. As discussed further below, these distal pocket interactions have been established to be a primary modulator of O_2 affinities among various Mb/Hbs.

All Mbs/Hbs proteins undergo the reversible O_2-binding reaction (1), and the equilibrium constants for this reaction are often expressed as $P_{1/2}$ or P_{50}, which represents the O_2 partial pressure in torr at which the O_2-binding sites are half-saturated. These values are inversely proportional to the O_2 dissociation constant; thus, a lower P_{50} value indicates a higher O_2 affinity. P_{50} values for Mbs/Hbs typically range between 1 and 10 torr, but values spanning the range of 0.01–100 torr have been reported.[15] The P_{50} value for sperm whale Mb ($\sim$0.65 torr) at neutral pH and room temperature corresponds to a dissociation constant for reaction (1) of $\sim$1 μM. The molecular source(s) of the 10^4-fold range of O_2 affinities among various Mb/Hbs are the subject of seemingly endless investigation and debate in the literature. A popular approach has been to measure the O_2-binding properties of engineered amino acid variants of Mb/Hb and to explain any alterations in these properties compared to the wild type in terms of structural alterations of the protein and/or the O_2-binding site. Indeed, atomic coordinates for well over 100 crystal structures of sperm whale Mb and its engineered amino acid variants in various oxidation and ligation states have been deposited in the Protein Data Bank. While the distal pocket interactions discussed above have clearly emerged as modulators of O_2 affinity in Mb/Hb from these studies, other features that potentially modulate the binding of O_2 and of other diatomic gases remain matters of contention. Both established and contentious features of gaseous diatomic ligand binding to Mb/Hb are described below.

8.10.2.1.4 The heme iron–dioxygen bond

Pauling and Coryell's classic magnetic susceptibility measurements[30] showed that, while deoxyHb is paramagnetic, oxyHb is diamagnetic, consistent with spin pairing of all iron and O_2 electrons. This result initiated controversies about both the geometry of and electronic distribution within the Fe$-O_2$ unit in oxyMb/Hb. The history of these controversies, including unsubstantiated

challenges to Pauling and Coryell's magnetic measurements on oxyHb, has been summarized elsewhere.[17,31] Weiss and Pauling proposed what turned out to be the correct $Fe-O_2$ geometry for oxyHb in 1964.[32,33] This question was not settled unambiguously, however, until the early 1980s by X-ray crystallography of oxyMb, which clearly showed that O_2 binds to the heme iron in a bent, end-on fashion, as illustrated in Figure 7. The reported $Fe-O-O$ angles are within the range of 115–160°,[25,28,34] with the highest-resolution structures tending towards the lower end of the range, as expected for end-on σ-type bonding of O_2 (cf. Figure 3).

Pauling and Coryell's measured magnetic moment, $\mu_{eff} = 5.5$/heme, for deoxyHb[30] is consistent with the spin only magnetic moment expected for the four unpaired d-electrons of high-spin Fe^{II} in an octahedral ligand field. The high-spin ferrous description of deoxyHb/Mb is supported by a wealth of spectroscopic and chemical evidence that has accumulated since the original magnetic measurements. The structural results on sperm whale Mb show that, upon conversion of the deoxy to the oxy form, the iron atom moves 0.3–0.5 Å closer to the mean plane through all the atoms of the porphyrin ring, and the iron–proximal histidine bond shortens slightly.[28] These structural changes are consistent with a decrease in the radius of the iron ion upon conversion of the deoxy to the oxy forms, and has been interpreted to indicate a change from high- to low-spin state of the iron, and/or oxidation of Fe^{II} in the deoxy forms to a higher formal oxidation state in the oxy forms. If the iron remains Fe^{II} in the oxy forms, the high- to low-spin conversion would result in its six d-electrons becoming completely spin paired. The pair of electrons in the filled π^* orbital of an effectively spin-singlet O_2 could then be donated to the dz^2 orbital on iron, as shown in Figure 3 (σ-type), in order to explain the observed diamagnetism. Back donation of d-electrons on iron into the other π^* orbital of O_2, as shown in Figure 3 (π-type), could also occur, leading to $Fe^{II}-O_2 \longleftrightarrow Fe^{IV}-O_2^{2-}$ resonance structures. Alternatively, if, upon O_2-binding, the high-to-low spin conversion of iron were accompanied by one electron transfer to the coordinated O_2, the resulting low-spin Fe^{III} would have one unpaired d-electron. This d-electron could be spin-paired with the remaining unpaired electron on the coordinated O_2^- via the π-type orbital overlaps shown in Figure 3, thereby achieving diamagnetism. These alternative descriptions both suggest some transfer of electron density from Fe^{II} to the coordinated O_2, which has been supported by subsequent studies.

Apart from the unusual temperature dependence of the ^{57}Fe Mössbauer quadrupole splitting,[35] which can be rationalized on the basis of heme/protein conformational dynamics, the diamagnetism of oxyMb/Hb originally reported by Pauling and Coryell in 1936 has held up to scrutiny remarkably well. The reported $O-O$ distances of bound O_2 in oxyHb and oxyMb range from 1.2 to 1.3 Å,[25,28,34] including the most recently reported oxyMb structure, which was solved at nearly atomic (1.0 Å) resolution.[28] When compared with those listed in Table 1, the $O-O$ distance seen in the oxyMb/Hb crystal structures is consistent with either a dioxygen or superoxide formalism for the bound O_2. Evidence favoring the superoxide formalism comes from vibrational spectroscopy, which gives $O-O$ stretching frequencies of the bound O_2 in the range 1,100–1,160 cm^{-1} for a variety of oxyMb/Hbs.[36–38] As can be seen from Table 1, this frequency range corresponds very closely to that for metal–superoxo complexes, and is well separated from the $O-O$ stretching frequencies of either O_2 or O_2^{2-}. Computational studies on oxyheme models indicate some partial negative charge on the bound O_2, consistent with the hydrogen bonding interactions shown in Figure 7.[39,40] A polar $Fe^{\delta+}-O_2^{\delta-}$ unit in oxyMb/Hb seems beyond dispute, and many bioinorganic chemists regard low-spin $Fe^{III}-O_2^-$ as the most accurate and useful representation of the electronic distribution. One should, nevertheless, keep in mind that the ferric–superoxo formalism represents only an approximation of the true electronic distribution.

8.10.2.1.5 Mechanism of dioxygen binding

As might be expected given its functional and physiological importance, the mechanism of O_2-binding to deoxyMb/Hb is among the most thoroughly scrutinized in biology. Historical reviews of the development of the kinetics methodology and the mechanism of O_2-binding are available.[13,41,42] The rate constants, k_{off}, for O_2 dissociation from deoxyMb/Hbs are typically measured by stopped-flow spectrophotometry, following mixing with an O_2 scavenging solution, while the association rate constants, k_{on}, for O_2-binding to deoxyMb/Hb are typically measured either by temperature-jump or laser flash photolysis. The intense and distinctive heme absorptions of the oxy- and deoxyMb/Hbs facilitate the flash photolysis experiments and also monitoring of reaction progress. For deoxyMb/Hbs from various vertebrates and invertebrates under ambient conditions,

the second-order rate constant for O_2 association, k_{on}, exhibits a range of $0.1–100 \times 10^6\,M^{-1}s^{-1}$, whereas the first-order rate constant, k_{off}, for O_2 dissociation exhibits a wider range: $10^{-3}–10^3\,s^{-1}$.[1,15,43] Typically, the ratio k_{on}/k_{off} is found to be in reasonably good agreement with the independently measured equilibrium association constants; that is, the measured k_{on} and k_{off} accurately reflect those for the equilibrium, reaction (1). Based on such kinetics data and crystal structures of numerous wild-type and engineered amino acid variants of sperm whale Mb,[1] the current understanding of the general mechanism of O_2 binding to mammalian Mbs has been summarized by Olson and Phillips,[44] as shown in Figure 8.

The mechanism is divided into four steps with five species, A through E. The intermediates B, C, and D are difficult to stabilize or trap and, therefore, their precise structures are less well established. The four steps leading from deoxy- to oxyMb consist of: (i) loss of a hydrogen-bonded water from the distal pocket; (ii) diffusion of O_2 through the protein matrix into the distal pocket, where the O—O axis is thought to be essentially parallel to the heme plane due to steric restrictions; (iii) formation of the heme Fe—O_2 bond and the associated movements of iron and proximal histidine ligand towards the heme plane; and (iv) formation of a hydrogen bond between the bound O_2 and distal histidine.

The hydrogen bond between the bound O_2 and distal histidine in oxyMb (structure E in Figure 8) was confirmed by neutron diffraction.[45] The pathway(s) of exchange of O_2 between the heme pocket and solvent remains a matter of contention.[42] The two sets of antiparallel arrows in the schematic structure of intermediate C in Figure 8 are meant to indicate two proposed pathways. One route leading directly to solvent requires only that the HisE7 side chain rotate away from the heme; the other hypothesis is that O_2 diffuses to and from the distal pocket by multiple hydrophobic pathways consisting of interconnected fluctuating and permanent cavities within the protein matrix. A collection of diffusive pathways is consistent with the observed rate constants for O_2-binding ($\sim 10^7\,M^{-1}s^{-1}$), the fluxional timescales of proteins in solution,[46,47] a library of randomly substituted amino acid variants of Mb that showed altered O_2-binding kinetics,[48] and cavities within the Mb protein matrix that can be occupied by xenon[49,50] and perhaps dioxygen.[28]
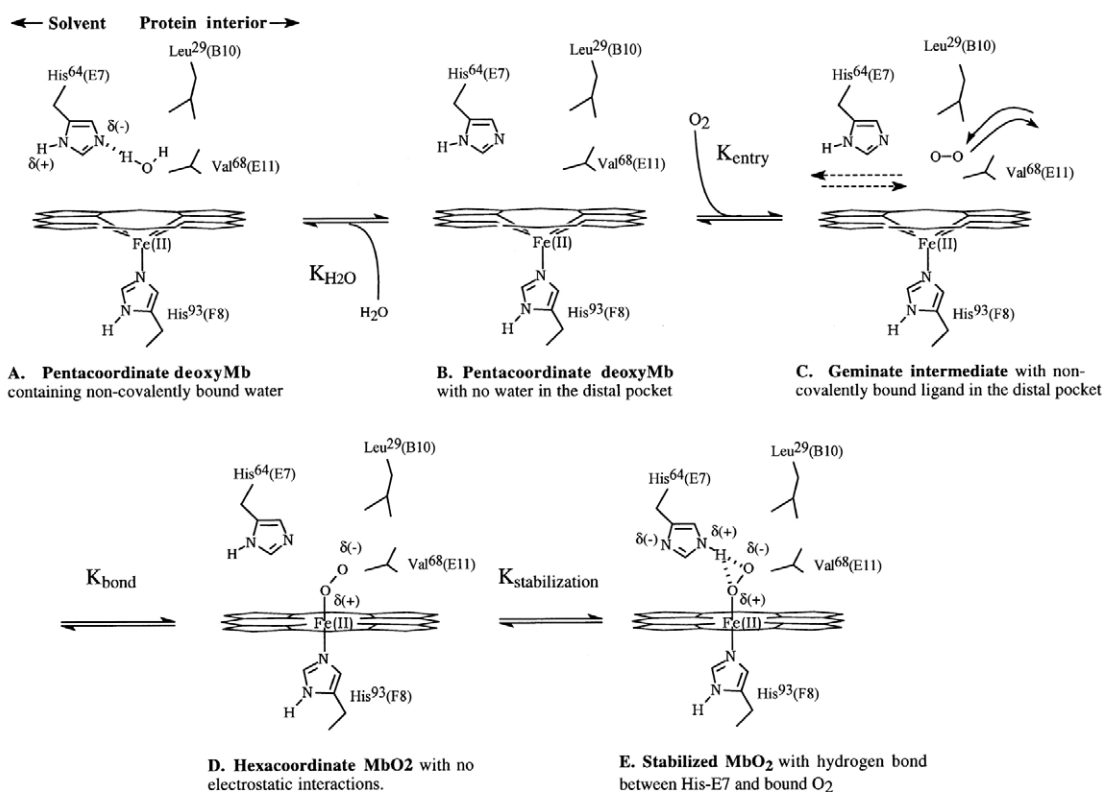
Figure 8 General mechanism for O_2-binding to sperm whale deoxyMb. Amino acid residues are labeled both by the name and number of the residue in the protein sequence (superscript), and in parentheses by a letter identifying the helical region from which the side chain protrudes followed by the number of the residue in that helical region (reproduced by permission of Olson and Phillips[44]).

Based on the flash photolysis results, it appears that, at room temperature, escape of O_2 from the distal pocket to the solvent plus entry of water (i.e., C to A in Figure 8) has about the same activation barrier as does "geminate recombination" of O_2 in the distal pocket with the heme (i.e., from C to E in Figure 4). Studies of a large number of engineered distal pocket amino acid variants show that the activation barrier to O_2 dissociation involves not only the inherent strength of the $Fe—O_2$ bond, but also the steric and electrostatic interactions of the $Fe—O_2$ unit within the distal pocket shown in Figure 8.[1] These interactions are discussed in more detail in the next subsection.

In multi-subunit Hbs, the globin structure prevents the close approach of hemes in adjacent subunits, and, thus, prevents μ-oxo dimer formation via reaction (2). However, another irreversible reaction, referred to as autoxidation, reaction (3), invariably occurs for all Mb/Hbs:[1]

$$\text{oxyMb/Hb} + H^+ \longrightarrow \text{metMb/Hb} + HO_2 \qquad (3)$$
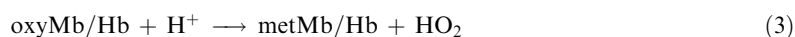
The "met" prefix refers to the ferric heme form of Mb/Hb, and, in fact, metMb/Hb is the thermodynamically stable oxidation state in an aerobic atmosphere. Reaction (3) typically occurs on the time scale of several hours to days at room temperature. MetMb/Hb reductases are present in tissues that keep the steady level of the met forms at a few percent or less.

8.10.2.1.6 Binding and discrimination of CO and NO

The ferrous heme within Mb and Hb forms stable complexes with at least two other gaseous diatomic molecules, namely, carbon monoxide and nitric oxide. Since both CO and NO are produced naturally in the body,[40,51] it is important for Mb/Hb to distinguish these two molecules from each other and from O_2. How does Mb/Hb discriminate three molecules of such similar size and polarity? Attempts to answer this question have occupied a number of investigators for many years, and several reviews on this topic are available.[1,40,44,52]

The debate about factors controlling discrimination between CO vs. O_2 affinities for deoxyMb/Hb has been particularly lively. The key observation spawning this debate is that synthetic pentacoordinate ferrous hemes in solution bind CO approximately 100,000 times more strongly than O_2, whereas Hb and Mb bind CO only about 100 times more strongly than O_2.[1] This lowering of the CO/O_2 affinity ratio by Hb and Mb compared to synthetic hemes, while insufficient to prevent the well-known toxicity of inhaled CO, does minimize interference with O_2-binding from CO generated by biological processes such as heme degradation. As expected from its strong ligand field, CO binding results in conversion to a low spin, diamagnetic six-coordinate ferrous complex, for both synthetic hemes and Mb/Hb (the sixth ligand being a nitrogenous base *trans* to the CO). The expected end-on binding of CO to iron through the carbon allows back donation into both empty π^* orbitals on CO from what would correspond to the d_{xz} and d_{yz} orbitals on iron in Figure 3, thereby favoring a linear $Fe—C—O$ geometry. Indeed, $Fe—C—O$ angles in several synthetic heme complexes vary from linearity by no more than about $10°$.[52] Until recently the "textbook" explanation for Mb/Hb's lowering of the CO/O_2 affinity ratio was that residues lining the distal O_2-binding pocket, particularly the conserved HisE7 (shown in Figure 7 for sperm whale Mb), sterically hindered attainment of the preferred linear $[Fe—C—O]^{2+}$ geometry observed in the synthetic heme–CO complexes. On the other hand, as discussed above, the $[Fe—O—O]^{2+}$ unit prefers to be bent, so that this steric restriction should be less of a hindrance to O_2-binding. Apparently confirming this explanation, the earlier, lower-resolution X-ray crystal structures of CO adducts of sperm whale Mb (MbCO) showed a bent $Fe—C—O$ unit with angles ranging from $20°$ to as much as $60°$ from linear (measured as the angle between the C—O bond axis and the normal to the average plane of the heme atoms). More recent single-crystal IR[53] and picosecond time scale solution IR[54] spectroscopies of MbCO, however, showed that the C—O vibrational dipole was nearly perpendicular to the heme plane, indicating a very-close-to-linear $Fe—C—O$ unit. This discrepancy between the earlier X-ray crystal structural and IR spectroscopic data was apparently resolved in 1999 by an X-ray structure of MbCO at nearly atomic resolution obtained at room temperature, which showed that the $Fe—C—O$ unit deviated from linearity by only $7 \pm 2°$. That is, as shown in Figure 9, the $Fe—C—O$ unit in MbCO is indeed very close to linear.[55] Comparison with a similarly high-resolution crystal structure of deoxyMb led to the conclusion that the lowered CO affinity of deoxyMb relative to synthetic hemes is due mostly to steric hindrance by distal pocket residues, particularly the distal histidine and valine side
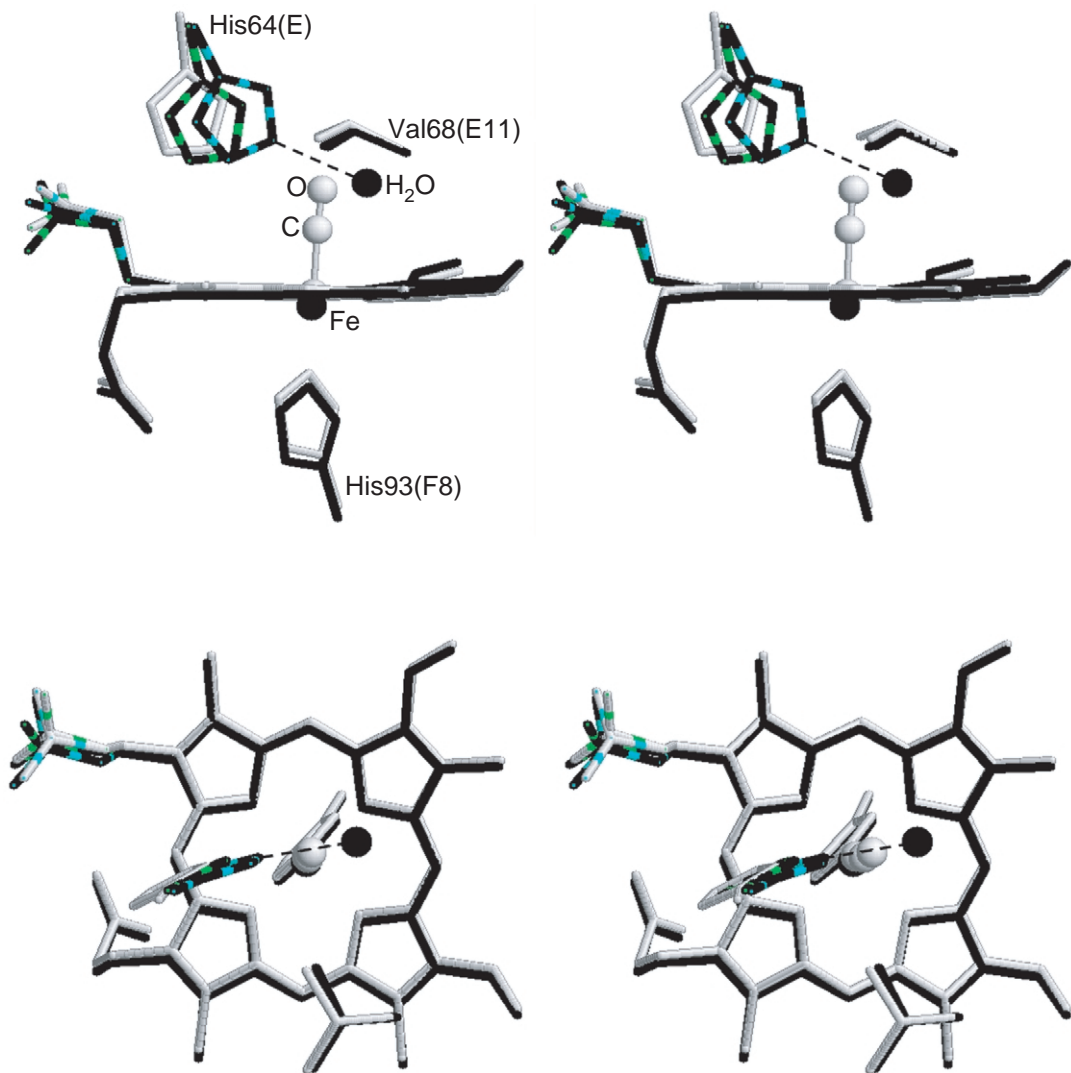
Figure 9 Stereo wireframe representations of hemes, proximal histidines, and distal pockets of the superposed deoxyMb (black) and MbCO (gray) room-temperature crystal structures[55] viewed approximately parallel (top) and perpendicular (bottom) to the heme planes. Drawings were generated using RASMOL[27] and coordinates from 1BZR and 1BZP deposited in the Protein Data Bank. The HisE7 side chain is interpreted to have two slightly different orientations in the deoxyMb crystal structure. A hydrogen bond between the closer HisE7 side chain orientation and the distal pocket water in deoxyMb is shown as a dashed line. One of the heme propionates is also disordered in both structures.

chains shown in Figure 9. These steric hindrances are relieved by reorientations of the heme and two surrounding helical regions in the CO adduct (cf. Figure 9). The energetic cost of these reorientations is then supposed to be responsible for the lower CO affinity of deoxyMb relative to synthetic hemes.[55]

However, the ~1,000-fold discrimination by deoxyMb towards O_2 and away from CO referred to above is due to the combination of a ~ten-fold decrease in CO affinity and a ~100-fold *increase* in O_2 affinity relative to synthetic hemes.[1] That is, the discrimination away from CO and towards O_2 appears to be due primarily to an increased O_2 affinity of the ferrous heme induced by the Mb polypeptide. Studies on a large number of site-directed Mb amino acid variants indicate that the increased O_2 affinity is due to a larger decrease in k_{off} than k_{on}, and that the decreased k_{off} is due to favorable interactions of the bound O_2 with distal pocket residues.[1] A distal pocket water in deoxyMb that is not coordinated to iron, but is hydrogen-bonded to the distal histidine side chain (cf. Figures 8 and 9) must be displaced upon binding of either O_2 or CO. In the case of O_2-binding, the energetic cost of this pocket water displacement is more than compensated by

formation of a hydrogen bond between the polar $Fe^{\delta+}-O-O^{\delta-}$ unit and the distal histidine (HisE7) side chain, as shown in Figures 7 and 8. In this distal pocket environment the less polar $Fe-C-O$ unit is relatively destabilized both because it cannot undergo the hydrogen bonding interaction with the distal histidine and also because it cannot so readily displace the pocket water. Thus, the current consensus is that the polar distal pocket is primarily responsible for discrimination of deoxyMb/Hb towards O_2 and away from CO.

The interaction of NO with Mb/Hb is more complicated. NO can bind to both ferric and ferrous hemes, can potentially function as either an oxidizing or reducing agent, and can also react with cysteine sulfhydryls on the protein.[57–61] The discussion here is confined to reactions of deoxy- and oxyMb/Hb with NO at the heme iron, which appear to be the most physiologically relevant.[56,62,63] These reactions are summarized in Figure 10.

The NO adducts of deoxyMb and deoxyHb (MbNO and HbNO), i.e., the $\{FeNO\}^7$ complexes in the notation of Enemark and Feltham,[64] have active site geometries very similar to that of oxyMb shown in Figure 7.[44] MbNO and HbNO contain six-coordinate, low spin (i.e., $S=1/2$ ground state) hemes with decidedly bent $Fe-N-O$ units (112–147°).[44,60,65] In MbNO the distal histidine epsilon nitrogen is within 2.8 Å of the coordinated NO nitrogen, indicative of a hydrogen bond. NO has a much higher affinity for deoxyMb/Hb than do either CO or O_2, due mostly do a greatly decreased k_{off}.[42,44] However, unlike O_2, engineered substitutions of the distal histidine have little or no effect on NO affinity of deoxyMb. This relative lack of effect of distal histidine substitution on NO affinity has been attributed to compensation of a tenfold increase in k_{off}, due to removal of the distal histidine hydrogen bonding interaction, by a tenfold increase in k_{on} due to lack of the distal pocket water in the deoxy forms of the distal-histidine substituted Mbs.[44,60] Despite the relatively high affinity of NO for deoxyMb/Hb, the sub-micromolar physiological concentrations of NO and the much higher concentrations of Mb and O_2 mean that, in oxygenated muscle tissue, Mb is predominantly in the oxy form.[56] However, at such low NO concentrations, its second-order reaction with O_2 is sufficiently slow to give NO a lifetime of several seconds, even in oxygenated tissues.[56] This lifetime is sufficient for reaction of oxyMb with NO, which occurs on the millisecond timescale at comparable concentrations, leading to metMb and nitrate.[66,67] The triangular portion of the scheme in Figure 10 has been proposed to be a physiologically relevant means of scavenging NO for both Mb and Hb.[56] The internal cavities within Mb identified by xenon binding[49,50] may facilitate entry of NO to the distal pocket for reaction with bound O_2, as shown in Figure 11. The mechanism of the reaction of oxyMb with NO appears to involve intermediate formation of peroxynitrite, consistent with the superoxide-like character of the bound O_2 discussed above.[67,68] A potential alternative pathway for nitrate formation, namely, electrophilic attack of non-coordinated O_2 on the coordinated NO of MbNO/HbNO,[63,69] apparently does not find experimental support.

A bacterial flavohemoglobin, which contains a globin domain fused to a flavin/NADH binding domain, functions enzymatically as a nitric oxide dioxygenase, using a catalytic cycle similar to that in Figure 10.[70,71] The role of this enzyme is apparently to detoxify nitric oxide produced by the body in response to bacterial infection. The distal pocket of flavohemoglobins more closely
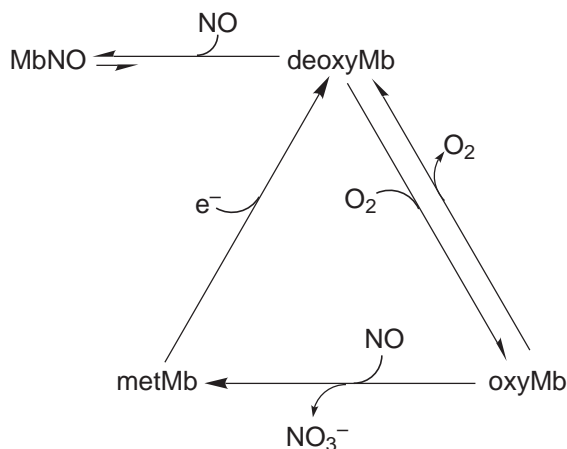
Figure 10 Schematic diagram depicting reactions of nitric oxide with deoxy- and oxyMb. These analogous reactions also apply to Hb (adapted from Brunori[56]).
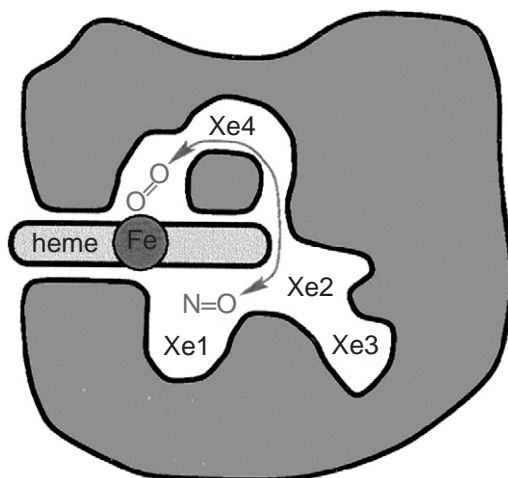
Figure 11 Cartoon of NO diffusion through xenon binding cavities and reaction with bound O_2 in oxyMb (reprinted from Frauenfelder *et al.*[51] with permission).

resembles that of the high O_2 affinity *Ascaris* Hbs, shown in Figure 7. The stronger hydrogen bonding interaction with the hydroxyl of the distal tyrosine apparently stabilizes the O_2 adduct, thereby minimizing inhibition by NO.

8.10.2.1.7 Cooperativity

Cooperativity in the context of multi-subunit, multi-active site O_2-binding proteins means simply that O_2-binding to one subunit increases the affinity of the remaining subunits for O_2. Cooperativity of O_2-binding to the mammalian Hb tetramer is manifested as a sigmoidally shaped binding curve, when plotted as fractional saturation (Y) of the O_2-binding sites vs. partial pressure of O_2 (P_{O2}), as shown in Figure 12A. The monomeric Mb exhibits no cooperativity in O_2-binding, and shows a hyperbolic binding curve. Figure 12A illustrates the physiological advantage of cooperativity. At low P_{O2} (venous pressure) typical of respiring muscle, O_2 can be delivered to the tissues via unloading from Hb to Mb, whereas, at high P_{O2} (arterial pressure) typical of the lungs, Hb can be saturated with O_2, which then circulates to the tissues.

Cooperativity in O_2-binding to mammalian Hbs was first recognized nearly 100 years ago, and attempts to investigate and explain this phenomenon have occupied a number of scientists ever since. Reviews of the history and current status of the understanding of cooperative O_2-binding to Hbs are available.[14,43,73,74] The Y vs. P_{O2} data have traditionally been analyzed using the so-called Hill Equation (4):

$$Y/(1 - Y) = K(P_{O2})^n \tag{4}$$

where K is the association constant, and the so-called Hill plot, shown in Figure 12B. The slope of the Hill plot is equal to the exponent, n, the Hill coefficient, in Equation (4). Non-cooperative binding, $n = 1$, is exhibited for Mb and also for Hb at either very low or very high P_{O2} (the dashed lines in Figure 12B). The maximum slope in the middle portion of the plot, $n_{max} = 2.8$ for human Hb, is typically cited as a measure of the extent of its cooperativity ($n_{max} = 4$ for "infinite," i.e., "all-or-nothing" cooperativity).

The crux of the question concerning cooperativity that has occupied investigators is: how can the data in Figure 12 for Hb be explained at a molecular level? This question became especially vexing after the crystal structure of human Hb was solved. As shown in Figure 13, in order to explain cooperativity, O_2-binding must be communicated between heme irons that are separated by 25–40 Å within the Hb tetramer. The first, and still largely successful, attempt to explain the cooperative O_2-binding to Hb was the so-called Monod–Wyman–Changeaux (MWC) model, which is illustrated schematically in Figure 14.[75] The key proposals of the MWC model are that two different conformations of the Hb tetramer differ in their O_2 affinity and that these two conformations are in equilibrium with each other. Thus, the proportion of low-affinity "tense"
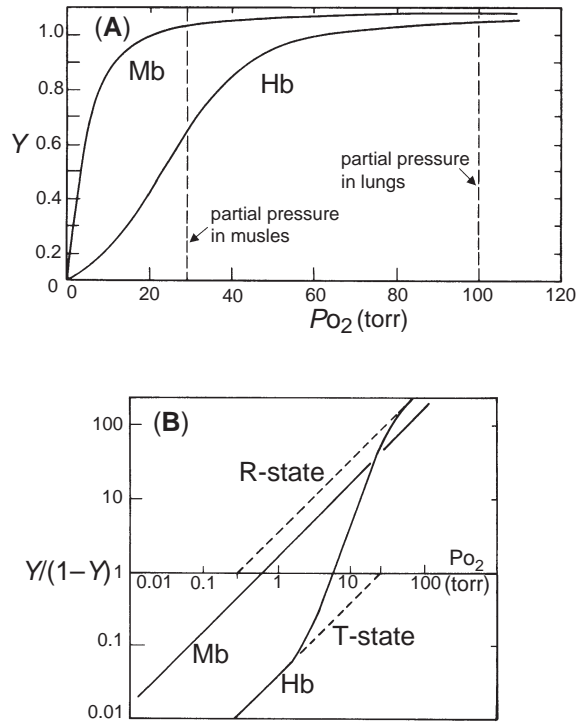
Figure 12 (A) Plots of fractional saturation of O_2 binding sites (Y) vs. partial pressure of O_2 (P_{O2}) for Mb (non-cooperative) and Hb (cooperative). (B) Hill plot for cooperative O_2 binding of Hb (plots are redrawn from Suslick and Reinert[72]).
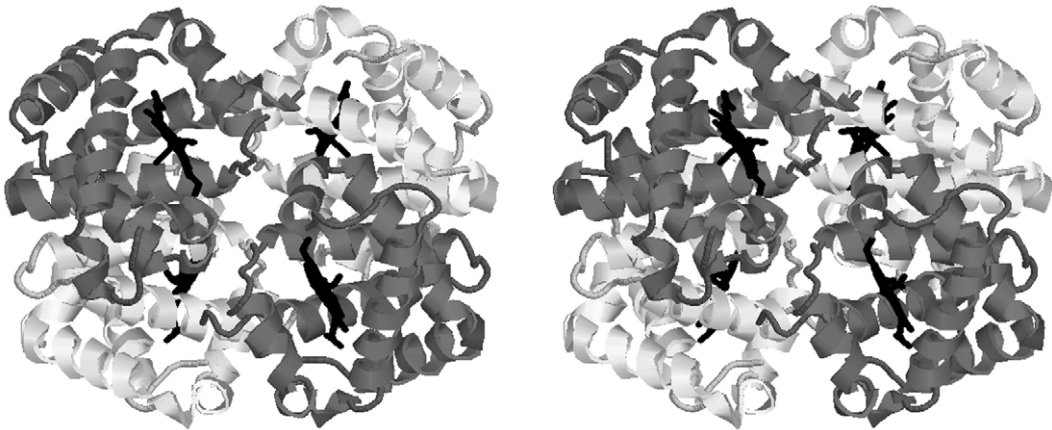
Figure 13 Stereo view of the human oxyHb tetramer. The subunits of the tetramer are associated in an approximately tetrahedral configuration, and the view is approximately along one of the pseudo two-fold rotation axes and perpendicular to the other two. The protein backbones are shown in ribbon representation. The backbones of the two subunits in the foreground (an $\alpha\beta$ pair) are colored darker than the two in the background. The heme groups are shown in wireframe representation and colored black (with bound O_2s omitted). For the $\alpha\beta$ subunit pairs, the intersubunit iron–iron distance is ~25 Å. Drawing was generated using RASMOL[27] and coordinates deposited in PDB ID 1HHO.[34]

(T) and high-affinity "relaxed" (R) conformations of the Hb tetramer is characterized by equilibrium constants, L_x, with $x = 1$–4 corresponding to the number of O_2 molecules bound per tetramer. (The model assumes that O_2-binding to individual subunits of the tetramer is random). By Le Chatelier's principle, therefore, binding of O_2 must shift the equilibrium towards the high-affinity, R state. Fits to O_2-binding curves of human Hb show $L_3, L_4 \gg L_0, L_1$, $L_2 \sim 1$, $P^T_{1/2} \sim 9$ torr, and $P^R_{1/2} \sim 0.25$ torr. That is, according to this model, the midpoint of the shift between
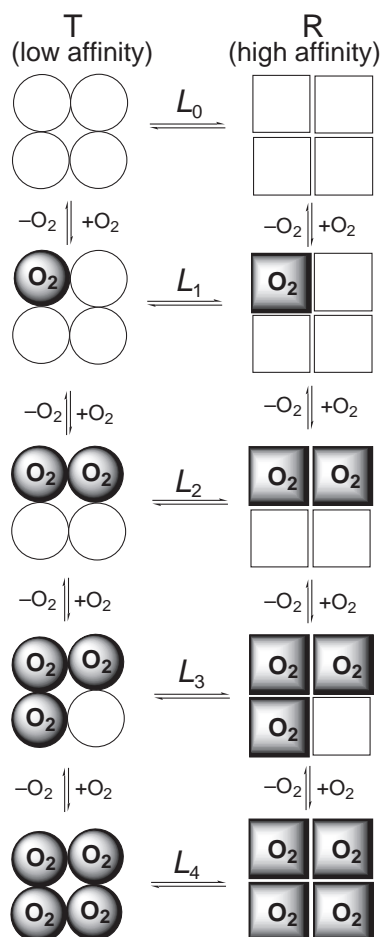
Figure 14 The MWC model explaining cooperative O_2 binding to Hb.

T and R states of the Hb tetramer occurs when two O_2 molecules are bound per tetramer, and the R state has a roughly 40-fold higher affinity for O_2 than does the T state. (These two limiting affinities correspond to the intersections of the dashed lines of the Hill plot in Figure 12B with the half-saturation line along the *x*-axis, i.e., where $Y/(1-Y) = 1$.)

Perutz first enunciated a molecular structural interpretation of the MWC model for cooperative O_2-binding to Hb in 1970,[76] and many aspects of his interpretation have withstood subsequent experimental scrutiny.[74,77] Figure 15 summarizes what are thought to be the key structural changes in the vicinity of the heme corresponding to the R/T transition. In the deoxy T state, the proximal HisNε—Fe bond is slightly off the heme normal axis, and the resulting steric interactions with the porphyrin ring prevent ligation of the proximal His unless the iron is out of the heme plane. Upon conversion to the oxy (R) state, the lateral movement of the F helix allows alignment of the HisNε—Fe with the heme normal, thus relieving the steric hindrance and allowing iron to move into the heme plane and towards the bound O_2. In the beta subunits (shown in Figure 15), the Val E11 side chain also moves away from a position that sterically hinders O_2-binding in the T state. The movement of the F helix causes breakage of salt bridges between alpha and beta subunits, thereby altering the orientation of alpha–beta subunit pairs with respect to each other.[14] The cooperative interaction energy, represented by the difference in O_2 affinities between T and R states listed above, amounts to only a few kcal mol^{-1}. Given the large number of atoms that shift positions upon T/R state interconversion, it has not been possible to unambiguously assign this relatively small interaction energy as being "stored" within a few bonds or other atomic interactions.

The breakage of salt bridges upon conversion to the R state releases protons, causing a decrease in O_2 affinity with decreasing pH—the so-called Bohr effect. Essentially, the R state is more acidic, and lower pH, therefore, shifts the R/T equilibrium towards the T state.[14] The Bohr effect
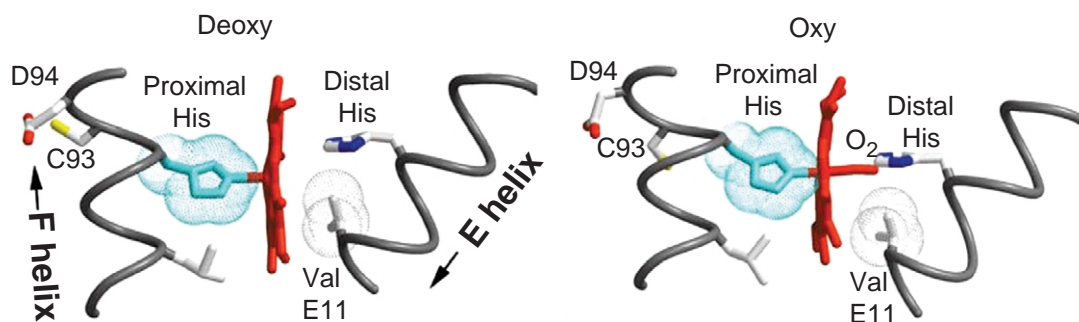
Figure 15 Structural changes in the vicinity of the heme associated with the T (deoxy) to R (oxy) transition for the beta subunits of human Hb.[34,78] Similar changes occur for the alpha subunits. The heme is shown approximately edge-on in red. Van der Waal's radii of the proximal His side chain atoms are shown in cyan and those of Val E11 in gray. Arrows indicate movements of the E and F helix upon transition from the T to R state. Two side chains at subunit interfaces that move upon the T/R transition are labeled by their one-letter amino acid symbols followed by their number in the amino acid sequence (drawing adapted from Royer *et al.*[43]).

has a well-established physiological benefit: it causes release of O_2 to rapidly respiring tissues, which accumulate dissolved CO_2, and thereby become acidic.

8.10.2.2   Di-iron Type: Hemerythrins and Myohemerythrins

8.10.2.2.1   *Early history and distribution of hemerythrins*

Of the three types of O_2-carrying proteins, the molecular details of O_2-binding to the active site of hemerythrin (Hr) were, chronologically, the next to be clarified. Several reviews are available discussing various aspects of Hr structure and function.[2,79–84] Hr most often occurs as an octamer of essentially identical O_2-binding subunits, although tetrameric, trimeric, and dimeric Hrs are also known.[80] Hr is thought to serve primarily as an O_2 storage reservoir in the relatively few phyla of marine invertebrates in which it occurs.[85,86] A monomeric counterpart, myoHr, fulfills a function more closely related to that of Mb and is confined to muscle tissues of the same marine invertebrates. The structure of the myoHr subunit and active site are both very similar to those of Hr.[80] The following discussion, therefore, applies, with very few exceptions, equally well to both Hr and myoHr.

   Despite its name, Hr contains no heme group. The protein does, however, contain tightly associated iron, evidence for which was presented as long ago as 1890,[87] and which was accurately quantitated in 1957 as two per bound O_2.[88,89] That Hr binds O_2 at a di-iron site, and, in the process, undergoes a reversible diferrous/diferric oxidation state change, was first proposed in 1955.[90] In fact, Hr was the first of a class of proteins found to contain non-heme, non-sulfur di-iron sites.[91]

8.10.2.2.2   *Protein structure*

The characteristic tertiary structure of Hr, first elucidated in 1975,[92] consists of a four-helix bundle surrounding a di-iron site, as shown in Figure 16A.[80,93] The Hr octamer consists of two squares of four 13.5-kDa subunits stacked atop one another in a 90°-offset, face-to-face fashion, which gives the octamer D_4 symmetry (cf. Figure 16B). A few Hrs consist of two different subunits in an $\alpha_4\beta_4$ composition,[94,95] but the configuration of alpha and beta subunits within the octamer is not known. A low-resolution structure of a trimeric Hr is also available.[80]

8.10.2.2.3   *The di-iron site and formulation of the O_2-binding reaction*

As shown in Figure 16C, the two iron atoms at the active site are bound directly to protein side chains: five histidines, one aspartate, and one glutamate. The carboxylate side chains of the latter two residues
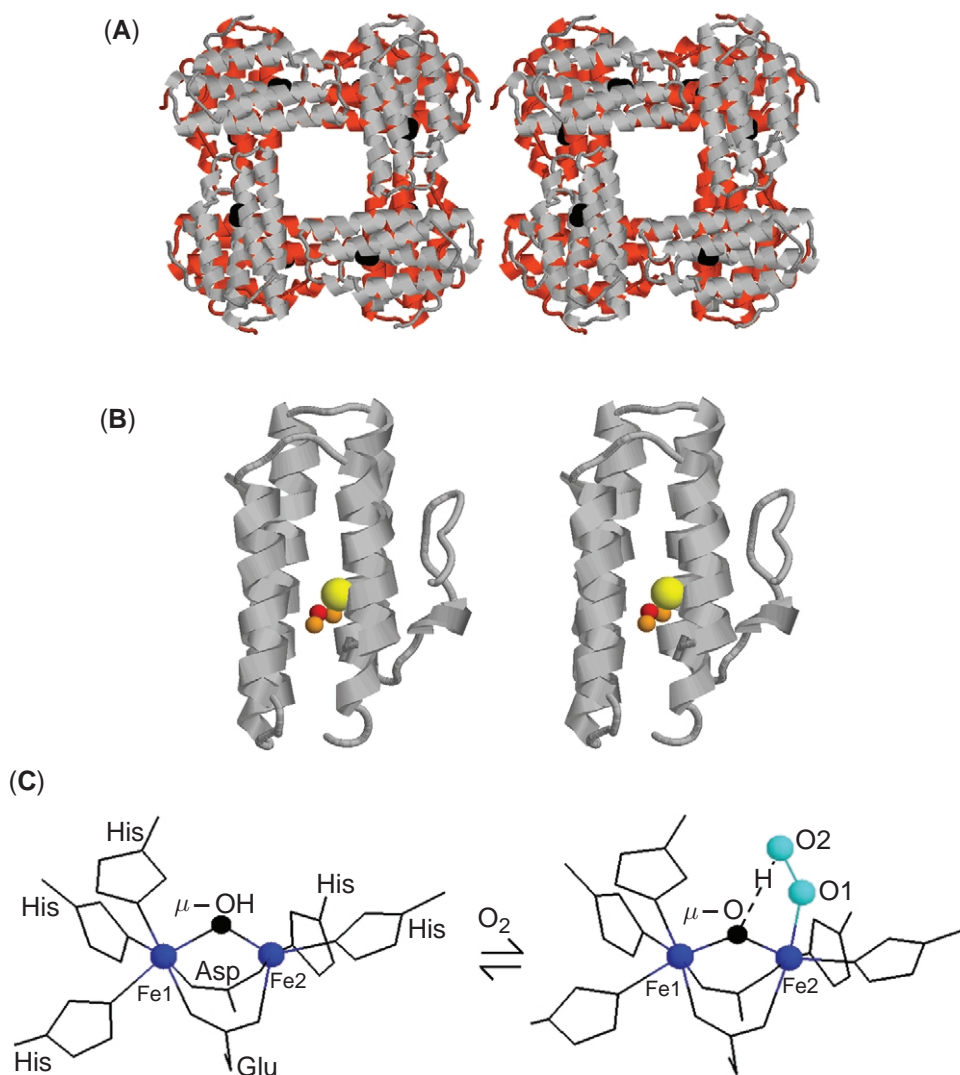
Figure 16 (A) Stereo view of the quaternary structure of an octameric Hr. (B) Stereo view of the tertiary structure of a Hr subunit. (C) The di-iron site structures of oxy- and deoxyHrs. Drawings were generated using RASMOL[27] and coordinates for *Phascolopsis gouldii* metHr ((A) and (B)) from 1I4Y[93] and for *T. dyscritum* oxy- and deoxyHrs (C) from 1HMO[96] in the Protein Data Bank. Protein backbones are traced in ribbon representation; iron atoms, oxo bridges, and O_2 are shown as spheres, and iron ligands are shown in wireframe representation. The hydrogen bond between the oxo bridge and bound O_2 is indicated as a dashed line. Although not visible in the crystal structure, the proton of this hydrogen bond is depicted as more closely associated with the bound O_2 than the oxo bridge for reasons discussed in the text.

bridge the two irons in a bidentate μ-1,3 fashion. The oxygenation reaction has the well-established formulation in reaction (5), i.e., hydroxo-bridged diferrous for deoxyHr and oxo-bridged diferric-hydroperoxo for oxyHr with both forms having two supporting carboxylate bridges:

$$[\text{Fe}^{\text{II}}(\mu-\text{OH})\text{Fe}^{\text{II}}] + \text{O2} \rightleftharpoons [\text{Fe}^{\text{III}}(\mu-\text{O})\text{Fe}^{\text{III}}\text{O}_2\text{H}^-] \tag{5}$$
$$\underset{\text{deoxy}}{} \qquad\qquad\qquad \underset{\text{oxy}}{}$$
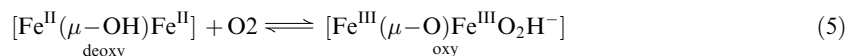
The deoxy and oxy structures in Figure 16C were first proposed in 1985, based on relatively low resolution X-ray crystal structures together with the spectroscopic and magnetic evidence discussed below.[97] Only one deoxy- and one oxyHr crystal structure each are currently available,[96] and relevant structural parameters of the di-iron sites from these structures are listed in Table 2. The averages listed in Table 2 avoid the tendency to over-interpret individual bond distances and angles at the relatively low resolution (2.0 Å) of these structures compared to those

Table 2 Pertinent distances (Å) and angles (°) of the di-iron sites in the X-ray crystal structures of *T. dyscritum* oxy and deoxyHrs.[a]

Distance or angle	Deoxy	Oxy
Fe1-Fe2	3.32	3.27
Fe-N(His)(average)	2.22	2.20
Fe-O(carboxylate)(average)	2.20	2.17
Fe-μ-O(bridge)(average)	2.02	1.84
Fe-O-Fe	111	125
Fe2-O1 (bound O_2)		2.15
Fe2-O1-O2 (bound O_2)[b]		130

[a] From Stenkamp.[80]   [b] From coordinates in 1HMO in the Protein Data Bank.[96]

of Mb. Nevertheless, it is apparent that the binding of O_2 occurs with little structural change or movement of the iron atoms and protein ligands.

From a bio-inorganic perspective, the most celebrated structural feature of Hr has been the diferric oxo-bridged unit. This unit was recognized in the 1960s as likely to be present in both the oxy and met forms, based on spectroscopic properties.[98] The spectroscopic feature most readily identified with the diferric oxo-bridged unit having a bent geometry is the presence of two electronic absorptions between 300 and 400 nm with $\varepsilon \sim 6{,}000\,M^{-1}cm^{-1}$ per di-iron site, as shown in Figure 17 for oxyHr. While initially controversial, the assignment of these transitions as oxo $\rightarrow Fe^{III}$ charge transfer has withstood the scrutiny of single-crystal electronic absorption, MCD, and resonance Raman spectroscopies.[79,99] The met form, which results from autoxidation of oxyHr (*vida infra*), also shows these characteristic oxo-bridged diferric charge transfer absorptions.

Iron-57 Mössbauer spectroscopy also clearly established that the best description of the irons in both oxy- and metHrs is high-spin Fe^{III},[83,100,101] but with magnetic behavior distinct from that of isolated ferric irons. A second characteristic feature of the diferric oxo-bridged unit is its ground state diamagnetism, due to antiferromagnetic coupling of the two high-spin ($S = 5/2$) Fe^{III}s. This coupling is attributed to superexchange via weak σ- and π-type orbital overlaps of d-orbitals on the irons and p-orbitals on the oxo bridge.[79] Consistent with such interactions, the diferric oxo-bridged unit is characterized by unusually short (1.8 Å) Fe$-$O distances, indicative of some multiple bond character.[102] The antiferromagnetic coupling is temperature dependent, due to a Boltzmann-weighted population of a ladder of higher-energy paramagnetic states ($S = 1$–5).
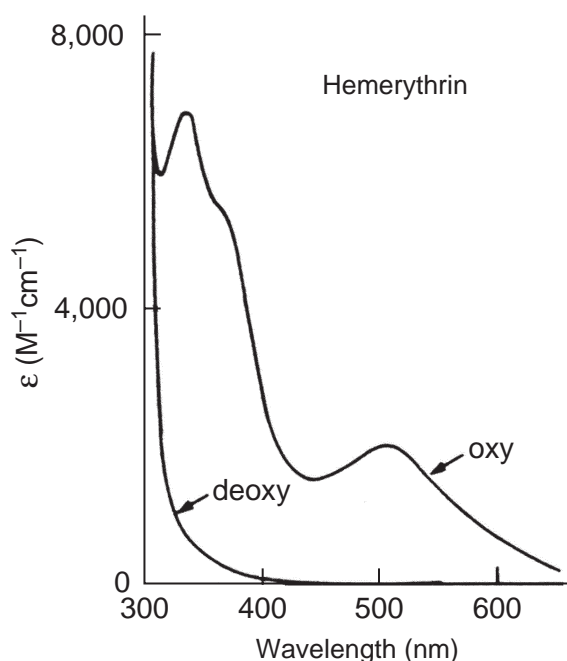
Figure 17 UV–vis absorption spectra of oxy and deoxyHrs from *Phascolopsis gouldii*.

From the temperature dependence of magnetic susceptibilties, the strength of this coupling, J, (expressed in the $-2J\mathbf{S}_1\cdot\mathbf{S}_2$ Heisenberg–Dirac–Van Vleck formalism) was reported as $-77\,\mathrm{cm}^{-1}$ for oxyHr and $-134\,\mathrm{cm}^{-1}$ for metHr in 1972.[103] Couplings of the latter magnitude are characteristic of the diferric-oxo bridged unit.[102] The hydrogen bonding interaction between the hydroperoxo and the oxo bridge of oxyHr (cf. Figure 16C) could be responsible for the lower $-J$ reported for oxyHr. Based on paramagnetic NMR shifts of the His ligand $N\delta$ protons, however, the ΔJ between oxy- and metHrs was judged to be smaller than the magnetic susceptibility measurements had indicated,[104] and supports the oxo-bridged formulation for oxyHr. Mössbauer spectroscopy also clearly indicated distinct environments for the two irons at the di-iron site of oxyHr,[83,105] as expected for the structure shown in Figure 16C.

The assignment of the less intense electronic absorption of oxyHr near 500 nm ($\varepsilon \sim 2{,}000\,\mathrm{M}^{-1}\mathrm{cm}^{-1}$ per di-iron site) shown in Figure 17 as a peroxo $\pi^* \rightarrow \mathrm{Fe}^{\mathrm{III}}$ charge transfer transition has also withstood rigorous scrutiny.[99] Resonance Raman excitation within this absorption band led to the discovery of an $\mathrm{O-O}$ stretching frequency at $844\,\mathrm{cm}^{-1}$.[106,107] Isotope labeling studies showed unequivocally that this frequency was due to the bound O_2 and also identified the corresponding $\mathrm{Fe-O}$ stretching frequency near $500\,\mathrm{cm}^{-1}$. Comparison to the $\mathrm{O-O}$ stretching frequencies in Table 1 clearly classifies the bound O_2 in Hr as a peroxo ligand, consistent with the two-electron oxidation of the di-iron site in reaction (5). Resonance Raman spectroscopy using a mixed $^{16}\mathrm{O}^{18}\mathrm{O}$ dioxygen molecule showed that the two bound oxygen atoms were in different environments, essentially ruling out a symmetrically bridging or side-on peroxo ligand.[84,108,109] Solvent deuterium isotope effects on the $\mathrm{O-O}$ stretching frequencies also support the hydrogen bonding interaction shown in Figure 16C.[110–112] The small, but measurable, oxygen isotope effect on O_2 affinity has also been interpreted to support the peroxo formulation in oxyHr.[113] Finally, resonance Raman excitation into the oxo $\rightarrow \mathrm{Fe}^{\mathrm{III}}$ charge transfer band of oxyHr enhances a vibrational mode at $486\,\mathrm{cm}^{-1}$, which shifts downward in $\mathrm{H}_2{}^{18}\mathrm{O}$ but not with $^{18}\mathrm{O}_2$. This frequency is assigned to the symmetric $\mathrm{Fe-O-Fe}$ stretch of the oxo bridge, and is close to (but distinct from) the corresponding $\mathrm{H}_2{}^{18}\mathrm{O}$-sensitive $\mathrm{Fe-O-Fe}$ stretch of metHr at $510\,\mathrm{cm}^{-1}$, which can be unambiguously assigned to the oxo bridge.[110,112] That is, oxyHr contains an oxo bridge similar to that of the met form. Thus, while the placement of the hydrogen-bonded proton between the peroxo and the oxo bridge has not been confirmed by X-ray or neutron diffraction, all of the spectroscopic, magnetic, and structural evidence discussed above supports the formulation for the Hr oxygenation reaction in Equation (5), and depicted in Figure 16D. That is, oxyHr contains a terminally coordinated hydroperoxo ligand hydrogen-bonded to the oxo bridge.

The diferrous nature of the deoxyHr active site was established by anaerobic iron chelation in the 1950s.[90] More difficult to establish was the nature of the magnetic coupling and the bridging solvent ligand between the iron atoms. Temperature-dependent magnetic circular dichroism (MCD) and paramagnetic $^1\mathrm{H}$ NMR measurements showed that the ground state of deoxyHr was diamagnetic, due to antiferromagnetic coupling between the two high spin ($S=2$) $\mathrm{Fe}^{\mathrm{II}}$. The magnitude of this coupling, $J = -15\,\mathrm{cm}^{-1}$,[114] closely matches that of a synthetic (μ-hydroxo)bis(μ-carboxylato)di-iron(II) complex, but is significantly stronger than that of a corresponding μ-aqua bridged core (in which the irons may actually be weakly ferromagnetically coupled).[79] The X-ray crystal structure of the deoxyHr active site was, therefore, interpreted as containing a hydroxo rather than aqua bridge (oxo-bridged diferrous complexes being unknown). The energies and intensities of the near-IR $d-d$ electronic transitions of deoxyHr support the crystallographically determined result of one six- and one five-coordinate ferrous iron.[114]

8.10.2.2.4 Mechanism of dioxygen binding

One striking feature of the oxygenation reaction shown in Figure 16 and Equation (5) is that, although both iron atoms formally undergo oxidation, O_2 appears to have direct, inner-sphere access to only the five-coordinate iron atom of deoxyHr. In this sense and in the end-on geometry and polar nature of the $\mathrm{Fe-O-O}$ unit, the oxy structure of Hr resembles that of the $\mathrm{Fe-O-O}$ unit of oxyMb/Hb. However, in contrast to Mb/Hb the O_2-binding pocket is lined exclusively with hydrophobic residues, as shown in Figure 18. Furthermore, no solvent molecules were observed within the O_2-binding pockets of either deoxy- or oxyHrs.[80] Both the hydrophobic nature and steric restrictions of the binding pocket favor the localized hydrogen bonding interaction of the bound O_2 with the oxo bridge. The relatively small structural changes and open
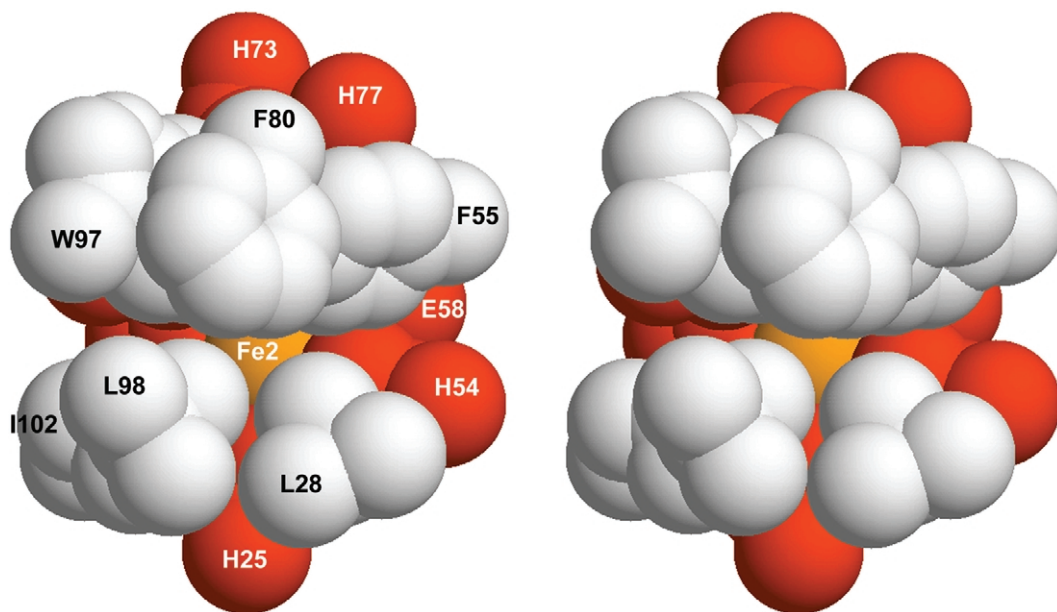
Figure 18 Space-filling representation of conserved amino acid side chains lining the O_2-binding pocket of *Themiste dyscritum* oxyHr. View is approximately parallel to the long axis of the four helix bundle and perpendicular to the Fe1−Fe2 axis, which is oriented vertically. Ligand side chains are shown in red, side chains lining the O_2-binding pocket in white. Obscured from view are the bridging carboxylates (in the rear), Fe1 and the oxo bridge (behind pocket side chains). Residues are labeled at their beta carbons by their one-letter amino acid code and number in the sequence. Fe2 labels the iron atom that binds the O_2, which is omitted for clarity. Drawing was generated using RASMOL[27] and coordinates from 1HMO in the Protein Data Bank.[96]

coordination site on Fe2 in deoxyHr (cf. Figure 16 and Table 2) seem designed for a facile O_2 association reaction, and this impression is borne out in the kinetics discussed below.

The large difference in visible and near-UV absorbances between deoxy and oxyHrs (cf. Figure 17) provides a convenient means of measuring rates of O_2 association and dissociation. Extensive kinetic studies on O_2 and other ligand binding to the Hr active site have been performed,[115–119] but unlike Mb/Hb, only one of the conserved O_2-binding pocket residues has so far been artificially substituted.[112,120,124] In addition to conventional stopped-flow techniques, these rates have been measured by laser flash photolysis[123,125] and temperature jump[115] methods. With few exceptions the rates measured by these various techniques are consistent with each other and with independently measured O_2 affinities.[112] The results of these kinetics studies are summarized in the pictorial formulation of the O_2-binding mechanism given in Figure 19.

With a single exception that has never been reproduced, no evidence for an intermediate species has ever been obtained during either O_2 association with deoxyHr or dissociation from oxyHr[112] (except perhaps for short-lived "geminate" dissociated states generated in low yields by laser flash photolysis[119]). Therefore, the bracketed species in Figure 19, if it exists as an inter-mediate rather than transition state, must be extremely short-lived. Based on computational studies, Brunhold and Solomon[126] proposed a concerted proton/electron transfer mechanism following the initial contact of O_2 with the di-iron site, in which the bracketed species shown in Figure 19 would not accumulate. The high second order rate constants (10^7−10^8 $M^{-1}s^{-1}$) and low activation enthalpies (a few kcal mol^{-1} or less[2,124]) for O_2 association with Hr are consistent with either rate-limiting diffusion through a fluctuating protein matrix or opening of a "gate" leading to the O_2-binding pocket (rate-determining diffusion of O_2 through solvent to the protein surface being ruled out by the lack of viscosity dependence[127]). One of the delta carbons of L98 in Figure 18 is nearly within van der Waal's contact with the terminal atom of the bound O_2, and this residue had been proposed to function as a steric "gate," whereby entry and exit of O_2 to the binding pocket would be limited by movements of this side chain.[120–122] Based on laser flash photolysis studies on oxyHr, opening of a "gate" was proposed to lead to escape of O_2 to solvent.[128] However, this opening occurred on a time scale of microseconds or less, which is much faster than the dissociation rates of any known Hr at room temperature (50–250 s^{-1}).[2,112,115] Furthermore,
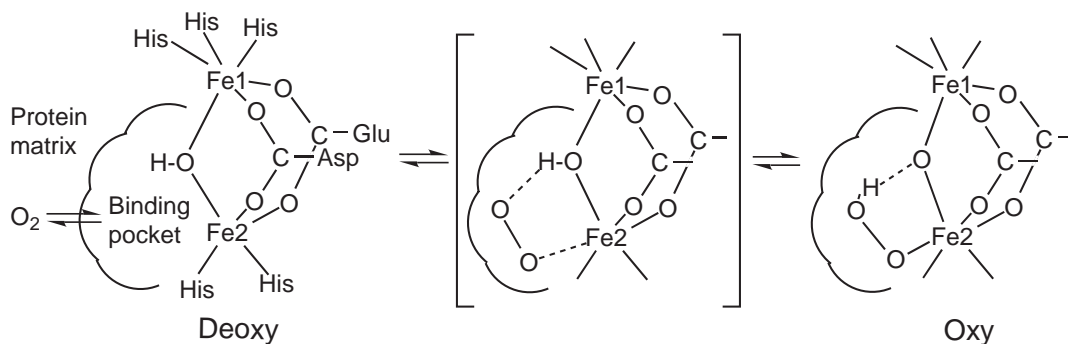
Figure 19 Schematic representation of steps in the O_2 binding mechanisms of Hr.

in order to accurately model the flash photolysis data, the gate was proposed to be permanently open in the deoxy form.[119] Mutations of L98 to residues with larger side chains did in some cases lead to decreases in O_2 association rates, presumably due to introduction of an artificial steric gate, i.e., partial occupancy of the binding pocket by the larger side chain. Mutations of L98 to residues with smaller side chains, however, did not lead to increases in O_2 association rates, as would be expected if L98 were functioning as a steric gate.[112,124] In addition, no solvent deuterium isotope effect on k_{on} was observed, despite the indication from resonance Raman that solvent deuterons have readily exchanged with the proton on the hydroperoxo. That is, no proton transfer, such as might occur through the intermediate bracketed in Figure 19, occurs in the rate-determining step for O_2 association. The concerted proton/electron transfer step referred to above would, therefore, have to occur *after* the rate-limiting step for O_2 association. This conclusion coupled with the lack of effect of the pocket residue substitutions on the kinetics is consistent with diffusion through the protein matrix up to the binding pocket being rate-limiting for O_2 association. The small positive activation volume measured for k_{on} also supports this mechanism.[129] Results of analogous kinetic studies on the other conserved residues surrounding the O_2-binding pocket illustrated in Figure 17 have not been reported, nor have preferred pathways of O_2 diffusion through the protein matrix, if they exist, been delineated. Unlike Mb/Hb, no internal cavities that accommodate atoms or molecules have been explicitly identified in crystal structures of Hr. All crystal structures of Hr do show a single water molecule inside the protein matrix that is hydrogen bonded to one of the Fe2 His ligands.[93] Pathways of entry of this internal water or of bulk solvent water into the O_2-binding pocket are not obvious from the crystal structures. The fluctuating nature of protein structures in solution[46,47] may mean that O_2 diffuses to the binding pocket of Hr via one or more transiently formed paths through the protein matrix.

Dioxygen dissociation rate constants for oxyHrs show relatively large activation energies, positive activation volumes, and a small solvent deuterium isotope effect ($k_H/k_D = 1.3–1.6$).[112,120,123,129,130] These parameters are consistent with Fe—O_2 bond weakening or breakage and some degree of proton transfer in the rate-determining step of O_2 dissociation. Once again, although substitutions at L98 with residues having larger side chains in some cases slowed the O_2 dissociation rates, substitutions with smaller side chains did not lead to increases in dissociation rates, suggesting that L98 does not sterically inhibit O_2 dissociation.[112,124] The L98Y variant of Hr showed a 200-fold slower O_2 dissociation rate and a much larger deuterium isotope effect ($k_H/k_D = 4$) on this rate relative to wild-type Hr.[124] These perturbations were ascribed to hydrogen bonding interactions of the tyrosyl hydroxyl with the bound O_2.[93]

8.10.2.2.5 *Autoxidation*

Hr undergoes slow autoxidation ($t_{1/2} \sim 18$ hours at pH 7 and room temperature), reactions (6a) and/or (6b),[117,120,124] producing metHr and hydrogen peroxide:

$$[Fe^{III}(\mu-O)Fe^{III}O_2H^-] + H^+ \longrightarrow [Fe^{III}(\mu-O)Fe^{III}] + H_2O_2 \qquad (6a)$$
$$\underset{oxy}{} \qquad\qquad\qquad \underset{met}{}$$

$$[Fe^{III}(\mu-O)\underset{oxy}{Fe^{III}O_2H^-}] + H_2O \longrightarrow [Fe^{III}(\mu-O)\underset{met}{Fe^{III}OH^-}] + H_2O_2 \qquad (6b)$$
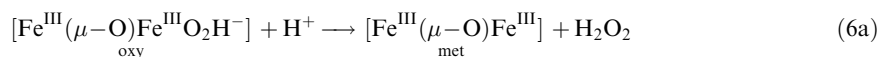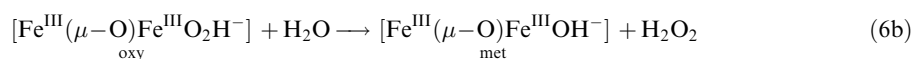
As with Mb/Hb, metHr is the thermodynamically stable form in aerobic solutions, and a metHr reductase has been reported.[131] The rate of autoxidation of oxyHr decreases by approximately tenfold with a one-unit decrease in pH in the acidic region, consistent with reaction (6a).[132] Certain exogenous anions, particularly azide, catalyze autoxidation of oxyHr by nucleophilic displacement of the peroxo ligand and/or by delivery of a proton to the coordinated peroxo. The slow rates of reactions (6a) and (6b) in the absence of these anions, however, indicate a substantial kinetic barrier to autoxidation. Presumably, autoxidation requires entry of solvent into the O_2-binding pocket of oxyHr, i.e., transient, simultaneous occupancy of the pocket by both bound O_2 and solvent. Consistent with this mechanism, the L98 variants of Hr in which either smaller or more polar side chains were substituted all led to significant increases in autoxidation rates.[93,112,120] Thus, the main function of L98 and the other hydrophobic residues shown in Figure 17 may be as hydrophobic and steric barriers to solvent-induced autoxidation.

8.10.2.2.6 Cooperative hemerythrins

Individual subunits of a Hr oligomer typically bind O_2 independently of each other, and with indistinguishable affinities; i.e., non-cooperatively. Two examples of cooperative Hrs are known, however, and these both consist of $\alpha_4\beta_4$ octamers.[94,95,133,134] Relative to Hb, the cooperativity in O_2-binding to these Hrs is modest with a Hill coefficient $n_{max} = 1.8–2.2$ and 1.4 kcal mol^{-1} of cooperative interaction energy, when analyzed in terms of higher- and lower-affinity R and T conformers.[134] Furthermore, the cooperativity is evident at pH 8, but not at pH 7, suggesting a deprotonation event is responsible for generating cooperative interactions. The small interaction energies and lack of detailed structural data on any $\alpha_4\beta_4$ Hr have made definitive atomic-level interpretation of these results impossible.

8.10.2.2.7 Mixed-valent forms

Mixed-valent $[Fe^{II}, Fe^{III}]$ forms of the Hr di-iron site, referred to as "semi-met," have been extensively characterized.[116,135–138] The semi-met forms can be prepared artificially either by one-electron oxidation of the deoxy form or one-electron reduction of the met form. Although they tend to disproportionate, the semi-met forms have sufficient kinetic stability ($t_{1/2}$ for disproportionation of several minutes) to be examined at room temperature and below. The semi-met forms show distinctive EPR spectra at <30 K arising from an $S = 1/2$ ground spin state due to antiferromagnetic coupling through what is presumed to be a hydroxo bridge. The semi-met forms prepared by reduction and oxidation have rhombic and axial EPR spectra, respectively, which has been interpreted in terms of a reversal of oxidation states of the two iron atoms and a protonation/deprotonation event.[135,138] A stable and reversible nitric oxide adduct of deoxyHr shows an $S = 1/2$ ground state, which has been interpreted as due to antiferromagnetic coupling between high spin Fe^{II} ($S = 2$) and high spin $\{FeNO\}^7$ ($S = 3/2$); the NO adduct is, thus, formulated as $[Fe^{II}(\mu\text{-OH})Fe^{III}NO^-]$.[139,140] No relevance of the semi-met forms to the O_2-binding reactions of Hr has been established, however. The plausible intermediate, $[Fe^{II}(\mu\text{-OH})Fe^{III}O_2^-]$, i.e., a "semi-met-superoxo" species, in the O_2 association/dissociation reactions, has never been detected. Furthermore, the semi-met form does not seem to be an intermediate during autoxidation.

8.10.2.2.8 Synthetic models

Accurate structural models of the (μ-oxo)bis(μ-carboxylato)di-iron(III) core of the Hr active site were first reported in 1983,[141,142] two years after an accurate structure of the metHr active site first appeared.[143] Since that time dozens of such structures have been reported,[102] an up-to-date compilation of which is beyond the scope of this chapter. Accurate models of the (μ-hydroxo)-bis(μ-carboxylato)di-iron (II) core of deoxyHr[144] and the corresponding mixed-valent core of semi-metHr[145,146] have also been prepared. The asymmetrical diferrous site of deoxyHr with one

six- and one five-coordinate iron (cf. Figure 16C), however, has proven difficult to reproduce synthetically, and, in fact, no such model that reversibly binds O_2 has yet been structurally authenticated. Diferrous complexes or enzymes with O,N-donor ligands and open or labile coordination sites on both irons have typically yielded metastable μ-1,2-peroxo complexes upon reaction with O_2.[79,91] One spectroscopically accurate model of the Hr oxygenation reaction has been reported. Exposure of a complex having a (μ-hydroxo)bis(μ-carboxylato)di-iron(II) core with one six- and one five-coordinate iron to O_2 at $-78\,^\circ$C generated a species with a UV–vis absorption spectrum strikingly similar to that of oxyHr and different from that of typical μ-1,2-peroxo complexes.[147,148] Resonance Raman excitation of the 470-nm absorption band of the oxygenated complex yielded an $^{18}O_2$-sensitive vibrational mode at $843\,cm^{-1}$, characteristic of a peroxo O−O stretch, and nearly identical to that of oxyHr. Iron-57 Mössbauer spectra indicated that the peroxo adduct was high-spin diferric. The O_2-binding in this complex was irreversible, and a crystal structure has not been reported.

8.10.2.3 Dicopper Type: Hemocyanins

The third known solution found by nature to the problem of reversible O_2-binding is the hemocyanins (Hcs).

8.10.2.3.1 *Early history and distribution*

Hcs are found extracellularly in the hemolymph (the fluid corresponding to blood) of two invertebrate phyla: arthropods and molluscs. These two phyla span a huge and diverse array of life forms, horseshoe crab and octopus being familiar examples from each.[86] Hcs are all large, multi-domain, multi-subunit proteins, and, due partly their large sizes, the structural and electronic aspects of O_2-binding to Hc were the most recent to be clarified among the O_2-carrying proteins. The presence of copper in Hc was apparently first reported in the blue blood of a snail in 1847, and the name, "hemocyanin" was coined in 1878, the "-cyanin" portion arising from the blue color of the oxygenated form.[149] A 2Cu:1O_2-binding stoichiometry was established by 1934[150], from which a dicopper site was inferred. Based on the color change, namely, colorless in the deoxy form to blue in the oxy form, it was recognized that oxidation of copper must be occurring during O_2-binding. Early formulations for the oxy state included $Cu^{II}(O_2{}^-)Cu^I$,[90] and a resonance structure among $[Cu^I(O_2)Cu^I] \longleftrightarrow [Cu^{II}(O_2{}^-)Cu^I] \longleftrightarrow [Cu^{II}(O_2{}^{2-})Cu^{II}]$.[149] A dicopper(II)–peroxo formulation has turned out to be the best description, based on the subsequently accumulated evidence discussed below.

8.10.2.3.2 *Protein structure and superstructure*

Molluscan and arthropodan Hcs have very different oligomeric structures, as illustrated in Figure 20A.[86,151,152] The molluscan Hcs form seven or eight $\sim$50 kDa domains in a single polypeptide chain, the domains being connected like "beads on a string". Each domain contains a dicopper site. Either ten or twenty of these $\sim$450-kDa subunits then form a cylindrical structure containing head-to-tail subunit pairs having molecular masses of 4,000 or 8,000 kDa, respectively. The arthropodan Hcs consist of $\sim$75-kDa subunits each containing a dicopper site, which assemble into hexamers having D_3 symmetry; these further assemble into aggregates containing as many as eight hexamers. The tertiary structure of one subunit of horseshoe crab Hc is shown in Figure 20B. From comparisons with the tertiary structures of Mb/Hb (Figure 6) and Hr (Figure 16), it is obvious that a much larger polypeptide surrounds the O_2-binding site in Hc. This comparison also emphasizes the dissimilarity in tertiary structures among the three types of O_2-carrying proteins.

8.10.2.3.3 *The dicopper site*

Despite the different oligomeric structures, molluscan and arthropodan Hcs contain very similar dicopper active sites. Two crystal structures are currently available for oxyHcs, one from the horseshoe crab, *L. polyphemus*, at 2.4 Å resolution,[153,154] and one from the mollusc, *Octopus*
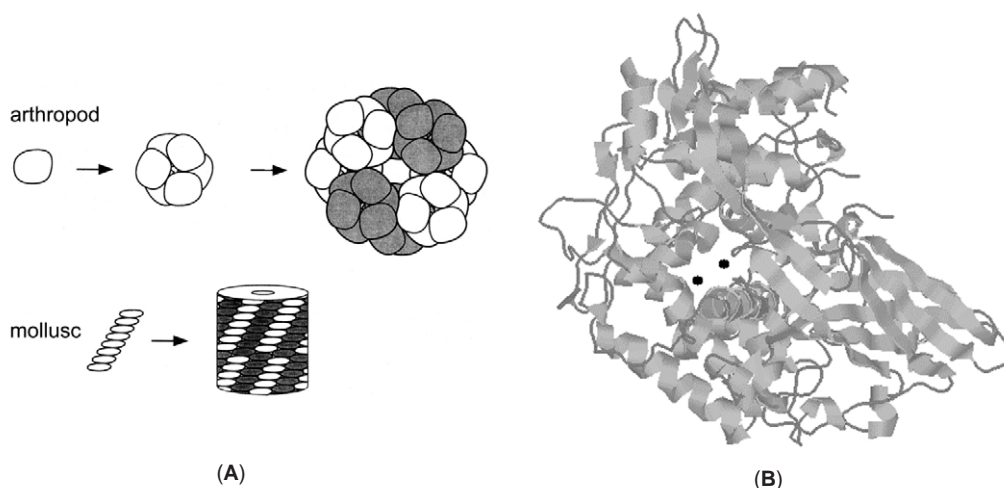
Figure 20 (A) Schematic diagrams depicting assembly of Hc oligomers.[151] (B) Ribbon drawing of the tertiary structure of *L. polyphemus* deoxyHc subunit surrounding the dicopper site (shaded spheres). Drawing was generated as described for the corresponding dicopper site in the legend to Figure 21.
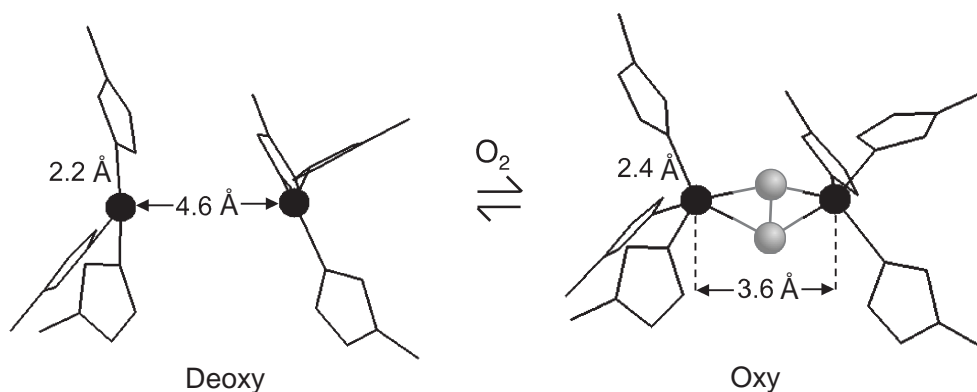
Figure 21 The dicopper sites of *L. polyphemus* deoxy and oxyHcs. Side chains of histidine ligands are shown in wireframe representation (with epsilon nitrogen ligands to Cu). Dark blue spheres represent coppers, and cyan spheres represent oxygens. Some representative interatomic distances are indicated. Drawings were

dofleini, at 2.3 Å resolution. Crystal structures are also available for deoxy forms of *L. polyphemus*[155] and another arthropod, *Panulirus interruptus*[156] at 2.2 and 3.2 Å resolutions, respectively. The dicopper sites are well-buried within the protein interior in both arthropodan and molluscan Hcs, and no solvent molecules appear to occupy the O_2-binding pockets, which are lined with hydrophobic residues. The only substantial difference between the dicopper site structures in molluscan vs. arthropodan Hcs is the presence of a thioether linkage from a cysteine residue to the $C\varepsilon 2$ of one of the His ligands in the molluscan Hcs. This linkage appears to have surprisingly little structural or functional effects on the O_2-binding properties.

The structures of the dicopper sites of the deoxy and oxy forms of *L. polyphemus* Hc are shown in Figure 21, along with pertinent distance information. Each of the Cu^I centers of deoxyHc has three histidine epsilon nitrogen ligands in a distorted trigonal planar coordination geometry, and the Cu^I–Cu^I separation is 4.6 Å. The coordination geometry of both Cu^{II} centers in oxyHc is best described as square-pyramidal with two bridging oxygens and two histidine nitrogens providing the equatorial ligands. The axial ligand is furnished by the third histidine nitrogen at a longer distance (2.4 Å) from the copper. The Cu^{II}–Cu^{II} distance has shortened by about 1 Å compared to the deoxy form and the dioxygen is coordinated in a symmetrical μ-η^2:η^2 mode with an essentially planar $[Cu_2O_2]^{2+}$ core.

This binding geometry and the formulation for the oxygenation reaction (7) are now considered to be well-established. This conclusion was arrived at, however, not so much from the two relatively

low-resolution X-ray crystal structures as from comparisons of spectroscopic and magnetic properties of the oxyHcs to those of synthetic dicopper–dioxygen complexes of known structure. Although it seemed clear that Cu^{II} must be involved, any structural and electronic formulation of the dicopper site of oxyHc also had to explain three distinctive and characteristic spectral properties (reviewed by Solomon *et al.*).[99,157] First, oxyHc shows no EPR spectrum, whereas magnetically isolated Cu^{II} (d^9) should show characteristic $S = 1/2$ EPR spectra. From magnetic susceptibility measurements, the singlet ground state was estimated to be $600\,cm^{-1}$ below the triplet state. Since EXAFS showed that the two copper atoms in oxyHc are $3.6\,\text{Å}$ apart,[158,159] such strong antiferromagnetic coupling is possible only via superexchange through a bridging ligand. Second, resonance Raman spectra identified an $^{18}O_2$-sensitive O—O stretching frequency at $750\,cm^{-1}$,[160,161] which seemed to confirm the dicopper(II)–peroxo description, but which is unusually low for a metal–peroxo complex (cf. Table 1). Third, oxyHc shows an intense electronic absorption at 350 nm ($\varepsilon \sim 20{,}000\,M^{-1}cm^{-1}$) and a less intense absorption at ~ 550 nm ($\varepsilon \sim 1{,}000\,M^{-1}cm^{-1}$) (the latter of which is responsible for the blue color), both of which are absent in the deoxy form. Based on analysis of the absorption and CD spectra and resonance Raman excitation profiles, these higher- and lower-energy absorptions were assigned to $O_2^{2-} \rightarrow Cu^{II}$ charge transfer transitions, presumably σ- and π-type, respectively, of a bridging peroxo.[99] With this spectroscopic and magnetic information in hand, the oxygenation reaction could be confidently formulated as reaction (7):

$$O_2 + \underset{\text{deoxy}}{Cu^I Cu^I} \rightleftharpoons \underset{\text{oxy}}{Cu^{II}(\mu - O_2^{2-})Cu^{II}} \tag{7}$$
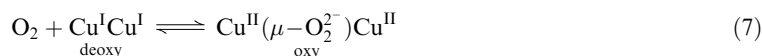
The preceding results, however, did not, by themselves, establish a unique structure for the dicopper site of oxyHc. In fact, it appears that the correct structure was never seriously considered prior to 1989. In that year, the complex, $[Cu(HB(3,5\text{-}i\text{-}Pr_2pz)_3)]_2(O_2)$ ($HB(3,5\text{-}i\text{-}Pr_2pz = $ hydrotris(3,5-diisopropyl-1-pyrazolyl)borate) was reported.[162] This complex was the first to show spectroscopic and magnetic properties that matched those of oxyHc almost exactly, including the low O—O stretching frequency, and its X-ray crystal structure provided the first example of a dicopper complex with a $\mu\text{-}\eta^2\text{:}\eta^2$ peroxo bridging geometry and planar $[Cu_2O_2]^{2+}$ core. By the time an X-ray crystal structure of oxyHc was published in 1994,[154] the $\mu\text{-}\eta^2\text{:}\eta^2$-peroxo and planar $[Cu_2O_2]^{2+}$ core structure in Figure 21 were already widely accepted, based on the original and several subsequent synthetic complexes with this geometry and distinctive spectroscopic properties.[163–165] Some of these synthetic complexes also bound O_2 reversibly. The unusually low O—O stretching frequency of the $\mu\text{-}\eta^2\text{:}\eta^2$ peroxo in the planar $Cu^{II}(O_2^{2-})Cu^{II}$ core was explained as due to the HOMO containing a considerable contribution from the peroxo σ_{2p}^* orbital, as shown in Figure 22.[166,167] This σ_{2p}^* orbital is usually too high in energy to contribute significantly to metal–dioxygen bonding, as noted by its absence from Figure 3B. This unusual π-acceptor interaction of the peroxo more than compensates for the strong σ donation from the in-plane peroxo π_{2p}^* orbital to d_{yz} orbitals on both coppers, the overlaps of which lead to the LUMO in Figure 22 (see also Chapter 8.15). This high-lying LUMO was suggested to be responsible for the intense, higher-energy electronic absorption at 350 nm, and, thus, supports its assignment as the in-plane peroxo $\pi_{2p}^* \rightarrow Cu^{II}$ (d_{xy}) charge transfer transition. The weaker absorption at 550 nm, giving rise to the blue color, was then assigned to the corresponding charge transfer transition from the perpendicular, essentially non-bonding peroxo π_{2p}^* to Cu^{II}.[99]

An apparent consequence of the relatively weak O—O bond in the $\mu\text{-}\eta^2\text{:}\eta^2$ peroxo $Cu^{II}(O_2^{2-})Cu^{II}$ core is that several of the synthetic complexes tend to undergo isomerization to a $Cu^{III}(\mu\text{-}O^{2-})_2)Cu^{III}$ core in which the O—O bond is completely cleaved.[168] This isomerization is apparently prevented in oxyHc by restrictions on the approach of the two copper centers imposed by the protein matrix. The bis(μ-oxo)bridged dicopper(III) complexes have Cu—Cu distances of $\sim 2.8\,\text{Å}$ compared to $\sim 3.6\,\text{Å}$ for the $\mu\text{-}\eta^2\text{:}\eta^2$ $Cu^{II}(O_2^{2-})Cu^{II}$ complexes. However, the preceding bonding description and $[Cu^{II}(\mu\text{-}O_2^{2-})Cu^{II}] \rightleftharpoons [Cu^{III}(\mu\text{-}O^{2-})_2)Cu^{III}]$ core isomerization in the synthetic complexes may have implications for the phenol hydroxylase activity exhibited by some hemocyanins and by the closely related enzyme, tyrosinase (see also Chapter 8.15).[157,169,170]

8.10.2.3.4 *Mechanism of dioxygen binding*

Hcs, at least in their aggregated forms, bind O_2 in a highly cooperative fashion, with Hill coefficients typically in the range, $n_{max} = 3$–5.[171–174] However, changing conditions, (pH, salt, etc.)
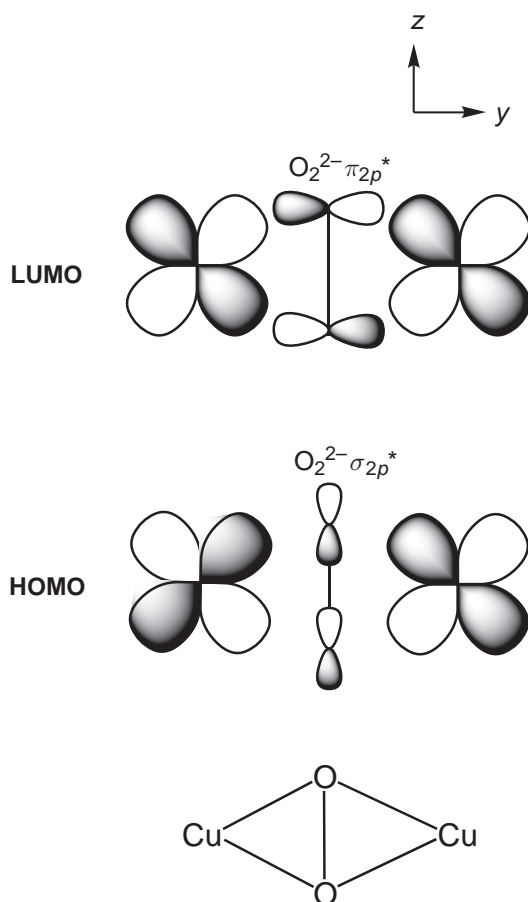
Figure 22 The HOMO and LUMO of the $\mu\text{-}\eta^2\text{:}\eta^2$ peroxo planar $[Cu_2O_2]^{2+}$ core at the active site of oxyHc.[166,167]

can have large effects on both O_2 affinity and on the extent of cooperativity in Hcs. Although attempts have been made to explain this cooperativity in terms of simple high- and low-affinity R and T conformers, as discussed above for Hb, more complicated models are often needed to accurately fit the O_2-binding curves.[153,154,171] These complications are undoubtedly due to both the conditional sensitivity mentioned above and the huge aggregates formed by many Hcs, which can potentially give rise to a large number of conformers. Hc aggregates larger than hexamers have so far defied atomic-level structural characterization.

Hc proteins are much larger per O_2-binding site than the other two types. Nevertheless, O_2 association and dissociation rates for Hcs are surprisingly similar to those of both Mb/Hbs and Hrs, that is, k_{on} on the order of $10^7 \, M^{-1} s^{-1}$ and k_{off} in the range of 10–100 s^{-1}.[115,130] Neither O_2 dissociation nor association rates show solvent deuterium isotope effects,[130] consistent with the absence of any proton transfer in the formulation of the O_2-binding equilibrium, reaction (7), and with the crystal structures of the dicopper sites, which show no water or hydrogen bonds to the dioxygen (cf. Figure 21). As for Mb/Hb and Hr, the high O_2 association rate constants are consistent with rate-limiting diffusion through the protein matrix. Examinations of the X-ray crystal structures have led to proposals of various paths for diffusion of O_2 from the protein surface through solvent-filled cavities to the dicopper site, all of which, however, appear to be obstructed in some way.[155,156] The difficulty of cloning and overexpressing Hcs in heterologous hosts has so far prevented examination of engineered amino acid variants.

Unlike the other two types of O_2-carrying proteins, the reaction of singlet Cu^I (d^{10}) with triplet O_2 is formally spin-forbidden. Based on a DFT study, Metz and Solomon[175] have proposed a concerted pathway, reproduced in Figure 23, for O_2-binding to the dicopper(I) site that overcomes the spin restriction by charge delocalization over the $[Cu_2O_2]^{2+}$ core, thereby lowering the energy difference between the singlet and triplet states. Neither the DFT calculations nor the kinetics of O_2-binding show any evidence for a superoxo intermediate, i.e., Cu^{II}–O_2^-–Cu^I. This
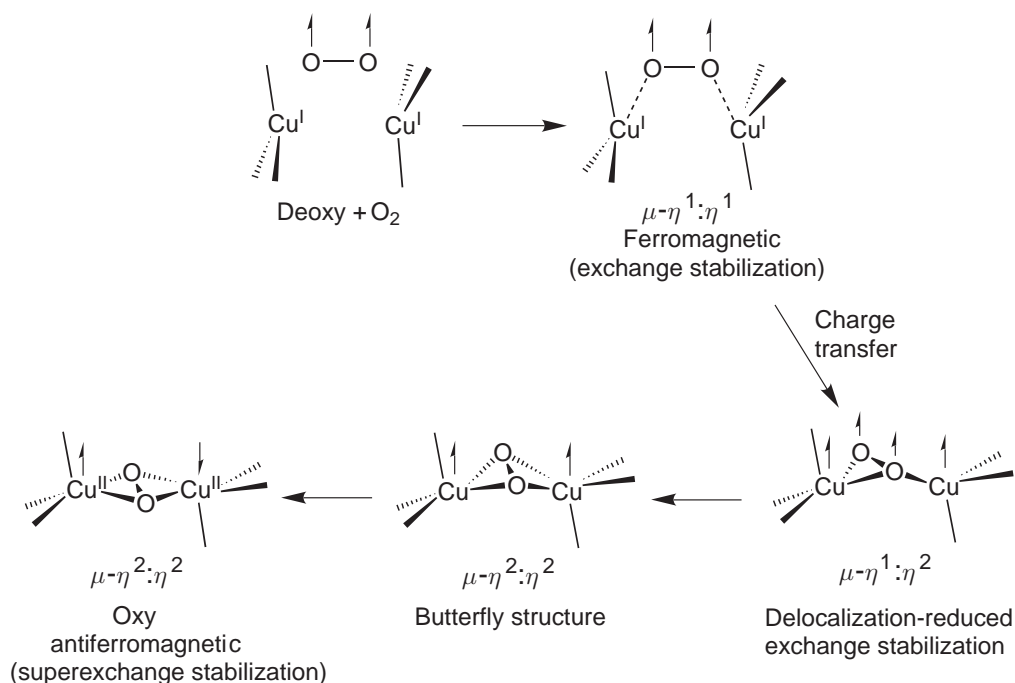
Figure 23 Concerted O_2 binding pathway proposed for Hc.[175] Half arrows indicate localization and signs of electron spins on the $[Cu_2O_2]^{2+}$ core.

negative result differs from O_2-binding to synthetic copper(I) model complexes, where a superoxide intermediate *is* observed on the way to the $\mu\text{-}\eta^2\text{:}\eta^2$ $Cu^{II}(O_2^{2-})Cu^{II}$ product.[165,168] The preorganized dicopper(I) site presumably favors the concerted two-electron transfer pathway shown in Figure 23. Metz and Solomon[175] also propose that the repulsive interaction energy caused by holding the two positively charged Cu^I centers of deoxyHc in close proximity within the low dielectric protein interior promotes the highly exothermic O_2-binding. This explanation also implies that longer and shorter Cu—Cu distances could be features of T and R state conformations with lower and higher O_2 affinities, respectively, and could thereby provide a mechanism for converting some of the negative enthalpy of O_2-binding into cooperative interaction energy.

8.10.3 O_2-, CO-, AND NO-SENSING METALLOPROTEINS

8.10.3.1 Types and Biological Roles

Relatively recently, it has become apparent that both higher and lower forms of life, including microorganisms, contain a separate class of metalloproteins that reversibly bind dioxygen or the related small gaseous molecules, nitric oxide and carbon monoxide. These proteins are typically found in relatively low intracellular concentrations and are meant to function not as carriers or storage proteins, but rather as sensors.[40,176,177] The sensing of one of these small gaseous molecules typically triggers a cascade of enzymatic reactions resulting in various metabolic responses, such as changes in blood pressure in humans or "swimming" away from dioxygen in the case of air-sensitive bacteria. The molecular mechanisms by which these sensing proteins specifically bind O_2, NO, or CO and transduce the binding energy are only beginning to be understood. Therefore, only short summaries are given here. Nearly all of the known examples are heme proteins. Only one potential example of a Hr-like O_2 sensor and no examples of Hc-like sensing proteins have been reported up to now.

8.10.3.2 NO Sensing: Guanylate Cyclase and Nitrophorin

Soluble guanylate cyclase (sGC) is a vertebrate protein consisting of two domains, one of which contains a heme. The ferrous heme domain binds nitric oxide, which activates the other domain

to catalyze conversion of guanosine triphosphate to cyclic guanosine monophosphate, a messenger in signaling pathways leading to smooth muscle relaxation and neurotransmission.[177,178] Spectroscopic studies indicate that the resting ferrous heme of sGC is five-coordinate with a proximal histidine ligand. This ferrous heme binds NO and CO, but surprisingly, not O_2, under aerobic conditions. There is currently no crystal structure of sGC, but spectroscopic and kinetics results suggest that a weak proximal histidine–iron bond and negative polarity of the distal heme pocket may discriminate against O_2-binding. In fact, the ferrous–nitrosyl heme adduct of sGC is five-coordinate, indicating cleavage of the proximal His—Fe bond upon binding NO.[178]

Some blood-sucking insects have apparently exploited the signaling cascade caused by sGC's response to NO. During a bloodmeal, these insects inject a heme protein called nitrophorin to transport NO from their salivary glands to the victims, resulting in vasodilation and reduced blood coagulation.[179] X-ray crystallography shows that nitrophorin has a five-coordinate heme with a proximal histidine ligand and open distal pocket in the resting state, but otherwise has no structural relation to the globin-type heme proteins. Nitrophorin binds and releases NO at a ferric rather than ferrous heme. The NO binds *trans* to the proximal histidine, forming a low-spin six-coordinate adduct. Ferric hemes, such as those in Mb and Hb, do bind NO reversibly, but this binding is followed by autoreduction.[61] The ferric heme–NO adduct is somehow stabilized against autoreduction in nitrophorin. Explanations for this stabilization have included protein-induced ruffling of the heme and expulsion of water together with closure of the distal pocket upon NO binding.[180,181] The ferric heme of nitrophorin also has a much lower reduction potential than does that of Mb. Nitrophorin may have evolved to stabilize the ferric heme as an alternative means of discriminating against binding of O_2 and CO, both of which have little or no inherent affinity for ferric hemes.

8.10.3.3   Regulation of Bacterial Gene Expression

8.10.3.3.1   *O_2 sensing: FixL and Dos*

FixL is a two-domain protein found in *Rhizobia*, the bacteria that colonize root nodules of leguminous plants. FixL functions as an O_2 sensor, regulating expression of genes associated with N_2 fixation.[176,177] The resting ferrous heme of the O_2-binding domain, which shows no homology to other known families of heme proteins, is five-coordinate with a distal histidine ligand. FixL binds O_2, NO, and CO reversibly, but with lower affinity than Mb and with much higher discrimination against CO.[177] X-ray crystal structures are available for several forms of FixL. Based on these structures, a mechanism has been proposed for selective binding of O_2 and signal transduction by FixL. A positively charged arginine side chain, which forms a salt bridge with a heme propionate in the ferrous resting state, moves to the heme distal pocket where it forms a hydrogen bond with the end-on bound O_2. NO and CO binding do not cause this movement of the arginine side chain, which remains salt-bridged to the heme propionate in these adducts.[176]

A related protein, Dos, is presumed to be an O_2 sensor in some bacteria, but its exact function is unknown. No structure is available, but spectroscopic data indicate that it differs from FixL in having a six-coordinate ferrous heme even in the absence of the gaseous diatomic ligands. The sixth ligand was recently identified as a thioether sulfur from a methionine residue, which is displaced upon binding of O_2, NO, or CO.[182] Like FixL, Dos strongly discriminates against CO relative to O_2-binding.

8.10.3.3.2   *CO sensing: CooA*

CooA is a CO-sensing heme protein found in a photosynthetic bacterium that can survive using oxidation of CO to CO_2 as its sole energy source. CooA induces transcription of several genes encoding enzymes in the CO oxidation pathway. It does so by binding to promoter regions on the DNA upstream of the genes, but only in the presence of CO.[176] Here again, CooA is a two-domain protein, one of which contains the heme. However, among the heme proteins that bind gaseous diatomic ligands, CooA is unique in several respects. Spectroscopic studies suggest that the heme is six-coordinate in both ferric and ferrous states, even in the absence of CO. X-ray crystallography revealed that in the ferrous state one of the axial ligands

is a histidine epsilon nitrogen, whereas in the ferric state, the histidine is replaced by a cysteine thiolate. The other axial ligand in both ferrous and ferric states is the amino nitrogen of a proline residue, the first reported example of such ligation. Spectroscopic studies indicate that this proline ligand is displaced upon CO binding, forming a six-coordinate adduct. However, no crystal structure of the CO adduct of CooA is yet available. NO apparently displaces both axial ligands and forms a five-coordinate complex with the ferrous heme that does not activate gene transcription. O_2 does not bind reversibly to ferrous CooA but rather causes rapid autoxidation to the ferric state.

8.10.3.4 Bacterial Aerotaxis

8.10.3.4.1 *O_2 sensing: HemAT*

Aerotaxis is the process by which bacteria and archaea "swim" up or down a concentration gradient of dissolved O_2. HemAT is the O_2-sensing heme protein in the complicated signaling cascade leading to aerotaxis in some bacteria and archaea. The heme binding domain of HemAT is a member of the globin family, and binds O_2 reversibly and with similar affinity to that of Mb.[176,183] No crystal structure is yet available.

8.10.3.4.2 *O_2 sensing: a hemerythrin-like protein*

The only example of a potential non-heme O_2-sensing metalloprotein reported up to now is DcrH from an anaerobic sulfate-reducing bacteria.[184] DcrH is homologous to a family of bacterial membrane-spanning chemotactic (chemo-sensing and transducing) proteins, but is unique in containing a Hr-like domain at its C-terminus. DcrH was, therefore, presumed to be involved in O_2 sensing, although its exact function remains to be determined. Because of the difficulty of isolating membrane-spanning proteins, the C-terminal Hr-like domain of DcrH, DcrH-Hr, was cloned and overexpressed separately. The heterologously expressed DcrH-Hr folded spontaneously into a helical protein containing an oxo-bridged diferric site, whose spectroscopic properties closely matched those of Hr. Based on UV–vis absorption spectra, exposure of the reduced (colorless, presumably diferrous) DcrH-Hr to air resulted in formation of an O_2 adduct very similar to that of oxyHr, although it autoxidized within a few minutes at room temperature.[184]

8.10.4 SUMMARY

For those sensing proteins containing heme, it is obvious even at this early stage that the molecular mechanisms for discriminating between the three gaseous diatomic ligands, O_2, NO, and CO, are quite distinct from those used by O_2-carrying heme proteins. Furthermore, the mechanisms used to explain cooperative O_2-binding to Hb cannot be used to explain signal transduction by the sensing proteins. The discovery of these sensing proteins thus represents an exciting new development in the area of O_2-binding proteins.

8.10.5 REFERENCES

1. Springer, B. A.; Sligar, S. G.; Olson, J. S.; Phillips, G. N. Jr. *Chem. Rev.* **1994**, *94*, 699–714.
2. Feig, A. L.; Lippard, S. J. *Chem. Rev.* **1994**, *94*, 759–805.
3. Vaska, L. *Acc. Chem. Res.* **1976**, *9*, 175–183.
4. Pecoraro, V. L.; Baldwin, M. J.; Gelasco, A. *Chem. Rev.* **1994**, *94*, 807–826.
5. Niederhoffer, E. C.; Timmons, J. A.; Martell, A. E. *Chem. Rev.* **1984**, *84*, 137–203.
6. Dickman, M. H.; Pope, M. T. *Chem. Rev.* **1994**, *94*, 569–584.
7. Busch, D. H.; Alcock, N. W. *Chem. Rev.* **1994**, *94*, 585–623.
8. Butler, A.; Clague, M. J.; Meister, G. E. *Chem. Rev.* **1994**, *94*.
9. Kitajima, N.; Moro-oka, Y. *Chem. Rev.* **1994**, *94*, 737–757.
10. Kurtz, D. M., Jr. *Essays Biochem.* **1999**, *34*, 85–100.
11. Kendrew, J. C.; Dickerson, R. E.; Strandberg, B. E.; Hart, R. G.; Davies, D. R.; Phillips, D. C.; Shore, V. C. *Nature* **1960**, *185*, 422–427.
12. Perutz, M. F.; Muirhead, H.; Cox, J. M.; Goaman, L. C. *Nature* **1968**, *219*, 131–139.

13. Antonini, E.; Brunori, M. *Hemoglobin and Myoglobin in their Reactions with Ligands*; North-Holland: Amsterdam, 1971.
14. Dickerson, R. E.; Geis, I. *Hemoglobin: Structure, Function, Evolution and Pathology*; Benjamin/Cummings: Menlo Park, CA, 1983.
15. Weber, R. E.; Vinogradov, S. N. *Physiol Rev* **2001**, *81*, 569–628.
16. Dolphin, D., Ed. *The Porphyrins*; Academic Press: New York, 1977; Vol. 1–7.
17. Momenteau, M.; Reed, C. A. *Chem. Rev.* **1994**, *94*, 659–698.
18. Collman, J. P.; Wang, Z. *Chemtracts, Inorg. Chem.* **2000**, *8*, 499–533.
19. Bellelli, A.; Lendaro, E.; Ippoliti, R.; Regan, R.; Gibson, Q. H.; Brunori, M. *Biochemistry* **1993**, *32*, 7635–7643.
20. Wang, J. H. *J. Am. Chem. Soc.* **1958**, *80*, 3168–3169.
21. Basolo, F.; Hoffman, B. M.; Ibers, J. A. *Acc. Chem. Res.* **1975**, *8*, 384–392.
22. Collman, J. P.; Gagne, R. R.; Reed, C. A.; Robinson, W. T.; Rodley, G. A. *Proc. Natl. Acad. Sci. USA* **1974**, *71*, 1326–1329.
23. Davies, M. J.; Mathieu, C.; A, P. *Adv. Inorg. Chem.* **1999**, *46*, 495–542.
24. Wittenberg, J. B.; Bolognesi, M.; Wittenberg, B. A.; Guertin, M. *J. Biol. Chem.* **2002**, *277*, 871–874.
25. Phillips, S. E. *J. Mol. Biol.* **1980**, *142*, 531–554.
26. Lamy, J. N.; Green, B. N.; Toulmond, A.; Wall, J. S.; Weber, R. E.; Vinogradov, S. N. *Chem. Rev.* **1996**, *96*, 3113–3124.
27. Sayle, R.; Milner-White, E. J. *Trends Biochem. Sci.* **1995**, *20*, 374–376.
28. Vojtechovsky, J.; Chu, K.; Berendzen, J.; Sweet, R. M.; Schlichting, I. *Biophys. J.* **1999**, *77*, 2153–2174.
29. Yang, J.; Kloek, A. P.; Goldberg, D. E.; Mathews, F. S. *Proc. Natl. Acad. Sci. USA* **1995**, *92*, 4224–4228.
30. Pauling, L.; Coryell, C. D. *Proc. Natl. Acad. Sci. USA* **1936**, *22*, 210–216.
31. Bytheway, I.; Hall, M. B. *Chem. Rev.* **1994**, *94*, 639–658.
32. Weiss, J. J. *Nature* **1964**, *202*, 83–84.
33. Pauling, L.; Weiss, J. J. *Nature* **1964**, *203*, 182–183.
34. Shaanan, B. *J. Mol. Biol.* **1983**, *171*, 31–59.
35. Boso, B.; Debrunner, P. G.; Wagner, G. C.; Inubushi, T. *Biochim. Biophys. Acta* **1984**, *791*, 244–251.
36. Potter, W. T.; Tucker, M. P.; Houtchens, R. A.; Caughey, W. S. *Biochemistry* **1987**, *26*, 4699–4707.
37. Miller, L. M.; Chance, M. R. *Biochemistry* **1995**, *34*, 10170–10179.
38. Das, T. K.; Couture, M.; Ouellet, Y.; Guertin, M.; Rousseau, D. L. *Proc. Natl. Acad. Sci. USA* **2001**, *98*, 479–484.
39. Rovira, C.; Kunc, K.; Hutter, J.; Ballone, P.; Parrinello, M. *J. Phys. Chem. A* **1997**, *101*, 8914–8925.
40. Spiro, T. G.; Jarzecki, A. A. *Curr. Opin. Chem. Biol.* **2001**, *5*, 715–723.
41. Gibson, Q. H. *J. Biol. Chem.* **1989**, *264*, 20155–20158.
42. Olson, J. S.; Phillips, G. N. Jr. *J. Biol. Chem.* **1996**, *271*, 17596.
43. Royer, W. E., Jr.; Knapp, J. E.; Strand, K.; Heaslet, H. A. *Trends Biochem. Sci.* **2001**, *26*, 297–304.
44. Olson, J. S.; Phillips, G. N., J. *J. Biol. Inorg. Chem.* **1997**, *2*, 544–552.
45. Phillips, S. E.; Schoenborn, B. P. *Nature* **1981**, *292*, 81–82.
46. Petsko, G. A. *Nat. Struct. Biol.* **1996**, *3*, 565–566.
47. Feher, V. A.; Baldwin, E. P.; Dahlquist, F. W. *Nat. Struct. Biol.* **1996**, *3*, 516–521.
48. Huang, X.; Boxer, S. G. *Nat. Struct. Biol.* **1994**, *1*, 226–229.
49. Schoenborn, B. P.; Watson, H. C.; Kendrew, J. C. *Nature* **1965**, *207*, 28–30.
50. Tilton, R. F., Jr.; Kuntz, I. D.; Petsko, G. A. *Biochemistry* **1984**, *23*, 2849–2857.
51. Frauenfelder, H.; McMahon, B. H.; Austin, R. H.; Chu, K.; Groves, J. T. *Proc. Natl. Acad. Sci. USA* **2001**, *98*, 2370–2374.
52. Slebodnick, C.; Ibers, J. A. *J. Biol. Inorg. Chem.* **1997**, *2*, 521–525.
53. Sage, J. T. *J Biol Inorg Chem* **1997**, *2*, 537–543.
54. Lim, M.; Jackson, T. A.; Anfinrud, P. A. *J. Biol. Inorg. Chem.* **1997**, *2*, 531–536.
55. Kachalova, G. S.; Popov, A. N.; Bartunik, H. D. *Science* **1999**, *284*, 473–476.
56. Brunori, M. *Trends Biochem. Sci.* **2001**, *26*, 209–210.
57. Jia, L.; Bonaventura, C.; Bonaventura, J.; Stamler, J. S. *Nature* **1996**, *380*, 221–226.
58. Witting, P. K.; Douglas, D. J.; Mauk, A. G. *J. Biol. Chem.* **2001**, *276*, 3991–3998.
59. Boffi, A.; Sarti, P.; Amiconi, G.; Chiancone, E. *Biophys. Chem.* **2002**, *98*, 209–216.
60. Brucker, E. A.; Olson, J. S.; Ikeda-Saito, M.; Phillips, G. N., Jr. *Proteins* **1998**, *30*, 352–356.
61. Addison, A. W.; Stephanos, J. J. *Biochemistry* **1986**, *25*, 4104–4113.
62. Joshi, M. S.; Ferguson, T. B. Jr.; Han, T. H.; Hyduke, D. R.; Liao, J. C.; Rassaf, T.; Bryan, N.; Feelisch, M.; Lancaster, J. R., Jr. *Proc. Natl. Acad. Sci. USA* **2002**, *16*, 10341–10346.
63. Muller, J. K.; Skibsted, C. H. *Chem. Rev.* **2002**, *102*, 1167–1178.
64. Enemark, J. H.; Feltham, R. D. *Coord. Chem. Rev.* **1974**, *13*, 339–406.
65. Harutyunyan, E. H.; Safonova, T. N.; Kuranova, I. P.; Popov, A. N.; Teplyakov, A. V.; Obmolova, G. V.; Valnshtein, B. K.; Dodson, G. G.; Wilson, J. C. *J. Mol. Biol.* **1996**, *264*, 152–161.
66. Doyle, M. P.; Hoekstra, J. W. *J. Inorg. Biochem.* **1981**, *14*, 351–358.
67. Eich, R. F.; Li, T.; Lemon, D. D.; Doherty, D. H.; Curry, S. R.; Aitken, J. F.; Mathews, A. J.; Johnson, K. A.; Smith, R. D.; Phillips, G. N., Jr.; Olson, J. S. *Biochemistry* **1996**, *35*, 6976–6983.
68. Herold, S.; Exner, M.; Nauser, T. *Biochemistry* **2001**, *40*, 3385–3395.
69. Ford, P. C.; Lorkovic, I. M. *Chem. Rev.* **2002**, *102*, 993–1018.
70. Gardner, P. R.; Gardner, A. M.; Martin, L. A.; Dou, Y.; Li, T.; Olson, J. S.; Zhu, H.; Riggs, A. F. *J. Biol. Chem.* **2000**, *275*, 31581–31587.
71. Gardner, A. M.; Martin, L. A.; Gardner, P. R.; Dou, Y.; Olson, J. S. *J. Biol. Chem.* **2000**, *275*, 12581–12589.
72. Suslick, K. S.; Reinert, T. J. *J. Chem. Ed.* **1985**, *62*, 974–983.
73. Edsall, J. T. *Fed. Proc.* **1980**, *39*, 226–235.
74. Eaton, W. A.; Henry, E. R.; Hofrichter, J.; Mozzarelli, A. *Nature Struct. Biol.* **1999**, *6*, 351–358.
75. Monod, J.; Wyman, J.; Changeux, J.-P. *J. Mol. Biol.* **1965**, *12*, 88–118.
76. Perutz, M. F. *Nature* **1970**, *228*, 726–739.
77. Perutz, M. F.; Wilkinson, A. J.; Paoli, M.; Dodson, G. G. *Annu. Rev. Biophys. Biomol. Struct.* **1998**, *27*, 1–34.

78. Fermi, G.; Perutz, M. F.; Shaanan, B.; Fourme, R. *J. Mol. Biol.* **1984**, *175*, 159–174.
79. Solomon, E. I.; Brunold, T. C.; Davis, M. I.; Kemsley, J. N.; Lee, S.-K.; Lehnert, N.; Neese, F.; Skulan, A. J.; Yang, Y.-S.; Zhou, J. *Chem. Rev.* **2000**, *100*, 235–350.
80. Stenkamp, R. E. *Chem. Rev.* **1994**, *94*, 715–726.
81. Kurtz, D. M., Jr. In *Advances in Comparative and Environmental Physiology 13. Blood and Tissue Oxygen Carriers*; Magnum, C. P., Ed.; Springer-Verlag: New York, 1992; Vol.13, pp 151–171.
82. Sanders-Loehr, J. In *Iron Carriers and Iron Proteins*; Loehr, T. M., Ed.; VCH: New York, 1989; pp 373–466.
83. Vincent, J. B.; Olivier-Lilley, G. L.; Averill, B. A. *Chem. Rev.* **1990**, *90*, 1447–1467.
84. Klotz, I. M.; Kurtz, D. M., Jr. *Acc. Chem. Res.* **1984**, *17*, 16–22.
85. Mangum, C. P. In *Advances in Comparative and Environmental Physiology 13. Blood and Tissue Oxygen Carriers*; Mangum, C. P., Ed.; Springer-Verlag: New York, 1992; Vol. 13, pp 173–192.
86. Terwilliger, N. B. *J. Exp. Biol.* **1998**, *201 (Pt. 8)*, 1085–1098.
87. Andrews, E. A. *J. Hopkins Univ. Circ.* **1890**, *9*, 65.
88. Klotz, I. M.; Klotz, T. A.; Fiess, H. A. *Arch. Biochem. Biophys.* **1957**, *68*, 284–299.
89. Boeri, E.; Ghiretti-Magaldi, A. *Biochim. Biophys. Acta* **1957**, *23*, 488–493.
90. Klotz, I. M.; Klotz, T. A. *Science* **1955**, *155*, 477–480.
91. Kurtz, D. M., Jr. *J. Biol. Inorg. Chem.* **1997**, *2*, 159–167.
92. Ward, K. B.; Hendrickson, W. A.; Klippenstein, G. L. *Nature* **1975**, *257*, 818–821.
93. Farmer, C. S.; Kurtz, D. M., Jr.; Liu, Z. J.; Wang, B. C.; Rose, J.; Ai, J.; Sanders-Loehr, J. *J. Biol. Inorg. Chem.* **2001**, *6*, 418–429.
94. Zhang, J. H.; Kurtz, D. M., Jr. *Biochemistry* **1991**, *30*, 9121–9125.
95. Kaminaka, S.; Takizawa, H.; Handa, T.; Kihara, H.; Kitagawa, T. *Biochemistry* **1992**, *31*, 6997–7002.
96. Holmes, M. A.; Trong, I. L.; Turley, S.; Sieker, L. C.; Stenkamp, R. E. *J. Mol. Biol.* **1991**, *218*, 583–593.
97. Stenkamp, R. E.; Sieker, L. C.; Jensen, L. H.; McCallum, J. D.; Sanders-Loehr, J. *Proc. Nat. Acad. Sci. USA* **1985**, *82*, 713–716.
98. Garbett, K.; Darnall, D. W.; Klotz, I. M.; Williams, R. J. P. *Arch. Biochem. Biophys.* **1969**, *135*, 419–434.
99. Solomon, E. I.; Tuczek, F.; Root, D. E.; Brown, C. A. *Chem. Rev.* **1994**, *94*, 827–856.
100. Garbett, K.; Johnson, C. E.; Klotz, I. M.; Okamura, M. Y.; Williams, R. J. *Arch. Biochem. Biophys.* **1971**, *142*, 574–583.
101. Okamura, M. Y.; Klotz, I. M.; Johnson, C. E.; Winter, M. R.; Williams, R. J. *Biochemistry* **1969**, *8*, 1951–1958.
102. Kurtz, D. M., Jr. *Chem. Rev.* **1990**, *90*, 585–606.
103. Dawson, J. W.; Wang, R. H.; Schredder, J. M.; Rossman, G. R.; Gray, H. B.; Hoenig, H. E. *Biochemistry* **1972**, *11*, 461–466.
104. Maroney, M. J.; Kurtz, D. M., Jr.; Nocek, J. M.; Pearce, L. L.; Que, L., Jr. *J. Am. Chem. Soc.* **1986**, *108*, 6871–6879.
105. Zhang, J. H.; Kurtz, D. M., Jr.; Xia, Y. M.; Debrunner, P. G. *Biochim. Biophys. Acta* **1992**, *1122*, 293–298.
106. Dunn, J. B. R.; Shriver, D. F.; Klotz, I. M. *Proc. Natl. Acad. Sci. USA* **1974**, *70*, 2852–2584.
107. Dunn, J. B.; Shriver, D. F.; Klotz, I. M. *Biochemistry* **1975**, *14*, 2689–2695.
108. Kurtz, D. M., Jr.; Shriver, D. F.; Klotz, I. M. *J. Am. Chem. Soc.* **1976**, *98*, 5033–5035.
109. Kurtz, D. M., Jr.; Shriver, D. F.; Klotz, I. M. *Coord. Chem. Rev.* **1977**, *24*, 145–178.
110. Shiemke, A. K.; Loehr, T. M.; Sanders-Loehr, J. *J. Am. Chem. Soc.* **1984**, *106*, 4951–4956.
111. Shiemke, A. K.; Loehr, T. M.; Sanders-Loehr, J. *J. Am. Chem. Soc.* **1986**, *108*, 2437–2443.
112. Xiong, J.; Phillips, R. S.; Kurtz, D. M., Jr.; Jin, S.; Ai, J.; Sanders-Loehr, J. *Biochemistry* **2000**, *39*, 8526–8536.
113. Tian, G.; Kninman, J. P. *J. Am. Chem. Soc.* **1993**, *115*, 8891–8897.
114. Solomon, E. I.; Zhang, Y. *Acc. Chem. Res.* **1992**, *25*, 343–352.
115. Petrou, A. L.; Armstrong, F. A.; Sykes, A. G.; Harrington, P. A.; Wilkins, R. G. *Biochim. Biophys. Acta* **1981**, *670*, 377–384.
116. Wilkins, R. G.; Harrington, P. C. *Adv. Inorg. Biochem.* **1983**, *5*, 51–85.
117. Wilkins, P. C.; Wilkins, R. G. *Coord. Chem. Rev.* **1987**, *79*, 195–214.
118. Zimmer, J. R.; Tachiiri, Y.; Takizawa, H.; Handa, T.; Yamamura, T.; Kihara, H. *Biochim. Biophys. Acta* **1986**, *874*, 174–180.
119. Lavalette, D.; Tetreau, C. In *Structure and Function of Invertebrate Oxygen Carriers*; Vinogradov, S. N., Kapp, O. H., Eds.; Springer-Verlag: NY, 1991; pp 191–198.
120. Lloyd, C. R.; Raner, G. M.; Moser, A.; Eyring, E. M.; Ellis, W. R., Jr. *J. Inorg. Biochem.* **2000**, *81*, 293–300.
121. Martins, L. J.; Hill, C. P.; Ellis, W. R., Jr. *Biochemistry* **1997**, *36*, 7044–7049.
122. Raner, G. M.; Martins, L. J.; Ellis, W. R., Jr. *Biochemistry* **1997**, *36*, 7037–7043.
123. Lloyd, C. R.; Eyring, E. M.; Ellis, W. R., Jr. *J. Am. Chem. Soc.* **1995**, *117*, 11993–11994.
124. Farmer, C. S.; Kurtz, D. M., Jr.; Phillips, R. S.; Ai, J.; Sanders-Loehr, J. *J. Biol. Chem.* **2000**, *275*, 17043–17050.
125. Alberding, N.; Lavalette, D.; Austin, R. H. *Proc. Nat. Acad. Sci. USA* **1981**, *78*, 2307–2309.
126. Brunold, T. C.; Solomon, E. I. *J. Am. Chem. Soc.* **1999**, *121*, 8288–8295.
127. Yedgar, S.; Tetreau, C.; Gavish, B.; Lavalette, D. *Biophys. J.* **1995**, *68*, 665–670.
128. Lavalette, D.; Tetreau, C. *Eur. J. Biochem.* **1988**, *177*, 97–108.
129. Projahn, H.-D.; Schindler, S.; van Eldik, R.; Fortier, D. G.; Andrew, C. R.; Sykes, A. G. *Inorg. Chem.* **1995**, *34*, 5935–5941.
130. Armstrong, G. D.; Sykes, A. G. *Inorg. Chem.* **1986**, *25*, 3135–3139.
131. Utecht, R. E.; Kurtz, D. M., Jr. *Biochim. Biophys. Acta* **1988**, *953*, 164–178.
132. Bradic, Z.; Conrad, R.; Wilkins, R. G. *J. Biol. Chem.* **1977**, *252*, 6069–6075.
133. Manwell, C. *Science* **1960**, *132*, 550–551.
134. Richardson, D. E.; Emad, M.; Reem, R. C.; Solomon, E. I. *Biochemistry* **1987**, *26*, 1003–1013.
135. Pearce, L. L.; Kurtz, D. M.; Xia, Y. M.; Debrunner, P. G. *J. Am. Chem. Soc.* **1987**, *109*, 7286–7293.
136. Thomann, H.; Bernardo, M.; McCormick, J. M.; Pulver, S.; Andersson, K. K.; Lipscomb, J. D.; Solomon, E. I. *J. Am. Chem. Soc.* **1993**, *115*, 8881–8882.
137. Derose, V. J.; Liu, K. E.; Kurtz, D. M., Jr.; Hoffman, B. M.; Lippard, S. J. *J. Am. Chem. Soc.* **1993**, *115*, 6440–6441.
138. McCormick, J. M.; Reem, R. C.; Solomon, E. I. *J. Am. Chem. Soc.* **1991**, *113*, 9066–9079.

139. Nocek, J. M.; Kurtz, D. M., Jr.; Sage, J. T.; Xia, Y. M.; Debrunner, P.; Shiemke, A. K.; Sanders-Loehr, J.; Loehr, T. M. *Biochemistry* **1988**, *27*, 1014–1024.
140. Rodriguez, J. H.; Xia, Y.-M.; Debrunner, P. G. *J. Am. Chem. Soc.* **1999**, *121*, 7846–7863.
141. Armstrong, W. H.; Lippard, S. J. *J. Am. Chem. Soc.* **1983**, *105*, 4837–4838.
142. Wieghardt, K.; Pohl, K.; Gebrt, W. *Angew. Chem., Int. Ed. Engl.* **1983**, *22*, 727–728.
143. Stenkamp, R. E.; Sieker, L. C.; Jensen, L. H. *Nature* **1981**, *291*, 263–264.
144. Chaudhuri, P.; Wieghardt, K.; Nuber, B.; Weiss, J. *Angew. Chem., Int. Ed. Engl.* **1985**, *24*, 778–779.
145. Bossek, U.; Hummel, H.; Wehhermuller, T.; Bill, E.; Wieghardt, K. *Angew. Chem., Int. Ed. Engl.* **1985**, *34*, 2642–2645.
146. Payne, S. C.; Hagen, K. S. *J. Am. Chem. Soc.* **2000**, *122*, 6399–6410.
147. Mizoguchi, T. J.; Lippard, S. J. *J. Am. Chem. Soc.* **1998**, *120*, 11022–11023.
148. Mizoguchi, T. J.; Kuzelka, J.; Spingler, B.; DuBois, J. L.; Davydov, R. M.; Hedman, B.; Hodgson, K. O.; Lippard, S. J. *Inorg. Chem.* **2001**, *40*, 4662–4673.
149. Lontie, R.; Witters, R. In *Inorganic Biochemistry*; Eichhorn, G. L., Ed.; Elsevier: New York, 1973; pp 344–358.
150. Redfield, A. C. *Biol. Rev. Biol. Proc. Cambridge Phil. Soc.* **1934**, *9*, 175–212.
151. Holm, R. H.; Kennepohl, P.; Solomon, E. I. *Chem. Rev.* **1996**, *96*, 2239–2314.
152. Cuff, M. E.; Miller, K. I.; van Holde, K. E.; Hendrickson, W. A. *J. Mol. Biol.* **1998**, *278*, 855–870.
153. Magnus, K. A.; Ton-That, H.; Carpenter, J. E. *Chem. Rev.* **1994**, *94*, 727–735.
154. Magnus, K. A.; Hazes, B.; Ton-That, H.; Bonaventura, C.; Bonaventura, J.; Hol, W. G. *Proteins* **1994**, *19*, 302–309.
155. Hazes, B.; Magnus, K. A.; Bonaventura, C.; Bonaventura, J.; Dauter, Z.; Kalk, K. H.; Hol, W. G. *Protein Sci.* **1993**, *2*, 597–619.
156. Volbeda, A.; Hol, W. G. *J. Mol. Biol.* **1989**, *209*, 249–279.
157. Solomon, E. I.; Baldwin, M. J.; Lowery, M. D. *Chem. Rev.* **1992**, *92*, 521–542.
158. Co, M. S.; Hodgson, K. O. *J. Am. Chem. Soc.* **1981**, *103*, 984–986.
159. Brown, J. M.; Powers, L.; Kincaid, B.; Larabee, J. A.; Spiro, T. G. *J. Am. Chem. Soc.* **1980**, *102*, 4210–4216.
160. Loehr, J. S.; Freedman, T. B.; Loehr, T. M. *Biochem. Biophys. Res. Commun.* **1974**, *56*, 510–515.
161. Freedman, T. B.; Loehr, J. S.; Loehr, T. M. *J. Am. Chem. Soc.* **1976**, *98*, 2809–2815.
162. Kitajima, N.; Fujisawa, K.; Moro-oka, Y. *J. Am. Chem. Soc.* **1989**, *111*, 8975–8976.
163. Kitajima, N.; Fujimoto, C.; Moro-oka, Y.; Hashimoto, S.; Kitagawa, T.; Toriumi, K.; Tatsumi, K.; Nakamura, A. *J. Am. Chem. Soc.* **1992**, *114*, 1277–1291.
164. Lynch, W. E.; Kurtz, D. M., Jr.; Wang, S.; Scott, R. A. *J. Am. Chem. Soc.* **1994**, *116*, 11030–11038.
165. Karlin, K. D.; Tolman, W. B.; Kaderli, S.; Zuberbuhler, A. D. *J. Mol. Catal. A: Chem.* **1997**, *117*, 215–222.
166. Ross, P. K.; Solomon, E. I. *J. Am. Chem. Soc.* **1990**, *112*, 5871–5872.
167. Ross, P. K.; Solomon, E. I. *J. Am. Chem. Soc.* **1991**, *1991*, 3246–3259.
168. Que, L., Jr.; Tolman, W. B. *Angew. Chem., Int. Ed. Engl.* **2002**, *41*, 1114–1137.
169. Decker, H.; Tuczek, F. *Trends Biochem. Sci.* **2000**, *25*, 392–397.
170. Nagai, T.; Osaki, T.; Kawabata, S. *J. Biol. Chem.* **2001**, *276*, 27166–27170.
171. van Holde, K. E.; Miller, K. I.; van Olden, E. *Biophys. Chem.* **2000**, *86*, 165–172.
172. Bridges, C. R. *J. Exp. Biol.* **2001**, *204*, 1021–1032.
173. Brouwer, M. In *Advances in Comparative and Environmental Physiology 13. Blood and Tissue Oxygen Carriers*; Mangum, C. P., Ed.; Springer-Verlag: New York, 1992; Vol.13, pp 1–21.
174. Brouwer, M.; Bonaventura, C.; Bonaventura, J. *Biochemistry* **1978**, *17*, 2148–2154.
175. Metz, M.; Solomon, E. I. *J. Am. Chem. Soc.* **2001**, *123*, 4938–4950.
176. Chan, M. K. *Curr. Opin. Chem. Biol.* **2001**, *5*, 216–222.
177. Rodgers, K. R. *Curr. Opin. Chem. Biol.* **1999**, *3*, 158–167.
178. Denninger, J. W.; Marletta, M. A. *Biochim. Biophys. Acta* **1999**, *1411*, 334–350.
179. Montfort, W. R.; Weichsel, A.; Andersen, J. F. *Biochim. Biophys. Acta* **2000**, *1482*, 110–118.
180. Roberts, S. A.; Weichsel, A.; Qiu, Y.; Shelnutt, J. A.; Walker, F. A.; Montfort, W. R. *Biochemistry* **2001**, *40*, 11327–11337.
181. Andersen, J. F.; Ding, X. D.; Balfour, C.; Shokhireva, T. K.; Champagne, D. E.; Walker, F. A.; Montfort, W. R. *Biochemistry* **2000**, *39*, 10118–10131.
182. Gonzalez, G.; Dioum, E. M.; Bertolucci, C. M.; Tomita, T.; Ikeda-Saito, M.; Cheesman, M. R.; Watmough, N. J.; Gilles-Gonzalez, M. A. *Biochemistry* **2002**, *41*, 8414–8421.
183. Aono, S.; Kato, T.; Matsuki, M.; Nakajima, H.; Ohta, T.; Uchida, T.; Kitagawa, T. *J. Biol. Chem.* **2002**, *277*, 13528–13538.
184. Xiong, J.; Kurtz, D. M., Jr.; Ai, J.; Sanders-Loehr, J. *Biochemistry* **2000**, *39*, 5117–5125.

8.11
Heme-peroxidases

B. MEUNIER
Laboratoire de Chimie de Coordination du CNRS, Toulouse, France

8.11.1 INTRODUCTION

Peroxidase activity was discovered by Schonbein in 1855 when treating guaiacol with hydrogen peroxide and plant extracts. Peroxidases are found in all plants and animals, and are essential for living systems.[1] They catalyze the abstraction of one or two electrons (usually two) via a single-electron transfer from an organic substrate, hydrogen peroxide being used as electron acceptor according to Equation (1):

$$AH_2 + H_2O_2 \xrightarrow{\text{peroxidase}} A + 2H_2O \tag{1}$$
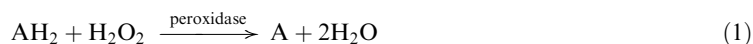
The prosthetic group of peroxidases is composed of a heme attached to the protein, usually via a histidine residue acting as proximal ligand. The activation of hydrogen peroxide by heme-peroxidase generates intermediate, high-valent, iron–oxo species that are able to abstract electrons from the different substrates. Horseradish peroxidase (the paradigm of plant peroxidases), ligninase, and manganese peroxidase are classical examples of heme-enzymes belonging to the superfamily of plant peroxidases.[2] Myeloperoxidase, lactoperoxidase, salivary peroxidase, and thyroid peroxidase are examples of human heme-peroxidases.[1] It must be noted that glutathione peroxidase, which catalyzes the elimination of peroxides in human blood, is a nonheme-enzyme with a selenium ion at the active site.[3] After each section on the structures and catalytic activities

of heme-peroxidases and heme-catalases, we will also provide a short survey on models of these heme-containing enzymes.

8.11.2   STRUCTURES AND CATALYTIC ACTIVITIES OF SELECTED HEME-PEROXIDASES

Within the scope of the present survey, we will limit the presentation of peroxidase structures and activities to some classical examples which have been extensively studied during recent decades: a plant peroxidase (horseradish peroxidase), a yeast peroxidase (cytochrome *c* peroxidase), three fungal peroxidases (chloroperoxidase, ligninase, and manganese peroxidase), and two human peroxidases (myeloperoxidase and thyroid peroxidase).

8.11.2.1   Horseradish Peroxidase (HRP)

A large number of publications on peroxidases have been devoted to horseradish peroxidase (HRP), and its properties in different oxidation states have been well studied.[4–6] Despite several efforts, a high-resolution X-ray structure of HRP was not obtained until 1997.[7] Horseradish peroxidase contains at least seven major isoenzymes, but the majority of the physico-chemical data have been obtained with the mixture of isoenzymes B and C (C being the major component in highly purified samples). The X-ray structure was solved for HRP-C, which was expressed in *E. coli* with a gene containing 309 amino-acid residues, only 306 of which are visible in the crystal structure. The prosthetic group of HRP consists of a ferric protoporphyrin IX with a histidine as proximal ligand (His-170) having an iron–nitrogen distance of 2.3 Å (Scheme 1). The proximal histidine (His-170) is separated from the Ca^{2+} site only by a threonine (Thr-171). In the active site are key conserved catalytic residues (arginine-38 with its guanidium acting as proton donor, and histidine-42 acting as base) for the activation of hydrogen peroxide; they are found in positions very similar to those in other heme-peroxidases with a pentacoordinated iron(III) center (see Figure 1 for a view of the active site).
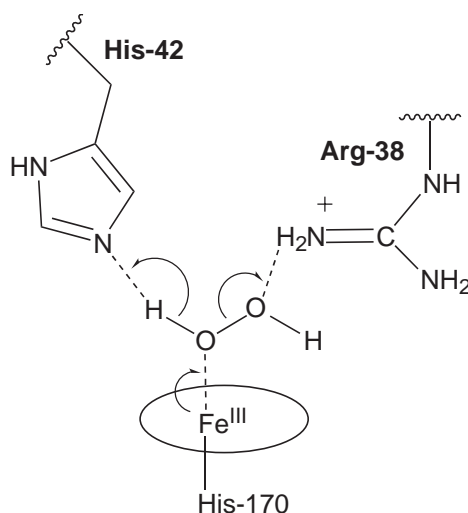
Scheme 1

The closest water molecule in the distal pocket is 3.2 Å away from the metal position. The structure shows the proximity of asparagine-70 to the distal histidine-42 and suggests its role in maintaining the basicity of His-42. That fact has been confirmed with a Val70Asn mutant that has a lower catalytic activity compared to the wild enzyme.[8,9]

A crystal structure of the peroxidase–substrate complex has been determined at 2.0 Å resolution and demonstrated the existence of an aromatic bonding pocket.[10] This hydrophobic distal pocket, containing a benzhydroxamic acid, is created by several phenylalanine residues (Phe-68, Phe-142, Phe-143, and Phe-179) and is close to His-42 and Arg-38. The shape of the distal cavity has been
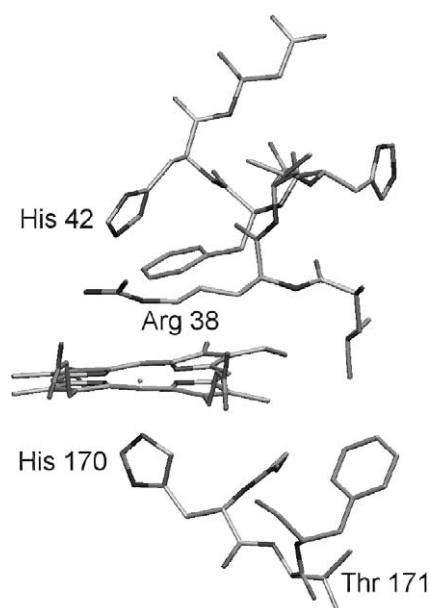
Figure 1 View of the active site of HRP with selected amino acids (for the complete X-ray structure, see ref. [10]).

investigated by proton NMR using the wild HRP and a mutant His42Ala. In this latter, modified enzyme, only small modifications of the distal pocket have been observed.[11]

The oxidation of HRP by hydrogen peroxide generates a reactive intermediate (called Compound I (Cpd I)) containing two redox equivalents (above the resting state of the native enzyme); one-electron reduction of this first high-valent intermediate generates compound II (Cpd II), Compounds I and II have a Soret band at 400 (broad) and 420 nm, respectively. Cpd I consists of an iron(IV)–oxo species with a radical cation on the porphyrin ring (Scheme 2). The formation of Cpd I has been monitored by stop-flow UV-visible spectroscopy and is a chemically controlled reaction, with a pre-equilibrium of the enzyme with a neutral molecule of H_2O_2 within the active site[12] which generates a ferric hydroperoxo intermediate (called compound 0) with a hyperporphyrin spectrum (for calculations on this intermediate, see refs. 13 and 14). A recent study performed on wild HRP and three mutants (His42Leu, Arg38Leu, and Arg38Gly) by rapid-scan stopped-flow and EPR has shown the formation of an iron–H_2O_2 intermediate, which serves as precursor of the Fe^{III}–OOH intermediate (Cpd 0).[15] At neutral pH values, His-42 is not protonated and acts as a base in the first deprotonation of hydrogen peroxide to generate Fe^{III}–OOH.

Compounds I and II have been characterized by X-ray absorption and Raman spectroscopy. Both methods demonstrated the presence of an iron(IV) oxo entity in both Cpds I and Cpd II, with a short Fe=O bond of 1.6 Å consistent with a ferryl structure.[16] Although it has been suggested that the Fe—O bond distance of Cpd II was longer: 1.9 Å at pH 7, and 1.7 at pH 10,[17] resonance Raman studies showed that Cpds I and II have Fe=O vibrations of comparable frequency, at 737 cm^{-1} and 776 cm^{-1}, respectively,[18] consistent with the ferryl description.

The additional oxidizing equivalent in Cpd I is stored on the porphyrin ligand, as a π-radical cation. This radical cation has a predominant $^2A_{2u}$ character, indicative of an electron abstraction from the a_{2u} orbital of the porphyrin ligand,[19] and is ferromagnetically coupled with the spin $S = 1$ of the ferryl state, as evidenced by EPR and Mössbauer studies.[20] With excess H_2O_2, an inactive intermediate compound III is formed, corresponding to an iron(III)–superoxo state and is equivalent to the addition of dioxygen to the ferrous state of HRP.[22] The redox potentials (E_0' values) of Cpds I and II are very similar and have been determined to be 0.88 V and 0.90 V, respectively for the couples Cpd I/Cpd II and Cpd II/ferric state.[21] Electrochemical data have been obtained on HRP by cyclic voltammetry, and provide new insights on the conversion of the catalytically active form to the inactive oxy-form (a superoxide anion bounded to an iron(III) center); these data are useful in biosensor applications for HRP.[23]
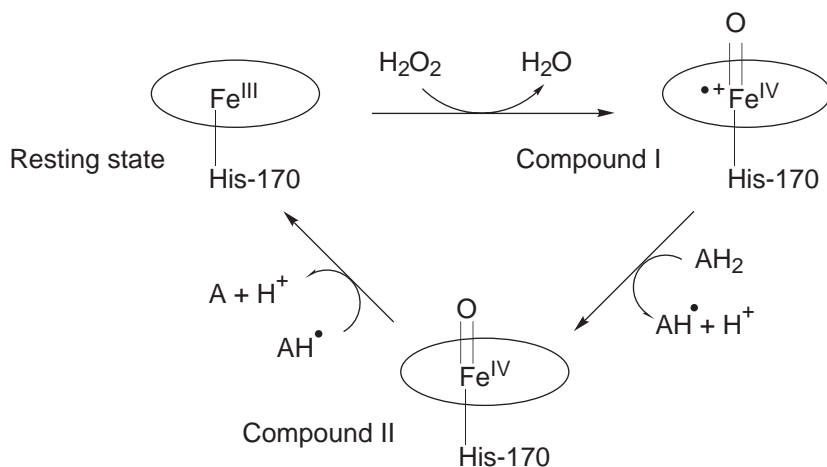
Scheme 2

The high-valent iron–oxo species of the reactive intermediates of HRP are not directly access-ible for many different substrates. Early studies on the alkylation of the *δ-meso* position of the heme-group by alkyl hydrazines have indicated that substrates approach the active site of HRP from a particular edge of the prosthetic group.[24] Substrate binding data have been obtained by proton NMR spectroscopy and molecular dynamics.[25–27] The X-ray structure of the binary complex HRP–ferulic acid provided accurate data on the binding of the ferulic substrate (a naturally occurring phenol in plant-cell walls) near the distal Arg-38 via a hydrogen bond.[10] This work also suggests that the water molecule produced from hydrogen peroxide after the generation of Cpd I remains in the active site, interacting via hydrogen bonds with ferulic acid, His-42, and Pro-139, and is liberated only after the oxidation of the phenolic substrate. This binding site of HRP must be considered as an open pocket that can accommodate a large range of substrates, explaining why this enzyme is such an efficient catalyst in the H_2O_2 oxidation of many different electron-donating molecules, so long as their redox potentials are compatible with those of Cpds I and II. For example, HRP has been used in the modeling of extra-hepatic oxidations (not oxygenation) of exogens (including many different drugs).[29]

Studies on the mechanism of the *O*-demethylation of aromatic substrates catalyzed by HRP have shown that the methyl group is removed as methanol (and not as formaldehyde, as in cytochrome P450-mediated oxidations).[30–32] This work has been useful in understanding the mechanism of lignin oxidation by ligninase, as some authors considered ligninase as an oxygen-ase, not as a peroxidase.

N-dealkylations are easily catalyzed by HRP, and its mechanism—whether or not an alpha-hydroxylamine is formed, as in P450-catalyzed dealkylations—has been controversial for many years.[1,32] Accurate kinetic isotope studies are in favor of a rate-determining electron-transfer step, followed by an H-atom transfer from the aminium radical-cation to the oxygen atom of the $Fe^{IV}=O$ species of Cpd II.[33] The formation of the aminium radical-cation by HRP–Cpd I has been confirmed with the use of *N*-cyclopropylamine derivatives; the cyclopropyl ring of the aminium radical-cation undergoes a ring-opening rearrangement to generate a radical cation, with the positive charge on the nitrogen iminium and a radical on the terminal methylene group.[34]

HRP is unable to oxidize styrene, unlike chloroperoxidase, which is able to catalyze the oxidation of this olefin to a mixture of the corresponding epoxide and phenylacetaldehyde.[35] How-ever, in the co-oxidation of styrene and 4-methylphenol, catalyzed by HRP, the epoxide results from the reaction with a hydroperoxide derived from the addition of dioxygen to a phenolic radical intermediate.[36] But a true peroxygenase activity can be obtained in the case of styrene with HRP mutants (His-42-Ala, His-42-Val, or Phe-41-Ala), indicating that substrate accessibility to the ferryl species is increased in these mutants.[37,38] The asymmetric oxidation of sulfides to sulfoxides, catalyzed by HRP, has been described by Colonna *et al.*,[39–41] with values of the enantiomeric excesses (ee) ranging from 30 to 68%. This reaction probably involves two one-electron oxidations rather than an oxygen-atom transfer from the high-valent iron–oxo intermedi-ates.[42] The HRP-catalyzed asymmetric sulfoxidation can be improved by changing the reaction medium from aqueous solution to nearly (99.7%) anhydrous organic solvents (methanol or

isopropanol). The higher substrate solubility and enzyme access largely compensate for the reduced intrinsic activity of HRP in alcohols.[43] However, the ee values are greatly enhanced when the sulfoxidation of thioanisole is performed in the presence of benzohydroxamic acid, a molecule forming a strong complex with HRP.[44]

Polyethylene-glycolated HRP has a reduced catalytic activity compared with the native enzyme, but this modification facilitates the study of the transient high-valent iron–oxo intermediates (the lifetime of Cpd I can be increased up to one hour at $-20\,^{\circ}\mathrm{C}$ in chlorobenzene).[45]

The viability of a sol–gel-encapsulated HRP has been demonstrated.[46] The sonication of the sol during the initial hydrolysis and condensation steps allows the incorporation of fragile biomolecules into the sol–gel matrix. The diffusion of substrates within the sol–gel matrix limits the catalytic activity of the encapsulated enzyme.

Novel peroxidases can be generated by screening *de novo* heme-proteins derived from a designed combinatorial library.[47] Turnover numbers as high as $17{,}000\,\mathrm{min}^{-1}$ have been obtained.

8.11.2.2 Chloroperoxidase (CPO)

Among all fungal peroxidases, chloroperoxidase (CPO) is one of the few enzymes that are able to catalyze the oxidative chlorination of substrates using H_2O_2 and Cl^- according to Equation (2) (myeloperoxidase MPO is another example):[48]

$$AH + H_2O_2 + Cl^- + H^+ \xrightarrow{\text{CPO}} ACl + 2H_2O \qquad (2)$$

This halogen-atom incorporation is catalyzed by CPO with substrates containing an activated carbon–hydrogen bond, such as β-diketones (chlorodimedone is a classical substrate for CPO activity assays). This heme-enzyme can be easily obtained and purified from the fungus *Caldariomyces fumago*. The big difference between CPO and HRP is the presence of a cysteine residue as proximal ligand (Cys-29 in CPO; see Figure 2).[49,50]

Furthermore, there is a manganese(II) ion bound to a heme-propionate and also surrounded by His-105, Glu-104, and Ser-108; this manganese ion might be the binding site for the chloride ion that has to be oxidized.[51] The role of the manganese ion in CPO might be similar to that of calcium in myeloperoxidase, which is located not too far from the heme (see Section 8.11.2.7 for details on myeloperoxidase).[52]

The addition of hydrogen peroxide to the ferric state of the enzyme generates CPO–Cpd I, the only detectable intermediate having an $Fe^{IV}{=}O$ bond with a Raman stretching band at
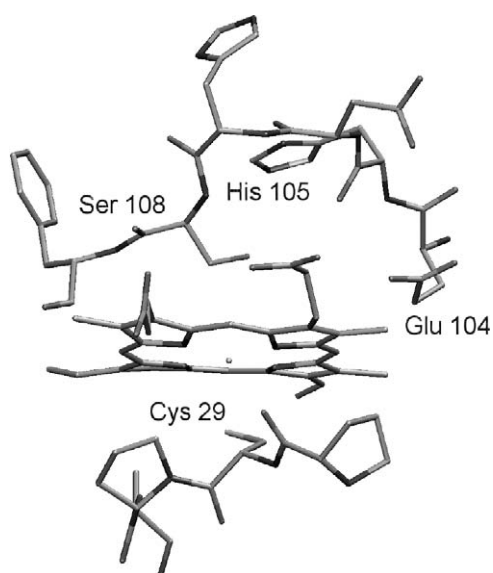
Figure 2 View of the active site of CPO with selected amino acids (for the complete X-ray structure, see ref. [51]).

790 cm^{-1}.[53,54] The radical-cation of Cpd I might be delocalized on the macrocycle or on the axial ligand (see ref. 55 for a proposal on the role of the S ligand in a high-valent cysteinato-heme-enzyme). The addition of chloride to Cpd I might generate an Fe^{III}–OCl entity, which in turn may effect the chlorination of substrates.[56] An alternative mechanism is the formation of free HOCl,[48] since the same mixture of chloroanisole isomers was observed in the chlorination of anisole by free HOCl or by a CPO-catalyzed reaction. A third possible mechanism involves the manganese site of CPO as the binding site of Cl$^-$. Because of the short distance between this Mn site and the heme, the bound chloride ion could be oxidized to Cl$^+$, which could attack the substrate present at the active site. Such a hypothesis would explain the absence of the formation of free HOCl during the CPO catalytic cycle, without invoking the formation of an iron(III) hypochlorito entity.

Chloroperoxidase is rendered inactive by the formation of an *N*-phenyl-heme in the oxidation of phenylhydrazine, or an *N*-alkyl-heme in the oxidation of terminal olefins.[57,58] These data suggest that various substrates have relatively easy access to the active site of CPO. In fact, this enzyme is able to catalyze the oxidation of a large range of substrates (tertiary amines, olefins, heterocycles, etc.). The mechanism of the *N*-demethylation of tertiary amines, catalyzed by CPO, probably involves an electron abstraction from the nitrogen atom, followed by a proton elimination of the methyl group (a primary isotope effect has been observed with a k_H/k_D value = 2.5). An alternative mechanism is the abstraction of an H atom from the methyl group, as observed for the hydroxylation reaction catalyzed by cytochrome P-450.[48] Chloroperoxidase is also able to catalyze the epoxidation of different olefins (styrene, propylene, allyl chloride).[45] The oxygen atom of the epoxide arises from the primary oxidant, as evidenced by the use of H$_2$^{18}O$_2$.[35] It has been demonstrated that CPO-catalyzed epoxidations of *cis*-disubstituted olefins are highly enantioselective, with enantiomeric excesses (ee values) ranging from 33% to 85%.[60] To avoid the irreversible degradation of CPO in the presence of H$_2$O$_2$, the concentration of the peroxide must be maintained as low as possible during the course of epoxidation. In these conditions, it has been possible to obtain 4,200 catalytic cycles with an ee value of 94% in the epoxidation of methylallyl propionate.[61] This CPO-catalyzed asymmetric epoxidation has been used in the synthesis of (*R*)-mevalonolactone,[62] and also with ω-bromo-2-methyl-1-alkenes.[63]

CPO is also able to catalyze the hydroxylation of allylic, benzylic, propargylic, and *cis*-cyclopropylmethanol derivatives with ee values ranging from 60% to 95%.[64–66] The CPO-catalyzed insertion of the oxygen atom into the C—H bonds in these hydroxylations might involve a very short-lived, carbon-centered radical intermediate, as checked with a hypersensitive radical probe (the lifetime of such a radical intermediate must be less than 3 ps).[67] CPO is also effective in converting oximes to halonitro compounds and ketones in a single step, in the presence of KCl or KBr and hydrogen peroxide.[68] No enantioselectivity has been observed during the formation of the nitro compounds, but the addition of co-solvents like dioxane or acetone increased the yield of the corresponding ketones.

The other useful reaction catalyzed by CPO is the enantioselective oxidation of sulfides to chiral sulfoxides with ee values of up to 90–95%.[40,69,70] Chiral sulfoxides are important synthons in the stereoselective synthesis of many natural products. Based on data obtained with a series of *para*-substituted thioanisoles, the proposed mechanism of the CPO-catalyzed S oxygenation involves an oxygen-atom transfer from compound I to the substrate, instead of a one-electron oxidation of the sulfide followed by the addition of H$_2$O$_2$ on the intermediate S radical-cation, as is proposed for sulfide oxidations catalyzed by HRP.[71]

Two novel heme-containing peroxidases with CPO activity have been discovered in marine worms: *Notomastus lobatus* chloroperoxidase (NCPO), catalyzing the halogenation of phenols; and *Amphitrite ornata* (DHP), performing the dehalogenation of halophenols to quinones.[72] Both enzymes contain a histidine residue as proximal ligand, and both are stable in their oxyferrous states (similarly to the Cpd III of HRP).[73]

8.11.2.3 Ligninase (LiP)

The possible development of the enzymatic degradation of lignin from wood pulp in the cellulose industry has stimulated many studies, since about 1980, on ligninolytic fungi. In particular, one fungus has focused the attention of several research groups in universities and industries: *Phanero-chaete chrysosporium*, which is able to degrade lignin by producing two extracellular peroxidases: ligninase (LiP) and manganese peroxidase (MnP). Both enzymes are able to oxidize lignin (the

ultimate degradation product of lignin being CO_2) via the formation of radical-cation intermediates on the substituted phenyl rings of this natural polymer resulting from the polymerization of *p*-coumarylic, coniferyl, or sinapylic alcohols (all these cinnamic alcohols are derived from phenylalanine).[74,75] The main target in lignin oxidation is the oxidation of the phenylpropanoid units, which constitute nearly 50% of the different linkages between the subunits of lignin. In particular, the oxidative cleavage of the C_α—C_β bond of these arylglycerol-β-arylether motifs is the key step in both the enzymatic and the chemical degradation of lignin. The C—C bond cleavage is triggered by the initial formation of radical-cation intermediates on the methoxylated aromatic rings constitutive of lignin.

Ligninase was independently purified by the groups of both Kirk and Gold in 1983.[76,77] Ligninase extracted from the extracellular fluid of ligninolytic cultures of *Phanerochaete chrysosporium* is a mixture of six isozymes, the major one (H8) having been used for most of the physico-chemical studies. LiP has a molecular weight of 42,000 Da, and this glycoprotein contains one iron–protoporphyrin IX entity as prosthetic group. Early studies on LiP, based on ^{18}O incorporation into oxidation products when performed under ^{18}O-labeled molecular oxygen, led to the classification of ligninase as an oxygenase.[78] However, further studies indicated that ^{18}O from labeled water was incorporated within the degradation products, as expected for a peroxidase-mediated oxidation (the initial radical-cation generated on methoxylated aromatic rings is highly electrophilic and reacts with water).[79]

The resting state of the enzyme is a high-spin iron(III) porphyrin with a histidine as proximal residue.[80] No water molecule is present as sixth ligand at room temperature. The X-ray structure of LiP confirms the presence of a proximal histidine (His-175), the conserved distal amino acids (His-47 and Arg-43), and a large pocket on the heme-edge.[81] The structure at 1.7 Å resolution reveals a long Fe–N(His) bond compared to regular peroxidases, suggesting that this weak Fe–N bond reduces the electron density on the heme itself and consequently contributes to the higher redox potential of LiP.[82] The overall folding of ligninase resembles that of cytochrome *c* peroxidase.

As for other peroxidases, a high-valent iron–oxo entity associated with a porphyrin π-radical-cation, Cpd I, is generated by the addition of hydrogen peroxide (see Scheme 3 for the catalytic cycle of LiP). This green compound (Soret band at 408 nm) has UV-visible and EPR characteristics similar to that of HRP–Cpd I.[83]
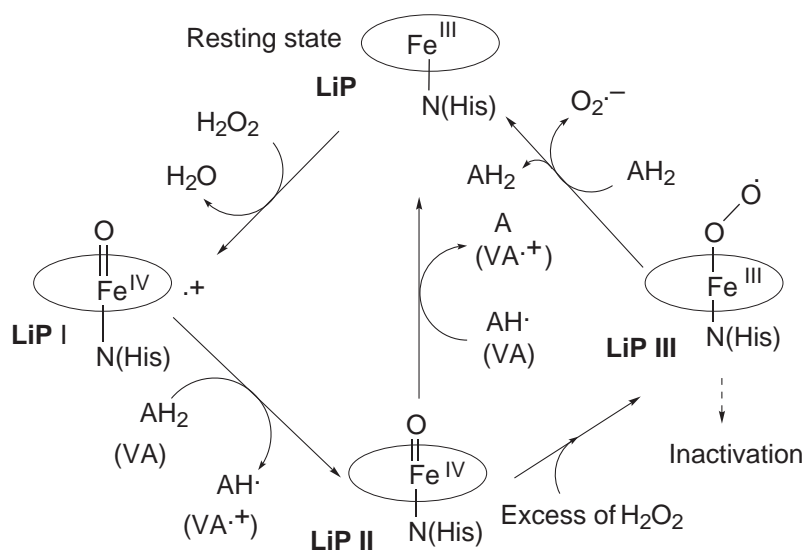
Scheme 3

The addition of 0.5 equivalent of a two-electron reducing agent like veratryl alcohol generates LiP–Cpd II (with a Soret band at 420 nm), which corresponds to the iron(IV)–oxo without oxidation of the porphyrin ligand. Site-directed mutations have demonstrated a key role for Trp-171 in veratryl alcohol oxidation, this amino acid being probably the location of an intermediate radical cation in the oxidation cascade.

Unexpectedly, LiP is a fragile enzyme when exposed to more than 20 equivalents of hydrogen peroxide: besides the two catalytically active forms (Cpds I and II), two inactive forms, LiP III and LiP III*, have been obtained in the presence of an excess of hydrogen peroxide or by addition of molecular oxygen to the reduced form of LiP (ferrous state).[85] The difference between these two inactive forms is due to the presence of an extra molecule of H_2O_2, probably in the vicinity of the prosthetic group in the case of LiP III*. Any adventitious electron transfer from the ferrous state of the enzyme to this extra hydrogen peroxide molecule would generate one hydroxyl radical, leading to an irreversible inactivation of LiP. The fragility of LiP in the presence of an excess of hydrogen peroxide has been the limiting factor for the industrial use of ligninase in delignification or in the oxidation of pollutants.

Veratryl alcohol is a secondary metabolite in delignification mediated by *Phanerochaete chrysosporium* and is a good substrate for ligninase, enhancing the rate of oxidations catalyzed by LiP. It has been proposed that veratryl alcohol, via the formation of its radical-cation, acts as a chemical mediator in the oxidative degradation of lignin. It mediates the transfer of electrons between the enzyme and lignin, two macromolecules being too large for perfect interactions (for kinetics and redox data, see refs. 86 and 87). Many oxidation products generated from veratryl alcohol by LiP/H_2O_2 have been identified, including veratraldehyde, two quinones (2-hydro-methyl-5-methoxy-1,4-benzoquinone and 2-methoxy-1,4-benzoquinone), and three lactones. Oxidation products of lignin-model dimers having an arylglycerol-3-arylether moiety have also been identified.[88,89] Experiments performed under $^{18}O_2$ and/or with $H_2^{18}O$ provided details on the mechanism of formation of these different oxidation products.[90]

One of the most interesting properties of ligninase is its capacity to oxidize various recalcitrant organic molecules. Microorganisms in soils and water convert many man-made chemicals into inorganic products.[91] Molecules resistant to biotransformation are subject to biomagnification and accumulation in plants or animal tissues. Among the compounds resistant to microbial degradation, DDT and lindane are two classical examples, both being slowly transformed by microbial reduction. *Phanerochaete chrysosporium* ligninase is able to oxidize trichlorophenols and benzodioxines.[92,93] It has been shown that the *Streptomyces viridosporium* T7A produces an extracellular ligninase ALiP–P3 that is also able to catalyze the degradation of 2,4-dichlorophenol.[94]

8.11.2.4 Manganese Peroxidase (MnP)

The culture medium of *Phanerochaete chrysosporium* contains another extracellular peroxidase, a manganese-dependent enzyme (four isozymes) that is unable to catalyze the oxidation of veratryl alcohol in the presence of H_2O_2.[95] Manganese peroxidase is a heme-glycoprotein of 46,000 Da which requires manganese(II) ions for its activity. The proximal ligand is a histidine. The X-ray structure indicates that three amino acids—Asp-179, Glu-35, and Glu-39—as well as a heme-propionate, are involved in the binding of a manganese(II) ion.[96] Site-directed mutations have indicated that Arg-177 is also involved in the binding of manganese(II) via a salt bridge with Glu-35, and that Glu-39 has a key role in the coordination of this transition-metal ion.[97,98] This peroxidase also has two calcium binding sites to prevent the thermal inactivation of the enzyme.[99] Additional disulfide bonds introduced in engineered MnP are able to enhance the stability of the recombinant enzyme.[100]

The native manganese peroxidase is oxidized by hydrogen peroxide to a Cpd I species similar to HRP–Cpd I. The Mn^{II} ion binds to the enzyme and reduces MnP–Cpd I to MnP–Cpd II. This latter, oxidized form of MnP is reduced to native MnP only by manganese(II), but not by phenols. The oxidation of Mn^{II} to Mn^{III} by MnP is dependent on the presence of chelating agents in the reaction mixture. These chelating agents, usually α-hydroxyacids such as lactate, succinate, malonate, have two different roles: they stimulate the catalytic activity by facilitating the dissociation of the enzyme–manganese complex via the chelation of Mn^{III}, and they stabilize the manganese ion in the oxidation state of III, since Mn^{III} salts have a tendency to dismutate to Mn^{II} and Mn^{IV}.[101] Pyrophosphate, a strong chelating agent of manganese salts, inhibits the MnP activity, suggesting that the enzymatic oxidation of manganese occurs with a free Mn^{II} ion. Since Mn^{III} chelates are able to oxidize only phenol derivatives, the main targets are essentially the phenolic residues of lignin (15% of the phenylpropane units of lignin have a free hydroxyl group in the para position).

A detailed study of a lignin-model dimer with a phenol function, such as 1-(3,5-dimethoxy-4-hydroxy-phenol)-2-(4-methoxy)propane-1,3-diol, indicated how this dimer was cleaved by MnP/H_2O_2/Mn^{II}.

Labeling studies with $^{18}O_2$ and $H_2{}^{18}O$ confirmed that the key step was the initial formation of a phenoxy radical.[102] Partial depolymerization of lignin by MnP has been observed *in vitro*.[103]

The ligninolytic activity of *Phanerochaete chrysosporium* is dependent on both enzymes, LiP and MnP, and also on the presence of molecular oxygen in the culture medium to facilitate the propagation of free-radical chain reactions. Otherwise, anaerobic conditions favor the recombination of lignin-centered radicals to generate new C—C or C—O bonds within lignin, leading to further reticulation of lignin, not to its degradation.

8.11.2.5   Cytochrome *c* Peroxidase (CCP)

CCP catalyzes the two-electron reduction of hydrogen peroxide to water by ferrous cytochrome *c*[104]:

$$2\,Fe^{II}\text{-cyt c} + H_2O_2 + 2\,H^+ \xrightarrow{\text{CCP}} 2\,Fe^{III}\text{-cyt c} + 2\,H_2O \tag{3}$$
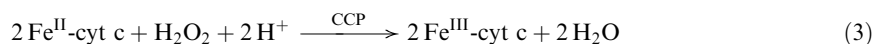
This process is integrated within the respiratory electron-transport chain involved in the mitochondria of cells. Yeast CCP is easy to purify and has been widely studied. The complex between CCP and cytochrome *c* was crystallized in 1992.[105] The electron-transfer pathway involves primarily Trp-191 and then Gly-192, Ala-193, and Ala-194. When Trp-191 is replaced by phenylalanine, the rate of the catalytic reaction is reduced by a factor of 1,000. Unlike other Cpd I formulations, CCP Cpd I consists of an iron(IV)–oxo and a radical-cation on Trp-191.

Besides a high-affinity binding site, a weaker binding site for a second cytochrome *c* molecule has been found by site-directed mutagenesis.[106] The crystal and solution structures of the proximal His-175-to-Gly protein mutant have been studied; peroxide activation is still possible, but the reaction with cytochrome *c* is inefficient due to alteration of the electron-transfer pathway.[107,108]

The crystal structure of *Nitrosomas europaea* cytochrome *c* peroxidase solved at 1.8 Å shows that this particular type of CCP enzyme contains two heme-motifs: one with high potential and Met and His as axial ligands, and the other with a low potential with two His as axial ligands. The latter is the reaction site with hydrogen peroxide.[109]

Surprisingly, the replacement of the distal histidine-52 in yeast CCP by a glutamine produces an enzyme that catalyzes the oxidation of hydrogen peroxide to superoxide anion. The reorganization of the peroxide binding site by the presence of the weakly basic amide favors the formation of a labile superoxide intermediate.[110] When the different redox-active amino acids of CCP—two tryptophans (Trp-51 and Trp-191) and six tyrosines (Tyr-36, Tyr-39, Tyr-42, Tyr-187, and Tyr-236)—are replaced by less oxidizable amino acids (as in ligninase), then the Cpd I of CCP is more stable, has a longer lifetime, and can be observed.[111] The presence of a potassium cation in the proximal heme-pocket has been confirmed by site-directed mutagenesis in the 192-199 loop located in the vicinity of Trp-191, the amino acid acting as an electron gate in the control of the electron flow from the ferrous cytochrome to the ferryl states of CCP.[112]

The distal pocket of CCP is accessible to small substrates like thioanisoles, which are oxidized to the corresponding sulfoxides with incorporation of an oxygen atom from hydrogen peroxide.[113] A weak asymmetric epoxidation has been observed with cis-β-methylstyrene. The monooxygenase activity of CCP can be modulated when introducing a second mutation requested to stabilize the S-coordination of cysteine in the replacement of the proximal histine by a cysteine residue.[114] CCP has been designed into a manganese peroxidase by site-directed mutagenesis, the easily oxidizable tryptophan-191 being replaced by a phenylalanine.[115,116]

8.11.2.6   Peroxidasic Activity of Hemoglobin (Hb) and Myoglobin (Mb)

Hemoglobin and myoglobin have been designed for the transport and storage, respectively, of molecular oxygen, and they are the essential reversible dioxygen binders for maintaining adequate oxygenation of tissues for the metabolism of many aerobic living systems. Both proteins contain an iron–protoporphyrin(IX) cofactor linked to a proximal histidine, and the binding of dioxygen is controlled by several amino acids in the distal pocket, as evidenced by different X-ray structures.[117–119] By inadvertent release from erythrocytes or tissues, hemoglobin and myoglobin can produce deleterious effects on cells and tissues. These heme-proteins are then able to be

activated by small amounts of hydrogen peroxide or lipid peroxides, acting then as regular peroxidases. This behavior was recognized 50 years ago for metmyoglobin by George and Irvine.[120] In the presence of hydrogen peroxide, both Hb and Mb are able to catalyze the oxidation of phenols, aminopyrines, and aromatic amines.[121] The formation and the reactivity of Compound I of myoglobin has been studied on mutants having the distal histidine-64 replaced by alanine, serine, or leucine.[122] When the distal threonine is replaced by an arginine, the peroxidase activity is also greatly enhanced.[123]

8.11.2.7 Myeloperoxidase (MPO)

This heme-enzyme is a covalently bound dimer of 140,000 Da present in polymorphonuclear leukocytes, neutrophils, phagocytes, eosinophils, and to a lesser degree in monocytes.[52] MPO has a strong antimicrobial activity that has been fully understood only since about 1980.[124,125] The X-ray structure of human myeloperoxidase confirms the presence of a proximal histidine and the histidine–arginine duo on the distal side. The prosthetic group is a protoporphyrin-IX derivative with modified hydroxyl–methyl groups on pyrroles A and C esterified with Glu-242 and Asp-94.[126] The kinetics of the two successive one-electron oxidations of 3,5,3′,5′-tetramethylbenzidine by MPO have been determined.[127] The high-valent iron–oxo entities of MPO (Cpds I and II) can also be reduced by chloride ions, leading to the generation of hypochlorous acid HOCl:

$$Cl^- + H_2O_2 \xrightarrow{\text{MPO}} HOCl + H_2O \tag{4}$$
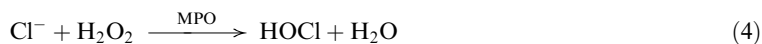
This potent toxic entity chlorinates protein amines, converts unsaturated lipids to chloro-hydrins, oxidizes free amino acids to aldehydes, and deactivates sulfhydryl groups. Additional chlorinations, such as that of low-density lipoprotein cholesterol, are due to Cl_2 generated by the reaction of HOCl with chloride at physiological pH.[128]

The MPO-catalyzed chlorination of membranes of exogenous microorganisms (bacteria, viruses, parasites, etc.) is a powerful antimicrobial activity generated at the contact of neutrophils with the microbes. However, MPO also contributes to the pathogenesis of several inflammatory and vascular disorders by converting free amino acids to reactive aldehydes.[129] It has been found that nitric oxide (the radical NO$^\bullet$) also plays a central role in these disorders. Activated MPO converts NO_2^- into NO_2Cl and $NO_2^{\bullet}$, both of which are able to nitrate tyrosine residues.[130] These MPO-mediated nitrations are enhanced by fluxes of nitric oxide.

8.11.2.8 Lactoperoxidase (LPO)

This peroxidase, present in milk, saliva, and tears, is involved in the bacterial defense through the oxidation of thiocyanate ions to the antibacterial species hypothiocyanate $OSCN^-$ and other higher oxyacids.[131] Thiocyanate, the physiological substrate of LPO, is present in secreted fluids in much higher concentrations than in blood plasma or in the extracellular space of tissues. LPO is a glycoprotein with a molecular weight of 78,000 Da and has a high content of carbohydrates (10%). Despite the absence of an X-ray structure for LPO, physico-chemical studies have shown that the bovine milk LPO-heme is a 1,5-bis(hydroxymethyl) derivative of heme *b*, linked to the protein by esterification with Glu-275 and Asp-125 as in MPO.[132]

LPO reacts with hydrogen peroxide to generate two different Cpd I derivatives: an iron(IV)–oxo with a porphyrin radical-cation, or with a radical on the protein. This second Cpd I is at the origin of the oligomerization of the protein via tyrosine–tyrosine linkages between Tyr-289 of different LPO units.[133] This oligomerization of LPO alters its ability to interact with macromolecular substrates. As observed for other mammalian peroxidases, the Cpd I of human LPO is a much better oxidant than HRP–Cpd I, whereas the redox potential of the Cpd II of LPO is lower compared to that of plant peroxidases.[134,135]

8.11.2.9 Thyroid Peroxidase (TPO)

This peroxidase catalyzes two important reactions in the thyroid hormone synthesis: (i) the iodination of tyrosines in thyroglobulin to yield protein-bound mono- and di-iodotyrosines

(thyroglobulin Tg contains more than 40 tyrosines per protein molecule); and (ii) the phenoxy–ether bond formation between two tyrosines of thyroglobulin to generate the thyroid hormones which are released by proteolysis of Tg (thyroxine T_4 and the triiodothyronine T_3).[136] Cpd I of TPO is highly efficient in the two-electron oxidation of iodide to iodonium, which quickly reacts with the tyrosine residues of the Tg protein. The presence of iodo substituents on halogenated tyrosines favors the C—O coupling reaction when oxidized by Cpd I of TPO.

Studies have shown that flavonoids are able to inhibit thyroid peroxidase. Flavonoids display diverse biological activities, e.g., anti-inflammatory, antiallergic, antiviral, antibacterial, and antioxidant effects, all of which are beneficial. Among the rare adverse effects of flavonoids, the TPO inhibition by oxidation of these benzopyrone derivatives should be noted. Quercetin is among the most powerful of the flavonoid-based inhibitors, the irreversible inhibition resulting from covalent attachment of an oxidized form of quercetin generated by TPO–Cpd I to TPO itself.[137] An overconsumption of flavonoids might play a role in the etiology of thyroid cancer. The antithyroid activity of minocycline, a tetracycline antibiotic, is also related to the fixation of this drug to TPO by covalent binding.[138] Finally, these modified TPO proteins might be the antigens in autoimmune thyroid diseases like Hashimoto's thyroiditis. The TPO-epitope is probably the C-terminal region of the peroxidase.[139,140]

8.11.2.10 KatG of *Mycobacterium tuberculosis*

This heme-peroxidase belongs to a class of enzymes called catalase-peroxidase, which are involved in the oxidative defense of bacterial and fungal cells. These KatG enzymes act primarily as catalase to remove hydrogen peroxide by dismutation.[141] The *Mycobacterium tuberculosis* KatG (dimer of 80 kDa) is homologous with CCP and plant peroxidases, though it is twice the length of these peroxidases as a result of gene duplication. Only one heme-binding consensus sequence is found in the *N*-terminal half. The structure of the catalase-peroxidase of *Haloarcula marismortui* confirms the presence of only one heme *b* in this type of enzyme.[142] At low peroxide concentrations, the Cpd I of KatG can be reduced by a suitable electron donor, resulting in a peroxidasic reaction appearing to be slower than the catalase reaction. No Cpd II has been detected during the reduction of KatG–Cpd I by a two-electron reductant.[143] The balance between peroxidase vs. catalase activity has been altered in favor of peroxidase activity by site-directed mutagenesis on KatG of *Escherichia coli* by changing Tyr-105 to a phenylalanine.[144]

The catalase-peroxidase of *Mycobacterium tuberculosis* (Mt-KatG) activates the antitubercular drug isoniazid (isonicotinic acid hydrazide, INH) making it the subject of intensive investigations. Since 1952, isoniazid has been used as a powerful drug against *M. tuberculosis* in both the therapeutic and the prophylatic chemotherapy of tuberculosis.[145] KatG oxidizes INH to an electrophilic species, probably the isonicotinoyl radical (as suggested by activation of the drug by the enzyme itself or biomimetic systems) which binds to, and deactivates, the NADH-specific enoyl-ACP (acyl carrier protein) reductase, an enzyme involved in the biosynthesis of mycolic acids of mycobacteria.[146–148] The oxidation of INH by KatG is enhanced by the presence of manganese(II) ions, suggesting that the peroxidase activity of this catalase-peroxidase is similar to that of manganese peroxidase from *Phanerochaete chrysosporium*.[149,150] Resistance to INH currently appears in more than 20% of drug-resistant tuberculosis cases. Cloning studies have found that mutations in, or deletion of, the gene of KatG results in the acquisition of isoniazid resistance.[151,152] Understanding the origin of INH resistance is an essential point in the fight against multidrug-resistant tuberculosis, since isoniazid is a cheap and easily affordable drug for developing countries.

8.11.3 A SHORT SURVEY OF PEROXIDASE MODELS WITH METALLOPORPHYRINS

For general reviews on the use of synthetic metalloporphyrins as heme-enzyme models, see refs. 153 and 154.

8.11.3.1 Models of Horseradish Peroxidase

Early peroxidase models were based on simple metal complexes or modified hemin derivatives.[155] Anionic metalloporphyrins adsorbed on ion-exchange resins have an efficient peroxidase activity,

which has been monitored by titration of the quinoid dye generated in the co-oxidation of 4-aminoantipyrine and phenol in the presence of hydrogen peroxide.[156] Oxidation of phenols and tertiary amines has been performed with different metalloporphyrins and various oxidants (not only hydrogen peroxide, but also alkylhydroperoxides, organic peracids, or aromatic amine *N*-oxides).[157–159] All these different metalloporphyrin complexes exhibit catalytic activities similar to those of peroxidases: oxidation of phenols, *N*-dealkylation of tertiary amines. Iron(III) or manganese(III) complexes of *meso*-tetrakis(2,6-dimethyl-3-sulfonatophenyl)porphyrin or *meso*-tetrakis(2,6-dichloro-3-sulfonatophenyl)porphyrin are suitable water-soluble peroxidase models, since these metalloporphyrins do not form μ-oxo dimers, neither do they aggregate due to steric hindrance created by the *ortho* substituents.

Microperoxidases-8 or -11 (MP-8 or MP-11) have been used as peroxidase models. These compounds consist of a peptide fragment (8 or 11 residues) containing a covalently bound heme, and are obtained by the enzymatic hydrolysis of cytochrome *c*.[160–162] MP-8 and -11 are able to catalyze the *N*-demethylation of amines and the oxidation of sulfides, in the same manner as peroxidases.

Artificial peroxidases have also been designed using the catalytic antibody strategy. The groups of Schultz and Harada initiated the field of antibody–metalloporphyrin complexes.[163,164] Immunization with *meso*-tetrakis(4-carboxyphenyl)porphyrin (TCPP) provides an antibody which binds very strongly to Mn^{III}-TCPP or to Fe^{III}TCPP.[165]

Peroxidase models based on metalloporphyrins have been used for the *in vitro* oxidation of drugs or drug candidates, since these biomimetic methods can be considered as a promising complementary approach to traditional techniques used to carry out oxidative activation of drugs (perfused organs, isolated cells, tissue homogenates, or purified enzymes). These biomimetic catalysts should facilitate the preparation and the isolation of reactive metabolites, due to the absence of proteins in the reaction mixture (electrophilic metabolites are usually trapped by nucleophilic sites of proteins). Several groups have developed the use of these metalloporphyrins in organic or aqueous solutions to catalyze the oxidation of drugs such as acetaminophen,[166] piperidine derivatives,[167] ellipticine derivatives,[168] lidocaine,[169] and an antagonist of a vasopressin receptor.[170] When using sterically hindered metalloporphyrins and monopersulfate as primary oxidant, the catalytic activities of these peroxidase-type oxidations are very close to that observed with horseradish peroxidase.[168]

The horseradish-catalyzed oxidation of luminol is widely used in the field of nonradioactive immunology assays. Iron and manganese porphyrins are also highly efficient catalysts when using perborate as oxidant. The chemiluminescence produced by nanomolar concentrations of Fe–TPPS can be over three times as strong as that produced by HRP, with a signal-to-noise ratio increasing up to 200.[171]

8.11.3.2 Models of Chloroperoxidase

Only a few reports have been devoted to the modeling of chloroperoxidase with metalloporphyrin catalysts. In the absence of protein around the active site to control the electron transfer, the oxidation of chloride ions competes with the direct oxidation of organic substrates by the high-valent metal–oxo species. The first CPO model was based on the association of $NaClO_2$ with an iron porphyrin, generating HOCl *in situ* which reproduced the main features of CPO-catalyzed chlorinations.[172] A second CPO model, using hydrogen peroxide and chloride ions, has been developed with an anionic manganese porphyrin supported on a cationic ion-exchange resin (the structures of these supported catalysts will be discussed in the next paragraph on ligninase models).[173] MnTMPS supported on a polyvinylpyridine polymer (PVP) was able to catalyze the oxidation of dimedone, a classical CPO substrate, to chlorodimedone.

A synthetic iron porphyrin with a thiolato ligand in the axial position has been oxidized by hydrogen peroxide in the presence of chloride. The shift of the Soret band from 408 nm to 404 nm might be due to the formation of a putative $Fe^{III}OCl$ entity which can generate free HOCl after protonation.[174] The kinetic parameters of halide oxidation by a high-valent manganese–oxo porphyrin complex have been reported.[175]

8.11.3.3 Models of Ligninase

This survey is limited to model systems based on synthetic water-soluble metalloporphyrins.[176–179] The activity of "$KHSO_5$/sulfonated metalloporphyrin" models has been checked with the usual

lignin-model molecules: veratryl alcohol and 1-(3,4-dimethoxyphenyl)-2-(2-methoxyphenoxy) propane-1,3-diol. Sterically hindered, water-soluble complexes are among the most efficient metalloporphyrin catalysts. The degradation products of lignin models are similar to those obtained in ligninase-catalyzed oxidations.[180,181]

Iron(III) *meso*-tetrakis(pentafluorophenyl)-β-tetrasulfonatoporphyrin is also an efficient catalyst for the oxidation of lignin models with hydrogen peroxide or magnesium monoperphthalate.[182] Sulfonated metalloporphyrins are also efficient catalysts in ligninase modeling when they are supported on ion-exchange resins. For example, FeTPPS or MnTPPS strongly interacts with the cationic Amberlite IRA 900 (an ion-exchange resin derived from polyvinylbenzene and bearing ammonium residues) to give solid-supported catalysts that are more stable than the corresponding soluble catalysts.[178] With a polyvinylpyridine (PVP) support, it has been possible to take advantage of the proximal effect of a pyridine ligand without free pyridine present in the reaction mixture.[183,184]

Ligninase models have been evaluated as catalysts for pollutant oxidation. Sulfonated iron or manganese porphyrin catalysts with $KHSO_5$ or H_2O_2 as primary oxidant were able to effectively promote the oxidative dechlorination of 2,4,6-trichlorophenol (TCP) to 2,6-dichlorobenzoquinone. Catalytic activities of up to 20 cycles s^{-1} were observed with monopersulfate as oxidant and a very low loading of FeTPPS catalyst (0.1–0.3% molar ratio with substrate).[185] Changing this oxidant for hydrogen peroxide resulted in a decrease in the catalytic activity. However, the limits of this catalytic reaction are set by a lower catalytic activity with H_2O_2, the cost of metalloporphyrins, and the absence of extensive oxidation of the generated quinones. Consequently, a biomimetic system able to degrade trichlorophenols should be based on a cheap and readily available catalyst with H_2O_2 as oxidant (the "clean" oxidant, water being the only by-product after oxidation); and, also, the oxidation of TCP should be able to generate ring-cleavage products and CO_2, as in biomineralization processes. We found that iron(III) tetrasulfonatophthalocyanine (FePcS) was able to catalyze the H_2O_2 oxidation of TCP according to the reaction conditions listed above.[186–188] With 3.7% of FePcS and five equivalents of H_2O_2 with respect to 2,4,6-trichlorophenol in a mixture of acetonitrile/buffered water (1/3, v/v) at pH 7, TCP was quantitatively converted at room temperature within a few minutes (TCP concentration = 2,000 ppm). The major TCP cleavage product was chloromaleic acid (yield = 24%) with chlorofumaric, maleic, and fumaric acids as minor products. Oxalic acid was also among the oxidation products of TCP.[188] The C_4-diacids resulting from the ring cleavage of TCP by FePcS/ H_2O_2 were also degraded by the catalytic system. The possible formation of carbon dioxide as the ultimate degradation product of these diacids was investigated by monitoring the release of labeled CO_2 during the oxidation of a (U-^{14}C)-TCP by FePcS/H_2O_2 in order to have a complete material balance of oxidation products.[187] After 90 min at room temperature, 11% of the initial radioactivity was recovered as CO_2.

Polyaromatics (anthracene and phenanthrene) have also been oxidized by FePcS/H_2O_2.[189] This catalytic system is highly influenced by the presence of an organic co-solvent and phosphate ions.[190,191] Iron tetra-amide complexes are also able to efficiently catalyze the oxidative cleavage of TCP with hydrogen peroxide at basic pH values.[192]

8.11.3.4 Models of Manganese Peroxidase

The modeling of a nonspecific peroxidase like ligninase is relatively simple compared to the design of metalloporphyrin catalysts able to selectively oxidize manganese(II) salts, in the presence of chelating agents and of easily oxidizable phenolic substrates. MnP has a manganese binding site able to control the selective oxidation of manganese(II) salts in the presence of phenols. Oxidation of Mn^{II} pyrophosphate to the corresponding Mn^{III} chelate was performed with catalytic amounts of iron- or manganese-sulfonated porphyrins.[193] As expected, sterically hindered iron complexes were the most active catalysts (8 cycles min^{-1} and 3 cycles min^{-1} for FeTDCPPS and FeTMPS, respectively). A striking feature of this metalloporphyrin-catalyzed oxidation of manganese pyrophosphate was the enhancement of the catalytic activity by the addition of limited amounts of methoxylated benzene derivatives acting as co-substrates: 1,2-dimethoxybenzene, 3,4-dimethoxybenzyl alcohol (veratryl alcohol), or 1,2,4-trimethoxybenzene. The catalytic activity of FeTMPS was strongly increased by 2–5% of one of these methoxylated benzenes. In order to mimic the manganese binding site of MnP, a metalloporphyrin bearing a manganese chelating ligand has been prepared.[194]

8.11.4 STRUCTURES AND CATALYTIC ACTIVITIES OF SELECTED HEME-CATALASES

Catalases, along with superoxide dismutases, are key enzymes for controlling the level of reduced oxygen species in living systems by catalyzing the dismutation of hydrogen peroxide and super-oxide anion.[195,196] Only heme-catalases will be presented in this article. Heme-catalases have an iron(III) protoporphyrin IX as prosthetic group, or modified porphyrins as in the two catalases of *E. coli* designated HPI and HPII.[197] Within peroxisomes of the same plant (sunflower), two catalases have been identified with different primary structures.[198] A particular case is the catalase-peroxidase KatG of *Mycobacterium tuberculosis*, which has been presented above, in Section 8.11.2.10.

Classical tetrameric heme-catalases are highly efficient catalysts for hydrogen peroxide dismutation to dioxygen and water at a very high rate of 10^5 cycles s^{-1}:

$$2\,H_2O_2 \xrightarrow{\text{catalase}} O_2 + 2\,H_2O \tag{5}$$

Catalase is also able to oxidize a few small molecules, in particular ethanol (the pro-*R*-hydrogen atom is stereospecifically removed as in the alcohol dehydrogenase-mediated oxidation).[199] Several heme-catalase three-dimensional structures are available: from the fungus *Penicillium vitale*,[200] from beef liver,[201] or from the bacterium *Micrococcus lysodeikticus*.[202] The proximal ligand site of these heme-catalases is occupied by a tyrosine residue (Tyr-357 and Tyr-339 in beef liver and bacterial catalases, respectively) with an Fe—O distance of 1.9 Å (see Figure 3).

The sixth coordination position of iron is occupied by a water molecule. The distal side of these catalases has the usual histidine and arginine residues found in heme-peroxidases and required for the heterolytic activation of hydrogen peroxide. In addition, the binding site of NADPH has been located.[202] All heme-catalases have a strong affinity for NADPH, which is necessary to reduce the Cpd II of catalase that does not take part in the catalytic cycle of the H_2O_2 dismutation, and in addition its accumulation would lead to the deactivation of the enzyme. Calculations suggest that the electron tunneling pathway between the heme and NADPH involves a tyrosine (Tyr-214) which is near the nicotinamide binding site.[203]

The oxidation of the iron(III) resting state of catalase by the first hydrogen peroxide molecule generates a high-valent metal–oxo species considered to be an iron(IV)–oxo with a radical-cation delocalized on the porphyrin ring, according to UV-visible, Raman, and EPR studies (see Scheme 4 for different intermediates of the catalytic cycle of catalase).[204,205]
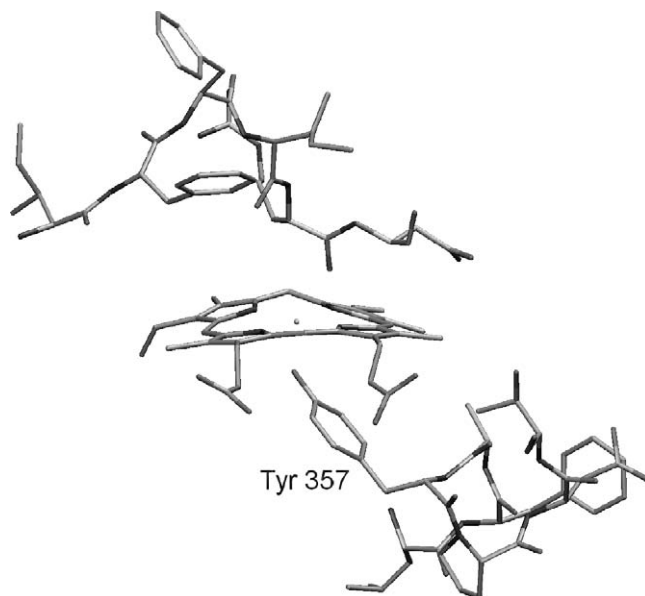
Figure 3 View of the active site of the beef catalase with selected amino acids (for the complete X-ray structure, see ref. [201]).

Differences between Cat–Cpd I and other peroxidase–Cpd I species have been noted: for example the exchange coupling between $S = 1$ of the Fe^{IV}–oxo and $S' = 1/2$ of the porphyrin radical-cation is ferromagnetic (not antiferromagnetic). The motion of the iron with respect to the heme plane has been monitored by time-resolved crystallography: the iron is 0.1 Å below, 0.3 Å above, and within the plane in the Cat resting state, Cat–Cpd I, and Cat–Cpd II, respectively.[206] In the absence of additional hydrogen peroxide, the catalase–Cpd I decays to generate a new species with a tyrosine radical.[207,208]

The addition of hydrogen peroxide to Cat–Cpd I might generate a putative intermediate with a hydroperoxo and a hydroxo ligand on the distal side (see Scheme 4). Labeling studies with doubly ^{18}O-labeled H_2O_2 proved that molecular oxygen is generated from the intact O—O bond in hydrogen peroxide.[209] Kinetic data indicated that the rate constant of Cpd I formation is $10^7 M^{-1} s^{-1}$, below the value for a simple diffusion-controlled bimolecular reaction $(10^{10} M^{-1} s^{-1})$.[210] Cat–Cpd II is generated by an adventitious reductant originating from the solvent or the protein matrix. The trajectories of hydrogen peroxide and water molecules within the main channel of catalase have been simulated by molecular mechanics.[211]
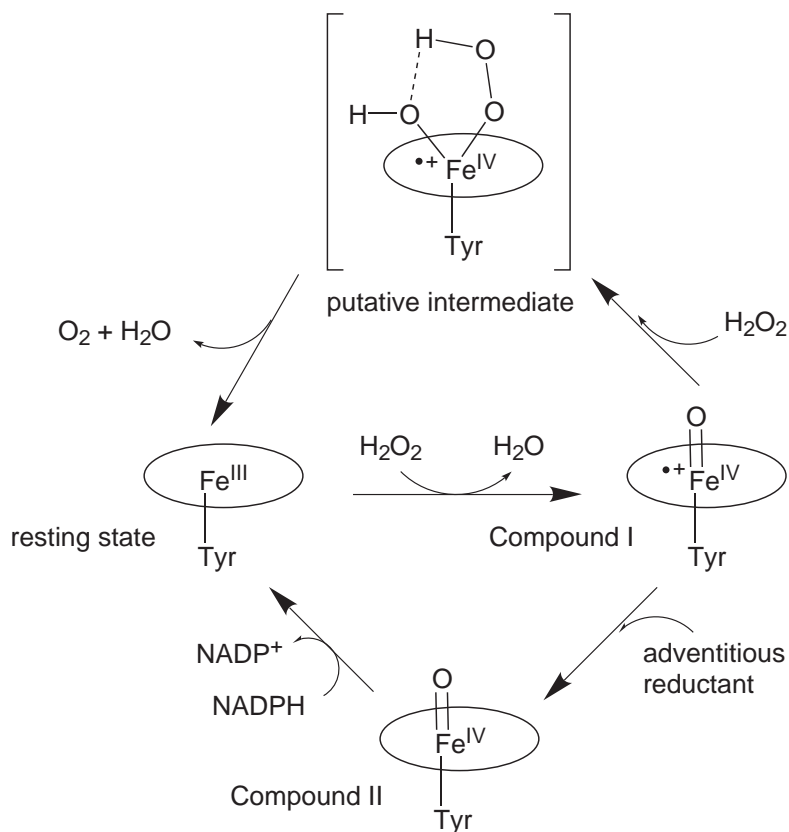
Scheme 4

8.11.5   SHORT SURVEY OF CATALASE MODELS WITH METALLOPORPHYRINS

Early studies of the catalytic decomposition of hydrogen peroxide have been performed with various iron(III) proto- and deuteroporphyrins, and also with metalloporphyrins soluble in organic solvents.[212] The formation of the analogue of Cat–Cpd I has been well studied with nonaggregating iron(III) or manganese(III) sulfonated porphyrins.[213,214]

The influence of the proximal ligand on the catalase activity of synthetic metalloporphyrins has been studied with complexes having an imidazole, an alkoxo, or a phenoxo ligand in the fifth coordination position.[215,216] Two reactions have been studied with these catalase models: (i) the catalytic dismutation of hydrogen peroxide, and (ii) the catalytic epoxidation of olefins. Manganese complexes were more efficient for both oxygenase and dismutase activities than the corresponding iron complexes. However, whereas complexes having a proximal nitrogen ligand

catalyzed both reactions (dismutation and oxygenation), metalloporphyrins with a proximal oxygen ligand catalyzed preferentially the dismutation of H_2O_2 in the case of manganese derivatives, and only this reaction in the case of iron complexes (the "true" models of catalase).[216]

Oxidant-mediated injuries to endothelial cells contribute to the pathogenesis of a variety of diseases (atherosclerosis, reperfusion injury after myocardial ischemia and stroke, adult respiratory distress syndrome, etc.) originating from hydrogen peroxide produced by inflammatory cells such as neutrophils. Consequently, in order to treat such disorders, catalase mimics based on manganese Schiff-base complexes have been developed as potential therapeutic agents. These manganese complexes have been successfully applied against the β-amyloid toxicity related to Alzheimer's disease,[217] the protection of rat kidneys from ischemia-reperfusion-induced damage,[218] and also for the prevention and suppression of autoimmune encephalomyelitis.[219] These catalase mimics are also able to significantly increase the mean lifespan of worms.[220]

Sulfonated metalloporphyrins adsorbed on ion-exchange resins are good catalase models and they can be recycled with a limited loss of catalytic activity.[221] Fe^{III} deuteroporphyrin linked to polylysine via the axial ligation of an amino side chain of the lysine residues can also catalyze the dismutation of hydrogen peroxide.[222]

In conclusion, the better understanding of molecular aspects of heme-peroxidases is the result of studies based on structural data obtained on the enzymes, mainly by crystallography, and from biomimetic models. Both approaches, molecular enzymology and biomimetic chemistry, strongly contributed to a remarkable increase in the knowledge of the properties of these enzymes within less than two decades. In the near future, genetic and chemical modifications of these proteins will provide new "à la carte" enzymes with man-defined activities.

ACKNOWLEDGEMENTS

8.11.6   REFERENCES

1. Everse, J.; Everse, K. E.; Grisham, M. B., Eds. *Peroxidases in Chemistry and Biology*; CRC Press: Boca Raton, FL, 1991; Vols. 1, 2.
2. Welinder, K. G. *Curr. Opin. Struct. Biol.* **1992**, *2*, 388–393.
3. Spallholz, J. E.; Boylan, L. M. In *Peroxidases in Chemistry and Biology*; Everse, J.; Everse, K. E.; Grisham, M. B., Eds., CRC Press: Boca Raton, FL, 1991; Vol. 1, pp 259–291.
4. Dunford, H. B. In *Peroxidases in Chemistry and Biology*; Everse, J.; Everse, K. E.; Grisham, M. B., Eds., CRC Press: Boca Raton, FL, 1991; Vol. 2, pp 1–24.
5. English, A. M.; Tsaprailis, G. *Adv. Inorg. Chem.* **1995**, *43*, 79–125.
6. Dawson, J. H. *Science* **1988**, *240*, 433–439.
7. Gadhede, M.; Schuller, D. J.; Henriksen, A.; Smith, A. T.; Poulos, T. L. *Nature Struct. Biol.* **1997**, *4*, 1032–1038.
8. Nagano, S.; Tanaka, M.; Ishimori, K.; Watanabe, Y.; Morishima, I. *Biochemistry* **1996**, *35*, 14251–14258.
9. Tanaka, M.; Nagano, S.; Ishimori, K.; Morishima, I. *Biochemistry* **1997**, *36*, 9791–9798.
10. Henriksen, A.; Schuller, D. J.; Meno, K.; Welinder, K. G.; Smith, A. T.; Gajhede, M. *Biochem.* **1998**, *37*, 8054–8060.
11. Asokan, A.; de Ropp, J. S.; Newmyer, S. L.; Ortiz de Montellano, P. R.; La Mar, G. N. *J. Am. Chem. Soc.* **2001**, *123*, 4243–4254.
12. Baek, H. K.; Van Wart, H. E. *Biochemistry* **1989**, *28*, 5714–5719.
13. Harris, D. L.; Loew, G. H. *J. Am. Chem. Soc.* **1996**, *118*, 10588–10594.
14. Wirstam, M.; Blomberg, M. R. A.; Siegbahn, P. E. M. *J. Am. Chem. Soc.* **1999**, *121*, 10178–10185.
15. Rodriguez-Lopez, J.; Lowe, D. J.; Hernandez-Ruiz, J.; Hiner, A. N. P.; Garcia-Canovas, F.; Thorneley, R. N. F. *J. Am. Chem. Soc.* **2001**, *123*, 11838–11847.
16. Penner-Hahn, J. E.; Eble, K. S.; McMurry, T. J.; Renner, M.; Balch, A. L.; Groves, J. T.; Dawson, J. H.; Hodgson, K. O. *J. Am. Chem. Soc.* **1986**, *108*, 7819–7825.
17. Chang, C. S.; Yamazaki, I.; Sinclair, R.; Khalid, S.; Powers, L. S. *Biochem.* **1993**, *32*, 923–928.
18. Paeng, K.-J.; Kincaid, J. R. *J. Am. Chem. Soc.* **1988**, *110*, 7913–7915.
19. Chuang, W.-J.; Van Wart, H. E. *J. Biol. Chem.* **1992**, *267*, 13293–13301.
20. Rutter, R.; Hager, L. P.; Dhonau, H.; Hindruch, M.; Valentine, M.; Debrunner, P. *Biochem.* **1984**, *23*, 6809–6816.
21. He, B.; Sinclair, R.; Copeland, B. R.; Makino, R.; Powers, L. S.; Yamazaki, I. *Biochem.* **1996**, *35*, 2413–2420.
22. Nakajima, R.; Yamazaki, I. *J. Biol. Chem.* **1987**, *262*, 2576–2581.
23. Dequaire, M.; Limoges, B.; Moiroux, J.; Savéant, J. M. *J. Am. Chem. Soc.* **2002**, *124*, 240–253.
24. Ator, M. A.; David, S. K.; Ortiz de Montellano, P. R. *J. Biol. Chem.* **1987**, *262*, 14954–14960.

25. Veitch, N. C.; Williams, R. J. P. *Eur. J. Biochem.* **1990**, *189*, 351–362.
26. Banci, L.; Bertini, I.; Bini, T.; Tien, M.; Turano, P. *Biochem.* **1993**, *32*, 5825–5831.
27. Banci, L.; Carloni, P.; Savellini, G. G. *Biochemistry* **1994**, *33*, 12356–12366.
28. Henriksen, A.; Smith, A. T.; Gadheje, M. *J. Biol. Chem.* **1999**, *274*, 35005–35011.
29. Meunier, B. *Biochimie* **1987**, *69*, 3–9.
30. Meunier, G.; Meunier, B. *J. Am. Chem. Soc.* **1985**, *107*, 2558–2560.
31. Meunier, G.; Meunier, B. *J. Biol. Chem.* **1985**, *260*, 10576–10582.
32. Meunier, B. In *Peroxidases in Chemistry and Biology*; Everse, J.; Everse, K. E.; Grisham, M. B., Eds., CRC Press: Boca Raton, FL, 1991; Vol. 2, pp 201–217.
33. Goto, Y.; Watanabe, Y.; Fukuzumi, S.; Jones, J. P.; Dinnocenzo, J. P. *J. Am. Chem. Soc.* **1998**, *120*, 10762–10763.
34. Shaffer, C. L.; Morton, M. D.; Hanzlik, R. P. *J. Am. Chem. Soc.* **2001**, *123*, 8502–8508.
35. Ortiz de Montellano, P. R.; Choe, Y. S.; DePillis, G.; Catalano, C. E. *J. Biol. Chem.* **1987**, *262*, 11641–11646.
36. Ortiz de Montellano, P. R.; Grab, L. A *Biochemistry* **1987**, *26*, 5310–5314.
37. Newmyer, S. L.; Ortiz de Montellano, P. R. *J. Biol. Chem.* **1995**, *270*, 19430–19438.
38. Savenkova, M. I.; Kuo, J. M.; Ortiz de Montellano, P. R. *Biochemistry* **1998**, *37*, 10828–10836.
39. Colonna, S.; Gaggero, N.; Carrea, G.; Pasta, P. *J. Chem. Soc., Chem. Comm.* **1992**, 357–358.
40. Casella, L.; Gullotti, M.; Ghezzi, R.; Poli, S.; Beringhelli, T.; Colonna, S.; Carrea, G. *Biochemistry* **1992**, *31*, 9451–9459.
41. Tanaka, M.; Ishimori, K.; Mukai, M.; Kitagawa, T.; Morishima, I. *Biochemistry* **1997**, *36*, 9889–9898.
42. Bacciochi, E.; Lanzalunga, O.; Malandrucco, S. *J. Am. Chem. Soc.* **1996**, *118*, 8973–8974.
43. Dai, L.; Klibanov, A. M. *Biotechnol. Bioeng.* **2000**, *5*, 353–357.
44. Das, P. K.; Caaveiro, J. M. M.; Luque, S.; Klibanov, A. M. *J. Am. Chem. Soc.* **2002**, *124*, 782–787.
45. Ozaki, S. I.; Inada, Y.; Watanabe, Y. *J. Am. Chem. Soc.* **1998**, *120*, 8020–8025.
46. Smith, K.; Silvernail, N. J.; Rodgers, K. R.; Elgren, T. E.; Castro, M.; Parker, R. M. *J. Am. Chem. Soc.* **2002**, *124*, 4247–4252.
47. Moffet, D. A.; Certain, L. K.; Smith, A. J.; Kessel, A. J.; Beckwith, K. A.; Hecht, M. H. *J. Am. Chem. Soc.* **2000**, *122*, 7612–7613.
48. Griffin, B. W. In *Peroxidases in Chemistry and Biology*; Everse, J.; Everse, K. E.; Grisham, M. B., Eds., CRC Press: Boca Raton, FL, 1991; Vol. 2, pp 85–137.
49. Blanke, S. R.; Hager, L. P. *J. Biol. Chem.* **1988**, *263*, 18739–18743.
50. Fann, Y.-C.; Gerber, N. C.; Osmulski, P. A.; Hager, L. P.; Sligar, S. G.; Hoffman, B. M. *J. Am. Chem. Soc.* **1994**, *116*, 5989–5990.
51. Sundaramoorthy, M.; Terner, J.; Poulos, T. L. *Structure* **1995**, *3*, 1367–1377.
52. Zeng, J.; Fenna, R. E. *J. Mol. Biol.* **1992**, *226*, 185–207.
53. Dunford, H. B.; Lambeir, A.-M.; Kashem, M. A.; Pickard, M. *Arch. Biochem. Biophys.* **1987**, *252*, 292–302.
54. Egawa, T.; Miki, H.; Ogura, T.; Makino, R.; Ishimura, Y.; Kitagawa, T. *FEBS Let.* **1992**, *305*, 206–208.
55. Bernadou, J.; Fabiano, A. S.; Robert, A.; Meunier, B. *J. Am. Chem. Soc.* **1994**, *116*, 9375–9376.
56. Wagenknecht, H.-A.; Woggon, W.-D. *Chem. Biol.* **1994**, *4*, 367–372.
57. Samokyszyn, V. M.; Ortiz de Montellano, P. R. *Biochem.* **1991**, *30*, 11646–11653.
58. Debrunner, P. G.; Dexter, A. F.; Schulz, C. E.; Xia, Y.-M.; Hager, L. P. *Proc. Natl. Acad. Sci. USA* **1996**, *93*, 12791–12798.
59. Geigert, J.; Lee, T. D.; Dalietos, D. J.; Hirano, D. S.; Neidleman, S. L. *Biochem. Biophys. Res. Commun.* **1986**, *136*, 778–782.
60. Allain, E. J.; Hager, L. P.; Deng, L.; Jacobsen, E. N. *J. Am. Chem. Soc.* **1993**, *115*, 4415–4416.
61. Dexter, A. F.; Lakner, F. J.; Campbell, R. A.; Hager, L. P. *J. Am. Chem. Soc.* **1995**, *117*, 6412–6413.
62. Lakner, F. J.; Hager, L. P. *J. Org. Chem.* **1996**, *61*, 3923–3925.
63. Lakner, F. J.; Cain, K. P.; Hager, L. P. *J. Am. Chem. Soc.* **1997**, *119*, 443–444.
64. Zaks, A.; Dodds, D. R. *J. Am. Chem. Soc.* **1995**, *117*, 10419–10424.
65. Hu, S.; Hager, L. P. *J. Am. Chem. Soc.* **1999**, *121*, 872–873.
66. Hu, S.; Dordick, J. S. *J. Org. Chem.* **2002**, *67*, 314–317.
67. Toy, P. H.; Newcomb, P.; Hager, P. L. *Chem. Res. Toxicol.* **1998**, *11*, 816–823.
68. Zaks, A.; Yabannavar, A. V.; Dodds, D. R.; Evans, C. A.; Das, P. R.; Malchow, R. *J. Org. Chem.* **1996**, *61*, 8692–8695.
69. Colonna, S.; Gaggero, N.; Manfredi, A.; Casella, L.; Gullotti, M.; Carrea, G.; Pasta, P. *Biochem.* **1990**, *29*, 10465–10468.
70. Colonna, S.; Gaggero, N. *Phosph. Sulf. Silicon* **1994**, *95–96*, 103–111.
71. Kobayashi, S.; Nakano, M.; Kimura, T.; Schaap, A. P. *Biochem.* **1987**, 5019–5022.
72. Franzen, S.; Roach, M. P.; Chen, Y. P.; Dyer, R. B.; Woodruff, W. H.; Dawson, J. H. *J. Am. Chem. Soc.* **1998**, *120*, 4658–4661.
73. Roach, M. P.; Chen, Y. P.; Woodin, S. A.; Lincoln, D. E.; Lovell, C. R.; Dawson, J. H. *Biochem.* **1997**, *36*, 2197–2202.
74. Wood, W. A.; Kellog, S. T., Eds.; *Biomass, Part B: Lignin, Pectin and Chitin. Methods in Enzymology*; Academic Press: New York, 1988; Vol. 161.
75. Labat, G.; Meunier, B. *Bull. Soc. Chim. Fr.* **1990**, *127*, 553–564.
76. Tien, M.; Kirk, T. K. *Science* **1983**, *221*, 661–663.
77. Glenn, J. K.; Morgan, M. A.; Mayfield, M. B.; Kuwahara, M.; Gold, M. H. *Biochem. Biophys. Res. Commun.* **1983**, *114*, 1077–1083.
78. Gold, M. H.; Kuwahara, M.; Chui, A. A.; Glenn, J. K. *Arch. Biochem. Biophys.* **1984**, *234*, 353–362.
79. Kersten, P. J.; Tien, M.; Kalyanaraman, B.; Kirk, T. K. *J. Biol. Chem.* **1985**, *260*, 2609–2612.
80. Andersson, A. L.; Renganathan, V.; Chui, A. A.; Loehr, T. M.; Gold, M. H. *J. Biol. Chem.* **1985**, *260*, 6080–6087.
81. Poulos, T. L.; Edwards, S. L.; Wariishi, H.; Gold, M. H. *J. Biol. Chem.* **1993**, *268*, 4429–4440.
82. Choinowski, T.; Blodig, W.; Winterhalter, K. H.; Piontek, K. *J. Mol. Biol.* **1999**, *286*, 809–827.
83. Khindaria, A.; Aust, S. D. *Biochem.* **1996**, *35*, 13107–13111.
84. Gelpke, M. D. S.; Lee, J.; Gold, M. H. *Biochem.* **2002**, *41*, 3498–3506.
85. Wariishi, H.; Gold, M. H. *J. Biol. Chem.* **1990**, *265*, 2070–2077.

86. Khindaria, A.; Yamazaki, I.; Aust, S. D. *Biochem.* **1995**, *34*, 16860–16869.
87. Schoemaker, H. E.; Lundell, T. K.; Hatakka, A. I.; Piontek, K. *FEMS Microbiol. Rev.* **1994**, *13*, 321–332.
88. Miki, K.; Renganathan, V.; Gold, M. H. *Biochem.* **1986**, *25*, 4790–4796.
89. Hammel, K. E.; Tien, M.; Kalyanaranam, B.; Kirk, T. K. *J. Biol. Chem.* **1985**, *260*, 8348–8353.
90. Miki, K.; Kondo, R.; Renganathan, V.; Mayfield, M. B.; Gold, M. H. *Biochem.* **1988**, *27*, 4787–4794.
91. Alexander, M. *Biodegradation and Bioremediation*; Academic Press: New York, 1994.
92. Bumpus, J. A.; Tien, M.; Wright, D.; Aust, S. D. *Science* **1985**, *228*, 1434–1436.
93. Joshi, D. K.; Gold, M. H. *Biochemistry* **1994**, *33*, 110969–10976.
94. Yee, D. C.; Wood, T. K. *Biotechnol. Prog.* **1997**, *13*, 53–59.
95. Kuwahara, M.; Glenn, J. K.; Morgan, M. A.; Gold, M. H. *FEBS Lett.* **1984**, *169*, 247–250.
96. Sundaramoorthy, M.; Kishi, K.; Gold, M. H.; Poulos, T. L. *J. Biol. Chem.* **1997**, *272*, 17574–17580.
97. Gelpke, M. D. S.; Moënne-Loccoz, P.; Gold, M. H. *Biochemistry* **1999**, *38*, 11482–11489.
98. Youngs, H. L.; Gelpke, M. D. S.; Li, D.; Sundaramoorthy, M.; Gold, M. H. *Biochem.* **2001**, *40*, 2243–2250.
99. Sutherland, G. R. J.; Aust, S. D. *Biochemistry* **1997**, *36*, 8567–8573.
100. Reading, N. S.; Aust, S. D. *Biochemistry* **2001**, *40*, 8161–8168.
101. Kishi, K.; Wariishi, H.; Marquez, L.; Dunford, H. B.; Gold, M. H. *Biochem.* **1994**, *33*, 8694–8701.
102. Wariishi, H.; Valli, K.; Gold, M. H. *Biochem.* **1989**, *28*, 6017–6023.
103. Wariishi, H.; Valli, K.; Gold, M. H. *Biochem. Biophys. Res. Commun.* **1991**, *176*, 269–275.
104. Bosshard, H. R.; Anni, H.; Yonetani, T. In *Peroxidases in Chemistry and Biology*; Everse, J.; Everse, K. E.; Grisham, M. B.; Eds., CRC Press: Boca Raton, FL, 1991; Vol. 2, pp 51–84.
105. Pelletier, H.; Kraut, J. *Science* **1992**, *258*, 1748–1755.
106. Leesch, V. W.; Bujons, J.; Mauk, A. G.; Hoffman, B. M. *Biochem.* **2000**, *39*, 10132–10139.
107. Sun, J.; Fitzgerald, M. M.; Goodin, D. B.; Loehr, T. M. *J. Am. Chem. Soc.* **1997**, *119*, 2064–2065.
108. Hirst, J.; Wilcox, S. K.; Ai J; Moënne-Loccoz, P.; Loehr, T. M.; Goodin, D. B. *Biochem.* **2001**, *40*, 1274–1283.
109. Shimizu, H.; Schuller, D. J.; Lanzilotta, W. N.; Sundaramoorthy, M.; Arciero, D. M.; Hooper, A. B.; Poulos, T. L. *Biochem.* **2001**, *40*, 13483–13490.
110. Bateman, L.; Léger, C.; Goodin, D. B.; Armstrong, F. A. *J. Am. Chem. Soc.* **2001**, *123*, 9260–9263.
111. Pfister, T. D.; Gengenbach, A. J.; Syn, S.; Lu, Y. *Biochemistry* **2001**, *40*, 14942–14951.
112. Bhaskar, B.; Bonagura, C. A.; Li, H.; Poulos, T. L. *Biochemistry* **2002**, *41*, 2684–2694.
113. Miller, V. P.; DePillis, G. D.; Ferrrer, J. C.; Mauk, A. G.; Ortiz de Montellano, P. R. *J. Biol. Chem.* **1992**, *267*, 8936–8942.
114. Sigman, J. A.; Pond, A. E.; Dawson, J. H.; Lu, Y. *Biochem.* **1999**, *38*, 11122–11129.
115. Wilcox, S. K.; Putnam, C. D.; Sastry, M.; Blankenship, J.; Chazin, W. J.; McRee, D. E.; Goodin, D. B. *Biochem.* **1998**, *37*, 16853–16862.
116. Gengenbach, A.; Syn, S.; Wang, X.; Lu, Y. *Biochem.* **1999**, *38*, 11425–11432.
117. Pauling, L. *Nature* **1964**, *203*, 182–183.
118. Kitagawa, T.; Ondrias, M. R.; Rousseau, D. L.; Ikeda-Saito, M.; Yonetani, T. *Nature* **1982**, *298*, 869–871.
119. Yang, J.; Kloek, A. P.; Goldberg, D. E.; Mathews, F. S. *Proc. Natl. Acad. Sci. USA* **1995**, *92*, 4224–4228.
120. George, P.; Irvine, D. H. *Biochem. J.* **1952**, *52*, 511–516.
121. Grisham, M. B.; In *Peroxidases in Chemistry and Biology*; Everse J.; Everse, K. E.; Grisham, M. B., Eds., CRC Press: Boca Raton, FL, 1991; Vol. 1, pp 335–344.
122. Matsui, T.; Ozaki, S. I.; Watanabe, Y. *J. Biol. Chem.* **1997**, *272*, 32735–32738.
123. Redaelli, C.; Monzani, E.; Santagostini, L.; Casella, L.; Sanangelantoni, A. M.; Pierattelli, R.; Banci, L. *ChemBioChem* **2002**, *3*, 226–233.
124. Klebanoff, S. In *Peroxidases in Chemistry and Biology*; Everse, J.; Everse, K. E.; Grisham, M. B., Eds., CRC Press: Boca Raton, FL, 1991; Vol. 1, pp 1–35.
125. Hurst, J. K. In *Peroxidases in Chemistry and Biology*; Everse, J.; Everse, K. E.; Grisham, M. B., Eds., CRC Press: Boca Raton, FL, 1991; Vol. 1, pp 37–62.
126. Blair-Johnson, M.; Fiedler, T.; Fenna, R. E. *Biochem.* **2001**, *40*, 13990–13997.
127. Marquez, L. A.; Dunford, H. B. *Biochem.* **1997**, *36*, 9349–9355.
128. Hazen, S. L.; Hsu, F. F.; Duffin, K.; Heinecke, J. W. *J. Biol. Chem.* **1996**, *271*, 23080–23088.
129. Hazen, S. L.; Hsu, F. F.; d'Avignon, A.; Heinecke, J. W. *Biochem.* **1998**, *37*, 6864–6873.
130. Eiserich, J. P.; Hristova, M.; Cross, C. E.; Jones, A. D.; Freeman, B. A.; Halliwell, B.; van der Vliet, A. *Nature* **1998**, *391*, 393–397.
131. Thomas, E. L.; Bozeman, P. M.; Learn, D. B. In *Peroxidases in Chemistry and Biology*; Everse, J.; Everse, K. E.; Grisham, M. B., Eds., CRC Press: Boca Raton, FL, 1991; Vol. 1, pp 123–142.
132. Rae, T. D.; Goff, H. M. *J. Biol. Chem.* **1998**, *273*, 27968–27977.
133. Lardinois, O. M.; Medzihradszky, K. F.; Ortiz de Montellano, P. R. *J. Biol. Chem.* **1999**, *274*, 35441–35448.
134. Monzani, E.; Gatti, A. L.; Profumo, A.; Casella, L.; Gullotti, M. *Biochem.* **1997**, *36*, 1918–1926.
135. Jantschko, W.; Furtmuller, P. G.; Allegra, M.; Livrea, M. A.; Jakopitsch, C.; Regelsberger, G.; Obinger, C. *Arch. Biochem. Biophys.* **2002**, *398*, 12–22.
136. Magnusson, R. P. In *Peroxidases in Chemistry and Biology*; Everse, J.; Everse, K. E.; Grisham, M. B., Eds., CRC Press: Boca Raton, FL, 1991; Vol. 1, pp 199–219.
137. Divi, R. L; Doerge, D. R. *Chem. Res. Toxicol.* **1996**, *9*, 16–23.
138. Doerge, D. R.; Divi, R. L.; Deck, J.; Taurog, A. *Chem. Res. Toxicol.* **1997**, *10*, 49–58.
139. Estienne, V.; Blanchet, C.; Niccoli-Sire, P.; Duthoit, C.; Durand-Gordet, J. M.; Geourjon, C.; Baty, D.; Carayon, P.; Ruf, J. *J. Biol. Chem.* **1999**, *274*, 35313–35317.
140. Charles, T.; Chapal, N.; Bresson, D.; Bes, C.; Giudicelli, V.; Lefranc, M. P.; Peraldi-Roux, S. *Immunogenetics* **2002**, *54*, 141–157.
141. Welinder, K. G. *Biochim. Biophys. Acta* **1992**, *1080*, 215–220.
142. Yamada, Y.; Fujiwara, T.; Sato, T.; Igarashi, N.; Tanaka, N. *Nature Struct. Biol.* **2002**, *9*, 691–695.
143. Chouchane, S.; Lippai, I.; Magliozzo, R. S. *Biochemistry* **2000**, *39*, 9975–9983.
144. Hillar, A.; Peters, B.; Pauls, R.; Loboda, A.; Zhang, H.; Mauk, A. G.; Loewen, P. C. *Biochem.* **2000**, *39*, 5868–5875.
145. Middlebrook, G. *Am. Rev. Tuberc.* **1954**, *69*, 471–472.

146. Quémard, A.; Dessen, A.; Sugantino, M.; Jacobs, W. R.; Sacchettini, J. C.; Blanchard, J. S. *J. Am. Chem. Soc.* **1996**, *118*, 1561–1562.
147. Bodiguet, J.; Nagy, J. M.; Brown, K.; Jamart-Grégoire, B. *J. Am. Chem. Soc.* **2001**, *123*, 3832–3833.
148. Nguyen, M.; Quémard, A.; Broussy, S.; Bernadou, J.; Meunier, B. *Antimicrob. Agents Chemother.* **2002**, *46*, 2137–2144.
149. Johnsson, K.; Froland, W. A.; Schultz, P. G. *J. Biol. Chem.* **1997**, *272*, 2834–2840.
150. Lei, B.; Wei, C. J.; Tu, S. C. *J. Biol. Chem.* **2000**, *275*, 2520–2526.
151. Morris, S.; Bai, G. H.; Suffys, P.; Portillo-Gomez, L.; Fairchok, M.; Rouse, D. *J. Infect. Dis.* **1995**, *171*, 954–960.
152. Heym, B.; Alzari, P. M.; Honore, N.; Cole, S. T. *Mol. Microbiol.* **1995**, *15*, 235–245.
153. Meunier, B. *Chem. Rev.* **1992**, *92*, 1411–1456.
154. Meunier, B.; Robert, A.; Pratviel, G.; Bernadou, J. In *The Porphyrin Handbook*; Kadish, K. M.; Smith, K.; Guilard, R., Eds., Academic Press: San Diego, CA, 2000; Vol. 4, Chap. 31, pp 119–187.
155. Jones, P.; Robson, T.; Brown, S. B. *Biochem. J.* **1973**, *135*, 353–359.
156. Takahashi, K.; Matsushima, A.; Saito, Y.; Inada, Y. *Biochem. Biophys. Res. Commun.* **1986**, *138*, 283–288.
157. Lindsay Smith, J. R.; Mortimer, D. N. *J. Chem. Soc., Chem. Commun.* **1985**, 64–65.
158. Traylor, T. G.; Lee, W. A.; Stynes, D. V. *Tetrahedron* **1984**, *40*, 553–568.
159. Bruice, T. C. *Acc. Chem. Res.* **1991**, *24*, 243–249.
160. Wang, J.-S.; Baek, H. K.; Van Wart, H. E. *Biochem. Biophys. Res. Commun.* **1991**, *179*, 1320–1324.
161. Nakamura, S.; Mashino, T.; Hirobe, M. *Tetrahedron Lett.* **1992**, *33*, 5409–5412.
162. Colonna, S.; Gaggero, N.; Carrea, G.; Pasta, P. *Tetrahedron Lett.* **1994**, *35*, 9103–9104.
163. Cochran, A. G.; Schultz, P. G. *J. Am. Chem. Soc.* **1990**, *112*, 9414–9415.
164. Harada, A.; Fukushima, H.; Shiotsuki, K; Yamaguchi, H.; Oka, F.; Kamachi, M. *Inorg. Chem.* **1997**, *36*, 6099–6102.
165. Quilez, R.; De Lauzon, S.; Desfosses, B.; Mansuy, D.; Mahy, J. P. *FEBS Lett.* **1996**, *395*, 73–76.
166. Bernadou, J.; Bonnafous, M.; Labat, G.; Loiseau, P.; Meunier, B. *Drug Met. Dispos.* **1991**, *19*, 360–365.
167. Masumoto, H.; Ohta, S.; Hirobe, M. *Drug Met. Dispos.* **1991**, *19*, 768–780.
168. Vidal, M.; Bonnafous, M.; Defrance, S.; Loiseau, P.; Bernadou, J.; Meunier, B. *Drug Met. Dispos.* **1993**, *21*, 811–817.
169. Carrier, M. N.; Battioni, P.; Mansuy, D. *Bull. Soc. Chim. Fr.* **1993**, *130*, 405–416.
170. Gaggero, N.; Robert, A.; Bernadou, J.; Meunier, B. *Bull. Soc. Chim. Fr.* **1994**, *131*, 706–712.
171. Adam, Y.; Bernadou, J.; Meunier, B. *New J. Chem.* **1992**, *16*, 525–528.
172. Wilson, I.; Bretscher, K. R.; Chea, C. K.; Kelly, H. C. *J. Inorg. Biochem.* **1983**, *19*, 345–357.
173. Labat, G.; Meunier, B. *J. Chem. Soc., Chem. Commun.* **1990**, 1414–1416.
174. Wagenknecht, H. A.; Woggon, W. D. *Angew. Chem. Int. Ed. Engl.* **1997**, *36*, 390–392.
175. Jin, N.; Bourassa, J. L.; Tizio, S. C.; Groves, J. T. *Angew. Chem. Int. Ed.* **2000**, *39*, 3849–3851.
176. Dolphin, D.; Nakano, T.; Maione, T. E.; Kirk, T. K.; Farrell, R. *Lignin Enzym. Microbiol. Degrad.* **1987**, *40*, 157–162 [Chem. Abst. 1988 109 69402u.]
177. Meunier, B.; Labat, G.; Séris, J. L., French patent 8,809,169, 1988. *Chem. Abstr.* **1990**, *113*, 152001r.
178. Labat, G.; Meunier, B. *New J. Chem.* **1989**, *13*, 801–804.
179. Labat, G.; Meunier, B. *J. Org. Chem.* **1989**, *54*, 5008–5011.
180. Hoffmann, P.; Robert, A.; Meunier, B. *Bull. Soc. Chim. Fr.* **1992**, *129*, 85–97.
181. Dolphin, D.; Traylor, T. G.; Xie, L. Y. *Acc. Chem. Res.* **1992**, *30*, 251–259.
182. Zhu, W.; Ford, W. T. *J. Mol. Cat.* **1993**, *78*, 367–378.
183. Labat, G.; Meunier, B. *C. R. Acad. Sci. Paris, Part II* **1990**, *311*, 625–630.
184. Pattou, D.; Labat, G.; Defrance, S.; Séris, J. L.; Meunier, B. *Bull. Soc. Chim. Fr.* **1994**, *131*, 78–88.
185. Labat, G.; Séris, J. L.; Meunier, B. *Angew. Chem. Int. Ed. Engl.* **1990**, *29*, 1471–1473.
186. Sorokin, A.; Séris, J. L.; Meunier, B. *Science* **1995**, *268*, 1163–1166.
187. Sorokin, A.; De Suzzoni-Dezard, S.; Poullain, D.; Noël, J. P.; Meunier, B. *J. Am. Chem. Soc.* **1996**, *118*, 7410–7411.
188. Meunier, B.; Sorokin, A. *Acc. Chem. Res.* **1997**, *30*, 470–476.
189. Sorokin, A.; Meunier, B. *Eur. J. Inorg. Chem.* **1998**, 1269–1281.
190. Hadasch, A.; Sorokin, A.; Rabion, A.; Fraisse, L.; Meunier, B. *Bull. Soc. Chim. Fr.* **1998**, *134*, 1025–1032.
191. Sanchez, M.; Hadasch, A.; Fell, R.; Meunier, B. *J. Catal.* **2001**, *202*, 177–186.
192. Gupta, S. S.; Stadler, M.; Noser, C. A.; Gosh, A.; Steinhoff, B.; Lenoir, D.; Horwitz, C. P.; Schramm, K. W.; Collins, T. J. *Science* **2002**, *296*, 326–328.
193. Defrance, S.; Séris, J. L.; Meunier, B. *New J. Chem.* **1992**, *16*, 1015–1016.
194. Policar, C.; Artaud, I.; Mansuy, D. *Inorg. Chem.* **1996**, *35*, 210–216.
195. Schonbaum, G. R.; Chance, B. In *The Enzymes*, Boyer, P. D., Ed.; Academic Press: New York, 1976; Vol. XIII, Chap. 7, pp 363–408.
196. Kimbrough, D. R.; Magoun, M. A.; Langfur, M. *J. Chem. Educ.* **1997**, *74*, 210–212.
197. Chiu, J. T.; Loewen, P. C.; Switala, J.; Gennis, R. B.; Timkovich, R. *J. Am. Chem. Soc.* **1989**, *111*, 7046–7050.
198. Kleff, S.; Sander, S.; Mielke, G.; Eising, R. *Eur. J. Biochem.* **1997**, *245*, 402–410.
199. Corrall, R. J. M.; Rodman, H. M.; Margolis, J.; Landau, B. R. *J. Biol. Chem.* **1974**, *249*, 3181–3182.
200. Vainshtein, B. K.; Melik-Adamyan, W. R.; Barynin, V. V.; Vagin, A. A.; Grebenko, A. I.; Borisov, V. V.; Bartels, K. S.; Fita, I.; Rossmann, M. G. *J. Mol. Biol.* **1986**, *188*, 49–61.
201. Fita, I.; Rossmann, M. G. *J. Mol. Biol.* **1985**, *185*, 21–37.
202. Murshudov, G. N.; Melik-Adamyan, W. R.; Grebenko, A. I.; Barynin, V. V.; Vagin, A. A.; Vainshtein, B. K.; Dauter, Z.; Wilson, K. S. *FEBS Lett.* **1992**, *312*, 127–131.
203. Olson, L. P.; Bruice, T. C. *Biochem.* **1995**, *34*, 7335–7347.
204. Dolphin, D.; Froman, A.; Borg, D. C.; Fajer, J.; Felton, R. H. *Proc. Natl. Acad. Sci. USA* **1971**, *68*, 614–618.
205. Benecky, M. J.; Frew, J. E.; Scowen, N.; Jones, P.; Hoffman, B. *Biochemistry* **1993**, *32*, 11929–11933.
206. Gouet, P.; Jouve, H. M.; Williams, P. A.; Andersson, I.; Andreoletti, P.; Nussaume, L.; Hadju, J. *Nature Struct. Biol.* **1996**, *3*, 951–956.
207. Ivancich, A.; Jouve, M. H.; Sartor, B.; Gaillard, J. *Biochem.* **1997**, *36*, 9356–9364.
208. Green, M. T. *J. Am. Chem. Soc.* **2001**, *123*, 9218–9219.
209. Jarnagin, R. C.; Wang, J. H. *J. Am. Chem. Soc.* **1958**, *80*, 786–787.

210. Jones, P.; Dunford, H. B. *J. Theor. Biol.* **1977**, *69*, 457–470.
211. Kalko, S. G.; Gelpi, J. L.; Fita, I.; Orozco, M. *J. Am. Chem. Soc.* **2001**, *123*, 9665–9672.
212. Traylor, T. G.; Xu, F. *J. Am. Chem. Soc.* **1987**, *109*, 6201–6202.
213. Zipplies, M. F.; Lee, W. A.; Bruice, T. C. *J. Am. Chem. Soc.* **1986**, *108*, 4433–4445.
214. Panicucci, R.; Bruice, T. C. *J. Am. Chem. Soc.* **1990**, *112*, 6063–6071.
215. Belal, R.; Momenteau, M.; Meunier, B. *J. Chem. Soc. Chem. Commun.* **1989**, 412–414.
216. Robert, A.; Loock, B.; Momenteau, M.; Meunier, B. *Inorg. Chem.* **1991**, *30*, 706–711.
217. Bruce, A. J.; Malfroy, B.; Baudry, M. *Proc. Natl. Acad. Sci. USA* **1996**, *93*, 2312–2316.
218. Gianello, P.; Saliez, A.; Bufkens, X.; Pettinger, R.; Misseleyn, D.; Hori, S.; Malfroy, B. *Transplantation* **1996**, *62*, 1664–1666.
219. Malfroy, B.; Doctrow, S. R.; Orr, P. L.; Tocco, G.; Fedeseyeva, E. V.; Benichou, G. *Cell. Immunol.* **1997**, *177*, 62–68.
220. Melov, S.; Ravenscroft, J.; Malik, S.; Gill, M. S.; Walker, D. W.; Clayton, P. E.; Wallace, D. C.; Malfroy, B.; Doctrow, S. R.; Lithgow, C. J. *Science* **2000**, *289*, 1567–1569.
221. Saito, Y.; Mifune, M.; Nakashima, S.; Kawaguchi, T.; Odo, J.; Tanaka, Y.; Chikuma, M.; Tanaka, H. *Chem. Pharm. Bull.* **1986**, *34*, 2885–2889.
222. Barteri, M.; Jones, P.; Mantovani, O. *J. Chem. Soc. Dalton Trans.* **1986**, 333–336.

8.12
Cytochrome P450

W. NAM
Ewha Womans University, Seoul, Korea

8.12.1 INTRODUCTION

Cytochromes P450 are a superfamily of cysteine thiolate-ligated heme-containing monooxygenase enzymes that catalyze the transfer of an oxygen atom from molecular oxygen into a wide variety of biological substrates, with the second oxygen atom being reduced by two electrons to a water molecule (Equation (1)).[1–10] Cytochrome P450 enzymes have been isolated from mammalian tissues, birds, fish, plants, insects, yeasts, bacteria, and other biological species, and the monooxygenases are known to participate in drug metabolism, biotransformation of naturally occurring molecules, and oxidative metabolism of xenobiotics.[8–10] The most often-encountered oxidation reactions by cytochromes P450 are hydroxylation, epoxidation, heteroatom oxidation, and heteroatom dealkylation:

$$RH + O_2 + 2e^- + 2H^+ \xrightarrow{\text{Cytochrome P450}} ROH + H_2O \qquad (1)$$
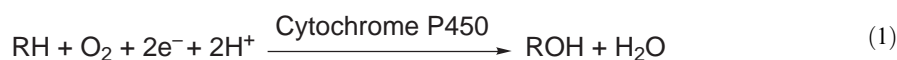
The first three-dimensional structure of cytochrome P450 was reported by Poulos in 1985, the soluble bacterial cytochrome P450cam isolated from the bacterium *Pseudomonas putida*.[11] The enzyme, which catalyzes the stereospecific hydroxylation of camphor to 5-exo-hydroxycamphor (Equation (2)), consists of a single polypeptide chain containing a heme *b* group (iron protoporphyrin IX) with a cysteine, Cys357, as an axial ligand (Figure 1). The heme *b* group bound to the protein by an iron-cysteinate bond is deeply embedded in the hydrophobic interior

$$(2)$$
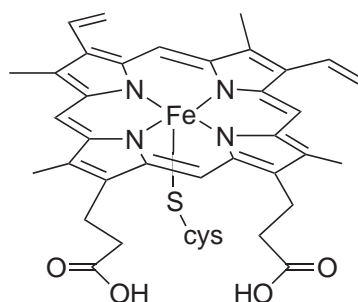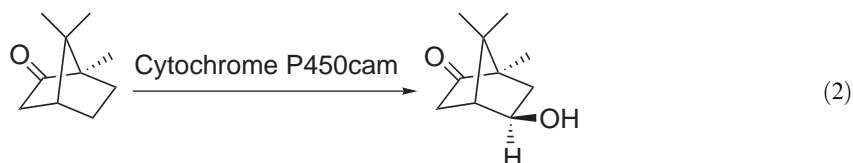
Figure 1 Iron(III) protoporphyrin IX with a cysteinate as an axial ligand.

to accommodate hydrophobic substrates. The name cytochrome P450 is derived from the fact that a red-shifted strong Soret band (high-energy π–π^* transition of the porphyrin ring) appears at 450 nm when CO binds to ferrous heme (Fe^{II}-CO). This spectral feature is caused by the strong electron-donating character of the cysteinate proximal ligand.[12,13] Other heme-containing proteins bearing a histidine proximal ligand exhibit a Soret band at 420 nm in the visible spectra of their Fe^{II}-CO adducts.[13]

One primary goal in cytochrome P450 research is to understand the mechanistic details of dioxygen activation and oxygen transfer reactions by the enzymes. Extensive mechanistic studies with cytochrome P450cam and iron porphyrin complexes resulted in the catalytic cycle of cytochrome P450 shown in Figure 2. In the resting, substrate-free state, cytochrome P450 contains a six-coordinate low-spin ferric state, (**1**), with water as the displaceable distal ligand. The binding of substrate to the resting state generates a five-coordinate high-spin ferric state, (**2**), which now has a vacant coordination site for dioxygen binding. Conversion of the low-spin ferric heme to the high-spin ferric heme shifts the redox potential ($E^{\circ\prime}$) from -300 mV to -170 mV,
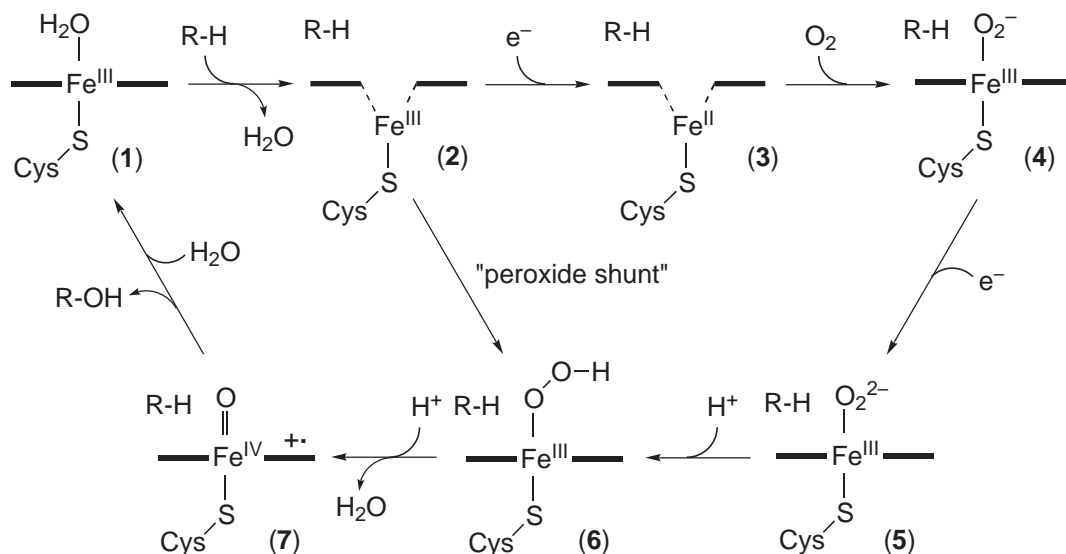
Figure 2 Proposed catalytic cycle of cytochrome P450.

thus facilitating the reduction of the ferric heme by reduced putidaredoxin ($E^{\circ'}$ of $-196\,\text{mV}$) to generate a five-coordinate high-spin ferrous heme, (**3**).[14] Dioxygen then binds to the ferrous heme to form the ferrous-dioxygen heme ($Fe^{II}\text{-}O_2$) or ferric-superoxo heme ($Fe^{III}\text{-}O_2^-$), (**4**). The electronic nature of (**4**) has been the subject of intense discussion, and the spectroscopic properties of (**4**) are most consistent with a ferric-superoxo complex ($Fe^{III}\text{-}O_2^-$). The O—O bond stretching and bending frequencies have been observed at $1{,}140\,\text{cm}^{-1}$ and $401\,\text{cm}^{-1}$, respectively, in the resonance Raman spectrum of P450cam, consistent with an η^1-superoxo ion coordinated to an iron(III) ion.[15]

In contrast to the four well-characterized states ((**1**)–(**4**) in Figure 2), evidence for the following three important states ((**5**)–(**7**) in Figure 2) has only recently been obtained. Addition of the second electron to (**4**), presumed to be the rate-limiting step in the catalytic cycle,[16] yields a ferric-peroxo species ($Fe^{III}\text{-}O_2^{2-}$), (**5**), which is then protonated to give a ferric-hydroperoxo complex, (**6**). Recently, the ferric–peroxo and ferric–hydroperoxo intermediates were generated by the radiolytic cryoreduction of the ferric–superoxo form of cytochrome P450cam, (**4**), with gradual temperature annealing and then characterized by EPR, ENDOR, and UV–vis spectroscopies.[17–19] The delivery of a second proton to the ferric–hydroperoxo species, (**6**), results in heterolytic O—O bond cleavage to release a water molecule and generate a formally oxoiron(V) species. This reactive species is better described as an oxoiron(IV) porphyrin π-cation radical intermediate, (**7**), which is equivalent to the high-valent intermediate, compound I, of horseradish peroxidase (HRP). Although the intermediate (**7**) is believed to be the most likely candidate for the reactive species that hydroxylates unactivated hydrocarbons in cytochromes P450, the characterization of this intermediate has been a challenge. Very recently, Schlichting and co-workers reported that the ferric–superoxo of cytochrome P450cam, (**4**), was converted by X-irradiation at cryogenic temperature into an intermediate that would be consistent with an oxoiron(IV) species.[20] In different studies, the oxidation of cytochromes P450 by *m*-chloroperbenzoic acid (*m*-CPBA) generated intermediates with UV–vis spectral features characteristic of an oxoiron(IV) porphyrin π-cation radical, (**7**).[21,22] The final step of the P450 reaction cycle is the transfer of an oxygen atom from (**7**) to the substrate to give the alcohol product followed by the regeneration of the resting, water-bound state, (**1**). In a reaction known as the "peroxide shunt," single oxygen atom donors such as hydrogen peroxide, alkyl hydroperoxides, peracids, and iodosylbenzenes can also be used to generate oxygenated products by bypassing the intermediates (**3**)–(**5**) in Figure 2.

8.12.2 METALLOPORPHYRINS AS MODELS FOR CYTOCHROME P450

8.12.2.1 Early History of Metalloporphyrins

In 1979, Groves and co-workers published the first article on the use of a synthetic iron(III) porphyrin complex, Fe(TPP)Cl (TPP = *meso*-tetraphenylporphyrin), in catalytic olefin epoxidation and alkane hydroxylation reactions by iodosylbenzene (PhIO).[23] Olefins were preferentially oxidized to the corresponding epoxides, and alcohols were obtained as major products in alkane hydroxylations (Equations (3) and (4)):

$$\text{(olefin)} + \text{PhIO} \xrightarrow{\text{Fe(TPP)Cl}} \text{(epoxide)} + \text{PhI} \qquad (3)$$

$$\text{C--H} + \text{PhIO} \xrightarrow{\text{Fe(TPP)Cl}} \text{C--OH} + \text{PhI} \qquad (4)$$
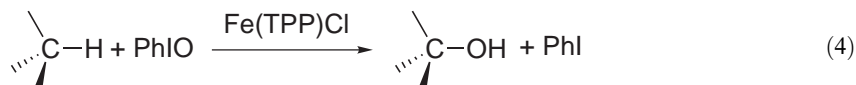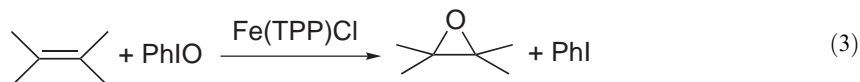
A remarkable feature of the Fe(TPP)Cl/PhIO system in olefin epoxidations was the stereospecific epoxidation of *cis*-stilbene and the high reactivity of *cis*-stilbene compared to *trans*-stilbene. With respect to the latter, *cis*-stilbene showed 15 times greater reactivity than *trans*-stilbene in intermolecular competitive epoxidation of *cis*- and *trans*-stilbenes by Fe(TPP)Cl and PhIO (Equation (5)).[24] The preference of *cis*-stilbene over *trans*-stilbene was ascribed to nonbonded interactions between the phenyl groups of *trans*-stilbene and the phenyl groups of the Fe(TPP)Cl catalyst. In the same year, Chang and Kuo reported that a green intermediate,

generated in the reaction of Fe(OEP)Cl (OEP = octaethyl-porphyrin) and an iodosylbenzene derivative, hydroxylated C—H bonds regiospecifically:[25]

$$\text{ratio of } cis\text{-oxide} : trans\text{-oxide} = 15:1$$

(5)
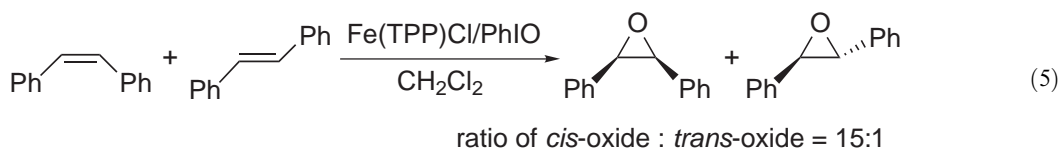
Other metalloporphyrins such as Mn(TPP)Cl and Cr(TPP)Cl were also investigated as catalysts in oxygenation reactions. Tabushi and co-worker were the first to use Mn(TPP)Cl as a catalyst in the oxygenation of hydrocarbons by molecular oxygen in the presence of sodium borohydride.[26] In 1980, Hill, Groves, and Meunier reported independently that Mn(TPP)Cl was an efficient catalyst in olefin epoxidation and alkane hydroxylation reactions by PhIO and NaOCl.[27–29] However, the chemistry of Mn(TPP)Cl was different from that of Fe(TPP)Cl. A significant amount of *trans*-stilbene oxide was obtained in *cis*-stilbene epoxidation by Mn(TPP)Cl, which was explained by the generation of a long-lived carbon radical.[28] In the case of Cr(TPP)Cl, Groves and Kruper isolated a high-valent chromium oxo porphyrin intermediate in the reaction of Cr(TPP)Cl and PhIO, and the intermediate showed an ability to epoxidize and hydroxylate hydrocarbons.[30] An important observation reported in the study was that the oxo ligand of the chromium oxo intermediate exchanged with labeled water, $H_2^{18}O$, and that when the intermediate reacted with an olefin in the presence of a small amount of $H_2^{18}O$, oxygen from the labeled water was incorporated into epoxide product.[30] In 1981, one of the most important papers in the history of metalloporphyrin chemistry was published by Groves and co-workers.[31] When Fe(TMP)Cl (TMP = *meso*-tetramesitylporphyrin) was reacted with *m*-CPBA in CH_2Cl_2—CH_3OH at $-78\,^\circ$C, a green intermediate was generated. On the basis of various spectroscopic measurements, this species was characterized to be an oxoiron(IV) porphyrin π-cation radical complex, $[(TMP)^{+\cdot}Fe^{IV}{=}O]^+$, identical to the compound I of peroxidases. In addition, this intermediate was capable of oxygenating olefins to yield the corresponding epoxide products. Furthermore, when the intermediate was treated with $H_2^{18}O$ prior to react with norbornene, the norbornene oxide product contained 99% ^{18}O (Scheme 1). The spectral similarity of the oxoiron(IV) porphyrin π-cation radical to the peroxidase compound I and the capability of oxygen atom transfer of the intermediate to organic substrates made this paper a milestone in the biomimetic studies of cytochromes P450.

8.12.2.2 First-, Second-, and Third-generation Metalloporphyrins

Metalloporphyrins containing the TPP ligand are called the first-generation metalloporphyrin catalysts. Although the first-generation metalloporphyrins associated with artificial oxidants such as PhIO, NaOCl, and $KHSO_5$ mimicked much of the chemistry of cytochrome P450, their catalytic activities became rapidly diminished by the extensive oxidative destruction of the porphyrin ligand and the formation of an inactive μ-oxo dimer (e.g., (TPP)Fe-O-Fe(TPP)). Such problems were overcome by introducing alkyl or halogen substituents on phenyl groups at the *meso*-positions of the TPP ligand, and these metalloporphyrins are called the second-generation metalloporphyrins. One important achievement of the second-generation metalloporphyrins was the increased catalytic activity toward substrate oxidation and the stability against oxidative destruction of porphyrin ligand.[32] Metalloporphyrins with halogenated substituents on the phenyl groups such as Fe(TPFPP)Cl (TPFPP = *meso*-tetrakis(pentafluorophenyl) porphyrin) and Fe(TDCPP)Cl (TDCPP = *meso*-tetrakis(2,6-dichlorophenyl)porphyrin) are particularly good examples (see Figure 3 for the structures).[33–36] Based on the lesson that introducing electron-withdrawing substituents on the *meso*-aryl rings enhanced the reactivity of metalloporphyrin catalysts, the third-generation metalloporphyrins were synthesized by placing electron-withdrawing substituents such as F, Cl, Br, and NO_2 on the β-pyrrole positions of the second-generation metalloporphyrins (Figure 3). Traylor and Dolphin reported independently that halogenation of the β-pyrrole positions of Fe(TDCPP)Cl markedly increased the catalytic efficiency and stability of the iron porphyrin catalysts in oxygenation reactions.[37,38] Ellis and Lyons also showed that these third-generation metalloporphyrins were efficient catalysts in the hydroxylation of alkanes

Structure of [(TMP)$^{+\bullet}$Fe^{IV}=O]$^+$

Scheme 1

Porphyrin	Ar group			Pyrrole
	R_1	R_2	R_3	X
TPP	H	H	H	H
TMP	CH_3	H	CH_3	H
TDCPP	Cl	H	H	H
TPFPP	F	F	F	H
TDCPβCl$_8$P	Cl	H	H	Cl
TDCPβBr$_8$P	Cl	H	H	Br
TPFPβF$_8$P	F	F	F	F
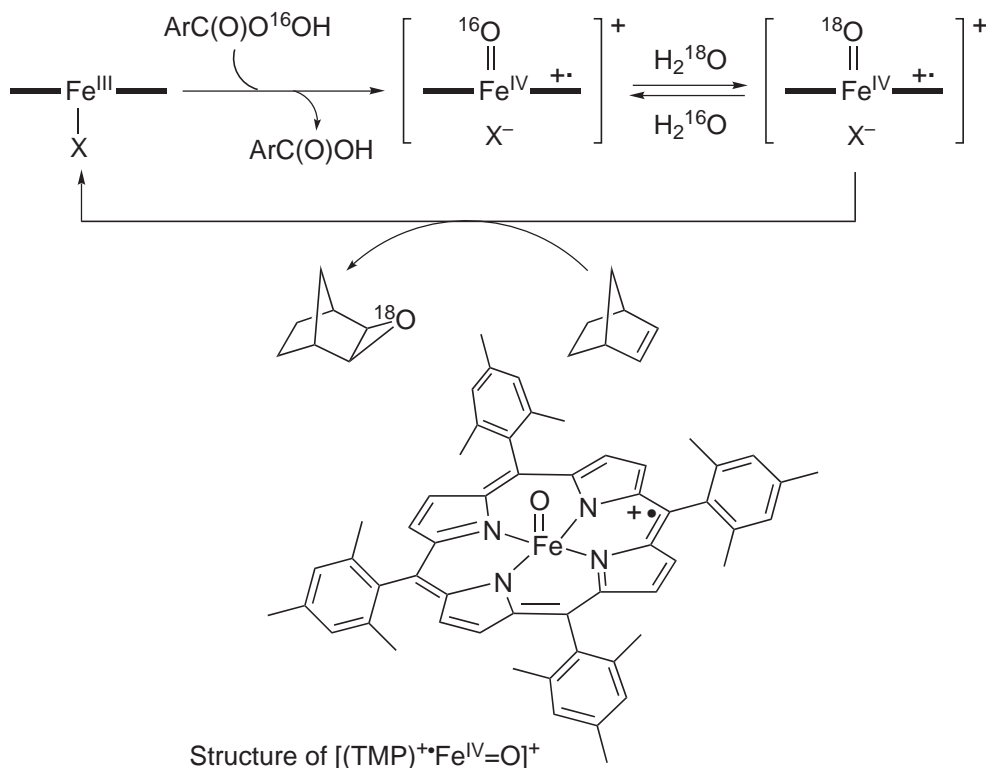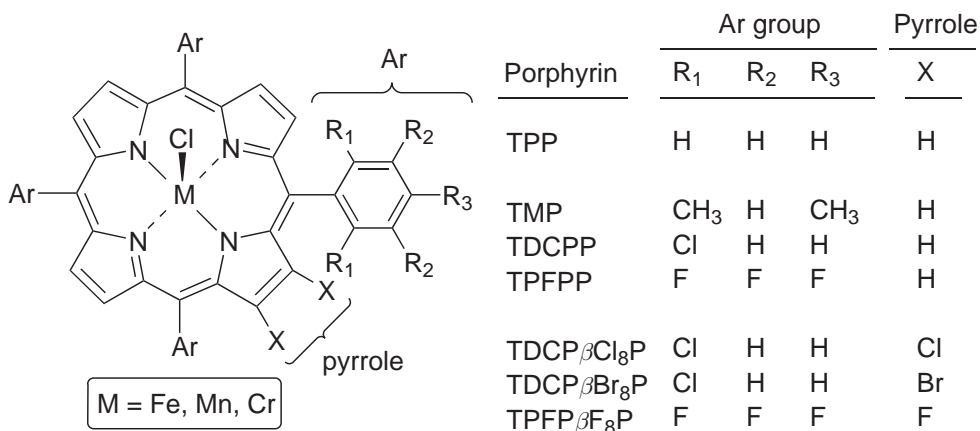
Figure 3 Structures of the first, second, and third-generation metalloporphyrins.

by air at room temperature and suggested that an oxoiron(IV) porphyrin was a reactive species responsible for alkane hydroxylations.[39] However, subsequent studies by Labinger, Gray, and co-workers demonstrated the involvement of a radical-chain mechanism in the alkane hydroxylations.[40] Recently, Mansuy and co-workers published that Fe(TDCPP)$^+$ and Mn(TDCPP)$^+$ complexes bearing β-nitro substituents were efficient catalysts in the oxygenation of hydrocarbons by H$_2$O$_2$.[41,42] In addition to the high catalytic property, the perhalogenated iron porphyrins showed a large positive shift in the iron(III)/iron(II) redox couple as well as severe saddling of the macrocyclic structure.[40]

8.12.2.3 Metalloporphyrins as Catalysts in Oxidation Reactions

Synthetic metalloporphyrins of Fe^{III}, Mn^{III}, Cr^{III}, and $Ru^{II,III,VI}$, especially with porphyrins bearing aryl-groups at *meso*-positions, have been used in a variety of oxidation reactions (Figure 4), with the intention of developing biomimetic catalysts which show regio-, stereo-, shape-, and enantioselectivity with a high efficiency under mild conditions.[5,43–47] Iron and manganese porphyrins are the most often used metalloporphyrins in the oxidation reactions, and the catalytic activity of chromium porphyrins is much inferior to those of iron-, manganese-, and ruthenium porphyrins. Ruthenium porphyrins have shown a high catalytic activity in olefin epoxidation and alkane hydroxylation, and the hydrocarbons are stereospecifically oxygenated with complete retention of configuration.[44] Although most of the metalloporphyrin-catalyzed oxidation reactions have been carried out in homogeneous solutions, polymer-supported metalloporphyrins such as metalloporphyrins anchored to organic or inorganic supports or encapsulated in zeolites have been used in heterogeneous oxidation reactions.[48] In addition to the oxidation reactions, metalloporphyrins, especially water-soluble manganese porphyrins, have been the subject of extensive studies in oxidative DNA cleavage and their interactions with DNA.[43]

A variety of oxidants including iodosylbenzenes, peracids, hypochlorite, periodate, ozone, potassium monoperoxysulfate, monoperoxyphthalate, pyridine *N*-oxides, nitrous oxide (N_2O), O_2 plus reductants, hydrogen peroxide, and alkyl hydroperoxides have been used as oxygen atom donors in catalytic oxidation reactions. The last two are considered to be the most important oxidants, since these are biologically relevant and environmentally clean. Therefore, the reactions of these oxidants with iron porphyrins have been the topic of continuing interest over the past two decades. In 1989, Traylor and co-workers published the first article on the epoxidation of olefins by an electron-deficient iron porphyrin complex, Fe(TDCPP)Cl, and hydroperoxides in a solvent mixture of CH_2Cl_2—CH_3OH—H_2O.[49,50] An oxoiron(IV) porphyrin π-cation radical intermediate, formed via O—O bond heterolysis in protic solvents, was proposed as the epoxidizing intermediate. The authors also proposed that the absence of oxygenated products often encountered in hydrocarbon oxygenations by iron porphyrin catalysts and hydroperoxides was the result of a fast reaction between oxoiron(IV) porphyrin π-cation radicals and hydroperoxides (Scheme 2, pathway A). The proposal was confirmed by carrying out competitive reactions of hydroperoxides and organic substrates with *in situ* generated oxoiron(IV) porphyrin
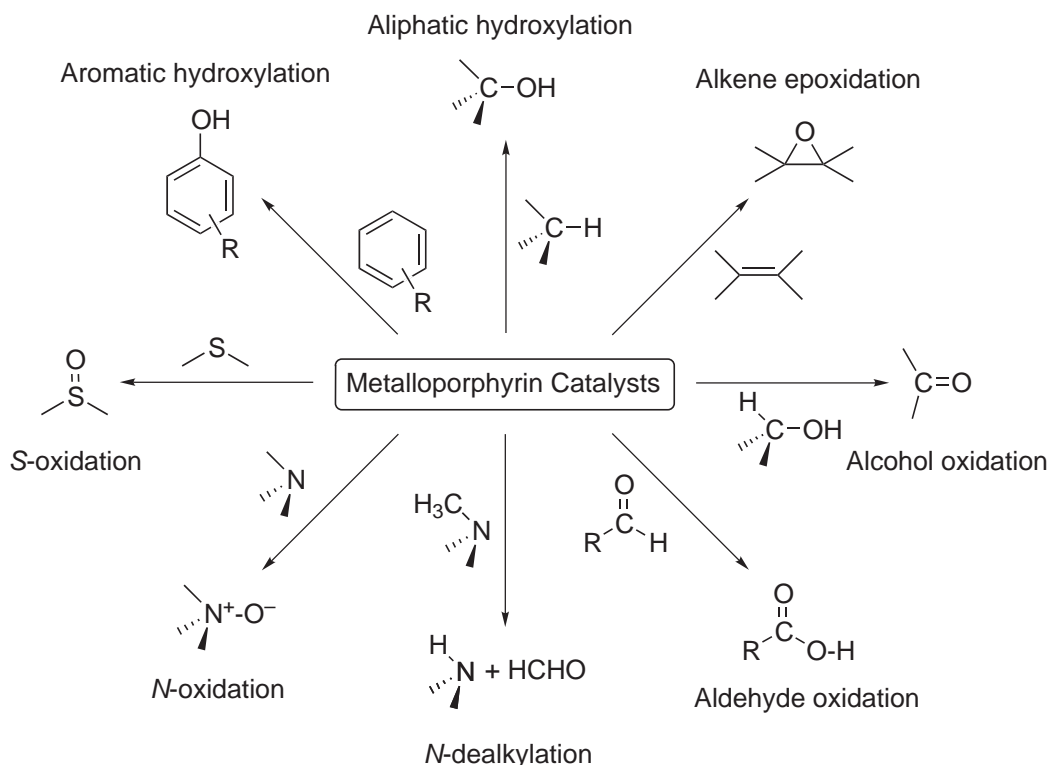
Figure 4 Metalloporphyrin-catalyzed oxidation reactions.

π-cation radical complexes.[51] In the reactions, oxoiron(IV) porphyrin π-cation radicals of electron-rich porphyrins reacted fast with ROOH (i.e., catalase and peroxidase type of chemistry; one-electron oxidation of ROOH) (Scheme 2, pathway A). On the other hand, oxoiron(IV) porphyrin π-cation radicals of electron-deficient porphyrins reacted fast with olefins to yield epoxide products (i.e., cytochrome P450 type of chemistry; oxygen atom transfer) (Scheme 2, pathway B). These results demonstrated that electron-deficient iron porphyrin complexes are better catalysts in hydrocarbon oxygenations by hydroperoxides, since these complexes can avoid the facile decomposition of oxoiron intermediates by ROOH (Scheme 2, pathway A). Indeed, highly electron-deficient iron(III) porphyrin complexes efficiently catalyze alkane hydroxylations by H_2O_2 in aprotic solvents.[41,42,52]
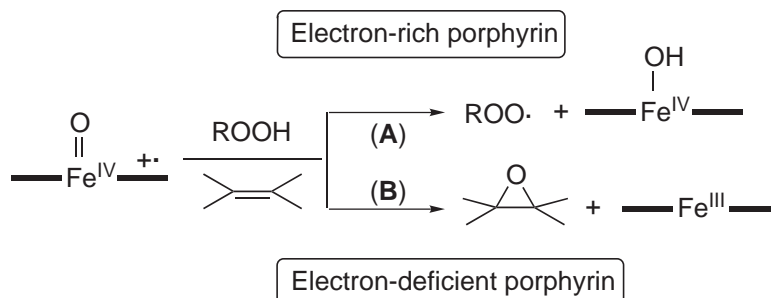
Scheme 2

Since an enormous number of articles have been published on metalloporphyrin-catalyzed oxidation reactions, it is impossible to cover all the published work in this chapter. Consequently, readers are referred to the excellent review articles or book chapters given in references,[1–7,43–47] especially a comprehensive review chapter by Meunier and co-workers.[43]

8.12.2.4 Labeled Water Experiments in Oxygenation Reactions

It is difficult to characterize reactive intermediates in catalytic oxygenation reactions by monooxygenase enzymes and their model compounds, since the intermediates are highly reactive and unstable in nature. Therefore, ^{18}O-labeled water experiments have been frequently carried out to obtain clues to identify the nature of reactive intermediates.[6,53] When labeled ^{18}O is incorporated from $H_2^{18}O$ into products, high-valent metal oxo complexes have been suggested as oxygenating species since the oxygen of the metal oxo species is believed to exchange with labeled water at a fast rate (Scheme 3).[30,31,54,55]
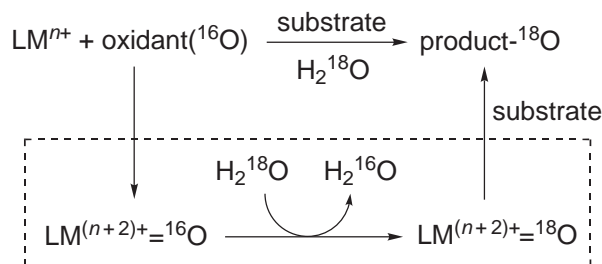
Scheme 3

Although the labeled water experiments have provided results in proposing the intermediacy of high-valent metal oxo complexes, this method led to an incorrect conclusion in the case of iodosylbenzene reactions.[56] In the oxygenation of hydrocarbons by PhIO catalyzed by metal complexes, high-valent metal oxo complexes were always proposed as reactive species because the source of oxygen in products was labeled water when the oxygenation reactions were carried out in the presence of $H_2^{18}O$. Even when a non-redox zinc complex was used as a catalyst, labeled oxygen from $H_2^{18}O$ was fully incorporated into oxygenated products.[56,57] On the basis of the latter result and the fact that the oxygen of iodosylbenzene coordinated to a manganese porphyrin

complex exchanges with labeled water,[58] it was concluded that, in iodosylbenzene reactions, oxygen exchange does not have to involve high-valent metal oxo intermediates and the ^{18}O-incorporation from $H_2^{18}O$ into products cannot be the evidence for the intermediacy of metal oxo complexes. An alternative mechanism was proposed in which iodosylbenzene exchanges its oxygen with labeled water after solid iodosylbenzene is dissolved and coordinated to a metal complex, (**8**), but before the high-valent metal oxo is formed or the oxygen atom is transferred to the substrate (Scheme 4).
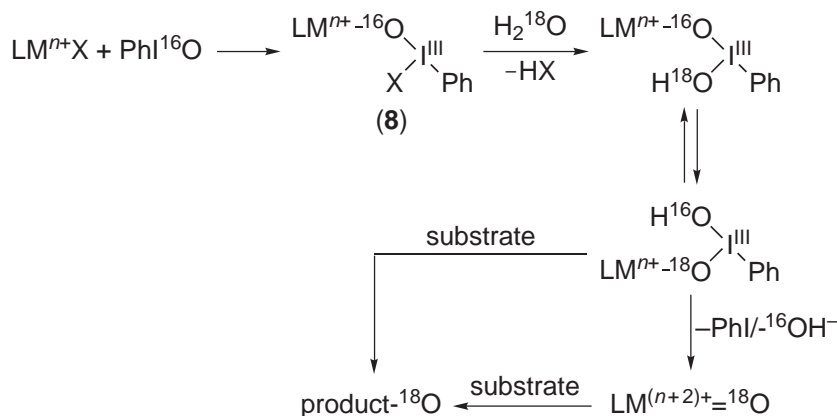
Scheme 4

As alluded to above, the rate of oxygen exchange between the metal oxo species and $H_2^{18}O$ (Scheme 5, pathway D) was believed to be much faster than that of oxygen transfer from the intermediate to organic substrates (Scheme 5, pathway C). Therefore, in the reactions where no or only a small amount of ^{18}O was incorporated from $H_2^{18}O$ into oxygenated products, the intermediacy of high-valent metal oxo species has often been ruled out. However, it turned out that the rate of ^{18}O-exchange between metal oxo intermediates and $H_2^{18}O$ (Scheme 5, pathway D) can be comparable or even slow relative to the reactions of the intermediates with substrates (Scheme 5, pathway C).[59,60] In addition, the ^{18}O-incorporation from $H_2^{18}O$ into oxygenated products was found to depend on reaction conditions such as the concentrations of substrate and $H_2^{18}O$,[59] the ease of substrate oxidation,[51] the electronic nature of porphyrin ligand,[51] the presence of axial ligand *trans* to the metal oxo moiety,[59,61,62] the oxidation state of high-valent metal(IV or V) oxo species,[61,63] and the temperature and pH of reaction solution.[53, 59,64] These factors affect the degree of ^{18}O-incorporation because:

(i) The reaction of a high-valent metal oxo intermediate with substrates (Scheme 5, pathway C) competes its exchange with isotopically labeled water (Scheme 5, pathway D).
(ii) The formation of a high-valent metal oxo intermediate from an oxidant-metal porphyrin adduct (Scheme 5, pathway B) competes with the oxygen atom transfer from the oxidant-metal porphyrin adduct to substrates (Scheme 5, pathway A).
(iii) The oxygen of metal oxo species exchanges with labeled water via "oxo-hydroxo tautomerism."[6,53]

The "oxo–hydroxo tautomerism" was proposed by Meunier and co-workers on the basis of the observation that 50% of oxygen in oxide product came from bulk $H_2^{18}O$ in the epoxidation of carbamazepine (CBZ) by a water-soluble manganese porphyrin complex, $Mn^{III}TMPyP$ (TMPyP = *meso*-tetrakis(4-*N*-methylpyridiniumyl)porphyrin), and $KHSO_5$ in aqueous solution (Equation (6)).[65] To explain the 50% ^{18}O-incorporation of labeled water into the oxide product, the authors proposed that an "oxo–hydroxo tautomerism" involves a rapid shift of two electrons and one proton from a hydroxo ligand to the *trans*-oxo species, leading to the transformation of the hydroxo ligand into an electrophilic oxo entity on the opposite side of the initial oxo species (Scheme 6). The "oxo–hydroxo tautomerism" is supported by the fact that ^{18}O-incorporation from $H_2^{18}O$ into products is completely prevented when the axial position opposite to the oxo group of high-valent metal oxo complexes is blocked by an axial ligand in metalloporphyrins and a cysteine thiolate ligand in cytochromes P450.[59,61,62,66]
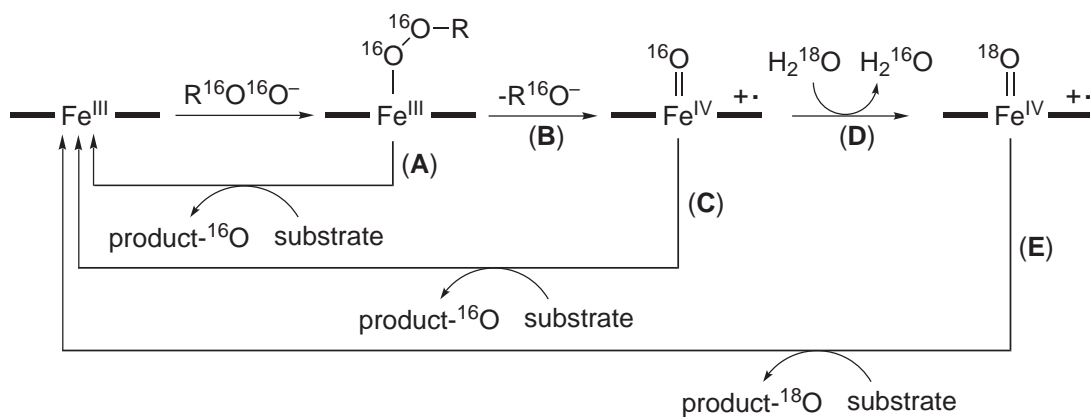
Scheme 5
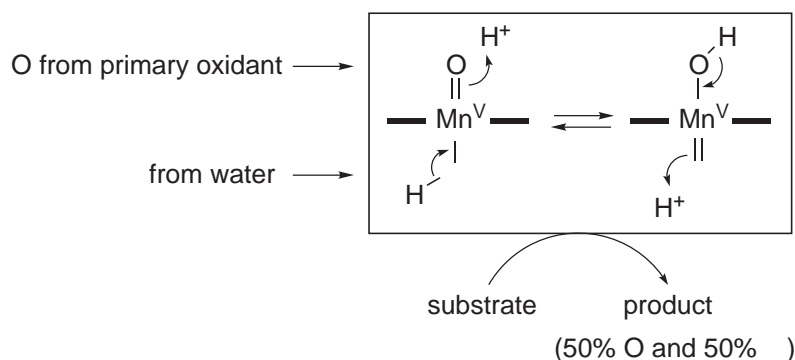
Scheme 6
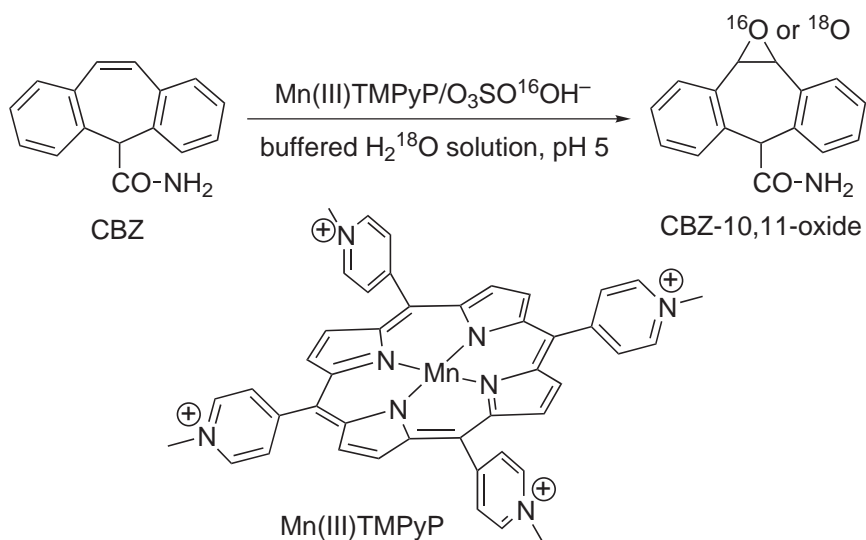
(6)

Very recently, Rietjens and co-workers proposed an alternative mechanism, "reversible compound I formation," to explain more than 90% ^{18}O-incorporation from bulk water into 4-aminophenol product in the hydroxylation of aniline by microperoxidase-8 (MP-8).[67,68] Since MP-8 contains histidine as an axial ligand, such a high oxygen incorporation from solvent water

into 4-aminophenol product cannot be explained by the "oxo–hydroxo tautomerism." Thus, the authors proposed that the oxygen exchange occurs via O—O bond formation between a high-valent metal oxo intermediate and a water molecule (Equation (7)):

$$
\overset{^{16}O}{\underset{Fe^{IV}}{\parallel}}{}^{+\cdot} \quad \underset{^{18}OH^-}{\overset{H_2{}^{18}O \quad H^+}{\rightleftharpoons}} \quad \overset{^{16}O\overset{^{18}OH}{\diagup}}{\underset{Fe^{III}}{\mid}}
$$

(7)
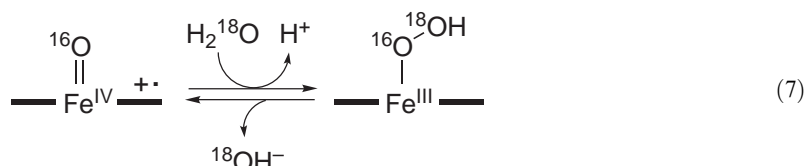
8.12.3   HIGH-VALENT OXOIRON PORPHYRINS

  High-valent oxoiron porphyrins refer to iron complexes of porphyrin ligands in which the oxidation state of the iron ion is higher than +3 and a terminal oxo group is bound to the iron center. The first high-valent oxoiron(IV) porphyrin π-cation radical complex was prepared by the oxidation of Fe(TMP)Cl with *m*-CPBA in CH_2Cl_2—CH_3OH at $-78\,^{\circ}C$.[31] The green species, formulated as $[(TMP)^{+\cdot}Fe^{IV}{=}O]^+$, has been well-characterized by various spectroscopic techniques such as UV–vis,[31] NMR,[31,69] EPR,[69] Mössbauer,[69,70] resonance Raman,[69,71] magnetic circular dichroisom,[72] and EXAFS spectroscopies.[73] The $[(TMP)^{+\cdot}Fe^{IV}{=}O]^+$ complex was also prepared using other oxidants such as ozone,[74] dimethyldioxirane,[75] and iodosylbenzene.[76]

8.12.3.1   Oxoiron(IV) Porphyrin Cation Radical Complexes

8.12.3.1.1   *Porphyrin ligand effects*

The success of generating $[(TMP)^{+\cdot}Fe^{IV}{=}O]^+$ as a model of compounds I of heme-containing enzymes prompted studies on the electronic effect of porphyrin ligands on the reactivities and spectroscopic properties of high-valent oxoiron(IV) porphyrin complexes.[77–79] As electron-deficient iron(III) porphyrin complexes are better catalysts in catalytic oxygenation reactions, oxoiron(IV) porphyrin π-cation radicals bearing electron-deficient porphyrin ligands show high reactivities in hydrocarbon oxygenations (Figure 5(b)).[51,80] For example, while $[(TPFPP)^{+\cdot}Fe^{IV}{=}O]^+$ complex hydroxylates alkanes rapidly and efficiently, $[(TMP)^{+\cdot}Fe^{IV}{=}O]^+$ is not capable of hydroxylating alkanes under the identical conditions.[51] In addition, oxoiron(IV) porphyrin π-cation radicals of electron-rich porphyrin ligands (e.g., $[(TMP)^{+\cdot}Fe^{IV}{=}O]^+$) react fast with hydroperoxides (Scheme 2, pathway A). On the other hand, oxoiron(IV) porphyrin π-cation radicals of electron-deficient porphyrin ligands (e.g., $[(TPFPP)^{+\cdot}Fe^{IV}{=}O]^+$) react faster with olefins than with hydroperoxides (Scheme 2, pathway B). These results demonstrate that the electronic nature of porphyrin ligands affects the reactivities of oxoiron(IV) porphyrin π-cation radicals significantly.[51]

  The electronic effect of porphyrin ligands on the spectroscopic properties of oxoiron(IV) porphyrin π-cation radicals has been investigated by placing electron-donating and electron-withdrawing substituents at *meso*- and pyrrole β-positions (Figure 5(b)).[69,80–83] The EPR spectra of oxoiron(IV) porphyrin π-cation radicals containing substituents at *meso*-positions exhibit typical $S=3/2$ EPR signals, indicating the strong ferromagnetic coupling between the ferryl iron and porphyrin radical spins.[82] As the electron-withdrawing power of the *meso*-substituent increases, the energy of the a_{2u} orbital would be stabilized relative to the a_{1u} orbital via the interaction of the aryl and porphyrin π-orbitals because of the large spin density at the *meso*-position in the a_{2u} orbital; there is instead a node at the *meso*-positions in the a_{1u} orbital (Figure 5a).[80,84] When the *meso*-substituent is highly electron-withdrawing such as pentafluorophenyl, the EPR spectrum exhibits a broad signal around $g=2$,[83] suggesting a weak ferromagnetic interaction between ferryl iron and porphyrin π-cation radical spins. The result further suggests that the a_{2u} orbital energy becomes lower and the HOMO of the porphyrin radical is switched from the a_{2u} radical state to the a_{1u} radical state (Figure 5(b)). The ^1H NMR spectra of oxoiron(IV) porphyrin π-cation radicals are sensitive to the electron-withdrawing power of *meso*-substituents.[80] The pyrrole proton signals shift upfield with the increase of the electronegativity of the *meso*-substituent, and the spectral change is interpreted with the mixing of the a_{2u} and a_{1u} orbitals due to the lowering the energy of the a_{2u} orbital relative to the a_{1u} orbital.[80]
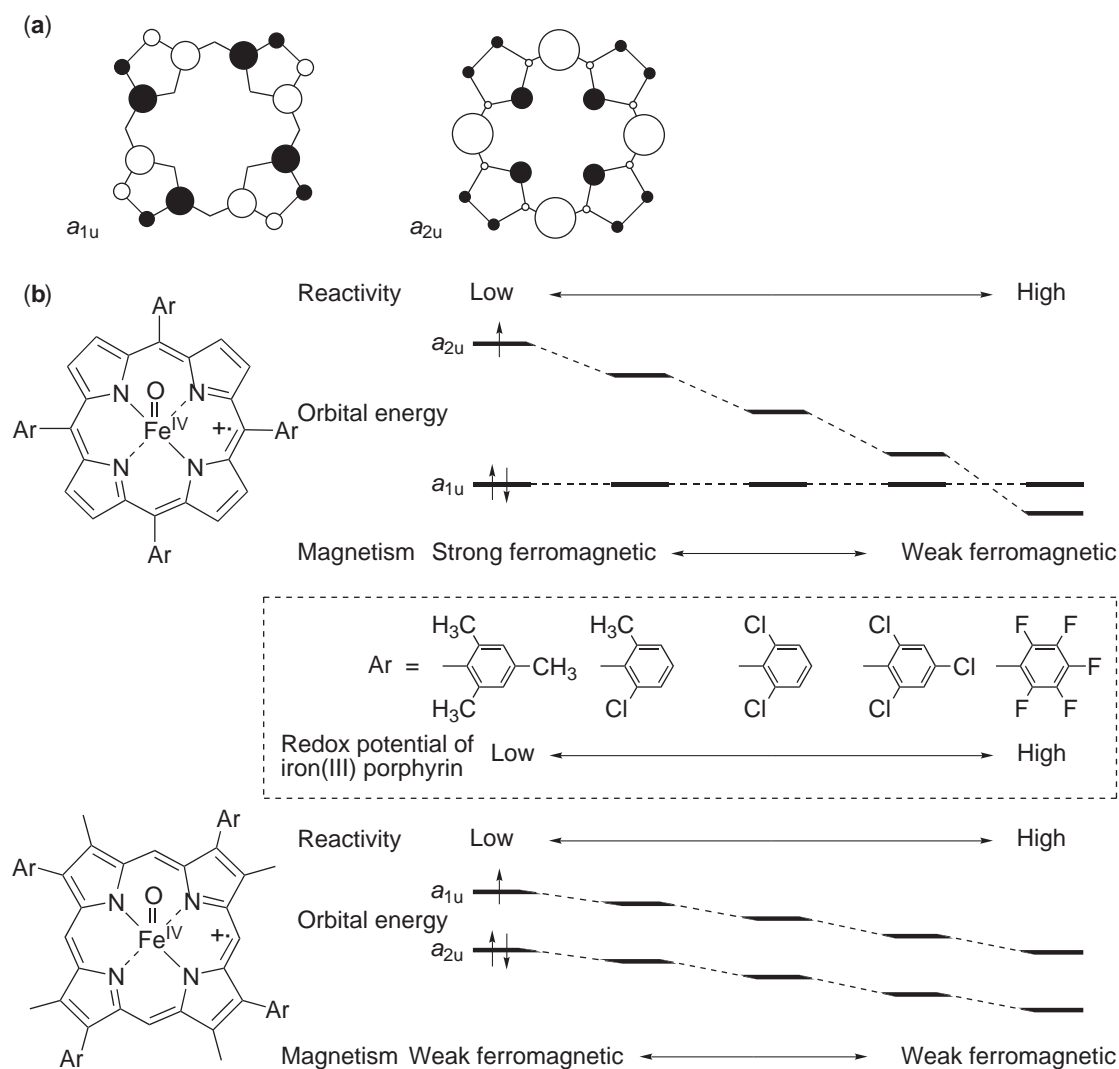
Figure 5 (a) Electron spin distribution of porphyrin atomic orbitals of a_{1u} (left) and a_{2u} (right) symmetries. Black and white circles represent signs of the upper lobe of the π-AOs. (b) Electron-withdrawing effects of the *meso*- and pyrrole β-substitued porphyrins on the reactivity and electronic structure of oxoiron(IV) porphyrin π-cation radicals (after Fujii).[52]

The electronic effects of pyrrole β-substituted porphyrins are different from those of *meso*-substituted porphyrins. The EPR spectra of oxoiron(IV) porphyrin π-cation radicals containing substituents at pyrrole β-positions show signals at $g_{\perp} \sim 3.1$ and $g_{||} \sim 2.0$,[82] which are similar to those of compounds I of *Micrococcus lysodeikticus* catalase and ascorbate peroxidase.[85,86] The ^{1}H-NMR spectra show large downfield shifts of β-methyl protons and small shifts of the *meso*-protons.[80] The EPR and ^{1}H-NMR spectral features indicate that the HOMO of the porphyrin radical is a_{1u} orbital and there is a weak ferromagnetic interaction between ferryl iron and porphyrin radical spins.[82] In addition, in contrast to the *meso*-substituted porphyrins, the electronic structure of oxoiron(IV) porphyrin π-cation radicals containing pyrrole β-substituents is not altered much by the electron-withdrawing pyrrole β-substituents because of the small spin densities of the a_{2u} and a_{1u} orbitals at the pyrrole β-positions and the slight stabilization of both orbitals by the electron-withdrawing substituents (Figure 5b).

8.12.3.1.2 *Axial ligand effects*

Axial ligands of heme-containing enzymes, such as a cysteine thiolate in cytochromes P450 and chloroperoxidases, a histidine imidazole in peroxidases, and a tyrosine phenolate in catalases, are

believed to play vital roles in generating and regulating the reactivities of high-valent oxoiron porphyrin intermediates.[87,88] Among the heme-containing enzymes, the unique monooxygenase activity of cytochromes P450 has been attributed to the presence of a cysteine thiolate ligand (see Figure 1). Thus, a variety of thiolate-coordinated heme models have been synthesized and studied in elucidating the role(s) of the thiolate ligand.[89] Early models were designed to mimic the physical properties of cytochromes P450 such as the appearance of a Soret band at 450 nm when iron(II) porphyrins bind to CO.[90,91] For an example, Collman and Groh synthesized iron(II) complexes of "mercaptan-tail" porphyrins (Figure 6a) that showed the resemblance of the spectral properties of the mercaptide-Fe(II)-CO to those of cytochrome P450 enzymes.[92] Another remarkable structural model was a picket fence iron porphyrin complex which showed a thermal stability of O_2 binding.[93] In the 1990s, Hirobe and co-workers synthesized an alkanethiolate-coordinated iron porphyrin complex (Swan Resting, SR complex), in which bulky groups on the RS^- coordination face were introduced to protect the thiolate ligation from oxidation (Figure 6b).[94,95] The SR complex was highly stable and retained its axial thiolate coordination during catalytic oxidations. Furthermore, the reactivities of the SR complex were different to the Fe(TPP)Cl complex but similar to cytochromes P450. For example, peroxyphenylacetic acid was heterolytically cleaved by the SR complex (Equation (8)), whereas homolytic O—O bond cleavage of peroxyphenylacetic acid was the predominant pathway when the catalyst was Fe(TPP)Cl (Equation (9)). The SR complex in alkane hydroxylation also showed a stronger hydrogen-abstraction ability than the chloride- or imidazole-ligated iron porphyrin complexes. In 2001, Naruta and co-workers synthesized iron porphyrin complexes bearing an alkanethiolate axial ligand and hydroxyl groups inside molecular cavities and demonstrated that the oxy form of the heme models was stabilized by the hydrogen bonding between the bound oxygen and the hydroxyl groups inside molecular cavities:[96]

$$PhCH_2CO_3H \xrightarrow[\text{benzene, 25 °C}]{\text{SR complex}} PhCH_2CO_2H + \text{compound I} \qquad (8)$$

$$PhCH_2CO_3H \xrightarrow[\text{benzene, 25 °C}]{\text{Fe(TPP)Cl}} [PhCH_2COO\cdot] + \text{compound II} \qquad (9)$$

$$\downarrow\downarrow$$

$$PhCH_3 + PhCH_2OH + PhCHO$$
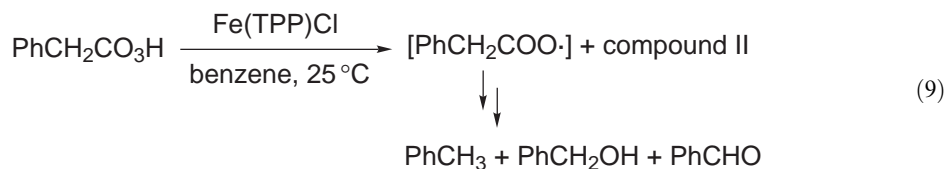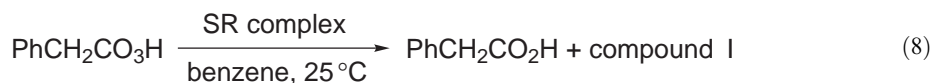
Compared to the many examples of iron(III) porphyrins with a thiolate axial ligand, the preparation of high-valent oxoiron porphyrins bearing a thiolate ligand has been less successful, probably, due to the easy oxidation of the thiolate ligand by oxidants. So far, only one oxo-iron(IV) porphyrin π-cation radical complex bearing a thiolate axial ligand has been prepared as a model of chloroperoxidase (Figure 6c).[97]
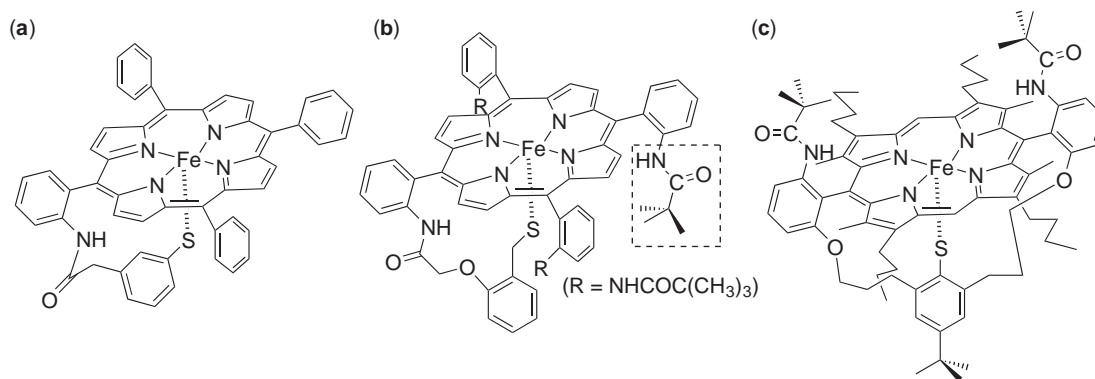
Figure 6 Structures of iron porphyrin complexes coordinating an axial thiolate ligand as models of cytochrome P450 enzymes.

Axial ligand effects on the reactivities and spectroscopic properties of oxoiron(IV) porphyrin π-cation radicals have been demonstrated with iron porphyrins bearing simple anionic ligands. Gross and co-workers reported that there is a pronounced axial ligand effect on the epoxidation of olefins by $(TMP)^{+\cdot}Fe^{IV}=O(X)$ complexes with different anionic ligands ($X = F^-$, MeOH, Cl^-, $MeCO_2^-$, $CF_3SO_3^-$, and ClO_4^-).[74,98] All of the $(TMP)^{+\cdot}Fe^{IV}=O(X)$ complexes except $(TMP)^{+\cdot}Fe^{IV}=O(ClO_4)$ epoxidize styrene to styrene oxide, and the rate of styrene epoxidation by the $(TMP)^{+\cdot}Fe^{IV}=O(X)$ complexes is in the order of $F^- \gg MeOH > Cl^- > MeCO_2^- \gg CF_3SO_3^-$. Gross, Kincaid, and co-workers also reported the effect of axial ligands on the spectroscopic properties of $(TMP)^{+\cdot}Fe^{IV}=O(X)$ complexes.[98,99] The EPR spectra of the $(TMP)^{+\cdot}Fe^{IV}=O(X)$ complexes show typical $S = 3/2$ signals irrespective of the axial ligands, whereas the ^{1}H-NMR β-pyrrole chemical shifts and resonance Raman $v(Fe=O)$ bands are sensitive to the nature of the axial ligands. According to the spectral data of ^{1}H-NMR and resonance Raman, the $(TMP)^{+\cdot}Fe^{IV}=O(X)$ complexes can be divided into two groups: one group with stronger electron donors such as F^-, Cl^-, and $MeCO_2^-$ and the other with weaker electron donors such as MeOH, $CF_3SO_3^-$, and ClO_4^-.[98,99]

8.12.3.2 Oxoiron(V) Porphyrins

Oxoiron(V) porphyrins, which are an isoelectronic form of oxoiron(IV) porphyrin π-cation radicals, have been reported in:

(i) the reaction of $[Fe(TDFPP)(F)_2]^-$ and *m*-CPBA in the presence of excess fluoride salt at $25\,^\circ C$;[100]
(ii) the addition of a small amount of MeOH to a CH_2Cl_2 solution of $[(TDCPP)^{+\cdot}Fe^{IV}=O]^+$ at $-90\,^\circ C$;[101] and
(iii) the reaction of $[Fe(TDCPP)]^+$ with F_5PhIO in the presence of a small amount of MeOH at $-90\,^\circ C$.[101]

The color of the oxoiron(V) porphyrins is red, and the UV-vis spectra of the complexes exhibit bands at $\sim$420 nm (Soret) and $\sim$540 nm. These features are very similar to those of $(Porp)Fe^{IV}=O$ species. The $(TDFPP)Fe^V=O(F)$ is stable even at room temperature, whereas $(TDCPP)Fe^V=O(OCH_3)$ is only stable at low temperature. The latter complex has shown a reactivity toward olefin epoxidation at $-90\,^\circ C$, but it reacts $\sim$10 times slower than $[(TDCPP)^{+\cdot}Fe^{IV}=O]^+$.[101] Although the spectroscopic and chemical properties, including ^{1}H NMR, EPR, magnetic susceptibility, iodometric titration, and the reactivity with organic substrates, of the red complexes are distinct from those of the corresponding oxoiron(IV) porphyrin and oxoiron(IV) porphyrin π-cation radical complexes,[100,101] the exact oxidation state of the iron ion of the red species is ambiguous. Very recently, Dey and Ghosh carried out density functional theory calculations on the oxoiron(V) porphyrin species and concluded that there is no true oxoiron(V) porphyrin species and an axial ligand set consisting of an oxide and a fluoride favors an oxoiron(IV) porphyrin π-cation radical as the ground state.[102]

8.12.3.3 Oxoiron(IV) Porphyrins

Oxoiron(IV) porphyrins, one oxidizing equivalent above the resting ferric state, are known as compound II in the catalytic cycle of peroxidases and catalases. The $(Porp)Fe^{IV}=O$ complexes can be generated by: (i) the homolytic O—O bond cleavage of $(Porp)Fe^{III}-O-O-Fe^{III}(Porp)$, which is formed by the addition of dioxygen to iron(II) porphyrins in the presence of a nitrogen base, (ii) the chemical oxidation of iron(III) porphyrins by *m*-CPBA and PhIO under certain circumstances, (iii) the electrochemical oxidation of hydroxoiron(III) porphyrins, and (iv) the reactions of iron(III) porphyrins with hydroperoxides (ROOH) in aqueous or organic solvents.[103] More detailed preparation methods and physical properties of various oxoiron(IV) porphyrin complexes are summarized in recent reviews.[77,79,103]

It has been considered that the oxoiron(IV) porphyrins are such poor oxidants that they can only oxygenate triphenylphosphine to triphenylphosphine oxide.[104] However, an olefin epoxidation by an oxoiron(IV) porphyrin complex was demonstrated by Groves and co-workers, in which $(TMP)Fe^{IV}=O$, prepared by ligand metathesis of $(TMP)^{+\cdot}Fe^{III}(ClO_4)_2$ over basic alumina,

reacted with olefins readily at room temperature.[105] As observed in oxomanganese(IV and V) porphyrin chemistry,[61] the reactivity pattern of the $(TMP)Fe^{IV}=O$ complex was very different from that of $[(TMP)^{+\cdot}Fe^{IV}=O]^+$. A nearly equimolar mixture of *cis-* and *trans-β*-methylstyrene oxide (*cis/trans* ratio of ~1.2) was produced in the epoxidation of *cis-β*-methylstyrene by $(TMP)Fe^{IV}=O$ (Equation (10)), whereas the $[(TMP)^{+\cdot}Fe^{IV}=O]^+$ complex afforded *cis-*oxide product predominantly (*cis/trans* ratio of ~11) (Equation (11)). In addition, a concave (upward) Hammett plot was observed in the reactions of $(TMP)Fe^{IV}=O$ with a series of substituted styrenes, whereas a linear Hammett plot with a large negative slope ($\rho = -1.9$) was obtained with the $[(TMP)^{+\cdot}Fe^{IV}=O]^+$ complex.[106] Other reactivity studies with $(Porp)Fe^{IV}=O$ complexes, such as the porphyrin ligand effect (Section 8.12.3.1.1),[51] have not yet been carried out in hydrocarbon oxygenation reactions:

$$(10)$$
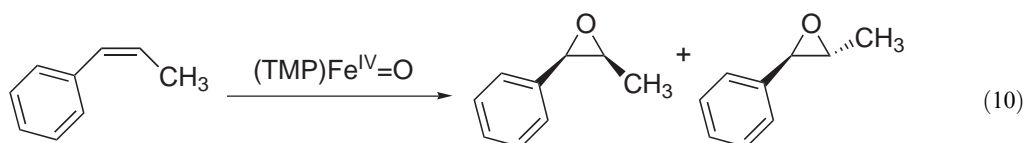
Ratio of *cis-*oxide : *trans-*oxide = 1.2:1

$$(11)$$
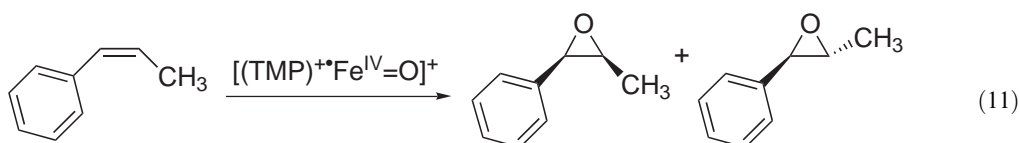
Ratio of *cis-*oxide : *trans-*oxide = 11:1

8.12.3.4   Mechanisms of Hydrocarbon Oxygenations

An early proposed mechanism of alkane hydroxylation by cytochrome P450 was a concerted insertion process in which an oxoiron(IV) porphyrin π-cation radical transfers its oxygen to unactivated C—H bonds via an insertion reaction (Scheme 7, concerted insertion pathway).[107] In the late 1970s, the currently most accepted "oxygen rebound" mechanism was enunciated by Groves and co-workers.[108] In the "oxygen rebound" mechanism (Scheme 7, cage-radical pathway), the oxoiron(IV) porphyrin π-cation radical abstracts a hydrogen atom from the substrate (R—H) to form a carbon radical and an Fe^{IV}-OH complex in a cage so that they cannot diffuse away from each other. These two species then recombine in the rebound step to produce the hydroxylated product and the resting state of the heme iron.[109,110] The "oxygen rebound"
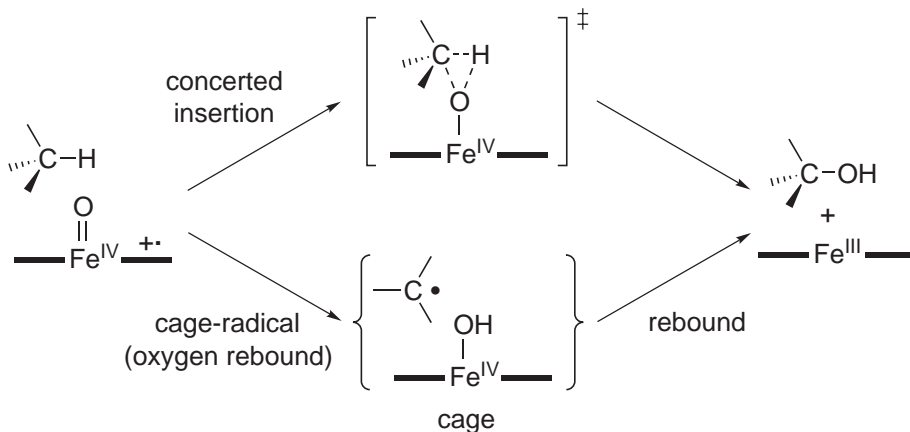
Scheme 7

mechanism was supported by numerous experimental observations such as high kinetic isotope effects,[108,111–115] partial positional or stereochemical scrambling,[116–118] and allylic rearrangements[119,120] in hydroxylation reactions by cytochromes P450 and iron porphyrin models. The formation of alkyl bromide in alkane hydroxylations by synthetic iron(III) porphyrins and oxidants in the presence of CCl_3Br was another piece of supporting evidence for the generation of a carbon radical in the "oxygen rebound" mechanism.[109,110]

The advent of "radical clock" substrates[121,122] in alkane hydroxylations by cytochromes P450 provided strong evidence for the involvement of carbon radicals and allowed the estimation of the rate of the oxygen rebound step. If a carbon radical is produced by a hydrogen atom abstraction of a "radical clock" substrate by an oxoiron(IV) porphyrin π-cation radical, the carbon radical either rebounds to the iron(IV)-OH complex to give an unrearranged alcohol product or rearranges to another ring-opened carbon radical which then rebounds to the iron(IV)-OH complex to yield the rearranged alcohol product (Scheme 8).[123] The ratio of unrearranged/rearranged alcohol products allows the calculation of the rate of oxygen rebound (k_{OH}) with the known rearrangement rate of the carbon radical (k_r). When Ortiz de Montellano and Stearns used bicyclo[2.1.0]pentane (**8**) as a radical clock in cytochrome P450-catalyzed hydroxylation reaction, a 7:1 mixture of unrearranged alcohol (**9**), and rearranged alcohol (**10**) was obtained (Scheme 8).[123] With the ratio and the rate of bicyclo[2.1.0]-2-yl radical rearrangement of $2 \times 10^9 \, s^{-1}$ (k_r), the rate of oxygen rebound (k_{OH}) was calculated to be $1.4 \times 10^{10} \, s^{-1}$. Very recently, Ortiz de Montellano, Groves, and co-workers reinvestigated the oxidation of norcarane ((**11**), $k_r = 2 \times 10^8 \, s^{-1}$) by four different cytochrome P450 enzymes and observed the formation of radical- and cation-derived rearrangement products (Equation (12)).[124] By calculating the relative amounts of unrearranged product (**12**) to radical-derived rearranged product (**13**) the oxygen rebound rate (k_{OH}) was calculated to be $\sim 2 \times 10^{10} \, s^{-1}$, a number very similar to that obtained in the oxidation of bicyclo[2.1.0]pentane.[123] The authors further suggested that the cation-derived product (**14**) was formed via an electron-transfer process:

Scheme 8

(12)
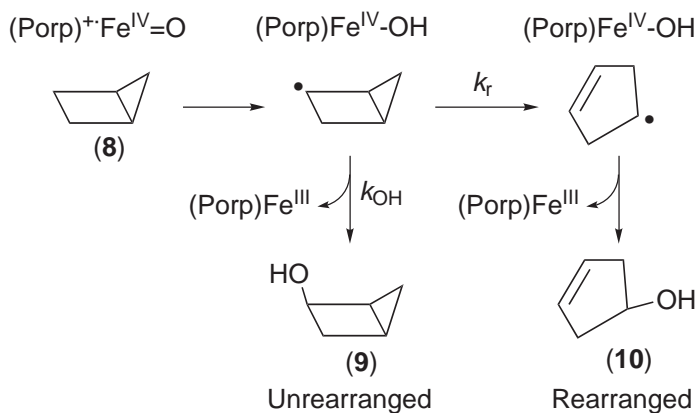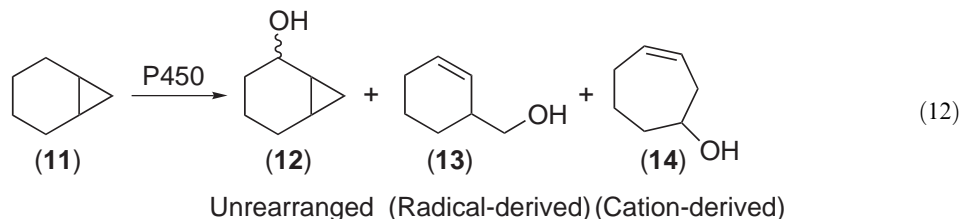
Despite the accumulated evidence for the "oxygen rebound" mechanism, recent results using more sophisticated and ultrafast "radical clocks" have challenged the "oxygen rebound" mechanism and revived the concerted insertion mechanism. Atkinson and Ingold used several radical clocks including phenyl-substituted cyclopropanes in P450-catalyzed hydroxylation reactions.[125]

Interestingly, the computed rates of the oxygen rebound step varied by nearly three orders of magnitude, depending on the "radical clock" substrates. In addition, there was no correlation between the amounts of rearranged products and the rate constants for radical rearrangements.[126,129] The latter phenomenon was explained with the generation of cationic species by an iron(III)-hydroperoxo intermediate (see Section 8.12.4.2).[129,130] A striking result of using hypersensitive radical probes such as (**15**) (Scheme 9), (*trans,trans*-2-*tert*-butoxy-3-phenylcyclopropyl) methane, and methylcubane was the incredibly fast oxygen rebound rate ($k_{OH} = \sim 1.4 \times 10^{13}\,s^{-1}$).[126–128] Thus, the lifetime of the radical species is in the range of 80–200 fs, and such an extremely short lifetime implies that the radical is not a true intermediate but a component of a reacting ensemble (or transition structure). Accordingly, a concerted nonsynchronous hydroxylation mechanism was invoked in which a "side-on" approach of an oxygen atom to the C—H bond was suggested as opposed to the linear C—H—O array of a conventional abstraction mechanism.[126–129]
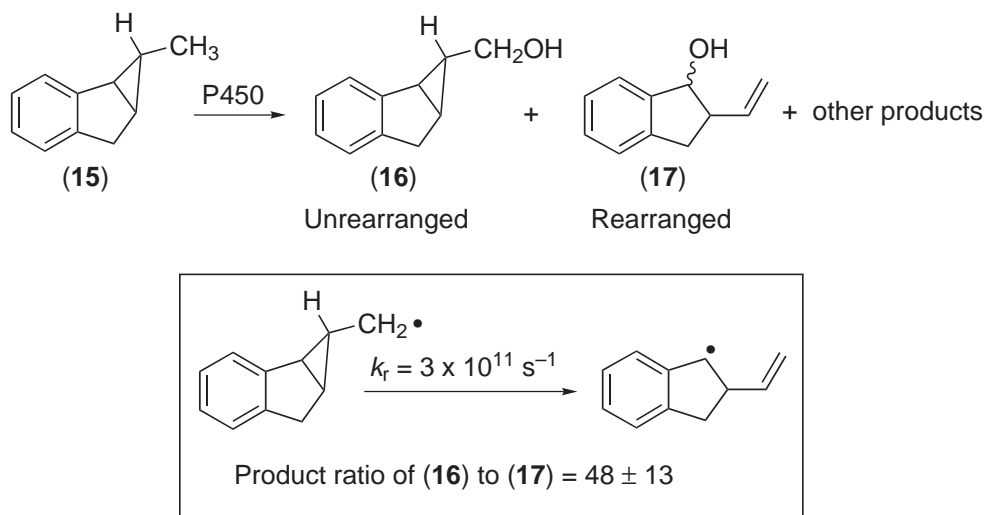
Scheme 9

Recent developments in theoretical calculations of compound I models have shed light on the structures and reactivities of oxoiron(IV) porphyrin π-cation radicals.[131–134] Notably, Shaik, Schwarz, and co-workers proposed a two-state reactivity (TSR) in C—H bond activation by a model for compound I of cytochromes P450.[134,135] As shown schematically in Figure 7, alkane hydroxylation proceeds by a two-state rebound mechanism of two closely lying spin states, the high-spin quartet state ($^4A_{2u}$) and low-spin doublet state ($^2A_{2u}$), of an oxoiron(IV) porphyrin π-cation radical. The C—H bond activation by the two spin states ($^4A_{2u}$ and $^2A_{2u}$) involves hydrogen abstraction-like transition states (^4TS_H and ^2TS_H) followed by the formation of carbon radical and iron(IV)-hydroxide intermediate clusters (^4C_I and ^2C_I). The low-spin intermediate cluster (^2C_I) collapses to the (Porp)Fe-alcohol product in a virtually barrierless fashion, making the low-spin process a nonsynchronous reaction with no true intermediate. On the other hand, the high-spin intermediate cluster (^4C_I) of iron(IV)-hydroxide and the alkyl radical undergoes rebound with a distinct transition state ($^4TS_{Reb}$) and a significant barrier, resulting in the existence of a true radical intermediate. Thus, the TSR scenario provides a reasonable reconciliation of the apparent contradiction between the oxygen rebound and concerted insertion mechanisms.[133–137]

Mechanisms for olefin epoxidation by oxoiron(IV) porphyrin π-cation radicals are not as well understood as those for alkane hydroxylations, and no major experimental advances have been made in the past decade. Possible intermediates that have been proposed in olefin epoxidations are depicted in Scheme 10: (i) a metallaoxetane (a), (ii) a carbon radical (b), (iii) a carbocation (c), (iv) an alkene-derived π-cation radical (d), and (v) a concerted oxygen insertion (e).[2,138] Most of the mechanisms were proposed on the assumption that oxoiron(IV) porphyrin π-cation radicals were generated as epoxidizing intermediates in catalytic epoxidation reactions, but recent studies provided evidence that multiple oxidants can be involved in olefin epoxidations (Section 8.12.4.2). So more experimental work, especially with *in situ* generated oxoiron(IV) porphyrin π-cation radicals,[139] is necessary to clarify the mechanisms of olefin epoxidations.
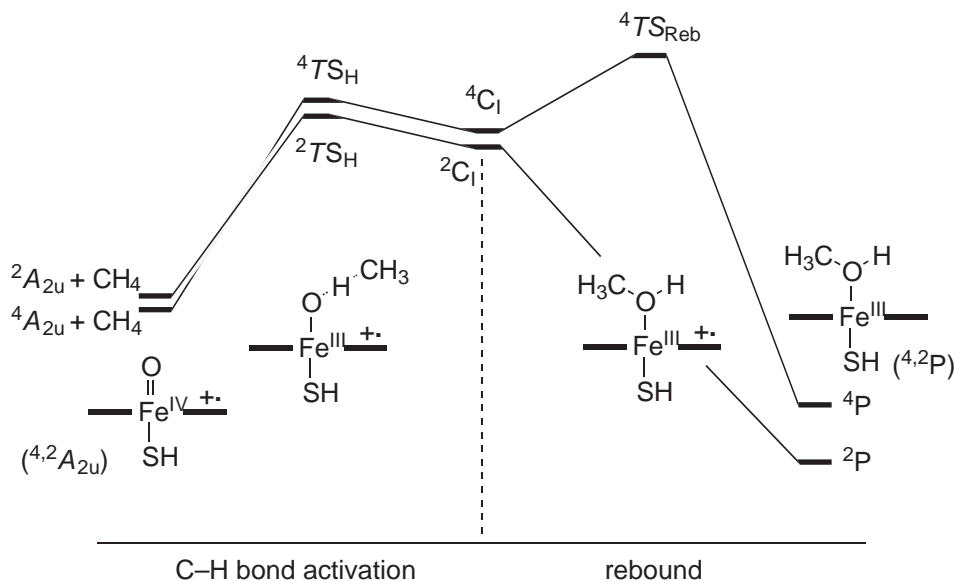
Figure 7 Schematic diagram for two-state rebound mechanism for methane hydroxylation by an oxoiron(IV) porphyrin π-cation radical (after Ogliaro *et al.*).[137]
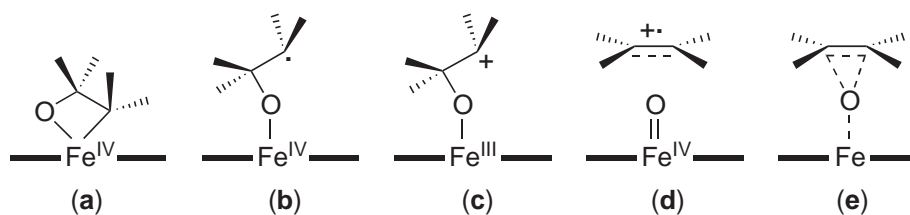
Scheme 10

8.12.4 MULTIPLE OXIDANTS IN OXYGEN TRANSFER REACTIONS

Elucidation of the nature of reactive intermediates in the catalytic oxygenation of hydrocarbons by cytochromes P450 and iron porphyrin models has remained of continuing interest to the bioinorganic chemistry community. It has been believed for a long time that oxoiron(IV) porphyrin π-cation radicals are the sole reactive species responsible for oxygen atom transfer in the catalytic oxygenation reactions. However, recent studies have revealed that multiple oxidants can be involved in oxygen transfer reactions and that the mechanism of oxygen atom transfer is much more complex than initially believed.[129,140–144] Figure 8 shows the structures and reactions of recently proposed reactive oxidants.

8.12.4.1 Multiple Oxidants in Cytochrome P450 Enzymes

The participation of ferric–peroxo species as the active oxidant has been proposed in many P450-catalyzed reactions. These include the aromatization of androgen to estrogen by cytochrome P450 aromatase, the deformylation of aldehydes by P450 2B4 and P450 2E1, the deformylation of lanosterol by lanosterol 14α-demethylase, the cleavage of the C-17 side chain of progesterone to form androstenedione by progesterone 17α-hydroxylase-17,20-lyase, and the transformation of L-arginine to L-citrulline by NO synthase (NOS).[1,4,7] Such ferric–peroxo species in the P450-mediated reactions act as nucleophiles, thereby attacking an aldehyde carbon or its analog. Evidence for the ferric–peroxo species behaving as nucleophiles has been obtained through mechanistic studies of the enzymes and their mutants.
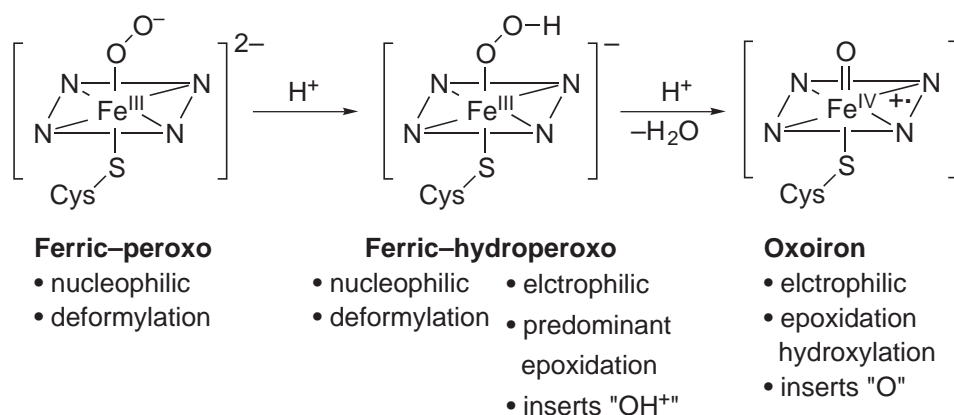
Figure 8 Multiple oxidants and their possible reactions in cytochromes P450-catalyzed oxygenation reactions (after Newcomb *et al.*).[130]

Cytochrome P450 aromatase catalyzes the conversion of human androgen to estrogens in three sequential oxidative reactions (Figure 9).[145] The first and second steps are typical P450-type hydroxylations, mediated by a high-valent oxoiron porphyrin species (Figure 9b). The third step is unusual in which oxidative deformylation of aldehydes affords an aromatized product and formic acid (Figure 9b). The nature of the active oxidant for the last step of the aromatization
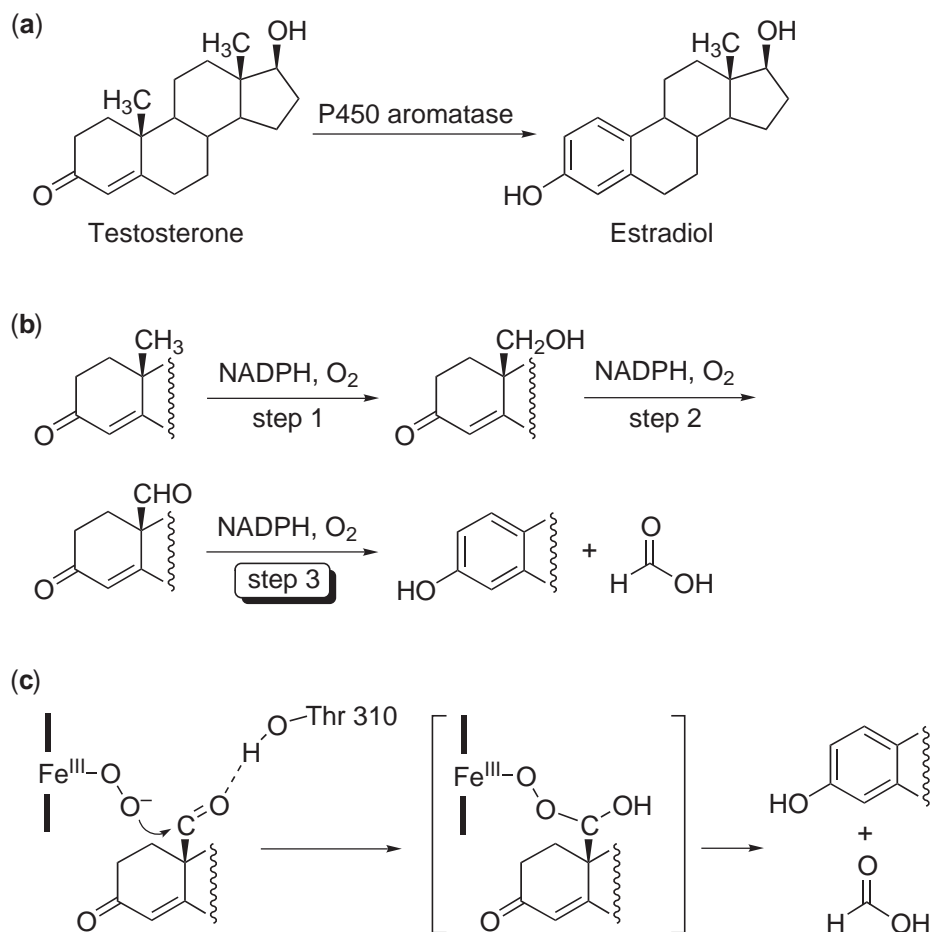
Figure 9 (a) Conversion of androgen to estrogen by cytochrome P450 aromatase. (b) Stepwise mechanisms. (c) A proposed mechanism of the third step in which ferric–peroxo species attacks aldehyde carbon via a nucleophilic reaction.

has been a topic of much debate for some time, and a ferric-peroxo species is believed to be the most likely candidate that attacks the C19 aldehyde to give an iron peroxohemiacetal intermediate (Figure 9c).[146–148]

The involvement of ferric–peroxo species in P450-mediated deformylation reactions was further evidenced from site-directed mutagenesis studies.[149] Cytochrome P450 2B4 catalyzes the hydroxylation of alkanes as well as the deformylation of aldehydes. A highly conserved threonine residue in the active site of the enzyme has been postulated to play a role in the activation of dioxygen to form a high-valent oxoiron species by serving as a link for proton delivery to the active site.[150,151] Thus, disruption of the proton delivery to the active site of P450 2B4 should result in the loss of substrate hydroxylation (Scheme 11, pathway A) and the enhancement of aldehyde deformylation (Scheme 11, pathway B). Coon and co-workers demonstrated that mutation of threonine 302 of P450 2B4 to alanine markedly decreased the hydroxylation of substrates and strikingly enhanced the deformylation of cyclohexane carboxaldehyde, leading to the conclusion that the ferric–peroxo species rather than a high-valent oxoiron species is the active oxidant for the deformylation reactions.[149]
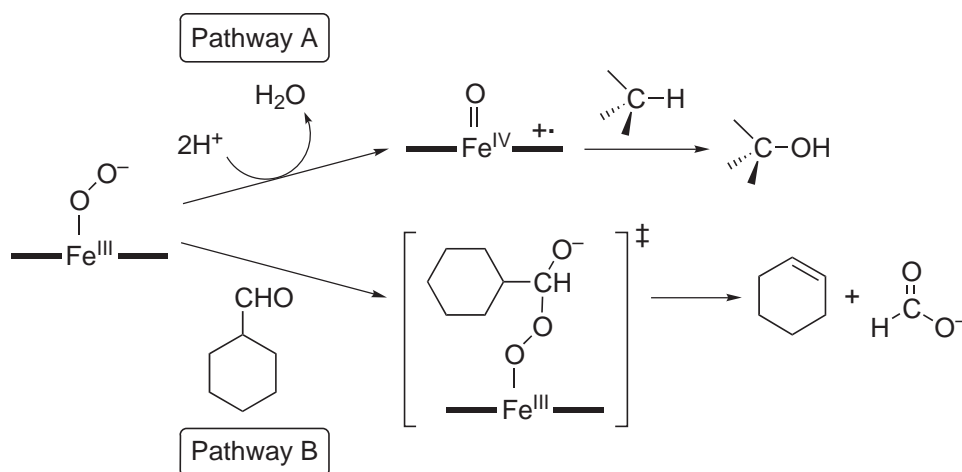
Scheme 11

In 1998, Coon and co-workers further examined the effect of site-directed mutagenesis of threonine to alanine on the epoxidation of olefins with P450 2B4, P450 2E1, and their respective mutants, 2B4 T302A and 2E1 T303A.[152] As discussed above, the threonine-to-alanine mutation interferes with proton delivery, inhibiting the conversion of a ferric–hydroperoxide species to a high-valent oxoiron species and a water molecule (Scheme 12a, pathway B) and resulting in the increase of the lifetime of a ferric–hydroperoxo species in the 2E1 T303A mutant.[150,151] As a result, epoxide formation by the ferric–hydroperoxo species would be increased (Scheme 12a, pathway A) and alcohol formation by the high-valent oxoiron species would be diminished (Scheme 12a, pathway C). Indeed, replacement of the threonine residue in P450 2E1 by alanine resulted in an increase of more than twofold in epoxidation along with a decrease in allylic oxidation. The authors proposed that two different species with electrophilic properties, ferric-hydroperoxo and high-valent oxoiron, effect olefin epoxidation. In the case of the ferric-hydroperoxo species, the distal oxygen in the hydroperoxide bound to the heme iron is transferred into olefins via a concerted mechanism (Scheme 12b).

More recently, the involvement of both ferric–hydroperoxo and oxoiron species in alkane hydroxylations has been proposed from the studies of the hydroxylation of hypersensitive radical probes with cytochromes P450 and their mutants.[130,153] The product distributions in the oxidation of the radical probe (**18**) by P450 2E1 and the 2E1 T303A mutant were different (Equation (13)); the amount of methyl group oxidation (hydroxylation, (**19**) and (**20**)) was not altered, but the phenyl group oxidation (epoxidation, (**21**)) markedly increased with the 2E1 T303A mutant.[153] The results were interpreted by invoking the existence of two distinct electrophilic oxidants in cytochrome P450-catalyzed hydroxylation reactions: one is a high-valent oxoiron species that gives mainly methyl group oxidation products ((**19**) and (**20**)) and the other is a ferric–hydroperoxo species which oxidizes the phenyl group to produce phenol (**21**).[153] The authors also
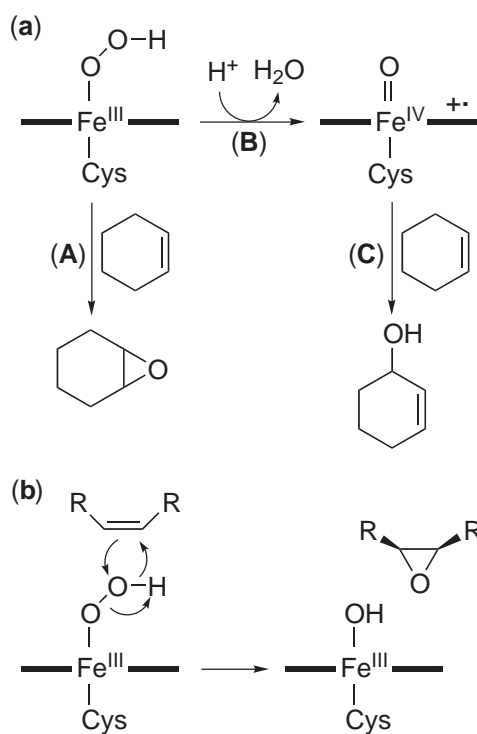
Scheme 12

proposed that alkane hydroxylations by the ferric–hydroperoxo and oxoiron species occur by insertion reactions and the hydroxylation by the ferric–hydroperoxo species proceeds via the insertion of OH^+ into the C—H bond (Scheme 15).[130] Evidence for the mechanism of OH^+ insertion was the formation of cation-derived product in the oxidation of probe (**22**) by P450s and their mutants (Scheme 13):

(13)
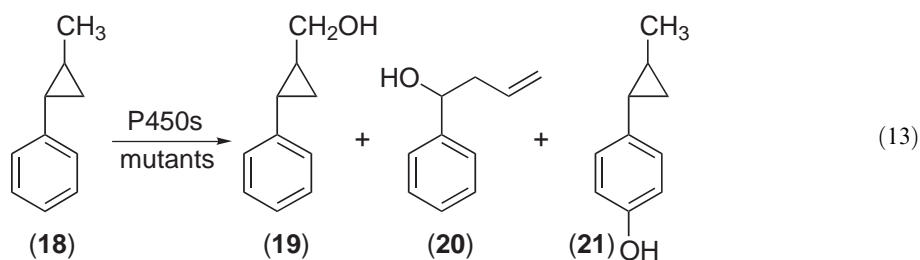
Ferric–hydroperoxo species as electrophilic oxidants has also been proposed in many enzyme systems such as the conversion of heme to α-*meso*-hydroxyheme by heme oxygenase,[154] aromatic *ipso*-substitution by P450,[155] and aniline *para*-hydroxylation by microperoxidase-8.[156]

8.12.4.2 Multiple Oxidants in Iron Porphyrin Models

The synthesis of a ferric–peroxo porphyrin complex, $[(Porp)Fe^{III}(O_2)]^-$, was first reported by Valentine and co-workers.[157] The ferric–peroxo species was prepared by reacting Fe(TPP)Cl or Fe(OEP)Cl with two equivalents of superoxide in the presence of crown ether in aprotic solvents such as acetonitrile or toluene. The first equivalent of superoxide reduces the ferric porphyrin to the ferrous porphyrin, and the second superoxide converts the ferrous porphyrin to the ferric-η^2-peroxo porphyrin complex (Equation (14)). The EPR spectrum of $[(OEP)Fe^{III}(O_2)]^-$ complex
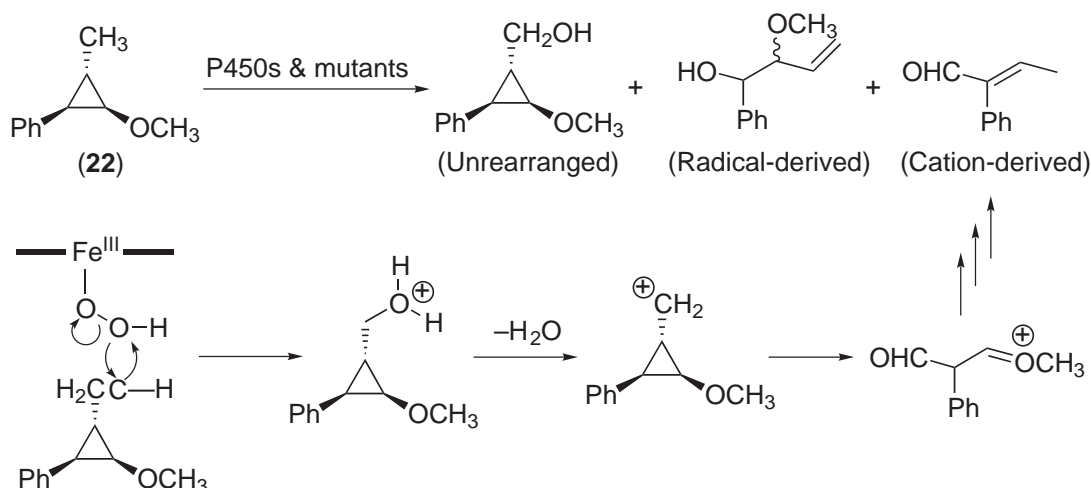
Scheme 13

showed signals at $g = 4$, $g = 8$ (weak), $g = 2$ (weak), indicating the presence of a high-spin rhombic ferric complex.[159] Other spectroscopic data including IR, EXAFS, D NMR, and Mössbauer indicate that the structure of the ferric–peroxo porphyrin complex is analogous to that of $[(TPP)Mn^{III}(O_2)]^-$ in which the peroxide ligand is bound in a side-on η^2 fashion.[158–160]

(14)

Proposed structure of (**23**)
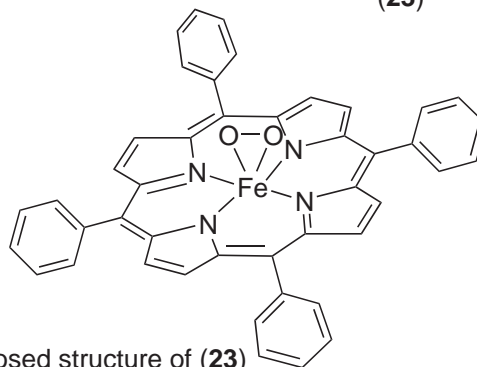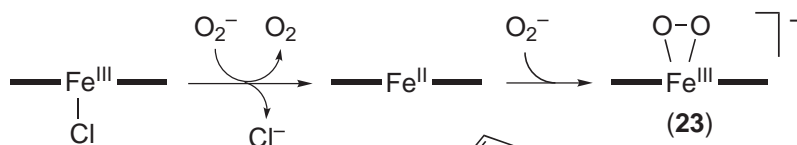
Early studies on the reactivity of the ferric–peroxo species demonstrated that the ferric–peroxo complexes do not give rise to the typical electrophilic reactions but display nucleophilic character in oxygen transfer reactions. When $[(Porp)Fe^{III}(O_2)]^-$ (Porp = TPP or TMP) was reacted with acetic anhydride, the formation of a peracetate-bound iron porphyrin intermediate, $(Porp)Fe^{III}$-$OOC(O)CH_3$, was detected.[161] Other examples of ferric–peroxo complexes reacting with electrophiles such as acyl halides, carbon dioxide, and sulfur dioxide have been reported in the early 1980s.[162,163] An important step toward establishing the nucleophilic character of ferric–peroxo complexes in olefin epoxidation reactions was achieved when Valentine and co-workers demonstrated that $[(Porp)Fe^{III}(O_2)]^-$ (Porp = TPP or TMP) complexes react with electron-deficient olefins (e.g., menadione) to give a high yield of menadione epoxide (Equation (15)).[164] The nucleophilicity of ferric–peroxo complexes was dependent on the electronic nature of porphyrin ligand and the presence of an axial ligand. For instance, a ferric–peroxo species of electron-deficient porphyrin ligand, $[(TPFPP)Fe^{III}(O_2)]^-$, does not epoxidize olefins.[165] Interestingly, when the $[(TPFPP)Fe^{III}(O_2)]^-$ complex binds DMSO as an axial ligand, the nucleophilicity

of the ferric–peroxo porphyrin is restored.[166] The authors proposed that the axial ligand acts as a switch to push the side-on peroxo ligand open and make the more nucleophilic end-on peroxo (Scheme 14).

$$(15)$$
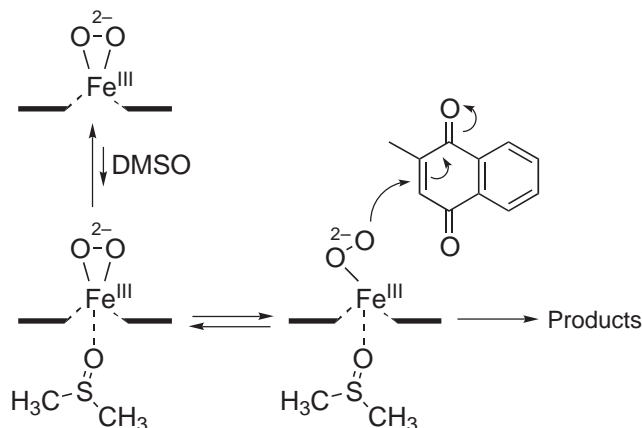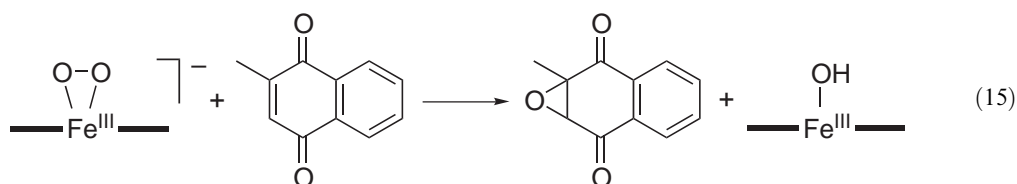
Scheme 14

One of the most intriguing questions that has attracted much attention from the mid-1990s is the existence of multiple oxidants in metal complex-catalyzed oxygenation reactions.[167–173] Since it is extremely difficult to identify the nature of reactive species directly in catalytic oxygenation reactions, indirect methods such as intermolecular competition reactions and isotopically labeled water experiments (Section 8.12.2.4) have been often used in suggesting the nature of reactive intermediates. In 1995, Watanabe and Morishima reported the results of competitive epoxidation of norbornylene and α-methylstyrene by iron porphyrin complexes and oxidants at $-78\,^{\circ}$C (Equation (16)).[167] In the reactions, the ratios of epoxide products varied depending on reaction conditions such as the electronic structure of iron porphyrin complexes (i.e., electron-rich and-deficient iron porphyrins), oxidants (i.e., peracids and iodosylbenzenes), and solvents (i.e., CH_2Cl_2 and toluene). In 2000, Nam and co-workers reported similar results in that the product ratios obtained in competitive epoxidations of *cis*- and *trans*-stilbenes depended markedly on the solvents (i.e., protic and aprotic solvents), the presence of a proton source in aprotic solvents, and the pK_a of protic solvents (Equation (17)).[168] By carrying out the competitive reactions with *in situ* generated oxoiron(IV) porphyrin π-cation radicals, the involvement of multiple oxidants (i.e., oxoiron(IV) porphyrin π-cation radical and oxidant-iron porphyrin complexes) was proposed. The olefin selectivity in the competitive epoxidation of *cis*- and *trans*-stilbenes was also found to depend on simple anionic ligands of iron porphyrin catalysts.[169] Groves and co-workers reported that the reaction of a mixture of *cis*- and *trans*-stilbenes with Fe(TPP)Cl and PhIO yielded 15 times more *cis*-stilbene oxide than *trans*-stilbene oxide (Section 8.12.2.1).[24] Interestingly, when the competitive epoxidation was carried out with the Fe(TPP)X complex containing a different anion such as triflate, the product ratio changed from 15 to 0.9 (Equation (18)).[169] The dependence of the product ratios on the anionic ligands of iron porphyrin catalysts was interpreted to indicate the generation of multiple oxidants, depending on the ligating nature of the anionic ligands.[169] In the competitive reactions, the selectivity for less hindered olefin by oxidant-iron porphyrin adducts was rationalized by the steric repulsion between the phenyl groups of *trans*-stilbene and those of the porphyrin ligand plus the bulky oxidant (e.g., an iodosylbenzene or acylperoxo group) bound to the iron porphyrin (Scheme 15).[167,168]

$$\text{(16)}$$

$$\text{(17)}$$
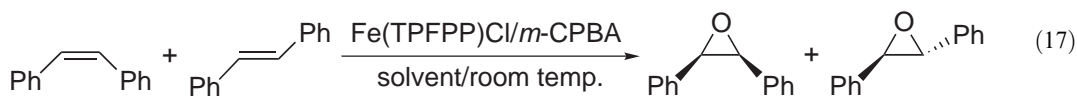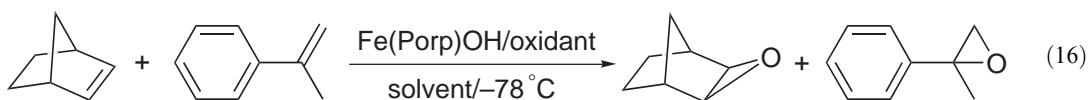
	aprotic solvent :	8	1
	protic solvent :	0.5	1
	$(\text{TPFPP})^{+\bullet}\text{Fe}^{IV}=\text{O}$:	0.5	1

$$\text{(18)}$$
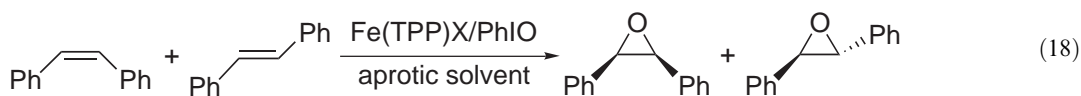
	$X^- = Cl^-$:	15	1
	$X^- = CF_3SO_3^-$:	0.9	1

The existence of multiple oxidants in alkane hydroxylations has also been proposed by Collman, Brauman, and co-workers.[170] They carried out intermolecular competitive hydroxylation of alkanes with various iodosylbenzenes in the presence of Fe(TPFPP)Cl and found that the oxidation rate ratios were different depending on iodosylbenzenes employed as terminal oxidants. The authors proposed iron–iodosylbenzene complexes as active oxidants responsible for the alkane hydroxylations. Nam and co-workers also reported that two distinct hydroxylating intermediates (i.e., an oxoiron(IV) porphyrin π-cation radical and an acylperoxo-iron porphyrin) participate in the catalytic hydroxylation of alkanes by Fe(TPFPP)X and *m*-CPBA, depending on the anionic ligands of the iron porphyrin catalyst.[171] A generalized reaction mechanism for the oxygenation of hydrocarbons by multiple oxidants is depicted in Scheme 16. If the O—X bond cleavage of (24) is fast (Scheme 16, pathway A), then (25) becomes the active oxidant. If the O—X bond cleavage of (24) is slow and the oxidizing power of (24) is strong enough to oxidize hydrocarbons, then (24) transfers its oxygen to organic substrates prior to the formation of (25) (Scheme 16, pathway B).

Finally, it should be pointed out that no direct evidence for the existence of multiple oxidants during catalytic oxygenation reactions has been obtained yet. Thus, determination of the "second oxidant"[174] structure and elucidation of its reactivities are the challenging targets that bioinorganic and biological chemists are working on with a great interest.
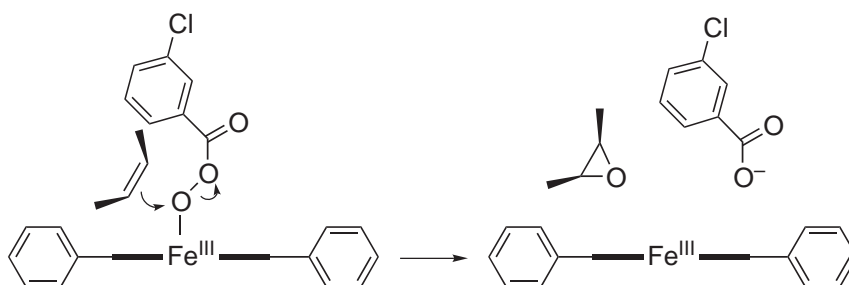
Scheme 15
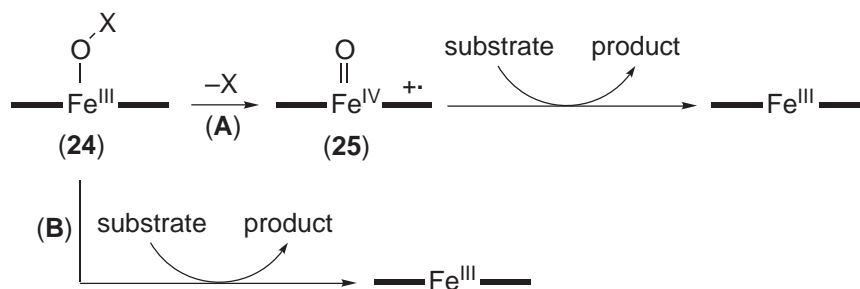
Scheme 16

8.12.5   CONCLUDING REMARKS

This chapter has focused on the discussion of how mechanistic developments/insights in iron porphyrin model research has helped our understanding of the dioxygen activation and oxygen atom transfer processes by cytochrome P450 enzymes. A tremendous amount of work has been accomplished over the past two decades on the synthesis of iron porphyrin complexes as synthetic analogues of the enzymes and use of the iron porphyrin models in biomimetic oxidation reactions, the isolation and characterization of oxoiron(IV) porphyrin intermediates, and the mechanistic details of O—O bond activation and oxygen transfer reactions. These studies have resulted in expanding the area of coordination chemistry and bringing new concepts of biomimetic reactions into inorganic and catalysis chemistry. Despite the great advances in understanding many aspects of cytochromes P450, continued extensive research is needed to clarify the currently unanswered questions in the enzyme mechanisms, such as the role(s) of the cysteine thiolate ligand, the mechanisms of O—O bond cleavage and oxygen atom transfer from oxoiron(IV) porphyrin π-cation radicals to organic substrates, and the existence of the "second oxidant" in catalytic oxygenation reactions. Without a doubt, the next decade promises some exciting discoveries to answer the current controversies and to develop industrially applicable biomimetic catalytic systems.

ACKNOWLEDGEMENTS

8.12.6   REFERENCES

1. Ortiz de Montellano, P. R., Ed. *Cytochrome P450: Structure, Mechanism, and Biochemistry*, 2nd ed.; Plenum: New York, 1995.
2. Traylor, T. G.; Traylor, P. S. In *Active Oxygen in Biochemistry*, Valentine, J. S.; Foote, C. S.; Greenberg, A.; Liebman, J. F., Eds.; Blackie: Glasgow, UK, 1995, pp 84–187.
3. Sono, M.; Roach, M. P.; Coulter, E. D.; Dawson, J. H. *Chem. Rev.* **1996**, *96*, 2841–2887.
4. Kadish, K.M.; Smith, K.M.; Guilard, R., Eds. *The Porphyrin Handbook*, Academic Press: San Diego, CA, 2000; Vol. 4.
5. McLain, J. L.; Lee, J.; Groves, J. T. In *Biomimetic Oxidations Catalyzed by Transition Metal Complexes,* Meunier, B., Eds.; Imperial College Press: London, 2000, 91–169.
6. Meunier, B.; Bernadou, J. *Struct. Bonding* **2000**, *97*, 1–35.
7. Wertz, D. L.; Valentine, J. S. *Struct. Bonding* **2000**, *97*, 37–60.
8. Guengerich, F. P. *Chem. Res. Toxicol.* **2001**, *14*, 611–650.
9. Omura, T. *Biochem. Biophys. Res. Commun.* **1999**, *266*, 690–698.
10. Mansuy, D. *Comp. Biochem. Physiol Part C.* **1998**, *121*, 5–14.

11. Poulos, T. L.; Finzel, B. C.; Gunsalus, I. C.; Wagner, G. C.; Kraut, J. *J. Biol. Chem.* **1985**, *260*, 16122–16130.
12. Omura, T.; Sato, R. *J. Biol. Chem.* **1964**, *239*, 2370–2378.
13. Dawson, J. H.; Sono, M. *Chem. Rev.* **1987**, *87*, 1255–1276.
14. Sligar, S. G. *Biochemistry* **1976**, *15*, 5399–5406.
15. Macdonald, I. D. G.; Sligar, S. G.; Christian, J. F.; Unno, M.; Champion, P. M. *J. Am. Chem. Soc.* **1999**, *121*, 376–380.
16. Brewer, C. B.; Peterson, J. A. *J. Biol. Chem.* **1988**, *263*, 791–798.
17. Davydov, R.; Makris, T. M.; Kofman, V.; Werst, D. E.; Sligar, S. G.; Hoffman, B. M. *J. Am. Chem. Soc.* **2001**, *123*, 1403–1415.
18. Denisov, I. G.; Makris, T. M.; Sligar, S. G. *J. Biol. Chem.* **2001**, *276*, 11648–11652.
19. Denisov, I. G.; Hung, S.-C.; Weiss, K. E.; McLean, M. A.; Shiro, Y.; Park, S.-Y.; Champion, P. M.; Sligar, S. G. *J. Inorg. Biochem.* **2001**, *87*, 215–226.
20. Schlichting, I.; Berendzen, J.; Chu, K.; Stock, A. M.; Maves, S. A.; Benson, D. E.; Sweet, R. M.; Ringe, D.; Petsko, G. A.; Sligar, S. G. *Science* **2000**, *287*, 1615–1622.
21. Kellner, D. G.; Hung, S.-C.; Weiss, K. E.; Sligar, S. G. *J. Biol. Chem.* **2002**, *277*, 9641–9644.
22. Egawa, T.; Shimada, H.; Ishimura, Y. *Biochem. Biophys. Res. Commun.* **1994**, *201*, 1464–1469.
23. Groves, J. T.; Nemo, T. E.; Myers, R. S. *J. Am. Chem. Soc.* **1979**, *101*, 1032–1033.
24. Groves, J. T.; Nemo, T. E. *J. Am. Chem. Soc.* **1983**, *105*, 5786–5791.
25. Chang, C. K.; Kuo, M.-S. *J. Am. Chem. Soc.* **1979**, *101*, 3413–3415.
26. Tabushi, I.; Koga, N. *J. Am. Chem. Soc.* **1979**, *101*, 6456–6458.
27. Hill, C. L.; Schardt, B. C. *J. Am. Chem. Soc.* **1980**, *102*, 6374–6375.
28. Groves, J. T.; Kruper, W. J., Jr.; Haushalter, R. C. *J. Am. Chem. Soc.* **1980**, *102*, 6375–6377.
29. Guilmet, E.; Meunier, B. *Tetrahedron Lett.* **1980**, *21*, 4449–4450.
30. Groves, J. T.; Kruper, W. J. Jr. *J. Am. Chem. Soc.* **1979**, *101*, 7613–7615.
31. Groves, J. T.; Haushalter, R. C.; Nakamura, M.; Nemo, T. E.; Evans, B. J. *J. Am. Chem. Soc.* **1981**, *103*, 2884–2886.
32. Dolphin, D.; Traylor, T. G.; Xie, L. Y. *Acc. Chem. Res.* **1997**, *30*, 251–259.
33. Chang, C. K.; Ebina, F. *J. Chem. Soc., Chem. Commun.* **1981**, 778–779.
34. Traylor, P. S.; Dolphin, D.; Traylor, T. G. *J. Chem. Soc., Chem. Commun.* **1984**, 279–280.
35. De Poorter, B.; Meunier, B. *Tetrahedron Lett.* **1984**, *25*, 1895–1896.
36. Renaud, J.-P.; Battioni, P.; Bartoli, J. F.; Mansuy, D. *J. Chem. Soc., Chem. Commun.* **1985**, 888–889.
37. Traylor, T. G.; Tsuchiya, S. *Inorg. Chem.* **1987**, *26*, 1338–1339.
38. Wijesekera, T.; Matsumoto, A.; Dolphin, D.; Lexa, D. *Angew. Chem., Int. Ed. Engl.* **1990**, *29*, 1028–1030.
39. Ellis, P. E., Jr.; Lyons, J. E. *Coord. Chem. Rev.* **1990**, *105*, 181–193.
40. Grinstaff, M. W.; Hill, M. G.; Labinger, J. A.; Gray, H. B. *Science* **1994**, *264*, 1311–1313.
41. Bartoli, J.-F.; Le Barch, K.; Palacio, M.; Battioni, P.; Mansuy, D. *Chem. Commun.* **2001**, 1718–1719.
42. Bartoli, J.-F.; Mouries-Mansuy, V.; Le Barch-Ozette, K.; Palacio, M.; Battioni, P.; Mansuy, D. *Chem. Commun.* **2000**, 827–828.
43. Kadish, K. M.; Smith, K. M.; Guilard, R., Eds. *The Porphyrin Handbook.* Academic Press: San Diego, CA, 2000, Vol. 4, Chapter 31, pp 119–187.
44. Kadish, K. M.; Smith, K. M.; Guilard, R., Eds. *The Porphyrin Handbook.* Academic Press: San Diego, CA, 2000, Vol. 4, Chapter 27, pp 17–40.
45. Kadish, K. M.; Smith, K. M.; Guilard, R., Eds. *The Porphyrin Handbook.* Academic Press: San Diego, CA, 2000, Vol. 4, Chapter 28, pp 41–63.
46. Montanari, F.; Casella, L., Eds. *Metalloporphyrin Catalyzed Oxidations*; Kluwer: Dordrecht, The Netherlands, 1994.
47. Sheldon, R. A., Ed., *Metalloporphyrins in Catalytic Oxidations*, Marcel Dekker: New York, 1994.
48. Lindsay Smith, J. R. In *Metalloporphyrins in Catalytic Oxidations*, Sheldon, R. A., Ed., Marcel Dekker: New York, 1994, 325–368.
49. Traylor, T. G.; Fann, W.-P.; Bandyopadhyay, D. *J. Am. Chem. Soc.* **1989**, *111*, 8009–8010.
50. Traylor, T. G.; Kim, C.; Richards, J. L.; Xu, F.; Perrin, C. L. *J. Am. Chem. Soc.* **1995**, *117*, 3468–3474.
51. Goh, Y. M.; Nam, W. *Inorg. Chem.* **1999**, *38*, 914–920.
52. Nam, W.; Goh, Y. M.; Lee, Y. J.; Lim, M. H.; Kim, C. *Inorg. Chem.* **1999**, *38*, 3238–3240.
53. Bernadou, J.; Meunier, B. *Chem. Commun.* **1998**, 2167–2173.
54. Goff, H.; Murmann, R. K. *J. Am. Chem. Soc.* **1971**, *93*, 6058–6060.
55. Murmann, R. K. *J. Am. Chem. Soc.* **1974**, *96*, 7836–7837.
56. Nam, W.; Valentine, J. S. *J. Am. Chem. Soc.* **1993**, *115*, 1772–1778.
57. Nam, W.; Valentine, J. S. *J. Am. Chem. Soc.* **1990**, *112*, 4977–4979.
58. Smegal, J. A.; Hill, C. L. *J. Am. Chem. Soc.* **1983**, *105*, 3515–3521.
59. Lee, K. A.; Nam, W. *J. Am. Chem. Soc.* **1997**, *119*, 1916–1922.
60. Groves, J. T.; Lee, J.; Marla, S. S. *J. Am. Chem. Soc.* **1997**, *119*, 6269–6273.
61. Groves, J. T.; Stern, M. K. *J. Am. Chem. Soc.* **1988**, *110*, 8628–8638.
62. Robert, A.; Meunier, B. *New J. Chem.* **1988**, *12*, 885–896.
63. Sorokin, A.; Meunier, B. *Eur. J. Inorg. Chem.* **1998**, 1269–1281.
64. Nam, W.; Kim, I.; Lim, M. H.; Choi, H. J.; Lee, J. S.; Jang, H. G. *Chem. Eur. J.* **2002**, *8*, 2067–2071.
65. Bernadou, J.; Fabiano, A.-S.; Robert, A.; Meunier, B. *J. Am. Chem. Soc.* **1994**, *116*, 9375–9376.
66. Hanna, I. H.; Krauser, J. A.; Cai, H.; Kim, M.-S.; Guengerich, F. P. *J. Biol. Chem.* **2001**, *276*, 39553–39561.
67. Primus, J.-L.; Teunis, K.; Mandon, D.; Veeger, C.; Rietjens, I. M. C. M. *Biochem. Biophys. Res. Commun.* **2000**, *272*, 551–556.
68. Haandel, M. J. H.; Primus, J.-L.; Teunis, C.; Boersma, M. G.; Osman, A. M.; Veeger, C.; Rietjens, I. M. C. M. *Inorg. Chim. Acta* **1998**, *275–276*, 98–105.
69. Jayaraj, K.; Terner, J.; Gold, A.; Roberts, D. A.; Austin, R. N.; Mandon, D.; Weiss, R.; Bill, E.; Müther, M.; Trautwein, A. X. *Inorg. Chem.* **1996**, *35*, 1632–1640.
70. Boso, B.; Lang, G.; McMurry, T. J.; Groves, J. T. *J. Chem. Phys.* **1983**, *79*, 1122–1126.
71. Hashimoto, S.; Mizutani, Y.; Tatsuno, Y.; Kitagawa, T. *J. Am. Chem. Soc.* **1991**, *113*, 6542–6549.

72. Jones, R.; Jayaraj, K.; Gold, A.; Kirk, M. L. *Inorg. Chem.* **1998**, *37*, 2842–2843.
73. Penner-Hahn, J. E.; Eble, K. S.; McMurry, T. J.; Renner, M.; Balch, A. L.; Groves, J. T.; Dawson, J. H.; Hodgson, K. O. *J. Am. Chem. Soc.* **1986**, *108*, 7819–7825.
74. Gross, Z.; Nimri, S. *Inorg. Chem.* **1994**, *33*, 1731–1732.
75. Wolowiec, S.; Latos-Grazynski, L. *Inorg. Chem.* **1998**, *37*, 2984–2988.
76. Nam, W.; Lim, M. H.; Oh, S.-Y. *Inorg. Chem.* **2000**, *39*, 5572–5575.
77. Fujii, H. *Coord. Chem. Rev.* **2002**, *226*, 51–60.
78. Gold, A.; Weiss, R. *J. Porph. Phthal.* **2000**, *4*, 344–349.
79. Weiss, R.; Bulach, V.; Gold, A.; Terner, J.; Trautwein, A. X. *J. Biol. Inorg. Chem.* **2001**, *6*, 831–845.
80. Fujii, H. *J. Am. Chem. Soc.* **1993**, *115*, 4641–4648.
81. Czarnecki, K.; Proniewicz, L. M.; Fujii, H.; Kincaid, J. R. *J. Am. Chem. Soc.* **1996**, *118*, 4680–4685.
82. Fujii, H.; Yoshimura, T.; Kamada, H. *Inorg. Chem.* **1996**, *35*, 2373–2377.
83. Fujii, H. *Chem. Lett.* **1994**, 1491–1494.
84. Terner, J.; Gold, A.; Weiss, R.; Mandon, D.; Trautwein, A. X. *J. Porph. Phthal.* **2001**, *5*, 357–364.
85. Benecky, M. J.; Frew, J. E.; Scowen, N.; Jones, P.; Hoffman, B. M. *Biochemistry* **1993**, *32*, 11929–11933.
86. Patterson, W. R.; Poulos, T. L.; Goodin, D. B. *Biochemistry* **1995**, *34*, 4342–4345.
87. Rietjens, I. *J. Biol. Inorg. Chem.* **1996**, *1*, 355–355.
88. Dawson, J. H. *Science* **1988**, *240*, 433–439.
89. Tani, F.; Matsu-ura, M.; Nakayama, S.; Naruta, Y. *Coord. Chem. Rev.* **2002**, *226*, 219–226.
90. Collman, J. P.; Sorrell, T. N. *J. Am. Chem. Soc.* **1975**, *97*, 4133–4134.
91. Chang, C. K.; Dolphin, D. *J. Am. Chem. Soc.* **1975**, *97*, 5948–5950.
92. Collman, J. P.; Groh, S. E. *J. Am. Chem. Soc.* **1982**, *104*, 1391–1403.
93. Schappacher, M.; Ricard, L.; Weiss, R.; Montiel-Montoya, R.; Bill, E.; Gonser, U.; Trautwein, A. *J. Am. Chem. Soc.* **1981**, *103*, 7646–7648.
94. Higuchi, T.; Shimada, K.; Maruyama, N.; Hirobe, M. *J. Am. Chem. Soc.* **1993**, *115*, 7551–7552.
95. Urano, Y.; Higuchi, T.; Hirobe, M.; Nagano, T. *J. Am. Chem. Soc.* **1997**, *119*, 12008–12009.
96. Tani, F.; Matsu-ura, M.; Nakayama, S.; Ichimura, M.; Nakamura, N.; Naruta, Y. *J. Am. Chem. Soc.* **2001**, *123*, 1133–1142.
97. Wagenknecht, H.-A.; Woggon, W.-D. *Angew. Chem., Int. Ed. Engl.* **1997**, *36*, 390–392.
98. Gross, Z. *J. Biol. Inorg. Chem.* **1996**, *1*, 368–371.
99. Czarnecki, K.; Nimri, S.; Gross, Z.; Proniewicz, L. M.; Kincaid, J. R. *J. Am. Chem. Soc.* **1996**, *118*, 2929–2935.
100. Nanthakumar, A.; Goff, H. M. *J. Am. Chem. Soc.* **1990**, *112*, 4047–4049.
101. Murakami, T.; Yamaguchi, K.; Watanabe, Y.; Morishima, I. *Bull. Chem. Soc. Jpn.* **1998**, *71*, 1343–1353.
102. Dey, A.; Ghosh, A. *J. Am. Chem. Soc.* **2002**, *124*, 3206–3207.
103. Weiss, R.; Gold, A.; Trautwein, A. X.; Terner, J. In *The Porphyrin Handbook*, Kadish, K. M.; Smith, K. M.; Guilard, R., Eds.; Academic Press: New York, 2000, Vol. 4, Chapter 29, pp 65–96.
104. Chin, D.-H.; La Mar, G. N.; Balch, A. L. *J. Am. Chem. Soc.* **1980**, *102*, 5945–5947.
105. Groves, J. T.; Gross, Z.; Stern, M. K. *Inorg. Chem.* **1994**, *33*, 5065–5072.
106. Groves, J. T.; Watanabe, Y. *J. Am. Chem. Soc.* **1986**, *108*, 507–508.
107. Shapiro, S.; Piper, J. U.; Caspi, E. *J. Am. Chem. Soc.* **1982**, *104*, 2301–2305 and references therein.
108. Groves, J. T.; McClusky, G. A.; White, R. E.; Coon, M. J. *Biochem. Biophys. Res. Commun.* **1978**, *81*, 154–160.
109. Groves, J. T. *J. Chem. Educ.* **1985**, *62*, 928–931.
110. Groves, J. T.; Nemo, T. E. *J. Am. Chem. Soc.* **1983**, *105*, 6243–6248.
111. Hjelmeland, L. M.; Aronow, L.; Trudell, J. R. *Biochem. Biophys. Res. Commun.* **1977**, *76*, 541–549.
112. Kadkhodayan, S.; Coulter, E. D.; Maryniak, D. M.; Bryson, T. A.; Dawson, J. H. *J. Biol. Chem.* **1995**, *270*, 28042–28048.
113. Iyer, K. R.; Jones, J. P.; Darbyshire, J. F.; Trager, W. F. *Biochemistry* **1997**, *36*, 7136–7143.
114. Manchester, J. I.; Dinnocenzo, J. P.; Higgins, L.; Jones, J. P. *J. Am. Chem. Soc.* **1997**, *119*, 5069–5070.
115. Sorokin, A.; Robert, A.; Meunier, B. *J. Am. Chem. Soc.* **1993**, *115*, 7293–7299.
116. Gelb, M. H.; Heimbrook, D. C.; Mälkönen, P.; Sligar, S. G. *Biochemistry* **1982**, *21*, 370–377.
117. White, R. E.; Miller, J. P.; Favreau, L. V.; Bhattacharyya, A. *J. Am. Chem. Soc.* **1986**, *108*, 6024–6031.
118. Traylor, T. G.; Hill, K. W.; Fann, W.-P.; Tsuchiya, S.; Dunlap, B. E. *J. Am. Chem. Soc.* **1992**, *114*, 1308–1312.
119. Groves, J. T.; Subramanian, D. V. *J. Am. Chem. Soc.* **1984**, *106*, 2177–2181.
120. Oliw, E. H.; Brodowsky, I. D.; Hörnsten, L.; Hamberg, M. *Arch. Biochem. Biophys.* **1993**, *300*, 434–439.
121. Griller, D.; Ingold, K. U. *Acc. Chem. Res.* **1980**, *13*, 317–323.
122. Newcomb, M. *Tetrahedron* **1993**, *49*, 1151–1176.
123. Ortiz de Montellano, P. R.; Stearns, R. A. *J. Am. Chem. Soc.* **1987**, *109*, 3415–3420.
124. Auclair, K.; Hu, Z.; Little, D. M.; Ortiz de Montellano, P. R.; Groves, J. T. *J. Am. Chem. Soc.* **2002**, *124*, 6020–6027.
125. Atkinson, J. K.; Ingold, K. U. *Biochemistry* **1993**, *32*, 9209–9214.
126. Newcomb, M.; Le Tadic, M.-H.; Putt, D. A.; Hollenberg, P. F. *J. Am. Chem. Soc.* **1995**, *117*, 3312–3313.
127. Newcomb, M.; Le Tadic-Biadatti, M.-H.; Chestney, D. L.; Roberts, E. S.; Hollenberg, P. F. *J. Am. Chem. Soc.* **1995**, *117*, 12085–12091.
128. Choi, S.-Y.; Eaton, P. E.; Hollenberg, P. F.; Liu, K. E.; Lippard, S. J.; Newcomb, M.; Putt, D. A.; Upadhyaya, S. P.; Xiong, Y. *J. Am. Chem. Soc.* **1996**, *118*, 6547–6555.
129. Newcomb, M.; Toy, P. H. *Acc. Chem. Res.* **2000**, *33*, 449–455.
130. Newcomb, M.; Shen, R.; Choi, S.-Y.; Toy, P. H.; Hollenberg, P. F.; Vaz, A. D. N.; Coon, M. J. *J. Am. Chem. Soc.* **2000**, *122*, 2677–2686.
131. Yoshizawa, K. *Coord. Chem. Rev.* **2002**, *226*, 251–259.
132. Ghosh, A. *J. Porph. Phthal.* **2001**, *5*, 187–189.
133. Harris, D. L. *Curr. Opin. Chem. Biol.* **2001**, *5*, 724–735.
134. Schröder, D.; Shaik, S.; Schwarz, H. *Acc. Chem. Res.* **2000**, *33*, 139–145.
135. Shaik, S.; Filatov, M.; Schröder, D.; Schwarz, H. *Chem. Eur. J.* **1998**, *4*, 193–199.
136. Ogliaro, F.; Harris, N.; Cohen, S.; Filatov, M.; de Visser, S. P.; Shaik, S. *J. Am. Chem. Soc.* **2000**, *122*, 8977–8989.

137. Ogliaro, F.; Filatov, M.; Shaik, S. *Eur. J. Inorg. Chem.* **2000**, 2455–2458.
138. Ostović, D.; He, G.-X.; Bruice, T. C. In *Metalloporphyrins in Catalytic Oxidations* Sheldon, R. A. Ed.; Marcel Dekker: New York, 1994, pp 29–68.
139. Gross, Z.; Nimri, S. *J. Am. Chem. Soc.* **1995**, *117*, 8021–8022.
140. Ortiz de Montellano, P. R.; De Voss, J. J. *Nat. Prod. Rep.* **2002**, *19*, 477–493.
141. Watanabe, Y. *J. Biol. Inorg. Chem.* **2001**, *6*, 846–856.
142. Bugg, T. D. H. *Curr. Opin. Chem. Biol.* **2001**, *5*, 550–555.
143. Vaz, A. D. N. *Curr. Drug Metab.* **2001**, *2*, 1–16.
144. Lewis, D. F. V.; Pratt, J. M. *Drug. Metab. Rev.* **1998**, *30*, 739–786.
145. Fishman, J. *Cancer Res.* **1982**, *42*, 3277–3280.
146. Akhtar, M.; Calder, M. R.; Corina, D. L.; Wright, J. N. *Biochem. J.* **1982**, *201*, 569–580.
147. Akhtar, M.; Lee-Robichaud, P.; Akhtar, M. E.; Wright, J. N. *J. Steroid Biochem Molec. Biol.* **1997**, *61*, 127–132.
148. Vaz, A. D. N.; Roberts, E. S.; Coon, M. J. *J. Am. Chem. Soc.* **1991**, *113*, 5886–5887.
149. Vaz, A. D. N.; Pernecky, S. J.; Raner, G. M.; Coon, M. J. *Proc. Natl. Acad. Sci. USA* **1996**, *93*, 4644–4648.
150. Martinis, S. A.; Atkins, W. M.; Stayton, P. S.; Sligar, S. G. *J. Am. Chem. Soc.* **1989**, *111*, 9252–9253.
151. Vidakovic, M.; Sligar, S. G.; Li, H.; Poulos, T. L. *Biochemistry* **1998**, *37*, 9211–9219.
152. Vaz, A. D. N.; McGinnity, D. F.; Coon, M. J. *Proc. Natl. Acad. Sci. USA* **1998**, *95*, 3555–3560.
153. Toy, P. H.; Newcomb, M.; Coon, M. J.; Vaz, A. D. N. *J. Am. Chem. Soc.* **1998**, *120*, 9718–9719.
154. Davydov, R.; Kofman, V.; Fujii, H.; Yoshida, T.; Ikeda-Saito, M.; Hoffman, B. M. *J. Am. Chem. Soc.* **2002**, *124*, 1798–1808.
155. Vatsis, K. P.; Coon, M. J. *Arch. Biochem. Biophys.* **2002**, *397*, 119–129.
156. Primus, J.-L.; Boersma, M. G.; Mandon, D.; Boeren, S.; Veeger, C.; Weiss, R.; Rietjens, I. M. C. M. *J. Biol. Inorg. Chem.* **1999**, *4*, 274–283.
157. McCandlish, E.; Miksztal, A. R.; Nappa, M.; Sprenger, A. Q.; Valentine, J. S.; Stong, J. D.; Spiro, T. G. *J. Am. Chem. Soc.* **1980**, *102*, 4268–4271.
158. Shirazi, A.; Goff, H. M. *J. Am. Chem. Soc.* **1982**, *104*, 6318–6322.
159. Burstyn, J. N.; Roe, J. A.; Miksztal, A. R.; Shaevitz, B. A.; Lang, G.; Valentine, J. S. *J. Am. Chem. Soc.* **1988**, *110*, 1382–1388.
160. VanAtta, R. B.; Strouse, C. E.; Hanson, L. K.; Valentine, J. S. *J. Am. Chem. Soc.* **1987**, *109*, 1425–1434.
161. Khenkin, A. M.; Shteinman, A. A. *J. Chem. Soc.Chem. Commun.* **1984**, 1219–1220.
162. Miksztal, A. R.; Valentine, J. S. *Inorg. Chem.* **1984**, *23*, 3548–3552.
163. Schappacher, M.; Weiss, R.; Montiel-Montoya, R.; Trautwein, A.; Tabard, A. *J. Am. Chem. Soc.* **1985**, *107*, 3736–3738.
164. Sisemore, M. F.; Burstyn, J. N.; Valentine, J. S. *Angew. Chem., Int. Ed. Engl.* **1996**, *35*, 206–208.
165. Selke, M.; Sisemore, M. F.; Valentine, J. S. *J. Am. Chem. Soc.* **1996**, *118*, 2008–2012.
166. Selke, M.; Valentine, J. S. *J. Am. Chem. Soc.* **1998**, *120*, 2652–2653.
167. Machii, K.; Watanabe, Y.; Morishima, I. *J. Am. Chem. Soc.* **1995**, *117*, 6691–6697.
168. Nam, W.; Lim, M. H.; Lee, H. J.; Kim, C. *J. Am. Chem. Soc.* **2000**, *122*, 6641–6647.
169. Nam, W.; Jin, S. W.; Lim, M. H.; Ryu, J. Y.; Kim, C. *Inorg. Chem.* **2002**, *41*, 3647–3652.
170. Collman, J. P.; Chien, A. S.; Eberspacher, T. A.; Brauman, J. I. *J. Am. Chem. Soc.* **2000**, *122*, 11098–11100.
171. Nam, W.; Lim, M. H.; Moon, S. K.; Kim, C. *J. Am. Chem. Soc.* **2000**, *122*, 10805–10809.
172. Wadhwani, P.; Mukherjee, M.; Bandyopadhyay, D. *J. Am. Chem. Soc.* **2001**, *123*, 12430–12431.
173. Suzuki, N.; Higuchi, T.; Nagano, T. *J. Am. Chem. Soc.* **2002**, *124*, 9622–9628.
174. Ogliaro, F.; de Visser, S. P.; Cohen, S.; Sharma, P. K.; Shaik, S. *J. Am. Chem. Soc.* **2002**, *124*, 2806–2817.

8.13
Nonheme Di-iron Enzymes

D. LEE and S. J. LIPPARD
Massachusetts Institute of Technology, Cambridge, MA, USA

8.13.1 INTRODUCTION

An emerging family of nonheme enzymes utilize carboxylate-rich ligand groups to hold two iron atoms in proximity.[1–6] Structural elucidation and mechanistic investigations of selected members of such enzymes since the early 1990s have fueled efforts to understand the underlying chemical principles of dioxygen activation occurring in their active sites. Well-characterized synthetic systems are now available that have complemented such efforts by providing simplified frameworks for spectroscopic, structural, and mechanistic studies.[5,7–9]

A structural module comprising tetra(carboxylato)di-iron(II) centers with two additional *N*-donor groups has been identified at the active sites of the hydroxylase component (MMOH) of soluble methane monooxygenase,[10–13] the R2 subunit of class I ribonucleotide reductase (RNR-R2),[14–16] and stearoyl–acyl carrier protein (ACP) Δ^9 desaturase (Δ9D).[17,18] Structural comparisons of these enzymes reveal striking architectural similarities involving an approximately 18 Å segment of a pseudo-*222*-symmetric four-helix bundle that encapsulates their di-iron active
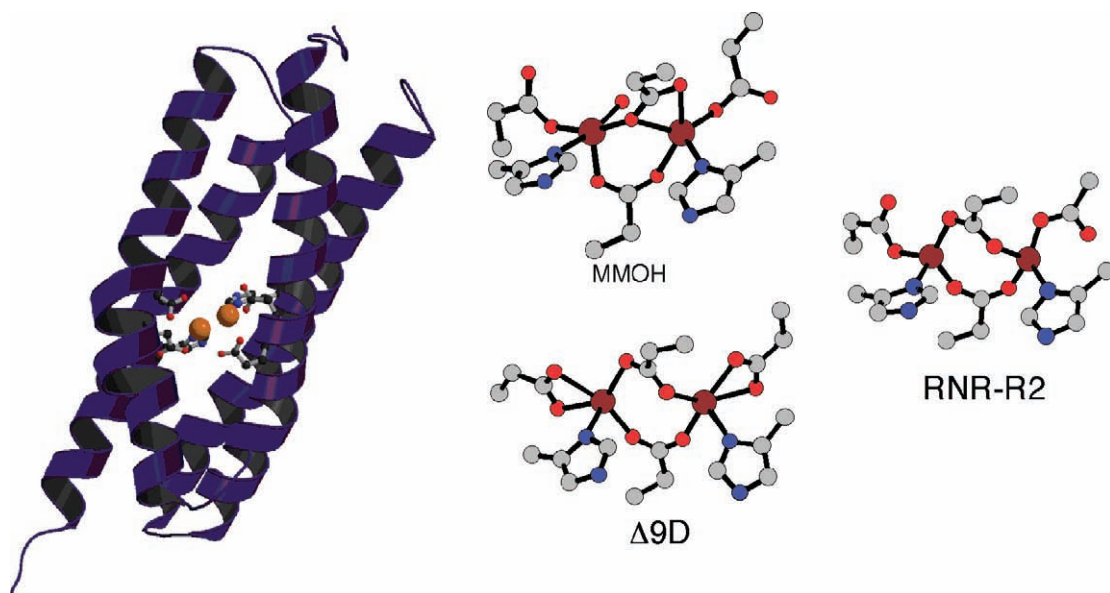
Figure 1 Ribbon diagram of four-helix bundle of MMOH from *M. capsulatus* (Bath) with the diiron active site depicted in ball-and-stick form (left). Ball-and-stick diagram of the MMOH, RNR-R2, and Δ9D active sites (right).

sites (Figure 1)[19] In the catalytic cycles of these enzymes, dioxygen binding to the coordinatively unsaturated di-iron(II) centers elicits a cascade of events involving controlled delivery of reducing equivalents affording metal-bound, O_2-derived fragments. Higher oxidation state intermediates evolve from essentially identical initial dioxygen-adduct(s) to carry out C—H activation, tyrosine oxidation, and desaturation of aliphatic fatty acid substrates. Together with the dioxygen carrier protein hemerythrin (Hr) discussed in Chapter 8.15, the reaction profiles of these carboxylate-bridged nonheme di-iron enzymes rival those of heme iron proteins, which utilize substantially less flexible metal cofactors.[20–23]

The low one-electron reduction potential and triplet ground spin-state of O_2 render reactions between dioxygen and organic substrates thermodynamically favorable but kinetically unfavorable.[24] The kinetic barrier can be surmounted by complexation of O_2 with paramagnetic transition metal centers.[1] Subsequent two-electron reduction and/or protonation of O_2-derived ligands provide the driving force for O—O bond cleavage that is typically accompanied by reorganization of the flexible primary coordination sphere. A tight coupling of the fundamental thermodynamic cycle of O_2 (Scheme 1)[25] with metal redox chemistry and ligand acid–base chemistry is crucial for the highly regulated dioxygen activation steps.
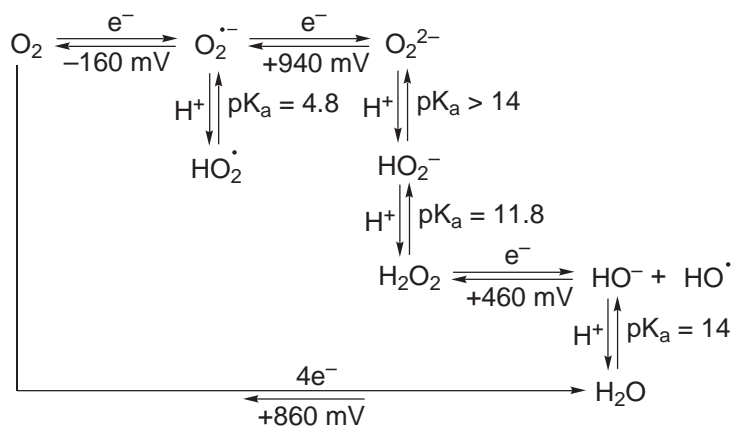
Redox potentials given vs. NHE

Scheme 1

8.13.2 METHANE MONOOXYGENASE HYDROXYLASE

8.13.2.1 Structure and Function

Methane monooxygenases (MMOs) catalyze the oxidation of methane to methanol (Equation 1):

$$CH_4 + O_2 + NADH + H^+ \longrightarrow CH_3OH + NAD^+ + H_2O \qquad (1)$$
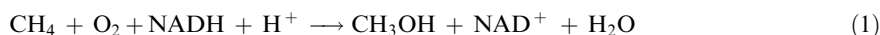
Found in methanotrophs that utilize methane as their sole source of carbon and energy, soluble MMO systems identified in two evolutionarily distinct classes of bacteria, *Methylococcus capsulatus* (Bath) and *Methylosinus trichosporium* OB3b, have been the most extensively studied.[10–12,26] In the MMO system, three proteins participate in the catalytic cycle, in which consumption of dioxygen and electrons and oxidation of hydrocarbon substrates are highly regulated. The hydroxylase protein methane monooxygenase hydroxylase (MMOH) is a $\sim$251 kDa protein that houses two carboxylate-bridged nonheme di-iron centers.[27–30] In the presence of substrates, two electrons per Fe_2 unit are supplied from a reductase protein MMOR to afford a fully reduced, di-iron(II) form of MMOH that activates dioxygen. The third protein MMOB regulates the catalytic process at various stages.

The active sites of MMOH are buried within the core of α-subunits in the $\alpha_2\beta_2\gamma_2$ dimeric structure. Four helices supply four Glu and two His residues that, along with solvent-derived ligands, coordinate to the dimetallic cofactor. For MMOH in the fully oxidized state, a triply bridged di-iron(III) core motif was identified crystallographically (Scheme 2).[13,27–30] Spectroscopic and structural data are consistent with the presence of hydroxo/aqua bridges that mediate weak antiferromagnetic (AF) interaction between high-spin iron(III) centers (Table 1).[6,13,14,17,18,27,29–61] Injection of two electrons elicits migration of the terminal monodentate Glu residue to a μ-1,1-bridging position and extrusion of solvent-derived single-atom bridging ligands to afford MMOH$_{red}$.[13,31] This carboxylate shift primes the metal center for reaction with a dioxygen molecule that approaches the di-iron(II) center distal to the two His groups.

8.13.2.2 Catalytic Cycle

The single-turnover reaction of MMOH$_{red}$ with O_2 has been monitored by time-resolved spectroscopic techniques. Stopped-flow optical spectroscopic and rapid freeze-quench (RFQ)
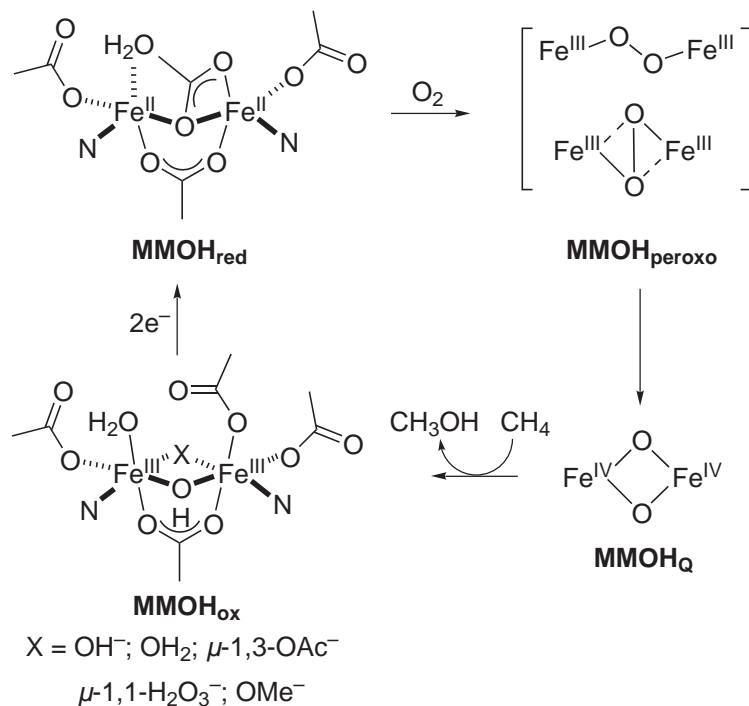
Scheme 2

Table 1 Structural and spectroscopic properties of MMOH, RNR-R2, $\Delta 9D$, and their O_2 reaction intermediates.

		Fe···Fe (Å)	λ_{max} (nm) (ε (M^{-1} cm^{-1}))	δ (ΔE_Q) (mm s^{-1})	ν_{O-O} ($\Delta\nu^a$) (cm^{-1})	ν_{Fe-O} ($\Delta\nu^a$) (cm^{-1})	J^b (cm^{-1})	g	References
MMOH (*M. capsulatus*)	H_{red}^{c}	3.3		1.3 (2.8)				15	31–33
	H_{ox}^{d}	3.1–3.4		0.51 (1.12)[e]; 0.50 (0.79)[e]; 0.47 (1.33)[f]; 0.72 (1.46)[f]					13,27,30,32
	H_{peroxo}		420 (4,000) 725 (1,800)	0.66 (1.51)					32,34–36
	H_Q		350 (3,600) 420 (7,200)	0.21 (0.68); 0.14 (0.55)					32,34,35
	$H_{Q_x}^{g}$			0.48 (−0.9); 0.14 (−0.6)					37
MMOH (*M. trichosporium* OB3b)	H_{red}^{c}			1.3 (3.0); 1.3 (2.7)			+ 0.35	16	38–41
	$H_{o_x}^{d}$	3.0		0.50 (1.16); 0.51 (0.87)			−7 ± 3		29,38,40
	H_{peroxo}		700 (2,500)	0.67 (1.51)					42,43
	H_Q	2.46[h]	330 (7,500) 430 (7,500)	0.17 (0.53)					43–46

		(B)	(C)	(D)	(E)	(F)	(G)	Ref
RNR-R2	$R2_{red}^{c}$	3.9		1.31 (3.24); 1.20 (2.92)				−0.5	14,47–49
	$R2_{ox}^{d}$	3.3	325 (9,400); 370 (7,200); 700 (1,500)	0.54 (1.64); 0.45 (2.41); 0.63 (1.58)					47,48,50,51
	$D84E\text{–}R2_{peroxo}^{i}$				890				6,52
	$D84E/W48F\text{–}R2_{peroxo}^{j}$		700 (1,800)	0.60 (1.48); 0.66 (1.67)	870 (−46)	458 (−16)^k; 499 (−22)^l			53,54
	X	2.5^h	360	0.55 (−0.9); 0.26 (−0.6)			2.007 1.999 1.994		55–57
Δ9D	$\Delta9D_{red}^{c}$	4.2		1.30 (3.04); 1.30 (3.36)				−1	17,18,58
	$\Delta9D_{ox}^{d}$		300–500 (8,000)	0.53 (1.54)^e; 0.50 (0.74)^f				<−30	58,59
	$\Delta9D_{peroxo}$		700 (1,200)	0.68 (1.90); 0.65 (1.06)	898 (−54)	442 (−17)^k; 490 (−19)^l			60,61

^{a} $\Delta\nu = (\nu$ of $^{16}O_2$-adduct$) - (\nu$ of $^{18}O_2$-adduct$)$. ^{b} $H = -2J\,S_1\cdot S_2$. ^{c} Fe(II)Fe(II) oxidation state. ^{d} Fe(III)Fe(III) oxidation state. ^{e} Species 1. ^{f} Species 2. ^{g} Cryoreductively generated Fe(III)Fe(IV) oxidation state. ^{h} Determined by EXAFS. ^{i} Peroxo from D84E mutant. ^{j} Peroxo from D84E/W48F mutant. ^{k} ν_{sym}. ^{l} ν_{asym}.

Mössbauer/EXAFS experiments identified sequential formation of dioxygen adducts at various iron oxidation levels. The first spectroscopically observable intermediate in the MMO reaction cycle is a (peroxo)di-iron(III) species displaying intense ligand-to-metal charge transfer (LMCT) bands at longer wavelengths (Table 1).[32,34–36,42] AF-coupling between iron(III) centers in this intermediate, MMOH$_{peroxo}$, results in an $S = 0$ ground state. An unusually large isomer shift of $0.66 \, \text{mm sec}^{-1}$ associated with MMOH$_{peroxo}$ is also shared by similar intermediates in the RNR-R2 and Δ9D reaction cycle (Table 1). They are formulated as (μ-1,2-peroxo)di-iron(III) species, based on vibrational spectroscopic evidence (*vide infra*). Subsequent reductive cleavage of the iron-bound O—O bond, in either a homolytic or protonation-assisted heterolytic fashion, affords a high-valent species MMOH$_Q$, which inserts one O$_2$-derived oxygen atom into the C—H bond of various hydrocarbon substrates including CH$_4$.[32,35,43–46] RFQ Mössbauer spectroscopic data point toward the presence of AF-coupled di-iron(IV) centers in MMOH$_Q$ (Table 1). A short Fe···Fe distance of 2.46 Å deduced from EXAFS data analysis implicates the presence of multiple single-atom bridging ligands derived from O$_2$ and protein side chains.[43] Mössbauer parameters of an iron(III)iron(IV) form of MMOH$_Q$, MMOH$_{Q_x}$, generated by cryoreduction[37] compare well with those of RNR-R2 intermediate X,[57] which has a similarly short Fe···Fe distance of 2.5 Å spanned by a single O$_2$-derived oxygen and carboxylate oxygen atoms (*vide infra*).[55]

Substrate probes have aided mechanistic understanding of the key C—H activation step in the MMOH reaction cycle. Chiral alkanes[62,63] and radical-clock substrate probes[64–68] were used to discriminate between radical recoil/rebound and nonsynchronous concerted insertion pathways. A short lifetime ($<150 \, \text{fs}$) estimated for the putative radical species derived from cyclopropane-based radical-clock substrates favors the latter process,[64,65] whereas partial racemization of chiral ethane substrate is consistent with the former scenario.[62] A unifying model was proposed, in which both recoil/rebound and concerted reaction channels are available for a bound radical intermediate and the partitioning between each trajectory is dependent on the substrate.[69] Formation of carbocation-derived products from certain probes implicates yet another route involving a formal OH$^+$ insertion.[67,68,70,71] Participation of multiple species capable of oxygen transfer is an emerging mechanistic view in both heme and nonheme systems, as exemplified by the studies of cP450s and their synthetic models.[72–74] Scheme 3 depicts various density functional theory (DFT) models of MMOH$_Q$ and their computed reaction pathways, which are reviewed in detail elsewhere.[2,5,6,12]
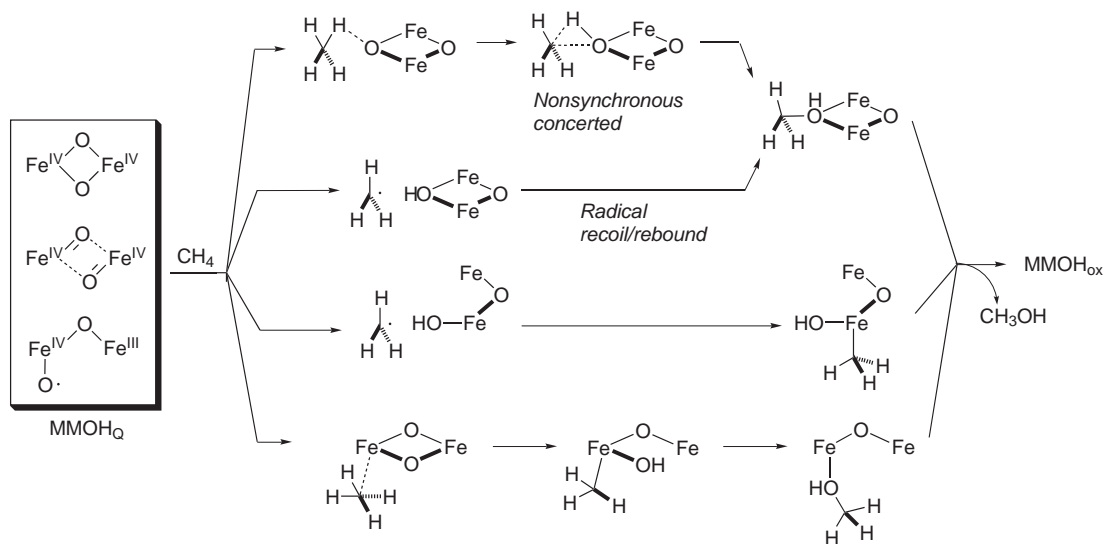
Scheme 3

8.13.3   RIBONUCLEOTIDE REDUCTASE R2 SUBUNIT

8.13.3.1   Structure and Function

Ribonucleotide reductases (RNRs) are ubiquitous enzymes that catalyze the conversion of ribonucleotides to deoxyribonucleotides.[15,16,75] Essential for DNA replication and repair, RNRs require

metallocofactors to initiate radical-based nucleotide reduction processes.[76] Class I RNRs isolated from *Escherichia coli* have a tetrameric structure comprising two homodimeric subunits, R1 and R2.[50,77] In the R2 subunit is housed a carboxylate-bridged nonheme di-iron center that reacts with dioxygen to afford a (μ-oxo)di-iron(III) cluster and a stable tyrosyl radical (Equation (2)):

$$Fe^{II}_2 + + O_2 + e^- \longrightarrow Fe^{III}-O-Fe^{III} + + OH^- \qquad (2)$$
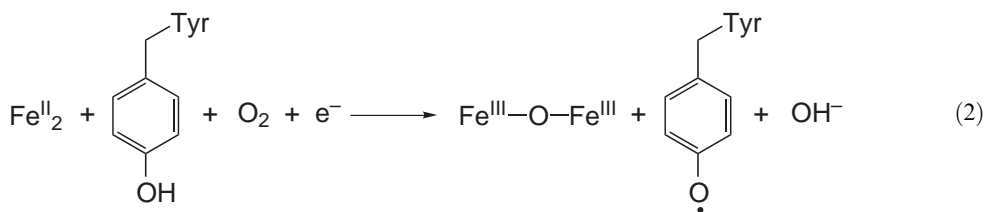
A subsequent long-range ($\sim$35 Å) proton-coupled electron transfer (PCET) generates a cysteine-derived thiyl radical in the substrate-binding R1 subunit, which initiates the catalytic cycle by abstracting a 3′ hydrogen from nucleoside diphosphates.[16,75,78] The X-ray structure of the RNR-R2 active site in the fully reduced state features a di(μ-carboxylato)di-iron(II) core having a long (3.9 Å) Fe$\cdots$Fe separation (Figure 1; Scheme 4).[14] Binding of monodentate Asp and Glu residues and two His imidazole groups completes the primary coordination sphere of each four-coordinate iron(II) center. A significant degree of ligand reorganization accompanies metal oxidation in RNR-R2, similarly to the observations made with MMOH. Notably, incorporation of an oxo bridging ligand induces shifting of one of the Glu groups from μ-1,3 bridging to monodentate terminal (Scheme 4). Coordination of two water molecules results in a coordinatively saturated di-iron(III) cluster in RNR-R2 in its resting state.[50] Important geometric and spectroscopic parameters of RNR-R2 are summarized in Table 1.

8.13.3.2 Mechanism of Cofactor Assembly

Assembly of the (μ-oxo)di-iron(III) and tyrosyl radical cofactor in RNR-R2 has been extensively studied. Reaction of the apoenzyme and iron(II) with dioxygen results in a putative peroxo species that rapidly collapses to intermediate X with injection of an external electron.[55–57,79–81] A $g = 2.00$ X-band EPR signal of X, which becomes anisotropic in Q-band (Table 1), displays hyperfine broadening upon the use of ^{57}Fe and ^{17}O-labeled O_2 and H_2O.[57] RFQ-ENDOR
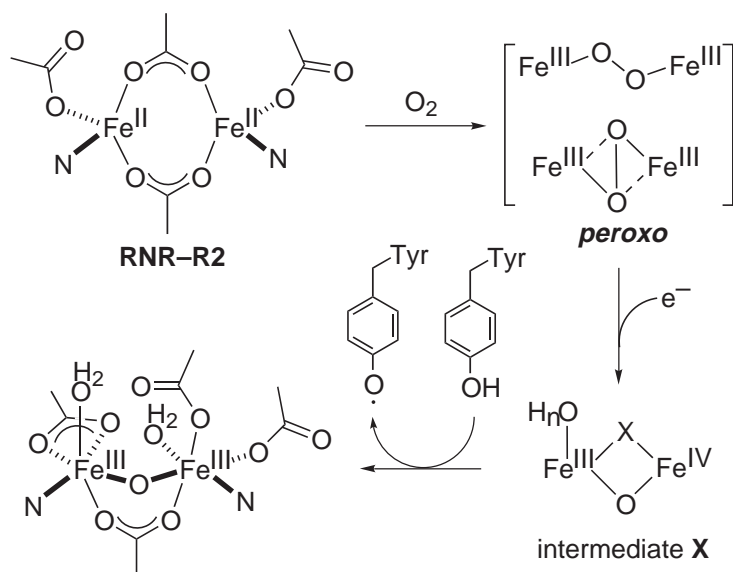
Scheme 4

spectroscopy established the formulation of X as $\{H_nO—Fe^{III}—O—Fe^{IV}\}$,[81] in which an O_2-derived oxo ligand mediates AF-coupling between high-spin (HS) iron(III) and (HS) iron(IV) atoms to afford a $S = 1/2$ ground spin state. The other oxygen atom ends up at a solvent-exchangeable terminal position on the iron(III) centers. Such an oxidation state assignment was substantiated further by Mössbauer data (Table 1), which suggest significant spin delocalization to the bridging oxo ligand. Oxidation of Tyr122 by PCET to the high-valent iron(III)iron(IV) unit generates the functionally requisite phenoxyl radical (Scheme 4).

By strategic replacement of key amino acid residues, the stability of the initial O_2-adduct was significantly enhanced, allowing spectroscopic characterization of a peroxo-type intermediate. In these RNR-R2 mutants, the distance of one carboxylate ligand group from its α-carbon was extended (RNR-R2-D84E) and the electron transfer (ET) pathway was blocked (RNR-R2-W48F/D84E).[52,54] Vibrational and Mössbauer spectroscopic evidence was consistent with the presence of a symmetric (μ-1,2-peroxo)di-iron(III) core in the O_2-adduct, which also displays broad absorption bands at ~700 nm (Table 1). Notably, the X-ray structure of the di-iron(II) form of the RNR-R2-D84E mutant bears a striking resemblance to the MMOH$_{red}$ active site.[82] Moreover, MMO-like monooxygenase activity was observed in certain RNR-R2 mutants, in which oxidizable Tyr or Phe residues were placed in the vicinity of the di-iron core.[53,83–85] These findings suggest a close structure–function relationship connecting the two functionally distinct enzymes.

8.13.4 STEAROYL–ACP Δ^9 DESATURASE

8.13.4.1 Structure and Function

Stearoyl–ACP Δ^9 desaturase, $\Delta9D$, is a soluble homodimeric protein.[86] In each 84 kDa subunit resides a carboxylate-bridged di-iron cluster that utilizes dioxygen to insert a *cis* double bond between the 9 and 10 position of stearoyl–ACP to afford oleoyl–ACP. The X-ray structure of a fully reduced form of $\Delta9D$ reveals a doubly carboxylate-bridged di-iron(II) core structurally related to MMOH and RNR-R2 (Figure 1).[17] Each five-coordinate iron atom has one bidentate carboxylate and one terminal histidine ligand. The Fe$\cdots$Fe separation is 4.2 Å. Although crystallographic information is not available for the di-iron(III) enzyme, UV-vis, resonance Raman, and Mössbauer data are consistent with the presence of a bridging oxo group that mediates AF coupling (Table 1).[58,59] X-ray absorption spectroscopy (XAS) and Mössbauer studies of oxidized $\Delta9D$ indicate the coexistence of two species, one with an oxo and the other with a hydroxo bridge.[87]

8.13.4.2 Substrate Binding and Dioxygen Activation

In the presence of stearoyl–ACP substrate, the geometric and electronic structure of the di-iron active site in $\Delta9D$ is strongly perturbed, as evidenced by circular dichroism (CD), MCD, and variable-temperature variable-field MCD studies.[18] Upon substrate binding, one iron atom remains five coordinate, whereas the other changes to four coordinate, providing an additional coordination site for O_2 binding. Such a geometric modulation alters the redox-active ground state orbitals and facilitates better overlap with the incoming dioxygen molecule. Enhanced O_2 reactivity was observed in the presence of the substrate, a finding analogous to the accelerated oxygenation of MMOH in the presence of the coupling protein, MMOB. Fully reduced $\Delta9D$ reacts with dioxygen to afford an initial adduct, the spectroscopic properties of which are consistent with those of a (μ-1,2-peroxo)di-iron(III) species (Table 1).[60,61] The remainder of the $\Delta9D$ reaction cycle, including the substrate oxidation step, is yet to be determined.

8.13.5 SYNTHETIC MODEL SYSTEMS

Prior to the structure determination of the nonheme di-iron enzymes described above, synthetic di-iron compounds had mainly served as benchmarks for calibrating spectral assignments made in the biological systems.[6,88–90] Since the early 1990s, details of the MMOH, RNR-R2, and $\Delta9D$ active sites have been mapped out by X-ray crystallography, providing blueprints for constructing synthetic surrogates. In the quest for minimal architectural motifs essential for function, significant advances

have been made in design, synthesis, and mechanistic understanding of the carboxylate-bridged nonheme di-iron complexes described below.

8.13.5.1 Carboxylate Shifts and Core Interconversion

Ligand migration within carboxylate-rich polynuclear clusters was first identified in synthetic compounds and termed *carboxylate shifts*.[91,92] Structural elucidation of nonheme di-iron enzymes at various oxidation levels substantiated the functional relevance of this concept.[13] A significant degree of structural flexibility, as reflected in the changes in Fe···Fe distances, is required when O_2 is activated during the reaction cycle. The versatility of carboxylates as ligands arises from the presence of four lone pair electrons disposed in an angle of approximately $120°$ with respect to the C—O vectors. Although the *syn* lone pairs preferentially bind metal ions owing to their enhanced basicity, examples exist whereby *anti* pairs are important participants in carboxylate shifts.[91] As depicted in Scheme 5, migration of carboxylate ligands can occur between bridging and terminal positions. Within this model, a conceptual linkage can be drawn between the μ-1,1 bridging, *syn,anti/syn,syn* μ-1,3 bridging, and mono/bidentate terminal coordination modes.

Flexible coordination of solvent-derived ligands has also been demonstrated. By appropriate choice of terminal ligands, a family of oxo/hydroxo-bridged di-iron(III) complexes was characterized, related by protonation and equation equilibria as depicted in Scheme 6.[93] Interconversion between different di-iron(III) cores was evidenced by various spectroscopic data, notable features and structural correlations of which were recently reviewed.[94] A conceptual comparison can be made to oxo–hydroxo tautomerism in heme iron chemistry, in which a solvent-derived oxygen atom can be incorporated into the primary coordination sphere and exchanged with the one derived from terminal oxidants.[95] Protonation of the $\{Fe_2O_2\}^{n+}$ core modulates donor strength and may elicit functionally required shifts in redox potential and ligand configuration.

8.13.5.2 Nonheme Di-iron Structural Models

Without steric confinement, kinetically labile iron-carboxylate units readily assemble into higher nuclearity species, a process assisted by single-atom bridging ligands.[96] Rapid ligand
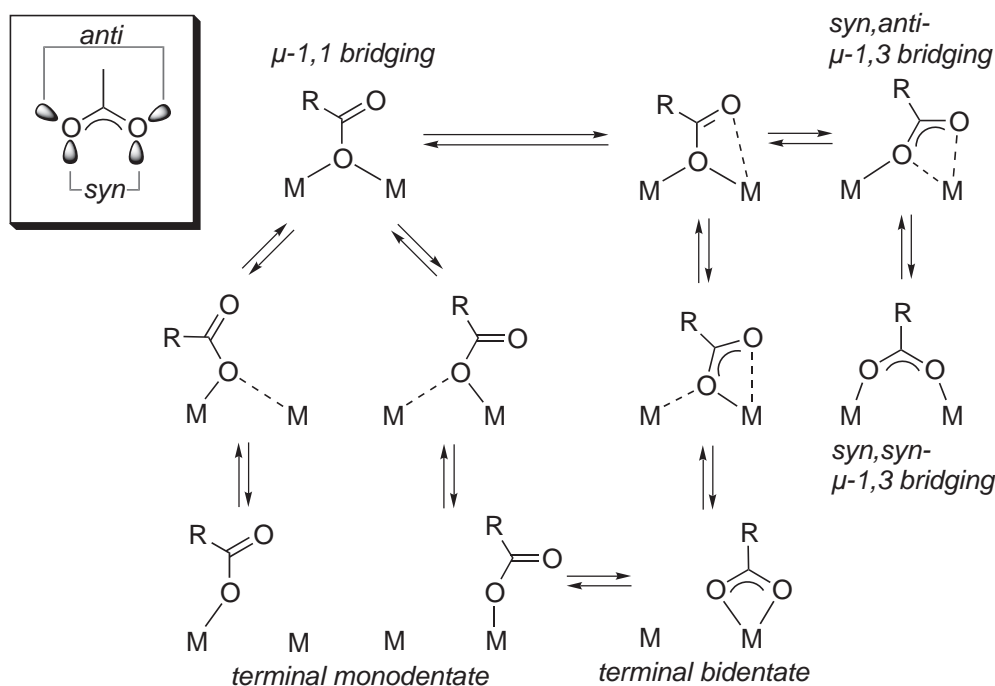
Scheme 5
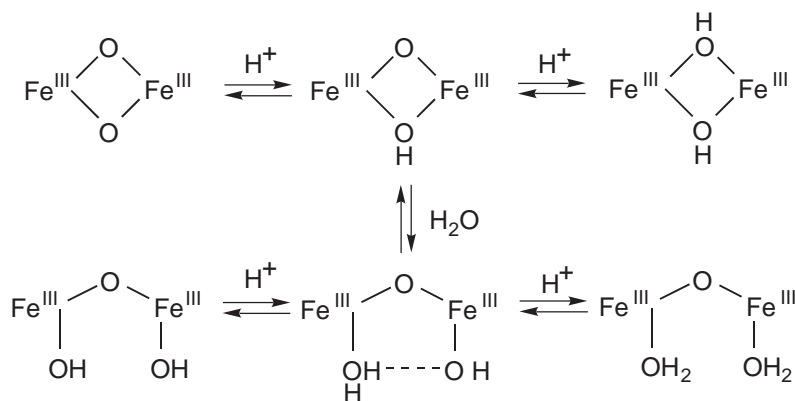
Scheme 6

substitution reactions at the metal centers increase the accessibility of energetically similar
coordination modes, resulting in the presence of multiple species at equilibrium in solution. In
such a situation, the product obtained is the thermodynamically most favorable one, which
often may not be the one of desired composition and geometry. Stabilizing discrete di-iron
units outside the well-shielded protein environment thus presents a formidable synthetic
challenge.[97] Early synthetic models of Hr, a dioxygen-carrier protein detailed in Chapter
8.15, utilized tridentate amine/imine ligands to gain control over the terminal coordination
sites. A discrete di-iron(II) complex [Fe$_2$(μ-OH)(μ-OAc)$_2$(Me$_3$TACN)$_2$]$^+$ (**1a**)[98,99] and its di-
iron(III) analogues [Fe$_2$(μ-O)(μ-OAc)$_2$L$_2$]$^{2+}$ (L = HBpz$_3^-$ (**2**), Me$_3$TACN (**1b**))[99–101] were
obtained in which the terminal coordination sites are effectively blocked by either Me$_3$TACN
or HBpz$_3^-$ ligands. Modeling of the anion-rich primary coordination in MMOH, RNR-R2,
and Δ9D active sites, however, requires the use of either low-denticity N-donor ligands or
specially designed carboxylate ligands having unique structural properties. Figure 2 shows
representative N-donor ligands and their abbreviations used in the compounds described
below.

8.13.5.2.1   Coordinatively saturated di(μ-carboxylato)di-iron(II) complexes

The doubly carboxylate-bridged di-iron(II) core structure in RNR-R2 and Δ9D was mimicked by
di-iron(II) complexes capped by tetradentate N-donor ligands. A coordinatively saturated di-iron(II)
complex [Fe$_2$(μ-OAc)$_2$(TPA)$_2$]$^{2+}$ (**3**) (Scheme 7) was assembled, in which a relatively long Fe···Fe
separation of 4.288(2) Å is spanned by two *syn,anti* μ-1,3 bridging carboxylate ligands.[102] In MeCN,
(**3**) dissociates into mononuclear iron(II) species, as revealed by its g = 9.3 EPR signal, and consumes
0.6(1) equiv. of dioxygen to afford a (μ-oxo)di-iron(III) complex. A mechanism for this autoxidation
was proposed in which a spectroscopically unobserved (peroxo)di-iron(III) intermediate is trapped by
another equivalent of ferrous precursor to yield two (μ-oxo)di-iron(III) molecules (see Section
8.13.5.5). A similar architectural feature is shared by doubly carboxylate bridged di-iron(II) com-
pounds [Fe$_2$(μ-OAc)$_2$(BPMEN)$_2$]$^{2+}$ (**4**)[103] and [Fe$_2$(μ-O$_2$CPh)$_2$(O$_2$CPh)$_2$(C$_5$H$_5$N)$_4$] (**5**) (Scheme 7),[104]
in which coordinatively saturated iron(II) centers are supported by N-rich ligand sets.
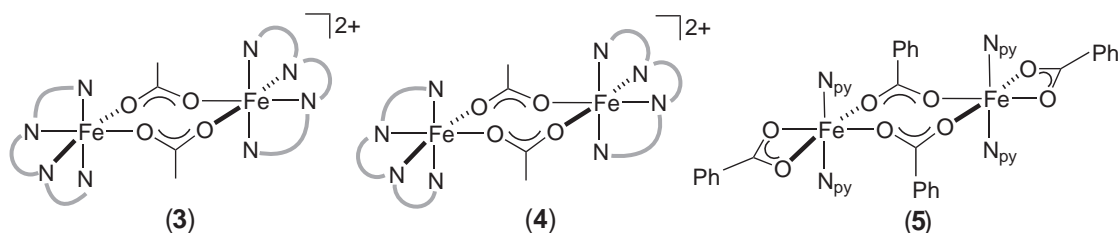
Scheme 7
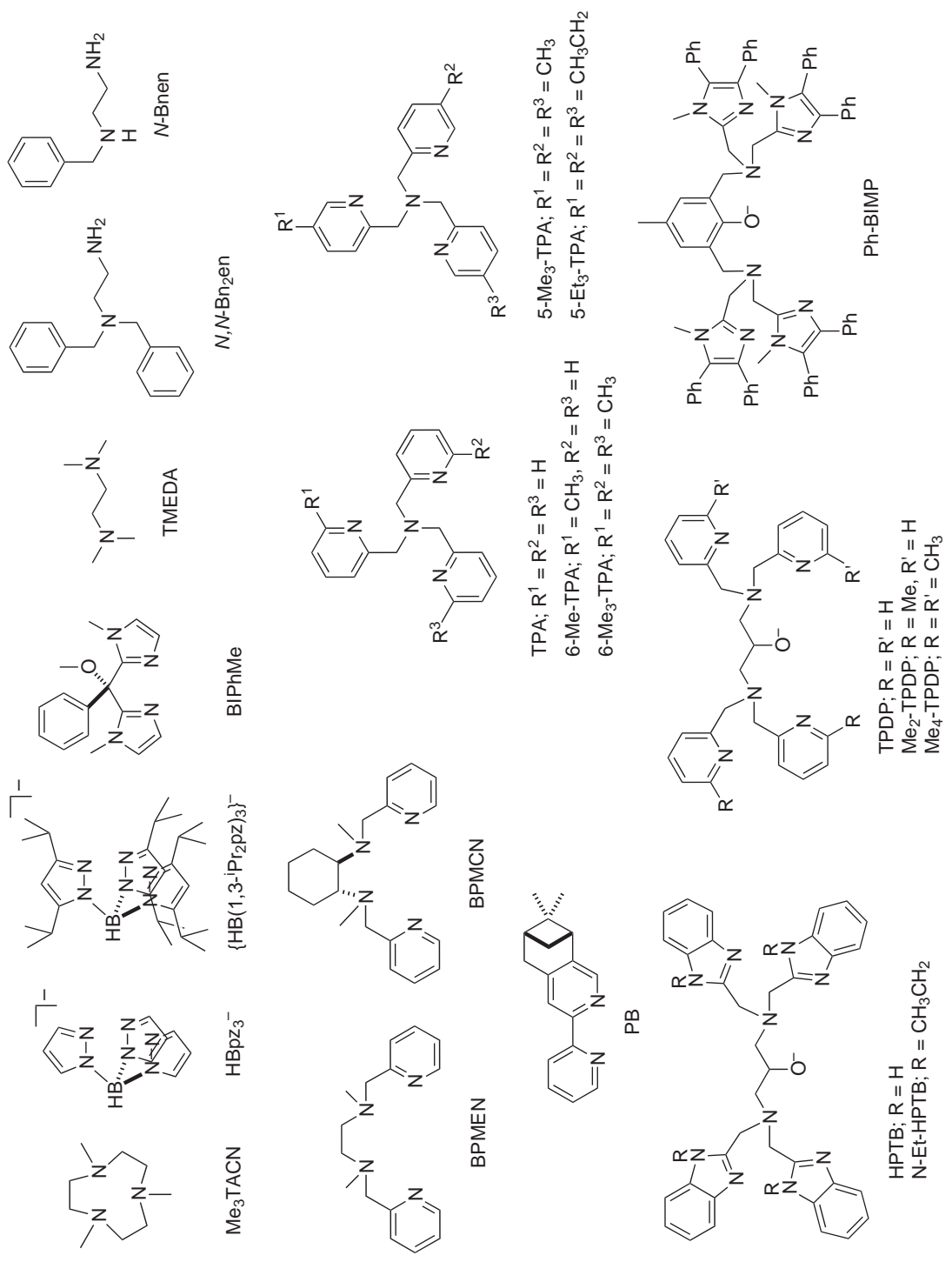
Figure 2 N-donor ligands used in nonheme di-iron model compounds and their abbreviations.

Scheme 8

8.13.5.2.2 Carboxylate-rich di-iron(II) complexes of monodentate or bidentate N-donor ligands

The asymmetric, anion-rich coordination of the MMOH active site was modeled by $[Fe_2(\mu\text{-}OH_2)$-$(\mu\text{-}OAc)_2(OAc)_3(C_5H_5N)_2]^-$ (**6**) (Scheme 8).[105,106] The triply bridging $\{(\mu\text{-}OH_2)(\mu\text{-}OAc)_2\}^{2-}$ unit in (**6**) is stabilized by hydrogen-bonding interactions between the bridging water molecule and two monodentate terminal carboxylate ligands. Both in the solid state and in solution, (**6**) displays a single sharp quadrupole doublet in its Mössbauer spectrum (Table 2), reflecting very similar electric field gradients (EFGs) at both iron sites.[105] Although stable in the presence of excess pyridine, the kinetically labile di-iron(II) center in (**6**) readily dissociates in MeCN and reassembles to afford a tri-iron(II) cluster $[Fe_3(OAc)_8]^{2-}$.[106] Air-oxidation of (**6**) resulted in mixed valence triiron or all-ferric tetrairon clusters. These observations clearly indicated that, without an effective steric shield or conformational rigidity, complexes of simple carboxylate/monodentate *N*-donor ligands rearrange to afford various iron-containing species in solution.

Depending on the denticity of the *N*-donor ligands and the number of carboxylate ligands, two distinct di-iron(II) core motifs are encountered. A hydroxo-bridged core is obtained for a di(carboxylato)di-iron(II) complex $[Fe_2(\mu\text{-}OH)(\mu\text{-}O_2CCF_3)_2(Me_3TACN)_2]^+$ (**7**), whereas a water-bridged core is accessed by a tetra(carboxylato)di-iron(II) complex $[Fe_2(\mu\text{-}OH_2)(\mu\text{-}O_2CCF_3)_2$-$(O_2CCF_3)_2(TMEDA)_2]$ (**8**) (Scheme 8).[107] As in (**6**), anion-rich primary coordination apparently attenuates the Lewis acidity of the metal centers, suppressing deprotonation of the bridging water molecule. The bridging water molecule in (**8**) is stabilized by hydrogen bonding with terminal monodentate carboxylate ligands on each metal center. ^1H and ^{19}F NMR techniques were used to probe the solution structure of these paramagnetic compounds. NMR spectra obtained for a mixture of H/D isotopomers are consistent with the solid-state structures determined by X-ray crystallography. The observed isotopomeric splitting was attributed to the ability of hydrogen bonding to bridging OH^- or H_2O to influence the stereochemistry of the resulting complex.[107] The two terminal carboxylate ligands in (**8**) can be exchanged with the dicarboxylate group in XDK (see below) to afford $[Fe_2(\mu\text{-}OH_2)(\mu\text{-}XDK)(O_2CCF_3)_2(TMEDA)_2]$ (**9**).[108] Selective and stepwise replacement of the terminal $CF_3CO_2^-$ ligands in (**8**) can also be achieved by addition of a bulky monocarboxylate ligand L^1 or XDK analogues, as monitored by ^{19}F NMR spectroscopy.[109]

An asymmetric di-iron(II) complex having an open terminal coordination site was prepared by using a bidentate *N*-donor ligand, BIPhMe, which supports the triply bridged di-iron(II) core in $[Fe_2(\mu\text{-}O_2CH)_3(O_2CH)(BIPhMe)_2]$ (**10a**) (Scheme 8).[110,111] The five- and six-coordinate iron(II) centers in (**10a**) are connected by one μ-1,1 and two μ-1,3 bridging ligands spanning an Fe···Fe distance of 3.5736(8) Å. Notably, the terminal formate ligand binds to iron via the less basic anti

Table 2 Structural and spectroscopic properties of nonheme diiron models.

Oxidation state	Compound	$Fe\cdots Fe$ (Å)	λ_{max} (ε) (nm (M^{-1} cm^{-1}))	$\delta(\Delta E_Q)$ (mm s^{-1})	ν_{O-O} $(\Delta\nu^d)$ (cm^{-1})	ν_{Fe-O} $(\Delta\nu^d)$ (cm^{-1})	J^b (cm^{-1})	g	References
Fe^{II}Fe^{II}	[Fe$_2$(μ-OAc)$_2$(TPA)$_2$]$^{2+}$ (**3**)	4.288(2)		1.12 (3.33)			−1		102
	[Fe$_2$(μ-OAc)$_2$[(μ-OH)$_2$(OAc)$_3$(C$_5$H$_5$N)$_2$] (**6**)	3.577(2)		1.30 (2.00)^c; 1.18 (2.96)^d			−0.2		105
	[Fe$_2$(μ-O$_2$CH)$_3$(O$_2$CH)(BIPhMe)$_2$] (**10a**)	3.5736(8)		1.26 (2.56); 1.25 (3.30)			−0.16(1)	~16	110,111
	[Fe$_2$(μ-O$_2$CPh)(μ-O$_2$CPh)(O$_2$CPh)(ImH)$_2$(MeOH)](**11a**)	3.609(4)		1.35 (3.04); 1.12 (2.83)			−0.51(2)		114
	[Fe$_2$(μ-XDK)(μ-O$_2$CCMe$_3$)(O$_2$CCMe$_3$)(N-MeIm)$_2$] (**12a**)	3.584(3)		1.34 (2.94); 1.15 (3.17)					114
	[Fe$_2$(μ-BXDK)(μ-O$_2$CPhCy)(O$_2$CPhCy)(C$_5$H$_5$N)$_2$] (**13a**)	3.5649(10)	~360	1.06 (2.56); 1.28 (3.01)^c; 1.10 (2.85); 1.34 (2.87)^d					118
	[Fe$_2$(μ-O$_2$CAr^{Tol})$_2$(O$_2$CAr^{Tol})$_2$(C$_5$H$_5$N)$_2$] (**15a**)	4.2189(10)	375 (1,100)	1.19 (3.02)			−0.9		120,125
	[Fe$_2$(μ-O$_2$CAr^{Tol})$_2$(O$_2$CAr^{Tol})$_2$(1-MeIm)$_2$] (**16**)	4.2029(10)^e; 4.1967(11)^f		1.19 (3.01)			−1.0		120,125
	[Fe$_2$(μ-O$_2$CAr^{Tol})$_4$(4-^{t}BuC$_5$H$_4$N)$_2$] (**17a**)	2.8229(9)	370 (1,400)	1.12 (3.05)					121,125
	[Fe$_2$(μ-O$_2$CAr^{Tol})$_2$(O$_2$CAr^{Tol})$_2$(N,N-Bn$_2$en)$_2$] (**18a**)	4.3598(8)		1.19 (2.90)					123,127
Fe^{III}Fe^{III}(μ-O$_2$)	[Fe$_2$(μ-O$_2$CPh)(TPDP)]$^{2+}$ (**28a**) + O$_2$		572 (2,060)		877, 893^{g,h} (−47)	453, 481^{g,i}			145
	[Fe$_2$(μ-O$_2$CPh)(Me$_4$-TPDP)]$^{2+}$ (**29a**) + O$_2$		616 (2,000)		918, 891^g	486, 450^g (−7~−8)			141
	[Fe$_2$(μ-O$_2$)(μ-O$_2$CPh)(Ph-BIMP)]$^{2+}$ (**30b**)	3.327(2)	500–800 (1,700)	0.58 (0.74); 0.65 (1.70)					146
	[Fe$_2$(μ-O$_2$CPh)(N-Et-HPTB)]$^{2+}$ (**31a**) + O$_2$		588 (1,500)		900 (−50)	476 (−16)			145
	[Fe$_2$(μ-O$_2$)(N-Et-HPTB(Ph$_3$P=O)$_2$]$^{3+}$ (**31b′**)	3.462(3)							147
	[Fe(O$_2$CPh)(HB(3,5-^{i}Pr$_2$pz)$_3$)] (**32a**) + O$_2$		682 (3,450)		876 (−49)	418 (−9)			148
	[Fe$_2$(μ-O$_2$)(μ-O$_2$CCH$_2$Ph)$_2$(HB(3,5-^{i}Pr$_2$pz$_3$))$_2$] (**33b**)	4.004(4)	694 (2,650)	0.66 (1.40)	888 (−46)	415 (−11)	−33		149
	[Fe$_2$(μ-BXDK)(μ-O$_2$CCMe$_3$)(O$_2$CCMe$_3$)(C$_5$H$_5$N)$_2$] (**34a**) + O$_2$		580 (1,200)		864				118
	[Fe$_2$(μ-BXDK)(μ-O$_2$CPhCy)(O$_2$CPhCy)(C$_5$H$_5$N)$_2$] (**13a**) + O$_2$		580 (1,500)		861 (−50)				118
	[Fe$_2$(μ-O$_2$CAr^{Mes})$_3$(O$_2$CAr^{Mes})(MeCN)$_2$] (**21a**) + O$_2$		540 (2,300)		885 (−14)				129
	[Fe$_2$(μ-O$_2$Cdxl)$_4$(C$_5$H$_5$N)$_2$] (**23a**) + O$_2$		500–550 (1,000–1,200)	0.65 (1.27); 0.71 (0.52)	822 (−43)		−25		133

Table 2 continued

Oxidation state	Compound	Fe···Fe (Å)	λ_{max} (ε) (nm (M^{-1} cm^{-1}))	$\delta(\Delta E_Q)$ (mm s^{-1})	ν_{O-O} $(\Delta\nu^a)$ (cm^{-1})	ν_{Fe-O} $(\Delta\nu^d)$ (cm^{-1})	J^b (cm^{-1})	g	References
	[Fe$_2$(μ-O)(O$_2$)(6-Me$_3$-TPA)$_2$]$^{2+}$ (**35b**)		490 (1,100); 640 (1,100)		848 ($-$46)	462 ($-$21)[j]; 531 ($-$21)[k]			151
	[Fe$_2$(μ-O)(O$_2$)(6-Me$_3$-TPA)$_2$]$^{2+}$ (**36b**)	3.14[l]	494 (1,100); 648 (1,200); 846 (230)	0.54 (1.68)	848 ($-$46)	462 ($-$21)			153
	[Fe$_2$(O$_2$)(O)(OAc)(HEXPY)]$^+$ (**37b**)		510 (1,300); 605 (1,310)	0.53 (1.67)	816 ($-$45)	472 ($-$17)	$-$55		155
	[Fe$_2$(μ-O)(PB)$_4$(H$_2$O)$_2$]$^{4+}$ (**38a**) + H$_2$O$_2$		680 (2,000)	0.49 (0.62)[m]; 0.43 (0.49); 0.23 (1.64)[n]	868 ($-$47)[m]; 806 ($-$46)[n]	483 ($-$23)[m]; 618 ($-$26)[n]			156,157
Fe^{III}Fe^{IV}(O)$_2$	[Fe$_2$(μ-O)$_2$(TPA)$_2$]$^{3+}$ (**39b**)		614 (5,500)						171
	[Fe$_2$(μ-O)$_2$(5-Me$_3$-TPA)$_2$]$^{3+}$ (**40b**)	2.683(1)	616 (5,200); 366 (7,900)	0.12(1) (0.49)				4.45; 3.90; 2.01	158,171
	[Fe$_2$(μ-O)$_2$(5-Et$_3$-TPA)$_2$]$^{3+}$ (**41b**)								159
	[Fe$_2$(O)$_2$(6-Me-TPA)$_2$]$^{3+}$ (**42b**)		350 (8,000)	0.48 (1.6); 0.08 (0.5)			<-40	2.00	160
	[Fe$_2$(μ-O)(O)(6-Me$_3$-TPA)$_2$]$^{3+}$ (**36d**)			0.50 (1.30); 0.10 (1.14)				1.999	151,153,161
	[Fe$_2$(μ-O$_2$CAr^{Tol})$_4$(4-^{t}BuC$_5$H$_4$N)$_2$] (**17a**) + O$_2$			0.56 (0.90); 0.19 (0.80)			<-100	1.986; 1.997; 2.011	121,126
Fe^{IV}Fe^{IV}(O)$_2$	[Fe$_2$(μ-O)$_2$(BPMCN)$_2$]$^{4+}$ (**43c**)	2.81[l]	656, 845	0.10 (1.75)			$|J|<2.5$		163

[a] $\Delta\nu$ = (ν of ^{16}O-labeled material) − (ν of ^{18}O-labeled material). [b] $\mathcal{H}=-2J\cdot S_1\cdot S_2$. [c] Solid sample. [d] Frozen solution sample. [e] Frozen solution sample. [f] 4,4-Coordinate isomer. [f] 5,5-Coordinate isomer. [g] Fermi doublet.
[h] Shifts to 834 cm^{-1} with ^{18}O$_2$. [i] Shifts to 444 cm^{-1} with ^{18}O$_2$. [j] ν_{sym}. [k] ν_{asym}. [m] Species (**38b**). [n] Species (**38b**).

electron lone pair. Upon exposure of (**10a**) to dioxygen, a green (μ-oxo)di-iron(III) complex [Fe$_2$(μ-O)(μ-O$_2$CH)$_2$(O$_2$CH)$_2$(BIPhMe)$_2$] (**10b**) was obtained in a nearly quantitative yield, in which an O$_2$-derived oxygen atom was incorporated as an oxo bridging group. The mechanistic implications of this conversion are described in Section 8.13.5.5.

8.13.5.2.3 Di-iron(II) complexes of dicarboxylate ligands XDK′

A cleft-shaped dinucleating ligand derived from Kemp's triacid, XDK,[112,113] and its analogues (XDK′)[114,115] have been used to stabilize coordinatively unsaturated di-iron(II) complexes. The robust doubly bridging units in XDK have reduced conformational degrees of freedom, lowering the entropic barrier to metal binding.[116] Consequently, discrete carboxylate-rich di-iron(II) complexes could be accessed without resorting to chelating *N*-donor ligands that often fill the terminal positions and preclude open coordination sites required for O$_2$ binding (Section 8.13.5.2.1). A versatile synthetic route was developed for XDK′ di-iron(II) complexes, which facilitated access to a wide variety of di-iron(II) compounds having ligand type and compositions exactly matching those in MMOH, RNR-R2, and Δ9D in their di-iron(II) states. Earlier attempts to access such units resulted in triply carboxylate-bridged di-iron(II) complexes [Fe$_2$(μ-XDK)(μ-O$_2$CPh)(O$_2$C-Ph)(ImH)$_2$(MeOH)] (**11a**) and [Fe$_2$(μ-PXDK)(μ-O$_2$CCMe$_3$)(O$_2$CCMe$_3$)(*N*-MeIm)$_2$] (**12a**) by self-assembly from iron(II) salts and ligand fragments.[114,117] A more efficient synthetic route was developed later, in which preassembled mononuclear iron(II) compounds [Fe(μ-XDK′)(NC$_5$H$_5$)$_2$] were prepared and subsequently allowed to react with [Fe(O$_2$CR)$_2$(NC$_5$H$_5$)$_n$] units generated *in situ*.[118] The resulting tetra(carboxylato)di-iron(II) complexes share the generic structural formula [Fe$_2$(μ-XDK′)(μ-O$_2$CR)(O$_2$CR)(NC$_5$H$_5$)$_2$]. Analogues having other *N*-donor ligands were also prepared. Different combinations of carboxylate and *N*-donor ligands could be accommodated within the {Fe$_2$(μ-XDK′)}$^{2+}$ platform, allowing analysis of the steric and electronic factors responsible for the resulting structures and reactivity properties. The XDK′ di-iron(II) complexes have one six-coordinate and one four- or five-coordinate iron atoms, the coordination number of the latter depending on the stereoelectronic demand of the ancillary carboxylate (RCO$_2^-$) and *N*-donor ligands. With an increase in the steric repulsion between RCO$_2^-$ and XDK′, as well as the *N*-donor strength, gradual shifts in RCO$_2^-$ coordination were observed.

As in RNR-R2 and Δ9D, very weak AF coupling was observed for (**11a**). Two inequivalent iron(II) centers in (**11a**) result in two overlapping quadrupole doublets in the Mössbauer spectra (Table 2). Essentially identical Mössbauer spectra were obtained for (**12a**) either in the solid state or in frozen THF solutions, indicating retention of structural integrity in solution. In contrast, the two distinct quadrupole doublets of solid [Fe$_2$(μ-BXDK)(μ-O$_2$CPhCy)(O$_2$CPhCy)(NC$_5$H$_5$)$_2$] (**13a**) become less resolved in frozen THF, indicating changes in the primary coordination sphere electronic environment. Migration of the carboxylate ligand may have afforded similar EFGs for the two iron(II) centers.

H$_2$XDK; R = CH$_3$
H$_2$PXDK; R = (CH$_2$)$_2$CH$_3$
H$_2$BXDK; R = CH$_2$C$_6$H$_5$

PhCyCO$_2$H

XDK′
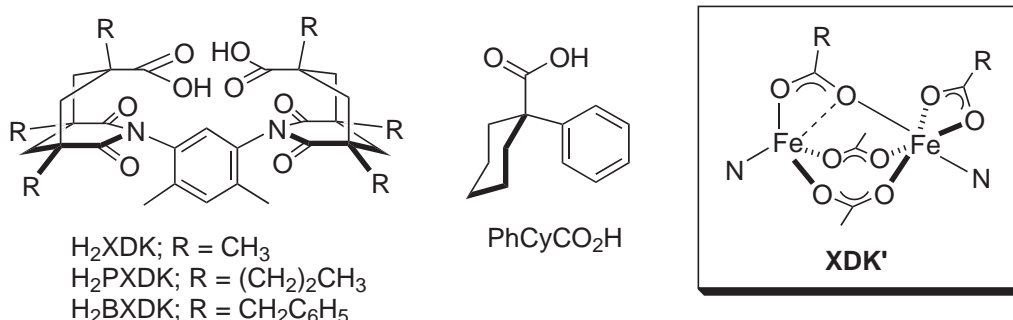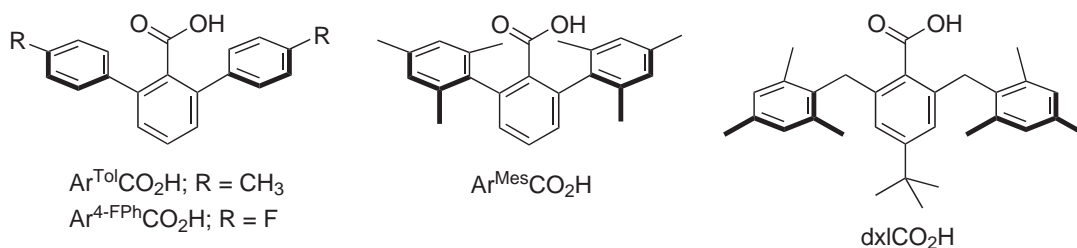
Scheme 9

Scheme 10

8.13.5.2.4 Di-iron(II) complexes of m-terphenyl carboxylate ligands

Sterically encumbered carboxylate ligands derived from a *m*-terphenyl framework support coordinatively unsaturated tetra(carboxylato)di-iron(II) complexes having two additional *N*-donor groups, affording ligand compositions identical to those in the nonheme di-iron enzyme active sites.[119] Steric crowding and the pseudo-C_2 symmetry within the ligands $Ar^{Tol}CO_2^-$, $Ar^{4-FPh}CO_2^-$, or $Ar^{Mes}CO_2^-$ (Scheme 10) promote *trans* disposition of the μ-1,3 bridging carboxylate ligands, similar to the situation in RNR-R2 and Δ9D.[120–131] Four interlocking carboxylate ligand modules in $[Fe_2(O_2CAr')_4L_2]$ ($Ar' = Ar^{Tol}$, Ar^{4-FPh}, Ar^{Mes}) emulate the hydrophobic cavity around the enzyme active sites and afford noncovalent interactions in the secondary coordination sphere (Figure 3).

The versatile synthetic precursor compounds $[Fe_2(\mu-O_2CAr')_2(O_2CAr')_2(THF)_2]$ ($Ar' = Ar^{Tol}$, Ar^{4-FPh}) facilitated the generation of a wide variety of $[Fe_2(O_2CAr')_4L_2]$ complexes by ligand substitution reactions.[120,125] By varying both carboxylate and *N*-donor ligands, either doubly bridged (*windmill*) or quadruply bridged (*paddlewheel*) di-iron(II) complexes were accessed. Windmill compounds $[Fe_2(\mu-O_2CAr^{Tol})_2(O_2CAr^{Tol})_2(NCMe)_2]$ (**14**), $[Fe_2(\mu-O_2CAr^{Tol})_2$-$(O_2CAr^{Tol})_2(NC_5H_5)_2]$ (**15a**), and $[Fe_2(\mu-O_2CAr^{Tol})_2(O_2CAr^{Tol})_2(1-MeIm)_2]$ (**16**) closely mimic the geometric properties of the catalytic sites in Δ9D and RNR-R2. Relatively long Fe···Fe distances of 3.9602(13)−4.2189(13) Å are spanned by two μ-1,3 bridging carboxylate ligands (Table 2). Either bidentate (for (**14**) and (**15a**)) or monodentate (for (**16**)) coordination of the terminal carboxylates and the presence of two *N*-donor ligands emulate the enzyme core structures (Figure 1). Paddlewheel di-iron(II) compounds such as $[Fe_2(\mu-O_2CAr^{Tol})_4(4-^tBuC_5H_4N)_2]$ (**17a**) display significantly shortened Fe···Fe distances ranging between 2.7277(7) and 2.8475(7) Å in the solid state. Further elaboration of the $Ar^{Tol}CO_2^-$ system afforded $[Fe_2(\mu-O_2CAr^{Tol})_2(O_2CAr^{Tol})_2$-$(N,N-Bn_2en)_2]$ (**18a**), in which oxidizable C—H bonds were installed in the form of two benzyl groups tethered to the ethylenediamine ligand.[123,127] The Mössbauer and magnetic parameters of (**15a**)–(**18a**) are comparable to those of the nonheme di-iron enzymes (Table 2).

Variable-temperature ^{19}F NMR spectroscopic studies of $[Fe_2(O_2CAr^{4-FPh})_4(THF)_2]$ (**19**) from $+20\,°C$ to $-80\,°C$ revealed dynamic interconversion between *windmill* and *paddlewheel* isomers via carboxylate shifts.[125] Structural characterization of two geometric isomers of (**19**), $[Fe_2(\mu-O_2CAr^{4-FPh})_2$-
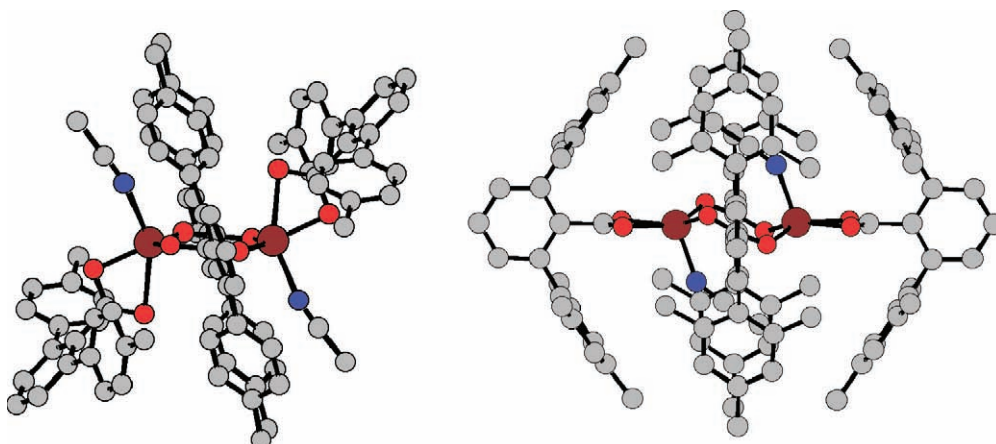
Figure 3 Structures of (**14**) (left) and (**21a**) (right) generated using the crystallographic coordinates.

windmill **paddlewheel**
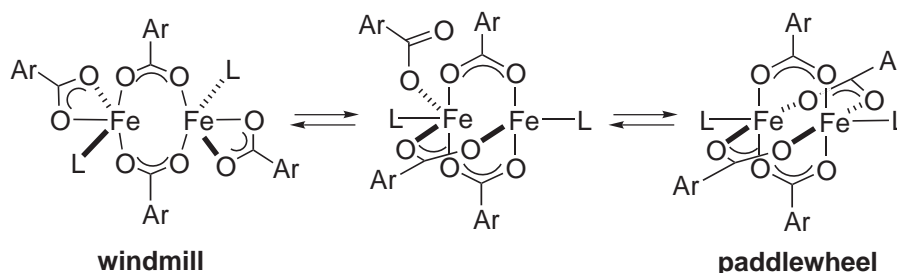
Scheme 11

$(O_2CAr^{4-FPh})_2(THF)_2]$ and $[Fe_2(\mu\text{-}O_2CAr^{4-FPh})_4(THF)_2]$, as well as the triply bridged di-iron(II) complex $[Fe_2(\mu\text{-}O_2CAr^{Tol})_3(O_2CAr^{Tol})(2,6\text{-lutidine})]$ (**20**), supports the mechanistic model depicted in Scheme 11. At lower temperatures, the solution population is dominated by the paddlewheel isomer, consistent with its favored energetics as determined by theoretical studies.[132] Possible mechanisms for the core interconversion were also examined by DFT calculations. Ligand migration within $[Fe_2(O_2CAr')_4L_2]$ facilitates opening of a coordination site for an incoming dioxygen molecule. A conceptual linkage can be drawn to the nonheme di-iron enzymes, in which similar carboxylate shifts may be elicited by binding of substrate (for $\Delta 9D$) or a coupling protein (for MMOH), and priming the di-iron(II) center for O_2 binding (*vide supra*).

Depending on the choice of N-donor ligand, either dinuclear or mononuclear iron(II) complexes can be assembled with $Ar^{Mes}CO_2^-$.[129,131] A di-iron(II) complex $[Fe_2(\mu\text{-}O_2CAr^{Mes})_2(O_2CAr^{Mes})_2\text{-}(NCMe)_2]$ (**21a**) was obtained, in which five-coordinate iron atoms are separated by 4.122(1) Å and bridged by two $\mu\text{-}1,3$ carboxylate ligands (Figure 3).[129] Two bidentate terminal carboxylates and two N-donor ligands fill the remaining coordination sites, as in the di-iron(II) forms of $\Delta 9D$ and $Ar^{Tol}CO_2^-$ complexes.[17,120,125] Notable structural disparity exists, however, between the $Ar^{Tol}CO_2^-$ and $Ar^{Mes}CO_2^-$ systems. Unlike $Ar^{Tol}CO_2^-$, significantly restricted aryl–aryl rotation in $Ar^{Mes}CO_2^-$ results in the orthogonal disposition of the four carboxylate ligands, an arrangement that minimizes interligand steric crowding (Figure 3). The iron atoms thus adopt square pyramidal geometry with MeCN as an axial ligand that can fill the crowded space walled in by the mesityl fragments. Use of N-donor ligands bigger than MeCN, such as pyridine or 1-MeIm, result in core disassembly to form mononuclear species.[131] The conformational rigidity in the $Ar^{Mes}CO_2^-$ groups can be reduced by adding methylene linkages between each adjacent aryl units. One such ligand, $dxlCO_2^-$, was used to assemble a series of paddlewheel di-iron(II) complexes $[Fe_2(\mu\text{-}O_2Cdxl)_4L_2]$ (L = THF (**22a**), C_5H_5N (**23a**), 1-MeIm (**24a**)) having less compact core structures.[133] Despite compositional and architectural similarities, the O_2 reaction chemistry of the $dxlCO_2^-$ di-iron(II) complexes (**22a**)–(**24a**) deviates significantly from that afforded by the $Ar^{Tol}CO_2^-$ compounds (**15a**) and (**17a**) (Section 8.13.5.3).

8.13.5.2.5 De novo *protein design*

The molecular middle ground between nonheme di-iron enzymes and their small molecule synthetic analogues has been explored by *de novo* protein design. A protein can be designed to fold into a predetermined tertiary structure without patterning the sequence after any natural protein.[134–136] A homodimer of two helix-loop-helix motifs was devised that assembles around a two-fold axis penetrating the center of the metal-binding site. In this approach, one helix in each monomer includes a Glu-Xxx-Xxx-His sequence, while the other contains a single Glu ligand. Placement of these residues in the appropriate sequence afforded a minimal idealized version of a di-iron protein, a 48-residue synthetic peptide DF1. DF1 binds zinc(II), cobalt(II), and iron(II), and the dizinc(II) form of DF1 (**25**) has been structurally characterized (Figure 4).[137] The metallopeptide (**25**) adopts the conformation of an antiparallel pair of helical hairpins and houses two zinc(II) ions bridged by two $\mu\text{-}1,3$ Glu residues. One His and one bidentate Glu group complete the coordination spheres, yielding symmetry-related five-coordinate metal centers, similarly to the di-iron(II) center in $\Delta 9D$. The metal···metal distance of 3.9 Å in (**25**) is close to the distances observed for $\Delta 9D$ and RNR-R2. The crystal structure also revealed the specific hydrogen-bonding interactions in the second coordination sphere.
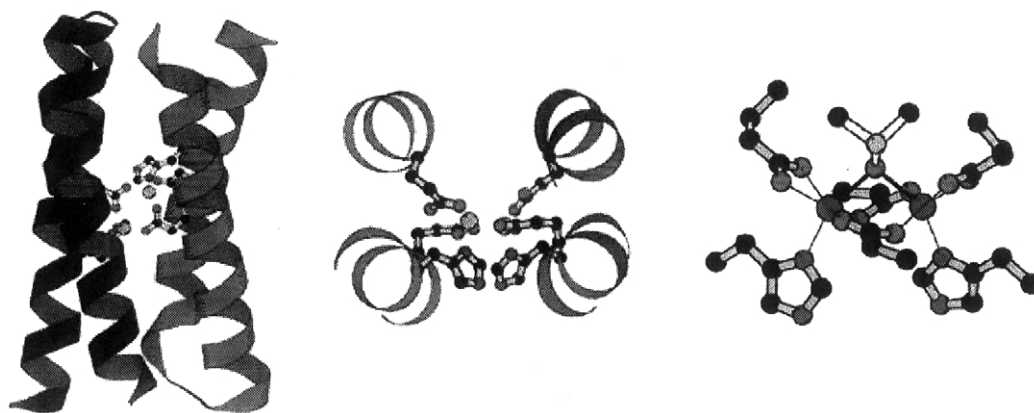
Figure 4 X-ray structures of (**25**) (left), dizinc(II) core of (**25**) (center), and dimanganese(II) core of (**27**) (right) (reproduced with permission from ref. 139; © 2001 American Chemical Society).

In order to enhance water solubility and promote substrate access to the dimetallic center, a structurally related second-generation protein, DF2, was prepared.[138] Unlike DF1, DF2 was expressed in *E. coli*, facilitating preparation of mutants and biosynthetic labeling for NMR spectroscopic studies. DF2 reconstituted with iron(II) (**26**) displays ferroxidase activity and affords a (μ-oxo)di-iron(III) core, as judged by UV-vis absorption features at 300–350 nm and 400–700 nm.[138,139] Addition of N_3^- or AcO^- induced spectral shifts, indicating ligand binding. An analogue of DF2 coordinates manganese(II) and the resulting metallopeptide (**27**) was structurally characterized.[139] The dimanganese(II) center in (**27**) lies at the bottom of a deep, water-filled pocket and adopts a geometry analogous to that of the dizinc(II) site in (**25**). An exogenous bridging ligand was also identified, the electron density of which was modeled as a μ-1,1 bridging DMSO. The Mn···Mn distances in the crystallographically independent dimers ranged between 3.6 Å and 3.9 Å. A heterotetrameric version of DF1, $A_aA_bB_2$, was constructed by noncovalent self-assembly of three different helices A_a, A_b, and B.[140] Upon exposure to O_2, $A_aA_bB_2$ loaded with iron(II) develops a strong ($\varepsilon = 1,000 \, M^{-1} \, cm^{-1}$) chromophore centered at 625 nm, properties reminiscent of those of (peroxo)di-iron(III) species (Tables 1 and 2).

8.13.5.3 Spectroscopic Models of Key O₂ Reaction Intermediates

The transient nature of spectroscopically detected reaction intermediates in the reaction cycle of nonheme di-iron enzymes makes it difficult to obtain detailed structural information. Characterization of biomimetic O_2-adducts derived from synthetic systems facilitates our understanding of the electronic and geometric structures of their biological counterparts.[6,90] Within synthetic platforms, (peroxo)di-iron(III) species can be accessed either by oxygenation of mono- or di-iron(II) complexes or by reaction of di-iron(III) complexes with hydrogen peroxide. Formation of high-valent iron(III)iron(IV) species proceeds either via biomimetic one-electron reduction of the (peroxo)di-iron(III) core or by one-electron chemical oxidation of a di-iron(III) precursor. Decomposition of an alkylperoxoiron(III) adduct can afford a di-iron(IV) species.

8.13.5.3.1 (Peroxo)di-iron(III) complexes

Dinucleating ligands having alkoxide or phenoxide bridging groups support (peroxo)di-iron(III) cores. Built on either 1,3-diaminopropan-2-oxide or 2,6-bis(aminomethyl)phenoxide spacer units, TPDP, HPTB, and BIMP ligand derivatives (Figure 2) allow systematic variations in ligand steric and electronic factors that modulate dioxygen binding affinity.[141–144]

In solution, dissociation of the H_2O ligand in $[Fe_2(\mu\text{-}O_2CR)(TPDP')(H_2O)_n]^{2+}$ (TPDP′ = TPDP (**28a**), Me₄-TPDP (**29a**)) generates 5,5-coordinate di-iron(II) complexes that react with dioxygen to afford (peroxo)di-iron(III) species (Table 2).[141,145] By increasing the number of α-methyl substituents on the pyridine rings (TPDP < Me₂-TPDP < Me₄-TPDP), the thermal stability of the dioxygen-adducts is enhanced. Steric shielding provided by the methyl groups apparently suppresses bimolecular decomposition. Decreased electron donation from the
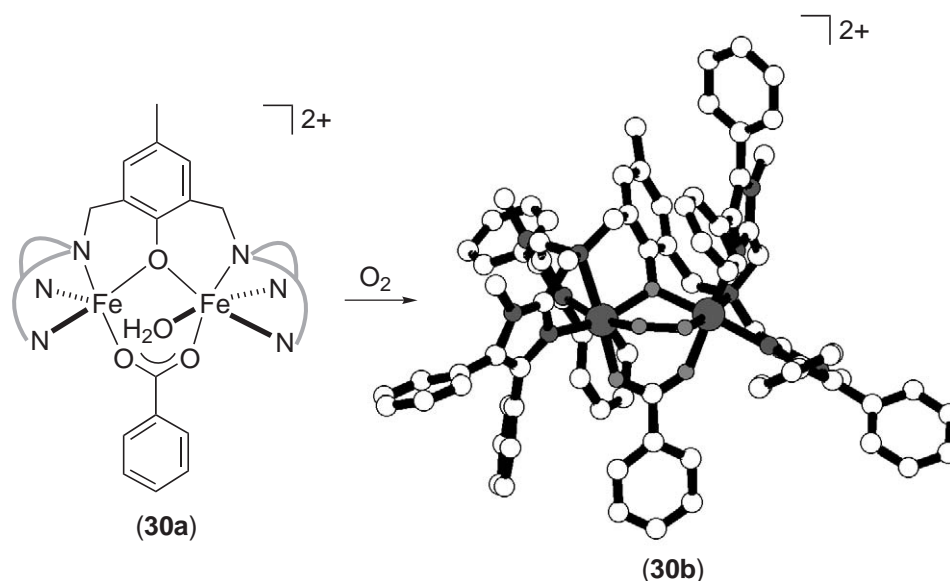
Scheme 12

sterically encumbered TPDP ligand derivatives is manifest in the oxidation potentials, which display positive shifts with increasing number of α-methyl groups, as well as in the elongated Fe—N distances observed in the homologous series.[141,143] With proper choice of ancillary ligands, oxygenation of the di-iron(II) complexes could be made reversible at low temperatures. Dioxygen affinity increases with better electron-donating carboxylate ligands ($C_6H_5CO_2^- > C_6F_5CO_2^- > CF_3CO_2^-$) in the Ph-TIDP di-iron(II) complexes.[143]

The sterically more encumbered Ph-BIMP ligand supports a (peroxo)di-iron(III) complex that is stable at room temperature.[146] Oxygenation of $[Fe_2(\mu\text{-}O_2CPh)(Ph\text{-}BIMP)]^{2+}$ (**30a**) in MeCN at 20 °C affords a dark green intermediate, characterized as a (μ-1,2-peroxo)di-iron(III) complex $[Fe_2(\mu\text{-}O_2)(\mu\text{-}O_2CPh)(Ph\text{-}BIMP)]^{2+}$ (**30b**) (Scheme 12; Table 2). Remarkably, oxygenation of (**30a**) is reversible, as demonstrated by its quantitative regeneration by boiling the MeCN solution of (**30b**) under N_2. Spectrophotometric titration of (**30b**) under partial O_2 pressure revealed a dioxygen affinity significantly ($\sim 2 \times 10^3 - 3 \times 10^4$ times) larger than those of either TPDP or Ph-TIDP di-iron(II) complexes. Preorganized ligand conformation apparently facilitates dioxygen binding, in which a minimal structural perturbation is introduced in the interconversion between oxy and deoxy forms. In contrast, a substantial shortening of the Fe $\cdots$ Fe distance would be required for the formation of (peroxo)di-iron(III) species from 1,3-diaminopropan-2-oxide supported di-iron(II) complexes, which have expanded Fe $\cdots$ Fe lengths ($> \sim 3.45$ Å).

A di-iron(II) complex $[Fe_2(\mu\text{-}O_2CPh)(N\text{-}Et\text{-}HPTB)]^{2+}$ (**31a**), structurally related to (**28a**)–(**30a**), irreversibly binds one equivalent of dioxygen at -60 °C in CH_2Cl_2 to afford an intensely purple-blue colored species (**31b**) (Table 2).[145] Substitution with more electron-donating carboxylate ligands results in a blue shift of the peroxide-to-iron(III) LMCT band, indicating that the carboxylate ligand remains coordinated upon O_2-adduct formation. The thermal stability of the O_2-adducts could be significantly enhanced in the presence of polar aprotic solvents such as DMSO, DMF, and N,N-dimethylacetamide, or by added $O=PPh_3$. Formal extrusion of the bridging $PhCO_2^-$ and coordination of two $O=PPh_3$ molecules to (**31b**) results in the formation of $[Fe_2(\mu\text{-}O_2)(N\text{-}Et\text{-}HPTB)(O=PPh_3)_2]^{3+}$ (**31b'**).[147] The X-ray structure of (**31b'**)·$(BF_4)_3$ has been determined, revealing the presence of a μ-1,2-peroxide ligand spanning a doubly bridged core with Fe $\cdots$ Fe $= 3.462(2)$ Å (Scheme 13).

A mononuclear iron(II) complex $[Fe(O_2CPh)\{HB(3,5\text{-}^iPr_2pz)_3\}]$ (**32a**) reacts with O_2 in toluene at -50 °C to afford an intense bluish green species (**32b**).[148] Binding of dioxygen can be reversible at -20 °C, as evidenced by cycling (> 10 times) between (**32a**) and (**32b**) with Ar-purging/O_2-exposure. Oxygenation at room temperature, however, resulted in an irreversible color change to reddish brown. Resonance Raman spectroscopy of (**32b**) revealed two isotope-sensitive vibrations assigned as ν_{O-O} and ν_{Fe-O} (Table 2), providing convincing evidence for the presence of a (μ-1,2-peroxo)di-iron(III) fragment. This proposal was supported further by the dioxygen uptake
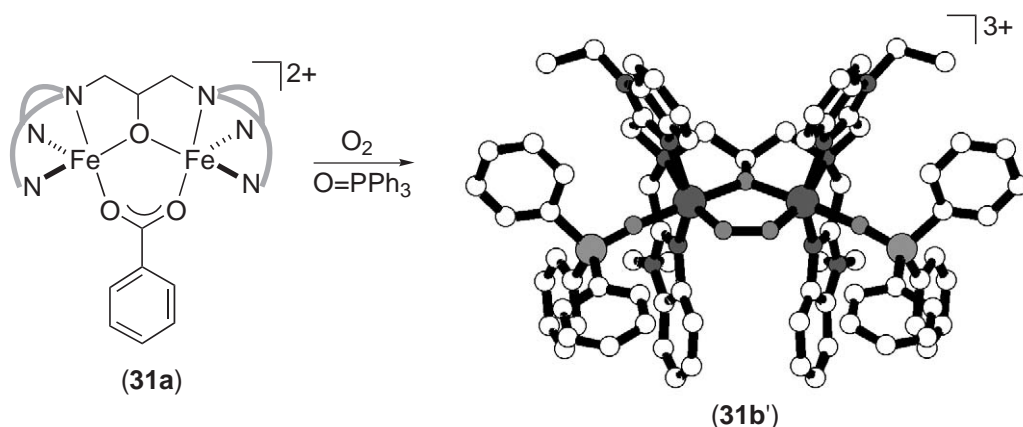
Scheme 13
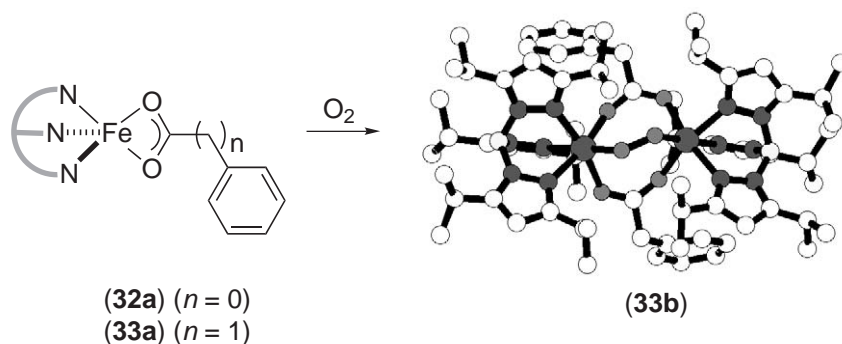
Scheme 14

stoichiometry of 2:1 for [Fe]:O_2. An AF interaction between two HS iron(III) centers resulted in a significantly narrower distribution of ^{1}H NMR signals compared with those of the paramagnetic HS iron(II) starting material. The structure of (**32b**) deduced from EXAFS analysis comprises a (μ-peroxo)di-iron(III) core with an Fe—O—O—Fe dihedral angle of $\sim 90°$ and Fe$\cdots$Fe separation of 4.3 Å. From the thermolysis of (**32b**) was obtained in low yield ($\sim 20\%$) a trinuclear iron(III) complex, [{HB(3,5-^{i}Pr$_2$pz)}Fe(μ-OH)(μ-O$_2$CPh)$_2$Fe(μ-O)(μ-O$_2$CPh)$_2$Fe{HB(3,5-^{i}Pr$_2$pz)}].

An analogue of (**32a**) having an α-phenylacetate ligand, [Fe(O$_2$CCH$_2$Ph){HB(3,5-^{i}Pr$_2$pz)}] (**33a**), reacts with O_2 in pentanes at $< -50\,°C$ to afford a thermally sensitive O_2-adduct [Fe$_2$(μ-O$_2$)-(μ-O$_2$CCH$_2$Ph)$_2${HB(3,5-^{i}Pr$_2$pz)}$_2$] (**33b**) having spectroscopic properties comparable to those of (**32b**) (Scheme 14; Table 2).[149] An X-ray structural determination of (**33b**) revealed a triply bridged di-iron(III) core, in which an Fe$\cdots$Fe distance of 4.004(4) Å is spanned by one μ-1,2 peroxide and two μ-1,3 carboxylate ligands. This arrangement differs from that proposed for (**32b**) from the EXAFS analysis. Notably, the Fe—O—O—Fe dihedral angle of 52.9° in (**33b**) distinguishes it from (**30b**) and (**31b'**), in which the presence of an additional single-atom bridge constrains the (μ-peroxo)di-iron(III) unit to near planarity. At 4.2 K, a frozen toluene solution of (**33b**) displays a Mössbauer spectrum with a sharp quadrupole doublet having $\delta = 0.66$ and $\Delta E_Q = 1.40\ \mathrm{mm\ s^{-1}}$. This unusually large isomer shift for a HS iron(III) center matches those of the peroxo intermediates in the catalytic cycles of MMOH and RNR-R2 (Table 1), suggesting the presence of similarly structured (peroxo)di-iron(III) units in the biological systems. Detailed spectroscopic and theoretical studies of (**32b**) were carried out.[150] The high ν_{O-O} of 876 cm^{-1} in (**32b**), compared with the values obtained for other (peroxo)di-iron(III) compounds (Table 2), results from substantial mechanical coupling between Fe—O and O—O stretching motions, not from a strong O—O bond. The coupling strength critically depends on the Fe—O—O bond angle. A π-bonding interaction between iron and peroxide ligand opens up the Fe—O—O angle, which

translates into increase in the O—O stretching frequency. The basic/nucleophilic character of the peroxide ligand was identified by DFT calculations.

XDK di-iron(II) complexes react with dioxygen to afford spectroscopically characterized (peroxo)di-iron(III) species. Compound (**11a**) converts to a deep green metastable intermediate (**11b**) upon reaction with O_2 in THF at $-78\,^\circ$C.[114] The development and decay of (**11b**) was traced with stopped-flow kinetic experiments. Buildup of a broad band was observed at 660 nm, a value reminiscent of the (μ-peroxo)di-iron(III) species. The significantly lower extinction coefficient ($\sim 170\,M^{-1}\,cm^{-1}$) of (**11b**) compared with those of well-characterized peroxo species (Table 2), however, indicates rapid decay of the chromophore before its full development. Use of a sterically more demanding ligand BXDK significantly enhanced the stability of the intermediate.[118] A blue intermediate (**34b**) ($\lambda_{max}\ \sim 580$ nm; $\varepsilon \sim 1{,}200\,M^{-1}\,cm^{-1}$) develops upon exposure of [$Fe_2(\mu$-BXDK$)(\mu$-$O_2CCMe_3)(O_2CCMe_3)(NC_5H_5)_2$] (**34a**) to dioxygen at $-78\,^\circ$C in solvents such as CH_2Cl_2, toluene, or THF. In conjunction with bulky carboxylate ligands such as $PhCyCO_2^-$ or 2,4,6-triisopropylbenzoate, the sterically less demanding XDK ligand can also stabilize analogous peroxo species under similar conditions. Dioxygen uptake (1.0 ± 0.1 equiv. O_2 per [Fe_2]), EPR ($S_{ground} = 0$ at 4.5 K), resonance Raman, and Mössbauer spectroscopic data are fully consistent with the formation of (peroxo)di-iron(III) species having inequivalent metal centers. Kinetic experiments conducted at $-77\,^\circ$C revealed first-order dependence of the peroxo formation on [Fe_2] and [O_2], indicating that the rate-determining step is bimolecular collision between the two reactants. An increase in the second-order rate constants with increasing steric demand of RCO_2^- and XDK′ implicates carboxylate shifts to open an O_2-binding site, processes facilitated by interligand steric crowding. Use of more electron-donating *N*-alkylimidazole derivatives significantly accelerated the oxygenation reaction. A mechanistic model was proposed, in which slow carboxylate shifts occur concomitant with O_2 binding. Rapid collapse of the initial adduct affords a (μ-peroxo)di-iron(III) species with inherent asymmetry rendered by the arrangement of the carboxylate ligands.[118]

The $Ar^{Mes}CO_2^-$-supported tetra(carboxylato)di-iron(II) complex (**21a**) reacts with O_2 in CH_2Cl_2 at $-50\,^\circ$C to afford a diamagnetic purple species (**21b**) (Table 2).[129] A resonance-enhanced vibration was observed at 885 cm^{-1}, which shifted by 14 cm^{-1} upon the use of $^{18}O_2$. Although (**21b**) was assigned as (μ-peroxo)di-iron(III) species, the observed $\Delta\nu_{O—O}$ of 14 cm^{-1} is significantly lower than that (51 cm^{-1}) expected from a diatomic oscillator. Although stable at $-50\,^\circ$C for up to 12 h, (**21b**) decays slowly ($t_{1/2} \sim 30$ h) to a brown species at 25 $^\circ$C. This unusual behavior was ascribed to the interdigitating ligand framework encapsulating the di-iron center. When oxygenation was conducted at $-30\,^\circ$C in the presence of excess ^iPrOH, a blue solution was obtained ($\lambda_{max} = 780$ nm; $\varepsilon \sim 2{,}000\,M^{-1}\,cm^{-1}$).[130] Depending on the crystallization conditions, two chemically equivalent but structurally distinct neutral iron(II)iron(III) complexes (**21c**) and (**21c′**) could be obtained, which share the structural formula of [$Fe_2(\mu$-$O^iPr)_2(\mu$-$O_2CAr^{Mes})$-($O_2CAr^{Mes})_2$] (Scheme 15). Notably, the orientation of the bridging isopropoxide ligand relative to the Fe—Fe vector affects the Fe···Fe separation, which translates into valence-delocalized and valence-trapped di-iron cores in (**21c**) and (**21c′**), respectively. Outer-sphere one-electron transfer from O_2 presumably affords the mixed valence species, which, in the presence of excess dioxygen, decomposes to form the di-iron(III) complex [$Fe_2(\mu$-$O^iPr)_2(O_2CAr^{Mes})_4$] (**21d**) by incorporating an additional $Ar^{Mes}CO_2^-$ ligand.[130]
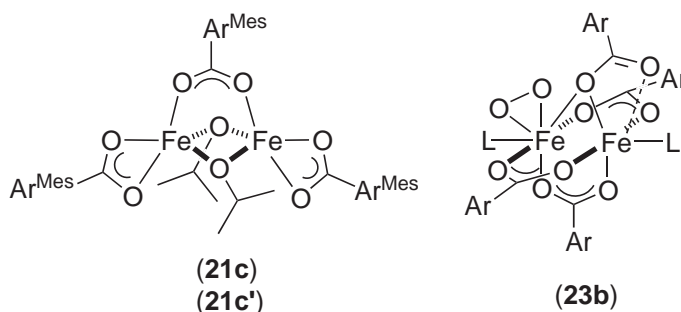
Scheme 15
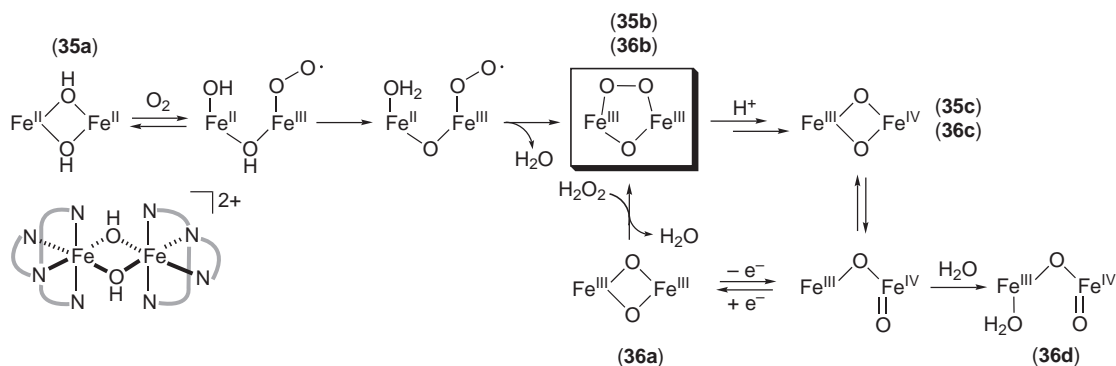
Scheme 16

Paddlewheel tetra(carboxylato)di-iron(II) complexes $[Fe_2(\mu-O_2Cdxl)_4L_2]$ (**22a**)–(**24a**) react with dioxygen at $-80\,^\circ$C to yield deep red-brown diamagnetic intermediates ($\lambda_{max} = 500$–550 nm; $\varepsilon = 1,000$–$1,200$ M^{-1} cm^{-1}).[133] Structural information obtained by resonance Raman and Mössbauer spectroscopy of (**23b**) (Table 2), derived from (**23a**), suggested an unusual $\{Fe^{III}-X-Fe^{III}(\eta^2-O_2)\}$ coordination mode as shown in Scheme 15.

Oxygenation of a coordinatively saturated di-iron(II) complex $[Fe_2(\mu-OH)_2(6\text{-Me}_3\text{-TPA})]^{2+}$ (**35a**) in CH$_2$Cl$_2$ at $-40\,^\circ$C leads to a diamagnetic green species (**35b**) (Scheme 16, Table 2) formulated as $[Fe_2(\mu-O)(O_2)(6\text{-Me}_3\text{-TPA})_2]^{2+}$ based on ESI-MS.[151,152] An essentially identical (peroxo)di-iron(III) species (**36b**) could be accessed by treating an MeCN solution of the di-iron(III) compound $[Fe_2(\mu-O)_2(6\text{-Me}_3\text{-TPA})_2]^{2+}$ (**36a**) at $-40\,^\circ$C with two equiv. of H$_2$O$_2$.[153] The spectroscopic properties displayed by this transient dark green species (**36b**) is also consistent with the (peroxo)di-iron(III) assignment (Table 2). The geometric parameters of Fe$\cdots$Fe $= 3.14$ Å and Fe—O $= 1.85$ Å deduced from EXAFS studies are consistent with the presence of a symmetric (μ-oxo)(μ-1,2-peroxo)di-iron(III) core.

A similar peroxide shunt route from a coordinatively saturated di-iron(III) complex $[Fe_2(\mu-O)(\mu-OAc)_2(HEXPY)]^{2+}$ (**37a**)[154] (HEXPY $=$1,2-bis[2-bis(2-pyridylmethyl)-6-pyridyl]ethane) resulted in the (peroxo)di-iron(III) species (**37b**) (Table 2),[155] which is stable at room temperature in the solid state. Elemental analysis and FAB-MS spectral data obtained for a dark purple species generated by treating (**37a**) with H$_2$O$_2$/Et$_3$N at $-30\,^\circ$C match those expected for $[Fe_2(O_2)(O)(OAc)(HEXPY)](OTf)\cdot 5H_2O$.

Reaction between a (μ-oxo)di-iron(III) complex and H$_2$O$_2$ at low temperatures generated two different (μ-peroxo)di-iron(III) species. Upon treating with 50 equiv. of H$_2$O$_2$ a MeCN solution of $[Fe_2(\mu-O)(PB)_4(H_2O)_2]^{4+}$ (**38a**) at $-40\,^\circ$C developed a broad CT band centered at 680 nm ($\varepsilon = 2,000$ M^{-1} cm^{-1}).[156,157] The appearance of two pairs of isotope-sensitive vibrations (Table 2) indicated the presence of two distinct peroxo species (**38b**) and (**38b**$'$) (Scheme 17). Analyses of field-dependent Mössbauer and multifrequency HF-EPR spectra indicated the presence of an $S = 0$ peroxo species arising from AF-coupled HS Fe^{III} centers, as well as an $S = 2$ peroxo species resulting from AF-coupling between LS Fe^{III} and HS Fe^{III} ions. This assignment was substantiated further by ESI-MS of (**38b**) and (**38b**$'$). A (peroxo)di-iron(III) species with such an asymmetric spin configuration has not been observed in biological systems.
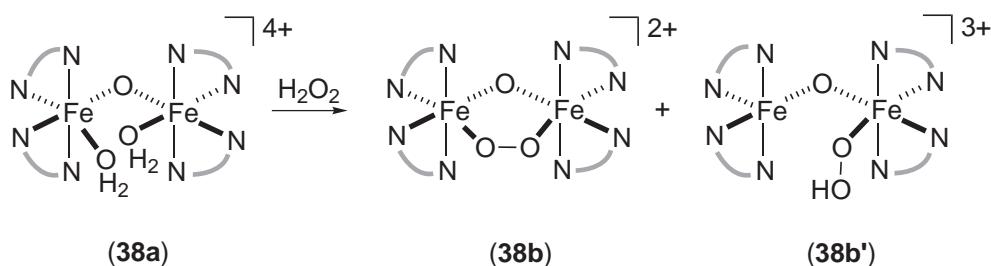
Scheme 17

8.13.5.3.2 *Iron(III)iron(IV) complexes: models of RNR-R2 intermediate X*

Although not biomimetic from a structural point of view, the tetradentate tripodal TPA ligand and its ring-alkylated or ring-fused derivatives (Figure 2) support iron(III)iron(IV) compounds relevant to intermediate X in the RNR-R2 reaction cycle. High-valent iron(III)iron(IV) species (**39b**)–(**41b**) were generated by treating the corresponding di-iron(III) precursor compounds $[Fe_2(\mu\text{-}O)(OH)(H_2O)(TPA')_2]^{3+}$ ($TPA' = TPA$ (**39a**), 5-Me$_3$-TPA (**40a**), 5-Et$_3$-TPA (**41a**)) with H_2O_2 in MeCN at $-40\,°C$.[158] A green solid material (**40b**) derived from (**40a**) was characterized spectroscopically. In (**40b**), the valence-delocalized, double exchange-coupled LS iron(III)–LS iron(IV) pair gave rise to an $S = 3/2$ ground spin state (Table 2). The formulation of (**40b**) as the $[Fe_2(O)_2(5\text{-Me}_3\text{-TPA})_2]^{3+}$ cation was consistent with the elemental analysis and ESI-MS. The presence of an $\{Fe_2(\mu\text{-}O)_2\}^{3+}$ rhombic core fragment in (**40b**) was indicated by the EXAFS data analysis, which required a Fe···Fe separation of 2.89 Å. Isotope-sensitive Fermi doublets associated with the Fe_2O_2 breathing mode appeared at $676\,cm^{-1}$ and $656\,cm^{-1}$ in the solution sample. A quasi-reversible one-electron reduction at $E_{1/2} = 0.96$ V (vs. NHE) was monitored by cyclic voltammetry of (**40b**).

Diffraction quality crystals were obtained for $[Fe_2(\mu\text{-}O)_2(5\text{-Et}_3\text{-TPA})_2](ClO_4)_3$ ((**41b**)·$(ClO_4)_3$).[159] The Fe···Fe distance of 2.683(1) Å in (**41b**) is significantly shorter than that (2.89 Å) determined by the EXAFS analysis of an analogue (**40b**),[158] which did not include contributions from the multicarbon shell at 2.87 Å. The Fe fitting parameters derived from this and other structurally characterized TPA complexes sharing the $\{Fe_2O_2(H)\}^{n+}$ motifs were used to reevaluate the EXAFS data of $MMOH_Q$ and RNR-R2 X. An Fe···Fe distance centered around 2.5 Å was obtained within an acceptable error range, validating the previous assignments. It was proposed that the core structures of $MMOH_Q$ and RNR-R2 intermediate X minimally consist of (μ-oxo) di-iron units and require additional bridging ligands to achieve such significant Fe···Fe shortening.[159]

Unlike the situation with TPA, 5-Me$_3$-TPA, or 5-Et$_3$-TPA di-iron compounds described above, the use of 6-Me-TPA (Figure 2) resulted in a high-valent iron(III)iron(IV) complex, in which AF coupling between HS iron sites afforded an $S = 1/2$ spin state. Oxidation of $[Fe_2(\mu\text{-}O)$-$(OH)(H_2O)(6\text{-Me-TPA})_2]^{3+}$ (**42a**) with H_2O_2 at $-40\,°C$ in MeCN afforded a brown species (**42b**) (Table 2), which was formulated as $[Fe_2(O)_2(6\text{-Me-TPA})_2]^{3+}$ based on ESI-MS.[160] A nearly isotropic $g = 2.00$ signal was displayed by (**42b**), which broadened upon the use of ^{57}Fe and ^{17}O. Field-dependent Mössbauer spectroscopy confirmed the presence of AF-coupled iron(III)iron(IV) species, the relevant parameters of which are listed in Table 2. A coupling constant of $< -40\,cm^{-1}$ was estimated from the temperature dependence of the EPR signal. These findings are consistent with the presence of a valence trapped HS Fe^{III}—HS Fe^{IV} site in (**42b**), analogous to that in RNR-R2 intermediate X.

Mechanistic models for the assembly of the iron(III)iron(IV) core were proposed from the studies of (**35a**) and (**36a**). As discussed in Section 8.13.5.3.1, reactions between (**36a**) and H_2O_2, or between (**35a**) and O_2, at low temperatures generated essentially identical (peroxo)di-iron(III) species (**36b**) and (**35b**), respectively (Scheme 16).[151–153] Upon decomposition, (**36b**) afforded a paramagnetic species (**36c**), the EPR and Mössbauer spectroscopic properties of which matched closely those associated with the iron(III)iron(IV) species (**42b**) (Table 2).[153] ESI-MS further supported the assignment of (**36c**) as $[Fe_2(O)_2(6\text{-Me}_3\text{-TPA})_2]^{3+}$. The conversion of (**36b**) to (**36c**) was facilitated by the presence of one equiv. $HClO_4$ and followed pseudo-first-order kinetics. In a similar manner, in the presence of one equiv. of $HClO_4$, (**35b**) decayed at $-30\,°C$ to a brown species (**35c**) (30% based on (**35a**)) having an isotropic EPR signal at $g = 1.999$, which significantly broadened upon doping with $H_2^{17}O$.[151] Similar observations were made with (**42b**) and RNR-R2 intermediate X,[57,160] which feature metal-based $S = 1/2$ paramagnetic centers. The decay of (**35b**) is coupled with the development of (**35c**), as monitored by the decrease in the 640 nm absorption and the increase in the $g \sim 2$ signal. Collectively, a biomimetic peroxo-to-X-type conversion was achieved in the TPA systems, although the source of an electron required for this process and its injection point along the reaction coordinate are yet to be delineated.

The spatial arrangement of the oxo ligands in $[Fe_2(O)_2(6\text{-Me}_3\text{-TPA})_2]^{3+}$, initially formulated as $[Fe_2(\mu\text{-}O)_2(6\text{-Me}_3\text{-TPA})_2]^{3+}$,[153] was investigated by vibrational spectroscopic studies. Compound (**36a**) could be reversibly oxidized to (**36c**) by cyclic voltammetry ($E_{1/2} = 0.41$ V vs. Fc/Fc$^+$) at $-40\,°C$ in MeCN.[161] Chemical oxidation of (**36a**) was achieved by using one equiv. of $(NBu)_4$-$Ce(NO_3)_6$ under similar conditions, affording a paramagnetic species with $S = 1/2$. ESI-MS revealed the presence of a $[Fe_2(O)_2(6\text{-Me}_3\text{-TPA})_2]^{3+}$ cation, along with its H_2O-adduct, $[Fe_2(O)_2(H_2O)(6\text{-Me}_3\text{-TPA})_2]^{3+}$, in the reaction products. The latter formulation was consistent

with the elemental analysis of the solid sample. Mössbauer spectroscopic studies revealed the presence of an HS iron(IV)—HS iron(III) couple (Table 2). The isomerization between $\{Fe_2(\mu\text{-}O)_2\}^{3+}$ and $\{Fe\text{—}O\text{—}Fe\text{=}O\}^{3+}$ cores was demonstrated by resonance Raman spectroscopic studies. A prominent vibration of (**36c**) at $840\,cm^{-1}$ shifts by $-5\,cm^{-1}$ upon the use of excess $H_2^{18}O$ in the reaction media, whereas a sample prepared with a doubly labeled di-iron(III) precursor $[Fe_2(\mu\text{-}^{18}O)_2(6\text{-}Me_3\text{-}TPA)_2]^{2+}$ displayed a downshift to $794\,cm^{-1}$. The latter vibration undergoes a $+3\,cm^{-1}$ shift upon the addition of excess $H_2^{16}O$. This spectroscopic behavior was explained by invoking two distinct oxo ligands in (**36d**) (Scheme 16) resulting from a ring-opening isomerization of the $\{Fe_2(\mu\text{-}O)_2\}^{3+}$ core. The bridging and terminal oxo ligands have markedly different propensity toward exchange with H_2O, properties that allow selective isotope labeling crucial for spectral assignments.

Parallel functional chemistry was observed with the structural models of RNR-R2 discussed in Section 8.13.5.2.4. The $Ar^{Tol}CO_2^-$ di-iron(II) complexes (**15a**) and (**17a**) react irreversibly with O_2 in CH_2Cl_2 at $-78\,^\circ C$ to afford dark green intermediates (**15b**) ($\lambda_{max} = 660\,nm$; $\varepsilon = 1,600\,M^{-1}\,cm^{-1}$) and (**17b**) ($\lambda_{max} = 670\,nm$; $\varepsilon = 1,700\,M^{-1}\,cm^{-1}$), respectively.[121,126] EPR and Mössbauer spectroscopic studies revealed the presence of equimolar amounts of valence-delocalized $Fe_2^{II,III}$ and valence-trapped $Fe^{III}Fe^{IV}$ species as major components of solution (**17b**) (Table 2). Deconvolution of the spectra corresponding to each paramagnetic species was aided by independent chemical synthesis and characterization of the $Fe_2^{II,III}$ components.[122,162] The intense visible absorptions of (**15b**) and (**17b**) arise from the intervalence charge transfer bands of $[Fe_2\text{-}(\mu\text{-}O_2C\text{-}Ar^{Tol})_4(NC_5H_5)_2]^+$ and $[Fe_2(\mu\text{-}O_2CAr^{Tol})_4(4\text{-}{}^tBuC_5H_4N)_2]^+$, respectively, which constitute ca. 45% of total $[Fe_2]$ as judged by redox titration with Cp^*_2Fe. The $Fe^{III}Fe^{IV}$ component (**17c**) in the mixture (**17b**) displays Mössbauer and EPR parameters characteristic of AF-coupled HS Fe^{III}—HS Fe^{IV} (Table 2) and comparable to those of RNR-R2 intermediate X and cryoreductively generated $MMOHQ_x$ (Table 1). A large coupling constant of $|2J| > 200\,cm^{-1}$ was estimated from EPR studies of the $g \sim 2$ signal. Along with the susceptibility of the di-iron core toward protonation, such a strong superexchange implicates the presence of at least one bridging oxo unit in the $\{Fe^{III}Fe^{IV}(O)_2\}^{3+}$ core fragment supported by $Ar^{Tol}CO_2^-$. A mechanistic model was proposed, in which doubly or triply bridged isomers of the di-iron(II) complex react with O_2 to afford an initial peroxo or Q-type adduct (Scheme 18).[126] One-electron reduction of this spectroscopically unobserved intermediate is coupled to one-electron oxidation of the paddlewheel di-iron(II) starting material that dominates the solution dynamics at low temperatures. The result is an equimolar mixture of di-iron(II,III) and iron(III)iron(IV) species. Thermal decomposition of (**15b**) and (**17b**) resulted in the formation of unprecedented quadruply bridged di-iron(III) complexes
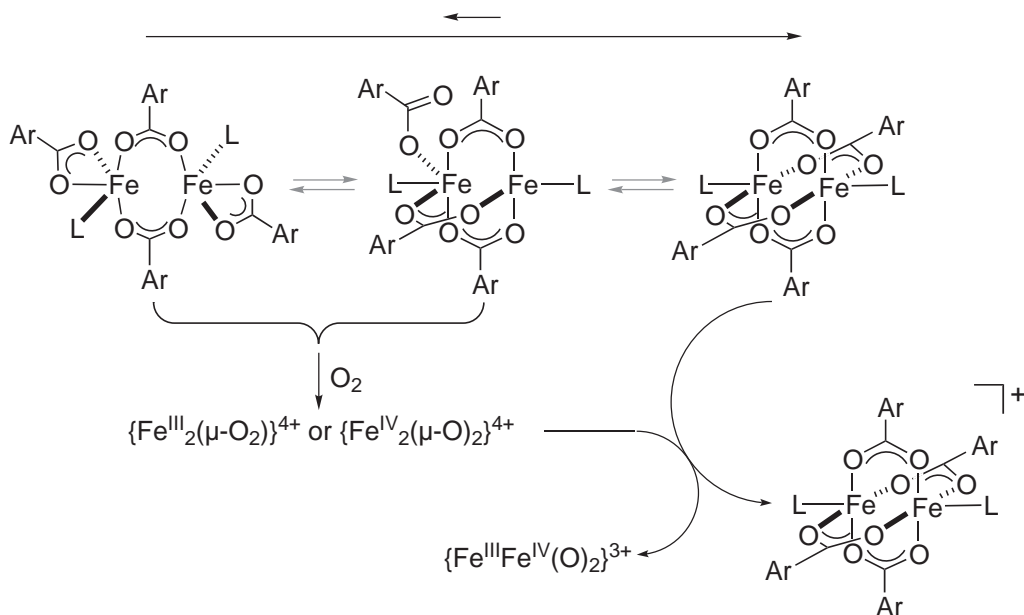
Scheme 18

$[Fe_2(\mu\text{-}OH)_2(\mu\text{-}O_2CAr^{Tol})_2(O_2CAr^{Tol})_2L_2]$ (L = C_5H_5N, 4-$^tBuC_5H_4N$) as isolated products. For these compounds, a weak F-coupling ($J \sim 0.7\,cm^{-1}$) between HS iron(III) centers was observed.

8.13.5.3.3 Di-iron(IV) complexes: models of MMOH intermediate Q

Oxidation of a mononuclear iron(II) complex afforded a spectroscopically characterized di-iron (IV) compound. Upon treating a CH_2Cl_2 solution of [Fe(BPMCN)(OTf)$_2$] (43a) with 10 equiv. of $^tBuO_2H$ at $-80\,°C$, a blue Fe^{III}—OO^tBu intermediate (43b) ($\lambda_{max} = 566\,nm$; $\varepsilon \sim 2,500\,M^{-1}cm^{-1}$) was generated, which gradually converted to another chromophore (43c) (Table 2).[163] At 4.2 K, a single sharp quadrupole doublet with $\delta = 0.10\,mm\,s^{-1}$ and $\Delta E_Q = 1.75\,mm\,s^{-1}$ was observed for a frozen solution sample of (43c), which was modeled with a symmetric exchange-coupled low-spin iron(IV)iron(IV) dimer with $|J| < 5\,cm^{-1}$. Resonance Raman spectra of the ^{18}O-labeled material established that the terminal oxygen atoms of two $^tBuO_2H$ units were incorporated in (43c). Oxygen-isotope-sensitive vibrations in the 600–$700\,cm^{-1}$ region substantiated further the presence of an $\{Fe_2(\mu\text{-}O)_2\}^{n+}$ core in (43c). Geometric parameters obtained by Fe K-edge EXAFS spectroscopy reveals short Fe···Fe and Fe—O scattering distances of 2.81 Å and 1.79 Å, respectively, values expected for such a rhombic unit. Based on these observations, (43c) was formulated as [Fe$_2$(μ-O)$_2$(BPMCN)$_2$](OTf)$_4$. The imine-rich primary coordination in (43c) renders the metal centers low-spin, electronic configurations different from those of the high-spin di-iron(IV) sites supported by carboxylate-rich residues in MMOH.

8.13.5.4 Functional Models

Significant efforts have been made to reproduce functional aspects of the nonheme di-iron enzymes. A few examples are now available in which well-characterized high-valent di-iron species participate in the key C—H/O—H activation steps. Differentiation of radical-free vs. free-radical processes is an important issue to be addressed for the catalytic systems that employ hydrogen peroxide or alkyl peroxides as terminal oxidants. In the following sections, selected nonheme di-iron systems that effect either stoichiometric or catalytic oxidation of organic substrates are described. Detailed accounts of Gif chemistry and Gif-type reagents can be found elsewhere.[164–166] Reviews of related C—H activation by Fenton-type processes are also available.[167–170]

8.13.5.4.1 C—H/O—H activation by well-characterized high-valent di-iron species

In MeCN at $-40\,°C$, low-spin iron(III)iron(IV) compounds [Fe$_2$(μ-O)$_2$(TPA)$_2$]$^{3+}$ (39b) and (40b) quantitatively oxidize 2,4-di-*tert*-butylphenol to the corresponding phenoxyl radical, which dimerizes to form the 2,2′-biphenol product.[171] Hydroxylation or desaturation of hydrocarbons can also be achieved by these high-valent species, which act as one-electron oxidants. A KIE of 20 was obtained for the second-order reaction between (39b) and ethylbenzene.[171] Activation of the benzylic C—H bond is a major component of the rate-determining step in both hydroxylation and desaturation, as demonstrated by product analysis. A mechanistic model was proposed
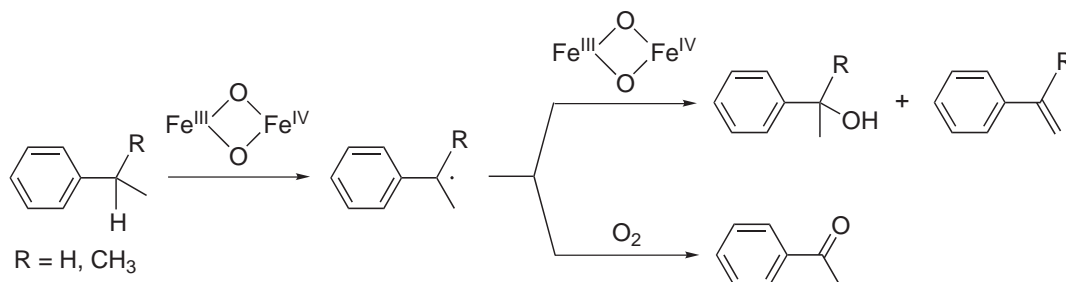
Scheme 19

(Scheme 19), in which a benzylic radical intermediate is generated from the rate-determining α-H abstraction by (**39b**). Subsequent reaction of this benzylic radical with a second equivalent of (**39b**), either by a formal oxygen rebound or by β-H abstraction, affords the corresponding alcohol or styrene, respectively. A competing reaction with O_2 produces the ketone product. Although the details of this partitioning in reaction pathways is yet to be elucidated, the high efficiency of this transformation (88% for cumene, based on consumption of two equiv. $Fe^{III}Fe^{IV}$ per conversion) highlights the functional relevance of this and related $\{Fe_2O_2\}^{n+}$ centers to biomimetic hydroxylation and desaturation reactions.

A high-spin iron(III)iron(IV) species (**35c**) quantitatively oxidizes 2,4,6-tri-*tert*-butylphenol to the corresponding phenoxyl radical.[151] An analogous functional mimic of RNR-R2 was achieved by the iron(III)iron(IV) species (**17c**) supported by $Ar^{Tol}CO_2^-$, which quantitatively oxidizes 2,4-di-*tert*-butylphenol to afford the biphenol coupling product.[126]

The high-valent di-iron(IV) species (**43c**) effects two-electron oxidation of strong C—H bonds.[163] At $-40\,^\circ$C and under Ar, (**43c**) reacts with adamantane to afford 1-adamantanol (56%) and 2-adamantanone (20%). With H_2O_2 as a terminal oxidant, however, (**43a**) and its sterically more demanding analogue [Fe(6-Me$_2$-BPMCN)(OTf)$_2$] (**44a**) catalyzes enantioselective epoxidation and *cis*-dihydroxylation of alkene substrates, demonstrating the metal-based nature of this transformation.[172] Apparently, the use of HOOH vs. ROOH significantly alters the pathways adopted by the Fe^{III}—OOR (R = alkyl or H) adduct. The origin of such a functional shift needs further clarification.

8.13.5.4.2 Stoichiometric and catalytic oxidation systems of biological relevance

Controlled delivery of reducing equivalents is an important prerequisite for any synthetic system mimicking the MMO catalytic cycle with O_2 as a terminal oxidant. For the enzyme, the sites of dioxygen activation and electron entry are physically separated. Tight regulation of electron and proton trafficking ensures that the high-valent reactive species should not be prematurely quenched before the key C—H activation step. Reproducing these aspects presents a formidable challenge for a synthetic system, for which every two electrons should be injected precisely at the end of each turnover. As in cP450 and its functional models, the peroxide shunt employing H_2O_2 or ROOH as terminal oxidants precludes the use of reducing agents to regenerate the di-iron(II) state upon completion of one turn of the catalytic cycle. For the catalytic systems that mimic the MMO reaction cycle using ROOH, distinguishing a metal-oxo-based two-electron oxidation from a radical-based one-electron oxidation has been a critical issue.

A (μ-oxo)di-iron(III) complex [Fe$_2$(μ-O)(H$_2$O)$_2$(TPA)$_2$]$^{4+}$ (**45**) catalytically oxidizes cyclohexane exclusively to cyclohexanol in MeCN at $25\,^\circ$C with $^tBuO_2H$ as a terminal oxidant.[173] An initially postulated mechanism based on a putative Fe^V=O species was re-investigated to reveal that the $^tBuO\cdot$ radical, not the high-valent iron-oxo species, is responsible for the key C—H bond activation step.[174,175] Hydrogen abstraction by ^tBuO generates a long-lived alkyl radical,
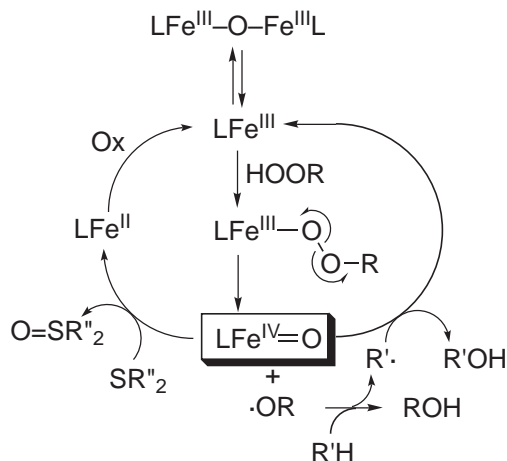
Scheme 20

which, in the absence of other trapping agents, reacts with the $Fe^{IV}=O$ species to afford the alcohol product (Scheme 20). Two-electron oxidation of thioanisole, cyclohexanol, and cyclooctene by (**45**) with 2-methyl-1-phenylprop-2-yl hydroperoxide (MPPH) as a terminal oxidant demonstrated that the same $Fe^{IV}=O$ species derived from (**45**) can be intercepted by suitable substrates in proximity.[176]

A synthetically applicable preparative scale epoxidation was achieved by a catalytic system comprising a mononuclear iron(II) complex $[Fe(BPMEN)(NCMe)_2]^{2+}$ (**46**) and H_2O_2.[177] Significantly enhanced catalytic performance was achieved by adding one equiv. of AcOH. Spectroscopic and X-ray crystallographic studies revealed that a (μ-oxo)(μ-carboxylato)di-iron(III) complex was assembled under the reaction conditions. The isolated dinuclear complex $[Fe_2(\mu\text{-}O)\text{-}(\mu\text{-}OAc)(BPMEN)_2]^{3+}$ (**47**) is as competent as (**46**)+AcOH in oxidizing 1-decene to 1,2-epoxidecane with H_2O_2 as a terminal oxidant. A wide range of aliphatically substituted alkenes proved to be excellent substrates. Notably, terminal alkenes, which are normally least reactive toward conventional electrophilic oxidants, convert to the corresponding epoxides within 5 min and in 60–90% isolated yields. With H_2O_2 as a terminal oxidant, a related mononuclear iron(II) complex $[Fe(5\text{-}Me_3\text{-}TPA)(NCMe)_2]^{2+}$ catalytically converts terminal and internal alkenes to a mixture of epoxides and diols in combined yields exceeding $\sim$70% (epoxide:diol = 1:3–4).[178] Under similar conditions, however, no catalytic activity was displayed by a series of $[Fe_2(\mu\text{-}O)(\mu\text{-}OAc)L_2]^{3+}$ compounds including (**47**).

The (peroxo)di-iron(III) species (**38b**) and (**38b'**)[157] effect enantioselective sulfoxidation of aryl sulfides.[156] In the catalytic reaction with H_2O_2 as a terminal oxidant, saturation kinetics were observed with respect to both $[H_2O_2]$ and [sulfide]. The peroxo species (**38b**)+(**38b'**) generated *in situ* at 0 °C decays in the presence of sulfide, following a saturation kinetics with respect to [sulfide]. For *p*-bromophenyl methyl sulfide, the ee approaches ca. 40%, providing compelling evidence for a metal-based oxidation pathway involving a (peroxo)di-iron(III)–sulfide binary complex embedded within chiral environment.

The tetradentate ligand L^2 derived from EDTA supports a tetrairon(III) cluster, which, in the presence of OAc^- and H_2O, dissociates to a spectroscopically characterized di-iron(III) complex $[Fe_2(\mu\text{-}O)(\mu\text{-}OAc)L^2_2]^-$ (**48**).[179,180] Upon reaction with O_2/ascorbate, (**48**) converts to a mononuclear iron(III) complex $[FeL^3(H_2O)]$ (**49**), in which the *ortho* position of one phenyl ring in L^2 was hydroxylated in 80% yield (Scheme 21). The same transformation could be effected with H_2O_2, following saturation kinetics indicative of pre-equilibrium binding of H_2O_2 to (**48**). Isotope-labeling experiments established that the oxygen atom in L^3 derives exclusively from O_2 in the former, and from H_2O_2 in the latter, system. No isotope scrambling with solvent H_2O was observed. A mechanistic model was proposed, in which putative peroxoiron species derived from either mononuclear iron(II) or di-iron(III) precursor compounds are trapped by a nucleophilic aryl ligand pendant.

Oxidizable ligand fragments could be installed within a tetra(carboxylato)di-iron(II) complex that match the MMOH primary coordination sphere ligand composition. One such compound (**18a**) reacts with O_2 to afford PhCHO in $\sim$60(5)% yield, following oxidative *N*-dealkylation of the benzyl pendant group on the diamine ligand *N,N*-Bn$_2$en (Scheme 22).[123,127] The origin of the oxygen atom incorporated into PhCHO was established by the use of $^{18}O_2$, which afforded

Scheme 21

(18a)

(18b)

MMOH$_{ox}$

CH$_2$Cl$_2$, r.t.

concerted C–H
insertion

radical

one electron N-oxidation
followed by proton
transfer

Fe^{II} Fe^{II}

Fe^{III} Fe^{III}

Fe^{IV} Fe^{III}

Fe^{IV} Fe^{IV}

Fe^{IV} Fe^{IV}

Fe^{III} Fe^{IV}

Fe^{III} Fe^{III}
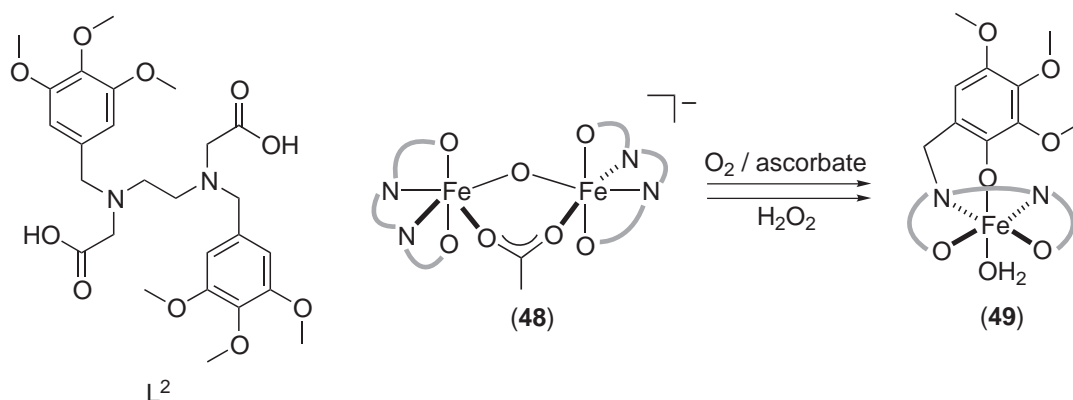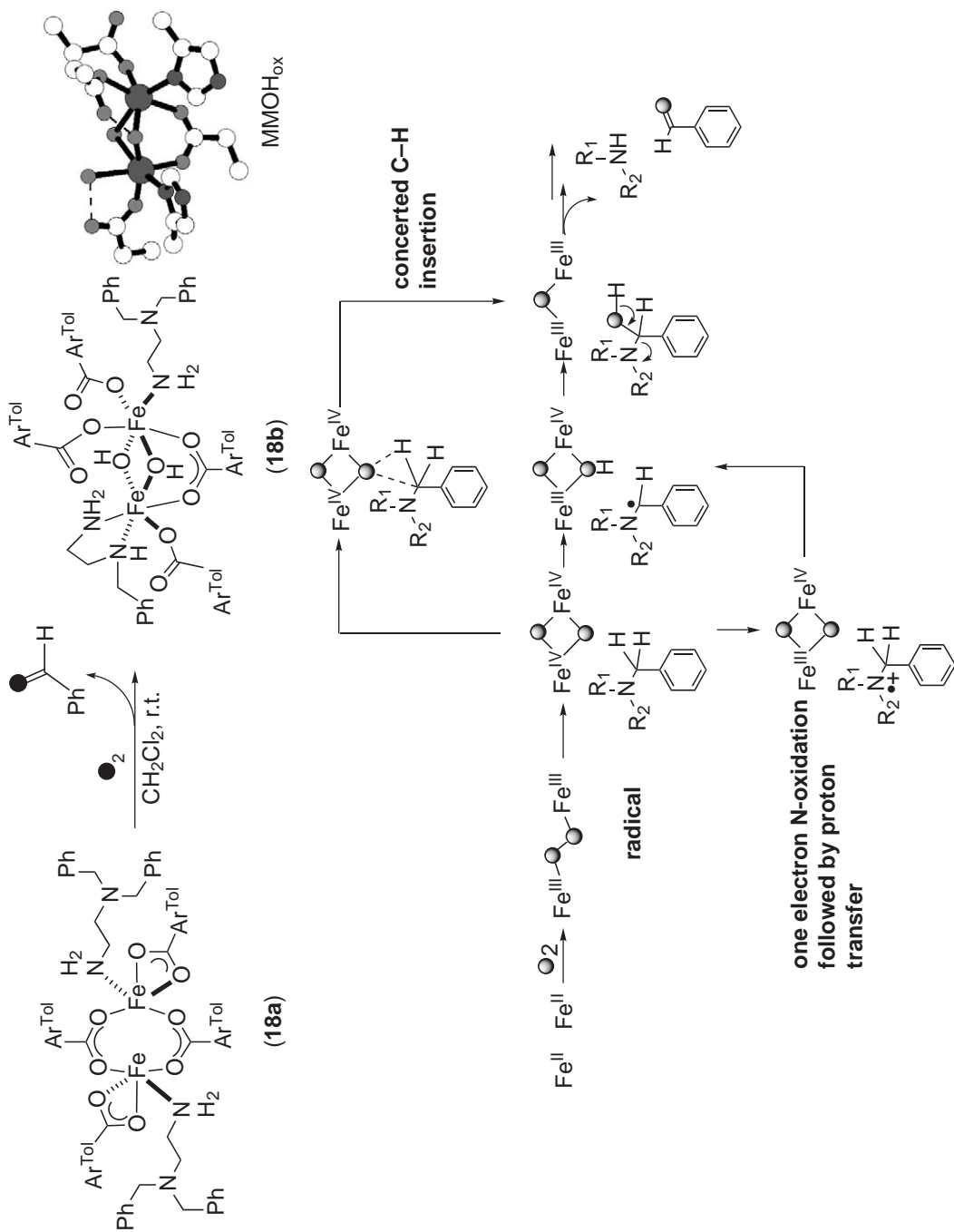
Scheme 22

$PhCH^{18}O$. Mechanistic models responsible for this transformation were proposed. Reaction manifolds involving putative di-iron(IV) species could be invoked that proceed via conventional radical recoil/rebound, concerted C—H insertion, or one-electron oxidation followed by proton transfer. As a result of such a transformation, a di-iron(III) compound $[Fe_2(\mu\text{-}OH)_2(\mu\text{-}O_2CAr^{Tol})\text{-}(O_2CAr^{Tol})_3(N,N\text{-}Bn_2en)(N\text{-}Bnen)]$ (**18b**) was assembled, in which the di(μ-hydroxo)(μ-carboxylato)-di-iron(III) core structure of MMOH in its resting state was reproduced for the first time on a nonpeptidyl ligand framework.

A di-iron system that delivers both O_2-derived oxygen atoms to the substrates would not require the use of sacrificial reducing equivalents, offering an ideal solution to atom-efficient catalysis. The di-iron(II) complex $[Fe_2(\mu\text{-}O_2CAr^{Tol})_2(NCMe)_2(Me_3TACN)_2]^{2+}$ (**50a**) reacts with O_2 in THF at $-78\,^{\circ}C$ to afford an intense blue-colored intermediate ($\lambda_{max} = 640\,nm$; $\varepsilon = 2,000\,M^{-1}\,cm^{-1}$) that decays to $[Fe_2(\mu\text{-}O)(\mu\text{-}O_2CAr^{Tol})_2(Me_3TACN)_2]^{2+}$ (**50b**) (Scheme 23).[128] With supply of O_2 under ambient conditions (1 atm, $25\,^{\circ}C$), (**50b**) catalyzes oxidation of Ph_3P to $Ph_3P=O$ with a remarkable efficiency of >2,000 turnovers. Details of the dioxygen reactivity of (**50a**), the oxo transfer reactivity of (**50b**), and the nature of the intervening O_2-adduct are yet to be understood. An analogue of (**50b**) having AcO^- ligands, (**1b**),[99] displays significantly reduced oxidation reactivity, implicating the importance of the sterically demanding carboxylate ligand $Ar^{Tol}CO_2^-$. Quantitative transfer of a bridging oxo ligand to PPh_3 was observed for the di-iron(III) complex $[Fe_2(\mu\text{-}O)(\mu\text{-}OH)(6\text{-}Me_3\text{-}TPA)_2]^{3+}$, which converts to a mononuclear iron(II) species following oxo transfer at $80\,^{\circ}C$.[181]

8.13.5.5 Mechanisms of Dioxygen Activation

Kinetic and spectroscopic studies have refined mechanistic models developed for dioxygen-activating nonheme di-iron compounds. As depicted in Scheme 24, reaction between a di-iron(II) center and dioxygen can proceed either via an outer-sphere one-electron transfer (pathway **I**) or via an inner-sphere two-electron transfer concomitant with dioxygen binding (pathway **II**). The latter route requires the formation of an intermediate (superoxo)iron(II)iron(III) species, which needs to be spectroscopically substantiated. Pathway **I** is favored by coordinatively saturated (μ-hydroxo)di-iron(II) complexes $[Fe_2(\mu\text{-}OH)(\mu\text{-}O_2CR)_2(Me_3TACN)_2]^+$ having sterically encumbered RCO_2^-.[182,183] Steric crowding impedes carboxylate shifts required to open a coordination site for incoming O_2 molecule, and the low oxidation potential of the metal center facilitates one-electron ET. The $Fe^{II}Fe^{III}$ species could be equally well accessed by one-electron chemical oxidation using H_2O_2 or trialkylamine N-oxides. Selected di-iron(II) complexes react with O_2 to afford (peroxo)di-iron(III) species via an associative rate-determining step, as manifest in the first-order dependence on $[O_2]$ and significantly negative $\Delta S^{\ddagger}$ values.[184,185] For five-coordinate metal centers, O_2 binding has a low barrier, whereas coordinatively saturated or sterically encumbered metal centers requires substantial ligand rearrangement. Dioxygen carriers have low barrier oxygenation pathways involving small activation entropy, whereas either a relatively high $\Delta H^{\ddagger}$ or a large negative $\Delta S^{\ddagger}$ is observed for dioxygen activators.[152] This behavior is consistent with the slower rate of dioxygen binding of the latter compared with the former.

In the absence of an effective steric shield, the (peroxo)di-iron(III) species reacts either with unoxidized di-iron(II) starting material or with another equivalent of the (peroxo)di-iron(III)
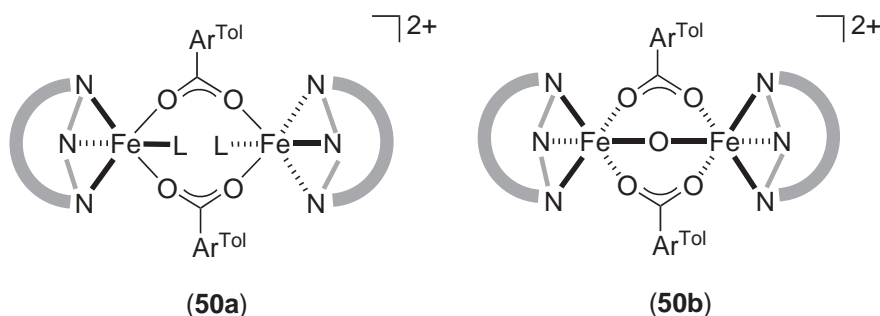
Scheme 23
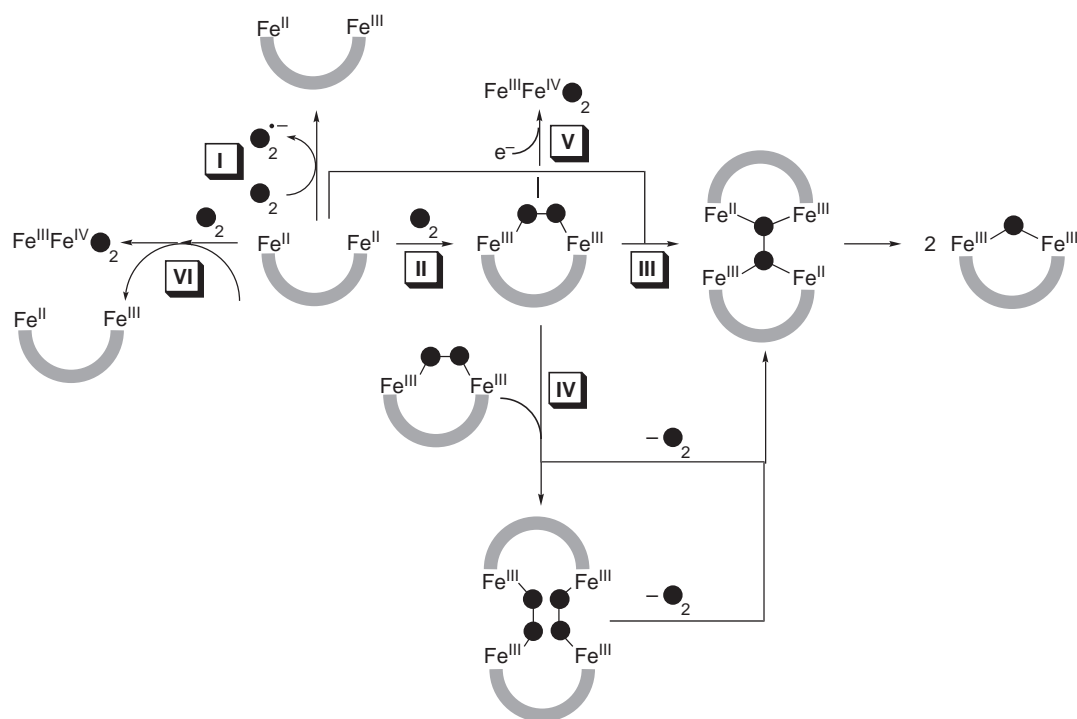
Scheme 24

molecule. A second-order dependence on [Fe$_2$] and first-order dependence on [O$_2$], consumption of 0.5 equiv. dioxygen, and complete incorporation of O$_2$-derived oxo groups in the final di-iron(III) products are consistent with pathway **III** of Scheme 24.[186] Cleavage of the O—O bond after the rate-determining formation of a tetranuclear iron–peroxide transition state affords two molecules of (μ-oxo)di-iron(III) products. A topologically related Fe$^{III}_4$–η^2:η^2-peroxo fragment was previously identified in larger polyiron clusters.[187] Pathway **IV** in Scheme 24 postulates (peroxo)tetrairon intermediates resulting from second-order decay of the (peroxo)di-iron(III) species. In this scenario, one equivalent of dioxygen is released to satisfy a stoichiometry of 0.5 equiv. O$_2$ per di-iron for the overall process.[185]

Injection of an external electron reductively activates the metal-bound peroxide ligand, affording high-valent iron(III)iron(IV) species. For the 6-Me$_3$-TPA system, stepwise conversion from di-iron(II) to iron(III)iron(IV) via (peroxo)di-iron(III) was observed (pathway **V**).[151] The source of the extra electron in a similar conversion was established only for the Ar^{Tol}CO$_2^-$ system.[121,125] Denoted as pathway **VI** in Scheme 24, the putative initial dioxygen adduct(s) react with the di-iron(II) starting material to afford an equimolar mixture of high-valent iron(III)iron(IV) and di-iron(II,III) species. This mechanistic model relates well to a recent proposal for the formation of RNR-R2 intermediate X.[188]

8.13.6 SUMMARY AND OUTLOOK

Significant progress has been made in understanding structure–function relationships in nonheme di-iron enzymes in the past decade. Mechanistic paradigms developed by direct studies of the biological systems have been calibrated further by theoretical studies. Access to discrete, low-coordination number di-iron(II) model complexes supported by carboxylate-rich ligand platforms has evolved an active research area. Structural and functional mimics of such enzymes are now in hand. Kinetic and thermodynamic stability rendered by *N*-rich multidentate ligands enabled stabilization and isolation of reactive high-valent di-iron intermediates of biological relevance. Steric shielding afforded by designer ligands prevents deleterious bimolecular decomposition of the reactive O$_2$-adducts, although controlled trafficking of electrons and protons still remains an

important issue to be solved for the systems to be made catalytic. Control of the chemo-, regio-, and stereoselectivity in the desired organic transformation is another challenge for the small molecules that apparently lack well-defined substrate binding sites. The robust tertiary structure afforded by *de novo* proteins offers an opportunity to construct highly simplified nonheme di-iron protein models in which both the primary and secondary coordination sphere can be tuned. A unified mechanistic view arising from these studies will undoubtedly benefit our understanding of biological O—O and C—H bond activation in the nonheme di-iron context.

ACKNOWLEDGMENTS

8.13.7 REFERENCES

1. Feig, A. L.; Lippard, S. J. *Chem. Rev.* **1994**, *94*, 759–805.
2. Wallar, B. J.; Lipscomb, J. D. *Chem. Rev.* **1996**, *96*, 2625–2657.
3. Que, L., Jr.; Dong, Y. *Acc. Chem. Res.* **1996**, *29*, 190–196.
4. Que, L., Jr. Oxygen Activation at Nonheme Iron Centers. In *Bioinorganic Catalysis*, 2nd ed.; Reedijk, J.; Bouwman, E., Eds.; Marcel Dekker: New York, 1999; pp 269–321.
5. Du Bois, J.; Mizoguchi, T. J.; Lippard, S. J. *Coord. Chem. Rev.* **2000**, *200–202*, 443–485.
6. Solomon, E. I.; Brunold, T. C.; Davis, M. I.; Kemsley, J. N.; Lee, S.-K.; Lehnert, N.; Neese, F.; Skulan, A. J.; Yang, Y.-S.; Zhou, J. *Chem. Rev.* **2000**, *100*, 235–349.
7. Que, L., Jr. *J. Chem. Soc., Dalton Trans.* **1997**, 3933–3940.
8. Westerheide, L.; Pascaly, M.; Krebs, B. *Curr. Opin. Chem. Biol.* **2000**, *4*, 235–241.
9. Tolman, W. B.; Spencer, D. J. E. *Curr. Opin. Chem. Biol.* **2001**, *5*, 188–195.
10. Valentine, A. M.; Lippard, S. J. *J. Chem. Soc., Dalton Trans.* **1997**, 3925–3931.
11. Lipscomb, J. D.; Que, L., Jr. *J. Biol. Inorg. Chem.* **1998**, *3*, 331–336.
12. Merkx, M.; Kopp, D. A.; Sazinsky, M. H.; Blazyk, J. L.; Müller, J.; Lippard, S. J. *Angew. Chem., Int. Ed.* **2001**, *40*, 2782–2807.
13. Whittington, D. A.; Lippard, S. J. *J. Am. Chem. Soc.* **2001**, *123*, 827–838.
14. Logan, D. T.; Su, X.-D.; Åberg, A.; Regnström, K.; Hajdu, J.; Eklund, H.; Nordlund, P. *Structure* **1996**, *4*, 1053–1064.
15. Sjöberg, B.-M. *Struct. Bonding (Berlin)* **1997**, *88*, 139–173.
16. Stubbe, J.; van der Donk, W. A. *Chem. Rev.* **1998**, *98*, 705–762.
17. Lindqvist, Y.; Huang, W.; Schneider, G.; Shanklin, J. *EMBO J.* **1996**, *15*, 4081–4092.
18. Yang, Y.-S.; Broadwater, J. A.; Pulver, S. C.; Fox, B. G.; Solomon, E. I. *J. Am. Chem. Soc.* **1999**, *121*, 2770–2783.
19. Summa, C. M.; Lombardi, A.; Lewis, M.; DeGrado, W. F. *Curr. Opin. Str. Biol.* **1999**, *9*, 500–508.
20. Sono, M.; Roach, M. P.; Coulter, E. D.; Dawson, J. H. *Chem. Rev.* **1996**, *96*, 2841–2887.
21. Stahl, S. S.; Lippard, S. J. Dioxygen and Alkane Activation by Iron-containing Enzymes. In *Iron Metabolism: Inorganic Biochemistry and Regulatory Mechanisms*; Ferreira, G. C.; Moura, J. J. G.; Franco, R., Eds.; Wiley-VCH: Weinheim, 1999; pp. 303–321.
22. Mansuy, D.; Battioni, P. Dioxygen Activation at Heme Centers in Enzymes and Synthetic Analogs. In *Bioinorganic Catalysis*; 2nd ed.; Reedijk, J.; Bouwman, E., Eds.; Marcel Dekker: New York, 1999; pp 323–354.
23. McLain, J. L.; Lee, J.; Groves, J. T. Biomimetic Oxygenations Related to Cytochrome P450: Metal-oxo and Metal-Peroxo Intermediates. In *Biomimetic Oxidations Catalyzed by Transition Metal Complexes*; Meunier, B., Ed., Imperial College Press: London, 2000; pp 91–169.
24. Valentine, J. S. Dioxygen Activation. In *Bioinorganic Chemistry*, Bertini, I.; Gray, H. B.; Lippard, S. J.; Valentine, J. S., Eds.; University Science Books: Mill Valley, CA, 1994; pp 253–313.
25. Pierre, J. L.; Fontecave, M. *Biometals* **1999**, *12*, 195–199.
26. Whittington, D. A.; Lippard, S. J. Methane Monooxygenase Hydroxylase. In *Handbook of Metalloproteins*; Messerschmidt, A.; Huber, R.; Poulos, T.; Wieghardt, K., Eds.; Wiley: Chichester, 2001; pp 712–724.
27. Rosenzweig, A. C.; Frederick, C. A.; Lippard, S. J.; Nordlund, P. *Nature* **1993**, *366*, 537–543.
28. Rosenzweig, A. C.; Lippard, S. J. *Acc. Chem. Res.* **1994**, *27*, 229–236.
29. Elango, N.; Radhakrishnan, R.; Froland, W. A.; Wallar, B. J.; Earhart, C. A.; Lipscomb, J. D.; Ohlendorf, D. H. *Protein Sci.* **1997**, *6*, 556–568.
30. Whittington, D. A.; Sazinsky, M. H.; Lippard, S. J. *J. Am. Chem. Soc.* **2001**, *123*, 1794–1795.
31. Rosenzweig, A. C.; Nordlund, P.; Takahara, P. M.; Frederick, C. A.; Lippard, S. J. *Chem. Biol.* **1995**, *2*, 409–418.
32. Liu, K. E.; Valentine, A. M.; Wang, D.; Huynh, B. H.; Edmondson, D. E.; Salifoglou, A.; Lippard, S. J. *J. Am. Chem. Soc.* **1995**, *117*, 10174–10185.
33. DeWitt, J. G.; Bentsen, J. G.; Rosenzweig, A. C.; Hedman, B.; Green, J.; Pilkington, S. J.; Papaefthymiou, G. C.; Dalton, H.; Hodgson, K. O.; Lippard, S. J. *J. Am. Chem. Soc.* **1991**, *113*, 9219–9235.
34. Liu, K. E.; Wang, D.; Huynh, B. H.; Edmondson, D. E.; Salifoglou, A.; Lippard, S. J. *J. Am. Chem. Soc.* **1994**, *116*, 7465–7466.
35. Valentine, A. M.; Stahl, S. S.; Lippard, S. J. *J. Am. Chem. Soc.* **1999**, *121*, 3876–3887.
36. Liu, K. E.; Valentine, A. M.; Qiu, D.; Edmondson, D. E.; Appelman, E. H.; Spiro, T. G.; Lippard, S. J. *J. Am. Chem. Soc.* **1995**, *117*, 4997–4998.

37. Valentine, A. M.; Tavares, P.; Pereira, A. S.; Davydov, R.; Krebs, C.; Hoffman, B. M.; Edmondson, D. E.; Huynh, B. H.; Lippard, S. J. *J. Am. Chem. Soc.* **1998**, *120*, 2190–2191.
38. Fox, B. G.; Hendrich, M. P.; Surerus, K. K.; Andersson, K. K.; Froland, W. A.; Lipscomb, J. D.; Münck, E. *J. Am. Chem. Soc.* **1993**, *115*, 3688–3701.
39. Hendrich, M. P.; Münck, E.; Fox, B. G.; Lipscomb, J. D. *J. Am. Chem. Soc.* **1990**, *112*, 5861–5865.
40. Fox, B. G.; Surerus, K. K.; Münck, E.; Lipscomb, J. D. *J. Biol. Chem.* **1988**, *263*, 10553–10556.
41. Fox, B. G.; Liu, Y.; Dege, J. E.; Lipscomb, J. D. *J. Biol. Chem.* **1991**, *266*, 540–550.
42. Lee, S.-K.; Lipscomb, J. D. *Biochemistry* **1999**, *38*, 4423–4432.
43. Shu, L.; Nesheim, J. C.; Kauffmann, K.; Münck, E.; Lipscomb, J. D.; Que, L., Jr. *Science* **1997**, *275*, 515–518.
44. Lee, S.-K.; Fox, B. G.; Froland, W. A.; Lipscomb, J. D.; Münck, E. *J. Am. Chem. Soc.* **1993**, *115*, 6450–6451.
45. Lee, S.-K.; Nesheim, J. C.; Lipscomb, J. D. *J. Biol. Chem.* **1993**, *268*, 21569–21577.
46. Brazeau, B. J.; Lipscomb, J. D. *Biochemistry* **2000**, *39*, 13503–13515.
47. Lynch, J. B.; Juarez-Garcia, C.; Münck, E.; Que, L., Jr. *J. Biol. Chem.* **1989**, *264*, 8091–8096.
48. Bollinger, J. M., Jr.; Tong, W. H.; Ravi, N.; Huynh, B. H.; Edmondson, D. E.; Stubbe, J. *J. Am. Chem. Soc.* **1994**, *116*, 8015–8023.
49. Pulver, S. C.; Tong, W. H.; Bollinger, M. J., Jr.; Stubbe, J.; Solomon, E. I. *J. Am. Chem. Soc.* **1995**, *117*, 12664–12678.
50. Nordlund, P.; Eklund, H. *J. Mol. Biol.* **1993**, *232*, 123–164.
51. Petersson, L.; Gräslund, A.; Ehrenberg, A.; Sjöberg, B.-M.; Reichard, P. *J. Biol. Chem.* **1980**, *255*, 6706–6712.
52. Bollinger, J. M., Jr.; Krebs, C.; Vicol, A.; Chen, S.; Ley, B. A.; Edmondson, D. E.; Huynh, B. H. *J. Am. Chem. Soc.* **1998**, *120*, 1094–1095.
53. Baldwin, J.; Voegtli, W. C.; Khidekel, N.; Moënne-Loccoz, P.; Krebs, C.; Pereira, A. S.; Ley, B. A.; Huynh, B. H.; Loehr, T. M.; Riggs-Gelasco, P. J.; Rosenzweig, A. C.; Bollinger, J. M., Jr. *J. Am. Chem. Soc.* **2001**, *123*, 7017–7030.
54. Moënne-Loccoz, P.; Baldwin, J.; Ley, B. A.; Loehr, T. M.; Bollinger, J. M., Jr. *Biochemistry* **1998**, *37*, 14659–14663.
55. Riggs-Gelasco, P. J.; Shu, L.; Chen, S.; Burdi, D.; Huynh, B. H.; Que, L., Jr.; Stubbe, J. *J. Am. Chem. Soc.* **1998**, *120*, 849–860.
56. Bollinger, J. M., Jr.; Tong, W. H.; Ravi, N.; Huynh, B. H.; Edmondson, D. E.; Stubbe, J. *J. Am. Chem. Soc.* **1994**, *116*, 8024–8032.
57. Sturgeon, B. E.; Burdi, D.; Chen, S.; Huynh, B. H.; Edmondson, D. E.; Stubbe, J.; Hoffman, B. M. *J. Am. Chem. Soc.* **1996**, *118*, 7551–7557.
58. Fox, B. G.; Shanklin, J.; Ai, J. Y.; Loehr, T. M.; Sanders-Loehr, J. *Biochemistry* **1994**, *33*, 12776–12786.
59. Fox, B. G.; Shanklin, J.; Somerville, C.; Münck, E. *Proc. Natl. Acad. Sci. USA* **1993**, *90*, 2486–2490.
60. Broadwater, J. A.; Ai, J.; Loehr, T. M.; Sanders-Loehr, J.; Fox, B. G. *Biochemistry* **1998**, *37*, 14664–14671.
61. Broadwater, J. A.; Achim, C.; Münck, E.; Fox, B. G. *Biochemistry* **1999**, *38*, 12197–12204.
62. Priestley, N. D.; Floss, H. G.; Froland, W. A.; Lipscomb, J. D.; Williams, P. G.; Morimoto, H. *J. Am. Chem. Soc.* **1992**, *114*, 7561–7562.
63. Valentine, A. M.; Wilkinson, B.; Liu, K. E.; Komar-Panicucci, S.; Priestley, N. D.; Williams, P. G.; Morimoto, H.; Floss, H. G.; Lippard, S. J. *J. Am. Chem. Soc.* **1997**, *119*, 1818–1827.
64. Liu, K. E.; Johnson, C. C.; Newcomb, M.; Lippard, S. J. *J. Am. Chem. Soc.* **1993**, *115*, 939–947.
65. Valentine, A. M.; Le Tadic-Biadatti, M.-H.; Toy, P. H.; Newcomb, M.; Lippard, S. J. *J. Biol. Chem.* **1999**, *274*, 10771–10776.
66. Choi, S.-Y.; Eaton, P. E.; Hollenberg, P. F.; Liu, K. E.; Lippard, S. J.; Newcomb, M.; Putt, D. A.; Upadhyaya, S. P.; Xiong, Y. *J. Am. Chem. Soc.* **1996**, *118*, 6547–6555.
67. Choi, S.-Y.; Eaton, P. E.; Kopp, D. A.; Lippard, S. J.; Newcomb, M.; Shen, R. *J. Am. Chem. Soc.* **1999**, *121*, 12198–12199.
68. Jin, Y.; Lipscomb, J. D. *Biochemistry* **1999**, *38*, 6178–6186.
69. Guallar, V.; Gherman, B. F.; Miller, W. H.; Lippard, S. J.; Friesner, R. A. *J. Am. Chem. Soc.* **2002**, *124*, 3377–3384.
70. Brazeau, B. J.; Austin, R. N.; Tarr, C.; Groves, J. T.; Lipscomb, J. D. *J. Am. Chem. Soc.* **2001**, *123*, 11831–11837.
71. Newcomb, M.; Shen, R.; Lu, Y.; Coon, M. J.; Hollenberg, P. F.; Kopp, D. A.; Lippard, S. J. *J. Am. Chem. Soc.* **2002**, *124*, 6879–6886.
72. Newcomb, M.; Toy, P. H. *Acc. Chem. Res.* **2000**, *33*, 449–455.
73. Nam, W.; Lim, M. H.; Moon, S. K.; Kim, C. *J. Am. Chem. Soc.* **2000**, *122*, 10805–10809.
74. Collman, J. P.; Chien, A. S.; Eberspacher, T. A.; Brauman, J. I. *J. Am. Chem. Soc.* **2000**, *122*, 11098–11100.
75. Stubbe, J. *Curr. Opin. Struct. Biol.* **2000**, *10*, 731–736.
76. Mulliez, E.; Fontecave, M. *Coord. Chem. Rev.* **1999**, *185–186*, 775–793.
77. Nordlund, P.; Sjöberg, B.-M.; Eklund, H. *Nature* **1990**, *345*, 593–598.
78. Licht, S. S.; Gerfen, G. J.; Stubbe, J. *Science* **1996**, *271*, 477–481.
79. Burdi, D.; Sturgeon, B. E.; Tong, W. H.; Stubbe, J.; Hoffman, B. M. *J. Am. Chem. Soc.* **1996**, *118*, 281–282.
80. Willems, J.-P.; Lee, H.-I.; Burdi, D.; Doan, P. E.; Stubbe, J.; Hoffman, B. M. *J. Am. Chem. Soc.* **1997**, *119*, 9816–9824.
81. Burdi, D.; Willems, J.-P.; Riggs-Gelasco, P.; Antholine, W. E.; Stubbe, J.; Hoffman, B. M. *J. Am. Chem. Soc.* **1998**, *120*, 12910–12919.
82. Voegtli, W. C.; Khidekel, N.; Baldwin, J.; Ley, B. A.; Bollinger, J. M., Jr.; Rosenzweig, A. C. *J. Am. Chem. Soc.* **2000**, *122*, 3255–3261.
83. Ormö, M.; deMaré, F.; Regnström, K.; Åberg, A.; Sahlin, M.; Ling, J.; Loehr, T. M.; Sanders-Loehr, J.; Sjöberg, B.-M. *J. Biol. Chem.* **1992**, *267*, 8711–8714.
84. Åberg, A.; Ormö, M.; Nordlund, P.; Sjöberg, B.-M. *Biochemistry* **1993**, *32*, 9845–9850.
85. Ormö, M.; Regnström, K.; Wang, Z.; Que, L., Jr.; Sahlin, M.; Sjöberg, B.-M. *J. Biol. Chem.* **1995**, *270*, 6570–6576.
86. Shanklin, J.; Somerville, C. *Proc. Natl. Acad. Sci. USA* **1991**, *88*, 2510–2514.
87. Shu, L.; Broadwater, J. A.; Achim, C.; Fox, B. G.; Münck, E.; Que, L., Jr. *J. Bioinorg. Chem.* **1998**, *3*, 392–400.
88. Vincent, J. B.; Olivier-Lilley, G. L.; Averill, B. A. *Chem. Rev.* **1990**, *90*, 1447–1467.
89. Kurtz, D. M., Jr. *Chem. Rev.* **1990**, *90*, 585–606.
90. Solomon, E. I.; Hanson, M. A. Bioinorganic Spectroscopy. In *Inorganic Electronic Structure and Spectroscopy*; Solomon, E. I.; Lever, A. B. P., Eds.; Wiley: New York, 1999; Vol. II, pp 1–129.

91. Rardin, R. L.; Tolman, W. B.; Lippard, S. J. *New J. Chem.* **1991**, *15*, 417–430.
92. Rardin, R. L.; Poganiuch, P.; Bino, A.; Goldberg, D. P.; Tolman, W. B.; Liu, S.; Lippard, S. J. *J. Am. Chem. Soc.* **1992**, *114*, 5240–5249.
93. Zheng, H.; Zang, Y.; Dong, Y.; Young, V. G., Jr.; Que, L., Jr. *J. Am. Chem. Soc.* **1999**, *121*, 2226–2235.
94. Que, L., Jr.; Tolman, W. B. *Angew. Chem., Int. Ed.* **2002**, *41*, 1114–1137.
95. Bernadou, J.; Meunier, B. *Chem. Commun.* **1998**, 2167–2173.
96. Lippard, S. J. *Angew. Chem., Int. Ed. Engl.* **1988**, *27*, 344–361.
97. Lippard, S. J. *Nature* **2002**, *416*, 587.
98. Chaudhuri, P.; Wieghardt, K.; Nuber, B.; Weiss, J. *Angew. Chem., Int. Ed. Engl.* **1985**, *24*, 778–779.
99. Hartman, J. R.; Rardin, R. L.; Chaudhuri, P.; Pohl, K.; Wieghardt, K.; Nuber, B.; Weiss, J.; Papaefthymiou, G. C.; Frankel, R. B.; Lippard, S. J. *J. Am. Chem. Soc.* **1987**, *109*, 7387–7396.
100. Armstrong, W. H.; Lippard, S. J. *J. Am. Chem. Soc.* **1983**, *105*, 4837–4838.
101. Armstrong, W. H.; Spool, A.; Papaefthymiou, G. C.; Frankel, R. B.; Lippard, S. J. *J. Am. Chem. Soc.* **1984**, *106*, 3653–3667.
102. Ménage, S.; Zang, Y.; Hendrich, M. P.; Que, L., Jr. *J. Am. Chem. Soc.* **1992**, *114*, 7786–7792.
103. Hazell, R.; Jensen, K. B.; McKenzie, C. J.; Toftlund, H. *J. Chem. Soc., Dalton Trans.* **1995**, 707–717.
104. Randall, C. R.; Shu, L.; Chiou, Y.-M.; Hagen, K. S.; Ito, M.; Kitajima, N.; Lachicotte, R. J.; Zang, Y.; Que, L., Jr. *Inorg. Chem.* **1995**, *34*, 1036–1039.
105. Coucouvanis, D.; Reynolds, R. A., III; Dunham, W. R. *J. Am. Chem. Soc.* **1995**, *117*, 7570–7571.
106. Reynolds, R. A., III; Dunham, W. R.; Coucouvanis, D. *Inorg. Chem.* **1998**, *37*, 1232–1241.
107. Lachicotte, R.; Kitaygorodskiy, A.; Hagen, K. S. *J. Am. Chem. Soc.* **1993**, *115*, 8883–8884.
108. Hagen, K. S.; Lachicotte, R.; Kitaygorodskiy, A.; Elbouadili, A. *Angew. Chem., Int. Ed. Engl.* **1993**, *32*, 1321–1324.
109. Hagen, K. S.; Lachicotte, R.; Kitaygorodskiy, *J. Am. Chem. Soc.* **1993**, *115*, 12617–12618.
110. Tolman, W. B.; Bino, A.; Lippard, S. J. *J. Am. Chem. Soc.* **1989**, *111*, 8522–8523.
111. Tolman, W. B.; Liu, S.; Bentsen, J. G.; Lippard, S. J. *J. Am. Chem. Soc.* **1991**, *113*, 152–164.
112. Rebek, J., Jr.; Marshall, L.; Wolak, R.; Parris, K.; Killoran, M.; Askew, B.; Nemeth, D.; Islam, N. *J. Am. Chem. Soc.* **1985**, *107*, 7476–7481.
113. Rebek, J., Jr. *Acc. Chem. Res.* **1990**, *23*, 399–404.
114. Herold, S.; Lippard, S. J. *J. Am. Chem. Soc.* **1997**, *119*, 145–156.
115. LeCloux, D. D.; Lippard, S. J. *Inorg. Chem.* **1997**, *36*, 4035–4046.
116. Watton, S. P.; Masschelein, A.; Rebek, J., Jr.; Lippard, S. J. *J. Am. Chem. Soc.* **1994**, *116*, 5196–5205.
117. Herold, S.; Pence, L. E.; Lippard, S. J. *J. Am. Chem. Soc.* **1995**, *117*, 6134–6135.
118. LeCloux, D. D.; Barrios, A. M.; Mizoguchi, T. J.; LIPPARD, S. J. *J. Am. Chem. Soc.* **1998**, *120*, 9001–9014.
119. Tolman, W. B.; Que, L., Jr. *J. Chem. Soc., Dalton Trans.* **2002**, 653–660.
120. Lee, D.; Lippard, S. J. *J. Am. Chem. Soc.* **1998**, *120*, 12153–12154.
121. Lee, D.; Du Bois, J.; Petasis, D.; Hendrich, M. P.; Krebs, C.; Huynh, B. H.; Lippard, S. J. *J. Am. Chem. Soc.* **1999**, *121*, 9893–9894.
122. Lee, D.; Krebs, C.; Huynh, B. H.; Hendrich, M. P.; Lippard, S. J. *J. Am. Chem. Soc.* **2000**, *122*, 5000–5001.
123. Lee, D.; Lippard, S. J. *J. Am. Chem. Soc.* **2001**, *123*, 4611–4612.
124. Lee, D.; Hung, P. -L.; Spingler, B.; Lippard, S. J. *Inorg. Chem.* **2002**, *41*, 521–531.
125. Lee, D.; Lippard, S. J. *Inorg. Chem.* **2002**, *41*, 2704–2719.
126. Lee, D.; Pierce, B.; Krebs, C.; Hendrich, M. P.; Huynh, B. H.; Lippard, S. J. *J. Am. Chem. Soc.* **2002**, *124*, 3993–4007.
127. Lee, D.; Lippard, S. J. *Inorg. Chem.* **2002**, *41*, 827–837.
128. Tshuva, E. Y.; Lee, D.; Bu, W.; Lippard, S. J. *J. Am. Chem. Soc.* **2002**, *124*, 2416–2417.
129. Hagadorn, J. R.; Que, L., Jr.; Tolman, W. B. *J. Am. Chem. Soc.* **1998**, *120*, 13531–13532.
130. Hagadorn, J. R.; Que, L., Jr.; Tolman, W. B.; Prisecaru, I.; Münck, E. *J. Am. Chem. Soc.* **1999**, *121*, 9760–9761.
131. Hagadorn, J. R.; Que, L., Jr.; Tolman, W. B. *Inorg. Chem.* **2000**, *39*, 6086–6090.
132. Baik, M.-H.; Lee, D.; Friesner, R. A.; Lippard, S. J. *J. Israel Chem. Soc.* **2002**, *41*, 173–186.
133. Chavez, F. A.; Ho, R. Y. N.; Pink, M.; Young, V. G., Jr.; Kryatov, S. V.; Rybak-Akimova, E. V.; Andres, H.; Münck, E.; Que, L., Jr.; Tolman, W. B. *Angew. Chem., Int. Ed.* **2002**, *41*, 149–152.
134. DeGrado, W. F.; Wasserman, Z. R.; Lear, J. D. *Science* **1989**, *243*, 622–628.
135. Bryson, J. W.; Betz, S. F.; Lu, H. S.; Suich, D. J.; Zhou, H. X.; O'Neil, K. T.; DeGrado, W. F. *Science* **1995**, *270*, 935–941.
136. Hill, R. B.; Raleigh, D. P.; Lombardi, A.; DeGrado, W. F. *Acc. Chem. Res.* **2000**, *33*, 745–754.
137. Lombardi, A.; Summa, C. M.; Geremia, S.; Randaccio, L.; Pavone, V.; DeGrado, W. F. *Proc. Natl. Acad. Sci. USA* **2000**, *97*, 6298–6305.
138. Pasternak, A.; Kaplan, J.; Lear, J. D.; DeGrado, W. F. *Protein Sci.* **2001**, *10*, 958–969.
139. Costanzo, L. D.; Wade, H.; Geremia, S.; Randaccio, L.; Pavone, V.; DeGrado, W. F.; Lombardi, A. *J. Am. Chem. Soc.* **2001**, *123*, 12749–12757.
140. Marsh, E. N. G.; DeGrado, W. F. *Proc. Natl. Acad. Sci. USA* **2002**, *99*, 5150–5154.
141. Hayashi, Y.; Kayatani, T.; Sugimoto, H.; Suzuki, M.; Inomata, K.; Uehara, A.; Mizutani, Y.; Kitagawa, T.; Maeda, Y. *J. Am. Chem. Soc.* **1995**, *117*, 11220–11229.
142. Suzuki, M. *Pure Appl. Chem.* **1998**, *70*, 955–960.
143. Sugimoto, H.; Nagayama, T.; Maruyama, S.; Fujinami, S.; Yasuda, Y.; Suzuki, M.; Uehara, A. *Bull. Chem. Soc. Jpn.* **1998**, *71*, 2267–2279.
144. Suzuki, M.; Furutachi, H.; Okawa, H. *Coord. Chem. Rev.* **2000**, *200–202*, 105–129.
145. Dong, Y.; Ménage, S.; Brennan, B. A.; Elgren, T. E.; Jang, H. G.; Pearce, L. L.; Que, L., Jr. *J. Am. Chem. Soc.* **1993**, *115*, 1851–1859.
146. Ookubo, T.; Sugimoto, H.; Nagayama, T.; Masuda, H.; Sato, T.; Tanaka, K.; Maeda, Y.; Okawa, H.; Hayashi, Y.; Uehara, A.; Suzuki, M. *J. Am. Chem. Soc.* **1996**, *118*, 701–702.
147. Dong, Y.; Yan, S.; Young, V. G., Jr.; Que, L., Jr. *Angew. Chem., Int. Ed. Engl.* **1996**, *35*, 618–620.
148. Kitajima, N.; Tamura, N.; Amagai, H.; Fukui, H.; Moro-oka, Y.; Mizutani, Y.; Kitagawa, T.; Mathur, R.; Heerwegh, K.; Reed, C. A.; Randall, C. R.; Que, L., Jr.; Tatsumi, K. *J. Am. Chem. Soc.* **1994**, *116*, 9071–9085.

149. Kim, K.; Lippard, S. J. *J. Am. Chem. Soc.* **1996**, *118*, 4914–4915.
150. Brunold, T. C.; Tamura, N.; Kitajima, N.; Moro-oka, Y.; Solomon, E. I. *J. Am. Chem. Soc.* **1998**, *120*, 5674–5690.
151. MacMurdo, V. L.; Zheng, H.; Que, L., Jr. *Inorg. Chem.* **2000**, *39*, 2254–2255.
152. Kryatov, S. V.; Rybak-Akimova, E. V.; MacMurdo, V. L.; Que, L., Jr. *Inorg. Chem.* **2001**, *40*, 2220–2228.
153. Dong, Y.; Zang, Y.; Shu, L.; Wilkinson, E. C.; Que, L., Jr.; Kauffmann, K.; Münck, E. *J. Am. Chem. Soc.* **1997**, *119*, 12683–12684.
154. Kodera, M.; Shimakoshi, H.; Nishimura, M.; Okawa, H.; Iijima, S.; Kano, K. *Inorg. Chem.* **1996**, *35*, 4967–4973.
155. Kodera, M.; Taniike, Y.; Itoh, M.; Tanahashi, Y.; Shimakoshi, H.; Kano, K.; Hirota, S.; Iijima, S.; Ohba, M.; Okawa, H. *Inorg. Chem.* **2001**, *40*, 4821–4822.
156. Duboc-Toia, C.; Ménage, S.; Ho, R. Y. N.; Que, L., Jr.; Lambeaux, C.; Fontecave, M. *Inorg. Chem.* **1999**, *38*, 1261–1268.
157. Hummel, H.; Mekmouche, Y.; Duboc-Toia, C.; Ho, R. Y. N.; Que, L., Jr.; Schünemann, V.; Thomas, F.; Trautwein, A. X.; Lebrun, C.; Fontecave, M.; Ménage, S. *Angew. Chem., Int. Ed.* **2002**, *41*, 617–620.
158. Dong, Y.; Fujii, H.; Hendrich, M. P.; Leising, R. A.; Pan, G.; Randall, C. R.; Wilkinson, E. C.; Zang, Y.; Que, L., Jr.; Fox, B. G.; Kauffmann, K.; Münck, E. *J. Am. Chem. Soc.* **1995**, *117*, 2778–2792.
159. Hsu, H.-F.; Dong, Y.; Shu, L.; Young, V. G., Jr.; Que, L., Jr. *J. Am. Chem. Soc.* **1999**, *121*, 5230–5237.
160. Dong, Y.; Que, L., Jr.; Kauffmann, K.; Münck, E. *J. Am. Chem. Soc.* **1995**, *117*, 11377–11378.
161. Zheng, H.; Yoo, S. J.; Münck, E.; Que, L., Jr. *J. Am. Chem. Soc.* **2000**, *122*, 3789–3790.
162. Lee, D.; DuBois, J. L.; Pierce, B.; Hedman, B.; Hodgson, K. O.; Hendrich, M. P.; Lippard, S. J. *Inorg. Chem.* **2002**, *41*, 3172–3182.
163. Costas, M.; Rohde, J.-U.; Stubna, A.; Ho, R. Y. N.; Quaroni, L.; Münck, E.; Que, L., Jr. *J. Am. Chem. Soc.* **2001**, *123*, 12931–12932.
164. Barton, D. H. R.; Doller, D. *Acc. Chem. Res.* **1992**, *25*, 504–512.
165. Barton, D. H. R. *Chem. Soc. Rev.* **1996**, *25*, 237–239.
166. Barton, D. H. R. *Tetrahedron* **1998**, *54*, 5805–5817.
167. Sawyer, D. T.; Sobkowiak, A.; Matsushita, T. *Acc. Chem. Res.* **1996**, *29*, 409–416.
168. Walling, C. *Acc. Chem. Res.* **1998**, *31*, 155–157.
169. MacFaul, P. A.; Wayner, D. D. M.; Ingold, K. U. *Acc. Chem. Res.* **1998**, *31*, 159–162.
170. Goldstein, S.; Meyerstein, D. *Acc. Chem. Res.* **1999**, *32*, 547–550.
171. Kim, C.; Dong, Y.; Que, L., Jr. *J. Am. Chem. Soc.* **1997**, *119*, 3635–3636.
172. Costas, M.; Tipton, A. K.; Chen, K.; Jo, D.-H.; Que, L., Jr. *J. Am. Chem. Soc.* **2001**, *123*, 6722–6723.
173. Kim, J.; Harrison, R. G.; Kim, C.; Que, L., Jr. *J. Am. Chem. Soc.* **1996**, *118*, 4373–4379.
174. MacFaul, P. A.; Ingold, K. U.; Wayner, D. D. M.; Que, L., Jr. *J. Am. Chem. Soc.* **1997**, *119*, 10594–10598.
175. Ingold, K. U.; MacFaul, P. A. Distinguishing Biomimetic Oxidations from Oxidations Mediated by Freely Diffusing Radicals. In *Biomimetic Oxidations Catalyzed by Transition Metal Complexes*; Meunier, B., Ed., Imperial College Press: London, 2000; pp 45–89.
176. Miyake, H.; Chen, K.; Lange, S. J.; Que, L., Jr. *Inorg. Chem.* **2001**, *40*, 3354–3538.
177. White, M. C.; Doyle, A. G.; Jacobsen, E. N. *J. Am. Chem. Soc.* **2001**, *123*, 7194–7195.
178. Ryu, J. Y.; Kim, J.; Costas, M.; Chen, K.; Nam, W.; Que, L., Jr. *Chem. Commun.* **2002**, 1288–1289.
179. Ménage, S.; Galey, J.-B.; Hussler, G.; Seité, M.; Fontecave, M. *Angew. Chem., Int. Ed. Engl.* **1996**, *35*, 2353–2355.
180. Ménage, S.; Galey, J.-B.; Dumats, J.; Hussler, G.; Seité, M.; Luneau, I. G.; Chottard, G.; Fontecave, M. *J. Am. Chem. Soc.* **1998**, *120*, 13370–13382.
181. Zang, Y.; Pan, G.; Que, L., Jr.; Fox, B. G.; Münck, E. *J. Am. Chem. Soc.* **1994**, *116*, 3653–3654.
182. Cohen, J. D.; Payne, S.; Hagen, K. S.; Sanders-Loehr, J. *J. Am. Chem. Soc.* **1997**, *119*, 2960–2961.
183. Payne, S. C.; Hagen, K. S. *J. Am. Chem. Soc.* **2000**, *122*, 6399–6410.
184. Feig, A. L.; Lippard, S. J. *J. Am. Chem. Soc.* **1994**, *116*, 8410–8411.
185. Feig, A. L.; Becker, M.; Schindler, S.; van Eldik, R.; Lippard, S. J. *Inorg. Chem.* **1996**, *35*, 2590–2601.
186. Feig, A. L.; Masschelein, A.; Bakac, A.; Lippard, S. J. *J. Am. Chem. Soc.* **1997**, *119*, 334–342.
187. Micklitz, W.; Bott, S. G.; Bentsen, J. G.; Lippard, S. J. *J. Am. Chem. Soc.* **1989**, *111*, 372–374.
188. Miller, M. A.; Gobena, F. T.; Kauffmann, K.; Münck, E.; Que, L., Jr.; Stankovich, M. T. *J. Am. Chem. Soc.* **1999**, *121*, 1096–1097.

8.14
Non-heme Mono-iron Enzymes

T. L. FOSTER and J. P. CARADONNA
Boston University, MA, USA

The discovery of oxygenase chemistry by Mason and Hayaishi in 1955 introduced the role of dioxygen as a biosynthetic reagent to the scientific community.[1,2] Since that time, many efforts have been made to better understand the means by which nature is able to overcome the significant kinetic barrier of O_2 activation in order to carry out oxygen atom insertion chemistry. These enzymes are found throughout the plant, animal, and microorganism kingdoms and are responsible for a wide variety of organic transformations.[2] Their role in biological processes such as neurotransmitter and hormone production and their potential to serve as models for synthetic catalysts have made them of tremendous importance from both a biological and industrial standpoint. This chapter focuses on the mononuclear iron-based oxygenases found in nature with an emphasis on the coordination environment of the metal and the role that model complexes have played in examining the structural and mechanistic details of the enzymes.

8.14.1   CATECHOL DIOXYGENASES

Catechol dioxygenases represent a class of soil residing, bacterial proteins that are responsible for the degradation of aromatic hydrocarbons to aliphatic molecules.[1] This family of proteins can be
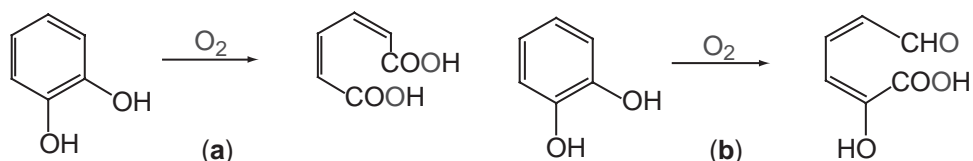
Figure 1 Modes of catechol dioxygenase cleavage.

further subdivided based on their mode of aromatic ring cleavage. The intradiol-cleaving catechol dioxygenases carry out a dioxygenation reaction in which each hydroxyl group of a catechol moiety is converted to a carboxylic acid functionality (Figure 1a). Alternately, extradiol-cleaving catechol dioxygenases generate one aldehyde and one carboxylic acid group, leaving one of the alcohol groups of the catechol in its original state (Figure 1b). In both cases, the oxidative cleavage of a carbon–carbon bond is carried out followed by the incorporation of both oxygen atoms of dioxygen into the organic substrate.[3]

The availability of X-ray quality crystals and suitable spectroscopic samples has enabled detailed investigations to be carried out into the active site structure of these iron-based proteins. Concurrently, several functional model systems have been developed that have aided in the elucidation of the mechanistic pathways involved in this family of enzymes.

8.14.1.1 Intradiol-cleaving Catechol Dioxygenases

The intradiol-cleaving catechol dioxygenases are unique among mononuclear, nonheme iron oxygenases in that they are the only ones to have a ferric ion as the active iron species. As such, the more common 2-His-1-carboxylate facial triad motif[4] is not conserved. Rather, coordination at the active site consists of two tyrosinate and two histidine residues, with a hydroxide anion occupying the fifth position in a trigonal bipyrimidal geometry (Figure 2a).[5] The paramagnetic nature of the ferric iron center has allowed extensive spectroscopic investigations of the coordination environment surrounding the iron active site. In fact, the crystal structure of protocatechuate 3,4-dioxygenase (3,4-PCD: E.C. 1.13.11.3) was obtained three years after original spectroscopic studies had predicted the exact coordination scheme outlined above.[6,7] The two tyrosinate residues were characterized using electronic spectroscopy ($\lambda_{max} \sim 460$ nm) and determined to be distinct based on distinguishable Raman excitations at ν_{CO} 1254 cm^{-1} and 1266 cm^{-1}.[8,9] Histidine ligation and the presence of a bound hydroxide ligand were both determined from XAS studies.[9–11] The high-spin ferric state of the metal was determined by

Figure 2 Schematic views of intradiol-cleaving dioxygenases.

EPR and Mössbauer spectroscopy.[12–15] These spectroscopic data are in perfect agreement with the results of single-crystal structural studies where the active site is located between the alpha and beta subunit with the endogenous ligand set arising exclusively from the beta subunit. This iron site is situated within a hydrophobic channel (proposed to be the substrate binding pocket) with the four endogenous ligands being the only bases located within the pocket.[5,6]

Upon substrate binding, the active site undergoes a structural rearrangement wherein both the axial tyrosinate and the hydroxide ligands are protonated and displaced from the iron center in order to allow binding of the catecholate substrate (Figure 3).[3] Substrate binding occurs without a change in the iron oxidation state as evidenced by the persistence of catecholato-to-Fe(III) charge transfer bands.[16–18] In fact, stopped-flow electronic and rapid-freeze-quench Mössbauer and EPR spectroscopic studies have allowed the identification of several intermediate species, all of which retain the spectral characteristics of the ferric ion.[14,15,19–21] In these studies, the ligand to metal charge transfer (LMCT) bands (associated with the Tyr408 residue) were monitored for a change in intensity and wavelength as a function of substrate binding. The binding of protocatechuate (PCA) to the iron center revealed an initial bleaching of the signal compared to the resting state of the enzyme, then three distinct changes are observed in the chromophore wherein each intermediate displays a commensurately more intense signal until the final chelated form of the iron(III)–PCA complex is observed. These changes reflect the *trans* effect on the Tyr408–Fe(III) bond wherein coordination via the negative, C4–O$^-$ moiety weakens the coordination at the *trans* position. For a detailed discussion regarding the possible structures of these intermediates, the reader is referred to the corresponding references.[8,21–23] These studies have also shown the reaction to proceed in an ordered, bimolecular fashion where the binding of substrate initiates the sequence. Thus the conclusion was made that the ferric state of the iron (which is unlikely to act as a dioxygen activator) serves to activate the catecholate substrate via the formation of the ferric–catecholato complex that can then react directly with molecular oxygen.

Figure 3 Proposed mechanism for intradiol-cleaving dioxygenases.

Figure 4 Products of catechol oxidation.

8.14.1.1.1 Model systems

Despite direct spectroscopic evidence of intermediates and the isolated crystal structures of various forms of the protein (i.e., resting state,[6,24] enzyme–substrate,[22,25] enzyme–substrate analogues[22] and enzyme–inhibitor),[23] the full mechanism by which this oxygenation reaction proceeds remains elusive. Key insights into the chemical pathway followed by this class of enzyme were, however, obtained from the investigation of functional model systems, which provided essential evidence for the accepted mechanism (Figure 3).[3] Initial studies made use of simple ferric salts in the presence of pyridine or bidentate, pi-acceptor ligands.[26–29] While turnover numbers were generally quite low (~2–10), product distribution did show the formation of intradiol (and extradiol) cleavage products, Figure 4.[3]

The reaction of iron salts in the ferrous and ferric oxidation states were monitored via UV–visible spectroscopy (LMCT bands of the iron–catecholate complex: $\lambda_{LMCT} = 550$ nm, 975 nm) in an effort to identify intermediates. It was noted that after addition of oxygen, there was no noticeable change in the electronic spectrum for the two salts.[26–30] Concurrently, the product distributions were shown to be comparable, regardless of the oxidation state of the metal. It was thus inferred that the oxidation state of the salt is inconsequential to the reaction pathway and that the mechanism proceeds through the same intermediate.[26–30] Isotopic labeling experiments were used to show that the oxidative processes were in fact occurring via an oxygenation pathway and not electron transfer processes followed by hydrolysis. While simple iron salts exhibit the ability to catalyze the conversion of catechol to the expected intradiol cleavage products, the turnover numbers are low and the selectivity of the reaction remains poor. As such, this first generation of model systems set the stage for the further understanding of the mechanistic pathways involved in the intradiol-cleaving dioxygenases.

The second class of model systems that were developed considered the fact that the iron center would require two readily accessible *cis*-coordination sites in order to allow for the bidentate binding motif of the catecholate while at the same time providing the appropriate distance for iron coordination of the intermediate peroxy intermediate.[3] Tripodal, tetradentate ligand systems were designed that incorporated alkyl amine groups with pendant pyridine, carboxylate or phenolate groups (Figure 5).[1] These ligands were not only capable of carrying out the oxygenation chemistry of their parent proteins in a selective and efficient fashion, but also afforded a further means of spectroscopic characterization in so far as they formed [Fe^III(L)catecholate] complexes that were easily isolated and characterized under anaerobic conditions.
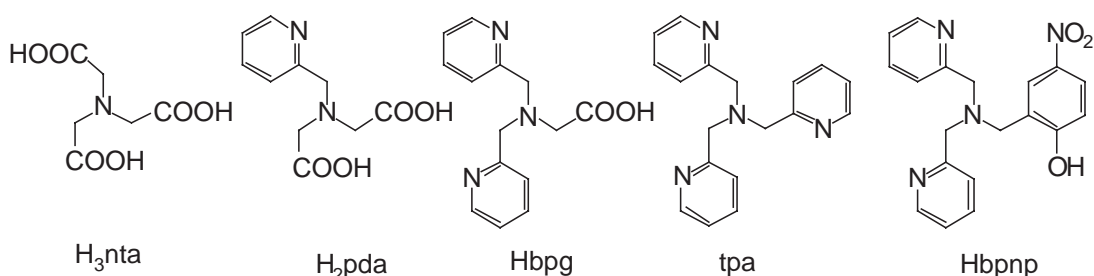
Figure 5 Tetradentate tripodal ligands for modeling intradiol-cleaving dioxygenases.
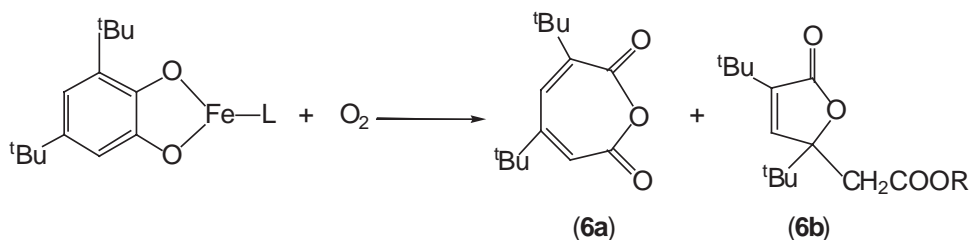
Figure 6 Reaction of model complexes with molecular oxygen.

The asymmetric bonding motif of the catecholate to the ferric ion in these complexes duplicates the binding motif in the enzyme–substrate structures that have been characterized. While the original belief that this asymmetry in Fe—O bond lengths was critical to the reactivity of the systems has since proven incorrect,[31,32] the complexes remain as functional models for the catechol dioxygenases due to both their structural and reactivity features. All complexes have been characterized as high-spin ferric catecholate complexes by UV–visible, EPR and NMR spectroscopy, and an examination of C—O bond length in these complexes shows all of the complexes to bind in the catecholate form with no semiquinonate character.[3]

It has also been observed that the covalency of the Fe—$O_{catecholate}$ bond is highly influenced by the substituents on the tripodal ligand. Specifically, the substitution of pyridines (tpa) for carboxylates (nta) greatly enhances the covalent nature of the Fe—$O_{catecholate}$ bond.[1] This can be observed in the NMR spectra due to the change in spin density and distribution as a result of mixing between the higher energy iron(III) semiquinonate state and the lower energy iron(III) catecholate ground state.[3] The result is an increase in the Lewis acidity of the iron catecholate complex and a marked increase in catechol turnover generating nearly quantitative conversion to product, Figure 6.[3] Thus it was inferred that the degree of Lewis acidity of the metal dictates the reactivity of the species. Stoichiometric reactions carried out by Que *et al.* on a series of $[Fe(L)(H_2dbc)]^+$ confirm these findings. Complexes showed an increase in the formation of the intradiol cleavage products as the ligand substituents become more electron donating, Table 1.[30] Spectroscopic data allowed for the correlation of electronic properties of the complexes with their reactivity. The reactivity of the complexes is readily followed by monitoring the disappearance of the LMCT bands upon exposure to oxygen. This decay was noted to proceed in a first-order fashion without the formation of any intermediary chromophore suggesting that the Fe(III)–catecholate complexes react directly with O_2.[31–33]

The preliminary conclusion regarding correlation between reactivity and Lewis acidity has since been revised and now states that rather than Lewis acidity, the accessibility of the reduced form of the metal (namely the iron(II) semiquinonate form) is the required feature in maximizing product formation. This was determined from an examination of analogous complexes with the redox inactive gallium(III) catecholate complex that showed no reactivity when exposed to dioxygen.[33] Consequently, the increase in reactivity observed in the more strongly covalent Fe—O_{cat} complexes has been explained by an increase in the iron(II) semiquinone character of the complex due to a transfer of electron density from the catecholate to the iron center (observable by NMR spectroscopy).[31,33] An examination of the spectral features of the catecholate complexes reveals a correlation between their reactivity and the LMCT band energies which represent transitions from the iron(III) catecholate state to the excited iron(II) semiquinonate form. This explanation, while not sufficient for all model systems, has been accepted as the general rule when predicting the reactivity of iron catecholate complexes.[31] A comparison between the enzyme–substrate complex (coordination sphere consists of two His, one Tyr and a catecholate) and the model systems (coordination sphere of four N atoms and the catecholate) also suggests that the Lewis acidity of

Table 1 Product Distribution from $[Fe(L)(H_2dbc)]^+$ Complexes with O_2 and H_2dbc.

Ligand	% **6a** & **6b**
H_3nta	84
H_2pda	95
Hbpg	97
tpa	98

the metal center is not a factor given that the enzyme exhibits a far greater reaction rate than those of the biomimetic complexes despite its greatly decreased Lewis acidity.

These elegant studies have led to the proposed mechanism illustrated in Figure 3. In this pathway, the first step, involving the loss of the tyrosinate and a water molecule, was demonstrated spectroscopically as mentioned earlier. While only the iron(III) catecholate complex is presented, it is important to remember that this species exists in equilibrium ($K_{eq} \sim 10^{-6}$) with the iron(II) semiquinonate tautomeric species.[34] Enzyme studies have suggested the ketonization of the C—O catecholate bond as a promoter in semiquinonate formation.[22,23,25,35] Subsequent to O_2 attack on the iron(II)-semiquinonate, the proposed mechanism suggests the formation of a short-lived alkylperoxy radical species prior to the formation of an alkylperoxy iron(III) intermediate, which in the enzyme is proposed to coordinate to the empty metal site that results upon substrate binding.[22,35] Structural basis for an alkylperoxo iron(III) species is derived from model complexes of iridium(III) catecholate containing triphos ligands.[36] Definitive isotopic labeling experiments have confirmed the Criegee rearrangement wherein the alkylperoxo species yields the muconic anhydride product and the iron(III) hydroxide species.[37,38] These studies utilized the $[Fe(H_3nta)(H_2dbc)]^{2-}$ model system and $^{18}O_2$. The results showed the incorporation of only one ^{18}O atom in the products as opposed to the dual insertion that would be expected from alternate pathways.[37] In more reactive systems, the formation of the anhydride (**6a**) is observed providing even more conclusive evidence for the Criegee rearrangement pathway.[37,38]

Koch and Kruger presented the first model system capable of carrying out both stoichiometric and catalytic cleavage ability.[32] The iron complex of L-N_4Me_2, Figure 7, carried out 70% product conversion to **6a** ($t_{reaction} = 3$ h, $P_{O2} = 1$ atm) and achieved catalytic turnover numbers of >50 in the presence of 1% catalyst. Product formation was monitored by ^1H NMR and showed the exclusive involvement of oxygenation pathways during product formation. Subsequently, additional model systems have been developed which have shown similar and increased reactivities.[3,39] The recurring theme throughout these is that the reactivity of the iron catecholate system with dioxygen governs the selectivity of oxygenation product versus side product (i.e., anhydride vs. benzoquinone).

8.14.1.2 Extradiol-cleaving Catechol Dioxygenases

The extradiol-cleaving dioxygenases exhibit the more commonly found coordination scheme involved in nonheme, mononuclear iron oxygenases. The common feature within the active sites of these proteins is the recurring 2-His-1-carboxylate motif surrounding a high-spin ferrous center.[4] The spectroscopically elusive nature of this iron species however has made characterization of these catechol dioxygenases rather difficult. Early studies were limited to Mössbauer spectroscopic investigations, but recent insights derived from spectroscopic and crystallographic studies over the past decade have supported a dramatic improvement in the understanding of the basic mechanism.[3] One of the better characterized catechol dioxygenases is 2,3-dihydroxybiphenyl 1,2-dioxygenase (DHBD: E.C. 1.13.11.39) which was crystallized in 1995 in the active hydrogencatecholato iron(II) form as well as the inactive Fe(III) form of the enzyme.[40] The overall geometry of the active site is that of a square pyramid consisting of two histidine and one glutamate residues with two water molecules occupying the remaining coordination sites around the ferrous ion (Figure 8a).[40] This structure with a vacant site trans to a His residue then undergoes a rearrangement upon substrate binding to yield a distinct square pyramidal structure with the vacant site trans to the Glu residue (Figure 8b).[1] The two water molecules have been
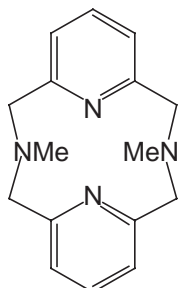
Figure 7 Structure of L-N_4Me_2 ligand.
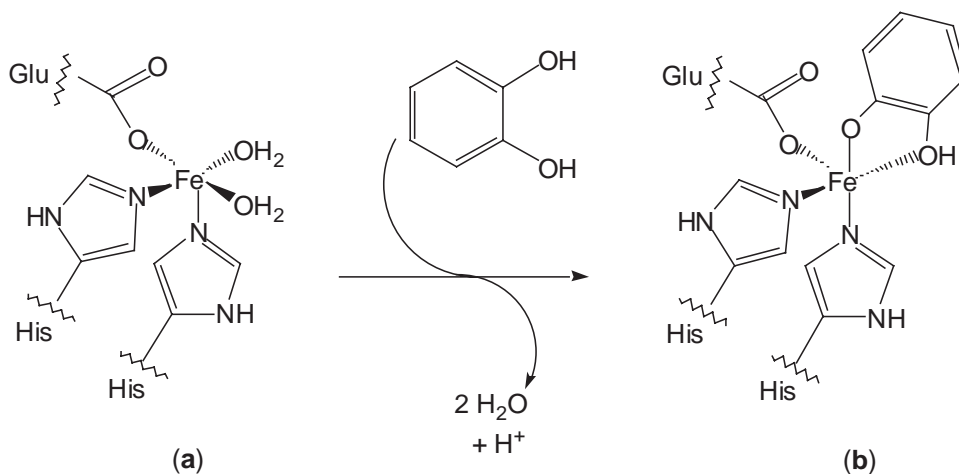
Figure 8 Schematic views of extradiol-cleaving dioxygenases.

displaced and the catecholate coordinates as a bidentate ligand trans to the two coordinated histidine residues. The square pyramidal geometry is supported by analysis of ligand field transitions in the electronic spectrum, while the retention of coordination number and geometry by XAS spectroscopy.[41–43] Due to its characteristic $S = 3/2$ EPR signal when bound to a ferrous ion, NO has been used as an O_2 surrogate to investigate the mechanistic pathways of these enzymes.[44] Studies have shown that NO has a specific binding site at the ferrous center and that the geometry of the enzyme substrate complex changes from five to six coordinate. Based on these data, the mechanism by which ring cleavage is carried out has been postulated (Figure 9) although further studies are ongoing to elucidate the finer points of the proposed scheme.

Unlike the intradiol catechol dioxygenases, the extradiol catechol dioxygenases retain all of their endogenous ligands throughout the catalytic cycle. It is suggested that substrate binding to the
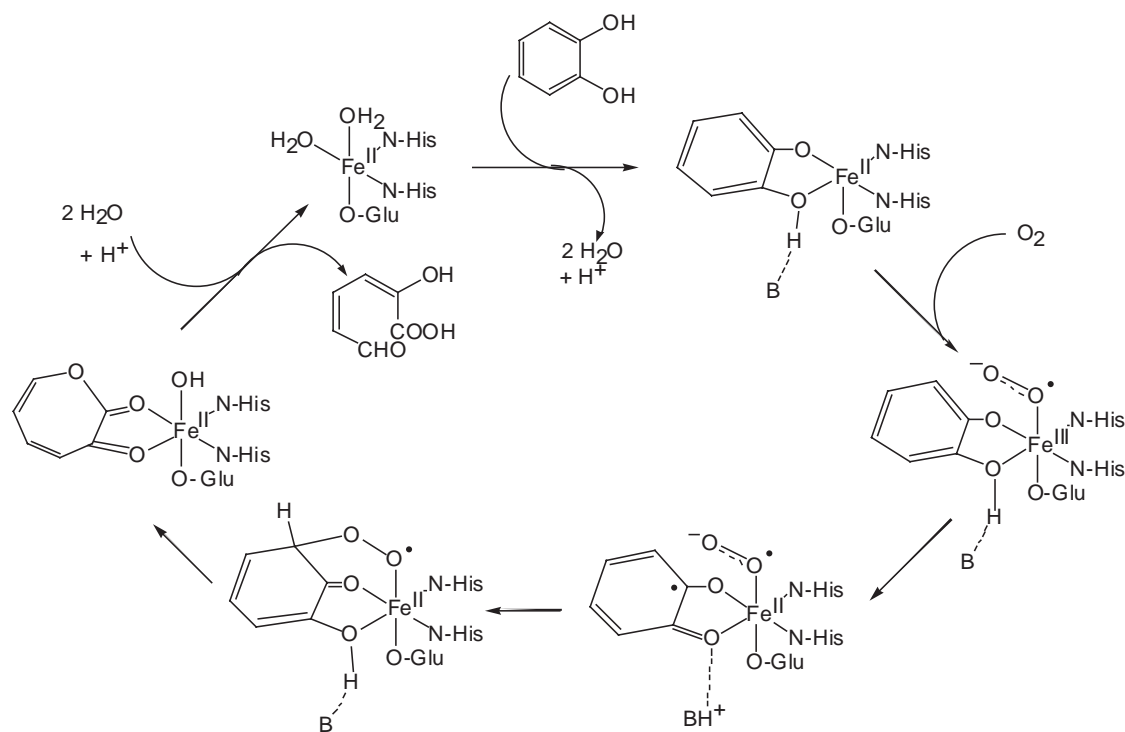
B: basic site along protein chain

Figure 9 Proposed mechanism for ring cleavage by extradiol dioxygenases.

ferrous center lowers the redox potential of the metal center, thereby making it a more favorable binding site for dioxygen. The facile transformation between the monohydrogencatecholato–super-oxo iron(II) species and the semiquinonato–superoxo iron(II) species has been supported by model complexes wherein a similar semiquinonato–superoxo rhodium(III) complex was observed.[45] This species can then more readily undergo a nucleophilic attack on the adjacent carbon of the enediol by the superoxide ion.[3] The alkylperoxo species then undergoes a Criegee rearrangement seen in the intradiol catechol dioxygenases to generate a seven membered 2,3-dioxolactone that upon hydrolysis affords the alpha-hydroxymuconic semialdehyde product.[3]

Important mechanistic studies were carried out by Bugg *et al.* that demonstrated support the proposed mechanism in Figure 9. These studies utilized isotopically labeled water ($H_2^{18}O$) to examine the Criegee rearrangement versus an intramolecular ring closure; the data support the Criegee rearrangement followed by the formation on an iron(II)-bound hydroxide or water molecule.[46] Secondly, a catecholate substrate containing a radical clock moiety (cyclopropyl group) was used to investigate the proposed formation of the semiquinonate radical species. Based on product distributions where the cyclopropyl group was observed to isomerize, the presence of a semiquinonate radical species was indeed confirmed to be form during the catalytic cycle.[47]

8.14.1.2.1 Model systems

Interestingly, the development of synthetic model systems to examining the mechanism of ring cleavage by extradiol catechol dioxygenases have proven far less promising than those for the intradiol-cleaving dioxygenases.[30] As previously mentioned, Funabiki's initial efforts involving ferrous and ferric salts in the presence of pyridine yielded extradiol cleavage products[30] but in low yield with no selectivity, and as such these reactions were not examined further with regards to their relevance as functional model systems for extradiol-cleaving dioxygenases. Chiou and Que then reported a structural model, $[Fe(6\text{-}Me_3\text{-tpa})(Hdbc)]^+$,[41,48] which mimicked the coordination mode of the catecholate to the iron in the enzyme–substrate complexes. However, it was unable to reproduce the extradiol cleavage oxygenation reaction. Instead, an electron transfer reaction occurred to produce the iron(III) catecholate complex $[Fe(6\text{-}Me_3\text{-tpa})(dbc)]^+$.[48]

The first example of a functioning model for this class of enzymes was developed by Dei and co-workers[34] and then further improved upon by Ito and Que.[49] A substoichiometric, yet significant yield of extradiol cleavage products (~29%) were observed when the complex [Fe(tacn)(dbc)Cl], Figure 10a, was reacted in stoichiometric quantities with dioxygen, Figure 10.[34] The two electron-oxidation product, dbq (di-tert-butylquinone), was also observed in ~50% yield. Itoh and Que later found that addition of pyridine and $AgBF_4$ increased the extradiol cleavage products to >98% yield.[49] As a result of their work, the mechanism in Figure 11 was proposed for the extradiol-cleavage dioxygenase model. The proposed pathway is based on two factors: first, the need for an open coordination site is taken care of by the removal of the chloride anion in the form of AgCl. This has been further substantiated in the reactions of iron(III) catecholate complexes containing the tridentate ligand hydridotris(3,5-di-*iso*-propyl-1-pyrazolyl)borate, Figure 12a, and a more sterically hindered ligand hydridotris(3-*tert*-butyl-5-*iso*-propyl-1-pyrazolyl)borate with dioxygen, Figure 12b.[50] The first complex releases a solvent molecule from its pseudooctahedral geometry to generate a square pyramidal iron (III) catecholate complex that affords an open coordination site, whereas the latter complex forms a trigonal bipyramidal iron(III) catecholate complex in which the open site is significantly hindered. As such, the complex is rendered stable to oxygen and no extradiol cleavage products are observed. Figure 12.[50] These studies support the proposed mechanism shown in Figure 9, wherein the biding of the substrate generates a square pyramidal intermediate with a nonhindered site for dioxygen binding and activation.

The second factor that led to the proposed mechanism in Figure 11 arose from the observation that in the absence of a coordinating pyridine ligand, the Lewis acidity of the complex is such that
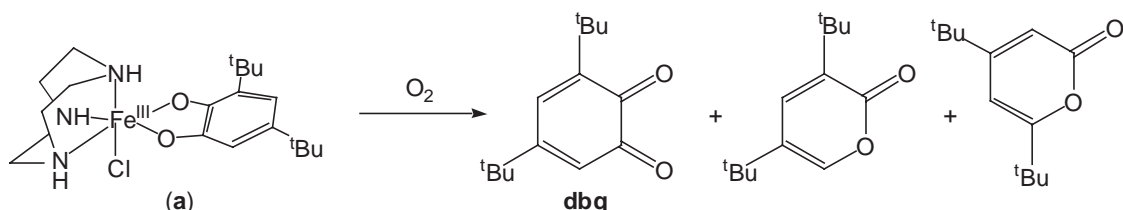
Figure 10 Reaction of extradiol dioxygenase model compound with dioxygen.
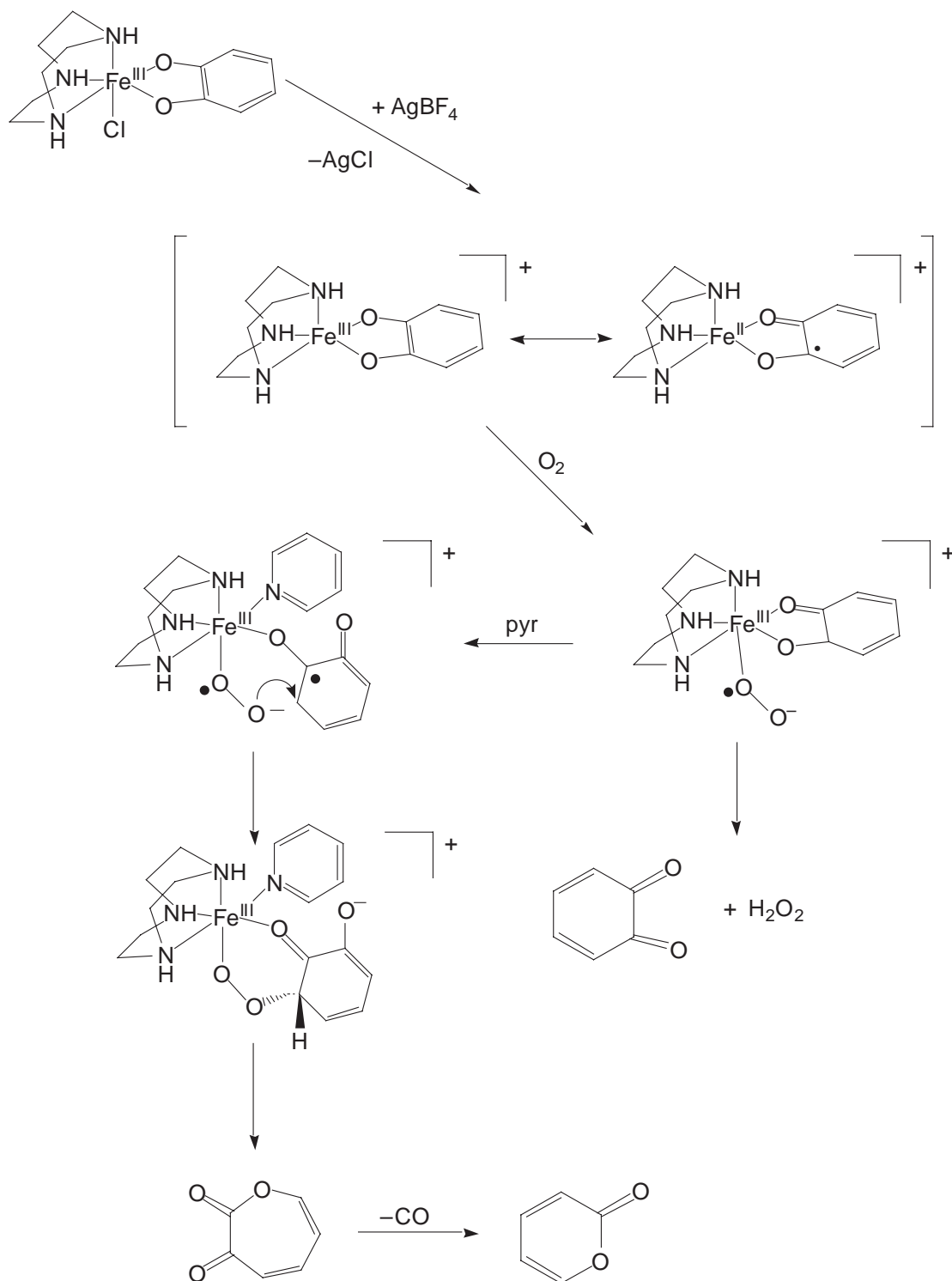
Figure 11 Proposed mechanism for model systems of extradiol dioxygenases.

a simple electron transfer process occurs to generate dbq and hydrogen peroxide as the sole products. The presence of a pyridine ligand creates a proximity between the superoxo species and the carbon atom adjacent to the enediol. Consequently, the difference between intradiol- and extradiol-cleavage mechanisms has been summarized as the difference in reactivity of the dioxygen species; that is, the nucleophilicity of the superoxide anion versus the electrophilicity of the oxygen molecule.[3] Functional model systems for the extradiol-cleaving dioxygenases remain a
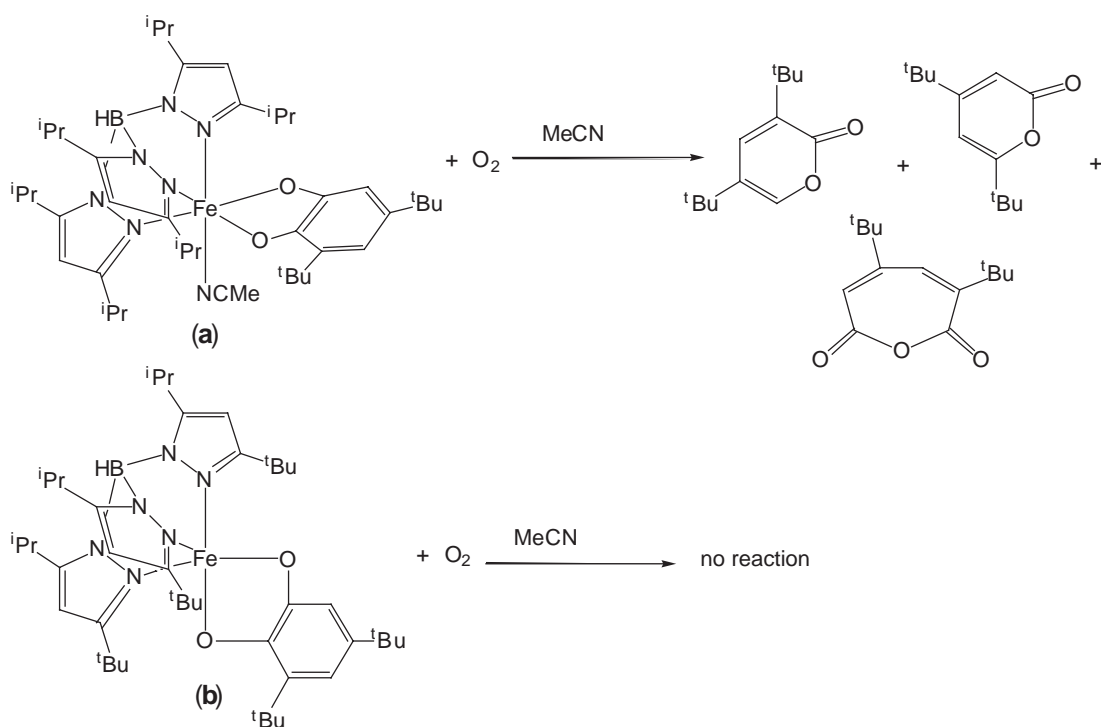
Figure 12   Importance of open coordination site for extradiol cleavage mechanism.

step behind their counterparts, the intradiol-cleaving dioxygenases. In particular, no iron(II) catecholate complexes have been reported to carry out the oxygenation chemistry of the enzymes. The development of model systems that proceed via the same pathway as the enzymes presents itself as the next challenge in the effective development of functional model systems.

8.14.2   2-OXOGLUTARATE-DEPENDENT ENZYMES

8.14.2.1   Introduction

2-oxoglutarate (2-OG)-dependent dioxygenases constitute the most diverse class of mononuclear, nonheme iron oxygenases due to both the number of enzymes that have been identified and the variety of biochemical transformations they perform.[51–53] Selected examples of their diverse utility are illustrated in Figure 13.[51] Most enzymes in this class catalyze the oxidative decarboxylation of 2-OG to generate the oxidant that transforms substrate into product. Plant forms of the enzymes are responsible for synthesizing signaling molecules, while in microorganisms, these enzymes act as catalysts in antibiotic synthesis and biodegradation. However other proteins not dependent on 2-OG have also been included in this family of enzymes due to their structural and functional characteristics. For example, 1-aminocyclopropane-1-carboxylic acid oxidase (ACCO), Figure 13c, utilizes ascorbate while isopenicillin N synthase (IPNS) uses no cosubstrate but rather carries out the four-electron oxidation of a tripeptide, Figure 13b.[51] Regardless of mechanistic features, common structural characteristics are conserved in all the enzymes.

8.14.2.2   Structure

A number of protein crystal structures has been obtained for this class of enzymes, including those of isopenicillin-N-synthase,[54] deacetoxycephalosporin C synthase (DAOCS) Figure 14,[55] and clavaminate synthase (CAS)[56] these structures are currently being studied with regards to the effect of structure on the regioselectivity exhibited by these enzymes.[56–60] For DAOCS the structure shows a jelly-roll motif with the active site situated in a shallow pocket on the edge of
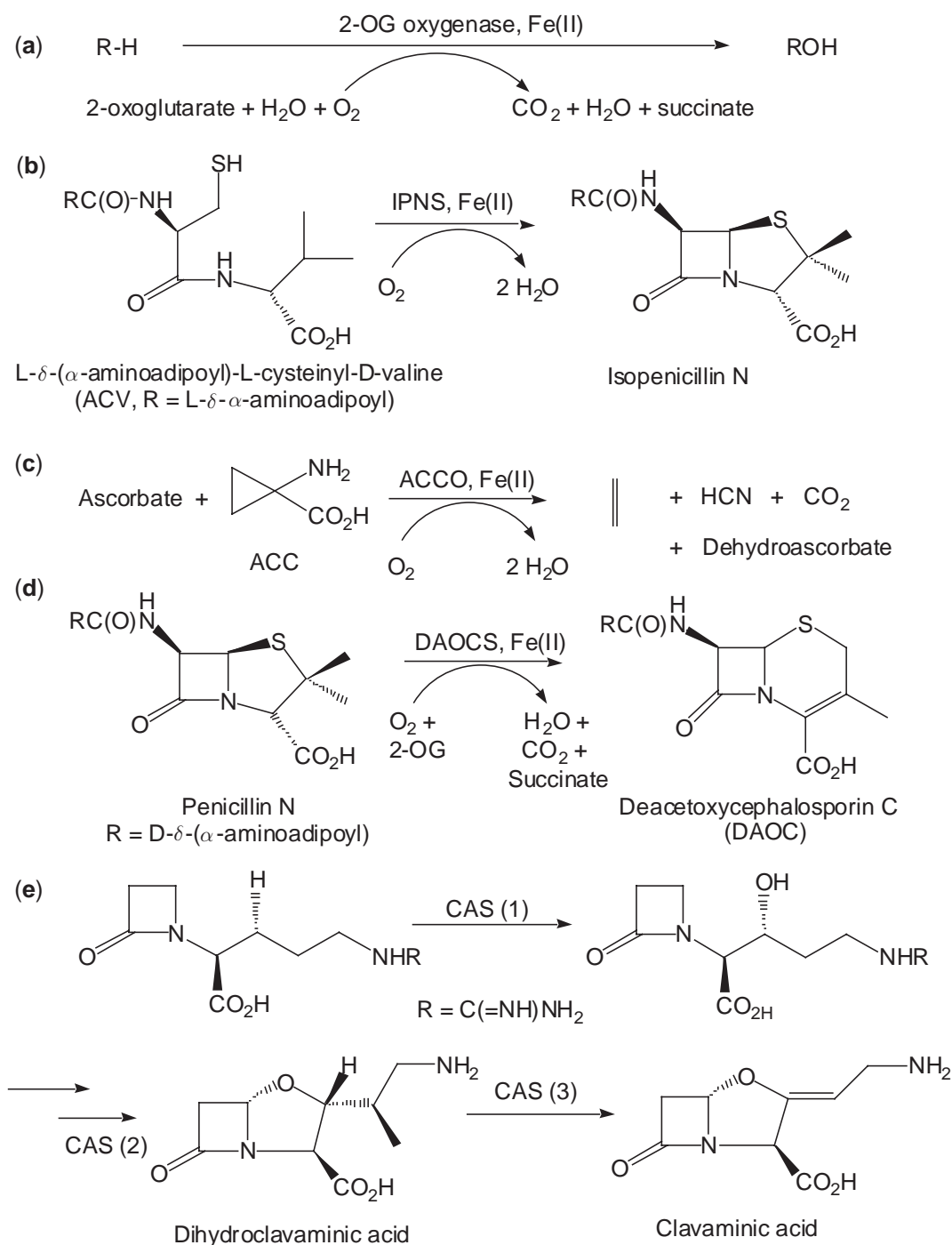
Figure 13 Reactions catalyzed by the 2-OG family.

a beta sheet. The ferrous iron site is coordinated by two histidine residues from the central beta sheet and an aspartate residue located at the end of a beta strand, Figure 14.[55] The active-site structure takes on a slightly distorted octahedral geometry with the 2-OG substrate bound directly to the metal center. As an added note, a conserved 'hinge' located at residues 298 and 302 has been proposed to play a role in regulation of the active site during certain steps of the catalytic pathway.[59] CAS has shown similar structural characteristics, the only major difference being a replacement of the coordinating aspartate by a glutamate side chain.[61] A possible explanation for this substitution is offered by Zhang *et al.* as providing additional flexibility to the enzyme such that it may carry out its role as a trifunctional enzyme, Figure 13e.[61] CD/MCD
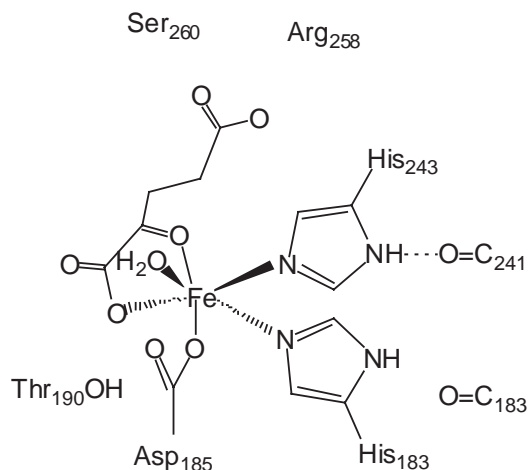
Figure 14   Active site for deacetoxycephalosporin C synthase.

studies on CAS show a change in coordination upon substrate binding (six to five coordinate), which would leave an open coordination site for dioxygen to bind at the ferrous center.[62,63] The binding of 2-OG is also different in CAS and DAOCS suggesting that the mode of O_2 binding and activation may also proceed via a different pathway provided there is no rearrangement in the binding motif of DAOCS upon binding of the primary substrate.[60]

8.14.2.3   Mechanism

Kinetic studies on the oxoglutarate-dependent enzymes suggest the orderly binding of 2-OG, the substrate, and then dioxygen.[64] These studies, combined with substrate analogue investigations have led to the mechanism proposed in Figure 15. This pathway proposes the binding of the substrate and O_2, as outlined above, in a sequential fashion followed by a two-electron oxidation of 2-oxoglutarate. This preliminary oxidation results in the decarboxylation of the glutarate moiety and the formation of a ferryl intermediate species. Subsequently, the primary substrate is oxidized by this highly electrophilic oxoferryl species to generate the hydroxylated alkane product.[55] An important feature in the reactivity of these enzymes is the release of a water ligand
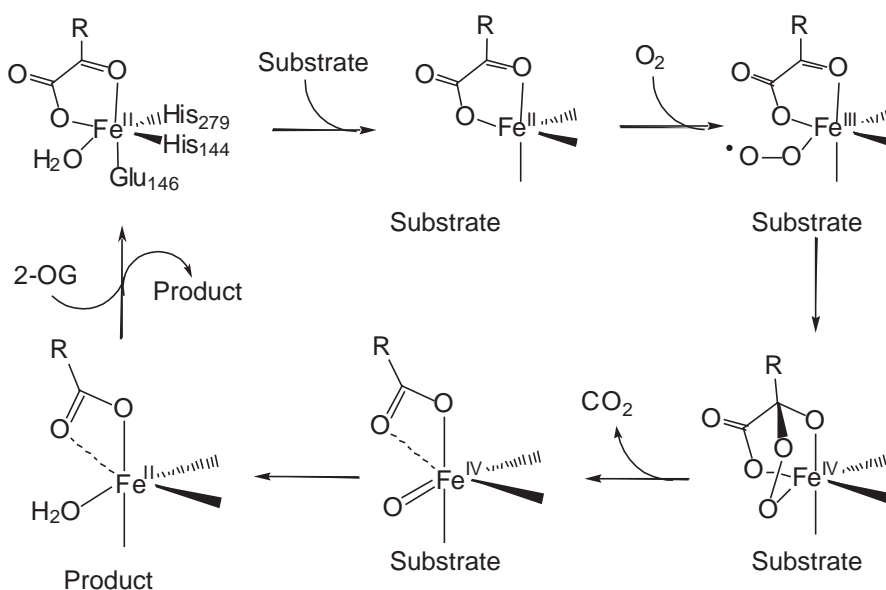
Figure 15   Proposed mechanism for 2-oxoglutarate-dependent enzymes.

upon substrate binding in order to open up the O_2 binding site. This process results in the one-electron oxidation of the ferrous center to the ferric oxidation state and the formation of a superoxide moiety on the metal center. Collapse of the superoxide with the cosubstrate and the subsequent decarboxylation is supported in studies where CO_2 is the first product formed throughout the reaction.[64] Indirect evidence for the formation of a ferryl intermediate has been found in studies by Baldwin and co-workers[59,65] While the role of the protein in determining substrate specificity is still being investigated, it is generally agreed that its role is minor outside of providing a suitable binding site for ferryl–substrate interaction.[51]

8.14.3 IPNS

While IPNS structurally (Figure 16) and evolutionarily falls within the same enzyme category as the 2-OG-dependent systems, it is unique in that it does not utilize the 2-OG cosubstrate seen in the previously discussed proteins. Rather, it catalyzes the four-electron oxidation of the tripeptide delta-(L-alpha-amino-delta-adipoyl)-L-cysteinyl-D-valine (ACV) to penicillin N via the complete reduction of O_2 to water. Although no spectroscopic intermediates in the reaction pathway of IPNS have been characterized in detail, kinetic studies have led to the mechanism proposed in Figure 17.[66,67] This pathway is based primarily on the results of structural characterizations and of enzymatic substrate analogue studies. The reaction is believed to proceed in two steps: formation of the beta-lactam ring followed by the formation of the thiazolidine ring. Evidence has been presented for the formation of radical substrate intermediates although no information supporting product racemization has been observed. As such, it has been postulated that the protein structure surrounding the active site must firmly dictate the positioning of the substrate on the metal center. The mechanism is then proposed to proceed via similar steps wherein O_2 binds in the trans position to the Asp_{216} residue and forms a superoxide species via the one-electron oxidation of the ferrous ion. This species then proceeds to form a metal-hydroperoxide species subsequent to formation of the β-lactam ring. Heterolytic cleavage of the peroxide moiety generates a high valent metal-oxo species that is in position to abstract the valine hydrogen atom from ACV, generating the thiazole ring present in the final product.

8.14.3.1 Model Systems

Several model systems have been developed in an effort to better understand the mechanistic pathways involved in the 2-OG-dependent enzymes. One of the first set of complexes was the $[Fe(II)(L)(BF)]^+$ series, where BF = benzoylformate, L = 6TLA or TPA, tris(6-methyl-2-pyridyl-methyl)-amine and tris(2-pyridyl-methyl)amine, respectively.[69,70] Both complexes reacted with O_2 to form decarboxylated products and could perform the oxidation of simple substrates such as phenol and phosphines, but no alkane oxidation was reported. The effects of substituents on the BF ligand on the rate of the reaction suggested the involvement of a nucleophilic mechanism, Figure 18.[69,70] Subsequent studies have also been carried out using a related complex with the tridentate Tp^{Ph2} (Tp^{Ph2} = hydrotris(3,5-diphenylpyrazol-1-yl)borate) ligand and a bidentate benzoylformate.[71,72] These complexes reacted with dioxygen to yield both benzoate (from oxidative decarboxylation) and a self-hydroxylation product from intramolecular attack of one of the phenyl rings on the ligand.[71]
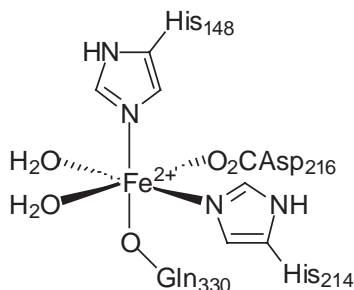
Figure 16 Schematic representation of IPNS active site.
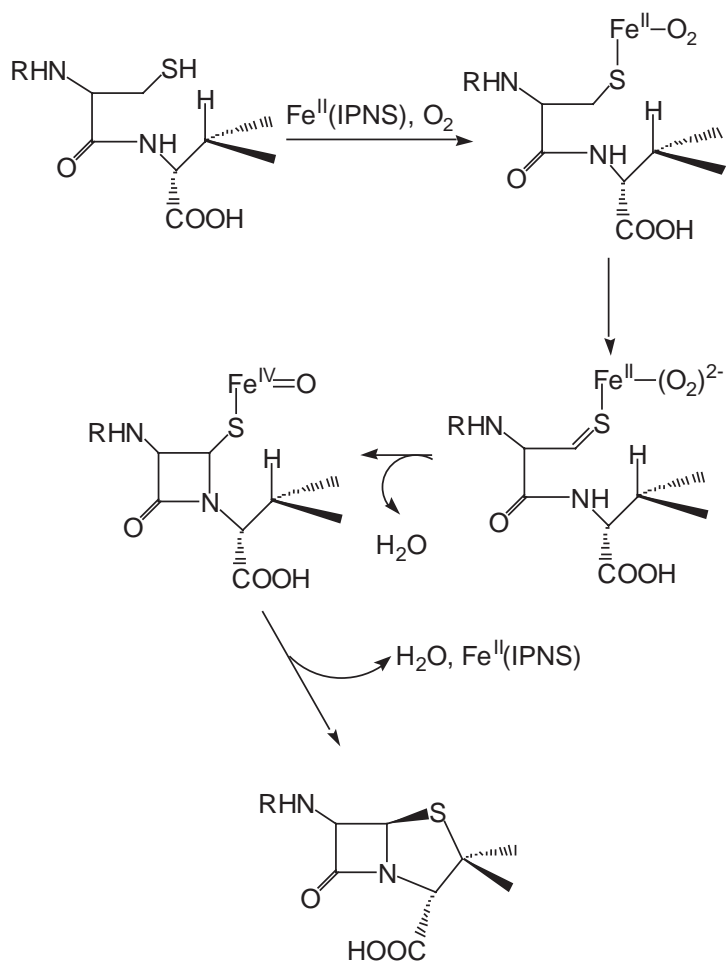
Figure 17 Proposed mechanism for isopenicillin N synthase.

The first model system shown capable of carrying out alkene oxidation was developed by Ha *et al.* using [Fe^{II}(BF)(Tp^{Me2})(CH$_3$CN)], Tp^{Me2} = hydrotris(3,5-dimethyl-1-pyrazoyl)borate.[72] This complex was shown to support the epoxidation of cyclohexene as well as the concomitant oxidation of the alkene to its corresponding allylic alcohol and ketone, Figure 19. Reactions recorded in the presence of radical scavengers showed no change in product distribution, indicating a radical free oxidation pathway. Interestingly, reaction of stilbenes with the iron catalyst showed only formation of the *cis* form of the epoxide, which suggested a sterically hindered transition state that would prevent formation of the trans isomer. Mechanistic studies implied the displacement of the acetonitrile solvent ligand prior to dioxygen bonding and the subsequent formation of a superoxide species. The bound superoxide anion could then react with the benzoylformate ligand to form the peroxy adduct which reacts with the olefin to generate the observed epoxide product. No spectroscopic studies have been reported that support the proposed intermediates and further mechanistic work on the system is required before the determination of a conclusive reaction pathway.

8.14.4 PTERIN-DEPENDENT AMINO ACID HYDROXYLASES

8.14.4.1 Introduction

The pterin-dependent amino acid hydroxylases (AAH) are a group of mononuclear, nonheme monooxygenases that catalyze the oxidation of aromatic amino acids necessary for the biosynthesis of a variety of neurotransmitters.[74,75] The three primary enzymes that have been
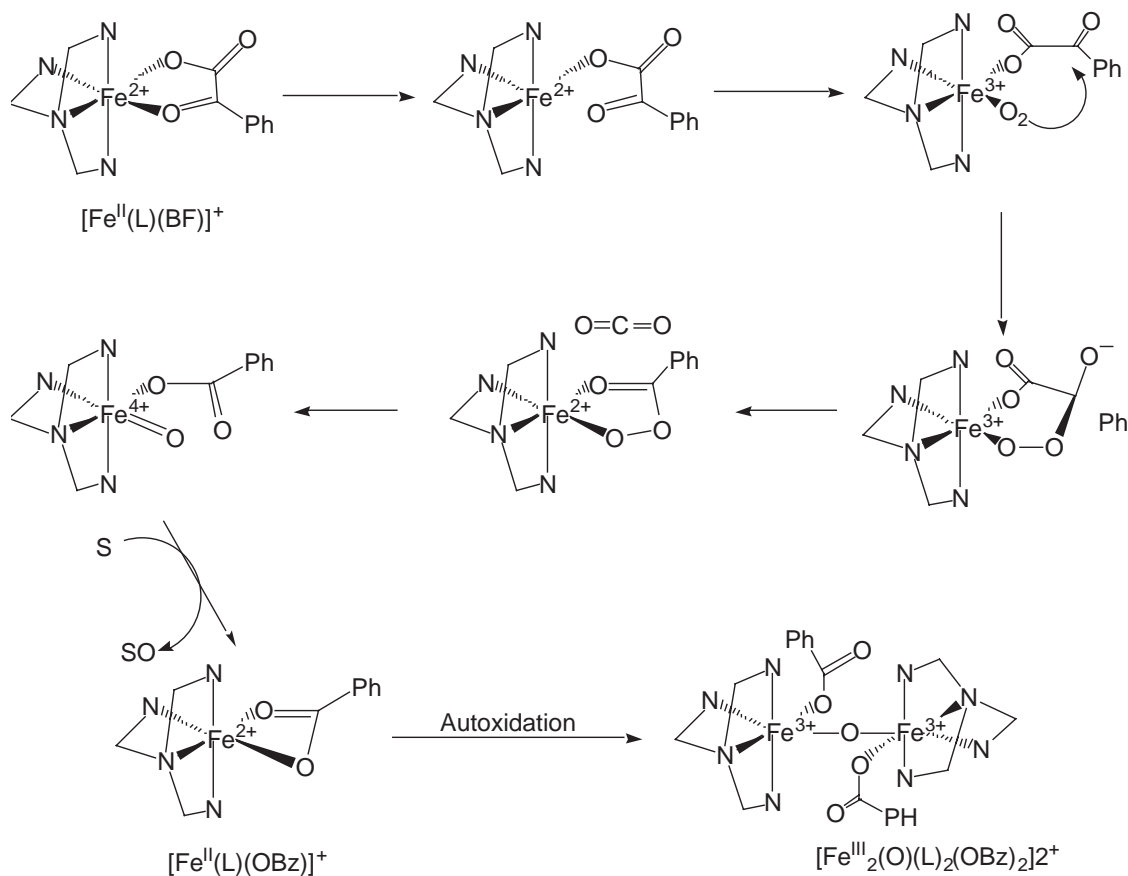
Figure 18 Proposed mechanism for the oxygenation of benozoylformateiron(II) complexes.

isolated and characterized are phenylalanine hydroxylase (PAH), tyrosine hydroxylase (TYRH) and tryptophan hydroxylase (TRPH). Other oxygenases of this class, anthranilate hydroxylase,[76] mandelate hydroxylase[77] and glyceryl-ether monooxygenase,[78] have been identified but have not been isolated or characterized in detail.[60] PAH, TYRH and TRPH utilize the $2e^-/2H^+$ reductant tetrahydrobiopterin (BH$_4$:(6(R)-L-erythro-5,6,7,8-tetrahydropterin) as cofactor, Figure 20.[60] PAH is the AAH that has been the most widely studied owing to its availability and
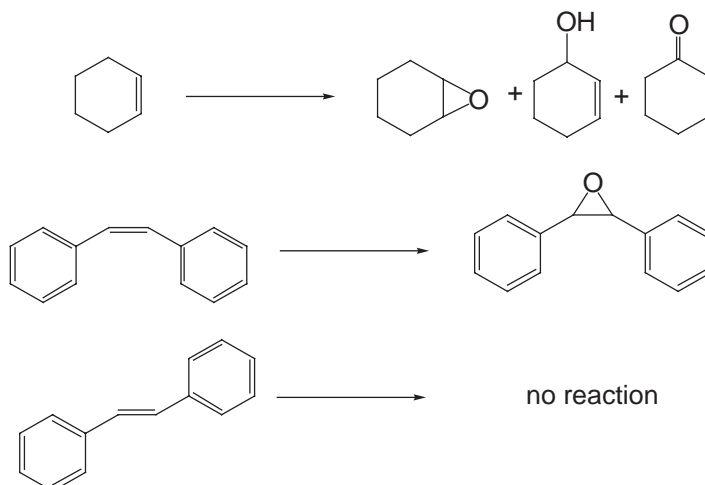
Figure 19 Olefin oxidation reactions of [Fe(BF)(Tp^{Me2})(CH$_3$CN)].
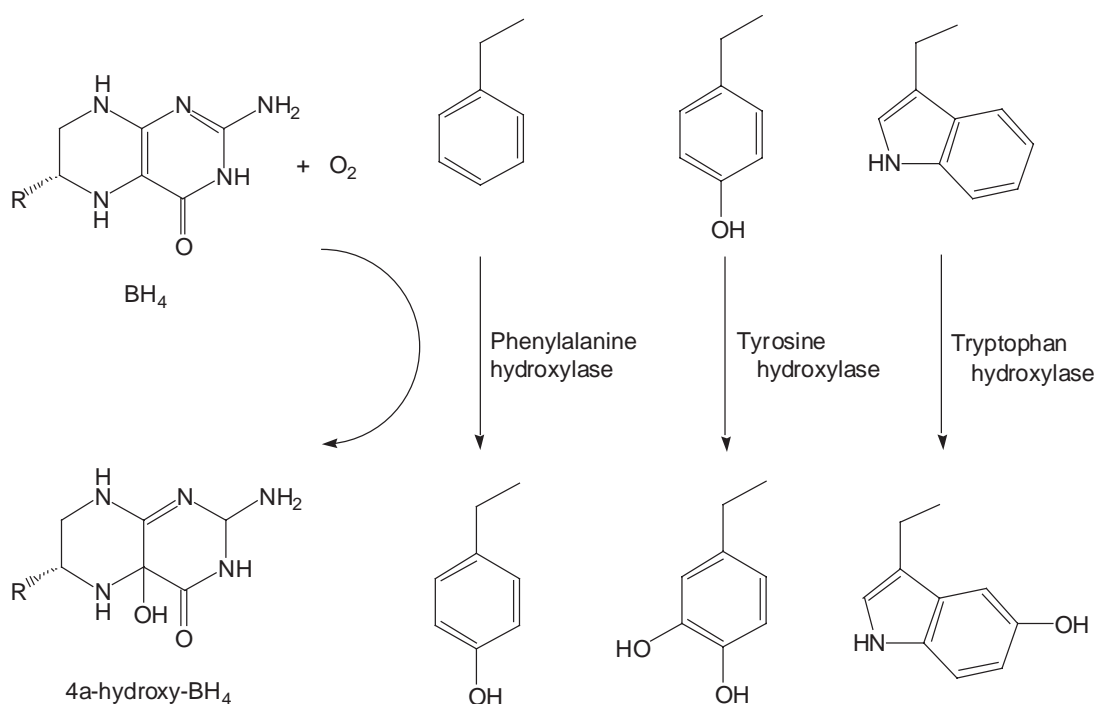
Figure 20 Transformation carried out by pterin-dependent hydroxylases.

stability. PAH is responsible for maintaining physiological L-Phe homeostasis. A disfunction of this enzyme results in the disease known as phenylketonuria (PKU), which if left untreated leads to severe mental retardation and premature death.[74] This disease represents one of the most common metabolic disorders of clinical significance in children. TYRH is the enzyme responsible for the formation of dihydroxyphenylalanine (L-dopa) whose physiological concentrations have been linked to disorders such as Parkinson's disease.[74] L-dopa is then converted to other neurotransmitters such as norepinephrine and epinephrine. Finally, TRPH converts the tryptophan amino acid to 5-hydroxy-tryptophan, which is the first step in the biosynthesis of the neurotransmitter serotonin.[74] Each of these proteins share a notable similarities in their sequences: 65% sequence identity and 80% sequence homology in the catalytic domains which contain the nonheme iron center.[75]

8.14.4.2 Active Sites for the Amino Acid Hydroxylases

Upon expression and purification, the proteins are retrieved in the inactive, ferric state due to the ease of oxidation of the ferrous center during isolation. It has been shown that the cofactor, BH_4, can act as a reductant for the ferric ion and as such, serves to maintain the protein in its active ferrous state for the enzymes PAH and TYRH.[79,80] Recent spectroscopic studies have shown the iron center in PAH to be coordinated in a distorted, octahedral geometry.[81,82] The catalytic domain has an α/β fold that makes a basket–like arrangement of helices and loops.0 The active site is situated ~10 Å away from the protein surface and is coordinated through three endogenous protein ligands: His_{285}, His_{290} and Glu_{330}, Figure 21a, thereby conserving the 2-His-1-carboxylate facial triad binding motif of mononuclear, nonheme oxygenases.[1] The crystal structure for tyrosine hydroxylase shows a square pyramidal arrangement wherein the 2-His-1-carboxylate motif occurs via coordination through the three endogenous protein ligands His_{331}, His_{335} and Glu_{375}, with two water molecules occupying the remaining coordination sites, Figure 21b.[75] This five-coordinate structure has recently been debated based on spectroscopic evidence for a six coordinate iron center[83] and current studies are attempting to resolve/explain the discrepancies between the crystallographic and spectroscopic data for the protein.

The AAH enzymes show remarkable specificity for their respective substrates; a characteristic governed by their regulatory domains. Each active site is situated within a hydrophobic pocket with negative electrostatic potential at the active site[75] offering a suitable binding environment for
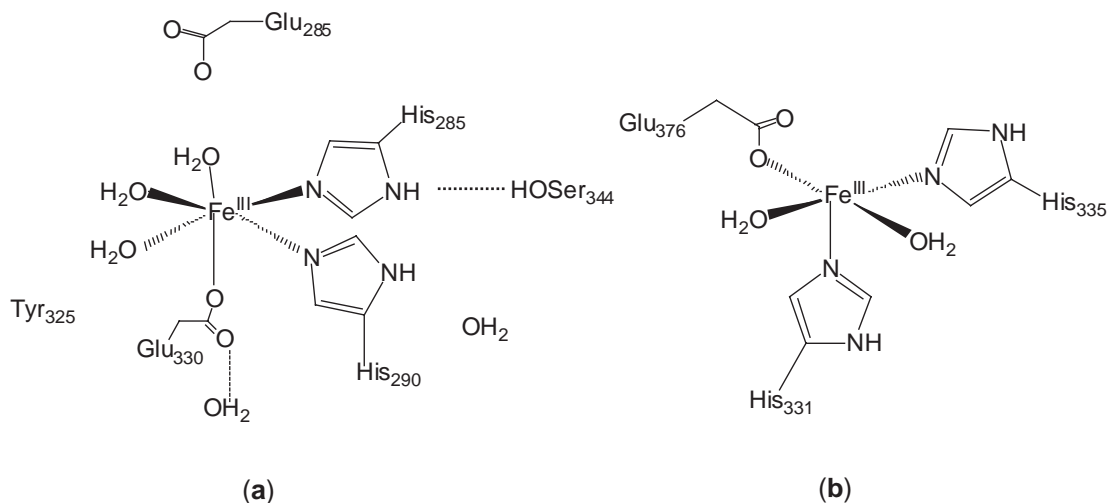
Figure 21 Iron coordination environments for PAH and TYRH.

amphipatic molecules such as substrates, the pterin cofactor or inhibitors. A major focus in the studies of these proteins involves elucidating the details surrounding the specific interactions between the substrate, cofactor and iron center.

8.14.4.3 Mechanism for Substrate Hydroxylation

The currently accepted mechanism by which substrate hydroxylation occurs in PAH is depicted in Figure 22.[74] MCD and XAS studies of the resting state inactive ferric and active ferrous enzymes indicate the presence of a slightly distorted six-coordinate iron site, a conclusion in agreement
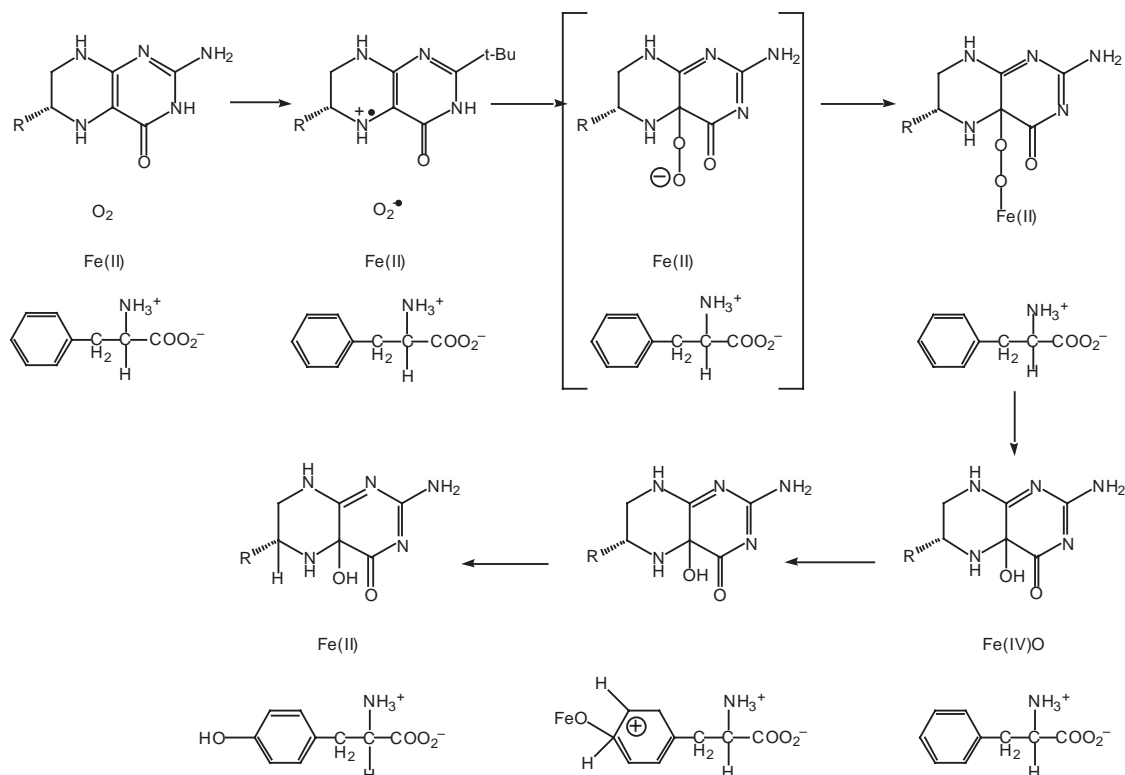
Figure 22 Proposed mechanism for phenylalanine hydroxylation by PAH.

with crystallographic studies of various truncated forms of oxidized PAH. This coordination environment is maintained in the presence of either cofactor alone or substrate alone.[84,85] However, prior to enzymatic turnover, PAH undergoes an allosteric activation induced by the binding of Phe to a site distinct from the catalytic site. Interestingly, once PAH is activated, the ferrous site adopts a square-pyramidal geometry caused by the loss of a single water ligand.[86] It is this form of the ferrous enzyme that is catalytically active. The proposed mechanism indicates that the initial reaction involves the interaction of dioxygen with the reduced pterin cofactor to afford the C4a-hydroperoxy-H_2biopterin species, a step that activates the kinetically inert O—O bond of dioxygen by converting it to an alkyl hydroperoxide moiety. It is important to note that there is no experimental evidence suggesting that either the reduced cofactor or the substrate molecule coordinates to the ferrous center in the active site. The next step is thought to involve the coordination of the alkylperoxide to the ferrous iron center[88] followed by subsequent heterolytic cleavage of the O—O bond to generate a high valent iron-oxo species and C4a-hydroxyl-H_2bio-pterin, a form of the cofactor observed during catalytic turnover. The analogy has been made between this iron oxo species and the one that has been postulated for heme systems such as cyt-P450.[89] Attack of the electrophilic ferryl species on the phenylalanine substrate then forms a cationic substrate intermediate[90] that, upon cleavage of the iron species, regenerates the ferrous ion leaving the hydroxylated product tyrosine.[74,91] The oxidation of Phe to Tyr is known to occur via a pathway that induces an NIH shift of para substituents on Phe (^2H, ^3H, Cl, CH_3), a process consistent with an oxygen atom transfer step. Interestingly, insights into the mechanism of wildtype PAH have allowed for a deeper understanding of the chemical basis of phenylketonuria as parallel spectroscopic and enzyme mechanistic studies on selected missense mutants that give rise to PKU in the human population have been reported. Such studies will enable the identification of the chemical basis of PKU.[92]

To date, no functional model systems have been developed to probe the reactivity and structural characteristics of the family of aromatic nonheme iron tetrahydropterin-dependent monooxygenases. Currently, all mechanistic information regarding the reaction pathways involved in PAH has been derived from *in vitro* studies on the protein. For a more detailed description of the evidence, the reader is directed to the accompanying references cited above.

8.14.5 LIPOXYGENASES

8.14.5.1 Introduction

Lipoxygenase (LO) enzymes have been isolated from plants, animals, fungi, algae, and cyanobacteria.[30] They have been shown to catalyze dioxygenation reactions wherein the 1,4-*cis-cis*-diene unit of a polyunsaturated fatty acid is converted to a hydroperoxide functionality, Figure 23.[60] The initial studies on these enzymes were traditionally carried out on the plant forms of the protein, namely soybean lipoxygenase (SLO), due to the fact that it is easily isolated and purified from plants. SLO exists in three isoforms (sLO-1, sLO-2 and sLO-3) that share homologous sequences.[60] In the latter part of the twentieth century, mammalian lipoxygenases became of great interest pharmaceutically due to their role in inflammatory processes.[93] Plant LOs catalyze the conversion of lineolic acids while mammalian LOs catalyze hydroperoxidation of arachidonic
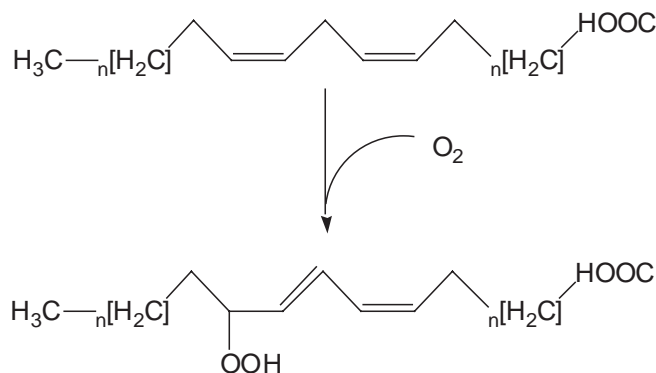
Figure 23 Dioxygenation reaction for lipoxygenases.

acids. All LOs have shown a remarkable conservation of sequence motifs and are concluded to have derived from a single evolutionary origin.

8.14.5.2 Structure

The isolated form of LO reveals a mononuclear, nonheme, high-spin ferrous center that is inactive until oxidized to the ferric state. The structure of the catalytic domain for SLO was debated for sometime owing to differences in reported crystal structures. The structure by Minor *et al.* proposed a five-coordination environment, where three histidine residues, the carboxylate from an isoleucine side chain, and an asparagine residue are coordinated to the metal center.[94] Alternatively, the structure solved by Boyington *et al.* revealed a four-coordinate site where there was no asparagine coordination to the metal center.[95] Recently, the crystal structure was resolved to 1.4 Å by Minor *et al.*[96] This form, depicted schematically in Figure 24a, is now recognized as the structure for the active sites of plant LOs.[60] These results indicate that the asparagine moiety is positioned too far from the ferrous center to act as a potential ligand yet does contribute to the rhombically distorted coordination sphere. The Asn, which is situated at 2.9 Å from the iron, would exhibit very weak bonding interactions and is proposed to account for the flexibility in the coordination sphere of ferrous sLOs.[97] The rabbit 15-LO enzyme, which was crystallized and solved to 2.4 Å resolution using an aryl inhibitor, shows a similar binding motif as observed in the plant LO enzyme.[98] Here, Asn_{694} is replaced by a coordinated histidine residue.

Although there are no water molecules observed in the immediate vicinity of the active site, it has been suggested that the binding of the aryl inhibitor displaces the originally coordinated water species (no crystal structures on the as isolated iron(III) protein have been resolved). The aryl inhibitor, while conformationally constrained and as such would not bind in the same mode as the arachidonic acid substrate, is thought to occupy the traditional substrate-binding site on the protein.[60] Furthermore it is offered as evidence that the carboxylate moiety on the acid interacts with a positively charged residue upon entering the channel to the active site.

To date, there are no published crystal structures for the substrate-bound, ferric form of LO enzymes. All spectroscopic evidence (XAS, MCD, CD) suggests a six coordinate species wherein the Asn694 may act as an iron ligand.[99–101] These results are interpreted to indicate that a hydroxide ion occupies the sixth coordination site in order to compensate for the increased charge on the metal ion after oxidation to the active species. Characterization of site-directed mutants of LO in which the Asn694 residue was altered to the noncoordinating alanine or threonine residue showed no activity whereas Asn694His mutations retained similar activities with wild-type protein further suggesting the coordination of the Asn to the ferric center. It is interesting to note, that the protein has an unusually high redox potential (+0.6 V) and the only suitable oxidant for the ferrous protein is the product of the reaction itself, the peroxy fatty acid.[60]
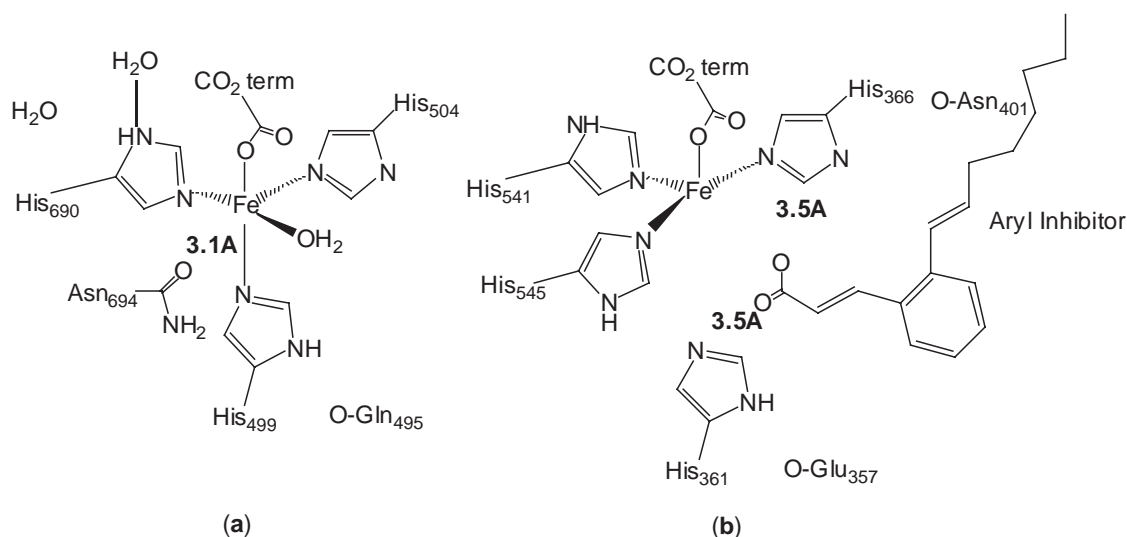
Figure 24 Iron coordination spheres of soybean and rabbit lipoxygenase.

8.14.5.3 Mechanism

The hydroperoxidation reactions of lipoxygenases are carried out with high regio- and stereoselectivity. Several pathways have been postulated for the mechanism of these specific hydroperoxidations, including substrate hydrogen atom abstraction, organo-iron complex formation, and protein radical site formation. The first of these proposed mechanisms has since become the accepted pathway and is outlined in Figure 25. In this mechanism, the hydroxide ligand on the ferric center carries out a hydrogen atom abstraction reaction generating a substrate radical and a ferrous iron center. This proposed mechanism accounts for the specificity of the reaction by proposing that the enzyme itself enforces a bent configuration upon the substrate such that attack by dioxygen occurs only at the desired site of peroxidation. Upon hydrogen atom transfer from the iron(II)-aqua unit to the substrate peroxy radical, the product is then generated and the active form of the enzyme is regained.

Another interesting feature of these enzymes is the formation of an intense purple intermediate upon the addition of excess hydroperoxy product.[102] It has been noted that this chromophore resembles the iron–alkylperoxo complexes previously characterized by Que and co-workers.[103] While no spectroscopic evidence has been obtained for the LO systems, such a complex would not be rationalized by the mechanism put forth in Figure 25 as the peroxy-substrate species would need to be positioned in a trans position to the iron.

8.14.5.4 Model Systems

Model complexes for LO have been investigated for almost 30 years. Chan *et al.* began with simple iron salts in phosphate buffers but were only able to obtain moderately stereospecific product yields.[104] Similar studies performed using the ferric-bleomycin compounds developed by Nagata *et al.*, where it was observed that the reaction of these complexes in phosphate buffer with lineolic acid yielded a mixture of monooxygenation and dioxygenation products.[105] Mascharak *et al.* have utilized $[Fe(PMA)]^{n+}$ complexes, Figure 26, to model the chemistry using both dioxygen and hydrogen peroxide. These complexes have been shown to proceed via a low-spin (hydroperoxo)–iron(III) intermediate, which was characterized by EPR spectroscopy. The reaction is proposed to proceed via the hydrogen atom abstraction pathway described earlier. The peroxidized lineolic acid radical species has been observed by UV spectroscopy.[106] Recently, Stack and co-workers have reported on a novel ligand system design that mimics the five
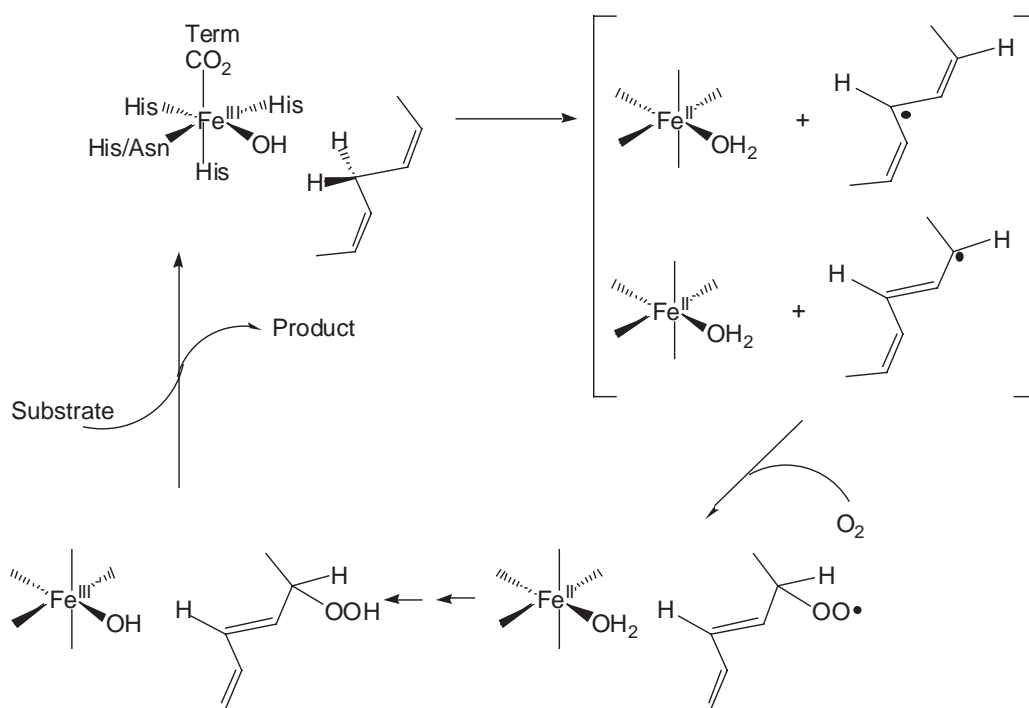
Figure 25 Proposed radical-based mechanism for lipoxygenase reaction.

$$n = 1, \quad X = Cl, \quad Solv = MeOH$$
$$n = 2, \quad X = (NO_3)_2, \quad Solv = DMSO$$
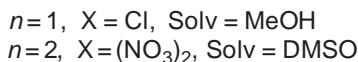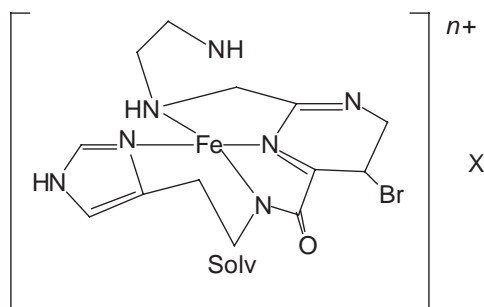
Figure 26 Structure for [Fe(PMA)] complex.

coordinate environment in LOs which can accommodate a sixth exogenous solvent ligand.[107] The ligand, 2,6-bis-((2-pyridyl)methoxymethane)pyridine, **PY5** (Figure 27), forms the high-spin, six-coordinate ferrous complex [Fe(**PY5**) (MeOH)](OTf)$_2$, Otf = CF$_3$SO$_3^-$ and is stable to air. In this system, the Lewis acidity of LOs is modeled and the short Fe—OMe bond distance reproduces that of the proposed ferric hydroxide species in activated LOs. The complex was shown capable of carrying out hydrogen atom abstraction on suitable diene substrates and isotopic substitution studies show the abstraction step to be the rate-determining step. This presents the first chemical precedence for the proposed RDS in the mechanism of LOs as well as setting the groundwork for further thermodynamic investigations regarding the mechanism.

More recent studies have focused on the characterization of the potential intermediate alkyl-peroxo–iron(III) species. Que and co-workers have synthesized [Fe(6-Me$_3$-TPA)(O$_2$CAr)]$^+$, 6-Me$_3$-TPA:tris(6-methyl-2-pyridylmethyl)amine, as a structural model for lipoxygenase.[108] This complex is an air stable iron(II) species that, upon reaction with peroxides, generates the metastable, purple intermediate species as witnessed upon the addition of excess product peroxide to the parent enzyme. The complex then decomposes via homolysis of the O—O bond to regenerate the original iron(II) species. The relevance of this pathway to the protein remains uncertain owing to the unlikelihood of an alkylperoxo intermediate being present within the currently accepted mechanism. Stack and Mayer have independently designed functional model systems wherein the hydrogen atom abstraction mechanism is witnessed as the rate-determining step for lineolic acid peroxidation reactions.[109,110] These systems have been utilized to examine the thermodynamic influences on C—H bond activation in lipoxygenase pathways.

8.14.6 ARENE DIOXYGENASES

8.14.6.1 Introduction

Arene dioxygenases, or Rieske dioxygenases (RDO), are enzymes that contain both a mono-nuclear, nonheme iron center as well as a Rieske-type, Fe$_2$S$_2$ cluster.[60] They have a wide-ranging
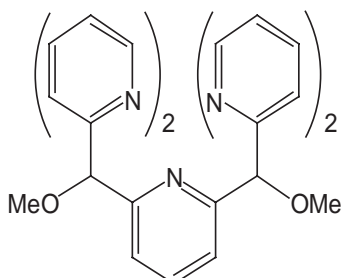
Figure 27 Structure of PY5 ligand.

substrate specificity, similar to those of the cytochrome P450's, yet they are the only class of proteins capable of carrying out the stereospecific, *cis*-dihydroxylation of aromatic compounds. Dioxygen and NAD(P)H are utilized in the catalytic cycle where the NAD(P)H serves as the redox partner for the electron-storing Rieske center. Their ability to degrade such biotoxic compounds as benzene, toluene, nitroaromatics, and halogenated polycyclic/aromatic compounds has made them of great interest to many researchers seeking to develop chiral synthons for biologically active chemicals or pharmaceuticals.[111]

8.14.6.2 Structure

The two most well-characterized RDO enzymes are phthalate dioxygenase (PDO) and naphthalene 1,2-dioxygenase (NDO).[112] The catalytic domain contains the mononuclear nonheme iron site, which is situated within a cavity of $\sim 30\,\text{Å}$ from the protein surface. The general coordination environment about each center is shown in Figure 28.[60] Recent studies have shown that Asp_{205}, which is engaged in second-sphere hydrogen bonding in order to stabilize the His_{208} residue, is in fact necessary for catalysis due to its role in the electron transfer from the Rieske center to the mononuclear site.[111] No structural changes in the protein are noted upon coordination of substrate to the active site, although spectroscopic studies reveal that the mononuclear site changes from five to six coordinate upon substrate binding to the ferrous center.[113,114] MCD studies suggested that in fact, the mononuclear center remains five coordinate throughout the entire cycle, but this conclusion may be influenced by difficulties in analyses due to having the Rieske center so close.[114] The Rieske domain is situated at about $12\,\text{Å}$ away from the catalytic center, which is within reasonable distance for a biological electron transfer process to occur.[115]

8.14.6.3 Mechanism

The proposed mechanism for RDO enzymes has arisen from steady-state kinetic experiments and single turnover experiments carried out by Ballou and Lipscomb, Figure 29.[116,117] The binding of the substrate occurs at the fully reduced enzyme center and enables the further activation of O_2 by the ferrous center. Production of the *cis*-dihydroxylated product generates the oxidized mono-
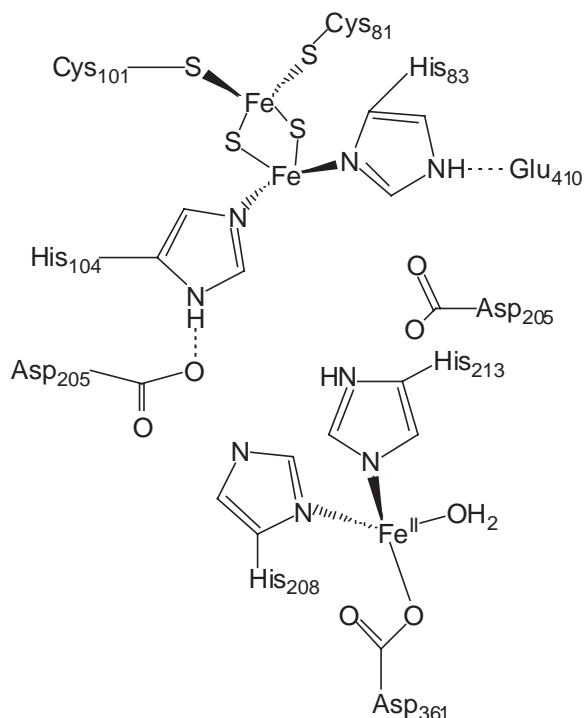
Figure 28 Coordination environment for naphthalene dioxygenase.
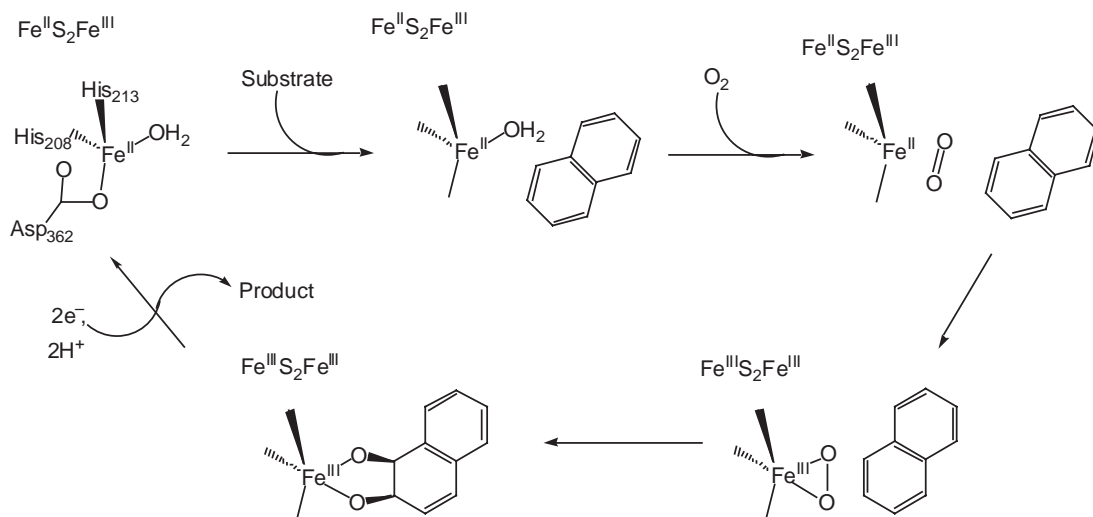
Figure 29 Proposed mechanism for the *cis*-dihydroxylation reaction of arene dioxygenases.

R = H, BPMCN
R = Me, 6-Me$_2$-BPMCN
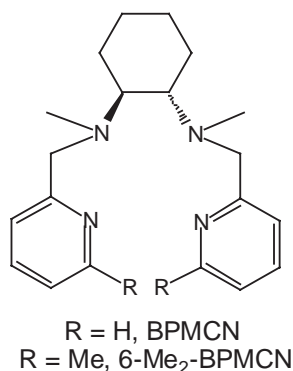
Figure 30 Tetradentate ligands used in models for Rieske dioxygenases.

nuclear and Rieske centers, which are subsequently reduced by two external electrons from the reductase component. New insight into the oxygen activation has recently been obtained by Eklund and Ramaswamy,[118] who report the first observed intermediate species for naphthalene dioxygenase where O$_2$ binds to the iron center in a side-on fashion. The side-on geometry puts the dioxygen directly in line with the target double bond and may account for the *cis* stereospecificity of dihydroxylation observed for these enzymes.

Recently, Chen, Costas, and Que have reported using iron complexes that catalyze olefin *cis*-dihydroxylations,[119] including those with linear tetradentate ligands containing a chiral diamine backbone, Figure 30, that carry out enantioselective oxidations.[120] It was found that the introduction of a 6-methyl substituent on the pyridine moiety can direct the catalytic pathway of the catalyst such that the primary oxygenation product is the dihydroxylated species. Altering these substituent groups allowed for enantioselective control over the hydroxylation pathway. While reaction conditions are not optimized (large excess of substrate are required) this system does suggest the possibility for the rational design of industrial catalysts capable of carrying out enantioselective, *cis*-dihydroxylation of olefins.

8.14.7 CONCLUDING REMARKS

Our understanding of mononuclear nonheme iron oxygenases has been greatly enhanced in the ten years prior to 2003 due to the explosion of protein crystallographic information on these enzymes and the development of functional model systems. As this manuscript was being completed, two papers on synthetic mononuclear oxoiron(IV) complexes were published, one of which reports the

first crystal structure of such a complex.[121,122] Since oxoiron(IV) species figure prominently in the mechanistic schemes proposed in this chapter, these later breaking results provide the first validation of such hypotheses. Clearly more progress in this sub-field can be expected in the near future.

8.14.8 REFERENCES

1. Que, L., Jr.; Ho, R. Y. N. *Chem. Rev.* **1996**, *96*, 2607–2624.
2. Sono, M.; Roach, M. P.; Coulter, E. D.; Dawson, J. H. *Chem. Rev.* **1996**, *96*, 2841–2887.
3. Meunier, B., Ed., *Biomimetic Oxidation Catalyzed by Transition Metal Complexes*; Imperial College Press: London, **2000**.
4. Hegg, E. L.; Que, L. Jr. *Eur. J. Biochem.* **1997**, *250*, 625–629.
5. Lipscomb, J. D.; Orville, A. M. *Met. Ions Biol. Sys.* **1992**, *28*, 243–298.
6. Ohlendorf, D. H.; Orville, A. M.; Lipscomb, J. D.; Weber, P. C. *Nature* **1988**, *336*, 403–405.
7. Pyrz, J. W.; Roe, A. L.; Stern, L. J.; Que, L. Jr. *J. Am. Chem. Soc.* **1985**, *107*, 614–620.
8. Que, L., Jr.; Epstein, R. M. *Biochemistry* **1981**, *20*, 2545–2549.
9. Siu, D. C.-T.; Orville, A. M.; Lipscomb, J. D.; Ohlendorf, D. H.; Que, L. Jr. *Biochemistry* **1992**, *31*, 10443–10448.
10. Felton, R. H.; Barrow, W. L.; May, S. W.; Sowell, A. L.; Goel, S.; Bunker, G.; Stern, E. A. *J. Am. Chem. Soc.* **1982**, *104*, 6132–6134.
11. True, A. E.; Orville, A. M.; Pearce, L. L.; Lipscomb, J. D.; Que, L. Jr. *Biochemistry* **1990**, *29*, 10847–10854.
12. Fujisawa, H.; Uyeda, M.; Kojima, Y.; Nozaki, N.; Hayaishi, O. *J. Biol. Chem.* **1972**, *247*, 4414–4421.
13. Whittaker, J. W.; Lipscomb, J. D.; Kent, T. A.; Münck, E. *J. Biol. Chem.* **1984**, *259*, 4466–4475.
14. Que, L. Jr.; Lipscomb, J. D.; Zimmermann, R.; Münck, E.; Orme-Johnson, N. R.; Orme-Johnson, W. H. *Biochim. Biophys. Acta* **1976**, *452*, 320–334.
15. Kent, T. A.; Münck, E.; Pyrz, J. W.; Widom, J.; Que, L. Jr. *Inorg. Chem.* **1987**, *26*, 1402–1408.
16. Que, L. Jr. *Coord. Chem. Rev.* **1983**, *50*, 73–108.
17. Felton, R. H.; Cheung, L. D.; Phillips, R. S.; May, S. W. *Biochem. Biophys. Res. Commun.* **1978**, *85*, 844–855.
18. Que, L., Jr.; Heistand II, R. H. *J. Am. Chem. Soc.* **1979**, *101*, 2219–2221.
19. Bull, C.; Ballou, D. P.; Otsuka, S. *J. Biol. Chem.* **1981**, *256*, 12681–12699.
20. Walsh, T.; Ballou, D. P.; Mayer, R.; Que, L. Jr. *J. Biol. Chem.* **1983**, *258*, 4422–4427.
21. Frazee, R. W.; Orville, A. M.; Dolbeare, K. B.; Yu, H.; Ohlendorf, D. H.; Lipscomb, J. D. *Biochemistry* **1998**, *37*, 2131–2144.
22. Orville, A. M.; Elango, N.; Lipscomb, J. D.; Ohlendorf, D. H. *Biochemistry* **1997**, *36*, 10039–10051.
23. Orville, A. M.; Lipscomb, J. D. *Biochemistry* **1997**, *36*, 14044–14055.
24. Ohlendorf, D. H.; Orville, A. M.; Lipscomb, J. D. *J. Mol. Biol.* **1994**, *244*, 586–608.
25. Elgren, T. E.; Orville, A. M.; Kelly, K. A.; Lipscomb, J. D.; Ohlendorf, D. H.; Que, L., Jr. *Biochemistry* **1997**, *36*, 11504–11513.
26. Funabiki, T.; Sakamoto, H.; Yoshida, H.; Tamara, K. *Chem. Commun.* **1979**, 754–755.
27. Funabiki, T.; Mizoguchi, A.; Sugimoto, T.; Yoshida, S. *Chem. Lett.* **1983**, 917–920.
28. Funabiki, T.; Mizoguchi, A.; Sugimoto, T.; Tada, S.; Tsuji, M.; Sakamoto, H.; Yoshida, S. *J. Am. Chem. Soc.* **1986**, *108*, 2921–2932.
29. Funabiki, T.; Konishi, T.; Kobayashi, S.; Mizoguchi, A.; Takano, M.; Yoshida, S. *Chem. Lett.* **1987**, *4*, 719–722.
30. Funabiki, T., Ed., *Oxygenases and Model Systems*; Kluwer Academic Publishers: Dordrecht, The Netherlands, **1997**; Vol. 19.
31. Jang, H. G.; Cox, D. D.; Que, L. Jr. *J. Am. Chem. Soc.* **1991**, *113*, 9200–9204.
32. Koch, W. O.; Kruger, H. J. *Angew. Chem. Int. Ed.* **1995**, *34*, 2671–2674.
33. Cox, D. D.; Que Jr, L. *J. Am. Chem. Soc.* **1991**, *110*, 8085–8092.
34. Dei, A.; Gatteschi, D.; Pardi, L. *Inorg. Chem.* **1993**, *32*, 1389–1395.
35. Orville, A. M.; Lipscomb, J. D.; Ohlendorf, D. H. *Biochemistry* **1997**, *36*, 10039–10051.
36. Barbaro, Y.; Shimo, H.; Kida, S. *Chem. Commun.* **1984**, 1611–1612.
37. White, L. S.; Nilsson, P. V.; Pignolet, L. H.; Que, L., Jr. *J. Am. Chem. Soc.* **1984**, *109*, 5373–5380.
38. Mayer, R. J.; Que, L., Jr. *J. Biol. Chem.* **1984**, *259*, 13056–13060.
39. Duda, M.; Pascaly, M.; Krebs, B. *Chem. Commun.* **1997**, 835–836.
40. Han, S.; Eltis, L. D.; Timmis, K. N.; Muchmore, S. W.; Bolin, J. T. *Science* **1995**, *270*, 976–980.
41. Shu, L.; Chiou, Y.-M.; Orville, A. M.; Miller, M. A.; Lipscomb, J. D.; Que, L., Jr. *Biochemistry* **1995**, *34*, 6649–6659.
42. Bertini, I.; Briganti, F.; Mangani, S.; Nolting, H. F.; Scozzafava, A. *FEBS Lett.* **1994**, *350*, 207–212.
43. Bertini, I.; Briganti, F.; Mangani, S.; Nolting, H. F.; Scozzafava, A. *Biochemistry* **1994**, *33*, 10777–10784.
44. Arciero, D. M.; Orville, A. M.; Lipscomb, J. D. *J. Biol. Chem.* **1985**, *260*, 14035–14044.
45. Bianchini, C.; Frediani, F.; Laschi, F.; Meli, A.; Vizza, F.; Zanello, P. *Inorg. Chem.* **1990**, *29*, 3402–3409.
46. Sanvoisin, J.; Langley, G. J.; Bugg, T. D. H. *J. Am. Chem. Soc.* **1995**, *117*, 7836–7837.
47. Spence, E. L.; Langley, G. J.; Bugg, T. D. H. *J. Am. Chem. Soc.* **1996**, *118*, 8336–8343.
48. Chiou, Y. M.; Que, L., Jr. *Inorg. Chem.* **1995**, *34*, 3577–3578.
49. Ito, M.; Que, L., Jr. *Angew. Chem. Int. Ed.* **1997**, *36*, 1342–1344.
50. Ogihara, T.; Hikichi, S.; Akita, M.; Moro-oka, Y. *Inorg. Chem.* **1998**, *37*, 2614–2615.
51. Schofield, C. J.; Zhang, Z. *Curr. Opin. Struct. Biol.* **1999**, *9*, 722–731.
52. Ryle, M. J.; Hausinger, R. P. *Curr. Opin. Chem. Biol.* **2002**, *6*, 193–201.
53. Prescott, A. G.; Lloyd, M. D. *Nat. Prod. Rep.* **2000**, *17*, 367–383.
54. Roach, P. L.; Clifton, I. J.; Fulop, V.; Harlos, K.; Barton, G. J.; Hajdu, J.; Andersson, I.; Scholfield, C. J.; Baldwin, J. E. *Nature* **1995**, *7*, 700–704.
55. Valegard, K.; Van Scheltinga, A. C. T.; Lloyd, M. D.; Hara, T.; Ramaswamy, S.; Perrakis, A.; Thompson, A.; Lee, H. J.; Baldwin, J. E.; Schofield, C. J.; Hajdu, J.; Andersson, I. *Nature* **1998**, *394*, 805–809.

56. Elson, S. W.; Baggaley, K. H.; Gillett, J.; Holland, S.; Nicholson, N. H.; Sime, J. T.; Woroniecki, S. R. *Chem. Commun.* **1998**, 1736–1738.
57. Elson, S. W.; Baggaley, K. H.; Gillett, J.; Holland, S.; Nicholson, N. H.; Sime, J. T.; Woroniecki, S. R. *Chem. Commun.* **1987**, 1739–1740.
58. Elson, S. W.; Baggaley, K. H.; Holland, S.; Nicholson, N. H.; Sime, J. T.; Woroniecki, S. R. *Bioorg. Med. Chem. Lett.* **1992**, *2*, 1503–1508.
59. Lloyd, M. D.; Merritt, K. D.; Lee, V.; Sewell, T. J.; Wha-Son, B.; Baldwin, J. E.; Schofield, C. J.; Elson, S. W.; Baggaley, K. H.; Nicholson, N. H. *Tetrahedron* **1999**, *55*, 10201–10220.
60. Bertini, I.; Sigel, A.; Sigel, H., Ed., *Handbook on Metalloproteins*; Marcel Dekker: New York, **2001**.
61. Zhang, Z. H.; Ren, J. S.; Stammers, D. K.; Baldwin, J. E.; Harlos, K.; Schofield, C. J. *Nat. Struct. Biol.* **2000**, *7*, 127–133.
62. Zhou, J.; Gunsior, M.; Bachmann, B. O.; Townsend, C. A.; Solomon, E. I. *J. Am. Chem. Soc.* **1998**, *120*, 13539–13540.
63. Pavel, E. G.; Zhou, J.; Busby, R. W.; Gunsior, M.; Townsend, C. A.; Solomon, E. I. *J. Am. Chem. Soc.* **1998**, *120*, 743–753.
64. Holme, E. *Biochemistry* **1975**, *14*, 4999–5003.
65. Baldwin, J. E.; Adlington, R. M.; Crouch, N. P.; Pereira, I. A. C. *Tetrahedron* **1993**, *49*, 7499–7518.
66. Long, A. J.; Clifton, I. J.; Roach, P. L.; Schofield, C. J.; Baldwin, J. E.; Hajdu, J. *FASEB J.* **1997**, *11*, 133. Suppl. 5.
67. Rowe, C. J.; Shorrock, C. P.; Claridge, T. D. W.; Sutherland, J. D. *Chem. Biol.* **1998**, *5*, 229–239.
68. Baldwin, J. E.; Bradley, M. *Chem. Rev.* **1990**, *90*, 1079–1088.
69. Chiou, Y. M.; Que, L., Jr. *J. Am. Chem. Soc.* **1995**, *117*, 3999–4013.
70. Chiou, Y. M.; Que, L., Jr. *Inorg. Chem.* **1995**, *34*, 3577–3578.
71. Hegg, E. L.; Ho, R. Y. N.; Que, L., Jr. *J. Am. Chem. Soc.* **1999**, *121*, 1972–1973.
72. Ho, R. Y. N.; Mehn, M. P.; Hegg, E. L.; Liu, A.; Ryle, M. J.; Hausinger, R. P.; Que, L., Jr. *J. Am. Chem. Soc.* **2001**, *123*, 5022–5029.
73. Ha, E. H.; Ho, R. Y. N.; Kisiel, J. F.; Valentine, J. S. *Inorg. Chem.* **1995**, *34*, 2265–2266.
74. Fitzpatrick, P. F. *Adv. Enz. Rel. Microbiol.* **2000**, *74*, 235–294.
75. Flatmark, T.; Stevens, R. C. *Chem. Rev.* **1999**, *99*, 2137–2160.
76. Kaufman, S. *Adv. Enz. Rel. Microbiol.* **1993**, *67*, 77–79.
77. Bhat, S.; Vaidyanathan, J. *J. Bacteriol.* **1976**, *127*, 1108–1118.
78. Kaufman, S.; Pollock, R. J.; Summer, G. K.; Das, A. K.; Hajra, A. K. *Arch. Biochem. Biophys.* **1990**, *1040*, 19–27.
79. Xia, T.; Gray, D. W.; Shiman, R. *J. Biol. Chem.* **1994**, *269*, 24647–24656.
80. Shiman, R.; Xia, T.; Hill, M. A.; Gray, D. W. *J. Biol. Chem.* **1994**, *269*, 24647–24656.
81. Loeb, K. E.; Westre, T. E.; Kappock, T. J.; Mitic, N.; Glasfeld, E.; Caradonna, J. P.; Hedman, B.; Hodgson, K. O.; Solomon, E. I. *J. Am. Chem. Soc.* **1997**, *119*, 1901–1915.
82. Meyer-Klaucke, W.; Winkler, H.; Schunemann, V.; Trautwein, A. X.; Nolting, H. F.; Haavik, J. *Eur. J. Biochem.* **1996**, *241*, 432–439.
83. Meyer-Klaucke, W.; Winkler, H.; Schunemann, V.; Trautwein, A. X.; Nolting, H. F.; Haavik, J. *Eur. J. Biochem.* **1996**, *241*, 432–439.
84. Kemsley, J. N.; Mitic, N.; Zaleski, K. L.; Caradonna, J. P.; Solomon, E. I. *J. Am. Chem. Soc.* **1999**, *121*, 1528–1536.
85. Loeb, K.; Westre, T.; Kappock, T. J.; Mitic, N.; Glasfeld, E.; Caradonna, J. P.; Hedman, B.; Hodgson, K.; Solomon, E. I. *J. Am. Chem. Soc.* **1998**, *119*, 1901–1915.
86. Wasinger, E. C.; Mitic, N.; Hedman, B.; Caradonna, J. P.; Solomon, E. I.; Hodgson, K. O. *Biochemistry* **2002**, *41*, 6211–6217.
87. Davis, M. D.; Kaufman, S. *J. Biol. Chem.* **1989**, *264*, 8585–8596.
88. Benkovic, S.; Wallick, D.; Bloom, L.; Gaffney, B. J.; Domanico, P.; Dix, T.; Pember, S. *Biochem. Soc. Trans.* **1985**, *13*, 436–438.
89. Guengerich, F. P.; MacDonald, T. L. *Acc. Chem. Res.* **1984**, *17*, 9–16.
90. Guroff, G.; Daly, J. W.; Jerina, D. M.; Renson, J.; Witkop, B.; Udenfriend, S. *Science* **1967**, *157*, 1524–1530.
91. Kappock, T. J.; Caradonna, J. P. *Chem. Rev.* **1996**, *96*, 2659–2756.
92. Kemsley, J. N.; Wasinger, E. C.; Datta, S.; Mitic, N.; Acharya, T.; Hedman, B.; Caradonna, J. P.; Hodgson, K. O.; Solomon, E. I. *J. Am. Chem. Soc.* **2003**, in press.
93. Samuelsson, B.; Dahlen, S.-E.; Lindgren, J. E.; Rouzer, C. A.; Serhan, C. N. *Science* **1987**, *237*, 1171–1176.
94. Minor, W.; Steczko, J.; Bolin, J. T.; Otwinowski, Z.; Axelrod, B. *Biochemistry* **1993**, *32*, 6320–6323.
95. Boyington, J. C.; Gaffney, B. J.; Amzel, L. M. *Science* **1993**, *260*, 1482–1486.
96. Minor, W.; Steczko, J.; Stek, B.; Otwinowski, Z.; Bolin, J. T.; Walter, R.; Axelrod, B. *Biochemistry* **1996**, *35*, 10687–10701.
97. Pavlosky, M. A.; Zhang, Y.; Westre, T. E.; Gan, Q. F.; Pavel, E. G.; Campochiaro, C.; Hedman, B.; Hodgson, K. O.; Solomon, E. I. *J. Am. Chem. Soc.* **1995**, *117*, 4316–4327.
98. Gilmor, S. A.; Villasenor, A.; Fletterick, R.; Sigal, E.; Browner, M. F. *Nat. Struct. Biol.* **1997**, *4*, 1003–1009.
99. Zhang, Y.; Gebhard, M. S.; Solomon, E. I. *J. Am. Chem. Soc.* **1991**, *113*, 5162–5175.
100. Scarrow, R. C.; Trimitsis, M. G.; Buck, C. P.; Grove, G. N.; Cowling, R. A.; Nelson, M. J. *Biochemistry* **1994**, *33*, 15023–15035.
101. Solomon, E. I.; Brunold, T. C.; Davis, M. I.; Kemsley, J. M.; Lee, S. K.; Lehnert, N.; Neese, F.; Skulan, A. J.; Yang, Y. S.; Zhou, J. *Chem. Rev.* **2000**, *100*, 235–349.
102. Nelson, M. J.; Cowling, R. A. *J. Am. Chem. Soc.* **1990**, *109*, 8107.
103. Zang, Y.; Elgren, T. E.; Dong, Y.; Que, L., Jr. *J. Am. Chem. Soc.* **1993**, *115*, 8107–8108.
104. Chan, H. W. S.; Newby, V. K.; Levett, G. J. *Chem. Commun.* **1978**, *82*, 756–757.
105. Nagata, R.; Morimoto, S.; Saito, I. *Tetrahedron Lett.* **1990**, *31*, 4485–4488.
106. Guajardo, R. J.; Mascharak, P. K. *Inorg. Chem.* **1995**, *34*, 802–808.
107. Goldsmith, C. R.; Jonas, R. T.; Stack, T. D. P. *J. Am. Chem. Soc.* **2002**, *124*, 83–96.
108. Kim, J.; Zang, Y.; Costas, M.; Wilkinson, H.; Que, L., Jr. *J. Biol. Inorg. Chem.* **2001**, *6*, 275–284.

109. Ogo, S.; Yamahara, R.; Roach, M.; Suenobu, T.; Aki, M.; Ogura, T.; Kitagawa, T.; Masuda, H.; Fukuzumi, S.; Watanabe, Y. *Inorg. Chem.* **2002**, *41*, 5513–5520.
110. Roth, J. P.; Mayer, J. M. *Inorg. Chem.* **1999**, *38*, 2760–2761.
111. Parales, R. E.; Parales, J. V.; Gibson, D. T. *J. Bacteriol.* **1999**, *181*, 1831–1837.
112. Harayama, S.; Kok, M.; Neidle, E. L. *Annu. Rev. Microbiol.* **1992**, *46*, 565–601.
113. Tsang, H.; Batier, C.; Ballou, D.; Penner-Hahn, J. *J. Biol. Inorg. Chem.* **1996**, *1*, 24–33.
114. Pavel, E.; Martins, L.; Ellis, W.; Solomon, E. I. *Chem. Biol.* **1994**, *1*, 173–183.
115. Page, N.; Moser, C.; Chen, X.; Dutton, P. *Nature* **1999**, *402*, 47–52.
116. Ballou, D. P.; Batie, C. *Prog. Clin. Biol. Res.* **1988**, *274*, 211–226.
117. Wolfe, M. D.; Parales, J. V.; Gibson, D. T.; Lipscomb, J. D. *J. Biol. Chem.* **2001**, *276*, 1945–1953.
118. Karlsson, A.; Parales, J. V.; Parales, R. E.; Gibson, D. T.; Eklund, H.; Ramaswamy, S. *Science* **2003**, *299*, 1039–1042.
119. Chen, K.; Costas, M.; Que, L., Jr., *J. Chem. Soc., Dalton Trans.* **2002**, *5*, 672–679.
120. Costas, M.; Tipton, A. K.; Chen, K.; Jo, D.-H.; Que, L., Jr. *J. Am. Chem. Soc.* **2001**, *123*, 6722–6723.
121. Rohde, J.-U.; In, J. H.; Lim, M. H.; Brennessel, W. W.; Bukowski, M. R.; Stubna, A.; Münck, E.; Nam, W.; Que, L., Jr. *Science* **2003**, *299*, 1037–1039.
122. Lim, M. H.; Rohde, J.-U.; Stubna, A.; Bukowski, M. R.; Costas, M.; Ho, R. Y. N.; Münck, E.; Nam, W.; Que, L., Jr. *Proc. Natl. Acad. Sci. USA* **2003**, *100*, 7, 3665–3670.

8.15
Dicopper Enzymes

S. ITOH
Osaka City University, Japan

8.15.1 INTRODUCTION

Copper-containing oxidases and oxygenases constitute one of the major classes of biocatalysts that participate in dioxygen processing.[1,2] They possess mononuclear, dinuclear, or trinuclear copper-active sites, many of which involve histidine imidazoles as supporting ligands.[3] Typical examples of the mononuclear copper-active site are found in dopamine β-monooxygenase (DβM, EC 1.14.17.1), peptidylglycine α-amidating monooxygenase (PAM, EC 1.14.17.3), and quercetin 2,3-dioxygenase (EC 1.13.11.24), which catalyze oxygenation of various organic substrates by molecular oxygen.[4,5] A series of copper-containing amine oxidases (EC 1.4.3.6), lysyl oxidase (EC 1.4.3.13), and galactose oxidase (EC 1.1.3.9) also contain a mononuclear copper-active site (Chapters 8.14 and 8.26). In these enzymes, the copper ion plays an essential role in the post-translational modification of an active site tyrosine to a novel organic cofactor, 2,4,5-trihydroxy-phenylalanine quinone (TPQ) in amine oxidases, lysine tyrosylquinone (LTQ) in lysyl oxidase, and Tyr–Cys (tyrosine cross-linked to cysteine via a thioether bond) in galactose oxidase.[4,6–11] Reoxidation of the reduced cofactors by molecular oxygen is also mediated by the copper ion in these enzyme-active sites.[4,11,12]

Dioxygen activation is also accomplished at the dinuclear copper-active sites in tyrosinases and catechol oxidases.[1,2,13–17] Tyrosinases (EC 1.14.18.1) are widely distributed throughout bacteria, fungi, plants, and animals, catalyzing the ortho-hydroxylation of phenols to catechols (phenolase activity, Equation (1)) and the oxidation of catechols to o-quinones (catecholase activity, Equation (2)).

These two processes are also referred as "cresolase activity" or "monophenolase activity" and "diphenolase activity," respectively. Such reactions represent the initial steps of vertebrate pigmentation (melanin biosynthesis) and the browning of fruits and vegetables.[1,2,14] Catechol oxidases (EC 1.10.3.1) are ubiquitous plant enzymes, which also catalyze the oxidation of a broad

range of catechols to the corresponding *o*-quinones (catecholase activity), but lack the phenolase activity. Although the crystal structure of tyrosinase has yet to be solved, chemical and spectroscopic investigations have unambiguously demonstrated that the structure of the dinuclear copper-active site in tyrosinase is very similar to those of catechol oxidase and the dioxygen carrier protein, hemocyanin, whose structures have been determined by X-ray crystallographic analysis.[18–24] In addition to these copper enzymes, there are some other copper-containing monooxygenases such as particulate methane monooxygenase (pMMO) and ammonia monooxygenase (AMO), in which the active site is believed to constitute a multi-copper reaction center. However, details about the active site structures and reaction mechanisms of pMMO and AMO are still unclear.[1,2]

$$+ \ O_2 \ + \ 2\,H^+ \ \longrightarrow \ \ \ + \ H_2O \qquad (1)$$

$$\longrightarrow \ \ \ + \ 2\,e^- \ + \ 2\,H^+ \qquad (2)$$
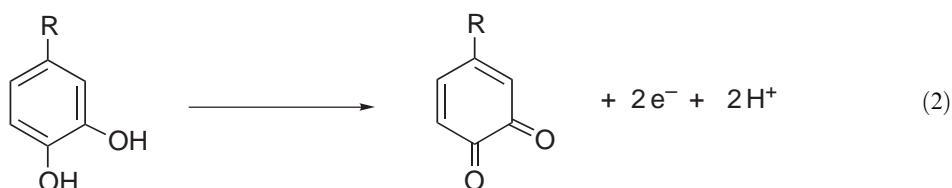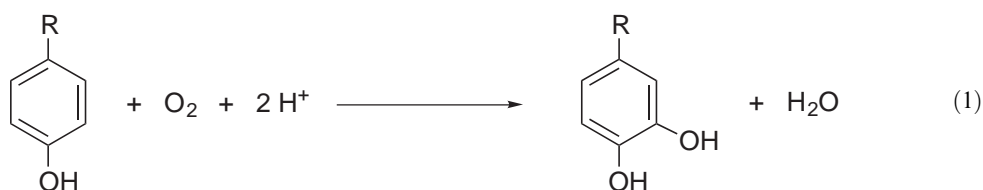
The purpose of this chapter is to summarize the information about the mechanism of dioxygen activation at the dinuclear copper-active sites in tyrosinase and catechol oxidase. Since a great deal of information about the enzymological and physiological studies of these enzymes is available in recent review articles,[1,2,13–15,17] the main attention of this chapter is focused on the chemistry that takes place in the active sites of the enzymes. Since structural and mechanistic studies of the enzymatic systems largely rely on model studies of copper–dioxygen reactivity, recent developments in the synthetic model chemistry are also included. Reversible dioxygen binding at the dinuclear copper site in hemocyanin and four-electron reduction of dioxygen to water at the trinuclear copper-reaction centers in multi-copper enzymes are described elsewhere (Chapters 8.10 and 8.17).

8.15.2 TYROSINASE AND CATECHOL OXIDASE

8.15.2.1 Active Site Structure

Tyrosinase is the most well-studied dicopper oxygenase, and the primary sequences of the cDNA for tyrosinases from *Streptomyces glaucescens*,[25] *Neurospora crassa*,[26] *Rona nigromaculata*,[27] *Mus musculus*,[28] and human melanocyte[29] have been reported. However, there is no crystal structure presently available for any tyrosinase. On the other hand, the crystal structures of sweet potato catechol oxidase in the resting dicopper(II) state (met form), the reduced dicopper(I) state (deoxy form), and a complex with the inhibitor, phenylthiourea, have been solved.[18] It is a monomeric 39 kDa enzyme with an overall elliptic shape which is composed primarily of α-helices.[18] The four-helix bundle in the core of the enzyme holds the catalytic dicopper center and is surrounded by two other α-helices and some short β-strands.[18] Each of the two active-site copper ions, termed CuA and CuB, is coordinated by three histidine imidazoles provided by the four helices of the α-bundle.[18] Interestingly, the imidazole ring of His 109, one of the supporting ligands of CuA, is covalently cross-linked to the sulfur atom of Cys 92, forming a novel thioether linkage as shown in Figure 1.[18] Such a His–Cys cross-link also exists in tyrosinase from *Neurospora crassa*[30] and in some
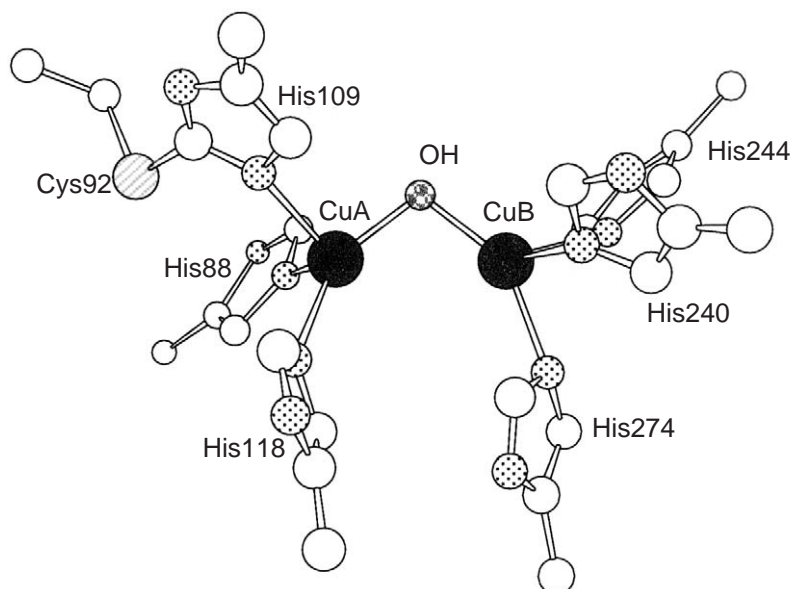
Figure 1 Active site structure of the resting dicopper(II) form of catechol oxidase from sweet potato.[18]

hemocyanins.[24,31] The His–Cys bridge may regulate the conformation of the imidazole rings during the catalytic cycle, but details about its function are not clear at present.

In the resting state (met form) of catechol oxidase, the two cupric ions are separated by 2.9 Å and are bridged by a hydroxide ion (Figure 1).[18] Both cupric ions exhibit a four-coordinate distorted trigonal pyramidal geometry with His 109 and His 240 in the apical positions for CuA and CuB, respectively.[18] These results are in agreement with the EXAFS data for the resting form of the enzyme[32] indicating a similar structure of the enzyme in solution. The EPR silence of the resting enzyme[32] reflects an antiferromagnetic interaction between the two cupric ions through the bridging hydroxide (Figure 1). EPR nondetectable met-tyrosinase probably has a similar active site structure with a hydroxide-bridging ligand between two cupric ions, although the EXAFS data on met-tyrosinase indicated a Cu—Cu distance of 3.4 Å that is longer than that of catechol oxidase (2.9 Å).[33] The overall structure of the active site of catechol oxidase is remarkably similar to that of met-hemocyanin.[15–19] Paramagnetic ^{1}H-NMR studies have provided additional information about the active site structure of met-tyrosinase.[34]

In the reduced state of catechol oxidase, the distance between the two cuprous ions is increased significantly to 4.4 Å, while the histidine residues move only slightly and no significant conformational change is observed for any other part of the enzyme (Figure 2).[18] The CuA site exhibits a distorted trigonal pyramidal geometry with one water molecule, while the CuB site has a three-coordinate T-shaped geometry.[18]

8.15.2.2 Peroxo Intermediates: Structure and Properties

Treatment of met-tyrosinase (EPR nondetectable dicopper(II) form) with hydrogen peroxide under aerobic conditions produces a characteristic absorption spectrum exhibiting an intense peak at 345 nm ($\varepsilon = \sim 18,000\,M^{-1}\,cm^{-1}$) together with a weak broad band at 600 nm ($\varepsilon = \sim 1,200\,M^{-1}\,cm^{-1}$).[35–39] The same species can be generated by reduction of the met form with hydroxylamine followed by oxygenation with O_2.[40] The oxygenated product is also EPR silent,[35,40] and provides a resonance-enhanced Raman band at 755 cm^{-1} with $^{16}O_2$ that shifts to 714 cm^{-1} upon $^{18}O_2$ substitution.[40] The spectroscopic features of oxy-tyrosinase are essentially the same as those of oxy-hemocyanin,[38] suggesting that the oxy-tyrosinase has a (μ-η^2:η^2-peroxo) dicopper(II) structure (**A** in Scheme 1) as in the case of oxy-hemocyanin.[22,41,42] Reaction of the met form of catechol oxidase with hydrogen peroxide also provides a similar absorption spectrum (343 nm ($\varepsilon = 6,500\,M^{-1}\,cm^{-1}$) and 580 nm ($\varepsilon = 450\,M^{-1}\,cm^{-1}$)) due to a similar peroxo dicopper(II) species.[32] An EXAFS study has shown that the Cu—Cu distance in the peroxo intermediate of catechol oxidase is 3.8 Å,[32] which is a little longer than that of oxy-hemocyanin (3.6 Å).[22,23]
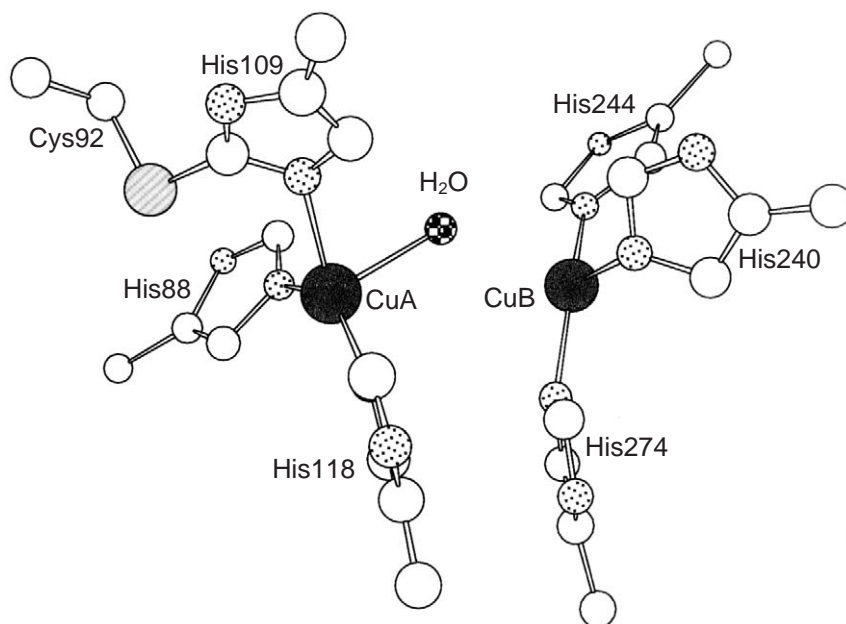
Figure 2 Active site structure of the deoxy dicopper(I) form of catechol oxidase from sweet potato.[18]
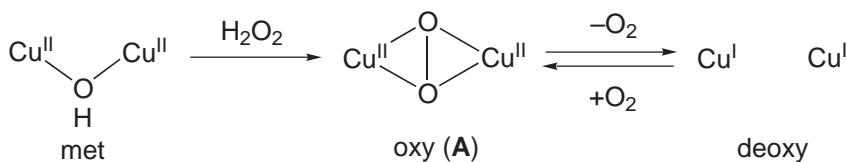
Scheme 1

Details about the spectroscopic characterization of the $(\mu\text{-}\eta^2\text{:}\eta^2\text{-peroxo})$ dicopper(II) complexes are presented later. It has been noted that the dioxygen binding of tyrosinase is reversible as in the case of oxy-hemocyanin (Scheme 1).[32,35,36] Thus, the oxy form of the enzyme is converted into the deoxy dicopper(I) state by releasing O_2 when the sample is placed under anaerobic conditions (Scheme 1).[35,36] Such a reversible dioxygen binding of tyrosinase, however, makes it difficult to study the single-turnover reaction between the peroxo species and substrates.

8.15.2.3   Enzymatic Reaction Pathways

Proposed reaction pathways of the phenolase and catecholase cycles are shown in Scheme 2.[1,2,14,16,17] As described above, oxygenation of the deoxy enzyme generates the oxy form of the enzyme having the $(\mu\text{-}\eta^2\text{:}\eta^2\text{-peroxo})$dicopper(II) structure (path (a)). Then, coordination of a phenolate (deprotonated form of the substrate) to one of the cupric ions of the peroxo intermediate occurs to give an oxy-P intermediate (P denotes phenolate substrate) (path (b)). This phenolate coordination step is what differentiates the enzymatic reactivity of tyrosinase and catechol oxidase from the mere dioxygen binding reaction of hemocyanin. A large difference in rate of displacement of the peroxide ligand in the oxy enzymes by exogenous ligands has been observed for tyrosinase relative to hemocyanin, demonstrating that the substrate accessibility is much higher in oxy-tyrosinase than in oxy-hemocyanin.[38,43,44] In this respect, findings of phenolase and catecholase activity in the activated hemocyanins are of great interest.[15,45] Arthropod hemocyanin has been shown to gain the catecholase activity in the presence of $NaClO_4$,[46] and the serine protease-treated hemocyanin from a chelicerate has also been demonstrated to exhibit both the phenolase and catecholase activities.[47] In the former case, perchlorate ion may induce a conformational change of the enzyme, allowing the substrate incorporation into the dinuclear copper-active site.[46] In the latter case, on the other hand, the cleavage of an *N*-terminal peptide by

Scheme 2
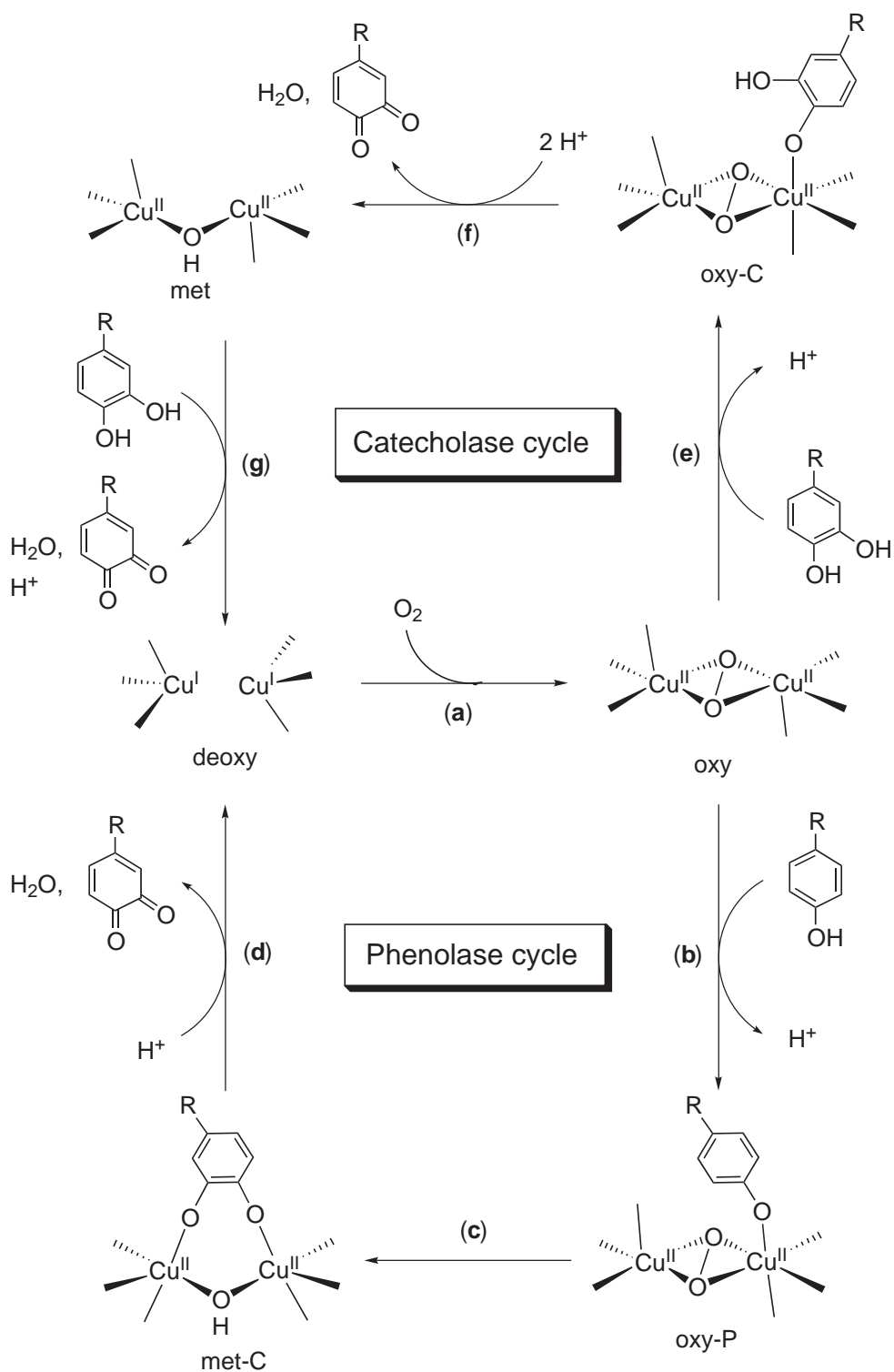
the limited proteolysis opens the entrance to the active site of the enzyme (highly conserved phenylalanine; Phe-49 in this case).[47] The substrate binding process has been examined in tyrosinase by using a substrate analogue (inhibitor) such as mimosine to demonstrate that it can bind to at least one copper ion and induce a geometric change of the copper center from a tetragonal to a

trigonal bipyramidal structure.[48,49] It has also been suggested that there are additional interactions between the aromatic ring of the inhibitor and the hydrophobic residues in the enzyme pocket, stabilizing the trigonal bipyramidal geometry.[49] Such a geometric change may be required for the following hydroxylation process (path (c)). Based on computer modeling using the X-ray structures of hemocyanin, the phenol substrate has been suggested to bind to the CuA site, inducing close contact of the ortho-position of the phenyl ring of the phenol substrate to one of the oxygen atoms of the peroxo ligand.[15,45] Such a conformation might be essential for the efficient aromatic hydroxylation in tyrosinase.

Hydroxylation of the bound phenolate (path (c)) then occurs to give the catecholate product that may coordinate to the dicopper(II) unit as a bridging ligand as shown in Scheme 2. An isotope-labeling experiment using $^{18}O_2$ has clearly demonstrated that the oxygen atom incorporated into the product derives from dioxygen.[50] Furthermore, kinetic experiments employing 3,5-ditritiated tyrosine have shown that there is little kinetic isotope effect, indicating that the C—H bond cleavage of the ortho-position of the aromatic ring is not involved in the rate-determining step.[51,52] Based on the model studies described later, this process is believed to involve rate-determining electrophilic attack of the peroxo group to the substrate arene ring.[53] Inner-sphere electron transfer in the met-C intermediate (C denotes catecholate product) generates the quinone product and the dicopper(I) deoxy site (path (d)), which further reacts with dioxygen to construct the phenolase cycle (Scheme 2).

In the catecholase cycle, both the oxy and met sites can react with catechol derivatives, oxidizing them to the corresponding quinones (paths (f) and (g) in Scheme 2).[54] Electron-donating substituents on the catechol ring have been shown to enhance the reactivity.[55] However, steric and polarity effects of the substituents may also be important for the observed difference in reactivity among the substrates.[54]

For the catecholase cycle of catechol oxidase, modeling of the substrate-binding process has been performed based on the X-ray structure of an inhibitor complex shown in Figure 3.[17,18] It has been proposed that the substrate binds to the CuB site of the oxy form of the enzyme, where one of the hydroxyl groups of the catechol substrate is deprotonated. A nearby Glu 236 has been suggested to be the proton acceptor from the substrate.[18] Hydrophobic interactions between the substrate and the amino acid residues Phe 261, Ile 241, and His 244 in the enzyme active site also have been postulated to contribute to the substrate binding.[18] In this model, the CuA site exhibits a square pyramidal geometry with His 88, His 118, and O_2^{2-} as the equatorial ligands and His 109 as the axial ligand, whereas the CuB site has an octahedral structure in which the equatorial
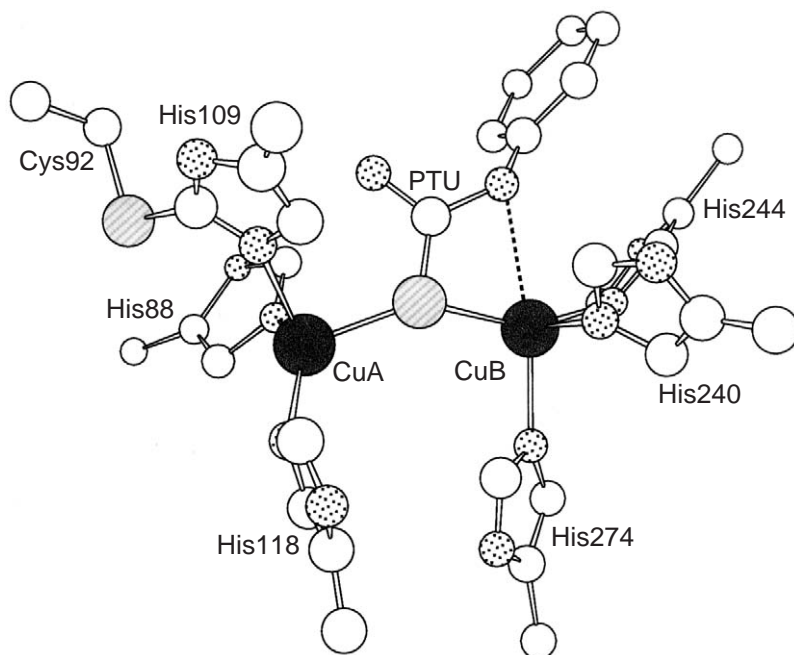
Figure 3 Active site structure of the inhibitor (phenylthiourea, PTU) bound catechol oxidase from sweet potato.[18]

plane is occupied by His 240, His 244, and O_2^{2-} and the axial positions are filled by the monodentate substrate and His 274. From this complex, electron transfer from the bound catecholate to the peroxide ligand and simultaneous O—O bond cleavage occur to produce the *o*-quinone product, water, and the met form of the enzyme (path (f)). The protonated Glu 236 and the second non-coordinating hydroxyl group of the substrate might donate protons to the peroxo ligand to promote O—O bond cleavage (step (f)). Another molecule of catechol then reacts with the resulting dicopper(II) site (met form) to give the deoxy dicopper(I) and another *o*-quinone product (path (g)), of which the former reacts with dioxygen to complete the catalytic cycles.[18]

Steady state kinetics as well as stopped-flow studies on the oxidation of phenol and catechol derivatives have so far been performed extensively.[14,53–66] However, detailed mechanistic information about the individual steps of phenolase and catecholase cycles has yet to be obtained due to the following side reactions: the self-inhibition by the phenol substrate (binding of phenols to the met form of the enzyme, not shown in Scheme 2), nonenzymatic intramolecular cyclization, disproportionation between the substrate and product, and polymerization of the product.

8.15.3 PARTICULATE METHANE MONOOXYGENASE AND AMMONIA MONOOXYGENASE

Particulate methane monooxygenases (pMMO) have been obtained from methanotrophic bacteria such as *Methylococcus capsulatus* (Bath),[67] *Methylosinus trichosporium* OB3b,[68] and *Methylomicrobrium album* BG8.[69] They catalyze the oxidation of methane to methanol as well as hydroxylation of *n*-alkanes and epoxidation of *n*-alkenes with five carbons or less by molecular oxygen.[1,2,70] The oxidation of chiral ethane ($CH_3C^1H^2H^3H$) by pMMO proceeds with complete retention of configuration, i.e., with 100% stereoselectivity, suggesting a concerted mechanism, where the C—H bond cleavage and the C—O bond formation occur simultaneously.[71]

Membrane-bound ammonia monooxygenase (AMO) has been isolated from ammonia-oxidizing bacteria,[1,2] and has recently been isolated from *Paracoccus denitrificans*.[72] This enzyme catalyzes not only oxygenation of ammonia to hydroxylamine but also hydroxylation and epoxidation of hydrocarbons.[1,2] pMMO and AMO have high sequence identity,[73] and are considered to be closely related to each other with respect to their structure and function.

Although soluble methane monooxygenases (sMMO) located in the cytoplasm of the bacterial cells have been well characterized in terms of their structure and reaction mechanism,[74,75] those of pMMO and AMO are poorly understood at present. This is due to difficulty in obtaining a pure enzyme that retains reactivity. It has so far been demonstrated that the enzymes contain up to ~15 copper ions per enzyme,[67,68,76] but only a type 2 copper(II) supported by three or four imidazole ligands can be detected by EPR.[69,77–79] The X-ray absorption and EPR studies have shown that many of the copper ions exist in the reduced copper(I) state and are arranged as clusters, which are believed to perform dioxygen activation and electron transfer.[80] In addition, the existence of a non-heme iron center has been suggested, although the catalytic role of such an iron center is not clear at present.[68,76,81]

8.15.4 MODEL COMPLEXES OF ACTIVE OXYGEN INTERMEDIATES

8.15.4.1 Dinuclear Copper(II) Peroxo Complexes

Copper(I) complexes supported by certain capping ligands react with molecular oxygen in a 2:1 ratio to afford dinuclear copper dioxygen (Cu_2/O_2) complexes. Such complexes can be regarded as structural and functional models of the reactive intermediates of tyrosinase and catechol oxidase. Numerous review articles on the subject have been published so far.[82–95]

The first structurally characterized dinuclear copper dioxygen complex was reported by Karlin and co-workers in 1988.[96] Reaction of the copper(I) complex supported by the tetradentate ligand TPA (tris(2-pyridylmethyl)amine, Scheme 3) with dioxygen at −80 °C in an organic solvent afforded a intensely purple-colored dinuclear copper(II) complex (**1**) having a *trans*-μ–1,2-peroxo bridge (Figure 4).[96] The penta-coordinate copper(II) ions exhibit a distorted trigonal bipyramidal geometry, where the equatorial ligands are the three pyridine nitrogens and one of the peroxo oxygen atoms and the aliphatic amine occupy the axial positions.[96] The O—O bond length of 1.43 Å is typical for a peroxo ligand (Table 1),[97] and the two cupric ions are antiferromagnetically
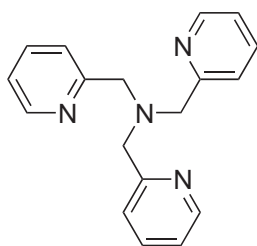
TPA
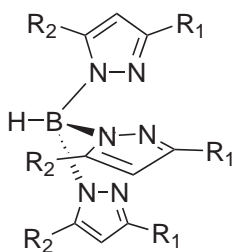
HB(3,5-i-Pr$_2$pz)$_3^-$: R$_1$ = R$_2$ = i-Pr
HB(3-CF$_3$-5-CH$_3$pz)$_3^-$: R$_1$ = CF$_3$, R$_2$ = CH$_3$
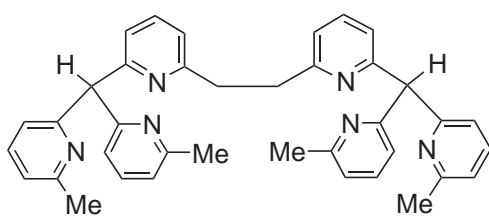
L^1
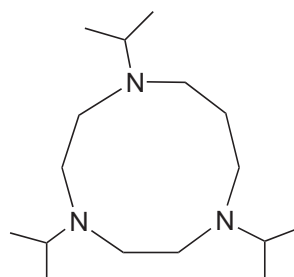
i-Pr$_3$TACD
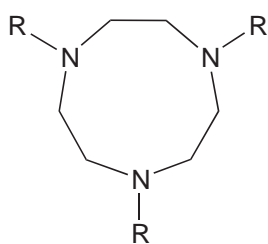
Bn$_3$TACN: R = −CH$_2$Ph
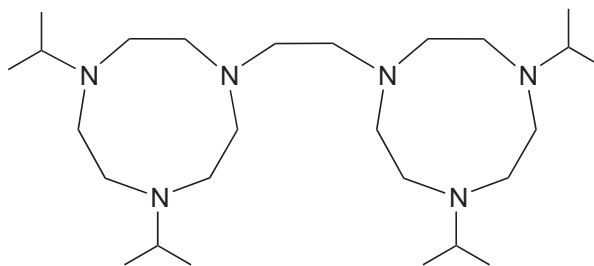
i-Pr$_4$DTNE
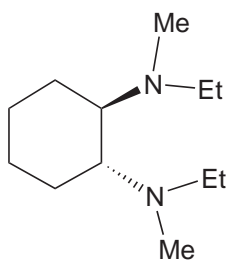
L$_{ME}$
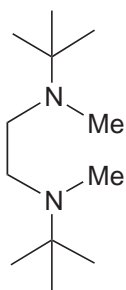
L^2
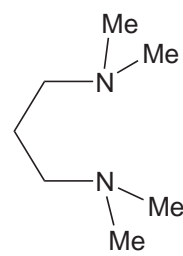
L$_{TMPD}$

Scheme 3
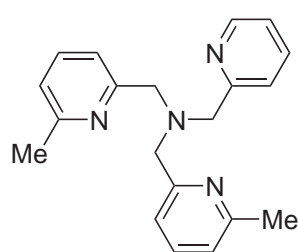
Me₂TPA
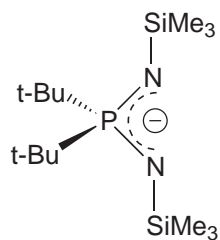
t-Bu₂P(NSiMe₃)₂⁻
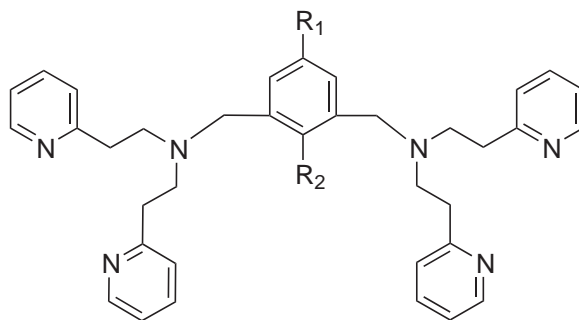
R1XYLR2
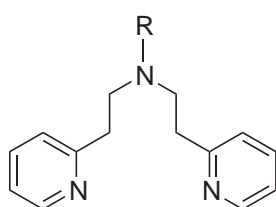
Py2R
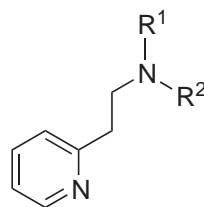
Py1R1,R2
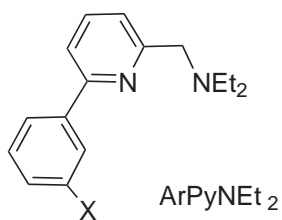
ArPyNEt₂

Scheme 3 continued

coupled through the end-on peroxo bridge, making the complex EPR-silent.[96] Broken-symmetry SCF-Xα-SW calculations have suggested that the electronic structure is dominated by the interaction of the peroxide π_σ^*-orbital (one of the antibonding π^*-orbitals of the O_2^{2-} ligand residing in the metal-peroxide plane) with the half-occupied copper d_{z^2}-orbitals.[98] Complex (**1**) exhibits
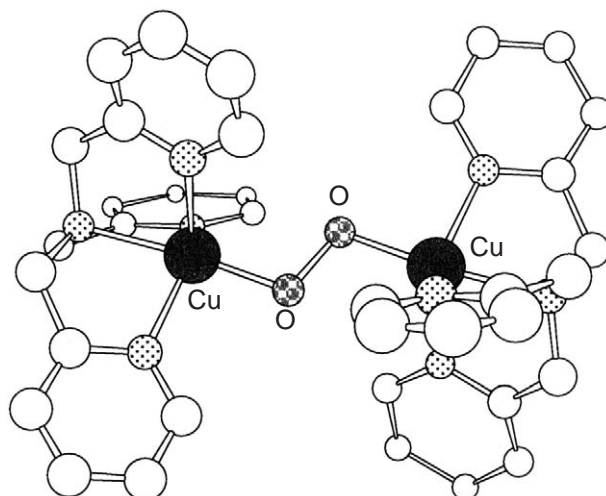
Figure 4 Chem 3D representation of the crystal structure of complex (**1**).[96]

resonance Raman bands at $832\,cm^{-1}$ ($788\,cm^{-1}$ with $^{18}O_2$) and $561\,cm^{-1}$ ($535\,cm^{-1}$ with $^{18}O_2$), which are assigned as the O—O and Cu—O stretching vibrational modes, respectively.[98] Peroxo-to-copper(II) charge-transfer bands appear at 525 nm ($\varepsilon = 11{,}500\,M^{-1}\,cm^{-1}$) and $\sim$590 nm ($7{,}600\,M^{-1}\,cm^{-1}$, shoulder), together with a *d–d* band at 1,035 nm ($160\,M^{-1}\,cm^{-1}$) due to trigonal bipyramidal copper(II) (Table 1).[96,98,99] These spectroscopic and structural features are significantly different from those of the oxy forms of hemocyanin, tyrosinase, and catechol oxidase, due to the different binding mode of the peroxo ligand in (**1**) and the proteins. Nonetheless, the (TPA)Cu^I precursor can bind dioxygen reversibly as in the case of the enzymes.[99] Similar (*trans*-μ-1,2-peroxo)dicopper(II) complexes have been generated using a series of tripodal tetradentate amine ligands, and the kinetics and thermodynamics of the reversible dioxygen binding process have been investigated in detail in some instances.[94,100–108] In general, the μ-peroxo dicopper(II) complex is formed through a mononuclear (superoxo)copper(II) intermediate, and room-temperature stability of the peroxo complex is precluded by a strongly negative reaction entropy.[104,109]

Adoption of tridentate instead of tetradentate ligands resulted in a drastically changed structure of the (μ-peroxo)dicopper(II) product. In initial studies by Kitajima and co-workers, a (μ-η^2:η^2-peroxo)dicopper(II) complex (**2**) was obtained as a deep purple solid when the copper(I) complex of a tridentate hydrotris(pyrazolyl)borate ligand (HB(3,5-i-Pr$_2$pz)$_3^-$, Scheme 3) was treated with dioxygen at $-78\,°C$ in acetone.[41,110] The crystal structure of (**2**) was determined by X-ray crystallographic analysis (Figure 5).[41,42] The same compound was obtained by the reaction of a bis(μ-hydroxo)dicopper(II) complex with the same ligand and H_2O_2 under similar reaction conditions.[42]

The O—O bond length of (**2**) is 1.41 Å, which is nearly the same as that of compound (**1**) (1.43 Å) (Table 1), but the Cu—Cu distance (3.56 Å) is significantly shorter than that in (**1**) (4.36 Å) due to the side-on peroxo bridging mode instead of the end-on type in (**1**).[41,42] Complex (**2**) exhibits a strong absorption feature at 349 nm ($\varepsilon = 21{,}000\,M^{-1}\,cm^{-1}$) together with a weak one at 551 nm ($790\,M^{-1}\,cm^{-1}$), which were assigned as peroxide-to-copper(II) charge-transfer transitions (Table 1).[111]

Table 1 The O—O bond length and the UV–vis and resonance Raman data of representative (μ-peroxo)dicopper(II) complexes that have been characterized by X-ray crystallography.

Complex	$d(O—O)$ (Å)	$\lambda_{max}\ (\varepsilon)$ (nm ($M^{-1}\,cm^{-1}$))	$\nu(^{16}O)\ (\nu(^{18}O))$ (cm^{-1})	
(**1**)[96]	1.432(6)	435 (1,700), 524 (11,300) 615 (5,800), 1035 (180)	O—O	832 (788)
(**2**)[41,42]	1.412(12)	349 (21,000), 551 (790)	O—O	741 (698)
(**3**)[122]	1.485(8)	360 (24,700), 532 (1,530)	O—O	760 (719)
(**4**)[119]	1.374(5)	380 (22,000), 520 (2,300)	O—O	739 (696)
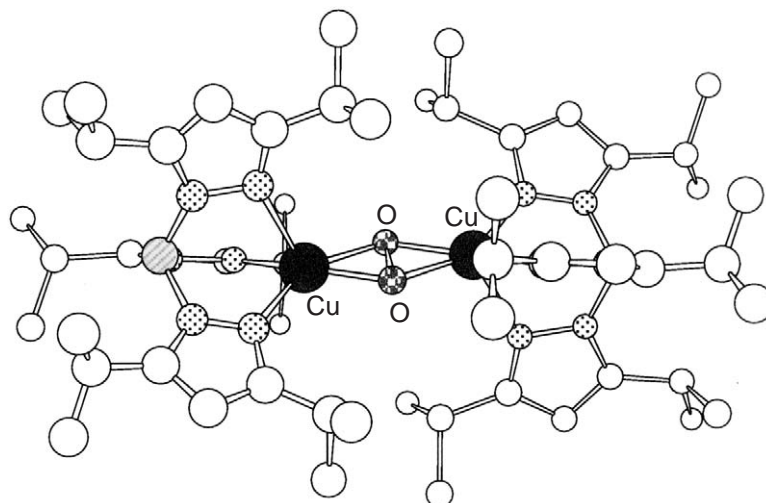
Figure 5 Chem 3D representation of the crystal structure of complex (**2**).[41]

The resonance Raman spectrum obtained by excitation into the low-energy charge-transfer band shows an O—O stretching vibration at 741 cm^{-1} that shifts to 698 cm^{-1} upon ^{18}O-substitution (Table 1).[41,42] The lower ν_{O-O} value of (**2**) indicates that the O—O bond of the side-on peroxo complex is significantly weakened as compared to that in the end-on peroxide (832 cm^{-1}). Compound (**2**) is also ESR-silent due to a strong antiferromagnetic interaction between the two cupric ions through the side-on peroxo bridge.[41,42] The similarity of the spectroscopic features of (**2**) and the oxy forms of the proteins strongly suggested that the peroxo state of the enzymes also possessed the side-on type binding mode. Indeed, five years after Kitajima's report (1989), the structure of oxy-hemocyanin was solved and it was concluded that oxy-hemocyanin has the same (μ-η^2:η^2-peroxo)dicopper(II) core as in (**2**).[22] The correct prediction of the active oxygen intermediate in the enzymatic system by the model studies represents one of the greatest successes in bioinorganic chemistry. Subsequently, (μ-η^2:η^2-peroxo)dicopper(II) complexes that exhibit similar spectroscopic features (UV–vis, resonance Raman, EPR) to those of (**2**) but which are supported by various capping ligands have been reported,[112–129] and some of these also have been structurally characterized (Table 1).[115,119,122,129]

The unique spectroscopic features of the (μ-η^2:η^2-peroxo)dicopper(II) core have been interpreted by Solomon *et al.* using broken-symmetry SCF-Xα-SW calculations.[1,16,130,131] The HOMO and LUMO for the (μ-η^2:η^2-peroxo)dicopper(II) complex are formed by the interaction of the peroxide valence orbitals with the half-occupied $d_{x^2-y^2}$ orbitals of the two copper(II) ions (Figure 6).[1,16] There is a strong σ-bonding interaction between the π_σ^*-orbital and the symmetric combination of d$_{x^2-y^2}$ orbitals (Cu($d_{x^2-y^2}$) + Cu($d_{x^2-y^2}$)) to form the LUMO.[1,16] Since, the peroxide ligand has four σ-donor orbitals to the two copper centers, the bonding/antibonding interaction becomes much larger than that in the end-on peroxo bridge, in which there are only two σ-donor interactions.[1,16] The larger σ-donor interaction in the side-on peroxo complex leads to a high energy for the peroxide π_σ^* to copper(II) charge-transfer transition ($\sim$350 nm) and a high intensity ($\sim$20,000 M^{-1} cm^{-1}) compared to those of the end-on counterparts ($\sim$530 nm, $\sim$10,000 M^{-1} cm^{-1}).[1,16] On the other hand, the interaction between the antisymmetric combination of d$_{x^2-y^2}$ orbitals (Cu($d_{x^2-y^2}$) $-$ Cu($d_{x^2-y^2}$)) and the high-energy unoccupied σ^*-orbital on the peroxide ligand comprise the HOMO, in which some π back-bonding of electron density from the copper centers into the σ^*-orbital of the peroxide occurs.[1,16] Since the σ^*-orbital is strongly anti-bonding with respect to the O—O bond, the π-electron back donation from the copper ions to the peroxide ligand weakens the O—O bond of the (μ-η^2:η^2-peroxo)dicopper(II) complex.[1,16] This is reflected in the significantly lower O—O bond stretching frequency ($\sim$740 cm^{-1}) of the side-on peroxide complex as compared to that of the end-on peroxide congener ($\sim$830 cm^{-1}).[1,16] In addition, very strong σ-donation (destabilization of the LUMO) and the π-electron back donation (stabilization of HOMO) leads to the large stabilization of the singlet ground state, which underlies the strong antiferromagnetic coupling between the two cupric ions.[1,16]

Interestingly, the thermal stability of the peroxo complexes supported by a relatively rigid dinucleating ligand L^1 (complex (**3**), Figure 7) and by the perfluorinated hydrotris (pyrazolyl)
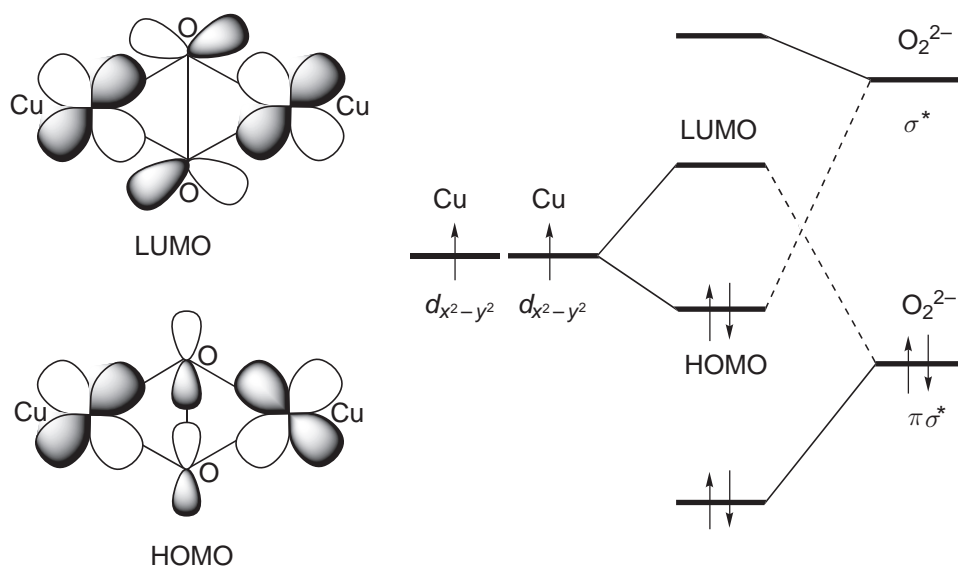
Figure 6 Electronic structure of the $(\mu\text{-}\eta^2\text{:}\eta^2\text{-peroxo})$dicopper(II) complex.[1,16]
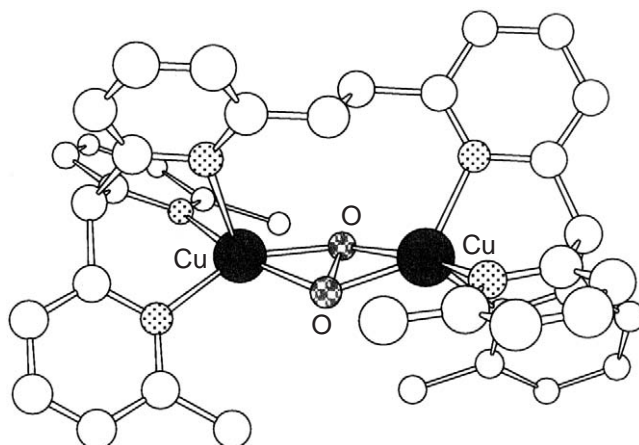
Figure 7 Chem 3D representation of the crystal structure of complex (**3**).[122]

borate ligand HB(3-CF$_3$-5-CH$_3$pz)$_3^-$ is significantly enhanced as compared to those of the others, so that they can be handled even at room temperature.[122,123] Furthermore, reversible dioxygen binding is accomplished using complex (**3**).[122] The square pyramidal geometry of each copper ion and the Cu$_2$O$_2$ core in (**3**) are relatively distorted as compared to those of complex (**2**), due to the steric restriction induced by the ligand strap of L^1 (Table 1). The conformation of the axial ligands in (**3**) is syn, whereas they are anti in (**2**). A perdeuterated macrocyclic ligand d_{21}-i-Pr$_3$ TADC (the isopropyl groups are deuterated, Scheme 3) also allowed them to isolate $(\mu\text{-}\eta^2\text{:}\eta^2\text{-peroxo})$ dicopper(II) complex (**4**).[119]

8.15.4.2 Bis(μ-oxo)dicopper(III) Complexes

Tolman and co-workers brought about another breakthrough in the Cu$_2$/O$_2$ chemistry in 1995.[90,92,132] Oxygenation of the copper(I) complex supported by 1,4,7-triazacyclononane ligand (TACN) carrying a bulky substituent such as benzyl group (Bn$_3$TACN, Scheme 3) at a low temperature ($-80\,^\circ$C) gave an unprecedented complex (**5**),[132] the X-ray structure of which was determined by adopting per-deuterated ligand d_{21}-Bn$_3$TACN.[133,134] It is a bis(μ-oxo)dicopper (III) complex as shown in Figure 8, in which each copper ion exhibits a distorted square pyramidal geometry with the N$_3$O$_2$ donor set. There is no covalent bond between the two
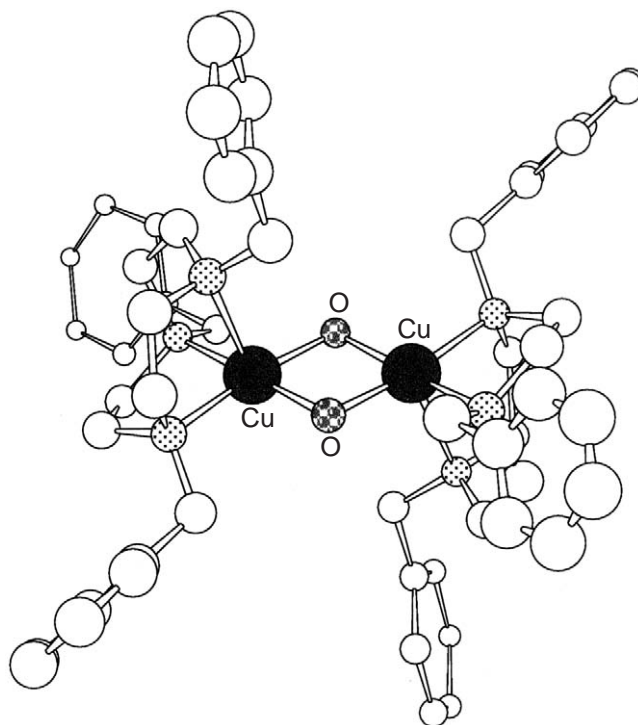
Figure 8 Chem 3D representation of the crystal structure of complex (**5**).[133,134]

oxygen atoms in the Cu_2O_2 core (O—O = 2.29 Å), while the Cu—Cu distance becomes significantly shorter (Cu—Cu = 2.79 Å) than that of the (μ-η^2:η^2-peroxo)dicopper(II) core (Cu—Cu = 3.56 Å) (Table 2).[133,134] The Cu—O (~1.80 Å) and Cu—N_{eq} (1.99 Å) bond lengths are also shorter than those of the corresponding bis(μ-hydroxo)dicopper(II) complexes (~1.94 Å, and ~2.06 Å, respectively).[133,134] These data are consistent with the high oxidation level of the bis(μ-oxo)dicopper(III) complex.[134] A bond valence sum (BVS) analysis of the crystallographic data strongly supports the copper(III) oxidation state of the complex.[134] The axial ligands, on the other hand, weakly coordinate to the copper ion with an anti-configuration (Cu—N_{ax} = ~2.30 Å).[134] Compound (**5**) exhibits two intense absorption bands at 318 nm (12,000 M^{-1} cm^{-1}) and 430 nm (14,000 M^{-1} cm^{-1}), and excitation of the lower-energy band resulted in intense resonance enhancement of Raman bands at 602 cm^{-1} and 612 cm^{-1} (with $^{16}O_2$), which collapsed into one band at 583 cm^{-1} upon $^{18}O_2$ substitution (Table 2).[134]

Since the initial report of (**5**), similar bis(μ-oxo)dicopper(III) complexes with a variety of ligands have been reported,[115,116,118,119,121,128,135–145] some of which [(d_{28}-i-Pr_4DTNE)Cu^{III}_2(μ-O)$_2$]$^{2+}$ (**6**),[135] [(L_{ME})$_2$$Cu^{III}_2$($\mu$-O)$_2$]$^{2+}$ (**7**),[137] [(Me_2TPA)$_2$$Cu^{III}_2$($\mu$-O)$_2$]$^{2+}$ (**8**),[141] and [(t-Bu_2P(NSiMe$_3$)$_2$$^-$)$_2$$Cu^{III}_2$($\mu$-O)$_2$]$^{2+}$ (**9**),[143] also have been characterized by X-ray crystallographic analysis (Table 2). In the absence of X-ray crystallographic information, the presence of the bis(μ-oxo)dicopper(III) core has also been deduced by X-ray absorption fine structure (EXAFS) spectroscopy.[115,134,138] The copper(III) oxidation state of the bis(μ-oxo) core has been confirmed directly by a Cu K-edge X-ray absorption spectroscopy (XAS) study on compound (**7**).[146] All complexes exhibit two intense

Table 2 The Cu—Cu distance and the UV–vis and resonance Raman data of representative bis(μ-oxo) dicopper(III) complexes that have been characterized by X-ray crystallography.

Complex	d(Cu—Cu) (Å)	$\lambda_{max}(\varepsilon)$ (nm (M^{-1} cm^{-1}))	$\nu(^{16}O)$ ($\nu(^{18}O)$) (cm^{-1})
(**5**)[134]	2.794(2)	318 (12,000), 430 (14,000)	602, 612 (583)
(**6**)[135]	2.783(1)	316 (13,000), 414 (14,000)	600 (582)
(**7**)[137]	2.743(1)	306 (21,000), 401 (28,000)	610 (587)
(**8**)[141]	2.758(4)	258 (36,000), 378 (19,000)	590 (564)
(**9**)[143]	2.906(1)	444 (~10,000)	Not reported
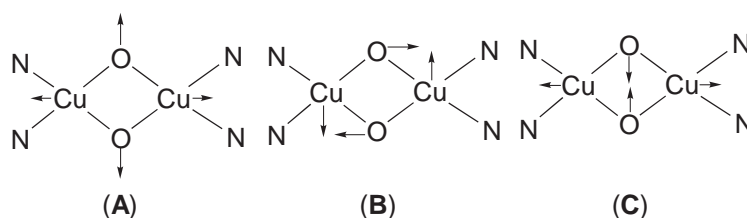
Figure 9 Main vibrational (A) core breathing mode, (B) pairwise stretching mode, and (C) core bending mode of the bis(μ-oxo)dicopper(III) core.[92]

oxo-to-copper charge transfer bands around 300 nm and 400 nm and an intense resonance Raman band at $\sim$600 cm^{-1}, which has been assigned to the core breathing mode of the bis(μ-oxo)dicopper unit (Figure 9).[147,148] The isotope shift of this band ($\nu(^{16}O_2) - \nu(^{18}O_2)$) is $20-30$ cm^{-1}.[92] In addition to the core breathing mode around 600 cm^{-1}, a weak Raman feature at $100-200$ cm^{-1} due to the core bending mode exists,[147] although little effort has so far been made to detect such a lower-energy frequency. In the case of an unsymmetric didentate ligand system,[136,139] a pairwise stretching mode around 600 cm^{-1} also has been detected. Furthermore, the bis(μ-oxo)dicopper(III) complexes are ESR-silent, consistent with the d^8 electronic configuration of the tetragonal copper(III) ions. Computational analyses of the bis(μ-oxo)dicopper(III) core have been performed using different donor sets at various levels of theory.[119,134,147,149–152] Details about the structure, spectroscopic features, and reactivity of the bis(μ-oxo)dicopper(III) complexes are summarized in a recent review article.[92]

8.15.4.3 Formation Mechanisms

So far, we have learned that copper(I) complexes with certain ligands react with molecular oxygen to produce three types of Cu$_2$/O$_2$ complexes. Tetradentate ligands usually provide the (*trans*-μ–1,2-peroxo)dicopper(II) complex, whereas the tridentate and didentate ligands afford the (μ-η^2:η^2-peroxo)dicopper(II) and/or the bis(μ-oxo)dicopper(III) complexes (Scheme 4). The ligand denticity might be the major factor that controls the different binding mode (end-on vs. side-on) in the peroxo dicopper(II) complexes. Since the copper(II) ion generally favors a five-coordinate geometry (square pyramidal and trigonal bipyramidal), the tetradentate ligand can provide only one vacant site available for the adduct formation with O$_2$, thus producing the end-on peroxo complex. On the other hand, the tridentate and didentate ligands can afford at least two vacant sites for the reaction with O$_2$, making it possible to form the side-on adduct. In this respect, it is interesting to note that all the dicopper enzymes so far known have tri-coordinate dicopper units, producing the (μ-η^2:η^2-peroxo)dicopper(II) as the common intermediate.
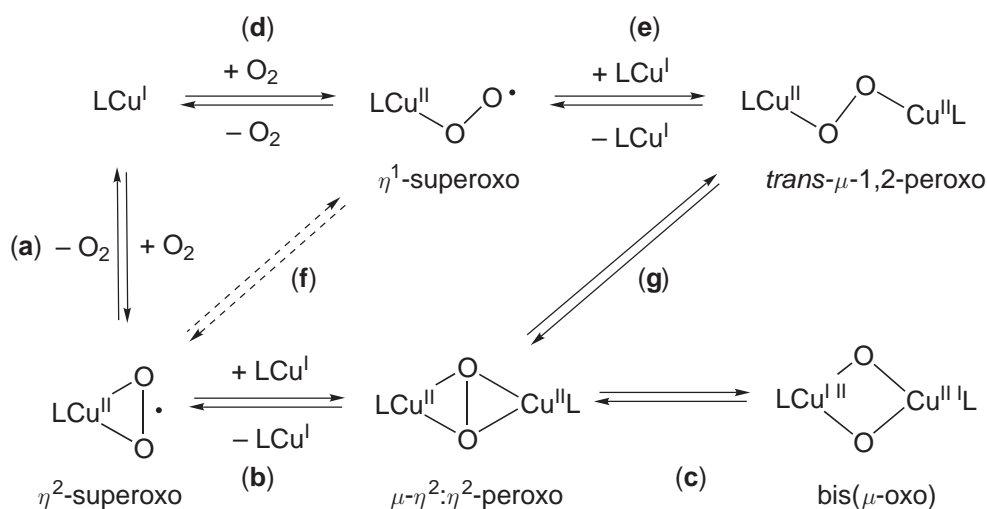
Scheme 4

In the model reactions, mononuclear copper(II)-superoxo complexes both in the end-on (η^1-superoxo) and side-on (η^2-superoxo) binding modes have been characterized in the reactions of copper(I) complexes and O_2.[100,102,104,153] Such mononuclear copper(II)-superoxo complexes could be the intermediates for the formation of dicopper(II)-peroxo complexes as illustrated in Scheme 4 (routes (a)–(b) and (d)–(e)), although direct evidence has yet to be obtained in order to confirm the postulated mechanism. Interconversions between the η^1- and η^2-superoxo frameworks (path (f)) and the (*trans*-μ–1,2-peroxo) and (μ-η^2:η^2-peroxo) bridging ligands (path (g)) are also possible depending on the ligand used. In fact, the pathway between the end-on and side-on peroxo ligand frameworks (path (g)) has been suggested to be involved in some instances.[154,155] Depending on the ligand structure used, the kinetics of the process of formation of the peroxo intermediate may be first or second order with respect to the copper complexes.[92,109,120,133] This difference has been attributed to a different rate-determining step; the (superoxo)copper(II) complex formation (path (a)) vs. the reaction between the superoxo complex and copper(I) precursor (path (b)). Computational studies on the dioxygen binding process in the dinuclear copper(I) site of the enzymes have been performed to provide insights into energetics as well as an intersystem crossing mechanism from triplet O_2 to the singlet (μ-peroxo)dicopper(II) species.[156–160]

It has been well established that the (μ-η^2:η^2-peroxo)dicopper(II) complex and the bis (μ-oxo)dicopper(III) complex can interconvert with each other (Scheme 4, path (c)).[90,133,161] The equilibrium position between the two species in solution has been demonstrated to be significantly influenced by the ligand structure, solvents, and counter anions.[90,128,133,161] Theoretical studies have indicated that the thermal stability of the two complexes are very close to each other and that the activation energy of the isomerization reaction is very small.[149–152,158] Although solvent and counter anion effects are not clearly understood, the ligand effects can be interpreted by taking into account the steric effect of the *N*-alkyl substituents as well as the electron donating ability of the supporting ligands. Namely, less hindered substituents allow closer contact of the two copper ions, stabilizing the bis(μ-oxo)dicopper core ($d_{Cu—Cu} = \sim 2.8\,\text{Å}$ vs. $d_{Cu—Cu} = \sim 3.5\,\text{Å}$ for the (μ-η^2:η^2-peroxo)dicopper(II) complex), and strongly σ-donating alkylamine ligands stabilize the higher oxidation state (Cu^{III}) in the bis(μ-oxo) complexes. It also has been proposed that the ligands that tend to give more tetragonal copper geometries tend to favor the bis(μ-oxo) complex, while ligands that favor more tetrahedrally distorted geometries favor the peroxo complex.[119] Thus, didentate ligands and tridentate alkylamine ligands tend to provide bis(μ-oxo)dicopper(III) complexes,[133,136–139,143–145] while tridentate aromatic ligands predominantly give (μ-η^2:η^2-peroxo) dicopper(II) complexes.[41,112–114,120,122–124,126,127] Recent studies have shown that subtle changes in the didentate ligands,[121,162] tridentate alkylamine ligand,[116,119] and tetradentate aromatic amine ligands[141] result in drastic changes in the structure of Cu_2/O_2 complexes.

8.15.5 MODEL REACTIONS

8.15.5.1 Oxygenation of Phenols (Model Reactions for Phenolase Reaction)

Many chemists have been fascinated by metalloenzyme-catalyzed oxygenation of various organic substrates with molecular oxygen. The phenolase activity of tyrosinase is one such reaction. Thus, great efforts have so far been made to develop oxygenation reactions of phenols by molecular oxygen catalyzed by various copper complexes. However, little information is available about the mechanistic details of such catalytic oxidation reactions.[163–170]

Karlin and co-workers have developed an aromatic ligand hydroxylation by O_2 using a dinuclear copper(I) complex supported by ^{H}XYL^H (Scheme 3, ^{R1}XYL^{R2} where $R^1 = R^2 = H$), where a hydroxylated ligand ^{H}XYL^{OH} was produced quantitatively.[171–173] Mechanistic studies of this and related systems have led to the following conclusions: (i) a migration of the aromatic methyl group occurred when ^{H}XYL^{CH3} was employed (NIH shift[174]), (ii) no kinetic deuterium isotope effect was observed (^{H}XYL^H vs. ^{H}XYL^D), (iii) electronic donating *p*-substituents accelerated the reaction rate (R^1 = t-Bu > H > F > NO$_2$ in ^{R1}XYL^H), and (iv) a side-on peroxo intermediate was detected in the case of ^{NO2}XYL^H.[113,175,176] These results suggest that the aromatic ligand hydroxylation reaction involves an electrophilic attack on the ligand arene ring by the (μ-η^2:η^2-peroxo) dicopper(II) intermediate.[113,175,176] Similar aromatic ligand hydroxylation reactions have been observed using a variety of *m*-xylyl dinucleating ligands.[112,118,177–187]

With respect to the intermolecular reaction between externally added phenols and (μ-η^2:η^2-peroxo) dicopper(II) complexes, however, most of the reactions reported so far afford the C—C coupling

dimer resulting from a phenoxyl radical as a major product (Scheme 5).[128,188–191] Such reactions are regarded as a model reaction of the phenolase activity of tyrosinase. Casella and co-workers recently reported that a (μ-η^2:η^2-peroxo)dicopper(II) complex can react with an exogenous phenolate to yield the corresponding catechol. However, the low yield of the product (20% based on the dicopper complex) has precluded kinetic and mechanistic investigation of this reaction.[124]
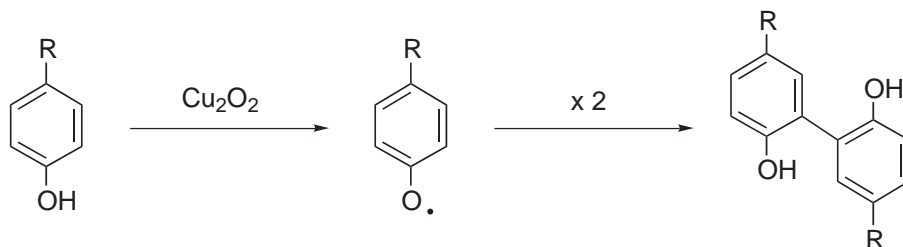

Scheme 5

Itoh and co-workers recently demonstrated that efficient catechol formation proceeds through the intermolecular reaction of a (μ-η^2:η^2-peroxo)dicopper(II) complex supported by the tridentate ligand Py2$^{Bn-d_2}$ (Scheme 3, Py2^R; R = Bn-d_2 = -CD$_2$Ph) with lithium salts of phenols.[192] Thus, the reaction of lithium salts of *p*-substituted phenols (*p*-X-C$_6$H$_4$OLi; X = t-Bu, Me, Cl, Br, and CO$_2$Me) with the (μ-η^2:η^2-peroxo)dicopper(II) complex at -80 °C resulted in formation of the corresponding catechols in good yields (>99%, 69%, 90%, 79%, and 60%, respectively, based on the peroxo complex), but neither the corresponding *o*-quinone derivatives nor the C—C and C—O coupling dimers were obtained from the final reaction mixture.[192] An isotope-labeling experiment using ^{18}O$_2$ confirmed that the origin of one of the two oxygen atoms of the product was molecular oxygen.[192] In contrast to such an efficient catechol formation by the peroxo complex, no catechol was formed when the bis(μ-oxo)dicopper(III) complex generated by using didentate ligand Py1$^{Et,Bn-d_2}$ (Scheme 3, Py1^{R1,R2}; R^1 = Bn-d_2, R^2 = Et) was employed under otherwise identical experimental conditions.[192]

The spectral changes for the oxidation of the lithium salt of *p*-chlorophenol at -94 °C in acetone is shown in Figure 10 as a typical example, where the characteristic absorption bands due to the (μ-η^2:η^2-peroxo)dicopper(II) complex at 364 nm and 530 nm decrease as the reaction proceeds.[192] The reaction obeys pseudo-first-order kinetics, and a plot of the pseudo-first-order rate constant k_{obs} against the substrate concentration afforded a Michaelis–Menten-type saturation curve (inset, Figure 10).[192] This result suggests formation of a complex of the substrate and the peroxo intermediate prior to the oxidation step. From the double reciprocal plot according to the equation, $1/k_{obs} = 1/k_{ox} + (1/K_f k_{ox})(1/[ArOLi])$, was obtained the formation constant K_f and the rate constant k_{ox} for the oxidation process as listed in Table 3. The absence of a C—C coupling product rules out an electron transfer pathway from the substrate to the peroxo intermediate to produce a free radical species.

As seen in Table 3, the reactivity of the substrate increases significantly with the increasing electron-donating ability of the *p*-substituent, whereas the K_f values are rather insensitive to the electronic effects of the *p*-substituents. In addition, no kinetic deuterium isotope effect was observed when *p*-Cl-C$_6$D$_4$OLi was used as the substrate instead of *p*-Cl-C$_6$H$_4$OLi.[192]

In the enzymatic mechanism of tyrosinase, an ongoing mechanistic debate concerns the timing of the O—O bond cleavage of the peroxo intermediate. Does it occur (i) before, (ii) simultaneous with, or (iii) after the C—O bond formation? In the case of mechanism (i), a bis(μ-oxo)dicopper (III) complex might be an active oxygen species. In Itoh's system, however, no catechol formation was detected in the intermolecular reaction of a phenolate and the bis(μ-oxo)copper(III) complex supported by Py1$^{Et,Bn-d_2}$.[192] In addition, the decay of a bis(μ-oxo)dinickel(III) complex supported by ^{H}XYL^H ligand (Scheme 3) did not yield any aromatic ligand hydroxylation product.[193] This result is in sharp contrast to the case of the (μ-η^2:η^2-peroxo)dicopper(II) complex with the same ligand, where quantitative aromatic ligand hydroxylation takes place.[171–173] On the other hand, if the O—O bond cleavage occurred after C—O bond formation (case iii), an (alkylperoxo) copper(II) type intermediate (R—O—O—Cu^{II}) would be involved as a key intermediate. Such a reactive species has been demonstrated to provide the quinone product directly.[167,194] In Itoh's
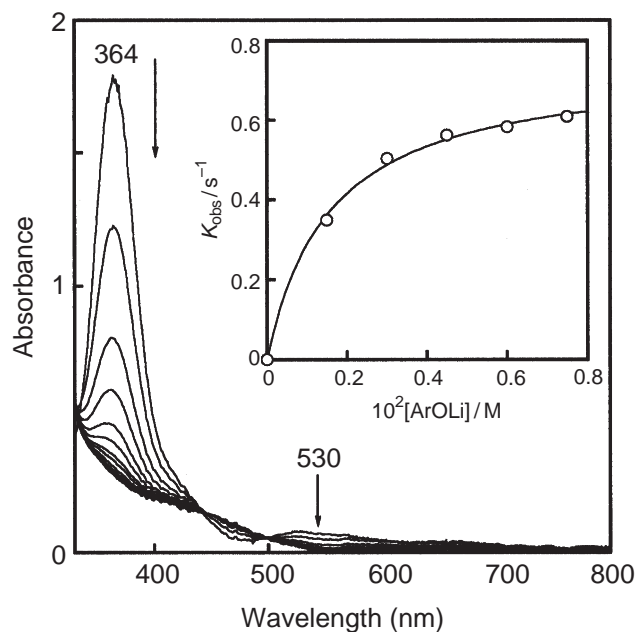
Figure 10 Spectral change for the reaction of $[Cu^{II}_2(\mu\text{-}O_2)(Py2^{Bn\text{-}d_2})_2]^{2+}$ (7.5×10^{-5} M) in acetone at $-94\,^\circ$C with lithium 4-chlorophenolate (1.5×10^{-3} M). Interval: 1.5 s. Inset: plot of k_{obs}^{-1} vs. $[p\text{-}Cl\text{-}C_6H_4\,OLi]^{-1}$.[192]

system, little of the corresponding quinone products were obtained, ruling out the possibility of mechanism (iii).[192] Thus, all the results are consistent with mechanism (ii). Namely, the oxygenation of exogenous phenolates to the corresponding catechols by the (μ-η^2:η^2-peroxo)dicopper(II) complex proceeds via an electrophilic aromatic substitution mechanism in a binary complex between the peroxo intermediate and the phenolate substrate, where the oxygenation of the substrate (C—O bond formation) occurs simultaneously with the O—O bond cleavage of the peroxo intermediate (Scheme 6). The electrophilic character of the (μ-η^2:η^2-peroxo)dicopper(II) complex has been well demonstrated by its reactivity pattern toward various external substrates.[189]

The density functional calculation (B3LYP) on the Cu$_2$/O$_2$ system with three imidazole ligands has suggested that the (μ-η^2:η^2-peroxo)dicopper(II) rather than the bis(μ-oxo)dicopper(III) is feasible as the active oxygen intermediate of tyrosinase.[195] Computational studies also have suggested the possible rearrangement of the (μ-η^2:η^2-peroxo) core to a (μ-η^1:η^2-peroxo) binding mode by coordination of a neutral phenol to one of the copper ions.[195] In the experimental systems, however, it is obvious that deprotonation of the substrate prior to the reaction is essential, since only the C—C coupling dimer was obtained when the phenol itself was used instead of the phenolate. Thus, the timing of deprotonation of the phenol substrate might also be an important mechanistic issue. Most of the results from the model studies so far described are consistent with the electrophilic aromatic substitution mechanism for the phenolase activity of a

Table 3 Formation constants (K_f) and rate constants (k_{ox}) for the reaction between $[Cu^{II}_2(Py2^{Bn\text{-}d_2})_2$-($\mu$-O$_2$)](PF$_6$)$_2$ and p-X-C$_6$H$_4$OLi in acetone at $-94\,^\circ$C.

X	K_f (M^{-1})	k_{ox} (s^{-1})
t-Bu	a	a
Me	a	a
Br	465	0.93
Cl	570	0.76
F	948	0.64
COMe	493	0.086
COOMe	940	0.083

a Too fast to be determined.

(μ-η^2:η^2-peroxo)dicopper(II) intermediate. On the other hand, aromatic ligand hydroxylation was observed upon decay of a bis(μ-oxo)dicopper(III) complex supported by ArPyNEt$_2$ (Scheme 7).[136] Since the calculations on dinuclear copper dioxygen complexes with other amine ligands argue for similar thermodynamic stabilities between the (μ-η^2:η^2-peroxo)dicopper(II) and the bis(μ-oxo) dicopper(III) cores,[119,149–152,158] the question of whether the bis(μ-oxo)dicopper(III) complex is capable of hydroxylating arenes is still an open one.
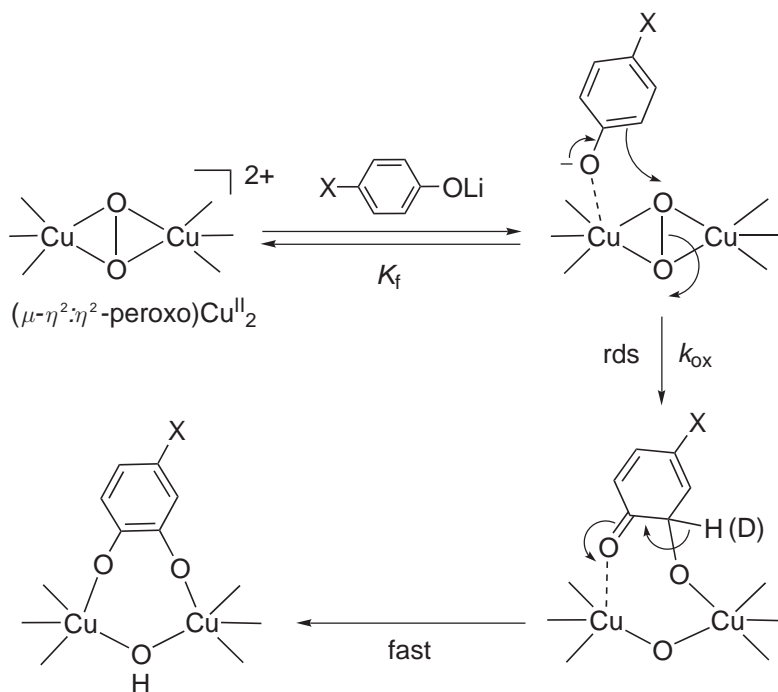
Scheme 6
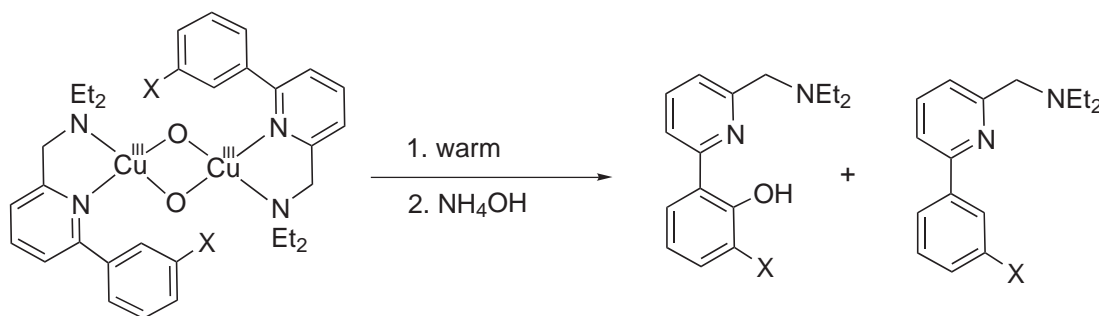
Scheme 7

As compared to the oxygenation reaction of phenols to catechols (phenolase reaction), dehydrogenation of catechols to the corresponding *o*-quinones (catecholase reaction) proceeds more readily. Thus, the catalytic activity of several tyrosinase and catechol oxidase models have been examined using 2,4-di-*tert*-butylcatechol (DTBC) as a substrate.[165,188,196–202] Direct reactions between the (μ-η^2:η^2-peroxo)dicopper(II) complexes and DTBC also have been studied at a low temperature,[124,188,203] and a semiquinone–copper(II) complex has been isolated and structurally characterized in one instance.[203]

8.15.5.2 Aliphatic C—H Bond Activation

Since the bis(μ-oxo)dicopper(III) complex was discovered in 1995,[133,134] the complex has attracted much attention as an active oxygen intermediate of the dicopper enzymes.[92] In this respect, an interesting feature of this complex is its reactivity toward aliphatic C—H bond activation. The bis(μ-oxo)dicopper(III) complexes so far reported have been shown to undergo C—H bond activation at the alkyl ligand substituent. In most cases, the C—H bond activation leads to an oxidative *N*-dealkylation of the ligand sidearm,[121,137,141,204] while an aliphatic ligand hydroxylation also takes place in some instances.[139,205] Kinetic studies, including (i) kinetic deuterium isotope effects (KIE), (ii) activation parameters ($\Delta H^{\ddagger}$ and $\Delta S^{\ddagger}$), and (iii) ligand substituent effects (Hammett study) as well as isotope labeling experiments using $^{18}O_2$, have suggested that the bis(μ-oxo)dicopper(III) complex exhibits a weakly electrophilic character and that the C—H bond activation reactions involve hydrogen atom abstraction by the bis(μ-oxo)dicopper(III) core followed by hydroxyl rebound or its concerted variant as shown in Scheme 8.[139,204] In a recent theoretical study, the transition state of the C—H bond activation process has been investigated in detail to support the proposed hydrogen atom abstraction mechanism.[206] The bis(μ-oxo)dinickel(III) complex supported by the tridentate ligand Py2^{Phe} (Phe = —CH$_2$CH$_2$Ph, Scheme 3) has also been shown to exhibit a similar reactivity involving aliphatic ligand hydroxylation via a similar mechanism.[193,207]
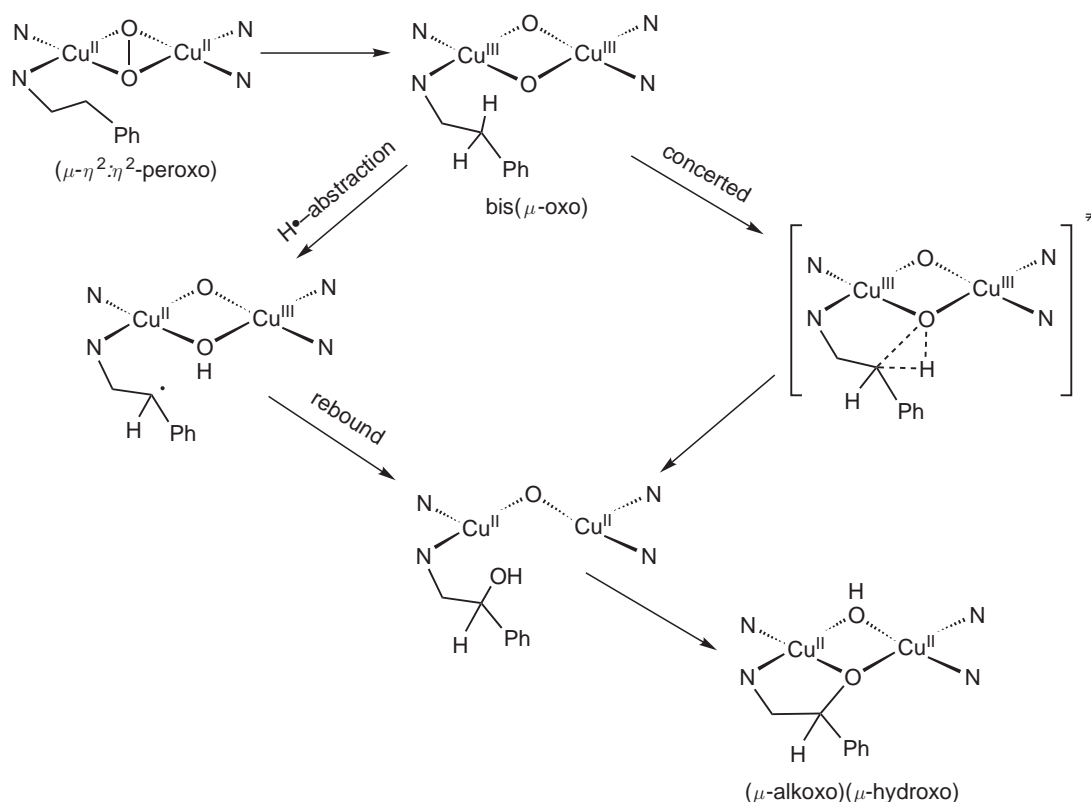
Scheme 8

An aliphatic ligand hydroxylation also proceeds upon decomposition of the (μ-η^2:η^2-peroxo) dicopper(II) complex supported by Py2^{Phe}.[208] Mechanistic studies indicated that the real active oxygen species is also a bis(μ-oxo)dicopper(III) complex derived from the peroxo intermediate, and that the O—O bond homolysis of the peroxo intermediate is the rate-determining step of the overall reaction.[120,121]

Examination of the intermolecular reaction between the bis(μ-oxo)dicopper(III) complex of didentate ligand Py1$^{Et,Bn-d_2}$ and an activated C—H bond such as in 10-methyl-9,10-dihydroacridine (AcrH$_2$) and 1,4-cyclohexadiene (CHD) has provided further insights into the chemistry of dinuclear copper dioxygen complexes. These substrates are efficiently converted into the

corresponding oxidation products, 10-methylacridinium ion (AcrH$^+$) and benzene, by the reaction with the bis(μ-oxo)dicopper(III) complex at $-94\,^\circ$C.[140] Interestingly, the reaction obeys second-order kinetics with respect to the copper complex even in the presence of a large excess of substrate.[140] In addition, a large primary kinetic deuterium isotope effect (KIE $= 22.7$) was obtained at $-94\,^\circ$C when AcrD$_2$ (AcrD$_2 =$ the 9,9-dideuterated analogue of AcrH$_2$) was used in place of AcrH$_2$.[140] Such a large primary kinetic deuterium isotope effect indicates that a tunneling hydrogen transfer process is involved in the rate-determining step of the C—H bond activation reaction.[209,210] The direct reaction between the bis(μ-oxo)dicopper(III) complex and AcrH$_2$ would afford a first-order dependence of the rate with respect to the concentration of each reactant, contrary to the observed experimental results.

A possible explanation for such an unusual kinetic behavior is the following. Disproportionation of two molecules of the bis(μ-oxo)dicopper(III) complexes may afford one molecule of (μ-oxo)(μ-oxyl radical)dicopper(III) (**A** in Scheme 9) and one molecule of bis(μ-oxo)Cu(II)Cu(III) (**B** in Scheme 9), the former of which may be the real active species for the C—H bond activation (hydrogen atom abstraction) of the substrates (Scheme 9).[140] Alternatively, two molecules of the bis(μ-oxo)dicopper(III) intermediate may function in unison (e.g., via a tetranuclear copper–oxo complex) to oxidize the substrate.[140]
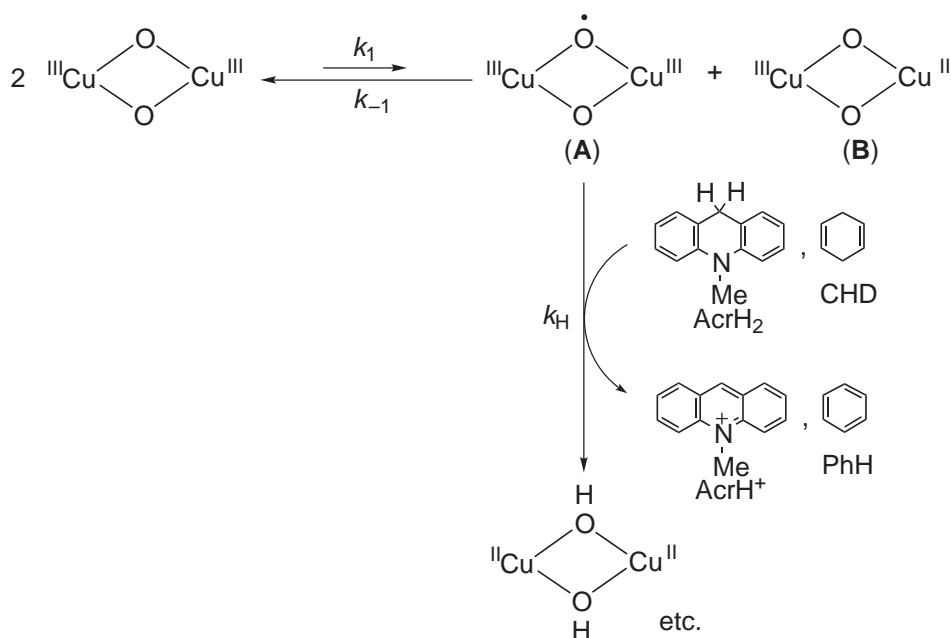
Scheme 9

8.15.5.3　Oxygen Atom Transfer Reaction

The (μ-η^2:η^2-peroxo)dicopper(II) complexes are able to transfer an oxygen atom to Ph$_3$P giving Ph$_3$P $=$ O.[128,189] In the system supported by an ethylenediamine ligand (L^2, Scheme 3) developed by Stack and co-workers, the oxygen atom transfer ability of the (μ-η^2:η^2-peroxo)dicopper(II) complex is much higher than that of the bis(μ-oxo) dicopper(III) congener supported by the same ligand.[128] On the other hand, Itoh and co-workers recently demonstrated that the bis(μ-oxo) dicopper(III) complex with the didentate ligand Py1$^{Et,Bn-d_2}$ can oxidize sulfides to sulfoxides more efficiently than the (μ-η^2:η^2-peroxo) dicopper(II) complex supported by the tridentate ligand Py2$^{Bn-d_2}$.[211] A detailed kinetic study of the sulfoxidation reaction suggested that the reaction proceeds via formation of binary complex (**X**) between the bis(μ-oxo) species and the substrate as illustrated in Scheme 10, although the structural details of the intermediate **X** have yet to be elucidated.[211] Dependence of the oxygen atom transfer rate on the one-electron oxidation potential of the sulfide substrates indicated that the reaction proceeds via direct oxygen atom transfer rather than an electron-transfer mechanism.[211] The coordination of exogenous substrates such as alcohols to the metal center of the bis(μ-oxo)dicopper(III) core supported by L$_{TMPD}$ (Scheme 3) has also been demonstrated to be a prerequisite for the dehydrogenation of the substrates.[138]

Thus, the difference in the reactivity between the (μ-η^2:η^2-peroxo)dicopper(II) complexes and the bis(μ-oxo)dicopper(III) complexes described above may be attributed in part to differences in accessibility of the substrates to the Cu_2/O_2 core.

$$Cu^{III} \overset{O}{\underset{O}{\diamondsuit}} Cu^{III} + R-S-R' \underset{k_{-1}}{\overset{k_1}{\rightleftharpoons}} X \overset{k_2}{\longrightarrow} \overset{O}{\overset{\|}{R-S-R'}}$$
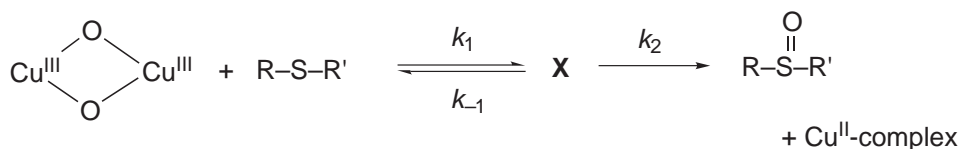
$$+ \ Cu^{II}\text{-complex}$$

Scheme 10

8.15.6 CONCLUDING REMARKS

In this chapter, the dioxygen activation mechanism at the dinuclear copper-active sites of tyrosinase and catechol oxidase has been surveyed. In both enzymes, a (μ-η^2:η^2-peroxo) dicopper(II) complex has been detected and characterized as a common reactive intermediate by several spectroscopic methods. In spite of longstanding efforts in the enzymological studies, mechanistic details of the enzymatic reactions (phenolase and catecholase activities) still remain ambiguous. On the other hand, recent developments in the model chemistry have provided a great deal of information about the structure and physicochemical properties as well as the reactivity of the peroxo intermediate and have advanced our understanding of the enzymatic reactions.

In addition to the (μ-η^2:η^2-peroxo)dicopper(II) complex, model studies have shown that a bis (μ-oxo)dicopper(III) complex can be easily generated by the O—O bond homolysis of the (μ-η^2:η^2-peroxo)dicopper(II) complex. The bis(μ-oxo)dicopper(III) complex exhibits different reactivity such as aliphatic C—H bond activation as well as oxygen atom transfer and dehydrogenation. Moreover, possible formation of a (μ-oxo)(μ-oxyl radical)dicopper(III) has also been suggested in some instances. Although such high-valent copper(III)–oxo species have yet to be detected in enzymatic systems, they can be a possible reactive intermediate of the pMMO and AMO reactions. These studies of Cu_2/O_2 chemistry provide significant insights into dioxygen activation mechanisms, not only in metalloenzymes but also in many catalytic oxidation reactions.

8.15.7 REFERENCES

 1. Solomon, E. I.; Sundaram, U. M.; Machonkin, T. E. *Chem. Rev.* **1996**, *96*, 2563–2605.
 2. Halcrow, M. A.; Knowles, P. F.; Phillips, S. E. V. In *Handbook on Metalloproteins*, Bertini, I.; Sigel, A.; Sigel, H., Eds.; Dekker: New York, 2001; pp 709–811.
 3. Holm, R. H.; Kennepohl, P.; Solomon, E. I. *Chem. Rev.* **1996**, *96*, 2239–2314.
 4. Klinman, J. P. *Chem. Rev.* **1996**, *96*, 2541–2561.
 5. Fusetti, F.; Schröter, K. H.; Steiner, R. A.; van Noort, P. I.; Pijning, T.; Rulebook, H. J.; Kalk, K. H.; Egmond, M. R.; Dijkstra, B. W. *Structure* **2002**, *10*, 259–268.
 6. McGuirl, M. A.; Dooley, D. M. *Curr. Opin. Chem. Biol.* **1999**, *3*, 138–144.
 7. Janes, S. M.; Mu, D.; Wemmer, D.; Smith, A. J.; Kaur, S.; Maltby, D.; Burlingame, A. L.; Klinman, J. P. *Science* **1990**, *248*, 981–987.
 8. Wang, S. X.; Mure, M.; Medzihradszky, K. F.; Burlingame, A. L.; Brown, D. E.; Dooley, D. M.; Smith, A. J.; Kagan, H. M.; Klinman, J. P. *Science* **1996**, *273*, 1078–1084.
 9. Choi, Y.-H.; Matsuzaki, R.; Suzuki, S.; Tanizawa, K. *J. Biol. Chem.* **1996**, *271*, 22598–22603.
10. Ito, N.; Phillips, S. E. V.; Stevens, C.; Ogel, Z. B.; McPherson, M. J.; Keen, J. N.; Yadav, K. D. S.; Knowles, P. F. *Nature* **1991**, *350*, 87–90.
11. Roger, M. S.; Baron, A. J.; McPherson, M. J.; Knowles, P. F.; Dooley, D. M. *J. Am. Chem. Soc.* **2000**, *122*, 990–991.
12. Dooley, D. M.; McGuirl, M. A.; Brown, D. E.; Turowski, P. N.; McIntire, W.; Knowles, P. F. *Nature* **1991**, *349*, 262–264.
13. Mayer, A. M.; Harel, E. *Phytochemistry* **1979**, *18*, 193–215.
14. Sánchez-Ferrer, Á.; Rodríguez-López, J. N.; García-Cánovas, F.; García-Carmona, F. *Biochim. Biophys. Acta* **1995**, *1247*, 1–11.
15. Decker, H.; Tuczek, F. *Trends Biochem. Sci.* **2000**, *25*, 392–397.
16. Solomon, E. I.; Chen, P.; Metz, M.; Lee, S.-K.; Palmer, A. E. *Angew. Chem. Int. Ed.* **2001**, *40*, 4570–4590.
17. Gerdemann, C.; Eicken, C.; Krebs, B. *Acc. Chem. Res.* **2002**, *35*, 183–191.
18. Klabunde, T.; Eicken, C.; Sacchettini, J. C.; Krebs, B. *Nat. Struct. Biol.* **1998**, *5*, 1084–1090.
19. Gaykema, W. P. J.; Hol, W. G. J.; Vereijken, J. M.; Soeter, N. M.; Bak, H. J.; Beintema, J. J. *Nature* **1984**, *309*, 23–29.
20. Volbeda, A.; Hol, W. G. J. *J. Mol. Biol.* **1989**, *209*, 249–279.

21. Hazes, B.; Magnus, K. A.; Bonaventura, C.; Bonaventura, J.; Dauter, Z.; Kalk, K. H.; Hol, W. G. J. *Proteins Sci.* **1993**, *2*, 597–619.
22. Magnus, K. A.; Hazes, B.; Ton-That, H.; Bonaventura, C.; Bonaventura, J.; Hol, W. G. J. *Proteins* **1994**, *19*, 302–309.
23. Magnus, K. A.; Ton-That, H.; Carpenter, J. E. *Chem. Rev.* **1994**, *94*, 727–735.
24. Cuff, M. E.; Miller, K. I.; van Holde, K. E.; Hendrickson, W. A. *J. Mol. Biol.* **1998**, *278*, 855–870.
25. Huber, M.; Hintermann, G.; Lerch, K. *Biochemistry* **1985**, *24*, 6038–6044.
26. Kupper, U.; Niedermann, D. M.; Travaglini, G.; Lerch, K. *J. Biol. Chem.* **1989**, *264*, 17250–17258.
27. Takase, M.; Miura, I.; Nakata, A.; Takeuchi, T.; Nishioka, M. *Gene* **1992**, *121*, 359–363.
28. Kwon, B. S.; Wakulchik, M.; Haq, A. K.; Halaban, R.; Kestler, D. *Biochem. Biophys. Res. Commun.* **1988**, *153*, 1301–1309.
29. Kwon, B. S.; Haq, A. K.; Pomerantz, S. H.; Halaban, R. *Proc. Natl. Acad. Sci. USA* **1987**, *84*, 7473–7477.
30. Lerch, K. *J. Biol. Chem.* **1982**, *257*, 6414–6419.
31. Gielens, C.; DeGeest, N.; Xin, X. Q.; Devreese, B.; VanBeeumen, J.; Préaux, G. *Eur. J. Biochem.* **1997**, *248*, 879–888.
32. Eicken, C.; Zippel, F.; Büldt-Karentzopoulos, K.; Krebs, B. *FEBS Lett.* **1998**, *436*, 293–299.
33. Woolery, G. L.; Powers, L.; Winkler, M.; Solomon, E. I.; Lerch, K.; Spiro, T. G. *Biochim. Biophys. Acta* **1984**, *788*, 155–161.
34. Bubacco, L.; Salgado, J.; Tepper, A. W. J. W.; Vijgenboom, E.; Canters, G. W. *FEBS Lett.* **1999**, *442*, 215–220.
35. Jolley, R. L. Jr.,; Evans, L. H.; Mason, H. S. *Biochem. Biophys. Res. Commun.* **1972**, *46*, 878–884.
36. Jolley, R. L. Jr.,; Evans, L. H.; Makino, N.; Mason, H. S. *J. Biol. Chem.* **1974**, *249*, 335–345.
37. Huber, M.; Lerch, K. *Biochemistry* **1988**, *27*, 5610–5615.
38. Himmelwright, R. S.; Eickman, N. C.; LuBien, C. D.; Lerch, K.; Solomon, E. I. *J. Am. Chem. Soc.* **1980**, *102*, 7339–7344.
39. Lerch, K. *FEBS Lett.* **1976**, *69*, 157–160.
40. Eickman, N. C.; Solomon, E. I.; Larrabee, J. A.; Spiro, T. G.; Lerch, K. *J. Am. Chem. Soc.* **1978**, *100*, 6529–6531.
41. Kitajima, N.; Fujisawa, K.; Moro-oka, Y. *J. Am. Chem. Soc.* **1989**, *111*, 8975–8976.
42. Kitajima, N.; Fujisawa, K.; Fujimoto, C.; Moro-oka, Y.; Hashimoto, S.; Kitagawa, T.; Toriumi, K.; Tatsumi, K.; Nakamura, A. *J. Am. Chem. Soc.* **1992**, *114*, 1277–1291.
43. Hepp, A. F.; Himmelwright, R. S.; Eickman, N. C.; Solomon, E. I. *Biochem. Biophys. Res. Commun.* **1979**, *89*, 1050–1057.
44. Himmelwright, R. S.; Eickman, N. C.; LuBien, C. D.; Solomon, E. I. *J. Am. Chem. Soc.* **1980**, *102*, 5378–5388.
45. Decker, H.; Dillinger, R.; Tuczek, F. *Angew. Chem. Int. Ed.* **2000**, *39*, 1591–1595.
46. Zlateva, T.; Di Muro, P.; Salvato, B.; Beltramini, M. *FEBS Lett.* **1986**, *384*, 251–254.
47. Decker, H.; Rimke, T. *J. Biol. Chem.* **1998**, *273*, 25889–25892.
48. Winkler, M. E.; Lerch, K.; Solomon, E. I. *J. Am. Chem. Soc.* **1981**, *103*, 7001–7003.
49. Wilcox, D. E.; Porras, A. G.; Hwang, Y. T.; Lerch, K.; Winkler, M. E.; Solomon, E. I. *J. Am. Chem. Soc.* **1985**, *107*, 4015–4027.
50. Mason, H. S.; Fowlks, W. L.; Peterson, E. W. *J. Am. Chem. Soc.* **1955**, *77*, 2914–2915.
51. Wood, B. J. B.; Ingraham, L. L. *Arch. Biochem. Biophys.* **1962**, *98*, 479–484.
52. Pomerantz, S. H. *J. Biol. Chem.* **1966**, *241*, 161–168.
53. Espín, J. C.; Varón, R.; Fenoll, L. G.; Gilabert, M. A.; García-Ruíz, P. A.; Tudela, J.; García-Cánovas, F. *Eur. J. Biochem.* **2000**, *267*, 1270–1279.
54. Rodríguez-López, J. N.; Fenoll, L. G.; García-Ruiz, P. A.; Varón, R.; Tudela, J.; Thorneley, R. N. F.; García-Cánovas, F. *Biochemistry* **2000**, *39*, 10497–10506.
55. Duckworth, H. W.; Coleman, J. E. *J. Biol. Chem.* **1970**, *245*, 1613–1625.
56. Ingraham, L. L. *J. Am. Chem. Soc.* **1957**, *79*, 666–669.
57. Kertesz, D.; Brunori, M.; Zito, R.; Antonini, E. *Biochim. Biophys. Acta* **1971**, *250*, 306–310.
58. Makino, N.; Mason, H. S. *J. Biol. Chem.* **1973**, *248*, 5731–5735.
59. Gutteridge, S.; Robb, D. *Eur. J. Biochem.* **1975**, *54*, 107–116.
60. García-Carmona, F.; García-Cánovas, F.; Iborra, J. L.; Lozano, J. A. *Biochim. Biophys. Acta* **1982**, *717*, 124–131.
61. Cabanes, J.; García-Cánovas, F.; Lozano, J. A. García-Carmona, F. *Biochim. Biophys. Acta* **1987**, *923*, 187–195.
62. Rodríguez-López, J. N.; Tudela, J.; Varón, R.; García-Carmona, F.; García-Cánovas, F. *J. Biol. Chem.* **1992**, *267*, 3801–3810.
63. Rodríguez-López, J. N.; Ros, J. R.; Varón, R.; García-Cánovas, F. *Biochem. J.* **1993**, *293*, 859–866.
64. Cooksey, C. J.; Garratt, P. J.; Land, E. J.; Pavel, S.; Ramsden, C. A.; Riley, P. A.; Smit, N. P. M. *J. Biol. Chem.* **1997**, *272*, 26226–26235.
65. Fenoll, L. G.; Rodríguez-López, J. N.; Varón, R.; García-Ruiz, P. A.; García-Cánovas, F.; Tudela, J. *Biophys. Chem.* **2000**, *84*, 65–76.
66. Fenoll, L. G.; Rodríguez-López, J. N.; García-Sevilla, F.; Tudela, J.; García-Ruiz, P. A.; Varón, R.; García-Cánovas, F. *Eur. J. Biochem.* **2000**, *267*, 5865–5878.
67. Nguyen, H.-H. T.; Elliott, S. J.; Yip, J. H.-K.; Chan, S. I. *J. Biol. Chem.* **1998**, *273*, 7957–7966.
68. Takeguchi, M.; Miyakawa, K.; Okura, I. *J. Mol. Catal. A* **1998**, *132*, 145–153.
69. Yuan, H.; Collins, M. L. P.; Antholine, W. E. *Biophys. J.* **1999**, *76*, 2223–2229.
70. Elliott, S. J.; Zhu, M.; Tso, L.; Nguyen, H.-H. T.; Yip, J. H.-K.; Chan, S. I. *J. Am. Chem. Soc.* **1997**, *119*, 9949–9955.
71. Wilkinson, B.; Zhu, M.; Priestley, N. D.; Nguyen, H.-H. T.; Morimoto, H.; Williams, P. G.; Chan, S. I.; Floss, H. G. *J. Am. Chem. Soc.* **1996**, *118*, 921–922.
72. Moir, J. W. B.; Crossman, L. C.; Spiro, S.; Richardson, D. J. *FEBS Lett.* **1996**, *387*, 71–74.
73. Semrau, J. D.; Christoserdov, A.; Lebron, J.; Costello, A.; Davagnino, J.; Kenna, E.; Holmes, A. J.; Finch, R.; Murrell, J. C.; Lidström, M. E. *J. Bacteriol.* **1995**, *177*, 3071–3079.
74. Merkx, M.; Kopp, D. A.; Sazinsky, M. H.; Blazyk, J. L.; Müller, J.; Lippard, S. J. *Angew. Chem. Int. Ed.* **2001**, *40*, 2782–2807.
75. Waller, B. J.; Lipscomb, J. D. *Chem. Rev.* **1996**, *96*, 2625–2657.
76. Zahn, J. A.; DiSpirito, A. A. *J. Bacteriol.* **1996**, *178*, 1018–1029.
77. Yuan, H.; Collins, M. L. P.; Antholine, W. E. *J. Am. Chem. Soc.* **1997**, *119*, 5073–5074.

78. Elliott, S. J.; Randall, D. W.; Britt, R. D.; Chan, S. I. *J. Am. Chem. Soc.* **1998**, *120*, 3247–3248.
79. Lemos, S. S.; Collins, M. L. P.; Eaton, S. S.; Eaton, G. R.; Antholine, W. E. *Biophys. J.* **2000**, *79*, 1085–1094.
80. Nguyen, H.-H. T.; Nakagawa, K. H.; Hedman, B.; Elliott, S. J.; Lidstrom, M. E.; Hodgson, K. O.; Chan, S. I. *J. Am. Chem. Soc.* **1996**, *118*, 12766–12776.
81. Zahn, J. A.; Arciero, D. M.; Hooper, A. B.; DiSpirito, A. A. *FEBS Lett.* **1996**, *397*, 35–38.
82. Karlin, K. D.; Tyeklár, Z. Eds. *Bioinorganic Chemistry of Copper*, Chapman & Hall: New York, 1993.
83. Fox, S.; Karlin, K. D. In *Active Oxygen in Biochemistry*, Valentine, J. S., Foote, C. S., Greenberg, A., Liebman, J. F., Eds.; Chapman & Hall: London, 1995; pp 188–231.
84. Sorrell, T. N. *Tetrahedron* **1989**, *45*, 3–68.
85. Kitajima, N.; Moro-oka, Y. *Chem. Rev.* **1994**, *94*, 737–757.
86. Ito, M.; Fujisawa, K.; Kitajima, N.; Moro-oka, Y. In *Oxygenases and Model Systems*, Funabiki, T., Ed.; Kluwer: Dordrecht, 1997; pp 345–376.
87. Kopf, M.-A.; Karlin, K. D. In *Biomimetic Oxidations Catalyzed by Transition Metal Complexes*, Meunier, B., Ed.; Imperial College Press: London, 1999; pp 309–362.
88. Karlin, K. D.; Zuberbühler, A. D. In *Bioinorganic Catalysis, Second Edition*, Reedijk, J., Bouwman, E., Eds.; Dekker: New York, 1999; pp 469–534.
89. Blackman, A. G.; Tolman, W. B. In *Metal Oxo and Metal-Peroxo Species in Catalytic Oxidations*, Meunier, B., Ed.; Springer: Berlin, 2000; pp 179–211.
90. Tolman, W. B. *Acc. Chem. Res.* **1997**, *30*, 227–237.
91. Holland, P. L.; Tolman, W. B. *Coord. Chem. Rev.* **1999**, *190–192*, 855–869.
92. Que, L. Jr.; Tolman, W. B. *Angew. Chem. Int. Ed.* **2002**, *41*, 1114–1137.
93. Mahadevan, V.; Gebbink, R. K.; Stack, T. D. P. *Curr. Opin. Chem. Biol.* **2000**, *4*, 228–234.
94. Schindler, S. *Eur. J. Inorg. Chem.* **2000**, 2311–2326.
95. Itoh, S.; Fukuzumi, S. *Bull. Chem. Soc. Jpn.* **2002**, *75*, 2081–2095.
96. Jacobson, R. R.; Tyeklar, Z.; Farooq, A.; Karlin, K. D.; Liu, S.; Zubieta, J. *J. Am. Chem. Soc.* **1988**, *110*, 3690–3692.
97. Gubelmann, M. H.; Williams, A. F. *Struct. Bonding (Berlin)* **1983**, *55*, 1–65.
98. Baldwin, M. J.; Ross, P. K.; Pate, J. E.; Tyeklár, Z.; Karlin, K. D.; Solomon, E. I. *J. Am. Chem. Soc.* **1991**, *113*, 8671–8679.
99. Tyeklár, Z.; Jacobson, R. R.; Wei, N.; Murthy, N. N.; Zubieta, J.; Karlin, K. D. *J. Am. Chem. Soc.* **1993**, *115*, 2677–2689.
100. Karlin, K. D.; Wei, N.; Jung, B.; Kaderli, S.; Niklaus, P.; Zuberbühler, A. D. *J. Am. Chem. Soc.* **1993**, *115*, 9506–9514.
101. Wei, N.; Murthy, N. N.; Tyeklár, Z.; Karlin, K. D. *Inorg. Chem.* **1994**, *33*, 1177–1183.
102. Lee, D.-H.; Wei, N.; Murthy, N. N.; Tyeklár, Z.; Karlin, K. D.; Kaderli, S.; Jung, B.; Zuberbühler, A. D. *J. Am. Chem. Soc.* **1995**, *117*, 12498–12513.
103. Karlin, K. D.; Lee, D.-H.; Kaderli, S.; Zuberbühler, A. D. *Chem. Commun.* **1997**, 475–476.
104. Karlin, K. D.; Kaderli, S.; Zuberbühler, A. D. *Acc. Chem. Res.* **1997**, *30*, 139–147.
105. Becker, M.; Heinemann, F. W.; Schindler, S. *Chem. Eur. J.* **1999**, *5*, 3124–3129.
106. Schatz, M.; Becker, M.; Thaler, F.; Hampel, F.; Schindler, S.; Jacobson, R. R.; Tyeklár, Z.; Murthy, N. N.; Ghosh, P.; Chen, Q.; Zubieta, J.; Karlin, K. D. *Inorg. Chem.* **2001**, *40*, 2312–2322.
107. He, C.; DuBois, J. L.; Hedman, B.; Hodgson, K. O.; Lippard, S. J. *Angew. Chem. Int. Ed. Engl.* **2001**, *40*, 1484–1487.
108. Bol, J. E.; Driessen, W. L.; Ho, R. Y. N.; Maase, B.; Que, Jr., L.; Reedijk, K. *Angew. Chem. Int. Ed.* **1997**, *36*, 998–1000.
109. Karlin, K. D.; Tolman, W. B.; Kaderli, S.; Zuberbühler, A. D. *J. Mol. Catal. A* **1997**, *117*, 215–222.
110. Kitajima, N.; Koda, T.; Hashimoto, S.; Kitagawa, T.; Moro-oka, Y. *J. Chem. Soc., Chem. Commun.* **1988**, 151–152.
111. Baldwin, M. J.; Root, D. E.; Pate, J. E.; Fujisawa, K.; Kitajima, N.; Solomon, E. I. *J. Am. Chem. Soc.* **1992**, *114*, 10421–10431.
112. Nasir, M. S.; Karlin, K. D.; McGowty, D.; Zubieta, J. *J. Am. Chem. Soc.* **1991**, *113*, 698–700.
113. Pidcock, E.; Obias, H. V.; Zhang, C. X.; Karlin, K. D.; Solomon, E. I. *J. Am. Chem. Soc.* **1998**, *120*, 7841–7847.
114. Pidcock, E.; Obias, H. V.; Abe, M.; Liang, H.-C.; Karlin, K. D.; Solomon, E. I. *J. Am. Chem. Soc.* **1999**, *121*, 1299–1308.
115. Pidcock, E.; DeBeer, S.; Obias, H. V.; Hedman, B.; Hodgson, K. O.; Karlin, K. D.; Solomon, E. I. *J. Am. Chem. Soc.* **1999**, *121*, 1870–1878.
116. Liang, H.-C.; Zhang, C. X.; Henson, M. J.; Sommer, R. D.; Hatwell, K. R.; Kaderli, S.; Zuberbühler, A. D.; Rheingold, A. L.; Solomon, E. I.; Karlin, K. D. *J. Am. Chem. Soc.* **2002**, *124*, 4170–4171.
117. Mahapatra, S.; Halfen, J. A.; Wilkinson, E. C.; Que, L. Jr.; Tolman, W. B. *J. Am. Chem. Soc.* **1994**, *116*, 9785–9786.
118. Mahapatra, S.; Kaderli, S.; Llobet, A.; Neuhold, Y.-M.; Palanché, T.; Halfen, J. A.; Young, V. G. Jr.; Kaden, T. A.; Que, L. Jr.; Zuberbühler, A. D.; Tolman, W. B. *Inorg. Chem.* **1997**, *36*, 6343–6356.
119. Lam, B. M. T.; Halfen, J. A.; Young, V. G. Jr.; Hagadorn, J. R.; Holland, P. L.; Lledós, A.; Cucurull-Sánchez, L.; Novoa, J. J.; Alvarez, S.; Tolman, W. B. *Inorg. Chem.* **2000**, *39*, 4059–4072.
120. Itoh, S.; Nakao, H.; Berreau, L. M.; Kondo, T.; Komatsu, M.; Fukuzumi, S. *J. Am. Chem. Soc.* **1998**, *120*, 2890–2899.
121. Taki, M.; Teramae, S.; Nagatomo, S.; Tachi, Y.; Kitagawa, T.; Itoh, S.; Fukuzumi, S. *J. Am. Chem. Soc.* **2002**, *124*, 124, 6367–6377.
122. Kodera, M.; Katayama, K.; Tachi, Y.; Kano, K.; Hirota, S.; Fujinami, S.; Suzuki, M. *J. Am. Chem. Soc.* **1999**, *121*, 11006–11007.
123. Hu, Z.; Williams, R. D.; Tran, D.; Spiro, T. G.; Gorun, S. M. *J. Am. Chem. Soc.* **2000**, *122*, 3556–3557.
124. Santagostini, L.; Gullotti, M.; Monzani, E.; Casella, L.; Dillinger, R.; Tuczek, F. *Chem. Eur. J.* **2000**, *6*, 519–522.
125. Gebbink, R. J. M. K.; Martens, C. F.; Kenis, P. J. A.; Jansen, R. J.; Nolting, H.-F.; Solé, V. A.; Feiters, M. C.; Karlin, K. D.; Nolte, R. J. M. *Inorg. Chem.* **1999**, *38*, 5755–5768.
126. Sorrell, T. N.; Allen, W. E.; White, P. S. *Inorg. Chem.* **1995**, *34*, 952–960.
127. Lynch, W. E.; Kurtz, D. M., Jr.; Wang, S.; Scott, R. A. *J. Am. Chem. Soc.* **1994**, *116*, 11030–11038.
128. Mahadevan, V.; Henson, M. J.; Solomon, E. I.; Stack, T. D. P. *J. Am. Chem. Soc.* **2000**, *122*, 10249–10250.

129. Hu, Z.; George, G. N.; Gorun, S. M. *Inorg. Chem.* **2001**, *40*, 4812–4813.
130. Ross, P. K.; Solomon, E. I. *J. Am. Chem. Soc.* **1990**, *112*, 5871–5872.
131. Ross, P. K.; Solomon, E. I. *J. Am. Chem. Soc.* **1991**, *113*, 3246–3259.
132. Mahapatra, S.; Halfen, J. A.; Wilkinson, E. C.; Pan, G.; Cramer, C. J.; Que, Jr., L.; Tolman, W. B. *J. Am. Chem. Soc.* **1995**, *117*, 8865–8866.
133. Halfen, J. A.; Mahapatra, S.; Wilkinson, E. C.; Kaderli, S.; Young, Jr., V. G.; Que, Jr., L.; Zuberbühler, A. D.; Tolman, W. B. *Science* **1996**, *271*, 1397–1400.
134. Mahapatra, S.; Halfen, J. A.; Wilkinson, E. C.; Pan, G.; Wang, X.; Young, Jr., V. G.; Cramer, C. J.; Que, Jr., L.; Tolman, W. B. *J. Am. Chem. Soc.* **1996**, *118*, 11555–11574.
135. Mahapatra, S.; Young, V. G. Jr.; Kaderli, S.; Zuberbühler, A. D.; Tolman, W. B. *Angew. Chem. Int. Ed.* **1997**, *36*, 130–133.
136. Holland, P. L.; Rodgers, K. R.; Tolman, W. B. *Angew. Chem. Int. Ed.* **1999**, *38*, 1139–1142.
137. Mahadevan, V.; Hou, Z.; Cole, A. P.; Root, D. E.; Lal, T. K.; Solomon, E. I.; Stack, T. D. P. *J. Am. Chem. Soc.* **1997**, *119*, 11996–11997.
138. Mahadevan, V.; DuBois, J. L.; Hedman, B.; Hodgson, K. O.; Stack, T. D. P. *J. Am. Chem. Soc.* **1999**, *121*, 5583–5584.
139. Itoh, S.; Taki, M.; Nakao, H.; Holland, P. L.; Tolman, W. B.; Que, Jr., L.; Fukuzumi, S. *Angew. Chem. Int. Ed.* **2000**, *39*, 398–400.
140. Taki, M.; Itoh, S.; Fukuzumi, S. *J. Am. Chem. Soc.* **2001**, *123*, 6203–6204.
141. Hayashi, H.; Fujinami, S.; Nagatomo, S.; Ogo, S.; Suzuki, M.; Uehara, A.; Watanabe, Y.; Kitagawa, T. *J. Am. Chem. Soc.* **2000**, *122*, 2124–2125.
142. Enomoto, E.; Aida, T. *J. Am. Chem. Soc.* **1999**, *121*, 874–875.
143. Straub, B. F.; Rominger, F.; Hofmann, P. *Chem. Commun.* **2000**, 1611–1612.
144. Funahashi, Y.; Nakaya, K.; Hirota, S.; Yamauchi, O. *Chem. Lett.* **2000**, 1172–1173.
145. Spencer, D. J. E.; Aboelella, N. W.; Reynolds, A. M.; Holland, P. L.; Tolman, W. B. *J. Am. Chem. Soc.* **2002**, *124*, 2108–2109.
146. DuBois, J. L.; Mukherjee, P.; Collier, A. M.; Mayer, J. M.; Solomon, E. I.; Hedman, B.; Stack, T. D. P.; Hodgson, K. O. *J. Am. Chem. Soc.* **1997**, *119*, 8578–8579.
147. Henson, M. J.; Mukherjee, P.; Root, D. E.; Stack, T. D. P.; Solomon, E. I. *J. Am. Chem. Soc.* **1999**, *121*, 10332–10345.
148. Holland, P. L.; Cramer, C. J.; Wilkinson, E. C.; Mahapatra, S.; Rodgers, K. R.; Itoh, S.; Taki, M.; Fukuzumi, S.; Que, L., Jr.; Tolman, W. B. *J. Am. Chem. Soc.* **2000**, *122*, 792–802.
149. Cramer, C. J.; Smith, B. A.; Tolman, W. B. *J. Am. Chem. Soc.* **1996**, *118*, 11283–11287.
150. Yoshizawa, K.; Ohta, T.; Yamabe, T. *Bull. Chem. Soc. Jpn.* **1997**, *70*, 1911–1917.
151. Liu, X.-Y; Palacios, A. A.; Novoa, J. J.; Alvarez, S. *Inorg. Chem.* **1998**, *37*, 1202–1212.
152. Flock, M.; Pierloot, K. *J. Phys. Chem. A* **1999**, *103*, 95–102.
153. Fujisawa, K.; Tanaka, M.; Moro-oka, Y.; Kitajima, N. *J. Am. Chem. Soc.* **1994**, *116*, 12079–12080.
154. Jung, B.; Karlin, K. D.; Zuberbühler, A. D. *J. Am. Chem. Soc.* **1996**, *118*, 3763–3764.
155. Halfen, J. A.; Young, V. G., Jr.; Tolman, W. B. *J. Am. Chem. Soc.* **1996**, *118*, 10920–10921.
156. Maddaluno, J.; Giessner-Prettre, C. *Inorg. Chem.* **1991**, *30*, 3439–3445.
157. Bernardi, F.; Bottoni, A.; Casadio, R.; Fariselli, P.; Rigo, A. *Inorg. Chem.* **1996**, *35*, 5207–5212.
158. Bérces, A. *Inorg. Chem.* **1997**, *36*, 4831–4837.
159. Metz, M.; Solomon, E. I. *J. Am. Chem. Soc.* **2001**, *123*, 4938–4950.
160. Takano, Y.; Kubo, S.; Onishi, T.; Isobe, H.; Yoshioka, Y.; Yamaguchi, K. *Chem. Phys. Lett.* **2001**, *335*, 395–403.
161. Cahoy, J.; Holland, P. L.; Tolman, W. B. *Inorg. Chem.* **1999**, *38*, 2161–2168.
162. Mirica, L. M.; Vance, M.; Rudd, D. J.; Hedman, B.; Hodgson, K. O.; Solomon, E. I.; Stack, T. D. P. *J. Am. Chem. Soc.* **2002**, *124*, 9332–9333.
163. Casella, L.; Gullotti, M.; Radaelli, R.; Di Gennaro, P. *J. Chem. Soc., Chem. Commun.* **1991**, 1611–1612.
164. Casella, L.; Monzani, E.; Gullotti, M.; Cavagnino, D.; Cerina, G.; Santagostini, L.; Ugo, R. *Inorg. Chem.* **1996**, *35*, 7516–7525.
165. Monzani, E.; Quinti, L.; Perotti, A.; Casella, L.; Gullotti, M.; Randaccio, L.; Geremia, S.; Nardin, G.; Faleschini, P.; Tabbí, G. *Inorg. Chem.* **1998**, *37*, 553–562.
166. Réglier, M.; Jorand, C.; Waegell, B. *J. Chem. Soc., Chem. Commun.* **1990**, 1752–1755.
167. Sayre, L. M.; Nadkarni, D. V. *J. Am. Chem. Soc.* **1994**, *116*, 3157–3158.
168. Iwata, M.; Emoto, S. *Tetrahedron Lett.* **1974**, 759–760.
169. Capdevielle, P.; Maumy, M. *Tetrahedron Lett.* **1982**, *23*, 1573–1576.
170. Chioccara, F.; Di Gennaro, P.; La Monica, G.; Sebastiano, R.; Rindone, B. *Tetrahedron* **1991**, *47*, 4429–4434.
171. Karlin, K. D.; Dahlstrom, P. L.; Cozzette, S. N.; Scensny, P. M.; Zubieta, J. *J. Chem. Soc., Chem. Commun.* **1981**, 881–882.
172. Karlin, K. D.; Gultneh, Y.; Hutchinson, J. P.; Zubieta, J. *J. Am. Chem. Soc.* **1982**, *104*, 5240–5242.
173. Karlin, K. D.; Hayes, J. C.; Gultneh, Y.; Cruse, R. W.; McKown, J. W.; Hutchinson, J. P.; Zubieta, J. *J. Am. Chem. Soc.* **1984**, *106*, 2121–2128.
174. Sheldon, R. A.; Kochi, J. K. *Metal-Catalyzed Oxidations of Organic Compounds* **1981**, Academic Press: New York.
175. Nasir, M. S.; Cohen, B. I.; Karlin, K. D. *J. Am. Chem. Soc.,* **1992**, *114*, 2482–2494.
176. Karlin, K. D.; Nasir, M. S.; Cohen, B. I.; Cruse, R. W.; Kaderli, S.; Zuberbühler, A. D. *J. Am. Chem. Soc.* **1994**, *116*, 1324–1336.
177. Casella, L.; Gullotti, M.; Pallamza, G.; Rigoni, L. *J. Am. Chem. Soc.* **1988**, *110*, 4221–4227.
178. Alzuet, G.; Casella, L.; Villa, M. L.; Carugo, O.; Gullotti, M. *J. Chem. Soc., Dalton Trans.* **1997**, 4789–4794.
179. Menif, R.; Martell, A. E.; Squattrito, P. J.; Clearfield, A. *Inorg. Chem.* **1990**, *29*, 4723–4729.
180. Gelling, O. J.; van Bolhuis, F.; Meetsma, A.; Feringa, B. L. *J. Chem. Soc., Chem. Commun.* **1988**, 552–554.
181. Sorrell, T. N.; Vankai, V. A.; Garrity, M. L. *Inorg. Chem.* **1991**, *30*, 207–210.
182. Sorrell, T. N.; Garrity, M. L. *Inorg. Chem.* **1991**, *30*, 210–215.
183. Ghosh, D.; Mukherjee, R. *Inorg. Chem.* **1998**, *37*, 6597–6605.

184. Gupta, R.; Mukherjee, R. *Inorg. Chim. Acta.* **1997**, *263*, 133–137.
185. Drew, M. G. B.; Trocha-Grimshaw, J.; McKillop, K. P. *Polyhedron* **1989**, *8*, 2513–2515.
186. Ryan, S.; Adams, H.; Fenton, D. E.; Becker, M.; Schindler, S. *Inorg. Chem.* **1998**, *37*, 2134–2140.
187. Fusi, V.; Llobet, A.; Mahía, J.; Micheloni, M.; Paoli, P.; Ribas, X.; Rossi, P. *Eur. J. Inorg. Chem.* **2002**, 987–990.
188. Kitajima, N.; Koda, T.; Iwata, Y.; Moro-oka, Y. *J. Am. Chem. Soc.,* **1990**, *112*, 8833–8839.
189. Paul, P. P.; Tyeklár, Z.; Jacobson, R. R.; Karlin, K. D. *J. Am. Chem. Soc.,* **1991**, *113*, 5322–5332.
190. Obias, H. V.; Lin, Y.; Murthy, N. N.; Pidcock, E.; Solomon, E. I.; Ralle, M.; Blackburn, N. J.; Neuhold, Y.-M.; Zuberbühler, A. D.; Karlin, K. D. *J. Am. Chem. Soc.,* **1998**, *120*, 12960–12961.
191. Halfen, J. A.; Young, V. G. Jr.; Tolman, W. B. *Inorg. Chem.,* **1998**, *37*, 2102–2103.
192. Itoh, S.; Kumei, H.; Taki, M.; Nagatomo, S.; Kitagawa, T.; Fukuzumi, S. *J. Am. Chem. Soc.* **2001**, *123*, 6708–6709.
193. Itoh, S.; Bandoh, H.; Nakagawa, M.; Nagatomo, S.; Kitagawa, T.; Karlin, K. D.; Fukuzumi, S. *J. Am. Chem. Soc.* **2001**, *123*, 11168–11178.
194. Mandal, S.; Macikenas, D.; Protasiewicz, J. D.; Sayre, L. M. *J. Org. Chem.,* **2000**, *65*, 4804–4809.
195. Siegbahn, P. E. M.; Wirstam, M. *J. Am. Chem. Soc.* **2001**, *123*, 11819–11820.
196. Kodera, M.; Shimakoshi, H.; Tachi, Y.; Katayama, K.; Kano, K. *Chem. Lett.* **1998**, 441–442.
197. Monzani, E.; Battaini, G.; Perotti, A.; Casella, L.; Gullotti, M.; Santagostini, L.; Nardin, G.; Randaccio, L.; Geremia, S.; Zanello, P.; Opromolla, G. *Inorg. Chem.* **1999**, *38*, 5359–5369.
198. Reim, J.; Krebs, B. *J. Chem. Soc., Dalton Trans.* **1997**, 3793–3804.
199. Rockcliffe, D. A.; Martell, A. E. *Inorg. Chem.* **1993**, *32*, 3143–3152.
200. Wegner, R.; Gottschaldt, M.; Görls, H.; Jäger, E.-G.; Klemm, D. *Chem. Eur. J.* **2001**, *7*, 2143–2157.
201. Gupta, M.; Mathur, P.; Butcher, R. J. *Inorg. Chem.* **2001**, *40*, 878–885.
202. Neves, A.; Rossi, L. M.; Bortoluzzi, A. J.; Szpoganicz, B.; Wiezbicki, C.; Schwingel, E.; Haase, W.; Ostrovsky, S. *Inorg. Chem.* **2002**, *41*, 1788–1794.
203. Berreau, L. M.; Mahapatra, S.; Halfen, J. A.; Houser, R. P.; Young, V. G., Jr.; Tolman, W. B. *Angew. Chem. Int. Ed.* **1999**, *38*, 207–210.
204. Mahapatra, S.; Halfen, J. A.; Tolman, W. B. *J. Am. Chem. Soc.* **1996**, *118*, 11575–11586.
205. Hayashi, H.; Uozumi, K.; Fujinami, S.; Nagatomo, S.; Shiren, K.; Furutachi, H.; Suzuki, M.; Uehara, A.; Kitagawa, T. *Chem. Lett.* **2002**, 416–417.
206. Cramer, C. J; Pak, Y. *Theor. Chem. Acc.* **2001**, *105*, 477–480.
207. Itoh, S.; Bandoh, H.; Nagatomo, S.; Kitagawa, T.; Fukuzumi, S. *J. Am. Chem. Soc.* **1999**, *121*, 8945–8946.
208. Itoh, S.; Kondo, T.; Komatsu, M.; Ohshiro, Y.; Li, C.; Kanehisa, N.; Kai, Y.; Fukuzumi, S. *J. Am. Chem. Soc.* **1995**, *117*, 4714–4715.
209. Bell, R. P. *The Tunneling Effect in Chemistry* **1980**, Chapman & Hall: London.
210. Kohen, A.; Klinman, J. P. *Acc. Chem. Res.* **1998**, *31*, 397–404.
211. Taki, M.; Itoh, S.; Fukuzumi, S. *J. Am. Chem. Soc.* **2002**, *124*, 998–1002.

8.16
Monocopper Oxygenases

M. A. HALCROW
University of Leeds, UK

8.16.1 INTRODUCTION

Monooxygenase enzymes catalyze the general reaction in Equation (1) ($x = 2$ or 3, depending on the hybridization state of the activated substrate carbon atom):

$$R_xC-H + O_2 + 2H^+ + 2e^- \rightarrow R_xC-OH + H_2O \qquad (1)$$
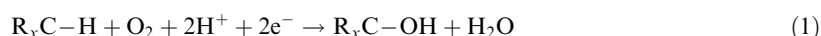
There are many enzymes that will carry out this chemistry, most of which contain iron[1] or copper[2–4] at their active sites. Generally speaking, the role of the metal ion in these proteins is to coordinate and reduce dioxygen, forming an activated oxygen species that is sufficiently electrophilic to attack the substrate C—H bond.

Three distinct classes of copper monoooxygenase have been discovered. First, tyrosinase catalyzes the oxidation of tyrosine and other phenols to *ortho*-quinones (Equation (2)):[2,3]

$$(2)$$
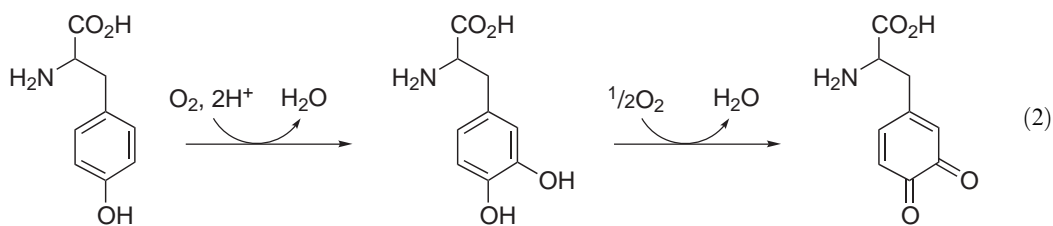
Second, dopamine-β-monooxygenase (DβM) and peptidylglycine α-hydroxylating monooxygenase (PHM), respectively, catalyze the reactions in Equations (3) and (4):[2,4]

$$(3)$$

and

$$(4)$$
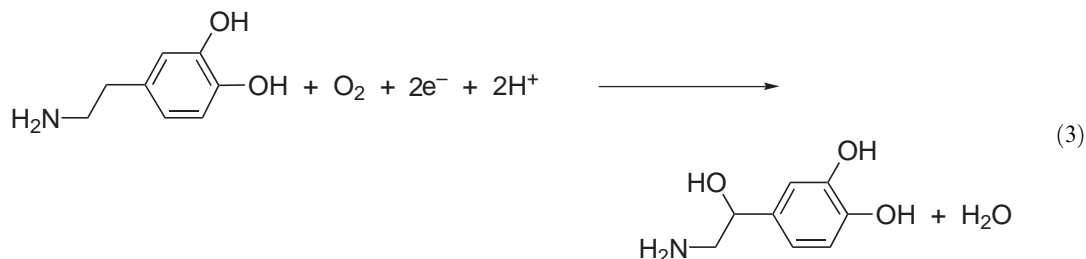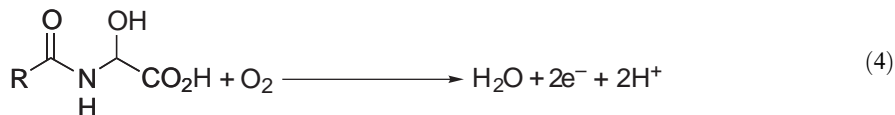
Finally, membrane-bound ("particulate") methane monooxygenase (pMMO) is a bacterial enzyme that effects the oxidation of methane to methanol (Equation (5)):[2,3]

$$CH_4 + O_2 + 2H^+ + 2e^- \rightarrow CH_3OH + H_2O \qquad (5)$$
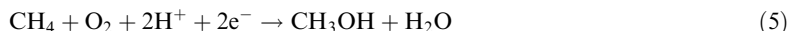
These three types of protein have very different active site structures, but perform essentially the same reaction on sequentially more demanding substrates (aryl C—H bonds are weaker than alkyl C—H bonds, while methane is the hardest hydrocarbon of all to functionalize[5]). It is an important question how nature has tuned the oxidizing power of the copper/dioxygen couple so precisely.

This chapter is concerned with monooxygenation reactions effected by monocopper centers in chemistry and biology. The enzymes DβM and PHM are the only known monooxygenase enzymes to have a monocopper active site, and are discussed together. A stoichiometric hydroxylation reaction at a monocopper biosite is also described, namely the conversion of tyrosine to 2,4,5-trihydroxyphenylalanine quinone during maturation of copper-containing amine oxidase. Finally, a copper-containing dioxygenase, quercetinase, is discussed. Selected structural and functional model chemistry relevant to all these proteins is highlighted. Other copper oxygenase enzymes are treated in Chapters 8.15 and 8.17 of this volume, while iron-containing oxygenases are discussed in Chapters 8.12, 8.13, and 8.14.

8.16.2 MONOOXYGENASE ENZYMES CONTAINING MONOCOPPER ACTIVE SITES

8.16.2.1 Dopamine β-Monooxygenase and Peptidylglycine α-Hydroxylating Monooxygenase

Dopamine β-monooxygenase (DβM, EC 1.14.17.1) is an enzyme found in mammalian brains that catalyzes the aerobic hydroxylation of dopamine to norepinephrine (Equation (3)).[4,6] Ascorbate is the physiological electron donor to the enzyme, so that two equivalents of ascorbate are

converted to dehydrosemiascorbate during turnover.[7] *In vivo*, DβM is mostly located within chromaffin granules, which are neurosecretory vesicles of the adrenal gland.[6] Both membrane-associated and soluble forms of DβM are found in these granules; most spectroscopic and mechanistic data for DβM have come from the soluble bovine enzyme. Both these forms have a quaternary structure derived from protein dimers, in which monomers of $M_r \approx 75$ kDa are covalently linked by a disulfide bridge.[8] These dimers in turn partially associate further into tetramers in solution, in a pH-dependent equilibrium; the tetrameric form is likely to be dominant *in vivo*.[9,10] Interestingly, the dimeric and tetrameric forms have different kinetic properties, for reasons that are unclear.[10] Each protein monomer of DβM contains 2 mol equivalents of copper.[11]

Peptidylglycine α-amidating enzyme (PAM, EC 1.14.17.3) is also found in the nervous systems of higher organisms.[4,12] The enzyme catalyzes the cleavage of the terminal acetate group from C-terminus glycyl peptides, through a two-step process that is accomplished at two different active sites within the same protein. First, a peptidylglycine α-hydroxylating monooxygenase (PHM, EC 1.4.17.3) domain within the protein monooxygenates the methylene carbon atom of the acetate group (Equation (4)).[4,12] Then, the resultant carbinolamide is cleaved by a different, peptidylamidoglycolate lyase (PAL, EC 4.3.2.5) domain to give the final product (Equation (6)).[13]

$$\underset{\substack{| \\ H}}{R-\overset{O}{\overset{||}{C}}-N-\overset{OH}{\underset{|}{C}}H-CO_2H} \longrightarrow R-\overset{O}{\overset{||}{C}}-NH_2 \;+\; \overset{O}{\overset{||}{C}}H-CO_2H \qquad (6)$$
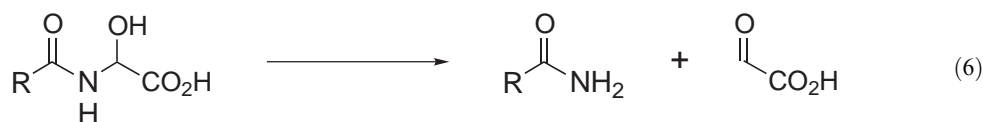
As for DβM, the electrons required to accomplish the PHM reaction (Equation (4)) are provided by two equivalents of ascorbate. Multiple forms of PAM are produced *in vivo*, with M_r of between 40 kDa and 100 kDa.[14] The soluble form of the enzyme, which has $M_r = 75$ kDa, has been the most studied. The catalytically active PHM and PAL domains of PAM can be produced separately from this protein, either by cleaving intact PAM or by using clones that produce only the relevant half of the polypeptide.[15,16] The PHM polypeptide contains two mole equivalents of copper;[17] however, PAL is a zinc enzyme,[13] and so is not discussed further here.

The PHM domain in peptidylglycine α-amidating enzyme shows 28% sequence identity to part of the amino acid sequence in DβM.[18] As described below, the spectroscopic and redox properties of the copper ions in DβM and PHM are also highly similar. Hence, although crystallographic data are only available for PHM, the active site structures and catalytic mechanisms of DβM and PHM are assumed to be similar. For this reason, they will be discussed together.

A crystal structure of the "catalytic core" (i.e., the part of the amino acid sequence that contains the two copper centers and the substrate binding site) of oxidized rat PHM at 2.3 Å resolution has been published.[19,20] This catalytic core gives indistinguishable EPR and copper EXAFS data to the complete PAM protein,[15] so that the crystallographic structures of the copper sites in the truncated protein should be the same as in the complete enzyme. The peptide is divided into two nine-stranded β-sandwich domains of about 150 residues each. These domains are separated by a hydrophobic cleft, which has an average width of 8 Å. The two copper ions lie on either side of this cleft, and are separated by 11 Å (Figure 1). One of these, termed "Cu$_H$" or "Cu$_A$" in the literature, is a T-shaped complex with three histidine ligands. The other copper ion, referred to as "Cu$_M$" or "Cu$_B$," has a trigonal pyramidal structure with two histidine and one water ligands in its basal plane, and a weak interaction of 2.68 Å to an apical methionine side-chain. Interestingly, the protein conformation in the crystal, and coordination geometries of Cu$_H$ and Cu$_M$, are barely perturbed following reduction of the copper ions with ascorbate.[20] The only notable structural changes between reduced and oxidized crystals are: contraction of one of the Cu—N bonds at Cu$_H$ upon reduction, so that the reduced center has a slightly more planar geometry; and a small movement of the water molecule coordinated to Cu$_M$. Finally, a 2.1 Å structure was obtained from a crystal of oxidized PHM catalytic core incubated with the substrate analogue *N*-α-acetyl-3,5-diiodotyrosylglycine.[20] The substrate molecule is bound within the inter-domain cleft, positioned so that the reactive methylene carbon atom is 4.3 Å from Cu$_M$, and oriented towards the Cu$_M$ water ligand (Figure 2). This is a suitable distance to allow the reactive C—H bond to interact with a peroxo or hydroperoxo ligand coordinated to Cu$_M$.

Interestingly, EXAFS measurements on DβM and PHM show some differences from these crystallographic structures. The oxidized proteins show 2–3 histidine plus 1–2 other O/N ligands per copper center, all at a distance of 1.97 Å; no S scatterer was detected in this state.[15,16,21–25] EXAFS data on ascorbate-reduced PHM showed one fewer O/N scatterers per dicopper protein
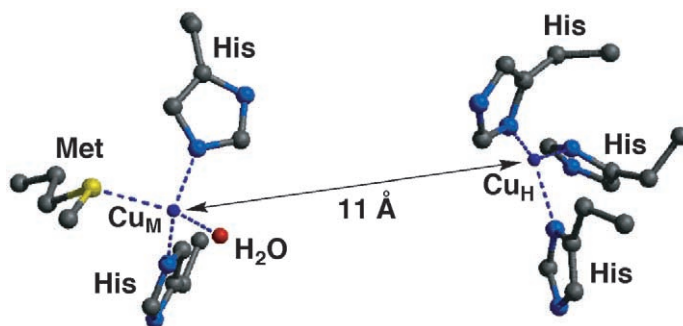
Figure 1 Structures of the copper centers in the catalytic core of PHM, as determined by protein X-ray crystallography.[19,20]

compared to oxidized PHM, together with 0.5 of a S/Cl scatterer at 2.27 Å.[16,22,24,25] This implies a substantial shortening of the Cu_M—S bond following reduction, which is not observed in the crystal. An identical result was obtained from the EXAFS of reduced half-apo DβM and PHM, in which the copper ion has been selectively removed from the Cu_H site.[26,27] It has been suggested that these different crystallographic and EXAFS structures may reflect the different pHs at which the two series of measurements were carried out.[20]

Oxidized DβM and PHM afford only one EPR signal, suggesting that the EPR properties of Cu_H and Cu_M are very similar.[28] This "averaged" spectrum is typical of a magnetically isolated type 2 copper(II) biosite but has varied slightly between proteins, with ($g_{\|} = 2.25$–2.29, $g_{\perp} = 2.05$, $A_{\|}\{^{63,65}Cu\} = 142$–162 G).[15,16,28–33] ESEEM spectra of oxidized DβM allowed the detection of histidine ligation to copper,[34] consistent with the crystallographic data.[19,20] Treatment with ascorbate causes reduction of both copper ions;[29,30,35] redox titrations have shown that Cu_H and Cu_M of DβM have very similar midpoint potentials, of $+350 \pm 40$ mV vs. nHe.[29,30] Both cyanide and azide can bind to both copper centers in oxidized DβM, although one copper site has a much greater affinity for these ions than the other.[33,36] However, in reduced DβM and PHM only Cu_M[26,27] can bind carbon monoxide[16,37–39] or isocyanides.[40,41] Both these adducts show IR spectra that are typical of terminal metal CO or RNC complexes,[26,27,37–41] while EXAFS spectra show that the methionine ligand is not displaced from the copper ion upon binding of these molecules.[26,27,38–40] The increased affinity of Cu_M for small molecules compared to Cu_H is consistent with the crystallographic conclusion, that Cu_M is the site of O_2 binding during catalysis.[20] However, the situation is complicated by the observation that, upon incubation of PHM with a substrate analog, Cu_H also becomes accessible to CO.[39] This is discussed in more detail below.

Reduction of oxidized Cu_H and Cu_M by ascorbate is rapid, and yields catalytically competent enzyme that can bind O_2 and organic substrate.[42,43] For PHM, an equilibrium ordered mechanism
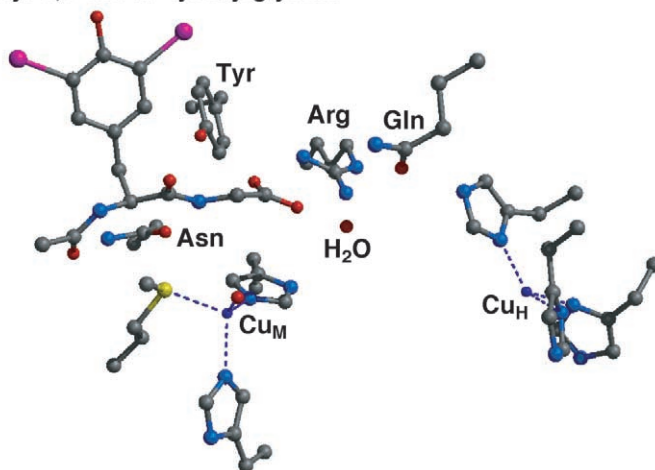
Figure 2 Binding of *N*-α-acetyl-3,5-diiodotyrosylglycine to the active site of PHM, as revealed by protein X-ray crystallography.[20]

was demonstrated, in which substrate binding to prereduced enzyme is followed by binding of O_2.[44] This contrasts with DβM, where binding of substrate and O_2 to the reduced enzyme can occur in a random order.[45] The rate-determining step of DβM catalysis is hydroxylation of the substrate C—H bond.[45] For PHM, substrate hydroxylation or product dissociation can be rate-limiting, depending on whether the PAL lyase domain is present in the protein.[43,44] DβM and PHM yield very similar intrinsic primary ^{2}H isotope effects of 10.6–10.9,[43,46] and α-secondary ^{2}H isotope effects of 1.2,[44,47] for substrate hydroxylation. For PHM, these two parameters are only slightly temperature dependent,[48] which is characteristic of non-classical kinetic behavior. These data imply that C—H cleavage occurs by a hydrogen atom transfer step, which has a substantial quantum mechanical tunneling component. A linear free-energy relationship with $\rho = -1.5$ was derived from hydroxylation of substituted phenylethylamine substrates by DβM, which is again typical of a radical-generating mechanism.[47] A free-energy analysis of individual steps of these reactions implied that the final step of the catalytic cycle is product dissociation from an inner-sphere complex to copper.[45,47] Finally, several mechanism-based inhibition studies have also indicated a free radical C—H oxygenation mechanism.[49–58]

The C—H hydroxylation step in the DβM catalytic cycle involves uptake of one proton per turnover.[45] This was used to infer the intermediacy of a copper hydroperoxide complex species in the hydroxylation reaction, generated by protonation of a bound dioxygen species. An intrinsic ^{18}O kinetic isotope effect of 1.025 has been measured for monooxygenation of dopamine by DβM;[59] importantly, the ^{18}O isotope effect for hydroxylation of a series of phenylethylamines by DβM increases as the reactivity of the substrates decreases.[59] These data suggest that O—O bond cleavage occurs *before* oxygen atom insertion into the substrate. This O—O cleavage event is not promoted by further reduction of the enzyme: peroxo complex by exogenous electron donors.[7] To accommodate these results, it was suggested that a tyrosine residue might donate an electron to a copper(II) hydroperoxo species, thus effecting O—O cleavage (Figure 3).[59] No tyrosyl radical has ever been directly detected in DβM or PHM under any conditions. However, treatment of oxidized DβM with hydrogen peroxide yields a protein-bound quinone residue, which could be circumstantial evidence for generation of a transient tyrosyl radical under these conditions.[60] Other mechanisms for DβM or PHM catalysis have also been proposed that avoid the need for a tyrosyl radical.[20,39,58] But these do not take account of the need to cleave the O—O bond prior to substrate hydroxylation.

Other aspects of the catalytic cycles of these enzymes are less clear-cut. One issue is how electron-transfer from Cu_H to Cu_M can take place, since crystallographically the shortest feasible electron-transfer pathway between the two copper sites is prohibitively long, at 24 amino acid residues.[20] Intriguingly, the crystal structure of the PHM catalytic core:substrate complex implies a potential pathway for electron transfer between the copper centers mediated by bound substrate. This led to the proposal that electron transfer between Cu_H and Cu_M is gated by substrate binding.[20] Alternatively, the fact that binding of carbon monoxide to Cu_H is promoted by substrate binding in PHM has led to another suggestion, that O_2 is reduced in two one-electron steps.[39] Under this scheme, O_2 first binds to, and is reduced by, Cu_H; then the resultant superoxide anion migrates to Cu_M through an as-yet-unidentified channel in the protein, where it is reduced further to the peroxide level.[39] As yet, there are no data available that would distinguish between these proposals. Another problem is the structure of the putative Cu_M hydroperoxo and/or Cu_M oxyl intermediates, which have never been directly observed and for which no spectroscopic or structural data are available.

8.16.2.2 Structural Models for the Cu_H Center: Three-coordinate Copper Complexes with All-nitrogen Ligation

The only known examples of synthetic three-coordinate copper(II) complexes are (**1**)–(**7**) (Scheme 1), which have near-planar Y-shaped geometries in the crystal with the Cu ion being displaced from the N_2X (X = Cl, O, S) donor plane by up to 0.22 Å (Figure 4).[61–63] These complexes are characterized by axial or slightly rhombic EPR spectra with a "normal" $g_\| > g_\perp > g_e$ pattern and a small hyperfine coupling to Cu; $g_\| = 2.17$–2.22, $g_\perp = 2.04$–2.05, $A_\|\{^{63,65}\text{Cu}\} = 90$–129 G.[61–64] It is uncertain how these data relate to the EPR spectrum of oxidized Cu_H, since accurate g and A values for this site have not been deconvoluted from those of Cu_M (see above). No compounds related to (**1**)–(**7**) containing an N_3 donor set that would more closely replicate the Cu_H site in its +2 oxidation state have yet been described.
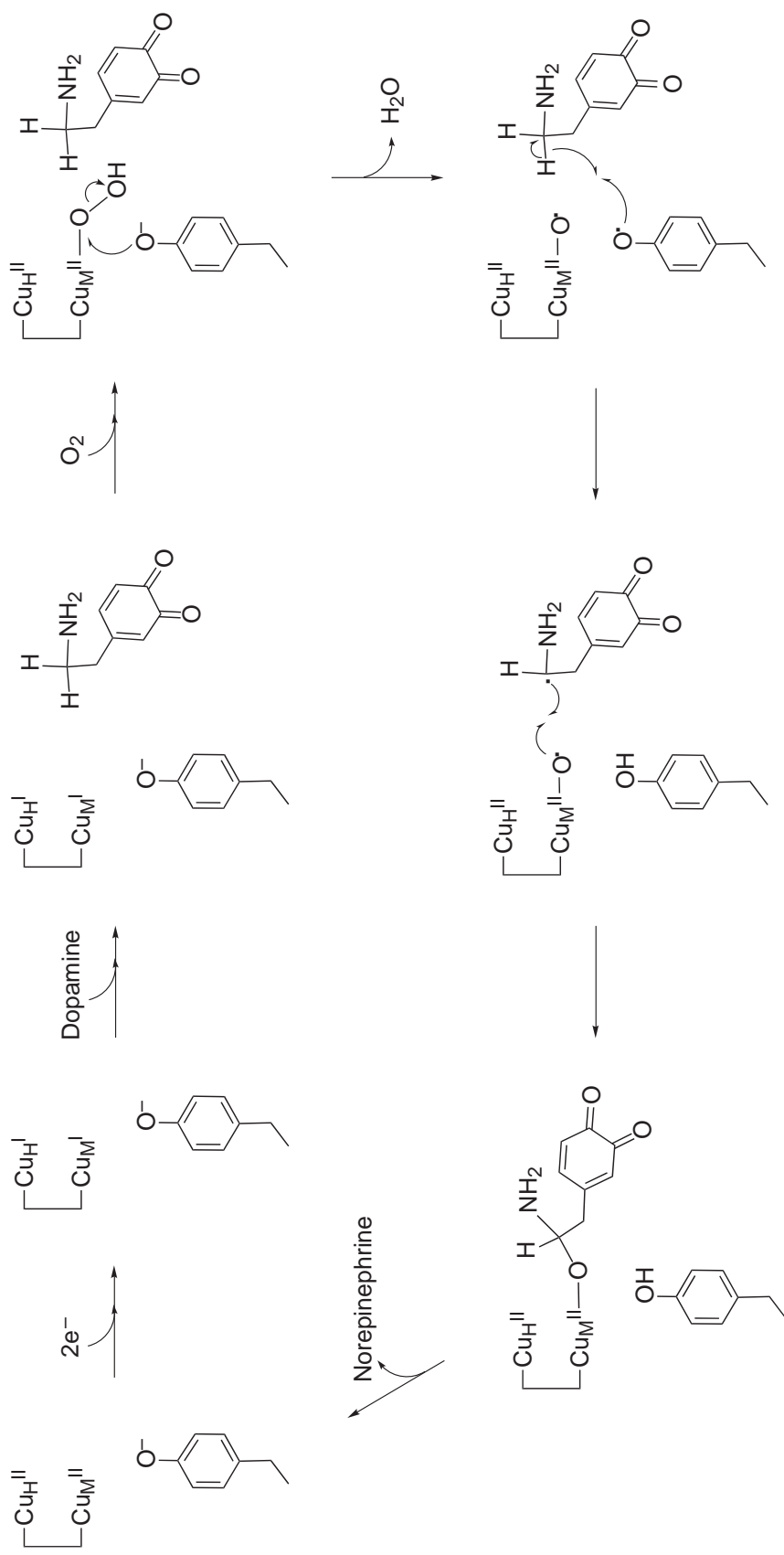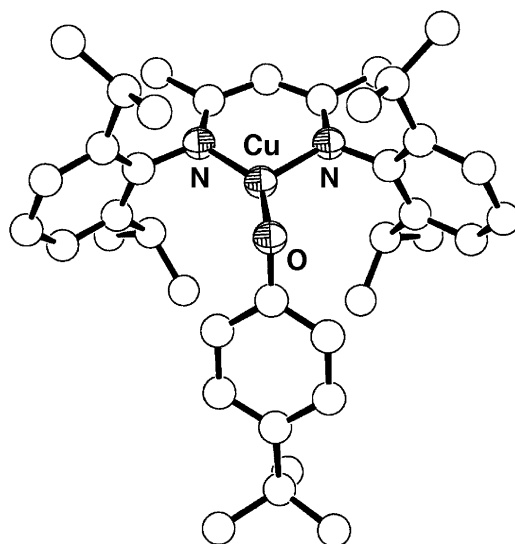
Figure 3 Proposed mechanism for dopamine hydroxylation by DβM, involving one-electron cleavage of a copper(II) hydroperoxide species by a tyrosine residue.[59,60]
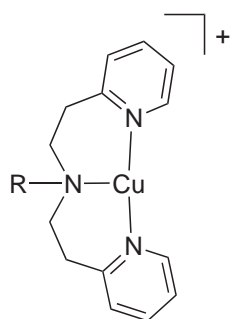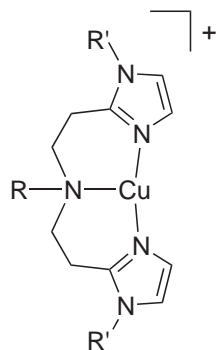
Scheme 1

R = Ph (**2**)
R = CH$_2$OCH$_3$(**3**)

X = H, R = Me, R' = H (**4**)
X = H, R = H, R' = OMe (**5**)
X = H, R = H, R' = tBu (**6**)
X = Cl, R = H, R' = tBu (**7**)
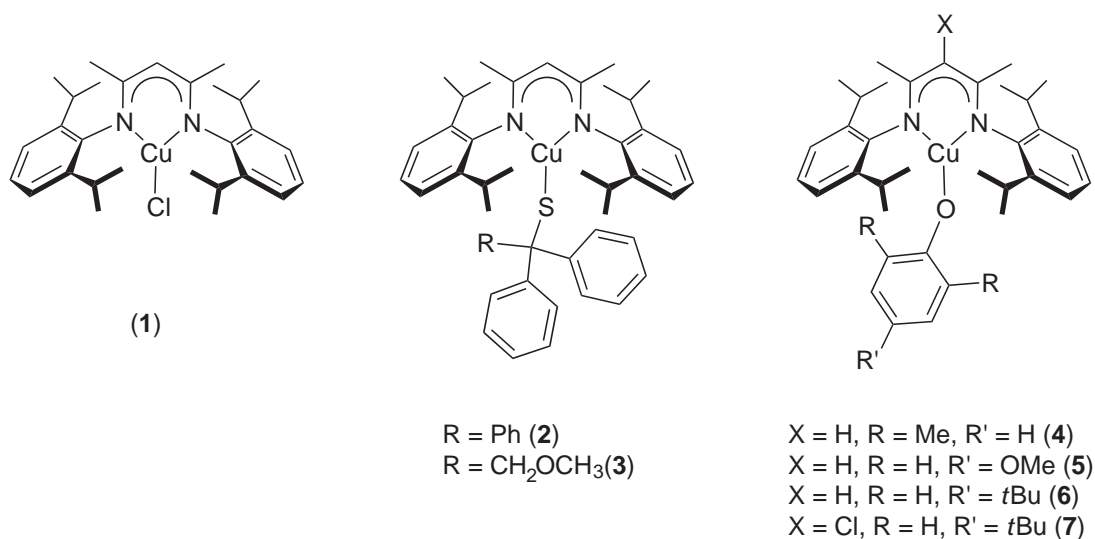
(**1**)

Figure 4 Single-crystal X-ray structure of (**6**), a three-coordinate copper(II) complex.[63] All hydrogen atoms have been omitted for clarity.

However, there is a large number of trigonal monocopper(I) complexes with a *tris*-N-donor set, which could provide insight into the chemistry of the reduced Cu$_H$ complex. Examples are known containing three monodentate ligands,[65–72] usually alkylated pyridines[65,66] or imidazoles.[69–72] Although crystal structures of these compounds always show approximately planar copper centers, their N–Cu–N angles can show substantial deviations from 120°.[65–68] Alternatively, a three-coordinate copper(I) ion may be bound by one bidentate and one monodentate ligand.[73–78] A planar Y-shaped geometry is most common for these compounds, owing to the limited bite angles of the chelating ligands; there is one T-shaped example, however.[76] Finally, the three N donors may be derived from one tridentate ligand. The coordination geometry of the copper ion here is dictated by the disposition of donors within the tridentate ligand. Most examples contain meridional *tris*-N-donor ligands, which form planar T-shaped copper(I) complexes (**8**)–(**31**) (Scheme 2). These most resemble the T-shaped geometry of the Cu$_H$ site, and are discussed in more detail below. There are also isolated examples containing tridentate cyclic ligands, which afford roughly C_{3v}-symmetric pyramidal (**32**)[79] or planar (**33**)[80] stereochemistries at copper (see below) (Scheme 3).

R = Me (**8**)
R = CH₂Ph (**9**)
R = C₂H₄Ph (**10**)
R = Ph (**11**)

R = H, R' = H (**12**)
R = H, R' = Me (**13**)
R = H, R' = CH₂Ph (**14**)
R = CH₂Ph, R' = H (**15**)
R = CH₂Ph, R' = Me (**16**)
R = CH₂Ph, R' = CH₂Ph (**17**)
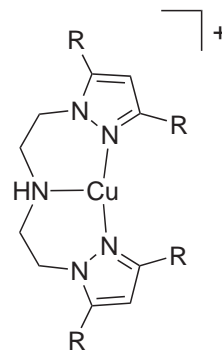
R = H (**18**)
R = Me (**19**)
R = *t*Bu (**20**)
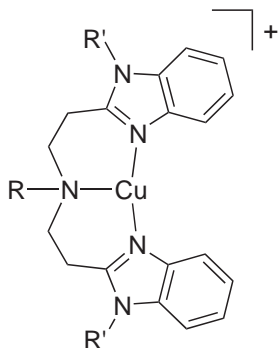
R = H, R' = H (**21**)
R = H, R' = Me (**22**)
R = CH₂Ph, R' = H (**23**)
R = CH₂Ph, R' = CH₂Ph (**24**)
R = C{O}Me, R' = Me (**25**)
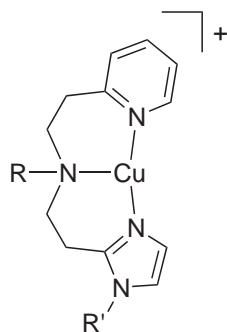
R = H, R' = *n*Bu (**26**)
R = CH₂Ph, R' = Me (**27**)
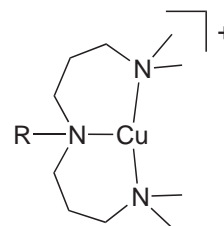
R = H (**28**)
R = Me (**29**)

(**30**)

(**31**)

Scheme 2

(32) **(33)**

Scheme 3

(A)

(B)
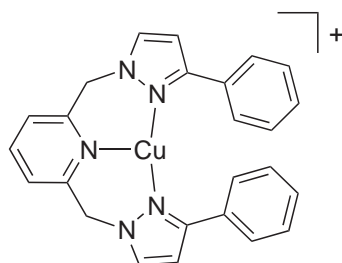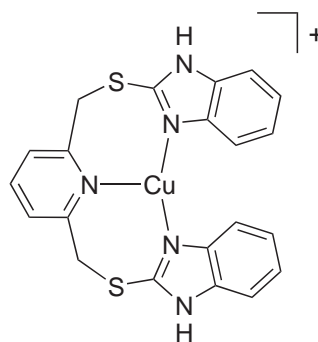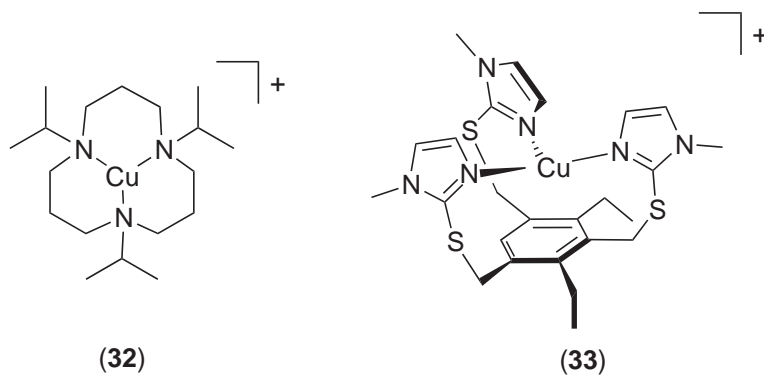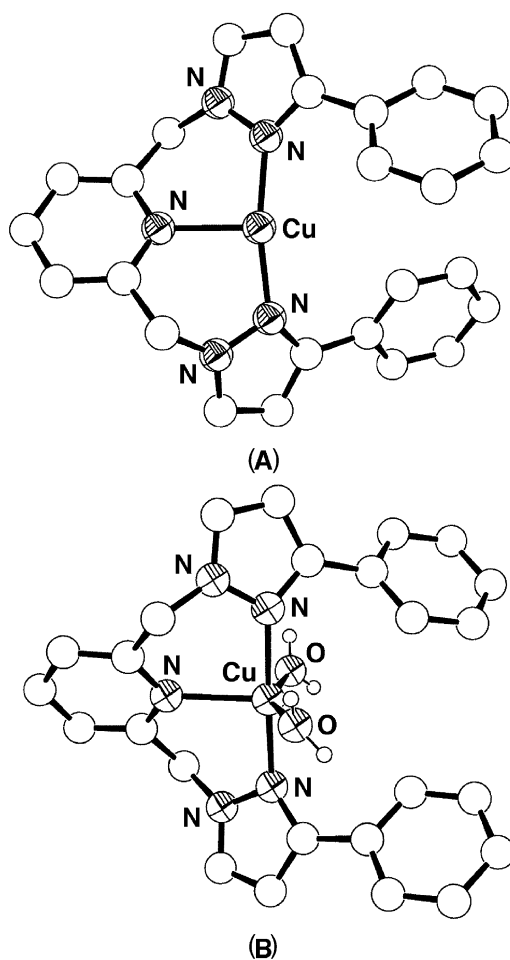
Figure 5 Single-crystal X-ray structures of [CuL]$^+$ (L = 2,6-*bis*{[3-phenylpyrazol-1-yl]methyl}pyridine) (**30**) (**A**) and [CuL(OH$_2$)$_2$]$^{2+}$ (**B**),[85] showing the increase in coordination number that typically occurs upon oxidation of a three-coordinate copper(I) center. All carbon-bound hydrogen atoms have been omitted for clarity.

The complexes (**9**),[81] (**11**),[82] (**13**),[83] (**28**),[84] (**29**),[84] (**30**),[85] and (**31**)[86] have all been structurally characterized, and show a T-shaped geometry with a "*transoid*" N–Cu–N angle of 143.03(13)–168.72(8)° (Figure 5A). In addition, although no crystal structure is available, (**19**) has been shown to be three-coordinate in the solid state by X-ray absorption spectroscopy.[90] While they have not been structurally characterized, salts of (**10**),[87] (**12**),[82] (**14**)–(**17**),[83,88] (**18**)–(**20**),[89–93] (**21**)–(**25**),[88,93–95] (**26**),[83] and (**27**)[88] containing weakly coordinating anions, are also assumed to be three-coordinate in the solid. In addition to these compounds, there are structurally characterized dicopper(I) complexes of ligands containing two independent *bis*(pyrid-2-ylethyl)amine[96–101] or *bis* (pyrazol-1-ylethyl)amine[102] domains linked by a hydrocarbon spacer. The individual Cu centers in these compounds are structurally essentially identical to those in (**8**)–(**11**) and (**18**)–(**20**). It is noteworthy that all of (**8**)–(**31**) contain six- or seven-membered chelate rings at copper. There is to date only one crystallographically authenticated three-coordinate copper(I) center, with two five-membered chelate rings linking three meridional N-donors.[103] Rather, meridional tridentate ligands containing five-membered chelate rings instead usually form copper(I) complexes that are either helical dimers,[104,105] or four-coordinate adducts containing an exogenous monodentate ligand.[103,106–111]

Despite being three-coordinate in the solid, (**18**)–(**20**),[89,91] (**30**),[85] (**31**)[86] or other compounds closely related to (**8**)–(**11**),[100,101,112–118] (**19**)[102] and (**30**)[85,119] will readily add a monodentate ligand such as Cl⁻, CO, MeCN, or PPh₃, or an endogenous alkene, imine, phenoxide, or thioether donor, to afford four-coordinate products. This affinity for a fourth donor mimics the ability of CO and isocyanides to bind to the Cu$_H$ site.[26,27,37–41] However, given the spectroscopic inertness of Cu(I), this affinity for exogenous ligands means that (**8**)–(**31**) cannot be assumed to be three-coordinate in solution, particularly in donor solvents such as MeCN. Compounds (**8**)–(**11**)[81,82,87] and copper(I) complexes of several other *N*-alkyl-*bis*(2-{pyrid-2-yl}ethyl)amines,[120–123] (**13**),[83,88] (**14**),[83,88] (**28**),[84] and (**29**)[84] react rapidly with O₂ in solution to form 2:1 Cu:O₂ adducts, that have been characterized in solution by manometry,[81–83,87] resonance Raman[84,87] and/or UV/vis spectroscopy[82–84,87,88] (Chapter 8.15). In contrast, (**12**),[88] (**15**)–(**17**),[88] (**21**)–(**25**),[88] (**30**),[85] and (**31**)[86] are air-stable in solution. There are no known monocopper superoxo or peroxo species derived from (**8**)–(**31**), or any other T-shaped copper(I) precursor, that might mimic the product of a putative reaction between Cu$_H$ and O₂ (see Section 8.16.4).

The Cu(II/I) couples shown by T-shaped copper(I) compounds of meridional *tris*-N-donor ligands are often chemically reversible, and show cyclic voltammograms consistent with fast electron transfer.[82,85,86,93,124] Since the copper(II) products generated by oxidation will expand their coordination numbers to four or five, through addition of solvent-derived ligands (Figure 5B),[85,86,93,120–124], this reversibility implies that the kinetics of exogenous ligand coordination to Cu(II), and decoordination from Cu(I), are rapid on the voltammetric timescale. The Cu(II/I) half-potential in these compounds can be sensitive to small changes in the donor properties of the tridentate ligand,[82,85,93] which makes it impossible to use these data to predict the effects of three-coordination on the oxidation potential of the reduced Cu$_H$ biosite.

Compound (**33**) is the only crystallographically characterized *tris*-imidazole-ligated copper(I) complex to adopt a near-regular trigonal planar geometry.[80] This complex is inert to ligand addition, does not react with O₂, and undergoes only a semi-reversible electrochemical oxidation to copper(II).[80] It is unclear how these properties would change following distortion of its coordination geometry from trigonal planar to the T-shaped structure in Cu$_H$. A T-shaped structure has been determined by EXAFS for [Cu(Me₂Im)₃]⁺ (Me₂Im = 1,2-dimethylimidazole);[72] interestingly, this complex reacts rapidly with O₂ in solution, whereas [Cu(Me₂Im)₂]⁺ is air-stable.[71,72] There are few other three-coordinate copper(I) *tris*-imidazole complexes.[69,70]

8.16.2.3   Structural Models for the Cu$_M$ Center

8.16.2.3.1   *Copper complexes with mixed nitrogen/thioether ligation*
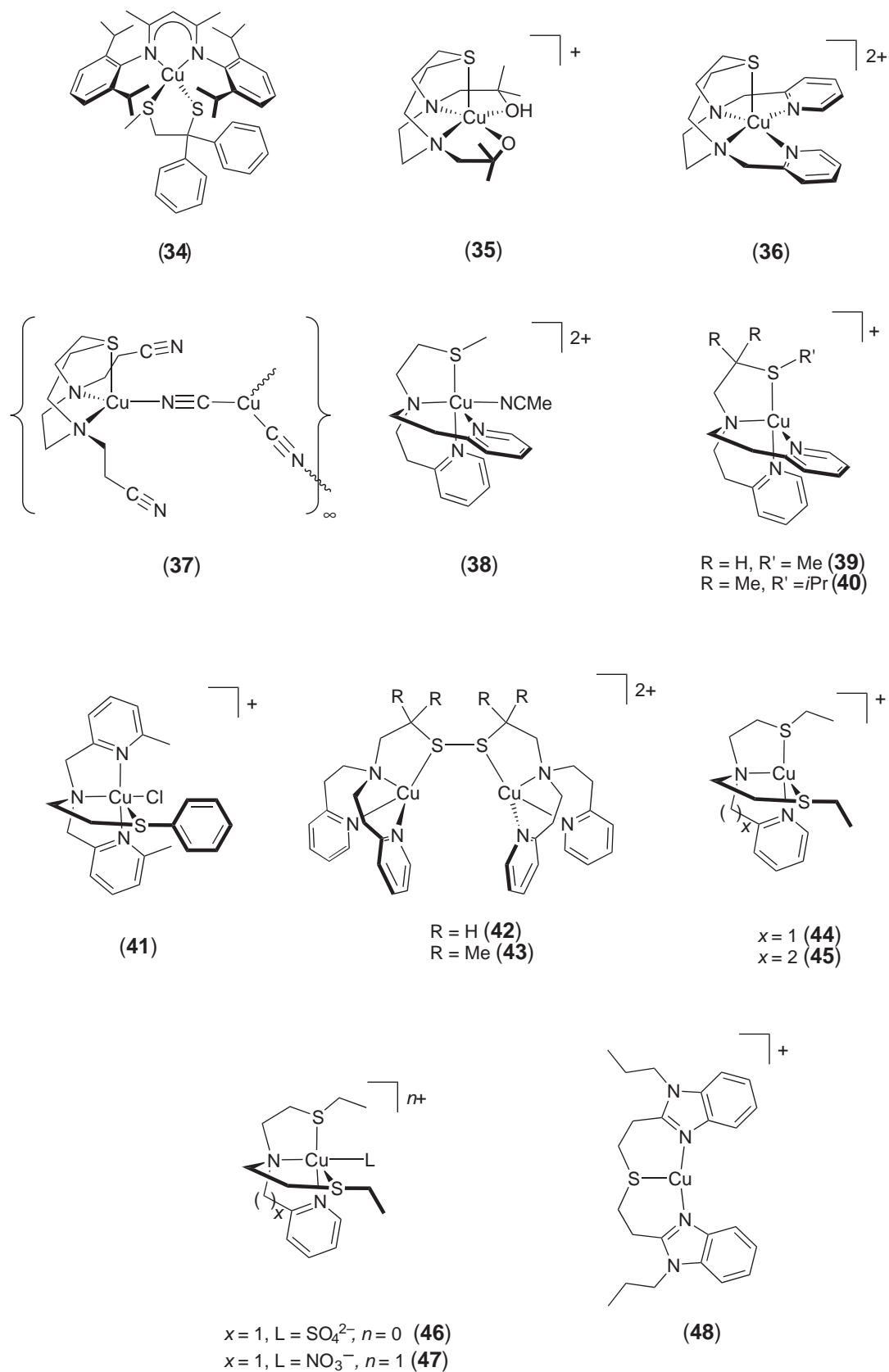
There are no synthetic copper(II) compounds with biological donors that adopt a coordination geometry analogous to that shown by Cu$_M$. The Cu$_M$ architecture of a trigonal pyramidal structure bearing a basal exogenous solvent ligand, and a very long apical Cu···S{thioether} distance, represents a formidable synthetic target in copper chemistry because of the strong

tendency of the copper(II) ion to form tetragonal or C_2-distorted tetrahedral complexes when four-coordinate. Hence, while there is a large number of known copper(II) complexes containing mixed nitrogen/thioether ligation, these give us little information about the chemistry to be expected of the Cu_M center. Hence, rather than provide a complete survey of a large and disparate series of complexes, this section concentrates on a smaller number of compounds with mixed N/S ligation that can yield conclusions about structural changes that might accompany redox at the Cu_M site.

The compound that most closely approximates the coordination geometry of Cu_M is (34) (Scheme 4),[62] which was originally targeted as a model of the type 1 cupredoxin active site (Chapter 8.4). This compound is closely related to complexes (1)–(7) already cited as models for Cu_H. The crystal structure of (34) shows a copper(II) ion with a flattened tetrahedral stereochemistry (Figure 6A). The Cu atom is displaced 0.484(2) Å above the $N_2S\{thiolate\}$ donor plane towards the thioether S donor, which results in an "apical" Cu—S{thioether} distance of 2.403(1) Å. This is at the short end of the range typically observed for apical or axial Cu(II)—S bonds. Unfortunately, the EPR spectrum of (34) ($g_1 = 2.15$, $g_2 = 2.06$, $g_3 = 2.01$, $A_1\{^{63,65}Cu\} = 98\,G$)[62] is very different from the "combined" EPR signal from $Cu_H + Cu_M$ ($g_\| = 2.25 - 2.29$, $g_\perp = 2.05$, $A_\|\{^{63,65}Cu\} = 142 - 162\,G$)[15,16,28–33] so that despite the structural similarities this is a poor model for the Cu_M biosite.
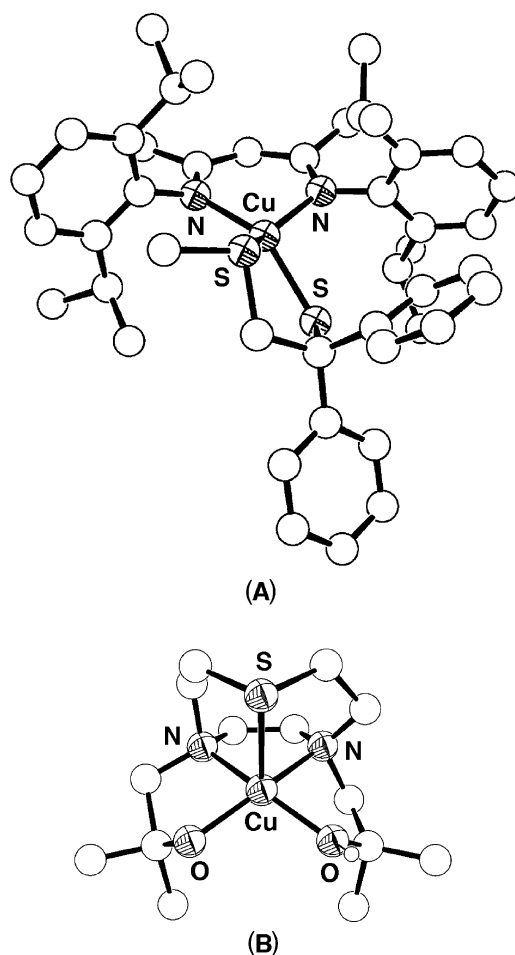
Figure 6 Single-crystal X-ray structures of (34) (A)[62] and (35) (B),[127] two copper(II) complexes with apical thioether donors whose molecular structures contain some features of the copper biosite. All hydrogen atoms have been omitted for clarity.

(**34**)   (**35**)   (**36**)

(**37**)   (**38**)   R = H, R' = Me (**39**)
                                                                                    R = Me, R' = *i*Pr (**40**)

(**41**)   R = H (**42**)   *x* = 1 (**44**)
                                          R = Me (**43**)   *x* = 2 (**45**)

x = 1, L = SO$_4^{2-}$, *n* = 0 (**46**)   (**48**)
x = 1, L = NO$_3^-$, *n* = 1 (**47**)

Scheme 4

One series of ligands that controllably provide an N_2S donor set with an apical thioether donor is small-ring diazathia macrocycles, of which 1,4-diaza-7-thiacyclononane ([9]aneN_2S) is the prototype. The parent ligand affords octahedral [Cu([9]ane$N_2S)_2$]$^{2+}$ with copper(II) salts of weakly coordinating anions.[125,126] However, several *N*-substituted derivatives of this macrocycle bearing donating side-arms controllably afford 1:1 complexes with copper(II), such as (**35**) (Figure 6B)[127] and (**36**) (Scheme 4).[128] Only one copper(I) complex of a [9]aneN_2S derivative has been structurally characterized, namely the coordination polymer (**37**) which contains a distorted tetrahedral copper(I) center.[129] The Cu—S bond lengths in (**35**), (**36**), and other square–pyramidal copper(II) complexes containing the [9]aneN_2S ligand framework are 2.486(4)–2.648(2) Å,[127,128,130–133] while the Cu(I)—S bond in (**37**) is 2.303(3) Å.[129] This shows that the weak apical Cu(II)—S interaction in these compounds has shortened significantly upon reduction, as was concluded from EXAFS (but not crystallographic) studies of the Cu_M center.

There are a small number of other mixed nitrogen/thioether-donor copper systems for which structural data in the +1 and +2 oxidation state are available (Scheme 4). Complex (**38**) was characterized crystallographically, and shows a square–pyramidal copper(II) ion with the S-donor in a basal, rather than apical, position.[134] EXAFS data for (**38**) and (**39**) suggest that the Cu—S bond is shortened upon reduction, from 2.34 Å in (**38**) to 2.16 Å in (**39**); the Cu—N distances are also shorter in the copper(I) complex.[134] The closely related (**41**)[135] has its S-donor in the apical position of a square pyramid, with a very long Cu(II)...S distance of 2.6035(3) Å; while, (**40**),[118] (**42**),[136] and (**43**)[117,118] show Cu(I)—S bonds of 2.228(6)–2.273(1) Å by crystallography. Similarly, the Cu(I)—S bonds in (**44**)[137] and (**45**),[138] at 2.230(5)–2.343(5) Å, are up to 0.23 Å shorter than for the trigonal bipyramidal copper(II) congeners (**46**)[137] and (**47**).[139] In contrast, the Cu(I)—S bond in (**48**) is 0.17 Å *longer* than for copper(II) complexes containing this tridentate ligand system, at 2.469(9) Å.[140,141] This is a consequence of the pseudo-linear geometry adopted by the copper(I) ion, resulting in a weaker Cu...S interaction.[140]

Although these data suggest that a Cu—S bond might be expected to shorten by up to 0.3 Å upon reduction from Cu(II) to Cu(I), these conclusions are complicated by the different coordination numbers and geometries that are virtually always present in copper complex redox pairs. Reflecting this complexity, a survey of all copper thioether complex crystal structures published in 1989 found that the mean Cu(I)—S and Cu(II)—S bond lengths were statistically indistinguishable, at 2.31(5) and 2.36(5) Å respectively.[142] To conclude, although it seems reasonable to expect a shorter Cu—S bond in reduced compared to oxidized Cu_M, it is impossible to predict how significant this difference should be.

8.16.2.3.2 *Copper(I) aqua complexes*

Another noteworthy feature of the structure of the Cu_M complex is the presence of a water ligand in its reduced state. Crystallographically authenticated copper(I) aqua complexes are rare,[143–148] and only two of the known examples are discrete monocopper compounds.[143,144] Each compound contains one water ligand per copper atom with a Cu(I)—O bond of between 2.167(7) Å and 2.307(14) Å, which is ca. 0.1–0.3 Å longer than is typically found in copper(II) complexes bearing a basal water ligand.[142] This change in bond length is consistent with the movement of the water ligand within the active site upon reduction of Cu_M.[20]

8.16.3 STOICHIOMETRIC C—H MONOOXYGENATION BY A COPPER BIOSITE

8.16.3.1 Cofactor Biosynthesis in Copper-containing Amine Oxidases

Copper-containing amine oxidase (CAO, EC 1.4.3.6) catalyzes the oxidation of primary amines by O_2 (Equation (7)):[2,4,149]

$$RCH_2NH_2 + O_2 + H_2O \rightarrow RCHO + NH_3 + H_2O_2 \tag{7}$$

The catalytic site of CAO contains a mononuclear, tetragonal [Cu(His)$_3$(OH$_2)_x$]$^{2+}$ ($x = 1$ or 2) center in its resting state, in close proximity to the protein-bound cofactor 2,4,5-trihydroxyphenyl-

alaninequinone (TPQ) (Scheme 5).[149–153] As discussed briefly in Section 8.16.4.1, the TPQ residue effects the amine oxidation during turnover, being itself reduced to an aminoquinol (TOPANH$_2$). The role of the CAO copper ion is to effect the biosynthesis of TPQ from tyrosine[154,155] and, possibly, to assist in the reoxidation of the aminoquinol reduced cofactor by O$_2$. The biosynthesis of TPQ in CAO is a self-processing event;[156] that is, it is performed by the pro-protein itself according to the stoichiometry in Equation (8),[157] without the need for any external cofactors apart from copper(II) and O$_2$.

Scheme 5

$$(8)$$
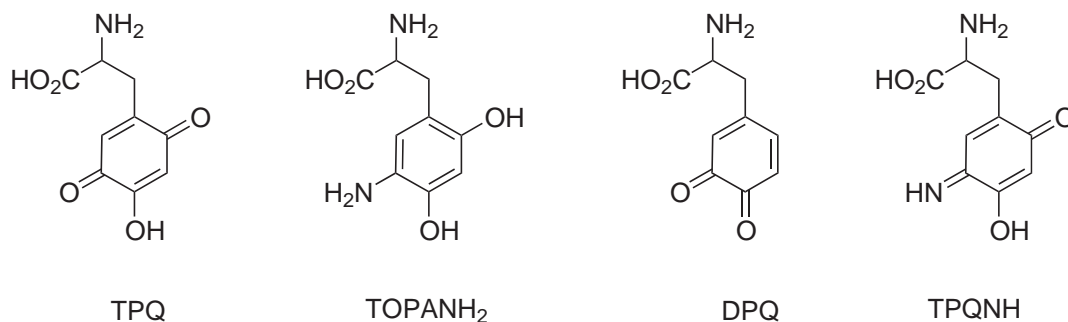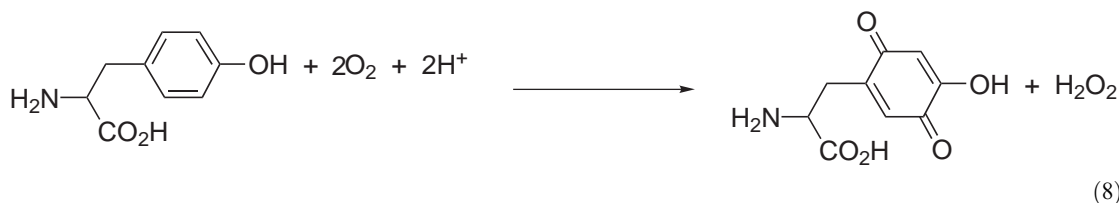
The mechanism of this transformation can be divided into two stages: monooxygenation and oxidation of tyrosine, to 3,4-dihydroxyphenylalanine quinone (DPQ; steps A–D of Figure 7); and, hydroxylation and oxidation of DPQ (steps F–H). A time-resolved crystallographic study of TPQ biosynthesis in a single crystal has confirmed the order of these events, showing that oxygenation of C3 of tyrosine occurs before oxygenation of C6.[158] The first of these processes represents the only known example of a *stoichiometric* monooxygenation of a C—H bond by a copper biosite.

Incubation of pro-CAO with copper(II) salts in air initially yields two species, which show absorptions at 350 nm and 380 nm that have been assigned to Tyr → Cu charge-transfer transitions.[159] The 380 nm band appears to be irrelevant to cofactor synthesis,[159] and probably arises from copper(II) ions[160] complexed to amino acids outside the active site. The 350 nm species is not obtained if pro-CAO is treated anaerobically with copper, although O$_2$ is not consumed during its aerobic formation.[159] Since there is no evidence for a Cu—O$_2$ bond in this species, this may imply the existence of a separate O$_2$-binding site remote from the copper ion, which would induce a protein conformational change in the presence of O$_2$ to allow the 350 nm complex to form.

The 350 nm intermediate in TPQ biogenesis has been proposed to contain a [Cu(His)$_3$(Tyr)] active site complex (Figure 7).[158,159] Consistent with this, a single-crystal structure of an unprocessed bacterial CAO containing zinc instead of copper shows a tetrahedral [Zn(His)$_3$(Tyr)]$^+$ center, with an unmodified tyrosine cofactor residue ligated to the Zn ion.[161] Formation of TPQ from the 350 nm species proceeds with first-order kinetics[159] and consumes one mole equivalent of O$_2$.[162] The reaction of the 350 nm intermediate with O$_2$ does not involve proton transfer, and is the rate-limiting step in TPQ biogenesis.[162] This reaction has been suggested to proceed via intramolecular Tyr → Cu electron transfer, yielding a copper(I) complex of a tyrosyl radical (step B of Figure 7).[159] Consistent with this, an inhibition study has shown that coordination of the precursor tyrosine side-chain to copper is a prerequisite for TPQ formation.[163] Once formed, the tyrosyl radical probably dissociates from the copper ion, to allow O$_2$ access to the copper center (step C). A similar sequence of substrate-to-metal electron transfer prior to O$_2$ activation
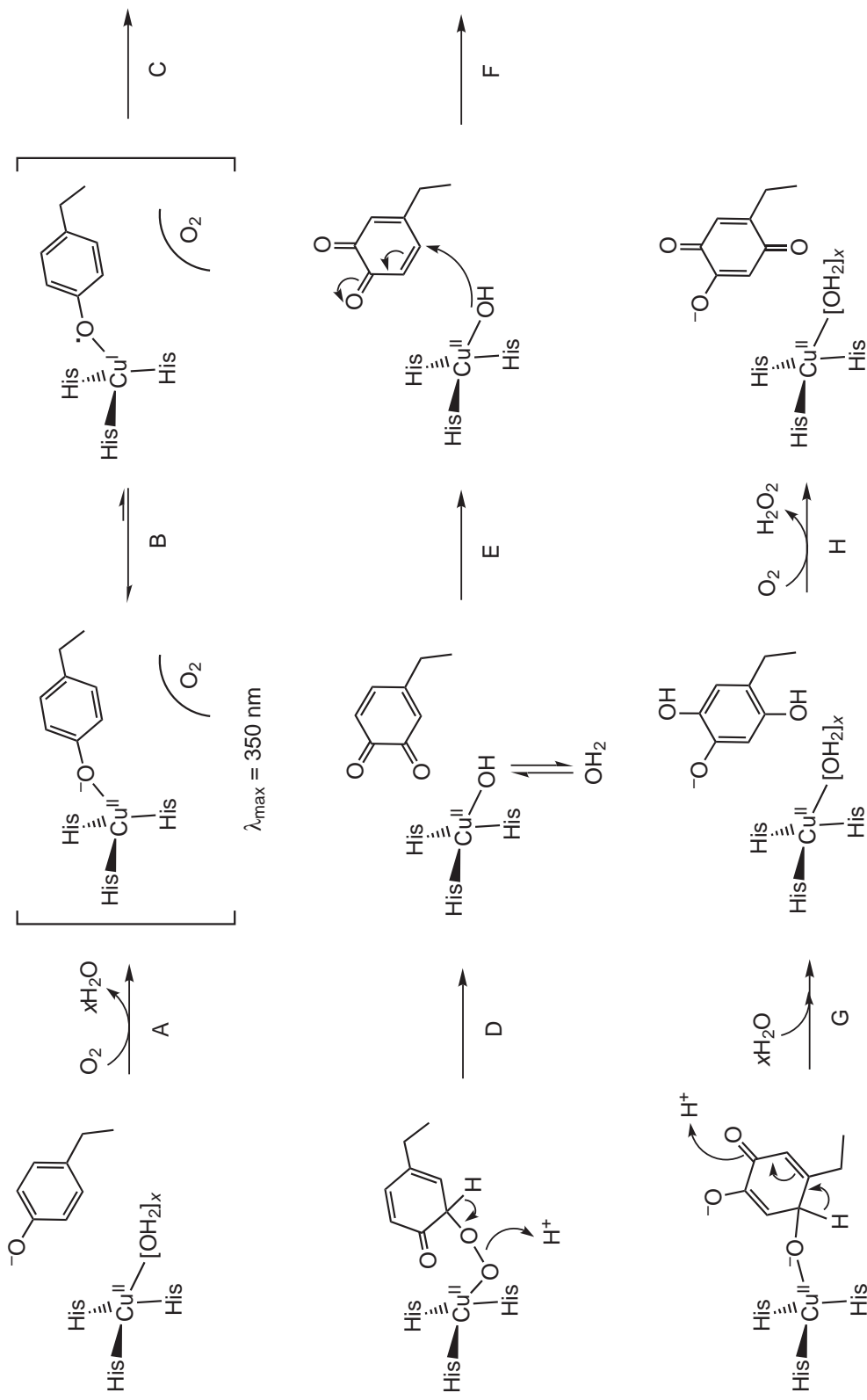
Figure 7 Currently preferred mechanism for biogenesis of the topaquinone cofactor in copper-containing amine oxidase.[162]

occurs in the catalytic cycles of iron-containing catechol dioxygenase enzymes (Chapter 8.14). The arylperoxo complex intermediate formed from step C would be structurally similar to the crystal-lographically characterized complex between CAO and O_2, which contains an asymmetric η^2–O species bridging between the Cu ion and TPQ ring (Section 8.16.4.1).[164] Hence, the arylperoxo species proposed in Figure 7 is sterically reasonable. It has been suggested that the arylperoxo intermediate could form directly from the 350 nm species without the intermediacy of step B.[165] No evidence to support this idea has been published, however.

Hydroxylation of the DPQ intermediate proceeds by nucleophilic attack of water at $C6$ of the quinone ring (step F of Figure 7).[166] The water nucleophile may be activated by coordination to the copper center, as shown in Figure 7, since DPQ is not hydrolyzed in neutral aqueous solution *in vitro*.[167–169] However, this would imply rotation of the DPQ ring by *ca.* 180° between the oxygenation and hydroxylation steps (step E), to allow a Cu-bound nucleophile to attack both $C2$ and $C5$ of the precursor tyrosine ring. In addition, steps E and F together must be slow compared to exchange of the Cu-bound hydroxide ion with exogenous water to permit incorporation of a water-derived O atom into the final product.

8.16.3.2   Model Studies Relevant to Topaquinone Biogenesis

8.16.3.2.1   *Oxidation of phenols by copper complexes*

There is one synthetic reaction that mimics complete TPQ biogenesis, where conversion of 4-*tert*butylphenol to 2-hydroxy-5-*tert*butylbenzoquinone is effected by $[Cu(Im)_4](ClO_4)_2$ (Im = imidazole).[170] This reaction proceeds in very low yields of <3%, and no mechanistic data were presented. The phenol monooxygenation in Figure 8 is also noteworthy, in that strong evidence was presented for the intermediacy of a copper arylperoxo intermediate (**49**) to account for migration of the *tert*butyl substituent.[171] This is directly analogous to the peroxo intermediate

(49)
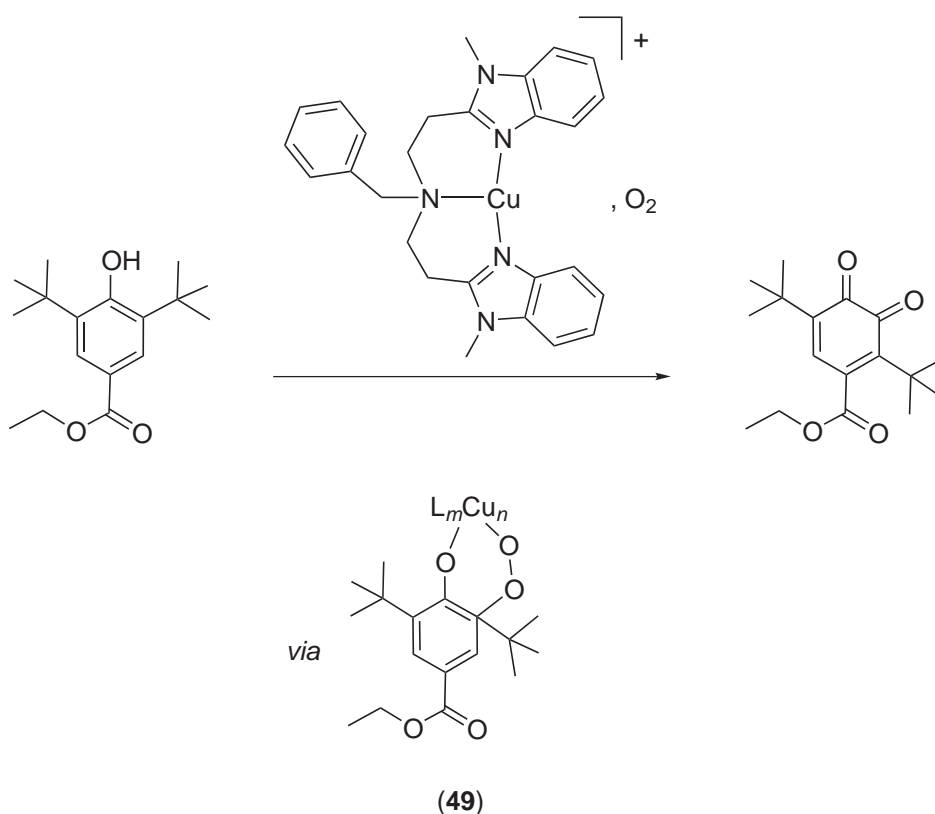
Figure 8   A copper-catalyzed oxidation of 2,4-*bis*(*t*-butyl)phenol, relevant to the mechanism of TPQ biosynthesis.[171]

proposed during the monooxygenation step of TPQ biosynthesis (step C of Figure 7). The undetected arylperoxo intermediate was proposed to contain one copper ion (i.e., (49), $n = 1$), by analogy with similar oxygenations effected by cobalt Schiff base complexes.[171] If so, however, then this must be formed by reaction of the precursor phenol with a dinuclear copper/oxygen adduct, which is the initial product of the reaction of this copper complex with O_2.[88]

The one-electron oxidation of tyrosine by a copper(II) center (step B of Figure 7) is modeled by two systems (Figure 9). Treatment of (1) with sodium 2,6-di(*tert*butyl)phenolate yields copper(I) products, which can be trapped with an isocyanide to give (50); 3,3′,5,5′-*tetrakis*(*tert*butyl)-4,4′-dibenzoquinone is formed in this reaction in its maximum theoretical yield of 25%.[63] Similar reactions using less sterically hindered phenolates instead yield the stable copper(II) phenoxide compounds (4)–(7).[63] Similarly, (51) and (52) decompose rapidly at room temperature to give 4,4-dibenzoquinone products.[172] The analog (53), bearing a 4-fluorophenoxide ligand, is thermally stable and was crystallographically characterized.[172] This complex has a coordination geometry and ligand donor set at copper that closely resembles that proposed for the "350 nm" intermediate in TPQ biogenesis (Figure 7). Both these reactions almost certainly involve intramolecular phenoxide → Cu one-electron transfer, yielding phenoxyl radicals which then

R = Me, R' = H (51)
R = *t*Bu, R' = H (52)
R = H, R' = F (53)

(51) and (52) only   R = Me or *t*Bu
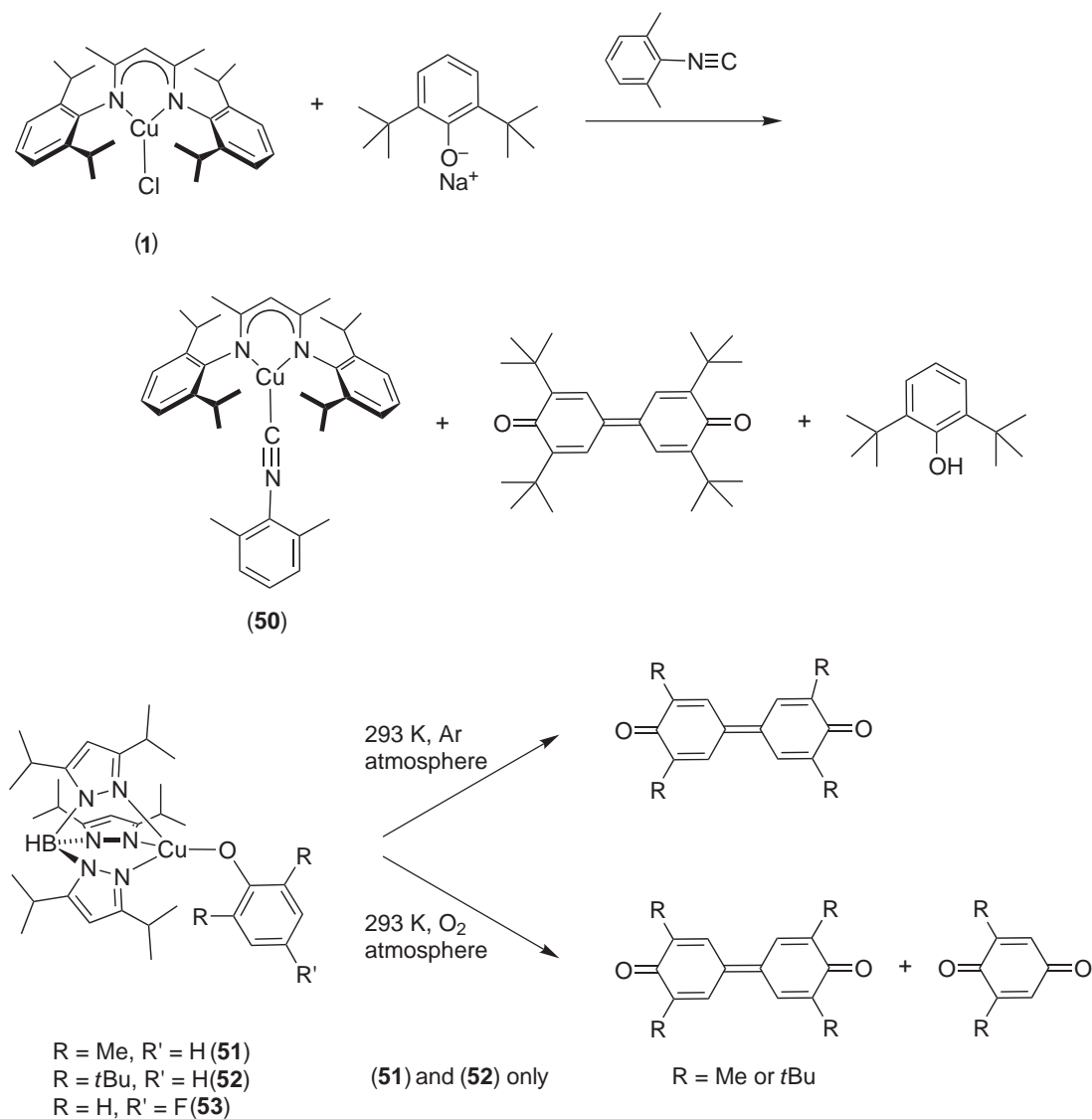
Figure 9 Two examples of the one-electron oxidation of phenols by copper(II) complexes, relevant to the mechanism of TPQ biosynthesis.[63,172]

rapidly dimerize. The catalytic dimerization of substituted phenols to either 2,2′-diphenols or 4,4′dibenzoquinones by the dicopper(II) complex (**54**) presumably proceeds by a similar mechanism.[173] All these observations provide direct precedents for step B of the TPQ biosynthesis mechanism (Figure 7).

(54)
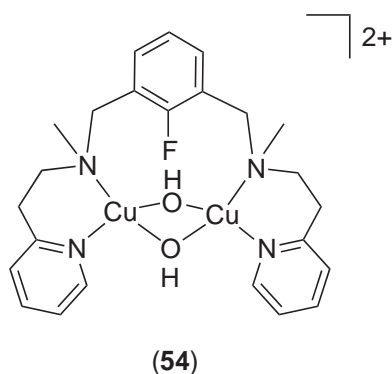
Interestingly, in the light of the above results, CuCl$_2$ complexes of some *tris*pyrazolylborate or 1,4,7-triazacyclononane derivatives are active catalysts for the polymerization of 4-fluorophenol[174] and 4-phenoxyphenols[175–180] to poly(1,4-phenylene)oxides. Using the results in Figure 9 as precedent,[172] these polymerizations have been proposed to proceed by coupling of phenoxyl radicals generated by the copper(II) catalysts.[175–180] However, a mechanistic study of an analogous polymerization of 2,6-dimethylphenol by [Cu(MeIm)$_4$](NO$_3$)$_2$ (MeIm = 1-methylimidazole) strongly favored an alternative nonradical mechanism, involving dicopper phenoxonium complex intermediates.[181–185] Hence, it is uncertain whether the copper-catalyzed polymerization of phenols provides additional precedent for free-radical reactivity arising from phenoxide → Cu electron transfer. A more detailed discussion of copper–phenoxyl radical chemistry is provided in Chapter 8.26.

8.16.3.2.2 Hydroxylation of orthoquinones in the presence and absence of copper

The hydroxylation of DPQ (steps F–H in Figure 7) is mimicked by the copper(II)-catalyzed aqueous autooxidation of 4-alkylcatechols to 2-alkyl-5-hydroxybenzoquinones (Figure 10).[169,186] The role of the catalyst here is to promote oxidation of the catechol precursor;[169,186] the subsequent hydrolysis step is promoted by base, but not by copper.[169] Interestingly, the "hydrolysis" is in fact a result of 1,4-addition of H$_2$O$_2$ to C5 of the catechol, rather than H$_2$O (Figure 10);[187] H$_2$O$_2$ is produced in the reaction mixture as a by-product of catechol oxidation. Hence, this apparently simple synthetic reaction does not accurately model the biogenesis of TPQ, in which the C2 O atom in the final product is derived from water.[166]
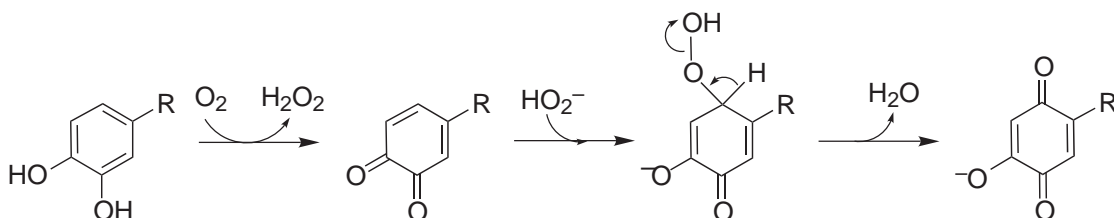
Figure 10   The mechanism of the aqueous autooxidation of catechols.[187]

8.16.4 MONOCOPPER OXYGEN CHEMISTRY

8.16.4.1 Other Monocopper Dioxygen Centers in Biology

In addition to the monocopper monooxygenases (DβM and PHM, Section 8.16.2.1) and amine oxidase (CAO, Section 8.16.3.1), there are two other known enzymes containing monocopper active sites, which react with oxygen or one of its reduced congeners. Galactose oxidase (GO, EC 1.1.3.9) catalyzes the aerobic oxidation of primary alcohols at a monocopper phenoxyl radical center (Equation (9)):[4,149]

$$RCH_2OH + O_2 \rightarrow RCHO + H_2O_2 \qquad (9)$$
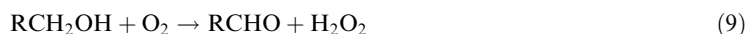
The second protein, copper/zinc superoxide dismutase (SOD, EC 1.15.1.1), catalyzes the disproportionation of O_2^- (Equation (10)) at a heterodimetallic Cu/Zn active site:[188,189]

$$2O_2{}^- + 2H^+ \rightarrow O_2 + H_2O_2 \qquad (10)$$

Although their structures are very different, the copper centers in DβM, PHM, CAO, GO, and SOD are all believed to interact with O_2 or O_2^- during turnover. However, characterization data are only available for the complex of O_2 and CAO at the time of writing; hence, only this species will be discussed here. The chemistry of GO is described in detail in Chapter 8.26, and of SOD in Chapter 8.19. The biosynthesis of the TPQ cofactor in CAO is discussed in Section 8.16.3.1.

The 2,4,5-trihydroxyphenylalanine quinone (TPQ) cofactor in CAO is the active oxidant for amine oxidation (Equation (7)), which proceeds by a ping-pong mechanism. The reductive half-reaction involves reduction of the TPQ residue by the substrate, yielding 5-amino-2,4-dihydroxy-phenylalanine (TOPANH$_2$), which must be reoxidized to TPQ in the oxidative half-reaction (Equation (11)), Scheme 5 complete the catalytic cycle:

$$TOPANH_2 + O_2 + H_2O \rightarrow TPQ + NH_3 + H_2O_2 \qquad (11)$$

The role of copper in the oxidative half-reaction has been debated for some years, since the Cu ion in CAO is redox active.[190–192] However, studies involving ^{18}O isotope effect measurements of CAO catalysis,[193] of the inhibition of CAO by CO,[192] and of substitution of the copper content of CAO with other metal ions,[194] have all implied that this site remains in its +2 oxidation state during normal turnover. That would mean that O_2 reacts with TOPANH$_2$ directly, without being activated by precoordination to Cu(I).

Crystals of *Escherichia coli* CAO were pre-reduced anaerobically with benzylamine, then exposed to O_2. This yielded a crystal structure at 2.1 Å resolution of a CAO/O_2/benzaldehyde complex, that gives an informative "snapshot" of the oxidative half-reaction (Figure 11).[164] The copper ion is approximately tetrahedral, with normal Cu—N bonds to the three histidine ligands and a long interaction of 2.8–3.0 Å to an approximately "side-on" η^2-O_2 molecule. Both O atoms of the O_2 molecule take part in hydrogen bonding; one is hydrogen-bonded to *O*2 of the TPQ
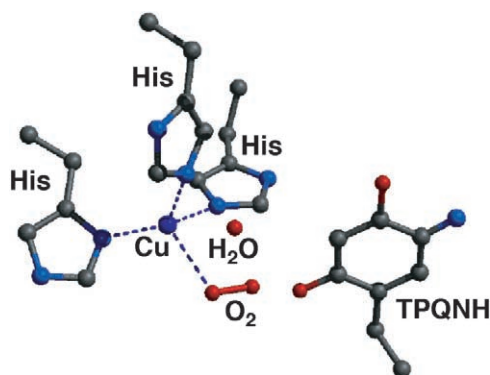
Figure 11 Structure of the complex between copper-containing amine oxidase and O_2, as determined by protein X-ray crystallography.[164]

residue, while the other atom interacts with a water molecule. Although there were no spectroscopic data to confirm this, the pattern of hydrogen bonding in the active site suggested that the O_2 moiety in the crystal was at the peroxide oxidation level. That is, oxidation of TOPANH$_2$ to TPQNH, and concomitant reduction of O_2 to $H_yO_2^{(2-y)-}$ ($y = 0$, 1 or 2), had already taken place in the crystal prior to data collection. The oxidation state of the Cu ion in the structure was uncertain. Given the long Cu$\cdots$O$_2$ interaction, and the direct O$_2\cdots$TPQ hydrogen bond, this structure gives no information about the importance of Cu/O$_2$ binding during the CAO oxidative half-reaction. Nonetheless, it represents the *only* direct experimental evidence to date for the reaction of a monocopper biosite with O_2.

8.16.4.2 Copper Superoxo Complexes

Treatment of Cu(I) or Cu(II) complexes with superoxide commonly results in disproportionation of the superoxide anion, according to Equation (10). Because of this, and the very high reactivity of the superoxide anion, there is thus far only one report of a superoxocopper species generated by reacting a Cu(II) precursor with O_2^-, that is long-lived enough to be detected.[195] The other known superoxocopper complexes have been generated by oxygenation of a Cu(I) precursor at low temperatures or, in one case, following reaction of a Cu(II) complex with H_2O_2.[196] Superoxide-containing species are sometimes detected as short-lived intermediates *en route* to dicopper(II) peroxo and/or dicopper(III) *bis*(oxo) complexes (Chapter 8.15).[197–201] Alternatively, where the superoxo complex is stable, this can be a result of steric protection that prevents attack of a second Cu center at the bound superoxide ion.[198,202,203]

Formation of unstable superoxocopper species in low-temperature oxygenation experiments has often been inferred from manometric determinations of a 1:1 Cu:O$_2$ adduct stoichiometry or stopped-flow kinetic data. The UV/vis spectra of the resultant copper(II) superoxo species each show an absorption at $\lambda_{max} = 352-416$ nm ($\varepsilon_{max} = 2{,}100-8{,}000\,mol^{-1}\,dm^3\,cm^{-1}$), which may arise from a $O_2^- \rightarrow$ Cu charge transfer transition (Table 1).[198,199,202–204] The most rigorous spectroscopic signature available for a copper superoxo complex is the O—O stretching vibration ($\nu_{O—O}$) of the superoxide ligand, measured by IR or resonance Raman spectroscopy. For the three monocopper superoxo compounds where this has been reported, $\nu_{O—O} = 1{,}112\,cm^{-1}$, $964\,cm^{-1}$, and $968\,cm^{-1}$ (Table 1).[202–204] This is higher than for comparable Cu(II)/η^1-O$_2$R$^-$ complexes (R = H, alkyl or acyl), by between $130\,cm^{-1}$ and $277\,cm^{-1}$ (Table 1).[135,205–207] All monocopper(II) superoxo complexes whose EPR or NMR spectra have been measured have been EPR-silent and/or diamagnetic, owing to strong antiferromagnetic coupling between the Cu(II) ion and O$_2^-$ ligand.[195,202–204,208]

Three isolable copper superoxo complexes have been reported, (**55**),[202] (**56**),[203,209] and (**57**),[204] which almost certainly contain different coordination modes of superoxide (Scheme 6). Low-resolution crystal structures of (**55**) and (**56**) showed copper centers that were best described as tetragonal, with a "side-on" coordinated η^2-O$_2^-$ ligand occupying two basal coordination sites (Figure 12).[202,209] The short O—O bond of 1.22(3) Å shown by (**55**) is consistent with a superoxo, rather than a peroxo, ligand; the O—O bond length derived for (**56**) was unreliable owing to
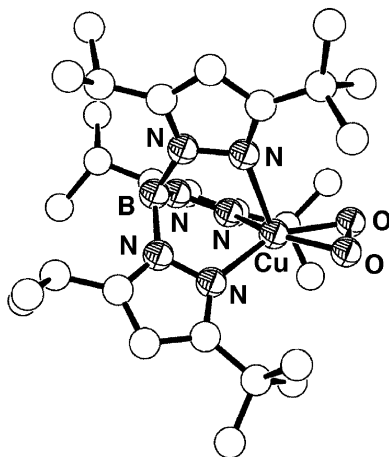
Figure 12 Single-crystal X-ray structure of (**55**),[202] a copper(II) superoxo complex. All hydrogen atoms have been omitted for clarity.

Table 1 Spectroscopic and structural data for monocopper superoxo, hydroperoxo, alkylperoxo, and acylperoxo complexes. Selected dicopper complexes are also listed for the purpose of comparison.

	Isolated	ν_{O-O} (cm^{-1})	$O_2^-\rightarrow Cu$ or $RO_2^-\rightarrow Cu$ λ_{max} (ε_{max}) (nm (mol^{-1} dm^3 cm^{-1}))	EPR spectrum g, $A\{^{63,65}Cu\}$, G	O–O bond length (Å)	References
[Cu(HB{pz^{tBu,iPr}}$_3$)(η^2-O$_2$)] (**55**)	Y	1,112[a]	352 (2,330)	Silent	1.22(3)	202
[Cu(acen')(η^2-O$_2$)] (**56**)	Y	968	385 (2,400)	Silent	[b]	203,209
[Cu(dpha)(NEt$_3$)(η^1-O$_2$)] (**57**)	Y	964	391 (2,100)[c]	Silent	[d]	204
[Cu(tppa)(η^1-O$_2$)]$^+$ [d]	N		315 (4,000)	Silent		208,211
[Cu(tetb)(η^1-O$_2$)]$^+$ (**58**)	N			Silent		195
[Cu(tmpa)(O$_2$)]$^+$	N		410 (4,000)			197,198
[Cu(tmpae)(O$_2$)]$^+$	N		415 (3,330)			199
[Cu(bqpa)(O$_2$)]$^+$	N		378 (8,200)			198,200
[Cu$_2$(μ-btmpa)(O$_2$)(NCEt)]$^{2+}$	N		416			199
[Cu$_2$(μ-btmpa)(O$_2$)$_2$]$^{2+}$	N		416 (8,900)			199
[Cu$_2$(μ-UN-O)(μ-O$_2$)]$^{2+}$ (**59**)	N		404 (5,400)			216
[Cu$_2$(μ-hexpy)(μ-OH)(η^1:η^1, μ-O$_2$)]$^{2+}$ (**60**)	N	1131	395 (8,000)	$g=2.0$ + half-field signal $g=2.04$		196
[Cu(HB{pz^{tBu,iPr}}$_3$)(η^1-O$_2$H)] (**64**)	N	843	556 (435), 604 ($\geq$1,180)	$g_\parallel=2.380$, $g_\perp=2.090$, $A_\parallel=44$		206
[Cu(bppa)(η^1-O$_2$H)]$^+$ (**69**)	Y	856	380 (890)	$g_\parallel=2.004$, $g_\perp=2.202$, $A_\parallel=109$, $A_\perp=75$	1.460(6)	205
[Cu(MeImPy$_2$)(η^1-O$_2$H)] (**70**)	N	849	380 ($\sim$1,500)	$g_\parallel=2.09$, $g_\perp=2.21$, $A_\parallel=80$, $A_\perp=94^e$		207
[Cu(MeImMe)(η^1-O$_2$H)] (**71**)	N	835,851[e]	380 ($\sim$1,500)	$g_\parallel=2.26$, $g_\perp=2.06$, $A_\parallel=155$		207
[Cu(MeImMe$_2$)(η^1-O$_2$H)] (**72**)	N	831	380 ($\sim$1,500)			207
[Cu(Py$_2$SPh)(η^1-O$_2$H)] (**73**)	N	881	357 (4,300)	$g_\parallel=2.24$, $g_\perp=2.06$, $A_\parallel=168$		135

Table 1 continued

	Isolated	ν_{O-O} (cm^{-1})	$O_2^- \rightarrow Cu$ or $RO_2^- \rightarrow Cu$ λ_{max} (ε_{max}) (nm (mol^{-1} dm^3 cm^{-1}))	EPR spectrum g, $A\{^{(63,65)}Cu\}$, G	O—O bond length (Å)	References
[Cu$_2$(μ-Py$_2$SSPy$_2$)(O$_2$H)$_x$]$^{2+}$ **(74)**	N	822, 836	325 (~6,400)	g = 2.0 + half-field signal		117, 118
[Cu$_2$(μ-UN-O)(μ-O$_2$H)]$^{2+}$ **(75)**	Y	892	395 (7,000)			116, 224
[Cu$_2$(μ-XYL-O)(μ-O$_2$H)]$^{2+}$ **(76)**	N		395 (8,000)			222, 223
[Cu$_2$(μ-Py$_2$Pz$_2$N$_6$O)(μ-O$_2$H)]$^{2+}$	N		400 (8,400)			225
[Cu$_2$(μ-Py$_2$DMP$_2$N$_6$O)(μ-O$_2$H)]$^{2+}$	N		395 (5,500)			225
[Cu(HB{pz^{iPr2}}$_3$)(O$_2$C{O}C$_6$H$_4$Cl-3]] **(61)**	N			$g_\parallel$ = 2.27, $g_\perp$ = 2.07, $A_\parallel$ = 160		219
[Cu(HB{pz^{iPr2}}$_3$)(η^1-O$_2$CMe$_2$Ph]] **(63)**	Y		506 (590), 572 ($\geq$3,815)	$g_\parallel$ = 2.316, $g_\perp$ = 2.097, $A_\parallel$ = 59	1.460(6)	206, 220
[Cu(HB{pz^{tBu,iPr}}$_3$)(η^1-O$_2$C^{t}Bu]] **(65)**	N		537 (855), 611 (5,000)	$g_\parallel$ = 2.336, $g_\perp$ = 2.076, $A_\parallel$ = 62		206
[Cu(HB{pz^{tBu,iPr}}$_3$)(η^1-O$_2$CMe$_2$Ph]] **(66)**	N		522 (655), 603 (5,410)	$g_\parallel$ = 2.350, $g_\perp$ = 2.076, $A_\parallel$ = 61		206
[Cu(tmpa)(O$_2$C{O}C$_6$H$_4$Cl-3)]$^+$ **(67)**	N			$g_\perp$ = 2.16, $A_\perp$ = 86^f		221
[Cu(Me$_2$Im)$_3$(O$_2$C{O}C$_6$H$_4$Cl-3)]$^+$ **(68)**	N		332 (950)	$g_\parallel$ = 2.26, $g_\perp$ = 2.04, $A_\parallel$ = 190		221
[Cu$_2$(μ-^{i}Pr$_3$tacnO$_2$)$_2$]$^{2+}$	Y	722	380 (2,800)	Silent		227
[Cu$_2$(μ-XYL-O)(η^1:η^1,μ-O$_2$C{O}C$_6$H$_4$Cl-3)]$^{2+}$	Y		395 (5,500–5,900)		1.462(12)	226

* Abbreviations used: acen^H = 2,4-bis([2,4,6-trimethylphenyl]imino)pentane; bppa = bis(6-{tertbutylcarboxamido}pyridyl-2-ylmethyl)(pyridyl-2-ylmethyl) amine; btmpa = 1,2-bis(6-{bis[pyridin-2-ylmethyl]aminomethyl}pyrid-3-yl)ethane; dphaH = 2,4-bis(tertbutyl)-6-(2-hydroxy-4,6-bis{tertbutyl}phenylimino)cyclohexa-2,4-dienone; hexpy = 1,2-bis(6-[bis{pyridin-2-ylmethyl}pyrid-2-yl]ethane; MeImMe = ((6-methylpyridin-2-yl}methyl)(pyridin-2-ylmethyl)({1-methylimidazol-4-yl}methyl)amine; Me$_2$Im = 1,2-dimethylimidazole; MeImMe$_2$ = bis((6-methylpyridin-2-yl]methyl) ({1-methylimidazol-4-yl]methyl)amine; MeImPy$_2$ = bis(pyridin-2-ylmethyl)({1-methylimidazol-4-yl}methyl)amine; ^{i}Pr$_3$tacnO$_2$H = 1-(1-{peroxomethyl}ethyl)-4,7-bis{isopropyl}-1,4,7-triazacyclononane; Py$_2$DMP$_2$N$_6$OH = 2,6-bis([{pyrid-2-ylethyl}{3,5-dimethylpyrazol-1-ylmethyl}amino]methyl)phenol; Py$_2$Pz$_2$N$_6$OH = 2,6-bis([{pyrazol-1-ylmethyl}amino]methyl)phenol; Py$_2$SPh = bis(pyridin-2-ylmethyl) (2-{phenylsulfanyl}ethyl)amine; Py$_2$S-SPy$_2$ = bis(2-[bis{pyrid-2-ylethyl}amino]prop-2-yl)disulfide; pz^{Bu,Ar}H = 3-tertbutyl-5-isopropylpyrazole; pz^{iPr2}H = 3,5-di-isopropylpyrazole; tetb = rac-5,5,7,12,12,14-hexamethyl-1,4,8,11-tetraazacyclotetradecane; tmpa = tris(pyridyl-2-ylmethyl)amine; tmpae = bis(pyridyl-2-ylmethyl)({5-methylcarboxypyrid-2-yl}methyl)amine; tppa = tris(6-{tertbutylcarboxamido}pyridyl-2-ylmethyl)amine; UN-OH = 2-(bis{pyrid-2-ylethyl}aminomethyl)-6-(bis{pyrid-2-ylethyl}amino)phenol; XYL-OH = 2,6-bis(bis{pyrid-2-ylethyl}aminomethyl)phenol.

^{a} A suggestion that this value of ν_{O-O} is erroneous,[203] is itself wrong. The transition ν_{O-O} = 1112 cm^{-1} for **(55)** has been confirmed by IR spectroscopy (E. I. Solomon, personal communication). ^{b} A O—O bond length of 1.44(2) Å was derived from a crystal structure of this compound, but is unreliable owing to disorder problems.[209] ^{c} The assignment of this band as a O$_2^-$ → Cu charge transfer band is uncertain, owing to the presence of other absorptions in the near-UV. ^{d} A putative crystal structure of this complex was in fact found to contain [Cu(tppa){OH}]$^+$. The assignment of this species therefore remains to be confirmed. ^{e} Solution contains a mixture of trigonal bipyramidal and square pyramidal monocopper hydroperoxo species. These were both observed in the EPR spectrum, although g and A values were not quoted. ^{f} g and A were not determined.

disorder. Interestingly, (**55**) and (**56**) exhibit rather different O—O vibrations, at $1,112\,\mathrm{cm}^{-1}$ and $968\,\mathrm{cm}^{-1}$, respectively (Table 1). DFT calculations indicated that the weaker O—O vibration for (**56**) reflects a substantial contribution of a Cu(III)/O_2^{2-} resonance form to the electronic structure of this complex.[209] The $^{16}O^{18}O^-$-containing isotopomer of (**56**) showed just one ν_{O-O} vibration by resonance Raman, consistent with an η^2-O_2^- coordination mode.[203] In contrast, the infrared spectrum of the $^{16}O^{18}O^-$-containing isotopomer of (**57**) shows two distinct ν_{O-O} peaks, which is strong evidence for an "end-on" η^1-O_2^- ligand.[204] Although no structural data are available, (**57**) most likely adopts a square pyramidal stereochemistry with an apical superoxide ligand. A similar structure was proposed for [Cu(tetb)(O_2)]$^+$ (**58**), which was detected spectrophotometrically in solutions containing [Cu(tetb)]$^{2+}$ and O_2^-;[195] and for adducts formed between O_2^- and copper(II) complexes of a series of tetradentate Schiff bases.[210] Compound (**56**) reacts stoichiometrically with some other Cu(I) species to form dicopper(III) *bis*(oxo) products (Chapter 8.15);[209] no other reactivity data for any of these superoxo complexes have yet been provided.

(**55**)

(**56**)

(**57**)

(**58**)

(**59**)

(**60**)
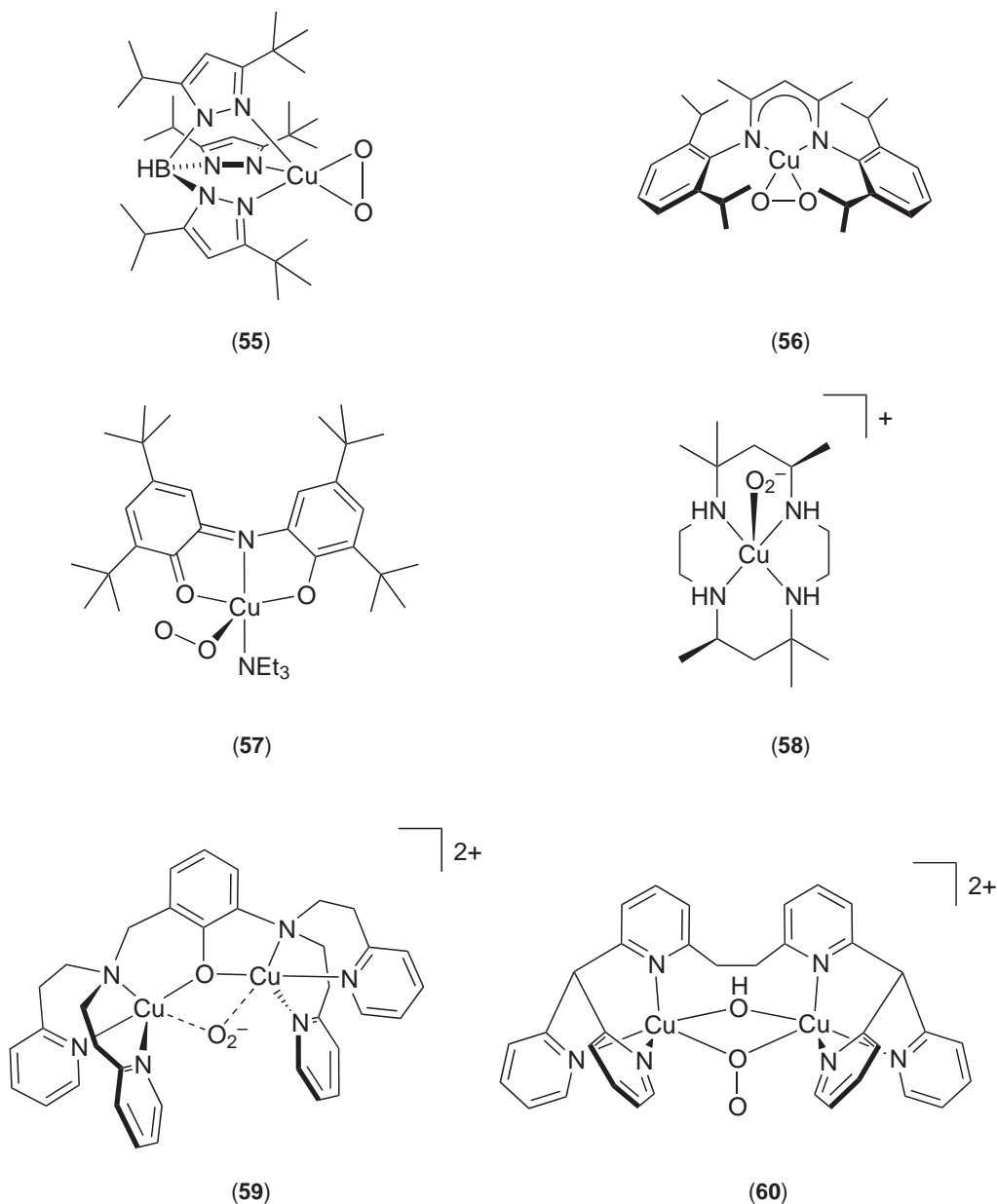
Scheme 6

A diamagnetic species assigned as $[Cu^{II}(tppa)(\eta^1-O_2)]^+$ (tppa = *tris*{6-[*tert*butylcarboxamido] pyrid-2-ylmethyl}amine) was obtained as the initial product of oxygenation of $[Cu^I(tppa)]^+$ at $-80\,°C$.[208,211] However, the resonance Raman spectrum of this complex could not be measured, while its UV/vis spectrum does not match those shown by copper superoxo complexes protected by similar *tris*(pyrid-2-yl)methylamine derivatives (Table 1).[197–200] A putative crystal structure of $[Cu^{II}(tppa)(\eta^1-O_2)]^{+}$[211] was reassigned by others as in fact containing $[Cu^{II}(tppa)(OH)]^+$,[212] which is a decomposition product of the initial low-temperature oxygenation product.[213] Hence, the existence of $[Cu^{II}(tppa)(\eta^1-O_2)]^+$ remains to be confirmed. A putative copper superoxo complex related to (**55**), but with a less sterically hindered *tris*pyrazolylborate ligand,[214] has been shown in fact to be a dicopper peroxo compound.[215]

Two dicopper(II) superoxo complexes, (**59**)[216] and (**60**),[196] have also been spectroscopically characterized in solution (Scheme 6). Both these compounds exhibit an apparent $O_2^- \rightarrow Cu$ charge transfer absorption in the same range as observed for the mononuclear complexes, and afford an EPR signal at 77 K showing $g \approx 2.04$ with no detectable hyperfine coupling, which is similar to the EPR spectra of superoxo complexes of diamagnetic metal ions.[217] Compound (**60**) shows $\nu_{O-O} = 1{,}131\,cm^{-1}$ by resonance Raman,[196] which is at the high end of the range shown by other copper superoxo complexes.[202–204] From these and other measurements, a structure containing a $\eta^1{:}\eta^1$, μ-O_2^- ligand was proposed for (**60**).[196] The coordination mode of superoxide in (**59**) was unclear.

8.16.4.3 Copper Hydroperoxo, Alkylperoxo, and Acylperoxo Complexes

As described in Chapter 8.15, there is a well-established chemistry of dicopper(II) peroxo complexes, which are the usual products of the oxygenation of Cu(I) precursors (Equation (12)):[218]

$$2[Cu^I L_n]^{m+} + O_2 \rightarrow [\{Cu^{II}L_n\}_2(\mu\text{-}O_2)]^{m+} \tag{12}$$
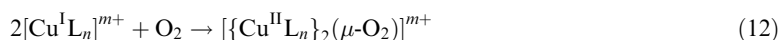
The driving force towards the formation of dinuclear products is the requirement for two electrons, to reduce dioxygen to the peroxide level. Since an individual Cu(I) center can only provide one electron under normal conditions, this makes the biomimetic synthesis of *mono*-copper peroxo compounds from O_2 a particular challenge. There are as yet no known mono-copper(II) complexes of the O_2^{2-} ligand, and only a small number that contain O_2R^- (R = H, alkyl, acyl; Table 1). These have all been synthesized by treatment of a Cu(II) complex with the relevant peroxide, rather than by oxygenation of Cu(I) species. Almost all known monocopper(II) peroxo complexes contain *tris*pyrazolylborates,[206,219,220] or *tris*(pyrid-2-ylmethyl)amine or related trip-odal amines,[117,118,135,205,207,221] as co-ligands. Although nominally a Cu(II) superoxo species, complex (**56**) contains a significant Cu(III) peroxo character by DFT calculations (Section 8.16.4.2).[209]

The first monocopper(II) peroxo compound to be reported was (**61**) (Scheme 7), although owing to its thermal sensitivity only its IR spectrum was reported.[219] The alkylperoxo analogues (**62**) and (**63**) were isolable in pure form, with (**63**) being characterized crystallographically (Figure 13).[220] The Cu center in (**63**) shows a distorted tetrahedral geometry containing a η^1-$Me_2PhCO_2^-$ ligand, with one long Cu—N bond and a very short Cu—O bond of 1.816(4) Å. These structural irregularities are a consequence of the Jahn–Teller distortion of the Cu(II) ion.[206] The O—O distance of 1.460(6) Å is consistent with an O—O single bond. Decomposition of (**62**) in pentane solution yields $tBuOOC_5H_{11}$ as a significant by-product, indicating that this complex decomposes by homolysis of the Cu—O bond, yielding $Bu^tOO\cdot$ radicals. Complex (**62**) anaerobically oxidizes PPh_3 to $OPPh_3$, C_4H_8SO (but not C_4H_8S) to $C_4H_8SO_2$, 2,4,6-*tert*butylphenol to its phenoxyl radical, and cyclohexene to 3,3′-bicyclohexene; under aerobic conditions, cyclohexene is instead oxidized to cyclohex-2-en-1-one. These reactions all probably proceed by radical mechanisms, involving $Bu^tOO\cdot$ and/or $Bu^tO\cdot$.[220] In contrast, the dicopper hydroperoxides (**75**)[116] and (**76**)[222] will oxygenate both PPh_3 and (for (**76**)) C_4H_8S.

More recently, a spectroscopic and theoretical study of (**63**), and the closely related (**64**)–(**66**) (Scheme 7), was undertaken.[206] Two $RO_2^- \rightarrow Cu$ charge transfer transitions were identified at $\lambda_{max} = 505$–556 nm ($\varepsilon_{max} = 590$–855 $mol^{-1}\,dm^3\,cm^{-1}$) and 572–611 (3,815–5,410; Table 1). The very high charge-transfer wavelengths in these compounds are a result of their distorted tetrahedral stereochemistry at copper, which allows very strong donation from an O—O π^*-orbital into the Cu $d_{x^2-y^2}$ orbital. The hydroperoxide complex (**64**) gave unambiguous O—O (ν_{O-O}) and C—O (ν_{C-O}) stretching vibrations at 843 cm^{-1} and 624 cm^{-1}, respectively, by resonance Raman. The vibrational spectra of (**63**), (**65**), and (**66**) were more complex, owing to mixing of

R = C{O}C6H4Cl-3 (**61**)
R = t Bu (**62**)
R = CMe₂Ph (**63**)

R = H (**64**)
R = t Bu (**65**)
R = CMe₂Ph (**66**)

(**67**)

(**68**)

(**69**)

R = R' = H (**70**)
R = H, R' = Me (**71**)
R = R' = Me (**72**)

(**73**)

(**74**)

x = 0(**75**)
x = 1(**76**)
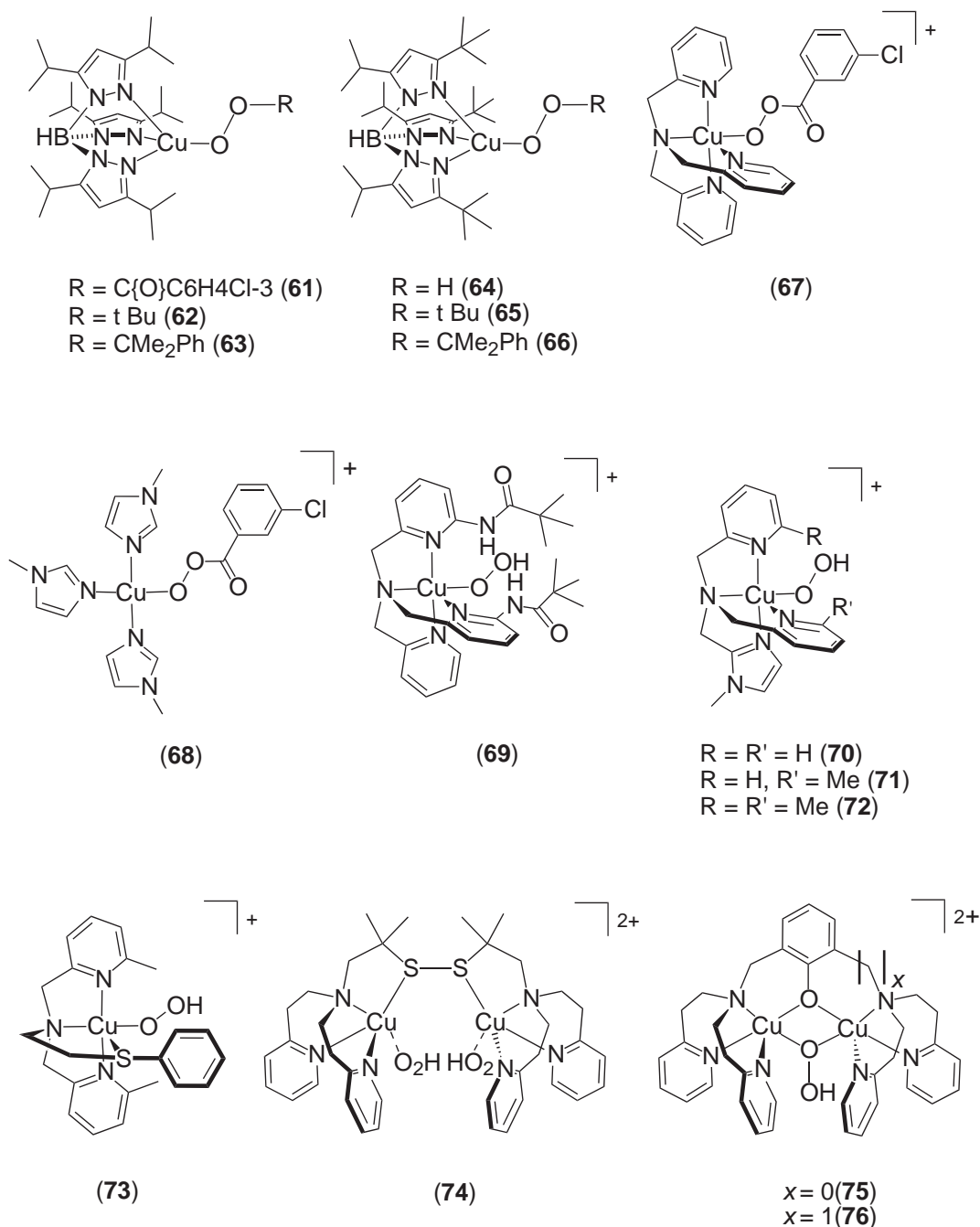
Scheme 7

O—O, C—O and C—C vibrations. DFT calculations confirmed that the RO_2^- ligands are strong
π-donors to the Cu ion, and implied that the peroxido moieties in (**63**)–(**66**) should be activated
towards electrophilic attack. However, reactions of these groups involving H atom abstraction or
O—O homolysis should be highly unfavourable, owing to the instability of the resultant copper
(III) oxo species.[206]

Several copper peroxo complexes containing *tris*(pyrid-2-ylmethyl)amine or related tripodal ligands
have been reported. In contrast to (**63**)–(**66**), these complexes are characterized by a $RO_2^- \rightarrow Cu$
charge transfer band at $\lambda_{max} = 332$–380 nm ($\varepsilon_{max} = 890$–4,300 mol⁻¹ dm³ cm⁻¹; Table 1);[135,205,207,221]
the values of $\nu_{O—O} = 831$–881 cm⁻¹ shown by (**69**)–(**73**) (Scheme 7, Table 1) [135,205,207] are similar
to those of the pyrazolylborate complexes, however. The single-crystal structure of (**69**) shows a
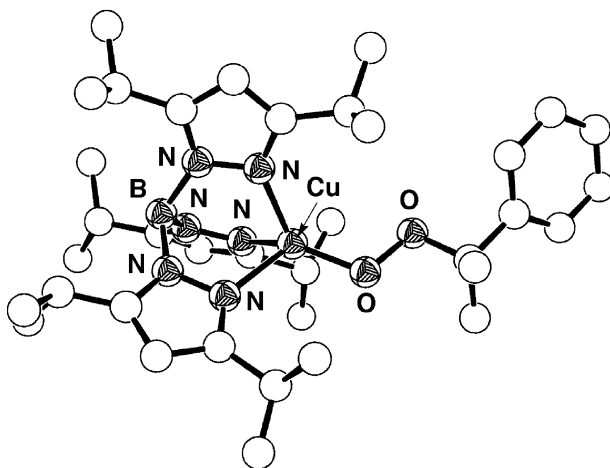
Figure 13 Single-crystal X-ray structure of (**63**),[220] a copper(II) alkylperoxo complex. All hydrogen atoms have been omitted for clarity.

trigonal bipyramidal Cu(II) center with a η^1-HO_2^- ligand that is sterically protected by the two *tert*butylamide substituents (Figure 14).[205] The hydroperoxide ligand shows a O—O bond length of 1.460(6) Å, while the coordinated O atom accepts hydrogen bonds from both of the carboxamide N—H groups. The EPR and *d-d* absorption spectra of (**69**)–(**73**) are all consistent with trigonal bipyramidal Cu(II) centers, suggesting that (**70**)–(**73**) have similar molecular structures to (**69**). The peroxide-specific UV/vis and resonance Raman data from (**67**) and (**69**)–(**73**) are very similar to those from dicopper complexes containing η^1-O_2R^- or η^1:η^1,μ-O_2R^- ligands such as (**74**) and (**75**).[116–118,222–226]

Complex (**73**) is particularly significant, since it is derived from a Cu(II) center bearing an N_2S donor set that closely replicates the $[Cu(his)_2(met)]^{+/2+}$ ligation of the Cu_M site of DβM and PHM.[135] The existence of (**73**) demonstrates that a thioether-ligated copper(II) ion can support a hydroperoxo ligand without undergoing oxidation of the sulfur donor. The arylsulfanyl substituent in (**73**) contributes significantly to its stability, since analogous ligands bearing alkylsulfanyl moieties did undergo oxidation of their thioether groups to sulfoxides and sulfones under the conditions used to prepare (**73**) from a Cu(II) precursor and H_2O_2.[135,136] One other copper(II) hydroperoxo complex with mixed N/S ligation has also been described (**74**), although the authors were unable to unambiguously establish whether it contains one or two O_2H^- ligands.[117,118]
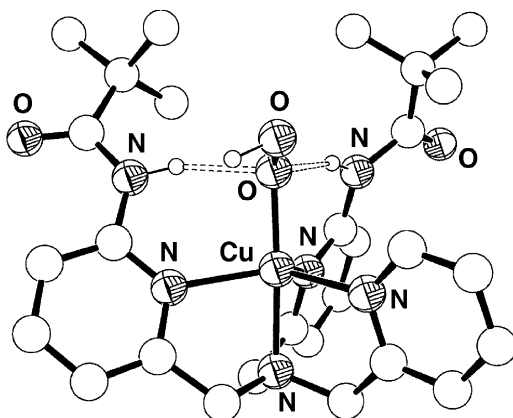
Figure 14 Single-crystal X-ray structure of (**69**),[205] a copper(II) hydroperoxo complex. All carbon-bound hydrogen atoms have been omitted for clarity.

8.16.5 OXYGENATION OF C—H BONDS RELATED TO COPPER MONOOXYGENASE CATALYSIS

8.16.5.1 Hydroxylation of C—H Bonds α- or β- to an Amine Group

There is one report of the copper-catalyzed oxidation of dopamine to norepinephrine (Equation (3)), which is accomplished in very low yields of <1% by copper sulfate, in air in the presence of aspartic acid. The active oxidant in this system was the hydroxyl radical, presumably generated by reductive cleavage of hydrogen peroxide by a copper(I) intermediate.[228] Several other instances of intramolecular hydroxylation of an aliphatic C—H bond α- or β- to an amine substituent have also been reported, and invoked as functional model chemistry for DβM or PHM.[120–123,222,229] However, all of these latter transformations involve dicopper peroxo or dicopper (*bis*)oxo oxidizing intermediates, which means that they cannot be directly related to the monocopper chemistry that must take place in the monocopper oxygenases.[229–231] There are, as yet, no examples of copper-effected hydroxylation reactions that have been shown unambiguously to proceed by a monocopper peroxo intermediate. Hence, there is a strong need for biomimetic data relevant to hydroxylation by a monocopper active site.

8.16.5.2 Peptide Amidation by Metal Complexes

Only a small number of examples of glycine-specific peptide hydroxylation by copper centers have been reported. The first example to accurately mimic the PHM reaction is shown in Equation (13):

$$(13)$$
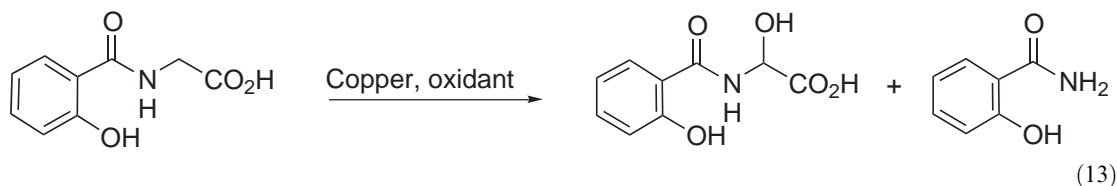
Three copper/oxidant combinations were used to carry out the reaction, including copper metal and O_2, and the copper complex of the precursor + trimethylamine oxide. The transformation was proposed to proceed by a radical rebound mechanism involving a monocopper oxo intermediate.[232] Similar results have been obtained by the oxidation of proteins, alkanes, or DNA by copper(II) complexes of *N*-alkylated-*bis*({pyrid-2-yl}methyl)amines, in the presence of H_2O_2. Efficient oxidation was only observed where the pendant group in these complexes contained a carboxamide function, such as (**77**)–(**79**) (Scheme 8). Other complexes containing carboxylic acid or ester pendants were inactive.[233–236] This was explained by the proposition that the active oxidant in these reactions was a copper(II) hydroperoxo complex, stabilized by hydrogen bonding of the peroxo ligand to the amide pendant (e.g., (**82**)). Interestingly, (**80**) and (**81**) are converted to (**78**) upon reaction with H_2O_2, which was taken as evidence for the formation of a monocopper hydroperoxide intermediate (**82**).[237] However, such a species has not been detected in this system.

A different version of the complete PAM reaction has been replicated in a series of 15 copper(II) complexes containing dipeptide moieties linked to a chelating ligand framework; (**83**) and (**84**) are two examples that were studied (Scheme 9).[238] Reaction of the complexes with persulfate or hexachloroiridate causes oxidative decarboxylation of the terminal carboxy group, forming a terminal imine function which is subsequently hydrolyzed to liberate formaldehyde. This generation of $CO_2 + HCHO$ is stoichiometrically equivalent overall to cleavage of glyoxalic acid (HC{O}CO₂H) from a *C*-terminal glycyl peptide (Equation (4)). However, the reactions progress by the initial oxidation of the copper centers to copper(III), which then intramolecularly induces decarboxylation without the need for ligand hydroxylation.[238] Therefore, this system is not mechanistically related to the chemistry of PHM as it is now understood. A similar, redox-induced degradation of an internal amide bond has been detected in copper complexes of tetraglycine[239] and a series of histidine-containing tripeptides.[240–242]

There are more examples of glycyl peptide hydroxylation effected by nickel(II)[243–248] and cobalt(III).[249] Many of these reactions require O_2[243–245,248,249] or a peroxide precursor,[246,247] and

x = 1, R = H (**77**)
x = 2, R = H (**78**)
x = 2, R = CH$_2$CO$_2$H (**79**)
x = 2, R = Me (**80**)
x = 2, R = Et (**81**)

Scheme 8

(**83**)   (**84**)
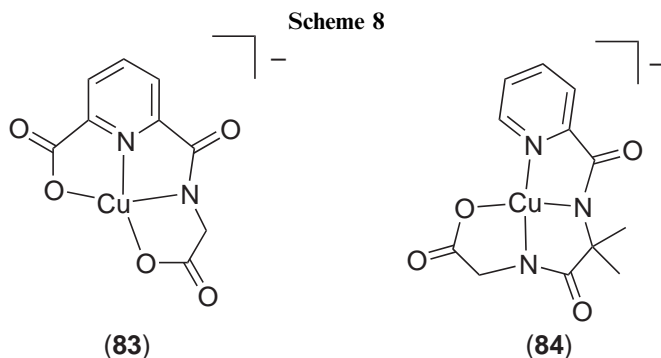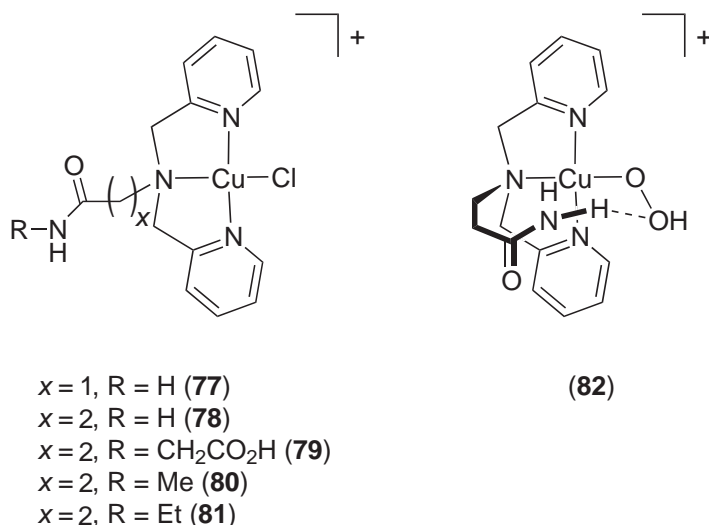
Scheme 9

are initiated by an oxidatively induced decarboxylation step. There are two recent reports where this is not the case, however, where a C—H monooxygenation mechanism related to PHM catalysis is likely;[248,249] in one of these, a radical rebound mechanism involving an (undetected) mononickel peroxo intermediate was proposed.[248]

8.16.6   A COPPER DIOXYGENASE ENZYME

8.16.6.1   Quercetinase

Several strains of the fungus *Aspergillus* can grow on flavonols like quercetin or rutin (a 3-*O*-glycosylated derivative of quercetin). It was demonstrated in the 1960s that whole-cell cultures of *Aspergillus flavus* convert quercetin into an insoluble depside according to Equation (14).[250–254]

Using radiolabeled substrates, it was demonstrated that *C*3 of quercetin was eliminated as CO,[252] and that both O atoms of O$_2$ are incorporated into the product at the *C*2 and *C*4 positions.[255] The quercetin-2,4-dioxygenase enzyme ("quercetinase," EC 1.13.11.) was isolated from this organism soon afterwards,[256,257] and was shown to require two mole equivalents of copper for activity.[258,259] Unfortunately, no further research on quercetinase was published between 1972 and 1999, when the enzyme was isolated from a second fungal strain *A. niger*, and the first spectroscopic character-ization of the protein undertaken.[260] Finally, the crystal structure of a third quercetinase, from *A. japonicus*, has very recently been published.[261] Hence, it has taken over forty years for an understanding of this unique copper-dependent dioxygenase to begin to develop. Quercetinase is often erroneously referred to as "quercetin-2,3-dioxygenase" in the literature.

$$(14)$$
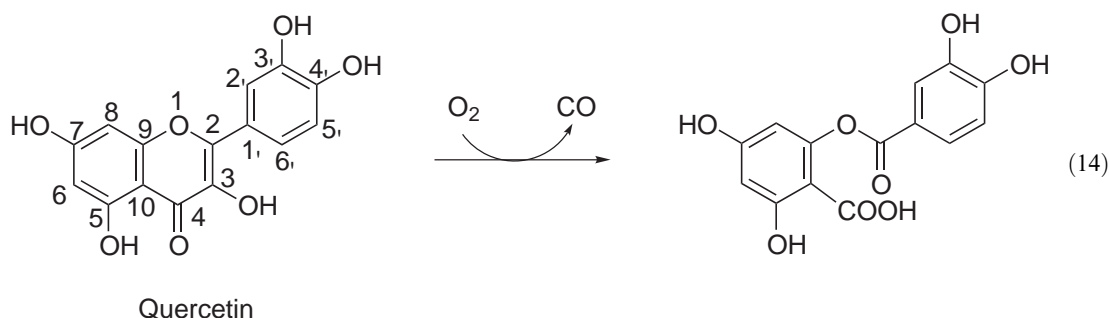
Quercetin

Interestingly, the three known quercetinases show some differences in their properties that have been reported to date. The *A. japonicus* quercetinase is an α_2 homodimer of total M_r 100 kDa and ca. 25% *N*-glycosylation by weight, which contains one Cu ion per subunit.[261] The *A. flavus* protein has a similar molecular weight and carbohydrate content,[256] and also contains 2 mol equivalents of copper.[258,259] However, the *A. niger* enzyme is a $\alpha\beta\gamma$ heterotrimer, of total M_r 148 kDa and a much higher degree of *N*-glycosylation at ca. 50%.[260] This protein contains 1.0–1.6 copper ions per trimeric molecule.[260] The EPR spectra of the as-isolated quercetinases also show some differences between the proteins. *A. japonicus* quercetinase shows two distinct signals in the low-field region, with $g_\parallel$ 2.330, $A_\parallel\{^{63,65}Cu\}$ 137 G and $g_\parallel$ 2.290, $A_\parallel\{^{63,65}Cu\}$ 125 G,[261] consistent with the heterogeneous active site structure present in the crystal structure of this protein (see below). However, the *A. niger* enzyme shows a single rhombic EPR peak with g_1 2.293, g_2 2.055, g_3 2.01, $A_1\{^{63,65}Cu\}$ 155 G, and $A_{2,3}\{^{14}N\}$ 13 G.[260] This latter coupling appears to be comprised of nine superhyperfine lines, which would indicate that the Cu center is ligated by four histidine donors. This is inconsistent with the crystal structure described below, however, and it is presently unclear how the *A. niger* quercetinase is related to the *A. flavus* and *A. japonicus* enzymes.

The single-crystal structure of *A. japonicus* quercetinase[261] shows the two protein monomers to be approximately C_2-symmetric, with two structurally similar domains sharing ca. 20% sequence identity and very similar tertiary structures that are mostly composed of antiparallel β-sheets. Unusually, the two monomers are covalently linked by a 7-unit heptasaccharide chain, as well as by a large number of hydrogen bonds covering a dimerisation interface of ca. 2000 Å^2. The active site lies within a hydrophobic cavity in one of these domains, ca. 10 Å from the protein surface but with access to the outside environment. The copper ion within the active site is ligated by three histidine residues and a water ligand, together with one partially occupied orientation of a disordered glutamate side-chain. Hence, the active site appears to exist as a mixture of approximately tetrahedral $[Cu(his)_3(OH_2)]^{2+}$ and trigonal bipyramidal $[Cu(his)_3(glu)(OH_2)]^+$ centers, in agreement with the heterogeneous EPR signal shown by this protein in solution (see above).[261] This represents the first example of carboxylate ligation to copper in a native copper protein. Using molecular modeling, a binding site for quercetin within the active site was proposed which involved its chelation to copper via *O*3 and *O*4, in agreement with earlier suggestions[262,263] and chemical precedent (see Section 8.16.6.2). The partially ligated glutamate ligand was dissociated from the copper ion in the model, and hydrogen-bonded to *O*3. This led to the suggestion that the deprotonation of *O*3 by this base might be an essential first step towards activating quercetin towards electrophilic attack by O$_2$.

There are no mechanistic data available for quercetinase beyond the labeling experiments mentioned above. However, from the data discussed in the following paragraphs it seems clear that the copper ion in quercetinase may not be involved in the binding or activation of O$_2$. Rather, it could activate the bound flavonol substrate in one of two ways. Chelation of the flavonol to the Lewis acidic Cu(II) ion may would decrease its pK_a, making it more susceptible to deprotonation and thus to electrophilic attack. Alternatively, intramolecular flavonolate $\rightarrow$ copper electron transfer may activate the substrate to attack by exogenous O$_2$ through a radical mechanism.

8.16.6.2 Functional Models for the Quercetinase Reaction

Many flavonols, including quercetin, will undergo the quercetinase reaction without a metal catalyst, under basic aerobic conditions in aqueous or aprotic solvents.[264–268] As in the enzymatic

reaction, under these conditions both O atoms from a single O_2 molecule are incorporated into the product, at $C2$ and $C4$.[267,268] The reaction is first order in flavonolate anion and O_2 and affords a linear free-energy relation using $4'$-substituted flavonols (fla^{h}H), with electron-donating "R" substituents giving faster reaction rates (Table 2).[266] EPR and spin-trapping experiments found no evidence of radical intermediates,[266] which was taken to support a mechanism involving base-promoted electrophilic attack at $C2$ by O_2 as the rate-determining step (Figure 15A).[269] The reaction exhibits a negative entropy of activation, consistent with such an associative rate-determining step (Table 2).[266]

fla^{R}H
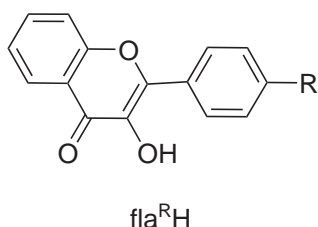
An attempt to induce a metal-free, radical-based oxygenation of quercetin with superoxide instead also resulted in an electrophilic oxygenation pathway via the initial protonation and disproportionation of superoxide.[270] However, aerobic flavonol oxidation can be induced by the free-radical initiators 2,2,6,6-tetramethylpiperidin-N-oxyl (TEMPO) or galvinoxyl.[271] The endoperoxide intermediate in Figure 15A is also believed to be formed under these conditions via the initial addition of O_2 to C2 of a transiently produced flavonoxyl radical. In contrast, reaction of 3-hydroxyflavones with photogenerated $^1O_2$ affords both depside and α-ketoacid products.[269,272] The latter can only be formed from an alternative mechanistic pathway, involving addition of O_2 to $C2$ and $C3$ of the substrate to afford a 1,2-dioxobutane intermediate (Figure 15B). Such a mechanism is not consistent with the labeling studies from the enzyme reaction, however, which demonstrated incorporation of O atoms from O_2 at $C2$ and $C4$, and loss of $C3$ as CO.[252,255]

Flavonolato complexes of Cu(II),[273–280] Cu(I),[281,282] Zn(II),[283–285] Ni(II)[286], and Co(III)[287] ((**85**)–(**97**)) (Scheme 10) have been structurally characterized, all of which show chelating fla^{R-} ligands binding through $O3$ and $O4$, as proposed for the quercetinase substrate complex (Figure 16). Many of these, and some other copper flavonolate complexes,[288] undergo the quercetinase transformation stoichiometrically upon heating in dmf solution. The products formed *in vitro* are copper complexes of the resultant benzoate derivatives obtained from *in situ* hydrolysis of the initially formed phenyl benzoate ester (Equation (15)).

^{18}O labeling studies of the oxygenation of the Cu(I) complex (**89**) gave identical results to those described earlier for quercetinase and metal-free flavonol oxygenolysis, confirming this reaction as a 2,4-dioxygenation.[282] All these stoichiometric transformations are second order, and show rather similar activation parameters to those derived for the basic oxygenation of free flavonol (Table 2). The rates of oxygenation of free and complexed flavonol are also very similar, all being within one order of magnitude of each other (Table 2). Hence, in the light of the mechanism of the oxygenation of [Co(salen)(fla^R)] in hot dmf (see below), it is uncertain whether these reactions involve oxygenation of copper-bound, or decoordinated, flavonolate anion.

Compounds (**89**)–(**92**) also carry out the oxygenation of flavonols catalytically. In contrast to the stoichiometric reactions, the orders of reaction and activation parameters for the catalytic transformations vary widely between systems (Table 2). Catalysis by [Cu^I(PPh$_3$)$_2$(fla^H)] (**89**),[289] [Cu^{II}(fla^H)$_2$] (**90**),[289] and [Cu^{II}(tmeda) (fla^H)$_2$][274] (tmeda = 1,2-*bis*(dimethylamino)ethane) is first order in substrate, catalyst, and O_2. Complexes (**89**) and (**90**) probably catalyze the reaction by the same mechanism, since (**89**) reacts with excess fla^{R}H in a catalytic mixture to form (**90**).[289] However, flavonol oxygenation catalyzed by (**92**) is zero- order in substrate, and shows rates and activation parameters very similar to those for stoichiometric flavonol oxygenation by the same complex (Table 2).[290] Finally, catalysis by [Cu(bipy)(fla^H)]$^+$ (bipy = 2,2$'$-bipyridine) (**85**) shows fifth-order kinetics, which was rationalized according to the mechanism in Figure 17.[274] In support of this scheme, it was shown that solutions of "[Cu^I(bipy)(fla^H)]" in fact contain a mixture of species, including [Cu^I(bipy)$_2$]$^+$ and the unusual, octahedral [Cu^I(fla^H)$_3$]$^{2-}$.[275] A separate study of a series of copper(II) flavonol complexes containing 2,2$'$-bipyridine or *tris*(pyrid-2-ylmethyl)amine derivatives as coligands showed that there was no simple correlation between the rate of stoichiometric oxygenation, and the Cu- or flavonol-based redox potentials, in these compounds.[276]

Table 2 Kinetic data for the oxygenation of flavonols and their complexes. Unless otherwise stated, all reactions were carried out in dimethylformamide (dmf) solution. All rate constants and activation parameters refer to oxygenation of the 4'-unsubstituted flavonol, $fla^R H$.

	Stoichiometric or catalytic	Order of reaction	$k\ (T, K)$	$\Delta H^{\ddagger}$ (kJ mol^{-1})	$\Delta S^{\ddagger}$ (J mol^{-1} K^{-1})	ρ	References
$fla^R H$, 1:1 dmso:H_2O	S	$[fla^{R-}][O_2]$	$4.5(1) \times 10^{-2}$ mol^{-1} dm^3 s^{-1} (353)	+59(4)	−110(11)	−0.50	266
$[Cu(fla^R)(bipy)]^+$ (**85**)	S^a						274
$[Cu(fla^R)(bipy)]^+$ (**85**)	C	$[fla^R H][complex]^2[O_2]^2$	$7.2(1) \times 10^{10}$ mol^{-4} dm^{12} s^{-1} (373)	+81(3)	+179(9)		274
$[Cu(fla^R)(PPh_3)_2]$ (**89**)	S	$[complex][O_2]$	$4.2(5) \times 10^{-3}$ mol^{-1} dm^3 s^{-1} (363)	+102(7)	−13(21)	−1.32	282
$[Cu(fla^R)(PPh_3)_2]$ (**89**)	C	$[fla^R H][complex][O_2]$	$8.0(9) \times 10^1$ mol^{-2} dm^6 s^{-1} (408)	+175(6)	+211(15)	−	289
$[Cu(fla^R)_2]$ (**90**)	S	$[complex][O_2]$	$8.7(15) \times 10^{-2}$ mol^{-1} dm^3 s^{-1} (373)	+53(6)	−138(11)	−0.63	278
$[Cu(fla^R)_2]$ (**90**)	C	$[fla^R H][complex][O_2]$	$2.0(1) \times 10^3$ mol^{-2} dm^6 s^{-1} (393)	+139(5)	+168(13)		289
$[Cu(fla^R)_2(tmeda)]$	C	$[fla^R H][complex][O_2]$					c
$[Cu(fla^R)(bpin)]$ (**91**)	C	$[fla^R H]^b$	6.6×10^{-5} s^{-1} (393)^b				280
$[Cu(fla^R)(Me_4dpta)]^+$ (**92**)	S	$[complex][O_2]$	$6.1(2) \times 10^{-3}$ mol^{-1} dm^3 s^{-1} (373)	+64(5)	−120(13)	−0.29	290
$[Cu(fla^R)(Me_4dpta)]^+$ (**92**)	C	$[complex][O_2]$	$4.2(2) \times 10^{-2}$ mol^{-1} dm^3 s^{-1} (403)	+71(6)	−97(15)		290
$[Zn(fla^R)(Me_4dpta)]^+$ (**93**)	S	$[complex][O_2]$	3.1×10^{-3} mol^{-1} dm^3 s^{-1} (373)	+75(5)	−96(13)	−0.83	301

* Abbreviations used: bipy = 2,2'-bipyridine; bpinH = 1,3-*bis*(pyrid-2-ylimino)isoindole; dmso = dimethylsulfoxide; Me₄dpta = *bis*(3-{dimethylamino}propyl)amine; tmeda = 1,2-*bis*(dimethylamino) ethane. ^{a} The kinetics of this reaction were complex, and could not be fitted to a simple rate law. ^{b} The order of this reaction in [complex] and [O₂] was not determined. ^{c} Unpublished data cited in ref. 274.
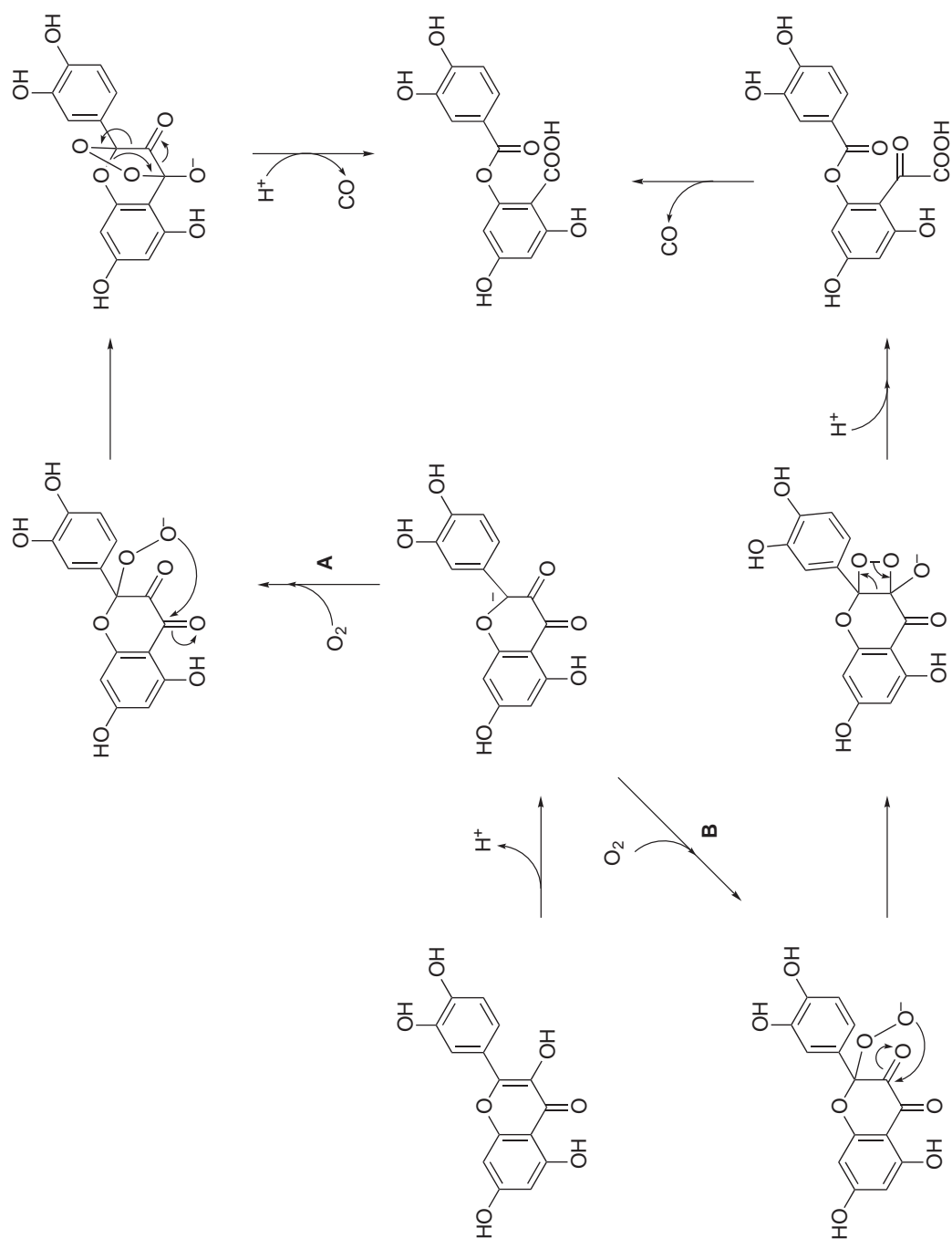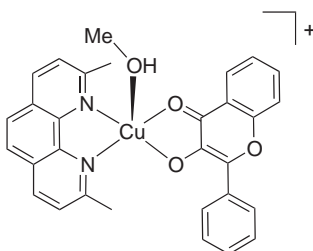
Figure 15 Two potential mechanisms for the quercetinase reaction (Equation (14)), involving 2,4-addition (**A**) and 2,3-addition (**B**) of dioxygen to the deprotonated substrate.[269]
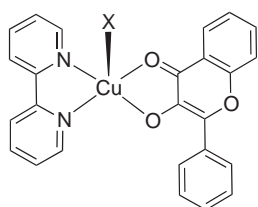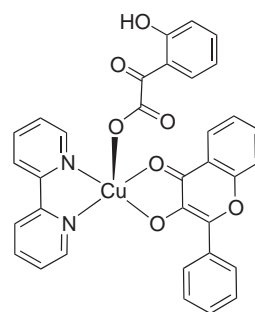
X⁻ = ClO₄⁻ (**85**)
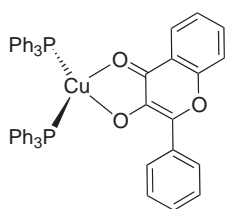X⁻ = NO₃⁻ (**86**)

(**87**)

(**88**)

(**89**)
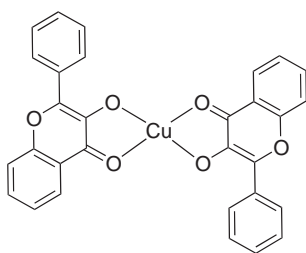
(**90**)
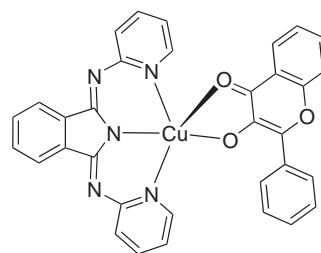
(**91**)
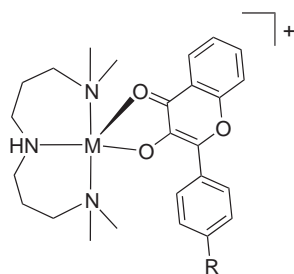
M = Cu, R = H (**92**)
M = Zn, R = H (**93**)
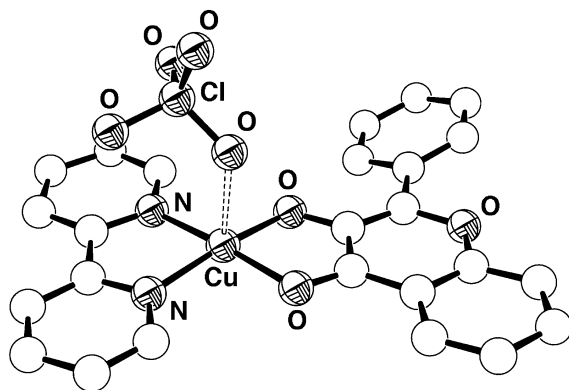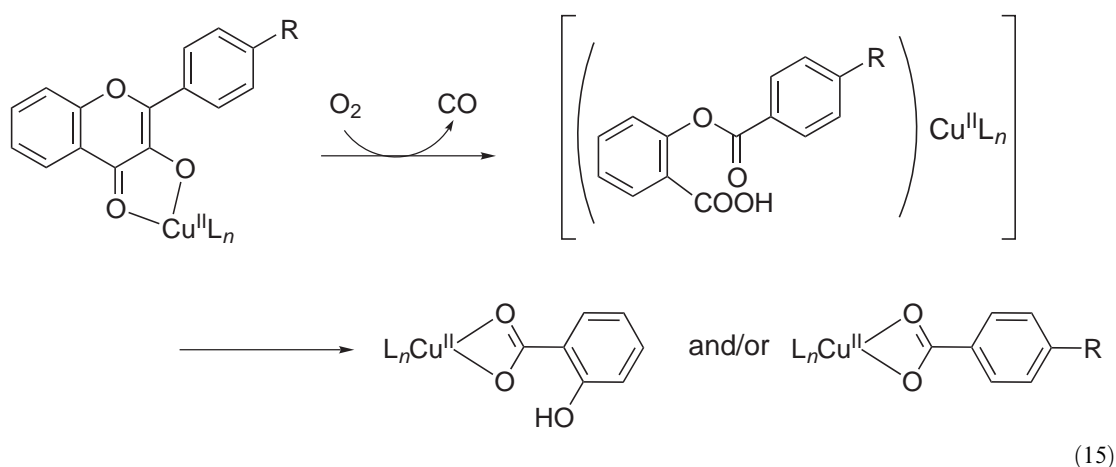M = Zn, R = OMe (**94**)
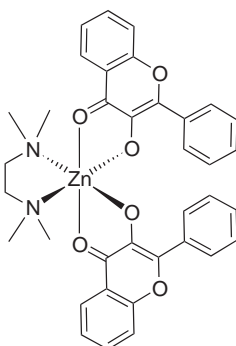
(**95**)
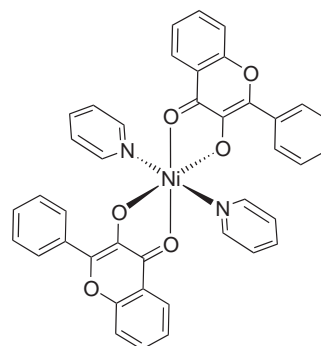
(**96**)
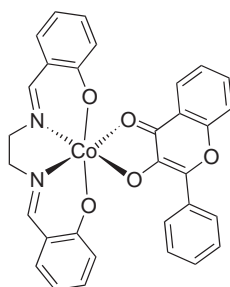
(**97**)

Scheme 10

Figure 16 Single-crystal X-ray structure of (**85**),[273] showing the *O*3, *O*4-coordinated flavonolate ligand. All H atoms have been omitted for clarity.


$$(15)$$

Interestingly, (**88**) was isolated following exposure of a solution of [Cu^I(bipy)(fla)] to air at 293 K, which implies the intermediacy of a 1,2-dioxobutane in this reaction (Figure 15B), rather than the more usual 2,4-endoperoxide species (Figure 15A).[275] No other mechanistic data from this reaction have been reported, however, and this suggestion was not incorporated into the mechanistic scheme for flavonol oxygenation catalysis by (**85**) (Figure 17).[274]

In contrast, reaction of quercetin or other flavonols with CuCl$_2$ in aerobic neutral or acid solution follows a different pathway.[291–293] In only one study was a depside isolated from this reaction, and only then as a minor product.[292] Rather, the reaction appears to result in simple two-electron oxidation of the flavonol, which then undergoes addition of solvent (Figure 18).[294] Similar or identical products are formed following oxidation of quercetin by periodate,[295] 2,2-di(4-*tert*octylphenyl)-1-picrylhydrazyl (DPPH),[296] or O$_2$ in the absence of base, or by its bulk electrochemical oxidation.[294,297]

In addition to copper, flavonol oxygenation has also been effected using cobalt(II)[287,298–300] or zinc(II)[301] centers. [Co^{II}(salen)] catalyzes the oxygenation of flavonols in dmf at 80 °C.[298] This reaction proceeds via a [Co^{III}(salen)(fla^R)] intermediate (**97**),[287,299] which then undergoes partial dissociation to [Co^{III}(salen)(dmf)$_2$]$^+$ and fla^{R-}.[300] Oxygenation of the resultant non-coordinated fla^{R-} anion proceeds by a non-radical mechanism[299,300] and is promoted by the cobalt(III) cation, which may assist in an intersystem crossing following initial attack of ^{3}O$_2$ at the substrate.[300] Complex (**93**) undergoes stoichiometric (but not catalytic) oxygenation of its flavonol ligand upon heating in dmf.[301] This reaction is first order in (**93**) and in O$_2$ only, and gives activation parameters that are very similar to those for (**92**) and the copper complexes in Table 2. In contrast to the [Co(salen)] system, O$_2^-$ was detected during oxidation of (**93**). Hence, it was proposed that the oxygenation followed a radical pathway, despite the
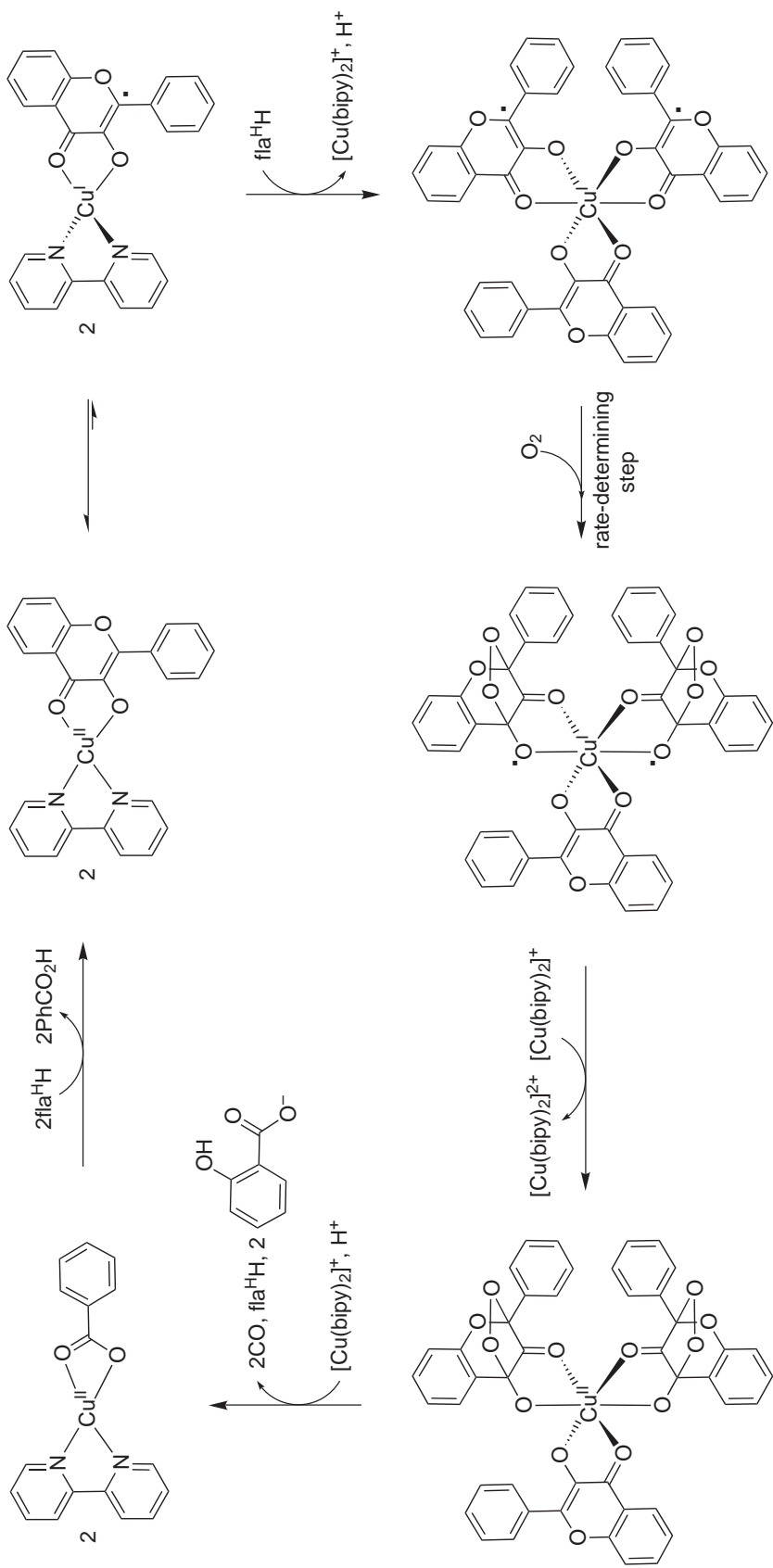
Figure 17 Proposed catalytic cycle for flavonol oxidation by [Cu(bipy)(fla^H)]^+ **(85)**.[274]
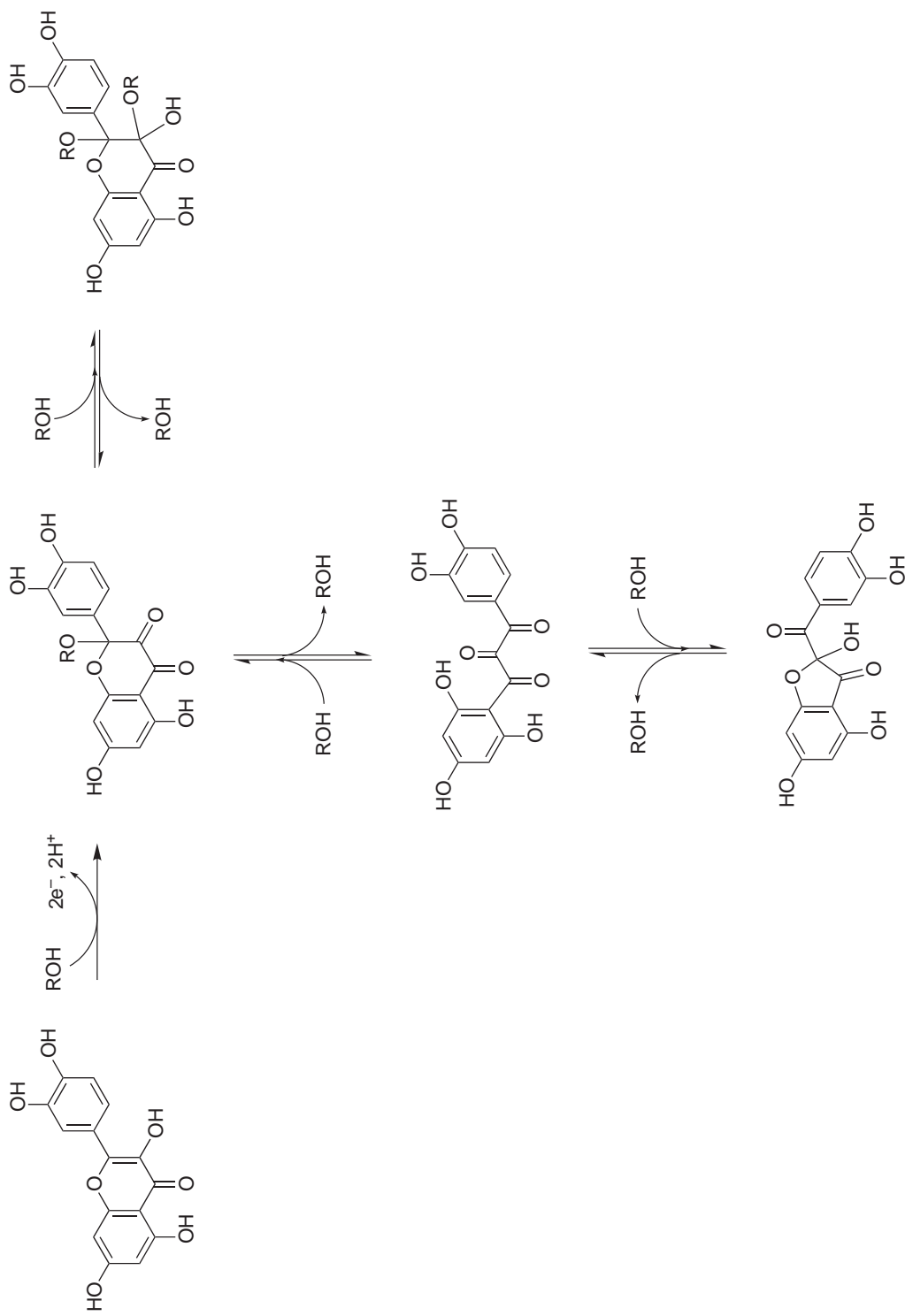
Figure 18 Mechanism of oxidation of flavonols in aqueous acid. [294]

redox-inertness of the Zn(II) ion.[301] NMR studies of (**95**) suggested that the flavonolate ligand remains coordinated in dmso solution.[285]

A mutant PHM enzyme has been reported, in which the only tyrosine residue close to the Cu_M site has been mutated to phenylalanine.[302] This mutant protein shows almost identical kinetic parameters for peptide hydroxylation as native PHM, which makes it unlikely that a tyrosine side-chain acts as electrondonor to O_2 during PHM (or DβM) catalysis, as previously proposed.[59] Mutation of one of the histidine ligands of the Cu_H centre of PHM to alanine affords a two-coordinate Cu_H site, whose CO-binding properties in the presence or absence of substrate are identical to those of the wild-type protein.[303] Recent mechanistic studies of the hydroxylation of aminoindane by DβM have been reviewed.[304] EXAFS[305] and EPR[306] studies of substrate-bound *A. japonicus* quercetinase, and crystal structures of the same protein with two different bound inhibitors,[307] have confirmed that quercetin complexes to the enzyme's active site, and showed that the Cu^{II} ion is not reduced upon substrate binding. Contrary to earlier predictions,[261] however, crystal structures of this quercetinase with two different bound substrates (including quercetin itself) showed *monodentate* flavonol coordination to copper, through the donor $O3$.[308] These structures imply that attack by O_2 at $C2$ of the flavonol ring is the first step of quercetinase catalysis.

A thorough spectroscopic and theoretical analysis of complex (**55**) (Figure 12) has appeared.[309] This showed that the previously reported UV/vis spectrum for this compound[202] (Table 1) is erroneous; the spectrum of (**55**) in the near-UV in fact shows weak absorptions at $\lambda_{max} = 383$ nm and 452 nm with $\varepsilon_{max} < 400$ dm^3 mol^{-1} cm^{-1}. The antiferromagnetic coupling between the Cu^{II} and O_2^- spins was measured at $2J \approx -1{,}500$ cm^{-1}.[309] A new example of a short-lived mono-Cu^{II} superoxo complex has been detected spectrophotometrically.[310] A new intermediate has been observed in the treatment of some Cu^{II} *bis*(2-{pyrid-2-yl}ethyl)amine complexes with H_2O_2 in the presence of Et$_3$N, which has been tentatively assigned to a η^2-O_2^{2-} complex of Cu^{II}.[310] A new example of a short-lived mono-Cu^{II} superoxo complex has been detected spectrophoto-metrically.[311]

8.16.7 REFERENCES

1. Sono, M.; Roach, M. P.; Coulter, E. D.; Dawson, J. H. *Chem. Rev.* **1996**, *96*, 2841–2887.
2. Halcrow, M. A.; Knowles, P. F.; Phillips, S. E. V. Copper Proteins in the Transport and Activation of Dioxygen, and the Reduction of Inorganic Molecules. In *Handbook on Metalloproteins*; Bertini, I., Sigel, A., Sigel, H., Eds.; Marcell Dekker: New York, 2001, Ch. 15, pp 709–762.
3. Solomon, E. I.; Sundaram, U. M.; Machonkin, T. E. *Chem. Rev.* **1996**, *96*, 2563–2605.
4. Klinman, J. P. *Chem. Rev.* **1996**, *96*, 2541–2561.
5. Crabtree, R. H. *J. Chem. Soc., Dalton Trans.* **2001**, 2437–2450.
6. Stewart, L. C.; Klinman, J. P. *Annu. Rev. Biochem.* **1988**, *57*, 551–592.
7. Stewart, L. C.; Klinman, J. P. *Biochemistry* **1987**, *26*, 5302–5309.
8. Wallace, E. F.; Krantz, M. J.; Lovenberg, W. *Proc. Natl. Acad. Sci. USA* **1973**, *70*, 2253–2255.
9. Saxena, A.; Hensley, P.; Osborne, J. C., Jr.; Fleming, P. J. *J. Biol. Chem.* **1985**, *260*, 3386–3392.
10. Stewart, L.; Klinman, J. P. *FEBS Lett.* **1999**, *454*, 229–232.
11. Klinman, J. P.; Krueger, M.; Brenner, M.; Edmondson, D. E. *J. Biol. Chem.* **1984**, *259*, 3399–3402.
12. Prigge, S. T.; Mains, R. E.; Eipper, B. A.; Amzel, L. M. *Cell. Mol. Life Sci.* **2000**, *57*, 1236–1259.
13. Bell, J.; Ash, D. E.; Snyder, L. M.; Kulathila, R.; Blackburn, N. J.; Merkler, D. J. *Biochemistry* **1997**, *36*, 16239–16246.
14. Stoffers, D. A.; Green, C. B.-R.; Eipper, B. A. *Proc. Natl. Acad. Sci. USA* **1989**, *86*, 735–739.
15. Eipper, B. A.; Quon, A. S. W.; Mains, R. E.; Boswell, J. S.; Blackburn, N. J. *Biochemistry* **1995**, *34*, 2857–2865.
16. Boswell, J. S.; Reedy, B. J.; Kulathila, R.; Merkler, D.; Blackburn, N. J. *Biochemistry* **1996**, *35*, 12241–12250.
17. Kulathila, R.; Consalvo, A. P.; Fitzpatrick, P. F.; Freeman, J. C.; Snyder, L. M.; Villafranca, J. J.; Merkler, D. *Arch. Biochem. Biophys.* **1993**, *311*, 191–195.
18. Southan, C.; Kruse, L. I. *FEBS Lett.* **1989**, *255*, 116–120.
19. Prigge, S. T.; Kolkehar, A. S.; Eipper, B. A.; Mains, R. E.; Amzel, L. M. *Science* **1997**, *278*, 1300–1305.
20. Prigge, S. T.; Kolkehar, A. S.; Eipper, B. A.; Mains, R. E.; Amzel, L. M. *Nature Struct. Biol.* **1999**, *6*, 976–983.
21. Hasnain, S. S.; Diakun, G. P.; Knowles, P. F.; Binsted, N.; Garner, C. D.; Blackburn, N. J. *Biochem. J.* **1984**, *221*, 545–548.
22. Scott, R. A.; Sullivan, R. J.; DeWolf, R.E., Jr.; Dolle, R. A.; Kruse, L. I. *Biochemistry* **1988**, *27*, 5411–5417.
23. Blumberg, W. E.; Desai, P. R.; Powers, L.; Freedman, J. H.; Villafranca, J. J. *J. Biol. Chem.* **1989**, *264*, 6029–6032.
24. Blackburn, N. J.; Hasnain, S. S.; Petingill, T. M.; Strange, R. W. *J. Biol. Chem.* **1991**, *266*, 23120–23127.
25. Blackburn, N. J.; Rhames, F. C.; Ralle, M.; Jaron, S. *J. Biol. Inorg. Chem.* **2000**, *5*, 341–353.
26. Reedy, B. J.; Blackburn, N. J. *J. Am. Chem. Soc.* **1994**, *116*, 1924–1931.
27. Jaron, S.; Blackburn, N. J. *Biochemistry* **2001**, *40*, 6867–6875.
28. Blackburn, N. J.; Concannon, M.; Shabiyan, S. K.; Mabbs, F. E.; Collison, D. *Biochemistry* **1988**, *27*, 6001–6008.
29. Walker, G. A.; Kon, H.; Lovenberg, W. *Biochim. Biophys. Acta* **1977**, *482*, 309–322.
30. Ljones, T.; Flatmark, T.; Skotland, T.; Petersson, L.; Backstrom, D.; Ehrenberg, A. *FEBS Lett.* **1978**, *92*, 81–84.
31. Skotland, T.; Petersson, L.; Backstrom, D.; Ljones, T.; Flatmark, T.; Ehrenberg, A. *Eur. J. Biochem.* **1980**, *103*, 5–11.

32. Klinman, J. P.; Kreuger, M.; Brenner, M.; Edmondson, D. E. *J. Biol. Chem.* **1984**, *259*, 3399–3402.
33. Obata, A.; Tanaka, H.; Kawazura, H. *Biochemistry* **1987**, *26*, 4962–4968.
34. McCracken, J.; Desai, P. R.; Papadopoulos, N. J.; Villafranca, J. J.; Peisach, J. *Biochemistry* **1988**, *27*, 4133–4137.
35. Freeman, J. C.; Villafranca, J. P.; Merkler, D. J. *J. Am. Chem. Soc.* **1993**, *115*, 4923–4924.
36. Blackburn, N. J.; Collison, D.; Sutton, J.; Mabbs, F. E. *Biochem. J.* **1984**, *220*, 447–454.
37. Blackburn, N. J.; Pettingill, T. M.; Seagraves, K. S.; Shigeta, R. T. *J. Biol. Chem.* **1990**, *265*, 15383–15386.
38. Pettingill, T. M.; Strange, R. W.; Blackburn, N. J. *J. Biol. Chem.* **1991**, *266*, 16996–17003.
39. Jaron, S.; Blackburn, N. J. *Biochemistry* **1999**, *38*, 15086–15096.
40. Reedy, B. J.; Murthy, N. N.; Karlin, K. D.; Blackburn, N. J. *J. Am. Chem. Soc.* **1994**, *116*, 9826–9831.
41. Rhames, F. C.; Murthy, N. N.; Karlin, K. D.; Blackburn, N. J. *J. Biol. Inorg. Chem.* **2001**, *6*, 567–577.
42. Brenner, M. C.; Klinman, J. P. *Biochemistry* **1989**, *28*, 4664–4670.
43. Takahashi, K.; Onami, T.; Noguchi, M. *Biochem. J.* **1998**, *336*, 131–137.
44. Francisco, W. A.; Merkler, D. J.; Blackburn, N. J.; Klinman, J. P. *Biochemistry* **1998**, *37*, 8244–8252.
45. Ahn, N.; Klinman, J. P. *Biochemistry* **1983**, *22*, 3096–3106.
46. Miller, S. M.; Klinman, J. P. *Biochemistry* **1983**, *22*, 3091–3096.
47. Miller, S. M.; Klinman, J. P. *Biochemistry* **1985**, *24*, 2114–2127.
48. Francisco, W. A.; Knapp, M. J.; Blackburn, N. J.; Klinman, J. P. *J. Am. Chem. Soc.* **2002**, *124*, 8194–8195.
49. Fitzpatrick, P. F.; Villafranca, J. J. *J. Biol. Chem.* **1986**, *261*, 4510–4518.
50. Bossard, M. J.; Klinman, J. P. *J. Biol. Chem.* **1986**, *261*, 16421–16427.
51. Goodhart, P. J.; Kruse, L. I. *Biochemistry* **1987**, *26*, 2576–2583.
52. Wimalasena, K.; May, S. W. *J. Am. Chem. Soc.* **1989**, *111*, 2729–2731.
53. Farrington, G. K.; Kumar, A.; Villafranca, J. J. *J. Biol. Chem.* **1990**, *265*, 1036–1040.
54. Kim, S. C.; Klinman, J. P. *Biochemistry* **1991**, *30*, 8138–8144.
55. Zabriskie, T. M.; Cheng, H.; Vederas, J. C. *J. Am. Chem. Soc.* **1992**, *114*, 2270–2272.
56. Sirimane, S. R.; May, S. W. *Biochem. J.* **1995**, *306*, 77–85.
57. Casara, P.; Ganzhorn, A.; Phillipo, C.; Chanal, M.-C.; Danzin, C. *Bioorg. Med. Chem.* **1996**, *6*, 393–396.
58. Driscoll, W. J.; König, S.; Fales, H. M.; Pannell, L. K.; Eipper, B. A.; Mueller, G. P. *Biochemistry* **2000**, *39*, 8007–8016.
59. Tian, G.; Berry, J. A.; Klinman, J. P. *Biochemistry* **1994**, *33*, 226–234.
60. Slama, P.; Jabre, P.; Tron, T.; Réglier, M. *FEBS Lett.* **2001**, *491*, 55–58.
61. Holland, P. L.; Tolman, W. B. *J. Am. Chem. Soc.* **1999**, *121*, 7270–7271.
62. Holland, P. L.; Tolman, W. B. *J. Am. Chem. Soc.* **2000**, *122*, 6331–6332.
63. Jazdzewski, B. A.; Holland, P. L.; Pink, M.; Young, V. G. , Jr.; Spencer, D. J. E.; Tolman, W. B. *Inorg. Chem.* **2001**, *40*, 6097–6107.
64. Randall, D. W.; George, S. D.; Holland, P. L.; Hedman, B.; Hodgson, K. O.; Tolman, W. B.; Solomon, E. I. *J. Am. Chem. Soc.* **2000**, *122*, 11632–11648.
65. Lewin, A. H.; Michl, R. J.; Ganis, P.; Lepore, U. *J. Chem. Soc., Chem. Commun.* **1972**, 661–662.
66. Habiyakare, A.; Lucken, E. A. C.; Bernardinelli, G. *J. Chem. Soc., Dalton Trans.* **1992**, 2591–2599.
67. Munakata, M.; Dai, J.; Maekawa, M.; Takayoshi, K.-S.; Fukui, J. *J. Chem. Soc., Chem. Commun.* **1994**, 2331–2332.
68. Schneider, W.; Bauer, A.; Schmidbaur, H. *Chem. Ber.* **1997**, *130*, 947–950.
69. Kitagawa, S.; Munakata, M. *Bull. Chem. Soc. Jpn.* **1986**, *59*, 2743–2750.
70. Sorrell, T. N.; Garrity, M. L.; Richards, J. L.; Pigge, C. F.; Allen, W. E. In *Bioinorganic Chemistry of Copper*, Karlin, K. D.; Tyeklár, Z., Eds.; Chapman and Hall: New York, 1993; pp 338–347.
71. Sanyal, I.; Strange, R. W.; Blackburn, N. J.; Karlin, K. D. *J. Am. Chem. Soc.* **1991**, *113*, 4692–4693.
72. Sanyal, I.; Karlin, K. D.; Strange, R. W.; Blackburn, N. J. *J. Am. Chem. Soc.* **1993**, *115*, 11259–11270.
73. Munakata, M.; Maekawa, M.; Kitagawa, S.; Matsuyama, S.; Masuda, H. *Inorg. Chem.* **1989**, *28*, 4300–4302.
74. Cole, A. P.; Root, D. E.; Mukherjee, P.; Solomon, E. I.; Stack, T. D. P. *Science* **1996**, *273*, 1848–1850.
75. Blake, A. J.; Hubberstey, P.; Li, W.-S.; Quinlan, D. J.; Russell, C. E.; Simpson, C. L. *J. Chem. Soc., Dalton Trans.* **1999**, 4261–4268.
76. Holland, P. L.; Rodgers, K. R.; Tolman, W. B. *Angew. Chem., Int. Ed. Engl.* **1999**, *38*, 1139–1142.
77. Bernardinelli, G.; Kubel-Pollack, A.; Ruttiman, S.; Williams, A. F. *Z. Kristallogr.* **1993**, *203*, 135–137.
78. Schneider, J. L.; Young, V.G., Jr.; Tolman, W. B. *Inorg. Chem.* **2001**, *40*, 165–168.
79. Lam, B. M. T.; Halfen, J. A.; Young, V. G. , Jr.; Hagadorn, J. R.; Holland, P. L.; Llédos, A.; Cucurull-Sánchez, L.; Novoa, J. J.; Alvarez, S.; Tolman, W. B. *Inorg. Chem.* **2000**, *39*, 4059–4072.
80. Voo, J. K.; Lam, K. C.; Rheingold, A. L.; Riordan, C. G. *J. Chem. Soc., Dalton Trans.* **2001**, 1803–1805.
81. Blackburn, N. J.; Karlin, K. D.; Concannon, M.; Hayes, J. C.; Gultneh, Y.; Zubieta, J. *J. Chem. Soc., Chem. Commun.* **1984**, 939–940.
82. Sanyal, I.; Mahroof-Tahit, M.; Nasir, M. S.; Ghosh, P.; Cohen, B. L.; Gultneh, Y.; Cruse, R. W.; Farooq, A.; Karlin, K. D.; Liu, S.; Zubieta, J. *Inorg. Chem.* **1992**, *31*, 4322–4332.
83. Sorrell, T. N.; Garrity, M. L.; Richards, J. L.; White, P. S. *Inorg. Chim. Acta* **1994**, *218*, 103–108.
84. Liang, H.-C.; Zhang, C. X.; Henson, M. J.; Sommer, R. D.; Hatwell, K. R.; Kaderli, S.; Zuberbühler, A. D.; Rheingold, A. L.; Solomon, E. I.; Karlin, K. D. *J. Am. Chem. Soc.* **2002**, *124*, 4170–4171.
85. Foster, C. L.; Kilner, C. A.; Thornton-Pett, M.; Halcrow, M. A. *Polyhedron,* **2002**, *21*, 1031–1041.
86. Balamurugan, R.; Palaniandavar, M.; Gopalan, R. S. *Inorg. Chem.* **2001**, *40*, 2246–2235.
87. Itoh, S.; Nakao, J.; Berreau, L. M.; Kondo, T.; Komatsu, M.; Fukuzumi, S. *J. Am. Chem. Soc.* **1998**, *120*, 2890–2899.
88. Sorrell, T. N.; Garrity, M. L. *Inorg. Chem.* **1991**, *30*, 210–215.
89. Sorrell, T. N.; Malachowski, M. R. *Inorg. Chem.* **1983**, *22*, 1883–1887.
90. Kau, L.-S.; Spira-Solomon, D. J.; Penner-Hahn, J. E.; Hodgson, K. O.; Solomon, E. I. *J. Am. Chem. Soc.* **1987**, *109*, 6433–6442.
91. Sorrell, T. N.; Borovik, A. S. *Inorg. Chem.* **1987**, *26*, 1957–1964.
92. Sorrell, T. N.; Borovik, A. S.; Caswell, D. S.; Grygon, C.; Spiro, T. G. *J. Am. Chem. Soc.* **1986**, *108*, 5636–5637.
93. Monzani, E.; Koolhaas, G. J. A. A.; Spandre, A.; Leggieri, E.; Casella, L.; Gullotti, M.; Nardin, G.; Randaccio, L.; Fontani, M.; Zanello, P.; Reedijk, J. *J. Biol. Inorg. Chem.* **2000**, *5*, 251–261.

94. Casella, L.; Carugo, O.; Gullotti, M.; Doldi, S.; Frassoni, M. *Inorg. Chem.* **1996**, *35*, 1101–1113.
95. Casella, L.; Monzani, E.; Gullotti, M.; Cavagnino, D.; Cerina, G.; Santagostini, L.; Ugo, R. *Inorg. Chem.* **1996**, *35*, 7516–7525.
96. Karlin, K. D.; Gultneh, Y.; Hutchison, J. P.; Zubieta, J. *J. Am. Chem. Soc.* **1982**, *104*, 5240–5242.
97. Karlin, K. D.; Hayes, J. C.; Gultneh, Y.; Cruse, R. W.; McKown, J. W.; Hutchison, J. P.; Zubieta, J. *J. Am. Chem. Soc.* **1984**, *106*, 2121–2128.
98. Blackburn, N. J.; Strange, R. W.; Reedijk, J.; Volbeda, A.; Farooq, A.; Karlin, K. D.; Zubieta, J. *Inorg. Chem.* **1989**, *28*, 1349–1357.
99. Nasir, M. S.; Jacobson, R. R.; Zubieta, J.; Karlin, K. D. *Inorg. Chim. Acta* **1993**, *203*, 5–7.
100. Karlin, K. D.; Tyeklár, Z.; Farooq, A.; Haka, M. S.; Ghosh, P.; Cruse, R. W.; Gultneh, Y.; Hayes, J. C.; Toscano, P. J.; Zubieta, J. *Inorg. Chem.* **1992**, *31*, 1436–1451.
101. Sanyal, I.; Murthy, N. N,; Karlin, K. D. *Inorg. Chem.* **1993**, *32*, 5330–5337.
102. Sorrell, T. N.; Malachowski, M. R.; Jameson, D. L. *Inorg. Chem.* **1982**, *21*, 3250–3252.
103. Schindler, S.; Szalda, D. J.; Creutz, C. *Inorg. Chem.* **1991**, *30*, 2255–2264.
104. Piguet, C.; Bernardinelli, G.; Hopfgartner, G. *Chem. Rev.* **1997**, *97*, 2005–2062 and refs. therein.
105. Albrecht, M. *Chem. Rev.* **2001**, *101*, 3457–3497 and refs. therein.
106. Shimazaki, Y.; Yokoyama, H.; Yamauchi, O. *Angew. Chem., Int. Ed. Engl.* **1999**, *38*, 2401–2403.
107. Tyeklár, Z.; Jacobson, R. R.; Wei, N.; Murthy, N. N.; Zubieta, J.; Karlin, K. D. *J. Am. Chem. Soc.* **1993**, *115*, 2677–2689.
108. Gagné, R. R.; Kreh, R. P.; Dodge, J. A.; Marsh, R. E.; McCool, M. *Inorg. Chem.* **1982**, *21*, 254–261.
109. Patch, M. G.; Choi, H.-K.; Chapman, D. R.; Bau, R.; McKee, V.; Reed, C. A. *Inorg. Chem.* **1990**, *29*, 110–119.
110. Pasquali, M.; Floriani, C.; Gaetani-Manfredotti, A.; Chiesi-Villa, A. *J. Am. Chem. Soc.* **1978**, *100*, 4918–4919.
111. Pasquali, M.; Floriani, C.; Gaetani-Manfredotti, A.; Chiesi-Villa, A. *Inorg. Chem.* **1979**, *18*, 3535–3542.
112. Karlin, K. D.; Haka, M. S.; Cruse, R. W.; Meyer, G. J.; Farooq, A.; Gultneh, Y.; Hayes, J. C.; Zubieta, J. *J. Am. Chem. Soc.* **1988**, *110*, 1196–1207.
113. Oshio, H. *J. Chem. Soc., Dalton Trans.* **1990**, 2985–2989.
114. Karlin, K. D.; Cruse, R. W.; Gultneh, Y.; Farooq, A.; Hayes, J. C.; Zubieta, J. *J. Am. Chem. Soc.* **1987**, *109*, 2668–2679.
115. Osako, T.; Tachi, Y.; Taki, M.; Fukuzumi, S.; Itoh, S. *Inorg. Chem.* **2001**, *40*, 6604–6609.
116. Mahroof-Tahir, M.; Murthy, N. N.; Karlin, K. D.; Blackburn, N. J.; Shaikh, S. N.; Zubieta, J. *Inorg. Chem.* **1992**, *31*, 3001–3003.
117. Ohta, T.; Tachiyama, T.; Yoshizawa, K.; Yamabe, T. *Tetrahedron Lett.* **2000**, *41*, 2581–2585.
118. Ohta, T.; Tachiyama, T.; Yoshizawa, K.; Yamabe, T.; Uchida, T.; Kitagawa, T. *Inorg. Chem.* **2000**, *39*, 4358–4369.
119. Manikandan, P.; Varghese, B.; Manoharan, P. T. *J. Chem. Soc., Dalton Trans.* **1996**, 371–376.
120. Itoh, S.; Kondo, T.; Komatsu, M.; Ohshiro, Y.; Li, C.; Kanehisa, N.; Kai, Y.; Fukuzumi, S. *J. Am. Chem. Soc.* **1995**, *117*, 4714–4715.
121. Blain, I.; Bruno, P.; Giorgi, M.; Lojou, E.; Lexa, D.; Réglier, M. *Eur. J. Inorg. Chem.* **1998**, 1297–1304.
122. Blain, I.; Giorgi, M.; De Riggi, I.; Réglier, M. *Eur. J. Inorg. Chem.* **2000**, 393–398.
123. Blain, I.; Giorgi, M.; De Riggi, I.; Réglier, M. *Eur. J. Inorg. Chem.* **2001**, 205–211.
124. Riklin, M.; Tran, D.; Laverman, L. E.; Ford, P. C. *J. Chem. Soc., Dalton Trans.* **2001**, 1813–1819.
125. Boeyens, J. C. A.; Dobson, S. M.; Hancock, R. D. *Inorg. Chem.* **1985**, *24*, 3073–3076.
126. Gahan, L. R.; Kennard, C. H. L.; Smith, G.; Mak, T. C. W. *Transition Met. Chem.* **1986**, *11*, 465–466.
127. Blake, A. J.; Danks, J. P.; Harrison, A.; Parsons, S.; Schooler, P.; Whittaker, G.; Schröder, M. *J. Chem. Soc., Dalton Trans.* **1998**, 2335–2340.
128. Wasielewski, K.; Mattes, R. *Acta Crystallogr., Sect. C* **1990**, *46*, 1826–1828.
129. Blake, A. J.; Danks, J. P.; Lippolis, V.; Parsons, S.; Schröder, M. *New J. Chem.* **1998**, *22*, 1301–1303.
130. Hancock, R. D.; Dobson, S. M.; Boeyens, J. C. A. *Inorg. Chim. Acta* **1987**, *133*, 221–231.
131. Weller, H.; Siegfried, L.; Neuburger, M.; Zehnder, M.; Kaden, T. A. *Helv. Chim. Acta* **1997**, *80*, 2315–2328.
132. Wasielewski, K.; Mattes, R. *Z. Naturforsch., Teil B* **1992**, *47*, 1795–1797.
133. Grillo, V. A.; Gahan, L. R.; Hanson, G. R.; Hambley, T. W.; Stranger, R.; Moubaraki, B.; Murray, K. S. *Aust. J. Chem.* **1999**, *52*, 861–866.
134. Champloy, F.; Benali-Chérif, N.; Bruno, P.; Blain, I.; Pierrot, M.; Réglier, M.; Michalowicz, A. *Inorg. Chem.* **1998**, *37*, 3910–3918.
135. Kodera, M.; Kita, T.; Miura, I.; Nakayama, N.; Kawata, T.; Kano, K.; Hirota, S. *J. Am. Chem. Soc.* **2001**, *123*, 7715–7716.
136. Itoh, S.; Nagagawa, M.; Fukuzumi, S. *J. Am. Chem. Soc.* **2001**, *123*, 4087–4088.
137. Karlin, K. D.; Dahlstrom, P. L.; Hyde, J. R.; Zubieta, J. *J. Chem. Soc., Chem. Commun.* **1980**, 906–908.
138. Karlin, K. D.; Dahlstrom, P. L.; Stanford, M. L.; Zubieta, J. *J. Chem. Soc., Chem. Commun.* **1979**, 465–467.
139. Karlin, K. D.; Dahlstrom, P. L.; Zubieta, J. *Transition Met. Chem.* **1981**, *6*, 314–315.
140. Dagdigian, J. V.; McKee, V.; Reed, C. A. *Inorg. Chem.* **1982**, *21*, 1332–1342.
141. Addison, A. W.; Burke, P. J.; Henrick, K.; Rao, T. N.; Sinn, E. *Inorg. Chem.* **1983**, *22*, 3645–3653.
142. Orpen, A. G.; Brammer, L.; Allen, F. H.; Kennard, O.; Watson, D. G.; Taylor, R. *J. Chem. Soc., Dalton Trans.* **1989**, S1–S83.
143. Olmstead, M. M.; Musker, W. K.; Kessler, R. M. *Transition Met. Chem.* **1982**, *7*, 140–146.
144. Munakata, M.; Kitagawa, S.; Ujimaru, N.; Nakamura, M.; Maekawa, M.; Matsuda, H. *Inorg. Chem.* **1993**, *32*, 826–832.
145. Naskar, J. P.; Hati, S.; Datta, D.; Tocher, D. A. *Chem. Commun.* **1997**, 1319–1320.
146. Naskar, J. P.; Chowdhury, S.; Drew, M. G. B.; Datta, D. *New J. Chem.* **2002**, *26*, 170–175.
147. Mykhalichko, B. M.; Mys′kiv, M. G. *Russ. J. Coord. Chem.* **1999**, *25*, 433–437.
148. Li, S.-L.; Mak, T. C. W.; Zhang, Z.-Z. *J. Chem. Soc., Dalton Trans.* **1996**, 3475–3483.
149. Halcrow, M. A.; Phillips, S. E. V.; Knowles, P. F. Amine Oxidases and Galactose Oxidase. In *Subcellular Biochemistry, Vol.35: Enzyme-Catalyzed Electron and Radical Transfer*; Holzenburg, A., Scrutton, N. S., Eds.; Plenum: New York, 2000; pp 183–231.

150. Parsons, M. R.; Convery, M. A.; Wilmot, C. M.; Yadav, K. D. S.; Blakeley, V.; Corner, A. S.; Phillips, S. E. V.; McPherson, M. J.; Knowles, P. F. *Structure* **1995**, *3*, 1171–1184.
151. Kumar, V.; Dooley, D. M.; Freeman, H. C.; Guss, J. M.; Harvey, I.; McGuirl, M. A.; Wilce, M. J. C.; Zubak, V. M. *Structure* **1996**, *4*, 943–955.
152. Wilce, M. C. J.; Dooley, D. M.; Freeman, H. C.; Guss, J. M.; Matsunami, H.; McIntire, W. S.; Ruggiero, C. E.; Tanizawa, K.; Yamaguchi, H. *Biochemistry* **1997**, *36*, 16116–16133.
153. Li, R.; Klinman, J. P.; Mathews, F. S. *Structure* **1998**, *6*, 293–307.
154. Dooley, D. M. *J. Biol. Inorg. Chem.* **1998**, *4*, 1–11.
155. Halcrow, M. A. *Angew. Chem., Int. Ed. Engl.* **2001**, *40*, 346–349.
156. Cai, D.; Klinman, J. P. *J. Biol. Chem.* **1994**, *269*, 32039–32042.
157. Ruggiero, C. E.; Dooley, D. M. *Biochemistry* **1999**, *38*, 2892–2898.
158. Kim, M.; Okajima, T.; Kishishita, S.; Yoshimura, M.; Kawamori, A.; Tanizawa, K.; Yamaguchi, H. *Nature Struct. Biol.* **2002**, *9*, 591–596.
159. Dove, J. E.; Schwartz, B.; Williams, N. K.; Klinman, J. P. *Biochemistry* **2000**, *39*, 3690–3698.
160. Ruggiero, C. E.; Smith, J. A.; Tanizawa, K.; Dooley, D. M. *Biochemistry* **1997**, *36*, 1953–1959.
161. Chen, Z.-W.; Schwartz, B.; Williams, N. K.; Li, R.; Klinman, J. P.; Mathews, F. S. *Biochemistry* **2000**, *39*, 9709–9717.
162. Schwartz, B.; Dove, J. E.; Klinman, J. P. *Biochemistry* **2000**, *39*, 3699–3707.
163. Schwartz, B.; Olgin, A. K.; Klinman, J. P. *Biochemistry* **2001**, *40*, 2954–2963.
164. Wilmot, C. M.; Hadju, J.; McPherson, M. J.; Knowles, P. F.; Phillips, S. E. V. *Science* **1999**, *286*, 1724–1728.
165. Williams, N. K.; Klinman, J. P. *J. Mol. Catal. B* **2000**, *8*, 95–101.
166. Nakamura, N.; Matsuzaki, R.; Choi, Y.-H.; Tanizawa, K.; Sanders-Loehr, J. *J. Biol. Chem.* **1996**, *271*, 4718–4724.
167. Mure, M.; Klinman, J. P. *J. Am. Chem. Soc.* **1993**, *115*, 7117–7127.
168. Rinaldi, A. C.; Rescigno, A.; Sollai, F.; Soddu, G.; Curreli, N.; Rinaldi, A.; Finazzi-Agrò, A.; Sanjust, E. *Biochem. Mol. Biol. Int.* **1996**, *40*, 189–197.
169. Rinaldi, A. C.; Porcu, C. M.; Oliva, S.; Curreli, N.; Rescigno, A.; Sollai, F.; Rinaldi, A.; Finazzi-Agrò, A.; Sanjust, E. *Eur. J. Biochem.* **1998**, *251*, 91–97.
170. Rinaldi, A. C.; Ponticelli, G.; Oliva, S.; Di Guilio, A.; Sanjust, E. *Bioorg. Med. Chem. Lett.* **2000**, *10*, 989–992.
171. Mandal, S.; Macikenas, D.; Protasiewicz, J. D.; Sayre, L. M. *J. Org. Chem.* **2000**, *65*, 4804–4809.
172. Fujisawa, K.; Iwata, Y.; Kitajima, N.; Higashimura, H.; Kubota, M.; Miyashita, Y.; Yamada, Y.; Okamoto, K.; Moro-oka, Y. *Chem. Lett.* **1999**, 739–740.
173. Gupta, R.; Mukherjee, R. *Tetrahedron Lett.* **2000**, *41*, 7763–7767.
174. Tsuchida, E.; Oyaizu, K.; Kumaki, Y.; Saito, K. Copper Complex Catalyst for Oxidative Polymerization of 4-Fluorophenol. WorldPat. Appl. WO/0121683, **2001**.
175. Higashimura, H.; Fujisawa, K.; Moro-oka, Y.; Kubota, M.; Shiga, A.; Terahara, A.; Uyama, H.; Kobayashi, S. *J. Am. Chem. Soc.* **1998**, *120*, 8529–8530.
176. Higashimura, H.; Kubota, M.; Shiga, A.; Fujisawa, K.; Moro-oka, Y.; Uyama, H.; Kobayashi, S. *Macromolecules* **2000**, *33*, 1986–1995.
177. Higashimura, H.; Fujisawa, K.; Moro-oka, Y.; Kubota, M.; Shiga, A.; Uyama, H.; Kobayashi, S. *J. Mol. Catal. A* **2000**, *155*, 201–207.
178. Higashimura, H.; Fujisawa, K.; Moro-oka, Y.; Kubota, M.; Shiga, A.; Uyama, H.; Kobayashi, S. *Appl. Catal. A* **2000**, *194–195*, 427–433.
179. Higashimura, H.; Fujisawa, K.; Namekawa, S.; Kubota, M.; Shiga, A.; Moro-oka, Y.; Uyama, H.; Kobayashi, S. *J. Polym. Sci. A* **2000**, *38*, 4792–4804.
180. Higashimura, H.; Fujisawa, K.; Moro-oka, Y.; Namekawa, S.; Kubota, M.; Shiga, A.; Uyama, H.; Kobayashi, S. *Macromol. Rapid. Commun.* **2000**, *21*, 1121–1124.
181. Baesjou, P. A.; Driessen, W. L.; Chulla, G.; Reedijk, J. *J. Mol. Catal. A* **1996**, *110*, 195–210.
182. Baesjou, P. A.; Driessen, W. L.; Chulla, G.; Reedijk, J. *J. Am. Chem. Soc.* **1997**, *119*, 12590–12594.
183. Baesjou, P. A.; Driessen, W. L.; Chulla, G.; Reedijk, J. *J. Mol. Catal. A* **1998**, *135*, 273–283.
184. Baesjou, P. A.; Driessen, W. L.; Chulla, G.; Reedijk, J. *Macromolecules* **1999**, *32*, 270–276.
185. Baesjou, P. A.; Driessen, W. L.; Chulla, G.; Reedijk, J. *J. Mol. Catal. A* **1999**, *140*, 241–253.
186. Rinaldi, A. C.; Porcu, C. M.; Curreli, N.; Rescigno, A.; Finazzi-Agrò, A.; Pedersen, J. Z.; Rinaldi, A.; Sanjust, E. *Biochem. Biophys. Res. Commun.* **1995**, *214*, 559–567.
187. Mandal, S.; Lee, Y.; Purdy, M. M.; Sayre, L. M. *J. Am. Chem. Soc.* **2000**, *122*, 3574–3584.
188. Bertini, I.; Mangani, S.; Viezzoli, M. S. *Adv. Inorg. Chem.* **1998**, *45*, 127–250.
189. Lyons, T. J.; Gralla, E. B.; Valentine, J. S. *Met. Ions Biol. Syst.* **1999**, *36*, 125–177.
190. Dooley, D. M.; McGuirl, M. A.; Brown, D. E.; Turowski, P. N.; McIntire, W. S.; Knowles, P. F. *Nature (London)* **1991**, *349*, 262–264.
191. Dooley, D. M.; Brown, D. E. *J. Biol. Inorg. Chem.* **1996**, *1*, 205–209.
192. Hirota, S.; Iwamoto, T.; Tanizawa, K.; Adachi, O.; Yamauchi, O. *Biochemistry* **1999**, *38*, 14256–14263.
193. Su, Q.; Klinman, J. P. *Biochemistry* **1998**, *37*, 12513–12525.
194. Mills, S. A.; Klinman, J. P. *J. Am. Chem. Soc.* **2000**, *122*, 9897–9904.
195. Nappa, M.; Valentine, J. S.; Miksztal, A. R.; Schugar, H. J.; Isied, S. S. *J. Am. Chem. Soc.* **1979**, *101*, 7744–7746.
196. Kodera, M.; Tachi, Y.; Hirota, S.; Katayama, K.; Shimakoshi, H.; Kano, K.; Fujisawa, K.; Moro-oka, Y.; Naruta, Y.; Kitagawa, T. *Chem. Lett.* **1998**, 389–390.
197. Karlin, K. D.; Wei, N.; Jung, B.; Kaderli, S.; Zuberbühler, A. D. *J. Am. Chem. Soc.* **1991**, *113*, 5868–5870.
198. Karlin, K. D.; Wei, N.; Jung, B.; Kaderli, S.; Niklaus, P.; Zuberbühler, A. D. *J. Am. Chem. Soc.* **1993**, *115*, 9506–9514.
199. Lee, D.-H.; Wei, N.; Murthy, N. N.; Tyeklár, Z.; Karlin, K. D.; Kaderli, S.; Jung, B.; Zuberbühler, A. D. *J. Am. Chem. Soc.* **1995**, *117*, 12498–12513.
200. Wei, N.; Murthy, N. N.; Chen, Q.; Zubieta, J. Karlin K. D. *Inorg. Chem.* **1994**, *33*, 1953–1965.
201. Itoh, S.; Nakao, H.; Berreau, L. M.; Kondo, T.; Komatsu, M.; Fukuzumi, S. *J. Am. Chem. Soc.* **1998**, *120*, 2890–2899.
202. Fujisawa, K.; Tanaka, M.; Moro-oka, Y.; Kitajima, N. *J. Am. Chem. Soc.* **1994**, *116*, 12079–12080.

203. Spencer, D. J. E.; Aboelella, N. W.; Reynolds, A. M.; Holland, P. L.; Tolman, W. B. *J. Am. Chem. Soc.* **2002**, *124*, 2108–2109.
204. Chaudhuri, P.; Hess, M.; Weyhermüller, T.; Wieghardt, K. *Angew. Chem., Int. Ed. Engl.* **1999**, *38*, 1095–1098.
205. Wada, A.; Harata, M.; Hasegawa, K.; Jitsukawa, K.; Masuda, H.; Mukai, M.; Kitagawa, T.; Einaga, H. *Angew. Chem., Int. Ed. Engl.* **1998**, *37*, 798–799.
206. Chen, P.; Fujisawa, K.; Solomon, E. I. *J. Am. Chem. Soc.* **2000**, *122*, 10177–10193.
207. Ohtsu, H.; Itoh, S.; Nagatomo, S.; Kitagawa, T.; Ogo, S.; Watanabe, Y.; Fukuzumi, S. *Inorg. Chem.* **2001**, *40*, 3200–3207.
208. Harata, M.; Jitsukawa, K.; Masuda, H.; Einaga, H. *Bull. Chem. Soc. Jpn.* **1998**, *71*, 637–645.
209. Aboelella, N. W.; Lewis, E. A.; Reynolds, A. M.; Brennessel, W. W.; Cramer, C. J.; Tolman, W. B. *J. Am. Chem. Soc.* **2002**, *124*, 10660, 10661.
210. Nishida, Y.; Unoura, K.; Watanabe, I.; Yokomizo, T.; Kato, Y. *Inorg. Chim. Acta* **1991**, *181*, 141–143.
211. Harata, M.; Jitsukawa, K.; Masuda, H.; Einaga, H. *J. Am. Chem. Soc.* **1994**, *116*, 10817–10818.
212. Berreau, L. M.; Mahapatra, S.; Halfen, J. A.; Young, V.G., Jr.; Tolman, W. B. *Inorg. Chem.* **1996**, *35*, 6339–6342.
213. Harata, M.; Jitsukawa, K.; Masuda, H.; Einaga, H. *Chem. Lett.* **1996**, 813–814.
214. Thompson, J. S. *J. Am. Chem. Soc.* **1984**, *106*, 4057–4059.
215. Kitajima, N.; Koda, T.; Fujisawa, K.; Fujimoto, C.; Hashimoto, S.; Kitagawa, T.; Moro-oka, Y. *J. Am. Chem. Soc.* **1991**, *113*, 5664–5671.
216. Mahroof-Tahir, M.; Karlin, K. D. *J. Am. Chem. Soc.* **1992**, *114*, 7599–7601.
217. Fukuzumi, S.; Ohkubo, K. *Chem. Eur. J.* **2000**, *6*, 4532–4535.
218. Blackman, A. G.; Tolman, W. B. *Struct. Bonding* **2000**, *97*, 180–211.
219. Kitajima, N.; Fujisawa, K.; Moro-oka, Y. *Inorg. Chem.* **1990**, *29*, 357–358.
220. Kitajima, N.; Katayama, T.; Fujisawa, K.; Iwata, Y.; Moro-oka, Y. *J. Am. Chem. Soc.* **1993**, *115*, 7872–7873.
221. Sanyal, I.; Ghosh, P.; Karlin, K. D. *Inorg. Chem.* **1995**, *34*, 3050–3056.
222. Karlin, K. D.; Ghosh, P.; Cruse, R. W.; Farooq, A.; Gultneh, Y.; Jacobson, R. R.; Blackburn, N. J.; Strange, R. W.; Zubieta, J. *J. Am. Chem. Soc.* **1988**, *110*, 6769–6780.
223. Karlin, K. D.; Cruse, R. W.; Gultneh, Y. *J. Chem. Soc., Chem. Commun.* **1987**, 599–600.
224. Root, D. E.; Mahroof-Tahir, M.; Karlin, K. D.; Solomon, E. I. *Inorg. Chem.* **1998**, *37*, 4838–4858.
225. Sorrell, T. N.; Vankai, V. A. *Inorg. Chem.* **1990**, *29*, 1687–1692.
226. Ghosh, P.; Tyeklár, Z.; Karlin, K. D.; Jacobson, R. R.; Zubieta, J. *J. Am. Chem. Soc.* **1987**, *109*, 6889–6891.
227. Halfen, J. A.; Young, V.G., Jr.; Tolman, W. B. *Inorg. Chem.* **1998**, *37*, 2102–2103.
228. Ito, S.; Takimura, M.; Sasaki, K. *Chem. Lett.* **1993**, 461–464.
229. Blain, I.; Pierrot, M.; Giorgi, M.; Réglier, M. *C. R. Acad. Sci. Paris, Ser. IIc* **2001**, *4*, 1–10.
230. Karlin, K. D.; Zuberbühler, A. D. Formation Structure and Reactivity of Copper Dioxygen Complexes. In *Bioinorganic Catalysis*, 2nd ed.; Reedijk, J.; Bouman, E., Eds.; Dekker: NewYork, 1999; pp. 469–532.
231. Que, L., Jr.; Tolman, W. B. *Angew. Chem., Int. Ed. Engl.* **2002**, *41*, 1114–1137.
232. Capdevielle, P.; Maumy, M. *Tetrahedron Lett.* **1991**, *32*, 3831–3834.
233. Okuno, T.; Ohba, S.; Nishida, Y. *Polyhedron* **1997**, *16*, 3765–3774.
234. Ishikawa, Y.; Ito, S.; Nishino, S.; Ohba, S.; Nishida, Y. Z. *Naturforsch Teil C* **1998**, *53*, 378–382.
235. Kobayashi, T.; Okuno, T.; Suzuki, T.; Kunita, M.; Ohba, S.; Nishida, Y. *Polyhedron* **1998**, *17*, 1553–1559.
236. Nishino, S.; Ishikawa, Y.; Nishida, Y. *Inorg. Chem. Commun.* **1999**, *2*, 438–441.
237. Nishino, S.; Kunita, M.; Kani, Y.; Ohba, S.; Matsushima, H.; Tokii, T.; Nishida, Y. *Inorg. Chem. Commun.* **2000**, *3*, 145–148.
238. Reddy, K. V.; Jin, S.-J.; Arora, P. K.; Sfeir, D. S.; Maloney, S. C. F.; Urbach, F. L.; Sayre, L. M. *J. Am. Chem. Soc.* **1990**, *112*, 2332–2340.
239. Rybka, J. S.; Kurtz, J. L.; Neubecker, T. A.; Margerum, D. W. *Inorg. Chem.* **1980**, *19*, 2791–2796.
240. de Meester, P.; Hodgson, D. J. *J. Am. Chem. Soc.* **1976**, *98*, 7086–7087.
241. McDonald, M. R.; Scheper, W. M.; Lee, H. D.; Margerum, D. W. *Inorg. Chem.* **1995**, *34*, 229–237.
242. McDonald, M. R.; Fredericks, F. P.; Margerum, D. W. *Inorg. Chem.* **1997**, *36*, 3119–3124.
243. Bossu, F. P.; Paniago, E. B.; Margerum, D. W.; Kirksey, S. T., Jr.; Kurtz, J. L. *Inorg. Chem.* **1978**, *17*, 1034–1042.
244. Sakurai, T.; Nakamura, A. *Inorg. Chim. Acta* **1979**, *34*, L243–L244.
245. Bal, W.; Djuran, M. I.; Margerum, D. W.; Gray, E. T., Jr.; Mazid, M. A.; Tom, R. T.; Nieboer, E.; Sadler, P. J. *J. Chem, Soc., Chem. Commun.* **1994**, 1889–1890.
246. Easton, C. J.; Eichinger, S. K.; Pitt, M. J. *J. Chem. Soc.Chem.Commun.* **1992**, 1295–1296.
247. Easton, C. J.; Eichinger, S. K.; Pitt, M. J. *Tetrahedron* **1997**, *53*, 5609–5616.
248. Haas, K.; Dialer, H.; Piotrowski, H.; Schapp, J.; Beck, W. *Angew. Chem, Int. Ed. Engl.* **2002**, *41*, 1879–1881.
249. Jitsukawa, K.; Irisa, T.; Einaga, H.; Masuda, H. *Chem. Lett.* **2001**, 30–31.
250. Hattori, S.; Noguchi, I. *Nature (London)* **1959**, *184*, 1145–1146.
251. Westlake, D. W. S.; Talbot, G.; Blakeley, E. R.; Simpson, F. J. *Can. J. Microbiol.* **1959**, *5*, 621–629.
252. Simpson, F. J.; Talbot, G.; Westlake, D. W. S. *Biochem. Biophys. Res. Commun.* **1960**, *2*, 15–18.
253. Westlake, D. W. S.; Roxburgh, J. M.; Talbot, G. *Nature (London)* **1961**, *189*, 510–511.
254. Simpson, F. J.; Narasimhachari, N.; Westlake, D. W. S. *Can. J. Microbiol.* **1962**, *9*, 15–25.
255. Krishnamurthy, H. G.; Simpson, F. J. *J. Biol. Chem.* **1970**, *245*, 1467–1471.
256. Oka, T.; Simpson, F. J.; Child, J. J.; Mills, S. C. *Can. J. Microbiol.* **1971**, *17*, 111–118.
257. Oka, T.; Simpson, F. J. *Can. J. Microbiol.* **1972**, *18*, 1171–1175.
258. Oka, T.; Simpson, F. J. *Biochem. Biophys. Res. Commun.* **1971**, *43*, 1–5.
259. Oka, T.; Simpson, F. J.; Krishnamurthy, H. G. *Can. J. Microbiol.* **1972**, *18*, 493–508.
260. Hund, H-K.; Breuer, J.; Lingens, F.; Hüttermann, J.; Kappl, R.; Fetzner, S. *Eur. J. Biochem.* **1999**, *263*, 871–878.
261. Fusetti, F.; Schröter, K. H.; Steiner, R. A.; van Noort, P. I.; Pijning, T.; Rozeboom, H. J.; Kalk, K. H.; Egmond, M. R.; Dijkstra, B. W. *Structure* **2002**, *10*, 259–268.
262. Thompson, M.; Williams, C. R.; Elliot, G. E. P. *Anal. Chim. Acta* **1976**, *85*, 375–381.
263. Takamura, K.; Ito, M. *Chem. Pharm. Bull.* **1977**, *25*, 3218–3225.
264. Nishinaga, A.; Tojo, T.; Teruo, M. *J. Chem. Soc. Chem. Commun.* **1973**, 9–10.

265. Nishinaga, A.; Tojo, T.; Tomita, H.; Matsuura, T. *J. Chem. Soc., Perkin Trans. 1* **1979**, 2511–2516.
266. Balogh-Hergovich, E.; Speier, G. *J. Org. Chem.* **2001**, *66*, 7974–7978.
267. Brown, S. B.; Rajananda, V. *Tetrahedron Lett.* **1981**, *22*, 4331–4334.
268. Brown, S. B.; Rajananda, V.; Holroyd, J. A.; Evans, E. G. V. *Biochem. J.* **1982**, *205*, 239–244.
269. Matsuura, T.; Matsushima, H.; Sakamoto, H. *J. Am. Chem. Soc.* **1967**, *89*, 6370–6371.
270. Kano, K.; Mabuchi, T.; Uno, B.; Esaka, Y.; Tanaka, T.; Iinuma, M. *J. Chem. Soc., Chem. Commun.* **1994**, 593–594.
271. Kaizer, J.; Speier, G. *J. Mol. Catal. A* **2000**, *171*, 33–36.
272. Matsuura, T.; Matsushima, H.; Nakashima, R. *Tetrahedron* **1970**, *26*, 435–443.
273. Lippai, I.; Speier, G.; Huttner, G.; Zsolnai, L. *Acta Crystallogr., Sect. C* **1997**, *53*, 1547–1549.
274. Lippai, I.; Speier, G. *J. Mol. Catal. A* **1998**, *130*, 139–148.
275. Lippai, I.; Speier, G.; Huttner, G.; Zsolnai, L. *Chem. Commun.* **1997**, 741–742.
276. Schweppe, F.; Sirges, H.; Pascaly, M.; Duda, M.; Nazikkol, C.; Steinforth, W.; Krebs, B. Transition-metal-catalyzed Oxyfunctionalization of Catechol and Flavonol Derivatives. In *Peroxide Chemistry,* Adam, W., Ed.; Wiley-VCH: New York, 2000; pp 232–248.
277. Balogh-Hergovich, E.; Speier, G.; Argay, G.; *J. Chem. Soc., Chem. Commun.* **1991**, 551–552.
278. Balogh-Hergovich, E.; Kaizer, J.; Speier, G.; Argay, G.; Párkányi, L. *J. Chem. Soc., Dalton Trans.* **1999**, 3847–3854.
279. Balogh-Hergovich, E.; Kaizer, J.; Speier, G.; Huttner, G.; Zsolnai, L. *Inorg. Chim. Acta* **2000**, *304*, 72–77.
280. Balogh-Hergovich, E.; Kaizer, J.; Speier, G.; Huttner, G.; Jacobi, A. *Inorg. Chem.* **2000**, *39*, 4224–4229.
281. Speier, G.; Fülöp, V.; Párkányi, L. *J. Chem. Soc., Chem. Commun.* **1990**, 512–513.
282. Balogh-Hergovich, E.; Kaizer, J.; Speier, G.; Fülöp, V.; Párkányi, L. *Inorg. Chem.* **1999**, *38*, 3787–3795.
283. Kaizer, J.; Kupan, A.; Pap, J.; Speier, G.; Reglier, M.; Michel, G. *Z. Kristallogr.* **2000**, *215*, 571–572.
284. Balogh-Hergovich, E.; Kaizer, J.; Speier, G.; Huttner, G.; Putsch, P. *Acta Crystallogr., Sect. C* **1999**, *55*, 557–558.
285. Annan, T. A.; Peppe, C.; Tuck, D. G. *Can. J. Chem.* **1990**, *68*, 423–430.
286. Farina, Y.; Yamin, B. M.; Fun, H.-K.; Yip, B.-C.; Teoh, S.-G. *Acta Crystallogr., Sect. C* **1995**, *51*, 1537–1540.
287. Hiller, W.; Nishinaga, A.; Rieker, A. *Z. Naturforsch, Teil B* **1992**, *47*, 1185–1188.
288. Balogh-Hergovich, E.; Kaizer, J.; Speier, G. *Inorg. Chim. Acta* **1997**, *256*, 9–14.
289. Balogh-Hergovich, E.; Kaizer, J.; Speier, G. *J. Mol. Catal. A* **2000**, *159*, 215–224.
290. Barhács, L.; Kaizer, J.; Pap, J.; Speier, G. *Inorg. Chim. Acta* **2001**, *320*, 83–91.
291. Utaka, M.; Takeda, A. *J. Chem. Soc., Chem. Commun.* **1985**, 1824–1826.
292. Balogh-Hergovich, E.; Speier, G. *J. Mol. Catal.* **1992**, *71*, 1–6.
293. Brown, J. E.; Khodr, H.; Hider, R. C.; Rice-Evans, C. A. *Biochem. J.* **1998**, *330*, 1173–1178.
294. Jungbluth, G.; Rühling, I.; Ternes, W. *J. Chem. Soc., Perkin Trans. 2* **2000**, 1946–1952.
295. Dangles, O.; Dufour, C.; Bret, S. *J. Chem. Soc., Perkin Trans. 2* **1999**, 737–744.
296. Dangles, O.; Fargeix, G.; Dufour, C. *J. Chem. Soc., Perkin Trans. 2* **1999**, 1387–1395.
297. Viborg Jørgensen, L.; Cornett, C.; Justesen, U.; Skibsted, L. H.; Dragsted, L. O. *Free Radical Res.* **1998**, *29*, 339–350.
298. Nishinaga, A.; Tojo, T.; Matsuura, T. *J. Chem. Soc., Chem. Commun.* **1974**, 896–897.
299. Nishinaga, A.; Numada, N.; Maruyama, K. *Tetrahedron Lett.* **1989**, *30*, 2257–2258.
300. Nishinaga, A.; Kuwashige, T.; Tsutsui, T.; Mashino, T.; Maruyama, K. *J. Chem. Soc., Dalton Trans.* **1994**, 805–810.
301. Barhács, L.; Kaizer, J.; Speier, G. *J. Mol. Catal. A* **2001**, *172*, 117–125.
302. Francisco, W. A.; Blackburn, N. J.; Klinman, J. P. *Biochemistry* **2003**, *42*, 1813–1819.
303. Jaron, S.; Mains, R. E.; Eipper, B. A.; Blackburn, N. J. *Biochemistry* **2002**, *41*, 13274–13282.
304. Blain, I.; Slama, P.; Giorgi, M.; Tron, T.; Réglier, M. *Rev. Mol. Biotech* **2002**, *90*, 95–112.
305. Steiner, R. A.; Meyer-Klaucke, W.; Dijkstra, B. W. *Biochemistry* **2002**, *41*, 7963–7968.
306. Kooter, I. M.; Steiner, R. A.; Dijkstra, B. W.; van Noort, P. I.; Egmond, M. R.; Huber, M. *Eur. J. Biochem* **2002**, *269*, 2971–2979.
307. Steiner, R. A.; Kooter, I. M.; Dijkstra, B. W. *Biochemistry* **2002**, *41*, 7955–7962.
308. Steiner, R. A.; Kalk, K. H.; Dijkstra, B. W. *Proc. Natl. Acad. Sci. USA* **2002**, *99*, 16625–16630.
309. Chen, P.; Root, D. E.; Campochiaro, C.; Fujisawa, K.; Solomon, E. I. *J. Am. Chem. Soc* **2003**, *125*, 466–474.
310. Weitzer, M.; Schindler, S.; Brehm, G.; Schneider, S.; Hörmann, E.; Jung, B.; Kaderli, S.; Zuberbühler, A. D. *Inorg. Chem* **2003**, *42*, 1800–1806.
311. Osako, T.; Nagamoto, S.; Tachi, Y.; Kitagawa, T.; Itoh, S. *Angew. Chem., Int. Ed. Engl* **2002**, *41*, 4325–4328.

8.17
Multimetal Oxidases

D.-H. LEE

Chonbuk National University, Chonju, South Korea

and

B. LUCCHESE and K. D. KARLIN

Johns Hopkins University, Baltimore, MD, USA

8.17.1 INTRODUCTION

In this chapter, we focus on the protein copper coordination chemistry in which dioxygen activation at heme-copper or multinuclear copper centers leads to the four-electron four-proton reduction of O_2 to water. These reactions are coupled to substrate oxidations as well as proton translocation in the case of cytochrome c oxidase. The last few years of the twentieth century saw considerable research advances in protein X-ray structures and insights into the O_2-binding and mechanisms of the reductive O—O cleavage process. We highlight here these structural and mechanistic advances, as well as aspects of synthetic model chemistry being carried out to mimic or provide additional insights into the fundamental metal–dioxygen chemistry involved.

8.17.2   CYCTOCHROME c OXIDASE

8.17.2.1   Introduction and Overview

Cytochrome *c* oxidases (C*c*Os) are important members of the superfamily of heme/copper-containing terminal oxidases, which play a central role in the respiratory metabolism of both eukaryotic organisms as well as some aerobic bacteria.[1–7] Various physiological donors provide electrons to dioxygen for reduction to water, a reaction that is coupled to vectorial proton translocation ("pump") across the membrane in a cycle aimed at energy production and storage. Some of the common features of the heme/copper oxidases are the strong sequence homology of their largest subunits and the presence of a bimetallic catalytic center consisting of a high-spin heme (heme a_3) and a closely associated copper ion (Cu_B) in their subunit I.[3] Additional metal centers are a low-spin heme (heme *a*) in subunit I and a dicopper center (referred to as Cu_A) located in subunit II (see Figure 1).

Electrons from cytochrome *c* are first transferred to the binuclear Cu_A center which displays a delocalized mixed-valence (Cu(1.5)–Cu(1.5)) electronic structure in its oxidized state (see Chapter 8.4).[8,9] Heme Fe_a is also another electron transfer center that is believed to be in rapid redox equilibrium with Cu_B.[1] Subsequent electron transfer occurs to subunit I and the binuclear heme a_3-Cu_B center, where molecular oxygen reduction occurs. During this process, four protons are supplied from the inner membrane. The free energy made available by this exergonic reaction drives the translocation ("pump") of four additional protons per O_2 molecule reduced from the "IN" side to the "OUT" side. The active transport of protons generates an electrochemical gradient across the membrane that ultimately drives ATP synthesis.

8.17.2.2   X-ray Structural Studies and Physical Properties

A number of X-ray structures of C*c*O derivatives are now available for the enzymes from *Paracoccus denitrificans*,[10–12] bovine heart,[13] the ba_3-type cytochrome *c* oxidase from
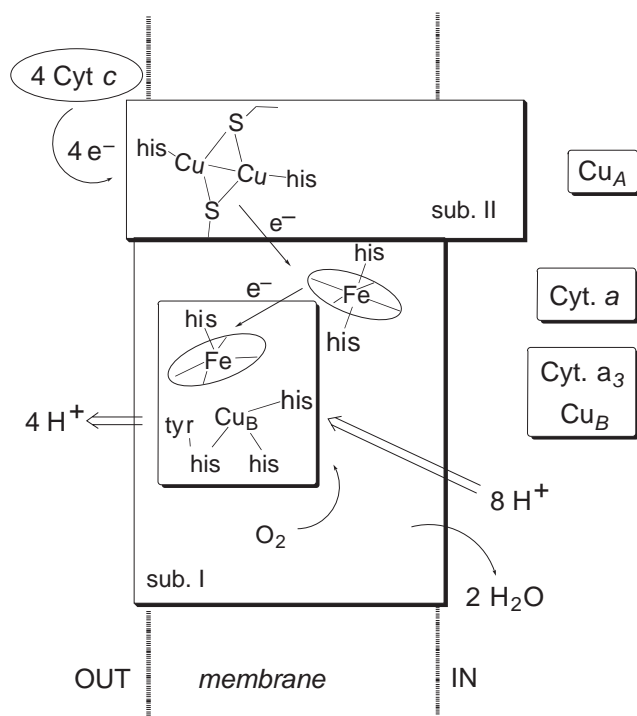
Figure 1   Schematic drawing of cytochrome *c* oxidase subunits I and II, the important metal centers, the general pathway for electron transfer from cytochrome *c*, and indications of the reaction stoichiometry and proton translocation chemistry.

T. *thermophilus*,[14] and from *Rhodobacter sphaeroides*.[15] In addition an *E. coli* ubiquinol oxidase, (utilzing ubiquinol rather then cytochrome *c* as physiological reductant) and lacking Cu_A, has been structurally characterized.[16] The bovine heart oxidase structures reveal 12 different subunits, two hemes, the coppers, plus magnesium and zinc.[13] By contrast, prokaryotes contain fewer subunits, usually up to four.

8.17.2.2.1 Heme a and Heme a₃-Cu_B center

Heme *a* contains a low-spin iron center which is coordinated by two axial histidines which are strictly conserved among heme-copper oxidases. The Cu_B center is ligated by three histidines with approximate trigonal planar geometry and the high-spin heme a_3 is bound to a histidine which is distal from the copper center (see Figure 2). In the X-ray structure of *P. denitrificans* C*c*O the shortest distance between the two hemes is 4.5 Å, while the iron–iron distance is 13.2 Å. The distances from the nearest copper ion of Cu_A to the iron atoms of heme *a* and a_3 are 19.5 Å and 22.2 Å, respectively (also see Figure 1).[10–12]

As Cu_B in fully oxidized enzymes is electron paramagnetic resonance (EPR)-silent, strong antiferromagnetic coupling between Fe^{III} ($S = 5/2$) and Cu^{II} ($S = 1/2$) leading to the formation of an $S = 2$ spin system has been proposed,[2] but alternative data or views suggesting weak coupling have been presented.[17,18] In support of antiferromagnetic coupling are magnetic susceptibility measurements[2,18] which early on led to the hypothesis of a bridged Fe^{III}—X—Cu^{II} moiety, with X possibly being an oxo, hydroxo, chloro, sulfido, cysteinato or imidazolato group.[19] In the initial enzyme X-ray structural reports for both bovine and *P. denitrificans* C*c*O, no bridging ligands were detectable. In the bovine enzyme the Fe–Cu distance is 4.5 Å.[13] Structural data on *P. denitrificans* C*c*O (Fe–Cu distance of 5.2 Å) suggest the presence of a water molecule bound to the heme a_3 iron and H-bonded to a hydroxide ion coordinated to Cu_B.[10,12] *T. Thermophilus* ba_3-C*c*O is described as a μ-X-bridged Fe—X—Cu complex with X = oxo, hydroxo, or water with Fe—X and Cu—X = 2.3 Å, while the Fe^{III}–Cu^{II} distance is 4.4 Å.[14] In *R. sphaeroides* C*c*O, there appears to be a hydroxide bound only to copper(II); Cu_B—OH^- = 2.0 Å while Fe_{a3-OH^-} = 3.6 Å.[15]

Yoshikawa and co-workers have obtained X-ray structural data on fully reduced, reduced CO-bound, oxidized with a putative μ-peroxo ligand, and azide-ligated oxidized forms.[13] Relative to oxidized forms, fully reduced enzymes do not appear to undergo major structural changes in Fe–Cu distance and protein residue ligation. The Fe^{II}–Cu^I distances are 5.2 Å (*P. denitrificans*)[12] and 5.19 Å (bovine heart),[12,13] but there are no detectable water-derived ligands between Cu_B and Fea_3.
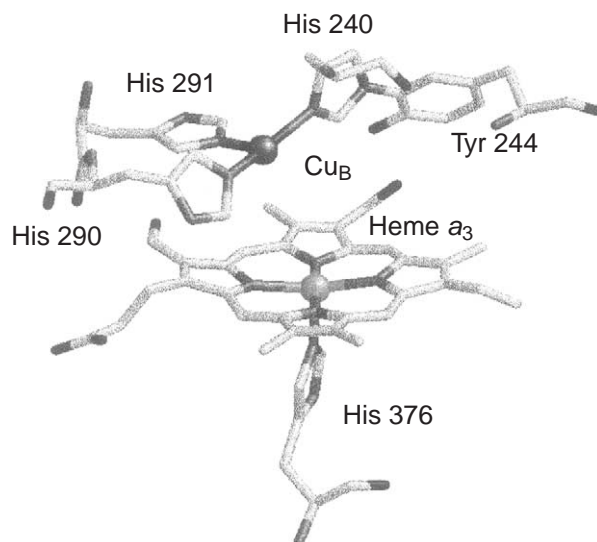
Figure 2 Bovine X-ray structure heme a_3-Cu_B active site for O_2-reduction, also indicating the cross-linked His–Tyr moiety.
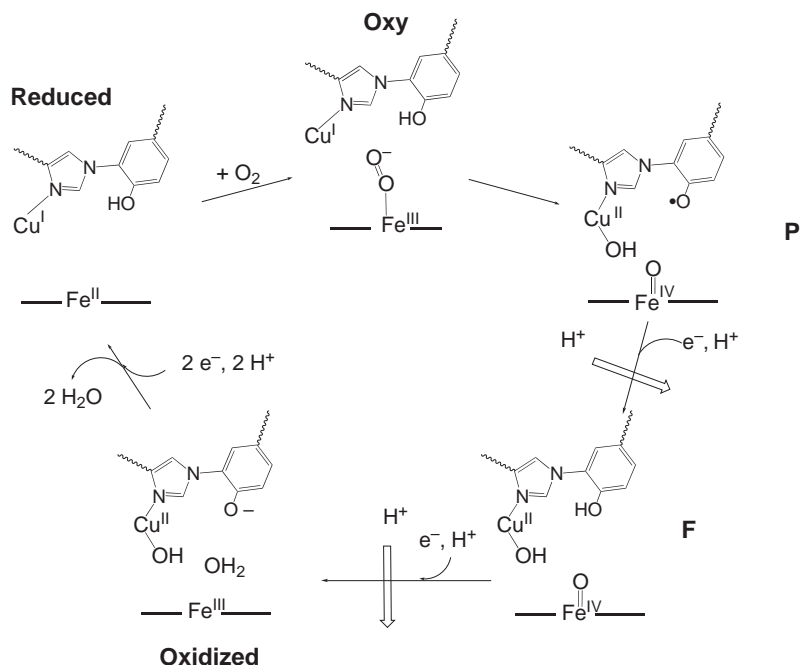
Figure 3 Proposed mechanism for O_2-reduction by the reduced heme a_3-Cu_B CcO ("mixed-valent") active site.

A remarkable aspect of the bimetallic center is that one of the three histidine residues coordinating Cu_B is covalently attached to a tyrosine side-chain (His-240 and Tyr-244, see Figure 2; His-276 and Tyr-280 in the bacterial structure), presumed to be the result of a post-translational modification.[20] The functional implications of this structure (or motif) for the O_2-reduction and/or proton pumping mechanism have yet to be fully elucidated, but most researchers suggest that the His–Tyr may donate a hydrogen atom (proton plus electron) to dioxygen, becoming a phenoxyl radical (see Figure 3).[6,21–24]

8.17.2.2.2 Cu_A Cys-bridged binuclear center

The coordination geometry around each metal center of the dinuclear Cu_A site, the most likely entry point of electrons from cyctochrome c, is distorted tetrahedral. Each copper ion is coordinated by two bridging cysteine thiolates and one terminal histidine; one Cu has a weaker (longer) methionine interaction, while similarly, a glutamate interacts with the other. The Cu–Cu distance is 2.4 Å in *T. thermophilus* and 2.7 Å in the bovine heart enzyme.[7,13] For a more detailed description of this site, see Chapter 8.4.

8.17.2.3 Dioxygen Reduction Mechanism

The present quite widely accepted view for the O_2-reduction cycle of two-electron reduced (so-called "mixed-valent") CcO is outlined in Figure 3;[7,23,25] variations in mechanistic interpretation occur for the reaction of O_2 with the fully (four-electron) reduced enzyme and uncertainties remain with respect to details. The detailed mechanism of proton pumping as related to the heme-copper O_2-reduction process is less certain and more controversial.[26–29]

Two electron transfers from cytochrome c substrate convert the inactive oxidized enzyme with Fe^{III}–Cu^{II} bimetallic site to an active Fe^{II}–Cu^{I} state "mixed-valent" form. The first intermediate in the reaction of O_2 is an adduct with cytochrome a_3, an Fe–O_2 moiety with $\nu_{Fe-O} = 572\,cm^{-1}$ (from resonance Raman (rR) spectroscopy) closely resembling those observed in oxyhemoglobin. It appears to involve a Fea_3^{III}–O_2^- in an end-on configuration, without any significant interaction with the Cu^I center,[2] consistent with the crystallographic data. The subsequent reaction was

previously assumed to involve formation of a peroxide species (thus designated **P**, see Figure 3). However, time-resolved rR spectroscopy (peak at $804\,cm^{-1}$) and mass spectroscopy using labeled $^{18}O_2$ have shown that the O—O bond is cleaved and the intermediate has the characteristics of an oxoferryl ($Fe^{IV}=O$) species.[25,30] Of the four electrons required for this step, two are supplied through the oxidation of the ferrous heme to the Fe^{IV} oxo-ferryl level while one comes from Cu_B (Cu^I to Cu^{II}). The fourth electron could in principle be provided by a one-electron oxidation of the heme a_3, but this possibility has been ruled out on the basis of optical spectra and Raman data.[2,31] As mentioned above, the proximal tyrosine (from Cu_B bound His–Tyr moiety) has thus been implicated as the source of the "missing" one electron reservoir.

8.17.2.4 C*c*O Model Compounds

Synthetically derived heme-copper heterobimetallic model complexes have previously concentrated on the resting oxidized state of the dinuclear center and the generation of mixed-metal Fe^{III}—X—Cu^{II} complexes where a bridging ligand (X) assembles two mononuclear precursors.[32] Karlin *et al.* showed that the reaction of O_2 with an equimolar mixture of $(F_8TPP)Fe^{II}$ (F_8TPP = tetrakis(2,6-difluorophenyl)porphyrin) (or an analogue with axial piperidine ligands) and $[(TMPA)Cu^I(CH_3CN)]^+$ (TMPA = tris(2-pyridylmethyl)amine)) produces a magnetically coupled μ-oxo-bridged $[(F_8TPP)Fe^{III}-(O^{2-})-Cu^{II}(TMPA)]^+$ complex (**1**) (Figure 4).[33] This species is of considerable interest since it is derived from a biomimetic reaction (i.e., from $O_2 + Fe^{II}Cu^I$). The X-ray structure of structure (**1**) reveals an essentially linear Fe^{III}-oxo-Cu^{II} arrangement (Fe—O—Cu angle of 178.2°), with very short Fe—O ($1.740\,\text{Å}$, similar to μ-oxo bridged iron-porphyrin dimers) and Cu—O ($1.856\,\text{Å}$) bond lengths. Magnetic measurements and Mössbauer spectroscopic data indicate that the compound has an overall $S=2$ ground state with the high-spin Fe^{III} ($S=5/2$) antiferromagnetically coupled through the oxo ligand to the $S=1/2$ Cu^{II} ion.[33,34] Complex (**1**) may also be isolated in an acid–base reaction by mixing $[(TMPA)Cu^{II}(CH_3CN)]^{2+}$ and the hydroxo-Fe^{III} complex, $(F_8TPP)Fe^{III}$-OH, in the presence of triethylamine as base.[19] Complex (**1**) is notably basic and may be reversibly protonated to give the hydroxo-bridged species, $[(F_8\text{-}TPP)Fe^{III}-(OH^-)-Cu^{II}(TMPA)]^+$. Such hydroxo-bridged analogues are possible candidates for resting state enzyme mimics, based on structural comparison and magnetic characterization.[19]

In a similar self-assembly approach Holm and co-workers prepared various Fe^{III}—X—Cu^{II} complexes that possess "unsupported" bridging groups (X = O^{2-}, OH^-, HCO_2^-, and CN^-).[35–37] Reactions of $[Fe(OEP)(OClO_3^-)]$ (OEP = octaethylporphyrinate(2−)) with $[Cu(Me_6tren)(OH)]^+$ (Me_6tren = tris(2-(dimethylamino)ethyl)amine) in the presence of a base lead to the complex $[(OEP)Fe\text{-}O\text{-}Cu(Me_6tren)]^+$.[38] An X-ray crystal structure analysis indicates a nearly linear arrangement of Fe—O—Cu (angle of 176.7°), properties of which closely match those observed for $[(F_8TPP)Fe^{III}-(O^{2-})-Cu^{II}(TMPA)]^+$. Synthetic models of the μ-CN$^-$ heme-copper moieties have also received considerable attention,[32,36] since such adducts can serve as site probes amenable to study by spectroscopic techniques including IR, UV–Vis, EPR, MCD, Mössbauer, and magnetic susceptibility measurements. They are also of importance in relation to cyanide toxicity, as irreversible binding at the binuclear site is linked to consequent inhibition of C*c*O. Using a variety
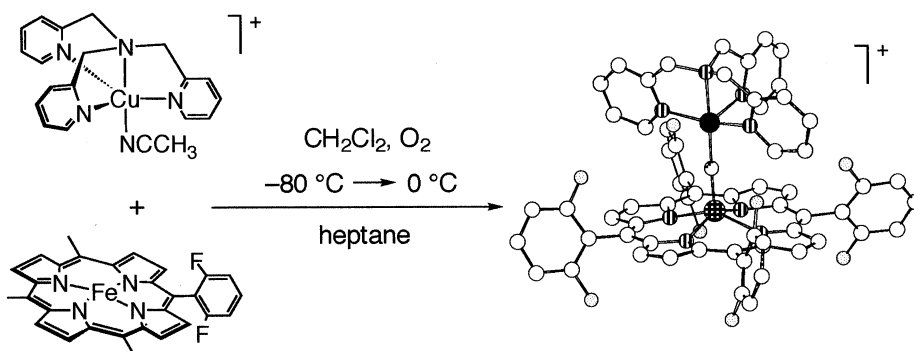
Figure 4 Reaction of copper(I) complex and reduced heme gives $[(F_8TPP)Fe^{III}-(O^{2-})-Cu^{II}(TMPA)]^+$ (**1**), in a crudely biomimetic reaction.
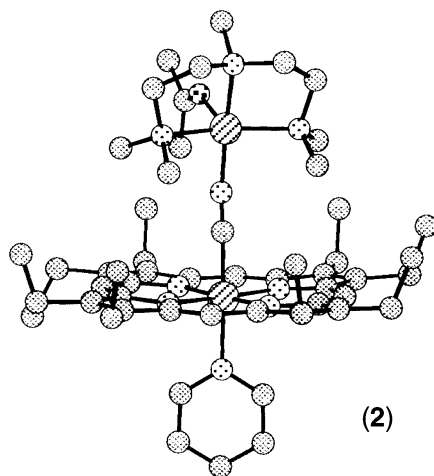
Figure 5 Structure of the μ-cyano-bridged heme-copper complex [(Py)(OEP)Fe^{III}-CN-Cu^{II}(Me$_5$dien) (OCMe$_2$)]$^{2+}$ (**2**), as a model for cyanide-poisoned cytochrome *c* oxidase.

of chelating tridentate or tetradentate ligands L, Holm and co-workers[35,36,39] generated a series of (OEP)(py)Fe^{III}-CN-Cu^{II}(L) complexes that feature ferromagnetically coupled low-spin Fe^{III} and Cu^{II} centers (i.e., $S = 1$). The cyanide stretching frequencies (ν_{CN}) increase with increasing Cu—N$_{CN}$—C$_{CN}$ angle and decreasing Cu–NC distance. The results establish with reasonable certainty the existence of the Fe^{III}-CN-Cu^{II} bridge motif in the cyanide treated oxidized enzyme. For the enzyme, ν_{CN} falls within a narrow range of 2,152–2,146 cm^{-1}. However, none of the structurally characterized model compounds display a ν_{CN} value exactly in this range, including [(Py)(OEP)Fe-CN-Cu(Me$_5$dien)(OCMe$_2$)]$^{2+}$ (**2**) ($\nu_{CN} = 2,175$ cm^{-1}), shown in Figure 5, or an analogous complex, [(Py)(F$_8$TPP) Fe^{III}-CN-Cu^{II}(TMPA)]$^{2+}$ ($\nu_{CN} = 2,170$ cm^{-1}).[40]

C*c*O models involving porphyrin complexes modified with covalently linked chelating ligands for copper ions have been developed to bring the Fe and Cu centers into close proximity and thus make reactivity studies more feasible. Collman and co-workers synthesized and characterized a series of "capped" porphyrins, for example with a 1,4,7-triazacyclonane (TACN) tethered to a Fe-porphyrin periphery by multiple linkers.[41] The reduced Fe^{II}/Cu^{I} complex (**3**) (see Figure 6) reacts with one equivalent of O$_2$ in the presence of an external base, 1,5-dicyclohexylimidazole, to generate an adduct.[42] Electrospray mass spectroscopy and redox titration measurements suggest that the oxygenated adduct could be a bridged peroxo species, but the rR spectroscopic data were inconclusive since the observed isotopic shift upon ^{18}O$_2$ substitution ($758 \rightarrow 740$ cm^{-1}) was smaller than expected.[42] This putative peroxide (dioxygen adduct) formed irreversibly, as indicated by the inability to displace O$_2$ by purging with either CO or Ar.
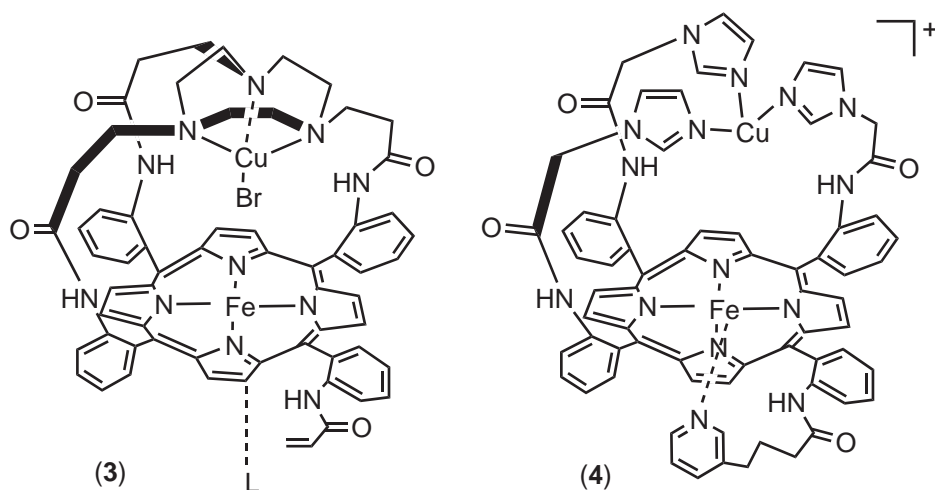

Figure 6 Heme-Cu model complexes of Collman and co-workers.[41,42]

Similar chemistry has been described with a closer structural analogue of the Fe_{a_3}/Cu_B active site, in which the copper coordination site is provided by three imidazole ligands, complex (**4**) in Figure 6.[43] This compound mediates the electrocatalytic four-electron reduction of O_2 in aqueous solution at physiological pH with no leakage of hydrogen peroxide, as similarly demonstrated with most of the previously reported TACN-based models. However, using tren-capped iron porphyrins (tren = tris(2-aminoethyl)amine) and new quinolinoyl picket porphyrins, Boitrel and co-workers[44] demonstrated efficient four-electron O_2-reduction with or without copper in the distal side of the porphyrin and whether or not a tailed nitrogen base was present. The authors suggest these observations are consistent with the formation of an important iron-peroxo intermediate (not Cu-ligated), which might also be relevant to the enzyme. In 2002 Collman, Boulatov and co-workers[45–47] employed an advanced generation model compound in studies comparing electrocatalytic activity with or without copper ion present; these researchers conclude that copper ion acts as a one-electron storage site, playing a critical role on the catalytic activity under diffusion-limited electron flux, being a readily accesible reductant. Under the conditions studied, the presence of copper ion (rather than with iron-only) suppresses superoxide-releasing autoxidation chemistry, decreases the susceptibility of the heme to inhibition by CN^- and CO; it accelerates O_2-binding, and it minimizes O—O bond homolysis in the reduction of H_2O_2.

The O_2-reacting model systems that Karlin and co-workers[48–54] have developed include those that use binucleating ligands such as ^{6}L, wherein a tripodal tetradentate TMPA (tris(2-pyridylmethyl)amine) moiety is covalently attached to a tetra-arylporphyrin (see Figure 7).[48,52] The complex $[(^6L)Fe^{II}Cu^I]^+$ (**5**) reacts with O_2 to give an adduct best described as a μ-peroxo Fe^{III}–(O_2^{2-})–Cu^{II} complex (**6**).[52] A peroxide O—O stretch appears at 787 cm^{-1} ($\Delta^{18}O_2$, 43 cm^{-1}) in the rR spectrum while ^{1}H-NMR spectroscopy shows downfield pyrrole and upfield Cu-ligand resonances indicative of a strongly coupled $S = 2$ system. Dioxygen uptake measurements indicate that 1 mol of O_2 is consumed per mole of complex (**5**) during the reaction. In the Matrix Assisted Laser Desorption-Time of Flight-Mass Spectrometry (MALDI-TOF-MS) pattern, a peak due to a compound with molecular weight corresponding to a molecule of Fe^{II}–Cu^I plus one of dioxygen is observed. Complex (**6**) is a possible model for an O_2-intermediate in CcO, as it is one of only a few discrete Fe—O_2—Cu adducts to have been described and is the first example of a high-spin heme-peroxo-Cu species. It thermally transforms to the μ-oxo species $[(^6L)Fe^{III}$–(O^{2-})–$Cu^{II}]^+$ (**7**), which has been structurally characterized (Figure 7).[48] In fact, essentially the same chemistry is observed with the individual components of the binucleating ligand system. Thus, $[Cu^I(TMPA)(MeCN)]^+$ reacts with $(F_8TPP)Fe^{II}$ (F_8TPP = tetrakis(2,6-difluorophenyl)porphrinate(2−)) and one equivalent of dioxygen to yield a heme-peroxo-copper complex $[(F_8TPP)Fe^{III}$–(O_2^{2-})–$Cu^{II}(TMPA)]^+$.[51] As possibly relevant to CcO O_2-reductive scission, the $\nu_{O—O}$ stretch here is noticably higher (807 cm^{-1}) compared to the value in the ^{6}L system (787 cm^{-1}), where ligand constraint induced structural alterations occur.[55] Karlin and co-workers have also studied Fe/Cu O_2-reactivity in systems wherein a tridentate (rather than tetradentate) copper-chelate is employed.[53,54] These also lead to low-temperature stable species described as heme-peroxo-copper adducts. Initial studies indicate that the $\nu_{O—O}$ stretch is still lower in these biomimetic systems with a tridentate ligand,[56,57] and that axial base donors for the heme may also be influential[58] in controlling the O—O bond strength.

Several other research groups are actively contributing in this field of CcO model chemistry. Naruta *et al.*[58] have reported tris(2-pyridylmethyl)amine Cu complex-linked iron *meso*-tetraphenylporphyrin derivatives and well-characterized Fe—(O_2)—Cu species that are similar to $[(^6L)Fe^{III}$–(O^{2-})–$Cu^{II}]^+$ (Structure (**7**)). A CcO model developed by Casella and co-workers is a natural porphyrin derivative, in which a polybenziimidazole residue for the Cu coordination site is attached to the propionic acid side chain of the deuteroporphyrin.[59] A new class of picket porphyrin, bearing covalently linked, axially placed tris(heterocycle) chelates for a copper ion, has been synthesized and characterized by Wilson and co-workers.[60]

Thus, great strides have been made in generating structural and crudely functional models for the heme-copper CcO active site. The latter involve either electrocatalytic O_2 reductions using heme-copper complexes with superstructured ligands, or O_2-reactivity studies aimed at how a proximate copper ion affects heme/O_2 reactions, or how a heme influences copper/O_2 reactivity. Such investigations can and will provide fundamental chemical, spectroscopic and mechanistic insights.
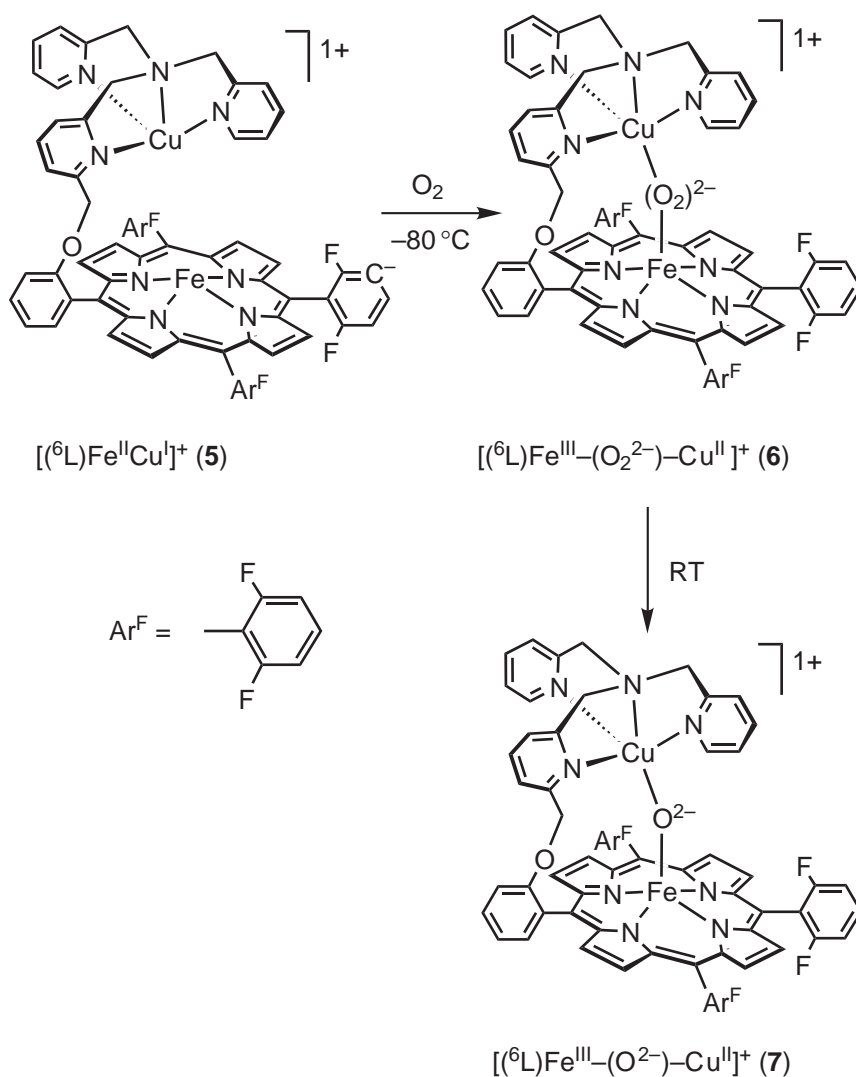
Figure 7 Heme-Cu dioxygen reactivity in a model system from Karlin and co-workers.[48,52]
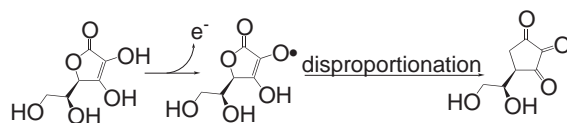
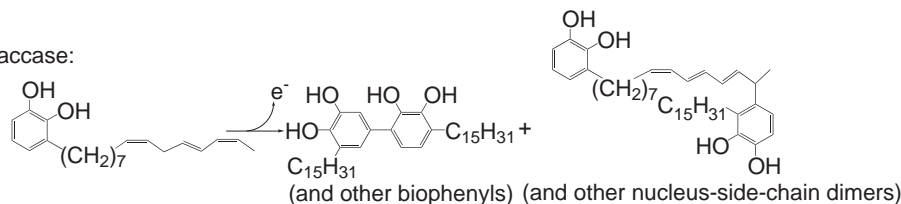## 8.17.3 "BLUE" COPPER OXIDASES

8.17.3.1 Protein Biochemistry

Multicopper oxidases[61–64] are defined by their homology with respect to spectroscopic features, amino acid sequence and reactivity. They are found both in plants and animals (humans among others). The currently well-defined members include ascorbate oxidase (AO), laccase (Lc), ceruloplasmin (Cp), Fet3 bilirubin oxidase (BO) and CueO. They all perform one-electron substrate oxidations, but the biological roles of these enzymes are either unclear or not unambiguously assigned. Examples of some of the enzyme reactions are given in Figure 8.

AO is widespread among plants and is also found in eubacteria and possibly in fungi.[63] In cells, most AO is associated with the cell wall.[63] A comparatively high level of specificity for L-ascorbate as substrate is observed, and oxidation to dehydroascorbate occurs via the disproportionation of the semidehydroascorbate radical. Other substrates are organic radicals, ferrocyanide, and substituted hydroquinones and leuco-2,6-dichlorophenol, which are oxidized to the respective *p*-quinones and the blue quinoid dye.[65] The rate of plant growth by way of cell elongation is strongly correlated to AO activity,[66] possibly via reaction of dehydroascorbate with cell wall components to cause the loosening of the cell wall itself,[66,67] or by suppression of lignin formation.[68] A role for AO in antioxidant defense also has been proposed[69] as it can scavenge organic radicals directly by
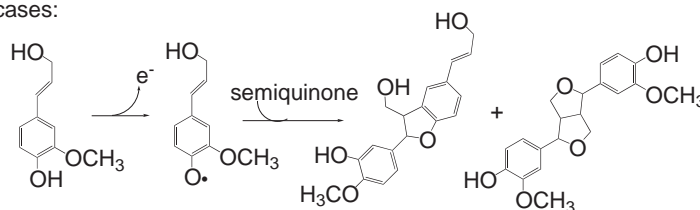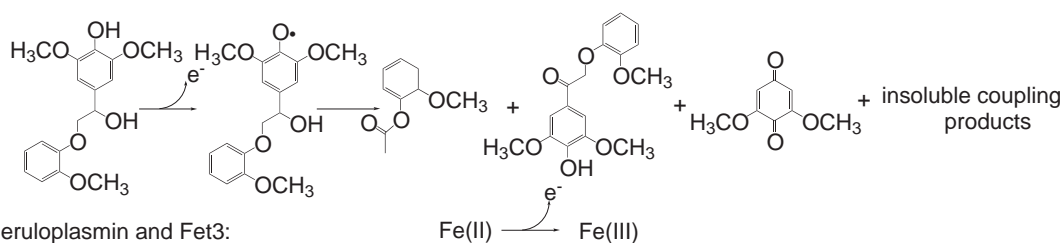
Ascorbate oxidase:

Rhus laccase:

(and other biophenyls) (and other nucleus-side-chain dimers)

Other plant laccases:

Fungal laccase:

Ceruloplasmin and Fet3:   Fe(II) $\xrightarrow{\text{e}^-}$ Fe(III)

Figure 8 Physiologically relevant reactions catalyzed by the blue copper oxidases (after Solomon and co-workers).[63]

accepting their extra electrons to reduce O_2 to water, or indirectly by producing the relatively harmless ascorbate radical which may quench free radical chains.

Laccases (Lcs) have been isolated from a variety of plant and fungal sources[63] and they are also reported to be widespread in bacteria.[70] Diphenol-oxidizing enzymes, thought to be Lcs, have also been found in insects.[71,72] Lcs are characterized by their low substrate specificity and they efficiently catalyze the one-electron oxidation of a wide variety of aromatic and inorganic species.[73,74] As most plant Lcs are able to oxidatively couple monolignols to dimers and tri-mers,[75–77] it has been proposed that they may be involved in lignin formation.[77] *R. Vernicifera* Lc (by far the most studied plant Lc), is unable to oxidize monophenols,[78] and is most likely not involved in lignin synthesis. It is present in large amounts in tree sap and catalyzes the aerobic polymerization of urushiol into lacquer in a process likened to the blood clotting response of animals.[73] Possible functions of fungal Lcs have been discussed elsewhere.[63]

Ceruloplasmin (Cp), secreted into the blood stream, appears to be ubiquitous in vertebrates. There is extensive *in vitro* evidence that Cp efficiently catalyzes the oxidation of Fe^{II} to Fe^{III} under near physiological conditions.[63,79] The role of Cp in iron metabolism is widely accepted and there is strong evidence for a secondary role in copper transport/regulation.[63,79] Defects in hepatic biosynthesis of Cp may result in diseases such as Wilson's disease.[79] There is conclusive evidence that Cp is the source for the copper found in cytochrome *c* oxidase and CuZn-SOD in cells.[63] Cp inhibition of Fenton chemistry-induced oxidative damage of deoxyribose, lipids, and DNA points to an antioxidant role,[80,81] which would explain the increase in Cp concentration in response to acute infection or inflammation.

Fet3 is found in the budding yeast, *Saccharomyces cerevisiae*, as a trans-membrane protein with a high degree of sequence homology with the other blue copper oxidases.[82–84] Like Cp, Fet3 can carry out the oxidation of Fe^{II} to Fe^{III}.[85] Fet3 is required for high affinity iron uptake.[82–84,86] Its role seems to be twofold, to correctly target the putative iron permease Ftr1 to the plasma membrane,[86,87] and also to oxidize Fe^{II} to Fe^{III} as a required step prior to the metal ion "relay" to Ftr1 for translocation.[88]

Bilirubin oxidase, purified and characterized from the fungus *Myrothecium verrucaria*,[89] has a strong amino acid sequence homology with the other blue copper oxidases[90] and point mutations studies on the supposed copper binding residues have confirmed its identity as a member of the enzymatic family.[91,92] *In vitro*, BO couples O_2-reduction to the oxidation of bilirubin to biliverdin. This catalytic activity has found clinical application in the diagnosis and treatment of jaundice and hyperbilirubinemia.

CueO (formerly YacK), identified as a homologue of Lc,[70] is found in the periplasmic space of *E. coli* and is known to be able to aerobically oxidize a wide variety of substrates, including 2,6-dimethoxyphenol, enterobactin (a catecholate siderophore produced by *E. coli*), and ferrous iron.[93,94] The biological role of CueO seems to be connected to copper regulation, probably effected not merely through copper binding.[95,96] An intriguing feature is that sizable CueO oxidase activity is observed only in the presence of excess copper. An X-ray structure is available.[97]

8.17.3.2 Spectroscopy and Copper Coordination

Spectroscopic, mechanistic, and X-ray structural insights (see Section 8.17.3.3) allow generalization of a number of features that apply to the entire family of the blue copper oxidases.

The minimum number of copper centers present in naturally occurring blue copper oxidases is four, all of which are in the oxidized, 2+ state in the resting (oxidized) enzymes. The T1 (type 1) or blue copper site (similar to that observed in blue electron-transfer proteins, e.g., plastocyanin and azurin) confers on solutions of these enzymes their characteristic color. It can either be tri- or tetracoordinate, but always includes two histidine and one cysteine residue. In the four-coordinate systems the last ligand is a weakly binding methionine which is "replaced" by the noncoordinating hydrophobic residues leucine or phenylalanine in the three-coordinate sites. T1 Cu exhibits an intense Cys-S $\rightarrow$ Cu^{II} LMCT absorption band in the 600 nm region ($\varepsilon \approx 5,000\,M^{-1}\,cm^{-1}$) that is responsible for the blue color. It is EPR active, displaying an unusually narrow hyperfine splitting $A_{||} = 43-95 \times 10^{-4}\,cm^{-1}$[163] that reflects the high degree of covalency (and electronic delocalization) of the Cu^{II}—S—Cys bond (see Chapter 8.4).

The T2 (or "normal") copper site has an unusual three-coordinate geometry with two histidines and a hydroxide (or a water molecule, indistinguishable by X-ray) ligands. It exhibits EPR parameters typical of normal (aqueous) copper ($A_{||} = 158-201 \times 10^{-4}\,cm^{-1}$)[63] and no intense (charge-transfer) features in the visible absorption spectrum.

The two remaining copper centers form the dinuclear T3 site in which each copper binds to three histidine ligands and a bridging hydroxo (or oxo) group in the oxidized state. The bimetallic cluster displays an absorption band at around 330 nm ($\varepsilon \approx 5,000\,M^{-1}\,cm^{-1}$) and is EPR silent, indicative of strong antiferromagnetic coupling, most likely due to the bridging ligand.

As first recognized via spectroscopic analyses by Solomon and colleagues[98] on *Rhus vernicifera* Lc, the T2 and T3 sites are located close to each other and form a trinuclear cluster, which functions as a unit and is the site of dioxygen binding and reduction to water. From the perspective of spectroscopic designation (T2 vs. T3 Cu moieties, especially in T2 depleted (T2D) protein derivatives), McMillin and colleagues[99] argue that, at least in *Polyporous versicolor* Lc, the T2 copper center is not the EPR active species in the trinuclear cluster and that ligand reorganization (of the eight His residues for three Cu ions) can occur. The role of the T1 Cu center is to harvest electrons (subsequently transferred intramolecularly to the T2/T3 site) through oxidation of the enzyme substrate. A highly conserved His–Cys–His motif comprises an electron-transfer pathway from the T1 Cu-Cys to each of the T3 His-Cu moieties (nine covalent, two coordination bonds, see Figure 9).

8.17.3.3 X-ray Structures

The first X-ray structure of a multicopper blue oxidase was reported by Messerschmidt and co-workers in 1989,[100] on an oxidized form of zucchini squash AO (now refined to 1.9 Å resolution,[101] Figure 9). It is a homodimer with each monomer containing the four-copper functional unit, as described above in the context of the spectroscopic data. A hydroxide (OH$^-$) or oxide (O^{2-}) was described as a T3 Cu bridging ligand; the average copper–copper distance in the T2/T3 site is 3.74 Å and the individual distances do not deviate by more than 0.16 Å from the mean value. The shortest distance between the type 1 copper center and the trinuclear site is 12.2 Å.
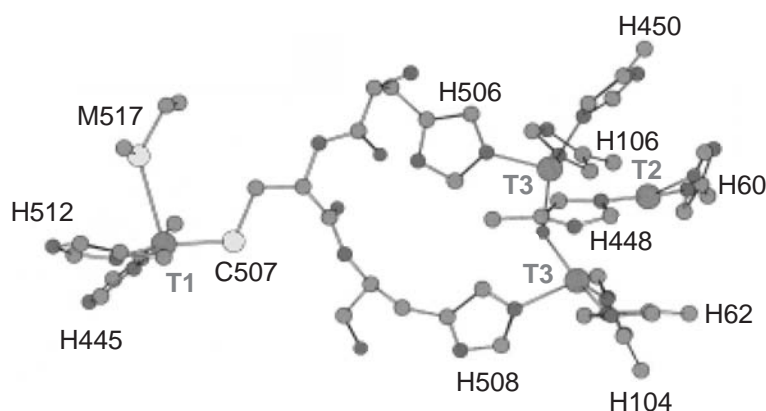
Figure 9 Crystal structure of the active site of resting (oxidized) ascorbate oxidase from *Cucurbita pepo medullosa* (after Solomon and co-workers).[62]

An X-ray structure (2.2 Å resolution) of a fully reduced AO[102] shows that the coordination environments and Cu–ligand distances of the T1 and T2 coppers are essentially unchanged compared to the oxidized enzyme. However, the O(H) bridging ligand is released from the T3 site, and the now tricoordinate copper centers in the T3 unit move apart (to 5.1 Å). In addition, the average distance among the T2/T3 metal ions grows to 4.5 Å. In a structure obtained by soaking AO with H_2O_2 (2.6 Å resolution),[102] the bridging OH ligand is replaced by a hydroperoxide (HOO$^-$) group that binds terminally to one T3 copper center. The existence of this structure influenced Messerschmidt to suggest its occurrence in the AO catalytic cycle, see below.

It has been shown by several groups that copper can be selectively removed from the blue copper oxidases, thereby causing a disappearance of the EPR signal assigned to the T2 copper. The so-called type-2 depleted (T2D) enzyme derivative is usually produced via the use of metal chelating reagents under reducing conditions.[64] Biochemical, spectroscopic, and enzyme mechanistic investigations[62–64] on the T2D forms of the multicopper oxidases are historically very important. Two X-ray structures of T2D enzymes have been obtained. T2D AO from zucchini squash,[103] *Cucurbita pepo medullosa* (2.5 Å resolution), displays removal of 1.3 copper ions per AO monomer. While T1 is not affected, Cu is lost from all three sites of the T2/T3 cluster with the T2 copper position being most affected. Complete disappearance of the EPR signal normally ascribed to the T2 site suggests that what is left is an EPR silent, antiferromagnetically coupled copper pair. T2D Lc from mushroom *Coprinus cinereus* (2.2 Å resolution)[104] does not display any concomitant loss of copper at the T3 site while the T2 copper is lost completely. His399, whose equivalent in resting AO is a T2 ligand, undergoes a conformational change so as to coordinate one of the T3 coppers (distance: 2.5 Å). In a 1.68 Å, 100 K structure,[105] this histidine is disordered with two contributing conformations. In one it displays the same orientation as in resting AO, but in the other it coordinates one of the T3 coppers. The bridging interaction between the T3 coppers is lost in both conformations.

X-ray structures of Lc from white rot fungus *Trametes versicolor* (2.4 Å[106] and 1.90 Å resolution[107]) have been determined. This is a monomeric protein, with four bound copper ions. As in all fungal Lcs it displays a tricoordinate T1 site. The lack of a fourth ligand, occupied now by a phenylalanine residue, is believed to cause the elevated redox potentials of fungal Lcs (to +700 to +800 mV from values of +300 to +400 mV in plant Lcs and AOs).[108–110] A 2,5-xylidine molecule is present in one of the structures,[106] in the the putative reducing cavity found adjacent to the T1 copper. It appears to be hydrogen-bonded with the T1 ligand His458 (as well as Asp206), suggesting that His458 is the "entrance door" for electron transfer from substrate to the T1 copper.

Native human Cp (3.0 Å resolution)[111,112] is a monomeric protein, comprised of a triangular array of six domains[113] and holds six or more copper centers per unit. A T1 copper center is found in domains 2, 4 and 6, while three copper ions are instead also located at the interface of domains 1 and 6 to form the T2/T3 trinuclear site. Domains 4 and 6 possess labile metal sites (see Figure 10) partially occupied by copper ions and in proximity (~10 Å) to the T1 sites. These are believed to be the sites of substrate (Fe^{II}) binding and oxidation. The T1 sites of domains 4 and 6 are four coordinate (with axial Met as the fourth ligand), whereas that of domain 2 is three coordinate. Spectroscopic evidence suggests that the latter is in a permanently reduced state.[114] The tertiary
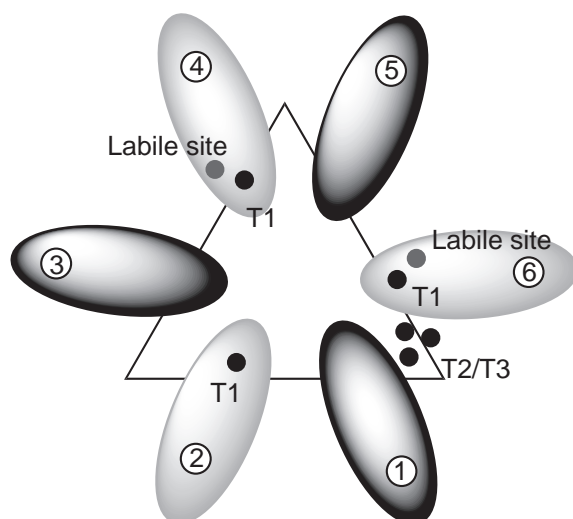
Figure 10   Schematic view of the crystal structure of human ceruloplasmin (after Zaitseva *et al.*[111]; Lindley *et al.*[112]).

structure of the protein constrains the distance between the T1 sites to be ~18 Å, well within electron-transfer range. Moreover, clear electron-transfer pathways between the metals exist. A hydroxide ion binds the T2 site and is hydrogen-bonded to the hydroxyl group of a tyrosine. As in oxidized AO (see above), a second hydroxide group bridges the T3 copper centers and His1020–Cys1021–His1022 in domain 6 affords a through-bond electron-transfer pathway between the T1 site of domain 6 and the T3 coppers.

8.17.3.4   Enzymatic O$_2$-derived Intermediates and Reaction Mechanism

Given the extent of similarity with regard to amino acid sequence, topography of the active site, spectroscopic features, and reactivity among all blue multicopper oxidases, it is usually assumed that the main features of the reaction mechanism are common to all members of the enzyme family. The catalytic pathway involves the rate-limiting one-electron oxidation of the substrate [62,115] coupled to (and driven by) the four-electron reduction of dioxygen to water. Laser-flash photo-lysis[116] or pulse radiolysis[117,118] studies on the rate of oxidation of substrates by AO have proven that the T1 copper is the primary electron acceptor from the reducing substrate. Anaerobic reduction of the resting T2/T3 site[117,118] is carried out through intramolecular electron transport from the T1 copper. Laccase, the simplest of the known blue copper oxidases, has been the enzyme of choice for most mechanistic studies.[115,119–131]

8.17.3.4.1   Native intermediate

When reduced native laccase reacts with dioxygen, an intermediate is formed with absorption features at 360 nm and 600 nm,[119] the latter of which is associated with the oxidation of the T1 site. Below 20 K this so-called "native" intermediate displays an EPR signal with an unusually low *g*-value centered at 1.94 which broadens when the intermediate is prepared with $^{17}O_2$.[120] No EPR signal that might be assigned to the oxidized T2 site is visible. ^{18}O isotope ratio mass spectrometry (IRMS) combined with ^{17}O-EPR studies show that one oxygen atom of the O$_2$ unit is present in the resting enzyme and is bound to the T2 copper.[131] Interpretation of the EPR spectrum of the native intermediate has been controversial. It has been suggested that it is due to a three-electron reduced oxyl or hydroxyl radical species bound to a reduced copper center.[120,132] However, X-ray absorption[121] and MCD[122] spectroscopic studies by Solomon and co-workers were interpreted to indicate that in the native intermediate all of the copper centers are oxidized and that the three T2/T3 centers are bridged by O^{2-} or OH^- groups. The unusual EPR signal observed is consistent with expectations, since an extensive bridging interaction leads to an $S = 1/2$ ground state, yet with delocalization over the three Cu^{II} (each $S = 1/2$) ions.[62,63]

The observed rate of decay of the native intermediate to the resting state of the enzyme and rate of reduction of the trinuclear copper cluster of the latter are both too slow to be consistent with being relevant to the actual enzyme catalytic turnover.[116,117,133] Reduction of the native intermediate is however rapid,[63] indicating that this is the most likely catalytically relevant oxidized species and that the usually discussed normal resting state is altogether bypassed in the reaction cycle.

8.17.3.4.2 *Peroxide-level intermediate*

Remarkably, reduced T2D Lc does not react with atmospheric O_2.[123] The behavior of the dinuclear T3 center thus contrasts starkly with that displayed by other reduced dinuclear copper sites of enzymes such as hemocyanin and tyrosinase or synthetic model dinuclear complexes (see Chapter 8.15).[134–136] These promptly perform a two-electron reduction of O_2 to the peroxide level (reversibly, in the case of hemocyanin).

However, T1Hg Lc, a derivative in which the T1 copper center has been replaced by a redox inert mercury ion,[124–126] does react with O_2 when the remaining trinuclear (T2/T3) center is reduced, producing an intermediate that displays UV-absorption features that are different from those of the native intermediate (see Figure 11).[128] The rate of formation of this adduct is essentially the same as that measured for the native intermediate.[127] Thus, this T1Hg intermediate may be a precursor of the native one and its formation may be rate determining in the overall process of O_2-reduction to H_2O.

IRMS indicates that two oxygen atoms are added to the active site upon formation of the T1Hg intermediate.[129] Circular dichroism spectra,[129] which probe the T3 site of this intermediate, display strong similarities with that of the oxidized, resting trinuclear copper cluster. Thus, both
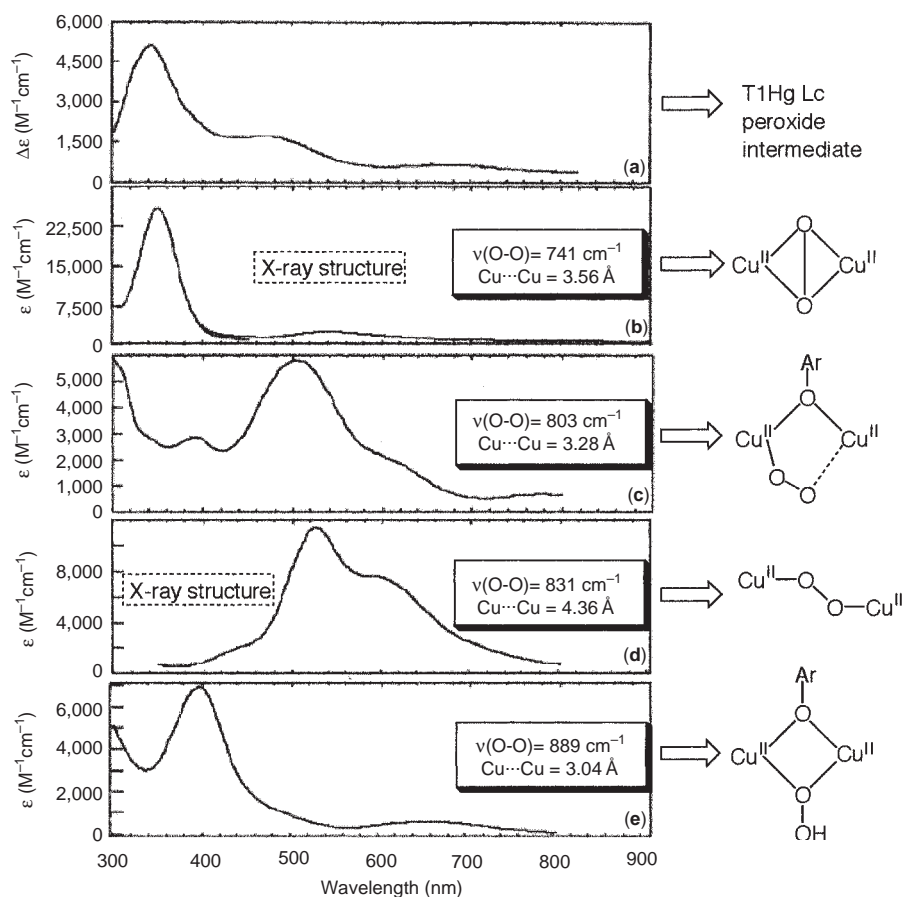
Figure 11 Absorption spectrum of T1Hg Lc oxygen intermediate/peroxide-level intermediate (a) compared to spectra of peroxo-dicopper(II) model complexes (b)–(e). Structural types indicated (after Solomon and co-workers).[63]

T3 coppers are oxidized. On the other hand, the absence of either low-temperature MCD or EPR signals[129] are consistent with a reduced T2 copper site. In summary, two electrons seem to have been transferred to dioxygen from the T3 coppers to generate a peroxide-level intermediate.

Magnetic-susceptibility measurements on the peroxide-level intermediate indicate that the two oxidized T3 centers are strongly antiferromagnetically coupled, indicative of the presence of a bridging ligand between them.[129] Furthermore, the Fourier transform of an EXAFS spectrum reveals an intense outer-shell peak at ~3.4 Å,[129] which is not present in the resting form of T1Hg Lc. This result implies that a bridging group is present between two copper centers that cannot be the μ-hydroxide of the resting enzyme. It was therefore concluded that a peroxide level species bridges the two copper ions.

In complementary experiments,[130] addition of H_2O_2 to the oxidized resting T1Hg Lc yielded a species that displayed the same EXAFS features as the peroxide-level intermediate. In this derivative, however, as opposed to the peroxide level intermediate, the T2 copper site is oxidized, allowing the use of EPR and low-temperature MCD spectroscopies to probe the coordination of the site. The data thus obtained, integrated with CD data (probing the T3 site), point to the formation of a peroxide bridge between the T2 site and one of the T3 coppers.

8.17.3.4.3 *Proposed mechanisms for O_2 reduction*

The two main proposed mechanisms for the catalytic cycle of O_2 reduction to H_2O, depicted in Figures 12 and 13, respectively, have been put forth by the groups of Messerschmidt[117] and Solomon.[62] Both involve the initial two-electron reduction of dioxygen to the peroxide level by the fully reduced enzyme. Messerschmidt's proposed peroxide-level intermediate, in contrast with Solomon's, does not involve the presence of a peroxide level bridging ligand (see Figure 13); a hydroperoxide ligand is instead proposed to bind terminally to one of the oxidized T3 copper ions (see Section 8.17.3.3). Solomon and co-workers, aside from a μ-hydroperoxo ligand bridging two copper ions, allow for the possibility of a peroxide moiety bridging all three copper ions (see Figure 13). Interestingly, an X-ray structure of a laccase derivative from *Melanocarpus albomyces*[137] reveals what appears to be an O_2 ligand spaced between all three T2/T3 copper ions (see Figure 14), although the Cu—O distances reported (2.4 to 2.6 Å) are not in line with strong bonding interactions.

The next step of the water reduction cycle, i.e., the formation of the native intermediate, is radically different in the two schemes. Solomon's mechanism requires a second two-electron reduction step—deemed necessary in order to overcome a large thermodynamic barrier for a one-electron process.[62,63] This step completes the reduction of O_2 to H_2O and leads to the formation of an "all-bridged" intermediate (see Figure 13). This intermediate is proposed to undergo reduction by the substrate (by way of the T1 center) to start a new catalytic cycle. Messerschmidt's proposal involves a sequence of two single-electron reduction steps. The first leads to the formation of an oxyl or hydroxyl radical bound to a reduced T3 copper center (in accordance with the earlier interpretations of the EPR signal), and with concomitant release of a water molecule. Further oxidation of this reduced copper ion and the release of a second molecule of water leads to the formation of the catalytically relevant all-oxidized intermediate which once fully re-reduced can commence a new catalytic cycle.

8.17.3.5 Synthetic Model Compounds

The chemistry of synthetic model compounds has been of great value in formulating and advancing hypotheses concerning O_2-chemistry in blue copper oxidases. This has been accomplished by comparing and contrasting structures and spectroscopy of O_2-adducts of ligand–copper(I) complexes with unstable or otherwise hard to probe natural enzyme intermediates or derivatives (i.e., peroxide level species).

8.17.3.5.1 *Models for the blue copper oxidase peroxide-level intermediate*

A mononuclear, terminal Cu^{II}-hydroperoxide complex has been obtained by Masuda and colleagues[138] through reaction at room temperature of the cupric complex of the tripodal ligand bis(6-pivalamide-2-pyridylmethyl)-(2-pyridylmethyl)amine with excess hydrogen peroxide in
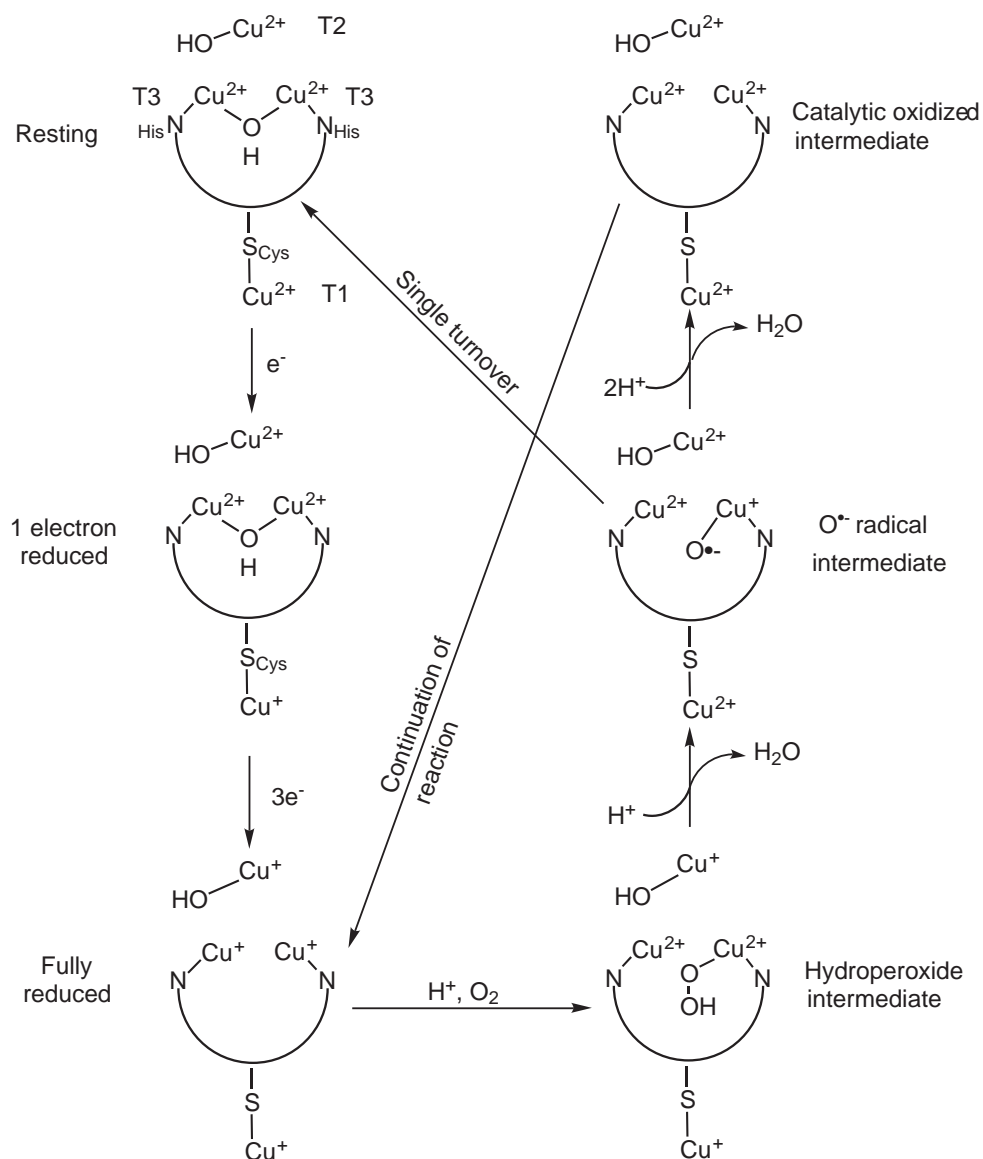
Figure 12 Messerchmidt's proposal for the mechanism of O_2 reduction to H_2O carried out by the blue copper oxidases (after Messerchmidt).[117]

acetonitrile. A crystal structure reveals a Cu^{II}—O—O—H moiety (Cu—O—O angle of 114.5°), stabilized by H-bonding to ligand N-H groups (see Figure 15). Absorbance features are: $\lambda_{max} = 380$ nm ($\varepsilon = 890\,M^{-1}\,cm^{-1}$), 660 nm ($\varepsilon = 150\,M^{-1}\,cm^{-1}$), and 830 nm ($\varepsilon = 250\,M^{-1}\,cm^{-1}$). Resonance Raman vibrational data show that $\nu(O—O) = 856\,cm^{-1}$, i.e., very similar to that of free hydrogen peroxide ($873\,cm^{-1}$).

A great deal more is known for binuclear systems, which are better for comparison to O_2 adducts within the trinuclear T2/T3 multicopper oxidase active site (see Figure 11). Mononuclear ligand–Cu(I) or dicopper(I) complexes with a binucleating ligand react with O_2 to yield peroxo or hydroperoxo-dicopper(II) complexes. These products have been characterized, often via low-temperature spectro-scopic studies (see Chapter 8.15). Kitajima's μ-η^2:η^2-peroxo (side-on peroxo) dicopper(II) adduct[139] shown in Figure 11(b) represents the formulation now known to exist in the O_2-carrier hemocyanin.[140] Another possible structure of a peroxo adduct is end-on. Two examples (Figure 11(c)[141] and 11(d)[142]) are known; in the former case a binucleating phenoxide supporting ligand leads to a terminal end-on geometry (probably no bridging of the peroxide ligand) marked by two LMCT transitions (~510 and 640 (sh) nm). In the latter, a mononucleating tripodal tetradentate ligand tris(2-pyridyl)methylamine leads to the bridged binuclear species shown. It appears spectroscopically similar, but in fact possesses

Figure 13 Solomon's proposal for the mechanism of O_2-reduction to H_2O carried out by the blue copper oxidases (after Solomon).[62]

Figure 14 Crystal structure of the T2/T3 cluster site of laccase from *Melanocarpus albomyces* (after Hakulininen *et al.*).[137]

Figure 15 A mononuclear, terminal Cu^{II}-hydroperoxide complex, obtained by Masuda and colleagues.[138]

more than the two peroxide derived LMCT bands. A μ-1,1-hydroperoxo dicopper adduct (Figure 11(e)) also has been reported.[143] Taking into account all the available protein spectroscopic data, Solomon and colleagues proposed a bridging hydroperoxo-dicopper adduct, like Figure 11(e), as one likely formulation for the Lc intermediate (see Figure 13).

8.17.3.5.2 Model systems involving trinuclear copper

A significant future challenge is to generate model synthetic systems where one forces three copper ions (like in the T2/T3 cluster) to participate in, or at least be in proximity for, O_2-derived chemistry and O—O reductive cleavage. Only a few relevant examples have been reported.

Stack and co-workers[144] discovered a new paradigm in copper(I)/O_2 chemistry, wherein a Cu^I/O_2 stoichiometry of 3:1 is observed when a copper(I) complex with *N*-permethylated (1*R*,2*R*)cyclohex-anediamine (**L**) reacts with O_2 at $-80\,^{\circ}C$ in dichloromethane. In this reaction, O—O cleavage occurs, and a (bis-μ_3-oxo)-$Cu^{II}_2Cu^{III}$ cluster forms (see Figure 16). Thus, four electrons are supplied to O_2 from three copper ions, similar to what occurs overall in multicopper oxidases, going from the fully reduced to the native intermediate (see Section 8.17.3.4.3). Spectroscopic,[144,145] structural,[144,145] and theoretical[146] evidence shows that no charge delocalization occurs in this trinuclear copper cluster; two metal centers possess a 2+ charge whereas the third is in its 3+ state.

Karlin and co-workers have designed several trinucleating ligands[147–151] for study in Cu^I_3/O_2 reactivity studies. For example, when a tricopper(I) complex of MES (Structure (**a**), Figure 17) is oxygenated, hydroxylation of the mesitylene ligand occurs.[149] A hexanuclear copper(II) product
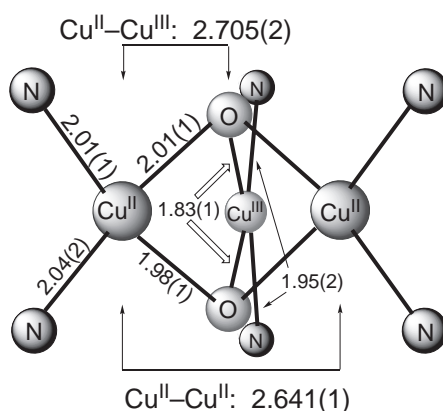
Figure 16 Schematic representation of the core of the crystal structure of $[L_3Cu_3O_3]^{3+}$.

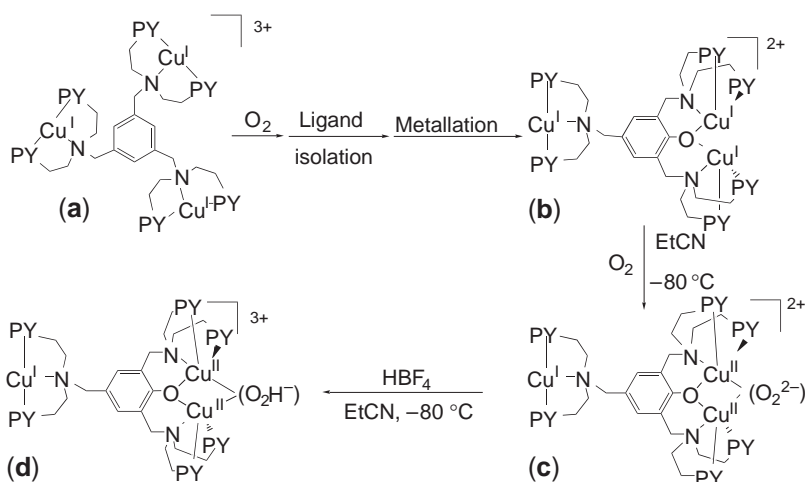**Figure 17** Trinuclear complex $[Cu^I_3(MES)]^{3+}$ (a) is hydroxylated in a reaction with dioxygen, leading to a new ligand tricopper(I) complex $[Cu^I_3(MES-O^-)]^{2+}$ (b). This reacts with O_2 giving peroxo(c) and hydroperoxo (d) dicopper(II) species.

was characterized, and as a result a new phenolic trinucleating MES-OH could be recovered. This allows generation of a trinuclear copper(I) complex (**b**) (see Figure 17), with unsymmetrical copper environments. [150] Low-temperature oxygenation in EtCN solvent, which inhibits O_2-reaction with the tridentate N_3–Cu^I moiety,[152] leads to a peroxo-dicopper(II) complex (**c**) (see Figure 17). This compound has spectroscopic features very similar to the phenoxide-bridged dicopper complex in Figure 11(c), but as a mixed-valent species it is a crude model for the laccase peroxo-level intermediate because a third copper(I) ion is present. In fact, the complex (**c**) can be further reacted (i.e., protonated) to give a μ-1,1-hydroperoxo product (**d**) (see Figure 17).

Although remarkable, neither of the systems reviewed in this last section has direct bearing or closely resembles the native intermediate of the laccase. Modeling of blue multicopper oxidase O_2 binding, O—O reductive cleavage, and fully understanding the role of protons and protonation levels remain a challenging research areas for the future.

NOTE ADDED IN PROOF

Naruta and Co-Workers (et al., *Angew. Chem. Int. Ed.*, 2003, *42*, 2788–2791) have obtained an important X-ray crystal structure of a heme-peroxo-Cu complex, a possible model compound relevant to cytochrome *c* oxidase activity (see Section 8.17.2.4). The structure has a bridged peroxo moiety, side-on (η^2-) with respect to the high-spin heme iron(III), but end-on (η^1-) with respect to the copper(II) ion.

8.17.4   REFERENCES

1. Babcock, G. T.; Wikström, M. *Nature* **1992**, *356*, 301–309.
2. Ferguson-Miller, S.; Babcock, G. T. *Chem. Rev.* **1996**, *96*, 2889–2907.
3. Calhoun, M. W.; Thomas, J. W.; Gennis, R. B. *Trends Biochem. Sci.* **1994**, *19*, 325–330.
4. Wikström, M. *Biochim. Biophys. Acta* **2000**, *1458*, 188–198.
5. Wikström, M.; Morgan, J. E.; Verkhovsky, M. I. *J. Bioenerg. Biomembr.* **1998**, *30*, 139–145.
6. Gennis, R. B. *Biochim. Biophys. Acta* **1998**, *1365*, 241–248.
7. Michel, H.; Behr, J.; Harrenga, A.; Kannt, A. *Annu. Rev. Biophys. Biomol. Struct.* **1998**, *27*, 329–356.
8. Sanders-Loehr, J. Case Study: The Cu_A Site of Cytochrome *c* Oxidase. In *Physical Methods in Bioinorganic Chemistry, Spectroscopy and Magnetism*; Que, L., Jr., Ed.; University Science Books: Sausalito, CA, 2000, pp 505–513, 525–526.
9. George, S. D.; Metz, M.; Szilagyi, R. K.; Wang, H.; Cramer, S. P.; Lu, Y.; Tolman, W. B.; Hedman, B.; Hodgson, K. O.; Solomon, E. I. *J. Am. Chem. Soc.* **2001**, *123*, 5757–5767.
10. Ostermeier, C.; Harrenga, A.; Ermler, U.; Michel, H. *Proc. Natl. Acad. Sci. USA* **1997**, *94*, 10547–10553.
11. Iwata, S.; Ostermeier, C.; Ludwig, B.; Michel, H. *Nature* **1995**, *376*, 660–669.
12. Harrenga, A.; Michel, H. *J. Biol. Chem.* **1999**, *274*, 33296–33299.
13. Yoshikawa, S.; Shinzawa-Itoh, K.; Nakashima, R.; Yaono, R.; Yamashita, E.; Inoue, N.; Yao, M.; Jei-Fei, M.; Libeu, C. P.; Mizushima, T.; Yamaguchi, H.; Tomizaki, T.; Tsukihara, T. *Science* **1998**, *280*, 1723–1729.
14. Soulimane, T.; Buse, G.; Bourenkov, G. P.; Bartunik, H. D.; Huber, R.; Than, M. E. *EMBO J.* **2000**, *19*, 1766–1776.
15. Svensson-Ek, M.; Abramson, J.; Larsson, G.; Tornroth, S.; Brzezinski, P.; Iwata, S. *J. Mol. Biol.* **2002**, *321*, 329–339.
16. Abramson, J.; Riistama, S.; Larsson, G.; Jasaitis, A.; Svensson-Ek, M.; Laakkonen, L.; Puustinen, A.; Iwata, S.; Wikstrom, M. *Nat. Struct. Biol.* **2000**, *7*, 910–917.
17. Oganesyan, V. S.; Butler, C. S.; Watmough, N. J.; Greenwood, C.; Thomson, A. J.; Cheesman, M. R. *J. Am. Chem. Soc.* **1998**, *120*, 4232–4233.
18. Day, E. P.; Peterson, J.; Sendova, M. S.; Schoonover, J.; Palmer, G. *Biochemistry* **1993**, *32*, 7855–7860.
19. Fox, S.; Nanthakumar, A.; Wikström, M.; Karlin, K. D.; Blackburn, N. J. *J. Am. Chem. Soc.* **1996**, *118*, 24–34.
20. Das, T. K.; Pecoraro, C.; Tomson, F. L.; Gennis, R. B.; Rousseau, D. L. *Biochemistry* **1998**, *37*, 14471–14476.
21. MacMillan, F.; Kannt, A.; Behr, J.; Prisner, T.; Michel, H. *Biochemistry* **1999**, *38*, 9179–9184.
22. Poulos, T. L.; Li, H.; Raman, C. S. *Curr. Opin. Chem. Biol.* **1999**, *3*, 131–137.
23. Babcock, G. T. *Proc. Natl. Acad. Sci. USA* **1999**, *96*, 12971–12973.
24. Proshlyakov, D. A.; Pressler, M. A.; DeMaso, C.; Leykam, J. F.; DeWitt, D. L.; Babcock, G. T. *Science* **2000**, *290*, 1588–1591.
25. Kitagawa, T. *J. Inorg. Biochem.* **2000**, *82*, 9–18.
26. Gennis, R. B. *Proc. Natl. Acad. Sci. USA* **1998**, *95*, 12747–12749.
27. Shultz, B. E.; Chan, S. I. *Annu. Rev. Biophys. Biomol. Struct.* **2001**, *30*, 23–65.
28. Zaslavsky, D.; Gennis, R. B. *Biochim. Biophys. Acta* **2000**, *1458*, 164–179.
29. Michel, H. *Biochemistry* **1999**, *38*, 15129–15140.
30. Fabian, M.; Wong, W. W.; Gennis, R. B.; Palmer, G. *PNAS* **1999**, *96*, 13114–13117.
31. Fabian, M.; Palmer, G. *Biochemistry* **1995**, *34*, 13802–13810.
32. Kitajima, N. *Adv. Inorg. Chem.* **1992**, *39*, 1–77.
33. Karlin, K. D.; Nanthakumar, A.; Fox, S.; Murthy, N. N.; Ravi, N.; Huynh, B. H.; Orosz, R. D.; Day, E. P. *J. Am. Chem. Soc.* **1994**, *116*, 4753–4763.
34. Nanthakumar, A.; Fox, S.; Murthy, N. N.; Karlin, K. D. *J. Am. Chem. Soc.* **1997**, *119*, 3898–3906.

35. Scott, M. J.; Holm, R. H. *J. Am. Chem. Soc.* **1994**, *116*, 11357–11367.
36. Holm, R. H. *Pure Appl. Chem.* **1995**, *67*, 217–224.
37. Kauffmann, K. E.; Goddard, C. A.; Zang, Y.; Holm, R. H.; Münck, E. *Inorg. Chem.* **1997**, *36*, 985–993.
38. Lee, S. C.; Holm, R. H. *J. Am. Chem. Soc.* **1993**, *115*, 11789–11798.
39. Lim, B. S.; Holm, R. H. *Inorg. Chem* **1998**, *37*, 4898–4908.
40. Corsi, D. M.; Murthy, N. N.; Young, J. V. G.; Karlin, K. D. *Inorg. Chem.* **1999**, *38*, 848–858.
41. Collman, J. P.; Schwenninger, R.; Rapta, M.; Bröring, M.; Fu, L. *Chem. Commun.* **1999**, 137–138.
42. Collman, J. P.; Herrmann, P. C.; Boitrel, B.; Zhang, X.; Eberspacher, T. A.; Fu, L.; Wang, J.; Rousseau, D. L.; Williams, E. R. *J. Am. Chem. Soc.* **1994**, *116*, 9783–9784.
43. Collman, J. P.; Rapta, M.; Bröring, M.; Raptova, L.; Schwenninger, R.; Boitrel, B.; Fu, L.; L'Her, M. *J. Am. Chem. Soc.* **1999**, *121*, 1387–1388.
44. Ricard, D.; Andrioletti, B.; Boitrel, B.; L'Her, M. *Chem. Commun.* **1999**, 1523–1524.
45. Boulatov, R.; Collman, J. P.; Shiryaeva, I. M.; Sunderland, C. J. *J. Am. Chem. Soc.* **2002**, *124*, 11923–11935.
46. Collman, J. P.; Boulatov, R.; Shiryaeva, I. M.; Sunderland, C. J. *Angew. Chem. Int. Ed. Engl.* **2002**, *41*, 4139–4142.
47. Collman, J. P.; Boulatov, R. *Angew. Chem. Int. Ed. Engl.* **2002**, *41*, 3487–3489.
48. Ju, T. D.; Ghiladi, R. A.; Lee, D.-H.; van Strijdonck, G. P. F.; Woods, A. S.; Cotter, R. J.; Young, J. V. G.; Karlin, K. D. *Inorg. Chem.* **1999**, *38*, 2244–2245.
49. Ghiladi, R. A.; Karlin, K. D. *Inorg. Chem.* **2002**, *41*, 2400–2407.
50. Ghiladi, R. A.; Kretzer, R. M.; Guzei, I.; Rheingold, A. L.; Neuhold, Y.-M.; Hatwell, K. R.; Zuberbühler, A. D.; Karlin, K. D. *Inorg. Chem.* **2001**, *40*, 5754–5767.
51. Ghiladi, R. A.; Hatwell, K. R.; Karlin, K. D.; Huang, H.-w.; Moenne-Loccoz, P.; Krebs, C.; Huynh, B. H.; Marzilli, L. A.; Cotter, R. J.; Kaderli, S.; Zuberbuehler, A. D. *J. Am. Chem. Soc.* **2001**, *123*, 6183–6184.
52. Ghiladi, R. A.; Ju, T. D.; Lee, D.-H.; Moënne-Loccoz, P.; Kaderli, S.; Neuhold, Y.-M.; Zuberbühler, A. D.; Woods, A. S.; Cotter, R. J.; Karlin, K. D. *J. Am. Chem. Soc.* **1999**, *121*, 9885–9886.
53. Kopf, M. A.; Karlin, K. D. *Inorg. Chem.* **1999**, *38*, 4922–4923.
54. Kopf, M.-A.; Neuhold, Y.-M.; Zuberbühler, A. D.; Karlin, K. D. *Inorg. Chem.* **1999**, *38*, 3093–3102.
55. Obias, H. V.; van Strijdonck, G. P. F.; Lee, D.-H.; Ralle, M.; Blackburn, N. J.; Karlin, K. D. *J. Am. Chem. Soc.* **1998**, *120*, 9696–9697.
56. Karlin, K. D. and co-workers, unpublished results.
57. Kim, E.; Helton, M. E.; Wasser, I. M.; Karlin, K. D.; Lu, S.; Huang, H.-w.; Moënne-Loccoz, P.; Incarvito, C. D.; Rheingold, A. L.; Honecker, M.; Kaderli, S.; Zuberbuehler, A. D. *Proc. Natl. Acad. Sci. USA* **2003**, *100*, 3623–3628.
58. Naruta, Y.; Sasaki, T.; Tani, F.; Tachi, Y.; Kawato, N.; Nakamura, N. *J. Inorg. Biochem.* **2001**, *83*, 239–246.
59. Casella, L.; Monzani, E.; Gullotti, M.; Gliubich, F.; De Gioia, L. *J. Chem. Soc., Dalton Trans.* **1994**, 3203–3210.
60. Thrash, T. P.; Wilson, L. J. *Inorg. Chem.* **2001**, *40*, 4556–4562.
61. Malkin, R.; Malmström, B. G. *Adv. Enzymol.* **1970**, *33*, 177–244.
62. Solomon, E. I.; Chen, P.; Metz, M.; Lee, S.-K.; Palmer, A. E. *Angew. Chem. Int. Ed. Engl.* **2001**, *40*, 4570–4590.
63. Solomon, E. I.; Sundaram, U. M.; Machonkin, T. E. *Chem. Rev.* **1996**, *96*, 2563–2605.
64. Messerschmidt, A. Ascorbate Oxidase. In *Handbook of Metalloproteins*; Messerschmidt, A.; Huber, R.; Poulos, T.; Wieghardt, K., Eds.; Wiley: New York, 2001, Vol. 1, pp 1345–1358.
65. Dayan, J.; Dawson, C. R. *Biochem. Biophys. Res. Commun.* **1976**, *73*, 451–4588.
66. Esaka, M.; Fujisawa, K.; Goto, M.; Kisu, Y. *Plant Physiol.* **1992**, *100*, 231–237.
67. Lin, L. S.; Varner, J. E. *Plant Physiol.* **1991**, *96*, 159–165.
68. Takahama, U.; Oniki, T. *Plant and Cell Physiology* **1994**, *35*, 257–266.
69. Buettner, G. R. *Arch. Biochem. Biophys.* **1993**, *300*, 535–543.
70. Alexandre, G.; Zhulin, I. B. *Trends Biotechnol.* **2000**, *18*, 41–42.
71. Barrett, F. M.; Andersen, S. O. *Insect Biochem.* **1981**, *11*, 17–23.
72. Thomas, B. R.; Yonekura, M.; Morgan, T. D.; Czapla, T. H.; Hopkins, T. L.; Kramer, K. J. *Insect Biochem.* **1989**, *19*, 611–622.
73. Malmstrom, B. G.; Andreasson, L. E.; Reinhammar, B. *The Enzymes,* 3rd ed. Boyer, P.D., Editor; Academic Press: New York, **1975**, *12*, 507–579.
74. Xu, F.; Shin, W.; Brown, S. H.; Wahleithner, J. A.; Sundaram, U. M.; Solomon, E. I. *Biochim. Biophys. Acta* **1996**, *1292*, 303–311.
75. Bao, W.; O'Malley, D. M.; Whetten, R.; Sederoff, R. R. *Science* **1993**, *260*, 672–674.
76. McDougall, G. J.; Stewart, D.; Morrison, I. M. *Phytochemistry* **1994**, *37*, 683–688.
77. Sterjiades, R.; Dean, J. F. D.; Gamble, G.; Himmelsbach, D. S.; Eriksson, K. E. L. *Planta* **1993**, *190*, 75–87.
78. Nakamura, W. *J. Biochem.* **1967**, *62*, 54–61.
79. Lindley, P. F. Ceruloplasmin. In *Handbook of Metalloproteins*; Messerschmidt, A.; Huber, R.; Poulos, T.; Wieghardt, K., Eds.; Wiley: New York, 2001, Vol. 1, pp 1369–1380.
80. Gutteridge, J. M. C.; Quinlan, G. J. *Biochim. Biophys. Acta* **1993**, *1156*, 144–150.
81. Gutteridge, J. M. C. *Clin. Sci.* **1991**, *81*, 413–417.
82. Yuan, D. S.; Stearman, R.; Dancis, A.; Dunn, T.; Beeler, T.; Klausner, R. D. *Proc. Natl. Acad. Sci. USA* **1995**, *92*, 2632–2636.
83. Askwith, C.; Eide, D.; Van Ho, A.; Bernard, P. S.; Li, L.; Davis-Kaplan, S.; Sipe, D. M.; Kaplan, J. *Cell* **1994**, *76*, 403–410.
84. De Silva, D. M.; Askwith, C. C.; Eide, D.; Kaplan, J. *J. Biol. Chem.* **1995**, *270*, 1098–1101.
85. De Silva, D.; Davis-Kaplan, S.; Fergestad, J.; Kaplan, J. *J. Biol. Chem.* **1997**, *272*, 14208–14213.
86. Stearman, R.; Yuan, D. S.; Yamaguchi-Iwai, Y.; Klausner, R. D.; Dancis, A. *Science* **1996**, *271*, 1552–1557.
87. Askwith, C. C.; de Silva, D.; Kaplan, J. *Molec. Microbiol.* **1996**, *20*, 27–34.
88. Hassett, R. F.; Yuan, D. S.; Kosman, D. J. *J. Biol. Chem.* **1998**, *273*, 23274–23282.
89. Murao, S.; Tanaka, N. *Agric. Biol. Chem.* **1981**, *45*, 2383–2384.
90. Koikeda, S.; Ando, K.; Kaji, H.; Inoue, T.; Murao, S.; Takeuchi, K.; Samejima, T. *J. Biol. Chem.* **1993**, *268*, 18801–18809.
91. Shimizu, A.; Kwon, J.-H.; Sasaki, T.; Satoh, T.; Sakurai, N.; Sakurai, T.; Yamaguchi, S.; Samejima, T. *Biochemistry* **1999**, *38*, 3034–3042.

92. Shimizu, A.; Sasaki, T.; Kwon, J. H.; Odaka, A.; Satoh, T.; Sakurai, N.; Sakurai, T.; Yamaguchi, S.; Samejima, T. *J. Biochem.* **1999**, *125*, 662–668.
93. Kim, C.; Lorenz, W. W.; Hoopes, J. T.; Dean, J. F. *J. Bacteriol.* **2001**, *183*, 4866–4875.
94. Grass, G.; Rensing, C. *Biochem. Biophys. Res. Commun.* **2001**, *286*, 902–908.
95. Grass, G.; Rensing, C. *J. Bacteriol.* **2001**, *183*, 2145–2147.
96. Outten, F. W.; Huffman, D. L.; Hale, J. A.; O'Halloran, T. V. *J. Biol. Chem.* **2001**, *276*, 30670–30677.
97. Roberts, S. A.; Weichsel, A.; Grass, G.; Thakali, K.; Hazzard, J. T.; Tollin, G.; Rensing, C.; Montfort, W. R. *Proc. Nat. Acad. Sci., USA* **2002**, *99*, 2766–2771.
98. Spira-Solomon, D. J.; Allendorf, M. D.; Solomon, E. I. *J. Am. Chem. Soc.* **1986**, *108*, 5318–5328.
99. Fraterrigo, T. L.; Miller, C.; Reinhammar, B.; McMillin, D. R. *J. Biol. Inorg. Chem.* **1999**, *4*, 183–187.
100. Messerschmidt, A.; Rossi, A.; Ladenstein, R.; Huber, R.; Bolognesi, M.; Gatti, G.; Marchesini, A.; Petruzzelli, R.; Finazzi-Agro, A. *J. Mol. Biol.* **1989**, *206*, 513–529.
101. Messerschmidt, A.; Ladenstein, R.; Huber, R.; Bolognesi, M.; Avigliano, L.; Petruzzelli, R.; Rossi, A.; Finazzi-Agro, A. *J. Mol. Biol.* **1992**, *224*, 179–205.
102. Messerschmidt, A.; Luecke, H.; Huber, R. *J. Mol. Biol.* **1993**, *230*, 997–1014.
103. Messerschmidt, A.; Steigemann, W.; Huber, R.; Lang, G.; Kroneck, P. M. H. *Eur. J. Biochem.* **1992**, *209*, 597–602.
104. Ducros, V.; Marek Brzozowski, A.; Wilson, K. S.; Brown, S. H.; Østergaard, P.; Schneider, P.; Yaver, D. S.; Pedersen, A. H.; Davies, G. J. *Nat. Struct. Biol.* **1998**, *5*, 310–316.
105. Ducros, V.; Brzozowski, A. M.; Wilson, K. S.; Ostergaard, P.; Schneider, P.; Svendson, A.; Davies, G. J. *Acta Crystallogr., Sect. D: Biol. Crystallogr.* **2001**, *D57*, 333–336.
106. Bertrand, T.; Jolivalt, C.; Briozzo, P.; Caminade, E.; Joly, N.; Madzak, C.; Mougin, C. *Biochemistry* **2002**, *41*, 7325–7333.
107. Piontek, K.; Antorini, M.; Choinowski, T. *J. Biol. Chem.* **2002**, *277*, 37663–37669.
108. Davies, G. J.; Ducros, V. Laccase. In *Handbook of Metalloproteins*; Messerschmidt, A., Huber, R., Poulos, T., Wieghardt, K., Eds.; Wiley: New York, 2001, Vol. 1, pp 1359–1368.
109. Karlsson, B. G.; Aasa, R.; Malmstroem, B. G.; Lundberg, L. G. *FEBS Lett.* **1989**, *253*, 99–102.
110. Guckert, J. A.; Lowery, M. D.; Solomon, E. I. *J. Am. Chem. Soc.* **1995**, *117*, 2817–2844.
111. Zaitseva, I.; Zaitsev, V.; Card, G.; Moshkov, K.; Bax, B.; Ralph, A.; Lindley, P. *J. Biol. Inorg. Chem.* **1996**, *1*, 15–23.
112. Lindley, P.; Card, G.; Zaitseva, I.; V., Z.; Reinhammar, B.; Selin-Lindgren, E.; Yoshida, K. *J. Biol. Inorg. Chem.* **1997**, *2*, 454–463.
113. Adman, E. T. *Adv. Protein Chem.* **1991**, *42*, 145–197.
114. Machonkin, T. E.; Zhang, H. H.; Hedman, B.; Hodgson, K. O.; Solomon, E. I. *Biochemistry* **1998**, *37*, 9570–9578.
115. Petersen, L. C.; Degn, H. *Biochim. Biophys. Acta* **1978**, *526*, 85–92.
116. Meyer, T. E.; Marchesini, A.; Cusanovich, M. A.; Tollin, G. *Biochemistry* **1991**, *30*, 4619–4623.
117. Kyritsis, P.; Messerschmidt, A.; Huber, R.; Salmon, G. A.; Sykes, A. G. *J. Chem. Soc., Dalton Trans.* **1993**, 731–735.
118. Farver, O.; Pecht, I. *Mol. Cryst. Liq. Cryst.* **1991**, *194*, 215–224.
119. Andreasson, L. E.; Branden, R.; Malmstrom, B. G.; Vanngard, T. *FEBS Lett.* **1973**, *32*, 187–189.
120. Aasa, R.; Branden, R.; Deinum, J.; Malmstrom, B. G.; Reinhammar, B.; Vanngard, T. *Biochem. Biophys. Res. Commun.* **1976**, *70*, 1204–1209.
121. Lee, S.-K.; DeBeer George, S.; Antholine, W. E.; Hedman, B.; Hodgson, K. O.; Solomon, E. I. *J. Am Chem. Soc.* **2002**, *124*, 6180–6193.
122. Clark, P. A.; Solomon, E. I. *J. Am. Chem. Soc.* **1992**, *114*, 1108–1110.
123. Kau, L.-S.; Spira-Solomon, A. J.; Penner-Hahn, J. E.; Hodgson, K. O.; Solomon, E. I. *J. Am. Chem. Soc.* **1987**, *109*, 6433–6442.
124. Morie-Bebel, M. M.; Menzie, J. L.; McMillin, D. R. *Biol. Inorg. Copper Chem., Proc. Conf. Copper Coord. Chem., 2nd* **1986**, *1*, 89–95.
125. Morie-Bebel, M. M.; Morris, M. C.; Menzie, J. L.; McMillin, D. R. *J. Am. Chem. Soc.* **1984**, *106*, 3677–3678.
126. Severns, J. C.; McMillin, D. R. *Biochemistry* **1990**, *29*, 8592–8597.
127. Cole, J. L.; Ballou, D. P.; Solomon, E. I. *J. Am. Chem. Soc.* **1991**, *113*, 8544–8546.
128. Cole, J. L.; Tan, G. O.; Yang, E. K.; Hodgson, K. O.; Solomon, E. I. *J. Am. Chem. Soc.* **1990**, *112*, 2243–2249.
129. Shin, W.; Sundaram, U. M.; Cole, J. L.; Zhang, H. H.; Hedman, B.; Hodgson, K. O.; Solomon, E. I. *J. Am. Chem. Soc.* **1996**, *118*, 3202–3215.
130. Sundaram, U. M.; Zhang, H. H.; Hedman, B.; Hodgson, K. O.; Solomon, E. I. *J. Am. Chem. Soc.* **1997**, *119*, 12525–12540.
131. Branden, R.; Deinum, J.; Coleman, M. *FEBS Lett.* **1978**, *89*, 180–182.
132. Aasa, R.; Branden, R.; Deinum, J.; Malmstrom, B. G.; Reinhammar, B.; Vanngard, T. *FEBS Lett.* **1976**, *61*, 115–119.
133. Farver, O.; Pecht, I. *Proc. Natl. Acad. Sci. USA* **1992**, *89*, 8283–8287.
134. Zhang, C. X.; Liang, H.-C.; Humphreys, K. J.; Karlin, K. D. Copper-Dioxygen Complexes and Their Roles in Biomietric Oxidation Reaction In *Catalytic Activation of Dioxygen by Metal Complexes*; Simandi, L., Ed.; Kluwer: Dordrecht, The Netherlands, 2002, Chapter 2, pp 79–121.
135. Karlin, K. D.; Zuberbühler, A. D. Formation, Structure, and Reactivity of Copper Dioxygen Complexes. In *Bioinorganic Catalysis: Second Edition, Revised and Expanded*; Reedijk, J., Bouwman, E., Eds.; Marcel Dekker: New York, 1999, pp 469–534.
136. Blackman, A. G.; Tolman, W. B. *Struct. Bonding (Berlin)* **2000**, *97*, 179–211.
137. Hakulinen, N.; Kiiskinen, L.-L.; Kruus, K.; Saloheimo, M.; Paananen, A.; Koivula, A.; Rouvinen, J. *Nat. Struct. Biol.* **2002**, *9*, 601–605.
138. Wada, A.; Harata, M.; Hasegawa, K.; Jitsukawa, K.; Masuda, H.; Mukai, M.; Kitagawa, T.; Einaga, H. *Angew. Chem. Int. Ed. Engl.* **1998**, *37*, 798–799.
139. Kitajima, N.; Fujisawa, K.; Morooka, Y.; Toriumi, K. *J. Am. Chem. Soc.* **1989**, *111*, 8975–8976.
140. Magnus, K. A.; Hazes, B.; Ton-That, H.; Bonaventura, C.; Bonaventura, J.; Hol, W. G. J. *Proteins: Struct., Funct., Genet.* **1994**, *19*, 302–309.
141. Karlin, K. D.; Cruse, R. W.; Gultneh, Y.; Farooq, A.; Hayes, J. C.; Zubieta, J. *J. Am. Chem. Soc.* **1987**, *109*, 2668–2679.

142. Karlin, K. D.; Ghosh, P.; Cruse, R. W.; Farooq, A.; Gultneh, Y.; Jacobson, R. R.; Blackburn, N. J.; Strange, R. W.; Zubieta, J. *J. Am. Chem. Soc* **1988**, *110*, 6769–6780.
143. Ghosh, P.; Tyeklár, Z.; Karlin, K. D.; Jacobson, R. R.; Zubieta, J. *J. Am. Chem. Soc.* **1987**, *109*, 6889–6891.
144. Cole, A. P.; Root, D. E.; Mukherjee, P.; Solomon, E. I.; Stack, T. D. P. *Science* **1996**, *273*, 1848–1850.
145. Root, D. E.; Henson, M. J.; Machonkin, T.; Mukherjee, P.; Stack, T. D. P.; Solomon, E. I. *J. Am. Chem. Soc.* **1998**, *120*, 4982–4990.
146. Daul, C.; Fernandez-Ceballos, S.; Ciofini, I.; Rauzy, C.; Schlapfer, C.-W. *Chem. Eur. J.* **2002**, *8*, 4392–4401.
147. Karlin, K. D.; Gan, Q.-F.; Farooq, A.; Liu, S.; Zubieta, J. *Inorg. Chim. Acta* **1989**, *165*, 37–39.
148. Frey, S. T.; Sun, H. H. J.; Murthy, N. N.; Karlin, K. D. *Inorg. Chim. Acta* **1996**, *242*, 329–338.
149. Karlin, K. D.; Gan, Q.-F.; Farooq, A.; Liu, S.; Zubieta, J. *Inorg. Chem.* **1990**, *29*, 2549–2551.
150. Karlin, K. D.; Gan, Q.-F.; Tyeklár, Z. *Chem. Commun.* **1999**, 2295–2296.
151. Humphreys, K. J.; Karlin, K. D.; Rokita, S. E. *J. Am Chem. Soc.* **2002**, *124*, 8055–8066.
152. Sanyal, I.; Mahroof-Tahir, M.; Nasir, S.; Ghosh, P.; Cohen, B. I.; Gultneh, Y.; Cruse, R.; Farooq, A.; Karlin, K. D.; Liu, S.; Zubieta, J. *Inorg. Chem.* **1992**, *31*, 4322–4332.
153. Naruta, *et al. Chem. Int. Ed.* **2003**, *42*, 2788–2791.

8.18
Molybdenum and Tungsten Enzymes

J. M. TUNNEY, J. MCMASTER, and C. D. GARNER
University of Nottingham, UK

8.18.1 INTRODUCTION

8.18.1.1 Perspective

Molybdenum is required as a trace element by all forms of life and is unique in being the only 4d transition metal that is utilized by biological systems. The relatively high concentration of molybdenum in seawater (10^{-5} g dm^{-3})[1] means that it is readily available for incorporation into biological systems, despite its relatively low terrestrial abundance. However, in the early stages of the evolution of life on this planet, molybdenum was probably not so readily available since it is present in the Earth's crust primarily as molybdenite, MoS_2, which is insoluble in water. In the presence of O_2 and water, MoS_2 is converted (Equation (1)) into molybdate, $[MoO_4]^{2-}$. Therefore, following the appearance of photosynthetic organisms and the subsequent production of O_2 on Earth some 2.7×10^9 years ago,[2] molybdenum would have become available for incorporation into biological systems:

$$2MoS_2 + 7O_2 + 2H_2O \rightleftharpoons 2[MoO_4]^{2-} + 4SO_2 + 4H^+ \tag{1}$$
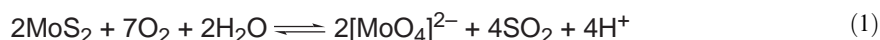
The first evidence that molybdenum is required for the metabolism of living systems was obtained in the 1930s, through studies of plants that established that it is essential for nitrogen fixation;[3] this special process is accomplished by the nitrogenase enzymes of bacteria and archaea

(Chapter 8.22). Dietary studies showed that molybdenum was an essential element for the normal growth and health of humans, animals, plants, and microorganisms. The first confirmation of the presence of molybdenum within an enzyme came in 1953 when dietary studies and atomic spectroscopy revealed its presence in hepatic and lactic xanthine oxidase.[4] Since then, extensive investigations have shown that molybdenum is an integral component of the active site of a large number (>40) of enzymes that catalyze important reactions in the carbon, nitrogen, sulfur, and selenium cycles of the biosphere.[5–8]

The majority of molybdenum enzymes catalyze a conversion, the net effect of which is oxygen atom transfer (OAT) to or from the substrate (Equation (2)), e.g., DMSO to DMS, sulfite to sulfate, an aldehyde to the corresponding carboxylic acid, or nitrate to nitrite. Crystallographic and spectroscopic investigations of molybdenum enzymes, combined with studies of relevant chemical systems, have allowed us to begin to understand the nature and the function of their catalytic centers.[5–40] In many cases protein crystallographic studies[41–64] have provided vital information concerning the nature of the active site, together with a clear perspective of its location within the protein assembly and the proximity of other functional groups:

$$X + H_2O \rightleftharpoons XO + 2H^+ + 2e^- \tag{2}$$
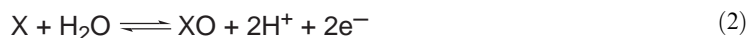
8.18.2 NATURE OF THE CATALYTIC CENTERS OF MOLYBDENUM OXIDOREDUCTASES

8.18.2.1 MPT

All molybdenum enzymes, with the notable exception of the nitrogenases (Section 8.18.3), involve a single metal atom bound to one or two molecules of a special ligand, originally named "molybdopterin" (MPT)[17] (Figure 1). However, as MPT also binds tungsten[65–74] (Section 8.18.3) this moiety is better named as the metal-binding pyranopterin ene-1,2-dithiolate, retaining the abbreviation MPT. MPT is comprised of a pterin, with pyrimidine and pyrazine rings, the latter being linked to a pyran ring that carries both an ene-1,2-dithiolate (dithiolene) that coordinates the Mo (or W) as a bidentate ligand and a $-CH_2OPO_3^{2-}$ group. In molybdenum–MPT enzymes isolated from prokaryotes (bacteria and archaea), the phosphate group may be part of a diphosphate linkage that forms a dinucleotide with adenine, guanine, cytosine, or hypoxanthine as the base. The form of MPT found in tungsten–MPT enzymes varies in a less predictable manner.

In each molybdenum–MPT[41–67] (and tungsten-MPT[69–74]) enzyme, the structure of the MPT is remarkably conserved; both the pyrazine and pyran rings are distinctly nonplanar and each of the three chiral carbon atoms of the pyran ring is in the (*R*)-configuration. The pyran ring adopts a half-chair conformation that deviates significantly from the plane of the pterin system. In the enzymes the best plane defined by the pyran ring is tilted ~40° from the plane of the pterin ring. However, the relationship between the rings is not precisely determined since there is some conformational flexibility in the way the pyran ring is tilted out of the plane of the conjugated part of the pterin. Additional conformational flexibility is present, in respect of the phosphorylated
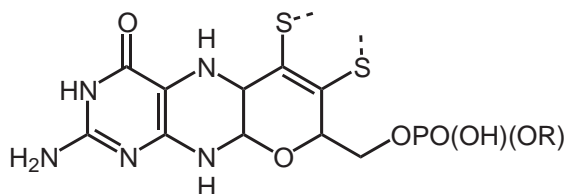
R = H (MPT); R = nucleoside

Figure 1   Structure of "molybdopterin"[17] or preferably the metal-binding pyranopterin ene-1,2-dithiolate (MPT); the phosphate group may be bound to a nucleotide.

hydroxymethyl side chain that leads to a wide variety of positions for the phosphate group relative to the pterin.

The polar (O, N, NH, and NH$_2$) groups of MPT participate extensively in the formation of hydrogen bonds to complementary groups of the polypeptide chain. The extent of this hydrogen bonding is significantly extended when the phosphate is bound to the dinucleotide (see Figure 1). This network of hydrogen bonds serves to appropriately locate the catalytically active center at a particular position within the polypeptide chain with respect to:

- the "funnel" in the protein "sheath," through which the substrate enters and product leaves;
- the "pocket" that binds the substrate in an orientation suitable for catalytic conversion to the particular product; and
- the electron transfer relay, involving the other redox active prosthetic groups, that leads to the site on the exterior of the protein where the redox partner binds.

There are several potential roles for MPT, including: cooperating with the metal–dithiolene center in the two-electron redox change required for catalysis; handling the protons involved in the OAT process (see Equation (2)); providing a route for electron transfer to or from the metal centre during turnover;[72,75] fine-tuning the redox potential of the metal center; and/or enhancing the OAT by strong S$\rightarrow$M σ- and π-donation.[76] With respect to the first of these aspects, it is important to note that in each crystallographic study the structure of MPT is apparently equivalent to the fully reduced state, i.e., a tetrahydropterin. This suggests that the pterin component of MPT is not involved in the redox changes that occur during catalysis. However, it should be noted that the opening of the pyran ring of MPT is likely to be facile and this ring-opened form (Figure 2) shows that, formally, MPT is a dihydropterin.[22]

The biosynthesis of molybdenum–MPT centers is an evolutionarily conserved pathway in archaea, eubacteria, and eukaryotes, including humans. This process is now reasonably well understood[8,77–83] and the structures of several proteins involved in the biosynthesis have been determined.[84–87] The metal is incorporated as the final stage and, in *Escherichia coli*, the *mod*-ABCD gene products are involved in the uptake of molybdate.[88] The ModA-C proteins comprise the molybdate transport system.[89] ModA is the initial binding protein and has a relatively high affinity for both molybdate and tungstate (4 µM and 7 µM, respectively);[90] the specificity of ModA to bind molybdate and tungstate (tungstate transport) but not sulfate or other anions is determined by the size of the binding pocket, in which the four oxo groups are held by hydrogen bonds to the amide and hydroxyl groups of the polypeptide chain.[91]

Molybdate is then delivered to ModB, located on the periplasmic side of the inner membrane; this protein, in concert with ModC, initiates the chemical transformation of the molybdenum and MoeA and MogA are believed to function in the addition of molybdenum to the dithiolene group of MPT.[92]

"Molybdenum cofactor deficiency" is a rare inborn error of metabolism and this can have serious consequences for the organism; this is well documented for humans for sulfite oxidase[93] (see Section 8.18.2.5), leading to severe neurological disorders, seizures, mental retardation, and death at an early age.[94] Therefore, it is encouraging that an MPT-free form of sulfite oxidase has been reconstituted with a *de novo* form of the "molybdenum cofactor" synthesized from molybdate and a biosynthethic precursor of MPT, "compound Z."[95]

8.18.2.2 Classification of Molybdenum–MPT Centers

Structural and spectroscopic studies of the oxidized state of the molybdenum–MPT enzymes have identified four types of molybdenum center (Figure 3) that provide a good basis for the classification of the molybdenum–MPT enzymes into families.[8]

- Members of the dimethylsulfoxide (DMSO) reductase family have the molybdenum ligated by two MPTs, one oxo group, and the donor atom from the side chain of an amino acid residue—Oγ of a serinyl residue (DMSO reductase or trimethylamineoxide (TMAO) reductase), Sγ of a cysteinyl residue (dissimilatory nitrate reductase), or Seγ of selenocysteinyl residue (formate dehydrogenase).
- Members of the sulfite oxidase family, including the assimilatory nitrate reductases, possess a *cis*-dioxo $\{MoO_2\}^{2+}$ center that is bound to one MPT, one hydroxo group, and a cysteinyl residue.

Fully oxidized pterin   Dihydropterin   Tetrahydropterin


MPT

Ring-opened MPT
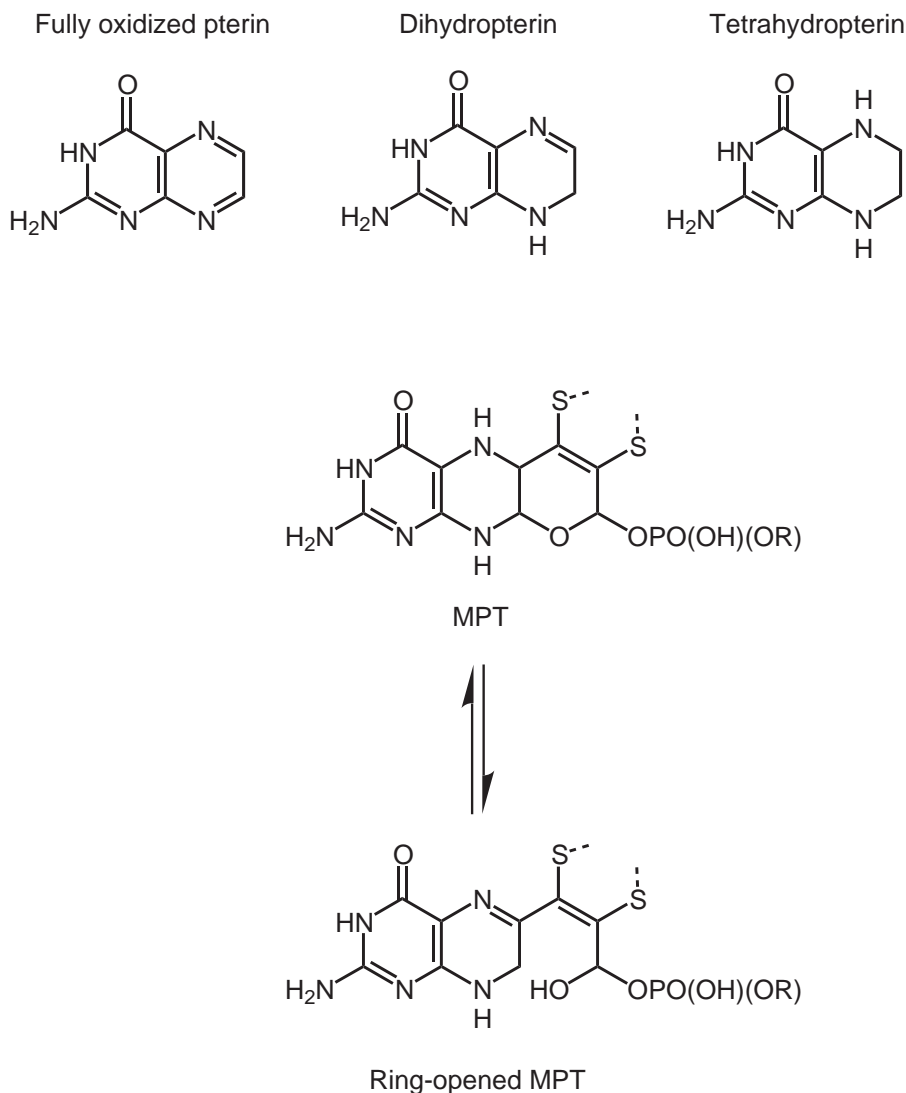
Figure 2 Oxidation levels of pterins and the opening of the pyran ring of MPT, showing that MPT is formally at the dihydropterin oxidation level.

- Members of the xanthine dehydrogenase/xanthine oxidase family, including the aldehyde oxidases, have a *cis*-oxo, sulfido $\{MoOS\}^{2+}$ center bound to one MPT and a hydroxo group.

Thus, unlike the nitrogenases, which possess an iron–molybdenum cofactor (FeMoco, Chapter 8.22), there is no unique "molybdenum cofactor" (or Moco) for the molybdenum–MPT enzymes. Rather there is a diverse collection of catalytic centers with the common features of a single molybdenum atom ligated by one or two MPTs, plus additional ligands, which can be an amino acid side chain, and/or one, two, or three small inorganic ligands—such as oxo, sulfido, or hydroxo groups.[8,96,97] Molybdenum–MPT enzymes of the same family generally possess a considerable homology in the sequence of their polypeptide chains and appear to employ a similar mechanism for catalysis. The former point illustrates that these molybdenum centers are produced under genetic control and the latter point demonstrates that reactivity at a metal center is greatly influenced by its coordination sphere.

There are some general points that can be made concerning the function of the catalytic centers of molybdenum-MPT enzymes. As noted in Section 8.18.1, these enzymes catalyze the two-electron oxidation or reduction of the substrate, often coupled to OAT (Equation (2)). Spectroscopic studies, notably EPR investigations of the Mo(V) state, have shown that the substrate
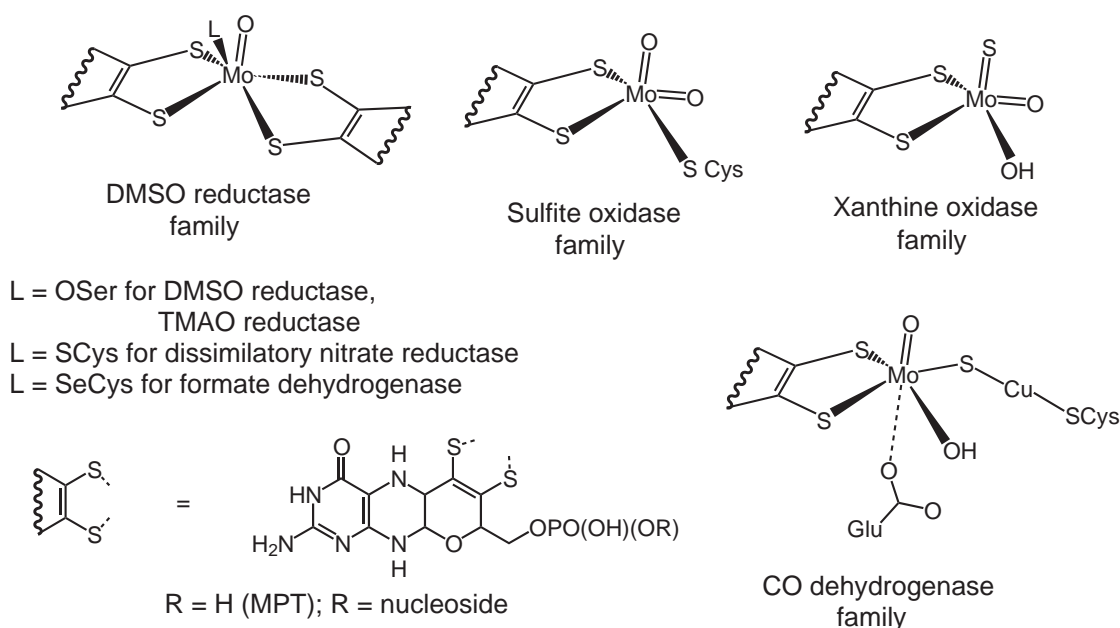
Figure 3 Structural basis for classifying the major families of the molybdenum–MPT enzymes.[8]

interacts directly with the metal center[98] and a substrate-bound form of the DMSO reductase from *Rhodobacter capsulatus* has been structurally characterized.[44] For oxidases, it is generally considered that catalysis involves the redox change from Mo(VI) to Mo(IV) with reductases utilizing the Mo(IV) to Mo(VI) redox change. In each case, the catalytically active state is regenerated by two, one-electron steps via an Mo(V) intermediate; e.g., reduction of an Mo(VI) center by an H^+/e^- addition converts an $Mo^{VI}=O$ group to Mo^V-OH; subsequent addition of H^+/e^- forms $Mo^{IV}-OH_2$.

Although the nature of the catalytic center and the molecular architecture of the various families of the molybdenum–MPT enzymes differ significantly, some general considerations apply.

- Each catalytic center is located in the interior of the molecule and the substrate approaches the center through a "funnel" through which the reaction product is removed.
- Prior to reaction, the substrate binds in a "pocket" immediately adjacent to the catalytic center in an orientation that facilitates the subsequent catalysis.
- In addition to the catalytic center, almost all of the molybdenum–MPT enzymes involve one (or several) other prosthetic group(s). These enzymes are organized in a manner analogous to an electrochemical cell: the site where oxidation occurs is the anode and the site where reduction occurs is the cathode; the redox active prosthetic groups are arranged to conduct electrons from the anode to the cathode; the external medium that supports the enzyme is analogous to a salt bridge.

For many of the molybdenum–MPT enzymes, the information available allows a mechanism to be proposed for the catalytic action; however, for every enzyme, further investigations are required to establish the precise details of the catalytic process.

8.18.2.3 The DMSO Reductase Family

DMSO reductases are common enzymes that catalyze the reduction (Equation (3)) of DMSO to DMS in bacteria and fungi that are present in the oceans and salt marshes. These enzymes are located in the periplasm and function in a respiratory chain that uses DMSO as the terminal electron acceptor and involves the transfer of two electrons from a cytochrome, to form DMS.[99] The activity of these enzymes can be linked to photosynthesis, for which they serve as a terminal electron acceptor. Although DMSO respiration ($\Delta G = -92\,kJ\,mol^{-1}$) does not provide as much

energy as O_2 respiration ($\Delta G = -218 \, kJ \, mol^{-1}$), it is more efficient than alcohol fermentation. These enzymes play a significant role in the global sulfur cycle since DMS is volatile and, in the atmosphere, is converted to methylsulfonate that acts to nucleate cloud formation.[100] Furthermore, the distinctive smell of DMS acts as a guide to certain seabirds who use it to locate productive regions of the ocean:[101]

$$DMSO + 2e^- + 2H^+ \rightleftharpoons DMS + H_2O \qquad (3)$$
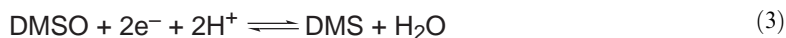
DMSO reductases have been purified and characterized from a range of sources.[25] The majority of investigations have been accomplished for the enzymes isolated from the purple phototrophic bacteria *Rhodobacter capsulatus*[99] and *Rhodobacter sphaeroides*.[102] These are the simplest of the known molybdenum–MPT enzymes, in that they are monomeric with a molecular weight of ~85 kDa and the molybdenum center is the sole prosthetic group. Thus, in contrast to the other molybdenum–MPT enzymes, these DMSO reductases lack Fe/S, heme, or flavin centers, although *E. coli* DMSO reductase[103,104] does contain an Fe_4S_4 center.

Several crystal structure determinations of the *Rhodobacter* DMSO reductases have been determined.[41–46] The polypeptide chain of 780 residues binds two MGD molecules (pterins P and Q) and one molybdenum. The polypeptide chain is folded into four, noncontiguous domains that link to form an ellipsoidal molecule with a "funnel-like" depression on one side. The molybdenum is located at the bottom of this funnel, close to the center of the molecule; the funnel is lined by aromatic residues, creating a hydrophobic pocket that facilitates the passage of DMSO and DMS to and from the active site, respectively. Both P-and Q-pterins are locked into the polypeptide by an extensive series of hydrogen bonds and there are significant conformational differences between the two pterins, notably in the deviation of the pyran ring from the plane of the pterin (P-pterin $\approx 30°$, Q-pterin 40–60°).

There has been some difficulty in defining the coordination geometry of the molybdenum in the *Rhodobacter* DMSO reductases, and detailed structural studies of oxidized DMSOR from *R. sphaeroides* at 1.3 Å[45] and *R. capsulatus*[46] have revealed a "plasticity" of the active site. In the former, the molybdenum center is discretely disordered and exists in both hexacoordinate and pentacoordinate environments. The hexacoordinated site (Figure 4) involves the metal bound to one oxo group (that is hydrogen bonded to Tyr114), the γ-oxygen of Ser147, and four sulfur atoms from the two MPTs; the six donor atoms form an irregular trigonal prism centered on the molybdenum. The pentacoordinated site involves the metal bound to two oxo groups, the γ-oxygen of Ser147, but only two sulfur atoms—those of pterin P, with the sulfurs of pterin Q (at 3.62 Å and 4.53 Å) being too far away to be considered bonded to the molybdenum. Molybdenum K-edge EXAFS[105,106] and resonance Raman spectra[107–109] are consistent with all four sulfur atoms being bound to the metal in the native enzyme. Thus, the structure shown in Figure 4 is generally accepted as the form of the molybdenum center in the oxidized state of the DMSO reductases. The results of crystallographic studies[45,46] demonstrate unequivocally that Hepes buffer leads to a significant change in the nature of the active site of the oxidized enzyme.[45,46]

A protein crystal structure has been reported for a form of the *R. capsulatus* DMSO reductase generated by addition of DMS to crystals of the enzyme.[44] The DMS binds to the oxo group, apparently producing DMSO bound to the reduced molybdenum center. This is depicted in Figure 5 as a des-oxo species, as formed by the addition of DMS to the mono-oxo center shown in Figure 4. The structures of the oxidized and reduced forms of the catalytic centers of the molybdenum DMSO reductases have stimulated an extensive range of coordination chemistry, directed at the production of their chemical analogues with some considerable success.[110–116]

Spectroscopic measurements on the *Rhodobacter* DMSO reductases are consistent with the oxidized state containing Mo(VI). The absence of prosthetic groups, other than the molybdenum–MPT center, facilitates spectroscopic studies of this center; e.g., the UV/visible spectrum of the oxidized enzyme has absorptions at 280 nm, 350 nm, 470 nm, 550 nm, and 720 nm and the dithionite reduced form has absorptions at 280 nm, 374 nm, 430 nm (sh), and 645 nm.[103] The Mo(V) state of the *R. capsulatus* enzyme, generated by titration of dithionite or reduced methyl viologen, has been investigated by MCD spectroscopy and the transitions observed assigned to ligand-to-metal charge transfer from the dithiolene sulfurs.[117] Reduction by dithionite produces a surprising number of Mo(V) EPR signals, suggesting some structural flexibility at the molybdenum center. Further reduction with dithionite produces an EPR-silent form, considered to contain Mo(IV).[118] ESEEM spectroscopy has been used to investigate the environment of the proton of the Mo^V–OH center of the DMSO reductase of *R. capsulatus*.[119]
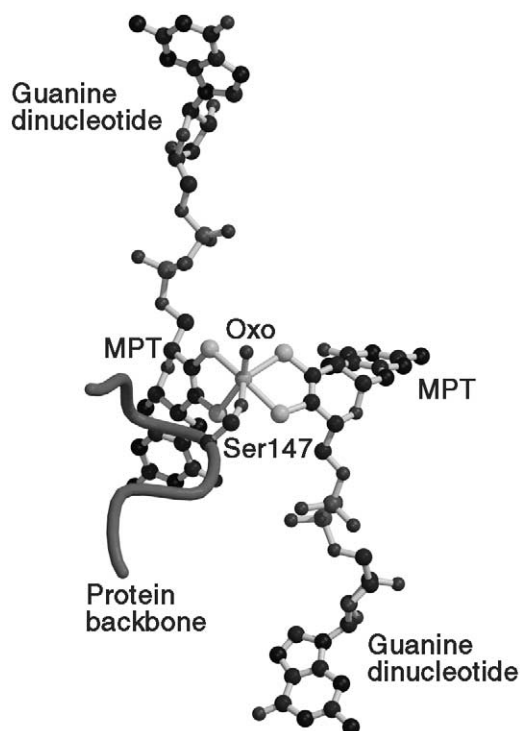
Figure 4 Structure of the molybdenum center of native, oxidized DMSO reductases.[45]

EPR potentiometric titrations of *R. sphaeroides* DMSO reductase at pH 7.0 and room temperature gave redox potentials of +144 mV for the Mo(VI)/Mo(V) couple and +160 mV for the Mo(V)/Mo(IV) couple.[102] The first cyclic voltammetric investigation of a molybdenum–MPT enzyme has been accomplished for *R. capsulatus* DMSO reductase.[120] In this study a reversible Mo(VI)/Mo(V) couple was observed at +161 mV and a reversible Mo(V)/Mo(IV) couple at −102 mV. The former couple exhibits a pH dependence of ca. −59 mV/pH unit consistent with an e$^-$/H$^+$ transfer (5 < pH < 9) and is taken to indicate the conversion of the Mo^{VI}=O group to a Mo^V–OH unit. The potential of the Mo(V)/Mo(IV) couple was constant for 5 < pH < 10, indicating that reduction of the Mo(V) does not involve protonation. This latter behavior contrasts with that of the *E. coli* DMSO reductase, for which each reduction involves coupled e$^-$/H$^+$ transfer.[121]
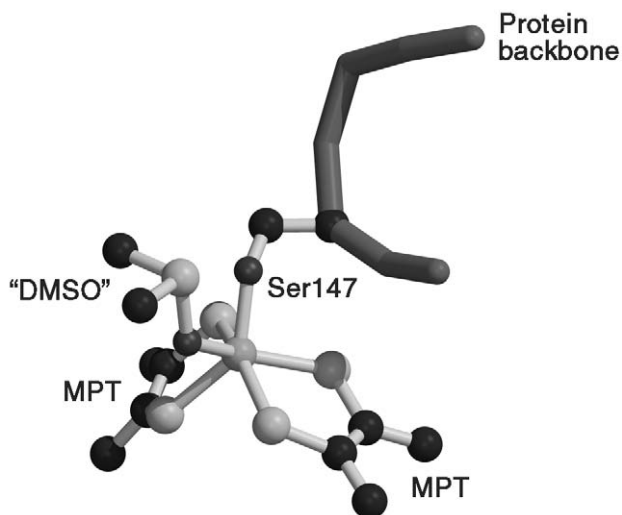
Figure 5 Structure of the molybdenum center of DMS-treated native DMSO reductase from *Rhodobacter capsulatus* (McAlpine *et al.*[44] but see text).

Catalytic and single-turnover experiments with the *R. sphaeroides* DMSO reductase, ^{18}O-labeled DMSO and 1,3,5-triaza-7-phosphatricyclo[3.3.1.1]decane as an oxygen atom acceptor have been used to demonstrate that the enzyme is an oxotransferase.[122] Complementary resonance Raman studies have been interpreted on the basis of a direct mechanism for OAT, with the active site cycling between mono-oxo-Mo(VI) and des-oxo-Mo(IV) forms via a DMSO-bound Mo(IV) intermediate. Both MPT dithiolene groups stay firmly attached to the molybdenum throughout the catalytic cycle.[108] However, EPR and UV/visible spectroscopic evidence has been interpreted on the basis of the species formed upon the addition of DMS to oxidized *R. capsulatus* DMSO reductase involving a Mo(V) center bound to a sulfur radical.[44]

A membrane-bound DMSO reductase has been identified in *E. coli*.[123] This enzyme is composed of three subunits: one containing the molybdenum–MPT catalytic center, which is essentially the same as those of the DMSO reductases of *R. capsulatus* and *R. sphaeroides*; a second containing four Fe_4S_4 clusters, to conduct electrons to the catalytic center; and a third that anchors the enzyme in the membrane and also contains the binding site for the external reductant, menaquinol.

The DMSO reductases are capable of catalyzing the reduction of a wide variety of substrates, including a range of sulfoxides. An interesting aspect of these reductions, doubtless a consequence of the chiral nature of the substrate-binding pocket, is the enantioselective reduction of a racemic mixture of chiral sulfoxides. Also, these enzymes catalyze the loss of an oxygen atom from a variety of *N*-oxides, including TMAO and pyridine-*N*-oxides, and chlorate, $[ClO_3]^-$. TMAO reductases possess a structure that is very similar to those of the DMSO reductases of *R. sphaeroides* and *R. capsulatus*, including an essentially identical catalytic center.[47,48]

A Tyr114 residue is present in the active site of DMSO reductase and biotin sulfoxide reductase,[124,125] but not TMAO reductase. This difference has been implicated in different substrate specificity of the enzymes, i.e., the DMSO reductases catalyze the reduction of both sulfoxides and amine oxides, but TMAO reductases will not catalyze the reduction of sulfoxides. To test this hypothesis, *E. coli* TMAO reductase was cloned and expressed at high levels and site-directed mutagenesis used to generate the Tyr114 Ala and Phe variants of *R. sphaeroides* DMSO reductase and to insert a Tyr residue into the equivalent position in TMAO reductase. Although all of the mutants turned over in a manner similar to their respective wild-type enzymes, mutation of Tyr114 in DMSO reductase resulted in: (i) a decreased specificity for *S*-oxides; (ii) an increased specificity for TMAO; and (iii) a loss in the ability of the oxidized enzyme to oxidize DMS. Also, insertion of Tyr into TMAO reductase resulted in a decreased preference for TMAO relative to DMSO.[126] Furthermore, a system for expressing site-directed mutants of the molybdenum DMSO reductase from *R. capsulatus* has been constructed and used to replace Tyr114 by Phe. The mutant has increased k_{cat} and K_m towards both DMSO and TMAO, compared to the native enzyme. Direct electrochemistry showed that the mutation did not affect the potential of the Mo(V)/Mo(IV) couple, but the midpoint potential of the Mo(VI)/Mo(V) couple was raised by ca. 50 mV.[127] Thus, the Tyr114 residue plays a critical role in the redox properties and OAT capability of the catalytic center of the DMSO reductases. As for the earlier mutagenesis,[126] it was found that the oxidation of DMS by the Phe114 mutant was significantly impaired, as compared to the native enzyme.[127] A DMS dehydrogenase, an enzyme that catalyzes the oxidation of DMS to DMSO, has been isolated from *Rhodovulum sulfidophilum*.[128]

8.18.2.4 Formate Dehydrogenases

Formate dehydrogenases catalyze the oxidation of formate to carbon dioxide (Equation (4)) and play an important role in the global fixation of carbon dioxide. Unusually for molybdenum–MPT enzymes, Equation (4) is not OAT but involves the cleavage of a C–H bond with the formation of a C=O bond. The majority of the formate dehydrogenases occur in aerobic microorganisms and they contain no molybdenum and depend on pyridine nucleotide for their activity. However, some formate dehydrogenases occur in anaerobic bacteria and involve molybdenum and other redox-active prosthetic groups.[25,129–134] The considerable similarity in the amino acid sequences of these formate dehydrogenases and members of the DMSO reductase family strongly suggests that these enzymes possess the same class of metal center[8] and this has been confirmed by the determination of the crystal structure of formate dehydrogenase H from *E. coli*.[49] This enzyme contains a single molybdenum center bound to two molybpterin guanine dinucleotide (MGD) cofactors and a selenocysteine (SeCys[140]), together with a Fe_4S_4 cluster. The structure was determined for the oxidized enzyme, with and without the inhibitor nitrite, and for the formate-reduced enzyme:

$$HCO^{2-} \rightleftharpoons CO_2 + H^+ + 2e^- \tag{4}$$
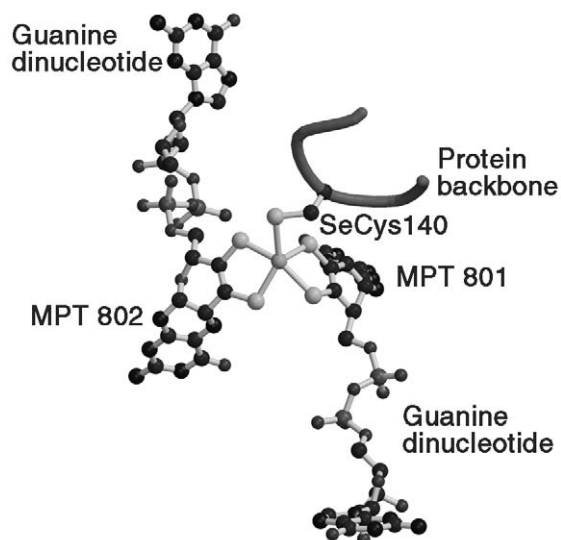
Figure 6 Structure of the Mo(IV) center of formate dehydrogenase H of *Escherichia coli*.[49]

The structure of the oxidized form of formate dehydrogenase H of *E. coli* involves a {Mo^{VI}O-(SeCys^{140})(MGD)$_2$} center and a Fe$_4$S$_4$ cluster. Formate binds to the oxidized enzyme and two electrons are transferred to the Mo(VI) to form a Mo(IV) center and, with the loss of H$^+$ and CO$_2$, the Mo(VI) center is regenerated by the removal of the two electrons via the Fe$_4$S$_4$ cluster. The coordination geometry of the Mo(IV) center (see Figure 6) is essentially square pyramidal, with the four sulfur atoms at the base, the Se at the apex and the Mo ca. 0.4 Å above the S_4 plane in the direction of the Se. The Mo(VI) center is bound to a sixth ligand, giving the metal an irregular trigonal prismatic coordination geometry; this ligand was modeled as a hydroxyl group with Mo–O ca. 2.2 Å. A similar geometry to the latter has been observed for the molybdenum center of formate dehydrogenase-N from *E. coli*.[50]

The protein crystallographic study[49] shows that nitrite binds directly to the molybdenum through one oxygen atom (Mo–O = 2.5 Å), displacing the hydroxyl ligand. When formate (HCO$_2$$^-$) is modeled into the nitrite-binding site, the C–H proton is <1.5 Å away from the selenium of SeCys^{140}, suitably poised for abstraction of hydride and formation of CO$_2$. This putative substrate binding site lies at the bottom of a deep crevice with Arg^{333} providing both a positive charge and a critical hydrogen bond to orient the substrate for oxidation.

The crystallographic results on the oxidized and reduced forms of formate dehydrogenase are in reasonable agreement with molybdenum *K*-edge EXAFS studies of the oxidized enzyme. These data were interpreted in terms of a coordination sphere containing four sulfur ligands at 2.36 Å, one oxygen at 2.11 Å, and one selenium at 2.62 Å. The coordination sphere changes little upon reduction to Mo(IV), the corresponding distances being 2.35 Å, 2.09 Å, and 2.62 Å. In contrast, the molybdenum *K*-edge EXAFS of the oxidised form of a mutant enzyme, in which SeCys^{140} → Cys, is consistent with a Mo=O bond at 1.72 Å plus five sulfur atoms at 2.42 Å. Selenium *K*-edge studies indicate the presence of a Se–S bond of length 2.19 Å, leading to the proposal that the active site contains a novel selenosulfide ligand.[135]

8.18.2.5 Dissimilatory Nitrate Reductases

Nitrate reductases are found in a wide range of eukaryotes and prokaryotes and have a crucial role in nitrogen assimilation and dissimilation (see Chapter 8.14). These enzymes catalyze the reaction shown in Equation (5); for the assimilatory nitrate reductases, this is followed by the reduction of nitrite to ammonia. Dissimilatory nitrate reductases [142–147] catalyze the reduction of nitrate to nitrite for respiration, to generate a transmembrane potential gradient.[25,136–142] The assimilatory nitrate reductases have a molybdenum center similar to that of sulfite oxidase (see

); however, the dissimilatory nitrate reductases are members of the DMSO reductase family:

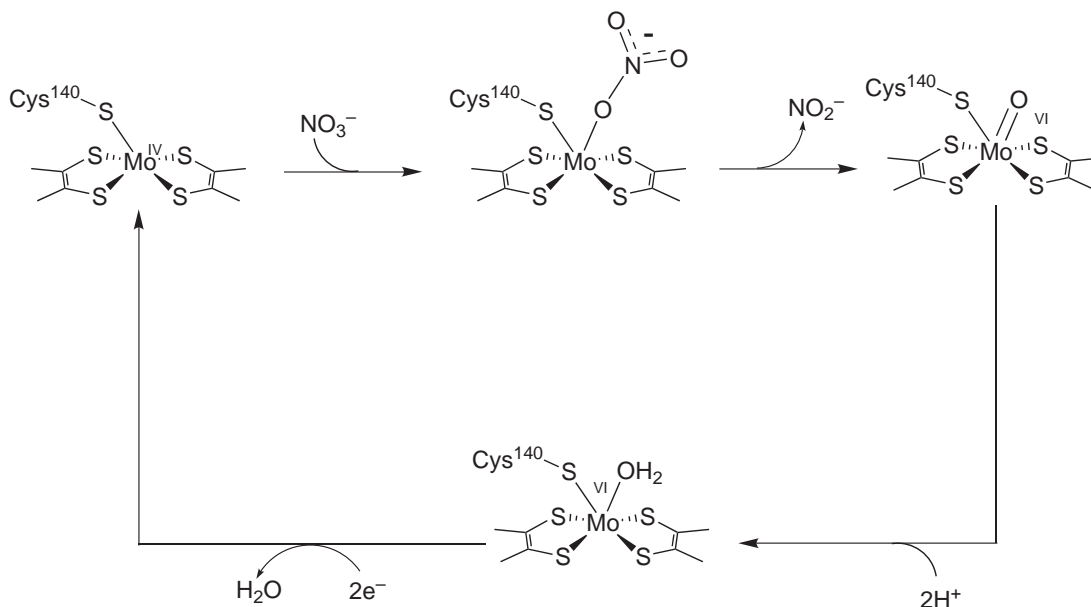$$NO_3^- + 2e^- + 2H^+ \rightleftharpoons NO_2^- + H_2O \qquad (5)$$

The structure of the oxidized form of the periplasmic dissimilatory nitrate reductase from *Desulfovibrio desulfuricans* ATCC 27774, an unusual sulfate-reducing bacterium that has the ability to grow with nitrate as the terminal electron acceptor of the respiratory chain, has been determined at 1.9 Å resolution.[51] The structure of this enzyme is very similar to that of formate dehydrogenase H from *E. coli*,[49,50] with the oxidized form involving a $\{Mo^{VI}O(SeCys^{140})(MGD)_2\}$ center, with an approximately trigonal prismatic coordination geometry, a heme, and an Fe_4S_4 cluster. The Mo(IV) center is suggested to have a similar structure to that of the Mo(VI) center, but without the O-donor ligand. Reduction of nitrate is suggested to occur by a mechanism (see Figure 7) that corresponds to that described for the DMSO reductases (Section 8.18.2.3). The nitrate binds to the $\{Mo^{IV}(SCys)(MGD)_2\}$ center and is anchored by an interaction with Arg^{354}; OAT then proceeds to form nitrite and the $\{Mo^{VI}O(SCys)(MGD)_2\}$ center. The latter would then be reduced to the catalytically active Mo^{IV} center by two e^-/H^+ steps; the electrons being transferred via an Fe_4S_4 cluster.

The nature of the molybdenum centers of several dissimilatory nitrate reductases has been investigated by K-edge EXAFS and by EPR spectroscopy[8,143,144] and the reduction potentials of the several redox-active centers in the *E. coli* nitrate reductase have also been determined by following the intensity of the "low pH" EPR signal as a function of the poised system potential.[145,146] The redox potentials of the Mo(VI/V) and Mo(V/IV) couples were determined as +220 mV and +180 mV, respectively, and the pH dependence of the potentials suggests that the redox processes involve coupled e^-/H^+ transfer.

Arsenite oxidase of *Alicaligenes faecalis* is comprised[52] of a large subunit that contains a molybdenum center that is very similar to that of the nitrate reductase, a Fe_3S_4 cluster, plus a smaller unit containing a Reiske-type Fe_2S_2 cluster.
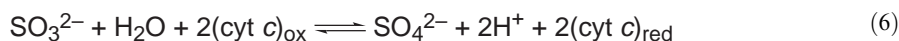
8.18.2.6   Sulfite Oxidases

Sulfite oxidases catalyze the physiologically vital oxidation of sulfite to sulfate, coupled to the reduction of two equivalents of ferricytochrome *c* (Equation (6)). This is the terminal reaction in

Figure 7   Proposed reaction mechanism for the reduction of nitrate to nitrite by the dissimilatory nitrate reductase of *Desulfovibrio desulfuricans* ATCC 2774.[51]

the oxidative degradation of the sulfur-containing amino acids cysteine and methionine. Also, the action of sulfite oxidase serves to remove excess sulfite from the body and this can occur because sulfite is used as a food preservative. The reducing equivalents associated with the oxidation of sulfite to sulfate are passed to cytochrome *c* and are then incorporated into the respiratory chain:

$$SO_3^{2-} + H_2O + 2(cyt\ c)_{ox} \rightleftharpoons SO_4^{2-} + 2H^+ + 2(cyt\ c)_{red} \qquad (6)$$

Sulfite oxidase is ubiquitous in animals[8,25,147–151] and has been isolated from plants;[151] the human,[150] rat,[149] and chicken liver[147] enzymes have been sequenced. In humans, a genetic deficiency of sulfite oxidase can occur for either or both of two reasons.[93,94] The first is a defect in the synthesis of MPT and this deficiency also affects the production of xanthine dehydrogenase and aldehyde oxidase. The second affects sulfite oxidase alone and is caused by mutations in the gene encoding for this enzyme. Individuals suffering from either genetic defect exhibit similar symptoms, including severe neurological abnormalities, mental retardation, and, in several cases, attenuated growth of the brain. The condition invariably results in death in infancy.

Amino acid sequence comparisons have shown that sulfite oxidase is related to the heme-containing assimilatory nitrate reductases with a 31% identity. Therefore, the nature of the crystal structure of chicken liver sulfite oxidase[53] has added relevance. The crystal structure of chicken liver oxidase at 1.9 Å resolution has revealed a dimeric enzyme with each monomer consisting of three domains and containing two prosthetic groups, a b_5-type heme and a molybdenum–MPT center (Figure 8). The latter is located deep in the second domain and the molybdenum is pentacoordinated with an approximately square pyramidal geometry. The metal site is comprised of an Mo=O = 1.7 Å group at the apex and a basal plane of two dithiolene sulfurs from the one MPT (Mo–S = 2.4 Å), Sγ from Cys[185] (Mo–S = 2.5 Å), and a water/hydroxo group (Mo–O = 2.3 Å). Unlike its eubacterial counterparts, the phosphate group of MPT of sulfite oxidase is not bound to a nucleotide. The Cys[185] residue is conserved in all sulfite oxidases and nitrate reductases, consistent with it behaving as a ligand to the molybdenum in all of these proteins. Site-directed mutagenesis, replacing Cys[185] with Ser, yields an inactive enzyme, showing that the cysteine is vital for catalytic activity.[150]

Analysis of the protein crystallographic data suggests that the form of the enzyme investigated was (at least partially) reduced, even though the enzyme was purified in the fully oxidized, Mo(VI)/Fe(III), form. It is probable that the molybdenum center was photoreduced during the exposure to X-rays necessary for the crystallographic investigation. Also, resonance Raman spectroscopy suggests the presence of a $\{Mo^{VI}O_2\}^{2+}$ center in the oxidized enzyme.[152] Sulfite is oxidized to sulfate by reacting with the Mo(VI) center and, in the crystal structure,[53] residual electron density adjacent to the water/hydroxo group was assigned to a mixture of sulfite and sulfate groups. The substrate binding pocket is formed by Arg[138], Arg[190], and Arg[450], Trp[204], and Tyr[322]. Another basic residue, Lys[200], although not within hydrogen bonding distance to the sulfate, contributes to the formation of the positively charged binding pocket, that is ideally suited for binding anions such as the substrate sulfite and the product sulfate. The four oxygen atoms of the sulfate are involved in an extensive hydrogen bonding network. The mechanism for oxidation
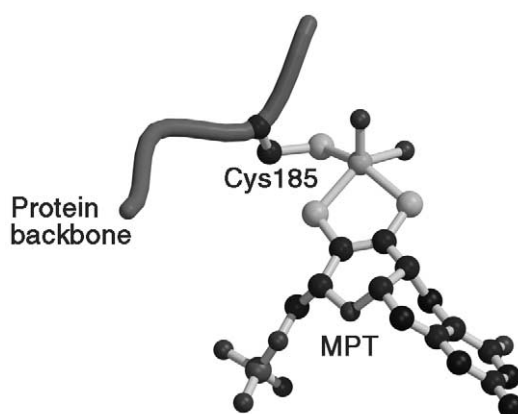

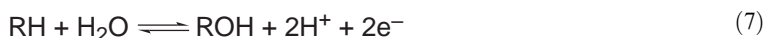**Figure 8** Structure of the oxidized form of the active site of chicken liver sulfite oxidase.[53]

sulfite has been investigated by extended Hückel calculations; the results favor direct attack of HSO_3^- at an $Mo^{VI}=O$ group.[153]

The Mo(IV) center is reoxidised via the cytochrome b_5 group and a comprehensive kinetic study of the turnover of chicken liver sulfite oxidase has been accomplished.[154] The Mo(V) state is an important stage of the catalytic cycle and this has been extensively probed, e.g., by MCD[155] and EPR[156,157] spectroscopy and the latter has led to the recognition of three distinct forms: high-pH, low-pH, and phosphate-inhibited forms. ESEEM measurements have shown that the high-pH form of sulfite oxidase probably involves a Mo^V–OH moiety.[158] Pulsed ENDOR spectra of the nonexchangeable protons in the vicinity of the Mo(V) center of high- and low-pH forms of native chicken liver and recombinant human sulfite oxidase have shown that the structures of their molybdenum centers are essentially identical.[159]

The potentials of the redox couples of sulfite oxidase have been determined; at pH 9.0, Mo(VI/V) = −57 mV, Mo(V/IV) = −233 mV, and heme Fe(III)/Fe(II) = 51 mV.[160] The value of both of the molybdenum redox couples increases significantly as the pH decreases, 9 > pH > 6, the Mo(VI/V) by 190 mV and the Mo(V/IV) by 150 mV, consistent with e^-/H^+ processes occurring for both couples. In contrast, the heme potential decreases by only 40 mV over the same pH range.

8.18.2.7 Xanthine Oxidases

Members of the xanthine oxidase family[2,21,25,161–165] are regarded as molybdenum hydroxylases since these enzymes catalyze hydroxylation reactions of the type shown in Equation (7) for purines, pyrimidines, pterins, and aldehydes. These enzymes generate the reducing equivalents in the course of the reaction and the oxygen atom incorporated into substrate derives from water:
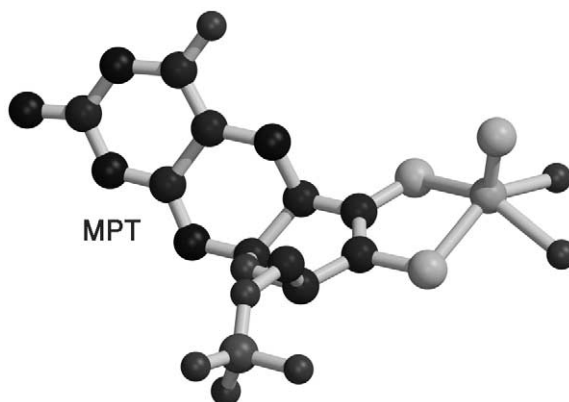
$$RH + H_2O \rightleftharpoons ROH + 2H^+ + 2e^- \qquad (7)$$

Milk xanthine oxidase is an archetypal enzyme that was originally described as aldehyde oxidase in 1902[166] and has subsequently served as a benchmark for the whole class of metal-loflavoproteins.[167] Xanthine oxidoreductases have been isolated from a wide range of organisms, from bacteria to man, and the molecular weight and nature of the redox centers is remarkably conserved.[8,168] Mammalian xanthine dehydrogenase and xanthine oxidase occur in the liver of animals and catalyze the oxidation of the last two steps of the formation of uric acid, the oxidation of hypoxanthine to xanthine and then to uric acid. The accumulation and crystallization of monosodium urate in joints or soft tissue is responsible for gout and an effective treatment is the administration of allopurinol that binds to the active site of the enzyme and, thus, inhibits the synthesis of uric acid.[61,169]

These enzymes are synthesized in the dehydrogenase form and exist mostly as such in the cell, but can be readily converted to the oxidase form by oxidation of sulfhydryl residues or by proteolysis. Xanthine dehydrogenase has a preference for NAD^+ reduction at the FAD reaction site, whereas xanthine oxidase fails to react with NAD^+ and exclusively uses dioxygen as the oxidant, leading to the formation of superoxide anion and hydrogen peroxide.[168]

The amino acid sequences of xanthine oxidoreductases from various sources have been determined.[164,165,168] The enzymes are comprised of ca. 1,330 amino acids and are highly homologous, e.g., the bovine milk enzyme (1,332 residues) shows a 90% sequence identity to the human liver enzyme (1,333 residues). The active form of these enzymes is a homodimer of molecular mass ca. 290 kDa and the structures of bovine milk xanthine dehydrogenase and xanthine oxidase have been solved at 2.1 Å resolution.[60] Each monomer is comprised of three domains: the N-terminal domain contains both Fe_2S_2 centers and is connected to the FAD-binding domain by a long segment of the polypeptide chain that was poorly resolved in the structure; the FAD domain is connected to a third domain by another linker segment that is also partially ordered; the third domain binds the molybdenum–MPT center close to the interfaces of the other two domains. The closest distance between the reaction centers of the different subunits is >50 Å, so it is unlikely that any inter-subunit electron transfer occurs. The reversible conversion of xanthine dehydrogenase to xanthine oxidase may be caused by the formation of a disulfide bond between Cys^{535} and Cys^{992}, leading to a significant conformational change of the protein.

At 2.1 Å resolution, the identity of the atoms bound to the molybdenum, beyond the two MPT sulfurs, cannot be determined unambiguously. The identity of these atoms was inferred from the
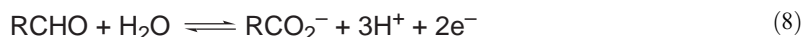
Figure 9 Structure of the oxidized form of the active site of bovine milk xanthine dehydrogenase and xanthine oxidase.[60]

results of earlier spectroscopic studies and by analogy to the molybdenum–MPT center in *Desulfovibrio gigas* aldehyde oxidase.[54–57] A striking feature of these enzymes is that they require an Mo=S group for their catalytic activity. In the oxidized form of the active xanthine dehydrogenase and xanthine oxidase (Figure 9), the molybdenum is considered to be bound to one MPT group, one Mo=O, one Mo=S, and one Mo–OH/H_2O group. Oxidation of substrates occurs at the molybdenum, leading to the reduction of Mo(VI) and the formation of Mo(IV); the latter is reoxidized by removing the two electrons via the Fe_2S_2 centers, then FAD, to an external oxidant. A wealth of spectroscopic information has been obtained concerning the nature of the molybdenum center in various forms of xanthine dehydrogenase and xanthine oxidase and to probe the nature of the catalytic process;[8,21,25,161,163,171–179] however, key details of the mechanism remain elusive.[180]

8.18.2.8 Aldehyde Oxidases

Aldehyde oxidases[181–185] catalyze the oxidation of aldehydes to carboxylic acids (Equation (8)) as a specific example of Equation (7):[8,25]

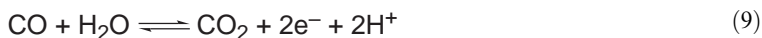$$RCHO + H_2O \rightleftharpoons RCO_2^- + 3H^+ + 2e^- \tag{8}$$

The aldehyde oxidase from the sulfate-reducing anaerobic bacterium *Desulfovibrio gigas* (MOP) is a member of the xanthine oxidase family and its crystal structure has been determined at various precisions[54–57] and finally at 1.28 Å resolution.[58] This enzyme is part of an electron transfer chain consisting of four proteins in *D. gigas* that links aldehyde oxidation to the production of dihydrogen.[186] MOP is a homodimer with 907 amino acid residues per monomer, organized as two Fe_2S_2 domains and an extended connecting peptide that leads to the molybdenum–MPT domain. The molybdenum–MPT center is buried in the protein and is accessible through a 15 Å deep tunnel that is funnel-shaped, wide at the upper rim, and narrowing toward the molybdenum and appears to allow passage of only small aliphatic aldehydes. MPT is present as a cytosine dinucleotide. The Mo(VI) center in the oxidized form of the desulfo enzyme is pentacoordinated by sulfur atoms from MPT (2.41(2) Å and 2.50(2) Å), two Mo=O groups (1.77(4) Å and 1.79(4) Å), and one Mo–OH_2/OH interaction at 2.024 Å.[58] Mo *K*-edge EXAFS and Mo(V) EPR spectra of desulfo-MOP indicate a close similarity of this molybdenum center to that of the desulfo form of xanthine oxidase, but the functional form of *both* of these enzymes is believed to require the presence of a Mo=S group.[171–177]

The structure of the aldehyde oxidase from *Desulfovibrio desulfuricans* ATCC 2774 has been determined at 2.8 Å resolution and the structural details found to be very similar to the corresponding aspects of MOP.[59]

The redox potentials for the Mo(VI)/Mo(V) and Mo(V)/Mo(IV) couples of the aldehyde oxidase obtained from rabbit liver have been measured as −359 mV and −351 mV, respectively.[187] Thus, like other molybdenum–MPT enzyme oxo-transferases, the center is poised for a two-electron process.

8.18.2.9 CO Dehydrogenases

Carbon monoxide (CO) is a trace gas and important scavenger for hydroxyl radicals in the atmosphere. The molybdenum-dependent CO dehydrogenases are found in aerobic CO-oxidizing bacteria, such as *Oligotropha carboxidovorans*, that use CO as the sole source of carbon. These bacteria live in the top few centimeters of the soil and metabolize about 20% of the total CO in the atmosphere and contribute to its regulation. The energy released on the oxidation of CO to CO_2 (Equation (9)) is used to synthesize ATP via a CO-insensitive respiratory chain that generates a proton gradient across the cytoplasmic membrane:[62–67]

$$CO + H_2O \rightleftharpoons CO_2 + 2e^- + 2H^+ \qquad (9)$$

The crystal structure of CO dehydrogenase from *O. carboxidovorans* has been determined.[62–64] This enzyme is a dimer with each monomer being composed of three proteins, the largest of which contains the molybdenum center. The active site contains a novel {MoSCu} moiety (see Figure 2) that is unique for the molybdenum–MPT enzymes. The coordination sphere of the Mo(VI) center also involves one MPT (as a cytosine dinucleotide), an Mo=O and an Mo–OH group, and a weakly bonded (Mo···O = 3.14 Å) oxygen from a glutamate residue. The copper is also coordinated to Cys^{388}, giving an approximately linear SCu^IS arrangement. Reduction to Mo(IV), as required for catalysis, causes relatively little structural change in the nature of the molybdenum center, except that it is considered that the two metals are linked by a monothiocarbonate group, formed from Mo–S–Cu, Mo–OH plus CO. The air-oxidized enzyme is EPR silent which seems to suggest that the copper remains as Cu(I) throughout the catalytic cycle.

The CO dehydrogenase from *O. carboxidovorans* also contains two Fe_2S_2 clusters and an FAD. The catalytic center is accessible through a narrow channel, 17 Å deep and 7 Å in diameter, that is lined with mainly hydrophobic groups. This channel allows access of CO and egress of CO_2, but will effectively discourage larger and/or polar molecules approaching the catalytic center.

8.18.3 NATURE OF THE CATALYTIC CENTERS OF TUNGSTEN OXIDOREDUCTASES

Tungsten enzymes occur in anaerobic micro-organisms, many of which are thermophilic.[188,189] Our understanding of the role of tungsten in biological systems has been transformed by recent discoveries.[30,38,68–73] Thus, several enzymes, each of which requires a tungsten–MPT center for activity, have been isolated and characterized. Virtually all of the tungsten–MPT enzymes catalyze the equivalent of aldehyde oxidation and the metal is invariably bound to two MPTs. Indeed, the first structural characterization of MPT was achieved for the aldehyde ferredoxin oxidoreductase of the hyperthermophilic archaeon *Pyrococcus furiosus*.[71]

This enzyme is a homodimer, in which each 605-residue subunit contains a Fe_4S_4 cluster and a tungsten–MPT center (see Figure 10). Further electron density at the site is suggestive of two *cis*-coordination sites that may be occupied by oxygen or by buffer-derived glycerol, a substrate analog, yielding a distorted trigonal prismatic coordination environment at the tungsten. No protein ligands are bound to the tungsten. The phosphate groups of the two MPTs are bound to the same Mg^{2+} ion. The Fe_4S_4 cluster is close to the tungsten ($\sim$10 Å) and is linked to one of the MPT ligands via the side chain of Arg^{76} that forms hydrogen bonds to an inorganic sulfur within the cluster and to two pterin oxygens. A second connection is provided by a hydrogen bond

Figure 10 Structure of the tungsten center of the aldehyde oxidoreductase from *Pyrococcus furiosus*.[71]

between the cluster ligand Sγ of Cys[494] and a pterin nitrogen. These pathways may allow electron transfer between the two centers and, as the Fe_4S_4 cluster is only 6 Å below the surface of the protein, it is a likely intermediary between the tungsten and the ferredoxin redox partner.

Unusually, the crystallography of AOR from *P. furiosus* preceded a thorough spectroscopic investigation of this protein. Many of the early spectroscopic investigations were carried out on an inactive form of the enzyme, called the red tungsten protein. Subsequent studies of the dithionite-reduced active enzyme showed the presence of 4–5 sulfur ligands at 2.40 Å, a single oxo group at 1.75 Å, and possibly an additional O/N contact at 1.97 Å.[190] These results clearly indicate the presence of one or two W=O groups and imply that the dioxo form of the enzyme is inactive. However, it should be noted that this enzyme has a considerable heterogeneity at the tungsten site, as revealed by the profusion of W(V) EPR signals attainable under different conditions, many corresponding to inactive forms of the enzyme. Also, ca. 30% of the as-prepared enzyme has the ability to cycle between W(IV)/(V)/(VI) at the physiologically relevant potentials associated with the active enzyme. Thus, the crystallographic and XAS studies probably represent an average structure of the tungsten center, rather than a single site.[191]

Formaldehyde ferredoxin oxidoreductases have ca. 40% sequence identity to their aldehyde counterparts, but can oxidize only C1–C3 aldehydes or <C6 dialdehydes.[192,193] The former have been isolated from the hyperthermophilic archaea *P. furiosus*[192] and *Thermococcus litoralis*[193] and shown to possess 92% sequence similarity. The structure of the formaldehyde ferredoxin oxido-reductases from *P. furiosus* has been solved to 1.75 Å resolution.[72] The enzyme is a homotetramer with subunits of 621 residues, each of which contains one Fe_4S_4 cluster and one tungsten–MPT center with two MPTs. The overall structure of this enzyme is very similar to that of the aldehyde ferredoxin oxidoreductase from *P. furiosus*,[71] except that the latter has a wider channel for access of substrate and egress of product. The tungsten is coordinated by the four sulfur atoms (W–S_{ave} = 2.5 Å) of the two MPTs and there are no protein side chains bound to the metal. One other ligand, assumed to be oxygen, is coordinated to the tungsten at ca. 2.1 Å. The phosphate groups of the two MPTs are linked by Mg^{2+} and Ca^{2+} ions.

Formate dehydrogenases (see Section 8.18.2.4) catalyze formate production (Equation (4)) and play a significant role in the global fixation of CO_2. The structure of the formate dehydrogenase from *Desulfovibrio gigas* has been determined.[73,74] The protein is comprised of two subunits of mass 110 kDa and 24 kDa; the larger subunit is similar to *E. coli* formate dehydogenase H[49,50] (Section 8.18.2.4) and to *D. desulfuricans* nitrate reductase[51] (Section 8.18.2.5) and contains the tungsten–MPT center and an Fe_4S_4 cluster. The tungsten is coordinated to the four sulfur atoms of two MPTs (as guanine dinucleotides), the selenium of SeCys[158], and one hydroxyl or sulfide ligand—the latter would be more compatible with putative reaction mechanisms.[73,74]

Several other tungsten–MPT enzymes have been identified;[30,38,68,188,189] tungsten has been shown to be capable of substituting for molybdenum in DMSO reductase of *R. capuslatus*,[194,195] and the knowledge available for tungsten centers in enzymes has stimulated a wealth of new coordination chemistry.[196–205] As a final and fascinating example, acetylene hydratase occurs in some acetylene-degrading bacteria such as *Pelobacter acetylinicus*.[206] The enzyme catalyzes the hydration of acetylene (ethyne) (Equation (10)); this is unique for the Mo–MPT and W–MPT enzymes in not involving a redox change of the substrate. The enzyme is a monomer of molecular weight ca. 80 kDa and contains one Fe_4S_4 cluster and one tungsten bound to two MPTs (as guanine dinucleotides):

$$C_2H_2 + H_2O \rightleftharpoons CH_3CHO \qquad (10)$$

8.18.4 REFERENCES

1. Lippard, S. J.; Berg, J. M. *Principles of Bioinorganic Chemistry;* University Science Books: Sausalito, CA, 1994; p 106.
2. Fraústo da Silva, J. J. R.; Williams, R. J. P. *The Biological Chemistry of the Elements;* Clarendon Press: Oxford, UK, 1991; p 513.
3. Bortels, H. *Zentralbl. Bakteriol. Parisitenkd. Infektionskr.* **1936**, *95*, 193–218.
4. DeRenzo, E. C; Kalieta, E.; Heytler, P.; Olsen, J. J.; Hutchings, B. L.; Williams, J. H. *J. Am. Chem. Soc.* **1953**, *75*, 753.
5. Spence, J. T. *Coord. Chem. Rev.* **1969**, *4*, 475–498.
6. Bray, R. C.; Swann, J. C. *Structure and Bonding* **1971**, *11*, 107–144.
7. Stiefel, E. I.; Coucouvanis, D.; Newton, W. E., Eds. *Molybdenum Enzymes, Cofactors and Model Systems;* ACS Symposium Series 535; American Chemical Society: Washington, DC, 1993.
8. Hille, R. *Chem. Rev.* **1996**, *96*, 2757–2816.

9. Howard, J. B.; Rees, D. C. *Chem. Rev.* **1996**, *96*, 2965–2982.
10. Burgess, B. K.; Lowe, D. J. *Chem. Rev.* **1996**, *96*, 2983–3011.
11. Johnson, M. K.; Rees, D. C.; Adams, M. W. W. *Chem. Rev.* **1996**, *96*, 2817–2839.
12. Hagen, W. R.; Arendson, A. F. *Structure and Bonding* **1996**, *90*, 161–192.
13. Collison, D.; Garner, C. D.; Joule, J. A. *Chem. Soc. Rev.* **1996**, *25*, 25–32.
14. Rees, D. C.; Hu, Y.; Kisker, C.; Schindelin, H. *J. Chem. Soc., Dalton Trans.* **1997**, 3909–3914.
15. Schindelin, H.; Kisker, C.; Rees, D. C. *JBIC* **1997**, *2*, 773–781.
16. Romão, M. J.; Rösch, N.; Huber, R. *JBIC* **1997**, *2*, 782–785.
17. Rajagopalan, K. V. *JBIC* **1997**, *2*, 786–789.
18. Kisker, C.; Schindelin, H.; Baas, D.; Retey, J.; Meckenstock, R. U.; Kroneck, P. M. H. *FEMS Microbiol. Rev.* **1998**, *22*, 503–521.
19. George, G. N. *JBIC* **1997**, *2*, 790–796.
20. Johnson, M. K.; Garton, S. D.; Oku, H. *JBIC* **1997**, *2*, 797–803.
21. Hille, R. *JBIC* **1997**, *2*, 804–809.
22. Enemark, J. H.; Garner, C. D. *JBIC* **1997**, *2*, 817–822.
23. McMaster, J.; Enemark, J. H. *Curr. Opin. Chem. Biol.* **1998**, *2*, 201–207.
24. Pilato, R. S.; Stiefel, E. I. In *Bioinorganic Catalysis;* Reedijk, J., Bouwman, E., Eds.; Marcel Dekker: New York, 1999; pp 81–152.
25. Garner, C. D.; Banham, R.; Cooper, S. J.; Davies, E. S.; Stewart, L. J. In *Handbook on Metalloproteins;* Bertini, I., Sigel, A., Sigel, H., Eds.; Marcel Dekker: New York, 2001; Chapter 22, pp 1023–1090.
26. Messerschmidt, A.; Huber, R.; Poulos, T.; Wieghardt, K., Eds. *Handbook of Metalloproteins*; Wiley: Chichester, UK, 2001; Vol. 2, pp 1023–1147.
27. Hille, R. *Trends Biochem. Sci.* **2002**, *27*, 360–367.
28. Mendel, R. R.; Hänsch, R. *J. Exp. Bot.* **2002**, *375*, 1689–1698.
29. Hille, R. In *Metal Ions in Biological Systems*; Sigel, A., Sigel, H., Eds.; Marcel Dekker: New York, 2002; Vol. 39, pp 187–226.
30. Dobbek, H.; Huber, R. In *Metal Ions in Biological Systems*; Sigel, A., Sigel, H., Eds.; Marcel Dekker: New York, 2002; Vol. 39, pp 227–263.
31. Mendel, R. R.; Schwarz, G. In *Metal Ions in Biological Systems*; Sigel, A., Sigel, H., Eds.; Marcel Dekker: New York, 2002, Vol. 39, pp 317–368.
32. Kroneck, P. M. H.; Abt, D. J. In *Metal Ions in Biological Systems*; Sigel, A., Sigel, H., Eds.; Marcel Dekker: New York, 2002, Vol. 39, pp 369–403.
33. Andreesen, J. R.; Fetzner, S. In *Metal Ions in Biological Systems*; Sigel, A., Sigel, H., Eds.; Marcel Dekker: New York, 2002, Vol. 99, pp 405–430.
34. Pai, E. F.; Nishino, T. In *Metal Ions in Biological Systems*; Sigel, A., Sigel, H., Eds.; Marcel Dekker: New York, 2002, Vol. 39, pp 431–454.
35. Lowe, D. J. In *Metal Ions in Biological Systems*; Sigel, A., Sigel, H., Eds.; Marcel Dekker: New York, 2002, Vol. 39, pp 455–479.
36. Kappl, R.; Hüttermann, J.; Fetzner, S. In *Metal Ions in Biological Systems*; Sigel, A., Sigel, H., Eds.; Marcel Dekker: New York, 2002, Vol. 39, pp 481–537.
37. Romão, M. J.; Cunha, C. A.; Brodino, C. D.; Moura, J. J. G. In *Metal Ions in Biological Systems*; Sigel, A., Sigel, H., Eds.; Marcel Dekker: New York, 2002, Vol. 39, pp 539–570.
38. Vorholt, J. A.; Thauer, R. K. In *Metal Ions in Biological Systems*; Sigel, A., Sigel, H., Eds.; Marcel Dekker: New York, 2002, Vol. 39, pp 571–619.
39. Enemark, J. H.; Cosper, M. M. In *Metal Ions in Biological Systems*; Sigel, A., Sigel, H., Eds.; Marcel Dekker: New York, 2002, Vol. 39, pp 621–654.
40. Gladyshev, V. N. In *Metal Ions in Biological Systems*; Sigel, A., Sigel, H., Eds.; Marcel Dekker: New York, 2002, Vol. 39, pp 655–672.
41. Schindelin, H.; Kisker, C.; Hilton, J.; Rajagopalan, K. V.; Rees, D. C. *Science* **1996**, *272*, 1615–1616.
42. Schneider, F.; Löwe, J.; Huber, R.; Schindelin, H.; Kisker, C.; Knäblein, J. *J. Mol. Biol.* **1996**, *263*, 53–69.
43. McAlpine, A. S.; McEwan, A. G.; Shaw, A. L.; Bailey, S. *JBIC* **1997**, *2*, 690–701.
44. McAlpine, A. S.; McEwan, A. G.; Bailey, S. *J. Mol. Biol.* **1998**, *275*, 613–623.
45. Li, H.-K.; Temple, C.; Rajagopalan, K. V.; Schindelin, H. *J. Am. Chem. Soc.* **2000**, *122*, 7673–7680.
46. Bray, R. C.; Adams, B.; Smith, A. T.; Bennett, B.; Bailey, S. *Biochemistry* **2000**, *39*, 11258–11269.
47. Knäblein, J.; Dobbek, H.; Ehlert, S.; Schneider, F. *Biol. Chem.* **1997**, *378*, 293–302.
48. Czjzek, M.; Dos Santos, J.-P.; Pommier, J.; Giordano, G.; Méjean, Haser R. *J. Mol. Biol.* **1998**, *284*, 435–447.
49. Boyington, J. C.; Gladyshev, V. N.; Khangulov, S. V.; Stadtman, T. C.; Sun, P. D. *Science* **1997**, *275*, 1305–1308.
50. Jormakka, M.; Törnroth, S.; Byrne, B.; Iwata, *Science* **2002**, *295*, 1863–1868.
51. Dias, J. M.; Than, M. E.; Humm, A.; Huber, R.; Bourenkov, G. P.; Bartunik, H. D.; Bursakov, S.; Calvete, J.; Caldeira, J.; Carneiro, C.; Moura, J. J. G.; Moura, I.; Romão, M. J. *Structure* **1999**, *7*, 65–79.
52. Ellis, P. J.; Conrads, T.; Hille, R.; Kuhn, P. *Structure* **2001**, *9*, 125–132.
53. Kisker, C.; Schindelin, H.; Pacheco, A.; Wehbi, W. A.; Garrett, R. M.; Rajagopalan, K. V.; Enemark, J. H.; Rees, D. C. *Cell* **1997**, *91*, 973–983.
54. Romão, M. J.; Barata, B. A. S.; Archer, M.; Lobeck, K.; Moura, I.; Carrondo, M. A.; LeGall, J.; Lottspeich, F.; Huber, R.; Moura, J. J. G. *Eur. J. Biochem.* **1993**, *215*, 729–732.
55. Theones, U.; Flores, O. L.; Neves, A.; Devreese, B.; VanBeumen, J. J.; Huber, R.; Romão, M. J.; LeGall, J.; Moura, J. J. G.; Rodrigues-Pousada, *Eur. J. Biochem.* **1994**, *220*, 901–910.
56. Romão, M. J.; Archer, M.; Moura, I.; Moura, J. J. G.; Schneider, M.; Hof, P.; Huber, R. *Science* **1995**, *270*, 1170–1176.
57. Huber, R.; Hof, P.; Duarte, R. O.; Moura, J. J. G.; Moura, I.; Liu, M.-Y.; LeGall, J.; Hille, R.; Archer, M.; Romão, M. J. *Proc. Natl. Acad. Sci. USA* **1996**, *93*, 8846–8851.
58. Rebelo, J.; Dias, J. M.; Huber, R.; Moura, J. J. G.; Romão, M. J. *JBIC* **2001**, *6*, 791–800.
59. Rebelo, J.; Maciero, S.; Dias, J. M.; Huber, R.; Ascenso, C. S.; Rusnak, F.; Moura, J. J. G.; Moura, I.; Romão, M. J. *J. Mol. Biol.* **2000**, *297*, 135–146.

60. Enroth, C.; Eger, B. T.; Okamoto, K.; Nishino, T.; Nishino, T.; Pai, E. *Proc. Natl. Acad. Sci. USA* **2000**, *97*, 10723–10728.
61. Truglio, J. J.; Theis, K.; Leimkühler, S.; Rappa, R.; Rajagopalan, K. V.; Kisker, C. *Structure* **2002**, *10*, 115–125.
62. Dobbek, H.; Gremer, L.; Meyer, O.; Huber, R. *Proc. Natl. Acad. Sci. USA* **1999**, *96*, 8884–8889.
63. Dobbek, H.; Gremer, L.; Kiefersauer, R.; Huber, R.; Meyer, O. *Proc. Natl. Acad. Sci. USA* **2002**, *99*, 15971–15976.
64. Gnida, M.; Ferner, R.; Gremer, L.; Meyer, O.; Meyer-Klaucke, W. *Biochemistry* **2003**, *42*, 222–230.
65. Hänzelmann, P.; Dobbek, H.; Gremer, L.; Huber, R.; Meyer, O. *J. Mol. Biol.* **2000**, *301*, 1221–1235.
66. Gremer, L.; Kellner, S.; Dobbek, H.; Huber, R.; Meyer, O. *J. Biol. Chem.* **2000**, *275*, 1864–1872.
67. Meyer, O.; Frunzke, K.; Mörsdorf, G. *Microbiol. Growth on C₁ Compounds* **1993**, 433–459.
68. Roy, R.; Adams, M. W. W. In *Metal Ions in Biological Systems*; Sigel, A., Sigel, H., Eds.; Marcel Dekker: New York, 2002, Vol. 39, pp 673–697.
69. Garner, C. D.; Stewart, L. J. In *Metal Ions in Biological Systems*; Sigel, A., Sigel, H., Eds.; Marcel Dekker: New York, 2002, Vol. 39, pp 699–726.
70. Stewart, L. J.; Bailey, S.; Bennett, B.; Charnock, J. M.; Garner, C. D.; McAlpine, A. S. *J. Mol. Biol.* **2000**, *299*, 593–600.
71. Chan, M. K.; Mukund, C.; Kletzin, A.; Adams, M. W. W.; Rees, D. C. *Science* **1995**, *267*, 1463–1469.
72. Hu, Y.; Faham, R.; Roy, R.; Adams, M. W. W.; Rees, D. C. *J. Mol. Biol.* **1999**, *285*, 899–914.
73. Raaijmakers, H.; Teixeira, S.; Dias, J. M.; Almendra, M. J.; Brondino, C. D.; Moura, I.; Moura, J. J. G.; Romão, M. J. *JBIC* **2001**, *6*, 398–404.
74. Raaijmakers, H.; Maciera, M.; Dias, J. M.; Teixeira, S.; Bursakov, S.; Huber, R.; Moura, J. J. G.; Moura, I.; Romão, M. J. *Structure* **2002**, *10*, 1261–1272.
75. Inscore, F. E.; McNaughton, R.; Wescott, B. L.; Helton, M. E.; Jones, R.; Dhawan, I. K.; Enemark, J. H.; Kirk, M. L. *Inorg. Chem.* **1999**, *38*, 1401–1410.
76. Izumi, Y.; Glaser, T.; Rose, K.; McMaster, J.; Basu, P.; Enemark, J. H.; Hedman, B.; Hodgson, K. O.; Solomon, E. I. *J. Am. Chem. Soc.* **1999**, *121*, 10035–10046.
77. Pateman, J. A.; Cove, B. M.; Rever, B. M.; Roberts, D. B. *Nature* **1963**, *201*, 58–64.
78. Rajagopalan, K. V. *Adv. Enzymol. Relat. Areas Mol. Biol.* **1991**, *64*, 215–289.
79. Liu, M. T. W.; Wuebbens, M. M.; Rajagopalan, K. V.; Schindelin, H. *J. Biol. Chem.* **2000**, *275*, 1814–1822.
80. Temple, C. A.; Rajagopalan, K. V. *J. Biol. Chem.* **2000**, *275*, 40202–40210.
81. Buchanan, G.; Kuper, J.; Mendel, R. R.; Schwarz, G.; Palmer, T. *Arch. Micobiol.* **2001**, *176*, 62–68.
82. Leimkühler, S.; Rajagopalan, K. V. *J. Biol. Chem.* **2001**, *276*, 22024–22031.
83. Gutzke, G.; Fischer, B.; Memdel, R. R.; Schwarz, G. *J. Biol. Chem.* **2001**, *276*, 36268–36274.
84. Lake, M. W.; Temple, C. A.; Rajagopalan, K. V.; Schindelin, H. *J. Biol. Chem.* **2000**, *275*, 40211–40217.
85. Stevenson, C. E. M.; Sargent, F.; Buchanan, G.; Palmer, T.; Lawson, D. M. *Structure* **2000**, *8*, 1115–1125.
86. Wuebbens, M. M.; Liu, M. T.; Rajagopalan, K. V.; Schindelin, H. *Structure* **2000**, *8*, 709–718.
87. Rudolph, M. J.; Wuebbens, M. M.; Rajagopalan, K. V.; Schindelin, H. *Nature, Structural Biol.* **2001**, *8*, 42–46.
88. Mouncey, N. J.; Mitchenall, L. A.; Pau, R. N. *J. Bacteriol.* **1995**, *177*, 5294–5302.
89. Grunden, A. M.; Shanmugam, K. T. *Arch. Microbiol.* **1997**, *168*, 345–354.
90. Rech, S.; Wolin, C.; Gunsalus, R. P. *J. Biol. Chem.* **1996**, *271*, 2557–2562.
91. Hu, Y.; Rech, S.; Gunsalus, R. P.; Rees, D. C. *Nature Structural Biol.* **1997**, *4*, 703–707.
92. Nichols, J.; Rajagopalan, K. V. *J. Biol. Chem.* **2002**, *277*, 24995–25000.
93. Johnson, J. L.; Coyne, K. E.; Rajagopalan, K. V.; Van Hove, J. L. K.; Mackay, M.; Pitt, J.; Bonech, A. *Am. J. Med. Genet.* **2001**, *104*, 169–173.
94. Johnson, J. L; Duran, M. *The Metabolic and Molecular Bases of Inherited Disease* Scriver, C. R. Beaudet, A. L., Sly, W. S., Valle, D., Ed., 8th ed. *Molybdenum Cofactor Deficiency and Isolated Sulfite Oxidase Deficiency* **2001**, 3163–3177. McGraw-Hill: New York.
95. Leimkühler, S.; Rajagopalan, K. V. *J. Biol. Chem.* **2001**, *276*, 1837–1844.
96. Kisker, C.; Schindelin, H.; Baas, D.; Retey, J.; Meckenstock, R. U.; Kroneck, P. *FEMS Microbiol. Rev.* **1998**, *22*, 503–521.
97. Schindelin, H.; Kisker, C.; Rajagopalan, K. V. *Adv. Prot. Chem.* **2001**, *58*, 47–94.
98. Bray, R. C. *Quart. Rev. Biophys.* **1988**, *21*, 299–329.
99. McEwan, A. G.; Ferguson, S. J.; Jackson, J. B. *Biochem. J.* **1991**, *274*, 305–307.
100. Lovelock, J. E.; MacIsaacs, D. P.; Bishop, R. E.; Bilous, P. T. *Nature* **1972**, *237*, 452–453.
101. Stiefel, E. I. *Science* **1996**, *272*, 1599–1600.
102. Bastian, N. R.; Kay, C. J.; Barber, M. J.; Rajagopalan, K. V. *J. Biol. Chem.* **1991**, *266*, 45–51.
103. Wiener, J. H.; MacIsaacs, D. P.; Bishop, R. E.; Bilous, P. T. *J. Bacteriol.* **1988**, *170*, 1505–1510.
104. Bilous, B. T.; Cole, S. T.; Anderson, W. F.; Weiner, J. H. *Mol. Microbiol.* **1988**, *2*, 785–795.
105. George, G. N.; Hilton, J.; Temple, C.; Prince, R. C.; Rajagopalan, K. V. *J. Am. Chem. Soc.* **1996**, *118*, 1113–1117.
106. George, G. N.; Hilton, J.; Temple, C.; Prince, R. C.; Rajagopalan, K. V. *J. Am. Chem. Soc.* **1999**, *121*, 1256–1266.
107. Finnegan, M. G.; Hilton, J.; Rajagopalan, K. V.; Johnson, M. K. *Inorg. Chem.* **1993**, *32*, 2616–2617.
108. Garton, S. D.; Hilton, J.; Oku, H.; Crouse, B. R.; Rajagopalan, K. V.; Johnson, M. K. *J. Am. Chem. Soc.* **1997**, *119*, 12906–12916.
109. Bell, A. F.; He, X.; Ridge, J. P.; Hanson, G. R.; McEwan, A. G.; Tonge, P. J. *Biochemistry* **2001**, *40*, 440–448.
110. Davies, E. S.; Beddoes, R. L.; Collison, D.; Dinsmore, A.; Docrat, A.; Joule, J. A.; Wilson, C. R.; Garner, C. D. *J. Chem. Soc., Dalton Trans.* **1997**, 3985–3996.
111. Tucci, G. C.; Donahue, J. P.; Holm, R. H. *Inorg. Chem.* **1998**, *37*, 1602–1608.
112. Donahue, J. P.; Lorber, C.; Nordlander, E.; Holm, R. H. *J. Am. Chem. Soc.* **1998**, *120*, 3259–3260.
113. Donahue, J. P.; Goldsmith, C. R.; Nadiminti, U.; Holm, R. H. *J. Am. Chem. Soc.* **1998**, *120*, 12869–12881.
114. Lim, B. S.; Donahue, J. P.; Holm, R. H. *Inorg. Chem.* **2000**, *39*, 263–273.
115. Lim, B. S.; Sung, K.-M.; Holm, R. H. *J. Am. Chem. Soc.* **2000**, *122*, 7410–7411.
116. Lim, B. S.; Holm, R. H. *J. Am. Chem. Soc.* **2001**, *123*, 1920–1930.
117. Benson, N.; Farrar, J. A.; McEwan, A. G.; Thomson, A. J. *FEBS Lett.* **1992**, *307*, 169–172.
118. Bennett, B.; Benson, N.; McEwan, A. G.; Bray, R. C. *Eur. J. Biochem.* **1994**, *225*, 321–331.

119. Raitsimring, A. M.; Astashkin, A. V.; Feng, C.; Enemark, J. H.; Nelson, K. J.; Rajagopalan, K. V. *JBIC* **2003**, *8*, 95–104.
120. Aguey-Zinsou, K.-F.; Bernhardt, P. V.; McEwan, A. G.; Ridge, J. P. *JBIC* **2002**, *7*, 879–883.
121. Anderson, L. J.; Léger, C.; Rothery, R.; Weiner, J. H.; Armstrong, F. A. *Biochemistry* **2001**, *40*, 3117–3126.
122. Schultz, B. E.; Hille, R. E.; Holm, R. H. *J. Am. Chem. Soc.* **1995**, *117*, 827–828.
123. Simala-Grant, J. L.; Wiener, J. H. *Eur. J. Biochem.* **1998**, *251*, 510–515.
124. Temple, C. A.; George, G. N.; Hilton, J. C.; George, M. J.; Prince, R. C.; Barber, M. J.; Rajagopalan, K. V. *Biochemistry* **2000**, *39*, 4046–4052.
125. Garton, S. D.; Temple, C. A.; Dhawan, I. K.; Barber, M. J.; Rajagopalan, K. V.; Johnson, M. K. *J. Biol. Chem.* **2000**, *275*, 6798–6805.
126. Johnson, K. E.; Rajagopalan, K. V. *J. Biol. Chem.* **2001**, *276*, 13178–13185.
127. Ridge, J. P.; Aguey-Zinsou, K.-F.; Bernhardt, P. V.; Brereton, I. M.; Hanson, G. R.; McEwan, A. G. *Biochemistry* **2002**, *41*, 15762–15769.
128. McDevitt, C. A.; Hugenholtz, P.; Hanson, G. R.; McEwan, A. G. *Mol. Microbiol.* **2002**, *44*, 1575–1587.
129. Zinoni, F.; Birkmann, T. C.; Stadtman, T. C.; Böck, A. *Proc. Natl. Acad. Sci. USA* **1986**, *83*, 4650–4654.
130. Berg, B. L.; Li, J.; Heider, J.; Heider, V. J. *J. Biol. Chem.* **1991**, *266*, 22380–22385.
131. Fleischmann, R. D.; Adams, M. D.; White, O.; Clayton, R. A.; Kirkness, E. F.; Kerlavage, A. R.; Bult, C. J.; Tomb, J.-F.; Dougherty, B. A.; Merrick, J. M.; McKenny, K.; Sutton, G.; FitzHugh, W.; Fields, C.; Gocayne, J. D.; Scott, J.; Shirley, R.; Liu, L-I.; Glodek, A.; Kelley, J. M.; Weidman, J. F.; Phillips, C. A.; Spriggs, T.; Hedblom, E.; Cotten, M. D.; Utterback, T. R.; Hanna, M. C.; Nguyen, D. T.; Saudek, D. M.; Brandon, R. C.; Fine, L. D.; Fitchman, J. L.; Fuhrman, J. L.; Geoghagen, N. S. M.; Gnehm, C. L.; McDonald, L. A.; Small, K. V.; Fraser, C. M.; Smith, H. O.; Venter, J. C. *et al. Science* **1995**, *269*, 496–512.
132. Bult, C. J.; White, O.; Olsen, G. J.; Zhou, L.; Fleischmann, R. D.; Sutton, G. G.; Blake, J. A.; FitzGerald, L. M.; Clayton, R. A.; Gocayne, J. D.; Kerlavage, A. R.; Dougherty, B. A.; Tomb, J.-F.; Adams, M. D.; Reich, C. I.; Overbeek, R.; Kirkness, E. F.; Weinstock, K. G.; Merrick, J. M.; Glodek, A.; Scott, J. L.; Geoghagen, N. S. M.; Weidman, J. F.; Fuhrmann, J. L.; Nguyen, D.; Utterback, T. R.; Kelley, J. M.; Peterson, J. D.; Sadow, P. W.; Hanna, M. C.; Cotton, M. D.; Roberts, K. M.; Hurst, M. A.; Kaine, B. P.; Borodovsky, M.; Klenk, H.-P.; Fraser, C. M.; Smith, H. O.; Woese, C. R.; Venter, J. C. *et al. Science* **1996**, *273*, 1058–1073.
133. Kunst, F.; Ogasawara, N.; Moszer, I.; Albertini, A. M.; Alloni, G.; Azevdo, V.; Bertero, M. G.; Bessières, P.; Bolotin, A.; Borchert, S.; Borriss, R.; Boursier, L.; Brans, A.; Braun, M.; Brignell, S. C.; Bron, S.; Brouillet, S.; Bruschi, C. V.; Caldwell, B.; Capuano, V.; Carter, N. M.; Choi, S.-K.; Codani, J.-J.; Connerton, I. F.; Cummings, N. J.; Daniel, R. A.; Denizot, F.; Devine, K. M.; Düsterhöft, A.; Ehrlich, S. D.; Emmerson, P. T.; Entain, K. D.; Errington, J.; Fabret, C.; Ferrari, E.; Fouliger, D.; Fritz, C.; Fujita, M.; Fujita, Fuma, S.; Galizzi, A.; Galleron, N.; Ghim, S.-Y.; Glaser, P.; Goffeau, J.; Golighty, E. J; Grandi, G.; Guiseppi, G.; Guy, B. J.; Haga, K.; Haiech, J.; Harwood, C. R.; Henaut, A.; Hilbert, H.; Holsappel, S.; Hosono, K.; Hullo, M.-F.; Itaya, M.; Jones, L.; Joris, B.; Karamata, D.; Kasahara, Y.; Klaerr-Blanchard, M.; Klein, C.; Kobayashi, Y.; Keotter, P.; Koningstein, G.; Krogh, S.; Kumano, M.; Kurita, K.; Lapidus, A.; Lardinois, S.; Lauber, J.; Lazarevic, V.; Lee, S.-M.; Levine, A.; Liu, H.; Masuda, S.; Mauël, C.; Médigue, C.; Medina, N.; Mellado, R. P.; Mizuno, M.; Moestl, D.; Nakai, S.; Noback, M.; Noone, D.; O'Reilly, M.; Ogawa, K.; Ogiwara, A.; Oudega, B.; Park, S.-H.; Parro, V.; Pohl, T. M.; Portetelle, D.; Porwollik, S.; Prescott, A. M.; Presecan, E.; Pujic, P.; Purnelle, B.; Rapoport, G.; Rey, M.; Reynolds, S.; Rieger, M.; Rivolta, C.; Rocha, E.; Roche, B.; Rose, M.; Sadaie, Y.; Sato, T.; Scanlan, E.; Schleich, S.; Schroeter, R.; Scoffone, F.; Sekiguchi, J.; Sekowska, A.; Seror, S. J.; Serror, P.; Shin, B.-S.; Soldo, B.; Sorokin, A.; Tacconi, E.; Takagi, T.; Takahashi, H.; Takemaru, K.; Tekeuchi, M.; Tamakoshi, A.; Tanaka, T.; Terpstra, P.; Tognoni, A.; Tosato, V.; Uchiyama, S.; Vanenbol, M.; Vannier, F.; Vassarotti, A.; Viari, A.; Wambutt, R.; Wedler, E.; Wedler, H.; Weitzenegger, T.; Winters, P.; Wipat, A.; Yamamoto, H.; Yamane, K.; Yasumoto, K.; Yata, K.; Yoshida, K.; Yoshikawa, H.-F.; Zumstein, E.; Yoshikawa, H.; Danchin, A. *et al. Nature* **1997**, *390*, 249–256.
134. Smith, D. R.; Doucette-Stamm, L. A.; Deloughery, C.; Lee, H.; Dubois, J.; Aldredge, T.; Bashirzadeh, R.; Blakely, D.; Cook, R.; Gilbert, K.; Harrison, D.; Hoang, L.; Keagle, P.; Lumm, W.; Pothier, B.; Qiu, D.; Spadafora, R.; Vicaire, R.; Wang, Y.; Wierzbowski, J.; Gibson, R.; Jiwani, N.; Caruso, A.; Bush, D.; Reeve, J. N. *et al. J. Bacteriol.* **1997**, *179*, 7135–7155.
135. George, G. N.; Colango, C. M.; Dong, J.; Scott, R. A.; Khagulov, S. V.; Gladyshev, V. N.; Stadtman, T. C. *J. Am. Chem. Soc.* **1998**, *120*, 1267–1273.
136. Blasco, F.; Iobbi, C.; Giordano, G.; Chippaux, M.; Bonnefoy, V. *Mol. Gen. Genet.* **1989**, *218*, 249–256.
137. Blasco, F.; Iobbi, C.; Raouchniak, J.; Giordano, G.; Bonnefoy, V.; Chippaux, M. *Mol. Gen. Genet.* **1990**, *222*, 104–111.
138. Andriesse, X.; Omata, T.; Hirano, A. *Mol. Gen. Genet.* **1993**, *236*, 193–202.
139. Bickel-Sandkötter, S.; Ufer, M. *Z. Naturforsch.* **1995**, *50*, 365–372.
140. Richardson, D. J.; Berks, B. C.; Reilly, A.; Willis, A. C.; Ferguson, S. J. *Biochem. J.* **1995**, *309*, 983–992.
141. Bursakov, S. A.; Liu, M.-Y.; Payne, W. J.; LeGall, J.; Moura, I.; Moura, J. J. G. *Anaerobe* **1995**, *1*, 55–60.
142. Nakazaki, N.; Muraki, A.; Naruo, K.; Okumura, S.; Shimpo, S.; Tekeuchi, C.; Wada, T.; Watanabe, A.; Yamada, M.; Yasuda, M.; Tabata, S. *DNA Res.* **1996**, *3*, 109–136.
143. Cramer, S. P.; Solomonson, L. P.; Adams, M. W. W.; Mortenson, L. E. *J. Am. Chem. Soc.* **1984**, *106*, 1467–1471.
144. George, G. N.; Turner, N. A.; Bray, R. C.; Morpeth, F. F.; Boxer, D. H.; Cramer, S. P. *Biochem. J.* **1989**, *259*, 693–700.
145. Vincent, S. P. *Biochem. J.* **1979**, *177*, 757–759.
146. Godfrey, C.; Greenwood, C.; Thomson, A. J.; Bray, R. C.; George, G. N. *Biochem. J.* **1984**, *224*, 601–608.
147. Neame, P. J.; Barber, M. J. *J. Biol. Chem.* **1989**, *264*, 20894–20901.
148. Johnson, J. L.; Garrett, R. M.; Graf, T. N.; Feigenbaum, A.; Rajagopalan, K. V. *Proc. Natl. Acad. Sci. USA* **1998**, *95*, 6394–6398.
149. Garrett, R. M.; Rajagopalan, K. V. *J. Biol. Chem.* **1994**, *269*, 272–276.
150. Garrett, R. M.; Bellissimo, D. B.; Rajagopalan, K. V. *Biochim. Biophys. Acta* **1995**, *1262* 147–149.
151. Eilers, T.; Schwarz, G.; Brinkmann, H.; Witt, C.; Richter, T.; Nieder, J.; Koch, B.; Hille, R.; Hänsch, R.; Mendel, R. R. *J. Biol. Chem.* **2001**, *276*, 46989–46994.

152. Garton, S. D.; Garrett, R. M.; Rajagopalan, K. V.; Johnson, M. K. *J. Am. Chem. Soc.* **1996**, *119*, 2590–2591.
153. Thapper, A.; Deeth, R. J.; Nordlander, E. *Inorg. Chem.* **1999**, *38*, 1015–1018.
154. Brody, S. M.; Hille, R. *Biochemistry* **1999**, *38*, 6668–6677.
155. Helton, M. E.; Pacheco, A.; McMaster, J.; Enemark, J. H.; Kirk, M. L. *J. Inorg. Biochem.* **2000**, *80*, 227–233.
156. Gutteridge, S.; Lamy, M. T.; Bray, R. C. *Biochem. J.* **1980**, *191*, 285–288.
157. Bray, R. C.; Gutteridge, S.; Lamy, M. T.; Wilkinson, T. *Biochem. J.* **1983**, *211*, 227–239.
158. Raitsimring, A. M.; Pacheco, A; Enemark, J. H. *J. Am. Chem. Soc.* **1998**, *119*, 11263–11278.
159. Astashkin, A. V.; Raitsimring, A. M.; Feng, C.; Johnson, J. L.; Rajagopalan, K. V.; Enemark, J. H. *J. Am. Chem. Soc.* **2002**, *124*, 6109–6118.
160. Spence, J. T.; Kipke, C. A.; Enemark, J. H.; Sunde, R. A. *Inorg. Chem.* **1991**, *30*, 3011–3015.
161. Bray, R. C. *Quart. Rev. Biophys.* **1988**, *21*, 299–329.
162. Romão, M. J.; Huber, R. *Structure and Bonding* **1998**, *90*, 69–95.
163. Ilich, P.; Hille, R. *J. Am. Chem. Soc.* **2002**, *124*, 6796–6797.
164. Ichida, K.; Ayama, Y.; Noda, K.; Minoshima, S.; Hosoya, T.; Sakai, O.; Shimizu, N.; Nishino, T. *Gene* **1993**, *133*, 279–284.
165. Berglund, L.; Rasmussen, J. T.; Anderson, M. D.; Rasmussen, M. S.; Peterson, T. E. *J. Dairy Sci.* **1996**, *79*, 198–204.
166. Schardinger, F. *Z. Untersuch. Nahrungs Genussmittel* **1902**, *5*, 1113–1121.
167. Massey, V.; Harris, C. M. *Biochem. Soc. Trans.* **1997**, *25*, 750–755.
168. Hille, R.; Nishino, T. *FASEB J.* **1995**, *9*, 995–1003.
169. Elion, G. B. *Science* **1989**, *244*, 41–47.
170. Olson, J. S.; Ballou, D. P.; Palmer, G.; Massey, V. *Biol. Chem.* **1974**, *249*, 4363–4382.
171. Turner, N.; Barata, B.; Bray, R. C.; Deistung, J.; LeGall, J.; Moura, J. J. G. *Biochem. J.* **1987**, *243*, 755–761.
172. Barata, B. A. S.; LeGall, J.; Moura, J. J. G. *Biochemistry* **1993**, *32*, 11559–11568.
173. Howes, B. D.; Bray, R. C. ;Richards R. L.; Turner, N.; Bennett, B.; Lowe, D. J. *Biochemistry* **1996**, *35*, 1432–1443.
174. Bray, R. C.; Bennett, B.; Burke, J. F.; Chovnick, A.; Doyle, W. A. *Biochem. Soc. Trans.* **1997**, *24*, 99–105.
175. Bordas, J.; Bray, R. C.; Garner, C. D.; Gutteridge, S.; Hasnain, S. S. *Biochem J.* **1980**, *191*, 499–508.
176. Hille, R.; George, G. N.; Eidsness, M. K.; Cramer, S. P. *Inorg. Chem.* **1989**, *28*, 4018–4022.
177. Turner, N. A.; Bray, R. C.; Diakun, G. P. *Biochem. J.* **1989**, *260*, 563–571.
178. Maiti, N. C.; Tomita, T.; Kitagawa, T.; Okamoto, K.; Nishino, T. *JBIC* **2003**, *8*, 327–333.
179. Manikandan, P.; Choi, E. Y.; Hille, R.; Hoffman, B. M. *J. Am. Chem. Soc.* **2001**, *123*, 2658–2663.
180. Ilich, P.; Hille, R. *J. Phys. Chem. B* **1999**, *103*, 5406–5412.
181. Calzi, M. L.; Raviolo, C.; Ghibaudi, E.; DeGioia, L.; Salmona, M.; Cazzaniga, G.; Kurosaki, M.; Garattini, E. *J. Biol. Chem.* **1995**, *270*, 31037–31045.
182. Wright, R. M.; Vaitaitis, G. M.; Wilson, C. M.; Repine, T. B.; Terada, L. S.; Repine, J. E. *Proc. Natl. Acad. Sci. USA* **1993**, *90*, 10690–10694.
183. Mahler, H. R.; Mackler, B.; Green, D. E.; Bock, R. M. *J. Biol. Chem.* **1954**, *210*, 465–480.
184. Tamaki, T.; Horinouchi, S.; Fukaya, M.; Okumura, H.; Kawamura, Y.; Beppu, T. *J. Biochem.* **1989**, *106*, 541–544.
185. Kim, S. W.; Luykx, D. M. A. M.; de Vries, S.; Duine, J. A. *Arch. Biochem. Biophys.* **1996**, *325*, 1–7.
186. Axley, M. J.; Grahame, D. A. *J. Biol. Chem.* **1991**, *266*, 13731–13736.
187. Brune, A.; Schink, B. *Arch. Microbiol.* **1992**, *157*, 417–424.
188. Johnson, M. K.; Rees, D. C.; Adams, M. W. W. *Chem. Rev.* **1996**, *96*, 2817–2835.
189. Hagen, W. R.; Arendson, A. F. *Struct. Bonding* **1996**, *90*, 161–192.
190. George, G. N.; Prince, R. C.; Mukund, S.; Adams, M. W. W. *J. Am. Chem. Soc.* **1992**, *114*, 3521–3523.
191. Koehler, B. P.; Mukund, S.; Conover, R. C.; Dhawan, I. K.; Roy, R.; Adams, M. W. W.; Johnson, M. K. *J. Am. Chem. Soc.* **1996**, *118*, 12391–12405.
192. Roy, R.; Mukund, S.; Schut, G.; Dunn, D. M.; Weiss, R.; Adams, M. W. W. *J. Bacteriol.* **1999**, *181*, 1171–1180.
193. Mukund, S.; Adams, M. W. W. *J. Biol. Chem.* **1993**, *268*, 13592–13600.
194. Stewart, L. J.; Bailey, S.; Bennett, B.; Charnock, J. M.; Garner, C. D.; McAlpine, A. S. *J. Mol. Biol.* **2000**, *299*, 593–600.
195. Stewart, L. J.; Bailey, S.; Collison, D.; Morris, G. A.; Preece, I.; Garner, C. D. *CHEMBIOCHEM* **2001**, *9*, 703–706.
196. Davies, E. S.; Aston, G. M.; Beddoes, R. L.; Collison, D. J.; Dinsmore, A.; Docrat, A.; Joule, J. A.; Wilson, C. R.; Garner, C. D. *J. Chem. Soc., Dalton Trans.* **1998**, 3647.
197. Lorber, C.; Donahue, J. P.; Goddard, A.; Nordlander, E.; Holm, R. H. *J. Am. Chem. Soc.* **1998**, *120*, 8102–8112.
198. Tucci, G. C.; Donahue, J. P.; Holm, R. H. *Inorg. Chem.* **1998**, *37*, 1602–1608.
199. Goddard, C. A.; Holm, R. H. *Inorg. Chem.* **1999**, *38*, 5389–5398.
200. Lim, B. S.; Sung, K.-M.; Holm, R. H. *J. Am. Chem. Soc.* **2000**, *122*, 7410–7411.
201. Miao, M.; Willer, M. W.; Holm, R. H. *Inorg. Chem.* **2000**, *39*, 2843–2849.
202. Sung, K.-M.; Holm, R. H. *Inorg. Chem.* **2000**, *39*, 1275–1281.
203. Sung, K.-M.; Holm, R. H. *Inorg. Chem.* **2001**, *40*, 4518–4525.
204. Sung, K.-M.; Holm, R. H. *J. Am. Chem. Soc.* **2001**, *123*, 1931–1943.
205. Sung, K.-M.; Holm, R. H. *J. Am. Chem. Soc.* **2002**, *124*, 4312–4320.
206. Meckenstock, R. U.; Krieger, R.; Ensign, S.; Kroneck, P. M. H.; Schink, B. *Eur. J. Biochem.* **1999**, *264*, 176–182.

8.19
Superoxide Processing

A.-F. MILLER

University of Kentucky, Lexington, KY, USA

8.19.1 THE SIGNIFICANCE OF SUPEROXIDE TO BIOLOGICAL UTILIZATION OF O_2

Dioxygen has an unpaired electron in each of the lowest-lying antibonding orbitals. Thus the kinetic barrier to reactivity associated with its triplet nature is compounded by the fact that the first electron gained in the course of its reduction must add to an antibonding orbital that is already populated. Nonetheless, life has contrived to exploit O_2's thermodynamic reactivity by entraining catalysts with multiple accessible spin states that permit conservation of spin at low energy cost, while also permitting accumulation of negative charge on O_2. Thus, upon binding to metal ions, effective electron transfer can occur with a decrease in the spin of O_2 but a compensating increase for the metal ion, which may be dissipated by spin–orbit coupling. Spin pairing and transfer of a second electron to superoxide ($O_2^{\bullet-}$) then produces the $S=0$ peroxide state.

Thus, not only in inorganic systems, but also in organic systems such as flavins, pterins, and xanthine,[1] the two spins of O_2 are formally separated before being paired (with other electrons) via the virtual or explicit intermediacy of $O_2^{\bullet-}$. Systems that stabilize the negatively charged $O_2^{\bullet-}$ and O_2^{2-} fragments further promote the reactivity of O_2. Thus, transition metal ions with their closely spaced electronic spin states, substantial spin–orbit coupling, and positive charge have been recruited time and again by biochemistry to activate O_2.

8.19.2 BIO-INORGANIC MODELS CONTAINING $O_2^{\bullet-}$

Stable complexes of $O_2^{\bullet-}$ provide fascinating glimpses of a crucial intermediate in O_2 metabolism and teach us about the electronics, structure, and reactivity of metal-bound superoxides. These have been reviewed relatively recently in articles focusing on superoxide as a ligand,[2] computational studies of superoxide complexes,[3] superoxide complexes with Mn,[4] Cr–Mo,[5] hemes,[6] and the spectroscopy of superoxide bound to dinuclear clusters,[7] as well as elsewhere in this series.

Complexes in which superoxide is bound end-on bent,[2,6,8] as well as side-on,[2,9,10] have been characterized. Significant unpaired electron spin density is often found to reside on the O_2 fragment.[2] Because $O_2^{\bullet-}$ is thermodynamically the most energetic oxidation state of O_2, considering only electronic ground states (Figure 1) $O_2^{\bullet-}$ complexes tend to attack a second metal ion, which they oxidize upon binding to form bridged peroxo complexes.[2,11] Thus, stable $O_2^{\bullet-}$ complexes are usually only formed from O_2 by metal ions limited to one-electron transfer or by hindered complexes in which coordinated $O_2^{\bullet-}$ does not have access to a second metal ion. A few binuclear superoxo complexes have nonetheless been reported.[12]

Superoxide generated in solution can be trapped and stabilized by binding to redox-inert metal ions such as Zn^{2+} and Sc^{3+}.[13] More commonly, however, complexes of $O_2^{\bullet-}$ are formed as a result of reaction of O_2 with a metal complex capable of donating electron density to it. In these cases, O_2 binding is not readily separable from its reduction, and release of the $O_2^{\bullet-}$ is accompanied by its reoxidation to O_2 in many cases. Thus, $Cr^{II}TPPpy$ reacts with O_2 to form a formal Cr^{III} adduct with $O_2^{\bullet-}$ in which the third unpaired electron of Cr^{III} is spin paired with the
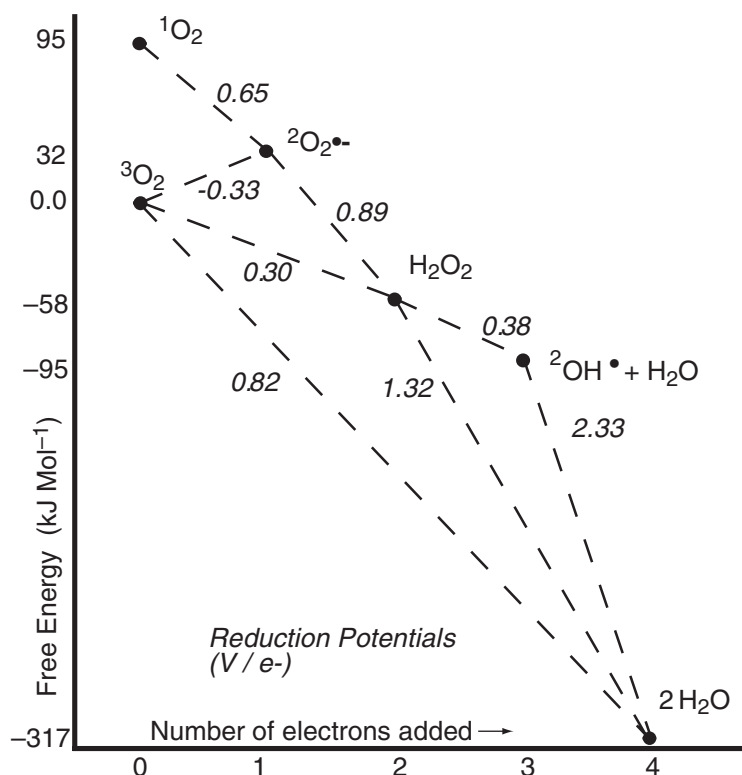
Figure 1 Free energies and reduction potentials of dioxygen and related compounds, adapted from Sawyer.[26] Reduction potentials are in italics, placed on the lines and are $E^{\circ\prime}$ values, at pH 7 K and 298 K, based on unit pressures of O_2 and unit concentrations of other species.

unpaired electron of $O_2^{\bullet-}$,[14] similar to the spin pairing invoked in production of diamagnetic oxy-hemoglobin and oxy-myoglobin.

Porphyrin–metal complexes are disproportionately represented among synthetic superoxide complexes due to the biological importance of O_2 carriers hemoglobin (Hb) and myoglobin (Mb), and the prevalence of cytochromes in oxygen-activating enzymes. Spin pairing between formally low-spin $S = 1/2$ Fe^{III} and $S = 1/2$ $O_2^{\bullet-}$ makes oxy-Hb diamagnetic.[6,8] This is the basis for extremely powerful magnetic resonance imaging methods used to determine the degree of oxygenation of tissues, based on the very different effects of high-spin deoxy-Hb (Fe^{II}–Hb, $S = 2$) and diamagnetic oxy-Hb ($O_2^{\bullet-}$–Fe^{III}–Hb, $S = 0$) on the nuclear relaxation times of protons in tissue.[15]

Both Hb and Mb are occasionally inactivated due to dissociation of coordinated $O_2^{\bullet-}$ without re-reduction of the Fe to Fe^{II}. Shimaka[16] has demonstrated that conversion of ($O_2^{\bullet-}$–Fe^{III}) oxy-Mb to met-Mb (Fe^{III}) can be understood in terms of displacement of bound $O_2^{\bullet-}$ by incoming bases including OH^- and H_2O present in the native aqueous environment. The fact that MbO_2 is oxidized to the met form only on a time scale of days, vs. minutes or less for free Fe^{II} porphyrin, reflects the isolation of the Fe porphyrin from redox-active species and its sequestration in a relatively non-polar protein matrix.

Superoxide complexes are also invoked as intermediates in the reactions of bleomycin,[17,18] catechol dioxygenases,[19] and cytochrome P450.[20] They can be expected to occur in cases where the redox cofactor consists of a single metal ion in the absence of other readily oxidizable cofactors.

8.19.3 SUPEROXIDE IN BIOLOGY

Superoxide is simply a fact of aerobic life. As much as 3% of the O_2 consumed biologically is only reduced as far as $O_2^{\bullet-}$,[21] normally as a result of electron leakage from the respiratory or photosynthetic electron transport chains.[22] Superoxide produced upon reperfusion of anoxic tissues is responsible for a substantial fraction of the damage sustained after ischemia and surgery (reviewed by McCord and Kehrer[23,24]). Superoxide retains the thermodynamic reactivity of O_2 without the kinetic restraints (superoxide reacts in radical chain reactions that conserve spin by producing another radical in each step), and in principle can act as either a reductant or an oxidant (Figure 1). Nonetheless, free $O_2^{\bullet-}$ is not a strong oxidant in practice, because its negative charge and electronic structure discourage acquisition of an additional electron. However, these same electrons make $O_2^{\bullet-}$ a good nucleophile, as well as a moderate reductant.[25] Superoxide can abstract weakly bound H atoms, leaving radical species which react rapidly with O_2, as in lipid peroxidation.[25] Moreover, the ability of $O_2^{\bullet-}$ to reduce metal ions such as Fe^{III} and Cu^{II}, in combination with the tendency of $O_2^{\bullet-} + H^+$ to disproportionate to produce H_2O_2, sets the stage for the reaction of H_2O_2 with Fe^{2+} or Cu^{1+} to yield extremely reactive $OH^{\bullet}$.[24,26] Thus, the most important biological consequences of $O_2^{\bullet-}$ are indirect, stemming not from the reactivity of $O_2^{\bullet-}$ itself, but the much higher reactivity of its progeny H_2O_2, $OH^{\bullet}$, HOCl, and ONO_2^- collectively known as reactive oxygen species (ROS). These, as well as $O_2^{\bullet-}$ itself, inactivate a number of FeS cluster-containing and other enzymes, including some essential to biosynthesis of sulfur-containing, aromatic and branched chain amino acids.[27,28] $OH^{\bullet}$ is indiscriminately reactive, abstracting H atoms from DNA bases, initiating strand breakage[29] and modifying amino acids[30] within a few Å of its site of formation, and thus primarily affecting metal-binding biomolecules. Reaction between $O_2^{\bullet-}$ and NO not only produces the very reactive oxidant ONO_2^- (peroxynitrite), but also consumes NO and thus interferes with NO-mediated signaling.[31] Indeed, ROS are now recognized to contribute to a great many degenerative conditions including arthritis, atherosclerosis, diabetes, reperfusion injury after ischemia, aging and cell death during infections, and the progress of AIDS (reviewed by Halliwell and Gutteridge[21]).

8.19.4 SUPEROXIDE-GENERATING SYSTEMS

8.19.4.1 NADPH Oxidase, the "Burst Oxidase"

Given the toxicity of ROS, it would have been remarkable if they had not been exploited to do intentional damage in some biological context. Indeed, the respiratory burst of neutrophils and macrophages is a crucial element of our antimicrobial arsenal.[33–35] Superoxide is produced by NADPH oxidase of activated phagocytic cells and can account for up to 90% of their O_2

consumption.[36] The redox-active cofactors are all bound by a transmembrane heterodimer of two closely associated components: gp91[phox] and p22[phox] (gp91[phox] = phagocyte oxidase glycoprotein of apparent molecular mass 91 kD, and p22[phox] = phagocyte oxidase protein of apparent molecular mass 22 kD).[37] However, additional cytoplasmic proteins are required for activity, including p47[phox], p67[phox], p40[phox], and a small GTPase called Rac (reviewed in references[33,34,38]). These are assembled in response to cellular stimulation by bacteria and activating chemicals. Individuals deficient in either (X-linked) gp91[phox], p47[phox], p67[phox], or g22[phox] have chronic granulomatous disease (CGD) and suffer abnormally frequent and severe bacterial and fungal infections.[39] NADPH oxidase catalyzes reduction of 2 O_2 by cytosolic NADPH and releases 2 $O_2^{\bullet-}$ outside the cell or into phagosomes (Figure 2). Consistent with the use of an obligate 2-electron reductant to effect 1-electron reduction of O_2, the catalytic core of NADPH oxidase (known as flavocytochrome b_{558}) contains one FAD along with two b-type cytochromes (Figure 2).[40] The cofactors are proposed to mediate electron transfer from NADPH to O_2 as follows: NADPH $\rightarrow$ FAD $\rightarrow$ heme A $\rightarrow$ heme B $\rightarrow$ O_2.[38,41] The NADPH binding site and FAD binding site have been located in gp91[phox] (Figure 2).[34,35,42] P67[phox] is required for electron transfer from NADPH to FAD[38] and His338 of gp91[phox] has been proposed to contact FAD and aid in electron transfer between it and the cytochromes (numbering is that of human NADH oxidase).[32,43]

The two cytochromes are proposed to reside within the membrane[37] bound by gp91[phox] via His101, His115, His209, and His222.[44] Sequence homology, comparable reduction potentials and spectral similarities among NADPH oxidases from different sources, *Saccharomyces cerevisiae* ferric reductase (FRE1), the FAD binding domain of ferredoxin-NADP$^+$ reductases (FNRs),[45] and the cytochrome b subunit of the mitochondrial cytochrome bc1 complex suggest a binding motif in which the cytochromes are bound stacked one above the other between a pair of helices, each with two histidines 12 or 13 residues apart.[37,44]

Resonance Raman and EPR spectroscopy indicate that both cytochromes are low spin, coordinated to two His residues in the resting state.[46,47] Upon activation of NADPH oxidase or exposure to the activator arachidonic acid, the oxidized cytochromes are partially converted to low-spin five-coordinate centers. The rate of butyl isocyanide binding to reduced NADPH oxidase increases dramatically, resulting in complete (though reversible) inhibition of $O_2^{\bullet-}$ production and changes to the EPR signals of both hemes.[48] Thus, at least one His ligand of each cytochrome is labile and might make way for coordination of O_2. Hence the path of electron flow may fork instead of running from one cytochrome to the next. Alternatively, binding of a regulator such as NO to one cytochrome could regulate $O_2^{\bullet-}$ production at the other.
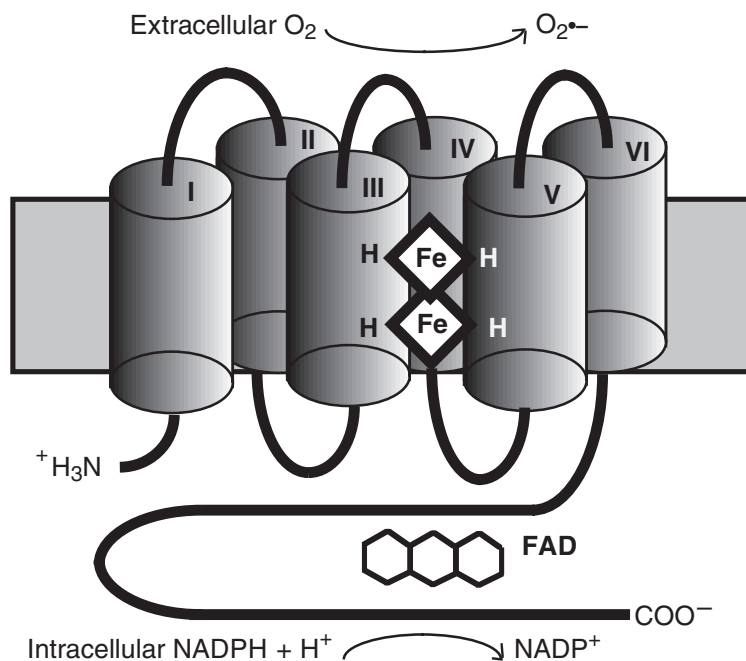
Figure 2 Cartoon of the structure of flavocytochrome b_{558} gp91[phox] of NADPH oxidase, adapted from Maturana *et al.*[190] The His ligands of the two cytochromes are indicated by H, and cylinders indicate transmembrane helices.

8.19.4.2 Nitric Oxide Synthase (NOS)

euronal nitric oxide synthase (nNOS) has been shown to catalyze $O_2^{\bullet-}$ formation when l-arginine (l-Arg) is scarce.[49,50] This appears to occur via electron transfer from the cytochrome to O_2 (as in NADPH oxidase). While inducible NOS (iNOS) has also recently been shown to produce $O_2^{\bullet-}$ in the absence of l-Arg, in this case the flavin cofactors appear to be responsible for reduction of O_2.[51] Endothelial nitric oxide synthase (eNOS) also produces $O_2^{\bullet-}$ but production of $O_2^{\bullet-}$ vs. $NO^{\bullet}$ is determined by the amount of fully reduced tetrahydrobiopterin (BH_4) available, with BH_4 suppressing $O_2^{\bullet-}$ in favor of $NO^{\bullet}$.[52] On a cautionary note, $O_2^{\bullet-}$ production by many systems may represent a non-physiological activity expressed only when native activity is compromised in some way.

8.19.4.3 Xanthine Oxidase

Under conditions of stress, the enzyme xanthine dehydrogenase is converted to xanthine oxidase, which uses $2\,O_2$ instead of NAD^+ to oxidize hypoxanthine and xanthine, and therefore releases $2O_2^{\bullet-}$. Thus, inhibitors of xanthine oxidase such as allopurinol are used to suppress inflammation associated with arthritis.[53] (Xanthine oxidase is discussed in more detail in Chapter 8.18)

8.19.5 OVERVIEW OF DEFENSES AGAINST SUPEROXIDE

It makes better biological sense to interrupt oxidative damage at the level of $O_2^{\bullet-}$ than further downstream, because scavenging $O_2^{\bullet-}$ depresses levels of all the reactive progeny simultaneously. Superoxide disproportionates rapidly at pHs approaching its pK of 4.8, but at more common physiological pHs, spontaneous disproportion is slower ($k \approx 2 \times 10^5\,s^{-1}$ at neutral pH). Therefore, in order to suppress $O_2^{\bullet-}$ to less than the lethal concentration of $\approx 10^{-10}\,M$, in the face of the estimated rate of $O_2^{\bullet-}$ formation of $5\,\mu M\,s^{-1}$[54], superoxide dismutase (SOD) and/or superoxide reductase (SOR) is probably present at $\approx 50\,\mu M$ in cells.[55] This may reflect the relatively high K_Ms of SOR and SOD ($\approx 100\,\mu M$, see below), which would decrease their efficiencies despite their very high second order rate constants of $k \approx 10^9\,M^{-1}s^{-1}$. A number of parasites and pathogens export SOD. This is believed to contribute to virulence, presumably because the exported SOD defends the pathogen against the burst of $O_2^{\bullet-}$ produced by phagocytic leukocytes.[56]

Superoxide can, in principle, be eliminated by oxidation, reduction, or disproportionation. The latter has the advantage of consuming two molecules of the offending substrate per reaction, but produces H_2O_2 as well as O_2, consistent with its dominance in aerobes (summarized in Table 1). $O_2^{\bullet-}$ oxidation to O_2 does not appear to be a prevalent strategy, possibly because the intracellular environment tends to be fairly reducing (ambient potentials $\approx -230\,mV$ for oxygen tension corresponding to 10% air-saturated[57]) so that most centers with an E_m sufficiently high to oxidize $O_2^{\bullet-}$ are normally reduced *in vivo*. Superoxide reduction is employed by strict anaerobes, either because the O_2 resulting from dismutation is toxic, or because the cell interior is so reducing that any enzyme oxidized by $O_2^{\bullet-}$ is rapidly re-reduced and would be subject to evolutionary optimization only for its ability to reduce $O_2^{\bullet-}$. SODs constitute robust stand-alone defenses, since they do not rely on any additional electron donor or acceptor, but utilize $O_2^{\bullet-}$ as both and consume two molecules of $O_2^{\bullet-}$ per turnover. The H_2O_2 they produce is normally consumed by catalases and peroxidases. Indeed, whereas moderate over-expression of SOD tends to be beneficial,[58] there are instances in which high levels of overexpression of SOD alone were found to be deleterious.[59] This may be because overexpressed SOD suppresses the $O_2^{\bullet-}$ concentration to the point that $O_2^{\bullet-}$ fails to activate the SoxR/S regulon and elicit overexpression of the several other enzymes besides SOD involved in minimizing oxidative damage.[59,60]

SODs have evolved on several independent occasions with the result that Cu,Zn–SOD is a completely different enzyme from Ni–SOD, and both are completely different from the Fe– and Mn–SODs (compare Figures 3 and 5). In contrast, Fe–SODs and Mn–SODs are strongly homologous to one another.[61] The different SODs are found in different organisms and associated with different cellular compartments in which $O_2^{\bullet-}$ is generated (Table 1). Notwithstanding its final destination, mitochondrial Mn–SOD is encoded by a nuclear gene.

Table 1 Comparison of the different types of superoxide dismutases and superoxide reductase.

Type of SOD or SOR	Metal content and ligation	Location	Oligomerization* monomer size	k_{cat} [a] (s^{-1})	K_M	Second order rate constant ($M^{-1}s^{-1}$)	Inhibition
Cu,Zn–SOD	$Cu^{I/II}(His_4)$, $Zn^{II}(His_3,Asp^-)$	Eukaryotic cytosol, peroxisomes, mitochondrial intermembrane space. Periplasm of Gram −ve bacteria, plant plastids, extracellular in mammals.	(1, 2, 4) *16 kD	0.9×10^6 [98]	3.5 mM at pH 9.3 and 5.5 °C [98]	2×10^9 at pH 7 and 25 °C [80]	pH <5, high pH pK ≈ 10.7, CN^-, N_3^-, NCO^-, H_2O_2
Fe–SOD	$Fe^{II/III}$ $(His_3,Asp^-$, $H_2O/OH^-)$	Prokaryotes, occasionally in cytoplasm of some protists, chloroplasts.	(1, 2) *22 kD	2.6×10^4 [120]	80 μM at pH 8.4 and 25 °C [120]	5×10^8 at pH 8, 25 °C [119]	pH ≤5, high pH pK ≈ 9, H_2O_2, N_3^-, F^- [120]
Mn–SOD	$Mn^{II/III}$ $(His_3,Asp^-$, $H_2O/OH^-)$	Mitochondria, peroxisomes of eukaryotes.	(2, 4) *22 kD	1.25–4×10^4 [147,148]	40–50 μM at pH = 9.3 and 2 °C [147]	5.6×10^8 at pH 8.9, 25 °C [189]	high pH pK ≈ 9.8, N_3^-, F^- [111]
Ni–SOD	$Ni^{II},Ni^{II/III}$ (Cys_4,His_2)	Fungi.	4*13 kD			1.3×10^9 at pH 7 [167]	CN^-, H_2O_2 [165]
SOR	$Fe^{II/III}(His_4,Cys,$ $(Glu))$	Strict anaerobes, archae.	4*14 kD			1.5×10^9 at pH 7.8, 25 °C [186]	pH <5.6, high pH pK ≈ 9.5, N_3^-, CN^-

[a] k_{cat} values are reported for the same conditions as those pertaining to K_M.

8.19.6 Cu,Zn-SOD CONTAINING SUPEROXIDE DISMUTASE

Cu,Zn-containing SODs (Cu,Zn–SODs) are known as the cytosolic and extracellular SODs of animals; however, they are also found in plants, animals, fungi and bacteria, and are encoded in several viral genomes.[25,62] In animals, Cu,Zn–SOD is also found in the nucleus, the mitochondrial intermembrane space, and lysosomes.[63] In plants, distinct Cu,Zn–SODs are found in the chloroplast and cytoplasm.[62] The prokaryotic Cu,Zn–SODs as a group are distinct from the eukaryotic Cu,Zn–SODs.[63] Recent reviews of Cu,Zn–SOD include those of Bordo and Bertini.[63,64]

8.19.6.1 Structure

As their name implies, Cu,Zn–SODs contain a $Cu^{I/II}$ and a Zn^{II} ion in each active site. The enzyme is most commonly a dimer of 16 kD monomers, although the human extracellular version is a homotetramer[65] and a few prokaryotic enzymes are monomers.[63] Monomeric versions of the human cytosolic enzyme have also been engineered.[66] In all structurally characterized cases, the monomers are single antiparallel β-barrel domains (Figure 3).[63,67] The active site is located on the exterior of the barrel at the base of a channel formed predominantly by loops. The Zn is completely occluded from solvent but the Cu has slight ($10\,\text{Å}^2$) solvent exposure.

In the oxidized state, the active site Cu^{II} ion is coordinated by four histidines: His44 (Nδ1), His46, His61, and His118 (Nε2, numbering of bovine Cu,Zn–SOD is used throughout) in a geometry intermediate between square–planar and trigonal–bipyramidal (Figure 4).[68–70] His61 also coordinates the Zn^{II} ion via Nδ1. The Zn ion is roughly tetrahedral and also coordinated by His69 and His78 (Nδ1) and Asp81$^-$.[63,68–70] Additional crucial residues include a buried Asp122$^-$ that hydrogen bonds to the His44 ligand of Cu and the His69 ligand of Zn, stabilizing the binuclear cluster, an Arg which is partially exposed to solvent near Cu, and a Cys whose participation in an S—S bond is held to be essential for correct active site structure and metal center maturation.[63] One molecule of solvent is coordinated to Cu^{II} based on NMR[71] and is visible in many crystal structures in the axial position, adjacent to Arg141.[68] However, some of the crystal structures purporting to describe the oxidized state may reflect varying contributions from reduced sites generated by X-ray photoreduction.[72]

The metal ions can be removed by dialysis against EDTA and reconstituted or replaced site-specifically.[73,74] Cu, E–SOD, Cu,Zn–SOD lacking the two Zn ions but with the two Cu ions in their correct sites, retains 80% of native activity at pH 6, indicating that neither the Zn ion nor the bridging His are essential at low pH.[75] Similarly, Cu,Co–SOD retains full activity[76] and native structure,[77] and thus affords very valuable spectroscopic probes of the Zn site. NMR studies of the Cu^{II},Co^{II}–SOD active site have been used to elucidate the effects of ligand binding and
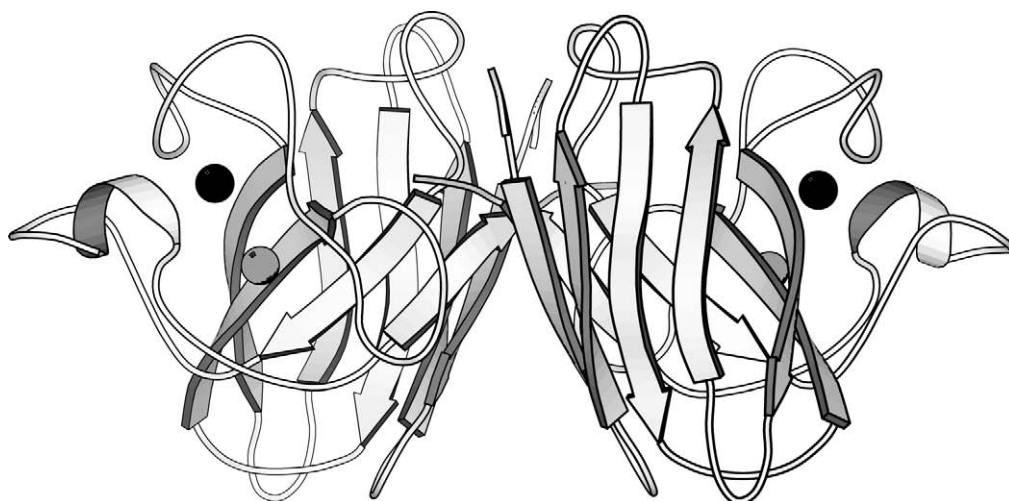
Figure 3 Ribbon of the Cu,Zn–SOD of bovine erythrocytes, based on the coordinates of Tainer *et al.*[69] (2SOD.pdb) All molecular structures are depicted using Molscript.[191]
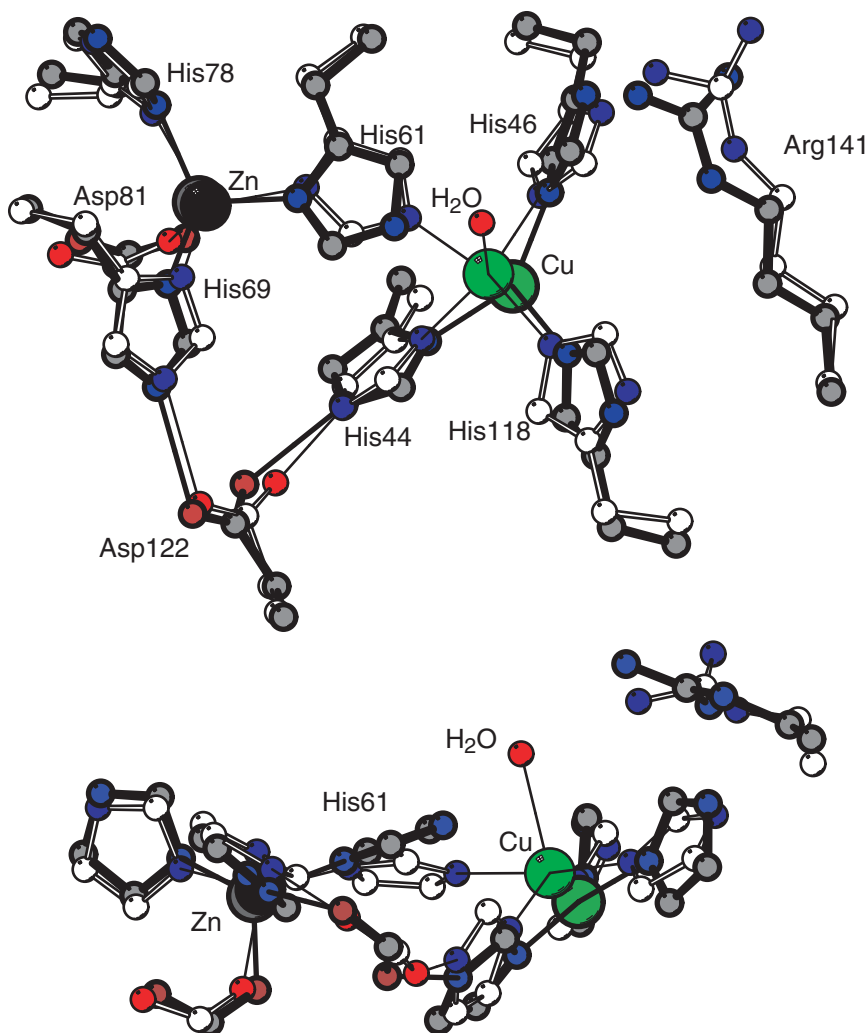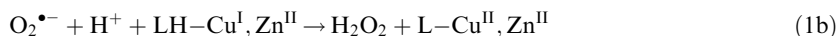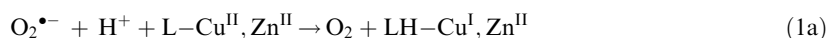
Figure 4 Active site of Cu,Zn–SOD, based on the oxidized-state coordinates of Tainer *et al.*[69] (2SOD.pdb, bovine erythrocytes) and the reduced state coordinates of Ogihara *et al.*[192] (1JCV.pdb, from yeast). The Cu ions are shown in green and Zn in black, other atoms are colored according to cpk. The reduced state structure is depicted using heavy bonds and darkened colors including C atoms in gray, the oxidized state structure is depicted with light bonds and light-colored atoms, including white C atoms.

mutations (reviewed by Bertini *et al.*[78]). Optical studies of Cu^I,Co^{II}–SOD were the first to indicate that the His61 bridge was broken upon Cu reduction (below).[79]

8.19.6.2 Mechanism and Insights from Spectroscopy

Superoxide dismutation appears to occur via two sequential reactions which are each first-order in superoxide, based on pulsed radiolysis.[80] Thus, the metal ion alternately accepts and donates an electron in conjunction with proton transfer.

$$O_2^{\bullet-} + H^+ + L{-}Cu^{II}, Zn^{II} \rightarrow O_2 + LH{-}Cu^I, Zn^{II} \tag{1a}$$

$$O_2^{\bullet-} + H^+ + LH{-}Cu^I, Zn^{II} \rightarrow H_2O_2 + L{-}Cu^{II}, Zn^{II} \tag{1b}$$

where L signifies the protein ligands to Cu and Zn.

The catalytic rate is limited by the rate of substrate diffusion into the active site under most conditions.[81] A constellation of conserved positively charged residues is credited with producing a positive electrostatic potential that "steers" $O_2^{\bullet-}$ into the active site, in accordance with
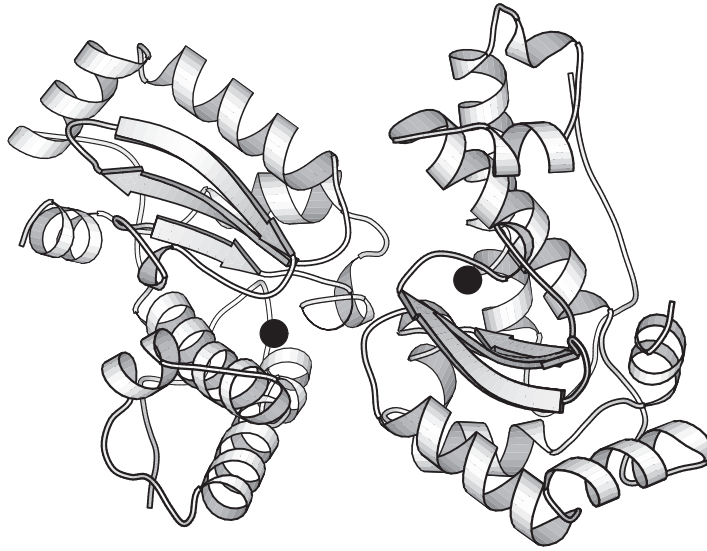
Figure 5 Ribbon structure of Fe–SOD, based on the coordinates 1ISB.pdb of Lah *et al.*[111] The Fe[III] ions are depicted by black spheres.

inhibition of catalytic activity by high ionic strength or modification of positively charged residues,[82,83] as well as calculations of Brownian dynamics.[84] Mutations decreasing the negative charge near the active site have produced enzymes with higher-than-native activity, including a *P. leiognathi* mutant Cu,Zn–SOD with $k_{cat}/K_M = 1 \times 10^{10}\,M^{-1}s^{-1}$, the highest of
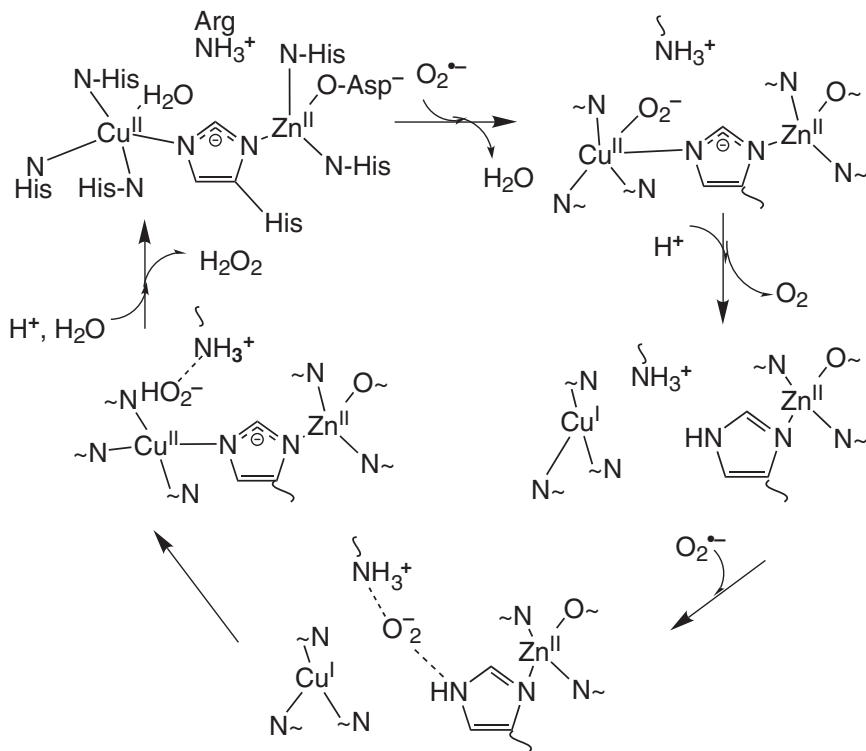
Scheme 1

any SOD.[85] However, the effects of such mutations on residues surrounding the active site are large only at low ionic strength, whereas at physiological ionic strength, Arg141 and the metal ions themselves are thought to explain most of the enhanced substrate diffusion into the active site.[86]

The green color of Cu^{II},Zn^{II}–SOD reflects its d–d band at 14,700 cm^{-1} (680 nm).[87,88] The appearance of a UV ligand-to-metal charge-transfer band upon binding N_3^- or SCN^-,[88] changes in the EPR signal induced by these and CN^-,[89] and X-ray crystal structures show that anions coordinate to Cu^{II} in a weak axial site, displacing water.[90] CN^- and N_3^- coordinate with quite different orientations, possibly due to steric interference between (larger) N_3^- and surrounding residues, as well as CN^-'s stronger ligand strength which gives it pre-eminence over the other ligands.[91] However, the fact that both bind in the position at which coordinated solvent is occasionally observed suggests that this is where $O_2^{\bullet-}$ binds too.[72,92] $O_2^{\bullet-}$ coordinated to Cu^{II} is proposed to be oxidized by inner sphere electron transfer to produce $Cu^I + O_2$, with the latter escaping from the active site since its neutrality robs it of electrostatic stabilization (Scheme 1, showing proposed detailed mechanism of CuZn–SOD, based on Bordo *et al.*[63] and Hart *et al.*[72] Proposed hydrogen bonds are shown as dashed lines.). Cu^I releases His61 to become trigonal planar[79,93,94] and His61 becomes protonated with a pK of 10.8 (Figure 4).[95]

Thus, Cu,Zn–SOD, takes up a proton.[94,96] Because proton uptake accompanies reduction of the metal ion, the total charge of the active site is conserved, and the second substrate to bind in the cycle benefits from the same overall electrostatic steering as the first. The second $O_2^{\bullet-}$ is proposed to hydrogen bond with Arg141 but not to coordinate directly to Cu^I based on infrared spectroscopy.[97] Outer sphere electron transfer is therefore inferred, coupled to proton transfer to nascent product from His61.[63] Re-binding of deprotonated His61 to the now-Cu^{II} site would aid in product displacement and/or discourage O_2H^- binding and restore the starting state of the active site (but see Fee and Bull[98]). Cu,Zn–SOD specific activity decreases at high pH with a pK of 10.7.[99] This could reflect in part release of Cu, but the decrease also coincides with the pK of 10.8 of His61 in reduced Cu,Zn–SOD.[95] Thus, low activity at high pH can be explained by competitive inhibition by OH^- binding to the oxidized state,[100] in conjunction with loss of a proton required for product formation by the reduced state. The solvent isotope effect of 3.6 also indicates that a proton transfer step contributes to the rate.[98]

Between pH 5 and 9.5, Cu,Zn–SOD activity is only very weakly pH dependent. This has been attributed to the His61 ligand to Cu and its bridge to Zn^{II}.[101] The pK of His61 is depressed from ≈14 to 10.8 due its coordination to Zn^{II}, enabling it to coordinate to Cu^{II} but not Cu^I.[102] Thus, it contributes to production of a favorable E_m for disproportionation of $O_2^{\bullet-}$, and couples proton transfer to electron transfer by taking up a proton upon Cu reduction. The Zn^{II} site also forces His61 to bind Cu^{II} in an equatorial position, and thus constrains most exogenous ligands including substrate to the weaker axial position. Product HO_2^- is presumably also only relatively weakly bound and readily displaced.[101]

Besides its role in forestalling aging by preventing oxidative damage, Cu,Zn–SOD has wider significance to human health. Some 10% of familial amyotrophic lateral sclerosis (FALS) cases are associated with mutation in the *SOD1* gene which encodes the cytoplasmic Cu,Zn–SOD.[103,104] Many different mutations have been identified, most of which are not believed to affect the active site directly.[105] Nonetheless, FALS victims are generally found to have lower-than-normal levels of total SOD activity.[106] Since introduction of a FALS-associated mutant Cu,Zn–SOD results in onset of FALS symptoms even for mice bearing the normal Cu,Zn–SOD gene, the mutant genes appear to have gained a new, dominant, and toxic phenotype.[107,108] Many FALS-associated mutant Cu,Zn–SODs were found to be less well metallated than similarly expressed WT Cu,Zn–SOD and significantly less stable.[105] Indeed, Fridovich has proposed that mutant Cu,Zn–SODs cause FALS by failing to enter the mitochondrial intermembrane space, embroiling heat shock proteins needed for other functions, and forming aggregates.[109]

8.19.7   Fe-CONTAINING SUPEROXIDE DISMUTASE

Fe-containing superoxide dismutase (Fe–SOD) is believed to be a relatively primitive SOD. It is constitutively expressed in many bacteria, and a few eukaryotes.[25] Fe–SOD has been the subject of a few relatively recent reviews.[110]

8.19.7.1 Structure

Fe–SODs are dimers of 22 kDa monomers (Figure 5) with a few monomeric exceptions.[25] Each subunit contains a single mononuclear Fe site in which Fe is coordinated by three His and one Asp⁻ residue as well as a molecule of solvent (Figure 6).[111] The solvent molecule is believed to be OH⁻ in (oxidized) Fe^{III}–SOD and H_2O in (reduced) Fe^{II}–SOD.[112] The Fe is trigonal–bipyramidal with coordinated solvent at one apex and His26 at the other. The ligating amino acids derive from both of the two domains of a given subunit, so that the metal center is effectively bound between the two (Figure 5). A His ligand in one active site (His160) donates a hydrogen bond to Glu159 from the other subunit, so that the two active sites are linked, and the electrostatic charge of the metal ion is neutralized over all by the coordinated solvent, the Asp⁻ ligand and this second sphere Glu⁻ (numbering of *E. coli* Fe–SOD is used throughout).[112,113] The active site also contains a universally conserved Tyr residue (Tyr34) which hydrogen bonds to a conserved Gln (Gln69) which in turn hydrogen bonds to the coordinated solvent (Figure 6). Although the coordinated solvent also hydrogen bonds to the ligand Asp⁻, Gln69 is its only link to the protein outside the active site.

All of the active site residues named above are enclosed in a shell of conserved aromatic side chains which have been proposed to insulate the active site from solvent and the surrounding protein.[114] Note, however, that they may also provide important insurance against irreversible inactivation of the enzyme by its toxic substrate and toxic product, both of which can be activated by Fe. These and the one-electron nature of the chemistry catalyzed by Fe–SOD put the active site amino acids at risk of oxidation and covalent modification by catalytic intermediates and by-products. However the radicals of the His, Tyr, Trp, and Phe residues that characterize SOD are generally more table than those of the non-polar aliphatic hydrophobic amino acids found in the interiors of typical proteins, and therefore may persist long enough for the next molecule of substrate to enter the active site and re-reduce them, rescuing the active site. Indeed, Trp and His side chains get modified in the course of inactivation by H_2O_2,[115] and mutation of Tyr34 to the higher-E_m residue Phe increases Fe-substituted Mn–SOD's susceptibility to inactivation.[118]
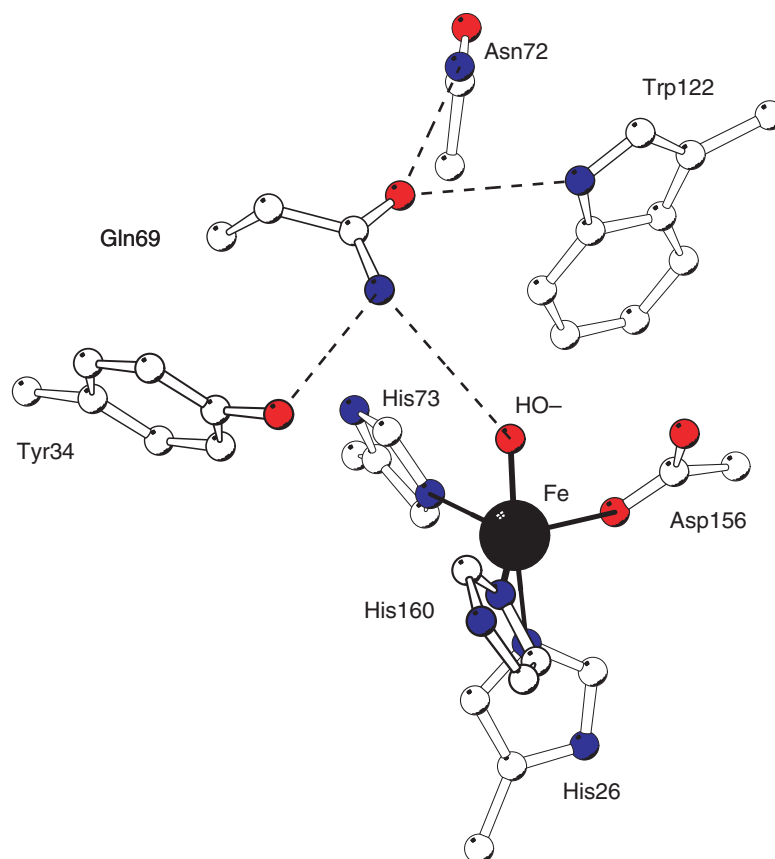
Figure 6 Active site of Fe^{III}–SOD, based on the coordinates of 1ISB.pdb Lah *et al.*[111] The Fe^{III} is in black and other atoms are colored according to cpk. Dashed lines indicate proposed hydrogen bonds.

8.19.7.2 Mechanism and Insights from Spectroscopy

Pulsed radiolysis studies indicate that the reaction proceeds via two sequential steps, both first order in $O_2^{\bullet-}$, in which $O_2^{\bullet-}$ is alternately oxidized to O_2 or reduced to H_2O_2 by the Fe ion.[119] Thus, the Fe cycles between the III and II states. Fe^{III}–SOD takes up a proton upon reduction throughout the pH range of activity,[120] and chemical precedent[112,121] as well as NMR studies (Miller *et al.*)[193] indicate that the proton is taken up by coordinated OH^- in the oxidized state to yield coordinated H_2O in the reduced state. Thus the reactions may be written:

$$O_2^{\bullet-} + H^+ + LFe^{III}(OH^-) \rightarrow O_2 + LFe^{II}(OH_2) \qquad (2a)$$

$$O_2^{\bullet-} + H^+ + LFe^{II}(OH_2) \rightarrow H_2O_2 + LFe^{III}(OH^-) \qquad (2b)$$

where L stands for the SOD protein, and the coordinated solvent molecule that couples proton transfer to electron transfer is in parentheses (Scheme 2, showing proposed detailed mechanism of Fe–SOD.).

The reaction proceeds with saturation kinetics with $k_{cat} = 2.6 \times 10^4\,s^{-1}$ and a K_M of $80\,\mu M$ for $O_2^{\bullet-}$ at pH $8.4\,^\circ C$ and $25\,^\circ C$,[120] consistent with the observed second order rate constant for consumption of $O_2^{\bullet-}$ of $k = 3 \times 10^8\,M^{-1}s^{-1}$.[122] Activity decreases at high pH with a pK of ≈ 9[120]
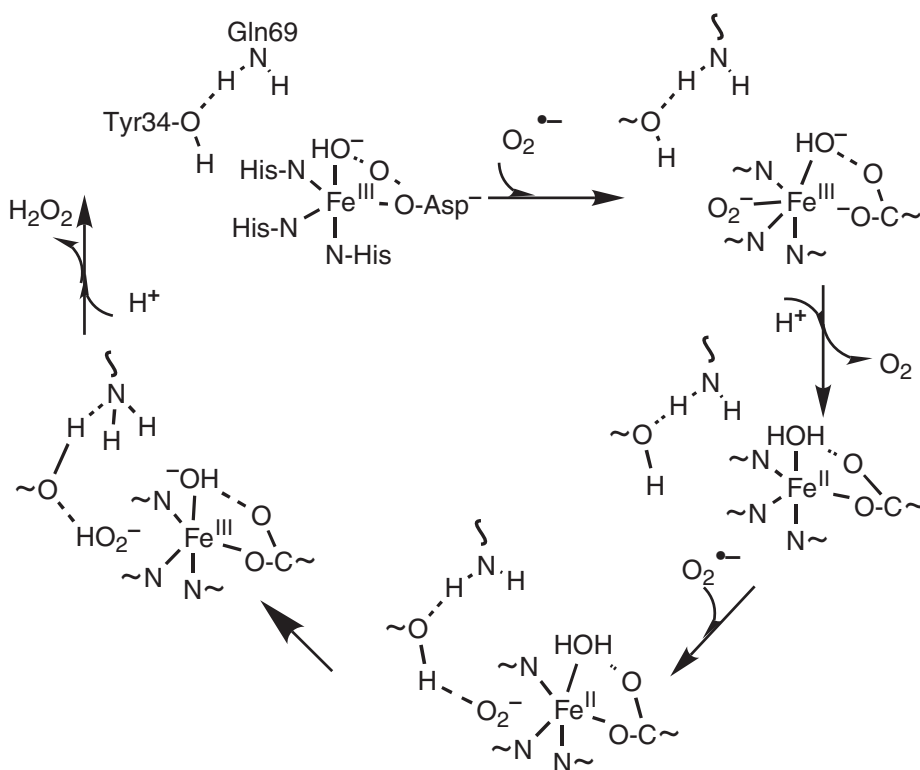
Scheme 2

that affects K_M but not k_{cat}.[122] The rate-limiting step is nonetheless indicated to involve a proton based on a solvent isotope effect of 3 for k_{cat} and because general acids accelerate the reaction by increasing k_{cat}.[120]

Fe is high-spin in both oxidation states, with and without substrate analogs bound.[123,124] Changes in the EPR signal and the appearance of a strong ligand-to-metal charge transfer band demonstrate that the competitive inhibitor N_3^- coordinates directly to Fe^{III}, as do F^- and OH^-.[120,123] (Other substrate analogs such as SCN^- and ClO_4^- inhibit via an outer sphere anion binding site.[120]) Superoxide is believed to coordinate directly to Fe^{III} in the equatorial plane, *trans* to the Asp^- ligand, to generate octahedral geometry[111] and oxidation of $O_2^{\bullet-}$ is

believed to occur via an inner sphere mechanism (Scheme 2). Considering that the coordination of Fe^{III} is oriented with the dominant (z)-axis defined by the axial ligand OH^-, the valence orbital is largely d_{xz}, which would overlap favorably with a π^*-orbital of incoming $O_2^{\bullet-}$,[125] providing a plausible mechanism for inner sphere electron transfer from an end-on bound $O_2^{\bullet-}$ (Scheme 3, showing proposed Fe^{III}–SOD d_{z_z} component of the redox-active orbital and its interaction with incoming $O_2^{\bullet-}$, based on crystal structures and DFT calculations.[111,125]). This is the reverse of the more familiar effective reduction of O_2 to $O_2^{\bullet-}$ upon binding to Fe^{II} in Mb and Hb, and suggests that $O_2^{\bullet-}$ does not engage in any H bonding in Fe^{III}–SOD, since that would raise the $O_2/O_2^{\bullet-}$ E_m. Thus, we propose that $O_2^{\bullet-}$ binds to Fe^{III} only, and due to Fe^{III}'s Lewis acidity, loses an electron.
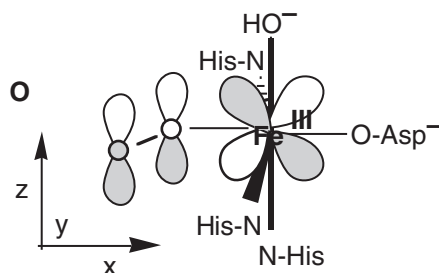
Scheme 3

In the second half of the catalytic cycle, Fe^{II} is reoxidized by $O_2^{\bullet-}$ in conjunction with proton transfer. This reaction is believed to proceed via outer-sphere electron transfer, since F^- binds to Fe^{II}–SOD but not in the inner sphere (Sorkin and Miller, unpublished),[124] but see ref. 194.

8.19.7.3 Protonation Steps Associated with Catalytic Activity

Reduction of $O_2^{\bullet-}$ is unfavorable on electrostatic and electronic grounds unless it is coupled to protonation. While the protons required for production of H_2O_2 derive ultimately from solvent,[120] active site residues are most likely to mediate proton transfer to nascent product as a means of accelerating this step. The most important candidates for the roles of proton donors are the coordinated H_2O (which will release a proton upon Fe^{II} oxidation) and Tyr34 (below).

Nevertheless, the pH dependence of activity does not appear to reflect a rate-limiting proton transfer since K_M but not k_{cat} is pH dependent.[120] The increase in K_M at high pH can be accounted for by two active site pKs. In the oxidized state, OH^- binds to Fe^{III} in competition with other anions and likely $O_2^{\bullet-}$, with a pK of 8.5,[120,126] and the reduced state displays a pK of 8.5 attributed to deprotonation of Tyr34.[127,128] Since F^- binding to Fe^{II}–SOD is inhibited by deprotonation of Tyr34,[129] it is possible that F^- and $O_2^{\bullet-}$ bind via Tyr34's OH proton, and that $O_2^{\bullet-}$ becomes partially protonated as part of binding. The pK of Tyr34 in Fe^{II}–SOD is quite low for a Tyr, at 8.5. To the extent that Tyr34 transfers its proton to $O_2^{\bullet-}$ as part of binding, $O_2^{\bullet-}$'s E_m will rise and favor its acquisition of an electron from Fe^{II}. Since $O_2^{\bullet-}$ is not coordinated to Fe^{II}, a hydrogen bond from Tyr34 to the distal O would not favor O—O bond breakage and production of $Fe^{IV}=O$. In contrast, in catechol dioxygenases such as 2,3-dihydroxybiphenyl 1,2-dioxygenase and cytochrome P450 which mediate O—O bond cleavage, O_2 is believed to bind to Fe at one end and form a hydrogen bond and/or accept a proton at the other.[20,130] The cost of substrate's not binding directly to the metal ion in Fe^{II}–SOD is decreased binding affinity, consistent with SOD's relatively high K_M. However, Tyr34's phenolic O is only 5.5 Å from Fe. In-line geometry, with a 1.35 Å O—$O^{\bullet-}$ bond[2] and a 2.7 Å hydrogen bond to $O_2^{\bullet-}$ places the proximal O 1.1 Å from Fe. Thus, $O_2^{\bullet-}$ is not expected to point directly towards Fe^{II}, and even at a 90° angle, electron transfer to the nearest O would not be rate limiting.

The rate-limiting step has been proposed to be displacement of the product and to involve a proton,[120] possibly transferred from coordinated solvent. It is unlikely that the proton acquired by departing H_2O_2 is one of the two that had been part of the coordinated H_2O molecule, but more likely that a proton released by coordinated solvent upon oxidation of Fe^{II} displaces another proton from the amide side chain of Gln69 towards Tyr34, which, being effectively deprotonated by $O_2^{\bullet-}$, would draw such a relay in just this direction (Scheme 2). Thus, it is

very likely that deprotonation of Fe^{II}–SOD's coordinated H_2O is coupled to protonation of nascent peroxide dianion, as well as electron transfer from Fe^{II}.

The coupling between proton transfer and electron transfer in this case would drive transfer of a proton from Tyr34 to $O_2^{\bullet-}$ despite the low pK of 4.8 of $HO_2^{\bullet}$ vs. Tyr34's pK of 8.5, by virtue of the effective pK of HO_2^{-}, of ≈ 24,[26] accessed as $O_2^{\bullet-}$ is reduced by Fe^{II}. The current proposal that $O_2^{\bullet-}$ is not coordinated to Fe^{II} has the advantage that the pK of $O_2^{\bullet-}$ would not be substantially depressed below 4.8, as it would be if $O_2^{\bullet-}$ were coordinated.

8.19.8 Mn-CONTAINING SUPEROXIDE DISMUTASE

Mn–SOD has been the focus of a great deal of recent activity, which has been reviewed by Whittaker and Tainer and co-workers, among others.[131,132]
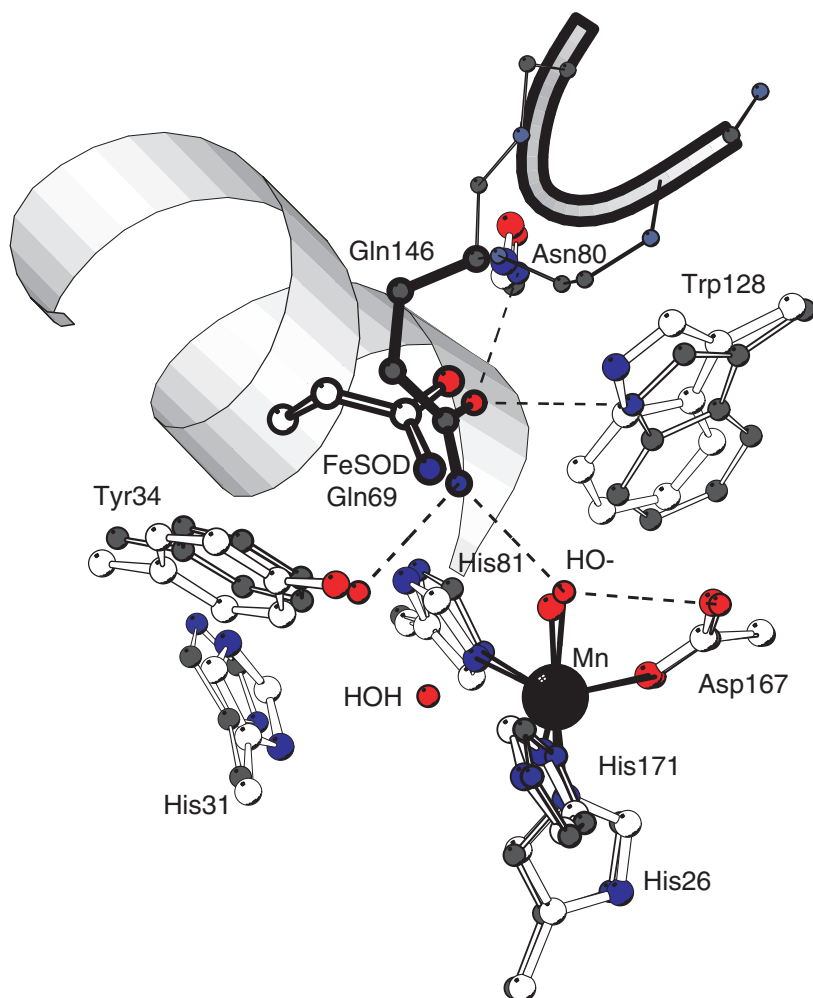
Figure 7 Overlay of the active sites of Mn–SOD and Fe–SOD. Mn–SOD is based on coordinates 1D5N.pdb[134] and depicted using narrower bonds, smaller atoms with dark cpk colors and dark grey C atoms. Fe^{III}–SOD is based on 1ISB.pdb,[111] and depicted using wider bonds and white C atoms. Also shown are a light gray cartoon section of the helix bearing Fe–SOD's Gln69 (analogous to residue 77 of Mn–SOD) and the second His ligand, as well as a dark gray tube depiction of the loop between β strands that bears Mn–SOD's Gln146 (analogous to residue 141 of Fe–SOD). All residue labels refer to *E. coli* Mn–SOD with the exception of Gln69, which refers to *E. coli* Fe–SOD. Backbone atoms are omitted for all residues except Gln146 of Mn–SOD, for which backbone C′, Cα, and N are shown, for itself and neighbors. For clarity the C$^{\alpha}$ of Asn80 is also omitted. Fe–SOD residues homologous to the Mn–SOD residues shown are His26, His31, Tyr34, Asn72, His73, Asp156, His160, and Trp122.
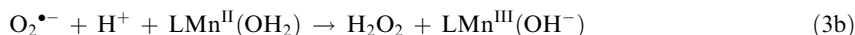
8.19.8.1 Structure

The overall structure of Mn–SOD is homologous with that of Fe–SOD.[111] Structurally characterized Mn–SODs are either dimers or tetrameric dimers of dimers. In the human Mn–SOD the dimers are held together by an association of two N-terminal helices from each participating monomer to form a 4-helix bundle.[133] This is quite different from the dimer/dimer interface of *T. thermophilus* or *E. coli* Mn–SOD.[111,113,134] In addition, one face of the *E. coli* Mn–SOD displays a large concentration of positive charge, which is proposed to be related to DNA binding and protection of the genome.[113] The active site of Mn–SOD is virtually super-imposable on that of Fe–SOD. All the coordinated amino acids are conserved (as is the coordinating solvent) and most of the second sphere residues are conserved as well, or conservatively replaced (Figure 7).[61,135] However, several subtle positional differences as well as the important differences between the electronic configurations of $Fe^{III/II}$ vs. $Mn^{III/II}$ result in subtle but potentially important differences in the detailed mechanism of Fe–SOD and Mn–SOD, including different anion binding geometries,[111,136] redox tuning[137,138] and pKs.[125,139] In particular, the side chain amide of the active site Gln is significantly closer to coordinated solvent in Mn–SOD than in Fe–SOD[111,113,134] and has been shown to be more strongly coupled to the metal ion,[140] suggesting that Gln146 of Mn–SOD donates a significantly stronger hydrogen bond to coordinated solvent than does Gln69 of Fe–SOD.[141]

8.19.8.2 Overall Course of the Reaction

As for Fe–SOD and Cu,Zn–SOD, a two-step reaction in which both steps are first-order in $O_2^{\bullet-}$ has been elucidated based on pulsed radiolysis.[142] A proton is taken up upon reduction,[193] as in Fe-SOD and consistent with computations[121] producing the following overall stoichiometry:

$$O_2^{\bullet-} + H^+ + LMn^{III}(OH^-) \rightarrow O_2 + LMn^{II}(OH_2) \tag{3a}$$

$$O_2^{\bullet-} + H^+ + LMn^{II}(OH_2) \rightarrow H_2O_2 + LMn^{III}(OH^-) \tag{3b}$$

where L stands for the SOD protein and the coordinated solvent is in parentheses.[121] Thus, the Fe–SODs and Mn–SODs are believed to have a lot in common, and it is not surprising that some homologous SODs have been identified that display catalytic activity with either Fe or Mn bound, for example:[143–145] These have been dubbed "cambialistic" with reference to the Latin *cambialis* for change[146] and are discussed further below.

Nonetheless, in addition to completing the reaction in Equation (3b), Mn–SOD from *Bacillus stearothermophilus, Thermus thermophilus*, and *Homo sapiens* all form an inactive intermediate (Figure 8),[142,147,148] whereas there is no evidence for the same behavior among Fe–SODs. Thus, for *T. thermopilus* Mn–SOD and moderately high $O_2^{\bullet-}$ concentrations, there is only a very short period of rapid superoxide consumption, amounting to approximately 80 $O_2^{\bullet-}$ per active site (the burst phase) before activity drops to a much lower rate which is proportional only to the enzyme concentration and independent of the $O_2^{\bullet-}$ concentration (the zero-order phase). This phase lasts until the $O_2^{\bullet-}$ concentration drops to less than 10 times the enzyme concentration. The duration of the burst phase reflects the rate at which Mn–SOD can release H_2O_2 vs. the rate of formation of the inhibited complex, whereas the catalytic rate observed during the zero-order phase is interpreted to reflect the rate of recovery from the inhibited state as well as H_2O_2 release.[147] Once the $O_2^{\bullet-}$ concentration is low, substrate binding rates become rate-determining and first-order behavior in $[O_2^{\bullet-}]$ is observed.[147] The product-inhibited complex can also be generated upon addition of H_2O_2 to $Mn^{III}SOD$[149] and appears to represent a six-coordinate Mn^{III} complex with O_2^{2-} or O_2H^-,[150] possibly bound side-on.[147] Its decay rate does not depend on pH,[148] however, mutation of Trp169 to Phe or mutation of Tyr34 to Phe increases the stability of the inhibited state (numbering of *E. coli* Mn–SOD).[149]

8.19.8.3 Mechanism and Insights from Spectroscopy

$O_2^{\bullet-}$ binding to Mn^{III}–SOD is believed to be an inner-sphere event,[111,151] but without net expansion of the coordination sphere at room temperature, based on absorbance and CD studies of the N_3^- complex.[150] However, below 200 K the N_3^- complex of *E. coli* Mn^{III}–SOD becomes
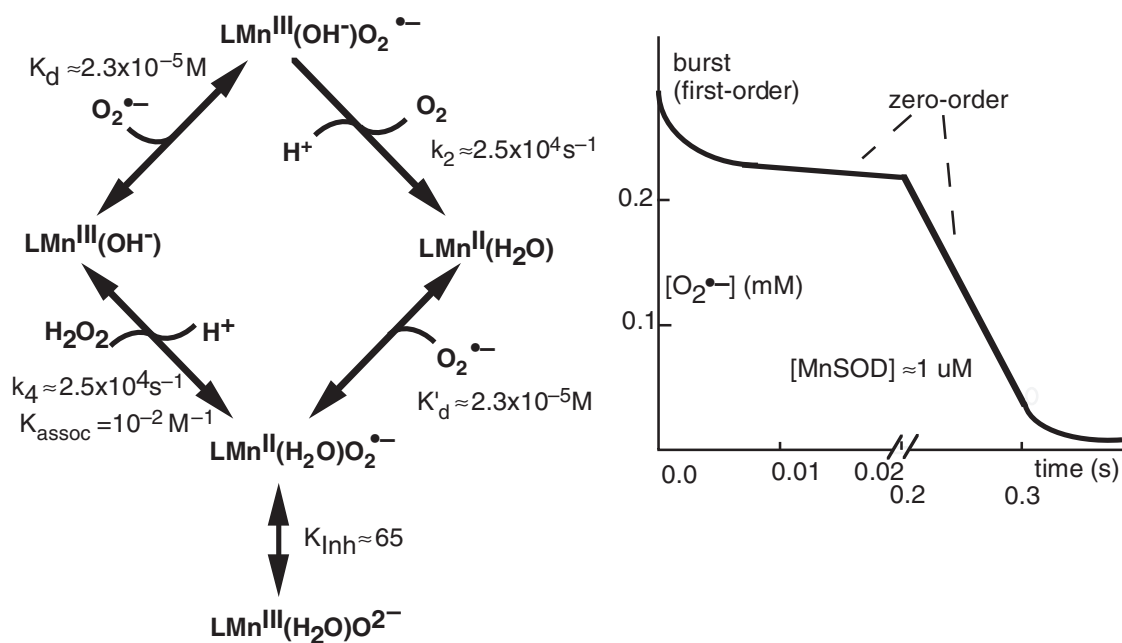
Figure 8 Overall mechanism of Mn–SOD and time course of catalyzed dismutation of $O_2^{\bullet-}$, adapted from Bull *et al.*[147] The Mn ion oxidation state and protonation state of the coordinated solvent are specified for each proposed intermediate. K_d is the dissociation constant for $O_2^{\bullet-}$ with Mn^{III}–SOD(OH$^-$) = k_{-1}/k_1; k_2 is the rate constant for the essentially irreversible oxidation of $O_2^{\bullet-}$ by Mn^{III}–SOD(OH$^-$) and dissociation of O_2; K'_d is the dissociation constant for $O_2^{\bullet-}$ with Mn^{II}–SOD(H$_2$O) = k_{-3}/k_3; k_4 is the rate constant for the reduction of $H^+ + O_2^{\bullet-}$ by Mn^{II}–SOD(H$_2$O) and dissociation of H_2O_2; K_{assoc}, a binding constant for H_2O_2, is defined as k_{-4}/k_4 for consistency with the K_ds; K_{Inh} is the equilibrium for formation of the inhibited state = k_5/k_{-5}. Rate constants, concentrations, and $O_2^{\bullet-}$ concentrations used for illustrative purposed are those of Bull *et al.*[147]

six coordinate.[150] In addition, mutation of Tyr34 to Phe results in formation of a six-coordinate N_3^- complex even at room temperature for *E. coli* Mn^{III}–SOD.[118] Thus, the five- and six-coordinate sites are not very different in energy and may very well both play roles in catalysis.[150] The Mn^{III} site is proposed to remain five-coordinate as a result of Asp$^-$ or OH$^-$ dissociation upon anion binding.[150] However, we favor displacement of coordinated OH$^-$ (Scheme 4). Tyr34 is inferred to participate in substrate binding based on the appearance of a hydrogen bonding interaction between Tyr34 and coordinated N_3^- in the N_3^-−Mn^{III}–SOD crystal structure and Tyr34's preferential modification by peroxynitrite.[111,152] However the N_3^-–Tyr34 bond is associated with movement of Tyr34,[111] mutation of Tyr to Phe actually raises the active site affinity for N_3^- rather than decreasing it[118] and N_3^- is substantially larger than the substrate. Thus, $O_2^{\bullet-}$ is unlikely to interact with Tyr34 in exactly the manner depicted by the crystal structure of the N_3^-.

Once bound, $O_2^{\bullet-}$ is oxidized by Mn^{III}. This would be favored by a high E_m for Mn. However, the E_m of Mn–SOD has been proposed to be depressed, in part by a strong hydrogen bond donated to coordinated solvent by Gln146, which would suppress the protonation of coordinated solvent which accompanies electron uptake.[137,140,141,193] Nonetheless, if substrate binding to Mn^{III} displaces the coordinated OH$^-$, this would relieve the E_m depression and favor oxidation of $O_2^{\bullet-}$ by Mn^{III}. Thus, electron transfer could be coupled to substrate binding via displacement of OH$^-$.

The Mn^{II} ion formed in reduced MnSOD is d^5 and likely prefers hexacoordination. Indeed, Mn^{II}−SOD appears to bind anions F$^-$ and N_3^- in the inner sphere based on EPR.[151] Thus, inner-sphere reduction of $O_2^{\bullet-}$ is inferred, in contrast to Fe–SOD. $O_2^{\bullet-}$ can presumably also interact with Tyr34 in this case as in Fe^{II}–SOD. However the two-pH-unit higher pK of Tyr34 (of 10.5) and the lower pK of coordinated $O_2^{\bullet-}$ would decrease the extent of proton transfer relative to the case in Fe^{II}–SOD. Electron transfer from Mn^{II} is also driven by the hydrogen bond from Gln146 to coordinated solvent, which favors coordinated OH$^-$ vs. H$_2$O, and thus the Mn^{III} state. This latter interaction also makes a proton from coordinated solvent available to $O_2^{\bullet-}$ enhance
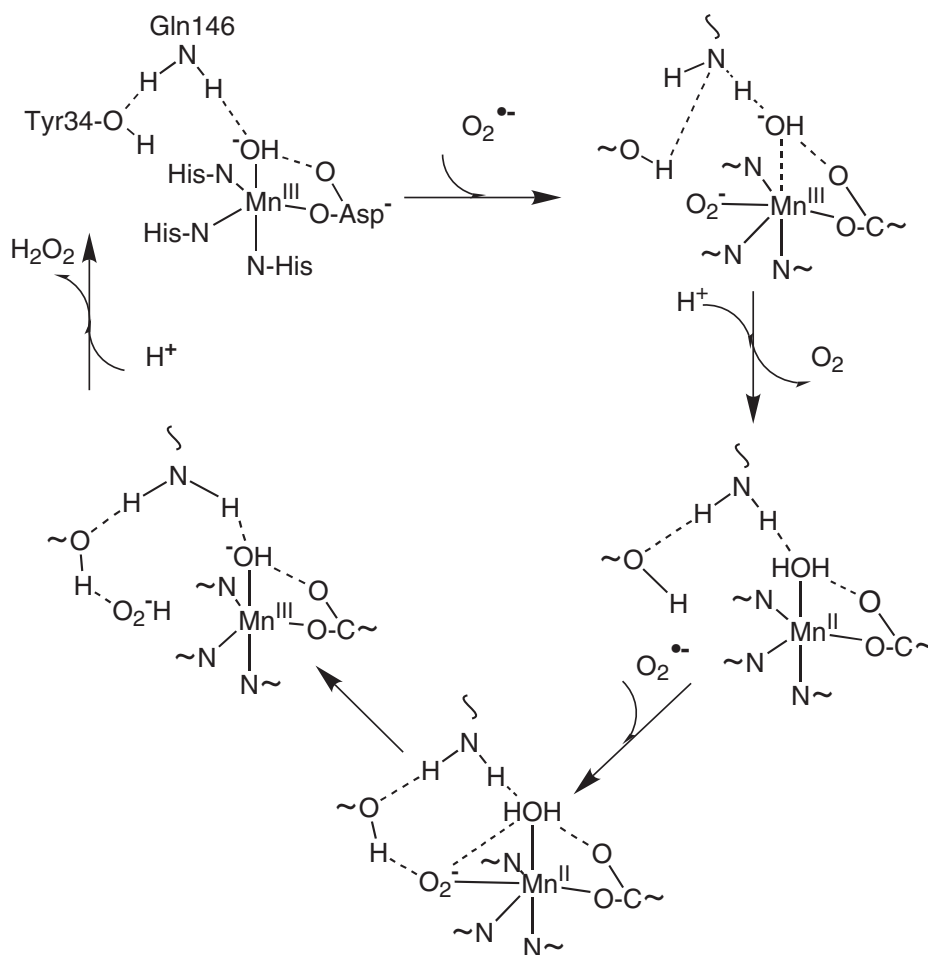
Gln146
Tyr34-O
His-N
His-N
Mn^{III}
N-His
O-Asp$^-$
$^-$OH
O
H
H
N
H
O$_2$$^{\bullet-}$

H$_2$O$_2$
H$^+$

Scheme 4

electron transfer to O$_2$$^{\bullet-}$. As Mn becomes oxidized to Mn^{III}, the coordinated solvent's pK drops and its proton is probably delivered to departing substrate, possibly via the active site hydrogen bond network.[118,153] Once Mn is oxidized it should recover its (Jahn–Teller) preference for pentacoordination, and only one of the newly deprotonated OH$^-$ or newly formed HO$_2$$^-$ should tend to stay bound. Based on simplistic consideration of the pKs of the relevant conjugated acids, 15.6 for H$_2$O and 11.8 for H$_2$O$_2$, respectively, coordinated hydroxide will tend to take precedence and hydroperoxide will normally be displaced. The longer lifetimes of the six-coordinate inhibited complexes of Y34F- and W169F-Mn–SOD[149] likely reflect at least in part relief of steric constraints, since Y34F-Mn^{III}–SOD has five-fold higher affinity for N$_3$$^-$ than wild-type Mn^{III}–SOD and forms a hexacoordinate N$_3$$^-$ complex even at room temperature.[118]

8.19.8.4 Protonation Steps Related to Activity, Mutation of Tyr34 or Gln146

Like that of Fe–SOD, the active site of Mn–SOD is affected by pH. However, the pK affecting the active site in the oxidized state has been assigned to ionization of Tyr34[139] (instead of binding of OH$^-$ as in Fe^{III}–SOD) and occurs at pH 9.5–10 (vs. 8.5–9).[118,153] This can be explained in part by the lower tendency of Mn^{III} than Fe^{III} to bind an additional ligand because Mn^{III} is a Jahn–Teller ion. The pK of Mn^{II}–SOD is assigned to Tyr34[139] as in Fe^{II}–SOD.[127,128] The pK of 10.5 is relatively normal for Tyr, in contrast to the depressed Tyr34 pK in Fe^{II}–SOD. The latter, however, is consistent with the different redox tuning produced by the Fe–SOD and Mn–SOD active sites (below). Mutation of Tyr34 only slightly affects activity[153] and the optical spectrum.[118]

It alters the pH behavior of Mn–SOD in both oxidation states, but both states remain pH dependent, possibly binding OH^- at very high pH.[125,139] In contrast, mutation of Gln146 decreases activity by two orders of magnitude and virtually eliminates substrate analog binding to Mn^{III}–SOD.[154] We interpret this as support for displacement of coordinated solvent (vs. Asp^-) in conjunction with anion binding to WT Mn^{III}–SOD at room temperature, since displaced OH^- would be stabilized by the hydrogen bond from Gln146. In the absence of Gln146, OH^- would tend to stay coordinated and anion binding would involve formation of the less-favored six-coordinate complex. Anion binding might also be abrogated by repositioning of Tyr34 in the absence of its hydrogen bond with Gln146.[154,155] Finally, the Q146N mutant of humports is fully reduced as isolated whereas WT Mn–SOD is predominantly oxidized.[155] This supports an important role in redox tuning for Gln146.[137,140,141]

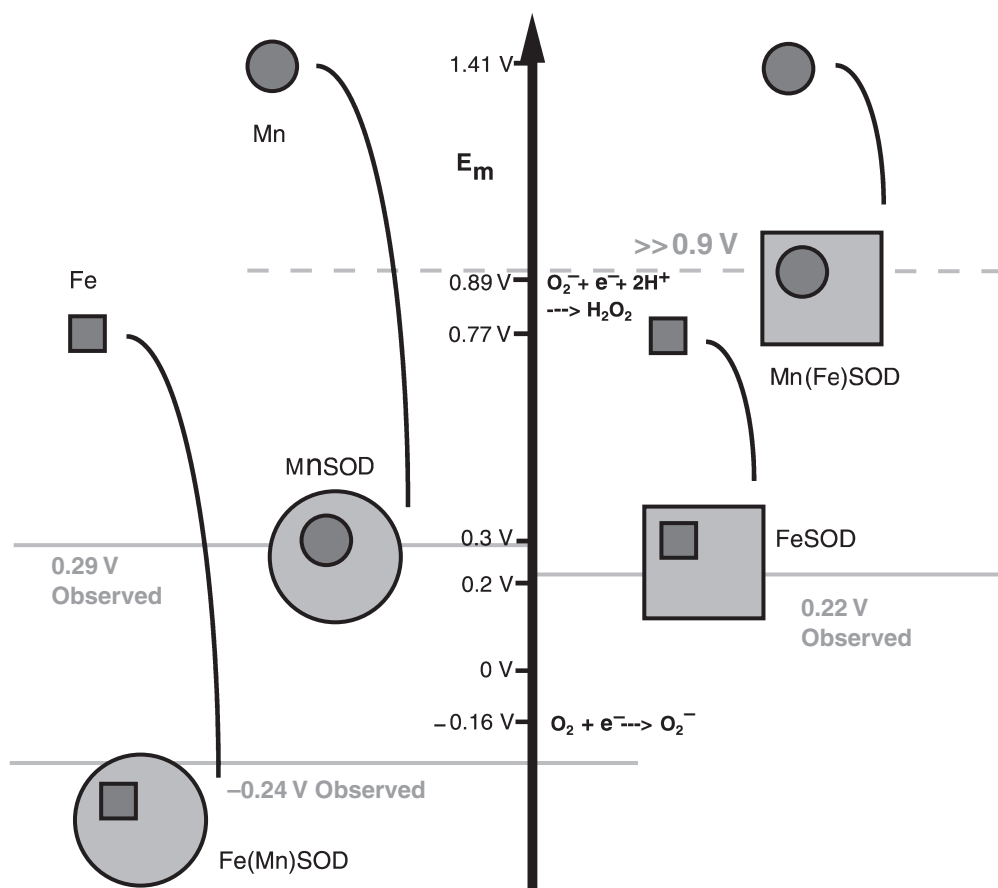### 8.19.8.5 Metal Ion Specificity in Fe–SOD and Mn–SOD

The cambialistic SODs of some anaerobes are active with either Fe or Mn bound, although their maximal activities tend to be less than those of metal ion-specific SODs.[143–146] Metal-specific Fe–SODs or Mn–SODs are inactive under normal conditions when prepared with the other metal ion bound.[156,157] This was considered perplexing given the virtual superimposability of the active sites of Fe–SODs and Mn–SODs, but given that the two sites should be optimized for different metal ions with different inherent E_ms and electronic configurations, it makes good sense that the sites should have distinctions that complement the differences between $Fe^{III/II}$ and $Mn^{III/II}$.[138] Understanding the subtle differences between Fe–SODs and Mn–SODs requires very detailed studies of both. Moreover, such studies should be performed on several different Fe–SODs and Mn–SODs in order for any differences to be generalized.

The biggest difference known to recur in many Fe–SODs and Mn–SODs is the identity and origin of the active site residue that hydrogen bonds to the coordinated solvent. In most Fe–SODs this residue is a Gln at position 69, in the second long helix of the first domain, one turn before the second His ligand (His73 of Fe–SOD, equivalent to His81 of Mn–SOD, Figure 7), although there are possible Fe–SODs with a His or Gln derived from position 146. In Mn–SODs and most cambialistic SODs, this residue is a Gln or His at position 146, in a loop between two β strands in the second domain[135] (see Edwards' discussion[154]). Thus, it is significant that mutation of the cambialistic SOD of *Porphyromonas gingivalis*, to remove the Gln69 characteristic of Fe–SODs and replace it with the Gln146 characteristic of Mn–SODs, increased the ratio of Mn-supported activity to Fe-supported activity.[145] Similarly, mutation of *E. coli* Mn–SOD to remove its active site Gln146 and replace it with the Gln69 characteristic of Fe–SOD resulted in a Mn–SOD with significant Fe-supported activity.[140] Single substitution of Gln146 of Mn–SOD also alters the Fe-supported activity and its pH dependence.[154]

For high-spin Mn the Mn^{II} oxidation state represents a half-filled d shell, whereas formation of high-spin Fe^{II} involves doubly populating a d-orbital, and is much less favorable. Thus, the III/II couple of Fe tends to have a significantly lower E_m than does that of Mn. This is confirmed by the examples of the hexa-aquo and EDTA complexes of Fe and Mn.[158] Nevertheless, both Mn–SOD and Fe–SOD must have E_ms midway between the E_ms characterizing the reduction and oxidation of $O_2^{\bullet-}$, in order to simultaneously optimize the rates of both half reactions. Thus, the E_ms of Fe–SODs as well as Mn–SODs are near 360 mV,[159] and the Mn–SOD protein must depress the potential of its bound metal ion much more than the Fe–SOD proteins need to (Figure 9).

Indeed, the E_m of Fe-substituted Mn–SOD was found to be almost 0.5 V lower than that of Fe–SOD,[137] and the E_m of Mn-substituted Fe–SOD appears to be at least 0.5 V higher than that of Mn–SOD,[138] although the accuracy of E_m measurements for SODs is severely limited ($\approx \pm 100$ mV) by the difficulty of achieving true equilibrium.[160] These lower (or higher)-than-native E_ms can explain the inactivity of Fe-substituted Mn–SOD (or Mn-substituted Fe–SOD). Spectroscopic comparisons,[161] the X-ray crystal structure,[162] and the fact that Fe-substituted Mn–SOD can still reduce (but not oxidize) $O_2^{\bullet-}$ demonstrate that the active site is not grossly disrupted and still reacts with substrate.[137] Inactivity related to a low E_m for Fe-substituted Mn–SOD is also consistent with Fe-substituted Mn–SOD's increased activity at lower pH[163] since the E_m should increase by 60 mV per pH unit to a closer-to-native value at lower pH.

The very large difference in redox tuning is reconciled with the virtual identity of the active sites by the proposal that the different origins of the active site Gln translate into significantly stronger hydrogen bonding to coordinated solvent from Mn–SOD's Gln146 than from Fe–SOD's
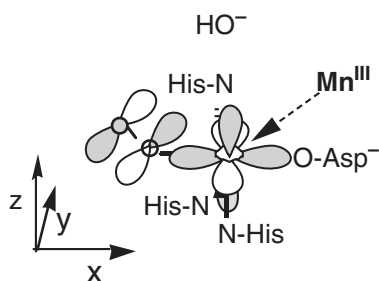
Figure 9 Cartoon of the reduction potentials of high-spin hexa-aquo $Fe^{III/II}$ vs. $Mn^{III/II}$ and the approximate different magnitudes of redox tuning required to bring them to the reduction potentials observed in *E. coli* Fe–SOD and Mn–SOD.[137,138] The potentials observed for Fe-substituted Mn–SOD (Fe(Mn)SOD) and Mn-substituted Fe–SOD (Mn(Fe)SOD) are also shown, and indicate that the magnitude of redox tuning applied by a given protein is the same whether Fe or Mn is bound.[137,138]

Gln69.[140,141] This would destabilize coordinated H_2O relative to OH^- in Mn–SOD, which in turn disfavors the Mn^{II} state relative to Mn^{III}.[140,141] Thus, Mn's E_m could be depressed more in the Mn–SOD protein. Since the compositions of the active site hydrogen bonding networks are the same, increased stabilization of OH^- at one end of the H bond network in Mn–SOD (depression of the pK of coordinated solvent) should come at the cost of less H bond donation to Tyr34, consistent with the much higher pK of Tyr34 in Mn^{II}–SOD than in Fe^{II}–SOD. Thus, the different E_m tuning is intimately related to the different active site pKs.

In fact, there are many additional mechanisms that could participate in differentially tuning the E_m in Mn-specific SODs vs. Fe-specific SODs. However, manipulation of the residue that hydrogen bonds to coordinated solvent can simultaneously address the different substrate binding modes needed to optimize electron transfer in the context of the different electronic configurations of $Fe^{III/II}$ and $Mn^{III/II}$.[125]

In $Fe^{III/II}$ the redox-active orbital is largely d_{xz}, which could form a favorable π-bonding interaction with a π^* valence orbital of $O_2^{\bullet-}$ approaching so as to bind end on, *trans* to Asp^- (Scheme 3). In contrast, the valence d_{z^2}-based orbital of a trigonal–bipyramidal $Mn^{III/II}$ with its z-axis directed at coordinated solvent would not overlap productively with $O_2^{\bullet-}$ approaching in the same way.[125] However, upon displacement of the coordinated solvent of Mn^{III}–SOD, and approach of incoming $O_2^{\bullet-}$, the site acquires planar character and the $d_{x^2-y^2}$ orbital becomes the valence orbital (z-axis still pointing towards departed coordinated solvent). This orbital would point towards incoming $O_2^{\bullet-}$ and could interact favorably with one of its π^*-orbitals if the $O_2^{\bullet-}$ bound in a bent configuration (as does N_3^-)[111] (Scheme 5, showing proposed Mn^{III}–SOD d_{z^2} component of the redox-active orbital of the resting active site (light gray) as well as the $d_{x^2-y^2}$ component of the redox-active orbital that would result upon dissociation of OH^-

(darker gray and white) and its interaction with incoming $O_2^{\bullet-}$, based on crystal structures and DFT calculations.[111,125]). Thus, the electronic configuration of $Mn^{III/II}$ does not appear to be poised for reactivity in the native enzyme, but could become reactive upon Gln146-supported dissociation of coordinated solvent.[125] A strong hydrogen bond from Gln146 to coordinated solvent in Mn–SOD could thus simultaneously depress E_m, facilitate displacement of OH^- upon substrate binding (and thus retention of Jahn–Teller stabilization plus temporary relief of E_m depression) and result in redefinition of the metal ion valence orbitals in such a way as to enhance reactivity and complement the different electronic configurations of high-spin $Mn^{III/II}$ vs. $Fe^{III/II}$.

Scheme 5

8.19.8.6 An Evolutionary Perspective

Thus, we envision that in an ancient reducing environment, Fe–SOD might have been prevalent as a defense against small radical ions present at low but still toxic concentrations due to low levels of O_2, high levels of ionizing radiation, and primitive metabolic activities involving single-electron transfer. The recruitment of Fe as the redox-active cofactor would have taken advantage of Fe's abundance in the Earth's crust. With the onset of evolution and accumulation of O_2, Fe's bioavailability would have decreased markedly due to oxidation, and toxicity associated with Fe would have increased significantly. Thus, versions of SOD able to use Mn instead of Fe would have conferred a competitive advantage and eventually replaced Fe–SOD in organisms most exposed to O_2.

Organisms employing Mn–SOD would have had to develop methods for acquiring Mn, which is scarcer than Fe. However, acquisition and storage of even Fe became metabolically costly in the modern aerobic environment, so scavenging Mn would not constitute a large *relative* disadvantage. Optimization of Mn-supported activity would likely have required lowering of the E_m and improvement of $O_2^{\bullet-}$ binding by the protein. As discussed above, both are accomplished in Mn–SOD via Gln146 (along with Tyr34). Thus, as is often observed for more modern enzymes, the protein appears more sophisticated and takes a more active role in supporting the chemistry in Mn–SOD than in Fe–SOD. This is accompanied at a genetic level by active regulation of Mn–SOD expression in response to $O_2^{\bullet-}$ levels and type of metabolism, whereas Fe–SOD is constitutively expressed.[164]

We also note that the change in metal ion specificity has been accomplished exclusively via the use of subtle changes in the *positions* of second sphere residues, or *very conservative* changes in their identities. This is consistent with the constraint that the evolutionary intermediates could not lack SOD activity altogether if the carrier organism were to survive.
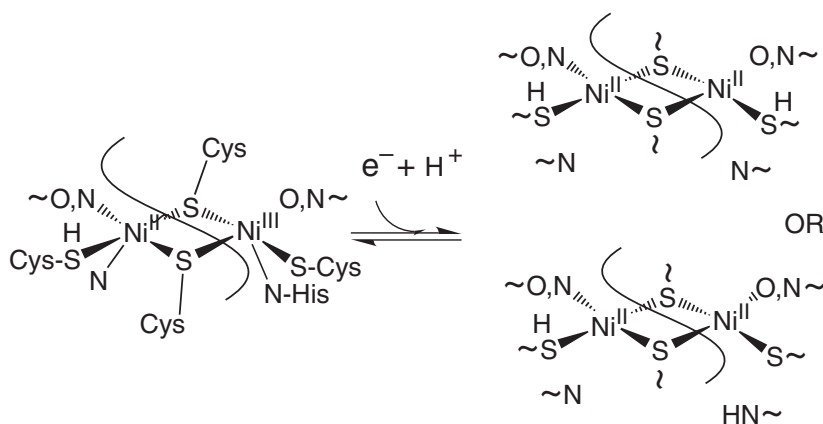
8.19.9 Ni-CONTAINING SUPEROXIDE DISMUTASES

Several species of *Streptomyces* possess a Ni-containing enzyme that has been purified on the basis of SOD activity.[165] This enzyme catalyzes dismutation of $O_2^{\bullet-}$ with rates comparable to those observed for the canonical SODs ($1.3 \times 10^9 \, M^{-1} s^{-1}$ on a per-Ni basis) and relatively independent of pH.[165] The enzyme appears to be cytoplasmic and as-isolated lacks the N terminal 14 amino acids.[166]

8.19.9.1 Structural Insights

Ni–SOD consists of a tetramer of 13.4 kD monomers containing a total of 4 Ni but less than 0.1 equivalent of Fe per subunit and negligible Zn, Mn, or Cu.[165] In the absence of a crystal structure, the nature of the active site has been elucidated spectroscopically. EXAFS of oxidized Ni–SOD indicates that each Ni ion is ligated by three S donors and two N/O donors, in a five-coordinate environment. However, each protein monomer has only two Cys and a Met, implying that either the Ni ions are bound by all of these, or in clusters. The latter is supported by the EPR signal of as-isolated enzyme which is characteristic of Ni^{III} but has intensity indicative of only 0.5 spins per Ni ion, suggesting a Ni^{III}/Ni^{II} cluster.[165,167] The proposed model therefore calls for a dimer of Ni bound at the interface between two protein monomers, by two bridging Cys and two terminal Cys, one of each originating from each of the two monomers. (Scheme 6, showing the proposed active site structures for the oxidized and reduced states of Ni–SOD, bound between two monomers, based on Maroney and co-workers.[167]) The EPR signal also displays super-hyperfine splitting characteristic of ligation by one axial ^{14}N (most likely from a His side chain[165]) and the EXAFS indicates loss of an N/O donor upon reduction in conjunction with a change in geometry to square planar, consistent with the known coordination preferences of Ni^{II} vs. Ni^{III}. Thus, Choudhoury *et al.* propose that the axial (His) ligand is released upon Ni reduction.[167]

Scheme 6

8.19.9.2 Proposed Mechanism

The enzyme is reduced to all-Ni^{II} by dithionite, suggesting a mechanism involving the $Ni^{III/II}$ couple.[165,167] Relevant thiolate-bridged dinuclear Ni model compounds display similar EPR spectra to that of Ni–SOD and have reduction potentials that would be competent for dismutation of superoxide.[168] Ni–SOD is relatively insensitive to N_3^-, but is inhibited by CN^- and H_2O_2, similar to Cu,Zn–SOD.[165]

Ni–SOD's high second order rate constant, higher than those of Fe–SOD or Mn–SOD, and its relative insensitivity to ionic strength, could reflect rapid outer-sphere electron transfer between Ni and $O_2^{\bullet-}$ in at least one half reaction.[167] The thiolate ligands with their diffuse *s*-orbitals would be very effective at mediating long-range outer-sphere electron transfer, yet an outer-sphere mechanism could minimize ligand oxidation by O_2 and H_2O_2. Finally, the thiolate ligands, or the His proposed to dissociate upon Ni reduction, are excellent candidates for coupling the necessary proton donation to the electron transfer events. Thus, a thiolate ligand in Ni,Fe-hydrogenase is proposed to acquire a proton upon Ni^{III} reduction.[169] The proposed ligand His of Ni–SOD could also acquire a proton upon dissociation from Ni in the course of Ni reduction, just as His61 does in Cu,Zn–SOD. This proton could then be transferred to a second $O_2^{\bullet-}$ to facilitate its reduction when Ni is reoxidized and rebinds the His (Scheme 6).

8.19.10 SUPEROXIDE REDUCTASES

Some anaerobes don't possess a SOD, but nonetheless have enzymatic defenses against oxidative stress in the form of the Fe-containing enzyme superoxide reductase (SOR) (Scheme 7, showing proposed mechanism of SOR, based on Abreu, Adams, and Kurtz.[170–172]). SORs catalyze the reduction of $O_2^{\bullet-}$ to H_2O_2:

$$O_2^{\bullet-} + LFe^{II} + 2H^+ \rightarrow H_2O_2 + LFe^{III} \tag{4}$$

where L represents the protein ligands to Fe. H_2O_2 is then proposed to be consumed by peroxidases or to react with reduced metabolites.[173] Thus this enzyme permits anaerobes to metabolize $O_2^{\bullet-}$ without generating O_2. The SOR from *Desulfoarculus baarsii* confers aerotolerance on SOD-deficient *E. coli*[174] and depresses intracellular $O_2^{\bullet-}$ concentrations to normal levels when over-expressed in *E. coli* lacking Mn–SOD and Fe–SOD.[175]
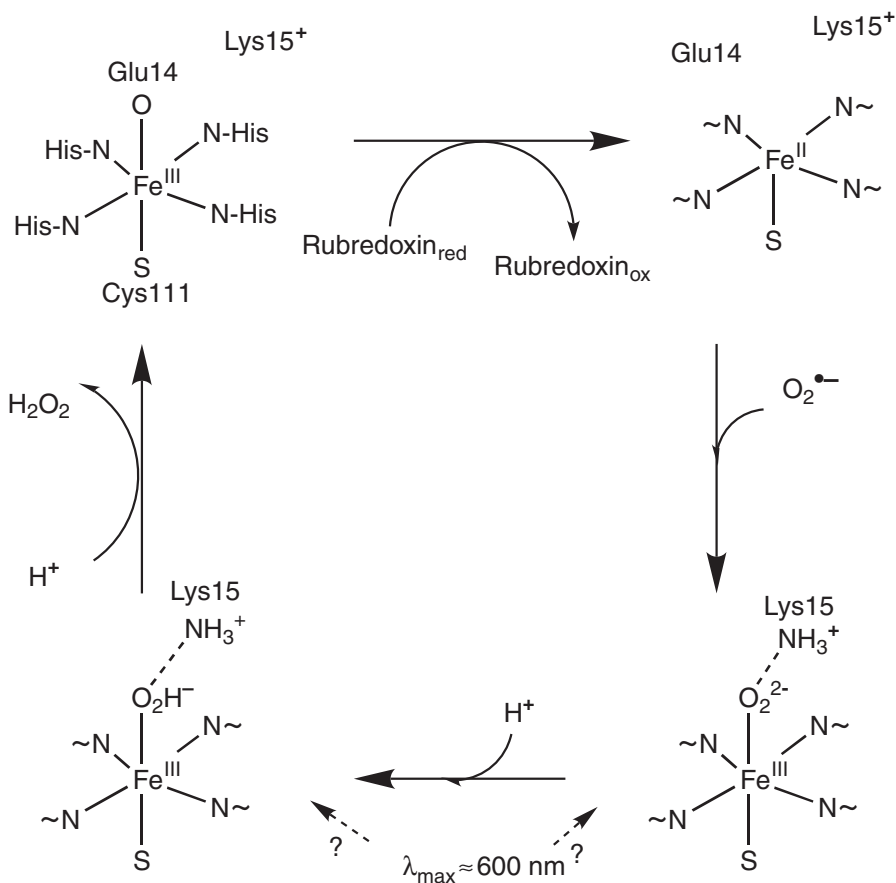
Scheme 7

Some SORs are reported to be able to oxidize $O_2^{\bullet-}$ slowly, as well as reduce it[176] but this has been argued not to be physiologically relevant.[171] SOR reacts with $O_2^{\bullet-}$ with a second order rate constant of $10^9 \, M^{-1}s^{-1}$ at 30 °C[177], whereas the rate for SOD activity of *Archaeoglobus fulgidus* SOR is $5 \times 10^6 \, M^{-1}s^{-1}$ (at 83 °C).[178] The fact that SOD activity is increased tenfold in E14V and E14Q mutants also suggests that this activity is not optimized in the wild-type protein, and therefore does not have important survival value (numbering of *Pyrococcus furiosus* is used throughout). However, the SOD activity could serve as a fall-back option in the event of prolonged oxidative stress in which NADH reserves became exhausted.[170]

8.19.10.1 Structure

SOR was first described as neelaredoxin[179] (from *neela*, the Sanskrit word for blue) or desulfoferrodoxin[180,181] and is found in all strict anaerobes whose genomes had been fully sequenced as of early 2002, including archea.[170] As isolated, the enzyme is a homotetramer and each subunit has its own active site (Figure 10). Both the "1Fe" (e.g., neelaredoxin) and "2Fe" types (e.g., desulfoferrodoxin) contain a novel mononuclear non-heme Fe site in which square–pyramidal Fe^{II} is coordinated by four equatorial His (three $N\varepsilon$ and one $N\delta$) and an axial Cys (Figure 11).[182,183] This is deemed to be the active site. The "2Fe" SORs such as desulfoferrodoxin contain an additional Fe-Cys$_4$ site[180] which is believed to mediate electron transfer to restore the first site to its Fe^{II} state between reactions with $O_2^{\bullet-}$. Upon oxidation, the active site Fe gains a conserved Glu ligand to become six-coordinate (Figure 11).[182] The active site also contains a conserved Lys only 6.6 Å from Fe that is proposed to participate in drawing substrate into the solvent-exposed active site, and possibly proton donation.[172]

### 8.19.10.2 Proposed Mechanism and Insights from Spectroscopy

The strong optical bands at 650 and 340 nm responsible for SOR's blue color are assigned to cysteinate S to Fe^{III} charge transfer.[184] The E_m is 200 mV,[179] with the result that the site remains reduced even after exposure to air. It is oxidized slowly by H_2O_2 but rapidly by $O_2^{\bullet-}$, possibly due to attraction between the positively charged active site and negatively charged $O_2^{\bullet-}$.[172]

$O_2^{\bullet-}$ is believed to coordinate directly to Fe^{II} based on the direct coordination of substrate analogs N_3^-, CN^-, and OH^- to the Fe^{III} of oxidized SOR, with displacement of the Glu47 ligand[184] and conversion of the axial EPR signal to one that is much closer to the rhombic limit.[184] Detailed spectroscopic analysis indicates an octahedral site with tetragonal compression along the axis of His47 and His16 when substrate analog is bound.[184] Similarly, CN^- and N_3^- coordinate to the Fe^{II} of reduced SOR to produce a six-coordinate site.[184]

Upon exposure of SOR to $O_2^{\bullet-}$, an intermediate characterized by an optical signal with λ_{max} near 600 nm is formed rapidly, with a rate that is first order in each of SOR and $O_2^{\bullet-}$ ($k \approx 10^9 \, M^{-1} s^{-1}$), independent of pH and without solvent isotope effect.[185,186] Thus, this signal is tentatively assigned to a hydroperoxo– or peroxo–Fe^{III} complex[185,186] and the step in which it is
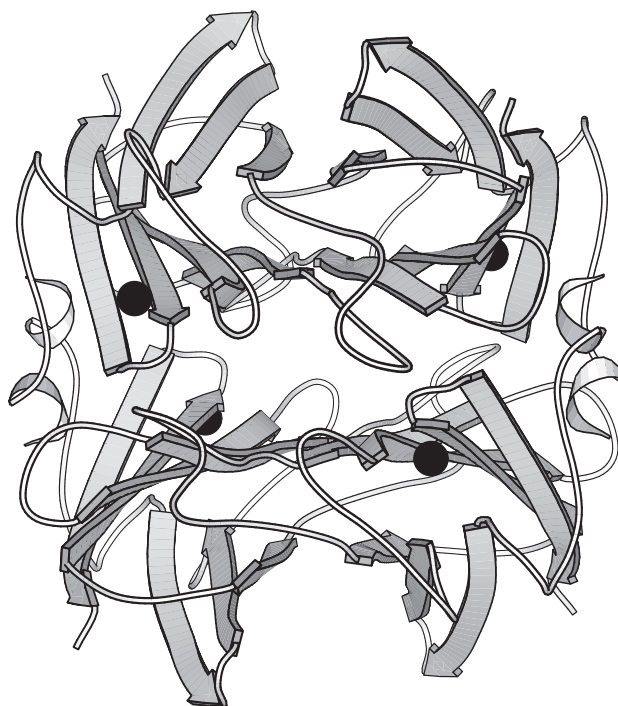
Figure 10 Ribbon structure of reduced SOR from *Pyrococcus furiosus*, based on the coordinates 1DQK.pdb of Yeh *et al.*[182] The Fe^{II} ions are depicted by black spheres.
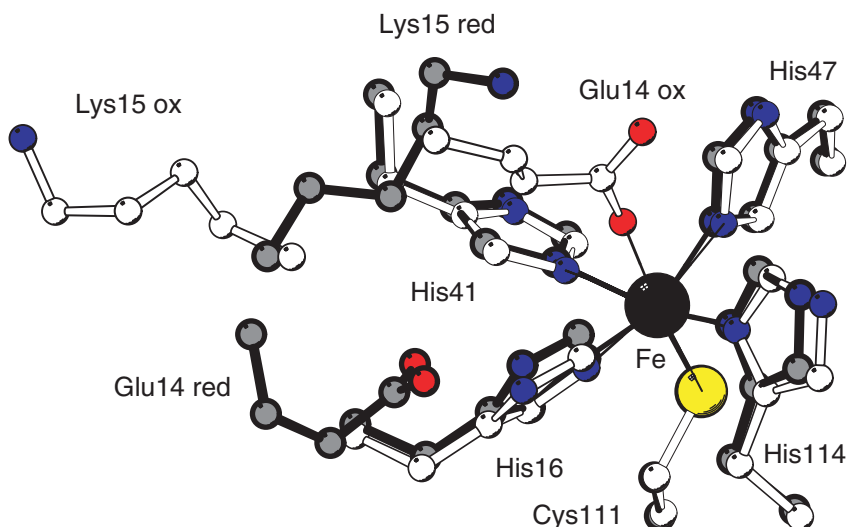
Figure 11 Overlay of the active sites of reduced and oxidized SOR. The reduced state structure determined at low temperature (1DQK.pdb[182]) is depicted using heavy lines, dark cpk colors and gray C atoms whereas the oxidized state structure (1DQI.pdb[182]) is depicted using light lines and white C atoms. The two residues that move most upon reduction are Glu14 and Lys15, which are labeled separately in each oxidation state. Fe is shown in back.

generated is presumed to constitute electron transfer from Fe^{II} to coordinated $O_2^{\bullet-}$. In *Treponema pallidum*, two intermediates are observed, one formed rapidly with $\lambda_{max} \approx 610$ nm as above, ascribed to an Fe^{III}–peroxo and a second formed from the first at a rate of $4,800\,s^{-1}$ with $\lambda_{max} \approx 670$ nm ascribed to an Fe^{III} hydroperoxo.[184,187] An Fe^{III} peroxo form of the active site has been characterized and vibrational features of the peroxo group documented,[188] although the optical band near 600 nm may also reflect cysteinyl-S-to-Fe^{III} charge transfer.[171,177,184] The same optical change is observed for the E14A mutant indicating that Glu14 is not required[172,187] (although it may serve to lower the E_m of SOR). Since reduction of $O_2^{\bullet-}$ would normally require that $O_2^{\bullet-}$ be at least partially protonated or coordinated to another Lewis acid, it seems likely that as part of binding, $O_2^{\bullet-}$ acquires a proton or at least a strong hydrogen bond, for example from Lys15.[187] Although the 600 nm intermediate is still formed in K15A SOR, its formation is 6 to 30 times slower than in wild-type and its decay is 4 times slower.[185,187]

The 600 nm intermediate decays slowly to the resting oxidized state, with a rate of $40\,s^{-1}$.[172] The rate of decay decreases at high pH and displays a solvent isotope effect of 2,[185] implying that it involves transfer of a proton. Thus, it is proposed to represent protonation and dissociation of the ferric-peroxo species.[172] The order in which the two Os are protonated is believed to be an important determinant of whether the O—O bond will be broken or not, with initial protonation at the distal O favoring bond cleavage as in cytochrome P450.[20] A salt bridge from Lys15 to the distal peroxy O could discourage protonation at that position and favor protonation of the coordinated O instead.

The axial Cys ligand has been proposed to play a pivotal role in defining the electronics of the Fe^{II} that underlie its reactivity, and in facilitating product dissociation as H_2O_2.[171] The intense optical transitions ($\varepsilon > 2,000\,M^{-1}\,cm^{-1}$) indicate good overlap of S and Fe-orbitals in both oxidation states, and the transitions have been interpreted to reflect π-type overlap between Sp and Fe d-orbitals.[184] Adams has argued that this molecular orbital would also interact with $O_2^{\bullet-}$ binding in *trans*, and since it would have substantial electron density contributed by S, it should be good at reducing $O_2^{\bullet-}$. However, as the electron density is transferred to nascent peroxide, it is expected to weaken both the axial ligand-Fe bonds, with the result that peroxide release is favored via the *trans* effect. Lys15 could play an important role in promoting this reactivity by aligning $O_2^{\bullet-}$ with the Fe and S.[171]

8.19.11   CONCLUDING REMARKS

With second order rate constants on the order of $10^9\,s^{-1}$, SODs and SORs are among the fastest enzymes known. This presumably reflects the strong thermodynamic driving force in their favor,

the simplicity of the reactions, and the apparent absence of gross structural rearrangement. Nonetheless, SOD and SOR incorporate many of the crucial elements of more complex redox catalysis: substrate specificity, electron transfer and proton transfer coupled to it. Thus, they are very attractive systems for studying redox catalysis. They also largely elude inactivation by their toxic substrate and product, and thus may serve as models for radical and oxidation-resistant proteins. The ability of SODs to evade side reactions is likely related to both their very fast turnover and their highly self-contained active sites (The second Fe site of 2Fe SORs may serve as an electron carrier to the activite site or a reservoir for another electron). The central chemistry of Fe–SODs and Mn–SODs is accomplished by the metal ion and the coordinated solvent molecule. In Cu,Zn–SODs the redox activity of the Cu ion is supported by proton uptake and release by a His residue, which is a part-time ligand of Cu and is also coordinated to the Zn. The His residue's oxidation-state-specific coordination of Cu contributes to redox tuning, as does the oxidation-state-specific protonation of coordinated solvent in Fe– and Mn–SOD. Likewise, the Glu ligand specific to the oxidized state of SOR may contribute to redox tuning and aid in product dissociation, as may release and rebinding of the coordinated solvent (or the Asp ligand) of Mn–SOD. Finally, the extreme simplicity and self-sufficiency of SODs, which recycle without recourse to any additional electron carriers, contrasts with the $O_2^{\bullet-}$ generating systems, in which the catalytic core is only one or two of many proteins required for activity. Most of the others appear to regulate activity and coordinate it with extracellular and intracellular signals. Thus, the SODs appear to be primitive enzymes, but highly effective in their role as a front-line defense against oxidative stress. Their efficiency, resistance to damage, and independence has contributed to the success of aerobic life.

ACKNOWLEDGEMENTS

8.19.12 REFERENCES

1. Walsh, C. *Enzymatic Reaction Mechanisms*; Freeman: New York, 1979.
2. Hill, H. A. O.; Tew, D. G. in *Comprehensive Coordination Chemistry*, Pergamon: Oxford, 1987, Vol. 2, pp. 315–332.
3. Bytheway, I.; Hall, M. B. *Chem. Rev.* **1994**, *94*, 639–658.
4. Pecoraro, V. L.; Baldwin, M. J.; Gelasco, A. *Chem. Rev.* **1994**, *94*, 807–826.
5. Dickman, M. H.; Pope, M. T. *Chem. Rev.* **1994**, *94*, 569–584.
6. Momenteau, M.; Reed, C. A. *Chem. Rev.* **1994**, *94*, 659–698.
7. Solomon, E. I.; Tuczek, F.; Root, D. E.; Brown, C. A. *Chem. Rev.* **1994**, *94*, 827–856.
8. Pauling, L.; Coryell, C. D. *Proc. Natl. Acad. Sci. U.S.A.* **1936**, *22*, 210–216.
9. Fujisawa, K.; Tanaka, M.; Moro-oka, Y.; Kitajima, N. *J. Am. Chem. Soc.* **1994**, *116*, 12079–12080.
10. Aboelella, N. W.; Lewis, E. A.; Reynolds, A. M.; Brennessel, W. W.; Cramer, C. J.; Tolman, W. B. *J. Am. Chem. Soc.* **2002**, *124*, 10660–10661.
11. Latos-Grazynski, L.; Cheng, R.-J.; La Mar, G. N.; Balch, A. N. *J. Am. Chem. Soc.* **1982**, *104*, 5992–6000.
12. Mahroof-Tahir, M.; Karlin, K. D. *J. Am. Chem. Soc.* **1992**, *114*, 7599–7601.
13. Fukuzumi, S.; Ohtsu, H.; Ohkubo, K.; Itoh, S.; Imahori, H. *Coord. Chem. Rev.* **2002**, *226*, 71–80.
14. Kellerman, R.; Hutta, P. J.; Klier, K. *J. Am. Chem. Soc.* **1974**, *96*, 5946–5947.
15. Ogawa, S.; Lee, T. M.; Kay, A. R.; Tank, D. R. *Proc. Natl. Acad. Sci. U.S.A.* **1990**, *87*, 9868–9872.
16. Shikama, K. *Coord. Chem. Rev.* **1988**, *83*, 73–91.
17. Ciriolo, M. R.; Magliozzo, R. S.; Peisach, J. *J. Biol. Chem.* **1987**, *262*, 6290–6295.
18. Burger, R. M.; Kent, T. A.; Horwitz, S. B.; Münck, E.; Peisach, J. *J. Biol. Chem.* **1983**, *258*, 1559–1564.
19. Bugg, T. D. H.; Lin, G. *Chem. Commun.* **2001**, *2001*, 941–952.
20. Sono, M.; Roach, M. P.; Coulter, E. D.; Dawson, J. H. *Chem. Rev.* **1996**, *96*, 2841–2887.
21. Halliwell, B.; Gutteridge, J. M. *Free Radicals in Biology and Medicine*; Oxford University Press: Oxford, 1999.
22. Messner, K. R.; Imlay, J. A. *J. Biol. Chem.* **1999**, *274*, 10119–10128.
23. McCord, J. M. *Am. J. Med.* **2000**, *108*, 652–659.
24. Kehrer, J. P. *Toxicology* **2000**, *149*, 43–50.
25. Miller, A.-F.; Sorkin, D. L. *Comments Mol. Cell. Biophys.* **1997**, *9*, 1–48.
26. Sawyer, D. T. *Oxygen Chemistry*; Oxford University Press: Oxford, 1991.
27. Benov, L.; Fridovich, I. *J. Biol. Chem.* **1999**, *274*, 4202–4206.
28. Flint, D. H.; Tuminello, J. F.; Emptage, M. H. *J. Biol. Chem.* **1993**, *268*.
29. Imlay, J. A.; Linn, S. *Science* **1988**, *240*, 1302–1309.
30. Stadtman, E. R. *Free Rad. Biol. Med.* **1990**, *9*, 315–325.
31. Nakozono, K.; Watanabe, N.; Sasaki, J.; Sato, T.; Inoue, M. *P.N.A.S.* **1991**, *88*, 10045–10048.

32. Maturana, A.; Arnaudeau, S.; Ryser, S.; Banfi, B.; Hossle, J. P.; Schlegel, W.; Krause, K.-H.; Demaurex, N. *J. Biol. Chem.* **2001**, *276*, 30277–30284.
33. Babior, B. M. *Blood* **1999**, *93*, 1464–1476.
34. Segal, A. W.; Shatwell, K. P. *Ann. N. Y. Acad. Sci.* **1997**, *832*, 215–222.
35. Rotrosen, D.; Yeung, C. L.; Leto, T. L.; Malech, H. L.; Kwong, C. H. *Science* **1992**, *256*, 1459–1462.
36. Root, R. K.; Metcalf, J. A. *J. Clin. Invest.* **1977**, *60*, 1266–1271.
37. Foubert, T. R.; Bleazard, J. B.; Burritt, J. B.; Gripentrog, J. M.; Baniulis, D.; Taylor, R. M.; Jesaitis, A. J. *J. Biol. Chem.* **2001**, *276*, 38852–38861.
38. Nishimoto, Y.; Motalebi, S.; Han, C.-H.; Lambeth, J. D. *J. Biol. Chem.* **1999**, *274*, 22999–23005.
39. Roos, D.; De Boer, M.; Kuribayashi, F.; Meischl, C.; Weening, R. S.; Segal, A. W.; Ahlin, A.; Nemet, K.; Hossle, J. P.; Bernatowska-Matuszkiewicz, E.; Middleton-Price, H. *Blood* **1996**, *87*, 1663–1681.
40. Cross, A.; Rae, J.; Curnutte, J. *J. Biol. Chem.* **1995**, *270*, 17075–17077.
41. Isogai, Y.; Shiro, Y.; Nasuda-Kouyama, A.; Iizuka, T. *J. Biol. Chem.* **1991**, *266*.
42. Lambeth, D. *Trends. Biochem. Sci.* **2000**, *25*, 459–460.
43. Yoshida, L. S.; Saruta, F.; Yshikawa, K.; Tatsuzawa, O.; Tsunawaki, S. *J. Biol. Chem.* **1998**, *273*, 27879–27886.
44. Biberstine-Kinkade, K. J.; DeLeo, F. R.; Epstein, R. I.; LeRoy, B. A.; Nauseef, W. M.; Dinauer, M. C. *J. Biol. Chem.* **2001**, *276*, 31105–31112.
45. Taylor, W. R.; Jones, D. T.; Segal, A. W. *Protein Sci.* **1993**, *2*, 1675–1685.
46. Hurst, J.; Loehr, T.; Curnutte, J.; Rosen, H. *J. Biol. Chem.* **1991**, *266*, 1627–1634.
47. Fujii, H.; Finnegan, M.; Miki, T.; Crouse, B.; Kakinuma, K.; Johnson, M. *FEBS Lett.* **1995**, *377*, 345–348.
48. Doussiere, J.; Gaillard, J.; Vignais, P. V. *Biochem.* **1996**, *35*, 13400–13410.
49. Pou, S.; Pou, W. S.; Bredt, D. S.; Snyder, S. H.; Rosen, G. M. *J. Biol. Chem.* **1992**, *267*, 24173–24176.
50. Heinzel, B.; John, M.; Klatt, P.; Bohme, E.; Mayer, B. *Biochem. J.* **1992**, *281*, 627–630.
51. Xia, Y.; Roman, L. J.; Masters, B. S. S.; Zweier, J. L. *J. Biol. Chem.* **1998**, *273*, 22635–22639.
52. Vasquez-Vivar, J.; Martasek, P.; Whitsett, J.; Joseph, J.; Kalyanaraman, B. *Biochem. J.* **2002**, *362*, 733–739.
53. Bulkley, G. B. *Surgery* **1993**, *113*, 479–483.
54. Imlay, J. A.; Fridovich, I. *J. Biol. Chem.* **1991**, *266*, 6957–6965.
55. Imlay, J. A. *J. Biol. Inorg. Chem.* **2002**, *7*, 659–663.
56. Tang, L.; Ou, X.; Henkle-Duhrsen, K.; Selkirk, M. E. *Infect. Immun.* **1994**, *62*, 961–967.
57. de Graef, M. R.; Alexeeva, S.; Snoep, J. L.; de Mattos, T. M. J. *J. Bacteriol.* **1999**, *181*, 2351–2357.
58. Gruber, M. Y.; Glick, B. R.; Thompson, J. E. *Proc. Natl. Acad. Sci. U.S.A.* **1990**, *87*, 2608–2612.
59. Liochev, S. I.; Fridovich, I. *J. Biol. Chem.* **1991**, *266*, 8747–8750.
60. Steinman, H. M.; Weinstein, L.; Brenowitz, M. *J. Biol. Chem.* **1994**, *269*, 28629–28634.
61. Smith, M. W.; Doolittle, R. F. *J. Mol. Evol.* **1992**, *34*, 175–184.
62. Fink, R. C.; Scandalios, J. G. *Arch. Biochem. Biophys.* **2002**, *399*, 19–36.
63. Bordo, D.; Pesce, A.; Bolognesi, M.; Stroppolo, M. E.; Falconi, M.; Desideri, A. In *handbook of metalloproteins*; John Wiley: Chichester, 2001, pp 128–1300.
64. Bertini, I.; Banci, L.; Piccioli, M. *Coord. Chem. Rev.* **1990**, *100*, 67–103.
65. Fridovich, I. *J. Biol. Chem.* **1997**, *272*, 18515–18517.
66. Banci, L.; Bertini, I.; Viezzoli, M. S.; Argese, E.; Orsega, E. F.; Chiu, C. Y.; Mullenbach, G. T. *J. Biol. Inorg. Chem.* **1997**, *2*, 295–301.
67. Richardson, J. S. *Nature* **1977**, *268*, 495–500.
68. Djinovic-Carugo, K.; Battistoni, A.; Carri, M.; Policelli, F.; Desideri, A.; Rotilio, G.; Coda, A.; Wilson, K.; Bolognesi, M. *Acta Crystallogr.* **1996**, *D52*, 176–188.
69. Tainer, J. A.; Getzoff, E. D.; Beem, K. M.; Richardson, K. S.; Richardson, D. C. *J. Miol. Biol.* **1982**, *160*, 181–217.
70. Kitagawa, Y.; Tanaka, N.; Hata, Y.; Kusunoki, M.; Lee, G.-P.; Katsube, Y.; Asada, K.; Aibara, S.; Morita, Y. *J. Biochem.* **1991**, *109*, 477–485.
71. Gaber, B. P.; Brown, R. D.; Koenig, S. H.; Fee, J. A. *Biochim. Biophys. Acta* **1972**, *271*, 1.
72. Hart, P. J.; Balbirnie, M. M.; Ogihara, N. L.; Nersissian, A. M.; Weiss, M. S.; Valentine, J. S.; Eisenberg, D. *Biochem.* **1999**, *38*, 2167–2178.
73. Beem, K. M.; Richardson, D. C.; Rajagopalan, K. V. *Biochem.* **1977**, *16*, 1930.
74. Fee, J. A.; Briggs, R. G. *Biochim. Biophys. Acta* **1975**, *400*, 439–450.
75. Valentine, J. S.; Pantoliano, M. W.; McDonnell, P. J.; Burger, A. J.; Lippard, S. J. *Proc. Natl. Acad. Sci. U.S.A.* **1979**, *76*, 4245.
76. McAdam, M.; Fielden, E. M.; Lavelle, F.; Calabrese, L.; Cocco, D.; Rotilio, G. *Biochem. J.* **1977**, *167*, 271–274.
77. Djinovik, K.; Coda, A.; Antolini, L.; Pelosi, G.; Desideri, A.; Falconi, M.; Rotilio, G.; Bolognesi, M. *J. Mol. Biol.* **1992**, *226*, 227–238.
78. Bertini, I.; Luchinat, C.; Piccioli, M. *Prog. NMR Spectrosc.* **1994**, *26*, 91–139.
79. Rotilio, G.; Calabrese, L.; Coleman, J. E. *J. Biol. Chem.* **1973**, *248*, 3855–3859.
80. Klug-Roth, D.; Fridovich, I.; Rabani, J. *J. Am. Chem. Soc.* **1973**, *95*, 2786–2790.
81. Fielden, E. M.; Roberts, P. B.; Bray, R. C.; Lowe, D. J.; Mautner, G. N.; Rotilio, G.; Calabrese, L. *Biochem. J.* **1974**, *139*, 49–60.
82. Cudd, A.; Fridovich, I. *J. Biol. Chem.* **1982**, *257*, 11443–11447.
83. Argese, E.; Viglino, P.; Rotilio, G.; Scarpa, M.; Rigo, A. *Biochemistry* **1987**, *26*, 3224–3228.
84. Sines, J. J.; Allison, S. A.; McCammon, J. A. *Biochem.* **1990**, *29*, 9403–9412.
85. Folcarelli, S.; Venerini, F.; Battistoni, A.; O'Neil, P.; Rotillio, G.; Desideri, A. *Biochem. Biophys. Res. Commun.* **1999**, *256*, 425–428.
86. Policelli, F.; Battistoni, A.; O'Neill, P.; Rotilio, G.; Desideri, A. *Protein Sci.* **1998**, *7*, 2354–2358.
87. McCord, J. M.; Fridovich, I. *J. Biol. Chem.* **1969**, *244*, 6049–6055.
88. Morpurgo, L.; Giovagnoli, C.; Rotilio, G. *Biochem. Biophys. Res. Commun.* **1973**, *322*, 204–210.
89. Rotilio, G.; Mondovi, B.; Morpurgo, L.; Calabrese, L.; Giovagnoli, C. *Biochemistry* **1972**, *11*, 2187–2192.
90. Djinovic Carugo, K. D.; Battistoni, A.; Carri, M. T.; Policelli, F.; Desideri, A.; Rotilio, G.; Coda, A.; Bolognesi, M. *FEBS Lett* **1994**, *349*, 93–98.

91. Lieberman, R. A.; Sands, R. H.; Fee, J. A. *J. Biol. Chem.* **1982**, *257*, 336–344.
92. Djinovic-Caruga, K.; Polticelli, F.; Desideri, A.; Rotilio, G.; Wilson, K.; Bolognesi, M. *J. Mol. Biol.* **1994**, *240*, 179–183.
93. Blackburn, N. J.; Hasnain, S. S.; Binsted, N.; Diakun, G. P.; Garner, C. D.; Knowles, P. F. *Biochem. J.* **1984**, *219*, 985–990.
94. Bertini, L.; Luchinat, C. *J. Am. Chem. Soc.* **1985**, *107*, 2178–2179.
95. Azab, H. A.; Banci, L.; Borsari, M.; Luchinat, C.; Sola, M.; Viezzoli, M. S. *Inorg. Chem.* **1992**, *31*, 4649–4655.
96. Fee, J. A.; DiCorleto, P. E. *Biochemistry* **1973**, *12*, 4893–4899.
97. Leone, M.; Cupane, M.; Militello, V.; Stroppolo, M. E.; Desideri, A. *Biochem.* **1998**, *37*, 4459–4464.
98. Fee, J. A.; Bull, C. *J. Biol. Chem.* **1986**, *261*, 13000–13005.
99. Banci, L.; Bertini, I.; Cabelli, D.; Hallewell, R. A.; Luchinat, C.; Viezzoli, M. S. *Inorg. Chem.* **1990**, *29*, 2398–2403.
100. Boden, N.; Holmes, M. C.; Knowles, P. F. *Biochem. J.* **1979**, *177*, 303–309.
101. Ellerby, L. M.; Cabelli, D. E.; Graden, J. A.; Valentine, J. S. *J. Am. Chem. Soc.* **1996**, *118*, 6556–6561.
102. Strothkamp, K. G.; Lippard, S. J. *J. Am. Chem. Soc.* **1982**, *104*, 852.
103. Deng, H.-X.; Hentati, A.; Tainer, J. A.; Iqbal, Z.; Cayabyab, A.; Hung, W.-Y.; Getzoff, E. D.; Hu, P.; Herzfeldt, B.; Roos, R. P.; Warner, C.; Deng, G.; Soriano, E.; Smyth, C.; Parge, H. E.; Ahmed, A.; Roses, A. D.; Hallewell, R. A.; Pericak-Vance, M. A.; Siddique, T. *Science* **1993**, *261*, 1047–1051.
104. Rosen, D. R.; Siddique, T.; Patterson, D.; Figlewicz, D. A.; Sapp, P.; Hentati, A.; Donaldson, D.; Goto, J.; O'Regan, J. P.; Deng, H.-X.; Rahmani, Z.; Krizus, A.; McKenna-Yasek, D.; Cayabyab, A.; Gaston, S. M.; Berger, R.; Tanzi, R. E.; Halperin, J. J.; Herzfeldt, B.; Van den Bergh, R.; Hung, W.-Y.; Bird, T.; Deng, G.; Mulder, D. W.; Smyth, C.; Laing, N. G.; Soriano, E.; Pericak-Vance, M. A.; Haines, J.; Rouleau, G. A.; Gusella, J. S.; Horvitz, H. R.; Brown, J. R. H. *Nature* **1993**, *362*, 59–62.
105. Rodriguez, J. A.; Valentine, J. S.; Eggers, D. K.; Roe, J. A.; Tiwari, A.; Brown, R. H. Jr.; Hayward, L. J. *J. Biol. Chem.* **2002**, *277*, 15932–15937.
106. Sendtner, M.; Thoenen, H. *Current Biol.* **1994**, *4*, 1036–1039.
107. Gurney, M. E.; Pu, H.; Chiu, A. Y.; Dal Canto, M. C.; Polchow, C. Y.; Alexander, D. D.; Caliendo, J.; Hentati, A.; Kwon, Y. W.; Deng, H. X.; Chen, W. J.; Zhai, P.; Sufit, R. L.; Siddique, T. *Science* **1994**, *264*, 1772–1775.
108. Ripps, M. E.; Huntley, G. W.; Hof, P. R.; Morrison, J. H.; Gordon, J. W. *Proc. Natl. Acad. Sci. U.S.A.* **1995**, *92*, 689–93.
109. Okado-Matsumoto, A.; Fridovich, I. *Proc. Natl. Acad. Sci. U.S.A.* **2002**, *99*, 9010–9014.
110. Miller, A.-F. In *Handbook of Metalloproteins*; K. Wieghardt, R.; Huber, T. L.; Poulos, A.; Messerschmidt, Eds; Wiley and Sons: Chichester, 2001, Vol. 1, pp. 668–682.
111. Lah, M. S.; Dixon, M. M.; Pattridge, K. A.; Stallings, W. C.; Fee, J. A.; Ludwig, M. L. *Biochemistry* **1995**, *34*, 1646–1660.
112. Stallings, W. C.; Metzger, A. L.; Pattridge, K. A.; Fee, J. A.; Ludwig, M. L. *Free Rad. Res. Comms.* **1991**, *12-13*, 259–268.
113. Edwards, R. A.; Baker, H. M.; Jameson, G. B.; Whittaker, M. M.; Whittaker, J. W.; Baker, E. N. *J.B.I.C.* **1998**, *3*, 161–171.
114. Stoddard, B. L.; Howell, P. L.; Ringe, D.; Petsko, G. A. *Biochemistry* **1990**, *29*, 8885–8893.
115. Yamakura, F. *Biochem. Biophys. Res. Commun.* **1984**, *122*, 635–641.
116. Berkowitz, J.; Ellison, G. B.; Gutman, D. *J. Phys. Chem.* **1994**, *98*, 2744–2765.
117. Bordwell, F. G.; Cheng, J.-P.; Harrelson, J. J. A. *J. Am. Chem. Soc.* **1988**, *110*, 1229–1231.
118. Whittaker, M. M.; Whittaker, J. W. *Biochemistry* **1997**, *36*, 8923–8931.
119. Lavelle, F.; McAdam, M. E.; Fielden, E. M.; Roberts, P. B.; Puget, K.; Michelson, A. M. *Biochem. J.* **1977**, *161*, 3–11.
120. Bull, C.; Fee, J. A. *J. Am. Chem. Soc.* **1985**, *107*, 3295–3304.
121. Han, W. G.; Lovell, T.; Noodleman, L. *Inorg. Chem.* **2002**, *41*, 205–218.
122. Fee, J. A.; McClune, G. J.; O'Neill, P.; Fielden, E. M. *Biochem. Biophys. Res. Commun.* **1981**, *100*, 377–384.
123. Slykhouse, T. O.; Fee, J. A. *J. Biological Chem.* **1976**, *251*, 5472–5477.
124. Whittaker, J. W.; Solomon, E. I. *J. Am. Chem. Soc.* **1988**, *110*, 5329–5339.
125. Jackson, T. A.; Xie, J.; Yikilmaz, E.; Miller, A.-F.; Brunold, T. C. *J. Am. Chem. Soc.* **2002**, *124*, 10833–10845.
126. Schmidt, M. *Eur. J. Biochem.* **1999**, *262*, 117–126.
127. Sorkin, D. L.; Miller, A.-F. *Biochemistry* **1997**, *36*, 4916–4924.
128. Sorkin, D. L.; Duong, D. K.; Miller, A.-F. *Biochemistry* **1997**, *36*, 8202–8208.
129. Sorkin D.L., Ph.D. thesis, The Johns Hopkins University (1999).
130. Han, S.; Eltis, L. D.; Timmis, K. N.; Muchmore, S. W.; Bolin, J. T. *Science* **1995**, *270*, 976–980.
131. Whittaker, J. W. In *Manganese and its Role in Biological Processes.*; A. Sigel, H. Sigel, Eds; Marcel Dekker: New York, 2000, Vol. 37, pp. 587–611.
132. Stroupe, M. E.; DiDonato, M.; Tainer, J. A. In *Handbook of Metalloproteins*; K. Wieghardt, R. Huber, T. L. Poulos, A. Messerschmidt, Eds; Wiley and Sons: Chichester, 2001, Vol. 2, pp. 941–951.
133. Borgstahl, G. E. O.; Parge, H. E.; Hickey, M. J.; Beyer, J. W. F.; Hallewell, R. A.; Tainer, J. A. *Cell* **1992**, *71*, 107–118.
134. Borgstahl, G. E. O.; Pokross, M.; Chehab, R.; Sekher, A.; Snell, E. H. *J. Mol. Biol.* **2000**, *296*, 951–959.
135. Parker, M. W.; Blake, C. C. F. *FEBS Lett.* **1988**, *229*, 377–382.
136. Xie, J.; Yikilmaz, E.; Miller, A.-F.; Brunold, T. C. *J. Am. Chem. Soc.* **2002**, *124*, 3769–3774.
137. Vance, C. K.; Miller, A.-F. *J. Am. Chem. Soc.* **1998**, *120*, 461–467.
138. Vance, C. K.; Miller, A.-F. *Biochemistry* **2001**, *40*, 13079–13087.
139. Maliekal, J.; Karapetian, A.; Vance, C.; Yikilmaz, E.; Wu, Q.; Jackson, T.; Brunold, T. C.; Spiro, T. G.; Miller, A.-F.; *J. Am. Chem. Soc.,* **2002**, *124*, 15064–15075.
140. Schwartz, A. L.; Yikilmaz, E.; Vance, C. K.; Vathyam, S.; Koder, R. L., Jr.; Miller, A.-F. *J. Inorg. Biochem.* **2000**, *80*, 247–256.
141. Yikilmaz, E.; Xie, J.; Miller, A.-F.; Brunold, T. C. *J. Am. Chem. Soc.* **2002**, *124*, 3482–3483.
142. Pick, M.; Rabani, J.; Yost, F.; Fridovich, I. *J. Am. Chem. Soc.* **1974**, *96*, 7329–7333.

143. Gregory, E. M.; Dapper, C. H. *Arch. Biochem. Biophys.* **1983**, *220*, 293–300.
144. Meier, B.; Barra, D.; Bossa, F.; Calabrese, L.; Rotilio, G. *J. Biol. Chem.* **1982**, *257*, 13977–13980.
145. Hiraoka, B. Y.; Yamakura, F.; Sugio, S.; Nakayama, K. *Biochem. J.* **2000**, *345*, 345–350.
146. Martin, M. E.; Byers, B. R.; Olson, M. O. J.; Salin, M. L.; Aruneaux, J. E. L.; Tolbert, C. *J. Biol. Chem.* **1986**, *261*, 9361–9367.
147. Bull, C.; Niederhoffer, E. C.; Yoshida, T.; Fee, J. A. *J. Am. Chem. Soc.* **1991**, *113*, 4069–4076.
148. Hsu, J.-L.; Hsieh, Y.; Tu, C.; O'Connor, D.; Nick, H. S.; Silverman, D. N. *J. Biol. Chem.* **1996**, *271*, 17687–17691.
149. Hearn, A. S.; Stroupe, M. E.; Cabelli, D. E.; Lepock, J. R.; Tainer, J. A.; Nick, H. S.; Silverman, D. S. *Biochemistry* **2001**, *40*, 12051–12058.
150. Whittaker, M. M.; Whittaker, J. W. *Biochemistry* **1996**, *35*, 6762–6770.
151. Whittaker, J. W.; Whittaker, M. M. *J. Am. Chem. Soc.* **1991**, *113*, 5528–5540.
152. Yamakura, F.; Taka, H.; Fujimura, T.; Murayama, K. *J. Biol. Chem.* **1998**, *273*, 14085–14089.
153. Guan, Y.; Hickey, M. J.; Borgstahl, G. E. O.; Hallewell, R. A.; Lepock, J. R.; O'Connor, D.; Hsieh, Y.; Nick, H. S.; Silverman, D. N.; Tainer, J. A. *Biochemistry* **1998**, *37*, 4722–4730.
154. Edwards, R. A.; Whittaker, M. M.; Whittaker, J. W.; Baker, E. N.; Jameson, G. B. *Biochemistry* **2001**, *40*, 15–27.
155. Hsieh, H.; Guan, Y.; Tu, C.; Bratt, P. J.; Angerhofer, A.; Lepock, J. R.; Hickey, M. J.; Tainer, J. A.; Nick, H. S.; Silverman, D. N. *Biochemistry* **1998**, *37*, 4731–4739.
156. Ose, D. E.; Fridovich, I. *J. Biol. Chem.* **1976**, *251*, 1217–1218.
157. Yamakura, F. *J. Biochem.* **1978**, *83*, 849–857.
158. Stein, J.; Fackler, J. P.; McClune, G. J.; Fee, J. A.; Chan, L. T. *Inorg. Chem.* **1979**, *18*, 3511–3519.
159. Barrette, J. W. C.; Sawyer, D. T.; Fee, J. A.; Asada, K. *Biochemistry* **1983**, *22*, 624–627.
160. Verhagen, M. F. J. M.; Meussen, E. T. M.; Hagen, W. R. *Biochim. Biophys. Acta* **1995**, *1244*, 99–103.
161. Vance, C. K.; Miller, A.-F. *Biochemistry* **1998**, *37*, 5518–5527.
162. Edwards, R. A.; Whittaker, M. M.; Whittaker, J. W.; Jameson, G. B.; Baker, E. N. *J. Am. Chem. Soc.* **1998**, *120*, 9684–9685.
163. Yamakura, F.; Kobayashi, K.; Ue, H.; Konno, M. *Eur. J. Biochem.* **1995**, *227*, 700–706.
164. Hassan, H. M.; Schrum, L. W. *FEMS Microbiol. Rev.* **1994**, *14*, 315–323.
165. Youn, H.-D.; Kim, E.-J.; Roe, J.-H.; Hah, Y. C.; Kang, S.-O. *Biochem. J.* **1996**, *318*, 889–896.
166. Kim, E.-J.; Chung, H.-J.; Suh, B.; Hah, Y. C.; Roe, J.-H. *Mol. Microbiol.* **1998**, *27*, 187–195.
167. Choudhury, S. B.; Lee, J.-W.; Davidson, G.; Yim, Y.-I.; Bose, K.; Sharma, M. L.; Kang, S.-O.; Cabelli, D. E.; Maroney, M. J. *Biochem.* **1999**, *38*, 3744–3752.
168. Maroney, M. J.; Pressler, M. A.; Mirza, S. A.; Whitehead, J. P.; Gurbiel, R. J.; Hoffman, B. M. *Adv. Chem. Ser.* **1995**, *246*, 21–60.
169. Dole, F.; Fournel, A.; Magro, V.; Hatchikian, E. C.; Bertrand, P.; Guigliarelli, B. *Biochem.* **1997**, *36*, 7847–7854.
170. Abreu, I. A.; Xavier, A. V.; LeGall, J.; Cabelli, D. E.; Teixeira, M. *J. Biol. Inorg. Chem.* **2002**, *7*, 668–674.
171. Adams, M. W. W.; Jenney, F. E., Jr.; Clay, M. D.; Johnson, M. K. *J. Biol. Inorg. Chem.* **2002**, *7*, 647–652.
172. Kurtz, D. M., Jr.; Coulter, E. D. *J. Biol. Inorg. Chem.* **2002**, *7*, 653–658.
173. Jenney, F. E., Jr.; Verhagen, M.; Cui, X.; Adams, M. W. W *Science* **1999**, *286*, 306–309.
174. Pianzzola, M. J.; Soubes, M.; Touati, D. *J. Bacteriol.* **1996**, *178*, 6736–6742.
175. Liochev, S. I.; Fridovich, I. *J. Biol. Chem.* **1997**, *272*, 25573–25575.
176. Silva, G.; Oliveira, S.; Gomes, C. M.; Pacheco, I.; Liu, M. Y.; Xavier, A. V.; Teixeira, M.; LeGall, J.; Rodrigues-Pousada, C. *Eur. J. Biochem.* **1999**, *259*, 235–243.
177. Abreu, I. A.; Saraiva, L. M.; Soares, C. M.; Teixeira, M.; Cabelli, D. E. *J. Biol. Chem.* **2001**, *276*, 38995–39001.
178. Abreu, I. A.; Saraiva, L. M.; Carita, J.; Huber, H.; Stetter, K. O.; Cabelli, D. E.; Teixeira, M. *Mol. Microbiol.* **2000**, *38*, 322–334.
179. Chen, L.; Sharma, P.; LeGall, J.; Mariano, A. M.; Teixeira, M.; Xavier, A. *Eur. J. Biochem.* **1994**, *226*, 613–618.
180. Brumlik, M. J.; Voordouw, G. *J. Bacteriol.* **1989**, *171*, 4996–5004.
181. Tavares, P.; Ravi, N.; Moura, J. J. G.; LeGall, J.; Huang, Y.-H.; Crouse, B. R.; Johnson, M. K.; Huynh, B. H.; Moura, I. *J. Biol. Chem.* **1994**, *269*, 10504–10510.
182. Yeh, A. P.; Hu, Y.; Jenney, F. E., Jr.; W, A. M. W.; Rees, D. C. *Biochem.* **2000**, *39*, 2499–2508.
183. Coehlo, A. V.; Matias, P.; Fülop, V.; Thomson, A.; Gonzalez, A.; Carrondo, M. A. *J. Biol. Inorg. Chem.* **1997**, *2*, 680–689.
184. Clay, M. D.; Jenney, F. E., Jr.; Hagedoorn, P. L.; George, G. N.; Adams, M. W. W.; Johnson, M. K. *J. Am. Chem. Soc.* **2002**, *24*, 788–805.
185. Emerson, J. P.; Coulter, E. D.; Cabelli, D. E.; Phillips, R. S.; Kurtz, D. M., Jr. *Biochem.* **2002**, *41*, 4348–4357.
186. Coulter, E. D.; Emerson, J. P.; Kurtz, D. M., Jr.; Cabelli, D. E. *J. Am. Chem. Soc.* **2000**, *122*, 11555–11556.
187. Lombard, M.; Houeé-Levin, C.; Touati, D.; Fontecave, M.; Niviere, V. *Biochem.* **2001**, *40*, 5032–5040.
188. Mathé, C.; Mattioli, T. A.; Horner, O.; Lombard, M.; Latour, J.-M.; Fontecave, M.; Niviere, V. *J. Am. Chem. Soc.* **2002**, *124*, 4966–4967.
189. McAdam, M. E.; Fox, R. A.; Lavelle, F.; Fielden, E. M. *Biochem. J.* **1977**, *165*, 71–79.
190. Yu, L.; Quinn, M.; Cross, A.; Dinauer, M. *Proc. Natl. Acad. Sci. U.S.A.* **1998**, *95*, 7993–7998.
191. Kraulis, P. J. *J. Appl. Cryst.* **1991**, *24*, 946–950.
192. Ogihara, N. L.; Parge, H. E.; Hart, P. J.; Weiss, M. S.; Goto, J. J.; Crane, B. R.; Tsang, J.; Slater, K.; Roe, J. A.; Valentine, J. S.; Eisenberg, D.; Tainer, J. A. *Biochemistry* **1996**, *35*, 2316–2321.
193. Miller, A.-F.; Padmakumar, K.; Sorkin, D. C.; Karapetian, A.; Vance, C. K. *J. Inorg. Biochem.* **2003**, *93*, 71–83.
194. Jackson, T. A.; Yikilmaz, E.; Miller, A.-F.; Brunold, T. C. *J. Am. Chem. Soc.* **2003**, *125*, accepted.

8.20
Oxygen Evolution

J. S. VRETTOS and G. W. BRUDVIG
Yale University, New Haven, CT, USA

8.20.1 INTRODUCTION

Oxygenic photosynthesis is the process by which green plants and cyanobacteria convert solar energy into the chemical potential used to produce carbohydrates from carbon dioxide and water, utilizing H_2O as an electron source and releasing O_2 as a by-product. The mechanism of photosynthetic oxygen evolution has been studied for a long time, but only in the past few years have detailed mechanisms been proposed. This is primarily due to the advent of increasingly higher resolution structures of the proteins involved in oxygenic photosynthesis and the development of chemical models that mimic the chemistry of oxygen evolution. In this chapter, we will focus on the bioinorganic chemistry of the active site of water oxidation, a tetranuclear manganese–oxo (Mn_4) cluster in the photosystem (PS) II protein complex. The present understanding of the structure of the Mn_4 cluster, its coordination environment, and its function will be reviewed. Structural and functional models of the Mn_4 cluster used to help understand results from PSII are discussed. Finally, proposals for the mechanism of water oxidation by PSII are presented.

8.20.1.1 The Photosystem II Protein Complex

The process of oxygenic photosynthesis is carried out in layers of flattened vesicles called thylakoids, membranes that contain the enzymes involved in the light reactions of photosynthesis. In cyanobacteria, thylakoids are formed by invaginations of the cell membrane, whereas in green plants thylakoids are housed in an organelle called the chloroplast. PSI and PSII and the cytochrome (Cyt) b_6f complex are the proteins involved in the light-dependent reactions of oxygenic photosynthesis, coupling the oxidation of water with the reduction of $NADP^+$, and the formation of a transmembrane proton gradient. This process begins in PSII with the oxidation of water and reduction of plastoquinone to plastoquinol. The plastoquinol delivers reducing equivalents to the Cyt b_6f complex, which transfers reducing equivalents to PSI via plastocyanin. PSI catalyzes the oxidation of plastocyanin and the reduction of ferrodoxin, which subsequently reduces $NADP^+$ to NADPH via NADP:ferrodoxin oxidoreductase. NADPH provides the reducing equivalents needed in the fixation of carbon.[1]

PSII is the multisubunit transmembrane complex located in the appressed regions of the thylakoid membrane that couples the four-electron oxidation of water to the reduction of two molecules of plastoquinone. Because of the size and complexity of PSII, it has proven difficult to obtain a high-resolution crystal structure of the protein. In the past, models of PSII have relied on analogy to the structure of the bacterial reaction center (BRC)[2,3] and the wealth of spectroscopic results available for PSII. Recently, however, a crystal structure at 3.8 Å resolution[4] was solved (Figure 1). At this resolution, the positions of the α helices, the tetrapyrrole portion of chlorophylls (chls) and hemes, and metal centers can be discerned, but not loop regions or individual amino acids. The main components of the electron-transfer chain are contained in a heterodimer composed of the D1 and D2 polypeptides. These include a pair of chl molecules (P_A and P_B), analogous to the special pair of bacteriochlorophylls in the BRC, flanked by a pair of chls (B_A and B_B) analogous to the voyeur bacteriochlorophylls of the BRC.[5] (It should be noted that B_A and B_B in PSII are chl *a* molecules and not bacteriochlorophylls.) Together, these four chls constitute the photoactive pigments of the reaction center.[6] Situated nearby are two pheophytins (Pheo). The binding pockets for a protein-bound plastoquinone (Q_A) and an exchangeable quinone (Q_B) are found at the stromal side of PSII, near the nonheme iron (Fe). Close to P_A on the lumenal side of the PSII is a redox-active tyrosine residue, Y161 of the D1 polypeptide (denoted Y_Z), which is a part of the oxygen-evolving complex (OEC). The OEC consists of Y_Z, the Mn_4 cluster, and Ca^{2+} and Cl^- ions and is the active site of water oxidation.[7–13]

8.20.1.2 Photochemistry of Water Oxidation

The energy required to oxidize water to O_2 is provided by visible photons, which are collected by an array of chls in light-harvesting proteins and funneled by energy-transfer mechanisms to the PSII reaction center chls. This excitation energy initiates electron transfer from the reaction center chls to $Pheo_A$ and subsequently to the membrane-bound quinone Q_A, yielding $P_A^{\bullet+} Q_A^{\bullet-}$.[6] To stabilize the charge-separated state, $Q_A^{\bullet-}$ is oxidized by Q_B and $P_A^{\bullet+}$ is reduced by Y_Z. On the electron acceptor side, $Q_A^{\bullet-}$ reduces Q_B to a semiquinone and subsequently to plastoquinol, after which Q_BH_2 leaves PSII and carries its stored reducing equivalents on to the next step in photosynthesis. On the electron donor side, the neutral radical $Y_Z^{\bullet}$ oxidizes the Mn_4 cluster. In the late 1960s, Joliot and Kok found that when dark-adapted PSII is subjected to a series of very
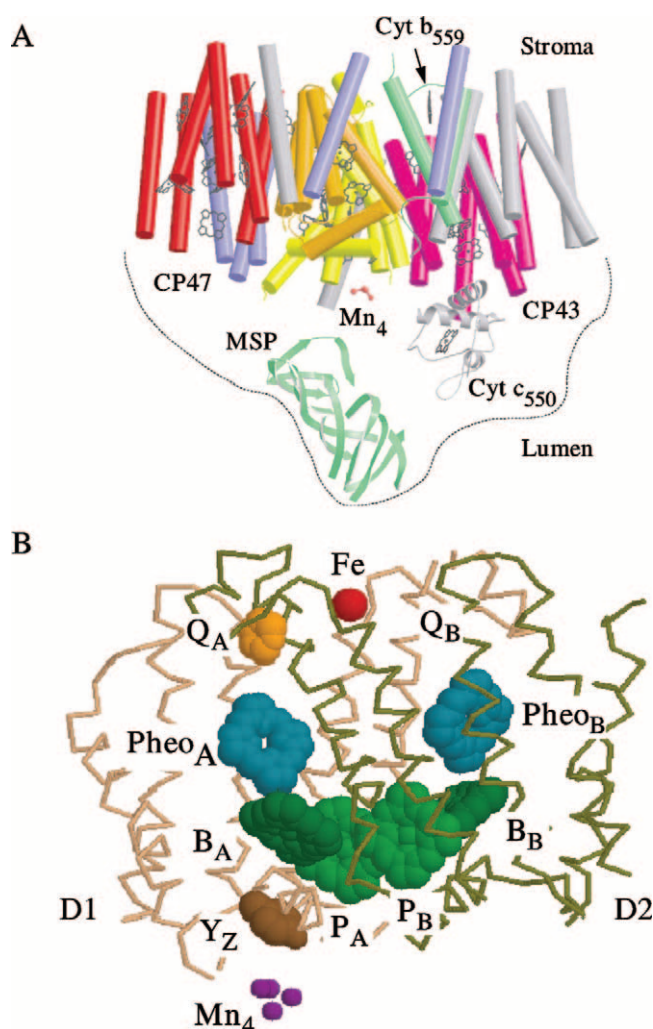
Figure 1 Model of the 3.8 Å crystal structure of PSII (PDB #1FE1).[4] Panel A depicts the major protein subunits, including the light-harvesting proteins CP47 (red) and CP43 (magenta), cyt b_{559} (light green), cyt c_{550} (gray), the manganese-stabilizing protein (MSP, green), and the D1 (yellow) and D2 (orange) polypeptides. The tetrapyrrole macrocycles of hemes and chl are shown in wireframe representation. Panel B highlights the cofactors in the heterodimer formed by D1 (beige) and D2 (olive), including the Mn_4 cluster (purple), Y_Z (brown), P_A and P_B (green), B_A and B_B (dark green), $Pheo_A$ and $Pheo_B$ (blue), Q_A (orange), and the nonheme Fe (red). Though not present in the crystal structure, the approximate location of Q_B is labeled, based on symmetry with Q_A.

short flashes of light, oxygen is evolved maximally on the third and then every fourth subsequent flash.[14,15] Later, they proposed the four-step S-state mechanism for O_2 evolution (Figure 2), in which each S-state represents the accumulation of an oxidizing equivalent on the Mn in PSII.[16] Because O_2 is produced on the third flash of light in the first sequence of flashes, they surmised that the S_1-state, and not S_0, was the dark-stable state. Protons are released into the thylakoid lumen during S-state advancement and O_2 is released spontaneously during the S_3 to S_0 conversion (Figure 2). It was in 1980 that direct evidence for sequential Mn oxidation was obtained using a variety of spectroscopic techniques, which will be discussed below.

8.20.2 THE Mn_4 CLUSTER AND OXYGEN-EVOLVING COMPLEX

8.20.2.1 Physical Characterization of the Oxygen-evolving Complex

The OEC is the site of water oxidation and consists of the Mn_4 cluster, Y_Z, and Ca^{2+} and Cl^- cofactors.[7–10,13] The exact arrangement of the Mn ions in the Mn_4 cluster is unknown, but a
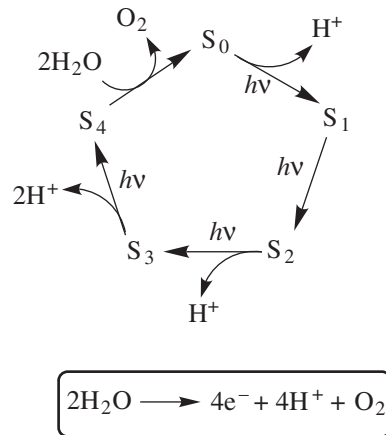
Figure 2 The S-state cycle, as proposed by Joliot and Kok.[16] In each light-driven step, the OEC is oxidized and an electron is transferred to $Y_Z^\bullet$.

topology is suggested based on the PSII crystal structure.[4] However, the PSII structure is not yet resolved well enough to distinguish the individual Mn ions in the electron density map or other metals such as Ca^{2+}. Most of what is known about the structure of the Mn_4 cluster and its coordination environment has been obtained by spectroscopic methods.

8.20.2.1.1 *X-ray absorption spectroscopy*

X-ray absorption spectroscopy (XAS) is well-suited for investigating the Mn_4 cluster because the X-ray absorption near-edge structure (XANES) and extended X-ray absorption fine structure (EXAFS) features report, respectively, on the average oxidation state of the manganese ions and their local environment. For the Mn_4 cluster, the edge region of the XAS is found at around 6,550 eV, which is typical of Mn complexes with +3 and +4 mean oxidation states.[17–19] The EXAFS extends beyond the edge to about 7,100 eV.[17,19–21]

An example of the XANES spectra obtained for the various S-states is shown in Figure 3. The pre-edge absorption at 6,540 eV is diagnostic of the symmetry and coordination of the Mn ions. For PSII, the weak pre-edge absorption indicates that the individual Mn ions are likely five- or six-coordinate in rather symmetric local environments.[19,22] The edge spectra report on the average oxidation state of the Mn_4 cluster. Generally, an increase in oxidation state will cause an increase in the edge energy, but changes in the geometry of the Mn_4 cluster or its ligand sphere will influence the magnitude of the shift.[21] There is general agreement on the oxidation state assignments for the XANES spectra of the low S-states, as follows: S_0 (2/3/4/4), S_1 (3/3/4/4), and S_2 (3/4/4/4).[10,23–28] However, there is some controversy over whether there is Mn-centered oxidation in the $S_2 \rightarrow S_3$ transition or ligand oxidation (to a radical), giving either (4/4/4/4)[23,28]
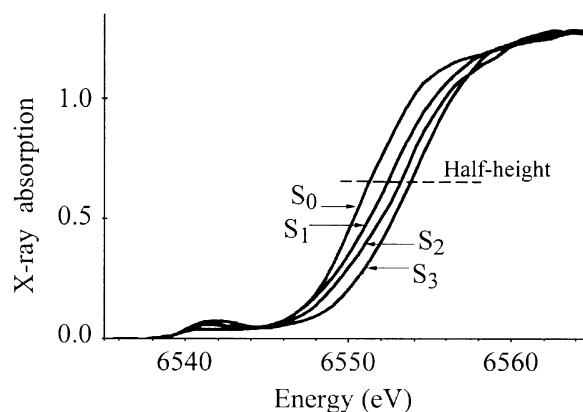
Figure 3 Mn K-edge XANES spectra of the Mn_4 cluster in various S-states.[17]

or (3/4/4/4)L[•24] as the S_3 oxidation state. This result is complicated by the observation that there may be structural rearrangements in the OEC on the $S_2 \rightarrow S_3$ transition[10,29] that may affect the XANES.

The EXAFS spectra of the Mn_4 cluster report on the distance to, and identity of, neighboring atoms in its coordination sphere. An example of the Fourier transform of the EXAFS for the S_1-state is shown in Figure 4.[30] Peak A, a convolution of apparent distances of 1.8 and 1.95–2.15 Å, indicates scattering from bridging or terminal O or N ligands. Peak B is assigned to 2–3 Mn—Mn scatterers at 2.72 Å. These features are diagnostic of di-μ-oxo-bridged manganese complexes, and there is general agreement on these assignments.[10,20,22,25,31–33] Peak C can be fit to contributions from both Mn and Ca at 3.3 Å, a distance characteristic of a mono-μ-oxo bridge between metal centers.[10,20,30,33,34] The dichroism of the 2.7 and 3.3 Å vectors has been investigated in oriented PSII samples. It was found that the 2.7 Å vectors are rather isotropic while the 3.3 Å vector forms an angle of $43 \pm 10°$ with the membrane normal.[35] A Ca—Mn distance of 4.2 Å has also been reported,[22] which is consistent with a mono-μ-oxo or carboxylato bridge between the metals. This distance is similar to that for the Mn—Ca separation in concanavalin A, the only other protein known to contain a Mn—Ca heteronuclear center.[36,37]

Based on the geometric constraints imposed by the EXAFS results, the structures shown in Figure 5 depict some of the possible topologies of the Mn_4 cluster. Coupled with the results from the X-ray crystal structure[4] and EPR[38,39] (discussed in Section 8.20.2.1.2), the three boxed structures are more likely candidates.

8.20.2.1.2 EPR

EPR spectra have been measured for the S_0–S_3-states, including an inhibited state in which the Mn_4 cluster is in the S_2-state and Y_Z is oxidized, denoted $S_2Y_Z^{•}$. EPR is very useful for studying the Mn_4 cluster because it can measure the oxidation states of Mn, the electronic coupling between Mn ions, and the distance from the Mn_4 cluster to other paramagnetic centers.

The multiline form of the S_2-state is the best characterized of the EPR signals arising from the OEC.[38,40–45] The spectrum, shown in Figure 6, arises from a $S = 1/2$ spin state and is 1,900 G wide with 18–20 lines centered at $g = 2$. The spectrum is indicative of an exchange-coupled cluster of mixed-valent Mn,[38,42,44,45] similar to that observed for mixed-valent Mn model complexes (discussed in Section 8.20.3.4). For example, an analogous multiline spectrum was generated by the one-electron reduction of a linear tetrameric $(Mn^{IV})_4$ di-μ-oxo-bridged model complex, which supports the oxidation state assignment (3/4/4/4) for the S_2-state.[46] Simulations of the EPR and electron spin echo-electron nuclear double resonance (ESE-ENDOR) spectra indicate that the S_2 multiline signal originates from a tetranuclear cluster in which the spin is delocalized over all four Mn ions, and not from a pair of isolated Mn_2 dimers nor a Mn monomer-plus-trimer
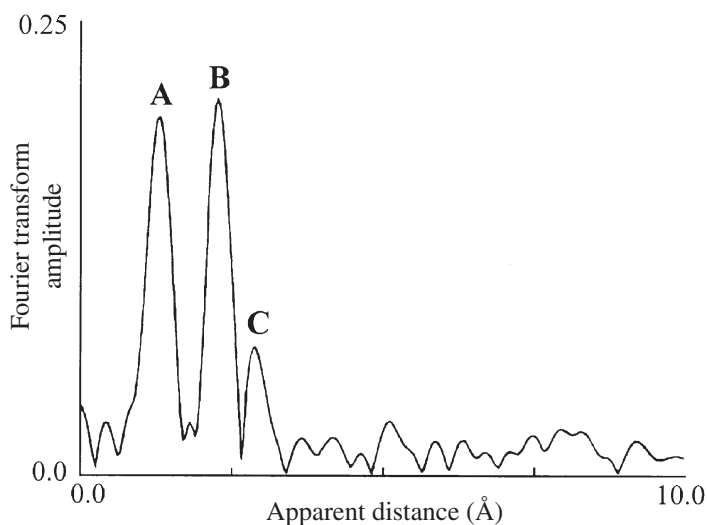
Figure 4 Fourier transform of the EXAFS arising from the XAS of the Mn_4 cluster.[30] Peak A indicates scattering from bridging or terminal O or N ligands at 1.80 and 1.95–2.15 Å. Peak B is assigned to Mn—Mn scattering at 2.72 Å. Peak C can be fit to contributions from both Mn and Ca at 3.3 Å.
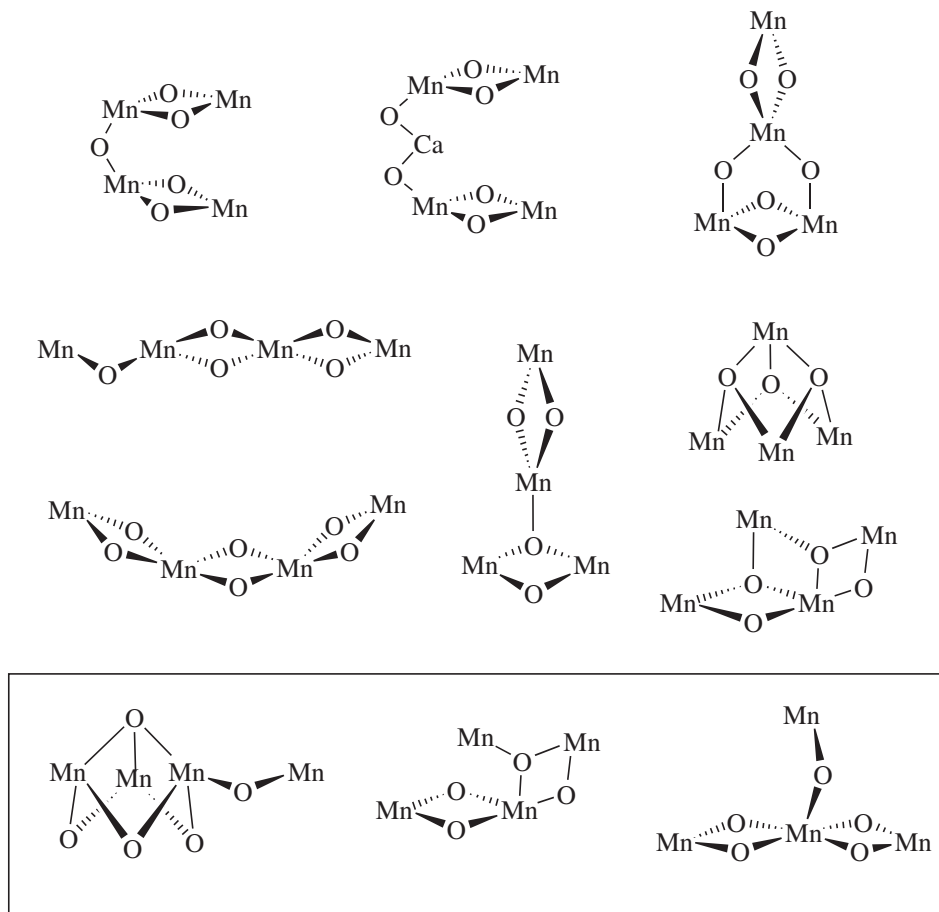
Figure 5 Possible structures of the Mn_4 cluster that satisfy the constraints from XAS.[19] In light of recent results from EPR and X-ray crystallography (discussed in the text), the three boxed structures represent more likely candidates for the actual topology of the Mn_4 cluster.

arrangement.[38,39,42,47,48] In the models of Britt and co-workers[38,48] and Kusunoki and co-workers,[39,45] three of the four Mn are strongly coupled (e.g., via di-μ-oxo bridges) with the fourth Mn more weakly coupled (e.g., via a mono-μ-oxo bridge), as depicted by the boxed structures in Figure 5.

An alternate form of the S_2-state can be prepared by illumination at 140 K that has an $S = 5/2$ ground state and an EPR signal centered at $g = 4.1$.[49–51] This "$g = 4.1$" S_2-state, shown in Figure 6, is relatively narrow, being 340 G wide with no resolved Mn-hyperfine lines (unless NH_3-treated and oriented on Mylar films).[43] The $g = 4.1$ S_2-state is the ground spin state of the Mn_4 cluster with altered couplings between Mn ions relative to those that give rise to $g = 2$ multiline form of the S_2-state.[52] The $g = 4.1$ form of S_2 can be converted from the multiline form (in otherwise untreated samples) by illumination with near-IR (NIR) light;[52,53] in some treated samples, such as chloride-depleted or -substituted PSII, it is the stable form of the S_2-state.[54] It is possible that the two forms of the S_2-state arise from a structural difference in the Mn_4 cluster that alters the magnitude of the weak coupling in the aforementioned models of Britt and co-workers[38,48] and Kusunoki and co-workers.[39,45]

Depletion of Ca^{2+} or Cl^-, or treatment with acetate, inhibits S-state advancement at the $S_2Y_Z^\bullet$-state.[55–61] The spectrum of this state, shown in Figure 7, is best simulated with a point-dipole interspin distance of ~ 8 Å between the Mn_4 cluster and $Y_Z^\bullet$.[62–65] This distance is potentially short enough to allow a Mn-bound water molecule proximal to Y_Z to hydrogen-bond directly to the phenol group.[66]

The S_0-state spectrum is shown in Figure 8. In S_0, the Mn_4 cluster has a ground spin state of $S = 1/2$ and its spectrum consists of 24–26 peaks, centered at $g = 2$, spanning 2,200–2,400 G.[67–69] The broader width of this spectrum compared to the S_2 multiline EPR signal may indicate the presence of a Mn^{II} ion in S_0, in agreement with interpretation of the XANES results. The S_1-state, with a ground spin state $S = 1$, has a signal detectable in parallel-mode EPR, shown in Figure 9.
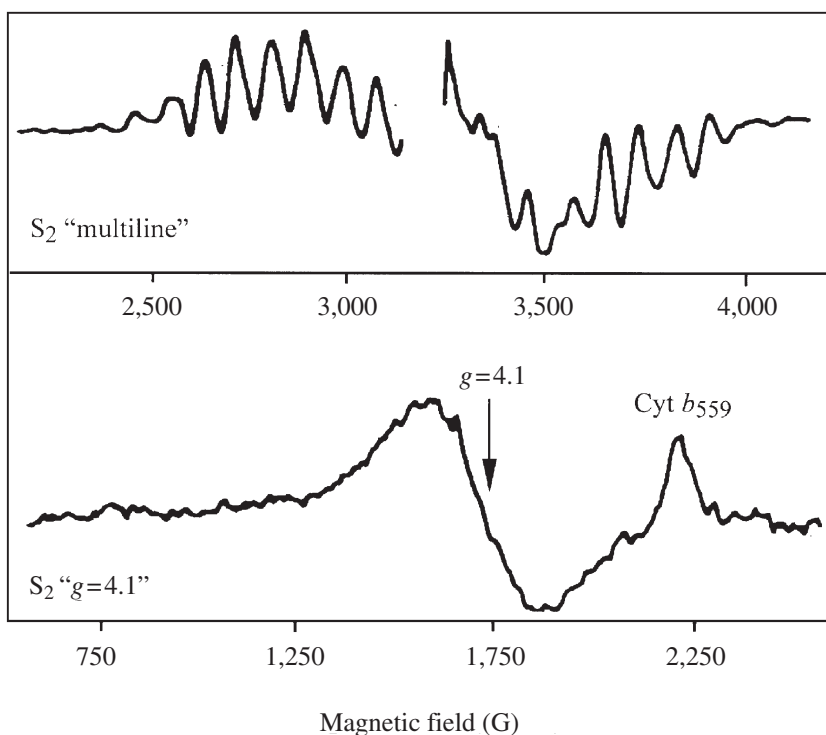
Figure 6 X-band EPR difference (S_2-minus-S_1) spectra of the S_2-state, showing the S_2 multiline (top) and $g = 4.1$ (bottom) signals arising from the $S = 1/2$ and $S = 5/2$ states of the Mn_4 cluster, respectively.[42] The contribution from $Y_D^\bullet$ at 3,200 G was deleted for clarity.
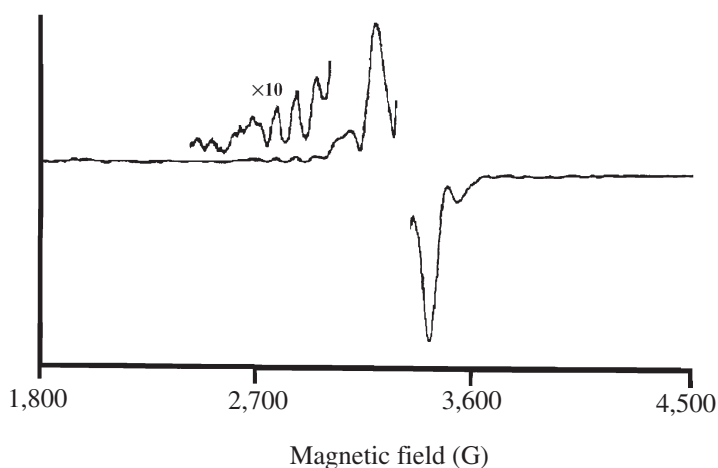

Figure 7 X-band "split" EPR spectrum of the $S_2Y_Z^\bullet$ state from acetate-treated PSII,[156] showing contributions from $Y_Z^\bullet$ and the S_2-state. The contribution from $Y_D^\bullet$ at 3,300 G was deleted for clarity.

It appears as a >18-line spectrum, 600 G wide, centered near $g = 12$.[70,71] Based on the number of lines and the temperature-dependence of the spectrum, it was concluded that all four manganese in the Mn_4 cluster contribute to the integer-spin state.

Finally, EPR signals arising from the S_3-state have been observed.[72,73] These broad signals resonate at $g = 8$ and 12 in parallel mode detection and can be simulated by an integer ($S = 1$) spin state of the Mn_4 cluster.[72] These signals also occur with formation of a split signal[73] at $g = 4$. The amplitudes of these signals decrease in the presence of small alcohols in a manner similar to the $g = 4.1$ S_2-state signal, as shown in Figure 10.[72,73] Because of this, it was suggested that the $g = 4.1$ form of the S_2-state may be the precursor of the low-field S_3 signals. Indeed, the S_3-state shows a response to NIR illumination that results in the formation of a broadened signal at $g = 2$, which may arise from the interaction of a modified form of the S_2-state with a radical.[72]
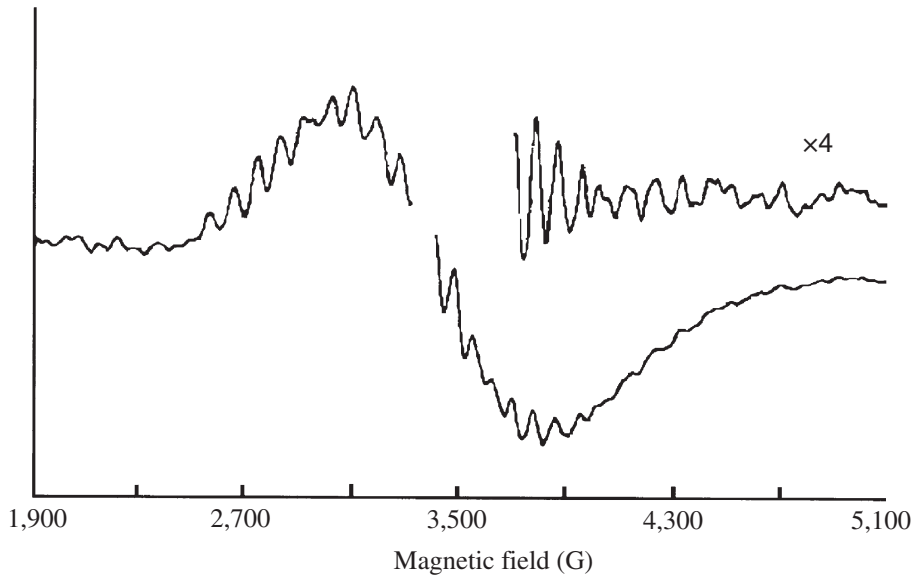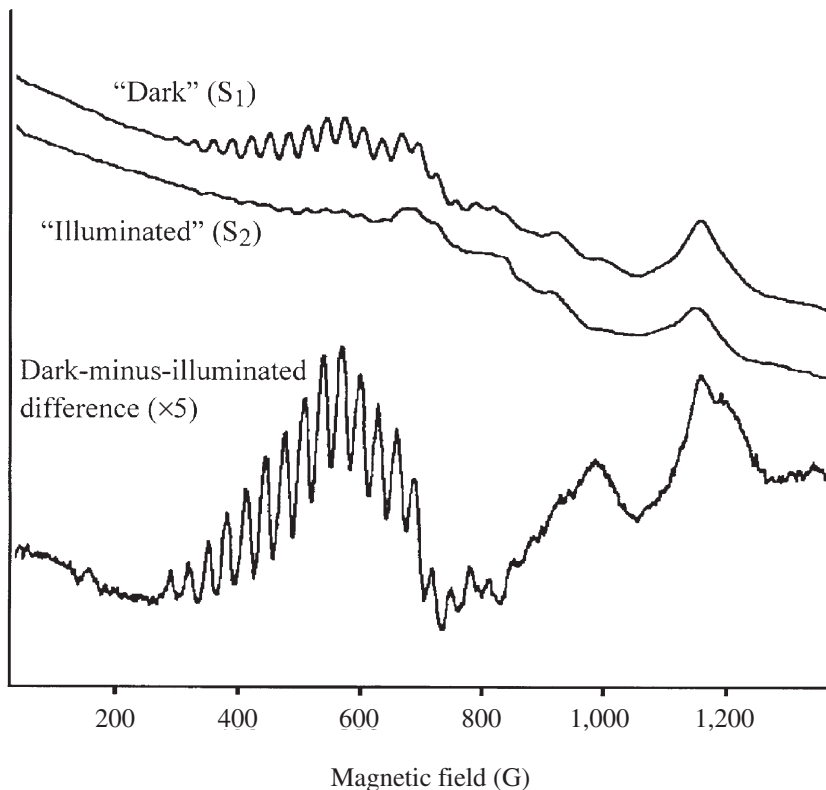
Figure 8 X-band EPR difference spectrum of the S_0-minus-S_1-states, showing the S_0-state in the presence of methanol (1.5% v/v).[67] The contribution from $Y_D^\bullet$ at 3,300 G was deleted for clarity.

8.20.2.1.3 *Electronic absorption spectroscopy*

By far, the dominant contributions to electronic absorption spectra of PSII arise from the pigment cofactors such as chl and carotenoids. Nonetheless, absorption features in the UV and NIR have been attributed to the Mn_4 cluster. The period-four oscillations in the UV associated with the S-state transitions[74–80] are shown in Figure 11 as difference spectra between successive

Figure 9 Parallel mode X-band EPR spectra of the S_1- and S_2-states and the S_1-minus-S_2 difference spectrum, showing the multiline signal from the S_1-state.[70]
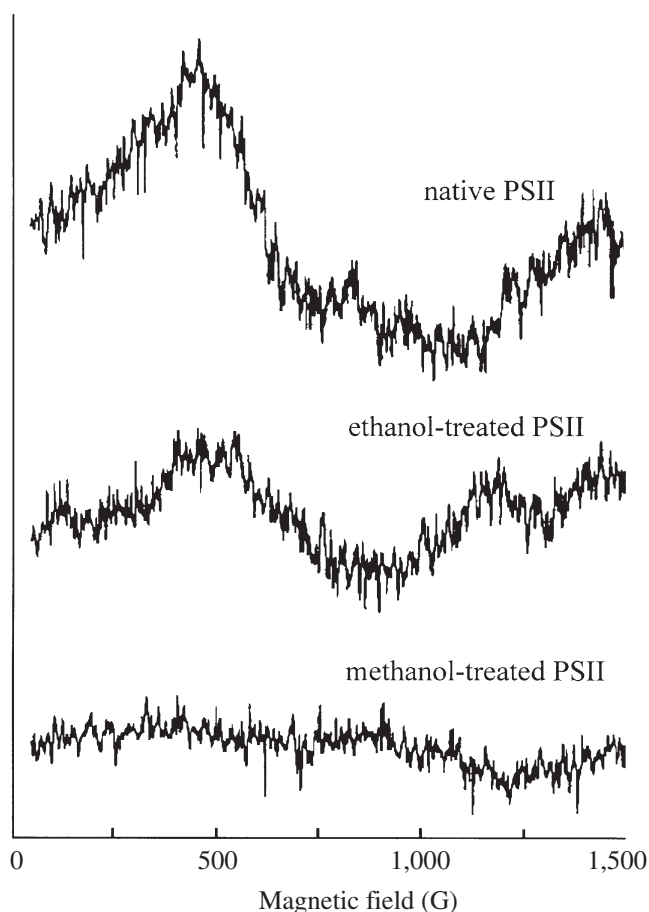
Figure 10 Parallel mode X-band EPR spectra of the S_3-state from native, ethanol-treated, and methanol-treated PSII.[72]

S-states. In particular, the feature near 350 nm with an absorbance amplitude sequence of $(+/+/+/-)$ is assigned to the Mn_4 cluster and not other UV absorbing species, such as the quinones.[75] The electronic nature of the absorption is unclear, although detailed analysis of the absorption spectra of model Mn–oxo complexes[81] suggests that these are metal-centered d–d or ligand-to-metal (oxo-to-Mn) charge transfer bands. This absorption feature is useful for monitoring the kinetics of S-state advancements, as it reports on the rate of reduction of $Y_Z^\bullet$ by the Mn_4 cluster.[82–87]

Another absorption assigned to the Mn_4 cluster, briefly mentioned above, occurs in the NIR, at around 820 nm.[52,53,72,88,89] The absorption of NIR light by the Mn_4 cluster has been shown to convert the multiline form of the S_2-state to the $g = 4.1$ form.[53] The action spectrum for this conversion and a direct NIR absorbance change for the $S_1 \rightarrow S_2$ transition are shown in Figure 12. The mechanism of this transformation is not understood, but the result may be changes in the ligand sphere of the Mn_4 cluster that alter the couplings between the Mn ions, thereby changing the ground spin state from $S = 1/2$ to $S = 5/2$. The nature of the electronic transition is also not clear. An intervalence Mn^{III}—Mn^{IV} charge-transfer or Mn^{III} spin state change has been proposed,[51,88] but it is unclear how an electronic transition could induce a stable change in the overall spin state of the Mn_4 cluster. One possibility is that the transition causes the photodissociation or rearrangement of ligands to the Mn_4 cluster, which then results in a change in the couplings between Mn ions.

8.20.2.1.4 Vibrational spectroscopy

Vibrational spectra are sensitive to qualities of metal complexes, such as changes in the mass of the ligands, that are key to understanding the mechanism of the OEC. For example, the change in mass of an aqua ligand to Mn that deprotonates to form hydroxide can be detected by vibrational
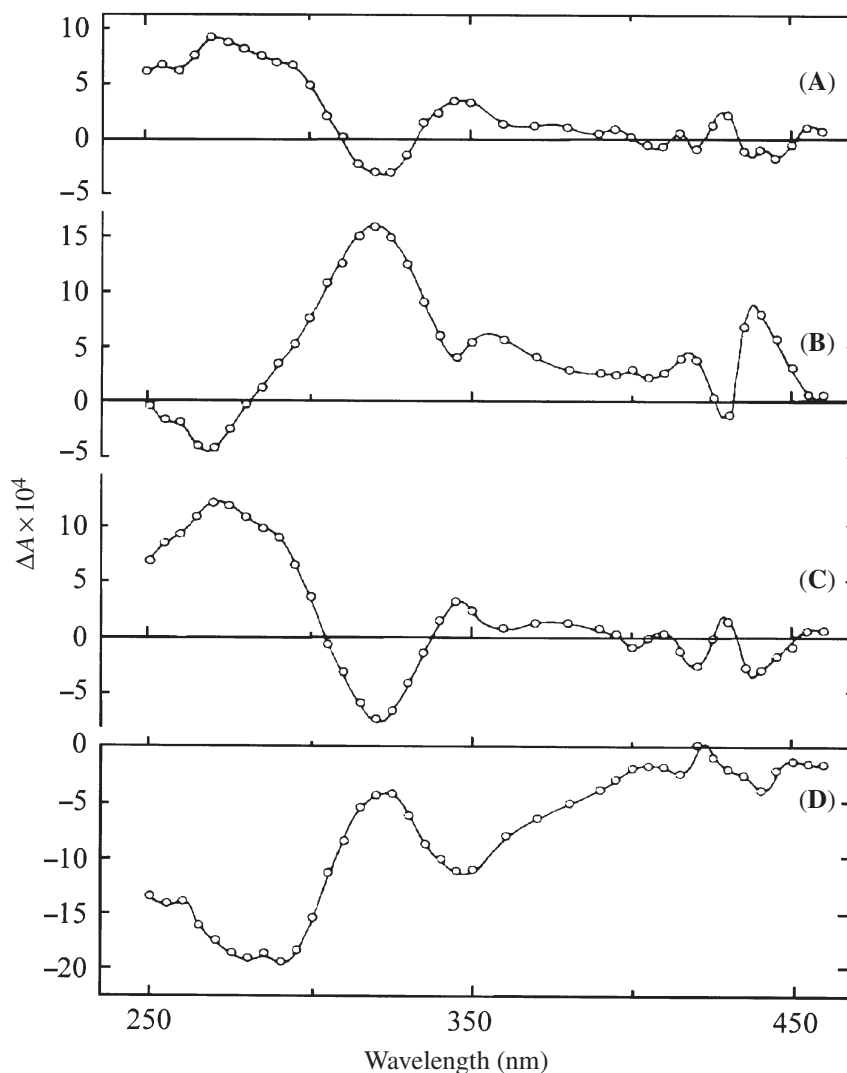
Figure 11 UV–visible absorption spectra associated with the $S_0 \rightarrow S_1$ (A), $S_1 \rightarrow S_2$ (B), $S_2 \rightarrow S_3$ (C), and $S_3 \rightarrow S_0$ (D) transitions of PSII.[75] The oscillations of the spectrum near 350 nm are thought to arise from absorption by the Mn_4 cluster.

spectroscopy. It is in the low-frequency region of the vibrational spectrum, from about 200–600 cm^{-1}, that vibrations involving the metal–ligand bonds of metal clusters are observed.[90] However, unlike high-frequency vibrational modes that are diagnostic of a single chemical moiety, low-frequency vibrations are usually the sum of contributions from the oscillation of several chemical bonds at once (vibrational coupling). Vibrational coupling can complicate the assignment of low-frequency vibrations from metal clusters because of the contributions of multiple oscillators to the observed vibrational modes. Alternatively, the high-frequency region of the IR spectrum reports on the structures of the ligands themselves (e.g., vibrations of carboxylic acid groups) and the amide backbone. High-frequency vibrations are generally localized on the oscillations of a chemical group and so are more easily assigned than low-frequency vibrations. In studies of PSII, difference spectra between successive S-states report on the specific structural changes that occur with each S-state advancement.

Infrared absorption spectroscopy has been extensively applied to studying the Mn_4 cluster.[91–103] The current instrumental limitations of IR absorption spectroscopy prevent great sensitivity in the low-frequency region, allowing spectra to be obtained only to ~350 cm^{-1} despite recent advances.[98] In addition, the overwhelming absorption of IR radiation by H_2O further complicates the acquisition of spectra of PSII. Nonetheless, several features in the 650–350 cm^{-1} region have been observed in S_2-minus-S_1 difference spectra of PSII.[96–99] In particular, a mode at 606 cm^{-1} is thought to arise from a Mn—O—Mn vibration.[97] This mode and others change when D1-Asp170
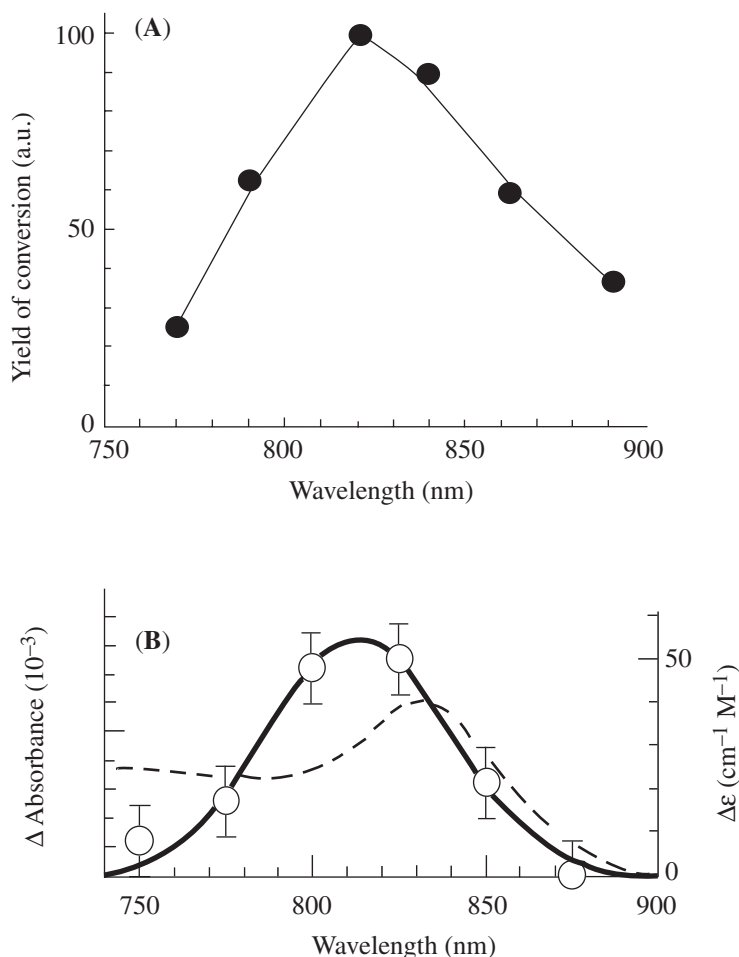
Figure 12 The effects of NIR light on the S_2-state of the Mn_4 cluster. Shown are (A) the action spectrum for the S_2 multiline to $g = 4.1$ conversion[53] and (B) a direct NIR absorbance change for the $S_1 \rightarrow S_2$ transition.[88] The dashed curve is the expected contribution from a chl cation radical in $\sim$1% of the centers.

is mutated to His, which suggests that Asp170 is a ligand to the Mn_4 cluster.[99] Many more IR investigations have focused on the high-frequency region of the spectrum, and have yielded information on protein conformational changes, the vibrations of amino acid groups, and O—H vibrations of substrate water molecules. FTIR spectra of the individual S-states formed by short successive flashes of light reveal dramatic protein conformational changes in the amide I-band and the stretching bands of carboxylato groups from amino acid side chains.[100] These changes showed a four-flash, period two oscillation, indicating that the changes that occur in the $S_1 \rightarrow S_2 \rightarrow S_3$ advances reverse in the $S_3 \rightarrow S_4 \rightarrow S_0$ conversion.[100,101] Contributions to the FTIR spectra from specific amino acids have been identified. A comparison of untreated and Ca^{2+}-depleted PSII S_2-minus-S_1 difference spectra show changes in features attributable to the carboxylato group of Asp or Glu amino acids.[93] FTIR spectra of PSII grown with ^{13}C-labeled tyrosine demonstrated a direct structural coupling between the Mn_4 cluster and a tyrosine residue that is most likely Y_Z.[94] Likewise, in PSII both bands that were globally labeled with ^{15}N and bands that were selectively labeled with ^{15}N-histidine, were observed in S_2-minus-S_1 difference spectra that indicate ligation of a histidine residue to the Mn_4 cluster.[102] By controlling the hydration state of films of PSII core complexes, FTIR spectra in the 3,000–4,000 cm^{-1} region were recorded that allowed contributions from active site water molecules to be observed in an S_2-minus-S_1 difference spectrum.[104]

Resonance Raman spectra of the Mn_4 cluster[89] have been obtained using excitation into the near-IR absorbance[53] at 820 nm. Low-frequency vibrations (300–600 cm^{-1}) were observed that were absent in Mn-depleted PSII samples. These signals were also lost after formation of the S_2-state, presumably because the absorbance feature giving rise to the resonance enhancement was shifted upon oxidation of the Mn_4 cluster. Several of the modes were sensitive to H_2O/D_2O substitution, making them candidates for vibrations involving aqua ligands to Mn.

8.20.2.2 Coordination Environment of the Mn$_4$ Cluster

So far in this chapter, the spectroscopic investigations of the structure of the Mn$_4$ cluster and its environment have been reviewed. Based on the sum of these results, some conclusions may be drawn regarding the structure of the OEC. It contains a tetrameric cluster of high valent Mn, with both strong and weak electronic couplings between the Mn ions. These are bridged by oxo ligands and possibly carboxylic acid groups of amino acids. Ca^{2+} and Cl$^-$ depletion or substitution affect the XAS and EPR spectra of the Mn$_4$ cluster, and so these ions are possibly part of the Mn ligand sphere. Vibrational spectroscopy has revealed the presence of water ligands and coupling between the Mn$_4$ cluster and both Ca^{2+} and Y$_Z$. Finally, Y$_Z$ is close enough to the Mn$_4$ cluster that it may be directly hydrogen-bonded to a terminal water ligand on Mn. Mechanistic implications of this structure will be discussed in Section 8.20.5.

8.20.2.2.1 Amino acid ligands

As mentioned, several amino acids have been identified as integral to the OEC. Based on the aforementioned spectroscopic results, Y$_Z$ is an intimate component of the OEC, and may be part of the secondary ligand sphere of the Mn$_4$ cluster. Both the rates of oxidation and reduction of Y$_Z$ are pH-dependent, with apparent pK_a values of ~8–10 and ~5–7.[105–107] The higher pK_a is assigned to that of Y$_Z$, while the other is assigned to a base that forms a hydrogen-bonded pair with Y$_Z$. The identification of this base as D1-H190 is strongly supported by site-directed mutagenesis studies.[105,108] It was found that in D1-H190 mutants, Y$_Z$ oxidation only occurs at high pH values, at which Y$_Z$ is already deprotonated.[105,106] Furthermore, the rates of P$_A^{\bullet +}$ reduction, Y$_Z$ oxidation, and Y$_Z^\bullet$ reduction in the mutants were all significantly enhanced by the addition of small organic bases, such as imidazole.[108] Together, the pH effects on the oxidation/reduction of Y$_Z$ in wild-type and D1-H190 mutant PSII suggest that H190 and Y$_Z$ form a hydrogen-bonded pair in which H190 is the proton acceptor for Y$_Z$. This implicates H190 in the water oxidation scheme, and thus includes H190 in the coordination environment of the Mn$_4$ cluster.

Site-directed mutagenesis has identified several other amino acids that may be either ligands to the Mn$_4$ cluster or Ca^{2+} or serve as proton acceptors involved in proton release during water oxidation.[109] Most of these amino acids have carboxylic acid side chains, which aid to stabilize high-valent Mn, generally constitute the coordination sphere of Ca^{2+}-binding sites, and can act as proton wires to shuttle protons out of the OEC. Mutations of D1-D59 and D1-D61, which are thought to ligate Ca^{2+}, result in centers that exhibit impaired oxygen-evolution capability.[110,111] Direct ligands to the Mn$_4$ cluster may include any of the following D1 residues: D170,[112,113] H332,[114–116] E333,[114–116] H337,[114–116] D342,[114–116] and A344 (the C-terminus).[117] Of particular interest are those mutations that support O$_2$ evolution or allow the assembly of the Mn$_4$ cluster, even if O$_2$ evolution is impaired. For example, replacement of D170 with amino acids that are Lewis bases yields PSII complexes that can assemble the Mn$_4$ cluster but have greatly reduced O$_2$-evolution rates.[113] Pulsed EPR spectra of PSII both globally ^{15}N-labeled and specifically labeled with ^{15}N-histidine demonstrated that a His residue is a ligand to the Mn$_4$ cluster.[118,119] In particular, D1-H332 is a likely candidate because H332E mutants assemble a Mn$_4$ cluster but evolve no O$_2$.[115] Instead, H332E mutants exhibit altered S$_2$ multiline EPR signals and are inhibited at the S$_2$Y$_Z^\bullet$-state under multiple turnover conditions. These results strongly suggest that D1-H332 ligates Mn and affects proton-coupled electron transfer (PCET) in the high S-states. The H332E mutant may either modulate the reduction potential of the OEC or change proton-coupled steps if, for example, H332 acts as a Lewis base.

8.20.2.2.2 Calcium

Calcium is required for water oxidation.[120–123] Depletion of Ca^{2+} from PSII results in inhibition of the S-state cycle at the S$_2$Y$_Z^\bullet$-state.[55,124] Activity can be restored to Ca^{2+}-depleted PSII by incubating the sample with millimolar concentrations of Ca^{2+} for extended periods of time.[121] Techniques used to characterize the Ca^{2+}-binding site in PSII include: steady-state activity measurements,[121,125] atomic absorption,[126] scintillation counting using ^{45}Ca^{2+},[127] the replacement of Ca^{2+} by metal ion inhibitors,[128–131] equilibrium measurements employing a Ca^{2+}-sensitive electrode,[132] EPR[55,56,124,129–131,133–135] and EXAFS.[22,33,34,136] From these results, there is general

agreement that 1 Ca^{2+}/PSII is required for water oxidation and this Ca^{2+} is tightly bound ($K_D \sim \mu M$) within the OEC.

Investigating the structure of the Ca^{2+} site in the OEC and its relationship with the Mn_4 cluster has proven to be difficult. As mentioned, EXAFS measurements indicate that Ca^{2+} may be quite close to the Mn_4 cluster, with Mn—Ca distances of 3.3 Å[20,136] and 4.2 Å[22] having been reported. The former distance is indicative of a structure with two single O-atom bridges between Mn and Ca, while the latter distance is consistent with a single μ-carboxylato or a halide bridge. Indeed, some FTIR data suggest that Ca^{2+} is coupled to the Mn_4 cluster through a carboxylato bridge.[93] Such a structure might be similar to that of the Mn—Ca heteronuclear site in concanavalin A, in which a μ-carboxylato bridge between Mn^{2+} and Ca^{2+} is provided by Asp10.[36,37]

It has been shown that Ca^{2+} binding is competitive with di- and trivalent metal ions,[121,128,129,131] and metal ion substitution has been employed to characterize the structure and function of Ca^{2+} in PSII. Measurements of the binding affinities of a series of di- and trivalent metal ions that compete for the Ca^{2+} site demonstrated that the Ca^{2+}-binding site is size-selective, preferentially binding metal ions with an ionic radius similar to that of Ca^{2+}.[128] Results of a $^{113}Cd^{2+}$ NMR study of Cd^{2+}-substituted PSII suggest that the Ca^{2+} site is composed of a symmetric array of ligands that may include oxygen and chlorine or nitrogen atoms.[137] Enhanced relaxation of the $^{113}Cd^{2+}$ NMR signal implies that the Ca^{2+} site may be close to the Mn_4 cluster. Of the many metals that compete with Ca^{2+}, only Sr^{2+} functionally replaces Ca^{2+}, while all others inhibit S-state advancement.[121,128,138] EPR studies of Ca^{2+}-depleted, lanthanide-substituted PSII show that the OEC cannot advance beyond the S_1-state[131,134] and that electron transfer from Y_Z to $P_A^{\bullet+}$ is affected.[135] However, illumination of Ca^{2+}-depleted PSII in the absence of competing metals allows the S-state cycle to advance to the $S_2Y_Z^{\bullet}$-state.[55,59,124] These results suggest that Ca^{2+} is intimately involved in the water oxidation cycle, possibly by participating in the organization of a hydrogen-bonding network in the OEC or binding one of the substrate water molecules necessary for O_2 formation.[66,122,128,139]

In the past, Ca^{2+} has usually been implicated in maintaining the structure of the OEC by stabilizing the Mn_4 cluster or organizing the local ligand environment.[122,138,140] However, many multivalent metal ions bind competitively with Ca^{2+} and several of these metals can replace Ca^{2+} in other proteins with no structural perturbations,[141,142] yet in PSII only Sr^{2+} yields a functional active site.[121,138] One might expect that if the role of Ca^{2+} were solely structural then more metal ions with structural properties similar to Ca^{2+}, e.g., Cd^{2+}, would at least partially restore activity, but this is not the case.[128] Lately, proposals have been put forth which progress the role of Ca^{2+} in water oxidation from a purely structural cofactor to being directly involved in tuning the properties of the Mn_4 cluster or binding one of the substrate water molecules.[13,139,143] In this respect, the role of Ca^{2+} is to act as a Lewis acid that tunes the potential of the Mn_4 cluster[143,144] or the reactivity of a substrate water molecule by adjusting its pK_a.[13,139] This would explain why only Sr^{2+} and no other cations functionally replace Ca^{2+}, because only Sr^{2+} has an electronegativity similar to Ca^{2+} and thus properly tunes the reactivity of a bound water molecule.[128]

8.20.2.2.3 Chloride

The nature of the involvement of Cl^- in O_2 evolution and its association with the Mn_4 cluster has been difficult to study. Cl^- is required for optimal O_2 evolution,[123,145–148] although there is evidence that rigorously Cl^--depleted samples retain 30–40% activity.[148,149] Studies of Cl^- binding in PSII isolated from spinach grown on $^{36}Cl^-$ show that one Cl^- binds to PSII with high affinity and is slow to exchange.[149,150] Cl^- is competitive with Br^-, NO_3^-, F^-, small primary amines, and acetate for binding to PSII,[58,145,149] but only Br^- and NO_3^- seem to be functional replacements. As with Ca^{2+}, the evidence that Cl^- is integral to the OEC and may be a ligand to the Mn_4 cluster mainly derives from spectroscopic studies. EXAFS spectra of F^--substituted PSII exhibit small changes in the 2.7 Å vectors assigned to Mn—Mn scattering.[151] Chloride ion depletion affects the magnetic properties of the S_2-state,[54] making the $g = 4.1$ form the stable form of S_2, and blocks the $S_2 \rightarrow S_3$ transition.[152] As in Ca^{2+}-depleted samples, in the absence of $Cl^{-153–155}$ or in acetate-treated samples[156–158] continuous illumination at 250 K produces the $S_2Y_Z^{\bullet}$-state. That depletion of Cl^- has effects on the Mn_4 cluster similar to Ca^{2+} depletion implicates Cl^- as a possible ligand to Mn, and suggests that Cl^- and Ca^{2+} may themselves be structurally coupled in the OEC.

8.20.2.2.4 *H₂O ligands and oxo bridges*

Oxygen ligands, in the form of carboxylato, oxo, and aqua or hydroxo groups, probably occupy most of the coordination sphere of Mn in the Mn_4 cluster. There is a total of 20–24 coordination sites available among the four Mn ions of the Mn_4 cluster, depending on whether they are five- or six-coordinate. Nitrogen ligands probably occupy only one or two of these sites,[115,118,119] and Cl^- may be another ligand, but this still leaves a large number of sites available. High-valent Mn is oxophilic, and so much of the remaining coordination sphere is likely to consist of O-donor ligands.

Carboxylato ligands are most likely contributed by amino acid side chains, as discussed in Section 8.20.2.2.1. The carboxylato group may coordinate as a mono- or bidentate ligand or as a μ-carboxylato bridge. The 2.7 and 3.3 Å distances observed in the EXAFS spectra are characteristic of di-μ-oxo and mono-μ-oxo bridges, respectively, between Mn ions. As shown in Figure 5, based on the EXAFS data there are ~4–5 μ-oxo bridges in the Mn_4 cluster, which would then account for 8–15 of the coordination sites on the Mn ions. Finally, H_2O ligands that are both ancillary ligands and substrate(s) bind to the Mn_4 cluster. Low-frequency resonance Raman spectra of PSII exhibit D_2O-sensitive bands which indicate that there are at least two aqua or hydroxo ligands to Mn.[89] The rates of exchange of the substrate waters have been measured and were found to exhibit a slow and a fast phase.[159] In these experiments, the rate of $H_2^{18}O$ incorporation into the product O_2 as a function of S-state was measured by mass spectrometry. The slow phase rate constants were 8, 0.021, 2.2, and 1.9 s^{-1} for S_0, S_1, S_2, and S_3, respectively, while the fast phase exhibited rates of >100 s^{-1} for S_0, S_1, and S_2 and 36.8 s^{-1} for S_3. These exchange rates are typical for water bound to metal ions, but in the absence of a structure of the OEC it is difficult to make specific assignments as to the binding site of these substrate water molecules.

Ammonia is an inhibitor of water oxidation and a substrate analog for H_2O, making it a useful probe for water in the OEC. Ammonia and other small primary amines have been shown to bind in competition with Cl^-,[145,147] so if Cl^- is a ligand to Mn then NH_3 may bind as an amido ligand in place of Cl^-. A second NH_3-binding site has been identified, which is accessible only to NH_3 and no other amines and which alters the magnetic properties of the S_2-state.[160] Electron spin echo envelope modulation (ESEEM) data on NH_3-treated PSII indicate that ammonia may form a μ-amido bridge between two Mn in place of a μ-oxo bridge.[161,162] Small alcohols also affect the magnetic properties of the Mn_4 cluster in the S_0, S_2, and S_3-states.[68,72,163] Although the issue is still unclear, alcohols may bind to the Mn_4 cluster in place of H_2O ligands.[164]

8.20.3 COORDINATION COMPLEXES AS STRUCTURAL AND FUNCTIONAL MODELS OF THE Mn₄ CLUSTER

To understand better the structure and function of the Mn_4 cluster, a variety of Mn–oxo complexes based on the di-μ-oxo-dimanganese motif have been synthesized. Their structures fall into a number of categories and employ many types of ligands, as discussed in Section 8.20.3.2.

Most models of the Mn_4 cluster are synthesized simply from Mn^{II} in the presence of ligands and oxidized to Mn^{III} or Mn^{IV}, which is required to achieve the acidity of the metal ions necessary to support μ-oxo bridges. A large number of high-potential oxidizing agents can be used, including MnO_4^- (also a source of Mn), Ce^{IV}, HSO_5^-, BrO_3^-, or simply atmospheric O_2. For complexes synthesized in organic solvents, such as CH_3CN, in which the aforementioned oxidants may not be soluble, tetrabutylammonium permanganate is typically used. The ligands employed should be oxidation resistant and sufficiently electron donating that they help stabilize high-valent Mn. Owing to the lability of Mn^{III}, it is commonly the case that a mixture of Mn and a given ligand in solution will yield a variety of Mn-oxo complexes if only subtle changes to the conditions of the synthesis are made; this is true for many of the complexes listed below. Often, a number of Mn–oxo complexes with different structures exist in solution at equilibrium, with the structure of the isolable Mn–oxo complex under thermodynamic control.[165] In some instances, relatively small changes in the synthesis, such as the choice of counterion or solvent,[166,167] result in significant differences in the structure of the Mn–oxo cluster that is isolated. In general, the Mn–oxo complexes that are good models of the Mn_4 cluster are not stable in solution for long periods of time because disproportionation reactions lead to insoluble forms of Mn, such as MnO_2. However, this problem can sometimes be overcome by the addition of an excess of ligand to the solution.[168]

8.20.3.1 Commonly Employed Ligands

As explained, ligands to high-valent Mn must be electron donating, and so most are nitrogen- or oxygen-based aliphatic, cyclic, or polypyridyl compounds that tolerate the oxidizing conditions necessary to assemble high-valent Mn–oxo complexes. Examples of commonly used bidentate, tridentate, tetradentate, and polydentate ligands are shown in Figures 13, 14, and 15, respectively. Of the bidentate ligands in Figure 13, bpy (**1**) has proven to be an extraordinarily fruitful ligand for the preparation of a number of Mn–oxo complexes.[167–177] The tridentate ligands (**7**), (**8**), and (**9**) shown in Figure 14 are of particular interest because when coordinated to a manganese ion having two μ-oxo bridges, an open coordination site is left available that can be occupied by ligands relevant to the biological Mn_4 cluster, such as H_2O and Cl^-.[178–180] Of the polydentate ligands shown in Figure 15, there is evidence that the Schiff-base salen ligand (**16**) is sufficiently electron donating to transiently form a $Mn^V{=}O$ species by the two-electron oxidation of the $[(salen)Mn^{III}]^+$ complex.[181]

### 8.20.3.2 Structures of Oxo-bridged Manganese Complexes

There are two goals in constructing bioinorganic models of any metalloenzyme active site: to reproduce the structure of the site, so that models are available for comparing experimental results from the protein to a well-characterized system, and to reproduce the function of the active site, so that the mechanism of the protein may be deduced and new catalysts developed. It is generally much simpler to build structural models than functional ones, because it is difficult to mimic the dynamic protein environment sufficiently well with simple ligands to achieve functionality. While there are many structural models of the Mn_4 cluster, there are very few that are capable of functionally reproducing the photo-induced electron transfer or water oxidation reactions of the OEC. While there are a large number of Mn–oxo complexes of varying oxidation state and nuclearity, we will focus on those that are relevant to the structure of the Mn_4 cluster.

Based on the EXAFS results, the Mn_4 cluster is composed of mono- and di-μ-oxo-dimanganese units with separations of 3.3 and 2.7 Å, respectively.[10,17,22] It is this structural motif that should be reproduced in Mn–oxo complexes that are models of the Mn_4 cluster. The most basic unit that mimics the structure of the Mn_4 cluster is, therefore, a mono- or di-μ-oxo-bridged Mn dimer, examples of which are shown in Figure 16. As can be seen from the list of complexes in Table 1, there have been many such Mn–oxo dimers synthesized. Invariably, complexes with the basic structures of (**22**), (**23**), and (**25**) in Figure 16 have Mn—Mn separations of 2.6–2.7 Å, independent of whether the oxidation states of the Mn are (3/4) or (4/4), which means that the di-μ-oxo-bridge and not the metal oxidation state determines the intermanganese distance. Alternatively, the mono-μ-oxo-bridged structures (**24**) and (**27**) have Mn—Mn separations of 3.1–3.3 Å. Mono-μ-oxo bridges are found in dinuclear complexes of Mn^{III}, whereas oxidation to the (3/4) or (4/4) states usually requires the formation of a di-μ-oxo bridge to stabilize the increased oxidation state
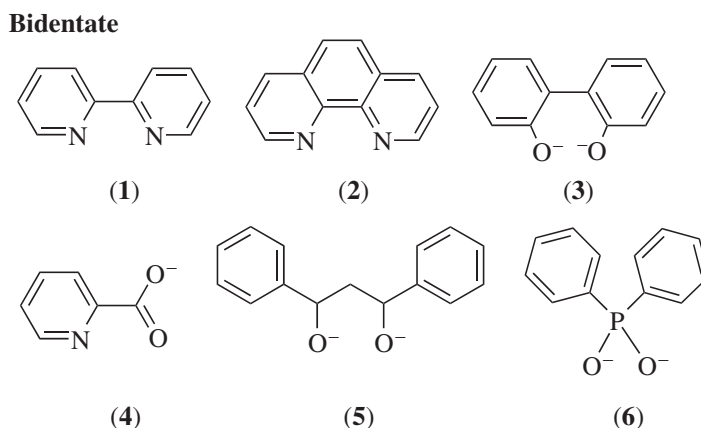
Bidentate

Figure 13 Bidentate ligands commonly used to synthesize Mn–oxo complexes: (**1**) 2,2′-bipyridine (bpy); (**2**) 1,10-phenanthroline (phen); (**3**) 2,2′-biphenolate (biphe); (**4**) picolinate (pic); (**5**) dibenzoylmethane (dbm); (**6**) diphenylphosphonate (dpp).

Tridentate
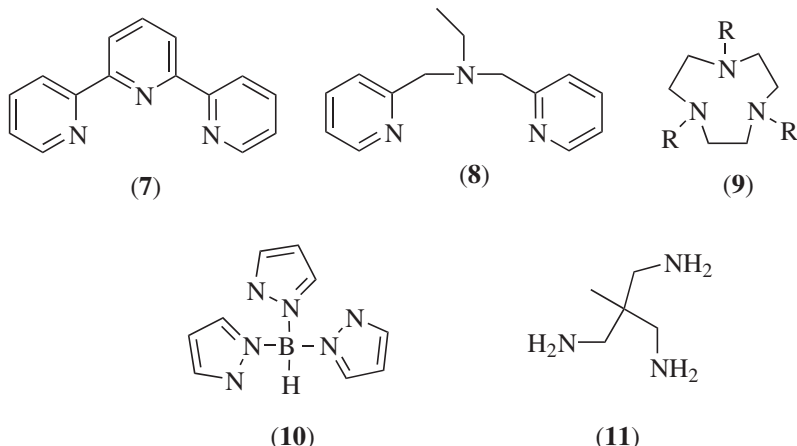
Figure 14 Tridentate ligands commonly used to synthesize Mn–oxo complexes: (**7**) 2,2′:6,2″-terpyridine (terpy); (**8**) *N,N-bis*(2-pyridylmethyl)ethylamine (bpea); (**9**) R = H, 1,4,7-triaza*cyclo*nonane (tacn); R = methyl, 1,4,7-trimethyl-1,4,7-triaza*cyclo*nonane (tmtacn); (**10**) hydro*tris*(pyrazol-1-yl)borate (HB(pz)₃); (**11**) 1,1,1-*tris*-(aminomethyl)ethane (tame).

of the metals. The mixed-valence complexes typically have trapped valences, evident by the observation of the Jahn–Teller axis of the Mn^{III} ion in the crystal structures of the complexes and also by the appearance of their EPR spectra, which are consistent with a valence-trapped system. In many complexes with available coordination sites, such as (**23**) and (**24**), acetato ligands fulfill the bridging coordination.

Trimeric Mn–oxo complexes are shown in Figure 17. While the basic Mn-acetate structure (**30**) is not a good model for the Mn₄ cluster, it has been very successfully utilized as a starting point to build more complex Mn–oxo structures.[182] The trimeric complexes (**28**) and (**29**) are based on a di-μ-oxo-bridged Mn motif, with the third Mn bridged to the others via mono-μ-oxo bridges. These structures are interesting because they contain both the short 2.7 Å distance and long 3.3 Å distance between Mn ions, and the H₂O ligands are bound to high-valent Mn^{IV} in the absence of acetato bridges. A notable difference between the basic structure of (**28**) *vs.* (**29**) is that in structure (**28**), the angle defined by the basal Mn and apical Mn through the mono-μ-oxo bridge is 180°,[165,183,184] but in (**29**) the angle is dramatically reduced to only 153°.[185] This causes a change in the *J* couplings between the apical and basal Mn from *J* = −50 cm⁻¹ in (**28**) to only −11 cm⁻¹ in (**29**) because the orbital overlap between the apical Mn and the base is reduced.[185]

Of greatest relevance to the structure of the Mn₄ cluster are the tetrameric complexes shown in Figure 18. These take the form of linear (**31**), adamantane (**32**), dimer-of-dimer (**33**), butterfly (**34**), cubane (**35**, **37**, **38**), and ladder (**36**) structures. However, while the topology of the ladder structure is interesting, there are no oxo bridges between Mn and so the couplings between Mn are less relevant to the Mn₄ cluster. The di-μ-oxo-bridged linear complex (**31**) contains all Mn^{IV},[186] but can be reduced in frozen solution by gamma-irradiation of the solvent to the (3/4/4/4) oxidation state. The EPR spectrum of this species closely resembles the S₂ multiline and so supports an oxidation state assignment of (3/4/4/4) for the S₂-state.[46] The adamantane complex (**32**) lacks di-μ-oxo bridges and so is not a good model for the topology of the Mn₄ cluster, but changes observed in the magnetic properties upon protonation of the oxo bridges may be relevant to studies of the OEC.[187] The dimer-of-dimers structure (**33**) was once a favored model for the Mn₄ cluster based on the EXAFS results,[30] but more recent EPR[38,39] results suggest that (**33**) is not a good match for the Mn₄ cluster. The butterfly core (**34**) is formed by a pair of "body" Mn connected by μ₃-oxo bridges that coordinate to two "wing" Mn. These complexes exhibit distances between Mn ions of 2.7 and 3.3 Å and are capable of coordinating a variety of physiologically relevant ligands. However, the oxidation states of the Mn ions do not exceed Mn^{III} in butterfly clusters and so are too low in comparison to the Mn₄ cluster. The distorted cubane clusters (**35**) and (**37**) are of interest spectroscopically because of the great number of substitutions that can be made in the corner of the cube.[19] The cubane cluster (**38**) has an all-oxygen coordination environment around each Mn ion. A mass change of (**32**) detected by mass spectrometry following illumination of (**38**) with UV radiation was interpreted to mean that O₂ was liberated from bridging μ-oxos, giving a butterfly structure.[188]

Tetradentate and Polydentate

(**12**)　　　　(**13**)　　　　(**14**)

(**15**)　　　　(**16**)

(**17**)

(**18**)　　　　(**19**)

(**20**)　　　　(**21**)
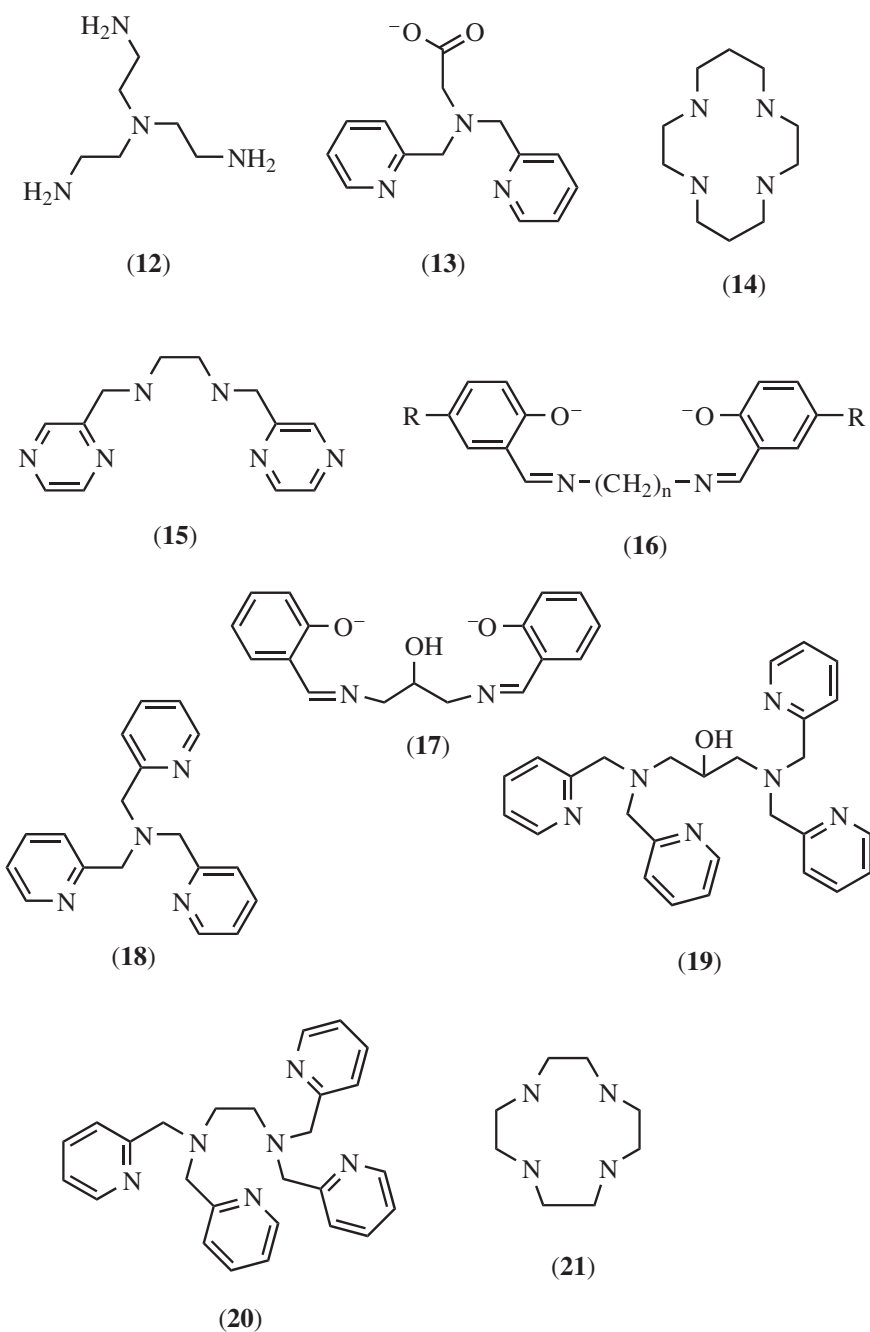
Figure 15 Tetradentate and polydentate ligands commonly used to synthesize Mn–oxo complexes: (**12**) *tris*(2-aminoethyl)amine (tren); (**13**) *N,N-bis*(2-pyridylmethyl)glycine (N$_3$O-py); (**14**) 1,4,8,11-tetraaza*cyclo*-tetradecane (cyclam); (**15**) *N,N′-bis*(pyrazinylmethyl)-1,2-ethanediamine (*bis*pyzen); (**16**) $n = 2$, R = H, *N,N′*-disalicylidene-1,2-ethylenediamine (salen); n = 2, R = butyl, *N,N′-bis*(5-t-butylsalicylidene)ethylenediamine (Bu-salen); n = 3, R = H, *N,N′-bis*(salicylidene)-1,3-propanediamine (salpn); n = 3, R = butyl, *N,N′-bis* (5-t-butylsalicylidene)propanediamine (Bu-salpn); (**17**) *N,N′*-disalicylidene-2-hydroxy-1,3-propanediamine (2-OHsalpn); (**18**) *tris*(2-pyridylmethyl)amine (tmpa); (**19**) *N,N,N′,N′*-tetrakis(2-pyridylmethyl)-2-hydroxy-1,3-propanediamine (tphpn); (**20**) *N,N,N′,N′*-tetrakis(2-pyridylmethyl)ethylenediamine (tpen); (**21**) 1,4,7,10-tetraaza*cyclo*dodecane (cyclen).

Dinuclear

(22)

(23)

(24)

(25)

(26)

(27)
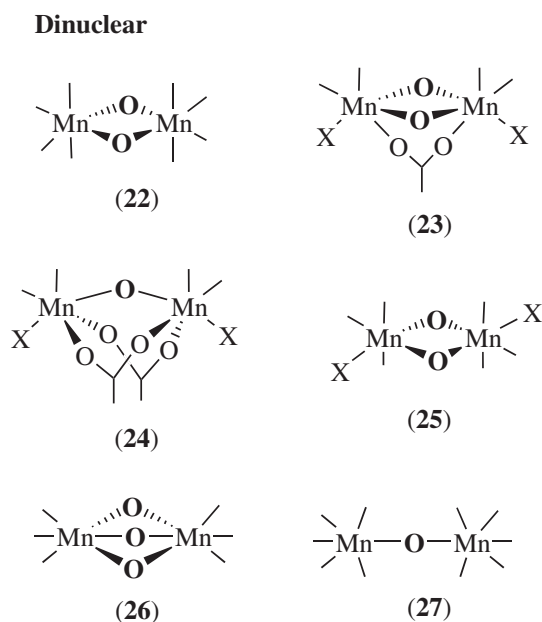
Figure 16 Examples of core structures of dinuclear manganese complexes. Bridging oxo ligands are in bold. Refer to Table 1 for details.

8.20.3.3 Models with Physiologically Relevant Ligands

Mn–oxo complexes which coordinate ligands that are also thought to bind to the Mn_4 cluster, such as H_2O, acetate, Cl^-, F^-, and Br^-, are of particular interest as structural models. Table 1 lists along with the basic structural types of Mn–oxo complexes the physiologically relevant ligands found to bind to them.

8.20.3.4 Use of Coordination Complexes to Characterize the Oxygen-evolving Complex

The characterization of model Mn–oxo complexes has been of great importance in interpreting results from the Mn_4 cluster. In this section, we will focus on spectroscopic investigations of structural models of the Mn_4 cluster and their application to results from PSII.

8.20.3.4.1 X-ray absorption spectroscopy

The study of Mn–oxo complexes relevant to the Mn_4 cluster by XAS gives information about the typical edge energies for various oxidation states of Mn[17] and also the average distance between Mn in Mn–oxo complexes of various topologies.[19,189,190] It has been observed in Mn–oxo complexes that, in the absence of any structural rearrangement, the K-edge energy increases by 2–4 eV per unit formal charge increase.[190] Because quantum chemical calculations have shown that the Mulliken charges of Mn ions do not correlate with formal oxidation state[191] and changes in metal–ligand bond lengths will affect the electron density on a given Mn, a correlation between the formal oxidation state of a Mn ion and the magnitude of the XAS edge shift is not straightforward. However, a bond valence sum approach, which predicts the average oxidation state of metals in a complex according to their metal–ligand bond lengths and empirically determined parameters, has correctly predicted oxidation states in a variety of well-characterized model complexes and metalloenzymes.[192] Application of this method to PSII predicts an average oxidation state of (3/3/4/4) for the S_1-state. In general, in the absence of structural effects, oxidation of the Mn_4 cluster should increase the edge energy by (3 eV/4 Mn) = 0.75 eV. While edge shifts anywhere from 0.6 eV to 2.3 eV are measured for the low S-state transitions,

Table 1 Mn–oxo complexes shown in Figures 16–18.

Complex	Ligands relevant to the OEC	Ancillary ligands[a]	References
Dinuclear			
(**22**)	μ-oxo		203,238–253
		bpy	168,176,254
		phen	168,255,256
		pic	257
		tren	206
		salpn	258–260
		*bis*picen	261–263
(**23**)	μ-oxo, μ-acetato, X = H$_2$O or Cl$^-$		264,265
		bpy	170,172,266
		bpea	180
		tpen	267
		tacn	268
(**24**)	μ-oxo, μ-acetato, X = H$_2$O or Cl$^-$		
		bpy	171,173
		phen	269
(**25**)[b]	μ-oxo, X = H$_2$O, F$^-$, Cl$^-$		
		terpy	178,179
		bpea	180
(**26**)	μ-oxo	tacn	270,271
(**27**)	μ-oxo, μ-hydroxo, μ-acetato		272–274
		5-NO$_2$saldien	275
		*bis*picen	276
		tacn	277
Trinuclear			
(**28**)	μ-oxo, X = H$_2$O or Cl$^-$		
		bpy	165,184
		phen	183
(**29**)	μ-oxo, X = OH$^-$, Cl$^-$, F$^-$	bpea	185
(**30**)	μ-oxo, μ-acetato, H$_2$O		283
Tetranuclear	(**31**)[c]	μ-oxo	bpy	46,174,175,186
	(**32**)	μ-oxo		
		tame	187
		bpea	203
		tacn	198,284
	(**33**)	μ-oxo	tphpn	285,286
	(**34**)	μ$_3$-oxo, carboxylato, Cl$^-$		282–286
		bpy	169,177,287–289
		phen	269,290
		pic	287,291,292
		dbm	293,294
	(**35**)	μ$_3$-oxo, Cl$^-$		295–297
		dbm	298
	(**36**)	acetato	hpdm	299
	(**37**)	μ$_3$-oxo, X = OAc$^-$, OMe$^-$, OH$^-$, N$_3^-$, F$^-$, Cl$^-$, Br$^-$	dbm	285,293,298,300–303
	(**38**)[d]	μ$_3$-oxo	dpp	188,304

[a] Only the more commonly used ligands, such as those depicted in Figures 13–15, are listed explicitly, while less frequently employed ligands are not.   [b] When terpy is used as a ligand and X = H$_2$O, the complex catalytically evolves O$_2$ by water oxidation using O-atom transfer reagents as primary oxidants.[178]   [c] EPR spectrum of one-electron reduced form of the linear tetramer with bpy ligands closely resembles that of the S$_2$ multiline spectrum of the Mn$_4$ cluster.[46]   [d] Mass change of 32 detected by mass spectrometry following illumination with UV radiation interpreted as O$_2$ liberation from bridging μ-oxos.[188]

Trinuclear

(28)   (29)

(30)
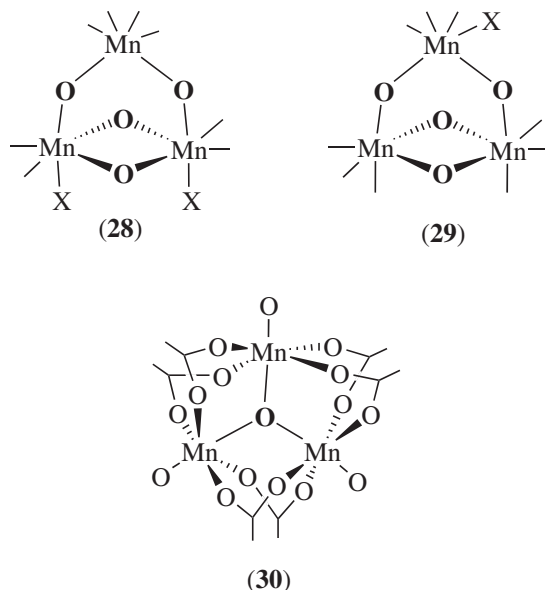
Figure 17 Examples of core structures of trinuclear manganese complexes. Bridging oxo ligands are in bold. Refer to Table 1 for details.

depending on the method of data analysis,[10,23–28] there is controversy regarding the magnitude of the shift in the $S_2 \rightarrow S_3$ transition, which calls into question whether there is Mn-centered[23,28] or ligand oxidation[24] in this step.

EXAFS studies of Mn–oxo compounds find that the Mn—Mn distance in di-μ-oxo-bridged dimers is always 2.65–2.75 Å, provided the oxo bridges are not protonated, while the Mn—O distance is found to be 1.8–1.9 Å.[22,193,194] The EXAFS spectra of the S_1-state indicate a shell of scatterers at 2.7 Å that is best modeled as originating from 2–3 pairs of Mn.[10,20,22,25,31–33] Mono-μ-oxo-bridged Mn dimers have longer Mn separations of 3.3 Å. The peak observed at 3.3 Å in the EXAFS of the S_1-state of the OEC can be fit to a contribution from Mn—Mn scattering, and so it is thought that there is one pair of Mn in the Mn_4 cluster coupled by a mono-μ-oxo bridge.[10,20,22,25,31–33]

8.20.3.4.2 Magnetic properties

Knowledge of the electronic exchange coupling in μ-oxo-bridged Mn complexes is important when trying to understand and model the spectra that arise from the Mn_4 cluster. The magnitude of the exchange coupling, J, can be calculated from the temperature dependence of the magnetic susceptibility. It has been found that superexchange coupling is more strongly mediated through di-μ-oxo bridges than in mono-μ-oxo bridges, and that antiferromagnetic coupling is more prevalent than ferromagnetic coupling in di-μ-oxo-dimanganese complexes.[195] Di-μ-oxo bridges typically give values of $|J|$ of 100–200 cm^{-1}, while mono-μ-oxo bridges give $|J|$ values of 3–10 cm^{-1}. In addition, direct exchange between the Mn centers may occur through the d_{xy} orbitals.[196] In di-μ-oxo dimers, a plot of the magnitude of $J/\cos \theta$, where θ is the angle between the two O—Mn—O planes (and hence the angle between the d_{xy} orbitals on the Mn ions), vs. $\exp(-r)$, where r is the Mn—Mn separation, shows a linear correlation.[195] This observation that J increases as the Mn—Mn separation decreases supports the idea that direct exchange is significant in di-μ-oxo-dimanganese complexes. Values of J for some representative dimanganese complexes are listed in Table 2.

The EPR spectra of dimanganese complexes can be understood in terms of a single J. However, in the case of a tetramer of Mn ions, there are six values of J to consider, and, depending on the symmetry of the complex, they may range from being all equivalent to completely inequivalent.

Tetranuclear
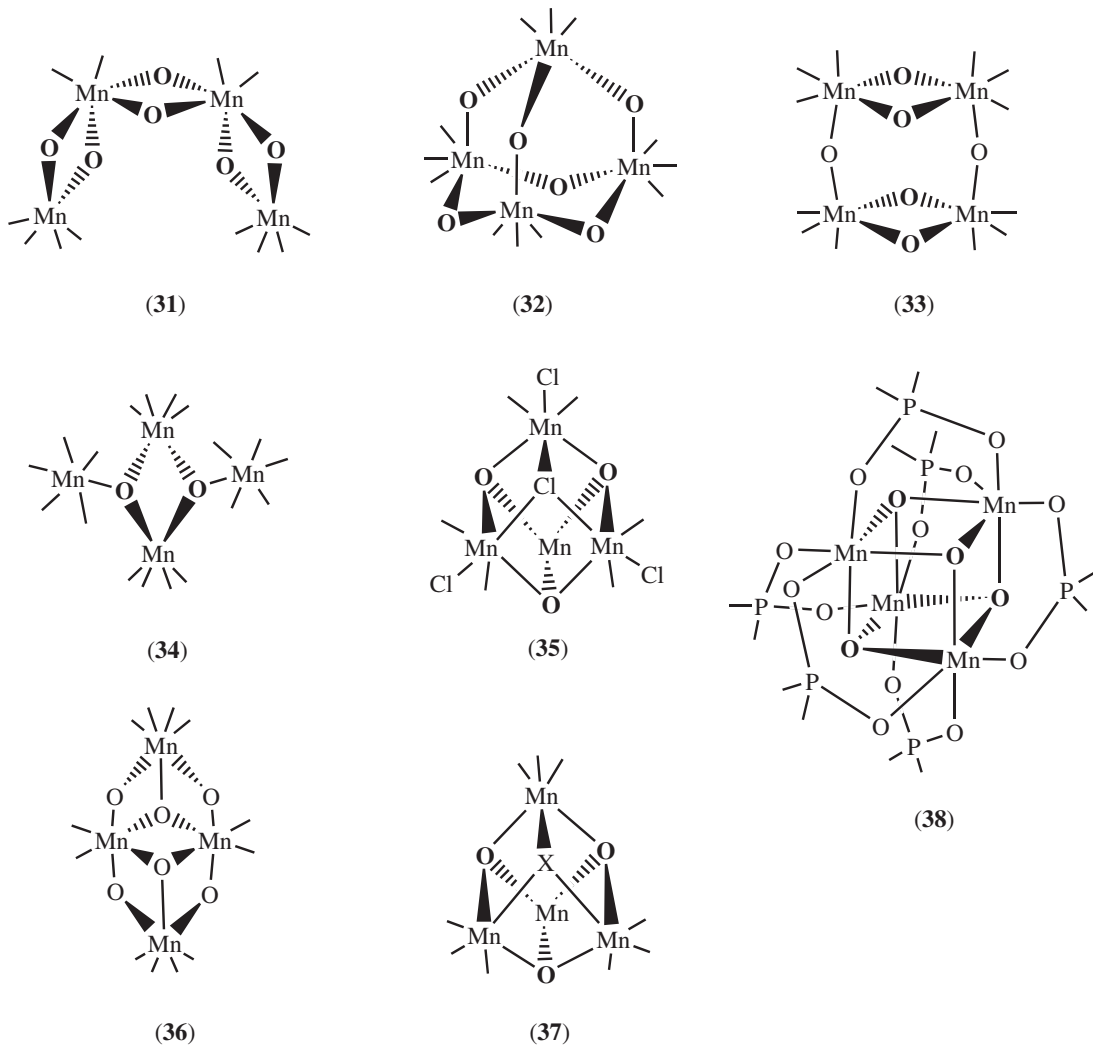
Figure 18 Examples of core structures of tetranuclear manganese complexes. Bridging oxo ligands are in bold. Refer to Table 1 for details.

The resultant overall spin state of the complex will depend on the magnitude and sign of the values of J. The couplings may result in spin frustration, a condition where Mn ions in a highly symmetric environment that are coupled either ferromagnetically or antiferromagnetically prevent a third coupled Mn ion from pairing with the others in the same manner; the spin of the third Mn is frustrated.

A comparison of the magnetic properties measured in tetrameric manganese complexes to those obtained from EPR studies of PSII gives insight into the structure of the Mn_4 cluster. The magnetic properties of the S_2-state of the Mn_4 cluster are discussed in the next section. It has been found that all butterfly complexes have weak antiferromagnetic couplings and their magnetic properties can be described by two J values, one for the coupling between the two "body" Mn ions and another for the coupling between the "body" Mn ions and the "wings".[169] In the cubane complex $[Mn_4(O)_3Cl_4(O_2CCH_3)_3(py)_3]$, two exchange couplings exist; one for the interactions between the three Mn^{III}—Mn^{IV} units and a second to describe the three Mn^{III}—Mn^{III} interactions.[197] The Mn^{III}—Mn^{IV} couplings are antiferromagnetic while the Mn^{III}—Mn^{III} couplings are ferromagnetic. In the case of the adamantane complexes $[Mn_4O_6L_4]^{4+}$ (L = tacn or tame), there are two weak antiferromagnetic exchange couplings between the Mn ions; the high symmetry of the complexes results in spin frustration.[187,198] In the linear complex $[Mn_4O_6(bpy)_4]^{4+}$, in which all the Mn^{IV} ions are antiferromagnetically coupled to give an $S = 0$ ground spin state, there are two equivalent couplings $J_{12} = J_{34}$ for the outer pairs of Mn ions, and

Table 2 Values of J, the Mn—Mn separation, and the dihedral O—Mn—O angle in dinuclear manganese complexes.

| Complex	J (cm^{-1})[a]	Mn—Mn (Å)	O—Mn—O dihedral angle (°)	References
$[Mn_2O_2(tmpa)_2]^{3+}$	−159	2.643	1.10	252
$[Mn_2O_2(tren)_2]^{3+}$	−146	2.679	0.80	206
$[Mn_2O_2(phen)_4]^{3+}$	−144	2.748	0.60	256
$[Mn_2O_2(bispicen)_2]^{3+}$	−140	2.659	0.00	245
$[Mn_2O_2(phen)_4]^{4+}$	−134	2.700	1.70	256
$[Mn_2O_2(bispicen)_2]^{4+}$	−125	2.672	0.00	245
$[Mn_2O_2(pic)_4]$	−87	2.747	0.00	257
$[Mn_2O_2(6\text{-}Me_2bispicen)_2]^{2+}$	−86	2.676	0.90	245
$[Mn_2O_2(bpy)_2(\mu\text{-}HPO_4)$ $(H_2PO_4)_2]^{3+}$	−39.5	2.702	11.60	249
$[Mn_2O(O_2CCH_3)_2(bpy)_2$ $(H_2O)_2]^{3+}$	−3.4	3.132		171
$[Mn_2O(O_2CCH_3)_2(bpy)_2$ $(N_3)_2]$	3.4	3.153		182
$[Mn_2O(O_2CCH_3)_2$ $(tmtacn)_2]^{2+}$	9.0	3.084		271

[a] For $H_{ex} = -2JS_1S_2$.

a second exchange coupling J_{23} for the inner pair. Reduction of this complex by one electron gives an $S = 1/2$ ground spin state best described by three antiferromagnetic exchange couplings for each of the nearest-neighbor interactions.[46] The X-band EPR spectrum of this complex is best simulated with the Mn[III] ion in a terminal position and is a close match to the spectrum of the S_2 multiline of the Mn_4 cluster.

8.20.3.4.3   EPR

In di-μ-oxo-bridged Mn complexes, the electron spins of the Mn ions are antiferromagnetically coupled via direct exchange or superexchange through the bridging oxo ligands. Therefore, typically only mixed-valence complexes with an odd number of spins are observed by conventional X-band EPR. For complexes with a $[Mn^{III}(O)_2Mn^{IV}]^{3+}$ core, a 16-line EPR spectrum centered at $g = 2$ is observed, as shown in Figure 19. The splittings arise from the hyperfine interaction with the Mn nuclear spin, which is $I = 5/2$. If the electron spin was delocalized over both Mn ions, then the hyperfine interactions would give a simple 11-line spectrum (number of lines $= 2nI + 1$, where $n = 2$). Instead, the hyperfine interactions are inequivalent, resulting in 36 hyperfine lines that overlap to give the observed 16-line spectrum. This result indicates that the spin is localized in a trapped-valence system. Occasionally, complexes with an even number of spins give rise to EPR spectra observable by conventional X-band EPR. In these cases, the zero-field splittings are small, on the order of the applied microwave quantum (~ 0.3 cm^{-1} at X-band). Such is the case for the complex $[Mn^{IV}(dtbsalpn)]_2DCBI^+$ ($H_2dtbsalpn = 1,3$-*bis*((3,5-di-*tert*-butyl-salicylidene)amino)propane, $H_3DCBI = 4,5$-dicarboxyimidazole).[199] This complex has an $S = 0$ ground state and $S = 1$, 2, and 3 excited states, where the ground state is separated from the triplet excited state by a zero-field splitting of only 0.9 cm^{-1}. Thus, at 5.5 K, transitions from the ground state to the triplet state give a spectrum observable by conventional EPR, and at higher temperatures more complicated features are seen as the higher spin states are occupied.

The S_2 multiline form of the Mn_4 cluster arises from an $S = 1/2$ ground spin state and is 1,900 G wide with 18−20 lines centered at $g = 2$. The spectrum is indicative of an exchange-coupled cluster of mixed-valent Mn. Few magnetic susceptibility measurements have been done on the Mn_4 cluster, so all information on its magnetic properties has been obtained through various continuous-wave (c.w.) and pulsed EPR techniques. Simulations of the spectra collected from an assortment of differently treated PSII samples yield calculated exchange and hyperfine coupling constants, initially based on values measured in model complexes, which can then be used to deduce possible structures for the Mn_4 cluster. Several groups have attempted to simulate the S_2 multiline spectrum. The model of Zheng and Dismukes is based on simulations of the
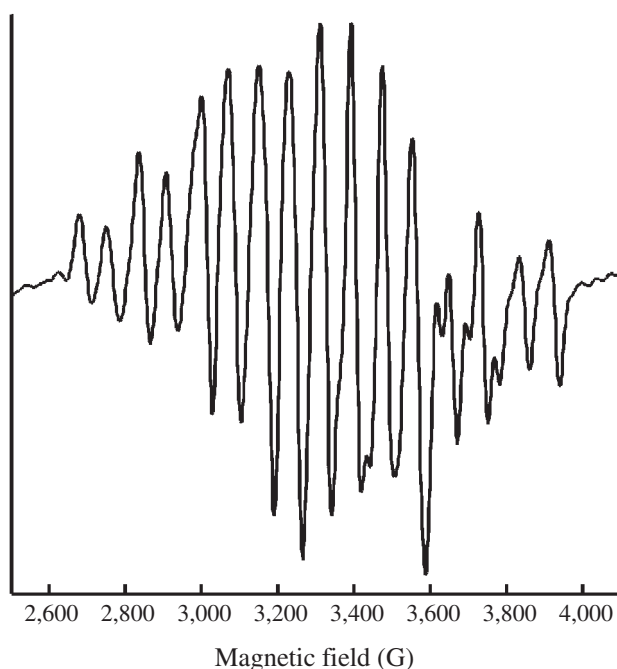
Figure 19 X-band EPR spectrum of 1 mM $[Mn_2(O)_2bpy_4]^{3+}$ in H_2O. Instrumental conditions: microwave frequency, 9.3 GHz; modulation frequency, 100 kHz; modulation amplitude, 20 G; microwave power, 1 mW; temperature, 10 K.

native, NH_3-treated and Ca^{2+}-depleted S_2 multiline signals obtained by c.w. EPR.[44] Their results were based on the dimer-of-dimers, distorted tetrahedral and distorted trigonal structural models and required one ferromagnetic and three antiferromagnetic couplings. The models assume an oxidation state assignment of (3/3/3/4) for the S_2-state, which is in contrast to the XAS data.[10,23–28] Alternatively, the work by Kusunoki and co-workers,[39,45,200] using an oxidation state of (3/4/4/4), simulated the c.w. EPR spectrum of the S_2-state using three strong and one weak antiferromagnetic exchange coupling. They proposed a distorted cubane based on a trimer/monomer motif. Finally, Britt and co-workers calculated parameters used to simulate both the c.w. EPR and ESE-ENDOR spectra of native, methanol- and NH_3-treated PSII in the S_2-state. They calculated hyperfine tensors consistent with a (3/4/4/4) oxidation state and three strong and one weak antiferromagnetic exchange couplings between the Mn ions. Their model of the Mn_4 cluster involves an arrangement of three Mn connected via di-μ-oxo bridges with the third connected via a mono-μ-oxo bridge to account for the strong and weak couplings.

Based on the simulations of the S_2 multiline signal, with three strong and one weak exchange couplings,[38,39] and including the results from EXAFS, it is postulated that three of the Mn ions in the Mn_4 cluster are connected via di-μ-oxo bridges with the third connected via a mono-μ-oxo bridge, as illustrated by the boxed structures in Figure 5. The number and type of oxo bridges between Mn in these models agrees with the EXAFS results.[10,20,22,25,31–33] Furthermore, these simulations assign the Mn oxidation states as (3/4/4/4). This assignment is supported by the one-electron reduced form of the linear di-μ-oxo-bridged Mn^{IV} tetramer (**31**), which has an EPR spectrum that is the closest match to the S_2 multiline spectrum in any model system.[46]

8.20.3.4.4 *Electronic absorption spectroscopy*

The Mn_4 cluster appears to have absorption features in the UV[74–80] and NIR.[52,53,72,88,89] The electronic absorption spectra of several complexes containing a $[Mn^{III}(O)_2Mn^{IV}]^{3+}$ core were investigated in detail using MCD spectroscopy in conjuction with resonance Raman and absorption spectroscopies.[81] The MCD spectra of the Mn–oxo complexes were recorded at 300–2,500 nm, deconvoluted, and the component peaks assigned. The majority of peaks corresponded to metal-centered *d–d* transitions and oxo-to-Mn^{IV} ligand-to-metal charge transfer (LMCT) bands. Although contributions from the other chromophores in PSII and low protein

concentration prevent a similar analysis of the Mn_4 cluster, it is likely that the Mn-associated features in the absorption spectrum of PSII have origins similar to the Mn–oxo model complexes.

8.20.3.4.5   *Vibrational spectroscopy*

As discussed above, IR absorption and Raman spectroscopies are proving to be useful tools in investigating the structure and coordination environment of the Mn_4 cluster. It is in the low-frequency region of the vibrational spectrum, 200–700 cm^{-1}, that metal–ligand vibrational modes are observed.[90] Hence, it is in this spectral region that information on the coordination environment of the Mn ions will be obtained. This frequency regime poses problems experimentally for IR absorption, but not for Raman measurements.[98] Assignments of the features observed in the vibrational spectra of the Mn_4 cluster depend on having well-characterized model systems for comparison. Unfortunately, detailed descriptions of the vibrational modes of Mn–oxo complexes are as of yet unavailable. The vibrations of the mono- and di-μ-oxo cores are the most well understood, which can be identified by ^{18}O-substitution. They occur in the 600–700 cm^{-1} range for di-μ-oxo cores and around 700 cm^{-1} (symmetric stretch) and 550 cm^{-1} (antisymmetric stretch) for mono-μ-oxo cores.[166,201–206] In complexes with bridging acetato ligands, the oxo core modes are coupled to oscillations of the acetato bridges. There appears to be no simple correlations between the oxidation states of the Mn ions and the frequencies of the oxo-core vibrational frequencies. This implies that the electronic effects of the ancillary ligands and the extent of vibrational coupling with other modes play important roles in determining the energies of the low-frequency vibrational modes. To date, there is still a lack of information regarding the vibrational modes of physiologically relevant ligands bound to Mn, such as Cl^- and H_2O, although much work is in progress in this area.

8.20.3.4.6   *Electrochemical properties*

Manganese is found in a wide range of oxidation states, from Mn^{II} to Mn^{VII}. High-valent Mn is a reasonably strong oxidant, with Mn^{III} and Mn^{IV} typically exhibiting reduction potentials near $\sim$1 V. This value will vary depending on the electronic properties of the ancillary ligands and the nuclearity of the complex. For the water oxidation process in PSII, a potential of more than 1 V is necessary to carry out the stepwise four-electron, four-proton oxidation of $2H_2O$ to O_2. Thus, with a range of accessible oxidation states and reduction potentials, manganese is well suited for this purpose. The reduction potentials for a variety of manganese complexes are listed in Table 3. The effects of the donor properties

Table 3   Reduction potentials (vs. SCE) for oxo-bridged manganese complexes.

Complex	$E_{1/2}$	$E_{1/2}$	References
	(3,3/3,4)	(3,4/4,4)	
$[Mn_2O_2(tmpa)_2]^{3+}$	0.24	1.04	252
$[Mn_2O_2(tren)_2]^{3+}$	0.08	0.83	206
$[Mn_2O_2(phen)_4]^{3+}$	0.33	1.29	256
$[Mn_2O_2(bpy)_4]^{3+}$	0.29	1.25	207
$[Mn_2O_2(bispicen)_2]^{3+}$	0.14	0.75	245
$[Mn_2O_2(cyclam)_2]^{3+}$	−0.12	1.00	205
$[Mn_2O_2(bispicen)_2]^{4+}$		1.00	245
$[Mn_2O_2(pic)_4]$	−0.47	0.66	257
$[Mn_2O_2(6-Me bispicen)_2]^{2+}$	0.57	1.34	245
$[Mn_2O_2(6-Me_2tmpa)_2]^{2+}$	0.68	1.45	245
$[Mn_2O_2(bpy)_2(\mu\text{-}HPO_4)(H_2PO_4)_2]^{3+}$		0.70	249
$[Mn_2O_2(salpn)_2]$		−0.39	258
$[Mn_2O_2(O_2CCH_3)(tpen)_2]^{2+}$		0.90	166
$[Mn_2O_2(O_2CCH_3)(bpea)_2]^{3+}$		0.93	185
$[Mn_2O(O_2CCH_3)_2(tmtacn)_2]^{2+}$	0.89	1.51	271
	(3,4,4/4,4,4)		
$[Mn_3O_4(bpy)_4(H_2O)]^{3+}$	0.36		165
$[Mn_3O_4(bpea)_3(OH)]^{3+}$	0.05		185
	(4,4,4,4/4,4,4,5)		
$[Mn_4O_6(tacn)_4]^{4+}$	1.32		271

of the ligands are easily discerned. For example, the reduction potentials for the (3,4/4,4) couple in [$Mn_2O_2L_2$] complexes range from 1.45 V (vs. SCE) with 6-Me$_2$tmpa as the ligand to −0.39 V with the strongly electron-donating salpn ligand. Complexes with increased nuclearity are generally easier to oxidize. For example, the (3,4,4/4,4,4) couple in [$Mn_3O_4(bpy)_4(H_2O)$]$^{3+}$ is only 0.36 V, which is on the order of the reduction potentials for the (3,3/3,4) couple in the dimeric complexes.

Many of the oxidation/reduction reactions of oxo-bridged Mn complexes are proton-coupled and thus pH-dependent.[207] For example, reduction of the complex [$Mn_2O_2(bpy)_4$]$^{3+}$ results in [$Mn_2O(OH)(bpy)_4$]$^{3+}$. However, reduction of [$Mn_2O_2(bis$picen)$_2$]$^{3+}$ is pH-independent because the μ-oxo bridges are not sufficiently basic in the (3/4) oxidation state to accept a proton. Further reduction of the (3/3) complex is proton-coupled because of the increased basicity of the μ-oxo bridges in this oxidation state. Given that the [Mn_2O_2] cores in both the bpy and *bis*picen complexes are similar, it can be deduced that the effects of the electron-donating properties of the ligands determine the basicity of the μ-oxo bridges and hence whether oxidation/reduction processes are proton-coupled. Such tuning of redox events by amino acid ligands of the Mn$_4$ cluster in the OEC may be important in adjusting the energetics of water oxidation.

8.20.3.5 Functional Models

Besides developing models to aid in understanding the structure of the Mn$_4$ cluster, there is great interest in biomimetic models that replicate the photo-induced oxidation of Mn and the chemistry of O−O bond formation. Progress in these areas is discussed in this section.

8.20.3.5.1 *Electron transfer in a ruthenium-linked manganese dimer*

Styring and co-workers have developed a photoactive triad composed of a ruthenium photosensitizer covalently joined to a dinuclear Mn site through a modified tyrosine linker.[208–215] Illustrated in Figure 20 are (A) the triad in the absence of Mn, showing the Ru(bpy) photosensitizer, the tyrosine linker, and the polypyridine Mn-binding site and (B) the triad with an assembled Mn dimer. In this system, the Ru(bpy) photosensitizer mimics $P_A^{\bullet+}$ and is electronically linked to the Mn cluster by the modified tyrosine moiety, much like Y_Z links the Mn$_4$ cluster to P_A in PSII. In


(A)   **(B)**
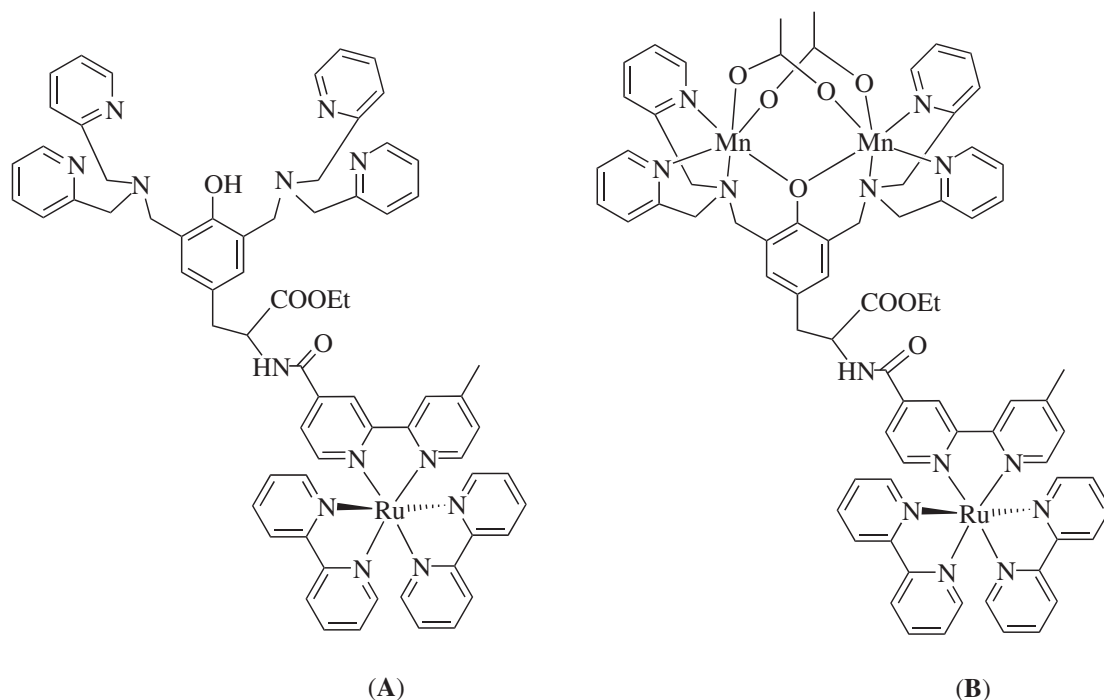
Figure 20 Biomimetic system for electron transfer in the OEC, consisting of a Ru(II) photosensitizer linked to a dinuclear Mn-binding site via a modified tyrosine linker.[212]

the absence of Mn, the Ru(bpy) group can photooxidize the tyrosine linker in a PCET step[210] with a pH-dependence similar to that for Y_Z oxidation in Mn-depleted PSII.[105–107] In the presence of Mn, the Ru(bpy) center can photooxidize the dinuclear Mn cluster from the (3/3) to the (3/4) oxidation state.[213] Experiments are in progress to improve the electron transfer rate and efficiency from the Mn cluster to the Ru(bpy) center and to oxidize the Mn beyond the (3/4) oxidation state, with the ultimate goal being to photochemically oxidize water using photogenerated high-valent Mn.

8.20.3.5.2 Catalytic oxygen evolution from a manganese dimer

Brudvig and co-workers have synthesized a homogeneous water oxidation catalyst that evolves O_2 from H_2O using O-atom transfer reagents as the primary oxidant.[178,216] While there are several reports of heterogeneous water oxidation catalysts, few are also structural models of the Mn_4 cluster and none have been well characterized. Many of these catalysts are Mn-based. These include suspensions of MnO_2 and phospholipid membranes containing Mn^{IV} that are thought to evolve O_2 in the presence of strong oxidants via a Mn^V species.[217,218] The complex $[(bpy)_2Mn(O)_2Mn(bpy)_2]^{3+}$ can act as a heterogeneous water oxidation catalyst[219,220] but with very low turnover. This is probably because in order for $[(bpy)_2Mn(O)_2Mn(bpy)_2]^{3+}$ to react with water, one of the arms of a bpy ligand must dissociate to allow water to bind to Mn. Alternatively, the complex $[(terpy)(H_2O)Mn^{III}(O)_2Mn^{IV}(OH_2)(terpy)]^{3+}$ (**39**) (shown in Figure 21) is a (3/4) di-μ-oxo dimer with terpy ligands that has an exchangeable coordination site where water can bind.[178] This is analogous to the only other known homogeneous water oxidation catalyst, $[(bpy)_2(H_2O)Ru(O)Ru(OH_2)(bpy)_2]^{4+}$.[221] The Ru dimer is capable of oxidizing water using a variety of oxidants and also electrochemically. Characterization of the Ru dimer was important because it demonstrated that the dimer is oxidized to a di-Ru^V=O species that is active in water oxidation.[222] This finding was significant because it supports the idea that a Mn^V=O species may be involved in the mechanisms of both (**39**) and the OEC (discussed in Section 8.20.5).[12,66,139,143,223,224]


(**39**)
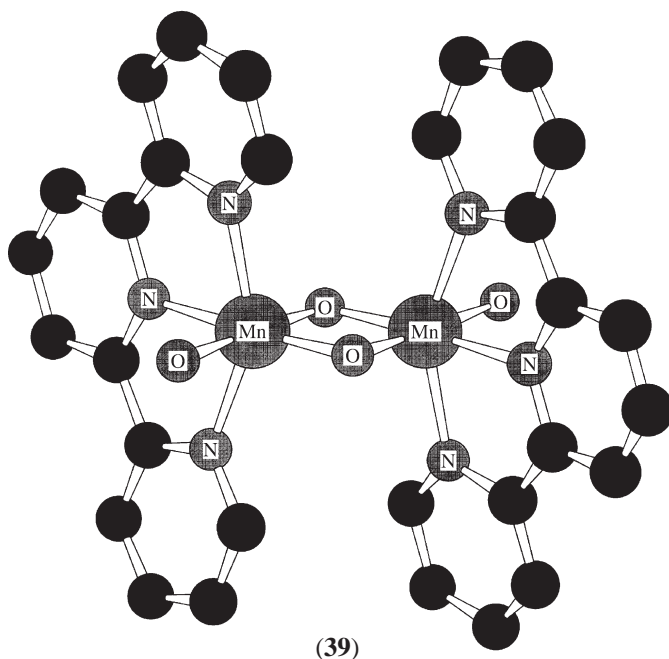
Figure 21 Crystal structure of $[(H_2O)(terpy)Mn(O)_2Mn(terpy)(OH_2)]^{3+}$, a homogeneous water oxidation catalyst.[178]

The di-manganese catalyst (**39**) catalyzes the oxidation of H_2O to O_2 using O-atom transfer reagents (XO) as the primary oxidants.[178,216] The proposed mechanism for the reaction of (**39**) with XO, such as HSO_5^- (oxone) and OCl^-, is shown in Figure 22. Kinetic measurements are consistent with the binding of XO to (**39**) in a preequilibrium. ^{18}O-labeling studies using $H_2^{18}O$ showed incorporation of the label into the product O_2, measured by mass spectrometry.[216] This observation supports the idea that the O−O bond forming step involves formation of a solvent-exchangable $Mn^V{=}O$ species (**41**).[178,216,225] Because the extent of ^{18}O-incorporation into the product O_2 was dependent on the relative concentrations of XO to (**39**), it was surmised that there are two competing pathways for O_2 formation.[216] When the concentration of XO is much greater than (**39**), then the mechanism is thought to involve the reaction of (**41**) with XO (Figure 22, left-hand pathway). Alternatively, when the concentration of XO is decreased, then (**41**) may react more readily with $H_2^{18}O$, giving more ^{18}O-label in the product O_2 (Figure 22, right-hand pathway). The possible participation of a $Mn^V{=}O$ species in O−O bond formation in the reaction of (**39**) with XO supports the proposals that a terminal $Mn{=}O$ species may also be active in the OEC.

8.20.4 ENERGETICS OF WATER OXIDATION

Thus far, we have investigated the coordination environment of the Mn_4 cluster and learned how model Mn–oxo coordination complexes contribute to understanding the structure and function of the OEC. In the following sections, we will focus on how the components of the OEC work
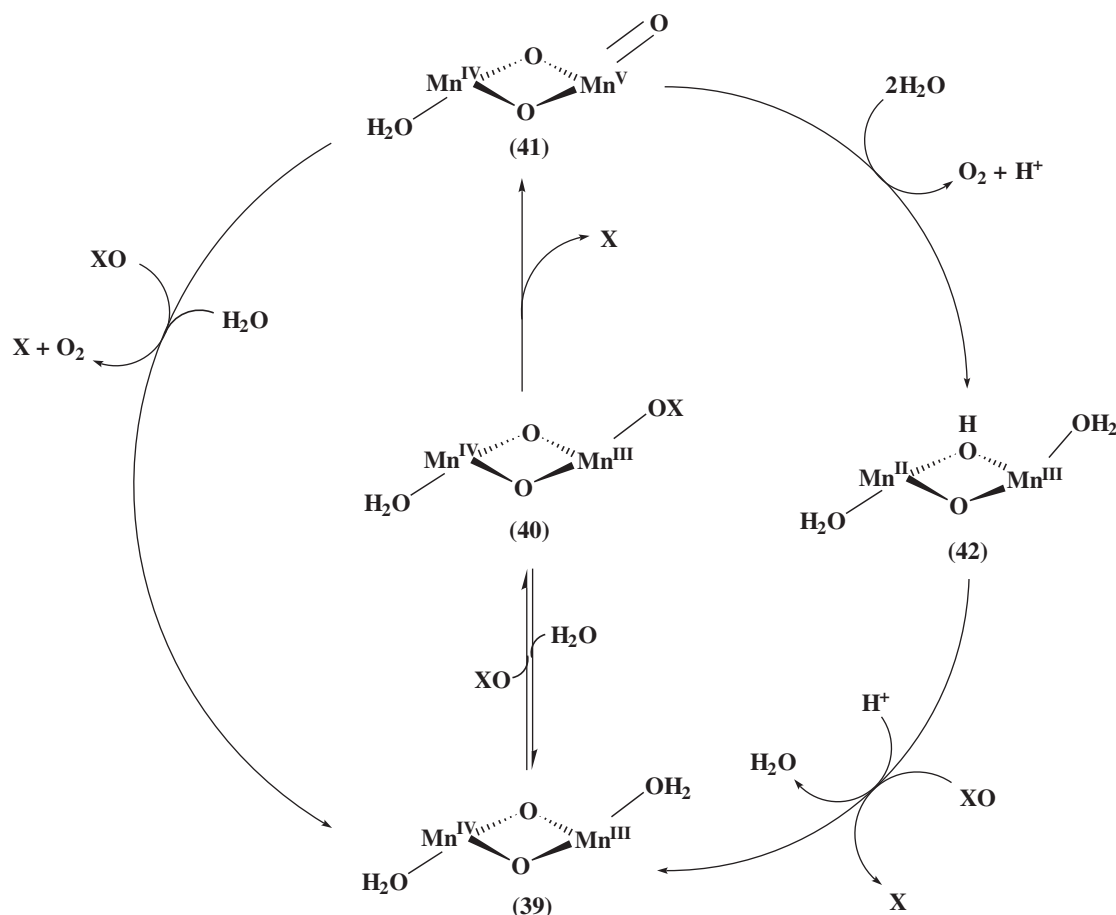
Figure 22 Proposed mechanism for O_2 evolution from $[(H_2O)(terpy)Mn(O)_2Mn(terpy)(OH_2)]^{3+}$. The terpy ligands have been omitted for clarity. In this mechanism, $[(H_2O)(terpy)Mn(O)_2Mn(terpy)(OH_2)]^{3+}$ (**39**) reacts with an O-atom transfer reagent (denoted XO, such as HSO_5^-) to form an adduct (**40**). Scission of the X–O bond forms a terminal-oxo species (**41**) that can react with either XO or H_2O to form O_2. Reaction of (**41**) with H_2O would be expected to form the (II/III) complex (**42**), which would be rapidly oxidized by XO back to (**39**).[216]

together to catalyze O_2 evolution from H_2O by considering the energetic requirements of water oxidation and proposals for the mechanism of O—O bond formation.

8.20.4.1   Thermodynamics and Kinetics

To oxidize H_2O to O_2, PSII must catalyze the breaking of four O—H bonds and the formation of an O—O bond. To achieve this, the Mn_4 cluster is oxidized stepwise by PCET reactions involving Y_Z. The thermodynamics and kinetics of these steps may reveal the mechanism of H_2O oxidation and O—O bond formation.

8.20.4.1.1   *Deuterium kinetic isotope and pH effects*

In Mn-depleted PSII, the rates for the oxidation and reduction of Y_Z are pH-dependent and exhibit kinetic deuterium isotope effects.[107,226,227] The rate of Y_Z oxidation increases as the pH is raised and becomes extremely rapid above pH 9. The measured pK_a values of 8–10 and 5–7[105,106] have been assigned, respectively, to those of Y_Z and its proposed proton acceptor, H190.[105,108] Therefore, at a pH > 9, Y_Z is deprotonated and so its oxidation is no longer proton-limited and occurs most rapidly. Furthermore, the k_H/k_D is only slightly greater than 1 under these conditions.[227] At pH values between 5 and 9, Y_Z oxidation is proton-coupled and proceeds normally, with a $k_H/k_D \sim 2.5$–3.5. However, at pH < 5, both Y_Z and H190 are protonated and so Y_Z oxidation is limited by proton transfer. In contrast to Y_Z oxidation, the rate of $Y_Z^{\bullet}$ reduction has a less pronounced k_H/k_D of 1.4–2.3,[227] and neither the measured rates nor the H/D effect correlate with pH. This suggests that, in the absence of the Mn_4 cluster, the reduction of $Y_Z^{\bullet}$ is not proton-limited, either because the tyrosinate anion Y_Z^{-} is formed (high pH) or because protons are readily available from solution (low pH).

The rates for the oxidation of Y_Z in Mn-containing PSII are insensitive to H/D effects, consistent with a structured pathway for PCET in contrast to Mn-depleted samples.[85,86,226,228] Alternatively, k_H/k_D for the reduction of $Y_Z^{\bullet}$ during S-state advancement is not constant, but rather varies with S-state.[83,85,86] The reported values are 1.4 ($S_0 \rightarrow S_1$), 1.4 ($S_1 \rightarrow S_2$), 2.3 ($S_2 \rightarrow S_3$), and 1.5 ($S_3 \rightarrow S_0$). The increase in k_H/k_D for the $S_2 \rightarrow S_3$ transition suggests a change in the mechanism of PCET in this step, which will be elaborated upon in Section 8.20.4.2.

8.20.4.1.2   *Activation energies*

As in the case of the H/D effects, the activation energies of the S-state transitions vary with each step. They have been measured to be 59.4 kJ mol^{-1} ($S_0 \rightarrow S_1$), 9.6 kJ mol^{-1} ($S_1 \rightarrow S_2$), and 26.8 kJ mol^{-1} ($S_2 \rightarrow S_3$).[82] As might be expected from those results, only the $S_1 \rightarrow S_2$ transition can occur at low temperature (140 K).[229] All the other S-state advancements require temperatures above 220 K,[41,230] where significant protein motions can still readily occur. These findings further support the notion that, in some S-state transitions, structural rearrangements within the OEC are required for PCET to proceed and that the mechanism of PCET may not be equivalent. Furthermore, it is thought that modifications to the OEC that result in the $S_2Y_Z^{\bullet}$-state,[55–59, 61,156,231] such as the depletion of Ca^{2+} or Cl^{-}, act by disrupting the hydrogen-bonding pathways required for efficient PCET to occur.[61]

8.20.4.2   Proton-coupled Electron Transfer

Based on the aforementioned results, it is clear that S-state advancement occurs by PCET mechanisms. Y_Z oxidation is expected to be proton-coupled, because oxidized Y_Z is a neutral radical.[232] At least some steps of water oxidation should be proton-coupled, because the O—H bonds in H_2O must be broken to make O_2. Based on the H/D isotope effects and the activation energies discussed above, the different observations described above can be explained by the models for PCET shown in Figure 23. The oxidation of Y_Z involves electron transfer to $P_A^{\bullet+}$ and deprotonation of the phenolic proton to H190, which subsequently must deprotonate to dissipate

Y$_Z$ Oxidation

Y$_Z$ Reduction

<table>
<tr><td>A</td><td>B</td></tr>
</table>
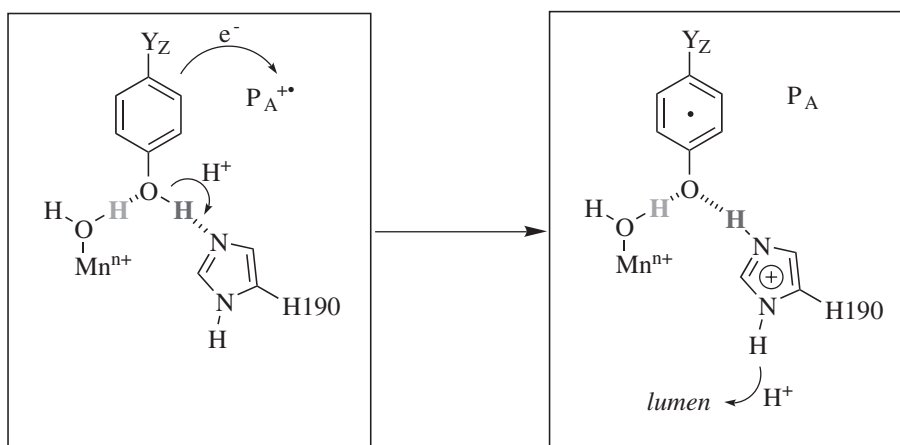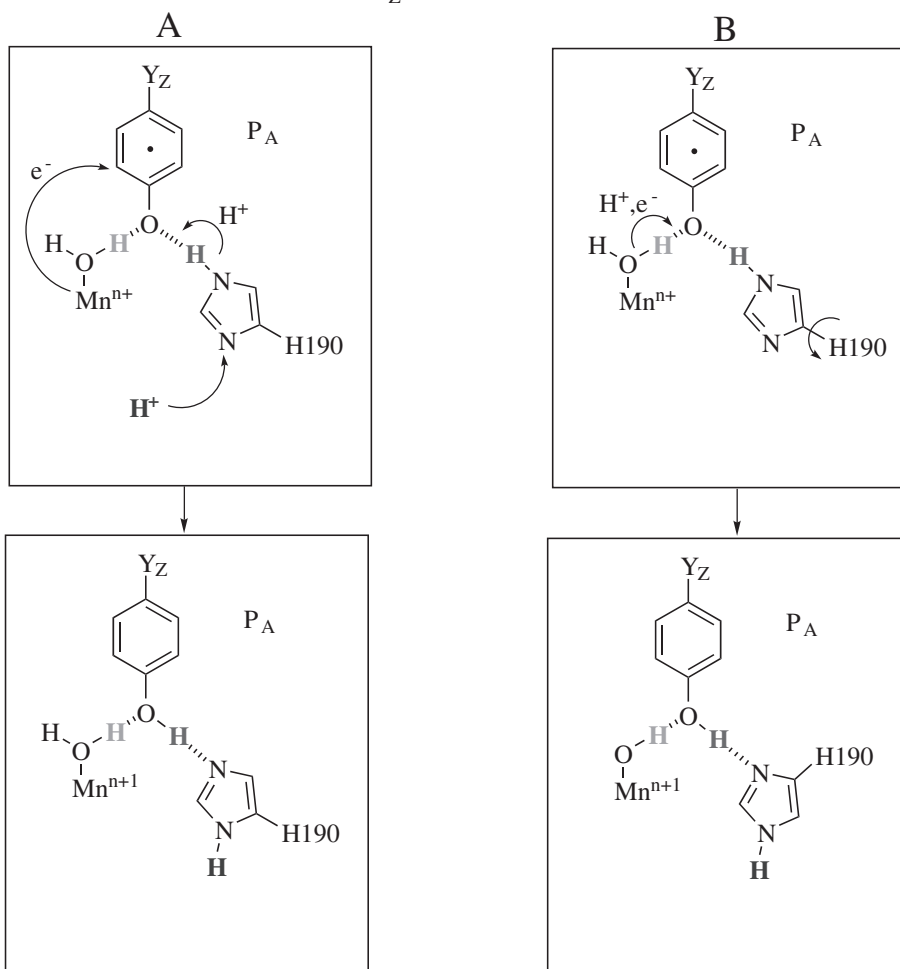
Figure 23 Proposed mechanisms for PCET during Y$_Z$ oxidation and reduction. Oxidation of Y$_Z$ by P$_A^{\bullet+}$ is accompanied by transfer of the phenolic proton to H190, the proposed hydrogen-bonding partner to Y$_Z$. Reduction of Y$_Z^{\bullet}$ can proceed via two pathways. In A, Y$_Z^{\bullet}$ is reduced by oxidizing the Mn$_4$ cluster and protonated by the return of the phenolic proton from H190. In turn, H190 is reprotonated by H$^+$. The net result is oxidation of the Mn$_4$ cluster by one electron. In B, Y$_Z^{\bullet}$ is reduced by an electron from the Mn$_4$ cluster and is protonated by a Mn-bound substrate water molecule.

the accumulated positive charge. However, the reduction of $Y_Z^\bullet$ can proceed via two pathways. In pathway A, $Y_Z^\bullet$ is reduced by the Mn_4 cluster and is protonated by the proton from H190. The net result is oxidation of the Mn_4 cluster. Alternately, $Y_Z^\bullet$ may be both reduced and protonated by the Mn_4 cluster by breaking an O—H bond in water ligated to Mn, as shown in pathway B (Figure 23). Based on comparison of the measured O—H bond dissociation energies of phenols and water bound to inorganic Mn model complexes, listed in Table 4, this mechanism is thermodynamically feasible.[233–236] In this case, the net result is oxidation of the Mn_4 cluster and the removal of a proton from water. Multiple concerted PCET steps by the mechanism shown in path B will lead to the formation of a Mn=O species, which has been proposed to be the key reactive species in O—O bond formation.[12,66,139,143,223,224]

8.20.5   PROPOSED MECHANISMS FOR WATER OXIDATION

The goal in understanding the structure of the coordination environment of the Mn_4 cluster is to relate that structure to the function of each of the components and the mechanism of O—O bond formation. The prevelant proposals for H_2O oxidation by the OEC are presented below.

8.20.5.1   Berkeley Model

The mechanism for water oxidation proposed by the group of Klein, Sauer, and Yachandra is shown in Figure 24.[10,237] The structure of the Mn_4 cluster is based on the results from EXAFS.[30] The mechanism involves successive oxidation of the Mn_4 cluster via pathway A in Figure 23 for all S-state transitions. The $S_2 \rightarrow S_3$ transition, however, results in ligand-centered oxidation of a bridging μ-oxo rather than Mn oxidation. O—O bond formation occurs by reaction of the bridging μ-oxyl radical with either outer-sphere H_2O or another oxo bridge. Precedent for O—O bond formation between bridging oxo groups comes from the bis(μ-oxo)dicopper complexes studied by Tolman and co-workers,[308] which form bridging μ-peroxy complexes. However, there is as yet no report of bridging μ-peroxy formation in model bis(μ-oxo)dimanganese complexes.

8.20.5.2   Babcock H-atom Abstraction Model

The mechanism of Babcock and co-workers was the first to suggest that pathway B in Figure 25 is involved in $Y_Z^\bullet$ reduction.[223] Contrary to the Berkeley model, in this mechanism pathway B occurs in all S-state transitions, each time removing both an electron from Mn and proton from H_2O. For this reason, the mechanism is known as the H-atom abstraction model, because the removal of both an electron from Mn and a proton from Mn-bound H_2O is similar to abstraction

Table 4 Homolytic bond dissociation energies for substituted phenols and Mn complexes with water and hydroxide ligands.

Compound	HBDE (kcal mol^{-1})[a]	References
Phenol	89.85	305
4-methyl-phenol	88.70	305
$Mn^{III}Mn^{IV}(salpn)_2(\mu\text{-O}, \mu\text{-OH})$	76.00	306
$Mn^{III}Mn^{IV}((3,5\text{-Cl-sal})pn)_2(\mu\text{-O}, \mu\text{-OH})$	77.00	306
$Mn^{III}Mn^{IV}((3,5\text{-NO}_2\text{-sal})pn)_2(\mu\text{-O}, \mu\text{-OH})$	79.00	306
$[Mn^{III}Mn^{III}(bpy)_4(\mu\text{-O}, \mu\text{-OH})]^{3+}$	84.00	307
$Mn^{III}Mn^{III}(2\text{-OH}(3,5\text{-Cl-sal})pn)OH_2$	89.00	233
$Mn^{III}Mn^{III}(2\text{-OHsalpn})OH_2$	85.00	233
$Mn^{III}Mn^{III}(2\text{-OH}(3,5\text{-t-Bu-sal})pn)OH_2$	82.00	233
$[Mn^{III}Mn^{IV}(2\text{-OH}(3,5\text{-Cl-sal})pn)OH_2]^+$	94.00	233
$Mn^{III}Mn^{IV}(2\text{-OHsalpn})OH_2^+$	89.00	233
$Mn^{III}Mn^{IV}(2\text{-OH}(3,5\text{-t-Bu-sal})pn)OH_2^+$	86.00	233

[a] Values for phenols were measured in DMSO, while values for the Mn complexes were measured in 16 M H_2O/CH_3CN.
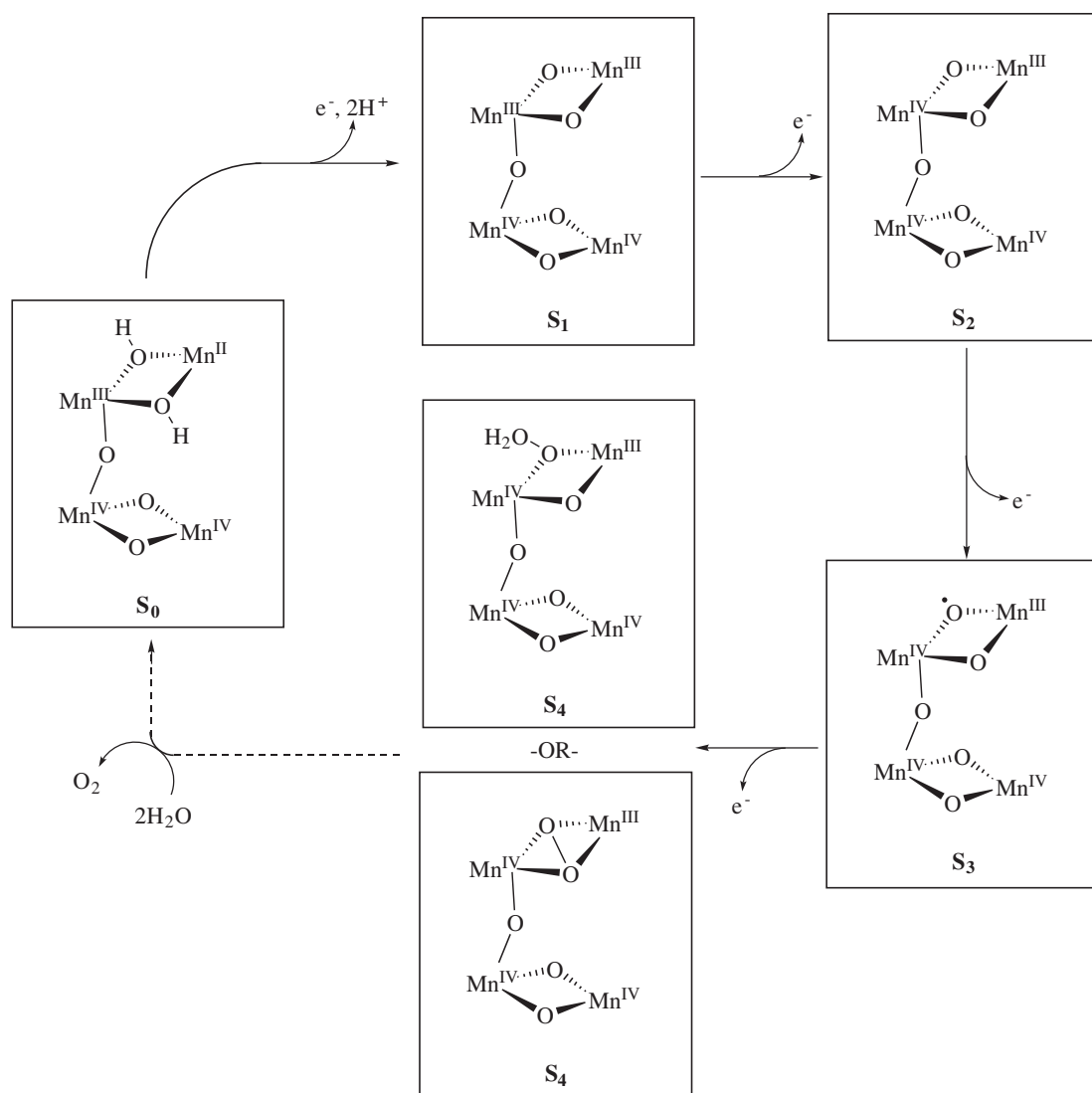
Figure 24 Proposed mechanism of water oxidation by Yachandra and co-workers.[10,237] Light-driven steps are indicated by solid arrows and spontaneous steps by dashed arrows. Reduction of $Y_Z^\bullet$ proceeds via mechanism A in Figure 23. The key intermediate in O—O bond formation is a bridging μ-oxyl radical formed in S_3 that reacts with either another μ-oxo or an outer-sphere H_2O molecule.

of an H-atom. Successive oxidations of the Mn_4 cluster by PCET path B leads to the formation of a terminal Mn^{IV}=O species that undergoes a nucleophilic attack by a Mn-bound hydroxide. This results in a transient peroxide in S_4 that is oxidized to O_2. Ca^{2+} is proposed to act as a docking site for Cl^-, which migrates from Ca^{2+} to coordinate to the Mn_4 cluster in the S_2-state to neutralize the increasing positive charge on Mn.

8.20.5.3 Mn–oxyl Radical Model

In the mechanism put forth by Siegbahn,[144] depicted in Figure 26, successive S-state advancements via PCET path B leads to the formation of a μ-oxyl radical. The mechanism is based largely upon density functional theory calculations. The role of Ca^{2+} is to polarize the Mn—O bonds and direct the placement of the radical. The O—O bond-forming step is as yet unclear in the density functional theory (DFT) calculations, but it appears to involve reaction of the oxyl radical with outer-sphere H_2O to form a hydroperoxide species that is oxidized to O_2.
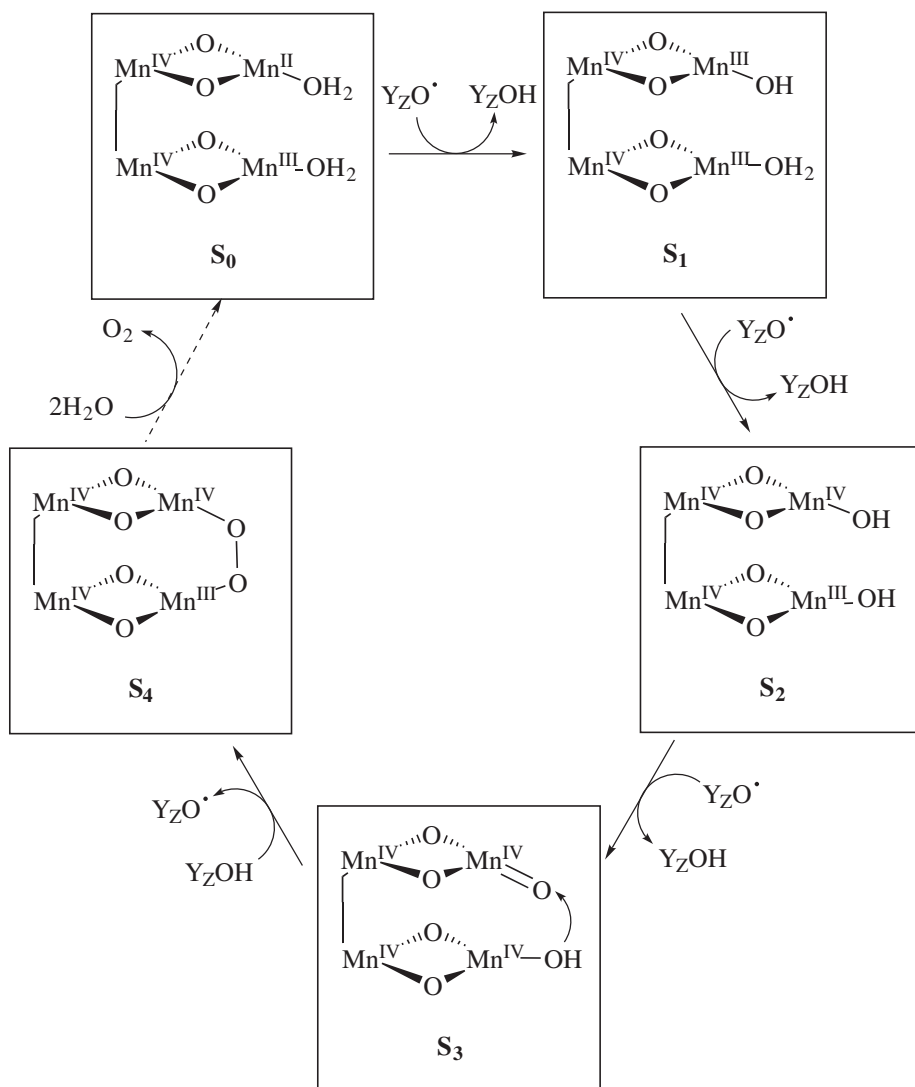
Figure 25 Proposed mechanism of water oxidation by Babcock and co-workers.[223] Light-driven steps are indicated by solid arrows and spontaneous steps by dashed arrows. In this cycle, $Y_Z^{\bullet}$ is reduced according to pathway B in Figure 23 in each S-state advancement. This forms a terminal-oxo $Mn=O$ in S_3 that reacts with Mn-bound hydroxide to form the O—O bond.

8.20.5.4 Electrophilic Mn–oxo Models

Based in part on an analysis of the reactivity of Ru and Mn oxidation catalysts, it seems that $Mn=O$ centers are electron deficient and subject to nucleophilic attack by reductants.[66] In the electrophilic $Mn=O$ models, the O—O bond-forming step involves nucleophilic attack by H_2O/ OH^- on a $Mn=O$ species. In the proposal by Pecoraro and co-workers,[139] the $S_0 \rightarrow S_1$ transition involves PCET path A, but the transitions of $S_2 \rightarrow S_3 \rightarrow S_4$ involve path B, as shown in Figure 27. This leads to the formation of Ca-bound OH^- and $Mn=O$ species. Nucleophilic attack of the OH^- on the $Mn=O$ forms a terminal hydroperoxide, which then displaces Cl^- on a second terminal Mn and is oxidized to O_2.

The mechanism of Brudvig and co-workers, shown in Figure 28, also involves a $Mn=O$ species.[13] S-state advancement from $S_0 \rightarrow S_1 \rightarrow S_2$ involves PCET path A. The large increases in activation energy and the deuterium kinetic isotope effect measured for the $S_2 \rightarrow S_3$ transition are taken to mean that there is a switch from path A to path B in this step, triggered by the increased net positive charge on the Mn_4 cluster in S_2. This leads to the formation of a $Mn^V=O$ species in S_4. Nucleophilic attack on the $Mn^V=O$ by a Ca-bound H_2O is prompted by

Figure 26 Proposed mechanism of water oxidation by Siegbahn.[144] Light-driven steps are indicated by solid arrows and spontaneous steps by dashed arrows. Reduction of $Y_Z^•$ by mechanism B in Figure 23 leads to the formation of a bridging μ-oxyl radical in S_3. Ca^{2+} aids in polarizing the Mn—O bonds to direct proton and electron transfer. The O—O bond-forming step involves reaction of the μ-oxyl radical with outer-sphere H_2O.

contraction of the Mn^V—Cl bond. This forms a hydroperoxide moiety that hydrogen-bonds to a bridging μ-O, analogous to the binding of O_2 in hemerythrin. Oxidation of the hydroperoxide reduces Mn and releases O_2.
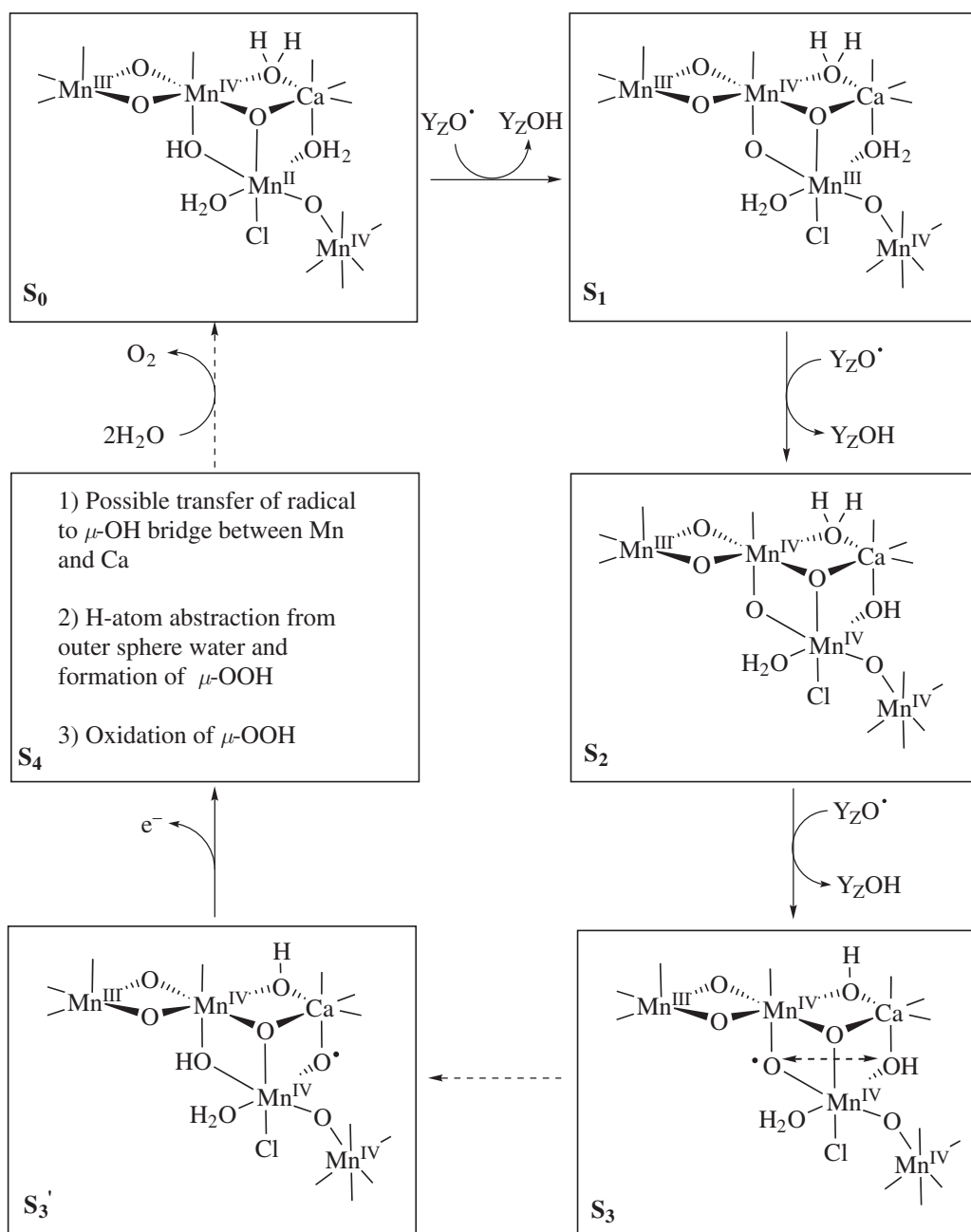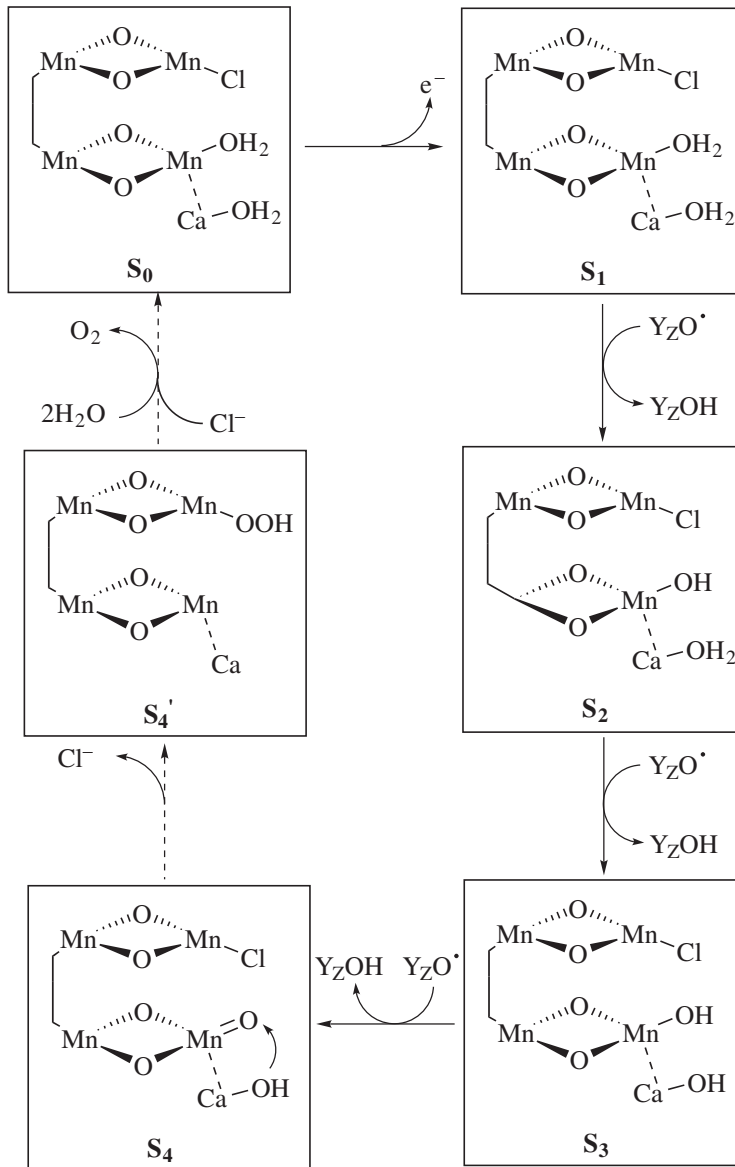
Figure 27 Proposed mechanism of water oxidation by Pecoraro and co-workers.[139] Light-driven steps are indicated by solid arrows and spontaneous steps by dashed arrows. Reduction of $Y_Z^\bullet$ by mechanism B in Figure 23 in $S_1 \rightarrow S_2 \rightarrow S_3$ forms a terminal Mn=O species. Nucleophilic attack on the Mn=O by a Ca-bound hydroxide forms hydroperoxide, which subsequently displaces Cl^- and is oxidized on another Mn center.

8.20.6 CONCLUSION

As can be seen, there is yet much to be learned about the coordination environment of the Mn_4 cluster in PSII. Until the crystal structure of PSII is refined to atomic resolution so that all of the amino acids and cofactors can be identified, spectroscopic and biochemical investigations remain the best methods to elucidate the structure and function of the OEC. Indeed, even after a detailed structure of the OEC is obtained, further work will be necessary to understand the mechanism of photosynthetic oxygen evolution.
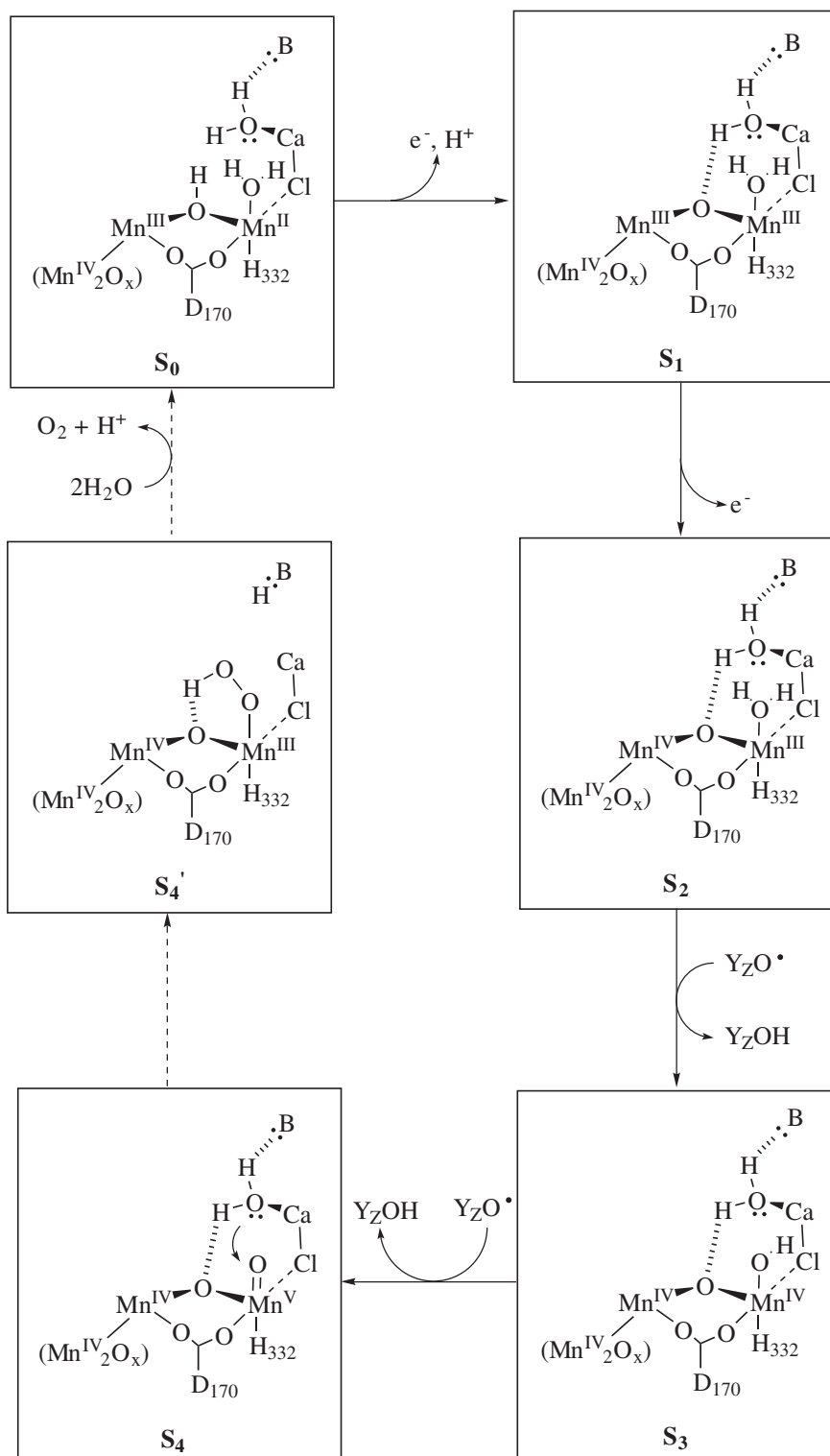
Figure 28 Proposed mechanism of water oxidation by Brudvig and co-workers.[13] Light-driven steps are indicated by solid arrows and spontaneous steps by dashed arrows. Reduction of $Y_Z^\bullet$ by mechanism A (Figure 23) in $S_0 \rightarrow S_1 \rightarrow S_2$ followed by mechanism B in $S_2 \rightarrow S_3 \rightarrow S_4$ forms a terminal $Mn^V{=}O$ species. Nucleophilic attack on the $Mn^V{=}O$ by a Ca-bound H_2O is directed by contraction of the Mn—Cl bond. This results in a bound hydroperoxide species, similar in structure to O_2 bound to hemerythrin, which is oxidized to O_2.

8.20.7 REFERENCES

1. Blankenship, R. E. *Molecular Mechanisms of Photosynthesis*, Blackwell Science, Oxford, **2002**.
2. Deisenhofer, J.; Epp, O.; Mikki, K.; Huber, R.; Michel, H. *J. Mol. Biol.* **1984**, *180*, 385–398.
3. Feher, G.; Allen, J. P.; Okamura, M. Y.; Rees, D. C. *Nature* **1989**, *339*, 111–116.
4. Zouni, A.; Witt, H. T.; Kern, J.; Fromme, P.; Krauß, N.; Saenger, W.; Orth, P. *Nature* **2001**, *409*, 739–743.
5. Michel, H.; Deisenhofer, J. *Biochemistry* **1988**, *27*, 1–7.
6. Diner, B. A.; Schlodder, E.; Nixon, P. J.; Coleman, W. J.; Rappaport, F.; Lavergne, J.; Vermaas, W. F. J.; Chisholm, D. A. *Biochemistry* **2001**, *40*, 9265–9281.
7. Debus, R. J. *Biochim. Biophys. Acta* **1992**, *1102*, 269–352.
8. Brudvig, G. W. *Adv. Chem. Ser.* **1995**, *246*, 249–263.
9. Rutherford, A. W.; Zimmermann, J.-L.; Boussac, A. In *The Photosystems: Structure, Function and Molecular Biology*; Barber, J., Ed.; Elsevier Science: Amsterdam **1992**, pp 179–229.
10. Yachandra, V. K.; Sauer, K.; Klein, M. P. *Chem. Rev.* **1996**, *96*, 2927–2950.
11. Diner, B. A.; Babcock, G. T. *Adv. Photosynth.* **1996**, *4*, 213–247.
12. Britt, R. D. In *Oxygenic Photosynthesis: The Light Reactions*; Ort, D. R.; Yocum, C. F., Eds.; Kluwer: Dordrecht, The Netherlands, 1996; Advances in Photosynthesis, Vol. 4, pp 137–159.
13. Vrettos, J. S.; Limburg, J.; Brudvig, G. W. *Biochim. Biophys. Acta* **2001**, *1503*, 229–245.
14. Joliot, P.; Joliot, A. *Biochim. Biophys. Acta* **1968**, *153*, 625–634.
15. Kok, B.; Forbush, B.; McGloin, M. *Photochem. Photobiol.* **1970**, *11*, 457–475.
16. Joliot, P.; Kok, B. In *Bioenergetics of Photosynthesis*; Govindjee, Ed.; Academic Press, New York, 1975, pp 387–412.
17. Dau, H.; Iuzzolino, L.; Dittmer, J. *Biochim. Biophys. Acta* **2001**, *1503*, 24–39.
18. Visser, H.; Anxolabéhère-Mallart, E.; Bergmann, U.; Glatzel, P.; Robblee, J. H.; Cramer, S. P.; Girerd, J.-J.; Sauer, K.; Klein, M. P.; Yachandra, V. K. *J. Am. Chem. Soc.* **2001**, *123*, 7031–7039.
19. Cinco, R.; Rompel, A.; Visser, H.; Aromi, G.; Christou, G.; Sauer, K.; Klein, M.; Yachandra, V. *Inorg. Chem.* **1999**, *38*, 5988–5998.
20. Cinco, R. M.; Robblee, J. H.; Rompel, A.; Fernandez, C.; Yachandra, V. K.; Sauer, K.; Klein, M. P. *J. Phys. Chem. B* **1998**, *102*, 8248–8256.
21. Penner-Hahn, J. E. *Struct. Bond.* **1998**, *90*, 1–36.
22. Penner-Hahn, J. E.; Fronko, R. M.; Pecoraro, V. L.; Yocum, C. F.; Betts, S. D.; Bowlby, N. R. *J. Am. Chem. Soc.* **1990**, *112*, 2549–2557.
23. Ono, T.-A.; Noguchi, T.; Inoue, Y.; Kusunoki, M.; Matsushita, T.; Oyanagi, H. *Science* **1992**, *258*, 1335–1337.
24. Roelofs, T. A.; Liang, W.; Latimer, M. J.; Cinco, R. M.; Rompel, A.; Andrews, J. C.; Sauer, K.; Yachandra, V. K.; Klein, M. P. *Proc. Natl. Acad. Sci. U.S.A.* **1996**, *93*, 3335–3340.
25. Riggs, P. J.; Mei, R.; Yocum, C. F.; Penner-Hahn, J. E. *J. Am. Chem. Soc.* **1992**, *114*, 10650–10651.
26. Bergmann, U.; Grush, M. M.; Horne, C. R.; DeMarois, P.; Penner-Hahn, J. E.; Yocum, C. F.; Wright, D. W.; Dubé, C. E.; Armstrong, W. H.; Christou, G.; Eppley, H. J.; Cramer, S. P. *J. Phys. Chem. B* **1998**, *102*, 8350–8352.
27. Goodin, D. B.; Yachandra, V. K.; Britt, R. D.; Sauer, K.; Klein, M. *Biochim. Biophys. Acta* **1984**, *767*, 209–216.
28. Iuzzolino, L.; Dittmer, J.; Dörner, W.; Meyer-Klaucke, W.; Dau, H. *Biochemistry* **1998**, *37*, 17112–17119.
29. Liang, W.; Roelofs, T. A.; Cinco, R. M.; Rompel, A.; Latimer, M. J.; Yu, W. O.; Sauer, K.; Klein, M. P.; Yachandra, V. K. *J. Am. Chem. Soc.* **2000**, *122*, 3399–3412.
30. Yachandra, V. K.; DeRose, V. J.; Latimer, M. J.; Mukerji, I.; Sauer, K.; Klein, M. P. *Science* **1993**, *260*, 675–679.
31. MacLachlan, D. J.; Hallahan, B. J.; Ruffle, S. V.; Nugent, J. H. A.; Evans, M. C. W.; Strange, R. W.; Hasnain, S. S. *J. Biochem.* **1992**, *285*, 569–576.
32. Kusunoki, M.; Takano, T.; Ono, T.; Noguchi, T.; Yamaguchi, Y.; Oyanagi, H.; Inoue, Y. In *Photosynthesis: from Light to Biosphere*; Mathis, P. Ed.; Kluwer: Dordrecht, The Netherlands 1995; Vol. II, pp 251–254.
33. Riggs-Gelasco, P. J.; Mei, R.; Ghanotakis, D. F.; Yocum, C. F.; Penner-Hahn, J. E. *J. Am. Chem. Soc.* **1996**, *118*, 2400–2410.
34. Latimer, M. J.; DeRose, V. J.; Mukerji, I.; Yachandra, V. K.; Sauer, K.; Klein, M. P. *Biochemistry* **1995**, *34*, 10898–10909.
35. Mukerji, I.; Andrews, J. C.; DeRose, V. J.; Latimer, M. J.; Yachandra, V. K.; Sauer, K.; Klein, M. P. *Biochemistry* **1994**, *33*, 9712–9721.
36. Naismith, J. H.; Emmerich, C.; Habash, J.; Harrop, S. *J. Acta Cryst.* **1994**, *D50*, 847–858.
37. Hardman, K. D.; Agarwal, R. C.; Freiser, M. J. *J. Mol. Biol.* **1982**, *157*, 69–86.
38. Peloquin, J. M.; Campbell, K. A.; Randall, D. W.; Evanchik, M. A.; Pecoraro, V. L.; Armstrong, W. H.; Britt, R. D. *J. Am. Chem. Soc.* **2000**, *122*, 10926–10942.
39. Hasegawa, K.; Ono, T.; Inoue, Y.; Kusunoki, M. *Bull. Chem. Soc. Jpn.* **1999**, *72*, 1013–1023.
40. Dismukes, G. C.; Siderer, Y. *FEBS Lett.* **1980**, *121*, 78–80.
41. Brudvig, G. W.; Casey, J. L.; Sauer, K. *Biochim. Biophys. Acta* **1983**, *723*, 366–371.
42. de Paula, J. C.; Beck, W. F.; Brudvig, G. W. *J. Am. Chem. Soc.* **1986**, *108*, 4002–4009.
43. Kim, D. H.; Britt, R. D.; Klein, M. P.; Sauer, K. *Biochemistry* **1992**, *31*, 541–547.
44. Zheng, M.; Dismukes, G. C. *Inorg. Chem.* **1996**, *35*, 3307–3319.
45. Hasegawa, K.; Kusunoki, M.; Inoue, Y.; Ono, T.-A. *Biochemistry* **1998**, *37*, 9457–9465.
46. Blondin, G.; Davydov, R. C. P.; Charlot, M.-F.; Styring, S.; Åkermark, B.; Girerd, J.-J.; Boussac, A. *J. Chem. Soc. Dalton* **1997**, 4069–4074.
47. Randall, D. W.; Sturgeon, B. E.; Ball, J. A.; Lorigan, G. A.; Chan, M. K.; Klein, M. P.; Armstrong, W. H.; Britt, R. D. *J. Am. Chem. Soc.* **1995**, *117*, 11780–11789.
48. Britt, R. D.; Peloquin, J. M.; Campbell, K. A. *Annu. Rev. Biophy. Biom.* **2000**, *29*, 463–495.
49. Casey, J. L.; Sauer, K. *Biochim. Biophys. Acta* **1984**, *767*, 21–28.
50. Haddy, A.; Dunham, W. R.; Sands, R. H.; Aasa, R. *Biochim. Biophys. Acta* **1992**, *1099*, 25–34.
51. Horner, O.; Rivière, E.; Blondin, G.; Un, S.; Rutherford, A. W.; Girerd, J.-J.; Boussac, A. *J. Am. Chem. Soc.* **1998**, *120*, 7924–7928.
52. Boussac, A.; Kuhl, H.; Un, S.; Rögner, M.; Rutherford, A. W. *Biochemistry* **1998**, *37*, 8995–9000.

53. Boussac, A.; Girerd, J.-J.; Rutherford, A. W. *Biochemistry* **1996**, *35*, 6984–6989.
54. Beck, W. F.; Brudvig, G. W. *Chem. Scripta* **1988**, *28A*, 93–98.
55. Boussac, A.; Zimmermann, J.-L.; Rutherford, A. W. *Biochemistry* **1989**, *28*, 8984–8989.
56. Andréasson, L.-E.; Vass, I.; Styring, S. *Biochim. Biophys. Acta* **1995**, *1230*, 155–164.
57. Wincencjusz, H.; Yocum, C. F.; van Gorkom, H. J. *Biochemistry* **1999**, *38*, 3719–3725.
58. Kühne, H.; Szalai, V. A.; Brudvig, G. W. *Biochemistry* **1999**, *38*, 6604–6613.
59. Hallahan, B. J.; Nugent, J. H. A.; Warden, J. T.; Evans, M. C. W. *Biochemistry* **1992**, *31*, 4562–4573.
60. Szalai, V. A.; Brudvig, G. W. *Biochemistry* **1996**, *35*, 1946–1953.
61. Szalai, V. A.; Brudvig, G. W. *Biochemistry* **1996**, *35*, 15080–15087.
62. Dorlet, P.; Di Valentin, M.; Babcock, G. T.; McCracken, J. L. *J. Phys. Chem. B* **1998**, *102*, 8239–8247.
63. Peloquin, J. M.; Campbell, K. A.; Britt, R. D. *J. Am. Chem. Soc.* **1998**, *120*, 6840–6841.
64. Lakshmi, K. V.; Eaton, S. S.; Eaton, G. R.; Frank, H. A.; Brudvig, G. W. *J. Phys. Chem. B* **1998**, *102*, 8327–8335.
65. Lakshmi, K. V.; Eaton, S. S.; Eaton, G. R.; Brudvig, G. W. *Biochemistry* **1999**, *38*, 12758–12767.
66. Limburg, J.; Szalai, V. A.; Brudvig, G. W. *J. Chem. Soc. Dalton* **1999**, 1353–1363.
67. Messinger, J.; Robblee, J. H.; Yu, W. A.; Sauer, K.; Yachandra, V. K.; Klein, M. P. *J. Am. Chem. Soc.* **1997**, *119*, 11349–11350.
68. Messinger, J.; Nugent, J. H. A.; Evans, M. C. W. *Biochemistry* **1997**, *36*, 11055–11060.
69. Åhrling, K. A.; Peterson, S.; Styring, S. *Biochemistry* **1997**, *36*, 13148–13152.
70. Campbell, K. A.; Peloquin, J. M.; Pham, D. P.; Debus, R. J.; Britt, R. D. *J. Am. Chem. Soc.* **1998**, *120*, 447–448.
71. Campbell, K. A.; Gregor, W.; Pham, D. P.; Peloquin, J. M.; Debus, R. J.; Britt, R. D. *Biochemistry* **1998**, *37*, 5039–5045.
72. Ionnidis, N.; Petrouleas, V. *Biochemistry* **2000**, *39*, 5246–5254.
73. Matsukawa, T.; Mino, H.; Yoneda, D.; Kawamori, A. *Biochemistry* **1999**, *38*, 4072–4077.
74. Dekker, J. P.; van Gorkom, H. J.; Brok, M.; Ouwehand, L. *Biochim. Biophys. Acta* **1984**, *764*, 301–309.
75. Dekker, J. P.; van Gorkom, H. J.; Wensink, J.; Ouwehand, L. *Biochim. Biophys. Acta* **1984**, *767*, 1–9.
76. Renger, G.; Hanssum, B. *Photosynth. Res.* **1988**, *16*, 243–259.
77. Saygin, Ö.; Witt, H. T. *Biochim. Biophys. Acta* **1987**, *893*, 452–469.
78. Saygin, Ö.; Witt, H. T. *FEBS Lett.* **1984**, *176*, 83–87.
79. Lavergne, J. *Biochim. Biophys. Acta* **1987**, *894*, 91–107.
80. Lavergne, J. *Biochim. Biophys. Acta* **1991**, *1060*, 175–188.
81. Gamelin, D. R.; Kirk, M. L.; Stemmler, T. L.; Pal, S.; Armstrong, W. H.; Penner-Hahn, J. E.; Solomon, E. I. *J. Am. Chem. Soc.* **1994**, *116*, 2392–2399.
82. Koike, H.; Hanssum, B.; Inoue, Y.; Renger, G. *Biochim. Biophys. Acta* **1987**, *893*, 524–533.
83. Bögershausen, O.; Haumann, M.; Junge, W. *Ber. Bunsenges. Phys. Chem.* **1996**, *100*, 1987–1992.
84. Karge, M.; Irrgang, K.-D.; Sellin, S.; Feinäugle, R.; Lui, B.; Eckert, H.-J.; Eichler, H. J.; Renger, G. *FEBS Lett.* **1996**, *378*, 140–144.
85. Karge, M.; Irrgang, K.-D.; Renger, G. *Biochemistry* **1997**, *36*, 8904–8913.
86. Haumann, M.; Bögershausen, O.; Cherepanov, D.; Ahlbrink, R.; Junge, W. *Photosynth. Res.* **1997**, *51*, 193–208.
87. Hundelt, M.; Haumann, M.; Junge, W. *Biochim. Biophys. Acta* **1997**, *1273*, 237–250.
88. Baxter, R.; Krausz, E.; Wydrzynski, T.; Pace, R. J. *J. Am. Chem. Soc.* **1999**, *121*, 9451–9452.
89. Cua, A.; Stewart, D. H.; Reifler, M. J.; Brudvig, G. W.; Bocian, D. F. *J. Am. Chem. Soc.* **2000**, *122*, 2069–2077.
90. Nakamoto, K. *Infrared and Raman Spectra of Inorganic and Coordination Compounds Part B: Applications in Coordination, Organometallic, and Bioinorganic Chemistry*, Wiley, New York, 1997.
91. Noguchi, T.; Ono, T. A.; Inoue, Y. *Biochemistry* **1992**, *31*, 5953–5956.
92. Noguchi, T.; Ono, T. A.; Inoue, Y. *Biochim. Biophys. Acta* **1995**, *1232*, 59–66.
93. Noguchi, T.; Ono, T. A.; Inoue, Y. *Biochim. Biophys. Acta* **1995**, *1228*, 189–200.
94. Noguchi, T.; Inoue, Y.; Tang, X.-S. *Biochemistry* **1997**, *36*, 14705–14711.
95. Smith, J. C.; Gonzalez, V. E.; Vincent, J. B. *Inorg. Chim. Acta* **1997**, *255*, 99–103.
96. Chu, H.-A.; Gardner, M. T.; O'Brien, J. P.; Babcock, G. T. *Biochemistry* **1999**, *38*, 4533–4541.
97. Chu, H.-A.; Sackett, H.; Babcock, G. T. *Biochemistry* **2000**, *39*, 14371–14376.
98. Chu, H.-A.; Hillier, W.; Law, N. A.; Babcock, G. T. *Biochim. Biophys. Acta* **2001**, *1503*, 69–82.
99. Chu, H.-A.; Debus, R. J.; Babcock, G. T. *Biochemistry* **2001**, *40*, 2312–2316.
100. Noguchi, T.; Sugiura, M. *Biochemistry* **2001**, *40*, 1497–1502.
101. Hillier, W.; Babcock, G. T. *Biochemistry* **2001**, *40*, 1503–1509.
102. Noguchi, T.; Inoue, Y.; Tang, X.-S. *Biochemistry* **1999**, *38*, 10187–10195.
103. Noguchi, T.; Sugiura, M. *Biochemistry* **2002**, *41*, 2322–2330.
104. Noguchi, T.; Sugiura, M. *Biochemistry* **2000**, *39*, 10943–10949.
105. Hays, A.-M.A.; Vassiliev, I. R.; Golbeck, J. H.; Debus, R. J. *Biochemistry* **1999**, *37*, 11851–11864.
106. Mamedov, F.; Sayre, R. T.; Styring, S. *Biochemistry* **1998**, *37*, 14245–14256.
107. Rappaport, F.; Lavergne, J. *Biochemistry* **1997**, *36*, 15294–15302.
108. Hays, A.-M. A.; Vassiliev, I. R.; Golbeck, J. H.; Debus, R. J. *Biochemistry* **1998**, *37*, 11352–11365.
109. Debus, R. J. *Met. Ions Biol. Syst.* **2000**, *37*, 657–711.
110. Qian, M.; Dao, L.; Debus, R. J.; Burnap, R. L. *Biochemistry* **1999**, *38*, 6070–6081.
111. Hundelt, M.; Hays, A.-M. A.; Debus, R. J.; Junge, W. *Biochemistry* **1998**, *37*, 14450–14456.
112. Chu, H.-A.; Nguyen, A. P.; Debus, R. J. *Biochemistry* **1995**, *34*, 5839–5858.
113. Nixon, P. J.; Diner, B. A. *Biochemistry* **1992**, *31*, 942–948.
114. Chu, H.-A.; Nguyen, A.-P.; Debus, R. J. *Biochemistry* **1995**, *34*, 5859–5882.
115. Debus, R. J.; Campbell, K. A.; Peloquin, J. M.; Pham, D. P.; Britt, R. D. *Biochemistry* **2000**, *39*, 470–478.
116. Nixon, P. J.; Diner, B. A. *Biochem. Soc. Trans.* **1994**, *22*, 338–343.
117. Nixon, P. J.; Trost, J. T.; Diner, B. A. *Biochemistry* **1992**, *31*, 10859–10871.
118. Tang, X. S.; Diner, B. A.; Larsen, B. S.; Gilchrist, M. L.; Lorigan, G. A.; Britt, R. D. *Proc. Natl. Acad. Sci. U. S. A.* **1994**, *91*, 704–708.

119. Britt, R. D.; Tang, X. S.; Gilchrist, M. L.; Lorigan, G. A.; Larsen, B. S.; Diner, B. A. *Biochem. Soc. Trans.* **1994**, *22*, 343–347.
120. Brand, J. J.; Becker, D. W. *J. Bioenerg. Biomembr.* **1984**, *16*, 239–249.
121. Ghanotakis, D. F.; Babcock, G. T.; Yocum, C. F. *FEBS Lett.* **1984**, *167*, 127–130.
122. Yocum, C. F. *Biochim. Biophys. Acta* **1991**, *1059*, 1–15.
123. Yocum, C. F. In *Manganese Redox Enzymes*; Pecoraro, V. L., Ed.; VCH: New York, 1992, pp 71–83.
124. Boussac, A.; Zimmermann, J.-L.; Rutherford, A. W. *FEBS Lett.* **1990**, *277*, 69–74.
125. Han, K.-C.; Katoh, S. *Biochim. Biophys. Acta* **1995**, *1232*, 230–236.
126. Kalosaka, K.; Beck, W. F.; Brudvig, G. W.; Cheniae, G. In *Current Research in Photosynthesis*; Baltscheffsky, M., Ed.; Kluwer: Dordrecht, The Netherlands, 1990; Vol. 1, pp 721–724.
127. Ädelroth, P.; Lindberg, K.; Andréasson, L.-E. *Biochemistry* **1995**, *34*, 9021–9027.
128. Vrettos, J. S.; Stone, D. A.; Brudvig, G. W. *Biochemistry* **2001**, *40*, 7937–7945.
129. Ono, T. J. *Inorg. Biochem.* **2000**, *82*, 85–91.
130. Burda, K.; Strzalka, K.; Schmid, G. H. Z. *Naturforsch.* **1995**, 220–230.
131. Ghanotakis, D. F.; Babcock, G. T.; Yocum, C. F. *Biochim. Biophys. Acta* **1985**, *809*, 173–180.
132. Grove, G.; Brudvig, G. W. *Biochemistry* **1997**, *37*, 1532–1539.
133. Astashkin, A. V.; Mino, H.; Kawamori, A.; Ono, T. *Chem. Phys. Lett.* **1997**, *272*, 506–516.
134. Bakou, A.; Buser, C.; Dandulakis, G.; Brudvig, G.; Ghanotakis, D. F. *Biochim. Biophys. Acta* **1992**, *1099*, 131–136.
135. Bakou, A.; Ghanotakis, D. F. *Biochim. Biophys. Acta* **1992**, *1141*, 303–308.
136. Latimer, M. J.; DeRose, V. J.; Yachandra, V. K.; Sauer, K.; Klein, M. P. *J. Phys. Chem. B* **1998**, *102*, 8257–8265.
137. Matysik, J.; Alia, ; Nachtegaal, G.; van Gorkom, H. J.; Hoff, A. J.; de Groot, H. J. M. *Biochemistry* **2000**, *39*, 6751–6755.
138. Boussac, A.; Rutherford, A. W. *Biochemistry* **1988**, *27*, 3476–3483.
139. Pecoraro, V. L.; Baldwin, M. J.; Caudle, M. T.; Hsieh, W.-Y.; Law, N. A. *Pure Appl. Chem.* **1998**, *70*, 925–929.
140. Ghanotakis, D. F.; Yocum, C. F. *Annu. Rev. Plant Phys.* **1990**, *41*, 255–276.
141. Bouckaert, J.; Loris, R.; Wyns, L. *Acta Cryst.* **2000**, *D56*, 1569–1576.
142. McPhalen, C. A.; Strynadka, N. C. J.; James, M. N. G. *Adv. Protein Chem.* **1991**, *42*, 77–144.
143. Siegbahn, P. E. M.; Crabtree, R. H. *J. Am. Chem. Soc.* **1999**, *121*, 117–127.
144. Siegbahn, P. E. M. *Inorg. Chem.* **2000**, *39*, 2923–2935.
145. Sandusky, P. O.; Yocum, C. F. *FEBS Lett.* **1983**, *162*, 339–343.
146. Sandusky, P. O.; Yocum, C. F. *Biochim. Biophys. Acta* **1986**, *849*, 85–93.
147. Sandusky, P. O.; Yocum, C. F. *Biochim. Biophys. Acta* **1984**, *766*, 603–611.
148. Lindberg, K.; Andréasson, L.-E. *Biochemistry* **1996**, *35*, 14259–14267.
149. Lindberg, K.; Vänngård, T.; Andréasson, L. E. *Photosynth. Res.* **1993**, *38*, 401–408.
150. Lindberg, K.; Wydrzynski, T.; Vänngård, T.; Andréasson, L. E. *FEBS Lett.* **1990**, *264*, 153–155.
151. DeRose, V. J.; Latimer, M. J.; Zimmermann, J. L.; Mukerji, I.; Yachandra, V. K.; Sauer, K.; Klein, M. P. *Chem. Phys.* **1995**, *194*, 443–459.
152. Wincencjusz, H.; van Gorkom, H. J.; Yocum, C. F. *Biochemistry* **1997**, *36*, 3663–3670.
153. Boussac, A.; Setif, P.; Rutherford, A. W. *Biochemistry* **1992**, *31*, 1224–1234.
154. vanVliet, P.; Rutherford, A. W. *Biochemistry* **1996**, *35*, 1829–1839.
155. Baumgarten, M.; Philo, J. S.; Dismukes, G. C. *Biochemistry* **1990**, *29*, 10814–10822.
156. Szalai, V. A.; Kühne, H.; Lakshmi, K. V.; Brudvig, G. W. *Biochemistry* **1998**, *37*, 13594–13603.
157. Force, D. A.; Randall, D. W.; Britt, R. D. *Biochemistry* **1997**, *36*, 12062–12070.
158. MacLachlan, D. J.; Nugent, J. H. A. *Biochemistry* **1993**, *32*, 9772–9780.
159. Hillier, W.; Messinger, J.; Wydrzynski, T. *Biochemistry* **1998**, *37*, 16908–16914.
160. Beck, W. F.; de Paula, J. C.; Brudvig, G. W. *J. Am. Chem. Soc.* **1986**, *108*, 4018–4022.
161. Britt, R. D.; Zimmermann, J. L.; Sauer, K.; Klein, M. P. *J. Am. Chem. Soc.* **1989**, *111*, 3522–3532.
162. Dau, H.; Andrews, J. C.; Roelofs, T. A.; Latimer, M. J.; Liang, W. C.; Yachandra, V. K.; Sauer, K.; Klein, M. P. *Biochemistry* **1995**, *34*, 5274–5287.
163. Zimmermann, J.-L.; Rutherford, A. W. *Biochemistry* **1986**, *25*, 4609–4614.
164. Force, D. A.; Randall, D. W.; Lorigan, G. A.; Clemens, K. L.; Britt, R. D. *J. Am. Chem. Soc.* **1998**, *120*, 13321–13333.
165. Sarneski, J. E.; Thorp, H. H.; Brudvig, G. W.; Crabtree, R. H.; Schulte, G. K. *J. Am. Chem. Soc.* **1990**, *112*, 7255–7260.
166. Pal, S.; Armstrong, W. H. *Inorg. Chem.* **1992**, *31*, 5417–5423.
167. Manchanda, R.; Brudvig, G. W.; Crabtree, R. H.; Sarneski, J. E.; Didiuk, M. *Inorg. Chim. Acta* **1993**, *212*, 135–137.
168. Cooper, S. R.; Calvin, M. *J. Am. Chem. Soc.* **1977**, *99*, 6623–6630.
169. Vincent, J. B.; Christmas, C.; Huffman, J. C.; Christou, G.; Chang, H. R.; Hendrickson, D. N. *J. Chem. Soc. Chem. Comm.* **1987**, *4*, 236–238.
170. Bashkin, J. S.; Schake, A. R.; Vincent, J. B.; Chang, H. R.; Li, Q. Y.; Huffman, J. C.; Christou, G.; Hendrickson, D. N. *J. Chem. Soc. Chem. Comm.* **1988**, 700–702.
171. Ménage, S.; Girerd, J.-J.; Gleizes, A. *J. Chem. Soc. Chem. Comm.* **1988**, 431–432.
172. Dave, B. C.; Czernuszewicz, R. S.; Bond, M. R.; Carrano, C. J. *Inorg. Chem.* **1993**, *32*, 3593–3594.
173. Vincent, J. B.; Tsai, H.-L.; Blackman, A. G.; Wang, S.; Boyd, P. D. W.; Folting, K.; Huffman, J. C.; Lobkovsky, E. B.; Hendrickson, D. N.; Christou, G. *J. Am. Chem. Soc.* **1993**, *115*, 12353–12361.
174. Philouze, C.; Blondin, G.; Girerd, J. J.; Guilhem, J.; Pascard, C.; Lexa, D. *J. Am. Chem. Soc.* **1994**, *116*, 8557–8565.
175. Dave, B. C.; Czernuszewicz, R. S. *New J. Chem.* **1994**, *18*, 149–155.
176. Wilson, C.; Larsen, F. K.; Figgis, B. N. *Acta Crystallogr. C* **1998**, *54*, 1797–1799.
177. Albela, B.; El Fallah, M. S.; Ribas, J.; Folting, K.; Christou, G.; Hendrickson, D. N. *Inorg. Chem.* **2001**, *40*, 1037–1044.
178. Limburg, J.; Vrettos, J. S.; Liable-Sands, L. M.; Rheingold, A. L.; Crabtree, R. H.; Brudvig, G. W. *Science* **1999**, *283*, 1524–1527.
179. Collomb, M. N.; Deronzier, A.; Richardot, A.; Pecaut, J. *New J. Chem.* **1999**, *23*, 351–353.

180. Pal, S.; Olmstead, M. M.; Armstrong, W. H. *Inorg. Chem.* **1995**, *34*, 4708–4715.
181. Feichtinger, D.; Plattner, D. A. *Angew. Chem. Int. Ed. Engl.* **1997**, *36*, 1718–1719.
182. Christou, G. *Acc. Chem. Res.* **1989**, *22*, 328–335.
183. Reddy, K. R.; Rajasekharan, M. V.; Arulsamy, N.; Hodgson, D. J. *Inorg. Chem.* **1996**, *35*, 2283–2286.
184. Auger, N.; Girerd, J. J.; Corbella, M.; Gleizes, A.; Zimmermann, J. L. *J. Am. Chem. Soc.* **1990**, *112*, 448–450.
185. Pal, S.; Chan, M. K.; Armstrong, W. H. *J. Am. Chem. Soc.* **1992**, *114*, 6398–6406.
186. Philouze, C.; Blondin, G.; Ménage, S.; Auger, N.; Girerd, J. J.; Vigner, D.; Lance, M.; Nierlich, M. *Angew. Chem. Int. Ed. Engl.* **1992**, *31*, 1629–1631.
187. Hagen, K. S.; Westmoreland, T. D.; Scott, M. J.; Armstrong, W. H. *J. Am. Chem. Soc.* **1989**, *111*, 1907–1909.
188. Ruettinger, W. F.; Ho, D. M.; Dismukes, G. C. *Inorg. Chem.* **1999**, *38*, 1036–1037.
189. DeRose, V. J.; Mukerji, I.; Latimer, M. J.; Yachandra, V. K.; Sauer, K.; Klein, M. P. *J. Am. Chem. Soc.* **1994**, *116*, 5239–5249.
190. Kirby, J. A.; Robertson, A. S.; Smith, J. P.; Thompson, A. C.; Cooper, S. R.; Klein, M. P. *J. Am. Chem. Soc.* **1981**, *103*, 5529–5537.
191. Blomberg, M. R. A.; Siegbahn, P. E. M.; Styring, S.; Babcock, G. T.; Åkermark, B.; Korall, P. *J. Am. Chem. Soc.* **1997**, *119*, 8285–8292.
192. Thorp, H. H. *Inorg. Chem.* **1992**, *31*, 1585–1588.
193. George, G. N.; Prince, R. C.; Cramer, S. P. *Science* **1989**, *243*, 789–791.
194. Guiles, R. D.; Yachandra, V. K.; McDermott, A. E.; Cole, J. L.; Dexheimer, S. L.; Britt, D. R.; Sauer, K.; Klein, M. P. *Biochemistry* **1990**, *29*, 486–496.
195. Manchanda, R.; Brudvig, G. W.; Crabtree, R. H. *Coord. Chem. Rev.* **1995**, *144*, 1–38.
196. Thorp, H. H.; Brudvig, G. W. *New J. Chem.* **1991**, *15*, 479–490.
197. Wang, S. Y.; Folting, K.; Streib, W. E.; Schmitt, E. A.; McCusker, J. K.; Hendrickson, D. N.; Christou, G. *Angew. Chem. Int. Ed. Engl.* **1991**, *30*, 305–306.
198. Wieghardt, K.; Bossek, U.; Gebert, W. *Angew. Chem. Int. Ed. Engl.* **1983**, *22*, 328–329.
199. Caudle, M. T.; Kampf, J. W.; Kirk, M. L.; Rasmussen, P. G.; Pecoraro, V. L. *J. Am. Chem. Soc.* **1997**, *119*, 9292–9298.
200. Hasegawa, K.; Ono, T.-A.; Inoue, Y.; Kusunoki, M. *Chem. Phys. Lett.* **1999**, *300*, 9–19.
201. Dave, B. C.; Czernuszewicz, R. S. *Inorg. Chim. Acta* **1998**, *281*, 25–35.
202. Dube, C. E.; Wright, D. W.; Pal, S.; Bonitatebus, P. J.; Armstrong, W. H. *J. Am. Chem. Soc.* **1998**, *120*, 3704–3716.
203. Torayama, H.; Nishide, T.; Asada, H.; Fujiwara, M.; Matsushita, T. *Polyhedron* **1998**, *17*, 105–118.
204. Hage, R.; Krijnen, B.; Warnaar, J. B.; Hartl, F.; Stufkens, D. J.; Snoeck, T. L. *Inorg. Chem.* **1995**, *34*, 4973–4978.
205. Brewer, K. J.; Calvin, M.; Lumpkin, R. S.; Otvos, J. W.; Spreer, L. O. *Inorg. Chem.* **1989**, *28*, 4446–4451.
206. Hagen, K. S.; Armstrong, W. H.; Hope, H. *Inorg. Chem.* **1988**, *27*, 967–969.
207. Manchanda, R.; Thorp, H. H.; Brudvig, G. W.; Crabtree, R. H. *Inorg. Chem.* **1991**, *30*, 494–497.
208. Hammarström, L.; Sun, L. C.; Åkermark, B.; Styring, S. *Spectroc. Acta A* **2001**, *57*, 2145–2160.
209. Sun, L. C.; Raymond, M. K.; Magnuson, A.; LeGourriérec, D.; Tamm, M.; Abrahamsson, M.; Kenéz, P. H.; Mårtensson, J.; Stenhagen, G.; Hammarström, L.; Styring, S.; Åkermark, B. *J. Inorg. Biochem.* **2000**, *78*, 15–22.
210. Sjödin, M.; Styring, S.; Åkermark, B.; Sun, L. C.; Hammarström, L. *J. Am. Chem. Soc.* **2000**, *122*, 3932–3936.
211. Hammarström, L.; Sun, L. C.; Åkermark, B.; Styring, S. *Catal. Today* **2000**, *58*, 57–69.
212. Sun, L. C.; Burkitt, M.; Tamm, M.; Raymond, M. K.; Abrahamsson, M.; LeGourriérec, D.; Frapart, Y.; Magnuson, A.; Kenéz, P. H.; Brandt, P.; Tran, A.; Hammarström, L.; Styring, S.; Åkermark, B. *J. Am. Chem. Soc.* **1999**, *121*, 6834–6842.
213. Magnuson, A.; Frapart, Y.; Abrahamsson, M.; Horner, O.; Åkermark, B.; Sun, L. C.; Girerd, J. J.; Hammarström, L.; Styring, S. *J. Am. Chem. Soc.* **1999**, *121*, 89–96.
214. Sun, L. C.; Berglund, H.; Davydov, R.; Norrby, T.; Hammarström, L.; Korall, P.; Börje, A.; Philouze, C.; Berg, K.; Tran, A.; Andersson, M.; Stenhagen, G.; Mårtensson, J.; Almgren, M.; Styring, S.; Åkermark, B. *J. Am. Chem. Soc.* **1997**, *119*, 6996–7004.
215. Magnuson, A.; Berglund, H.; Korall, P.; Hammarström, L.; Åkermark, B.; Styring, S.; Sun, L. C. *J. Am. Chem. Soc.* **1997**, *119*, 10720–10725.
216. Limburg, J.; Vrettos, J. S.; de Paula, J. C.; Crabtree, R. H.; Brudvig, G. W. *J. Am. Chem. Soc.* **2001**, *123*, 423–430.
217. Shafirovich, V. Y.; Khannanov, N. K.; Shilov, A. E. *J. Inorg. Biochem.* **1981**, *15*, 113–129.
218. Luneva, N. P.; Knerelman, E. I.; Shafirovich, V. Y.; Shilov, A. E. *J. Chem. Soc. Chem. Comm.* **1987**, 1504–1505.
219. Ramaraj, R.; Kira, A.; Kaneko, M. *Chem. Lett.* **1987**, 261–264.
220. Ramaraj, R.; Kira, A.; Kaneko, M. *Angew. Chem. Int. Edit.* **1986**, *25*, 825–827.
221. Gersten, S. W.; Samuels, G. J.; Meyer, T. J. *J. Am. Chem. Soc.* **1982**, *104*, 4029–4030.
222. Hurst, J. K.; Zhou, J.; Lei, Y. *Inorg. Chem.* **1992**, *31*, 1010–1017.
223. Hoganson, C. W.; Babcock, G. T. *Science* **1997**, *277*, 1953–1956.
224. Tommos, C.; Hoganson, C. W.; Di Valentin, M.; Lydakis-Simantiris, N.; Dorlet, P.; Westphal, K.; Chu, H.-A.; McCracken, J.; Babcock, G. T. *Curr. Opin. Chem. Biol.* **1998**, *2*, 244–252.
225. Bernadou, J.; Meunier, B. *J. Chem. Soc. Chem. Comm.* **1998**, 2167–2173.
226. Christen, G.; Seeliger, A.; Renger, G. *Biochemistry* **1999**, *38*, 6082–6092.
227. Diner, B. A.; Force, D. A.; Randall, D. W.; Britt, R. D. *Biochemistry* **1998**, *37*, 17931–17943.
228. Christen, G.; Renger, G. *Biochemistry* **1999**, *38*, 2068–2077.
229. de Paula, J. C.; Innes, J. B.; Brudvig, G. W. *Biochemistry* **1985**, *24*, 8114–8120.
230. Styring, S.; Rutherford, A. W. *Biochim. Biophys. Acta* **1988**, *933*, 378–387.
231. Tang, X.-S.; Randall, D. W.; Force, D. A.; Diner, B. A.; Britt, R. D. *J. Am. Chem. Soc.* **1996**, *118*, 7638–7639.
232. Tommos, C.; Tang, X.-S.; Warncke, K.; Hoganson, C. W.; Styring, S.; McCracken, J.; Diner, B. A.; Babcock, G. T. *J. Am. Chem. Soc.* **1995**, *117*, 10325–10335.
233. Caudle, M. T.; Pecoraro, V. L. *J. Am. Chem. Soc.* **1997**, *119*, 3415–3416.
234. Bordwell, F. G.; Cheng, J.-P. *J. Am. Chem. Soc.* **1991**, *113*, 1736–1743.
235. Mayer, J. M. *Accounts Chem. Res.* **1998**, *31*, 441–450.
236. Bakac, A. *J. Am. Chem. Soc.* **2000**, *122*, 1092–1097.

237. Robblee, J. H.; Cinco, R. M.; Yachandra, V. K. *Biochim. Biophys. Acta* **2001**, *1503*, 7–23.
238. Frapart, Y. M.; Boussac, A.; Albach, R.; Anxolabéhère-Mallart, E.; Delroisse, M.; Verlhac, J. B.; Blondin, G.; Girerd, J. J.; Guilhem, J.; Cesario, M.; Rutherford, A. W.; Lexa, D. *J. Am. Chem. Soc.* **1996**, *118*, 2669–2678.
239. Suzuki, M.; Senda, H.; Kobayashi, Y.; Oshio, H.; Uehara, A. *Chem. Lett.* **1988**, 1763–1766.
240. Torayama, H.; Asada, H.; Fujiwara, M.; Matsushita, T. *Chem. Lett.* **1996**, 1067–1068.
241. Torayama, H.; Asada, H.; Fujiwara, M.; Matsushita, T. *Polyhedron* **1998**, *17*, 3859–3874.
242. Plaksin, P. M.; Palenik, G. J.; Stoufer, R. C.; Mathew, M. *J. Am. Chem. Soc.*, **1972**, *94*, 2121, 2122.
243. Gallo, E.; Solari, E.; Re, N.; Floriani, C.; ChiesiVilla, A.; Rizzoli, C. *J. Am. Chem. Soc.* **1997**, *119*, 5144–5154.
244. Schindler, S.; Walter, O.; Pedersen, J. Z.; Toftlund, H. *Inorg. Chim. Acta* **2000**, *303*, 215–219.
245. Goodson, P. A.; Oki, A. R.; Glerup, J.; Hodgson, D. J. *J. Am. Chem. Soc.* **1990**, *112*, 6248–6254.
246. Goodson, P. A.; Glerup, J.; Hodgson, D. J.; Michelsen, K.; Pedersen, E. *Inorg. Chem.* **1990**, *29*, 503–508.
247. Law, N. A.; Kampf, J. W.; Pecoraro, V. L. *Inorg. Chim. Acta* **2000**, *297*, 252–264.
248. Goodson, P. A.; Hodgson, D. *J. Inorg. Chem.* **1989**, *28*, 3606–3608.
249. Sarneski, J. E.; Didiuk, M.; Thorp, H. H.; Crabtree, R. H.; Brudvig, G. W.; Faller, J. W.; Schulte, G. K. *Inorg. Chem.* **1991**, *30*, 2833–2835.
250. Iikura, H.; Nagata, T. *Inorg. Chem.* **1998**, *37*, 4702–4711.
251. Ramalakshmi, D.; Rajasekharan, M. V. *Acta Crystallogr. B* **1999**, *55*, 186–191.
252. Towle, D. K.; Botsford, C. A.; Hodgson, D. J. *Inorg. Chim. Acta* **1988**, *141*, 167–168.
253. Asada, H.; Ozeki, M.; Fujiwara, M.; Matsushita, T. *Chem. Lett.* **1999**, 525–526.
254. Jensen, A. F.; Su, Z. W.; Hansen, N. K.; Larsen, F. K. *Inorg. Chem.* **1995**, *34*, 4244–4252.
255. Manchanda, R.; Brudvig, G. W.; Degala, S.; Crabtree, R. H. *Inorg. Chem.* **1994**, *33*, 5157–5160.
256. Stebler, M.; Ludi, A.; Burgi, H. B. *Inorg. Chem.* **1986**, *25*, 4743–4750.
257. Libby, E.; Webb, R. J.; Streib, W. E.; Folting, K.; Huffman, J. C.; Hendrickson, D. N.; Christou, G. *Inorg. Chem.* **1989**, *28*, 4037–4040.
258. Gohdes, J. W.; Armstrong, W. H. *Inorg. Chem.* **1992**, *31*, 368–373.
259. Aurangzeb, N.; McAuliffe, C. A.; Pritchard, R. G.; Watkinson, M.; Bermejo, M.; Garciadeibe, A.; Sousa, A. *Acta Crystallogr. C* **1993**, *49*, 1945–1947.
260. Larson, E.; Lah, M. S.; Li, X. H.; Bonadies, J. A.; Pecoraro, V. L. *Inorg. Chem.* **1992**, *31*, 373–378.
261. Collins, M. A.; Hodgson, D. J.; Michelsen, K.; Towle, D. K. *J. Chem. Soc. Chem. Comm.* **1987**, 1659–1660.
262. Horner, O.; Charlot, M. F.; Boussac, A.; Anxolabéhère-Mallart, E.; Tchertanov, L.; Guilhem, J.; Girerd, J. J. *Eur. J. Inorg. Chem.* **1998**, 721–727.
263. Glerup, J.; Goodson, P. A.; Hazell, A.; Hazell, R.; Hodgson, D. J.; McKenzie, C. J.; Michelsen, K.; Rychlewska, U.; Toftlund, H. *Inorg. Chem.* **1994**, *33*, 4105–4111.
264. Schafer, K. O.; Bittl, R.; Zweygart, W.; Lendzian, F.; Haselhorst, G.; Weyhermuller, T.; Wieghardt, K.; Lubitz, W. *J. Am. Chem. Soc.* **1998**, *120*, 13104–13120.
265. Mok, H. J.; Davis, J. A.; Pal, S.; Mandal, S. K.; Armstrong, W. H. *Inorg. Chim. Acta* **1997**, *263*, 385–394.
266. Reddy, K. R.; Rajasekharan, M. V.; Padhye, S.; Dahan, F.; Tuchagues, J. P. *Inorg. Chem.* **1994**, *33*, 428–433.
267. Pal, S.; Gohdes, J. W.; Wilisch, W. C. A.; Armstrong, W. H. *Inorg. Chem.* **1992**, *31*, 713–716.
268. Wieghardt, K.; Bossek, U.; Zsolnai, L.; Huttner, G.; Blondin, G.; Girerd, J. J.; Babonneau, F. *J. Chem. Soc. Chem. Comm.* **1987**, 651–653.
269. Ruiz, R.; Sangregorio, C.; Caneschi, A.; Rossi, P.; Gaspar, A. B.; Real, J. A.; Munoz, M. C. *Inorg. Chem. Commun.* **2000**, *3*, 361–367.
270. Koek, J. H.; Russell, S. W.; vanderWolf, L.; Hage, R.; Warnaar, J. B.; Spek, A. L.; Kerschner, J.; DelPizzo, L. *J. Chem. Soc. Dalton* **1996**, 353–362.
271. Wieghardt, K.; Bossek, U.; Nuber, B.; Weiss, J.; Bonvoisin, J.; Corbella, M.; Vitols, S. E.; Girerd, J. J. *J. Am. Chem. Soc.* **1988**, *110*, 7398–7411.
272. Horner, O.; Anxolabéhère-Mallart, E.; Charlot, M. F.; Tchertanov, L.; Guilhem, J.; Mattioli, T. A.; Boussac, A.; Girerd, J. *J. Inorg. Chem.* **1999**, *38*, 1222–1232.
273. Bossek, U.; Hummel, H.; Weyhermuller, T.; Wieghardt, K.; Russell, S.; van der Wolf, L.; Kolb, U. *Angew. Chem. Int. Edit.* **1996**, *35*, 1552–1554.
274. Oberhausen, K. J.; Obrien, R. J.; Richardson, J. F.; Buchanan, R. M.; Costa, R.; Latour, J. M.; Tsai, H. L.; Hendrickson, D. N. *Inorg. Chem.* **1993**, *32*, 4561–4565.
275. Kipke, C. A.; Scott, M. J.; Gohdes, J. W.; Armstrong, W. H. *Inorg. Chem.* **1990**, *29*, 2193–2194.
276. Arulsamy, N.; Glerup, J.; Hazell, A.; Hodgson, D. J.; McKenzie, C. J.; Toftlund, H. *Inorg. Chem.* **1994**, *33*, 3023–3025.
277. Darovsky, A.; Kezerashvili, V.; Coppens, P.; Weyhermüller, T.; Hummel, H.; Wieghardt, K. *Inorg. Chem.* **1996**, *35*, 6916–6917.
278. Hessel, L. W.; Romers, C. *Recl. Trav. Chim. Pays-Bas* **1969**, *88*, 545–552.
279. Zhang, L.; Yan, S. P.; Li, C. H.; Liao, D. Z.; Jiang, Z. H.; Cheng, P.; Wang, G. L.; Weng, L. H.; Leng, X. B. *J. Chem. Crystallogr.* **2000**, *30*, 251–254.
280. Kirk, M. L.; Chan, M. K.; Armstrong, W. H.; Solomon, E. I. *J. Am. Chem. Soc.* **1992**, *114*, 10432–10440.
281. Chan, M. K.; Armstrong, W. H. *J. Am. Chem. Soc.* **1991**, *113*, 5055–5057.
282. Boskovic, C.; Folting, K.; Christou, G. *Polyhedron* **2000**, *19*, 2111–2118.
283. Bouwman, E.; Bolcar, M. A.; Libby, E.; Huffman, J. C.; Folting, K.; Christou, G. *Inorg. Chem.* **1992**, *31*, 5185–5192.
284. Wemple, M. W.; Tsai, H. L.; Wang, S. Y.; Claude, J. P.; Streib, W. E.; Huffman, J. C.; Hendrickson, D. N.; Christou, G. *Inorg. Chem.* **1996**, *35*, 6437–6449.
285. Wang, S. Y.; Huffman, J. C.; Folting, K.; Streib, W. E.; Lobkovsky, E. B.; Christou, G. *Angew. Chem. Int. Ed. Engl.* **1991**, *30*, 1672–1674.
286. Kulawiec, R. J.; Crabtree, R. H.; Brudvig, G. W.; Schulte, G. K. *Inorg. Chem.* **1988**, *27*, 1309–1311.
287. Wemple, M. W.; Coggin, D. K.; Vincent, J. B.; McCusker, J. K.; Streib, W. E.; Huffman, J. C.; Hendrickson, D. N.; Christou, G. *J. Chem. Soc. Dalton* **1998**, 719–725.
288. Vincent, J. B.; Christmas, C.; Chang, H. R.; Li, Q. Y.; Boyd, P. D. W.; Huffman, J. C.; Hendrickson, D. N.; Christou, G. *J. Am. Chem. Soc.* **1989**, *111*, 2086–2097.

289. Christmas, C.; Vincent, J. B.; Huffman, J. C.; Christou, G.; Chang, H. R.; Hendrickson, D. N. *J. Chem. Soc. Chem. Comm.* **1987**, 1303–1305.
290. Tomida, S.; Matsushima, H.; Koikawa, M.; Tokii, T. *Chem. Lett.* **1999**, 437–438.
291. Libby, E.; Folting, K.; Huffman, C. J.; Huffman, J. C.; Christou, G. *Inorg. Chem.* **1993**, *32*, 2549–2556.
292. Libby, E.; McCusker, J. K.; Schmitt, E. A.; Folting, K.; Hendrickson, D. N.; Christou, G. *Inorg. Chem.* **1991**, *30*, 3486–3495.
293. Wang, S. Y.; Wemple, M. S.; Yoo, J.; Folting, K.; Huffman, J. C.; Hagen, K. S.; Hendrickson, D. N.; Christou, G. *Inorg. Chem.* **2000**, *39*, 1501–1513.
294. Wang, S. Y.; Tsai, H. L.; Hagen, K. S.; Hendrickson, D. N.; Christou, G. *J. Am. Chem. Soc.* **1994**, *116*, 8376–8377.
295. Wemple, M. W.; Tsai, H. L.; Folting, K.; Hendrickson, D. N.; Christou, G. *Inorg. Chem.* **1993**, *32*, 2025–2031.
296. Hendrickson, D. N.; Christou, G.; Schmitt, E. A.; Libby, E.; Bashkin, J. S.; Wang, S. Y.; Tsai, H. L.; Vincent, J. B.; Boyd, P. D. W.; Huffman, J. C.; Folting, K.; Li, Q. Y.; Streib, W. E. *J. Am. Chem. Soc.* **1992**, *114*, 2455–2471.
297. Li, Q.; Vincent, J. B.; Libby, E.; Chang, H. R.; Huffman, J. C.; Boyd, P. D. W.; Christou, G.; Hendrickson, D. N. *Angew. Chem. Int. Ed. Engl.* **1988**, *27*, 1731–1733.
298. Wang, S. Y.; Tsai, H. L.; Libby, E.; Folting, K.; Streib, W. E.; Hendrickson, D. N.; Christou, G. *Inorg. Chem.* **1996**, *35*, 7578–7589.
299. Brechin, E. K.; Yoo, J.; Nakano, M.; Huffman, J. C.; Hendrickson, D. N.; Christou, G. *Chem. Commun.* **1999**, 783–784.
300. Wemple, M. W.; Adams, D. M.; Hagen, K. S.; Folting, K.; Hendrickson, D. N.; Christou, G. *J. Chem. Soc. Chem. Comm.* **1995**, 1591–1593.
301. Wemple, M. W.; Adams, D. M.; Folting, K.; Hendrickson, D. N.; Christou, G. *J. Am. Chem. Soc.* **1995**, *117*, 7275–7276.
302. Aromi, G.; Wemple, M. W.; Aubin, S. J.; Folting, K.; Hendrickson, D. N.; Christou, G. *J. Am. Chem. Soc.* **1998**, *120*, 5850–5851.
303. Wang, S.; Tsai, H. L.; Streib, W. E.; Christou, G.; Hendrickson, D. N. *J. Chem. Soc. Chem. Comm.* **1992**, 1427–1429.
304. Ruettinger, W. F.; Campana, C.; Dismukes, G. C. *J. Am. Chem. Soc.* **1997**, *119*, 6670–6671.
305. Lind, J.; Shen, X.; Eriksen, T. E.; Merényi, G. *J. Am. Chem. Soc.* **1990**, *112*, 479–482.
306. Baldwin, M. J.; Pecoraro, V. L. *J. Am. Chem. Soc.* **1996**, *118*, 11325–11326.
307. Thorp, H. H.; Sarneski, J. E.; Brudvig, G. W.; Crabtree, R. H. *J. Am. Chem. Soc.* **1989**, *111*, 9249–9250.
308. Halfen, J. A.; Mahapatra, S.; Wilkinson, E. C.; Kademi, S.; Young, V. G. Jr.; Gue, L. Jr.; Zuberbühler, A. D.; Tolman, W. B. *Science* **1996**, *271*, 1397–1400.

8.21
Hydrogen Activation

I. P. GEORGAKAKI and M. Y. DARENSBOURG
*Texas A & M University, College Station, Texas, USA*

8.21.1 INTRODUCTION

The popularity of research into the science of hydrogenases enlists biologists, chemists, biophysicists, as well as agriculture, medical, and technological communities. It is also evidenced by a multitude of reviews, so many that a review of the reviews is required as preamble to that which follows. The biology of hydrogenases, "Classification and Phylogeny of Hydrogenases," written by P. M. Vignais, B. Billoud, and J. Meyer is addressed in terms of cellular function, sequence homologies and genome sequences, biosynthesis, and localization in cells.[1] This comprehensive review both establishes the phylogenetic distinctiveness of the two classes of metal-containing hydrogenases, iron-only ([Fe]H_2ase) and nickel–iron ([NiFe]H_2ase) hydrogenases, and attempts to simplify the nomenclature of H_2ase-encoding genes.[1]

The historically important compendium, "The Bioinorganic Chemistry of Nickel," was written within a few years of the discovery of nickel in [NiFe]H_2ase.[2] It places the biochemistry of [NiFe]H_2ase within the context of other Ni-containing enzymes and presents the spectral, especially EPR, and biological data that encouraged bioinorganic chemists to enter the area of chemical models. Published in 1988,[2] this was prior to knowledge of protein crystal structures. An equally significant and excellent text edited by Richard Cammack, Michel Frey, and Robert Robson titled "Hydrogen as a Fuel" appeared in 2001 and contains up-to-the-minute descriptions of hydrogenase structures, spectroscopies, origins, evolution and biodiversity, and the potential for hydrogenase in biotechnology.[3] It describes in detail the important biochemical experiments for isolation and characterization, including electrochemistry and redox titrations to establish the various redox levels wherein H_2 production and uptake occurs.
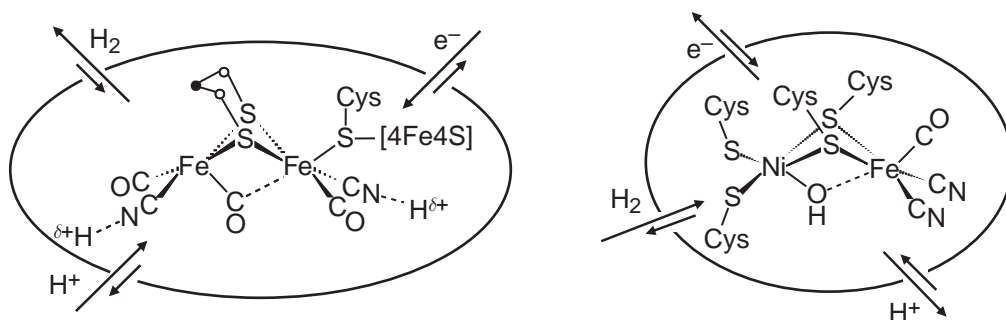
Figure 1 Generalized active site structures of the metallohydrogenases, showing entry points of e^-, H_2, and H^+.

The last topic, relating to fuel cells and future technologies, is treated in a popular manner in "Tomorrow's Energy: Hydrogen Fuel Cells and the Prospects for a Cleaner Planet" by Peter Hoffmann.[4] At the other extreme of the applications approach is "The Modern Inorganic Chemistry Series," which published "Metal Dihydrogen and σ-Bond Complexes" by Gregory Kubas in 2001.[5] Chapter 10 of that book presents a review of the chemistry behind the activation of hydrogen and related small molecules by metalloenzymes. Of the numerous shorter reviews, especially recommended is Michel Frey's "Hydrogenases: Hydrogen-Activating Enzymes".[6] One of us co-authored a review devoted to the organometallic iron sites in hydrogenases in 2000, which serves as background to the unique $Fe(CO)_n(CN)_{3-n}$ sites found in both metallohydrogenases, and the chemistry possible with a probably primordial precursor, $(\mu\text{-}S_2)Fe_2(CO)_6$.[7] Schröder *et al.* reviewed models appropriate to [NiFe]H$_2$ase in 2001.[8] The focus of the discussion presented below is the chemist's view of the active sites of hydrogenases, and the coordination chemistry displayed in their structures, that might provide clues as to mechanism of action.

The development of electrocatalysts for H_2 production which might mimic the hydrogenases has been a recurring theme in inorganic chemical research over the past half-century. It was not until the last decade (1995 →), however, that synthetic chemists were gifted with a set of plans for the construction of the active sites of metallohydrogenases. This was the decade of hydrogenase protein crystallography. As mentioned above, a wealth of precursor work from a diverse and international pool of biologists, spectroscopists, and biochemists aided in the rapid incorporation of the emerging structural features into a comprehensive view of the mechanism of hydrogenase activity. This view was articulated with clarity and in depth by the crystallographers themselves, whose publications demonstrated extensive scope and knowledge of the field. About the structures of [NiFe] and Fe-only hydrogenases, it is expressed no better than in Richard Cammack's words:[3] "The structures of the metal-containing hydrogenases reflect, in an unexpectedly literal way, the different components of the reaction:"

$$2H^+ + 2e^- \rightleftharpoons H_2 \qquad (1)$$

Thus the cartoons of Figure 1, which generalize the active site structures of [NiFe][9–15] and Fe–H$_2$ases[16–19], cannot do justice to the amazing work of the protein crystallographers who established the paths of electron transfer (a line of iron–sulfur clusters characteristically spaced by $\sim$12.5 Å), proton transfer (an obvious chain of H^+ hand-off sites involving amino acid carboxyl, amines, hydroxyls, etc. as donor–acceptor groups), and an H_2 access route (a hydrophobic channel shown to be filled with xenon in one crystal structure[20] and similarly observed in all H$_2$ase structures).[21]

Neglecting the complexities of the protein *sans* active site and its interactions with ancillary protein is, of course, a dangerous business. Nevertheless, our expertise is with coordination chemistry, which is the point of interest of this volume. Hence, the following comments are directed towards analysis of the active sites of hydrogenases which facilitate the simplest of reactions in all of chemistry.

## 8.21.2 THE ROLES OF TRANSITION METALS IN H$_2$ ACTIVATION: A PRIMER OF η^2-H$_2$ COMPLEXES AND THEIR REACTIVITY

The isolation and full characterization of dihydrogen complexes by Gregory Kubas in 1984 represents a pivotal point in coordination chemistry.[22] Other discoveries soon followed and the three examples selected for Figure 2 represent various impacts of these mononuclear complexes on fundamental understanding.
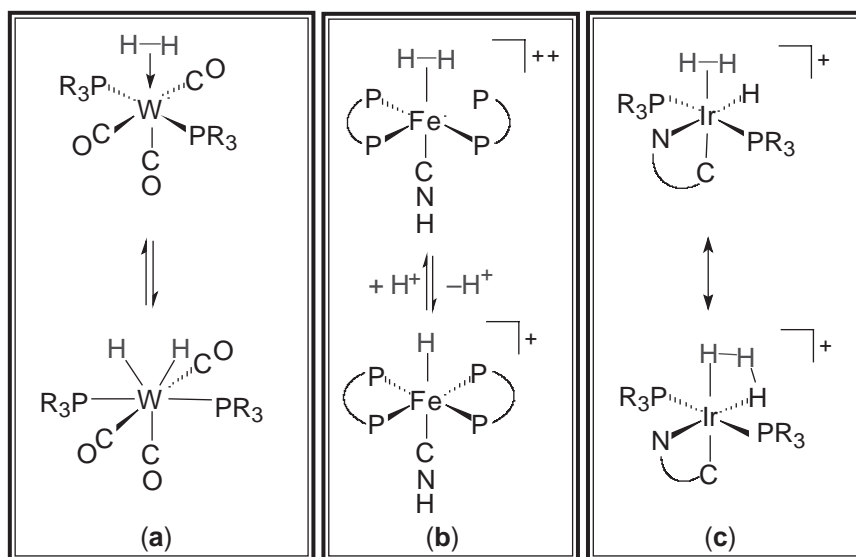
Figure 2 Common η^2-H$_2$ complexes characterized by: (a) Kubas,[23] (b) Morris,[24] and (c) Crabtree.[27]

Note that the stable η^2-H$_2$ complexes presented are all d^6 octahedral complexes involving zero-valent W^0, divalent Fe^{II}, and trivalent Ir^{III}. In such complexes the metal–dihydrogen ligand interactions, H$_2$ σ-donor/metal σ-acceptor and metal π-donor/H$_2$ σ*-acceptor, are balanced so as to lend stability, Scheme 1.

σ-donor σ*-acceptor M^{2+}(H$^-$)$_2$
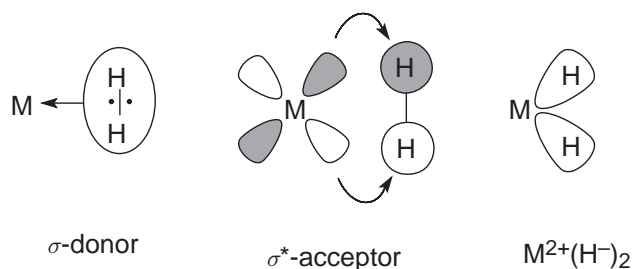
Scheme 1

Insufficient σ-accepting capability of the metal results in H$_2$ loss; excessive π-donor capability from the metal to the η^2-H$_2$ results in full oxidative addition. This latter balance was well demonstrated by the Kubas-type complexes of zero-valent group 6 metals, $(\eta^2$-H$_2)$M(L)$_5$, L = CO, PR$_3$, which showed the equilibrium position depicted in Figure 2 to be controlled by M and the donor ability of PR$_3$.[23] With R = i-Pr, both the η^2-H$_2$ complex and the oxidative addition product, a tungsten(II)dihydride, are in solution simultaneously. In several reviews Kubas noted that the most important factor that determined where the dihydrogen complex lies along the $(\eta^2$-H$_2)$M$^n \rightleftharpoons$ M^{n+2}(H)$_2$ reaction coordinate was the ligand *trans* to the η^2-H$_2$ binding position.[23]

For iron(II), the balance that leads to stable η^2-H$_2$ complexes is demonstrated in the octahedral [trans-$(\eta^2$-H$_2)$(diphos)$_2$(L)Fe]^n (n = +1, L = CN; or +2, L = CNH or CO) complexes of Morris.[24] As indicated by the acidity of the Morris-type complexes, the σ-acceptor ability of Fe^{II} dominates the $(\eta^2$-H$_2)$Fe bonding and facilitates heterolytic cleavage. The enhancement of the acidity of metal-bound H$_2$ over free H$_2$ (pKa of free H$_2$ in THF = ca. 50)[25,26] is in cases a factor of 10, with examples showing acidity equal to that of triflic acid! As heterolytic cleavage is the process whereby H$_2$ is activated by metallohydrogenases, the fundamental properties of Morris' Fe^{II} complexes are of ultimate interest.

The third example given in Figure 2 demonstrates an η^2-H$_2$ complex of Ir^{III} from Crabtree's group that is stabilized by interactions with a terminal hydride ligand as a trihydrogen species.[27] This internal ligand interaction presents an avenue for H/D exchange in H$_2$/D$_2$ mixtures under anhydrous conditions.

8.21.3   ELECTROCHEMICAL PROCESSES: WORKING HYPOTHESES FOR H$_2$ PRODUCTION AND UPTAKE CYCLE

The scope of η^2-H$_2$ interaction and resultant chemistries at monometallic sites is summarized in Figure 3. This is the generally accepted mechanism for an H$^+$/e$^-$-coupled H$_2$ utilization process which for Fe^{II}, for example, would involve on deprotonation of the (η^2-H$_2$) Fe complex, formation of an [Fe^{II}–H]$^-$ followed by oxidation to [Fe^{III}–H]^o. On deprotonation of this species, the original two electrons of the H$_2$ moiety are formally shifted to the Fe; i.e., removal of H$^+$ from [Fe^{III}–H]^o is formally a reductive elimination, generating Fe^I. From Fe^I another electron is removed and another H$_2$ binds to Fe^{II}. This electrochemical mechanism is of the CECE type (Chemical–Electrochemical–Chemical–Electrochemical). While the last two steps might be switched, yielding a CEEC mechanism, there is little doubt of the order of the first two steps.

The reversibility of the electrochemical box mechanism offers an explanation of H/D exchange in H$_2$/D$_2$O or D$_2$/H$_2$O mixtures, a process that is carried out by the enzyme and sometimes used as an activity assay. [28,29] Addition of a deuteron from D$_2$O to the M–H$^-$ generates HD and HOD. Alternatively, deprotonation by D$_2$O and reprotonation of MH$^-$ by [D$_2$OH]$^+$ can also yield HD and HOD.

Notably with a single metal site and innocent ligands, there is an oxidation-state range of 2 units during the course of H$_2$ oxidation or H$^+$ reduction to H$_2$. While binding and heterolytic cleavage of H$_2$ does not change the metal's oxidation state, subsequent extractions of the electrons from the M–H$^-$ results in oxidation-state changes as noted in Figure 3. Note that it is not necessary that moieties bearing each of the three oxidation states be stable and observable. Nevertheless, in the case of [NiFe]H$_2$ase, EPR and redox titration experiments led to the suggestion that such states existed, covering a range of Ni^I to Ni^{III}.[30] This presented coordination chemists with a conundrum, as careful studies found no examples of a single set of ligand donors that could support such states at the positive potentials (-200 to -350 mV) and within the narrow range of biological nickel, ca. 200 mV. Typical ranges for classical coordination complexes are 2 V. That is, the soft donor (organometallic-like) ligand sets which stabilize Ni^I, destabilize Ni^{III}; and the harder donors of "classical" coordination chemistry which stabilize Ni^{III}, destabilize the Ni^I oxidation state. The difference between the Ni$^{I/II}$ and Ni$^{II/III}$ couples stays fairly constant at ca. 2 V in model complexes.

Prior to the X-ray crystal structures of the metallohydrogenases and the discovery of the binuclear active sites, the oxidation-state enigma was addressed in the literature by mechanisms of H$_2$ activation invoking ligand-based cysteine-S reactivity, in conjunction with metal redox changes and H$^+$/e$^-$-coupled processes, Figure 4.[31] Additionally, the prospect of a second metal interaction with the nickel-bound cysteine sulfurs, changing them from RS$^-$ anionic donors to softer, phosphine-like metalated RSM′, was suggested as a capable redox switch, the former stabilizing the Ni$^{III/II}$ couple and the latter permitting access to the Ni$^{II/I}$ couple, Figure 5.[32] This conclusion was based on electrochemical measurements of N$_2$S$_2$Ni complexes and metalated derivatives which provided precedents for such redox changes.

These redox level issues have not been solved, despite the discovery of the more complicated coordination complexes of the binuclear active sites which might offer greater versatility. Binuclear sites provide the possibility of sharing the two-electron changes by two metals; but whether this occurs is not established. The clear result of the protein crystal structures is that the target-model complexes for the active sites are well defined. The next section describes the active sites of [NiFe] and [Fe]H$_2$ases.
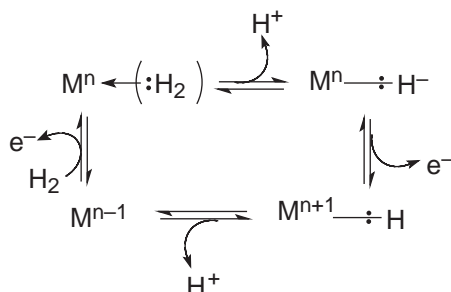
Figure 3   Generally accepted mechanism for H$^+$/e$^-$-coupled H$_2$ utilization process on a transition metal.
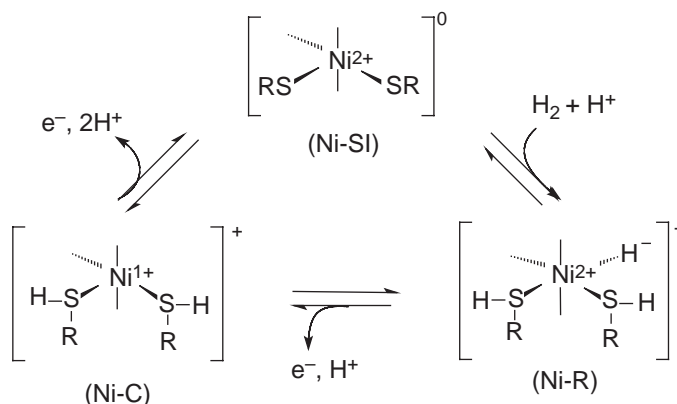
Figure 4 Lindahl's mechanism for H_2 uptake by Ni-cysteine site.[31]
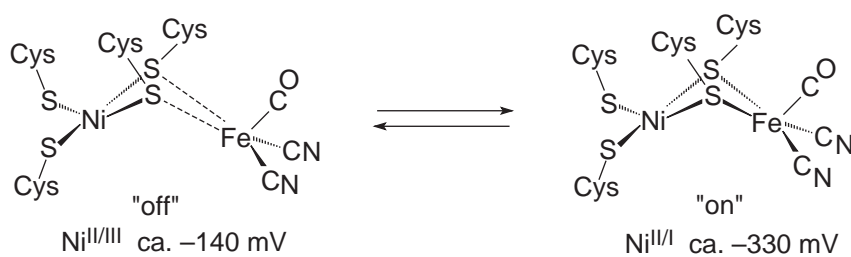
Figure 5 Hypothesis for accessibility of Ni^I/Ni^{III} redox states due to the off/on interaction of the $Fe(CO)(CN)_2$ unit with the Ni-thiolate.[32]

8.21.4 COORDINATION SPHERES OF Ni AND Fe IN THE BINUCLEAR ACTIVE SITES OF [NiFe] AND [Fe]H₂ASES

Figure 1, as well as Figures 6 and 7, gives the stick drawings of the active site structures of [NiFe][9–15] and [Fe]H₂ase.[16–19] From five different bacterial sources, six independent protein crystal-structure determinations find that the common features of the [NiFe] binuclear site are a pyramidal $Fe(CO)(CN)_2$ unit which is incorporated into an octahedron in the oxidized form of the enzymes, with inclusion of the two cysteine sulfurs which bridge to the nickel. Additional terminal cysteines on nickel yield *cis*-dithiolates in a distorted tetrahedral array. In the *Desulfomicrobium baculatum* source, a selenocysteine replaces one of the terminal cysteines as shown in Figure 6b.[11] This [NiFeSe]H₂ase is less susceptible to oxidation and thus permits examination of the reduced state of the enzyme. It differs from the oxidized form, Figure 6a,[9–10] by the absence of the bridging OH^- group and in the decrease in the Ni···Fe distance of ca. 0.4 Å. A recently reported structure of [NiFe]H₂ase derived from the CO-inhibited form of *D. vulgaris Miyazaki* F enzyme yielded the active-site structure, Figure 6c, which shows the exogeneous CO bound to Ni in a bent Ni–CO arrangement.[15] Note that the three diatomic ligands on Fe are not definitely
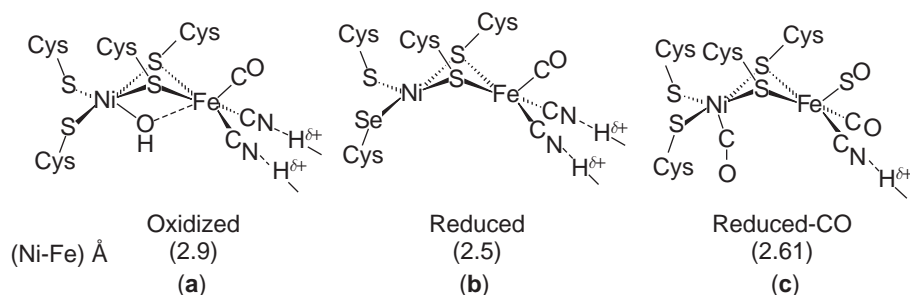
Figure 6 Structures of the (a) oxidized (*D. gigas*);[9,10] (b) reduced (*Dm. baculatum*);[11] and (c) reduced-CO-bound (*D. vulgaris Miyazaki F*)[15] forms of the active site of [NiFe]H₂ase. Ni···Fe distances are given in parentheses in Å.
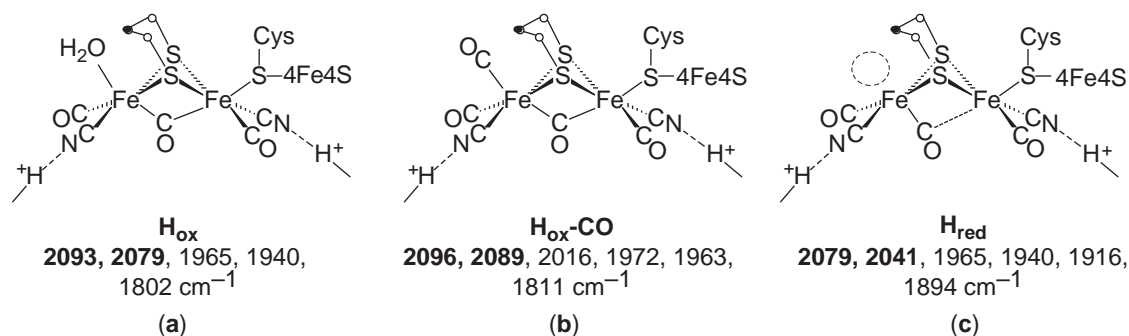
Figure 7 Structures and $\nu(CX)$ IR spectral positions of the (a) oxidized, H_{ox},[16] and (b) CO-inhibited form, H_{ox}–CO,[19] from CpI, and (c) reduced form, H_{red},[17,18] from DdH of [Fe]H$_2$ase active site. (Fe···Fe distances are 2.6 Å for all states).

assigned, but most likely are two basal CN and an apical CO, as in the other [NiFe]H$_2$ases. An SO ligand was proposed for one of the terminal diatomics in earlier studies of the Miyazaki enzyme, but confirmatory vibrational spectroscopy studies are not available.

Structures 7a–7c of Figure 7 are of [Fe]H$_2$ase active sites from different isolations.[16–19] They all show a binuclear iron site that is covalently bound to the protein by only one cysteine ligand. The stabilization of the active site in the protein environment is further supported by H-bonds from the cyanides similar to the [NiFe]H$_2$ases. The two iron atoms are separated by 2.6 Å and are connected by a dithiolate bridging unit in which the sulfurs are linked by three light atoms. As of this writing the exact nature of this three-light-atom bridge has not been resolved, as protein crystallography cannot distinguish among C, O, and N at the resolution level. The SCys bridges the 2Fe2S cluster to a 4Fe4S cluster, which solves a long-standing mystery of the "unusual" 6Fe6S hydrogen-producing, or H-cluster. The distinctly organometallic 2Fe2S cluster bound to the 4Fe4S cluster has a bridging CO ($\nu(CO) \cong 1{,}800\,cm^{-1}$) in the case of structures 7a[16] and 7b,[19] the oxidized forms, while the μ-CO becomes terminal (or only slightly semi-bridging) in the reduced form in which the site *trans* to it appears to be open, structure 7c.[17,18] The oxidized, CO-inhibited form shows the exogenous CO molecule has displaced the H$_2$O molecule in the oxidized form, structure 7b.

A hydrophobic channel which leads from the protein to this side of the binuclear site is taken as further support that this vacancy or CO-binding site is the site of H$_2$ activation (H$_2$-binding or H$_2$ evolution). As this site is close to basic protein residues (a nearby lysine forms a hydrogen bond with the CN$^-$ ligand and, at a more oxidized stage, a cysteine residue is H-bonded to H$_2$O bound at this site), heterolytic splitting of an η^2-H$_2$, with the formation of an Fe-bound hydride, is expected to be facilitated. Oxidation would then lead to another H$^+$ abstraction from the Fe–H by a base. Conversely, H$_2$ formation could also take place at this site; combination of a proton with the reduced cluster would form a hydride bound to the Fe, which upon further protonation would form η^2-H$_2$.

8.21.5 SPECTROSCOPIC STUDIES

While the above crystallographic definition of the active sites provides a clear picture of the biological organometallic catalysts in terms of structural features related to the chemistry of the enzyme, information concerning the possible redox states comes more directly from other sources. The experimentally determined states of the enzyme based on spectroscopic studies using infrared, Mössbauer, and EPR spectroscopies are discussed below.

8.21.5.1 [NiFe]Hydrogenase

As both metalloproteins are active in mixed-valent states, EPR spectroscopy has been used as a primary tool for correlating enzyme activity with redox levels. With the discovery of triply bonded diatomic ligands in the active sites, the powerful tool of vibrational spectroscopy has been applied to all redox levels, including EPR-silent forms. A detailed review of the correlation of EPR signals, FTIR absorptions, and enzyme activity in the [NiFe]H$_2$ases is available.[33] Earlier

interpretation has concluded a redox-stable Fe^{II} unit with the redox activity in the active site localized on nickel, involving $Ni^{III} \rightleftharpoons Ni^{II} \rightleftharpoons Ni^{I}$ oxidation couples. The incongruity of such drastically different coordination environment requirements for these states has led to a two-state hypothesis of oscillations between $Ni^{III} \rightleftharpoons Ni^{II} \rightleftharpoons Ni^{III}$, as mentioned above. Maroney and Bryngelson further advanced an argument that the NiFe binuclear site acts as a unit to delocalize a single-electron redox center which is not amenable to oxidation-state assignments on individual metals.[33] Consistent with this, the range in $\nu(CX)$ values shifts (ca. $40\,cm^{-1}$ for the $\nu(CO)$) indicates significant differences in the electronic environment of Fe in $[NiFe]H_2$ase.

8.21.5.2 [Fe]-only Hydrogenase

FTIR experiments carried out in the active site of $[Fe]H_2$ase from *Desulfovibrio desulfuricans* (DdH) found three different oxidation levels based on the stretching frequencies of the diatomic ligands (CO, CN^-). A summary of these redox states is presented as follows:[18,34]

$$H_{as-isolated} \xrightarrow[+\,e^-]{-535mV} H_{red} \xrightarrow[-\,e^-]{-285mV} H_{ox} \xrightarrow{CO} H_{ox}-CO \qquad (2)$$
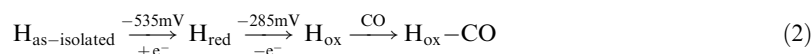
The IR spectrum in the diatomic ligand region of the as-isolated enzyme form DdH shows two bands ($2,107$, $2,087\,cm^{-1}$) that correspond to CN^- ligands, two ($2,007$, $1,983\,cm^{-1}$) in the region of the terminally bound CO, and one ($1,847\,cm^{-1}$) that is assigned as a semi-bridging or bridging CO. Note that this form is more oxidized than the H_{ox} whose representation and IR spectrum is given in Figure 7. Upon reduction at $-535\,mV$ the IR spectrum shows a more complicated pattern, whose dominant feature is the shift of the $1,847$ peak to $1,894\,cm^{-1}$ (well within the region of a terminal CO) with a major increase in its intensity.[18] The magnitude of this intensity increase results in a band pattern that is unexplained.

Based on this result and consistent with the available active-site structure, determined by protein crystallography, the main consequence of the reduction is the movement of the bridging CO to a terminal position. For example, the Fe···Fe distance is constant at $2.6\,\text{Å}$ within the limits of the structure resolution. Re-oxidation at $-285\,mV$ results in a spectrum with a pattern similar to that of the as-isolated state with all the adsorptions shifted to lower wave numbers (the peak at $1,847\,cm^{-1}$ shifts to $1,802\,cm^{-1}$, where a fully bridging CO would appear).[18] This spectrum is very similar to that of the corresponding oxidized $[Fe]H_2$ase isolated from *Clostridium pasteurianum* I (CpI)[35] in terms of pattern and position of the bands, indicating the structural homology of the two active sites isolated from different sources. This H_{ox} state of the enzyme binds exogenous CO to the distal Fe center forming the so-called CO-inhibited form, H_{ox}–CO, Figure 7. The binding of CO shifts the stretching frequencies of all the diatomic ligands to higher wave numbers, as expected from the π-accepting character of CO.

Recent infrared studies on H_{ox}–CO from CpI found that irradiation at cryogenic temperatures resulted in $\nu(CX)$ band pattern changes that indicated CO loss.[35] That is, photolysis resulted in the disappearance of either the $\nu(CO)$ band that corresponds to the exogenous CO ($T < 150\,K$) or that of the bridging CO ($T < 80\,K$). However, whether the CO in the bridging position is actually removed, or one of the terminal COs is lost and the bridging CO becomes terminally bound to one Fe center, is questionable. A rotation of the "free" end of this site could switch the bridging CO to terminal (a fluxional process common in $Fe^{I}Fe^{I}$ model complexes)[36] consistent with the disappearance of the low-frequency $\nu(CO)$ band and the observed band pattern. Whether or not the H-bonding to CN^- prevents such a rotation is also an issue, although the energy of an H bond is considerably lower than the $Fe(CO)_2L$ unit rotational barrier that has been found for the models.

Based on the stretching frequencies of the diatomic ligands as a valid measure of the electron density around the metal centers, and compared to $Fe^{I}Fe^{I}$ model complexes, as discussed below, the above study would suggest low-valent Fe centers are present in the $[Fe]H_2$ase active site. Mössbauer spectra were originally interpreted in terms of a paramagnetic $Fe^{III}Fe^{II}$ stage in the oxidized form, and $Fe^{II}Fe^{II}$ in the diamagnetic reduced form, even though the possibility of $Fe^{II}Fe^{I}$ and $Fe^{I}Fe^{I}$, respectively, was not excluded.[37] However, the above infrared studies strongly suggest $Fe^{II}Fe^{I}$ and $Fe^{I}Fe^{I}$ oxidation-level assignments for the oxidized and the reduced state of the enzyme, respectively. EPR spectroscopy also finds the oxidized form of the enzyme (H_{ox}) to be a mixed-valent paramagnetic state, while the reduced is diamagnetic.[38,39] The metal–metal bond of $Fe^{I}Fe^{I}$ binuclear complexes accounts for the diamagnetism of the latter. The binding of

CO is a characteristic feature of the H_{ox} state, which changes its EPR signal from rhombic ($g = 2.10$) to axial ($g = 2.07$) upon CO binding, in a process that is associated with localization of the spin on one Fe center.

8.21.6 A COMPARISON OF THE ACTIVE SITES OF [NiFe] AND [Fe]H$_2$ASE

Despite the different origins or a distinct phylogenetic tree of the two classes of metallohydrogenases, they have several aspects of structural features (coordination environment) and reactivity in common. The most obvious are listed here:

  (i)   metal–metal distances within range of orbital overlap and bonding;
 (ii)   square-pyramidal $(\mu\text{-SR})_2\text{Fe(CO)}_x\text{(CN)}_{3-x}$ units;
(iii)   the presence of a third μ-L position dependent on the redox level of the enzyme;
 (iv)   distortion from the known ground-state geometries in both structures: about the Ni(SR)_4 unit in the [NiFe] enzyme, and overall geometrical anomalies in the dinuclear FeFe unit in [Fe] hydrogenase;
  (v)   both are enzymatically active in a paramagnetic, mixed-valent state.

Discordant features are also found:

  (i)   a more obvious result of the oxidation level in [NiFe] as contrasted to [Fe]H$_2$ase (greater Ni···Fe distance changes as compared to Fe···Fe);
 (ii)   the nature of the bridging sulfur moiety, protein attached for [NiFe] but a μ-SRS cofactor in [Fe]H$_2$ase heretofore undetected in nature;
(iii)   the obvious open site on Fe(CX)$_3$ in [Fe]H$_2$ase is filled by CO in the CO-inhibited form of the enzyme. Exogenous CO binds to Ni in the [NiFe]H$_2$ase.

It should be noted that, while hydrogenases can perform the oxidation of molecular hydrogen reversibly, they are typically committed to either H$_2$ uptake ([NiFe]) or H$_2$ production ([Fe] only) in any given organism or metabolic path.

Such commonalities and differences set the stage for the design of model complexes. Assuming that functional models should have at least some structural features in common with the active sites, dithiolate-bridged binuclear complexes have been targeted. Nevertheless, isolated monometallic units have provided both spectroscopic and functional reference points. Selected examples of both are presented below.

8.21.7 [NiFe]H$_2$ASE ACTIVE-SITE MODEL COMPLEXES

Figure 8 presents examples of small-molecule models which have proven useful as reference points for structural, spectroscopic, or functional features of [NiFe]H$_2$ase. The simple $(\eta^5\text{-C}_5\text{H}_5)$-Fe(CO)(CN)$_2^-$ organometallic, structure 8a,[40] presents a rigid model of the Fe^{II}(CO)(CN)$_2$ pyramidal unit. Despite its extreme organometallic character, i.e., devoid of any thiolate ligands, the two cyanides and one CO provided an exact spectral match for the oxidized, as-isolated, form of *D. gigas* [NiFe]H$_2$ase,[41] (ν(CO), enzyme, *model* = 1,947, 1,949 and ν(CN), enzyme, *model* = 2,093, 2,083, 2,094, 2,088 cm^{-1}). Furthermore, examination of the ν(CX) band positions as influenced by better electron donors $(\eta^5\text{-C}_5\text{Me}_5)$, H-bonding, counter-ion, and solvent effects provided baseline reference points for correlation with different states of the enzyme. This was done in an elegant way with the Density Functional Theory computations of Niu, Thomson, and Hall.[42] Via the correlation of calculated CO and CN bond lengths with ν(CO) and ν(CN) values referenced to the model compounds, the structures of possible active-site states such as **A**, **B**, and **C** were evaluated. Significantly, the folding and unfolding of the Ni$(\mu\text{-SR})_2$Fe core was found to be important to the ability to bind H$_2$ to the d^6 Fe^{II} center.

Complexes 8b[43] and 8c[44], Figure 8, better mimic the chemical composition of the iron portion of the active site. As a result of the anionic charge, their ν(CX) IR absorptions are much lower than those in the active site. As the anionic charge would be neutralized by nickel binding, an NiFe heterobimetallic should give a more spectroscopically compatible model. Complex 8c was also prepared as the amidosulfido derivative.[45] A six-coordinate complex
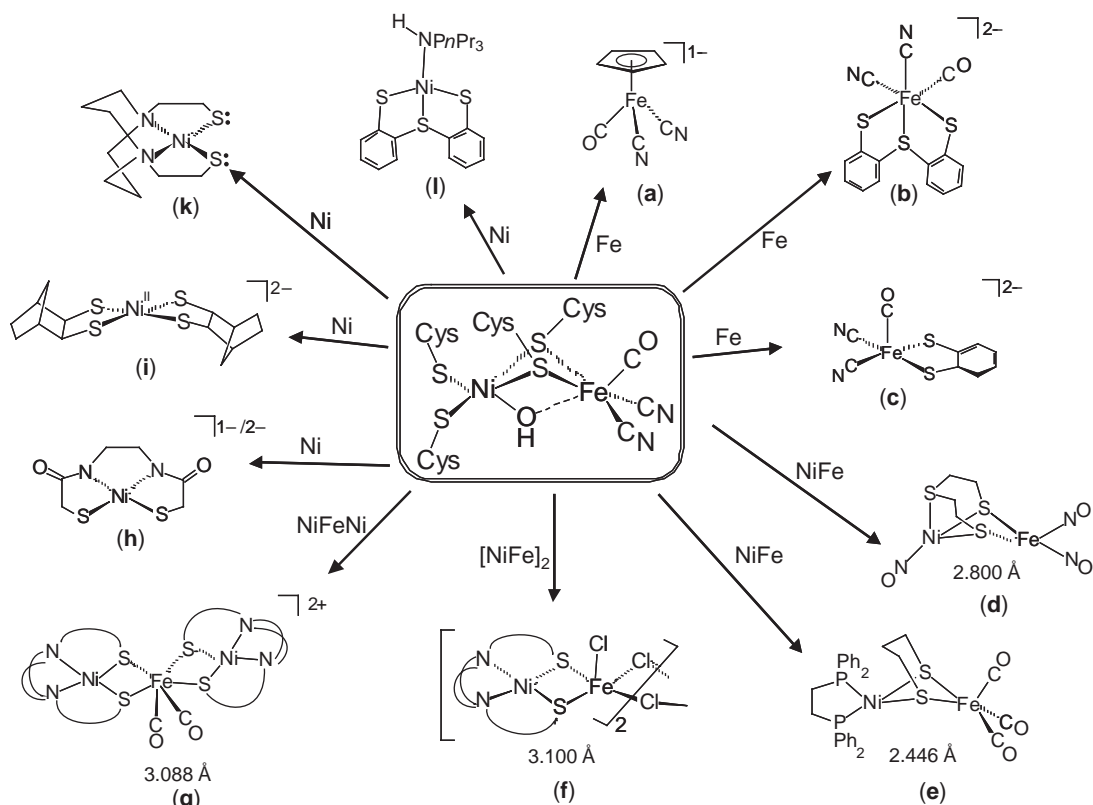
Figure 8 Selected models of [NiFe]H$_2$ase active site (references given in text).

[PS$_3$Fe(CO)(CN)]$^{2-}$, structure **D**,[46] containing a PS$_3$ tripodal ligand demonstrated the possibility of Fe^{II} → Fe^{III} redox changes in the same ligand set, with increases of ν(CN) by ca. 30 cm^{-1} and ν(CO) of ca. 100 cm^{-1}. As there are few examples of Fe^{III}–CO species, the observation provides a precedent for the possibility of such an oxidation state in the enzyme. However, the change in ν(CN) and ν(CO) is double that seen in the enzyme with any redox-level changes. Whereas prior to the reports of the protein crystal structures there were few NiFe heterobimetallic complexes reported in the chemical literature, several have been prepared as synthetic analogues in the meantime. The synthetic approach in general is to use a *cis*-dithiolate of nickel to serve as a metallothiolate ligand to an iron(II) source. A perusal of structures 8d–8g [8,47–49] demonstrates the necessity for a butterfly or folded (μ-SR)$_2$NiFe core to achieve Ni$\cdots$Fe distances within the range of the enzyme (2.6–2.9 Å). Interestingly, the shortest distance is achieved with the propane-dithiolate (μ-SRS) bridge complex in 8e.[8]
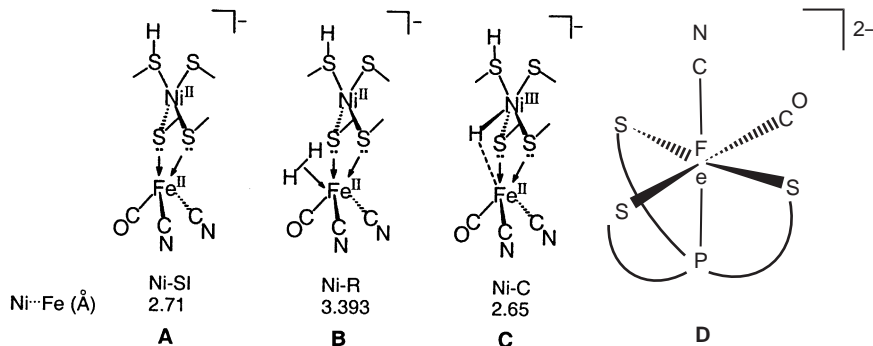
The monomeric nickel dithiolates, structures 8h–8l, have yielded electrochemical data relating to the three-oxidation-state hypothesis expressed in the Introduction. Complexes 8h–8k show S-based reactivity, including the S-based uptake and binding of gaseous molecules, SO$_2$, O$_2$, and I$_2$ in complex 8k.[50–53] Complex 8h[54] was used in an intensive analysis of requirements to achieve the
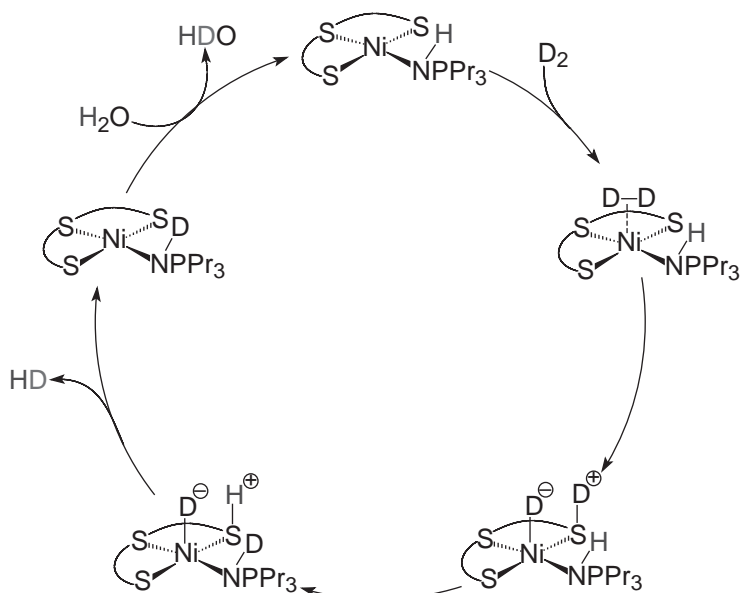
Figure 9 Proposed mechanism of D_2/H^+ exchange catalyzed by complex **8(l)**.[56]

very positive values for the $Ni^{II/III}$ couple, the tetra-anionic ligand affording $Ni^{II/III}$ at -0.34 V. The dianionic Ni^{II} tetrathiolate, **8i**,[55] was shown to undergo $Ni^{II/III}$ oxidation at -0.46 V vs. SCE. Complex **8(l)**[56] acts as a functional model that avoids the oxidation-state difference by offering evidence for heterolytic H_2 cleavage using a thiolate ligand as internal base for the heterolytic splitting of nickel-bound H_2 (Figure 9).

8.21.8   [Fe]H$_2$ASE ACTIVE-SITE MODEL COMPLEXES

The possibility of low-valent $Fe^I Fe^I$ in the reduced state of the enzyme is especially appealing in view of the structural similarity of this active site to well-studied, easily prepared, classical organometallic $Fe^I Fe^I$ complexes of the type $(\mu\text{-SR})_2[Fe(CO)_3]_2$.[57] This similarity has inspired research into the synthesis of new complexes based on the low-valent organometallic, modified in such a way to better mimic the main features of the enzyme active site.

The parent organometallic model complex for [Fe]H$_2$ase is $(\mu\text{-SCH}_2\text{CH}_2\text{CH}_2\text{S})[Fe(CO)_3]_2$ or $(\mu\text{-pdt})[Fe(CO)_3]_2$, whose structural overlay shows a match in the 2Fe2S core and in the three-atom bridge (Figure 10).[58] The slight mismatch of the central atom of the S-to-S linker is ascribed to the constraint of the active site in the protein environment, if the co-factor is propanedithiolate. An alternate and appealing explanation is that an N heteroatom might exist in that position, specifically for its capability to serve as an internal base to facilitate the shuttle of protons from the nearby $(\eta^2\text{-H}_2)Fe$ or to Fe–H$^-$ in the H_2 production process. Note that in the enzyme there is a bridging or semi-bridging CO ligand that makes the geometry around each iron atom octahedral (or pseudo-octahedral), while in the $Fe^I Fe^I$ models each iron is a five-coordinate, pseudo-square pyramid. This difference most likely reflects a different oxidation state of the Fe atoms in the active-site structure ($Fe^{II} Fe^I$) compared to the low-valent $Fe^I Fe^I$ model, $(\mu\text{-pdt})[Fe(CO)_3]_2$.
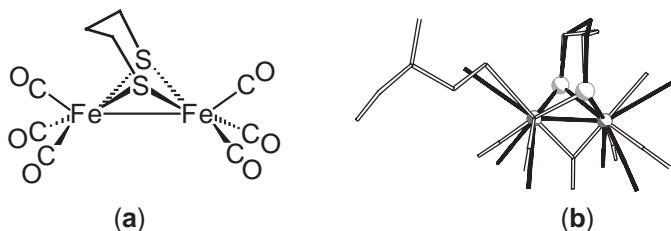
Figure 10   (a) Stick drawing structure of $(\mu\text{-pdt})[Fe(CO)_3]_2$, and (b) overlay of $(\mu\text{-pdt})[Fe(CO)_3]_2$ with the oxidized active-site structure.
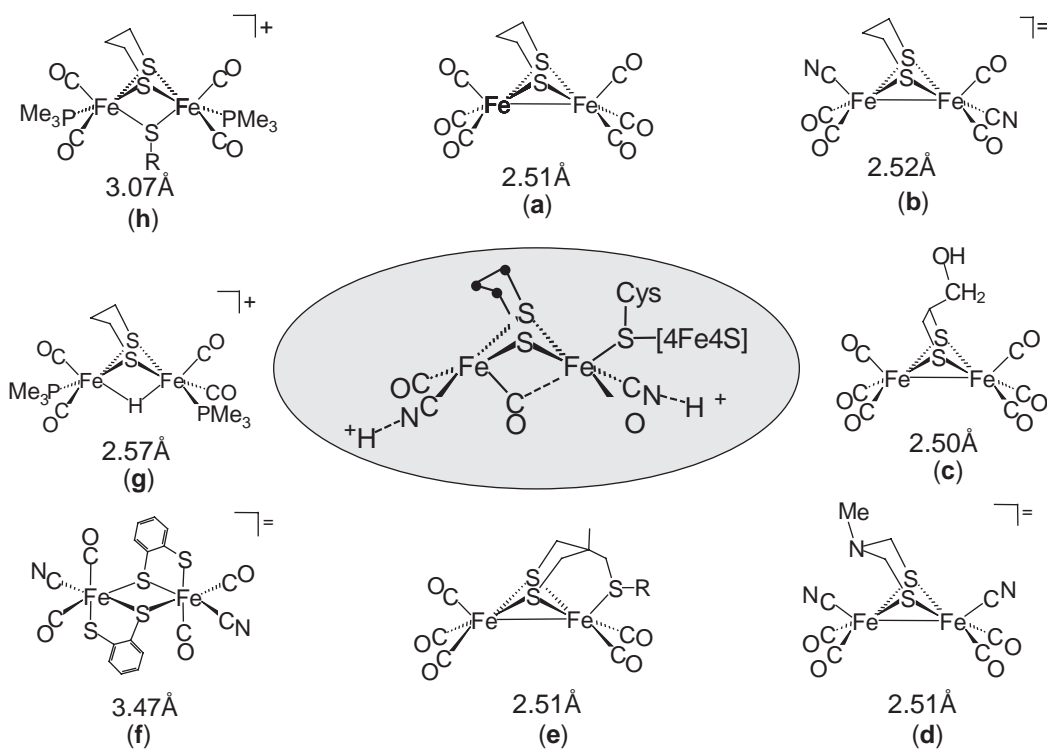
Figure 11 Selected Fe^{I}Fe^I and Fe^{II}Fe^{II} models of the active site of [Fe]H$_2$ase (references given in text).

Figure 11 shows a collection of Fe^{I}Fe^I and Fe^{II}Fe^{II} models that have been structurally characterized. Description of the differences of the models 11a and 11b with the active site is that the former are two edge-bridged square pyramids with Fe–Fe bond density underneath the two basal planes. The enzyme active site has one of these square pyramids inverted with respect to the other, a structure that is only seen (computed) in models as a transition state.[36,59] Such a high-energy structure would have an inherent open site, ready, if Fe^{II}, to take up the dihydrogen molecule; or, if Fe^0, to oxidatively add a proton.

Substitution of CO by CN$^-$ in complex 11a yields the dicyanide derivative (μ-pdt) [Fe(CO)$_2$(CN)]$_2^{2-}$, 11b,[58,60,61] which has one CN$^-$ ligand on each Fe atom, providing a model with a coordination composition and environment more similar to the active site of the enzyme. The dithiolate bridge can be functionalized as shown in Figure 11c.[62] Advances in the synthetic S-to-S bridge have also yielded a di-(thiomethyl)-amine (dtma)-bridged diiron hexacarbonyl complex as an analogue to the proposed CH$_2$N(H)CH$_2$ linker in the enzyme active site. The X-ray crystal structure of its dicyanide derivative has been determined, Figure 11d,[63] showing that the central nitrogen atom in the amine group adopts a planar geometry which decreases its basic character. This is an attractive model, since its synthesis can be obtained based on a biologically relevant route; i.e., by condensation of small molecules, HCHO and NH$_3$.[64]

Another significant contribution to the synthesis of models of [Fe]H$_2$ase is shown in Figure 11e.[65] This modified propanedithiolate-bridged 2Fe2S cluster that allows the coordination of the thioether S atom, attached to the bridge, gives rise to a 2Fe3S cluster with the two Fe centers being non-equivalent. The cyanide substitution of this complex gives the dicyanide derivative, in which the thioether group has dissociated.[66] One-electron oxidation of this dicyanide Fe^{I}Fe^I complex gives spectroscopic evidence for the formation of a mixed-valent Fe^{II}Fe^I complex with a bridging CO, structure **E**.[67] As indicated by its infrared stretching frequencies and its EPR signal, this complex provides a good spectroscopic model for the oxidized, CO-inhibited form of the enzyme, H$_{ox}$–CO.

E
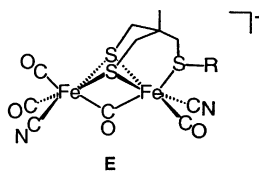
Even though the active site of [Fe]H$_2$ase is known to exist in several oxidation levels, its structure can be largely reproduced by the Fe^{I}Fe^I models presented above, convincingly indicating that low-valent iron, including the Fe^{I}Fe^I oxidation state assignment with the potential of an Fe—Fe bond, would be structurally consistent with a biological catalytic site, with the distortions mentioned above readily accessible. This conclusion is precedent setting, in that until now all biological iron was assumed to be in the Fe^{III} or Fe^{II} oxidation states. The synthesis of mixed-valent Fe^{II}Fe^I complexes is not easily achieved; however, the interactions that might be possible at an Fe^{II} site within a binuclear complex might be observed in Fe^{II}Fe^{II} complexes that are available. Thus, the Fe^{II}Fe^{II} complex presented in Figure 11f[47], generated from a mononuclear Fe^{II} precursor, has ν(CO) and ν(CN) stretching frequencies similar to the oxidized, as-isolated form of the enzyme. However, because it is an edge-bridged bioctahedron with four terminal ligands on each Fe atom, the Fe$_2$S$_2$ core is flat and diamond-shaped. It has an Fe$\cdots$Fe separation of 3.47 Å that is considerably longer than the enzyme active site (2.6 Å). Unfortunately this complex cannot be induced to lose ligands and fold into the butterfly core (Figure 11).

Another bidentate system, involving less biologically relevant S-to-P chelating ligands, with the butterfly core in Fe^{I}Fe^I as well as Fe^{II}Fe^{II} derivatives, is shown in Equation (3):[68]

$$(3)$$
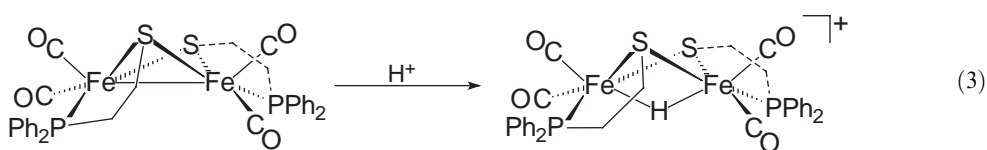
The latter synthetic approach towards the synthesis of Fe^{II}Fe^{II} complexes involves binuclear oxidative addition of an electrophile (H$^+$ or SMe$^+$) to the Fe^{I}Fe^I structural models, resulting in the formation of Fe^{II}(μ-H)Fe^{II} or Fe^{II}(μ-SMe)Fe^{II}, Figures 11g[69] and 11h.[70] The presence of good donor ligands such CN$^-$ or PMe$_3$ that would stabilize the Fe^{II}Fe^{II} redox level is necessary for such a process to occur. Unfortunately, protonation of the dicyanide complex (μ-pdt)[Fe(CO)$_2$(CN)]$_2^{2-}$ is complicated due to the basicity of the cyanide nitrogen, whose protonation leads to decomposition products. Success is achieved with the PMe$_3$ analogues. (Interestingly, PMe$_3$ is nearly as good a donor as is the anionic cyanide ligand!)[69,71,72] The face-bridged bioctahedra, with three terminal ligands on each iron, maintain closer Fe$\cdots$Fe distances compared to the diamond-core Fe^{II}Fe^{II} complex presented in Figure 11f. The close proximity of the two metals, which is similar to the [Fe]H$_2$ase active site, is maintained by the bridging hydride but not by the SMe bridge. Should a CO ligand insert into the Fe—Fe bond in place of SMe$^+$ (as is known for SO$_2$), one would expect a shorter Fe$\cdots$Fe distance, along with an analogue of the CO-inhibited form, Figure 7b.

Table 1 lists the Fe$\cdots$Fe distances and the infrared ν(CO) and ν(CN) stretching frequencies of the enzyme active site in different redox levels, together with several of the models described above. From this table it is clear that Fe^{I}Fe^I models are good mimics for the diamagnetic reduced state of the enzyme, and Fe^{II}Fe^I for the mixed-valent, paramagnetic, oxidized CO-inhibited form. The Fe^{II}Fe^{II} matches the as-isolated form (inactive and more oxidized).

Table 1 Fe$\cdots$Fe distances and infrared data of the active site of [Fe]H$_2$ase form DdH[18] and some of the models of Figure 11.

Di-iron species	Fe$\cdots$Fe (Å)	ν(CN), ν(CO) (cm^{-1})
[Fe]H$_2$ase, as isolated		**2107**, **2087**, 2007, 1983, 1847
[Fe]H$_2$ase, CO-inhibited	2.6	**2096**, **2089**, 2016, 1972, 1963, 1811
[Fe]H$_2$ase, reduced	2.6	**2079**, 2041, 1965, 1940, 1916, 1894
Fe^{I}Fe^I		
(μ-pdt)[Fe(CO)$_3$]$_2$, Figure 11a	2.51	2072, 2033, 1993
Figure 11b	2.52	**2076**, 1964, 1924, 1885
Fe^{II}Fe^I		
Structure **E**		**2107**, **2083**, 2030, 1978, 1945, 1910, 1790
Fe^{II}Fe^{II}		
Figure 11f	3.47	**2101**, 1960, 2013
Figure 11h	2.58	2029, 1989

8.21.9 FUNDAMENTAL PROPERTIES OF Fe^{I}Fe^I MODEL COMPLEXES

Low-valent Fe^{I}Fe^I complexes of the type $(\mu\text{-SRS})[\text{Fe(CO)}_3]_2$ are very attractive as active-site synthetic analogues, in that they are associated with fundamental properties related to the structure and the chemistry of [Fe]H$_2$ase active site that can be summarized as follows: (i) they undergo CN$^-$ substitution reactions with remarkable regioselectivity, to result in the dicyanide derivatives;[36] (ii) they show fluxionality or intramolecular site exchange at Fe(CO)$_3$ units;[36] and (iii) they have a highly reactive Fe—Fe bond that reacts with electrophiles such as H$^+$ or SMe$^+$ to form Fe$^{II}(\mu\text{-H})$Fe^{II} or Fe$^{II}(\mu\text{-SMe})$Fe^{II} complexes, respectively.[69,70]

8.21.9.1 Activity Assay Models

The basis for hydrogenase activity assays typically involves H$_2$ uptake indicated by H/D exchange in H$_2$/D$_2$O mixtures and H/D scrambling in H$_2$/D$_2$ mixtures, presumably via H$_2$O mediation. Based on such test reactions, the binuclear Fe$^{II}(\mu\text{-H})$Fe^{II} complexes serve as functional models of [Fe]H$_2$ase in the catalytic isotopic scrambling of D$_2$/H$_2$O and H$_2$/D$_2$ mixtures.[69,71] During the processes, all of which require photolysis, Fe$^{II}(\mu\text{-H})$Fe^{II} becomes Fe$^{II}(\mu\text{-D})$Fe^{II}, indicating involvement of the bridging hydride in the isotope-exchange mechanism. Proposed intermediates such as structures **F** and **G** call upon the μ-H to shift to a terminal position and serve as an internal base, under anhydrous conditions, to deprotonate the proximate $(\eta^2\text{-H}_2)$Fe^{II} moiety. A weak external base such as H$_2$O can also deprotonate the acidic $(\eta^2\text{-H}_2)$Fe^{II} intermediate. Complex Fe$^{II}(\mu\text{-SMe})$Fe^{II} also demonstrates H$_2$ (or D$_2$) uptake and heterolytic cleavage by D$_2$O (or H$_2$O), indicating that a built-in hydride is not needed for H/D exchange in D$_2$/H$_2$O or H$_2$/D$_2$/H$_2$O mixtures.[70] The singular requirement for these processes is an open site on an Fe^{II}, necessary for H$_2$ binding in an η^2 coordination mode. This H$_2$ activation is an important characteristic that further links the models to [Fe]H$_2$ase.

8.21.9.2 Electrocatalytic Generation of H$_2$

A more recent and technologically relevant advance in this area of research has come from the use of such Fe^{I}Fe^I models to produce H$_2$ electrocatalytically. The Fe^{I}Fe^I complexes modified by better donor ligands can be protonated, to give Fe$^{II}(\mu\text{-H})$Fe^{II} species which, at relatively mild potentials and in the presence of a strong acid, release H$_2$. An example of this type of electro-generation of H$_2$ was first published by Rauchfuss and co-workers and it is presented as a CCEE electrocatalytic mechanism in Scheme 2.[73]

Scheme 2

F

G

E = H or SMe
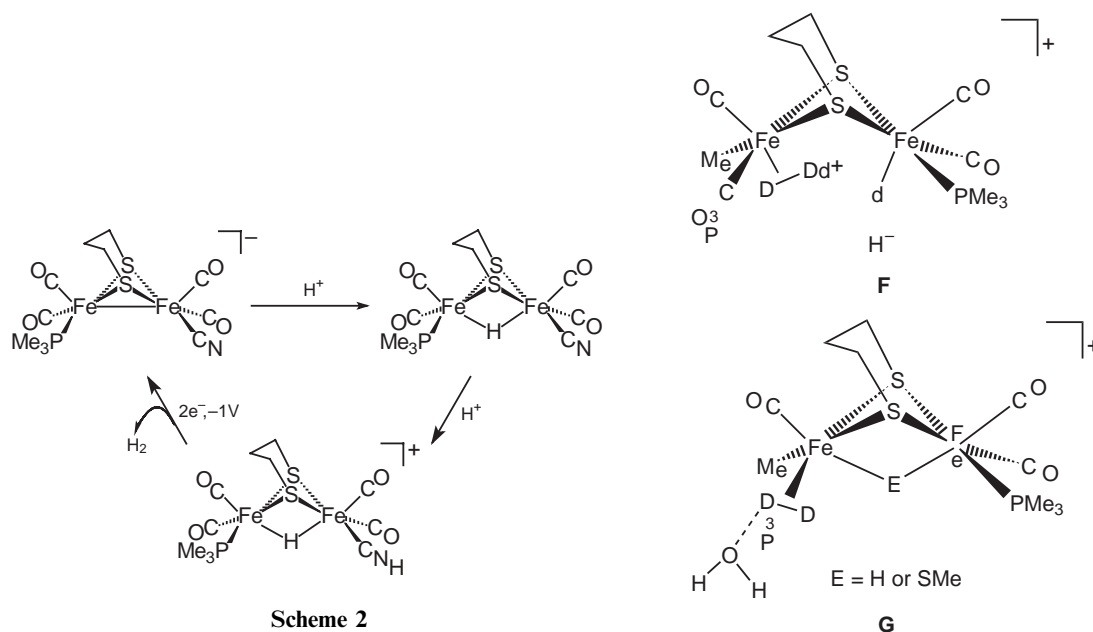
Alternatively, we have found a lower-valent pathway for the electrogeneration of H_2 by Fe^IFe^I complexes of the type $(\mu\text{-SRS})[Fe(CO)_2(PMe_3)]_2$, Scheme 3, which utilizes weak acid at more negative potentials.[74] The difference from the above pathway is that the latter describes electrogeneration of H_2 at an Fe^0Fe^I oxidation level, while the former utilizes an $Fe^{II}Fe^I$ intermediate.
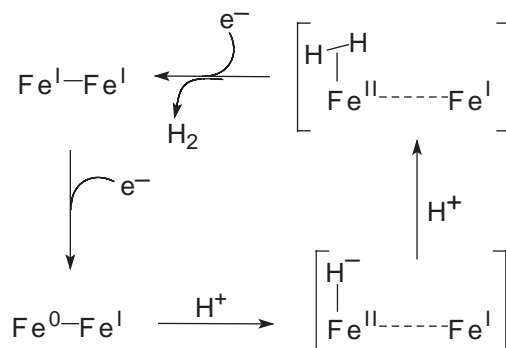
Scheme 3

8.21.10 THEORETICAL CALCULATIONS OF H_2 ACTIVATION

8.21.10.1   [Fe]-only Hydrogenase

The structural definition of a hydrophobic channel that leads to the open site of the distal Fe atom, suggesting that this is the site of hydrogen binding or evolution, has been supported by density functional theory (DFT) calculations that provide valid possibilities for the mechanistic pathway of H_2 activation by these sites. These studies use structural models to predict possible oxidation states and structures of the intermediates of the catalytic mechanism. Recent DFT studies by Cao and Hall[75] used the complex $[(H_2O)(CO)(CN)Fe(\mu\text{-pdt})(\mu\text{-CO})Fe(CO)(CN)(CH_3S)]^{n-}$ to compute H_2 activation by this structural model. This model combines all the features of the first coordination sphere of the active site, except the bridging cysteine to 4Fe4S cluster that was modeled as SMe. The results suggest a catalytic mechanism in which H_2 binds weakly to the distal Fe center in the Fe^IFe^{II} oxidation level, which is then oxidized to form a stable $(\eta^2\text{-}H_2)Fe^{II}Fe^{II}$ intermediate, **1**. As presented in Scheme 4, H_2 heterolytic cleavage takes place at this $Fe^{II}Fe^{II}$ species, resulting in a proton transfer to a CN^- or a bridging thiolate S with the formation of a terminally bound H^-. Deprotonation of the metal-bound hydride reduces the
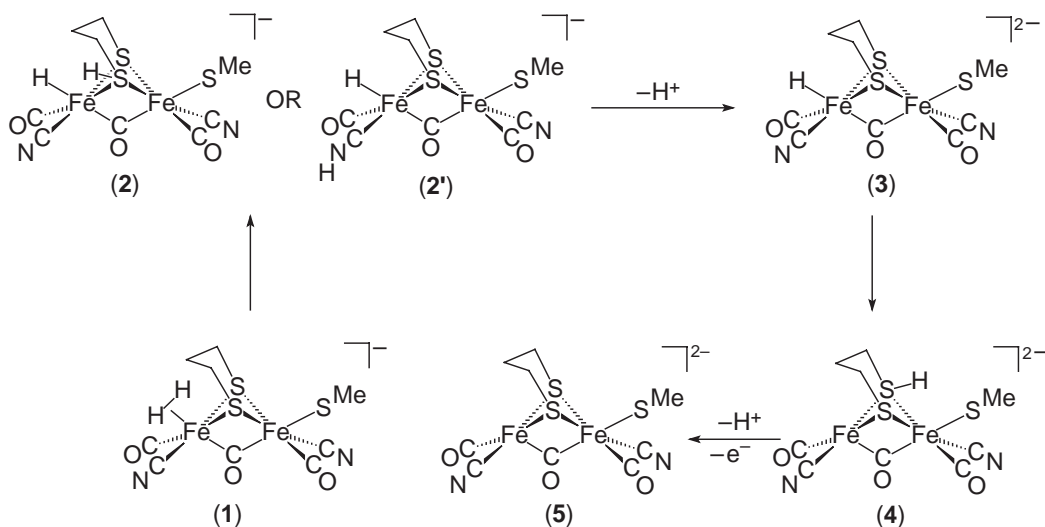
Scheme 4

metals by two electrons (one electron per metal). This two-electron reduction shared by the two metals gives a reasonable explanation for the requirement of a dinuclear active site. The protonation of the CN^- is kinetically unfavorable, with an activation energy of 37.8 kcal mol^{-1}, but thermodynamically favorable (**2′** is 0.3 kcal mol^{-1} more stable than **1**), while the protonation of the bridging thiolate finds a lower activation barrier (17.4 kcal mol^{-1}) but forms a much less stable product, **2**, that lies 15.3 kcal mol^{-1} higher than the reactant, **1**.

The possibility that the central atom of the S-to-S linker might be nitrogen, as suggested by Fontecilla-Camps and co-workers,[18] has been computed by Fan and Hall[76] to provide another low-energy alternative site for H^+ abstraction, with a lower activation barrier of 6.53 kcal mol^{-1}, as compared to 32.3 kcal mol^{-1} for protonation of the pdt-S, Scheme 5. However, product **2a′** is 2.62 kcal mol^{-1} less stable than **1a**, while **2a** is 6.10 kcal mol^{-1} more stable.

Although a hydrophobic channel that leads from the surface of the protein to the open site on the distal Fe supports the idea that this should be the site for H_2 binding, De Gioia and co-workers[77] reported a theoretical study that shows the heterolytic H_2 cleavage taking place at the proximal Fe center (Scheme 6). In the De Gioia model, SMe^- represents the cysteine which connects the 2Fe site to the 4Fe4S cluster. The activation energy for the heterolytic splitting of H_2 in such a fashion is calculated to be 5.3 kcal mol^{-1}, while the bridging hydride product lies 2.4 kcal mol^{-1} higher in energy than the η^2-H_2 complex, **1b**.
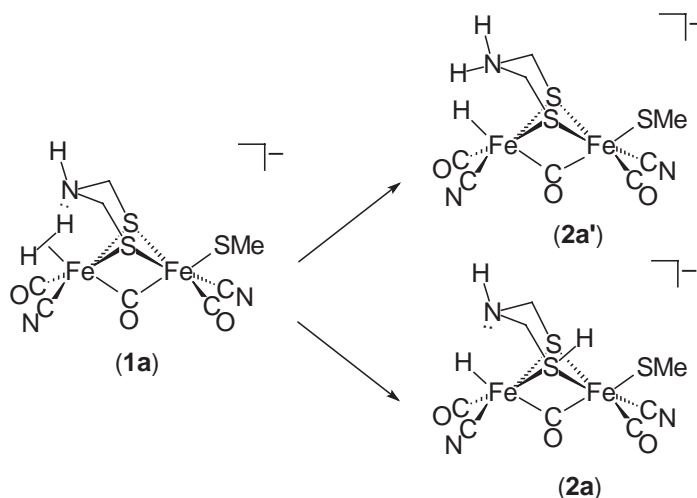
Scheme 5
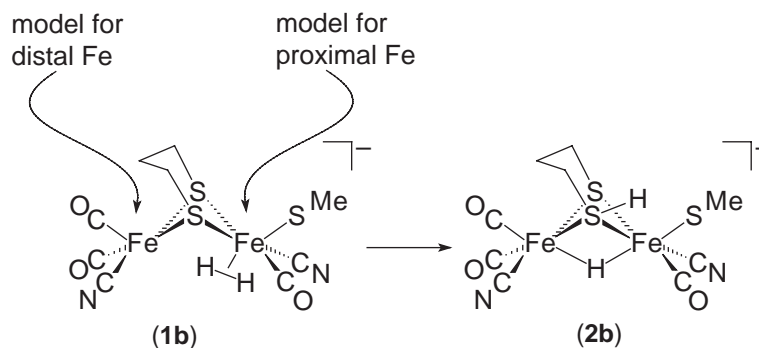
Scheme 6

A similar model, again using a terminal SMe^- to represent the cysteine that connects the 2Fe unit to the 4Fe4S cluster, was employed by Liu and Hu[78] in their attempts to characterize the possible structures of the active site of [Fe]H_2ase at different redox levels. According to their study, the fully oxidized, inactive, and EPR-silent state of the enzyme was satisfied by an $Fe^{II}Fe^{II}$ model with a terminally bound OH^- group on the distal Fe. The oxidized active state of the

enzyme was suggested to be Fe^IFe^{II}, with a vacant site on the distal Fe where the spin was localized, reproducing well the experimental observation of CO binding at this Fe center in the CO-inhibited form of the enzyme. The fully reduced, EPR-silent state was found to be a mixture of Fe^IFe^I with protonated amine group of the dithiolate bridge and its rearranged $Fe^{II}Fe^{II}$ form, with a terminal H^- ligand on the distal Fe.

According to the above possible redox states, a possible pathway which shows the changes that occur during H_2 metabolism at the active site of $[Fe]H_2$ase was suggested. This process, Scheme 7,[78] involves the protonation of the oxidized active state, $Fe^{II}Fe^I(OH)$, to release a H_2O molecule creating an open site at the Fe^I center, which can be further protonated upon reduction to yield the reduced state Fe^IFe^I or $Fe^{II}Fe^{II}(H)$. Either of these two forms of the reduced state can release H_2 upon protonation and reduction and give back the $Fe^{II}Fe^I$ oxidized state.
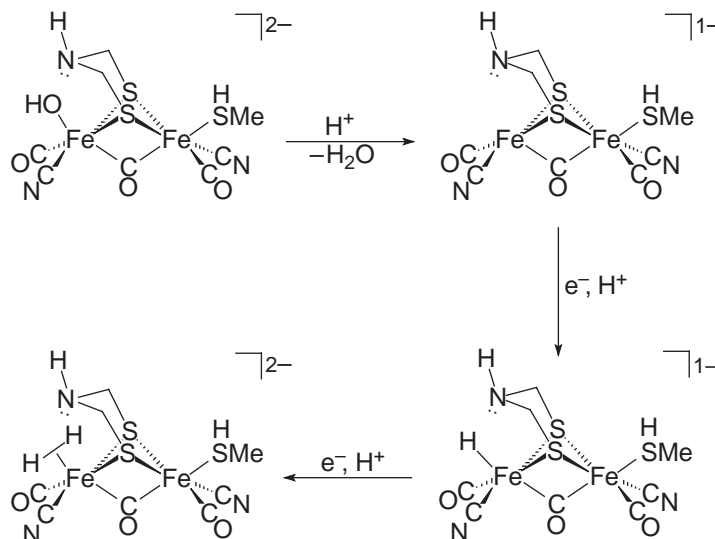
Scheme 7

The above theoretical studies based on structural models, and their possible involvement in H_2 activation or production, give some insight into the possible redox levels of the active site. However, they focus only on the active center. They do not consider at all the protein environment which is crucial to the reactions that this site promotes, i.e., the availability of energetically favorable pathways for proton and electron transfer in and out of this active site. Nevertheless, these theoretical calculations have reproduced some of the spectroscopic features (i.e., stretching frequencies) of synthetic models, which lends confidence to the reliability of the computations. A reasonable agreement in all these calculations is that H_2 binds to an Fe^{II} center and not Fe^I, which is consistent with the experimental fact that the mixed-valent active form of the enzyme has at least one Fe in the $+2$ oxidation state. This is also in agreement with the formation of stable η^2-H_2 complexes of d^6 metals.

8.21.10.2 [NiFe] Hydrogenase

Calculations have been carried out on simplified models of the active site of [NiFe] hydrogenase in order to investigate the different active or inactive forms of the enzyme.[79] Due to the lack of crystal structures of all the different redox states (there are at least seven that have been identified spectroscopically) of the enzyme, theoreticians have computed different possibilities for these states based on their primary spectroscopic features. Mechanistic conclusions for H_2 activation processes at these sites have been made using the proposed calculated structures.

The model in the first theoretical study used SH groups to mimic the S–Cys used by the enzyme. A mechanism proposed by Pavlov *et al.*[80,81] involved H_2 binding to the Fe atom, with subsequent heterolytic cleavage to yield a protonated thiol group and a hydride that was transferred from the Fe to the Ni atom. A similar mechanism was suggested by Pavlov *et al.*

proposing that the splitting of H_2 that takes place at the Fe atom, to protonate a bridging thiolate and form a bridging hydride. This protonated thiolate was subsequently moved to terminally bound thiol to Fe atom, as described in Scheme 8.
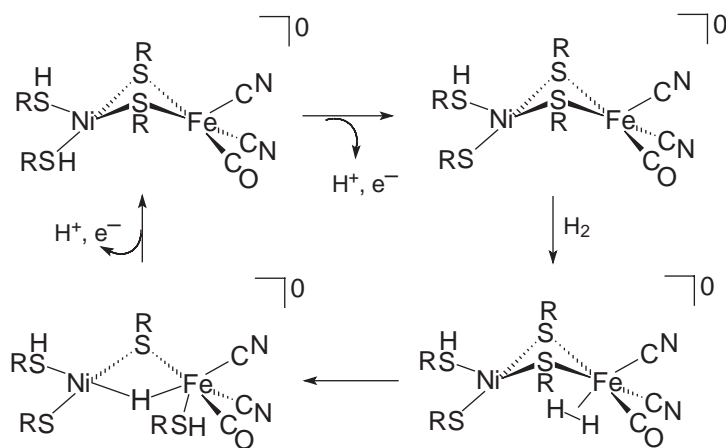
Scheme 8

By comparing the spectroscopic features of the enzyme various redox states and using similar models, Amara et al.[82] derived a catalytic mechanism of [NiFe] hydrogenase with the active forms of the site. Their mechanism is presented in Scheme 9.
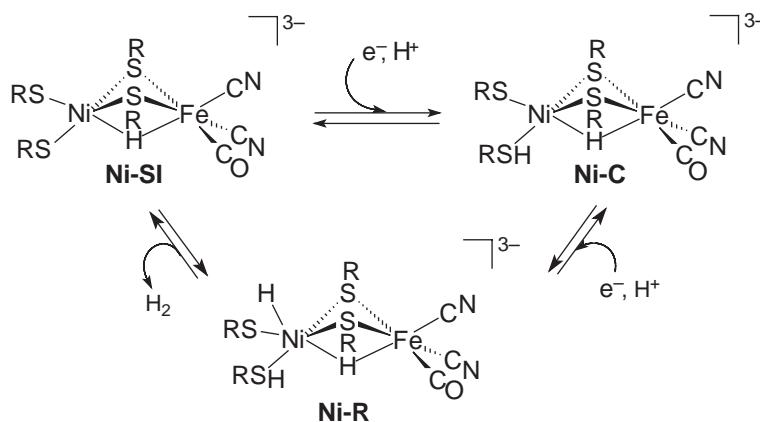
Scheme 9

Scheme 10 presents another H_2 activation cycle, computed by Niu, Thomson, and Hall[42] for the different redox levels of *D. gigas* [NiFe]H_2ase that participate in the enzymatic reaction. It involves H_2 binding at the Fe^{II} center of an $Ni^{II}Fe^{II}$ species that is suggested to be a model for the Ni–R state. One-electron oxidation yields a Ni^{III} species that cleaves H_2 heterolytically to form a bridging hydride modeled as the Ni–C state. Further deprotonation and oxidation gives back the $Ni^{II}Fe^{II}$ (Ni–Si(b)) state that originally binds H_2.

8.21.11 CONCLUDING REMARKS

The power of protein crystallography that has defined the stationary active-site structures of the metallohydrogenases, corroborating and fulfilling decades of development by biochemists and biophysicists, has set a stage whereby theoreticians may make a prominent contribution to the next step of delineating mechanism of action. As the catalytic sites are isolated within the protein folds, as solvation shells about the coordination spheres are fixed by the protein, and
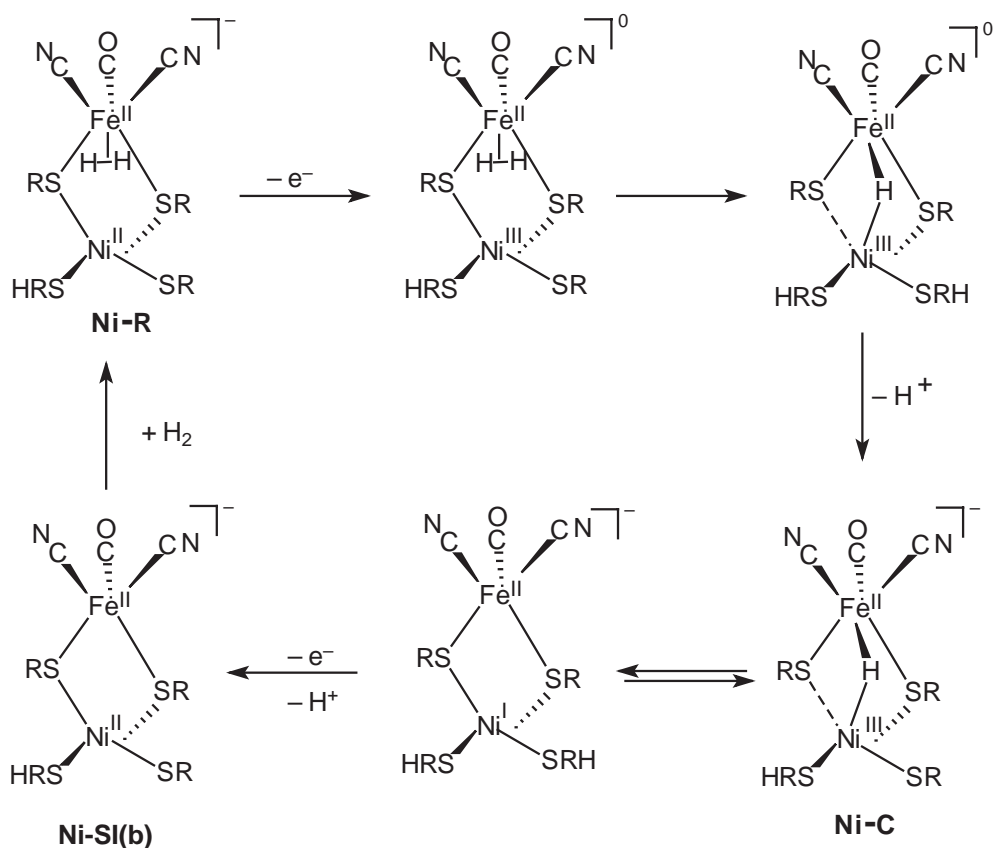
Scheme 10

as spectroscopic signatures may be referenced to well-characterized small-molecule models, theoreticians are provided with a rich opportunity to expand their computational approach, from first-coordination-sphere, gas-phase models to a significantly real reaction scenario. The iteration involves theoretical models chosen as carefully, and interpreted as carefully, as the design of thermodynamically stable small-molecule models in the chemist's laboratory. The eventual prediction of properties required for small-molecule catalysts similar to the metallo-hydrogenases is a goal worthy of intense study in both camps. Additional reviews are in references 83 and 84.

8.21.12 REFERENCES

1. Vignais, P. M.; Billoud, B.; Meyer, J. *FEBS Microbiol. Rev.* **2001**, *25*, 455–501.
2. Lancaster, J. R., Jr. *The Bioinorganic Chemistry of Nickel*; VCH: New York, 1988.
3. Cammack, R.; Frey, M.; Robson, R. *Hydrogen as a Fuel*; Taylor and Francis: London, 2001.
4. Hoffmann, P. *Tomorrow's Energy: Hydrogen, Fuel Cells, and Prospects for a Cleaner Planet*; MIT Press: Cambridge, MA, 2001.
5. Kubas, G. J. *Metal Dihydrogen and σ-Bond Complexes*; Kluwer Academic/Plenum; New York, 2001.

6. Frey, M. *ChemBioChem*. **2002**, *3*, 153–160.
7. Darensbourg, M. Y.; Lyon, E. J.; Smee, J. J. *Coord. Chem. Rev*. **2000**, *206–207*, 533–561.
8. Marr, A. C.; Spencer, D. J. E.; Schröder, M. *Coord. Chem. Rev*. **2001**, *219–221*, 1055–1074.
9. Volbeda, A.; Charon, M.-H.; Piras, C.; Hatchikian, E. C.; Frey, M.; Fontecilla-Camps, J. C. *Nature* **1995**, *373*, 580–586.
10. Volbeda, A.; Garcin, E.; Piras, C.; De Lacey, A. L.; Fernandez, V. M.; Hatchikian, E. C.; Frey, M.; Fontecilla-Camps, J. C. *J. Am. Chem. Soc*. **1996**, *118*, 12989–12996.
11. Garcin, E.; Vernède, X.; Hatchikian, E. C.; Volbeda, A.; Frey, M.; Fontecilla-Camps, J. C. *Structure* **1999**, *7*, 557–566.
12. Higuchi, Y.; Yagi, T.; Yasuoka, N. *Structure* **1997**, *5*, 1671–1680.
13. Higuchi, Y.; Ogata, H.; Miki, K.; Yasuoka, N.; Yagi, T. *Structure* **1999**, *7*, 549–556.
14. Volbeda, A.; Montet, Y.; Vernède, X.; Hatchikian, E. C.; Fontecilla-Camps, J. C. *Int. J. Hydrogen Energy* **2002**, *27*, 1449–1461.
15. Ogata, H.; Mizoguchi, Y.; Mizuno, N.; Miki, K.; Adachi, S.-I.; Yasuoka, N.; Yagi, T.; Yamauchi, O.; Hirota, S.; Higuchi, Y. *J. Am. Chem. Soc*. **2002**, *124*, 11628–11635.
16. Peters, J. W.; Lanzilotta, W. N.; Lemon, B. J.; Seefeldt, L. C. *Science*. **1998**, *282*, 1853–1858.
17. Nicolet, Y.; Piras, C.; Legrand, P.; Hatchikian, C. E.; Fontecilla-Camps, J. C. *Structure* **1999**, *7*, 13–23.
18. Nicolet, Y.; De Lacey, A. L.; Vernède, X.; Fernandez, V. M.; Hatchikian, E. C.; Fontecilla-Camps, J. C. *J. Am. Chem. Soc*. **2001**, *123*, 1596–1601.
19. Lemon, B. J.; Peters, J. W. *Biochemistry*. **1999**, *38*, 12969–12973.
20. Montet, Y.; Amara, P.; Volbeda, A.; Vernède, X.; Hatchikian, E. C.; Field, M. J.; Frey, M.; Fontecilla-Camps, J. C. *Nat. Struct. Biol*. **1997**, *4*, 523–526.
21. Nicolet, Y.; Cavazza, C.; Fontecilla-Camps, J. C. *J. Inorg. Biochem*. **2002**, *91*, 1–8.
22. Kubas, G. J.; Ryan, R. R.; Swanson, B. I.; Vergamini, P. J.; Wasserman, H. J. *J. Am. Chem. Soc*. **1984**, *106*, 451–452.
23. Kubas, G. J. *Acc. Chem. Res*. **1988**, *21*, 120–128.
24. Forde, C. E.; Landau, S. E.; Morris, R. H. *J. Chem. Soc., Dalton Trans*. **1997**, 1663–1664.
25. Abdur-Rashid, K.; Fong, T. P.; Greaves, B.; Gusev, D. G.; Hinman, J. G.; Landau, S. E.; Lough, A. J.; Morris, R. H. *J. Am. Chem. Soc*. **2000**, *122*, 9155–9171.
26. Fong, T. P.; Forde, C. E.; Lough, A. J.; Morris, R. H.; Rigo, P.; Rocchini, E.; Stephan, T. *J. Chem. Soc., Dalton Trans*. **1999**, 4475–4486.
27. Crabtree, R. H.; Lavin, M.; Bonneviot, L. *J. Am. Chem. Soc*. **1986**, *108*, 4032–4037.
28. Farkas, A.; Farkas, L.; Yudkin, J. *Proc. Roy. Soc. (London)* **1934**, *B115*, 373.
29. Krasna, A. I.; Rittenberg, D. *J. Am. Chem. Soc*. **1954**, *76*, 3015–3020.
30. Barondeau, D. P.; Roberts, L. M.; Lindahl, P. A. *J. Am. Chem. Soc*. **1994**, *116*, 3442–3448.
31. Roberts, L. M.; Lindahl, P. A. *Biochemistry* **1994**, *33*, 14339–14350.
32. Musie, G.; Farmer, P. J.; Tuntulani, T.; Reibenspies, J. H.; Darensbourg, M. Y. *Inorg. Chem*. **1996**, *35*, 2176–2183.
33. Maroney, M. J.; Bryngelson, P. A. *J. Biol. Inorg. Chem*. **2001**, *6*, 453–459.
34. De Lacey, A. L.; Stadler, C.; Cavazza, C.; Hatchikian, E. C.; Fernandez, V. M. *J. Am. Chem. Soc*. **2000**, *122*, 11232–11233.
35. Chen, Z.; Lemon, B. J.; Huang, S.; Swartz, D. J.; Peters, J. W.; Bagley, K. A. *Biochemistry* **2002**, *41*, 2036–2043.
36. Lyon, E. J.; Georgakaki, I. P.; Reibenspies, J. H.; Darensbourg, M. Y. *J. Am. Chem. Soc*. **2001**, *123*, 3268–3278.
37. Popescu, C. V.; Münck, E. *J. Am. Chem. Soc*. **1999**, *121*, 7877–7884.
38. Pereira, A. S.; Tavares, P.; Moura, I.; Moura, J. J. G.; Huynh, B. H. *J. Am. Chem. Soc*. **2001**, *123*, 2771–2782.
39. Bennett, B.; Lemon, B. J.; Peters, J. W. *Biochemistry* **2000**, *39*, 7455–7460.
40. Lai, C.-H.; Lee, W.-Z.; Miller, M. L.; Reibenspies, J. H.; Darensbourg, D. J.; Darensbourg, M. Y. *J. Am. Chem. Soc*. **1998**, *120*, 10103–10114.
41. De Lacey, A. L.; Hatchikian, E. C.; Volbeda, A.; Frey, M.; Fontecilla-Camps, J. C.; Fernandez, V. M. *J. Am. Chem. Soc*. **1997**, *119*, 7181–7189.
42. Niu, S.; Thomson, L. M.; Hall, M. B. *J. Am. Chem. Soc*. **1999**, *121*, 4000–4007.
43. Sellmann, D.; Geipel, F.; Heinemann, F. W. *Chem. Eur. J*. **2002**, *8*, 958–966.
44. Rauchfuss, T. B.; Contakes, S. M.; Hsu, S. C. N.; Reynolds, M. A.; Wilson, S. R. *J. Am. Chem. Soc*. **2001**, *123*, 6933–6934.
45. Liaw, W.-F.; Lee, N.-H.; Chen, C.-H.; Lee, C.-M.; Lee, G.-H.; Peng, S.-M. *J. Am. Chem. Soc*. **2000**, *122*, 488–494.
46. Hsu, H.-F.; Koch, S. A.; Popescu, C. V.; Münck, E. *J. Am. Chem. Soc*. **1997**, *119*, 8371–8372.
47. Liaw, W.-F.; Chiang, C.-Y.; Lee, G.-H.; Lai, C.-H.; Darensbourg, M. Y. *Inorg. Chem*. **2000**, *39*, 480–484.
48. Mills, D. K.; Reibenspies, J. H.; Darensbourg, M. Y. *Inorg. Chem*. **1990**, *29*, 4364–4366.
49. Lai, C.-H.; Reibenspies, J. H.; Darensbourg, M. Y. *Angew. Chem. Int. Ed. Engl*. **1996**, *35*, 2390–2393.
50. Farmer, P. J.; Solouki, T.; Mills, D. K.; Soma, T.; Russel, D. H.; Reibenspies, J. H.; Darensbourg, M. Y. *J. Am. Chem. Soc*. **1992**, *114*, 4601–4605.
51. Darensbourg, M. Y.; Tuntulani, T.; Reibenspies, J. H. *Inorg. Chem*. **1994**, *33*, 611–613.
52. Lyon, E. J.; Musie, G.; Reibenspies, J. H.; Darensbourg, M. Y. *Inorg. Chem*. **1998**, *37*, 6942–6946.
53. Grapperhaus, C. A.; Darensbourg, M. Y. *Acc. Chem. Res*. **1998**, *31*, 451–459.
54. Krüger, H.-J.; Peng, G.; Holm, R. H. *Inorg. Chem*. **1991**, *30*, 734–742.
55. Fox, S.; Wang, Y.; Silver, A.; Millar, M. *J. Am. Chem. Soc*. **1990**, *112*, 3218–3220.
56. Sellmann, D.; Geipel, F.; Moll, M. *Angew. Chem. Int. Ed. Engl*. **2000**, *39*, 561–563.
57. Seyferth, D.; Womack, G. B.; Gallagher, M. K.; Cowie, M.; Hames, B. W.; Fackler, Jr., J. P.; Mazany, A. M. *Organometallics* **1987**, *6*, 283–294.
58. Lyon, E. J.; Georgakaki, I. P.; Reibenspies, J. H.; Darensbourg, M. Y. *Angew. Chem. Int. Ed. Engl*. **1999**, *38*, 3178–3180.
59. Georgakaki, I. P.; Thomson, L. M.; Lyon, E. J.; Hall, M. B.; Darensbourg, M. Y. *Coord. Chem. Rev*. **2003**, *238–239*, 255–266.
60. Schmidt, M.; Contakes, S. M.; Rauchfuss, T. B. *J. Am. Chem. Soc*. **1999**, *121*, 9736–9737.
61. Le Cloirec, A.; Best, S. P.; Borg, S.; Davies, S. C.; Evans, D. J.; Hughes, D. L.; Pickett, C. J. *Chem. Commun*. **1999**, 2285–2286.
62. Razavet, M.; Le Cloirec, A.; Davies, S. C.; Hughes, D. L.; Pickett, C. J. *J. Chem. Soc., Dalton Trans*. **2001**, 3551–3552.

63. Lawrence, J. D.; Li, H.; Rauchfuss, T. B.; Bénard, M.; Rohmer, M.-M. *Angew. Chem., Int. Ed. Engl.* **2001**, *40*, 1768–1771.
64. Li, H.; Rauchfuss, T. B. *J. Am. Chem. Soc.* **2002**, *124*, 726–727.
65. Razavet, M.; Davies, S. C.; Hughes, D. L.; Pickett, C. J. *Chem. Commun.* **2001**, 847–848.
66. George, S. J.; Cui, Z.; Razavet, M.; Pickett, C. J. *Chem. Eur. J.* **2002**, *8*, 4037–4046.
67. Razavet, M.; Borg, S. J.; George, S. J.; Best, S. P.; Fairhurst, S. A.; Pickett, C. J. *Chem. Commun.* **2002**, 700–701.
68. Zhao, X.; Hsiao, Y.-M.; Lai, C.-H.; Reibenspies, J. H.; Darensbourg, M. Y. *Inorg. Chem.* **2002**, *41*, 699–708.
69. Zhao, X.; Georgakaki, I. P.; Miller, M. L.; Yarbrough, J. C.; Darensbourg, M. Y. *J. Am. Chem. Soc.* **2001**, *123*, 9710–9711.
70. Georgakaki, I. P.; Miller, M. L.; Darensbourg, M. Y. *Inorg. Chem.* **2003**, *42*, 2489–2494.
71. Zhao, X.; Georgakaki, I. P.; Miller, M. L.; Mejia-Rodriguez, R.; Chiang, C.-Y.; Darensbourg, M. Y. *Inorg. Chem.* **2002**, *41*, 3917–3928.
72. Gloaguen, F.; Lawrence, J. D.; Schmidt, M.; Wilson, S. R.; Rauchfuss, T. B. *J. Am. Chem. Soc.* **2001**, *123*, 12518–12527.
73. Gloaguen, F.; Rauchfuss, *J. Am. Chem. Soc.* **2001**, *123*, 9476–9477.
74. Chong, D.; Georgakaki, I. P.; Miller, M. L.; Mejia-Rodriguez, R.; Darensbourg, M. Y. *Dalton Trans.* **2003**, 4158–4163.
75. Cao, Z.; Hall, M. B. *J. Am. Chem. Soc.* **2001**, *123*, 3734–3742.
76. Fan, H.-J.; Hall, M. B. *J. Am. Chem. Soc.* **2001**, *123*, 3828–3829.
77. Bruschi, M.; Fantucci, P.; De Gioia, L. *Inorg. Chem.* **2002**, *41*, 1421–1429.
78. Liu, Z.-P.; Hu, P. *J. Am. Chem. Soc.* **2002**, *124*, 5175–5182.
79. Siegbahn, P. E. M.; Blomberg, M. R. A.; Pavlov, M. W.; Crabtree, R. H. *J. Biol. Chem.* **2001**, *6*, 460–466.
80. Pavlov, M.; Siegbahn, P. E. M.; Blomberg, M. R. A.; Crabtree, R. H. *J. Am. Chem. Soc.* **1998**, *120*, 548–555.
81. Pavlov, M.; Blomberg, M. R. A.; Siegbahn, P. E. M. *Int. J. Quantum Chem.* **1999**, *73*, 197–207.
82. Amara, P.; Volbeda, A.; Fontecilla-Camps, J. C.; Field, M. J. *J. Am. Chem. Soc.* **1999**, *121*, 4468–4477.
83. Darensbourg, M. Y.; Lyon, E. J.; Zhao, X.; Georgakaki, I. P. *Proc. Natl. Ac. Sci.* **2003**, *100*, 3683–3688.
84. Evans, D. J.; Pickett, C. J.; *Chem. Soc. Rev.* **2003**, *32* (advance article).

8.22
Nitrogen Fixation

P. L. HOLLAND
University of Rochester, NY, USA

8.22.1 INTRODUCTION

The process of dinitrogen reduction, or "fixation," has captured the attention of generations of chemists for a number of reasons. Agricultural production is often limited by the amount of available nitrogen. Despite the fact that aerobic organisms are surrounded by nitrogen in the form of N_2, plants and animals are unable to use this molecule to synthesize nitrogen-containing building blocks like nucleic acids and amino acids. In the crowded world in which we live

today, we are dependent on nitrogen fixation by microorganisms and by industry for roughly equal amounts of fixed nitrogen (about 2×10^{13} g yr^{-1}).[1] Most of the vast industrial output of N_2-derived chemicals (NH_4^+ and NO_3^- in great part) is used for fertilizer, and the need for cheap fixed nitrogen for crops is often cited as a motivation for N_2 fixation research. This view is becoming untenable, though, because (i) the Haber process for reducing nitrogen (see Section 8.22.1.2.1) is inexpensive already and (ii) the high solubility of ammonia and nitrates, combined with a lack of restraint in application of fertilizer, is causing undesirable environmental effects including bacterial blooms and nitrite poisoning. It is questionable whether industry and the environment have much to gain from the technology for additional N_2-fixing capacity.

Another motivation for nitrogen fixation research is the quest to conquer an unusually difficult chemical challenge. The triple bond in N_2 has a strength of 944 kJ mol^{-1}, making it one of the strongest bonds known. In addition to this thermodynamic stability, there are kinetic difficulties in reacting with N_2 because it is nonpolar and interacts weakly with most compounds. For these reasons, the cleavage of N_2 is a demonstration of the power of chemists over the compounds they manipulate.

Incorporation of the nitrogen atoms of N_2 into alkaloids and other bioactive organic compounds is another motivation for research into N_2 activation, because N_2 is a cheap and plentiful raw material. In certain instances, this has been possible: for example, a method for incorporating N_2 into pyrrole (through a series of tungsten complexes) is known.[2] The N_2 chemistry leading to N-containing organic compounds has been reviewed.[3,4] The synthesis of anilines and related organics from N_2, aryl halides, and reductant using a titanium catalyst has been reported.[5,6]

Successful approaches to nitrogen fixation have always depended on coordination chemistry. Studies on the binding and transformations of N_2 at characterized transition metal complexes were initiated in the 1960s,[7] and amazing progress has occurred since the publication of *Comprehensive Coordination Chemistry* (*CCC*, 1987, Volume 6, Section 62.1.14.1, pp. 718–725). A number of excellent reviews are available, and these cover the subject in a variety of perspectives and depths.[8–26] Because of the breadth of the field, this chapter is not all-inclusive. It focuses on nature's solution to the nitrogen fixation problem, describing our current understanding (to the end of 2002) of the metal clusters of the nitrogenase enzymes, supplemented by model complexes closely related to these clusters. Opportunities for continued research are described. This review should provide for bioinorganic chemists a coordination chemist's perspective on relevant questions in nitrogenase research, and for coordination chemists a summary of the insights into nitrogen fixation that can be gained through study of the nitrogenase enzyme system.

8.22.1.1 Binding of N_2 to Transition Metals

Dinitrogen binds to metals in several different ways (Figure 1), depending on the particular metal, its oxidation state, and ancillary ligands. The most common are end-on terminal and end-on/end-on, in which one or both N_2 lone pairs interact with metal orbitals to form a σ-bond. End-on binding has been found for most transition metals. In this geometry, the π^*-orbitals of the N_2 unit can interact with metal *d*-orbitals in a π-backbonding interaction like that found in metal–CO complexes. Both σ-donation and π-backbonding are substantially diminished in N_2 relative to
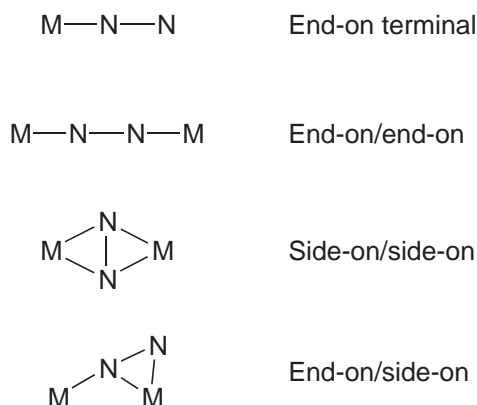
Figure 1 Binding modes for N_2.

CO, and therefore N_2 is a relatively poor ligand. As a result, N_2 will only displace very weak ligands, except at a strongly π-backbonding metal (low-valent, second or third row).

A quantitative method for evaluating the extent of backbonding is through the N—N stretching frequency, which correlates with the N—N bond length.[27] There is less backbonding (higher N—N stretching frequency) for more electronegative and higher-valent transition metals, and more backbonding (lower N—N stretching frequency) for electropositive, lower-valent transition metals. In the context of nitrogen fixation, note that low-valent early and middle transition metals back-bond most strongly, and most effectively destabilize the N—N bond and shift electron density onto the N_2 moiety. However, the weakening of the N—N bond and the reactivity of the N_2 ligand do not necessarily correlate.[15,16]

Side-on/side-on binding is found with group 1–4 metals, lanthanides, and actinides. One complex of this type is $[\{(thf)_3Li\}_2(\mu-\eta^2:\eta^2-N_2)]^{n+}$ (**1**), which may be a dication[28] or a monocation.[29] Complexes like this generally result from the reaction of a d^1 transition metal complex with N_2, and conceptually may be envisioned as the result of electron transfer to N_2. Such complexes are known for Sm,[30,31] U,[32,33] Dy,[34] Tm,[35] Pr,[36] and Nd.[37] Several group 4 complexes of this type have been isolated, some in metallocene systems[38,39] and others with amido ligands.[40–44] The extent of N—N weakening (as measured by the N—N distance or the N—N stretching frequency in Raman spectra) varies from very little (Sm) to weaker than an N—N single bond (Zr).[45] Late-metal complexes with transient side-on N_2 ligands have been identified. There is crystallographic evidence for a metastable side-on osmium–N_2 complex that is formed by photolysis of a single crystal of its end-on isomer.[46] A metastable side-on rhenium–N_2 complex can be generated thermally, as shown by the intramolecular scrambling of label in CpRe $(CO)_2(^{14}N\equiv^{15}N)$.[47]
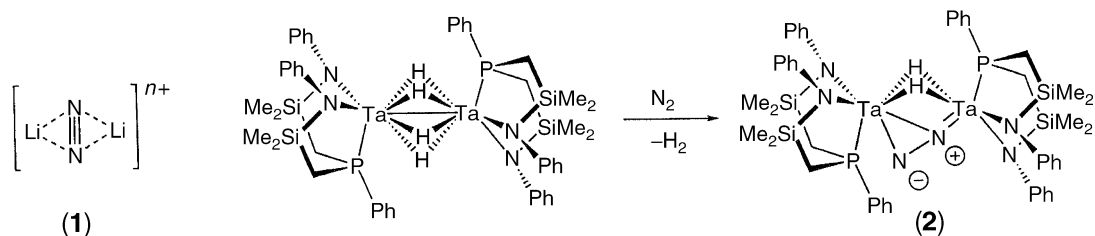
In other complexes, N_2 is bound both end-on and side-on. In some end-on/side-on complexes, each metal plays its customary role, with an alkali metal bound side-on and a late transition metal bound end-on.[48–50] In one very unusual compound, though, lithium atoms are at the ends of N_2 and nickel coordinates to the side.[51] In some homometallic clusters, N_2 is bound end-on to some metals and side-on to others.[52,53] One of the best-characterized examples of end-on/side-on binding is in $[(NPN)Ta]_2(N_2)$ (**2**),[54,55] in which the unsymmetric binding of N_2 activates it toward reaction.[56]

8.22.1.2 Major Nonbiological Advances in Nitrogen Activation

8.22.1.2.1 Heterogeneous catalysis

It was at the beginning of the twentieth century that Haber and co-workers developed the catalytic nitrogen reduction system that would earn him a Nobel prize. The best catalyst for this process (Equation (1)) is produced by H_2 reduction of Fe, K, and Al oxides.[57] Using this catalyst, large-scale N_2 reduction is performed at about 500 K to attain reasonable rates. At such high temperatures and atmospheric pressure, the equilibrium constant for Equation (1) is very small, so high pressures (>100 atm) are used. The N_2 molecule is thought to bind to the solid catalyst at sites with exposed second- or third-layer iron atoms,[58,59] and lies nearly parallel to the surface in the α form that is the precursor to N—N cleavage.[60,61] There is increasing evidence that surface defects are important in the catalytic reaction:[62]

$$N_2 + 3H_2 \longrightarrow 2NH_3 \tag{1}$$

In an effort to find a catalyst that operates at lower temperatures and pressures, work on heterogeneous catalysts for hydrogen reduction of N_2 has continued. One strategy has been to use the heavier group 8 metals Ru and Os,[63,64] and Ba instead of K.[65] Another strategy has been to use different mixtures of transition metals in the catalyst. For example, ternary nitrides of Mo with Fe, Co, or Ni have higher activity than the commercial iron catalyst.[66,67] A third type of method uses titanium oxides, with light[68–70] or electrochemical potential[71,72] as the driving force. These approaches are especially exciting because they do not require H_2 as a reducing agent, eliminating the need for fossil fuels in N_2 fixation (industrial H_2 is derived from reforming of alkanes).

8.22.1.2.2   Homogeneous catalysis

Early exciting results showed that simple transition metal salts can catalyze N_2 reduction by strongly reducing metals.[7,10,73,74] Some of these reactions give more than 1 mol of NH_3 per mole of transition metal, showing that the transition metal plays a catalytic role. However, since the early 1980s we have learnt few of the important intermediates or the mechanism(s) of reduction. In one of the most active iron systems, $FeCl_3 + PhLi$, a compound was isolated from a catalytic mixture and crystallographically identified as the very unusual "rectangular planar" iron(0) complex $[Ph_4Fe]^{4-}$.[75] Re-evaluation shows that the crystal structure actually corresponds to $[trans\text{-}Ph_4FeH_2]^{4-}$, which is inactive toward N_2.[76] In a general sense, it seems likely that some of the reported N_2 reductions are catalyzed by colloidal zerovalent metals, and some observations of NH_3 may arise from decomposition of electrolyte or other added reagents. Careful mechanistic studies into these very complicated reactions are needed.

8.22.1.2.3   Stoichiometric N_2 cleavage by coordination complexes

An impressive synthetic advance is the complete cleavage of the N—N bond of N_2 by well-characterized, isolable compounds. The three-coordinate molybdenum(III) tris-anilide complex (3a) reacts quantitatively with 0.5 equivalents of N_2 at ambient temperature to give the molybdenum(VI) nitride (5a).[77,78] There is no evidence that analogous tris-alkoxomolybdenum(III) and tris-thiolatomolybdenum(III) complexes can cleave N_2, although the alkoxide can cleave N_2 in combination with the anilide.[79,80] Steric effects play an important role, as the related anilide complex (3b) does not split N_2.[81,82] The mechanism of the reaction involves the formation of a transient triplet Mo—N≡N—Mo intermediate (4a) that has been characterized by EXAFS and Raman spectroscopies.[78] Interestingly, the MNNM core of (4a) has a "zigzag" structure that is conducive to NN bond cleavage.[83] The reaction is more rapid in the presence of one-electron reducing agents.[81] The driving force for the formation of (5a) is the strong Mo≡N bond $(650\,kJ\,mol^{-1})$.[84] In another low-coordinate system, reaction of $MoCl_4{\cdot}dme$ with 4 M equivalents of mesityl Grignard reagent gives $[Mes_3\,Mo{=}N{=}N{=}MoMes_3]$, which can be photolyzed to yield a nitride product from N_2 cleavage.[85]

R = *t*-Bu (**3a**); 1-adamantyl (**3b**)   (**4a**)   (**5a**)
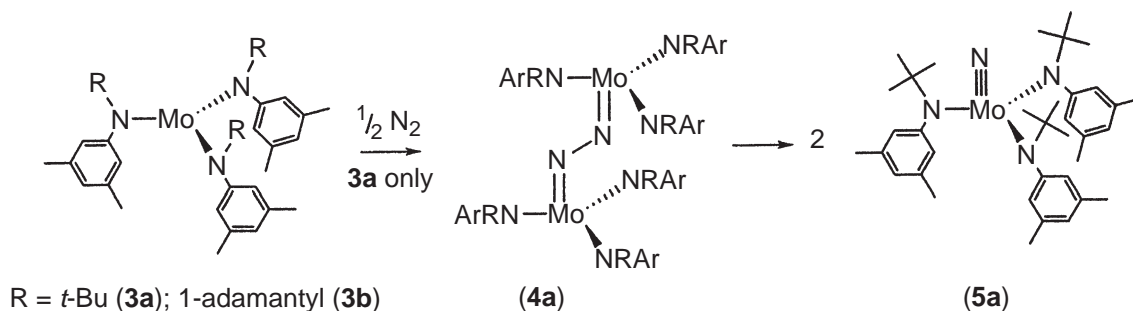
In other systems, N—N cleavage gives bis(μ-nitrido)dimetal "diamond cores" as the products of N_2 cleavage. A reduced niobium complex of calix[4]arene reduces N_2 in the presence of sodium metal, and a number of intermediates can be isolated.[86,87] A related tridentate aryloxide ligand also splits N_2 to give a diamond core with lithium ions bound to the nitrides.[88] A vanadium diamidoamine complex reacts with N_2 to give a product with a similar core structure, which may be further reduced by potassium graphite to a compound with one unpaired electron.[89] This

reaction has been evaluated using density functional theory.[90] A uranium product from N_2 cleavage (**6**) was shown to have a diamond core using X-ray crystallography.[91]

(6)
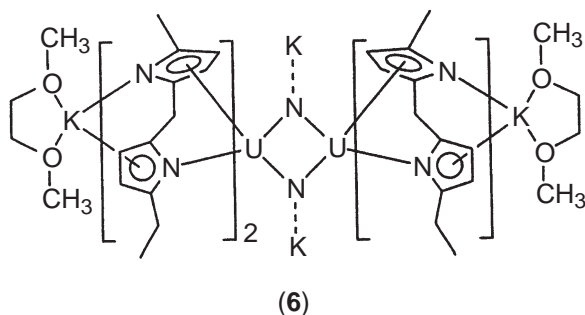
Electron-rich ligands based on phosphines and deprotonated amines have given a number of unprecedented complexes and reactions. The side-on/side-on $(P_2N_2)Zr-N_2$ complex (**7**) reacts with H_2 to give (**8**), which has a bridging hydride and a bridging $\mu\text{-}\eta^2\text{:}\eta^2\text{-}N_2H$ ligand, as shown by NMR, neutron crystallography, and vibrational spectra.[92,93] This represents the first example of direct reaction of H_2 with coordinated N_2 to form N—H bonds. *Ab initio* computational studies of this reaction have been reported.[93,94] The same (P_2N_2) ligand, when coordinated to Nb, gives an end-on/end-on N_2 complex, in which the N—N bond may be cleaved.[95] Using a related tridentate ligand, the Ta–N_2 compound (**2**) is produced by displacement of H_2 from a polyhydride complex (analogous to the displacement of H_2 from the FeMoco in the Thorneley–Lowe scheme, Section 8.22.3.1.1).[54,55] The N_2 ligand is polarized by the unsymmetric binding, and attracts electrophiles at the nonbridging nitrogen atom, leading to functionalization and/or N—N cleavage.[55,56]

(7)   **(8)**
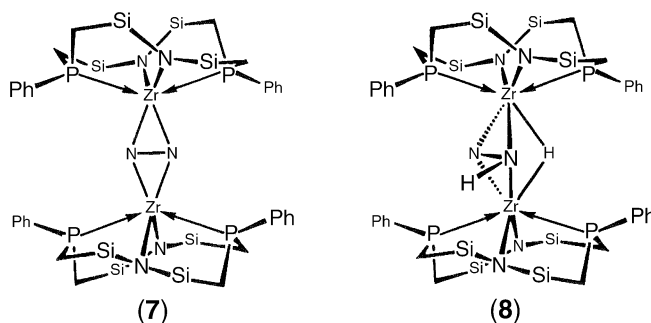
Triamidoamine ("N_3N") ligands have been useful in supporting molybdenum–dinitrogen complexes that are amenable to N_2 functionalization and cleavage.[96] $[(N_3N)Mo(N_2)]^{n-}$ ($n = 0, 1$) complexes like (**9**) are nucleophilic at the terminal nitrogen atom, and react with protons and electrophiles at this position.[97] Using extremely bulky N_3N ligands, it is possible to reduce N_2 to ammonia stoichiometrically.[98,99] These classical approaches have been supplemented by a strategy in which acidic metal–dihydrogen complexes are used as the proton source for producing NH_3 from coordinated N_2.[100–103] Because of the possibility of multimetallic dihydrogen–dinitrogen complexes on the FeMoco of nitrogenase (see Section 8.22.3.2), these reactions hold special interest.

(9)
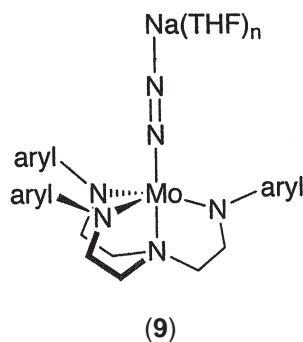
What characteristics in a complex lead to N_2 activation? The metal is typically very donating, and π-donor ligands are useful in enhancing the transfer of electrons to the N_2 unit. Adoption of a nonlinear MNNM geometry is likely to be important; this can be achieved through bending an end-on/end-on dimer, or through a side-on interaction with one or more metals. One interesting approach to evaluating the barrier for N—N cleavage is based on the study of N—N coupling, because the principle of microscopic reversibility implies that the mechanism of this reaction will apply also to N—N cleavage. Thus, it is notable that osmium nitride complexes can couple to form dinitrogen.[104] This coupling reaction is speeded by using two different metals, suggesting that an asymmetric metal environment lowers the barrier to N—N formation and cleavage reactions.[105] In a related result, a relative of the Mo tris-anilide complexes (**3**) gives a Mo—N_2—Nb system that can be reduced to split N_2.[106] Considering the recent successes in heterogeneous reactions using mixed metals, the study of heterobimetallic systems appears to be a fruitful direction for continued research.

8.22.1.3 Nitrogenase

The term "nitrogenase" refers to a class of similar enzymes that catalyze the reduction of dinitrogen to ammonium ion using protons, electrons, and ATP (which is hydrolyzed to ADP). This reaction is shown in Equation (2), where $n \geq 1$. These enzymes are produced by anaerobic and aerobic bacteria and archaea ("diazatrophs"), which were responsible for the bulk of bioavailable nitrogen before the advent of the Haber process on the modern scale. The most agriculturally relevant of these microorganisms live symbiotically with leguminous plants, providing the plant with fixed nitrogen in return for other nutrients and protection from oxygen. Other diazatrophs are free-living, and have been found widely in soils and oceans:

$$N_2 + (6 + 2n)H^+ + (6 + 2n)e^- + (12 + 4n)MgATP \longrightarrow 2NH_3 + nH_2 + (12 + 4n)MgADP +$$
$$(12 + 4n)\text{phosphate} \qquad (2)$$
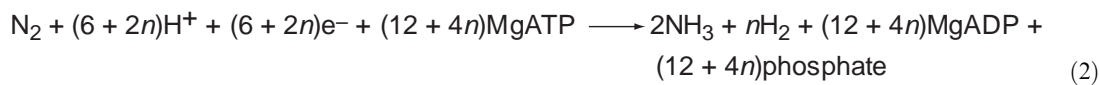
Active cell-free extracts of nitrogenase were isolated in 1960,[107] and since then the study of these enzymes has posed a great challenge to biochemists. One substantial barrier is that the enzymes are sensitive to oxidation, and must be handled in an oxygen-free environment, often in the presence of a reductant (typically dithionite). In addition, the metal content of the enzyme varies depending on the growth conditions. With sufficient [Mo], the main product, "MoFe nitrogenase," contains iron and molybdenum. The other "alternative" nitrogenases (Section 8.22.4) are expressed only under Mo-poor conditions, and have similar structure and high sequence homology. Another discovery is a superoxide-dependent nitrogenase, which is not yet understood at a level sufficient for discussion of its coordination chemistry.[108] The bulk of this chapter addresses MoFe nitrogenase, because it is by far the best understood, and results on alternative nitrogenases are viewed through the lens of MoFe nitrogenase chemistry.

MoFe nitrogenase consists of several proteins. The "Fe protein" (encoded by the *nifH* gene) is a 64 kDa homodimer, and the "MoFe protein" is made up of two different kinds of subunits (encoded by the *nifD* and *nifK* genes) in an $\alpha_2\beta_2$ tetramer of roughly 250 kDa. These are often numbered 2 and 1, respectively, along with the organism name: for example, Av2 is the Fe protein from *A. vinelandii*; Cp1 is the MoFe protein from *C. pasteurianum*. The metal-containing cofactors will be discussed in detail below. X-ray crystallography shows that the metal sites within the two $\alpha\beta$ units of the MoFe protein are distant (>70 Å) from each other, so it is usually assumed that each $\alpha\beta$ unit functions independently. There is consensus that the role of the Fe protein is to bind to the MoFe protein, hydrolyze ATP, and use the resultant energy to transfer electrons to the MoFe protein, the site of N_2 reduction. Dissociation of the Fe protein from the MoFe protein is the overall rate-limiting step in nitrogenase catalysis.

It is interesting and possibly mechanistically significant that nitrogenase enzymes also function naturally as hydrogenases. In the absence of N_2, protons are reduced to H_2 without loss in subsequent nitrogenase activity. However, even under saturating concentration of N_2, a substantial amount of H_2 is produced. A convenient measure of nitrogenase versus hydrogenase activity is the number of electrons devoted to N_2 reduction as a fraction of total electrons consumed. Under optimal conditions, FeMo nitrogenase uses 75% of electrons for nitrogen reduction (1:1 ratio of N_2 consumed/H_2 produced), but the alternative nitrogenases are less efficient, putting

only a quarter of their electrons into N_2. Hydrogen production is usually regarded as "leaking" of electrons from an imperfect N_2 reduction system, although the 1:1 limiting ratio in FeMo nitrogenase has also been attributed to a necessary part of the reaction mechanism, as discussed in Section 8.22.3.1.1.

8.22.2 METAL SITES IN NITROGENASE AND SYNTHETIC MODEL COMPLEXES

There are three catalytically necessary metal–sulfur clusters in iron–molybdenum nitrogenase: the Fe_4S_4 cluster in the Fe protein (Section 8.22.2.1), the P cluster (Section 8.22.2.2), and the FeMo cofactor (Section 8.22.2.3). Each one will be discussed separately, along with relevant coordination complexes.

8.22.2.1 Fe Protein

8.22.2.1.1 *Function and structure*

The Fe protein (also called *nifH* after the gene that encodes it) is the vehicle for a 4Fe/4S cubane-type cluster (Figure 2), in which the tetrahedral coordination at each iron atom is completed by a cysteine residue. The Fe protein is a homodimer, and the cluster lies at the interface between the two units, held by Cys97 and Cys132 from each subunit. The X-ray crystal structure of the Fe protein shows that the iron–sulfur cluster is exposed to solvent, a feature that presumably assists in acquisition of electrons from its natural electron donors (flavodoxin or ferredoxin).[109,110]

The Fe protein is the only known reductant that successfully induces the MoFe protein to catalyze N_2 reduction. The redox potential of the biologically important $Fe_4S_4^{2+}/Fe_4S_4^{1+}$ couple depends on the presence or absence of nucleotide substrates: it is -0.30 V without nucleotides, -0.43 V in the presence of ATP, and -0.49 V in the presence of ADP.[24] This trend is consistent with a role where the Fe protein accepts an electron, and nucleotide binding and hydrolysis trigger electron donation. Because it is more effective than reductants with lower redox potentials, it is likely that binding between the Fe and MoFe proteins is accompanied by some conformational change that opens an efficient electron transfer pathway. The structural details have been elucidated using X-ray crystallography of nitrogenase inhibited with $ADP \cdot AlF_4^-$, which binds in the ATP site and stabilizes the docked Fe protein/MoFe protein complex.[111] The structure shows that deep-seated conformational changes in the Fe protein upon binding[112] place the Fe_4S_4 cluster about 14 Å from the P cluster (see Section 8.22.2.2) of the MoFe protein. In addition, the bound complex has hydrogen bonding interactions between the peptide backbone of the MoFe protein and the sulfides of the cluster. The direct source of the shift of potential may derive from specific hydrogen bonding interactions, or from a change in the polarity of the environment of the cluster. Redox potentials of iron–sulfur clusters in organic solution are typically much lower than those for the same site in water, suggesting that movement of the cluster from the surface to the interior of the protein upon nucleotide binding could make it a stronger reductant.[113]

Under standard *in vitro* conditions with dithionite as reductant, the Fe_4S_4 cluster is in the reduced $Fe_4S_4^{1+}$ state. Interestingly, the $Fe_4S_4^{1+}$ cluster can be reduced by titanium(III), chromium(II), or radiolytic reduction to an $Fe_4S_4^0$ (all-ferrous) form, an oxidation level that is
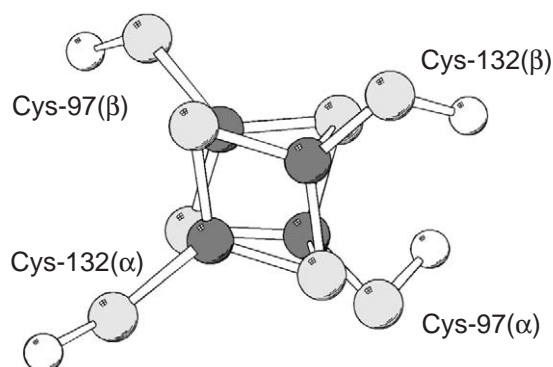
Figure 2 Fe_4S_4 cluster of the Fe protein. Coordinates from Schlessman *et al.*[110]

unusual for Fe_4S_4 clusters.[114,115] The structure of the $Fe_4S_4{}^0$ form has been determined using X-ray crystallography at moderate resolution (2.25 Å).[116] The structure shows that the coordination of the cluster does not change upon reduction. The Fe_4S_4 cluster expands slightly, and the cysteine ligands attract seven hydrogen bond donors, presumably to dissipate the substantial negative charge on the cluster. Predicted metrical details also come from preliminary density functional calculations.[121]

Because nitrogenase catalysis consumes less ATP and shows no induction period with Ti(III) as reductant, it has been suggested that the $Fe_4S_4{}^0$ oxidation level could be physiologically relevant.[117,118] This proposal suggests that the Fe_4S_4 cluster transfers pairs of electrons rather than undergoing single electron transfer events, consistent with the fact that all nitrogenase substrates are reduced by multiples of two electrons. However, the relevance of the all-ferrous state *in vivo* is controversial: a study indicates that the redox potential of the $Fe_4S_4{}^{1+}/Fe_4S_4{}^0$ couple in Av2 is -0.79 V, too low for reduction by any of the possible natural reductants, and not at -0.46 V as earlier reported.[119] The lower value is more reasonable, based on the differences between $Fe_4S_4{}^{2+}/Fe_4S_4{}^{1+}$ and $Fe_4S_4{}^{1+}/Fe_4S_4{}^0$ redox potentials in model complexes,[120] and on the results of density functional calculations.[121]

Numerous synthetic Fe_4S_4 cubanes with thiolate ligation like that of the Fe protein cluster are known in the $Fe_4S_4{}^{2+}$ and $Fe_4S_4{}^{1+}$ states (synthetic Fe_4S_4 complexes are discussed in Section 8.22.2.2.4). These have been studied mostly in nonaqueous environments, and have $Fe_4S_4{}^{2+}/Fe_4S_4{}^{1+}$ potentials at -0.7 V to -1.3 V. In a few cases, it has been possible to reduce the clusters further to the $Fe_4S_4{}^0$ level in cyclic voltammetry experiments, but no all-ferrous Fe_4S_4 model compounds have been isolated.[120,122,123] It is possible that synthetic strategies using small peptides that incorporate protein-like hydrogen bonding interactions may stabilize the substantial negative charge on a $Fe_4S_4\text{-}(SR)_4{}^{4-}$ unit and enable the isolation of this type of synthetic compound in the future.

8.22.2.1.2   *Spectroscopy*

At the $Fe_4S_4{}^{1+}$ oxidation level, the Fe_4S_4 cluster is in a mixture of $S = 1/2$ and $S = 3/2$ states.[124–128] Electron paramagnetic resonance studies, magnetism, Mössbauer, and MCD studies have led to this conclusion, although the details of this spin crossover/admixture are not clear.[18]

As the $Fe_4S_4{}^0$ state is not stable in synthetic compounds, spectroscopists have taken advantage of the accessibility of Fe protein in the all-ferrous state to understand the spectroscopic characteristics of this novel oxidation level. The parallel-mode EPR spectrum shows a resonance at $g_{eff} = 16.4$ from a ground state $S = 4$ spin multiplet, and the electronic absorption spectrum has a band at 490 nm that gives the all-ferrous protein a pink color.[129,130] EXAFS shows iron–iron distances of 2.53 Å and 2.77 Å, consistent with a tetragonally distorted tetrahedron with substantial Fe—Fe bonding interactions.[131] However, the results of EPR and Mössbauer investigations suggest that one of the four iron sites is different from the other three, inconsistent with any C_2-symmetric structure.[115] The X-ray crystal structure is not of high enough resolution to distinguish between these distortions.[116]

8.22.2.2   MoFe Protein: P Cluster

8.22.2.2.1   *Function and structure*

The P cluster is an Fe_8S_7 cluster that lies at the interface of the α- and β-subunits of the MoFe protein. It is situated about 15 Å from the site at which the Fe protein binds and about the same distance from the FeMoco, suggesting a role in electron transfer. This idea was first supported by a tandem EPR/kinetics study, in which the (small) characteristic spectroscopic change observed corresponds to the rate of FeMoco reduction.[132] More direct evidence comes from the observation in a mutant of a characteristic EPR signal that disappears during turnover and then returns.[133] Therefore, the P cluster is generally viewed as a gateway for electron transfer into the catalytic FeMoco center. The P cluster is observed in several redox states: the most common are called P^{2+} (or P^{OX}), P^{1+}, and P^N (fully reduced).

X-ray crystallography in the reduced P^N form shows that it is a double cubane in which one sulfide is shared by both cubanes. Figure 3a shows the model from Av1 at 1.16 Å resolution.[154] This structural feature is also present in the Kp1 structure.[134] The bridging sulfur atom is six
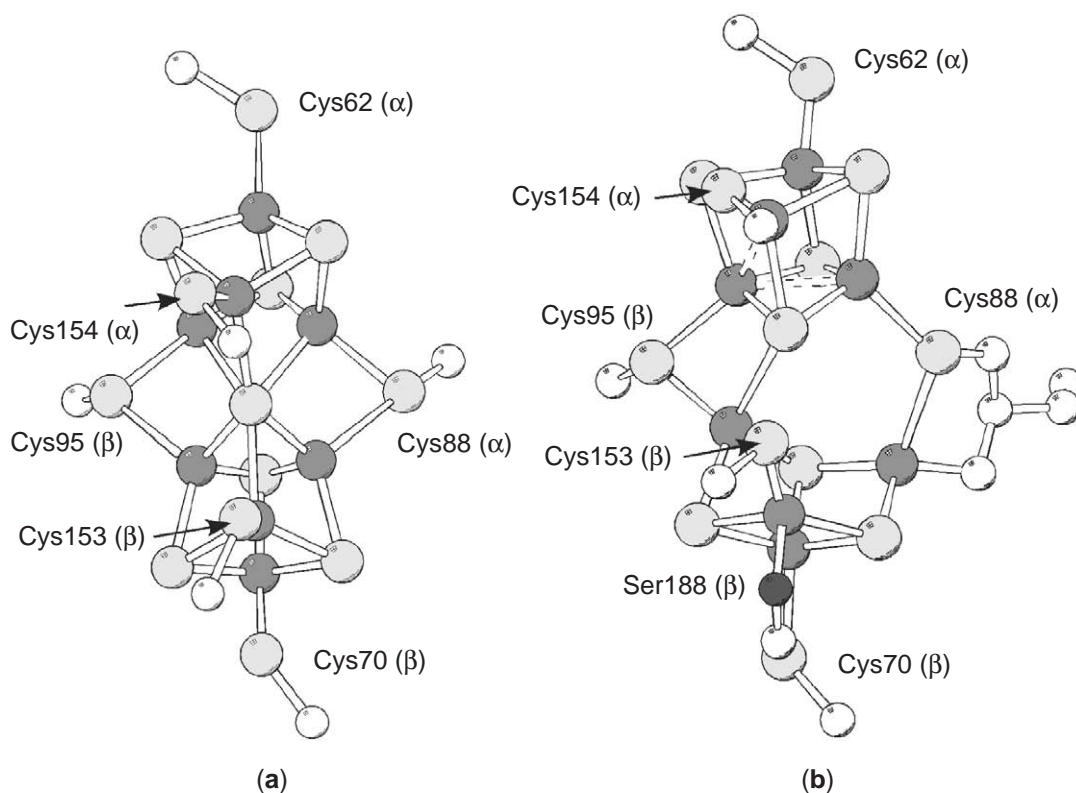
Figure 3 P cluster of the MoFe protein in two different oxidation states: (a) P^N; (b) P^{OX}. Carbon and nitrogen atoms are shown in white. Coordinates from Einsle *et al.*[154] and Peters *et al.*[136]

coordinate, and the six bonds to this sulfur atom have equivalent lengths in the highest-resolution Kp1 and Av1 structures. The two cubane units are also bridged by the sulfur atoms from Cys88 (α) and Cys95 (β), and the remaining coordination sites are filled by Cys residues from both subunits.

Upon transformation to P^{OX} (the P^{OX}/P^N redox potential is roughly $-0.3\,V$),[21,135] there is a structural change where the two cubanes move apart, replacing two of the bonds to the central sulfide with O and N atoms from Ser188 (β) and the protein backbone of Cys88 (α), respectively (Figure 3b shows the model of P^{OX} from Av1 at 2.03 Å resolution).[136] It is reasonable that these "hard" donors stabilize a more oxidized state of the redox center; however, the exact redox level of the iron atoms in the P cluster in the aforementioned states is not yet known. The presence of natural amide and alkoxide donors to an iron–sulfur cluster, as in P^{OX}, is unusual because iron–sulfur clusters are typically coordinated by cysteine thiolate ligands. In addition to their "hard" character, the high pK_a values for the N and O donors admit the possibility that they may be protonated, i.e., a pH change may be mechanistically important in controlling the redox activity. Indeed, the potential of the P^{OX}/P^{1+} redox couple is pH dependent.[135] Mutation of Ser188 (β) to Gly does not alter the redox potential: this leaves the amide, a coordinated Cys, or some proton-mediated conformational change as potential pH-sensitive contributors to function.[24] A crystal structure indicates that the coordinated amide nitrogen is not planar, suggesting that it might be protonated.[134]

The redox-coupled conformational change and the two-electron change from P^N to P^{OX} has led most researchers to view the P cluster as a diode and/or capacitor for electron flow into the FeMoco. This hypothesis explains the ability of the nitrogenase protein to build up sufficient reducing equivalents at one site (the FeMoco) to accomplish the difficult reduction of N_2. However, more work is necessary to establish the ways in which the protein controls the rate and direction of electron transfer.[24]

8.22.2.2.2 Spectroscopy

Fe *K*-edge EXAFS of FeMoco-deficient MoFe protein gives a picture of the P^N and P^{OX} states that is generally consistent with crystallography, although the presence of a large number of iron

atoms in similar environments makes it difficult to distinguish specific distances.[137] It is interesting, though, that very short (2.42 Å and 2.57 Å) Fe—Fe distances consistently were obtained in the refinements of the P^{OX} and P^N states, respectively.

The P^N state is diamagnetic, as shown by its EPR silence and the lack of response of its Mössbauer signal to a magnetic field.[138] This restrains the possible oxidation states to an even number of both iron(II) and iron(III) ions, but the exact oxidation level of the eight-metal cluster is not known. Mössbauer studies also suggest a primarily (if not exclusively) iron(II) formulation of P^N.[139] Either an Fe^{II}_8 or an $Fe^{II}_6Fe^{III}_2$ formulation seems reasonable, because it is possible to oxidize the cluster to P^{OX}, which is thought to have $S = 3$ or 4 and be two electrons more oxidized than P^N (redox potential $= -0.31$ V). The integer-spin formulation of P^{OX} is supported by a characteristic signal in parallel-mode EPR spectra.[140,141]

An intermediate oxidation level can be identified in redox titrations below physiological pH: this is P^{1+}, which has a $S = 1/2$–$5/2$ mixed spin state.[142] This may arise from mixtures of isomers in which Ser188 (β) is bound or not, from states in which the "hole" is on different halves of the cluster, or in which different cysteinates are cleaved.[134] It has been possible to stabilize this state with a mutation Ser188Cys in which the electron-rich thiolate shifts the redox potentials to lower values.[133] The P^{OX}/P^{1+} redox couple is pH dependent, as noted above. Another redox state, P^{3+}, has also been identified, and it also is apparently a mixed spin state with $S = 7/2$ and $1/2$.[143] In the *R. capsulatus* enzyme, though, neither P^{1+} nor P^{3+} is mixed.[144] Clearly, additional work is necessary to understand the electronic structure of this cluster and its interplay with geometric structure and electron transfer.

8.22.2.2.3 *Model complexes*

It is now possible for synthetic chemists to create iron–sulfur clusters that mimic the unusual distribution of iron atoms in P^N. The first stable double cubanes with thiolate bridges like those in the P cluster were created in 1997.[145] The challenge of making a μ_6-sulfido bridge was conquered with the complex $[(Cl_4cat)_6(Et_3P)_6Mo_6Fe_{20}S_{30}]^{6-}$, in which there are Fe_6Mo_2 units.[146] A smaller cluster with similar structural analogies to P^N is $[(Cl_4cat)_4 (Et_3P)_4Mo_4Fe_{12}S_{20}K_3(DMF)]^{5-}$ (**10**), which contains two $[(catecholate)(phosphine)Mo]_2Fe_6S_9{}^{2-}$ units bridged by two μ_2-sulfide bridges and three potassium ions.[147] Although the Fe_6S_9 $[Mo(catecholate)(phosphine)]_2$ fragments have octahedral molybdenum atoms in place of the outer iron atoms, there is a clear analogy with P^N, in which two bound cubanes are connected by μ-sulfide. Mössbauer and magnetization data support a primarily ferrous environment in (**10**). Finally, monomeric clusters (**11**) ($[Tp_2M_2Fe_6S_9]^{n-}$; M = Mo, $n = 3$; M = V, $n = 4$) are stabilized by the tris(pyrazolyl)borate ligand, showing that the cluster topology found in P^N can exist as a free entity in solution.[148] Complex (**11b**) has metrical parameters that are truly close to P^N, with an r.m.s. deviation of only 0.33 Å for the M_8S_9 core.

(**10**)   (**11a**)(Mo, 3–), (**11b**)(V, 4–)
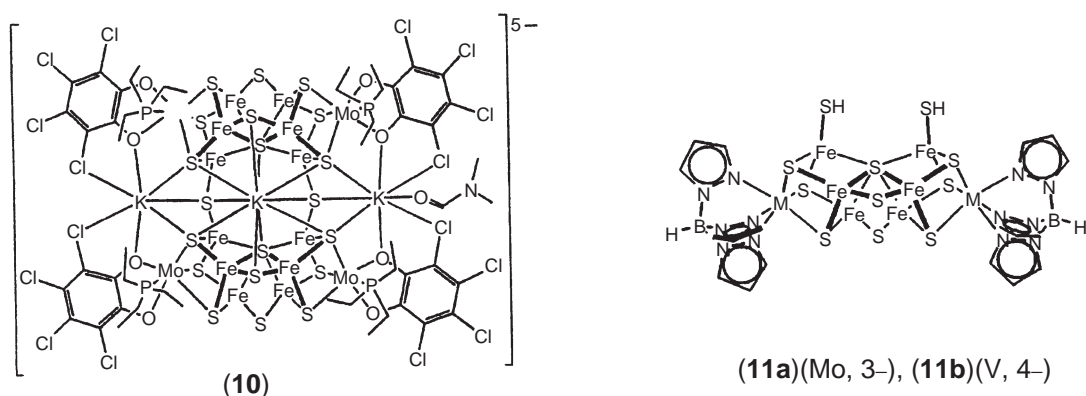
The synthesis of (**11**) shows that the P^N geometry can spontaneously assemble from a cubane synthon, hydrosulfide, and reducing agent. The Fe protein is essential in the natural synthesis of working MoFe protein (see Section 8.22.5), suggesting that a similar reductive cluster fusion could

be relevant in the biosynthetic pathway. What challenges in model complexes for P^N remain? The above clusters have not been synthesized with only iron. Apparently, the octahedral coordination at the terminal Mo sites is beneficial for steering the Fe_3 units into appropriate fused clusters. Also, the synthetic compounds have μ_2-sulfide bridges instead of thiolates (cysteinate residues in the protein).

8.22.2.3 MoFe Protein: FeMo Cofactor

8.22.2.3.1 *Function and structure*

The iron–molybdenum cofactor of nitrogenase is one of the most fascinating exhibits in bioinorganic chemistry, because it is here that the enzyme somehow catalytically cleaves the strong triple bond of N_2 to give ammonia. As noted in Section 8.22.1.2, human ingenuity has not yet devised a catalytic method for this process that is comparably effective at room temperature and atmospheric pressure. Therefore, coordination chemists can gain valuable lessons in bond cleavage and catalysis from this metal cluster, its surroundings, and its metal-substituted analogues.

The iron–molybdenum cofactor ("FeMoco" or "M cluster") is widely accepted to be the site of N_2 binding and reduction. Mutations near this site, or the absence of homocitrate (from *nifV⁻* mutants) greatly affect the catalytic specificity and activity. The enzyme is inactive if the biosynthetic machinery for FeMoco synthesis is removed, but becomes active if "extracted FeMoco" (see Section 8.22.2.3.4) is added. The characteristic EPR signal for the FeMoco changes under turnover conditions, and, as shown below, some substrates have been shown to bind at the FeMoco.

The FeMoco has been observed in three redox states. When the enzyme is isolated in the presence of dithionite, the FeMoco is in the M^N ("native") form. Most crystallographic studies have taken place on enzyme in which the FeMoco is in the M^N state. M^{OX} can be generated by one-electron oxidation of M^N with dyes, and can be reactivated by reduction. The M^{OX}/M^N redox potential is dependent on the organism from which the nitrogenase is derived, lying in the range 0 mV to -180 mV.[149] The X-ray crystal structure of MoFe protein with the FeMoco in the M^{OX} state shows no major differences from M^N.[134,136] M^R is the turnover state of the enzyme, corresponding to one-electron reduction of M^N, and has not been crystallographically analyzed because it is only observed during catalytic turnover.

The basic structure of the FeMoco in the M^N state (Figure 4) is a $MoFe_7S_9$ cluster, lying deep within the α subunit, that has superficial similarity to the P^N cluster. However, in the FeMoco there are fewer protein-derived ligands: a cysteine thiolate (Cys275) binds to the terminal iron site, and the central bridges are sulfides rather than thiolates. The molybdenum atom is octahedrally
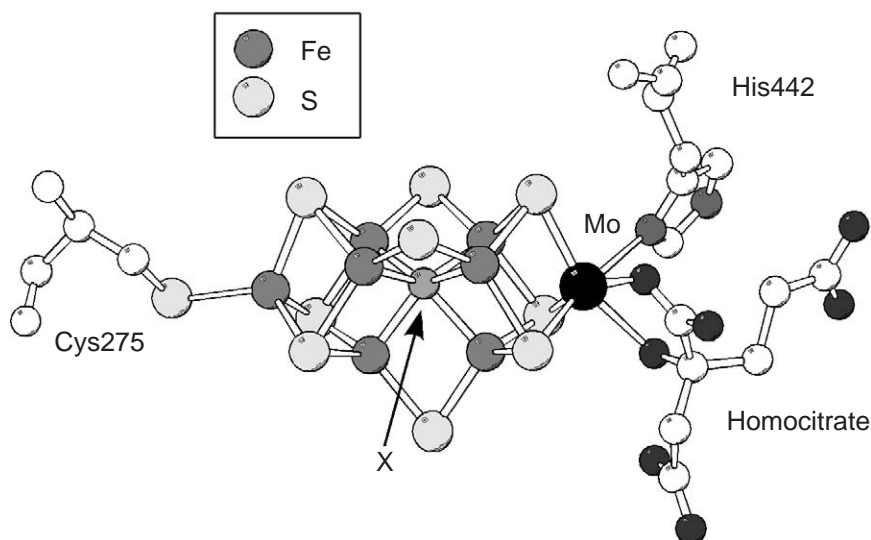
Figure 4 Iron–molybdenum cofactor (FeMoco) of the MoFe protein. Carbon and nitrogen atoms are shown in white. Coordinates from Einsle *et al.*[154]
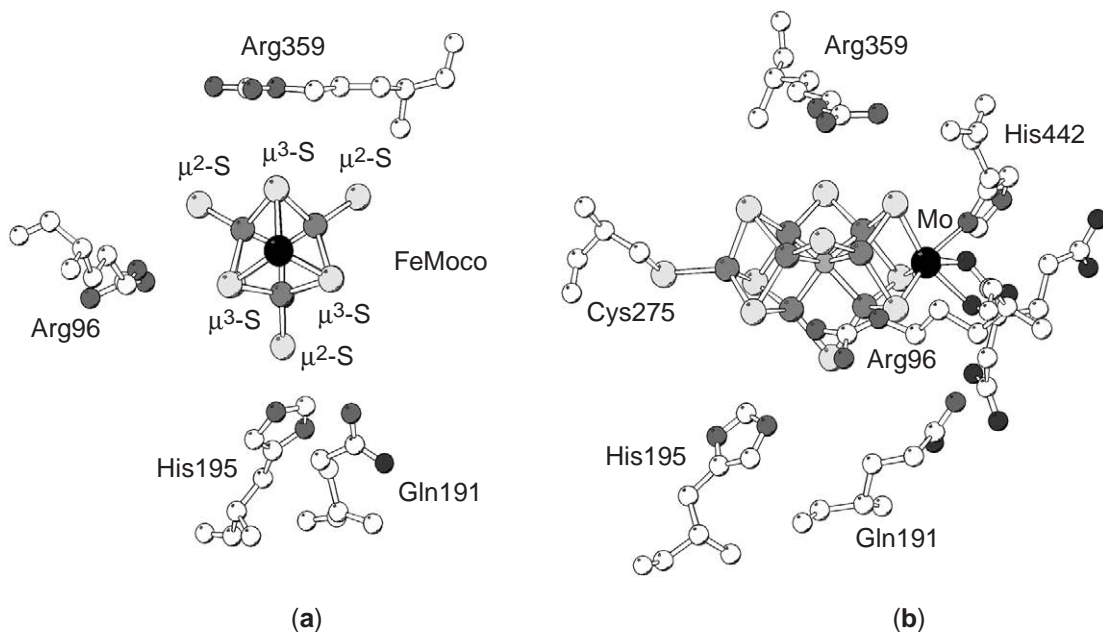
Figure 5 FeMoco with nearby residues that could potentially coordinate and/or form hydrogen bonds with intermediates. Carbon and nitrogen atoms are shown in white: (a) front view; (b) side view. Coordinates from Einsle *et al.*[154]

coordinated by three μ_3-sulfides, His442, and (*R*)-homocitric acid (2-hydroxy-1,2,4-butanetricar-boxylic acid). Homocitrate, the deprotonated form of the acid, coordinates through the alcohol oxygen (which may or may not be deprotonated) and in a monodentate fashion through the central carboxylate. One of the remaining carboxylates has a hydrogen bond to Gln191 (Figure 5b); the others are surrounded by water molecules. A theoretical study suggests that the histidine imidazole could be deprotonated at the uncoordinated ε position.[150]

The FeMoco is surrounded by a number of very close amino acid residues. Figure 5a shows M^N along with several residues that have metal-binding and/or hydrogen-bonding capabilities. His195 is close enough for a direct hydrogen-bonding interaction with a nucleophilic μ_2-sulfide bridge. Two arginine residues also are quite close to the central region of the cluster, and may be involved in proton delivery to the FeMoco. The positive charges on these residues are also likely to affect the behavior of the FeMoco, through direct interaction with N_2 or intermediates, or through electrostatic modification of the redox potential. There is a substantial "pool" of water molecules in the vicinity of the homocitrate ligand. Channels through which protons can approach and ammonia can leave have been located using theoretical calculations.[151,152]

8.22.2.3.2 *Atoms in the belt region*

The six iron atoms in the center of the cofactor (the "belt" or "waist" region) are unusual. Based on crystallography with moderate resolution, admirers of the FeMoco (the author included) long held the unlikely belief that the six iron atoms were three-coordinate, because the only visible ligands are the three bridging sulfides in a roughly trigonal planar arrangement. This rare coordination geometry in synthetic compounds is invariably enforced by very large ligands (see Section 8.22.2.3.5), and therefore it is surprising that three-coordination would persist in the presence of potentially coordinating Arg and His residues. The $\sim$2.6 Å Fe—Fe distances between adjacent iron atoms (Figure 6) could represent enough iron–iron bonding that the iron atoms are not electronically unsaturated.[153] Iron–iron bonds can also be seen as a storage site for electrons.

Our view of the FeMoco changed drastically in 2002. Crystallographic analysis to 1.16 Å resolution of *A. vinelandii* MoFe protein shows that there is a light atom X (C, N, or O) between the six iron atoms, whose presence had been masked by systematic termination errors that are inherent in Fourier analysis of diffraction data.[154] This discovery is consistent with numerous data that are more difficult to explain with the "three-coordinate" model. First, each of the six
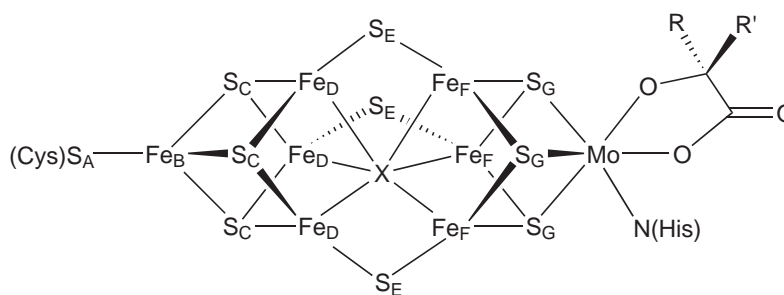
Figure 6

belt iron atoms slightly deviates from its S_3-coordination plane toward the *inside* of the cluster, to make the bond to X. Second, the distance from X to each belt iron atom is 2.0 Å, a reasonable bond distance for an Fe—N, Fe—C, or Fe—O bond. (This distance is too short for X to be sulfur, and the thermal parameters of the iron atoms are symmetric, indicating full occupancy of X.) Third, the unusual lack of coordination from the protein surroundings is explained because the iron atoms are not actually three-coordinate in the isolated form. Finally, the presence of a structural stabilizer like X explains why the FeMoco can be chemically extracted from the protein without extensive changes in the geometric and electronic structure (see Section 8.22.2.3.4). Therefore, the belt iron atoms in the FeMoco have a four-coordinate trigonal pyramidal geometry.

Figure 6 and Table 1 show the current model of the FeMoco. The electron density for X in the X-ray crystal structure is most consistent with a nitrogen atom,[154] but C and O models are within experimental error. Theoretical calculations reproduce the Fe—X bond lengths most accurately with X = N.[155] X has been postulated to be a nitride derived from splitting of N_2, and therefore the resting state of the catalyst would represent an FeMoco that has completed part of the nitrogen reduction.[154] This is consistent with the observation that N_2 uptake only occurs after addition of three or four electrons to the resting state (see Section 8.22.3.1.1). However, spectroscopic investigations show that added $^{15}N_2$ is not incorporated into the cluster during turnover, ruling out the identification of X as a nitride that originates from the catalytic reduction of N_2.[156] Therefore, the available data suggest that X fulfills a structural role, although much remains to be done to delineate its identification and function in N_2 reduction.

Synthetic compounds show precedents for C, N, and O atoms that bridge six transition metals. Hexanuclear nitrides are known for most transition metals in groups 8 and 9, and there are a few in which all six atoms are iron.[157,158] Most of these clusters have an octahedral arrangement of metal atoms, and Fe—(μ_6-N) distances are 1.84–1.89 Å. Trigonal prismatic arrangements of metals around a nitride are less common, but one example is $[Co_6N(CO)_{15}]^-$, in which the μ_6-nitrido ligand was characterized by ^{15}N NMR spectroscopy.[159] The many μ_6-oxo complexes typically have M—O distances greater than 2.0 Å. Synthetic iron–carbide clusters are known having carbide ligands with varying coordination numbers up to 6, but it is unclear how carbide could be formed in nitrogenase.[160,161] Therefore, there are precedents for C, N, and O atoms fulfilling the high-coordinate bridging role of X, but N seems most likely at this early stage. It is notable that the metal atoms in the synthetic clusters invariably have strong-field ligands (primarily carbonyl) and are low spin, and therefore may not be directly comparable with the low coordination number and weak-field sulfide ligands found in the FeMoco. A review has recently appeared.[350]

Table 1   Average bond lengths (standard deviation) of the FeMoco from the 1.16 Å structure of Av1.[154] Distances in Å. Labels in Figure 6.

Fe_B—S_A	2.27(1)	Fe_B—Fe_D	2.67(1)
Fe_B—S_C	2.28(1)	Fe_D—Fe_D	2.65(2)
Fe_D—S_C	2.27(2)	Fe_D—Fe_F	2.59(2)
Fe_D—S_E	2.23(1)	Fe_F—Fe_F	2.62(2)
$Fe_{D,F}$—X	2.00(3)	Fe_F—Mo	2.70(3)
Fe_F—S_E	2.22(1)	Mo—O(carbox)	2.20(1)
Fe_F—S_G	2.23(1)	Mo—O(alkox)	2.18(1)
Mo—S_E	2.34(1)	Mo—N(His)	2.30(1)

Another view of the FeMoco compares it to bulk metals with interstitial carbide, nitride, or oxide in the lattice. It is difficult to draw clear analogies between the band electronic structure of solids (through which oxide, nitride, and carbide materials are understood) and the localized interactions in the FeMoco, although theoretical calculations should give progress along these lines.

It should be stressed that, although the dithionite-reduced M^N form of the FeMoco has been crystallographically characterized, M^N does not bind N_2. Several reducing equivalents (from the Fe protein, presumably through the P cluster) are required before N_2 binds. Some metrical changes undoubtedly accompany the full reduction, and these may be substantial. Once a complete picture of the FeMoco (including the identification of X) is established, *ab initio* calculations[121] will have a significant impact on our understanding.

8.22.2.3.3   *Spectroscopy*

Iron and molybdenum EXAFS data on M^N complement those from X-ray crystallography, and are consistent with the heavy-atom (Mo, Fe, S) distances found there.[162–164] Iron EXAFS interpretation is difficult because of the large number of iron atoms, including those from the P cluster, a situation in which overlapping shells complicate the interpretation of the data. It is possible to locate a 3.7–3.8 Å Fe—Fe distance that is characteristic of a cross-cluster distance in the crystallographic FeMoco structure, and incompatible with the geometry of other iron–sulfur clusters.[164] EXAFS data on the one-electron-reduced form M^R have been interpreted as showing a *decrease* (0.04 Å) in the average Fe—Fe distance upon reduction of the cluster from M^N to M^R.[165] This is unusual behavior for an iron–sulfur cluster, because they generally expand upon reduction. More detailed structural information on M^R is not known, and structurally nothing is known about the more reduced forms of the FeMoco that actually bind N_2.

The M^N forms of wild-type MoFe proteins have an EPR signature that has been assigned to the FeMoco because the P cluster is diamagnetic under these conditions. The signal is unusual, with components near $g = 4.3$, 3.65, and 2, and it arises from the ground state Kramer's doublet of an $S = 3/2$ spin system with small rhombicity and positive axial zero-field splitting.[166–170] This signal is coupled to the iron part of the cofactor[171,172] and also to Mo,[173] as shown by ENDOR. The signal disappears under turnover conditions (with Fe protein present), but the Mössbauer spectrum remains magnetic, showing that M^R has integer spin.[174,175] The ground state of M^{OX} is diamagnetic, as shown by Mössbauer and MCD spectroscopies.[176,177]

The determination of precise oxidation states has been troublesome because of the extensive spin coupling within the FeMoco. The molybdenum atom in M^N is thought to be low-spin Mo(IV), based on ENDOR[178] and X-ray absorption[163] measurements. Assigning the iron oxidation states as $Mo^{4+}/6Fe^{2+}/1Fe^{3+}$ (or $Mo^{4+}/5Fe^{2+}/2Fe^{2.5+}$) is more consistent with ^{57}Fe ENDOR measurements.[179] However, a $Mo^{4+}/4Fe^{2+}/3Fe^{3+}$ formulation better rationalizes the Mössbauer isomer shifts.[180] All of the oxidation state conclusions, as well as *ab initio* evaluations of the oxidation state problem,[181] need to be re-evaluated using a model of FeMoco with the central X.

The M^N to M^R transition causes only small changes in the ^{57}Fe Mössbauer isomer shifts, suggesting that the reduction from M^N to M^R may be at molybdenum.[180] Interestingly, a second reduced state, M^I, can be generated by radiolytic reduction of M^N: it may have a different site of reduction (the coupled iron sites) or a difference in conformation (M^R is observed under turnover conditions in the presence of Fe protein, but M^I comes directly from M^N). Another reduced state has been observed by rapid-freeze EPR spectroscopy of turnover solutions.[182] The time course of its formation suggests that it arises from a three-electron reduced species, but its $S = 3/2$ signal is inconsistent with all three reducing equivalents residing at the FeMoco.

Advanced EPR measurements have also given information about coupling to nearby residues. ESEEM modulations indicating ^{14}N coupling to the $S = 3/2$ signal have been observed in wild-type Av1 but not in some mutants.[183–185] Although these were originally assigned to nearby amino acid residues (His or Gln), the potential presence of the μ-nitride complicates the interpretation. The presence of this modulation is not perfectly correlated with the ability of the mutant to turn over N_2, arguing against assignment of the modulation as nitrogen from turnover N_2.

The various timescales available in spectroscopic measurements are a potential route to discovering the dynamic properties of the FeMoco. Because of the few points of attachment between the cofactor and the protein, and the many steps necessary to cleave the N—N bond and form six N—H bonds, the cluster dynamics are likely to be mechanistically important. EPR measurements

of the MoFe protein have been interpreted as showing significant flexibility in the FeMoco.[186] Much remains to be learned in this area, especially in the correlation between dynamics and redox level.

8.22.2.3.4 Extracted FeMoco

The presence of only two connections between the FeMoco and the MoFe protein suggests that it might be possible to remove the cluster, and it was shown in 1977 that the FeMoco could be extracted from the protein.[187,188] This "extracted FeMoco" does not reduce nitrogen without the MoFe protein. The most widely used method for extraction is that of McLean *et al.* in which the protein is bound to DEAE-cellulose instead of acid denaturation.[189] The solvent of choice for extracting FeMoco is *N*-methylformamide (NMF), although DMF and acetonitrile can also be used.[190] The resultant NMF solutions of extracted FeMoco can be reduced with dithionite to give an $S = 3/2$ EPR signal much like that in the M^N state of the holo enzyme. Although the signal is somewhat broader, it sharpens upon the addition of thiophenol, which presumably coordinates to the unique iron atom previously bound to cysteine.[169] EXAFS confirms that the analogue selenophenol binds to this unique iron in a terminal position.[191,192] Most importantly, FeMoco-deficient mutants of the MoFe protein can be treated with solutions of extracted FeMoco to give fully active MoFe protein. Therefore, if there is some structural change in the FeMoco upon extraction, its reversibility suggests that it is not extreme. Mo EXAFS measurements show that extracted FeMoco may have one less Fe atom near the molybdenum than Cp1 or Av1.[193,194] The Fe EXAFS of extracted FeMoco contains a peak at 3.7 Å, which is characteristic of the distance between nonadjacent belt iron atoms in the protein-bound FeMoco.[195] Therefore, the available evidence leans toward a model in which the FeMoco has a similar structure to that crystallographically characterized in the MoFe protein, but there may be differences.

What is the constitution of the FeMoco in the absence of protein? Homocitrate remains attached, as demonstrated by the activity of reconstituted MoFe protein. Because the extraction is only effective in coordinating solvents, one assumes that the sites on Mo and Fe previously occupied by His and Cys are replaced by neutral solvent molecules. NMF binding is supported by IR spectroscopy.[196] Extracted FeMoco has a negative charge, as shown by binding and electrophoresis.[189,197,198] The exact charge is unknown, and guessing requires a choice of iron oxidation states and of X, which have not been unambiguously determined. In one possibility for an M^N-like state where the formula is [(homocitrate)$Mo^{4+}Fe_4^{2+}Fe_3^{3+}NS_9(NMF)_2$], the overall charge on the formula unit is -4, where two of the four negative charges are on the pendant carboxylates of homocitrate and the others are on the cluster. The overall charge becomes one unit more negative if thiolate replaces solvent.

The solution behavior of extracted FeMoco is further complicated by aggregation, and a combination of cooperative thiol binding curves and small-angle X-ray scattering suggests an aggregation state of up to 12.[199,200] In a related result, after treatment with Bu_4NPF_6, desalting, and evaporation of NMF, the cofactor may be re-extracted into organic solvents such as acetonitrile, acetone, dichloromethane, tetrahydrofuran, and even benzene.[201] Solubility in such nonpolar solvents is surprising considering the substantial negative charge on the cluster, and it seems likely that ion pairing is present. Note that the re-extracted solutions in these nonpolar solvents have EPR signals at $g = 2$ rather than the expected $S = 3/2$ signals, suggesting some change in electronic structure from aggregation or structural reorganization.

Despite the air and water sensitivity of extracted FeMoco, it is thermally quite stable compared to many synthetic iron–sulfur clusters. A coordination chemist might wonder why, then, solutions of extracted FeMoco have not yielded X-ray quality crystals. Complicating issues include: (i) extracted FeMoco solutions always contain some salts and impurities, (ii) the solutions are extremely air sensitive, and sensitive to excess water, (iii) roughly 1 kg of bacteria is required to make 6–7 mg of extracted FeMoco,[17] and (iv) the reversible aggregation phenomena described above.

In order to bypass these structural difficulties, Henderson and co-workers have used a different method to probe the coordination environment of the extracted FeMoco, where the rate constant for the displacement of NMF with thiol (about $50 \, s^{-1}$ in unmodified NMF solutions) "reports" changes in the cluster.[202] This binding is reversible, as shown by ^{19}F NMR studies of *p*-trifluoromethylthiophenol,[203] and because the rate has a first-order dependence on [FeMoco] and a zero-order dependence on [thiol], substitution follows a dissociative mechanism. Assumption of a linear free energy relationship implies that the cluster electronics can be evaluated through the "strength" of the Fe—NMF bond. The assumptions in this approach will break down if there is any change in mechanism or aggregation state of the rate-determining solvent dissociation. Using

this strategy, they have shown that citrate and homocitrate do not modify the Fe—NMF bond until histidine is added.[204] Molecular mechanics investigations show that the change in Fe—NMF strength from histidine could be due to hydrogen bonding between the histidine and homocitrate. Extension of this idea to the FeMoco in the MoFe protein suggests that the flexibility of homocitrate allows it to swing away from the Mo atom, forming a metastable intermediate with lower coordination number at Mo that could bind N_2.

Extracted FeMoco is not active for the reduction of N_2. However, it has been observed to reduce protons to H_2 electrochemically.[205] It also reacts with "alternative substrates" (Section 8.22.3.3): for example, it binds multiple molecules of cyanide.[206] It will catalyze the reduction of acetylene to ethylene and ethane by metal amalgam reducing agents.[207,208] In an interesting observation, N_2 is a competitive inhibitor of acetylene reduction, providing the first evidence for N_2 binding at extracted FeMoco.[209,210]

8.22.2.3.5 Model complexes

Structural models are discussed here, and reactivity models are discussed in Section 8.22.3. An excellent review on model complexes recently appeared.[351]

One of the great challenges of synthetic inorganic chemistry is the artificial synthesis of the FeMoco. There are no synthetic complexes that contain the metal–sulfur connectivity found in the FeMoco. However, because the FeMoco is stable in NMF solution, it is likely that this task is feasible, and hopefully the imminent identification of the central atom will lead to such a synthesis. Notably, there is one octacobalt cluster that mimics the belt $(\mu_3$-ligand$)_6(\mu_2$-ligand$)_3M_6$ cluster geometry of the FeMoco, with imido ligands instead of sulfido ligands.[211] However, no central atom corresponding to X was found.

Despite the lack of success in FeMoco synthesis, the quest for the FeMoco has motivated the study of numerous iron–molybdenum–sulfur clusters.[212–214] $MoFe_3S_4$ cubanes represent half of the FeMoco, and therefore have been extensively studied. Catecholates are often used to model the homocitrate ligand; tetrachlorocatecholate (Cl$_4$-cat) is common, but other acids are also used.[215]

Carbonyl-capped MoFe clusters include $[(Cl_4\text{-cat})MoFe_3S_3(PEt_3)_2(CO)_6]$[216] and its pyridine adduct $[(Cl_4\text{-cat})(py)MoFe_3S_3(PEt_3)_2(CO)_6]$ (**12**).[153,217] Cluster (**12**) has molybdenum in a NO_2S_3 environment similar to that of the Mo atom in the FeMoco. The distribution of metal–metal distances in these clusters evidences substantial metal–metal bonding beyond that shown in the illustration, suggesting that Fe—Fe and/or Fe—Mo bonding could be important in the electronic structure and electron storage function of the FeMoco. Many Fe_3MoS_4 clusters have terminal chloride ligands completing the coordination at the iron sites. This leads to closer models because the weak-field chloride ligand gives a tetrahedral iron geometry that more closely resembles the S_4 tetrahedral coordination in typical biological iron-sulfide sites. The complex $[(Cl_4\text{-cat})MoFe_3S_4Cl_3(CH_3CN)]^{2-}$ [218] is a convenient precursor, because the acetonitrile ligand may be replaced by N donors,[219] and the catecholate may be replaced by other bidentate O donors.[215,220] Other synthetic approaches to clusters of this type are from $Fe(PEt_3)_2Cl_2$ and binuclear Mo/Fe compounds,[221] or from edge-bridged double cubanes.[222]

The synthesis of double clusters bridged by μ_2-sulfide has been more challenging, because triply and quadruply bridging sulfides are more common.[223] μ_2-Sulfide bridges between cubanes are supported by a second bridging ligand in (**13**),[224,225] and unsupported in (**14**) and its heterometal analogues.[226,227] To create a $MoFe_7$ core (a "compositional analogue" of the FeMoco) using this strategy, it is necessary to couple a $MoFe_3$ cube with a Fe_4 cube, which has also been accomplished.[226]

In the above compounds, the structural motif is the M_4S_4 cubane, but these closed structures will not incorporate three μ_2-sulfide bridges easily. A different self-assembly route leads to MoFe clusters that have a different composition but do contain a sulfur-voided cubane held by three μ_2-sulfides. The clusters $MFe_4S_6L_5$ are shown as (**15**).[228,229] Their $Fe_4(\mu_3\text{-S})_3(\mu_2\text{-S})_3$ portions structurally resemble the part of the FeMoco farthest from molybdenum. These pentametallic clusters have been used to calibrate Fe EXAFS of the FeMoco.[228] Another important aspect of these clusters is that three iron atoms have trigonal pyramidal geometry like the belt iron atoms of the FeMoco, with three sulfides in the "basal" positions and a phosphine in the axial position. A series of "basket" clusters (**16**) also has trigonal pyramidal iron atoms (see also Section 8.3.5.2).[230,231] Although the geometry of these iron atoms is appropriate, the axial ligands are on the outside of the clusters rather than the inside like the FeMoco. Efforts to replace these phosphines with an oxide or nitride ligand may be rewarded with complexes that mimic this feature of the FeMoco.

(12)

PP = Me₂PCH₂CH₂PMe₂

(13)

(14)

M = Mo, V

(15)

(16)
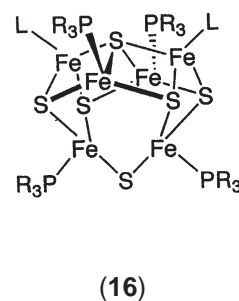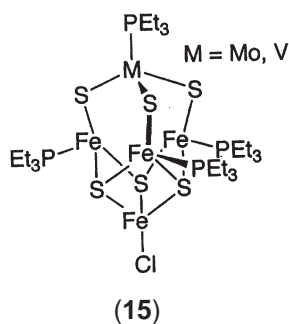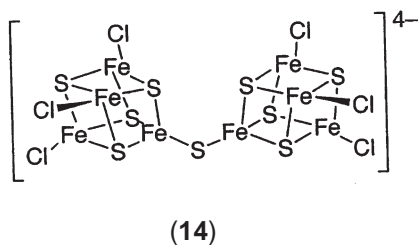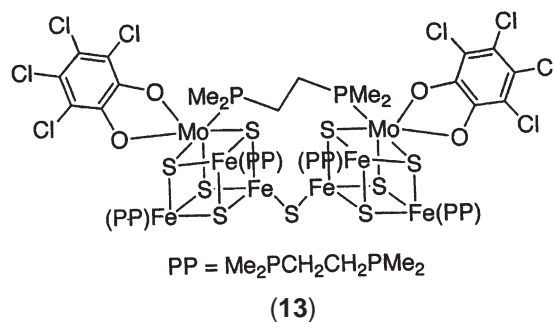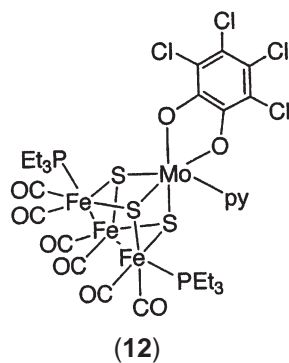
Because of the difficulty in rationally creating clusters with a given geometry, many modeling efforts have concentrated on mononuclear synthetic complexes with specific features from the FeMoco. Octahedral molybdenum(IV) complexes are common, but interestingly there are no crystallographically characterized mononuclear Mo(IV) complexes with an α-hydroxy carboxylate ligand. There are some precedents for mononuclear Mo(VI) oxo complexes with such ligands.[232–235] Note that high-valent Mo complexes do not interact with N_2; the octahedral molybdenum complexes that are active toward N_2 binding and activation are generally in oxidation states of $+3$ or less.[4,7]

An unusual feature of the FeMoco is the possibility of trigonal iron(II), and this feeds a more general interest in the behavior of coordinatively unsaturated iron atoms that may be formed during N_2 reduction. There are not many three-coordinate iron(II) complexes (see Section 8.22.3.1.4) and only $[Fe(SC_6H_2\text{-}2,4,6\text{-}^tBu_3)_3]^-$ **(17)** has all-sulfur ligation that most closely resembles the FeMoco.

(17)
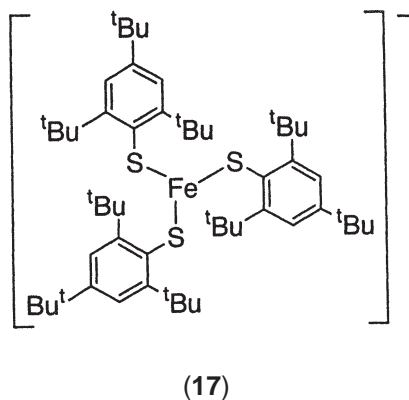
Accordingly, the Mössbauer parameters of this thiolate complex have been compared to the FeMoco.[180,236,237] A systematic approach to the Mössbauer parameters of three-coordinate iron complexes comes from a series of complexes maintained in a three-coordinate geometry by a bulky β-diketiminate ligand.[238] Because one of the three ligands can be changed over a wide range of electronic properties, it is possible to understand trends in the quadrupole splitting with assistance from detailed theoretical analysis. The synthesis of a trigonal pyramidal iron (II) monomer has also been reported.[352]

8.22.3 INTERACTION WITH SUBSTRATES

8.22.3.1 Dinitrogen

8.22.3.1.1 *Kinetic models*

Studying the binding and transformations of N_2 at the FeMoco is extremely difficult. No substrates bind to the crystallographically characterized M^N form.[239] When the enzyme is reduced, it is not stable, and reduces protons to dihydrogen. Likewise, it has not been possible to observe spectroscopically any enzyme intermediates in which N_2 is demonstrably bound to the FeMoco. Therefore, it is not straightforward to measure rate constants for the individual transformations. However, by global fitting of changes in UV–visible spectra and uptake/release under a wide variety of conditions, Lowe and Thorneley have formulated a kinetic scheme that rationalizes the combined kinetics.[127,240,241] The "Thorneley–Lowe" scheme is shown in Figure 7. In this scheme, "E" states are numbered to indicate the total number of electrons transferred from the Fe protein since the resting state. Therefore, E_0 represents M^N and E_1 represents M^R.

   Several features of the Thorneley–Lowe scheme are notable. (i) Several reductions of the MoFe protein occur before N_2 binds. This is an absolute requirement of any kinetics model, based on the kinetics of uptake of N_2 by the enzyme, and shows that the crystallographically characterized form of the FeMoco is not directly relevant to N_2 binding. (ii) Electrons are added one at a time, and the additional charge is balanced by protonation of the cluster. These protons presumably come from the pool of nearby water molecules and/or from the positively charged His and Arg residues near the FeMoco. The model does not specify whether these hydrogen atoms are hydride ligands to the metals, or protonated sulfide/homocitrate. (iii) N_2 displaces H_2 at the cluster. This well-precedented substitution reaction would provide a coordination site for N_2. It also explains why H_2 is always formed along with NH_3, and the inhibition of N_2 reduction by H_2, because H_2 release is an integral part of the reaction mechanism. (iv) Hydrazine can be released at the E_4 state. This follows the important observation that, if quenched under specific turnover conditions,
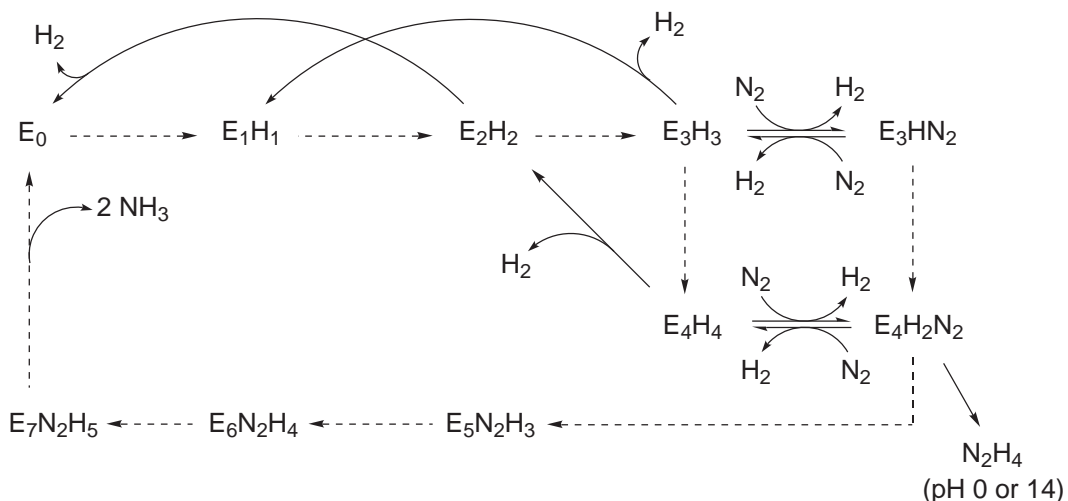
Figure 7 Thorneley–Lowe kinetics scheme for reduction of N_2 by nitrogenase. Dashed lines represent reduction by Fe protein, which is accompanied by protonation (after Burgess and Lowe[18]).

hydrazine is released from the enzyme.[242] However, if hydrazine is added under an argon atmosphere, it is not reduced, showing that free hydrazine is not an intermediate. Because the amount of hydrazine released upon quenching decreases with a rate constant identical to that for production of NH_3, it is likely that the hydrazine precursor is also a precursor of NH_3. There are a multitude of potential hydrazine precursor/FeMoco complexes, and free diazene (H_2N_2) can disproportionate to N_2 and N_2H_4, further complicating mechanistic conclusions based on hydrazine release.

In considering the mechanism, one should also consider the following data:[243] (i) there is no $^{14}N/^{15}N$ kinetic isotope effect, but this is perhaps mechanistically irrelevant because Fe protein dissociation, not a chemical step, is rate determining; (ii) reduction of $^{14}N_2/^{15}N_2$ mixtures gives no $^{14}N^{15}N$, showing that N—N cleavage is not reversible; (iii) NH_3 is not an inhibitor, nor is labeled NH_3 incorporated into any products; (iv) nitrogenase does not reduce diazene or hydrazine, indicating that partially reduced N/H species are likely to be enzyme bound.

The Thorneley–Lowe scheme highlights the intimate connection between proton transfer, electron transfer, and N_2 binding and reduction. Aspects of proton reduction and H_2 transformations are discussed in Section 8.22.3.2.

8.22.3.1.2 Potential binding modes for N_2

Many binding modes are possible for N_2 at the FeMoco. Although others are conceivable, the most chemically reasonable are illustrated in Figure 8: (a) end-on binding to the molybdenum atom; (b) the center of the cluster; (c) end-on binding to a single iron atom; (d) bridging between multiple iron atoms. Each will be considered in the context of relevant coordination complexes.

8.22.3.1.3 Molybdenum binding models

Mode (a). Mechanistic models in which N_2 binds at molybdenum are supported by the extensive coordination chemistry of molybdenum with N_2.[244] In a dramatic demonstration of the ability of molybdenum to activate N_2 toward protonation, Chatt produced NH_3 in up to 90% yield from octahedral Mo—N_2 and W—N_2 complexes using sulfuric acid.[245] Many studies since then have shown stepwise addition of hydrogen atoms to the terminal nitrogen atom N_2 fragments coordinated to metals in groups 5–7.[3,246] The model N_2 complexes are generally in the zero oxidation state when they bind N_2, and the molybdenum atom in the FeMoco is believed to be $+4$, at least in the M^N state. Therefore, if the "activating" reductions of the FeMoco take place at the molybdenum atom, this would encourage N_2 binding at Mo. A tungsten model system can produce ammonia from N_2 with electrochemical reduction.[247]

Because the molybdenum atom in the M^N state is octahedral and coordinatively saturated, it is normally postulated that one of the N/O ligands is lost (probably by protonation) in order to clear a coordination site for N_2 binding. (Dissociation is not absolutely necessary, because Mo can reach coordination numbers higher than six.) Molecular mechanics shows that a protonated carboxylate of homocitrate could find hydrogen-bonding partners, supporting the idea that it could dissociate.[204] Density functional calculations also indicate that protonation of the carboxylate can give five-coordinate molybdenum, as shown in Figure 8a.[248,249] A protonated carboxylic acid could act as a "proton delivery system," transferring protons to N_2 in a favorable geometry.[250] These models explain why nitrogenase with organic acids other than (*R*)-homocitrate is more than 10 times less active for N_2 reduction.[251]

There are other data that are harder to explain with a molybdenum-based model. The most problematic is that molybdenum is not necessary for N_2 fixation: as described below, there are V-substituted nitrogenases as well as active nitrogenases with no metal but iron (see Section 8.22.4). It is also difficult to explain the huge differences in reaction rate and product distribution upon mutation of residues near the iron belt but distant from the molybdenum atom. Neither of these problems is fatal to the molybdenum model, because a few octahedral vanadium and iron N_2 complexes produce ammonia upon protonation. In such models, distant belt-area mutations presumably cause a change in the hydrogen bonding network around the Mo site. Thus it is tenable to hold that all nitrogenases react with N_2 at the octahedral metal site in the M cluster.

The study of $MoFe_3S_4$ "cubane" clusters (Section 8.22.2.3.5) has not yielded N_2 adducts, although some iron–sulfur and molybdenum–iron–sulfur clusters may be catalysts for the electrolytic reduction of N_2.[252] Coucouvanis and co-workers have discovered that a number of Mo/Fe cubanes catalyze the reduction of hydrazines and diazenes to ammonia and/or amines.[253–256]
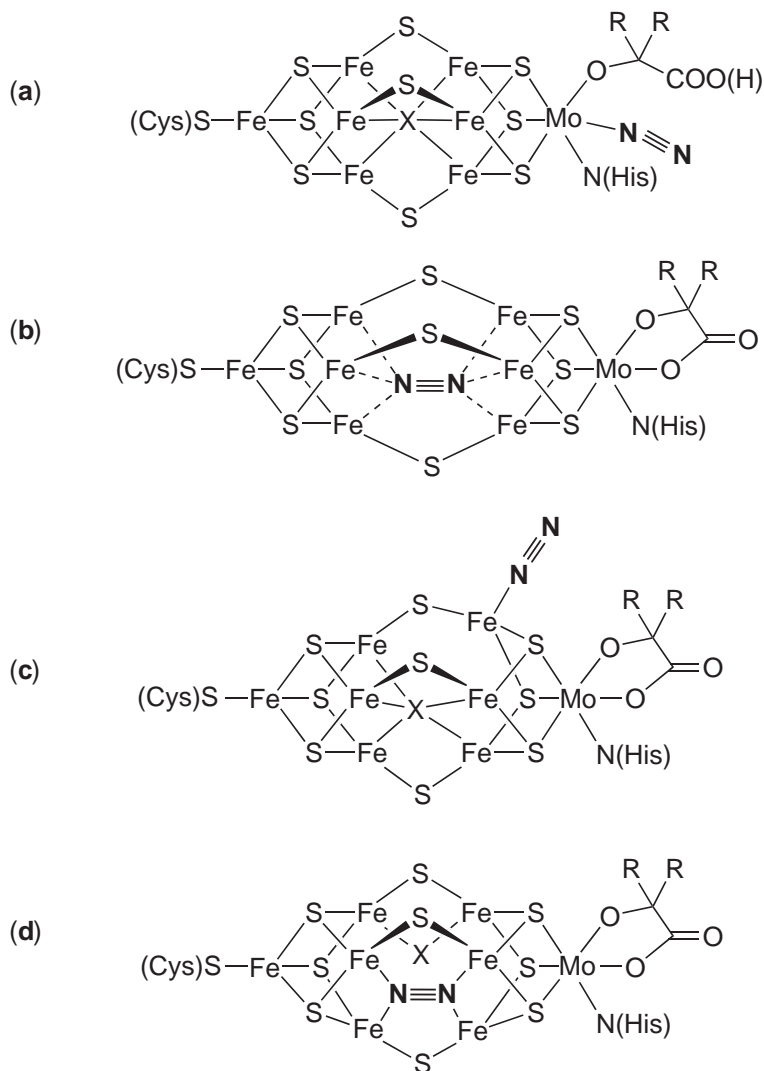
Figure 8 Some possible binding modes for N_2 to the FeMoco: (a) end-on binding to the molybdenum atom; (b) the center of the cluster; (c) end-on binding to a single iron atom; (d) bridging between multiple iron atoms.

These reactions occur at the Mo site of the cubane. On this basis, they have proposed an N_2 reduction mechanism where initial N_2 binding and reduction occurs at the belt region (i.e., mode (d)) and then a partially reduced fragment migrates to molybdenum for cleavage of the final N—N bond.[250] A different bimetallic mechanism has been proposed on the basis of density functional calculations, in which initial protonation of a molybdenum–dinitrogen complex gives an Mo=N—NH$_2$ intermediate that bridges to a belt iron for final N—N cleavage.[257]

8.22.3.1.4 Iron binding models

Mode (b). This coordination geometry is aesthetically pleasing, because the six reducing equivalents for N_2 reduction come from the six belt iron atoms. N—N cleavage has been observed from a model complex with six gold atoms bound to an N_2^{4-} unit.[258] However, there are no synthetic precedents for iron binding N_2 in this way, and the cavity (i.e., the spot marked by X) in the FeMoco is not large enough to accommodate N_2 (at least in the M^N form).[259,260] The idea of mode (b) was raised again as a possible precursor to an N_2-derived nitride as X, but ESEEM and ENDOR now suggest that X is not a nitride derived from turnover nitrogen, as noted above. One is tempted to discount the possibility of internal binding, but the nucleophilicity of an oxide/

nitride/carbide ligand and the unknown flexibility of the FeMoco mean that participation of an internal atom (even if it is not derived from N_2) is not inconceivable, because X could transiently form a bond with N_2 or an N_2-derived intermediate.

Mode (c). One can imagine that multiple-electron reduction of M^N breaks a bond between X and one of the belt iron atoms, causing the affected iron atom(s) to change from four-coordinate in M^N to three-coordinate in M^R. This would cause the affected iron atom(s) to become coordinatively unsaturated and therefore activated toward N_2 binding.

A number of octahedral and trigonal bipyramidal iron–dinitrogen complexes have been crystallographically characterized, either with terminal end-on N_2 or bridging end-on/end-on N_2.[261–269] These are low-spin complexes in the Fe(0) or Fe(II) oxidation state. Their N—N bond distances and N—N stretching frequencies suggest that their N—N bonds are not weakened as much as those in analogous complexes of molybdenum or other low-valent transition metals to the left of iron in the periodic table.[270–272] Accordingly, there are no examples of stepwise proton addition to an iron-bound N_2 ligand akin to the well-characterized precedents with early transition metals. The typical mode of reactivity upon protonation is dissociation of N_2.[265] However, there are a few dinitrogen and dinitrogen–hydride complexes of octahedral iron that release hydrazine and/or ammonia upon protonation.[266,269,273–275] The active intermediates in the iron-promoted nitrogen reduction are unknown.[274]

Considering that the iron atoms in the FeMoco are high spin and less than five coordinate, the consideration of mode (c) is hindered by the near absence of N_2 complexes of three- or four-coordinate iron. No iron–sulfur clusters have been reported to bind dinitrogen, nor has any complex of iron with sulfur ligands. A three-coordinate complex with an FeS_3 coordination sphere (**17**) is known, but it does not bind dinitrogen.[236] This may be a steric problem, because (**17**) has not been reported to bind any fourth ligands. A very unusual complex has three-coordinate iron(II) coordinated to three N_2 ligands that each bridge to molybdenum (**18**).[276,277] A low-coordinate iron–dinitrogen complex (**19**) has N_2 bound to only low-coordinate iron.[278] Substantial weakening of the N—N bond shows that low-coordinate, high-spin iron can have a substantial backbonding interaction with N_2. The geometry of (**19**) is probably not directly relevant to the FeMoco, because (**19**) is trigonal planar including the N_2 ligand, whereas a belt iron atom would be tetrahedral after N_2 binding. However, a related dinitrogen complex that is four-coordinate at each iron atom is also stable.[279] More low-coordinate iron compounds are necessary to elucidate the binding parameters and spectroscopic signatures of N_2 bound to low-coordinate iron.

$N_3N = (Me_3SiNCH_2CH_2)_3N$

(**18**)

Ar = 2,6-diisopropylphenyl

(**19**)
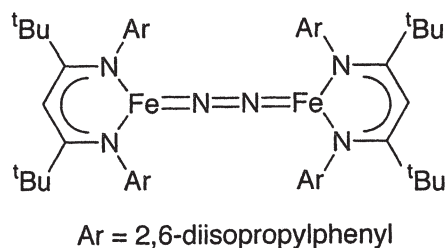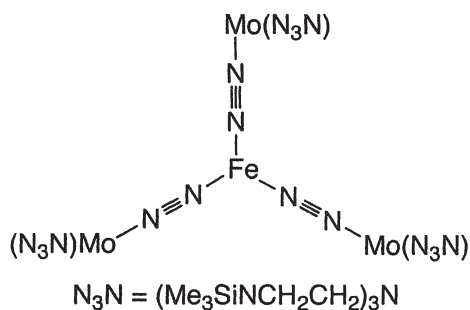
Mode (d). Here, N_2 is bound to a four-iron "face" of the FeMoco. Proponents of this binding mode cite some of the advantages found for mode (b), in that multiple reduced iron atoms may interact simultaneously with N_2. Site-directed mutagenesis of amino acids immediately surrounding the belt of the FeMoco has drastic effects on the substrate specificity and nitrogen-reducing ability of nitrogenase, directly implicating this area of the cofactor in binding. These studies have been summarized.[24]

There are no synthetic complexes with iron bound to N_2 in mode (d). The polymetallic iron–N_2 complexes that are known have linear end-on/end-on coordination, a binding mode that is difficult to imagine in the FeMoco. Side-on/end-on binding could be accommodated by the FeMoco geometry, and precedents exist for other transition metals (see Sections 8.22.1.1 and 8.22.1.2.3). An interesting series of diazene complexes have been isolated that have N_2H_2 ligands bridging two iron atoms, in which the N-bound hydrogen atoms are stabilized by hydrogen bonding to thiolate ligands.[280] These were used to propose a FeMoco model in which a μ_2-sulfide bridge

opens and N_2 binds between two adjacent iron belt atoms. This model would be strengthened by well-characterized examples of interconversion between bridging and terminal iron sulfides. Synthetic iron complexes with different binding modes and with more than two iron atoms are necessary to properly evaluate the feasibility of mode (d) in the FeMoco.

8.22.3.2   Protons

Nitrogenase enzymes act as hydrogenases in the absence of N_2. The mechanism of this simpler reaction might be expected to give insight into proton delivery to the FeMoco for use in ammonia production as well. However, it is possible that H_2 is not formed by the same mechanism in the presence and absence of N_2! This surprising conclusion is based on the observation that added D_2 gas exchanges with protons to give HD in the presence of N_2, but no HD is formed in the absence of N_2. In addition, H_2 is an inhibitor of N_2 reduction, but it does not inhibit its own production. H_2 production always accompanies N_2 reduction, even under a very high pressure of N_2. These combined results suggest that H_2 evolution may be an integral part of the N_2 reduction mechanism, consistent with the Thorneley–Lowe kinetics scheme. However, H_2 formation in the absence of N_2 or with mutated MoFe protein shows that the FeMoco can devote electrons to H_2 production when conditions are not appropriate for N_2 reduction. There is substantial controversy, then, regarding the mechanistic significance of H_2 formation in the enzyme. Standard methods, such as Arrhenius plots and H/D kinetic isotope effects, are ineffective because N—H formation occurs after the rate-determining step, and because ammonia protons exchange with water. No protonated forms of the FeMoco have been identified, leaving chemists and biochemists with theoretical approaches and synthetic models to inform their mechanistic curiosity. Molecular modeling has been used to evaluate the routes for proton transport to different sites of the FeMoco.[151,281] There is a water-filled channel from the exterior of the protein leading to the homocitrate ligand and to two of the three belt μ_2-sulfide bridges.

There are several potential sites at which protons could bind. First, homocitrate could be protonated, which is considered in Section 8.22.2.3.4. This process could weaken a Mo—O bond and clear a coordination site for N_2 binding, or give an acidic carboxylic acid that could deliver the proton to N_2.

The sulfide ligands of the cluster are also expected to attract protons. The Brønsted basicity of the extracted FeMoco has been evaluated using the kinetic method described in Section 8.22.2.3.4, suggesting that the first pK_a of the cluster is about 8.[282] A similar pK_a of 9 comes from the pH variation in rates of H_2 evolution and acetylene reduction by the holo enzyme.[283] The protonation of the FeMoco also has been evaluated with *ab initio* calculations, showing that, as expected, the μ_2-sulfides should be more basic than the μ_3-sulfides.[249] This work showed the best proton binding position to be the center of the FeMoco, undoubtedly a result of the omission of the central X atom in the theoretical model. The sulfur atoms of synthetic FeS clusters can also act as bases,[284] and the protonated forms may play a role in redox chemistry.[285]

Reduced metals are Brønsted bases, forming hydride ligands through formal two-electron oxidation of the metal. The resulting hydride complexes can attract additional protons to form complexes with η^2-H_2 ligands. Molecular H_2 binds relatively strongly to low-valent, unsaturated molybdenum complexes, and less strongly to iron.[286,287] As a result, a number of mechanistic models incorporating molybdenum–dihydrogen complexes have been proposed.[18] In these models, the dihydrogen ligand is displaced by N_2 in agreement with (i) the Thorneley–Lowe kinetics model and (ii) the inhibition of N_2 reduction by H_2. In another potential role for an H_2 ligand, model studies have shown that coordinated H_2 ligands can act as acids toward coordinated N_2, as discussed in Section 8.22.1.2.3. The belt iron atoms are also potential protonation sites, and low-coordinate iron complexes with hydride ligands have the ability to cleave multiple bonds.[288]

An argument for HD formation on bound diazene complexes has been elucidated.[289] This idea is based on iron and ruthenium diazene complexes that readily exchange the protons from their μ-N_2H_2 ligands with free H_2.

8.22.3.3   Unnatural Substrates

Because of the difficulty in analyzing reactions of N_2, and because of the complete lack of spectroscopic evidence for N_2 adducts, biochemists have sought other substrates that could give

insight into the workings of the FeMoco. Fortunately, nitrogenase reduces a number of "alternative" substrates that have double or triple bonds. These include alkynes, cyanide, isocyanides, nitrous oxide, azide, nitriles, CE_2 (E = O or S), allene, and cyclopropene. The product distributions and reaction kinetics have been reviewed,[18,243,290] and will be considered here to the extent that they give insight into the potential sites of N_2 binding and transformations.

Consideration of inhibitors that are not substrates is useful because they presumably bind to the FeMoco without being reduced. H_2 inhibits N_2 reduction, but does not inhibit reduction of protons or any alternative substrates. This could indicate either that the mechanism for N_2 reduction is different than those for reduction of protons and alternative substrates, or that N_2 is held weakly and is more easily inhibited. Carbon monoxide inhibits N_2 reduction, as well as all substrates except protons. It binds to the FeMoco under turnover conditions after a short lag time, and EPR shows two different adducts that are termed lo-CO and hi-CO.[291] The relative intensities of these signals depends on [CO], with lo-CO predominant at 0.08 atm CO and hi-CO predominant at 0.5 atm CO. The lag time could indicate a structural change in the FeMoco prior to binding. ENDOR studies with isotopic labeling show that lo-CO has one CO ligand on the FeMoco, and hi-CO has two CO ligands on the FeMoco.[292,293] A combination of ENDOR and IR spectroscopies suggests that the lo-CO carbonyl may be in a bridging or semibridging mode but the hi-CO carbonyls are terminally bound,[294,295] and that the oxidation state does not change upon CO binding.[179] It is not known whether the CO ligands are bound to the same metal atom, but ENDOR measurements on ^{57}Fe-labeled FeMoco suggest that CO ligands are bound to iron. The model chemistry of high-spin iron–carbonyl complexes is almost nonexistent, but interestingly an isolated tetrahedral iron(I) carbonyl complex has ν_{CO} at $1,907 \, cm^{-1}$, near the band in lo-CO ($1,904 \, cm^{-1}$).[296]

Terminal alkynes are reduced to alkenes by nitrogenase. This "hydrogenation" of C_2D_2 gives *cis*-dideuteroethylene: the stereospecificity indicates that any intermediates remain cofactor bound, and argues against the presence of σ-acetylide intermediates. With the use of mutants at Arg277 and His195, it has been possible to observe EPR and ENDOR signals that arise from C_2H_2 bound directly to the FeMoco.[297,298] Again, multiple-bound forms are detected, suggesting that there are at least two binding sites on the FeMoco. Some of these sites are the same as the CO binding sites.[299] The substrate specificity and stereospecificity of the reduction can be altered by mutations at Gly69, Val70, Arg96, and His195, suggesting that the binding site(s) are in the belt region of the FeMoco.[300–302] The data are most easily accommodated through a model in which acetylene binds to multiple iron atoms,[300] and relative changes in N_2 and acetylene reduction abilities suggest that the binding site is a four-iron face capped by Val70.[303]

Model complexes containing $MoFe_3S_4$ cubane cores perform the analogous reduction of acetylene to ethylene, which occurs at the molybdenum site of the cluster.[304,305] However, as noted above, the bulk of the available evidence suggests that acetylene binds at an iron site of the FeMoco.[306] Many mononuclear iron–hydride complexes react with alkynes to give *cis*-addition products, and there are precedents for the reaction of alkynes with iron clusters.[307–309]

Cyanide and nitriles are reduced to alkanes and ammonia with nitrogenase and reductant. (Cyanide is in equilibrium with HCN in aqueous solution.) Cyanide binds to the $S = 3/2$ state of the extracted FeMoco in solution,[203,310,311] but not to the M^N state of holo-MoFe protein.[239] Cyanide binds to mutants with changes in the belt region, as is evident from ^{13}C ENDOR signatures.[302] Kinetics data suggest that cyanide binds to a more oxidized state of the FeMoco than N_2 does, and a lag time may indicate a rearrangement.[312]

8.22.4 ALTERNATIVE NITROGENASES

When nitrogen-fixing bacteria such as *A. vinelandii* are grown in a Mo-deficient environment, they maintain much of their nitrogen-fixing ability, suggesting that there is a non-Mo pathway to nitrogen reduction. In several cases, it has been possible to isolate and characterize the "alternative nitrogenases" that are responsible for this activity. These are made up of an Fe protein with an electron transfer role, a catalytic protein with P and M clusters, and additional subunits. The iron–vanadium and iron-only alternative nitrogenases have been reviewed.[313,314]

These enzymes are somewhat less active toward N_2 than the molybdenum-dependent nitrogenase. However, recall that (i) protein dissociation is usually rate limiting, and (ii) proton reduction competes with nitrogen reduction. Therefore, it is likely that the activation barriers are similar for nitrogen reduction by the different nitrogenases. There is high sequence homology (and invariably

conservation of the M ligands Cys275 and His442) and correspondence of kinetic and spectro-scopic signatures between the different kinds of nitrogenase. The simplest model consistent with the data is that all three (FeMo, FeV, and Fe-only) nitrogenases have eight-metal M cofactors at which N_2 is reduced, with a similar structure to the FeMoco. The similarity in activity, then, may indicate that the octahedral site on the cofactor serves to "tune" the properties of the cluster.

8.22.4.1   Iron–Vanadium Nitrogenase

Iron–vanadium nitrogenase was isolated in 1986.[315,316] Its nitrogen-reducing activity is 1/3–1/2 of that for molybdenum nitrogenase, and the VFe protein is spectroscopically different from the analogous MoFe protein. There is no X-ray crystal structure of any component of iron–vanadium nitrogenase.

   The P clusters are similar to those from iron–molybdenum nitrogenase, with a number of accessible oxidation states with analogous EPR signals.[317] The M center of the VFe protein is thought to be an FeVco analogous to the FeMoco in the molybdenum enzyme. The FeVco has an EPR signal with resonances at $g = 5.4$ and 5.8. This signal has been attributed to an $S = 3/2$ spin system with higher rhombicity than the FeMoco, and a small negative zero-field splitting.[318] Interestingly, the EPR signal shows no coupling to ^{51}V ($I = 7/2$), suggesting that the spin density is largely on the iron part of the cofactor. Despite this difference in electronic structure, the Mössbauer and MCD characteristics of the M center are similar between the MoFe and VFe proteins.[319,320] The strongest evidence for similarity in the cofactors comes from V and Fe EXAFS measurements on VFe protein, which show striking similarities to those for the MoFe protein, including the characteristic 3.7–3.8 Å iron–iron distance that has been assigned as a cross-belt distance in the FeMoco.[164,321,322]

   There are notable reactivity differences between iron–vanadium and iron–molybdenum nitro-genases. Iron–vanadium nitrogenase allocates electrons less effectively, producing at least three molecules of H_2 for every molecule of N_2 reduced. The mechanism may be similar, as evidenced by production of hydrazine under similar quenching conditions that are effective for Mo nitro-genase.[323] Acetylene is reduced to mixtures of ethylene and ethane by iron–vanadium nitrogenase, whereas iron–molybdenum nitrogenase forms only ethylene.[324,325]

   It is possible to extract the FeVco from iron–vanadium nitrogenase using NMF, and to produce apo-VFe protein, leading to interesting studies on "hybrid" VFe and MoFe proteins in which the unnatural cofactor has been inserted.[326–328] There is agreement that VFe protein reconstituted with FeVco regains its full activity, and that VFe protein reconstituted with FeMoco can reduce acetylene and protons. Some workers have found that VFe protein/FeMoco will reduce N_2, but others find no N_2 reduction activity. MoFe protein/FeVco is also active, and reduces acetylene to ethylene and ethane, behavior characteristic of iron–vanadium nitrogenase.

   Cuboidal iron–vanadium–sulfur clusters have been synthesized in an effort to understand the role of vanadium in this enzyme, and to delineate the differences between clusters with Mo and V in the same position.[329–333] The model compounds do not bind or reduce N_2 or other nitrogenase substrates.[332] However, some iron–vanadium–sulfur clusters will reduce hydrazine to ammonia.[250] In a systematic evaluation of the metal M in double cubane clusters $[M_2Fe_6S_8(SEt)_9]^{3-}$ (M = V, Nb, Mo, W, Re), it was found that the reduction potential is lower, and the ^{57}Fe Mössbauer isomer shift higher, for Mo relative to V.[334] However, the ^{57}Fe isomer shifts are similar between MoFe and VFe proteins, suggesting that protein interactions (especially hydrogen bonding) are likely to play an important role in determining the electron density at the iron atoms in the FeMoco and FeVco.[319,333]

8.22.4.2   Iron-only Nitrogenase

Progress in the biochemistry and spectroscopy of iron-only nitrogenase has occurred, with the most active, pure preparations reported in 1997.[335] Mössbauer and EXAFS results support electronic and structural analogy between the eight-iron cluster in this enzyme (the "FeFeco") and the FeMoco.[336] One notable difference is that the FeFeco is diamagnetic in its dithionite-reduced form, and thus corresponds to M^{OX} in the MoFe protein. Therefore, the oxidation states are thought to be $Fe(II)_4Fe(III)_4$ or $Fe(II)_6Fe(III)_2$, in analogy to the two most likely oxidation

state assignments for the FeMoco (Section 8.22.2.3.3). EPR spectra of the FeFeco and P clusters of the Fe-only enzyme are substantially more complicated than those of the MoFe system.[337,338]

The reactivity of iron-only nitrogenase is more similar to iron–vanadium nitrogenase than iron–molybdenum nitrogenase. Substantial amounts of H_2 are produced during N_2 reduction, and acetylene is reduced to mixtures of ethylene and ethane.[335] Clearly, much remains to be learned about this enzyme.

8.22.4.3 Other Heterometal-containing Nitrogenases

There are reports of nitrogenases containing tungsten,[339] manganese,[340,341] and chromium.[342,343] Hopefully these will be followed with more detailed studies to verify the role of the heterometal, along with spectroscopy and activity measurements.

8.22.5 BIOSYNTHESIS OF THE NITROGENASE COFACTORS

Another active area of research aims to identify the biochemical pathway through which the unusual P and M clusters are formed. A brief overview of a leading biosynthetic model[344] is presented here.

The proteins encoded by *nif* genes (for FeMo nitrogenase) and *vnf* (for FeV nitrogenase) work together to produce the FeMoco and FeVco, respectively. Each protein is named after the *nif* gene that encodes it. *nifV* is responsible for homocitrate synthesis from acetyl-coenzyme A and α-ketoglutarate, and *nifV* deletion mutants have been used to substitute other carboxylic acids for homocitrate as noted in Section 8.22.2.3.1. *nifU* and *nifS* mobilize Fe and S, respectively, for assembly of an Fe—S cluster on *nifB*. This cluster, called the FeBco, is diamagnetic and has not been thoroughly characterized. The next step is transfer to *nifNE*, at which Mo (with the help of *nifX*)[345,346] and homocitrate are added to form the FeMoco. *nifH* (the Fe protein, Section 8.22.2.1) plays a role at this stage, presumably as a reductant. The essential role of *nifNE* has been disputed.[347] The bioinorganic chemistry of *nifNE* is likely to yield substantial insights into the construction and possible conformations of the FeMoco.

Finally, the FeMoco is transferred to *nifDK* (apo-MoFe protein) to form the holo-MoFe protein with the help of ATP and several proteins: *nifH*, γ, and GroEL.[348] The X-ray crystal structure of *nifDK* shows a positively charged channel through which FeMoco could enter.[349] The *vnf* system for synthesis of the FeVco is thought to be similar to the *nif* system, with added assistance in the last step by *vnfG*, a third subunit of VFe nitrogenase that is necessary for activity.

8.22.6 CONCLUSION

Our understanding of both synthetic and biochemical nitrogen reduction has made great strides since publication of *CCC* (1987). In Haber's 1918 Nobel speech, he said: "Nitrogen bacteria teach us that Nature, with her sophisticated forms of the chemistry of living matter, still understands and utilizes methods which we do not as yet know how to imitate." This is still true, but there is hope that we may yet understand and replicate its activity in the laboratory.

ACKNOWLEDGMENTS

8.22.7 REFERENCES

1. Falkowski, P. G. *Nature* **1997**, *387*, 272–275.
2. Seino, H.; Ishii, Y.; Hidai, M. *J. Am. Chem. Soc.* **1994**, *116*, 7433–7434.
3. Hidai, M.; Mizobe, Y. *Chem. Rev.* **1995**, *95*, 1115–1133.
4. Hidai, M. *Coord. Chem. Rev.* **1999**, *185–186*, 99–108.

5. Hori, K.; Mori, M. *J. Am. Chem. Soc.* **1998**, *120*, 7651–7652.
6. Ueda, K.; Sato, Y.; Mori, M. *J. Am. Chem. Soc.* **2000**, *122*, 10722–10723.
7. Chatt, J.; Dilworth, J. R.; Richards, R. L. *Chem. Rev.* **1978**, *78*, 589–625.
8. Gambarotta, S. *J. Organomet. Chem.* **1995**, *500*, 117–126.
9. Richards, R. L. *Coord. Chem. Rev.* **1996**, *154*, 83–97.
10. Bazhenova, T. A.; Shilov, A. E. *Coord. Chem. Rev.* **1995**, *144*, 69–145.
11. Hidai, M. *Coord. Chem. Rev.* **1999**, *185–186*, 99–108.
12. Hidai, M.; Mizobe, Y. In *Molybdenum and Tungsten: Their Roles in Biological Processes*; Sigel, A., Sigel, H., Eds.; Marcel Dekker: New York, 2002; pp 121–161.
13. Leigh, G. J. *Acc. Chem. Res.* **1992**, *25*, 177–181.
14. Sellmann, D.; Utz, J.; Blum, N.; Heinemann, F. W. *Coord. Chem. Rev.* **1999**, *190–192*, 607–627.
15. Tuczek, F.; Lehnert, N. *Angew. Chem., Int. Ed.* **1998**, *37*, 2636–2638.
16. Fryzuk, M. D.; Johnson, S. A. *Coord. Chem. Rev.* **2000**, *200–202*, 379–409.
17. Burgess, B. K. *Chem. Rev.* **1990**, *90*, 1377–1406.
18. Burgess, B. K.; Lowe, D. J. *Chem. Rev.* **1996**, *96*, 2983–3011.
19. Howard, J. B.; Rees, D. C. *Chem. Rev.* **1996**, *96*, 2965–2982.
20. Eady, R. R. *Chem. Rev.* **1996**, *96*, 3013–3030.
21. Smith, B. E. *Adv. Inorg. Chem.* **1999**, *47*, 159–218.
22. Smith, B. E.; Eady, R. R. *Eur. J. Biochem.* **1992**, *205*, 1–15.
23. Evans, D. J.; Henderson, R. A.; Smith, B. E. In *Bioinorganic Catalysis*, 2nd ed.; Reedijk, J., Bouwman, E., Eds.; Marcel Dekker: New York, 1999; pp 153–207.
24. Christiansen, J.; Dean, D. R.; Seefeldt, L. C. *Annu. Rev. Plant Physiol. Plant Mol. Biol.* **2001**, *52*, 269–295.
25. Burris, R. H. *J. Biol. Chem.* **1991**, *266*, 9339–9342.
26. Pau, R. N. *Adv. Inorg. Biochem.* **1994**, *10*, 49–70.
27. Cohen, J. D.; Mylvaganam, M.; Fryzuk, M. D.; Loehr, T. M. *J. Am. Chem. Soc.* **1994**, *116*, 9529–9534.
28. Ho, J.; Drake, R. J.; Stephan, D. W. *J. Am. Chem. Soc.* **1993**, *115*, 3792–3793.
29. Bazhenova, T. A.; Kulikov, A. V.; Shestakov, A. F.; Shilov, A. E.; Antipin, M. Y.; Lyssenko, K. A.; Struchkov, Y. T.; Makhaev, V. D. *J. Am. Chem. Soc.* **1995**, *117*, 12176–12180.
30. Evans, W. J.; Ulibarri, T. A.; Ziller, J. W. *J. Am. Chem. Soc.* **1988**, *110*, 6877–6879.
31. Jubb, J.; Gambarotta, S. *J. Am. Chem. Soc.* **1994**, *116*, 4477–4478.
32. Roussel, P.; Scott, P. *J. Am. Chem. Soc.* **1998**, *120*, 1070–1071.
33. Cloke, F. G. N.; Hitchcock, P. B. *J. Am. Chem. Soc.* **2002**, *124*, 9352–9353.
34. Evans, W. J.; Allen, N. T.; Ziller, J. W. *Angew. Chem., Int. Ed.* **2002**, *41*, 359–361.
35. Evans, W. J.; Allen, N. T.; Ziller, J. W. *J. Am. Chem. Soc.* **2001**, *123*, 7927–7928.
36. Campazzi, E.; Solari, E.; Floriani, C.; Scopelliti, R. *Chem. Commun.* **1998**, 2603–2604.
37. Evans, W. J.; Zucchi, G.; Ziller, J. W. *J. Am. Chem. Soc.* **2003**, *125*, 10–11.
38. Gynane, M. J. S.; Jeffery, J.; Lappert, M. F. *J. Chem. Soc., Chem. Commun.* **1978**, 34–36.
39. Chirik, P. J.; Henling, L. M.; Bercaw, J. E. *Organometallics* **2001**, *20*, 534–544.
40. Duchateau, R.; Gambarotta, S.; Beydoun, N.; Bensimon, C. *J. Am. Chem. Soc.* **1991**, *113*, 8986–8988.
41. Beydoun, N.; Duchateau, R.; Gambarotta, S. *J. Chem. Soc., Chem. Commun.* **1992**, 244–246.
42. Fryzuk, M. D.; Haddad, T. S.; Rettig, S. J. *J. Am. Chem. Soc.* **1990**, *112*, 8185–8186.
43. Fryzuk, M. D.; Haddad, T. S.; Mylvaganam, M.; McConville, D. H.; Rettig, S. J. *J. Am. Chem. Soc.* **1993**, *115*, 2782–2792.
44. Cohen, J. D.; Fryzuk, M. D.; Loehr, T. M.; Mylvaganam, M.; Rettig, S. J. *Inorg. Chem.* **1998**, *37*, 112–119.
45. Cohen, J. D.; Mylvaganam, M.; Fryzuk, M. D.; Loehr, T. M. *J. Am. Chem. Soc.* **1994**, *116*, 9529–9534.
46. Fomitchev, D. V.; Bagley, K. A.; Coppens, P. *J. Am. Chem. Soc.* **2000**, *122*, 532–533.
47. Cusanelli, A.; Sutton, D. *Organometallics* **1996**, *1*, 1457–1464.
48. Jonas, K.; Brauer, D. J.; Krüger, C.; Roberts, P. J.; Tsay, Y. H. *J. Am. Chem. Soc.* **1976**, *98*, 74–81.
49. Hammer, R.; Klein, H. F.; Friedrich, P.; Huttner, G. *Angew. Chem.* **1977**, *89*, 499–500.
50. Klein, H. F.; Hammer, R.; Wenninger, J.; Friedrich, P.; Huttner, G. *Z. Naturforsch. B* **1978**, *33*, 1267–1273.
51. Krüger, C.; Tsay, Y.-H. *Angew. Chem.* **1973**, *85*, 1051–1052.
52. Pez, G. P.; Apgar, P.; Crissey, R. K. *J. Am. Chem. Soc.* **1982**, *104*, 482–490.
53. Ganesan, M.; Gambarotta, S.; Yap, G. P. A. *Angew. Chem., Int. Ed.* **2001**, *40*, 766–769.
54. Fryzuk, M. D.; Johnson, S. A.; Rettig, S. J. *J. Am. Chem. Soc.* **1998**, *120*, 11024–11025.
55. Fryzuk, M. D.; Johnson, S. A.; Patrick, B. O.; Albinati, A.; Mason, S. A.; Koetzle, T. F. *J. Am. Chem. Soc.* **2001**, *123*, 3960–3973.
56. Fryzuk, M. D.; MacKay, B. A.; Johnson, S. A.; Patrick, B. O. *Angew. Chem., Int. Ed.* **2002**, *41*, 3709–3712.
57. Jennings, J. R., Ed., *Catalytic Ammonia Synthesis: Fundamentals and Practice*, Plenum: New York, 1991.
58. Falicov, L. M.; Somorjai, G. A. *Proc. Natl. Acad. Sci. USA* **1985**, *82*, 2207–2211.
59. Strongin, D. R.; Carrazza, J.; Bare, S. R.; Somorjai, G. A. *J. Catal.* **1987**, *103*, 213–215.
60. Grunze, M.; Golze, M.; Hirschwald, W.; Freund, H. J.; Pulm, H.; Seip, U.; Tsai, M. C.; Ertl, G.; Küppers, J. *Phys. Rev. Lett.* **1984**, *53*, 850–853.
61. Freund, H. J.; Bartos, B.; Messmer, R. P.; Grunze, M.; Kuhlenbeck, H.; Neumann, M. *Surf. Sci.* **1987**, *185*, 187–202.
62. Egeberg, R. C.; Dahl, S.; Logadottir, A.; Larsen, J. H.; Norskøv, J. K.; Chorkendorff, I. *Surf. Sci.* **2001**, *491*, 183–194.
63. Ozaki, A. *Acc. Chem. Res.* **1981**, *14*, 16–21.
64. Bielawa, H.; Hinrichsen, O.; Birkner, A.; Muhler, M. *Angew. Chem., Int. Ed.* **2001**, *40*, 1061–1063.
65. Hagen, S.; Barfod, R.; Fehrmann, R.; Jacobsen, C. J. H.; Teunissen, H. T.; Ståhl, K.; Chorkendorff, I. *Chem. Commun.* **2002**, 1206–1207.
66. Jacobsen, C. J. H. *Chem. Commun.* **2000**, 1057–1058.
67. Jacobsen, C. J. H.; Dahl, S.; Clausen, B. S.; Bahn, S.; Logadottir, A.; Norskøv, J. K. *J. Am. Chem. Soc.* **2001**, *123*, 8404–8405.
68. Schrauzer, G. N.; Guth, T. D. *J. Am. Chem. Soc.* **1977**, *99*, 7189–7193.
69. Hoshino, K. *Chem. Eur. J.* **2001**, *7*, 2727–2731.

70. Rusina, O.; Eremenko, A.; Frank, G.; Strunk, H. P.; Kisch, H. *Angew. Chem., Int. Ed.* **2001**, *40*, 3993–3995.
71. Marnellos, G.; Stoukides, M. *Science* **1998**, *282*, 98–100.
72. Kordali, V.; Kyriacou, G.; Lambrou, C. *Chem. Commun.* **2000**, 1673–1674.
73. Shilov, A. E. In *Treatise on Dinitrogen Fixation*; Hardy, R. W. F., Bottomley, F., Burns, R. C., Eds.; Wiley-Interscience: New York, 1979; 31–108.
74. Shilov, A. E. *New J. Chem.* **1992**, *16*, 213–218.
75. Bazhenova, T. A.; Lobkovskaya, R. M.; Shibaeva, R. P.; Shilov, A. E.; Shilova, A. K.; Gruselle, M.; Leny, G.; Tchoubar, B. *J. Organomet. Chem.* **1983**, *244*, 265–272.
76. Jefferis, J. M.; Girolami, G. S. *Organometallics* **1998**, *17*, 3630–3632.
77. Laplaza, C. E.; Cummins, C. C. *Science* **1995**, *268*, 861–863.
78. Laplaza, C. E.; Johnson, M. J. A.; Peters, J.; Odom, A. L.; Kim, E.; Cummins, C. C.; George, G. N.; Pickering, I. J. *J. Am. Chem. Soc.* **1996**, *118*, 8623–8638.
79. Laplaza, C. E.; Johnson, A. R.; Cummins, C. C. *J. Am. Chem. Soc.* **1996**, *118*, 709–710.
80. Agapie, T.; Odom, A. L.; Cummins, C. C. *Inorg. Chem.* **2000**, *39*, 174–179.
81. Peters, J. C.; Cherry, J.-P. F.; Thomas, J. C.; Baraldo, L.; Mindiola, D. J.; Davis, W. M.; Cummins, C. C. *J. Am. Chem. Soc.* **1999**, *121*, 10053–10067.
82. Hahn, J.; Landis, C. R.; Nasluzov, V. A.; Neyman, K. M.; Rösch, N. *Inorg. Chem.* **1997**, *36*, 3947–3951.
83. Cui, Q.; Musaev, D. G.; Svensson, M.; Sieber, S.; Morokuma, K. *J. Am. Chem. Soc.* **1995**, *117*, 12366–12367.
84. Cherry, J.-P. F.; Johnson, A. R.; Baraldo, L. M.; Tsai, Y.-C.; Cummins, C. C.; Kryatov, S. V.; Rybak-Akimova, E. V.; Capps, K. B.; Hoff, C. D.; Haar, C. M.; Nolan, S. P. *J. Am. Chem. Soc.* **2001**, *123*, 7271–7286.
85. Solari, E.; Da Silva, C.; Iacono, B.; Hesschenbrouck, J.; Rizzoli, C.; Scopelliti, R.; Floriani, C. *Angew. Chem., Int. Ed.* **2001**, *40*, 3907–3909.
86. Zanotti-Gerosa, A.; Solari, E.; Giannini, L.; Floriani, C.; Chiesi-Villa, A.; Rizzoli, C. *J. Am. Chem. Soc.* **1998**, *120*, 437–438.
87. Caselli, A.; Solari, E.; Scopelliti, R.; Floriani, C.; Re, N.; Rizzoli, C.; Chiesi-Villa, A. *J. Am. Chem. Soc.* **2000**, *122*, 3652–3670.
88. Kawaguchi, H.; Matsuo, T. *Angew. Chem., Int. Ed.* **2002**, *41*, 2792–2794.
89. Clentsmith, G. K. B.; Bates, V. M. E.; Hitchcock, P. B.; Cloke, F. G. N. *J. Am. Chem. Soc.* **1999**, *121*, 10444–10445.
90. Bates, V. M. E.; Clentsmith, G. K. B.; Cloke, F. G. N.; Green, J. C.; Jenkin, H. D. L. *Chem. Commun.* **2000**, 927–928.
91. Korobkov, I.; Gambarotta, S.; Yap, G. P. A. *Angew. Chem., Int. Ed.* **2002**, *41*, 3433–3436.
92. Fryzuk, M. D.; Love, J. B.; Rettig, S. J.; Young, V. G. *Science* **1997**, *275*, 1445–1447.
93. Basch, H.; Musaev, D. G.; Morokuma, K.; Fryzuk, M. D.; Love, J. B.; Seidel, W. W.; Albinati, A.; Koetzle, T. F.; Klooster, W. T.; Mason, S. A.; Eckert, J. *J. Am. Chem. Soc.* **1999**, *121*, 523–528.
94. Basch, H.; Musaev, D. G.; Morokuma, K. *J. Am. Chem. Soc.* **1999**, *121*, 5754–5761.
95. Fryzuk, M. D.; Kozak, C. M.; Bowdridge, M. R.; Patrick, B. O.; Rettig, S. J. *J. Am. Chem. Soc.* **2002**, *124*, 8389–8397.
96. Schrock, R. R. *Acc. Chem. Res.* **1997**, *30*, 9–16.
97. Greco, G. E.; Schrock, R. R. *Inorg. Chem.* **2001**, *40*, 3861–3878 and references therein.
98. O'Donoghue, M. B.; Davis, W. M.; Schrock, R. R. *Inorg. Chem.* **1998**, *37*, 5149–5158.
99. Yandulov, D. V.; Schrock, R. R. *J. Am. Chem. Soc.* **2002**, *124*, 6252–6253.
100. Nishibayashi, Y.; Iwai, S.; Hidai, M. *Science* **1998**, *279*, 540–542.
101. Nishibayashi, Y.; Iwai, S.; Hidai, M. *J. Am. Chem. Soc.* **1998**, *120*, 10559–10560.
102. Nishibayashi, Y.; Takemoto, S.; Iwai, S.; Hidai, M. *Inorg. Chem.* **2000**, *39*, 5946–5957.
103. Nishibayashi, Y.; Wakiji, I.; Hirata, K.; DuBois, M. R.; Hidai, M. *Inorg. Chem.* **2001**, *40*, 578–580.
104. Ware, D. C.; Taube, H. *Inorg. Chem.* **1991**, *30*, 4605–4610.
105. Seymore, S. B.; Brown, S. N. *Inorg. Chem.* **2002**, *41*, 462–469.
106. Mindiola, D. J.; Meyer, K.; Cherry, J.-P. F.; Baker, T. A.; Cummins, C. C. *Organometallics* **2000**, *19*, 1622–1624.
107. Carnahan, J. E.; Mortenson, L. E.; Mower, H. F.; Castle, J. E. *Biochim. Biophys. Acta* **1960**, *44*, 520–535.
108. Ribbe, M.; Gadkari, D.; Meyers, O. *J. Biol. Chem.* **1997**, *272*, 26627–26633.
109. Georgiadis, M. M.; Komiya, H.; Chakrabarti, P.; Woo, D.; Kornuc, J. J.; Rees, D. C. *Nature* **1992**, *257*, 1653–1659.
110. Schlessman, J. L.; Woo, D.; Joshua-Tor, L.; Howard, J. B.; Rees, D. C. *J. Mol. Biol.* **1998**, *280*, 669–685.
111. Schindelin, H.; Kisker, C.; Schlessman, J. L.; Howard, J. B.; Rees, D. C. *Nature* **1997**, *387*, 370–376.
112. Grossman, J. G.; Hasnain, S. S.; Yousafzai, F. K.; Eady, R. R. *J. Biol. Chem.* **2001**, *276*, 6582–6590.
113. Jang, S. B.; Seefeldt, L. C.; Peters, J. W. *Biochemistry* **2000**, *39*, 641–648.
114. Watt, G. D.; Reddy, K. R. N. *J. Inorg. Biochem.* **1994**, *53*, 281–294.
115. Yoo, S. J.; Angove, H. C.; Burgess, B. K.; Hendrich, M. P.; Münck, E. *J. Am. Chem. Soc.* **1999**, *121*, 2534–2545.
116. Strop, P.; Takahara, P. M.; Chiu, H.-J.; Angove, H. C.; Burgess, B. K.; Rees, D. C. *Biochemistry* **2001**, *40*, 651–656.
117. Erickson, J. A.; Nyborg, A. C.; Johnson, J. L.; Truscott, S. M.; Gunn, A.; Nordmeyer, F. R.; Watt, G. D. *Biochemistry* **1999**, *38*, 14279–14285.
118. Nyborg, A. C.; Johnson, J. L.; Gunn, A.; Watt, G. D. *J. Biol. Chem.* **2000**, *275*, 39307–39312.
119. Guo, M.; Sulc, F.; Ribbe, M. W.; Farmer, P. J.; Burgess, B. K. *J. Am. Chem. Soc.* **2002**, *124*, 12100–12101.
120. Zhou, C.; Raebiger, J. W.; Segal, B. M.; Holm, R. H. *Inorg. Chim. Acta* **2000**, *300–302*, 892–902.
121. Noodleman, L.; Lovell, T.; Liu, T.; Himo, F.; Torres, R. A. *Curr. Opin. Chem. Biol.* **2002**, *6*, 259–273.
122. Cambray, J.; Lane, R. W.; Wedd, A. G.; Johnson, R. W.; Holm, R. H. *Inorg. Chem.* **1977**, *16*, 2565–2571.
123. Henderson, R. A.; Sykes, A. G. *Inorg. Chem.* **1980**, *19*, 3103–3105.
124. Hagen, W. R.; Eady, R. R.; Dunham, W. R.; Haaker, H. *FEBS Lett.* **1985**, *189*, 250–254.
125. Onate, Y. A.; Finnegan, M. G.; Hales, B. J.; Johnson, M. K. *Biochim. Biophys. Acta* **1993**, *1164*, 113–123.
126. Watt, G. D.; McDonald, J. W. *Biochemistry* **1985**, *24*, 7226–7231.
127. Lowe, D. J.; Thorneley, R. N. F. *Biochem. J.* **1984**, *224*, 895–901.
128. Lindahl, P. A.; Day, E. P.; Kent, T. A.; Orme-Johnson, W. H.; Münck, E. *J. Biol. Chem.* **1985**, *260*, 11160–11173.
129. Angove, H. C.; Yoo, S. J.; Burgess, B. K.; Münck, E. *J. Am. Chem. Soc.* **1997**, *119*, 8730–8731.
130. Yoo, S. J.; Angove, H. C.; Burgess, B. K.; Münck, E.; Peterson, J. *J. Am. Chem. Soc.* **1998**, *120*, 9704–9705.

131. Musgrave, K. B.; Angove, H. C.; Burgess, B. K.; Hedman, B.; Hodgson, K. O. *J. Am. Chem. Soc.* **1998**, *120*, 5325–5326.
132. Lowe, D. J.; Fisher, K.; Thorneley, R. N. *Biochem. J.* **1993**, *292*, 93–98.
133. Chan, J. M.; Christiansen, J.; Dean, D. R.; Seefeldt, L. C. *Biochemistry* **1999**, *38*, 5779–5785.
134. Mayer, S. M.; Lawson, D. M.; Gormal, C. A.; Roe, S. M.; Smith, B. E. *J. Mol. Biol.* **1999**, *292*, 871–891.
135. Lanzilotta, W. N.; Christiansen, J.; Dean, D. R.; Seefeldt, L. C. *Biochemistry* **1998**, *37*, 11376–11384.
136. Peters, J. W.; Stowell, M. H.; Soltis, S. M.; Finnegan, M. G.; Johnson, M. K.; Rees, D. C. *Biochemistry* **1997**, *36*, 1181–1187.
137. Musgrave, K. B.; Liu, H. I.; Ma, L.; Burgess, B. K.; Watt, G.; Hedman, B.; Hodgson, K. O. *J. Biol. Inorg. Chem.* **1998**, *3*, 344–352.
138. Zimmermann, R.; Münck, E.; Brill, W. J.; Shah, V. K.; Henzl, M. T.; Rawlings, J.; Orme-Johnson, W. H. *Biochim. Biophys. Acta* **1978**, *537*, 185–207.
139. McLean, P. A.; Papaefthymiou, V.; Orme-Johnson, W. H.; Münck, E. *J. Biol. Chem.* **1987**, *262*, 12900–12903.
140. Surerus, K. K.; Hendrich, M. P.; Christie, P. D.; Rottgardt, D.; Orme-Johnson, W. H.; Münck, E. *J. Am. Chem. Soc.* **1992**, *114*, 8579–8590.
141. Pierik, A. J.; Wassink, H.; Haaker, H.; Hagen, W. R. *Eur. J. Biochem.* **1993**, *212*, 51–61.
142. Tittsworth, R. C.; Hales, B. J. *J. Am. Chem. Soc.* **1993**, *115*, 9763–9767.
143. Hagen, W. R.; Eady, R. R.; Dunham, W. R.; Haaker, H. *FEBS Lett.* **1985**, *189*, 250–254.
144. Siemann, S.; Schneider, K.; Dröttboom, M.; Müller, A. *Eur. J. Biochem.* **2002**, *269*, 1650–1661.
145. Huang, J.; Goh, C.; Holm, R. H. *Inorg. Chem.* **1997**, *36*, 356–361.
146. Osterloh, F.; Sanakis, Y.; Staples, R. J.; Münck, E.; Holm, R. H. *Angew. Chem., Int. Ed.* **1999**, *38*, 2066–2070.
147. Osterloh, F.; Achim, C.; Holm, R. H. *Inorg. Chem.* **2001**, *40*, 224–232.
148. Zhang, Y.; Zuo, J.-L.; Zhou, H.-C.; Holm, R. H. *J. Am. Chem. Soc.* **2002**, *124*, 14292–14293.
149. O'Donnell, M. J.; Smith, B. E. *Biochem. J.* **1978**, *173*, 831.
150. Szilagyi, R. K.; Musaev, D. G.; Morokuma, K. *Inorg. Chem.* **2001**, *40*, 766–775.
151. Durrant, M. C. *Biochem. J.* **2001**, *355*, 569–576.
152. Szilagyi, R. K.; Musaev, D. G.; Morokuma, K. *J. Mol. Struct. (Theochem)* **2000**, *506*, 131–146.
153. Coucouvanis, D.; Han, J.; Moon, N. *J. Am. Chem. Soc.* **2002**, *124*, 216–224.
154. Einsle, O.; Tezcan, F. A.; Andrade, S. L. A.; Schmid, B.; Yoshida, M.; Howard, J. B.; Rees, D. C. *Science* **2002**, *297*, 1696–1700.
155. Dance, I. *Chem. Commun.* **2003**, 324–325.
156. Lee, H.-I.; Benton, P. M. C.; Laryukhin, M.; Igarashi, R. Y.; Dean, D. R.; Seefeldt, L. C.; Hoffman, B. M., *J. Am. Chem. Soc.* **2003**, *125*, 5604–5605.
157. Della Pergola, R.; Garlaschelli, L.; Manassero, M.; Sansoni, M.; Strumolo, D.; Fabrizi de Biani, F.; Zanello, P. *J. Chem. Soc., Dalton. Trans.* **2001**, 2179–2183.
158. Pergola, R. D.; Bandini, C.; Demartin, F.; Diana, E.; Garlaschelli, L.; Stanghellini, P. L.; Zanello, P. *J. Chem. Soc., Dalton. Trans.* **1996**, 747–754.
159. Martinengo, S.; Ciani, G.; Sironi, A.; Heaton, B. T.; Mason, J. *J. Am. Chem. Soc.* **1979**, *101*, 7095–7097.
160. Tachikawa, M.; Sievert, A. C.; Muetterties, E. L.; Thompson, M. R.; Day, C. S.; Day, V. W. *J. Am. Chem. Soc.* **1980**, *102*, 1725–1727.
161. Tachikawa, M.; Muetterties, E. L. *Prog. Inorg. Chem.* **1981**, *28*, 203–238.
162. Chen, J.; Christiansen, J.; Campobasso, N.; Bolin, J. T.; Tittsworth, R. C.; Hales, B. J.; Rehr, J. J.; Cramer, S. P. *Angew. Chem., Int. Ed. Engl.* **1993**, *32*, 1661–1594.
163. Liu, H. I.; Filipponi, A.; Gavini, N.; Burgess, B. K.; Hedman, B.; Di Cicco, A.; Natoli, C. R.; Hodgson, K. O. *J. Am. Chem. Soc.* **1994**, *116*, 2418–2423.
164. Chen, J.; Christiansen, J.; Tittsworth, R. C.; Hales, B. J.; George, S. J.; Coucouvanis, D.; Cramer, S. P. *J. Am. Chem. Soc.* **1993**, *115*, 5509–5515.
165. Christiansen, J.; Tittsworth, R. C.; Hales, B. J.; Cramer, S. P. *J. Am. Chem. Soc.* **1995**, *117*, 10017–10024.
166. Palmer, G.; Multani, J. S.; Cretney, W. V.; Zumft, W. G.; Mortenson, L. E. *Arch. Biochem. Biophys.* **1972**, *153*, 325–332.
167. Münck, E.; Rhodes, H.; Orme-Johnson, W. H.; Davis, L. C.; Brill, W. J.; Shah, V. K. *Biochim. Biophys. Acta* **1975**, *400*, 32–53.
168. Smith, B. E.; Lowe, D. J.; Bray, R. C. *Biochem. J.* **1973**, *135*, 331–341.
169. Rawlings, J.; Shah, V. K.; Chisnell, J. R.; Brill, W. J.; Zimmermann, R.; Münck, E.; Orme-Johnson, W. H. *J. Biol. Chem.* **1978**, *253*, 1001–1004.
170. Zimmermann, R.; Münck, E.; Brill, W. J.; Shah, V. K.; Henzl, M. T.; Rawlings, J.; Orme-Johnson, W. H. *Biochim. Biophys. Acta* **1978**, *537*, 185–207.
171. Lowe, D. J.; Eady, R. R.; Thorneley, R. N. F. *Biochem. J.* **1978**, *173*, 277–290.
172. Hoffman, B. M.; Venters, R. A.; Roberts, J. E.; Nelson, M.; Orme-Johnson, W. H. *J. Am. Chem. Soc.* **1982**, *104*, 4711–4712.
173. Hoffman, B. M.; Roberts, J. E.; Orme-Johnson, W. H. *J. Am. Chem. Soc.* **1982**, *104*, 860–862.
174. Huynh, B. H.; Henzl, M. T.; Christner, J. A.; Zimmermann, R.; Orme-Johnson, W. H.; Münck, E. *Biochim. Biophys. Acta* **1980**, *623*, 124–138.
175. Orme-Johnson, W. H.; Hamilton, W. D.; Jones, T. L.; Tso, M. Y. W.; Burris, R. H.; Shah, V. K.; Brill, W. J. *Proc. Natl. Acad. Sci. USA* **1972**, *69*, 3142–3145.
176. Huynh, B. H.; Münck, E.; Orme-Johnson, W. H. *Biochim. Biophys. Acta* **1979**, *576*, 192–203.
177. Johnson, M. K.; Thomson, A. J.; Robinson, A. E.; Smith, B. E. *Biochim. Biophys. Acta* **1981**, *671*, 61–70.
178. Venters, R. A.; Nelson, M. J.; McLean, P. A.; True, A. E.; Levy, M. A.; Hoffman, B. M.; Orme-Johnson, W. H. *J. Am. Chem. Soc.* **1986**, *108*, 3487–3498.
179. Lee, H.-I.; Hales, B. J.; Hoffman, B. M. *J. Am. Chem. Soc.* **1997**, *119*, 11395–11400.
180. Yoo, S. J.; Angove, H. C.; Papaefthymiou, V.; Burgess, B. K.; Münck, E. *J. Am. Chem. Soc.* **2000**, *122*, 4926–4936.
181. Lovell, T.; Li, J.; Liu, T.; Case, D. A.; Noodleman, L. *J. Am. Chem. Soc.* **2001**, *123*, 12392–12410.
182. Fisher, K.; Newton, W. E.; Lowe, D. J. *Biochemistry* **2001**, *40*, 3333–3339.

183. Thomann, H.; Bernardo, M.; Newton, W. E.; Dean, D. R. *Proc. Natl. Acad. Sci. USA* **1991**, *88*, 6620–6623.
184. DeRose, V. J.; Kim, C.-H.; Newton, W. E.; Dean, D. R.; Hoffman, B. M. *Biochemistry* **1995**, *34*, 2809–2814.
185. Lee, H.-I.; Thrasher, K. S.; Dean, D. R.; Newton, W. E.; Hoffman, B. M. *Biochemistry* **1998**, *37*, 13370–13378.
186. George, G. N.; Prince, R. C.; Bare, R. E. *Inorg. Chem.* **1996**, *35*, 434–438.
187. Shah, V. K.; Brill, W. J. *Proc. Natl. Acad. Sci. USA* **1977**, *74*, 3249–3253.
188. Burgess, B. K.; Jacobs, D. B.; Stiefel, E. I. *Biochim. Biophys. Acta* **1980**, *614*, 196–209.
189. McLean, P. A.; Wink, D. A.; Chapman, S. K.; Hickman, A. B.; McKillop, D. M.; Orme-Johnson, W. H. *Biochemistry* **1989**, *28*, 9402–9406.
190. Lough, S. M.; Jacobs, D. L.; Lyons, D. M.; Watt, G. D.; McDonald, J. W. *Biochem. Biophys. Res. Comm.* **1986**, *139*, 740–746.
191. Harvey, I.; Strange, R. W.; Schneider, R.; Gormal, C. A.; Garner, C. D.; Hasnain, S. S.; Richards, R. L.; Smith, B. E. *Inorg. Chim. Acta* **1998**, *275–276*, 150–158.
192. Conradson, S. D.; Burgess, B. K.; Newton, W. E.; Di Cicco, A.; Filipponi, A.; Wu, Z. Y.; Natoli, C. R.; Hedman, B.; Hodgson, K. O. *Proc. Natl. Acad. Sci. USA* **1994**, *91*, 1290–1293.
193. Cramer, S. P.; Gillum, W. O.; Hodgson, K. O.; Mortenson, L. E.; Stiefel, E. I.; Chisnell, J. R.; Brill, W. J.; Shah, V. K. *J. Am. Chem. Soc.* **1978**, *100*, 3814–3819.
194. Conradson, S. D.; Burgess, B. K.; Newton, W. E.; Mortenson, L. E.; Hodgson, K. O. *J. Am. Chem. Soc.* **1987**, *109*, 7507–7515.
195. Arber, J. M.; Flood, A. C.; Garner, C. D.; Gormal, C. A.; Hasnain, S. S.; Smith, B. E. *Biochem. J.* **1988**, *252*, 421–425.
196. Walters, M. A.; Chapman, S. K.; Orme-Johnson, W. H. *Polyhedron* **1986**, *5*, 561–565.
197. Huang, H. Q.; Kofford, M.; Simpson, F. B.; Watt, G. D. *J. Inorg. Biochem.* **1993**, *218*, 59–75.
198. Yang, S. S.; Pan, W. H.; Friesen, G. D.; Burgess, B. K.; Corbin, J. L.; Stiefel, E. I.; Newton, W. E. *J. Biol. Chem.* **1982**, *257*, 8042–8048.
199. Eliezer, D.; Frank, P.; Gillis, N.; Newton, W. E.; Doniach, S.; Hodgson, K. O. *J. Biol. Chem.* **1993**, *268*, 20953–20957.
200. Frank, P.; Angove, H. C.; Burgess, B.; Hodgson, K. O. *J. Biol. Inorg. Chem.* **2001**, *6*, 683–697.
201. Wink, D. A.; McLean, P. A.; Hickman, A. B.; Orme-Johnson, W. *Biochemistry* **1989**, *28*, 9407–9412.
202. Smith, B. E.; Durrant, M. C.; Fairhurst, S. A.; Gormal, C. A.; Grönberg, K. L. C.; Henderson, R. A.; Ibrahim, S. K.; Le Gall, T.; Pickett, C. J. *Coord. Chem. Rev.* **1999**, *185–186*, 669–687.
203. Conradson, S. D.; Burgess, B. K.; Holm, R. H. *J. Biol. Chem.* **1988**, *263*, 13743–13749.
204. Grønberg, K. L. C.; Gormal, C. A.; Durrant, M. C.; Smith, B. E.; Henderson, R. A. *J. Am. Chem. Soc.* **1998**, *120*, 10613–10621.
205. Gall, T. L.; Ibrahim, S. K.; Gormal, C. A.; Smith, B. E.; Pickett, C. J. *Chem. Commun.* **1999**, 773–774.
206. Richards, A. J.; Lowe, D. J.; Richards, R. L.; Thomson, A. J.; Smith, B. E. *Biochem. J.* **1994**, *297*, 373–378.
207. Bazhenova, T. A.; Bazhenova, M. A.; Petrova, G. N.; Shilova, A. K.; Shilov, A. E. *Russ. Chem. Bull.* **1998**, *47*, 861–867.
208. Bazhenova, T. A.; Bazhenova, M. A.; Petrova, G. N.; Mironova, S. A. *Kinet. Catal.* **2002**, *43*, 351–362.
209. Bazhenova, T. A.; Bazhenova, M. A.; Petrova, G. N.; Shilov, A. E. *Kinet. Catal.* **1999**, *40*, 942–943.
210. Bazhenova, M. A.; Bazhenova, T. A.; Petrova, G. N.; Mironova, S. A. *Kinet. Catal.* **2002**, *43*, 592–602.
211. Link, H.; Fenske, D. *Z. Anorg. Allg. Chem.* **1999**, *625*, 1878–1884.
212. Coucouvanis, D. *Acc. Chem. Res.* **1981**, *14*, 201–209.
213. Coucouvanis, D. *Acc. Chem. Res.* **1991**, *24*, 1–8.
214. Holm, R. H. *Adv. Inorg. Chem.* **1992**, *38*, 1–71.
215. Demadis, K. D.; Coucouvanis, D. *Inorg. Chem.* **1995**, *34*, 436–448.
216. Tyson, M. A.; Coucouvanis, D. *Inorg. Chem.* **1997**, *36*, 3808–3809.
217. Han, J.; Coucouvanis, D. *J. Am. Chem. Soc.* **2001**, *123*, 11304–11305.
218. Palermo, R. E.; Singh, R.; Bashkin, J. K.; Holm, R. H. *J. Am. Chem. Soc.* **1984**, *106*, 2600–2612.
219. Mosier, P. E.; Kim, C. G.; Coucouvanis, D. *Inorg. Chem.* **1993**, *32*, 2620.
220. Coucouvanis, D.; Demadis, K. D.; Kim, C. G.; Dunham, R. W.; Kampf, J. W. *J. Am. Chem. Soc.* **1993**, *115*, 3344–3345.
221. Han, J.; Koutmos, M.; Al Ahmad, S.; Coucouvanis, D. *Inorg. Chem.* **2001**, *40*, 5985–5999.
222. Demadis, K. D.; Campana, C. F.; Coucouvanis, D. *J. Am. Chem. Soc.* **1995**, *117*, 7832–7833.
223. Osterloh, F.; Segal, B. M.; Achim, C.; Holm, R. H. *Inorg. Chem.* **2000**, *39*, 980–989.
224. Challen, P. R.; Koo, S. M.; Kim, C. G.; Dunham, W. R.; Coucouvanis, D. *J. Am. Chem. Soc.* **1990**, *112*, 8606–8607.
225. Han, J.; Coucouvanis, D. *Inorg. Chem.* **2002**, *41*, 2738–2746.
226. Huang, J.; Mukerjee, S.; Segal, B. M.; Akashi, H.; Zhou, J.; Holm, R. H. *J. Am. Chem. Soc.* **1997**, *119*, 8662–8674.
227. Huang, J.; Holm, R. H. *Inorg. Chem.* **1998**, *37*, 2247–2254.
228. Nordlander, E.; Lee, S. C.; Cen, W.; Wu, Z. Y.; Natoli, C. R.; Di Cicco, A.; Filipponi, A.; Hedman, B.; Hodgson, K. O.; Holm, R. H. *J. Am. Chem. Soc.* **1993**, *115*, 5549–5558.
229. Cen, W.; MacDonnell, F. M.; Scott, M. J.; Holm, R. H. *Inorg. Chem.* **1994**, *33*, 5809–5818.
230. Reynolds, M. S.; Holm, R. H. *Inorg. Chem.* **1988**, *27*, 4494–4499.
231. Snyder, B. S.; Reynolds, M. S.; Holm, R. H.; Papaefthymiou, G. C.; Frankel, R. B. *Polyhedron* **1991**, *10*, 203–213.
232. Knobler, C. B.; Wilson, A. J.; Hider, R. N.; Jensen, I. W.; Penfold, B. R.; Robinson, W. T.; Wilkins, C. J. *J. Chem. Soc., Dalton. Trans.* **1983**, 1299–1303.
233. Cervilla, A.; Llopis, E.; Ribera, A.; Domenech, A.; White, A. J. P.; Williams, D. J. *J. Chem. Soc., Dalton. Trans.* **1995**, 3891–3895.
234. Zhou, Z.-H.; Wan, H.-L.; Tsai, K.-R. *J. Chem. Soc., Dalton. Trans.* **1999**, 4289–4290.
235. Zhou, Z.-H.; Wan, H.-L.; Tsai, K.-R. *Inorg. Chem.* **2000**, *39*, 59–64.
236. MacDonnell, F. M.; Ruhlandt-Senge, K.; Ellison, J. J.; Holm, R. H.; Power, P. P. *Inorg. Chem.* **1995**, *34*, 1815–1822.
237. Sanakis, Y.; Power, P. P.; Stubna, A.; Münck, E. *Inorg. Chem.* **2002**, *41*, 2690–2696.
238. Andres, H.; Bominaar, E. L.; Smith, J. M.; Eckert, N. A.; Holland, P. L.; Münck, E. *J. Am. Chem. Soc.* **2002**, *124*, 3012–3025.

239. Howes, B. D.; Fisher, K.; Lowe, D. J. *Biochem. J.* **1994**, *297*, 261–264.
240. Thorneley, R. N. F.; Lowe, D. J. In *Molybdenum Enzymes*; Spiro, T. G., Ed.; Wiley: New York, 1985; pp 221–284.
241. Wilson, P. E.; Nyborg, A. C.; Watt, G. D. *Biophys. Chem.* **2001**, *91*, 281–304.
242. Thorneley, R. N. F.; Eady, R. R.; Lowe, D. J. *Nature* **1978**, *272*, 557–558.
243. Hardy, R. W. F. In *Treatise on Dinitrogen Fixation*; Hardy, R. W. F., Bottomley, F., Burns, R. C., Eds.; Wiley-Interscience: New York, 1979; pp 515–568.
244. Pickett, C. J. *J. Biol. Inorg. Chem.* **1996**, *1*, 601–606.
245. Chatt, J.; Pearman, A. J.; Richards, R. L. *Nature* **1975**, *253*, 39–40.
246. Anderson, S. N.; Fakley, M. E.; Richards, R. L.; Chatt, J. *J. Chem. Soc., Dalton. Trans.* **1981**, 1973–1980.
247. Pickett, C. J.; Ryder, K. S.; Talarmin, J. *J. Chem. Soc., Dalton. Trans.* **1986**, 1453–1457.
248. Szilagyi, R. K.; Musaev, D. G.; Morokuma, K. *Inorg. Chem.* **2001**, *40*, 766–775.
249. Lovell, T.; Li, J.; Case, D. A.; Noodleman, L. *J. Am. Chem. Soc.* **2002**, *124*, 4546–4547.
250. Coucouvanis, D. *J. Biol. Inorg. Chem.* **1996**, *1*, 594–600.
251. Imperial, J.; Hoover, T. R.; Madden, M. S.; Ludden, P. W.; Shah, V. K. *Biochemistry* **1989**, *28*, 7796–7799.
252. Tanaka, K.; Hozumi, Y.; Tanaka, T. *Chem. Lett.* **1982**, 1203–1206.
253. Coucouvanis, D.; Mosier, P. E.; Demadis, K. D.; Patton, S.; Malinak, S. M.; Kim, C. G.; Tyson, M. A. *J. Am. Chem. Soc.* **1993**, *115*, 12193–12194.
254. Demadis, K. D.; Coucouvanis, D. *Inorg. Chem.* **1994**, *33*, 4195–4197.
255. Demadis, K. D.; Malinak, S. M.; Coucouvanis, D. *Inorg. Chem.* **1996**, *35*, 4038–4046.
256. Malinak, S. M.; Simeonov, A.; Mosier, P. E.; McKenna, C. E.; Coucouvanis, D. *J. Am. Chem. Soc.* **1997**, *119*, 1662–1667.
257. Durrant, M. C. *Inorg. Chem. Commun.* **2001**, *4*, 60–62.
258. Shan, H.; Yang, Y.; James, A. J.; Sharp, P. R. *Science* **1997**, *275*, 1460–1462.
259. Chan, M. K.; Kim, J.; Rees, D. C. *Science* **1993**, *260*, 792–794.
260. Rees, D. C.; Chan, M. K.; Kim, J. *Adv. Inorg. Chem.* **1994**, *40*, 89–119.
261. Hills, A.; Hughes, D. L.; Jimenez-Tenorio, M.; Leigh, G. J. *J. Organomet. Chem.* **1990**, *391*, C41–C44.
262. Kandler, H.; Gauss, C.; Bidell, W.; Rosenberger, S.; Bürgi, T.; Eremenko, I. L.; Veghini, D.; Orama, O.; Burger, P.; Berke, H. *Chem. Eur. J.* **1995**, *1*, 541–548.
263. Berke, H.; Bankhardt, W.; Huttner, G.; Von Seyerl, J.; Zsolnai, L. *Chem. Ber.* **1981**, *114*, 2754–2768.
264. Wiesler, B. E.; Lehnert, N.; Tuczek, F.; Neuhausen, J.; Tremel, W. *Angew. Chem., Int. Ed.* **1998**, *37*, 815–817.
265. Hirano, M.; Akita, M.; Morikita, T.; Kubo, H.; Fukuoka, A.; Komiya, S. *J. Chem. Soc., Dalton. Trans.* **1997**, 3453–3458.
266. George, T. A.; Rose, D. J.; Chang, Y.; Chen, Q.; Zubieta, J. *Inorg. Chem.* **1995**, *34*, 1295–1298.
267. Leal, A. D.; Tenorio, M. J.; Puerta, M. C.; Valerga, P. *Organometallics* **1995**, *14*, 3839–3847.
268. Komiya, S.; Akita, M.; Yoza, A.; Kasuga, N.; Fukuoka, A.; Kai, Y. *J. Chem. Soc., Chem. Commun.* **1993**, 787–788.
269. Hills, A.; Hughes, D. L.; Jimenez-Tenorio, M.; Leigh, G. J.; Rowley, A. T. *J. Chem. Soc., Dalton. Trans.* **1993**, 3041–3049.
270. Franke, O.; Wiesler, B. E.; Lehnert, N.; Tuczek, F. *Z. Anorg. Allg. Chem.* **2002**, *628*, 2395–2402.
271. Deeth, R. J.; Langford, S. A. *J. Chem. Soc., Dalton. Trans.* **1995**, 1–4.
272. Duarte, H. A.; Salahub, D. R.; Haslett, T.; Moskovits, M. *Inorg. Chem.* **1999**, *38*, 3895–3903.
273. Leigh, G. J.; Jimenez-Tenorio, M. *J. Am. Chem. Soc.* **1991**, *113*, 5862–5863.
274. Hall, D. A.; Leigh, G. J. *J. Chem. Soc., Dalton. Trans.* **1996**, 3539–3541.
275. Leigh, G. J. *Acc. Chem. Res.* **1992**, *25*, 177–181.
276. O'Donoghue, M. B.; Zanetti, N. C.; Davis, W. M.; Schrock, R. R. *J. Am. Chem. Soc.* **1997**, *119*, 2753–2754.
277. O'Donoghue, M. B.; Davis, W. M.; Schrock, R. R.; Reiff, W. M. *Inorg. Chem.* **1999**, *38*, 243–252.
278. Smith, J. M.; Lachicotte, R. J.; Pittard, K. A.; Cundari, T. R.; Lukat-Rodgers, G.; Rodgers, K. R.; Holland, P. L. *J. Am. Chem. Soc.* **2001**, *123*, 9222–9223.
279. Smith, J. M.; Lachicotte, R. L.; Holland, P. L., unpublished results.
280. Sellmann, D.; Sutter, J. *Acc. Chem. Res.* **1997**, *30*, 460–469.
281. Szilagyi, R. K.; Musaev, D. G.; Morokuma, K. *Theochem* **2000**, *506*, 131–146.
282. Almeida, V. R.; Gormal, C. A.; Grönberg, K. L. C.; Henderson, R. A.; Oglieve, K. E.; Smith, B. E. *Inorg. Chim. Acta* **1999**, *291*, 212–225.
283. Pham, D. N.; Burgess, B. K. *Biochemistry* **1993**, *32*, 13725–13731.
284. Henderson, R. A.; Oglieve, K. E. *J. Chem. Soc., Chem. Commun.* **1994**, 377–379.
285. Hirst, J.; Jameson, G. N. L.; Allen, J. W. A.; Armstrong, F. A. *J. Am. Chem. Soc.* **1998**, *120*, 11994–11999.
286. Helleren, C. A.; Henderson, R. A.; Leigh, G. J. *J. Chem. Soc., Dalton. Trans.* **1999**, 1213–1220.
287. Basallote, M. G.; Durán, J.; Fernández-Trujillo, M. J.; Máñez, M. A. *J. Organomet. Chem.* **2000**, *609*, 29–35.
288. Smith, J. M.; Lachicotte, R. L.; Holland, P. L. submitted for publication.
289. Sellmann, D.; Fursattel, A.; Sutter, J. *Coord. Chem. Rev.* **2000**, *200–202*, 545–561.
290. Leigh, G. J.; McMahon, C. N. *J. Organomet. Chem.* **1995**, *500*, 219–225.
291. Cameron, L. M.; Hales, B. J. *Biochemistry* **1998**, *37*, 9449–9456.
292. Pollock, R. C.; Lee, H.-I.; Cameron, L. M.; DeRose, V. J.; Hales, B. J.; Orme-Johnson, W. H.; Hoffman, B. M. *J. Am. Chem. Soc.* **1995**, *117*, 8686–8687.
293. Christie, P. D.; Lee, H.-I.; Cameron, L. M.; Hales, B. J.; Orme-Johnson, W. H.; Hoffman, B. M. *J. Am. Chem. Soc.* **1996**, *118*, 8707–8709.
294. Lee, H.-I.; Cameron, L. M.; Hales, B. J.; Hoffman, B. M. *J. Am. Chem. Soc.* **1997**, *119*, 10121–10126.
295. George, S. J.; Ashby, G. A.; Wharton, C. W.; Thorneley, R. N. F. *J. Am. Chem. Soc.* **1997**, *119*, 6450–6451.
296. Kisko, J. L.; Hascall, T.; Parkin, G. *J. Am. Chem. Soc.* **1998**, *120*, 10561–10562.
297. Shen, J.; Dean, D. R.; Newton, W. E. *Biochemistry* **1997**, *36*, 4884–4894.
298. Sørlie, M.; Christiansen, J.; Dean, D. R.; Hales, B. J. *J. Am. Chem. Soc.* **1999**, *121*, 9457–9458.
299. Lowe, D. J.; Fisher, K.; Thorneley, R. N. *Biochem. J.* **1990**, *272*, 621–625.
300. Benton, P. M. C.; Christiansen, J.; Dean, D. R.; Seefeldt, L. C. *J. Am. Chem. Soc.* **2001**, *123*, 1822–1827.
301. Mayer, S. M.; Niehaus, W. G.; Dean, D. R. *Dalton* **2002**, 802–807.

302. Benton, P. M. C.; Mayer, S. M.; Shao, J.; Hoffman, B. M.; Dean, D. R.; Seefeldt, L. C. *Biochemistry* **2001**, *40*, 13816–13825.
303. Christiansen, J.; Cash, V. L.; Seefeldt, L. C.; Dean, D. R. *J. Biol. Chem.* **2000**, *275*, 11459–11464.
304. Laughlin, L. J.; Coucouvanis, D. *J. Am. Chem. Soc.* **1995**, *117*, 3118–3125.
305. Coucouvanis, D.; Demadis, K. D.; Malinak, S. M.; Mosier, P. E.; Tyson, M. A.; Laughlin, L. J. *J. Mol. Catal. A* **1996**, *107*, 123–135.
306. Conradson, S. D.; Burgess, B. K.; Vaughn, S. A.; Roe, A. L.; Hedman, B.; Hodgson, K. O.; Holm, R. H. *J. Biol. Chem.* **1989**, *264*, 15967–15974.
307. Albertin, G.; Antoniutti, S.; Del Ministro, E.; Bordignon, E. *J. Chem. Soc., Dalton. Trans.* **1992**, 3203–3208.
308. MacLaughlin, S. A.; Doherty, S.; Taylor, N. J.; Carty, A. J. *Organometallics* **1992**, *11*, 4315–4325.
309. Hogarth, G.; Lavender, M. H. *J. Chem. Soc., Dalton. Trans.* **1994**, 3389–3396.
310. Richards, A. J.; Lowe, D. J.; Richards, R. L.; Thomson, A. J.; Smith, B. E. *Biochem. J.* **1994**, *297*, 373–378.
311. Grönberg, K. L. C.; Gormal, C. A.; Smith, B. E.; Henderson, R. A. *Chem. Commun.* **1997**, 713–714.
312. Lowe, D. J.; Fisher, K.; Thorneley, R. N. F.; Vaughn, S. A.; Burgess, B. K. *Biochemistry* **1989**, *28*, 8460–8466.
313. Eady, R. R. *Adv. Inorg. Chem.* **1991**, *36*, 77–102.
314. Eady, R. R. *Chem. Rev.* **1996**, *96*, 3013–3030.
315. Robson, R. L.; Eady, R. R.; Richardson, T. H.; Miller, R. W.; Hawkins, M.; Postgate, J. R. *Nature* **1986**, *322*, 388–390.
316. Hales, B. J.; Case, E. E.; Morningstar, J. E.; Dzeda, M. F.; Mauterer, L. A. *Biochemistry* **1986**, *25*, 7251–7255.
317. Tittsworth, R. C.; Hales, B. J. *Biochemistry* **1996**, *35*, 479–487.
318. Morningstar, J. E.; Hales, B. J. *J. Am. Chem. Soc.* **1987**, *109*, 6854–6855.
319. Ravi, N.; Moore, V.; Lloyd, S. G.; Hales, B. J.; Huynh, B. H. *J. Biol. Chem.* **1994**, *269*, 20920–20924.
320. Morningstar, J. E.; Johnson, M. K.; Case, E. E.; Hales, B. J. *Biochemistry* **1987**, *26*, 1795–1800.
321. Arber, J. M.; Dobson, B. R.; Eady, R. R.; Stevens, P.; Hasnain, S. S.; Garner, C. D.; Smith, B. E. *Nature* **1987**, *325*, 372–374.
322. Arber, J. M.; Dobson, B. R.; Eady, R. R.; Hasnain, S. S.; Garner, C. D.; Matsushita, T.; Nomura, M.; Smith, B. E. *Biochem. J.* **1989**, *258*, 733–737.
323. Dilworth, M. J.; Eady, R. R. *Biochem. J.* **1991**, *277*, 465–468.
324. Dilworth, M. J.; Eady, R. R.; Robson, R. L.; Miller, R. W. *Nature* **1987**, *327*, 167–168.
325. Dilworth, M. J.; Eady, R. R.; Eldridge, M. E. *Biochem. J.* **1988**, *249*, 745–751.
326. Smith, B. E.; Eady, R. R.; Lowe, D. J.; Gormal, C. *Biochem. J.* **1988**, *250*, 299–302.
327. Moore, V. G.; Tittsworth, R. C.; Hales, B. J. *J. Am. Chem. Soc.* **1994**, *116*, 12101–12102.
328. Chatterjee, R.; Allen, R. M.; Ludden, P. W.; Shah, V. K. *J. Biol. Chem.* **1996**, *271*, 6819–6826.
329. Kovacs, J. A.; Holm, R. H. *J. Am. Chem. Soc.* **1986**, *108*, 340–341.
330. Carney, M. J.; Kovacs, J. A.; Zhang, Y. P.; Papaefthymiou, G. C.; Spartalian, K.; Frankel, R. B.; Holm, R. H. *Inorg. Chem.* **1987**, *26*, 719–724.
331. Kovacs, J. A.; Holm, R. H. *Inorg. Chem.* **1987**, *26*, 711–718.
332. Ciurli, S.; Holm, R. H. *Inorg. Chem.* **1989**, *28*, 1685–1690.
333. Hauser, C.; Bill, E.; Holm, R. H. *Inorg. Chem.* **2002**, *41*, 1615–1624.
334. Cen, W.; Lee, S. C.; Li, J.; MacDonnell, F. M.; Holm, R. H. *J. Am. Chem. Soc.* **1993**, *115*, 9515–9523.
335. Schneider, K.; Gollan, U.; Dröttboom, M.; Selsemeier-Voigt, S.; Müller, A. *Eur. J. Biochem.* **1997**, *244*, 789–800.
336. Krahn, E.; Weiss, B. J. R.; Kröckel, M.; Groppe, J.; Henkel, G.; Cramer, S. P.; Trautwein, A. X.; Schneider, K.; Müller, A. *J. Biol. Inorg. Chem.* **2002**, *7*, 37–45.
337. Müller, A.; Schneider, K.; Knüttel, K.; Hagen, W. R. *FEBS Lett.* **1992**, *303*, 36–40.
338. Siemann, S.; Schneider, K.; Dröttboom, M.; Müller, A. *Eur. J. Biochem.* **2002**, *269*, 1650–1661.
339. Hales, B. J.; Case, E. E. *J. Biol. Chem.* **1987**, *262*, 16205–16211.
340. Huang, J. F.; Dong, Z. G.; Wang, D. Y.; Lu, Y. B.; Zhang, H. F.; Wang, Y. P.; Han, Y.; Dai, X. H. *Acta Botanica Sinica* **2001**, *43*, 375–379.
341. Huang, J. F.; Wang, D. Y.; Dong, Z. G.; Wang, Z. P.; Zhang, H. F.; Lu, Y. B.; Xu, X. M.; Zhao, Y. *Acta Botanica Sinica* **2001**, *43*, 918–922.
342. Huang, J. F.; Dong, Z. G.; Zhang, H. F.; Lu, Y. B.; Zhao, Y.; Wang, Z. P. *Acta Botanica Sinica* **2002**, *44*, 297–300.
343. Zhang, H. F.; Wang, Y. P.; Lu, Y. B.; Zhao, Y.; Dai, X. H.; Dong, Z. G.; Huang, J. F. *Acta Botanica Sinica* **2002**, *44*, 400–404.
344. Rangaraj, P.; Rüttimann-Johnson, C.; Shah, V. K.; Ludden, P. W. In *Prokaryotic Nitrogen Fixation: A Model System for Analysis of a Biological Process*; Horizon Scientific Press: Wymondham, UK, 2000; pp 55–79.
345. Rangaraj, P.; Rüttimann-Johnson, C.; Shah, V. K.; Ludden, P. W. *J. Biol. Chem.* **2001**, *276*, 15968–15974.
346. Rangaraj, P.; Ludden, P. W. *J. Biol. Chem.* **2002**, *277*, 40106–40111.
347. Siemann, S.; Schneider, K.; Behrens, K.; Knochel, A.; Klipp, W.; Müller, A. *Eur. J. Biochem.* **2001**, *268*, 1940–1952.
348. Ribbe, M. W.; Burgess, B. K. *Proc. Natl. Acad. Sci. USA* **2001**, *98*, 5521–5525.
349. Schmid, B.; Ribbe, M. W.; Einsle, O.; Yoshida, M.; Thomas, L. M.; Dean, D. R.; Rees, D. C.; Burgess, B. K. *Science* **2002**, *296*, 352–356.
350. Lee, S. C.; Holm, R. H. *Proc. Natl. Acad. Sci. USA* **2003**, *100*, 3595–3600.
351. Barriére, F. *Coord. Chem. Rev.* **2003**, *236*, 71–89.
352. Ray, M.; Golombek, A. P.; Hendrick, M. P.; Young, V. G.; Borovik, A. S. *J. Am. Chem. Soc.* **1996**, *118*, 6084–6085.

8.23
Zinc Hydrolases

S. AOKI and E. KIMURA
Hiroshima University, Japan

8.23.1 INTRODUCTION

Most of the monometallic hydrolases contain the zinc(II) ion in their catalytic centers as an essential metal ion. Typical zinc(II) hydrolases include carboxypeptidase (CPD), thermolysin, β-lactamase, phosphomonoesterase (such as alkaline phosphatase (AP)), phosphodiesterase, phosphotriesterase, matrix metalloproteinase (MMP), and carbonic anhydrase (CA).[1–12]

The reasons why Zn^{2+} ions are used for hydrolytic enzymes almost exclusively over other metals come from specific Zn^{2+} properties, such as: (i) zinc is more abundant than nickel, cadmium, iron, copper, etc.; (ii) Zn^{2+} does not have any redox activity; (iii) Zn^{2+} is a strong Lewis acid and binds strongly with oxyanions; (iv) the coordination number of Zn^{2+} ion is not rigid, but instead is flexible (between four and six),[1,8,11] which is essential for hydrolytic processes

involving expansion of the coordination sphere. The energy difference between four- and six-coordinated Zn^{2+} ions is only about 0.4 kcal mol^{-1}. For comparison, the six-H_2O-coordinated Mg^{2+} ion $((Mg[H_2O]_6)^{2+})$ is 9 kcal mol^{-1} more stable than four-coordinated Mg^{2+} $(Mg[H_2O]_4)$, according to *ab initio* molecular orbital calculations;[13] (v) The ligands (in particular, substrates and products) attached to Zn^{2+} are rather labile with respect to other divalent transition-metal ions such as nickel.

Technical advances have greatly helped to study the structure and reaction mechanisms of zinc(II) enzymes by X-ray crystal-structure analysis, site-directed mutagenesis, and spectroscopic analysis such as NMR experiments. The design of inhibitors which are useful as drugs requires a knowledge of enzyme reaction mechanisms. Moreover, specific enzyme inhibitors help the study of mechanisms. Along with these methodologies, artificial zinc(II) complexes having similar zinc(II)-coordination environments to those of native enzymes have been proven to be useful in elucidating why zinc(II) atoms are essential at the active sites of enzymes, including hydrolases. In this chapter, representative zinc(II) enzymes and their inhibitors and model systems will be focused upon, with emphasis on recent (1990 ∼ 2001) developments.

8.23.2 ZINC(II) ENZYME CLASSIFICATION BY COORDINATING AMINO ACIDS

There are three types of Zn^{2+}-enzyme binding sites: catalytic, cocatalytic,[1–12] and structural.[1,2,9,14–18] There are more than seven dozen three-dimensional structural references to Zn^{2+} enzymes.[10] Contrary to an earlier classification according to reaction type,[8] it may now be useful to classify zinc(II) enzymes according to the Zn^{2+}-coordinating amino acids, which come from analogous gene expression. Typical classified families are shown in Table 1.[10] The protein data bank (PDB) numbers of each enzyme are provided in ref. 10, and these permit prediction of zinc binding sites and thereby zinc functions from DNA sequences without having expressed proteins.

Most of the catalytic sites of zinc enzymes are tetrahedrally or trigonal-bipyramidally coordinated by four or five amino-acid residues, typically His (N), Glu (O), Asp (O), and Cys (S) (Scheme 1). These ligands are generally separated by amino-acid spacers,[10] with the spacer length being fairly common and characteristic to each family. Water is always a ligand to catalytic zinc(II). The Zn^{2+}-bound H_2O may be activated by Zn^{2+} alone, or together with a base form of an active-site amino acid at neutral pH, to provide the hydroxide ions for nucleophilic attack toward the electrophilic substrates. The Zn^{2+}–H_2O may also be poised for displacement with other strong ligands or inhibitors: e.g., iodide ion, sulfonamide, alcohol, thiol, phosphates, or phenol. The varying structure of the active site implies that the amino-acid ligands, their spacing, and secondary interactions with neighboring amino acids are all critical for the Zn^{2+} enzyme mechanism.

In carboxypeptidases[89,90] and thermolysins,[91] the Zn^{2+} ligands are two histidines and one Glu CO_2^-, separated by a different number of amino-acid spacers. The Zn^{2+}–H_2O activated by Glu CO_2^- is involved in catalysis. Human leucotriene A_4 hydrolase,[30] *Clostridium botulinum* neurotoxin A,[32,33] and VanX D-Ala-D-Ala carboxypeptidase[35] belong to the thermolysin family, although they do not necessarily catalyze peptidase reactions.

In astacin[36,37] and MMPs,[11] Zn^{2+} ions are bound to three His's as in carbonic anhydrases (CAs). However, a nearby Glu CO_2^- residue is required to act as a nucleophile or general base for the Zn^{2+}-bound water (like CPD).

CA provides the best-defined example of an ionized Zn^{2+}-bound water mechanism.[92–96] Thr199 and orientation residues such as Glu106, and proton shuttle residues such as His64, are needed to make CA the fastest biological catalyst. 6-Pyruvoly-tetrahydropterin synthase,[81,82] *E. coli* fuculose-1-phosphate aldolase,[84–86] and *E. coli* fructose-1,6-bisphosphate aldolase[87,88] belong to the CA family, although the reactions these enzymes are involved in are different.

8.23.3 PROGRESS IN UNDERSTANDING MECHANISMS OF ZN^{2+}–HYDROLASES

In the 1990s and early 2000s, X-ray crystal-structure studies of enzymes and enzyme–substrate (or inhibitor or product) complexes have deepened our knowledge of enzyme mechanisms. The studies with mutant enzymes have also contributed to understanding the role of essential amino acids at the active sites.

Table 1 Catalytic zinc sites (Zn–L1,L2,L3,L4,L5) of representative Zn^{2+} enzymes (referred from ref. 10).
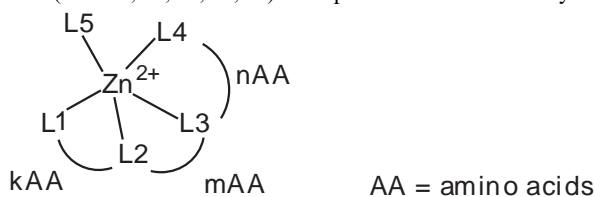
Enzymes	L1	k	L2	m	L3	n	L4	L5	References
Carboxypeptidase (CPD) Family									
Bovine A	His	2	$Glu_{2b\alpha}$	123	His_β(C)		H_2O		19,20
Bovine B	His	2	Glu	123	His		H_2O		21
Rat A_2	His	2	Glu	123	His		H_2O		22
Human A_2	His	2	$Glu_{2b\alpha}$	124	His_β		H_2O		23
Avian D	His	2	$Glu_{2b\alpha}$	103	His_β		H_2O		24
Bovine CPD A	His	2	$Glu_{2b\alpha}$	123	His_β		H_2O		25
Human CPD A_2	His	2	Glu	123	His_β		H_2O		26
Thermolysin Family									
Bacillus thermoproteolyticus	His_α	3	His_α	19	Glu_α(C)		H_2O		27
Pseudomonas aeruginosa	His_α	3	His_α	19	Glu_α		H_2O		28
Staphylococcas aureus	His_α	3	His_α	19	Glu_α		H_2O		29
Human leucotriene A_4 hydrolase	His_α	3	His_α	18	Glu_α(C)		H_2O		30
Human neutral endoprotease	His_α	3	His_α	58	Glu_α(C)		H_2O		31
Clostridium botulinum neurotoxin A	His_α	3	His_α	34	Glu_L(C)		H_2O		32,33
Streptomyces albus G DD-CPD	His_α	6	His_α	35	His_β(C)		H_2O		34
D-Ala-D-Ala carboxy-peptidase (VanX)	His_α	6	His_α	60	His_β(C)		H_2O		35
Astacin Superfamily Serratia Family	His_α	3	His_α	5	His		H_2O	Tyr	36,37
Pseudomonas aeruginosa alkaline protease	His_α	3	His_α	5	His(C)		H_2O	Tyr	38,39
Serratia marcescens Metalloprotease	His_α	3	His_α	5	His		H_2O	Tyr	40
Snake Venom Protease Family									
Crotalus adamanteus (or adamalysin II)	His_α	3	His_α	5	His(C)		H_2O		41,42
Human TNF-α-converting enzyme (TACE)	His_α	3	His_α	5	His		H_2O		43
MMP Family									
Human fibroblast collagenase (MMP-1)	His_α	3	His_α	5	His(C)		H_2O		44
Human fibroblast collagenase (MMP-1)	His_α	3	His_α	5	His		H_2O		45,46
Human matrilysin (MMP-7)	His_α	3	His_α	5	His		H_2O		47
Human stromelysin-1 (MMP-3)	His_α	3	His_α	5	His		H_2O		48–50
Human stromelysin-1 (MMP-3)	His_α	3	His_α	5	His		H_2O		51,52

Table 1 continued

Enzymes	L1	k	L2	m	L3	n	L4	L5	References
Human progelatinase (MMP-2)	His_α	3	His_α	5	His(C)	200	Cys_β(N)		53
Human collagenase-3 (MMP-13)	His_α	3	His_α	5	His		H_2O		54,55
Murine adenosine	His	1	His_α	196	His_β(C)		H_2O		56,57
E. coli cytidine deaminase	Cys_α	2	$Cys_{b\alpha}$	26	$His_{\,b\alpha}$(N)		H_2O		58,59
E. coli peptide deformylase	His_α	3	His_α	41	Cys(N)		H_2O		60–62
E. coli colicin E7 DNAse	$His_{a\alpha}$	3	His_α	24	His_β(N)		H_2O		63
Human GTP cyclohydrolase I	Cys_β	2	$His_{2b\alpha}$	41	$Cys_{a\beta}$(C)		H_2O		64
Bacteriophage T7 lysozome	$Cys_{2b\beta}$	7	His_β	104	His_β (N)		H_2O		65
β-Lactamase Family									
Bacillus cereus	$His_{2\alpha\beta}$	1	His	60	His(C)		H_2O		66–69
Pseudomonas aeruginosa	$His_{2\alpha\beta}$	1	His	59	His(C)		H_2O		70
E. coli alkaline phosphatase	Asp_α	3	His_α	80	His(C)		H_2O		71,72
Bacillus cereus phospholipase C	Glu_α	3	His_α	13	His_α(N)		H_2O		73
Penicillum citrinum P1 nuclease	$Asp_{a\alpha}$	3	His_α	12	His(N)		H_2O		74
Hepatitis C virus proteinase	Cys	1	Cys	45	Cys_β(C)		H_2O		75,76
CA Family									
Homo Sapiens CA I	His_β	1	His_β	22	His_β(C)		H_2O		77
Homo Sapiens CA II	His_β	1	His_β	22	His_β(C)		H_2O		78
Bovine CA III	His_β	1	His_β	22	His_β(C)		H_2O		79
Murine CA IV	His_β	1	His_β	22	His_β(C)		H_2O		80
Rat 6-pyruvoyl-tetrahydropterin synthase	His_β	1	His_β	24	His_β(N)		H_2O		81,82
E. coli 5-amino-aevulinate dehydratase	$Cys_{a\beta}$	1	Cys	7	Cys(N)		H_2O	Glu_L	83
E. coli fuculose-1-phosphate aldolase	His_β	1	$His_{\alpha\beta}$	60	$His_{b\beta}$(C)		H_2O	Glu_L	84–86
E. coli fructose-1,6-bisphosphate aldolase	His_β	115	$His_{\alpha\beta}$	38	$His_{b\beta}$		H_2O		87,88

[a] The number of amino acids as a spacer between ligands L1 and L2 is k, that between L2 and L3 is m, and that between L3 and L4 is n. The symbols N and C indicate that L3 is located on the amino(N) or the carboxy (C) side of L2, respectively. The subscripts α, β, refer to the α- or 3_{10} helix and β-sheet structure which supplies the ligand. The letter subscript L is an amino-acid sequence of <5 residues between two structural elements. The subscripts a and b indicate the ligand is either one (or two, 2) residues after or before the secondary structural element.

8.23.3.1 Carboxypeptidase Family

The carboxypeptidase family of exopeptidases and the thermolysin family of endopeptidases are the most studied examples of carboxylate-assisted Zn^{2+}-bound water catalysis.[4,8,11,90,91] The Zn^{2+}-containing bovine pancreatic carboxypeptidase A and B (CPDA and B) were two of the earliest identified Zn^{2+} metalloenzymes. They catalyze the degradation of food proteins leading to amino acids such as Phe, Trp, Lys, and Arg, complementing the actions of chymotrypsin, pepsin, and trypsin. X-ray crystal structures of CPDA-inhibitor complexes, spectroscopic studies of inhibitor and substrate binding of Co^{II}-substituted enzymes,[89,97] and XAFS studies of the effect of pH and inhibitor binding on the Zn^{2+} coordination sphere[98] have provided evidence for a mechanism involving Zn^{2+}–OH_2 and a general acid/base role for Glu270, assisted by the guanidinium of Arg127 for the anionic transition state. A Glu carboxylate similarly activates Zn^{2+}–OH_2 in thermolysin.[91]
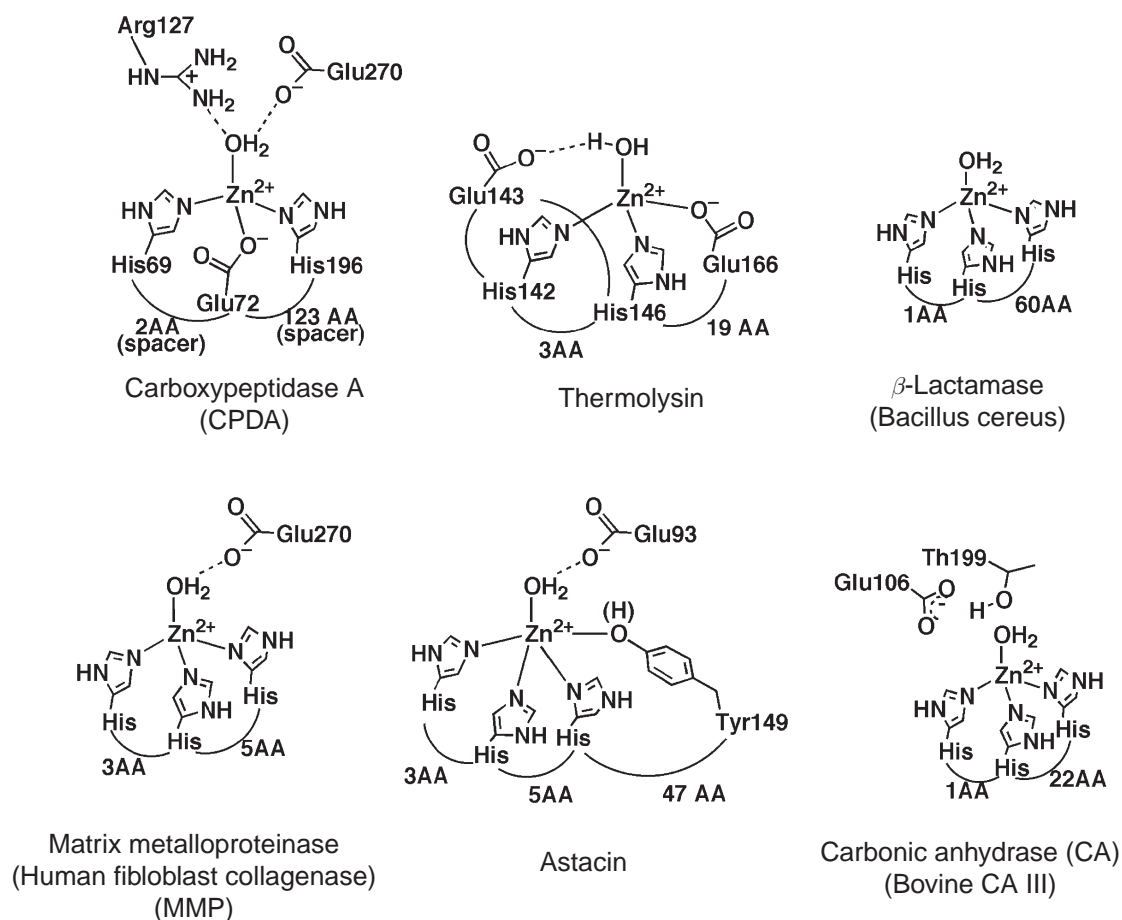
Scheme 1

Scheme 2 shows the proposed mechanism of CPDA.[11,90] The catalytic Zn^{2+} site of CPDA is comprised of His69, Glu72, His196, and a water molecule. The first two ligands are separated by a short spacer of two residues in a seven-amino-acid loop region between a β-sheet and/or α-helix, while His196 is the last residue in a β-pleated sheet extending from amino acids 191 and 196. This site is highly conserved throughout the extended CPD family. In the precatalytic Michaelis complex with the substrate, the carbonyl oxygen is hydrogen-bonded to Arg127 to assist nucleophilic attack by the Zn^{2+}-bound H_2O (or OH^-) activated by Glu270 (Scheme 2a). The anionic tetrahedral transition state is stabilized by chelation to Zn^{2+} and interaction with Arg127, and protonated by Glu270 (Scheme 2b) to give the CPDA-product complex (Scheme 2c). The interactions of the substrate with Arg145, Arg127, and the carbonyl oxygen of Ser197 were confirmed by X-ray crystal structure analysis.[99,100] A modified mechanism has been proposed, which includes interactions of the nitrogen of the scissile peptide bond with Glu270 and Tyr248, as shown in Scheme 2d and 2e.[91]

8.23.3.2 Thermolysin Family

The structure of the active site of thermolysins is similar to that of carboxypeptidases, although the amino-acid spacers and the overall tertiary structures of these two enzymes are different.[91] The Zn^{2+} ion in thermolysin from *Bacillus thermoproteolyticus* is coordinated by His142, His146, Glu166, and a water molecule in a tetrahedral geometry (Scheme 3). The position of Glu143 is almost superimposable on Glu270 of CPDA (Scheme 2), suggesting that Glu143 similarly functions as the general acid/base in catalysis and that the chemical and stereochemical combination

Scheme 2

of the Zn^{2+} ion and these two Glu CO_2^- (Glu143 of thermolysin and Glu270 of CPDA) is crucial to the hydrolytic activities (Schemes 3a–3c). His231 of thermolysin and Tyr248 of CPDA are considered to be proton donors.[91] However, the replacement of Tyr248 of CPDA had little effect on enzymatic activity, suggesting that Tyr248 is not always required for substrate hydrolysis.

Comparison of the ligands to Zn^{2+} in human leukotriene A_4 hydrolase[101,102] with those in thermolysin allowed its classification as a thermolysin type (Table 1). Although the hydrolase reaction involved is different (Scheme 4), nucleophilic attack at the substrate by Zn^{2+}–OH_2 is a common feature.

VanX is a carboxypeptidase that hydrolyzes the amide bond of a dipeptide, D-alanyl-D-alanine (D-Ala-D-Ala).[35,103] This enzyme is essential for vancomycin-resistant enterococci (VRE), because it produces peptidoglycan precursors terminating in D-alanyl-D-lactate (D-Ala-D-Lac) in place of D-Ala-D-Ala, resulting in a 100-fold decrease in the affinity with vancomycin.[104,105] Scheme 5 depicts a proposed mechanism of VanX, where the active-site structure is similar to those of CPDA and thermolysin. The Zn^{2+}-bound H_2O activated by Glu181 attacks

Scheme 3

Scheme 4

the carbonyl carbon polarized by zinc(II) (Scheme 5a) to give a tetrahedral intermediate, which is stabilized by Zn^{2+} and Arg71 (Scheme 5b). Glu181 gives the proton to the nitrogen that is hydrogen bonded to the carbonyl oxygen of Tyr109 (Scheme 5c) prior to the cleavage of the peptide bond (Scheme 5d).

Angiotensin-converting enzyme (ACE) is also a zinc(II) dipeptidase, responsible for the formation of an octapeptide angiotensin II (Asp–Arg–Val–Tyr–Ile–His–Pro–Phe) by hydrolyzing the dipeptide (His-Leu) at the C-terminus of a decapeptide, angiotensin I (Asp–Arg–Val–Tyr–Ile–His–Pro–Phe–His–Leu).[106,107] ACE is a key enzyme for the rennin–angiotensin blood-pressure-controlling system. Although the crystal structure of ACE has not as yet been determined, the DNA sequence of ACE is homologous to that of thermolysin.[107]
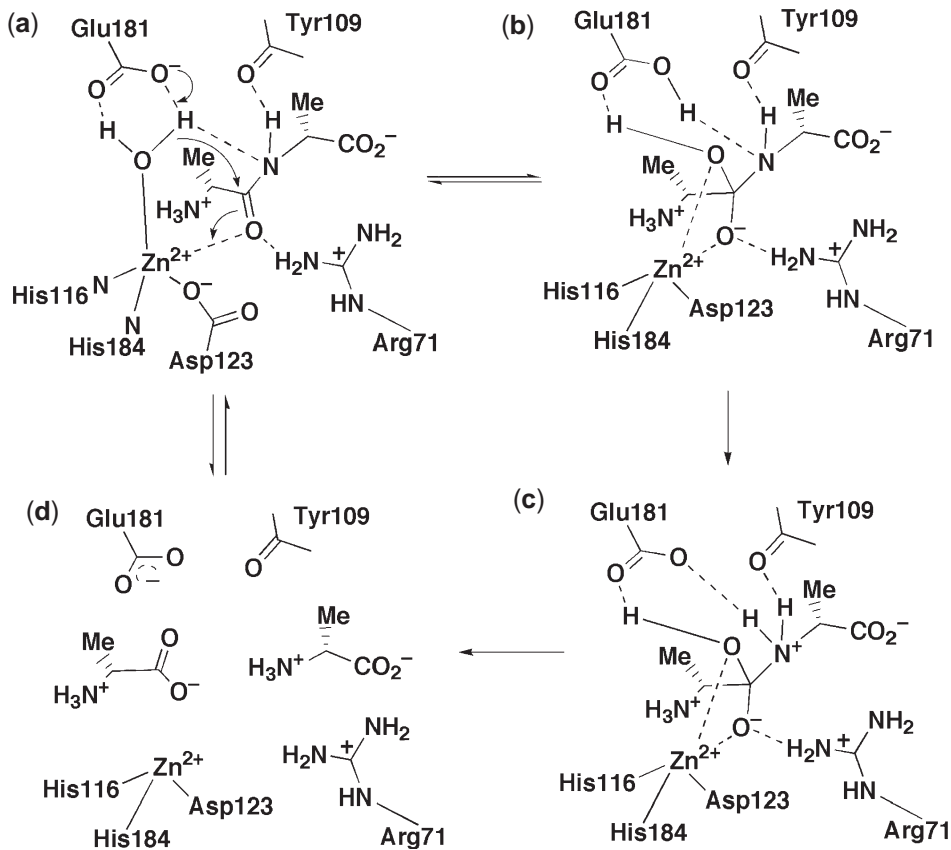
Scheme 5

8.23.3.3 Astacin Superfamily

This superfamily is named after Astacus protease, or astacin, which was identified as a Zn^{2+} protease in 1988.[108] The consensus Zn^{2+}-binding site amino-acid sequence within astacin is HExxHxxGxxH, which also was found in some metalloproteinases; these were divided into four subclasses, comprising 33 proteases, in this superfamily.[109] Representative structures of enzymes from the four common subfamilies were characterized, i.e., (i) serratia family; (ii) snakevenom protease family; (iii) MMP family; and (iv) β-lactamase family. The tumor necrosis factor α-converting enzyme (TACE) forms a member of the second subgroup.

In contrast to the structure of CPDA or thermolysin, the Zn^{2+} ion in serratia has the fifth ligand, Tyr149, as shown in Scheme 6. The Zn^{2+}–O(Tyr149) length is 2.75 Å in the solid state.[110–112] Since Tyr149 is located in a similar position to His231 of thermolysin (Scheme 3), it is considered that these two amino-acid residues have a similar function. Glu93 in astacin may work to shuttle protons between the Zn^{2+}-bound water and the nitrogen atom of the scissile peptide bond (Schemes 6b–6d) in analogy to Glu270 of CPDA and Glu143 of thermolysin.

8.23.3.3.1 MMP family

MMP are structurally similar to the serratia family but without Tyr at the Zn^{2+} active center. They mediate the breakdown of the extracellular matrix, which is associated with normal tissue remodeling processes during pregnancy, wound healing, and angiogenesis.[113–116] Therefore, MMPs are potential targets for therapeutic drugs against inflammatory, malignant, and degenerative diseases.[117]

A proposed mechanism for MMP catalysis is depicted in Scheme 7.[117,118] The Zn^{2+} ion is coordinated by three His(218, 222, and 228) and one water molecule. A Glu carboxylate
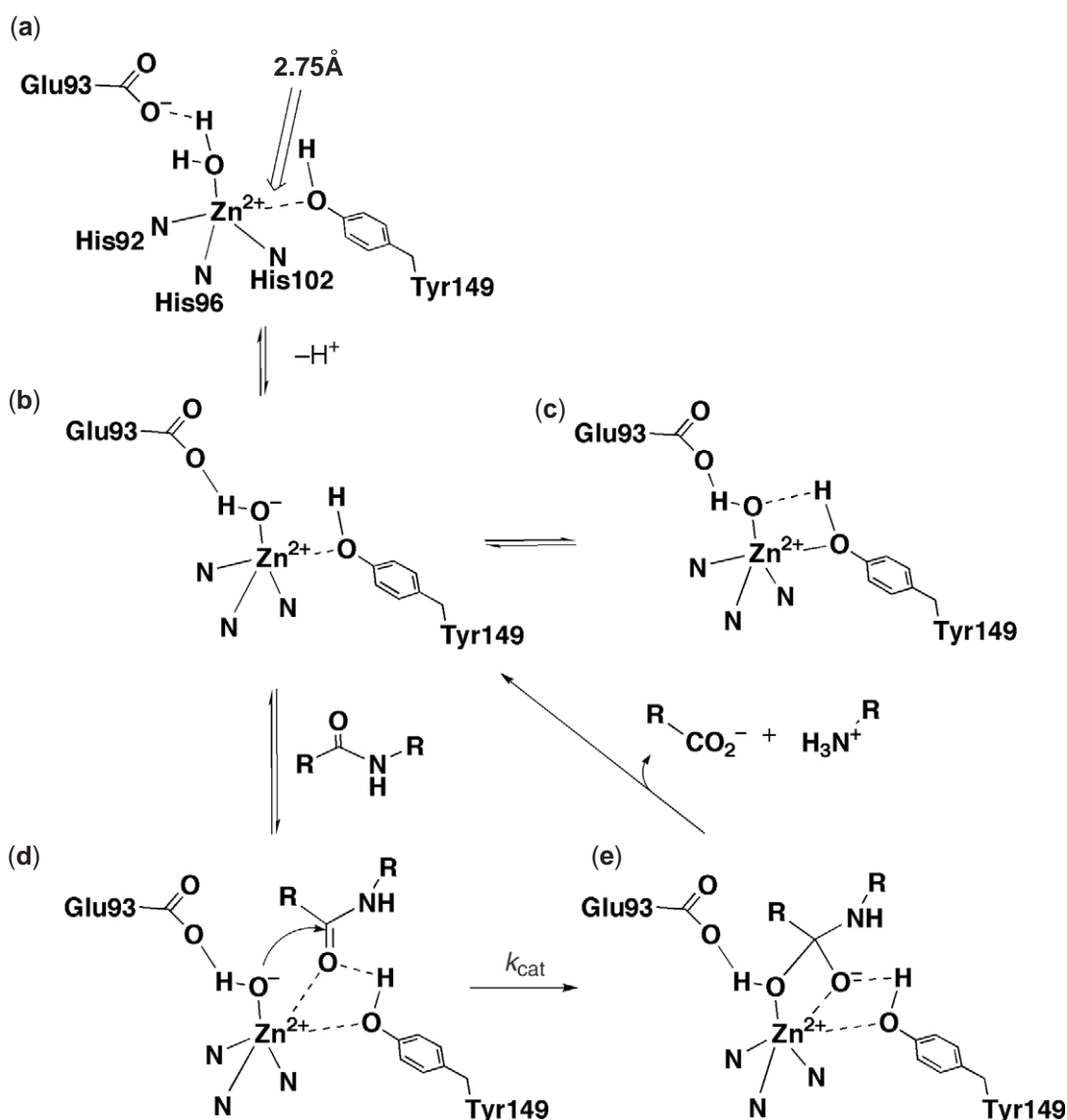
Scheme 6

(e.g., Glu219 in MMP-1 (fibroblast collagenase) or Glu198 in MMP-8 (neutrophil collagenase)) acts as a base to activate Zn^{2+}-bound water (Scheme 7a) like Glu270 in CPDA, Glu143 in thermolysin, and Glu93 in astacin. It is proposed that the scissile amide carbonyl oxygen coordinates to the Zn^{2+} ion. A proton transferred from Zn^{2+}-bound water to Glu219 is again shuttled onto the nitrogen atom of the scissile amide (Scheme 7b) that is then cleaved (Scheme 7c). A conserved Ala182 stabilizes positive charge at the nitrogen of the scissile amide.

  E. coli cytidine deaminase (CDA) is an enzyme that catalyzes hydrolytic deamination of cytidine to uridine (or from 2′-deoxycytidine to 2′-deoxyuridine) (Scheme 8).[119,120] This enzyme is considered to be a member of the MMP family, although the Zn^{2+}-binding site contains two Cys and one His residues. On the basis of the X-ray crystal structure of a transition-state analogue complex,[58,59] a mechanism was proposed as shown in Scheme 8, in which Glu104 serves multiple roles: the deprotonation of the Zn^{2+}-bound water and simultaneous protonation to N3 of the substrate (Scheme 8a), stabilization of the first tetrahedral transition state (Scheme 8b), and protonation of the leaving amino group at the 4-position of the substrate in the second tetra-hedral intermediate (Scheme 8c).[119,120] Upon elimination of NH_3, an E–P complex is formed (Scheme 8d) and the enzyme goes into the next turnover. The deamination mechanism of *E. coli*
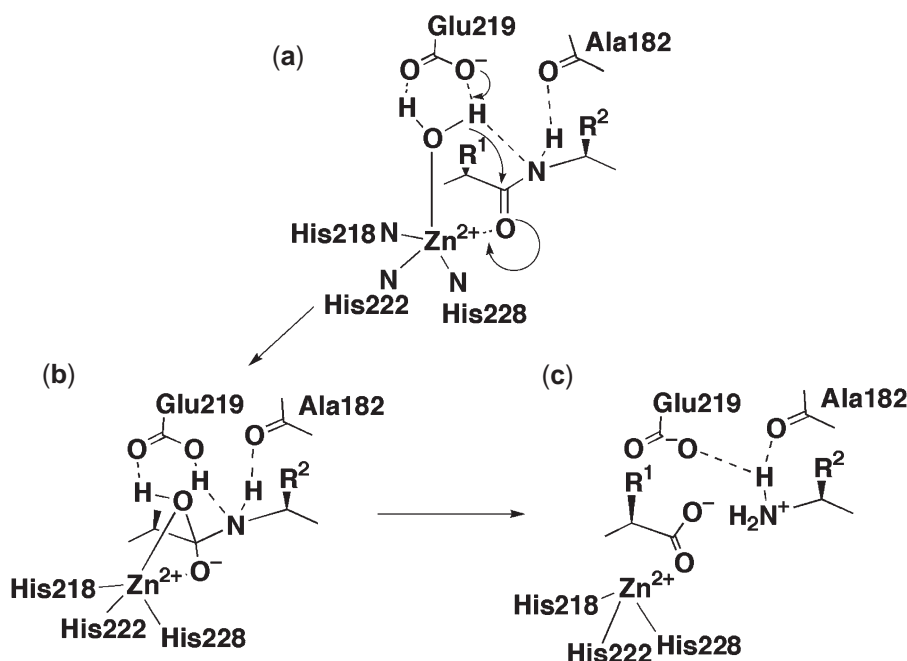
Scheme 7

adenosine deaminase (ADA) is considered to be similar.[10] However, the Zn^{2+}-binding site of ADA contains three His residues. The difference in Zn^{2+} ligands and tertiary structures of ADA and CDA led to the proposal that the common features in the transition-state stabilization arose from convergent evolution.[58]

8.23.3.3.2 β-Lactamase family

β-Lactamases are bacterial enzymes, some of which play a crucial role in the resistance of pathogens to β-lactam antibiotics. They are grouped into four classes (A, B, C, and D).[121–126] Classes A, C, and D are serine enzymes using serine as a nucleophile,[125] which are excluded in this text. Class B β-lactamases include mononuclear zinc(II)-β-lactamases[127–131] and dinuclear zinc(II)-β-lactamases.[131–134] A Zn^{2+}-containing β-lactamase II hydrolyzes the β-lactam ring of a variety of penicillins (e.g., benzylpenicillin) and cephalosporins. At pH 7 and 30 °C, the half-life of benzylpenicillin bound to β-lactamase II is ca. 0.5 ms. The first structure of the *B. cereus* enzyme showed one Zn^{2+} coordinated by His86, His88, and His149, and a water in a tetrahedral arrangement.[66,67] Scheme 9 represents a proposed mechanism for the monozinc(II)-β-lactamase reaction with benzylpenicillin.[130] Two pK_a values, pK_{a1} and pK_{a2}, of β-lactamase were found to be 5.6 and were assigned to a Zn^{2+}-bound water (Scheme 9a and 9b), and Asp90 carboxylic acid (Schemes 9c and 9d). The mechanism involves the binding of the substrate carbonyl to Zn^{2+} (Scheme 9c), nucleophilic attack of the Zn^{2+}-bound HO^- to the carbonyl carbon of the substrate (Scheme 9c), and subsequent stabilization of the oxyanion by Zn^{2+} (Schemes 9d and 9e).[124,125,130]

Alkaline phosphatase (AP) from *Escherichia coli* is a homodimeric, nonspecific phospho-monoesterase consisting of 449 amino acids, two Zn^{2+} ions, and one Mg^{2+} ion (Table 1).[135–142] One Zn^{2+} (Zn^{2+}(1) in Scheme 10) is coordinated by two His and one Asp and is proposed to provide the catalytically required Zn^{2+}–OH_2. The *E. coli* AP is a prototype for all alkaline phosphatases (especially the mammalian phosphatases) and is functionally related to the phosphoesterases, such as phospholipase C from *Bacillus* cereus[73] and P1 nuclease from *Penicillum citrinum*.[74] Scheme 10 shows a proposed mechanism for AP.[143] In Schemes 10a and 10b, the formation of an AP–$ROPO_3^{2-}$ complex involves coordination of a phosphate oxygen to Zn^{2+}(1) and additional interactions between the RO group of the substrate and Zn^{2+}(2), as well as hydrogen bonds to the guanidinium group of Arg166. The Zn^{2+}(2)–bound Ser102 occupies the
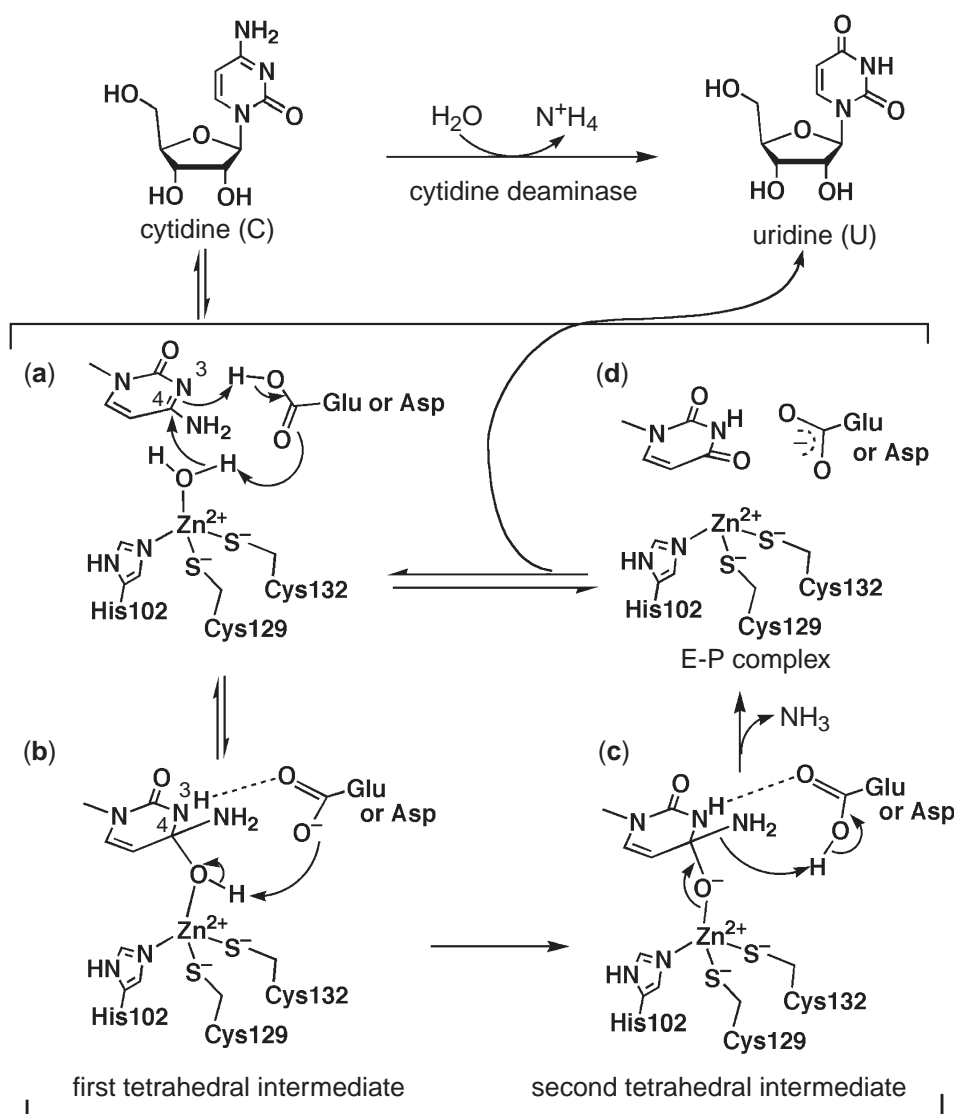
Scheme 8

position opposite to the leaving OR group (Schemes 10b and 10c). By nucleophilic attack of Ser102 on $ROPO_3^{2-}$, the P—OR bond is cleaved and the AP–PO_4^{2-} complex (E–P intermediate) is formed, in which PO_4^{2-} is stabilized by Arg166. At alkaline pH, the Zn^{2+}–bound water (or hydroxide) attacks the covalent E–P intermediate forming the noncovalent E·PO_4^{3-} (or E·HPO_4^{2-}) complex (Scheme 10c and 10d). Recently, a revised mechanism involving Mg^{2+} was proposed.[142]

8.23.3.4 CA Family

CA is the well-studied classic Zn^{2+} enzyme.[92–96] CA catalyzes the reversible formation of bicarbonate and a hydrogen ion from water and carbon dioxide. So far, seven human CA isozymes have been identified: CA I–VII, which are expressed in varying amounts in different tissues and cell locations. All the isozymes have at least 31% amino-acid homology and CA I–III share 58–60% amino-acid identity.
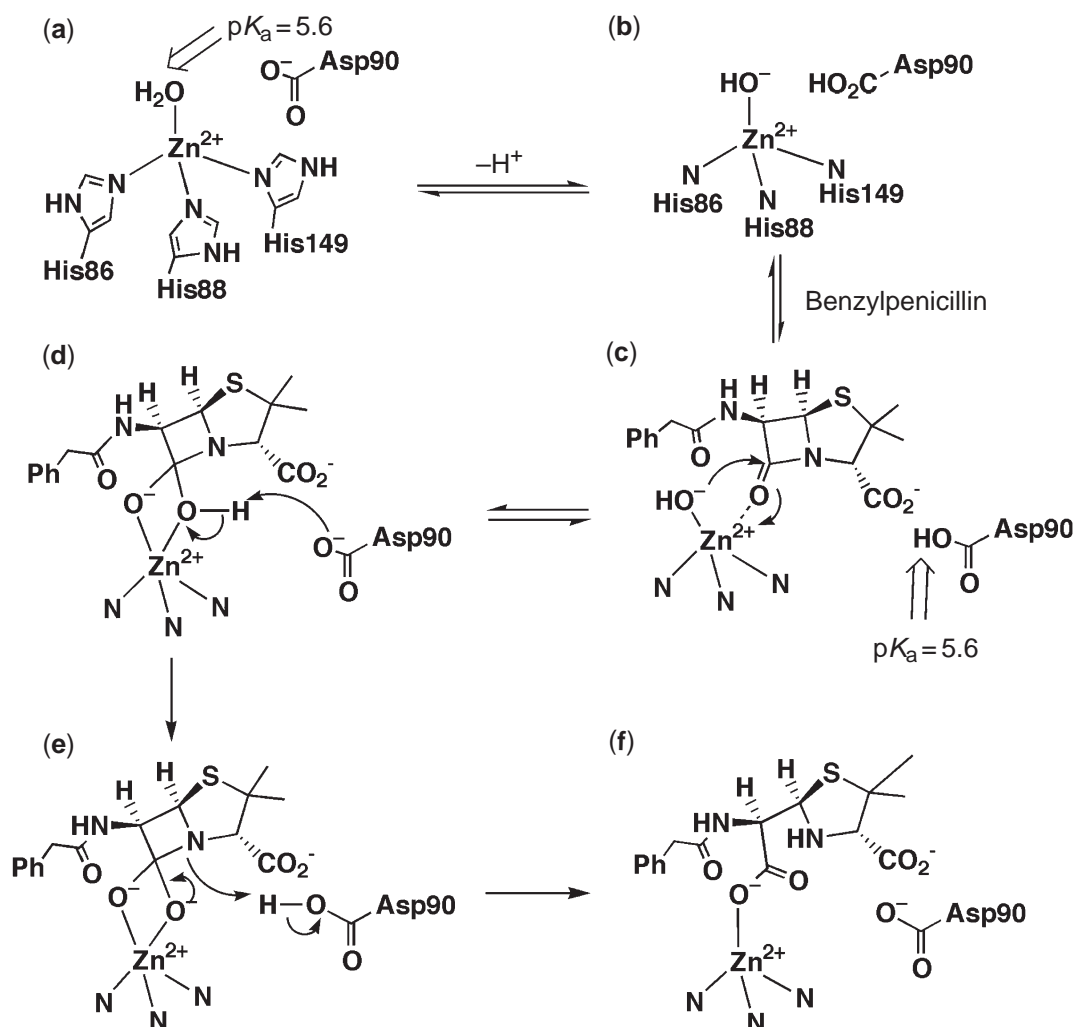
Scheme 9

In general, the catalytic unit, $Zn(His)_3$, is buried in a hydrophobic cavity. Three His moieties are hydrogen-bonded to the amide oxygen (side chain) of Gln92, the amide oxygen of the Asn244 backbone, and the Glu117 carboxylate, respectively (Scheme 11).[11,143] The deprotonation of a Zn^{2+}-bound H_2O (Scheme 11a) to a distinct Zn^{2+}-bound OH^- (Scheme 11b) occurs with a pK_a value of 6.9, which may be facilitated by the base-relaying of Glu106 and Thr199. The Zn^{2+}-bound OH^- attacks CO_2 (Scheme 11c) that is bound in a hydrophobic pocket constructed by Val143, Val121, Trp209, and Leu198, to yield HCO_3^- ion, stabilized by coordination to Zn^{2+} (Scheme 11d). Upon release of HCO_3^-, the Zn^{2+}-bound H_2O is regenerated.

Aldolases II are lyases that catalyze reversible aldol reactions and yet are classified in the CA family because of their common amino-acid ligands (Table 1). Aldolases consist of two types. The type-I aldolases, which primarily are found in animals and higher plants, activate donor substrates, typically dihydroxyacetone phosphate (DHAP), via formation of a Schiff base with a lysine side chain as an intermediate (Schemes 12a and 12b). The type-II aldolases, which occur in yeasts and *Escherichia coli*, utilize the zinc(II) ion[144–146] to polarize the carbonyl group (Schemes 12c and 12e). The X-ray crystal structure of the type-II fuculose-1-phosphate (Fuc–1-P) aldolase revealed that the zinc(II) ion is coordinated by three imidazole groups of His(92, 94, 155) and one carboxylate of Glu73. On the basis of the X-ray crystal structure of Fuc–1-P aldolase complexed with phosphoglycolohydroxamate (PGH), which is a substrate analogue and an efficient inhibitor, a role of the zinc(II) ion was proposed in which it stabilizes the enediolate–DHAP intermediate. All the observations have also suggested a role for zinc(II) in polarizing the
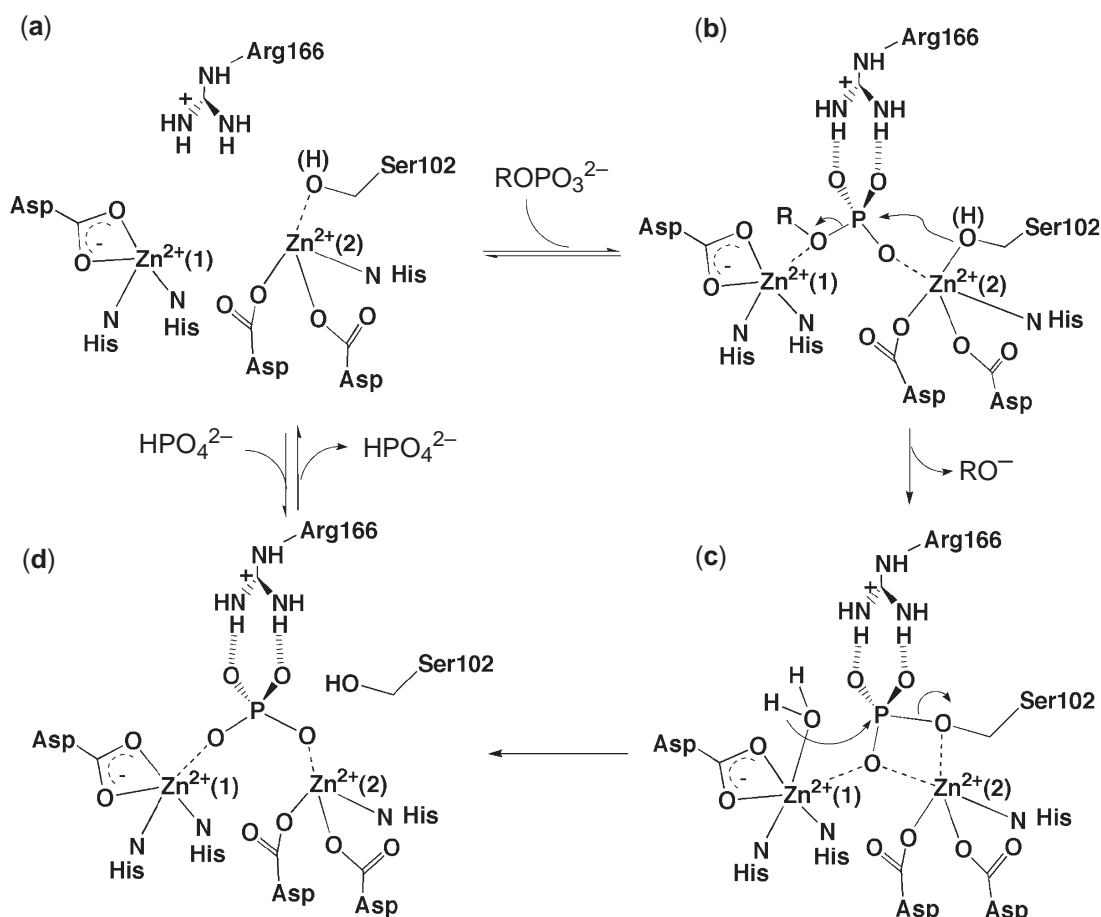
Scheme 10

carbonyl bond to increase the acidity of the α-methylene protons, so as to be readily abstracted by the carboxylate of Glu73 (Scheme 12c).

8.23.3.5 Other Zinc(II) Hydrolases

8.23.3.5.1 Histone deacetylase (HDAC)

Histone deacetylase (HDAC) is an enzyme that hydrolyzes acetylated lysines in histone proteins to change the conformation of the nucleosome (a complex of histone protein with nucleus DNA) and hence regulates gene expression.[147–150] The X-ray crystal structure of a HDAC homologue complexed with a specific inhibitor revealed that a Zn^{2+} ion in the active site is coordinated by Asp168, His170, Asp258, and a water molecule in a tetrahedral geometry. With the presence of an Asp–His charge-relay system, a mechanism is proposed for the deacetylation reaction as shown in Scheme 13.[151]

8.23.3.5.2 Anthrax lethal factor

The lethal factor (LF) of anthrax, which is responsible for the pathogenesis of anthrax, was found to possess highly specific protease acitivities against mitogen-activated protein kinase kinases (MAPKKs) family, leading to inhibition of one or more signaling pathways.[152,153] The X-ray crystal-structure analysis revealed that the anthrax LF comprises four domains: domain I
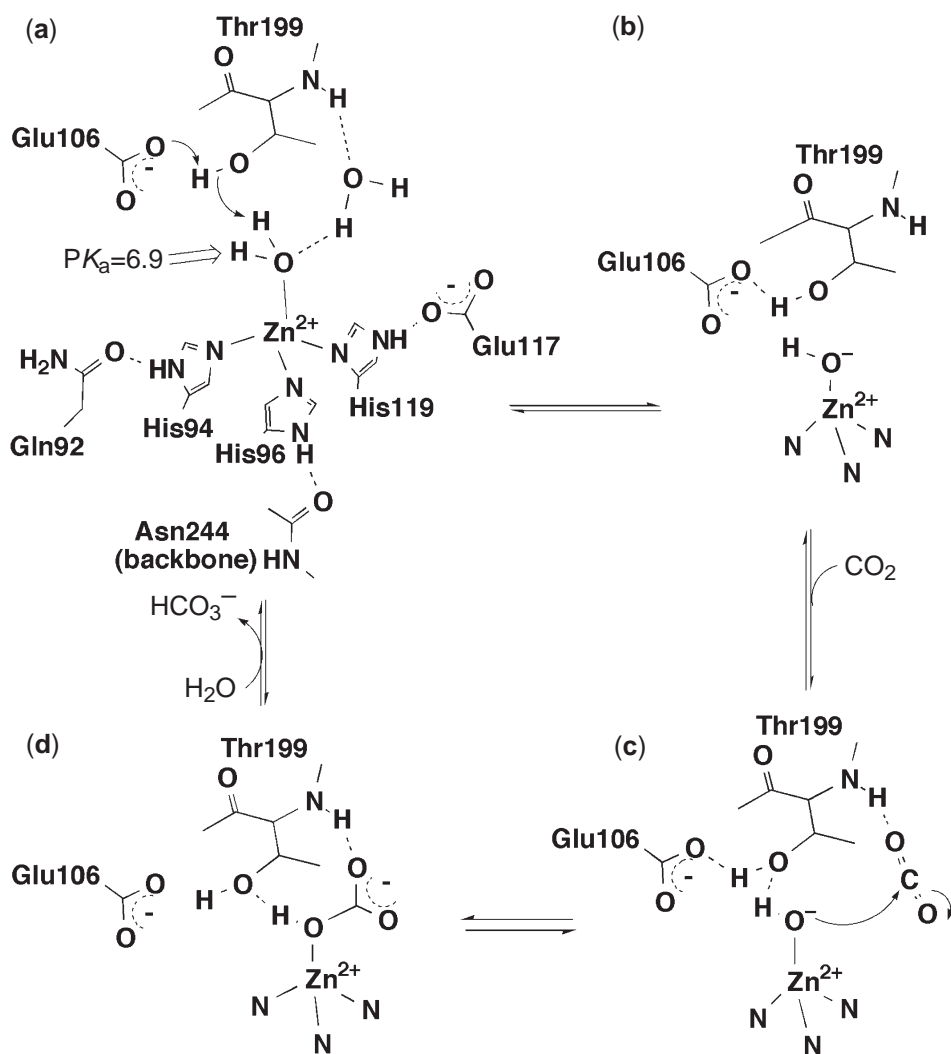
Scheme 11

binds the membrane-translocating component of anthrax toxin; domains II, III, and IV make a deep groove that captures the substrate, the *N*-terminal sequence of MAPKK-2.[154] Among these four domains, the domain IV possesses Zn^{2+} metalloproteinase activity. The Zn^{2+} ion is coordinated by His686, His 690, Glu735, and a water molecule, and resembles the active Zn^{2+} site of carboxypeptidases (Scheme 14). Glu687 from the HExxH motif is located 3.5 Å from the Zn^{2+}-bound water, implying that it functions as a general base to activate the Zn^{2+}-bound water. The hydroxy group of Tyr728 hydrogen bonds to the Zn^{2+}-bound water from the opposite side of Glu687. Tyr728 possibly acts as a general acid to activate the amino group of the substrate.

Moreover, the crystal structure of the complex of the anthrax LF with an intact natural substrate (Met–Leu–Ala–Arg–Arg–Lys–Pro–Val–Leu–Pro–Ala–Leu–Thr–Ile–Asn–Pro) was solved (Scheme 14), where the main-chain peptide bond between Ala11 and Leu12 is to be cleaved. The amino-acid residue nearest to the Zn^{2+} ion was Pro10, about 6 Å away from the Zn^{2+}-bound water, a fact suggesting that this structure represents a "precleavage" complex.

8.23.4 DEVELOPMENT OF Zn^{2+} HYDROLASE INHIBITORS

Specific inhibitors for Zn^{2+} hydrolases have been very actively developed, mostly on the basis of the acquired information on the structures of the active centers. They are extremely helpful in
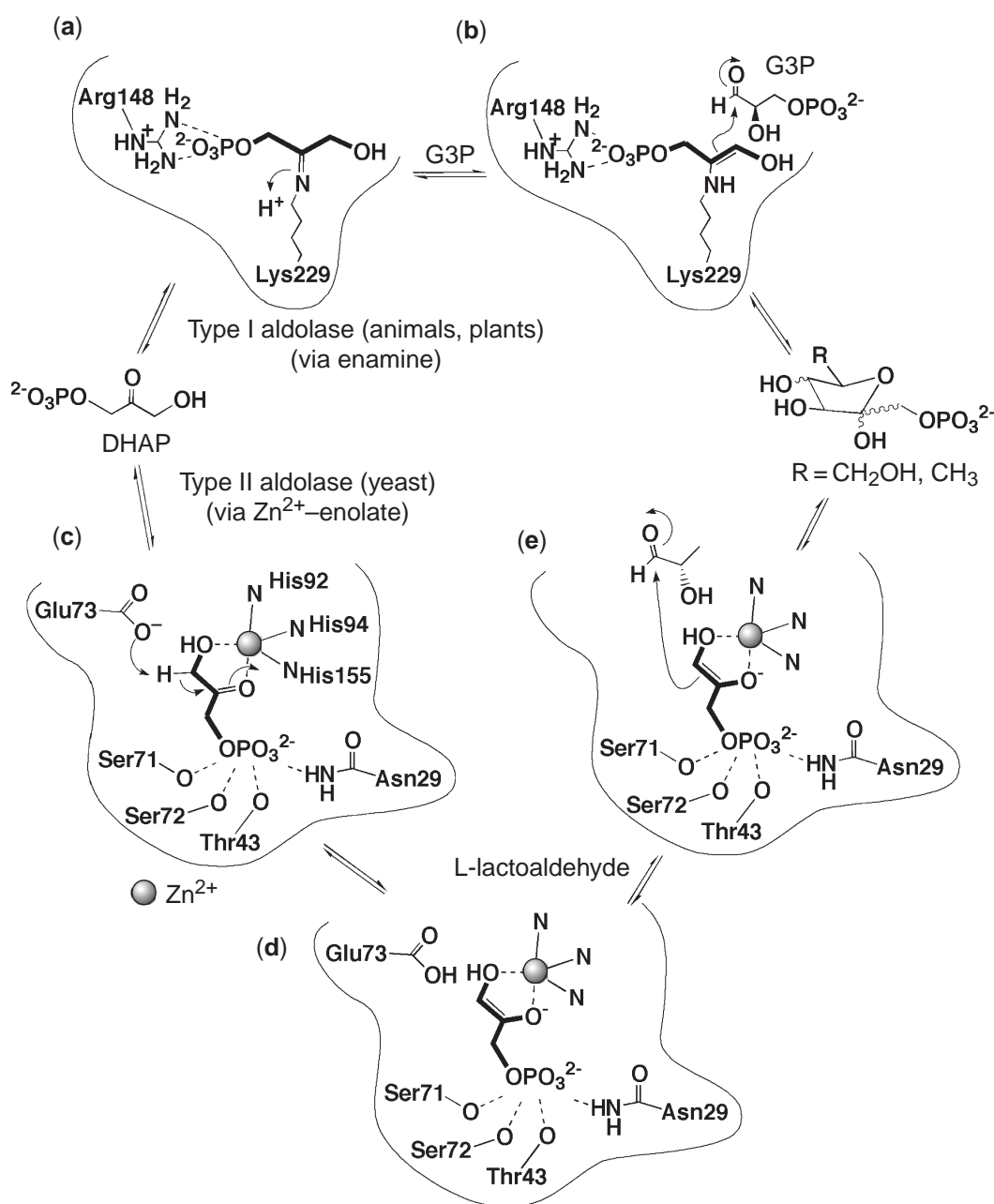
Scheme 12

understanding more detailed mechanisms and, moreover, they may be good drugs against diseases involving Zn^{2+} enzymes.[155–159]

8.23.4.1 Carboxypeptidase Inhibitors

The commercially most successful zinc(II) carboxylase inhibitors include captopril (**1**), enalapril (**2a**), enalaprilat (**2b**) (the diacid metabolite of **2a**), and trandolapril (**3**).[155–158,160–162] For structures of these drugs, see Scheme 15. They all act against the ACE that converts angiotensin I to angiotensin II. These compounds have been used for years as successful orally active drugs to reduce high blood pressure by decreasing the ACE activities that play a major role in the
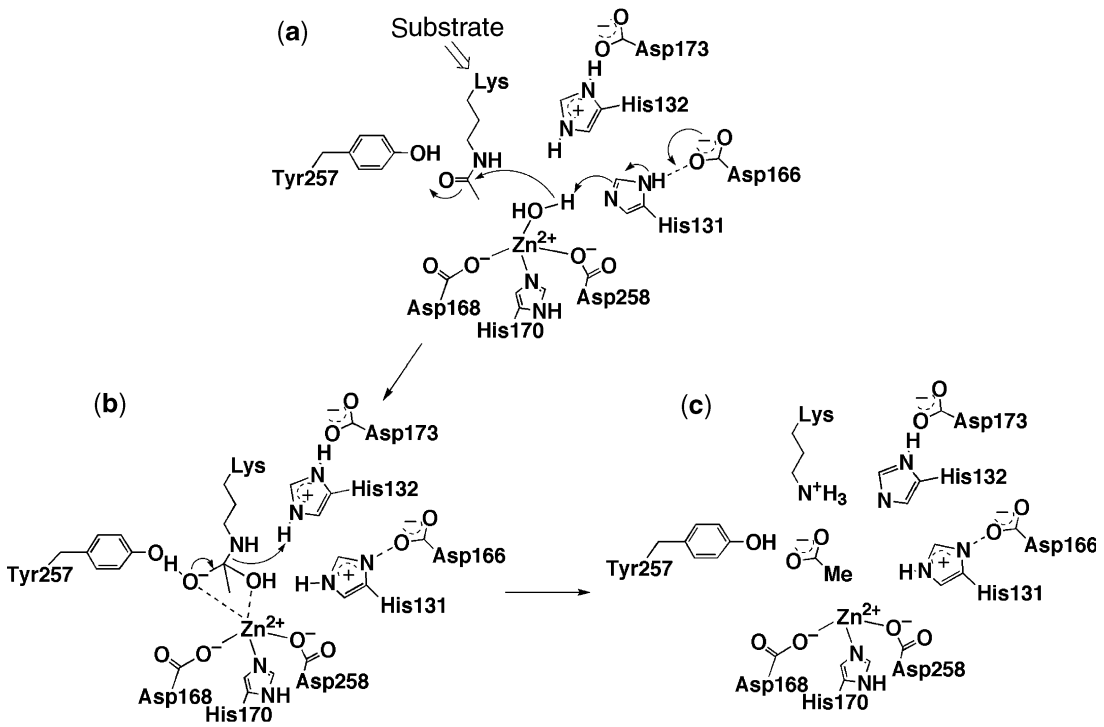
Scheme 13
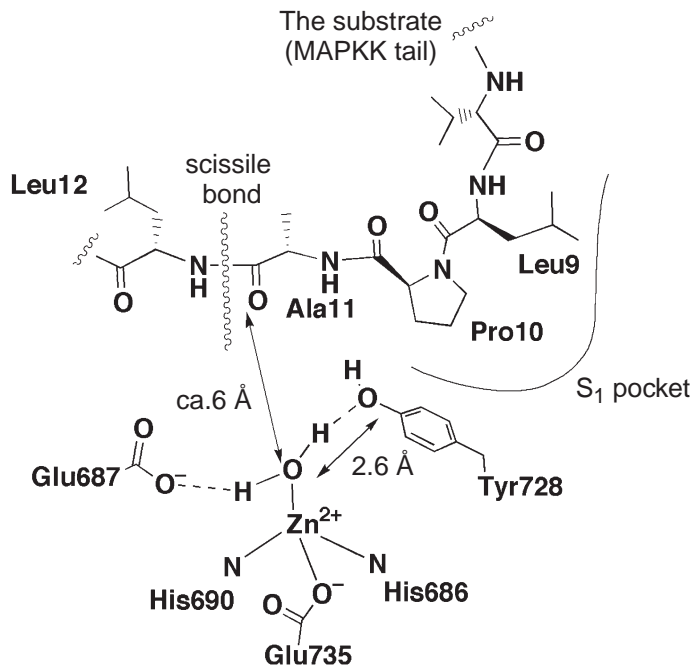
Scheme 14

renin–angiotensin blood regulating system (the half-inhibitory concentrations (IC$_{50}$) are marked in Scheme 16). It is remarkable that these drugs were developed without detailed structural knowledge about ACE, and the discovery of the original ACE inhibitor captopril (**1**) by Ondetti *et al.* is a legendary story.[160–162] The interaction of the substrate (angiotensin I) and the
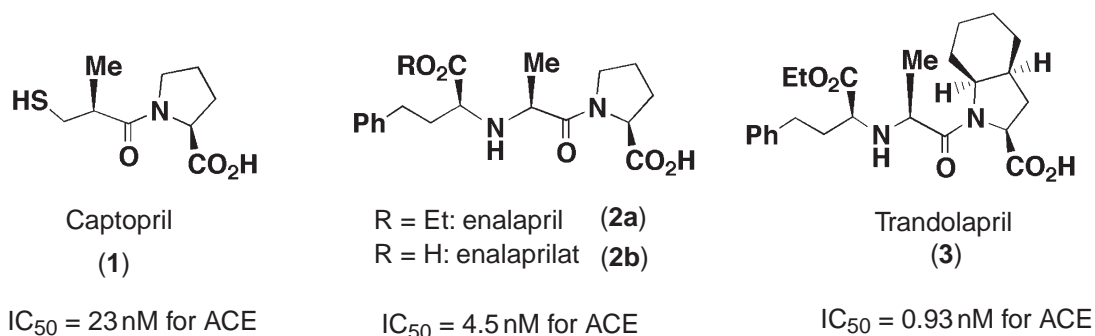
Scheme 15
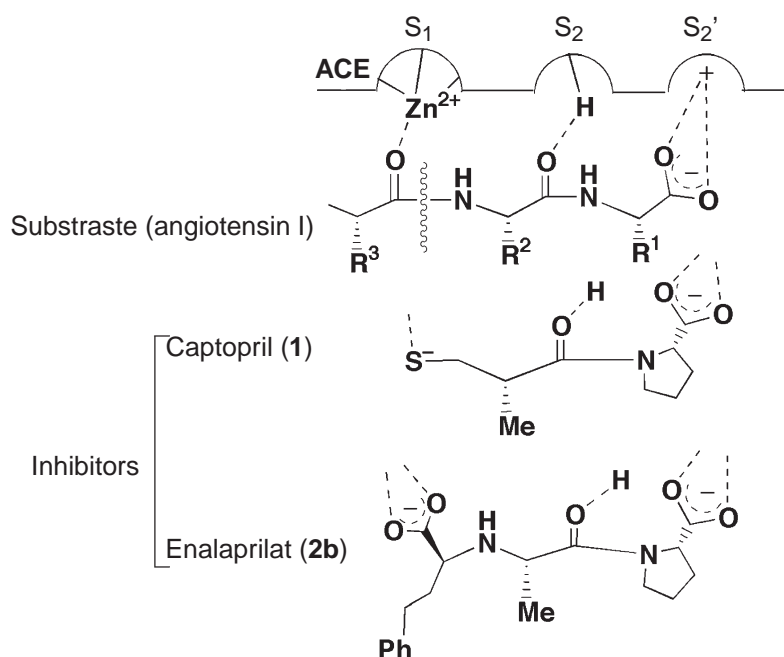
Scheme 16

inhibitors with the active site of ACE was hypothesized to be as shown in Scheme 16. The original design of captopril (**1**) was inspired by Byer's independent report of D-benzylsuccinic acid (**4**) being a selective inhibitor of CPDA,[163] where a carboxylate binds to Zn^{2+} and a benzyl side chain fits to the hydrophobic pocket of CPD (Scheme 17).[157,158]

Since the discovery of D-benzylsuccinic acid (**4**), all the inhibitors for CPDA comprise the 2-phenylpropanoic acid platform (**5**) (Scheme 17).[164–173] Bartlett *et al.* have synthesized a tripeptide analogue (**5a**) as a potent CPDA inhibitor having K_i of 1 pM.[164,165] Kim's group developed novel irreversible inhibitors such as 2-benzyl-3,4-epoxybutanoic acid (**5c**).[166–170] An X-ray crystal structure of (**5c**)-treated CPDA showed a covalent bond modification of the essential Glu270, which arose from the activation of the epoxide moiety by coordination to Zn^{2+} of CPDA (Scheme 18a).[164] Mobashery's group synthesized 2-benzyl-3-iodopropanoic acid (**5d**) that inactivates CPDA irreversibly.[171] The iodo moiety of (**5d**) could be activated by coordination to a Zn^{2+} ion (Scheme 18b). A crystal structure of the (**5d**)-treated CPDA showed that Glu270 is alkylated by one enantiomer (corresponding to D-Phe) of (**5d**).[172] The hydroxam derivative (**5e**) was also reported.[173]

CPD

Substrate

Inhibitors
(D-benzylsuccinic acid (**4**))

(**5a**) $K_i = 1\,pM$

(**5b**) (racemic) $K_i = 11\,nM$

(**5c**)   ((2*S*, 3*R*) form)$K_i = 0.19\,mM$
((2*R*,3*S*) form)$K_i = 0.34\,mM$
(irreversible inhibitor)

(**5d**) (racemic) $K_i = 2.0\,mM$
(irreverisible inhibitor)

(**5e**)   ((*R*)-form) $K_i = 0.6\,\mu M$
((*S*)-form) $K_i = 5.0\,\mu M$
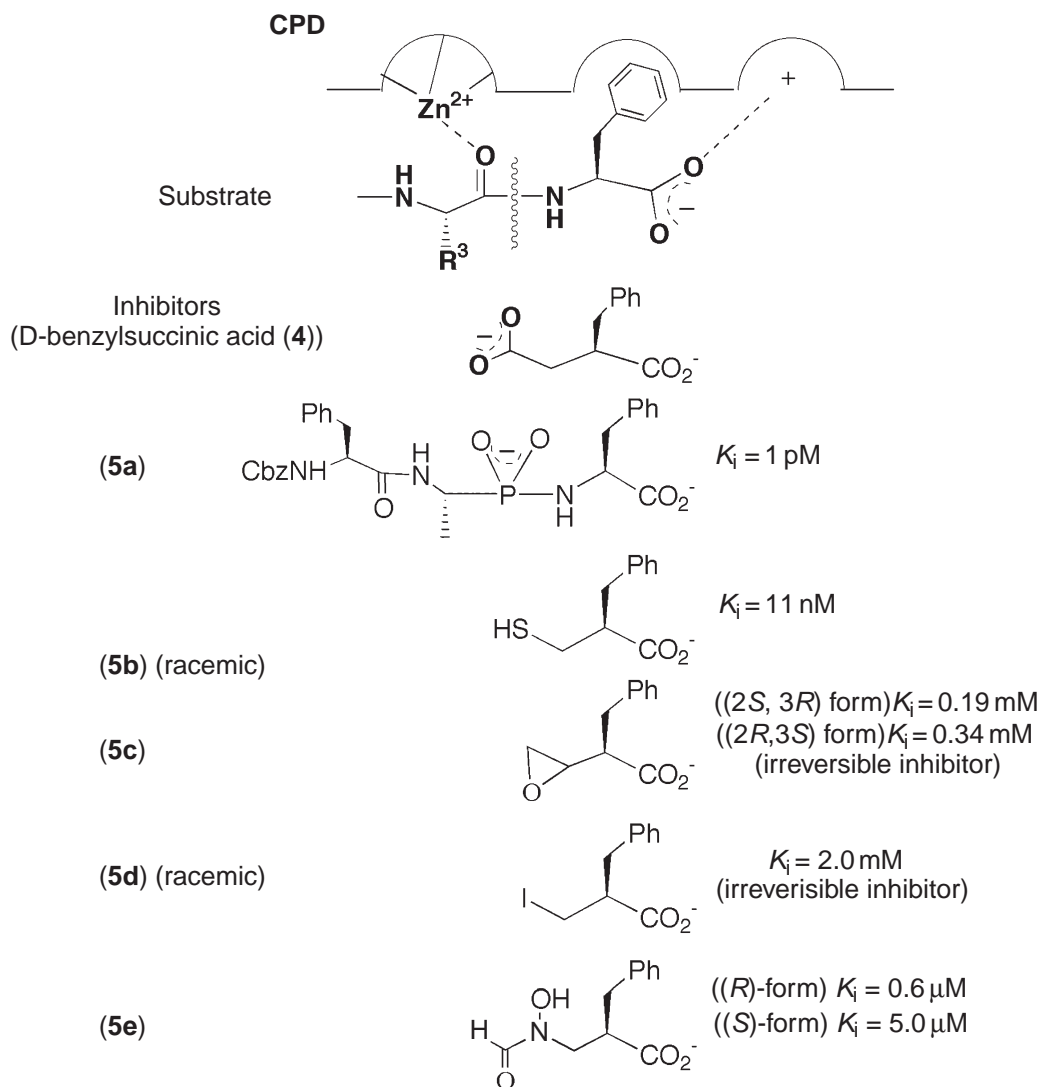
Scheme 17

8.23.4.2 Thermolysin Inhibitors

The structure of thermolysin has also been extensively studied and its inhibitors were reviewed by Matthews.[91] The tripeptide analogues, Cbz–Phe[P]–L–Leu–L–Ala (**6**) ($K_i = 68\,pM$)[174] and Cbz–Gly[P]–L–Leu–L–Leu (**7**) ($K_i = 9.1\,nM$)[175] (Phe[P] and Gly[P] depict the phosphonic acid analogues of Phe and Gly, respectively) are potent inhibitors for thermolysin. Recent advances in computer chemistry, with structural information of enzymes from X-ray crystal-structure analysis and NMR experiments, made possible the "structure-based" design of enzyme inhibitors. For instance, macrocyclic thermolysin inhibitors such as (**8**) were rationally designed. Among all the possible diastereomers synthesized, (*S*,*S*)-(**8**) was the most potent ($K_i = 4\,nM$) against thermolysin (Scheme 19).[176,177]

For investigation of the enzymatic mechanism of VanX and for the design of the anti-VRE drugs, potential inhibitors have been developed. The basic idea for the design of VanX inhibitors (as well as other hydrolase inhibitors) was to mimic a tetrahedral reaction transition state (**10**), which would bind to the active site to block the access of the native substrate (Scheme 20). A phosphinate compound (**11**) was designed as a transition state analogue of (**10**). Note that the K_i value was time-dependent; the K_i value was $1.5\,\mu M$ immediately and $0.47\,\mu M$ subsequently after addition of VanX solution, indicating slow binding of (**11**) to VanX.[178]

Scheme 18

$((S,S)\text{-}\mathbf{8})$
$K_i = 4\,\text{nM}$
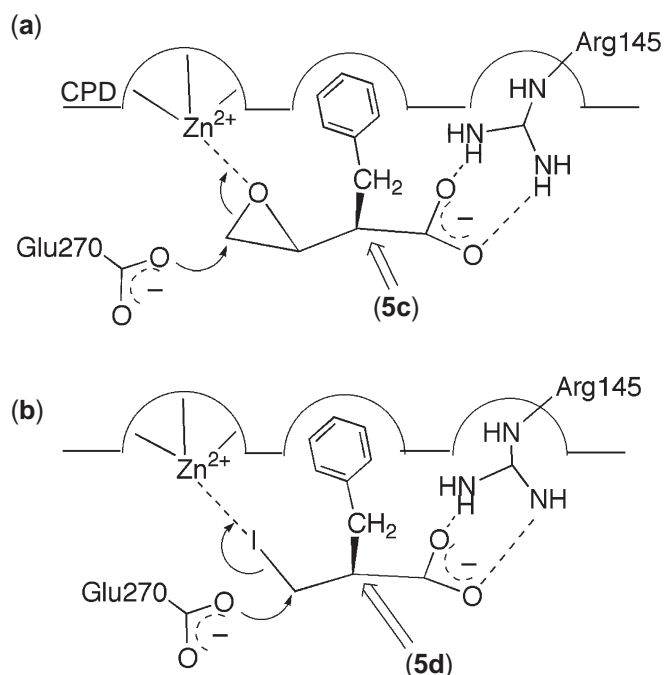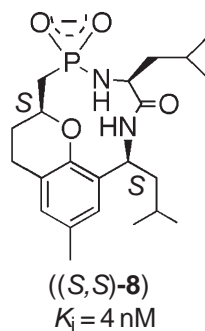
Scheme 19

8.23.4.3 MMP Inhibitors

MMP inhibitors are promising clinical agents which may halt or slow the progression of diseases such as osteoarthritis, tumor metastatsis, corneal ulceration, cancer, or inflammation.[117,157–159,179] Although most of the MMP inhibitors obtained from natural sources contain a peptide backbone, structural information on MMP has made *de novo* design of nonpeptide inhibitors possible.[117,157,159] The huge number of MMP inhibitors can be classified into two categories (Scheme 21).[159] Class I inhibitors (**14**) include succinamide carboxylates and hydroxamates having two sp^3 carbons between a Zn^{2+}-binding function (ZBF) and the first peptide bond (**11**). The compounds in class I are designed by replacing the peptide bond with a ZBF–CH_2 group, such that the ZBF is geometrically positioned to coordinate to Zn^{2+} by analogy to the oxygens of the primary tetrahedral intermediate (**12**). A typical example is marimastat (**14a**) (ZBF = (C=O)NHOH). Class II inhibitors (**15**) contain three sp^3-hybridized atoms, such as carboxyalkyl α-amino amides (X = NH) and glutaramide carboxylates (X = CH_2), between the ZBF and the first peptide bond, as exemplified by (**15a**). The compounds in this class mimic the interactions of the secondary tetrahedral intermediate (**13**).
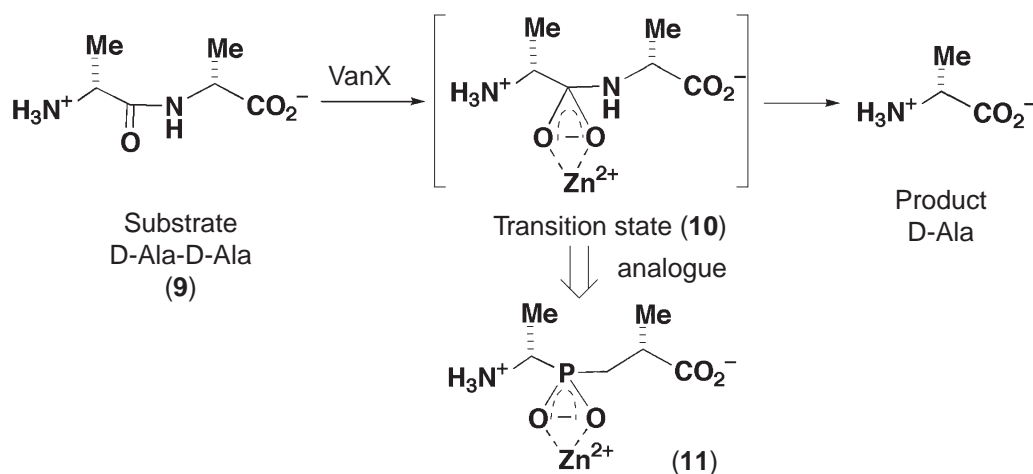
Scheme 20

8.23.4.4 Metallo β-Lactamase Inhibitors

For inhibitors of monomeric zinc(II) β-lactamases, there are few examples such as N-(2′-mercapto-ethyl)-2-phenylacetamide (16) with K_i being ca. 0.1 mM against the monomeric zinc(II) β-lacta-mase from *Bacteroides cereus*.[130] For dimeric zinc(II) β-lactamases, 4-morpholinoethane sulfonic acid (MES) (17), which is one of Good's buffer compounds,[180] was found to be an inhibitor against *B. fragilis* ($K_i = 23$ mM).[181] Various biphenyl tetrazole derivatives such as (18) are inhibitors having K_i of micromolar order against *B. fragilis* (Scheme 22).[182]

8.23.4.5 CA Inhibitors

Strong inhibitors of CA are mostly aromatic sulfonamides.[183–187] Acetazolamide (19), with K_i of 6 nM against human carbonic anhydrase II (HCA II), is therapeutically prescribed as a diuretic drug.[92–95,184] The X-ray crystal-structure analysis of the HCA II–acetazolamide complex con-firmed that the N-deprotonated amide binds to Zn^{2+} in the active site (20) (Scheme 23).[187] Trifluoroacetohydroxamic acid, an inhibitor for HCA II, was found to coordinate to Zn^{2+} via N-deprotonated hydroxamate and fluoride ((21) in Scheme 23).[188]

Whitesides *et al.* have screened libraries of aromatic sulfonamides (22) attached to various amino-acid AA_1 and AA_2 side chains using electrospray ionization-mass (ESI-MS) spectrometry (Scheme 24).[189] Among two libraries containing 289 compounds from L-amino acids and 256 compounds from D-amino acids, the tightest binding inhibitor (23) ($AA_1 = AA_2 = $ L-Leu) was discovered.

Combinatorial chemistry for drug discovery is now extensively used.[190–193] Huc *et al.* have developed combinatorial chemistry based on dynamic equilibration, in which a set of four amines and three aldehydes (attached to aromatic carboxylates, sulfonates, or sulfonamides) are mixed to yield 12 imines reversibly and these reaction mixtures were reduced.[193] When this reaction was carried out in the presence of CA, the chemical yield derived from an aromatic sulfonamide derivative was almost doubled, implying that CA worked as a template to choose the best ligand.

8.23.4.6 HDAC Inhibitors

Butylic acid (24),[194] trichostatin A (25),[194] tripoxin B (27a),[196–198] and depudecin (28)[199] were discovered to be selective inhibitors for HDACS (Scheme 25). The mechanism of HDAC has been speculated as shown in Scheme 13 by using inhibitors (25) and suberoylanilide hydroxamic acid (26).[151] The hydroxamic acid groups of (25) and (26) were found to chelate the Zn^{2+} ion in the active site as a bidentate ligand. The epoxide moiety in the side chain of (27a) was considered to react with amino acids in the active site of HDAC. CHAP1 (27b) containing a hydroxamic acid
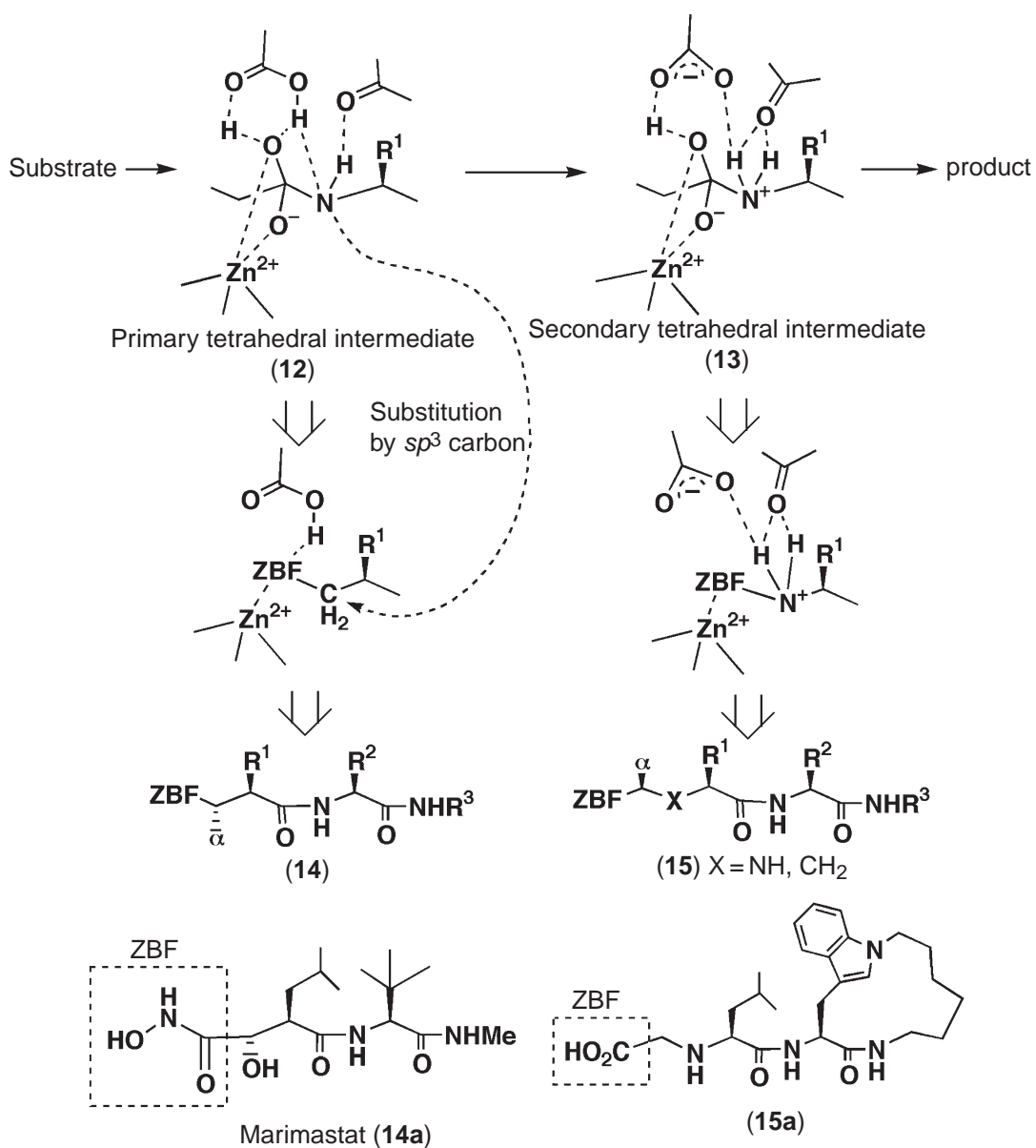
Scheme 21
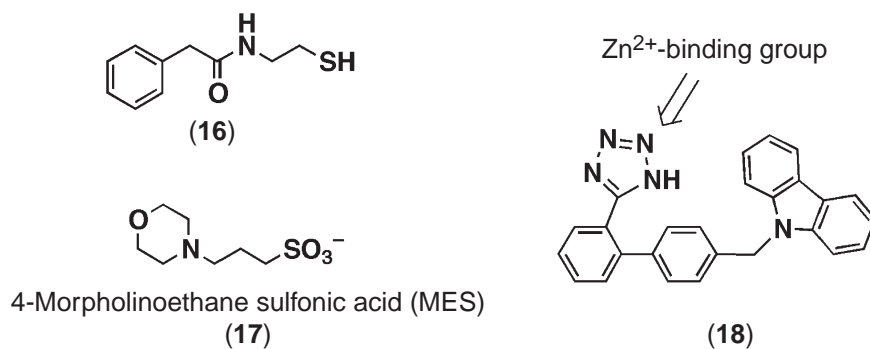
Scheme 22
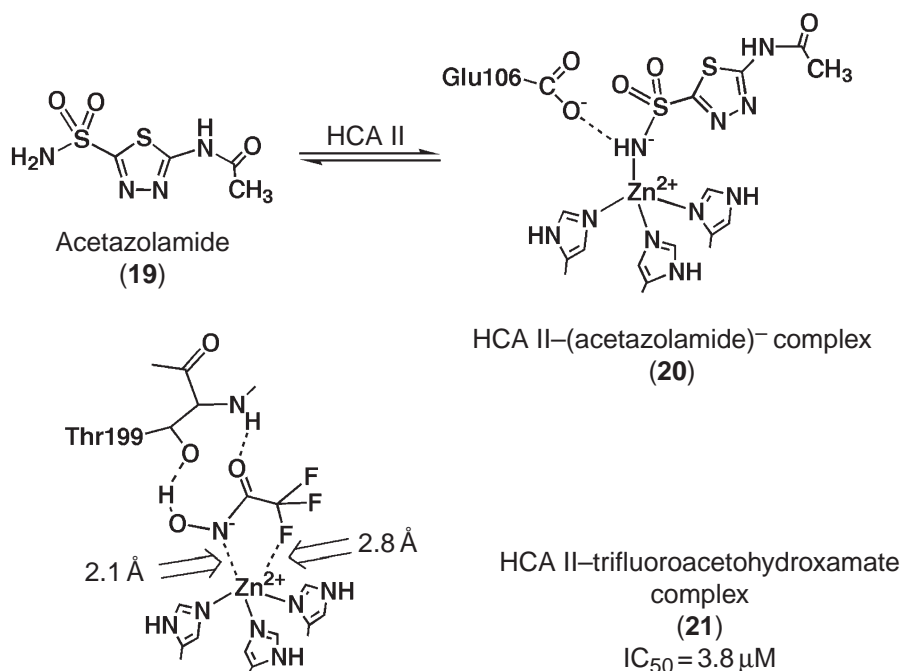
Scheme 23
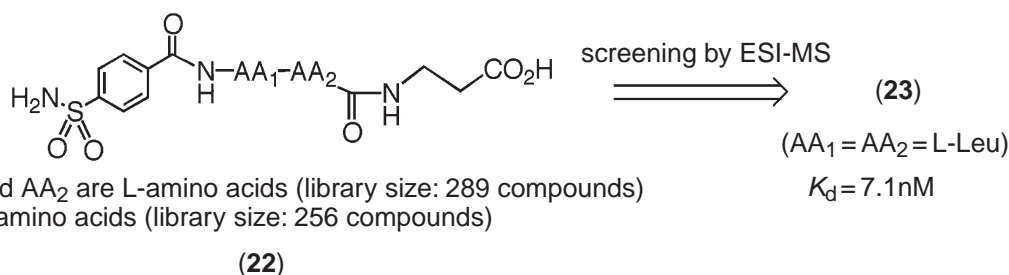
Scheme 24

group has been reported to be a potent HDAC inhibitor, having IC_{50} of 1.9 nM, 2.7 nM, and 19 nM against HDAC1, HDAC4, and HDAC6, respectively.[200]

8.23.4.7 Serine Protease Inhibitors by Zinc(II)

A new concept for the development of serine protease inhibitors by Zn^{2+} chelation has been reported (1998).[201] Inhibition of serine proteases may be therapeutically useful, since they also play important roles in disease. The active sites of serine proteases consist of a catalytic triad of Ser195, His57, and Asp102 residues (**29**) (numbering for bovine trypsin) (Scheme 26).

Bis(5-amidino-2-benzimidazolyl)methane (BABIM) (**30**) is a serine protease inhibitor having K_i of 19 µM (against trypsin) at pH 8.2 in the presence of 1.0 mM EDTA. Addition of Zn^{2+} at concentrations as low as 100 nM increased the affinity of BABIM for trypsin to K_i of 5.0 nM (i.e., by 3,800-fold). The X-ray crystal structure analysis of the trypsin–BABIM–Zn^{2+} complex (**31**) disclosed that His57 and Ser195 (maybe deprotonated) of trypsin, as well as two deprotonated nitrogen atoms from each of the two benzimidazoles of BABIM, coordinate to Zn^{2+} tetrahedrally in the S_1 (subsite 1) pocket. The BABIM in the trypsin–BABIM–Zn^{2+} complex

Butylic acid
(**24**)

Tricostatin A
(**25**)

Trapoxin B

(**27a**): R =

(**27b**): R = CHAP1

Suberoylanilide hydroxamic acid
(**26**)

Depudecin
(**28**)

Scheme 25

A catalytic triad of serine protease (trypsin)
(**29**)

bis(5-amidino-2-benzimidazolyl)methane
(BABIM) (**30**)

+ Zn^{2+}

trypsin–(**30**)–Zn^{2+} complex
(**31**)
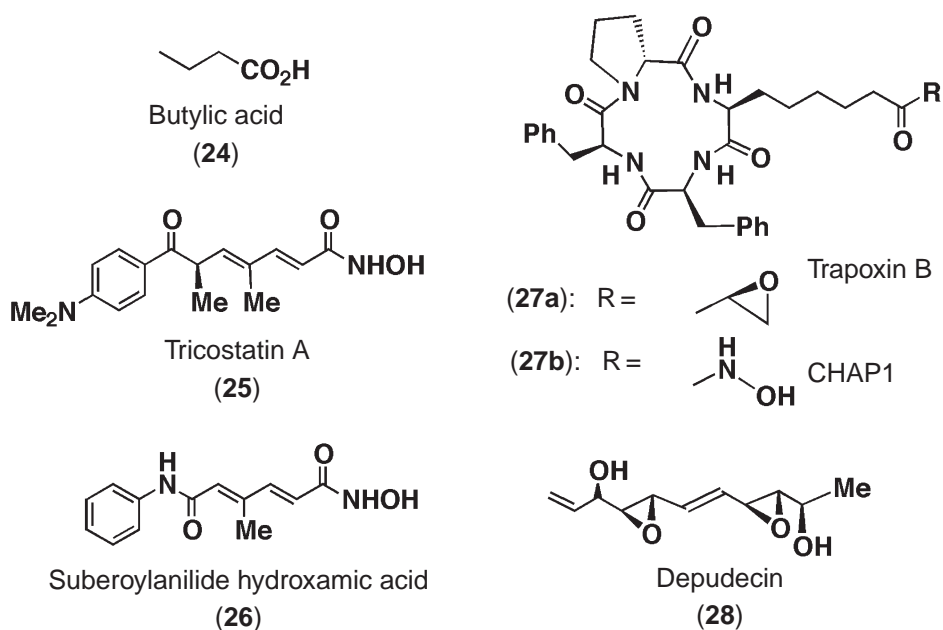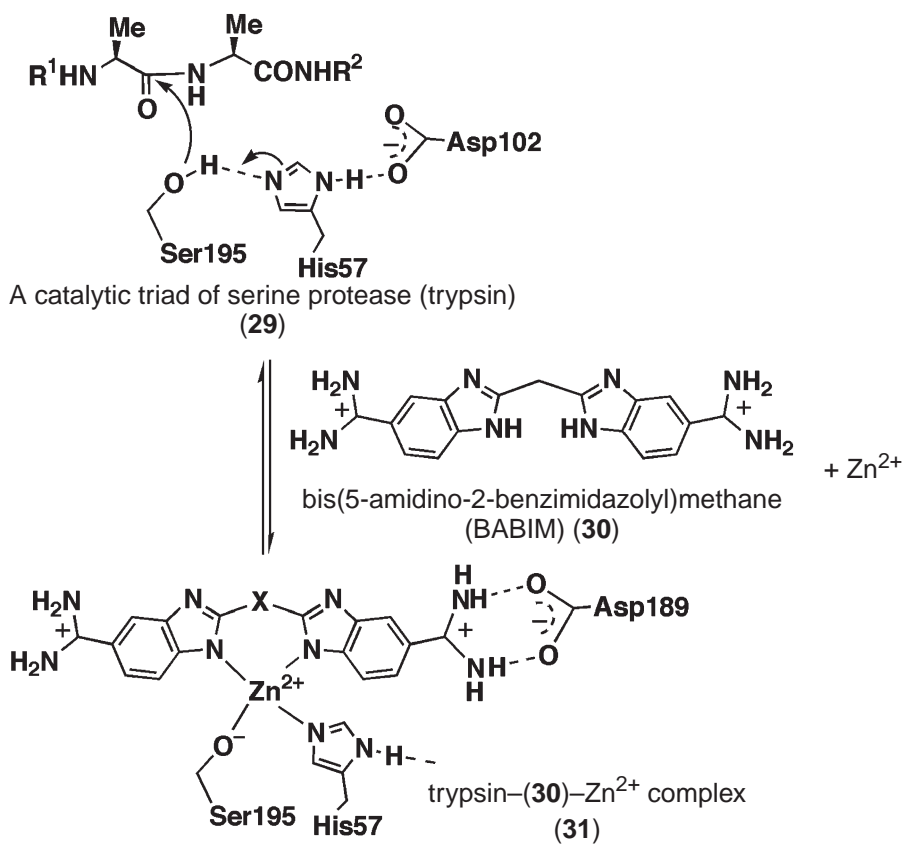
Scheme 26

(**31**) is almost superimposable on that in the trypsin–BABIM complex without Zn^{2+}, suggesting that Zn^{2+} enhances the affinity of BABIM for its target. Interestingly, inhibition by BABIM against other serine proteases such as chymotrypsin or chymase is much weaker. These proteases have an uncharged side chain at position 189, so there is no additional interaction with the amidinium moiety of BABIM (Scheme 26), thus resulting in weaker inhibition.[201]

8.23.5   MODEL SYSTEMS FOR MONONUCLEAR ZINC(II) ENZYMES

8.23.5.1   CA Models

In all the above Zn^{2+} enzymes, the Zn^{2+}-bound H_2O is activated by the Zn^{2+} ion with various degrees of assistance from a proximate general base such as Glu, for deprotonation or polarization for nucleophilic attack at the electrophilic substrates. With a pK_a value of ~ 6.9, the Zn^{2+}-bound H_2O in CA is deprotonated to attack at substrate CO_2 to produce the hydrated HCO_3^- in the simplest electrophilic reaction. Apparently, the Zn^{2+} complex of the three neutral imidazole ligands is sufficiently Lewis acidic to activate the coordinated H_2O. Targeting CA is probably the easiest entry to the model study of Zn^{2+} enzymes.

A number of simple zinc(II) complexes have been designed in order to gain basic knowledge of Zn^{2+} ion chemistry in the zinc(II) hydrolases.[202–213] Most of them feature tridentate or tetradentate ligands with vacant sites. In 1975, Wooley reported the first well-defined zinc(II) complex (**33**) with a macrocyclic tetramine as a model for CA (Scheme 27).[214,215] It was demonstrated that the Zn^{2+}-bound HO^- species is a reactant that attacks CO_2 to afford HCO_3^-, with a second-order rate constant for hydration, k^h_{cat}, of $2 \times 10^2 \, M^{-1} \, s^{-1}$ at $25\,^\circ C$. On the basis of the pH-dependent hydration rates, a pK_a value of 8.1 was assigned to the Zn^{2+}-bound H_2O, which was lower than the values of 9–10 for H_2O bound to free Zn^{2+}.
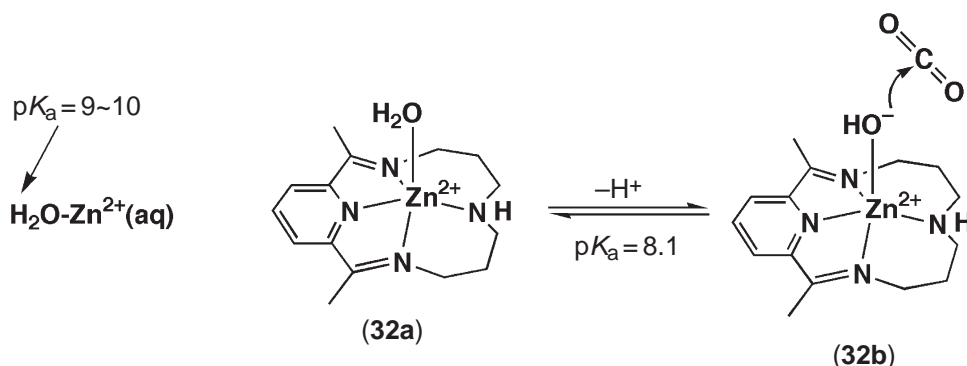
Scheme 27

In 1990, the zinc(II) complex of 1,5,9-triazacyclododecane (Zn^{2+}–[12]aneN$_3$) (**33**) was found to be more structurally and functionally relevant to the active center of CA (Scheme 28).[216–223] Its basic form (**33b**) was isolated as a trimeric complex ((**33b**)$_3$·HClO$_4$·(ClO$_4$)$_3$) from pH 8 aqueous solution.[216] The X-ray structure of this complex, which contained three (**33b**) molecules, disclosed a tetrahedral coordination environment about the zinc center, with a Zn^{2+}–OH^- length of 1.94 Å at the fourth coordination site, shorter than the Zn^{2+}—N bonds (average 2.02 Å). It dissociates into monomeric (**33b**) in aqueous solution.[216] Potentiometric pH titration measurements were used to show that the Zn^{2+}-bound H_2O in (**33a**) is deprotonated to give (**33b**) with a pK_a value of 7.3 at $25\,^\circ C$ and $I = 0.1$ (NaClO$_4$). The data are interpreted to indicate that (**33**) is a strong anion binder; i.e., hydroxide anion binds with a log K_s value of 6.4 (at $I = 0.2$), where K_s is the affinity constant. The Zn^{2+}–OH^- species (**33b**) turned out to be a good nucleophile and showed CA-like catalytic activity in the hydration of acetaldehyde (at $0\,^\circ C$), as well as in the hydrolysis of an unactivated ester, methyl acetate (at $25\,^\circ C$). The second-order rate (first order in [(**33a**)] and [acetaldehyde or CH_3CO_2Me]) constant-pH plots were sigmoidal, yielding the kinetic pK_a values of 7.3 at $25\,^\circ C$, which are identical to the thermodynamic pK_a values of 7.3.
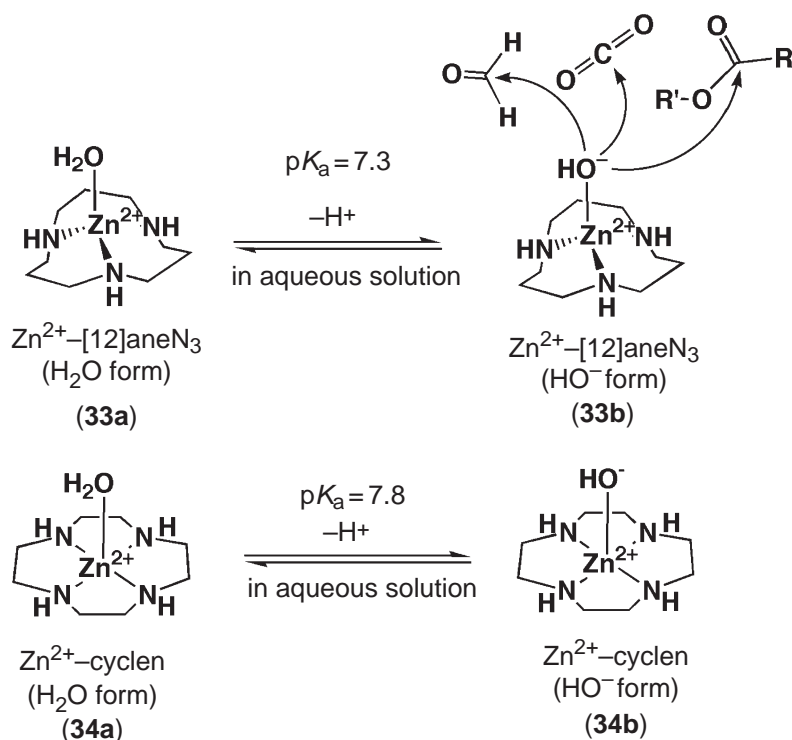
Scheme 28

The catalytic hydration of CO_2 also occurred with (**33**) and followed pH-dependent, second-order kinetics. Enzymatic CO_2 hydration and the reverse (HCO_3^- dehydration) were mimicked by (**33**).[217] The reaction was followed by measuring the evolution of OH^- for the reaction ($HCO_3^- \rightarrow CO_2 + OH^-$). The CO_2 hydration rates (the second-order constant is k^h_{cat}) decreased and HCO_3^- dehydration rates (the second-order constant is k^d_{cat}) increased with lowering pH (Figure 1). The kinetic data agreed with the reaction shown in Equation (1), being first order in [(**33b**)] and [HCO_3^-]. The second-order constant k^d_{cat} for HCO_3^- dehydration was found to be $5 M^{-1}s^{-1}$ and the kinetically obtained pK_a value for (**33a**)–(**33b**)+H^+ was 7.3 at 25 °C. Conclusions for the HCO_3^- dehydration with the catalyst (**33**) were: (i) the reactive species is the zinc(II)–OH_2 form, and (ii) substitution of the zinc(II)-bound H_2O by HCO_3^- is rate determining.
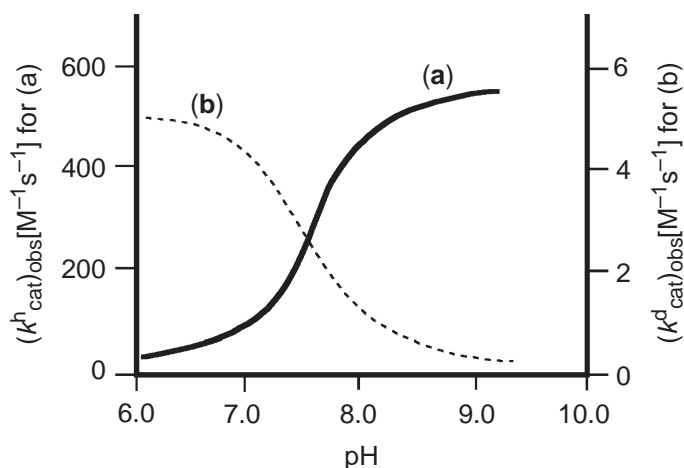
Figure 1 The rate–pH profile for (a) a CO_2 hydration; (b) HCO_3^- dehydration, catalyzed by Zn^{2+}–[12]aneN$_3$ (**33**).

Although the magnitudes of k^h_{cat} and k^d_{cat} differed significantly, the two pH-dependent rate curves (Figures 1a and 1b) are symmetrical (with scales adjusted) with an inflection point at pH ca. 7.4, a value close to the pK_a value of 7.3. Thus, the macrocyclic complex (33) was the first to mimic the pH-dependent behavior of reversible CO_2 hydration catalyzed by CA. This fact implies that in CA, too, the CO_2 hydration/HCO_3^- dehydration should be essentially controlled by the zinc(II)–OH^-/zinc(II)–OH_2 equilibrium at the active center.

A zinc(II) complex of the 12-membered macrocyclic tetraamine, cyclen (1,4,7,10-tetraazacyclo-dodecane) (34), was later shown to be a useful Zn^{2+}-enzyme model, although the pK_a value (7.8) of the Zn^{2+}-bound water (for (34a) → (34b) + H^+) was a little higher than that (7.3) for the triamine complex (33) (Scheme 28).[218] These findings demonstrated that simple zinc(II) complexes can be used to activate H_2O at physiological pH for catalytic reactions, in analogy to the monometallic zinc(II) enzymes.

A series of tris(pyrazolyl)hydroborate zinc(II)–OH^- complexes (such as (35)) was synthesized to model the catalytic center of CA and other Zn^{2+} enzymes.[224–238] Indeed, the zinc(II)–OH^- in (35b) was highly nucleophilic to CO_2, carboxylesters, activated amides (β-lactam or CF_3CONH_2), and phosphonates. Those reactions, were run in organic solvents and, therefore, were stoichio-metric. The high nucleophilicity of (35b) was attributed to monomeric character of the zinc(II)-bound OH^- due to steric hindrance and the hydrophobic environment. The pK_a value for (for (35a) → (35b) + H^+) was estimated to be 6.5 ± 0.4.[209] The zinc(II) complex (35b) reacted with CO_2 to yield a bridging carbonato complex (37), possibly via formation of (36) (Scheme 29).[228,234] Thermodynamic and kinetic parameters for CO_2 hydration and CO_3^- dehydration reactions in water-containing solvents were reported.
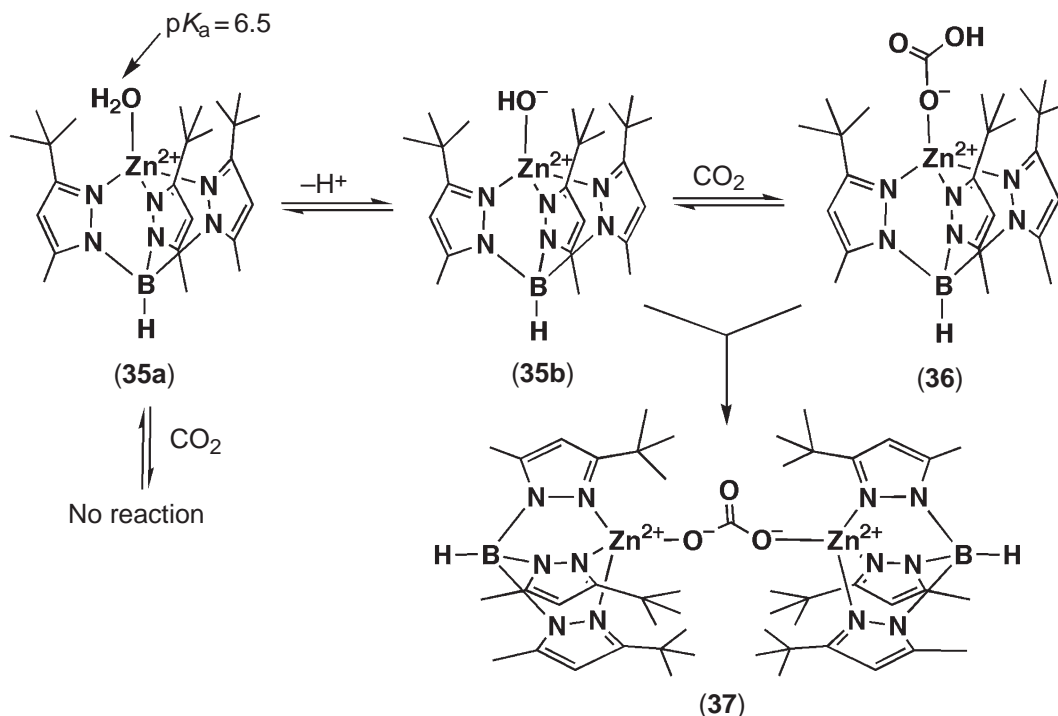
Scheme 29

A similarly water-insoluble Zn^{2+} complex of a tris(3,5-diisopropyl-1-pyrazolyl)hydroborate (38) reacted with CO_2 instantaneously to give the (μ-carbonato)-dizinc(II) complex (39), where the binding mode of the bicarbonate bridge was different from that of (37) (Scheme 30).[239,240] CO_2 hydration was also reported for the water-soluble Zn^{2+} complexes such as (40).[241]
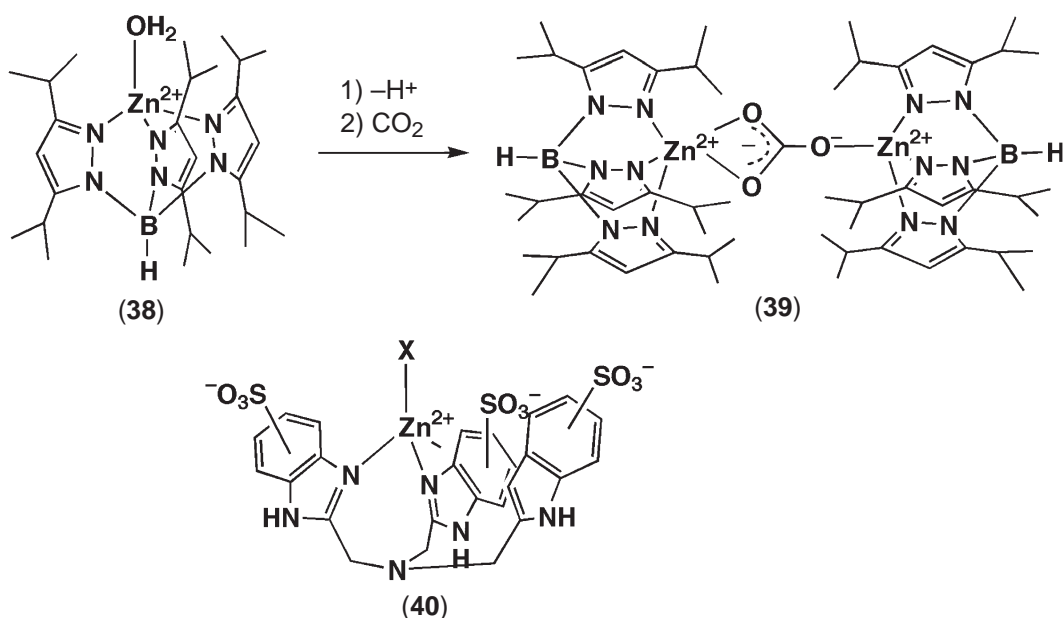
Scheme 30

8.23.5.2 Peptidase Models

Amide bonds are extremely stable and their half-life for hydrolysis in neutral aqueous solution is estimated to be seven years.[242] Zinc(II)–OH$^-$ species (derived from mononuclear Zn^{2+} complexes) alone are incapable of hydrolyzing amide bonds. Rather, Zn^{2+}–OH$^-$ species may often act as a base to deprotonate amides.[243]

There are only a few dinuclear Zn^{2+} complexes known to exhibit peptidase activity. A dimeric Zn^{2+} complex (**41**) was reported to hydrolyze L-Leu-4-nitropyhenylanilide (Scheme 31).[244] The reaction was first order with respect to the substrate and the catalyst (**41**). The other dimeric Zn^{2+} complex (**42**) cleaves a peptide bond of Gly–Gly.[245] It was proposed that the amide carbonyl of Gly–Gly coordinates to one of the Zn^{2+} ions in (**42**) to be activated for hydrolysis by the other Zn^{2+}–OH$^-$. For other metals, several complexes of Cu^{2+}, Ni^{2+}, Pd^{2+}, and Co^{3+} were shown to cleave amide bonds.[210, 246–251] It is of interest to note that while carboxamides are substrates for CPD, they are inhibitors for CA.[252] A recent model study has addressed this issue.[243]
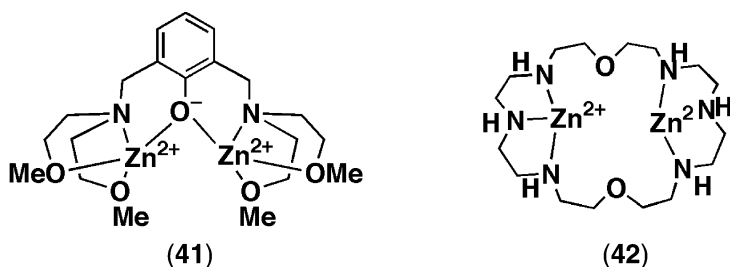
Scheme 31

8.23.5.3 Phosphatase Models

As described in Section 8.23.3.5, many phosphatases are dinuclear metalloenzymes with Zn^{2+}, Fe^{3+}, Mn^{2+}, Mg^{2+}, etc. Typically, alkaline phosphatases (AP) are dimetallic Zn^{2+} hydrolases.

As shown in Scheme 10, Ser102 of AP is apparently activated by Zn^{2+} to attack at phosphate substrates polarized by another Zn^{2+} ion.

The interaction and hydrolysis of phosphate esters were mimicked by the CA models, (33)[253] and (34),[254] and an alcohol-pendant Zn^{2+} complex (45)[255] (Schemes 32 and 33). It was found that (33) and (34) hydrolyzed bis(4-nitrophenyl) phosphate (BNPP) to give stable complexes (43) and (44) of the product, mono(4-nitrophenyl) phosphate (4-NPP). The second-order rate constants are $8.5 \times 10^{-5}\,M^{-1}\,s^{-1}$ and $2.1 \times 10^{-5}\,M^{-1}\,s^{-1}$, respectively, at 25 °C (Scheme 32). An alcohol-pendant Zn^{2+} complex (45) provided a model for the Zn^{2+}-activated serine of AP (see Scheme 10).[255] An alkoxide group in (45b) attacked BNPP to give a phosphorylserine intermediate (46), which was susceptible to further hydrolysis by the intramolecular Zn^{2+}-bound hydroxide in (46b) to give (47) (Scheme 33). For the first step, the alcohol group is deprotonated by the proximate Zn^{2+} ($pK_a = 7.5$) to an alkoxide complex (45b), which was 125 times more effective as nucleophile to the phosphate substrate than was the Zn^{2+}-activated water of the reference compound (34). For the subsequent step, the nucleophilic Zn^{2+} species (46c) was generated with a pK_a value of 9. This intramolecular hydrolysis is 45,000 times faster than the intermolecular hydrolysis of ethyl 4-nitrophenyl phosphate (ENP) with (34b). These results imply an advantage of the intramolecular arrangement of two Zn^{2+} ions in AP (as shown in Scheme 10) over mononuclear Zn^{2+} hydrolases. Toward any mononuclear Zn^{2+} phosphatase model, phosphomonoesters were not substrates, but instead were inhibitors, as shown by isolation of the stable complexes (43), (44), and (47). The tris(pyrazolyl)-hydroborate complexes such as (35) and (38) hydrolyze phosphodiesters to phosphomonoesters, which similarly bind to Zn^{2+} to become inert to further hydrolysis.[233,239]
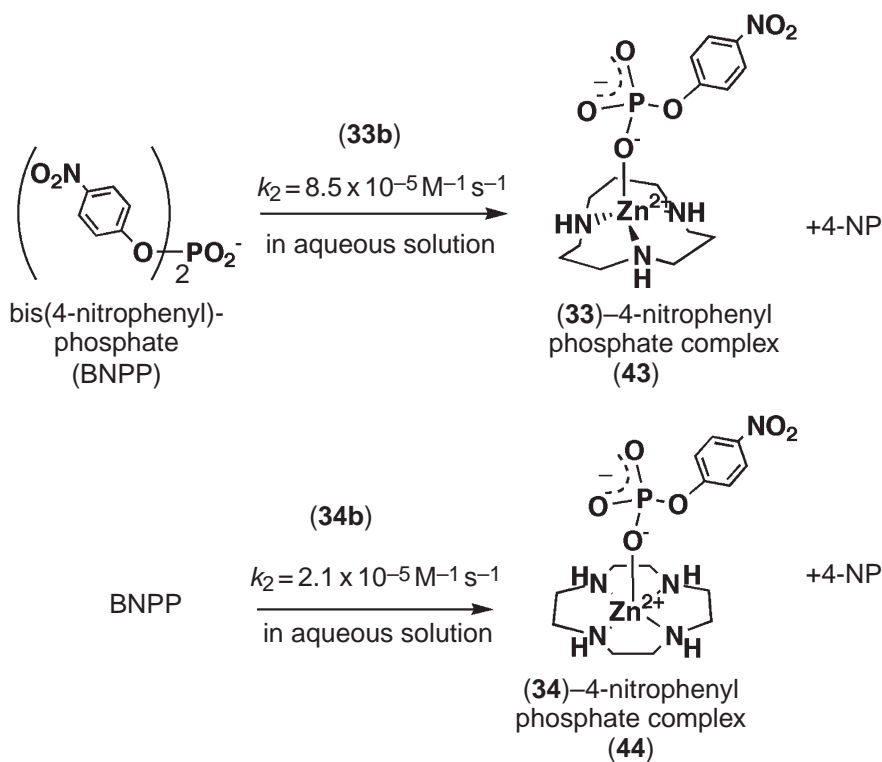
Scheme 32

The requirement of the dimetallic complexes to hydrolyze phosphomonoesters was demonstrated by a dizinc(II) cryptate (48) with an alkoxide-bridge (Scheme 34).[256] Complex (48) reacted with phosphomonoesters such as mono(4-nitrophenyl) phosphate (4-NPP) at pH 5–7 in aqueous solution. It should be noted that (48) reacts with 4-NPP exclusively, not with diester, BNPP, nor triester, tris(4-nitrophenyl) phosphate (TNPP). A second-order dependence of the rate constant (first order with respect to both [(48)] and [(4-NPP)] was determined. The rate–pH profile exhibited a bell-shaped relationship with the maximum rate at pH 5.9. On the basis of X-ray crystal-structure analysis of (48) and (50), a mechanism was proposed (Scheme 34). Initially, two O^- donors of 4-NPP interact with the two Zn^{2+} ions, which are suitably separated (3.42 Å) (49).

Concomitantly, two of the axial NH groups of (**49**) begin to dissociate and attack the phosphorus atom of the activated 4-NPP, to displace 4-nitrophenolate and yield stable (**50**). These reactions have analogies to the alkaline phosphatase reactions shown in Scheme 10, where the Zn^{2+}-bound Ser102 reacts with the incoming phosphomonoester.
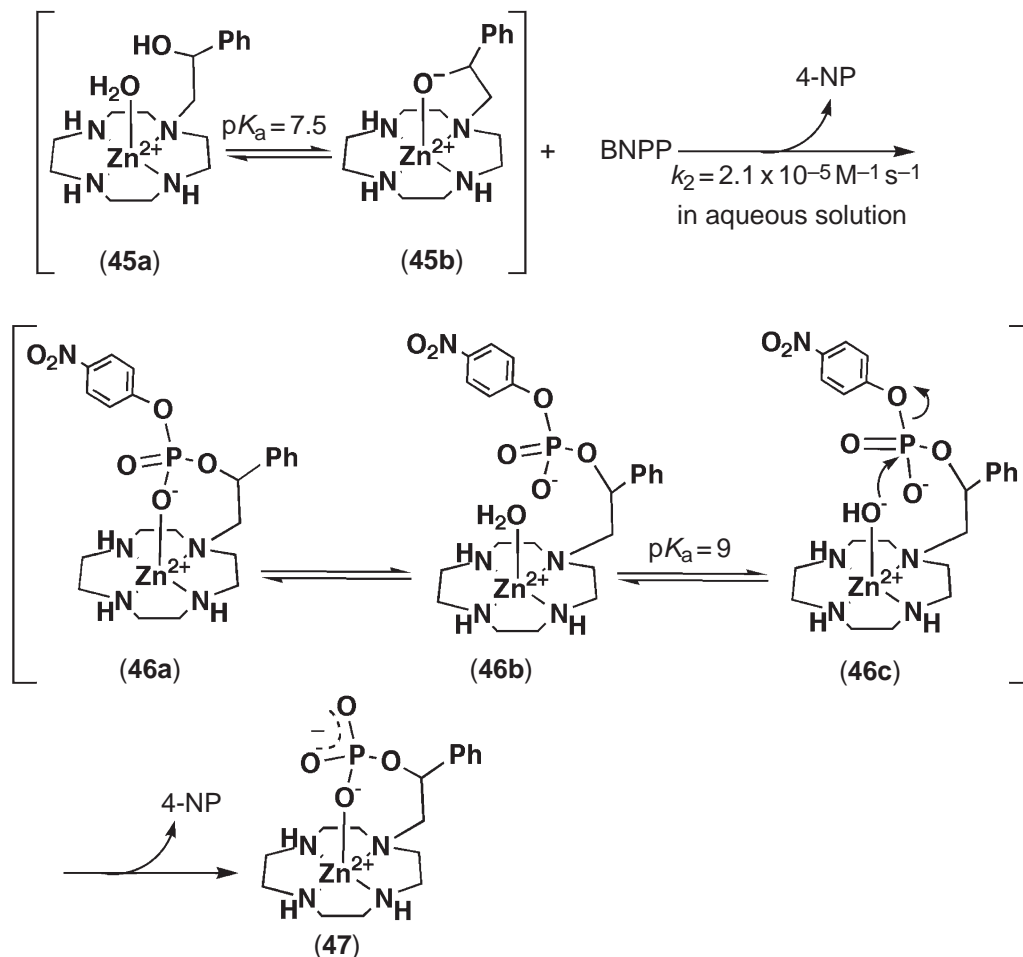
Scheme 33
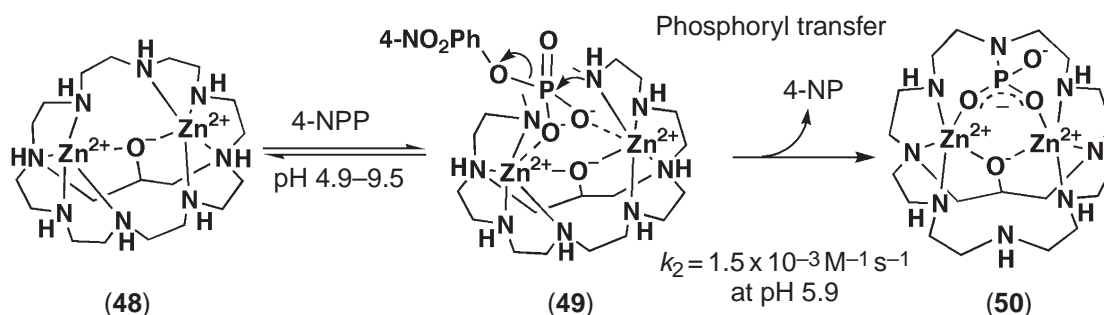
Scheme 34

Many metal complexes have been designed and synthesized as catalysts for transesterification of phosphate diesters to model mechanisms of RNases. Typical examples are monomeric Zn^{2+} complexes (**53**)[257] and (**54**)[258] and dimetallic Zn^{2+} complexes such as (**55**)[259] (Scheme 35). For (**53**), the pseudo-first-order rate constant, k, for hydrolysis of BPP and for transesterification of

2-hydroxypropyl 4-nitrophenyl phosphate (HPNP) (**51**) yielding (**52**) was 1.5×10^2 h^{-1} in 10% DMSO solution at pH 7.0 and 37 °C. Among dinuclear Zn^{2+} macrocyclic complexes tested, the dimeric Zn^{2+} complexes (**55**), in which two Zn^{2+} ions are well separated, were found to be the best catalysts for the hydrolysis of BPP and HPNP. A trinuclear Zn^{2+} complex (**56**) was reported to promote transesterification of adenyl(3′-5′)adenosine (ApA).[260,261] For models utilizing other metal complexes, see references [262–269].

2-hydroxypropyl 4-nitrophenyl phosphate
(HPNP)(**51**)

(**52**)

(**53**)   R=H,

(**55**)

(**54**)   (**56**)
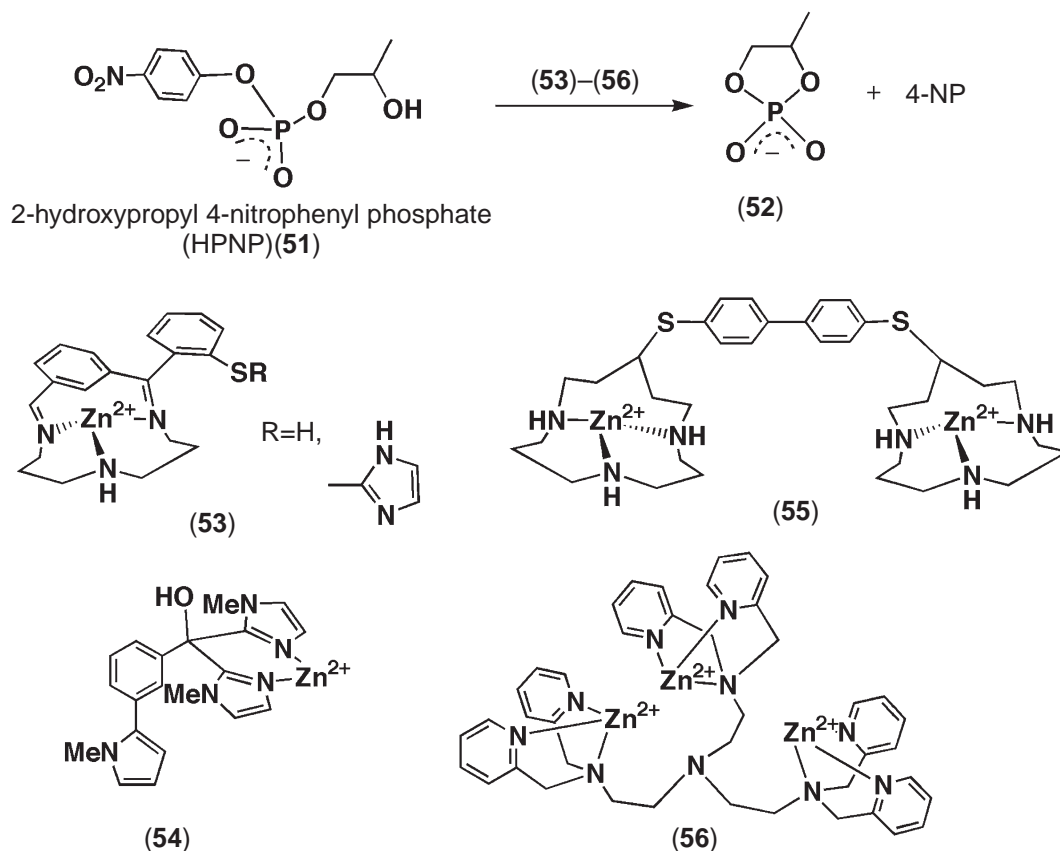
Scheme 35

8.23.5.4 *β*-Lactamase Models

The coordinating ligands to Zn^{2+} in *β*-lactamases (Scheme 9) are essentially similar to those of CA (Scheme 11). In addition to acting as a CA model, Zn^{2+}–cyclen (**34**) was found to catalyze the hydrolysis of *N*-benzylpenicillin (Scheme 36).[270] Interestingly, (**34**) also catalyzed epimerization of the hydrolyzed product, (5*R*)-benzylpenicilloate, to (5*S*)-benzylpenicilloate, unlike the enzymatic reaction.

With relevance to dimetallic zinc(II) *β*-lactamases, a dinuclear zinc(II) complex (**57**) was designed and synthesized (Scheme 37).[271,272] It has been found that (**57**) catalyzes a hydrolysis of nitrocefin, a substrate for the dimetallic zinc(II) *β*-lactamase from *B. fragilis*, to give a complex (**58**) of the hydrolyzed product and (**57**).

8.23.5.5 Type-II Aldolase Models

Zn^{2+} complexes[273,274] have been prepared that model type-II aldolases, which catalyze reversible aldol addition reactions. Enolizations are essential for the carbon–carbon bond formation in an aldol reaction, and Zn^{2+} may play a role in such processes. For example, activation of the carbonyl of DHAP in the active site of type-II aldolases was performed by a Zn^{2+} complex of 1-(4-bromophenacyl)-cyclen (**59**) (Scheme 38).[273] The pK_a value for the acidic protons of the carbonyl α-position was 8.4.
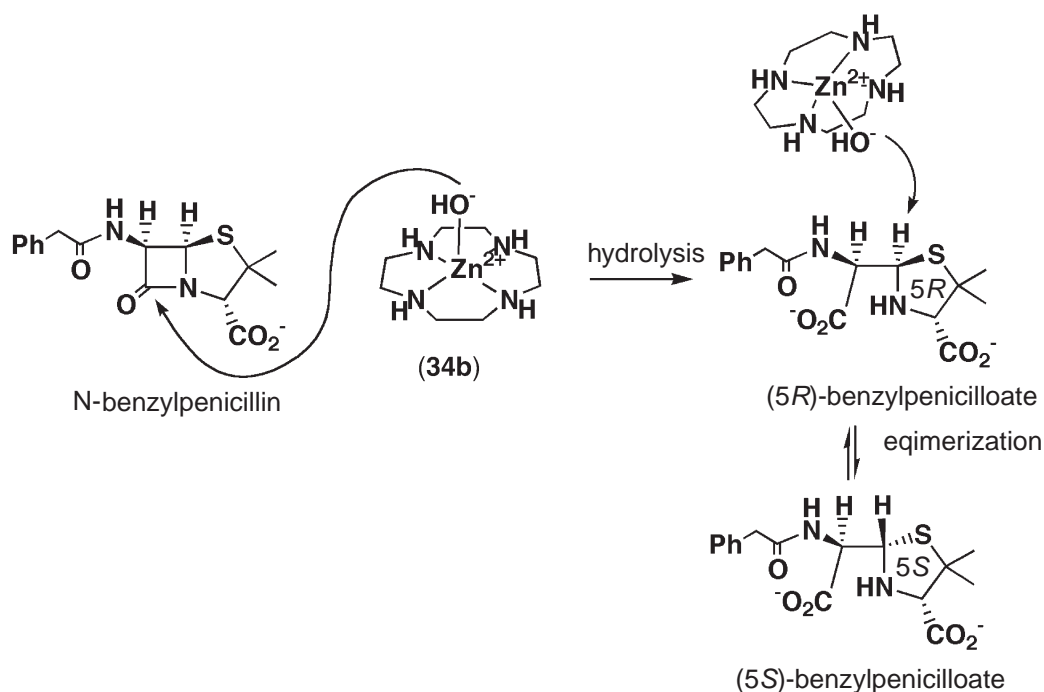
Scheme 36
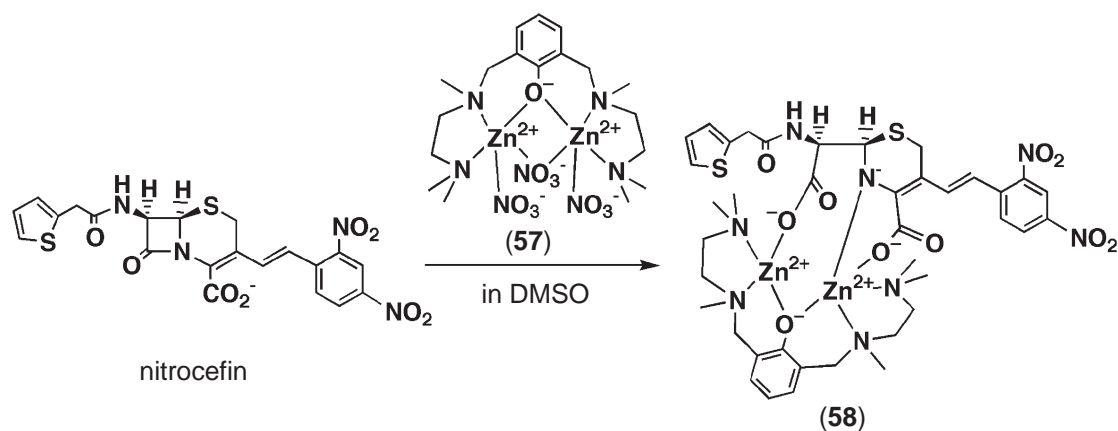
Scheme 37

The deprotonation yielded an enolate complex (**60a**) and a Zn^{2+}–OH^- species (**60b**) in a 23:77 ratio in aqueous solution. The results imply that the Zn^{2+}-coordination of the carbonyl group of DHAP certainly facilitates enolization by lowering the pK_a of ca. 19 to a physically feasible pH.

8.23.5.6 More Recent Developments

8.23.5.6.1 CA-mimetic zinc(II) fluorophores

The concentration of free Zn^{2+} within cells varies from about 1 nM in the cytoplasm of many cells, to about 1 mM in some vesicles. As the significance of Zn^{2+} physiology and homeostasis has
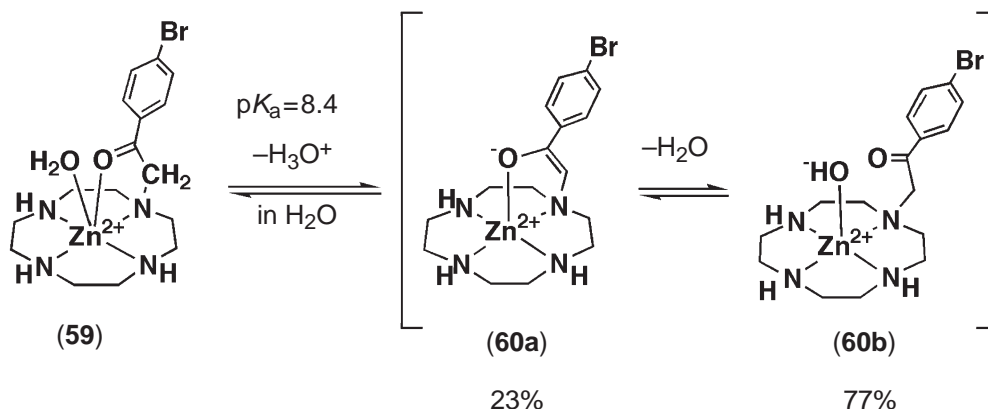
Scheme 38

increased, the need for useful zinc fluorophores to quantify trace Zn^{2+} flux in biological dynamics has become more urgent.

In a development since the first discovery of sulfonamides as inhibitors of CA,[183] Chen and Kernohan studied the interaction of bovine erythrocyte CA with dansylamide (**61**) and saw a highly fluorescent complex (**62**) with a dissociation constant K_d of 2.5×10^{-7} M at pH 7.4 (Scheme 39).[184]
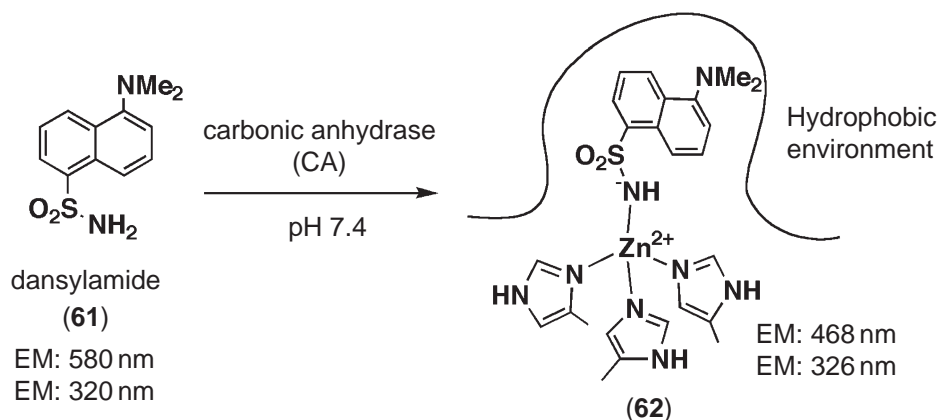
Scheme 39

By combining established knowledge of CA-sulfonamide complexes[185–188,275,276] and CA-model Zn^{2+} complexes,[216–222,252–256,277] a new type of selective and efficient zinc fluorophore, a dansylami-doethylcyclen (**63**), was designed (Scheme 40).[278–282] The 1:1 complexation constant for (**64**) (log $K = \log ([Zn^{2+}-H_{-1}L]/[L \cdot 2H^+][Zn^{2+}])$) was as large as 20.8 M^{-1} at 25 °C with $I = 0.10$ (NaNO$_3$) as determined from potentiometric pH titrations.[278] The response of (**63**) (5 μM) to Zn^{2+} (0.1–5 μM) (at 528 nm) was linear until it reached a 1:1 $[Zn^{2+}]/[63]$ ratio, and then became a plateau. Alternatively, Cu^{2+} linearly diminished the fluorescence emission until complete quenching at $[Cu^{2+}]/[63] = 1$, although Cu^{2+} forms the most stable five-coordinate complex $Cu^{2+}-H_{-1}L$ (log $K = \log ([Cu^{2+}-H_{-1}L]/[Cu^{2+}][H_{-1}L]) > 30$ at 25 °C). New macrocyclic Zn^{2+} fluorophores have been found, including anthrylmethyl-cyclen (**65**),[283–286] Zinquin (**66**),[287–289] ACF-1 and -2 (**67a** and **67b**),[290] or Zinpyr-1 (**68**)[291,292] (Scheme 41).[281]

8.23.5.6.2 *Artificial receptors by Zn^{2+} enzyme models*

As substrates and inhibitors, phosphate anions bind as reversibly monodentate ligands to zinc(II) ions in CPA,[293] alkaline phosphatase,[139] phospholipase C,[73] or alkaline phosphatase A.[222] The
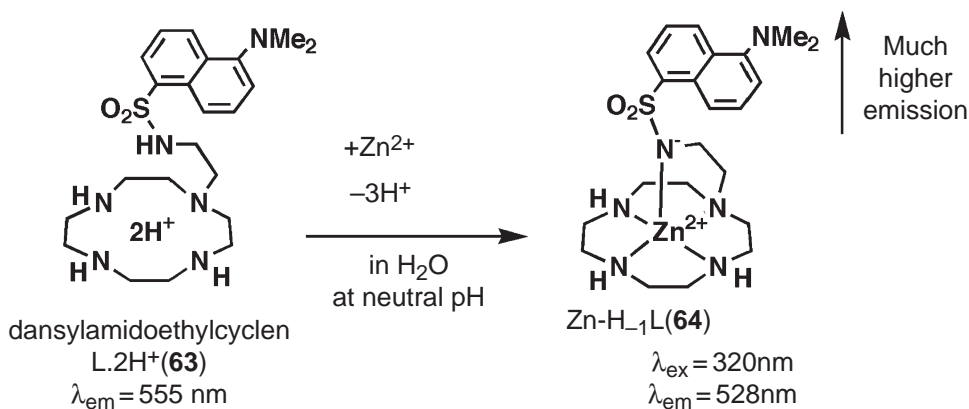
Scheme 40
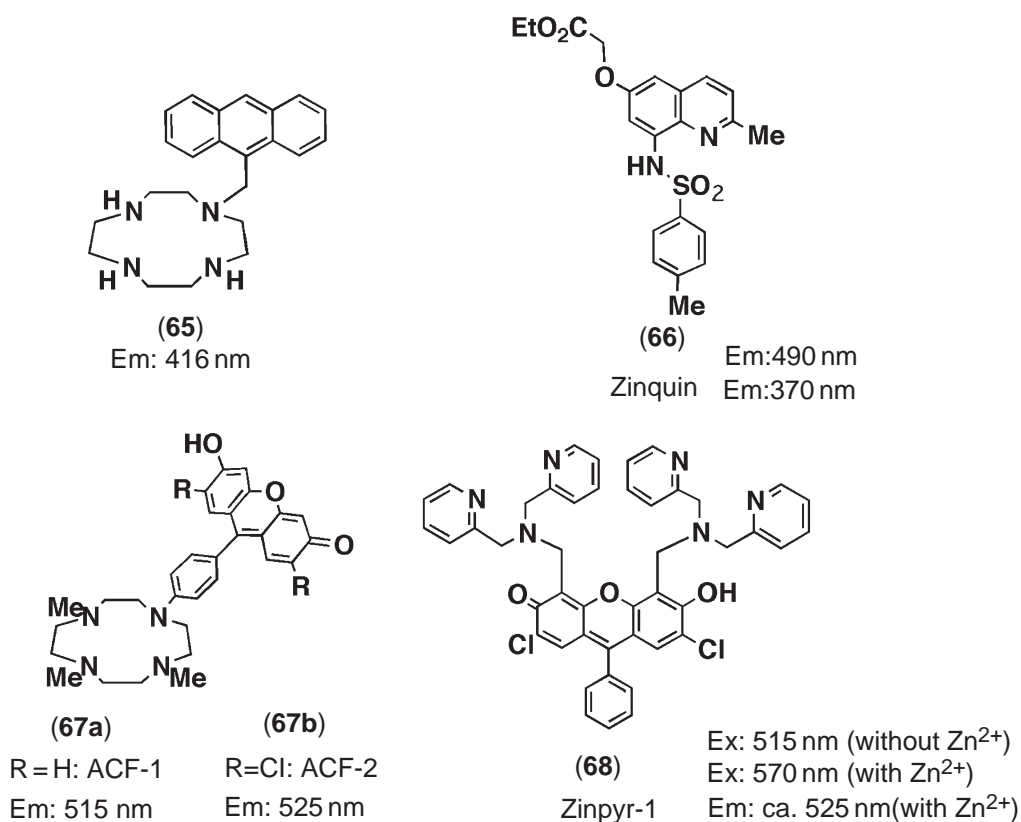
Scheme 41

zinc(II)-enzyme-model complexes, (**33**) and (**34**), likewise strongly bind to dianionic phosphates such as HPO_4^{2-}, phenyl phosphate (PP), and 4-nitrophenyl phosphate (4-NPP) to yield 1:1 complexes (**43**) and (**44**), while metal-free cyclen (similarly dicationic with two protons ($L \cdot 2H^+$) at neutral pH) ineracted only weakly with these phosphate dianions. The 1:1 complexation constant log K_s for (**44**) was 3.1 in aqueous solution with $I = 0.2$ (NaClO$_4$) at 25 °C (Scheme 42).[218] A bis(Zn^{2+}–cyclen) complex linked with a *m*-xylene spacer (**69**)[294] and tris(Zn^{2+}–cyclen) (**70**)[295] are much better phosphate receptors, with log K_s of 4.0 and 5.8 (with 4-NPP).[296,297]

PP   : R = H
4-NPP : R = NO$_2$

(34)

Zn^{2+}–cyclen–phosphate^{2-} complex
(44)

m-bis(Zn^{2+}–cyclen)
(69)

tris(Zn^{2+}–cyclen)
(70)
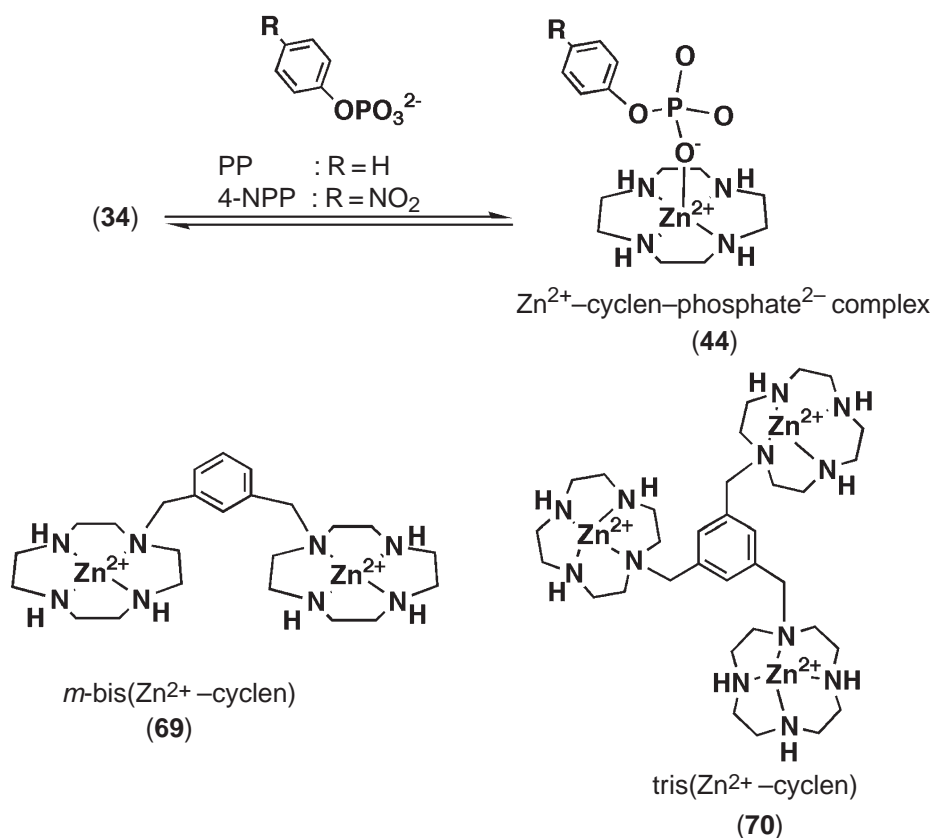
Scheme 42

8.23.5.6.3 Guanidine coordination to Zn^{2+}-enzyme-model complex in aqueous solution at neutral pH

Contrary to a prevalent perception that an arguinine residue always acts as a protonated guanidinium cation in an enzyme, a neutral form of guanidine was discovered to coordinate to Zn^{2+} in a cyclen functionalized with a guanidinylethyl pendant (71) (p$K_a > 12$).[298] The guanidinium was deprotonated in the vicinity of Zn^{2+} with pK_a of 5.9 to yield ZnL (72b). Moreover, the Zn^{2+}-bound guanidine in (72b) was displaced by a phosphate monoester in aqueous solution at pH ~ 5.5 to form (73) via Zn^{2+}–OH$_2$ species (Zn(L·H$^+$)H$_2$O) (72a) (Scheme 43). These findings with the Zn^{2+}-enzyme model suggest transient coordination of arguinine residues in the transition state of the Zn^{2+}-promoted phosphatase reaction.

8.23.6 SUMMARY

We have reviewed recent (1990–2001) reports on the structures and mechanisms of monomellic hydrolases (and homologues) that mostly contain zinc(II). To help study the reactions of the Zn^{2+} enzyme and elucidate the essential roles of Zn^{2+} ions, inhibitors and model systems have been studied. More hydrolases (including zinc(II) hydrolases) are likely to be found to add to the currently classified list of enzyme families. Recently applied techniques, including site-directed mutagenesis, X-ray crystal-structure analysis, and other analytical methodologies have led to clearer understanding of the enzyme activities. It is interesting that, despite the different amino-acid ligands for different enzymes that have variable functions, the catalytic Zn^{2+} commonly plays the same acid role to activate the Zn^{2+}-bound H$_2$O to perform as a nucleophile.

Hydrolase inhibitors are potentially important as therapeutic agents to treat diseases that involve these hydrolases. The inhibitors further help in the study of reaction mechanisms. Development of β-lactamase inhibitors or MMP inhibitors is urgently needed in the fight against
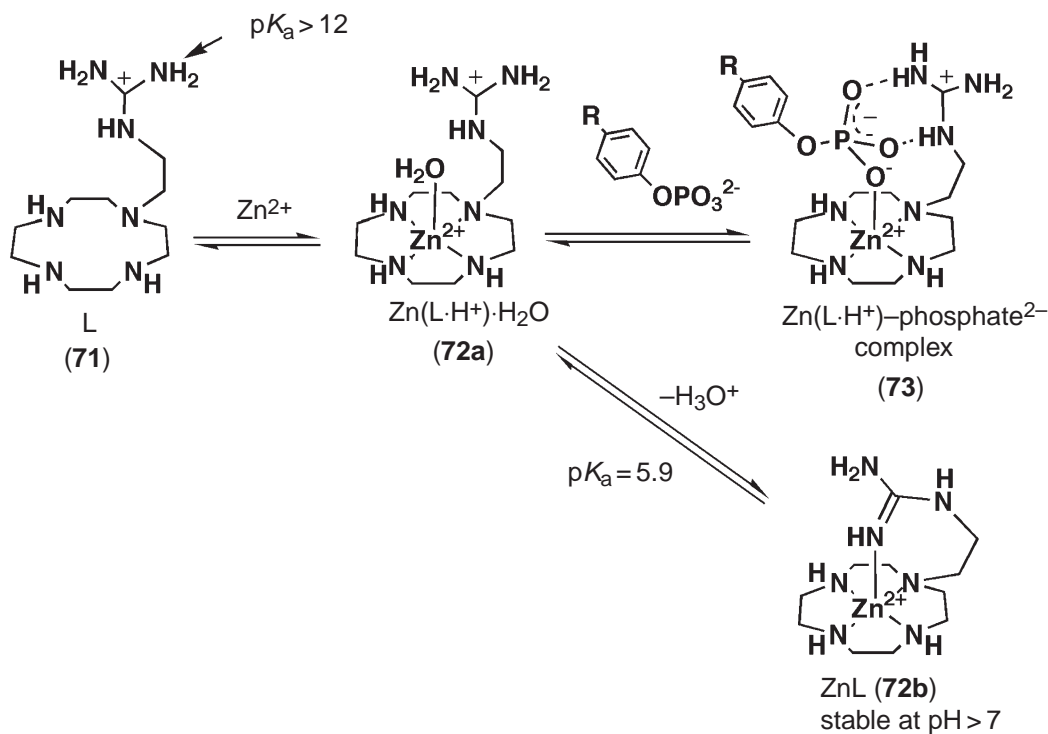
Scheme 43

bacterial resistance or cancers. In addition to random drug screening, computer chemistry and combinatorial screening methodologies based on the knowledge of these enzymes will accelerate drug discovery.

We have also presented recent developments in the study of Zn^{2+}-enzyme-model complexes as a means toward shedding light on the intrinsic roles of Zn^{2+} in enzymes. Advances in Zn^{2+} coordination chemistry since the 1990s have been contributing to the design of useful and versatile Zn^{2+}-enzyme models that have allowed accurate measurements of Zn^{2+} acidities in aqueous solution. Until the advent of macrocyclic ligands, it was extremely difficult to obtain Zn^{2+} complexes that were stable enough to sustain pH 4–10 measurement in aqueous solution. Further elaborate ligand design is likely to lead not only to elucidation of enzyme mechanism, but also to the development of new catalytic reactions, analytical techniques, or drugs.

8.23.7 REFERENCES

1. Fraústo da Silva, J.; Williams, R. J. P. *The Biological Chemistry of the Elements*, Clarendon Press: Oxford, 1991; Chapter 11, pp 299–318.
2. Lippard, S. J.; Berg, J. M. *Principles of Bioinorganic Chemistry*; University Science Books: Mill Valley, CA, 1994.
3. Walsh, C. T. *Enzymatic Reaction Mechanisms*; W. H. Freeman: New York, 1977.
4. Barrett, A. J.; Rawlings, N. D.; Woessner, J. F., Eds; *Handbook of Proteolytic Enzymes*; Academic Press: London, 2000.
5. Chlebowski, J. F.; Coleman, J. E. In *Metal Ions in Biological Systems*; Sigel, H., Ed.; Marcel Dekker: New York, 1976, Vol. 6, pp 1–140.
6. Vallee, B. L.; Auld, D. S. *Biochemistry* **1990**, *29*, 5647–5659.
7. Vallee, B. L.; Auld, D. S. *Proc. Natl. Acad. Sci., USA* **1990**, *87*, 220–224.
8. Vallee, B. L.; Falchuk, K. H. *Physiol Rev.* **1993**, *73*, 79–118.
9. Vallee, B. L.; Auld, D. S. *Acc. Chem. Res.* **1993**, *26*, 543–551.
10. Auld, D. S. *BioMetals* **2001**, *14*, 271–313.
11. Lipscomb, W. N.; Styräter, N. *Chem. Rev.* **1996**, *96*, 2375–2433.
12. Coleman, J. E. *Curr. Opin. Chem. Biol.* **1998**, *2*, 222–234.
13. Bock, C. W.; Glusker, J. P. *Inorg. Chem.* **1993**, *32*, 1242–1250.
14. Berg, J. M. *Acc. Chem. Res.* **1995**, *28*, 14–19.
15. Berg, J. M.; Shi, Y. *Science* **1996**, *271*, 1081–1085.
16. Berg, J. M.; Godwin, H. A. *Ann. Rev. Biophys. Biomol. Struct.* **1997**, *26*, 357–371.

17. Junker, M.; Rodgers, K. K.; Coleman, J. E. *Inorg. Chim. Acta* **1998**, *275–276*, 481–492.
18. Cox, E. H.; McLendon, G. L. *Cur. Opin. Chem. Biol.* **2000**, *4*, 162–165.
19. Quiocho, F. A.; Lipscomb, W. N. *Adv. Protein Chem.* **1971**, *25*, 1–78.
20. Bukrinsky, J. T.; Bjerrum, M. J.; Kadziola, A. *Biochemistry* **1998**, *37*, 16555–16564.
21. Schmitt, M. F.; Herriotto, J. R. *J. Mol. Biol.* **1976**, *103*, 175–190.
22. Faming, Z.; Kobe, C. B.; Stewart, B.; Rutter, W. J.; Goldsmith, E. J. *J. Biol. Chem.* **1991**, *266*, 24606–24612.
23. Reverter, D.; Fernandez-Catalan, C.; Baumagartner, R.; Pfander, R.; Huber, R.; Bode, W.; Vendrell, J.; Holak, T. A.; Aviles, F. X. *Nat. Struct. Biol.* **2000**, *7*, 322–328.
24. Gomis-Ruth, F. X.; Kress, L. F.; Bode, W. *EMBO J.* **1999**, *18*, 5817–5826.
25. Gomis-Ruth, F. X.; Gomez, M.; Bode, W.; Huber, R.; Aviles, F. X. *EMBO J.* **1995**, *14*, 4387–4394.
26. Garcia-Saez, I.; Reverter, D.; Vendrell, J.; Aviles, F. X.; Coll, M. *EMBO J.* **1997**, *16*, 6906–6913.
27. Matthews, B. W.; Weaver, L. H.; Kester, W. R. *J. Biol. Chem.* **1974**, *249*, 8030–8044.
28. Thayer, M. M.; Flaherty, K. M.; McKay, D. B. *J. Biol. Chem.* **1991**, *266*, 2864–2871.
29. Banbula, A.; Potempa, J.; Travis, J.; Fernandez-Catalan, C.; Mann, K.; Huber, R.; Bode, W.; Medrano, F. *Structure* **1998**, *6*, 1185–1193.
30. Thunnissen, M. M.; Nordlund, P.; Haeggstrom, J. Z. *Nat. Struct. Biol.* **2001**, *8*, 131–135.
31. Oefner, C.; D'Arcy, A.; Hennig, M.; Winkler, F. K.; Dale, G. E. *J. Mol. Biol.* **2000**, *296*, 341–349.
32. Lacy, D. B.; Tepp, W.; Cohen, A. C.; DasGupta, B. R.; Stevens, R. C. *Nat. Struct. Biol.* **1998**, *5*, 898–902.
33. Lacy, D. B.; Stevens, R. C. *J. Mol. Biol.* **1999**, *291*, 1091–1104.
34. Ghuysen, J. M. In *Antibiotic Inhibition of Bacterial Cell Surface Assembly and Function*: Actor, P., Daneo-Moore, L., Higgins, M. L., Salton, M. R. J., Eds.; American Society for Microbiology: Washington DC, 2000, pp 268–284.
35. Bussiere, D. E.; Pratt, S. D.; Katz, L.; Severin, J. M.; Holzman, T.; Park, C. H. *Mol. Cell* **1998**, *2*, 75–84.
36. Bode, W.; Gomis-Ruth, F. X.; Huber, R.; Zwilling, R.; Stocker, W. *Nature* **1992**, *358*, 164–167.
37. Grams, F.; Dive, V.; Yiotakis, A.; Yiallouros, I.; Vasiliou, S.; Zwilling, R.; Bode, W.; Stöcker, W. *Nat. Struc. Biol.* **1996**, *3*, 671–675.
38. Baumann, U.; Wu, S.; Flaherty, K. M.; McKay, D. B. *EMBO J.* **1993**, *12*, 3357–3364.
39. Miyatake, H.; Hata, Y.; Fujii, T.; Hamada, K.; Morihara, K.; Katsube, Y. *J. Biochem.* **1995**, *118*, 474–479.
40. Baumann, U.; Bauer, M.; Létoffé, S.; Delepelaire, P.; Wandersman, C. *J. Mol. Biol.* **1995**, *248*, 653–661.
41. Gomiz-Ruth, F. X.; Kress, L. F.; Bode, W. *EMBO J.* **1993**, *12*, 4151–4157.
42. Gomiz-Ruth, F. X.; Kress, L. F.; Kellermann, J.; Mayr, I.; Lee, X.; Huber, R.; Bode, W. *J. Mol. Biol.* **1994**, *239*, 513–544.
43. Maskos, K.; Fernandez-Catalan, C.; Huber, R.; Bourenkov, G. P.; Bartunik, H.; Ellestad, G. A.; Reddy, P.; Wolfson, M. F.; Rauch, C. T.; Castner, B. J.; Davis, C. H. R.; Petersen, M.; Fitzner, J.N.; Cerretti D. P.; March, C. J.; Paxton, R. J.; Black, R. A.; Bode, W. *Proc. Natl. Acad. Sci. USA* **1998**, *95*, 3408–3412.
44. Lovejoy, B.; Cleaby, A.; Hassell, A. M.; Longley, K.; Luther, M. A.; Weigl, D.; McGeehan, G.; McElroy, A. B.; Drewry, D.; Lambert, M. H.; Jordan, S. R. *Science* **1994**, *263*, 375–377.
45. Moy, F. J.; Chanda, P. K.; Cosmi, S.; Pisano, M. R.; Urbano, C.; Wilhelm, J.; Powers, R. *Biochemistry* **1998**, *37*, 1495–1504.
46. Moy, F. J.; Chanda, P. K.; Chen, J. M.; Cosmi, S.; Edris, W.; Skotnicki, J. S.; Wilhelm, J.; Powers, R. *Biochemistry* **1999**, *38*, 7085–7096.
47. Browner, M. F.; Smith, W. W.; Castelhano, A. L. *Biochemistry* **1995**, *34*, 6602–6610.
48. Gooley, P. R.; O'Connell, J. F.; Marcy, A. I.; Cuca, G. C.; Salowe, S. P.; Bush, B. L.; Hermes, J. D.; Esser, C. K.; Hagmann, W. K.; Springer, J. P.; Johnson, B. A. *Nat. Struct. Biol.* **1994**, *1*, 111–118.
49. Li, Y. C.; Zhang, X.; Melton, R.; Ganu, V.; Gonnella, N. C. *Biochemistry* **1998**, *37*, 14048–14056.
50. Van Doren, S. R.; Kurochkin, A. V.; Hu, W.; Ye, W. Z.; Johnson, L. L.; Hupe, D. J.; Zuiderweg, E. R. *Protein Sci.* **1995**, *4*, 2487–2498.
51. Chen, L.; Rydel, T. J.; Gu, F.; Dunaway, C. M.; Pikul, S.; Dunham, K. M.; Bartlett, B. L. *J. Mol Biol.* **1999**, *293*, 545–557.
52. Dharnaraj, V.; Ye, Q. Z.; Johnson, L. L.; Hupe, D. J.; Ortwine, D. F.; Dunbar, J. B., Jr; Rubin, J. R.; Pavlovsky, A.; Humblet, C.; Blundell, T. L. *Structure* **1996**, *4*, 375–386.
53. Morgunova, E.; Tuuttilla, A.; Bergmann, U.; Isupov, M.; Lindqvist, Y.; Schneider, G.; Tryggvason, K. *Science* **1999**, *284*, 1667–1670.
54. Moy, F. J.; Chanda, P. K.; Chen, J. M.; Cosmi, S.; Edris, W.; Levin, J. I.; Powers, R. *J. Mol. Biol.* **2000**, *302*, 671–689.
55. Botos, I.; Meyer, E.; Swanson, S. M.; Lemaître, V.; Eeckhout, Y.; Meyer, E. F. *J. Mol. Biol.* **1999**, *292*, 837–844.
56. Wang, Z.; Quiocho, F. A. *Biochemistry* **1998**, *37*, 8314–8324.
57. Wilson, D. K.; Rudolph, F. B.; Quiocho, F. A. *Science* **1991**, *252*, 1278–1284.
58. Betts, L.; Xiang, S.; Short, S. A.; Wolfenden, R.; Carter, C. W., Jr., *J. Mol. Biol.* **1994**, *235*, 635–656.
59. Xiang, S.; Short, S. A.; Wolfenden, R.; Carter, C. W., Jr. *Biochemistry* **1995**, *34*, 4516–4523.
60. Chan, M. K.; Gong, W.; Rajagopalan, P. T.; Hao, B.; Tsai, C. M.; Pei, D. *Biochemistry* **1997**, *36*, 13904–13909.
61. Becker, J. W.; Marcy, A. I.; Rokosz, L. L.; Axel, M. G.; Burbaum, J. J.; Fitzgerald, P. M.; Cameron, P. M.; Esser, C. K.; Hagmann, W. K.; Hermes, J. D. *Protein Sci.* **1995**, *4*, 1966–1976.
62. Meinnel, T.; Blanquet, S.; Dardel, F. *J. Mol. Biol.* **1996**, *262*, 375–386.
63. Ko, T. P.; Liao, C. C.; Ku, W. Y.; Chak, K. F.; Yuan, H. S. *Structure* **1999**, *7*, 91–102.
64. Auerbach, G.; Herrmann, A.; Baracher, A.; Bader, G.; Gutlich, M.; Fischer, M.; Neukamn, M.; Garrido-Franco, M.; Richardson, J.; Nar, H.; Huber, R.; Bacher, A. *Proc. Natl. Acad. Sci. USA* **2000**, *97*, 13567–13572.
65. Cheng, X.; Zhang, X.; Pflugrath, J. W.; Studier, F. W. *Proc. Natl. Acad. Sci. USA* **1994**, *91*, 4034–4038.
66. Carfi, A.; Pares, S.; Duee, E.; Galleni, M.; Duez, C.; Frere, J. M.; Dideberg, O. *EMBO J.* **1995**, *14*, 4914–4921.
67. Carfi, A.; Duee, E.; Paul-Soto, M. R.; Galleni, M.; Frere, J. M.; Dideberg, O. *Acta Cryst. D.* **1998**, *54*, 45–57.
68. Carfi, A.; Duee, E.; Galleni, M.; Frere, J. M.; Dideberg, O. *Acta Cryst. D.* **1998**, *54*, 313–323.
69. Fabiane, S. M.; Sohi, M. K.; Wan, T.; Payne, D. J.; Bateson, J. H.; Mitchell, T.; Sutton, B. J. *Biochemistry* **1998**, *37*, 12404–12411.
70. Concha, N. O.; Janson, C. A.; Rowling, P.; Pearson, S.; Cheever, C. A.; Clarke, B. P.; Lewis, C.; Galleni, M.; Frere, J. M.; Payne, D. J.; Bateson, J. H.; Abdel-Meguid, S. S. *Biochemistry* **2000**, *39*, 4288–4298.

71. Stec, B.; Hehir, M. H. J.; Brennan, C.; Nolte, M.; Kantrowitz, E. R. *J. Mol. Biol.* **1998**, *277*, 647–662.

72. Kim, E. E.; Wyckoff, H. W. *J. Mol. Biol.* **1991**, *218*, 449–464.

73. Hough, E.; Hansen, L. K.; Birknes, B.; Jynge, K.; Hansen, S.; Hordvik, A.; Little, C.; Dodson, E.; Derewenda, Z. *Nature* **1989**, *338*, 357–360.

74. Volbeda, A.; Lahm, A.; Sakiyama, F.; Suck, D. *EMBO J.* **1991**, *10*, 1607–1618.

75. Love, R. A.; Parge, H. E.; Wickersham, J. A.; Hostomsky, Z.; Habuka, N.; Moomaw, E. W.; Adachi, T.; Hostomska, Z. *Cell* **1996**, *87*, 331–342.

76. Yan, Y.; Li, Y.; Munshi, S.; Sardana, V.; Cole, J. L.; Sardana, M.; Steinkuehler, C.; Tomei, L.; De Francesco, R.; Kuo, L. C.; Chen, Z. *Protein Sci.* **1998**, *7*, 837–847.

77. Kannan, K. K.; Notstrand, B.; Fridborg, K.; Lovgren, S.; Ohlsson, A.; Petef, M. *Proc. Natl. Acad. Sci. USA* **1975**, *72*, 51–55.

78. Liljas, A.; Kannan, K. K.; Bergsten, C.; Waara, I.; Fridbrg, K.; Strandberg, B.; Carlbom, U.; Jarup, L.; Lovgren, S.; Petef, M. *Nat. New. Biol.* **1972**, *235*, 131–137.

79. Eriksson, A. E.; Liljas, A. *Proteins* **1993**, *16*, 29–42.

80. Stams, T.; Nair, S. K.; Okuyama, T.; Waheed, A.; Sly, W. S.; Christianson, D. W. *Proc. Natl. Acad. Sci. USA* **1996**, *93*, 13589–13594.

81. Burgisser, D. M.; Thony, B.; Redweik, U.; Hess, D.; Heizmann, C. W.; Huber, R.; Nar, H. *J. Mol. Biol.* **1995**, *253*, 358–369.

82. Ploom, T.; Thony, B.; Yim, J.; Lee, S.; Nar, H.; Leimbacher, W.; Richardson, J.; Huber, R. Auerbach G. *J. Mol. Biol.* **1999**, *286*, 851–860.

83. Erskine, P. T.; Norton, E.; Cooper, J. B.; Lambert, R.; Coker, A.; Lewis, G.; Spencer, P.; Sarwar, M.; Wood, S. P.; Warren, M. J. *Biochemistry* **1999**, *38*, 4266–4276.

84. Fessner, W.-D.; Schneider, A.; Held, H.; Sinerius, G.; Walker, C.; Hixon, M.; Schloss, J. V. *Angew. Chem. Int. Ed. Engl.* **1996**, *35*, 2219–2221.

85. Dreyer, M. K.; Schulz, G. E. *J. Mol. Biol.* **1996**, *259*, 458–466.

86. Joerger, A. C.; Mueller-Dieckmann, C.; Schulz, G. E. *J. Mol. Biol.* **2000**, *303*, 531–543.

87. Hall, D. R.; Leonard, G. A.; Reed, C. D.; Watt, I.; Berry, A.; Hunter, W. N. *J. Mol. Biol.* **1999**, *287*, 383–394.

88. Zgiby, S.; Plater, A. R.; Bates, M. A.; Thomson, G. J.; Berry, A. *J. Mol. Biol.* **2002**, *315*, 131–140.

89. Auld, D. S.; Vallee, B. L. Neuberger, H.Brocklehurst, K. Eds.; *Hydrolytic Enzymes* **1987**, 201. Elsevier: Amsterdam.

90. Christiansen, D. W.; Lipscomb, W. N. L. *Acc. Chem. Res.* **1989**, *222*, 62–69.

91. Mattews, B. W. *Acc. Chem. Res.* **1988**, *21*, 333–340.

92. Botre, F.; Gros, G.; Storey, B. T. *Carbonic Anhydrase* **1991**, VCH: New York.

93. Deutsch, H. F. *Int. J. Biochem.* **1987**, *19*, 101–113.

94. Silverman, D. N.; Lindskog, S. *Acc. Chem. Res.* **1988**, *21*, 30–36.

95. Christianson, D. W.; Fierke, C. A. *Acc. Chem. Res.* **1996**, *29*, 331–339.

96. Sly, W. S.; Hu, P. Y. *Ann. Rev. Biochem.* **1995**, *64*, 375–401.

97. Bertini, I.; Luchinat, C.; Messori, L.; Monnanni, R. *Biochemistry* **1988**, *27*, 8318–8325.

98. Auld, D. S. *Structure and Biology* **1997**, *89*, 29–50.

99. Christianson, D. W.; Lipscomb, W. N. *Proc. Natl. Acad. Sci. USA* **1985**, *82*, 6840–6844.

100. Christianson, D. W.; Lipscomb, W. N. *J. Am. Chem. Soc.* **1986**, *108*, 4998–5003.

101. Samuelsson, B.; Dahlén, S.-E.; Lindgren, J. Å.; Rouzer, C. A.; Serhan, C. N. *Science* **1987**, *237*, 1171–1177.

102. Medina, J. F.; Wetterholm, A.; Radmark, O.; Shapiro, R.; Haeggström, J. Z.; Vallee, B. L.; Samuelsson, B. *Proc. Natl. Acad. Sci. USA* **1991**, *88*, 7620–7624.

103. Dideberg, O.; Charlier, P.; Dive, G.; Joris, B.; Frere, J. M.; Ghuysen, J. M. *Nature* **1982**, *299*, 469–470.

104. Healy, V. L.; Park, I.-S.; Walsh, C. T. *Chem. Biol.* **1998**, *5*, 197–207.

105. Lessard, I. A. D.; Walsh, C. T. *Chem. Biol.* **1999**, *6*, 177–187.

106. Yang, H. Y. T.; Erdös, E. G.; Levin, Y. *Biochem. Biophys. Acta* **1970**, *214*, 374–376.

107. Soubrier, F.; Alhenc-Gelas, F.; Hubert, C.; Allegrini, J.; John, M.; Tregear, G.; Corvol, P. *Proc. Natl. Acad. Sci. USA* **1988**, *85*, 9386–9390.

108. Stöcker, W.; Wolz, R. L.; Zwilling, R.; Strydom, D. J.; Auld, D. S. *Biochemistry* **1988**, *27*, 5026–5032.

109. Auld, D. S. *Faraday Discuss.* **1992**, *93*, 117–120.

110. Mock, W. L.; Yao, J.; Ming, L.-J. *Biochemistry* **1997**, *36*, 4949–4958.

111. Park, H. I.; Park, L.-J. *J. Inorg. Biochem.* **1998**, *72*, 57–62.

112. Park, H. I.; Ming, L.-J. *J. Biol. Inorg. Chem.* **2002**, *7*, 600–610.

113. MacDougall, J. R.; Matrisian, J. M. *Cancer Metastasis Rev.* **1995**, *14*, 351–362.

114. Chandler, S.; Miller, K. M.; Clements, J. M.; Luryh, J.; Corkill, D.; Anthonyh, D. C. C.; Adams, S. E.; Gearing, A. J. H. *J. Neuroimmun.* **1997**, *72*, 155–161.

115. Johnson, L. L.; Dyer, R.; Hupe, D. J. *Curr. Opin. Chem. Biol.* **1998**, *2*, 466–471.

116. Massova, I.; Kotra, L. P.; Fridman, R.; Mobashery, S. *FASEB J.* **1998**, *12*, 1075–1095.

117. Whittaker, M.; Floyd, C. D.; Brown, P.; Gearing, A. J. H. *Chem. Rev.* **1999**, *99*, 2735–2776.

118. Lovejoy, B.; Hassell, A. M.; Luther, M. A.; Weigl, D.; Jordan, S. R. *Biochemistry* **1994**, *33*, 8207–8217.

119. Carlow, D.C.; Carter, C.W.; Mejlhede, N.; Neuhard, J.; Wolfenden, R. *Biochemistry* **1999**, *38*, 12258–12265.

120. Mejlhede, N.; Neuhard, J. *Biochemistry* **2000**, *39*, 7984–7989.

121. Frere, J.-M. *Mol. Microbiol.* **1995**, *16*, 385–395.

122. Matagne, A.; Dubus, A.; Galleni, M.; Frere, J.-M. *Natl. Prod. Rep.* **1999**, *16*, 1–19.

123. Bush, K. *Clin. Infect. Dis.* **1998**, *27*, S48–S53.

124. Page, M. I.; Laws, A. P. *J. Chem. Soc., Chem. Commun.* **1998**, 1609–1617.

125. Wang, Z.; Fast, W.; Valentine, A. M.; Benkovic, S. J. *Curr. Opin. Chem. Biol.* **1999**, *3*, 614–622.

126. Wright, G. D. *Chem. Biol.* **2000**, *7*, R127–R132.

127. Bicknell, R.; Schäffer, A.; Waley, S. G.; Auld, D. S. *Biochemistry* **1986**, *25*, 7208–7215.

128. Sutton, B. J.; Artymicuk, P. J.; Corder-Borboa, A. E.; Little, C.; Phillips, D. C.; Waley, S. G. *Biochem. J.* **1987**, *248*, 181–188.

129. Suárez, D.; Merz, K. M., Jr. *J. Am. Chem. Soc.* **2001**, *123*, 3759–3770.

130. Bounaga, S.; Laws, A. P.; Galleni, M.; Page, M. I. *Biochem. J.* **1998**, *331*, 703–711.
131. Paul-Soto, R.; Bauer, R.; Frere, J.-M.; Galleni, M.; Meyer-Klaucke, W.; Nolting, H.; Rossolini, G.; deSeny, M. D.; Hernandez-Valladares, M.; Zeppezauer, M.; Adolph, H.-W. *J. Biol. Chem.* **1999**, *274*, 13242–13249.
132. Wang, Z.; Fast, W.; Benkovic, S. J. *J. Am. Chem. Soc.* **1998**, *120*, 10788–10789.
133. Wang, Z.; Benkovic, S. J. *J. Biol. Chem.* **1998**, *273*, 22402–22408.
134. Wang, Z.; Fast, W.; Benkovic, S. J. *Biochemistry* **1999**, *38*, 10013–10023.
135. Butler-Ransohoff, J. E.; Kendall, D. A.; Kaiser, E. T. In *Metal Ions in Biological Systems,* Sigel H., Sigel, A. Eds.; Marcel Dekker: New York, 1976, Vol. 25, pp 395–415.
136. Sträter, N.; Lipscom, W. N.; Klabunde, T.; Krebs, B. *Angew. Chem. Int. Ed. Engl.* **1996**, *35*, 2025–2055.
137. Wilcox, D. E. *Chem. Rev.* **1996**, *96*, 2435–2458.
138. Kim, E. E.; Wyckoff, H. W. *Clin. Chim. Acta* **1989**, *186*, 175–188.
139. Coleman, J. E. *Ann. Rev. Biophys. Biomol. Struct.* **1992**, *21*, 441–483.
140. Holtz, K. M.; Stec, B.; Kantrowitz, E. R. *J. Biol. Chem.* **1999**, *274*, 8351–8354.
141. Holtz, K. M.; Kantrowitz, E. R. *FEBS Lett.* **1999**, *462*, 7–11.
142. Stec, B.; Holtz, K. M.; Kantrowitz, E. R. *J. Mol. Biol.* **2000**, *299*, 1303–1311.
143. Linskog, S.; Lilias, A. *Curr. Opin. Struct. Biol.* **1993**, *3*, 915–920.
144. Wong, C.-H.; Whitesides, G. M. *Enzymes in Synthetic Organic Chemistry* **1994**, Pergamon: Oxford.
145. Fessner, W.-D.; Walter, C. *Topics in Current Chemistry* **1996**, *184*, 97–194.
146. Machajewski, T. D.; Wong, C.-H. *Angew. Chem. Int. Ed. Engl.* **2000**, *39*, 1352–1374.
147. Yoshida, M.; Kijima, M.; Kita, M.; Beppu, T. *J. Biol. Chem.* **1990**, *265*, 17174–17179.
148. Yoshida, M.; Horinouchi, S.; Beppu, T. *BioEssays* **1995**, *17*, 423–430.
149. Hassig, C. A.; Tong, J. K.; Schreiber, S. L. *Chem. Biol.* **1997**, *4*, 783–789.
150. Hassig, C. A.; Schreiber, S. L. *Curr. Opin. Chem. Biol.* **1997**, *1*, 300–308.
151. Finnin, M. S.; Doninglan, J. R.; Cohen, A.; Richon, V. M.; Rifkind, R. A.; Marks, P. A.; Breslow, R.; Pavietich, N. P. *Nature* **1999**, *401*, 188–193.
152. Duesbery, N. S.; Webb, C. P.; Leppla, S. H.; Gordon, V. M.; Klimpel, K. R.; Copeland, T. D.; Ahn, N. G.; Oskarsson, M. K.; Fukusawa, K.; Paull, K. D.; Vande Woude, G. F. *Science* **1998**, *280*, 734–737.
153. Dixon, T. C.; Meselson, M.; Guillemin, J.; Hanna, P. C. *New Engl. J. Med.* **1999**, *341*, 815–826.
154. Pannifer, A. D.; Wong, T. Y.; Schwarzenbacher, R.; Renatus, M.; Petosa, C.; Bienkowska, J.; Lacy, D. B.; Collier, R. J.; Park, S.; Leppla, S. H.; Hanna, P.; Liddington, R. C. *Nature* **2001**, *414*, 229–233.
155. Silverman, R. B. *The Organic Chemistry of Drug Design and Drug Action* **1992**, Academic Press: San Diego, CA.
156. Ahnfelt-Rönne, I. In *A Textbook of Drug Design and Development,* 2nd ed., Korgsgaard-Larsen, P., Liljefors, T., Madsen, U., Eds.; Harwood Academic: Amsterdam, The Netherlands,1996, pp 289–326.
157. Leung, D.; Abbenante, G.; Fairlie, D. P. *J. Med. Chem.* **2000**, *43*, 305–341.
158. Gante, J. *Angew. Chem. Int. Ed. Engl.* **1994**, *33*, 1699–1720.
159. Babine, R. E.; Bender, S. L. *Chem. Rev.* **1997**, *97*, 1359–1472.
160. Ondetti, M. A.; Rubin, B.; Cushman, D. W. *Science* **1977**, *196*, 441–444.
161. Cushman, D. W.; Cheung, H. S.; Sabo, E. F.; Ondetti, M. A. *Biochemistry* **1977**, *16*, 5484–5491.
162. Ondetti, M. A.; Condon, M. E.; Reid, J.; Sabo, E. F.; Cheung, G. S.; Cushman, D. W. *Biochemistry* **1979**, *18*, 1427–1430.
163. Byers, L. D.; Wolfenden, R. *Biochemistry* **1973**, *12*, 2070–2078.
164. Hanson, J. E.; Kaplan, A. P.; Bartlett, P. A. *Biochemistry* **1989**, *28*, 6294–6305.
165. Kaplan, A. P.; Bartlett, P. A. *Biochemistry* **1991**, *30*, 8165–8170.
166. Kim, D. H.; Kim, K. B. *J. Am. Chem. Soc.* **1991**, *113*, 3200–3202.
167. Yun, M.; Park, C.; Kim, S.; Nam, D.; Kim, S. C.; Kim, D. H. *J. Am. Chem. Soc.* **1992**, *114*, 2281–2282.
168. Ryu, S.-E.; Choi, H.-C.; Kim, D. H. *J. Am. Chem. Soc.* **1997**, *119*, 38–41.
169. Kim, D. H.; Jin, Y. *Bioorg. Med. Chem. Lett.* **1999**, *9*, 691–696.
170. Han, M. S.; Ryu, C. H.; Chung, S. J.; Kim, D. H. *Org. Lett.* **2000**, *2*, 3149–3152.
171. Tanaka, Y.; Grapsas, I.; Dakoji, S.; Cho, Y. J.; Mobashery, S. *J. Am. Chem. Soc.* **1994**, *116*, 7475–7480.
172. Massova, I.; Martin, P.; de Mel, S.; Tanaka, Y.; Edwards, B.; Mobashery, S. *J. Am. Chem. Soc.* **1996**, *118*, 12479–12480.
173. Mock, W. L.; Cheng, H. *Biochemistry* **2000**, *39*, 13945–13952.
174. Bartlett, P. A.; Marlowe, C. K. *Science* **1987**, *235*, 569–571.
175. Tronrud, D. E.; Holden, H. M.; Matthews, B. W. *Science* **1987**, *235*, 571–574.
176. Morgan, B. P.; Scholtz, J. M.; Ballinger, M. D.; Zipkin, I. D.; Bartlett, P. A. *J. Am. Chem. Soc.* **1991**, *113*, 297–307.
177. Morgan, B. P.; Holland, D. R.; Matthews, B. R.; Bartlett, P. A. *J. Am. Chem. Soc.* **1994**, *116*, 3251–3260.
178. Wu, Z.; Walsh, C. T. *Proc. Natl. Acad. Sci. USA* **1995**, *92*, 11603–11607.
179. Cawston, T. E. *Pharm. Ther.* **1996**, *70*, 163–182.
180. Segel, I. H. *Biochemical Calculations* 2nd ed. **1976**, Wiley: New York.
181. Fitzgerald, P. M. D.; Wu, J. K.; Toney, J. H. *Biochemistry* **1998**, *37*, 6791–6800.
182. Toney, J. H.; Fitzgerald, P. M. D.; Grover-Shamama, N.; Olson, S. H.; May, W. J.; Sundelof, J. G.; Vanderwall, D. E.; Cleary, K. A.; Grant, S. K.; Wu, J. K.; Kozarich, J. W.; Pompliano, D. L.; Hammond, G. G. *Chem. Biol.* **1998**, *5*, 185–196.
183. Mann, T.; Keilin, D. *Nature* **1940**, *146*, 164–165.
184. Chen, R. F.; Kernohan, J. C. *J. Biol. Chem.* **1967**, *242*, 5813–5823.
185. Nair, S. K.; Krebs, J. F.; Christianson, D. W.; Fierke, C. A. *Biochemistry* **1995**, *34*, 3981–3989.
186. Nair, S. K. Elbau D.; Christianson, D. W. *J. Biol. Chem.* **1996**, *271*, 1003–1007.
187. Huang, S.; Xue, Y.; Sauer-Eriksson, E.; Chirica, L.; Lindskog, S.; Jonsson, B.-H. *J. Mol. Biol.* **1998**, *283*, 301–310.
188. Scolnick, L. R.; Clements, A. M.; Liao, J.; Crenshaw, L.; Hellberg, M.; May, J.; Dean, T. R.; Christianson, D. W. *J. Am. Chem. Soc.* **1997**, *119*, 850–851.
189. Gao, P. J.; Cheng, X.; Chen, R.; Sigal, G. B.; Bruce, J. E.; Schwartz, B. L.; Hofstadler, S. A.; Anderson, G. A.; Smigh, R. D.; Whitesides, G. M. *J. Med. Chem.* **1996**, *39*, 1949–1955.
190. Ganesan, A. *Angew. Chem. Int. Ed. Engl.* **1998**, *37*, 2828–2831.

191. Lehn, J.-M. *Chem. Eur. J.* **1999**, *5*, 2455–2463.
192. Cousins, G. R. L.; Poulsen, S.-A.; Sanders, J. K. M. *Curr. Opin. Chem. Biol.* **2000**, *4*, 270–279.
193. Huc, I.; Lehn, J.-M. *Proc. Natl. Acad. Sci. USA* **1997**, *94*, 2106–2110.
194. Riggs, M. G.; Whittaker, R. G.; Neumann, J. R.; Ingram, V. M. *Nature* **1977**, *268*, 426–465.
195. Takahashi, I.; Miyaji, H.; Yoshida, T.; Sato, S.; Mizukami, T. *J. Antibiotics* **1996**, *49*, 453–457.
196. Kijima, M.; Yoshida, M.; Sugita, K.; Horinouchi, S.; Beppu, T. *J. Biol. Chem.* **1993**, *268*, 22429–22435.
197. Taunton, J.; Hassig, C. A.; Schreiber, S. L. *Science* **1996**, *272*, 408–411.
198. Taunton, J.; Collins, J. L.; Schreiber, S. L. *J. Am. Chem. Soc.* **1996**, *118*, 10412–10422.
199. Kwon, H. J.; Owa, T.; Hassig, C. A.; Shimada, J.; Schreiber, S. L. *Proc. Natl. Acad. Sci. USA* **1998**, *95*, 3356–3561.
200. Furumai, R.; Komatsu, Y.; Nishino, N.; Khochbin, S.; Yoshida, M.; Horinouchi, S. *Proc. Natl. Acad. Sci. USA* **2001**, *98*, 87–92.
201. Katz, B. A.; Clark, J. M.; Finer-Moore, J. S.; Jenkins, T. E.; Johnson, C. R.; Ross, M. J.; Luong, C.; Moore, W. R.; Stroud, R. M. *Nature* **1998**, *391*, 608–612.
202. Chin, J. *Acc. Chem. Res.* **1991**, *24*, 145–152.
203. Suh, J. *Acc. Chem. Res.* **1992**, *25*, 275–286.
204. Suh, J.; Park, T. H.; Hwang, B. K. *J. Am. Chem. Soc.* **1992**, *114*, 5141–5146.
205. Breslow, R. *Acc. Chem. Res.* **1995**, *28*, 146–153.
206. Kimura, E.; Koike, T. In *Comprehensive Supramolecular Chemistry*; Reinhoudt, D. N., Ed; Pergamon: Tokyo, 1996; Vol. 10, pp 429–444.
207. Kimura, E.; Koike, T. *J. Chem. Soc., Chem. Commun.* **1998**, 1495–1500.
208. Kimura, E.; Koike, T. In *Bioinorganic Catalysis*, Reedijk, J., Bouwman, E., Eds; Marcel Dekker: New York, 1999, pp 33–54.
209. Vahrenkamp, H. *Acc. Chem. Res.* **1999**, *32*, 589–596.
210. Krämer, R. *Coord. Chem. Rev.* **1999**, *182*, 243–261.
211. Bashkin, J. K. *Curr. Op. Chem. Biol.* **1999**, *3*, 752–758.
212. Parkin, G. *J. Chem. Soc., Chem. Commun.* **2000**, 1971–1985.
213. Parkin, G. In *Metal Ions in Biological Systems;* Marcel Dekker: New York, 2001; Vol. 38; p. 411–460.
214. Woolley, P. *Nature* **1975**, *258*, 677–682.
215. Woolley, P. *J. Chem. Soc., Perkin Trans.* **1977**, *2*, 318–324.
216. Kimura, E.; Shiota, T.; Koike, T.; Shiro, M.; Kodama, M. *J. Am. Chem. Soc.* **1990**, *112*, 5805–5811.
217. Zhang, X.; van Eldik, R.; Koike, T.; Kimura, E. *Inorg. Chem.* **1993**, *32*, 5749–5755.
218. Koike, T.; Kimura, E. *J. Am. Chem. Soc.* **1991**, *113*, 8935–8941.
219. Kimura, E.; Koike, T. *Comments Inorg. Chem.* **1991**, *11*, 285–301.
220. Kimura, E.; Koike, T.; Shionoya, M. In *Structure and Bonding: Metal Sites in Proteins and Models*; Sadler, J. P., Ed.; Springer: Berlin, 1997; 89, pp 1–28.
221. Kimura, E. *Yakugaku-Zasshi* **1996**, *116*, 587–605.
222. Kimura, E. *Yakugaku-Zasshi* **2002**, *122*, 219–236.
223. Bazzicalupi, C.; Bencini, A.; Bianchi, A.; Fusi, V.; Giorgi, C.; Paolettti, P.; Valtancoli, B.; Zanchi, D. *Inorg. Chem.* **1997**, *36*, 2784–2790.
224. Alsfasser, R.; Powell, A. K.; Vahrenkamp, H. *Angew. Chem. Int. Ed. Engl.* **1990**, *29*, 898–899.
225. Alsfasser, R.; Trofimenko, S.; Looney, A.; Parkin, G.; Vahrenkamp, H. *Inorg. Chem.* **1991**, *30*, 4098–4100.
226. Chaudhuri, P.; Stockheim, C.; Wieghardt, K.; Peck, W.; Gregorzik, R.; Vahrenkamp, H.; Nuber, B.; Weiss, J. *Inorg. Chem.* **1992**, *31*, 1451–1457.
227. Alsfasser, R.; Ruf, M.; Trofimenko, S.; Vaherenkamp, H. *Chem. Ber.* **1993**, *126*, 703–710.
228. Ruf, M.; Weis, K.; Vahrenkamp, H. *J. Am. Chem. Soc.* **1999**, *118*, 9288–9294.
229. Ruf, M.; Vahrenkamp, H. *Chem. Ber.* **1996**, *129*, 1025–1028.
230. Ruf, M.; Vahrenkamp, H. *Inorg. Chem.* **1996**, *35*, 6571–6578.
231. Brand, V.; Rombach, M.; Vahrenkamp, H. *J. Chem. Soc., Chem. Commun.* **1998**, 2717–2718.
232. Ruf, M.; Weis, K.; Vahrenkamp, H. *Inorg. Chem.* **1997**, *36*, 2130–2137.
233. Weis, K.; Rombach, M.; Ruf, M.; Vahrenkamp, H. *Eur. J. Inorg. Chem.* **1998**, 263–270.
234. Looney, A.; Han, R.; McNeill, K.; Parkin, G. *J. Am. Chem. Soc.* **1993**, *115*, 4690–4697.
235. Kimblin, C.; Allen, W. E.; Parkin, G. *J. Chem. Soc., Chem. Commun.* **1995**, 1813–1815.
236. Bergquist, C.; Parkin, G. *J. Am. Chem. Soc.* **1999**, *121*, 6322–6323.
237. Kuchta, M. C.; Parkin, G. *J. Chem. Soc., Dalton Trans.* **1998**, 2279–2280.
238. Ghosh, P.; Parkin, G. *J. Chem. Soc., Dalton Trans.* **1998**, 2281–2283.
239. Hikichi, S.; Tanaka, M.; Moro-oka, Y.; Kitajima, N. *J. Chem. Soc., Chem. Commun.* **1992**, 814–815.
240. Kitajima, N.; Hikichi, S.; Tanaka, M.; Moro-oka, Y. *J. Am. Chem. Soc.* **1993**, *115*, 5496–5508.
241. Nakata, K.; Shimomura, N.; Shiina, N.; Izumi, M.; Ichikawa, K.; Shiro, M. *J. Inorg. Biochem.* **2002**, *89*, 255.
242. Kahne, D.; Still, W. C. *J. Am. Chem. Soc.* **1988**, *110*, 7592–7534.
243. Kimura, E.; Gotoh, T.; Aoki, S.; Shiro, M. *Inorg. Chem.* **2002**, *41*, 3239–3248.
244. Sakiyama, H.; Mochizuki, R.; Sugawara, A.; Sakamoto, M.; Nishida, Y.; Yamasaki, M. *J. Chem. Soc., Dalton Trans.* **1999**, 997–1000.
245. Bordignon Luiz, M. T.; Szpoganicz, B.; Rizzoto, M.; Basellote, M. G.; Martell, A. E. *Inorg. Chim. Acta* **1999**, *287*, 134–141.
246. Rana, T. M.; Meares, C. F. *J. Am. Chem. Soc.* **1990**, *112*, 2457–2459.
247. Zhu, L.; Qin, L.; Parac, T. N.; Kostic, N. M. *J. Am. Chem. Soc.* **1994**, *116*, 5218–5224.
248. Parac, T. N.; Kostic, N. M. *J. Am. Chem. Soc.* **1996**, *118*, 51–58.
249. Chen, X.; Zhu, L.; You, X.; Kostic, N. M. *J. Biol. Inorg. Chem.* **1998**, *3*, 1–8.
250. Parac, T. N.; Ullmann, G. M.; Kostic, N. M. *J. Am. Chem. Soc.* **1999**, *121*, 3127–3135.
251. Hegg, E. L.; Burstyn, J. N. *J. Am. Chem. Soc.* **1995**, *117*, 7015–7016.
252. Kimura, E. *Acc. Chem. Res.* **2001**, *34*, 171–179.
253. Kimura, E.; Nakamura, I.; Koike, T.; Shionoya, M.; Kodama, Y.; Ikeda, T.; Shiro, M. *J. Am. Chem. Soc.* **1994**, *116*, 4764–4771.

254. Koike, T.; Kajitani, S.; Nakamura, I.; Kimura, E.; Shiro, M. *J. Am. Chem. Soc.* **1995**, *117*, 1210–1219.
255. Kimura, E.; Kodama, Y.; Koike, T.; Shiro, M. *J. Am. Chem. Soc.* **1995**, *117*, 8304–8311.
256. Koike, T.; Inoue, M.; Kimura, E.; Shiro, M. *J. Am. Chem. Soc.* **1996**, *118*, 3091–3099.
257. Breslow, R.; Berger, D.; Huang, D.-L. *J. Am. Chem. Soc.* **1990**, *112*, 3686–3687.
258. Chu, F.; Smith, J.; Lynch, V. M.; Anslyn, E. V. *Inorg. Chem.* **1995**, *34*, 5689–5690.
259. Chapman, W. H., Jr.; Breslow, R. *J. Am. Chem. Soc.* **1995**, *117*, 5462–5469.
260. Yashiro, M.; Ishikubo, A.; Komiyama, M. *J. Chem. Soc., Chem. Commun.* **1995**, 1793–1794.
261. Yashiro, M.; Ishikubo, A.; Komiyama, M. *J. Chem. Soc., Chem. Commun.* **1997**, 83–84.
262. Chin, J. *Curr. Opin. Chem. Biol.* **1997**, *1*, 514–521.
263. Chin, J. *Acc. Chem. Res.* **1999**, *32*, 485–493.
264. Trawick, B. N.; Daniher, A. T.; Bashkin, J. K. *Chem. Rev.* **1998**, *98*, 939–960.
265. Cowan, J. A. *Chem. Rev.* **1998**, *98*, 1067–1087.
266. Kimura, E. *Curr. Opin. Chem. Biol.* **2000**, *4*, 207–213.
267. Young, M. J.; Chin, J. *J. Am. Chem. Soc.* **1995**, *117*, 10577–10578.
268. Williams, N. H.; Lebuis, A.-M.; Chin, J. *J. Am. Chem. Soc.* **1999**, *121*, 3341–3348.
269. Wall, M.; Linkletter, B.; Williams, D.; Lebuis, A.-M.; Hynes, R. C.; Chin, J. *J. Am. Chem. Soc.* **1999**, *121*, 4710–4711.
270. Koike, T.; Takamura, M.; Kimura, E. *J. Am. Chem. Soc.* **1994**, *116*, 8443–8449.
271. Kaminskaia, N. V.; Spingler, B. Lippard S. J. *J. Am. Chem. Soc.* **2000**, *122*, 6411–6422.
272. Kaminskaia, N. V.; Spingler, B. Lippard S. J. *J. Am. Chem. Soc.* **2001**, *123*, 6555–6563.
273. Kimura, E.; Gotoh, T.; Koike, T.; Shiro, M. *J. Am. Chem. Soc.* **1999**, *121*, 1267–1274.
274. Ruf, M.; Weis, K.; Brasack, K.; Vahrenkamp, H. *Inorg. Chim. Acta* **1996**, *250*, 271–281.
275. Elbaum, D.; Nair, S. K.; Patchan, M. W.; Thompson, R. B.; Christianson, D. W. *J. Am. Chem. Soc.* **1996**, *118*, 8381–8387.
276. Thompson, R. B.; Maliwal, B. P. *Anal. Chem.* **1998**, *70*, 1749–1754.
277. Koike, T.; Kimura, E.; Nakamura, I.; Hashimoto, Y.; Shiro, M. *J. Am. Chem. Soc.* **1992**, *114*, 7338–7345.
278. Koike, T.; Watanabe, T.; Aoki, S.; Kimura, E.; Shiro, M. *J. Am. Chem. Soc.* **1996**, *118*, 12696–12703.
279. Kimura, E. *S. Afr. J. Chem.* **1997**, *50*, 240–248.
280. Kimura, E.; Koike, T. *Chem. Soc. Rev.* **1998**, *27*, 179–184.
281. Kimura, E.; Aoki, S. *BioMetals* **2001**, *14*, 191–204.
282. Koike, T.; Abe, T.; Takahashi, M.; Ohtani, K.; Kimura, E.; Shiro, M. *J. Chem. Soc., Dalton Trans.* **2002**, 1764–1768.
283. Huston, M. E.; Akkaya, M. E. U.; Czarnik, A. W. *J. Am. Chem. Soc.* **1989**, *111*, 8735–8737.
284. Vance, D. H.; Czarnik, A. W. *J. Am. Chem. Soc.* **1994**, *116*, 9397–9398.
285. Czarnik, A. W. *Acc. Chem. Res.* **1994**, *27*, 302–308.
286. Czarnik, A. W. *Fluorescent Chemosensors for Ion and Molecule Recognition*; American Chemical Society: Washington, DC, 1993.
287. Zalewski, P. D.; Forbes, I. J.; Betts, W. H. *Biochem. J.* **1993**, *296*, 403–408.
288. Zalewskik, P. D.; Forbes, I. J.; Seamark, R. F.; Borlinghaus, R.; Betts, W. H.; Lincoln, S. F.; Ward, A. D. *Curr. Biol.* **1994**, *1*, 153–161.
289. Truong-Tran, A. Q.; Carter, J.; Ruffin, R. E.; Zalewski, P. D. *BioMetals* **2001**, *14*, 315–330.
290. Hirano, T.; Kikuchi, K.; Urano, Y.; Higuchi, T.; Nagano, T. *Angew. Chem. Int. Ed. Engl.* **2000**, *39*, 1052–1054.
291. Walkup, G. K.; Burdette, S. C.; Lippard, S. J.; Tsien, R. Y. *J. Am. Chem. Soc.* **2000**, *112*, 5644–5645.
292. Burdette, S. C.; Walkup, G. K.; Spingler, B.; Tsien, R. Y.; Lippard, S. J. *J. Am. Chem. Soc.* **2001**, *123*, 7831–7841.
293. Mangani, S.; Ferraroni, M.; Oriori, P. *Inorg. Chem.* **1994**, *33*, 3421–3423.
294. Fujioka, H.; Koike, T.; Yamada, N.; Kimura, E. *Heterocycles* **1996**, *42*, 775–787.
295. Kimura, E.; Aoki, S.; Koike, T.; Shiro, M. *J. Am. Chem. Soc.* **1997**, *119*, 3068–3076.
296. Kimura, E.; Koike, T.; Aoki, S. *J. Synth. Org. Chem. Jpn* **1997**, *55*, 1052–1061.
297. Aoki, S.; Kimura, E. *Rev. Mol. Biotech.* **2002**, *90*, 129–155.
298. Aoki, S.; Iwaida, K.; Hanamoto, N.; Shiro, M.; Kimura, E. *J. Am. Chem. Soc* **2002**, *124*, 5256–5257.

8.24
Dinuclear Hydrolases

B. A. AVERILL
University of Toledo, OH, USA

8.24.1 INTRODUCTION

Phosphate ester and amide bonds are ubiquitous in biochemistry, because they provide the linkages that hold together two of the most important types of biological polymers, nucleic acids and proteins. Phosphate ester bonds are also present in important intracellular components such as nucleotides, while phosphorylation/dephosphorylation of amino acid residues in proteins plays a crucial role in biological signal transduction. In addition, amide bonds are important components of many biologically active small molecules, including peptide hormones and antibiotics. Although hydrolysis of both phosphate ester and amide bonds is thermodynamically spontaneous at pH 7, the kinetic stability of these units represents a major chemical challenge. Living organisms have overcome this challenge by evolving efficient and specific catalysts for the hydrolysis of phosphate esters and amides. Many, but by no means all, of the enzymes that carry out such reactions utilize metal ions as Lewis acids to promote the reactions. As illustrated in Figure 1 for a phosphate ester, in principle a metal ion can accelerate the rate of hydrolysis in three different ways: (i) by coordinating to the substrate to enhance its electrophilicity and neutralize the developing negative charge in the transition state; (ii) by coordinating to the nucleophile (water), thus lowering its pK_a and increasing the effective concentration of the nucleophile; and (iii) by coordinating to and stabilizing the negatively charged leaving group. As we shall see in this review, examples of all of these modes of catalysis are well established.
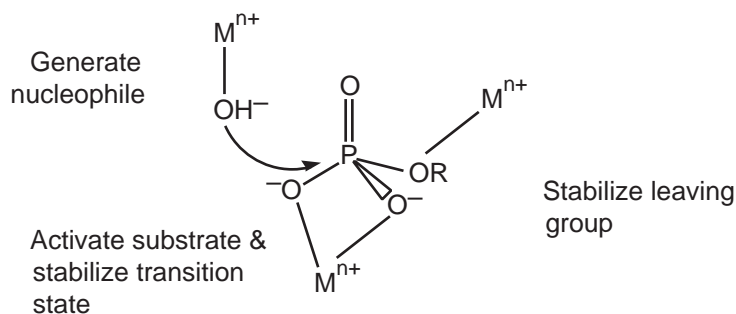
Figure 1 Schematic drawing of the various ways in which metal ions can, in principle, facilitate hydrolysis of a phosphate ester: by providing a coordinated nucleophile, activating the substrate and stabilizing the transition state, and stabilizing the laving group. Similar factors are operative for hydrolysis of amide bonds.

Many hydrolytic metalloenzymes contain only a single metal ion at their active sites; the properties of these systems are discussed in Chapter 8.22. Because the effects of multiple modes of catalysis tend to be multiplicative rather than additive,[1] however, many enzymes utilize two or more metal ions simultaneously to give maximal acceleration of the catalyzed reaction. Such enzymes are the topic of this section. This review will focus on recent developments in this rapidly growing subfield of bioinorganic chemistry. More detailed discussions of the older literature are available in the authoritative reviews by Sträter *et al.*[2] and Wilcox.[3] These earlier reviews were organized by the type of substrate (i.e., phosphate esters vs. amides). In contrast, the present review is organized by the type of metal center present, in order to emphasize the structural and mechanistic similarities between catalysts that utilize similar centers to catalyze different reactions. Hydrolysis of both amides and phosphate esters appears invariably to proceed via an associative mechanism. The nucleophile attacks either the sp^2 carbonyl carbon to give a tetrahedral intermediate or the tetrahedral phosphorus atom to generate a trigonal bipyramidal transition state in which the leaving group is opposite the nucleophile, resulting in inversion of configuration at phosphorus.[4] Given these mechanistic similarities, the utilization of similar constellations of metal ions and acidic or basic groups to facilitate these superficially disparate reactions is not particularly surprising, and comparisons are likely to prove informative.

We shall begin with enzymes that have binuclear centers containing two divalent metal ions, focusing initially on metalloenzymes that contain tightly bound metal ions, where the nature of the physiologically relevant form of the enzyme is not in question. We will then proceed to metal-activated enzymes that also utilize dinuclear metal centers, whose metal ions are less tightly bound and hence are often lost during purification. As we shall see, such enzymes often exhibit comparable activity with a range of metal ions. Consequently, spectroscopic, mechanistic, and structural studies on many of these systems have frequently been performed with metal ions that may not be representative of the form of the enzyme present *in vivo*, which may well depend upon the relative concentrations of metal ions present in a particular intracellular compartment. Subsequently, we will examine the properties of enzymes that contain trivalent–divalent dinuclear metal centers at their active sites, which constitute an important and as yet largely unappreciated class. Given the fact that two metal ions often appear to be better than one, it is not surprising that some enzymes appear to utilize a "the more, the merrier" approach to substrate hydrolysis. We will therefore conclude by considering a few well-characterized examples of metalloenzymes that utilize three or more metal ions simultaneously in catalysis.

In all cases, we will proceed in the following order: (i) a brief discussion of the basic reaction that is catalyzed and the properties of the protein, including the metal ions likely to be present under physiological conditions; (ii) a description of the structural properties of the di- or trimetal active site in the absence and presence of inhibitors, as inferred from spectroscopic, site-directed mutagenesis, and crystallographic studies; and (iii) a discussion of the most recent proposals regarding the enzyme mechanism, as derived from a combination of structural and kinetic studies. Given the great increase in the number of structure determinations in recent years, the discussions will focus much more heavily on structural vs. spectroscopic results than did previous reviews.

Throughout the discussions, we will utilize two of the conventions used by Wilcox in his earlier review.[3] First, because the protonation state of water-derived ligands is difficult to establish directly and depends greatly on both the pH and the identity and environment of the metal ion, we will generally describe such ligands as "water/hydroxide," recognizing that in certain cases

the ligand could actually even be an oxide ion. As we shall see, in many cases the level of structural detail is now such that the major source of controversy is *which* water (hydroxide) of those present at the active site acts as the nucleophile that attacks the substrate that is hydrolyzed. Second, due to a similar uncertainty in the protonation state of phosphate and phosphate esters, which again depends upon the pH, the metal ion to which they are bound, and the local environment, we will not attempt to distinguish between the various possibilities, unless there is unambiguous experimental evidence in support of one or more of the alternatives.

8.24.2 HYDROLASES USING DIVALENT–DIVALENT DIMETAL CENTERS

As noted above, the precise identity of the metal ions used by an enzyme *in vivo* is often problematical, especially for those enzymes whose low affinity for their native metal ions results in their being lost during purification. Nonetheless, it is clear that certain hydrolytic metallo-enzymes contain particular metal ions, which raises the interesting question of how the properties of a given metal ion make it peculiarly suited for catalyzing a particular reaction. As we shall see below, for example, urease contains two Ni^{II} ions as isolated, and forms containing other metal ions such as Mn^{II} are much less active. In contrast, arginase, which catalyzes a reaction that is superficially very similar to that of urease, generally contains Mn^{II} as isolated, and achieves maximal activity with two Mn^{II} per subunit. Unlike urease, however, arginase exhibits significant activity when reconstituted with a variety of other metal ions, including Ni^{II}! Similarly, amino-peptidases are known that contain either two Zn^{II} or, in one possible case, two Co^{II} ions. In addition, two series of Ser/Thr protein phosphatases are known, one of which utilizes a binuclear Mn^{II} center, while the other utilizes a trivalent–divalent dinuclear center containing Fe^{III} and either Zn^{II} or Fe^{II}. Do systems such as these represent independent biochemical solutions to the same chemical problem using randomly selected metals, in which the observed metal ions simply reflect the evolutionary history of the system? Or do the properties of the metal ions somehow make them uniquely suited for these reactions, resulting in evolutionary pressure that selects against other metals? It seems clear that, in many systems at least, it is a gross oversimplification to view the metal ions as Lewis acids whose role in catalysis is dictated simply by their charge-to-radius ratios.

In this section, we will begin with a consideration of urease, for which a great deal of spectroscopic, kinetics, and structural information is now available, and which in many ways is a paradigm that illustrates the interplay between mechanistic, spectroscopic, and structural studies. We will then proceed to systems containing dinuclear zinc, manganese, and cobalt centers, which will be discussed in considerably less detail. We will not, however, consider enzymes that employ dimagnesium centers in catalysis.[5,6] These constitute a rapidly growing group, which includes ribonucleases,[7] endonucleases,[8] exonucleases,[9] inositol poly- and monophosphate and fructose-1,6-bisphosphate phosphatases,[10] and ribozymes.[11] Although these are biologically and in some cases medically important systems, the spectroscopic invisibility of magnesium makes the study of such enzymes a rather separate area, with little overlap of techniques with those typically used to study enzymes containing transition metal ions. The interested reader is referred to the lead references cited above and to Chapter 8.5.

8.24.2.1 Urease, a Dinickel Hydrolase

Urease allows bacteria, fungi, and higher plants to utilize urea as a nitrogen source for growth; it catalyzes the hydrolysis of urea to ammonia and carbamate, which subsequently hydrolyzes spontaneously to ammonia and bicarbonate (Equation (1)):

$$\underset{H_2N}{\overset{O}{\underset{\displaystyle }{\overset{\displaystyle \|}{C}}}}\!\!\underset{NH_2}{} + H_2O \longrightarrow NH_4^+ + NH_2CO_2^D \xrightarrow{\;H_2O\;} 2\,NH_4^+ + CO_2 \qquad (1)$$
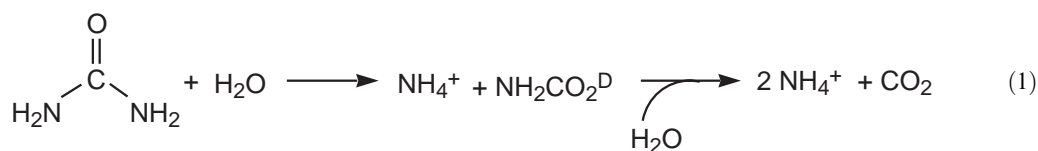
Urease from jack beans was the first enzyme to be crystallized, and based on his chemical analysis of the crystalline enzyme, Sumner in 1926 made the revolutionary proposal that enzymes

were pure proteins that contained only amino acids.[12] In 1975, however, Zerner *et al.* demonstrated convincingly that urease was in fact a nickel enzyme that contained two nickel atoms per catalytic site.[13,14] Subsequent studies have demonstrated that the enzyme consists of an α_6 hexamer, with one active site per 90.4-kDa subunit.[15] Initial kinetics and spectroscopic studies were carried out on the jack bean enzyme, but most recent work has focused on bacterial enzymes, particularly those from *Klebsiella aerogenes*, *Bacillus pasteurii*, and, most recently, *Helicobacter pylori*. Although the latter are trimers of asymmetric trimers, with an overall $(\alpha\beta\gamma)_3$ architecture and two nickel atoms per α subunit, they exhibit >50% sequence homology to the jack bean enzyme.[16,17] In addition, all spectroscopic data reported to date indicate that there are no significant differences between the Ni sites of the bacterial and plant enzymes.[18]

Most surprisingly, the activity of apo-urease cannot be restored by reconstitution with most other divalent metal ions, such as Zn^{II}, Co^{II}, and Cu^{II}, although Mn^{II} gives Å2% of the activity of the reconstituted Ni^{II} enzyme.[19,20] The unique role played by nickel in urease is emphasized by the fact that three other proteins are required for incorporation of nickel into urease[21]. In addition, a fourth protein binds nickel and appears to function as a metallochaperone that provides nickel for insertion into urease.[22,23] Carbon dioxide is also required for nickel binding to apo-urease,[24] which is explained by the incorporation of CO_2 into a carbamylated Lys side chain that bridges the two metal ions (see below). Not surprisingly, CS_2 can replace CO_2 to give a nickel-containing protein that presumably has a bridging dithiocarbamate ligand, but this form of the enzyme is completely inactive.[25] Of the other species examined, only vanadate could replace CO_2 in the activation process, giving an active enzyme with kinetic properties essentially identical to those of the wild-type enzyme; this form of the enzyme presumably contains a vanadylated Lys residue in which the vanadate bridges the two nickels.[25]

X-ray structure determinations of three bacterial ureases have now been reported, as have those of a number of mutant enzymes and enzyme–inhibitor complexes. All structures of the native enzymes agree on the basic protein architecture: the enzyme is a trimer of $\alpha\beta\gamma$ trimers with threefold symmetry.[26–28] The α subunit (60.3 kDa) is the largest and consists of two domains, the larger of which is an $(\alpha/\beta)_8$ barrel that contains the dinuclear nickel center. All three structures also contain a mobile flap that covers the active site and contains residues that interact with the active site.

In the first structure reported, that of *K. aerogenes* urease at 2.2 Å resolution,[26] the dinickel site was well resolved, with the two nickel ions separated by 3.5 Å and bridged by the carbamylated lysine residue. Adjacent to the dinickel site was a small, solvent-filled cavity approximately the size of a urea molecule. A more recent structure determination of the *B. pasteurii* enzyme, with slightly better resolution (2.0 Å) and a more complete data set, gave a detailed picture of the active site and the solvent structure in the cavity.[27] As shown in Figure 2, the two nickel ions are 3.5 Å apart, bridged by the bidentate lysine carbamylate and a water/hydroxide. In addition, Ni1 is coordinated by two histidine imidazoles and a water/hydroxide to give a distorted square pyramidal coordination geometry, while Ni2 is coordinated by two histidine imidazoles, a monodentate aspartate carboxylate, and a water/hydroxide, giving a distorted octahedral coordination geometry. These coordination geometries are consistent with a variety of spectroscopic results.[18]
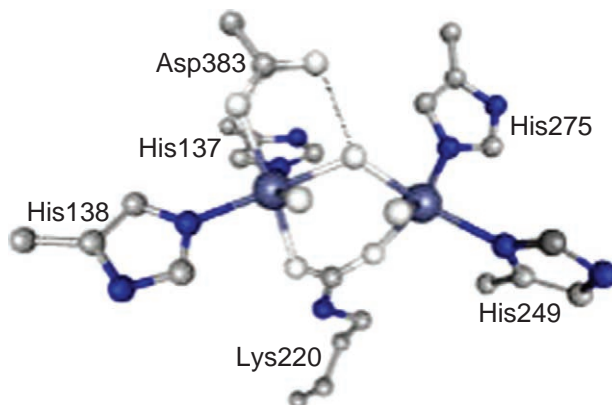
Figure 2 The active site of native urease from *Bacillus pasteurii* (pdb 2UBP). Nickel atoms are in dark gray, carbon atoms in light gray, oxygen atoms in white, and nitrogen atoms in black. Hydrogen bonding interactions are indicated as dashed lines.

In addition, the structure shows the presence of a fourth water molecule hydrogen-bonded to the other three water/hydroxide ligands and to a sulfate ion from the crystallization buffer. Given the importance of water in the reaction that is catalyzed, the presence of an ordered and fully occupied array of water (hydroxide) in the cavity is likely to be relevant to the catalytic mechanism.

Nickel can be removed from urease by dialysis at low pH in the presence of complexing agents to give an apoenzyme; the apoenzyme can also be isolated from bacteria in which one or more of the genes necessary for nickel insertion have been deleted. The structure of apo-urease from *K. aerogenes* shows several important features.[29] As expected, the nickel ions are absent, and a single well-ordered water molecule is hydrogen bonded to the two histidine imidazoles that are ligands to Ni2 in the native enzyme. In addition, the carbamyl group on the active site lysine is also absent if nickel is not present. Most importantly, the basic architecture of the active site is essentially unchanged, indicating that the protein provides a rigid array of amino acid residues that coordinate to the nickel ions with minimal structural rearrangement.

The structures of more than a dozen different mutants of *K. aerogenes* urease have been determined at atomic resolution, some at multiple pHs and/or in the presence of inhibitors.[29–31] Together with the observed effects of the mutations on the kinetics of the enzyme, these structures have yielded important insights into the function of many of the residues at or near the active site.

For example, His320 has variously been proposed to act as a general acid in catalysis[32] or as a hydrogen bond acceptor that stabilizes an incipient positive charge on the urea.[27] Conversion of His320 to Ala, Asn, or Gln gives a 10^5 decrease in k_{cat}, with little change in K_m. For the His320Ala mutant, it is clear that changes in the positions of the waters in the active site result in a major change in coordination geometry at Ni1, which becomes pseudotetrahedral.[29,31] Thus, it remains unclear whether His320 functions as an acid or base in catalysis or whether it simply helps to order the water cluster and ensure the correct geometry at Ni1.

His219 does not interact directly with the active site or its cluster of waters, but it does point directly at the active site cavity with its presumably protonated $N\varepsilon$ atom, suggesting that it can hydrogen-bond to the urea oxygen and polarize the C=O bond. Mutation of this residue to Ala, Asn, or Gln results in a 2–20-fold decrease in k_{cat} and an 80–1,000-fold increase in K_m, consistent with it playing an important role in both substrate binding and catalysis, but *not* via acid or base chemistry. The structures of these mutants show only modest changes in the conformation of the flap and the water cluster.[29,31]

Other mutations result in major changes in the structure of the active site and, predictably, completely abolish activity. For example, removal of one of the histidine ligands to Ni2 in the His134Ala mutant produces an inactive enzyme with a mononuclear active site.[33] Similarly, replacement of Lys217, which in its carbamylated form provides the bridging ligand between the nickel ions, with other residues such as Cys, Glu, or Ala gave inactive enzymes containing no nickel. These mutants could, however, be "rescued" by prolonged incubation with Ni^{2+} and acids such as formate, which were shown to replace the carbamate in bridging the nickel ions, resulting in enzymes with modest activity.[34]

Perhaps the most informative structural studies have been those on inhibited forms of the enzyme, which include one containing a potential transition state analogue. A variety of kinetics and spectroscopic data, including EXAFS[35] and the observation of strong antiferromagnetic coupling between the nickels,[36] had demonstrated that thiolates were competitive inhibitors that bound to and bridged the nickel ions. This was confirmed by the structure of the β-mercaptoethanol-inhibited enzyme from *B. pasteurii*, which showed that the thiolate replaced the bridging water; the β-OH of the alcohol forms a chelate with Ni1.[37] A similar geometry is observed for the enzyme complexed with acetohydroxamate, in which the hydroxamate oxygen bridges the two nickels, and the carbonyl oxygen coordinates to Ni1. Phosphate, which is a relatively weak, pH-dependent competitive inhibitor of urease ($K_i = 0.1$ mM and 50 mM at pH 5 and 7, respectively), is found to form a complex in which three oxygen atoms are coordinated to the dinickel center: one O atom bridges the two metal ions, while two other O atoms form chelates to Ni1 and Ni2, respectively, with the fourth O atom pointing into the solvent channel.[38] Analysis of the hydrogen bonding suggests that phosphate binds as $H_2PO_4^-$. Finally, treatment of urease with phenylphosphorodiamidate, $(PhO)PO(NH_2)_2$, results in hydrolysis of the phenyl phosphate moiety to yield enzyme containing coordinated diamidophosphate, $(H_2N)_2PO_2^-$, which appears to be a transition state analog. The diamidophosphate binds to the dinickel center very similarly to phosphate, with one bridging O atom, the second O atom coordinated to Ni1, and one -NH_2 bound to Ni2.

Let us now turn to a consideration of the mechanisms that have been proposed for hydrolysis of urea by urease. Due to the extreme stability afforded by its resonance energy, hydrolysis of urea is a difficult reaction, with an estimated half-life of 3–4 yr at 38 °C and pH 7. Yet urease accelerates the reaction by a factor of at least 10^{14}, making it one of the most proficient enzymes known. Such a tremendous catalytic enhancement implies a truly extraordinary stabilization of the transition state, and a number of specific proposals have been made as to how this might occur. The first proposed mechanism was due to Zerner and co-workers,[39] who suggested that one nickel acted to activate urea and one to activate water (Figure 3(A)), with the protein providing a carboxylate to stabilize a positive charge on one of the urea nitrogen atoms as well as a general acid (a cysteine?) and a general base.

More recently, a modified version of this same mechanism has been suggested based on the structural and kinetics results on the *K. aerogenes* enzyme.[32] The key features of this proposal are the interaction of urea with both nickel ions and the presence of a reverse protonation scheme. In this scheme, a protonated His320 acts as a general acid, while the less acidic water coordinated to Ni2 is deprotonated and acts as the nucleophile that attacks the urea coordinated to Ni1. Thus, it is proposed that the active form of the enzyme consists of the one molecule in approximately $10^{2.5}$ that contains both a deprotonated water ligand (estimated $pK_a \approx 9.0$) and a protonated His320 (estimated $pK_a \approx 6.5$). Such a reverse protonation scheme results in both a stronger acid and a more potent nucleophile, which in this model accounts for the ability of urease to overcome the lack of basicity of urea (estimated $pK_a \approx -2$) and its inertness to nucleophilic attack. Thus, if this model is correct, the actual k_{cat}/K_m value for urease is approximately $10^{8.5}$ rather than 10^6, i.e., very near the diffusion-controlled limit.

Most recently, an alternative mechanism has been proposed based on the structural results for the phosphate and diamidophosphate complexes of the *B. pasteurii* enzyme.[18,27] This proposal, which is also supported by computational studies in which inhibitors and potential transition states were docked into the active site,[40] is shown schematically in Figure 3B. The key features of this mechanism are binding of urea in a bridging bidentate mode and the identity of the nucleophile that attacks the urea carbonyl group: the bridging hydroxide, which also acts as the required general acid. In addition, His320 is proposed to act as a general base that stabilizes
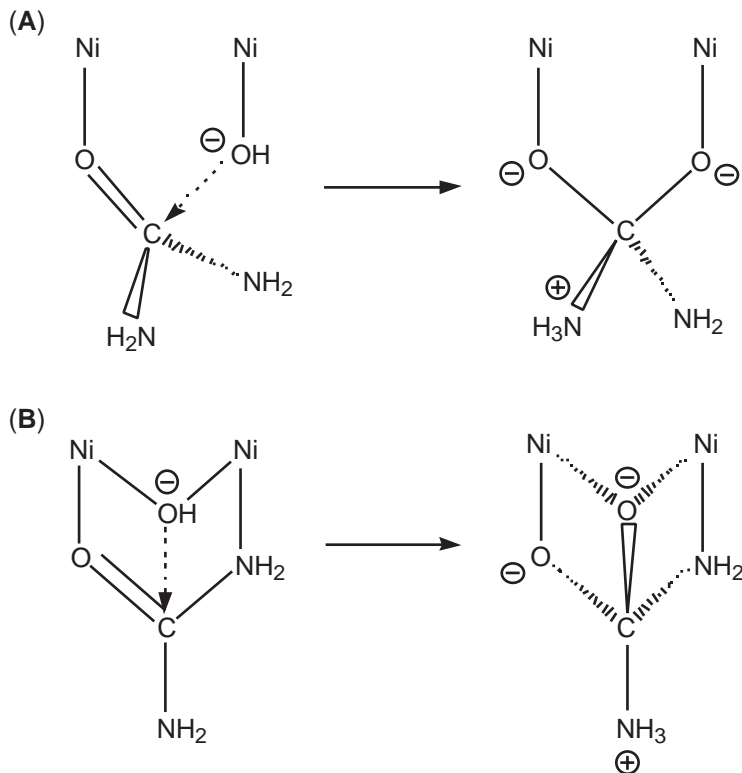
Figure 3   The two limiting mechanisms for urease: (A) attack of a monodentate hydroxide coordinated to one Ni on urea coordinated to the other, and (B) concerted attack of a bridging hydroxide on a bidentate bridging urea.

the developing positive charge on the transition state. Recent results on inhibition of the *K. aerogenes* enzyme by fluoride, which is a slow-binding inhibitor that binds only to a protonated form of the enzyme, have been interpreted in terms of fluoride replacing the bridging hydroxide.[41] These results are consistent with a bridging *oxide* derived from the bridging hydroxide as the nucleophile. The bridging hydroxide can be replaced by fluoride only when protonated to give a more labile bridging water. This proposal thus results in a picture very similar to that shown in Figure 3B, with the main point of remaining contention being the immediate source of the proton that is transferred to urea: His320 vs. the bridging hydroxide. It is clear that we now have a rather complete understanding of the mechanism of urease, which we shall utilize frequently as a paradigm in our discussion of other dinuclear hydrolases.

8.24.2.2 Dizinc Hydrolases

Hydrolytic enzymes that contain dinuclear zinc sites are known that hydrolyze both phosphate ester and amide bonds, and the number of such enzymes is growing rapidly.[42] Although each of the major types of enzyme to be discussed contains a distinctive protein fold that is unrelated to those of the other dizinc hydrolases, the active sites of these diverse enzymes exhibit a number of structural similarities, which suggests a convergent evolution of similar metal binding sites in otherwise unrelated proteins (analogous to the relationship between the mononuclear zinc hydrolases, thermolysin and carboxypeptidase A). In addition, as we shall see, some of the dizinc hydrolases exhibit structural similarities to other metalloenzymes (including urease), suggesting an evolutionary process in which they have diverged from a common ancestor.

8.24.2.2.1 *Phosphotriesterase*

We will begin with phosphotriesterase, which is an unusual (if not unique) enzyme in that it has no naturally occurring substrates. The enzyme was originally isolated from soil bacteria that were able to hydrolyze and detoxify a wide variety of organophosphate insecticides and nerve toxins. A typical reaction is the hydrolysis of the insecticide paraoxon, shown in Equation (2):

$$
\text{EtO}-\overset{\overset{\displaystyle O}{\|}}{\underset{\underset{\displaystyle OEt}{|}}{P}}-O-\!\!\left\langle\bigcirc\right\rangle\!\!-NO_2 + H_2O \longrightarrow \text{EtO}-\overset{\overset{\displaystyle O}{\|}}{\underset{\underset{\displaystyle OEt}{|}}{P}}-OH \; + \; HO-\!\!\left\langle\bigcirc\right\rangle\!\!-NO_2
$$

$$\tag{2}$$
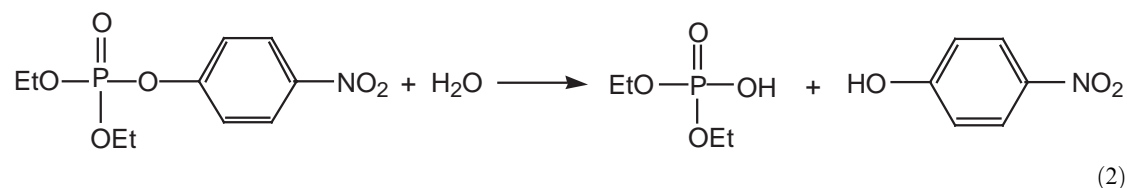
In addition, phosphotriesterase is a relatively efficient catalyst for the hydrolysis of chemical warfare agents such as Sarin and VX. Because of its obvious relevance in bioremediation and detoxification of potential chemical warfare agents, this enzyme has been the object of intense investigation.[43] By far the best-characterized example is the enzyme from *Pseudomonas diminuta* (henceforth abbreviated as PTE), on which almost all the relevant experiments have been performed. PTE is a dimeric protein with a subunit molecular weight of 20 kDa. It is isolated with up to two Zn bound per subunit, suggesting that zinc is the physiologically relevant metal ion. It is, however, possible to remove the bound zinc by treatment with *o*-phenanthroline to give an apoenzyme, which can be reconstituted with a variety of divalent metal ions, including cobalt, nickel, cadmium, manganese, and copper. All of these derivatives contain 2 mol of divalent metal per subunit, and all except the copper derivative exhibit significant enzymatic activity.[44] As for a number of zinc enzymes, the dicobalt derivative is actually a somewhat better catalyst than the presumed native dizinc form. In fact, the order of catalytic efficiency for the substituted species is $Co^{2+}–Co^{2+} > Ni^{2+}–Ni^{2+} > Cd^{2+}–Cd^{2+} > Zn^{2+}–Zn^{2+} > Mn^{2+}–Mn^{2+}$,[45] which shows no obvious correlation with the charge to radius ratio of the metal ions.

High-resolution (1.3 Å) crystal structures of the dizinc, dicadmium, dimanganese, and zinc–cadmium forms of PTE are now available,[46] which reinforce and expand upon many of the conclusions derived from earlier lower resolution structure determinations[47–49] and studies of the EPR spectra of the dimanganese[50] and dicopper enzymes.[44] In particular, the two metal ions
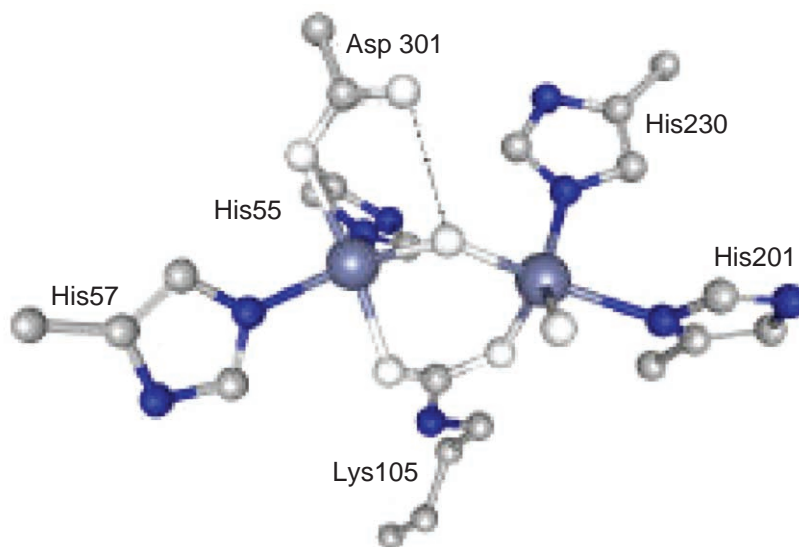
Figure 4   The active site of phosphotriesterase (pdb 1HZY). The zinc ions are in dark gray, carbon atoms in light gray, oxygen atoms in white, and nitrogen atoms in black. Hydrogen bonding interactions are indicated as dashed lines.

are located in close proximity to one another at the C-terminal end of an $(\alpha\beta)_8$ barrel structure. As shown in Figure 4, in the native enzyme the zinc ions are bridged by a water or hydroxide, as well as a carbamylated lysine residue like that found in urease. In addition, both zincs are coordinated by two histidine imidazoles each, with an aspartate carboxylate also coordinated to one zinc and a water to the other, giving distorted trigonal bipyramidal sites.[46] Detailed quantum mechanical calculations on the PTE active site have been carried out, and emphasize the importance of additional water molecules in the vicinity of the active site.[51,52]

Both the overall protein architecture and the structure of the dinuclear center of phosphotriesterase are very similar to those of the nickel-binding domain of urease (cf. Figure 2), suggesting a possible evolutionary relationship between these enzymes. Unlike urease, however, which requires a set of accessory proteins for insertion of nickel, apo-phosphotriesterase readily incorporates zinc in the presence of CO_2 to give the fully functional enzyme.[53] Although the $(\alpha\beta)_8$ barrel motif is a common feature in the structure of a wide variety of proteins, the elliptical barrel axis of the $(\alpha\beta)_8$ barrel of phosphotriesterase and the urease nickel-binding domain are rather rare. Only two other proteins with similar structures known[26]: adenosine deaminase, which contains a single zinc ion in place of the dinuclear zinc or nickel site,[54] and a protein of unknown function from *Escherichia coli* called phosphotriesterase homology protein (PHP), which contains a dinuclear zinc center very similar to that of phosphotriesterase, but in which a glutamate carboxylate replaces the carbamylated lysine as a bridging ligand.[55] Sequence alignments reveal the presence of homologues to PHP in both pathogenic microorganisms and in mammals,[55] but in no case has a physiological function been established. The fact that all other known members of this class of proteins are hydrolytic metalloenzymes strongly suggests that PHP also catalyzes a hydrolytic reaction, as did the presumed ancestor of this family of enzymes.

A variety of mutagenesis experiments has been performed to characterize the requirements for catalytic activity.[56] Conversion of Asp253, which is hydrogen-bonded to the His230 ligand to the more exposed zinc, to Asn had essentially no effect on catalytic activity, but replacement of this residue by Ala caused a 500-fold decrease in activity. These results were interpreted in terms of a role for the Asp in orienting the His ligand properly for binding to the dizinc site, rather than in terms of the Asp functioning as a proton donor or acceptor in the catalytic mechanism. The aspartate ligand to the five-coordinate zinc (Asp301) is clearly crucial: replacement by either coordinating residues (His, Asn, Cys) or a noncoordinating residue (Ala) caused a 10^2-10^4 decrease in activity. Finally, replacement of the carbamylated Lys residue by Arg, Met, Glu, or Ala caused (10^3-10^5)-fold decreases in activity. In some cases, activity could be partially restored by incubation with bicarbonate or acetate, suggesting that these exogenous ligands can replace the bridging carbamate, as with urease.
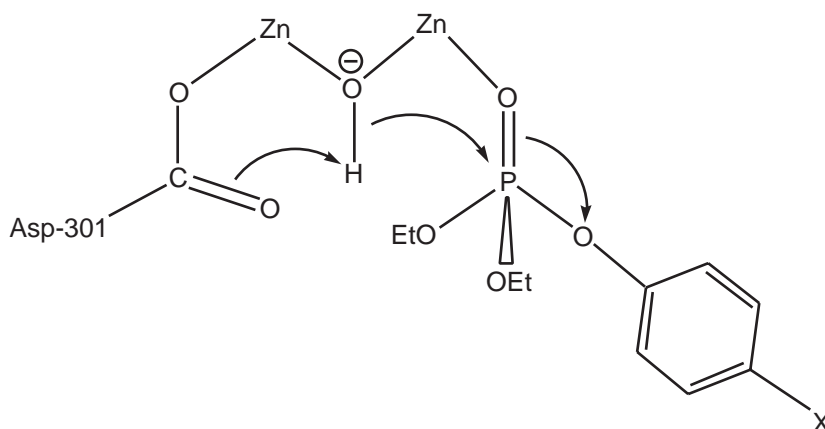
Figure 5 Working model for the initial catalytic complex of substrate with the dizinc center of phospho-triesterase. One zinc ion polarizes and activates the substrate, and nucleophilic attack of the bridging hydroxide is facilitated by the non-coordinated O atom of the Asp301 ligand to the other zinc ion.

The crystal structure of the complex of PTE with a nonhydrolyzable substrate analogue, diethyl 4-methylbenzylphosphonate, has shown that there are three distinct binding pockets adjacent to the dinuclear center.[49] These have been termed the *small*, the *large*, and the *leaving group* pockets, respectively, based upon their ability to accommodate substituents of varying size. The arrangement of these pockets nicely accounts for the selectivity observed in hydrolysis of chiral phosphate triesters with substituents of different size, and site-directed mutagenesis has been employed to alter the stereochemical preferences of the enzyme in a rational way.[57] Most importantly for a consideration of the enzymatic mechanism, the structure of the diethyl 4-methylbenzylphosphonate complex shows that the phosphoryl oxygen atom is 3.5 Å from the more solvent-exposed zinc ion. A mechanism that successfully accounts for the available experimental data is shown in Figure 5. It involves electrophilic activation of the phosphoryl group by coordination to the tetrahedral zinc ion, followed by nucleophilic attack of the bridging hydroxide, perhaps facilitated by the second oxygen atom of the coordinated aspartate carbonyl, to generate the *p*-nitropheno-late leaving group directly, followed by dissociation of the diethylphosphate product. ^{18}O isotope effects suggest that the transition state is highly associative, with the incoming nucleophile in close contact with the phosphorus atom when the leaving group is ejected.[58] There is no evidence for other proton donors or acceptors in the vicinity of the active site, and the only pK_a observed in the pH profile of the enzyme is at ≈ 6, which can be attributed to protonation of the bridging hydroxide.[43] This mechanism also nicely accounts for the fact that the enzyme can be irreversibly inactivated by suicide substrates such as diethyl 1-hexynyl phosphate and diethyl 1-bromovinyl phosphate. In each case, nucleophilic attack by water/hydroxide is postulated to form a ketene intermediate, which reacts rapidly with an enzyme nucleophile.[59]

8.24.2.2.2 Aminopeptidases

Aminopeptidases catalyze the hydrolytic removal of the N-terminal amino acid of peptides and proteins. Examples with differing specificities occur in virtually all organisms that have been examined, where they play essential roles in protein degradation. Particularly noteworthy are the methionine aminopeptidases, which remove the N-terminal Met residue resulting from initiation of protein synthesis, as is required in many cases for protein transport. Depending upon the subtype and the biological source, aminopeptidases are known that utilize mononuclear Co^{2+} or Fe^{2+} centers, dinuclear zinc centers (in some of which one zinc is not absolutely necessary for catalysis), dinuclear manganese centers, and dinuclear cobalt centers. The proline aminopepti-dases or prolidases provide examples of both of the latter, and will be discussed in the following sections.

This section will focus on the structure and properties of the two best characterized examples of aminopeptidases that contain dinuclear zinc centers, both of which happen to be leucine amino-peptidases: the enzymes from bovine lens (blLAP) and the marine bacterium *Aeromonas proteo-lytica* (AAP). Despite the fact that they catalyze the same reaction with comparable efficiencies,
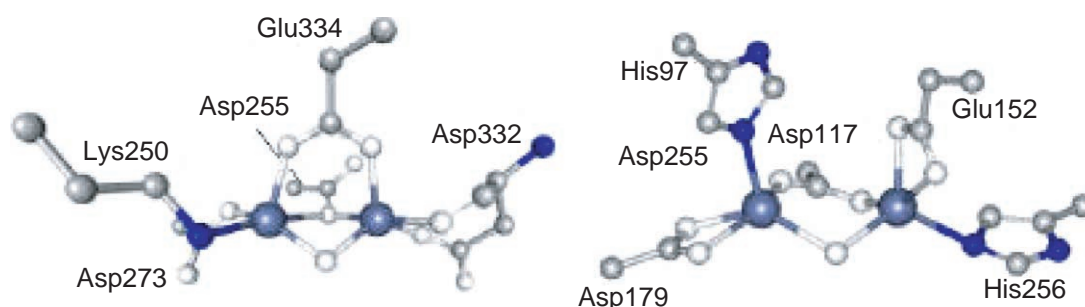
Figure 6 The active site structures of (left) bovine lens leucine aminopeptidase (pdb 1LAM) and (right) *Aeromonas proteolytica* leucine aminopeptidase (pdb 1AMP). The zinc ions are in dark gray, carbon atoms in light gray, oxygen atoms in white, and nitrogen atoms in black. Hydrogen bonding interactions are indicated as dashed lines.

these two enzymes show no sequence homology, have very different subunit masses and degrees of oligomerization, and, as shown in Figure 6, exhibit completely different structures for the dinuclear zinc center.

blLAP is a hexamer of identical 54 kDa subunits, each of which contains a dinuclear zinc site. Recent crystal structures of unligated blLAP[60] as well as its complexes with two transition state analogues, L-leucinal[60] and L-leucinephosphonic acid,[61] have revealed the structure of the zinc complex and its interaction with substrate. As shown on the left in Figure 6, the two zinc ions are 3.0 Å apart, and are bridged by a bidentate glutamate carboxylate, a monodentate aspartate carboxylate, and a water/hydroxide. Coordination of an aspartate carboxylate oxygen and the amide carbonyl oxygen of the same residue to Zn(1) and of an aspartate carboxylate oxygen and a lysine amino group to Zn(2) result in approximately square pyramidal coordination geometries for both metal ions, with the vacant sites in both coordination spheres on the same side of the dinuclear center. Given the substantial asymmetry in the dinuclear center, it is not surprising that the two metal-binding sites exhibit different affinities and metal ion exchange kinetics. The zinc in site 1 is readily replaced by other metal ions such as Mg^{2+}, Mn^{2+}, or Co^{2+}, while the zinc in site 2 can only be replaced by Co^{2+} under more forcing conditions. All of the metal-substituted forms cited retain catalytic activity, although they exhibit significant differences in kinetics parameters.

Our understanding of the catalytic mechanism of blLAP is largely derived from crystallographic studies of the structures of the enzyme with naturally occurring inhibitors and the transition state analogues mentioned above. It is clear from first principles[62] that hydrolysis of a peptide is most likely to occur via addition of water to the amide carbonyl to produce a tetrahedral *gem*-diolate intermediate, which then collapses to products as shown in Equation (3). The major issues to be resolved are how the amide is activated for nucleophilic attack and how the required hydroxide is provided at neutral pH. It is clear from the structure of the uncomplexed enzyme that coordination of the substrate to the vacant coordination sites on the adjacent zinc ions could be used to activate the amide carbonyl, while the bridging hydroxide represents a potential nucleophile that could attack the coordinated amide carbonyl. These predictions are nicely borne out by the structures of blLAP with both L-leucinal[60] and L-leucinephosphonic acid.[61] As shown in Figure 7, L-leucinal binds to Zn2 via the amino group, while the bridging hydroxide has apparently added to the aldehyde carbon to give a *gem*-diolate that remains coordinated to Zn1 via both oxygen atoms. A nearby lysine residue is apparently poised to donate a proton to the nitrogen of the amide bond to facilitate its cleavage. The structure of blLAP with L-leucinephosphonic acid is virtually identical, with the aldehyde-derived *gem*-diolate replaced by the phosphonate group. A network of hydrogen-bonded water molecules is also present, as shown in Figure 7. These offer additional possibilities for facilitating proton transfer during catalysis to ensure that the products are released in appropriate protonation states. The mechanism of blLAP has also been examined via a quantum chemical/molecular mechanical approach.[62] The calculations largely confirm the mechanism outlined above, but suggest that the bridging hydroxide is in equilibrium with a terminal hydroxide coordinated to Zn1, which due to its increased nucleophilicity is the actual nucleophile.
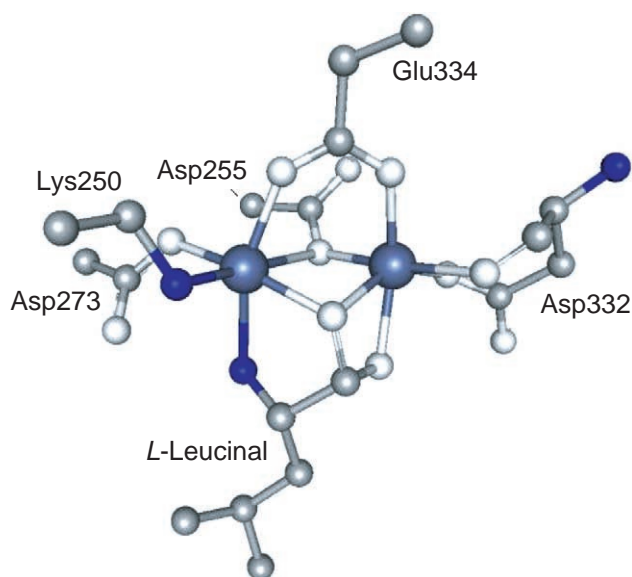
Figure 7 Drawing of the complex of bovine lens leucine aminopeptidase with the transition state analogue *L*-leucinal. Note the coordination mode of the *gem*-diolate in the bottom center. The spheres labeled 1 and 2 are the zinc ions.

$$(3)$$
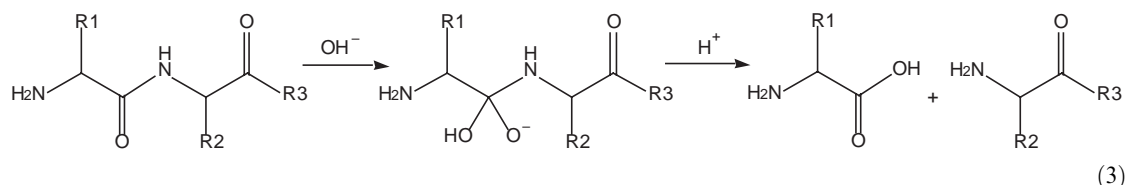
In distinct contrast to blLAP, the enzyme from *A. proteolytica* (AAP)[63] is a 29.5 kDa monomer that is secreted into the growth medium, presumably as a means of generating nutrients for bacterial growth via hydrolysis of peptides and proteins in the growth medium. AAP is isolated with two zinc ions per protein, removal of which completely abolishes activity. One or both of the zinc ions can be replaced by other divalent metals such as Co^{2+}, Ni^{2+}, and Cu^{2+} to produce enzymes that are significantly more active than the wild type, but the activity of these substituted forms depends dramatically upon both the nature of the metal and the order of addition. For example, the $Ni^{2+}Zn^{2+}$ form (prepared by adding the metal ions in that order) is 100 times more active than the wild type. Most importantly, however, it is clear that the activity of AAP containing only a *single* zinc ion is $\approx 80\%$ that of the dizinc form, and that this activity cannot be explained by the presence of a mixture of the dizinc and apo forms of the enzyme. Thus, AAP represents an intriguing mechanistic conundrum, in that it is apparently almost equally effective as a catalyst when it contains either one or two zinc ions.

Crystal structures of native AAP[64] and its complexes with a hydroxamate inhibitor,[65] the transition state analogue L-leucinephosphonic acid,[66] and the buffer Tris[67] have now been reported. As shown on the right in Figure 6, the structure of the dinuclear zinc site is very different from that in blLAP, but bears a number of resemblances to the active site of phosphotriesterase. For example, both AAP and PTE contain five-coordinate zinc sites bridged by a water/hydroxide and a bidentate carboxylate (in this case, an aspartate rather than a lysine carbamate). The major difference between the AAP and PTE centers is the higher symmetry of the AAP site, with both zincs coordinated by one histidine imidazole and an asymmetrically bidentate carboxylate from Glu (Zn1) or Asp (Zn2). In addition, a Glu carboxylate is hydrogen-bonded to the bridging water/hydroxide in AAP. Compared to the blLAP active site, AAP has a doubly vs. a triply bridged dinuclear site, lacks lysine residues in or near the active site, and has an essentially symmetrical structure. The structure of a phenylalanine hydroxamate complex, in which the hydroxylamine O atom bridges the two zincs while the carbonyl oxygen coordinates to Zn2, demonstrated that typical inhibitors bind directly to

the dinuclear active site.[65] The structure of the L-leucinephosphonic acid complex, which as noted above, acts as a presumed transition state analogue, was more informative regarding the enzymatic mechanism. Not unexpectedly, the mode of coordination of L-leucinephosphonic acid to AAP is quite similar to that observed for blLAP. The major difference is that the phosphonate binds in a bidentate bridging mode to AAP vs. a monodentate bridging mode for blLAP, with an additional phosphonate O atom coordinated to Zn1. In both cases, the amino group of the phosphonate interacts with Zn2. Both structures imply that the *gem*-diolate intermediate is stabilized by interactions with both metal ions.

Based upon the crystallographic results, inhibition studies,[68] studies on the binding of a variety of leucine analogs,[69] and spectroscopic studies on the binding of inhibitors to mixed-metal forms of the enzyme,[66,70,71] a detailed mechanism for AAP catalysis has been proposed.[63] As shown in Figure 8, it is proposed that the amide carbonyl oxygen of the substrate binds first to Zn1, followed by coordination of the amino group to Zn2. Converting the bridging hydroxide to a terminal ligand to Zn1 allows it to attack the amide carbonyl to give the *gem*-diolate intermediate, which then breaks down to products, with the previously N-terminal leucine the last product to leave the active site. In contrast, the mechanism for hydrolysis of substrates by AAP containing a single metal ion remains obscure. It seems likely, however, that the carboxylate ligand to the absent Zn2 interacts with the substrate amino group to facilitate binding.

It is worth noting at this point that several other hydrolytic enzymes are now known or strongly suspected to have active sites resembling that of AAP. For example, the structure of a *Pseudomonas* carboxypeptidase G_2 (CPG$_2$) that catalyzes the hydrolytic removal of glutamates from folates reveals the existence of a dinuclear zinc site identical in all respects to that of AAP.[72] In addition, the sequence of glutamate carboxypeptidase II (GCP II), which cleaves glutamate from N-acetyl-L-aspartyl-L-glutamate (NAAG) in the nervous system, exhibits very high sequence homology with CPG$_2$ and AAP.[73] CPG II also requires two zinc ions for activity, strongly suggesting an active site similar to that of AAP. Other potentially related enzymes include the N-succinyl-L,L-diaminopimelic acid desuccinylases, which catalyze a key step in lysine biosynthesis by a number of pathogenic bacteria, and which exhibit significant sequence simila-
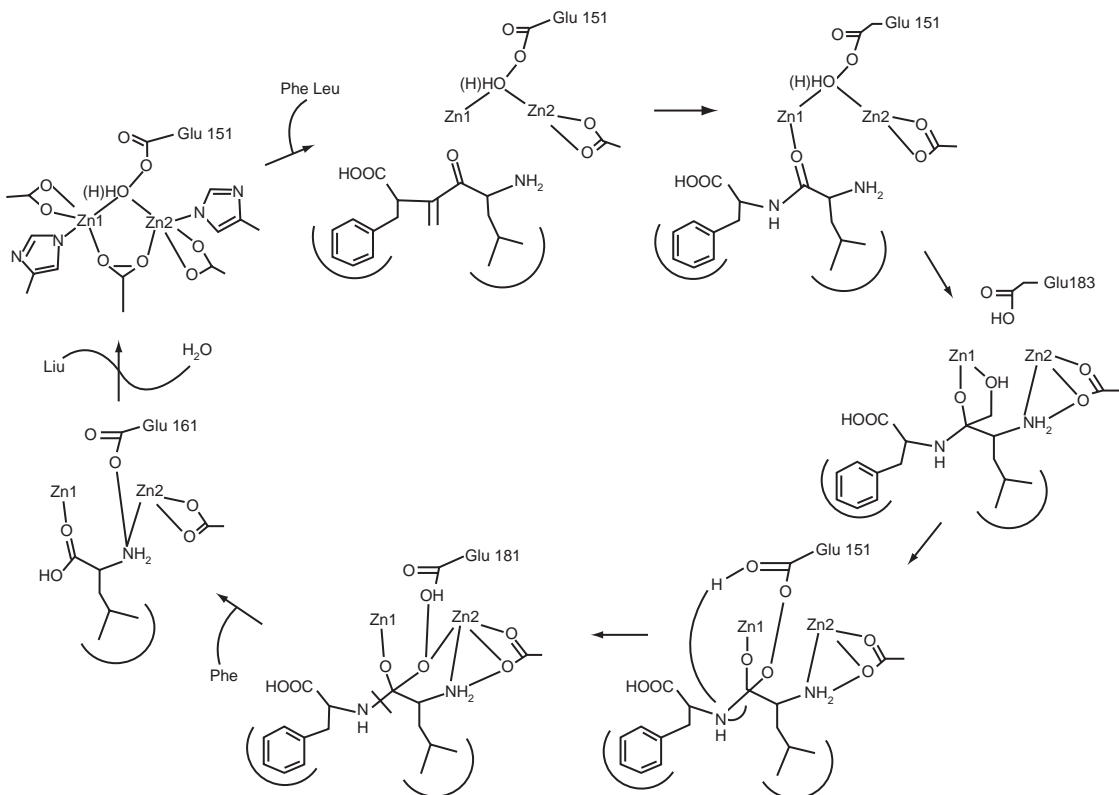

Figure 8 Mechanism of peptide hydrolysis proposed for the leucine aminopeptidase from *Aeromonas proteolytica*. Protein ligands to the dizinc site are shown only in the first panel (at top left) (reproduced with permission from ref. 66).

rities to AAP and CPG$_2$.[63] The fact that thiol-containing analogues of AAP substrates act as high-affinity, slow-binding inhibitors of AAP[74,75] suggests that some of the basic chemistry developed for AAP may be applicable to these related and medically highly important enzymes.

8.24.2.2.3 Metallo-β-lactamases

Microbial production of β-lactamases is one of the major factors in the rise in antibiotic resistance in bacteria. Of the four known classes of β-lactamases, only the class B enzymes are metalloenzymes, while the rest utilize an active site serine in a mechanism that involves formation of an acyl-enzyme intermediate. As we shall see, the metallo-β-lactamases utilize a completely different mechanism and have rather different properties. Most importantly, they are not inhibited by classic β-lactamase inhibitors such as clavulanic acid, which makes them particularly relevant in the proliferation of β-lactam-resistant pathogens. As a result, these enzymes have been the focus of a great deal of recent scientific attention.[76]

The basic reaction catalyzed by β-lactamases is the hydrolytic opening of the β-lactam ring (Equation (4)). Metallo-β-lactamases typically have a broad substrate specificity, and hence they are able to efficiently hydrolyze virtually all of the clinically important variants of the β-lactam framework, corresponding to different R, R′, and X groups in the structure in Equation (4):

$$\text{(4)}$$
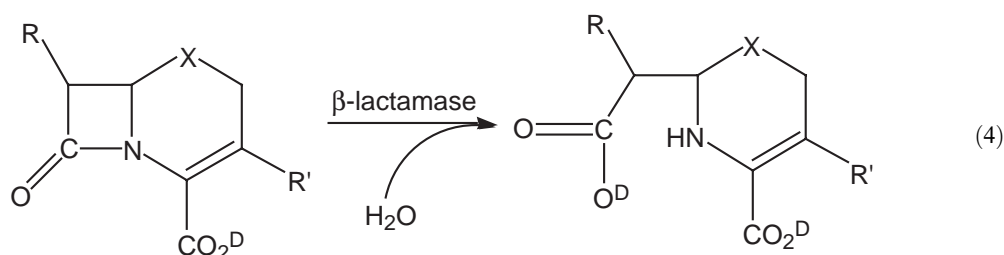
Analysis of a large number of amino acid sequences indicates that all metallo-β-lactamases are apparently related, although overall sequence homologies vary substantially. Most importantly, all known sequences exhibit a consensus sequence that contains all of the ligands to the metal sites: His–X–His–X–Asp–X$_i$–His–X$_j$–Cys–X$_k$–His, where X can be any amino acid and $i = 55$–74, $j = 18$–24, and $k = 37$–41.[76] Despite these similarities, the number and roles of the bound zinc ions vary greatly. For example, the enzymes from *Bacteroides fragilis*,[77,78] *Stenotrophomonas maltophilia* (L1)[79] and *Shigella flexneri* JS19622[80] have two high affinity zinc sites, while the superficially similar enzyme from *Bacillus cereus* has one high affinity zinc site and one low affinity site;[81] as a result, the monozinc enzyme may be the physiologically relevant form. Both the *B. cereus* and *S. maltophilia* enzymes have been shown to be catalytically active in the monozinc form, although the activity is somewhat lower than that of the dizinc forms.[81–83] Most perplexingly, however, the enzymes from *Aeromonas hydrophila* and *A. veronii* are most active with a single zinc, and are actually inactivated by binding of a second zinc.[84] Thus, there is clearly substantial variability in the nature of the catalytically active zinc sites in these enzymes.

To date, crystal structures of various forms of metallo-β-lactamases have been reported from four organisms: *B. cereus*, *B. fragilis*, *S. maltophilia*, and *Pseudomonas aeruginosa*.[76,85,86] All show a similar protein architecture, which consists of an αββα sandwich structure, with two β-sheets covered by two α-helices on each side. In all cases, the zinc binding site is located between the β-sheets near one edge of the sandwich, at the bottom of a wide and shallow groove that can accommodate a variety of β-lactam substrates. The structure of the dizinc site of the enzyme from *B. fragilis*[87] is typical, and is shown in Figure 9. As in all structurally characterized dizinc enzymes, one zinc (Zn1) is tetrahedrally coordinated by three histidine imidazoles and a bridging water/hydroxide. The other zinc (Zn2) is trigonally bipyramidally coordinated, with the bridging water/hydroxide, a histidine imidazole, and a cysteine thiolate in the equatorial plane and an aspartate carboxylate and a terminal water in the axial positions. In the structure of the *S. maltophilia* enzyme, however, in which the conserved Cys residue is replaced by a Ser in the amino acid sequence, the cysteine ligand to Zn2 is replaced by a second histidine imidazole rather than the corresponding serine hydroxyl. In enzymes containing only a single zinc, the zinc is located in the Zn1 binding site.[88]
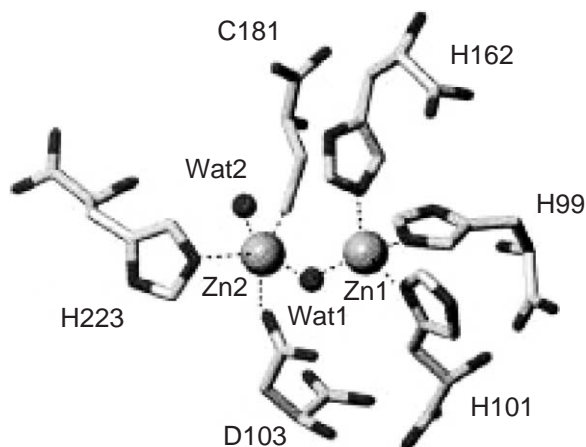
Figure 9 The structure of the active site of *Bacillus cereus* metallo-β-lactamase showing the bridging and terminal water/hydroxides (reproduced with permission from S. B. D. Scrofani, *et al. Biochemistry* **1999**, *38*, 14508).
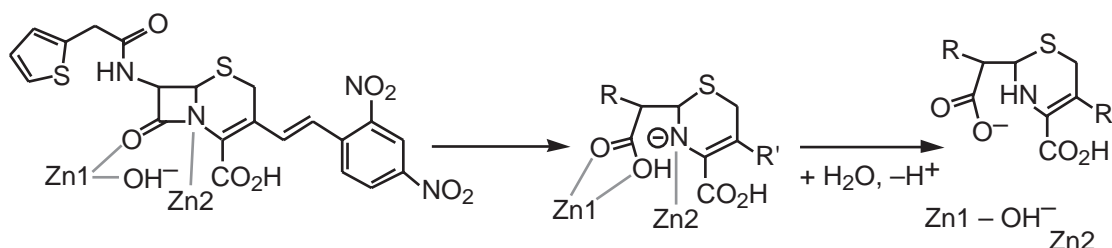
Figure 10 Proposed catalytic mechanism for hydrolysis of nitrocefin by the metallo-β-lactamase from *Bacillus fragilis*.

Based on a variety of kinetics and spectroscopic studies, a mechanism has been proposed for the monozinc *B. cereus* enzyme that involves attack of a coordinated hydroxide on the coordinated β-lactam carbonyl, followed by proton-assisted cleavage of the CN bond.[89] In contrast, pre-steady-state studies of the hydrolysis of nitrocefin, a chromophoric substrate, by the dizinc enzymes from both *B. fragilis*[90–92] and *S. maltophilia*[93] have revealed the existence of a relatively long-lived intermediate. The observed optical spectrum is most consistent with the N-deprotonated form of the product, presumably stabilized by coordination to the second zinc, as shown in Figure 10.[76] The lack of pH dependence between pH 5.25 and 10 indicates both that the pK_a of the water coordinated to Zn1 is <5.25, which is extraordinarily low, and that no other catalytically important groups have pK_as in this range. Consequently, it appears as if protonation of the cleaved intermediate is the rate-limiting step in the catalytic mechanism of the dizinc enzymes.

8.24.2.2.4   Related systems

In the preceding sections, the existence of enzymes related to phosphotriesterase and leucine aminopeptidase has been pointed out at the appropriate points. In addition, there exists a substantial number of as yet more poorly characterized enzymes that are likely to also contain dizinc sites, some of which may well be similar to those discussed above. This short section will briefly describe a few additional enzymes that are either known to or may eventually be shown to contain a dizinc center.

One enzyme that certainly contains a dizinc center in at least some cases is glyoxylase II, which catalyzes the hydrolytic cleavage of *S*-D-lactoylglutathione to lactate and glutathione. Formation of the substrate by isomerization of the hemimercaptal produced by spontaneous reaction of 2-oxoaldehydes such as methylglyoxal with glutathione is catalyzed by glyoxylase I, which is known to be a zinc-dependent enzyme. Together, these two enzymes provide a system for

detoxifying 2-oxoaldehydes, which are cytotoxic by-products of glucose and lipid metabolism, by conversion to the corresponding hydroxyacids. Both glyoxalase II and aryl sulfatase contain a zinc-binding motif virtually identical to that in metallo-β-lactamases, suggesting that they might well be zinc proteins.[94] This suggestion was supported by initial results on the overexpressed glyoxalase II from *Arabidopsis thaliana*, which convincingly demonstrated the presence of two tightly bound zinc ions per 29 kDa protein.[95] The presence of zinc is essential for the activity and the stability of the enzyme, but the instability of the apoenzyme precluded its reactivation by added Zn^{2+}. A subsequent crystal structure determination of the human enzyme confirmed the presence of a dizinc center, but also showed that the structure of the center exhibited a number of significant differences from those in the metallo-β-lactamases.[96] One zinc (Zn1) is indeed coordinated by three histidine residues that are homologous to the Zn1 ligands in the metallo-β-lactamases, but the two zinc ions are bridged by a water/hydroxide plus a monodentate aspartate carboxylate that replaces the cysteine ligand to Zn2. The second zinc (Zn2) is coordinated by the expected aspartate and histidine ligands, but in addition a second histidine has replaced the coordinated water. Thus, each zinc is coordinated by four protein ligands plus a bridging water/hydroxide. The structure of the "native" enzyme also has a bidentate cacodylate ligand bridging the two zincs, which results in a distorted octahedral coordination for both metals. The structure of the complex of the enzyme with glutathione and an *S*-acylglutathione derivative were also determined, and show that the carbonyl oxygen of the thioester group interacts with Zn2. As a result, it has been suggested that the enzymatic mechanism involves nucleophilic attack of the bridging hydroxide on the coordinated thioester carbonyl to give a *gem*-diolate intermediate, which breaks down to glutathione and the 2-hydroxyacid. Whether all glyoxalase II enzymes contain dizinc centers has been brought into question by a recent report that the wild-type *A. thaliana* enzyme actually contains an FeZn center.[97] Apparently the work supporting the initial report of a dizinc center in this enzyme[95] was actually carried out on a mutant form of the enzyme in which an arginine was replaced by a tryptophan. The authors have shown that the mutant does indeed bind two zincs, but that the wild-type enzyme definitely contains one Fe and one Zn per mole, and that it is substantially more active than mutants that contain dizinc centers. It seems clear that further work will be require to resolve the issue of the identity and/or diversity of the metal ions present in these enzymes from diverse sources.

Another enzyme that exhibits significant sequence homology to the metallo-β-lactamases is the product of the *ElaC* gene in *E. coli*. Analysis of recombinant protein, which is a dimer of 36 kDa subunits, has shown that it contains two zinc ions per subunit.[98] In addition, a preliminary Zn K-edge EXAFS study was consistent with the presence of a dinuclear zinc site with a Zn–Zn distance of 3.3 Å and an average first coordination shell consisting of two histidine ligands, one carboxylate, and 1.5 O atoms from water/hydroxide. These parameters are in reasonable agreement with an active site structure similar to that of the metallo-β-lactamases and glyoxalase II.

A family of putative dizinc enzymes that appear to be related to the Co^{2+}-containing methionine aminopeptidases (Section 8.24.2.4) are the tripeptidases known as the PepT gene products. The fact the same five amino acid residues that are known to bind Co^{2+} in the dinuclear cobalt site of *E. coli* methionine aminopeptidase are conserved in the amino acid sequences of PepT proteins initially suggested that PepT was a cobalt enzyme. The enzyme from *Bacillus subtilis* is, however, isolated with substoichiometric contents of zinc (0.26 Zn/49-kDa monomer) but no cobalt, and its activity is substantially enhanced by addition of exogenous zinc ions.[99] The enzyme is also activated by added Co^{2+}, but a three-fold higher concentration of cobalt than zinc is required to obtain the same activation. These data, together with the greater facility of refolding in the presence of Zn^{2+} vs. Co^{2+}, suggest that PepT is indeed a zinc protein, perhaps analogous to some of the metallo-β-lactamases in having one low affinity site and one high affinity site.

8.24.2.3 Dimanganese Hydrolases

Due to its high-spin d^5 electronic configuration, the Mn^{2+} ion has a spherical distribution of *d*-electrons. Together with its similarity in ionic radius to Mg^{2+} (0.86 Å vs. 0.97 Å, respectively), this property makes the Mn^{2+} ion a good and widely used replacement for Mg^{2+} in biological reactions that require loosely bound divalent cations. Because both Mn^{2+} and Mg^{2+} bind to protein residues primarily via electrostatic interactions, which are neither highly directional nor highly specific, most protein binding sites for these metal ions exhibit rather low affinities. As a result, the metal ions are often lost during purification, resulting in the isolation of an inactive

metal-free protein to which metals must be added to restore activity. Thus, even if a particular enzyme contains bound Mn^{2+} ions *in vivo*, it is difficult or impossible to know this from the isolated protein. In many cases, Mn^{2+} binds to proteins that are known to utilize other metal ions *in vivo*, with restoration of some or all of the enzymatic activity. Consequently, in most cases it is usually very difficult to state with any degree of certainty that a given enzyme is indeed a manganese enzyme. This situation has greatly limited the number of well-characterized manganese enzymes. In only one case is an enzyme isolated from its natural sources in the absence of added manganese that retains all or part of its manganese content: arginase. In all other cases where the presence of dimanganese centers has been convincingly demonstrated by crystallographic or spectroscopic studies, the enzyme has been incubated with substantial concentrations of Mn^{2+} (typically 1 mM) during the crystal growth or titrated with Mn^{2+} prior to the spectroscopic measurement. Consequently, the discussion of dimanganese hydrolases will focus on the properties of arginase. A brief summary of the essential features of two other crystallographically characterized enzymes with dimanganese sites will conclude this section.

8.24.2.3.1 *Arginase*

Arginase catalyzes the hydrolytic cleavage of L-arginine to L-ornithine and urea (Equation (5)). Arginase is most familiar as the enzyme that is responsible for the last step in the urea cycle, which is catalyzed by the type 1 isoform of the enzyme in the cytosol of the liver. In addition, however, the type 2 isoform of arginase is found in the mitochondria of many other tissues; its function is apparently to produce ornithine for the synthesis of proline, glutamate, and polyamines. Because arginine is also the substrate of nitric oxide synthase, it is clear that tissue NO levels are controlled by the relative flux of arginine through arginase vs. NO synthase. Thus, any factor that decreases the rate of the arginase reaction is likely to increase the rate of NO synthesis. In fact, it has recently been demonstrated that a specific arginase inhibitor, *S*-(2-boronylethyl)-L-cysteine, results in increased NO-mediated smooth muscle relaxation in extracts of human penile corpus cavernosum tissue, which is required for penile erection.[100]

$$(5)$$
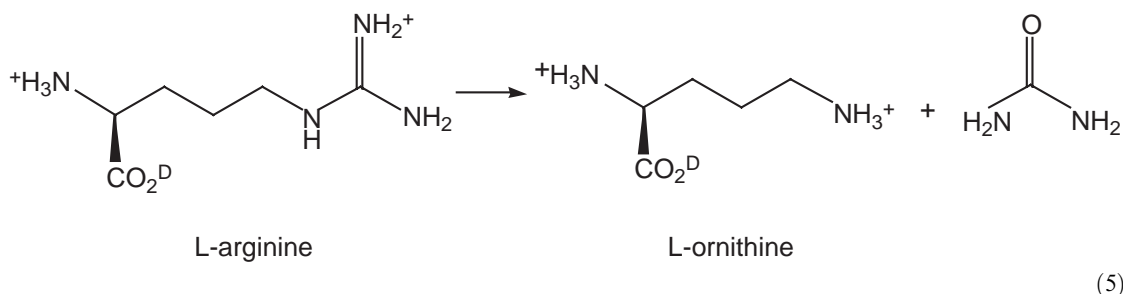
Both isoforms of arginase exist as trimers of 35 kDa subunits, and their amino acid sequences are Å50% identical. As isolated, arginase from rat liver typically contains three Mn^{2+} ions per trimer, and maximum catalytic activity is achieved with a total of six Mn^{2+} per trimer. The EPR spectrum of arginase is complex, but the ^{55}Mn hyperfine splitting of only 45 G, approximately one-half of normal mononuclear Mn^{2+} complexes, is convincing evidence for the presence of an antiferromagnetically coupled manganese dimer.[101] This hypothesis was confirmed by the crystal structure of the rat liver enzyme, which demonstrated that the dinuclear manganese centers are bound at the bottom of a 15 Å deep cleft in each monomer, with the metal ligands provided by residues on one edge of the β-sheet of the α/β structure.[102] The Mn^{2+} ions are 3.3 Å here apart, and are bridged by a monodentate aspartate carboxylate, a bidentate aspartate carboxylate, and a water/hydroxide. In addition, one Mn^{2+} (Mn_B) is coordinated by a histidine imidazole and a bidentate aspartate carboxylate, resulting in a distorted octahedral coordination geometry. The other manganese (Mn_A) is also coordinated by a histidine imidazole and a monodentate aspartate carboxylate (which is hydrogen bonded to the bridging hydroxide), resulting in a square pyramidal coordination geometry (Figure 11). Not surprisingly, mutation of one of the His ligands to the dimanganese center to an Asn residue greatly diminishes metal binding, protein stability, and catalytic activity.[103] In addition, mutation or chemical modification of a nearby His residue
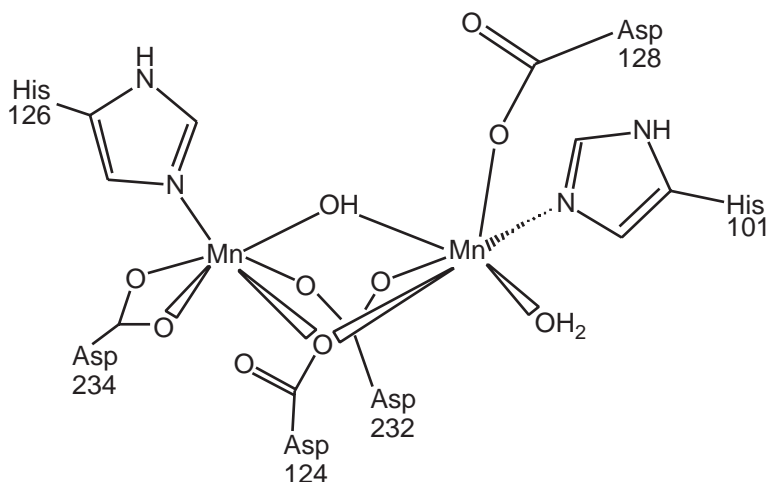
Figure 11 Schematic drawing of the active site of native rat liver arginase.

(His141) has no effect on the binding constant (K_M) for arginine, but decreases k_{cat} (10–20)-fold, suggesting that this residue is catalytically important even though it is not a metal ligand.[104]

Recent structures of arginase complexed with the products L-ornithine and urea, the competitive inhibitors N^ω-hydroxy-L-arginine and N^ω-hydroxy-*nor*-L-arginine, and the transition state analogue S-(2-boronylethyl)-L-cysteine[105] have provided important insights into the enzyme mechanism. In the product complex, the ornithine δ-NH_3^+ group is hydrogen bonded to the bridging hydroxide, and the urea carbonyl oxygen atom is coordinated to the open site on Mn_A.[106] In addition, there are extensive hydrogen bonding contacts to both the bound ornithine, which occupies the cleft in the protein structure, and to urea. Both of the N-hydroxyarginines bind to the enzyme in essentially the same way, although there are differences in the hydrogen bonding interactions. Most importantly, in both cases the N-hydroxy group replaces the bridging hydroxide. Finally, in the structure of the transition state analogue S-(2-boronylethyl)-L-cysteine, one of the boronic acid hydroxy groups also replaces the bridging hydroxide, while a second boronic acid hydroxy group is coordinated to the vacant site on Mn_A. The rest of the inhibitor binds in the active site cleft in a manner similar to ornithine. Based on the structural and kinetics data, a mechanism has been proposed for arginase that involves nucleophilic attack of the bridging hydroxide on the guanidinium carbon of arginine to form a tetrahedral intermediate. Sequential proton transfers mediated by the monodentate aspartate ligand to Mn_A and His141 are proposed to result in collapse of this intermediate with loss of ornithine to give urea coordinated to Mn_A, which then dissociates. The most unusual feature of this mechanism is the almost complete lack of any means of activating the rather unreactive guanidinium group toward nucleophilic attack; the only interaction with the protein that is suggested is with the carboxylate of a nearby glutamate residue. Perhaps this results in (partial) proton transfer to give a neutral guanidine that is the actual electrophile that is attacked?

8.24.2.3.2 Related systems

The crystal structures of two other hydrolytic enzymes that contain a dimanganese center have been reported. The first is the protein serine/threonine protein phosphatase 2C[107] (now referred to as a member of the PPM family of serine/threonine-specific protein phosphatases), whose dimanganese center is shown schematically in Figure 12. This structure is very unusual in the relatively small number of protein ligands to the metal center: only two monodentate aspartate carboxylates coordinate to one manganese and a single main chain peptide carbonyl to the other, as well as a bridging aspartate carboxylate. The other five metal ligands (one bridging and two terminal on each manganese) are water molecules or hydroxide ions. Most importantly, the reported crystal structure is that of the phosphate complex, but even the reaction product phosphate does not bind to the dimanganese center, interacting instead with coordinated water molecules and an arginine residue. Although detailed mechanistic studies on these enzymes have not yet been reported, the features noted above strongly suggest the possibility of an unusual mechanism, in which the
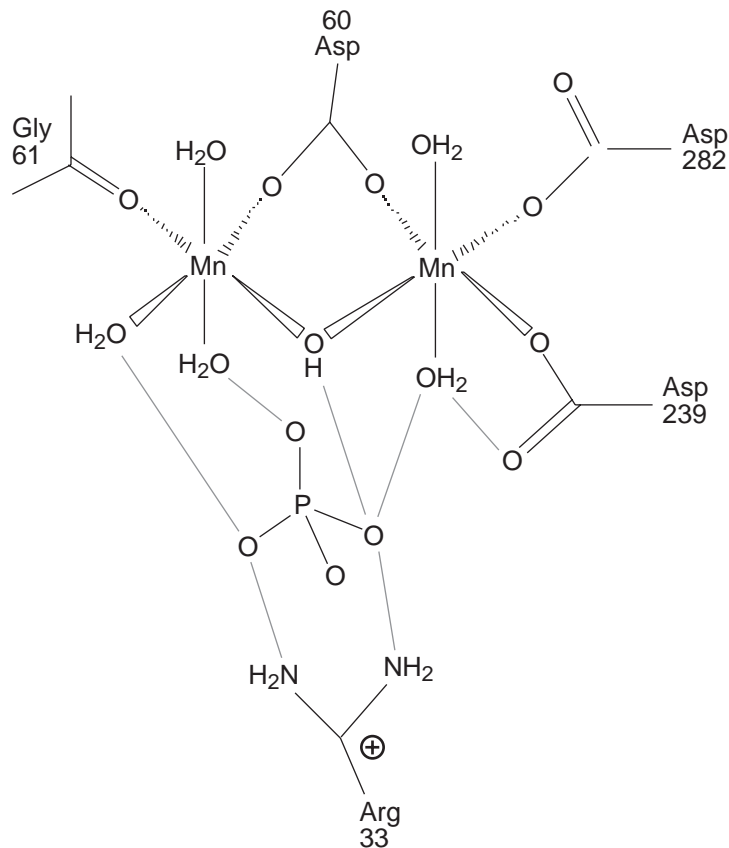
Figure 12 Schematic drawing of the active site of human protein phosphatase 2C.

phosphate ester interacts only with coordinated water molecules rather than the metal.[108] The biochemistry of this enzyme will be discussed along with that of the other protein serine/threonine-specific protein phosphatases below in Section 8.24.3.2.

The proline-specific aminopeptidase P(AMPP) specifically hydrolyzes the N-terminal amino acid from peptides in which the penultimate residue is a proline. It was earlier shown that AMPP from *E. coli* was activated by both Mn^{2+} and Co^{2+}, and EPR and EXAFS spectra of the Mn^{2+}-reconstituted enzyme were consistent with the presence of a dinuclear Mn^{2+} center.[109] Subsequently, the crystal structure of the enzyme were showed that it did indeed contain a dinuclear manganese center.[110] The enzyme is a dimer of dimers of identical 49.5 kDa subunits, and the manganese binding site is located on the inner surface of a domain consisting of a curved six-stranded β-sheet whose outer surface is covered by seven α-helices. The dinuclear manganese site is bridged by a water/hydroxide and two carboxylate residues (one from Glu, one from Asp), with a Mn–Mn distance of 3.3 Å. In addition, one Mn is coordinated by a bidentate aspartate carboxylate to give square pyramidal coordination, and the other is coordinated by a histidine imidazole, a monodentate glutamate carboxylate, and a terminal water/hydroxide in a distorted octahedral arrangement. This structure and the arrangement of the protein ligands in the amino acid sequence are very similar to those in a structurally characterized dicobalt methionine aminopeptidase that will be discussed in the next section. The existence of virtually identical active sites and the ease with which metal ions can be exchanged in these enzymes naturally raises the question of whether they in fact utilize different metal ions for catalysis *in vivo*.

8.24.2.4 Dicobalt Hydrolases

Methionine aminopeptidases (MAPs) are the only enzymes for which substantial evidence has been presented that they contain dicobalt centers in their native state. As noted above, by hydrolytic removal of the N-terminal Met residue due to initiation of protein synthesis, methionine aminopeptidases play a crucial role in all known organisms. The importance of MAPs is

demonstrated by the fact that deletion of the gene coding for MAP in *E. coli*, *Salmonella typhimurium*, or *Saccharomyces cerevisiae* is lethal to the cells. Two classes of MAP are known to exist.[111] The type 1 enzymes are generally found in prokaryotes and are monomeric 30 kDa proteins. In contrast, the eukaryotic and archaeal type 2 enzymes are generally larger due to insertion of a 62 amino acid sequence near the C-terminus.

At first sight, the evidence for the presence of a catalytically active dicobalt center in MAPs is indeed convincing: the crystal structures of three different MAPs have been reported (the type 1 MAP from *E. coli*[112] and the type 2 MAPs from humans[113] and the hyperthermophile *Pyrococcus furiosus*).[114] All three structures contain virtually identical catalytic domains that contain a bis(μ-η-1,2-carboxylato)(μ-aquo/hydroxo)dicobalt unit with a Co–Co distance of about 3 Å. In addition, one cobalt (Co1) is coordinated by a bidentate aspartate carboxylate, while the other (Co2) is coordinated by a monodentate glutamate carboxylate, a histidine imidazole, and a water/hydroxide,[115] resulting in a distorted trigonal bipyramidal coordination geometry for Co1 and a distorted octahedral geometry for Co2.

Based on the structures of the native and inhibited forms of *E. coli* MAP,[115,116] a catalytic mechanism has been proposed that is in good agreement with detailed kinetics studies of recombinant human MAP.[117] In this mechanism, the α-amino group of the substrates replaces the terminal water/hydroxide ligand to Co2, after which the bridging hydroxide attacks the carbonyl carbon of the amide, which is activated by interaction with Co1.

Although this mechanism is both intuitively rather satisfying and analogous to the catalytic mechanisms of other enzymes discussed previously, there is mounting evidence that it may not be correct due to the fact that the identity and number of metal ions in the active site is incorrect. Studies of the interaction of *E. coli* MAP with divalent metal ions have shown that it is activated by Zn^{2+}, but not by Co^{2+}.[118] The affinity of the enzyme for the second Co^{2+} is ≈ 2.5 mM, however, which is much too high to be physiologically relevant, and binding of the second Co^{2+} actually *decreases* enzymatic activity. Both EXAFS and EPR studies of *E. coli* MAP in the presence of one and two equivalents of Co^{2+} gave no evidence for the presence of a dinuclear $(Co^{2+})_2$ unit in solutions containing 1 mM MAP and 2 mM Co^{2+}, consistent with the low affinity of the enzyme for the second Co^{2+}.[119] In addition, it has been shown that Fe^{2+} can also activate MAP, and that the affinity of the enzyme for Fe^{2+} is actually slightly higher than that for Co^{2+}.[120] Complementary whole cell studies on metal contents during overexpression of MAP are also consistent with its formulation as an iron enzyme.[120] Similar results have been reported for the type 2 MAP from *P. furiosus*, indicating that both the type 1 and type 2 enzymes share a common metal center and, presumably, catalytic mechanism that is as yet unknown. Thus, a variety of lines of evidence now suggest strongly that methionine aminopeptidases are mononuclear iron enzymes, rather than dicobalt enzymes, although a consensus on this point has not yet been achieved. This turnaround in our view of an important set of enzymes emphasizes the point made above regarding the difficulties in identifying the identity and number of the presumed physiologically relevant metals in enzymes that contain labile metal ions.

With this cautionary note in mind, we should note that a related enzyme, prolidase from *P. furiosus*, has also been reported to be a dicobalt enzyme.[121] In contrast to the aminopeptidases discussed above, prolidase specifically cleaves dipeptides containing a C-terminal proline. Prolidase is present in humans and a variety of bacteria, and appears to be identical to the enzyme previously known as organophosphorus acid anhydrolase, which can hydrolyze and detoxify organophosphorus nerve agents.[122] A function in hydrolyzing peptides, rather than nerve agents that have only been known for a few decades, seems much more probable for these enzymes, which are found in both eukaryotes and prokaryotes. Whether prolidases actually utilize a dinuclear cobalt site in catalysis will require further investigation.

8.24.3 HYDROLASES USING TRIVALENT–DIVALENT DIMETAL CENTERS

As should be clear from the previous discussion, enzymes that utilize dinuclear active sites containing two divalent metal ions are both numerous and diverse, and the range of chemical reactions that they catalyze includes a variety of substrates containing both phosphate ester and amide bonds. In contrast, enzymes that utilize a mixed-valence dinuclear center that contains one divalent and one trivalent center exhibit much less diversity in all respects: identity of the metal ions, nature of the reactions catalyzed, and overall protein structure. As we shall see, all such enzymes known to date contain Fe^{III} plus either Fe^{II}, Zn^{II}, or Mn^{II}, the only physiological

reaction they catalyze is dephosphorylation of proteins containing phosphoserine, -threonine, and possibly -tyrosine residues, and their catalytic domains all consist of a $\beta\alpha\beta\alpha\beta$ fold that contains a phosphoesterase signature motif, Asp–X–{Gly/His}–X_m–Gly–Asp–XX–{Tyr/X}–X_n–Gly–Asn–His–{Glu/Asp}. Many additional enzymes are known that contain this motif, but which do not utilize a trivalent–divalent dinuclear metal center. Examples of the latter include 5′-nucleotidase and the phage λ protein phosphatase, which will be discussed at the end of this section.
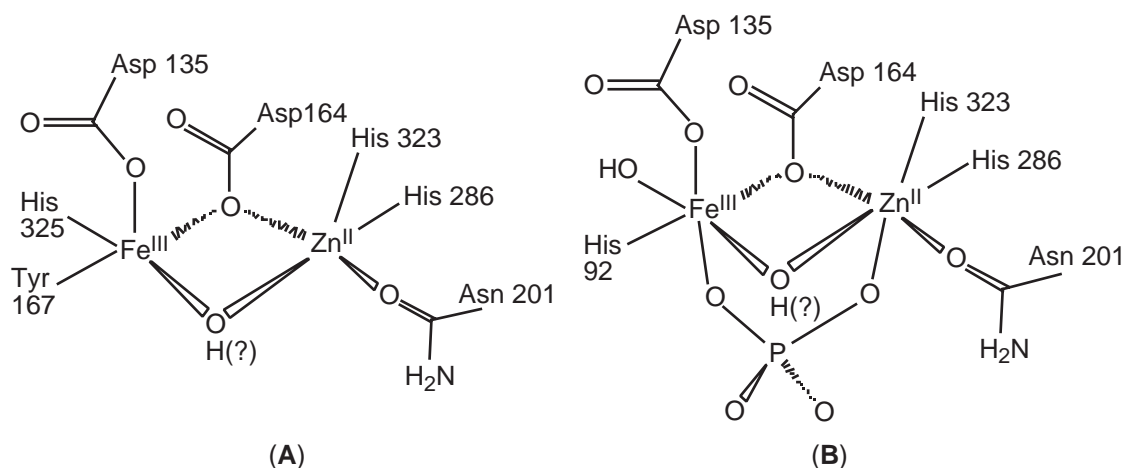
8.24.3.1 Purple Acid Phosphatases

Purple acid phosphatases (PAPs)[123–125] are also called tartrate-resistant acid phosphatases (TRAPs) or type 5 acid phosphatases (Acp 5s) in the biomedical literature.[126] PAPs are typically glycoproteins with a low pH optimum (5–6) for enzymatic activity. They are insensitive to inhibition by tartrate, and exhibit an intense pink or purple color. PAPs have been isolated from mammalian, plant, and microbial sources, and differ in metal content. Essentially nothing is known about the physiological function of PAP in plants, and its function in many mammalian systems remains to be elucidated. Mammals appear to contain only a single copy of the gene encoding PAP, yet its expression levels vary tremendously in different tissues.[127] As a result, only two physiological roles are well established. High levels of uteroferrin (Uf) are present in the intrauterine fluids of pregnant sows, whose high pH makes a role as a phosphatase unlikely. Consequently, Uf has been suggested to play a role in transporting iron to the developing fetus.[128,129] In contrast, osteoclasts secrete PAP (along with cathepsin K, which is presumably responsible for its proteolytic activation) into the acidified space between the osteoclast and the bone surface, where PAP appears to facilitate bone resorption. PAP may help anchor the osteoclast to the bone by dephosphorylation of osteopontin,[130,131] and it may also dephosphorylate bone matrix phosphoproteins. A role in bone resorption is supported by the phenotype of double knockout mice that lack both copies of the PAP gene: such mice exhibit osteopetrosis, with short, thick bones whose tissue has not been extensively remodeled.[132] PAP is also expressed in other cells of the mononuclear phagocyte system, including monocytes and macrophages,[133] where its lysosomal location suggests a role in degradation of proteins arising from phagocytosis of bacteria and/or senescent erythrocytes. Recently, however, a number of tantalizing observations have been reported that suggest a much wider set of physiological functions for PAP. For example, it has been shown that PAP is expressed at high levels in antigen-presenting dendritic cells in epithelial tissues (skin, gut, lung, thymus, spleen),[134,135] and that mice lacking PAP exhibit a compromised immune response.[133] Most intriguing, however, is the observation that high levels of PAP are expressed in the trigeminal ganglion, brain, and spinal cord of rats, suggesting a significant role in the nervous system.[136]

Plant PAPs are dimers of 55 kDa subunits that contain either 1 Zn and 1 Fe (kidney bean PAP and one isoform of sweet potato PAP) or 1 Fe and 1 Mn per subunit (a second isoform of sweet potato PAP).[137–140] The crystal structure of the kidney bean enzyme has been determined,[141,142] and shows that the metal ions are located between and at the edge of the sandwiched β-sheets, at the bottom of a shallow depression in the protein surface. As shown schematically in Figure 13A, the metal ions are bridged by a monodentate aspartate carboxylate and a water/hydroxide. In addition, the zinc is coordinated by two histidine imidazoles and an asparagine side-chain amide oxygen, while a histidine imidazole, a monodentate aspartate carboxylate, and a tyrosine phenolate are coordinated to the iron. In the kidney bean PAP structure, two additional terminal solvent-derived ligands were modeled into the otherwise open coordination sites on the metal ions to give distorted octahedral geometries for both metal ions.

Mammalian PAPs are monomers with a molecular mass of 36 kDa; all appear to contain a dinuclear oxo- or hydroxo-bridged iron center at the active site. Crystal structures of two different forms of rat bone PAP[143,144] and one form of PAP from porcine uterine fluids[145] have been reported, and show that the structures are virtually identical to that of the catalytic domain of kidney bean PAP. The structure of the dinuclear metal site in the mammalian enzymes is indistinguishable from that shown in Figure 13A for the kidney bean enzyme, except for replacement of Zn^{2+} by Fe^{3+}; the diferric form is stabilized by the presence of a bridging phosphate ion in two of the structures and a bound sulfate in the other. Particularly noteworthy is the presence in all structures of a tyrosinate ligand to the trivalent metal and an O-bonded Asn amide ligand to the divalent metal site. The characteristic purple color of these enzymes is due to a low-energy ligand-to-metal charge transfer band from the tyrosinate to the ferric ion, while the

Figure 13 Schematic drawings of the active sites of (A) kidney bean purple acid phosphatase and (B) the phosphate complex of calcineurin.

asparagine ligand plays a crucial role in proteolytic activation of PAP,[146,147] which is presumed to be a physiologically relevant regulatory mechanism. It seems clear that the distribution of negatively charged residues favors Fe^{3+} binding to the trivalent site, while the preponderance of neutral ligands favors binding of divalent metal ions at the other site, thus insuring the proper asymmetric distribution of the metal ions. To date, no metals other than Ca have been reported to be present in microbial PAPs, which have received very little attention.

The best characterized PAPs are those from bovine spleen (BSPAP) and porcine uterine fluids (uteroferrin or Uf), which exhibit >90% homology in their amino acid sequences[148,149] and congruent spectroscopic properties.[123–125] Studies on these two systems have been largely complementary in nature, and have led to the following conclusions. (i) Both enzymes exist in inactive oxidized ($Fe^{III}-Fe^{III}$) and active reduced ($Fe^{III}-Fe^{II}$) forms; at $T < 30$ K the latter exhibits a $g' = 1.7$ EPR signal diagnostic of the mixed-valence dinuclear center.[150–152] (ii) The purple or pink color is due to a tyrosinate-to-ferric iron charge transfer transition, whose intensity and energy is modulated by oxidation state, protein conformation, anion binding, etc.[151,153,154] (iii) The Fe atoms in the oxidized enzyme are relatively strongly coupled magnetically ($-2J \sim 80 \, cm^{-1}$), while those in the reduced form are much more weakly coupled ($-2J \sim 10–20 \, cm^{-1}$), consistent with protonation of a bridging (oxo? hydroxo?) ligand upon reduction.[151,155,156] (iv) Isotropically shifted NMR resonances are consistent with coordination of one Tyr phenoxide and one His imidazole to the ferric site and one His imidazole to the ferrous site in the reduced form.[156–158] (v) Phosphate forms a tight 1:1 complex with the oxidized form of the enzyme, which involves coordination of phosphate to the Fe ions in a bidentate bridging mode.[159] (vi) Tetrahedral oxoanions such as phosphate and molybdate bind to the mixed-valence di-iron center in the reduced form of the enzymes.[160–162] (vii) The Fe^{II} in the reduced enzyme can be replaced by Zn^{II} with 100% retention of activity,[160,163,164] as well as by other divalent metal ions such as Co^{II}. The Fe^{III} can be replaced by Ga^{3+} or Al^{3+} with retention of activity.[165]

The use of a mixed-valent, dinuclear iron site, similar to those in hemerythrin and ribonucleotide reductase,[124,166,167] to catalyze a nonredox reaction such as phosphate ester hydrolysis is novel and unexpected for a variant of the familiar oxo(hydroxo)-bridged diiron center. In contrast to the general agreement that exists regarding the spectroscopic and physical properties of the PAPs, their kinetics properties and especially their mechanism of action remain controversial. Much of the disagreement stems from the different pH dependences of the catalytic activity of BSPAP and Uf, which is due to the fact that the former is isolated in a proteolytically activated form while the latter is not. Proteolysis results in a substantial increase in optimal pH in addition to an increase in catalytic activity at the optimal pH.[146] Current data suggest that many of the spectroscopic studies described in the literature were performed on a catalytically inactive form of the enzyme.[168] As a result, the roles of the trivalent and divalent metal ions in catalysis and in particular the identity of the nucleophilic hydroxide that directly attacks the phosphate ester[169] remain unresolved.

The three most likely mechanistic possibilities for catalysis of phosphate ester hydrolysis by PAPs are shown in Figure 14. Each mechanism utilizes a different hydroxide as the nucleophile: a
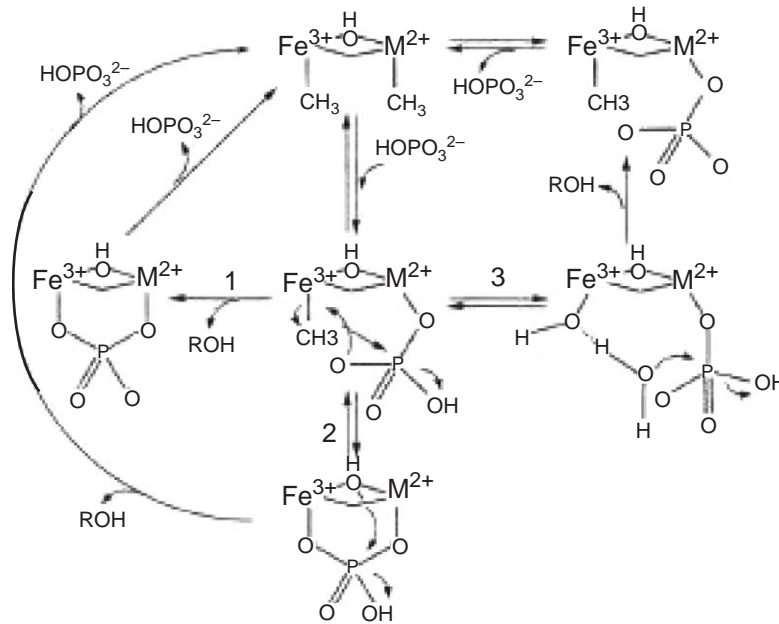
Figure 14 Catalytic mechanisms proposed for the purple acid phosphatases: (1) attack of a terminal hydroxide on the Fe^{3+} on a monodentate phosphate ester substrate coordinated to the divalent metal site; (2) attack of the bridging hydroxide on a bridging phosphate ester; (3) attack of a hydroxide ion generated in the second coordination sphere of the Fe^{3+} on a monodentate phosphate ester.

terminal OH^- on the Fe^{3+}; an OH^- in the second coordination sphere of the Fe^{3+}; or the bridging OH^-, respectively. Mechanism 1 is based on analogy to the rather well-established mechanism of the Zn-containing alkaline phosphatases, and utilizes the greater Lewis acidity of Fe^{3+} vs. Zn^{2+} to generate a metal-bound OH^- nucleophile at pH < 7, well below the pH range accessible with a divalent transition metal. In this case, the phosphate ester substrate is assumed to bind to the divalent metal site, which acts as a Lewis acid to activate it for nucleophilic attack.[141,170] Mechanism 2 invokes the bridging hydroxide as nucleophile, and is based on a plausible mechanism for hydrolysis of urea by urease[31] and a variety of spectroscopic studies of Uf.[171,172] This mechanism assumes that phosphate binds to the mixed-valent dinuclear center in the same way as it does to the diferric center, and it has most recently been invoked to explain the failure to observe a terminal hydroxide or water bound to the Fe^{3+} by ENDOR spectroscopy.[173] It is, however, not consistent with results regarding the pH dependence of phosphate or substrate binding in steady-state and pre-steady-state kinetics studies,[168] and it seems unlikely to be able to account for the high activity of the AlZn form of PAP.[174] Mechanism 3 utilizes the Fe^{3+}-bound OH^- only as a base to generate a nucleophilic hydroxide in the second coordination sphere of the Fe^{3+}. It is analogous to a plausible mechanism for the nitrile hydratases, which contain mono-nuclear *low-spin* Fe^{3+} or Co^{3+} centers.[175,176] The rates of ligand exchange of these metal ions are expected to be too slow to account for catalysis, if breaking a bond between the kinetically inert trivalent metal and the product were part of the mechanistic pathway. This mechanism was invoked to explain the fact that the $Al^{3+}Zn^{2+}$ form of BSPAP is as active a catalyst as the $Fe^{3+}Fe^{2+}$ or $Fe^{3+}Zn^{2+}$ forms, despite the 100-fold lower rate of ligand exchange for Al^{3+} vs. Fe^{3+}.[174] Regardless of which mechanism is correct, the ability to replace Fe^{2+} by Zn^{2+} and vice versa, with full retention of activity, suggests that it is likely to be applicable to both the dinuclear iron site in the mammalian PAPs and the FeZn site in the plant PAPs. In all cases, the key feature appears to be the use of a trivalent–divalent dinuclear site for phosphate ester hydrolysis.

8.24.3.2 Protein Phosphatases 1, 2A, and 2B

Protein phosphatases (PPs) are a class of mammalian regulatory enzymes that catalyze the dephosphorylation of phosphoserine and phosphothreonine residues in proteins.[177,178] Specific processes known to be controlled by protein phosphatases include glycogen metabolism, muscle contraction, mitosis, and transduction of hormonal signals. In the last 15 years, it has become

clear that protein phosphatases are as important as protein kinases in regulating a wide variety of metabolic processes via dephosphorylation-induced conformational changes with concomitant increases or decreases in the activity of key enzymes.

The known protein phosphatases can be divided into two types, based on their inhibition by two endogenous heat stable proteins (inhibitors 1 and 2) and their preference for dephosphorylating the β vs. α subunits of phosphorylase kinase.[179,180] Phosphoprotein phosphatase 1 (PP1), which is inhibited by inhibitors 1 and 2 and preferentially dephosphorylates the β-subunit of phosphorylase kinase, consists of a 38 kDa catalytic subunit complexed with either a larger glycogen-binding subunit, myosin, or inhibitor 1 or 2, depending on the source. The type 2 enzymes, which are insensitive to inhibitors 1 and 2 and preferentially dephosphorylate the α-subunit of phosphorylase kinase, are further divided into three classes. PP2A is a cytosolic enzyme that possesses broad reactivity, and contains a ca. 36 kDa catalytic subunit. PP2B, also known as calcineurin (CaN), is a Ca- and calmodulin-binding enzyme that dephosphorylates several brain-specific phosphoproteins; it consists of a 60 kDa catalytic subunit and a smaller Ca-binding 19 kDa regulatory subunit.[181] In contrast, PP2C consists of a single 46 kDa subunit. The catalytic subunits of PP1, PP2A, and PP2B are apparently closely related; the amino acid sequences deduced from the corresponding DNAs show >50% homology,[180,182] placing all of these enzymes into the so-called PPP superfamily of phosphoprotein phosphatases; the PPPs are among the most evolutionarily conserved proteins known.[177,182] The PP2B sequence appears to be the result of fusion of a protein analogous to the PP1 and PP2A catalytic subunits with another domain that is responsible for binding its regulatory subunit, CaNB. In contrast, the amino acid sequence of PP2C is not related to those of the other PPs, and based on its sequence PP2C is a member of the evolutionarily unrelated PPM superfamily of phosphoprotein phosphatases. It contains a dimanganese center, which was discussed in Section 8.24.2.3.2.

The physiological importance of protein phosphatases is indicated by the fact that calcineurin is the primary intracellular target of two different immunosuppressant drugs, cyclosporin and FK506. The complex of cyclosporin with its endogenous binding protein, cyclophilin, and the complex of FK506 with its binding protein, FKBP, form a tight complex with the CaN catalytic/regulatory subunit complex, which results in complete inhibition of protein phosphatase activity *in vitro* with phosphoprotein substrates.[183,184] CaN activity appears to be essential for both T cell receptor and interleukin-2 (IL-2) receptor signaling pathways. Its inhibition by the drug-binding protein complexes interferes with the translocation of a nuclear activating factor, resulting in inhibition of DNA translation in T-lymphocyte nuclei and preventing the immunoglobulin E (IgE)-stimulated release of secretory granules containing tissue inflammation mediators such as histamine.[183,184] Most intriguingly, the immunosuppressant-inhibited form of CaN is actually *twice* as active as the uninhibited form toward small molecule substrates such as *para*-nitrophenyl phosphate.[184] This finding suggests that inhibition is due to steric blockage of access of phosphoprotein substrates to the active site, rather than to binding to the active site.

For many years, no relationship was suspected between the PAPs and PPs, despite the seminal report by King and Huang in 1984 of the presence of equimolar Fe and Zn in bovine brain calcineurin.[185] In particular, the amino acid sequences of PPs and PAPs show no evidence whatsoever for an evolutionary relationship between these two classes of enzymes. Based on the existence of regions of the amino acid sequences of PAPs vs. PP1s, PP2As, and PP2Bs that had highly conserved patterns of potential metal ligands, however, in 1990 it was proposed that calcineurin and the homologous PP1s and PP2As would prove to be metalloenzymes with FeZn active site structures similar to those of the plant PAPs.[186] This hypothesis was abundantly confirmed by the publication in 1995 of *two* structures of bovine brain CaN,[187,188] whose dinuclear metal site is shown schematically in Figure 13B. Comparison of this structure to that of the active site of kidney bean PAP in Figure 13A demonstrates that the two structures are highly congruent, with one significant difference: the TyrO$^-$ ligand to the Fe^{3+} has effectively been replaced by a water-derived species, presumably a terminal hydroxide ion. In particular, the unusual O-bonded Asn ligand to the divalent metal site is present in both structures, as are the two conserved His residues near the dinuclear site that are postulated to be involved in substrate binding. In addition, the CaN structure clearly shows the presence of *two* terminal water-derived species on the trivalent metal: one is that which effectively replaces the TyrO$^-$ ligand, and the other corresponds to the terminal ferric-hydroxide proposed to act as the nucleophile or base in the PAP mechanism. Two crystal structures have also been reported for PP1s,[189,190] and show active site structures that are essentially identical to that of CaN. Unfortunately, however, the identity and the oxidation state of the metal ions in the PP1 structures are unclear, with Fe, Mn, and Co reported as possibilities. In both structures, the metal ions were regarded as divalent, but

there is no evidence in the structures to support this assignment. Unexpectedly, given the differences in amino acid sequences between PAPs and PPs, the two sets of enzymes have very similar protein folds and virtually identical locations of the active site within these folds.

Given the similarity in active site structures, one might expect extensive mechanistic similarities between the PAPs and PPPs as well. Unfortunately, however, there is as yet no evidence that this is the case. A major reason is the lack of published mechanistic studies on PPPs. The only such studies have reported that hydrolysis of phosphate esters by CaN occurs via an unprecedented random two-step mechanism, in which either the alcohol product or phosphate is released first.[191] In addition, general agreement regarding the oxidation states of the metal ions in the PPP active sites is lacking. An elegant series of studies on bovine brain calcineurin has shown that the Zn^{2+} in CaN can be replaced by Fe^{2+} to give an active enzyme with a g' 1.7 EPR signal that is virtually identical to that of the mixed-valent form of the mammalian PAPs.[192,193] Nonetheless, data have been reported showing that superoxide dismutase protects CaN against inactivation by superoxide, which has been interpreted as favoring the presence of an $Fe^{2+}Zn^{2+}$ dinuclear center in the active form of CaN.[194] Given the tendency of O_2^- to act as a one-electron *reductant* in promoting Fenton-type chemistry of H_2O_2, however, it seems more likely that O_2^- is actually inactivating CaN by *reducing* the ferric ion. This point must be unambiguously established before a detailed chemical mechanism can be considered. Several studies have, however, suggested that calcineurin is subject to redox regulation *in vivo*, due either to a change in the oxidation state of the iron or redox-active cysteine residues.[195,196]

8.24.3.3 Related Systems

Two other well-characterized hydrolytic enzymes are known that also possess a very similar $\beta\alpha\beta\alpha\beta$ protein structure, together with the phosphoesterase signature motif and a dinuclear metal center: the phage λ protein phosphatase (λPP) and the 5′-nucleotidase (5′-NT) from *E. coli*.[237] Despite the existence of active sites that are either identical (λPP) or very similar (5′-NT) to those in PP1 and PP2B, these two enzymes apparently utilize a dinuclear center containing two divalent metal ions (Mn^{2+} in λPP, Zn^{2+} in 5′-NT) rather than a trivalent–divalent center.

Of these two enzymes, λPP is the better characterized biochemically. Although its physiological function remains obscure, it represents in many ways a minimal model for a PPP, and, more importantly, it lacks the biological complexity of the mammalian enzymes with regard to regulatory subunits, calcium activation, etc. The enzyme is isolated as an inactive apoenzyme that requires the presence of two Mn^{2+} ions for activity. The binding constant for the second Mn^{2+} is about 100 times weaker than for the first. The enzyme fully loaded with Mn^{2+} exhibits an EPR spectra due to an exchange-coupled Mn^{2+} dimer,[197] and this spectrum is perturbed by phosphonoacetohydroxamic acid and tetrahedral oxoanions that are competitive inhibitors of the enzyme, suggesting that substrates are hydrolyzed at the dinuclear site.[198] The crystal structure of λPP[199] shows that the identity and arrangement of the protein ligands to the dinuclear active site are essentially identical to those in PP2B, which clearly contains Fe^{3+} and Zn^{2+}. It remains unclear why the λPP active site prefers to bind two *divalent* metal ions rather than a trivalent/divalent pair as in the PAPs and the PPs. The crystal structure also contains two types of coordinated sulfate ions in different molecules within the asymmetric unit, which may model the interaction with phosphate and phosphate esters. One sulfate is coordinated to Mn2 (the manganese coordinated to two histidines and an asparagine amide) in a monodentate fashion, but the other sulfate provides a triply bridging ligand to the active site: one O atom is bridging the metals, one O atom is coordinated to Mn1, and a third O atom is coordinated to Mn2. Based on this sulfate binding mode, a mechanism for the action of λPP has been proposed that is very similar to Mechanism 2 discussed above for the PAPs. In this mechanism, the phosphate ester coordinated to Mn2 is attacked by the bridging hydroxide to give a triply bridged phosphate intermediate. Heavy atom isotope effect studies indicate that the transition state is a dissociative one, involving significant P—O bond cleavage.[200] Finally, site-directed mutagenesis studies have recently identified the Mn2 site as the high affinity binding site.[201] This led to the suggestion that the resting enzyme contains a single Mn^{2+} ion in the Mn2 site, and that the second Mn^{2+} is derived from binding of a Mn^{2+} complex of the phosphate ester substrate.

In contrast, 5′-NT is an enzyme that has been known since the 1960s, but its chemistry has not been examined as extensively. 5′-NT was initially characterized as a periplasmic UDP-sugar hydrolase. As such, its likely function is to cleave UDP-glucose in the environment into uridine,

phosphate, and glucose-1-phosphate, which after further hydrolysis can be transported across the cell membrane as a nutrient. In addition, it has a relatively nonspecific 5′-nucleotidase activity. The corresponding mammalian enzymes are located of the cell surface, where they apparently hydrolyze extracellular nucleotides as part of a signaling process.
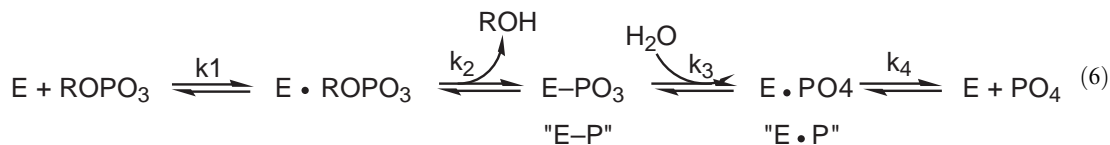
8.24.4 HYDROLASES USING TRIMETAL CENTERS

As noted in the introduction, the effects of multiple modes of catalysis are often multiplicative rather than simply additive. Consequently, it is not surprising that a number of hydrolytic metalloenzymes have evolved that utilize a constellation of three metal ions in catalysis. Perhaps not coincidentally, all well-characterized examples of this class catalyze the hydrolytic cleavage of phosphate ester or phosphoric acid anhydride bonds, which represent a difficult and long-standing chemical problem. In every case but one, the metal ions in the trimetal centers are all zinc. As we shall see, alkaline phosphatase utilizes a Zn_2Mg trinuclear center. It should be pointed out that in the older literature[2,3] many of the enzymes discussed in this section have been described as containing dinuclear metal centers. Only in the last few years has it become clear that three metal ions are present and participate in catalysis by these systems.

8.24.4.1 Alkaline Phosphatase

It is likely that alkaline phosphatase has the longest history and is the most intensively investigated hydrolytic enzyme discussed in this chapter. Because most of the published work has, however, been discussed in detail in earlier reviews, this discussion will be limited to a very brief summary of the most salient features and the latest findings. Alkaline phosphatases are zinc-dependent enzymes that are rather nonspecific and exhibit maximal catalytic activity at alkaline pH (>7.5). The enzyme is found in all organisms examined to date, and in humans the level of serum alkaline phosphatase activity is a clinically important indicator of a variety of disease states.

Several lines of evidence made it clear very early on that the hydrolytic reaction proceeds via a phosphorylated enzyme intermediate, designated as E–P in Equation (6) (which ignores the state of protonation of the phosphate and phosphoryl groups). For example, the enzyme is able to catalyze transphosphorylation reactions, in which the phosphoryl group of the substrate is transferred to acceptors such as alcohols rather than water. Moreover, the stereochemistry at phosphorus was retained when chiral phosphate substrates were examined, consistent with consecutive nucleophilic attack by a protein group on the phosphate ester substrate and by water on the phosphorylated enzyme. At pH >7.5 dissociation of phosphate from the enzyme (k_4) is the rate-limiting step in the mechanism, while breakdown of the E–P intermediate is rate-limiting at pH <7.5. In addition, the product phosphate is a potent competitive inhibitor of the enzyme, with $K_i \approx 1\,\mu M$, which has greatly complicated analysis of the kinetics:[202]

$$E + ROPO_3 \underset{}{\overset{k_1}{\rightleftharpoons}} E \cdot ROPO_3 \overset{ROH}{\underset{}{\overset{k_2}{\rightleftharpoons}}} \underset{"E-P"}{E-PO_3} \overset{H_2O}{\underset{}{\overset{k_3}{\rightleftharpoons}}} \underset{"E \cdot P"}{E \cdot PO4} \overset{k_4}{\rightleftharpoons} E + PO_4 \quad (6)$$

The best-characterized alkaline phosphatase is the enzyme from *E. coli*, which is a homodimer of 47 kDa subunits. Each subunit contains two Zn^{2+} ions and one Mg^{2+} ion, but the metal ions can be readily removed and replaced by other divalent metal ions. The enzyme containing Mg^{2+}, Co^{2+}, or Mn^{2+} in the zinc sites has a substantially lower catalytic activity, and the Cd_2Mg enzyme has a greatly reduced value of k_3, such that the E·P species accumulates.

Recent high-resolution crystal structures of the wild-type *E. coli* enzyme and its complex with phosphate[203] have enhanced our initial understanding of the enzyme mechanism, which was based on earlier lower-resolution structures of the same forms plus the E–P form of the cadmium-substituted enzyme. In all cases, the zinc ions are separated by about 4.0 Å, and there are no protein ligands bridging the two zincs. The magnesium ion is located 4.8 Å from the less solvent-exposed zinc (Zn2), to which it is linked by a bridging bidentate aspartate carboxylate, and 7.1 Å

from the more exposed zinc (Zn1). In the native enzyme, Zn1 is five-coordinate, with two histidine imidazoles, a bidentate aspartate carboxylate, and a water molecule as ligands. In contrast, Zn2 is tetrahedrally coordinated, with one histidine imidazole, two monodentate aspartate carboxylates (one of which bridges Zn2 and Mg), and the oxygen of the active site serine, Ser102, as ligands. A variety of evidence suggests that the oxygen of Ser102 is deprotonated, resulting in a coordinated alkoxide. The active site also contains two ordered water molecules that are hydrogen bonded to Ser102 and other residues in and around the active site. In the phosphate complex, the phosphate group replaces the water on Zn1 and acts as a bidentate bridge between the two zinc ions. The Ser102 side chain is disordered over two conformations, with relative occupancies of 60% and 40%, respectively. The major conformation has the Ser102 side chain coordinated to Zn2 adjacent to the phosphate oxygen, while in the minor conformation Ser102 is not coordinated to zinc. The fact that the occupancy of the Mg site in the phosphate complex was only 60%, the same as that of the major Ser102 conformation, suggests that the presence of Mg is required for coordination of Ser102 to Zn2 for formation of the nucleophilic alkoxide that attacks the substrate.

All of these features have been incorporated in a revised proposal for the catalytic mechanism that emphasizes the key role of the Mg^{2+} ion in generating the deprotonated Ser102 hydroxyl that is the actual nucleophile in the initial phosphoryl transfer. As shown in Figure 15, initial in-line attack of Ser102 results in inversion of configuration at phosphorus to give a covalent serine phosphate ester, which is then attacked by a hydroxide coordinated to Zn1 to give the phosphate complex, again with inversion of configuration at phosphorus.

Both arylsulfatases and phosphodiesterases are members of a protein superfamily that includes alkaline phosphatase, and the crystal structure of an arylsulfatase shows the presence of a metal binding site that is homologous to that of alkaline phosphatase, although it contains only a single
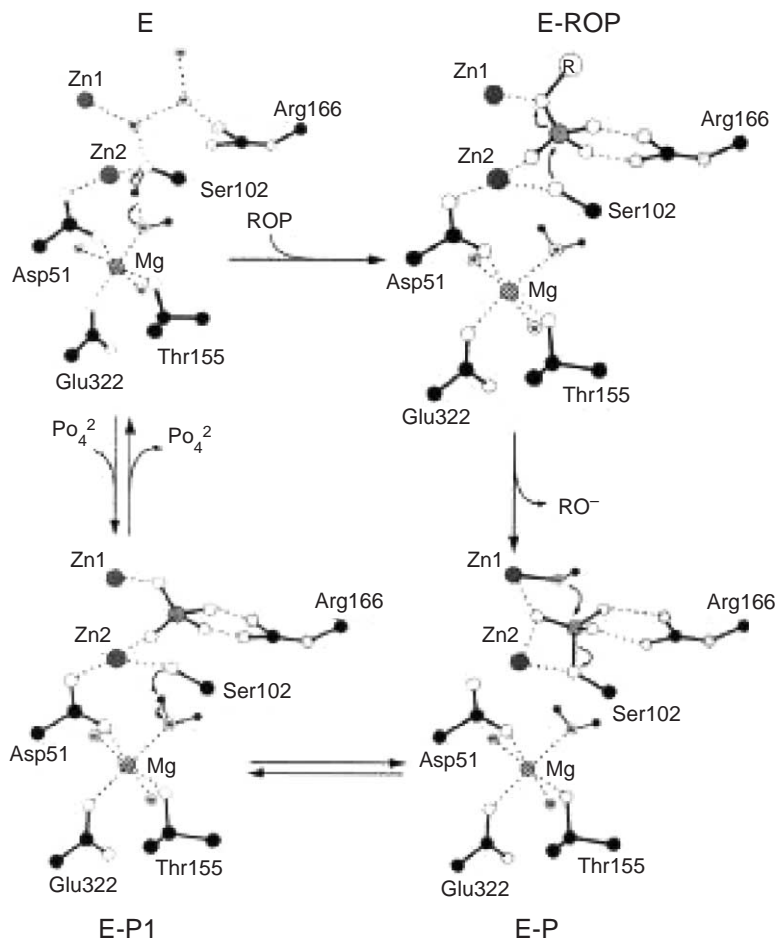

Figure 15 The three-metal-ion catalytic mechanism proposed for alkaline phosphatase (reproduced with permission from ref. 203).

metal ion (Ca^{2+}). The fact that alkaline phosphatase has recently been found to exhibit measurable levels of both arylsulfatase[204] and phosphodiesterase[205] activity with activated aryl sulfates and phosphate diesters suggests the existence of at least a vestigial functional relationship between the active sites of these three enzymes.

8.24.4.2   Phospholipase C

Phospholipases C (PLCs) catalyze the hydrolytic cleavage of the headgroup of phospholipids to give diacylglycerols (DAGs) and the phosphorylated headgroup (Equation (7)). As such, they play essential roles in signaling pathways that utilize inositol triphosphate and DAGs as second messengers. Mammals contain a family of phospholipases C, individual members of which exhibit specificity for hydrolysis of phosphatidylinositol, phosphatidylcholine, etc. Because of the difficulty in cloning and isolating pure samples of the mammalian enzymes, most studies on these enzymes have focused on the more tractable PLC from *Bacillus cereus* as a model:[206]

$$(7)$$
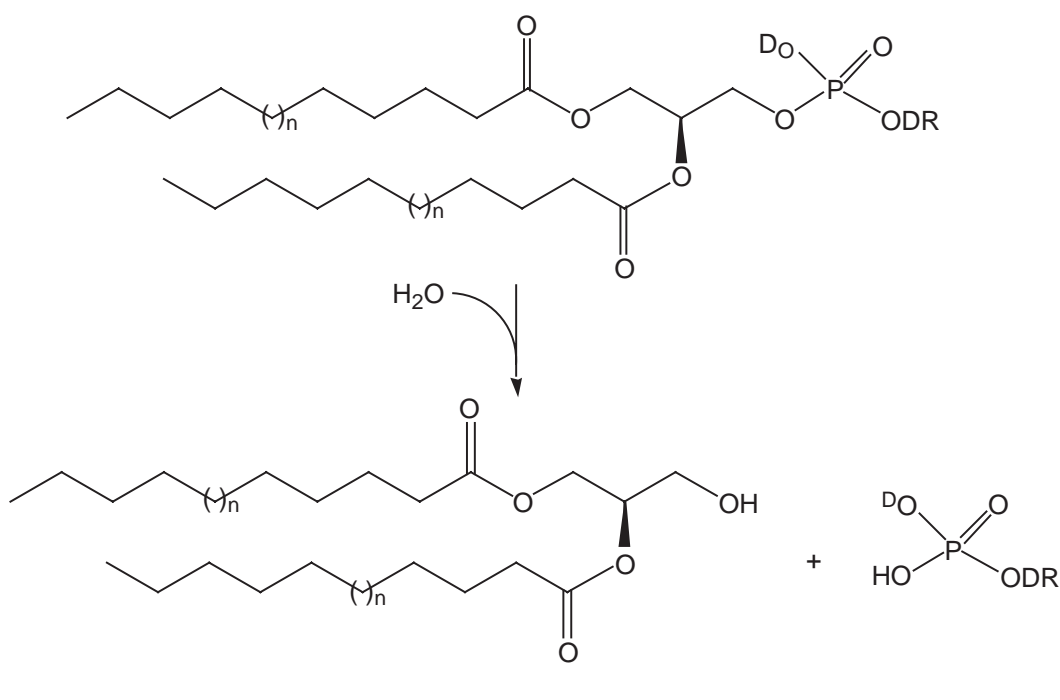
B. cereus PLC exists as a 28 kDa monomer that has a high affinity for two Zn^{2+} ions and a lower affinity for a third. The zinc ions can be replaced by other divalent metal ions, such as Co^{2+}, Mn^{2+}, and Mg^{2+}, to give reconstituted PLC with decreased activity and altered substrate specificity. Systematic studies of alternative substrates and inhibitors have shown that the positively charged choline headgroup is important for substrate recognition and binding. Replacement of the oxygen atom in the bond that is cleaved by sulfur results in a poor substrate, while replacement of the oxygen by NH, CH_2, or CF_2 results in competitive inhibitors. The corresponding dithiophosphate analog is a potent inhibitor of the enzyme, as are dithioxanthates with large hydrophobic chains, 7-hydroxytropolone, and *N,N'*-dihydroxyureas,[207] presumably due to coordination to one or more of the active site zinc ions.

The crystal structure of the native enzyme provided the first indication of the presence of a trinuclear zinc active site, which is located in a cleft in the surface of the largely α-helical protein.[208] Two zinc ions (Zn1 and Zn3) are 3.6 Å apart, and are bridged by a bidentate aspartate carboxylate and a water/hydroxide. In addition, Zn1 is ligated by two histidine imidazoles and a monodentate aspartate carboxylate, while Zn1 is coordinated by a histidine imidazole and the amino group and amide carbonyl oxygen of the N-terminal tryptophan, resulting in distorted trigonal bipyramidal coordination geometry for each. The third zinc ion (Zn2) is 6.0 Å from Zn1 and 4.7 Å from Zn3, with no bridging ligands. Two histidine imidazoles, a monodentate gluta-
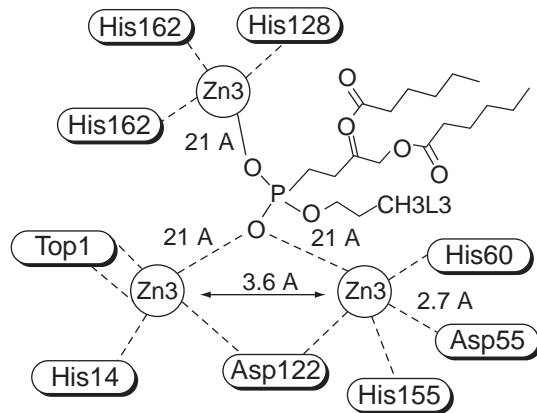
Figure 16 Schematic drawing of the active site of *Bacillus cereus* phospholipase C complexed with a phosphonate substrate analog inhibitor (reproduced by permission of Springer from Hergenrother and Martin[206]).

mate carboxylate, and two terminal water/hydroxide groups give a trigonal bipyramidal coordination geometry. In addition, crystal structures of the complexes of PLC with phosphate, a weak competitive inhibitor, and a phosphonate substrate analogue have been reported, and have provided details on how the substrate is likely to interact with the trinuclear site.[209,210] Both structures show that the trinuclear zinc site surrounds the phosphate or phosphonate group, which bridges Zn1 and Zn3 via one phosphate or phosphonate oxygen and coordinates to Zn2 via a second (Figure 16).

Based on the available structural data and a wide range of site-directed mutagenesis[211–213] and mechanistic[214] studies, a relatively detailed mechanism has been proposed.[206] Most surprisingly, given the plethora of metal ions potentially available to provide an activated hydroxide nucleophile, this mechanism (Figure 17) invokes an amino acid residue (Asp55) as the general base that interacts with a noncoordinated water molecule to generate a hydroxide ion, which attacks the phosphodiester directly. In this mechanism, the role of the metal ions is simply to activate the substrate for nucleophilic attack and to position it properly.
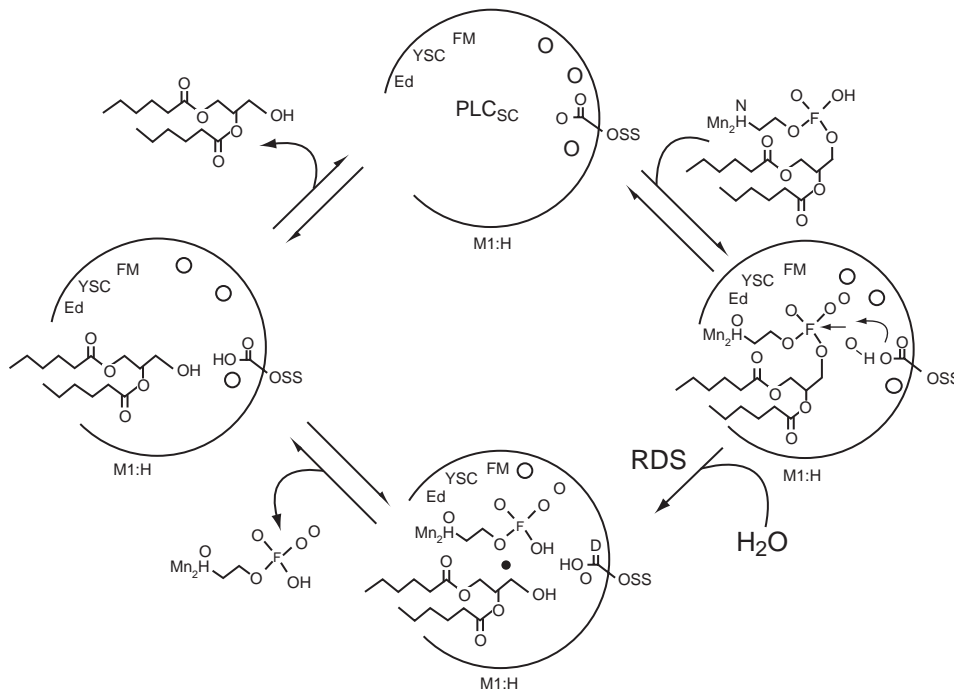
Figure 17 Proposed catalytic mechanism for phospholipase C. Zinc ions are indicated as filled circles (reproduced by permission of Springer from Hergenrother and Martin[206]).

Nuclease P1 is a 36 kDa phosphodiesterase isolated from *Penicillium citrinum*; it cleaves the bond between the 3′-hydroxyl and the 5′-phosphate of single-stranded RNA and DNA, as well as acting as a phosphomonoesterase that cleaves terminal 3′-phosphate groups. Although no sequence homology between P1 and PLC has been reported, the crystal structure of P1 shows that it contains a trinuclear zinc active site that is virtually identical to that of PLC, including the unusual coordination mode of the N-terminal tryptophan.[215] The only difference is that the monodentate glutamate ligand to Zn2 in PLC is replaced by a monodentate aspartate ligand in P1. Despite these structural similarities, the mode of interaction with nonhydrolyzable substrate analogues is significantly different for P1 vs. PLC.[215,216] Most importantly, the phosphoryl group of the phosphodiester binds only to Zn2, and the water/hydroxide bridging Zn1 and Zn3 is intact. Based on the structural studies, a very different mechanism has been proposed for P1, in which the bridging hydroxide is the nucleophile that attacks the phosphorus atom of the phosphodiester.[216] Given the extreme structural similarities, the likelihood of such different catalytic mechanisms being operative for the two enzymes seems low. It is clear that further studies, especially on P1, are in order.

8.24.4.3 Inorganic Pyrophosphatase

Soluble inorganic pyrophosphatase (PPase) is essential for growth of all known organisms. As shown in Equation (8), it catalyzes the simple hydrolytic cleavage of pyrophosphate to two phosphates. This reaction is essential because many key biosynthetic reactions release pyrophosphate rather than phosphate from nucleotide triphosphates, and the subsequent hydrolysis of pyrophosphate makes such reactions functionally irreversible, as well as providing a substantial additional thermodynamic driving force:

$$[O_3POPO_3]^{4-} + H_2O \longrightarrow 2HPO_4^{2-} \tag{8}$$

Two completely unrelated families of PPases are known.[217] The family I enzymes are by far the most common, and are found in eubacteria, archaeabacteria, fungi, plants, and animals. In contrast, only a few organisms, including *B. subtilis*[218] and *Streptococcus mutans*,[219] are known to contain the family II enzymes. The family I enzymes show extensive amino acid sequence homologies, even though they vary greatly in subunit size and degree of oligomerization. For example, the two best-characterized examples are the enzymes from *E. coli* and *Saccharomyces cerevisiae*, which exist as a hexamer of 20 kDa subunits and a dimer of 32 kDa subunits, respectively. Despite these differences, the active sites of these two enzymes are essentially superimposable. Most surprisingly, the active site of the unrelated family II enzyme is also very similar. All PPases require the presence of divalent metal ions for activity. The physiological metal ion may well be Mg^{2+}, which gives the highest activity, but Mn^{2+}, Co^{2+}, and Zn^{2+} also activate the enzyme.

The core of all structurally characterized family I PPases is a twisted five-stranded β-barrel, and the active site is located on the top surface of the barrel.[220] The resting enzyme contains two Mn^{2+} ions separated by about 3.5 Å, bridged by a bidentate aspartate carboxylate and possibly a water/hydroxide. Manganese in the M1 site, which has the highest affinity for divalent metal ions, is also coordinated by two additional monodentate aspartate carboxylates and two water/hydroxide molecules, giving an essentially octahedral coordination geometry. The manganese in the M2 site has only one protein ligand, the bridging aspartate carboxylate, with its octahedral coordination completed by water/hydroxide molecules that are hydrogen bonded to groups lining the active site. Crystal structures are now also available for apo-, mono-, and tri-metallated forms of the family I PPases,[221,222] the enzymes complexed with phosphate,[220,223] sulfate,[224] and pyrophosphate (in the inactive dicalcium form)[225], as well as of active site mutants.[226] The structural data, together with mutagenesis,[227–231] inhibition,[229] and quantum chemical studies,[232] are consistent with a picture in which the resting form of the enzyme contains two metal ions in the M1 and M2 sites, with one or two additional metals (either Mg^{2+} or Mn^{2+}) accompanying the binding of substrate or phosphates to occupy the M3 and M4 sites. The M3 site is 5.6 Å from M1 and 5.4 Å from M2, while the M4 site is 3.72 Å from M1, 6.2 Å from M2, and 4.9 Å from M3. Superposition of the active site structure of the fully metallated yeast PPase on that of the phosphate complex of alkaline phosphatase shows a great deal of similarity, with M1 and M2 corresponding to the zinc sites and M4 to the Mg site in alkaline phosphatase.

The structure of the complex of yeast PPase containing four Mn^{2+} and two phosphate ions[220] is particularly informative with regard to mechanism, in that it represents the structure of the enzyme immediately following hydrolysis of pyrophosphate, but before dissociation of either product. The working hypothesis for the enzyme mechanism is shown in Figure 18. Although four metal ions are shown, the mechanism has been described as a three metal ion mechanism, because only three of the metals are postulated to be involved in the actual catalytic mechanism. In this mechanism, the nucleophilic hydroxide bridging M1 and M2 attacks one end of the bound pyrophosphate, which is bound and activated by interactions with a tyrosine and the positively charged side chains of one arginine and two lysine residues. The role of M3 is to provide a coordinated water molecule that can act as a general acid to protonate the phosphate leaving group. In addition, however, M4 is shown as interacting with one oxygen atom of both phosphates, so this may represent an example of metal ion stabilization of the leaving group as well, making this in effect a four metal ion mechanism.

As noted previously, the family II PPases are not related to the family I enzymes in amino acid sequence. The crystal structure of the family II enzyme from *S. mutans* has recently been reported,[219] and as expected there is no similarity in protein architecture between the two types of enzyme. The family II PPase consists of a two-domain structure, with a 189-residue N-terminal α/β domain connected to a 14-residue C-terminal α/β domain by a short linker. The active site lies at the domain interface and, most surprisingly, it is almost superimposable on the active site of the family I enzymes, with Mn^{2+} ions in the M1 and M2 sites, and Mg^{2+} in the M3 site. The major difference is that the family II structure lacks a metal binding site corresponding to M4. In addition, the active site contains two histidine residues, which are conserved in all family II PPase
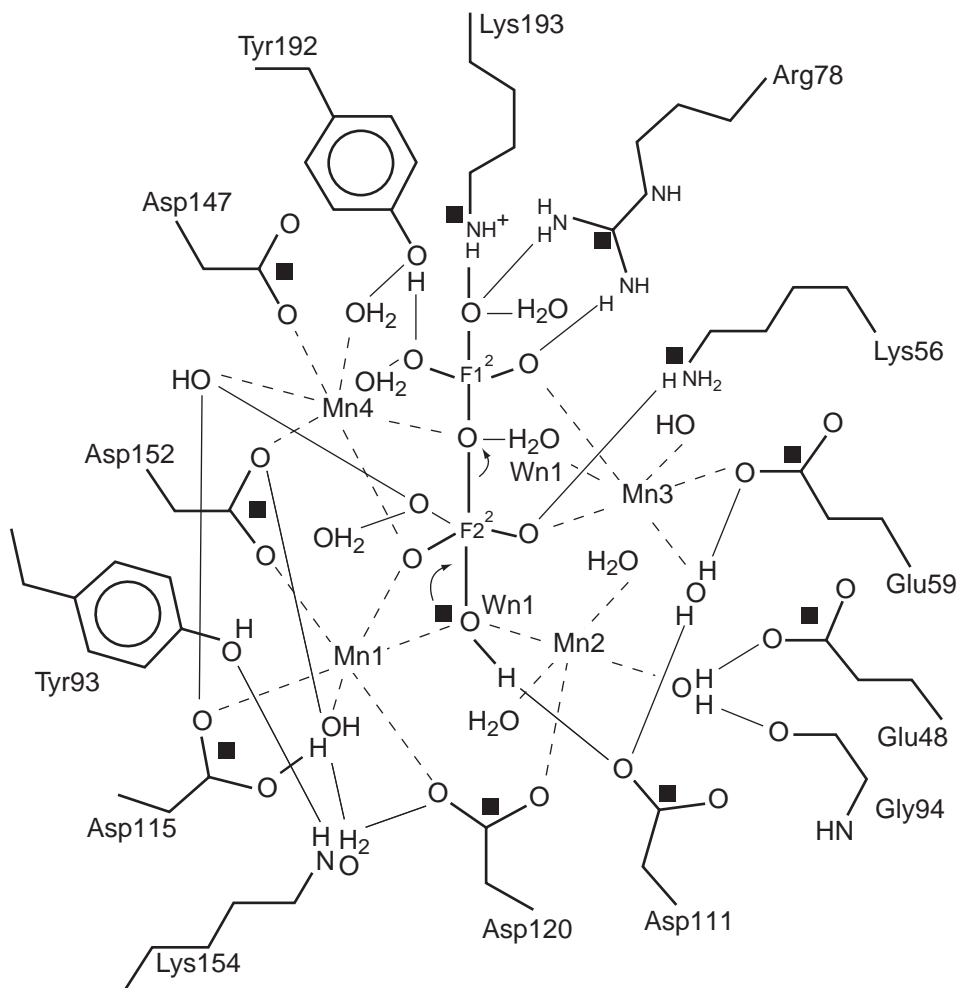
Figure 18 Proposed interactions during hydrolysis of inorganic pyrophosphate by the tetrametal active site of yeast inorganic pyrophosphatase (reproduced with permission from ref. 220).

sequences. The presence of one histidine imidazole ligand to both M1 and M2 may account for the apparent preference of the family II enzymes for Mn^{2+} rather than Mg^{2+}. M1 and M2 are bridged by a bidentate aspartate carboxylate group, a water/hydroxide, and a bidentate bridging sulfate group, similarly to the family I structures. In addition, M1 is coordinated by a bidentate aspartate carboxylate, while M2 is coordinated by two monodentate aspartate carboxylates, giving both metal ions roughly octahedral coordination. The extreme similarity of active site structures in unrelated proteins suggests that the two PPase families are examples of convergent evolution of active site structure, which seems likely to extend to a convergence of mechanism as well.

Finally, both microorganisms and higher animals produce aminoacylases, enzymes that catalyze the hydrolytic cleavage of N-acyl amino acids to produce the parent organic acid and an amino acid. In mammals, the function of these enzymes is apparently to detoxify amino acid derivatives of xenobiotics, while in bacteria they appear to play a role in catabolism of protein substrates for cell growth. Because individual aminoacylases are usually specific for either D or L forms of N-acylamino acids, they are used widely in industry for the production of optically pure amino acids; in fact, they are in the top 10 enzymes with biotechnological applications. Despite this, fundamental knowledge of these enzymes is rather sparse. Recently, however, it has been demonstrated that the aminoacylase from the hyperthermophilic archaeon *Pyrococcus furiosus* is a zinc enzyme.[233] The enzyme is a homotetramer of 42 kDa subunits, each of which contains 1 ± 0.5 Zn atoms as isolated. Removal of zinc with EDTA abolished activity, which could largely be restored by incubation with Zn^{2+} (and, to a lesser extent, with Co^{2+}). The reconstituted zinc enzyme contained 2.85 ± 0.5 zinc atoms per subunit, suggesting that aminoacylases may eventually be shown to be the first example of an enzyme that utilizes a trinuclear zinc site to cleave amide bonds.

8.24.5 CONCLUSIONS

In the preceding discussion, examples of enzymes have been described that utilize di-, tri-, and possibly tetranuclear active sites to catalyze the hydrolysis of phosphate ester and amide bonds, two of the most difficult chemical problems facing biological systems. In doing so, they employ all of the conceivable modes of catalysis discussed in the introduction: generation of a coordinated nucleophile, electrophilic activation of substrate and transition state stabilization, and even (in, e.g., inorganic pyrophosphatase) stabilization of a leaving group. The most common mode of catalysis by far, however, is activation of solvent to produce a hydroxide nucleophile, followed by substrate activation. It would seem that leaving group stabilization is generally a less effective catalytic strategy, and consequently it is employed only in addition to the other modes of catalysis if an additional metal ion can be brought to bear.

In the systems described above, the presence of bridging ligands is the rule rather than the exception. The most common bridging ligand is a bidentate carboxylate (or carbamate in urease and phosphotriesterase), which is often accompanied by a bridging water/hydroxide. Given the effect of metal ion coordination on the pK_a of water, the latter are likely to be hydroxides at physiological pHs. Most of the structurally characterized dinuclear active sites exhibit significant asymmetry due to differences in the number and kind of ligands to the two metals. In some cases, the mechanisms proposed for the enzymes exploit this asymmetry to assign separate roles for the two metals. For example, one metal delivers a coordinated nucleophile to a substrate that is activated by coordination to the adjacent metal. Although the existence of clearly separated roles for the two metals was previously thought to be a pervasive mechanistic theme in these enzymes,[2,3] the flood of structural data in recent years has focused attention on a more cooperative mode of operation, in which the responsibility for providing the catalytically important nucleophile or activating the substrate is shared by two metal ions.

In particular, bridging hydroxides have been proposed as the nucleophile for many of the reactions discussed above. At first sight, coordination of hydroxide to two metal ions might well be expected to drastically decrease its nucleophilicity. Formally, a hydroxide coordinated to two Lewis acids is analogous to the H_3O^+ ion, which is not known for its nucleophilic character. Nonetheless, a great deal of structural and mechanistic data has been accumulated in recent years that supports the use of a bridging hydroxide as the nucleophile in a number of well-characterized enzymatic reactions, such as that catalyzed by urease. The details as to why coordination of hydroxide to two metal ions does not abolish its nucleophilicity will probably have to be

established by detailed quantum mechanical calculations, which should be approaching feasibility given the increased sophistication of such methods and the increasing availability of high-resolution protein structures to use as a starting point.

In addition, it should be clear that identifying the physiologically relevant metal ions in metal-activated enzymes with relatively low affinities for metal ions poses a particularly challenging problem. The case studies presented above make it clear that neither the metal ion that gives the greatest enzymatic activity upon reconstitution *in vitro* nor the metal ion that gives the best crystals for diffraction experiments can be assumed to be the metal ion responsible for the catalytic activity *in vivo*. Elucidation of the identity of the physiologically relevant metal ion requires a multi-facetted approach, and it may not be possible to do so unambiguously in all cases.

Finally, it seems likely that the enzymes discussed in this chapter represent only the tip of the iceberg in terms of the breadth of reactions catalyzed by enzymes containing di- and trinuclear metal centers. The explosion of information on protein sequences due to completion of the various genome projects and increasingly sophisticated bioinformatics and molecular biology techniques are likely to result in a dramatic increase in the number and kinds of such systems in the near future.

A phospholipase D from *Streptomyces chromofuscus* has recently been reported to be an Fe^{3+}-dependent enzyme with possible structural and mechanistic similarities to the purple acid phosphatases.[238]

8.24.6 REFERENCES

1. Williams, N. H.; Takasaki, B.; Wall, M.; Chin, J. *Acc. Chem. Res.* **1999**, *32*, 485–493.
2. Sträter, N.; Lipscomb, W. N.; Klabunde, T.; Krebs, B. *Angew. Chem., Intl. Ed. Eng.* **1996**, *35*, 2025–2055.
3. Wilcox, D. E. *Chem. Rev.* **1996**, *96*, 2435–2458.
4. Knowles, J. R. *Annu. Rev. Biochem.* **1980**, *49*, 877–919.
5. Cowan, J. A. *BioMetals* **2002**, *15*, 225–235.
6. Cowan, J. A. *Chem. Rev.* **1998**, *98*, 1067–1088.
7. Cowan, J. A.; Ohyama, T.; Howard, K.; Rausch, J. W.; Cowan, S. M. L.; Le Grice, S. F. J. *J. Biol. Inorg. Chem.* **2000**, *5*, 67–74.
8. Klumpp, K.; Doan, L.; Roberts, N. A.; Handa, B. *J. Biol. Chem.* **2000**, *275*, 6181–6188.
9. Hamdan, S.; Carr, P. D.; Brown, S. E.; Ollis, D. L.; Dixon, N. E. *Structure* **2002**, *10*, 535–546.
10. Stieglitz, K. A.; Johnson, K. A.; Yang, H.; Roberts, M. F.; Seaton, B. A.; Head, J. F.; Stec, B. *J. Biol. Chem.* **2002**, *277*, 22863–22874.
11. Shan, S.-O.; Kravchuk, A. V.; Piccirilli, J. A.; Herschlag, D. *Biochemistry* **2001**, *40*, 5161–5171.
12. Sumner, J. B. *J. Biol. Chem.* **1926**, *69*, 435–441.
13. Dixon, N. E.; Gazzola, C.; Blakeley, R. L.; Zerner, B. *J. Am. Chem. Soc.* **1975**, *97*, 4131–4133.
14. Dixon, N. E.; Gazzola, C.; Watters, J. J.; Blakeley, R. L.; Zerner, B. *J. Am. Chem. Soc.* **1975**, *97*, 4130–4131.
15. Takishima, K.; Suga, T.; Mamiya, G. *Eur. J. Biochem.* **1988**, *175*, 151–165.
16. Mulrooney, S. B.; Hausinger, R. P. *J. Bacteriol.* **1990**, *172*, 5837–5843.
17. Moersdorf, G.; Weinmann, P.; Kaltwasser, H. EMBL Data Library, 1994.
18. Ciurli, S.; Benini, S.; Rypniewski, W. R.; Wilson, K. S.; Miletti, S.; Mangani, S. *Coord. Chem. Rev.* **1999**, *190–192*, 331–355.
19. Park, I.-S.; Hausinger, R. P. *Biochemistry* **1996**, *35*, 5345–5352.
20. Yamaguchi, K.; Cosper, N. J.; Stålhandske, C.; Scott, R. A.; Pearson, M. A.; Karplus, P. A.; Hausinger, R. P. *J. Biol. Inorg. Chem.* **1999**, *4*, 468–477.
21. Moncrief, M. B. C.; Hausinger, R. P. In *Mechanisms of Metallocenter Assembly*; Hausinger, R. P.; Eichhorn, G. L.; Marzilli, L. G., Eds.; VCH: New York, 1996; Vol. 11; pp 151–171.
22. Hausinger, R. P. *J. Biol. Inorg. Chem.* **1997**, *2*, 279–286.
23. Ciurli, S.; Safarov, N.; Miletti, S.; Dikiy, A.; Christensen, S. K.; Kornetzky, K.; Bryant, D. A.; Vandenberghe, I.; Devreese, B.; Samyn, B.; Remaut, H.; Van Beeumen, J. *J. Biol. Inorg. Chem.* **2002**, *7*, 623–631.
24. Park, I.-S.; Hausinger, R. P. *Science* **1995**, *267*, 1156–1158.
25. Yamaguchi, K.; Hausinger, R. P. *Biochemistry* **1997**, *36*, 15118–15122.
26. Jabri, E.; Carr, M. B.; Hausinger, R. P.; Karplus, P. A. *Science* **1995**, *268*, 998–1004.
27. Benini, S.; Rypniewski, W. R.; Wilson, K. S.; Miletti, S.; Ciurli, S.; Mangani, S. *Structure* **1999**, *7*, 205–216.
28. Ha, N.-C.; Oh, S.-T.; Sung, J. Y.; Cha, K. A.; Lee, M. H.; Oh, B.-H. *Nature Struct. Biol.* **2001**, *8*, 505–509.
29. Jabri, E.; Karplus, P. A. *Biochemistry* **1996**, *35*, 10616–10626.
30. Pearson, M. A.; Michel, L. O.; Hausinger, R. P.; Karplus, P. A. *Biochemistry* **1997**, *36*, 8164–8172.
31. Pearson, M. A.; Park, I.-S.; Schaller, R. A.; Michel, L. O.; Karplus, P. A.; Hausinger, R. P. *Biochemistry* **2000**, *39*, 8575–8584.
32. Karplus, P. A.; Pearson, M. A.; Hausinger, R. P. *Acc. Chem. Res.* **1997**, *30*, 330–337.
33. Park, I.-S.; Michel, L. O.; Pearson, M. A.; Jabri, E.; Karplus, P. A.; Wang, S.; Dong, J.; Scott, R. A.; Koehler, B. P.; Johnson, M. K.; Hausinger, R. P. *J. Biol. Chem.* **1996**, *271*, 18632–18637.
34. Pearson, M. A.; Schaller, R. A.; Michel, L. O.; Karplus, P. A.; Hausinger, R. P. *Biochemistry* **1998**, *37*, 6214–6220.
35. Wang, S.; Lee, M. H.; Hausinger, R. P.; Clark, P. A.; Wilcox, D. E.; Scott, R. A. *Inorg. Chem.* **1994**, *33*, 1589–1593.

36. Finnegan, M. G.; Kowal, A. T.; Werth, M. T.; Clark, P. A.; Wilcox, D. E.; Johnson, M. K. *J. Am. Chem. Soc.* **1991**, *113*.
37. Benini, S.; Rypniewski, W. R.; Wilson, K. S.; Ciurli, S.; Mangani, S. *J. Biol. Inorg. Chem.* **1998**, *3*, 268–273.
38. Benini, S.; Rypniewski, W. R.; Wilson, K. S.; Ciurli, S.; Mangani, S. *J. Biol. Inorg. Chem.* **2001**, *6*, 778–790.
39. Dixon, N. E.; Riddles, P. W.; Blakeley, R. L.; Zerner, B. *Can. J. Chem.* **1980**, *58*, 1335–1344.
40. Musiani, F.; Arnofi, E.; Casadio, R.; Ciurli, S. *J. Biol. Inorg. Chem.* **2001**, *6*, 300–314.
41. Todd, M. J.; Hausinger, R. P. *Biochemistry* **2000**, *39*, 5389–5396.
42. Coleman, J. E. *Curr. Opin. Chem. Biol.* **1998**, *2*, 222–234.
43. Raushel, F. M.; Holden, H. M. *Adv. Enzymol.* **2000**, *74*, 51–93.
44. Chae, M. Y.; Omburo, G. A.; Lindahl, P. A.; Raushel, F. M. *Arch. Biochem. Biophys.* **1995**, *316*, 765–772.
45. Omburo, G. A.; Kuo, J. M.; Mullins, L. S.; Raushel, F. M. *J. Biol. Chem.* **1992**, *267*, 13278–13283.
46. Benning, M. M.; Shim, H.; Raushel, F. M.; Holden, H. M. *Biochemistry* **2001**, *40*, 2712–2722.
47. Benning, M. M.; Kuo, J. M.; Raushel, F. M.; Holden, H. M. *Biochemistry* **1994**, *33*, 15001–15007.
48. Benning, M. M.; Kuo, J. M.; Raushel, F. M.; Holden, H. M. *Biochemistry* **1995**, *34*, 7973–7978.
49. Vanhooke, J. L.; Benning, M. M.; Raushel, F. M.; Holden, H. M. *Biochemistry* **1996**, *35*, 6020–6025.
50. Chae, M. Y.; Omburo, G. A.; Lindahl, P. A.; Raushel, F. M. *J. Am. Chem. Soc.* **1993**, *115*, 12173–12174.
51. Krauss, M. *J. Chem. Inform. Comp. Sci.* **2001**, *41*, 8–17.
52. Krauss, M.; Olsen, L.; Antony, J.; Hemmingsen, L. *J. Phys. Chem. B* **2002**, *106*, 9446–9453.
53. Shim, H.; Raushel, F. M. *Biochemistry* **2000**, *39*, 7357–7364.
54. Wilson, D. K.; Rudolph, F. B.; Quiocho, F. A. *Science* **1991**, *252*, 1278–1284.
55. Buchbinder, J. L.; Stephenson, R. C.; Dresser, M. J.; Pitera, J. W.; Scanlan, T. S.; Fletterick, R. J. *Biochemistry* **1998**, *37*, 5096–5106.
56. Kuo, J. M.; Chae, M. Y.; Raushel, F. M. *Biochemistry* **1997**, *36*, 1982–1988.
57. Chen-Goodspeed, M.; Sogorb, M. A.; Wu, F.; Hong, S.-B.; Raushel, F. M. *Biochemistry* **2001**, *40*, 1325–1331.
58. Anderson, M. M.; Shim, H.; Raushel, F. M.; Cleland, W. W. *J. Am. Chem. Soc.* **2001**, *123*, 9246–9253.
59. Hong, S.-B.; Mullins, L. S.; Shim, H.; Raushel, F. M. *Biochemistry* **1997**, *36*, 9022–9028.
60. Sträter, N.; Lipscomb, W. N. *Biochemistry* **1995**, *34*, 14792–14800.
61. Sträter, N.; Lipscomb, W. N. *Biochemistry* **1995**, *34*, 9200–9212.
62. Schürer, G.; Horn, A. H. C.; Gedeck, P.; Clark, T. *J. Phys. Chem. B* **2002**, *106*, 8815–8830.
63. Holz, R. C. *Coord. Chem. Rev.* **2002**, *232*, 5–26.
64. Chevrier, B.; Schalk, C.; D'Orchymont, H.; Rondeau, J.-M.; Moras, D.; Tarnus, C. *Structure* **1994**, *2*, 283–291.
65. Chevrier, B.; D'Orchymont, H.; Schalk, C.; Tarnus, C.; Moras, D. *Eur. J. Biochem.* **1996**, *237*, 393–398.
66. Stamper, C.; Bennett, B.; Edwards, T.; Holz, R. C.; Ringe, D.; Petsko, G. *Biochemistry* **2001**, *40*, 7035–7046.
67. Desmarais, W. T.; Bienvenue, D. L.; Bzymek, K. P.; Holz, R. C.; Petsko, G. A.; Ringe, D. *Structure* **2002**, *10*, 1063–1072.
68. Chen, G.; Edwards, T.; D'souza, V. M.; Holz, R. C. *Biochemistry* **1997**, *36*, 4278–4286.
69. Bienvenue, D. L.; Gilner, D.; Holz, R. C. *Biochemistry* **2002**, *41*, 3712–3719.
70. Bennett, B.; Holz, R. C. *Biochemistry* **1997**, *36*, 9837–9846.
71. Bennett, B.; Holz, R. C. *J. Am. Chem. Soc.* **1997**, *119*, 1923–1933.
72. Rowsell, S.; Pauptit, R. A.; Tucker, A. D.; Melton, R. G.; Blow, D. M.; Brick, P. *Structure* **1997**, *5*, 337–347.
73. Speno, H. S.; Luthi-Carter, R.; Macias, W. L.; Valentine, S. L.; Joshi, A. R. T.; Coyle, J. T. *Mol. Pharmacol.* **1999**, *55*, 179.
74. Huntington, K. M.; Bienvenue, D. L.; Wei, Y.; Bennett, B.; Holz, R. C.; Pei, D. *Biochemistry* **1999**, *38*, 15587–15596.
75. Bienvenue, D. L.; Bennett, B.; Holz, R. C. *J. Biol. Inorg. Chem.* **2000**, *78*, 43–54.
76. Wang, Z.; Fast, W.; Valentine, A. M.; Benkovic, S. J. *Curr. Opin. Chem. Biol.* **1999**, *3*, 614–622.
77. Crowder, M. W.; Wang, Z.; Franklin, S. L.; Zovinka, E. P.; Benkovic, S. J. *Biochemistry* **1996**, *35*, 12126–12132.
78. Wang, Z.; Benkovic, S. J. *J. Biol. Chem.* **1998**, *273*, 22402–22408.
79. Crowder, M. W.; Walsh, T. R.; Banovic, L.; Pettit, M.; Spencer, J. *Antimicrob. Agents Chemother.* **1998**, *42*, 921–926.
80. O'Hara, K.; Haruta, S.; Sawai, T.; M, T.; Iyobe, S. *FEMS Microbiol. Lett.* **1998**, *162*, 201–206.
81. Orellano, E. G.; Girardini, J. E.; Cricco, J. A.; Ceccarelli, E. A.; Vila, A. J. *Biochemistry* **1998**, *37*, 10173–10180.
82. Paul-Soto, R.; Hernandez-Valladares, M.; Galleni, M.; Bauer, R. *FEBS Lett.* **1998**, *438*, 137–140.
83. Paul-Soto, R.; Bauer, R.; Frère, J.-M.; Galleni, M.; Meyer-Klaucke, W.; Nolting, H.; Rossolini, G. M.; de Seny, D.; Hernandez-Valladares, M.; Zeppezauer, M.; Adolph, H.-W. *J. Biol. Chem.* **1999**, *274*, 13242–13249.
84. Valladares, M. H.; Felici, A.; Weber, G.; Adolph, H.-W.; Zeppezauer, M.; Rossolini, G. M.; Amicosante, G.; Frère, J.-M.; Galleni, M. *Biochemistry* **1997**, *36*, 11534–11541.
85. Concha, N. O.; Janson, C. A.; Rowling, P.; Pearson, S.; Cheever, C. A.; Clarke, B. P.; Lewis, C.; Galleni, M.; Frere, J.-M.; Payne, D. J.; Bateson, J. H.; Abdel-Meguid, S. S. *Biochemistry* **2000**, *39*, 4288–4298.
86. Ullah, J. H.; Walsh, T. R.; Taylor, I. A.; Emery, D. C.; Verma, C. S.; Gamblin, S. J.; Spencer, J. *J. Mol. Biol.* **1998**, *284*, 125–136.
87. Concha, N. O.; Rasmussen, B. A.; Bush, K.; Herzberg, O. *Structure* **1996**, *4*, 823–836.
88. Carfi, A.; Pares, S.; Duee, E.; Galleni, M.; Duez, C.; Frere, J.; Dideberg, O. *EMBO J.* **1995**, *14*, 4914–4921.
89. Bounaga, S.; Laws, A. P.; Galleni, M.; Page, M. I. *Biochem. J.* **1998**, *331*, 703–711.
90. Wang, Z.; Fast, W.; Benkovic, S. J. *J. Am. Chem. Soc.* **1998**, *120*, 10788–10789.
91. Wang, Z.; Fast, W.; Benkovic, S. J. *Biochemistry* **1999**, *38*, 10013–10023.
92. Fast, W.; Wang, Z.; Benkovic, S. J. *Biochemistry* **2001**, *40*, 1640–1650.
93. McManus-Munoz, S.; Crowder, M. W. *Biochemistry* **1999**, *38*, 1547–1553.
94. Melino, S.; Capo, C.; Dragani, B.; Aceto, A.; Petruzzelli, R. *Trends Biochem. Sci.* **1998**, *23*, 381–382.
95. Crowder, M. W.; Maiti, M. K.; Banovic, L.; Makaroff, C. A. *FEBS Letters* **1997**, *418*, 351–354.
96. Cameron, A. D.; Ridderström, M.; Olin, B.; Mannervik, B. *Structure* **1999**, *7*, 1067–1078.
97. Zang, T. M.; Hollman, D. A.; Crawford, P. A.; Crowder, M. W.; Makaroff, C. A. *J. Biol. Chem.* **2001**, *276*, 4788–4795.
98. Vogel, A.; Schilling, O.; Niecke, M.; Bettmer, J.; Meyer-Klaucke, W. *J. Biol. Chem.* **2002**, *277*, 29078–29085.
99. Cha, M. H.; Yong, W. M.; Lee, S. M.; Lee, Y. S.; Chung, I. Y. *Molec. Cells* **2000**, *10*, 423.

100. Kim, N. N.; Cox, J. D.; Baggio, R. F.; Emig, F. A.; Mistry, S. K.; Harper, S. L.; Speicher, D. W.; Morris, S. M.; Ash, D. E.; Traish, A.; Christianson, D. W. *Biochemistry* **2001**, *40*, 2678–2688.
101. Khangulov, S. V.; Pessiki, P. J.; Barynin, V. V.; Ash, D. E.; Dismukes, G. C. *Biochemistry* **1995**, *34*, 2015–2025.
102. Kanyo, Z. F.; Scolnick, L. R.; Ash, D. E.; Christianson, D. W. *Nature* **1996**, *383*, 554–557.
103. Scolnick, L. R.; Kanyo, Z. F.; Cavalli, R. C.; Ash, D. E.; Christianson, D. W. *Biochemistry* **1997**, *36*, 10558–10565.
104. Carvajal, N.; Olate, J.; Salas, M. O. N.; Uribe, E.; López, V.; Herrera, P.; Cerpa, J. *Arch. Biochem. Biophys.* **1999**, *371*, 202–206.
105. Colleluori, D. M.; Ash, D. E. *Biochemistry* **2001**, *40*, 9356–9362.
106. Cox, J. D.; Cama, E.; Colleluori, D. M.; Pethe, S.; Boucher, J.-L.; Mansuy, D.; Ash, D. E.; Christianson, D. W. *Biochemistry* **2001**, *40*, 2689–2701.
107. Das, A.; Helps, N.; Cohen, P.; Barford, D. *EMBO J.* **1996**, *15*, 6798–6809.
108. Rusnak, F. *Metal Ions Biol. Syst.* **2000**, *37*, 305–343.
109. Zhang, L.; Crossley, M. J.; Dixon, N. E.; Ellis, P. J.; Fisher, M. L.; King, G. F.; Lilley, P. E.; MacLachlan, D.; Pace, R. J.; Freeman, H. C. *J. Biol. Inorg. Chem.* **1998**, *3*, 470–483.
110. Wilce, M. C. J.; Bond, C. S.; Dixon, N. E.; Freeman, H. C.; Guss, J. M.; Lilley, P. E.; Wilce, J. A. *Proc. Natl. Acad. Sci. USA* **1998**, *95*, 3472–3477.
111. Arfin, S.; Kendall, R.; Hall, L.; Weaver, L.; Stewart, A.; Matthews, B.; Bradshaw, R. *Proc. Natl. Acad. Sci. USA* **1995**, *92*, 7714–7718.
112. Roderick, S. L.; Matthews, B. W. *Biochemistry* **1993**, *32*, 3907–3912.
113. Liu, S.; Widom, J.; Kemp, C. W.; Crews, C. M.; Clardy, J. *Science* **1998**, *282*, 1324–1327.
114. Tahirov, T. H.; Oki, H.; Tsukihara, T.; Ogasahara, K.; Yutani, K.; Ogata, K.; Izu, Y.; Tsunasawa, S.; Kato, I. *J. Mol. Biol.* **1998**, *284*, 101–124.
115. Lowther, W. T.; Orville, A. M.; Madden, D. T.; Lim, S.; Rich, D. H.; Matthews, B. W. *Biochemistry* **1999**, *38*, 7678–7688.
116. Lowther, W. T.; Zhang, Y.; Sampson, P. B.; Honek, J. F.; Matthews, B. W. *Biochemistry* **1999**, *38*, 14810–14819.
117. Yang, G.; Kirkpatrick, R. B.; Ho, T.; Zhang, G.-F.; Liang, P.-H.; Johanson, K. O.; Casper, D. J.; Doyle, M. L.; Marino, J. P.; Thompson, S. K.; Chen, W.; Tew, D. G.; Meek, T. D. *Biochemistry* **2001**, *40*, 10645–10654.
118. D'souza, V. M.; Bennett, B.; Copik, A. J.; Holz, R. C. *Biochemistry* **2000**, *39*, 3817–3826.
119. Cosper, N. J.; D'souza, V. M.; Scott, R. A.; Holz, R. C. *Biochemistry* **2001**, *40*, 13302–13309.
120. D'souza, V. M.; Holz, R. C. *Biochemistry* **1999**, *38*, 11079–11085.
121. Ghosh, M.; Grunden, A. M.; Dunn, D. M.; Weiss, R.; Adams, M. W. W. *J. Bacteriol.* **1998**, *180*, 4781–4789.
122. Cheng, T.; Harvey, S.; Chen, G. *Appl. Environ. Microbiol.* **1996**, *62*, 1636–1641.
123. Klabunde, T.; Krebs, B. *Struct. Bonding* **1997**, *89*, 177–198.
124. Vincent, J. B.; Olivier-Lilley, G. L.; Averill, B. A. *Chem. Rev.* **1990**, *90*, 1447–1467.
125. Vogel, A.; Spener, F.; Krebs, B.; Purple Acid Phosphatase. In *Handbook of Metalloproteins*; Messerschmidt, A.; Huber, R.; Wieghardt, K.; Poulos, T., Eds.; Wiley Interscience: New York, 2001; Vol. 1; pp 752–767.
126. Vincent, J. B.; Averill, B. A. *FASEB J.* **1990**, *4*, 3009–3014.
127. Oddie, G. W.; Schenk, G.; Angel, N. Z.; Walsh, N. G. L. W.; DeJersey, J.; Cassady, A. I.; Hamilton, S. E.; Hume, D. A. *Bone* **2000**, *27*, 575–584.
128. Buhi, W. C.; Ducsay, C. A.; Bazer, F. W.; Roberts, R. M. *J. Biol. Chem.* **1982**, *257*, 1712–1723.
129. Ducsay, C. A.; Buhi, W. C.; Bazer, F. W.; Roberts, R. M. *Biol. Reprod.* **1982**, *26*, 729–743.
130. Ljusberg, J.; EkRylander, B.; Andersson, G. *Biochem. J.* **1999**, *343*, 63–69.
131. Reinholt, F. P.; Hultenby, K.; Oldberg, A.; Heinegard, D. *Proc. Natl. Acad. Sci. USA* **1990**, *87*, 4473–4475.
132. Hayman, A. R.; Jones, S. J.; Boyde, A.; Foster, D.; Colledge, W. H.; Carlton, M. B.; Evans, M. J.; Cox, T. M. *Development* **1996**, *122*, 3151–3162.
133. Bune, A. J.; Hayman, A. R.; Evans, M. J.; Cox, T. J. *Immunology* **2001**, *102*, 103–113.
134. Hayman, A. R.; Bune, A. J.; Bradley, J. R.; Rashbass, J; Cox, T. M. *J. Histochem. Cytochem.* **2000**, *48*, 219–227.
135. Hayman, A. R.; Bune, A. R.; Cox, T. J. *J. Anatomy* **2000**, *196*, 433–441.
136. Lang, P.; M, S.; G, A. *J Histochem. Cytochem.* **2001**, *49*, 379–396.
137. Beck, J. L.; McConachie, L. A.; Summors, A. C.; Arnold, W. N.; de Jersey, J.; Zerner, B. *Biochim. Biophys. Acta* **1986**, *869*, 61–68.
138. Hefler, S. K.; Averill, B. A. *Biochem. Biophys. Res. Comm.* **1987**, *146*, 1173–1177.
139. Schenk, G.; Ge, Y. B.; Carrington, L. E.; Wynne, C. J.; Searle, I. R.; Carroll, B. J.; Hamilton, S.; deJersey, J. *Arch. of Biochem. Biophys.* **1999**, *370*, 183–189.
140. Schenk, G.; Guddat, L. W.; Ge, Y.; Carrington, L. E.; Hume, D. A.; Hamilton, S.; de Jersey, J. *Gene* **2000**, *250*, 117–125.
141. Klabunde, T.; Sträter, N.; Fröhlich, R.; Witzel, H.; Krebs, B. *J. Mol. Biol.* **1996**, *259*, 737–748.
142. Sträter, N.; Klabunde, T.; Tucker, P.; Witzel, H.; Krebs, B. *Science* **1995**, *268*, 1489–1492.
143. Lindqvist, Y.; Johansson, E.; Kaija, H.; Vihko, P.; Schneider, G. *J. Mol. Biol.* **1999**, *291*, 135–147.
144. Uppenberg, J.; Lindqvist, F.; Svensson, C.; EkRylander, B.; Andersson, G. *J. Mol. Biol.* **1999**, *290*, 201–211.
145. Guddat, L. W.; McAlpine, A. S.; Hume, D.; Hamilton, S.; de Jersey, J.; Martin, J. L. *Structure* **1999**, *7*, 757–767.
146. Funhoff, E. G.; Klaassen, C. E. H. W.; Samyn, B.; Van Beeumen, J.; Averill, B. A. *ChemBioChem* **2001**, *2*, 355–363.
147. Funhoff, E. G.; Ljusberg, J.; Wang, Y.; Andersson, G.; Averill, B. A. *Biochemistry* **2001**, *40*, 11614–11622.
148. Hunt, D. F.; Yates, J. R.; Shabanowitz, J.; Zhu, N.-Z.; Zirino, T.; Averill, B. A.; Daurat-Larroque, S. T.; Shewale, J. G.; Roberts, M. R.; Brew, K. *Biochem. Biophys. Res. Comm.* **1987**, *144*, 1154–1160.
149. Ketcham, C. M.; Roberts, R. M.; Simmen, R. C. M.; Nick, H. S. *J. Biol. Chem.* **1989**, *264*, 557–563.
150. Antanaitis, B. C.; Aisen, P.; Lilienthal, H. R. *J. Biol. Chem.* **1983**, *258*, 3166–3172.
151. Averill, B. A.; Davis, J. C.; Burman, S.; Zirino, T.; Sanders-Loehr, J.; Loehr, T. M.; Sage, J. T.; Debrunner, P. G. *J. Am. Chem. Soc.* **1987**, *109*, 3760–3767.
152. Debrunner, P. G.; Hendrich, M. P.; de Jersey, J.; Keough, D. T.; Sage, J. T.; Zerner, B. *Biochim. Biophys. Acta* **1983**, *745*, 103–106.
153. Antanaitis, B. C.; Strekas, T.; Aisen, P. *J. Biol. Chem.* **1982**, *257*, 3766–3770.
154. Vincent, J. B.; Crowder, M. W.; Averill, B. A. *Biochemistry* **1991**, *30*, 3025–3034.

155. Day, E. P.; David, S. S.; Peterson, J.; Dunham, W. R.; Bonvoison, J. J.; Sands, R. H.; Que, L., Jr. *J. Biol. Chem.* **1988**, *263*, 15561–15567.
156. Lauffer, R. B.; Antanaitis, B. C.; Aisen, P.; Que, L., Jr. *J. Biol. Chem.* **1983**, *258*, 14212–14218.
157. Scarrow, R. C.; Pyrz, J. W.; Que, L., Jr. *J. Am. Chem. Soc.* **1990**, *112*, 657–665.
158. Wang, Z.; Ming, L.-J.; Que, L., Jr.; Vincent, J. B.; Crowder, M. W.; Averill, B. A. *Biochemistry* **1992**, *31*, 5263–5268.
159. Kauzlarich, S. M.; Teo, B. K.; Zirino, T.; Burman, S.; Davis, J. C.; Averill, B. A. *Inorg. Chem.* **1986**, *25*, 2781–2785.
160. David, S. S.; Que, L., Jr. *J. Am. Chem. Soc.* **1990**, *112*, 6455–6463.
161. Doi, K.; McCracken, J.; Peisach, J.; Aisen, P. *J. Biol. Chem.* **1988**, *263*, 5757–5763.
162. Wang, D. L.; Holz, R. C.; David, S. S.; Que, L., Jr.; Stankovich, M. T. *Biochemistry* **1991**, *30*, 8187–8194.
163. Davis, J. C.; Averill, B. A. *Proc. Natl. Acad. Sci. USA* **1982**, *79*, 4623–4627.
164. Keough, D. T.; Dionysius, D. A.; de Jersey, J.; Zerner, B. *Biochem. Biophys. Res. Comm.* **1980**, *94*, 600–605.
165. Merkx, M.; Averill, B. A. *Biochemistry* **1998**, *37*, 8490–8497.
166. Que, L., Jr.; True, A. E. *Progr. Inorg. Chem.* **1990**, *38*, 97–200.
167. Sanders-Loehr, J.; Binuclear Iron Proteins. In *Iron Carriers and Iron Proteins*; Loehr, T. M., Ed.; VCH: New York, 1989; pp 375–466.
168. Merkx, M.; Pinkse, M. W. H.; Averill, B. A. *Biochemistry* **1999**, *38*, 9914–9925.
169. Mueller, E. G.; Crowder, M. W.; Averill, B. A.; Knowles, J. R. *J. Am. Chem. Soc.* **1993**, *115*, 2974–2975.
170. Dietrich, M.; Münstermann, D.; Suerbaum, H.; Witzel, H. *Eur. J. Biochem.* **1991**, *199*, 105–113.
171. Wang, X.; Randall, C. R.; True, A. E.; Que, L., Jr. *Biochemistry* **1996**, *35*, 13946–13954.
172. Wang, X. D.; Ho, R. Y. N.; Whiting, A. K.; Que, L., Jr. *J. Am. Chem. Soc.* **1999**, *121*, 9235–9236.
173. Smoukov, S. K. Q.; Luca, ; Wang, ; Xuedong, ; Doan, ; Peter, E.; Hoffman, ; Brian, M.; Que, L., Jr. *J. Am. Chem. Soc.* **2002**, *124*, 2595–2603.
174. Merkx, M.; Averill, B. A. *J. Am. Chem. Soc.* **1999**, *121*, 6683–6689.
175. Huang, W. J.; Jia, J.; Cummings, J.; Nelson, M.; Schneider, G.; Lindqvist, Y. *Structure* **1997**, *5*, 691–699.
176. Payne, M. S.; Wu, S. J.; Fallon, R. D.; Tudor, G.; Stieglitz, B.; Turner, I. M.; Nelson, M. J. *Biochemistry* **1997**, *36*, 5447–5454.
177. Barford, D.; Das, A. K.; Egloff, M.-P. *Annu. Rev. Biophys. Biomol. Struct.* **1998**, *27*, 133–164.
178. Rusnak, F.; Yu, L.; Mertz, P. *J. Biol. Inorg. Chem.* **1996**, *1*, 388–396.
179. Ballou, L. M.; Fischer, E. H. *The Enzymes* **1986**, *17*, 311–361. Academic Press.
180. Cohen, P. *Annu. Rev. Biochem.* **1989**, *58*, 453–508.
181. Rusnak, F.; Mertz, P. *Physiol. Rev.* **2000**, *80*, 1483–1521.
182. Cohen, P. *J. Biol. Chem.* **1989**, *264*, 21435–21438.
183. Liu, J.; Albers, M. W.; Wandless, T. J.; Luan, S.; Alberg, D. G.; Belshaw, P. J.; Cohen, P.; MacKintosh, C.; Klee, C. B.; Schreiber, S. L. *Biochemistry* **1992**, *31*, 3896–3901.
184. Liu, J.; Farmer, J. D., Jr.; Lane, W. S.; Friedman, J.; Weissman, I.; Schreiber, S. L. *Cell* **1991**, *66*, 807–815.
185. King, M. M.; Huang, C. Y. *J. Biol. Chem.* **1984**, *249*, 8847–8856.
186. Vincent, J. B.; Averill, B. A. *FEBS Lett.* **1990**, *263*, 265–268.
187. Kissinger, C. R.; Parge, H. E.; Knighton, D. R.; Lewis, C. T.; Pelletier, L. A.; Tempczyk, A.; Kalish, V. J.; Tucker, K. D.; Showalter, R. E.; Moomaw, E. W.; Gastinel, L. N.; Habuka, N.; Chen, X.; Maldonado, F.; Barker, J. E.; Bacquet, R.; Villafranca, J. E. *Nature* **1995**, *378*, 641–644.
188. Griffith, J. P.; Kim, J. L.; Kim, E. E.; Sintchak, M. D.; Thomson, J. A.; Fitzgibbon, M. J.; Fleming, M. A.; Caron, P. R.; Hsiao, K.; Navia, M. A. *Cell* **1995**, *82*, 507–522.
189. Egloff, M. P.; Cohen, P. T. W.; Reinemer, P.; Barford, D. *J. Mol. Biol.* **1995**, *254*, 942–959.
190. Goldberg, J.; Huang, H.-B.; Kwon, Y.-G.; Greengard, P.; Nairn, A. C.; Kuriyan, J. *Nature* **1995**, *376*, 745–753.
191. Martin, B. L.; Graves, D. J. *J. Biol. Chem.* **1986**, *261*, 14545–14550.
192. Yu, L.; Golbeck, J.; Yao, J.; Rusnak, F. *Biochemistry* **1997**, *36*, 10727–10734.
193. Yu, L.; Haddy, A.; Rusnak, F. *J. Am. Chem. Soc.* **1995**, *117*, 10147–10148.
194. Wang, X.; Culotta, V. C.; Klee, C. B. *Nature* **1996**, *383*, 434–437.
195. Rusnak, F.; Reiter, T. *Trends Biochem. Sci.* **2000**, *25*, 527–529.
196. Reiter, T. A.; Abraham, R. T.; Choi, M.; Rusnak, F. *J. Biol. Inorg. Chem.* **1999**, *4*, 632–644.
197. Rusnak, F.; Yu, L.; Todorovic, S.; Mertz, P. *Biochemistry* **1999**, *38*, 6943–6952.
198. Reiter, N. J.; White, D. J.; Rusnak, F. *Biochemistry* **2002**, *41*, 1051–1059.
199. Voegtli, W. C.; White, D. J.; Reiter, N. J.; Rusnak, F.; Rosenzweig, A. C. *Biochemistry* **2000**, *39*, 15365–15374.
200. Hoff, R. H.; Mertz, P.; Rusnak, F.; Hengge, A. C. *J. Am. Chem. Soc.* **1999**, *121*, 6382–6390.
201. White, D. J.; Reiter, N. J.; Sikkink, R. A.; Yu, L.; Rusnak, F. *Biochemistry* **2001**, *40*, 8918–8929.
202. O'Brien, P. J.; Herschlag, D. *Biochemistry* **2002**, *41*, 3207–3225.
203. Stec, B.; Holtz, K. M.; Kantrowitz, E. R. *J. Mol. Biol.* **2000**, *299*, 1323–1331.
204. O'Brien, P. J.; Herschlag, D. *J. Am. Chem. Soc.* **1998**, *120*, 12369–12370.
205. O'Brien, P. J.; Herschlag, D. *Biochemistry* **2001**, *40*, 5691–5699.
206. Hergenrother, P. J.; Martin, S. F. *Top. Curr. Chem.* **2001**, *211*, 131.
207. Martin, S. F.; Follows, B. C.; Hergenrother, P. J.; Franklin, C. L. *J. Org. Chem.* **2000**, *65*, 4509–4514.
208. Hough, E.; Hansen, L. K.; Birkness, B.; Jynge, K.; Hansen, S.; Hordvik, A.; Little, C.; Dodson, E.; Derewenda, Z. *Nature* **1989**, *338*, 357–360.
209. Hansen, S.; Hansen, S. H.; Hough, E. *J. Mol. Biol.* **1992**, *225*, 543–549.
210. Hansen, S.; Hough, E.; Svensson, L. A.; Wong, Y.-L.; Martin, S. F. *J. Mol. Biol.* **1993**, *234*, 179–187.
211. Martin, S. F.; Follows, B. C.; Hergenrother, P. J.; Trotter, B. K. *Biochemistry* **2000**, *39*, 3410–3415.
212. Martin, S. F.; Hergenrother, P. J. *Biochemistry* **1998**, *37*, 5755–5760.
213. Martin, S. F.; Spaller, M. R.; Hergenrother, P. J. *Biochemistry* **1996**, *35*, 12970–12977.
214. Martin, S. F.; Hergenrother, P. J. *Biochemistry* **1999**, *38*, 4403–4408.
215. Volbeda, A.; Lahm, A.; Sakiyama, F.; Suck, D. *EMBO J.* **1991**, *10*, 1607–1618.
216. Romier, C.; Dominguez, R.; Lahm, A.; Dahl, O.; Suck, D. *Proteins: Struct., Funct., Genet.* **1998**, *32*, 414–424.
217. Sivula, T.; Salminen, A.; Parfenyev, A. N.; Pohjanjoki, P.; Goldman, A.; Cooperman, B. S.; Baykov, A. A.; Lahti, R. *FEBS Lett.* **1999**, *454*, 75–80.

218. Shintani, T.; Uchiumi, T.; Yonezawa, T.; Salminen, A.; Baykov, A. A.; Lahti, R.; Hachimori, A. *FEBS Lett.* **1998**, *439*, 263–266.
219. Merckel, M. C.; Fabrichniy, I. P.; Salminen, A.; Kalkkinen, N.; Baykov, A. A.; Lahti, R.; Goldman, A. *Structure* **2001**, *9*, 289–297.
220. Heikinheimo, P.; Lehtonen, J.; Baykov, A.; Lahti, R.; Cooperman, B. S.; Goldman, A. *Structure* **1996**, *4*, 1491–1508.
221. Kankare, J.; Salminen, T.; Lahti, R.; Cooperman, B. S.; Baykov, A. A.; Goldman, A. *Biochemistry* **1996**, *35*, 4670–4677.
222. Harutyunyan, E. H.; Oganessyan, V. Y.; Oganessyan, N. N.; Avaeva, S. M.; Nazarova, T. I.; Vorobyeva, N. N.; Kurilova, S. A.; Huber, R.; Mather, T. *Biochemistry* **1997**, *36*, 7754–7760.
223. Harutyunyan, E.; Kuranova, I.; Vainshtein, B.; Hohne, W.; Lamzin, V.; Dauter, Z.; Teplyakov, A.; Wilson, K. *Eur. J. Biochem.* **1996**, *239*, 220–228.
224. Avaeva, S.; Kurilova, S.; Nazarova, T.; Rodina, E.; Vorobyeva, N.; Sklyankina, V.; Grigorjeva, O.; Harutyunyan, E.; Oganessyan, V.; Wilson, K.; Dauter, Z.; Huber, R.; Mather, T. *FEBS Lett.* **1997**, *410*, 502–508.
225. Samygina, V. R.; Popov, A. N.; Rodina, E. V.; Vorobyeva, N. N.; Lamzin, V. S.; Polyakov, K. M.; Kurilova, S. A.; Nazarova, T. I.; Avaeva, S. M. *J. Mol. Biol.* **2001**, *314*, 633–645.
226. Tuominen, V.; Heikinheimo, P.; Kajander, T.; Torkkel, T.; Hyytiä, T.; Käpylä, J.; Lahti, R.; Cooperman, B. S.; Goldman, A. *J. Mol. Biol.* **1998**, *284*, 1565–1580.
227. Efimova, I. S.; Salminen, A.; Pohjanjoki, P.; Lapinniemi, J.; Magretova, N. N.; Cooperman, B. S.; Goldman, A.; Lahti, R.; Baykov, A. A. *J. Biol. Chem.* **1999**, *274*, 3294–3299.
228. Hyytiä, T.; Halonen, P.; Salminen, A.; Goldman, A.; Lahti, R.; Cooperman, B. S. *Biochemistry* **2001**, *40*, 4645–4653.
229. Pohjanjoki, P.; Fabrichniy, I. P.; Kasho, V. N.; Cooperman, B. S.; Goldman, A.; Baykov, A. A.; Lahti, R. *J. Biol. Chem.* **2001**, *276*, 434–441.
230. Rodina, E. V.; Vainonen, Y. P.; Vorobyeva, N. N.; Kurilova, S. A.; Nazarova, T. I.; Avaeva, S. M. *Eur. J. Biochem.* **2001**, *268*, 3851–3857.
231. Zyryanov, A. B.; Pohjanjoki, P.; Kasho, V. N.; Shestakov, A. S.; Goldman, A.; Lahti, R.; Baykov, A. A. *J. Biol. Chem.* **2001**, *276*, 17629–17634.
232. Heikinheimo, P.; Tuominen, V.; Ahonen, A.-K.; Teplyakov, A.; Cooperman, B. S.; Baykov, A. A.; Lahti, R.; Goldman, A. *Proc. Natl. Acad. Sci. USA* **2001**, *98*, 3121–3126.
233. Story, S. V.; Grunden, A. M.; Adams, M. W. W. *J. Bacteriol.* **2001**, *183*, 4259–4268.
234. Galperin, M. Y.; Bairoch, A.; Koonin, E. V. *Protein Sci.* **1998**, *7*, 1829–1835.
235. Lukatela, G.; Krauss, N.; Theis, K.; Selmer, T.; Geiselmann, V.; Von Figura, K.; Saenger, W. *Biochemistry* **1998**, *37*, 3654–3664.
236. Bond, C. S.; Clements, P. R.; Ashby, S. J.; Collyer, C. A.; Harrop, S. J.; Hopwood, J. J.; Guss, J. M. *Structure* **1997**, *5*, 277–289.
237. Knöfel, T.; Sträter, N. *J. Mol. Biol.* **2001**, *309*, 239–254.
238. Zambonelli, C.; Roberts, M. F. *J. Biol. Chem.* **2003**, *278*, 13706–13711.

8.25
Bioorganometallic Chemistry of Cobalt and Nickel

C. G. RIORDAN
University of Delaware, Newark, DE, USA

8.25.1 INTRODUCTION

The phrase "bioorganometallic chemistry" is rather nebulous, conjuring different visions to various communities of scientists. In the strictest terms it is defined as the study of biological species that contain a direct metal-to-carbon bond. The significance and role of the organometallic fragment can vary widely. Such species are of great importance in enzymology, where they often serve as components of a metalloprotein active site; in the environment, where volatile organometallics are toxic to life and require remediation; and in medicinal applications, where robust organometallic fragments provide markers for diagnostic and therapeutic treatments. "Bioorganometallic" has been used with increasing frequency since about 1980.[1] While the term is appropriate to describe the CO-inhibited form of heme proteins such as carbonmonoxymyoglobin, this chapter focuses more narrowly on the enzymology of metalloproteins and cofactors in
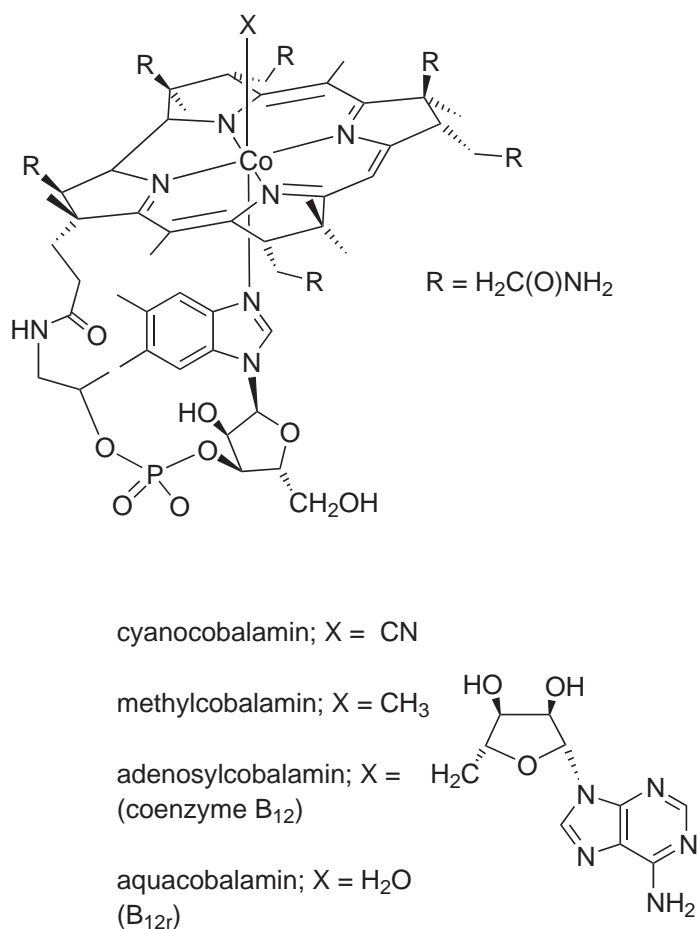
which the making and breaking of metal–carbon bonds appears seminal to catalysis. This definition also excludes the fascinating hydrogenases that contain $Fe(CO)(CN)_2$ fragments at their active sites.[2–5] Coordination chemistry relevant to the H_2ase proteins is surveyed separately in Chapter 8.10. The cobalt-containing B_{12} cofactor, methylcob(III)alamin and the nickel-containing proteins, methyl reductase, CO dehydrogenase, and acetyl coenzyme A synthase, are an intriguing set of biomolecules that manipulate one-carbon units in a diverse set of chemical transformations necessary for autotrophic growth of certain microorganisms. The archae (phylogenetically distinct from bacteria) includes acetogenic and methanogenic bacteria that produce acetate and methane, respectively, as the end products of their metabolism. A unique group of organic and inorganic cofactors are found in the proteins of these organisms. Their beginnings have been proposed as tracing back to primordial conditions near the origin of life. Specifically, Wachtershauser has demonstrated that Ni–Fe–S slurries catalyze C—C, C—N, and C—S bond formation under hydrothermal conditions.[6–10]

This chapter focuses on the role of organocobalt and organonickel species as competent intermediates in a range of enzymatic transformations. The text is organized by enzyme, with each section beginning with a summary of the relevant structural biology (where available) and enzymology to frame the discussion for the structural and reactivity model chemistry that follows.

8.25.1.1 ORGANOCOBALT SPECIES

8.25.1.2 Enzymology

The cobalt-containing B_{12} cofactors (cobalamins) hold a significant place in the historical development of metallobiochemistry. First isolated from liver in 1948 as a red, crystalline compound, vitamin B_{12} (cyanocobalamin) was structurally characterized in the landmark X-ray studies of Hodgkin.[11] The enormous complexity of the vitamin's structure and subsequent elucidation of the compositions and structures of the biologically active coenzyme B_{12} (adenosylcobalamin) and methyl B_{12} (methylcobalamin) ushered in the area of bioorganometallic chemistry (Figure 1). The latter two species represent the first characterized examples of metal–carbon, σ-bonded organometallic units found in nature. Despite intense efforts over the last few decades to elucidate the structure of other purported metal–carbon intermediates in enzymological cycles, the B_{12} cofactors remain the only bona fide species of this class to be identified.[12] Adenosylcobalamin and methylcobalamin are cofactors for very different protein classes and chemical transformations. Adenosylcobalamin-dependent reactions are characterized as 1,2-rearrangements in which substrate is converted to product via the transposition of substituents, hydrogen, and a heteroatom group, on adjacent carbons, Scheme 1.[13] The enzymes of this class may be grouped into the aminomutases (β-lysine-5,6-aminomutase, D-α-lysine-5,6-aminomutase, D-ornithine-4,5-aminomutase leucine-2,3-aminomutase), the carbon-skeleton mutases (methylmalonyl-CoA mutase, glutamate mutase, 2-methyleneglutarate mutase, isobutyryl mutase), and the dehydratases (propanol and glycerol dehydratase, ethanolamine ammonia lyase). Each of these reactions proceeds with good stereochemical control.[13] There is also a member of the ribonucleotide reductases (RTPR) that is coenzyme B_{12}-dependent.[14] The last reaction, while chemically distinct from the others since it involves reduction of ribonucleotide triphosphates to the corresponding deoxyribonucleotide triphosphates, appears to be initiated by a similar mechanism to the 1,2-rearrangement reactions. In the generally accepted mechanism for the adenosylcobalamin-dependent reactions, initiation involves homolysis of the cobalt–carbon bond generating the 5'-deoxyadenosyl radical and the cob(II)alamin cofactor (B_{12r}).[15,16] The carbon radical is the "active" catalyst for the reaction and abstracts the migrating hydrogen atom from the substrate. The resultant substrate radical rearranges to form the product radical, which abstracts a hydrogen atom from the 5'-deoxyadenosine. In these transformations it is suggested that the cob(II)alamin is not directly involved in the rearrangements.[17,18] In the RTPR reaction, cobalt–carbon bond homolysis is kinetically coupled to hydrogen-atom abstraction from a cysteine residue of the protein; no distinct 5'-deoxyadenosyl radical is involved.[19] The resulting cysteine radical (thiyl radical) initiates ribonucleotide triphosphate reduction via hydrogen-atom abstraction from the substrate. Clearly, there is chemical similarity between the RTPR and 1,2-migration reactions catalyzed by coenzyme B_{12}.

cyanocobalamin; X = CN

methylcobalamin; X = CH_3

adenosylcobalamin; X =
(coenzyme B_{12})

aquacobalamin; X = H_2O
(B_{12r})

R = $H_2C(O)NH_2$

Figure 1 Compositions and structures of the biologically active coenzyme B_{12} (adenosylcobalamin) and methyl B_{12} (methylcobalamin).

X = migrating group
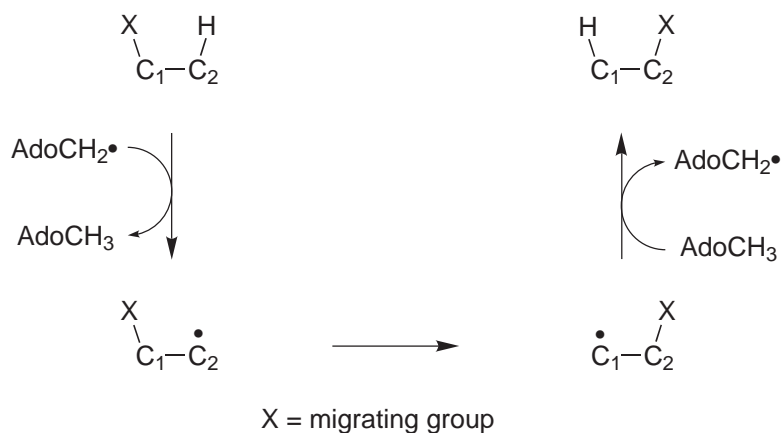
Scheme 1

In contrast, methylcobalamin-dependent reactions, which include methionine synthase, and anaerobic methyl transferases found in acetogens and methanogens, appear to involve heterolysis of the cobalt–methyl bond.[15] In the best studies of these proteins, methionine synthase, the B_{12} cofactor, serves as an intermediate in the shuttling of a methyl group equivalent (CH_3^+) from methyl tetrahydrofolate to homocysteine in the final step of the biosynthetic pathway of

methionine synthesis, Scheme 2.[20] In two sequential nucleophilic displacement reactions, the methyl group is transferred first from methyl tetrahydrofolate to cob(I)alamin, yielding methyl cob(III)alamin, then to homocysteine to liberate methionine and regenerate cob(I)alamin. The latter species has been termed a "supernucleophile" due to its remarkable reactivity in this reaction class. Stereochemical studies have corroborated the proposed sequential S_N2 methyl-transfer steps. Details of this reaction remain to be elucidated, including the mechanism by which methyl tetrahydrofolate and homocysteine are "activated" for catalysis. Matthews has implicated a mononuclear zinc site in methionine synthase as requisite for homocysteine binding and activation.[21] The differential modes of cobalt–carbon bond cleavage in methylcobalamin and adenosylcobalamin have been rationalized by the significant differences in the thermodynamic cobalt–carbon bond dissociation energies (BDEs).[15] Halpern developed a kinetic approach to elucidating the homolytic BDE for metal–carbon species.[22,23] When applied to coenzyme B_{12}, a value of about $130 \, kJ \, mol^{-1}$ was obtained independently by the Halpern and Finke groups.[24,25] The exact value depends slightly on a variety of conditions, including the identity of the *trans* axial ligand—so-called base-on or base-off forms—and the solvent, which results in considerable radical-cage effects.[26] These issues are outlined in detail in Section 8.25.3.1. In contrast, the BDE for methyl B_{12} is approx. $155 \, kJ \, mol^{-1}$.[27] The higher value is apparently sufficient to preclude cobalt–carbon homolysis in methylcobalamin-mediated reactions, and to allow for the heterolytic pathway to operate in methyl transferases.
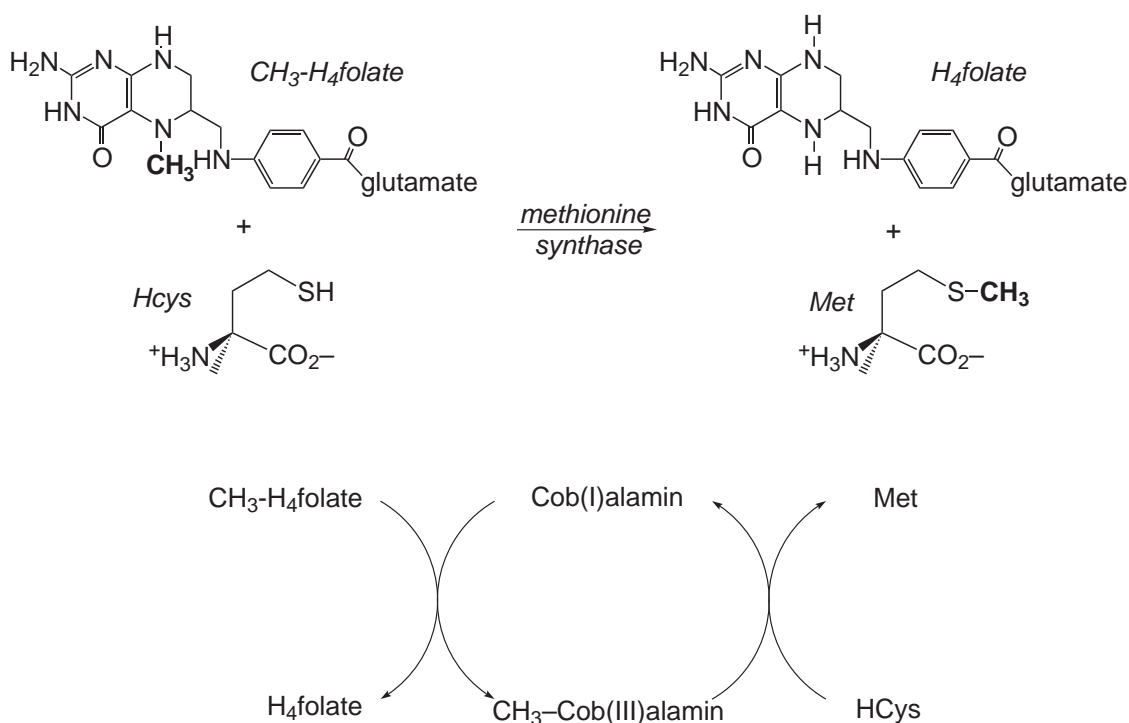
Scheme 2

Despite enormous progress in understanding B_{12}-mediated reactions, several seminal questions remain. Two issues of great interest are the molecular mechanism of cobalt–carbon bond activation in coenzyme B_{12} and the function of the *trans* axial ligand in catalysis. While the cobalt–carbon bond of coenzyme B_{12} is relatively weak, it must be further "activated" by a factor of two (in terms of BDE) upon enzyme complexation to yield bond homolysis rates consistent with enzyme turnover rates. The role of the *trans* axial base has received a great deal of attention. The novel 5,6-dimethylbenzimidazole donor has been postulated to play a key role in catalysis (Figure 1). It has been suggested that the coordinated base represents a mechanochemical trigger for labilizing the cobalt–carbon bond via distortion of the corrin macrocycle.[16,24] This mechanism has received renewed scrutiny following the first X-ray structure of an organocobalamin bound to its requisite enzyme. Drennan *et al.* established that methylcobalamin binds to methionine synthase with the 5,6-dimethylbenzimidazole away from the cobalt replaced with a protein His

in the *trans* axial position.[28] This so-called "base-off, His-on" species has been observed for other structurally characterized proteins: for example, methylmalonyl CoA mutase.[29] However, there are also examples of the corrinoid bound to a protein in the base-on form. Drennan and Stubbe have reported one such structure for RTPR.[30] The two topics of cobalt–carbon bond activation and *trans* axial base effects are often intertwined, and each provides an excellent opportunity for the coordination chemist to evaluate the properties via suitable model chemistry.

8.25.2 ORGANOCOBALAMINS: STRUCTURAL MODELS

The inorganic scientific community has been deeply interested in the synthesis of model complexes for the B_{12} cofactors since the elucidation of the structure of vitamin B_{12} in the 1960s. Indeed, as small-molecule cofactors, coenzyme B_{12} and its organocobalt relatives may serve as "model" complexes themselves, to the extent that they may be probed with spectroscopic, structural, and reactivity techniques common to the preparative chemist. General features common to all organocobalamin-model complexes are a tetradentate ligand(s) that occupies the equatorial plane, an axial organic ligand (R = alkyl or aryl), and (often, but not always) an axial base, L, for example, pyridine or imidazole, (**1**). Within this setting, a large number of such complexes have been prepared. The enormity of the field, coupled with space limitations, prevents a complete review of all such complexes. To this end, there are a number of excellent monographs and review articles that are appropriate for the reader.[31–33] Herein, the synthesis and structure of organocobalt-model complexes will be organized, based on their structure type. Specific groups are defined based on the tetradentate ligand(s) used.

8.25.2.1 Organocobalt[III]-model Complexes

The most common tetradentate ligands used to model the B_{12} corrin-ring structure are the bis(dimethylglyoximes) (abbreviated $(DH)_2$, or cobaloxime when including the metal), the products of Schiff-base condensation of *o*-salicylaldehyde and a variety of diamines, abbreviated SALEN, the mixed Schiff base–oxime ligands (Costa-type), porphyrins, and saturated tetraaza-macrocyles such as cyclam. Each ligand provides four equatorial donors, typically all nitrogens, except for the SALEN type, with varying degrees of ligand flexibility. The ligands are easily accessible synthetically from commercial reagents. The preparative procedures allow for the facile incorporation of a wide range of substituents at various ligand positions. This provides the advantage of systematic assessment of structure–function relationships. Furthermore, the equatorial ligands support Co in the three oxidation states necessary for B_{12} mimicry.[34,35]

The cobaloximes represent the largest class of organocobalt complexes prepared to date (2002). The bis(dimethylglyoxime) framework constitutes a pseudomacrocycle in which protons are bridged between partially ionized N-hydroxyl groups, (**2**). Introduction of strong acids results in protonation of the ligand and decomposition of the cobaloxime. Addition of boron Lewis acids, such as BF_3 or BPh_3, yields the macrocyclic complexes in which the BR_2 unit replaces the protons bridging two oxygens. As expected, these complexes are not acid sensitive. Although less common, there are examples of glyoximato complexes where the methyl substituents have been replaced with other substituents, such as a ferrocenyl moiety.[36]

The Co(SALEN) complexes are attractive organocobalt-model complexes due to their ready preparation via Schiff-base condensation of a diamine and *o*-salicylaldehyde, (**3**).[37] The limitation of these resultant species is the N_2O_2 ligand field, rather than the desired N_4 donor. Variations of the condensation protocol have resulted in the preparation of related complexes suitable for organocobalt synthesis.

Costa introduced a class of B_{12} analogs, commonly referred to as Costa-type complexes.[38–40] These organocobalt complexes have tetradentate N_4 donors that are mixed Schiff base-oxime derivatives, (**4**). The species differ from the dimethylglyoxime-supported complexes in that one half of the oximate pseudomacrocycle is replaced by a carbon group, most commonly a propyl linker. The Costa ligand is a monoanion, the same ligand charge as the corrin of cobalamin derivatives. An important consequence is that the resulting organocobalt[III] complexes are cationic, typically found with noncoordinating anions. Comparative studies have documented that the

length of the carbon linker dictates the puckering of the chelate ligand, with a butyl chain resulting in greater distortion.[41]
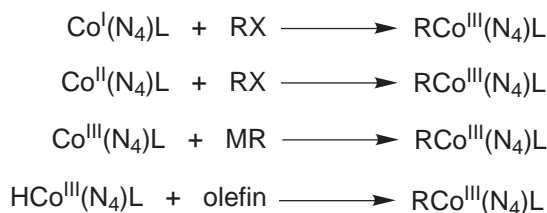
Organocobalamin analogs have been prepared that incorporate the porphyrin macrocycle as the tetradentate ligand that mimics the corrin structure.[42,43] Given the enormous attention and interest in porphyrin complexes of the transition metals, a large number of synthetic porphyrins are available. However, most of the B_{12}-model studies have utilized two derivatives, octaethyl-porphyrin (OEP) and tetraphenylporphyrin (TPP). Due to the aromaticity of the macrocycle, its structure is more rigidly planar. This contrasts with the flexible nature of the dimethylglyoxime, SALEN, and Costa-type equatorial ligands. These structural differences have allowed for comparative studies, designed to elucidate the relationship between conformational flexibility in the corrin ring and function/reactivity in organocobalt Co—C bond-activation processes. Beyond the porphyrins, other N_4 tetradentate macrocycles have been the focus of B_{12} mimicry, (**5**).[44–46]

$E = N, O$

(1)

$X = H, BR_2$

(2)

(3)

(4)

(5)
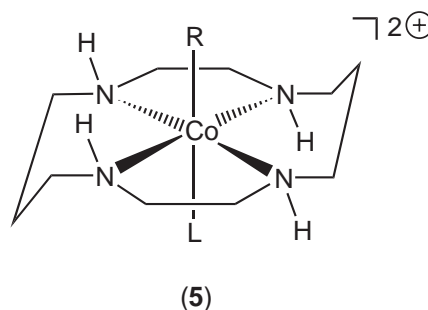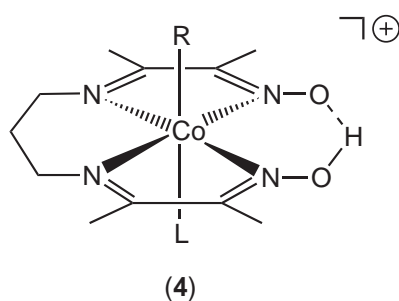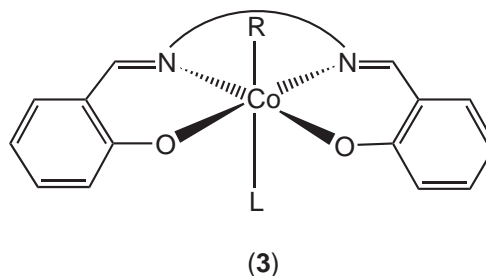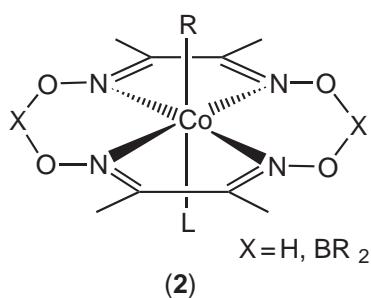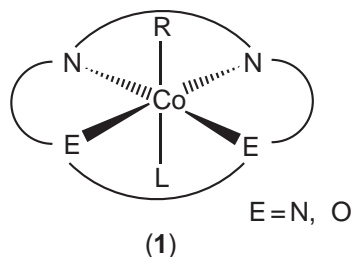
### 8.25.2.2 Methods of Synthesis of Organocobalamins and Models

There are a number of synthetic routes appropriate for the preparation of organocob(III)alamins and their model complexes.[35] Some of these procedures are of biological relevance, for example, alkylation of B_{12s} (cob(I)alamin species). This formal oxidative addition procedure has been applied to a large number of cobalt systems and is widely applicable. In most instances the reaction is a formal S_N2 process, whereby stereochemical inversion at carbon is observed. Other protocols have no biological analogy, such as metathetical replacement of a halide for alkyl anion on Co^{III}. The synthetic procedures detailed in Scheme 3 are generally useful for cobalamins, cobaloximes, and other B_{12}-model systems. The resulting organocobalt complexes are quite stable

in aqueous media due to their low-polarity Co—C bonds. This property contrasts with other organometallic compounds that tend to be hydrolytically sensitive. The synthetic routes have proven of great utility in synthetic organic chemistry for manipulating and forming C—C bonds. However, these issues are outside the scope of this chapter. The reader is referred to several reviews for detailed descriptions of the utility of organocobalt complexes in organic synthesis.[47–49]

$$Co^I(N_4)L \ + \ RX \longrightarrow RCo^{III}(N_4)L$$

$$Co^{II}(N_4)L \ + \ RX \longrightarrow RCo^{III}(N_4)L$$

$$Co^{III}(N_4)L \ + \ MR \longrightarrow RCo^{III}(N_4)L$$

$$HCo^{III}(N_4)L \ + \ olefin \longrightarrow RCo^{III}(N_4)L$$

Scheme 3

The Co^I form of these species has been termed a "supernucleophile," because of its rapid oxidation by alkyl halides to the corresponding organocobalt species, reacting 10^6 times faster than $[Co(CN)_5]^{2-}$ or $[Co(CO)_4]^-$ with MeI.[50] Standard preparative conditions involve *in situ*, reductive generation of the supernucleophile from Co^{II} precursors and $NaBH_4$, followed by addition of the organic halide. Aqueous reactions proceed smoothly under basic conditions. In most instances, these reactions appear to occur by an S_N2 path, although evidence for an electron-transfer mechanism has been suggested for the 2-substituted cyclohexyl halides.[51] The predominant S_N2 path provides convenient entry to regio- and stereochemically pure organo-cobalt species that may be utilized for subsequent mechanistic studies. The radical clock substrate 1-bromo-5-hexene reacts with $[Co(dmgBF_2)_2py]^-$ to generate (5-hexenyl)$Co(dmgBF_2)_2py$ cleanly, consistent with either a clean S_N2 displacement or generation of a radical with a short lifetime,

(5-hexenyl)Co(dmgBF₂)₂py
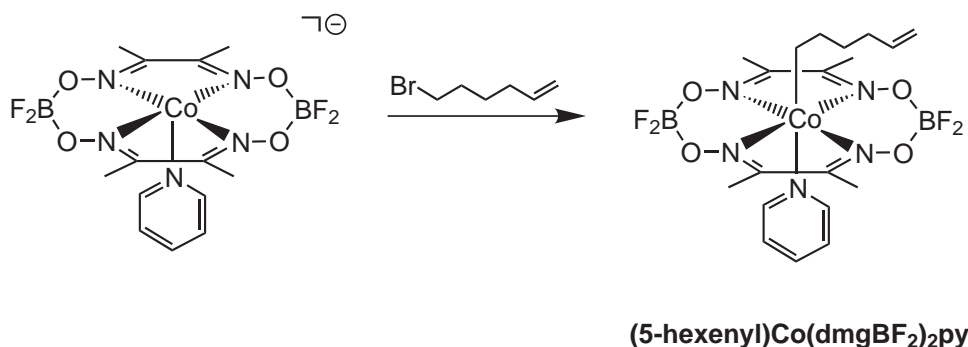
Scheme 4

Scheme 4.[52] Other routes to generate organocobalt complexes derive from Co^{II} or Co^{III} precursors. Derivatives of the former oxidation state react with alkyl halides via a radical route involving initial halide abstraction.[53] Consequently, loss of stereochemical integrity is problematic in this approach. Two useful procedures using Co^{III} precursors are transmetalation using main-group organometallics, and olefin insertion into Co^{III} hydrides. The relatively strong and low-polarity Co—C bond formation serves to drive the former reactions. Nonetheless, this route is of limited utility for organocobalamin preparation, as the organoalkalis are not stable in aqueous media. The final preparative approach entails olefin insertion into Co^{III}–H. The latter species is often formed *in situ* from Co^{II} and H_2. Reaction of (*E*)-PhCH=CHMe with $[CoH(dmg)_2py]$ yields the two diastereomers expected from *cis* and *trans* addition across the olefinic bond.[54] The stereochemistry of the products supports a mechanism initiated by H-atom abstraction followed by radical recombination. The coordinatively saturated Co^{III} complex is likely to operate via such a dissociative mechanism. While olefin insertion into metal hydrides is an attractive protocol, it is not available to the cofactor itself. Hydridocob(III)alamin is strongly acidic and exists only at

very low pH.[55,56] This observation serves to highlight the important distinction between nucleophilicity and basicity. B_{12s} are supernucleophiles, yet poor Bronsted bases. Such disparate properties may be important for several B_{12}-dependent reactions, including methinone synthase. It has been postulated that methylation of B_{12s} by methyl-H_4folate occurs only following protonation of the folate at N_5. In this instance, the B_{12s} could abstract either H^+ or Me^+. Only the latter, productive transformation is observed.

Systematic evaluation of the structures of B_{12}-model complexes has been described, with a focus on trends in ground-state molecular structures, specifically correlating cobalt–carbon bond distances with substituent effects. In the series of $[MeCo(DH)_2PR_3]$ complexes there is a strong correlation between the Co—P bond length and the size of the phosphine, the latter determined by its Tolman cone angle.[57] The larger phosphines also impact the equatorial ligands by producing a puckering of the two DH donors with respect to one another. This distortion results in the metal ion being displaced from the plane of the four nitrogens, towards the neutral axial ligand. These distortions range from $0.0035\,\text{Å}$ to $0.011\,\text{Å}$.[57,58] At parity of equatorial and *trans* axial ligands, a series of organocobalt complexes exhibit Co—C bond lengths consistent with the steric requirements of the alkyl ligand. The bond lengths increase in the order: Me < primary < secondary < tertiary.[32,59] There is also the common inductive effect of the *trans* axial ligand influencing the length of the Co—C bond.

Marzilli employed resonance Raman spectroscopy to elucidate factors that determine the strength of the Co—C bond as reflected in the ν(Co—C) frequency.[60–62] For a series of Costa-type complexes with an axial methyl group, the ν(Co—C) ranged from $455\,\text{cm}^{-1}$ to $505\,\text{cm}^{-1}$ in a predictable manner. The stronger *trans*-influence axial ligands, e.g., PMe_3 and CD_3, resulted in the lowest-energy vibrations. Steric effects of the *trans* axial ligand are also reflected in the ν(Co—C) frequency, with larger ligands exhibiting lower stretching values. This trend has been rationalized as reflecting a steric destabilization of the Co—C bond due to puckering of the equatorial ligand(s).

The application of Co XAS techniques to organocobalamins and their models has been reported.[63] Several of the results appear controversial, with a very recent (2001) methodological study presented that explains the origin of the controversies.[64] Proposals to improve EXAFS structure-parameter refinement by first-shell filtering, and the importance of mapping techniques in this regard, have been described.

8.25.3 ORGANOCOBALAMINS: REACTIVITY MODELS

8.25.3.1 Determination of Cobalt–Carbon Bond Dissociation Energies

It appears that the key to differential reactivity between methylcob(III)alamin (heterolysis) and adenosylcob(III)alamin (homolysis) is the striking difference in the homolytic BDE, the former possessing a Co—C bond that is ca. $29\,\text{kJ}\,\text{mol}^{-1}$ stronger.[15] While there are a number of other variables at work that result in a remarkable level of protein-controlled catalysis for coenzyme B_{12}-dependent enzymes, a great deal of insight may be achieved by understanding the fundamental aspects of Co—C bond activation in the isolated cofactors.[26] Halpern pioneered a number of kinetic and thermodynamic approaches to quantitative measurement of metal–carbon homolytic BDE.[22,23] The most widely applied method is kinetic in its approach, relying upon selective, competitive trapping of the carbon-based radical following reversible homolysis, Scheme 5. The choice of radical trap is paramount, as it must react selectively; reaction with the organocobalt reagent or cob(II)alamin needs to be precluded. Finke introduced the use of nitroxide traps, e.g., TEMPO, that meet these requirements.[65] Inherent in this approach is the assumption of a diffusion-controlled back reaction between B_{12r} and the adenosyl radical, which has been confirmed directly and indirectly. The most compelling kinetic evidence for reversible homolysis is provided by observation of an inverse dependence of rate on $[B_{12r}]$, although this is not established routinely. Using this method, the groups of Halpern[24] and Finke[25] independently reported adenosylcob(III)alamin BDEs of $109\,\text{kJ}\,\text{mol}^{-1}$ and $130\,\text{kJ}\,\text{mol}^{-1}$, respectively. Halpern's initial report did not include the minor contribution that comes from heterolysis, a point highlighted by Finke. Later Halpern attributed the differences in the values to solvent viscosity differences, as Finke's initial studies were conducted in ethylene glycol.[66] However, further studies by Finke confirmed a value of $130\,\text{kJ}\,\text{mol}^{-1}$ in both ethylene glycol and water.[67] Caged-radical

effects, which are sensitive to solvent viscosity, are significant in organocobalamin homolysis. The quantitative assessment of cage effects is described by the cage efficiency factor, F_c. The application and significance of this phenomenon has been thoroughly treated by Finke.[26,68]
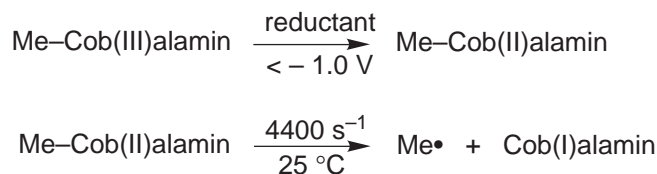
$$RCo^{III}(N_4)L \underset{k_{-1}}{\overset{k_1}{\rightleftharpoons}} Co^{II}(N_4)L + R\bullet$$

$$R\bullet + Trap \xrightarrow{k_2} R–Trap$$
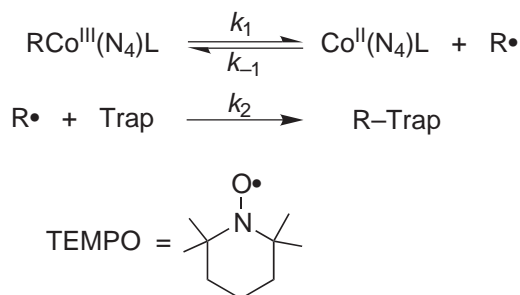
TEMPO =

Scheme 5

While the TEMPO reagent is highly effective in trapping the adenosyl radical, approximately 2% of the products of thermolysis may be attributed to heterolysis, namely aquocob(III)alamin, adenine, and 2,3-dihydroxy-4-pentenal. The product yield is independent of trap concentration, leading to the conclusion that the heterolysis products are not derived from an initial homolysis event. Heterolysis product formation is temperature dependent, with 10% observed at 358 K and only 3% at 383 K.[69] More recently, Halpern has identified and quantitated pH-dependent and -independent hydrolysis pathways for coenzyme B_{12} and related organocobalamins. The latter complexes differ systematically in the substitution on the adenosyl fragment. The hydrolysis routes are depurination (major) and ribose ring-opening (minor), facilitated by protonation at the ribofuranosyl oxygen.[70]

The effect of the 5,6-dimethylbenzimidazole base on homolysis in coenzyme B_{12} is significant. For the adenosylcob(III)inamide, the so-called base-off form, the BDE is approx. 4 kJ mol^{-1} greater than in the base-on form.[71] This small difference translates into a significant homolysis-rate acceleration of ca. 1,000 for the base-on vs. base-off coenzymes. Important to the interpretation of these data is a complete understanding of the thermodynamics of 5,6-dimethylbenzimidazole binding. For the equilibrium at room temperature in terms of base-off/base-on, the thermodynamic parameters are $\Delta H^0 = -32 \text{ kJ mol}^{-1}$ and $\Delta S^0 = -84.5 \text{ J mol}^{-1} \text{ K}^{-1}$.[72,73] Consequently, in general, most of the homolytic reactivity is observed to proceed via the base-on form due to the 4 kJ mol^{-1} lower BDE.

The so-called dmb base-off, protein His base-on form has been studied in an analogous manner by Finke. Motivated by the protein crystal structures of MeCbl bound to methionine synthase and AdoCbl bound to methylmalonyl-CoA mutase showing protein His axial coordination, AdoCbi ligated by N-methylimidazole and other nitrogenous bases was assayed.[74] Thermodynamic parameters for N-methylimidazole binding to AdoCbi reveal aspects of base binding among the aromatic nitrogen bases tested, with a more favorable $\Delta H^0 = -33 \text{ kJ mol}^{-1}$ and a compensatingly less favorable entropy, $\Delta S^0 = -117 \text{ J mol}^{-1} \text{ K}^{-1}$. Importantly, thermolysis yielded a high amount (50%) of Co—C heterolysis compared to that observed with dmb as axial ligand (2%). The N-methylimidazole accelerated the rate of Co—C bond homolysis eightfold, relative to AdoCbl.

The Co—C BDE in methylcob(III)alamin is 155 kJ mol^{-1}, significantly stronger than in adenosylcob(III)alamin. The 29 kJ mol^{-1} difference translates into a diminution of 10^6 (or more) in the rate of homolysis. Furthermore, due to the small size of the methyl substituent, there appears to be no obvious mechanical mechanism by which a protein could further activate the Co—C bond. In all cases studied to date, it appears that methylcobalamin operates via heterolysis, cleaving the Co—CH_3 bond to yield B_{12s} and the equivalent of a methyl carbocation. The *trans* axial base plays a critical role in controlling reactivity. Base coordination promotes homolysis, whereas when the ligand is not present the Co—CH_3 is more susceptible to nucleophilic attack.[75] One-electron reduction of alkylcob(III)alamins is an effective means to promote homolysis. Such reductions increase the rate of homolysis by a factor approaching 10^{12} by effectively reducing the Co—C bond order, Scheme 6. However, Finke has detailed why reduction most certainly is not the genesis of the biochemical activation of the organocobalamins.[76] One reason is that the potentials required to reduce coenzyme B_{12} of less than -1 V are inaccessible to physiological reductants.

$$\text{Me–Cob(III)alamin} \xrightarrow[< -1.0 \text{ V}]{\text{reductant}} \text{Me–Cob(II)alamin}$$

$$\text{Me–Cob(II)alamin} \xrightarrow[25\,^\circ\text{C}]{4400\ \text{s}^{-1}} \text{Me}\bullet \ + \ \text{Cob(I)alamin}$$

Scheme 6

Despite the relatively low BDE value determined for AdoCbl, the B_{12}-dependent enzymes still must provide a remarkable level of rate acceleration for catalysis. At $25\,^\circ\text{C}$ the rate of cofactor bond homolysis is $10^{-9\pm1}$ s^{-1}, which is ca. $10^{12\pm1}$ slower than the turnover rates for three different coenzyme-dependent proteins, diol dehydratase, ethanolamine ammonia-lyase, and ribonucleotide triphosphate reductase.[26] The latter enzyme operates by what has been described as "molecule-assisted homolysis," in which Ado·radical generation is coupled to (or concerted with) thiol S—H bond homolysis.[19] Despite the subtle and important differences among these proteins, the enormous magnitude of enzyme-promoted rate acceleration translates into a $\Delta\Delta G^{\ddagger}$ value of approx. $67\,\text{kJ}\,\text{mol}^{-1}$. Significantly, the quantitative assessment of the rate acceleration was made possible only through the chemical precedent studies of Halpern and Finke, a point emphasized by Finke. The details of protein-induced rate acceleration have been presented and discussed elsewhere.[71] In short, the role of the axial base, unto itself, may account for only a factor of 10^2 in rate acceleration.

A number of elegant, systematic studies of model complexes have led to an understanding of the relationship between organocobalt structural features and Co—C BDEs. As expected, the identity of the alkyl substituent is a significant determinant of the BDE. The general trend, which holds for all organometallic complexes for which quantitative BDEs are available, is: aryl > methyl > primary > secondary > tertiary. The ordering parallels that for C—H bond energies, but anomalies may exist for larger groups. For example, in an early study Halpern reported Co–C BDEs for the series of complexes RCo(saloph)py.[77,78] Bond dissociation values determined in pyridine (to eliminate complications from axial base dissociation equilibria) were $105\,\text{kJ}\,\text{mol}^{-1}$ (Et), $92\,\text{kJ}\,\text{mol}^{-1}$ (Bn), $84\,\text{kJ}\,\text{mol}^{-1}$ (Pr^i), and $75\,\text{kJ}\,\text{mol}^{-1}$ (Np). The results suggest that the primary Np is at least as sterically demanding as a secondary alkyl, Pr^i.

To elucidate the role of the size and basicity of the *trans* axial ligand in dictating Co—C BDEs, Halpern examined a series of R—Co$^{\text{III}}$ (R = Bn, CH(Me)Ph) complexes with phosphine axial ligands.[79,80] One series of complexes contained octaethylporphyrin (OEP) as the equatorial ligand, (**6**). A second series employed dimethylglyoxime. The derivatives containing OEP as ligand showed a correlation between the Co—Bn BDE and the pK_a of the five phosphine ligands, with values ranging from $100\,\text{kJ}\,\text{mol}^{-1}$ (PPh$_3$) to $124\,\text{kJ}\,\text{mol}^{-1}$ (PCy$_3$) (Figure 2).[80] The more basic phosphines give rise to the larger BDEs, due to their ability to preferentially stabilize the higher oxidation state, RCo$^{\text{III}}$ vs. Co$^{\text{II}}$, the latter resulting from homolysis. For these derivatives a correlation did not exist between BDE and phosphine size, as defined by the Tolman cone angle. However, for the dimethylgloxime-supported complexes, the correlation was between BDE and phosphine cone angle (Figure 3). The smallest phosphine examined, PMe$_2$Ph, showed the strongest Co—Bn bond, $127\,\text{kJ}\,\text{mol}^{-1}$, whereas the large PCy$_3$ yielded a much weaker bond, $95\,\text{kJ}\,\text{mol}^{-1}$. In these complexes the larger phosphines destabilize the Co—C bond, lengthening and weakening it via a conformational distortion that forces the equatorial ligand upward towards the Bn group. The more rigid OEP ligand acts effectively as a "barrier," shielding the Bn group from steric perturbations imposed by the axial ligand. The mechanical modulation of the Co—C bond induced by the corrin macrocycle conformational distortions has been suggested as a rationale for the presence of the corrin, rather than a porphyrin in the B_{12} cofactors.

### 8.25.3.2 Chemical Models for Specific Enzymatic Processes

8.25.3.2.1 Methionine synthases

The methionine synthases represent a paradigm in organocobalamin biochemistry. The cobalamin-dependent protein, Met H, catalyzes the transfer of a methyl group from methyl-H$_4$folate to Hcys via a MeCbl intermediate. Biophysical evidence is in accord with a mechanism involving
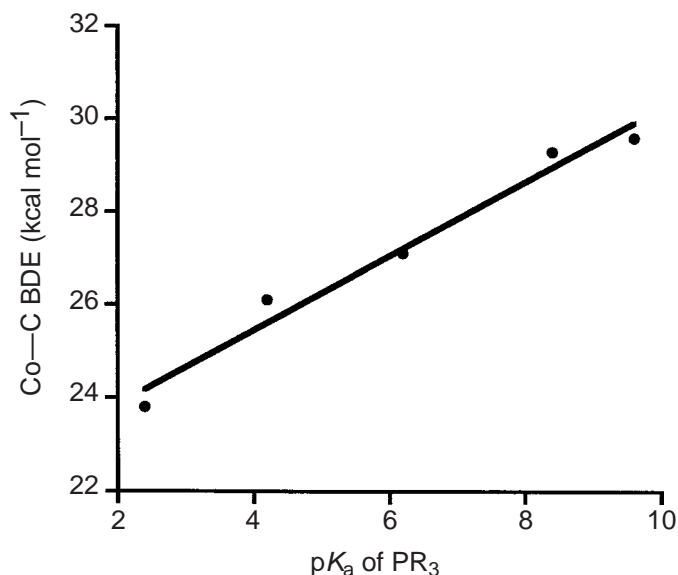
Figure 2 Correlation between the Co—Bn BDE and the pK_a of five phosphine ligands.

sequential S_N2 transfers, resulting in net retention of stereochemistry at the transferred carbon. Despite this detailed understanding of the enzymology, small-molecule precedents for the suggested elementary steps are largely lacking. Several key studies demonstrate alkyl transfer from the activated N—C bonds of quaternary ammonium and methylpterinium salts.[81,82] Methyl transfer from these reagents to the Co^I forms of cobaloximes and cobalamin produced the methyl-transfer products, Mecob(III)aloxime and MeCbl, in moderate yields. C-13 labelling of the methyl groups confirmed transfer of the assumed alkyl substituent. Bn and *p*-substituted Bn groups are also transferred from alkyl ammonium salts to Co^I. Early reports of thiol-promoted Co—C bond rupture under neutral or acidic conditions appear to be irreproducible.[83–85] More recently, the five-coordinate phthalocyanine (Pc) species MeCo(Pc) was shown to methylate thiophenylate in dimethylacetamide solution.[86] The reaction was rapid, occurring on the millisecond timescale. The observed rate constant saturated at high [PhS$^-$] is consistent with a mechanism requiring equilibrium coordination of the thiolate ligand to MeCo(Pc). Similarly, MeCbl incubated with β-mercaptoethanol or dithiothreitol (DTT) generated the thioether product, in accord with methyl
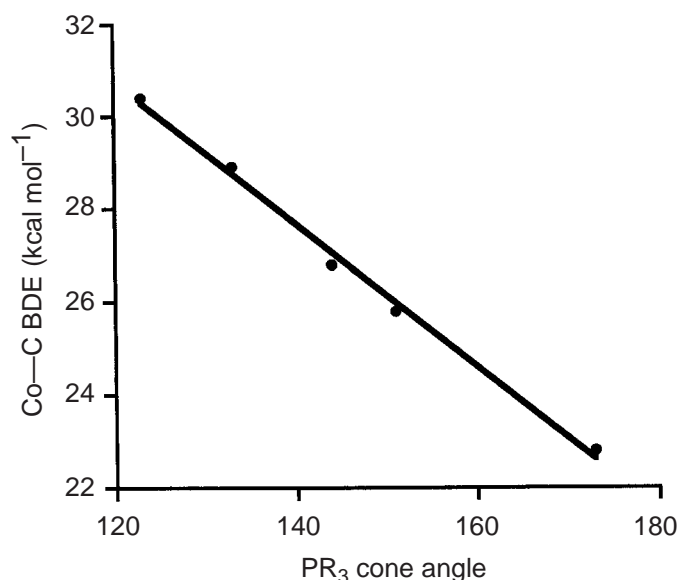

Figure 3 Correlation between BDE and phosphine cone angle.
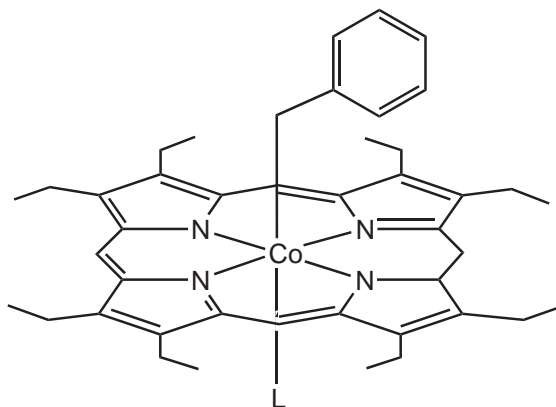
(6)

transfer and cob(II)alamin production.[86] The reactions are slow ($t_{1/2} = 1.5$ hr at 43 °C) and exhibit pH-dependent rates, consistent with the thiolate anion serving as the nucleophile. Optical spectroscopy confirmed cob(I)alamin as the initial product of heterolytic cleavage, with competing follow-up reactions leading to cob(II)alamin.

It has been proposed that thiolate ligation *trans* to the methyl group (displacing dmb) in MeCbl and its models could provide an effective means of labilizing the alkyl susbtituent for nucleophilic attack. This hypothesis appears not to be valid, as there was no evidence for thiol ligation to MeCbl upon reaction with DTT. Furthermore, methyl transfer was inhibited by thiolate coordination to Co in MeCo(Pc).[86] Marzilli prepared a series of model complexes with EtS^- bound *trans* to the alkyl group, **(7)**.[85] None of these complexes was active towards Co—C bond rupture. Pentafluorophenylthiolato-Cbl has also been characterized.[87] Nonetheless, Tada and co-workers have demonstrated that Co thiolates may be alkylated directly by methyl ammonium salts.[88] Phenylthiolatocobaloxime, prepared from cob(II)aloxime and phenyl disulfide, was methylated by $PhNMe_3^+I^-$ in 60% yield. Investigation of four derivatives differing in the *para* substituents of the arylthiolato ligand led to the proposal of a radical mechanism for thioanisole formation, initiated by Co—S bond homolysis.
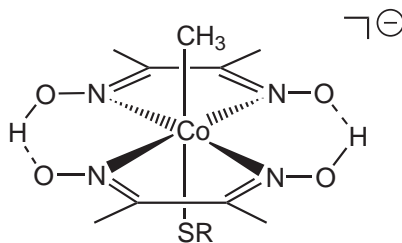
RS = EtS, 3,5-Me$_2$PhS, 4-MePhSO$_2$, Pr^{i}OCS

(7)

8.25.3.2.2 *Ribonucleotide triphosphate reductases*

Finke has established a chemical precedent for the proposed mechanism for thiyl radical formation in the B$_{12}$-dependent ribonucleotide reductase.[89] Thermolysis of AdoCbl with excess β-mercaptoethanol under anaerobic conditions yielded 90% Co—C homolysis and 10% heterolysis, as determined by product characterization. The homolysis products were 5′-deoxyadenosine, cob(II)alamin, and the disulfide 2,2′-dithiodiethanol. Kinetic studies established a zero-order dependence on thiol at high [RSH], consistent with rate-limiting Co—C homolysis and formation of a discrete Ado· that subsequently abstracts an H atom from the thiol. Consequently, the

isolated cofactor mechanism appears distinct from the enzyme-promoted pathway. The latter appears to couple Co—C bond homolysis and H-atom abstraction from Cys S—H.[19]

### 8.25.3.2.3 Cobalt participation in 1,2-migrations

Numerous studies aimed at elucidating the participation/nonparticipation of Co in the AdoCbl-dependent 1,2-migrations have been detailed. The majority of the chemical and enzymatic stereochemical evidence is in accord with noninvolvement of the cob(II)alamin. Leading studies by Halpern[17] and Finke[18] argue against metal participation in the rearrangement step, in favor of protein-bound radicals. Kinetic and mechanistic studies of the rearrangement of the radicals (8), in competition with trapping by tin hydrides, yielded rates sufficiently fast to be kinetically competent in the enzymatic reactions.[16,17] For example, the thioester substrate (8) (X = SEt), a model for the radical intermediate in methylmalonyl-CoA mutase, rearranged with a rate constant of $23\,s^{-1}$ at 60.5 °C. Finke prepared organocobalt models with organic, Costa-type ligands designed to produce diol radicals upon Co—C bond homolysis, (9).[18,90] Such species led only to a nonproductive redox side-reaction product, inconsistent with the enzymatic reaction. Alternatively, thioester 1,2-migrations have been promoted by cobaloxime model complexes, with Co—S ligation proposed as the origin of the increased yield of rearranged product.[91]

(8)   (9)
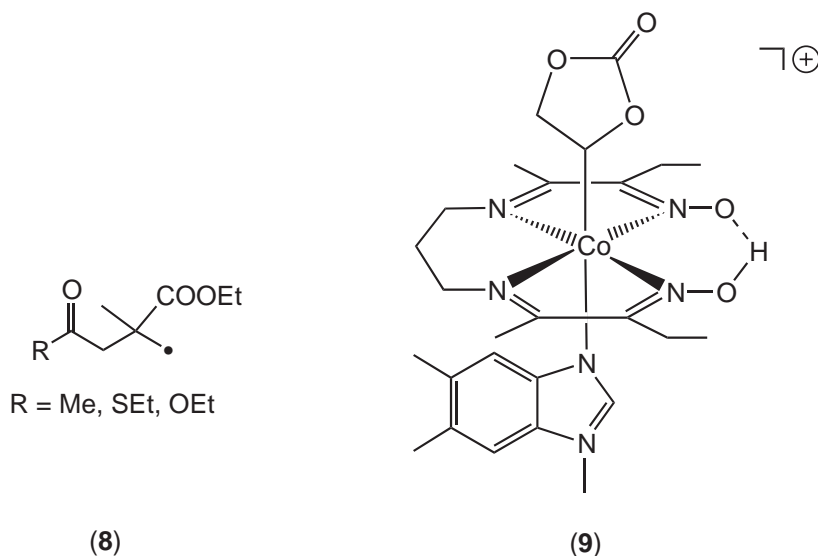
Methylcorrinoids are competent for the efficient methylation of alkyl radicals. Thermolysis of 2′-bis(ethoxycarbonyl)propylcobalamin and methylcobalamin at 70 °C led to formation of cob(II)alamin and the organic products 2-ethyl-2-methylmalonic acid diethyl ester and 2,2-dimethylmalonic acid diethyl ester.[92] The former product was generated with quantitative deuterium incorporation from CD_3cob(III)alamin. The proposed mechanism involves homolytic substitution on methylcob(III)alamin by the 2′-bis(ethoxycarbonyl)propyl radical, resulting in net methyl-radical abstraction, a process calculated to be highly exothermic ($\Delta H \sim -201\,kJ\,mol^{-1}$). The stereochemical course of the reaction should result in net inversion at the methyl carbon, although this has not been demonstrated. The reaction may serve as a precedent for several biosynthetic methylations, such as the antibiotic thienamycin synthesis.[93]

Thermolysis of the coenzyme B_{12}-model complex, (10), led to an equilibrium mixture of the BnCo species and the Bn-migration macrocyclic complex, Scheme 7, without formation of bibenyl.[94,95] Surprisingly, the reaction proceeds intermolecularly via Co—C bond homolysis, leading to the free radicals Bn• and Co^{II}. The latter, stable species is termed a "persistent" radical, thus allowing for the observed chemical selectivity of greater than 10^5 for the observed equilibrium species over bibenzyl. These observations represent a seminal example of Fischer's internal suppression of fast reactions, which requires that one of the radical intermediates formed be more persistent than the others, and the persistent and transient species must be formed at equal rates.[96] Both criteria are met, as the Co^{II} complex is quite stable and Co—C homolysis ensures that both radicals are formed simultaneously.

(10)
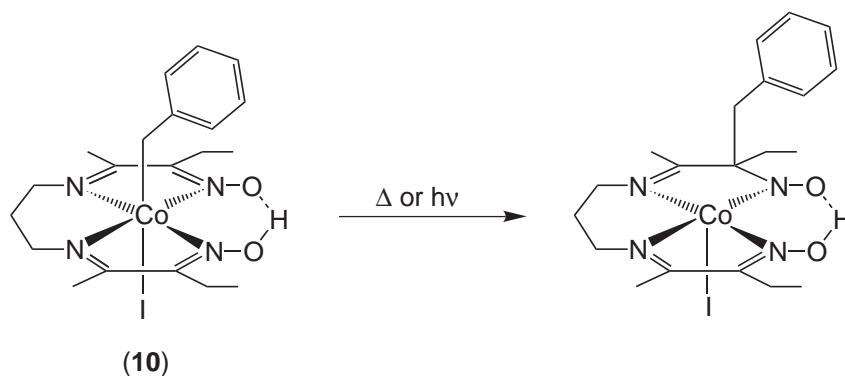
Scheme 7

8.25.4 NICKEL-CONTAINING PROTEINS

8.25.4.1 Methyl Reductase (MCR)

8.25.4.1.1 Enzymology

Methane production in the biosphere resulting from the microbial decomposition of organic materials is estimated to be more than 10^9 tons annually.[97,98] This process, termed methanogenesis, is catalyzed by a diverse group of organisms called achaebacteria (arche from the Greek "origin"). These are thought to be some of the oldest organisms on the planet, even older than the more extensively studied eubacteria, which include *E. coli* and cyanobacteria. Methanogens are obligate anaerobes; they die when exposed to oxygen. Consequently, they are found in a range of exotic, anaerobic habitats including the rumen and lower intestinal tracts of animals, sewage digestors, landfills, freshwater sediments, hydrothermal vents, and coastal marine sediments.[99]

The diversity of methanogens lies in the range of C_1 donors that they utilize to synthesize methane. Approximately two-thirds of the methane produced in Nature results from the reduction of the methyl group of acetate. About one-third derives from the reduction of carbon dioxide. With each of these substrates, hydrogen or formate provides the reducing equivalents. Methane is also produced in much smaller amounts from methanol, methylamines, and even dimethyl sulfide as the methyl donors.[98] The unifying theme of these different pathways is that a methyl equivalent is reduced to methane in the final, energy-conserving step in the catalytic cycle. A unique set of cofactors, found only in methanogenic archea, is responsible for these novel transformations.[98,100]
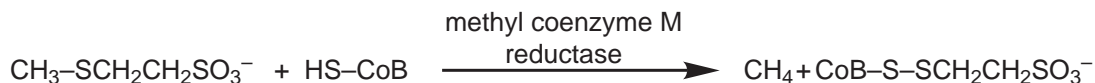
The reduction of CO_2 to methane requires eight electrons and results in the production of two equivalents of water:

$$CO_2 + 4H_2 \rightarrow CH_4 + 2H_2O \tag{1}$$

The reduction proceeds stepwise in a series of four two-electron reductions, with the electrons coming indirectly from hydrogen. The resulting C_1 fragments are cofactor-bound throughout the reduction process. While the overall reaction from CO_2 is exergonic by $131 \, kJ \, mol^{-1}$, the major energy-generating step is the final reduction of the methyl group to methane, $\Delta G^0 = -45 \, kJ \, mol^{-1}$. The enzyme responsible for methyl-group reduction is methyl coenzyme M reductase, a 300-kD enzyme that is a functional dimer.[101] The overall reaction catalyzed is shown in Scheme 8. The cofactors for the enzyme are 2-(methylthio)ethanesulfonic acid (CH_3CoM), the thiol (7-mercaptoheptanoyl)threonine phosphate (HS–HTP or coenzyme B), and cofactor 430 (F_{430}) (Figure 4). CH_3CoM is the methyl-group donor common to all methanogens. F_{430} is the nickel-containing prosthetic group of MCR, so named because it is the chromophore with an absorbance maximum at 430 nm ($\varepsilon = 23{,}300 \, M^{-1}$ per Ni) responsible for methane production.[102–104] Several inactive states of MCR have been crystallographically characterized at high resolution (1.16 Å).[105] These results show that each Ni cofactor is buried deeply in the protein matrix, accessible via a 50 Å-long substrate channel. The Ni is ligated in the equatorial

plane by four nitrogens, provided by the reduced pyrrole rings of the corrinoid macrocycle. Similar ligation has been observed for the isolated cofactor.[106,107] There is an additional glutamine axial ligand, Gln147, provided by the protein. This structure leaves a single axial ligation site available. The orientation of the F_{430} binding requires that the remaining site be exposed at the bottom of the substrate access channel. Kinetic studies suggest that both MeCoM and CoB bind to MCR prior to methane formation.[108]

$$CH_3–SCH_2CH_2SO_3^- \ + \ HS–CoB \ \xrightarrow[\text{reductase}]{\text{methyl coenzyme M}} \ CH_4 + CoB–S–SCH_2CH_2SO_3^-$$

Scheme 8

Two mechanistic proposals for methane formation invoke discrete methylnickel intermediates. Both pathways require redox chemistry promoted by Ni^I/Ni^{II} (and possibly Ni^{III}) interconversions. In the first mechanistic scheme, Berkessel proposed that CoB is oxidized to its thiyl radical form, which subsequently attacks the thioether sulfur of MeCoM generating a sulfuranyl radical.[109] This unusual species then transfers its methyl group to F_{430}, generating the methylnickel species via a radical pathway. In an alternate mechanism proposed by Thauer and based on his laboratory's crystallographic studies, CoB provides a proton to MeCoM.[105] This electrophilic species is then attacked by a nucleophilic Ni^I form of F_{430}, generating a methylnickel^{III} intermediate. Both mechanisms provide for the incorporation of solvent hydrogen in the methane, as demonstrated in reactions conducted in D_2O, via water protonation of the methylnickel intermediate. A third, provocative proposal, based on density functional theory by Siegbahn and Crabtree, does not invoke a methylnickel intermediate.[110] Rather, Ni^I reduction of MeCoM generates Ni^{II}–CoM and a free methyl radical. The methyl radical is quenched via hydrogen-atom transfer from CoB.

8.25.4.1.2 MCR: structural models

The macrocycle of F_{430} is unique in biology and has been termed a "hydrocorphinoid," because it has an oxidation state similar to that of the **corr**in found in the B_{12} cofactors. That is, it is more reduced than the porphyrin. However, its overall connectivity—four pyrrolic rings adjoined by single carbon linkers—is analogous to the ubiquitous porphyrin. A number of structural studies have examined the isolated F_{430} cofactor which is extracted from MCR in the Ni^{II} state, albeit in part as the 12,13-diepimer.[106,111,112] Most studies to date (2002) have focused on the methanolysis product, F_{430M}, due to increased stability and solubility relative to the isolated cofactor. F_{430M} undergoes two reversible, one-electron redox processes in organic media. An oxidation in acetonitrile occurs at 1.45 V (vs. NHE), while a reduction is observed at -0.66 V (in THF).[113] ESR spectral properties are consistent with the assignment of the redox processes as nickel-based. That is, the oxidized species is Ni^{III}, while the reduced is formulated as Ni^I. These observations are in contrast to the redox properties of Ni porphyrin complexes, which show complicated oxidative
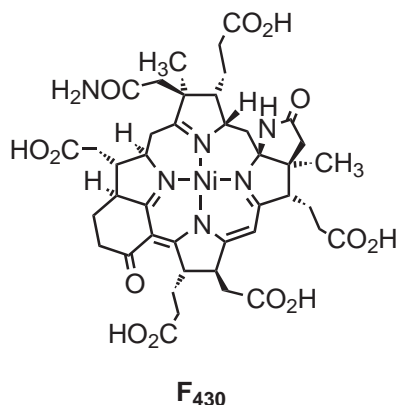
Figure 4 Cofactor 430 (F_{430}).

and reductive electrochemical behavior.[114] These latter processes are ascribed to a combination of nickel- and ligand-centered events, with the location of the odd electron identifiable by ESR spectroscopy and sensitive to the exact nature and substitution pattern of the macrocycle. Other reduced tetrapyrrolic macrocycles bind Ni^{II} and show interesting electrochemical properties. This work has been reviewed.[115] Most relevant for modeling of F_{430} are derivatives of the *iso*-bacteriochlorin framework, as the Ni complexes show interesting and novel reactivity. [Ni(OEiBC)]$^-$, (**11**), generated by sodium amalgam reduction in THF or acetonitrile, produced violet solutions that presented ESR spectral parameters similar to those of reduced F_{430} or F_{430M}, (g∥ = 2.20, g⊥ = 2.07, and A^N = 9.8 G).[116–118] This species is quite stable under anaerobic conditions with respect to disproportonation to Ni^{II} and Ni^0. It represents the first stable Ni^I complex of an aromatic macrocycle; the other species demonstrate Ni^{II}–ligand radical anion structures.
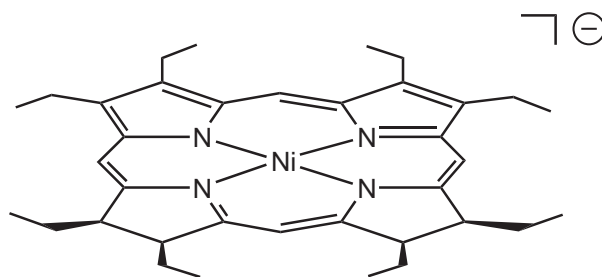
Ni(OEiBC)$^-$

(**11**)

(i) MeCoM and thioether binding to Ni macrocycles

MeCoM is the functionalized thioether that is the key substrate for MCR-catalyzed methane formation. Reductive cleavage of the $S—CH_3$ bond is the energy-deriving step in methanogenesis. Therefore, synthetic studies directed toward understanding the interaction of Ni complexes with thioethers in general, and MeCoM in particular, have been described. Thioethers are notoriously weak donor ligands and show little tendency to bind Ni^{II} unless the donor is part of a larger chelate ligand structure. For example, observable binding of aliphatic thioethers to Ni(tmc)$^{2+}$ (tmc = 1,4,8,11-tetramethyl-1,4,8,11-tetraazacyclotetradecane) requires high concentrations of the sulfide.[119] The equilibrium binding constant for Me_2S is $0.10 M^{-1}$ at 25 °C in acetone. Aryl sulfides including Ph_2S and thioanisole do not bind under similar conditions. The aryl substituents are electron withdrawing, resulting in diminished electron density at sulfur. There is no evidence of thioethers ligating to the corresponding Ni^I species, Ni(tmc)$^+$. Furthermore, disulfides do not bind the tmc complexes in either the Ni^I or Ni^{II} oxidation states. Berkessel has prepared a series of Schiff base-SALEN and thio-SALEN ligands possessing ether and thioether substituents as potential donors of five ligands to Ni^{II}.[109,120] One complex, (**12**), shows a weak Ni—S interaction at 2.575(2) Å, too long for a significant bonding interaction. Furthermore, the diamagnetic behavior of the complexes is most consistent with square-planar ligation. Nonetheless, the oxidation potential of the thioether-appended complexes, E_{ox}, is ca. 800 mV (vs. Ag/Ag$^+$), and was interpreted as Ni-based followed by intramolecular electron transfer from the thioether to the Ni^{III} species. Support for this proposal includes the observation that the oxidative electrochemistry of the untethered, four-coordinate complex did not change in solutions containing up to 18 mM thioanisole. The 14-membered macrocyclic complexes of Ni^{II} with tethered thioanisolyl groups, (**13**), also showed no evidence of thioether interaction with the metal ion.[121] Sodium amalgam reduction in DMF generated a small amount of methane, implicating nickel-based reactivity.

Surprisingly, the ligation aptitude of MeCoM has been little studied. MeCoM binds Ni(tmc)$^{2+}$ avidly.[119] NMR and IR spectral analysis were consistent with the proposed mode of binding as through the sulfonate end group, (**14**). In acetone, the inherent preference for sulfonate vs. thioether ligation was determined to be greater than 10^7. It was suggested that *in vivo*, the sulfonate is involved in hydrogen bonding with residues near the active site of MCR, which
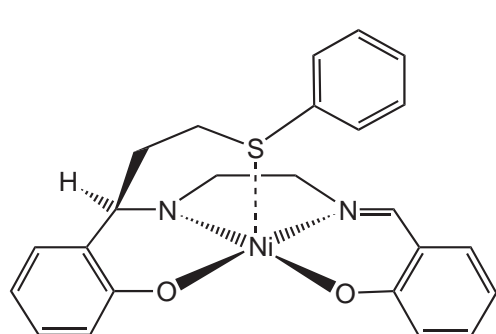
(12)
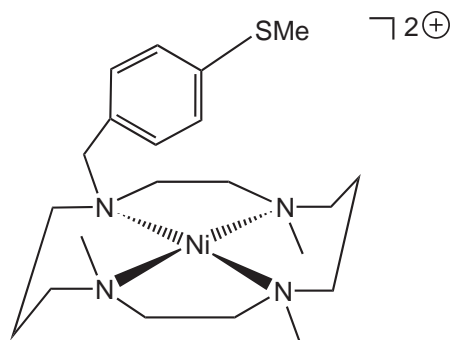
(13)

deactivates this group towards binding to Ni and probably directs the thioether of the substrate towards the Ni ion. The binding of CoM, the thiol form of the MeCoM substrate, to a series of Ni^{II} complexes has been assayed by optical and electrochemical methods. Bispyridyl thioether ligands formed six-coordinate Ni^{II} complexes, with water serving as the additional ligands, (15).[122] When incubated with the sodium salt of CoM, the *d–d* electronic bands red shift by 100–200 nm. The reductive electrochemistry of the complexes is subtly sensitive to CoM. In methanol, the one-electron reduction shifted positive by 63 to 74 mV in the presence of one equivalent of CoM. These series of observations were ascribed to CoM binding to the Ni species via the thiolate sulfur. A similar coordination of CoM to the Ni ion in F_{430} was observed crystallographically by Thauer in one inactive form of MCR.[105]
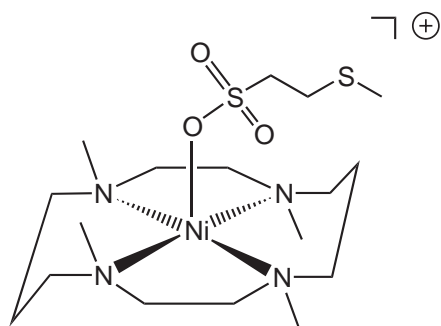
(14)
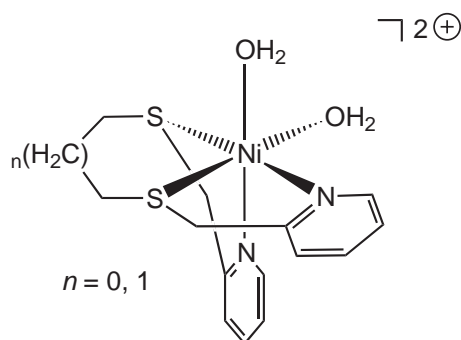
(15)

(ii) Ni–Me models

Proposed mechanisms for methane generation from MeCoM catalyzed by MCR point to the intermediacy of a methylnickel intermediate. Such species with the metal in either the +2 or +3 oxidation state have been proposed. While the organometallic chemistry of nickel has a rich and long history, pioneered by Wilke,[123] such species in the more relevant coordination spheres of azamacrocycles are surprisingly limited. Lin and Juan have demonstrated that reaction of F_{430M} with $(CD_3)_2Mg$ generated the brown, five-coordinate methylnickel^{II} complex characterized by its diagnostic, and paramagnetically shifted, CD_3—Ni resonances.[124] Such characteristics are appropriate for a high-spin, triplet ($S=1$) ground-state structure. At $-40\,^{\circ}C$, the resonance appears at $-490\,\text{ppm}$. The temperature dependence of this signal's chemical shift follows the Curie law, with a ^2H hyperfine coupling constant of $-0.85\,\text{MHz}$. The species decays slowly at $-20\,^{\circ}C$. The CD_3—Ni^{II} form of F_{430M} suffers rapid protonolysis by CF_3SO_3H, even at $-78\,^{\circ}C$. It appears

that intermolecular exchange of the axial methyl group either is slow on the NMR timescale, or does not occur. The electronic structure of CD_3—Ni^{II} F_{430M} appears quite similar to that of the synthetic complex $[Ni(tmc)CH_3]^+$, (**16**), first reported by Barefield.[125] This species, a rare example of a high-spin organonickel[II] complex, has paramagnetic proton (and ^2H for the CD_3 derivative) NMR spectral properties close to those of the methylated cofactor. The room-temperature chemical shift of the CD_3—Ni protons occurs at -299 pm. This signal's temperature dependence also follows the Curie law, yielding a ^2H hyperfine coupling constant of -0.65 MHz. The synthetic complex enjoys a greater thermal stability, showing no decomposition over weeks in solution or years in the solid state. $[Ni(tmc)CH_3]^+$ degrades rapidly in the presence of electrophiles, including H^+, SO_2, and CO_2. The molecular structure of $[Ni(tmc)CH_3]$ $(B(C_6H_3(CF_3)_2)_4)$ has been determined by X-ray diffraction.[52] The crystal structure consists of discrete ions with no close interionic contacts. The Ni-ion geometry is square pyramidal, with four basal Ni—N distances averaging to 2.15(2) Å and an apical Ni—CH_3 distance of 2.04(1) Å. The Ni—N distances are in accord with the high-spin Ni^{II} description, as deduced in a number of $[Ni(tmc)X]^+$ derivatives. Given the high congruity between the NMR properties of this complex and CD_3—Ni^{II} F_{430M}, the former serves as an appropriate structural model for the proposed methylnickel intermediate in MCR.
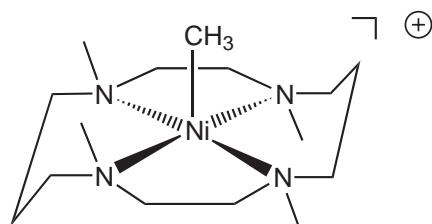
$$[Ni(tmc)Me]^+$$

(**16**)

Alternative approaches to the preparation of organonickel complexes supported by azamacrocycles include the oxidative addition of organohalides to Ni^I precursors and the reaction of alkyl radicals, generated by pulse radiolysis, with Ni^{II} complexes. Bakac and Espenson characterized a series of derivatives of the type $[Ni(tmc)R]^+$, analogous to the methyl complex prepared by Barefield, via electroreduction of $[Ni(tmc)]^{2+}$, in the presence of various alkyl halides in basic, aqueous solution.[126,127] In addition to insightful mechanistic studies, which led to the proposal of organonickel intermediates, the authors characterized these derivatives by electronic absorption spectroscopy. In a related system, examined independently by Castro[128] and Stolzenberg,[129,130] $[Ni(OEiBC)]^-$ was reacted with alkyl halides (RX). The saturated (RH and RR) and unsaturated (R–H) organic products derived from alkyl halide reduction were formed. Stolzenberg interpreted the results in the context of a mechanism involving Ni^{III}–R intermediates, although no such species were detected in the reactions.[130] Alkene isomerization during the reduction of long-chain alkyl bromides lended support for their formation. Castro proposed an alternate mechanism that did not include Ni—C bond formation.[128] In the reaction of alkyl radicals, generated by pulse radiolysis, with $[Ni(cyclam)]^{2+}$, Ni^{III}–R intermediates were formed with rate constants of $10^8 M^{-1} s^{-1}$.[131,132] The optical absorption spectrum of $[Ni(cyclam)CH_3]^{2+}$ displayed bands at ca. 300, 350, and 520 nm, similar to those reported for other Ni^{III} complexes. The Ni^{III}–R species were short lived, decomposing by a variety of pathways involving Ni—C bond homolysis driven by the stability of the Ni^{II} form. In general it appears that the Ni^{II}–R species are thermodynamically more robust than the corresponding Ni^{III}–R analogs, although relevant, quantitative Ni—R BDE are lacking. Such measurements would be of significant utility in developing a foundation for understanding MCR and ACS catalysis, as well as in Ni-mediated cross-coupling reactions.

8.25.4.1.3 MCR: reactivity models

In an early mechanistic study that assayed a variety of MeCoM substrate analogs for MCR activity, Gunsalus and co-workers developed a beautiful structure–function correlation that

continues to guide mechanistic frameworks.[133,134] The choice of substrate analogs was designed to address aspects of MeCoM structure by deconvoluting the native substrate into specific subunits: the terminal alkyl, the heteroatom connected to the alkyl group, and the terminal sulfonate. Taking each in turn, EtCoM and CF_2HCoM were found to be active, while PrCoM, cyclo PrCoM, and CF_3CoM were inactive. $CH_2{=}CHCH_2CoM$ was a potent inhibitor. These results highlighted the conformational restriction of the F_{430} active site that would permit activation of methyl and ethyl thioethers, but not the larger propyl and cyclopropyl analogs. To elucidate the role of the thioether heteroatom, the corresponding ether and selenoether analogs were studied. The former was deduced to be a weak inhibitor of MCR, while the latter was an efficient substrate leading to methane formation. The high degree of sensitivity to the heteroatom was taken to infer Ni–heteroatom coordination as a requisite step in catalysis. Additionally, inductive effects of the alkyl substituent, as demonstrated for the CF_2H and CF_3 analogs, appear to implicate thioether coordination to Ni. In the landmark study of Floss and co-workers, the stereochemical outcome of MeCoM reduction was elucidated. Using the chiral substrates (*R*)- and (*S*)-[1-^{2}H, ^{3}H]ethylCoM, it was determined that the reduction to the chiral ethane proceeded with net inversion of stereochemistry at carbon.[135,136] The result is in agreement with several mechanistic proposals that entail displacement of the sulfur atom of the methyl (ethyl) group by nucleophilic Ni^I, leading to inversion followed by protonolysis of the alkyl–Ni bond, which would be expected to proceed with retention. The stereochemical outcome is at odds with alternate schemes that invoke methyl radicals of sufficient lifetime to invert and, therefore, yield racemized products.

(i) Reactions of the isolated cofactor F_{430M}

Since the isolated cofactor F_{430M} can be efficiently reduced to the Ni^I state and that oxidation level has been proposed to be catalytically competent, Juan and Pfaltz pursued its reaction chemistry with thioethers and more active electrophilic methylating agents.[137] Ni^I F_{430M} does not interact with MeCoM or Me_2S. However, it does cleanly generate methane in good yields from methyl iodide, methyl tosylate, or trimethylsulfonium hexafluorophosphate. Kinetic analysis of the latter transformation, which results in greater than 100 turnovers, indicated first-order dependence on both F_{430M} and sulfonium ion, without build-up of any detectable intermediates. However, an incubation period for methane production of ca. 1 hour was generally noted. In the presence of excess propanethiol, no delay was observed and methane formation followed pseudo-first-order kinetics, with a log dependence of the initial rate on propanethiol concentration. Deuterium labeling studies indicated the source of the fourth hydrogen as a proton, and that free methyl radicals are not involved. Reaction with methyl iodide is much faster and evidence for a CH_3–Ni^{II} intermediate has been provided.[124]

(ii) Methane generation from synthetic nickel complexes

An informative kinetic analysis of the reaction of alkyl halides with the Ni^I azamacrocycle, [Ni(tmc)]$^+$, by Bakac and Espenson established that such reduced Ni species were competent in activating carbon electrophiles via Ni—C bond formation.[127] The proposed two-step mechanism involves rate-limiting, one-electron reduction of the alkyl halide, either via outer-sphere electron transfer or halogen-atom transfer, followed by rapid trapping of the carbon-centered radical by a second [Ni(tmc)]$^+$, Scheme 9. Support for the mechanism includes the overall 2 Ni: 1 RX stoichiometry, the reactivity order within a series of alkyl halides (methyl < primary < secondary) secondary) which parallels the relative stability of the carbon radicals, and the trapping of the carbon radical $CH_2CH(CH_2)_3CH_2^•$ in competition with its unimolecular cyclization. The detectable [Ni(tmc)R]$^+$ complexes are unstable for most alkyl substituents, decomposing by a variety of Ni—C bond cleavage pathways including hydrolysis, reaction with excess alkyl halide, cyclization, or fragmentation. Importantly, and distinct from the corresponding Ni^{III} [Ni(tmc)R]$^+$ species, bond homolysis is not a degradation pathway. The mechanism of formation of the Ni^{II} alkyls appears at odds with the results of Floss' chiral CH_3CH_2CoM experiment, which indicated inversion of stereochemistry at carbon, since free-radical trapping is expected to proceed with racemization.[136] [Ni(tmc)]$^+$ activates disulfides to the corresponding thiolato complexes,

[Ni(tmc)SR]$^+$ (R = Et, Ph), via a similar electron-transfer mechanism, but it does not react with less activated sulfur-containing molecules including thioethers nor, specifically, MeCoM.[119]

$$[Ni(tmc)]^+ \; + \; RX \longrightarrow [Ni(tmc)X]^+ \; + \; R\bullet$$

$$[Ni(tmc)]^+ \; + \; R\bullet \longrightarrow [Ni(tmc)R]^+$$
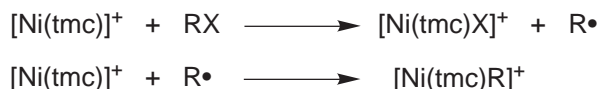
Scheme 9

The reaction of carbon electrophiles with the seemingly related Ni^I macrocycle, [Ni(OEiBC)]$^-$, provided contrasting results. While the stoichiometry remained the same at two Ni for each alkyl halide, the relative rates of reaction for a series of alkyl halides and alkyl tosylates showed the opposite trend; methyl > primary > secondary > tertiary.[128,130] This trend is consistent with rate-limiting nucleophilic attack (S$_N$2) at carbon to generate organonickel^{III} species, [Ni(OEiBC)R]. This pathway resembles the activity of cobalt^I complexes, including B$_{12s}$, with carbon electrophiles. In fact, Castro has suggested that [Ni(OEiBC)]$^-$ is a more reactive nucleophile than B$_{12s}$, termed a "supernucleophile" based on its higher rates of reaction, ca. 2,000 times, with identical alkyl halides.[128] Based on product distributions, the decomposition of the resulting Ni^{III}–R species involves homolysis, hydrogen-atom eliminations, and reductions to Ni^{II}–R species. While there was no spectroscopic evidence for the Ni^{III}–R intermediates, isomerization of alkenes did occur, strongly implicating organonickel and hydridonickel intermediates. Hydrogen incorporation in alkane products resulted from reaction with protic sources, as indicated by labeling studies. An alternate mechanism proposed by Castro invokes a three-electron nucleophile. leading to a transformation described as S$_N$2 with no bond formation (NBF). While the S$_N$2 component explains the observed rate trends, the organic product distribution is more complex that that expected from purely "free" carbon-radical-derived products. In either case, it seems the odd-electron Ni^I species is participating in the alkyl halide reductions as a nucleophile, presumably using the HOMO (dz^2) rather than the SOMO (dx^2-y^2).

The Ni^{II} complex of 1,4,7,10,13-pentaazacyclohexadecane-14,16-dionate, (**17**), was reported to be active in liberating methane from MeCoM in water, with concomitant formation of the CoM disulfide.[138,139] Addition of an oxidant such as I$_2$ or NaClO makes the reaction catalytic in Ni. The proposed mechanism includes thioether ligation to Ni and oxidation to Ni^{III} coupled with methane formation, leading to a Ni^{III}–CoM thiolate species. Control studies using the alternate Ni amine complexes of tetraethylenepentamine (tetren) or 1,4,8,11-tetraazacyclotetradecane-5,7-dionate, or even Ni^{II} acetate, did not convert MeCoM to methane under similar conditions. The 1,4,7,10,13-pentaazacyclohexadecane-14,16-dionate ligand was implicated as uniquely activating MeCoM. Subsequently, in a careful analysis reported by Stolzenberg, authentic samples of the Ni complex were incapable of cleaving MeCoM.[140,141] Only when unpurified, technical-grade tetren was used in the ligand synthesis could methane be liberated from MeCoM. One of the ligand contaminants was identified as 1,4,7,10-tetraazacyclotridecane-11,13-dionate, and its Ni complex was also ineffective in promoting the reaction. The role and identity of the impurity(ies) responsible for the high activity in the original report remain unidentified. Therefore, the precedent of Ni^{III}-model complexes in MeCoM activation remains in doubt.
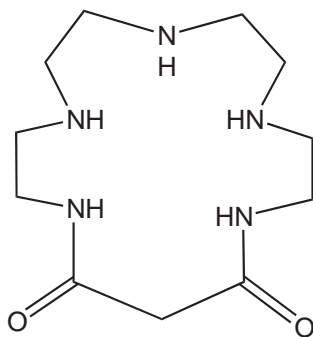

(**17**)

Stolzenberg demonstrated that the low-valent, heterogeneous sources of Ni, Raney nickel and nickel boride, yield methane from MeCoM.[140] The former reaction is quantitative, while in the latter, the catalyst preferentially cleaves the S—CH$_2$ bond of MeCoM. Attempts to prepare homogeneous catalysts derived from Ni macrocycles and sodium borohydride proved ineffective.

Meyerstein and co-workers reported that Ni^{I} tetraazamacrocycles generated radiolytically from Ni^{II} precursors produced methane from MeCoM. At pH 7.4 only traces of methane were detected, while at pH 9.4 the yield was over 10%.[142] Control experiments established that MeCoM scavenges methyl radicals via a mechanism that does not produce methane as the major product. Both Ni^{II}–CH$_3$ and Ni^{III}–CH$_3$ intermediates were postulated.

The mechanism of reductive degradation of the Ni thioether/thiolate complex, (**18**), prepared by Sellmann[143] was described by Kovacs.[144] Compound (**18**) displays a quasi-reversible reduction wave at −1.16 V (vs. SCE in DMF). Chemical reduction with sodium naphthalenide in THF was optimum with two equivalents of reductant, and led to formation of [Ni(bdt)$_2$]$^{2-}$ (bdt = benzene-1,2-dithiolate), ethylene, polyethylene, and ethylene sulfide. The proposed mechanism involved initial reduction to Ni^{I}, for which ESR evidence was presented ($g = 2.056$, 2.036, 2.001) followed by internal electron transfer leading to sequential C—S bond homolyses. Control experiments confirmed that the degradation required Ni.

Several models systems have been reported to cleave sulfur–carbon bonds under photolytic conditions. In two systems designed to evaluate the merits of the Berkessel mechanism that invokes sulfuranyl radical intermediates, methane production from thioethers has been observed. Tada and Masuzawa photolyzed Ni^{II}Sp–C$_6$H$_4$CH$_3$ complexes supported by azamacrocycles with 350 nm wavelength light in the presence of thioanisole.[145] Methane and the mixed disulfide p-TolSSPh were produced when the Ni catalyst was cationic, such as (**19**). Neutral complexes such as Ni(DH)$_2$ and Ni(TPP) (TPP = tetraphenylporphyrin) showed no activity. The methane production was not quantified and disulfide yields ranged from 1.3% to 24%, depending on the Ni complex. Irradiation of solutions containing an equivalent amount of a nitroxide-radical trap gave 12% yield of the thiyl radical-derived product, RN–S(O)p-Tol, supporting the involvement


NiL$_{S5}$

(**18**)

(**19**)
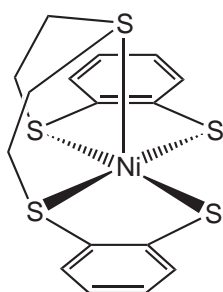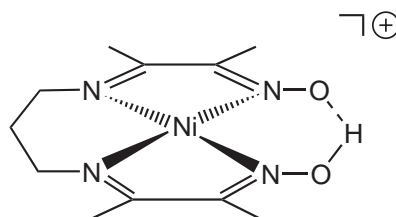
of thiyl radicals in methane production. The proposed mechanism consists of homolysis of the Ni–Sp-Tol to generate Ni^{I} and thiyl radical. The radical is then trapped by thioanisole to yield the sulfuranyl radical, which subsequently delivers a methyl substituent to Ni^{I}. The regiochemical preference for methyl rather than aryl transfer from the sulfuranyl radical may have steric origins, with attack of Ni^{I} on methyl being more favored.

Pfaltz, Jaun, and co-workers developed a related system that utilized photochemical homolysis of Ni^{II}–thiolate bonds to generate sulfuranyl radical intermediates, via an intramolecular cyclization involving a Ni-bound aliphatic thioether, Scheme 10.[146] Methane yields ranged from 2.5% to 48%. These authors repeated the Tada and Masuzawa photochemical experiments in order to quantitate methane formation. While they succeeded in reproducing methane and disulfide formation, the methane yields in the presence of Ni complex (0.3–1.4%) were consistently much lower than in the absence of Ni.

Darensbourg and co-workers found that the [Ph$_2$P(o-C$_6$H$_4$)SCH$_3$]$_2$Ni(0) complex degrades under ambient light to the corresponding dithiolate Ni^{II} species, [Ph$_2$P(o-C$_6$H$_4$)S]$_2$Ni, Scheme 11.[147,148] The transformation involves methyl radicals that were trapped by the nitroxide, TEMPO, and a Ni^{I} derivative characterized by ESR spectroscopy (10 K, $g = 2.08$).
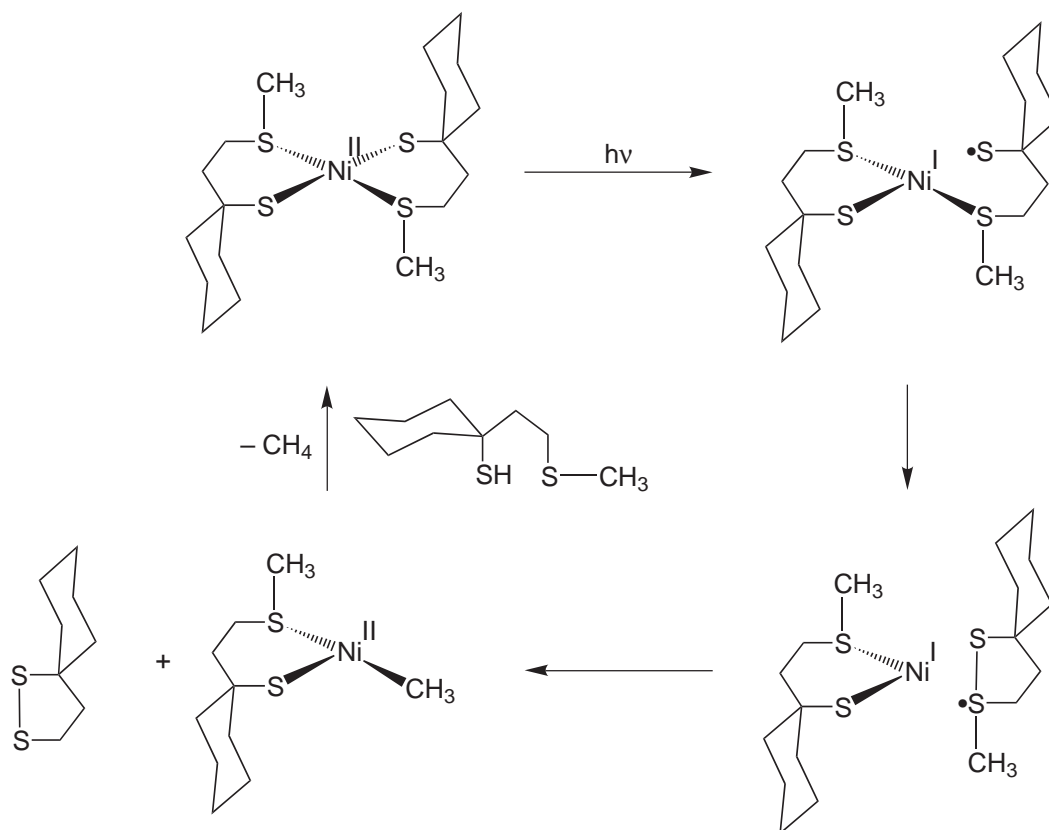
Scheme 10
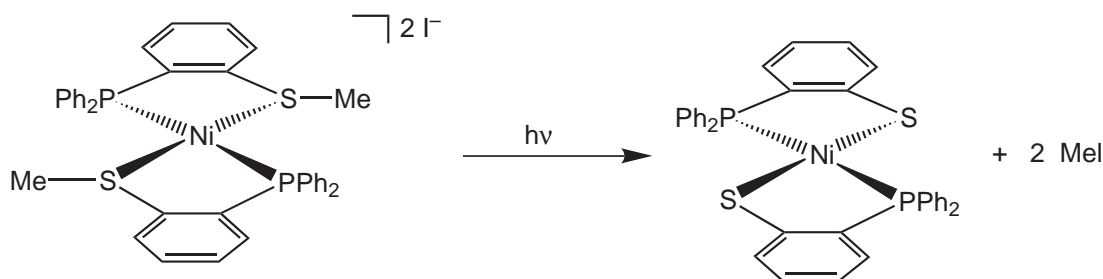
Scheme 11

The efficiency of MCR-catalyzed C—S bond rupture prompted Liebeskind to evaluate sulfonium salts and thioglycolic reagents as substrates in metal-catalyzed cross-coupling reactions.[149] The sulfonium salt participated in Pd-promoted cross-coupling reactions with organoboron and organotin reagents.[150] The nickel catalyst $Ni(dppf)Cl_2$ (dppf = 1,1'-bis(diphenylphosphino)ferrocene) was active for cross-coupling of organozinc reagents with the sulfonium salts.[150] Clearly, this reagent bears no resemblance to the F_{430} cofactor. The range of substrates useful in the reactions includes a broad spectrum of benzylic and heterobenzylic sulfonium salts, extending the scope of the cross-coupling to an important class of substrates. Similar carbon–carbon bond-forming reactions were promoted by $Ni(PMePh_2)_2Cl_2$, in which one of the substrates was either S-substituted organoCoM or thioglycolate derivatives.[151] Control experiments pointed to the requirement of the heteroatom group (sulfonate or carboxylate) chelating zinc, although the transmetalation appeared to proceed via an external organozinc species.

8.25.4.2 Carbon Monoxide Dehydrogenase (COdH)

8.25.4.2.1 *Enzymology*

Carbon monoxide dehydrogenases (COdH) catalyze the interconversion of CO and CO_2:

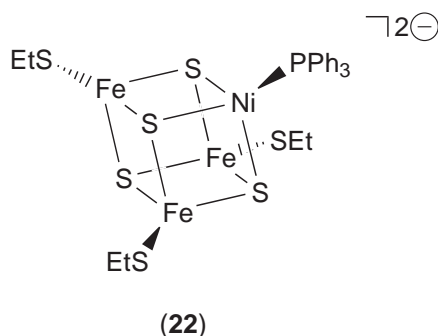$$CO + H_2O \rightleftharpoons CO_2 + 2H^+ + 2e^- \tag{2}$$

and are found in a wide range of microorganisms, including acetogenic, methanogenic, and phototrophic bacteria. These enzymes may be divided into two classes: monofunctional enzymes that catalyze only the COdH reaction; and bifunctional enzymes that, in addition to the COdH activity, promote the acetyl CoA synthase reaction (ACS)

$$CH_3\text{—cob(III)alamin} + CO + HSCoA \rightleftharpoons CH_3C(O)SCoA + \text{cob(I)alamin} \tag{3}$$
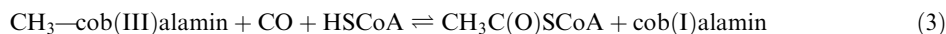
The latter class has been found in acetogens and methanogens.[12,152] The monofunctional proteins include both anaerobic phototrophs and aerobic molybdopterin-containing proteins. The active sites and mechanism of action of the anaerobic and aerobic COdH proteins are quite distinct. The latter utilize the molybdopterin cofactor, as found in a number of oxygen-atom-transfer proteins, and appear similar mechanistically to those proteins. The aerobic COdHs have been reviewed separately,[153,154] do not fall under the coverage of this review, and consequently will not be discussed here. All known anaerobic COdHs contain a NiFeS active site (termed the C cluster) for the CO-to-CO_2 transformation. The unique composition of the C cluster has resulted in numerous biophysical studies designed to establish the cluster's electronic and molecular structures.[12,155] A complicating aspect of the protein that has hampered these investigations is the structural diversity of the metal sites. The two most extensively interrogated proteins from this perspective are from the acetogenic organism, *Moorella thermoacetica* (formerly *Clostridium thermoaceticum*), and a purple non-sulfur bacterium, *Rhodospirilium rubrum*. The former contains 2 Ni ions, 11–14 Fe ions, and 14 acid-labile sulfides per α/β unit; while the latter contains 2 Ni ions, 10 Fe ions, and 10 acid-labile sulfides per functional dimer. In principle, since *M. thermoacetica* contains the active sites for COdH (C cluster) and ACS (A cluster), and *R. rubrum* the site only for COdH, "difference" spectroscopy should be useful in teasing out the structures of the different metal sites. However, in practice this remains challenging. Structural models consistent with spectroscopic data from ESR, ENDOR, Ni XAS, Mössbauer experiments propose the C cluster to be a novel, $[Fe_4S_4]$ ferredoxin-like, cuboidal cluster, linked via a bridging residue to a unique iron site. The bridge has been suggested to be sulfur-based, i.e., either a Cys residue or S^{2-}. However, protein crystallographic reports for proteins from two different monofunctional organisms (no ACS activity) proposed models of the C cluster of unprecedented structure, (**20**) and (**21**).[156,157] Each can be viewed generally as a cuboidal $NiFe_3S_4$ cluster tethered to an additional iron ion, exo to the cube (previously denoted as ferrous component II (FCII) due to its unique spectroscopic features[158]). Each metal of the cuboidal cluster is ligated by a Cys residue. The unique exo iron is bound by one His and one Cys residue. There are differences between the active sites of the two structural models. In the protein from the thermophilic *Carboxydothermus hydrogenoformans*, there is a fifth sulfide within the C cluster that bridges the unique iron and the nickel ions, (**20**).[157] This position in the *R. rubrum* structure, (**21**), is occupied by a bridging Cys residue.[156] Additional electron density at Ni has been modeled as an exogenous, small-molecule ligand, not believed to be substrate, completing a six-coordinate site. Lastly, in the *C. hydrogenoformans* the $NiFe_3S_4$ cube is distorted significantly, such that one nickel-to-sulfide distance is beyond bonding distance. This results in an essentially square-planar Ni ligation sphere. The remaining iron ions and sulfides in the protein are organized into typical ferredoxin Fe_4S_4 clusters, termed B and D, which provide a clear electron-transfer path in the functional dimer. Each dimer contains two B and C clusters, one per subunit, and a single D cluster that occupies a position at the interface between the two polypeptide chains. The recent structural insights of the active-site C cluster provided by crystallography will undoubtedly provide fodder for reexamination and interpretation of the biophysical data previously evaluated in the context of a Ni–X–Fe_4S_4 model. Furthermore, the unexpected cluster motif will renew interest in the preparation of appropriate structural and functional small-molecule analogs.
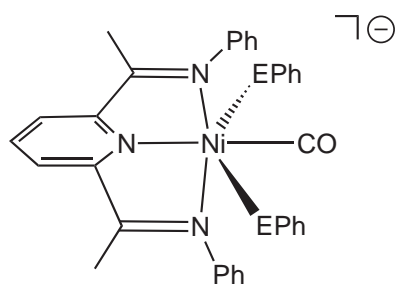
(20)　　　　　COdH Cluster C　　　　　(21)

The conversion between CO and CO_2 catalyzed by COdH is compositionally similar to the industrial water-gas-shift reaction. A key difference is that the latter generates dihydrogen, rather than protons and electrons. Nonetheless, mechanistic proposals for COdH catalysis have found inspiration in the industrial transformation. Given the structural complexity and the presumed rational evolution of the C cluster for its intended function, mechanisms typically involve bimetallic pathways. The bimetallic mechanism invokes a Lewis-acid role for the unique iron to serve as the site for metal hydroxide formation.[158] The Ni ion serves as the site for CO binding. The key step then becomes the bimetallic migratory insertion that generates the metallocarboxylic acid. Subsequent general base deprotonation, followed by CO_2 liberation, results in a formal, two-electron reduction at the C cluster. While several proposals have been presented to describe the appropriate electronic structure of the reduced forms of the C cluster and to explain associated ESR signals, the exact nature of this catalytic species remains in question. A very similar bimetallic mechanistic proposal that reverses the roles of the unique iron and nickel has been described, in which generation of Ni–OH and Fe–CO intermediates leads to an Fe-bound carboxylic acid.[12,159] Ludden and coworkers have suggested an alternative pathway that includes the generation of nickel hydride species, although details of the mechanism are vague.[160,161] Nickel hydrides are ubiquitous in organometallic chemistry,[162] and metal hydrides are invoked as intermediates in the water-gas-shift reaction. This proposal also invokes an endogenous CO ligand (nonsubstrate) that appears consistent with X-ray diffraction results described previously.[156]

8.25.4.2.2 *COdH structural models*

In the light of the recent crystallographic models proposed for the C cluster, heterocubanes of the type $NiFe_3S_4$ represent the most accurate structural models to date. Holm and co-workers prepared a series of such clusters in the early 1990s via a synthetic route that utilized the linear Fe_3S_4 cluster as an appropriate precursor.[163–166] Reductive activation with Ni(0) sources such as $Ni(PPh_3)_4$ facilitated metal-ion incorporation. The resulting cuboidal cluster $[NiFe_3S_4(PPh_3)(SEt)_3]^{2-}$, (22), has been characterized crystallographically, as have several other $NiFe_3X_4$ (X = S or Se) derivatives.[165,166] The clusters show trigonal symmetry, with unexceptional Fe–S distances and a quite short Ni–P distance of 2.18 Å. ESR ($g = 4.36, 3.26, 1.86$) and Mössbauer ($\delta = 0.47, \Delta E_Q = -0.90$) spectroscopic parameters, as well as the temperature dependence of the magnetic susceptibility, are consistent with a $S = 3/2$ ground state arising from antiparallel coupling of a $S = 5/2$ Fe_3S_4 fragment to a $S = 1$ Ni site. Ni incorporation also has a dramatic influence on the reduction potential of the cuboidal cluster, $[NiFe_3S_4(SEt)_4]^{2-}$, which is reduced at 300 mV more negative potential than the similarly charged $[Fe_4S_4(SEt)_4]^{2-}$ species. Comparison of the Ni EXAFS data for the synthetic $NiFe_3S_4$ complexes with that for the protein from *R. rubrum* led to the conclusion that a $NiFe_3S_4$ cluster was not an accurate model for the C cluster.[164] The cluster $[NiFe_3S_4(PPh_3)(SEt)_3]^{2-}$ showed rich ligand-substitution behavior, with the nickel site PPh3 being replaced by other phosphines including bidentate ligands, thiolates, isocyanides, and cyanide.[163] Under CO, cluster redistribution was observed that led to the identifiable formation of the $[Fe_4S_4(SEt)_4]^{2-}$ cluster. To date (2003), there are no examples of synthetic $NiFe_4S_5$ clusters in a synthetic system.

$$\neg 2\ominus$$

(**22**)

While nickel carbonyl chemistry can be traced back to Mond in the 1890s,[167] biomimetic Ni—CO species remain rather uncommon, particularly because the Ni^{II} and Ni^{III} oxidation states rarely bind CO to yield characterizable adducts. It has long been assumed that the lower-lying d manifold found for the higher Ni oxidation states is not favorable in promoting the efficient π–back donation required to stabilize such species. However, given interest in CO adducts of COdH, ACS, and the NiFe H$_2$ases, considerable preparative advances have been made. Ni^{I} azamacro-cycles are well known as yielding adducts upon exposure to CO, whereas the corresponding Ni^{II} species are not carbonylated.[168,169] There are a number of Ni^{I}—CO complexes that possess biologically relevant sulfur-supporting ligands. Mascharak and co-workers described the carbonylate, $[Ni(DAPA)(EPh)_2(CO)]^-$, (**23**), where E is S or Se formed via carbonylation of the Ni^{I} species generated *in situ*.[170–172] The notable spectroscopic feature of the anionic complex are the high ν_{CO} feature at $2,024\,cm^{-1}$. Ni^{I}—CO adducts supported by thioether ligation have been reported, including several derivatives characterized by X-ray diffraction. The tbp cation, $[Ni(NS_3tBu)(CO)]^+$ $(NS_3tBu = N(CH_2CH_2S'Bu)_3)$, (**24**), displays a ν_{CO} band at $2,026\,cm^{-1}$ which is surprisingly similar to the value above, reflecting compensating electron-density effects.[173,174] The analogous phosphino complex, $[Ni(np_3)(CO)]^+$ $(np_3 = N(CH_2CH_2PPh_2)_3)$, pre-pared earlier by Sacconi, exhibited a ν_{CO} band at $1988\,cm^{-1}$ for the BPh_4^- salt, and $2,020\,cm^{-1}$ and $2,032\,cm^{-1}$ when the counter anion was BF_4^-.[175] Surprisingly, the analogous Ni^{II} dicationic CO complexes featuring amino (np$_3$) and phosphino (pp$_3$) tetradentate tripodal ligands have been reported. The ν_{CO} energy is at an expected higher energy for the dication and is insensitive to the *trans* axial ligand, N or P.[176] The pseudotetrahedral, neutral Ni^{I} complex, $[PhTt^{tBu}]Ni(CO)$, (**25**), displays a carbonyl band at $1999\,cm^{-1}$.[177] A Ni^{I} thiolate/thioether complex, $[Ni(tpttd)]^-$, (**26**), was prepared via *in situ* reduction and shown to bind CO reversibly by electrochemical and IR measurements (ν_{CO} at $1,940\,cm^{-1}$).[178]
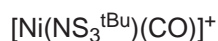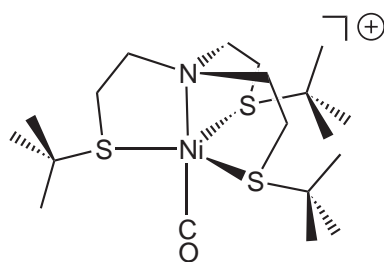
More interesting, given the paucity of examples, are the Ni^{II} carbonyl complexes.[179] Crabtree and Eisenstein have provided a theoretical framework in which to consider the electronic and structural requirements for Ni^{II}—CO formation.[180] Following analysis of known complexes (at that time), they concluded that π-donor ligands such as halides and thiolates can increase electron density at Ni^{II} sufficiently to permit it to behave like the more electron-rich Ni^{I} counterpart. Indeed, in recent years several very interesting Ni^{II}—CO adducts that bear thiolate supporting ligands have been described. Millar and Koch reported the tbp complex $[Ni(PS3^*)(CO)]^-$ $(PS^*3 = tris(3\text{-phenyl-2-thiophenyl})phosphine)$, (**27**), in which the apical CO gives rise to an IR stretch at $2,029\,cm^{-1}$, a remarkably high value for a Ni^{II} species.[181] Liaw has reported a series of structurally-defined, square-planar Ni^{II} derivatives, $[Ni(CO)(SPh)_n\,(SePh)_{3-n}]^-$, that display ν_{CO} at energies of $2,020\,cm^{-1}$ to $2,030\,cm^{-1}$.[182] The complexes were prepared via a novel route involving ER^-/Cp^- exchange, followed by R_2E_2 oxidative addition from $CpNi(CO)_2$.[183] COdH-related reactivity of these fascinating Ni^{II} species has yet to be described.

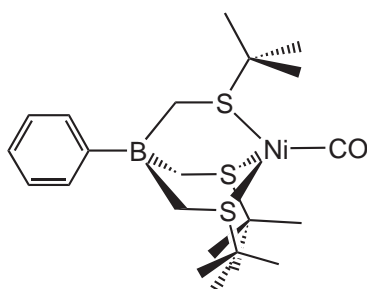### 8.25.4.2.3 COdH reactivity models

Nickel azamacrocyclic complexes are quite active in the aqueous, electrochemical reduction of CO_2 to CO.[184–186] Kinetic studies point to an electrode-adsorbed Ni species as the active catalyst. The proposed mechanism of reduction involves η^1–CO_2 ligation stabilized by H-bonding to the amine protons, followed by sequential electron- and proton-transfer steps.[185] In DMF, the major product is formate instead of CO. An alternative pathway proposed for the same reaction
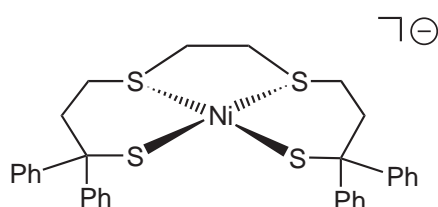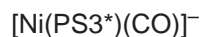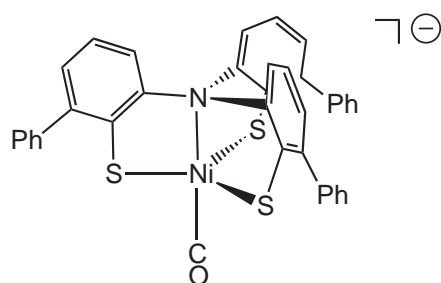
[Ni(DAPA)(EPh)$_2$(CO)]$^-$

(**23**)

[Ni(NS$_3{}^{tBu}$)(CO)]$^+$

(**24**)

[PhTt^{tBu}]Ni(CO)

(**25**)

[PhNi(tpttd)]$^-$

(**26**)

[Ni(PS3*)(CO)]$^-$

(**27**)

promoted photochemically invokes a Ni—H intermediate that inserts CO_2, with the subsequent step being protonation of the Ni–formate.[187] Insertion of CO_2 into a Ni—H has been demonstrated independently.[188]

Biomimetic CO_2 reduction promoted by Ni complexes has been reported by Tommasi.[189] The isolable and previously characterized Ni(0) adduct, Ni(PCy$_3$)$_2$(CO$_2$), reacted with thiols to liberate Ni(PCy$_3$)$_2$(CO)$_2$, Ni(PCy$_3$)$_2$(SR)$_2$, and water. The authors suggest single-electron transfer from PhSH to the Ni(0)–CO$_2$ adduct, followed by proton transfer, as the key mechanistic steps in CO_2 reduction. Lower yields resulted when using HCl or H$_2$S in place of PhSH, consistent with proton

transfer not being the rate-limiting step. Increased product yields under a CO_2 atmosphere were indicative of reversible CO_2 binding and suggested that initial reduction was a Ni-mediated process.

Lu and Crabtree described a Ni-based catalytic model system that operates in the reverse direction, i.e., CO oxidation to CO_2.[190,191] The square-planar Ni^{II} complexes are dimeric in the solid state and contain N, S, O donors with phenoxy bridges, (**28**). The dimers convert CO to CO_2 catalytically in aqueous media at room temperature, using methyl viologen (MV^{2+}) as the electron acceptor. H_2 is not a product, thus differentiating this transformation from the water-gas-shift reaction. The activity is specific for Ni; the analogous Fe^{II}, Co^{II}, Cu^{II}, and Zn^{II} derivatives do not effect the reaction. Rate measurements point to pseudo-first-order dependence on catalyst, CO, H_2O, and MV^{2+}. The transformation is pH dependent, with a rate/pH profile that shows sigmoidal behavior with an inflection point at pH 7.6. Analogous to the enzyme, the functional model is inhibited at low pH, by MeI, and by CN^-. The proposed mechanism invokes a monomer as the active species that binds CO, which is subsequently attacked by a water-derived nucleophile to yield the nickel carboxylic acid. This species is then deprotonated (pK_a of 7.6) in a fast step that may be coupled to electron transfer to MV^{2+}. The resulting Ni^I species reduces the second MV^{2+} to close the catalytic cycle.

A Ni^{II} amido complex supported by a thioether/thiolate chelating ligand that promotes the desoxygenation of CO, CO_2, and SO_2 has been described, (**29**).[192] The product, NCO, and mechanism of CO_2 reduction involving CO_2 insertion into the Ni—N bond, bear no resemblance to the enzymatic process.
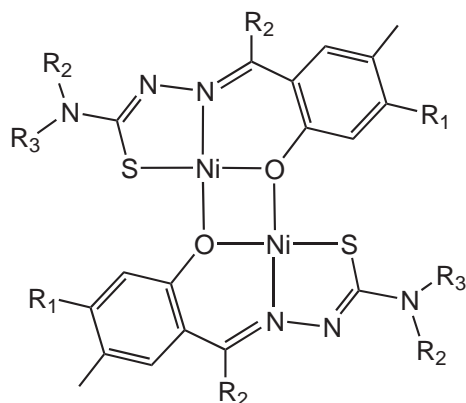

(**28**)
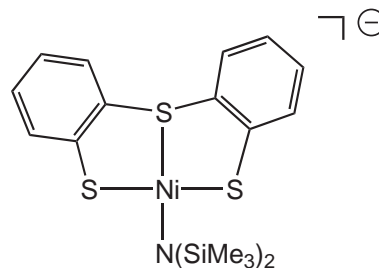
(**29**)

### 8.25.4.3 Acetyl Coenzyme A Synthase (ACS)

8.25.4.3.1 Enzymology

Acetyl coenzyme A synthase is a NiFeS protein that catalyzes the assembly/disassembly of acetate from the constituents of a methyl group (equivalent), CO, and the thiol, coenzyme A (CoA) (Equation (3)). The reversibility of the transformation allows a convenient *in vitro* assay

$$CH_3C(O)SCoA + {}^{13}CO \rightleftharpoons CH_3{}^{13}C(O)SCoA + CO \qquad (4)$$
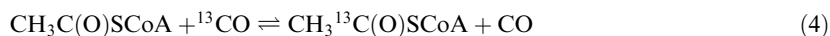
that permits the incorporation of labeled CO into acetyl CoA. All known ACS enzymes are bifunctional in that they contain the clusters necessary for, and possess, CODH activity.[12,193] As CO is a substrate for both CodH and ACS reactions in these bifunctional enzymes, it is perhaps not surprising that a proteinaceous "CO tunnel" has been described, independently by Lindahl[194,195] and Ragsdale.[196] Through this tunnel CO can pass from the C cluster, where it is generated by CO_2 reduction, to the A cluster (ACS active site) without leaving the macromolecule. Acetogenic bacteria assemble acetyl CoA as part of their autotrophic growth processes. Methanogenic archae can grow on acetate as an alternate carbon source (rather than CO_2), under which conditions they decompose acetyl CoA and utilize the methyl group to derive energy in methane

production via MCR catalysis.[12,197] The active-site cluster for ACS catalysis, the A cluster, is proposed to have a novel Ni–X–Fe$_4$S$_4$ structure, (**30**), based on its ESR, EXAFS, ENDOR, and Mössbauer features.[198–201] Very recently, two X-ray structures have been reported that depict a more complicated active site cluster composition with varying metal occupation at one position.[202] The primary, and compelling, evidence for a cluster in which the Ni and Fe$_4$S$_4$ are coupled was provided in a landmark ESR experiment with the CO-reduced form of the A cluster, termed A$_{red}$—CO.[203,204] This state exhibits a slow-relaxing rhombic signal with *g*-values of 2.08, 2.07, and 2.03. The signal shows hyperfine broadening when the enzyme was grown on either ^{61}Ni or ^{57}Fe, or when reduced under ^{13}CO. Clearly, the unpaired spin density reported by the ESR signal has some contribution from each of the above nuclei. Nonetheless, the CO ligand appears to be bound to only one metal, i.e., in a nonbridging position, based on the ν_{12CO} value of 1,995 cm^{-1}.[205] The two subunits of CODH/ACS from *M. thermoacetica* have been dissociated under detergent conditions to provide a clearer view of the A cluster, which is contained in the α subunit. This subunit contains only one Ni and four Fe, with spectroscopic features similar to the A cluster in the intact $\alpha_2\beta_2$ holoenzyme (which contains 2 Ni and 12 Fe).[200] Ni EXAFS of the α subunit was modeled as a distorted square-planar Ni site, with two sulfur ligands at 2.19 Å and two oxygen/nitrogen ligands at 1.89 Å.
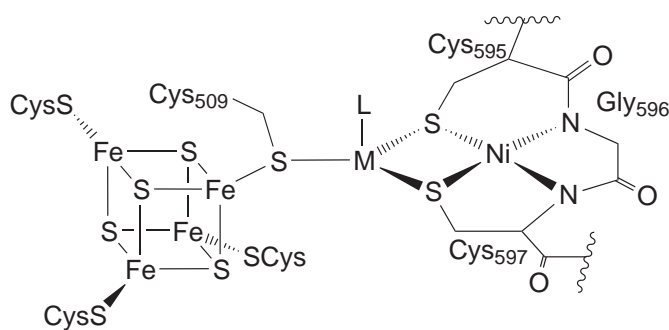
ACS Cluster A

(**30**)

As with the comparison between CODH catalysis and the water-gas-shift reaction, the ACS-promoted assembly of acetate finds parallel in the industrial Monsanto acetic acid synthesis reaction. The latter process is catalyzed by a low-valent, Rh-based monomer, with the clear involvement of organometallic intermediates in the elementary steps.[206] ACS catalysis is proposed to involve unprecedented, biological organometallic intermediates. Two redox states of the A cluster have been unequivocally assigned. A$_{ox}$ represents the as-isolated, inactive form that must be reduced to yield a catalytically competent protein. Reduction of A$_{ox}$ with CO yields A$_{red}$—CO, the state characterized by its unique ESR signal and terminal CO mode in the FT-IR. Two mechanisms currently under intense investigation propose disparate roles for the A$_{red}$—CO state. Ragsdale has put forth a mechanism in which A$_{red}$—CO is an intermediate and the first step is reductive carbonylation of the A$_{ox}$ state to A$_{red}$—CO.[193] The latter is assigned a structure of Ni^I—CO. This species is subsequently methylated by methylcobalamin to yield a Ni^{III}(CH$_3$)(CO) intermediate (not detected) and Cob(I)alamin. In *M. thermoacetica* the cobalamin is the cofactor for a unique protein termed the corrinoid iron–sulfur protein (CFeSP). The Ni oxidation-state assignments assume an S$_N$2-type methyl transfer, as has been invoked in numerous methylcobalamin alkylations, e.g., methionine syntheses.[20] Ragsdale invokes internal electron transfer, followed by a classic CH$_3$/CO migratory insertion to generate a Ni^{II}–acetyl species (also not observed). The final step involves attack by CoA to generate the thioester bond. This could proceed in either of two ways. Direct sulfur nucleophilic attack on the metal–acetyl would generate the product. Alternatively, CoA could first ligate to the A cluster, then generate the thioester via a formal C—S reductive elimination. In favor of the latter process, there is spectroscopic evidence for CoA binding to the A cluster.[207,208] Both C—S bond-forming pathways have model chemistry precedents.[174,209,210] The mechanism accounts for the observed stereochemical outcome of chiral methyl probe experiments. Using chiral CHDT–H$_4$folate, Floss found conversion to acetate with retention of stereochemistry.[211] Net retention is explained by invoking two S$_N$2-like steps, with each proceeding by inversion at the methyl carbon. The first inversion is methyl transfer from H$_4$folate to the Co^I of the CFeSP, and the second is transfer from CFeSP to the A cluster.
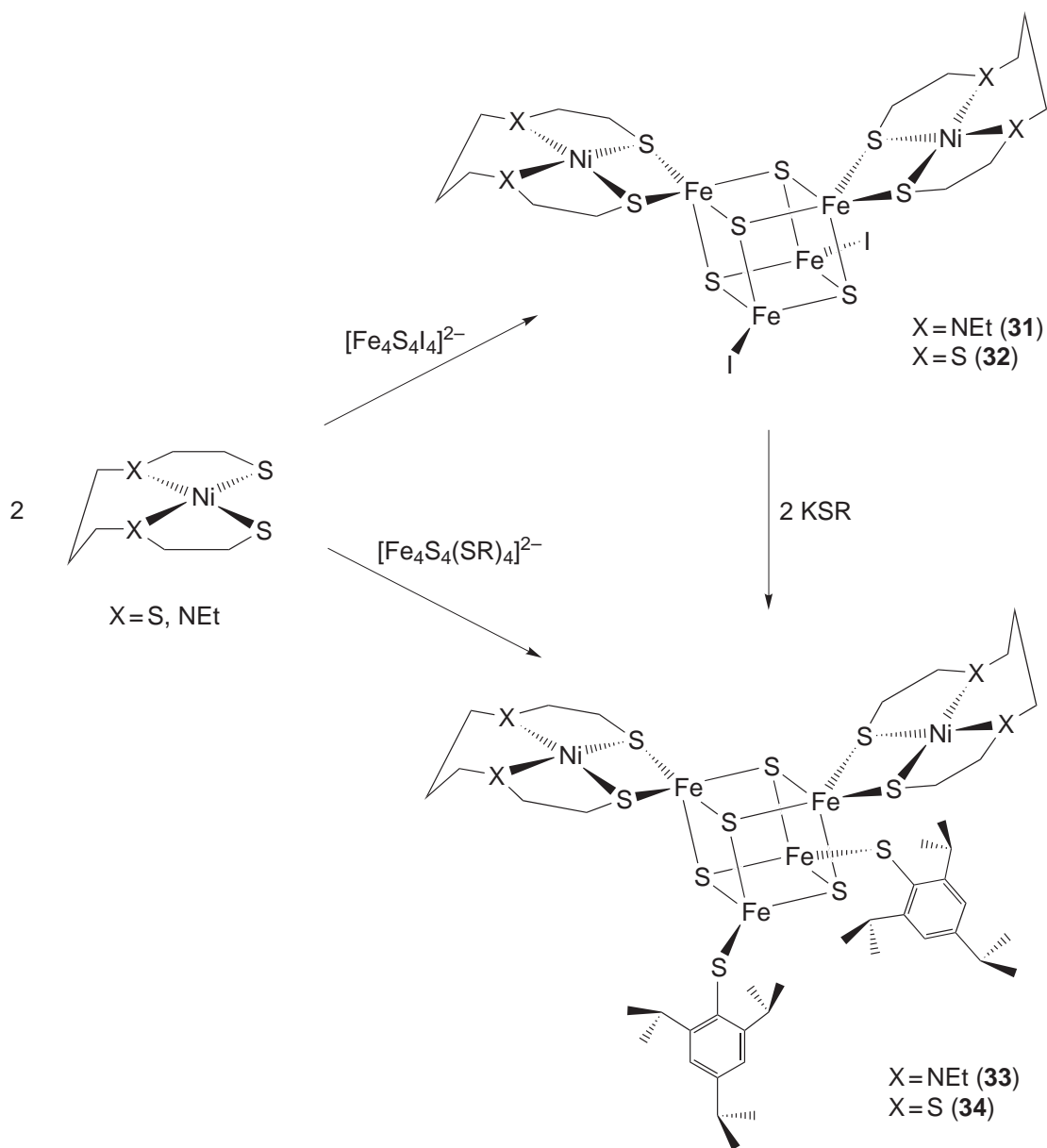
Lindahl has proposed an alternative mechanism for acetyl–CoA synthesis in which the A_{red}—CO state is not an intermediate but, instead, is a competitive inhibitor with a K_d of 180 μM.[212,213] The mechanism, based on extensive kinetic studies, invokes a unique two-electron redox site, termed the D site (not to be confused with the more recently described D cluster in COdH), as seminal to catalysis. Although the specific identity of this site remains unknown, it is proposed to be a low potential, −540 mV, two-cysteine/cystine site. The mechanism begins with a two-electron reduction of the D site (D_{ox} to D_{red}), yielding a reduced form of ACS with Ni in the +2 oxidation state. Methyl transfer from CFeSP to Ni is closely followed by, or coupled to, oxidation of the D site, yielding Ni^{II}—CH$_3$ with D_{ox}. CO then binds to Ni and inserts to generate a Ni^{II}–acetyl species, which is subsequently attacked by CoA to generate the product. In this transformation, the D site increases electron density at Ni in some manner, thus permitting Ni^{II} to be an effective nucleophile for the transmethylation. The mechanism requires an ordered binding of methyl, followed by CO, while accounting for the stereochemical outcome of the chiral methyl experiments.

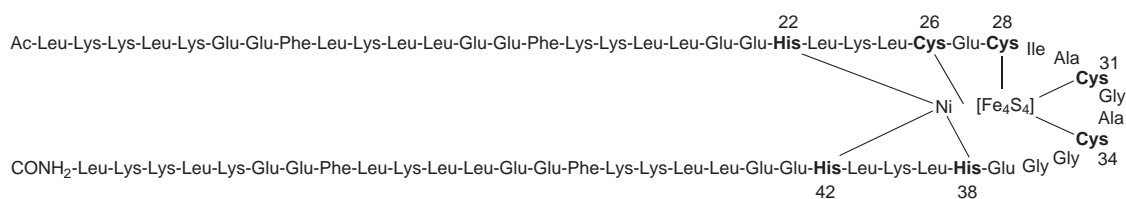### 8.25.4.3.2 *Structural models of the A cluster*

Prior to crystallographic studies of anaerobic COdH proteins, the C and A clusters were proposed to have very similar Ni–X–Fe$_4$S$_4$ compositions. Furthermore, given that CO is a substrate common to both sites, synthetic chemistry and reactivity studies directed toward active-site structural models of NiFe$_4$S$_4$ clusters were motivated to mimic both chemistries. The coordination chemistry of Ni—CO complexes relevant to these proteins was reviewed in Section 8.25.4.2.2 above. The focus here is on structural models that include Ni ions attached to Fe$_4$S$_4$ clusters. Saak and Pohl have prepared the most relevant small-molecule analogs to date, using a convergent synthetic strategy, Scheme 12.[214,215] They successfully coupled a series of monomeric Ni complexes to [Fe$_4$S$_4$X$_4$]$^{2-}$ (X = SR, I) using bridging thiolates to link the nickel and the cubane. This metalloligand approach, in which *cis* disposed thiolates of a chelating ligand bridge to a different metal ion, has precedents in similar Ni thiolate complexes that bridge to other Fe sites.[216,217] The complexes that form are of the stoichiometry 2 Ni per Fe$_4$S$_4$ and yield neutral complexes, the latter attribute provides the driving force for formation of the 2:1 species. A 1 Ni per Fe$_4$S$_4$ complex has been described, and its structure determined at low resolution. The 2:1 complexes are best described with a localized electron distribution of 2 Ni^{II} complexes bound to a [Fe$_4$S$_4$]$^{2+}$ cubane. The cluster with NiN_2S_2 ligation is electrochemically reduced at −1040 mV and oxidized at 0 mV and 485 mV (vs. SCE). The first two processes are cubane-based, and the last tentatively assigned as oxidation of one of the two Ni^{II} sites to Ni^{III}. Several of the derivatives have been characterized crystallographically.[214] In each, the Ni ion resides in a square-planar geometry, with thiolate bridging to the Fe$_4$S$_4$ unit. The nature of the bridging unit is quite different among the three crystallographically characterized complexes, ranging from symmetric bidentate thiolate coordination (Fe—S distances, 2.533(2) and 2.464(2) Å) in [{Ni(EtN$_2$S$_2$)}$_2$Fe$_4$S$_4$I$_2$] (EtN$_2$S$_2$ = N,N′-diethyl-3,7-diazanonane-1,9-dithiolate), (**31**), to asymmetric bridging in two complexes possessing arylthiolate ligation at the two Fe positions, [{Ni(EtN$_2$S$_2$)}$_2$Fe$_4$S$_4$(Stip)$_2$] (tip = 2,4,6-tri*iso*propylphenyl), (**33**), (Fe—S, 2.361(5) and 2.941(5) Å) and [{Ni(S$_4$)}$_2$Fe$_4$S$_4$(Stip)$_2$] (S$_4$ = 3,7-dithianonane-1,9-dithiolate), (**34**), (Fe—S, 2.460(3) and 2.662(4) Å). The differences in bridging modes have been ascribed to electronic properties of the Fe$_4$S$_4$ unit, rather than to steric forces imposed by the larger Stip ligands. Nonetheless, in solution the bridges are symmetric on the NMR timescale. Other notable features of the structures are the Ni–Fe separations ranging from 2.8 Å–3.0 Å and short Ni–S(sulfide) contacts of 3.2 Å–3.4 Å. In the C cluster of COdH, the exo iron forms a bond with one of the sulfides in the NiFe$_3$S$_4$ core. Reactivity studies, beyond the aforementioned electrochemical analyses, have not been reported.

An alternate synthetic strategy employed by Holm and LaPlaza entails stabilizing Ni–Cys–Fe$_4$S$_4$ structures within a peptide construct.[218–220] This modeling approach is an attractive and compelling alternative to the more classic synthetic analog approach that utilizes organic ligands or single amino acid residues, and is particularly suited for more complex metal-cluster compositions. A series of helix-loop-helix 63-mer peptides, (**35**), that contained ferredoxin consensus binding motifs in the loop region, were developed and incorporate previous design elements.[218] The sequences were modified to introduce binding sites for single Ni ions in a position that would utilize one of the Fe$_4$S$_4$ cluster Cys ligands as a bridge to the Ni ion. In solution the peptides form stable dimers of high helical content. Presumably the dimerization is driven, by four-helix bundle formation. Two constructs that proved successful resulted in N$_2$S$_2$ (His$_2$Cys$_2$) and N$_3$S (His$_3$Cys) Ni coordination. Incorporation of Fe$_4$S$_4$ cubane clusters was accomplished by incubating the

2

X = S, NEt

$[Fe_4S_4I_4]^{2-}$

$[Fe_4S_4(SR)_4]^{2-}$

2 KSR

X = NEt (**31**)
X = S (**32**)

X = NEt (**33**)
X = S (**34**)

Scheme 12
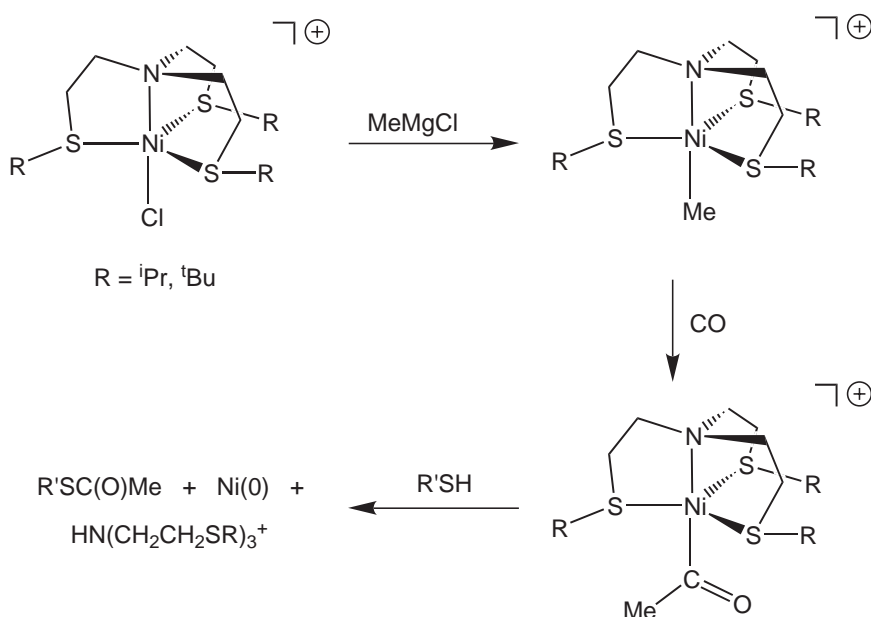
peptides with the performed cluster, $[Fe_4S_4(SCH_2CH_2OH)_4]^{2-}$. Electronic absorption, Mössbauer, and iron EXAFS data supported the conclusion that the cubane binds the peptide intact.[220] Nickel[II] binding was deduced by Ni ion content (atomic absorption), difference electronic absorption spectroscopy, and Ni K-edge spectra and EXAFS. The related Co–Cys–Fe$_4$S$_4$ peptides were also prepared and examined by Co EXAFS. While the Ni (and Co) EXAFS analysis is complicated by a minority population (20%) of six-coordinate Ni with low Z ligands, i.e., non-sulfur, it seems clear that the Ni binds predominantly in the designed sites with distorted square-planar geometry based on characteristic pre-edge features. In the His$_2$Cys$_2$ and His$_3$Cys peptides, best fits were found for Ni—N distances of 1.92–1.96 Å and Ni—S of ~2.20 Å. These distances are in accord with four-coordinate sites; five- and six-coordinate sites would yield significantly longer bond lengths. The population of an alternate Ni binding site is the result of equilibrium Ni binding to the designed peptide site, as determined by denaturation studies. The determined binding constants for the designed sites are $4.4 \times 10^5\,M^{-1}$ for the His$_2$Cys$_2$ peptide, and $2.7 \times 10^5\,M^{-1}$ for the His$_3$Cys peptide.[219]

Ac-Leu-Lys-Lys-Leu-Lys-Glu-Glu-Phe-Leu-Lys-Leu-Leu-Glu-Glu-Phe-Lys-Lys-Leu-Leu-Glu-Glu-**His**-Leu-Lys-Leu-**Cys**-Glu-**Cys** Ile   Ala   31

CONH$_2$-Leu-Lys-Lys-Leu-Lys-Glu-Glu-Phe-Leu-Lys-Leu-Leu-Glu-Glu-Phe-Lys-Lys-Leu-Leu-Glu-Glu-**His**-Leu-Lys-Leu-**His**-Glu Gly

Cys Gly Ala **Cys** Gly 34

Ni [Fe$_4$S$_4$]

22 26 28 42 38

(35)

8.25.4.3.3 *ACS reactivity models*

Given the mechanistic models of Ragsdale and Lindahl, coupled with the extensive organo-metallic chemistry of nickel (as compared with limited organometallic examples of Fe$_4$S$_4$ clusters), much effort has centered on reactivity analogs of ACS that involve relevant transformations at mononuclear nickel sites. Using a tripodal [NS$_3^R$] donor ligand possessing a tertiary amine and thioether sulfur donors with large (R = ^{i}Pr or ^{t}Bu) substituents, Holm has prepared a series of five-coordinate, trigonal-bipyramidal complexes, [NS$_3^R$]Ni(L), and demonstrated most of the proposed elementary steps of acetyl CoA production.[173,174] The chloro complex, [NS$_3$]Ni(L), which is dimeric for R = iPr and monomeric when R = tBu, provides entry into the other derivatives. Of most relevance to ACS catalysis is the series of transformations, outlined in Scheme 13, that initiates with replacement of the chloride with a methyl group, generating [NS$_3^R$]Ni(CH$_3$) via the action of a Grignard reagent. One of the diamagnetic organonickel complexes has been characterized crystallographically.[174] In [NS$_3^{iPr}$]Ni(CH$_3$) the notable feature is a relatively short Ni—C bond distance of 1.94 Å. Carbonylation of [NS$_3^{iPr}$]Ni(CH$_3$) proceeded smoothly at low temperature to yield the acetyl derivatives, presumably by a mechanism involving CO coordination followed by migratory insertion. However, no intermediates were detected. Lastly, addition of sulfur-based nucleophiles to [[NS$_3^R$]Ni(C(O)CH$_3$) liberated the corresponding thioesters, along with protonated [NS$_3^R$] ligand and metallic Ni. Thioester yields were dependent on the identity of the thiol, with more acidic thiols (PhSH and PhCH$_2$SH) reacting much faster (than EtSH). Surprisingly, the complex supported by the more crowded ligand, [NS$_3^{tBu}$]Ni(C(O)CH$_3$), reacted faster at parity of thiol. The reaction results in a two-electron reduction at Ni, and because the [NS$_3^R$] ligand cannot stabilize Ni(0), it precipitates. The formation of the C—S bond could proceed either by nucleophilic attack at the acetyl carbon, or by thiolate coordination followed by a formal reductive elimination.


R = ^{i}Pr, ^{t}Bu

R'SC(O)Me + Ni(0) + HN(CH$_2$CH$_2$SR)$_3^+$

Scheme 13

In a subsequent study from the same laboratory, square-planar complexes were targeted as appropriate to establish the feasibility of the latter C—S bond-forming pathway. Specifically, $Ni(bpy)(SAr)(CH_3)$ (bpy = 2,2'-bipyridyl) was produced by protonolysis of $Ni(bpy)(CH_3)_2$ with the corresponding arylthiol.[209] The alkyl-thiolate species reacted with one equivalent of CO to generate the first stable acetyl-thiolate derivatives of Ni, one of which was characterized crystallographically. Addition of subsequent CO (three equivalemts) produced the thioester and a Ni(0) species, $Ni(bipy)(CO)_2$. This transformation demonstrates that *cis*-disposed acetyl and thiolate ligands can coexist at a single Ni site, and can reductively eliminate thioester under suitable conditions. Nonetheless, thiolate-ligand exchange is rapid, as demonstrated by equilibration between $Ni(bpy)(SAr)(CH_3)$ and $Ni(bpy)(SAr')(CH_2CH_3)$ to a mixture of four components through intermolecular pathways. Along this line, Hillhouse demonstrated[210] and Holm confirmed[209] that the cyclic alkyl-thiolate, complex (**37**), was carbonylated to γ-thiobutyrolactone. Other reports described analogous generation of metallacyclic alkyl-thiolates that yield cyclic thialactones via the intermediacy of well-characterized acetyl-thiolates.[221]

Sellmann has reported a Ni—CH$_3$ complex, (**38**), supported by sulfur-only ligation that is carbonylated to the acetyl complex.[222] The acetyl complex was unstable under the conditions employed with respect to ketone and thioester formation, although these products were not identified. In a further study, the complete reaction sequence of ACS catalysis was demonstrated using a mixed dithioether/dithiolate ligand, (**39**).[221] The key step was Na/Hg amalgam reduction of the Ni^{II} species, that resulted in reductive C—S bond cleavage to generate the Ni^{II} cyclic trimer possessing tethered alkyl substituents. These substituents underwent carbonylation and cyclic thioester reductive elimination steps similar to those described above.[209,210]

(**37**)   (**38**)   (**39**)

Formation of Ni—CH$_3$ species by the more likely biological route of Ni-based nucleophilic attack on a methyl electrophile has been demonstrated.[223] The Ni^{II} complex, (**40**), supported by thioether and phosphine ligation, was reduced to the Ni^0 adduct *in situ*. It was then oxidized to the Ni^{II}CH$_3$ and Ni^{II}(C(O)CH$_3$) species by reaction with CH$_3$I and CH$_3$C(O)Cl, respectively. These low-spin, square-pyramidal complexes contain apical organic ligands and are related by CO insertion/extrusion, which was rapid even at $-60\,^\circ$C, precluding kinetic analysis.

Although acetyl formation at monomeric metal sites occurs predominantly by methyl migration to the carbonyl, free-radical pathways also have been established.[224] Bimetallic complexes that participate in CH$_3$/CO migratory insertion, and therefore serve as precedent for ACS, are not common.[225] Darensbourg provided an unequivocal example of enhanced migratory insertion rates provided by a second metal.[226] The rate of acetyl formation in $CH_3FeW(CO)_9^-$ is over an order of magnitude faster than for the corresponding monomer, $CH_3Fe(CO)_4^-$. The W site serves as an internal Lewis acid to activate the carbonyl for methyl migration. Similar bimolecular enhancements has been documented for the carbonylation of the ZrMo dimer, (**41**), leading to a bridging acetyl group.[227]

(**40**)   (**41**)

The remarkable biological transfer of a methyl group from one metal to another in ACS catalysis has been modeled using a monomeric Ni^I complex, $[Ni(tmc)]^+$.[52,228]

$$CH_3Co(dmgBF_2)_2py + 2Ni(tmc)^+ \rightarrow Co(dmgBF_2)_2py^- + [Ni(tmc)CH_3]^+ + Ni(tmc)^{2+} \qquad (5)$$

$RCo(dmgBF_2)_2L$ reacted with two equiv. of $[Ni(tmc)]^+$ to rapidly yield $[Ni(tmc)R]^+$, $[Ni(tmc)]^+$, and $Co(dmgBF_2)_2L^-$. Methyl-transfer rates were on the order of $10^3–10^4 M^{-1} s^{-1}$, as determined by stopped-flow kinetic methods. These rates were correlated with the reduction potential of $RCo(dmgBF_2)_2L$. The mechanism proposed, Scheme 14, begins with rate-determining reduction of the organocobalt derivatives by the N;^{I} complex, followed by Co—R bond homolysis.[229] Reactions utilizing the radical clock probe 5-hexenyl-Co^{III} yielded methylcyclopentane, consistent with intervention of the hexenyl radical. Methyl ligation to Ni tetraazamacrocycles has been analyzed computationally at the Hartree–Fock level.[230] Results are in general agreement with the above experimentally-derived mechanism. Methyl radical addition to $Ni^I[cyclam]$ yielding Ni^{II}—CH_3 is clearly exothermic, with $\Delta E = -552 \text{ kJ mol}^{-1}$ to -564 kJ mol^{-1} for formation of the triplet product. Conversely, methyl-radical addition to $Ni^{II}[cyclam]$ to generate Ni^{III}—CH_3 is strongly endothermic, with $\Delta E = 271 \text{ kJ mol}^{-1}$ for formation of the high-spin product and $\Delta E = 456 \text{ kJ mol}^{-1}$ for the low-spin product, consistent with the great instability of such species determined experimentally. Interestingly, and of potential enzymatic relevance, the calculations suggest that methyl-cation addition to $Ni(I)[cyclam]$ generating Ni^{III}—CH_3 is energetically favored, again with the formation of the high-spin product providing a more exothermic path. However, much of the energy derived in the last reaction results from the fact that the gas-phase calculations place an unsolvated methyl cation at an exceedingly high energy, 837 kJ mol^{-1} above the methyl radical. Clearly, in solution this extreme driving force is not present.
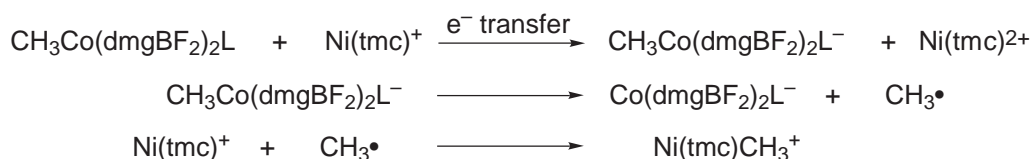
Scheme 14

Studies designed to probe the feasibility of the Lindahl D site mechanism, in which a remote, two-electron redox site is oxidized upon alkylation of a Ni^{II} center to yield a Ni^{II}—CH_3 species, are lacking and provide an attractive direction for future studies. Most relevant is the observation by Maroney of a Ni^{II} dimer, (**42**), that upon exposure to iodine forms a ligated disulfide through the quantitative oxidation of two thiolate ligands (per Ni).[231]
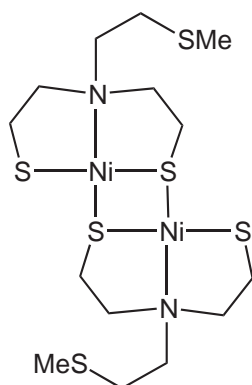
(**42**)

8.25.5   REFERENCES

1. (a)Top, S.; Jaouen, G.; Vessteres, A.; Abjean, J.-P.; Davoust, D.; Rodger, C. A.; Sayer, B. G.; McGlinchey, M. J. *Organometallics*, **1985**, *4*, 2143–2150.
   (b)Halpern, J. *Pure Appl. Chem.* **1986**, *58*, 575–584.
2. Nicolet, Y.; Cavazza, C.; Fontecilla-Camps, J. C. *J. Inorg. Biochem.* **2002**, *91*, 1–8.
3. Frey, M. *Chembiochem.* **2002**, *3*, 153–160.
4. Adams, M. W. W.; Stiefel, E. I. *Curr. Opin. Chem. Biol.* **2000**, *4*, 214–220.
5. Fontecilla-Camps, J. C.; Ragsdale, S. W. In *Advances in Inorganic Chemistry*. Academic Press 1999; Vol. 47, pp 283–333.
6. Huber, C.; Wachtershauser, G. *Science* **1998**, *281*, 670–672.
7. Huber, C.; Wachtershauser, G. *Science* **1997**, *276*, 245–247.
8. Wachtershauser, G. *Proc. Natl. Acad. Sci. USA*. **1994**, *91*, 4283–4287.
9. Keller, M.; Blochl, E.; Wachtershauser, G.; Stetter, K. O. *Nature* **1994**, *368*, 836–838.
10. Blochl, E.; Keller, M.; Wachtershauser, G.; Stetter, K. O. *Proc. Natl. Acad. Sci., USA* **1992**, *89*, 8117–8120.
11. Hodgkin, D. C., Ed., *Vitamin B12* **1979**, de Grutyer: W., Berlin.
12. Ragsdale, S. W.; Kumar, M. *Chem. Rev.* **1996**, *96*, 2515–2540.
13. Golding, B. T.; Anderson, R. J.; Ashwell, S.; Edwards, C. H.; Garnett, I.; Kroll, F.; Buckel, W. In *Vitamin B12 and B12-Proteins*; Kräutler, B.; Arigoni, D.; Golding, B. T., Eds.; Wiley-VCH: Weinheim, Germany, 1996; pp 201–216.
14. Fontecave, M.; Mulliez, E. In *Chemistry and Biochemistry of B12*; Banerjee, R., Ed.; Wiley: New York, 1999; pp 731–756.
15. Kräutler, B. In *Vitamin B12 and B12-Proteins*; Kräutler, B.; Arigoni, D.; Golding, B. T., Eds.; Wiley-VCH: Weinheim, Germany, 1996; pp 201–216.
16. Halpern, J. *Science* **1985**, *227*, 869–875.
17. Wollowitz, S.; Halpern, J. *J. Am. Chem. Soc.* **1988**, *110*, 3112–3120.
18. Wang, Y.; Finke, R. G. *Inorg. Chem.* **1989**, *28*, 983–986.
19. Lawrence, C. C.; Stubbe, J. *Curr. Opin. Chem. Biol.* **1998**, *2*, 650–655.
20. Drennan, C. L.; Dixon, M. M.; Hoover, D. M.; Jarrett, J. T.; Goulding, C. W.; Matthews, R. G.; Ludwig, M. L. In *Vitamin B12 and B12-Proteins*; Kräutler, B.; Arigoni, D.; Golding, B. T., Eds.; Wiley-VCH: Weinheim, Germany, 1996; pp 133–156.
21. Matthews, R. G.; Goulding, C. W. *Curr. Opin. Chem. Biol.* **1997**, *1*, 332–339.
22. Halpern, J. *Acc. Chem. Res.* **1982**, *15*, 238–244.
23. Halpern, J. *Polyhedron* **1988**, *7*, 1483–1490.
24. Halpern, J.; Kim, S. H.; Leung, T. W. *J. Am. Chem. Soc.* **1984**, *106*, 8317–8319.
25. Finke, R. G.; Hay, B. P. *Inorg. Chem.* **1984**, *23*, 3041–3043.
26. Finke, R. G. In *Vitamin B12 and B12-Proteins*; Kräutler, B.; Arigoni, D.; Golding, B. T., Eds.; Wiley-VCH: Weinheim, Germany, 1996; pp 383–402.
27. Kräutler, B. In *Cobalt, B12-Enzymes and Coenzymes, Encyclopedia of Inorganic Chemistry*; King, R. B., Ed., Wiley: Chichester, UK, 1994; Vol. 2, p. 697.
28. Drennan, C. L.; Huang, S.; Drummond, J. T.; Matthews, R. G.; Ludwig, M. L. *Science* **1994**, *266*, 1669–1674.
29. Mancia, F.; Keep, N. H.; Nakagawa, A.; Leadlay, P. F.; McSweeney, S.; Rasmussen, B.; Bosecke, P.; Diat, O.; Evans, P. R. *Structure* **1996**, *4*, 339–350.
30. Sintchak, M. D.; Arjara, G.; Kellogg, B. A.; Stubbe, J.; Drennan, C. L. *Nat. Struct. Biol.* **2002**, *9*, 293–300.
31. Dolphin, D.; *Vitamin B12*. Wiley: New York, 1984.
32. Brescianipahor, N.; Forcolin, M.; Marzilli, L. G.; Randaccio, L.; Summers, M. F.; Toscano, P. J. *Coord. Chem. Rev.* **1985**, *63*, 1–125.
33. Randaccio, L. *Comm. Inorg. Chem.* **1999**, *21*, 327–376.
34. Randaccio, L.; Pahor, N. B.; Zangrando, E.; Marzilli, L. G. *Chem. Soc. Rev.* **1989**, *18*, 225–250.
35. Toscano, P. J.; Marzilli, L. G. *Prog. Inorg. Chem.* **1983**, *31*, 105–204.
36. Ertas, M.; Koray, A. R.; Ahsen, V.; Bekaroglu, O. *J. Organomet. Chem.* **1986**, *317*, 301–306.
37. Costa, G.; Mestroni, G.; Stefani, L. *J. Organomet. Chem.* **1967**, *7*, 493.
38. Costa, G.; Mestroni, G.; Tauzher, G.; Stefani, L. *J. Organomet. Chem.* **1966**, *6*, 181–187.
39. Finke, R. G.; Smith, B. L.; McKenna, W. A.; Christian, P. A. *Inorg. Chem.* **1981**, *20*, 687–693.
40. Costa, G. *Coord. Chem. Rev.* **1972**, *8*, 63.
41. Choo, P. L.; Mulichak, A. M.; Jones, R. W.; Bacon, J. W.; Pett, V. B.; Zacharias, D. E. *Inorg. Chim. Acta* **1990**, *171*, 183–192.
42. Gridnev, A. A.; Ittel, S. D.; Fryd, M.; Wayland, B. B. *Organometallics* **1993**, *12*, 4871–4880.
43. Woska, D. C.; Wayland, B. B. *Inorg. Chim. Acta* **1998**, *270*, 197–201.
44. Endicott, J. F.; Ferraudi, G. J. *J. Am. Chem. Soc.* **1977**, *99*, 243–245.
45. Endicott, J. F.; Netzel, T. L. *J. Am. Chem. Soc.* **1979**, *101*, 4000–4002.
46. Bakac, A.; Espenson, J. H. *J. Am. Chem. Soc.* **1984**, *106*, 5197–5202.
47. Welker, M. E. *Curr. Org. Chem.* **2001**, *5*, 785–807.
48. Jacobsen, E. N. *Acc. Chem. Res.* **2000**, *33*, 421–431.
49. Tada, M. *Rev. Heteroatom. Chem.* **1999**, *20*, 97–144.
50. Pearson, R. G.; Figdore, P. E. *J. Am. Chem. Soc.* **1980**, *102*, 1541–1547.
51. Okabe, M.; Tada, M. *Chem. Lett.* **1980**, 831–834.
52. Ram, M. S.; Riordan, C. G.; Yap, G. P. A.; Liable-Sands, L.; Rheingold, A. L.; Marchaj, A.; Norton, J. R. *J. Am. Chem. Soc.* **1997**, *119*, 1648–1655.
53. Espenson, J. H.; McDowell, M. S. *Organometallics* **1982**, *1*, 1514–1518.
54. Derenne, S.; Gaudemer, A.; Johnson, M. D. *J. Organomet. Chem.* **1987**, *322*, 229–238.
55. Schrauzer, G. N.; Holland, R. J. *J. Am. Chem. Soc.* **1971**, *93*, 4060.
56. Smith, E. L.; Mervyn, L. *Biochemical Journal* **1963**, *86*, P2.
57. Sweany, R. L. In *Comprehensive Organometallic Chemistry II*, Elsevier Science: Tarrytown, NY, 1995, Vol. 8, Chap. 1, p 1.

58. Geremia, S.; Mari, M.; Randaccio, L.; Zangrando, E. *J. Organomet. Chem.* **1991**, *408*, 95–104.
59. Parker, W. O.; Brescianipahor, N.; Zangrando, E.; Marzilli, L. G.; Randaccio, L. *Inorg. Chem.* **1985**, *24*, 3908–3913.
60. Nie, S. M.; Marzilli, P. A.; Marzilli, L. G.; Yu, N. T. *J. Am. Chem. Soc.* **1990**, *112*, 6084–6091.
61. Puckett, J. M.; Mitchell, M. B.; Hirota, S.; Marzilli, L. G. *Inorg. Chem.* **1996**, *35*, 4656–4662.
62. Hirota, S.; Polson, S. M.; Puckett, J. M.; Moore, S. J.; Mitchell, M. B.; Marzilli, L. G. *Inorg. Chem.* **1996**, *35*, 5646–5653.
63. Giorgetti, M.; Berrettoni, M.; Conti, P.; DiCicco, A.; Marassi, R.; Ascone, I. *Organometallics* **1996**, *15*, 3491–3495.
64. Fonda, E.; Michalowicz, A.; Randaccio, L.; Tauzher, G.; Vlaic, G. *Eur. J. Inorg. Chem.* **2001**, 1269–1278.
65. Finke, R. G.; Smith, B. L.; Mayer, B. J.; Molinero, A. A. *Inorg. Chem.* **1983**, *22*, 3677–3679.
66. Geno, M. K.; Halpern, J. *J. Chem. Soc., Chem. Commun.* **1987**, 1052–1053.
67. Hay, B. P.; Finke, R. G. *Polyhedron* **1988**, *7*, 1469–1481.
68. Garr, C. D.; Finke, R. G. *J. Am. Chem. Soc.* **1992**, *114*, 10440–10445.
69. Hay, B. P.; Finke, R. G. *J. Am. Chem. Soc.* **1986**, *108*, 4820–4829.
70. Jensen, M. P.; Halpern, J. *J. Am. Chem. Soc.* **1999**, *121*, 2181–2192.
71. Hay, B. P.; Finke, R. G. *J. Am. Chem. Soc.* **1987**, *109*, 8012–8018.
72. Waddington, M. D.; Finke, R. G. *J. Am. Chem. Soc.* **1993**, *115*, 4629–4640.
73. Brown, K. L.; Evans, D. R. *Inorg. Chem.* **1994**, *33*, 6380–6387.
74. Sirovatka, J. M.; Finke, R. G. *J. Am. Chem. Soc.* **1997**, *119*, 3057–3067.
75. Wassenaar, R. W.; Daas, P. J. H.; Geerts, W. J.; Keltjens, J. T.; vanderDrift, C. *J. Bacteriol.* **1996**, *178*, 6937–6944.
76. Martin, B. D.; Finke, R. G. *J. Am. Chem. Soc.* **1990**, *112*, 2419–2420.
77. Ng, F. T. T.; Rempel, G. L.; Halpern, J. *J. Am. Chem. Soc.* **1982**, *104*, 621–623.
78. Tsou, T. T.; Loots, M.; Halpern, J. *J. Am. Chem. Soc.* **1982**, *104*, 623–624.
79. Geno, M. K.; Halpern, J. *J. Am. Chem. Soc.* **1987**, *109*, 1238–1240.
80. Ng, F. T. T.; Rempel, G. L.; Halpern, J. *Inorg. Chim. Acta* **1983**, *77*, L165–L166.
81. Hilhorst, E.; Iskander, A. S.; Chen, T.; Pandit, U. K. *Tetrahedron* **1994**, *50*, 8863–8870.
82. Hilhorst, E.; Iskander, A. S.; Chen, T.; Pandit, U. K. *Tetrahedron Lett.* **1993**, *34*, 4257–4260.
83. Brown, K. L.; Kallen, R. G. *J. Am. Chem. Soc.* **1972**, *94*, 1894.
84. Hogenkamp, H. P. C.; Bratt, G. T.; Sun, S. *Biochemistry* **1985**, *24*, 6428–6432.
85. Polson, S. M.; Hansen, L.; Marzilli, L. G. *Inorg. Chem.* **1997**, *36*, 307–313.
86. Galezowski, W.; Lewis, E. S. *J. Phys. Org. Chem.* **1994**, *7*, 90–95.
87. Hsu, T. L. C.; Brasch, N. E.; Finke, R. G. *Inorg. Chem.* **1998**, *37*, 5109–5116.
88. Tada, M.; Kambe, T.; Inouye, Y. *Chem. Comm.* **1998**, 41–42.
89. Sirovatka, J. M.; Finke, R. G. *J. Inorg. Biochem.* **2000**, *78*, 149–160.
90. Anderson, R. J.; Ashwell, S.; Garnett, I.; Golding, B. T. *Perkins Trans. I* **2000**, 4488.
91. Tada, M.; Kaneko, K. *Chem. Lett.* **1995**, 843–844.
92. Mosimann, H.; Krautler, B. *Angew. Chem., Int. Ed. Engl.* **2000**, *39*, 393–395.
93. Houck, D. R.; Kobayashi, K.; Williamson, J. M.; Floss, H. G. *J. Am. Chem. Soc.* **1986**, *108*, 5365–5366.
94. Daikh, B. E.; Finke, R. G. *J. Am. Chem. Soc.* **1991**, *113*, 4160–4172.
95. Daikh, B. E.; Finke, R. G. *J. Am. Chem. Soc.* **1992**, *114*, 2938–2943.
96. Fischer, H. *J. Am. Chem. Soc.* **1986**, *108*, 3925–3927.
97. Chistoserdova, L.; Vorholt, J. A.; Thauer, R. K.; Lidstrom, M. E. *Science* **1998**, *281*, 99–102.
98. Thauer, R. K. *Microbiology* **1998**, *144*, 2377–2406.
99. Ferry, J. G. *Crit. Rev. Biochem. Mol. Biol.* **1992**, *27*, 473–503.
100. Wolfe, R. S. *Trends Biochem. Sci.* **1985**, *10*, 396–399.
101. Wackett, L. P.; Honek, J. F.; Begley, T. P.; Shames, S. L.; Niederhoffer, E. C.; Hausinger, R. P.; Orme-Johnson, W. H.; Walsh, C. T. In *The Bioinorganic Chemistry of Nickel*; Lancaster, J. R. , Ed.; VCH: New York, 1988; p 249–274.
102. Ellefson, W. L.; Whitman, W. B.; Wolfe, R. S. *Proc. Natl. Acad. Sci. USA* **1982**, *79*, 3707–3710.
103. Wolfe, R. S. *Biochem. Soc. Symp.* **1992**, 41–49.
104. Telser, J. *Structure and Bonding* **1998**, *91*, 31–63.
105. Ermler, U.; Grabarse, W.; Shima, S.; Goubeaud, M.; Thauer, R. K. *Science* **1997**, *278*, 1457–1462.
106. Kratky, C.; Fassler, A.; Pfaltz, A.; Krautler, B.; Jaun, B.; Eschenmoser, A. *J. Chem. Soc., Chem. Commun.* **1984**, 1368–1371.
107. Farber, G.; Keller, W.; Kratky, C.; Jaun, B.; Pfaltz, A.; Spinner, C.; Kobelt, A.; Eschenmoser, A. *Helv. Chim. Acta* **1991**, *74*, 697–716.
108. Grabarse, W.; Mahlert, F.; Duin, E. C.; Goubeaud, M.; Shima, S.; Thauer, R. K.; Lamzin, V.; Ermler, U. *J. Mol. Biol.* **2001**, *309*, 315–330.
109. Berkessel, A. *Bioorganic Chem.* **1991**, *19*, 101–115.
110. Pelmenschikov, V.; Blomberg, M. R. A.; Siegbahn, P. E. M.; Crabtree, R. H. *J. Am. Chem. Soc.* **2002**, *124*, 4039–4049.
111. Hamilton, C. L.; Ma, L.; Renner, M. W.; Scott, R. A. *Biochim. Biophys. Acta* **1991**, *1074*, 312–319.
112. Fassler, A.; Kobelt, A.; Pfaltz, A.; Eschenmoser, A.; Bladon, C.; Battersby, A. R.; Thauer, R. K. *Helv. Chim. Acta* **1985**, *68*, 2287–2298.
113. Jaun, B. *Helv. Chim. Acta* **1990**, *73*, 2209–2217.
114. Renner, M. W.; Fajer, J. *J. Biol. Inorg. Chem.* **2001**, *6*, 823–830.
115. Halcrow, M. A.; Christou, G. *Chem. Rev.* **1994**, *94*, 2421–2481.
116. Renner, M. W.; Furenlid, L. R.; Barkigia, K. M.; Forman, A.; Shim, H. K.; Simpson, D. J.; Smith, K. M.; Fajer, J. *J. Am. Chem. Soc.* **1991**, *113*, 6891–6898.
117. Stolzenberg, A. M.; Stershic, M. T. *J. Am. Chem. Soc.* **1988**, *110*, 6391–6402.
118. Stolzenberg, A. M.; Stershic, M. T. *Inorg. Chem.* **1987**, *26*, 3082–3083.
119. Ram, M. S.; Riordan, C. G.; Ostrander, R.; Rheingold, A. L. *Inorg. Chem.* **1995**, *34*, 5884–5892.
120. Berkessel, A.; Bats, J. W.; Schwarz, C. *Angew. Chem., Int. Edit. Engl.* **1990**, *29*, 106–108.
121. Schmid, C. L.; Kempf, C.; Taubert, A.; Neuburger, M.; Zehnder, M.; Kaden, T. A.; Bujno, K.; Bilewicz, R. *Helv. Chim. Acta* **1996**, *79*, 1011–1020.

122. Pandiyan, T.; Enriquez, M. A. R.; Bernes, S.; de Bazua, C. D. *Polyhedron* **1999**, *18*, 3383–3390.
123. Jolly, P. W.; Wilke, G. In *The Organic Chemistry of Nickel* **1974**, Academic Press: New York.
124. Lin, S.-K.; Juan, B. *Helv. Chim. Acta* **1991**, *74*, 1725.
125. D'Aniello, M. J.; Barefield, E. K. *J. Am. Chem. Soc.* **1976**, *98*, 1610–1611.
126. Ram, M. S.; Bakac, A.; Espenson, J. H. *Inorg. Chem.* **1986**, *25*, 3267–3272.
127. Bakac, A.; Espenson, J. H. *J. Am. Chem. Soc.* **1986**, *108*, 713–719.
128. Helvenston, M. C.; Castro, C. E. *J. Am. Chem. Soc.* **1992**, *114*, 8490–8496.
129. Stolzenberg, A. M.; Stershic, M. T. *J. Am. Chem. Soc.* **1988**, *110*, 5397–5403.
130. Lahiri, G. K.; Schussel, L. J.; Stolzenberg, A. M. *Inorg. Chem.* **1992**, *31*, 4991–5000.
131. Sauer, A.; Cohen, H.; Meyerstein, D. *Inorg. Chem.* **1988**, *27*, 4578–4581.
132. Vaneldik, R.; Cohen, H.; Meshulam, A.; Meyerstein, D. *Inorg. Chem.* **1990**, *29*, 4156–4158.
133. Gunsalus, R. P.; Romesser, J. A.; Wolfe, R. S. *Biochemistry* **1978**, *17*, 2374–2377.
134. Rospert, S.; Voges, M.; Berkessel, A.; Albracht, S. P. J.; Thauer, R. K. *Eur. J. Biochem.* **1992**, *210*, 101–107.
135. Floss, H. G.; Lee, S. S. *Acc. Chem. Res.* **1993**, *26*, 116–122.
136. Ahn, Y. H.; Krzycki, J. A.; Floss, H. G. *J. Am. Chem. Soc.* **1991**, *113*, 4700–4701.
137. Jaun, B.; Pfaltz, A. *J. Chem. Soc., Chem. Commun.* **1988**, 293–294.
138. Drain, C. M.; Sable, D. B.; Corden, B. B. *Inorg. Chem.* **1990**, *29*, 1428–1433.
139. Drain, C. M.; Sable, D. B.; Corden, B. B. *Inorg. Chem.* **1988**, *27*, 2396–2398.
140. Stolzenberg, A. M.; Zhang, Z. *Inorg. Chem.* **1997**, *36*, 593–600.
141. Zhang, Z.; Petersen, J. L.; Stolzenberg, A. M. *Inorg. Chem.* **1996**, *35*, 4649–4655.
142. Zilbermann, I.; Golub, G.; Cohen, H.; Meyerstein, D. *Inorg. Chim. Acta* **1994**, *227*, 1–3.
143. Sellmann, D.; Funfgelder, S.; Pohlmann, G.; Knoch, F.; Moll, M. *Inorg. Chem.* **1990**, *29*, 4772–4778.
144. Cha, M. Y.; Shoner, S. C.; Kovacs, J. A. *Inorg. Chem.* **1993**, *32*, 1860–1863.
145. Tada, M.; Masuzawa, Y. *Chem. Commun.* **1997**, 2161–2162.
146. Signor, L.; Knuppe, C.; Hug, R.; Schweizer, B.; Pfaltz, A.; Jaun, B. *Chem. Eur. J.* **2000**, *6*, 3508–3516.
147. Kim, J. S.; Reibenspies, J. H.; Darensbourg, M. Y. *Inorg. Chim. Acta* **1996**, *250*, 283–294.
148. Kim, J. S.; Reibenspies, J. H.; Darensbourg, M. Y. *J. Am. Chem. Soc.* **1996**, *118*, 4115–4123.
149. Liebeskind, L. S.; Srogl, J.; Savarin, C.; Polanco, C. *Pure Appl. Chem.* **2002**, *74*, 115–122.
150. Srogl, J.; Allred, G. D.; Liebeskind, L. S. *J. Am. Chem. Soc.* **1997**, *119*, 12376–12377.
151. Srogl, J.; Liu, W. S.; Marshall, D.; Liebeskind, L. S. *J. Am. Chem. Soc.* **1999**, *121*, 9449–9450.
152. Maroney, M. J.; Davidson, G.; Allan, C. B.; Figler, J. *Structure and Bonding* **1998**, *91*, 1–65.
153. Hille, R. *J. Biol. Inorg. Chem.* **1996**, *1*, 397–404.
154. Vorholt, J. A.; Thauer, R. K. In *Molybdenum and Tungsten: Their Roles in Biological Processes*. Marcel Dekker 2002; Vol. 39, pp 571–619.
155. Lindahl, P. A. *Biochemistry* **2002**, *41*, 2097–2105.
156. Drennan, C. L.; Heo, J. Y.; Sintchak, M. D.; Schreiter, E.; Ludden, P. W. *Proc. Natl. Acad. Sci. USA* **2001**, *98*, 11973–11978.
157. Dobbek, H.; Svetlitchnyi, V.; Gremer, L.; Huber, R.; Meyer, O. *Science* **2001**, *293*, 1281–1285.
158. DeRose, V. J.; Telser, J.; Anderson, M. E.; Lindahl, P. A.; Hoffman, B. M. *J. Am. Chem. Soc.* **1998**, *120*, 8767–8776.
159. Qiu, D.; Kumar, M.; Ragsdale, S. W.; Spiro, T. G. *Science* **1994**, *264*, 817–819.
160. Staples, C. R.; Heo, J.; Spangler, N. J.; Kerby, R. L.; Roberts, G. P.; Ludden, P. W. *J. Am. Chem. Soc.* **1999**, *121*, 11034–11044.
161. Heo, J.; Staples, C. R.; Telser, J.; Ludden, P. W. *J. Am. Chem. Soc.* **1999**, *121*, 11045–11057.
162. Darensbourg, M. Y.; Ludvig, M.; Riordan, C. G. *Inorg. Chem.* **1989**, *28*, 1630–1634.
163. Ciurli, S.; Ross, P. K.; Scott, M. J.; Yu, S. B.; Holm, R. H. *J. Am. Chem. Soc.* **1992**, *114*, 5415–5423.
164. Tan, G. O.; Ensign, S. A.; Ciurli, S.; Scott, M. J.; Hedman, B.; Holm, R. H.; Ludden, P. W.; Korsun, Z. R.; Stephens, P. J.; Hodgson, K. O. *Proc. Natl. Acad. Sci. USA* **1992**, *89*, 4427–4431.
165. Zhou, J.; Scott, M. J.; Hu, Z.; Peng, G.; Munck, E.; Holm, R. H. *J. Am. Chem. Soc.* **1992**, *114*, 10843–10854.
166. Ciurli, S.; Yu, S. B.; Holm, R. H.; Srivastava, K. K. P.; Munck, E. *J. Am. Chem. Soc.* **1990**, *112*, 8169–8171.
167. Mond, L. *J. Chem. Soc.* **1890**, *57*.
168. Kelly, C. A.; Mulazzani, Q. G.; Blinn, E. L.; Rodgers, M. A. J. *Inorg. Chem.* **1996**, *35*, 5122–5126.
169. Jung, H. J.; Bang, H.; Suh, M. P. *Bull. Kor. Chem. Soc.* **2001**, *22*, 523–526.
170. Marganian, C. A.; Vazir, H.; Baidya, N.; Olmstead, M. M.; Mascharak, P. K. *J. Am. Chem. Soc.* **1995**, *117*, 1584–1594.
171. Baidya, N.; Olmstead, M. M.; Mascharak, P. K. *J. Am. Chem. Soc.* **1992**, *114*, 9666–9668.
172. Baidya, N.; Olmstead, M. M.; Whitehead, J. P.; Bagyinka, C.; Maroney, M. J.; Mascharak, P. K. *Inorg. Chem.* **1992**, *31*, 3612–3619.
173. Stavropoulos, P.; Carrie, M.; Muetterties, M. C.; Holm, R. H. *J. Am. Chem. Soc.* **1990**, *112*, 5385–5387.
174. Stavropoulos, P.; Muetterties, M. C.; Carrie, M.; Holm, R. H. *J. Am. Chem. Soc.* **1991**, *113*, 8485–8492.
175. Sacconi, L.; Ilardi, C. A.; Alli, C.; Nobini, F. *Inorg. Chem.* **1975**, *14*, 1380–1386.
176. Miedaner, A.; Curtis, C. J.; Wander, S. A.; Goodson, P. A.; DuBois, D. L. *Organometallics* **1996**, *15*, 5185–5190.
177. Schebler, P. J.; Mandimutsira, B. S.; Riordan, C. G.; Liable–Sands, L.; Incarvito, C. D.; Rheingold, A. L. *J. Am. Chem. Soc.* **2001**, *123*, 331–332.
178. Yamamura, T.; Sakurai, S.; Arai, H.; Miyamae, H. *J. Chem. Soc., Chem. Commun.* **1993**, 1656–1658.
179. Bishop, J. J.; Davison, A. *Inorg. Chem.* **1971**, *10*, 832.
180. Macgregor, S. A.; Lu, Z.; Eisenstein, O.; Crabtree, R. H. *Inorg. Chem.* **1994**, *33*, 3616–3618.
181. Nguyen, D. H.; Hsu, H. F.; Millar, M.; Koch, S. A.; Achim, C.; Bominaar, E. L.; Munck, E. *J. Am. Chem. Soc.* **1996**, *118*, 8963–8964.
182. Liaw, W.-F.; Horng, Y.-C.; Ou, D.-S.; Ching, C.-Y.; Lee, G.-H.; Peng, S.-M. *J. Am. Chem. Soc.* **1997**, *119*, 9299–9300.
183. Liaw, W.-F.; Chen, C.-H.; Lee, C.-M.; Lee, G.-H.; Peng, S.-M. *J. Chem. Soc., Dalton Trans.* **2001**, 138–143.
184. Collin, J. P.; Jouaiti, A.; Sauvage, J. P. *Inorg. Chem.* **1988**, *27*, 1986–1990.
185. Beley, M.; Collin, J. P.; Ruppert, R.; Sauvage, J. P. *J. Am. Chem. Soc.* **1986**, *108*, 7461–7467.

186. Collin, J. P.; Sauvage, J. P. *Coord. Chem. Rev.* **1989**, *93*, 245–268.
187. Craig, C. A.; Spreer, L. O.; Otvos, J. W.; Calvin, M. *J. Phys. Chem.* **1990**, *94*, 7957–7960.
188. Darensbourg, D. J.; Darensbourg, M. Y.; Goh, L. Y.; Ludvig, M.; Wiegreffe, P. *J. Am. Chem. Soc.* **1987**, *109*, 7539–7540.
189. Tommasi, I.; Aresta, M.; Giannoccaro, P.; Quaranta, E.; Fragale, C. *Inorg. Chim. Acta* **1998**, *272*, 38–42.
190. Lu, Z.; Crabtree, R. H. *J. Am. Chem. Soc.* **1995**, *117*, 3994–3998.
191. Lu, Z.; White, C.; Rheingold, A. L.; Crabtree, R. H. *Angew. Chem., Int. Ed. Engl.* **1993**, *32*, 92–94.
192. Sellmann, D.; Geipel, F.; Heinemann, F. W. *Chem. Eur. J.* **2000**, *6*, 4279–4284.
193. Ragsdale, S. W.; Riordan, C. G. *J. Biol. Inorg. Chem.* **1996**, *1*, 489–493.
194. Maynard, E. L.; Lindahl, P. A. *J. Am. Chem. Soc.* **1999**, *121*, 9221–9222.
195. Maynard, E. L.; Lindahl, P. A. *Biochemistry* **2001**, *40*, 13262–13267.
196. Seravalli, J.; Ragsdale, S. W. *Biochemistry* **2000**, *39*, 1274–1277.
197. Maroney, M. J. *Curr. Opin. Chem. Biol.* **1999**, *3*, 188–199.
198. Ralston, C. Y.; Wang, H. X.; Ragsdale, S. W.; Kumar, M.; Spangler, N. J.; Ludden, P. W.; Gu, W.; Jones, R. M.; Patil, D. S.; Cramer, S. P. *J. Am. Chem. Soc.* **2000**, *122*, 10553–10560.
199. Munck, E.; Popescu, C. V. *Hyperfine Interact.* **2000**, *126*, 59–67.
200. Xia, J.; Dong, J.; Wang, S.; Scott, R. A.; Lindahl, P. A. *J. Am. Chem. Soc.* **1995**, *117*, 7065–7070.
201. Xia, J. Q.; Hu, Z. G.; Popescu, C. V.; Lindahl, P. A.; Munck, E. *J. Am. Chem. Soc.* **1997**, *119*, 8301–8312.
202. Subsequent to submission of this manuscript, two reports of the crystal structure of ACS from *M. thermoacetica* have appeared. The composition of the active site cluster A is more complex than originally proposed and different in each report. The reader is directed to (a) Doukov, T. I.; Iverson, T. M.; Seravalli, J.; Ragsdale, S. W.; Drennan, C. L. *Science* **2002**, *298*, 567–572; (b) Darnault, C.; Volbeda, A.; Kim, E. J.; Legrand,, P.; Vernene, X.; Lindahl, P. A.; Fontecilla-Camps, J. C. *Nat. Struct. Biol.* **2003**, *10*, 271–279.
203. Gorst, C. M.; Ragsdale, S. W. *J. Biol. Chem.* **1991**, *266*, 20687–20693.
204. Fan, C. L.; Gorst, C. M.; Ragsdale, S. W.; Hoffman, B. M. *Biochemistry* **1991**, *30*, 431–435.
205. Kumar, M.; Ragsdale, S. W. *J. Am. Chem. Soc.* **1992**, *114*, 8713–8715.
206. Collman, J. P.; Hegedus, L. S.; Norton, J. R.; Finke, R. G. *Principles and Applications of Organotransition Metal Chemistry* **1987**, University Science Books: Mill Valley, CA.
207. Shanmugasundaram, T.; Kumar, G. K.; Wood, H. G. *Biochemistry* **1988**, *27*, 6499–6503.
208. Ragsdale, S. W.; Wood, H. G. *J. Biol. Chem.* **1985**, *260*, 3970–3977.
209. Tucci, G. C.; Holm, R. H. *J. Am. Chem. Soc.* **1995**, *117*, 6489–6496.
210. Matsunaga, P.; Hillhouse, G. L. *Angew. Chem. Int. Ed. Engl.* **1994**, 1748.
211. Raybuck, S. A.; Bastian, N. R.; Zydowsky, L. D.; Kobayashi, K.; Floss, H. G.; Ormejohnson, W. H.; Walsh, C. T. *J. Am. Chem. Soc.* **1987**, *109*, 3171–3173.
212. Barondeau, D. P.; Lindahl, P. A. *J. Am. Chem. Soc.* **1997**, *119*, 3959–3970.
213. Tan, X. S.; Sewell, C.; Lindahl, P. A. *J. Am. Chem. Soc.* **2002**, *124*, 6277–6284.
214. Osterloh, F.; Saak, W.; Pohl, S. *J. Am. Chem. Soc.* **1997**, *119*, 5648–5656.
215. Osterloh, F.; Saak, W.; Haase, D.; Pohl, S. *J. Chem. Soc., Chem. Commun.* **1996**, 777–778.
216. Lai, C.-H.; Reibenspies, J. H.; Darensbourg, M. Y. *Angew. Chem. Int. Ed. Engl.* **1996**, *35*, 2390.
217. Colpas, G. J.; Day, R. O.; Maroney, M. J. *Inorg. Chem.* **1992**, *31*, 5053–5055.
218. Laplaza, C. E.; Holm, R. H. *J. Am. Chem. Soc.* **2001**, *123*, 10255–10264.
219. Laplaza, C. E.; Holm, R. H. *J. Biol. Inorg. Chem.* **2002**, *7*, 451–460.
220. Musgrave, K. B.; Laplaza, C. E.; Holm, R. H.; Hedman, B.; Hodgson, K. O. *J. Am. Chem. Soc.* **2002**, *124*, 3083–3092.
221. Sellmann, D.; Häussinger, D.; Knoch, F.; Moll, M. *J. Am. Chem. Soc.* **1996**, *118*, 5368–5374.
222. Sellmann, D.; Schillinger, H.; Knoch, F.; Moll, M. *Inorg. Chim. Acta* **1992**, *198*, 351.
223. Hsiao, Y. M.; Chojnacki, S. S.; Hinton, P.; Reibenspies, J. H.; Darensbourg, M. Y. *Organometallics* **1993**, *12*, 870–875.
224. Arafa, I.; Shin, K.; Goff, H. *J.Am. Chem. Soc.* **1988**, *110*, 5228–5229.
225. Markham, J.; Tolman, W.; Menard, K.; Cutler, A. *J. Organomet. Chem.* **1985**, *294*, 45–58.
226. Arndt, L. W.; Bancroft, B. T.; Darensbourg, M. Y.; Janzen, C. P.; Kim, C. M.; Reibenspies, J.; Varner, K. E.; Youngdahl, K. A. *Organometallics* **1988**, *7*, 1302–1309.
227. Longato, B.; Norton, J. R.; Huffman, J. C.; Marsella, J. A.; Caulton, K. G. *J. Am. Chem. Soc.* **1981**, *103*, 209–210.
228. Ram, M. S.; Riordan, C. G. *J. Am. Chem. Soc.* **1995**, *117*, 2365–2366.
229. Lexa, D.; Saveant, J. M. *J. Am. Chem. Soc.* **1976**, *98*, 2652–2658.
230. De Gioia, L.; Fantucci, P. *Inorg. Chim. Acta* **1998**, *273*, 379–387.
231. Kumar, M.; Day, R. O.; Colpas, G. L.; Maroney, M. J. *J. Am. Chem. Soc.* **1989**, *111*, 5974–5976.

8.26
Metal–Radical Arrays

W. B. TOLMAN
University of Minnesota, Minneapolis, MN, USA

8.26.1   INTRODUCTION

Protein radicals, defined here as free radicals situated on amino acid or modified amino acid groups linked to a protein covalently, are involved in many enzymatic processes. The chemistry of such species has been surveyed in several comprehensive review articles.[1–5] Metal-containing cofactors are situated in close proximity to, and invariably are responsible for the generation of, protein radicals. In many instances, the radicals are transient species that react with substrate essentially independently of the metal site (e.g., cobalamins, see Chapter 8.25). In other cases, the metal site both generates and stabilizes the protein radical, and is intimately involved in the reactions it performs. These reactions often entail mechanistically novel multielectron redox processes that result from the close interplay between metal center and organic radical. The metal–radical interactions also result in interesting electronic structures, as revealed by physical/ spectroscopic studies of the proteins and of related synthetic complexes. A central issue in this regard concerns ligand "innocence," namely, whether the electron "hole" is localized solely on the ligand or the metal, or is delocalized between them. This issue has been explored extensively in many contexts, including complexes of hemes (see Chapters 8.11 and 8.12), dioxolenes (catecholate/semiquinone/quinone),[6,7] and related ligands with imino and/or thiolate donors located at the 1 and/or 2-positions on aromatic rings.[8–15]

The focus of this chapter is on those few examples of protein metal–radical arrays that have been reported in which the radical is stabilized by the metal, the metal and radical components function synergistically, and the array is sufficiently stable to have been subjected to detailed spectroscopic and structural analysis. One case is the conjoined ("proximal") Cu^{II}-tyrosyl radical in galactose and glyoxal oxidase (Figure 1a). Another example is the tyrosyl radical located at a nonbonding distance ("distal") to the diferric cluster in ribonucleotide reductase (Figure 1b). A third case involves a tryptophan radical distal to the oxyferryl site in cytochrome *c* peroxidase (Figure 1c). In the following discussion of these arrays, the current level of understanding of the
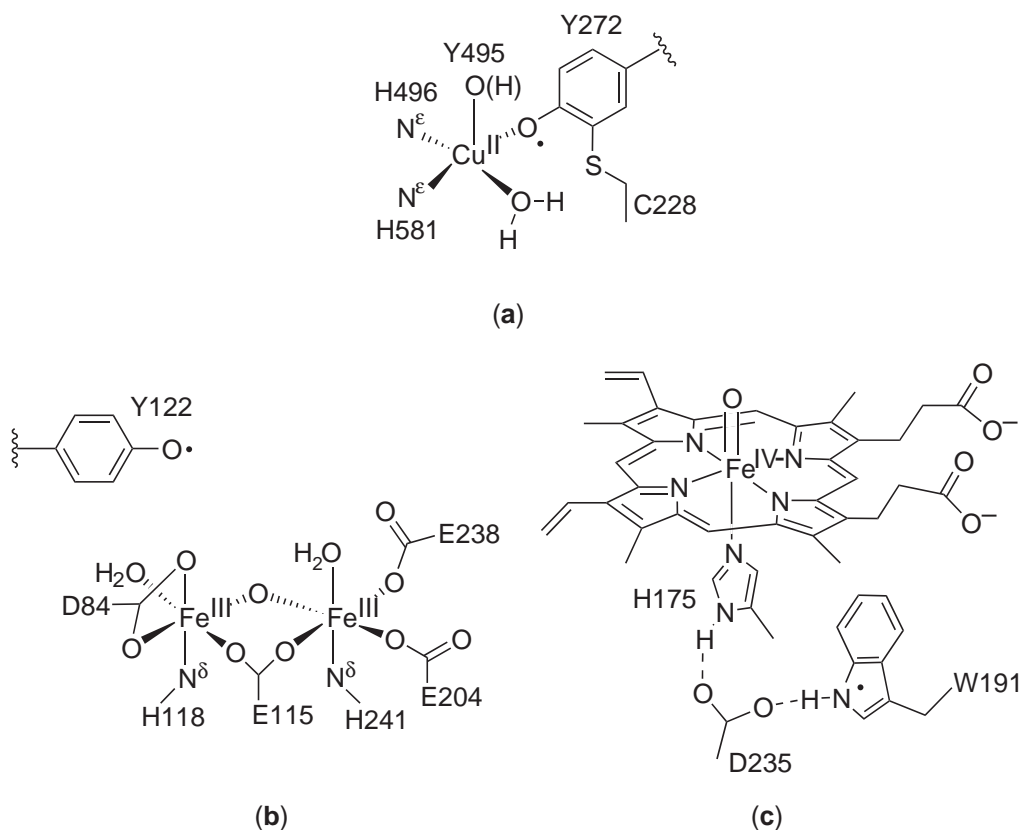
Figure 1 Drawings of the stable well-characterized metal–radical arrays in (a) galactose oxidase, (b) R2 subunit of the class I ribonucleotide reductase, and (c) cytochrome *c* peroxidase.

biological system derived from direct spectroscopic, structural, and functional probes is presented. Selected studies of synthetic complexes relevant to the protein sites will then be described, where applicable. An overriding emphasis will be placed on the structural and functional significance of the metal–radical interaction. Important metal–radical arrays in proteins that do not fall within the narrow scope of this article but are discussed elsewhere in this volume include the ubiquitous oxyferryl/porphyrin cation radical implicated in heme iron biochemistry (see Chapters 8.11 and 8.12), the Mn_4 cluster/tyrosyl radical assembly in the photosystem II oxygen evolving complex (see Chapter 8.20), and the Cu/tyrosyl and semiquinone radical intermediates proposed for amine oxidase cofactor biogenesis and catalysis (see Chapter 8.16).

8.26.2 Cu^{II}-TYROSYL RADICAL IN GALACTOSE AND GLYOXAL OXIDASE

8.26.2.1 Protein Structure and Properties

The fungal enzyme galactose oxidase (GAO) catalyzes the reaction shown in Equation (1) at a monocopper active site:[16–21]

$$RCH_2OH + O_2 \rightarrow RCHO + H_2O_2 \tag{1}$$
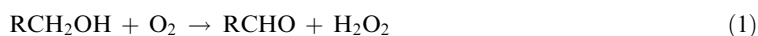
Peroxidases excreted by the fungus use the H_2O_2 produced by GAO to degrade lignin. Glyoxal oxidase is a related enzyme that has been shown to have an active site similar to GAO and to generate H_2O_2, but by oxidizing an aldehyde instead of an alcohol (Equation (2)):[22–24]

$$RCHO + H_2O + O_2 \rightarrow RCO_2H + H_2O_2 \tag{2}$$
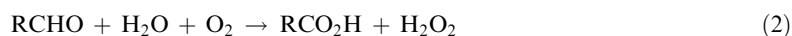
Both reactions are two-electron processes, which initially led to the proposal that the copper site cycled between the Cu^I and Cu^{III} oxidation states.[25,26] Subsequent work showed that instead of using the Cu^{III} state, the active form contains a Cu^{II}-tyrosyl radical, so that individual sites prone to one-electron redox (Cu^I/Cu^{II} and tyrosinate/tyrosyl radical) act together to catalyze the overall two-electron process.

The GAO active site structure was revealed by X-ray crystallography on a sample that presumably[16] is poised at the Cu^{II}-tyrosinate redox level ("inactive," pH 4.5, 1.7 Å resolution, Figure 2).[27–30] The square pyramidal coordination sphere is occupied by two histidine imidazo-lyls, acetate (from the buffer), and a modified tyrosinate (Y272) in the basal positions, with an axial tyrosine residue (Y495) that is probably protonated (Cu—$O = 2.7$ Å). A cysteine (C228) is linked via $S\gamma$ covalently to $C\varepsilon$ of Y272, and a tryptophan residue (W290) is located within π-stacking distance (3.4 Å) of the Y272-C228 unit. Recent evidence shows that the bond linking Y272 and C228 forms through a Cu^{II}- and O_2-dependent self-processing reaction,[31,32] placing GAO within an emergent class of proteins that incorporate post-translationally modified, redox active amino acid cofactors.[33]

Spectroscopic data support location of the radical in GAO on the Y272-C228 unit. The first indication came from UV-vis, EPR, and ENDOR studies of a one-electron oxidized form of Cu-depleted (apo) GAO, which showed the formation of a thioether-modified tyrosyl radical.[34–36] This radical was found to be quite stable, as reflected by the oxidation potential of about $+0.4$ V (vs. normal hydrogen electrode (NHE))[37] which is significantly less than that of other tyrosine/tyrosyl radical couples (cf. $+0.93$ V for free tyrosine[38] or $+1.0$ V for the tyrosyl residue near the diiron site in ribonucleotide reductase,[39] *vide infra*). Possible origins of this unusual stability that have been considered are the thioether substituent,[40] the nearby W290,[29] and/or other unspecified protein environmental effects.[1] Coordination of this radical to Cu^{II} was then proposed for the
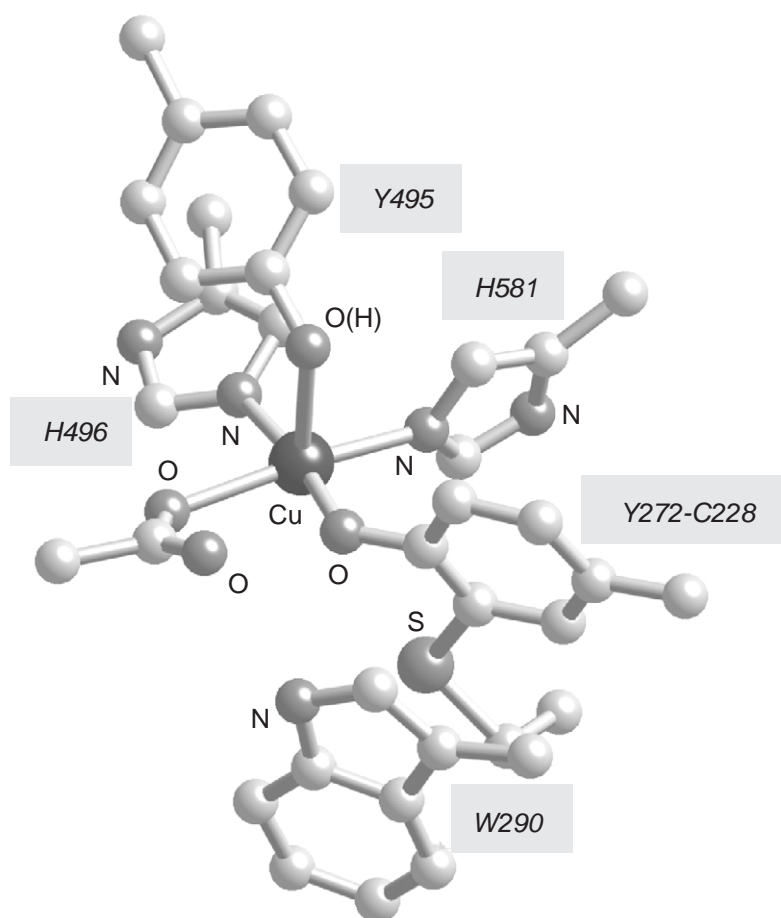
Figure 2 Representation of the X-ray crystal structure of the GAO active site (pdb 1GOF, pH 4.5).
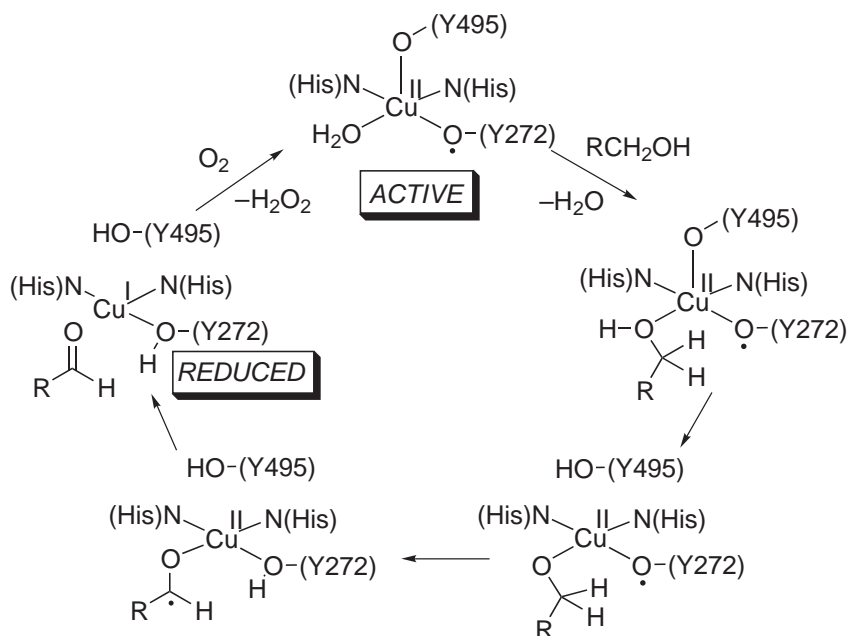
Figure 3 Proposed mechanism for alcohol oxidation by GAO.

"active" form of the enzyme, which may be generated by one-electron oxidation of the inactive state. The latter form exhibits properties expected for a Cu^{II}-tyrosinate, including:

(i)   an axial EPR signal for an $S = 1/2$ system localized on Cu^{II},[19,20,41–43] and
(ii) X-ray absorption spectral (XAS) data consistent with the presence of copper in the +2 state.[43,44]

In contrast, the active form is EPR silent, yet exhibits X-ray absorption near-edge data nearly identical to that of the inactive state and clearly indicative of Cu^{II}. Antiferromagnetic coupling between a coordinated tyrosyl radical and d^9 Cu^{II} rationalizes these results; magnetic susceptibility measurements indicate an energy difference of 200 cm^{-1} between the $S = 0$ ground and the higher spin first excited state.[19,20] UV–vis and resonance Raman spectroscopic data further support the structural assignment for the active form. In particular, vibrational modes due to a coordinated tyrosinate (e.g., 1,246 cm^{-1}, 1,499 cm^{-1}, and 1,603 cm^{-1})[45] and a tyrosyl radical (1,487 cm^{-1} and 1,595 cm^{-1}) were identified in resonance Raman spectra.[46]

The Cu^{II}-tyrosyl radical form of GAO plays a central role in the proposed catalytic "ping-pong" mechanism (Figure 3).[42,47–53] After binding of the substrate alcohol to the Cu^{II} center, proton transfer to the axial Y495 is suggested, resulting in loss of this ligand. This role of Y495 is supported by the results of azide titration and kinetics studies of wild-type GAO and a mutant (Y495F).[42,46,54] Rate-determining hydrogen atom abstraction from the coordinated alcoholate (specifically the pro-S hydrogen for β-D-galactopyranosides)[55] by the Y272 radical then proceeds to yield a bound ketyl radical anion, support for which has been provided by inhibition studies using β-haloethanol substrates.[56] Intramolecular electron transfer follows to generate the aldeyhyde product and the Cu^{I} ("reduced") form of the enzyme. The observation of significant deuterium kinetic isotope effects (KIEs, $k_H/k_D = 10$–22) supports the rate-limiting nature of the hydrogen atom transfer,[49] although variation of the KIE as a function of substrate structure has been suggested to indicate partial rate limitations by the prior proton transfer and/or subsequent single electron transfer steps.[51] The large magnitude and temperature dependence of the KIE suggests a tunneling contribution to the rate of hydrogen atom transfer,[49] a phenomenon documented for a number of other enzymes.[57] Finally, the GAO catalytic cycle is completed by reaction of the "reduced" form with O$_2$ to yield H$_2$O$_2$, presumably through the intermediacy of an as yet unobserved 1:1 Cu/O$_2$ adduct.

8.26.2.2 Synthetic Metal-phenoxyl Radical Complexes

Extensive studies of synthetic complexes comprising a phenoxyl radical coordinated to a metal ion have provided detailed insights into geometric features, spectroscopic signatures, electronic

structures, and reactivity, much of which is relevant to the active site chemistry of galactose and glyoxal oxidase.[58–60] Before discussing copper-containing systems that are most pertinent to the enzymes, we discuss selected systems with other metal ions that have yielded much fundamental and useful knowledge. In general, metal-phenoxyl radical complexes have been prepared through oxidation of metal-phenolates. To engender sufficient stability for characterization of the metal-phenoxyl radical unit, the phenolates are typically incorporated into multidentate chelate ligands, with substituents required at the *ortho-* and *para-* positions.[61] These substituents may be varied, but in general if simple methyl groups are used the phenoxyl radicals are prone to decompose via quinone methide formation; thus, *t*-butyl, methoxy, and/or thioalkyl groups have been employed most often.

8.26.2.2.1 Noncopper systems

The most thoroughly studied class of phenoxyl radical complexes was prepared by oxidation of first-row transition metal complexes of the type of macrocyclic phenolate ligands shown in Figure 4. Studies of those compounds that contain Ga^{III}, Sc^{III}, and Zn^{II} have been particularly useful for differentiating and establishing the properties of coordinated vs. uncoordinated phenoxyl radicals. Due to their closed shell nature, these ions are both spectroscopically "silent" and redox inactive, thus enabling the properties of phenoxyl radicals in their complexes to be seen "unmasked" from those of the metal ion. Data for oxidized forms of the complexes [L^RM] ((**1**)–(**4**) are illustrative).[62] These compounds undergo three reversible one-electron oxidations at approximately equally spaced
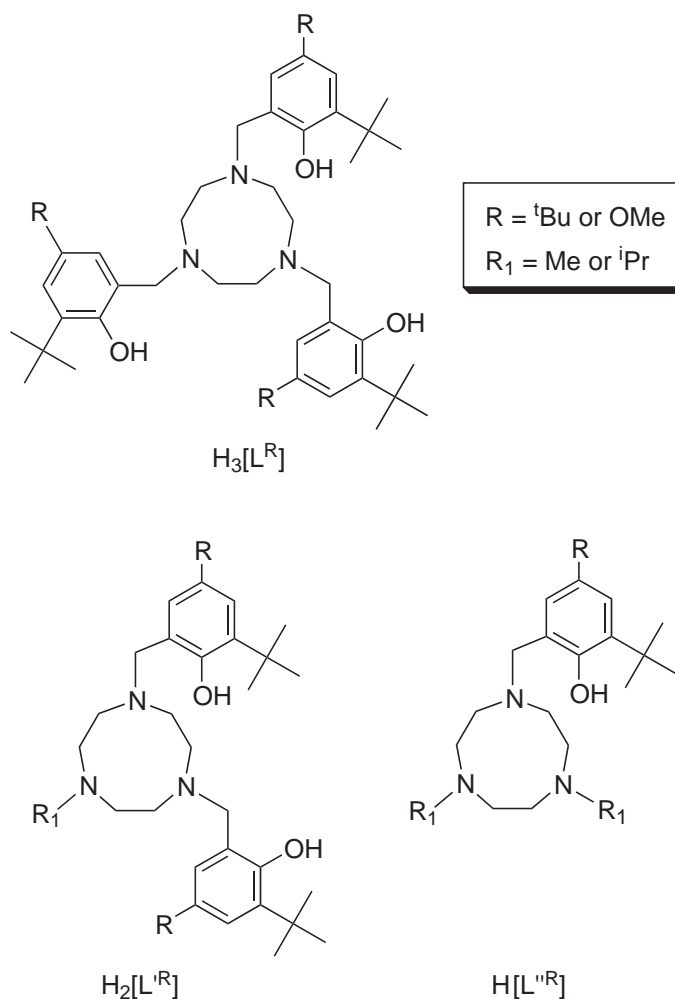
Figure 4 Protonated forms of macrocyclic phenolate ligands used to prepare metal-phenoxyl radical complexes.

potentials (Figure 5 and Table 1) which were ascribed to ligand-based processes (Equation (3), $M = Ga^{III}$ or Sc^{III}):[62]

$$[(L^R)M] \underset{+e^-}{\overset{-e^-}{\rightleftharpoons}} [(L^R\cdot)M]^+ \underset{+e^-}{\overset{-e^-}{\rightleftharpoons}} [(L^R\cdot\cdot)M]^{2+} \underset{+e^-}{\overset{-e^-}{\rightleftharpoons}} [(L^R\cdot\cdot\cdot)M]^{3+} \qquad (3)$$
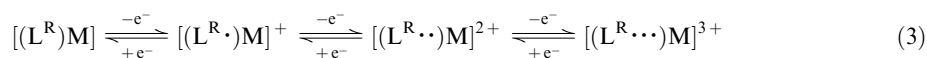
As expected, the potentials decreased (phenolates more readily oxidized) when methoxy substituents were present (R = OMe, Table 1). Successive generation of species with one, two, and three phenoxyl radicals was supported by UV–vis spectroscopy on MeCN solutions generated by controlled potential coulometry at −30 °C. Intense bands between 400–430 nm were observed that are particularly diagnostic of phenoxyl radicals ($\pi \to \pi^*$ transition). Proof for coordination of the phenoxyl radical(s) to the metal ion in these compounds was obtained through EPR spectroscopy. For example, X-band EPR spectra of the $S = 1/2$ 1-electron oxidized species [(L^{Bu}M]$^+$ (1$^+$) and (3$^+$), M = Sc^{III} and Ga^{III}, respectively) and analogs deuterated at the benzylic positions showed hyperfine coupling to the metal ion nuclei ($^{71/69}$Ga, $I = 3/2$, 0.23/0.29 mT; ^{45}Sc, $I = 7/2$, 0.12 mT).[62] These results indicate electron spin delocalization onto the metal ion through direct phenoxyl radical binding. Equivalent hyperfine coupling to the benzylic hydrogens also was observed, indicating delocalization or electron hopping of the monoradical amongst the three phenolate positions on
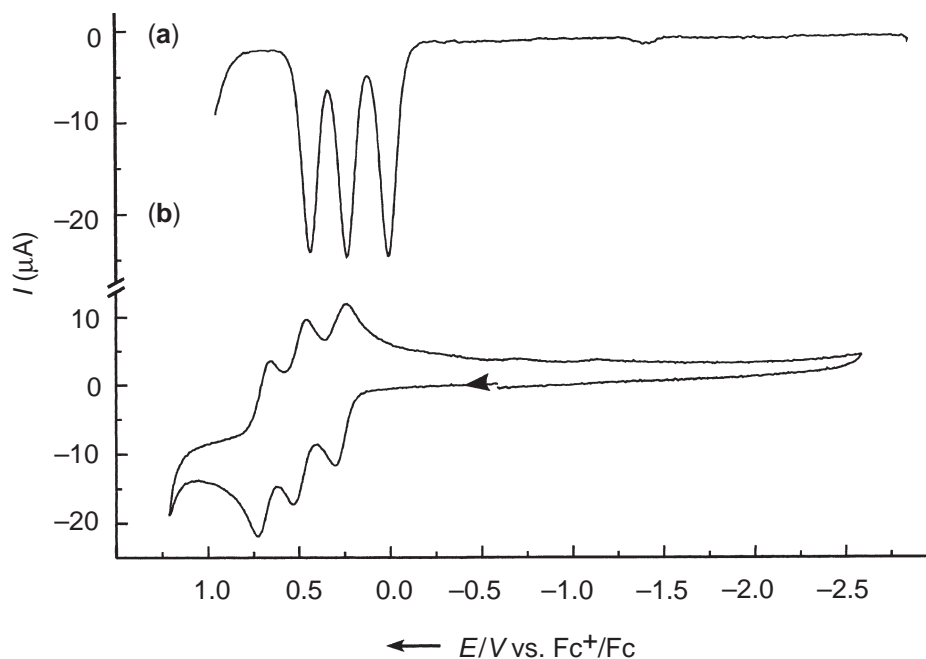
Figure 5 (a) Square-wave voltammogram of [L^{OMe}Ga] ((4), MeCN, 0.1 M Bu$_4$NPF$_6$, frequency 30 Hz, pulse height 2.5×10^{-2} V, glassy carbon electrode). (b) Cyclic voltammogram of [L^{OMe}Sc] (2), MeCN, 0.1 M Bu$_4$NPF$_6$, scan rate 200 mV s^{-1}, 298 K, glassy carbon electrode) (reproduced by permission of Wiley-Interscience from Adam *et al.*[62]).

Table 1 Redox potentials for selected complexes [L$^{RR'}$M].[a]

Entry	Complex	$E^1_{1/2}$	$E^2_{1/2}$	$E^3_{1/2}$	References
1	[L^{Bu2}Ga]	0.87	0.62	0.35	62
2	[L^{BuOMe}Ga]	0.43	0.23	0.01	62
3	[L^{BuOMe}Sc]	0.69	0.47	0.27	62
4	[L^{BuOMe}Fe]	0.63	0.38	0.14	62
5	[L^{BuOMe}Co]	0.43	0.18	−0.10	66
6	[L^{BuOMe}Cr]	−0.03	0.24	0.45	67

[a] For ligand structures and nomenclature, see Figure 4. The potentials are reported vs. the ferrocene/ferrocenium couple and refer to the processes described by Equation (3). Conditions: 0.10 M [N(Bu^n)$_4$(PF$_6$)] in MeCN, 298 K, glassy carbon electrode, Ag/AgCl reference electrode, 200 mV s^{-1}.

the EPR time scale (ca. 10^{-8} sec). Isotropic signals with hyperfine coupling to benzylic hydrogens also were observed in spectra of a number of Zn^{II}-phenoxyl radical complexes, including with ligands other than those shown in Figure 4.[63–65] For example, the EPR spectrum of a Zn^{II} species derived from ligand (**8**), $[Zn^{II}(\mathbf{8}^{\cdot})NO_3]^+$, exhibited such coupling, as well as significant delocalization of spin density onto the thioether substituent.[65] Studies of $[(L^{OMe\cdot\cdot})Zn]^+$ ($R_1 = Et$) comprising two phenoxyl radicals revealed weak antiferromagnetic coupling between them ($J = -3.2\,cm^{-1}$, $H = -2JS_1{\cdot}S_2$).[64]

	R	M^{III}
(**1**)	^tBu	Sc
(**2**)	OMe	Sc
(**3**)	^tBu	Ga
(**4**)	OMe	Ga
(**5**)	OMe	Fe
(**6**)	OMe	Co
(**7**)	OMe	Cr

(**8**)
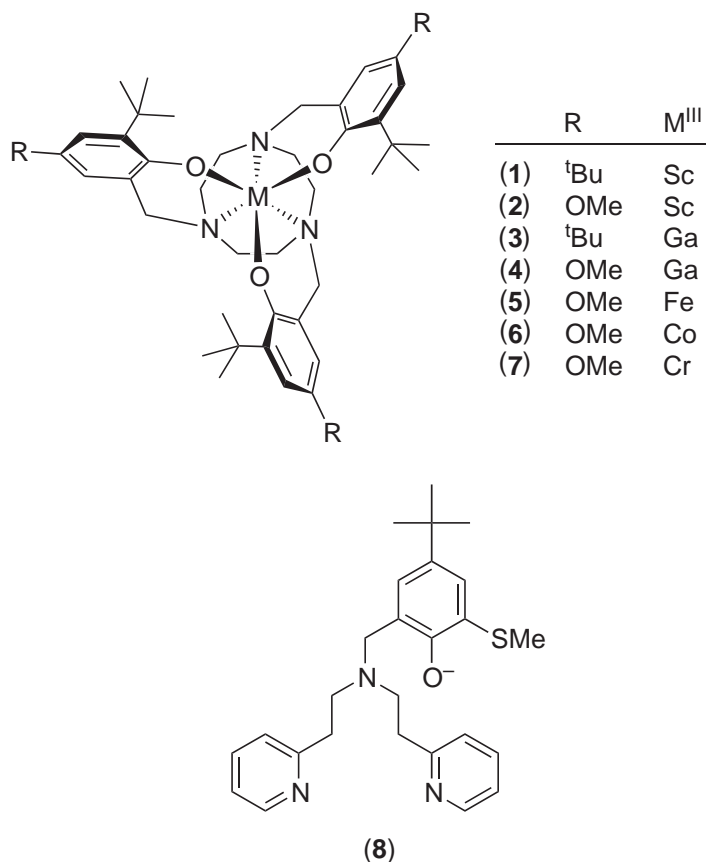
In a comparison of the series of isostructural, neutral complexes (**2**) and (**4**)–(**7**) of the identical ligand L^{OMe} with $M = Co^{III}$,[66] Cr^{III},[67] Fe^{III},[62] Ga^{III},[62] or Sc^{III},[62] the redox potentials for each of the successive ligand-based oxidations were found to vary with the nature of the metal ion (Table 1). A correlation was drawn between these potentials and the strength of the metal-phenolate bonding interaction in the trisphenolate $[(L^{OMe})M]$, as illuminated by two parameters, Δ and α. The term Δ reflects the covalency of the M^{III}-O(phenolate) interaction (i.e., degree of π-bonding), and is obtained by subtracting the sum of the ionic radii of the metal ion and an O^{2-} ion from the actual M^{III}-O(phenolate) bond distance determined by X-ray crystallography. This term increases as the metal ion becomes more electron withdrawing (e.g., has empty or partially filled π-acceptor t_{2g} orbitals) and indicates greater phenolate $\pi \to M^{III}$ donation. The degree of π-bonding is also reflected by α, the angle between two phenolate donors, which is $\sim 90°$ for M—O single bonds and increases with increasing π-donation.[68,69] The correlation of Δ and α with redox potentials is illustrated by their plots versus $E^3_{1/2}$ values ($[(L^{OMe\cdot\cdot\cdot})M]^{3+}/[(L^{OMe\cdot\cdot\cdot})M]^{2+}$ couples) shown in Figure 6. In sum, more electron withdrawing metal ions have stronger M—O bonds, which results in the coordinated phenolate being more difficult to oxidize.

The metrical details of a coordinated phenoxyl radical have been determined through an X-ray crystal structure of $[L^{(OMe\cdot)}Cr](ClO_4){\cdot}3MeCN$;[67] the only other metal-phenoxyl radical complex to be structurally defined by X-ray diffraction is a Cu^{II} species,[70] which is discussed in Section 8.26.2.2.2. The phenoxyl ring is readily identified in the structure by the difference between its bond distances and those of the other two phenolate ligands, as well as those of the phenolate ligands in the precursor $[L^{OMe}Cr]{\cdot}2MeCN$ (Figure 7). The distances in the phenoxyl ring
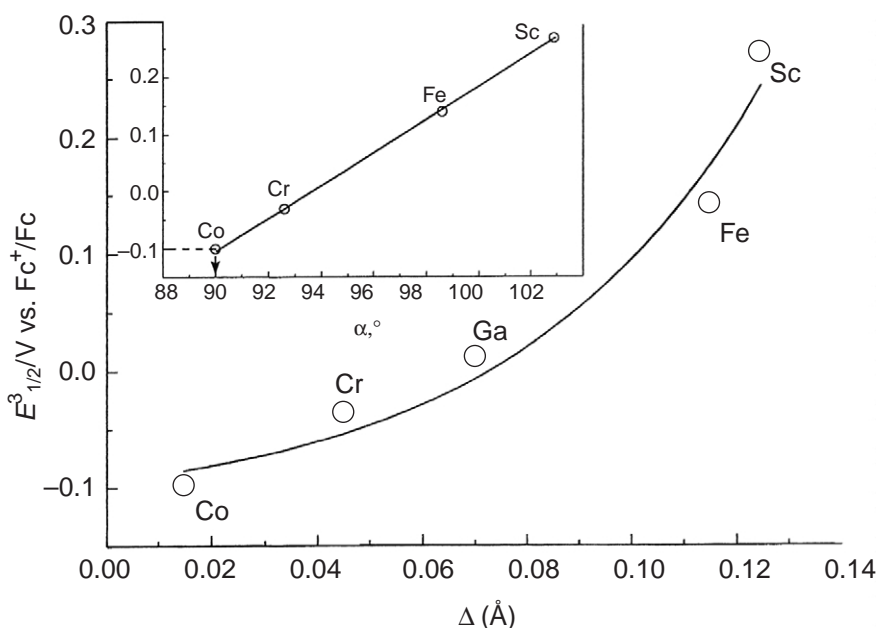
Figure 6 Plot of the redox potential for the $[(L^{OMe})M]^{+/0}$ couple, $E_{1/2}^3$, versus the value of Δ, the difference between the ionic radii of M^{III} and O^{2-} and the experimentally determined M—O bond distance. The dependence of $E_{1/2}^3$ on the O—M—O bond angle, α, in $[L^{OMe}M]$ is shown in the inset (reproduced by permission of Wiley-Interscience from *Prog. Inorg. Chem*, **2001**, *50*, (51–216).

correspond to the indicated quinoid resonance structure, and compare favorably to those calculated for the free phenoxyl[71–74] and *p*-methoxyphenoxyl[71] radicals (Figure 7c).

Resonance Raman spectroscopy has been shown to a particularly effective tool for differentiating between coordinated and uncoordinated phenoxyl radicals.[71] Excitation into the 400–430 nm $\pi \rightarrow \pi^*$ transition of metal-phenoxyl radical complexes leads to resonant enhancement of bands at $\sim$1,500 cm^{-1} and $\sim$1,600 cm^{-1}. By analogy to experimental and calculated vibrational spectra for free phenoxyl radicals (e.g., PhO·),[71,72,75–77] these bands have been assigned as ν_{7a} and ν_{8a} modes, respectively. These modes, which primarily comprise C_{ortho}–C_{meta} (ν_{7a}) and C_1–O_1 (ν_{8a}) stretching vibrations, have been shown to be sensitive indicators of phenoxyl radical complex geometric and electronic structural properties. First, a high value of ν_{8a} correlates with a shorter C_{ortho}–C_{meta} distance, indicating greater semiquinoid character in the ring. A more useful measure is the frequency difference ($\nu_{8a} - \nu_{7a}$), which is large (>90 cm^{-1}) in complexes with coordinated phenoxyl radicals and notably smaller than the value for free phenoxyl radicals. The basis for this effect has been analyzed for a series of complexes with a variety of metal ions,[71] and it was shown
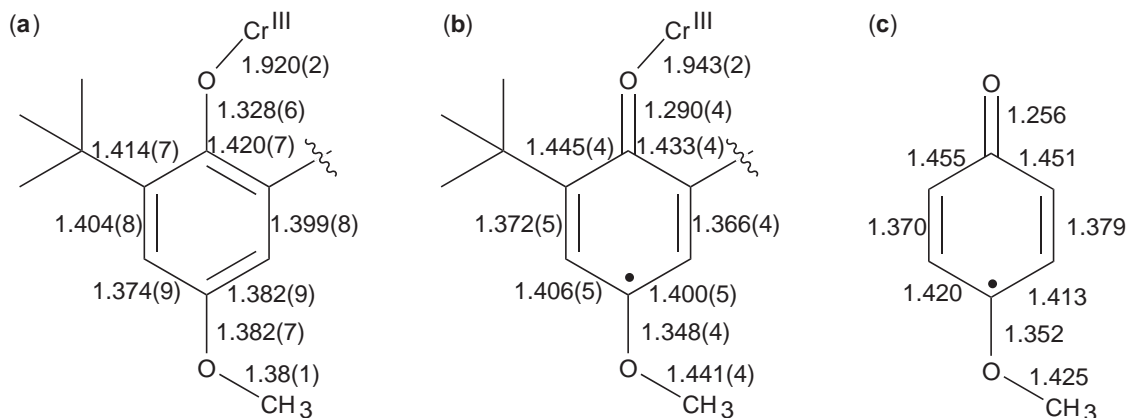
Figure 7 Selected bond distances from X-ray crystal structures for (a) the Cr^{III}-phenolate portion of $[L^{OMe}Cr]\cdot 2MeCN$ **(7)** and (b) the Cr^{III}-phenoxyl radical portion of $[(L^{OMe}\cdot)Cr](ClO_4)\cdot 3MeCN$ $(7^+ClO_4^-)$.[67] The calculated bond distances in the *p*-methoxyphenoxyl radical are shown in (c).[71]
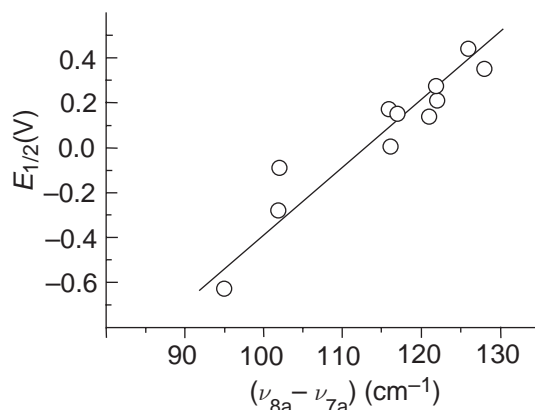
Figure 8 Correlation of the first redox potential $E_{1/2}$ for complexes of $H_x(L^{OMe})^{x-3}$ ($x = 0-2$) and the frequency difference of the observed vibrational modes ($\nu_{8a} - \nu_{7a}$) of the coordinated phenoxyls (reproduced by permission of American Chemical Society from Schnepf *et al.*[71]).

that the difference ($\nu_{8a} - \nu_{7a}$) correlates with the redox potential of the phenolate ligand and the nature of the metal–O(phenoxyl) interaction. In brief, a higher reduction potential for the phenoxyl/phenolate couple (i.e., stronger M—O(phenolate) bond and larger Δ value, *vide supra*) correlates with decreased spin density at O_1 and C_{ortho} and greater semiquinoid character in the phenoxyl radical. This relation might lead one to predict a corresponding increase in both ν_{8a} and ν_{7a}. The latter is delicately balanced by substituent effects, however, resulting in the difference ($\nu_{8a} - \nu_{7a}$) being the most useful marker, such that a larger difference corresponds to a larger $E_{1/2}$ and greater electron withdrawal by the metal ion via M—O bonding (Figure 8).

The existence of magnetic coupling between the ligand radical and unpaired electrons on a metal ion has been revealed in studies of phenoxyl radical complexes of Mn,[62,78] Fe,[62,79,80] and Ni.[78] For example, EPR studies of (**9**) showed a $S_{total} = 3/2$ resulting from antiferromagnetic exchange between a high-spin Mn^{III} ion ($S = 2$) and the phenoxyl ($S = 1/2$).[78] In another illustration, variable temperature magnetic susceptibility, Mössbauer, and EPR data for $[(L^{OMe\cdot})Fe]^+$ (**5**$^+$) indicated a $S_{total} = 2$ via coupling of the radical spin to the high-spin Fe^{III} ($S = 5/2$), and a J value of $-80\,cm^{-1}$ was determined ($H = -2JS_1 \cdot S_2$).[79] Ferromagnetic coupling of the radical in (**10**) to the octahedral Ni^{II} ion ($S = 1$) was shown to give rise to $S_{total} = 3/2$.[78] In general, the magnetic behaviors of these and other species resemble those of related metal-semiquinone complexes,[6,7] and provide further support for coordination of the phenoxyl radical to the metal ion.
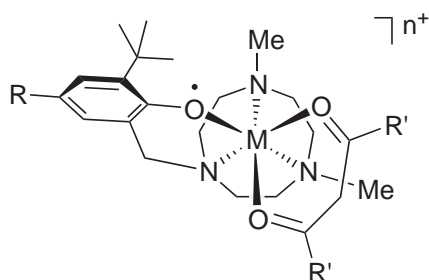
(**9**) ($M = Mn^{III}$, $n = 2$)
(**10**) ($M = Ni^{II}$, $n = 1$)
(**11**) ($M = Cu^{II}$, $n = 1$)
R' = Ph or Bu

8.26.2.2.2 Structures and properties of copper-phenoxyl radicals

Chemical or electrochemical oxidation of a variety of Cu^{II}-phenolate complexes has led to the formation of mononuclear Cu^{II}-phenoxyl radical species (**11**),[81] (**12**)–(**14**),[82,83] (**15**)–(**18**),[84] (**19**),[85,86] (**20**),[87] (**21**),[88] $[(8\cdot)Cu(NO_3)]^+$,[89] $[(22\cdot)Cu]^+$,[90,91] and $[(23)(23\cdot)Cu]^+$.[70] A dicopper complex

with two phenoxyl radicals, (**24**), also has been prepared.[92] While the presence of appropriate substituents on the phenoxyl ring resulted in sufficient stability in solution at low temperature to enable their identification by spectroscopic means, decomposition at ambient temperature was still problematic in most cases. Typical spectral features attributable to a coordinated phenoxyl radical (Table 2) include an intense $\pi \to \pi^*$ absorption band ($\lambda_{max} \sim 400\,\text{nm}$) and diagnostic peaks in Raman spectra (ν_{7a} and ν_{8a} at $\sim 1,500\,\text{cm}^{-1}$ and $\sim 1,600\,\text{cm}^{-1}$, respectively), as well as EPR data indicative of magnetic coupling of the radical with the Cu(II) ion. The observed coupling may be antiferromagnetic, leading to an $S_{tot} = 0$ ground state (cf. (**12**) or [(**23**)(**23·**)Cu]$^+$, for which variable temperature magnetic susceptibility data indicate $J = -6.1\,\text{cm}^{-1}$, $H = -2JS_1S_2$),[70] or ferromagnetic, resulting in $S_{tot} = 1$ (cf. (**11**)).[81] Which of these situations is adopted depends on the relative orientations of the relevant magnetic orbitals ($d_{x^2-y^2}$ on Cu^{II}, π on phenoxyl), as schematically depicted in Figure 9.[81] With this magnetostructural correlation, a 10° change in the angle β from 27.4° in the phenolate precursor of (**12**) to 17.6° in the precursor of (**11**) was used to rationalize the observed switch in the exchange coupling for the two Cu^{II}-radical species, from
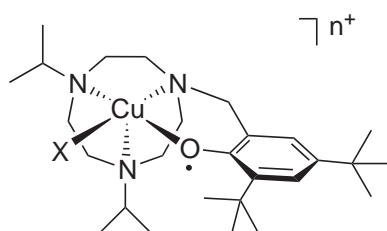
(**12**) (X = Cl$^-$, n = 1)
(**13**) (X = CH$_3$CN, n = 2)
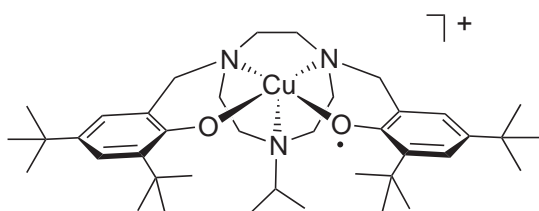
(**14**)
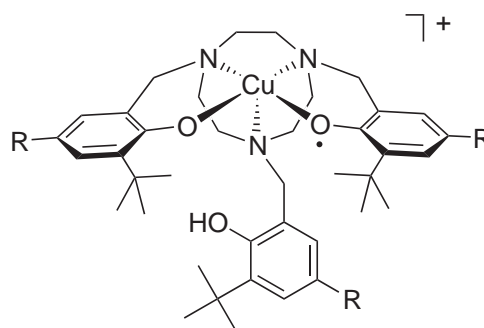
(**15**) (R = ^{t}Bu)
(**16**) (R = OMe)
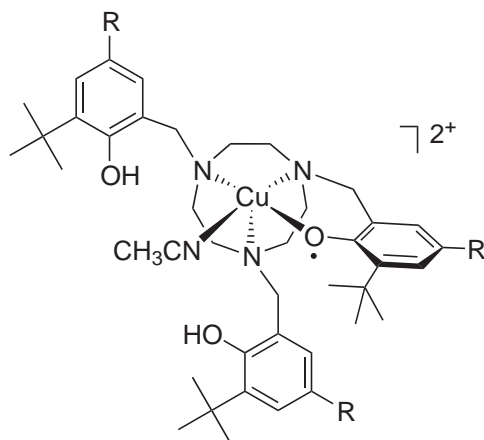
(**17**) (R = ^{t}Bu)
(**18**) (R = OMe)
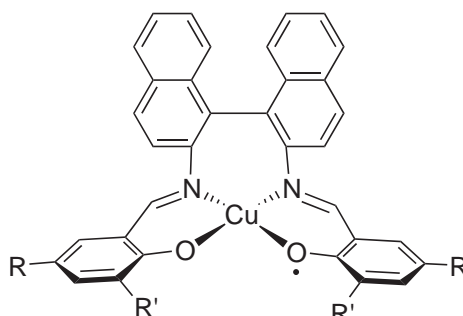
(**19**)
(R' = ^{t}Bu, SPh, S^{i}Pr, or Br;
R = ^{t}Bu or Br)

antiferromagnetic (**12**) to ferromagnetic (**11**). The observed $S=0$ ground state for GAO was rationalized similarly ($\alpha \sim 129°$ and $\beta \sim 75°$).
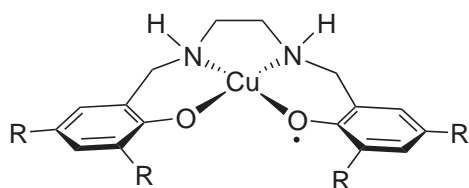
(**20**) (R = ^{t}Bu)
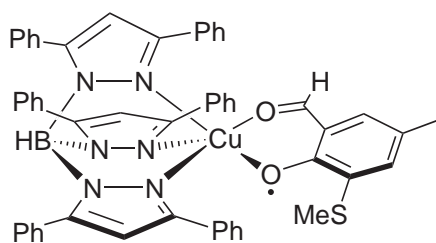
(**21**)
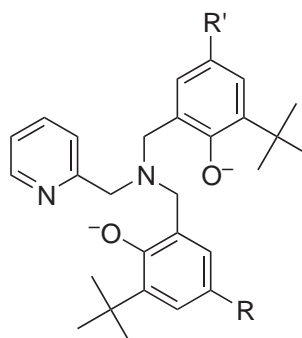
(**22**)

(R = R' = ^{t}Bu or

R = OMe, R' = NO$_2$)
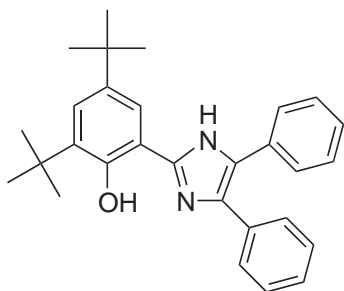
(**23**)
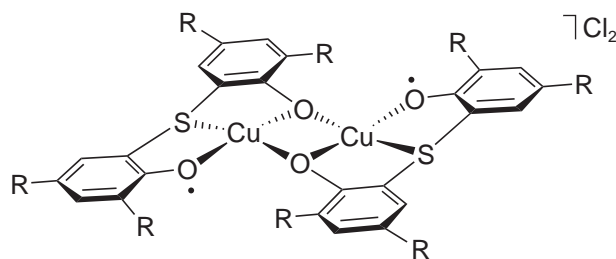
(**24**) (R = ^{t}Bu)

Table 2 Selected spectroscopic data for Cu^{II}-phenoxyl radical complexes.[a]

Complex	Electronic absorption(λ_{max})[b]	Raman peak[c]	References
(**11**)[d]	391 (3,200), 411 (4,000), 477 (990)	1,509, 1,602	81
(**13**)	410 (4,000), 422 (sh, 3,800), 672 (1,000)	1,497, 1,600	82,83
(**14**)	398 (3,900), 568 (2,200), 646 (2,200)	1,495, 1,599	83
(**15**)	402 (2,800), 548 (br, 1,400), 650 (br, 1,300)	1,497, 1,590	84
(**16**)	414 (4,300), 600 (sh)	1,497, 1,614	84
(**18**)	411 (6,100), 432 (7,600)	1,494, 1,620	84
(**20**)	403 (2,500), 440 (2,500), 610 (4,800)	e	87
(**21**)	419 (4,400), 907 (1,200), 1037 (1,100)	e	88
[(**8**˙)Cu(NO$_3$)]$^+$	415 (1,790), 867 (550)	1,512, 1,589	89
[(**22**˙)Cu]$^{+f}$	439 (16,700), 620 (600)	1,488, 1,612	90
[(**23**)(**23**˙)Cu]$^+$	401 (9,200), 514 (4,000), 715 (5,600)	e	70
(**24**)	404 (8,000)	1,451, 1,579, 1,594, 1,606	92

[a] Only selected values are reported; see the indicated reference for full listings. [b] Values reported in nm, with extinction coefficients in parentheses (M^{-1}cm^{-1}). [c] Raman shift reported in cm^{-1}. [d] Data reported for case where R' = Bu. [e] Not reported. [f] Data reported for case where R = R' = Bu^t.

	α	β	S_{tot}
	180°	0°–90°	1
	~130°	90°	0
	~130°	0°	1
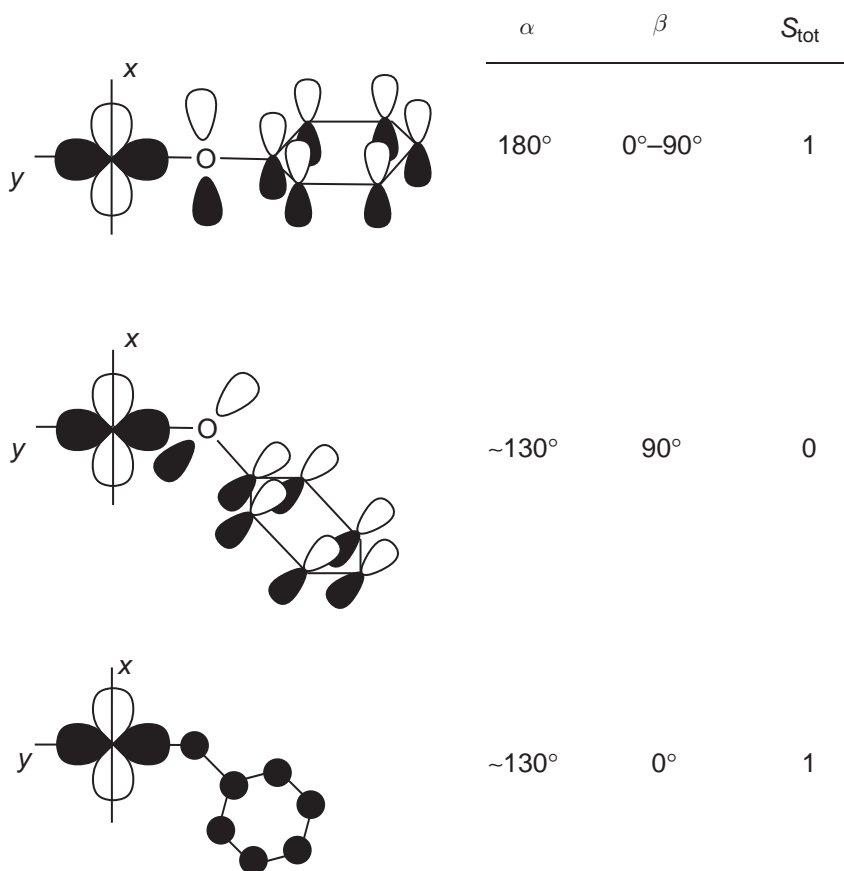
Figure 9 Relative orientations of the magnetic orbitals on Cu$^{\text{II}}$ ($d_{x^2-y^2}$) and a coordinated phenoxyl radical (half-occupied π) that result in the expected overall spin state (S_{tot}). The angles α and β are defined as follows: $\alpha =$ Cu—O—C bond angle, $\beta =$ dihedral angle between the x, y plane and the phenoxyl ring plane (reproduced by permission of Wiley-Interscience from Müller *et al.*[81]).

The only Cu$^{\text{II}}$-phenoxyl radical complex to have been structurally defined by X-ray crystallography is [(**23**)(**23·**)Cu]BF$_4$·2CH$_2$Cl$_2$ (Figure 10).[70] The radical is localized on one ligand, as evident from a comparison of bond distances within the two ring systems in the same molecule. In particular, a significant lengthening of the Cu—O bond (1.850(3) Å in (**23**) to 1.948(3) Å in (**23·**)) and concomitant shortening of the C—O distance (1.322(5) Å in (**23**) to 1.264(5) Å in (**23·**)) corresponds to formation of a Cu$^{\text{II}}$-phenoxyl radical with a semiquinoid structure (**25**), analogous to that determined for the Cr$^{\text{III}}$ species derived from (**7**) (Figure 7). The apparent stability of [(**23**)(**23·**)Cu]$^+$ that enabled the structure determination is exceptional, and may be traced to the lack of benzylic hydrogens on (**23**) that would be prone to abstraction upon radical formation.

(**25**)
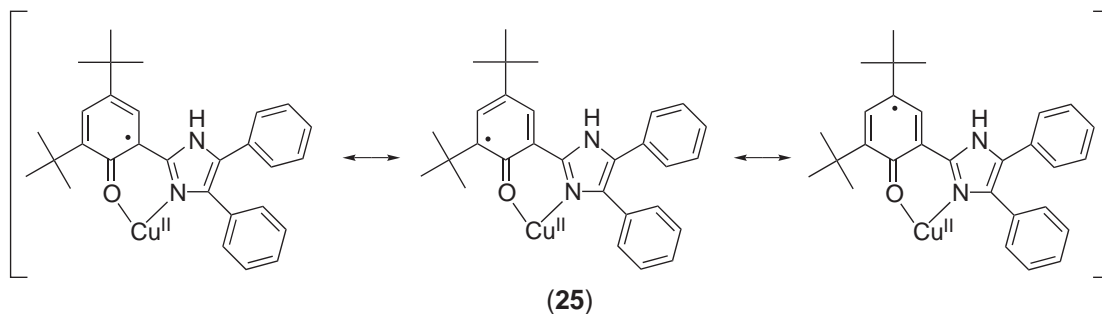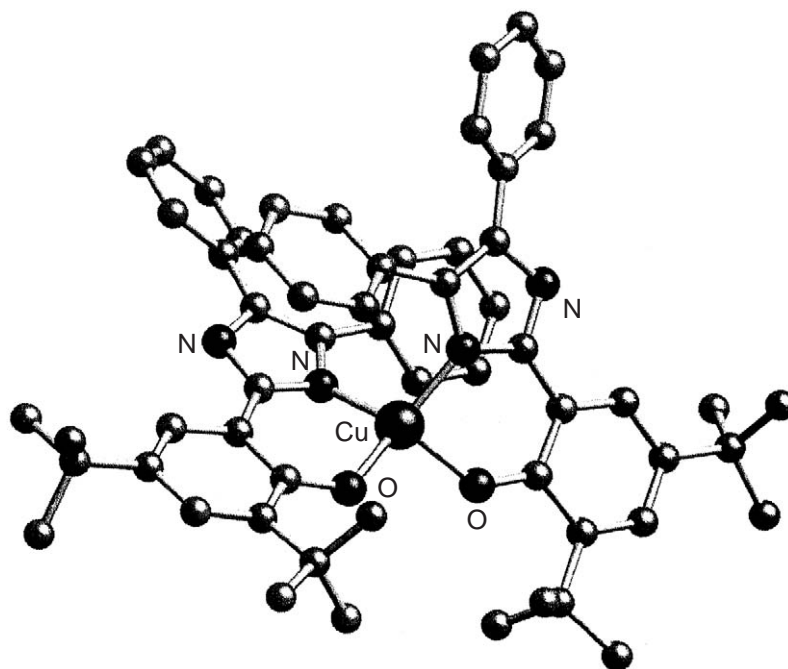
Figure 10 Drawing of the cationic portion of the X-ray crystal structure of [(**23**)(**23·**)Cu]BF$_4$·2CH$_2$Cl$_2$, with hydrogen atoms and solvate molecules omitted for clarity.[70]

8.26.2.2.3 *Reactivity of copper-phenoxyl radicals*

In studies of the reactivity of copper-phenoxyl radical species, particular emphasis has been placed on performing alcohol oxidations, either stoichiometrically or catalytically, and by using O$_2$ as the final oxidant. One goal has been to obtain mechanistic insights into GAO function. In addition, the GAO reaction sequence has been used as inspiration for the development of new chemical catalysts for alcohol oxidations and H$_2$O$_2$ generation (a "bioinorganic success story").[93]

In an initial illustration of the capability of synthetic systems to model GAO function, a complex (**26**) comprising *syn*-phenolate and benzylalkoxide ligands was shown to yield benzaldehyde upon electrochemical oxidation.[82] The X-ray structure of (**26**) (Figure 11) revealed interaction of a benzylic hydrogen with the phenolate oxygen atom, suggesting that the system is poised for hydrogen atom abstraction by the putative phenoxyl radical suggested to arise in the oxidation process. The reaction sequence closely replicates that hypothesized for the enzyme. A similar intermediate species with an alkoxide coordinated to a Cu^{II}-phenoxyl radical was suggested to be involved in the reaction of excess benzyl alcohol with [(**8·**)Cu(NO$_3$)]$^+$, which yielded benzaldehyde and a Cu^I product(s).[89] Rate-controlling hydrogen atom abstraction was invoked on the basis of kinetic studies, which showed overall second-order behavior (first order in substrate and in the complex) and a kinetic isotope effect of 6.8 when the rates of oxidation of PhCD$_2$OH and PhCH$_2$OH were compared. A second order dependence on the complex concentration was observed for the analogous system incorporating redox-inactive Zn^{II}, and a different mechanism involving a dinuclear intermediate with two phenoxyl radicals was invoked in order to rationalize the kinetic results and the requirement for two oxidizing equivalents to produce the benzaldehyde product.

In an early report of a catalytic alcohol oxidation system, (**27**) was treated with KOH under O$_2$ in neat primary alcohol substrate (EtOH, Pr^{n}OH, or hydroxyacetone). As many as 12 turnovers to aldehyde product were observed (10 h).[94] Similar turnovers of LiOCH$_2$Ph to benzaldehyde were obtained with the Cu^{II}-phenoxyl radical species (**19**) (R = SPh).[85] Complex (**20**) also converted primary alcohols to aldehydes with turnover numbers of ~32.[87] Higher turnover numbers (cf. 300 per day) were found using [(**22·**)Cu]$^+$ (R = OMe, R′ = NO$_2$).[91] Of particular relevance to the GAO mechanism, exposure of a mixture of (**22**)H$_2$ and CuCl to O$_2$ resulted in the generation of H$_2$O$_2$.

Even more pertinent to GAO are systems that couple the conversion of O$_2$ to H$_2$O$_2$ with the oxidation of alcohols. This was accomplished with (**19**) (R′ = Bu^t or SPh) or its reduced forms (Cu^I-phenolate or Cu^{II}-phenolate) in the presence of base and O$_2$, which resulted in the catalytic
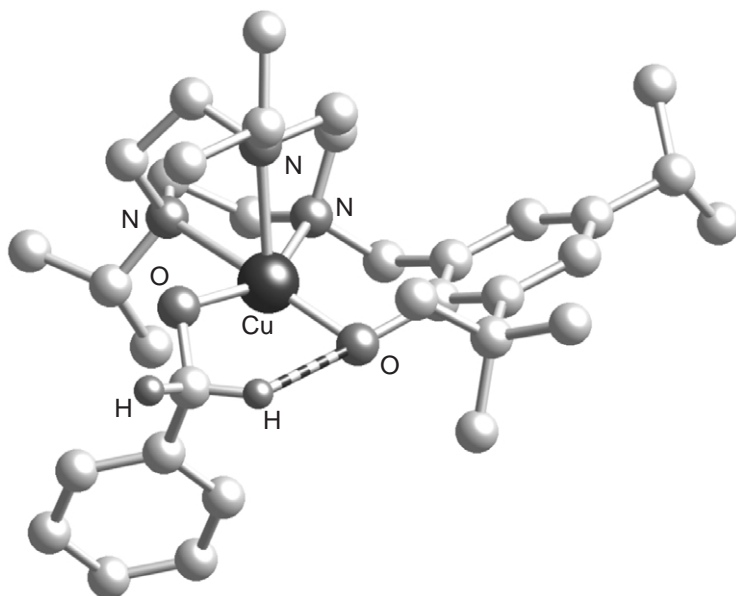
Figure 11 X-ray crystal structure of (**26**), with all hydrogen atoms except for those at the benzylic position of the benzyl alkoxide ligand omitted for clarity.[82]

conversion of allylic or benzylic alcohols to the respective aldehydes and an equivalent amount of H_2O_2.[86] A mechanism for this process was proposed (Figure 12), with supporting evidence including a competitive H/D kinetic isotope effect of 5.3 and a Hammett ρ value of -0.14 for variously substituted benzyl alcohols. These data are consistent with rate-determining hydrogen atom abstraction from a Cu^{II}-phenoxyl/alkoxide intermediate, as suggested for GAO.

(**26**)   (**27**)
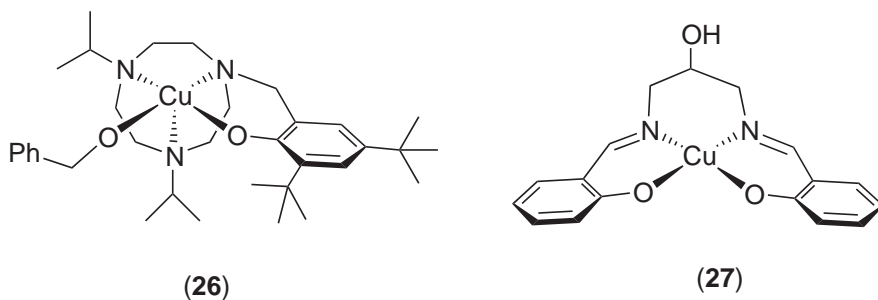
Complex (**24**) is a more powerful catalyst, capable of oxidizing EtOH and secondary alcohols like 2-propanol with O_2 to yield H_2O_2.[92] Primary alcohols yield primarily aldehyde product, but the secondary alcohols generally afford C—C coupling products (1,2-glycols). On the basis of the results of kinetics experiments, hydrogen atom abstraction was shown to be rate-determining. Interestingly, and unlike in GAO, Cu^I/Cu^{II} redox cycling was not invoked in the proposed mechanism (Figure 13); instead, the two phenoxyl radicals provide the necessary oxidizing equivalents. A similar pathway was suggested for 1,2-glycol formation, but involving coordination and hydrogen atom abstraction from two substrate molecules (one at each Cu^{II}) followed by C—C coupling, rather than ketone/aldehyde formation.

Although Cu^{II}-phenoxyl radicals are not involved *per se*, efficient catalysis of alcohol oxidation by O_2 with release of H_2O_2 has been reported using related Cu^{II}- and Zn^{II}-iminosemiquinone systems.[95,96] The proposed catalytic cycles for these systems resemble those noted above, and thus further illustrate useful "bio-inspired" chemical processes. For example, rapid alcohol oxidation is promoted by (**28**), and the mechanism shown in Figure 14 was proposed.[95] Interestingly, the O_2 adduct (**29**) (Figure 14) was isolated, either by treating (**28**) with H_2O_2 or by reacting the ligand with a Cu^I source followed by exposure to O_2. End-on coordination of superoxide in (**29**) was proposed on the basis of FTIR data on complex derived from the mixed isotopomer $^{18}O^{16}O$. The observation of (**29**) and its conversion to (**28**) and H_2O_2 elegantly model the O_2-activation phase of the GAO catalytic cycle in a system that is catalytically active for alcohol oxidation. Methanol oxidation is effected by
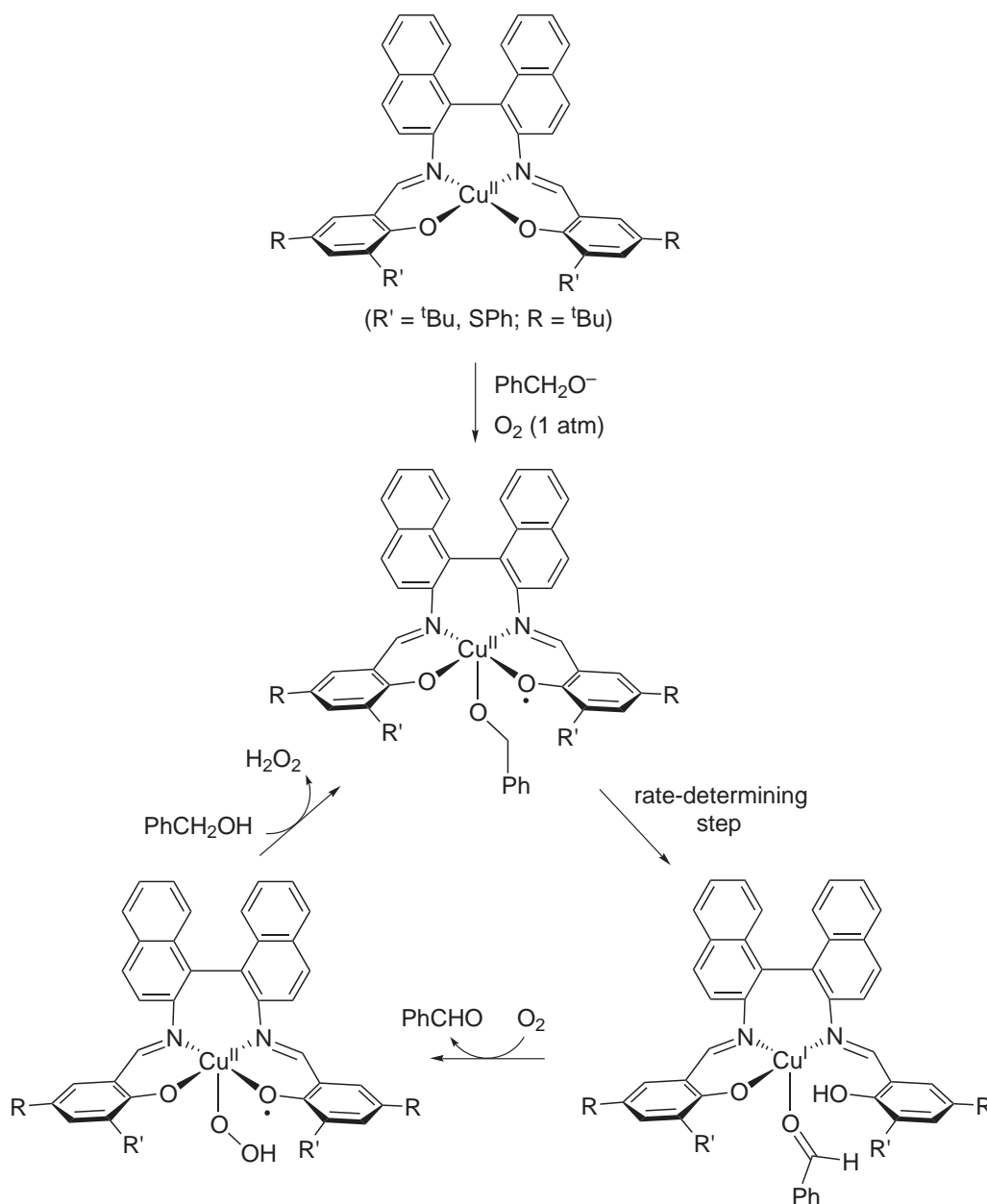
Figure 12 Proposed mechanism for catalytic alcohol oxidation with concomitant evolution of H_2O_2 using the system based on (**19**).[86]

(**28**), and a large kinetic isotope effect of 54 for the oxidation of CD_3OH was measured, indicative of a tunneling contribution to the hydrogen atom transfer step akin to that identified in GAO.[96]

8.26.3 DIFERRIC CLUSTER-TYROSYL RADICAL IN RIBONUCLEOTIDE REDUCTASE

The ribonucleotide reductases (RNRs) catalyze the deoxygenation of nucleotides in the rate-determining step of the biosynthesis of DNA. These enzymes have been categorized into three classes, each of which incorporates a metal site that initiates nucleotide reduction via processes that involve free radicals, in particular cysteinyl radicals.[97] Extensive studies of these processes have provided detailed insights into their mechanisms, as described in comprehensive reviews.[1,98–100] Here we focus on the most thoroughly characterized class I enzymes,[1,98,101] which in their resting state contain a stable tyrosyl radical in close proximity, but not directly coordinated, to a diiron cluster.
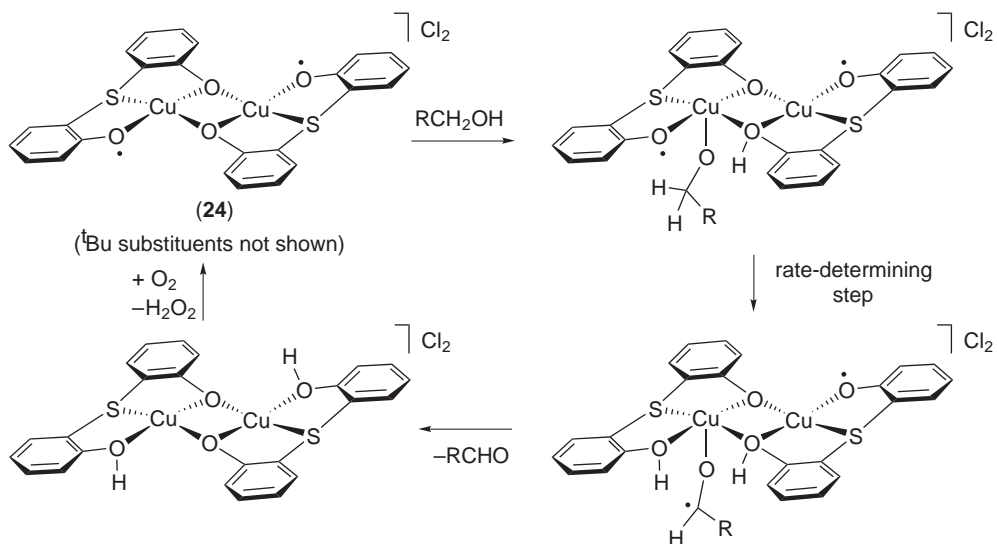
Figure 13 Proposed mechanism for the catalytic oxidation of primary alcohols using (**24**).[92]
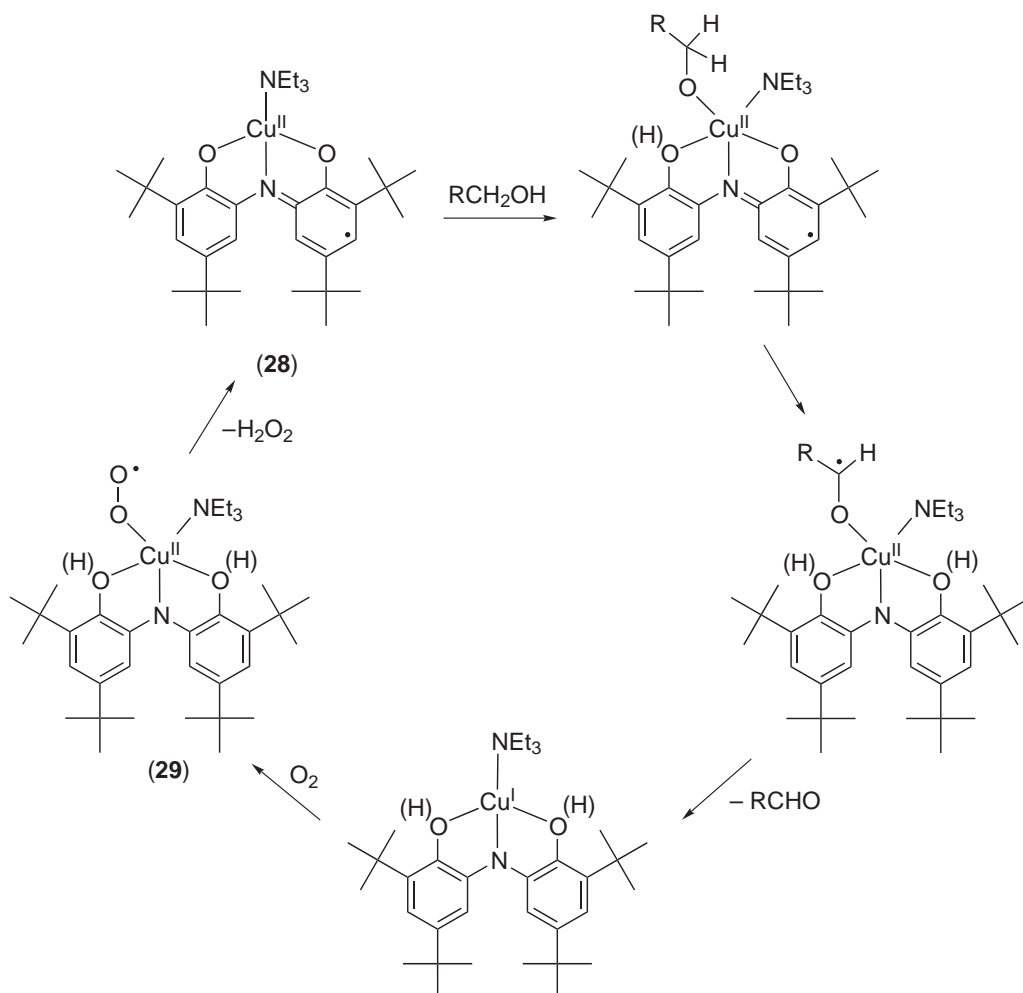
Figure 14 Proposed mechanism for the catalytic oxidation of alcohols using (**28**).[95]

8.26.3.1 Protein Structure and Properties

The class I RNRs exist as homodimers, with the R1 protein being responsible for nucleotide reduction and the R2 protein housing the diiron-tyrosyl array. The tyrosyl radical in R2 (Y122 in the *E. coli* enzyme) has been characterized through EPR and ENDOR spectroscopy studies, which have led to a detailed description of its spin density distribution.[102–104] This distribution is similar to those determined for other tyrosyl radicals in proteins (e.g., $Y_D\cdot$ and $Y_Z\cdot$ in photosystem II (see Chapter 8.20) despite differences in their environments and functions. Insight into the structure of the nearby diiron cluster was obtained primarily through studies of the met form, in which the tyrosyl radical is reduced but the metal atoms are at the Fe^{III} oxidation level. Combined Mössbauer,[105,106] resonance Raman,[107] and magnetic susceptibility data[108] indicate an antiferromagnetically coupled (μ-oxo)(μ-carboxylato)-diiron (III) unit ($J = -108$ cm^{-1}), which was further defined by X-ray crystallography for enzymes from several organisms (Figure 15).[109–112] The structure of the diiron portion is similar to that identified for other nonheme diiron enzymes, as discussed in Chapter 8.13. Importantly, the oxygen atom of tyrosine Y122 is located 5.3 Å from one iron atom in the *E. coli* enzyme;[109,110] a longer distance of ~7 Å with an intervening water molecule was identified in the enzymes from other organisms.[111,112] These distances are presumed to be similar in the diiron-tyrosyl radical form, a notion corroborated by EPR relaxation and line broadening data that indicate magnetic exchange interactions between the diiron center and the radical.[104,113] This diiron-tyrosyl radical form is generated by the reaction of the diiron(II) site with O_2,[114] an intriguing process that involves unusual oxidized intermediates (including a $Fe^{III}Fe^{IV}$ species) that have been the subject of intense study (see Chapter 8.13). The tyrosyl radical that is produced in this process then functions to generate a cysteinyl radical 35 Å distant in the R1 protein, where nucleotide reduction then ensues. The precise pathway by which this catalytically important R1 radical is created continues to be investigated.[1,115,116]

8.26.3.2 Model Complexes

A number of ligands comprising protected phenols, exemplified by (**30**)[117] and (**31**),[118] have been complexed to metal ions and oxidized in attempts to generate compounds with uncoordinated phenoxyl radicals. In most cases, UV-vis, IR, and/or EPR spectroscopic evidence was provided in support of phenoxyl radical formation, but in few cases were the compounds isolated as pure solids, and no X-ray structural data is available. A survey of these systems has been published.[119]

In efforts more directly aimed at modeling the diiron-tyrosyl radical array in RNR, the stable radical ligand (**32**) was prepared and its coordination chemistry probed.[120,121] Reaction of (**32**) with $[Fe_2O(XDK)(MeOH)_5(H_2O)](NO_3)_2$ yielded a crystalline product formulated as (**33**) on the basis of elemental analysis, UV-vis, resonance Raman, magnetic susceptibility, and EPR data. Notably, the presence of the (μ-oxo)(μ-carboxylato)diiron(III) unit and the phenoxyl radicals in (**33**) were indicated by features at 524 cm^{-1} and 1504 cm^{-1} in the Raman spectrum that are due to the Fe—O—Fe and ν_{7a} modes, respectively. SQUID and EPR saturation-recovery data ($g = 2.00$ signal) showed that the high spin Fe^{III} ions are antiferromagnetically coupled ($J = -115$ cm^{-1}),
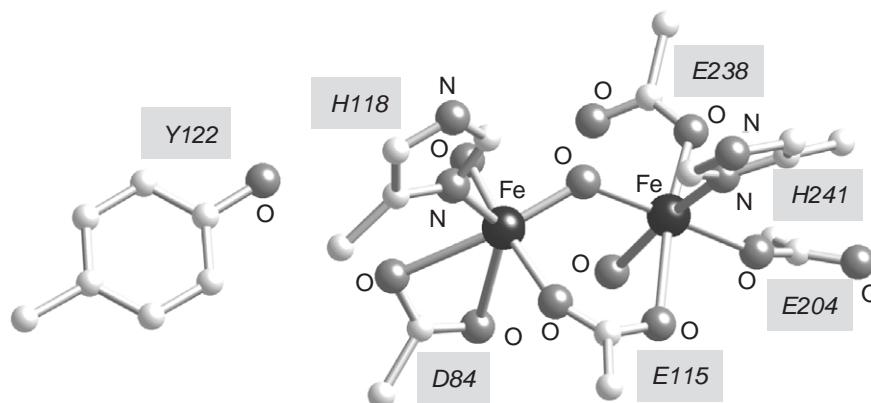
Figure 15 View of the diiron-tyrosine unit in the met form of the class I RNR from *E. coli* (pdb 1RIB).[110]
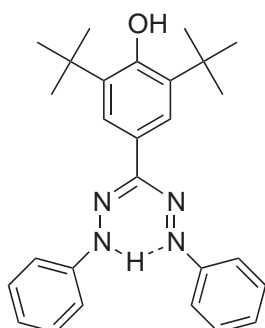
(30)
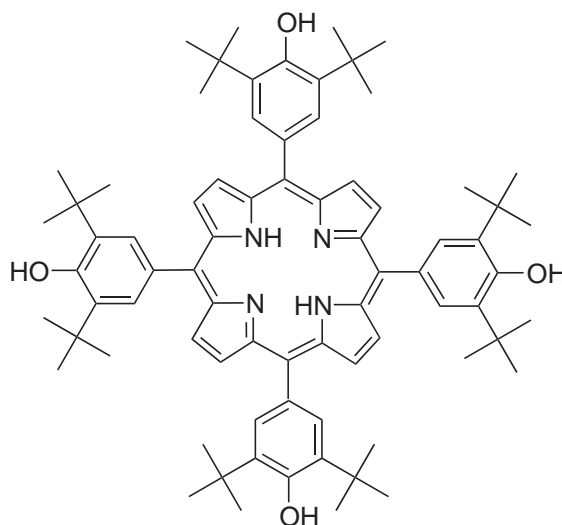
(31)

and that at temperatures less than 40 K the phenoxyl radicals exhibit Curie behavior. A comparison of the spin-lattice relaxation behavior of the radical EPR signal in the temperature range 6.7–115 K with that of a Zn^{II} reference complex indicated little magnetic interaction between the radical and the diferric center, but enhanced relaxation of the diiron complex was observed at higher temperatures that was attributed to population of the $S = 1$ excited state of the FeOFe unit. Despite many important similarities between (33) and the diiron-tyrosyl radical array in RNR, "there is no significant exchange interaction due to spatial overlap between the phenoxyl radical and the diferric center" in (33),[120] consistent with a greater distance between these units (estimated to be ~13.5 Å) than in the enzyme.
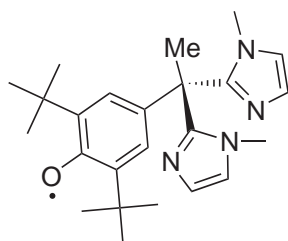
(32)
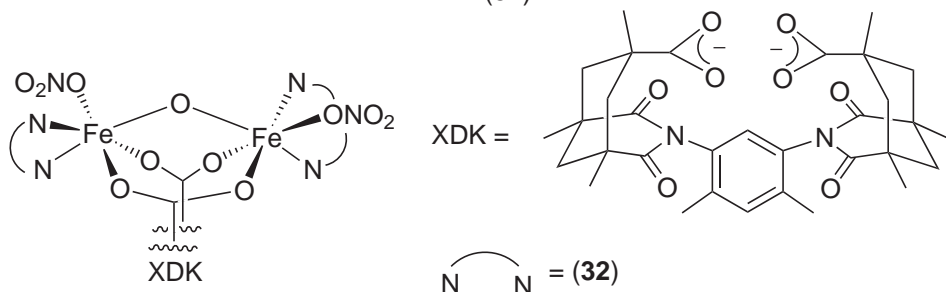
(33)

8.26.4 FERRYL-TRYPTOPHAN RADICAL IN CYTOCHROME *C* PEROXIDASE

One of the earliest metal–radical arrays to have been identified in biology[122] is the so-called "compound ES" state of cytochrome *c* peroxidase (C*c*P), a heme enzyme of the type described
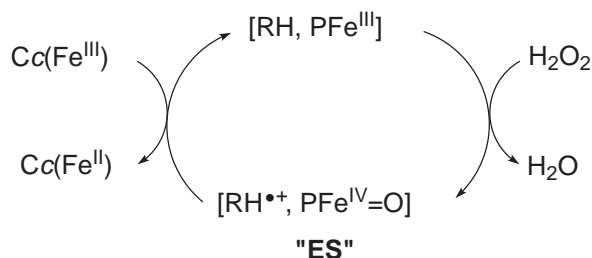
Figure 16 Scheme showing the generation and catalytic function of intermediate ES in cytochrome c peroxidase (P = porphyrin, RH = indole portion of W191, Cc = cytochrome c).

more fully in Chapter 8.11. Compound ES is a catalytically relevant two-electron oxidized form of CcP that is generated by the reaction of H_2O_2 with the resting ferric-heme state (Figure 16). The CcP catalytic cycle is completed by two successive interprotein single electron transfers between ES and the biological partner, the Fe^{II} form of cytochrome c. Formally, ES is equivalent to compound I of horseradish peroxidase (HRP), in which the two oxidizing equivalents are stored in a system comprising a $S = 1$ oxyferryl coupled to a porphyrin cation radical, $[P^{+\cdot}, Fe^{IV}=O]$.[123] While ES also contains an oxyferryl unit, the second oxidizing equivalent is not stored on the porphyrin, but instead resides as a cation radical on an amino acid residue. The involvement of this residue in the electron transfer function of CcP is discussed elsewhere;[1,124] here, we focus on the identification of the residue and its stabilization.

X-ray crystallographic studies of both the resting Fe^{III} [125,126] and ES[127,128] forms showed several residues near the heme-iron site that would be reasonable sites for the radical: M171, W51, and W191 (Figure 17). Through analysis of EPR spectra of mutants in which these residues were replaced, M171 and W51 were ruled out as radical sites, leaving W191 as the sole candidate.[129–133] However, the EPR signal of ES is unusually broad for an aromatic π-radical and extends to g values below 2.0. This anomalous signal was further investigated using multifrequency EPR and ENDOR spectroscopy.[134,135] Analysis of the data led to a specific model in which a protonated $S = 1/2$ W191 cation radical (hydrogen bonded to D235, Figure 17) is weakly exchange coupled to the $S = 1$ oxyferryl, with the broad EPR signal resulting from a distribution of protein conformations that yields a range of J values ($-0.049\,\text{cm}^{-1}$ to $+0.098\,\text{cm}^{-1}$).

The W191$^{+\cdot}$ in ES is quite stable ($t_{1/2} \sim 6\,\text{h}$),[136] as reflected by a reduction potential of $+650\,\text{mV}$,[137] approximately 350 mV less positive (radical cation more stable) than free tryptophan or tryptophan cation radicals ($E^0 = 1.01–1.15\,\text{V}$).[138] The negative electrostatic potential provided by the nearby, hydrogen-bonded aspartate residue (D235) is deemed responsible for stabilizing W191$^{+\cdot}$.[137] Moreover, similar hydrogen bonding interactions between D235 and the proximal H175 are thought to stabilize the oxyferryl unit (Figure 17). Thus, the oxyferryl, W191$^{+\cdot}$, and intervening H175-D235 residues represent a novel metal–radical assembly that is stabilized by synergistic interactions and that plays a central functional role in directional electron transfer using H_2O_2 as terminal oxidant.[139]

8.26.5 CONCLUSION

The three metal–radical arrays described in this article are particularly well-characterized members of a broader class of biological and synthetic systems that incorporate redox active metals and organic radicals.[1–7] Such systems are uniquely disposed to perform multielectron redox chemistry through the synergistic involvement of the multiple sites. Our understanding of this chemistry will continue to be augmented by interdisciplinary studies of both the biomolecules and synthetic molecules, as illustrated by the research on the GAO, RNR, and CCP sites. Thus, examinations of synthetic models have provided detailed insights into metal–radical array structures, spectroscopic features, and reactivity, while design of new small molecule catalysts has been inspired by the knowledge of the biochemical systems, particularly in the case of GAO, and potentially for other systems as well. More metal–radical arrays with potentially unique properties are sure to be discovered or constructed through such interdisciplinary and cooperative approaches.
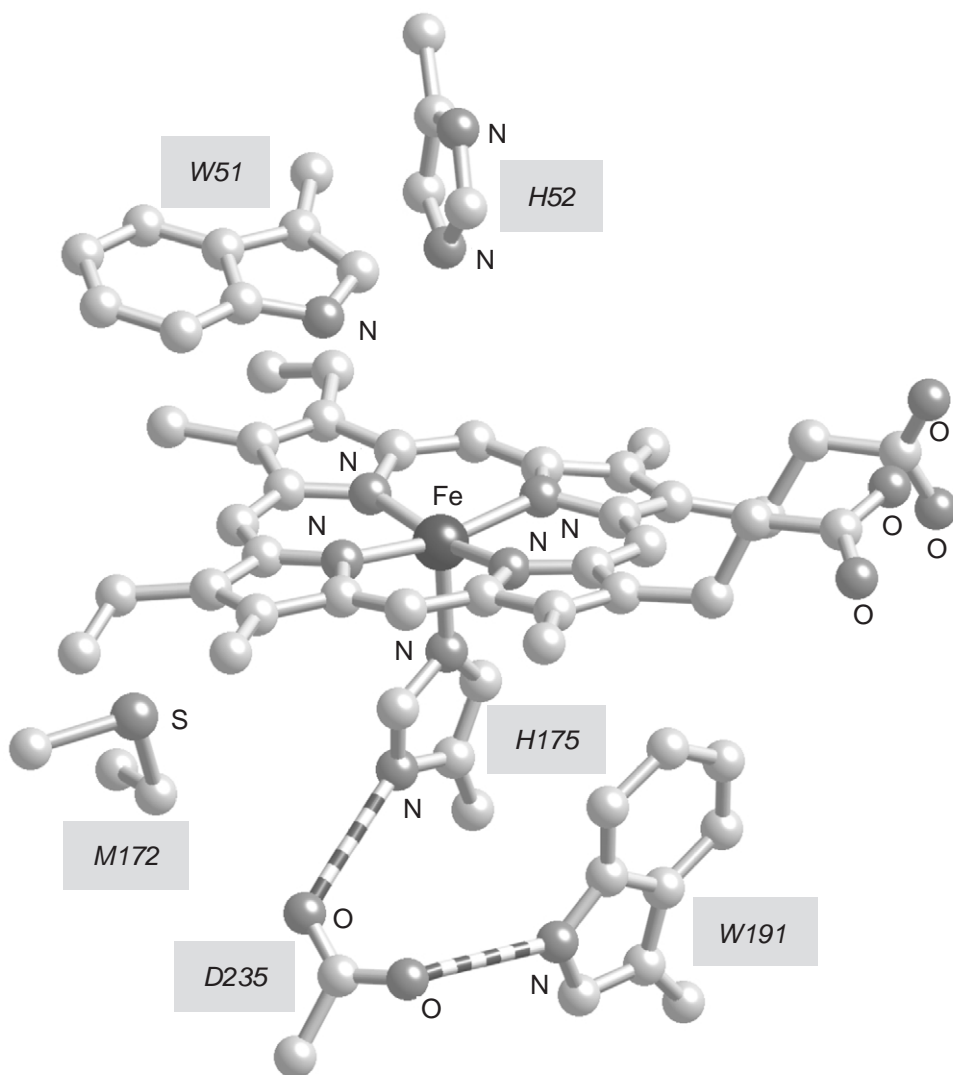
Figure 17   The active site of cytochrome *c* peroxidase (resting ferric form, pdb 1CCP).[126]

ACKNOWLEDGEMENTS

8.26.6   REFERENCES

1. Stubbe, J.; van der Donk, W. A. *Chem. Rev.* **1998**, *98*, 705–762.
2. Stubbe, J. A. *Annu. Rev. Biochem.* **1989**, *58*, 257–285.
3. Frey, P. A. *Chem. Rev.* **1990**, *90*, 1343–1357.
4. Sigel, H.; Sigel, A., Eds., *Metalloenzymes Involving Amino Acid Residue and Related Radicals*; Marcel Dekker: New York, 1994, Vol. 30.
5. Fontecave, M.; Pierre, J. L. *Bull. Soc. Chim. Fr.* **1996**, *133*, 653–660.
6. Pierpont, C. G.; Lange, C. W. *Prog. Inorg. Chem.* **1994**, *41*, 331–442.
7. Pierpont, C. G. *Coord. Chem. Rev.* **2001**, *216–217*, 99–125.
8. Chaudhuri, P.; Verani, C. N.; Bill, E.; Bothe, E.; Weyhermüller, T.; Wieghardt, K. *J. Am. Chem. Soc.* **2001**, *123*, 2213–2223.
9. Chun, H. P.; Chaudhuri, P.; Weyhermüller, T.; Wieghardt, K. *Inorg. Chem.* **2002**, *41*, 790–795.
10. Herebian, D.; Bothe, E.; Bill, E.; Weyhermüller, T.; Wieghardt, K. *J. Am. Chem. Soc.* **2001**, *123*, 10012–10023.

11. Chun, H.; Verani, C. N.; Chaudhuri, P.; Bothe, E.; Bill, E.; Weyhermüller, T.; Wieghardt, K. *Inorg. Chem.* **2001**, *40*, 4157–4166.
12. Chun, H.; Weyhermüller, T.; Bill, E.; Wieghardt, K. *Angew. Chem., Int. Ed. Engl.* **2001**, *40*, 2489–2492.
13. Herebian, D.; Ghosh, P.; Chun, H.; Bothe, E.; Weyhermüller, T.; Wieghardt, K. *Eur. J. Inorg. Chem.* **2002**, 1957–1967.
14. Sun, X.; Chun, H.; Hildenbrand, K.; Bothe, E.; Weyhermüller, T.; Neese, F.; Wieghardt, K. *Inorg. Chem.* **2002**, *41*, 4295–4303.
15. Bachler, V.; Olbrich, G.; Neese, F.; Wieghardt, K. *Inorg. Chem.* **2002**, *41*, 4179–4193.
16. Whittaker, J. W. The Free Radical-Coupled Copper Active Site of Galactose Oxidase. In *Metalloenzymes Involving Amino Acid Residue and Related Radicals*; Sigel, H.; Sigel, A., Eds., Marcel Dekker: New York, 1994, Vol. 30, pp 315–360.
17. Knowles, P. F.; Ito, N. Galactose Oxidase. In *Perspectives in Bioinorganic Chemistry*; Jai Press: London, 1994; Vol. 2, pp 207–244.
18. Borman, C. D.; Saysell, C. G.; Sokolowski, A.; Twitchett, M. B.; Wright, C.; Sykes, A. G. *Coord. Chem. Rev.* **1999**, *190–192*, 771–779.
19. Whittaker, J. W. Spectroscopic Studies of Galactose Oxidase. In *Methods in Enzymology, Redox-Active Amino Acids in Biology*, Klinman, J. P., Ed., Academic Press: San Diego, CA, 1995; Vol. 258, pp 262–277.
20. Whittaker, J. W.; Whittaker, M. M. *Pure Appl. Chem.* **1998**, *70*, 903–910.
21. Halcrow, M.; Phillips, S.; Knowles, P. Amine oxidases and galactose oxidase. In *Subcellular Biochemistry, Vol. 35: Enzyme-Catalyzed Electron and Radical Transfer*; Holzenburg, A.; Scrutton, N. S., Eds., Plenum: New York, 2000; pp 183–231.
22. Whittaker, M. M.; Kersten, P. J.; Nakamura, N.; Sanders-Loehr, J.; Schweizer, E. S.; Whittaker, J. W. *J. Biol. Chem.* **1996**, *271*, 681–687.
23. Whittaker, M. M.; Kersten, P. J.; Cullen, D.; Whittaker, J. W. *J. Biol. Chem.* **1999**, *274*, 36226–36232.
24. Kersten, P. J. *Proc. Natl. Acad. Sci. USA* **1990**, *87*, 2936–2940.
25. Dyrkacz, G. R.; Libby, R. D.; Hamilton, G. A. *J. Am. Chem. Soc.* **1976**, *98*, 626–628.
26. Hamilton, G. A.; Adolf, P. K.; de Jersey, J.; DuBois, G. C.; Dyrkacz, G. R.; Libby, R. D. *J. Am. Chem. Soc.* **1978**, *100*, 1899–1912.
27. Ito, N.; Phillips, S. E. V.; Stevens, C.; Ogel, Z. B.; McPherson, M. J.; Keen, J. N.; Yadav, K. D. S.; Knowles, P. F. *Nature* **1991**, *350*, 87–90.
28. Ito, N.; Phillips, S. E. V.; Stevens, C.; Ogel, Z. B.; McPherson, M. J.; Keen, J. N.; Yadav, K. D. S.; Knowles, P. R. *Faraday Discuss. Chem. Soc.* **1992**, *93*, 75–84.
29. Ito, N.; Phillips, S. E. V.; Yadav, K. D. S.; Knowles, P. F. *J. Mol. Biol.* **1994**, *238*, 794–814.
30. Ito, N.; Knowles, P. F.; Phillips, S. E. V. X-ray crystallographic studies of cofactors in galactose oxidase. In *Methods in Enzymology, Redox-Active Amino Acids in Biology*, Klinman, J., Ed., Academic Press: San Diego, CA, 1995; Vol. 235–262.
31. Rogers, M. S.; Baron, A. J.; McPherson, M. J.; Knowles, P. F.; Dooley, D. M. *J. Am. Chem. Soc.* **2000**, *122*, 990–991.
32. Firbank, S. J.; Rogers, M. S.; Wilmot, C. M.; Dooley, D. M.; Halcrow, M. A.; Knowles, P. F.; McPherson, M. J. *Proc. Natl. Acad. Sci. USA* **2001**, *98*, 12932–12937.
33. Okeley, N. M.; van der Donk, W. A. *Chem. Biol.* **2000**, *7*, R159–R171.
34. Babcock, G. T.; El-Deeb, M. K.; Sandusky, P. O.; Whittaker, M. M.; Whittaker, J. W. *J. Am. Chem. Soc.* **1992**, *114*, 3727–3734.
35. Gerfen, G. J.; Bellew, B. F.; Griffin, R. G.; Singel, D. J.; Ekberg, C. A.; Whittaker, J. W. *J. Phys. Chem.* **1996**, *100*, 16739–16748.
36. Himo, F.; Babcock, G. T.; Eriksson, L. A. *Chem. Phys. Letters* **1999**, *313*, 374–378.
37. Whittaker, M. M.; Whittaker, J. W. *J. Biol. Chem.* **1990**, *265*, 9610–9613.
38. Harriman, A. *J. Phys. Chem.* **1987**, *91*, 6102–6104.
39. Silva, K. E.; Elgren, T. E.; Que, L., Jr.; Stankovich, M. T. *Biochemistry* **1995**, *34*, 14093–14103.
40. Itoh, S.; Hirano, K.; Furuta, A.; Komatsu, M.; Ohshiro, Y.; Ishida, A.; Takamuku, S.; Kohzuma, T.; Nakamura, N.; Suzuki, S. *Chem. Lett.* **1993**, 2099–2102.
41. Whittaker, M. M.; Whittaker, J. W. *J. Biol. Chem.* **1988**, *263*, 6074–6080.
42. Whittaker, M. M.; Whittaker, J. W. *Biophys. J.* **1993**, *64*, 762–772.
43. Knowles, P. F.; Brown, R. D., III; Koenig, S. H.; Wang, S.; Scott, R. A.; McGuirl, M. A.; Brown, D. E.; Dooley, D. M. *Inorg. Chem.* **1995**, *34*, 3895–3902.
44. Clark, K.; Penner-Hahn, J. E.; Whittaker, M.; Whittaker, J. W. *Biochemistry* **1994**, *33*, 12553–12557.
45. Que, L., Jr. Metal-Tyrosinate Proteins. In *Biological Applications of Raman Spectroscopy*; Spiro, T. G., Ed. Wiley: New York, 1988; Vol. 3, pp 491–521.
46. McGlashen, M. L.; Eads, D. D.; Spiro, T. G.; Whittaker, J. W. *J. Phys. Chem.* **1995**, *99*, 4918–4922.
47. Wachter, R. M.; Branchaud, B. P. *J. Am. Chem. Soc.* **1996**, *118*, 2782–2789.
48. Borman, C. D.; Saysell, C. G.; Sykes, A. G. *J. Biol. Inorg. Chem.* **1997**, *2*, 480–487.
49. Whittaker, M. M.; Ballou, D. P.; Whittaker, J. W. *Biochemistry* **1998**, *37*, 8426–8436.
50. Wachter, R. M.; Branchaud, B. P. *Biochim. Biophys. Acta* **1998**, *1384*, 43–54.
51. Whittaker, M. M.; Whittaker, J. W. *Biochemistry* **2001**, *40*, 7140–7148.
52. Rothlisberger, U.; Carloni, P.; Doclo, K.; Parrinello, M. *J. Biol. Inorg. Chem.* **2000**, *5*, 236–250.
53. Himo, F.; Eriksson, L. A.; Maseras, F.; Siegbahn, P. E. M. *J. Am. Chem. Soc.* **2000**, *122*, 8031–8036.
54. Reynolds, M. P.; Baron, A. J.; Wilmot, C. M.; Phillips, S. E. V.; Knowles, P. F.; McPherson, M. J. *Biochem. Soc. Trans.* **1995**, *23*, 510S.
55. Maradufu, A.; Cree, G. M.; Perlin, A. S. *Can. J. Chem.* **1971**, *49*, 3429–3437.
56. Wachter, R. M.; Montague-Smith, M. P.; Branchaud, B. P. *J. Am. Chem. Soc.* **1997**, *119*, 7743–7749.
57. Kohen, A.; Klinman, J. P. *Acc. Chem. Res.* **1998**, *31*, 397–404.
58. Chaudhuri, P.; Wieghardt, K. *Prog. Inorg. Chem.* **2001**, *50*, 151–216.
59. Jazdzewski, B. A.; Tolman, W. B. *Coord. Chem. Rev.* **2000**, *200–202*, 633–685.
60. Itoh, S.; Taki, M.; Fukuzumi, S. *Coord. Chem. Rev.* **2000**, *198*, 3–20.
61. Altwicker, E. R. *Chem. Rev.* **1967**, *67*, 475–531.

62. Adam, B.; Bill, E.; Bothe, E.; Goerdt, B.; Haselhorst, G.; Hildenbrand, K.; Sokolowski, A.; Steenken, S.; Weyhermüller, T.; Wieghardt, K. *Chem. Eur. J.* **1997**, *3*, 308–319.
63. Sokolowski, A.; Müller, J.; Weyhermüller, T.; Schnepf, R.; Hildebrandt, P.; Hildenbrand, K.; Bothe, E.; Wieghardt, K. *J. Am. Chem. Soc.* **1997**, *119*, 8889–8900.
64. Bill, E.; Müller, J.; Weyhermüller, T.; Wieghardt, K. *Inorg. Chem.* **1999**, *38*, 5795–5802.
65. Itoh, S.; Taki, M.; Takayama, S.; Nagatomo, S.; Kitagawa, T.; Sakurada, N.; Arakawa, R.; Fukuzmi S. *Angew. Chem., Int. Ed. Engl.* **1999**, *38*, 2774–2776.
66. Sokolowski, A.; Adam, B.; Weyhermüller, T.; Kikuchi, A.; Hildenbrand, K.; Schnepf, R.; Hildebrandt, P.; Bill, E.; Wieghardt, K. *Inorg. Chem.* **1997**, *36*, 3702–3710.
67. Sokolowski, A.; Bothe, E.; Weyhermüller, T.; Wieghardt, K. *J. Chem. Soc., Chem. Commun.* **1996**, 1671–1672.
68. Auerbach, A.; Eckert, U.; Wieghardt, K.; Nuber, B.; Weiss, J. *Inorg. Chem.* **1990**, *29*, 938–944.
69. Auerbach, U.; Weyhermüller, T.; Wieghardt, K.; Nuber, B.; Bill, E.; Butzlaff, C.; Trautwein, A. X. *Inorg. Chem.* **1993**, *32*, 508–519.
70. Benisvy, L.; Blake, A. J.; Collison, D.; Davies, E. S.; Garner, C. D.; McInnes, E. J. L.; McMaster, J.; Whittaker, G.; Wilson, C. *Chem. Commun.* **2001**, 1824–1825.
71. Schnepf, R.; Sokolowski, A.; Müller, J.; Bachler, V.; Wieghardt, K.; Hildenbrandt, P. *J. Am. Chem. Soc.* **1998**, *120*, 2352–2364.
72. Qin, Y.; Wheeler, R. A. *J. Am. Chem. Soc.* **1995**, *117*, 6083–6092.
73. Himo, F.; Graslund, A.; Eriksson, L. A. *Biophys. J.* **1997**, *72*, 1556–1567.
74. Adamo, C.; Subra, R.; Di Matteo, A.; Barone, V. *J. Chem. Phys.* **1998**, *109*, 10244–10254.
75. Mukherjee, A.; McGlashen, M. L.; Spiro, T. G. *J. Phys. Chem.* **1995**, *99*, 4912–4917.
76. Chipman, D. M.; Liu, R.; Zhou, X.; Pulay, P. *J. Chem. Phys.* **1994**, *100*, 5023–5035.
77. Qin, Y.; Wheeler, R. A. *J. Chem. Phys.* **1995**, *102*, 1689–1697.
78. Müller, J.; Kikuchi, A.; Bill, E.; Weyhermüller, T.; Hildebrandt, P.; Ould-Moussa, L.; Wieghardt, K. *Inorg. Chim. Acta* **2000**, *297*, 265–277.
79. Snodin, M. D.; Ould-Moussa, L.; Wallmann, U.; Lecomte, S.; Bachler, V.; Bill, E.; Hummel, H.; Weyhermüller, T.; Hildebrandt, P.; Wieghardt, K. *Chem. Eur. J.* **1999**, *5*, 2554–2565.
80. Hockertz, J.; Steeken, S.; Wieghardt, K.; Hildebrandt, P. *J. Am. Chem. Soc.* **1993**, *115*, 11222–11230.
81. Müller, J.; Weyhermüller, T.; Bill, E.; Hildebrandt, P.; Ould-Moussa, L.; Glaser, T.; Wieghardt, K. *Angew. Chem., Int. Ed. Engl.* **1998**, *37*, 616–619.
82. Halfen, J. A.; Young, V. G., Jr.; Tolman, W. B. *Angew. Chem., Int. Ed. Engl.* **1996**, *35*, 1687–1690.
83. Halfen, J. A.; Jazdzewski, B. A.; Mahapatra, S.; Berreau, L. M.; Wilkinson, E. C.; Que, L., Jr.; Tolman, W. B. *J. Am. Chem. Soc.* **1997**, *119*, 8217–8227.
84. Sokolowski, A.; Leutbecher, H.; Weyhermüller, T.; Schnepf, R.; Bothe, E.; Bill, E.; Hildebrandt, P.; Wieghardt, K. *J. Biol. Inorg. Chem.* **1997**, *2*, 444–453.
85. Wang, Y.; Stack, T. D. P. *J. Am. Chem. Soc.* **1996**, *118*, 13097–13098.
86. Wang, Y.; DuBois, J. L.; Hedman, B.; Hodgson, K. O.; Stack, T. D. P. *Science* **1998**, *279*, 537–540.
87. Saint-Aman, E.; Ménage, S.; Pierre, J.-L.; Defrancq, E.; Gellon, G. *New J. Chem.* **1998**, 393–394.
88. Halcrow, M. A.; Chia, L. M. L.; Liu, X.; McInnes, E. J. L.; Yellowlees, L. J.; Mabbs, F. E.; Scowen, I. J.; McPartlin, M.; Davies, J. E. *J. Chem. Soc., Dalton Trans.* **1999**, 1753–1762.
89. Itoh, S.; Taki, M.; Takayama, S.; Nagatomo, S.; Kitagawa, T.; Sakurada, N.; Arakawa, R.; Fukuzmi, S. *Angew. Chem., Int. Ed. Engl.* **1999**, *38*, 2774–2776.
90. Zurita, D.; Gautier-Luneau, I.; Ménage, S.; Pierre, J.-L.; Saint-Aman, E. *J. Biol. Inorg. Chem.* **1997**, *2*, 46–55.
91. Thomas, F.; Gellon, G.; Gautier-Luneau, S.; Saint-Aman, E.; Pierre, J.-L. *Angew Chem., Int. Ed. Engl.* **2002**, *41*, 3047–3050.
92. Chaudhuri, P.; Hess, M.; Flörke, U.; Wieghardt, K. *Angew. Chem., Int. Ed. Engl.* **1998**, *37*, 2217–2220.
93. Krüger, H.-J. *Angew. Chem., Int. Ed. Engl.* **1999**, *38*, 627–631.
94. Kitajima, N.; Whang, K.; Moro-oka, Y.; Uchida, A.; Sasada, Y. *J. Chem. Soc., Chem. Commun.* **1986**, 1504–1505.
95. Chaudhuri, P.; Hess, M.; Weyhermüller, T.; Wieghardt, K. *Angew. Chem., Int. Ed. Engl.* **1999**, *38*, 1095–1098.
96. Chaudhuri, P.; Hess, M.; Muller, J.; Hildenbrand, K.; Bill, E.; Weyhermuller, T.; Wieghardt, K. *J. Am. Chem. Soc.* **1999**, *121*, 9599–9610.
97. The designation of a fourth class that contains Mn is controversial. See, for example: Huque, Y.; Fieschi, F.; Torrents, E.; Gibert, I.; Eliasson, R.; Reichard, P.; Sahlin, M.; Sjöberg, B.-M. *J. Biol. Chem.* **2000**, *275*, 25365–25371.
98. Stubbe, J. *Adv. Enzymol.* **1990**, *63*, 349–419.
99. Stubbe, J.; van der Donk, W. A. *Chem. Biol.* **1995**, *2*, 793–801.
100. Licht, S.; Stubbe, J. Mechanistic Investigations of Ribonucleotide Reductases. In *Comprehensive Natural Products Chemistry*. Barton, D.; Nakanishi, K., Eds., Elsevier: New York, 1999; Vol. 5, pp 163–203.
101. Fontecave, M.; Nordlund, P.; Eklund, H.; Reichard, P. *Adv. Enzymol.* **1992**, *65*, 147–183.
102. Gerfen, G. J.; Bellew, B. F.; Un, S.; Bollinger, J. M., Jr.; Stubbe, J.; Griffin, R. G.; Singel, D. J. *J. Am. Chem. Soc.* **1993**, *115*, 6420–6421 and references therein.
103. Hoganson, C. W.; Sahlin, M.; Sjöberg, B.-M.; Babcock, G. T. *J. Am. Chem. Soc.* **1996**, *118*, 4672–4679 and references therein.
104. Bar, G.; Bennati, M.; Nguyen, H.-H. T.; Ge, J.; Stubbe, J.; Griffin, R. G. *J. Am. Chem. Soc.* **2001**, *123*, 3569–3576.
105. Atkin, C. L.; Thelander, L.; Reichard, P.; Lang, G. *J. Biol. Chem.* **1973**, *248*, 7464–7472.
106. Lynch, J. B.; Juarez-Garcia, C.; Münck, E.; Que, L., Jr. *J. Biol. Chem.* **1989**, *264*, 8091–8096.
107. Sjöberg, B.-M.; Loehr, T. M.; Sanders-Loehr, J. *Biochemistry* **1982**, *21*, 96–102.
108. Petersson, L.; Gräslund, A.; Ehrenberg, A.; Sjöberg, B.-M.; Reichard, P. *J. Biol. Chem.* **1980**, *255*, 6706–6712.
109. Nordlund, P.; Sjöberg, B.-M.; Eklund, H. *Nature* **1990**, *345*, 593–598.
110. Nordlund, P.; Eklund, H. *J. Mol. Biol* **1999**, *232*, 123–164.
111. Eriksson, M.; Jordan, A.; Eklund, H. *Biochemistry* **1998**, *37*, 13359.
112. Högbom, M.; Huque, Y.; Sjöberg, B.-M.; Nordlund, P. *Biochemistry* **2002**, *41*, 1381–1389.
113. Sahlin, M.; Petersson, L.; Gräslund, A.; Ehrenberg, A.; Sjöberg, B.-M.; Thelander, L. *Biochemistry* **1987**, *26*, 5541–5548.

114. For example, see: Yun, D.; Krebs, C.; Gupta, G. P.; Iwig, D. F.; Huynh, B. H.; Bollinger J. M., *J. Biochemistry* **2002**, *41*, 981–990, and references therein.
115. Ekberg, M.; Pötsch, S.; Sandin, E.; Thunnissen, M.; Nordlund, P.; Sahlin, M.; Sjöberg, B.-M. *J. Biol. Chem.* **1998**, *273*, 21003–21008.
116. Siegbahn, P. E. M.; Eriksson, L.; Himo, F.; Pavlov, M. *J. Phys. Chem. B* **1998**, *102*, 10622–10629.
117. Pokhodenko, V. D.; Melezhik, A. V.; Vovk, D. N. *Sov. J. Coord. Chem. (Engl. Transl.)* **1982**, *8*, 667–671.
118. Melezhik, A. V.; Pokhodenko, V. D. *J. Org. Chem. USSR (Engl. Transl.)* **1982**, *18*, 912–917.
119. Goldberg, D. P.; Lippard, S. J. Modeling Phenoxyl Radical Metalloenzyme Active Sites. In *Mechanistic Bioinorganic Chemistry,* Thorp, H. H.; Pecoraro, V. L., Eds., American Chemical Society: Washington, D.C., 1995; Vol. 246, pp 61–81.
120. Goldberg, D. P.; Watton, S. P.; Masschelein, A.; Wimmer, L.; Lippard, S. J. *J. Am. Chem. Soc.* **1993**, *115*, 5346–5347.
121. Goldberg, D. P.; Koulougliotis, D.; Brudvig, G. W.; Lippard, S. J. *J. Am. Chem. Soc.* **1995**, *117*, 3134–3144.
122. Yonetani, T.; Schleyer, H.; Ehrenberg, A. *J. Biol. Chem.* **1966**, *241*, 3240–3243.
123. Poulos, T. M.; Fenna, R. E. Peroxidases: Structure, Function and Engineering. In *Metal Ions in Biological Systems*; Sigel, H.; Sigel, A., Eds.; Marcel Dekker: New York, 1994; Vol. 30, pp 25–75.
124. Millett, F.; Durham, B. *Biochemistry* **2002**, *41*, 11315–11324 and references therein.
125. Finzel, B. C.; Poulos, T. L.; Kraut, J. *J. Biol. Chem.* **1984**, *259*, 13027–13036.
126. Wang, J.; Mauro, J. M.; Edwards, S. L.; Oatley, S. J.; Fishel, L. A.; Ashford, V. A.; Xuong, N.-H.; Kraut, J. *Biochemistry* **1990**, *29*, 7160–7173.
127. Edwards, S. L.; Xuong, N. H.; Hamlin, R. C.; Kraut, J. *Biochemistry* **1987**, *26*, 1503–1511.
128. Fulop, V.; Phizackerley, R. P.; Soltis, S. M.; Clifton, I. J.; Wakatsuki, S.; Erman, J.; Hajdu, J.; Edwards, S. L. *Structure* **1994**, *2*, 201–208.
129. Goodin, D. B.; Mauk, A. G.; Smith, M. *Proc. Natl. Acad. Sci. USA* **1986**, *83*, 1295–1299.
130. Fishel, L. A.; Farnum, M. F.; Mauro, J. M.; Miller, M. A.; Kraut, J.; Liu, Y.; Tan, X.; Scholes, C. P. *Biochemistry* **1991**, *30*, 1986–1996.
131. Goodin, D. B.; Mauk, A. G.; Smith, M. *J. Biol. Chem.* **1987**, *262*, 7719–7724.
132. Mauro, J. M.; Fishel, L. A.; Hazzard, J. T.; Meyer, T. E.; Tollin, G.; Cusanovich, M. A.; Kraut, J. *Biochemistry* **1988**, *27*, 6243–6256.
133. Scholes, C. P.; Liu, Y.; Fishel, L. A.; Farnum, M. F.; Mauro, J. M.; Kraut, J. *Isr. J. Chem.* **1989**, *29*, 85–92.
134. Houseman, A. L. P.; Doan, P. E.; Goodin, D. B.; Hoffman, B. M. *Biochemistry* **1993**, *32*, 4430–4443.
135. Huyett, J. E.; Doan, P. E.; Gurbiel, R.; Houseman, A. L. P.; Sivaraja, M.; Goodin, D. B.; Hoffman, B. M. *J. Am. Chem. Soc.* **1995**, *117*, 9033–9041.
136. Erman, J. E.; Yonetani, T. *Biochim. Biophys. Acta* **1975**, *393*, 350–357.
137. Miller, M. A.; Han, G. W.; Kraut, J. *Proc. Natl. Acad. Sci. USA* **1994**, *91*, 11118–11122.
138. Solar, S.; Getoff, N.; Surdhar, P. S.; Armstrong, D. A.; Singh, A. *J. Phys. Chem.* **1991**, *95*, 3639–3643.
139. Goodin, D. B.; McRee, D. E. *Biochemistry* **1993**, *32*, 3313–3314.

8.27
Iron–Sulfur Clusters in Enzyme Catalysis

J. B. BRODERICK
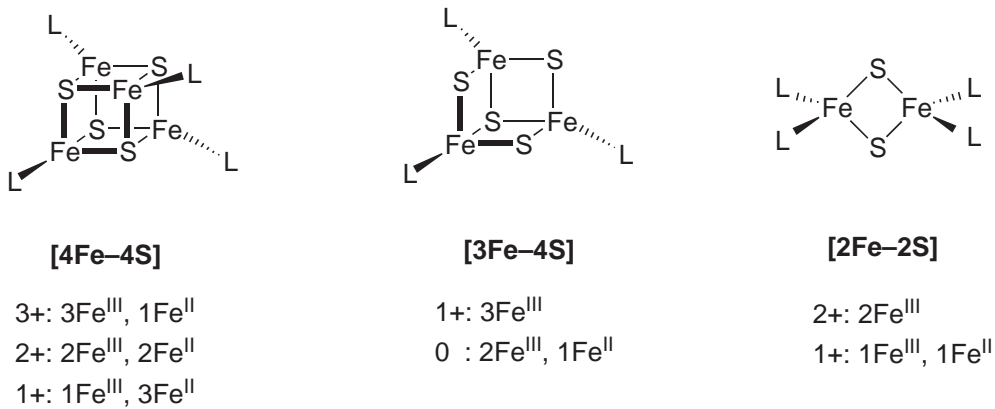*Michigan State University, East Lansing, Michigan, USA*

8.27.1 INTRODUCTION

8.27.1.1 Roles for Iron–Sulfur Clusters in Biology

Iron–sulfur clusters are among the most ubiquitous and diverse metal-containing structures in biology. Since the early 1960s they have been known for their role in electron transfer, including most notably in the ferredoxins, the mitochondrial electron transport chain, and photosynthesis.[1–3] Electron transfer is perhaps the most obvious role for these clusters, due to the presence of at least two redox states readily accessible under normal biological conditions for most types of Fe–S clusters. The role of iron–sulfur clusters in electron transport is covered in detail elsewhere (see Chapter 8.3).

In addition to electron transport, however, a number of other roles have emerged for these clusters, reflecting the fascinating diversity of chemistry accessible to iron–sulfur clusters.[2,3] For

[4Fe–4S]

3+: 3Fe^{III}, 1Fe^{II}

2+: 2Fe^{III}, 2Fe^{II}

1+: 1Fe^{III}, 3Fe^{II}

[3Fe–4S]

1+: 3Fe^{III}

0 : 2Fe^{III}, 1Fe^{II}

[2Fe–2S]

2+: 2Fe^{III}

1+: 1Fe^{III}, 1Fe^{II}

Figure 1 The three most common types of biological iron–sulfur clusters, with the common oxidation states indicated for each. For biological iron–sulfur clusters, cluster oxidation states are typically stated as the sum of the charges on the iron ions and the sulfide ions, ignoring the charges on the exogenous ligands (L in this figure). The *nominal* oxidation states of the iron ions in each cluster are indicated, although it should be emphasized that delocalized mixed-valent states are common in these clusters.

example, iron–sulfur clusters function in regulatory roles,[4] turning gene expression on or off in response to levels of iron (the iron-responsive element-binding protein or IRE-BP),[5,6] oxygen (the FNR protein),[7–9] or superoxide (SoxR).[10–12] Evidence also points to an essential *structural* role for iron–sulfur clusters in several enzymes, including the DNA repair enzymes endonuclease III[13] and MutY.[14] Iron–sulfur clusters can also be used directly in catalysis of redox chemistry on small molecules, as they are, for example, in carbon monoxide dehydrogenase,[15] hydrogenase (see Chapter 8.21), and nitrogenase (see Chapter 8.22). The focus of this chapter will be on recent developments towards understanding the role of the coordination chemistry of iron–sulfur clusters in enzymatic catalysis, with an emphasis on systems in which coordination of substrate to the iron–sulfur cluster has been demonstrated.

8.27.1.2   Types of Catalytic Biological Iron–Sulfur Clusters

The common types of iron–sulfur clusters in biology have been discussed elsewhere (see Chapter 8.3), as have the more complex clusters involved in chemistry such as nitrogen fixation (see Chapter 8.22). Although the [2Fe–2S], [3Fe–4S], and [4Fe–4S] structural types (Figure 1) are common in biology, only the [4Fe–4S] cluster is currently known to be directly involved in enzymatic catalysis. A common feature among catalytic [4Fe–4S] clusters is the presence of a site-differentiated cluster, with one iron in a unique position coordinated by a noncysteinyl ligand. This unique iron is the site of coordination of substrate during enzymatic catalysis, as will be discussed in further detail in the following sections.

8.27.2   ACONITASE

8.27.2.1   Background and Early Studies

Aconitase (citrate(isocitrate)hydro-lyase) catalyzes the isomerization of citrate and isocitrate via *cis*-aconitate, as shown in Figure 2. The reaction is stereospecific, as shown, with the hydration reactions occurring in a *trans* orientation across the double bond.[16–18] Also as shown, the H$^+$
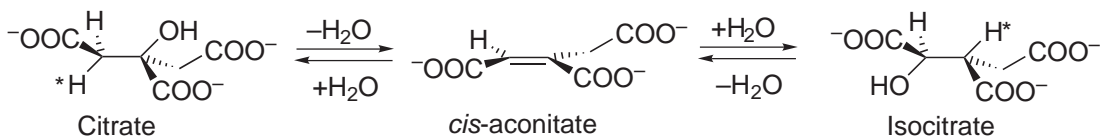
Figure 2 The reactions catalyzed by aconitase.

removed during dehydration does not readily exchange with solvent, and therefore can reappear on the adjacent carbon during the rehydration reaction.[19] Citrate and isocitrate are intermediates in what is known as the citric acid cycle (or alternatively the TCA (tricarboxylic acid) or Krebs cycle), a central process of energy metabolism in aerobic organisms. Aconitase was first suggested to be an iron enzyme in 1951, when it was shown that it could be re-activated by addition of iron(II) and a reducing agent.[20] The form of the iron and its role in catalysis was not known at the time, although it was suggested that binding of substrate to the iron might facilitate catalysis.[20]

8.27.2.2 The Iron–Sulfur Cluster of Aconitase

Aconitase was first suggested to have an iron–sulfur cluster by virtue of the presence of acid-labile sulfide,[21] as well as a $g = 2.01$ EPR signal,[22,23] in the purified protein. The iron–sulfur cluster giving rise to this $g = 2.01$ signal was later shown to be a $[3Fe–4S]^+$ cluster, and was characteristic of inactive enzyme.[24–27] Activation by addition of iron and reductant, or by addition of reductant alone, provided the enzymatically active aconitase, although in the latter case only approximately 75% of full activity was obtained.[28] As the active form of aconitase was subsequently shown to be the $[4Fe–4S]^{2+}$ form,[24] addition of iron and reductant provided the iron needed to occupy the fourth metal site in the cluster, while addition of reductant alone resulted in rearrangement of the clusters, labilizing iron to allow reassembly of [4Fe–4S] clusters in 3/4 of the cluster sites.

It is of interest to note that yet another known cluster type has been observed in aconitase. When the as-isolated, $[3Fe–4S]^+$ form of aconitase is placed in alkaline conditions (pH > 9), the enzyme becomes purple and develops a distinctive UV–visible spectrum[29] which had previously been observed for $[Fe_3S_4(SEt)_4]^{3-}$, a linear three-iron cluster.[30] EPR and Mössbauer studies confirmed the presence of a linear three-iron cluster in purple aconitase.[29] Biochemical studies suggested that, unlike in the case of the cuboidal cluster, the linear 3Fe cluster was coordinated by four cysteinyl ligands.[31] Two of the ligands to the cuboidal cluster (C421 and C424) are retained in the linear cluster, while the third original cysteine ligand (C358) is lost. Two cysteines from an adjacent helix (C250 and C257) provide the other two ligands to the linear cluster. X-ray crystallographic studies of aconitase with the cuboidal cluster show that formation of the linear 3Fe cluster and the ligand replacement involved in this transformation require a fairly significant structural reorganization of the protein.[32]

8.27.2.3 The Unique Iron Site

That aconitase is isolated with a cuboidal $[3Fe–4S]^+$ cluster,[33] rather than the catalytically active $[4Fe–4S]^{2+}$ cluster, suggested that one of the irons in the $[4Fe–4S]^{2+}$ cluster is more labile than the others. Stoichiometric oxidation of $[4Fe–4S]^{2+}$/aconitase with ferricyanide also results in quantitative formation of the $[3Fe–4S]^+$ cluster of aconitase, while addition of Fe^{2+} and a thiol reagent regenerates the $[4Fe–4S]^{2+}$ cluster.[28,34] Studies with a series of iron isotopes demonstrated that iron used to reconstitute the $[3Fe–4S]^+$ enzyme was found only in the unique labile site,[28] and thus this site-specific labeling could be used to investigate the unique site.[35] For example, addition of $^{57}Fe^{II}$ to natural-abundance $[3Fe–4S]^+$-aconitase allowed Mössbauer spectroscopic characterization of the unique site.[35] Alternatively, ^{57}Fe-enriched aconitase could be oxidized to generate the $[3Fe–4S]^+$ form, and then ^{56}Fe could be substituted into the unique site.[24] In this way the labile site (Fe_a) and the three nonlabile sites (Fe_b) could be probed independently, and it was demonstrated that each had unique Mössbauer parameters, as shown in Table 1.[35] Therefore, the labile site was spectroscopically distinct from the three iron sites that constitute the $[3Fe–4S]^+$ cluster.[35]

The presence of a labile iron site, together with the lack of evidence for the liberation of a free sulfhydryl upon converting the [4Fe–4S] to the [3Fe–4S] form,[36] as well as the evidence that only three cysteine residues were protected from labeling in both the [3Fe–4S] and [4Fe–4S] forms of aconitase,[37] suggested that the labile iron was coordinated by a noncysteinyl ligand. EPR line broadening in $H_2^{17}O$ had shown the presence of an exchangeable solvent in the vicinity of the cluster, and subsequent ENDOR studies in $H_2^{17}O$ demonstrated coordination of solvent to the cluster.[38] ^2H ENDOR spectra of aconitase in ^2H_2O reveal only a single type of exchangeable proton coupled to the cluster, indicating that the solvent is bound as hydroxide rather than water.[38] Thus the coordination environment of the cluster in the absence of substrate can be depicted as shown in Figure 3, with the unique site coordinated by a solvent-derived hydroxyl.

**Table 1** Mössbauer parameters for the iron sites in aconitase.[a]

Sample	ΔE_Q (mm s^{-1})	δ (mm s^{-1})	References
[4Fe–4S]$^{2+}$ aconitase			
Fe$_a$	0.83	0.46	35
Fe$_b$	1.30	0.44	24
Fe$_a$ + citrate	1.26	0.84	35
	1.83	0.89	
Fe$_b$ + citrate	1.15	0.44	35
[4Fe–4S]$^{+}$ aconitase			
Fe$_a$	+2.6	1.00	39
Fe$_{b1}$	−2.6	0.64	39
Fe$_{b2}$ = Fe$_{b3}$	+1.15	0.49	39
Reference values			
Fe^{III}S$_4$ [b]		∼0.25	
Fe^{II}S$_4$ [b]		∼0.70	
Typical [4Fe-4S]$^{2+}$		∼0.45	

[a] Fe$_a$ refers to the unique iron site. Fe$_b$ refers to the three other iron sites in the [4Fe–4S] cluster. For each set of data, only the indicated site is labeled with ^{57}Fe. Indicated parameters are for $T = 4$ K. [b] For the localized valence states in an iron–sulfur cluster.

Addition of substrate had a dramatic effect on the Mössbauer parameters of the unique (Fe$_a$) site, but not the Fe$_b$ sites (Table 1).[35,39] The unique site in the presence of citrate shows two new doublets with parameters given in Table 1. It was suggested, and then later supported on the basis of rapid-freeze-quench Mössbauer experiments,[39] that the two doublets arose from binding of isocitrate and citrate due to substrate turnover during sample preparation.[39] This conclusion was confirmed by Mössbauer spectroscopy of structurally characterized single crystals of aconitase with isocitrate bound, which showed a single doublet.[40] Regardless of the differences in the Mössbauer parameters upon binding citrate vs. isocitrate, in both cases the addition of substrate results in a dramatic perturbation of the Mössbauer parameters of the Fe$_a$ (Table 1), to parameters that are no longer consistent with an iron in a tetrahedral sulfur environment, or even a tetrahedral iron with one thiolate replaced by a nonsulfur ligand.[41] The Mössbauer results instead pointed to the Fe$_a$ going to five- or six-coordinate upon binding of substrate, suggesting that substrate was coordinating to the unique Fe$_a$.[35]

Further evidence for direct interaction of the substrate with the cluster was provided by EPR spectroscopy.[35] Although the catalytically most active state of aconitase is the EPR-silent [4Fe–4S]$^{2+}$, this state could be reduced to the [4Fe–4S]$^{+}$ state for examination by EPR. The [4Fe–4S]$^{+}$ state of aconitase appears to retain approximately 30% activity, and exhibits a rhombic EPR signal with $g = 2.06$, 1.93, 1.86, which is perturbed upon addition of substrates or analogs to a more rhombic signal with $g = 2.04$, 1.85, and 1.78.[34] The increased rhombicity upon addition of substrate supported the conclusions from Mössbauer spectroscopy,[35] that addition of substrate causes one iron site to become distinct from the other three sites in the cluster.

Mössbauer spectroscopy of the [4Fe–4S]$^{+}$ aconitase in the presence of substrate shows an even more dramatic effect on the unique site than in the case of [4Fe–4S]$^{2+}$ aconitase, with the Fe$_a$ parameters indicating largely ferrous character and a localized valence at this site (Table 1).[39] The Fe$_b$ sites also differentiate, with two (Fe$_{b2}$ and Fe$_{b3}$) essentially unaffected by substrate addition, and the third (Fe$_{b1}$), which shows increased ferrous character. That both the Fe$_a$ and Fe$_{b1}$ sites show increased ferrous character, while the Fe$_{b2}$ and Fe$_{b3}$ sites are essentially unchanged upon substrate binding, requires that electron density be withdrawn either from the bound substrate or
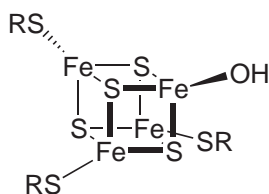
Figure 3 The coordination environment of the [4Fe–4S] cluster of aconitase as predicted based on biochemical and spectroscopic measurements. The coordinating cysteine residues are indicated as RS^{-}.

from the cluster sulfides upon substrate binding.[39] The former possibility would be consistent with the role of the cluster in Lewis acid catalysis (*vide infra*). [57]Fe-ENDOR spectroscopy of the site-specifically labeled cluster confirmed these Mössbauer results: four inequivalent iron sites were observed, with the Fe_a undergoing dramatic perturbations upon substrate binding, while the three Fe_b sites show only minor changes.[42]

8.27.2.4 The Role of the Unique Iron Site in Catalysis

8.27.2.4.1 *Mode of substrate binding to the unique site*

A series of elegant [17]O-ENDOR experiments using substrates site-specifically labeled with [17]O provided a clear picture of the interaction of substrate with the unique iron site of the [4Fe–4S] cluster of aconitase.[43] By a combination of enzymatic and chemical means, citrate specifically [17]O-labeled at the α- and β-carboxyls, and isocitrate labeled at the γ-carboxyl, were synthesized. Nitroisocitrate was similarly labeled at the α-carboxyl and hydroxyl, or at the hydroxyl alone, with [17]O. ENDOR spectroscopic studies of these labeled substrates bound to aconitase provided clear evidence for the two proposed modes of substrate binding. In the case of [17]O-labeled citrate, only samples with label at the Cβ carboxylate showed coupling (15 MHz) to the [4Fe–4S]$^+$ cluster. Nitroisocitrate, an analogue of isocitrate that is incapable of binding in the citrate mode, showed coupling from [17]O labels at both the hydroxyl (9 MHz) and the carboxyl (13 MHz) at the Cα position. These results provided evidence for both the citrate mode (i.e., coordination through the hydroxyl and carboxyl at Cβ) and the isocitrate mode (coordination through the hydroxyl and carboxyl at Cα) of substrate binding to the unique iron site of aconitase.[43]

As stated previously, [4Fe–4S]$^+$-aconitase in H$_2$[17]O exhibits an [17]O ENDOR signal, demonstrating solvent coordination to the unique site.[38] This [17]O ENDOR signal is also observed after addition of substrate, suggesting that substrate binding does not displace the bound solvent.[38] Instead, the coordination number of the unique iron is expanded upon substrate binding to accommodate the two additional oxygen ligands. This suggestion is supported by the Mössbauer results described previously, which provided evidence for an increase in coordination number of the Fe_a site.[35,39] A schematic representation of substrate binding to the active site of aconitase, derived from the ENDOR studies just described, is shown in Figure 4.

8.27.2.4.2 *X-ray structural studies of aconitase*

Aconitase was initially crystallized in the [3Fe–4S]$^+$ form, and these crystals could be converted to the [4Fe–4S]$^{2+}$ form by addition of ferrous ammonium sulfate.[32] Alternatively, anaerobic crystallization methods were used to crystallize the [4Fe–4S]$^{2+}$ form directly.[40] The iron–sulfur cluster of aconitase sits within a solvent-filled cleft in the protein structure and is coordinated by Cys 358, Cys 421, and Cys 424. The [3Fe–4S]$^+$ cluster shows the typically cuboidal geometry, with the open iron site directed toward the active site cleft.[32] Conversion to the active [4Fe–4S]$^{2+}$ form results in almost no structural perturbation, with the extra iron atom simply being inserted into the vacant site in the cluster. The fourth iron is tetrahedrally coordinated, but with a solvent hydroxide rather than a cysteine as the fourth ligand. (The electron density clearly reveals a bound solvent, and previous ENDOR studies[38] had demonstrated that the bound species was associated with only a single proton.)
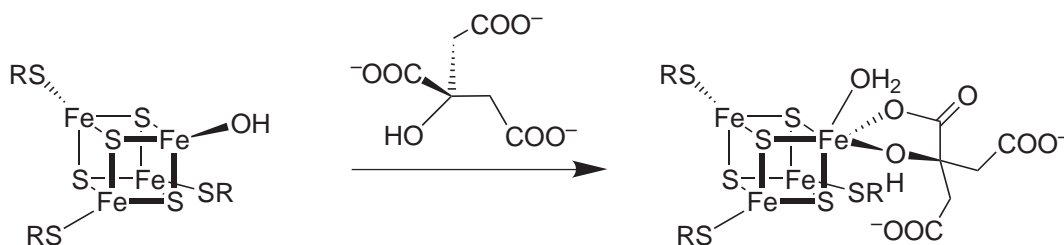
Figure 4 Citrate binding to the active site [4Fe–4S] cluster of aconitase, as deduced from ENDOR measurements.
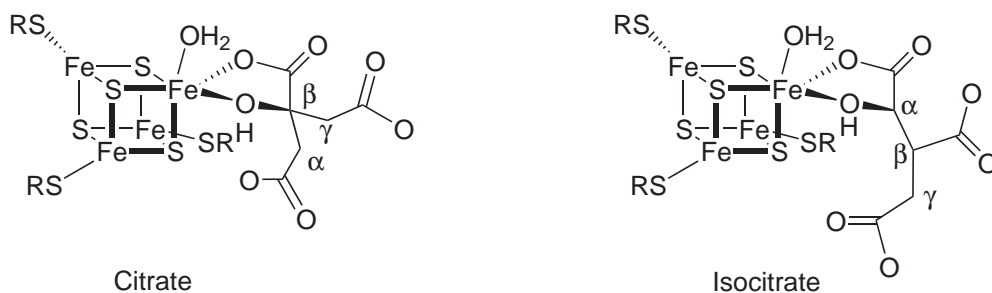
Figure 5   Binding of citrate and isocitrate to the catalytic [4Fe–4S] cluster.

The X-ray crystallographic studies also confirmed the previous spectroscopic results indicating that substrate binds to this unique iron site.[40,44–46] Although the equilibrium mixture of substrates should contain 0.88:0.04:0.08 citrate:*cis*-aconitate:isocitrate, when crystals were grown in the presence of *cis*-aconitate, only isocitrate was observed to be bound to the cluster.[40] The isocitrate bound form was also obtained when crystals were grown in the presence of citrate. The structures show that isocitrate coordinates to the unique iron via one oxygen of the Cα-carboxylate and the hydroxyl group on Cα.[40] A water is also coordinated to the unique iron in the enzyme–substrate complex, as was previously shown by ENDOR.[38] Although six-coordinate, the unique iron environment is distorted from octahedral, with S–Fe–S angles averaging 101° and O–Fe–O angles averaging 74°.[40] The unique iron is also displaced by approximately 0.2 Å from the site it would occupy in a typical [4Fe–4S] cluster.

As crystals with citrate bound in the active site could not be obtained, crystals with the analogue nitrocitrate were characterized.[40] The structure shows that nitrocitrate binds to the unique iron via the carboxylate and hydroxyl groups of Cβ. This structure confirmed the binding modes deduced from spectroscopic methods, in which isocitrate binds through carboxyl and hydroxyl moieties on Cα, while citrate binds through the same groups on Cβ.[43] In other words, the two binding modes (denoted the citrate mode and the isocitrate mode) are related by a twofold axis of rotation about the Cα—Cβ bond (Figure 5).

The observation that isocitrate and nitrocitrate bind with the carboxyl and hydroxyl of Cα and Cβ, respectively, bound to the unique site, and that the binding modes are related by a twofold axis of rotation about the Cα—Cβ bond, requires that the Cγ carboxyl be situated in opposite orientations in these two binding modes (Figure 5). As *cis*-aconitate is the intermediate product from which both citrate and isocitrate are formed, this requires that *cis*-aconitate be able to bind in two different orientations, which have been called the citrate mode and the isocitrate mode.[44,47] Dual binding modes for *cis*-aconitate would also be required to explain the *trans* addition/elimination of H$_2$O across the double bond, as shown in Figure 2.[19] Use of the substrate analogue α-methyl-*cis*-aconitate, which is converted only to α-methyl-isocitrate, provided further evidence for these dual binding modes.[45,46] The binding of this substrate analogue is nearly identical to that of isocitrate, with the α-carboxylate coordinated to the unique iron of the cluster.

8.27.2.4.3   Catalytic mechanism of aconitase

Together, the biochemical, spectroscopic, and structural data suggest a mechanism for aconitase in which the unique iron site of the [4Fe–4S] cluster serves as a Lewis acid in catalysis, binding and polarizing substrate to facilitate the dehydration/rehydration reactions. The use of an iron–sulfur cluster in a nonredox role, as well as its function in binding substrates, was novel and unexpected, and was the first indication of the remarkable diversity of these clusters in functions beyond electron transfer.

The overall catalytic mechanism of aconitase is shown in Figure 6. Starting with citrate or isocitrate as substrate, substrate binding occurs via coordination of the carboxylate and hydroxyl of Cβ or Cα, respectively, to the unique iron of the [4Fe–4S]$^{2+}$ cluster. In doing so, substrate does not displace the coordinated hydroxyl, although the ENDOR studies demonstrate that the hydroxyl becomes protonated upon substrate binding.[38] Therefore, the unique iron of the [4Fe–4S] cluster goes from four-coordinate, with three μ_3-bridging sulfides and a hydroxyl ligand, to six-coordinate, with three μ_3-bridging sulfides, a water, and the carboxylate and hydroxyl of substrate, coordinated to the iron. This change in coordination number was shown by ENDOR
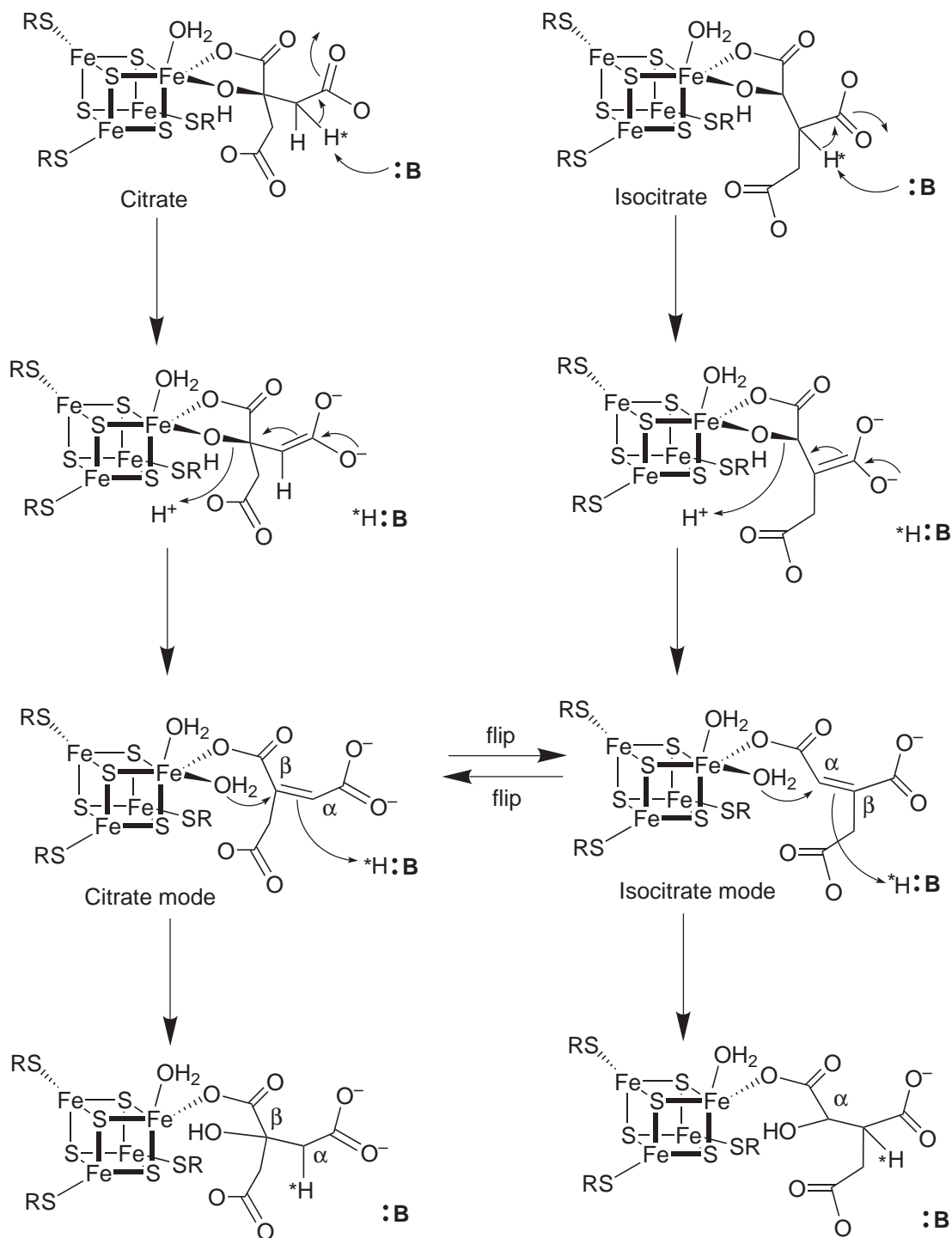
Figure 6 Catalytic mechanism of aconitase starting from citrate (left) or isocitrate (right).

and by X-ray crystallographic studies,[38,40,44] and is consistent with the dramatically altered Mössbauer parameters upon substrate binding.[35,39]

Once substrate is bound, a base in the active site, thought to be the alkoxide form of serine 642,[40] abstracts a proton from either $C\alpha$ (in the case of citrate) or $C\beta$ (in the case of isocitrate). This proton abstraction produces initially a carbanion intermediate, depicted here as the *aci*-acid. The fact that the nitro analogs of the substrates are both good structural mimics of the putative *aci*-acid intermediates and are also good inhibitors of aconitase provides additional evidence for the intermediacy of the *aci*-acid intermediates. The collapse of the *aci*-acid intermediate ultimately

results in the protonation (by His 101) and elimination of the Cβ (citrate) or Cα (isocitrate) hydroxyl as water, leaving *cis*-aconitate as the other product. Both the water and the *cis*-aconitate remain bound to the unique iron of the [4Fe–4S] cluster.

As discussed previously, enzymatic action of aconitase on *cis*-aconitate can produce either citrate or isocitrate, and it is the mode of binding of *cis*-aconitate in the enzyme active site that determines the product of the reaction.[40,44,47] The involvement of two modes of *cis*-aconitate binding in aconitase was first suggested by kinetic studies,[47] and later supported by the detailed spectroscopic and structural studies that gave so much insight into the aconitase mechanism (*vide supra*). The two modes of *cis*-aconitate binding, termed the citrate mode and the isocitrate mode, are related by a twofold axis of rotation about the Cα—Cβ bond, as shown in Figure 6. Once *cis*-aconitate is formed in the active site, it can dissociate and re-bind in either conformation, or alternatively it can be displaced by another *cis*-aconitate molecule binding in either orientation. The *cis*-aconitate bound in the active site can then be hydrated by the water bound to the unique site, as shown in Figure 6. If *cis*-aconitate is bound in the citrate mode, Cβ is closest to the iron-bound water and thus water adds to this position, producing citrate. Alternatively, if *cis*-aconitate is bound in the isocitrate mode, Cα is closest to the iron-bound water and hydroxyl adds to this position. In either case, the pK_a of the bound water is lowered by coordination to the unique iron of the cluster, making water a better nucleophile in the reaction. Coordination of the *cis*-aconitate also makes Cα or Cβ (depending on binding mode) a better electrophile. Attack of the bound water/hydroxyl at Cα or Cβ is accompanied by protonation at Cβ or Cα, respectively, to produce isocitrate or citrate, respectively, as shown in Figure 6. The protonation accompanying water/hydroxyl attack appears to occur via Ser 642, the same residue that, in its alkoxyl form, abstracted a proton from citrate or isocitrate to initiate the reaction. In fact, remarkably, tritium-labeling experiments have shown that the proton abstracted from substrate to initiate the reaction is not readily exchangeable, and is returned to the product upon completion of the reaction.[19]

Thus, the overall mechanism for aconitase involves an iron–sulfur cluster acting as a Lewis acid, coordinating the organic substrates and water, stabilizing reaction intermediates, and making water a better nucleophile and the double bond in *cis*-aconitate a better electrophile. This is a remarkable role for an iron–sulfur cluster, since the cluster itself does not change redox state during catalysis. In fact, other than the unique iron site, none of the rest of the cluster is involved in catalysis in any obvious way. Why nature chose to utilize a relatively complex, labile, and biosynthetically expensive species like an iron–sulfur cluster to perform hydrolytic chemistry, the type of chemistry that in other biological systems is adequately performed by mononuclear metal centers, is an intriguing question. It has been suggested that the cluster provides a unique scaffold that allows the iron to undergo the dramatic changes in coordination number required by the proposed mechanism.[40] However, this may not be an adequate explanation, since mononuclear iron enzymes are known which can accommodate up to three exogenous ligands for catalysis.[48]

8.27.2.5 Aconitase and Iron Homeostasis

Perhaps one of the most surprising developments regarding aconitase is its relationship to cellular iron homeostasis. Two types of aconitase are present in cells: mitochondrial aconitase, responsible for the key role in the Krebs cycle as discussed previously, and cytosolic aconitase, which was shown in the 1990s to be the same protein as the iron-responsive protein (IRP, also known as the iron-responsive element-binding protein, IRE-BP).[5,49] IRP is a protein that senses iron levels in the cell and translates this information into increased or decreased production of ferritin, the iron-storage protein, and transferrin, the iron-transport protein, as well as other iron-regulated genes.[6,50] IRP binds to the messenger RNA (mRNA) of ferritin and transferrin (or other proteins) under low iron conditions; in the case of ferritin mRNA the binding is at the 5′ end of the mRNA and prevents further synthesis of ferritin, which is not needed under low iron conditions. In the case of transferrin, IRP binding is at the 3′ end of the mRNA and prevents degradation of the mRNA, therefore allowing more transferrin synthesis, which results in more iron being transported into the cell. Under high iron levels, IRP does not bind to either ferritin or transferrin mRNA, and as such it allows synthesis of ferritin, needed under high iron conditions, and prevents further synthesis of transferrin, since the transferrin mRNA is rapidly degraded in the absence of IRP binding. It had been known for some time that the binding or lack of binding of IRP to mRNA was related not to the presence or absence of IRP, but rather to its redox state

and/or its state of metallation. Subsequent detailed studies into IRP and its identification as the cytosolic aconitase revealed the difference between "active" and "inactive" IRP: IRP incapable of mRNA binding contained a [4Fe–4S] or [3Fe–4S] cluster, with the former showing significant aconitase activity, while IRP capable of mRNA binding contained no iron–sulfur cluster and no aconitase activity.[5,49] Thus IRP/c-aconitase presented one of the first examples of an iron–sulfur cluster as a sensor, in which building up or destruction of the cluster was used as a signal for required metabolic changes. The IRP/c-aconitase is also an unusual example of a dual function metalloregulatory protein/metalloenzyme. The mechanism by which the [4Fe–4S] cluster of IRP/c-aconitase is degraded and re-synthesized in response to changing iron levels in the cell, however, is still not well understood, although cluster degradation has been suggested to involve reaction with NO.[6]

8.27.2.6 Other Hydrolytic Enzymes Containing [4Fe–4S] Clusters

Several additional enzymes have been identified that appear to be related to aconitase in the sense that they use an iron–sulfur cluster to catalyze dehydratase reactions (see Figure 7).[51] Among these are isopropylmalate isomerase, which catalyzes a key reaction in leucine biosynthesis, has sequence homology with aconitase,[52] and has spectroscopic features of a [4Fe–4S] cluster that can be converted to a [3Fe–4S] cluster.[53] Fumarase A also contains a catalytically essential [4Fe–4S] cluster, which can be converted to a [3Fe–4S] cluster upon oxidation, suggesting the presence of a unique iron site.[54] Dihydroxyacid dehydratase,[55] maleic acid hydratase,[56] tartrate dehydratase,[57] serine dehydratase,[58,59] and phosphogluconate dehydratase[60] also appear to belong to this group of [4Fe–4S] cluster-containing dehydratase enzymes. In all these cases it is thought that the [4Fe–4S] cluster contains a unique iron site whose function is to coordinate and activate substrate for turnover. In addition to the enzymes just mentioned, several others have been proposed to belong to the [4Fe–4S]-dehydratase group of enzymes.[51]
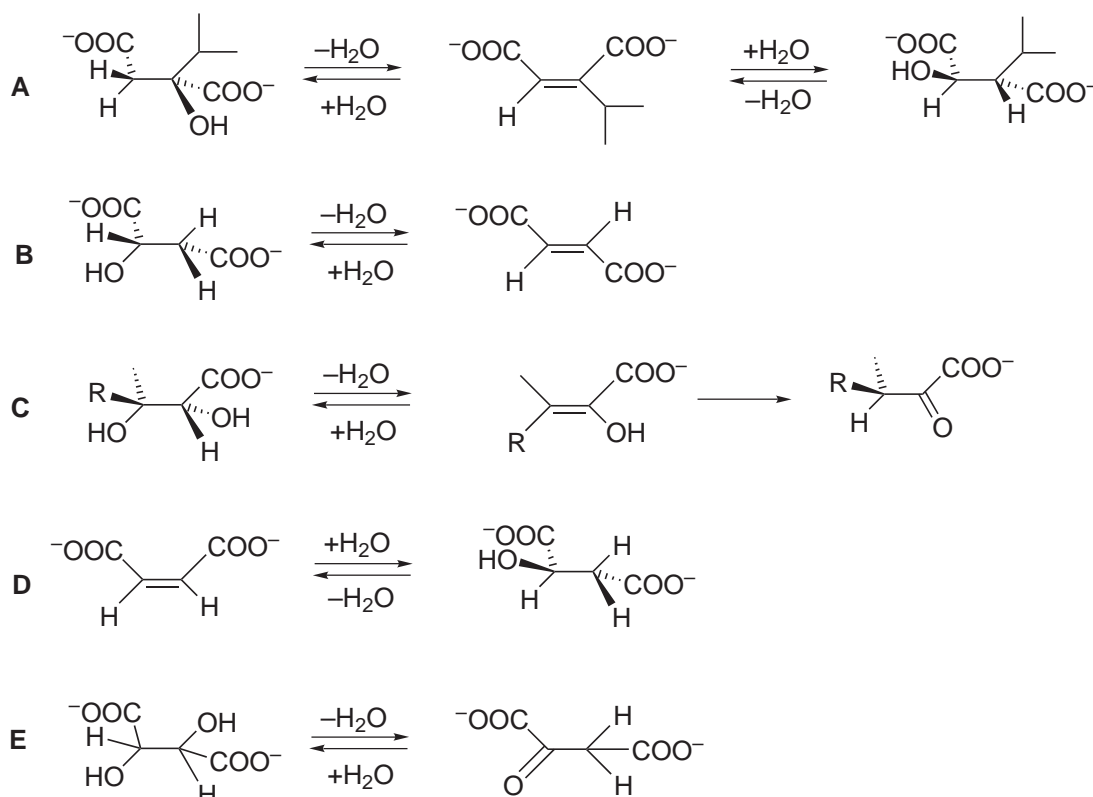
Figure 7 Other dehydratases that may use a [4Fe–4S] cluster in an analogous manner to aconitase. A. Isopropylmalate isomerase. B. Fumarase. C. Dihydroxyacid dehydratase. D. Maleic acid hydratase. E. Tartrate dehydratase.

8.27.3 S-ADENOSYLMETHIONINE-DEPENDENT RADICAL ENZYMES

8.27.3.1 Introduction to the Radical-SAM Superfamily

The recently identified "radical-SAM"[61] superfamily comprises a diverse group of enzymes which at first glance bear little resemblance to aconitase and the related dehydratases. However, as we shall see, the radical-SAM enzymes, like aconitase, appear to use a unique iron site in a [4Fe–4S] cluster to coordinate substrate. A common feature of the members of the radical-SAM super-family is the presence in the amino acid sequence of a characteristic cluster-binding motif (CX_3CX_2C) containing only three cysteines, and evidence suggests that these three cysteines alone are responsible for cluster binding.[62] The presence of only three cysteines in the cluster-binding motif is reminiscent of aconitase and related enzymes in that it suggests the presence of a unique, noncysteinyl-coordinated iron in a [4Fe–4S] cluster, although the putative noncysteinyl ligand has not been identified for any of the enzymes in this family.

The radical-SAM superfamily is so-called because its members catalyze radical reactions and utilize S-adenosylmethionine (SAM or AdoMet) as a required cofactor or co-substrate.[61] These enzymes also contain catalytically essential iron–sulfur clusters.[62] The best-studied members of this family, including lysine aminomutase, pyruvate formate-lyase activating enzyme, anaerobic ribonucleotide reductase, lipoate synthase, and biotin synthase, were being investigated long before the superfamily was named, and have provided important clues to the catalytic mechanism and the role of the iron–sulfur cluster and AdoMet.[62] Additional members of this family are being identified and isolated at a fairly rapid pace. In fact, the bioinformatics approach that was used to identify the superfamily has revealed hundreds of other putative members throughout the phylogenetic kindgom, from simple unicellular organisms to humans.[61]
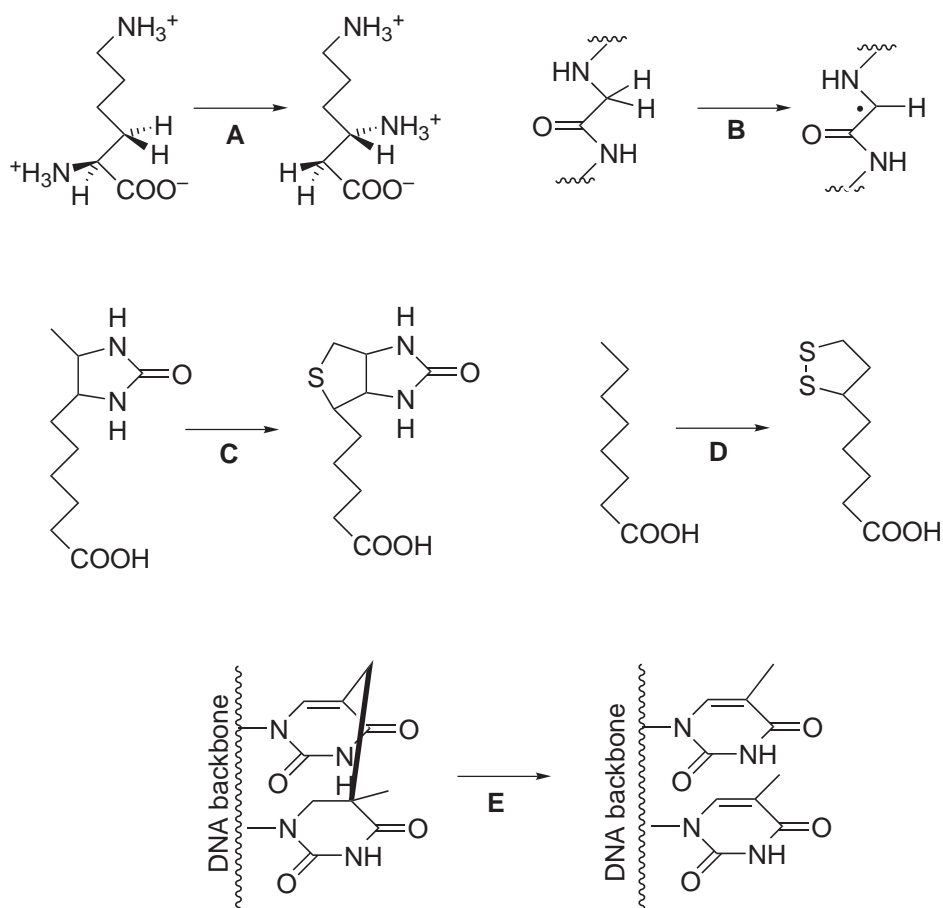
8.27.3.1.1 Lysine 2,3-aminomutase

Lysine 2,3-aminomutase, known alternatively as LAM or KAM, catalyzes a rearrangement reaction of lysine, the interconversion of L-lysine and L-β-lysine (Figure 8A). The reaction, which is catalytic in AdoMet, is directly analogous to rearrangement reactions catalyzed by coenzyme B12-dependent enzymes,[63–66] and in fact in both the B12 and the AdoMet-dependent enzymes the key initial step in catalysis is the abstraction of a hydrogen atom to yield a substrate radical intermediate.[67,68] In the case of the B12-dependent enzymes, the hydrogen atom is abstracted by a B12-derived 5′-deoxyadenosyl radical intermediate generated via homolytic Co—C bond cleavage. In the case of the AdoMet-dependent lysine aminomutase, the hydrogen atom is abstracted by an AdoMet-derived 5′-deoxyadenosyl radical. Such a radical mechanism was originally proposed by Moss and Frey,[69] and later supported experimentally by the observation of a kinetically competent lysine radical,[70–72] as well as by the spectroscopic observation of an allylic analogue of the putative 5′-deoxyadenosyl radical intermediate.[73,74] This intriguing parallel between the B12 and the AdoMet-dependent radical enzymes, the intermediacy of a 5′-deoxyadenosyl radical, extends to other members of the radical-SAM superfamily as well. In addition to the requirement for an iron–sulfur cluster and AdoMet, LAM also requires pyridoxal 5′-phosphate, which forms an adduct with the substrate during turnover.

8.27.3.1.2 Pyruvate formate-lyase activating enzyme

Pyruvate formate-lyase activating enzyme (PFL-AE) was identified early on as an iron-dependent protein required to activate pyruvate formate-lyase (PFL) for its essential function in anaerobic glucose metabolism in bacteria, the conversion of pyruvate and coenzyme-A (CoA) to formate and acetyl-CoA.[75–77] The activation of PFL for this central function involves the generation of a stable and catalytically essential glycyl radical,[76] which is generated under anaerobic conditions by PFL-AE (Figure 8B) and is quenched once conditions become increasingly oxic (PFL is not needed under aerobic conditions) by the PFL deactivating enzyme.[78] The activation of PFL by PFL-AE, unlike the LAM reaction, involves the *stoichiometric* consumption of AdoMet, which is converted to methionine and 5′-deoxyadenosine by reductive cleavage of the sulfur–carbon bond of AdoMet.[76] Isotopic labeling studies showed early on that the hydrogen atom abstracted from the glycyl residue of PFL ended up at the 5′-carbon of 5′-deoxyadenosine,[79] thereby implicating

Figure 8 Reactions catalyzed by the radical-SAM superfamily. A. Lysine 2,3-aminomutase. B. Activating enzymes. C. Biotin synthase. D. Lipoic acid synthase. E. Spore photoproduct lyase.

an intermediate adenosyl radical in catalysis. The nature of the iron requirement for PFL-AE remained a mystery until PFL-AE was identified as an iron–sulfur protein.[80]

8.27.3.1.3 Anaerobic ribonucleotide reductase activating enzyme

The anaerobic ribonucleotide reductase (aRNR), like pyruvate formate-lyase, is a bacterial enzyme that operates only under anaerobic conditions. Like PFL, aRNR must be activated for catalysis, which involves the generation of a stable glycyl radical on the enzyme (Figure 8B).[81,82] The aRNR activating enzyme, once considered to be merely the β_2 subunits of an $\alpha_2\beta_2$ holoenzyme,[83] is now known to function catalytically with respect to the aRNR (i.e., the α_2 component).[84] However, the activase (β_2) is tightly associated with the reductase (α_2), unlike the activating enzyme of PFL-AE, which is not tightly associated with PFL. The aRNR activating enzyme has been shown to contain an iron–sulfur cluster and to utilize AdoMet in catalysis, converting it stoichiometrically to methionine and 5'-deoxyadenosine.[85,86]

8.27.3.1.4 Biotin synthase and lipoate synthase

The biotin and lipoate synthases catalyze similar reactions, the insertion of sulfur into unactivated C—H bonds to generate essential cofactors (Figures 8C and 8D). The substrate in the case of biotin synthase is dethiobiotin, with a single sulfur inserted into two C—H bonds to generate the tetrahydrothiophene ring of biotin. In the case of lipoate synthase, two atoms of sulfur are inserted, one each into the C—H bonds at positions 6 and 8 of octanoic acid to produce dihydrolipoate, which is typically isolated in the oxidized form shown in Figure 8D. (The actual

substrate of lipoate synthase is not free octanoic acid, but octanoate bound to acyl-carrier protein (octanoyl-ACP).[87]) Both biotin synthase[88] and lipoate synthase[89,90] have been shown to contain iron–sulfur clusters, and both require AdoMet for catalysis.[87,91] In the case of biotin synthase, there is evidence for hydrogen atom transfer from substrate into deoxyadenosine, thereby implicating an intermediate 5′-deoxyadenosyl in the catalytic mechanism.[92] The deoxyadenosyl radical presumably abstracts a hydrogen atom from substrate to generate a substrate radical intermediate, to which sulfur is added. Evidence points to an iron–sulfur cluster being the source of the added sulfur, as is discussed further in Section 8.27.3.4.

8.27.3.1.5   Spore photoproduct lyase

Spore photoproduct lyase (SPL) catalyzes the repair of UV-induced DNA damage in *Bacillus*, and possibly other spore-forming microorganisms (Figure 8E).[93–95] It has been shown to contain an iron–sulfur cluster and to utilize AdoMet in catalysis.[96,97] Like lysine aminomutase but unlike the other radical-SAM enzymes discussed above, SPL appears to use AdoMet catalytically; i.e., AdoMet is not consumed during substrate turnover.[98] Evidence for a radical mechanism of DNA repair has been obtained, as repair of damaged DNA labeled at C-6 of thymine results in specific label transfer into AdoMet, suggesting that C-6 H atom abstraction by a 5′-deoxyadenosyl radical intermediate is the initial step in DNA repair.[98]

8.27.3.2   Properties of the Iron–Sulfur Clusters

As stated previously, a common feature among the radical-SAM enzymes is the presence of a distinctive three-cysteine cluster-binding motif,[62] as was also seen in aconitase. This conserved cluster-binding motif leads to similarities in the cluster properties among the members of this family. As will be discussed in more detail below, the [4Fe–4S] cluster is now known to be the catalytically relevant cluster. However, a distinctive feature of the clusters in these enzymes is their lability; thus, the literature on these enzymes provides evidence for [2Fe–2S] clusters, cuboidal and linear [3Fe–4S] clusters, and [4Fe–4S] clusters in a variety of oxidation states.[62] This cluster lability, though somewhat confusing in the early literature on these enzymes, is reminiscent of aconitase, in which all these cluster forms were also observed. However even among the radical-SAM enzymes the degree of cluster lability is quite variable.[62]

Pyruvate formate-lyase activating enzyme is the member of the radical-SAM family whose cluster properties are most similar to those of aconitase. The cluster in pyruvate formate-lyase activating enzyme is quite labile, and in fact until 1997 it was not known that the enzyme contained an iron–sulfur cluster, as all preparations to that time had been done aerobically, under which conditions the cluster falls apart.[75] It was initially reported that PFL-AE contained a mixture of [2Fe–2S] and [4Fe–4S] clusters,[80] and subsequent reconstitution studies of the apo enzyme provided evidence for a [4Fe–4S] cluster.[99] Further studies showed that anaerobic isolation resulted in purification of a form of PFL-AE that contained primarily $[3Fe–4S]^+$ clusters, which upon reduction converted to [4Fe–4S] clusters.[100,101] This reductive cluster conversion from $[3Fe–4S]^+$ to $[4Fe–4S]^{2+}$ clusters *even in the absence of added iron* was remarkably reminiscent of aconitase (see Section 8.27.2.2), and suggested a labile cluster site. Adding to the similarity to aconitase, Mössbauer spectroscopy provided evidence for a linear [3Fe–4S] cluster in PFL-AE isolated under appropriate conditions.[101] Therefore all of the cluster forms previously identified in aconitase were also found in PFL-AE, and like aconitase it appeared to be relatively simple to interconvert between these cluster forms.[101]

The other members of the radical-SAM family have shown some, but not all, of the cluster properties observed for PFL-AE. For example, evidence for both $[2Fe–2S]^{2+}$ and $[4Fe–4S]^{2+}$ clusters have been reported for both biotin synthase[102–104] and lipoate synthase.[89,90,104] In fact, the [2Fe–2S] cluster in biotin synthase is quite stable, and thus biotin synthase can be purified aerobically with the [2Fe–2S] cluster intact,[88] and then reconstituted anaerobically to generate the [4Fe–4S] cluster.[102–105] No significant amount of $[3Fe–4S]^+$ cluster has been observed in biotin synthase, although lipoate synthase appears to contain some $[3Fe–4S]^+$ depending on isolation conditions.[87]

It had been previously proposed that the reductive cluster conversions (in the absence of added iron) in the radical-SAM enzymes occurred by cluster "cannibalization," as had also been

proposed for aconitase. That is, reduction results in labilization of the metal–ligand bonds, essentially releasing iron and sulfide which can then reassemble into the thermodynamically favored cluster form under reducing conditions. Direct evidence for such release and reabsorption of iron and sulfide during reductive cluster conversions was provided for biotin synthase,[106] supporting this general mechanism of cluster conversion in the radical-SAM enzymes.

In contrast to these examples is lysine aminomutase, in which the only significant cluster form observed is the [4Fe–4S] form, although a [3Fe–4S] cluster can be generated upon oxidation.[107] However, no [2Fe–2S] cluster has been reported for this enzyme. LAM is also the only member of this family in which a [4Fe–4S]$^{3+}$ cluster has been observed.[107] The iron–sulfur cluster in spore photoproduct lyase has not been characterized, although some evidence for [4Fe–4S] and [3Fe–4S] forms has been obtained.[97]

In summary, the common CX$_2$CX$_3$C cluster-binding motif found in the radical-SAM enzymes confers some common properties to the clusters in these enzymes, including cluster lability. However, the details of the lability and the precise cluster forms observed vary from enzyme to enzyme.

8.27.3.3 Involvement of the Clusters in Radical Catalysis

The variety of clusters observed in these enzymes, and the cluster lability, led to difficulties in determining unequivocally the active cluster form and oxidation state. Fontecave and co-workers showed that, in the absence of the aRNR (also known as the α_2 domain), the aRNR-AE (or β_2 domain) in the [4Fe–4S]$^+$ state reacts with AdoMet to generate methionine concomitant with cluster oxidation, with a stoichiometry of 2–3 methionines per cluster oxidized.[85] Although this is not the physiologically relevant reaction of radical generation on aRNR, it does demonstrate the ability of the [4Fe–4S]$^+$-aRNR-AE to reductively cleave AdoMet. Later studies on aRNR confirmed the stoichiometry of approximately two methionines produced per [4Fe-4S]$^+$ oxidized, although for aRNR-AE in the presence of the aRNR only one methionine, along with 0.5–0.9 glycyl radicals, was produced per [4Fe–4S]$^+$ oxidized.[86]

Evidence for the [4Fe–4S]$^+$ cluster as the active form of lysine aminomutase was obtained by Frey and co-workers, who showed by a combination of EPR spectroscopy and enzyme assays that the [4Fe–4S]$^+$-LAM generated in the presence of AdoMet was catalytically active.[108] Unlike aRNR-AE, however, LAM catalyzes a *reversible* reductive cleavage of AdoMet, and thus methionine production and cluster oxidation could not be monitored as evidence of turnover. It is of interest to note that in the case of LAM, the presence of AdoMet facilitates reduction to the [4Fe–4S]$^+$ state; very little [4Fe–4S]$^+$ cluster is produced by the reduction of LAM with dithionite in the absence of AdoMet, while the presence of AdoMet or its analogue S-adenosylhomocysteine dramatically increases the quantity of [4Fe–4S]$^+$ produced.[108] It is not clear whether the presence of AdoMet affects the redox potential of the cluster or whether some other effect, such as accessibility of the cluster by the reductant, is at work.

The most direct demonstration of the involvement of the [4Fe–4S]$^+$ cluster in radical catalysis by the radical-SAM enzymes was obtained in the case of PFL-AE.[109] PFL-AE was reduced from the [4Fe–4S]$^{2+}$ to the [4Fe–4S]$^+$ state using photoreduction in the presence of 5-deazariboflavin. EPR samples of the enzyme in the presence of AdoMet alone show increasing amounts of [4Fe–4S]$^+$ with increasing times of illumination. (Unlike the aRNR-AE, PFL-AE does not reductively cleave AdoMet at an appreciable rate in the absence of the other substrate, PFL.) Parallel samples to which PFL had been added (addition was performed in the dark to eliminate the exogenous reductant) showed increasing quantities of a glycyl radical EPR signal with increasing illumination time. Spin quantitation of the EPR signals from the parallel PFL-AE/AdoMet and PFL-AE/AdoMet/PFL samples demonstrated a 1:1 correspondence between the amount of [4Fe–4S]$^+$ in the former to the amount of glycyl radical in the latter.[109] Furthermore, the [4Fe–4S]$^+$ EPR signal disappears upon addition of PFL and generation of the glycyl radical, thereby suggesting that the [4Fe–4S]$^+$ cluster is oxidized to [4Fe–4S]$^{2+}$. It was proposed that the [4Fe–4S]$^+$ cluster provided the electron necessary for reductive cleavage of AdoMet to generate methionine and the putative 5′-deoxyadenosyl radical intermediate.[109]

Together, the results described for aRNR-AE, LAM, and PFL-AE point to the [4Fe–4S]$^+$ cluster as the catalytically active cluster, and they point to a role for this cluster in providing the electron necessary for reductive cleavage of AdoMet, either reversibly (as in the case of LAM) or irreversibly (as in the cases of the two activating enzymes), as illustrated in Figure 9.[62] Therefore,
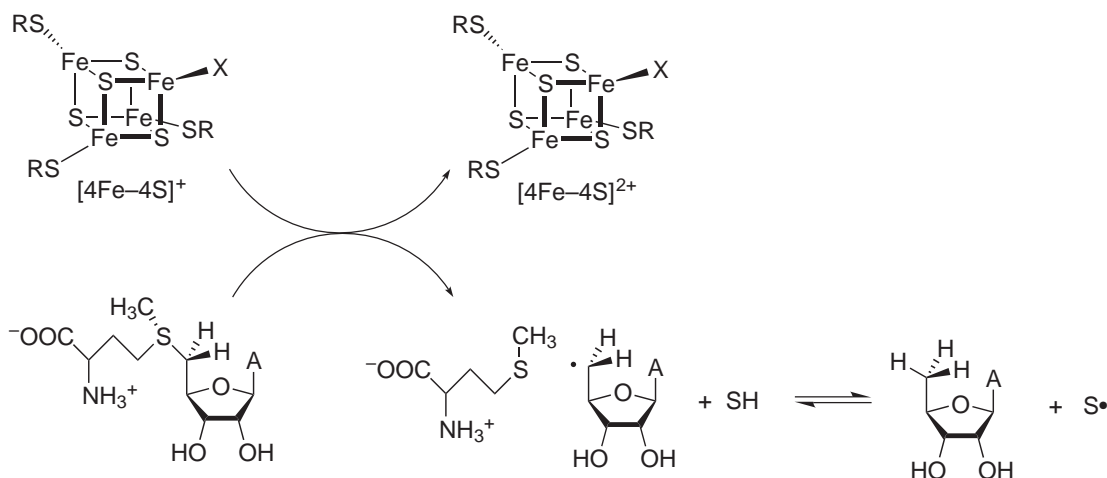
Figure 9 A generalized reaction scheme for the radical-SAM enzymes. The $[4Fe–4S]^+$ provides the electron necessary for the reductive cleavage of AdoMet to generate the intermediate adenosyl radical. The adenosyl radical abstracts a hydrogen atom from substrate (SH) to initiate the radical reaction.

although many of the cluster properties of the radical-SAM enzymes are similar to those of aconitase, the precise role of the cluster in catalysis is not. In aconitase, the $[4Fe–4S]^{2+}$ cluster serves as a Lewis acid, binding and activating substrate for the dehydratase reaction, but not acting in a redox role. In contrast, the cluster in the radical-SAM enzymes is a redox-active cluster, with the reduced $[4Fe–4S]^+$ state being catalytically active. The oxidized $[4Fe–4S]^{2+}$ state is produced either as an intermediate (e.g., LAM) or a product (e.g., aRNR-AE and PFL-AE) as AdoMet is used catalytically or stoichiometry, respectively.

8.27.3.4 Interaction of S-Adenosylmethionine with the Clusters

The involvement of a $[4Fe–4S]^+$ cluster and its role in reductive cleavage of AdoMet led to the question of precisely *how* the $[4Fe–4S]^+$ cluster was involved in catalysis. Based on the evidence described in the previous section, it was conceivable that the cluster served as a remote electron-transfer center, reducing AdoMet via long-range electron transfer to generate an AdoMet radical which subsequently underwent reductive C—S bond cleavage. Alternatively, the cluster might interact directly with AdoMet to mediate this unusual radical generation reaction. A number of pieces of evidence had hinted at the possibility that AdoMet interacted directly with the cluster, including the observation of dramatic changes in the EPR signal line shape of the $[4Fe–4S]^+$ upon addition of AdoMet[110,111] and increased ability to reduce the cluster in the presence of Ado-Met.[108]

Additional evidence for a close association between AdoMet and the $[4Fe–4S]$ cluster in the radical-SAM enzymes came from selenium K-edge X-ray absorption studies of lysine amino-mutase in the presence of the cleaved cofactor S-adenosyl-L-selenomethionine (Se-AdoMet).[112] Selenium EXAFS of the LAM/Se-AdoMet complex itself did not show a close contact to an iron of the cluster. However, in the presence of DTT and the substrate analog *trans*-4,5-dehydrolysine, the cofactor was cleaved to deoxyadenosine and selenomethionine, and a close (2.7 Å) contact to an iron of the $[4Fe–4S]$ cluster was observed in the selenium EXAFS.[112] This led the authors to propose a close association between AdoMet and the $[4Fe–4S]$ cluster of LAM, with the sulfonium sulfur situated near to the presumed unique iron site of the cluster (Figure 10). Substrate binding would then bring AdoMet closer to the iron–sulfur cluster, allowing electron transfer from the cluster and ultimately sulfur–carbon bond cleavage, which would leave methionine in close contact with the unique iron site (Figure 10).

Electron-nuclear double resonance (ENDOR) studies of PFL-AE complexed to specifically isotopically labeled AdoMets has revealed the details of the interaction between AdoMet and the cluster in this enzyme.[111–113] Deuterium ENDOR spectra of PFL-AE in the $[4Fe–4S]^+$ state complexed with methyl-D$_2$-AdoMet showed a pair of peaks centered at the deuteron Larmor frequency and split by the hyperfine coupling to the spin of the cluster.[111] Examination of the field-dependence of the coupling showed that it was dipolar in nature, and gave an estimation of the
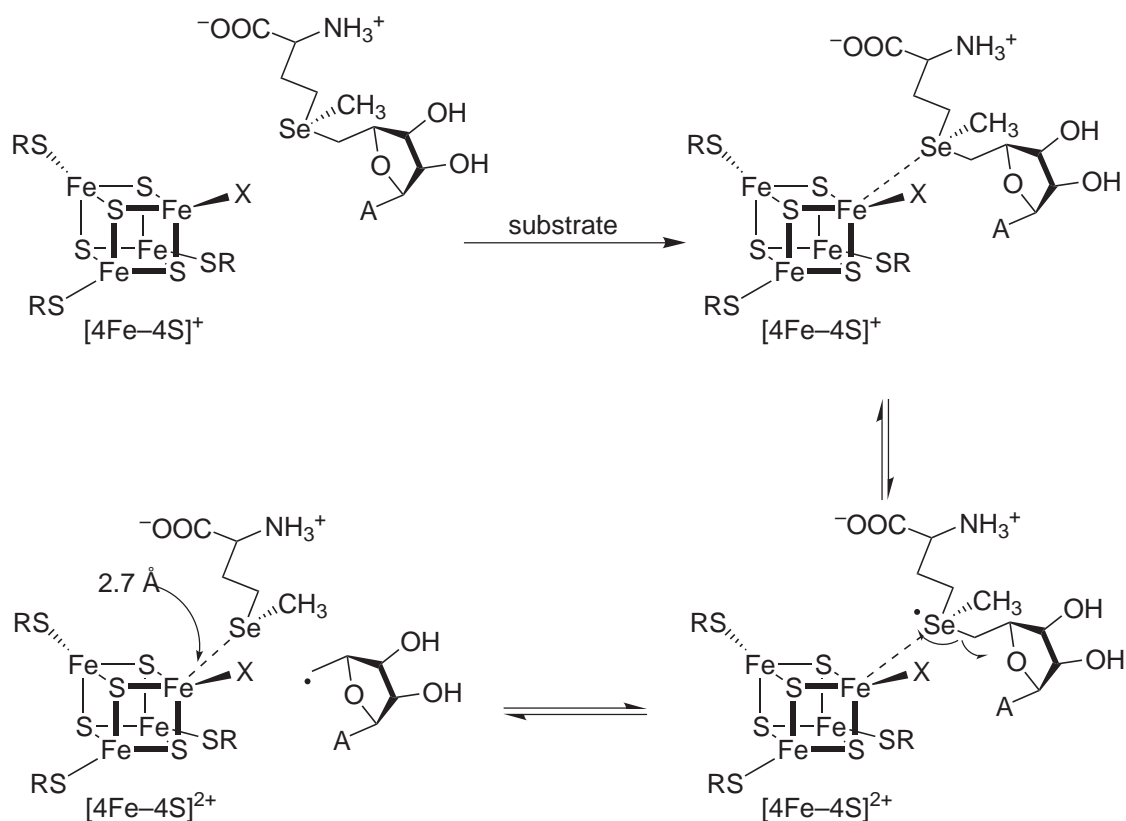
Figure 10 Interaction of AdoMet with the iron sulfur cluster in LAM to generate the intermediate deoxyadenosyl radical. Adapted from ref. 112.

distance from the nearest deuteron to the closest iron of the cluster of approximately 3.0–3.8 Å.[111] Fully consistent results were obtained from ^{13}C-ENDOR studies of [4Fe-4S]$^+$/PFL-AE in the presence of AdoMet labeled at the methyl carbon with [13]C.[111] In this case the estimated distance to the nearest iron of the cluster was 4–5 Å, and the coupling could best be modeled through a combination of through-space and through-bond contributions. The presence of isotropic through-bond contributions to the ^{13}C coupling requires that there be some orbital overlap, in order to provide a pathway for delocalization of unpaired spin density from the cluster. Due primarily to electrostatic considerations, it was proposed that the orbital overlap occurs via a close association of the AdoMet sulfonium with one of the μ_3-bridging sulfides of the cluster (Figure 11).[111]

The results just described probed the interaction of AdoMet with the catalytically active [4Fe-4S]$^+$ cluster of PFL-AE. Interaction of AdoMet with the oxidized [4Fe-4S]$^{2+}$ cluster cannot be probed directly using ENDOR spectrsocopy, since the [4Fe-4S]$^{2+}$ cluster is diamagnetic. In order to probe the interaction with the 2+ cluster, therefore, PFL-AE in the [4Fe-4S]$^{2+}$ state was mixed
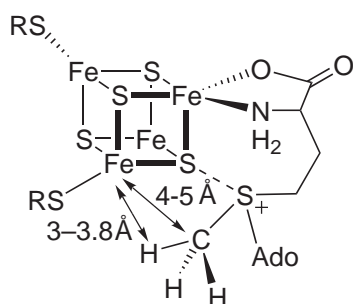
Figure 11 The interaction of AdoMet with the [4Fe-4S] cluster of PFL-AE as deduced from ^{2}H, ^{13}C, ^{17}O, and ^{15}N ENDOR measurements and ^{54}Fe Mössbauer studies.

with isotopically labeled AdoMet, and then frozen. At 77 K, with the samples frozen in the conformation of the 2+ state, the samples were γ-irradiated to cryoreduce the clusters to the 1+ state. Both ^{2}H and ^{13}C-ENDOR with methyl-labeled AdoMet give essentially identical results to those for the $[4Fe–4S]^+$/PFL-AE/AdoMet complex, suggesting that AdoMet interacts with both oxidation states of the cluster in essentially the same manner.[111]

The proposal that the sulfonium of AdoMet interacts with a μ_3-bridging sulfide of the cluster left open the question of the role for the putative unique iron site. A unique iron site was in fact demonstrated in PFL-AE via specific isotopic labeling of the unique iron site with ^{57}Fe, in the same way described previously for aconitase (see Section 8.27.2.3), which allowed probing of the unique site by Mössbauer spectroscopy.[114] The Mössbauer parameters for this unique site in the absence of AdoMet were typical for iron in $[4Fe–4S]^{2+}$ clusters (Table 2). Addition of AdoMet, however, dramatically altered the Mössbauer parameters (Table 2). The new parameters are inconsistent with coordination of a sulfur to the unique site, but are consistent with an increase in coordination number of the unique iron to 5 or 6, and/or coordination of an ionic ligand.[114] Thus it was proposed that the carboxylate of AdoMet coordinated to the unique iron site of the cluster.[114]

Further ENDOR studies have confirmed such an interaction with the unique site, and point to a role for the unique iron in anchoring AdoMet for catalysis.[113] ENDOR studies with the carboxylate labeled with ^{17}O show a strong coupling (12.2 MHz) to the $[4Fe–4S]^+$ cluster, much like what was observed with aconitase with ^{17}O-labeled substrate (13–15 MHz).[43] This ^{17}O coupling in the PFL-AE/AdoMet complex is consistent with a direct coordination of the carboxylate to the unique iron site of the $[4Fe–4S]^+$ cluster. ^{13}C-ENDOR with the carboxylate carbon labeled with ^{13}C also showed coupling (0.71 MHz) to the cluster, confirming the coordination of the carboxylate group. By comparison, a coupling of 1 MHz was observed for aconitase in the presence of substrate labeled with ^{13}C at the carboxyl group.[43] A broad ENDOR signal observed at $\sim$8 MHz in $[4Fe–4S]^+$/PFL-AE samples made with natural abundance AdoMet disappears in samples in which AdoMet was labeled with ^{15}N at the amino position, while a new signal appears corresponding to an ^{15}N coupling of 5.8 MHz.[113] This coupling of the amino nitrogen to the cluster clearly demonstrates that the amino group of AdoMet is also coordinated to the unique iron of the cluster.

The picture that emerges from the ENDOR results is one in which AdoMet forms a classical five-member ring N/O chelate with the unique iron of the [4Fe–4S] cluster, as shown in Figure 11.[113] This is analogous to the chelation of substrate hydroxyl and carboxyl to the unique iron in aconitase.[43] The sulfonium of AdoMet is thus anchored in place, closely associated with one of the μ_3-bridging sulfides of the cluster, for an inner-sphere electron transfer from the cluster to AdoMet to initiate catalysis.[113] Therefore, although the presence of a unique site in the [4Fe–4S] cluster and the chelation of substrate to that unique site are common features of aconitase and PFL-AE, the role for the unique site appears to be distinctly different in these two enzymes. In aconitase, the unique site is a catalytic site, binding and activating substrate for the dehydratase reaction. In PFL-AE, the unique site is an anchor, holding substrate in place so that the reactive end of the substrate, the sulfonium, is positioned properly for the subsequent chemistry to occur.

The evidence for coordination of AdoMet to the unique iron site in PFL-AE leads to the question of how these results relate to the interaction of AdoMet in the other radical-SAM enzymes. As described previously, the EXAFS evidence for LAM points to an entirely different type of interaction, in which the sulfonium is closely associated with the unique iron site, rather than a μ_3-bridging sulfide.[112] The potentially different modes of interaction between AdoMet and the [4Fe–4S] cluster in these two enzymes may reflect a key difference between these two enzymes: in PFL-AE, AdoMet is consumed as a substrate during turnover, while in LAM AdoMet is a

Table 2 Mössbauer parameters for the unique site of PFL-AE.[a]

Sample	ΔE_Q (mm s^{-1})	δ (mm s^{-1})	*References*
$[4Fe–4S]^{2+}$ PFL-AE			
$[4Fe–4S]^{2+}$ [b]	1.15	0.45	101
	1.00	0.45	101
Fe_a [c]	1.12	0.42	114
Fe_a [c] + AdoMet	1.15	0.72	114

[a] Data recorded at 4.2 K. [b] All sites are labeled with ^{57}Fe. [c] Only the unique site is labeled with ^{57}Fe.

catalytic cofactor. Perhaps these different modes of interaction will be found to be characteristic of the distinct ways AdoMet is used by the radical-SAM enzymes, with the enzymes using AdoMet stoichiometrically (aRNR-AE, biotin synthase, lipoate synthase) showing a PFL-AE-type interaction and the enzymes using AdoMet catalytically (e.g., spore photoproduct lyase) showing LAM-type interaction. Further detailed studies on the radical-SAM enzymes will be required to address this intriguing question.

8.27.3.5 A Second Iron–Sulfur Cluster in Biotin Synthase

It should be noted that recent evidence points to a second iron–sulfur cluster being present in catalytically active biotin synthase. Using a combination of spectroelectrochemical studies and enzymatic assays, Jarrett and co-workers have shown that the form of biotin synthase present in typical anaerobic assays of the enzyme contains one $[4Fe–4S]^{2+}$ and one $[2Fe–2S]^{2+}$ cluster.[105] These results have been further substantiated by Mössbauer spectroscopic experiments that provide evidence for two distinct cluster binding sites in biotin synthase.[115] Jarrett and co-workers have also shown that the $[2Fe–2S]^{2+}$ cluster is degraded during turnover.[116] Together, these results are interpreted as the requirement for two distinct clusters for catalysis by biotin synthase.[116] The [4Fe–4S] cluster, like the related clusters in the other radical-SAM enzymes, is thought to be the catalytic cluster, generating an adenosyl radical intermediate via reductive cleavage of AdoMet. The [2Fe–2S] cluster has been proposed to be the sulfur donor in the biotin synthase reaction, which is consistent with previous suggestions that an iron–sulfur cluster was the source of the sulfur for biotin synthesis.[117–119] Whether similar results will be obtained with lipoic acid synthase, which also catalyzes a sulfur insertion reaction, remains to be determined.

8.27.4 REFERENCES

1. Johnson, M. K. Iron sulfur proteins In *Encyclopedia of Inorganic Chemistry*; King, R. B., Ed., Wiley: Chichester, U.K., 1994, pp 1896–1915.
2. Beinert, H.; Holm, R. H.; Münck, E. *Science* **1997**, *277*, 653–659.
3. Beinert, H. *J. Biol. Inorg. Chem.* **2000**, *5*, 2–15.
4. Rouault, T. A.; Klausner, R. D. *Trends Biochem. Sci.* **1996**, *21*, 174–177.
5. Haile, D. J.; Rouault, T. A.; Harford, J. B.; Kennedy, M. C.; Blondin, G. A.; Beinert, H.; Klausner, R. D. *Proc. Natl. Acad. Sci. U.S.A.* **1992**, *89*, 11735–11739.
6. Hentze, M. W.; Kühn, L. C. *Proc. Natl. Acad. Sci. U.S.A.* **1996**, *93*, 8175–8182.
7. Khoroshilova, N.; Beinert, H.; Kiley, P. *Proc. Natl. Acad. Sci. U.S.A.* **1995**, *92*, 2499–2503.
8. Khoroshilova, N.; Popescu, C.; Münck, E.; Beinert, H.; Kiley, P. J. *Proc. Natl. Acad. Sci. U.S.A.* **1997**, *94*, 6087–6092.
9. Popescu, C. V.; Bates, D. M.; Beinert, H.; Münck, E.; Kiley, P. J. *Proc. Natl. Acad. Sci. U.S.A.* **1998**, *95*, 13431–13435.
10. Hidalgo, E.; Ding, H.; Demple, B. *Trends Biochem. Sci.* **1997**, *22*, 207–210.
11. Demple, B. *Science* **1998**, *279*, 1655–1656.
12. Ding, H.; Demple, B. *Proc. Natl. Acad. Sci. U.S.A.* **1997**, *94*, 8445–8449.
13. Cunningham, R. P.; Asahara, H.; Bank, J. F.; Scholes, C. P.; Salerno, J. C.; Surerus, K.; Münck, E.; McCracken, J.; Peisach, J.; Emptage, M. H. *Biochemistry* **1989**, *28*, 4450–4455.
14. Porello, S. L.; Cannon, M. J.; David, S. S. *Biochemistry* **1998**, *37*, 6465–6475.
15. Drennan, C. L.; Heo, J.; Sintchak, M. D.; Schreiter, E.; Ludden, P. W. *Proc. Natl. Acad. Sci. U.S.A.* **2001**, *98*, 11973–11978.
16. Gawron, O.; Glaid, A. J. III; LoMonte, A.; Gary, S. *J. Am. Chem. Soc.* **1958**, *80*, 5856–5860.
17. England, S.; Breiger, H. H. *J. Biol. Chem.* **1960**, *235*, 1510–1516.
18. Gawron, O.; Glaid, A. J. III; Fondy, T. P. *J. Am. Chem. Soc.* **1961**, *83*, 3634–3640.
19. Rose, I. A.; O'Connell, E. L. *J. Biol. Chem.* **1967**, *242*, 1870–1879.
20. Dickman, S. R.; Cloutier, A. A. *J. Biol. Chem.* **1951**, *188*, 379–388.
21. Kennedy, S. C.; Rauner, R.; Gawron, O. *Biochem. Biophys. Res. Commun.* **1972**, *47*, 740–745.
22. Ruzicka, F. J.; Beinert, H. *Biochem. Biophys. Res. Commun.* **1974**, *58*, 556–563.
23. Ruzicka, F. J.; Beinert, H. *J. Biol. Chem.* **1978**, *253*, 2514.
24. Kent, T. A.; Dreyer, J. L.; Kennedy, M. C.; Huynh, B. H.; Emptage, M. H.; Beinert, H.; Münck, E. *Proc. Natl. Acad. Sci. U.S.A.* **1982**, *79*, 1096–1100.
25. Beinert, H.; Emptage, M. H.; Dreyer, J. L.; Scott, R. A.; Hahn, J. E.; Hodgson, K. O.; Thomson, A. J. *Proc. Natl. Acad. Sci. U.S.A.* **1983**, *80*, 393–396.
26. Beinert, H.; Thomson, A. J. *Arch. Biochem. Biophys.* **1983**, *222*, 333–361.
27. Rydén, L.; Öfverstedt, L. G.; Beinert, H.; Emptage, M. H.; Kennedy, M. C. *J. Biol. Chem.* **1984**, *259*, 3141–3144.
28. Kennedy, M. C.; Emptage, M. H.; Dreyer, J.-L.; Beinert, H. *J. Biol. Chem.* **1983**, *258*, 11098–11105.
29. Kennedy, M. C.; Kent, T. A.; Emptage, M.; Merkle, H.; Beinert, H.; Münck, E. *J. Biol. Chem.* **1984**, *259*, 14463–14471.
30. Hagen, K. S.; Watson, A. D.; Holm, R. H. *J. Am. Chem. Soc.* **1983**, *105*, 3905–3913.
31. Plank, D. W.; Kennedy, M. C.; Beinert, H.; Howard, J. B. *J. Biol. Chem.* **1989**, *264*, 20385–20393.

32. Robbins, A. H.; Stout, C. D. *Proc. Natl. Acad. Sci. U.S.A.* **1989**, *86*, 3639–3643.
33. Kent, T. A.; Dreyer, J.-L.; Emptage, M. H.; Moura, I.; Moura, J. J. G.; Huynh, B. H.; Xavier, A. V.; LeGall, J.; Beinert, H.; Orme-Johnson, W. H.; Münck, E. Evidence for a novel three-iron center in two ferredoxins and aconitase. In *Symposium on Interaction between Iron and Proteins in Oxygen and Electron Transport*; Ho, C., Ed.; Elsevier: North Holland, Amsterdam, 1982, pp 371–374.
34. Emptage, M. H.; Dreyer, J.-L.; Kennedy, M. C.; Beinert, H. *J. Biol. Chem.* **1983**, *258*, 11106–11111.
35. Emptage, M. H.; Kent, T. A.; Kennedy, M. C.; Beinert, H.; Münck, E. *Proc. Natl. Acad. Sci. U.S.A* **1983**, *80*, 4674–4678.
36. Kennedy, M. C.; Beinert, H. *J. Biol. Chem.* **1988**, *263*, 8194–8198.
37. Plank, D. W.; Howard, J. B. *J. Biol. Chem.* **1988**, *263*, 8184–8189.
38. Werst, M. M.; Kennedy, M. C.; Beinert, H.; Hoffman, B. M. *Biochemistry* **1990**, *29*, 10526–10532.
39. Kent, T. A.; Emptage, M. H.; Merkle, H.; Kennedy, M. C.; Beinert, H.; Münck, E. *J. Biol. Chem.* **1985**, *260*, 6871–6881.
40. Lauble, H.; Kennedy, M. C.; Beinert, H.; Stout, C. D. *Biochemistry* **1992**, *31*, 2735–2748.
41. Debrunner, P. G.; Münck, E.; Que, L.; Schulz, C. E. Recent Moessbauerre sults of someiron sulfur proteins and model complexes. In *Iron Sulfur Proteins*; Lovenberg, W., Eds.; Academic Press: New York, 1977, Vol. III, pp 381–417.
42. Werst, M. M.; Kennedy, M. C.; Houseman, A. L.; Beinert, H.; Hoffman, B. M. *Biochemistry* **1990**, *29*, 10533–10540.
43. Kennedy, M. C.; Werst, M.; Telser, J.; Emptage, M. H.; Beinert, H.; Hoffman, B. M. *Proc. Natl. Acad. Sci. U.S.A.* **1987**, *84*, 8854–8858.
44. Lauble, H.; Kennedy, M. C.; Beinert, H.; Stout, C. D. *J. Mol. Biol.* **1994**, *237*, 437–451.
45. Lauble, H.; Stout, C. D. *Proteins: Struct., Funct., Genet.* **1995**, *22*, 1–11.
46. Lauble, H.; Kennedy, M. C.; Emptage, M. H.; Beinert, H.; Stout, C. D. *Proc. Natl. Acad. Sci. U.S.A.* **1996**, *93*, 13699–13703.
47. Gawron, O.; Mahajan, K. P. *Biochemistry* **1966**, *5*, 2343–2350.
48. Que, L., Jr.; Ho, R. Y. N. *Chem. Rev.* **1996**, *96*, 2607–2624.
49. Haile, D. J.; Rouault, T. A.; Tang, C. K.; Chin, J.; Harford, J. B.; Klausner, R. D. *Proc. Natl. Acad. Sci. U.S.A.* **1992**, *89*, 7536–7540.
50. Theil, E. C. *J. Biol. Chem.* **1990**, *265*, 4771–4774.
51. Flint, D. H.; Allen, R. M. *Chem. Rev.* **1996**, *96*, 2315–2334.
52. Roncero, M. I. G.; Jepsen, L. P.; Stroeman, P.; van Heeswijck, R. *Gene* **1989**, *84*.
53. Emptage, M. H. Yeast isopropylmalate isomerase as an iron sulfur protein. In *Biosynthesis of Branched Chain Amino Acids, Proc. Workshop*; Barak, Z. E., Chipman, D. M. and Schloss, J. V., Ed.; VCH, 1988, pp 315–328.
54. Flint, D. H.; Emptage, M. H.; Guest, J. R. *Biochemistry* **1992**, *31*, 10331–10337.
55. Flint, D. H.; Emptage, M. H.; Finnegan, M. G.; Fu, W.; Johnson, M. K. *J. Biol. Chem.* **1993**, *268*, 14732–14742.
56. Dreyer, J.-L. *Eur. J. Biochem.* **1985**, *150*, 145–154.
57. Kelly, J. M.; Scopes, R. K. *FEBS Lett.* **1986**, *202*, 274–276.
58. Hofmeister, A. E. M.; Albracht, S. P. J.; Buckel, W. *FEBS Lett.* **1994**, *351*, 416–418.
59. Grabowski, R.; Buckel, W. *Eur. J. Biochem.* **1991**, *199*, 89–94.
60. Rodriquez, M.; Wedd, A. G.; Scopes, R. K. *Biochem. Mol. Biol. Int.* **1996**, *38*, 783–789.
61. Sofia, H. J.; Chen, G.; Hetzler, B. G.; Reyes-Spindola, J. F.; Miller, N. E. *Nucleic Acids Res.* **2001**, *29*, 1097–1106.
62. Cheek, J.; Broderick, J. B. *J. Biol. Inorg. Chem.* **2001**, *6*, 209–226.
63. Dolphin, D. *B12* **1982**, *1 and 2* Wiley: New York.
64. Banerjee, R. *Biochemistry* **2001**, *40*, 6191–6198.
65. Marsh, E. N. G. *Essays Biochem.* **1999**, *34*, 139–154.
66. Ochiai, E.-I. *Met. Ions Biol. Sys.* **1994**, *30*, 255–278.
67. Frey, P. A. *Chem. Rev.* **1990**, *90*, 1343–1357.
68. Frey, P. A. *Annu. Rev. Biochem.* **2001**, *70*, 121–148.
69. Moss, M.; Frey, P. A. *J. Biol. Chem.* **1987**, *262*, 14859–14862.
70. Ballinger, M. D.; Reed, G. H.; Frey, P. A. *Biochemistry* **1992**, *31*, 949–953.
71. Ballinger, M. D.; Frey, P. A.; Reed, G. H. *Biochemistry* **1992**, *31*, 10782–10789.
72. Chang, C. H.; Ballinger, M. D.; Reed, G. H.; Frey, P. A. *Biochemistry* **1996**, *35*, 11081–11084.
73. Magnusson, O. T.; Reed, G. H.; Frey, P. A. *J. Am. Chem. Soc.* **1999**, *121*, 9764–9765.
74. Magnusson, O. T.; Reed, G. H.; Frey, P. A. *Biochemistry* **2001**, *40*, 7773–7782.
75. Conradt, H.; Hohmann-Berger, M.; Hohmann, H.-P.; Blaschkowski, H. P.; Knappe, J. *Arch. Biochem. Biophys.* **1984**, *228*, 133–142.
76. Knappe, J.; Neugebauer, F. A.; Blaschkowski, H. P.; Gänzler, M. *Proc. Natl. Acad. Sci U.S.A.* **1984**, *81*, 1332–1335.
77. Knappe, J.; Elbert, S.; Frey, M.; Wagner, A. F. V. *Biochem. Soc. Trans.* **1993**, *21*, 731–734.
78. Kessler, D.; Leibrecht, I.; Knappe, J. *FEBS Lett.* **1991**, *281*, 59–63.
79. Frey, M.; Rothe, M.; Wagner, A. F. V.; Knappe, J. *J. Biol. Chem.* **1994**, *269*, 12432–12437.
80. Broderick, J. B.; Duderstadt, R. E.; Fernandez, D. C.; Wojtuszewski, K.; Henshaw, T. F.; Johnson, M. K. *J. Am. Chem. Soc.* **1997**, *119*, 7396–7397.
81. Eliasson, R.; Pontis, E.; Fontecave, M.; Gerez, C.; Harder, J.; Jörnvall, H.; Krook, M.; Reichard, P. *J. Biol. Chem.* **1992**, *267*, 25541–25547.
82. Mulliez, E.; Fontecave, M.; Gaillard, J.; Reichard, P. *J. Biol. Chem.* **1993**, *268*, 2296–2299.
83. Ollagnier, S.; Mulliez, E.; Gaillard, J.; Eliasson, R.; Fontecave, M.; Reichard, P. *J. Biol. Chem.* **1996**, *271*, 9410–9416.
84. Tamarit, J.; Mulliez, E.; Meier, C.; Trautwein, A.; Fontecave, M. *J. Biol. Chem.* **1999**, *274*, 31291–31296.
85. Ollagnier, S.; Mulliez, E.; Schmidt, P. P.; Eliasson, R.; Gaillard, J.; Deronzier, C.; Bergman, T.; Gräslund, A.; Reichard, P.; Fontecave, M. *J. Biol. Chem.* **1997**, *272*, 24216–24223.
86. Padovani, D.; Thomas, F.; Trautwein, A. X.; Mulliez, E.; Fontecave, M. *Biochemistry* **2001**, *40*, 6713–6719.
87. Miller, J. R.; Busby, R. W.; Jordan, S. W.; Cheek, J.; Henshaw, T. F.; Ashley, G. W.; Broderick, J. B.; Cronan, J. E., Jr.; Marletta, M. A. *Biochemistry* **2000**, *39*, 15166–15178.
88. Sanyal, I.; Cohen, G.; Flint, D. H. *Biochemistry* **1994**, *33*, 3625–3631.
89. Busby, R. W.; Schelvis, J. P. M.; Yu, D. S.; Babcock, G. T.; Marletta, M. A. *J. Am. Chem. Soc.* **1999**, *121*, 4706–4707.

90. Ollagnier-de Choudens, S.; Fontecave, M. *FEBS Lett.* **1999**, *453*, 25–28.
91. Sanyal, I.; Gibson, K. J.; Flint, D. H. *Arch. Biochem. Biophys.* **1996**, *326*, 48–56.
92. Escalettes, F.; Florentin, D.; Bui, B. T. S.; Lesage, D.; Marquet, A. *J. Am. Chem. Soc.* **1999**, *121*, 3571–3578.
93. Munakata, N.; Rupert, C. S. *J. Bacteriol.* **1972**, *111*, 192–198.
94. Munakata, N.; Rupert, C. S. *Mol. Gen. Genet.* **1974**, *130*, 239–250.
95. Wang, T. C.; Rupert, C. S. *Photochem. Photobiol.* **1977**, *25*, 123–127.
96. Rebeil, R.; Sun, Y.; Chooback, L.; Pedraza-Reyes, M.; Kinsland, C.; Begley, T. P.; Nicholson, W. L. *J. Bacteriol.* **1998**, *180*, 4879–4885.
97. Rebeil, R.; Nicholson, W. L. *Proc. Natl. Acad. Sci. U.S.A.* **2001**, *98*, 9038–9043.
98. Cheek, J.; Broderick, J. B. *J. Am. Chem. Soc.* **2002**, *124*, 2860–2861.
99. Külzer, R.; Pils, T.; Kappl, R.; Hüttermann, J.; Knappe, J. *J. Biol. Chem.* **1998**, *273*, 4897–4903.
100. Broderick, J. B.; Henshaw, T. F.; Cheek, J.; Wojtuszewski, K.; Trojan, M. R.; McGhan, R.; Smith, S. R.; Kopf, A.; Kibbey, M.; Broderick, W. E. *Biochem. Biophys. Res. Commun.* **2000**, *269*, 451–456.
101. Krebs, C.; Henshaw, T. F.; Cheek, J.; Huynh, B.-H.; Broderick, J. B. *J. Am. Chem. Soc.* **2000**, *122*, 12497–12506.
102. Duin, E. C.; Lafferty, M. E.; Crouse, B. R.; Allen, R. M.; Sanyal, I.; Flint, D. H.; Johnson, M. K. *Biochemistry* **1997**, *36*, 11811–11820.
103. Bui, B. T. S.; Florentin, D.; Marquet, A.; Benda, R.; Trautwein, A. X. *FEBS Lett.* **1999**, *459*, 411–414.
104. Ollagnier-de Choudens, S.; Sanakis, Y.; Hewitson, K. S.; Roach, P.; Baldwin, J. E.; Münck, E.; Fontecave, M. *Biochemistry* **2000**, *39*, 4165–4173.
105. Ugulava, N. B.; Gibney, B. R.; Jarrett, J. T. *Biochemistry* **2001**, *40*, 8343–8351.
106. Ugulava, N. B.; Gibney, B. R.; Jarrett, J. T. *Biochemistry* **2000**, *39*, 5206–5214.
107. Petrovich, R. M.; Ruzicka, F. J.; Reed, G. H.; Frey, P. A. *Biochemistry* **1992**, *31*, 10774–10781.
108. Lieder, K.; Booker, S.; Ruzicka, F. J.; Beinert, H.; Reed, G. H.; Frey, P. A. *Biochemistry* **1998**, *37*, 2578–2585.
109. Henshaw, T. F.; Cheek, J.; Broderick, J. B. *J. Am. Chem. Soc.* **2000**, *122*, 8331–8332.
110. Liu, A.; Gräslund, A. *J. Biol. Chem.* **2000**, *275*, 12367–12373.
111. Walsby, C. J.; Hong, W.; Broderick, W. E.; Cheek, J.; Ortillo, D.; Broderick, J. B.; Hoffman, B. M. *J. Am. Chem. Soc.* **2002**, *124*, 3143–3151.
112. Cosper, N. J.; Booker, S. J.; Ruzicka, F.; Frey, P. A.; Scott, R. A. *Biochemistry* **2000**, *39*, 15668–15673.
113. Walsby, C. J.; Ortillo, D.; Broderick, W. E.; Broderick, J. B.; Hoffman, B. M. *J. Am. Chem. Soc.* **2002**, *124*, 11270–11271.
114. Krebs, C.; Broderick, W. E.; Henshaw, T. F.; Broderick, J. B.; Huynh, B. H. *J. Am. Chem. Soc.* **2002**, *124*, 912–913.
115. Ugulava, N. B.; Surerus, K. K.; Jarrett, J. T. *J. Am. Chem. Soc.* **2002**, *124*, 9050–9051.
116. Ugulava, N. B.; Sacanell, C. J.; Jarrett, J. T. *Biochemistry* **2001**, *40*, 8352–8358.
117. Bui, B. T. S.; Florentin, D.; Fournier, F.; Ploux, O.; Méjean, A.; Marquet, A. *FEBS Lett.* **1998**, *440*, 226–230.
118. Gibson, K. J.; Pelletier, D. A.; Turner, I. M. Sr. *Biochem. Biophys. Res. Commun.* **1999**, *254*, 632–635.
119. Bui, B. T. S.; Escalettes, F.; Chottard, G.; Florentin, D.; Marquet, A. *Eur. J. Biochem.* **2000**, *267*, 2688–2694.

8.28
Denitrification

R. R. EADY

John Innes Centre, Norwich, UK

and

S. S. HASNAIN

CLRC Daresbury Laboratory, Warrington, UK

8.28.1 INTRODUCTION

Denitrification is the process in which some microorganisms couple respiratory ATP synthesis to the reduction of nitrate and nitrite, via the gaseous N oxide products NO and N_2O, to N_2. These reactions form an important step in the global nitrogen cycle, with agronomic (losses of soil N available for crop growth), environmental (generation of the greenhouse gas N_2O), and medical impact. The causative agents of bacterial meningitis (*Neisseria meningitidis*)[1] and gonorrhea (*N. gonorrhoeae*)[2] have the potential to denitrify during infection which may alleviate nitrosative stress generated by host defenses.

The individual reactions of denitrification are catalyzed by distinct reductases that variously contain Mo, Fe, Cu, or heme centers. Sequence comparisons show these reductases to be highly conserved between different denitrifyers, and that in some cases they are members of subclasses of superfamilies of enzymes. The chemistry is that of small-molecule binding and activation and coupled electron–proton transfer in one- or two-electron reductions. The crystallographic structures of many of the enzymes involved in denitrification have been determined. This has revealed the chemical nature of the electron transfer and catalytic centers of these enzymes, and in some instances their interaction with substrates and inhibitors. New metallocenters, and novel roles for others, have been revealed by these studies. The development of chemical models for Fe- and Cu-mediated transformations of nitrite to NO and the subsequent formation of N_2O have been stimulated by this area of biological research.

By drawing on the extensive body of available spectroscopic data we intend to highlight the additional insight these data give to enzyme function/mechanism. We shall also indicate the role of spectroscopy in the "refinement" of crystallographically derived models of metal centers particularly when the resolution of the crystallographic structure is only modest, and when the functional state of the enzyme (or metal centers) is not well defined in the particular crystal from which the crystallographic data were collected. This review is necessarily space constrained, and reference to early work cannot be all-inclusive; thus appropriate review references are cited.

8.28.1.1 Terminology

Denitrification is defined as the use of nitrate or nitrite as oxidants in electron transport pathways involving energy-generating proton translocation, *with the concomitant evolution of gas* (NO, N_2O, or N_2). This definition excludes the majority of nitrate-respiring bacteria that are only capable of reducing nitrate to nitrite during anaerobic growth. The energy source for growth is usually an organic compound, but H_2, NH_4^+, SO_4^-, or even Fe^{II} can be used.[3] The range of organisms has been extended to the actinomycetes[4] that denitrify nitrate or nitrite to form N_2O as the product, and to fungi, extending this ability to the eukaryotes.[3,5] Denitrification occurs most commonly under anaerobic or microaerophilic conditions when reducing equivalents derived from the oxidation of the energy source for growth are diverted from the reduction of oxygen to the reduction of N oxides.[6]

8.28.1.2 Biochemistry of Denitrification

The genes for the five N oxide reductases and a number of ancillary proteins required for reductase activity have been identified, indicating that denitrification involves some 50 genes. The sequence similarity of some of the reductase genes with other enzymes has provided insight into their relationship with other enzymes. For example, nitric oxide reductase (NOR) is a member of the superfamily of heme/Cu cytochrome oxidases, and the C-terminal region of nitrous oxide reductase (N_2OR) has strong homology with cytochrome *c* oxidase subunit II containing the Cu_A binding site.[3,5,6] It has been proposed that denitrification predated aerobic respiration.[7]
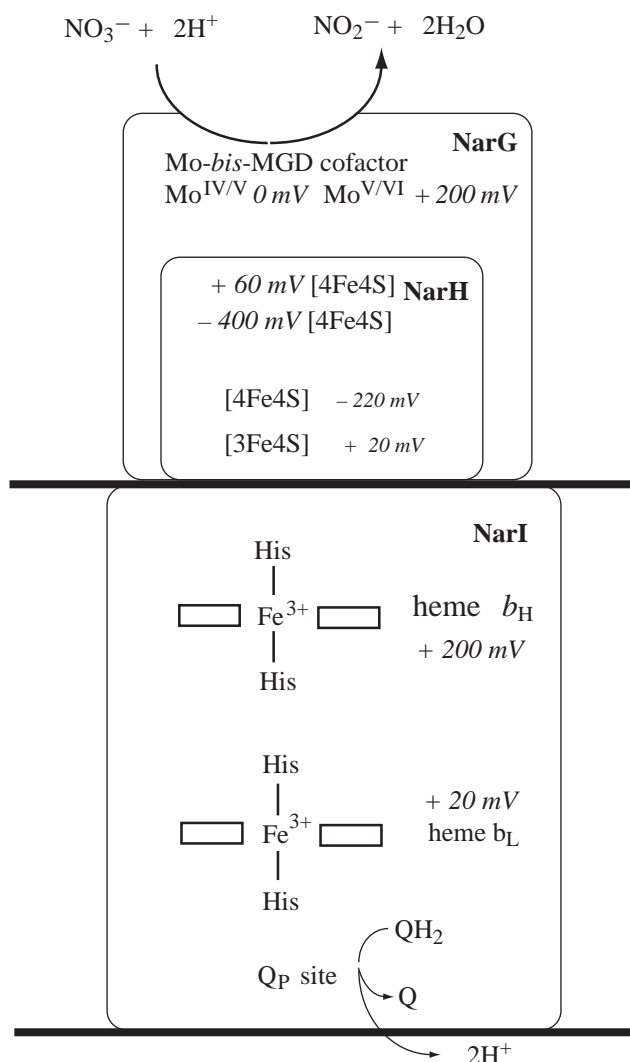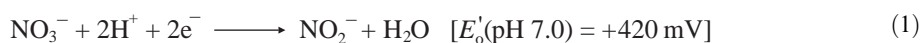
8.28.2 NITRATE REDUCTASE

Two types of dissimilatory nitrate reductase (NR) have been characterized in denitrifying bacteria, being either membrane-bound or soluble enzymes. Nitrate reduction by membrane-bound NR (encoded by *nar*) occurs in the cytoplasm and is involved in energy conservation, in contrast

to the periplasmic respiratory NRs (encoded by *nap*) that are energy dissipating. The Mo in both types of NR is bound in a modified molybdopterin cofactor at the active site, (molybdopterin guanine dinucleotide, MGD) in which two guanosine monophosphate molecules are bound to form a bis-MGD center.

8.28.2.1 Summary of Properties

Nitrate reductases catalyze the reduction of nitrate by an oxo-transfer mechanism to the Mo ion of the bis-MGD center (Equation (1)). Membrane-bound NRs encoded by *narGHJI* are members of a superfamily of bacterial [FeS]/MGD cofactor-containing enzymes and sequence comparisons indicate them to be members of the DMSO reductase family.[8,9] NR has been solubilized from the membrane and purified from a number of denitrifyers.[6] The enzymes are trimers containing heme *b*, tightly bound menaquinone-9, one [3Fe4S], and three [4Fe4S] centers which form the electron transfer pathway to the catalytic Mo atom of the MGD center. The global organization of these centers is shown in Figure 1:

$$NO_3^- + 2H^+ + 2e^- \longrightarrow NO_2^- + H_2O \quad [E_o'(pH\ 7.0) = +420\ mV] \tag{1}$$

Figure 1 Schematic of the arrangement of the redox centers of *E. coli* nitrate reductase.

The periplasmic NRs are heterodimeric enzymes encoded by *napAB* that are coupled to quinol oxidation by a membrane-bound tetra *c*-type cytochrome, encoded by *napC*. These enzymes do not have a role in energy conservation. In some organisms, e.g., *P. pantotrophicus*[10] and *Pseudomonas* sp. Strain G-179,[11] they are essential for anaerobic denitrification; however, it is clear that this enzyme has a range of physiological functions and is found in nondenitrifying organisms.[12]

Periplasmic NRs are closely related to formate dehydrogenase;[6] the larger subunit contains a [4Fe4S] center (in contrast to the analogous subunit of the membrane-bound NRs) and a bis-MGD cofactor center. The smaller subunit is a *c*-type cytochrome. The enzymes from *P. pantotrophicus* and *P. denitrificans* have been extensively studied using a range of spectroscopic techniques.

The nitrate reductases are discussed in more detail in Chapter 8.18.

8.28.3 NITRITE REDUCTASE

Two classes of dissimilar nitrite reductase (NiR) are known, one containing heme cd_1 and the other containing Cu; both classes catalyze the reaction of Equation (2):

$$NO_2^- + 2H^+ + e^- \longrightarrow NO + H_2O \quad [E_o'(pH\ 7.0) = +370\ mV] \tag{2}$$
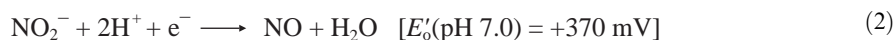
Structural studies of both types of enzyme have been extensive, and in the case of the heme NiRs a considerable body of kinetic data has been reported. Reviews of these enzymes and model coordination compounds relevant to substrate binding and reactivity have been published.[5,6,13–15]

8.28.3.1 Heme cd_1 NiR

This highly conserved class of cd_1 heme-containing NiR, present in some two-thirds of denitrifying bacteria, has been isolated and characterized from a number of sources. Structural studies of these enzymes are extensive; they present unexpected differences in heme ligation when isolated from different organisms, and extensive changes in conformation on redox state or the binding of ligands.[13]

These enzymes are homodimeric periplasmic proteins (encoded by *nirS*) that contain two different heme groups per monomer. One is a *c*-type heme bound via a Cys–X–X–Cys–His motif and has a role in electron transfer; the other, a noncovalently linked d_1 heme, is an unusual ferric-dioxoisobacteriochlorin, restricted to this class of enzyme and forms the active site. The biosynthetic pathway of heme d_1 is unique among the tetrapyrroles in having oxo, methyl, and acrylate side chains, involving some seven *nir* genes.[5] The E_m values of heme d_1 model complexes are ~200 mV lower than iron porphyrins.

The heme-containing NiRs are bifunctional, capable of the one-electron reduction of nitrite to NO, the two-electron reduction of hydroxylamine to NH_3, and the four-electron reduction of oxygen to water. Since the physiological role has been shown to be the reduction of nitrite, reactivity towards oxygen is not considered here. The formation of NO as the product of the reduction of the physiological substrate nitrite poses a mechanistic problem of avoiding the formation of dead-end, stable NO ferrous heme species.

8.28.3.1.1 Structure

The X-ray structures of oxidized and reduced NiRs from *P. pantotrophus*[16,17] and *Ps. aeruginosa*[18,19] and the mixed valence $c^{2+}d_1^{3+}$ states of PsNiR[20] have been determined. In addition, structures of the nitrite/NO, CN, CO, and O_2-bound species have been reported[19,21–25] providing an excellent basis for understanding events that occur during catalysis.

The crystal structures show the subunit of the $c\ d_1$ heme-containing NiR dimer to be comprised of two domains, a cytochrome *c*-like domain containing a covalently bound heme *c* and a rigid eight-bladed *β*-propeller domain containing a noncovalently bound heme d_1 (Figure 2). This heme, which forms the active site, is in a central tunnel of the *β*-propeller domain making a large number of contacts with both the polypeptide chain and buried water molecules. The shape of the d_1 heme

is not constrained by these interactions and the ring is nearly planar. The heme *c* environment is predominantly hydrophobic with the propionate side chains being solvent exposed; this center has a role in electron transfer from physiological electron donor (reduced pseudoazurin or *c*-type cytochromes) to the d_1 heme. The structures show the hemes to be angled at 60° with a heme/heme edge separation of ~12 Å, an arrangement leading to the expectation of rapid electron transfer between centers. However, as discussed below, this is not always observed.

The structure of oxidized PpNiR at 1.55 Å resolution reveals unexpected His/His ligation of heme *c*, with His69 and His17 as the axial ligands.[16] Heme d_1 is six-coordinate (6-c) with Tyr25 as a distal ligand and His200 as the sixth ligand. Tyr25 is located on an N-terminal arm of the heme *c* domain that extends into the heme *d* domain of the same monomer. The distal side of the heme d_1 pocket contains two conserved histidine residues, His345 and His388, with a presumed role in substrate binding or protonation. EPR and MCD data are consistent with the crystallographic assignment of heme ligation.[26]

On reduction of the crystals of PpNiR, unprecedented changes in heme ligation occur. The d_1 heme loses Tyr25 as a ligand and the heme *c* domain undergoes an extensive reorganization resulting in a ligand switching of heme *c*, with His17 being replaced by Met106. This conformational change and associated changes in heme *c* ligation result in essentially the same fold as seen in *oxidized* PaNiR (discussed below). The dissociation of Tyr25 from the distal face of the d_1 heme leaves it five coordinate ready to bind substrate, consistent with EPR and MCD data.

Crystallization of ascorbate-reduced PpNiR under anaerobic conditions resulted in a different crystal form where the heme *c* domain had a significantly different conformation from earlier structures resulting from rigid body domain movement.[27] The heme *c* of this conformation was a typical heme *c* with His/Met ligation that was unchanged on oxidation. The d_1 heme was five-coordinate with His200 as the proximal ligand. The conformational plasticity of the heme *c* ligation is consistent with an NMR study of the isolated heme *c* domain of PpNiR.[28] This showed that in the reduced state the heme ligation was His/Met as seen in reduced crystals of the intact enzyme. However, oxidation of heme *c* in the isolated domain resulted in an equilibrium mixture of His/Met and His/His ligation, with His/Met predominating.[28]

(a)

Heme *c*
Heme d_1

(b)
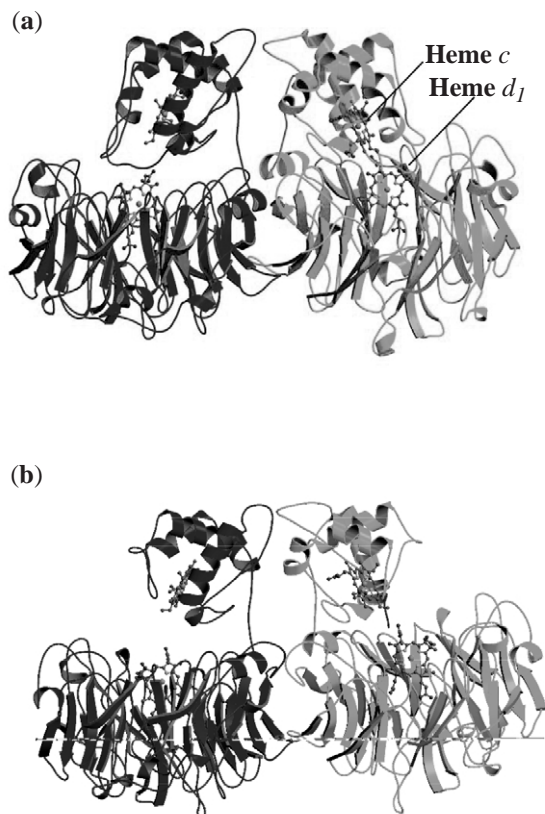
Figure 2 Structures of (a) oxidized and (b) reduced PpNiR.

The subsequent determination of the structure of PaNiR at 2.15 Å resolution revealed differences in the ligation of both hemes. Although the d_1 heme domain is essentially the same as that of PpNiR, the topology of the cytochrome c domain and ligands of the c heme are different.[18] The heme c ligands of PaNiR are His51/Met88 in both oxidized and reduced enzyme, rather than the atypical His/His and redox-dependent ligand switching seen in PpNiR. In addition, the distal ligand of heme d_1 is a hydroxyl group rather than Tyr. The coordinated hydroxyl group is H-bonded to Tyr10, but this residue is provided by the N terminus from the c domain of a different monomer in contrast to PpNiR. Mutagenesis of this Tyr residue has no effect on activity, so it is not required to promote dissociation of NO from the enzyme.[20] Comparative EPR and MCD studies of PsNiR indicated that like PaNiR the heme c had His/Met ligation.[26] These authors have suggested that the His/His ligation of heme c represented a resting state of the PpNiR.

8.28.3.1.2 Mechanistic implications

The change in ligation of the heme c of PpNiR on reduction is important for catalysis since the enzyme was inactive with pseudoazurin as electron donor and prereduction of the enzyme with dithionite was required to activate the enzyme.[29] Once activated, the enzyme undergoes redox cycling maintaining His/Met ligation of heme c. On exhaustion of reductant the enzyme reverted to the "as isolated" coordination environment within 20 min. Relaxation of the enzyme to the "as isolated" conformation was prevented by nitrite (but not a variety of other anions) indicating the specificity of the heme d_1 for its substrate.[30] The stable ferric NO_2^- d_1 heme complex surprisingly was EPR silent and heme c retained His/Met coordination.

Time-resolved studies of PpNiR during turnover using single-crystal microspectrophotometry and X-ray crystallography, together with freeze-quench, have allowed structural rearrangements of the enzyme to be identified and reaction intermediates to be trapped.[21] Nitrite was shown to bind to the reduced heme by N rather than O, and is H-bonded to both His245 and His388, potential sources of the protons required for nitrite reduction.

A heme-bound NO product with an Fe—NO bond angle of 131° and an Fe—N distance of 2.0 Å was assigned to a ferric species, since the planarity of the heme d_1 was that of the oxidized enzyme and crystals could undergo repeated catalytic cycling. This indicates that a long-lived ferrous NO adduct was not formed under these conditions. The position of Tyr25 was different in the NO- and nitrite-bound structures and it was proposed[16] to have a role in assisting displacement of NO, although this cannot be a general role for Tyr in the distal pocket since mutagenesis of this residue of PaNiR did not affect activity.[31] In these structures the heme c had His/His ligation characteristic of the oxidized enzyme, consistent with microspectrophotmetric measurements that both hemes were oxidized in the NO-bound structure.

Crystallographic studies[19] of NO bound to PaNiR formed by diffusing NO into reduced crystals showed that the conserved His residues in the distal pocket interacted with the O atom of the bound NO. The Fe—N distance was 0.2 Å shorter than for PpNiR, consistent with a different oxidation state of the heme d_1. Tyr10 that H bonds to the hydroxide bound to the heme d_1 of the oxidized enzyme is rotated away from the active site. Mutational studies of the two conserved His residues of the distal pocket of PaNiR showed that they are important for activity and in preventing the formation of dead-end species with NO bound to ferrous heme d_1.[32] These mutations also resulted in large changes in the topology of the heme c domain. His369 has also been shown to form a hydrogen bond to CN bound to heme d_1 and appears to play a dominant role in controlling the binding of anionic ligands.[33]

8.28.3.1.3 Heme–heme electron transfer

The redox coupling of the two hemes shows different degrees of complexity in these enzymes. *Pseudomanas nautica* (PnNiR) shows ideal behavior and E_m values for heme c and heme d_1 are +234 mV and +199 mV, respectively.[34] In contrast, PpNiR shows strong heme–heme interaction resulting in hysteretic behavior attributed to kinetically gated, conformationally dependent cooperatitvity in two-electron transfer reactions.[35]

The heme–heme separations in PpNiR and RaNiR are similar, but internal electron transfer occurs at very different rates. Pulse radiolysis studies show the rapid reduction of heme c in both enzymes but the subsequent electron transfer to heme d_1 occurs at a rate of $3 s^{-1}$ in PaNiR compared with $1.4 \times 10^3 s^{-1}$ in PpNiR.[36,37] The authors argue that this difference is too large to

be accounted for by a difference in redox potentials of the hemes in the two enzymes, even if His/His ligation of heme c was retained in PpNiR. The slow rate was proposed to arise from a coordination change associated with electron transfer from heme c to heme d_1. The suggested loss of the hydroxide from heme d_1 of PaNiR on reduction, as the coordination change responsible was consistent with the 10^4 increase in the rate of electron transfer observed in the presence of CN, which binds to both oxidized and reduced heme d_1, removing the requirement for a ligand exchange to facilitate electron transfer.[37] Further support was provided in a crystallographic freeze-quench study of the mixed valence $c^{2+}d_1{}^{3+}$ species of PaNiR showing the ligating hydroxide was retained.[20] This study also showed that reduction of the heme c did not trigger conformational changes around heme d_1 as had been suggested earlier.[19]

In the case of PpNiR, heme d_1 can accept an electron without displacement of Tyr25 from the Fe ion and rapid electron transfer is observed.[37] In pulse radiolysis experiments the rate of internal electron transfer was not changed in the presence of nitrite and an intermediate (presumed to be an NO-bound oxidized heme d_1 species) formed within 2 s. Thus the structural differences that result in different rates of primary electron transfer (i.e., the first intramolecular electron transfer following reduction of the oxidized enzyme) appear to be the presence of hydroxide versus Tyr as the axial ligand to heme d_1.

Laser photodissociation of both reduced PaNiR—CO and PaNiR$c^{3+}d_1{}^{2+}$–CO results in the formation of a conformationally unrelaxed transient[38] that undergoes rapid structural relaxations before rebinding of CO occurs. In the transient $c^{3+}d_1{}^{2+}$ species the reduction of heme c by heme d_1 is fast, with a rate constant of $2.5 \times 10^4\,\mathrm{s}^{-1}$. However, rebinding of CO to the relaxed mixed valence $c^{2+}d_1{}^{3+}$ species was slow with a rate constant of $0.25\,\mathrm{s}^{-1}$ proposed to be due to the rate-limiting electron transfer from heme c to heme d_1. Slow rates of electron transfer are consistent with pulse radiolysis studies and the rate determined with reduced azurin as electron donor.[31] The fast structural reorganization of both PaNiR and PsNiR on photodissociation of CO is not dependent on the presence of the N-terminal extension since it is lacking in PsNiR.[38,39]

The kinetics of CO photodissociation and rebinding to PpNiR showed a biphasic recovery.[25] The slower phase of rebinding of the neutral ligand CO to heme d_1 was associated with proton release and it was proposed that if this occurred when NO bound, electron transfer may be modulated to prevent reduction of heme d_1 before dissociation of NO. A comparison of the structures of reduced PpNiR and the NiR—CO complex revealed changes in the puckering of d_1 heme and the H-bonding network.[25]

8.28.3.1.4 Mechanistic studies

Resonance Raman studies of CO and NO bound to PaNiR showed unusually high stretching frequencies compared with other hemoproteins due to the different electronic properties of d_1 heme.[40] Nitrite binds to heme d_1 in both ferrous and ferric oxidation states but has a higher affinity for ferrous Fe with K_d values of approximately 1 μM and 2.5 mM, respectively.[30,32] Extensive evidence for the formation of an electrophilic heme–nitrosyl species derived from nitrite (formulated as Fe^{II}–NO^+ or Fe^{III}–NO) based on isotope exchange with ^{18}O-labeled water into NO, nitrosyl transfer to N nucleophiles, and FTIR studies of the interaction of NO with oxidized PsNiR.[41] In the latter study a band at 1,910 cm^{-1} was assigned to a ferric NO heme complex. This species is considered as the key intermediate in the mechanism for nitrite reduction.[41]

The transient kinetics of NiR turnover has been studied using stopped-flow absorbance, rapid-quench EPR, and time-resolved FTIR spectroscopy. Stopped-flow/quenched EPR showed that nitrite binds to the ferrous heme d_1 of PaNiR and was reduced to NO within the dead time of the apparatus to form an EPR-silent ferric NO heme d_1 complex.[42] The subsequent transient with a rate constant of 1 s^{-1} was assigned to electron transfer from heme c to heme d_1. The final species corresponded to the EPR-detectable NO–heme d_1 complex of fully reduced enzyme. A later study[33] detected the mixed valence heme c^{3+}–heme $d_1{}^{2+}$NO species at 6 ms after mixing before formation of the fully reduced NO complex.

Similar experiments with PpNiR together with time-resolved FTIR showed significant differences.[43] Nitrite bound to heme d_1 and was rapidly reduced to form an EPR-detectable ferrous NO–heme d_1 complex with oxidized heme c. The rate constant for electron transfer was estimated to be 500 s^{-1}. In a slower phase FTIR showed development of a band at 1,913 cm^{-1} formed with a rate constant of 38 s^{-1}. The energy of this band is consistent with a heme–Fe^{II}–NO^+ species, and close to those of model compounds of ferric heme d_1 with NO and N-methyl imidazole.[44]
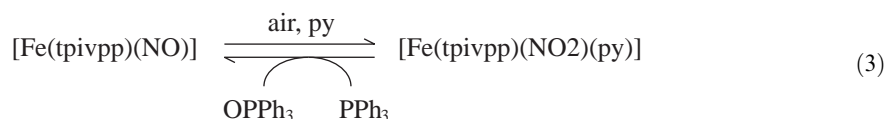
Surprisingly, given the highly reactive nature of this species[45] it remained stable for 15 min. Optical and EPR changes concomitant with the formation of the heme–Fe^{II}–NO^+ species corresponded to the redistribution of electrons to give ~50% mixture of species of heme c^{3+}–heme d_1^{2-}–NO and of heme c^{2+}–heme d_1^{2+}–NO^+. These changes were attributed to different geometries of NO binding, possibly within different subunits of the dimer, consistent with the asymmetric distribution of intermediates detected in turnover of PpNiR in crystals.[21] No spectroscopic evidence for the rebinding of Tyr25 to heme d_1 was obtained.

A proposed reaction mechanism based on these structural and kinetic data is shown in Figure 3. Nitrite binding to reduced heme d_1 is followed by transfer of an electron and two protons from

Figure 3 Scheme for the reaction mechanism of PpNiR.

the conserved His residues to form water and an enzyme-bound ferric nitrosyl intermediate. This intermediate is unstable and the NO dissociates before re-reduction of heme d_1 occurs in order to prevent the formation of the dead end ferrous NO complex. As discussed above, an unresolved problem with this mechanism is that no transient kinetic study has revealed catalytically competent rates of NO release from the enzyme. A quantum mechanical analysis[46] of steps in the reduction of nitrite also indicated the potential for isomerization of the $Fe^{II}-NO^+$ species to the heme–Fe^{III}–NO species, as proposed from FTIR studies.[43]

8.28.3.1.5 Model studies

A series of Fe^{II} and Fe^{III} porphyrin complexes in which NO and/or NO_2^- is the axial ligand have been synthesized and characterized by Scheidt and co-workers.[14] The Fe^{III} complexes are unstable; the bound nitrite is activated and undergoes O atom transfer reactions to a variety of acceptor molecules to form a stable Fe^{II}–NO species.[14,48]

The conversion of the coordinated nitrosyl of the picket fence porphyrin complex [Fe(tetra($\alpha,\alpha,\alpha,\alpha$-*o*-pivalamidophenyl)porphyrinato)(NO)] to nitrite provides the first unambiguous demonstration of a nitrosyl-to-nitrite conversion at an iron porphyrin center.[49] The reaction of Equation (3) occurs in air in the presence of pyridine, and is biomimetic since the starting complex is formed on reduction with triphenylphosphine. The picket fence pocket appears to be crucial for the stabilization of the NO product in air, since nonpicket fence NO porphyrins were shown to form oxo dimers readily:

$$[\text{Fe(tpivpp)(NO)}] \; \underset{\text{OPPh}_3 \quad \text{PPh}_3}{\overset{\text{air, py}}{\rightleftharpoons}} \; [\text{Fe(tpivpp)(NO2)(py)}] \qquad (3)$$

Limited data for Fe^{II} nitrite complexes are available. They do not undergo O atom transfer reactions but [Fe^{II} (tetra($\alpha,\alpha,\alpha,\alpha$-*o*-pivalamidophenyl)porphyrinato)(NO)] reacts with an excess of NO to form the mixed $Fe^{II}(NO)(N_2O)$ complex via a proposed reactive nitrite intermediate.[14]

8.28.3.2 Copper NiR

Copper-containing NiRs have been isolated and characterized from a range of denitrifyers (both Gram positive and negative bacteria and fungi) and been the subject of extensive spectroscopic and structural studies.[5,14,15,47] One development has been the recognition of a new class of membrane-bound NiR isolated from *N. gonorrhoeae*.[50] This enzyme has a low sequence identity (30%) but a similar structure to the soluble enzymes. The major difference is an N-terminal extension, which is embedded in the membrane via a palmityl group.

The structures of the enzymes from *Achromobacter cycloclastes*,[51,52] *Alcaligenes faecalis* S6,[53,54] *Alcaligenes xylosoxidans*,[55–58] and the soluble domain of NiR from *N. gonorrhoeae*[50] have been determined.

The family of enzymes encoded by *NirA* has highly conserved amino acid sequences with 60–80% identity. In addition to their physiological role, reduction of nitrite to NO, these enzymes also catalyze the slow formation of N_2O by reaction of an enzyme-bound intermediate with NO. Activity is inhibited by CN, CO, and N_3^-.

Depending on the organism from which they are isolated, Cu—NiR is blue (e.g., AxNiR, NgNiR) or green (e.g., AcNiR, AfNiR). The color arises from a (Cys) S—Cu charge transfer transition, characteristic of type 1 Cu centers, giving rise to absorption bands at 600 nm and 450 nm. The ratio of these bands depends on the geometry of the center and determines the color of the enzyme.

The oxidized enzymes have EPR spectra comprised of overlapping contributions from type 1 and type 2 Cu centers. Features arising from the hyperfine structure of the type 2 center are resolved at low field. The isolation of a species of NiR depleted in the type 2 Cu (T2DNiR) has enabled difference spectroscopy to be used in EPR, ENDOR, and EXAFS studies to probe the active site type 2 center of the holoenzyme.

The consensus view of CuNiR function, and that considered here, is that the reduction of nitrite occurs at the type 2 Cu center. However, enzyme deficient in type 2 Cu has consistently been reported to have an NiR activity, up to 60% of the wild-type under some conditions,[59] and nitrite has been shown to bind to T2DAxNiR.[60] The difficulty of retaining a type 2 site geometry and environment (proposed to be required for activity), other than the loss or removal of Cu from the native enzyme, has made it difficult to exclude the possibility that the observed activity is due to residual Cu in the type 2 center. The proposal that T2DNiR has activity is controversial.

8.28.3.2.1 Structure

These enzymes are trimeric periplasmic proteins, $M_r \sim 109$ kDa encoded by *NirA*, except NgNiR as noted above. Each monomer contains a type 1 copper center (His$_2$, Met, Cys) which has a role in electron transfer from physiological electron donors to the catalytic type 2 copper centers (His$_3$H$_2$O). The type 2 copper centers are located at the interface of two subunits (Figure 4). The Cu ions are some 12.6 Å apart and are directly connected by the adjacent residues His129 and Cys130. A second connection between the sites is provided by the chain His89 to His94 (AxNiR numbering), which also carries the putative proton donating group at the active site, Asp92 (Figure 5). The global structures of the green and blue NiRs are very similar (C$_\alpha$ rmsd are 0.6 Å), with each monomer consisting of two domains with Greek key β-barrels, typical of the cupredoxin fold found in azurins. A surprising finding from a comparison of the structures of the blue AxNiR and the green AfNIR was the difference in surface charge of -30 e for the two proteins, which sequence comparisons show to be 68% homologous, but was not obvious from the composition similarity.[56]

8.28.3.2.2 Type 1 Cu electron transfer centers

The type 1 Cu ion is ligated with a distorted trigonal geometry with two His and the Cys as the strong planar ligands, with a weaker axial Met ligand (Figure 5). The structure determination of

Figure 4 Structure of AxNiR.
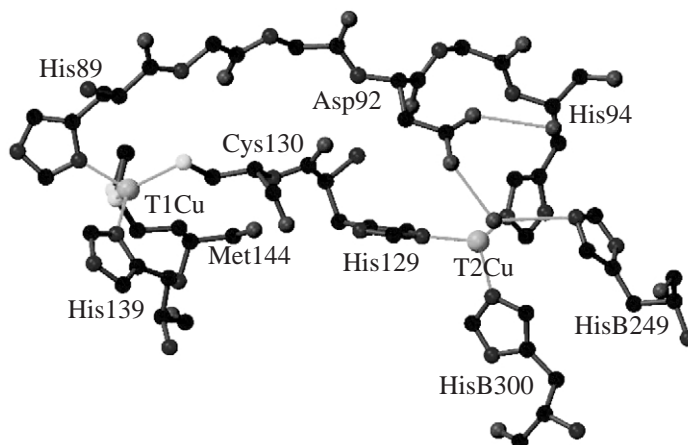
Figure 5 Organization of the Cu centers of AxNiR.

the blue AxNiR[56,57] showed the difference in spectroscopic properties of type 1 Cu centers of the blue and green enzymes to arise from a difference in the angular organization of Met in the site. These differences result in a more trigonal rather than flattened tetrahedral geometry of green NiRs, in agreement with density functional calculations.[61] The E_m of the type 1 centers of different NiRs are ~240 mV. As observed in azurins, one of the His residues (His139 in AxNiR) is exposed to the solvent providing a route for electron transfer from the physiological redox partner, azurin or pseudoazurin to blue and green NiRs, respectively.

8.28.3.2.3 Type 2 Cu catalytic centers

The type 2 Cu ion is ligated by two His residues from one monomer, a His residue from a second monomer, and an exogenous ligand H_2O (OH^- or Cl^-). The near tetrahedral arrangement of the ligands is unusual, since type 2 Cu is similar to that of the Zn site of carbonic anhydrase and thermolysin.[62] Q-band ENDOR of RsNiR is consistent with the strong hyperfine coupling of two histidine nitrogen atoms and a more weakly coupled histidine nitrogen.[63] The site is located at the bottom of a channel, ~13 Å deep, directly exposed to the solvent. The channel is lined with hydrophobic residues and the carboxylate of the conserved Asp in the hydrophobic pocket is H-bonded to the H_2O bound to the Cu and to a H_2O bridged to the imidazole of the conserved His residue (Figure 5). This bridging network completes a solvent network leading to the surface of the enzyme. The bridging H_2O donates a proton to Asp98 and is a proton acceptor from positively charged His255. These residues and the water bound between them are the probable sources of the protons required for nitrite reduction. The proposed protonation state of Asp98 is consistent with a FTIR pH-dependence study of CO bound to the type 2 center.[64]

  EPR and ^1H, $^{14,15}N$ ENDOR studies of AxNiR[65] and RsNiR[63] have shown that nitrite binds to the type 2 Cu center and perturbs the ligation of the Cu to displace a proton. This is consistent with EXAFS data for AxNIR, that show nitrite binding causes the average Cu—His distance to increase[66] by 0.08 Å. These spectroscopic data are complemented by crystallographic studies of AfNiR,[67] AxNiR,[55,56,68] and AcNiR[53] that show nitrite displaces the ligated H_2O to bind to the Cu asymmetrically via both O atoms. The conserved Asp of the hydrophobic pocket H-bonds to the bound substrate and has a presumptive role in facilitating proton transfer to the bound substrate. Binding of nitrite monitored by changes in the EPR of the type 2 center shows tighter binding at pH 5.2 compared with pH 7.5, consistent with activity pH profiles.[69] The lower activity at high pH may arise from the inability of nitrite to displace OH^- from the active site.[70]

8.28.3.2.4 Role of active site aspartate and histidine residues

The superposition of Asp98 and His255 on catalytically important residues of Cu_2Zn_2 carbonic anhydrase led to a suggested role important for NiR catalysis.[66,71] These two residues have been

mutagenized in AxNiR,[72,73] and structurally characterized in AfNiR[74,75] and AxNiR.[76] The conserved His residue has been mutated in RsNiR.[63]

The mutant proteins show substantial decreases of (100–1,000)-fold in NiR activity when assayed with Methyl Viologen as electron donor. Surprisingly, the D92 N and D92E mutants of AxNiR had significant activity with reduced azurin.[73] These differences could arise from an altered conformation of NiR when complexed with azurin, resulting in an increased accessibility to the active site or reorganization of the water network.

The crystal structure of the AfNiR-D98 N mutant showed that the side chain ofAsn98 was reoriented resulting in the loss of the H bond to the H_2O bound at the active site Cu, but was still H-bonded to His255. A role for negatively charged Asp98 in directing the binding and protonation of nitrite in the native enzyme was proposed, consistent with kinetic studies of the comparable mutants of AxNiR.[72]

In both mutants an additional H_2O in the pocket restored H bonding from the H_2O ligand of the Cu to the substituted residues in position 255. The position of the additional H_2O would obstruct the binding of nitrite, consistent with steady-state assays that show an increase in the apparent K_m for nitrite.[72]

Nitrite soaking of crystals of the oxidized D98 N mutant revealed that nitrite bound weakly, emphasizing the importance of the H bond of bound substrate to Asp98 in the wild-type enzyme. The oxidized H255 N mutant showed that nitrite did not displace the bound H_2O ligand, nor the additional H_2O, but bound in a novel monodentate mode via a single O atom.[75] The structure of the Cu, with a distorted square pyramidal geometry is similar to a synthetic analogue.[77] Surprisingly, in both mutants nitrite remained bound to the *reduced* enzymes and it was proposed that the novel monodentate binding mode of nitrite with retention of the H_2O ligand mimicked the electronic and structural properties of a catalytic intermediate of wild-type NiR. An equally surprising finding was the incorporation of Cu from the crystallization mother liquor into the type 1 site of the His255N[NO_2^-] enzyme generated a unique binuclear center with similarities to a Cu_A site.

8.28.3.2.5 Internal electron transfer

Pulse radiolysis studies show that the rapid reduction of the type 1 centers is followed by a partial reoxidation as an electron is transferred to the type 2 Cu centers. The extent of reoxidation is determined by the relative redox potentials of the two centers. In the presence of nitrite the reaction (Equation (4)) proceeds to completion and the type 1 center becomes fully reoxidized. Typical values for k_{ET} for both green (AcNiR) and blue (AxNiR) at pH 7 are $1.4 \times 10^3 \, s^{-1}$, which decreases by 50% in the presence of nitrite.[78] The rapid rate of reduction of the type 1 center was unaffected by pH but k_{ET} showed a marked pH dependence and at pH 6 the rate was $2 \times 10^3 \, s^{-1}$ and was unchanged by nitrite.[79] Curves for the pH k_{ET} dependence were essentially the same as the pH activity curve suggesting that two proton dissociations with pK_a values of ~5 and ~7 play an important role in both processes. Studies with AxNiR mutants Asp98Ala and His255Ala showed that these residues in wild-type NiR control the rate of electron transfer from the type 1 to the type 2 center by the formation of an H-bonding network:[79]

$$\text{T1Cu(II) T2Cu(II)} + e^- \longrightarrow \text{T1Cu(I) T2Cu(II)} \xrightarrow{k_{ET}} \text{T1Cu(II) T2Cu(I)} \tag{4}$$
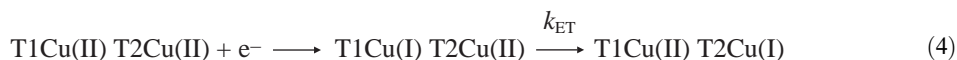
These residues clearly have a role controlling electron transfer in addition to the provision of protons required for nitrite reduction, consistent with the proposal that structural change around the type 2 Cu center gated internal electron transfer.[80] Control of the timing of the delivery of electrons to the type 2 center is critical in CuNiR function since nitrite has a very low affinity for the reduced center.[66] The driving force for electron transfer in isolated CuNiR is low due to the small difference in the E_m values of the two Cu centers.[6] In the case of RsNiR, electron transfer is thermodynamically unfavorable since the type 2 center with $E_m > 200 \, mV$ is some 50 mV more negative that the electron donor type 1 center.[63] Presumably changes in the electronic state of the center that occurs when nitrite binds results in an increase in redox potential of the site to facilitate electron transfer.

8.28.3.2.6 Mechanistic studies

Comparative EPR, EXAFS, and UV–visible spectroscopy of reduced and oxidized AxNiR showed that the reduced type 2 center lacked the H_2O ligand seen in the oxidized state.[66] In addition, azide, a competitive inhibitor, could no longer bind to the active site of the reduced enzyme. Together with crystallographic data for AfNiR showing low occupancy of nitrite in crystals of the reduced enzyme,[67] these data strongly suggest that the reduced type 2 center does not bind nitrite. This is consistent with the observation that reduction of AxNiR in the absence of nitrite inactivates the enzyme.[66]

Reaction schemes for CuNiR have been proposed where binding of nitrite asymmetrically via both O atoms to the oxidized type 2 center triggers electron transfer from the reduced type 1 center. Inorganic model systems[14] show Cu^{II} preferentially binds nitrite via O (as in oxidized NiR), but the complexes are nonmimetic, whereas Cu^{I} binds nitrite via N and reacts with acid to form NO and H_2O. Clearly these preferred binding modes can be modulated in the protein environment as indicated by the monodentate binding via a single O atom to Cu^{I} in a reduced type 2 Cu center. However, although there are no structural or spectroscopic data suggestive of N coordination of nitrite to CuNiR, N coordination of an intermediate has supporting data.

One proposed mechanism[81] for CuNiR, which parallels catalysis by the well-characterized heme NiRs, involves the formation of a $Cu^{I}-NO^+$ intermediate formed by protonation of bound nitrite followed by the abstraction of an oxygen atom to form OH^-. Although the $Cu^{I}-NO^+$ intermediate has not been observed directly, the formation of N_2O, a minor product of nitrite reduction by AfNiR,[82] has been attributed to the reaction of a Cu nitrosyl intermediate with NO to form N_2O. Consistent with this, large amounts of $^{14/15}N_2O$ were formed[83] during turnover in the presence of ^{15}N-labeled nitrite and ^{14}N-labeled NO.

The importance of the conserved His and Asp residues and associated H_2O molecules of the active site pocket in substrate binding and catalysis has led to proposed reaction schemes involving general acid–base catalysis with[55] or without[52,59] the formation of a Cu nitrosyl species (Figures 6A and 6B, respectively).

In both mechanisms, nitrite binding involves the displacement of H_2O to form a $Cu^{II}-NO^{2-}$ complex. The water departs as OH^- leaving the Asp residue protonated. Reduction of the type 2 center then results in the breakage of the O—N bond of nitrite proximal to the Asp residue, which protonates the cleaved oxygen to form OH^-. The enzyme at this stage has a type 2 center with NO bound, $Cu^{I}-NO^+$ (or $Cu^{II}-NO\cdot$).

The structure of the AfNiRH255 N mutant with both nitrite and H_2O bound to the active site Cu^{II} has led to the proposal that a transient in catalysis may be a Cu^{II} $OH^-\cdot NO$ species prior to this step.[75] Protonation of the OH^- at the active site by His255 via the bridging water and release of NO regenerates the active site (Figure 6A). In a variant of this reaction scheme, a proton from Asp is transferred to nitrite to form a Cu^{I} NOOH intermediate.[72] The subsequent internal electron transfer and protonation of this species by His255 yields NO and Cu^{II} H_2O regenerating the type 2 center for further catalysis.[84] Neither of these proposed mechanisms involves the putative nitrosyl intermediate.[81]

In an alternative scheme (Figure 6B), the species $Cu^{I}-NO^+$ undergoes linkage isomerization to form a Cu^+-N-NO^+ species.[55] By analogy with reactions of model systems[85] this would facilitate catalysis via the putative $Cu^{I}-NO^+$ intermediate[81] and NO formation would occur by the decomposition of the unstable $Cu^{II}-NO\cdot$ species formed by internal electron transfer. A proposal[53] involving a $Cu^{I}-ON^+$ species appears less likely since it is without chemical precedent. Further studies are required to resolve the mechanism, and the controversial issue of the activity of T2DNiR.

8.28.3.2.7 Model studies

The first structurally characterized mononuclear Cu^{I} nitrite complex with biomimetic activity was $[(L^{i-Pr})Cu(NO_2)]$ (L^{i-Pr} = 1,4,7-triisopropyl-1,4,7-triacyclononane) in which nitrite binds in an η^1-N mode[85,86] (Figure 7). On treatment with acetic acid or the Lewis acid $Me_3SiO_3SCF_3$, this complex yielded NO and $L^{i-Pr}Cu(O_2CCH_3)_2$ or $L^{i-Pr}Cu(O_3SCF_3)_2$, respectively.

A series of Cu^{I} and Cu^{II} compounds with tridentate ligands incorporating benzimidazole or pyrazole have also been synthesized and structurally characterized.[14,87] Their nitrite binding and biomimetic properties were investigated and the Cu^{II} complexes were shown to bind nitrite with high affinity; either through one or both O atoms depending on the stereochemical feature
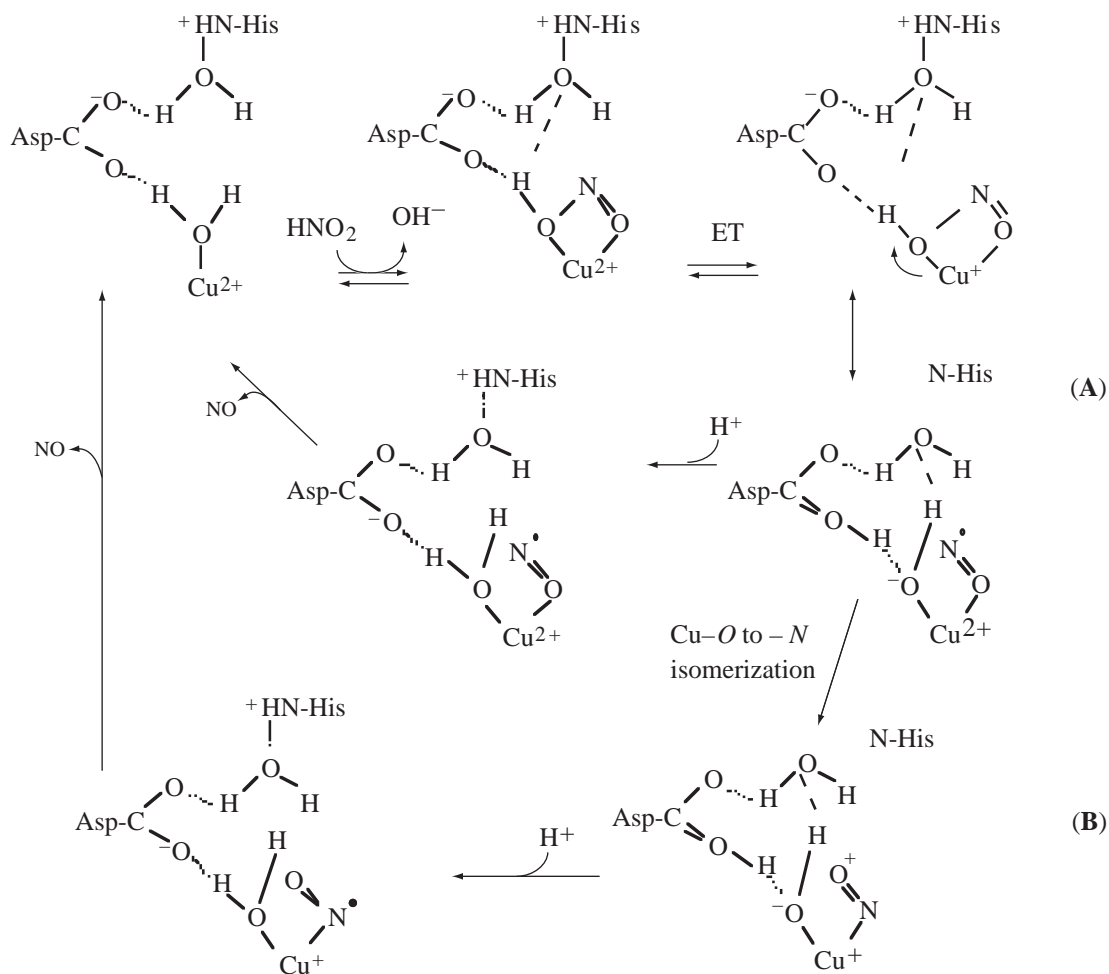
Figure 6 Proposed mechanisms for CuNiR.
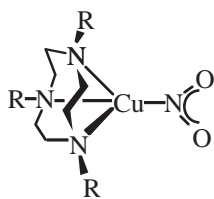
Figure 7 Stable mononuclear η^1-*N*-nitrite Cu^I complex with biomimetic activity.

imposed by the coordination environment. The Cu^I complexes showed biomimetic activity and in the presence of nitrite and protons form the Cu^{II} complex and NO. The complex with bis[2-(1-methylbenzimidazol-2-yl)ethyl]amine ligation to the Cu was the most effective (Figure 8) and spectroscopic studies were consistent with a rapid protonation of the bound nitrite preceding
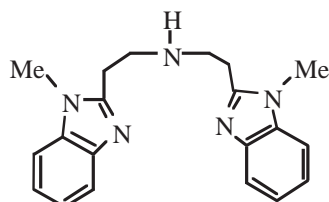
Figure 8 Cu^I complex with N-donor ligands is an effective CuNiR model.

electron transfer, via a mechanism involving dehydration of a diprotonated nitrite to form the nitrous acidium ion ($H_2NO^+_2$).

Nitrous acid was the only observable intermediate even at low temperature and conditions designed to maximize the accumulation of other species. The mode of binding of nitrite to the Cu^I species is not known but the authors suggest that coordination through the N atom would facilitate *O*-protonation and loss of water.[87] Both N and O modes of binding have been shown for [(tris((2-pyridyl)-methyl)-amine)$Cu^{II}(NO_2)](PF_6)$ complexes where, depending on the solvent, interconversion between ligation modes occurs. The O binding mode of nitrite is asymmetric η^2-O,O′ in these complexes.

8.28.4 BACTERIAL NITRIC OXIDE REDUCTASE

Irrespective of the bacterial species from which they are isolated these enzymes have the same heme/nonheme iron active site that catalyzes N—N bond formation in the reaction of Equation (5). However, some nitric oxide reductases (NORs) exhibit a different subunit composition and type of center involved in electron transfer to the active site. The prototype bacterial NOR, isolated from Gram-negative organisms *P. stuzeri*, *Pa. halodenitrifcans*, and *P. denitrificans*, is dimeric with the subunits encoded by *norBC*.[5,6,88–90] These are membrane-bound enzymes containing both nonheme and heme iron, and despite their sequence homology with heme copper oxidases, prototype bacterial NOR does not contain copper. No structure of the bacterial NORs has been determined so the homology modeling and spectroscopy provide the basis for the nature and organization of the redox centers these enzymes contain:

$$2NO + 2e^- + 2H^+ \longrightarrow N_2O + H_2O \quad [E'_o(pH\ 7.0) = +1.18\ V] \tag{5}$$
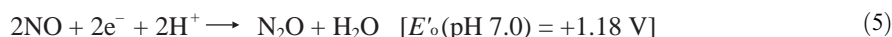
The dimeric NOR from *Bacillus azotoformans* contains a Cu_A center located in the smaller subunit, in place of the *c*-type heme of prototype NOR. Menahydroquinone, but not cytochrome *c*, functions as electron donor.[91]

A second variant, the enzyme from *Ralstonia eutropha* H16 (previously *Alcaligenes eutrophus* H16), is monomeric (encoded by *norB*) and lacks the small subunit that binds the electron donating centers of the other enzymes.[92] Residues proposed to ligate hemes *b* and Fe_B are conserved in *norB* of *R. eutropha* and the enzyme contains heme *b* and nonheme Fe in a 2:1 ratio. The enzyme has an extended N-terminus of 280 amino acids that is essential for activity, with a proposed role in allowing quinols rather than cytochrome *c* to function as electron donor. These NORs, which are also membrane bound, have biochemical and spectral properties indicating that the catalytic center is the same as in prototype NOR.

8.28.4.1 Prototype NOR Containing Heme *c*, Heme *b*, and Nonheme Fe

Although NOR may be associated with additional subunits *in vivo*,[3] fully functional NOR preparations isolated following detergent treatment of membranes are dimeric. The smaller subunit (NorC, 17 kD) is predicted to have a single transmembrane helix at the N terminus that anchors the periplasmic C terminus to the membrane. This subunit has a single Cys–Xaa–Xaa–Cys–His heme *c* binding motif. The larger subunit (NorB, 53 kD) is predicted to have 12 transmembrane helices and carries the low-spin bis-His coordinated heme *b* and the dinuclear heme b_3–Fe_B center. DNA sequence comparisons of NorB with subunit I of CcO show that NOR is a divergent member of the superfamily of the respiratory heme/copper oxidases. The structure of CcO shows the active site to be a high-spin heme located ~5 Å from a copper ion (Cu_B) forming a magnetically interacting dinuclear center.[93] As described below, the analogous center of prototype NORs forming the catalytic center is a high-spin b-type heme (heme b_3) and a nonheme iron center (Fe_B).

Prototype NORs have been solubilized and purified from a number of sources.[5,6] The most extensively studied, and discussed here, are those of *Ps. stuzeri*, *P. halodenitrificans*, and *P. denitrificans*. EPR and variable-temperature MCD studies of oxidized PsNOR showed the presence of three 6-c heme groups with distinct axial coordination.[90,95]

Two of these are magnetically isolated low-spin ferric heme *c* and heme *b*, which have IR transitions characteristic of bis-His and His-Met ligation. The third heme, b_3, has unusual temperature-dependent spin state and EPR and MCD spectroscopic features consistent with

His/OH coordination. This differs from the penta coordination assigned to heme b_3 of oxidized PdNOR from room temperature resonance Raman data.[95]

The high-spin ferric heme b Fe and Fe$_B$ are strongly antiferromagnetically coupled which results in both metal centers being EPR silent.[88,90,94] The nature of this interaction was defined in a resonance Raman study of oxidized PdNOR.[96] When incubated with ^{18}O-labeled water the ^{16}O–^{18}O difference spectrum showed a vibration at $\sim 830\,cm^{-1}$ reduced in intensity. Comparison with the model porphyrin compound[97] tris(2-(^{5}L)Fe^{III}–O–Fe^{III}–Cl)$^+$ identified the ν_{as} band as arising from a (Fe—O—Fe) grouping with a Fe—Fe separation of $\geq 3.5\,\text{Å}$. No effect of D$_2$O on the spectra was observed, suggesting that the oxo-bridge is not protonated. On reduction of the center the bridging oxygen leaves as water and the high-spin heme Fe coordinates to histidine, resulting in a site poised to bind NO.[96]

8.28.4.1.1 Structural model

A structural model for NorB has been proposed, based on the crystal structure of *R. denitrificans* CcO and the conserved primary structures of three NorB sequences from different organisms.[3,6] Although the overall sequence homology is only 18%, the six His residues that bind the heme and Cu$_B$ of CcO are conserved. Constraints for the relative positions of these His ligands of the high- and low-spin hemes and the Cu$_A$ (Fe$_B$) centers were applied, which allowed a model based on multiple alignment of the sequences to be developed. The two hemes are nearly perpendicular to the membrane surface, and the nonheme Fe$_B$ linked via an oxo-bridge to the high-spin Fe ion heme b_3. Because the preferred coordination geometry of Fe^{III} is octahedral or penta/hexa geometry the additional ligands are proposed to be conserved Gln residues.[6] Mutagenesis of PdNOR has shown two of these residues to be important for activity with a suggested role, not in ligation, but in proton delivery or as a base involved in NO redox chemistry.[98] Electron cryo-microscopy of two-dimensional crystals of PdNOR shows similarities with CcO indicating a common molecular architecture.[89] A schematic of the structure of NOR is shown in Figure 9.

The topology of the redox centers is consistent with electron transfer rates described in Section 8.28.4.1.3. Since the rate of recombination of CO with NOR is some three orders of magnitude faster than with the active site of CcO, this suggests a more open environment of the heme in NOR. CO binds to the ferrous heme b_3 to form a 6-c low-spin adduct.[99] Laser flash photolysis results in cleavage of the Fe—CO bond, followed by recombination of the CO at a rate of $k_{on} = 1.7 \times 10^8\,M^{-1}\,s^{-1}$. In contrast, the rate of formation of the initial CO adduct of NOR is much slower ($k_{on} = 1.2 \times 10^5\,M^{-1}\,s^{-1}$) possibly due to the displacement of a distal heme ligand (OH$^-$/H$_2$O) to allow binding of CO.

8.28.4.1.2 Mechanistic studies

Studies of ligand binding to NOR and the kinetics of these processes benefit from comparative studies on heme copper oxidases of known structure. Spectroscopic studies suggest that the spin-coupled dinuclear iron center, comprised of the heme b_3–Fe$_B$ entity, is the active site of NOR, and the low-spin hemes b and c have a role in electron transfer to the active site.
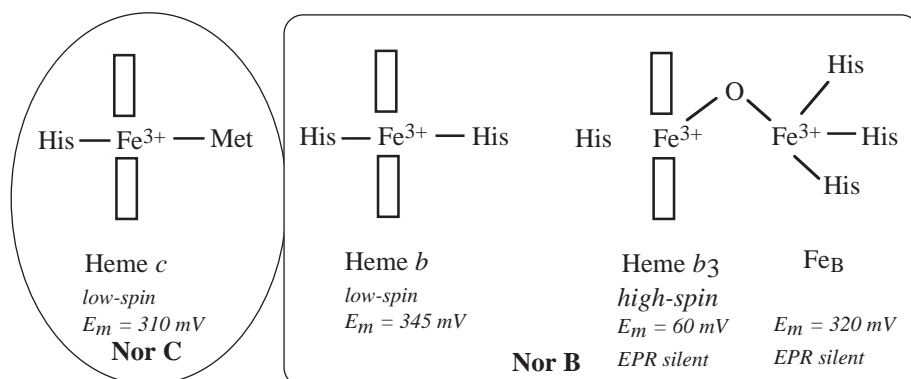

Figure 9 Schematic of the organization of the redox centers of prototype NOR.

The addition of NO to ascorbate-reduced NOR results in the formation of two strong EPR signals at $g = 2$ and 4 due to the disruption of the magnetic coupling of the ferrous high-spin heme and the ferrous Fe_B atom. The complex signal at $g = 2$ with a peak at $g = 2.08$ is typical of nitrosyl ferroheme. The other signal, with $g = 4.11$, 3.95, and 2.0, was assigned to a $S = 3/2$ spin system arising from a nonheme Fe^{II} NO adduct. Thus, under turnover conditions the two ferrous iron atoms at the active site both bind NO, behaving like mononuclear centers.[100]

The kinetics of NO binding to heme b_3 has been determined by optical flow-flash methods, in which the reaction is initiated by the photolysis of CO bound to heme b_3.[89] In the first phase of the subsequent reaction with NO (after 2 μs) a spectral species characteristic of ligand binding to a high-spin heme is formed. It has been suggested that NO partitions into the lipid phase generating higher localized [NO] around the enzyme and that Fe_B provides a second binding site, consistent with EPR data.

8.28.4.1.3 Heme–heme electron transfer

Equilibrium titration of PdNOR showed the E_m value of Fe_B was 320 mV, that of heme b_3 was +60 mV, and those of heme c and heme b were +310 mV and +340 mV, respectively.[100] The rates of intramolecular electron transfer between the redox centers of NOR have been investigated using the "electron backflow" technique.[89] The photolysis of CO bound to the high-spin heme b_3 results in a decrease in E_m of the heme to its basal value, causing a transient redistribution of electrons with the other redox centers before CO rebinding occurs. Time-resolved optical spectroscopy and electrometric changes in membrane potential[89] induced by photolysis of the CO-bound mixed-valence state of PdNOR reconstituted into proteoliposomes indicate that the pathway of electron transfer is similar to that of the heme Cu oxidases, consistent with the modeling studies discussed above. Electrons are accepted from external donors by heme c, transferred to the low-spin heme d ($k_{obs} = 3 \times 10^4 \, s^{-1}$), and then to heme b_3 of the binuclear center ($k_{obs} > 10^6 \, s^{-1}$). This technique revealed that Fe_B remained reduced and that electron backflow involved only the heme centers.

The separation of the redox potentials has enabled the three-electron reduced state with Fe^{III} heme b_3 of PdNOR to be characterized spectroscopically.[100] It was proposed that the thermodynamic barrier presented by the lower potential of heme b_3 prevents the two-electron reduction of the binuclear center to avoid the formation of a stable inactive Fe^{II}–heme b_3 NO• adduct. However, a much smaller difference between E_m of heme c and heme b_3 was deduced from the equilibrium constant for electron transfer between the two hemes in the electron backflow experiments[101] indicating that, as with CcO, the redox centers exhibit negative cooperativity. Thus reduction of the redox center with the lowest E_m is more difficult when the other centers are already reduced resulting in an apparent decrease of E_m of the center.

8.28.4.1.4 Substrate reduction

Two modes of binding of NO have been considered, one involving binding of two NO molecules to a single metal site (the "*cis*" mechanism) and the other involving binding of NO to both metals of a binuclear site (the "*trans*" mechanism). The former mode clearly applies in the case of catalysis by FoP450nor, where only a single heme site is present (see Section 8.28.5) and it has also been proposed for bacterial NORs. Spectroscopic studies of the reaction of NO with cytochrome bo_3 were consistent with the formation of a $Cu_B^{II}(NO)_2$ species.[102] The role of heme o_3 in the subsequent formation of N_2O was proposed to be that of abstraction of an O atom to form an oxyferryl species, a mechanism that avoids the formation of a stable $Fe^{II}NO$ species. The close relationship of cytochrome bo_3 with NOR led to the proposal that these enzymes share a common mechanism for N_2O formation,[103] and due to the relatively low E_m of heme b_3 relative to hemes c and b formation of a stable $Fe^{II}NO$ would be minimized.

EPR changes on binding NO to reduced PdNOR were consistent with both ferrous iron atoms of the binuclear heme b_3 Fe_B binding NO.[89] A "*trans*" catalytic cycle for PdNOR has been proposed in which heme b of the reduced catalytic center has His ligation. On binding two NO molecules cleavage of the Fe—His bond occurs.[95] On elimination of N_2O from the Fe^{II}–NO::NO–Fe^{II} species the two Fe atoms are oxidized and become bridged by an oxo group. On reduction by internal electron transfer the bridging ligand is lost and is replaced by the original His ligand[96] (see Figure 10). This scheme apparently conflicts with the report that the rapid initial binding of NO to heme b_3 (within 2 μs, studied by flash-flow) does not significantly perturb the proximal His
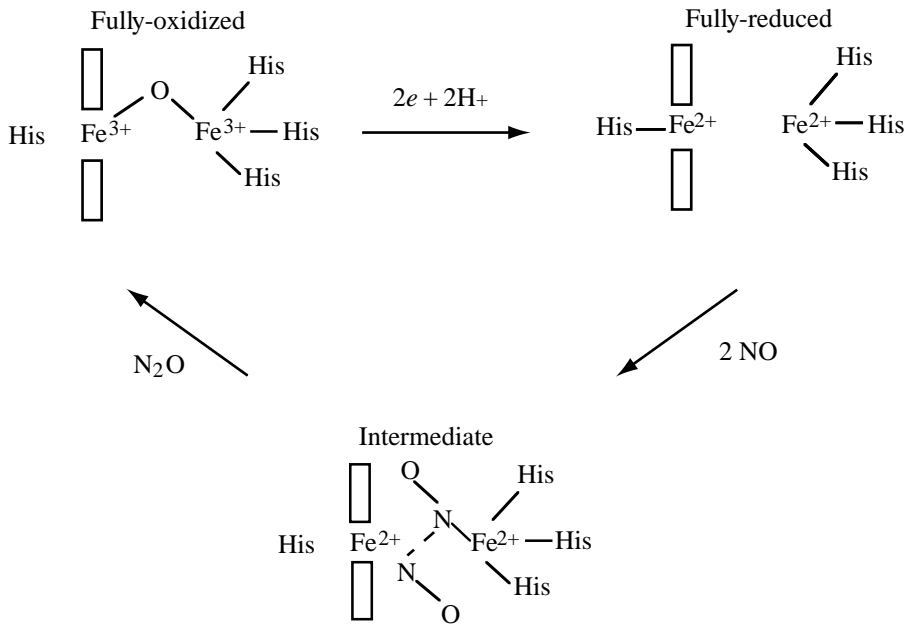
Figure 10 Proposed structures of the catalytic site of NOR during turnover.

heme ligand.[101] However, it is possible that a transient 6-c species with His/NO ligation is formed as has been reported for the interaction of NO with guanylate cyclase[104] and cytochrome c'.[105]

Electrometric and spectrophotometric time-resolved studies of proton and electron flow in PdNOR used "flow-flash" laser activation of the CO–heme b_3, fully reduced enzyme to initiate turnover both in proteoliposomes and of soluble preparations.[101] Subsequent changes in potential generated by the movement of charge across the membrane dielectric in proteoliposomes were complex, and were fitted to a sequential reaction model with six phases. Under these conditions fully reduced NOR has sufficient electrons for two turnover events, and the primary event is most likely to involve the reduced active site. The first rapid change was the formation of a ferrous heme b_3–NO adduct ($k_{obs} = 5 \times 10^5\,\mathrm{s}^{-1}$) and a suggested binding of NO to Fe_B. This observation is not consistent with a "*cis*" model analogous to that involving Cu_A proposed for CcO.[103]

8.28.4.1.5 Model studies

A good structural and functional model of the heme/nonheme di-iron center of the active site of the prototype NOR has been developed and characterized by Karlin and co-workers.[14,97,106] The complexes consist of a binucleating ligand ^{5}L with a tetradentate tris(2-pyridylmethyl)amine moiety tethered to a synthetic tetraarylporphyrin (with three 2,6-difluorophenyl meso substituents; see Figure 11). As discussed above, the resonance Raman spectra of the oxidized compound show features in common with NOR supporting the assignment of the active site as oxo-bridged in the oxidized enzyme.

Reduction of the $[(^5L)\,Fe^{III}$—O—Fe^{III}—Cl]$^+$ complex results in the loss of the oxo-bridge to form $[(^5L)\,Fe^{II} \cdots Fe^{II}$–Cl]$^+$, which shows reactivity towards NO. At low [NO], N_2O is formed and the original oxo-bridged complex reformed, providing a good functional model for NOR function (Figure 11). At high [NO] the reaction is more complex producing a stable ferrous nitrosyl adduct and NO_2 in addition to N_2O. Details regarding the site(s) at which NO binds to the complex are not available, since no stable intermediates could be trapped at $-80\,^\circ$C.

8.28.5 FUNGAL P450-CONTAINING NITRIC OXIDE REDUCTASE

Many strains of fungi have been shown to denitrify, extending this ability, long believed to be restricted to bacteria, to eukaryotes. In the best-characterized organisms, *Fusarium oxysporum*

$[(^5L)Fe^{III}–O–Fe^{III}–Cl]^+$

Structural model
for oxidized NOR
catalytic site

$[(^5L)Fe^{III} \cdots Fe^{III}–Cl]^+$

Structural model
for reduced NOR
catalytic site, loss of the
Fe–Fe oxo bridge

Stable ferrous nitrosyl species
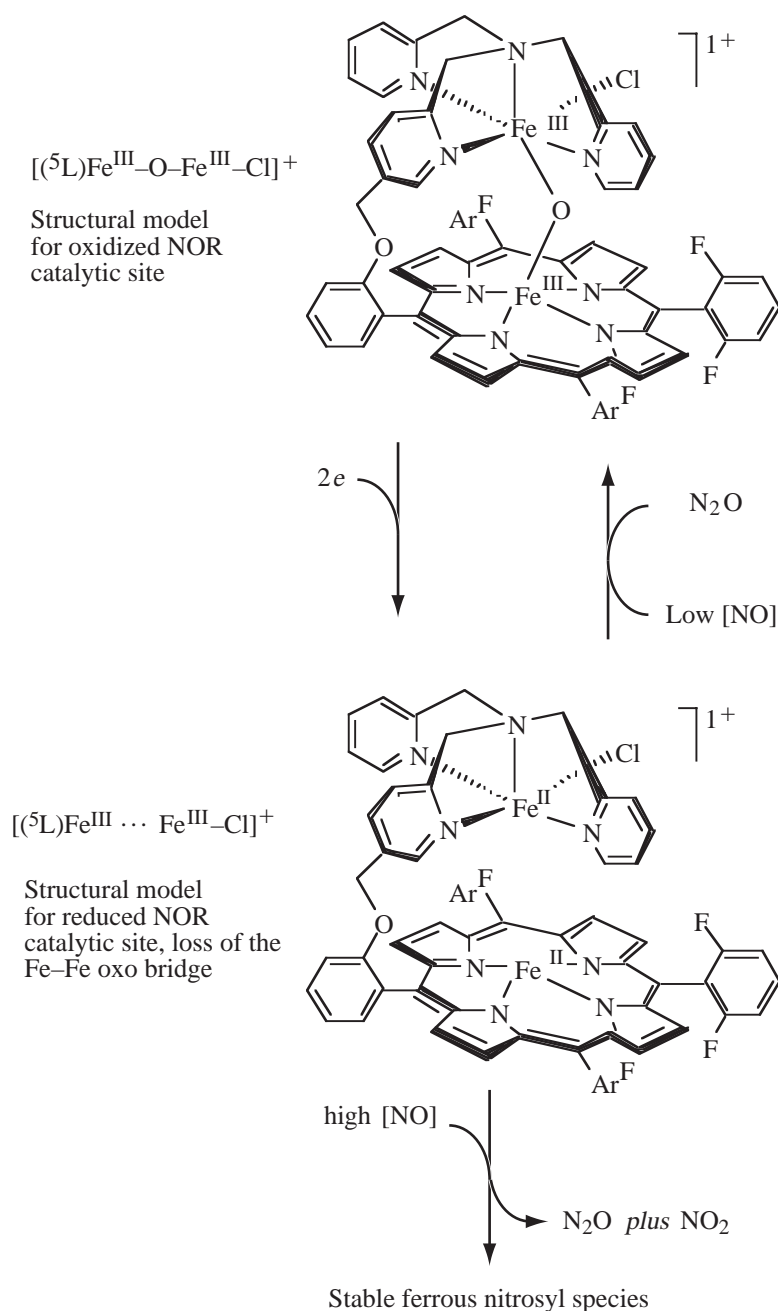
Figure 11   Functional heme/nonheme diiron complex models for NOR activity.

and *Clindrocarpon tonkinense*, the enzymes are mitochondrial and denitrification is coupled to the formation of ATP.[107]

The enzymology of NO reduction by fungi is unrelated to the bacterial enzymes, but with up to 40% homology is a member of the cytochrome P450 monooxygenase superfamily, and is specifically designated as P450nor.[108]

The NO reductase of *F. oxysporum* (FoP450nor) is soluble, monomeric ($M_r = 46,000$) and contains one protoheme as prosthetic group. Activity is specific for NADH which functions as a direct electron donor to the enzyme which catalyses the reaction of Equation (6):

$$2NO + NADH + H^+ \longrightarrow N_2O + NAD^+ + H_2O \qquad (6)$$

The EPR spectrum of the enzyme at 4 K exhibits both high-spin ($g = 8$) and low-spin ($g = 2.3$, 2.25, and 1.91) features, consistent with Cys as the fifth axial ligand of the heme iron. The midpoint potential of -350 mV is significantly lower than other P450 cytochromes. The enzyme has been the subject of extensive spectroscopic studies and crystal structures of the enzyme with NO, CO, and native enzyme have been determined.

8.28.5.1   Structure

The structure the ferric resting state of FoP450nor[109] shown in Figure 12 is essentially the same as has been found for the monooxygenase P450. The heme is located between proximal and distal helices, with the thiolate of Cys352 coordinated as the proximal ligand to the heme iron with a Fe—S bond distance of 2.17 Å. Compared with the P450 structures, the distal heme pocket is more open to the solvent, which may account for faster binding rates for CO and NO to P450nor.

The global structure of the ferrous CO complex of FoP450nor is unchanged compared with the ferric resting state.[109] However, the distribution of H_2O molecules in the distal pocket is altered. Since the ferric NO complex is isoelectronic and isosteric in Fe coordination to the ferrous CO adduct, this difference in H-bonding has been proposed to account for the difference in reactivity between the ferric resting state and the ferric NO adduct towards NADH, which can only reduce the latter species. The importance of this H-bonding network has been shown by mutagenesis of heme pocket residues forming a H-bonded network connecting the active site with the solvent to play a critical role in catalysis.

The structures of the ferric NO adduct of FoP450nor and mutant enzymes have been determined under cryogenic conditions at 1.7 Å resolution, allowing the NO binding mode and H-bond network to be defined.[110] As with CO, the binding of NO does not perturb the global structure of the enzyme. The bound NO is highly ordered in a slightly bent conformation with an Fe—NO angle of 161° and an Fe—NO bond length of 1.63 Å, consistent with earlier EXAFS data.[111] The Fe atom is essentially in plane with the heme. The electron density on the Fe-bound NO was proposed to be relatively high, corresponding to a formal electronic state of "Fe^{3+}–NO." This assignment of a neutral NO entity is consistent with IR data indicating an N—O stretching band at $1851\,cm^{-1}$ and the slow autoreduction rate of the ferric FoP450nor NO adduct.

The higher-resolution structures of the wild-type ferric FoP450nor NO adduct shows the presence of two H-bond networks from the heme pocket to the solvent, only one of which was apparent in the lower resolution structures of the native and ferrous CO adduct. In this structure
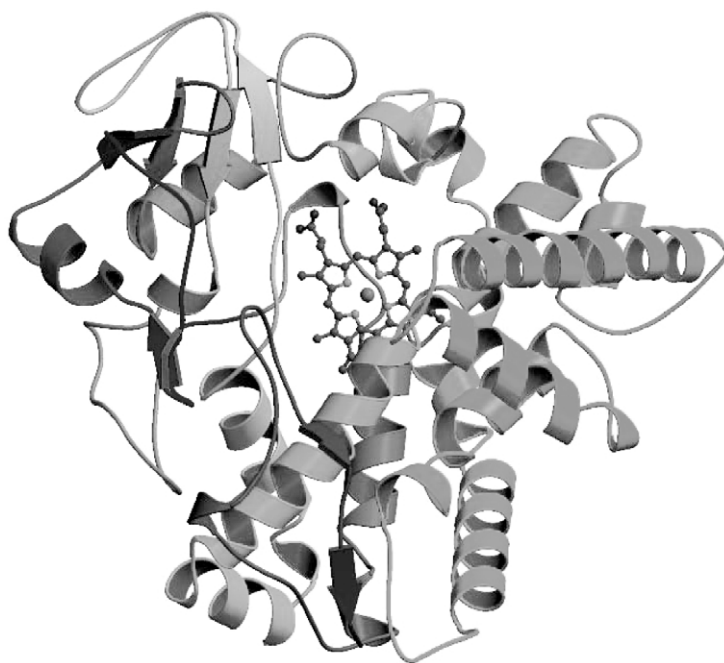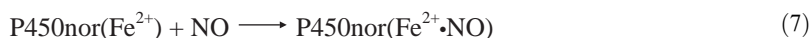

Figure 12   Structure of FoP450nor.

a water molecule at the heme end of the networks is 3.31 Å from the bound NO and is essential for proton delivery required for NO reductase activity.

8.28.5.2 Mechanistic Studies

In formulating a mechanism for FoP450nor two observations have to be taken into account. First, activity is not inhibited by CO, implying that the external ligand-free state of the Fe^{2+} is not an intermediate in the catalytic cycle. Second, NADH does not react with the ligand-free Fe^{2+} state, but does reduce the Fe^{3+}·NO adduct, presumably as a consequence of an NO-mediated conformational change in the enzyme.

The optical absorption spectra of the stable Fe^{2+}, Fe^{3+}, and Fe^{3+}·NO species were determined,[112] and stopped-flow rapid scan, flash photolysis, and low-temperature spectroscopic methods have been applied to study the reactions of Equations (7)–(9). The species P450nor(Fe^{2+}·NO) formed in reaction (7) was characterized by stopped-flow as having a diminished Soret absorbance at 434 nm and a single broad band at 558 nm. Formation of this species was complete within the dead time of the stopped-flow apparatus, even at 10 °C and [NO] of 5 μM, allowing a limit for k, the rate constant for formation of this species, to be estimated as larger than $10^7 \, M^{-1} \, s^{-1}$.

The rate constant for NO binding to P450nor(Fe^{3+}) to form P450nor(Fe^{3+}·NO) (reaction (8)) was determined by monitoring the decay in absorbance at 434 nm as rebinding occurred following laser photodissociation of the P450nor(Fe^{3+}·NO) adduct:

$$\text{P450nor}(Fe^{2+}) + \text{NO} \longrightarrow \text{P450nor}(Fe^{2+}\text{·NO}) \tag{7}$$

$$\text{P450nor}(Fe^{3+}) + \text{NO} \longrightarrow \text{P450nor}(Fe^{3+}\text{·NO}) \tag{8}$$

$$\text{P450nor}(Fe^{3+}\text{·NO}) + \text{NADH} \longrightarrow \text{Intermediate?} \tag{9}$$
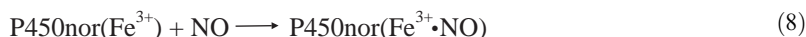
The reduction of P450nor(Fe^{3+}·NO) by NADH (reaction (9)) was followed by rapid-scan spectroscopy. The reaction resulted in the shift of the Soret from 431 nm to form a transient species with Soret at 444 nm and a broad visible absorption at 544 nm, which then decayed to form a species with a peak at 413 nm. These spectral changes are consistent with the intermediate giving rise to the 444 nm band decaying to form P450norFe^{3+}. The spectral characteristics of the intermediate formed by reduction of P450nor(Fe^{3+}·NO) with NADH (peaks at 445 nm and 544 nm) are different from those of P450nor(Fe^{2+}·NO) formed by the reduction of P450nor (Fe^{3+}·NO) by dithionite (peaks at 434 nm and 558 nm).

The formation of the intermediate species was [NADH] dependent and a second-order rate constant of $0.9 \times 10^6 \, M^{-1} \, s^{-1}$ was determined. Under limiting [NO] (equivalent to the enzyme concentration) the decay of the intermediate was independent of [NADH] and a single-order rate constant of $0.027 \, s^{-1}$ was obtained. This rate is too slow to account for the high turnover rate of the enzyme, and it is apparent that excess NO accelerates this reaction since at higher [NO] (~mM) the spectrum of the intermediate was not observed. Under these conditions the absorbance changes corresponded to the direct conversion of P450nor(Fe^{3+}·NO) to P450nor(Fe^{3+}).

Since NADH is a two-electron donor, it was suggested that the intermediate is formed by the two-electron reduction of P450nor(Fe^{3+}·NO), formally to the $(Fe^{3+}\text{·NO})^{2-}$ state, a species without precedent in hemeoprotein chemistry. This is regarded as the key intermediate precursor leading to N—O bond cleavage and N—N bond formation to form N_2O. The electronic structure of the intermediate has been probed by time-resolved resonance Raman spectroscopy.[113] The low-frequency regions of P450nor(Fe^{3+}·NO) and P450nor(Fe^{2+}·NO) spectra showed $^{15/14}$NO-sensitive lines at 530 nm and 544 nm, respectively. These were absent in the spectrum of the intermediate, but were replaced with a new line at 596 nm that was assigned to a ν_{Fe-NO} stretching mode by comparison with model systems. The Fe—NO was assigned a bent conformation since the isotope shift of $10 \, cm^{-1}$ is larger than that of $5 \, cm^{-1}$ shown by a linear Fe—NO unit. From these studies the structure $Fe^{2+}(NO)^-H^+$ was proposed, in which a negative charge delocalized over the bound
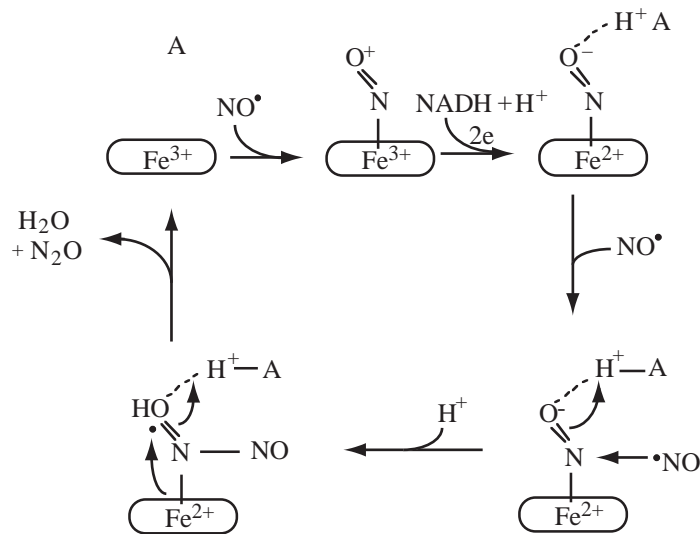
Figure 13 Proposed reaction mechanism for P450nor.

NO moiety is stabilized by H-bonding to the ordered water network discussed above. This novel structure enables a reaction mechanism in which a second NO molecule attacks the N atom of the intermediate to form a transient hyponitrite ($HONNO^-$) in which N—N bond formation occurs. This species rapidly decomposes to yield N_2O and H_2O, the N—O bond cleavage step. Based on these data the authors proposed the scheme shown in Figure 13 for the catalytic cycle of P450nor.

The more usual reactivity of NADH in functioning as a hydride donor has led to the modified proposal[81] that hydride transfer to a Fe^{II}–NO^+ complex would form HNO coordinated to the heme. The reaction of NO with this species would form N_2O and regenerate the ferric heme site for further catalysis.

8.28.5.3 Model Studies

The formation of N_2O at a heme center as in P450nor requires the orientation of two NO entities bound in such a way as to facilitate N—N coupling. Bent nitrosyl ligands (as seen in the structure of the ferric P450nor–NO adduct) are subject to electrophilic attack at the nitrogen lone pair by free NO to form a hyponitrite species. On reduction and protonation this species decomposes to give $(N_2O_2)^{2-}$ which rapidly decomposes to give N_2O and H_2O to regenerate Pt^{II}. This mechanism, shown in Figure 14, was proposed from earlier kinetic studies of the palladium-catalyzed formation of N_2O from NO in aqueous solution with $CuCl_2$ as reductant.[14,114]
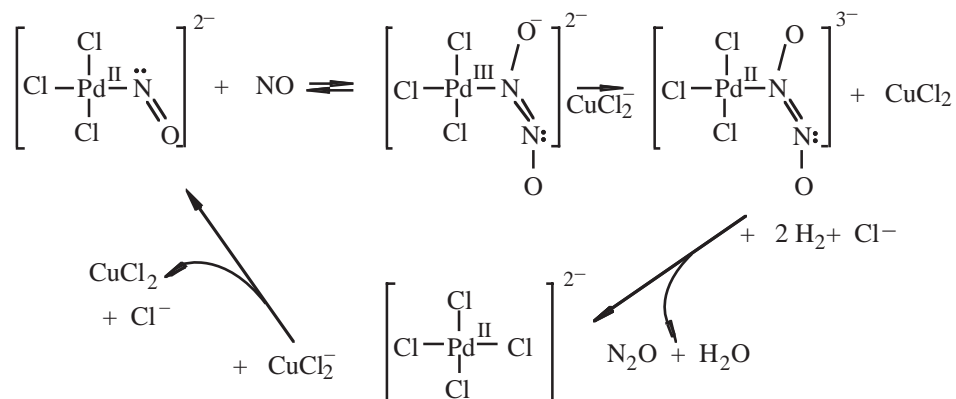
Figure 14 Reaction scheme for the formation of N_2O by the heterophilic attack of a bound nitrosyl species.

8.28.6 NITROUS OXIDE REDUCTASE

Nitrous oxide reductases are soluble, periplasmic Cu-containing enzymes encoded by *nos*Z that catalyze the final step in denitrification (Equation (10)). This reaction is difficult chemistry, since N_2O is a poor ligand for transition metals, is kinetically inert, and none of the known metal/N_2O complexes have been structurally characterized.[6] No Cu/N_2O chemistry, other than that associated with N_2OR, has been reported:

$$N_2O + 2e^- + 2H^+ \longrightarrow N_2 + H_2O \quad [E'_o \text{ (pH 7.0)} = +1.77 \text{ V}] \tag{10}$$

The gene-derived sequences of N_2OR from several species show sequence identity ranging from 50% to 90%. The C-terminal domains have the conserved sequence motif $H(X)_{34}C(X)_3C(X)_3H(X)_2M$, involved in ligation of the binuclear Cu_A center of CcO.[5,6]

N_2OR purified from eight organisms are homodimers of ~66 kDa, typically containing eight Cu atoms per dimer. However, the Cu content is variable. Since the crystal structures of N_2OR reveal each subunit to have a Cu_A center and a novel tetranuclear Cu_Z catalytic center, a fully active enzyme has 12 Cu atoms per dimer.

A number of distinct forms of N_2OR with different colors and activities have been characterized, depending on oxidation state and degree of anaerobicity maintained during purification.[5] The most active purple form has an intense absorption band at 540 nm, which characterizes the oxidized enzyme. These differences have been shown to be due to the presence of multiple forms of the catalytic center.[115] The aerobic purification of N_2OR from *Ps. nautica* 617 avoiding freeze-thaw cycles gave preparations containing 10.7 ± 1.7 Cu/dimer.[116] Similar values were subsequently reported for PdN_2OR, PaN_2OR, and PsN_2OR.[117,118]

8.28.6.1 Structure

Before the structures were elucidated, the redox centers present in N_2OR had been studied extensively by a wide range of spectroscopic techniques. Resonance Raman, multifrequency EPR, ENDOR, ^1H NMR, EXAFS, and MCD spectroscopies were interpreted in terms of two multinuclear Cu centers.[5,6,119] Comparative studies of native N_2OR and on mutated species lacking one of the centers led to the consensus view that two types binuclear Cu centers were present, Cu_A with a role in electron transfer from the endogenous electron donor, and a catalytic Cu_Z center.

The structure of the reduced blue form of PnN_2OR was solved at 2.4 Å resolution[116,120] and subsequently for PdN_2OR at 1.6 Å resolution.[118] The two structures are very similar, with each N_2OR monomer being composed of two domains, an N-terminal catalytic domain forming a β-propeller and the C-terminal domain forming a cupredoxin fold containing the Cu_A center (Figure 15). The catalytic Cu_Z center is located at one end of the pseudo-seven-fold axis of the propeller as is found for the active sites of other enzymes with this fold. An internal solvent channel runs though the axis of the propeller. The dimer is so arranged such that the Cu_A center
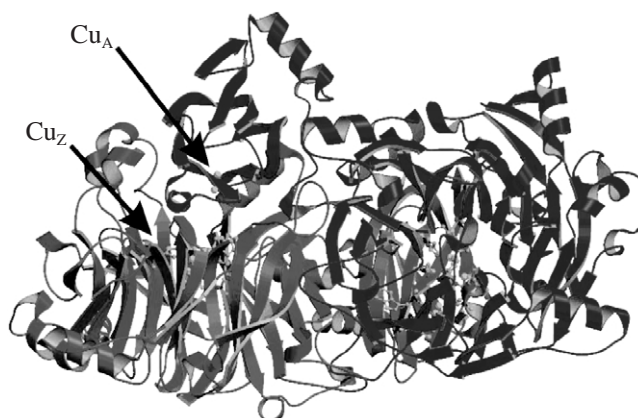

Figure 15 Structure of PnN_2OR.

of one monomer is closest to the Cu_Z center of the second monomer. This cluster separation is $\sim10\,\text{Å}$, compared with the $\sim40\,\text{Å}$ for the centers of a single monomer, strongly suggesting that electron transfer from the Cu_A center to the active site occurs across the subunit interface.

8.28.6.2 Electron Transfer Cu_A Center

The structure of the Cu_A site of PnN_2OR shows the two Cu ions to be linked in a distorted square planar geometry by the $S\gamma$ atoms of Cys561 and Cys565. In addition, each Cu is ligated by the $N\delta$ atom of a His residue, and the coordination is completed by the carbonyl oxygen of a tryptophan residue to one Cu and the $S\gamma$ atom of a Met residue to the other (Figure 16). The unusual seven-line EPR signal of N_2OR has been attributed to the delocalization of an unpaired electron between two Cu nuclei of the Cu_A center. The average Cu—Cu distance of $2.47\,\text{Å}$ is in agreement with EXAFS distances of $2.5\,\text{Å}$, suggesting Cu—Cu bonding interactions, as has been shown in EXAFS and MCD studies for CcO and inorganic Cu_A models.[121,122] The structure of the Cu_A center of N_2OR (Figure 16) is very similar to those of CcO[93,123] and the menaquinonol NO reductase of *B. azotoformans*.[91] Resonance Raman data for N_2OR are consistent with Cys and His ligation, and MCD optical transitions from the paramagnetic sites were assigned to Cys–S–Cu charge transfer bands. This resulted in a model in which two of the Cu atoms per monomer were arranged in a mixed valence center with $S = 1/2$ with a core structure $2Cu^{1.5+}2S_{Cys}2N_{His}$. The blue color of the crystals of PnN_2OR indicates the Cu_A centers are reduced.

8.28.6.3 Catalytic Cu_Z Center

Based on the analysis of EPR, optical, and MCD data, the catalytic Cu_Z center was proposed to be a second binuclear Cu center with cysteine ligation.[6,7,119] The absence of sufficient conserved Cys residues in sequences of N_2OR to bind two thiolate-bridged dinuclear centers led to the suggested involvement[118,120] of conserved His residues, as subsequently revealed by the structures.

The first crystal structure modeled Cu_Z as four Cu ions arranged in the shape of a distorted terahedron ligated by seven histidine residues (conserved in all N_2OR sequences). Three of the Cu ions (Cu1, Cu2, Cu3) were coordinated by two His residues each, the fourth (Cu4) by one His residue and a water or OH^-. The terminal Cu (Cu1) was coordinated by a second OH^-. In the original model at $2.4\,\text{Å}$ resolution a third OH^- was placed in a bridging mode making bonding contacts with all four Cu ions with distances ranging from $2.15\,\text{Å}$ to $2.38\,\text{Å}$. Although ^1H NMR studies had shown the association of at least two histidine residues with this center,[124] the all histidine/OH ligation pattern in this novel structure was surprising, since earlier spectroscopic studies were consistent with sulfur ligation in Cu_Z with significant Cu—S bonding.

A major step in resolving this incompatibility was the unexpected discovery that PsN_2OR and $PapN_2OR$ contained acid-labile sulfide present at $\sim1.7 \pm 0.4$ atoms per dimer, not found in mutated protein lacking Cu_Z centers.[117] Resonance Raman data for PsN_2OR indicated that Cu_Z contained a Cu—S bond.[117] A prominent band at $382\,\text{cm}^{-1}$ was sensitive to the substitution of ^{32}S by ^{34}S (isotope shift $-5.8\,\text{cm}^{-1}$), but not by isotopic substitution of ^{63}Cu by ^{65}Cu or

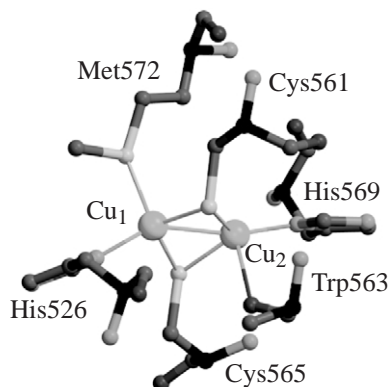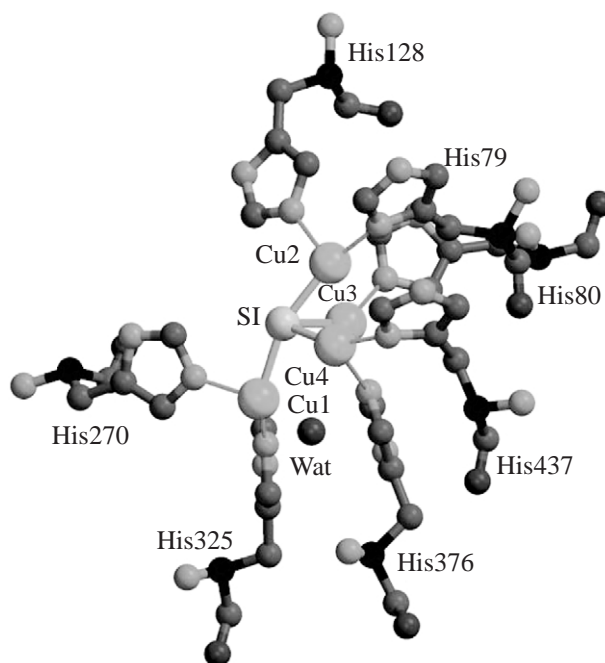**Figure 16**   Structure of the Cu_A center of PnN_2OR.

Figure 17 Structure of the catalytic Cu$_Z$ center of PnN$_2$OR.

incorporation of [^{15}N]-labeled histidine. This band was assigned to a Cu—S vibrational mode associated with Cu$_Z$, since it was present in a mutant form of PsN$_2$OR lacking the Cu$_A$ centers. No sulfide or Raman band was detected in mutant forms of N$_2$OR lacking Cu$_Z$ centers. Optical, magnetic, and resonance Raman properties showed the sulfide must occupy a bridging position between two Cu ions.[117,125] Subsequently PnN$_2$OR and PdN$_2$OR were also shown to contain comparable amounts of sulfide.[118]

Refinement of PdN$_2$OR at 1.6 Å resolution allowed reassignment of the bridging electron density to sulfur, consistent with the spectroscopic and biochemical data (Figure 13). The refined model for PnN$_2$OR also showed the density previously assigned to a OH$^-$/oxygen liganded to Cu1was lost, but that associated with Cu4, close to Cu1, was retained.

This novel class of copper–sulfur cluster, designated as a μ_4-sulfide bridged tetranuclear Cu$_Z$ center[126] (see Figure 17), has average distances of Cu1—Cu3 and Cu1—Cu4 of 3.1 Å, but those for Cu2—Cu3 and Cu2—Cu4 are shorter at 2.55 Å. This short Cu—Cu separation is similar to that found in Cu$_A$ centers suggesting metal–metal bonding occurs in both types of center. A combination of spectroscopic data and density functional calculations has been used to develop a detailed bonding description of the ground and excited states of the cluster.[126,127] These indicate that the Cu$_Z$ center is an $S = 1/2$ spin system with Cu oxidation states of 1Cu^{II}/3Cu^I. The single electron hole resides mostly on Cu1 but is partially delocalized onto Cu2 via a super-exchange pathway mediated by the bridging sulfide. The Cu$_Z$ center is the first biological example of a Cu–sulfide cluster, although a synthetic [3FeCu–4S] cubane cluster has been reported.[128]

8.28.6.4 Mechanistic Implications

Although the binding of N$_2$O has not been observed experimentally, density functional calculations suggest a role for Cu1 and Cu4 in this process, since these Cu ions have open coordination positions orientated to the exchangable water/OH$^-$. A bridging mode of binding of N$_2$O is favored with the O atom interacting with Cu1, the predominantly oxidized Cu in the cluster.[127] This binding was suggested to provide a strategy for overcoming the reaction barrier for the reduction of N$_2$O by facilitating the two-electron transfer; directly from Cu4 and also from Cu2 by a super-exchange pathway involving the bridging sulfide. It has also been proposed that the bridging sulfide may accept the O atom from N$_2$O to form a sulfoxide intermediate prior to reduction to H$_2$O.[117] Mechanistic studies of N$_2$OR are hindered by the sluggish response of the centers on redox changes and the lack of a spectroscopic fingerprint for substrate binding.

8.28.7 PERSPECTIVE

There have been exciting advances in the enzymology and biomimetic chemistry of the reactions of denitrification. With the exception of the heme/nonheme NOR we now have knowledge of the structures of the catalytic centers of the enzymes responsible for the activation of nitrite and its reduction via NO and N_2O to N_2. These structures, in combination with spectroscopic data and structures of enzymes with substrates and inhibitors bound, have guided the formulation of reaction schemes for several of these systems. Such schemes have benefited greatly from the development of chemical model complexes with structural and biomimetic properties that give insight to potential reactivity of metal-bound NO_x species. Further advances will require better models and understanding of the nature of the intermediates during enzymatic catalysis and how access of proton and electron delivery to the active sites is controlled. This is particularly so for the development of models for N_2O binding and activation at Cu centers which remains a major challenge. The continuing interest in the area of NO_x chemistry by both chemists and biologists together with the application of emerging techniques will enable these developments to be realized.

8.28.8 REFERENCES

1. Anjum, M. F.; Stevanin, T. M.; Read, R. C.; Moir, J. W. B. *J. Bacteriol.* **2002**, *184*, 2987–2993.
2. Knapp, J. S.; Clark, V. L. *Infect. Immun.* **1984**, *46*, 176–181.
3. Zumft, W. G. The Denitrifying Procaryotes. In *The Prokaryotes*; 2nd ed.; Balows, A., Truper, E. A., Dorkin, M., Harder, W., Scheifer, K.-H., Eds.; Springer Verlag: New York, 1996; pp 554–582.
4. Shoun, H.; Kano, M.; Baba, K.; Takaya, N.; Matsuo, M. *J. Bacteriol.* **1998**, *180*, 4413–4415.
5. Zumft, W. G. *Microbiol. Molec. Biol. Rev.* **1997**, *61*, 533–616.
6. Berks, B. C.; Ferguson, S. J.; Moir, J. W. B.; Richardson, D. J. *Biochim. Biophys. Acta* **1995**, *1232*, 97–173.
7. Saraste, M.; Castresana, J. *FEBS Lett.* **1994**, *341*, 1–4.
8. Hillie, R. *Chem. Rev.* **1995**, *96*, 2757–2816.
9. Garner, C. D.; Banham, R.; Cooper, S. J.; Davies, E. S.; Stewart, L. J. In *Handbook of Metalloproteins*; Bertini, I., Sigal, A., Sigal, H., Eds.; Marcel Dekker: New York, 2001; pp 1023–1090.
10. Bell, L. C.; Richardson, D. J.; Ferguson, S. J. *FEBS Lett.* **1992**, *265*, 85–87.
11. Bedzyk, L.; Wang, T.; Ye, R. W. *J. Bacteriol.* **1999**, *181*, 2802–2806.
12. Richardson, D. J. *Microbiology* **2000**, *146*, 551–571.
13. Allen, J. W. A.; Ferguson, S. J.; Fulop, V. In *Handbook of Metalloproteins*; Messerschmidt, A., Huber, R., Poulos, T., Wieghardt, K., Eds.; Wiley: New York, 2001; pp 424–439.
14. Wasser, I. M.; deVries, S.; Moënne-Loccoz, P.; Schröder, I.; Karlin, K. K. *Chem. Rev.* **2002**, *102*, 1201–1234.
15. Cutruzzolà, F. *Biochim. Biophys. Acta* **1999**, *141*, 231–249.
16. Fülop, V.; Moir, J. W. B.; Ferguson, S. J.; Hadju, J. *Cell* **1995**, *81*, 369–377.
17. Baker, S. C.; Saunders, N. F. W.; Willis, A. C.; Ferguson, S. J.; Hadju, J.; Fülop, V. *J. Mol. Biol.* **1997**, *269*, 440–455.
18. Nurizzo, D.; Silvistrini, M.-C.; Mathieu, M.; Cutruzzolà, F.; Bourgeois, D.; Fülop, V.; Hajdu, J.; Brunori, M.; Tegoni, M.; Cambillau, C. *Structure* **1997**, *5*, 1157–1171.
19. Nurizzo, D.; Cutruzzolà, F.; Arese, M.; Bourgeois, D.; Brunori, M.; Cambillau, C.; Tegoni, M. *Biochemistry* **1998**, *37*, 13987–13996.
20. Nurizzo, D.; Cutruzzola, F.; Arese, M.; Bourgeois, D.; Brunori, M.; Cambillau, C.; Tegoni, M. *J. Biol. Chem.* **1999**, *274*, 14997–15004.
21. Williams, P. A.; Fülop, V.; Garman, E. F.; Saunders, N. F. W.; Ferguson, S. J.; Hajdu, J. *Nature* **1997**, *389*, 406–412.
22. Jafferji, A.; Allen, W. A.; Ferguson, S. J.; Fülop, V. *J. Biol. Chem.* **2000**, *275*, 25089–25094.
23. Sun, W.; Arese, M.; Brunori, M.; Nurizzo, D.; Brown, K.; Cambilliau, C.; Tegoni, M.; Cutruzzolà, F. *Biochem. Biophys. Res. Commun.* **2002**, *291*, 1–7.
24. Sjögren, T.; Hajdu, J. *J. Biol. Chem.* **2001**, *276*, 13072–13076.
25. Sjögren, T.; Svensson-Elk, M.; Hajdu, J.; Brzezinski, R. *Biochemistry* **2000**, *39*, 10967–10974.
26. Cheesman, M. R.; Ferguson, S. J.; Moir, J. W. B.; Richardson, D. J.; Zumft, W. G.; Thomson, A. J. *Biochemistry* **1997**, *36*, 16267–16276.
27. Sjögren, T.; Hajdu, J. *J. Biol. Chem.* **2001**, *31*, 29450–29455.
28. Steensma, E.; Gordon, E.; Oster, L. M.; Ferguson, S. J.; Hajdu, J. *J. Biol. Chem.* **2001**, *276*, 5846–5855.
29. Allen, J. W. A.; Watmough, N. J.; Ferguson, S. J. *Nature Struct. Biol.* **2000**, *7*, 885–888.
30. Allen, J. W. A.; Higham, C. W.; Zajicek, R. S.; Watmough, N. J.; Ferguson, S. J. *Biochem. J.* **2002**, *366*, 883–888.
31. Cutruzzolà, F.; Arese, M.; Grasso, S.; Bellelli, A.; Tegoni, M.; Brunori, M. *FEBS Lett.* **1997**, *412*, 365–369.
32. Cutruzzolà, F.; Brown, K.; Wilson, E. K.; Bellelli, A.; Arese, M.; Tegoni, M.; Cambillau, C.; Brunori, M. *Proc. Natl. Acad. Sci. USA* **2001**, *98*, 2232–2237.
33. Sun, W.; Arese, M.; Brunori, M.; Nurizzo, D.; Brown, K.; Cambilliau, C.; Tegoni, M.; Cutruzzolà, F. *Biochem. Biophys. Res. Commun.* **2002**, *291*, 1–7.
34. Besson, S.; Carnerio, C.; Moura, I.; Fauque, G. *Anaerobe* **1995**, *1*, 219–226.
35. Koppenhöffer, A.; Turner, K. L.; Allen, J. W. A.; Chapman, S. K.; Ferguson, S. J. *Biochemistry* **2000**, *39*, 4243–4249.
36. Kobayashi, K.; Koppenhöffer, A.; Ferguson, S. J.; Tagawa, S. *Biochemistry* **1997**, *36*, 13611–13616.
37. Kobayashi, K.; Koppenhöffer, A.; Ferguson, S. J.; Watmough, N. J.; Tagawa, S. *Biochemistry* **2001**, *40*, 8542–8547.
38. Wilson, E. K.; Bellini, A.; Liberti, S.; Arese, M.; Grasso, S.; Cutruzzola, F.; Brunori, M.; Brzezinski, P. *Biochemistry* **1999**, *38*, 7556–7564.

39. Wilson, E. K.; Bellini, A.; Cutruzzolà, F.; Zumft, W. G.; Guterrez, A.; Scrutton, N. S. *Biochem. J.* **2001**, *355*, 39–43.
40. Das, T. K.; Wilson, E. K.; Curruzzolà, F.; Brunori, M.; Rousseau, D. L. *Biochemistry* **2001**, *40*, 10774–1078.
41. Wang, Y.; Averill, B. A. *J. Am. Chem. Soc.* **1996**, *118*, 3972–3973.
42. Silvestrini, M. C.; Tordi, M. G.; Musci, G.; Brunori, M. *J. Biol. Chem.* **1990**, *265*, 11783–11787.
43. George, S. J.; Allen, J. W. A.; Ferguson, S. J.; Thorneley, R. N. F. *J. Biol. Chem.* **2000**, *43*, 33231–33237.
44. Ozaawa, S.; Sakamoto, E.; Ichikawa, T.; Watanabe, Y.; Morishima, I. *Inorg. Chem.* **1995**, *34*, 6362–6370.
45. Olsen, L. W.; Schaeper, D.; Lacon, D.; Kadish, K. M. *J. Am. Chem. Soc.* **1983**, *104*, 2042–2044.
46. Ranghino, G.; Scorza, E.; Sjögren, T.; Williams, P. A.; Ricci, M.; Hadju, J. *Biochemistry* **2000**, *39*, 10958–10966.
47. Suzuki, S.; Kataoka, K.; Yamaguchi, K.; Inoue, T.; Kai, Y. *Coord. Chem. Rev.* **1999**, *190*, 192–245.
48. Castro, C. E. *J. Am. Chem. Soc.* **1996**, *118*, 3984–3985.
49. Cheng, L; Powell, D. R.; Kahn, M. A.; Richter-Addo, G. B. *Chem. Commun.* **2000**, 2301–2302.
50. Boulanger, M. J.; Murphy, M. E. P. *J. Mol. Biol.* **2002**, *315*, 1111–1127.
51. Godden, J. W.; Turley, S.; Teller, D. C.; Adman, E. T.; Lui, M. Y.; Payne, W. J.; LeGall, J. *Science* **1991**, *253*, 438–442.
52. Adman, E. T.; Godden, J. E.; Turley, S. *J. Biol. Chem.* **1995**, *270*, 27458–27474.
53. Kukimoto, M.; Nishiyama, M; Murphy, M. E. P.; Turley, S.; Adman, E. T. *Biochemistry* **1994**, *33*, 5246–5252.
54. Murphy, M. E. P.; Turley, S.; Kukimoto, M.; Nishiyama, M.; Horinouchi, S.; Sasaki, H.; Tankurra, M.; Adman, E. T. *Biochemistry* **1995**, *34*, 12107–12117.
55. Dodd, F. E.; Hasnain, S. S.; Abraham, Z. H. L.; Eady, R. R.; Smith, B. E. *Acta Crystallogr. D.* **1998**, *53*, 406–418.
56. Dodd, F. E.; Van Beeumen, J.; Eady, R. R.; Hasnain, S. S. *J. Mol. Biol.* **1998**, *282*, 369–382.
57. Inoue, T.; Gotowda, M.; Deligeer.; Kataoka, K.; Yamaguchi, K.; Suzuki, S.; Watanabe, H.; Kai, Y. *J. Biochem.* **1998**, *124*, 876–879.
58. Ellis, M. J.; Dodd, F. E.; Strange, R. W.; Prudêncio, M.; Sawers, G.; Eady, R. R.; Hasnain, S. S. *Acta Crystallogr.* **2001**, *D57*, 1110–1118.
59. Kataoka, K.; Furusawa, H.; Takagi, K.; Yamaguchi, K.; Suzuki, S. *J. Biochem.* **2000**, *127*, 345–350.
60. Abraham, Z. H. L.; Smith, B. E.; Howes, B. D.; Lowe, D. J.; Eady, R. R. *Biochem. J.* **1997**, *324*, 511–516.
61. LaCroix, L. B.; Shadle, S. E.; Wang, Y. N.; Averill, B. A.; Hedman, B; Hodgson, K. O.; Solomon, E. I. *J. Am. Chem. Soc.* **1996**, *188*, 7755–7768.
62. Strange, R. W.; Dodd, F. E.; Abraham, Z. H. L.; Grossman, J. G.; Brüser, T.; Eady, R. R.; Smith, B. E.; Hasnain, S. S. *Nature Struct. Biol.* **1995**, *2*, 287–292.
63. Veselov, A.; Olesen, K.; Sienkiewicz, A.; Shapleigh, J. P.; Schole, C. P. *Biochemistry* **1998**, *37*, 6095–6105.
64. Zhang, H.; Boulanger, M. J.; Mauk, A. G.; Murphy, M. E. P. *J. Phys. Chem.* **2000**, *B104*, 10738–10742.
65. Howes, B. D.; Abraham, Z. H. L.; Lowe, D. J.; Brüser, T.; Eady, R. R.; Smith, B. E. *Biochemistry* **1996**, *33*, 2171–3177.
66. Strange, R. W.; Murphy, L. M.; Dodd, F. E.; Abraham, Z. H. L.; Eady, R. R.; Smith, B. E.; Hasnain, S. S. *J. Mol. Biol.* **1999**, *287*, 1001–1009.
67. Murphy, M. E. P.; Turley, S.; Adman, E. T. *J. Biol. Chem.* **1995**, *270*, 27458–27474.
68. Suzuki, S.; Horikoshi, T.; Kohzuma, T. *Biochem. Biophys. Res. Commun.* **1999**, *255*, 427–430.
69. Abraham, Z. H. L.; Smith, B. E.; Howes, B. D.; Lowe, D. J.; Eady, R. R. *Biochem. J.* **1997**, *324*, 511–516.
70. Ellis, M. J.; Dodd, F. E.; Strange, R. W.; Prudêncio, M.; Sawers, G.; Eady, R. R.; Hasnain, S. S. *Acta Crystallogr.* **2001**, *D57*, 1110–1118.
71. Strange, R. W.; Dodd, F. E.; Abraham, Z. H. L.; Grossman, J. G.; Bruser, T.; Eady, R. R.; Smith, B. E.; Hasnain, S. S. *Nature Struct. Biol.* **1995**, *2*, 287–292.
72. Kataoka, K.; Furusawa, H.; Takagi, K.; Yamaguchi, K.; Suzuki, S. *J. Biochem.* **2000**, *127*, 345–350.
73. Prudêncio, M.; Eady, R. R.; Sawers, G. *Biochem. J.* **2001**, *353*, 259–266.
74. Boulanger, M. J.; Kukimoto, M.; Nishiyama, M.; Horinouchi, S.; Murphy, M. E. P. *J. Biol. Chem.* **2000**, *275*, 23957–23964.
75. Boulanger, M. J.; Murphy, M. E. P. *Biochemistry* **2001**, *40*, 9132–9140.
76. Ellis, M. J.; Prudêncio, M.; Dodd, F. E.; Strange, R. W.; Sawers, G.; Eady, R. R.; Hasnain, S. S. *J. Mol. Biol.* **2002**, *316*, 51–64.
77. Halfen, J. A.; Tolman, W. B. *J. Am. Chem. Soc.* **1994**, *116*, 5475–5476.
78. Kobayashi, K.; Tawaga, S.; Deligeer.; Suzuki, S. *J. Biochem.* **1999**, *126*, 408–412.
79. Suzuki, S.; Furusawa, H.; Kataoka, K.; Yamaguchi, K.; Kobayashi, K.; Tagawa, S. *Inorg. React. Mechanisms* **2000**, *2*, 129–135.
80. Farver, O.; Eady, R. R.; Abraham, Z. H. L.; Pecht, I. *FEBS Lett.* **1998**, *436*, 239–224.
81. Averill, B. A. *Chem. Rev.* **1996**, *96*, 2952–2964.
82. Hulse, C. L.; Averill, B. A.; Teijde, J. M. *J. Am. Chem. Soc.* **1989**, *111*, 2322–2323.
83. Jackson, M. N.; Tiejde, J. M.; Averill, B. A. *FEBS Lett* **1991**, *291*, 41–44.
84. Suzuki, S.; Kataoka, K.; Yamaguchi, K. *Acc. Chem. Res.* **2000**, *33*, 728–753.
85. Halfen, J. A.; Mahapatra, E. C.; Wilkinson, A. J.; Gengenbach, V. G.; Young, V. G., Jr.; Que, L., Jr.; Tolman, W. B. *J. Am. Chem. Soc.* **1996**, *118*, 763–776.
86. Halfen, J. A.; Mahapatra, S.; Olmstead, M. M.; Tolman, W. B. *J. Am. Chem. Soc.* **1994**, *116*, 2173–2174.
87. Monzani, E.; Anthony, G. J.; Koolhaas, A.; Spandre, A.; Leggieri, E.; Casella, L.; Gullotti, M.; Nardin, G.; Randaccio, L.; Fontani, M.; Zanello, P.; Reedijk, J. *J. Biol. Inorg. Chem.* **2000**, *5*, 251–261.
88. Girsh, P.; de Vries, S. *Biochim. Biophys. Acta* **1997**, *1318*, 202–208.
89. Hendriks, J.; Warne, A.; Gohlke, U.; Haltia, T.; Ludovici, C.; Lüben, M.; Saraste, M. *Biochemistry* **1998**, *37*, 13102–13109.
90. Sakurai, N.; Sakurai, T. *Biochemistry* **1997**, *36*, 13809–13815.
91. Suharti, S; Strampraad, M. J. F.; Schröder, I.; de Vries, S. *Biochemistry* **2001**, *40*, 2632–2639.
92. Cramm, R.; Pohlmann, A.; Friedrich, B. *FEBS Lett.* **1999**, *460*, 6–10.
93. Iwata, S.; Ostermeier, C.; Ludwig, B.; Michel, H. *Nature* **1995**, *376*, 660.
94. Cheesman, M. R.; Zumft, W. G.; Thomson, A. J. *Biochemistry* **1998**, *37*, 3994–4000.
95. Moënne-Loccoz, P.; de Vries, S. *J. Am. Chem. Soc.* **1998**, *120*, 5147–5152.

96. Moënne-Loccoz, P.; Richter, O.-H.; Huanng, H.-W.; Wasser, I. M.; Ghiladi, R. A.; Karlin, K. D.; de Vries, S. *J. Am. Chem. Soc.* **2000**, *122*, 9344–9345.
97. Martens, C. F.; Murthy, N. N.; Obias, H. V.; Karlin, K. D. *J. Chem. Soc. Chem. Commn.* **1996**, 629–630.
98. Butland, G.; Spiro, S.; Watmough, N. J.; Richardson, D. J. *J. Bacteriol.* **2001**, *183*, 189–199.
99. Hendriks, J. H. M.; Prior, L.; Baker, A. R.; Thomson, A. J.; Saraste, M.; Watmough, N. J. *Biochemistry* **2001**, *40*, 13361–13369.
100. Grönberg, K. L.; Roldàn, M. D.; Prior, L.; Butland, G.; Cheesman, M. R.; Richardson, D. J.; Spiro, S.; Thomson, A. J.; Watmough, N. J. *Biochemistry* **1999**, *38*, 13780–13786.
101. Hendriks, J. H.; Jasaitis, A.; Saraste, M.; Verkhovsky, M. I. *Biochemistry* **2002**, *41*, 2331–2340.
102. Butler, C. S.; Seward, H. E.; Greenwood, C.; Thomson, A. J. *Biochemistry* **1997**, *36*, 16259–16266.
103. Watmough, N. J.; Cheeseman, M. R.; Butler, C. S.; Little, R. H.; Greenwood, C.; Thomson, A. J. *J. Bioenerg. Biomembr.* **1998**, *30*, 55–62.
104. Zhao, Y.; Brandish, P. E.; Ballou, D. P.; Marletta, M. A. *Proc. Natl. Acad. Sci. USA* **1999**, *96*, 14753–14758.
105. Andrew, C. R.; George, S. J.; Lawson, D. M.; Eady, R. R. *Biochemistry* **2002**, *41*, 2352–2360.
106. Ju, T. D.; Woods, A. S.; Cotter, R. J.; Moënne-Loccoz, P.; Karlin, K. D. *Inorg. Chim. Acta* **2000**, *297*, 362–372.
107. Kobayashi, M.; Matsuo, Y.; Takimoto, A.; Suzuki, S.; Maruo, F.; Shoun, H. *J. Biol. Chem.* **1996**, *271*, 16263–16267.
108. Nakahara, K.; Tanimoto, T.; Hatano, K.; Usuda, K.; Shoun, H. *J. Biol. Chem.* **1993**, *268*, 8350–8355.
109. Park, S.-Y.; Shimizu, H.; Adachi, S.; Nakagawa, A.; Tanka, I.; Nakahara, K.; Obayashi, E.; Nakamura, H.; Iizuka, T.; Shiro, Y. *Nature Struct. Biol.* **1997**, *4*, 827–832.
110. Shimizu, H.; Obayashi, E.; Gomi, Y.; Arakawa, H.; Park, S.-Y.; Nakamura, H.; Adachi, S.; Shoun, H.; Shiro, Y. *J. Biol. Chem.* **2000**, *275*, 4816–4826.
111. Obayashi, E.; Tsukamoto, K.; Adach, S.; Takahashi, S.; Nomura, M.; Iizuka, T.; Shoun, H.; Shiro, Y. *J. Am. Chem. Soc.* **1997**, *119*, 7807–7816.
112. Shiro, Y.; Fujii, M.; Iizuka, T.; Adach, S.; Tsuamoto, K.; Nakahara, K.; Shoun, H. *J. Biol. Chem.* **1995**, *270*, 1617–1623.
113. Obayashi, E.; Takahashi, S.; Shiro, Y. *J. Am. Chem. Soc.* **1998**, *120*, 12964–12965.
114. MacNeil, J. H.; Berseth, P. A.; Bruner, E. L.; Perkins, T. L.; Wadia, Y.; Westwood, G.; Trolger, W. C. *J. Am. Chem. Soc.* **1997**, *119*, 1668–1675.
115. Rasmussen, T.; Berks, B. C.; Butt, J. N.; Thomson, A. J. *Biochem. J.* **2002**, *364*, 807–815.
116. Prudêncio, M.; Pereira, A. S.; Taveres, P.; Besson, S.; Cabito, I.; Brown, K.; Samyn, B.; Devreese, B.; Van Beemen, J.; Rusnak, F.; Fauque, G.; Moura, J. J. G.; Tegoni, M.; Cambillau, C.; Moura, I. *Biochemistry* **2000**, *39*, 3899–3907.
117. Rassmussen, T.; Berks, B. C.; Sanders-Loehr, J.; Dooley, D. M.; Zumft, W. G.; Thomson, A. J. *Biochemistry* **2000**, *39*, 12753–12567.
118. Brown, K.; Djinovic-Carugo, K.; Haltia, T.; Cabrito, I.; Saraste, M.; Moura, J. J.; Moura, I.; Tegoni, M.; Cambillau, C. *J. Biol. Chem.* **2000**, *52*, 41133–41136.
119. Farrar, J. A.; Zumft, W. G.; Thomson, A. J. *FEBS Lett.* **1991**, *294*, 11–15.
120. Brown, K.; Tegoni, M.; Prudêncio, M.; Pereira, A. S.; Besson, S.; Moura, J. J.; Moura, I.; Cambillau, C. *Nature Struct. Biol.* **2000**, *7*, 191–195.
121. Williams, K. R.; Gamelin, D. R.; LaCroix, L. B.; Houser, R.; Tolman, W. B.; de Vries, S.; Hedman, B.; Hodgson, K. O.; Solomon, E. I. *J. Am. Chem. Soc.* **1997**, *119*, 613–614.
122. Gamelin, D. R.; Randall, D. W.; Hay, M. T.; Houser, R.; Mulder, T. C.; Canters, G. W.; de Vries, S.; Tolman, W. B.; Lu, Y.; Solomon, E. I. *J. Am. Chem. Soc.* **1998**, *120*, 5246–5263.
123. Tsukihara, T.; Aoyama, H.; Yamashita, E.; Tomizaki, T; Yamaguchi, H.; Shinawa-Itoh, K.; Yaono, R.; Yoshikawa, S. *Science* **1995**, *269*, 1069–1074.
124. Holz, R. C.; Alvarez, M. L.; Zumft, W. G.; Dooley, D. M. *Biochemistry* **1999**, *38*, 11164–11171.
125. Alvarez, M. L.; Jingyuan, A.; Zumft, W. G.; Sanders-Loehr, J.; Dooley, D. M. *J. Am. Chem. Soc.* **2001**, *123*, 576–586.
126. Chen, P.; Cabrito, I.; Moura, J. J. G.; Moura, I.; Solomon, E. I. *J. Am. Chem. Soc.* **2002**, *124*, 10497–10507.
127. Chen, P.; George, S. D.; Cabrito, I.; Antholine, W. E.; Moura, J. J. G.; Moura, I.; Hedman, B.; Hodgson, K.; Solomon, E. I. *J. Am. Chem. Soc.* **2002**, *124*, 744–745.
128. Butt, J.; Niles, J.; Armstrong, F. A.; Breton, J.; Thomson, A. J. *Struct. Biol.* **1994**, *1*, 427–433.

8.29
DNA and RNA as Ligands

V. J. DEROSE, S. BURNS, N.-K. KIM, and M. VOGT
Texas A & M University, TX, USA

8.29.1 INTRODUCTION

8.29.1.1 Background: Roles of Metals in DNA and RNA Structure and Function

Nucleic acids exhibit a diversity of structures and play many different roles in controlling gene expression.[1–3] Deoxyribonucleic acid (DNA) is predominantly found in chromosomes, where it is stored in the form of double-stranded helices that may be further highly condensed around protein cores. DNA is transcribed by polymerase enzymes into ribonucleic acid (RNA), which has diverse functions and cellular locations. RNA plays a dominant role in gene expression as protein-encoding messenger RNA (mRNA). The ribosome, the protein-RNA machine that translates messenger RNA into proteins, contains ribosomal RNA (rRNA) and catalyzes amide bond formation between amino acids transported on transfer RNAs (tRNA). There are many other RNA–protein complexes, including the spliceosome, signal recognition particle, telomerase, and more. In a few systems self-splicing "catalytic" RNAs perform chemical reactions in the absence of proteins.[3,4] In the cell cycle, the structures of both DNA and RNA are dynamic, being subject to chemical modifications and temporal formation of nucleic acid–protein complexes.

As described below, nucleic acids are anionic polymers with phosphodiester linkages, nitrogen-containing heterocyclic bases, and sugar moieties. Thus, nucleic acids contain many potential coordination sites for metal ions. Cations, monovalent and divalent, can be important for structure and function in both RNA and DNA.[2–6] The most biologically relevant ions are likely Na^I, K^I, and Mg^{II}, based on estimated cellular concentrations of greater than 1–100 mM for each ion. Other metal ions including Mn^{II}, Co^{II}, and Cd^{II} can sometimes substitute for Mg^{II} in supporting nucleic acid folding and function *in vitro*. Nucleic acids are targets of metal-based therapeutic agents, the most well-known being the Pt^{II} anticancer compounds.[7] RNA and DNA polymerases perform phosphoryl transfer chemistry catalyzed by Mg^{II} and Zn^{II}.[8,9] Several nucleases, enzymes that cleave nucleic acids, also use these ions in catalysis. Artificial nucleases have been designed as coordination compounds with different metals including Zn^{II}, Cu^{II}, and lanthanides.[10,11] Coordination compounds of nearly all metals with nucleic acid bases have been prepared for purposes of studying metal toxicity or molecular recognition.

Information about metal interactions with RNA and DNA comes from functional studies and also from structural investigations, including X-ray crystallography, NMR spectroscopy, optical spectroscopies, and measurements of thermodynamic stability. Metal ions have been localized in several X-ray crystal structures of canonical DNA duplexes.[12] Metal sites were elucidated in early X-ray structures of tRNA which, like other RNA molecules, has a more complex folded structure. More recently, many metal sites have been revealed in X-ray crystal structures of ribozymes, RNA molecules that perform chemical reactions, and in some cases metals have been proposed to be cofactors in these reactions.[5] Finally, from very recent X-ray crystal structures, hundreds of embedded metal ions are predicted within the RNA components of the enormous ribosomal subunits.[13] An interesting aspect of such structures is also the use of heavy-metal coordination compounds for the purposes of X-ray phasing.

In this chapter, we will describe the coordination properties of nucleic acids, including the consequences on metal interactions of the polyanionic nature of oligonucleotides and the supramolecular structure of the double-helix. Types of metal sites found in other structures such as G-quartets and complex RNA folds will be described. Small coordination compounds between metals and nucleotides, the monomeric units of polymeric DNA and RNA, have been widely studied and also are included in this review. While the majority of material included in the review is derived from X-ray crystallographic studies, some information from spectroscopy and other physical methods is included where illuminating.

8.29.2 NUCLEIC ACIDS AS LIGANDS

8.29.2.1 Overview of DNA/RNA Structure

Nucleic acids, historically named as the acidic compounds isolated from cell nuclei, are polymers composed of sugar, base, and phosphate groups. Each monomeric unit of an oligonucleotide consists of a B-D-ribose or B-D-deoxyribose sugar with three points of attachment: a glycosidic linkage to a base at the 1′ position; a phosphodiester at the 3′ position; and a phosphodiester at the 5′ position (see Figure 1). Four bases, two purines and two pyrimidines, provide the sole encoding of structural diversity. The major differences between RNA and DNA are the presence
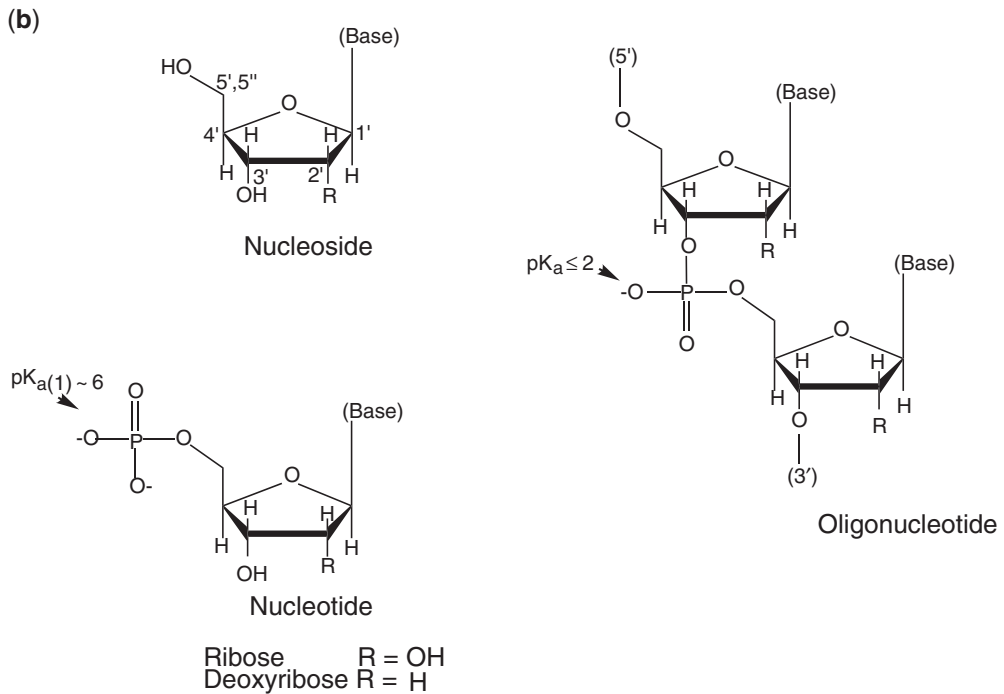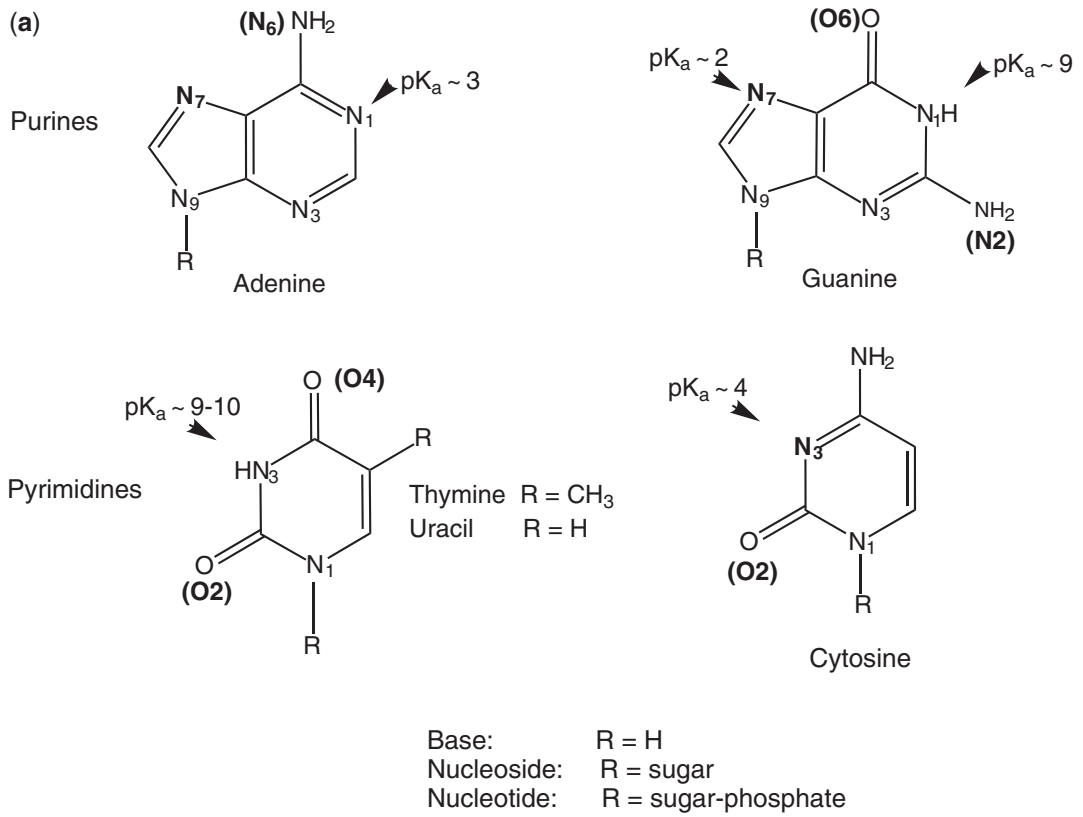
Figure 1 The chemical units of nucleic acids. (a) The purine and pyrimidine nucleobases. (b) Nucleosides, nucleotides, and an oligonucleotide. Approximate pK_a values taken from Bloomfield *et al.*[2]

in RNA of the 2′-OH substituent and substitution of uracil for thymine. Considering the approximate pK_a values given in Figure 1, it can be seen that at neutral pH the only species expected to carry a net charge would be the phosphodiester groups, with pK_a values of less than 2. Thus, oligonucleotides are negatively charged polymers.

Both DNA and RNA can form double-helical structures that are thermodynamically driven by stacking between the hydrophobic bases (see Figure 2). The double helix is most stable with the canonical Watson–Crick base pairing such that adenine (A) forms hydrogen bonds with thymine (T) (or uracil, U, in RNA), and guanine (G) pairs with cytosine (C) (see Figure 3). Within double-helical RNA or DNA, the planes of the sugar and base are roughly perpendicular to each other and the phosphodiester groups form a negatively charged backbone, exposed to solvent.

The double helix can be envisioned as a twisted ladder wherein the front and back edges of each ladder step are the edges of the base-pairs. As seen in Figures 3 and 4, the ladder is asymmetric because the width of the "step" is shorter on one edge. This "minor groove" edge includes the pyrimidine O2-keto and purine N3 imino groups. The "major groove" edge includes purine N7 imino nitrogens, which are not involved in hydrogen bonding and are common metal ion ligands. Metal coordination properties of the double-helical duplex structures depend on the width of the
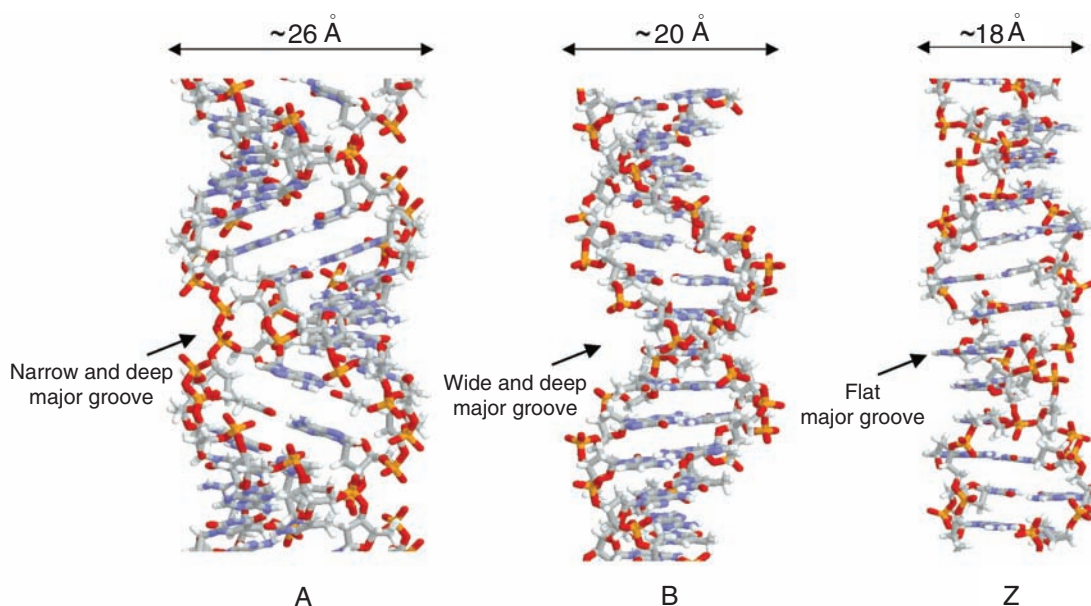
Figure 2 The three standard forms of nucleic acid duplexes: A-form, generally found in RNA duplexes; B-form, standard for DNA duplexes; and the rare Z-form, which can be stabilized by transition metal ions. $(ACGT)_5$ $(A + B\text{-form})$ and $(CG)_{10}$ (Z-form) duplexes built with the Biopolymer module of InsightII.
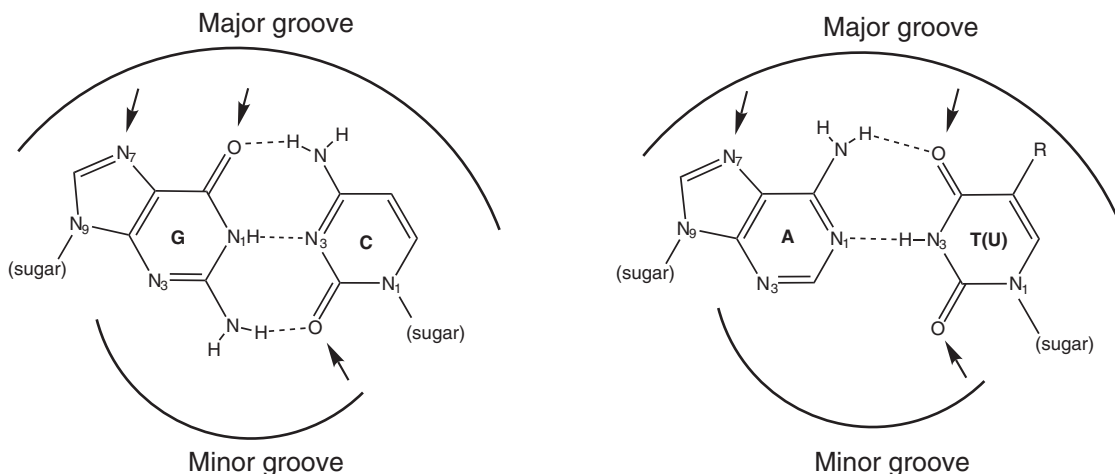
Figure 3 Canonical Watson–Crick base pairs found in nucleic acid duplexes. Arrows indicate the most common metal coordination sites in major and minor grooves.
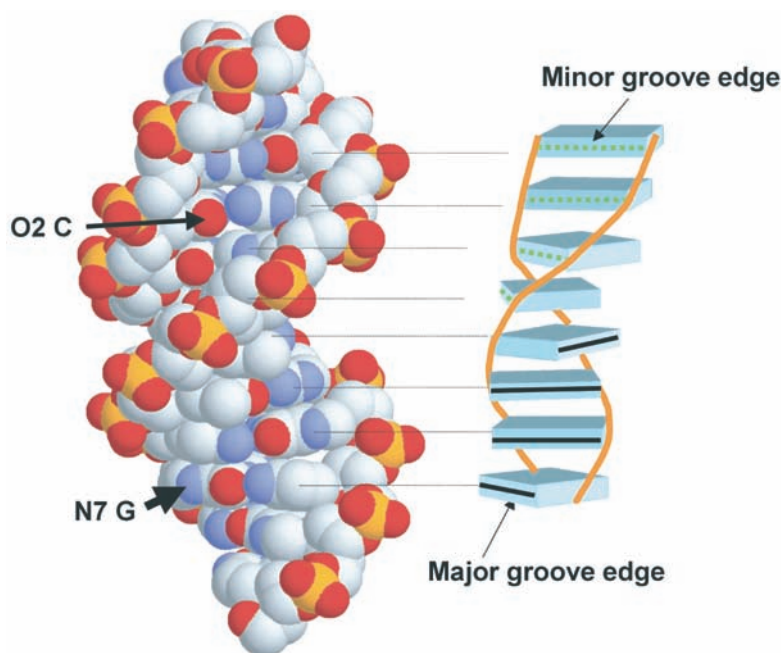
Figure 4 Space-filling model of a B-form duplex (left). Arrows highlight common minor groove cytosine O2 keto oxygen and major groove guanine N7 imino nitrogen ligands. The schematic (right) shows the phosphodiester backbone as solid lines and base-pairs as rectangles, with the minor and major groove faces indicated by dotted and solid lines, respectively.

grooves, which are bordered by the phosphodiester groups, and the accessibility of ligand positions on the buried nucleic acid bases.

Seven dihedral angles describe the conformation of each nucleotide unit, including the conformation of the sugar and phosphodiester bond groups. Changes in these angles, predominantly in sugar conformation, propagate in the polymer. Three major forms of double-helical structures, B-, A-, and Z-forms, are most commonly described and these differ in the sugar conformations, distances between phosphodiester groups, and dimensions of the major and minor grooves (Figure 2). DNA is predominantly found in B-form conformations but can be induced to A-and Z-forms depending on conditions of cations and humidity. The 2′-OH of RNA favors a C3′-*endo* conformation that propagates predominantly to create A-form double-helical geometries. As described below, different helical geometries influence metal coordination not only through accessibility of potential ligands, but also via electrostatic properties generated from the closely-spaced phosphodiester groups. Conversely, metal coordination can dramatically alter helical properties; examples include the influence of cisplatin on widening the minor groove of B-form DNA, and the ability of Ni^{II} to convert B- to Z-form, where purine N7 positions are most exposed.

Both DNA and RNA can form structures other than the double helix, with RNA generating the predominant examples. RNA generally functions as a single strand whose folded structure consists of double-helical regions and also extra-helical regions with a more complex nature. The complex structure in RNA often involves the hydrogen-bond donor/acceptor properties of the 2′-OH positions. Thus, in addition to the known metal-binding positions in the major and minor grooves of both DNA and RNA helices, additional metal sites are also found in RNA that include nonhelical regions where phosphate oxygen and base heteratoms come into close proximity.

8.29.2.2 Ligand Properties of Bases, Nucleosides, and Nucleotides

The pK_a values for many nucleic acid–base derivatives have been measured potentiometrically and provide one measure of the propensity of a site to bind metals. The pK_a values in Figure 1 are for the nucleosides, the derivatives with sugars attached at the purine N9 and pyrimidine N1 positions. As described by Martin,[14] there is in general an excellent correlation between the pK_a values of the pyridine-like positions of the purines (N1 of A,G) and pyrimidines (N3 of C,T,U) and the affinities of these sites for metal ions. Substitution at other sites on the

nucleosides does not affect this correlation. The imidazole-like N7 positions of A and G also show a strong correlation between pK_a and metal ion affinity.

Since metal binding and protonation are linked events, the distribution of nucleoside species that are metallated at different sites is pH dependent. The vast majority of oligonucleotide-metal complexes demonstrate metal coordination to the guanine N7 position that is deprotonated at neutral pH, sometimes with additional interactions to the O6 keto oxygen atom. In adenine and adenosine, however, the pK_a of N1 is $\sim$3 and greater than that of N7. At neutral pH, metal coordination to adenine N1 and N7 positions has been measured to be nearly equally populated in, for example, slowly exchanging Pt compounds. As noted below, in standard nucleic acid duplexes the N7 position of purines are more likely metal sites, since the N1 positions are involved in hydrogen bonding. In the pyrimidines, both keto oxygens and N3 positions provide potential metal ligands. For thymine and uracil, deprotonation of N3 at high pH is required to render N3-nitrogen metal complexes. Although the exocyclic amino nitrogens, in particular N6 of adenine, N2 of guanine, and N4 of cytosine, appear to be promising ligands, the lone pairs of these amines are donated back into the heterocyclic ring systems. The 2′- and 3′-hydroxyl groups on the furanose sugars of nucleosides are potential ligands but have rarely been found coordinated to metals in characterized complexes except under conditions of high pH, where 2′-,3′-O$^-$ ribonucleoside chelates can be formed.

Building towards models relevant for polymeric DNA and RNA, nucleotides contain a phosphate attached at the 5′ or 3′ position. The 5′-nucleotides are most commonly studied, for which the phosphate has a p$K_a \sim 6$ for the first protonation step. Unless otherwise noted, throughout this chapter "nucleotide" will refer to the 5′-phosphate linkage. In nucleotides, metal–phosphate coordination competes with metal–base interactions. Chelate complexes with both phosphate and base coordination can occur when sterically allowed. Thus, transition metal complexes with purine monophosphates tend to exhibit metal coordination to the base N7 position, with apparent hydrogen bonding of coordinated waters to the phosphate. By contrast, more ionic Mg^{II} binds preferentially to the phosphate groups in nucleotide monophosphates. In di- and tri-phosphate complexes such as metal–ATP compounds, the proximity of multiple phosphates generally favors polyphosphate chelate complexes with metal ions.

8.29.2.3 Ligand Properties of Oligonucleotides: Overview

Metal association with oligonucleotides has been examined in systems ranging from 10-nucleotide base-paired duplexes to 300–400 nucleotide RNA molecules. At neutral pH, these oligonucleotides carry one negative charge per phosphate group. The consequence of multiple, closely spaced negative charges is the creation of an ionic "atmosphere" around nucleic acids. As described below, this atmosphere leads to an association of hydrated counterions that may not include direct coordination contacts with the nucleic acid. Within the supramolecular architecture of double helices, however, some sites on the nucleic acid bases are accessible for binding to metal ions. In addition, metal-binding pockets with appropriately placed ligands including both phosphate and base coordination sites are found in more complex nucleic acid structures. As described below, the thermodynamic affinities of metals for these specific sites include factors such as coulombic attraction between the metal ion and negatively charged regions of the nucleic acid and penalties for dehydration of the ion, in addition to metal–ligand bond enthalpies.

8.29.3 TYPES OF NUCLEIC ACID–CATION INTERACTIONS

Metal-binding sites in nucleic acids can have a range of thermodynamic and kinetic properties. Based on theory and experiment, Draper and Misra[6] have emphasized three types of association of cations with nucleic acids that provide useful starting categories (see Figure 5):

(a) "territorial" binding, a mobile charged layer of hydrated cations associated with the nucleic acid polyanion;
(b) nonspecific "site-binding," association of hydrated cations with pockets of negative electrostatic potential created by the nucleic acid structure; and
(c) specific "site-binding," in which at least one cation aqua ligand is replaced by a ligand from the nucleic acid.
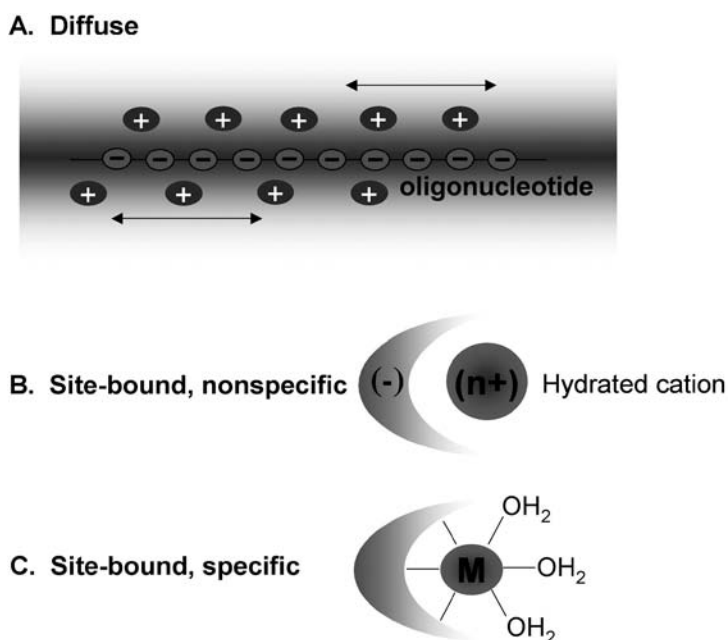
Figure 5 Three general types of cation interactions with nucleic acid oligonucleotides (after Misra and Draper[6]).

The bulk of this chapter will describe metal sites in category (c), which are specific metal sites that have been localized in X-ray or spectroscopic studies of nucleic acid structures. In order to put these sites into perspective within the complexities of a nucleic acid polyanion, this section provides a brief description of all three categories.

8.29.3.1 Nucleic Acids are Polyelectrolytes: Counterion Condensation Theory

A formal theoretical model for the association of cations with polyelectrolytes is provided by counterion condensation theory. In its ideal form this theory assumes a linear polyanionic chain consisting of regularly spaced charges and of infinite length, in a medium of constant dielectric constant.

Three important properties of the ions involved in counterion condensation are the following. First, the cations are considered to maintain full hydration and to be "territorially" or diffusely bound, meaning that they are mobile, not localized on the nucleic acid. Second, the effective concentration of cations in this mobile layer becomes independent of the bulk at a relatively low threshold concentration. Third, because of charge–charge repulsion, the effective compensation of negative charge on the nucleic acid by the cation counterions is modeled to be slightly less than 1:1. Evidence for these properties has been derived for DNA oligomers using NMR spectroscopy, among other techniques.[2] A final and critical point concerning metal interactions with nucleic acids is that the *apparent* affinity of a metal ion for a site will depend on the counterion atmosphere. For example, the apparent affinity of a divalent ion for a specific site will decrease with increasing concentrations of background monovalent ions. Moreover, the entropic cost of displacing the counterion atmosphere must be considered when metals bind to specific sites in RNA and DNA. These factors lead to relatively low apparent affinities of specific metal ion sites in oligonucleotides in comparison with metal sites found in proteins or small-molecule inorganic complexes.

The assumption that is made in formal counterion condensation theory of a linear, infinitely long oligonucleotide chain breaks down for shorter oligonucleotides and complex RNA structures with irregular shapes. The properties of ion atmospheres for such structures have more recently been modeled using Poisson–Boltzmann-type electrostatic models.[15]

8.29.3.2 Nonspecific Site-binding

Metal sites in nucleic acids are sometimes predicted from measurements of functional properties, such as stability of the folded structure, that depend on the presence of specific classes of cations. The classic example of such a site is found in folding studies of transfer RNA (tRNA), whose tertiary structure is stabilized by addition of divalent cations such as Mg^{II}, Ca^{II}, or Mn^{II} (see Figure 6).[15,16] The stabilities of RNA and DNA duplexes are always increased by addition of monovalent and divalent cations. Tertiary structure, however, generally creates regions with close association of phosphates and other groups that may accommodate an ion of a particular size and charge properties. Such metal sites may be categorized as "site-bound" or "localized" on the nucleic acid. "Localized" ions may provide sufficient population to be observable in X-ray
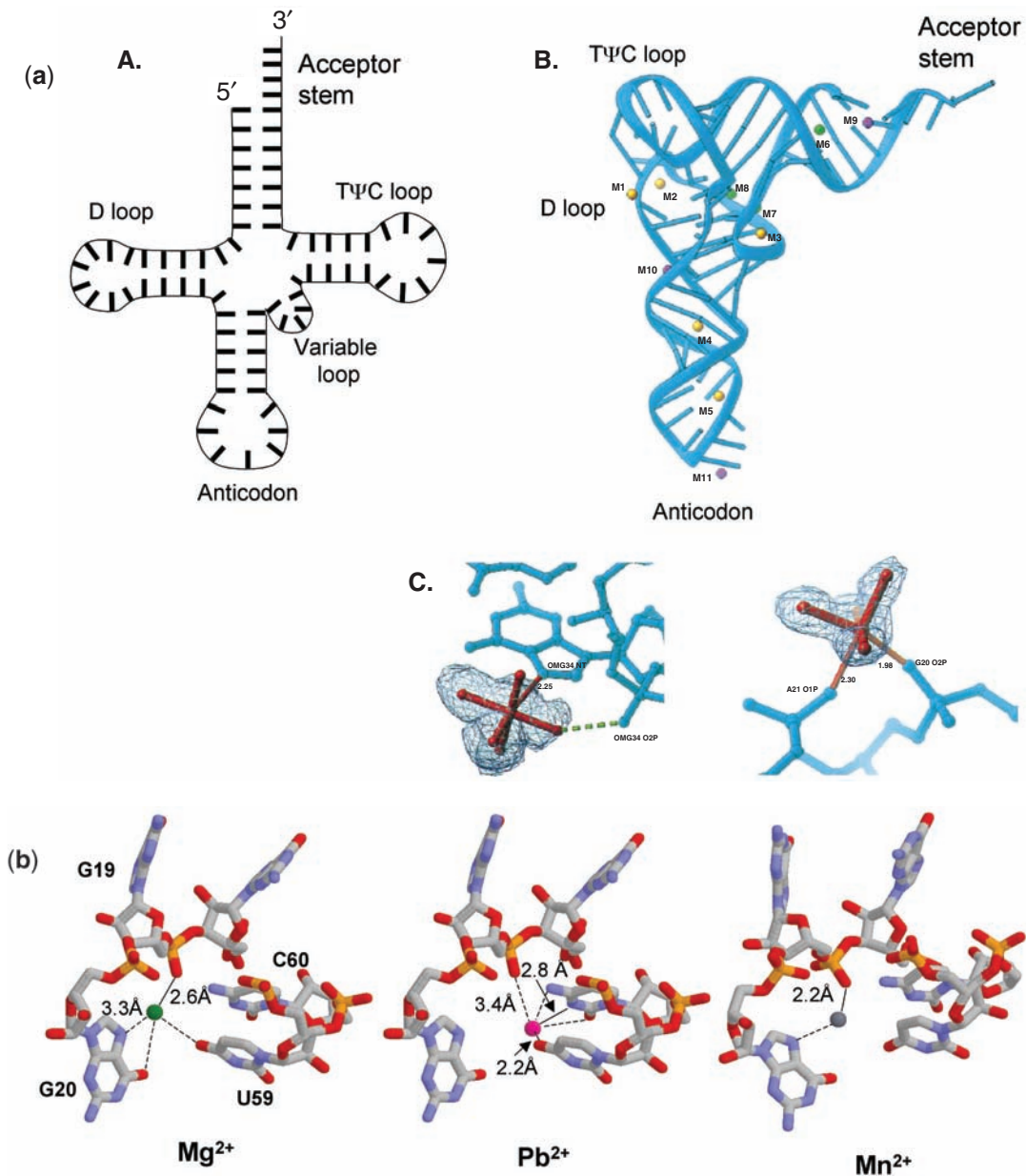
Figure 6 Structure and metal sites of yeast tRNA^{Phe}. (a) The secondary structure (A), ribbon diagram of folded RNA (B), and two specific metal sites (C) (reproduced by permission of Cambridge University Press from Shi and Moore[16], vol. 6, pp 1091–1109). (b) Metal site M2 at the intersection of the D and TΨC loop (PDB 1EHZ (Mn, 1.9 Å resolution) (reproduced by permission of Cambridge University Press from Shi and Moore[16], vol. 6, pp 1091–1109) and 1TN2 (Pb/Mg, 3.0 Å resolution, after Brown *et al.*[170]). The Pb^{II} occupancy is estimated as less than 50%. Dashed lines indicate distances estimated to be less than 4 Å.

crystallography of nucleic acids, but the sites may not require dehydration of the cation. In addition, "localized" metal sites observed by X-ray crystallography may not always correspond to sites of functional importance, i.e., metal sites whose population actually stabilizes the folded nucleic acid.

8.29.3.3 Specific Site-binding

Sites in which metal ions exchange aqua ligands for ligands from the RNA or DNA have been found in several X-ray crystal structures and predicted from spectroscopic measurements. Examples of these sites, the main topic of this chapter, include binding of cisplatin to DNA, metal sites in ribozymes, some metal sites in tRNA (Figure 6), and many other cases. It is important to note that for RNA and DNA oligomers, the thermodynamic affinity of metal ions for RNA or DNA ligands depends not only on the structure of the chelating site and the thermodynamics of bond formation, but also on the balancing factors of metal ion dehydration, displacement of other cations from the site, and transfer of the ion from the counterion condensation layer. These effects have recently been treated theoretically and in at least one case, compared favorably with experimental measurements.[15] An important result from such calculations is that when the unfavorable contributions are taken into account, there is rarely sufficient stabilizing energy to compensate for full dehydration of the cation in the nucleic acid site. *Thus, metal ions in specific sites in RNA and DNA rarely have lost more than two to three aqua or other exogeneous ligands in exchange for ligands from the nucleic acid.* An exception to this is a highly, dehydrated K^I site in a ribosomal RNA domain, described in Section 8.29.4.2. It should be kept in mind that the *apparent* thermodynamic affinities for such sites in nucleic acids depend on the background of other cations and also contain a substantial electrostatic contribution from the site on the nucleic acid.

In the following sections of this chapter, metal sites in nucleic acids and small molecules are categorized by metal type. In each section, known structures of sites in RNA and DNA are described, and results of small-molecule models are summarized.

8.29.4 MONOVALENT IONS: GROUP I AND THALLIUM(I)

The positions of low-Z cations in crystal structures of nucleic acids are often difficult to determine even at high resolution.[12,17] One reason for this difficulty is that monovalent ions such as Na^I and K^I can have irregular coordination geometries, and Na^I has an electron density that is similar to that of a water molecule.[18] Disorder and low occupancies also contribute to the difficulty of localizing cations in oligonucleotide structures, and have been a particular challenge for structural characterization of Na^I ions. These observations are consistent with an overall picture of monovalent cations predominantly contributing to a mobile counterion atmosphere in oligonucleotides. There are, however, a few examples demonstrating localized monovalent ion sites in DNA and RNA structures and in small nucleotide complexes. In addition to X-ray crystallography, a number of techniques including NMR spectroscopy and dynamics calculations have been used to characterize cation binding in nucleic acid duplexes. In some cases it has been suggested that the long residence times of Na^I ions in certain sites has an influence on duplex structure, which in turn may influence biological function.[19,20]

8.29.4.1 Sodium

Sodium ions have been proposed to bind to N3 of guanine or adenine and the O2 of cytosine or thymine in the minor groove of the DNA dodecamer referred to as the Dickerson-Drew-B-DNA dodecamer.[21] This sequence, the subject of several X-ray crystal structures extending to sub-Ångstrom resolution, contains a run of A:T base pairs known as an A-tract. All monovalent cation sites are only partially occupied in these structures. Because sodium ions are difficult to distinguish from water molecules using crystallographic techniques, a bond-valence sum approach was employed in the analysis by Williams and co-workers, who proposed that the DNA minor

groove was partially occupied by sodium and water molecules.[21] Analysis of a higher-resolution crystal structure of the same B-DNA dodecamer by Egli and co-workers found no evidence for sodium ions in the minor groove.[20] However, a series of other monovalent ions including K^I, Cs^I, Rb^I, and Tl^I have been shown to partially occupy similar sites at the ApT step of this dodecamer (*vide infra*).

G-quartets are an interesting class of supramolecular structures formed by certain oligonucleotide sequences containing runs of guanines. These structures can form stacked quadruplexes or tetraplexes of guanine bases. Each tetraplex consists of four nearly planar hydrogen-bonded guanine bases, with the sugar and phosphodiester groups remaining on the outside of the structure (see Figure 7). The structure contains a central pore in which guanine O6 ligands point towards the center, creating specific ion binding sites. Monovalent ions stabilize and can cause conformational changes in G-quartets.[22,23]

Sodium ions bind to O6 of guanines in the centers of $d(G_4T_4G_4)$ and $[d(TG_4T)]_4$ G-quartets.[22–24] The 0.95 Å resolution structure of $[d(TG_4T)]_4$ shows a line of seven dehydrated Na^I ions positioned in the central core of the eight stacked guanine tetraplexes (Figure 7). Most of the Na^I ions are positioned between tetraplexes, garnering eight O6 ligands from tetraplexes above and below the ion with Na^I–O distances of 2.2–3.7 Å. At the end of the quadruplexes the Na^I ions sit in the center of the plane of the guanine bases and have square pyramidal geometries, with four O6 ligands and an additional aqua ligand. Coordination to the O2 atom of thymine has also been observed in G-quartets.[23]

Several crystal structures of nucleotide model complexes have revealed Na ions coordinating to base, sugar, phosphate, and aqua ligands with distances of 2.2–2.9 Å.[25] A complex with 5-bromocyditine monophosphate shows dehydrated Na^I in a distorted octahedral environment, bridging two nucleotides through the cytosine O2 and N3 positions from each base with additional coordination to phosphate oxygen ligands.[26] In the case of purines, sodium can coordinate directly to the N7 of adenine or guanine or the O6 of guanine at distances ranging from 2.5 Å to 2.7 Å.[25,27]

Coordination of Na^I to the O2 of uracil was observed in the early structure of Na_2ApU (sodium adenylyl-3′-5′-uridine), which found Watson–Crick base pairing between dinucleotide units and a resulting pseudohelical structure. Foreshadowing results from later structures of full duplexes, partially hydrated Na^I coordinates to uracil O2 positions that are 4 Å apart in the "minor groove" of this mini-helical structure.[25] "Minor groove" binding was not observed in the related structure of sodium GpC, suggesting steric hindrance by the guanine N2 exocyclic amino groups.
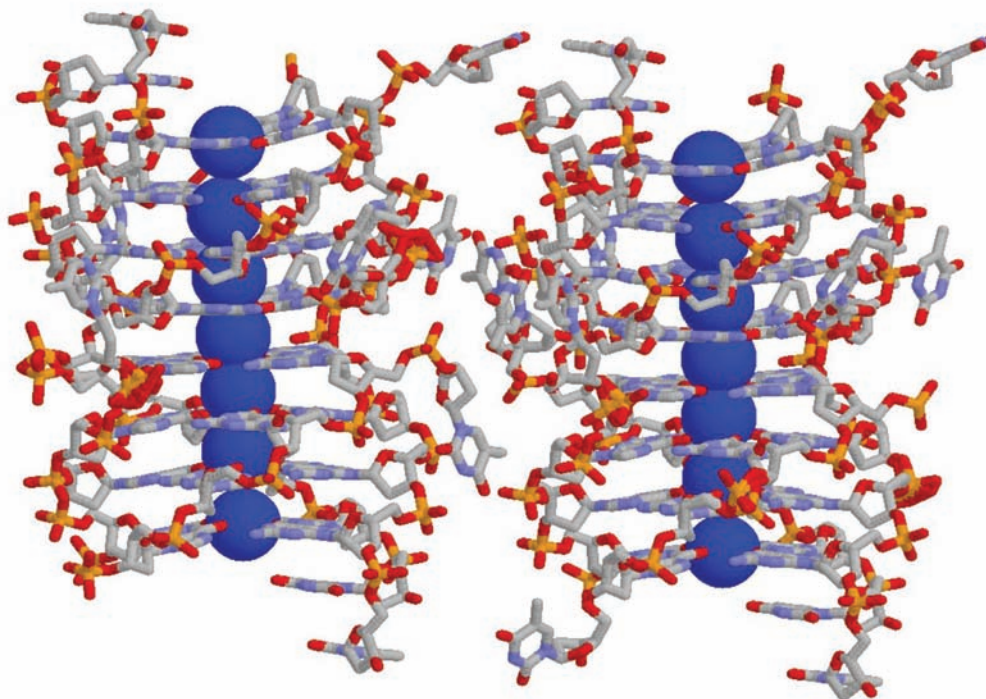
Figure 7 Na^I ions in central channel of DNA G-quartets or tetraplexes (d(TGGGT)) (PDB 352D, 0.95Å resolution, after Phillips *et al.*[24]). Two molecules from the asymmetric unit are shown. Na^I, K^I, Pb^I, and other ions coordinate multiple guanine O6 positions in the stacked quartets.

Coordination of Na^I to phosphate oxygens is commonly observed with bond distances in the range of 2.3–2.8 Å.[25,27] Additional ligands can include the sugar O2′ and O3′ positions,[25] as well as one example in (5′-ATPNa$_2$) of coordination to the sugar O4′.[28] In nearly all of these crystal structures, the sodium ions are either partially or completely surrounded by water oxygen atoms demonstrating the difficulty of dehydrating this ion.

8.29.4.2 Potassium, Thallium

Like Na^I, K^I ions bind to O6 of guanines in $d(G_4T_4G_4)$ and $[d(G_3T_4G_3)]_2$ G-quartets.[22–24] Coordination to the O2 atom of thymine has also been observed in these G-quadruplexes.[23] Unlike Na^I, the ionic radius of K^I is too large to coordinate in the plane of the terminal G-quartet, which may affect the stability of the structure.[22]

Tl^I has been shown to be a useful K^I mimic because both ions have similar ionic radii and irregular coordination geometries, but the higher electron density of Tl^I allows it to be located more readily by X-ray crystallography.[18] The Tl^I crystal structure of the Dickerson-Drew-B-dodecamer revealed 13 partially occupied (10–35%) Tl^I sites.[18] These sites were distributed between the minor groove in the A-tract part of the helix and the major groove of the G-tract segment. In the G-tract major groove of the dodecamer, Tl^I binds both N7 and O6 atoms of each guanine with ligand distances of 2.3–3.1 Å. In the A-tract minor groove Tl^I binds the adenine N3 and O2 of thymines, and the sugar O4′ positions, with bond lengths of 2.5–3.2 Å. A terminal π-cation interaction of Tl^I with the face of a cytosine base is suggested.[18] In general, the coordination of the Tl^I ion in these sites is a distorted octahedral with as many as four inner-sphere or direct contacts to the nucleic acid. Structural analysis of the dodecamer is consistent with DNA bending towards localized cations within the crystal structure.[18]

Specific sites for K^I have been observed in at least two complex RNA structures, and are considered important for function in both. In the 160-nucleotide P4–P6 domain of the *Tetrahymena* group I intron, a K^I ion is coordinated below the AA platform within the tetraloop receptor.[29] Thallium was also used as a potassium mimic to determine the coordination of the ion. Tl^I binds directly to the N7 and O6 of G227, the O4 of U228, the pro-R_p phosphate oxygen of A226, and the O2′ of the sugar of A225, with bond lengths in the range of 2.4–2.7 Å.[29] This monovalent ion appears to organize the AA platform of the tetraloop receptor in order to enhance tertiary interactions with the tetraloop.[29] Since potassium, rather than thallium, is a physiologically relevant ion, it is believed that potassium binds in this site *in vivo*.

A crystal structure of a 58 nucleotide ribosomal RNA fragment was found to contain a K^I site buried in a pocket of the RNA, bound to six phosphate oxygen atoms with an average ligand distance of 3.0 Å (Figure 8).[30] To confirm the potassium ion site, again Tl^I was used as a mimic. The Tl^I-substituted structure also has six phosphate oxygen atoms from four nucleotides. The site
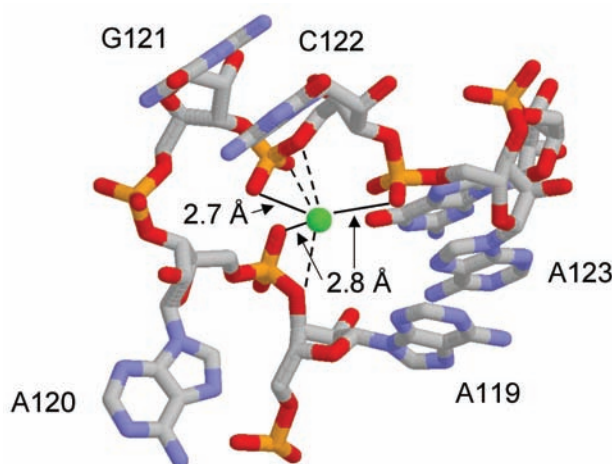
Figure 8 A K^I ion buried in a pocket of a 58-nucleotide ribosomal 23S RNA domain binds six phosphate oxygen atoms with an average distance of 3 Å. Dotted lines indicate distances of 3.0–3.3 Å (PDB 1HC8, 2.8 Å resolution, after Conn *et al.*[30]).

is shielded from solvent, creating an unusual mainly dehydrated monovalent cation near to six RNA-derived ligands. It has been shown that the monovalent cation binding site must be occupied for this 58 nt rRNA to fold.[30] This site represents an excellent example of an RNA–cation interaction that has been both structurally and functionally characterized.

A crystal structure of (nitrato)(1-methylcytosine)thallium(I) demonstrates Tl[I] interactions with N3 and O2 atoms of cytosine with distances ranging from 2.9 Å to 3.1 Å, and is different from the complex made with Ag[I] (*vide infra*).[31] Each Tl[I] ion is chelated by an N3/O2 pair from two cytosines, and an additional O2 of two additional cytosines. The Tl[I] has three additional oxygen ligands from nitrate making it an eight-coordinate complex.[31]

8.29.4.3 Rubidium, Caesium

Like K[I] and presumably Na[I], Rb[I] ions bind to the central ApT step in the minor groove of the Dickerson-Drew-B-DNA dodecamer.[32] The Rb[I] site is partially occupied, and has a coordination sphere that consists of seven oxygen atoms, with four DNA-derived ligands and three aqua ligands. The ion is coordinated to the O(2) atoms of two thymines and to two O4′ sugar positions with distances ranging from 2.8 Å to 3.5 Å.

Analysis of the Cs[I] form of the Dickerson-Drew-B-DNA dodecamer suggests lower occupancies of Cs[I] for this ApT site.[20,32]

An anomalous diffraction analysis of an A-form-DNA decamer demonstrated success of that method in locating Rb[I], Cs[I], and K[I] in three types of sites.[33] This study also demonstrated that the occupancies of the monovalent ion sites can be highly dependent on crystallization conditions. Two sites including coordination to phosphate O atoms and to 3′-OH positions from more than one duplex, with average cation to O distances of 2.9 Å to 3.2 Å, were observed. The third site was found in the major groove of the decamer, with apparent direct contacts to thymine O4 and guanine N6 positions as well as at least five additional aqua ligands.

8.29.5 GROUP IIA: MAGNESIUM/CALCIUM/STRONTIUM/BARIUM

Mg[II] has a relatively high cellular concentration and generally supports folding and activity in nucleic acids. Several nucleic acid X-ray crystal structures have been modeled with sites that exhibit direct coordination of Mg[II] to RNA or DNA ligands. The relatively low electron density and uncertainty in hydration of Mg[II] make deriving such models from low-resolution structures of nucleic acids challenging. In some cases, substitution with a heavier transition metal has confirmed the site, although as noted below in comparison with Mg[II] the transition metals often exhibit a slight shift in coordination mode, and occupation of additional sites. The vast majority of Mg[II] sites involve coordination to phosphodiester groups, but there are a few predictions of Mg[II]–nitrogen ligation to base imino nitrogen positions.

Eight Mg[II] sites are located in the 1.9 Å resolution crystal structure of tRNA[Phe],[16] three of which had not been located in previous studies.[34] Of these sites, only two involve direct contacts between Mg[II] and the RNA and both of these are through phosphate oxygens. The "M1" tRNA[Phe] site has two monodentate phosphate ligands, and "M2" has just one (Figure 6a). When substituted with Mn[II] or Co[II], additional metal sites and slight changes in coordination are observed (Figure 6b, and see Sections 8.29.6.2 and 8.29.6.4).

One of the highest-resolution nucleic acid crystal structures with localized Mg[II] sites is the 5S ribosomal RNA Loop E motif, solved to 1.5 Å resolution[35] (See Figure 9). Four high-occupancy Mg[II] ions are modeled into the structure of this 23 nucleotide motif, two of which appear to create a "binuclear" site with a 2.7 Å Mg[II]–Mg separation. Each ion of the binuclear site has monodentate coordination to a phosphate oxygen with a 2.1 Å Mg[II]–O distance, and the site is modeled with three bridging aqua ligands whose protonation states are undetermined (see Figure 9).

The 160-nucleotide P4–P6 subdomain of the large group I intron ribozyme requires Mg[II] or other divalent cations to fold, and also has at least one specific K[I] site mentioned above. The crystal structure of this RNA revealed several sites in which Mg[II] binds in complex folded regions of the molecule.[36,37] A recent 2.2 Å resolution structure of this RNA located 12 Mg[II] sites with confidence, six of which were fully hydrated and six of which coordinated to at least one RNA ligand.[37] Two of the Mg[II] ions in this motif each have three RNA ligands from phosphodiester oxygen atoms and three aqua ligands (see Figure 10). With three inner-sphere RNA ligands, these
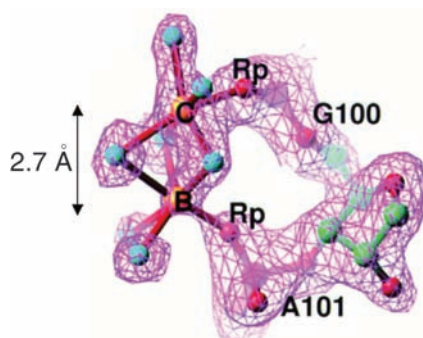
Figure 9 A "binuclear" Mg^{II} site predicted from the 1.5 Å resolution X-ray crystal structure of the loop E subdomain from 5S ribosomal RNA. Phosphodiester-ligated Mg^{II} ions bridged by aqueous ligands are shown as spheres labeled B and C (PDB 354D) (reproduced with permission from *Cell*, **1997**, *91*, 705–712; © 1997, Cell Press).
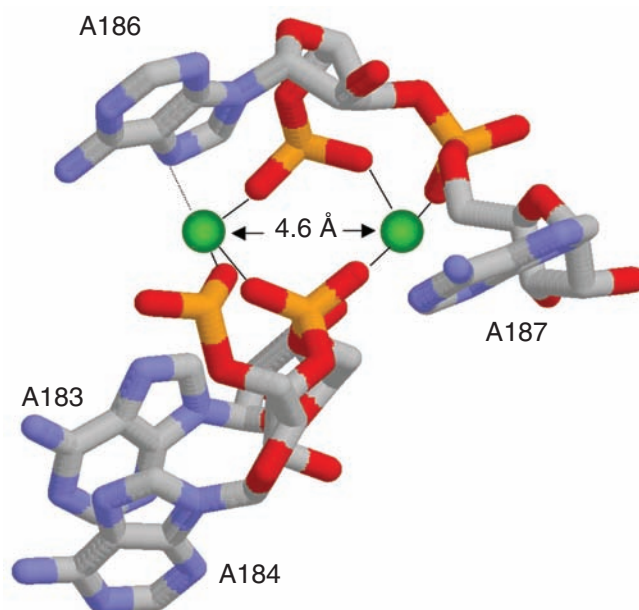
Figure 10 Binuclear Mg^{II} site from the P4–P6 subdomain of the group I intron RNA. The equivalent structure with Mn^{II} has been solved (PDB 1HR2, 2.25 Å resolution, after Juneau *et al.*[37]).

sites represent the most dehydrated Mg^{II} ions modeled in a nucleic acid structure. The two Mg^{II} ions are bridged by one of the phosphodiester groups, resulting in a 4.6 Å Mg^{II}–Mg^{II} distance. In this structure, another Mg^{II} ion binds to a guanine N7, a rare example of Mg^{II}–N7 coordination, and the O6 positions from a neighboring guanine.

A well-refined Ba^{II} site was located with 50% occupation in a short eight-nucleotide RNA duplex from a 5S rRNA subdomain. Direct coordination of Ba^{II} to guanine N7 and O6 positions and an adenine N7 was observed, albeit with relatively long bond lengths suggesting facile displacement by water ligands.[38]

Ca^{II} and Sr^{II} have both been observed to coordinate sugar 2′,3′-OH positions at the ends of helices.[39,40] Ca^{II} is generally modeled as being six- or seven-coordinate, and has also been found bound predominantly to phosphate oxygens in RNA structures.[39,41,43] Coordination of Ca^{II} O6 to keto oxygens and inino N7 of G has been observed in DNA duplexes.[42,43]

8.29.6 TRANSITION METALS

The majority of described metal–nucleotide or oligonucleotide complexes come from studies with transition metals, predominantly those late in the series. Because of similar ionic radius and

geometric preferences, Mn^{II} has long been used as a heavy-atom substitute for Mg^{II} in studies of DNA and RNA. Chromium(III) is a ligand exchange-inert analogue useful in investigating Mg^{II}–nucleotide interactions. Nucleic acid complexes with other transition metals such as Cu^{II} and Ni^{II} have been explored to better understand their basic properties, and as a basis for understanding toxicity of certain metals. The purine N7 position becomes more available for coordination in Z-form DNA than in B-form DNA, and so certain late-transition metals can cause conversion between B- and Z-form helices.

8.29.6.1   Chromium

Chromium(III) is oxophilic and can occupy sites in nucleotide complexes similar to those bound by Mg^{II}. Since Cr^{III}–nucleotide complexes are relatively inert, however, they do not support the phosphoryl transfer chemistry catalyzed by Mg^{II} in polymerases or other nucleotide-dependent enzymes. Thus, Cr^{III}–nucleotide complexes have been used to study structure and mechanism, particularly in polymerases. As one example, a co-crystal of DNA polymerase β with Cr^{III}–dTTP substrate shows Cr^{III} occupying one site in the two metal binding active site as a replacement of Mg^{II}.[44] In this structure, Cr^{III} binds to the β,γ-phosphate oxygens of the 5′-dTTP substrate.

8.29.6.2   Manganese

Mn^{II} has often been employed as a substitute for Mg^{II} to investigate potential metal binding sites in nucleic acids. High-spin Mn^{II} is similar but not identical to Mg^{II} in properties such as ionic radius, enthalpy of hydration, and coordination preferences.[45] Since the earliest crystal structures of tRNA it has been observed that some sites may be occupied by either divalent Mg or Mn, but that coordination details may differ between the two ions (Figure 6b). The most common difference is that the indirect interactions of hydrated Mg^{II} ions with RNA that are mediated by aqua ligands are sometimes replaced by direct coordination between Mn and a phosphate or nucleic acid base position.

A 10-nt RNA duplex containing sheared G:A basepairs was shown to have an Mn^{II} ion bound to the N7 of a guanine residue and the phosphate oxygen of the preceding adenosine residue.[46] A similar site is found in the hammerhead ribozyme between the phosphate of A9 and the N7 position of G10.1 (Figure 11).[47] This site in the hammerhead ribozyme has been investigated by EPR methods and has an apparent affinity of $\sim 10^5$ M^{-1} in 0.1 M NaCl, pH 7.[48] In the complex folded structure of the group I P4-P6 RNA, it was found that Mn^{II} replaced Mg^{II} at all sites that included innersphere coordination to the RNA, but not at all sites bound by hexahydrated Mg^{II}.[37]

In complex with GMP, Mn^{II} coordinates the guanine N7 and five H_2O molecules with a possible through-water interaction to the phosphate group (Figure 12).[49] The bis(ATP)$_2$ Mn^{II} complex exhibits chelation of the metal with six oxygen atoms from the α, β, and γ phosphates of two ATP molecules.[51,77] The Mn^{II}–CMP complex crystallized as a polymeric chain with four oxygens from three phosphates and two cytosine O2 oxygen donors bound to each Mn^{II} ion.[52]
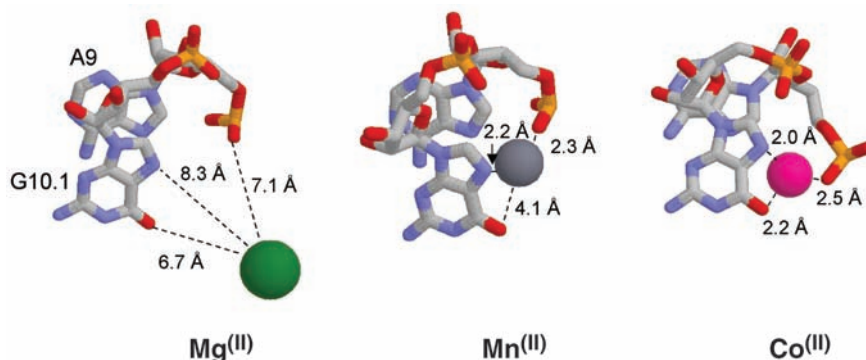
Figure 11   The structure of the A9/G10.1 metal site in the hammerhead ribozyme from crystals soaked in Mg^{II} (PDB 301D, 3.0 Å resolution), Mn^{II} (300D, 3.0 Å resolution, after Scott *et al.*[64]), or Co^{II} (379D, 3.1 Å resolution, after Murray *et al.*[65]).
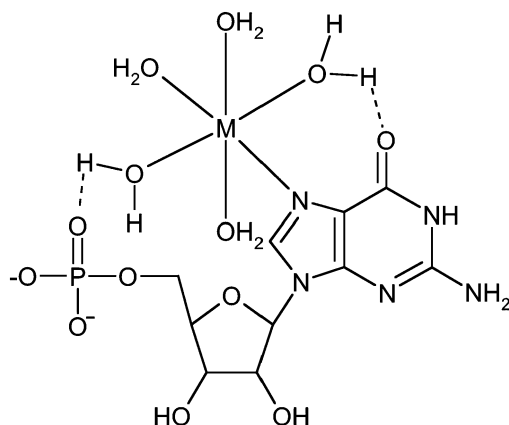
Figure 12 General scheme for transition metals in complex with 5′-guanosine monophosphate (GMP). Mn^{II}, Co^{II}, Cd^{II}, Fe^{II} coordinate to the N7 position of the guanine residue and are commonly hydrogen-bonded to the phosphate through a metal-aqua ligand (after de Meester *et al.*[49]).

The structure of a biscytosine Mn^{II} complex also shows *trans*-coordination of Mn^{II} to the O2 positions of both cytosine bases and four water molecules in octahedral geometry.[53]

8.29.6.3 Iron

The Fe^{II}–GMP complex $[Fe(5′\text{-}GMP)(H_2O)_5]$ is isostructural with that of Mn^{II} (Figure 12),[54] but no X-ray crystal structures of Fe^{II} in an oligonucleotide have yet been reported.

8.29.6.4 Cobalt

Cobalt(II) is considered a "borderline" metal and may interact with phosphate oxygen and nitrogen or oxygen atoms in the base moiety.[55] In oligonucleotides, Co^{II} most often coordinates to the N7 atom of purine bases via inner-sphere or outer-sphere interactions. For example, penta-aqua Co^{II} binds to the major groove N7 guanine positions in the structure of a short DNA duplex interacting with an intercalating agent, presumably stabilizing the duplex structure.[56]

The 1:1 and 1:2 complexes of Co^{II} with 5′-GMP show octahedral coordination to Co^{II} through the N7 atoms of one or two guanine bases with additional aqua ligands.[57,58] An octahedral bis-adenine Co^{II} complex has been reported with *trans* coordination to the adenine N9 positions.[59] Differing from observations with Mn^{II}, Co^{II} coordinates to the N3 imino nitrogen of cytosine forming a distorted tetrahedral geometry,[60,61] whereas the distorted tetrahedral Co^{II} complex with 5′-CMP includes the N3, two oxygen atoms from two different phosphate groups, and a water molecule.[62] Cytosine O2 coordination is also observed with Co^{II}.[60] With dATP, Co^{II} coordinates to the α- and γ-phosphate oxygens.[63]

At least two studies have investigated Co^{II} replacement of Mg^{II} in complex RNA structures. Both of these studies demonstrate that, as with Mn^{II}, Co^{II} generally occupies the same site in RNA but with subtle differences in ligand environment. More so than Mn^{II}, these studies suggest that Co^{II} also occupies additional sites over those located for Mg^{II}; one reason may be that the stronger electron density for Co^{II} allows this ion to be more easily located by X-ray diffraction. In tRNA, Mg^{II} was located in eight sites, Mn^{II} in one additional site (nine total), and an additional two sites were located using Co^{II} (11 total).[16] An example of ion-dependant differences is found for metals occupying the tRNA site denoted M2. While Mg^{II} exhibits direct coordination to the phosphate oxygen of G19 and through-water coordination to N7 of G20, Co^{II} switches to direct coordination of the base and a through-water interaction with phosphate.

Similar properties are found in structure determinations of Co^{II}-soaked crystals of the hammer-head ribozyme. In the hammerhead RNA structures, Mg^{II} ions have been located in five sites, Mn^{II} ions in six sites,[64] and Co^{II} ions in eight sites.[65] As described above for Mg^{II} and Mn^{II}, the coordination details of the A9/G10.1 site, which consists of phosphate/N7 ligands, changes with

metal type (see Figure 11). For both transition metal ions, direct coordination to the guanine N7 position and also the phosphate is observed whereas Mg^{II} exhibits innersphere coordination only to the A9 phosphate. Three sites in the Co^{II}-hammerhead structure are not observed for Mg^{II} or Mn^{II}; two of these involve coordination to a guanine N7 and one Co^{II} ion is modeled to bind to a guanine N3.[65]

8.29.6.5 Nickel

Ni^{II} can convert DNA duplexes containing alternating purine and pyrimidine bases from B- to Z-helix forms, via interactions between Ni^{II} and the more exposed guanine N7 positions in Z-form DNA. In a B-form DNA duplex, it has been observed that Ni^{II} binds only N7 of guanine bases rather than that of adenine bases, presumably due to the higher basicity of the guanine N7 position. Internal major-groove N7 positions may not be accessible to aquated Ni^{II}. In studies with DNA duplexes containing guanines at both internal and terminal positions, Ni^{II} coordinated only to the terminal guanine positions.[66–69]

Like Co^{II}, Ni^{II} coordinates to the α- and γ-phosphate oxygens of dATP.[63] Ni^{II} forms octahedral complexes with nucleotides, predominantly binding to the N7 atom of purine bases.[50,70–74] The $[Ni(en)_2(Cyt)_2]^{2+}$ complex exhibits *trans* coordination of two Cyt O2 atoms to the Ni^{II} ions in a slightly distorted octahedral structure.[75]

8.29.6.6 Copper

A crystal structure of a Z-form DNA duplex gives evidence for at least partial occupancy of six Cu^{II} sites, near to every guanine N7 position (Figure 13). One site with strong occupancy was modeled as a six-coordinate octahedral $[Cu^{II}(H_2O)_5]^{2+}$ ion with the guanine N7 position as an axial ligand.[76] Five other Cu^{II} ions were also observed to interact with the N7 of other guanine residues in the duplex, but had lower occupancy levels and the ligands for these Cu^{II} ions could be only partially determined.
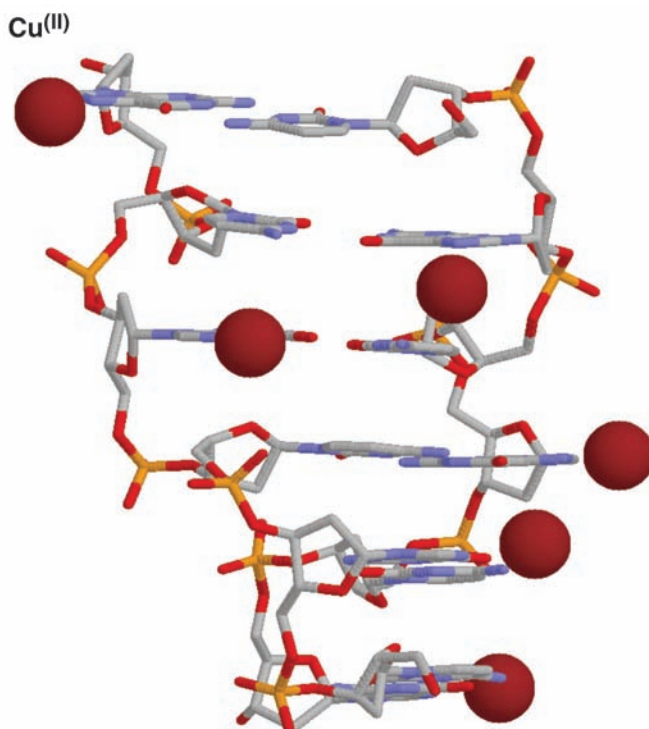
Figure 13 Six Cu^{II} atoms observed interacting with the exposed N7 position of guanine bases in a Z-form DNA duplex with sequence d(CGCGCG) (PDB 1D39, 1.2 Å resolution, after Kagawa *et al.*[76]).
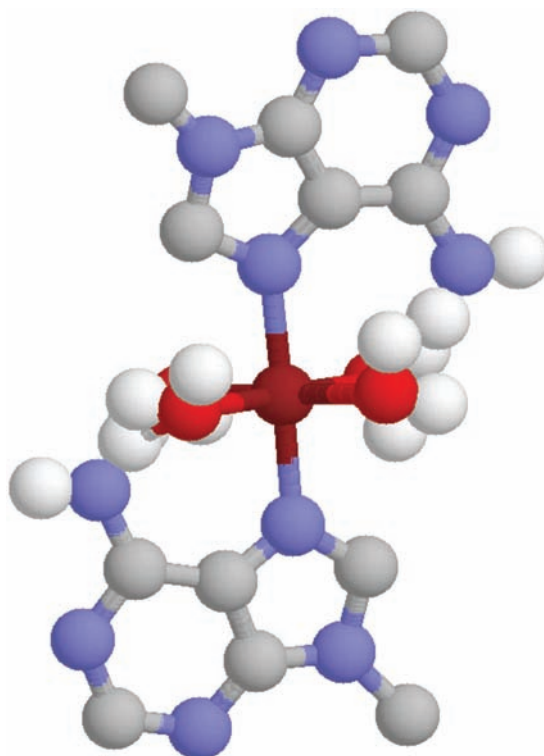
Figure 14 The Cu^{II}−bis-adenine complex [Cu(Ad)$_2$(H$_2$O)$_2$]$^{2+}$ showing axial coordination to N7 and hydrogen-bonding of Cu^{II} aqua ligands to the exocyclic N6 amines (after Sletten *et al.*[78]).

There is a comparatively rich literature on Cu^{II} complexes with nucleic acid bases and nucleotides. Mono- and bis-adenine complexes with Cu^{II} exhibit N7 coordination (Figure 14),[78] as does the bis-guanine complex.[79] With cytosine, both N3 and O2 positions are found to coordinate Cu^{II}.[80,81] At high pH, [Cu^{II}(NH$_3$)$_2$]$^{2+}$ has also been observed in square planar geometry bound to the deprotonated N3 positions of two thymine residues in *trans* geometry.[82] A square planar bis-uracil Cu^{II} complex also exhibits *trans* coordination to the nucleobase O4 positions.[83] In the polymeric 1:1 Cu^{II}:GMP complex, Cu^{II} coordinates the guanine N7 position and a phosphate oxygen from a neighboring GMP.[84] Cu^{II}−(GMP)$_2$ has also been observed in octahedral geometry with tetragonal distortion, with two guanine N7 and two aqua ligands in the plane of the Cu^{II} and two axial H$_2$O ligands.[85]

8.29.6.7 Zinc, Cadmium

The influence of added Zn^{II} on structure and stability of DNA has long been a topic of interest.[86–89] In spite of the importance of Zn^{II} in biochemistry, and the common use of the analogue Cd^{II}, few of structures of nucleic acid complexes with these ions are available. Many Zn^{II}- or Cd^{II}-nucleotide models have been characterized.

The structure of a B-form 10-nucleotide duplex (d(CGCAATTGCG)) with a covalently linked peptidyl tail has been solved in the presence of Zn^{II}.[90] As observed in similar studies with Ni^{II}, in this duplex Zn^{II} binds to the N7 positions of terminal guanine residues, but not to the purine positions internal to the duplex although these might be expected to be accessible in the major groove. One Zn^{II} is also modeled to coordinate four 5′-terminal phosphate ligands from four neighboring duplexes, with two additional aqua ligands. This Zn^{II} site apparently stabilizes association of the four duplexes.[90]

A comparison of hammerhead ribozyme structures solved in the presence of 0.1 M Zn^{II}, Co^{II}, or Cd^{II} shows that in addition to other sites also occupied by Mg^{II}, the transition metals bind at an additional site within ~2.5 Å of the N7 of position G5, a position relatively exposed to solvent.[65] A Cd^{II} site including guanine N7 and a rare sugar 2′-OH as ligands has been modeled in a 2.6 Å structure of a 23S rRNA subdomain bound to ribosomal protein L11;[91] a different structure of this same RNA was also found to contain a K^{I} site[30] (see Section 8.29.4.2).

Except for one example in which Zn^{II} binds to the N3 atom of an adenine base derivative,[92] Zn complexes with purine bases exhibit N7 coordination with remaining sites occupied by exogeneous ligands.[93–96] Zinc binds to N3 of cytosine.[97] It may also form a polymeric structure by tetrahedrally binding to N3 and O2 atoms of different cytosines alternatively bridged by a hydroxyl group.[98] The larger Cd^{II} ion can asymmetrically chelate the cytosine N3 and O2 in a bidentate manner.[99] Both ions coordinate to base positions and phosphate oxygens from different molecules of CMP.[99–101]

8.29.7   TRANSITION METALS: SECOND AND THIRD ROW

The Pt^{II} anticancer agents[7] and other potential therapeutic properties[102] drive interest in complexes of these nonbiological metals with nucleic acids. In addition to standard nucleobase coordination modes, the heavy metals can facilitate deprotonation of and bind to exocyclic amino groups. Coordination compounds of Ru, Rh, and Re have been used in the study of electron transfer properties of DNA;[103,104] because these mainly involve outer-sphere recognition of the nucleic acid, they are not reviewed here.

8.29.7.1   Molybdenum

No structures of Mo complexed to an oligonucleotide have been reported. However, it has been reported that the polyoxomolybdates have a potent *in vivo* antitumor activity.[176] In an interesting pentamolybdate complex with AMP, $[(AMPH)_2Mo_5O_{15}]^{2-}$, five octahedral MoO_6 complexes form a planar ring with the two 5′-AMP capping above and below the ring, bridging Mo units via the phosphate groups. Each metal is bound to two phosphate oxygens of 5′-AMP, two bridging oxides, and two terminal oxo groups.[105]

8.29.7.2   Ruthenium

The complexes of (η^6-arene)Ru^{II} with purine bases and nucleotides have been reported. In the cyclic trimer $[\{Ru(\eta^6\text{-}p\text{-Me-C}_6H_4Pr^i)(5'\text{-AMP})\}_3]$, each 5′-AMP bridges two Ru^{II} ions via $\mu\text{-}1\kappa N^1{:}2\kappa^2 N^6,N^7$ coordination mode.[106] In the case of guanine, steric hindrance from the N2 exocyclic amino group blocks such extensive bridging and reaction of $[Ru(\eta^6\text{-C}_6H_6)(H_2O)_3]^{2+}$ with 9-ethylguanine leads to a displacement of two aqua ligands by guanine N7 groups. Mixed amino acid–base compounds have been examined as a part of an investigation of potential antitumor properties of Ru^{II} complexes. When $[Ru(\eta^6\text{-C}_6H_6)(\text{L-ala})Cl]$ and $[Ru(\eta^6\text{-C}_6H_6)(\text{L-ala-Me})Cl_2]$ complexes are tested with 9-ethylguanine, the nucleobase N7 displaces Cl in the former, but the single amino acid ligand in the latter.[107]

8.29.7.3   Silver

Ag^I complexes with all purine and pyrimidine bases are known. Ag^I forms a binary 2:1 complex with 9-ethylguanine through N7 coordination.[108] A distorted trigonal planar Ag^I is reported for a complex in which Ag is coordinated to both the N7 atom of 9-methyladenine and the N3 atom of 1-methylcytosine, with the remaining site occupied by a water molecule.[109] An intermolecular hydrogen bond is observed between O2 of 1-methylcytosine and N6 exocyclic amine of 9-methyladenine. In dimers with 1-methylcytosine, an Ag^I ion is strongly coordinated to both the O2 atom of one cytosine base and the N(3) atom of the other base forming a centrosymmetric eight-membered ring.[110] In an interesting example of a heterometallic, mixed-nucleobase complex,[111] *cis*-$(NH_3)_2Pt^{II}$ is bound to N3 of a uracil and N3 of a cytosine base in square planar geometry, and an Ag^I ion bridges O(4) of the uracil and O2 of the cytosine, with a water and nitrate completing the strongly distorted tetrahedral Ag^I coordination sphere.

8.29.8 PLATINUM AND PALLADIUM

8.29.8.1 Platinum

Due to the anticancer activity of some amine-coordinated Pt^{II} compounds, there has been extensive interest in the complexes of Pt^{II} with oligonucleotides and nucleotides. These Pt^{II} complexes normally have square planar geometry and, in the case of bases and dinucleotides, can template more extensive supramolecular structures. Certain *cis*-Pt^{II} complexes are highly effective anticancer agents, the most famous being cisplatin or *cis*-diamminedichloroplatinum(II) and a related compound, carboplatin, *cis*-diammine(cyclobutane-1,1-dicarboxylato)platinum(II). There have been extensive studies of the coordination properties of Pt^{II} compounds with nucleic acid bases to further understand the effect of these drugs on DNA structure and function.[7]

When exposed to DNA, *cis*-Pt(Cl$_2$)(NH$_3$)$_2$ exchanges labile chloro ligands with the N7 positions of adjacent guanine bases (GpG) (Figure 15) or, with less frequency, A–G steps (ApG).[7] The crystal and NMR structures of [Pt^{II}(NH$_3$)$_2$]$^{2+}$ with *cis*-coordination to two N7 sites of adjacent guanine bases in a double-stranded DNA dodecamer duplex have been reported (Figure 16).[112] The binding of Pt^{II} does not interfere with base pairing of the nucleotides, but brings the N7 positions of the guanine bases into closer proximity than in the native duplex. This distortion has significant structural consequences, including a bend in the DNA towards a narrowed major groove and widening of the minor groove. A junction between helical forms is produced, wherein regions 5′- to the Pt^{II} lesion adopt an overall A-form structure, with a wider minor groove, whereas standard B-form helix is maintained 3′- to the site. In the crystal structure, the overall bend of the DNA duplex was determined to be 34° at the Pt^{II} coordination site.[113] Hydrogen bonding is predicted between a Pt^{II} ammine ligand and the phosphate 5′- to the Pt^{II} site. These distortions in DNA structure provide a possible basis for protein recognition of cisplatin-bound DNA sites, and the structure of one such complex is described below.

The X-ray crystallographic model of the cisplatin-DNA dodecamer shows the Pt^{II} atom to be displaced from the planes of the guanine rings by ∼1 Å in an apparently strained configuration. In the less constrained Pt^{II} adducts of a GpG dinucleotide (Figure 15) and CpGpG trinucleotide, the guanine bases have a large dihedral angle of greater than 70°, and the Pt^{II} atom is not displaced from the guanine ring planes.[114,115] Thus, the distortion in Pt^{II} geometry observed in the dodecamer double helix appears to be a consequence of the constraints imposed by more extensive base stacking in the duplex. A similar distortion in Pt^{II} geometry was observed in the X-ray crystal structure of a DNA adduct with oxaliplatin, a related platinum anticancer compound.[116] Solution NMR studies of a cisplatin-modified 9-nucleotide duplex were modeled with normal geometry about the Pt^{II}, and suggest dynamics in the region of the lesion site.[117] In addition to structures of duplexes with intrastrand cisplatin cross-links, the structure of two duplexes cross-linked via an *interstrand* cisplatin adduct has been reported. The Pt^{II} cross-link is between two guanine residues on separate helices and causes significant distortion of the helices.[118]
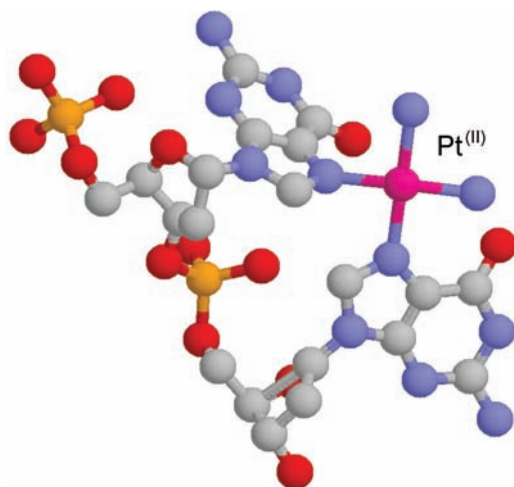
Figure 15 The coordination of *cis*-diamminodichloro Pt^{II} (cisplatin) to adjacent guanine residues in a dinucleotide disrupts base stacking, with a 76–88° angle between d(pGpG) guanine bases (after Sherman *et al.*[114]).
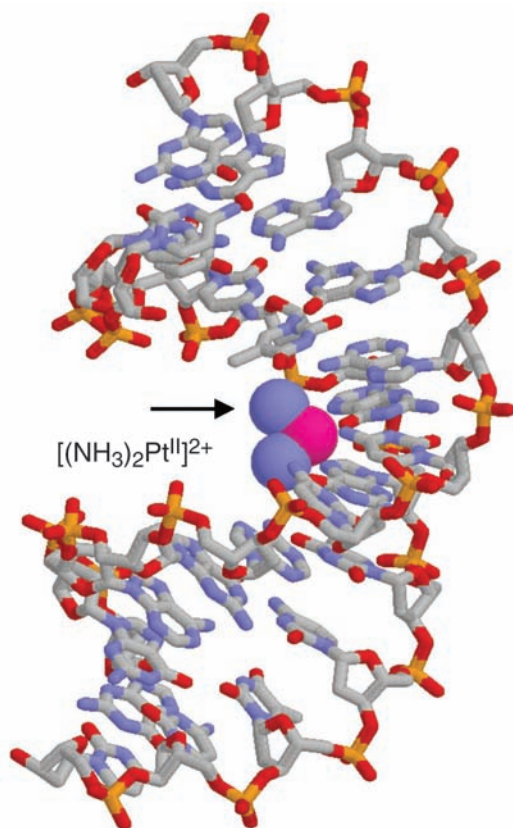
Figure 16 Cisplatin coordinated to two adjacent G residues causing a bend of ~26° in the DNA structure towards the major groove. Structure of DNA duplex d(CCTCTG*G*TCTCC) and d(GGAGACCAGAGG), where G*G* is the Pt binding site (PDB 1AIO, 2.6 Å resolution, after Takahara *et al.*[112]).

The structure of a cisplatin-modified 16-nucleotide DNA duplex with an intrastrand G–G cross-link bound to an high mobility group (HMG) protein domain has been reported.[119] In this structure, the *cis*-diamminoplatinum(II) unit coordinates to adjacent guanine bases and causes distortions of the DNA duplex that are generally similar, but not identical, to those observed in the duplexes as described above. Interestingly, in this complex an aromatic phenylalanine residue from the protein intercalates between the adjacent guanine bases of the Pt^{II} adduct. The Pt^{II} ion has a regular coordination geometry and is in the plane of the guanine bases, which are at a dihedral angle of greater than 70° that is apparently stabilized by the hydrophobic interaction from the intercalated Phe residue.

Several square planar Pt^{II} complexes with bases, nucleosides, and nucleotides have been characterized. A series of guanine-derived complexes have been prepared with both *cis*- and *trans*-geometries. These complexes generally show Pt^{II} coordination to the N7 position[120,121] except when that position is blocked and coordination to the N1 position can be observed.[122] In the case of adenine, Pt^{II} coordination to both N7 and N1 is feasible. The crystal structure of bis-adenine Pt^{II} bound to the N7 position with *trans*-geometry has been reported.[123] The mono-, bis-, and tris-cytosine Pt^{II} complexes all exhibit coordination to the N3 position.[124–126] A number of mixed-base compounds have been prepared.[127–133]

The regular square planar nature of Pt^{II} compounds has led to a series of molecules with extended "supramolecular" structures enforced by the relatively rigid metal–ligand geometries, and supported by hydrogen-bonding between bases. Because the metal–base vectors are nearly at right angles, platination of both N7 and N1 positions of purines can create the corner of a square molecule.[123,128] A U-shaped quartet has been created in a [Pt^{II}]$_3$ complex with two guanines and two adenines (see Figure 17). In this complex, a *trans*-[Pt^{II}(CH$_3$NH$_2$)$_2$]$^{2+}$ ion bridges two adenines via their N1 positions. Each adenine also has an N7-coordinated trans-Pt^{II}(NH$_3$)$_2$$^{2+}$ cation, creating corners that are linked to the N7 of a guanine forming a U-shaped quartet.[128] Interestingly, the quartet could be "closed" via coordination of Hg^{II} to exocyclic amines on both adenine and guanine ligands.
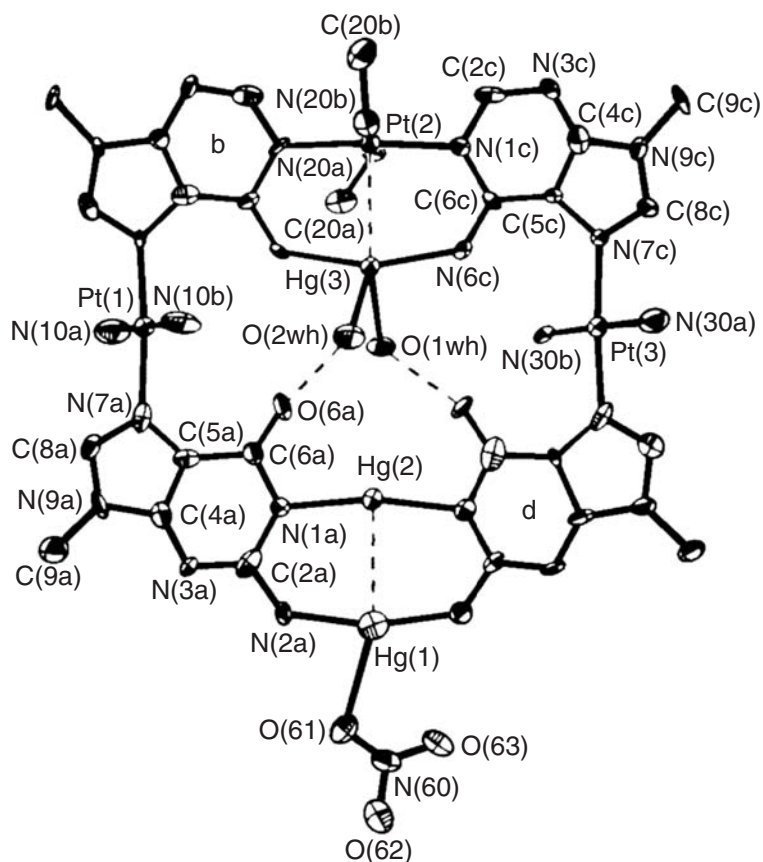
Figure 17 Adenine/guanine tetraplex templated by trans-Pt^{II} coordination and closed with Hg^{II} ions. The cation of *trans,trans,trans*-{(CH$_3$NH$_2$)$_2$PtHg(H$_2$O)$_2$[(*N1,N6*-9-MeA-*N7*)(NH$_3$)$_2$Pt(*N7*-9-MeG$_2$ *N1,N2*)]$_2$Hg$_2$ (ONO$_2$)}(NO$_3$)$_5$·13H$_2$O is shown (reproduced with permission from *Inorg. Chem.* **1998**, *37*, 5044–5045; © 1998, American Chemical Society).

In an example of molecular recognition templated by Pt^{II}, the tris-guanine [Pt^{II}(NH$_3$)]$^{2+}$ cation includes a head-to-head arrangement of two N7-coordinated guanines, the Watson–Crick faces of which are available to interact with a second tris-guanine [Pt^{II}(NH$_3$)]$^{2+}$ cation via several hydrogen-bonding interactions.[134]

8.29.8.2 Palladium

Palladium(II) generally forms isostructures with Pt^{II} complexes, but with reaction kinetics that are ~10^4 times faster than those of Pt^{II}.[135] The greater lability of Pd^{II} compounds has led to some unique ligand isomerization reactions in complexes with nucleic acid bases.

The reaction of [Pd(en)Cl$_2$] with 5′-GMP produces [Pd(en)(5′-GMP-*N7*)$_2$], (en = ethylene-1,2-diamine) in which GMP moieties are coordinated through their N7 positions to Pd^{II} and significant hydrogen bonding is observed between the GMP phosphates and ethylenediamine ligand NH positions.[135] An unusual N3-coordination is observed in the complex of adenine base with a Pd^{II} phenanthroline derivative.[136] In this dinuclear compound, adenine bridges two Pd^{II}-phen complexes (phen = 1,10-phenanthroline) bound to the N3 and N9 positions. The mononuclear complex exhibits some DNA nicking behavior that is attributed to destabilization of the glycosidic bond due to metal ion coordination at N3.

Palladium(II) normally coordinates to the N3 atoms of the cytosine base forming a square planar geometry.[137–141] An unexpected isomerization from *trans*- to *cis*-coordination of ammine ligands about Pd^{II} occurs when *trans*-[Pd^{II}(NH$_3$)$_2$(H$_2$O)$_2$]$^{2+}$ is added to the mononuclear *trans*-Pd^{II}(NH$_3$)$_2$(1-methyl cytosine)$_2$(NO$_3$)$_2$. The resulting bridged dinuclear Pd^{II} complex has two *cis*-[Pd^{II}(NH$_3$)$_2$]$^{2+}$ units bridged by cytosines through their to both N3 and deprotonated N4

exocyclic amine groups. The complex is isomorphous with the analogous bridged Pt^{II} species,[137] which is made from *cis*-diammino Pt^{II} starting materials with no apparent isomerization about Pt^{II}. These compounds show unusual coordination to deprotonated exocyclic amino groups, whose pK_a values are nominally considered to be greater than 13.

Models for cross-linking between proteins and nucleic acids have been prepared in which dipeptide-coordinated Pd^{II} completes its square-planar coordination sphere through N7 coordination to a guanine base.[142,143] Macrocyclic organopalladium crown ether complexes also have been used in molecular recognition of nucleobases including cytosine or adenine via σ-interactions between Pd^{II} and the nucleobase nitrogen ligands, π-stacking interactions between substrates and aromatic rings in the macrocyclic complexes, and hydrogen bonding of bases to ether oxygen atoms.[144–146]

8.29.9   TUNGSTEN, RHENIUM, GOLD, AND MERCURY

8.29.9.1   Tungsten, Rhenium

Deprotonated uracil or thymine bases can be coordinated to $W(CO)_5(THF)$ or $W(CO)_5(MeOH)$ organometallic complexes by a ligand displacement reaction.[147,148] Due to steric interaction between the tungsten complex and pyrimidine bases, only the N1 atom of each pyrimidine base is bound to the central metal forming a distorted octahedral coordination geometry. In this case, it has been observed that ring nitrogen atoms play a role as π-donor ligands and facilitate CO dissociation to $W(CO)_4(pyr)$ (pyr = pyrimidine).

The crystal structure of $[Re^Ibipy(CO)_3(9\text{-ethylguanine})]^+$ coordinated to a guanine base has been reported, with a 2.220 Å distance between Re^I and the guanine N7.[149] The electronic properties of the nucleobase strongly affect the luminescent properties of the Re complex.

8.29.9.2   Gold

Au^I and Au^{III} have been used to model interactions between gold and DNA, and a crystal structure for a metal–nucleotide interaction has been reported.[150] In trichloro(1-methylcytosinato) gold(III), three Cl$^-$ and the N3 atom of 1-methylcytosine are coordinated to the Au^{III} ion producing a nearly square-planar geometry. Due to steric hindrance, the cytosine ring is placed almost perpendicular to the $AuCl_3$ plane.

8.29.9.3   Mercury

In at least one case, methylmercury has been used as a heavy-atom derivative for phasing in an RNA crystal structure.[91] Although it has been generally proposed that mercury would bind nitrogen donor atoms of heterocyclic bases or pyrimidine keto oxygens,[151–153] in this case coordination to uracil N3 (presumably deprotonated) was suggested, as had been previously observed in a thymine model compound.[154] As predicted, in model compounds Hg^{II} interacts with both purine and pyrimidine N-donors. Methylmercury(II) coordinates to either N1 or N3 of cytosine base forming linear complexes.[155] Moreover, multiple methylmercury(II) ions can be simultaneously bound to N1, N3, and the N4 exocyclic amine groups of cytosine, forming 2:1 or 3:1 metal:base complexes.[155] Monomeric 5-chloromercurio-2′-deoxyuridine, an intermediate in the synthesis of 5-substituted pyrimidine nucleoside derivatives, is also known.[156]

In a dimeric mercuric chloride complex, di-μ-chloro bis[chloro(1-methylcytosine-O,N3)Hg^{II}], each of the Hg^{II} ions has asymmetric coordination to cytosine in a bidentate mode (N3, 2.17 Å; O2, 2.84 Å) with very distorted trigonal bipyramidal geometries.[157] Mercury(II) was observed to have a weak *trans* coordination to O4 of two different uracil bases forming a distorted octahedral geometry with the remaining sites filled with chloride ligands.[158] The coordination of guanine bases to Hg^{II} is only through the N7 atoms of the bases.[159,160]

8.29.10 DIMETAL COMPLEXES

Metal–metal bonded compounds have been examined as therapeutic agents that may target nucleic acids. Often bridged by carboxylate groups in the equatorial positions, the dimetal centers can have a bond order of one to four. The coordination properties of these dimetal units allow binding to bases as part of the bridging unit, or coordination to the axial positions of the complex. Axial coordination is observed predominantly for adenine, where it is favored due to hydrogen bonding between the N6 exocyclic NH_2 and the bridging carboxylate oxygen of the dimetal center.[161] With guanine, this interaction would be repulsive due to the O6 carbonyl oxygen. Antitumor activity has been observed for some dimetal complexes.[162]

8.29.10.1 Rh$_2$ and Ru$_2$

A four carboxylate-bridged $[Rh_2]^{4+}$ complex with a metal–metal single bond has been observed to link two tRNA^{Phe} molecules by coordination to two adenosine residues through the axial positions of the metals.[163] Due to the low resolution of the crystal structure, only one axial ligand to the N1 of an adenine was assigned. The crystal structure of a bis-adenosine $[Rh_2^{II}]^{4+}$ complex shows coordination through the axial position to the N7 position of both bases.[164] A dirhodium complex has also been prepared with bis-guanine bridging of the dimetal center, in which each Rh atom is coordinated to the guanine O6 and N7 in either a head-to-tail or head-to-head arrangement.[165,166] The equivalent $(Ru_2)^{4+}$ head-to-tail bis-guanine complex has been prepared.[166] The bis-adenine $(Rh_2)^{4+}$ compound has also been characterized with N7 and N6 positions bridging the dimetal center in a head-to-tail arrangement.[161] In this compound, a protonic shift is observed from the N6 exocyclic amine to the adenine N1 position, apparently reflecting a change in pK_a induced by metal coordination to the adenine N7.

The NMR-derived structure of $[Rh_2(OAc)_2\{[d(pGpG)]\}]$ has been reported and is nearly isostructural with the analogous cisplatin adduct (see Figure 18).[167]

8.29.10.2 Mo$_2$

$[Mo_2]^{4+}$ with a metal–metal quadruple bond has shown bis-adenine coordination in a bidentate N7, N6 bridging mode and head-to-head arrangement.[168] The bis-guanine complex has also been prepared, showing coordination to O6 and N7 in head-to-head arrangement as observed for the dirhodium complex (see Figure 19).[166]

8.29.11 LEAD AND TERBIUM

Due to the toxicity of Pb, there is interest in understanding interactions of this ion with nucleic acids. The relatively low pK_a for aqua ligands coordinated to Pb^{II} gives rise to enhanced strand cleavage for certain sites in RNA. Three Pb^{II} ions were observed to bind to yeast phenylalanine
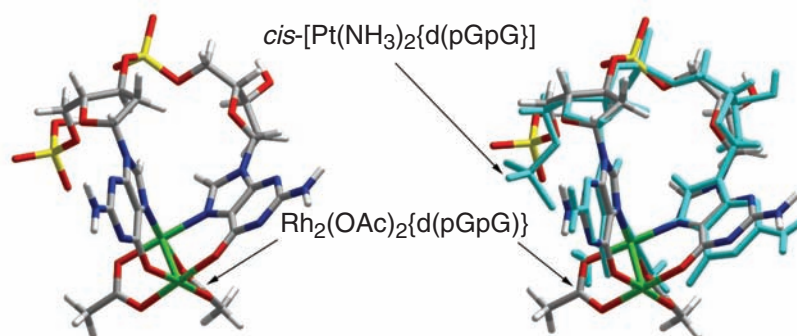
Figure 18 Comparison of dinucleotide d(pGpG) adducts with $[Pt(NH_3)_2]^{2+}$ and dirhodium $[Rh_2(OAc)_2]^{2+}$ compounds (reproduced with permission from *J. Amer. Chem. Soc.* **2003**, in press; © 2003, American Chemical Society).
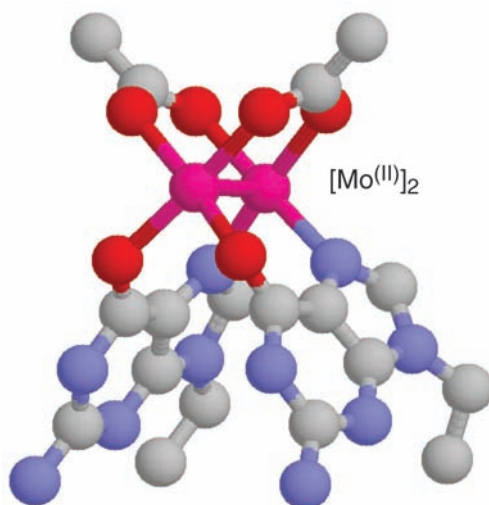
Figure 19 $[Mo_2(O_2CMe)_2(9\text{-etGH})_2(L)_2]^{2+}$ dimolybdenum complex with two guanines in head-to-head arrangement (axial $L = MeCN$ ligands omitted for clarity) (after Day *et al.*[168]).

tRNA.[169,170] Pb^{II} occupies Mg^{II} ion sites but with accommodation for its larger ionic radius and "softer" ligand preferences. In one $tRNA^{Phe}$ site, Pb^{II} is observed coordinated to the O4 of U59, the N3 and O2 of C60, and to have through-water coordination to a phosphate group. Mg^{II} and Mn^{II} also coordinate at this site, but are shifted in the binding pocket to make different inner-sphere and through-water interactions (Figure 6b). This site undergoes Pb^{II}-specific cleavage.

Another RNA molecule that undergoes Pb^{II}-specific cleavage activity has been "evolved" from random pools of RNA sequences and structurally characterized. The crystal structure of this lead-dependent ribozyme[171] has been solved in a mixture of Mg^{II}, Pb^{II}, and Ba^{II} to 2.7 Å resolution, and demonstrates the potential plasticity of some metal sites in RNA. In this structure, one Pb^{II} ion binds in a bidentate manner to G42 through N7 (3.1 Å) and O6 (3.5 Å), and also coordinates O4 of a uracil. Barium(II) also binds to this site in a similar manner, whereas a second RNA molecule in the asymmetric unit has a slightly different local structure with hydrated Mg^{II} occupying the same site.

In a guanine quadruplex, Pb^{II} ions were observed to bind between two G-quartet planes at a mean distance of 2.66 Å to the O6 position of all eight guanines.[172] In comparison with K^I, Pb^{II} is more stabilizing based on closer inter-guanine distances in the G-quartet plane and a smaller separation between the planes.

Terbium(III) binds to metal sites in nucleic acids, but often inhibits function apparently due to its higher charge.[173] Moreover, this metal also has luminescence properties that are useful for investigating metal binding sites of biomolecules. Tb^{III} is suggested to inhibit the hammerhead ribozyme by competing with a functional Mg^{II} ion, creating a nonproductive complex. An X-ray crystal structure of Tb^{III} bound to the hammerhead ribozyme shows three Tb^{III} ions interacting with the RNA at sites otherwise occupied by Mg^{II}.[174] Two Tb^{III} sites are located in stem I and stem III and show outer-sphere interactions with the RNA. However, the third Tb^{III} interacts with the face of a guanosine(G5) in the catalytic core of the ribozyme, approximately 10 Å from the cleavage site. Through luminescence studies, the relative affinities of several ions for this site were determined based on competition with Tb^{III}.[175]

8.29.12 REFERENCES

1. Voet, D.; Voet, J. *Biochemistry*, 2nd ed.; Wiley: New York, 1995.
2. Bloomfield, V. A.; Crothers, D. M.; Tinoco, I. Jr., Ignacio *Nucleic Acids Structures, Properties, and Functions* University Science Books: Sausalito, CA, 2000.
3. *The RNA World*; 2nd ed.; Cold Spring Harbor: New York, 1999.
4. DeRose, V. J. *Chem. Biol.* **2002**, *9*, 961–969.
5. Pyle, A. M. *J. Biol. Inorg. Chem.* **2002**, *7*, 679–690.
6. Misra, V. K.; Draper, D. E. *Biopolymers* **1998**, *48*, 113–135.
7. Jamieson, E.; Lippard, S. J. *Chem. Rev.* **1999**, *99*, 2467–2498.
8. Lipscomb, W. N.; Sträter, N. *Chem. Rev.* **1996**, *96*, 2375–2433.

9. Wilcox, D. E. *Chem. Rev.* **1996**, *96*, 2435–2458.
10. Sreedhara, A.; Cowan, J. A. *J. Biol. Inorg. Chem.* **2001**, *6*, 337–347.
11. Williams, N. H.; Takasaki, B.; Wall, M.; Chin, J. *Acc. Chem. Res.* **1999**, *32*, 485–493.
12. Egli, M. *Chem. Biol.* **2002**, *9*, 277–286.
13. Ramakrishnan, V.; Moore, P. B. *Curr. Opin. Struct. Biol.* **2001**, *11*, 144–154.
14. Martin, R. B. *Acc. Chem. Res.* **1985**, *18*, 32–38.
15. Misra, V. K.; Shiman, R.; Draper, D. E. *Biopolymers* **2003**, *69*, 118–136.
16. Shi, H.; Moore, P. B. *RNA* **2000**, *6*, 1091–1105.
17. Soler-Lopez, M.; Malinina, L.; Subirana, J. A. *J. Biol. Chem.* **2000**, *275*, 23034–23044.
18. Howerton, S. B.; Sines, C. C.; VanDerveer, D.; Williams, L. D. *Biochemistry* **2001**, *40*, 10023–10031.
19. Hud, N. V.; Polak, M. *Curr. Opin. Struct. Biol.* **2001**, *11*, 293–301.
20. Tereshko, V.; Minasov, G.; Egli, M. *J. Am. Chem. Soc.* **1999**, *121*, 470–471.
21. Shui, X. Q.; McFail-Isom, L.; Hu, G. G.; Williams, L. D. *Biochemistry* **1998**, *37*, 8341–8355.
22. Keniry, M. A. *Biopolymers* **2001**, *56*, 123–146.
23. Horvath, M. P.; Schultz, S. C. *J. Mol. Biol.* **2001**, *310*, 367–377.
24. Phillips, K.; Dauter, Z.; Murchie, A. I. H.; Lilley, D. M. J.; Luisi, B. *J. Mol. Biol.* **1997**, *273*, 171–182.
25. Katti, S. K.; Seshadri, T. P.; Viswamitra, M. A. *Acta Crystallogr., Sect. B: Struct. Sci.* **1981**, *B37*, 1825–1831.
26. Mande, S. S.; Seshadri, T. P.; Viswamitra, M. A. *Acta Crystallogr., Sect. C: Cryst. Struct. Commun.* **1994**, *C50*, 876–879.
27. Sugawara, Y.; Kamiya, N.; Iwasaki, H.; Ito, T.; Satow, Y. *J. Am. Chem. Soc.* **1991**, *113*, 5440–5445.
28. Kennard, O.; Isaacs, N. W.; Motherwell, W. D. S.; Coppola, J. C.; Wampler, D. C.; Lawson, A. C.; Watson, D. G. *Proc. Roy. Soc. London Series A,* **1971**, *325*, 401–436.
29. Basu, S.; Rambo, R. P.; Strauss-Soukup, J.; Cate, J. H.; Ferre-D'Amare, A. R.; Strobel, S. A.; Doudna, J. A. *Nat. Struct. Biol.* **1998**, *5*, 986–992.
30. Conn, G. L.; Gittis, A. G.; Lattman, E. E.; Misra, V. K.; Draper, D. E. *J. Mol. Biol.* **2002**, *318*, 963–973.
31. Renn, O.; Preut, H.; Lippert, B. *Inorg. Chim. Acta* **1991**, *188*, 133–137.
32. Tereshko, V.; Minasov, G.; Egli, M. *J. Am. Chem. Soc.* **1999**, *121*, 3590–3595.
33. Tereshko, V.; Wilds, C. J.; Minasov, G.; Prakash, T. P.; Maier, M. A.; Howard, A.; Wawrzak, Z.; Manoharan, M.; Egli, M. *Nucleic Acids Res.* **2001**, *29*, 1208–1215.
34. Westhof, E.; Sundaralingam, M. *Biochemistry* **1985**, *25*, 4868–4878.
35. Correll, C. C.; Freeborn, B.; Moore, P. B.; Steitz, T. A. *Cell* **1997**, *91*, 705–712.
36. Cate, J. H.; Gooding, A. R.; Podell, E.; Zhou, K.; Golden, B. L.; Kundrot, C. E.; Cech, T. R.; Doudna, J. A. *Science* **1996**, *273*, 1678–1685.
37. Juneau, K.; Podell, E.; Harrington, D. J.; Cech, T. R. *Structure* **2001**, *9*, 221–231.
38. Perbandt, M.; Vallazza, M.; Lippmann, C.; Betzel, C.; Erdmann, V. A. *Acta Crystallogr., Sect. D* **2001**, *D57*, 219–224.
39. Xiong, Y.; Deng, J.; Sudarsanakumar, C.; Sundaralingam, M. *J. Mol. Biol.* **2001**, *313*, 573–582.
40. Mueller, U.; Schübel, H.; Sprinzl, M.; Heinemann, U. *RNA* **1999**, *5*, 670–677.
41. Ippolito, J. A.; Steitz, T. A. *Proc. Natl. Acad. Sci. USA* **1998**, *95*, 9819.
42. Kielkopf, C. L.; Ding, S.; Kuhn, P.; Rees, D. C. *J. Mol. Biol.* **2000**, *296*, 787–801.
43. Minasov, G.; Tereshko, V.; Egli, M. *J. Mol. Biol.* **1999**, *291*, 83–99.
44. Arndt, J. W.; Gong, W.; Zhong, X.; Showalter, A. K.; Liu, J.; Dunlap, C. A.; Lin, Z.; Paxson, C.; Tsai, M. D.; Chan, M. K. *Biochemistry* **2001**, *40*, 5368–5375.
45. Feig, A. L. *Met. Ions Biol. Syst.* **2000**, *37*, 157–82.
46. Baeyens, K. J.; De Bondt, H. L.; Pardi, A.; Holbrook, S. R. *Proc. Natl. Acad. Sci. USA* **1996**, *93*, 12851–12855.
47. Pley, H. W.; Flaherty, K. M.; McKay, D. B. *Nature* **1994**, *372*, 68–74.
48. Morrissey, S. R.; Horton, T. E.; DeRose, V. J. *J. Am. Chem. Soc.* **2000**, *122*, 3473–3481.
49. de Meester, P.; Goodgame, D. M. L.; Jones, T. J.; Skapski, A. C. *Biochem. J.* **1974**, *139*, 791–792.
50. Collins, D. A.; de Meester, P.; Goodgame, D. M. L.; Skapski, A. C. *Biochim. Biophys. Acta* **1975**, *402*, 1–6.
51. Grant, C. V.; Frydman, V.; Frydman, L. *J. Am. Chem. Soc.* **2000**, *122*, 11743–11744.
52. Aoki, K. *J. Chem. Soc., Chem. Commun.* **1976**, 748–749.
53. De Munno, G.; Medaglia, M.; Armentano, D.; Anastassopoulou, J.; Theophanides, T. *J. Chem. Soc., Dalton Trans.* **2000**, 1625–1629.
54. Capparelli, M. V.; Goodgame, D. M. L.; Hayman, P. B.; Skapski, A. C. *Inorg. Chem. Acta* **1986**, *125*, L47–L49.
55. Wilkinson, G.; Gillard, R. D.; McCleverty, J. A. *Comprehensive Coordination Chemistry*; Pergamon: Oxford, UK, 1987.
56. Adams, A.; Guss, J. M.; Collyer, C. A.; Denny, W. A.; Wakelin, L. P. G. *Nucleic Acids Res.* **2000**, *28*, 4244–4253.
57. de Meester, P.; Goodgame, D. M. L.; Jones, T. J.; Skapski, A. C. *C.R. Acd. Sci., Ser. C* **1974**, *279*, 667.
58. Poojary, M. D.; Manohar, H. *Chem. Commun.* **1982**, 533–534.
59. de Meester, P.; Skapski, A. C. *J. Chem. Soc., Dalton Trans.* **1973**, 1596–1601.
60. Munno, G. D.; Medaglia, M.; Armentano, D.; Anastassopoulou, J.; Theophanides, T. *J. Chem. Soc., Dalton Trans.* **2000**, 1625–1629.
61. Qui, D. T.; Bagieu, M. *Acta Crystallogr., Sect. C: Cryst. Struct. Commun.* **1990**, *46*, 1645–1647.
62. Clark, G. R.; Orbell, J. D. *Acta Crystallogr., Sect. B: Struct. Sci.* **1978**, *B34*, 1815–1822.
63. Pelletier, H.; Sawaya, M. R.; Wolfle, W.; Wilson, S. H.; Kraut, J. *Biochemistry* **1996**, *35*, 12762–12777.
64. Scott, W. G.; Murray, J. B.; Arnold, J. R. P.; Stoddard, B. L.; Klug, A. *Science* **1996**, *274*, 2065–2069.
65. Murray, J. B.; Terwey, D. P.; Maloney, L.; Karpeisky, A.; Usman, N.; Beigelman, L.; Scott, W. G. *Cell* **1998**, *92*, 665–673.
66. Abrescia, N. G. A.; Malinina, L.; Fernandez, L. G.; Huynh-Dinh, T.; Neidle, S.; Subirana, J. A. *Nucleic Acids Res.* **1999**, *27*, 1593–1599.
67. Abrescia, N. G. A.; Malinina, L.; Subirana, J. A. *J. Mol. Biol.* **1999**, *294*, 657–666.
68. Abrescia, N. G. A.; Huynh-Dinh, T.; Subirana, J. A. *J. Biol. Inorg. Chem.* **2002**, *7*, 195–199.
69. Shih, H. C.; Tang, N.; Burrows, C. J.; Rokita, S. E. *J. Am. Chem. Soc.* **1998**, *120*, 3284–3288.
70. Sheldrick, W. S. *Z. Naturforsch., Teil B* **1982**, *37*, 1070–1074.
71. Begum, N. S.; Poojary, M. D.; Manohar, H. *J. Chem. Soc., Dalton Trans.* **1988**, 1303–1307.

72. de Meester, P.; Goodgame, D. M. L.; Skapski, A. C.; Smith, B. T. *Biochim. Biophys. Acta* **1974**, *340*, 113–115.
73. Garcia-Raso, A.; Fiol, J. J.; Badenas, F.; Cons, R.; Terron, A.; Quiors, M. *J. Chem. Soc., Dalton Trans.* **1999**, 167–173.
74. Fiol, J. J.; Terron, A.; Calafat, A. M.; Moreno, V.; Aguilo, M.; Solans, X. *J. Inorg. Biochem.* **1989**, *35*, 191–214.
75. Cervantes, G.; Fiol, J. J.; Terrón, A.; Moreno, V.; Alabart, J. R.; Aguiló, M.; Gómez, M.; Solans, X. *Inorg. Chem.* **1990**, *29*, 5168–5173.
76. Kagawa, T. F.; Geierstanger, B. H.; Wang, A. H. J.; Ho, P. S. *J. Biol. Chem.* **1991**, *266*, 20175–20184.
77. Sabat, M.; Cini, R.; Haromy, T.; Sundaralingam, M. *Biochemistry* **1985**, *24*, 7827–7833.
78. Sletten, E.; Ruud, M. *Acta Crystallogr., Sect. B: Struct. Sci.* **1975**, *B31*, 982–985.
79. Sletten, E.; Fløgstad, N. *Acta Crystallogr., Sect. B: Struct. Sci.* **1976**, *B32*, 461–466.
80. Valle, G.; Ettorre, R.; Peruzzo, V. *Acta Crystallogr., Sect. C: Cryst. Struct. Commun.* **1996**, *C52*, 626–628.
81. Panfil, A.; Terron, A.; Fiol, J. J.; Quiros, M. *Polyhedron* **1994**, *13*, 2513–2518.
82. Parvez, M.; Birdsall, W. J. *Acta Crystallogr., Sect. C: Cryst. Struct. Commun.* **1994**, *C50*, 540–542.
83. Cartwright, B. A.; Goodgame, M.; Johns, K. W.; Skapski, A. *Biochem. J.* **1978**, *175*, 337–339.
84. Clark, G. R.; Orbell, J. D.; Aoki, K. *Acta Crystallogr., Sect. B: Struct. Sci.* **1978**, *B34*, 2119–2128.
85. Sheldrick, W. S. *Acta Crystallogr., Sect. B: Struct. Sci.* **1981**, *B37*, 1820–1824.
86. Shin, Y. A.; Eichhorn, G. L. *Biochemistry* **1968**, *7*, 1026–1032.
87. Fazakerley, G. V. *Nucleic Acids Res.* **1984**, *12*, 3643–3648.
88. Lohrmann, R.; Bridson, P. K.; Orgel, L. E. *Science* **1980**, *208*, 1464–1465.
89. Butzow, J. J.; Eichhorn, G. L. *Biopolymers* **1965**, *3*, 95–107.
90. Soler-Lopez, M.; Malinina, L.; Tereshko, V.; Zarytova, V.; Subirana, J. A. *J. Biol. Inorg. Chem.* **2002**, *7*, 533–538.
91. Wimberly, B. T.; Guymon, R. G.; McCutcheon, J. P.; White, S. W.; Ramakrishnan, V. *Cell* **1999**, *97*, 491–502.
92. Shipman, M. A.; Price, C.; Gibson, A. E.; Elsegood, M. R. J.; Clegg, W.; Houlton, A. *Chem. Eur. J.* **2000**, *6*, 4371–4378.
93. Shionoya, M.; Ikeda, T.; Kimura, E.; Shiro, M. *J. Am. Chem. Soc.* **1994**, *116*, 3848–3859.
94. Miller, S. K.; VanDerveer, D. G.; Marzilli, L. G. *J. Am. Chem. Soc.* **1985**, *107*, 1048–1055.
95. Taylor, M. R.; Vilkins, L. M.; McCall, M. J. *Acta Crystallogr., Sect. C: Cryst. Struct. Commun.* **1989**, *C45*, 1625–1626.
96. Taylor, M. R.; McCall, M. J. *Acta Crystallogr., Sect. A: Found. Crystallogr.* **1975**, *31*, S42.
97. Beauchamp, A. L. *Inorg. Chem. Acta* **1984**, *91*, 33–38.
98. Fusch, E. C.; Lippert, B. *J. Am. Chem. Soc.* **1994**, *116*, 7204–7209.
99. Aoki, K.; Saenger, W. *J. Inorg. Biochem.* **1984**, *20*, 225–245.
100. Stigler, R. D.; Kollat, P.; Stezowski, J. J. *Acta Crystallogr., Sect. A: Found. Crystallogr.* **1984**, *40*, C70.
101. Miller, S. K.; Marzilli, L. G.; Dõrre, S.; Kollat, P.; Stigler, R.-D.; Stezowski, J. J. *Inorg. Chem.* **1986**, *25*, 4272–4277.
102. Clarke, M. J. *Coord. Chem. Rev.* **2002**, *232*, 69–93.
103. Thorp, H. H. *Adv. Inorg. Chem.* **1995**, *43*, 127–77.
104. Erkkila, K. E.; Odom, D. T.; Barton, J. K. *Chem. Rev.* **1999**, *99*, 2777–2796.
105. Inoue, M.; Yamase, T. *Bull. Chem. Soc. Jpn.* **1996**, *69*, 2863–2868.
106. Korn, S.; Sheldrick, W. S. *J. Chem. Soc., Dalton Trans.* **1997**, 2191–2199.
107. Sheldrick, W. S.; Heeb, S. *Inorg. Chim. Acta* **1990**, *168*, 93–100.
108. Menzer, S.; Hillgeris, E. C.; Lippert, B. *Inorg. Chim. Acta* **1993**, *210*, 167–171.
109. Menzer, S.; Sabat, M.; Lippert, B. *J. Am. Chem. Soc.* **1992**, *114*, 4644–4649.
110. Kistenmacher, T. J.; Rossi, M.; Marzilli, L. G. *Inorg. Chem.* **1979**, *18*, 240–244.
111. Schöllhorn, H.; Thewalt, U.; Lippert, B. *Inorg. Chem. Acta* **1987**, *135*, 155–159.
112. Takahara, P. M.; Rosenzweig, A. C.; Frederick, C. A.; Lippard, S. J. *Nature* **1995**, *377*, 649–652.
113. Takahara, P. M.; Frederick, C. A.; Lippard, S. J. *J. Am. Chem. Soc.* **1996**, *118*, 12309–12321.
114. Sherman, S. E.; Gibson, D.; Wang, A. H. J.; Lippard, S. J. *Science* **1985**, *230*, 412–417.
115. Admiraal, G.; van der Veer, J.; de Graaff, R. A. G.; den Hartog, J. H. J.; Reedijk, J. *J. Am. Chem. Soc.* **1987**, *109*, 592–594.
116. Spingler, B.; Whittington, D. A.; Lippard, S. J. *Inorg. Chem.* **2001**, *40*, 5596–5602.
117. Marzilli, L. G.; Saad, J. S.; Kuklenyik, Z.; Keating, K. A.; Xu, Y. *J. Am. Chem. Soc.* **2001**, *123*, 2764–2770.
118. Coste, F.; Malinge, J.-M.; Serre, L.; Shepard, W.; Roth, M.; Leng, M.; Zelwer, C. *Nucleic Acids Res.* **1999**, *27*, 1837–1846.
119. Ohndorf, U. M.; Rould, M. A.; He, Q. C.; Pabo, C. O.; Lippard, S. J. *Nature* **1999**, *399*, 708–12.
120. Terzis, A.; Mentzafos, D. *Inorg. Chem.* **1983**, *22*, 1140–1143.
121. Cramer, R. E.; Dahlstrom, P. L.; Seu, M. J. T.; Norton, T.; Kashiwagi, M. *Inorg. Chem.* **1980**, *19*, 148–154.
122. Sigel, R. K. O.; Sabat, M.; Freisinger, E.; Mower, A.; Lippert, B. *Inorg. Chem.* **1999**, *38*, 1481–1490.
123. Schreiber, A.; Lüth, M. S.; Erxleben, A.; Fusch, E. C.; Lippert, B. *J. Am. Chem. Soc.* **1996**, *118*, 4124–4132.
124. Lippert, B.; Lock, C. J. L.; Speranzini, A. *Inorg. Chem.* **1981**, *20*, 335–342.
125. Orbell, J. D.; Marzilla, L. G.; Kistenmacher, T. J. *J. Am. Chem. Soc.* **1981**, *103*, 5126–5133.
126. Faggiani, R.; Lock, C. J. L.; Lippert, B. *Inorg. Chem. Acta* **1985**, *106*, 75–79.
127. Schröder, G.; Sabat, M.; Baxter, I.; Kozelka, J.; Lippert, B. *Inorg. Chem.* **1997**, *36*, 490–493.
128. Lüth, M. S.; Freisinger, E.; Glahé, F.; Lippert, B. *Inorg. Chem.* **1998**, *37*, 5044–5045.
129. Faggaini, R.; Lippert, B.; Lock, C. J. L.; Speranzini, R. A. *Inorg. Chem.* **1982**, *21*, 3216–3225.
130. Sigel, R. K. O.; Freisinger, E.; Metzger, S.; Lippert, B. *J. Am. Chem. Soc.* **1998**, *120*, 12000–12007.
131. Beyerle-Pfnur, R.; Brown, B.; Faggaini, R.; Lippert, B.; Lock, C. J. L. *Inorg. Chem.* **1985**, *24*, 4001–4009.
132. Hegmans, A.; Sabat, M.; Baxter, I.; Freisinger, E.; Lippert, B. *Inorg. Chem.* **1998**, *37*, 4921–4928.
133. Lippert, B.; Pfab, R.; Neugebauer, D. *Inorg. Chem. Acta* **1979**, *37*, L495–497.
134. Freisinger, E.; Meier, S.; Lippert, B. *J. Chem. Soc., Dalton Trans.* **2000**, 3274–3280.
135. Barnham, K. J.; Bauer, C. J.; Djuran, M.; Mazid, M. A.; Rau, T.; Sadler, P. J. *Inorg. Chem.* **1995**, *34*, 2826–2832.
136. Suggs, J. W.; Dube, M. J.; Nichols, M. *Chem. Commun.* **1993**, 307–309.
137. Krumm, M.; Mutikainen, I.; Lippert, B. *Inorg. Chem.* **1991**, *30*, 884–890.
138. Holthenrich, D.; Zangrando, E.; Pichierri, F.; Randaccio, L.; Lippert, B. *Inorg. Chem. Acta* **1996**, *248*, 175–179.

139. Sinn, E.; Flynn, C. M.; Martin, R. B. *Inorg. Chem.* **1977**, *16*, 2403–2406.
140. Cosar, S.; Janik, M. B. L.; Flock, M.; Freisinger, E.; Farkas, E.; Lippert, B. *J. Chem. Soc., Dalton Trans.* **1999**, 2329–2336.
141. Khan, B. T.; Mohan, K. M.; Khan, S. R. A.; Venkatasubramanian, K.; Satyanarayana, T.; Swamy, G. Y. S. K. *Polyhedron* **1996**, *15*, 63–67.
142. Wienken, M.; Zangrando, E.; Randaccio, L.; Menzer, S.; Lippert, B. *J. Chem. Soc., Dalton Trans.* **1993**, 3349–3357.
143. Wienken, M.; Kiss, A.; Sóvágó, I.; Fusch, E. C.; Lippert, B. *J. Chem. Soc., Dalton Trans.* **1997**, 563–568.
144. Kickham, J. E.; Loeb, S. J. *Inorg. Chem.* **1994**, *33*, 4351–4359.
145. Kickham, J. E.; Loeb, S. J.; Murphy, S. L. *Chem. Eur. J.* **1997**, *3*, 1203–1213.
146. Kickham, J. E.; Loeb, S. J.; Murphy, S. L. *J. Am. Chem. Soc.* **1993**, *115*, 7031–7032.
147. Darensbourg, D. J.; Draper, J. D.; Larkins, D. L.; Frost, B. J.; Reibenspies, J. H. *Inorg. Chem.* **1998**, *37*, 2538–2546.
148. Darensbourg, D. J.; Frost, B. J.; Larkins, D. L.; Reibenspies, J. H. *Eur. J. Inorg. Chem.* **2000**, 2487–2495.
149. Oriskovich, T. A.; White, P. S.; Thorp, H. H. *Inorg. Chem.* **1995**, *34*, 1629–1631.
150. Holowczak, M. S.; Stancl, M. D.; Wong, G. B. *J. Am. Chem. Soc.* **1985**, *107*, 5789–5790.
151. Gruenwedel, D. W.; Davidson, N. *J. Mol. Biol.* **1966**, *21*, 129–144.
152. Gruenwedel, D. W.; Davidson, N. *Biopolymers* **1967**, *5*, 847–861.
153. Eichhorn, G. L.; Clark, P. *J. Am. Chem. Soc.* **1963**, *85*, 4020–4024.
154. Kosturko, L. D.; Folzer, C.; Stewart, R. F. *Biochemistry* **1974**, *13*, 3949–3952.
155. Beauchamp, A. L.; Simard, M. *Acta Crystallogr., Sect. A: Found. Crystallogr.* **1984**, *40*, C67.
156. Toma, P. H.; Dalla Riva Toma, J. M.; Bergstrom, D. E. *Acta Crystallogr., Sect. C: Cryst. Struct. Commun.* **1993**, *49*, 2047–2049.
157. Authier-Martin, M.; Beauchamp, A. L. *Can. J. Chem.* **1977**, *55*, 1213–1217.
158. Carrabine, J. A.; Sundaralingum, M. *Biochemistry* **1971**, *10*, 292–299.
159. Canty, A. J.; Tobias, R. S.; Chaichit, N.; Gatehouse, B. M. *J. Chem. Soc., Dalton Trans.* **1980**, 1693–1697.
160. Authier-Martin, M.; Hubert, J.; Rivest, R.; Beauchamp, A. L. *Acta Crystallogr., Sect. B: Struct. Sci.* **1978**, *34*, 273–276.
161. Catalan, K. V.; Hess, J. S.; Maloney, M. M.; Mindiola, D. J.; Ward, D. L.; Dunbar, K. R. *Inorg. Chem.* **1999**, *38*, 3904–3913.
162. Keppler, B. K.; Henn, M.; Juhl, U. M.; Berger, M. R.; Nieble, R.; Wagner, F. E.; *Prog. Clin. Biol. Med.* **1989**, *10*, 41–69.
163. Rubin, J. R.; Sundaralingam, M. *J. Biomol. Struct. Dyn.* **1984**, *2*, 525–530.
164. Rubin, J. R.; Haromy, T. P.; Sundaralingam, M. J. *Acta Crystallogr., Sect. C: Cryst. Struct. Commun.* **1991**, *C47*, 1712–1714.
165. Dunbar, K. R.; Matonic, J. H.; Saharan, V. P.; Crawford, C. A.; Christou, G. *J. Am. Chem. Soc.* **1994**, *116*, 2201–2202.
166. Crawford, C. A.; Day, E. F.; Saharan, V. P.; Folting, K.; Huffman, J. C.; Dunbar, K. R.; Chistou, G. *Chem. Commun.* **1996**, 1113–1114.
167. Dunbar, K. R.; Chifotides, H. T.; Koshlap, K. M.; Thomson, L. M. *J. Am. Chem. Soc.* **2002**, in press.
168. Day, E. F.; Crawford, C. A.; Folting, K.; Dunbar, K. R.; Christou, G. *J. Am. Chem. Soc.* **1994**, *116*, 9339–9340.
169. Rubin, J. R.; Sundaralingam, M. *J. Biomol. Struct. Dyn.* **1983**, *1*, 639–646.
170. Brown, R. S.; Dewan, J. C.; Klug, A. *Biochemistry* **1985**, *24*, 4785–4801.
171. Wedekind, J. E.; McKay, D. B. *Nat. Struct. Biol.* **1999**, *6*, 261–268.
172. Kotch, F. W.; Fettinger, J. C.; Davis, J. T. *Org. Lett.* **2000**, *2*, 3277–3280.
173. Horrocks, W. D. J. *Methods Enzymol.* **1993**, *226*, 495–538.
174. Feig, A. L.; Scott, W. G.; Uhlenbeck, O. C. *Science* **1998**, *279*, 81–84.
175. Feig, A. L.; Panek, M.; Horrocks, W. D.; Uhlenbeck, O. C. *Chem. Biol.* **1999**, *6*, 801–810.
176. Yamase, T.; Fujita, H.; Fukushima, K. *Inorg. Chim. Acta* **1988**, *151*, 15–18.

8.30
Appendix to Volume 8

JON A. McCLEVERTY
University of Bristol, Bristol, UK
and
THOMAS J. MEYER
Los Alamos National University, Los Alamos, New Mexico, USA

This appendix provides access to original chapters from Comprehensive Coordination Chemistry (published in 1987) that are relevant to this volume of Comprehensive Coordination Chemistry II (CCC2) but that are not cited by a specific chapter in CCC2.

For further details please see the end of the Preface under the General Information tab.

PDF 1. Chapter 62.1 Coordination Compounds in Biology